THE ESSENTIAL CANDU

A Textbook on the **CANDU Nuclear Power Plant Technology**

The Essential CANDU

A textbook on the CANDU Nuclear Power Plant Technology

Blank page

The Essential CANDU

A textbook on the CANDU Nuclear Power Plant Technology

CANDU (short for CANada Deuterium Uranium)
www.unene.ca/education/candu-textbook

Editor-in-Chief: Wm. J. Garland, Professor Emeritus, McMaster University, Hamilton, Ontario

Citations: Since the contents of this web-based textbook are subject to change without notice, it is important that the date of retrieval be included in the citation. To cite the textbook, the following form is suggested:

> The Essential CANDU, A Textbook on the CANDU Nuclear Power Plant Technology, Editor-in-Chief Wm. J. Garland, <chapter, page, etc, as appropriate>, University Network of Excellence in Nuclear Engineering (UNENE), ISBN 0-9730040. Retrieved from https://www.unene.ca/education/candu-textbook on <insert date of retrieval>.

UNENE,
c/o Department of Engineering Physics, Bldg. JHE A315
McMaster University
Hamilton, Ontario, CANADA L8S 4L7
Tel: (905) 525-9140 ext. 20168
URL: http://www.unene.ca
Email: unene@mcmaster.ca

Library of Congress Cataloging in Publication data:
UNENE
The Essential CANDU.

Includes bibliographical references.
Nuclear reactors – Design and construction
Nuclear Engineering
Nuclear fission

ISBN 0-9730040

First Edition
Printed in Canada

Dedication

This textbook is dedicated to the students of CANDU everywhere.

Disclaimer

UNENE assumes no liability for use or misuse of the textbook contents. While due care is taken to ensure the contents are accurate, UNENE does not make any warranty, expressed or implied, or assume any legal liability or responsibility for the accuracy, completeness, or usefulness of any information contained herein.

Table of Contents

Preface

There has long been a need for a CANDU[1] nuclear power plant textbook suitable for students, educators, trainers and working professionals at a target level of senior undergraduate year university engineering and science. The aim is to provide a concise, and consistently told, root storyline that will enable those new to CANDU, whether a student, a manager, a teacher / trainer, a journalist or a discipline area specialist, to learn about CANDU as an overall system and to delve into any specific area as desired. This supports the agile deployment of personnel into the industry and redeployment throughout the industry. Early on it was decided that the textbook would be public domain available online in pdf form under the UNENE banner along with associated prerequisite material and further reading. This web material can be copied to CDs for distribution or printed in book form, yet is easily updated and expanded. It is to be a living document appearing in the form of editions for revision tracking purposes.

The Essential CANDU is a textbook about nuclear science and engineering pertaining to CANDU reactors using CANDU as the reference design. This distinguishes it from comparable textbooks based on PWR reactors. This is not a product description of CANDU per se. The book will emphasize theory over other aspects of nuclear science.

This is a textbook about CANDU nuclear reactor and power plant engineering, not just the reactor physics of the core. While it is true that the reactor is certainly the distinguishing feature of the plant, it is hardly the whole story. Within the Nuclear Steam Supply System (NSSS) there are some 225 systems, but only a few can be covered explicitly in the book. This is a book about the nuclear and related bits that constitute the key bits that define nuclear engineering, not the many associated disciplines per se.

CANDU 6 was chosen as the reference design. Specifically it was agreed that Pt. Lepreau (post refurbishment) would be used as the default reference design. This does not preclude reference to multi-unit designs, single-unit variants and future designs as appropriate.

It is the root story line that glues a textbook together and guides what material is to be emphasized or deemphasized. The steam generator (and the associated heat duty diagram) is the central node of the station. It is the steam generator that dominates the overall plant dynamics. The primary side temperature floats on top of the steam drum temperature with just enough ΔT to transfer the heat from the primary side to the secondary side as discussed in Chapter 6. If the drum pressure (hence temperature) jumps, the primary side jumps to suit, affecting primary temps, fuel temps, margins, reactivity feedbacks, etc. But clearly the overall system behavior is very much dependent on the characteristics and limits of the various sub-systems and components. In short, reactor physics – the inevitable focus of typical reactor texts – is important to be sure and is covered herein. But there is so much more to a nuclear plant than reactor physics that we would be remiss in telling the CANDU story if we were to overlook the broader

1 CANDU (short for CANada Deuterium Uranium)

picture.

There are a number of existing documents and products that cover significant parts of the CANDU story. UNENE itself hosts a dozen or so graduate level courses that are significant resources for preparing a CANDU textbook. See www.unene.ca for details on those courses. And of course there are many other existing university nuclear and nuclear related courses in Canada and elsewhere (see for instance http://nuclearcanada.ca). The CANTEACH repository at http://canteach.candu.org contains a large number of legacy CANDU documents, albeit largely descriptive. Significant training, design, analysis and operation documents exist within AECL (and now Candu Energy) , Ontario Power Generation, Bruce Power, the CNSC and other organizations comprising the Canadian nuclear enterprise. *The Essential CANDU*, with its educational focus is complementary to all that.

As Editor-in-Chief it has been my pleasure to work with the authors as they laboured well beyond expectations. I have worked for years on course development with Ben Rouben and Dorin Nichita on reactor physics, Nik Popov on thermalhydraulics, Victor Snell on safety, and George Bereznai on plant systems and operations. It is truly satisfying to see the fruits of that labour appearing in the form of this text. On a more administrative level I have worked with Robin Chaplin (thermodynamics), Derick Lister and Willy Cook (Chemistry and Corrosion), Jin Jiang (Electrical) as they developed and delivered courses for UNENE. From its inception in 2000, UNENE has been a world class and world leading nuclear network. The aforementioned people are part of the UNENE team. Their research and educational contributions are a big part of that success. Guy Marleau (reactor physics), Al Hepburn (I&C), Ed Waller (Health Physics), Milan Gacesa and Mukesh Tayal (Fuel topics), and Ms. Diane Damario (Fuel Handling) are all well known in their areas. It was a pleasure to work with them on this project. Old and new colleagues and friends - it is an honour to have worked with them all.

Of course it is not just the authors that deserve special mention. As they would readily attest, it took many creative and hard working professionals to build our Canadian Nuclear Enterprise – generations of them going all the way back to the early roots of CANDU. They are the past and present colleagues, professors, managers, researchers, students and others that form our foundation and upon whose work we are but modest reporters. Two particular subsets of those are the reviewers of this text and the Working Group for this project. Scholars and authors in their own right, they have overseen and guided the development of this work. It was a comforting 'defense in depth'. The reviewers are acknowledged at the end of each chapter. We wish to sincerely thank the following Working Group members for their guidance and technical oversight:

- George Bereznai (University of Ontario Institute of Technology)
- Basma Shalaby (UNENE)
- John Luxat (McMaster University)
- Mahesh Pandey (University of Waterloo)
- Jatin Nathwani (University of Waterloo)
- Esam Hussein (University of Regina)

I have worked with each of the Working Group members as colleagues on and off over the years going back to the 70's. George, Basma, others and I bemoaned the lack of a comprehensive

CANDU textbook from the beginning. George and I even mapped out our vast plans (with half-vast ideas) and did manage over time to guide a number of courses through to completion, as did other professors. The interactions and the innumerable chats with these and many other colleagues through the years collectively set the backdrop for this textbook. But it was Basma, when stepping in as President of UNENE as I stepped out, who said: “Come on Bill. Let’s go.” And so, we did. Thanks Basma for that final prod.

This textbook, as large and comprehensive as it is, is far from complete. Each topic is a book, perhaps several books, on its own. I hope it at least encourages others to build on this modest start. It is worth noting too that the written word, try as we might, does not capture well the tacit knowledge, the working knowledge, that the working professionals have. This textbook is but a humble complement to that. The very process of creating this textbook, however, creates a learning environment for the authors and we found a considerable sharing of expertise as we prepared the chapters. This will apply to future authors as well. So, “Come on, let’s go.”

Finally, what can we say of our long suffering families but a truly heartfelt thanks. We shall be forever in your debt. Thank you all.

Bill Garland
Professor Emeritus
Department of Engineering Physics
McMaster University

Acknowledgments

We wish to sincerely thank the following Steering Committee member organizations for their financial support and access to technical information, without which this project would not have been possible:

Ontario Power Generation (OPG)
Bruce Power Inc. (BP)
Atomic Energy of Canada Limited (AECL-CRL)
Korea Hydro & Nuclear Power Company (KHNP)
Societatea Nationala “Nuclearelectrica” – S.A. (SNN)
Third Qinshan Nuclear Power Company (TQNPC)
AMEC-Nuclear Safety Solutions Limited (AMEC-NSS)
Canadian Nuclear Safety Commission (CNSC)
Canadian Nuclear Society (CNS)
Hydro Quebec (HQ)
Kinectrics (Kinectrics)
New Brunswick Power Nuclear (NBPN)
SNC-Lavalin (SNC-Lavalin)
University Network of Excellence in Nuclear Engineering (UNENE)

We wish to acknowledge and thank CANDU Owners Group Inc. (COG), especially Henry Chan and John Sowagi, for administrative support. Thank you Henry for stepping up to the plate and securing sponsorship.

PROLOGUE

CANDU in Context

prepared by
Dr. William J. Garland, Professor Emeritus,
Department of Engineering Physics,
McMaster University, Hamilton, Ontario, Canada

Summary:

Herein, we introduce the CANDU reactor by first looking at the broad social context to see why we need nuclear power. Then we take a look at the Nuclear Reactor in a nutshell, giving a quick overview to provide some context for the details found in this textbook.

Table of Contents

List of Figures

1 Energy in Society

Let's step back to take a glimpse of the context into which CANDU must be placed. The simple fact is that we are here. And there are a lot of us - some 7 billion in the year 2013 and our population is destined to hit 10 billion in a few generations. On the premise that life is worth living (and most of us think that way, otherwise our population wouldn't be growing), it follows that we should make the best of the situation. Quality of life is, thus, a worthy and meaningful pursuit. To achieve and maintain a reasonable quality of life requires energy. Access to energy is an enabling force, empowering society and individuals. In short, it is fundamental to our existence. Energy is not a panacea for the strife of life, to be sure; but without it, there would be no life at all.

One has only to reflect on early societies to appreciate the central role that access to energy has played in our development. Food and water are essential commodities for the human race. To supply these in adequate quantities to society has always been a challenge. Ancient civilizations have met this challenge with remarkable feats of engineering such as those at Angkor Wat and Machu Picchu. The Roman aqueducts such as the Pont du Gard also demonstrate significant ingenuity to provide a single commodity. Most of these were built using human power only, which limited the rate of implementation and hence development. This changed with the industrial revolution when first water power and then steam power became a source of energy to assist in the supply of food and water as well as clothing and transport. This supply of energy enabled society to implement new ideas and advance technology at a greater rate and to sustain an increase in population. Thus the human race became dependent upon another essential commodity, namely energy.

It is well established that for the prosperity of any nation, a plentiful supply of cheap energy is the key to economic growth. Countries where energy in some form or another is readily available have become wealthy. Others have had to use their ingenuity to provide this resource. Over time natural resources become depleted and new resources have to be found or developed. Some key resources which have sustained society are wood, coal, oil and now uranium. Although uranium may not generally be considered an essential resource some countries currently cannot do without it.

A suitable environment is an important factor for human survival. People are adaptable and various sectors of humanity have managed to live in all parts of the world from the frigid Arctic to the burning deserts. Hardships in these regions can be alleviated with a supply of energy enabling increased development and access to more resources. In essence, an artificial environment has been created in which to live. The human race is becoming more and more dependent upon such an artificial environment or inner environment which includes heating and air conditioning and promotes productivity. This requires increasing dependence on energy. On the other hand there is the outer environment into which waste products from the inner environment and energy production are dumped. No matter how good the inner environment the outer environment still needs protection to sustain humanity.

The development of technology has put increasing stress on the outer environment but has also provided the means to protect it. In the generation of power and the use of energy through fossil fuels, various solid pollutants such as fly ash and gaseous pollutants such as sulphur dioxide and nitrogen oxide are produced. The former have been significantly reduced by the

use of electrostatic precipitators and fabric filters in coal fired plants and the latter by the implementation of alternative fuels to eliminate smog and the development of on board diagnostic systems to reduce automobile emissions. Nevertheless, the outer environment is adversely impacted by the extensive use of fossil fuels. The only practical and economic way that these effects can be reduced is by burning less hydrocarbon fuel.

This problem of energy use and power production can be overcome by using electrical energy to replace hydrocarbon fuels and generating this energy by water and wind as well as by the nuclear fission of uranium. Most sites for hydro power have already been developed, and future development in this area is limited by possible detrimental local environmental effects. Wind power is intermittent and variable so that, beyond a certain capacity relative to the grid capacity, the electrical grid becomes unstable. Moreover, reserve capacity has to be provided for the loss of wind power. This leaves nuclear power as the only choice for long term base load energy production with minimal impact on the environment. There are no carbon dioxide emissions from nuclear power, and a relatively small amount of radioactive waste is produced. By recycling this waste the very long lived transuranic products can be returned to the reactor to be destroyed leaving only the shorter life fission products to be stored. A huge advantage of nuclear energy is the vast amount of energy obtained from a very small amount of uranium. Nuclear power is the only existing option for large scale power production that transcends the limitations of nonrenewable alternatives (such as coal, oil and gas) and renewable alternatives (wind, solar and biomass). To be sure, there are many local, national and international issues that flavour the ultimate choice of energy source, but nuclear should not be dismissed. The consequences would be dire.

We conclude, then, that nuclear should be part of the energy mix now and in the future, that is, we have a functional requirement for nuclear energy.

2 First some basics

2.1 Fission

To make sense of nuclear reactor design in general, and CANDU design in particular, the reader needs to have some familiarity with a few key nuclear concepts and phenomena. In a nutshell, slow neutrons (called thermal neutrons) can initiate a fission of uranium 235 (U-235), an isotope of uranium that occurs in nature. This is illustrated in Figure 1. Natural uranium that is mined from the ground is 0.7% U-235 and 99.3% U-238. The results of fission are fission products that are radioactive, gamma radiation, fast (or energetic) neutrons and heat. The fast neutrons have a low probability of inducing further fissions, and hence have a low probability of generat-

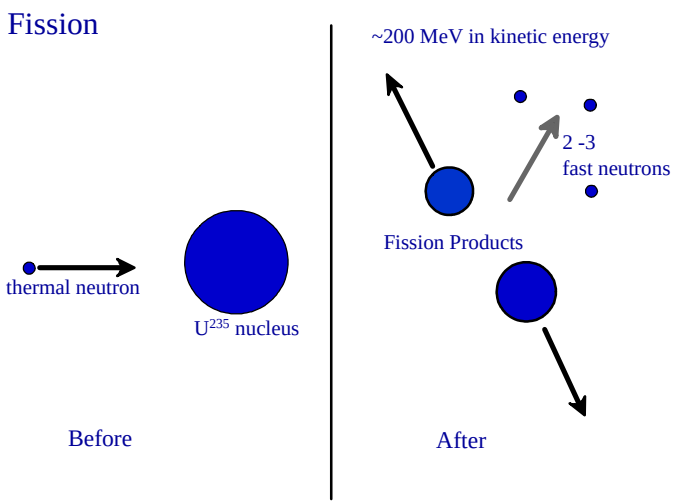

Figure 1 Fission

ing more neutrons and thus sustaining a chain reaction. So the neutrons need to be slowed down (i.e., thermalized or moderated), which is done by using a moderator such as water. The heat generated needs to be removed. The process is controlled by controlling the number of neutrons since the number of fissions per second (and hence the heat produced) is proportional to the number of neutrons present to induce the fissions.

From this the basic functional requirements of a reactor are directly derived. Needed are:

- a fuel such as U-235
- a moderator to thermalize (i.e., slow down) the fast neutrons
- a coolant to remove the heat
- a control system to control the number of neutrons
- a shielding system to protect equipment and people from radiation
- a system that pulls all this together into a workable device.

In the following, these requirements are discussed in turn to gain some insight on how and why CANDUs (and other reactor types) are built the way they are.

2.2 The fuel: the source of energy by the fission process

The probability of neutron capture leading to fission is larger for slow neutrons than for fast neutrons. Hence, most practical reactors are "thermal" reactors, that is, they utilize the higher thermal cross sections. Possible fuels include some of the various isotopes of uranium (U) and plutonium (Pu). The only naturally occurring fuel with suitable properties of significant quantities is U-235, hence most reactors use this fuel.

Naturally occurring uranium is composed of 0.7% U-235. The rest is U-238. This percentage is too low to sustain a chain reaction when combined with most practical moderators. Hence either, the probability of fission must be enhanced or the moderator effectiveness must be enhanced. One group of reactor types (PWR, BWR, AGR, RBMK, HTGR) enrich the fuel (a costly task) and use a cheap moderator (ordinary water or graphite).

Alternatively, natural uranium (relatively cheap) is used with an excellent but expensive moderator (heavy water). This is the CANDU approach. Which is better? There is no simple answer. Both work. In engineered systems, there are always tradeoffs and the final design has to be viewed in the overall context of the end-use environment.

2.3 The moderator: slowing down those speedy neutrons

The best moderator to slow down a speedy neutron is something that is the same size as the neutron itself. This is true because if a neutron hit a massive target, it would just bounce off in a different direction but with little loss in energy like a hard ball against a wall. If the neutron hit an object much smaller that itself, it would just continue on virtually unaffected. But if it hit a hydrogen atom, which is just a proton and an electron, that is almost exactly the mass of a neutron, it could lose all its energy in one collision, just like in a game of billiards. However, hydrogen does absorb neutrons as well which runs counter to the need to preserve these precious neutrons so that they can cause fission. The deuterium isotope of hydrogen, at twice the mass of hydrogen, is almost as good a slowing down agent but, since it already has an extra

neutron in the nucleus, it has a very low absorption probability. So, overall, deuterium is a far better moderator than hydrogen. By using deuterium in the form of heavy water, natural uranium can be used as a fuel. If ordinary water is used, the fuel must be enriched in U-235. Other possible moderators include graphite or beryllium and gases such as carbon dioxide and helium. A good moderator has a high scattering cross section, a low absorption cross section and slows down the neutron in the least number of collisions. Figure 2 illustrates the fission and moderation processes.

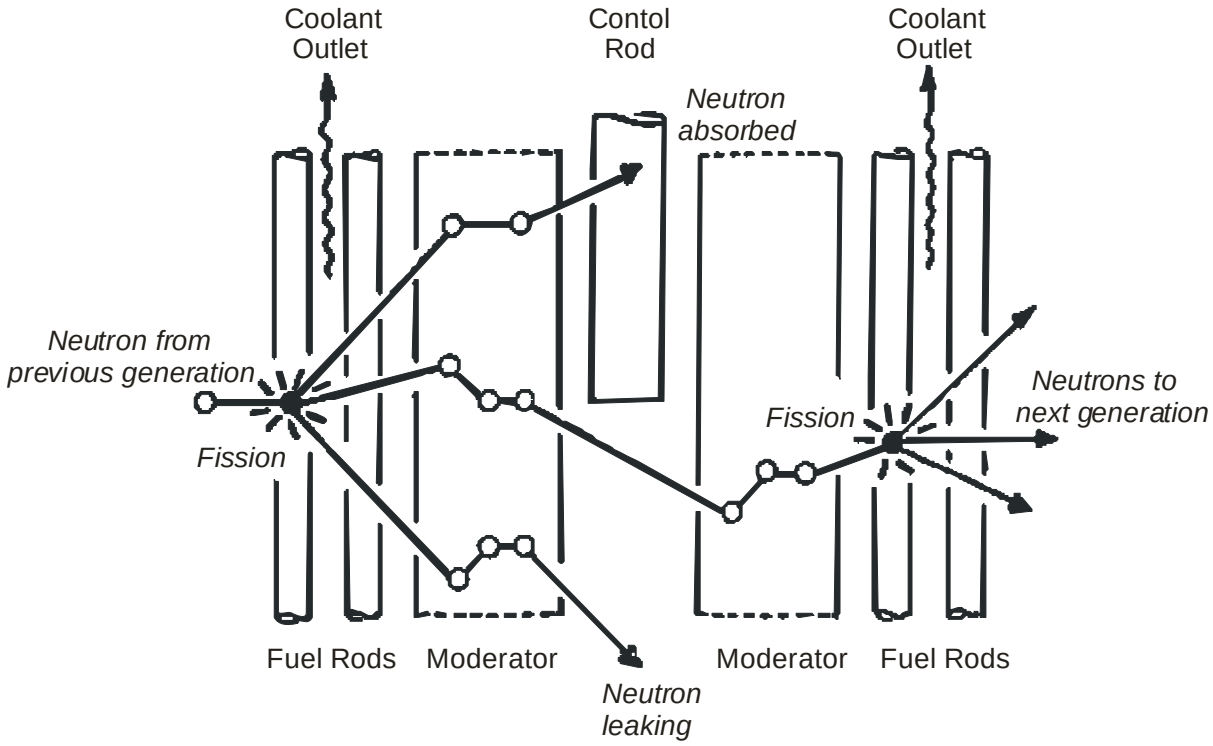

Figure 2 Nuclear reactor components

2.4 The coolant: to take away the heat generated by fissioning

The fissioning process generates energy, predominately in the form of kinetic energy of the fission products which, after a few collisions with the immediately surrounding material matrix, manifests itself as heat. A coolant (commonly) is passed over the fuel to remove this heat so that it can be used productively for energy generation. So far, we have fuel, moderator and coolant. We can conceptualize our CANDU as in the illustrations in Figure 3, below.

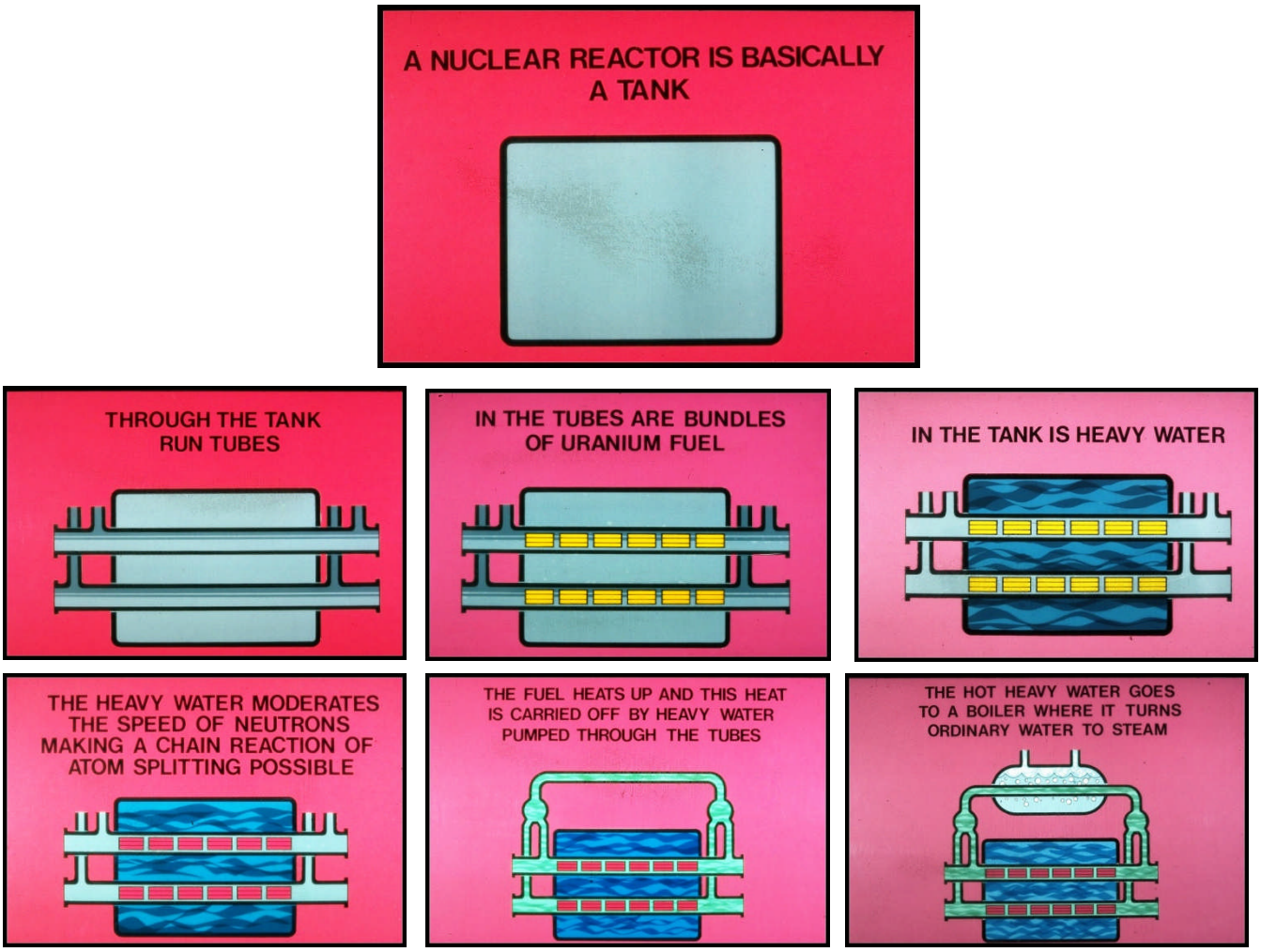

Figure 3 A Conceptual CANDU

We typically use the 'heat engine' process to turn this heat into a more useable (that is, flexible, transportable, convenient, etc.) form of energy. As illustrated in Figure 4, this heat is used to boil water and the resulting steam drives a turbine which drives an electrical generator. Electricity is a very convenient form of energy - today it is so ubiquitous that it is hard to image life without it.

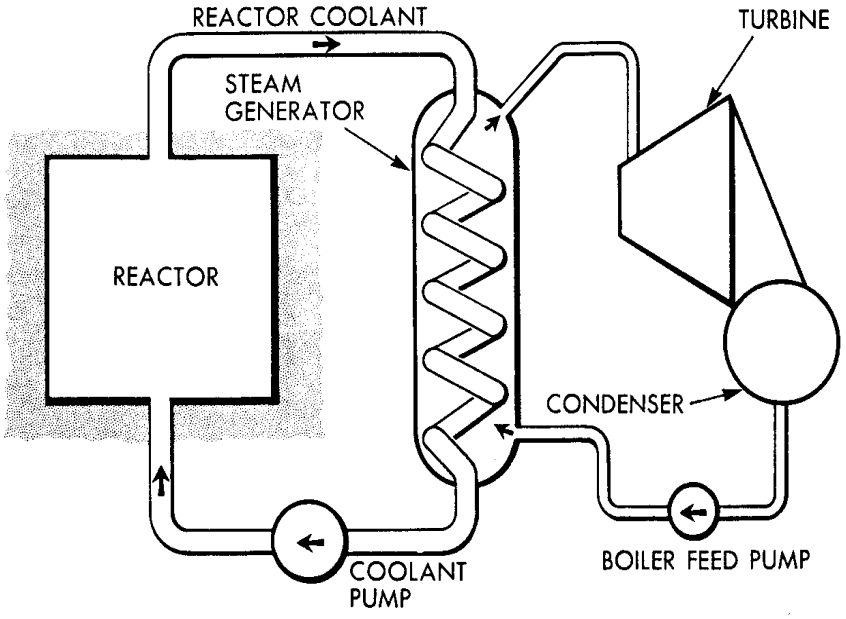

Figure 4 Basic power reactor schematic

2.5 Control: staying within desired and safe limits of power

Control of the fissioning process is achieved most easily by simply adding or removing neutron absorbers. Materials such as cadmium readily absorb neutrons and can be conveniently formed into solid rods. So by having a number of these control rods partially inserted into the moderator tank (also called the calandria) amongst the fuel and moderator in guide tubes, the neutron population can be controlled.

Hence the fissioning process and the resultant heat output can be controlled. For safety's sake, in CANDUs, these control rods and the associated control system electronics and measurement devices are built for reliable, fail-safe operation, are highly redundant, and employ additional safety concepts such as group separation.

2.6 Shielding: providing protection from radiation

Uranium isotopes are not very radioactive by themselves and do not constitute a direct radiation hazard. You can safely hold a fresh CANDU fuel bundle in your hands. Your biggest concern would be dropping it on your toes since a typical bundle weighs about 20 kg or so. It is the fissioning process that creates the nasty radioactive fission products. These ARE dangerous and must be kept isolated from us. Radiation takes on a number of forms. Alpha and beta particles are energetic charged particles that cannot penetrate solids to any significant degree. So as long as the radioactive fission products are contained by a fuel sheath or some other pipe or wall, there is no concern. Neutrons are not charged and can penetrate solid walls. We protect ourselves from them by thick walls that slow down and absorb the neutrons. Combinations of hydrogenous materials (like water and hydrocarbons) and absorbing materials (like boron and cadmium) make good neutron shields. Gamma radiation, essentially very energetic photons (ordinary light is low energy photons), are best stopped by dense material like lead and concrete. So constructing good shielding is not an onerous task, but it is an important one. Like in the control systems, safety is enhanced by redundancy. In this case, this means layering the shielding systems, one inside the other like a Russian doll set.

2.7 The system that pulls it all together

The various requirements related to fuel, moderation, cooling, control and shielding to conceive a stylized CANDU are pulled together as illustrated in figure 5. At the heart of the plant is the reactor core containing the fuel and the moderator. Heat generated there is transported away by the cooling system to the conventional side of the plant (steam generator, turbine and electrical generator).

Recall the layered, defense-in-depth approach wherein the radioactive fission products are kept from the environment by multiple protective barriers, culminated by the outer containment shell.

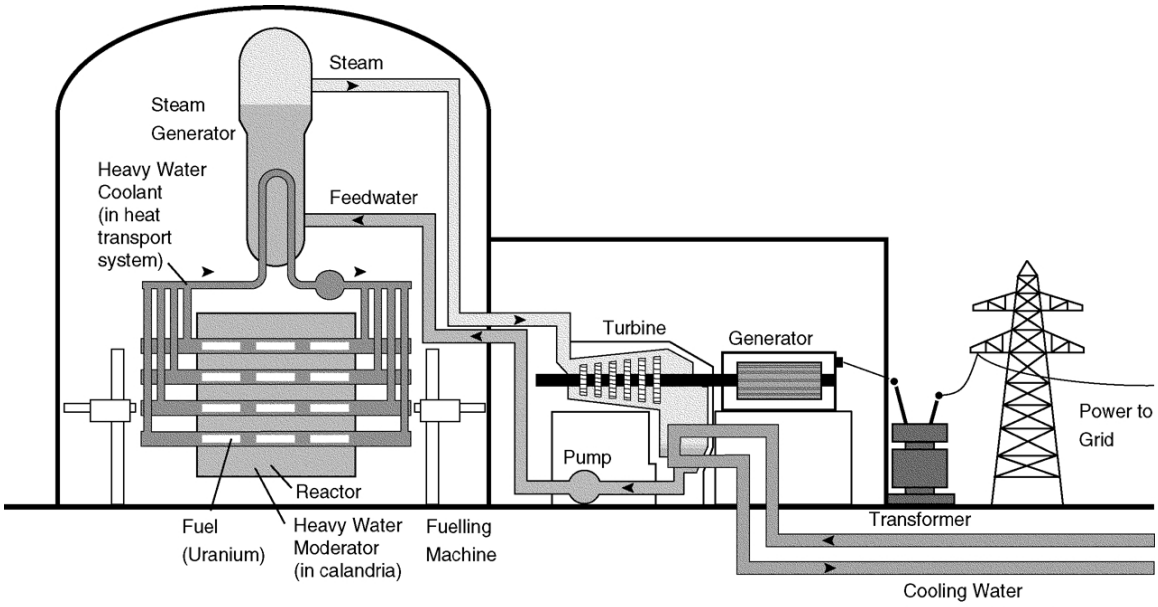

Figure 5 The overall CANDU nuclear plant

Obviously, a real CANDU is far more complex than the illustrations and designing a nuclear plant is not a trivial exercise. There are many systems and sub-systems that interact.

3 Textbook Organization

Presenting educational material on a complex physical system such as a nuclear power plant is problematic in that some knowledge of the physical plant is needed in order to give context to the physical phenomena studied, yet some knowledge of the physical phenomena is needed to make sense of the physical plant. So some iteration in presentation is unavoidable and, from a learning perspective, will prove helpful.

So we begin in the introductory chapters by putting the CANDU reactor in a societal context, give a very brief look at how the reactor functions, provide some historical context, and describe how it has evolved. From this the reader will appreciate enough of what a CANDU as a physical system entails to give context to the more in-depth chapters that follow.

The flow of the Chapters 3 to 11 is dictated by the focus on the Process Systems and the flow of power from the core to the grid. Subsequently Chapters 12 to 19 explore various key topics that arise directly as a result of the energy generating process.

The very core of the subject, literally is the fuel. The process (i.e. fissioning) aspects of the fuel and associated moderator are the subject of Chapters 3, 4 and 5 which cover the basic nuclear processes and the reactor physics topics of statics and dynamics. This sets the nature of the beast, as it were.

From both a process perspective and a safety perspective, cooling the reactor core and transporting the heat energy generated by the core is centrally important. Thermalydraulic Design and Analysis is covered by Chapters 6 and 7.

The overall plant dynamics are not so much determined by the dynamics of the individual components and systems such as the reactor core or heat transport system since each of these systems is controlled to keep each system within its own operating envelop. Overall plant dynamics is more characterized by how these systems interact with each other and is the subject of the chapters on Plant Systems (8) and Plant Operations (9).

Then a closer look at reactor and process system Instrumentation and Control (10) and Electrical Systems (11) is given.

Radiation is generated and so must be understood, quantified and handled (Chapter 12 Radiation Protection and Environmental Safety).

Fissioning is inherently an exponential process and entails substantial decay heat even after shutdown. Hence Safety (13) and Regulations and Licensing (16) are central issues.

The nuclear environment can be a harsh and demanding one. Physical integrity must be maintained over the long life of the plant, day in, day out. Hence Materials (14) and Chemistry (14) are key subjects.

The process characteristics of fuel as they relate to fissioning and heat transfer are treated in the early chapters. But there is much more to say about fuel, specifically its physics characteristics that enable it to perform so well under conditions that are so demanding. This is the

subject of Chapter 17. The forward looking topics of Fuel cycles and storage and disposal are the subjects of Chapters 18 and 19 and are a fitting way to end our introductory textbook on the Essential CANDU.

4 Further reading

- The Virtual Nuclear Tourist at http://www.virtualnucleartourist.com/ - a very popular site run by Joe Gonyeau, a dedicated nuclear engineer.
- The CANTEACH website at https://canteach.candu.org/ - be sure to visit the site library for extensive information on CANDU reactors.

CHAPTER 1

Introduction to Nuclear Reactors

prepared by
Dr. Robin Chaplin

***Summary**:*

This chapter provides a top-level introduction to nuclear reactors and surveys the world reactor situation. The various commercial large power producing reactors are identified and described against a brief background of nuclear reactor principles and key reactor components. The progressive expansion of nuclear power production is put into perspective in the global context. The operation of nuclear plants with respect to changing grid system demand is explained with some constraints identified. The chapter concludes with a brief review of safety and risk which are critical aspects in the design and operation of nuclear plants.

Table of Contents

List of Figures

List of Tables

1 Nuclear Reactor Principles

1.1 Fission Energy

All atoms consist of a nucleus of protons and neutrons surrounded by a cloud of electrons. Generally, for elements of low atomic mass numbers, there are equal numbers of neutrons and protons in the nucleus because this arrangement represents the most stable configuration. As the atomic mass number increases, however, the increasing weak repulsive forces of similarly charged protons in the nucleus are compensated for by an increasing number of neutrons which contribute additional strong nuclear forces that bind adjacent protons and neutrons together. Therefore, at high atomic mass numbers, there are approximately one and one-half times as many neutrons as protons in the nucleus, as shown in Figure 1.

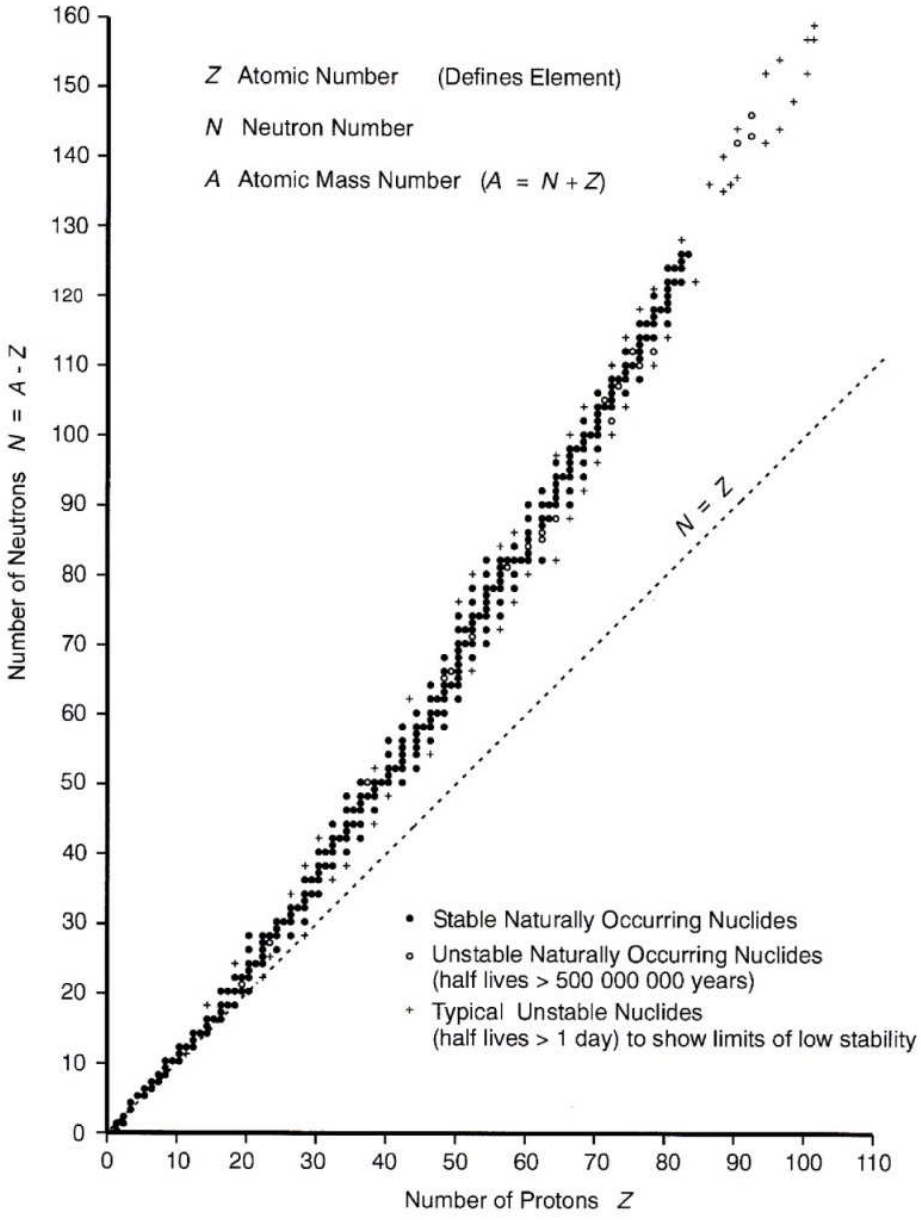

Figure 1 Range of stable and unstable nuclides

Should an element of high atomic mass number split, during a fission process, into two elements of lower atomic mass number, not as many neutrons will be required to create a stable configuration, and the surplus neutrons will be released.

The nucleons (neutrons and protons) in the nucleus are bound together by nuclear forces. When a nucleus is assembled, the binding energy attracting the individual nucleons is released. Conversely, energy is required to separate individual nucleons from one another or from the nucleus. This is analogous to the attraction of magnets to one another, but with a different type of force. This binding energy is a maximum per nucleon for elements near the middle of the range of atomic mass numbers and is somewhat less for elements with high atomic mass numbers, as shown in Figure 2. This means that, if a heavy element fissions or splits into two mid-range elements, the nucleons are bound together with a greater amount of binding energy per nucleon. The surplus energy is released as the nucleons come together more strongly. This is analogous to masses with potential energy falling into deeper holes and releasing this energy. Because of the well-known relationship between mass and energy, the release of binding energy is accompanied by a very slight decrease in the total mass of the constituents.

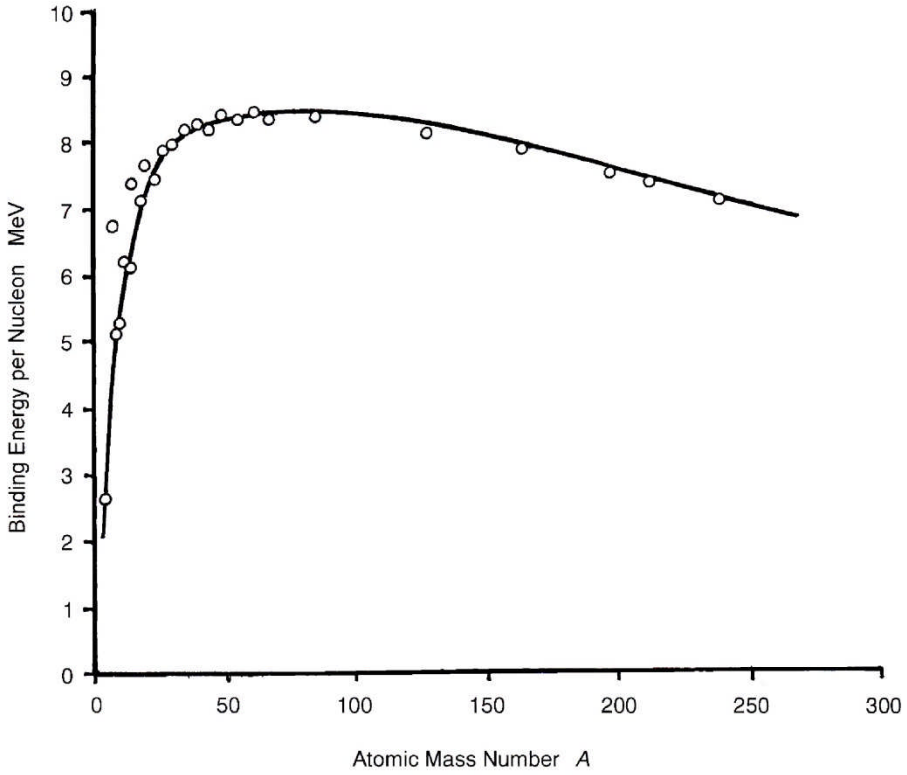

Figure 2 Binding energy per nucleon

Elements with high atomic mass numbers are unstable and become more so as the atomic mass number increases. If a neutron is added to the nucleus of a very heavy element, the additional binding energy brought into the nucleus may excite it to the extent that it fissions. This occurs in two isotopes of uranium and two isotopes of plutonium. Of these four fissile materials, only uranium-235 is naturally occurring. Furthermore natural uranium contains only 0.7 percent of U-235. Nevertheless, uranium-235 is the primary fuel of all commercial power producing nuclear reactors.

When a U-235 nucleus fissions, the release of binding energy amounts to about 200 MeV, or 32 x 10^{-12} J. Although a very small amount, this translates into a heat production rate of 950 MW if 1 kg of U-235 is totally consumed per day. In a typical nuclear power plant operating on a conventional steam cycle, this could be converted into an electrical power output of about 300 MW.

1.2 Nuclear Reactor Principles

Some heavy elements, such as uranium-235, can be induced to fission by adding a neutron to their nuclei. When fission occurs, the resultant lighter elements do not require as many neutrons in their nuclei to maintain a stable configuration and, on average, between two and three surplus neutrons are released. These neutrons can cause further fissioning of other U-235 nuclei and so establish a chain reaction. Such a reaction can be allowed to diverge, as in an atomic bomb, or be controlled, as in a nuclear reactor. Under steady state conditions, just one neutron on average from each fission should go on to produce another fission event.

When fission occurs, the release of energy drives the lighter elements or fission products and the surplus neutrons away from one another at high velocity. Most of the energy is thus transformed into kinetic energy carried by the fission products. As heavy strongly charged particles, they do not travel any significant distance and dissipate their kinetic energy in the fuel by interaction with other atoms, thus increasing the temperature of the fuel. The high energy fast neutrons, being uncharged, readily pass through the fuel and other reactor materials.

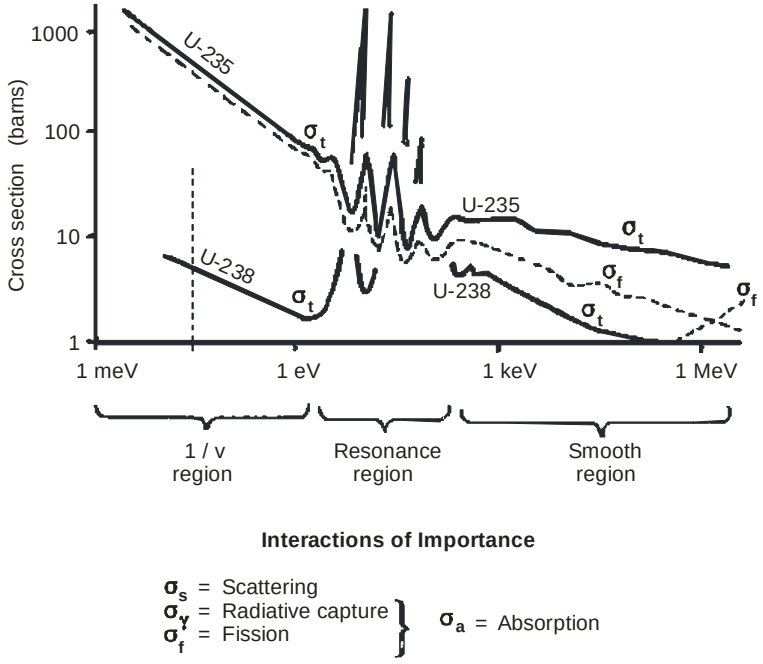

Figure 3 Fission and absorption characteristics of uranium

There are varying probabilities that they will be absorbed by different nuclei. The probability of absorption by another U-235 nucleus to cause fission increases if the neutron velocity is reduced, and therefore reducing neutron energies is advantageous. Figure 3 shows the variation of the fission cross section, that is, the probability of a fission reaction, of U-235 versus neutron energy as a dotted line. The probability increases by a factor of nearly 500 as the neutron energy is reduced from the fissioning release energy to the natural energy of neutrons in the local environment, a process known as thermalization. This can be achieved by allowing the

neutrons to experience a series of non-absorbing collisions with light nuclei, which during an elastic collision receive some of the energy from the neutrons. The resulting low energy slow neutrons are then absorbed in U-235 nuclei to cause further fissions. Some elements that can slow down or moderate neutrons effectively without significant absorption are hydrogen, deuterium, helium, beryllium, and carbon. Hence, light water (H_2O), heavy water (D_2O), and graphite (C) all make good moderators in nuclear reactors.

The solid lines in Figure 3 show the total probability of absorption (resulting in both fission and capture) in U-235 and U-238. In the resonance region (where neutron and nucleus frequencies coincide) are large spikes with very high probability of capture for U-238, so it is best to avoid this region during the neutron slowing down process. This can be achieved to some degree by ensuring that the moderation process is carried out away from the fuel. This leads to a reactor consisting of a matrix of fuel elements within the moderator with a discrete distance between fuel elements. Furthermore, to promote heat transfer from the fuel, the fuel elements themselves consist of bundles of small fuel rods. This is illustrated diagrammatically in Figure 4.

Most of the heat from fission is generated by dissipation of the kinetic energy of the fission products. Because this occurs in the fuel near the point of fission, it follows that the fuel becomes the main source of heat in the reactor. To maintain a thermodynamic cycle to produce work, this heat must be removed continuously as it is produced. A suitable coolant is therefore required to flow over the fuel elements and remove the heat. The coolant must not readily absorb neutrons and must have suitable thermal properties. Coolants such as light water, heavy water, helium, and carbon dioxide meet these requirements.

Finally, to ensure steady state operation, the number of neutrons allowed to go on to produce fission must be the same as the number in preceding generations of neutrons. To achieve the required balance, the reactor as a whole is designed to generate excess neutrons in each generation and to have a system for absorbing the excess so as to maintain and control the reactor at a steady load. This also enables the number of neutrons in successive generations to be increased when more power is required or to be decreased when power must be reduced. Such control is usually achieved by having movable neutron-absorbing control rods partially inserted into the reactor. By fully inserting the control rods, the reactor can be shut down.

Therefore, a typical nuclear reactor consists of the following main components as shown in Figure 4:

- Fuel in which fission occurs and heat is generated
- Moderator to reduce the energy of the neutrons
- Coolant to remove the heat from the fuel elements
- Control rods to maintain the proper neutron balance.

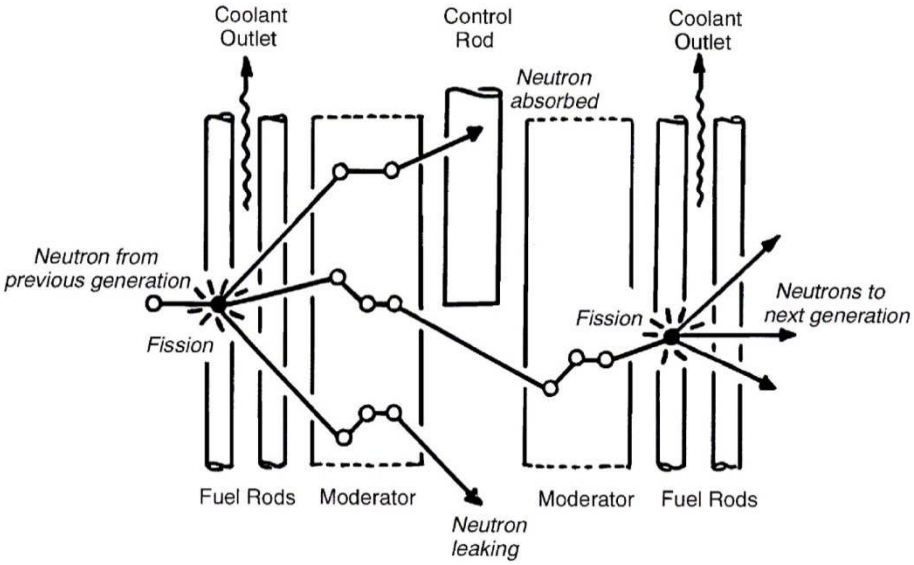

Figure 4 Nuclear reactor components

These components are usually arranged in a two-dimensional matrix so that neutrons generated by fission in one fuel rod pass through the moderator before entering the next fuel rod. The spacing of the fuel rods depends upon the moderator properties and the distance required to reduce the energy of the neutrons. The fuel rods are made small enough to promote heat removal and are surrounded by coolant. Often the coolant serves as a moderator as well. The control rods are made to penetrate between the fuel rods to capture excess neutrons effectively. Naturally, some neutrons leak through the boundaries of the system, and many are absorbed by the reactor materials or in the fuel without causing fission, meaning that the control rods do not have to absorb a significantly large number of neutrons compared with the number causing fission. The actual configuration of the matrix and the spacing of the fuel rods depend upon the fuel and moderator characteristics.

2 Reactor Types

2.1 Prototype Reactors

As nuclear reactors developed around the key elements of fuel, moderator, and coolant, many different types were proposed and constructed as demonstration models in an endeavour to prove their technical and commercial viability. Some designs had serious technical problems, while others had uniquely advanced features. However, due to arbitrary political decisions, one or two good designs did not go beyond the prototype stage, while others with insurmountable technical difficulties were abandoned. Nevertheless, some prototypes did operate successfully for many years, providing valuable technical and operational experience while producing power. Ultimately, the field narrowed to certain proven designs which were adopted on a commercial basis. Currently, there are six main types, which are listed below in order of numbers in service. The first five have proven to be commercially viable, while the sixth can be considered to be still in the prototype stage, but to hold promise for the future as a reactor which can breed new fissile fuel:

PWR	Pressurized Water Reactor
BWR	Boiling Water Reactor
PHWR	Pressurized Heavy Water Reactor (CANDU)
GCR	Gas Cooled Reactor
LGR	Liquid Graphite Reactor
LMFBR	Liquid Metal Fast Breeder Reactor.

2.2 Commercial Reactors

The reactors listed above will be described briefly in the following paragraphs for comparison, starting with the simplest concept.

2.2.1 Boiling water reactor (BWR)

The boiling water reactor consists of a pressure vessel containing the fuel rods in vertical elements, with each element surrounded by a channel. The channels are flooded with light water which serves as the moderator and coolant. Pumps circulate water upwards through the channels, and steam is generated within the channels. The exit steam quality is about 13%, and the steam is separated from the water in cyclone separators above the reactor core. This saturated steam is sent directly to the steam turbines.

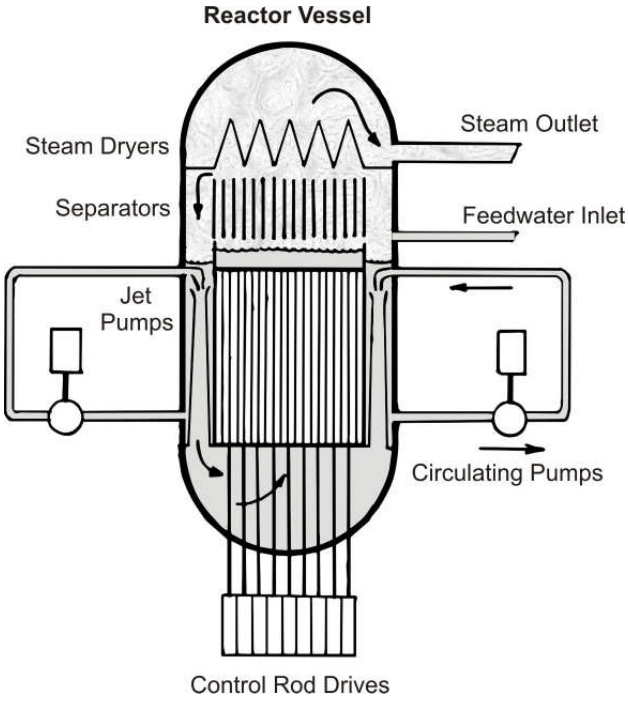

Figure 5 Diagrammatic cross section of a typical BWR

This simple direct cycle has the disadvantage that steam from the reactor is passed through the turbine and the condensate is returned through the feedwater heaters, making the whole steam circuit slightly radioactive during operation. A simplified diagram of a boiling water reactor is given in Figure 5.

2.2.2 Pressurized water reactor (PWR)

The pressurized water reactor overcomes the problem of a slightly radioactive steam circuit by having an intermediate heat exchanger to separate the reactor coolant circuit from the turbine steam circuit. Steam is generated in this steam generator and is sent to the turbine as saturated steam under conditions similar to those in the boiling water reactor. The reactor coolant circuit is maintained at high pressure to prevent any boiling in the reactor and operates at a slightly higher temperature than the BWR to promote heat transfer to the secondary steam circuit. Because no boiling occurs in the reactor core, it is more compact and does not require channels. The fuel rods of the individual elements form a continuous vertical matrix in the core. This is flooded with an upward flow of circulating light water which serves as coolant and moderator. A simplified diagram of a pressurized water reactor is given in Figure 6.

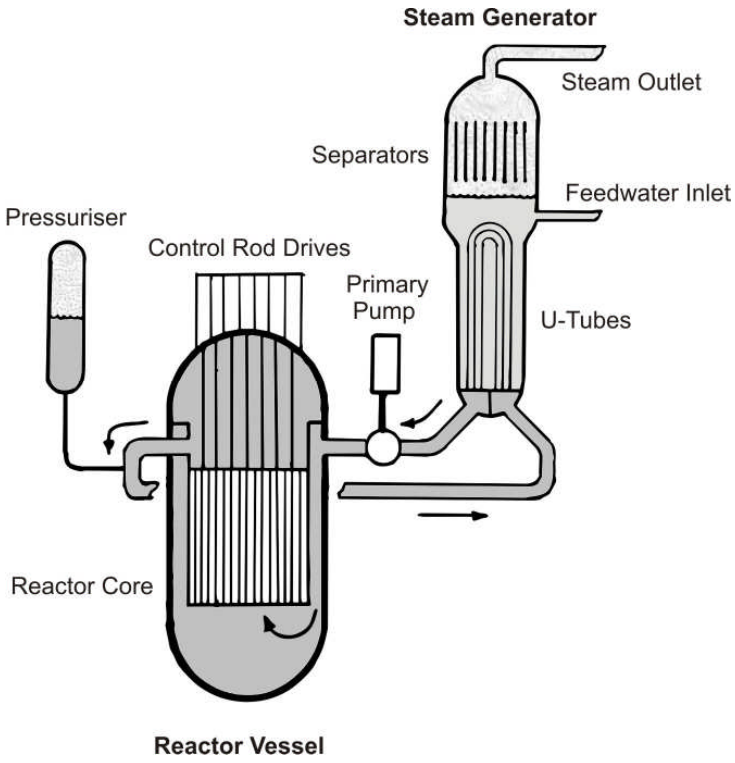

Figure 6 Diagrammatic cross section of a typical PWR

2.2.3 Pressurized heavy water reactor (PHWR) (CANDU)

The pressurized heavy water reactor is similar to the pressurized water reactor in that it has a primary coolant circuit and secondary steam circuit with a steam generator producing saturated steam. The reactor, however, is different in that it has individual pressure tubes passing horizontally through the reactor core. Fuel rods in the form of bundles are contained within these pressure tubes. The heavy water coolant flows through these tubes and is then circulated through the steam generator. The pressure tubes are surrounded on the outside by heavy water at low pressure and low temperature, which serves as the moderator. This is contained in a large vessel or calandria at ambient pressure. The advantage of this system is that it does not require a very heavy pressure vessel as in the BWR and PWR. The Canadian version is known as the CANDU. Other variations such as the steam generating heavy water reactor (SGHWR) had light water coolant and vertical channels and generated steam in the core. A simplified diagram

of a pressurized heavy water reactor is given in Figure 7.

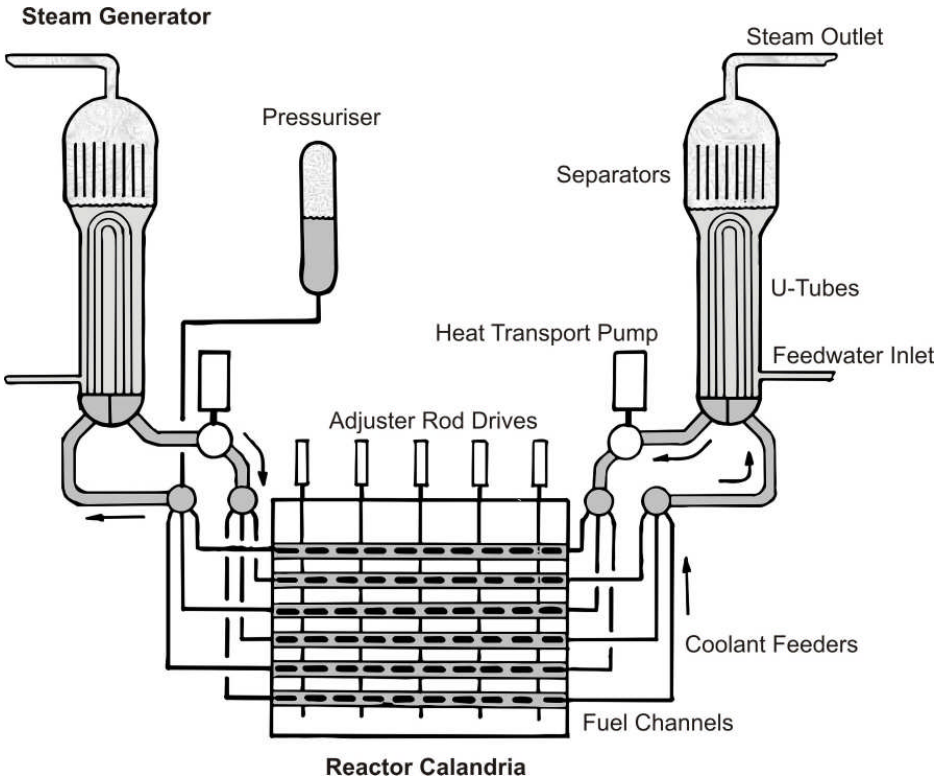

Figure 7 Diagrammatic cross section of a typical PHWR (CANDU)

2.2.4 Gas cooled reactor (GCR)

The gas cooled reactor, like the pressurized water reactor, has separate reactor coolant and steam generating circuits with an intermediate steam generator. The coolant, however, is gas, which enables higher coolant temperatures to be achieved. This enables superheated steam to be generated and a high efficiency steam circuit similar to that of a fossil fuel fired plant to be used. Due to the high temperatures and large core volume required with a gas coolant, graphite is more suitable than water as a moderator. This is installed in the form of blocks with holes to form channels into which the fuel elements are placed and through which the gas coolant flows. The early reactors of this type were known as Magnox from the type of fuel used, and later ones were called advanced gas cooled reactors (AGRs), which run at higher temperatures with a different type of fuel. By changing the coolant from carbon dioxide to helium, even higher temperatures could be achieved, hence the designation *high temperature reactor* (HTR). This type gave the ultimate advantage of large gas cooled reactors, which have a cycle efficiency as high as any fossil fuel fired plant.

Later developments in this field, such as the pebble bed modular reactor (PBMR), use a direct cycle, with the helium coolant passing directly to a helium turbine with the promise of even better cycle efficiency. A simplified diagram of an advanced gas cooled reactor is given in Figure 8.

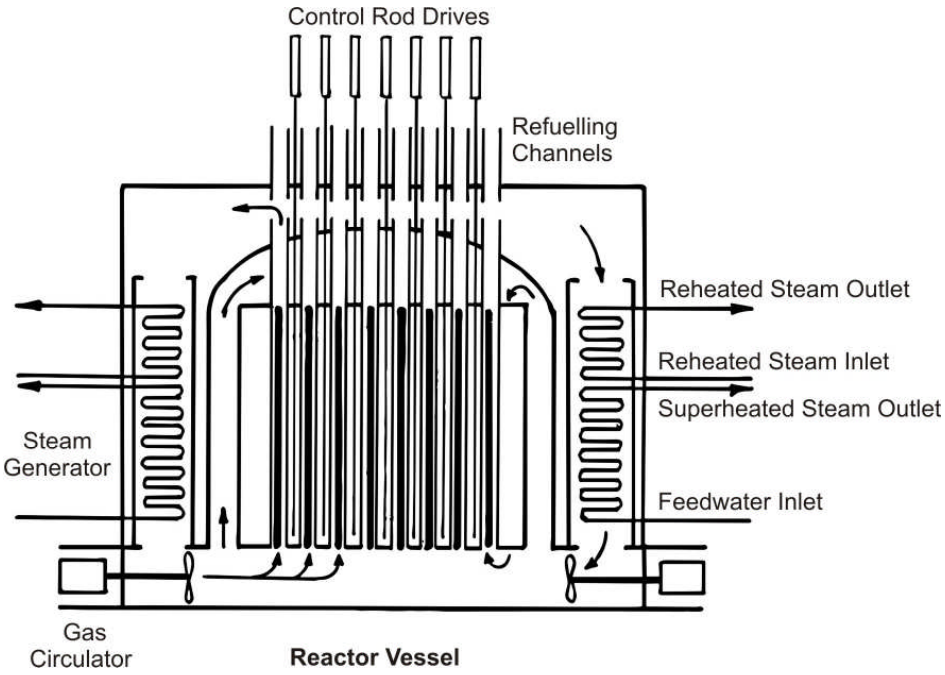

Figure 8 Diagrammatic cross section of a typical AGR

2.2.5 Liquid graphite reactor (LGR)

The liquid graphite reactor has a graphite block core similar to that of a gas cooled reactor. Pressure tubes similar to those of the pressurized heavy water reactor pass through vertical holes in the graphite, which serves as the moderator. Fuel elements made up of clusters of rods are located within these vertical tubes, and light water coolant flows upwards over the fuel and within the tubes. Boiling occurs in the fuel as in the boiling water reactor. The resulting steam is separated from the water in an external drum and the water recirculated. As with the boiling water reactor, saturated steam is sent to the turbine. This type of reactor of Russian design is known as the RBMK. A simplified diagram of a liquid graphite reactor is given in Figure 9.

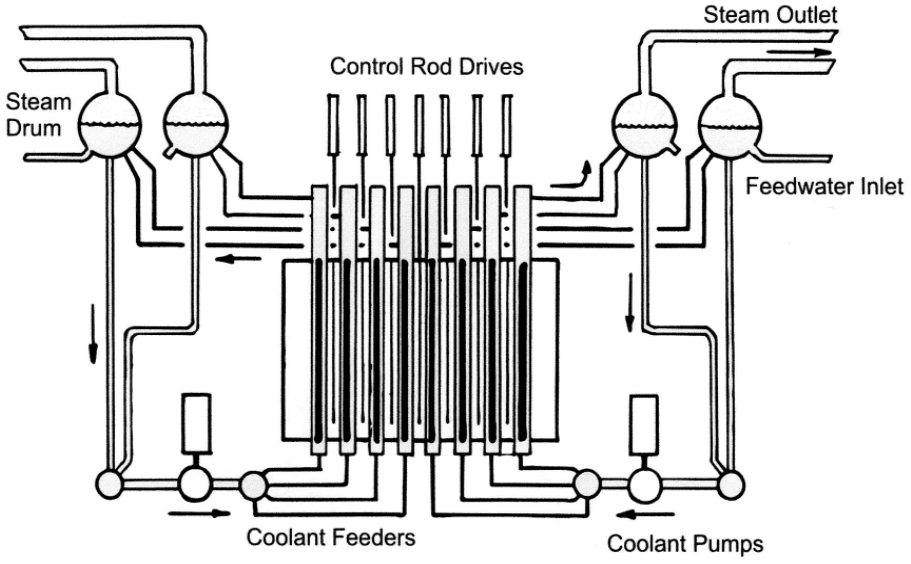

Figure 9 Diagrammatic cross section of a typical RBMK (LGR)

2.2.6 Liquid metal fast breeder reactor (LMFBR)

The liquid metal fast breeder reactor is different from the others in many ways. The coolant is a liquid metal, usually sodium, which flows directly over the fuel rods of the vertical fuel elements in an upward direction. The heat carried in this primary circuit is transferred to a secondary sodium circuit in a heat exchanger. This secondary circuit then transfers the heat to the steam circuit in a steam generator. Because sodium remains a liquid at high temperatures without being pressurized, heavy pressure vessels are not required, and high temperature superheated steam can be produced to provide good cycle efficiency. There is no moderator to reduce the energy of the neutrons, hence the term "fast", and surplus neutrons are used to convert non-fissile material into fissile fuel, hence the term "breeder". This type of reactor has not yet reached the commercially viable stage, and therefore there is no typical design.

3 World-Wide Commercial Power Reactors

3.1 Reactor Development

Following the Second World War, the development of nuclear reactors followed different paths in different countries depending upon the facilities developed during the war and the perceived military needs of certain countries following the war. The first nuclear reactors served to generate plutonium-239, another fissile material formed when uranium-238, the major constituent of natural uranium, absorbs excess neutrons. Pu-239 could be easily separated from the original uranium fuel and was needed for atomic bombs. U-235 is also used in nuclear weapons, but is difficult to separate from U-238.

The United States had isotope separation facilities for uranium and therefore was able to pursue the development of light water reactors requiring the use of uranium fuel slightly enriched in U-235. The United Kingdom did not have such facilities and therefore was forced to develop reactors using natural uranium. Canada had developed expertise in heavy water technology as a result of the war effort and was therefore well positioned to develop heavy water moderated reactors also using natural uranium.

When using natural uranium as a fuel, the low concentration of U-235 and the absorption of neutrons in U-238 necessitate use of a moderator with an extremely low absorption cross section to establish a continuous chain reaction. Only heavy water (deuterium and oxygen) and graphite (carbon) have the required physical and neutron properties. This led Britain to develop graphite moderated natural uranium metal fueled reactors with carbon dioxide as a coolant. Later, when they had uranium enrichment facilities, they were able to switch to uranium dioxide as the fuel. Canada, which had supplies of heavy water, was able to develop heavy water moderated natural uranium dioxide fueled reactors. Heavy water is the only moderator that can be used directly with natural uranium dioxide fuel to sustain the required fission chain reaction. Although heavy water is an excellent moderator, especially with respect to neutron absorption, it is very expensive to separate from ordinary water. If enriched uranium is available, as was the case in the United States, there is wider scope in the choice of a moderator because more neutron absorption can be tolerated. Therefore, light water (hydrogen and oxygen) can be used as a moderator. An advantage of light water as a moderator is that it is very effective per unit distance in slowing down neutrons, leading to a smaller moderator volume and a more compact reactor than with the other moderators. However, light water has the inherent disadvantage of absorbing a greater fraction of neutrons than graphite or heavy

water.

Of the three moderators mentioned above, graphite is the least effective in reducing neutron energy and requires the largest volume. Graphite moderated reactors are therefore the largest, leading to high capital costs. Considering capital cost, moderator costs, and enriched fuel supply and cost, all three of these became economically viable in their respective countries, and commercial reactors for power plants subsequently evolved.

Over time, enriched uranium became more easily available, and commercial reactors were sold to other countries which did not have fuel enrichment resources, leading to a free choice of reactors. It is of interest to review the world use of nuclear reactors for electric power production.

3.2 Commercial Reactors in Service

Table 1 shows the number, type, and output of reactors operating and committed or under construction in different countries. The first column under the two latter headings is for reactors currently in service and the second column for those reactors to be added in the coming years. This table is representative of current commercial technology because most prototype and early commercial reactors have served their useful life and been decommissioned.

Table 1 Nuclear reactors in service and planned*

BWR–Boiling (Light) Water Reactor
GCR–Gas Cooled Reactor
LGR–Light Water Graphite Reactor
LMFBR–Liquid Metal Fast Breeder Reactor
PWR–Pressurized (Light) Water Reactor
PHWR–Pressurized Heavy Water Reactor

Country	Reactor Type	Number Operational + Planned		Existing Capacity + New Capacity (MWe)	
Argentina	PHWR	2	1	935	692
Armenia	PWR	1		375	
Belgium	PWR	7		5 885	
Brazil	PWR	2	1	1 901	1 275
Bulgaria	PWR	2	2	1 906	2 000
Canada	PHWR	22		15 137	
China	PWR	12	41	9 748	42 230
	PHWR	2		1 300	
	GCR		1		200
	LMFBR		1		20
Czech Republic	PWR	6		3 678	
Finland	PWR	2	1	976	1 600
	BWR	2		1 740	
France	PWR	58	1	63 130	1 600
Germany	PWR	7		9 486	
	BWR	2		2 572	
Hungary	PWR	4		1 889	
India	PWR		2		1 834
	BWR	2		300	
	PHWR	18	4	4 091	2 560
	LMFBR		1		500
Iran	PWR	1		915	
Japan	PWR	24		19 286	
	BWR	26	2	24 818	2 756
Kazakhstan	LMFBR	1		70	

Country	Reactor Type	Number Operational + Planned		Existing Capacity + New Capacity (MWe)	
Mexico	BWR	2		1 300	
Netherlands	PWR	1		487	
Pakistan	PWR	2	1	600	300
	PHWR	1		125	
Romania	PHWR	2	3	1 300	1 869
Russia	PWR	16	11	11 914	9 810
	LGR	15		10 219	
	LMFBR	1	1	560	750
Slovakia	PWR	4	2	1 816	810
Slovenia	PWR	1		666	
South Africa	PWR	2		1 800	
South Korea	PWR	17	7	15 975	8 600
	PHWR	4		2 722	
Spain	PWR	6		6 004	
	BWR	2		1 510	
Sweden	PWR	3		2 799	
	BWR	7		6 504	
Switzerland	PWR	3		1 700	
	BWR	2		1 538	
Taiwan	PWR	2		1 780	
	BWR	4	2	3 104	2 600
Turkey	PWR		4		4 600
Ukraine	PWR	15	3	13 107	2 850
United Arab Emirates	PWR		4		5 600
United Kingdom	PWR	1		1 188	
	GCR	17		8 732	
United States	PWR	69	8	68 459	8 990
	BWR	35	2	34 935	2 700

* Adapted from Nuclear News, March 2012

It is evident from Table 1 that certain types of reactors became dominant in certain countries, particularly in those developing their own reactors, for example, PWRs and BWRs in the United States, GCRs in the United Kingdom, PHWRs in Canada, and LGRs in Russia. However, in later years, certain types of reactors have been favoured by countries without their own developmental program, leading to the spread of some of these types to other countries. The PWR, however, has become the most common type and is currently produced by various manufactur-

ers around the world.

3.3 Recent Past and Near Future

Table 2 gives a summary of the situation at the beginning of 2012. It shows that PWRs make up 61% of operational reactors and 67% of total nuclear capacity, due mainly to their larger size relative to PHWRs and GCRs.

Table 2 Nuclear reactors in service in 2012*

Reactor Type	Number in Service	%	Total Capacity (MWe)	%
PWR	267	61	246 555	67
BWR	84	19	78 321	21
PHWR	51	12	25 610	7
GCR	17	4	8 732	2
LGR	15	4	10 219	3
LMFBR	1	0	560	0
TOTAL	435	100	369 997	100

*Adapted from Nuclear News, March 2012.

A similar review done in 1998 indicated that during the intervening 14 years, the number of reactors in service had only increased by two, but that total capacity had increased by 11%. This was due primarily to the decommissioning of smaller older reactors which had reached the end of their economic life. It does not reflect a lack of new plants coming on-line because the number of PWRs increased by 17, even though 10 were taken out of service during this period.

Looking forward over 10 years to 2022, Table 3 shows the total number of reactors currently in service and committed for commissioning or construction. Although the table does not consider possible decommissioning of some reactors, it also does not take account of new orders which will be completed before 2022. In this context, it should be noted that 80% of new construction is due to be on-line by 2017, leaving time for new commitments which will likely overcompensate for possible decommissionings.

Table 3 shows a dramatic increase of 25% and 29% respectively in the number of reactors in service and available capacity over the following 10 years.

Table 3 Projected reactors in service in 2022*

Reactor Type	Number in Service	Change (%)	Total Capacity (MWe)	Change (%)
PWR	356	+33	339 569	+38
BWR	90	+7	86 377	+10
PHWR	59	+16	30 722	+20
GCR	18	+6	8 932	+2
LGR	15	0	10 219	0
LMFBR	5	+400	2 076	+271
TOTAL	543	+25	477 895	+29

*Adapted from Nuclear News, March 2012

3.4 Status of Large Reactors

Table 4 New large reactors (1000 MWe and greater)*

Country	Reactor Type	Number Committed	New Capacity (MWe)
Brazil	PWR	1	1 275
Bulgaria	PWR	2	2 000
China	PWR	38	36 400
Finland	PWR	1	1 600
France	PWR	1	1 600
Russia	PWR	6	6 900
South Korea	PWR	7	8 600
Taiwan	PWR	2	2 600
Turkey	PWR	4	4 600
United Arab Emirates	PWR	4	5 600
United States	PWR	8	8 990
	BWR	2	2 700

*Data extracted from Nuclear News, March 2012

Most reactors currently under construction or on order are of large capacity, that is, 1000 MWe or greater. Considering only reactors of this size, Table 4 shows the type of reactor, total capacity, and country where these are being built or to be built.

For comparison, the number of large units taken out of service to date is given in Table 5. This

table shows the capacity, date taken out of service, and number of years in service.

Table 5 Decommissioned large reactors (1000 MWe and greater)*

Country	Reactor Type	Capacity (MWe)	Date	Years of Service
France	LMFBR	1 200	1998	12
Germany	PWR	1 219	2001	14
	BWR	1 346	2011	27
	PWR	1 345	2011	32
	PWR	1 240	2011	34
	PWR	1 167	2011	36
United States	PWR	1,095	1992	16
	PWR	1 040	1998	24
	PWR	1 040	1998	25
TOTAL		10 692		220

*Data extracted from Nuclear News, March 2012

The average service life of these excluding the LMFBR is 26 years. Typically with refurbishment the life expectancy of such reactors would be at least double this.

4 Power Production

4.1 Energy Transfer

Heat, energy, and work all have the same units (joules), but somewhat different meanings, and power is the rate of doing work (watts). What is important is that not all heat can be converted into work. Although the first law of thermodynamics states that all work can be dissipated as heat, the second law states that not all heat can be converted into work. In a typical water cooled nuclear plant (CANDU, PWR and BWR) approximately 30% of the heat released by the fuel is ultimately converted into electrical energy. The rest must be discharged as low grade (low temperature) heat.

During the fission process, heat is generated in the fuel. This heat is removed by the reactor coolant flowing over the fuel rods and transported in the primary circuit to the steam generator, where it flows inside the tubes and its heat is transferred to the secondary circuit through the walls of the tubes in the steam generator. Water in the secondary circuit outside the tubes absorbs this heat and is converted into steam under saturated conditions. This steam is passed to the turbine where it expands to low pressure while being directed onto the turbine blades and in so doing transfers its energy to the turbine rotor. The rotor drives the electrical generator which produces electric power. The exhaust steam is condensed by cooling water passing through the condenser tubes and in so doing discharges the bulk of the heat which cannot be converted into work. The condensate is returned to the steam generator after being preheated in the feedwater heating system. A simple flow diagram for a nuclear plant is shown in Figure 10. Note that in the BWR and RBMK, steam is generated directly in the reactor, so there is no

separate steam generator.

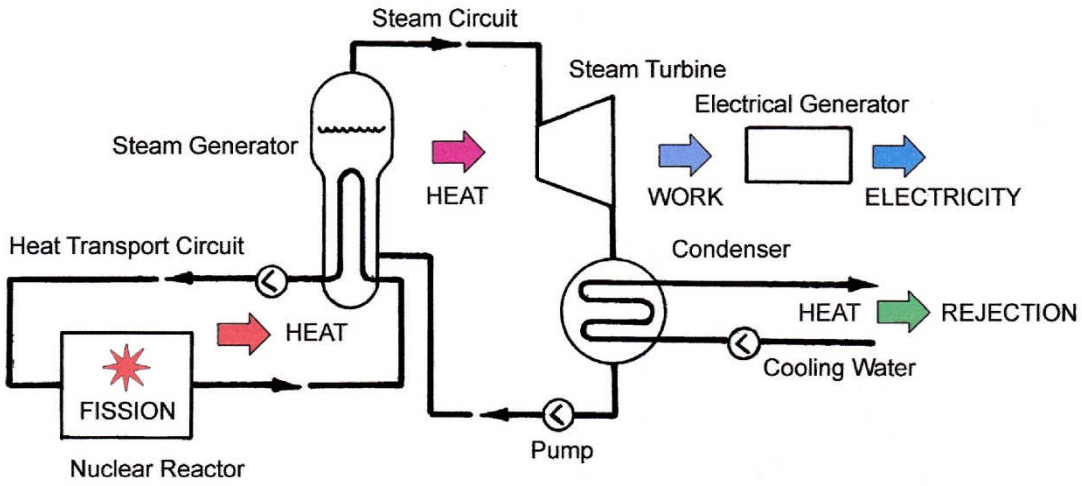

Figure 10 Simplified flow diagram of a nuclear plant

4.2 Power Output

Consider a very simple system with a nuclear reactor, steam generator, and turbine generator supplying electric power to an isolated electrical grid, as shown in Figure 11. This power must be generated at the moment it is required by the consumers connected to the grid. Power production must follow demand exactly, and any mismatch will cause the grid frequency to fall or rise as demand increases or decreases. A basic control system works as follows to maintain appropriate power output from the plant. In the event of an increase in demand the mismatch will cause the grid frequency to fall. Because the turbine generator is synchronized to the grid, its speed will drop accordingly. This will be sensed by the turbine governor which will open the governor valves to admit more steam to increase the power output of the turbine generator. The additional flow of steam to the turbine will cause a reduction in steam pressure in the steam generator. This in turn will be sensed by the reactor regulating system which will withdraw control rods from the reactor core until the increased fission rate generates sufficient additional heat to restore the steam generator pressure. In the event of a decrease in demand the reverse occurs. This is known as the reactor following or turbine leading mode of operation (or normal mode in some plants because it is a natural way of maintaining stable conditions).

Such a system, however, cannot maintain a specified frequency (60 Hz in North America) exactly without large unstable oscillations, and therefore a certain speed droop is incorporated into the turbine governor. This enables a progressive increase in governor valve opening (steam flow) as the turbine speed (grid frequency) falls. A typical droop setting is 4%, which means that, if the turbine was initially at zero load and full speed, its speed would have to drop to 96% before the governor valve would be fully open. Such a speed is not acceptable for the turbine due to possible blade vibration, nor to the grid due to loss in speed of connected motors. Therefore, the governor is adjusted to bring the speed back to 100% at full load. In the event of a turbine trip or load reduction to zero under these conditions, the reverse would occur, and the turbine speed would rise to 104% of full speed.

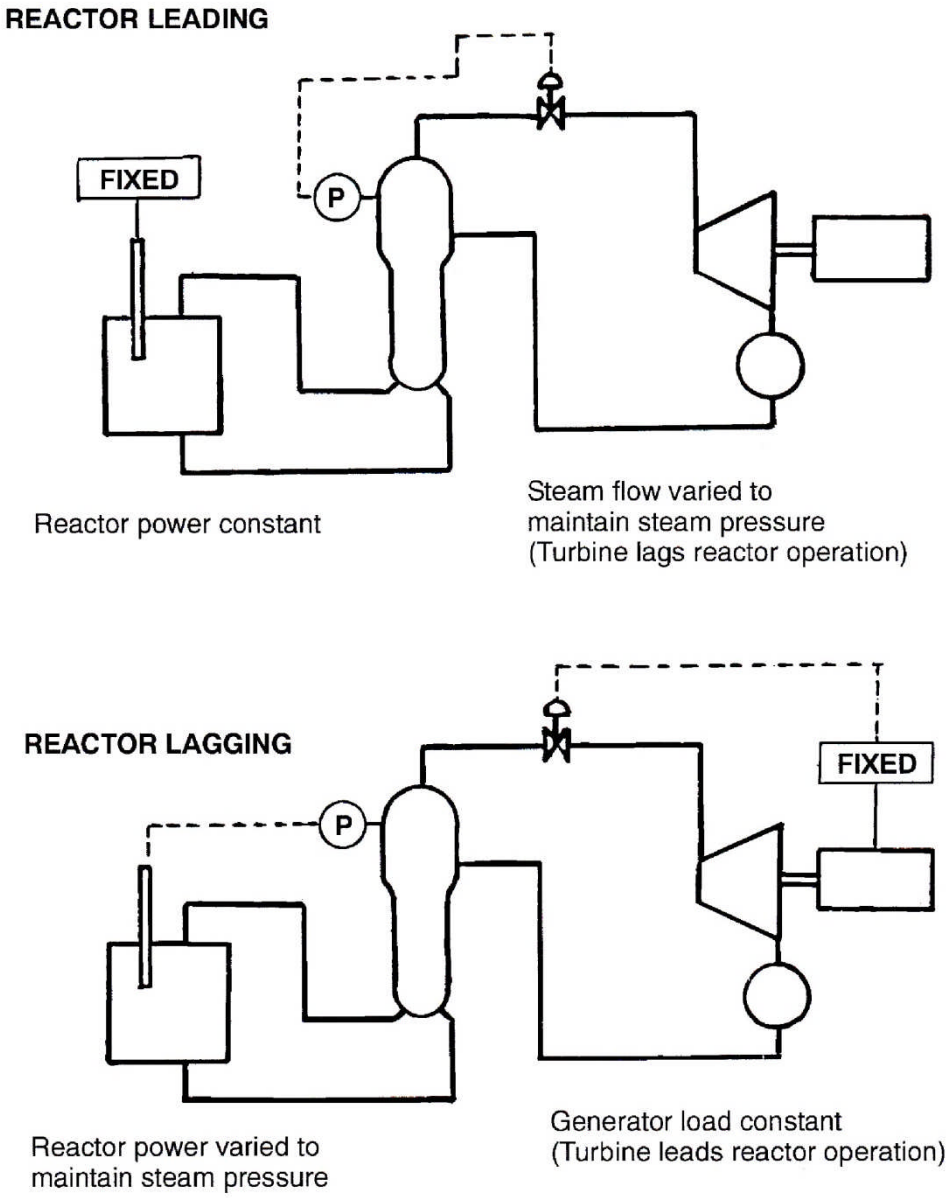

Figure 11 Lagging and leading plant operation

In the mode of operation just described, the nuclear reactor output follows the electrical grid demand, and therefore its power level oscillates continuously. This can have adverse effects depending upon the type and design of the reactor. Excessive oscillations impose temperature transients on the fuel, which can cause premature failures of the fuel cladding. Large oscillations near full power can cause power limits to be exceeded, thus tripping the reactor and losing power production as well as imposing restart transients on it and the turbine. Due to high capital cost and low fuel cost it is desirable to run nuclear reactors at full power most of the time. An alternative mode of operation is therefore often used at nuclear plants where the reactor power output is fixed. This is known as reactor leading or turbine lagging operation. To maintain stable operation, the reactor power is controlled at a given value by measuring the neutron flux and adjusting the control rods accordingly. Pressure in the steam generator must be maintained at the proper value to ensure stable conditions in the reactor coolant circuit. This is done by opening or closing the turbine governor valves to control steam flow from the

generators. The turbine then delivers power according to the steam flow and the generator sends this power into the grid system regardless of the grid frequency. The grid frequency must then be controlled by other turbine generators which feed into the grid system and operate in the turbine leading mode.

By referring to the figure showing the two modes of operation, it can be seen that steam generator pressure is a key control parameter in both modes. This highlights the importance of the steam generator, where a balance of heat input and heat output must be maintained to maintain pressure. Furthermore, the difference in temperature between the primary coolant and the secondary working fluid determines the rate of heat transfer. Hence the reactor coolant temperature is determined by saturation temperature and thus by steam generator pressure.

4.3 Operating Constraints

During operation, parts of the reactor, steam system, and turbine are subject to high temperatures. If these parts have thick walls or have a substantial solid mass they will likely suffer thermal stress during the heating and cooling that arises during startup and shutdown and also during load transients. If a thick component is heated on one side, that side will tend to expand. If the side is constrained by the still cold base material so that it cannot expand an internal stress will be set up. The reverse happens during cooling. Therefore, large rigid components which are subject to transient and uneven heating and cooling will suffer low cycle fatigue damage and may ultimately fail. This effect can be minimized by slow heating and cooling to reduce temperature differences in single components such as reactor pressure vessels, steam generators, steam pipes, turbine casings and turbine rotors. This means that all these components must be preheated slowly before startup and the unit must be loaded slowly. Similarly, load changes on the unit should be carried out slowly. This requirement imposes operating restrictions on reactors and turbines. Generally, the larger the unit, the longer the time to start it up and load it. This makes large units less flexible in operation than smaller units.

In the reactor, temperature transients in the fuel cause structural changes within the fuel and stress on the cladding and therefore must be minimized to avoid premature fuel failures. In the turbine, uneven heating and cooling of the rotor can cause bending, which in turn causes excessive vibration and in the extreme case contact with the casing and therefore must be monitored very carefully.

A nuclear reactor is also subject to xenon transients which may inhibit operation for a certain period. When the load on a reactor is suddenly reduced, xenon, a fission product that absorbs neutrons very strongly, builds up in the fuel and may force a reactor shutdown. The xenon eventually decays after about 40 hours, and the reactor can be restarted. During this time, there is a loss in electrical power production, and the larger the unit, the more serious is this loss in revenue generating output.

4.4 Fuel Burnup

As the fuel in the reactor is used up, the concentration of uranium-235 decreases. This reduces the number of fissions occurring with a given number of neutrons. Furthermore, some of the fission products produced absorb neutrons, thus reducing the number of neutrons available to produce fission. These changes can be accommodated by withdrawing the control rods from

the reactor and allowing more neutrons to be available in the fuel. After a long period of operation, however, such changes can no longer be accommodated, and the fuel may have become depleted in U-235 to the point where a continuous chain reaction can no longer be sustained. At this point, the reactor has to be refuelled with fresh fuel.

With reactors that are partially refuelled once a year, the control rods do not provide an adequate range of control, and therefore a soluble neutron absorber is added in small quantities to the moderator. Its concentration is gradually reduced over time to compensate for fuel burnup. Some reactors are designed for continuous on-load refuelling. This is advantageous because the effects of fuel burnup and fission product production are negligible with regard to overall reactor conditions.

5 Safety and Licensing

5.1 Radiation Hazards

Many types of radiation, both natural and human generated, are encountered in everyday life. Even the human body contains radioactive materials. This radiation can be divided into two categories. The first is electromagnetic radiation, which is assumed to travel in waves of discrete frequencies, for example, X-rays, γ-rays, and UV rays. The second is particulate radiation consisting of high-energy particles moving at high velocity, such as α-particles, β-particles, neutrons, etc. Charged particles such as α-particles and β-particles are easily stopped by ionization of surrounding material, but γ-rays and neutrons can be very penetrating due to their low interaction with most materials.

Radiation causes damage to biological structures such as cells. However, cells are in a continual state of dying and being replaced, so such damage is naturally repaired provided that it is not excessive. Of concern though is possible damage to DNA structures and subsequent genetic effects. For this reason exposure to radiation is controlled much more rigidly than exposure to toxic materials and dangerous chemicals. Although γ-rays and neutrons can penetrate the human body, α-radiation and β-radiation are generally damaging only if materials that emit these particles are ingested or come into contact with skin.

In the core of a nuclear reactor, the fission process produces neutrons and highly reactive fission products which emit α-particles and β-particles as well as γ-radiation as they decay to stable isotopes. Neutrons and γ-rays are emitted from the core, but are attenuated to low and safe levels by adequate shielding around the reactor. The fission products are held within the fuel and therefore do not pose a hazard unless released to the environment through leakage from the fuel or rupture of the fuel.

During operation of a nuclear plant, small amounts of leakage inevitably occur because some fission products are gaseous and attenuation cannot eliminate all radiation. Therefore, the entire operational area within and surrounding the plant as well as the local environment is continuously monitored to ensure that radiation is kept well within safe limits and usually kept much lower.

In the event of a serious accident, for example, fuel overheating and rupture of reactor components, the design of all reactors makes provision for barriers to contain these fission products and prevent their release to the environment. Such barriers may not be perfect, and some radioactive products may be released. If people in the surrounding area ingest such products,

they will be subject to α-radiation or β-radiation emitted by these products, along with some γ-radiation resulting from the decay process. The design of the plant has, as a key objective, the provision of safety devices and containment barriers to ensure that radiation exposure to the public is kept well below acceptable limits in the event of an accident.

5.2 Risk Assessment

Humankind is subject to many risks, both natural and human generated. These risks have been analyzed, and if the severity of an accident is compared with the probability of its occurrence, it is generally found that the probability of an accident occurring is much higher if the number of deaths per accident is low (motor vehicle accidents) than if the number of deaths is high (air-craft accidents). Because the consequences of a serious nuclear accident (for example, the Chernobyl accident) can be very severe, the probability of its occurrence must be kept very low. This puts great pressure on the nuclear industry to minimize the risk of serious accidents to levels far below those of other industries. The result is that the nuclear industry is the most regulated of all industries. Highly sophisticated design and accident analysis techniques and requirements are in place to ensure public safety.

5.3 Licensing Principles

All nuclear plants are subject to a rigorous licensing process by an independent regulatory authority to ensure safety of operating personnel and the general public and to ensure that there are no detrimental effects to the surrounding environment. All aspects of the plant are checked and assessed with regard to the effects of possible failures of key components. Initially this assessment was based on the maximum credible accident due to a single failure. In the event of the worst possible accident, the likely damage to the plant was assessed and the containment barriers reviewed to determine the likely amount of radioactive fission product release to the environment. This release was to be kept below specified values. This concept did not take account of the possible (though very unlikely) failure of a component deemed not to fail, nor did it take account of multiple minor failures which could have a cumulative or cascading effect, causing an otherwise unpredicted failure of a key component.

The modern approach, based on the probability of failure of a key component and the consequences of such a failure, overcomes the shortcomings mentioned above. A component deemed not to fail can be given a very low but still finite probability of failure. Moreover, multiple components which are all associated with one type of accident can each be given a certain probability of failure, and hence the probability of simultaneous failure can be assessed. Ultimately the entire plant can be assessed to determine the probability of an accident leading to a certain release of radioactive fission products. Hence, the safety of the surrounding environment and population can be ensured to a very high degree, that is, a very low probability of damage to the environment or excessive radiation exposure to the population.

The transition to a probabilistic approach as opposed to the deterministic method was initially difficult due to a lack of statistical data and because certain failures could have different root causes. However, as the industry has matured, more statistical data have become available from test results and operating experience. Nevertheless, the process remains complex.

Another consideration is the relative importance of component failure and human error. A quick analysis done many years ago indicated that roughly half of various incidents and accidents in operating nuclear plants around the world were caused by human error and roughly

half by component failure. Many component failures could be ascribed to human error during component design or manufacture. Rigorous quality control, quality assurance, and quality management procedures can minimize manufacturing and construction defects. Proper training, assessment, and licensing of plant operators can minimize human error during operation. This all contributes to a lower risk of accident and increased safety in nuclear plants.

A further development in the nuclear industry is the concept of passive safety. This means that in the event of a failure leading to accident conditions, the reactor will naturally revert to a safe shutdown condition and maintain that condition with minimal operator intervention, even in the event of the loss of key services. Some newer designs, for example, can maintain reactor cooling after shutdown by natural coolant circulation and natural heat convection to the environment.

6 Problems

1 Explain why the fission of very heavy elements results in release of neutrons as well as production of excess energy.

2 Explain the purpose of the key components of a nuclear reactor and show how these are arranged to ensure adequate heat removal and satisfactory control.

3 Describe the key similarities and differences between a CANDU and a PWR as well as between a CANDU and a BWR.

4 Explain how fission heat is converted into electrical energy and identify all key interfaces and points of energy conversion in the process.

7 Bibliography

[Cameron1982] I. R. Cameron, *Nuclear Fission Reactors*, Plenum Press, New York, 1982.

[El-Wakil1982] M. M. El-Wakil, *Nuclear Energy Conversion*, 3rd ed., American Nuclear Society, La Grange Park, IL, USA, 1982.

[Foster1983] A. R. Foster and R. L. Wright, *Basic Nuclear Engineering*, 4th ed., Prentice-Hall, Englewood Cliffs, NJ. USA, 1983.

[Glasstone1994] S. Glasstone and A. Sesonske, *Nuclear Reactor Engineering: Volume 2, Reactor Systems Engineering,* 4th ed., Chapman & Hall, New York, NY, USA, 1994.

[Knief1992] R. A. Knief, *Nuclear Engineering,* 2nd ed., Hemisphere Publishing Corporation, Washington, DC, USA.

[Lamarsh2001] J. R. Lamarsh and A. J. Baratta, *Introduction to Nuclear Engineering*, 3rd ed., Prentice-Hall, New Jersey, USA, 2001.

8 Acknowledgments

The following reviewers are gratefully acknowledged for their hard work and excellent comments during the development of this Chapter. Their feedback has much improved it. Of course the responsibility for any errors or omissions lies entirely with the author.

Bob Tapping
Jeremy Whitlock
Bhaskar Sur
Terry Rogers
George Bereznai

Thanks are also extended to Diana Bouchard for expertly editing and assembling the final copy.

Historical Background

prepared by
Dr, Robin Chaplin
Professor of Power Plant Engineering (retired)
University of New Brunswick

Summary:

A review of the historical background for the development of nuclear energy is given to set the scene for the discussion of CANDU reactors.

Table of Contents

List of Figures

1 Growth of Science and Technology

The rate of technology increase has accelerated as technology itself has increased, leading to a sort of exponential growth. Energy growth is a good example of this phenomenon. Water power developed relatively slowly, steam power somewhat more quickly, electrical power even more rapidly, and nuclear power very rapidly. In the case of nuclear energy, collaboration between scientists in different countries initially spurred the discovery of various nuclear particles. Then the Second World War provided an incentive to harness the fission process, and later the rapid growth in demand for new energy after the war provided the need for nuclear power. Within the time span of roughly half a century, an entirely unknown source of energy had become a major producer of commercial electric power. In addition, an entirely new and sophisticated technology had been developed.

Before about 1900, most scientific work in this field was related to electricity. Then in the next two decades following the discovery of radiation and its characteristics, various pieces of the nuclear puzzle began to come together. Only by 1920 was the basic structure of the atom understood, and the existence of the neutron was confirmed in 1932. This was a pivotal discovery because the neutron is the key element in establishing a fission chain reaction. Just ten years later, in 1942, the first self-sustaining chain reaction was established, and by 1956 the technology had advanced to the point where a nuclear fission reactor could produce electric power on a commercial scale.

In reviewing this evolution of nuclear energy, it is important to note the recognition given to the researchers responsible for these discoveries. The Nobel Prize is the most prestigious award given to such advances in the scientific field. Some twenty Nobel Prizes in nuclear and radiation physics and nuclear chemistry or closely related fields were awarded over a fifty-year period from 1901, the year of the first Nobel Prize.

To appreciate these advances in technology properly, it is convenient to consider a timeline of achievement with key advances shown and to link these with some renowned scientists. A timeline of these discoveries is shown in Figure 1.

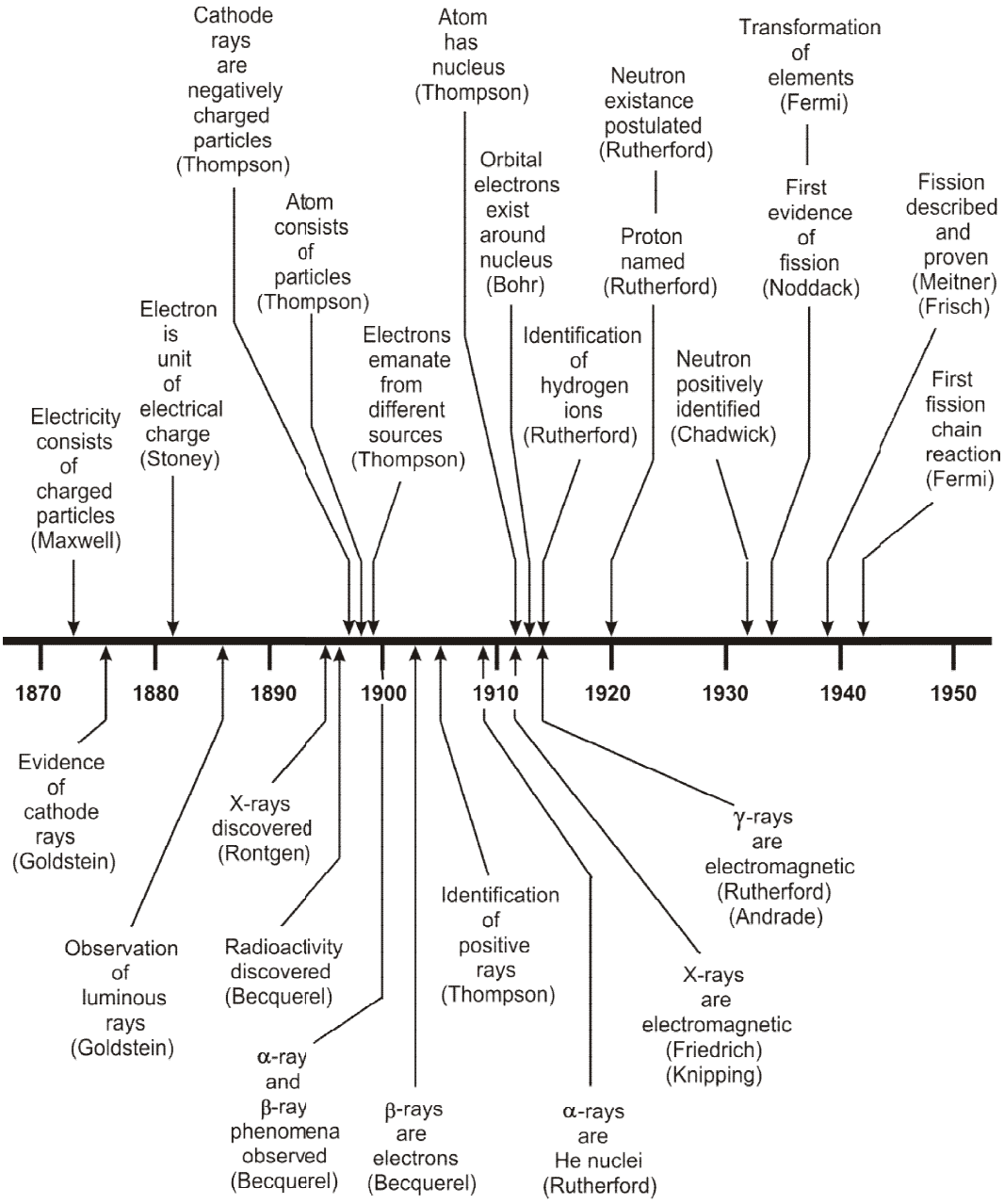

Figure 1 Timeline of significant discoveries

2 Renowned Scientists

Many researchers in different countries around the world have contributed to this new field of science. Several collaborated with one another or worked or were trained in another's laboratory. Each contributed a piece of the puzzle. Those making a significant advancement in this field were awarded Nobel Prizes. Some 20 prizes were awarded over a fifty-year period, demonstrating the importance of this field of science.

The Nobel Prizes awarded in Physics and Chemistry in the nuclear field from 1901 to 1951 with the recipients and a statement of their contribution, as obtained from the *Nobel Foundation Official Web Site,* are listed below.

1901 Physics: *Wilhelm Conrad Roentgen*
"In recognition of the extraordinary services he has rendered by the discovery of the remarkable rays subsequently named after him"

1903 Physics: *Antoine Henri Becquerel*
"In recognition of the extraordinary services he has rendered by his discovery of spontaneous radioactivity"
Pierre Curie, Marie Curie (née Sklodowska)
"In recognition of the extraordinary services they have rendered by their joint researches on the radiation phenomena discovered by Professor Henri Becquerel"

1906 Physics: *Joseph John Thomson*
"In recognition of the great merits of his theoretical and experimental investigations on the conduction of electricity by gases"

1908 Chemistry: *Ernest Rutherford*
"For his investigations into the disintegration of the elements, and the chemistry of radioactive substances"

1911 Chemistry: *Marie Curie (née Sklodowska)*
"In recognition of her services to the advancement of chemistry by the discovery of the elements radium and polonium, by the isolation of radium and the study of the nature and compounds of this remarkable element"

1918 Physics: *Max Karl Ernst Ludwig Planck*
"In recognition of the services he rendered to the advancement of Physics by his discovery of energy quanta"

1921 Physics: *Albert Einstein*
"For his services to Theoretical Physics, and especially for his discovery of the law of the photoelectric effect"

1922 Physics: *Niels Henrik David Bohr*
"For his services in the investigation of the structure of atoms and of the radiation emanating from them"

1923 Physics: *Robert Andrews Millikan*
"For his work on the elementary charge of electricity and on the photoelectric effect"

1927 Physics: *Arthur Holly Compton*
"For his discovery of the effect named after him"
Charles Thomson Rees Wilson
"For his method of making the paths of electrically charged particles visible by condensation of vapour"

1929 Physics: *Prince Louis-Victor Pierre Raymond de Broglie*
"For his discovery of the wave nature of electrons"

1932 Physics: *Werner Karl Heisenberg*
"For the creation of quantum mechanics, the application of which has, inter alia, led to the discovery of the allotropic forms of hydrogen"

1933 Physics: *Erwin Schrödinger*, *Paul Adrien Maurice Dirac*
"For the discovery of new productive forms of atomic theory"

1935 Physics: *James Chadwick*
"For the discovery of the neutron"

1938 Physics: *Enrico Fermi*
"For his demonstrations of the existence of new radioactive elements produced by neutron irradiation, and for his related discovery of nuclear reactions brought about by slow neutrons"

1939 Physics: *Ernest Orlando Lawrence*
"For the invention and development of the cyclotron and for results obtained with it, especially with regard to artificial radioactive elements"

1944 Chemistry: *Otto Hahn*
"For his discovery of the fission of heavy nuclei"

1945 Physics: *Wolfgang Pauli*
"For the discovery of the Exclusion Principle, also called the Pauli Principle"

1951 Physics: *Sir John Douglas Cockcroft*
Ernest Thomas Sinton Walton
"For their pioneer work on the transmutation of atomic nuclei by artificially accelerated atomic particles'

1951 Chemistry: *Edwin Mattison McMillan, Glenn Theodore Seaborg*
"For their discoveries in the chemistry of the transuranium elements"

3 Significant Achievements

Three scientists and their respective discoveries tend to stand out in the development of nuclear physics as applied to energy production. Niels Bohr developed a model to describe the structure of the atom, James Chadwick established the existence of neutrons, and Enrico Fermi directed the construction of the first reactors. All these achievements were the result of extensive work in analyzing the results and further developing the ideas of other researchers and collaborators. Extracts of their biographies from the *Nobel Foundation Official Web Site* are given below.

3.1 Niels Bohr

In the autumn of 1911 he made a stay at Cambridge, where he profited by following the experimental work going on in the Cavendish Laboratory under Sir J.J. Thomson's guidance, at the same time as he pursued his own theoretical studies. In the spring of 1912 he was at work in Professor Rutherford's laboratory in Manchester, where just in those years such an intensive scientific life and activity prevailed as a consequence of that investigator's fundamental inquiries into the radioactive phenomena. Having there carried out a theoretical piece of work on the absorption of alpha rays which was published in the *Philosophical Magazine,* 1913, he passed on to a study of the structure of atoms on the basis of Rutherford's discovery of the atomic nucleus. By introducing conceptions borrowed from the Quantum Theory as established by Planck, which had gradually come to occupy a prominent position in the science of theoretical physics, he succeeded in working out and presenting a picture of atomic structure that, with later improvements (mainly as a result of Heisenberg's ideas in 1925), still fitly serves as an elucidation of the physical and chemical properties of the elements.

3.2 James Chadwick

In 1932, Chadwick made a fundamental discovery in the domain of nuclear science: he proved the existence of *neutrons*—elementary particles devoid of any electrical charge. In contrast with the helium nuclei (alpha rays) which are charged, and therefore repelled by the considerable electrical forces present in the nuclei of heavy atoms, this new tool in atomic disintegration need not overcome any electric barrier and is capable of penetrating and splitting the nuclei of even the heaviest elements. Chadwick in this way prepared the way towards the fission of uranium 235 and towards the creation of the atomic bomb. For this epoch-making discovery he was awarded the Hughes Medal of the Royal Society in 1932, and subsequently the Nobel Prize for physics in 1935.

3.3 Enrico Fermi

In 1934, Fermi evolved the β-decay theory, coalescing previous work on radiation theory with Pauli's idea of the neutrino. Following the discovery by Curie and Joliot of artificial radioactivity (1934), he demonstrated that nuclear transformation occurs in almost every element subjected to neutron bombardment. This work resulted in the discovery of slow neutrons that same year, leading to the discovery of nuclear fission and the production of elements lying beyond what was until then the Periodic Table.

In 1938, Fermi was without doubt the greatest expert on neutrons, and he continued his work on this topic on his arrival in the United States, where he was soon appointed Professor of Physics at Columbia University, N.Y. (1939-1942).

Upon the discovery of fission, by Hahn and Strassmann early in 1939, he immediately saw the possibility of emission of secondary neutrons and of a chain reaction. He proceeded to work with tremendous enthusiasm, and directed a classical series of experiments which ultimately led to the atomic pile and the first controlled nuclear chain reaction. This took place in Chicago on December 2, 1942, on a squash court situated beneath Chicago's stadium. He subsequently played an important part in solving the problems connected with the development of the first atomic bomb. (He was one of the leaders of the team of physicists on the Manhattan Project for the development of nuclear energy and the atomic bomb).

4 Nuclear Fission

Before 1939, there was no evidence to suggest the practical usefulness of atomic energy. In 1934, Enrico Fermi had reported that, when uranium was subjected to a stream of neutrons, elements of higher mass number were formed. These transuranic elements attracted the interest of other researchers, who discovered elements of unexpected mass numbers in the products. Otto Hahn and Friedrich Strassmann noted in 1938 that the masses of two of these products added up to the mass of the uranium atom plus a neutron. Subsequently, in early 1939, Lise Meitner and Otto Frisch were able to explain in a published report that "it seems possible that the uranium nucleus has only small stability of form and may, after neutron capture, divide itself into two nuclei of roughly equal size". This was called *fission*, the term which was commonly used in biology to describe the division of living cells. Otto Frisch soon after proved, as they had predicted, that the particles released had strong ionizing power. This was also confirmed by several other researchers. Furthermore, these fission fragments were found to be ejected at high velocity and to possess radioactive properties. Most of the confirmatory work of this new revelation was completed within three months of the initial publication of the theory of nuclear fission. This subsequently was generally referred to as "splitting the atom".

Lise Meitner and Otto Frisch estimated that the amount of energy release in a single fission process was in the order of 200 MeV, far greater than any other known nuclear reaction. This can be shown by comparing the masses of the fission products with the masses of the original nucleus plus a neutron and converting this difference to energy.
It soon became evident, as had been mentioned by Enrico Fermi, that neutrons should be emitted during fission due to the general structure of the atoms of uranium and the fission products. This was subsequently confirmed by different researchers.

5 Nuclear Energy

It had already been recognized that mass could be converted into energy and that so-called sub-atomic particles existed within atoms. When nuclear fission by neutrons was discovered and found to produce further neutrons along with fission fragments, the possibility of a branching chain of fissions became a real prospect. If these occurred in a rapid sequence, given the amount of energy released in each fission event, the result could be a catastrophic explosion. At

that time, interest became focused on the possibility of a powerful atomic bomb. Subsequently, from 1940 on, all further work related to the use of nuclear energy to produce an atomic bomb took place in secrecy. The limits to this possibility became evident with further research that showed that a nuclear chain reaction could be sustained only in uranium-235 and plutonium-239. The former could be separated by gaseous diffusion and the latter created by a controlled neutron chain reaction. Both methods required extensive equipment to produce even small amounts.

The production of Pu-239 required an operating nuclear reactor with suitable fuel and moderator to establish a chain reaction with U-235 in which neutrons were produced, some of which would be absorbed in U-238 to create Pu-239. To construct a reactor in which a controlled chain reaction would occur, Enrico Fermi and Leo Szilard realized that a heterogeneous system of lumps of uranium embedded in graphite blocks in a lattice formation would be required. The first experimental lattice was erected in 1941 at Columbia University under the supervision of Fermi and followed by a larger one shortly thereafter, but impurities in the materials prevented a chain reaction from being initiated. Towards the end of 1942, sufficient amounts of pure materials were available, and a sufficiently large pile of graphite blocks and lumps of uranium was built at the University of Chicago to establish a continuous self-sustaining chain reaction on December 2, 1942.

The next step was an enormous scale-up to the plutonium production plants at Hanford Works, where sufficient plutonium was produced to enable the first atomic bomb to be tested on July 16, 1945. Concurrently, a huge gaseous diffusion plant was built at Oak Ridge to separate U-235 from U-238 and so create highly enriched uranium for a second atomic bomb.

6 Acknowledgments

The following reviewers are gratefully acknowledged for their hard work and excellent comments during the development of this Chapter. Their feedback has much improved it. Of course the responsibility for any errors or omissions lies entirely with the author.
Bob Tapping
Jeremy Whitlock
Bhaskar Sur
Terry Rogers
George Bereznai
Thanks are also extended to Diana Bouchard for expertly editing and assembling the final copy.

CHAPTER 2

Genealogy of CANDU Reactors

prepared by
Dr. Robin Chaplin

Summary:

This chapter discusses the historical beginnings and evolution of the CANDU reactor. The research and prototype reactors leading to the CANDU design are described with some of their principle technical parameters. Reasons for the choice of key parameters are given. This leads into a review of the evolution of the design of increasingly larger commercial CANDU reactors. The CANDU 6 reactor design has been chosen as a reference and a brief description of its main components with typical design parameters follows with a comparison with the CANDU 9 reactor. The chapter includes a note on the advantages of the CANDU reactor compared with other water cooled reactors and a general review of reactor safety as applicable to most water cooled reactors. It concludes with some technical details of the proposed Advanced CANDU reactor for comparison with existing commercial CANDU reactors.

Table of Contents

List of Figures

List of Tables

1 Canadian Historical Review

1.1 Canadian Nuclear Beginnings

During the first part of the 20th Century, significant discoveries were made in the field of nuclear physics and chemistry, leading to the splitting of the atom and release of energy. Canada became an important player in the development of nuclear technology during and after World War II as a result of the Allied war effort to develop the atomic bomb. Although not directly involved in the development of the bomb, Canada contributed a significant amount of related nuclear research.

Canadian history in nuclear physics essentially started in 1898 when Ernest Rutherford, a New Zealand born British scientist, was appointed Professor of Experimental Physics at McGill University. His early work here was related to radioactivity, and he won a Nobel Prize for this contribution to scientific knowledge in 1908. One of his students, John Cockcroft, who received a Nobel Prize jointly with Ernest Walton in 1951, subsequently came to Canada in 1944 to direct the Montreal Laboratory which had been set up in 1942 as a joint British-Canadian effort. In the intervening period, much fundamental research had been done, and consideration was then being given to the design and building of a reactor which would require more extensive laboratories to be located at Chalk River.

Concurrent work in the United States had led to the building of the first nuclear reactor, in which a self-sustaining nuclear reaction took place in 1942. This reactor was built of graphite blocks in which were distributed lumps of uranium. It was known as a pile due to the method of construction.

During the war years, emphasis in the United States was directed towards the development of the atomic bomb. This required highly enriched uranium or plutonium. Whereas the former required extensive isotope separation facilities, the latter could be created from non-fissile uranium in a reactor and chemically separated from the spent fuel. There was therefore a concerted effort in the United States to build suitable reactors. Therefore, after the war, nuclear research was also directed towards the design of reactors for power production.

After the war, Britain, without enrichment facilities and with no source of heavy water, followed the route of graphite moderated natural uranium reactors to produce plutonium for nuclear weapons, while at the same time developing reactors for power production. As a result, Calder Hall became the first commercial nuclear power plant in the world when the first of four 60 MWe units was connected to the grid on 27 August 1956. It continued to operate until 2003. In the United States, with uranium enrichment facilities in place, the focus was on the development of light water moderated reactors using enriched uranium. Such reactors were highly suitable for submarine propulsion because the reactors were very compact. Furthermore, the vessels could remain submerged for extended periods and could operate extensively between refuellings. The expertise thus developed in steam system components for submarine propulsion greatly influenced and facilitated the design of Canadian power reactors. Canada had supported the war effort by research related to heavy water physics and therefore had the expertise to direct its efforts into the development of heavy water moderated reactors using natural uranium as fuel. In summary, each country focused its efforts in different directions depending upon its relative expertise and resources.

Work in Canada was directed towards use of heavy water as a moderator, and to test the

concept, a Zero-Energy Experimental Pile known as ZEEP was built at Chalk River. It was essentially an aluminum cylinder 2 m in diameter and 2.5 m in height surrounded by blocks of graphite. Uranium metal rods clad in aluminum were hung vertically from the top, and heavy water could be pumped in slowly at the bottom. ZEEP was completed and went critical on 5 September 1945, with almost exactly the amount of heavy water that had been predicted by theory. It was the first nuclear reactor to operate outside the United States. This confirmed the design parameters that would be used for the fuel rod lattice for the first functional reactor, designated NRX. ZEEP, however, continued to be used in later years for experimental studies of neutron behaviour.

2 Canadian Research Reactors

2.1 Small Research Reactors

The Zero-Energy Experimental Pile or ZEEP, which had an operating power of just 1 W, enabled tests to be carried out to determine the characteristics of heavy water and uranium lattices. It was also used to determine the neutron energy spectrum in various regions of a fuel bundle.

A larger version of ZEEP, known as ZED-2, was used for studies of fuel and irradiation effects as well as a variety of possible lattices for power reactors. Fuel bundle designs from 7-element to 37-element assemblies were tested to determine their performance.

The Pool Test Reactor, or PTR, was constructed, as its name implies, near the bottom of a deep pool of light water. Because this light water was both moderator and coolant, slightly enriched uranium had to be used as fuel. This arrangement with an easily accessible core made it possible to shuttle samples of fuel and other materials in and out of the reactor core to determine their effect on reactivity as well as to study short term radiation effects on materials.

2.2 The NRX Reactor

The first Canadian nuclear reactor to be designed to operate with a positive power output due to its generation of excess heat was the NRX. This reactor started operation in 1947 with a design thermal power rating of 10 MW, which was increased to 42 MW by 1954. At the time of its construction, it was the most powerful nuclear research reactor in the world and became the most intense source of neutrons available anywhere. It also suffered one of the first major nuclear reactor accidents in the world (power excursion to 80 MW and partial core meltdown), but was rebuilt and restarted within two years. It continued in service until 1993, which was quite a remarkable achievement for an experimental reactor.

The NRX reactor consisted of a vertical cylindrical aluminum calandria with a diameter of 8 m and a height of 3 m. The calandria contained the heavy water moderator. The core consisted of a hexagonal array of approximately 175 tubes with a diameter of 60 mm. These tubes held fuel elements, control rods, and experimental devices. Of these, 12 held control rods made of steel tubes containing boron carbide powder. The fuel elements consisted of uranium metal rods 3.1 m in length and 31 mm in diameter sheathed in aluminum. Each was surrounded by an aluminum tube through which flowed cooling water from the Ottawa River. An air flow in the gap between the calandria tube and the coolant tube was maintained to limit heat flow to the moderator to maintain it at a low temperature.

The key technical parameters for the NRX reactor are given in Table 1. The modern CANDU

reactor has all these key elements in a similar but horizontal arrangement.

Table 1 Technical data for NRX

Parameter	Characteristic
Reactor shape	cylindrical
Reactor orientation	vertical
Calandria diameter	8 m
Calandria height	3 m
Fuel channel arrangement	vertical hexagonal array
Number of fuel channels	~175
Fuel channel diameter	60 mm
Fuel channel material	aluminum
Fuel	uranium metal
Fuel rod length	3.1 m
Fuel rod diameter	31 mm
Fuel rod mass	55 kg
Fuel cladding material	aluminum
Moderator	heavy water
Moderator quantity	14 m^3
Coolant	light water
Coolant flow	250 kg/s
Annulus gas	air
Annulus flow	8 kg/s
Control rods	steel tubes containing boron carbide

2.3 The NRU Reactor

The National Research Universal (NRU) Reactor was a significantly advanced version of the NRX. Design was started in 1949 after NRX had been put into operation, and it started self-sustained operation in 1957, some 10 years after NRX. It was designed for a thermal output of 200 MW using natural uranium, but was converted to 60 MW using highly enriched uranium in 1964 and converted again to 135 MW using low enriched uranium in 1991. The NRU supported the Canadian Neutron Beam Centre and served as a test bed for the development of the CANDU reactor. Like NRX, it was when built the most powerful source of neutrons in the world and became the world's leading supplier of radioactive isotopes. It suffered an accident in 1958 when a fuel rod caught fire on removal from the reactor and caused radioactive contamination within the building and to a lesser degree on the surrounding site. As with NRX, the NRU was designed to use natural uranium as fuel and heavy water as moderator, but was cooled by heavy water. With a view to later commercial power applications, it was designed for on-load refuel-

ling.

3 Development of the CANDU Reactor

3.1 The NPD Reactor

The Nuclear Power Demonstration or NPD Reactor was partially modelled on the NRU reactor and was intended to be the first Canadian nuclear power reactor and a prototype for the CANDU design. Design work commenced in 1955, with the important components being designed and fabricated by Canadian General Electric. As a power producer, it had to operate at high temperatures sufficient to generate steam to drive a power producing turbine. These requirements presented some unique technical challenges due to the pressures under which the systems would have to operate. The design electrical output was to be 22 MW. Use of heavy water as a coolant and on-load refuelling had been proven with the NRU reactor, but the higher temperatures and pressures had to be accommodated by some significant changes. Firstly, the fuel was changed from uranium metal to uranium dioxide, which could withstand higher temperatures and was dimensionally stable over long irradiation periods. Secondly, the fuel cladding was changed from aluminum to zirconium alloy, which could also withstand higher temperatures and was corrosion resistant as well as being essentially transparent to neutrons. Thirdly, the fuel channels rather than the calandria were pressurized, leading to a pressure tube design rather than a pressure vessel design, and these pressure tubes would be of zirconium alloy. The pressure tube design led to further considerations to accommodate on-load refuelling. With horizontal pressure tubes rather than vertical tubes as in the NRX and NRU reactors, the fuel could be made into easily handled bundles which could be pushed in from one end and recovered from the other during refuelling while the reactor was at full power. Several unique safety features, such as safety shutdown systems with testability during operation, decay heat removal by natural circulation after shutdown, and a containment to prevent the release of radioactive material in the event of an accident, were incorporated. The NPD reactor started operation in 1962 and was taken out of service in 1987, by which time it had fulfilled its original purpose as a prototype and would have required re-tubing. It had also been an important training centre for future CANDU nuclear plant operators.

3.2 Douglas Point

The Douglas Point plant was the first full-scale CANDU nuclear generating station and was built on the shores of Lake Huron where the Bruce Nuclear Power Complex is now located. The proposed electrical output was 200 MW, and approval was given in 1959. It was basically a scale-up of the NPD reactor with similar design and components. It delivered power to the Ontario Hydro electrical grid system from 1967 until 1984, when replacement of the pressure tubes became necessary and could not be justified on economic grounds. Valuable experience was gained on this plant which was subsequently applied to later CANDU nuclear power plants.

4 Commercial CANDU Reactors

4.1 Commercial Reactor Development

The design of the CANDU reactor began with the Nuclear Power Demonstration (NPD) plant. Certain parameters had to be established within the constraints of existing technology. Basically, the reactor had to be fuelled with natural uranium, with heavy water as a moderator. This required a heterogeneous core arrangement with an array of fuel channels through which coolant flowed. Initial studies suggested a fuel channel cross section of 50 cm^2, which translated into a standard size fuel channel 3.25 in (83 mm) in diameter. To promote good heat transfer from the fuel, a modified hexagonal array of 19 rods or elements was chosen. The minimum spacing between rods based on laboratory testing was determined to be 0.050 in (1.27 mm). Based on irradiation testing, uranium dioxide was shown to have better dimensional stability and corrosion resistance than uranium metal at high burnup levels. This choice did, however, reduce the uranium concentration in the fuel and increased the need for good neutron economy. Zirconium had been selected as fuel cladding due to its corrosion resistance and low neutron absorption, but the quantity of it around the fuel had to be reduced as much as possible. Although a cladding thickness of 0.020 in (0.51 mm) was recommended by the tube supplier, further experimental work led to a thickness of 0.015 in (0.38 mm) and later to 0.013 in (0.33 mm). This resulted in collapsible cladding where the tube wall was compressed onto the fuel once in service.

A major decision was to adopt a pressure tube design rather than a pressure vessel design to avoid the difficulty of constructing a sufficiently large vessel for a heavy water moderated reactor. Zirconium alloy pressure tubes had sufficient neutron transparency to make this possible. A further major decision was to orient the fuel channels horizontally instead of vertically to facilitate on-load refuelling. The fuel could be made in the form of bundles which could be pushed through the channels with no need to link them together. These decisions on reactor configuration made the CANDU unique with regard to other commercial reactor developments. Although some were designed with pressure tubes or separate fuel bundles, only the CANDU has horizontal fuel channels.

With a selected fuel channel length of 4 m, the next question was the optimum number of fuel bundles. A significant advantage of separate fuel bundles was that the entire fuel channel need not be refuelled at one time. Low burnup fuel could be retained while new fuel was added. An analysis of diminishing returns indicated that having more than eight bundles would not yield any advantage, assuming a cosine neutron flux distribution along the fuel channel. This gave a fuel bundle length of 50 cm in a 4 m long fuel channel. This translated into a standard fuel bundle length of 19.5 in (495 mm), which was adopted for future CANDU reactors.

A fuelling machine was required at each end of the fuel channel. One supplied fresh fuel from one end, while the other received spent fuel at the other end. They had to connect to each fuel channel in turn and remove and re-insert closure plugs at the beginning and end of the refuelling process. The fuel configuration in the form of separate bundles facilitated the design of these machines because they did not have to handle a very long fuel assembly. In fact, the design of the fuel string and machines was dictated by the space available in the rock excavation, which had been dimensioned on the assumption that the reactor would have a vertical orientation. Of necessity, therefore, the fuelling machines were designed each with a rotating

magazine with slots to hold each bundle separately. A significant advantage of this arrangement was that fuelling could take place from either end of the reactor. Such bi-directional fuelling made it possible to balance the tendency for flux skewing in a partially refuelled channel by fuelling in the opposite direction in an adjacent channel. In the NPD design, coolant flowed in the direction opposite to the fuelling direction, so that the fuel bundles were held in place by the flow of coolant. This established the characteristic bi-directional coolant flow in CANDU reactors.

The calandria vessel and calandria tubes were of aluminum. Initially, there was no spacer between the calandria tubes and the fuel channel pressure tube, but as the design for Douglas Point evolved, a single spacer in the form of an Inconel wire garter spring was introduced. This enabled the pressure tubes to withstand the effect of creep sag. The calandria had a light water neutron reflector surrounding it in a radial direction. To bring about a shutdown, the heavy water moderator could be rapidly drained into a dump tank, which for a small reactor was an effective way of ensuring safe shutdown in the event of an accident.

The heat transport system which removed heat from the reactor core and generated steam in a steam generator required pumps to circulate the coolant. Originally, completely enclosed canned pumps were proposed, but these were later changed to conventional vertical pumps with shaft seals. These had the advantage of being able to incorporate a flywheel to provide increased rotational inertia, which would extend the rundown period after a power failure and enable extra core cooling during the initial stages of high decay heat. The steam generator design was based on those being designed for United States nuclear submarines. It consisted essentially of a U-shaped horizontal heat exchanger in which the heavy water coolant transferred heat to the light water of the steam system. Because the latter operated at a lower pressure, some steam was generated around the tubes. Risers and downcomers circulated the steam and water mixture to a steam drum and returned the water to the heat exchanger. The long circular horizontal steam drum was similar to that of a conventional fossil fuel fired boiler and had internal cyclones for effective steam separation. The overall configuration required inlet and outlet headers at each end of the reactor to accommodate bi-directional coolant flow. The former were supplied by three 50% capacity pumps, and the latter delivered coolant to a single steam generator.

The NPD reactor was followed very closely by the Douglas Point reactor, the latter being essentially an enlarged version capable of operating like a commercial power plant and producing electric power to the grid system on a commercial scale. The site chosen was on Lake Huron, where there was an adequate supply of cooling water to sustain large scale power production. The most significant change was an upgrade in power from 20 MW electrical to 200 MW electrical. This naturally required a larger and more robust calandria, and therefore the structural material was changed from aluminum alloy to stainless steel and the calandria tubes from aluminum alloy to zirconium alloy. Because stainless steel is a stronger neutron absorber than aluminum, the calandria diameter was further enlarged to accommodate an internal heavy water reflector instead of an external light water reflector. The axial shields were moved inwards so that the fuel channel end fittings would be outside the shield and therefore more easily accessible.

The increased size of the Douglas Point reactor required fuel channels with a length of 5 m. This meant more fuel bundles per channel. The one-eighth length fuel bundle was based on a cosine flux distribution, but with flux flattening, such short lengths were not required, and one

third length bundles would give virtually optimum fuel burnup. Because the same standard length fuel bundles would be used, the fuelling machines were therefore redesigned to handle two bundles in each slot. This enabled the magazine to be smaller in diameter, but able to accommodate 39 in (991 mm) of fuel with each fuel movement. Other changes in fuelling-machine design provided positive control from both ends of the fuel channel during refuelling and enabled refuelling in the same direction as coolant flow. The advantage of this was that fresh fuel, which would give a higher local power output, would be in contact with cooler water when only part of the fuel channel had been refuelled.

The larger output required increased steam generating capabilities. Furthermore, the longer reactor put the inlet and outlet of each channel further apart. Therefore, it was decided to put steam generators and circulating pumps at each end of the reactor. The same concept of separate heat exchangers and steam drums was retained, but instead of one horizontal heat exchanger, several vertical hairpin tube exchangers were used to feed a single steam drum in a way similar to that in which steam is generated in the water walls of a fossil fuel fired boiler. The multiple smaller heat exchangers could be replaced more easily than a single large one should tube problems arise. With steam generators and circulating pumps at each end of the reactor and with bi-directional flow, the "figure of eight" configuration for the heat transport system was established for this and all future CANDU reactors. A further feature of Douglas Point was the introduction of horizontal inlet and outlet headers above the highest fuel channels, but below the steam generators and circulating pumps. This would enable the system to be partially drained for maintenance on the circulating pumps and steam generators while still maintaining fuel cooling to remove decay heat. In normal operation, pressure was maintained in the heat transport system by a feed-and-bleed system to minimize heavy water inventory.

Pickering was the first large scale multi-unit commercial CANDU plant. This was yet a further scale-up from the 200 MW Douglas Point plant to a 4 x 500 MW plant. The 500 MW electrical unit size was consistent with that of the coal fired units on the Ontario Hydro system. Significant changes to the reactor included longer and wider fuel channels to accommodate the increased fuel inventory. The fuel channels were 6 m in length instead of 5 m. Rather than increasing the number of fuel channels excessively, it was decided to increase the diameter to a nominal 4 in (102 mm) while retaining the fuel element or rod diameter. This resulted in fuel bundles with 28 instead of 19 elements. This required a fuel channel 4.07 in (103 mm) in diameter to maintain the standard minimum element spacing, which was maintained by pads brazed to the element cladding. This then became the standard for all future CANDU reactors. The end shields were redesigned, and the annular space between the pressure tube and calandria tube filled with inert gas to minimize the risk of corrosion.

A further change was the adoption of a double "figure of eight" coolant loop with two hydraulically independent loops. This had the advantage of limiting the consequences of a loss of coolant accident due to a pressure tube or feeder tube break because the fuel channels in half the reactor would remain flooded without the need for emergency coolant injection. The moderator dump system for emergency shutdown was retained, but due to the time needed to drain the large calandria, it was supplemented with gravity operated shutoff rods. The latter system was able to handle most reactor trips, and therefore a dump arrest system was added to prevent dumping, enabling a faster reactor restart for such non-accident related trips.

The larger reactor introduced the possibility of flux oscillation, in which the peak flux wanders from one region of the reactor to another, induced by xenon transients. To overcome this, the

reactor was divided into 14 zones, each with a neutron flux detector and a chamber in which an appropriate amount of light water could act as a stronger neutron absorber than the surrounding heavy water moderator and thus achieve local flux control. This regional neutron flux control system became a standard feature of all subsequent CANDU reactors.

An innovative change was the introduction of vertical steam generators which incorporated the vertical U-tube heat exchange surface and steam separation cyclones into a single vessel with provision for water recirculation and feedwater preheating. This design became the standard for CANDU reactors and many pressurized light water reactors, or PWRs.

For a multi-unit station, the concept of a containment surrounding each reactor was maintained and extended by linking the separate containments to a common vacuum building. In the event of a major reactor accident and release of steam inside any containment, the vacuum building would act to suck out and condense the steam, thus establishing a negative pressure in the containment to prevent egress of radioactive material.

Bruce was the next large multi-unit nuclear generating station to be built. This involved a change in the heat transport system. In previous designs, the outlet conditions of the fuel channels varied due to the different power ratings of the channels across the reactor core. To create more uniform conditions at the channel outlets, the central core region required a greater degree of subcooling at the inlet. This was accomplished by having separate preheaters outside some steam generators rather than integral preheaters and passing coolant for the central region only through these preheaters. This complicated the flow system, but obtained better matching of coolant outlet conditions. Another change was made to the steam generators, where the large U-tube heat exchanger as used in Pickering was retained, but without the integral upper steam separating section. Instead, a single long horizontal steam drum was attached to the top of all steam generators at each end of the reactor. The larger water-steam interface reduced level control problems, but introduced thermal stress problems. This design was used on Bruce A, while Bruce B reverted to the separate integral design as used at Pickering.

Studies had indicated that a moderator dump system was too slow for a large reactor, and therefore this was eliminated in favour of faster acting gravity shutoff rods. Because dumped moderator would not be available for channel cooling in the event of loss of coolant, a new system was developed for the next generation of reactors, but applied at Bruce. This was the injection of high pressure water into the heat transport system headers from gas pressurized storage tanks. For Bruce, the initial supply pressure was 800 lbf/in^2 (5.52 MPa), but this was reduced to 600 lbf/in^2 (4.14 MPa) in subsequent reactors.

A further safety issue arose with regard to the shutdown system. Bearing in mind that the CANDU design is a neatly balanced configuration of fuel and moderator, any disruption of this configuration will render the reactor subcritical and inoperable. In the event of failure of the shutdown system to operate in an overpower situation, the reactor would disassemble and shut itself down. Further consideration of the core disassembly philosophy led to addition of a second shutdown system which would remove the need to consider core disassembly for licensing purposes. Because the shutoff rods operated in a vertical plane, a new system operating entirely independently on a horizontal plane was developed. Solid rods were considered, but might suffer mechanical interference, so liquid rods were favoured. However, their effect would be too localized, so liquid dispersion in the moderator was the ultimate choice. By

injecting neutron absorbing gadolinium nitrate solution into the moderator through an array of nozzles in the reactor core, a very quick shutdown could be ensured. This system was driven by helium in pressurized storage tanks and became standard on all CANDU reactors. Because removal of the gadolinium nitrate from the moderator was a lengthy process, this became the secondary shutdown system, while the shutoff rods remained the primary shutdown system which operates first in adverse transient conditions requiring a reactor trip.

The next generation of CANDU units included Point Lepreau and Gentilly-II as well as a number of overseas plants. A design for single unit stations was needed for these to be attractive to small utilities. The major change was the requirement for a single large containment for the reactor and heat transport system, including the steam generators, which would condense released steam and contain radioactive products in the event of a large break and loss of coolant accident. Other changes followed a natural evolution in reactor design. The fuel bundles were modified from 28 to 37 element bundles by using smaller diameter elements. The increased heat transfer surface thus created enabled a power increase from 500 MW to 600 MW electrical, while reducing the number of fuel channels from 390 to 380. This reactor therefore became known as the CANDU 600. Furthermore, from 12 steam generators and 16 coolant pumps at Pickering, the design had evolved to 4 steam generators and 4 coolant pumps. Experience in steam generator design had enabled larger components to be built. Comprehensive testing had shown that some boiling could be permitted within the fuel channels, thus increasing substantially the heat removal capability of the coolant. Darlington followed the design of the CANDU 600, but with a degree of scaling up. The heat transport system maintained the same arrangement of two loops in a figure-of-eight configuration, with each loop having a steam generator and a circulating pump at each end. For increased output, the reactor was designed for 480 fuel channels instead of 380. For future reactors of this size, a change in the figure-of-eight arrangement has been proposed. Instead of the two loops being in separate halves of the reactor, they would be interleaved alternately between adjacent channels throughout the reactor. The advantage of this would be to avoid a flux tilt and power pulse in the event of a loss of coolant accident in one loop while still maintaining the advantages of the two loop concept.

4.2 CANDU Reactors in Service

Table 2 lists the CANDU reactors in service in Canada with their commercial service start dates. Of these, Point Lepreau and Gentilly 2 are both CANDU 600 or CANDU 6 reactors, which was the basic reference design for reactors sold abroad. Table 3 lists CANDU 6 reactors in operation in foreign countries. In this text, Point Lepreau has been selected as the reference plant because it is typical of CANDU reactors on a worldwide basis.

Table 2 Canadian CANDU reactors: capacity and service date

Country	Station Name	Gross (MWe)	Net (MWe)	Service Date
Canada	Pickering 1	542	515	1971
Canada	Pickering 2	542	515	1971
Canada	Pickering 3	542	515	1972
Canada	Pickering 4	542	515	1973
Canada	Bruce 1	836	781	1977
Canada	Bruce 2	836	781	1977
Canada	Bruce 3	836	781	1978
Canada	Bruce 4	836	781	1979
Canada	Point Lepreau*	680	635	1983
Canada	Gentilly 2*	675	635	1983
Canada	Pickering 5	540	516	1983
Canada	Pickering 6	540	516	1984
Canada	Pickering 7	540	516	1985
Canada	Pickering 8	540	516	1986
Canada	Bruce 5	877	822	1985
Canada	Bruce 6	877	822	1984
Canada	Bruce 7	877	822	1986
Canada	Bruce 8	877	822	1987
Canada	Darlington 1	935	881	1992
Canada	Darlington 2	935	881	1990
Canada	Darlington 3	935	881	1993
Canada	Darlington 4	935	881	1993

*CANDU-6 Reactor

Table 3 Foreign CANDU 6 reactors: capacity and service date

Country	Station Name	Gross (MWe)	Net (MWe)	Service Date
Argentina	Embalse 1	648	600	1984
China	Quinshan 4	700	640	1984
China	Quinshan 5	700	640	2002
Romania	Cernavoda 1	706	655	1996
Romania	Cernavoda 2	706	655	2007
South Korea	Wolsong 1	679	629	1983
South Korea	Wolsong 2	700	650	1997
South Korea	Wolsong 3	700	650	1998
South Korea	Wolsong 4	700	650	1999

4.3 Direct Steam Generation

Some reactors, such as the boiling water reactor or BWR, generate steam within the reactor core. Due to the cost of heavy water and the formation of tritium, heavy water cannot be used in the steam cycle because some leakage from this cycle is inevitable. Therefore, light water must be used as the coolant. The CANDU with its separate moderator and coolant circuits (unlike the light water PWR and BWR reactors in which the moderator and coolant are the same and in a single loop) can be adapted for direct steam generation by using heavy water as moderator in the calandria and light water as coolant in the fuel channels. Some boiling already occurs in CANDU fuel channels, and this can be increased with vertical channels, where the natural buoyancy effect enhances the forced circulation generated by the circulating pumps. Steam is separated in horizontal steam drums similar to those in the early CANDU reactors. Hence, we have the heavy water-light water reactor, or HWLWR.

The most successful of these was the 100 MWe Steam Generating Heavy Water Reactor, or SGHWR, built in the United Kingdom. This reactor operated as a commercial prototype and produced reliable power to the national grid system from 1968 to 1990, when it reached the end of its design life. It had some novel design aspects, including direct injection of emergency coolant into the centres of the fuel bundles in the event of a loss of coolant accident, and served as a testing ground for various types of fuel. Because light water, which absorbs more neutrons than heavy water, was used as coolant, slightly enriched uranium in the form of uranium dioxide was required. The steam became slightly radioactive due to formation of nitrogen-16 in the reactor, and therefore certain precautions had to be taken by operational and maintenance staff when working around the steam turbine and feedwater system. Gentilly-1, a similar Canadian design, designated the CANDU Boiling Water Reactor or CANDU-BWR and also known as the CANDU Boiling Light Water Reactor or CANDU BLW, was modelled on the SGHWR, but fuelled with natural uranium. Built for an output of 250 MWe, first power was produced in 1971, and full power was achieved in 1972. However, it did not operate successfully. The reactor had a strong positive power coefficient of reactivity when additional voidage due to steam formation in the coolant channels occurred. Although this could be corrected by absorber rods in the core, the reactor remained difficult to control, and its operation was sporadic

due to other problems such as condenser corrosion. It was shut down in 1979 and eventually decommissioned in 1984.

5 The Current CANDU Reactor Design

5.1 Plant Arrangement

The general arrangement of the plant is shown in Figure 1. The active part of the reactor is cylindrical in shape and set horizontally. The moderator is contained in the calandria, which is about 6.0 m long and about 7.6 m in diameter for the CANDU 6. Because of the low internal pressure in the calandria, the thickness of its shell and its tubes needs to be sufficient only to be structurally sound and to support the weight of the moderator. Only the pressure tubes located within the calandria tubes are pressurized. These pressure tubes, which contain the fuel and through which the coolant flows, are arranged horizontally in an axial direction. The coolant is fed to and from the pressure tubes by feeder tubes, which in turn are connected to headers situated above the reactor. The headers in turn are connected to steam generators in which heat from the coolant is used to generate steam. Circulating pumps, usually known as heat transport pumps, drive the coolant around the primary circuit. A pressurizer maintains pressure in the primary system to suppress large scale boiling and maintain operating temperatures.

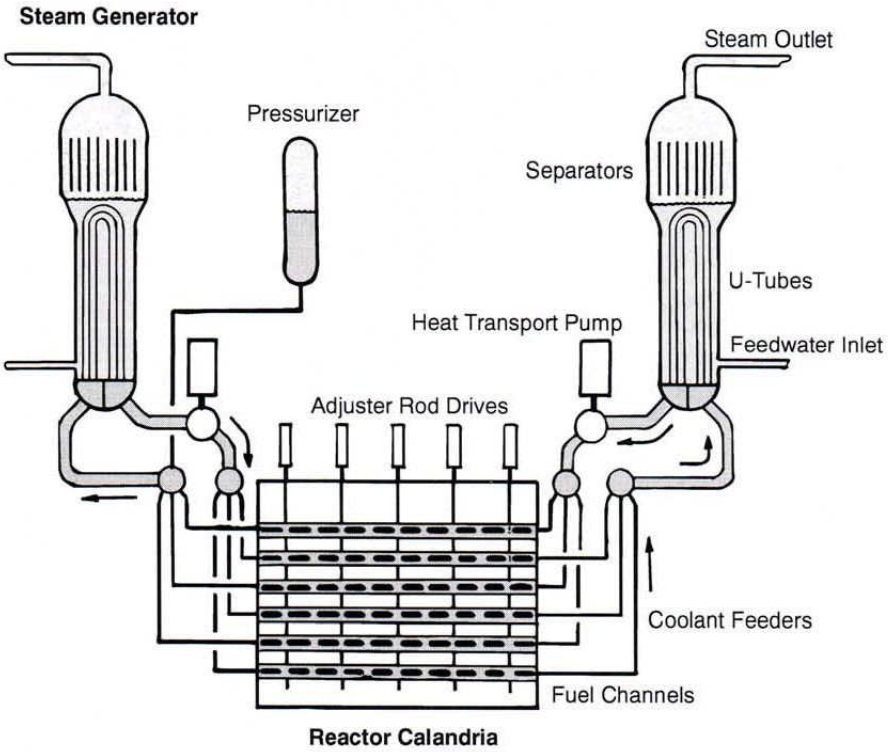

Figure 1 Diagrammatic cross section of a typical CANDU (PHWR)

The moderator absorbs some energy from the neutrons as they are slowed down and also receives some heat by conduction and radiation through the annulus gas between the pressure tubes and calandria tubes as well as conduction through the tubes themselves. The low con-

ductivity of the annulus gas provides the greatest resistance to heat transfer. Cooling of the moderator is therefore required to maintain a temperature of about 70°C, which means that a circulating and cooling system is required. This is shown diagrammatically in Figure 2.

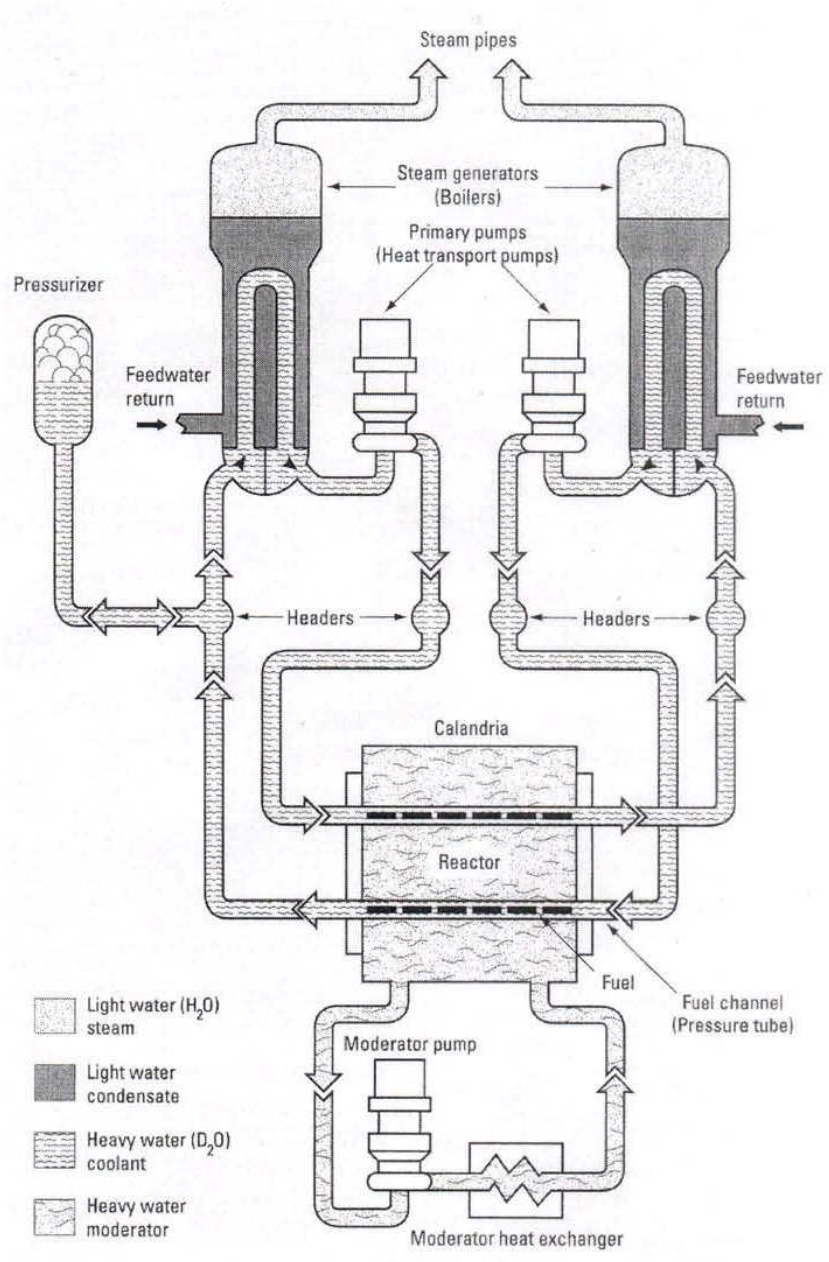

Figure 2 Moderator and coolant circuits

One characteristic when using heavy water as a moderator is that the neutron slowing down distance is relatively long. This determines the spacing between the fuel channels because neutrons need to be able to reach thermal equilibrium with the moderator before entering the next fuel channel. Too short a distance results in under-moderation and too long a distance in

over-moderation. CANDU reactors are slightly over-moderated, but while this has some disadvantages, it does provide additional space between the fuel channels for various control devices. Over-moderation enables additional neutrons to be absorbed in the moderator, and when voidage occurs in the fuel channels, fewer neutrons are absorbed, thus increasing the number of neutrons and giving a positive void coefficient of reactivity which must be counteracted in other ways. With a separate calandria, the moderator temperature can be kept relatively low compared with the fuel and coolant. This is advantageous in reducing neutron energy and promoting the fission process due to the increased fission cross section of uranium at lower temperatures. In all CANDU reactors, the moderator in the calandria is maintained at atmospheric pressure and a temperature of about 70°C.

5.2 Fuel Channel Conditions

In the CANDU reactor, coolant enters the fuel channels of the core in a subcooled state, but not excessively subcooled. It leaves the most highly rated fuel channels with a vapour content of a few percent, with boiling having occurred. The lower rated channels have little or no boiling. In this way, nearly constant reactor coolant outlet temperatures can be maintained even though some channels produce more heat than others. Furthermore, the outer channels with the lowest rating can have their flow slightly restricted to enhance their coolant outlet temperatures. Note in this context that for good thermodynamic efficiency, the cycle working fluid should receive heat at the highest possible temperature. Hence, the reactor primary coolant should be at the highest possible temperature so that it can supply heat to the secondary working fluid at a suitably high temperature as well. Limited boiling in some fuel channels of a CANDU reactor enables the average temperature of the coolant entering the steam generators to be very near saturated conditions. An alternative view of the above review is that, by allowing some boiling to occur in the fuel channels, the pressure of the primary circuit can be lower while still maintaining desired steam generator temperatures. This has significant benefits in the design and manufacture of a rather complex primary system with multiple pressure tubes and feeder pipes.

Within individual fuel channels where boiling does occur, conditions are not uniform across the fuel bundles. The circular arrangement of fuel elements in each bundle leads to irregularly shaped and sized coolant channels. More boiling occurs in narrow channels than in wider ones. The horizontal arrangement of the fuel bundles also creates non-uniform mixing between the coolant channels because the lighter vapour tends to migrate upwards, resulting in some vertical segregation of vapour and liquid across the channel. Although turbulence, particularly at the abutting ends of fuel bundles, tends to equalize conditions, some fuel pins are subject to more boiling than others. Boiling does enhance heat transfer, but excessive vapour is detrimental, and therefore fuel sheath temperatures do vary slightly across any particular fuel bundle.

5.3 Comparison of CANDU Reactors

The CANDU reactor has evolved progressively and has been marketed in several other countries. Three standardized versions, CANDU 300, CANDU 600, and CANDU 900, with different capacities were developed. These are now known as CANDU 3, CANDU 6, and CANDU 9 respectively. The original numbers indicate roughly the electrical output in megawatts, but later developments have enabled much greater outputs to be achieved by the respective models. Table 4 gives key technical parameters and shows the range in outputs available from these

three models built up with similar basic components.

Although the CANDU 6, for example Point Lepreau, is representative of CANDU reactors in general and most existing CANDU reactors are of this capacity, the CANDU 3 and CANDU 9, for example Bruce and Darlington, were marketed as alternate capacities to suit smaller or larger electrical utility systems respectively. The CANDU 9 is very similar to the CANDU 6, being simply larger in diameter and with increased heat transport capacity. It therefore has the benefit of economies of scale. The CANDU 3, however, was a novel development to minimize the adverse effects of economies of scale, but no examples have been built. It is like a half CANDU 6 with a single loop instead of a "figure of eight" loop with two steam generators at one end and two heat transport pumps at the other, thus maintaining essentially the same size components as the CANDU 6. Coolant flow is in one direction only, and only one refuelling machine is used, which is located at the coolant outlet end so that coolant flow aids the discharge of fuel bundles. A comparison of these three basic designs is given in Table 4. The technical parameters given in Table 4 and those given in Section 6 were extracted from the Atomic Energy of Canada publication "Technical Summary CANDU Nuclear Generating Station" which gives the parameters for the 600 MW and 950 MW units (subsequently the CANDU 6 and CANDU 9). The complete tabulated parameters are given in Appendix C to this chapter. Since publication these parameters have been revised as new developments have allowed the design to evolve particularly with regard to channel power. The parameters given for CANDU 9 (950 MW unit) are therefore not representative of the latest plants for example Darlington which has a lesser number of fuel channels each of which have a higher power rating. However Appendix C is useful for comparison of the two unit sizes and serves well for educational purposes as the data is based on the same design philosophy. A later AECL publication in 1997 "CANDU Technical Summary" gives some technical parameters for the CANDU 6 but not for the CANDU 9.

As the CANDU design evolved with the proposed Bruce B and the later Darlington nuclear plants these were nominally in the 800 MW range resulting in the CANDU 8 design. The AECL publication in 1989 "CANDU 8 Technical Outline" lists the net output of Bruce B as 825 MW and of Darlington as 881 MW. Subsequently the terminology was rationalized as in Appendix B "CANDU: The Evolution". This shows the development of the CANDU up to the four-unit CANDU 600 MW class (Pickering) and the subsequent division into the single-unit CANDU 6 or 700 MW class (Point Lepreau onwards) and the four-unit CANDU 900 MW class (Bruce A & B and Darlington) with the further development of the single-unit CANDU 9 also 900 MW class.

5.4 Power Density

Power density is a measure of how much power is generated per unit volume of core. Generally, the higher the power density, the more compact is the reactor and the lower the capital cost. In all reactors, therefore, there is an incentive firstly to maintain a high neutron flux (to achieve a high heat release rate) right across the reactor core and secondly to maintain a high heat flux (to achieve a high heat removal rate) everywhere in the reactor.

All CANDU reactors contain roughly the same amount of in-core fuel per channel, but the major differences are in the fuel bundles themselves and in the number of channels. The total design power output of a CANDU reactor can be fixed by selecting an appropriate number of fuel channels for the reactor. In a CANDU 3 reactor there are 232 fuel channels, in the CANDU 6 reactor the number of channels is increased to 380, while in the CANDU 9 reactor there are 600 fuel channels.

A new development is the Advanced CANDU Reactor, known as the ACR, which uses slightly enriched uranium as fuel and light water as coolant. This has the benefit of significantly reducing the heavy water inventory. In the proposed ACR, the power density is increased by a smaller calandria diameter, but with an increased number of elements in the fuel bundle and a smaller channel pitch, resulting in a more compact reactor.

Table 4 Comparison of CANDU reactor types

Parameter	Units	CANDU 3	CANDU 6	CANDU 9
Moderator		D_2O	D_2O	D_2O
Coolant		D_2O	D_2O	D_2O
Number of fuel channels		232	380	600
Fuel		UO_2	UO_2	UO_2
Number of elements in bundle		37	37	37
Number of bundles in channel		12	12	12
Number of steam generators		2	4	8
Number of heat transport pumps		2	4	4
Reactor outlet pressure	MPa	10.0	10.3	10.3
Reactor outlet temperature	°C	310	312	312
Reactor coolant flow rate	kg/s	5 300	7 600	13 500
Steam pressure	MPa	4.7	4.7	5.1
Steam temperature	°C	260	260	265
Steam flow rate	kg/s	700	1 050	1 610
Total fission heat	MW	1 441	2 156	3 394
Net heat to steam cycle	MW	1 390	2 060	3 347
Gross turbine generator output	MW	470	676	1 121
Net electrical output	MW	450	626	1 031

6 CANDU Technical Parameters

6.1 Reference Plant

Point Lepreau has been chosen as the reference for this text because it is a typical CANDU 6 reactor. Technical parameters for other CANDU reactors are given here for comparison to show the main differences, but other chapters will generally refer to Point Lepreau characteristics. Figure 3 shows an external view of Point Lepreau. Appendix A shows a cutaway view of a CANDU 6 reactor plant.

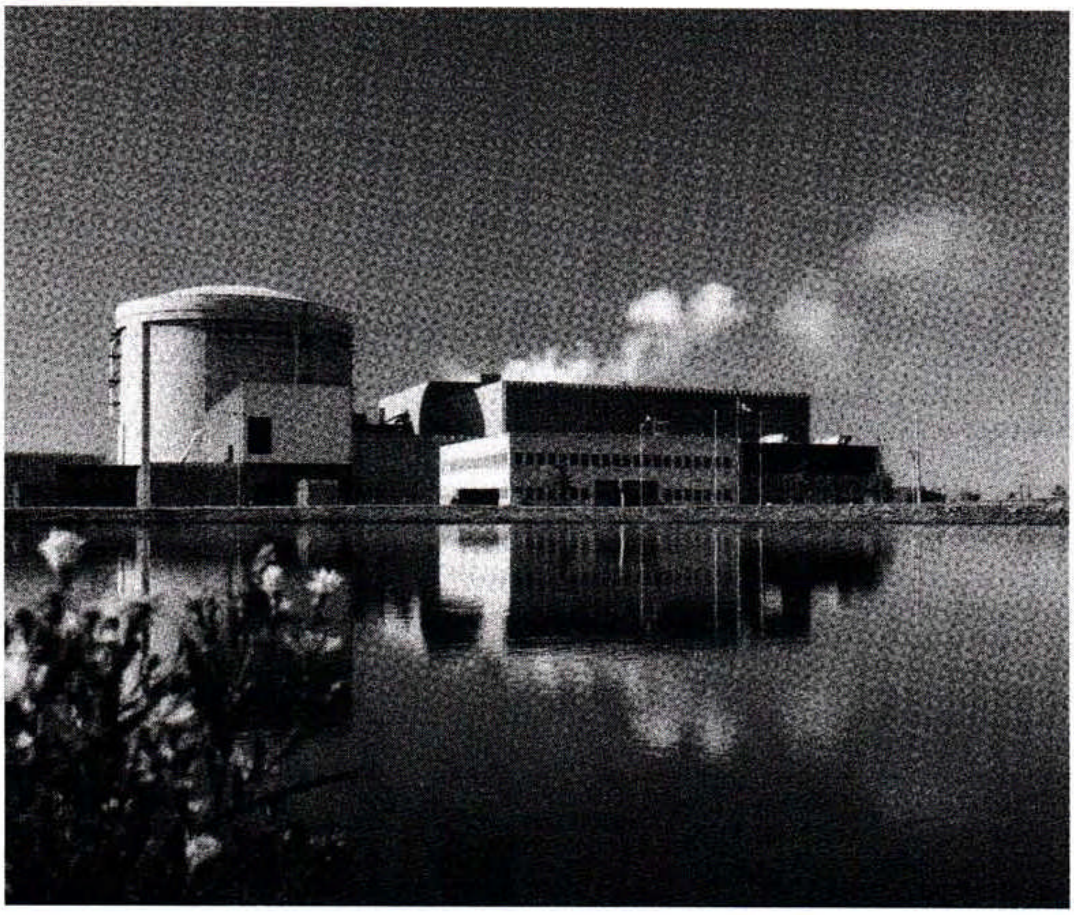

Figure 3 Point Lepreau nuclear generating station

6.2 Reactor Core Arrangement

The reactor core is cylindrical, but is set horizontally, as shown in Figure 4, with horizontal fuel channels. The heavy water moderator is contained in a cylindrical calandria with multiple tubes set in a square array and in an axial direction so that the moderator surrounds all the tubes.

Pressure tubes containing the fuel bundles pass through the calandria tubes. Heavy water coolant under a pressure of about 10 MPa flows through the pressure tubes to remove heat from the fuel bundles. Because the coolant is heavy water, there is minimal absorption of neutrons. Each pressure tube contains twelve fuel bundles, each of which has 37 fuel elements arranged in a circular pattern, as shown in Figure 5. The fuel elements consist of zirconium-alloy tubes filled with natural uranium dioxide pellets. A feature of the CANDU is that individual fuel channels can be refuelled while the reactor is at full power by pushing new fuel elements in at one end of the pressure tube and removing spent fuel elements at the other end, using special refuelling machines which can be attached to the ends of any pressure tube.

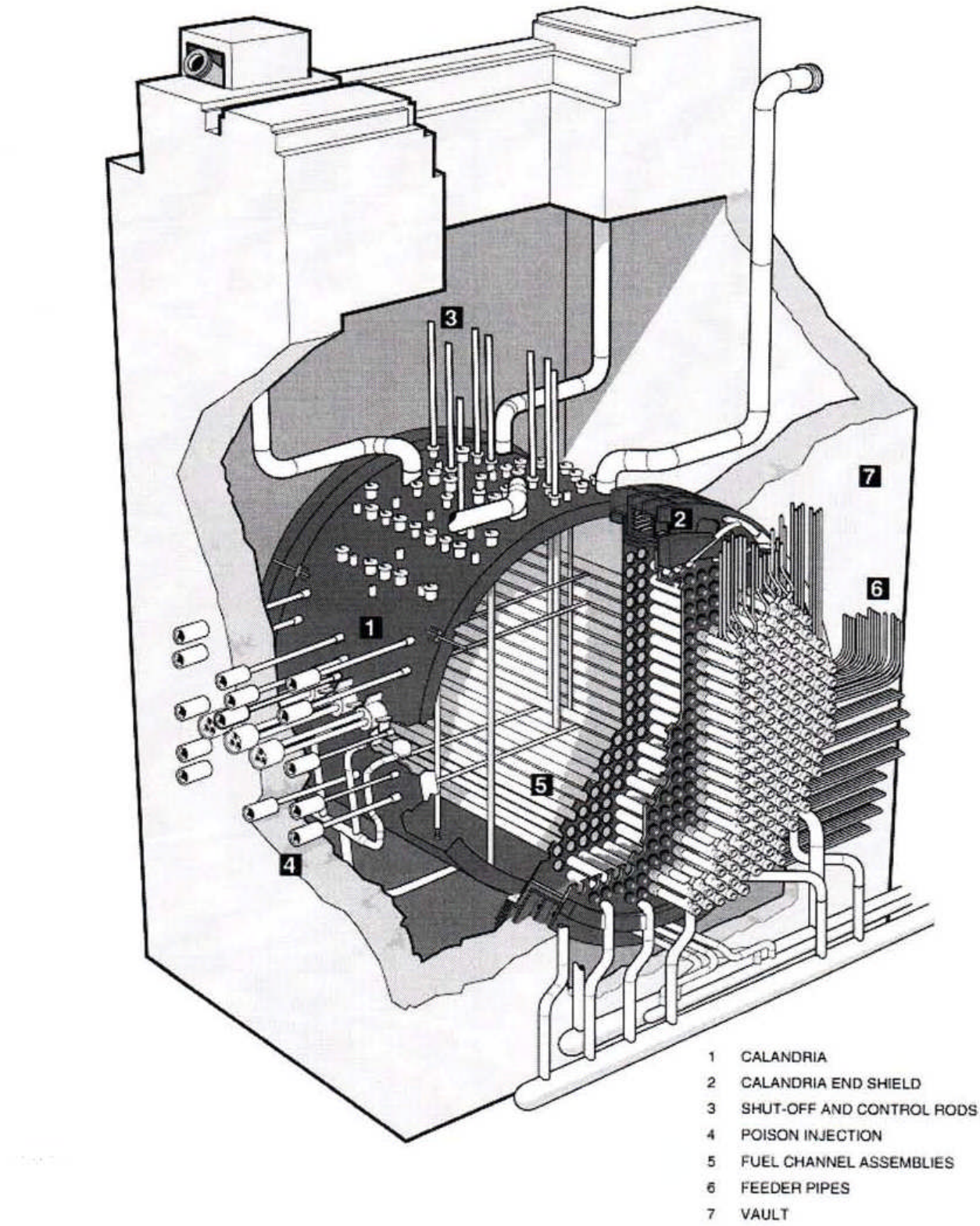

Figure 4 Reactor vault and assembly

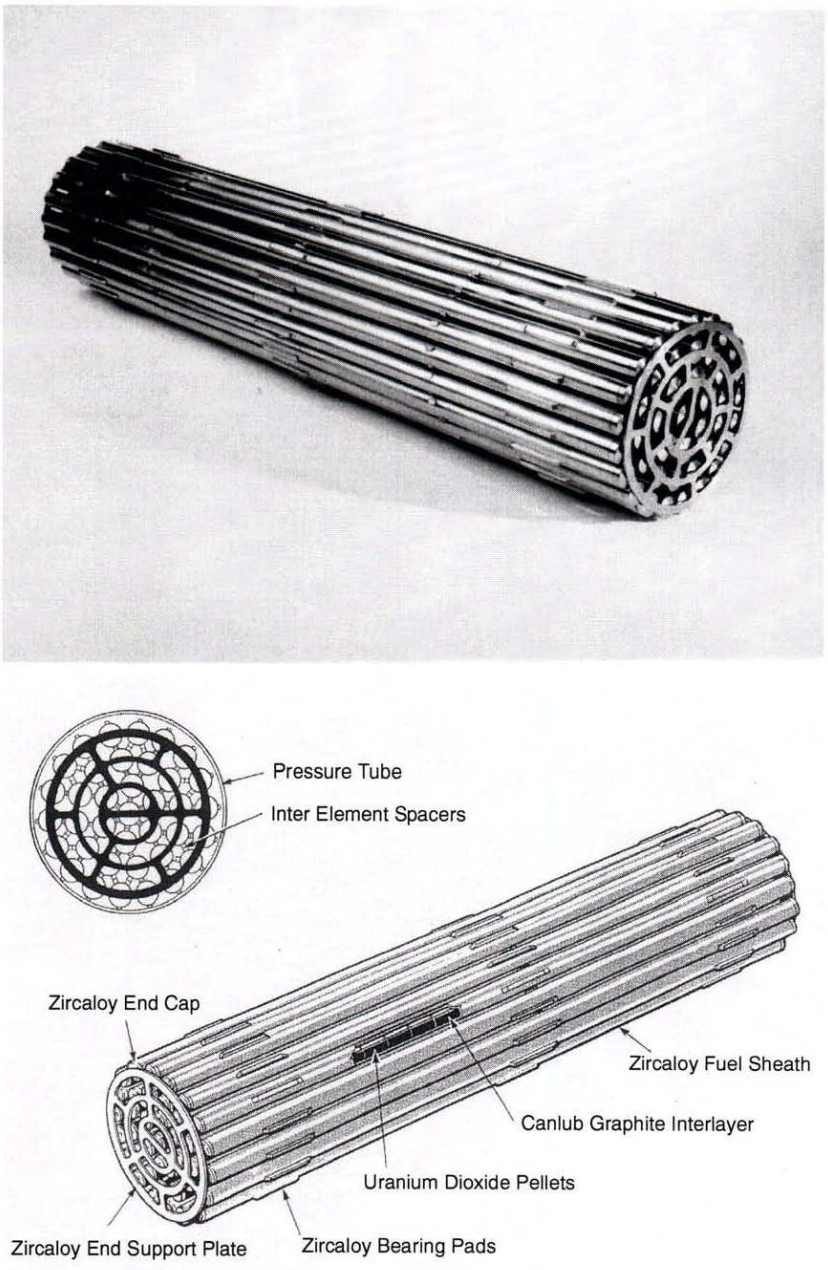

Figure 5 37-element fuel bundle

Control of the reactor is achieved by varying the amount of light water in special liquid level tubes in separate control zones in the calandria and by manipulation of control rods which are inserted into special vertical channels within the calandria and pass at right angles between the calandria tubes. Typical parameters for 600 MWe (electrical) and 950 MWe (electrical) CANDU reactor cores are given in Table 5.

Table 5 CANDU core parameters

Parameter	CANDU 600	CANDU 900
Number of fuel channels in core	380	600
Number of fuel bundles per channel	12	12
Number of fuel elements per bundle	37	37
Number of pellets per rod	30	30
Fuel pellet material	UO_2 sintered	UO_2 sintered
Fuel cladding material	Zircaloy-4	Zircaloy-4
Fuel channel array	square	square
Fuel channel lattice pitch	286 mm	286 mm
Fuel element configuration	circular	circular
Fuel bundle length	495 mm	495 mm
Fuel bundle diameter	102.4 mm	102.4 mm
Fuel element diameter	13.08 mm	13.08 mm
Fuel pellet diameter	12.16 mm	12.16 mm
Mass of uranium dioxide in core	95 Mg	153 Mg
Mass of uranium in core	84 Mg	135 Mg
Fuel type	natural U	natural U
Average core power density	~ 11 MW/m^3	~ 11 MW/m^3
Active core length	5.94 m	5.94 m
Extrapolated core length	6.06 m	6.06 m
Equivalent core diameter	6.27 m	7.90 m
Total core fission power	2 180 MW	3 394 MW
Total core thermal power	2 060 MW	3 237 MW
Maximum channel power	6.5 MW	6.5 MW
Maximum bundle power	0.8 MW	0.8 MW
Active heat transfer area	~ 3 430 m^2	~ 5 420 m^2
Average heat flux	~ 600 kW/m^3	~ 600 kW/m^3
Maximum heat flux	~ 1 000 kW/m^3	~ 1 000 kW/m^3

The reactor core includes monitoring and control devices to measure neutron flux and to modify the flux profile if required to obtain the best power distribution. Safety devices to bring about rapid shutdown, such as the shutoff rods and poison injection system, are also built into the core. The general arrangement of these is shown in Figure 6, and their locations are shown in the three views given in Figures 7, 8, and 9.

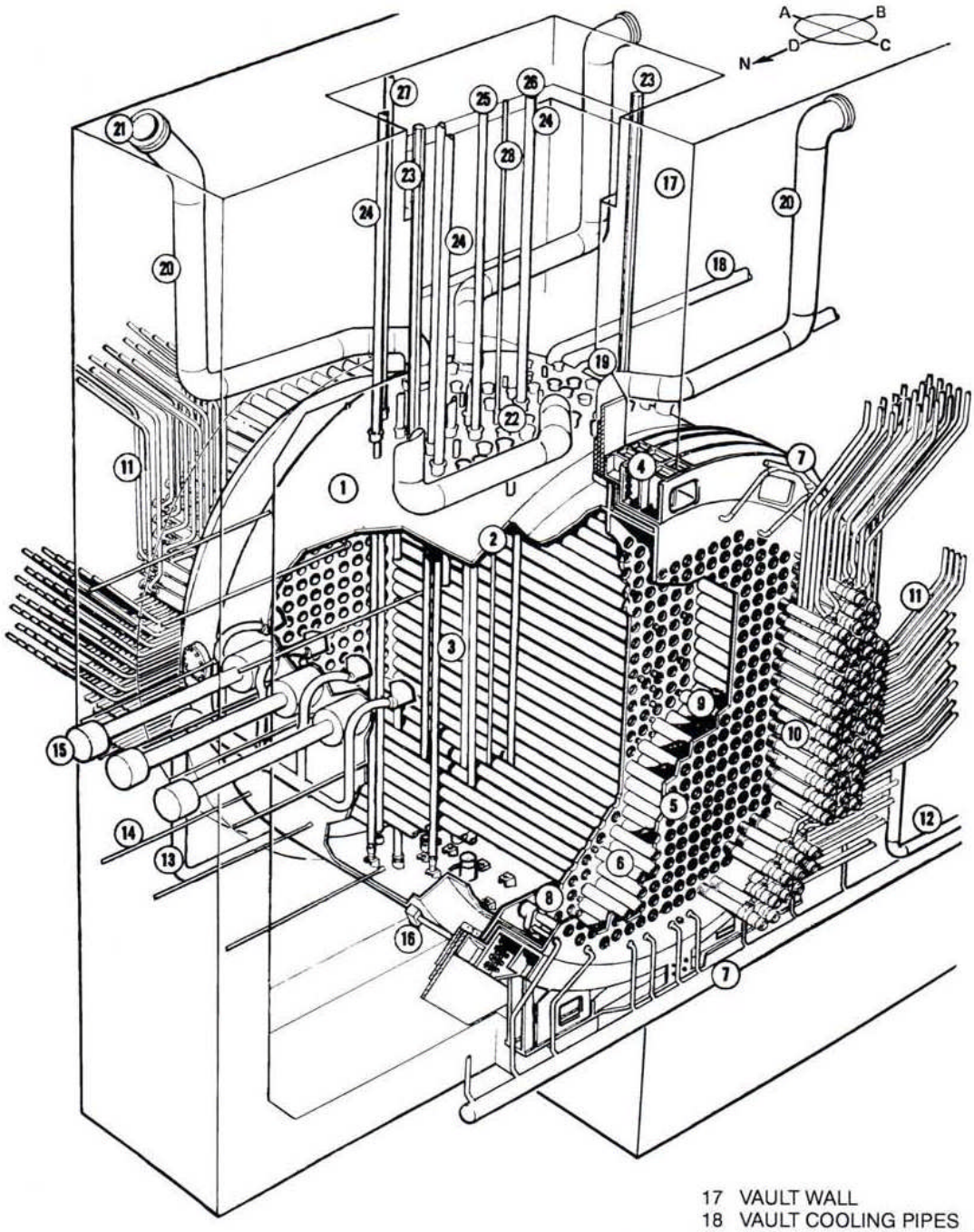

1 CALANDRIA
2 CALANDRIA SHELL
3 CALANDRIA TUBES
4 EMBEDMENT RING
5 FUELLING TUBESHEET
6 END SHIELD LATTICE
7 END SHIELD COOLING PIPES
8 INLET OUTLET STRAINER
9 STEEL BALL SHIELDING
10 END FITTINGS
11 FEEDER PIPES
12 MODERATOR OUTLET
13 MODERATOR INLET
14 FLUX MONITOR AND POISON INJECTION
15 ION CHAMBER
16 EARTHQUAKE RESTRAINT
17 VAULT WALL
18 VAULT COOLING PIPES
19 MODERATOR OVERFLOW
20 ACCIDENT DISCHARGE PIPE
21 RUPTURE DISC
22 REACTIVITY CONTROL ROD NOZZLES
23 VIEWING PORT
24 SHUTOFF ROD
25 ADJUSTER ROD
26 CONTROL ABSORBER ROD
27 ZONE CONTROL ROD
28 VERTICAL FLUX MONITOR

Figure 6 CANDU 6 reactor assembly

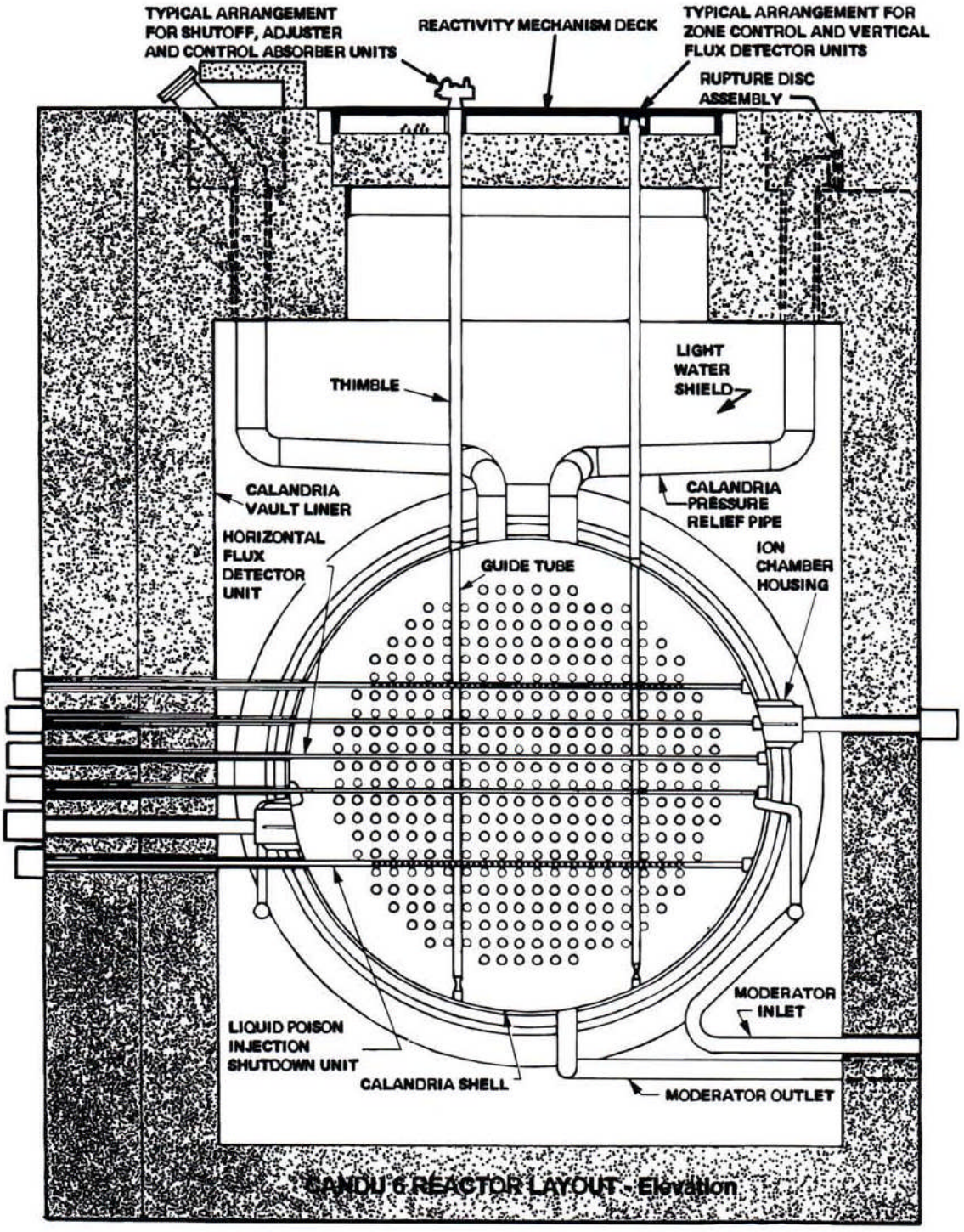

Figure 7 Reactor cross section

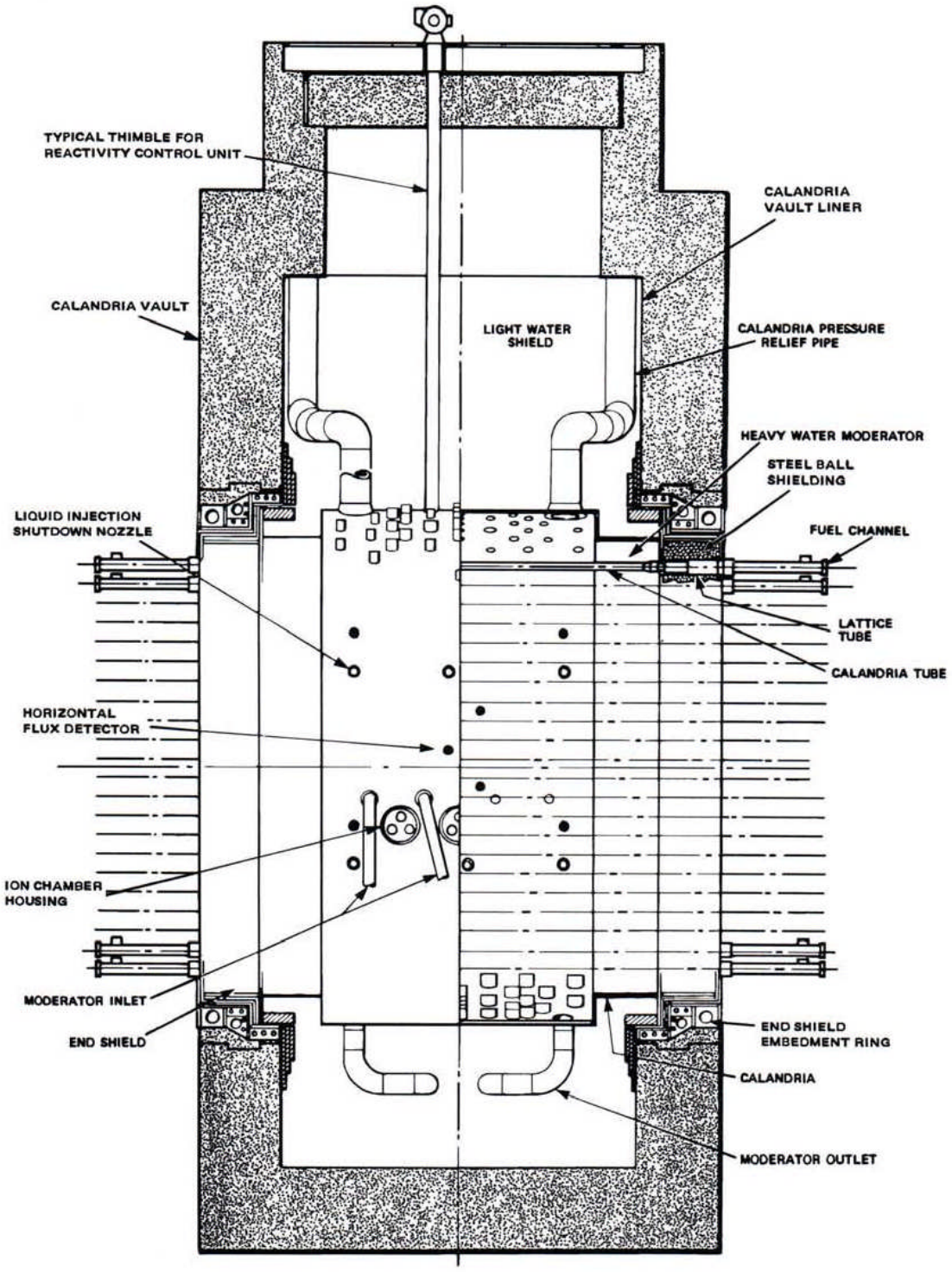

Figure 8 Reactor longitudinal section

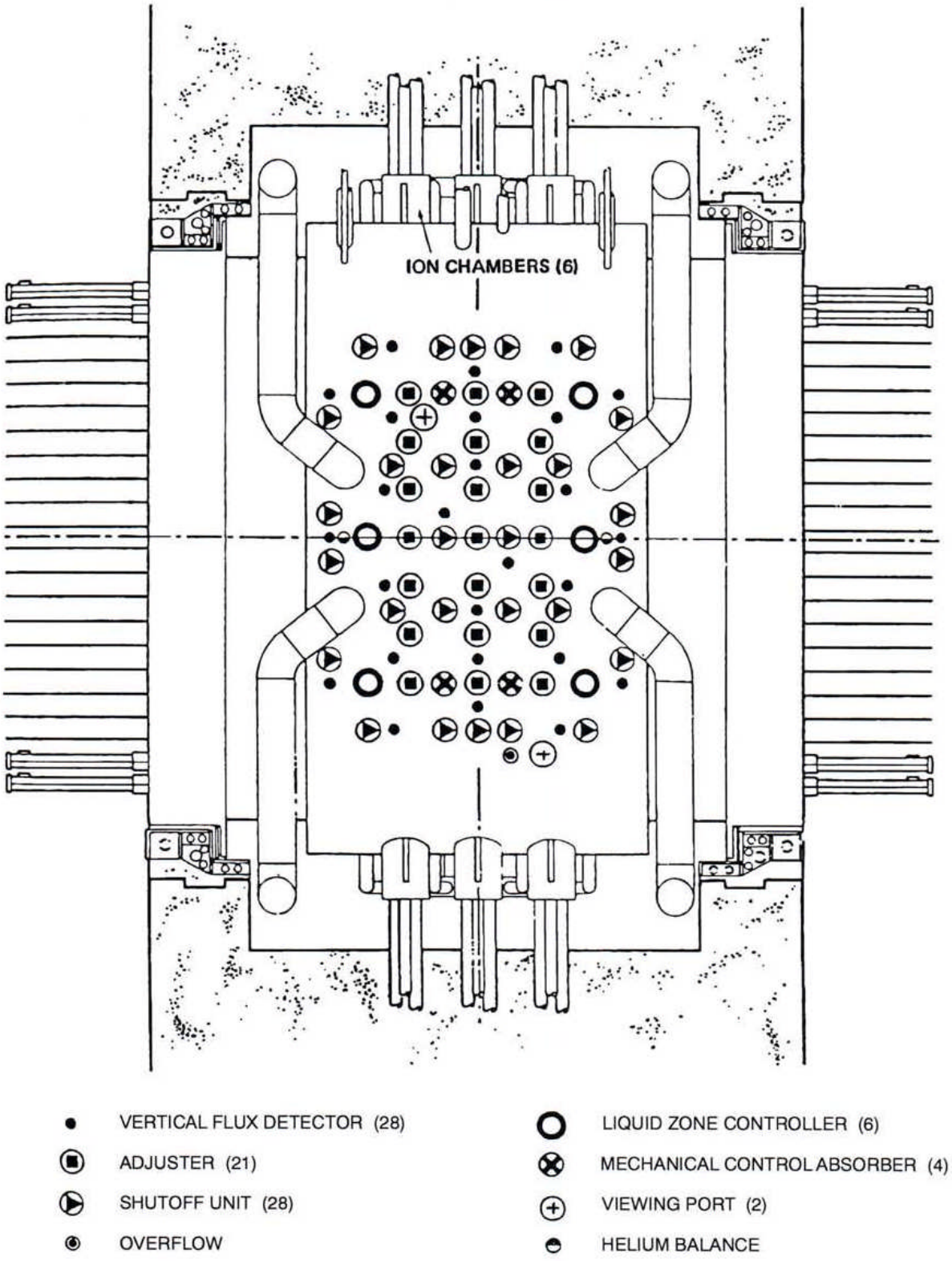

Figure 9 Reactor plan view

6.3 Coolant Loop Arrangement

The pressure tubes contain heavy water coolant at about 10 MPa and form part of the coolant

loop. Flow in the pressure tubes is arranged to be in opposite directions in adjacent fuel channels. Thus, at each end of the reactor, there are sets of inlets and outlets to and from each fuel channel, as shown in Figure 10. To carry the coolant to and from each of these inlets and outlets, small diameter feeder tubes are used, as shown in Figure 11. These are linked to twin common headers above each end of the reactor core. Coolant from the outlet headers at each end passes to the steam generators, then through the coolant pumps and back to the inlet headers at the same end of the reactor core. After a second pass through the fuel channels, the coolant passes to steam generators and coolant pumps at the other end of the reactor core. The complete coolant loop thus has a double figure-of-eight configuration. Typically, there are two steam generators and two coolant pumps at each end of the reactor core, making a total of four of each. Although each pair of steam generators and its associated coolant loop has a separate figure-of-eight configuration, the headers are cross-connected so that the whole system operates at the same pressure. Pressure is maintained by a single pressurizer connected to one of the coolant loops. The pressurizer is a tall cylindrical vessel containing half water and half steam and maintained at saturation conditions. By varying the temperature in the vessel with heaters or water sprays, the pressure in the entire coolant system can be controlled. Typical parameters for 600 MWe (electrical) and 950 MWe (electrical) CANDU coolant systems are given in Table 6. Full technical details are given in Appendix C Single Unit Station Data.

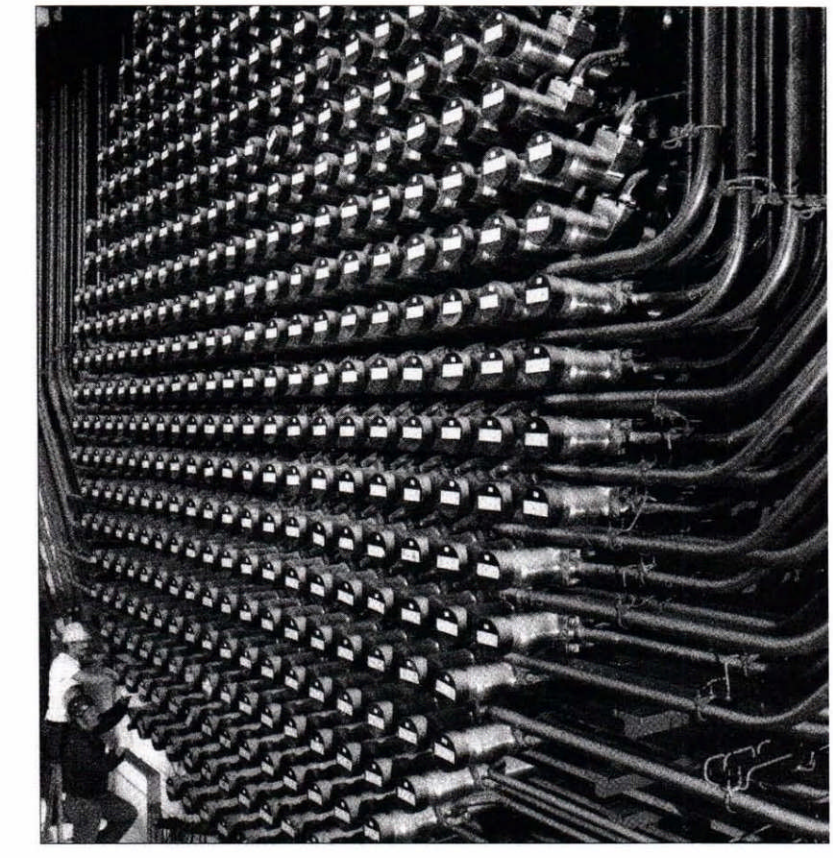

Figure 10 Fuel channel end fittings on reactor face

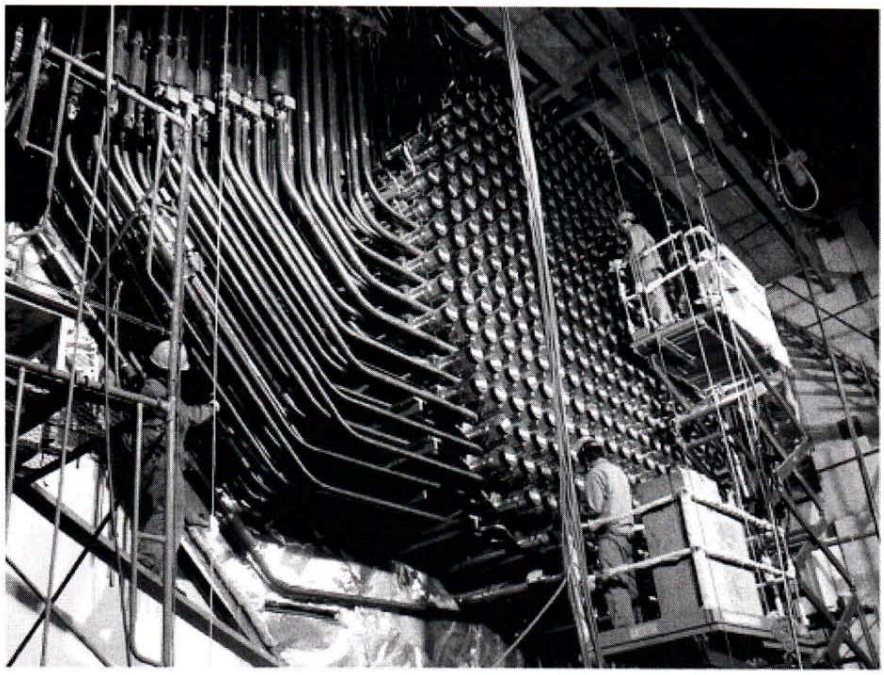

Figure 11 Feeder tube assembly on reactor face

Table 6 CANDU coolant system parameters

Parameter	CANDU 600	CANDU 900
Number of pressure tubes	380	600
Pressure tube material	Zirconium-niobium alloy	Zirconium-niobium alloy
Pressure tube diameter (ID)	103.38 mm	104 mm
Number of primary pumps	4	4
Pump flow rate (each)	2.228 m^3/s	3.959 m^3/s
Pump total heat (each)	215 m	245 m
Coolant flow rate through core	7 600 kg/s	13 500 kg/s
Coolant inlet temperature	267°C	266°C
Coolant outlet temperature	312°C	312°C
Coolant inlet pressure	11.04 MPa	11.17 MPa
Coolant outlet pressure	10.03 MPa	10.29 MPa

6.4 Steam Generators

The purpose of the steam generators is to transfer heat from the primary coolant system to the secondary steam system and thus supply the required heat to operate the steam cycle. Like those of the PWR, the steam generators are tube or surface heat exchangers, with high pressure coolant passing inside the tubes and lower pressure steam being generated on the outside of the tubes. The steam pressure is typically 5 MPa. The usual configuration is a vertical cylinder with inverted U-tubes in the lower part and steam-water separators in the upper part, as shown diagrammatically in Figure 12. Steam generated within the tube bundle rises and promotes natural circulation. At the top of the vessel, the steam-water mixture passes through cyclone type primary separators where the steam is separated from the circulating water. The water returns down an annulus between the tube bundle and the steam generator shell. The separated steam passes through secondary separators or steam dryers to remove moisture and so improve its quality before passing out at the top of the vessel. Incoming feedwater enters at the bottom of the steam generator. This cooler feedwater is confined within baffles and made to flow in a criss-cross manner over that part of the tube bundle near the primary coolant outlet. In this way, the feedwater temperature is raised to saturation conditions before mixing with the circulating water in the steam generator. This arrangement improves thermodynamic performance, but limits the range of temperature at which feedwater can be introduced to the steam generator. A sudden drop in feedwater temperature during normal operating conditions could cause thermal shock to the vessel and tubes. Typical parameters for 600 MWe (electrical) and 950 MWe (electrical) CANDU reactor steam generators are given in Table 7.

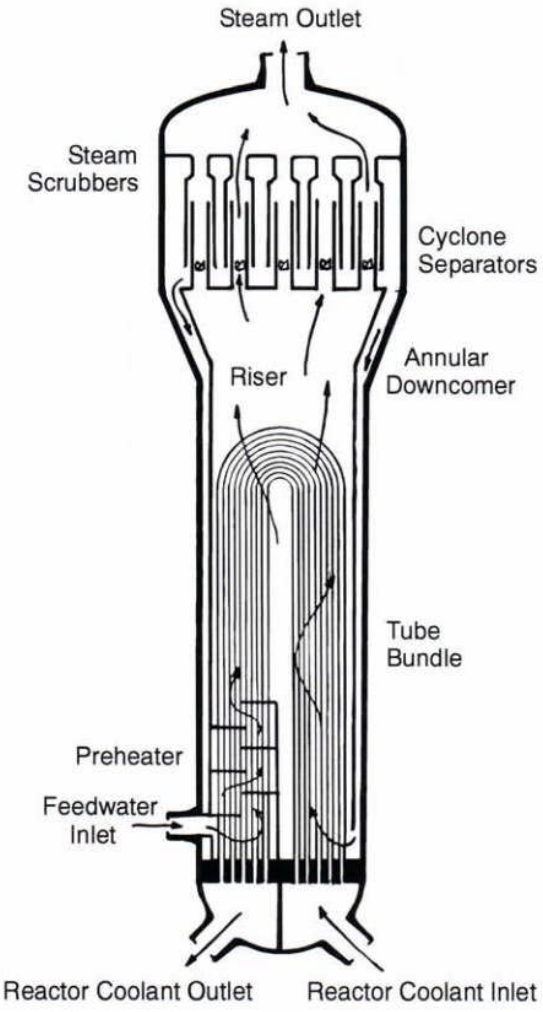

Figure 12 Steam generator for CANDU system

Table 7 CANDU steam generator parameters

Parameter	CANDU 600	CANDU 900
Number of steam generators	4	8
Heat transfer capacity (total)	2 064 MW	3 258 MW
Primary side water flow (total)	7 600 kg/s	13 500 kg/s
Primary side operating pressure	~ 10 MPa	~ 10 MPa
Primary side inlet temperature	312°C	312°C
Primary side outlet temperature	~ 267°C	~ 266°C
Secondary side steam flow (total)	1 047 kg/s	1 612 kg/s
Secondary side feedwater flow (total)	959 kg/s	1 536 kg/s
Secondary side operating pressure	4.69 MPa	5.07 MPa
Secondary side inlet temperature	187°C	177°C
Secondary side outlet temperature	260°C	265°C
Steam outlet wetness	0.25%	0.25%
Number of tubes (each)		4 663
Heat transfer area per steam generator		~ 3 066 m^3
Tube diameter (OD)	22.23 mm	15.9 mm
Tube material	Inconel 600	Incoloy 800

6.5 Steam Turbines

Each CANDU unit has a single steam turbine and electrical generator on a single shaft. The steam turbine consists of a high pressure turbine receiving saturated steam from the steam generators and three low pressure turbines receiving steam, after moisture separation and reheating, from the high pressure turbine. Saturated steam from the steam generator is used for reheating, and the reheated steam becomes superheated at the lower pressure. This is required to avoid too high a moisture content in the turbine exhaust. Three low pressure turbines are required due to the large increase in steam specific volume as it expands to condenser conditions. Figure 13 shows the 600 MW steam turbine at Point Lepreau viewed from the steam inlet end, with the steam inlet valves and high pressure turbine in the foreground and the low pressure turbines further back. Figure 14 shows the same turbine from the electrical output end, with the exciter and generator in the foreground and the low pressure turbines behind them. Typical parameters for 600 MW (electrical) and 950 MW (electrical) steam turbines are given in Table 8.

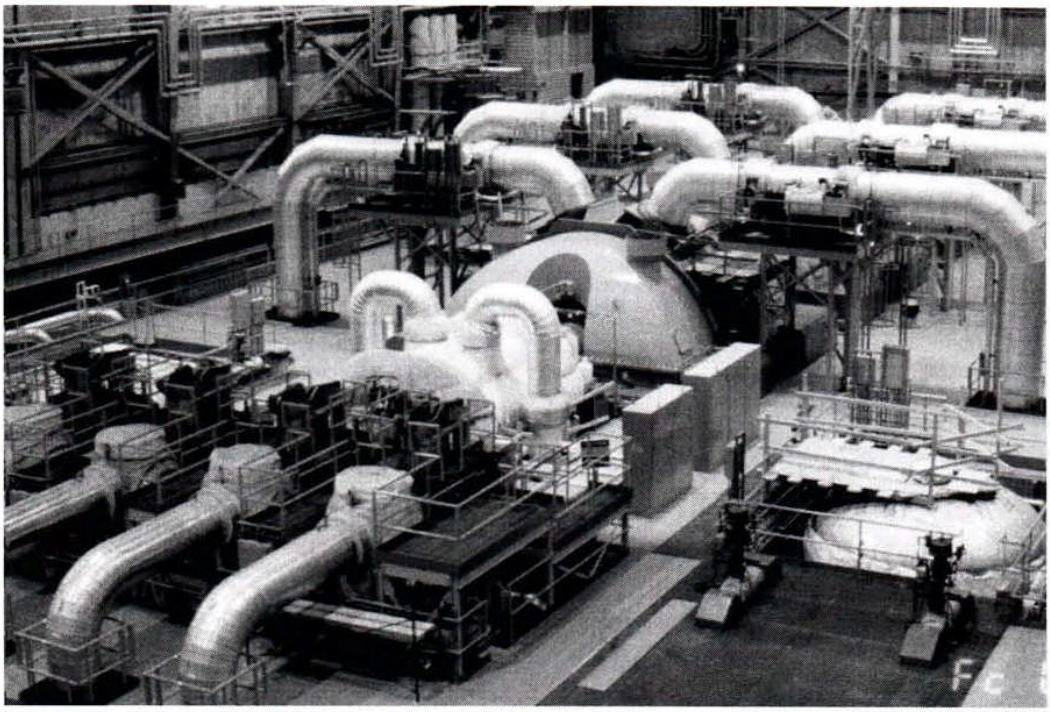

Figure 13 600 MW steam turbine for nuclear unit

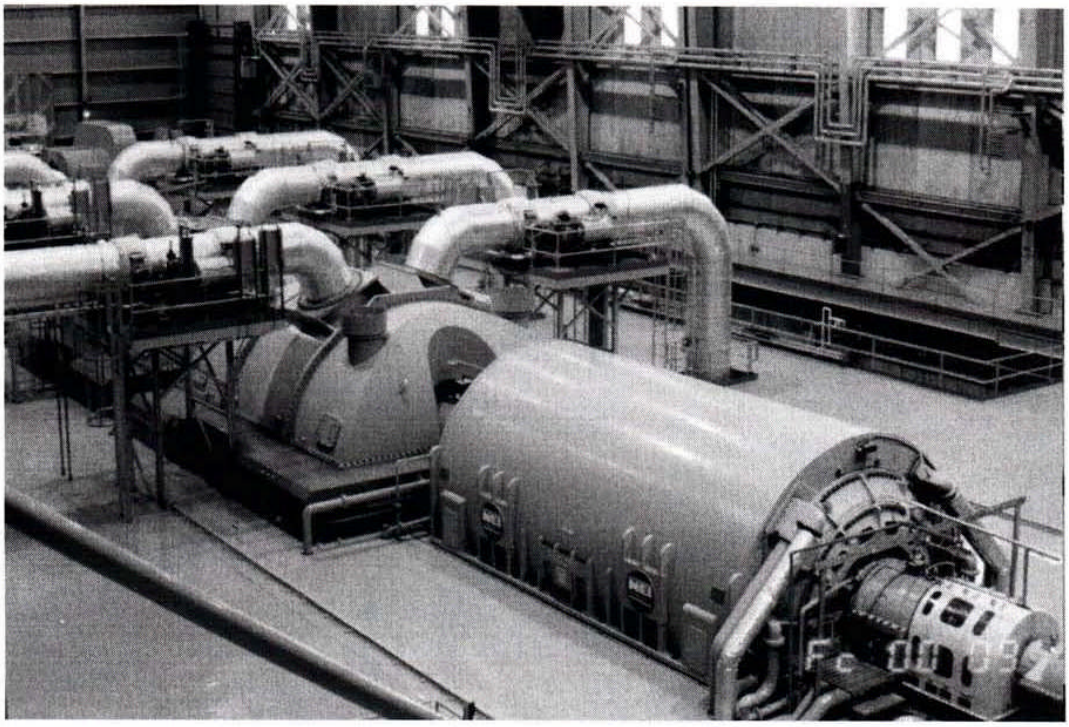

Figure 14 Turbine generator for nuclear unit

Table 8 Steam turbine parameters

Parameter	CANDU 600	CANDU 900
Number of HP cylinders	1 double flow	1 double flow
Number of LP cylinders	3 double flow	3 double flow
Main steam flow rate	1 047 kg/s	1 612 kg/s
Live steam flow to valves	957 kg/s	1 533 kg/s
Live steam flow to reheater	90 kg/s	77 kg/s
HP steam inlet pressure	4.55 MPa	4.93 MPa
HP steam inlet temperature	258°C	263°C
HP steam exhaust pressure	0.665 MPa	0.545 MPa
HP steam exhaust quality	88.2%	86.5%
LP steam inlet pressure	0.588 MPa	0.500 MPa
LP steam inlet temperature	242°C	247°C
LP steam exhaust quality	89.5%	91.0%
Steam cycle efficiency	32.8%	34.4%
Electrical generator gross output	678 MW	1 121 MW

6.6 Technical Data

The technical data in this chapter were obtained from various sources, including references in the bibliography and public relations brochures from Atomic Energy of Canada Limited, and therefore are not necessarily applicable to a particular nuclear power plant. Some data may be inconsistent or in conflict due to evolution of the design or to differences between design and operational data. Furthermore, some missing data were deduced by simple calculation for illustrative purposes and are indicated as an approximate value, meaning that what is presented is typical rather than specific.

7 Possible CANDU Reactor Development

7.1 CANDU Advantages

Refuelling can be done while the reactor is on power by pushing new fuel bundles in at one end of a fuel channel while spent fuel bundles are removed at the other end. This allows the CANDU reactors to achieve high capacity factors compared with those reactors which have to be shut down periodically for refuelling. Figure 15 shows a typical annual analysis of capacity factors for CANDU reactors and other light water reactors in the early years of their life before major maintenance or refurbishment became necessary. This shows that in that year in the top 25 reactors worldwide, with regard to capacity factor performance, there are proportionately twice as many CANDU reactors listed as in the general population of water cooled reactors. One year within the first ten years of operation Point Lepreau was actually ranked first on this list. This was due to only one short planned annual shutdown for routine maintenance of systems not able to be accessed during normal operation during the initial years of operation.

Furthermore the relative simplicity of the fuel bundles and the use of natural uranium leads to low fuel costs for CANDU reactors. With no heavy reactor pressure vessel and the possibility of modular construction the erection time of a CANDU reactor can be shorter than that of some other reactor systems. Having been developed to use natural uranium in conveniently small fuel bundles, the CANDU reactor has the ability of utilizing low enriched fuel from other sources such as light water reactors and also blended fuel from nuclear weapons. This makes it attractive as part of a fuel reprocessing and recycling scheme involving different nuclear plants and facilities.

The refurbishment of CANDU reactors has been proven. Steam generators and reactor pressure tubes can be replaced. This has the potential of effectively doubling the life of the plant enabling it to operate efficiently for 50 to 60 years. The overall capital investment including the cost of refurbishment can make the CANDU reactor an attractive investment for bulk base load power production.

AECL EACL

The Top Twenty-five

Lifetime World Power Reactor Performance to September 30, 1995* *from among 370 reactors over 150 MW*

Rank	Country	Unit	Type	Year of First Power	Capacity Factor %†
1	Germany	Emsland	PWR	1988	91.4
2	Germany	Neckar 2	PWR	1989	89.2
3	Canada	Point Lepreau	CANDU	1982	88.3
4	Germany	Grohnde	PWR	1984	88.1
5	Canada	Pickering 8	CANDU	1986	88.0
6	Canada	Pickering 7	CANDU	1984	87.6
7	Belgium	Tihange 3	PWR	1985	87.5
8	Finland	Loviisa 2	PWR	1980	86.8
9	Hungary	Paks 2	PWR	1984	86.2
10	Switzerland	Beznau 2	PWR	1971	85.7
11	Germany	Philippsburg 2	PWR	1984	85.5
12	Hungary	Paks 4	PWR	1987	85.4
13	Canada	Darlington 3	CANDU	1992	85.4
14	Canada	Darlington 4	CANDU	1993	85.2
15	Hungary	Paks 3	PWR	1986	85.2
16	Canada	Pickering 6	CANDU	1983	84.6
17	Switzerland	Gösgen	PWR	1979	84.2
18	Germany	Gralenrheinfeld	PWR	1981	83.9
19	Finland	TVO 1	BWR	1978	83.8
20	Spain	Cofrentes	BWR	1984	83.7
21	Spain	Trillo 1	PWR	1988	83.3
22	Spain	Almaraz 2	PWR	1983	83.2
23	Finland	Loviisa 1	PWR	1977	83.2
24	Korea	Wolsong 1	CANDU	1982	83.2
25	Finland	TVO 2	BWR	1980	83.1

*Source: Nuclear Engineering International

† Capacity Factor = actual electricity generation / perfect electricity generation

Figure 15 Typical capacity factors of CANDU and other reactors

7.2 Future Prospects

Future prospects for the CANDU reactor are good. About one third of CANDU reactors in operation are of the CANDU 6 type and all have performed well. The few larger reactors have also provided good service. A CANDU reactor would be a good choice for any future nuclear

reactors built in Canada. However it would be in competition with light water reactors especially the PWR where later designs are under construction.

Of particular note is the modular construction proposed for new reactors. The advantage that this modular construction offers is a decreased construction time and hence lower costs. It also allows specific parts of the reactor to be more easily replaced during the life of the plant.

New fuel bundles with 43 fuel elements have been developed and tested. The increased surface area and smaller diameter elements resulting from this change allow for increased heat transfer and hence more power per bundle. Such design developments are able to reduce the capital and operating costs of the current CANDU system.

7.3 Safety Aspects

The primary way to avoid reactor accidents is through use of duplicate safety systems, core cooling systems, and engineered safeguards built into the reactor design. The CANDU reactor has evolved to be inherently safe, with consideration given to all conceivable accidents. Accidents to early reactors, as mentioned earlier, have highlighted the need for very conservative and safe design requirements.

In case of an adverse transient which could lead to a potential accident, there are two independent shutdown systems. The SDS1 system consists of mechanical shutoff rods which drop into the core by gravity when a trip signal is received. The SDS2 system consists of an array of nozzles which inject gadolinium nitrate under gas pressure into the moderator on receipt of a trip signal.

In the event of loss of coolant from the reactor heat transport system, an emergency core cooling system injects cooling water into the headers to ensure a water supply to maintain fuel cooling. This is backed up by alternative systems to maintain cooling for an extended period.

Use of multiple pressure tubes instead of a single large pressure vessel permits thinner walls and simpler manufacture to the required pressure threshold. Any leaks can be detected by monitoring moisture content and pressure in the gap between the pressure tube and the calandria tube, which is done on a continuous basis. When detected, a faulty pressure tube can be readily replaced.

The heavy water moderator and reflector in the calandria surrounding the pressure tubes are at a relatively low temperature compared with that of the coolant flowing in the pressure tubes. Because of this lower temperature, the moderator and reflector act as an energy sink in case of certain reactor accidents. This heat sink is an important feature in the CANDU design because it means that if the emergency core cooling system fails, some heat can be transferred from the fuel to the moderator. The calandria itself is surrounded by light water in the reactor vault, thus creating an additional short term heat sink for the moderator.

Most important are the engineered safeguards that protect the public from possible release of fission products in the event of a component failure. As in most nuclear power plants, there are four barriers that prevent the release of significant quantities of fission products to the environment. These barriers are: the fuel itself, the fuel cladding, the primary heat transport system boundary, and the containment building.

The first barrier is the uranium dioxide fuel, which is chemically inert even in high temperature water and has a high melting point. Even under high temperature conditions, about 99% of all

radioactivity is trapped in the uranium dioxide matrix. This means that almost all solid fission products are contained in the fuel under normal non-melting conditions.

The second barrier is the fuel cladding, which is a zirconium alloy sheath. This sheath is designed to withstand the stress associated with fuel expansion and buildup of trapped fission gases. Zirconium would be subject to damage should dryout and elevated temperatures occur in the fuel channel. Provided the fuel bundles are kept flooded with coolant during accident conditions, this barrier will remain intact.

The third barrier is the primary heat transport system boundary. This provides containment for the coolant, which may contain fission products in the event of fuel cladding leakage. The primary circuit is a closed loop and does not allow any fission products to go any further unless it in turn has a leak.

The fourth and final barrier to fission product release is the prestressed low leakage concrete containment building. The building is maintained under a slightly negative pressure and is lined with a plastic coating which limits the leakage of fission products in the event of overpressure due to an accident. In addition, air exchange filters in the ventilation system remove any fission products in the circulating air which is discharged to the atmosphere.

7.4 The Advanced CANDU Reactor

A possible new development of the CANDU reactor is the Advanced CANDU Reactor (ACR 1000), with a nominal net electrical output of 1000 MWe. The general arrangement is very much the same as the basic CANDU reactor, as shown in Figure 16, but some significant technical changes have been included.

These reactors have been designed so that they can be built within a four-year period and have an expected plant life of 60 years, with an overall lifetime capacity factor of over 90%. They use light water instead of heavy water as coolant, thus simplifying several supporting auxiliary systems. This necessitates use of low enrichment fuel to compensate for increased neutron absorption in the coolant. The fuel bundles are of the CANFLEX 43 element design, as shown in Figure 17, which provides increased power output per bundle and hence per channel. This design has fuel elements of two different sizes. There are 8 central elements 13.5 mm in diameter and 35 outer elements 11.5 mm in diameter. A quick comparison between the CANDU 6 and Darlington Generating Station shows the general trend of the conventional CANDU design towards larger capacities, while a comparison between Darlington and the ACR 1000 shows somewhat of a reversal of this trend with current technical changes. Table 9 shows some key technical parameters which illustrate this trend.

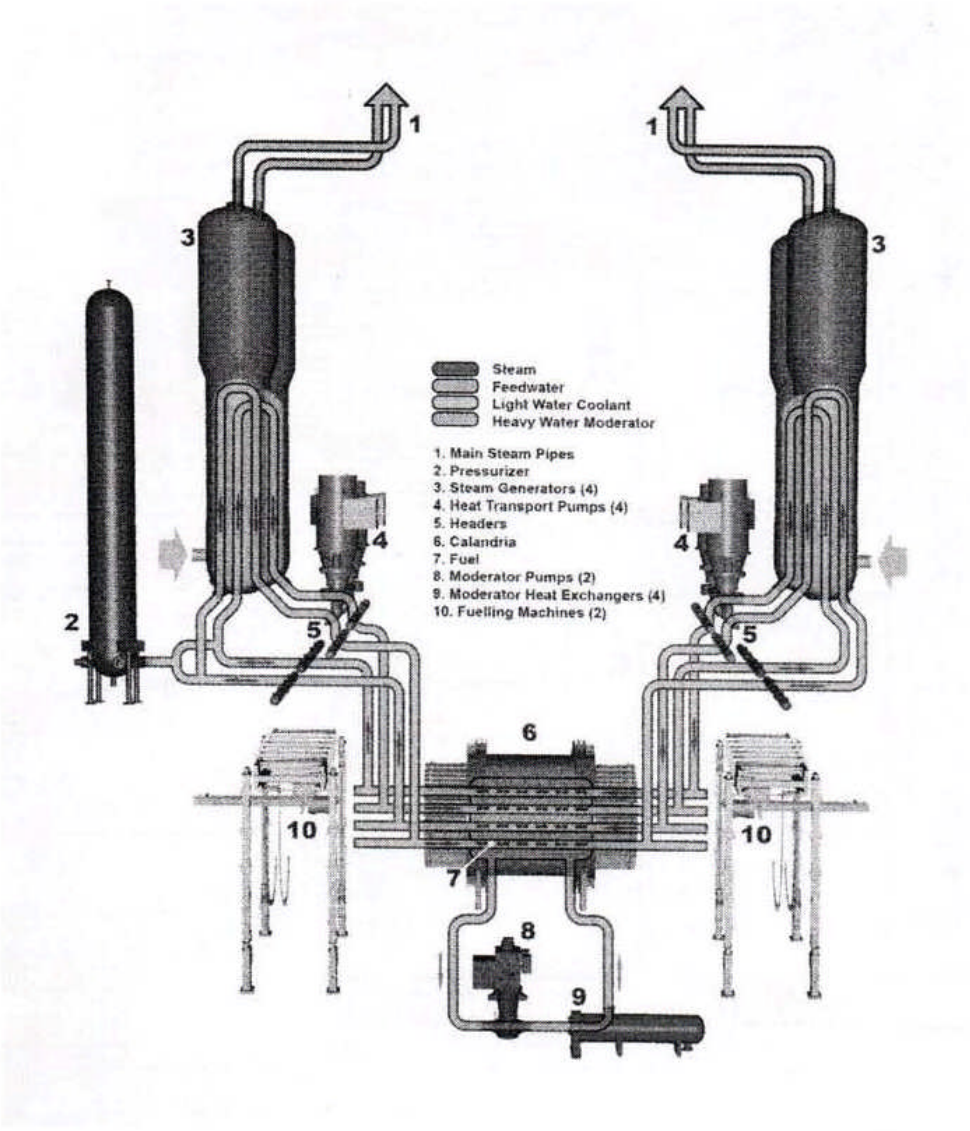

Figure 16 ACR 1000 nuclear systems schematic

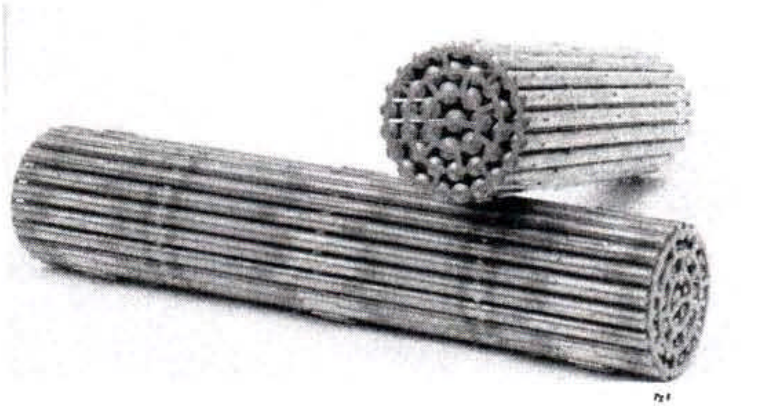

Figure 17 ACR CANFLEX fuel bundles

Table 9 Advanced CANDU reactor parameter comparison

Parameter	Units	CANDU 6	Darlington	ACR 1000
Reactor power output	MWt	2 064	2 657	3 187
Moderator		D_2O	D_2O	D_2O
Coolant		D_2O	D_2O	H_2O
Fuel		Nat UO_2	Nat UO_2	Enriched UO_2
Heavy water inventory in moderator	Mg	265	312	250
Heavy water inventory in coolant	Mg	192	280	0
Number of fuel channels		380	480	520
Number of bundles per fuel channel		12	13	12
Number of elements per bundle		37	37	43
Fuel burnup	MWd/tU	7 500	7 791	20 000
Calandria diameter	m	7.6	8.5	7.5
Lattice pitch	mm	286	286	240
Pressure tube wall thickness	mm	4	4	6.5
Inlet header pressure	MPa	11.2	11.3	12.5
Inlet header temperature	°C	260	267	275
Outlet header pressure	MPa	9.9	9.9	11.1
Outlet header temperature	°C	310	310	319
Maximum channel flow	kg/s	28	27	28
Number of heat transport pumps		4	4	4
Pump motor rating (each)	MWe	6.7	9.6	10.0
Pump rated flow (each)	m^3/s	2.228	3.240	4.300
Number of steam generators		4	4	4
Tube diameter	mm	15.9	15.9	17.5
Steam pressure	MPa	4.6	5.0	5.9
Steam temperature	°C	260	265	276
Steam quality	%	99.75	99.75	99.90
Net power to turbine generator	MWt	2 060	2 650	3 180
Steam cycle efficiency		35.3	35.3	~ 36.6
Gross electrical power output	MWe	728	935	1 165
Net electrical power output	MWe	666	881	1 085
Turbine inlet steam temperature	°C	258	263	273
Final feedwater temperature	°C	187	177	217
Condenser vacuum	kPa	4.9	4.2	4.9

The table clearly shows the evolution of the ACR 1000. The 43-element fuel bundle provides an average channel power of 6.13 MW (12 bundles) as opposed to 5.43 MW (12 bundles) and 5.54 MW (13 bundles). This in turn enables fewer channels to be used for an equivalent output, resulting in a smaller reactor for the same output. Furthermore, the channel pitch has been

reduced by 16% resulting in an even smaller reactor. The overall result is that the ACR 1000 reactor is about the same size as the CANDU 6, as illustrated in Figure 18. The heavy water inventory has been reduced accordingly. The light water coolant eliminates a pressurized heavy water circuit altogether, thereby effecting a further and major saving in inventory and heavy water support systems. The low enriched uranium increases the burnup by a factor of about 2.5 and consequently decreases the amount of spent fuel. An additional reserve water system provides a passive safety feature, making this a Generation III+ design. Other than these important changes, there are many small improvements in the general operating conditions of the heat transport system and steam cycle, giving an improvement in overall efficiency from 35.3% to 36.6%, which ultimately saves on fuel consumption.

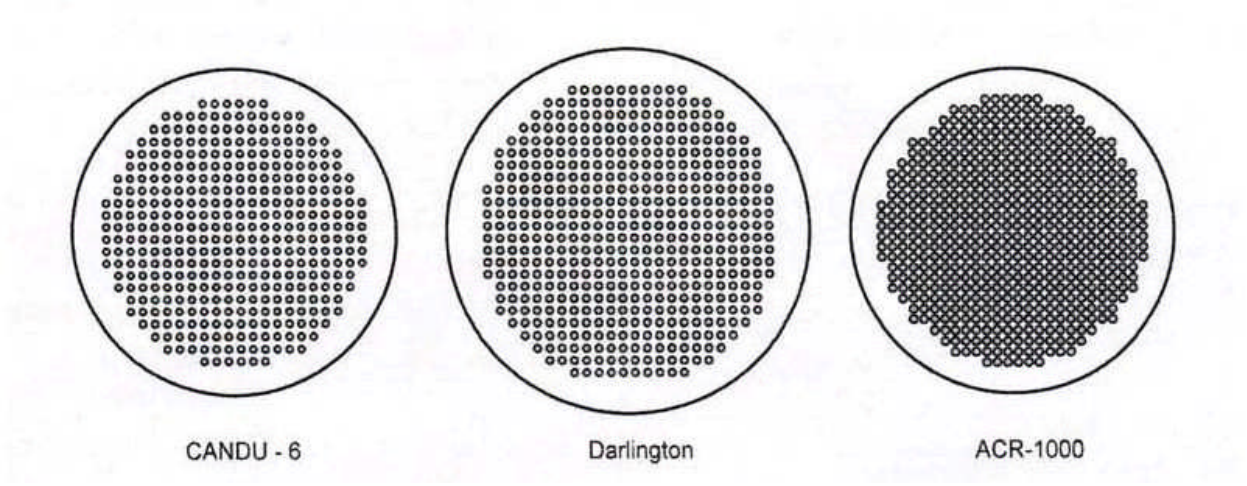

Figure 18 Comparison of core sizes

8 Problems

1 Sketch a typical figure-of-eight CANDU heat transport system showing all key components and describe the functions of these components.

2 Sketch a typical CANDU reactor core and show in the sketch where, with respect to the fuel channels, the various control devices are installed. Identify the devices and state their purpose.

3 Describe the structure and characteristics of a CANDU fuel channel and the fuel within the channel. Describe also what happens in the fuel channel as the coolant flows through it.

4 Sketch a CANDU steam generator showing the key components and explain the function of each component and why they are arranged in this particular configuration.

9 References and Bibliography

[AECL1989] Atomic Energy of Canada Limited, CANDU 8 Technical Outline. September 1989.

[AECL1989] Atomic Energy of Canada Limited, *CANDU 3 Technical Outline*, Document Number 74-01010-TED-001, Revision 9, 1989.

[AECL1991] Atomic Energy of Canada Limited, *Technical Summary CANDU Nuclear Generating Station*. 1991.

[AECL1997] Atomic Energy of Canada Limited, CANDU Technical Summary, 1997.

[AECL1997a] Atomic Energy of Canada Limited, *Canada Enters the Nuclear Age*, AECL, McGill-Queen's University Press, 1997.

[AECL1997b] Atomic Energy of Canada Limited, *CANDU 6 Technical Outline*, Document Reference CO/MISC-0131, Revision 1, 1997.

[AECL2007] Atomic Energy of Canada Limited, *ACR 1000 Technical Summary*. 2007.

[Brooks1993] Brooks, G. L., *A Short History of the CANDU Nuclear Power System*, Ontario Hydro Demand/Supply Hearing, Canada, January 1993.

[Brooks2001a] Brooks, G. L., *CANDU Origins and Evolution – Part 2 of 5 – Why CANDU*, AECL Retirees Group, Canada, February 2001. [CANTEACH, https://canteach.candu.org]

[Brooks2001b] Brooks, G. L., *CANDU Origins and Evolution – Part 3 of 5 – 'Figure of Eight' Heat Transport System Arrangement*, AECL Retirees Group, Canada, February 2001. [CANTEACH, https://canteach.candu.org]

[Brooks2001c] Brooks, G. L., *CANDU Origins and Evolution – Part 4 of 5 – Emergency Core Cooling Systems*, AECL Retirees Group, Canada, February 2001. [CANTEACH, https://canteach.candu.org]

[Brooks2001d] Brooks, G. L., *CANDU Origins and Evolution – Part 5 of 5 – Origins and Evolution of the Second Shutdown System*, AECL Retirees Group, Canada, February 2001. [CANTEACH, https://canteach.candu.org]

[Chaplin1973] Chaplin, R. A., "The Winfrith Steam Generating Heavy Water Reactor", *South African Mechanical Engineer*, May 1973.

[Chaplin2006a] Chaplin, R. A., "Pressurized Heavy Water Reactors", Chapter 3.6.2.3 in *Nuclear Energy and Reactors*, Encyclopedia of Life Support Systems by UNESCO, EOLSS Publishers, Oxford, UK, 2006.

[Chaplin2006b] Chaplin, R. A., "Heavy Water Light Water Reactors", Chapter 3.6.2.4 in *Nuclear Energy and Reactors*, Encyclopedia of Life Support Systems by UNESCO, EOLSS Publishers, Oxford, UK, 2006.

[Dyke2006] Dyke, J. M. and Garland, W. J., "Evolution of CANDU Steam Generators – A Historical View", Canada, May 2006. [CANTEACH, https://canteach.candu.org]

[Foster2001] Foster, J. S. & Brooks, G. L., *CANDU Origins and Evolution – Part 1 of 5 – An Overview of the Early CANDU Program*, AECL Retirees Group, Canada, February 2001. [CANTEACH, https://canteach.candu.org]

[Laurence1980] Laurence, G. C., Early Years of Nuclear Research in Canada. AECL, Chalk River

ON, May 1980.

10 Acknowledgements

Acknowledgements are extended to Atomic Energy of Canada Limited and to NB Power for use of information, diagrams and photographs to support the text of this chapter.

The following reviewers are gratefully acknowledged for their hard work and excellent comments during the development of this Chapter. Their feedback has much improved it. Of course the responsibility for any errors or omissions lies entirely with the author.

Bob Tapping
Jeremy Whitlock
Bhaskar Sur
Terry Rogers
George Bereznai

Thanks are also extended to Diana Bouchard for expertly editing and assembling the final copy.

Genealogy of CANDU Reactors: Appendices

prepared by

Dr. Robin Chaplin

Table of Contents

Appendix A – Cutaway View of CANDU 6 Reactor Plant

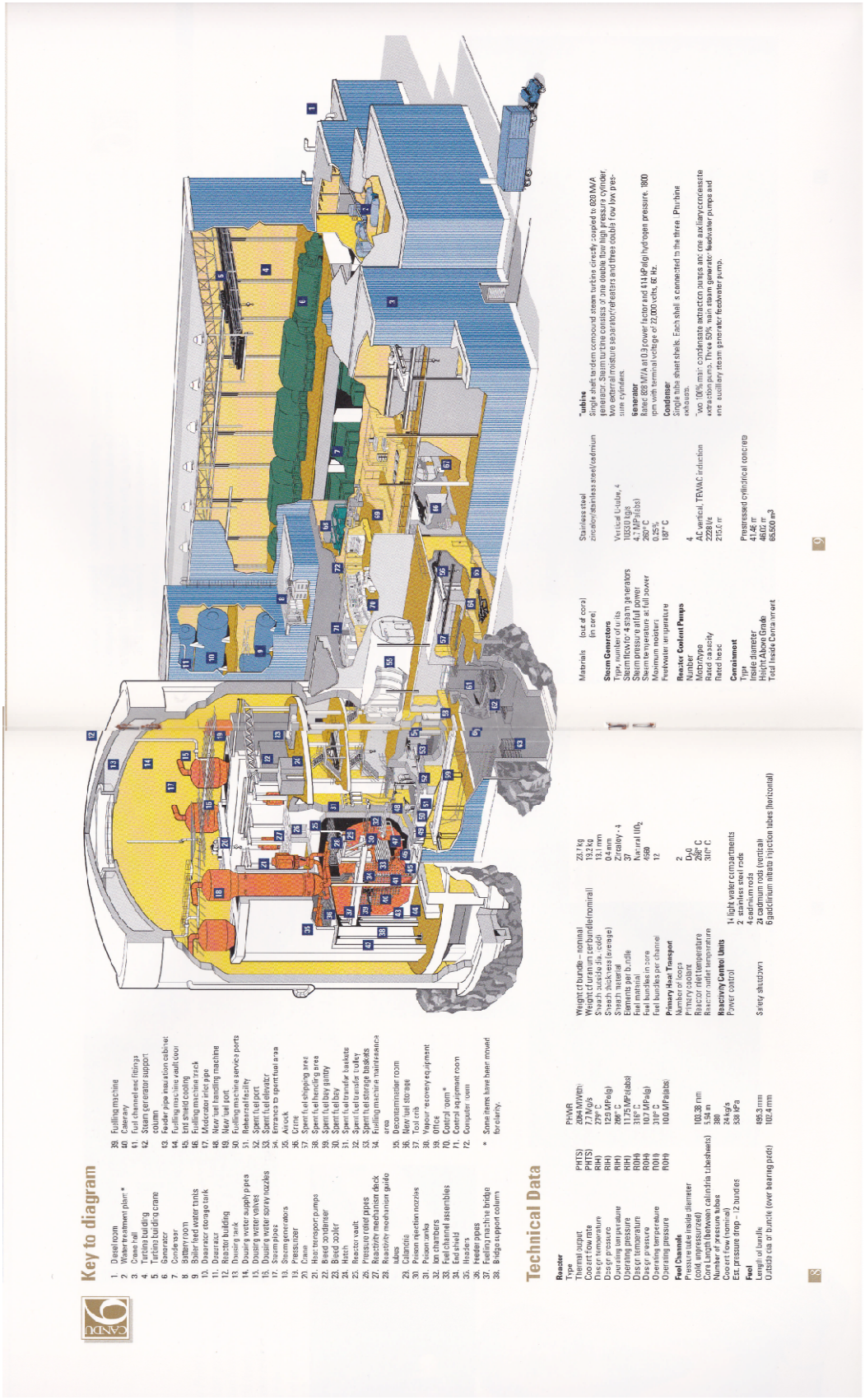

Appendix B – CANDU Evolution

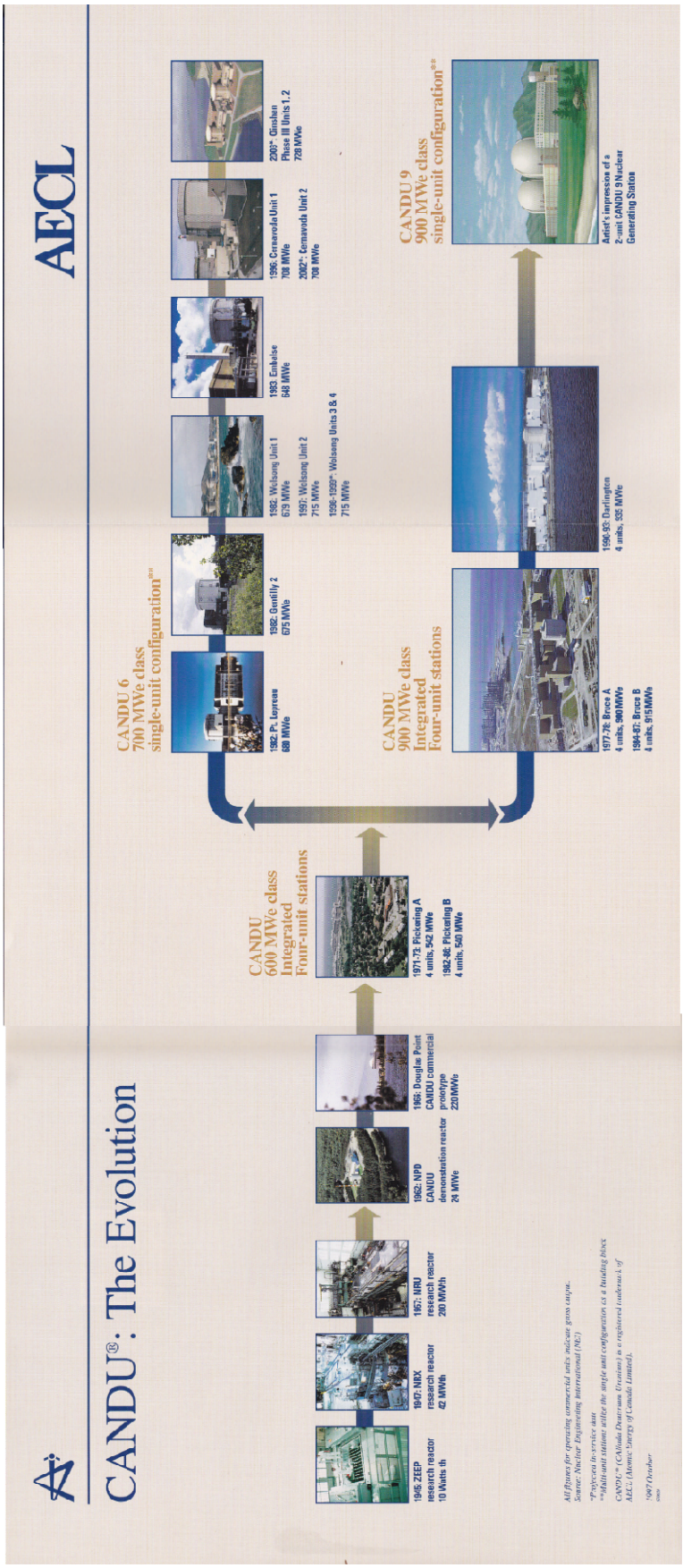

Appendix C – Single Unit Station Data (5 pages)

The data presented are typical values for 600 MW and 950 MW CANDU nuclear generating stations. Actual values for a specific customer and site are dependent upon the turbine generator design and condenser cooling water temperature.

	600 MW		950 MW	
HEAT GENERATION BALANCE				
Fission Power Distribution:				
Heat Generation In:				
Fuel	2029.7	MW(th)	3192	MW(th)
Sheaths and Bundle Structure	7.24	MW(th)	11.4	MW(th)
Coolant	12.2	MW(th)	19.2	MW(th)
Pressure Tubes	12.23	MW(th)	19.2	MW(th)
Total (Fuel Channels)	2061.4	MW(th)	3242	MW(th)
Moderator	78.3	MW(th)	123	MW(th)
Reflector	4.4	MW(th)	8.6	MW(th)
Calandria Tubes	4.3	MW(th)	6.7	MW(th)
Calandria Shell	2.1	MW(th)	3.5	MW(th)
Tubesheets	1.4	MW(th)	3.7	MW(th)
End Shields	0.6	MW(th)	1.1	MW(th)
Other Calandria Components (Including Reactivity Mechs. and Guide Tubes)	2.4	MW(th)	3.4	MW(th)
Shields, Structures Outside Calandria and End Shields	1	MW(th)	1.5	MW(th)
Total (Other Reactor Components)	94.5	MW(th)	152	MW(th)
Total Fission Heat	2155.9	MW(th)	3394	MW(th)
HEAT TRANSFER BALANCE (PRIMARY)				
Heat Transport System:				
Heat from fuel channels	2061.4	MW(th)	3242	MW(th)
Heat Loss to Moderator	3	MW(th)	5	MW(th)
Heat Loss to End Shields	2.4	MW(th)	3.6	MW(th)
Total Heat Loss (Mod. and Shields)	5.4	MW(th)	8.6	MW(th)
Net Fission Heat to Coolant	2056	MW(th)	3233.4	MW(th)
Heat Loss to H.T. Piping	3	MW(th)	4.5	MW(th)
Heat Loss to H.T. Auxiliaries	6	MW(th)	8.9	MW(th)
Total Heat Loss	9	MW(th)	13.4	MW(th)
Net Fission Heat to Steam Generators	2047	MW(th)	3220	MW(th)
Pump Energy Appearing in Coolant	17	MW(th)	38	MW(th)
Total Heat Transferred to Steam Generators	2064	MW(th)	3258	MW(th)

	600 MW		950 MW	
Moderator System:				
Heat Generated in Moderator	*78.3*	*MW(th)*	*123*	*MW(th)*
Heat Generated in Reflector	4.4	MW(th)	8.6	MW(th)
Heat Generated in Calandria Tubes	4.3	MW(th)	6.7	MW(th)
Heat Generated in Guide Tubes and Reactivity Mechanisms	2.4	MW(th)	3.4	MW(th)
Heat from Fuel Channels	3	MW(th)	5	MW(th)
Heat from Calandria Shell and Tubesheets	1.6	MW(th)	2.6	MW(th)
Total Fission Heat to Moderator	94	MW(th)	149	MW(th)
Heat Loss to Moderator Piping	0.3	MW(th)	0.2	MW(th)
Net Fission Heat to Moderator	93.7	MW(th)	149	MW(th)
Pump Energy Appearing in Moderator	0.7	MW(th)	1.5	MW(th)
Net Heat to Moderator	94.4	MW(th)	150	MW(th)
Shield Cooling System:				
Heat from Calandria Shell & Tubesheet	1.9	MW(th)	4.6	MW(th)
Heat from End Shields	0.6	MW(th)	1.1	MW(th)
Heat from Thermal Shield Structures Outside Calandria/End Shields	1	MW(th)	1.5	MW(th)
Heat from Fuel Channels	2.4	MW(th)	3.6	MW(th)
Net Fission Heat to Shield System	5.9	MW(th)	11	MW(th)
Auxiliary Systems:				
Heat from Heat Trans. Aux.	6	MW(th)	6.9	MW(th)
Heat from Heat Trans. Piping	3	MW(th)	4.5	MW(th)
Heat from Moderator Piping	0.3	MW(th)	0.2	MW(th)
Net Fission Heat to Aux. Systems	9.3	MW(th)	14	MW(th)
Summation:				
Net Fission Heat to Steam Generators	2047	MW(th)	3220	MW(th)
Net Fission Heat to Moderator	93.7	MW(th)	149	MW(th)
Net Fission Heat to Shield System	5.9	MW(th)	11	MW(th)
Net Fission Heat to Aux. Systems	9.3	MW(th)	14	MW(th)
Total Fission Heat	2155.9	MW(th)	3394	MW(th)

	600 MW	950 MW
HEAT TRANSFER BALANCE (SECONDARY)		
Net Heat Input to Turbine Cycle	2060.3 MW(th)	3347 MW(th)
Generator Output — Nominal	675.7 MW(e)	1121 MW(e)
Heat Rejected by T/G	1384.6 MW(th)	2226 MW(th)
UNIT ENERGY BALANCE		
Generator Output (Gross — Nominal)	675.7 MW(e)	1121 MW(e)
Station Service Power (Estimated)	50 MW(e)	90 MW(e)
Generator Output (net)	625.7 MW(e)	1031 MW(e)
EFFICIENCY (TYPICAL)		
Efficiency of Fission Heat Conservation and Transmission to Steam Generators	94.9% (2047/2155.9 x 100)	94.9% (3220/3394 x 100)
Overall Station Efficiency	29% (625.7/2155.9 x 100)	30.4% (1031/3394 x 100)
REACTOR PHYSICS AND DYNAMICS		
The following data is valid for certain typical conditions assumed in reactor physics design. Actual values are dependent upon design for a specific customer.		
Core Data		
Number of cells	380	600
Cell Array	Square	Square
Lattice Pitch	28.6 cm	28.6 cm
Core Radius (Effective)	314.3 cm	395.2 cm
Core Length	594.4 cm	594.4 cm
Extrapolated Length	606 cm	606 cm
Average Reflector Thickness at Mid Point	65.46 cm	70 cm
Total Fission Power	2180 MW	3394 MW
Total Thermal Power	2060 MW	3237 MW
Nominal Channel Power	5.5 MW	5.5 MW
Nominal Bundle Power	800 kW	800 kW
Equilibrium Xenon Load	28 mk	28.2 mk
FUEL		
General:		
Fuel	Compacted and sintered natural UO_2 pellets	Compacted and sintered natural UO_2 pellets
Form	Fuel bundle assembly of 37 elements	Fuel bundle assembly of 37 elements

	600 MW	950 MW
Weight		
Total weight of UO_2 in reactor	95 Mg	153 Mg
Total weight of U in reactor	84 Mg	135 Mg
Pellets:		
Quantity (approx./element)	30	30
Form	Cylindrical pellets with concave dished ends	Cylindrical pellets with concave dished ends
Diameter (nominal)	12.16 mm	12.16 mm
Stack length (nominal)	480 mm	480 mm
Element assembly:		
Material	Zircaloy-4	Zircaloy-4
Weight	2.319 kg	2.319 kg
Outside diameter	13.08 mm	13.08 mm
Bundle assembly:		
Quantity in reactor	4560	7200
Quantity per fuel channel	12	12
Length of bundle	495 mm	495 mm
Outside diameter	102.4 mm	102.4 mm
Weight of bundle	23.5 kg	23.5 kg
REACTIVITY DEVICE WORTHS		
Total Zone Control Worth	7.5 mk	8.1 mk
Total Adjuster Worth	15 mk	16.4 mk
Total Mechanical Control Absorber Worth	10.5 mk	7.1 mk
Total Static Worth of Shutoff Units	80 mk	67.3 mk
Total Worth of Poison Injection	600 mk	600 mk
REACTOR BUILDING		
Form	Upright cylinder with flat base and double dome	Upright cylinder with flat base and double dome
Material	Reinforced pre-stressed concrete	Reinforced pre-stressed concrete
Diameter (inside)	41.45 m (136 ft)	52.0 m (170 ft)
(Outside)	43.59 m (143 ft)	54.2 m (178 ft)
Height (Basement to inside top of dome	51.21 m (168 ft)	64.5 m (212 ft)
Design Pressure	124.1 kPa(g) (18 psig)	138 kPa(g) (20 psig)
Wall thickness	1.07 m (3.5 ft)	1.1 m (3.6 ft)

	600 MW	950 MW
Reactor Containment		
Net Building Air Volume	48 477 m^3 (1 712 000 ft^3)	106 000 m^3 (3 743 000 ft^3)
Base slab thickness	1.68 m (5.51 ft)	3m (9.84 ft)
Wall height (not incl. dome)	42.3 m (138.8 ft)	54.0 m (177.2 ft)
Thickness of dome at crown	0.60 m (1.97 ft)	0.61 m (2 ft)
Ring beam thickness	2.20 m (7.2 ft)	1.9 m (6.2 ft)
Ring beam height	4.3 m (14.1 ft)	4.3 m (14.1 ft)
Internal dome thickness	0.39 m (1.25 ft)	0.4 m (1.3 ft)
REACTOR		
Type	Horizontal pressure tube	Horizontal pressure tube
coolant	Pressurized heavy water (D_2O)	Pressurized heavy water (D_2O)
Moderator	Heavy Water (D_2O)	Heavy Water (D_2O)
Inlet Temperature	49°C (120°F)	51°C (123°F)
Outlet Temperature	77°C (170°F)	66°C (151°F)
Moderator Flow Rate	940 L/s (12 400 lgpm)	2200 L/s (29 000 lgpm)
Cooling Capacity	120 MW(th)	155 MW(th)
Fuel	Natural UO_2	Natural UO_2
Number of Channels	380	600
Reactivity Control:		
Main Method	On power refuelling and moderator poison control	On power refuelling and moderator poison control
Trim	H_2O zone control assemblies and vertical control absorber rods	H_2O zone control assemblies and vertical control absorber rods
Poison Override	Vertical adjuster rods	Vertical adjuster rods
Shutdown:		
System no. 1	Spring-augmented gravity-accelerated shutoff rods	Spring-augmented gravity-accelerated shutoff rods
System no. 2	Moderator poison injection	Moderator poison injection
Flux Flattening:		
Axial	Vertical adjuster rods	Vertical adjuster rods
Radial	Differential fuelling and vertical adjuster rods	Differential fuelling and vertical adjuster rods
Flux Control	H_2O Zone Control	H_2O Zone Control

	600 MW	950 MW
FUEL CHANNEL ASSEMBLIES		
Quantity	380	600
Length:		
Overall including end fittings	10.82 m (35.5 ft)	11.15 m (36.6 ft)
Channel Flow (maximum)	24 kg/s (190 000 lb/h)	26.5 kg/s (210 000 lb/h)
Inlet temperature*	266.6°C (511.8°F)	266.2°C (511.1°F)
Outlet temperature*	312°C (594°F)	312°C (594°F)
Inlet pressure*	11.04 MPa(a) (1601 psia)	11.17 MPa(a) (1620 psia)
Outlet pressure*	10.3 MPa(a) (1494 psia)	10.29 MPa(a) (1492.9 psia)
Pressure Tubes		
Quantity	380	600
Material	Zirconium/ Niobium Alloy	Zirconium/ Niobium Alloy
Length Trimmed for Installation (approx.)	6.30 m (20.66 ft)	6.32 m (20.75 ft)
Inside Diameter, Minimum	103.38 mm (4.07 in)	104 mm (4.09 in)
Wall Thickness, Minimum	4.19 mm (0.165 in)	
STEAM GENERATORS		
Name	Primary Heat Transport System Steam Generator	Primary Heat Transport System Steam Generator
Quantity	4	8
Type	Vertical U-tube with integral steam drums and preheater	Vertical U-tube with integral steam drums and preheater
Heat transferred*	2064 MW(th)	3258 MW(th)
Heat transfer area per steam generator	3127 m^2 (34 200 ft^2)	3066 m^2 (33 000 ft^2)
Fluid	D_2O	D_2O
Flow Rate**	7.6 Mg/s (60.3 x 10^6 lb/h)	13.5 Mg/s (107.1 x 10^6 lb/h)
Shell Side Data:		
Fluid	H_2O	H_2O
Steam Flow**	1.047 Mg/s (8.31 x 10^6 lb/h)	1.612 Mg/s (12.79 x 10^6 lb/h)
Feedwater Flow**	959 kg/s (7.615 x 10^6 lb/h)	1536 kg/s (12.19 x 10^6 lb/h)
Blowdown Flow** (continuous)	1.00 kg/s (8000 lb/h)	2.0 kg/s (15 900 lb/h)

* Maximum power channel at 100% power (measured at fuel)
** total for four steam generators (600 MW) total for eight steam generators (950 MW)

	600 MW	950 MW
Feedwater inlet temperature	187°C (368°F)	177°C (350°F)
Pressure at drum nozzle	4.69 MPa(a) (681 psia)	5.07 MPa(a) (735 psia)
Temperature at drum nozzle	260°C (500°F)	265°C (509°F)
Quality at drum nozzle	99.75%	99.75%
HEAT TRANSPORT PUMPS		
Quantity	4	4
Type	Vertical, centrifugal, single suction double discharge	Vertical, centrifugal, single suction double discharge
Duty	Continuous	Continuous
Fluid	D_2O	D_2O
Flow Rate	2228 L/s (29 400 Igpm)	3959 L/s (52 256 Igpm)
Temperature	266°C (511°F)	266°C (511°F)
Head	215 m (705 ft)	245 m (803 ft)
REACTIVITY CONTROL		
Shut-Off Units (Shutdown System No. 1)		
Quantity	28	38
Shutoff Rods:		
Type	Stainless steel-clad cadmium tube	Stainless steel-clad cadmium tube
Insertion Sequence	Simultaneous drop, spring augmented, gravity-accelerated	Simultaneous drop, spring augmented, gravity-accelerated
Static Reactivity Worth, approx.	-60 milli-k (28 rods)	-67.3 milli-k (36 rods)
Drive Mechanism:		
Rod Insertion mechanism	Free-wheeling winch and cable	Free-wheeling winch and cable
Rod deceleration system	Rotary hydraulic damper on winch	Rotary hydraulic damper on winch
Withdrawal mechanism	Motor & gear train engaged to winch by a dc electro-magnetic friction clutch	Motor & gear train engaged to winch by a dc electro-magnetic friction clutch
Liquid Injection Shutdown System (Shutdown System No. 2)		
Quantity	6	8
Type	Horizontal nozzle tubes inject liquid poison directly into moderator when system is actuated	Horizontal nozzle tubes inject liquid poison directly into moderator when system is actuated
Poison	Gadolinium nitrate in D_2O (8000ppm solution)	Gadolinium nitrate in D_2O (8000ppm solution)
Reactivity worth		
Short term (after 2 sec.)	-55 mk (min.)	
Long term (after 1 min.)	-300 mk (min.)	
Liquid Zone Control Units		
Quantity	6 (4 x 2 compartments and 2 x 3 compartments)	8 (4 x 3 compartments and 4 x 2 compartments)
Reactivity Worth, approx. maximum	- 7.5 milli-k	- 8.1 milli-k
Type	Vertical through-tubes, divided into compartments that can be partially or completely filled with light water.	Vertical through-tubes, divided into compartments that can be partially or completely filled with light water.
Mechanical Control Absorber Units		
Absorber Rods:		
Quantity	4	4
Type	Stainless steel-clad cadmium tube	Stainless steel-clad cadmium tube
Insertion Sequence + Method:		
Reactor Stepback	Simultaneous, free drop, gravity acceleration	Simultaneous, free drop, gravity acceleration
Reactor Setback	Simultaneous, motor driven	Simultaneous motor driven
Withdrawal Sequence + Method	Simultaneous, motor driven	Simultaneous motor driven
Insertion & Withdrawal Time	Variable (130 sec minimum)	Variable (150 sec minimum)
Reactivity Worth, approx.	-10 milli-k	-7.1 milli-k
Adjuster Units		
Quantity	21	27
Absorber Element:		
Type	Variable thickness tube plus centre rod	Variable thickness tube plus centre rod
Material	Stainless Steel	Stainless Steel
Withdrawal and Insertion Sequence	1 bank at a time	1 bank at a time
Withdrawal or Insertion Time, Each Bank	60 ± 5 seconds	60 ± 5 seconds
Poison Override Time	30 minutes	30 minutes
Total Reactivity Worth, approx.	- 15 milli-k	- 16.4 milli-k

	600 MW	950 MW
Moderator Liquid Poison System		
Long Term Reactivity Control: Poison	Boric Anhydride	Boric Anhydride
Solubility Limit in D_2O at 20°C (68°F)	27 g/L	27 g/L
Concentration of Boron in the Moderator to simulate -28.5 mk*	3.5 ppm	3.5 ppm
Concentration of Poison in the Poison Tank	10.56 g/L	10.56 g/L
Rate of Poison Solution Addition to Achieve -0.75 mk/min	117 mL/s (1.54 lgpm)	170 mL/s (2.24 lgpm)
Startup Reactivity Control: Poison	Gadolinium Nitrate Hexahydrate	Gadolinium Nitrate Hexahydrate
Solubility Limit in D_2O at 25°C (77°F)	2.35 kg/L	2.35 kg/L
Concentration of Gadolinium in the Moderator to Simulate -28.5mk*	0.89 ppm	0.89 ppm
Concentration of Poison in the Poison Tank	3.99 g/L	3.99 g/L
Rate of Poison Solution Addition to Achieve -0.75 mk/min	78.1 mL/s (1.03 lgpm)	113 mL/s (1.49 lgpm)
Vertical Flux Detector Units		
No. of Assemblies	26	28
Type	Factor sealed, encapsulated, multi-detector assembly; self-powered, platinum and vanadium detectors	Factory sealed, encapsulated, multi-detector assembly; self-powered platinum and vanadium detectors
Horizontal Flux Detector Units		
No. of Assemblies	7	14
Type	Factory sealed, encapsulated, multi-detector assembly; self-powered, platinum and vanadium detectors	Factory sealed, encapsulated, multi-detector assembly; self-powered, platinum and vanadium detectors
TURBINE GENERATOR AND AUXILIARIES		
Design temperature of circulating water 22°C (71.6°F)		
Generator gross output	675.7 MW(e)	1121 MW(e)
Turbine cycle heat rate	10 937 kJ/kWh	10 460 kJ/kWh
Steam cycle gross efficiency	32.8%	34.4%
Main steam flow, MCR	1047 kg/s (8,310 x 10^3 lb/h)	1612 kg/s (12 794 x 10^3 lb/h)
Turbine Generator		
Live steam flow to valves	957 kg/s	1532.5 kg/s
Live steam flow to reheater	89.9 kg/s	77.2 kg/s(2nd Stage)
Live steam pressure at valves	4.55 MPa(a) (660 psia)	4.93 MPa(a) (715 psia)
Live steam temperature at valves	258°C (496.6°F)	263°C (505.4°F)
Pressure of HP exhaust steam	665.3kPa(a) (96.5 psia)	545.4 kPa(a) (79.1 psia)
Quality of HP exhaust steam	88.24%	86.5%
Inlet pressure of LP steam	588.4 kPa(a) (85.3 psia)	500 kPa(a) (72.6 psia)
Inlet temperature of LP steam	242.2C (468.68°F)	247.4°C (477.3°F)
Quality of LP exhaust steam	89.5%	91.0%
Turbine generator speed	1800 rpm	1800 rpm
Number of HP cyclinders	1, double flow	1, double flow
Number of LP cylinders	3, double flow	3, double flow
Number of moisture separators	4	2
Number of reheaters	2	2
Numbers and diameter of steam inlets	4 x 61 cm (4 x 24 in)	4 x 61 cm (4 x 24 in)
Generator Type	Direct coupled, hydrogen/water cooled	Direct coupled, hydrogen/water cooled

* -28.5 mk is the reactivity required to compensate for complete absence of equilibrium xenon in the reactor fuel.

CHAPTER 3

Nuclear Processes and Neutron Physics

prepared by
Dr. Guy Marleau
École Polytechnique de Montréal

Summary:

In this section, we first describe the nucleus, including its composition and the fundamental forces that affect its behaviour. Then, after introducing the concepts of radioactivity and nuclear decay, we discuss the various interactions between radiation and matter that can take place in and around a nuclear reactor. We finish with a presentation of neutron physics for fission reactors.

Table of Contents

List of Figures

List of Tables

1 Introduction

Energy production in an operating nuclear reactor is mainly the result of fission reactions initiated by neutrons. Following these reactions, radiation is produced in the form of alpha particles, electrons (β-particles), photons, and neutrons, as well as a large number of unstable nuclei (including actinides and fission products) that may decay, thereby producing additional radiation and energy. The neutrons generated directly in the fission reaction as well as those resulting from fission product decay are a key factor in maintaining and controlling the chain reaction as discussed in Chapters 4 and 5. Radiation also has an impact on the properties of the various materials in the core as well as on living cells. It is therefore important to understand how radiation interacts with matter if one needs, for example, to evaluate the radiotoxicity of burned fuel (Chapter 19) or to determine the kind of barrier that must be put in place to protect the public, the environment, or the personnel in a nuclear power plant (Chapter 12). Moreover, the energy produced by these decays contributes to heating the fuel, whether it is still in the reactor or in the spent fuel pools. The aim of this chapter is to provide the reader with an overview of the nuclear processes that take place in and around a reactor.

1.1 Overview

Several very important processes take place simultaneously in a nuclear reactor, including neutron slowdown as a result of collisions with nuclei, nuclear fission, and decay of radioactive nuclei with radiation emissions that subsequently lose energy or are absorbed.

To understand how all these physical processes take place, it is important to possess a general knowledge of the physics of the nucleus, including its composition and the fundamental forces that affect its behaviour. Although one rarely uses a description of the nucleus in terms of elementary particles and their interaction in power-reactor applications, such a description provides a practical background for a study of nuclear structure. In fact, the nucleus is such a complex object that it can be described only through simplified models that provide useful information. For example, the liquid drop model (Section 2.4) gives an empirical description of how one can extract energy from a nucleus by breaking it into smaller components (fission or decay) or by combining nuclei (fusion). These models are also used to predict the stability of a nucleus under various decay processes, the energy associated with its excited states, and the associated gamma-ray spectrum. In Section 2, an overview of the structure of the nucleus is provided, starting from a fundamental description and progressing to more practical models. We will also introduce some language specific to nuclear physics that will be useful throughout this book.

The majority of the fission reactions taking place in a reactor are initiated following the absorption of a neutron by a heavy nucleus. Radioprotection also involves the interaction between radiation, in the form of alpha particles, electrons, photons, and neutrons, and matter. Two important points must then be addressed before describing the physics of neutrons in a nuclear reactor: the source of this radiation and its behaviour over time, and the interaction of the emitted particles with matter. Therefore, Section 3 is divided into three parts: it starts with a description of radioactivity and the decay of nuclei, continues with a description of the interaction of ionizing radiation with matter (everything but neutrons), which is a very important topic for radiation protection studies, and ends with a brief discussion of the interaction of neutrons with matter.

The last section of this chapter is dedicated to the nuclear chain reaction. It starts by giving an extensive description of the fission reaction and discusses the need to slow down neutrons. This is followed by a description of the neutron transport equation that can be used to characterize the behaviour of neutrons inside a reactor.

1.2 Learning Outcomes

The goal of this chapter is for the reader to:

- Understand the fundamental forces in nature and the structure of the nucleus;
- Learn how to compute the mass of a nucleus based on the liquid drop model and to evaluate the energy released by the fission and fusion processes;
- Understand how to evaluate the activity and radio-toxicity of spent fuel;
- Become familiar with nuclear cross-section databases for neutrons and ionization radiation and the computation of reaction rates between particles and matter;
- Recognize the need to slow down neutrons in thermal reactors and to evaluate the effectiveness of a moderator.

2 Structure of the Nucleus

2.1 Fundamental Interactions and Elementary Particles

Four forces, or interactions, are currently sufficient to understand and explain nature from particle physics to astrophysics, including chemical and biological processes. These forces are classified relative to their intensity at the nuclear level (distances of the order of 1 fm) as follows:

- The strong force: responsible for the cohesion of the proton as well as the nucleus. This force is always attractive.
- The electromagnetic force: governs the physics of the atom and the associated chemical and biological processes. This force can be both attractive and repulsive.
- The weak force: responsible for the existence of the neutron as well as many other radioactive nuclei. This force is always attractive.
- The gravitational force: governs the large-scale structure of the universe. This force ensures the stability of the solar system as well as the fact that people can keep their feet on the ground. This force is always attractive.

From the point of view of physics, these forces arise from the specific intrinsic properties of the particles on which they act. For example, the electromagnetic force arises between two particles that have electric charges, while the gravitational force appears between two particles with masses (or more generally, between two particles with energy). For the strong force, the so-called "colour" of the particle plays a role equivalent to that of electric charge in electromagnetic interactions, while the weak force is the result of the interaction of two particles having a "weak" charge. **Table 1** provides a brief description of the general properties of the four fundamental forces, where the α's are dimensionless coupling constants related to the intensity of the interaction and the spatial dependence of the force is expressed in powers of r, the distance between the two interacting particles [Halzen1984]. For example, the electromagnetic force between two particles of charge ze and Ze is given by:

$$|\vec{F}(\vec{r})| = \left(\frac{e^2}{4\pi\varepsilon_0}\right)\frac{zZ}{|r|^2} = (\alpha_e \hbar c)\frac{zZ}{|r|^2}, \quad (1)$$

where $e = 1.6 \times 10^{-19}$ C is the charge of an electron, $\varepsilon_0 = 8.854 \times 10^{-12}$ F/m is the electric permittivity of vacuum, $\hbar = 1.0546 \times 10^{-34}$ J × s is the reduced Planck constant, and $c = 2.9979 \times 10^{8}$ m/s is the speed of light. For the gravitational force, the coupling constant is expressed in terms of proton masses. One can immediately see that the range of the gravitational and electromagnetic forces is substantially larger than that of the weak force due to their $\frac{1}{r^2}$ dependence. Accordingly, the weak force is important only when two particles with weak charges are in close contact. On the other hand, the strong (colour) force remains significant irrespective of the distance between particles with colour charge. This observation led to the concept of colour confinement, meaning that it is impossible to isolate a particle having a net colour charge different from zero [Halzen1984].

Table 1 Properties of the four fundamental forces

Force	Equivalent charge	Coupling constant	Spatial dependence
Strong	Colour charge	$\alpha_s \approx 1$	$\approx r^0$
Electromagnetic	Electric charge	$\alpha_e \approx 1/137$	r^{-2}
Weak	Weak charge	$\alpha_w \approx 10^{-6}$	r^{-5} to r^{-7}
Gravitational	Mass	$\alpha_G \approx 10^{-39}$	r^{-2}

In the standard model of particle physics [Halzen1984, Le Sech2010], these forces are represented by 12 virtual particles of spin 1 called "gauge bosons":

- the massless photon that carries the electromagnetic interaction;
- eight massless gluons that carry the strong (colour) force;
- three massive bosons ($W^{\pm}$ and Z^0) that mediate the weak interaction.

These bosons are exchanged between the 12 "physical fermions" (spin $1/2$ particles) that make up all the matter in the universe:

- six light fermions or leptons that have a weak charge. Three of these have no electric charge (the neutrinos), while three are charged (electron, muon, and tau);
- six heavy fermions or quarks that have colour, weak, and electric charges. These fermions cannot exist freely in nature because of colour confinement and must be combined in triplets of quarks or quark-antiquark pairs to form respectively baryons (protons, neutrons) and mesons (pion, kaon) that have no net colour charge.

Table 2 Properties of leptons and quarks

Leptons			Quarks		
Particle	Mass (GeV/c^2)	Charge	Particle	Mass (GeV/c^2)	Charge
e	0.000511	-1	u	≈ 0.003	$2/3$
ν_e	$< 2.5 \times 10^{-9}$	0	d	≈ 0.006	$-1/3$
μ	0.1057	-1	c	≈ 1.2	$2/3$
ν_μ	< 0.000170	0	s	≈ 0.1	$-1/3$
τ	1.7777	-1	t	≈ 173	$2/3$
ν_τ	< 0.018	0	b	≈ 4.1	$-1/3$

Table 2 provides a description of the main properties of leptons and quarks with the masses given in GeV/c^2, with 1 GeV/c$^2 \approx 1.782661 \times 10^{-27}$ kg, and the charges in terms of the charge of one electron [Le Sech2010].

2.2 Protons, Neutrons, and the Nuclear Force

The two lightest baryons that can be created out of a quark triplet are the positively charged proton, which is composed of two u quarks and one d quark, and the neutral neutron, made up of two d quarks and one u quark. These are present in the nucleus of all the elements present naturally in the universe. The main properties of the proton and the neutron are provided in **Table 3** [Basdevant2005]. One can immediately see that the masses of the proton and neutron are very large compared with those of the u and d quarks. In fact, most of their mass is a result of the strong colour force (gluon interaction). One can also observe that protons are stable, while neutrons are unstable and decay relatively rapidly into protons through the weak interaction. A second observation is that the magnetic moment, which is created by the movement of charged particles, is negative for the neutron. This confirms, at least partially, the theory that neutrons are made of quarks because even though the neutron is neutral, the distribution of charge inside it is not uniform.

Table 3 Main properties of protons and neutrons.

Property	Proton	Neutron
Mass (GeV/c^2)	$m_p = 0.938272$	$m_n = 0.939565$
Charge (electron charge)	1	0
Magnetic moment (μ_N)	$\mu_p = 2.792847$	$\mu_n = -1.913042$
Spin	1/2	1/2
Mean-life (s)	$\tau_p > 10^{36}$	$\tau_n = 881.5$

Although the proton and neutron have a neutral colour, they interact through the nuclear force, which is a residual of the strong colour force. However, instead of exchanging gluons directly, as do the quarks inside the proton or neutron, they interact by exchanging of virtual pion. As a result, the nuclear force is much weaker than the strong force in the same way that

the Van der Waals force between neutral atoms is weaker than the electromagnetic force. Moreover, in contrast to the strong colour force, the magnitude of the nuclear force decreases rapidly with distance, the nuclear interaction being given approximately by the Yukawa potential:

$$V_{Yukawa}(r) = -\alpha_N \hbar c \frac{e^{-\frac{m_\pi c r}{\hbar}}}{r}, \tag{2}$$

where m_π is the mass of the pion (140 MeV/c^2) and $\alpha_N \approx 14.5$ is a constant that controls the strength of the nuclear interactions between baryons (protons or neutrons). The minus sign here indicates that the resulting force ($\vec{F} = -\vec{\nabla}V$) is always attractive. This potential is identical for proton-proton, proton-neutron, and neutron-neutron interactions.

The strength of this force at short distances is so intense that it can compensate for the repulsive electromagnetic force between protons, leading to the formation of bonded nuclei as well as inhibiting neutron decay. For example, the helium nucleus, which is composed of two protons and two neutrons, is stable. Similarly, the stable deuteron is composed of one proton and one neutron. The absence in nature of a nucleus composed of two protons is not a result of the fact that the electromagnetic force is greater than the strong force, but rather due to the exact structure of the nuclear force. In addition to having a spatial behaviour provided by the Yukawa potential, this potential is also spin-dependent and repulsive between particles with anti-parallel spins (a nucleus with two protons having parallel spins is not permitted because of Pauli's exclusion principle). This also explains why stable nuclei containing only neutrons are not seen in nature.

2.3 Nuclear Chart

As indicated in the previous section, not all combinations of neutrons and protons can lead to bonded states. **Figure 1** provides a list of all bonded nuclei [Brookhaven2013, KAERI2013]. The points in red represent stable nuclei, while those in green indicate radioactive nuclei. The straight black line indicates nuclei having the same number of neutrons and protons. Note that this chart is quite different from the periodic table, where the classification of the elements is based on the number of electrons surrounding the nucleus. Because the number of electrons surrounding the nucleus is identical to Z, the number of protons inside the nucleus, each element corresponds to a combination of the nuclei that are found on a horizontal line of the nuclear chart. The nomenclature used to classify these nuclei is the following:

- The number of protons in the nucleus is used to identify the element. For example, all nuclei with $Z = 8$ are known as oxygen (atomic symbol O), independently of the number of neutrons present in the nucleus.
- For a given element, the specific isotope is identified by $A = Z + N$, where A is known as the mass number and N is the number of neutrons in the nucleus. For example, oxygen-17, denoted by ^{17}O, corresponds to an oxygen atom where the nucleus has eight protons and nine neutrons. Instead of the notation $^{N+Z}$X, with X the element associated with Z, the notation $^{N+Z}_{Z}$X is also found in the literature.
- Two other terms are less frequently used: isobars, corresponding to nuclei having the same mass numbers, but different values for Z and N; and isotones, corresponding to nuclei having the same number of neutrons, but a different number of protons.

Several conclusions can be reached from **Figure 1**:

- Isotopes containing a small number of protons ($Z < 20$) will generally be stable only if N and Z are nearly equal. If the difference $|N - Z|$ is slightly too large, the nucleus becomes unstable. For combination of protons and neutrons with large values of $|N - Z|$, no nuclei can be formed.
- For nuclei with values of Z ranging from 20 to 82, the number of excess neutrons ($N - Z$) required to create bonded nuclei increases steadily. One can also observe that for a specific value of Z, several stable nuclei can be produced with different numbers of neutrons.
- No stable nucleus exists with $Z > 83$, although some radioactive nuclides with $Z < 93$ can still be found in nature because they decay at a very slow rate. No isotope with Z above 92 remains in nature.

Approximately 3200 bonded nuclei have been identified, out of which 266 are stable. The stability of a nucleus is ensured by the presence of a sufficient number of neutrons to compensate for the effect of the Coulomb force between protons. Because the nuclear force acts only at short distances, while the Coulomb force has a longer range, additional neutrons are required when the radius R of the nucleus increases because of the presence of more nucleons (protons and neutrons):

$$R \propto A^{1/3} R_0, \tag{3}$$

where R_o is the average radius of a single nucleon.

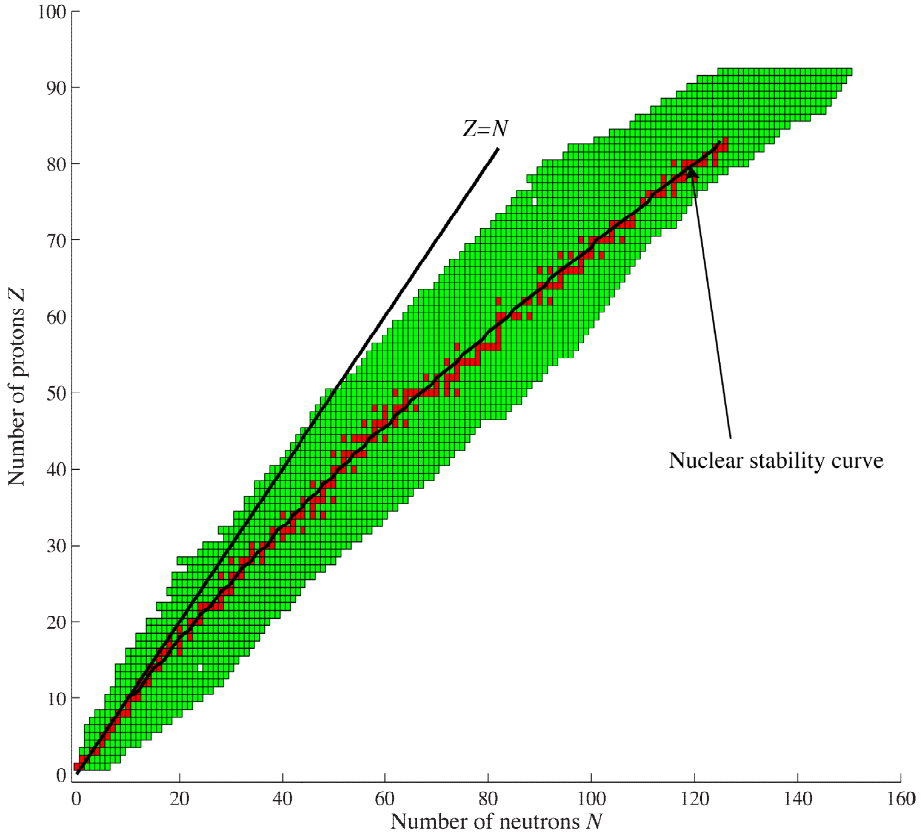

Figure 1 Nuclear chart, where N represents the number of neutrons and Z the number of protons in a nucleus. The points in red and green represent respectively stable and unstable nuclei. The nuclear stability curve is also illustrated.

The stability of a nucleus does not only depend on the number of nucleons it contains but also on how these protons and neutrons are paired. For example, out of the 266 stable nuclei:

- 159 contain an even number of protons and of neutrons,
- 53 have an even number of protons, but an odd number of neutrons,
- 50 have an odd number of protons and an even number of neutrons, and
- only 4 are made up of an odd number of protons and of neutrons.

In addition, for values of Z or N equal to 8, 20, 50, 82, and 126, the number of stable nuclei is very high. These numbers are known as "magic numbers". They suggest that the neutrons and protons, just like electrons in atoms, are more tightly bonded when they fill a quantum energy shell (see Section 2.5).

The mass m_{N+Z_X} of a nucleus produced by combining Z protons and N neutrons is less than the sum of the masses of its constituents:

$$m_{N+Z_X} = Z\ m_p + Nm_n - AB/c^2, \tag{4}$$

where $B > 0$, the average binding energy per nucleon, is the result of the negative potential that binds the nucleons inside the nuclei. As can be seen in **Figure 2**, where a plot of B as a function of A is provided for stable nuclei, B first increases rapidly for low mass numbers, reaching a maximum around $A = 60$, and then decreases slowly with A. This means that, on the average, nucleons are more tightly bonded inside nuclei having intermediate values of A ($20 < A < 120$) than for very low or very high values.

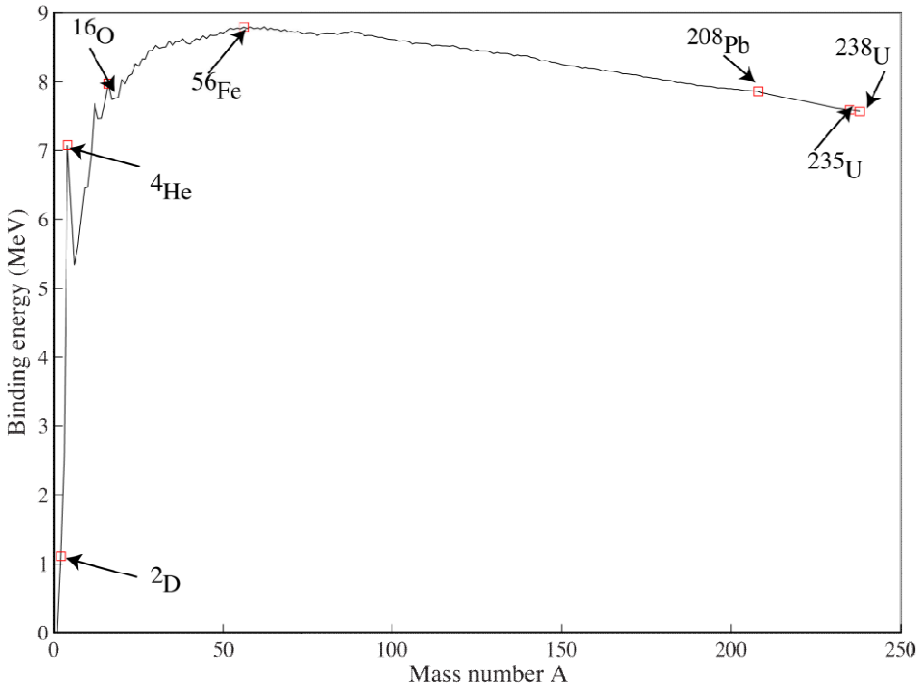

Figure 2 Average binding energy per nucleon (MeV) as a function of the mass number (number of nucleons in the nucleus).

Information on the atomic mass of over 3000 isotopes is available in [Livermore2013]. Note that the atomic mass is different from the nuclear mass of an isotope because it includes both the mass and the binding energy of the Z electrons gravitating around the nucleus. One simple way to compute the atomic mass is using

$$M_{{}^{N+Z}X} \approx Z\ M_{{}^{1}H} + Nm_n - AB/c^2, \tag{5}$$

where the mass of the proton has been replaced by that of the hydrogen atom, which includes the electron mass as well as its binding energy. The approximation sign comes from the fact that the binding energy of each of the Z electrons around a heavy nucleus is different from that of a single electron attached to a proton in the hydrogen atom.

Finally, the natural composition of a given element will include stable as well as some radioactive isotopes. Assuming that the relative atomic abundance of isotope i of atomic mass M_i in the natural element is γ_i, then the mass of the natural element is given by:

$$M_X = \sum_i \gamma_i M_i. \tag{6}$$

In reactor physics, one often works with the mass (or weight) fraction for the abundance of an isotope, defined as:

$$w_i = \frac{\gamma_i M_i}{M_X}. \tag{7}$$

For completeness, one can compute the isotopic concentration N_X of an element (atoms/cm^3) with atomic mass M_X (g/moles) and density ρ (g/cm^3) using:

$$N_X = \frac{\rho}{M_X}\ \mathbb{N}_A, \tag{8}$$

where $\mathbb{N}_A = 6.022 \times 10^{23}$ atoms/moles is the Avogadro number. The concentration of isotope i is then given by:

$$N_i = \gamma_i \frac{\rho}{M_X}\ \mathbb{N}_A = \gamma_i N_X. \tag{9}$$

More information related to the isotopic contents of natural elements can be found in [KAERI2013, WebElements2013].

2.4 Nuclear Mass and the Liquid Drop Model

As discussed in Section 2.3, the mass of the nucleus is smaller than its classical mass (the mass of its constituents) because the strong force linking the nucleons reduces the global energy of the nuclear system, the binding energy being related to the missing mass Δm_X according to

$$\Delta m_X c^2 \approx AB. \tag{10}$$

This missing mass is very difficult to compute based on theoretical models because the form of the nuclear potential is known only approximately and because quantum models involving more than two particles in interaction cannot be solved exactly. For evaluation of the missing mass, one generally relies on a semi-empirical model known as the liquid drop model. The main assumption used in this model is that the nuclear force is identical for protons and neutrons.

The liquid drop model first assumes that each of the A nucleons in the nucleus sees the same nuclear potential [Basdevant2005]. Moreover, this potential is independent of the number of nucleons in the nucleus. This second assumption can be justified by the fact that the range of the nuclear force is small, and therefore each nucleon feels the effect of only the limited

number of nucleons that are close by. Accordingly, the contribution to the missing mass from the A nucleons is given by:

$$\Delta m_V c^2 = a_V A, \tag{11}$$

where the constant a_V ≈15.753 MeV has been determined experimentally. This contribution is known as the volume effect because the volume of a nucleus can be assumed to be proportional to the number of nucleons it contains. This term would be sufficient if the nucleus had an infinite size. However, this is not the case, and the protons and neutrons that are located near the boundary of the nucleus will interact with a smaller number of nucleons. If the surface of the nucleus is given by $4\pi R^2 \propto A^{2/3}$, one can assume that the $A^{2/3}$ nucleons near the outer surface of the nucleus see a reduced uniform potential. This leads to a negative surface contribution to the mass defect of the form:

$$\Delta m_S c^2 = -a_S A^{2/3}, \tag{12}$$

where a_S ≈17.804 MeV.

Until now, only the nuclear force has been taken into account. However, the protons present inside the nucleus repel each other through the Coulomb force, thereby decreasing the binding energy. Because the potential associated with this force is long-range ($V(R) \propto 1/R \propto 1/A^{1/3}$), each of the Z protons will interact with the remaining $Z-1$ protons, leading to a contribution of the form:

$$\Delta m_C c^2 = -a_C \frac{Z(Z-1)}{A^{1/3}} \approx -a_C \frac{Z^2}{A^{1/3}}, \tag{13}$$

where only the dominant term in Z has been preserved, and a_C ≈0.7103 MeV.

It can be observed in the nuclear chart that stable nuclei with a low mass number generally contain an equal number of protons and neutrons. As the number of excess neutrons or protons in a nucleus increases, it becomes more and more unstable until no bonded state can be produced. This means that nuclear binding should decrease as a function of $|N-Z| = |A-2Z|$, the form of the contribution being

$$\Delta m_A c^2 = -a_A \frac{(A-2Z)^2}{A}, \tag{14}$$

where a_A ≈23.69 MeV is known as the asymmetry term. The nuclear chart also shows that few stable nuclei with an odd number of neutrons and protons (odd-odd nuclei) can be found in nature, while the number of isotopes with an even number of protons and neutrons (even-even nuclei) dominates. This means that the binding energy should be large for even-even and small for odd-odd nuclei. Assuming that the contribution to the missing mass presented previously remains valid only for odd-even or even-odd nuclei (A odd), an additional empirical correction of the form

$$\Delta m_P c^2 = (-1)^Z a_P \frac{(1+(-1)^A)}{2A^{3/4}} \tag{15}$$

is required. Here, a_P ≈33.6 MeV is known as the pairing term.

The final formula for the missing mass is therefore

$$\Delta m_X c^2 \approx a_V A - a_S A^{\frac{2}{3}} - a_C \frac{Z^2}{A^{\frac{1}{3}}} - a_A \frac{(A-2Z)^2}{A} + (-1)^Z a_P \frac{(1+(-1)^A)}{2A^{3/4}}, \quad (16)$$

which is known as the Bethe-Weizsäcker or semi-empirical mass formula (SEMF). Even if this mechanistic model is relatively simple, it provides a very good approximation to the mass of the nuclei found in nature. It can also be used to determine the value of A that minimizes the mass of a nucleus for a specific value of Z, thereby maximizing the probability that it is stable. Neglecting the pairing term, one then obtains

$$\mathrm{Z}(\mathrm{A}) = \frac{4Aa_A + A(m_n - m_p)c^2}{8a_A + 2a_C A^{\frac{2}{3}}}. \quad (17)$$

This equation, which is also illustrated in **Figure 1** (the nuclear stability curve), closely follows the nuclear stability profile.

The main weakness of the liquid drop model is its lack of predictive power. For example, it neither explains the presence of "magic numbers", nor the gamma-ray absorption spectrum, nor the decay characteristics of different nuclei. These explanations can be obtained only by looking at the interactions between protons and neutrons using quantum theory, as explained in the next section.

2.5 Excitation Energy and Advanced Nuclear Models

All chemists and physicists are familiar with atomic "magic numbers", even though the explicit term is rarely used. For example, the number of electrons in noble gases could be considered "magic" because these gases are odourless, colourless, and have very low chemical reactivity. For such atoms, all the states associated with principal quantum energy levels 1 to n are occupied by electrons (closed or filled shells). In addition, the absorption (emission) spectrum of light by different atoms is the result of electrons being excited (de-excited) from one electronic shell to another. One can therefore expect nuclear magic numbers to have a similar nature, namely, that only specific energy levels are permitted for the protons and neutrons when they are bonded inside a nucleus (which would explain also the photon emission and absorption spectra). These energy levels are not uniformly distributed, but occur in bands called *shells*. The fact that all the quantum states in a shell (a neutron or proton shell) are occupied by a nucleon increases the stability of the nucleus compared to nuclides with partially filled shells.

To obtain the energy levels permitted for protons and neutrons inside the nucleus, one needs to solve the quantum-mechanics Schrödinger equation for A strongly coupled nucleons [Griffiths2005]. However, when trying to solve this equation, two problems arise:

- the Schrödinger equation has no analytic solution for problems where three or more particles are coupled;
- the interaction potential between nucleons is not known exactly.

As a result, this many-body problem is generally simplified using the following assumptions that are inherent to the shell model [Basdevant2005]:

- each nucleon in the nucleus is assumed to move independently without being affected by the displacement of other nucleons;

- a nucleon moves in a potential $V(r)$ that is relatively uniform inside the nucleus and increases sharply near its outer surface, namely when $r \approx R$ (mean field approximation).

Note that in this model, there are no one-to-one interactions between the nucleons. This means that instead of solving the Schrödinger equation for A strongly coupled nucleons, the problem is reduced to the solution of A independent Schrödinger equations for a single nucleon with an averaged potential. The conventional nuclear potential used in the shell model is the Saxon-Wood potential (see **Figure 3**), which has the form [Basdevant2005]:

$$V(r) = -V_0 \left(\frac{1}{1+e^{(r-R)/R}} \right), \tag{18}$$

where V_0 ≈30 MeV is the potential depth and $R \propto A^{1/3}$ is the radius of the nucleus in fm.

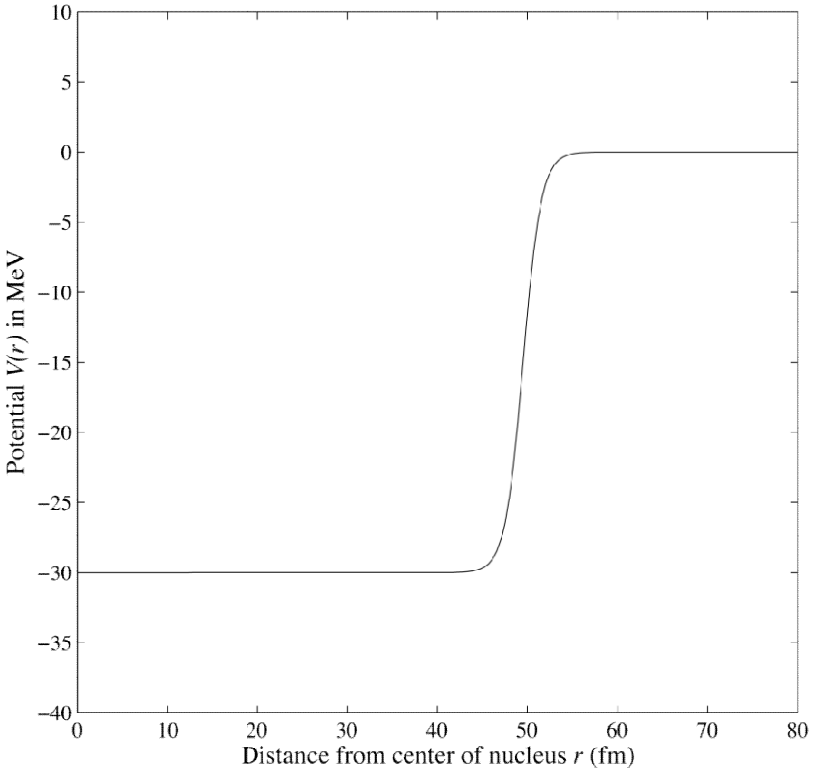

Figure 3 Saxon-Wood potential seen by nucleons inside the uranium-235 nucleus.

The energy levels are then very similar to those associated with the harmonic potential, namely

$$E_N = \frac{\hbar\sqrt{2V_0}}{R\sqrt{m_n}} \left(N + \frac{3}{2} \right), \tag{19}$$

where m_n is the mass of a nucleon (proton or neutron), $N = (2n + l - 2) = 0,1,2,\cdots$ with $n = 1,2,\cdots$ the principal quantum number, and $l = 0,1,2,\cdots$ the angular momentum quantum number that takes into account spin-orbit coupling. In general, one assumes that the energy is independent of the magnetic quantum number m. The spin j of each of the nucleons, which is important when determining the probability of interaction between a nucleus (spin J) and other particles, is a combination of its internal spin and its angular momentum:

$$j = \left(l \pm \frac{1}{2} \right). \tag{20}$$

The energy states of the shell model are presented in **Table 4**, whereas the association between the magic numbers and these states is illustrated in **Figure 4**.

The model is never used to evaluate the mass of nuclei (the SEMF model is used for this purpose), but it is useful for classifying the energy levels of excited nuclei (denoted as $({}^{N+Z}_{Z}\mathrm{X})^{*}$) and for determining the magic numbers.

Table 4 Energy states in the shell model, where *g* is the degeneracy level of a state.

N	0	1	2	2	3	3	4	4	4
n	1	1	1	2	1	2	1	2	3
l	0	1	2	0	3	1	4	2	0
g	2	6	10	2	14	6	16	10	2
orbital	1s	1p	1d	2s	1f	2p	1g	2d	3s

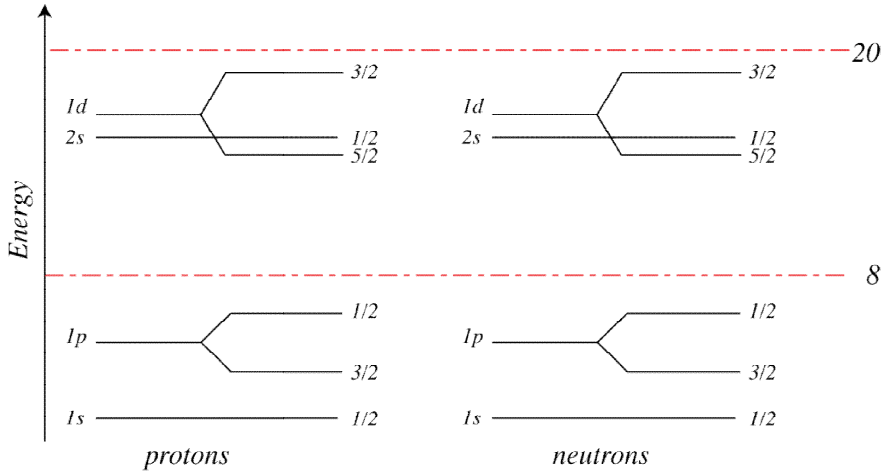

Figure 4 Shell model and magic numbers.

The second model that is often used is the collective model of the nucleus. Here, instead of looking at the motion of the individual nucleons, one considers the overall rotation and vibration movement of the nucleus. The justification for this model is that most nuclei take the shape of an ellipsoid (only nuclei that contain magic numbers of protons and neutrons are spherical). Distorted nuclei can then acquire rotational and vibrational motions, to which quantized energy levels can be associated. In classical mechanics, the energy of a rotating solid having a moment of inertia I and an angular momentum J is given by [Basdevant2005, Wong2004]:

$$E = \frac{J^2}{2I}, \tag{21}$$

In quantum mechanics, the angular momentum is quantized, with the energy levels being given by

$$E_J = \hbar^2 \frac{J\left(J+1\right)}{2I}, \tag{22}$$

with $J = 0,1,2,\cdots$. For nucleus having an ellipsoid shape, only even values of J are allowed, and the energies satisfy the following relation:

$$E_2 = \frac{3}{10}E_4 = \frac{1}{17}E_6 = \frac{1}{12}E_8, \tag{23}$$

with

$$E_2 = \frac{15\hbar^2}{2MR^2}, \tag{24}$$

where M and R are respectively the mass and radius of the nucleus. These energy levels are generally much smaller than those associated with the shell model.

2.6 Nuclear Fission and Fusion

Let us look back at **Figure 2**, where the average binding energy per nucleon is provided as a function of mass number. As mentioned previously, this curve indicates that the total binding of one heavy nuclide containing $A > 180$ nucleons, which is given by

$$E_A = AB\left(A\right), \tag{25}$$

is larger than that of two identical nuclides containing $A/2$ protons and neutrons:

$$2E_{A/2} = AB\left(\frac{A}{2}\right) > E_A. \tag{26}$$

In physical terms, this means that two lighter nuclides generally represent a lower energy state than a heavier nucleus. Accordingly, a spontaneous reaction where the heavy nuclide, H, breaks down into two smaller components (L_1 and L_2) is permitted from an energy-conservation point of view, with the energy released by the reaction given by $E_{L_1} + E_{L_2} - E_H$. This spontaneous reaction, called fission, has been observed experimentally for long-lived actinides such as $^{232}\mathrm{Th}$, $^{235}\mathrm{U}$, and $^{238}\mathrm{U}$, even though this is not their preferential decay mode (seven in 10^9 decays of $^{235}\mathrm{U}$ follow this path). For example, the spontaneous fission reaction

$$^{235}_{92}U \Rightarrow 2\,^{1}_{0}n + \,^{133}_{50}Sn + \,^{100}_{42}Mo, \tag{27}$$

which releases 116 MeV, has been observed.

A second observation is that, even if a spontaneous fission reaction is very improbable, the fission process can be initiated externally by an absorption collision between a projectile and a heavy nuclide. For example, the neutron-induced reaction,

$$^{1}_{0}n + \,^{235}_{92}U \Rightarrow 3^{1}_{0}n + \,^{133}_{50}Sn + \,^{100}_{42}Mo, \tag{28}$$

is possible even with very low-energy neutrons and produces the same amount of energy as the spontaneous fission reaction above. This reaction is facilitated by the fact that the main

interaction between the neutron and a nucleus is the attractive nuclear force. The fact that several neutrons are generally produced following such reactions finally leads to the concept of a controlled chain reaction, if sufficient neutrons are produced following a fission reaction to initiate another fission reaction. The conditions required to achieve and maintain such a chain reaction are discussed in Section 4.

Figure 2 also indicates that the nucleons inside very light nuclides are loosely bonded compared to intermediate-mass nuclei. Combining two such nuclides could therefore result in a nucleus that is more strongly bonded, again releasing energy. This process is called nuclear fusion. Examples of such exothermal fusion reactions are

$$ {}_1^2H + {}_1^3H \Rightarrow {}_0^1n + {}_2^4He, \tag{29} $$

$$ {}_1^2H + {}_2^3He \Rightarrow {}_1^1H + {}_2^4He, \tag{30} $$

which release respectively 17.6 and 18.3 MeV in the form of kinetic energy for the final fusion products. Producing such reactions is much more difficult than neutron-induced fission because the two initial nuclides have positive charges and must overcome the Coulomb force to come into close contact. This can be achieved by providing sufficient kinetic energy (plasma temperature) for a sufficient long time (confinement) to ensure that the energy released by fusion is greater than the energy required to reach these conditions (the break-even point). The two main technologies that are currently able to attain the conditions necessary for controlled nuclear fusion are based respectively on confinement by magnetic fields (Tokamak) and inertial confinement (fusion by laser).

3 Nuclear Reactions

From the nuclear chart (**Figure 1**), it is clear that only 266 nuclides are stable. This means that most of the bonded nuclei that can be created will decay. This raises two questions:

- How do they decay?
- How are they created?

Another observation is that if one succeeds in creating a nucleus (stable or not), it may not necessarily be in its fundamental (ground) energy state (see Section 2.5). These are the main questions to answer in the first part of this section. We start by discussing the decay process before continuing with a description of nuclear reactions. The second topic involves the interaction of particles with matter, with most of these particles being produced during the decay process.

3.1 Radioactivity and Nuclear Decay

Nuclear decay, the emission of radiation from an unstable nucleus or radioisotope, is a stochastic process controlled by the laws of statistics and physics. Therefore, it cannot take place unless several fundamental quantities are conserved [Basdevant2005, Smith2000]:

- total energy (including mass, which is a form of energy according to special relativity);
- linear momentum;
- angular momentum;
- electric charge;
- leptonic charge; and
- baryonic charge.

The latter two are required because of the intrinsic properties of quarks and leptons. For common nuclear reactions, these last two conservation relations can be translated to:

- conservation of electrons and neutrinos where the electron and the neutrino have a leptonic charge of +1 and the positron (anti-electron) and anti-neutrino have a leptonic charge of -1; and
- conservation of the total number of protons plus neutrons (mass number).

A decay process transforms, through emission of particles, a parent nucleus into a more stable daughter nucleus (a nucleus with a lower mass where the nucleons are more strongly bonded or equivalently have a lower mass). In fact, if one considers a nucleus at rest that decays according to the following reaction:

$$ {}^{A}_{Z}X \Rightarrow {}^{B}_{W}Y + \sum_{i=1}^{N} {}^{C_i}_{V_i}b, \tag{31} $$

then total energy conservation implies that

$$ m_{{}^{A}_{Z}X}c^2 = \left(m_{{}^{B}_{W}Y}c^2 + T_{{}^{B}_{W}Y}\right) + \sum_{i=1}^{N}\left(m_{{}^{C_i}_{V_i}b}c^2 + T_{{}^{C_i}_{V_i}b}\right), \tag{32} $$

where T is the kinetic energy of the different decay products. This reaction can take place spontaneously only if

$$ T_{{}^{B}_{W}Y} + \sum_{i=1}^{N} T_{{}^{C_i}_{V_i}b} = m_{{}^{A}_{Z}X}c^2 - m_{{}^{B}_{W}Y}c^2 - \sum_{i=1}^{N} m_{{}^{C_i}_{V_i}b}c^2 > 0, \tag{33} $$

$$ Z = W + \sum_{i=1}^{N} V_i, \tag{34} $$

$$ A = B + \sum_{i=1}^{N} C_i, \tag{35} $$

that is, when the energy balance is favourable (the last two equations are for mass number and charge conservation). For a nucleus in an excited state, the daughter nucleus will often be the same as the parent nucleus, but at a different energy level (ground or lower-lying excited state), the secondary particle being a photon (a γ-ray because the photon is produced following a nuclear reaction).

Nuclear decay is characterized by a constant λ defined according to [Smith2000, Nikjoo2012]:

$$ \lambda = \lim_{\Delta t \to 0} \frac{-\Delta N(t) \big/ N(t)}{\Delta t}, \tag{36} $$

where $N(t)$ is the number of nuclei present at time t, $\Delta N(t)$ is the change (negative because of the decay process) in the number of nuclei after time Δt, and λ is known as the decay constant. This definition leads to the Bateman equation [Bell1982]:

$$ \frac{dN(t)}{dt} = -\lambda N\left(t\right) + S(t), \tag{37} $$

where $S(t)$ represents the net rate of production of nuclei (from the decay of other nuclei or from nuclear reactions). One can also define

$$A(t) = \lambda N(t), \tag{38}$$

the activity of a radionuclide that represents the number of decays per second taking place at time t. This activity is generally stated in Becquerels (Bq), where 1 Bq corresponds to one decay per second. For the case where $S(t) = 0$, the solution to the Bateman equation has the form

$$N(t_0 + \Delta t) = N(t_0)e^{-\lambda \Delta t}, \tag{39}$$

where $N(t_0)$ is the number of nuclei at time t_0.

Two other concepts related to decay constants are also commonly used. The mean life, τ, defined as

$$\tau = \frac{1}{\lambda}, \tag{40}$$

represents the average time required for the final number of nuclei to reach a value of $N(t_0)/e$:

$$N(t_0 + \tau) = \frac{N(t_0)}{e}. \tag{41}$$

Similarly, the half-life, $t_{1/2}$,

$$t_{1/2} = ln(2)\tau = \frac{ln(2)}{\lambda}, \tag{42}$$

represents the average time required for the initial number of nuclei to decrease to a value of $N(t_0)/2$.

For some radionuclides, several decay reactions (decay channels) may be observed, each being characterized by a specific relative production yield Y_j such that

$$\sum_{j=1}^{J} Y_j = 1. \tag{43}$$

The decay constant associated with each channel is given by $\lambda_i = \lambda Y_i$. For example, potassium-40 ($^{40}_{19}\mathrm{K}$), which has a mean life of 1.805×10^9 years, decays 89.28% of the time into calcium-40 ($Y_{^{40}_{20}\mathrm{Ca}} = 0.8928$) and 10.72% of the time into argon-40 ($Y_{^{40}_{18}\mathrm{Ar}} = 0.1072$).

Note that the decay constant, λ, associated with a reaction can be evaluated using Fermi's second golden rule [Schiff1968]:

$$\lambda = \sum_f \int \frac{2\pi}{\hbar} \left| \langle f | H' | i \rangle \right|^2 \rho(f, \Xi)\, d\Xi, \tag{44}$$

where $|i\rangle$ is the wave function associated with the initial state, $\langle f|$ is the wave function associated with a final state, and H' is the interaction potential associated with the reaction. The integral is over phase space $d\,\Xi$, with the term $\rho(f, \Xi)$ being the density of state for the final wave function.

The most common decay reactions are the following:

γ-ray emission for an excited nucleus:

$$({}^{A}_{Z}\mathrm{X})^{*} \Rightarrow {}^{A}_{Z}\mathrm{X} + \gamma. \quad (45)$$

Internal conversion for an excited nucleus:

$$({}^{A}_{Z}\mathrm{X})^{*} \Rightarrow [{}^{A}_{Z}\mathrm{X}]^{+} + e_{-}. \quad (46)$$

This process corresponds to the direct ejection of an orbital electron leaving the nucleus in an ionized state ($[{}^{A}_{Z}\mathrm{X}]^{+}$).

β^{-} decay (weak interaction) for a nucleus containing too many neutrons:

$${}^{A}_{Z}\mathrm{X} \Rightarrow [{}^{A}_{Z+1}\mathrm{Y}]^{+} + e_{-} + \bar{\nu}. \quad (47)$$

Neutron emission (nuclear interaction) for a nucleus having a very large neutron excess:

$${}^{A}_{Z}\mathrm{X} \Rightarrow {}^{A-1}_{Z}\mathrm{X} + {}^{1}_{0}n. \quad (48)$$

β^{+} decay (weak interaction) for a nucleus containing too many protons:

$${}^{A}_{Z}\mathrm{X} \Rightarrow [{}^{A}_{Z-1}\mathrm{Y}]^{-} + e_{+} + \nu. \quad (49)$$

Orbital electron capture (weak interaction) for a nucleus containing too many protons:

$${}^{A}_{Z}\mathrm{X} \Rightarrow {}^{A}_{Z-1}\mathrm{Y} + \nu. \quad (50)$$

Proton emission (nuclear interaction) for a nucleus having a very large proton excess:

$${}^{A}_{Z}\mathrm{X} \Rightarrow [{}^{A-1}_{Z-1}\mathrm{Y}]^{-} + {}^{1}_{1}p = {}^{A-1}_{Z-1}\mathrm{Y} + \mathrm{H}^{1}_{1}. \quad (51)$$

This process corresponds to the ejection of an atom of hydrogen.

α-emission for heavy nuclei (nuclear interaction):

$${}^{A}_{Z}\mathrm{X} \Rightarrow [{}^{A-4}_{Z-2}\mathrm{Y}]^{2-} + {}^{4}_{2}\alpha = {}^{A-4}_{Z-2}\mathrm{Y} + {}^{4}_{2}\mathrm{He}. \quad (52)$$

This process corresponds to the ejection of an atom of helium.

Spontaneous fission for heavy nuclei (nuclear interaction):

$${}^{A}_{Z}\mathrm{X} \Rightarrow C\ {}^{1}_{0}n + {}^{B}_{Y}\mathrm{F} + {}^{A-B-C}_{Z-Y}\mathrm{G}. \quad (53)$$

This process corresponds to the fragmentation of a heavy nucleus into two or more smaller nuclei with the emission of several neutrons.

For heavy or very unstable nuclei (see, for example, **Figure 5** for uranium-238), several of these reactions must often take place before a stable isotope is reached.

The Janis software from OECD-NEA can be used to retrieve and process the decay chain for all isotopes [OECD-NEA2013].

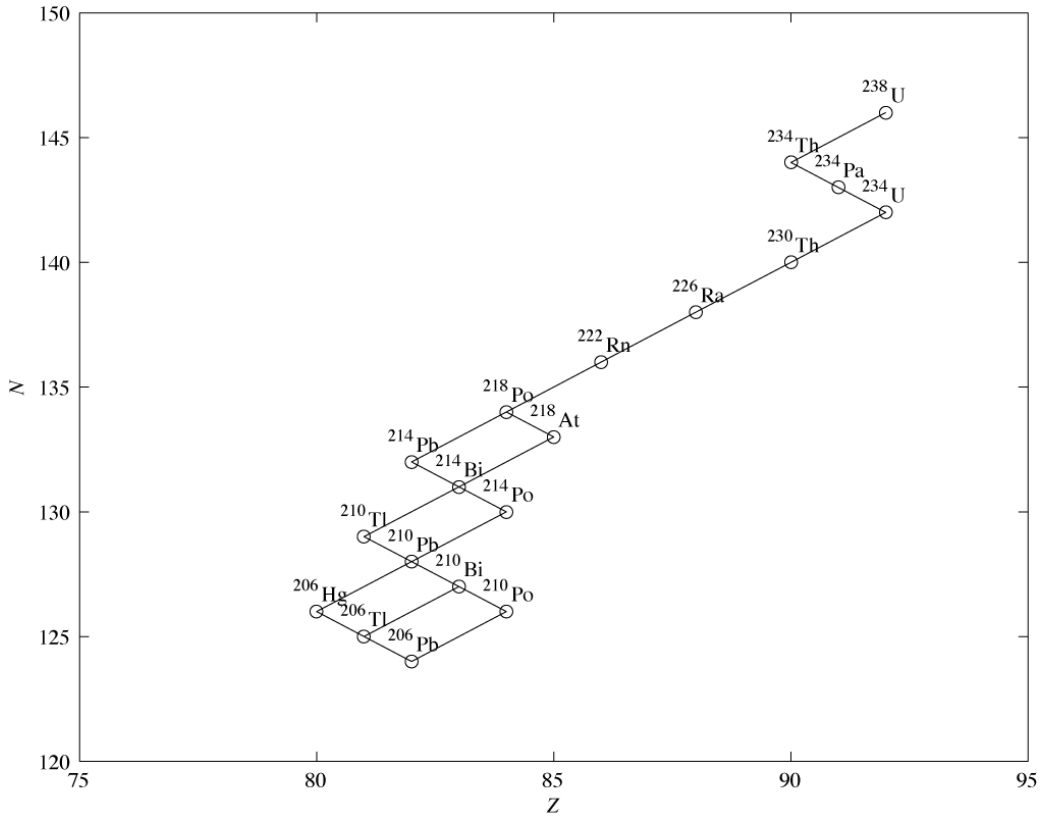

Figure 5 Decay chain for uranium-238 (fission excluded). The type of reaction (β or α-decay) can be identified by the changes in N and Z between the initial and final nuclides.

3.2 Nuclear Reactions

As we saw in the previous section, several types of particles are produced through decay of radioactive nuclides. These particles have kinetic energy, and as they travel through matter, they interact with orbital electrons and nuclei. A nuclear reaction takes place if these particles produce after a collision one or more nuclei that are different from the original nucleus (an excited state of the original nucleus or a new nucleus). Otherwise, the collision gives rise to a simple scattering reaction where kinetic energy is conserved.

For the case where charged particles are traveling through a material, scattering collisions with the orbital electrons or the nucleus are mainly observed (also called potential scattering). More rarely, the charged particles are captured by the nucleus to form a compound nucleus (a very short-lived, semi-bonded nucleus) that can decay through various channels.

Similarly, the electric and magnetic fields associated with the photons interact mostly with the nucleus or the orbital electrons. They can also initiate nuclear reactions after being absorbed in the nucleus. Finally, neutrons rarely interact with electrons because they are neutral particles and the electrons are not affected by the nuclear force (electromagnetic interaction with the quarks inside the nucleon, magnetic interactions with unpaired electrons, and weak interactions are still present). However, they can be scattered (nuclear potential scattering) or absorbed (nuclear reaction) by the nucleus. Again, this absorption can lead to the formation of a very unstable compound nucleus that will decay rapidly.

The main nuclear reactions of photons, electrons, neutrons, and charged heavy particles with nuclei are often the inverses of the decay reactions presented earlier:

γ – ray absorption:

$$\gamma + {}^{A}_{Z}X \Rightarrow \left({}^{A}_{Z}X\right)^{*}. \tag{54}$$

γ-ray scattering (elastic and inelastic):

$$\gamma + {}^{A}_{Z}X \Rightarrow \left({}^{A}_{Z}X\right)^{*} + \gamma^{*}. \tag{55}$$

electron capture:

$$e_{-} + {}^{A}_{Z}X \Rightarrow \left[{}^{A}_{Z-1}Y\right]^{+} + \nu + \gamma. \tag{56}$$

positron capture:

$$e_{+} + {}^{A}_{Z}X \Rightarrow \left[{}^{A}_{Z+1}Y\right]^{-} + \bar{\nu} + \gamma \tag{57}$$

proton capture:

$$p^{1}_{1} + {}^{A}_{Z}X \Rightarrow \left[{}^{A+1}_{Z+1}Y\right]^{-} + \gamma. \tag{58}$$

α capture:

$$\alpha^{4}_{2} + {}^{A}_{Z}X \Rightarrow \left[{}^{A+4}_{Z+2}Y\right]^{2-} + \gamma. \tag{59}$$

neutron capture:

$${}^{1}_{0}n + {}^{A}_{Z}X \Rightarrow {}^{A+1}_{Z}X + \gamma. \tag{60}$$

neutron scattering (elastic and inelastic):

$${}^{1}_{0}n + {}^{A}_{Z}X \Rightarrow \left({}^{A}_{Z}X\right)^{*} + {}^{1}_{0}n + \gamma. \tag{61}$$

photon-induced fission:

$$\gamma + {}^{A}_{Z}X \Rightarrow C\,{}^{1}_{0}n + {}^{B}_{Y}F + {}^{A-B-C}_{Z-Y}G + \gamma. \tag{62}$$

neutron-induced fission:

$${}^{1}_{0}n + {}^{A}_{Z}X \Rightarrow C\,{}^{1}_{0}n + {}^{B}_{Y}F + {}^{A+1-B-C}_{Z-Y}G + \gamma. \tag{63}$$

These reactions must obey the same conservation laws as those described earlier for the decay reaction. For most reactions (except elastic scattering), the final nucleus will be in a highly excited state and will decay rapidly by γ-ray emission (prompt photons).

The probability that any given reaction will take place between a nucleus and a particle is represented by the microscopic cross section σ. Much like the decay constant, the cross sections have a quantum mechanical interpretation and can be expressed in terms of the wave function $|i\rangle$ associated with the initial state (the product of the wave functions of the projectile and the nucleus), the wave function $\langle f|$ associated with the final state, and H', the interaction potential. The differential cross section is then given by Fermi's first golden rule, which can be written as:

$$\frac{d\sigma}{d\Xi} = \frac{2\pi V}{\hbar v_i}\left\langle \left| f|H^{'}|i\right\rangle \right|^{2} \rho(f), \tag{64}$$

where V is the volume of the system, v_i is the velocity of the projectile (assuming that the initial nucleus is at rest), and $\rho(f)$ is again the density of states in the phase space Ξ for final particles. The cross section, which is then the integration over the final phase space of the differential cross section, has units of surface. The most common unit used for the microscopic cross section is the barn (b), with $1\ \mathrm{b} = 10^{-24}\ \mathrm{cm}^2 = 10^{-28}\ \mathrm{m}^2$.

These cross sections are very difficult to evaluate explicitly because of the complexity of the wave functions (the wave function for a nucleus is the product of the wave functions of all the nucleons in the nucleus bonded by the nuclear potential) and the interaction potential. These are generally evaluated experimentally, and the results are stored in evaluated nuclear data files. A software package such as Janis can be used to retrieve and analyze these cross sections [OECD-NEA2013]. For computational reactor physics, the NJOY program is generally used to process the cross-section databases for neutron-induced reactions [MacFarlane2010].

3.3 Interactions of Charged Particles with Matter

As mentioned earlier, charged particles traveling through matter interact mainly with atomic electrons because they are much more numerous than nuclei (Z electrons for a nucleus with atomic number Z) and also because the wave functions associated with these electrons have a very large spatial extension (the size of an atom) compared to that associated with the nucleus.

Heavy particles, such as protons, α-particles, and ions, are scattered by the Coulomb potential produced by the electron, with the cross section given by the Mott scattering formula [Leroy2009, Bjorken1964]. As a result, a heavy particle loses a very small quantity of energy and momentum to secondary electrons and travels mainly in a straight line as it slows down. The secondary electrons, on the other hand, can gain enough energy to be knocked loose from the atom, leaving it in an ionized state.

For electrons and positrons traveling through matter, the problem is somewhat more complex. The cross section for electron-electron collisions is given by the Möeller scattering formula, while Bhabha scattering is used for positron-electron collisions [Leroy2009, Bjorken1964]. Positrons lose, on average, half their energy in collision with atomic electrons, and their trajectory is somewhat erratic. Positron-electron annihilation reactions can also take place, producing two γ-rays. Finally, the electrons and positrons that are accelerated in the strong electromagnetic field of a heavy nucleus lose some of their energy by γ-ray emission due to synchrotron radiation (also known as Bremsstrahlung) [Leroy2009, Bjorken1964].

One can approximate the energy loss of a particle of charge z and mass m inside a material of density ρ, atomic number Z, and atomic mass M using the continuous slowing-down approximation (CSDA), where one assumes that the particle is interacting constantly with an electron gas of density n given by

$$n = Z\frac{\rho}{M}\,\mathbb{N}_A. \tag{65}$$

The energy loss per unit distance traveled by the particle inside the material ($-dE/dx$), known as the stopping power, is then given by the Bethe-Block formula [Smith2000, Leroy2009]:

$$\left(-\frac{dE}{dx}\right)_{collision} = 4\pi n\frac{\left(z\alpha_e\hbar c\right)^2}{mv^2}\left(L\left(v\right)-F\left(v\right)\right), \tag{66}$$

where v is the speed of the particle and $L(v)$ the stopping number, which can be written as

$$L = ln\left(\frac{2mv^2}{I(1-(v/c)^2)}\right)-(v/c)^2, \tag{67}$$

where I is the mean excitation potential for the atomic electrons in this material. The correction term, $F(v)$, takes into account the fact that the atomic electrons are bonded as well as other quantum effects. For electrons, one must also consider the energy lost by synchrotron radiation, which is given approximately by [Leroy2009]:

$$\left(-\frac{dE}{dx}\right)_{radiation} \approx Zn\frac{\alpha_e^3\hbar^2}{m_e}, \tag{68}$$

where m_e is the mass of the electron. Here, it is assumed that the kinetic energy of the electrons $T_e \ll m_e c^2$.

For heavy particles (protons, α-particles), nuclear slowing-down, $(-dE/dx)_{\text{nuclear}}$, becomes important when they reach a low energy.

The CSDA range R of a particle is defined as the distance (path of flight) that it must travel to lose all its kinetic energy. It is computed as

$$R = \int_0^T \frac{1}{\left(-\frac{dE}{dx}\right)_{total}} dE, \tag{69}$$

where T is the initial kinetic energy of the particle and

$$\left(-\frac{dE}{dx}\right)_{total} = \left(-\frac{dE}{dx}\right)_{collision} + \left(-\frac{dE}{dx}\right)_{radiation} + \left(-\frac{dE}{dx}\right)_{nuclear}. \tag{70}$$

These CSDA expressions are helpful to understand the general behaviour of particles slowing down in a material. However, for practical applications, tabulated values for $-dE/dx$ and R are more useful. This type of information for electrons, protons, and α-particles can be found on-line for various elements and different material compositions on the National Institute of Standard and Technology Web sites [Berger2013a]. The databases available are:

- ESTAR, for electrons;
- PSTAR, for protons;
- ASTAR, for α-particles.

For heavy particles, this site also provides information on nuclear stopping power. Also note that the stopping power and range are defined in a somewhat different way from the notation above. The following expressions are used instead:

$$-dE/dx(\text{MeV}\times\text{cm}^2/\text{g}) = -\frac{1}{\rho}dE/dx(\text{MeV}/\text{cm}) \tag{71}$$

and

$$R(\text{g}/\text{cm}^2) = \rho R(\text{cm}) \tag{72}$$

because these are the conventional units used in radiation shielding studies. Note that the number of electron/ion pairs produced per unit distance in a material is given approximately by

$$\frac{dn_{pairs}}{dx} = \frac{1}{W}\left(-\frac{dE}{dx}\right)_{total}, \tag{73}$$

where W is the average energy required to ionize an atom in this material.

3.4 Interactions of Photons with Matter

The behaviour of photons as they travel in a material is somewhat different from that of charged particles, which lose their kinetic energy mainly by continuously interacting with electrons and nuclei, the Coulomb field being a long-range force. The photon is the quantum particle that carries the energy $E = h\nu$ and momentum $\vec{p} = \vec{n}h/\lambda$ of an electromagnetic field of frequency ν and wavelength $\lambda = c/\nu$ travelling in direction $\vec{n}$. Depending on its wavelength, the photon behaves as a wave (diffraction and interference for low-energy photons) or as a particle (photoelectric effect for high-energy photons) when it interacts with matter. Here, we will consider only the interactions with matter of the relatively high-energy photons ($E > 1$ keV) found in nuclear reactors. In this case, the photon behaves as a particle that is first absorbed by the atomic electrons or the nucleus. Following this absorption, secondary particles can be produced, including photons (scattering reactions), electrons and positrons (pair creation), and neutrons (photonuclear reaction).

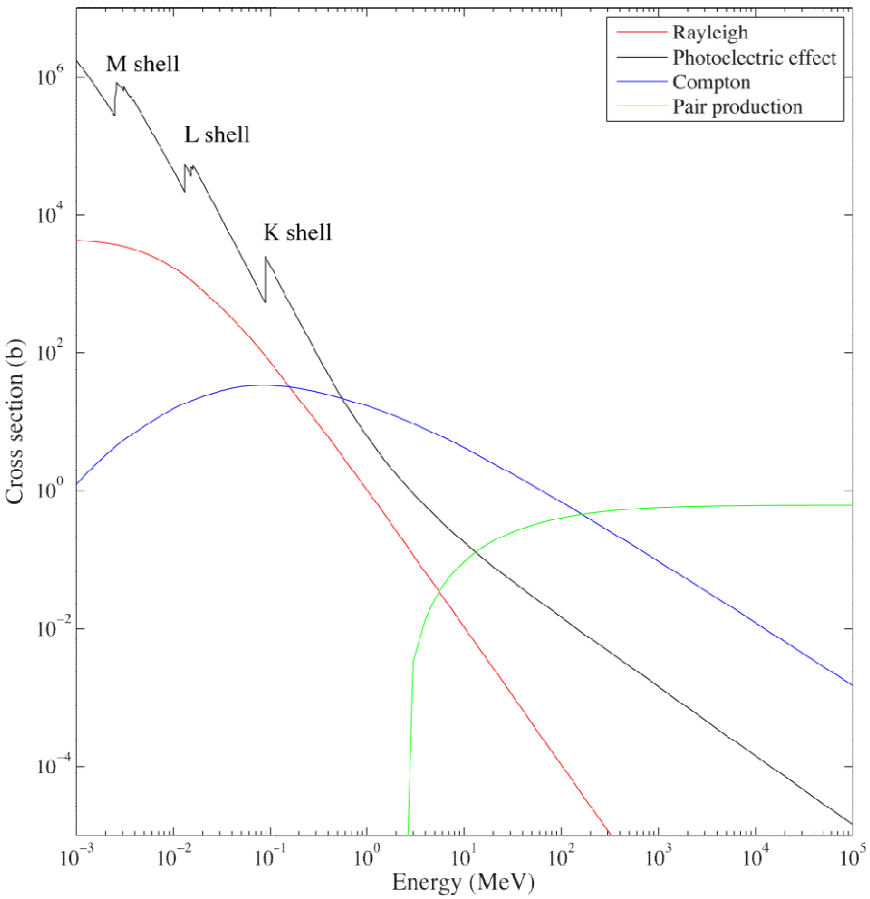

Figure 6 Microscopic cross section of the interaction of a high-energy photon with a lead atom.

The five main reactions taking place between high-energy photons and matter that are of interest in nuclear reactor-related studies are:

- Photoelectric effect;
- Rayleigh scattering;
- Compton scattering;
- Pair production; and
- Photonuclear reactions.

With each such reaction is associated a macroscopic cross section $\Sigma_{m,x}(E)$ representing the probability per unit distance travelled by a photon of energy E that an interaction of type x has taken place in material m. The macroscopic cross section takes into account the probabilities of interaction both between single photons and between particles and the fact that the material contains $N_{m,i}$ particles of type i per unit volume:

$$\Sigma_{m,x}(E) = \sum N_{m,i}\sigma_{i,x}(E), \tag{74}$$

where $\sigma_{i,x}(E)$ is the microscopic cross section of the interaction of a photon of energy E with a particle of type i through reaction x (see Section 3.2). The total microscopic photon cross section can be expressed as:

$$\sigma(E) = \sigma_{Photoelectric}(E) + \sigma_{Rayleigh}(E) + \sigma_{Compton}(E) + \sigma_{Pair\ production}(E) + \sigma_{Photonuclear}(E). \tag{75}$$

Examples of microscopic cross sections for the interaction of photons with a lead atom are presented in **Figure 6.**

Let us now describe in detail the five reactions contributing to $\sigma(E)$ and discuss their respective dependences on the energy of the incident photon.

3.4.1 Photoelectric effect

This effect is illustrated in **Figure 7**. A photon with an energy $E = h\nu$ that is greater than the binding energy W of atomic electrons around the nucleus is absorbed. Following this absorption, the electron becomes free, leaving behind an ion. The energy balance for this reaction is

$$T_e + T_N = E - W, \tag{76}$$

where T_e is the kinetic energy of the final electron and T_N that of the recoil nucleus (generally very small compared with T_e).

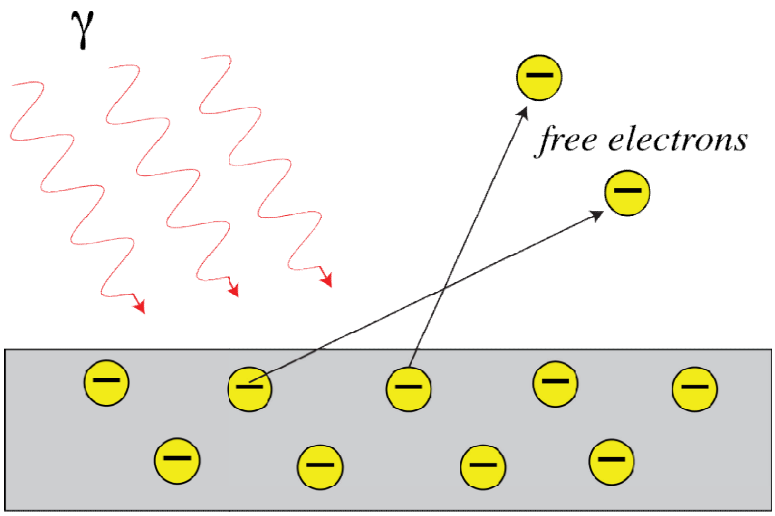

Figure 7 Photoelectric effect.

From quantum mechanics, the binding energy of electrons around a nucleus of charge Ze can be approximated using [Griffiths2005]:

$$W_n = \frac{13.61\, Z^2}{n^2} eV, \tag{77}$$

where $n = 1$ for K-shell electrons, 2 for L-shell electrons, and so on. Therefore, as the energy of the photon decreases, the electrons in the more tightly bonded shells (K, L, and M shells) are successively excluded, producing a large drop in the photoelectric cross section when the energy falls below W_n (see **Figure 6**). The evaluation of this cross section is therefore very difficult, and only approximate relations are available. For a K-shell electron, one can use [Leroy2009]:

$$\sigma_{Photoelectric,K}\left(E\right) \approx \frac{32\sqrt{2}\pi Z^5 \alpha_e^6 \left(m_e c^2\right)^{\frac{3}{2}}}{3\left(E\right)^{\frac{7}{2}}} \left(\hbar c\right)^2, \tag{78}$$

which is valid, within 2%, for photon with energies ranging from 100 keV to 200 MeV. The total photoelectric cross section (the sum over all energy shells) is given approximately by [Leroy2009]:

$$\sigma_{Photoelectric}\left(E\right) \approx \sigma_{Photoelectric,K}\left(E\right) \times \left(1 + 0.01481\left(\ln\left(Z\right)\right)^2 - 0.000788\left(\ln\left(Z\right)\right)^3\right). \tag{79}$$

Clearly, this cross section decreases rapidly with photon energy. It is dominant only for photons of energies less than a few tenths of an MeV.

Several processes can take place after this reaction. If the electron ejected from the atom was initially in the valence band, the ionized atom is in its ground state, and no further radiation emission is observed. When electrons coming from more tightly bonded energy levels are ejected, the ionized atom is left in an excited state. This excited ion can then decay to its ground state by two different means. First, an electron in a much higher energy state (i.e., a valence electron) can emit a photon and fill the vacant energy level. The electron can also come from a slightly higher energy level, leaving the ion in a less excited state that will further decay before reaching its ground state. When the photons emitted in these successive decays

are absorbed by less-bonded electrons, so-called soft Auger electrons are ejected from the atom, producing an Auger electron cascade.

3.4.2 Rayleigh scattering

This elastic scattering reaction takes place when a photon, after being absorbed by a bound atomic electron, is re-emitted with the same energy, but in a different direction, by the electron, returning the atom to its original state [Leroy2009, Jauch1976]. The cross section for this reaction is very difficult to evaluate because it depends strongly on the wave function of the bonded electrons surrounding the nucleus. It is generally written as an integral of the form

$$\sigma_{Rayleigh}\left(E\right)=\pi\left(\frac{\alpha_e\hbar c}{m_e c^2}\right)^2\int_0^{\pi}\left(1+\cos^2\left(\theta\right)\right)\left[F\left(E,\theta,Z\right)\right]^2\sin\left(\theta\right)d\,\theta, \tag{80}$$

where $F(E,\theta,Z)$ is the atomic form factor that represents the effect of the Z electrons surrounding the nucleus on the scattering of a photon at an angle θ with respect to the initial photon direction. Several theoretical expressions for $F(E,\theta,Z)$ are available in the literature for different values of Z and various energy ranges. For example, when the photon energy is greater than 100 keV, the main contributors to Rayleigh scattering are the electrons in the K-shell, and the relativistic Bethe-Levinger form factor is used [Hubbell1975]:

$$F\left(E,\theta,Z\right)=\frac{\sin(2\gamma\text{atan}(Q))}{\gamma Q\left(1+Q^2\right)^{\gamma}}, \tag{81}$$

with

$$Q\left(E,\theta,Z\right)=\frac{2E\sin(\theta/2)}{\alpha_e Z m_e c^2}, \tag{82}$$

$$\gamma\left(Z\right)=\sqrt{1+\left(\alpha_e Z\right)^2}. \tag{83}$$

Because Rayleigh scattering is never the dominant photon reaction (see **Figure 6**) for the photon energy range considered in nuclear reactors, its contribution to the total cross section is often neglected.

3.4.3 Compton scattering

The Compton effect is the incoherent inelastic scattering of a photon by an electron that is weakly bonded to a nucleus (see **Figure 8**). Here, a photon with momentum $\vec{k}$ ($\left|\vec{k}\right|=h\nu/c=E/c$) is scattered at an angle θ with respect to its original direction, with the final momentum of the photon being $\vec{k}'$. The electron is then ejected with a kinetic energy T_e, obtained by conservation of momentum and energy:

$$T_e=E^2\left(\frac{(1-\cos\theta)}{m_e c^2+E(1-\cos\theta)}\right), \tag{84}$$

where the binding energy of the electron is assumed to be small compared to the photon energy, and the recoil energy carried by the nucleus is neglected. For a nearly free electron, the cross section for this reaction is given by the Klein-Nishina formula, which can be written as

$$\sigma_{Compton}(E) = \frac{\pi}{\varepsilon}\left(\frac{\alpha_e \hbar c}{m_e c^2}\right)^2 \left[ln(1+2\varepsilon)\left(1 - \frac{2(1+\varepsilon)}{\varepsilon^2}\right) + \frac{1}{2} + \frac{4}{\varepsilon} - \frac{1}{2(1+2\varepsilon)^2}\right], \quad (85)$$

with $\varepsilon = E/(m_e c^2)$ This cross section decreases with energy, but much more slowly than for the photoelectric effect. It dominates the photoelectric reaction for energies above approximately 0.5 MeV.

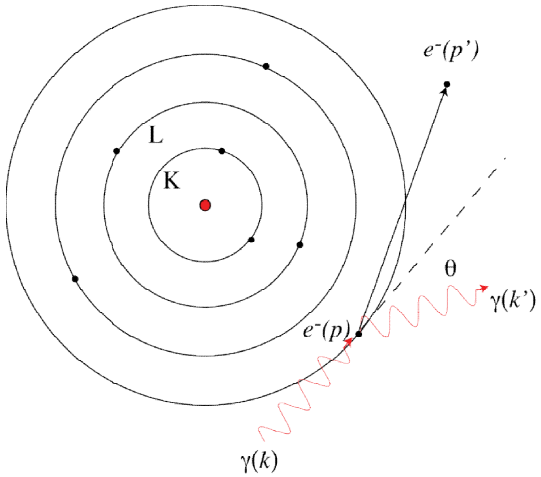

Figure 8 Compton effect.

3.4.4 Pair production

A photon with energy $E = h\nu > 2m_e c^2$ traveling through the Coulomb field of a nucleus of charge Z (or an electron) can be converted into an electron-positron pair. After the reaction, the nucleus carries a small part of the kinetic energy of the photon, with the bulk of the energy being transferred in the form of mass and kinetic energy to the pair. For photon energies in the range found in nuclear reactors, the cross section for this reaction is given approximately by [Leroy2009]:

$$\sigma_{Pair\ production}(E) \approx \alpha_e Z^2 \left(\frac{\alpha_e \hbar c}{m_e c^2}\right)^2 \left[\frac{28}{9}\ln(2\varepsilon) - \frac{218}{17} + \frac{129}{20\varepsilon}\right], \quad (86)$$

with $\varepsilon = E/(m_e c^2)$. This cross section vanishes for $E < 1.02$ MeV and is larger than the Compton cross section above a few MeV.

3.4.5 Photonuclear reactions

Photonuclear reactions are the result of photons being absorbed by a nucleus to form an excited nucleus, which gets rid of its energy through different decay processes, namely the emission of a secondary photon, the ejection of one or more nucleons (protons and neutrons), the ejection of α-particles, or through a fission reaction. Photonuclear reactions occur only above a threshold, which lies between 7 and 9 MeV for heavy nuclides, but is considerably lower for very light isotopes (1.666 MeV and 2.226 MeV respectively for beryllium and deuterium). The absorption cross sections for these reactions (see **Figure 9**) are generally very difficult to evaluate, and only approximate expressions are available.

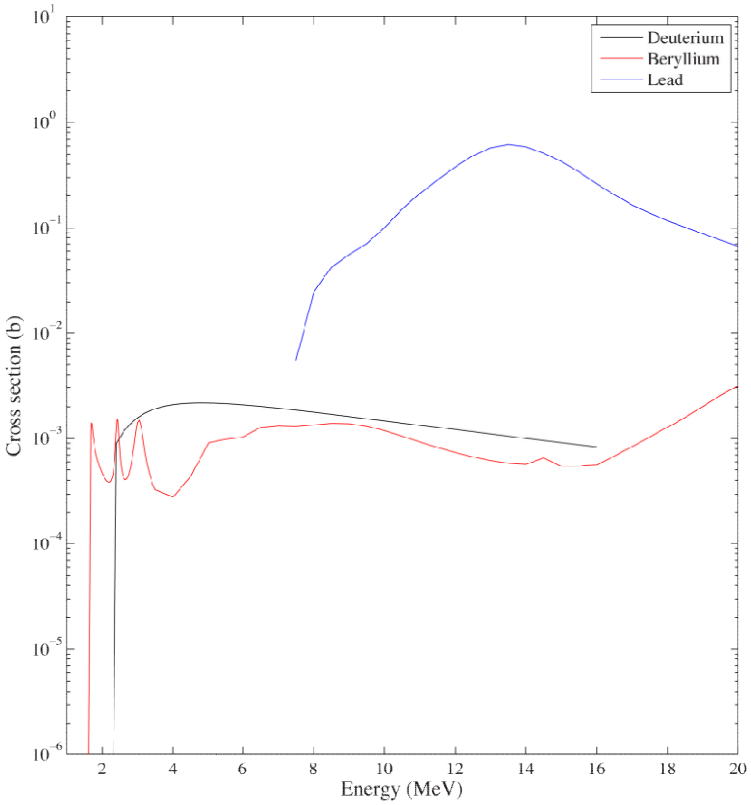

Figure 9 Photonuclear cross sections for deuterium, beryllium, and lead.

For deuterium, which is important to CANDU reactors because they use large amounts of heavy water, the expression [Leroy2009]

$$\sigma_{^2D,Photonuclear}(E) \approx C_{^2D} \frac{\left(\sqrt{E-2.226}\right)^3}{E^3} \tag{87}$$

is often used, where E, the photon energy, is given in MeV, $C_{^2\mathrm{D}}$ varies between 0.061 and 0.0624, and $\sigma_{\mathrm{D}}(E)$ is in barns. The end result of such a photonuclear reaction is a hydrogen atom and a fast neutron that can initiate a fission reaction (see Section 2.6).

Tabulated values for Rayleigh scattering (coherent scattering), photoelectric effect, Compton scattering (incoherent scattering), and pair production cross sections with different atoms or materials and for energies ranging from 1 keV to 100 GeV are available on-line on the Web site of the National Institute of Standards and Technology (NIST) [Berger2013b]. For photonuclear reactions, the energy-dependent cross sections for various isotopes can be obtained using the OECD-NEA Janis software [OECD-NEA2013].

For each reaction presented above, the photons first transfer all their energy to an electron or a nucleus following a collision. As a result, starting with $n(E,\vec{r},\vec{\Omega})$ photons of energy E and direction $\vec{\Omega}$ incident at point $\vec{r}$ on a material of uniform macroscopic cross section $\Sigma(E)$, the number of initial photons $n(E,\vec{r}+s\vec{\Omega},\vec{\Omega})$ still present after a distance s has been crossed is given by [Basdevant2005]:

$$n\left(E,\vec{r}+s\vec{\Omega},\vec{\Omega}\right) = n\left(E,\vec{r},\vec{\Omega}\right)e^{-\Sigma(E)s}. \tag{88}$$

The number of photons therefore decreases exponentially with distance. This behaviour is similar to what is observed when light is attenuated by passing through a material with a linear attenuation coefficient $\mu(E) = \Sigma(E)$. Secondary photons produced with energy E and direction $\vec{\Omega}$ following the absorption of photons of energy E' and direction $\vec{\Omega}'$ will also contribute to the total population of photons at point $\vec{r} + s\vec{\Omega}$. The equation that describes the photon population in a material, assuming a constant neutron incident population, is the static photon transport equation, which takes the form [Pomraning1991]:

$$\vec{\Omega} \cdot \vec{\nabla}\, n\left(E, \vec{\Omega}, \vec{r}\right) = -\Sigma\left(E\right) n\left(E, \vec{\Omega}, \vec{r}\right) + \int dE' \int d\vec{\Omega}'\, \Sigma_s\left(E' \to E, \vec{\Omega}' \to \vec{\Omega}\right) n\left(E', \vec{\Omega}', \vec{r}\right), \qquad (89)$$

where $\Sigma_s\left(E' \to E, \vec{\Omega}' \to \vec{\Omega}\right)$ is the differential scattering cross section representing the probability that the absorption of a photon of energy E' and direction $\vec{\Omega}'$ produces a photon of energy E and direction $\vec{\Omega}$.

3.5 Interactions of Neutrons with Matter

Neutron interaction with matter is the result of the nuclear force, although weak and electromagnetic interactions, the latter being the result of anomalous magnetic moment, are also possible. As a result, only neutron-nucleus interactions are generally considered, including

- elastic potential scattering with cross section σ_{elastic};
- inelastic scattering with cross section $\sigma_{\text{inelastic}}$;
- neutron absorption with cross section $\sigma_{\text{absorption}}$; and
- spallation reactions, $\sigma_{\text{spallation}}$.

In the first three reactions, the neutron interacts with the nucleus as a whole. In spallation reactions, the neutrons interact directly with the nucleons in the nucleus. The latter reaction can take place only when the energy of the incident neutron $E_{n,i}$ is sufficiently high (threshold reactions with $E_{n,i} > 0.1$ MeV), and therefore $\sigma_{\text{spallation}}$ is either neglected, because it is too small, or simply included in the absorption cross section. The probability that the neutron interacts with a nucleus is then given by the total cross section, σ, where

$$\sigma(E_{n,i}) = \sigma_{absorption}(E_{n,i}) + \sigma_{scattering}(E_{n,i}), \qquad (90)$$

$$\sigma_{scattering}\left(E_{n,i}\right) = \sigma_{elastic}\left(E_{n,i}\right) + \sigma_{inelastic}\left(E_{n,i}\right). \qquad (91)$$

Elastic potential scattering is an interaction in which kinetic energy is conserved and the neutron does not penetrate the nucleus. As a result, the neutron is slowed down, transferring part of its energy to the nucleus. For a collision between a neutron with an initial kinetic energy $E_{n,i}$ and a nucleus of mass M_X at rest, the final neutron kinetic energy $E_{n,f}$ (momentum and energy conservation) will be given by [Bell1982]:

$$E_{n,f} = \frac{E_{n,i}}{\left(1+A\right)^2}\left(A^2 + 1 + 2A\cos\vartheta\right), \qquad (92)$$

where $A = M_X/m_n$ and ϑ, the scattering angle for the final neutron in the of mass system, is related to the scattering angle in the laboratory system θ by

$$\cos\theta = \frac{A\cos\vartheta + 1}{\sqrt{\left(A^2 + 1 + 2A\cos\vartheta\right)}}. \qquad (93)$$

On average, the neutron will lose an energy ΔE:

$$\Delta E = \frac{(1-\alpha)}{2} E_{n,i}, \tag{94}$$

$$\alpha = \frac{(A-1)^2}{(A+1)^2}, \tag{95}$$

after each collision. Because ΔE decreases as A increases, neutron slowing-down (also called moderation) is more efficient when scattering collisions with light rather than heavy nuclei are involved.

For low-energy neutrons, the potential scattering cross section in the centre of mass system is nearly constant and has the form [Bell1982]:

$$\sigma = 4\pi R^2, \tag{96}$$

where R is the nuclear radius for this material. At higher energy, one can use Fermi's golden rules to obtain an approximation for $\sigma(E)$ of the form

$$\sigma(E) = 4\pi \frac{\hbar^2 \sin^2 \delta}{2 m_n E}, \tag{97}$$

where δ represents the phase shift of the neutron wave function in isotropic scattering.

Inelastic scattering and absorption reactions generally proceed by creation of a compound nucleus:

$$n + {}^{A}_{Z}X \Rightarrow \left({}^{A+1}_{Z}X\right)^{*} \Rightarrow n' + \left({}^{A}_{Z}X\right)^{*}, \tag{98}$$

$$n + {}^{A}_{Z}X \Rightarrow \left({}^{A+1}_{Z}X\right)^{*} \Rightarrow \textit{other decay channels}. \tag{99}$$

The creation of the compound nucleus is a resonant reaction because the resulting weakly bonded nucleus can exist only if it corresponds to an excitation state of ${}^{A+1}_{Z}\mathrm{X}$. The lifetime of this excited nucleus is generally very short ($\tau \approx 10^{-16}$ s), and with each decay channel k, including inelastic scattering, is associated a resonance width given by [Bell1982]:

$$\Gamma_k = \frac{\hbar}{\tau_k}, \tag{100}$$

with τ_k being the mean life for decay through this channel. The total resonance width for the creation of the excited nucleus Γ is then given by

$$\Gamma = \sum \Gamma_k. \tag{101}$$

For light nuclei, $\Gamma_{\text{inelastic}} \gg \Gamma_{\text{absorption}}$, and the inelastic scattering process dominates. For heavy nuclei, the reverse is true (absorption dominates). The resonance widths for inelastic scattering also increase with energy, the explicit dependence being

$$\Gamma_{inelastic}(E) = \Gamma_n(E) = \Gamma_0 \sqrt{E}, \tag{102}$$

where Γ_0 is a constant that depends on the nucleus considered.

The probability (cross section) for the creation of a compound nucleus with resonant energy E_0 is given by

$$\sigma_{{}^{A+1}_{Z}X}(E) = (2l+1)\frac{\pi\hbar^2}{2mE}\left(\frac{\Gamma_n(\mathrm{E})\Gamma}{(E-E_0)^2+\left(\frac{\Gamma}{2}\right)^2}\right), \tag{103}$$

where l is the orbital-angular-momentum quantum number. For a nucleus that decays through channel k, the cross section is

$$\sigma_k(E) = \sigma_{{}^{A+1}_{Z}X}(E)\frac{\Gamma_k}{\Gamma}. \tag{104}$$

Note that at low energy ($E \ll E_0$), $\Gamma_n = \Gamma_0\sqrt{E}$,

$$\sigma_k(E) \approx (2l+1)\frac{\pi\hbar^2\Gamma_0\Gamma_k}{2m\sqrt{E}} = \frac{\sigma_0}{v}, \tag{105}$$

and the cross section is a function of $1/v$, with v being the incoming neutron velocity.

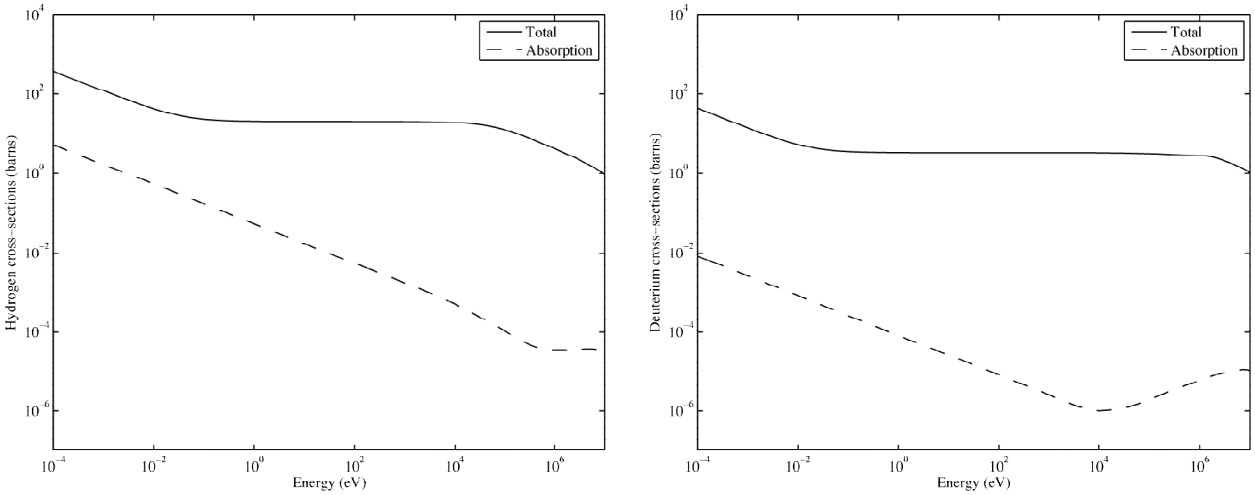

Figure 10 Cross sections for hydrogen (left) and deuterium (right) as functions of energy.

Examples of cross sections for light (hydrogen and deuterium) and heavy nuclei ($^{235}_{92}$U and $^{238}_{92}$U) are presented in **Figure 10** and **Figure 11**. For light nuclides, the scattering process clearly dominates. One can also observe that the total cross section of hydrogen is about ten times larger than that of deuterium (better scattering nucleus for neutron moderation). With absorption representing 10% of the total cross section of hydrogen, one out of ten collisions will lead to neutron capture. For deuterium, the ratio of neutron absorptions to collisions is closer to 1%, making this isotope a better neutron moderator overall. For heavy nuclides, the absorption reaction is the most prevalent and exhibits a very large number of resonances. At very high energy, these resonances do not disappear, but are so closely packed that they produce a nearly continuous cross section.

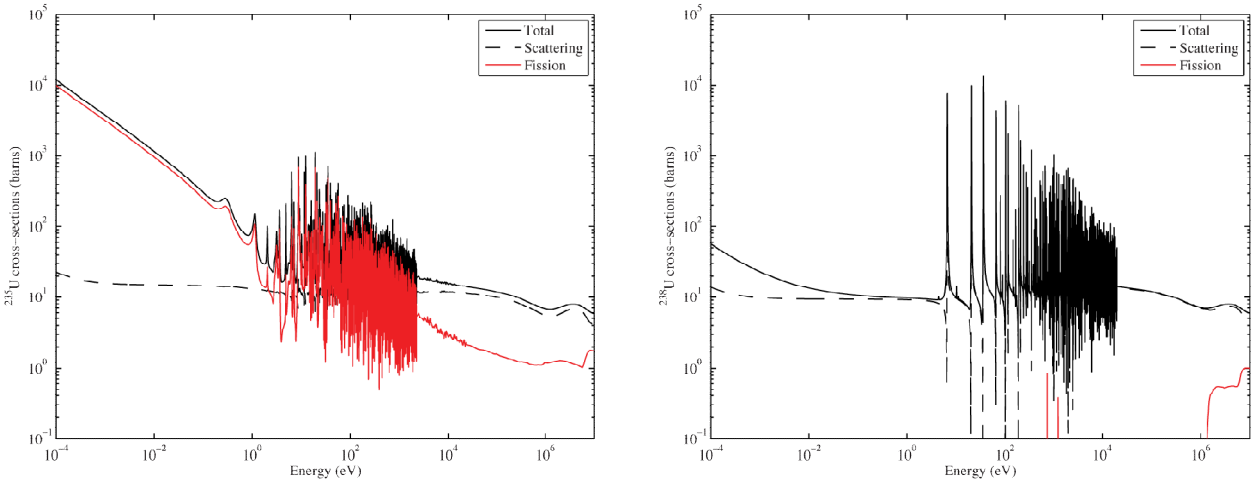

Figure 11 Cross sections for $^{235}_{92}\mathrm{U}$ (left) and $^{238}_{92}\mathrm{U}$ (right) as functions of energy.

The derivations above are valid only if one assumes that the nucleus is at rest. This is clearly not the case for material having temperatures $T > 0$, because atoms acquire an average kinetic energy that is proportional to the temperature of their medium. The resulting effect on the cross sections can be taken into account for a material at temperature T using [Bell1982]:

$$\sigma_k(E,T) = \frac{1}{\sqrt{2mE}} \int \left|\vec{v}_n - \vec{v}_X\right| \sigma_k\left(\left|\vec{v}_n - \vec{v}_X\right|\right) p(E_X)\, dE_X, \tag{106}$$

where $\vec{v}_n$ and $\vec{v}_\mathrm{X}$ are the velocity of the neutron and the nucleus respectively. Here, $p(E_\mathrm{X})dE_\mathrm{X}$ is the Maxwell-Boltzmann distribution, which represents the probability of finding a nucleus with energy E in the range $E_\mathrm{X} < E < E_\mathrm{X} + dE_\mathrm{X}$ due to thermal motion:

$$p(E_X)\, dE_X = \frac{2\pi}{(\pi k_B T)^{3/2}} \sqrt{E_X}\, e^{-E_X/(k_B T)} dE_X, \tag{107}$$

where k_B is the Boltzmann constant. This thermal motion of nuclei has no impact on cross sections exhibiting $1/v$ behaviour (i.e., absorption cross sections of hydrogen at low energy). At low neutron energies, the scattering cross section for light nuclides also exhibits $1/v$ behaviour and is not affected by this transformation, although the energy distribution of the final neutrons resulting from these collisions will be such that they end up in thermal equilibrium with the nuclides in the medium [Bell1982].

The thermal motion of atoms also changes the form of resonant cross sections by reducing the height of the resonance while increasing its width (see **Figure 12**). This widening of the resonance is known as the Doppler effect.

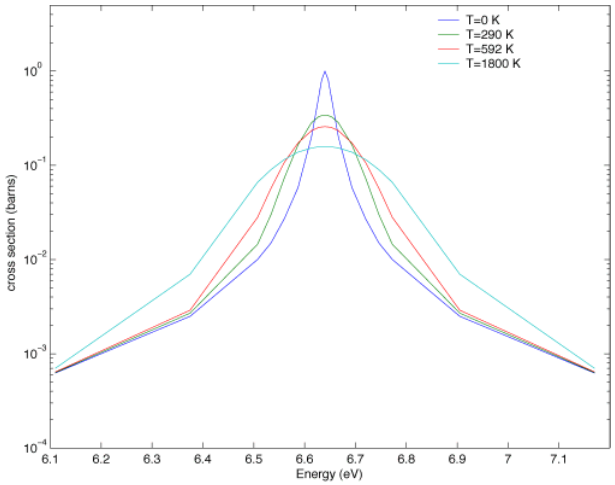

Figure 12 Effect of temperature on U^{238} absorption cross section around the 6.64-eV resonance.

The neutron-nucleus interaction cross sections are very complex and in most cases are evaluated using a combination of theory and experiment. They are generally tabulated in evaluated nuclear data files that can be read by nuclear calculation software (NJOY, for example) [MacFarlane2010]. They can also be extracted on-line from nuclear databases or off-line using the Janis software [KAERI2013, Livermore2013, OECD-NEA2013].

Once the energy-dependent cross sections are known, one can easily evaluate the number of reactions of type x per second (the reaction rate $R_{m,x}(v)$) taking place inside a region of volume V containing N_m nuclei per cm^3 of a material m (cross section $\sigma_{m,x}(v)$) with a population of $n(v)$ neutrons per cm^3 having a velocity $v = \sqrt{2E_n/m}$:

$$R_{m,x}(v) = V\frac{N_m\sigma_{m,x}(v)n(v)}{v} = V\Sigma_{m,x}(v)\phi(v), \tag{108}$$

where $\phi(v) = n(v)/v$ is the neutron flux and $\Sigma_{m,x}(v) = N_m\sigma_{m,x}(v)$ the macroscopic cross section for a reaction of type x in this material.

4 Fission and Nuclear Chain Reaction

The concept of controlled energy production in a nuclear reactor is based on three fundamental ideas that were discussed in Sections 2.6, 3.1, and 3.2, namely:

- energy is released if a heavy nucleus is fragmented into lighter nuclei, the fragmentation process being called nuclear fission;
- the spontaneous nuclear fission process, which has a very low yield for several heavy nuclei, generates neutrons in addition to the light nuclei as end products;
- the nuclear fission process can be initiated by neutrons and photons.

Accordingly, a neutron of kinetic energy T_n travelling through a medium containing heavy nuclei at rest could initiate a fission reaction:

$${}_o^1n + {}_Z^AX \Rightarrow C\,{}_o^1n + {}_Y^BF + {}_{Z-Y}^{A-B-C+1}G. \tag{109}$$

The kinetic energy T_R released by this reaction is then

$$T_R = T_n + (1-C)m_nc^2 + m_{{}_Z^AX}c^2 - m_{{}_Y^BF}c^2 - m_{{}_{Z-Y}^{A-B-C+1}G}c^2, \tag{110}$$

with part of the energy carried by the neutrons and the lighter nuclei. These lighter nuclei rapidly lose their energy in matter (see Section 3.3), thereby producing heat that is removed by the coolant and transformed to electricity.

Not all the neutrons produced after this reaction initiate a fission reaction. A number of them are absorbed by material without producing a fission reaction. Others simply leave the system (with or without collisions). Provided that on average a single neutron per fission reaction can initiate a new fission, a controlled exothermal chain reaction can be established. Establishing such a chain reaction looks relatively simple; however, this is far from the case, as shown in the following subsections.

4.1 Fission Cross Sections

The probability of fission is given by the value of the fission cross sections associated with a nucleus and depends on the energy of the neutron that initiates the reaction. All isotopes with atomic number $Z > 90$ are fissionable (have a non-zero probability of undergoing fission following the capture of a neutron). **Table 5** compares the average energy, U, required to initiate a fission reaction in different nuclei with the energy, Q, available in the compound nucleus after a neutron with a vanishing kinetic energy has been captured. For nuclei containing an even number of protons and an odd number of neutrons, $Q > U$. Such isotopes are called fissile isotopes because the internal energy of the compound nucleus resulting from neutron capture is sufficient to surmount the potential barrier for fission even when the incident neutrons are very slow ($T_n \approx 0$). For isotopes with $Q < U$, the fission barrier can be overcome only using neutrons with relatively high kinetic energy. Fission for these nuclei is a threshold reaction.

Table 5 Comparison of the energy, *U*, required for a fission reaction in a compound nucleus with the energy, *Q*, available after a neutron collision with different isotopes.

Isotope	$\boldsymbol{Q}$(MeV)	$\boldsymbol{U}$(MeV)
$^{232}_{90}$Th	5.1	5.9
$^{233}_{92}$U	6.6	5.5
$^{235}_{92}$U	6.4	5.8
$^{238}_{92}$U	4.9	5.9
$^{239}_{94}$Pu	6.4	5.5

As shown in **Figure 13**, the energy dependence of the fission cross sections for $^{235}_{92}$U and $^{238}_{92}$U reflects the behaviour described above. The probability that a neutron of energy $E_n < 1.0$ MeV will collide with $^{238}_{92}$U and result in a fission reaction is very low. For $^{235}_{92}$U, there is no lower limit on the neutron energy, and the fission probability increases as the energy of the neutron decreases. The neutron capture cross section (neutron absorption followed by photon emission) for $^{238}_{92}$U dominates at low energy, while for $^{235}_{92}$U, it remains relatively small compared to the fission cross section (approximately 10%) over the full energy range. As a result, most neutron absorption in $^{235}_{92}$U will lead to fission followed by production of new neutrons (neutrons are regenerated). For $^{238}_{92}$U, a collision with a neutron having energy below

the fission threshold will lead to a net neutron loss. As a result, the natural uranium fuels used in CANDU reactors (0.72 atomic% of $^{235}_{92}\mathrm{U}$) will be much less reactive (prone to fission) than the enriched fuels (enrichment factors ϵ ranging from 2.5 to 5 atomic% of $^{235}_{92}\mathrm{U}$) used in light water reactors (LWR).

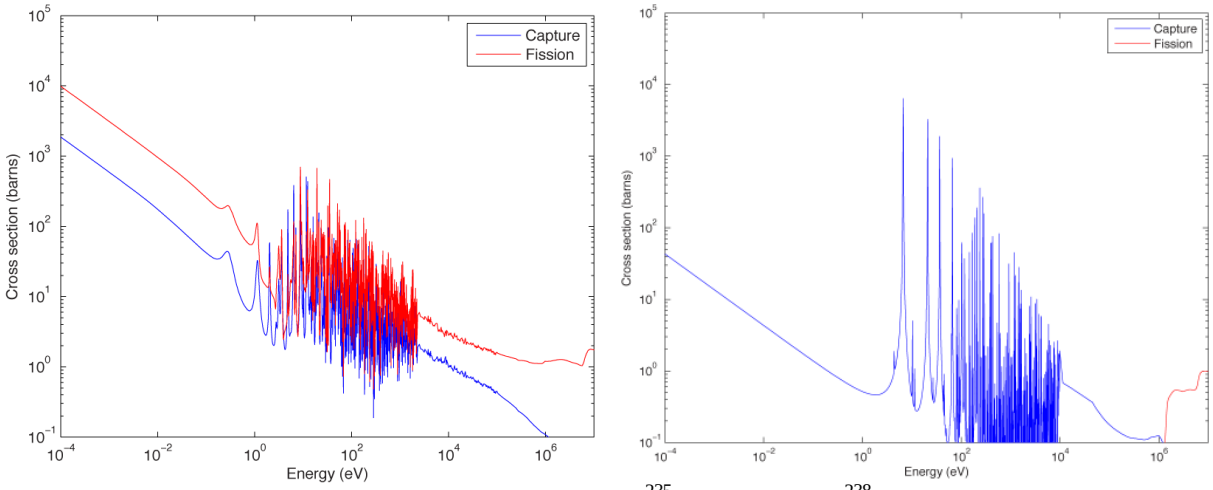

Figure 13 Capture and fission cross sections of $^{235}_{92}\mathrm{U}$ (left) and $^{238}_{92}\mathrm{U}$ (right) as functions of energy.

4.2 Fission Products and the Fission Process

The fission process generally produces two light nuclei, called fission products, although three or more nuclei can also be generated. The relative rate of production of a given nuclide I, called the fission yield, is denoted by Y_I and satisfies

$$\sum_I Y_I = 2, \tag{111}$$

assuming that only two nuclei are produced by each fission reaction. As one can see in **Figure 14**, where the fission yields of all the nuclei resulting from the fission of $^{235}_{92}\mathrm{U}$ are plotted as a function of their mass number, the fission process favours the production of relatively light nuclides ($90 < A < 105$) combined with heavier isotopes ($130 < A < 145$).

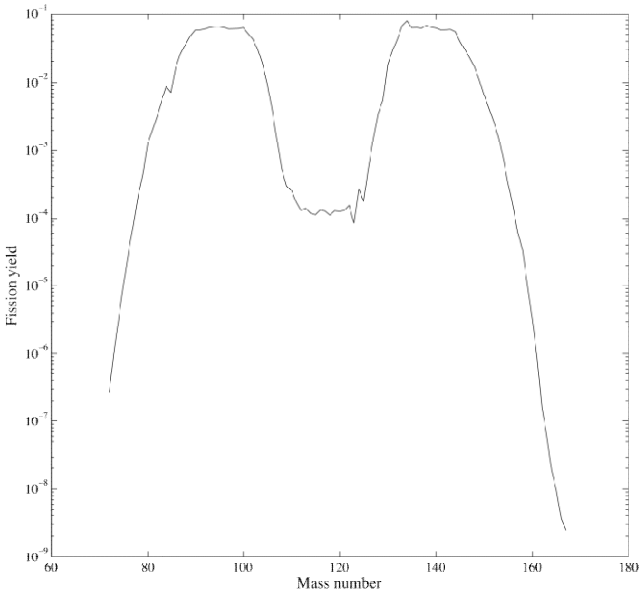

Figure 14 Relative fission yield for $^{235}_{92}\mathrm{U}$ as a function of mass number.

The average number υ of neutrons emitted by the fission process (see **Table 6**) is relatively small compared to the neutron excess $N - Z > 40$ required for heavy isotopes to exist. The value of υ for a given reaction depends on the nature of the fissile nuclides, the fission products released, and the energy of the neutrons. Most fission products are therefore very neutron-rich and unstable. They will reach stability through two main processes: β^- decay and neutron emission. All the transformations that take place within 10^{-14}s of the fission reaction are generally included in the so-called prompt contribution (prompt neutrons, prompt electrons, and prompt photons). Particles produced on a longer time scale (from milliseconds to minutes) due to decay of isotopes with longer mean lifetimes are called delayed.

Table 6 Average numbers of neutrons produced by the fission of common heavy nuclides.

Isotope	$\boldsymbol{\upsilon}(\boldsymbol{E_n}$<1 eV)	$\boldsymbol{\upsilon}(\boldsymbol{E_n}$>1 MeV)
$^{232}_{90}$Th	0	2.2
$^{233}_{92}$U	2.50	2.6
$^{235}_{92}$U	2.43	2.6
$^{238}_{92}$U	0	2.6
$^{239}_{94}$Pu	2.89	3.1

The fission reaction (see Section 2.6) also releases a large amount of kinetic energy (on the order of 200 MeV) that is distributed between fission products, neutrons, γ-rays, etc. (see **Table 7**). Clearly, the fission products carry most of the energy, and because of their very short range in matter, this energy heats the nuclear fuel. Similarly, the charged electrons (β^- particles) also lose most of their energy in the fuel. The highly penetrating γ-rays will end up depositing their energy in the reactor structures, while the weakly interacting neutrinos will generally be lost to the environment. Finally, for LWR and CANDU reactors, only a very small

part of the neutron energy will be transferred to the fuel in the form of heat, with most of it being lost to the environment (mostly through slowing-down in the moderator).

Table 7 Distribution of kinetic energy among the particles produced by a fission reaction.

Particles	Kinetic energy (MeV)
Fission products	168
Prompt γ-rays	7
Delayed γ-rays	7
Electrons	8
Neutrinos	12
Neutrons	7
Total	207

Note that the data presented in **Table 7** represent average values, meaning that the neutrons produced in the fission process have an energy distribution. The probability that a neutron of energy E_n is produced in the fission process, which is known as the fission spectrum, $\chi(E_n)$, is often approximated by the Watt relationship [Watt1952]:

$$\chi\left(E_n\right) = Ce^{-aE_n}\sinh\left(\sqrt{bE_n}\right), \tag{112}$$

where a and b are constants associated with the isotope undergoing fission and depend weakly on the incident neutron energy. The normalization factor C is defined so that

$$\int_0^\infty \chi\left(E_n\right) dE_n = 1 \tag{113}$$

and has the value

$$C = \frac{2a^{2/3}e^{-b/4a}}{\sqrt{\pi b}}. \tag{114}$$

This fission spectrum for $^{235}_{92}\mathrm{U}$ is illustrated in **Figure 15**. Clearly, most of the neutrons are released with energies greater than 1 MeV and can initiate fission reactions with fissionable material. However, the fission cross section for this energy range is relatively low (see **Figure 13**), and fissions at such energies are highly improbable. Nevertheless, a controlled chain reaction that relies mainly on fast fission can be achieved in so-called "fast neutron reactors", where $^{239}_{94}\mathrm{Pu}$ is often used because of its large fission cross section for high-energy neutrons. The alternative to fast neutron reactors is moderated reactors, in which the fast neutrons are slowed down to energies where the fission cross section is significantly larger (below 1 eV). This is the concept used in "thermal neutron reactors", which are discussed in the next section.

Now, let us look at the properties of fission products. These nuclides have intermediate masses and vanishing fission cross sections. However, they can have very large neutron-capture cross sections and thereby can have a considerable negative impact on the neutron population in the fuel where they are produced. For this reason, they are often called neutron poisons. Examples of poisons that have a large impact on nuclear-reactor operation are $^{135}_{54}\mathrm{Xe}$ ($\sigma_a = 3.1 \times 10^6$ b) and $^{149}_{62}\mathrm{Sm}$ ($\sigma_a = 6.1 \times 10^4$ b). A second observation is that most of these nuclides are unstable and decay naturally through one of the reactions described in Section 3.1. These reactions produce both particles, including delayed neutrons, and energy that is often deposited in the fuel. These delayed neutrons play an important role in the control of nuclear reactors, as will be explained in Chapter 5. Moreover, energy will still be produced in the fuel for a long time after the controlled fission reaction has been stopped, due to the decay of fission products. This is the main source of the heat produced in neutron-irradiated nuclear fuels (some energy is also produced through photonuclear fission). This residual heat is removed from shut-down reactors and irradiated fuel pools by continuously circulating the coolant.

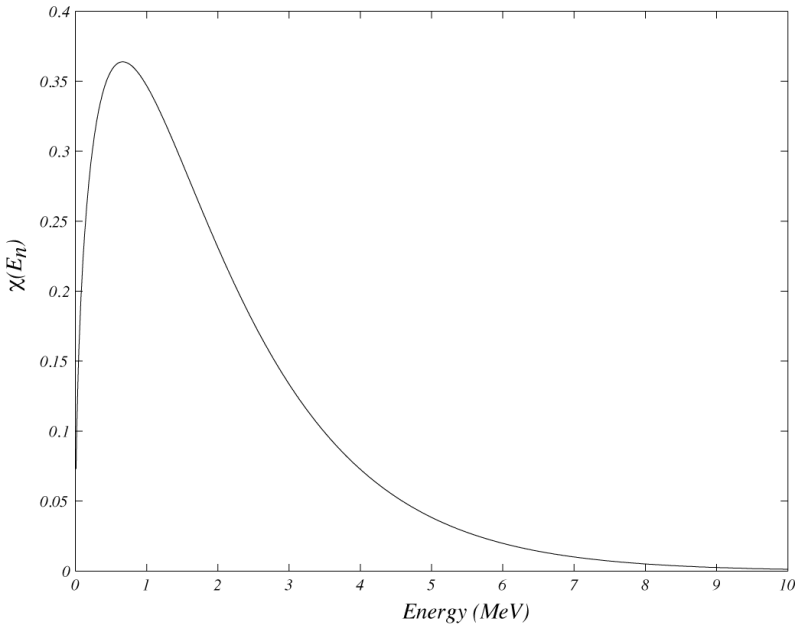

Figure 15 Fission spectrum for $^{235}_{92}\mathrm{U}$.

Finally, we must address the problem of the changes in the composition of a material exposed to a neutron flux. In Section 3.1, we introduced the Bateman equation, which takes the form [Smith2000, Nikjoo2012, Magill2005]:

$$\frac{dN_I(t)}{dt} = -\lambda_I N_I(t) - L_I(t) + P_I(t), \tag{115}$$

where $N_I(t)$ is the concentration of isotope I in the material and the net source $S(t)$ is now divided into a production $P_I(t)$ and a loss $L_I(t)$ term. The loss term, from sources other than decay, is the result of a neutron being absorbed (captured) by isotope I:

$$L_I(t) = N_I(t)\int_0^\infty \sigma_{I,absorption}(E)\phi(E)\,dE, \tag{116}$$

where $\phi(E)$ is the neutron flux. The production term has two contributions: decay from other nuclei, and transformation of a different nucleus into I following a neutron-induced nuclear reaction:

$$P_I(t) = \sum_J Y_{J,I}^d \lambda_J N_J(t) + \sum_J \sum_x Y_{J,I}^x N_J(t) \int_0^\infty \sigma_{J,x}(E)\phi(E)dE, \quad (117)$$

where $Y_{J,I}^d$ is the yield for the production of isotope I from the decay of isotope J, while $Y_{J,I}^x$ is the isotope I production yield from a reaction of type x (fission, capture, etc.) between a neutron and isotope J.

4.3 Nuclear Chain Reaction and Nuclear Fission Reactors

The previous sections have introduced all the concepts required to design a conceptual nuclear fission reactor:

- The nuclear fuel contains heavy isotopes that are broken into lighter nuclides (fission products) following a neutron-induced fission reaction. Such a reaction also generates energy and secondary neutrons that can be used to maintain a chain reaction.
- Most of the energy released as a result of the fission process is carried away by the fission products and deposited in the fuel because of the short range of these nuclei.
- The secondary neutrons produced in the fission process are fast neutrons.
- These neutrons can lose their energy through scattering collisions with the various materials present in our conceptual reactor. Neutron slowing-down by collisions with light isotopes is more efficient than by collision with heavy isotopes (see Section 3.5).
- This energy deposition increases the temperature of the fuel, which must then be cooled to make use of the heat and avoid damage to the reactor. For a power reactor, this heat is collected in a coolant (generally gas or liquids circulating around the fuel) and used to generate electricity.

Now let us look at the fuel and coolant materials that are the most readily available.

Three heavy fissionable isotopes are present in nature: $^{232}_{90}\mathrm{Th}$, $^{238}_{92}\mathrm{U}$, and $^{235}_{92}\mathrm{U}$. Of these, only $^{235}_{92}\mathrm{U}$ is fissile by neutrons of all energies. Because the density of thorium is 11,000 kg/m^3 and it has a microscopic fission cross section of 0.1 barn for 1 MeV neutrons, the mean free path of a neutron for fission in this material is 3.5 m. The mean free path for neutron capture in thorium is very similar in magnitude. Therefore, nearly half the 2.2 neutrons emitted by fission in thorium will be lost to unproductive capture. For $^{238}_{92}\mathrm{U}$, which represents 99.27% of all the atoms found in natural uranium (density of 18,000 kg/m^3), the odds are slightly better, with mean free paths for fission and capture respectively of 50 and 300 cm and fewer neutrons emitted per fission are lost to capture.

The main advantage of $^{235}_{92}\mathrm{U}$, even though it represents only 0.72% of natural uranium composition, is that its fission cross section is quite high (1000 barns at 0.01 eV), giving a mean free path for fission of 2 cm. The capture cross section of $^{235}_{92}\mathrm{U}$ at this energy is also six times smaller than the fission cross section. It is possible to decrease the mean free path for fission with $^{235}_{92}\mathrm{U}$ by increasing its relative concentration in uranium-based fuel (fuel enrichment). The ratio of capture to fission in uranium-enriched fuels remains small even if the fuel contains a large amount of $^{238}_{92}\mathrm{U}$ (capture cross section less than 1 barn).

The heat produced in the fuel can then easily be extracted by conventional means (by circulating a fluid such as water). The main problem is to slow down the secondary fission neutrons to low energies (< 1 eV) while ensuring that few are lost by capture inside other materials or by leaving the reactor. A neutron slowing-down material, the moderator, must therefore be introduced into the reactor to serve this purpose.

Table 8 Maximum values of the elastic scattering and absorption cross sections for $^{1}_{1}\mathrm{H}$, $^{2}_{1}\mathrm{D}$, and $^{12}_{6}\mathrm{C}$ in the energy range 0.1 eV < E <0.1 MeV.

Isotope	$\sigma_{\text{scattering}}$ (b)	$\sigma_{\text{absorption}}$ (b)
$^{1}_{1}\mathrm{H}$	18	0.17
$^{2}_{1}\mathrm{D}$	3.4	0.00025
$^{12}_{6}\mathrm{C}$	4.6	0.0016

For this moderator, two questions are of prime importance: what should be its composition, and where should it be located? The first question is easily answered by combining the kinetics of the neutron-nucleus collision and a survey of the scattering and absorption cross sections of the most promising candidates. In Section 3.5, we concluded that the slowing-down efficiency of a nucleus increases as its mass number decreases, which points to the use of light nuclides as moderators. The most promising candidates are the isotopes of hydrogen and carbon that are readily available in water and graphite. **Table 8** provides the maximum values of the elastic scattering and absorption cross sections for $^{1}_{1}\mathrm{H}$, $^{2}_{1}\mathrm{D}$, and $^{12}_{6}\mathrm{C}$ in the energy range $0.1\ \mathrm{eV} < E < 0.1\ \mathrm{MeV}$. As one can see, $^{1}_{1}\mathrm{H}$ is the best moderator if one does not take into account its absorption cross section. However, up to one in ten collisions of a neutron with $^{1}_{1}\mathrm{H}$ could lead to absorption (for 1eV neutrons). On the other hand, even if the number of collisions required to slow down neutrons using $^{2}_{1}\mathrm{D}$ and $^{12}_{6}\mathrm{C}$ is significantly higher (the distance the neutron will travel between collisions is longer), less than 0.007% of the collisions with $^{2}_{1}\mathrm{D}$ and 0.03% of the collisions with $^{12}_{6}\mathrm{C}$ (1 eV neutron) lead to capture. Accordingly, if one wants to build a core that is compact, a $^{1}_{1}\mathrm{H}$-based moderator is a requirement (light water, for example in LWR); otherwise the best candidate is a moderator that contains large concentrations of $^{2}_{1}\mathrm{D}$ (heavy water in CANDU).

Now let us try to answer the question of the spatial distribution of this moderator. Two very different options can be considered: a homogeneous mixture of fuel and moderator, and small isolated fuel elements placed strategically in the moderator. Again, the answer to this question can be inferred from **Figure 13**. The neutrons in a homogeneous mixture of fuel and moderator materials have a large chance of colliding with fuel isotopes as they are slowing down. This means that neutrons with energies in the "resonance" range ($4\ \mathrm{eV} < E < 10\ \mathrm{keV}$) will be in direct contact with fuel nuclides. Because their capture cross sections at resonance energies increase, often by several orders of magnitude with respect to the background value, neutron capture will have a detrimental effect on the number of neutrons that can reach energies below 1 eV. On the other hand, by separating different fuel elements by a sufficient amount of moderating materials to ensure that a maximum number of neutrons escape the resonance energy range, one decreases neutron loss by capture and increases the probability of fission.

These are the general physics considerations that led to current reactor designs, including the pressurized water (PWR) and CANDU reactors. In the next section, we conclude this chapter by introducing the neutron transport equation, which provides a means to evaluate numerically the neutron population in the reactor and to determine whether a given reactor concept can lead to a sustained chain reaction. This equation also provides the neutron flux that is required to follow the evolution of the fuel and the fission products in the reactor using the Bateman equation.

4.4 Reactor Physics and the Transport Equation

When designing a nuclear power reactor, physicists have two main objectives:

- controlling the nuclear chain reaction;
- extracting the energy produced inside the fuel to avoid damage to the core and to use this energy to produce electricity.

Because most of the energy produced in a nuclear reactor is the result of the fission process, the power produced in the core can be expressed by:

$$P(t) = \int_V d^3r \int_0^\infty dE \sum_J \kappa_J \Sigma_{f,J}(\vec{r},t,E) \int_{4\pi} \phi(\vec{r},t,E,\vec{\Omega}) d^2\Omega, \tag{118}$$

where V is the reactor volume, $\phi(\vec{r},t,E,\vec{\Omega})$ is the flux of neutrons with energy E and direction $\vec{\Omega}$ at a point $\vec{r}$ in space and a time t, and $\Sigma_{f,J}(\vec{r},t,E)$ is the macroscopic fission cross section for isotope J given by

$$\Sigma_{f,J}(\vec{r},t,E) = N_J(\vec{r},t)\sigma_{f,J}(E), \tag{119}$$

where $N_J(\vec{r},t)$ is the time-dependent concentration of J, the solution of the flux-dependent Bateman equations (see Section 4.2). Finally, κ_J represents the average energy produced by the fission of isotope J, which we assume to be energy-independent.

Now let us consider the flux, which is a measure of the neutron population in the reactor (Section 3.5). For a given time interval dt, the change of the neutron population $dn(\vec{r},t,E,\vec{\Omega}) = d\phi(\vec{r},t,E,\vec{\Omega})/v$ due to loss of neutrons by collisions is [Bell1982, Duderstadt1979, Hébert2009, Lewis1993]:

$$L_C(\vec{r},t,E,\vec{\Omega})dt = -\Sigma(\vec{r},t,E)\phi(\vec{r},t,E,\vec{\Omega})dt, \tag{120}$$

where Σ is the total cross section and $L_C(\vec{r},t,E,\vec{\Omega})$ the rate of collision per unit volume of neutrons with energy E and direction $\vec{\Omega}$ at point $\vec{r}$ and time t. This term includes both absorbed and scattered neutrons. Some neutrons will be lost to migration when the net flow of neutrons reaching a region in space of volume d^3r is different from that leaving this same region. This rate of neutron loss due to migration is given by

$$L_M(\vec{r},t,E,\vec{\Omega})dt = -\vec{\Omega}\cdot\vec{\nabla}\phi(\vec{r},t,E,\vec{\Omega})dt, \tag{121}$$

meaning that neutrons, which can be considered to form a gas, tend to move towards regions of low neutron population (the kinetic theory of gas). Neutron with energy E and direction $\vec{\Omega}$ can also be produced in this region of space due to scattering of neutrons with different directions and energies:

$$S_S\left(\vec{r},t,E,\vec{\Omega}\right)dt=\int_0^{\infty}dE'\int_{4\pi}d^2\Omega'\,\Sigma_s\left(\vec{r},t,E'\rightarrow E,\vec{\Omega}'\rightarrow\vec{\Omega}\right)\phi\left(\vec{r},t,E',\vec{\Omega}'\right)dt, \tag{122}$$

where $\Sigma_s(\vec{r},t,E'\rightarrow E,\vec{\Omega}'\rightarrow\vec{\Omega})$ is the probability (also known as the double differential scattering cross section) that a neutron of energy E' moving in direction $\vec{\Omega}'$ is scattered in direction $\vec{\Omega}$ with energy E. For the case where fission takes place, the neutron production rate is

$$S_F\left(\vec{r},t,E,\vec{\Omega}\right)dt=\sum_j\chi_j(E)\int_0^{\infty}dE'\;\;\nu_j\Sigma_{f,J}(\vec{r},t,E')\int_{4\pi}d^2\Omega'\phi(\vec{r},t,E',\vec{\Omega}')dt, \tag{123}$$

where $\chi_j(E)$ is the fission spectrum and ν_j the average number of neutrons produced by fission of isotope J. Neutron productions from other sources $S_E\left(\vec{r},t,E,\vec{\Omega}\right)$ can also be added to the balance, for example, sources for other types of nuclear reactions (photonuclear fission and photoneutron production in ${}^2_1\mathrm{D}$) or flux-independent contributions from the decay of radioactive isotopes.

The global neutron population will then satisfy the following balance equation:

$$\frac{1}{v}\frac{d\phi\left(\vec{r},t,E,\vec{\Omega}\right)}{dt}=L_C\left(\vec{r},t,E,\vec{\Omega}\right)+L_M\left(\vec{r},t,E,\vec{\Omega}\right)+S_S\left(\vec{r},t,E,\vec{\Omega}\right)+S_F\left(\vec{r},t,E,\vec{\Omega}\right)+S_E\left(\vec{r},t,E,\vec{\Omega}\right), \tag{124}$$

which is known as the Boltzmann transport equation. If one assumes that the cross sections are nearly constant over time (the change in the composition of the materials in the reactor varies substantially only over long time periods) and that the core is at static equilibrium (the flux remains constant), one obtains the following time-independent neutron transport equation [Lewis1993]:

$$\vec{\Omega}\cdot\vec{\nabla}\phi\left(\vec{r},E,\vec{\Omega}\right)+\Sigma\left(\vec{r},E\right)\phi\left(\vec{r},E,\vec{\Omega}\right)=$$

$$\int_0^{\infty}dE'\int_{4\pi}d^2\Omega'\;\Sigma_s\left(\vec{r},E'\rightarrow E,\vec{\Omega}'\rightarrow\vec{\Omega}\right)\phi\left(\vec{r},E',\vec{\Omega}'\right)+\frac{1}{k}\sum_j\chi_j\left(E\right)\int_0^{\infty}dE'\;\;\nu_j\Sigma_{f,J}\left(\vec{r},E'\right)\int_{4\pi}d^2\Omega'\phi\left(\vec{r},E',\vec{\Omega}'\right), \tag{125}$$

where k is known as the multiplication factor. It is inserted in the transport equation to modify the fission rate in such a way as to reach this static equilibrium. When $k=1$, equilibrium is achieved, and the reactor is critical. For $k<1$, the reactor is sub-critical, and neutron generation is insufficient to compensate for losses, whereas for $k>1$, the reactor is super-critical, and neutron production exceeds losses.

For reactor calculations, where fission reactions take place only inside the core, boundary conditions of the form

$$\phi\left(\vec{r}_B,E,\vec{\Omega}\right)=0\;\;\text{for}\;\vec{\Omega}\cdot\vec{N}<0 \tag{126}$$

are generally imposed on the transport equation. Here, the point $\vec{r}_B$ is on the outer boundary of the reactor, with $\vec{N}$ being a unit vector normal to this boundary and directed outwards. This condition simply means that no neutrons will enter the reactor from the outside.

The static transport equation is an eigenvalue equation, with k being the inverse of the eigenvalue. Therefore, the neutron flux is the eigenvector for this equation and is only defined

to within a normalization constant. Therefore, if $\phi(\vec{r}, E, \vec{\Omega})$ is a solution, so is $a\phi(\vec{r}, E, \vec{\Omega})$, with a an arbitrary constant. For reactor calculations, the normalization constant is directly related to the power produced in the core.

Solving the transport problem is not trivial, even for very simple cases (static, one velocity neutrons in one dimension). In Chapters 4 (static) and 5 (time-dependent), approximation to and simplification of the transport equation commonly used in reactor simulations will be discussed. One should then be able to extract, from the solutions of the resulting simplified equations, information useful for the design, operation, and control of nuclear reactors.

5 Bibliography

[Basdevant2005] J.-L. Basdevant, R. James, S. Michel, *Fundamentals in Nuclear Physics*. Springer, New York, 2005.

[Bell1982] G. I. Bell, S. Glasstone, *Nuclear Reactor Theory*. Robert E. Krieger, Malabar, 1982.

[Berger2013a] M. J. Berger, J. S. Coursey, M. A. Zucker, J. Chang, J., *ESTAR, PSTAR, and ASTAR: Computer Programs for Calculating Stopping-Power and Range Tables for Electrons, Protons, and Helium Ions*, http://physics.nist.gov/Star, visited April 2013.

[Berger2013b] M. J. Berger, J. H. Hubbel, S. M. Seltzer, J. Chang, J. S. Coursey, R. Sukumar, D. S. Zucker, K. Olsen, *XCOM: Photon Cross Section Database*, http://www.nist.gov/pml/data/xcom, visited April 2013.

[Bjorken1964] J. D. Bjorken, S. D. Drell, *Relativistic Quantum Mechanics*, McGraw-Hill, New York, 1964.

[Brookhaven2013] National Nuclear Data Center at Brookhaven National Laboratory: http://www.nndc.bnl.gov/chart/, visited April 2013.

[Griffiths2005] D. J. Griffiths, *Introduction to Quantum Mechanics*, Pearson Canada, Toronto, 2005.

[Duderstadt1979] J. J. Duderstadt, W. R. Martin, *Transport Theory*. Wiley, New York, 1979.

[Halzen1984] F. Halzen, A. Martin, *Quarks and Leptons: An Introductory Course in Modern Particle Physics*. Wiley, New York, 1984.

[Hébert2009] A. Hébert, *Applied Reactor Physics*. Presses Internationales Polytechnique, Montréal, QC, 2009.

[Hubbell1975] J. H. Hubbell, W. J. Veigele, E. A. Briggs, R. T. Brown, D. T. Cromer, and R. J. Howerton, "Atomic form factors, incoherent scattering functions, and photon scattering cross sections", *J. Phys. Chem. Ref. Data*, 4, 471-538, 1975.

[Jauch1976] J. M. Jauch, F. Rohrlich, *The Theory of Photons and Electrons*. Springer-Verlag, New York, 1976.

[KAERI2013] Nuclear Data Center at Korea Atomic Energy Research Institute: http://atom.kaeri.re.kr/ton/, visited April 2013.

[Leroy2009] C. Leroy, P.-G. Rancoita, *Principle of Radiation Interaction in Matter and Detection*, 2nd edition. World Scientific, Singapore, 2009.

[Le Sech2010] C. Le Sech, C. Ngô, *Physique nucléaire : Des quarks aux applications*. Dunod, Paris, 2010.

[Lewis1993] E. E. Lewis and W. F. Miller, Jr., *Computational Methods of Neutron Transport,* 2nd edition. Wiley, New York, 1993.

[Livermore2013] *Isotope Evaluation at Lawrence Livermore National Laboratory*: http://ie.lbl.gov/toi2003/MassSearch.asp, visited April 2013.

[MacFarlane2010] R. E. MacFarlane, A. C. Kahler, "Methods for Processing ENDF/B-VII with NJOY", *Nuclear Data Sheets*, 111, 2739-2890, 2010.

[Magill2005] J. Magill and J. Galy, *Radioactivity, Radionuclides, Radiation*. Springer: Heidelberg, 2005.

[Nikjoo2012] H. Nikjoo, S. Uehara, D. Emfietzoglou, *Interaction of Radiation with Matter*. CRC Press, Boca Raton, FL, 2012.

[OECD-NEA2013] OECD-NEA Janis 3.0, *Java-Based Nuclear Data Display Program.* https://www.oecd-nea.org/janis, visited April 2013.

[Pomraning1991] G. C. Pomraning, *Linear Kinetic Theory and Particle Transport in Stochastic Mixtures*. World Scientific, London, 1991.

[Schiff1968] L. I. Schiff, *Quantum Mechanics*. McGraw-Hill, New York, 1968.

[Smith2000] F. A. Smith, *A Primer of Applied Radiation Physics*. World Scientific, Singapore, 2000.

[Watt1952] B. E. Watt, "Energy spectrum of neutrons from thermal fission of ^{235}U", *Phys. Rev.* 87, 1037-1041, 1952.

[WebElements2013] *WebElements: The Periodic Table on the Web*. http://www.webelements.com/isotopes.html, visited April 2013.

[Wong2004] S. S. M. Wong, *Introductory Nuclear Physics*. Wiley-VCH, Weinheim, 2004.

6 Summary of Relationship to Other Chapters

This chapter explains the structure of the nucleus and introduces the various interactions of charged particles, photons, and neutrons with matter. It also defines the basic quantities and concepts needed to study the fission chain reaction and to approach the analysis of reactors. The Bateman equations are presented and used in other chapters to evaluate the rate of evolution of fuel composition. The Boltzmann transport equation, which provides a way to evaluate the neutron population in a nuclear reactor, is also introduced. This is the fundamental equation from which the neutron diffusion equation used in Chapters 4 and 5 is derived.

Chapter 4 starts with the static transport equation to derive the time-independent neutron-diffusion equation for the analysis of steady-state (time-independent) neutron distributions either in the presence of external sources or in fission reactors. It also discusses the evolution of the fuel composition in an operating reactor based on the coupled solution of the transport and Bateman equations using a quasi-static approximation.

Chapter 5 covers the time-dependent neutron-diffusion equations and studies the phenomena of fast-neutron kinetics, fission-product poisoning, reactivity coefficients, etc., in reactors.

Chapter 12 deals with radioprotection and uses the concept defined in the present chapter for the interactions of charged particles, photons, and neutrons with matter with the goal of reducing the damage to living tissues.

Chapter 19 examines the behaviour of fuel after irradiation in a nuclear reactor, particularly its composition and the residual energy that it produces.

7 Problems

1. Evaluate the intensity of the electromagnetic force acting between two protons in an atom of helium.
2. Determine the atomic mass of natural chlorine if it is composed of 75.77 %atomic $^{35}_{17}\mathrm{Cl}$ and 24.23 %atomic $^{37}_{17}\mathrm{Cl}$.
3. What is the atomic concentration of $^{235}_{92}\mathrm{U}$ in a sample of uranium oxide ($\mathrm{UO_2}$) of density ρ=10.4 g /cm^3 enriched at a level of 3.5 %weight?
4. Using the semi-empirical mass formula, evaluate the atomic mass of $^{56}\mathrm{Fe}$ and compare with the exact value.
5. What is the ground state energy level of a neutron in the Saxon-Wood potential for $^{238}_{92}\mathrm{U}$?
6. Complete the following nuclear reactions and determine the net energy in MeV released by these reactions:
   a) $^{2}_{1}H+^{3}_{1}H=^{A}_{Z}X+^{1}_{0}n$
   b) $^{1}_{0}n+^{241}_{96}Cm=^{A}_{Z}X+^{90}_{36}Kr+3^{1}_{0}n$
7. What is the activity of one gram of potassium-40?
8. Assuming that the activity of a sample of water due to tritium is 100 Bq, determine the mass of tritium in this sample. What will be the activity of this sample after three years?
9. Using the information available on the ESTAR web site, plot the CSDA range in cm for an electron in dry air at sea level as a function of its energy for 100 keV <E < 10 MeV.
10. Draw the deuterium cross section for photonuclear reactions as a function of energy in the range 2.23 MeV < E < 10MeV (here assume $C_{^2D} = 0.062$). Compare with the deuterium cross section for neutron radiative capture at 300 K in the same energy range.
11. How many collisions are required on average to slow down a neutron to half its speed (1/4 of its energy) through elastic collisions with deuterium nuclei?
12. Evaluate the potential scattering cross section for oxygen and hydrogen at low energy.
13. A CANDU bundle contains 19.5 kg of natural uranium (enrichment of 0.711 %weight). Compute the fission rate in a bundle due to $^{235}_{92}\mathrm{U}$ if it is exposed to a flux of 10^{14} neutrons/cm^2/s of energy E=0.01 eV.
14. Show that the mean free path of 1 MeV neutrons in thorium is 3.5 m.

8 Acknowledgments

Reviewers Marv Gold and Esam Hussein are gratefully acknowledged for their hard work and excellent comments during the development of this Chapter. Their feedback has much improved it. Of course the responsibility for any errors or omissions lies entirely with the author.

Thanks are also extended to Diana Bouchard for expertly editing and assembling the final copy.

CHAPTER 4

Reactor Statics

Prepared by
Dr. Benjamin Rouben, 12 & 1 Consulting, Adjunct Professor, McMaster University & University of Ontario Institute of Technology (UOIT)
and
Dr. Eleodor Nichita, Associate Professor, UOIT

***Summary**:*

This chapter is devoted to the calculation of the neutron flux in a nuclear reactor under special steady-state conditions in which all parameters, including neutron flux, are constant in time. The main calculation method explored in this chapter is the neutron-diffusion equation. Analytical solutions are derived for simple neutron-diffusion problems in one neutron energy group in systems of simple geometry. Two-group diffusion theory and the approximate representation of the diffusion equation using finite differences applied to a discrete spatial mesh are introduced. The rudimentary reactor-physics design of CANDU reactors is presented. The two-step approach to neutronics calculations is presented: multi-group lattice transport calculations, followed by full-core, few-group diffusion calculations. Finally, the chapter covers fuel-property evolution with fuel burnup and specific features of CANDU neutronics resulting from on-line refuelling.

Table of Contents

List of Figures

1 Introduction

1.1 Overview

This chapter is devoted to the calculation of the neutron flux[1] in a nuclear reactor under special steady-state conditions in which all parameters, including neutron flux, are constant in time. The position-, energy-, and angle-dependent steady-state neutron-transport equation is derived by writing the detailed neutron-balance equation. This is done in Chapter 3 of the book. However, it is also done here for completeness. The steady-state diffusion equation is subsequently derived using a linear approximation of the angular dependence of the neutron flux. Multi-group neutron-energy discretization is also introduced.

Analytical solutions are derived for simple neutron diffusion problems. First, the one-group diffusion equation is solved for a uniform non-multiplying medium in simple geometries. Subsequently, the one-group diffusion equation is solved for a uniform multiplying medium (a homogeneous "nuclear reactor") in simple geometries. The importance of neutron leakage and the concepts of criticality and the neutron cycle are introduced.

Of course, real reactors are almost never homogeneous, and rarely can neutron energies be accurately represented by a single energy group. However, two energy groups are often sufficient to represent neutron diffusion in a thermal reactor because most of the fissions are induced by thermal neutrons. This chapter therefore proceeds to introduce two-group diffusion theory and the approximate representation of the diffusion equation using finite differences applied to a discrete spatial mesh. The latter enables the treatment of non-uniform reactor cores.

Following this treatment of the basic theory of neutron transport and diffusion, the rudimentary reactor-physics design of CANDU reactors is presented, and the associated neutron energy spectrum is discussed. Subsequently, more general core modelling concepts are presented, including the two-step approach to neutronics calculations: multi-group lattice transport calculations, followed by full-core, few-group diffusion calculations. The final section in the chapter concentrates on fuel-property evolution with fuel burnup and specific features of CANDU neutronics resulting from on-line refuelling.

1.2 Learning Outcomes

The goal of this chapter is for the student to understand:

- The neutron transport resulting from the detailed neutron balance;
- The neutron-diffusion equation resulting from the linear approximation of the angular dependence of the neutron flux;
- Analytical solutions of the diffusion equation in simple geometries for both multiplying and non-multiplying media;

1 In this document, the term "neutron flux" is used to denote the quantity $\phi = n\upsilon$, where n is neutron density and υ is neutron speed. The units of flux are $1 \cdot cm^{-2} \cdot s^{-1}$ or $1 \cdot m^{-2} \cdot s^{-1}$. Some newer texts use the term flux density or fluence rate. All three terms refer to the same physical quantity.

- The concepts of neutron cycle, criticality, and buckling;
- Energy discretization of the diffusion equation using neutron energy groups and spatial discretization using finite differences;
- The two steps of neutronics calculations: lattice-cell transport calculations and full-core diffusion calculations; and
- Basic design elements of CANDU reactors and their implications for the physical attributes of such reactors.

2 Neutron Diffusion Theory

2.1 Time-Independent Neutron Transport

The time-independent neutron-transport equation is an equation in six variables: three variables $\vec{r}$ for the position of the neutron in the reactor, two variables $\hat{\Omega}$ for the direction of neutron motion, and one variable *E* for neutron energy (we could also use neutron speed v instead of *E*, because there is a one-to-one relationship between v and *E*).

Because we are dealing with time independence (i.e., reactor statics), the neutron-transport equation expresses the fact that the number of neutrons at any position, moving in any direction, and with any energy, is unchanging over time. In other words, if we consider a differential volume in the six-dimensional variable space, i.e., $d\vec{r}d\hat{\Omega}dE$ about $\left(\vec{r},\hat{\Omega},E\right)$, the rate of neutrons "entering" the differential volume must be equal to the rate of neutrons "exiting" the differential volume.

To write the equation, we must therefore consider all phenomena by which neutrons enter or exit the differential volume or are created or destroyed within the volume. The phenomena which we must consider are:

- Neutron production by nuclear fission;
- Neutron scattering, which can change the neutron's energy and/or its direction of motion;
- Neutron absorption;
- Neutron spatial leakage into or out of the differential volume.

[Note: Another process for neutron production is the (n, 2n) nuclear reaction. However, this reaction produces many fewer neutrons than fission and is neglected here.]

The rates at which neutrons enter or exit the differential volume by virtue of these various phenomena, expressed per unit differential volume per second, are given one by one in the following equations.

The rate of birth of neutrons by fission is given by:

$$\frac{\chi(E)}{4\pi}\int_{E'}\int_{\hat{\Omega}'} \nu\Sigma_f(\vec{r},E')\phi\left(\vec{r},\hat{\Omega}',E'\right)d\hat{\Omega}'dE', \tag{1}$$

where

- $\nu\Sigma_f(\vec{r},E')$ is the neutron-yield cross section at position $\vec{r}$ for fissions induced by neutrons of energy *E'*;

- $\phi\left(\vec{r},\hat{\Omega}',E'\right)$ is the angular flux of neutrons at position, of energy *E'*, and moving in direction $\hat{\Omega}'$; and
- $\chi(E)$ is the fraction of all fission neutrons born with energy *E*. Note: In this chapter, for simplicity, a single fission spectrum $\chi(E)$ is used for fissions induced in all nuclides, whereas in reality the fission spectrum should be taken as different for different nuclides. This fully correct treatment is what is done in Chapter 3.

Note: In the above equation, delayed neutrons are not referred to separately. The neutron production rate includes both prompt and delayed neutrons. This is acceptable because it can be shown that in (true) steady state, accounting separately for delayed-neutron production reduces in any case to the above expression.

The rate of production of neutrons from an "external" source (not related to fissions in the reactor fuel) is given by:

$$S\left(\vec{r},E\right), \tag{2}$$

where $S\left(\vec{r},E\right)$ is the external source strength for neutrons of energy *E* at position $\vec{r}$.

Note: We will assume that the source is isotropic.

The rate of neutron gain from neutrons entering the differential volume by scattering from other neutron directions of motion or other neutron energies is given by:

$$\int_{E'}\int_{\hat{\Omega}'}\Sigma_s\left(\vec{r},E'\to E,\hat{\Omega}'\to\hat{\Omega}\right)\phi\left(\vec{r},\hat{\Omega}',E'\right)d\hat{\Omega}'\,dE', \tag{3}$$

where $\Sigma_s\left(\vec{r},E'\to E,\hat{\Omega}'\to\hat{\Omega}\right)$ is the cross section for scattering neutrons from energy *E'* to energy *E* and from direction $\hat{\Omega}'$ to direction $\hat{\Omega}$.

The rate of neutron loss from absorption and from neutrons exiting the differential volume by scattering is given by:

$$\Sigma_t\left(\vec{r},E\right)\phi\left(\vec{r},\hat{\Omega},E\right), \tag{4}$$

where $\Sigma_t\left(\vec{r},E\right)$, the total cross section at position $\vec{r}$ for neutrons of energy *E,*

$$=\Sigma_a\left(\vec{r},E\right)+\iint\Sigma_s\left(\vec{r},E\to E',\hat{\Omega}\to\hat{\Omega}'\right)d\hat{\Omega}'\,dE',$$

where $\Sigma_a\left(\vec{r},E\right)$ is the absorption cross section.

The net rate of neutron spatial leakage (i.e., diffusion) **out** of the differential volume is given by:

$$\vec{\nabla}\cdot\vec{J}\left(\vec{r},\hat{\Omega},E\right), \tag{5}$$

where $\vec{J}\left(\vec{r},\hat{\Omega},E\right)$ is the angular current at position $\vec{r}$ of neutrons moving in direction $\hat{\Omega}$ with energy *E*.

Note: Because $\vec{J}\left(\vec{r},\hat{\Omega},E\right)=\phi\left(\vec{r},\hat{\Omega},E\right)\hat{\Omega}$, the neutron leakage [Eq. (5)] can also be written as:

$$\hat{\Omega}\cdot\vec{\nabla}\phi\left(\vec{r},\hat{\Omega},E\right). \tag{6}$$

Taking into account all the above rates, the neutron balance can then be expressed in the **time-**

independent neutron-transport equation as follows:

$$\frac{1}{4\pi}S(\vec{r},E)+\frac{\chi(E)}{4\pi}\int_{E'}\int_{\hat{\Omega}'}\nu\Sigma_f(\vec{r},E')\phi(\vec{r},\hat{\Omega}',E')d\hat{\Omega}'dE'+\int_{E'}\int_{\hat{\Omega}'}\Sigma_s(\vec{r},E'\to E,\hat{\Omega}'\to\hat{\Omega})\phi(\vec{r},\hat{\Omega}',E')d\hat{\Omega}'dE' \\ -\Sigma_t(\vec{r},E)\phi(\vec{r},\hat{\Omega},E)-\vec{\nabla}\cdot\vec{J}(\vec{r},\hat{\Omega},E)=0. \qquad (7)$$

Note again that for simplicity a single fission spectrum $\chi(E)$ has been used here. See Chapter 3 for the fully correct treatment. The second term of the equation can be simplified because the fission cross section does not depend on $\hat{\Omega}'$, so that the integral over $\hat{\Omega}'$ in the second term reduces to the angle-integrated flux, and Eq. (7) becomes:

$$\frac{1}{4\pi}S(\vec{r},E)+\frac{\chi(E)}{4\pi}\int_{E'}\nu\Sigma_f(\vec{r},E')\phi(\vec{r},E')dE'+\int_{E'}\int_{\hat{\Omega}'}\Sigma_s(\vec{r},E'\to E,\hat{\Omega}'\to\hat{\Omega})\phi(\vec{r},\hat{\Omega}',E')d\hat{\Omega}'dE' \\ -\Sigma_t(\vec{r},E)\phi(\vec{r},\hat{\Omega},E)-\vec{\nabla}\cdot\vec{J}(\vec{r},\hat{\Omega},E)=0, \qquad (7)'$$

where $\phi(\vec{r},E')=\int_{\hat{\Omega}'}\phi(\vec{r},\hat{\Omega}',E')d\hat{\Omega}'$ is the total (angle-integrated) flux of neutrons with energy *E* at position $\vec{r}$.

The neutron-transport equation (7) or (7)' is an exact statement of the general steady-state neutron-balance problem. However, it can immediately be seen that it is very complex: in addition to its dependence on six independent variables, it is an integrodifferential equation. Because of its complexity, this equation cannot be solved analytically except for problems in the very simplest geometries, and real problems require numerical solution by computer.

Note that when there is no external source *S*, the equation appears to be a linear homogeneous equation, which does not generally have a solution (except a trivial zero solution for the flux) for arbitrary values of the nuclear properties. In this case, a solution can be found by modifying the nuclear properties. Mathematically, this can be done by modifying the yield cross section $\nu\Sigma_f$ by dividing it by a quantity, k_{eff}, which can be selected to ensure a non-trivial solution. This quantity k_{eff} is called the multiplication constant.

Two general categories of codes exist to solve the neutron-transport equation: **deterministic codes** (which solve the equation directly by numerical means) and **Monte Carlo codes** (where stochastic methods are used to model a very large number—typically millions or even hundreds of millions—of neutron births and their travel and event histories, from which the multiplication constant and flux and power distributions can be evaluated using appropriate statistics of these histories). Although the application of either type of transport computer code to full-core reactor models requires very significant computer resources and execution time to achieve a high degree of accuracy, both methods, especially Monte Carlo codes, have seen much greater application in whole-reactor analysis in the last decade or so. While core-wide pin-power reconstruction and time-dependent kinetics calculations are still beyond reach, static eigenvalue calculations and global flux and power distributions can now be carried out routinely using Monte Carlo codes. However, detailed discussion of either type of transport code will not be covered in the present work.

The traditional way of attacking neutronics problems in reactors has been to solve the transport equation numerically in relatively small regions (such as a basic lattice cell or a small collection

of cells) to compute region-averaged properties, and then to use these to solve the full-core reactor problem with a simplified version of the transport equation, the neutron-diffusion equation. This computational scheme is discussed in greater detail in Section 9.

2.2 Fick's Law and Time-Independent Neutron Diffusion

To derive a simplified version of the neutron-transport equation, we note that, because the fission and total cross sections do not depend on the neutron direction of motion $\hat{\Omega}$ (i.e., "nuclei do not care from which direction neutrons interact with them"), and also because the most important quantity in reactor physics is the fission rate (which determines power production), it may be very effective to try to obtain an equation which is independent of $\hat{\Omega}$ and which involves only the angle-integrated flux $\phi(\vec{r},E)$ [also called the integral flux].

To achieve this, we can attempt to remove the neutron direction of motion by simply integrating Eq. (7)′ over $\hat{\Omega}$. Let us see what this gives, term by term. The first two terms in (7)′ do not contain $\hat{\Omega}$, and because the integral of $\hat{\Omega}$ over a sphere is 4π, their integrals, which we can call T_1 and T_2, can be written directly as:

$$T_1 = S(\vec{r},E) \tag{8}$$

$$T_2 = \chi(E)\int_{E'} \nu\Sigma_f(\vec{r},E')\phi(\vec{r},E')dE'. \tag{9}$$

Similarly, integrating the fourth term gives a result that depends on the integral flux only:

$$T_4 = \int_{\hat{\Omega}} \Sigma_t(\vec{r},E)\phi(\vec{r},\hat{\Omega},E)d\hat{\Omega} = \Sigma_t(\vec{r},E)\phi(\vec{r},E). \tag{10}$$

Integrating the third term gives a more complex relation:

$$T_3 = \int_{\hat{\Omega}}\int_{E'}\int_{\hat{\Omega}'} \Sigma_s(\vec{r},E'\to E,\hat{\Omega}'\to\hat{\Omega})\phi(\vec{r},\hat{\Omega}',E')d\hat{\Omega}'dE'd\hat{\Omega}. \tag{11}$$

We can, however, simplify T_3 by noting that, because no absolute direction in space is "special", the scattering cross section Σ_s cannot depend on the absolute directions $\hat{\Omega}$ and $\hat{\Omega}'$, but only on the scattering angle between the directions of the incoming and scattered neutrons, or even more specifically on the cosine μ of that angle, i.e., on $\mu \equiv \hat{\Omega}'\cdot\hat{\Omega}$. Using this fact, we can then simplify the integral in Eq. (11) by integrating over $\hat{\Omega}$ first (actually over μ, because Σ_s does not depend on the "azimuthal" angle of scattering, and integrating over that azimuthal angle simply gives 2π). The result is then a product of two integrals:

$$\begin{aligned} T_3 &= \int_{E'}\int_{\hat{\Omega}'} \phi(\vec{r},E'\to E,\hat{\Omega}')d\hat{\Omega}'\int_{\mu} 2\pi\Sigma_s(\vec{r},E'\to E,\mu)d\mu dE' \\ &= \int_{E'} \phi(\vec{r},E')\Sigma_s(\vec{r},E'\to E)dE', \end{aligned} \tag{12}$$

where we have defined

$$\Sigma_s(\vec{r},E'\to E) = 2\pi\int_{\mu} \Sigma_s(\vec{r},E'\to E,\mu)d\mu. \tag{13}$$

Equation (12) is a useful result because it depends on the integral flux $\phi(\vec{r},E')$ only.

For the fifth term, we get:

$$T_5 = \int_{\hat{\Omega}} \vec{\nabla}\cdot\vec{J}\left(\vec{r},E,\hat{\Omega}\right)d\hat{\Omega}\left[=\int_{\hat{\Omega}}\hat{\Omega}\cdot\nabla\phi\left(\vec{r},E,\hat{\Omega}\right)d\hat{\Omega}\right] \\ = \vec{\nabla}\cdot\vec{J}\left(\vec{r},E\right), \tag{14}$$

where

$$\vec{J}\left(\vec{r},E\right) = \int \vec{J}\left(\vec{r},E,\hat{\Omega}\right)d\hat{\Omega} \tag{15}$$

is the current of neutrons of energy *E* at position $\vec{r}$.

Unfortunately, this result is not at all of the form we would like, i.e., it is not at all expressible in terms of the integral flux, because it is clear that integrating a function of the vector quantity $\vec{J}(\vec{r},E,\hat{\Omega})$ over $\hat{\Omega}$ will obviously give in general a result totally unrelated to the integral flux $\phi(\vec{r},E)$!

In summary, integrating Eq. (7)′ over $\hat{\Omega}$ gives:

$$S\left(\vec{r},E\right)+\chi\left(E\right)\int_{E'}\nu\Sigma_f\left(\vec{r},E'\right)\phi\left(\vec{r},E'\right)dE'+\int_{E'}\Sigma_s\left(\vec{r},E'\to E\right)\phi\left(\vec{r},E'\right)dE' \\ -\Sigma_t\left(\vec{r},E\right)\phi\left(\vec{r},E\right)-\vec{\nabla}\cdot\vec{J}\left(\vec{r},E\right)=0, \tag{16}$$

but the last term on the left-hand side (the leakage term) has thwarted our efforts to achieve an equation in the integral flux only.

However, one approximation which is often used in diffusion problems (diffusion of one material through another) can help us here. This approximation, called Fick's Law, applies in low-absorption media if the angular flux varies at most linearly with angle and if the neutron source is isotropic [already assumed in writing Eq. (7)]. Under these conditions it states that **the current** $\vec{J}(\vec{r},E)$ is in the direction in which the integral flux $\phi(\vec{r},E)$ decreases most rapidly, i.e., it is proportional to the negative gradient of $\phi(\vec{r},E)$:

$$\vec{J}\left(\vec{r},E\right) = -D\left(\vec{r},E\right)\nabla\phi\left(\vec{r},E\right), \tag{17}$$

where the quantity $D(\vec{r},E)$ is called the diffusion coefficient and can be written as $1/(3\Sigma_{tr})$, with Σ_{tr} being the neutron transport cross section.

The reader is referred to Appendix A (Reactor Statics) of this chapter for the derivation of Fick's Law. Here, we will continue to derive the final form of the neutron-diffusion equation.

Equation (17), when substituted into Eq. (16), finally gives an equation in the integral flux only, **the time-independent neutron-diffusion equation**:

$$S\left(\vec{r},E\right)+\chi\left(E\right)\int_{E'}\nu\Sigma_f\left(\vec{r},E'\right)\phi\left(\vec{r},E'\right)dE'+\int_{E'}\Sigma_s\left(\vec{r},E'\to E\right)\phi\left(\vec{r},E'\right)dE'- \\ \Sigma_t\left(\vec{r},E\right)\phi\left(\vec{r},E\right)+\vec{\nabla}\cdot D\left(\vec{r},E\right)\nabla\phi\left(\vec{r},E\right)=0 \tag{18}$$

The time-independent neutron-diffusion equation is much simpler than the neutron-transport equation and can be used to solve for the flux in specially prepared full-core reactor models. Note that the out-leakage term (the last term on the left-hand side) has a positive sign, even though this term nominally represents a loss of neutrons; the + sign arises as a result of the – sign in relationship (17) between the current vector and the flux gradient.

Before the diffusion equation can be used, it is important to understand that Fick's Law is only an approximation; it is valid only in low-neutron-absorption media, when the integral flux does not vary too quickly and when angular flux varies weakly with angle (at most linearly). Therefore, Fick's Law is not an especially good approximation in the vicinity of strong absorbers, where the spatial flux variation is very large, or, for the same reason, near interfaces between regions with large variations in nuclear properties or near external surfaces.

2.3 Diffusion Boundary Condition with Vacuum at a Plane Boundary

To solve the diffusion equation, which is a second-order partial differential equation, throughout the reactor volume, we need to define boundary conditions at the surface of the reactor.

The vacuum boundary conditions in transport theory are quite clear: the angular current (or angular flux) at the boundary must be zero for any direction pointing to the inside of the reactor (assuming that the reactor has no re-entrant surface):

$$\phi\left(\vec{r},\hat{\Omega},E\right)=0 \tag{19}$$

for $\vec{r}$ at the boundary and any $\hat{\Omega}$ such that $\mu \equiv \hat{\Omega}\cdot\hat{e}<0,$ where $\hat{e}$ is the unit outgoing normal at $\vec{r}$.

This condition cannot be applied in diffusion theory, which depends on the integral flux only, because we have lost all the directional information of the angular flux. In diffusion theory, we need boundary conditions, at most, on the integral flux and its gradient. The conditions can be generalized to demand that the **total rate of incoming neutrons** be zero. We will now proceed to derive the boundary conditions used in diffusion theory.

We first derive a general relationship between the angular flux and the current using the approximation that the angular flux is linear in angle. Linearity in angle means that the angular flux can be written as a linear function of the *x*-, *y*-, and *z*-components of the angle $\hat{\Omega}$:

$$\phi\left(\hat{\Omega}\right)=a+b_x\Omega_x+b_y\Omega_y+b_z\Omega_z, \tag{20}$$

where a, b_x, b_y, b_z are constants which can be determined in terms of the integral flux and current.

Let us first consider the integral flux $\phi=\int_\Omega \phi\left(\hat{\Omega}\right)d\hat{\Omega}$. From Eq. (20),

$$\phi = a\int_\Omega d\hat{\Omega}+b_x\int_\Omega \Omega_x d\hat{\Omega}+b_y\int_\Omega \Omega_y d\hat{\Omega}+b_z\int_\Omega \Omega_z d\hat{\Omega}. \tag{21}$$

The first integral in Eq. (21) has value 4π, whereas the others have value 0 (it is clear that in integrating a single component of the angle over all solid angles, the + and – components cancel out). This means that $\phi = 4\pi a$, which implies that

$$a = \frac{\phi}{4\pi}. \tag{22}$$

Now let us consider the current:

$$\vec{J} = \int_{\Omega} \phi\left(\hat{\Omega}\right)\hat{\Omega}d\hat{\Omega}. \tag{23}$$

From Eq. (20),

$$\vec{J} = a\int_{\Omega} \hat{\Omega}d\hat{\Omega} + b_x\int_{\Omega} \Omega_x\hat{\Omega}d\hat{\Omega} + b_y\int_{\Omega} \Omega_y\hat{\Omega}d\hat{\Omega} + b_z\int_{\Omega} \Omega_z\hat{\Omega}d\hat{\Omega}. \tag{24}$$

It is clear that the first integral in Eq. (24) is zero, for the same reason that the + and – components cancel out. Consider the other integrals in Eq. (24), for instance, $\int_{\Omega} \Omega_x\hat{\Omega}d\hat{\Omega}$. This is a vector integral, and only the *x*-component will survive because $\int_{\Omega} \Omega_x\Omega_y\left(or\ \Omega_z\right)d\hat{\Omega} = 0$, for the same reason, cancellation.

On the other hand, the *x*-component gives $\int_{\Omega} \Omega_x^2 d\hat{\Omega}$, which can easily be shown to be equal to $4\pi/3$ [by symmetry, it must be equal to $\int_{\Omega} \Omega_z^2 d\hat{\Omega} = 2\pi\int_{-1}^{1} \mu^2 d\mu = \frac{2\pi}{3}\mu^3\Big|_{-1}^{1} = \frac{4\pi}{3}$].

Therefore, we can conclude that

$$\vec{J} = \frac{4\pi}{3}\left(b_x\hat{i} + b_y\hat{j} + b_z\hat{k}\right), \tag{25}$$

i.e.,

$$b_x = \frac{3}{4\pi}J_x \tag{26}$$

(and similarly for *y* and *z*).

Now, substituting Eqs. (22) and (26) into Eq. (20),

$$\phi\left(\hat{\Omega}\right) = \frac{\phi}{4\pi} + \frac{3}{4\pi}\left(J_x\Omega_x + J_y\Omega_y + J_z\Omega_z\right) = \frac{\phi}{4\pi} + \frac{3}{4\pi}\vec{J}\cdot\hat{\Omega}. \tag{27}$$

Let us now apply Eq. (27) at a plane boundary with vacuum. Assume that the boundary plane is perpendicular to the *z*-axis and the polar axis is the outward normal to the boundary, i.e., the unit vector $\hat{k}$ in the positive *z*-direction. The total rate of incoming neutrons is:

$$\int_{\Omega^-} \vec{J}\left(\hat{\Omega}\right)\cdot\hat{k}d\hat{\Omega}, \tag{28}$$

where the integral over the "half-space" Ω^- means integrating over the entire azimuthal angle α (i.e., over 2π), but only over half the polar angle θ, i.e., over θ from $\pi/2$ to π (or over $\mu \equiv \cos\theta$ from -1 to 0).

Using Eq. (27), the total rate of incoming neutrons is:

$$\int_{\Omega^-} \phi\left(\hat{\Omega}\right)\hat{\Omega}\cdot\hat{k}d\hat{\Omega} = \int_{\Omega} \left(\frac{\phi}{4\pi} + \frac{3}{4\pi}\vec{J}\left(\hat{\Omega}\right)\cdot\hat{\Omega}\right)\hat{\Omega}\cdot\hat{k}d\hat{\Omega}. \tag{29}$$

Because $\hat{\Omega}\cdot\hat{k} = \Omega_z = \mu$, then, in the integral of the second term, only the part involving Ω_z will

survive (for the same reason stated before), and:

Total rate of incoming neutrons = $\frac{\phi}{4\pi} * 2\pi * \int_{-1}^{0} \mu d\mu + \frac{3}{4\pi} * 2\pi * \vec{J} \cdot \hat{k} * \int_{-1}^{0} \mu^2 d\mu = -\frac{\phi}{4} + \frac{\vec{J} \cdot \hat{k}}{2}$.

Applying Fick's Law and setting the total rate of incoming neutrons to 0 gives:

$$-\frac{\phi}{4} - \frac{D}{2}\vec{\nabla}\phi \cdot \hat{k} = 0, \text{ i.e., } -\frac{D}{2}\frac{d\phi}{dz} - \frac{\phi}{4} = 0 \tag{30}$$

$$\Rightarrow \frac{1}{\phi}\frac{d\phi}{dz}\bigg|_{boundary} = -\frac{1}{2D},$$

which can be written as

$$-\frac{1}{d_{extr}},$$

which leads to

$$d_{extr} = 2D = \frac{2}{3\Sigma_{tr}}, \tag{31}$$

$$d_{extr} = 2D = \frac{2}{3\Sigma_{tr}}, \tag{32}$$

where Σ_{tr} is the transport cross section.

Actually, a more advanced analysis gives a slightly higher, more correct value for d_{extr}:

$$d_{extr} = 2.1312\,D = \frac{2.1312}{3\Sigma_{tr}} = \frac{0.7104}{\Sigma_{tr}}. \tag{33}$$

Equations (30)-(33) result in a zero net incoming current at the physical boundary.

The geometric interpretation of Eq. (30) is that the relative neutron flux near the plane boundary has a slope of -1/d_{extr}, i.e., the flux would extrapolate linearly to 0 at a distance d_{extr} beyond the boundary. This is often stated as "the flux goes to 0 at an extrapolation distance d_{extr} beyond the boundary". Such an interpretation is not literally correct: the flux cannot go to zero in a vacuum, because there are no absorbers to remove the neutrons; the flux only **appears** to be heading to the zero value at the extrapolation point. In fact, instead of using the "slope" version (30), the boundary condition is often applied by "extending" the reactor model to the extrapolation point and demanding a zero flux at that point.

Now, typical values for the diffusion coefficients *D* in CANDU reactors are ≅ 1 cm, and therefore the extrapolation distance d_{extr} is of the order of 2–3 cm. For systems of large dimension, e.g., large power reactors which are several metres in size, the extrapolation distance is sometimes neglected if a slightly approximate answer is sufficient.

[Note: Equation (33) applies in principle to plane boundaries only. Slightly different formulas for the extrapolation distance would apply to curved boundaries; however, the difference is small unless the radius of curvature of the boundary is of the same order of magnitude as d_{extr}.]

2.4 Energy Discretization: The Multi-Group Diffusion Equation

Neutron energy *E* is of course a continuous variable. However, the diffusion equation (18) with continuous *E* is not usually solved as is. Instead, the equation is rewritten in "multi-group" form by subdividing the energy range into a number *G* of intervals, called energy "groups" and labelled with *g* from 1 to *G* (*g* =1 corresponding to the interval with the highest energies and *g* = *G* to the interval with the lowest energies). In each group *g*, the continuous flux $\phi(\vec{r},E)$ is replaced by an average group flux, $\phi_g(\vec{r})$.

The nuclear cross sections in each group are assumed to have been appropriately averaged over the corresponding energy intervals. In multi-group notation, the cross sections and variables are written as follows:

$$\begin{aligned}
&S(\vec{r},E) \Rightarrow S_g(\vec{r}) \\
&\chi(E) \Rightarrow \chi_g \\
&\nu\Sigma_f(\vec{r},E) \Rightarrow \nu\Sigma_{f,g}(\vec{r}) \\
&\Sigma_s(\vec{r},E' \to E) \Rightarrow \Sigma_{s,g'\to g}(\vec{r}) \\
&\Sigma_t(\vec{r},E) \Rightarrow \Sigma_{t,g}(\vec{r}) \\
&D(\vec{r},E) \Rightarrow D_g(\vec{r}).
\end{aligned}$$

The multi-group diffusion equation then takes the form:

$$S_g(\vec{r}) + \chi_g \sum_{g'=1}^{G} \nu\Sigma_{f,g'}(\vec{r})\phi_{g'}(\vec{r}) +$$

$$\sum_{g'=1}^{G} \Sigma_{s,g'\to g}(\vec{r})\phi_{g'}(\vec{r}) - \Sigma_{t,g}(\vec{r})\phi_g(\vec{r}) + \vec{\nabla}\cdot D_g(\vec{r})\nabla\phi_g(\vec{r}) = 0,\ g = 1,\ldots,G.$$

3 One-Group Diffusion in a Uniform Non-Multiplying Medium

We will start the analysis of systems with simple systems and increase complexity gradually. Assume that all neutrons are lumped into a single energy group, i.e., *G* = 1. There is then no need for the subscript *g*. With a single energy group, the notion of scattering **across** groups has no meaning, and the "incoming scattering" term in Σ_s cancels the "outgoing scattering" term inherent in the total cross section Σ_t (another way of saying this is that the "out-scattering" and "in-scattering" terms cancel one another if there is only one group). This means that we can drop the second term in the diffusion equation and write Σ_a instead of Σ_t in the third term.

In this section, we will deal with neutron diffusion in non-multiplying media, i.e., in media where the fission cross section is zero and the neutron flux is driven by an external neutron source. This type of problem is sometimes called a "source-sink" problem. We will assume that the medium is uniform outside the source, and also that it is infinite in size. Uniform properties also mean that the diffusion coefficient can be taken outside the divergence operator. With these assumptions, the diffusion equation becomes:

$$\begin{aligned}
&S(\vec{r}) - \Sigma_a\phi(\vec{r}) + D\vec{\nabla}\cdot\vec{\nabla}\phi(\vec{r}) = 0, \\
&or\ S(\vec{r}) - \Sigma_a\phi(\vec{r}) + D\nabla^2\phi(\vec{r}) = 0.
\end{aligned} \tag{34}$$

3.1 Plane Source

We take the source as an infinite plane source, which we can place, without loss of generality, in the *y-z* plane. In this case, the flux is a function of *x* only, $\phi(x)$, and the Laplacian can be written as:

$$\nabla^2 = \frac{d^2}{dx^2}.$$

The diffusion equation **outside the source**, i.e., for any *x* different from 0, becomes:

$$D\frac{d^2\phi(x)}{dx^2} - \Sigma_a\phi(x) = 0. \tag{35}$$

We can simplify this equation by dividing by *D*. If we define

$$L^2 = \frac{D}{\Sigma_a}, \tag{36}$$

called the diffusion area (and *L* called the diffusion length), the equation becomes:

$$\frac{d^2\phi(x)}{dx^2} - \frac{1}{L^2}\phi(x) = 0. \tag{37}$$

For $x > 0$, Eq. (37) has mathematical solutions $\exp(x/L)$ and $\exp(-x/L)$, which give a general solution:

$$\phi(x) = Ae^{x/L} + Ce^{-x/L}.$$

However, the term $e^{x/L}$ goes to ∞ as $x \to \infty$ and therefore cannot be part of a physically acceptable solution for $x > 0$. The solution for $x > 0$ must then be $\phi(x) = Ce^{-x/L}$.

By left-right symmetry, we can see that the full solution for any *x* must be

$$\phi(x) = Ce^{-|x|/L}, \tag{38}$$

with *C* being a constant which we can determine from the boundary condition at $x = 0$.

If *S* is the source strength per unit area of the plane, then the number of neutrons crossing outwards per unit area in the positive *x*-direction must tend to $S/2$ as $x \to 0$. Therefore,

$$\lim_{x\to 0}\left[J(x)\right] = \frac{S}{2}$$
$$\Rightarrow \lim_{x\to 0}\left[-D\frac{d\phi(x)}{dx}\right] = \frac{S}{2}$$
$$\Rightarrow \lim_{x\to 0}\left[\frac{CD}{L}e^{-x/L}\right] = \frac{S}{2}$$
$$\Rightarrow \frac{CD}{L} = \frac{S}{2},\ i.e.,\ C = \frac{SL}{2D}.$$

The neutron flux outside the source is then finally:

$$\phi(x) = \frac{SL}{2D} e^{-|x|/L}. \tag{39}$$

It is interesting to try to interpret the "physical" meaning of the diffusion area L^2. Let us calculate the **mean square distance** that a neutron travels in the *x*-direction from the source (at *x* = 0) to its absorption point. We can do this by averaging x^2 with the absorption rate $\Sigma_a\phi$ as a weighting function:

$$\overline{x}^2 = \frac{\int_0^\infty x^2 \Sigma_a \phi dx}{\int_0^\infty \Sigma_a \phi dx}.$$

With the form (39) for the flux, we can evaluate the integrals and show that

$$< x^2 >= 2L^2,$$

i.e., we can interpret L^2 as one-half the square of the average distance (in one dimension) between the neutron's birth point and its absorption point.

3.2 Point Source

Let us now take the source as a single point source, assumed isotropic. Without loss of generality, we can place the source at the origin of co-ordinates, $\vec{r} = 0$.

To solve for the flux in this geometry, we need to write the Laplacian ∇^2 in spherical co-ordinates. In view of the spherical symmetry of the problem, there is no dependence on angle (whether polar or azimuthal), the flux is a function of radial distance *r* only, i.e., $\phi(r)$, and the Laplacian is then:

$$\nabla^2 \equiv \frac{1}{r^2}\frac{d}{dr}\left(r^2 \frac{d}{dr}\right) = \frac{d^2}{dr^2} + \frac{2}{r}\frac{d}{dr}. \tag{40}$$

The diffusion equation outside the source, i.e., for all points except the origin, is then:

$$\begin{aligned} &D\nabla^2\phi(r) - \Sigma_a\phi(r) = 0, \\ &i.e.,\ D\left[\frac{d^2\phi}{dr^2} + \frac{2}{r}\frac{d\phi}{dr}\right] - \Sigma_a\phi(r) = 0, \end{aligned} \tag{41}$$

$$\begin{aligned} &D\nabla^2\phi(r) - \Sigma_a\phi(r) = 0, \\ &i.e.,\ D\left[\frac{d^2\phi}{dr^2} + \frac{2}{r}\frac{d\phi}{dr}\right] - \Sigma_a\phi(r) = 0, \end{aligned} \tag{42}$$

$$\frac{d^2\phi(r)}{dr^2} + \frac{2}{r}\frac{d\phi(r)}{dr} - \frac{1}{L^2}\phi(r) = 0. \tag{43}$$

To solve this equation, we can write ϕ in the form $\phi(r) = \frac{\psi(r)}{r}$. Then, in terms of ψ, Eq. (43) becomes:

$$\frac{\frac{d\psi(r)}{dr}}{r} - \frac{\psi(r)}{r^2},$$

$$\frac{d^2\phi(r)}{dr^2} = \frac{\frac{d^2\psi(r)}{dr^2}}{r} - \frac{\frac{d\psi(r)}{dr}}{r^2} - \frac{\frac{d\psi(r)}{dr}}{r^2} + \frac{2\psi(r)}{r^3}.$$

.

Substituting these forms into Eq. (43) results in the simpler form:

$$\frac{d^2\psi(r)}{dr^2} - \frac{1}{L^2}\psi(r) = 0. \tag{44}$$

Equation (44) has mathematical solutions exp(*r*/*L*) and exp(-*r*/*L*), which give a general solution:

$$\psi(r) = Ae^{r/L} + Ce^{-r/L}$$

$$\Rightarrow \phi(r) = A\frac{e^{r/L}}{r} + C\frac{e^{-r/L}}{r}.$$

Now, the term $\frac{e^{r/L}}{r} \to \infty$ as $r \to \infty$ and therefore cannot be part of a physically acceptable solution. The solution must then be

$$\phi(r) = C\frac{e^{-r/L}}{r}, \tag{45}$$

with C being a constant which remains to be determined. To determine *C*, we can use the continuity condition at the origin.

If *S* is the source strength, then the number of neutrons crossing the surface of a small sphere outwards must tend to *S* as the sphere's radius tends to 0, and therefore:

$$\lim_{r\to 0}\left[4\pi r^2 J(r)\right] = S$$

$$\Rightarrow \lim_{r\to 0}\left[4\pi r^2\left(-D\frac{d\phi}{dr}\right)\right] = S$$

$$\Rightarrow \lim_{r\to 0}\left[4\pi r^2\left(-CD\left(\frac{-\frac{r}{L}e^{-r/L} - e^{-r/L}}{r^2}\right)\right)\right] = S$$

$$\Rightarrow 4\pi CD = S, \; i.e., \; C = \frac{S}{4\pi D}.$$

The neutron flux outside the source is then, finally:

$$\phi(r) = \frac{S}{4\pi D}\frac{e^{-r/L}}{r}. \tag{46}$$

Again, it is interesting to interpret the physical meaning of the diffusion area L^2. Let us calculate the mean square distance that a neutron travels outwards from the source (at *r* = 0) to its

absorption point. We can do this by averaging r^2 with the absorption rate $\Sigma_a\phi$ as a weighting function:

$$\overline{r^2} = \frac{\int_0^\infty r^2 \Sigma_a \phi 4\pi r^2 dr}{\int_0^\infty \Sigma_a \phi 4\pi r^2 dr}.$$

With the form (46) for the flux, we can evaluate the integrals and show that

$$< r^2 > = 6L^2, \tag{47}$$

i.e., we can interpret L^2 as one-sixth of the square of the average distance outwards between the neutron's birth point and its absorption point.

3.3 Flux Curvature in Source-Sink Problems and Neutron In-Leakage

Let us consider the "out-leakage" term (call it $Leak_{out}$) in the above examples.

$Leak_{out}$ ≡ leakage out per differential physical volume $d\vec{r} = \vec{\nabla}\cdot\vec{J} = -\vec{\nabla}\cdot D(\vec{r})\nabla\phi(\vec{r})$. Applying this to the flux from a plane source (Eq. 39) gives, for $x > 0$:

$$Leak_{out} = -D\nabla^2\left(\frac{SL}{2D}e^{-x/L}\right) = -\left(\frac{S}{2L}\right)e^{-x/L} < 0.$$

We can also show that $Leak_{out} < 0$ for $x < 0$. If we apply the formula to the flux from a point source (Eq. 46):

$$Leak_{out} = -D\nabla^2\left(\frac{S}{4\pi D}\frac{e^{-r/L}}{r}\right) = -D\left(\frac{d^2}{dr^2}+\frac{2}{r}\frac{d}{dr}\right)\left(\frac{S}{4\pi D}\frac{e^{-r/L}}{r}\right), \text{ which we can show}$$

$$= -\frac{S}{4\pi L^2}\frac{e^{-r/L}}{r} < 0.$$

We see that in all cases, $Leak_{out} < 0$, i.e., the leakage is inwards (in-leakage) at any point outside the source. This can actually be seen in the general case from

$$S(\vec{r}) - \Sigma_a\phi(\vec{r}) + D\nabla^2\phi(\vec{r}) = 0,$$

stated earlier as Eq. (34), which for any point outside the source gives $-D\nabla^2\phi(\vec{r}) = -\Sigma_a\phi(\vec{r}) < 0$. In other words, we can say that any point outside an external source in a non-multiplying medium sees a positive flux curvature and neutron in-leakage, **i.e., any differential volume is a net sink or absorber of neutrons:**

Positive flux curvature ≡ neutron in-leakage.

4 One-Group Diffusion in a Uniform Multiplying Medium with No External Source

We will now switch to the analysis of reactor systems with no external source, meaning that all neutrons are produced by neutron-induced nuclear fission. In this section, as in the previous one, we will start by assuming that all neutrons are lumped into a single energy group, i.e., G =

1. There is then, again, no need for the subscript *g*. Also, as explained in Section 3, we can drop the term in Σ_s and replace Σ_t by Σ_a.

The neutron-diffusion equation in this case is:

$$\nu\Sigma_f\phi(\vec{r}) - \Sigma_a\phi(\vec{r}) + D\nabla^2\phi(\vec{r}) = 0. \tag{48}$$

A very important point to note is that without the external source, this is a linear homogeneous equation in the flux (if the properties are truly constant and independent of the flux). This means that if we find one solution of the equation, then any multiple is also a solution. Therefore, the absolute value of the flux cannot possibly be deduced from the diffusion equation (incidentally, not from the transport equation either). This is totally different from problems with external sources, which drive the absolute value of the flux.

4.1 Uniform Infinite Reactor in One Energy Group

Let us first assume a uniform reactor, infinite in size. This assumption makes all points in space "equivalent", which means that the neutron flux ϕ would also have to be constant throughout space. Moreover, there can be no leakage from one point to another; therefore, the leakage term can be dropped from the equation.

The equation in the infinite uniform multiplying medium is then:

$$\nu\Sigma_f\phi - \Sigma_a\phi = 0. \tag{49}$$

This equation is interesting. The only solution is a trivial solution, i.e., a null flux, $\phi = 0$, **unless**

$$\nu\Sigma_f = \Sigma_a. \tag{50}$$

In other words, unless the composition of the medium is exactly balanced so that Eq. (50) is satisfied, the uniform infinite reactor cannot really operate in steady state (except in a trivial zero-flux situation). We can call Eq. (50) the **criticality condition** for a uniform infinite reactor.

What happens if the criticality condition in Eq. (50) is not satisfied? Then there is no non-trivial solution, but is this all that we can say? Actually, we can ensure that there is always a non-trivial solution if we modify Eq. (49) by "tuning" the neutron-yield cross section by dividing it by a new "modifying factor" which we call k_∞, as in:

$$\frac{\nu\Sigma_f}{k_\infty}\phi - \Sigma_a\phi = 0. \tag{51}$$

A non-trivial solution of Eq. (51) can always be guaranteed by selecting the value of k_∞ as:

$$k_\infty = \frac{\nu\Sigma_f}{\Sigma_a}. \tag{52}$$

What this means is that if the composition of the uniform infinite reactor is modified from the original composition by dividing the neutron-yield cross section by k_∞ defined as in Eq. (52), the **modified** uniform infinite reactor can then be operated in steady state with a non-zero flux; this modified reactor is now **critical**. What is the value of the flux? We can see from Eq. (51) that with the modified neutron-yield cross section, the flux can have **any** value; in other words, the critical uniform infinite reactor can operate at any flux (and therefore power) value! This is a direct consequence of the (apparent) homogeneity of the equation (i.e., the equation is of the

form $\boldsymbol{F}\phi = 0$, with $\boldsymbol{F}$ an arbitrary operator independent of the flux).

Comparing Eqs. (50) and (51), the criticality condition for a uniform infinite reactor can be seen to be:

$$k_\infty \equiv \frac{\nu\Sigma_f}{\Sigma_a} = 1 \tag{53}$$

for criticality. The deviation of k_∞ from 1 tells us **how far** the reactor with the original composition ($\nu\Sigma_f, \Sigma_a$) is from criticality. k_∞ is called the **infinite reactor multiplication constant** and can have the following values:

$k_\infty < 1$: the infinite reactor is said to be subcritical;
$k_\infty = 1$: the infinite reactor is critical;
$k_\infty > 1$: the infinite reactor is said to be supercritical.

The physical interpretation of k_∞ can be stated as follows:

$$k_\infty \equiv \frac{\nu\Sigma_f}{\Sigma_a} = \frac{\nu\Sigma_f\phi}{\Sigma_a\phi} = \frac{\text{neutron production rate}}{\text{neutron loss rate}}. \tag{54}$$

A quantity related to k_∞, but "centred" at 0 instead of at 1, is the "reactivity", ρ_∞, defined as:

$$\rho_\infty = 1 - \frac{1}{k_\infty}. \tag{55}$$

Therefore:

$k_\infty < 1 \Rightarrow \rho_\infty < 0$: the infinite reactor is subcritical
$k_\infty = 1 \Rightarrow \rho_\infty = 0$: the infinite reactor is critical
$k_\infty > 1 \Rightarrow \rho_\infty > 0$: the infinite reactor is supercritical.

Real-life reactors are designed to be operated at critical or very close to critical. Therefore, in most situations, we would expect k_∞ to be very close to 1 and ρ_∞ to be very close to 0. As a result, while ρ_∞ (and k_∞) are absolute, dimensionless numbers, a new fractional "unit" of 1 milli-k (or mk) is defined for reactivity, where:

$$1 \text{ mk } = \ 0.001. \tag{56}$$

For example, ρ_∞ = + 2 mk (or – 1 mk) means that ρ_∞ = +0.002 (or – 0.001). Another reactivity unit, "pcm" ≡ 0.01 mk, is commonly used in Europe.

4.2 Uniform Finite Reactors in One Energy Group

We will now analyze uniform reactors of finite size (at least in some dimensions). The nuclear properties are assumed uniform throughout the reactor, but not all points in the reactor are equivalent spatially (some are further from or closer to the reactor boundary), so that the flux is a function of space, $\phi(\vec{r})$, and also the leakage term must remain in the diffusion equation:

$$\nu\Sigma_f\phi(\vec{r}) - \Sigma_a\phi(\vec{r}) + D\nabla^2\phi(\vec{r}) = 0,$$

presented earlier as Eq. (48). This can be rewritten as:

$$-D\nabla^2\phi(\vec{r}) = \nu\Sigma_f\phi(\vec{r}) - \Sigma_a\phi(\vec{r}). \tag{57}$$

The left-hand side of Eq. (57) is the leakage out of the "point" $\vec{r}$. If we integrate Eq. (57) over the volume *V* of the reactor:

$$-\int_V D\nabla^2\phi(\vec{r})\,d\vec{r} = \left(\nu\Sigma_f - \Sigma_a\right)\int_V \phi(\vec{r})\,d\vec{r}. \tag{58}$$

The left-hand side of Eq. (58) is the **total leakage out of the reactor**. This of course must be positive: neutrons can only go **out of** the reactor, not **into** it, because there are no sources of neutrons outside which can "feed" neutrons into the reactor. Therefore, if Eq. (58) is true as is, the right-hand side must be positive, and because the integral of the flux must also be positive, so must the quantity $(\nu\Sigma_f - \Sigma_a)$. We can therefore write Eq. (57) as:

$$\begin{aligned} -\nabla^2\phi(\vec{r}) &= \frac{\nu\Sigma_f - \Sigma_a}{D}\phi(\vec{r}) \\ i.e., -\nabla^2\phi(\vec{r}) &= B_g^2\phi(\vec{r}), \end{aligned} \tag{59}$$

where we have defined

$$B_g^2 = \frac{\nu\Sigma_f - \Sigma_a}{D}. \tag{60}$$

The quantity B_g^2, as it appears in Eq. (59), is called the **geometrical buckling** of the reactor. Its physical meaning can be understood by rewriting Eq. (60) as:

$$B_g^2 = -\frac{\nabla^2\phi(\vec{r})}{\phi(\vec{r})}. \tag{61}$$

In other words, **the geometrical buckling is the negative relative curvature of the neutron flux**. Because we have established that B_g^2 is definitely positive, this means that the flux curvature is negative (see Figure 1), and in fact, in view of Eq. (59), **the relative curvature is uniform (and negative) in a homogeneous finite reactor**. Note that this statement is strictly true for homogeneous reactors only. In real reactors, the relative flux curvature (and the buckling) can vary and even change sign.

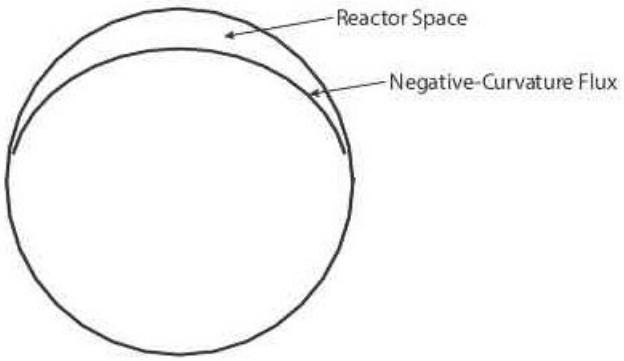

Figure 1 Negative flux curvature in homogeneous reactor

Because the neutron flux curvature/geometrical buckling must "bend" the flux to bring it to 0

almost at the reactor boundary (actually, at an extrapolation distance d_{extr} beyond the physical boundary), it is clear that the flux curvature will be large for reactors of small dimensions and small if the reactor dimensions are large. Therefore, B_g^2 in Eq. (59) is purely a geometrical quantity.

Returning now to Eq. (57) and using the definition of geometrical buckling, the diffusion equation for homogeneous reactors can be rewritten as:

$$\nu\Sigma_f\phi(\vec{r}) - \Sigma_a\phi(\vec{r}) - DB_g^2\phi(\vec{r}) = 0. \tag{62}$$

This equation has the same characteristics as Eq. (49). The only solution is a null flux, $\phi(\vec{r}) = 0$, **unless**

$$\nu\Sigma_f = \Sigma_a + DB_g^2. \tag{63}$$

In other words, unless the composition of the reactor is exactly balanced so that Eq. (63) is satisfied, the uniform reactor cannot really operate in steady state (except in a trivial zero-flux situation). We can call Eq. (63) the **criticality condition** for a uniform finite reactor.

What happens if the criticality condition Eq. (63) is not satisfied? Then there is no non-trivial solution. However, just as we did for the infinite medium, we can ensure that there is always a non-trivial solution if we modify Eq. (62) by tuning the neutron-yield cross section by dividing it by a similar parameter, called k_{eff}, as in:

$$\frac{\nu\Sigma_f}{k_{eff}}\phi(\vec{r}) - \Sigma_a\phi(\vec{r}) - DB_g^2\phi(\vec{r}) = 0. \tag{64}$$

A non-trivial solution of Eq. (64) can always be guaranteed by selecting the value of k_{eff} as:

$$k_{eff} = \frac{\nu\Sigma_f}{\Sigma_a + DB_g^2}, \tag{65}$$

which can also be written as:

$$B_g^2 = \frac{\dfrac{\nu\Sigma_f}{k_{eff}} - \Sigma_a}{D}. \tag{66}$$

This means that if the composition of the uniform reactor is modified from the original composition by dividing the neutron-yield cross section by k_{eff} defined as in Eq. (65), the **modified** uniform reactor can then operate in steady state (i.e., as a **critical** reactor) with a non-zero flux. Again, as in the infinite medium, the flux in the modified critical reactor can have **any** value, that is, the critical uniform reactor can operate at any flux (and therefore power) value!

In summary, the **criticality condition** for a uniform finite reactor is:

$$k_{eff} \equiv \frac{\nu\Sigma_f}{\Sigma_a + DB_g^2} = 1 \tag{67}$$

or

$$B_g^2 = \frac{\nu\Sigma_f - \Sigma_a}{D} = \frac{\frac{\nu\Sigma_f}{\Sigma_a} - 1}{\frac{D}{\Sigma_a}} = \frac{k_\infty - 1}{L^2}. \tag{68}$$

Equation (67) is clearly a generalization of the criticality condition Eq. (53) for the infinite medium, where the buckling was 0, i.e., $B_g^2 = 0$ (flat flux). The deviation of k_{eff} from 1 tells us **how far** the reactor with the original composition $(\nu\Sigma_f, \Sigma_a, D)$ is from criticality.

Equation (68) is intriguing. The left-hand side, B_g^2, is a geometrical quantity, as already noted. The right-hand side, on the other hand, is a function of the nuclear properties only and is not a geometrical quantity. It is nonetheless called a "buckling", the **material buckling:**

$$B_m^2 = \frac{k_\infty - 1}{L^2}. \tag{69}$$

In view of this, the criticality condition for a uniform reactor in one neutron-energy group can be expressed as:

$$\text{Geometrical Buckling} = \text{Material Buckling}, \;\; B_g^2 = B_m^2. \tag{70}$$

The physical interpretation of k_{eff} can be obtained from:

$$k_{eff} \equiv \frac{\nu\Sigma_f}{\Sigma_a + DB_g^2} = \frac{\nu\Sigma_f \phi(\vec{r})}{\Sigma_a \phi(\vec{r}) + DB_g^2 \phi(\vec{r})} = \frac{\text{neutron production rate}}{\text{neutron loss rate (by absorption and leakage)}}. \tag{71}$$

This ratio of production to loss is **the same at any point in a homogeneous reactor** and is of course then also the same as the ratio of the reactor-integrated production and loss.

Incidentally, Eq. (64), a linear equation with a boundary condition (zero flux at the extrapolation distance beyond the boundary), is mathematically an **eigenvector problem**, which can best be seen by rewriting the equation in the form:

$$\left(\Sigma_a + DB_g^2\right)\phi(\vec{r}) = \lambda \nu\Sigma_f \phi(\vec{r}), \tag{72}$$

where

$$\lambda \equiv \frac{1}{k_{eff}} \tag{73}$$

is the eigenvalue of the problem.

Eigenvalues of eigenvector problems can take on only distinct, non-continuous values. This tells us that k_{eff} cannot have just any value, but it can have only a certain number of distinct values. Later, we will see that the "physical" k_{eff} is the largest of these distinct values.

4.3 Uniform Finite Reactors in Various Geometries

Equations (67) and (68) relate the reactor multiplication constant to the reactor properties and to geometrical buckling, but we do not yet have a value for the buckling or for the distribution of the neutron flux in the reactor. In this section, we will solve for the flux distribution and for the value of the reactor multiplication constant k_{eff} for reactors of various geometries (and we

can therefore also derive the value of the buckling). We will do this by showing how to solve the diffusion equation in the following form [rewritten from Eq. (59)]:

$$\nabla^2\phi(\vec{r}) + B_g^2\phi(\vec{r}) = 0. \tag{74}$$

4.3.1 Infinite slab reactor

Let us consider a reactor in the shape of a slab of physical width *a* in the *x*-direction and infinite in the *y*- and *z*-directions. The reactor is centred at *x* = 0; see Figure 2. This is a one-dimensional problem, meaning that ϕ is a function of *x* only. The Laplacian reduces to $\frac{d^2}{dx^2}$, and the diffusion equation (74) is now:

$$\frac{d^2\phi(x)}{dx^2} + B_g^2\phi(x) = 0. \tag{75}$$

This equation has mathematical solutions $\phi(x) \propto \sin(B_g x)$ and $\phi(x) \propto \cos(B_g x)$. However, by left-right symmetry, $\sin(B_g x)$ is not a viable solution (because the flux would be negative in half the space). Therefore, the only physical solution must have the form $\phi(x) = A\cos(B_g x)$, where *A* is a constant.

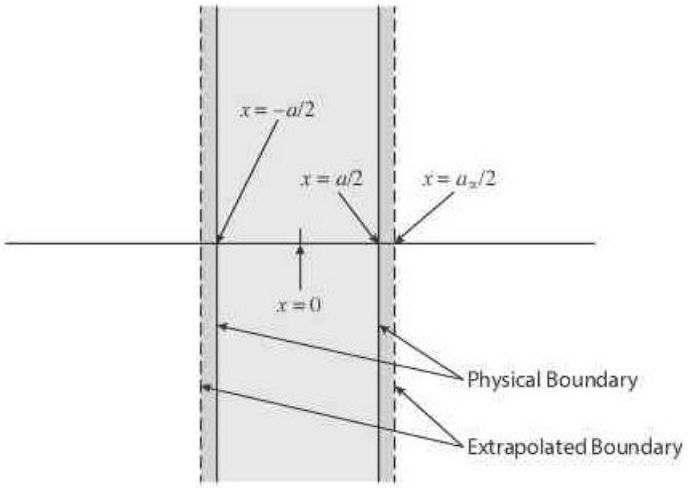

Figure 2 Infinite-slab reactor

However, we must also satisfy the boundary condition for the problem, which is $\phi\left(\frac{a_{ex}}{2}\right) = 0$, where a_{ex} is the "extrapolated width" and $x = a_{ex}/2$ is the point at which the flux appears to go to zero. Therefore, we must have $A\cos\left(B_g\frac{a_{ex}}{2}\right) = 0$, which means that the values of B_g are limited to $B_g = \frac{n\pi}{a_{ex}}$, where *n* = any odd integer.

While any odd integer value of *n* gives a mathematical solution of Eq. (75), only *n* = 1 is a physically acceptable solution, because higher values of *n* would give cosine functions which would

become negative for some values of *x* before returning to 0 at a_{ex} (see Figure 3). Therefore, the final solution for the flux distribution in an infinite slab reactor is

$$\phi(x) = A\cos\left(\frac{\pi x}{a_{ex}}\right), \tag{76}$$

and the buckling is

$$B_g^2 = \left(\frac{\pi}{a_{ex}}\right)^2. \tag{77}$$

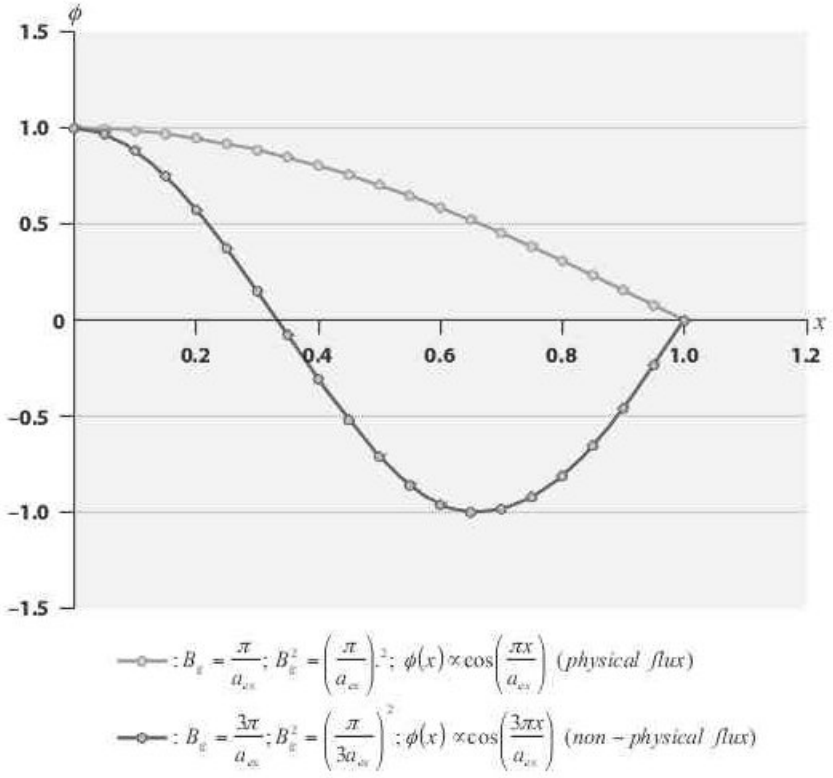

Figure 3 Flux with physical and unphysical values of buckling

Note: The value of buckling which gives the only physical solution is the smallest of the mathematically possible values, and the corresponding value of k_{eff} for the physical solution is the largest of the mathematically possible values (i.e., the physical eigenvalue is the smallest of the possible values).

Equation (76) gives the flux **distribution** in the reactor. However, the amplitude *A*, which gives the absolute value of the flux, cannot be obtained from the diffusion equation, as noted at the beginning of Section 4. To find *A*, an extraneous condition has to be imposed, for instance the actual value of the flux at a point, or the total power of the reactor, or the power in some region of the reactor.

For example, if we assume a value *P* for the power per unit area of the *y-z* plane and note that E_f is the energy released per fission (typically 200 MeV $\cong 3.2*10^{-11}$ joules), we have:

$$P = E_f \Sigma_f \int_{-a/2}^{a/2} \phi(x)\,dx = E_f \Sigma_f \int_{-a/2}^{a/2} A_1 \cos\left(\frac{\pi x}{a_{ex}}\right) dx$$

$$\text{i.e., } P = \frac{a_{ex}}{\pi} E_f \Sigma_f A \sin\left(\frac{\pi x}{a_{ex}}\right)\Bigg|_{-a/2}^{a/2} = 2A\frac{a_{ex}}{\pi} E_f \Sigma_f \sin\left(\frac{\pi a}{2a_{ex}}\right)$$

$$\therefore A = \frac{\pi P}{2a_{ex} E_f \Sigma_f \sin\left(\frac{\pi a}{2a_{ex}}\right)},$$

and the absolute flux in the slab is

$$\phi(x) = \frac{\pi P}{2a_{ex} E_f \Sigma_f \sin\left(\frac{\pi a}{2a_{ex}}\right)} \cos\left(\frac{\pi x}{a_{ex}}\right). \tag{78}$$

If the extrapolation distance is ignored, i.e., $a_{ex} = a$, this reduces to:

$$\phi(x) = \frac{\pi P}{2aE_f \Sigma_f} \cos\left(\frac{\pi x}{a}\right). \tag{79}$$

4.3.2 Infinite cylindrical reactor

We now consider a reactor in the shape of a uniform cylinder of physical radius *R* and of infinite length in the axial (*z*) direction, as shown in Figure 4. The problem is independent of the azimuthal angle, and the flux is a function of the *r* variable only.

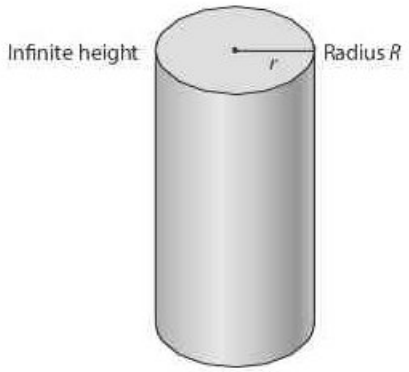

Figure 4 Infinite-cylinder reactor

The Laplacian can now be written as

$$\frac{1}{r}\frac{d}{dr}\left(r\frac{d}{dr}\right),$$

and the diffusion equation (74) becomes:

$$\frac{1}{r}\frac{d}{dr}\left(r\frac{d\phi(r)}{dr}\right)+B_g^2\phi(r)=0$$
$$i.\text{e.,}\ \frac{d^2\phi(r)}{dr^2}+\frac{1}{r}\frac{d\phi(r)}{dr}+B_g^2\phi(r)=0. \tag{80}$$

This differential equation is actually well known to mathematicians: it is called Bessel's equation of order 0, and its mathematical solutions are the ordinary Bessel functions of the first and second kind, $J_0(Br)$ and $Y_0(Br)$ respectively; see Figure 5.

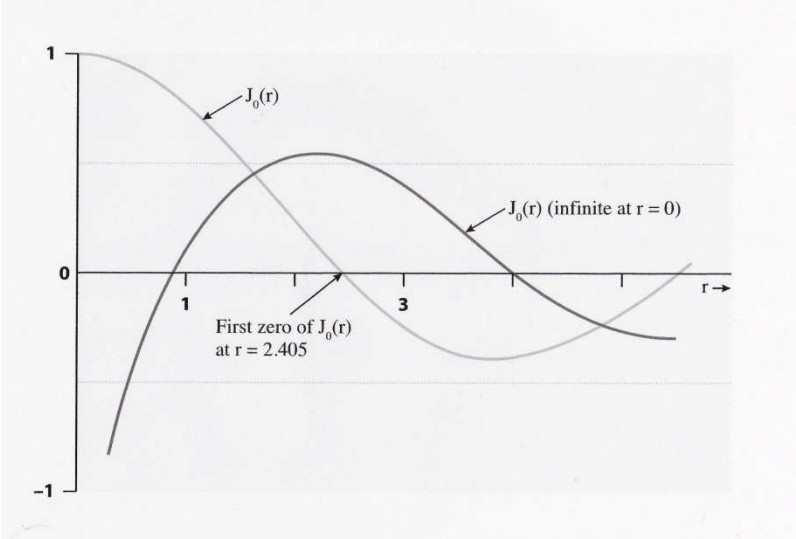

Figure 5 Ordinary Bessel functions of first and second kind

From Figure 5, we can see that $Y_0(Br)$ goes to $-\infty$ as $r \rightarrow 0$ and is therefore not acceptable as a physical solution for the neutron flux. The only solution is then:

$$\phi(r)=AJ_0(B_g r). \tag{81}$$

The flux must go to 0 at the extrapolated radial boundary R_{ex}, i.e., we must have:

$$J_0(B_g R_{ex})=0. \tag{82}$$

Figure 5 shows that $J_0(r)$ has several zeroes, called r_i: the first is at $r_1 \cong 2.405$, and the second at $r_2 \cong 5.6$. However, because the neutron flux cannot have regions of negative values, the only physically acceptable value for B_g is

$$B_g=\frac{2.405}{R_{ex}}. \tag{83}$$

As a result, the flux in the infinite cylinder is given by:

$$\phi(r)=AJ_0\left(\frac{2.405r}{R_{ex}}\right), \tag{84}$$

and the buckling for the infinite cylinder is

$$B_g^2 = \left(\frac{2.405}{R_{ex}} \right)^2 . \tag{85}$$

If we use the reactor power *P* per unit axial height to determine *A* and neglect the extrapolation distance, the following value is obtained:

$$A = \frac{0.738P}{E_f \Sigma_f R^2}, \tag{86}$$

and the absolute flux is

$$\phi(r) = \frac{0.738P}{E_f \Sigma_f R^2} J_0 \left(\frac{2.405r}{R} \right). \tag{87}$$

4.3.3 Parallelepiped reactor

We now look at a fully finite reactor geometry (i.e., the reactor is finite in every dimension, and is uniform): the parallelepiped of sides *a*, *b*, *c* (see Figure 6). In this case, we use the Cartesian co-ordinate system, and the flux is written as $\phi(\vec{r}) \equiv \phi(x, y, z)$. The diffusion equation becomes:

$$\frac{d^2\phi(x,y,z)}{dx^2} + \frac{d^2\phi(x,y,z)}{dy^2} + \frac{d^2\phi(x,y,z)}{dz^2} + B_g^2\phi(x,y,z) = 0. \tag{88}$$

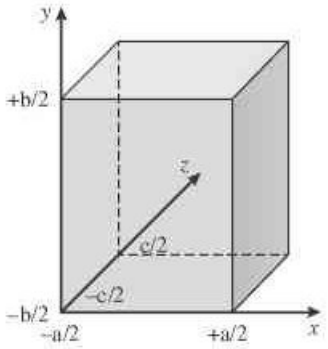

Figure 6 Rectangular-parallelepiped reactor

To solve this equation, we try a **separable** form for the neutron flux, i.e.,

$$\phi(x,y,z) = f(x)g(y)h(z), \tag{89}$$

where *f*, *g*, and *h* are functions to be determined. Substituting form (89) into Eq. (88), we get:

$$\frac{d^2 f(x)}{dx^2} g(y)h(z) + f(x)\frac{d^2 g(y)}{dy^2} h(z) + f(x)g(y)\frac{d^2 h(z)}{dz^2} + B_g^2 f(x)g(y)h(z) = 0. \tag{90}$$

Dividing the equation by *f*(*x*)*g*(*y*)*h*(*z*):

$$\frac{1}{f(x)}\frac{d^2 f(x)}{dx^2} + \frac{1}{g(y)}\frac{d^2 g(y)}{dy^2} + \frac{1}{h(z)}\frac{d^2 h(z)}{dz^2} = -B_g^2. \tag{91}$$

The left-hand side of Eq. (91) is a sum of three terms which are functions only of *x*, *y*, and *z*

respectively. The right-hand side is a constant. The only way in which this can happen is if each of the three terms on the left-hand side is a constant on its own, i.e., if we can write:

$$\frac{1}{f(x)}\frac{d^2 f(x)}{dx^2} = -B_x^2,\ \ \frac{1}{g(y)}\frac{d^2 g(y)}{dy^2} = -B_y^2,\ \ \frac{1}{h(z)}\frac{d^2 h(z)}{dz^2} = -B_z^2, \tag{92}$$

where $B_x^2,\ B_y^2,\ B_z^2$ are constants and

$$B_x^2 + B_y^2 + B_z^2 = B_g^2. \tag{93}$$

Each of the equations in (92), e.g.,

$$\frac{1}{f(x)}\frac{d^2 f(x)}{dx^2} = -B_x^2 \Rightarrow \frac{d^2 f(x)}{dx^2} + B_x^2 f(x) = 0, \tag{94}$$

is exactly the same equation as for the slab reactor, with the same solution

$$f(x) \propto \cos(B_x x), \tag{95}$$

where

$$B_x = \frac{\pi}{a_{ex}}. \tag{96}$$

The full solution for the neutron flux in the parallelepiped reactor is therefore:

$$\phi(x,y,z) = A\cos\left(\frac{\pi x}{a_{ex}}\right)\cos\left(\frac{\pi y}{b_{ex}}\right)\cos\left(\frac{\pi z}{c_{ex}}\right). \tag{97}$$

The quantities

$$B_x^2 = \left(\frac{\pi}{a_{ex}}\right)^2,\ B_y^2 = \left(\frac{\pi}{b_{ex}}\right)^2,\ B_z^2 = \left(\frac{\pi}{c_{ex}}\right)^2, \tag{98}$$

are called the "partial bucklings" in the three directions, and the total buckling is

$$B_g^2 = \left(\frac{\pi}{a_{ex}}\right)^2 + \left(\frac{\pi}{b_{ex}}\right)^2 + \left(\frac{\pi}{c_{ex}}\right)^2. \tag{99}$$

If we normalize the flux to the total fission power *P* of the reactor and neglect the extrapolation distance, we can show that the normalization constant, *A*, is given by

$$A = \frac{\pi^3 P}{8abcE_f\Sigma_f}. \tag{100}$$

4.3.4 Finite-cylinder reactor

In the case of a finite-cylinder uniform reactor of radius *R* and height *H* (see Figure 7), we use the cylindrical co-ordinate system to write the flux as $\phi(\vec{r}) \equiv \phi(r,z)$. The Laplacian can be written as:

$$\nabla^2 = \frac{d^2}{dr^2} + \frac{1}{r}\frac{d}{dr} + \frac{d^2}{dz^2}, \tag{101}$$

and the diffusion equation becomes

$$\frac{d^2\phi(r,z)}{dr^2} + \frac{1}{r}\frac{d\phi(r,z)}{dr} + \frac{d^2\phi(r,z)}{dz^2} + B_g^2\phi(r,z) = 0. \tag{102}$$

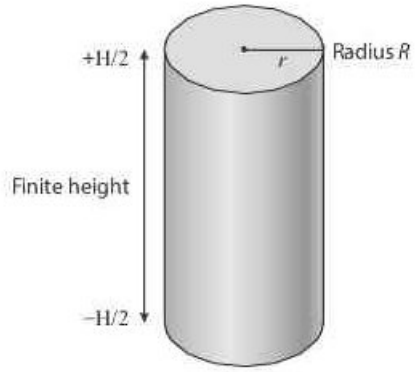

Figure 7 Finite-cylinder reactor

To solve this equation, we again try a **separable** form for the neutron flux, i.e.,

$$\phi(r,z) = f(r)g(z), \tag{103}$$

where *f* and *g* are functions to be determined. Substituting Eq. (103) into Eq. (102), we get:

$$\frac{d^2f(r)}{dr^2}g(z) + \frac{1}{r}\frac{df(r)}{dr} + f(r)\frac{d^2g(z)}{dz^2} + B_g^2 f(r)g(z) = 0. \tag{104}$$

Let us divide this equation by $f(r)g(z)$:

$$\frac{1}{f(r)}\frac{d^2f(r)}{dr^2} + \frac{1}{f(r)}\frac{1}{r}\frac{df(r)}{dr} + \frac{1}{g(z)}\frac{d^2g(z)}{dz^2} = -B_g^2. \tag{105}$$

The left-hand side of Eq. (105) is the sum of a function of *r* and a function of *z*. The right-hand side is a constant. The only way in which this can happen is if the parts in *r* and *z* are each individually equal to a constant, i.e., if we can write:

$$\frac{1}{f(r)}\frac{d^2f(r)}{dr^2} + \frac{1}{f(r)}\frac{1}{r}\frac{df(r)}{dr} = -B_r^2, \quad \frac{1}{g(z)}\frac{d^2g(z)}{dz^2} = -B_z^2, \tag{106}$$

where B_r^2, B_g^2 are constants and

$$B_r^2 + B_g^2 = B_g^2. \tag{107}$$

The equations in (106) have been seen before; they are the same equations as for the infinite cylinder and the slab reactor respectively and therefore have the same solutions:

$$f(r) \propto J_0(B_r r), \quad g(z) \propto \cos(B_z z), \tag{108}$$

where

$$B_r = \frac{2.405}{R_{ex}} \quad \text{and} \quad B_z = \frac{\pi}{H_{ex}}, \tag{109}$$

where R_{ex} and H_{ex} are the extrapolated radius and the extrapolated axial dimension of the reactor. The full solution for the neutron flux in the finite-cylinder reactor is therefore:

$$\phi(r,z) = AJ_0\left(\frac{2.405r}{R_{ex}}\right)\cos\left(\frac{\pi z}{H_{ex}}\right), \tag{110}$$

$$B_r^2 = \left(\frac{2.405}{R_{ex}}\right)^2,\ B_z^2 = \left(\frac{\pi}{H_{ex}}\right)^2 \tag{111}$$

are called the radial and axial bucklings respectively, and the total buckling is

$$B_g^2 = \left(\frac{2.405}{R_{ex}}\right)^2 + \left(\frac{\pi}{H_{ex}}\right)^2. \tag{112}$$

If we normalize the flux to the total fission power P of the reactor and neglect the extrapolation distance, we can show that the normalization constant is:

$$A = \frac{3.63P}{\pi R^2 H E_f \Sigma_f}. \tag{113}$$

4.3.5 Spherical reactor

The last geometry we will look at is a spherical uniform reactor of radius R. We use the spherical co-ordinate system, and because there is spherical symmetry, the flux can be written as $\phi(\vec{r}) \equiv \phi(r)$. The Laplacian can be written as:

$$\nabla^2 = \frac{1}{r^2}\frac{d}{dr}\left(r^2\frac{d}{dr}\right), \tag{114}$$

and the diffusion equation becomes

$$\frac{1}{r^2}\frac{d}{dr}\left(r^2\frac{d\phi(r)}{dr}\right) + B_g^2\phi(r) = 0. \tag{115}$$

Let us try to represent $\phi(r)$ in the form

$$\phi(r) = \frac{\psi(r)}{r}, \tag{116}$$

where the function $\psi(r)$ is to be determined. Equation (115) then reduces to:

$$\frac{1}{r^2}\left[\frac{d}{dr}\left\{r^2\left(-\frac{1}{r^2}\psi(r)+\frac{1}{r}\frac{d\psi(r)}{dr}\right)\right\}\right]+B_g^2\frac{\psi(r)}{r}=0$$

$$\text{i.e., } \frac{1}{r^2}\left[\frac{d}{dr}\left\{-\psi(r)+r\frac{d\psi(r)}{dr}\right\}\right]+B_g^2\frac{\psi(r)}{r}=0$$

$$\text{i.e, } \frac{1}{r^2}\left[-\frac{d\psi(r)}{dr}+\frac{d\psi(r)}{dr}+r\frac{d^2\psi(r)}{dr^2}\right]+B_g^2\frac{\psi(r)}{r}=0,$$

which finally reduces to

$$\frac{d^2\psi(r)}{dr^2}+B_g^2\psi(r)=0. \tag{117}$$

The general solution of this equation is:

$$\psi(r)=A\sin\left(B_g r\right)+C\cos\left(B_g r\right),$$

which gives

$$\phi(r)=A\frac{\sin\left(B_g r\right)}{r}+C\frac{\cos\left(B_g r\right)}{r}. \tag{118}$$

However, the cosine term goes to ∞ as $r \rightarrow 0$, which is physically not acceptable, whereas the sine term is acceptable because it has a finite limit as $r \rightarrow 0$ (as can be verified using L'Hôpital's rule). Therefore, the final solution for the spherical reactor is

$$\phi(r)=A\frac{\sin\left(B_g r\right)}{r},$$

where, for the same reason as in the other geometries (to guarantee no negative flux), B_g must take the lowest allowable value, i.e.,

$$B_g=\frac{\pi}{R_{ex}}, \tag{119}$$

so that finally

$$\phi(r)=A\frac{\sin\left(\frac{\pi r}{R_{ex}}\right)}{R}. \tag{120}$$

If we normalize the flux by imposing a value P for the total fission power of the reactor and neglect the extrapolation distance, we find that:

$$\begin{aligned} P &= 4AR^2E_f\Sigma_f \\ \Rightarrow A &= \frac{P}{4R^2E_f\Sigma_f}. \end{aligned} \tag{121}$$

4.4 Flux Curvature and Neutron Out-Leakage

Let us consider the "out-leakage" term (call it $Leak_{out}$) in the above examples: $Leak_{out} \equiv$ outleak-

age per differential physical volume $d\vec{r} = \vec{\nabla} \cdot \vec{J} = -\vec{\nabla} \cdot D(\vec{r}) \nabla \varphi(\vec{r})$. Applying this to the flux in a uniform slab reactor (Eq. 76) gives, for $x > 0$:

$$Leak_{out} = -D\nabla^2 \left(A\cos\left(\frac{\pi x}{a_{ex}}\right)\right) = +DA\left(\frac{\pi}{a_{ex}}\right)^2 \cos\left(\frac{\pi x}{a_{ex0}}\right) > 0.$$

We can similarly show for all other uniform reactors that $Leak_{out} > 0$. This can actually be seen in the general case from $\nu\Sigma_f \phi(\vec{r}) - \Sigma_a \phi(\vec{r}) + D\nabla^2 \phi(\vec{r}) = 0$ (presented earlier as Eq. (48)), which for any point in the **uniform** reactor gives $-D\nabla_2 \phi(\vec{r}) = (\nu\Sigma_f - \Sigma_a)\phi(\vec{r}) = DB^2 \phi(\vec{r}) > 0$. This means that we can say that any point in a uniform reactor sees neutron out-leakage (i.e., any differential volume is a source of neutrons).

Note again that the above finding applies to uniform reactors, not to all reactors in general. Real reactors may have regions which are net sinks of neutrons, where the flux curvature is positive and where there is a net in-leakage of neutrons. The general rule that we can infer from the above and also from what we learned in source-sink problems is that:

Positive flux curvature ≡ Net neutron in-leakage, while

Negative flux curvature ≡ Net neutron out-leakage.

5 Reactors in Two Neutron-Energy Groups with No External Source

5.1 The Neutron Cycle and the Four-Factor Formula

Neutrons born in fission have high energy (see the sketch of their energy distribution in Figure 8).

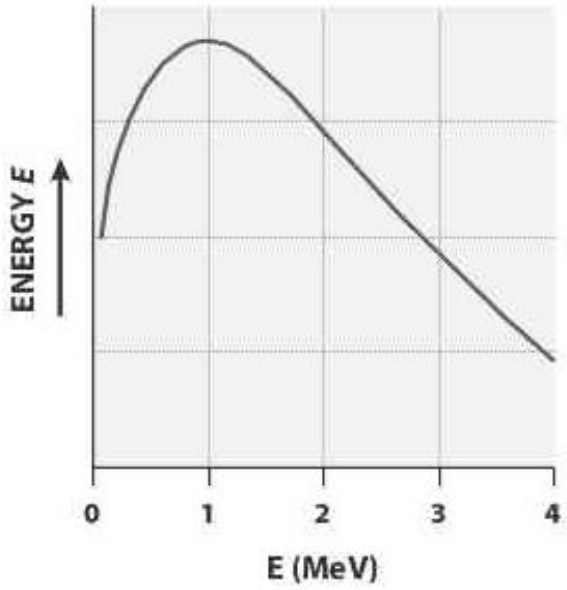

Figure 8 Energies of fission neutrons

It can be seen that the peak in their energy distribution is ~0.73 MeV. A 1-MeV neutron has a speed of ~13,800 km/s: fission neutrons are **fast** neutrons. There are essentially no fission neutrons born with thermal energies ≤~1 eV; the reference thermal energy is 0.025 eV, speed 2,200 m/s, T = 293.6 K.

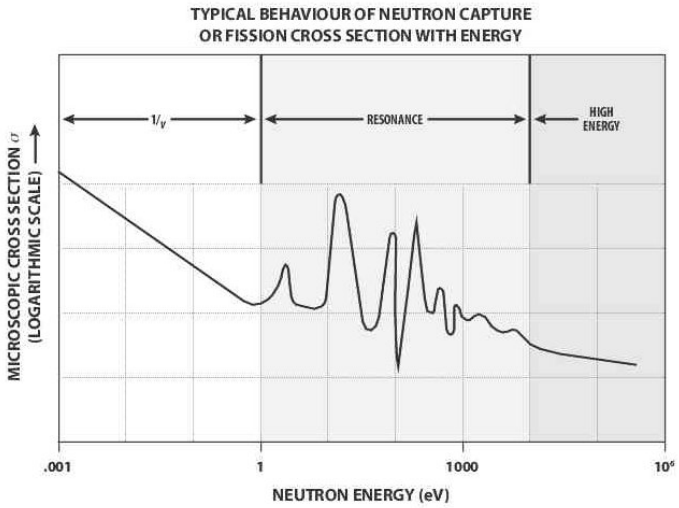

Figure 9 Sketch of cross section versus neutron energy

However, the probability of neutrons inducing fission in fissile nuclei (such as ^{235}U) is orders of magnitude larger for thermal neutrons (with energies of a small fraction of 1 eV) than for fast neutrons (see Figure 9). This is why thermal reactors (such as CANDU reactors) use a neutron moderator (such as heavy water in CANDU) to slow neutrons down. This leads to the neutron cycle in thermal reactors: neutrons are born "fast" (i.e., with relatively high energy, typically in the range of MeV) and are "encouraged" to slow down to the thermal range, where they induce more fissions. Of course, fast neutrons do induce a small number of fissions; in fact, only fast neutrons can fission non-fissile nuclides (e.g., ^{238}U), because there is usually a minimum energy threshold for such fission to occur. Moreover, while following the cycle, neutrons can also escape (leak out of the reactor) or be captured in non-productive absorptions at any energy, in particular in the "resonance range" (between ~1 eV and ~10^5 eV), where many strong resonance-absorption peaks (mostly leading to non-productive captures) exist. To reduce resonance capture, most power reactors are designed with the fuel lumped into (mostly) cylindrical elements in fuel-rod assemblies (inside fuel channels in the case of CANDU) surrounded by a moderator. Note also that some up-scattering (increase in neutron energy on collision with a nucleus) can occur in the neutron cycle; this is much less than the rate of down-scattering (moderation) of neutrons, and the up-scattering cross section is sometimes neglected. The neutron cycle in a thermal reactor and with no up-scattering (i.e., scattering from a low-energy group to a high-energy group neglected) is illustrated in Figure 10.

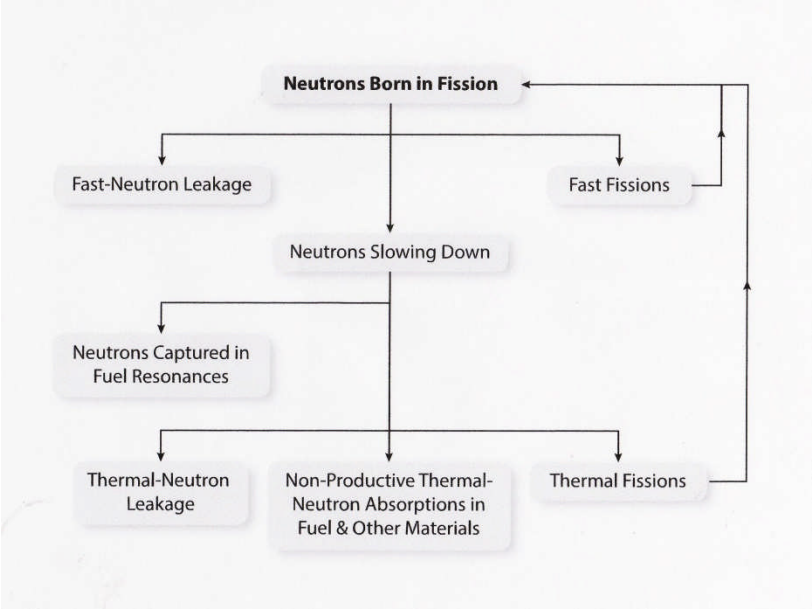

Figure 10 Neutron cycle in thermal reactor

We can derive an equation for the infinite-lattice multiplication constant k_∞ by "following" the various phases of the neutron cycle in the "neutron-generation" view, as follows:

- Imagine that ***N*** neutrons are born in thermal fissions in one generation (each thermal fission produces about 2.5 neutrons on average).
- There will also be some neutrons born in fast fissions in the same generation. Define ε as the ratio of the total number of fission neutrons born in both fast and thermal fissions to the number born in thermal fissions. ε is called the **fast-fission ratio** ($\varepsilon > 1$). Therefore the total number of fast neutrons is now $N\varepsilon$.
- These neutrons start to slow down, but some are captured in non-productive resonances. If we define ***p* as the resonance-escape probability** (***p*** < 1), the number of neutrons which survive to thermal energies is now $N\varepsilon p$.
- These thermal neutrons can be absorbed in fuel or in non-fuel components of the medium. If we define ***f*** as the ratio of thermal neutrons absorbed in fuel nuclides to the total number of thermal neutrons absorbed in this same generation, then the number of neutrons absorbed in fuel in the current generation is $N\varepsilon pf$; ***f*** is called the **fuel utilization** ($f \leq 1$).
- Some of the neutrons absorbed in fuel may induce more fissions, and some may not. Define η as the average number of fission neutrons released per thermal absorption event in the fuel. Then the total number of fission neutrons born (in this new generation!) from these thermal fissions is now $N\varepsilon pf\eta$. η is called the **reproduction factor ($\eta > 1$)**.
- We have now gone around the cycle one full time, and we can compare the number of neutrons in the same phase in successive generations: the ratio in successive generations is k_∞, given by:

$$k_\infty = \frac{N\varepsilon pf\eta}{N} = \varepsilon pf\eta. \tag{122}$$

5.2 The Two-Energy-Group Model

The neutron energy range in the neutron cycle is very wide, eight or nine orders of magnitude (from ~10 MeV to ~0.01 eV). From this it is obvious that the one-neutron-energy-group diffusion treatment, while very instructive, cannot be very accurate. Because a very large majority of fissions are induced by thermal neutrons and the fission rate is the most important rate to calculate correctly (because it is essentially the heat-production rate), a two-energy-group treatment is often sufficiently accurate in diffusion calculations. The nuclear properties in two groups must of course be obtained by proper averaging of the detailed many-group properties determined by a transport-theory calculation. Next, we will analyze the two-energy-group model.

5.3 Neutron Diffusion Equation in Two Energy Groups

With two energy groups, we will need:

- Two fluxes $\phi_1(\vec{r})$ and $\phi_2(\vec{r})$, with index 1 for the fast (sometimes called the slowing-down) group and index 2 for the thermal group;
- Two absorption cross sections, $\Sigma_{a1}(\vec{r})$ and $\Sigma_{a2}(\vec{r})$;
- Two neutron-yield cross sections, $\nu\Sigma_{f1}(\vec{r})$ and $\nu\Sigma_{f2}(\vec{r})$, acting on the fast and thermal fluxes respectively;
- Down-scattering and up-scattering cross sections, $\Sigma_{1\to2}(\vec{r})$ and $\Sigma_{2\to1}(\vec{r})$ respectively;
- Two diffusion coefficients, $D_1(\vec{r})$ and $D_2(\vec{r})$.

The diffusion equation for two energy groups is actually two equations, one for each group. There must be neutron balance in each group. As previously indicated, all neutrons are born in the fast group:

$$\nu\Sigma_{f1}(\vec{r})\phi_1(\vec{r}) + \nu\Sigma_{f2}(\vec{r})\phi_2(\vec{r}) + \Sigma_{2\to1}(\vec{r})\phi_2(\vec{r}) - \Sigma_{a1}(\vec{r})\phi_1(\vec{r}) - \Sigma_{1\to2}(\vec{r})\phi_1(\vec{r}) + \vec{\nabla}\cdot D_1(\vec{r})\nabla\phi_1(\vec{r}) = 0, \tag{123}$$

$$\Sigma_{1\to2}(\vec{r})\phi_1(\vec{r}) - \Sigma_{a2}(\vec{r})\phi_2(\vec{r}) - \Sigma_{2\to1}(\vec{r})\phi_2(\vec{r}) + \vec{\nabla}\cdot D_2(\vec{r})\nabla\phi_2(\vec{r}) = 0. \tag{124}$$

5.4 Uniform Infinite Medium in Two Energy Groups

As we did in one energy group, let us first assume a uniform reactor, infinite in size. Again, all points in space are "equivalent", which means that the neutron fluxes are constant through space and there is no leakage from one point to another; therefore the leakage terms can be dropped from the equations.

The diffusion equations (123) and (124) in the infinite uniform multiplying medium then become:

$$\begin{aligned} \nu\Sigma_{f1}\phi_1 + \nu\Sigma_{f2}\phi_2 + \Sigma_{2\to1}\phi_2 - \Sigma_{a1}\phi_1 - \Sigma_{1\to2}\phi_1 &= 0 \\ \Sigma_{1\to2}\phi_1 - \Sigma_{a2}\phi_2 - \Sigma_{2\to1}\phi_2 &= 0, \end{aligned}$$

which can be written as a linear homogeneous system of two equations:

$$\left(\nu\Sigma_{f1}-\Sigma_{a1}-\Sigma_{1\to2}\right)\phi_1+\left(\nu\Sigma_{f2}+\Sigma_{2\to1}\right)\phi_2=0 \tag{125}$$

$$\Sigma_{1\to2}\phi_1-\left(\Sigma_{a2}+\Sigma_{2\to1}\right)\phi_2=0. \tag{126}$$

Now, this system can have a non-trivial flux solution if and only if the determinant of the flux coefficients is zero, i.e.:

$$-\left(\nu\Sigma_{f1}-\Sigma_{a1}-\Sigma_{1\to2}\right)\left(\Sigma_{a2}+\Sigma_{2\to1}\right)-\left(\nu\Sigma_{f2}+\Sigma_{2\to1}\right)\Sigma_{1-2}=0. \tag{127}$$

Satisfying the criticality condition, Eq. (127), requires a very fine balance between the nuclear properties. What if that balance is not achieved and Eq. (127) is not satisfied? Then there is no non-trivial solution, i.e., we do not have a real operating infinite-medium reactor. However, we can ensure that there is always a non-trivial solution if we "tune" the neutron-yield cross sections by dividing them by a parameter, k_∞ (to be determined). The diffusion equations then become:

$$\left(\frac{\nu\Sigma_{f1}}{k_\infty}-\Sigma_{a1}-\Sigma_{1\to2}\right)\phi_1+\left(\frac{\nu\Sigma_{f2}}{k_\infty}+\Sigma_{2\to1}\right)\phi_2=0 \tag{128}$$

$$\Sigma_{1\to2}\phi_1-\left(\Sigma_{a2}+\Sigma_{2\to1}\right)\phi_2=0, \tag{129}$$

and the criticality condition is:

$$\left(\frac{\nu\Sigma_{f1}}{k_\infty}-\Sigma_{a1}-\Sigma_{1\to2}\right)\left(\Sigma_{a2}+\Sigma_{2\to1}\right)-\left(\frac{\Sigma_{f2}}{k_\infty}+\Sigma_{2\to1}\right)\Sigma_{1\to2}=0. \tag{130}$$

From Eq. (130), we can determine the value that k_∞ must have for criticality:

$$k_\infty=\frac{\nu\Sigma_{f1}\left(\Sigma_{a2}+\Sigma_{2\to1}\right)+\nu\Sigma_{f2}\Sigma_{1\to2}}{\Sigma_{a1}\Sigma_{a2}+\Sigma_{a1}\Sigma_{2\to1}+\Sigma_{a2}\Sigma_{1\to2}}. \tag{131}$$

As before, we can define the reactivity as

$$\rho_\infty=1-\frac{1}{k_\infty}.$$

The difference of k_∞ from unity (or of ρ_∞ from 0) tells us how far from critical the original uniform medium is.

When the fast-fission and up-scattering cross sections are neglected, the form obtained for k_∞ is simpler and instructive:

$$k_{\infty,\,no\,up-scattering\,\&\,no\,fast\;fission}=\frac{\nu\Sigma_{f2}}{\Sigma_{a2}}\frac{\Sigma_{1\to2}}{\Sigma_{a1}+\Sigma_{1\to2}}. \tag{132}$$

The second factor in Eq. (132),

$$\frac{\Sigma_{1\to2}}{\Sigma_{a1}+\Sigma_{1\to2}},$$

gives the probability that fast neutrons will down-scatter relative to their probability of being absorbed or down-scattered; i.e., it is the probability of fast neutrons surviving to thermal

energies, which is simply the **resonance-escape probability *p*** in Eq. (122). The first factor in Eq. (132) is the number of fission neutrons produced per thermal absorption, i.e., it is the **reproduction factor** η.

Another important quantity to determine in the two-group model, which has no meaning in the one-group treatment, is the ratio of group fluxes. In the uniform infinite medium, this can be obtained most simply from Eq. (129):

$$\frac{\phi_2}{\phi_1} = \frac{\Sigma_{1\to 2}}{\Sigma_{a2} + \Sigma_{2\to 1}}. \tag{133}$$

Note that the criticality condition (130) ensures that the same value would be obtained from Eq. (128).

5.5 Uniform Finite Reactors in Two Energy Groups

We now analyze uniform finite reactors. The diffusion equations are now:

$$\nu\Sigma_{f1}\phi_1(\vec{r}) + \nu\Sigma_{f2}\phi_2(\vec{r}) + \Sigma_{2\to 1}\phi_2(\vec{r}) - \Sigma_{a1}\phi_1(\vec{r}) - \Sigma_{1\to 2}\phi_1(\vec{r}) + D_1\nabla^2\phi_1(\vec{r}) = 0 \tag{134}$$

$$\Sigma_{1\to 2}\phi_1(\vec{r}) - \Sigma_{a2}\phi_2(\vec{r}) - \Sigma_{2\to 1}\phi_2(\vec{r}) + D_2\nabla^2\phi_2(\vec{r}) = 0. \tag{135}$$

We can try to find a solution for the flux which is separable in space and energy, i.e., where the two-row flux vector

$$\Phi(\vec{r}) \equiv \begin{pmatrix} \phi_1(\vec{r}) \\ \phi_2(\vec{r}) \end{pmatrix}$$

can be written as a group-dependent amplitude times a group-independent flux shape. If we can solve the equation with such a solution, then it is a good solution:

$$\begin{pmatrix} \phi_1(\vec{r}) \\ \phi_2(\vec{r}) \end{pmatrix} = \begin{pmatrix} A_1\psi(\vec{r}) \\ A_2\psi(\vec{r}) \end{pmatrix}. \tag{136}$$

Substituting Eq. (136) into Eq. (135), we get:

$$(\Sigma_{1\to 2}A_1 - \Sigma_{a2}A_2 - \Sigma_{2\to 1}A_2)\psi(\vec{r}) + D_2A_2\nabla^2\psi(\vec{r}) = 0, \tag{137}$$

and if we divide by $\psi(\vec{r})$:

$$\frac{\nabla^2\psi(\vec{r})}{\psi(\vec{r})} = -\frac{\Sigma_{1\to 2}A_1 - \Sigma_{a2}A_2 - \Sigma_{2\to 1}A_2}{D_2A_2}. \tag{138}$$

The right-hand side of Eq. (138) is a single number, independent of space, which we can write as $-B^2$. [Note: We would have reached a similar conclusion if we had substituted Eq. (136) into Eq. (134).] Equation (138) is analogous to Eq. (61), i.e., B^2 is a group-independent geometric buckling that is applicable to both the fast and the thermal groups:

$$\nabla^2\phi_g(\vec{r}) = -B^2\phi_g(\vec{r}),\ g = 1,2. \tag{139}$$

Because this is exactly the same equation as we found with one energy group, the flux distribution in two groups is exactly the same as in one energy group: i.e., a product of cosines in a

parallelepiped reactor, an axial cosine times a radial Bessel function in a cylindrical reactor, and a sine-over-r function in a spherical reactor. The only new quantity is the ratio of the group fluxes!

Let us now return to the criticality conditions for a finite reactor. Substituting Eq. (139) into Eqs. (134) and (135) gives a linear homogeneous system, and therefore we can divide the yield cross sections by k_{eff} as usual to ensure a non-trivial solution:

$$\left(\frac{\nu\Sigma_{f1}}{k_{eff}} - \Sigma_{a1} - \Sigma_{1\to 2} - D_1 B^2\right)\phi_1(\vec{r}) + \left(\frac{\nu\Sigma_{f2}}{k_{eff}} + \Sigma_{2\to 1}\right)\phi_2(\vec{r}) = 0 \tag{140}$$

$$\Sigma_{1\to 2}\phi_1(\vec{r}) - (\Sigma_{a2} + \Sigma_{2\to 1} + D_2 B^2)\phi_2(\vec{r}) = 0. \tag{141}$$

The criticality condition for finite reactors in two energy groups is found by equating the determinant of this system to zero, which yields:

$$k_{eff} = \frac{\nu\Sigma_{f1}\left(\Sigma_{a2} + \Sigma_{2\to 1} + D_2 B^2\right) + \nu\Sigma_{f2}\Sigma_{1\to 2}}{\left(\Sigma_{a1} + D_1 B^2\right)\left(\Sigma_{a2} + \Sigma_{2\to 1} + D_2 B^2\right) + \Sigma_{1\to 2}\left(\Sigma_{a2} + D_2 B^2\right)}. \tag{142}$$

If we consider the simpler case obtained by neglecting up-scattering and fast fission, as we did following Eq. (131), we get:

$$\begin{aligned} k_{eff,\,no\,up-scattering\,\&\,no\,fast\,fission} &= \frac{\nu\Sigma_{f2}\Sigma_{1\to 2}}{\left(\Sigma_{a1} + D_1 B^2\right)\left(\Sigma_{a2} + D_2 B^2\right) + \Sigma_{1\to 2}\left(\Sigma_{a2} + D_2 B^2\right)} \\ &= \frac{\nu\Sigma_{f2}\Sigma_{1\to 2}}{\left(\Sigma_{a1} + \Sigma_{1\to 2} + D_1 B^2\right)\left(\Sigma_{a2} + D_2 B^2\right)}. \end{aligned} \tag{143}$$

The ratio of Eq. (143) to Eq. (132) gives the effect of leakage:

$$\frac{k_{eff}}{k_\infty} = \frac{\dfrac{\nu\Sigma_{f2}\Sigma_{1\to 2}}{\left(\Sigma_{a1} + \Sigma_{1\to 2} + D_1 B^2\right)\left(\Sigma_{a2} + D_2 B^2\right)}}{\dfrac{\nu\Sigma_{f2}\Sigma_{1\to 2}}{\Sigma_{a2}\left(\Sigma_{a1} + \Sigma_{1\to 2}\right)}} = \frac{\Sigma_{a1} + \Sigma_{1\to 2}}{\Sigma_{a1} + \Sigma_{1\to 2} + D_1 B^2}\frac{\Sigma_{a2}}{\Sigma_{a2} + D_2 B^2}. \tag{144}$$

The first factor is the ratio of (fast absorption + down-scattering) to (fast absorption + down-scattering + fast leakage). Therefore, the first factor represents the fast non-leakage probability, which we can call P_{1NL}. In the same way, the second factor represents the thermal non-leakage probability, P_{2NL}. Therefore, Eq. (144) is equivalent to

$$k_{eff} = k_\infty P_{1NL} P_{2NL}, \tag{145}$$

and the total non-leakage probability is

$$P_{NL} = P_{1NL} P_{2NL}. \tag{146}$$

If we use the four-factor formula for k_∞, then Eq. (146) becomes a **six-factor formula** for k_{eff}:

$$k_{eff} = \varepsilon p f \eta P_{1NL} P_{2NL}. \tag{147}$$

6 Solution for Neutron Flux in a Non-Uniform Reactor

For uniform (homogeneous) reactors of various geometries, we were able to solve the diffusion equation analytically and find closed forms for the neutron-flux distribution. However, real reactors are not homogeneous. The steady-state neutron-diffusion equation must then be solved numerically. This section shows one method for doing this in the two-neutron-energy group case.

We start with the two-group neutron-diffusion-equation system, Eqs. (123) and (124), which we rewrite with the required k_{eff} added as a divisor to the fission cross sections (6.1):

$$(\nu\Sigma_{f1}(\vec{r})\phi_1(\vec{r}) + \nu\Sigma_{f2}(\vec{r})\phi_2(\vec{r}))/k_{eff} + \Sigma_{2\to1}(\vec{r})\phi_2(\vec{r}) - \Sigma_{a1}(\vec{r})\phi_1(\vec{r}) -$$

$$\Sigma_{1\to2}(\vec{r})\phi_1(\vec{r}) + \vec{\nabla}\cdot D_1(\vec{r})\nabla\phi_1(\vec{r}) = 0 \tag{148}$$

$$\Sigma_{1\to2}(\vec{r})\phi_1(\vec{r}) - \Sigma_{a2}(\vec{r})\phi_2(\vec{r}) -$$

$$\Sigma_{2\to1}(\vec{r})\phi_2(\vec{r}) + \vec{\nabla}\cdot D_2(\vec{r})\nabla\phi_2(\vec{r}) = 0. \tag{149}$$

All cross sections in a lattice cell are homogenized (averaged spatially within the cell) and condensed to two groups using a multi-group transport code for each lattice cell, but in a real reactor, they must also incorporate the effects of reactivity devices superimposed upon the basic lattice.

6.1 Finite-Difference Form of the Neutron-Diffusion Equation

The simplest method for solving the neutron-diffusion equation in a non-homogeneous reactor starts by developing a finite-difference form of the equations.

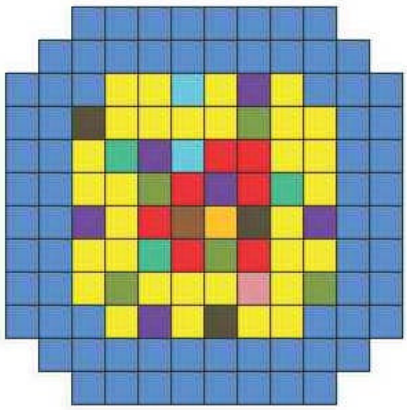

Figure 11 Face view of very simple reactor model

Consider a two-dimensional view of a reactor model, where each spatial dimension has been subdivided into intervals (see Figure 11). The model is then a collection of homogeneous cells (which may generally all have different nuclear properties). These cells can be basic lattice cells or subdivisions of these cells. The finite-difference method then consists of solving for the flux distribution at a single point in each cell, the centre of the cell in the mesh-centred formulation, which we will use here.

Let us look at one of these cells (which we label with a superscript C for Central) and its six nearest neighbours in the three directions, labelled with a superscript *n* = 1 to 6 (1 to 4 in *x*-*y* geometry). We get the finite-difference form of the diffusion equation if we integrate Eqs. (148) and (149) over the volume of cell C:

$$\int_C \left[\frac{\nu\Sigma_{f1}^C \phi_1(\vec{r}) + \nu\Sigma_{f2}^C \phi_2(\vec{r})}{k_{eff}} + \Sigma_{2\to1}^C \phi_2(\vec{r}) - \left(\Sigma_{a1}^C + \Sigma_{1\to2}^C\right)\phi_1(\vec{r}) + \vec{\nabla}\cdot D_1^C \nabla\phi_1(\vec{r}) \right] d\vec{r} = 0 \qquad (150)$$

$$\int_C \left[\Sigma_{1\to2}^C \phi_1(\vec{r}) - \left(\Sigma_{a2}^C + \Sigma_{2\to1}^C\right)\phi_2(\vec{r}) + \vec{\nabla}\cdot D_2^C \nabla\phi_2(\vec{r}) \right] d\vec{r} = 0. \qquad (151)$$

where we have dropped the dependence on $\vec{r}$ for the properties because the cells are homogeneous.

There are two types of integrals in Eqs. (150) and (151). The first type does not involve the divergence operator "$\vec{\nabla}\cdot$". In these integrals, the (homogeneous) cross sections can be taken out of the integral sign, for example:

$$\int_C \Sigma_{a2}^C \phi_2(\vec{r}) = \Sigma_{a2}^C \int_C \phi_2(\vec{r})\, dr.$$

For the integral on the right-hand side, the approximation is made that the integral is equal to the value of the flux at the centre of the cell multiplied by the volume $V^C \equiv \Delta x^C \Delta y^C \Delta z^C$ of the cell ($\Delta x^C, \Delta y^C, \Delta z^C$ being the dimensions of the cell in *x*, *y*, and *z*). Then:

$$\int_C \Sigma_{a2}^C \phi_2(\vec{r}) = \Sigma_{a2}^C \phi_2^C V^C. \qquad (152)$$

The second type of integral has the divergence operator in the integrand. This type of integral simply represents the leakage out of cell C to its neighbours. By Gauss's theorem, the volume integral over the divergence is equal to a surface integral, for example,

$$\int_C \vec{\nabla}\cdot D_1^C \nabla\phi_1(\vec{r})\, d\vec{r} = \int_S D_1^C \nabla\phi_1(\vec{r})\cdot\hat{n}\, ds = \int_S \vec{J}_1 \cdot \hat{n}\, ds, \qquad (153)$$

where *S* is the surface of the cell, $\hat{n}$ is the outer normal to the surface, and by Fick's Law, $\vec{J}_1$ is the net outward current at a point on the surface of the cell.

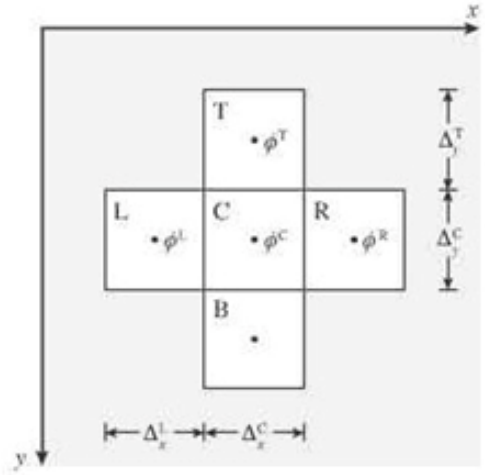

Figure 12 Flux in a cell and in immediate neighbours

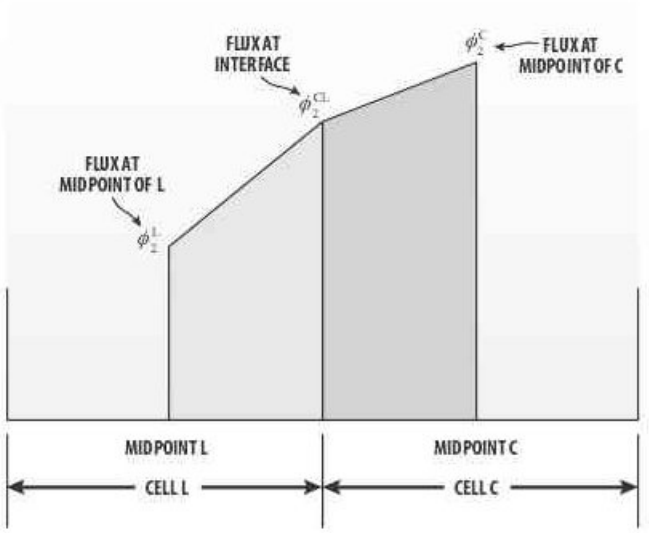

Figure 13 Linear treatment of flux in central cell and one neighbour

Because the cell has six faces, the surface integral is evaluated over the six interfaces between cell C and its six neighbours, *n* = 1-6. If we take as an example the face towards the cell with the lowest *x*-value (*n* = 1) for cell C, we can evaluate the surface integral of the current in the fast group over that face (which we call face C1) as follows. First, denote the group-1 flux at the centre of the face by ϕ_1^{C1} (see Figure 12). Then let us assume that the flux is linear between the centre of the cell and the centre of the face (see Figure 13). Then the group-1 current from cell C to its neighbouring cell 1, at the centre of the face, is:

$$J_{1,C\to 1} = -D_1^C \frac{d\phi_1^C}{dx} = -D_1^C \frac{\left[\phi_1^C - \phi_1^{C1}\right]}{\frac{1}{2}\Delta x^C}. \tag{154}$$

Similarly, the group-1 current from cell 1 to cell C is:

$$J_{1,1\to C} = -D_1^1 \frac{\left[\phi_1^{C1} - \phi_1^1\right]}{\frac{1}{2}\Delta x^1}. \tag{155}$$

However, the current must be continuous at the face, i.e.,

$$J_{1,1\to C} = J_{1,C\to 1}. \tag{156}$$

Then by equating Eqs. (154) and (155) and solving for the interface flux, we find that:

$$\phi_1^{C1} = \frac{D_1^C \Delta x^1 \phi_1^C + D_1^1 \Delta x^C \phi_1^1}{D_1^C \Delta x^1 + D_1^1 \Delta x^C}. \tag{157}$$

We can then substitute this into Eq. (155) and calculate the current at the centre of the face:

$$J_{1,C\to 1} = -D_1^C \frac{\left[\phi_1^C - \phi_1^{C1}\right]}{\frac{1}{2}\Delta x^C} = -\frac{2D_1^C D_1^1 \left(\phi_1^C - \phi_1^1\right)}{D_1^C \Delta x^1 + D_1^1 \Delta x^C}. \tag{158}$$

If we assume that the average current over the face is equal to the current at the centre of the face, the total current over face C1 is:

$$\int_{C1} \vec{J}_1 \cdot \hat{n} ds = -\frac{2D_1^C D_1^1 \Delta y^C \Delta z^C}{D_1^C \Delta x^1 + D_1^1 \Delta x^C} \left(\phi_1^C - \phi_1^1 \right) \equiv A_1^{C1} \left(\phi_1^C - \phi_1^1 \right), \tag{159}$$

where A_1^{C1} is a coupling coefficient:

$$A_1^{C1} = -\frac{2D_1^C D_1^1 \Delta y^C \Delta z^C}{D_1^C \Delta x^1 + D_1^1 \Delta x^C}. \tag{160}$$

A very similar process can of course be performed for all six faces between cell C and its neighbours. The total outward current in Eq. (153) is then:

$$\int_S \vec{J}_1 \cdot \hat{n} ds = \sum_{n=1}^{6} A_1^{Cn} \left(\phi_1^C - \phi_1^n \right). \tag{161}$$

Using all the above results, the finite-difference neutron-diffusion Eqs. (150) and (151) then become:

$$\frac{\nu\Sigma_{f1}^C \phi_1^C + \nu\Sigma_{f2}^C \phi_2^C}{k_{eff}} V^C + \Sigma_{2\to1}^C \phi_2^C V^C - \left(\Sigma_{a1}^C + \Sigma_{1\to2}^C \right) \phi_1^C V^C + \sum_{n=1}^{6} A_1^{Cn} \left(\phi_1^C - \phi_1^n \right) = 0 \tag{162}$$

$$\Sigma_{1\to2}^C \phi_1^C V^C - \left(\Sigma_{a2}^C + \Sigma_{2\to1}^C \right) \phi_2^C V^C + \sum_{n=1}^{6} A_2^{Cn} \left(\phi_2^C - \phi_2^n \right) = 0. \tag{163}$$

These equations couple cell C to its closest neighbours. These and similar equations for all the other cells in the model make up a coupled system of linear homogeneous equations for the fluxes at the centres of the cells. If there are *N* cells in the model, the system is composed of 2*N* equations. To solve this coupled system, we need also the boundary conditions at the model edges, which we look at now.

The edge cells have neighbour cells only towards the "interior" of the model. In directions outward from the model, the diffusion boundary condition with vacuum is that the flux goes to zero at the extrapolation distance beyond the boundary.

However, we can express the boundary condition in the same form as Eqs. (162) and (163) by creating a "dummy" neighbour cell of width 2 d_{extr}, where d_{extr} is the extrapolation length = 2.1312 D^C [see Eq. (33)] and forcing the flux to be zero at the extrapolation distance (see Figure 14).

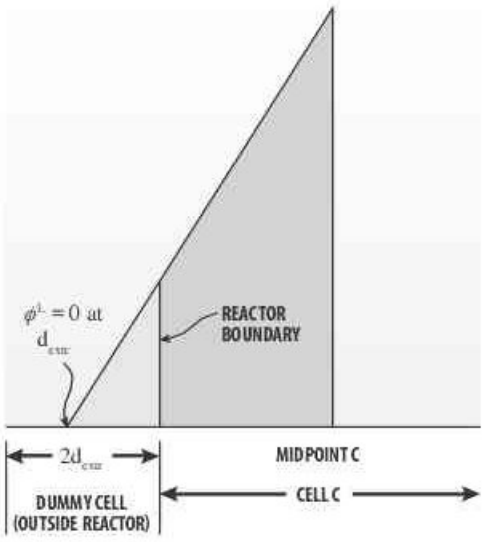

Figure 14 Flux in cell at reactor boundary

6.2 Iterative Solution of the Neutron-Diffusion Equation

The finite-difference neutron-diffusion-equation system described above is a coupled set of 2*N* homogeneous equations, where *N* is the number of real cells in the model. However, actually we seem to have (2*N* + 1) unknowns: two values of flux for each of the *N* cells, plus the value of k_{eff}. In fact, however, there are only 2*N* unknowns because the overall flux normalization is arbitrary in the homogeneous diffusion equation and only relative fluxes can be determined. The absolute flux normalization factor must be determined using an extraneous condition such as the total reactor fission power.

In real-life reactors, the number of cells *N* is very large (typically tens of thousands). Consequently, the system of equations can be solved only by iterative techniques. The first step is that a flux guess must be selected; this can be as simple as a "flat" flux distribution, i.e., the same value in all cells. A first guess must also be made for k_{eff}; for instance, we can use the guess $k_{eff} = 1$.

Once a flux guess has been established, the flux iterations can begin. At each iteration, the computer program progresses from cell to cell in the *x*-direction, the *y*-direction, and finally the *z*-direction, with each cell considered as the central cell C. The two equations (162) and (163) are solved simultaneously to obtain the fluxes in cell C, ϕ_1^C and ϕ_2^C, using the latest values of the fluxes in the neighbouring cells. As the sweep progresses through the cells, all the fluxes are updated and used as the latest flux values when the cells are called upon as neighbours. During this sweep, the value of k_{eff} is kept constant. However, when a full sweep over all reactor cells (a "full iteration") is completed, the value of k_{eff} is updated. It can be recalculated from the definition of the reactor multiplication constant:

$$k_{eff} = \frac{\text{Neutron Production}}{\text{Neutron Absorption} + \text{Neutron Leakage}}$$
$$= \frac{\int_{\vec{r}} [\nu\Sigma_{f1}(\vec{r})\phi_1(\vec{r}) + \nu\Sigma_{f2}(\vec{r})\phi_2(\vec{r})]d\vec{r}}{\int_{\vec{r}} \left[\Sigma_{a1}(\vec{r})\phi_1(\vec{r}) + \Sigma_{a2}(\vec{r})\phi_2(\vec{r}) + \vec{\nabla}\cdot\vec{J}_1(\vec{r}) + \vec{\nabla}\cdot\vec{J}_2(\vec{r})\right]d\vec{r}},$$

where the latest fluxes from the latest iteration are used and the integrals are evaluated as sums over the cells.

One iteration is not sufficient to obtain a self-consistent solution of the entire system of finite-difference equations. We must repeat the iterations until the fluxes converge, i.e., until the relative difference in flux in each cell from one iteration to the next is very small, smaller than an accepted tolerance, typically ~10^{-5}. A convergence criterion is also needed for k_{eff}; typically, a difference of 0.001 or 0.01 mk from one iteration to the next is used. Once convergence has been reached, we have the sought-after solution for the flux shape, i.e., we have the unnormalized (relative) flux distribution. To find the absolute values for the flux, we can normalize the flux distribution to the total reactor fission power, for example.

7 Energy Dependence of Neutron Flux

In Section 4, we studied the spatial dependence of the neutron flux in one energy group in uniform reactors. In Sections 5 (uniform reactors) and 6 (non-uniform reactors), we studied how to determine the neutron flux both in space and in two energy groups. But what can be said about the variation of the neutron flux with energy when treated as a continuous variable (not just in two groups)? We examine this in the present section.

When we consider the range of neutron energies from ~1 (or a few) MeV down to a fraction of 1 eV, we can subdivide the flux energy spectrum into three broad regions (note that the region boundaries cannot be considered "sharp"):

- Fission-neutron energies (>~0.5 MeV)
- Slowing-down (or moderation) range (~0.5 MeV - ~0.625 eV)
- Thermal range (< ~0.625 eV)

We will look at the variation of neutron flux with energy in these three regions in turn.

7.1 The Fission-Neutron Energy Range

This range consists of energies above ~0.5 MeV, up to several MeV, with a maximum flux magnitude around 0.7 MeV. The energy distribution ("spectrum") of neutrons in this range is determined by experimental measurement. It is found to be well approximated by:

$$\chi(E) = 0.453e^{-1.036E}\sinh\sqrt{2.29E}, \tag{164}$$

where E is in MeV (see Figure 15). [Note: In Chapter 3, the Watt spectrum is used.]

Note that this is a distribution of the number of neutrons, but the flux can be obtained simply by multiplying by the neutron speed υ (not to be confused with ν, the fission neutron yield).

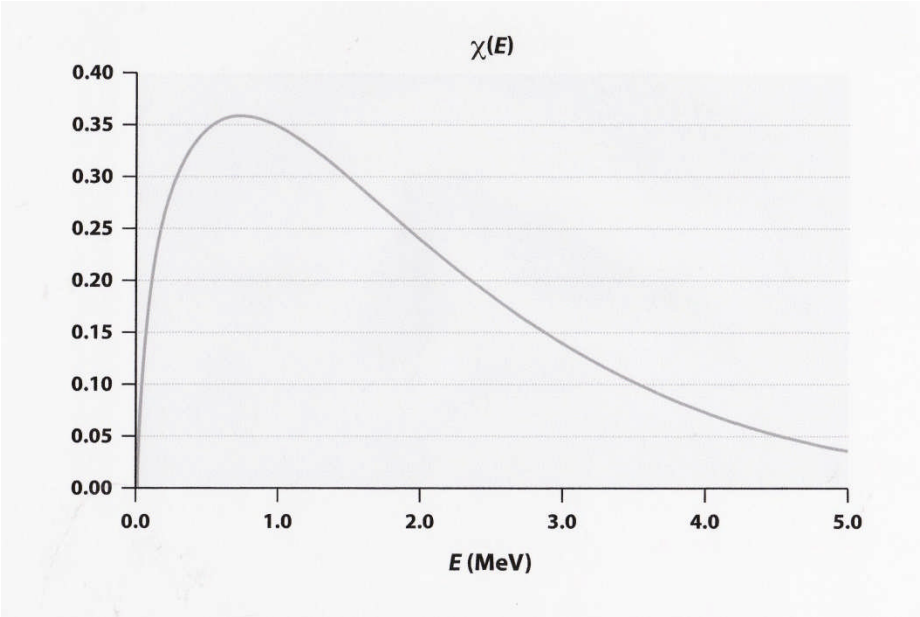

Figure 15 Energy distribution of fission neutrons

7.2 The Thermal Energy Range

Next, let us look at the thermal energy range, with neutron energies less than ~0.625 eV. Here, the neutrons are in thermal-equilibrium balance with the ambient medium at temperature *T*.

Analogously to the atoms in an ideal gas at thermal equilibrium, the neutron population has a Maxwellian (or approximately Maxwellian) distribution. In terms of flux:

$$\phi(E) = \frac{E}{(kT)^2} e^{-\frac{E}{kT}}. \tag{165}$$

Room temperature is by convention taken as T = 293.6 K = 20.4°C, which gives kT = 0.0253 eV. The energy value $E = kT$ is the most probable neutron energy in a Maxwellian flux distribution, and the corresponding "thermal neutron" speed is:

$$v(kT = 0.0253eV) = 2200\ m/s. \tag{166}$$

7.3 The Slowing-Down Energy Range

The slowing-down energy range is intermediate between the fission-energy range and the thermal-energy range. This is the most complex range because of its very broad size and the highly complex resonance scheme presented to neutrons by heavy nuclides, e.g., ^{238}U.

Therefore, especially when considering neutron absorption in the resonance range in fuel, neutron slowing-down can be very difficult to calculate and is now mostly done by numerical computation using complex lattice codes. However, under certain approximations, it is possible to derive an analytic form for the energy distribution of neutrons as they slow down in the moderator through collisions with light nuclei.

7.3.1 Slowing down in a hydrogen moderator

The simplest case is slowing down in hydrogen. Using analysis of the kinematics of neutron

collisions with hydrogen nuclei, the slowing-down flux $\phi(E)$ in hydrogen can be derived. It can be shown that below the lower boundary E_s of the fission-neutron energy range and neglecting neutron absorption relative to scattering (a fairly good approximation), the slowing-down flux is inversely proportional to energy E:

$$\phi(E) = \frac{S}{E\Sigma_s}, \tag{167}$$

where S is the fission source and Σ_s is the scattering cross section (assumed to be independent of energy).

This provides an important, simple, basic formula for the slowing-down spectrum, even if it is somewhat of an approximation. Another way of interpreting this relationship is that the product $E\phi(E)$ is nearly constant with energy below E_s.

7.3.2 Slowing down in a non-hydrogenous moderator

The analysis of the slowing-down spectrum in a non-hydrogenous moderator is more complex, but under similar approximations, the same form of the slowing-down flux can be found:

$$\phi(E) = \frac{S}{E\xi\Sigma_s}, \tag{168}$$

This has the same form as in hydrogen, with an additional factor of ξ in the denominator. ξ is the average lethargy gain per collision, where the lethargy u is defined as:

$$u = \ln\left(\frac{E_s}{E}\right). \tag{169}$$

Refer to Chapter 3 for greater detail.

7.3.3 Relaxing the no-absorption approximation

If the absorption cross section is no longer neglected, but is assumed to vary smoothly with energy (i.e., in the absence of resonances), the 1/E flux spectrum can be modified to:

$$\phi(E) = \frac{S}{E\Sigma_t(E)} \exp\left(-\int_E^{E_s} \frac{\Sigma_a(E')}{\Sigma_t(E')}\frac{dE'}{E'}\right). \tag{170}$$

The exponential factor in Eq. (170) represents the probability that the neutron survives slowing down to energy E; i.e., it is the resonance-escape probability to energy E, which we can denote as $p(E)$.

From the general form of the slowing-down flux, the following simplified statements about the product $E\phi(E)$ can be deduced:

- If absorption is neglected, and under the assumption that the scattering cross section does not depend on energy, $E\phi(E)$ is constant (flat) with E.
- If absorption is included, and assuming a smooth variation of the absorption cross section with E, then $E\phi(E)$ will decrease smoothly for decreasing E.

These statements are shown in graphical form in Figure 16.

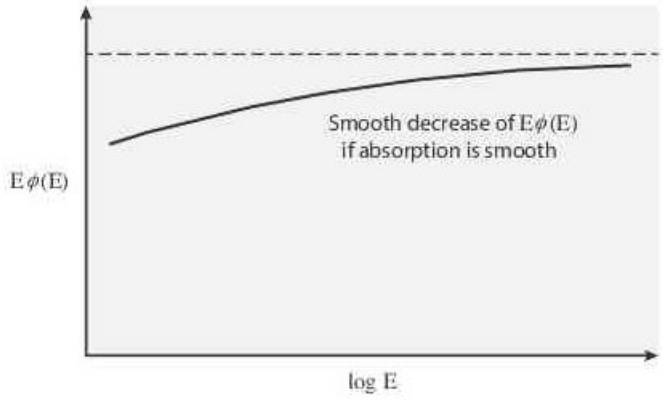

Figure 16 Variation of flux with energy if absorption is smooth

7.3.4 Slowing down in the presence of resonances

Let us now consider absorption resonances. At a resonance energy, the neutron flux decreases significantly because of the very high absorption cross section at that energy.

As a result of the dip in flux, the absorption rate in the resonance (which is proportional to the flux) is reduced relative to the absorption rate with the "background" flux value at energies above and below the resonance, i.e., the product $\Sigma_a \phi$ is smaller than if the flux were unaffected. This is called "resonance self-shielding".

On account of resonances, then, the slowing-down flux will be distorted relative to the smooth curve in the previous subsection, as shown in Figure 17.

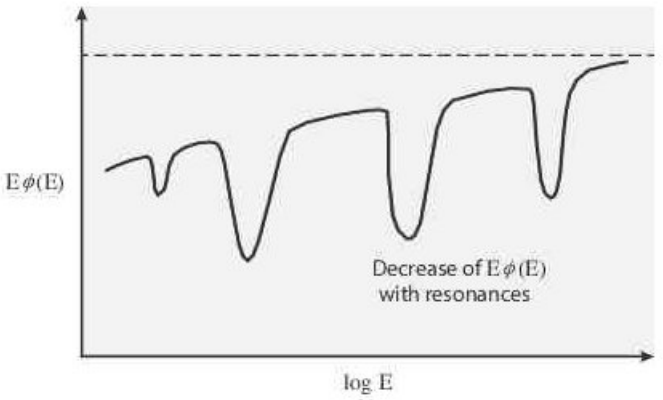

Figure 17 Variation of flux with energy in the presence of resonances

7.4 Neutron Flux over the Full Energy Range

With the results in the previous subsections, we are able to "piece together" the neutron flux over the energy range from fission energies to the thermal range, using:

- the fission spectrum at energies above about 500 keV;

- the slowing-down spectrum to about 0.625 eV. [Note that in the thermal energy range, neutrons can gain as well as lose energy in collisions. To be consistent with the approximation of no up-scattering in the derivation of the slowing-down spectrum, the "boundary" between thermal and epithermal energies should be selected sufficiently high to ensure negligible up-scattering from the thermal region to the epithermal region. This is one reason for the typical choice of 0.625 eV, which is about 25 times the most probable energy of 0.025 eV at room temperature, as the lower energy boundary of the epithermal range.]
- the Maxwellian spectrum at thermal energies. [Note that it is not a perfect Maxwellian, being distorted somewhat by neutron absorption].

The piecing together of the neutron-flux portions in the various energy regions is shown in the sketch in Figure 18.

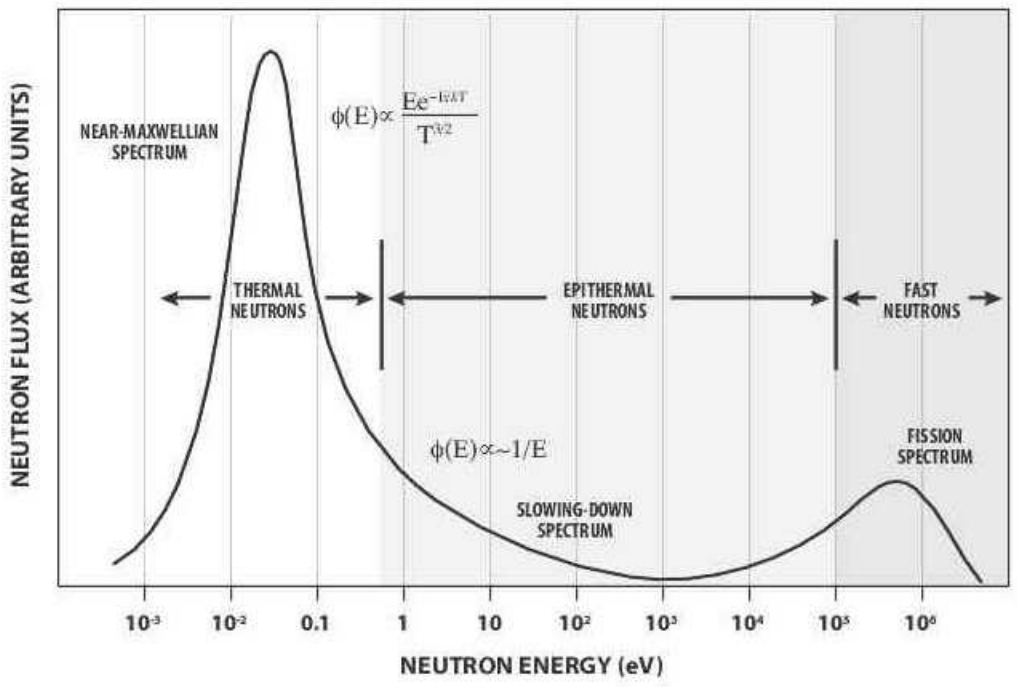

Figure 18 Sketch of flux variation over full energy range

8 Basic Design of Standard CANDU Reactors

In this section, we look at the basic features of the standard CANDU reactor design. The CANDU design is based on the following design principles and the rationale for each:

- **Use natural uranium (NU) as fuel.** The reason for this choice is that Canada has substantial, high-grade, domestic uranium mineral resources and, for a reactor cooled and moderated by heavy water (D_2O), it is not necessary to use enriched uranium fuel. Developing a uranium-enrichment industry is extremely expensive, primarily because of the sophisticated technology involved as well as the costs associated with the stringent materials safeguards, physical security, and criticality safety requirements associated with enriched nuclear materials. Moreover, the production cost of uranium-isotope enrichment is also high using current technology, in part due to the energy requirements. Consequently, natural-uranium

fuel is much cheaper and simpler to fabricate than enriched-uranium fuel.

- **Use heavy water (D_2O) as neutron moderator and reactor coolant.** The fission chain reaction cannot be self-sustaining with light water (H_2O) as moderator and NU as fuel. The reason is that normal hydrogen (H) has a fairly large absorption cross section for thermal neutrons. Hence, light water robs neutrons from the chain reaction, and the fuel must be enriched to restore a self-sustaining balance between neutron production and capture. On the other hand, deuterium (D), or heavy hydrogen, has a very small neutron-absorption cross section and enables the use of NU fuel: heavy water provides high **neutron economy**. Although D_2O is very expensive to produce due to the low abundance of D relative to H in nature, the large mass difference between D and H makes separation relatively easy to achieve using chemical technology processes, and, unlike enriched fuel, the D_2O retains its favourable nuclear properties for the full life of the reactor.
- **Use a pressure-tube rather than a pressure-vessel design.** The coolant takes heat away from the fuel (to create steam and produce electricity in a turbine generator) and becomes very hot. If we want to keep the coolant liquid (or to limit boiling to a small amount), we must pressurize it (to about 100 atmospheres, ~10 MPa). Therefore, a pressure boundary must be provided. In light-water reactors (LWRs) a large, thick, steel pressure vessel is used that surrounds the entire reactor core. The first prototype CANDU reactor [Nuclear Power Demonstration (NPD), the first reactor to produce electricity in Canada (about 20 MWe)], was initially conceived with a pressure-vessel design. However, using D_2O as the moderator results in a larger vessel than for an LWR, because the smaller scattering cross section of D_2O (compared to that of H_2O) requires a larger moderator volume. Concerns were expressed about the huge size of the pressure vessels which would be required for larger CANDU reactors, because such vessels would be difficult to fabricate and very expensive. The design of NPD, and that of all later CANDU reactors, was therefore changed to a pressure-tube design, in which the pressure boundary occurs in a small, relatively thin, fuel channel that surrounds each fuel assembly module and its associated coolant. A pressure-tube design was made possible only by emerging research on zirconium, which showed that zirconium had a very small neutron-absorption cross section and would be a very good candidate metal for the pressure tubes. Using steel, with its much larger absorption cross section, would not permit a working pressure-tube design for a reactor using natural-uranium fuel. The pressure-tube design has the additional safety feature that the break of one pressure tube is more manageable than the break of a large pressure vessel.

Some additional CANDU design features and some consequences of the design decisions are explored here:

- The natural-uranium lattice has low excess reactivity because the fuel is not enriched. This is a safety advantage because it limits the amount of reactivity increase available in an accident. It is also another rationale for adopting a pressure-tube design which allows on-power refuelling of the reactor to sustain the core reactivity without shutting down the reactor. Otherwise, batch refuelling of a CANDU reactor in a pressure vessel would be required every few months, which would lower its capacity factor on account of the lost operating time during refuelling and during the associated, time-consuming, shutdown/cool-down and start-up/heat-up transients.
- CANDU NU fuel achieves a discharge burnup in the ~7,500–~9,500 MW.d/Mg(U) range, depending on the specific reactor design. This is much lower than the dis-

charge burnup in LWRs (~30,000–50,000 MW.d/Mg(U)). However, considering fuel enrichment for LWRs (about 3.5%–5% ^{235}U) and the depleted-uranium tailings which are discarded, CANDU reactors are more efficient than LWRs and extract ~25% more energy per Mg of mined natural uranium.

- The pressure-tube design means that the main reactor vessel (the calandria) is not pressurized. The moderator is insulated from the hot coolant by placing a calandria tube concentric with each pressure tube, with an insulating gas in the intermediate (annulus) space. The moderator can be maintained relatively cool at ~70°C by circulating it in its own heat-exchanger circuit, which means that more of the neutrons will have lower thermal energies than in an LWR and consequently will more readily induce fission in fissile nuclides, e.g., ^{235}U and ^{239}Pu.
- CANDU reactivity devices are located interstitially between pressure tubes and are therefore in a benign (low-temperature and unpressurized) environment, which is a safety advantage. CANDU reactivity devices are not subject to being ejected from the reactor by coolant pressure.
- Heavy water is used as coolant instead of light water in all operating CANDU reactors for additional neutron economy. Light water was used as coolant in the Gentilly-1 prototype, and organic coolant was used in the Whiteshell Reactor (WR-1) engineering test unit, both of which are no longer in operation. Light water is also used as coolant in the proposed Advanced CANDU Reactor (ACR) design, to reduce capital costs associated with heavy water, and also in the Supercritical-Water-Cooled Reactor (SCWR) design.
- All operating CANDU reactors have horizontal pressure tubes (the Gentilly-1 prototype and the WR-1 had vertical pressure tubes). This orientation promotes symmetry because coolant can be circulated in opposite directions in alternate tubes (i.e., using bi-directional coolant flow), making average neutronics conditions essentially identical at the two ends of the reactor (unlike the situation in LWRs). With vertical pressure tubes, the gradient in coolant temperature and density as the coolant picks up heat and moves upward makes the neutronic and thermal-hydraulic conditions asymmetric.
- Horizontal pressure tubes also facilitate bi-directional refuelling (i.e., fuelling in opposite directions in adjacent channels), which further promotes symmetry. When the fuel is manufactured as short (~50-cm-long) fuel bundles which can easily be pushed through the pressure tube from either end, the associated fuelling machines will also be short, less cumbersome, and require less radiation shielding. With vertical tubes, the entire fuel string (consisting of a vertical stack of perhaps 12 or 13 bundles) would have to be removed from the top of the reactor, so that a very long fuel assembly would have to be used (together with a long and heavy transfer flask), or short fuel bundles would have to be connected to a common stringer.
- Whereas the loss of moderator shuts any (thermal) reactor down, the loss of coolant in a CANDU reactor does not have the same effect because the coolant is separated from the moderator. Instead, the loss of coolant in operating CANDU reactors generates a positive reactivity insertion (called the coolant void reactivity, or CVR); this is due to a number of spectral effects which change mostly the fast-fission factor and the resonance-escape probability. As a consequence, a loss-of-coolant accident in CANDU results in a positive power pulse, which must be quickly turned around by

shutdown-system action to avoid overheating the fuel. In fact, the postulated large-loss-of-coolant accident (LLOCA) scenario is the reason for the adoption of redundancy in CANDU shutdown capability design. CANDU reactors have two fast shutdown systems, which are physically and logically independent of one another and each fully capable of shutting the reactor down from any credible configuration. Shutdown system 1 consists of cadmium shut-off rods which fall under gravity (initially spring-assisted) into the reactor from above. Shutdown system 2 consists of the injection of a solution of neutron-absorbing gadolinium (a high neutron absorber) under high pressure through nozzles directly into the moderator.

- The lattice pitch (distance between the centres of neighbouring tubes) in all operating CANDU reactors is 28.575 cm. This is not the optimum value in the sense of maximizing the lattice reactivity (therefore minimizing the refuelling rate and maximizing the average fuel discharge burnup), which is closer to 34 cm or so. However, the larger volume of D_2O moderator would result in a higher capital cost; the shorter pitch was selected to minimize the levellized unit-energy cost. A shorter lattice pitch of 24 cm was selected for the ACR (to reduce moderator cost, among other reasons), but the reduced moderation would not allow the chain reaction to be self-sustaining with natural-uranium fuel, and the ACR would need to use enriched fuel.
- The "workhorse" control devices in all operating CANDU reactors are "liquid" zone controllers. These control 14 compartments in which amounts of light water (used for its much higher neutron-absorption cross section than heavy water) can be varied uniformly across all compartments to control reactivity or to shape the power distribution differentially.

9 CANDU Reactor Physics Computational Scheme

Because of the strong heterogeneity of reactor lattices (see the example of the CANDU basic lattice cell in Figure 19) and because nuclear fuel is a strong neutron absorber, the diffusion equation cannot be used in reactors based on the detailed lattice geometry. For cases where it is not desired to apply neutron transport in full-core reactor models, a two-stage or three-stage process has been developed to enable calculation of the neutron flux and the power distribution using the diffusion equation. This process is illustrated here for CANDU reactors.

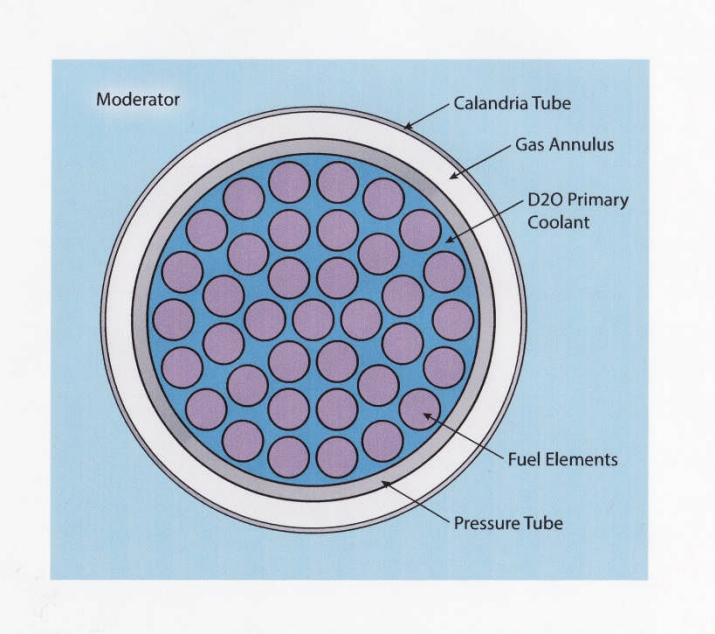

Figure 19 CANDU basic lattice cell

The computational scheme for CANDU neutronics consists of three stages. Separate computer programs have been developed to perform the calculations corresponding to each stage. The three stages are:

- lattice-cell calculation
- reactivity-device (supercell) calculation
- finite-core calculation.

9.1 Lattice Calculation

The first stage involves solving for the flux distribution in the basic lattice cell, which consists of the fuel, coolant, pressure and calandria tubes, and moderator, but no reactivity devices (see Figure 19). This calculation is performed using a deterministic multi-group neutron transport code such as WIMS-AECL. Then the transport code averages the nuclear properties (for absorption, moderation, fission, etc.) over the cell according to the calculated reaction rates in each sub-region of the lattice cells to determine the effective neutronic properties of the whole lattice cell (i.e., few (typically 2)-group macroscopic cross sections and diffusion coefficients). This averaging (homogenization) of the properties of the basic lattice cell dilutes the strong absorption of the fuel with the much weaker absorption in the moderator. With these homogenized properties, Fick's Law becomes a good approximation over most of the reactor model, and the diffusion equation can be used to calculate the full-core neutron-flux and power distributions. The lattice properties govern the neutron-multiplying behaviour of the reactor lattice, and therefore they must be obtained for all ages of the reactor fuel, i.e., the transport code must perform a "depletion" calculation to evolve the lattice-cell neutronic properties to reflect the changes in the nuclide composition of the fuel with irradiation/burnup. The lattice properties must also reflect any modified configurations of the lattice. For example, if the coolant is assumed "voided" in a hypothetical loss-of-coolant accident, or the temperature of the material in a sub-region is assumed to change, then the lattice properties must change accordingly.

9.2 Reactivity-Device Calculation

This type of calculation determines the effect of a reactivity device on the nuclear properties in its vicinity. This effect is expressed in the form of "incremental" cross sections which are added to the (unperturbed) homogenized properties of neighbouring lattice cells in a modelled volume around the device, called a "supercell"; see Figure 20.

For instance, shutoff-rod incremental cross sections dictate the local efficacy of the shutoff rods in absorbing neutrons and shutting down the fission chain reaction. The incremental cross sections of a device are obtained by calculating the differences in the supercell homogenized properties between the case when the device is inserted into the supercell and the case when it is withdrawn from it. The incremental cross sections are added to the lattice-cell cross sections in the modelled volume around the device's position in the reactor core, when that particular device is inserted.

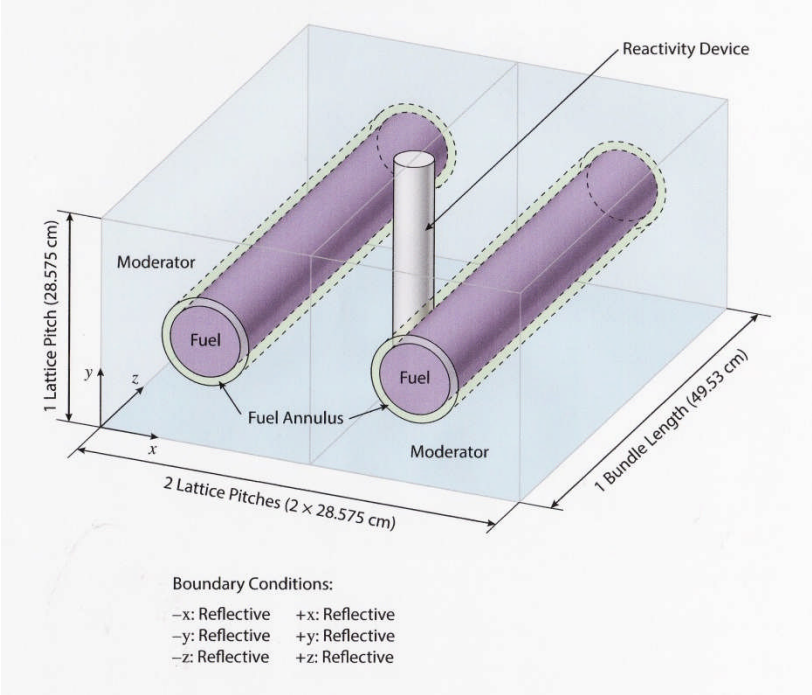

Figure 20 Supercell for calculating device incremental cross sections

Because the supercell also contains highly absorbing material, transport theory must again be used. CANDU reactivity devices are perpendicular to the fuel channels. Therefore, realistic supercell models are three-dimensional, and as a result supercell calculations are best done using the DRAGON transport code, which can perform calculations in three dimensions.

9.3 Full-Core Calculation

In the final stage, a full-core reactor model is assembled. The full-core model must incorporate, for each cell in the reactor, the homogenized unperturbed-lattice-cell cross sections which apply there, together with the incremental cross sections of nearby reactivity devices in their appropriate locations. The model therefore consists of homogenized basic-lattice cells on which are superimposed homogenized subcells representing reactivity devices. One of many such "device model areas" is shown in Figure 21; in the white subcells, the nuclear cross sections are obtained by summing the basic-cell properties and the appropriate device incremental properties.

A full, 3-D reactor model constructed in this way is used to calculate the three-dimensional flux and power distributions in the core. Because homogenized properties are used, few-group diffusion theory can be applied to the full-core reactor model.

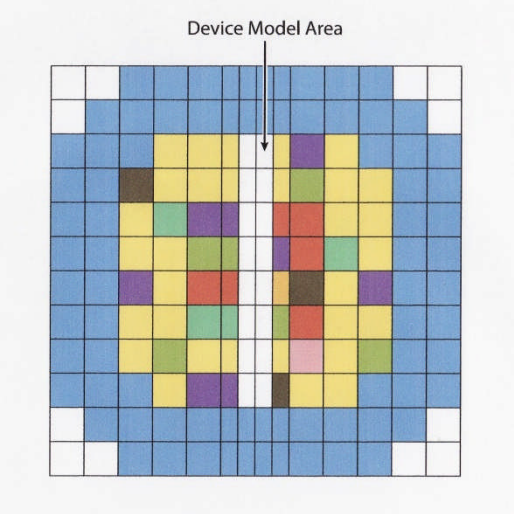

Figure 21 Simple model with superimposed reactivity device

10 Evolution of Lattice Properties

When nuclear fuel is "burned" in a reactor, changes occur in the material composition of the fuel. These changes are generally called "fuel (isotopic) depletion". In this section, we look at how the properties of the CANDU lattice evolve with fuel irradiation (or burnup).

The following changes occur cumulatively in CANDU nuclear fuel with time:

- The ^{235}U depletes (i.e., its concentration, which starts at 0.72 atom% for fresh natural uranium, decreases).
- Fission products accumulate; most of these are radioactive, and many have a significant neutron-absorption cross section.
- ^{239}Pu is produced by neutron absorption in ^{238}U and two subsequent beta decays:

$$^{238}\mathrm{U} + \mathrm{n} \rightarrow {}^{239}\mathrm{U}^{*} \rightarrow {}^{239}\mathrm{Np} + \beta$$

$$^{239}\mathrm{Np} \rightarrow {}^{239}\mathrm{Pu} + \beta.$$

- ^{235}Pu participates strongly in the fission chain reaction (because it is fissile, like ^{235}U), but while it continues to be created at about the same rate from ^{238}U, its net rate of increase slows.
- Further neutron absorptions lead from ^{239}Pu to ^{240}Pu (non-fissile), and then to ^{241}Pu (fissile).
- Other higher actinides are also formed (e.g., curium, americium).
- The total fissile fraction in the fuel (^{235}U + ^{239}Pu + ^{241}Pu) decreases monotonically. The evolution of the concentration of these three nuclides is shown in Figure 22.

A typical graph of reactivity ρ_∞ of the infinite CANDU lattice versus fuel irradiation, obtained from a cell calculation using a transport code, is shown in Figure 23. The following points are of note:

- The fresh-fuel infinite lattice (where the fuel has not yet received any irradiation) has a high reactivity (~78 mk when the ^{135}Xe and other saturating fission products have built up). To achieve a steady state in the infinite lattice with fresh fuel, a corresponding amount of negative reactivity must be added to the lattice [e.g., by dissolving a neutron poison (i.e., a material with a large neutron absorption cross section) in the moderator] to suppress the initial supercriticality.
- The reactivity starts to decrease immediately on account of ^{235}U depletion.
- It then starts to increase for a while, on account of production of ^{239}Pu, which is slightly more effective than ^{235}U. Note the slight delay due to the ^{239}Np ~2-day half-life.
- However the rate of increase of reactivity slows (because the net rate of plutonium production decreases), and the reactivity proceeds through a maximum, called the plutonium peak, with increasing burnup (note that this is not a peak in ^{239}Pu concentration, but in lattice-cell reactivity!).
- Following the plutonium peak, the reactivity decreases monotonically on account of the continuing depletion of ^{235}U and the continuing accumulation of fission products.
- The infinite lattice reaches zero reactivity at an irradiation corresponding to a burnup of ~6,700 MW.d/Mg(U).
- A homogeneous infinite lattice with fuel beyond that burnup would be subcritical.

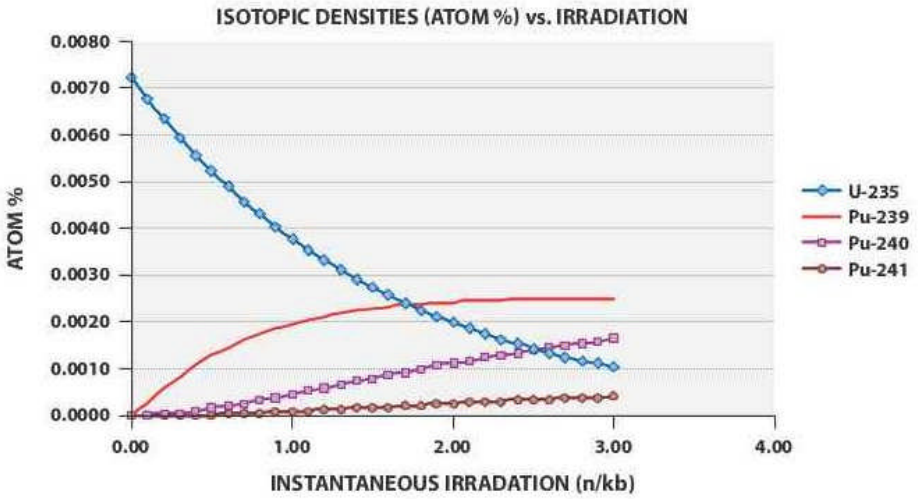

Figure 22 Evolution of fuel isotopic densities

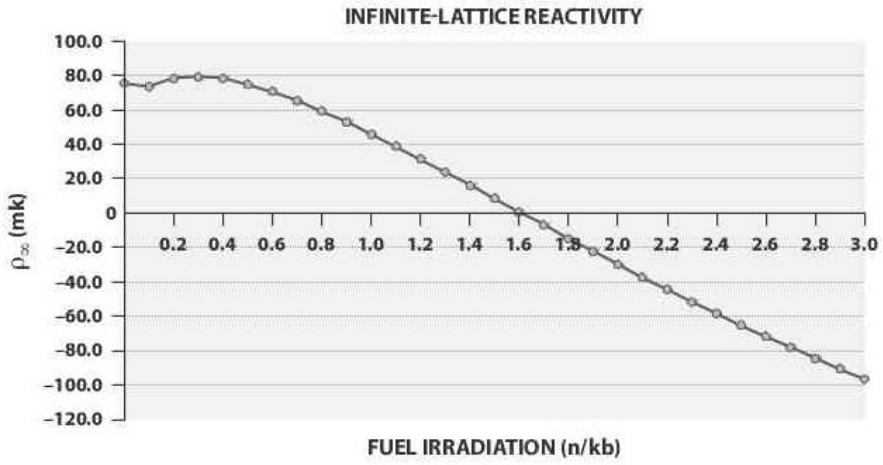

Figure 23 Infinite-lattice reactivity vs. irradiation

However, remember that the infinite lattice does not experience reactivity losses due to neutron leakage; moreover, it does not account for neutron absorption in all the reactivity devices within the core. Consequently, a homogeneous reactor with all fuel at the same irradiation would reach zero reactivity at a much lower burnup than the infinite lattice.

In the CANDU-6 reactor, leakage is about -30 mk, and the average in-core reactivity-device load is ~-18 mk. Therefore, an estimate of the reactivity ρ_{eff} of a finite homogeneous CANDU-6 reactor can be obtained by subtracting 48 mk from the reactivity of the infinite lattice; see Figure 24.

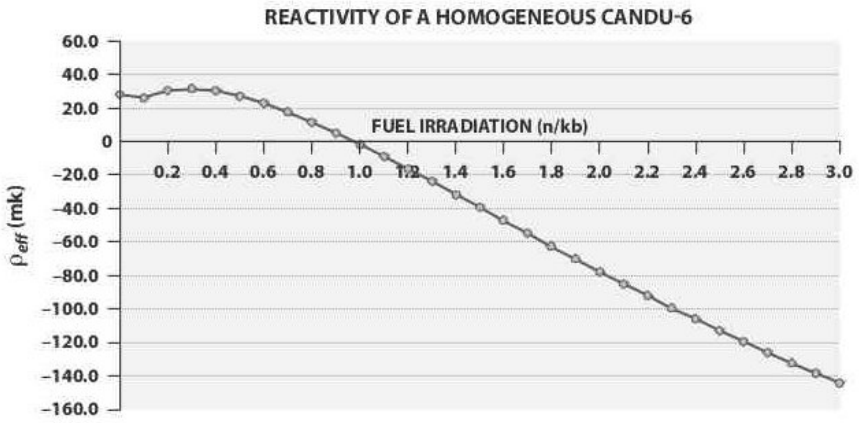

Figure 24 Finite-reactor reactivity vs. irradiation

In a homogeneous reactor, a significant amount of additional negative reactivity (~30 mk) is required to suppress the initial supercriticality. A homogeneous CANDU-6 would reach zero reactivity at an irradiation corresponding to a burnup of ~4,000 MW.d/Mg(U). A homogeneous CANDU-6 with fuel beyond that burnup would be subcritical [note that the argument is hypothetical in any case because a homogeneous finite reactor would not remain homogeneous with burnup]. Therefore, if the CANDU-6 were to be batch-refuelled, the discharge burnup would be only ~4,000 MW.d/Mg(U).

However, CANDU reactors are refuelled on-power, and therefore there is always (except near start of life) a mixture of fresh fuel and fuel with high irradiation. The fuel with high irradiation has negative "local reactivity", but this is compensated for by the positive local reactivity of low-irradiation fuel. The proper mixture of fuel in this inhomogeneous reactor (obtained by the proper rate of daily refuelling) maintains the reactor critical day-to-day. Physically, the older fuel does the job of reducing the high reactivity of the young fuel, a job which moderator poison does in the batch-refuelled reactor. The difference is that whereas the poison is just a "parasitic" absorber, the older fuel does provide fissions and therefore additional energy.

The mixture of new and old fuel makes it possible to drive the discharge burnup to a much higher value than that deduced from the "homogeneous" reactivity curve. We can guess (or calculate) approximately how far we can drive the exit burnup by determining what value gives equal "positive" and "negative" areas "under" the reactivity curve [this tells us where the average ρ_{eff} would be 0]; see Figure 25.

From the figure, we can see that positive and negative areas are equal when the average exit (or discharge) burnup to which we can take the fuel with daily refuelling is ~7,500 MW.d/Mg(U). This is almost twice the discharge-to-burnup value attainable in the "batch-refuelled" reactor and represents quite a benefit provided by on-power refuelling!

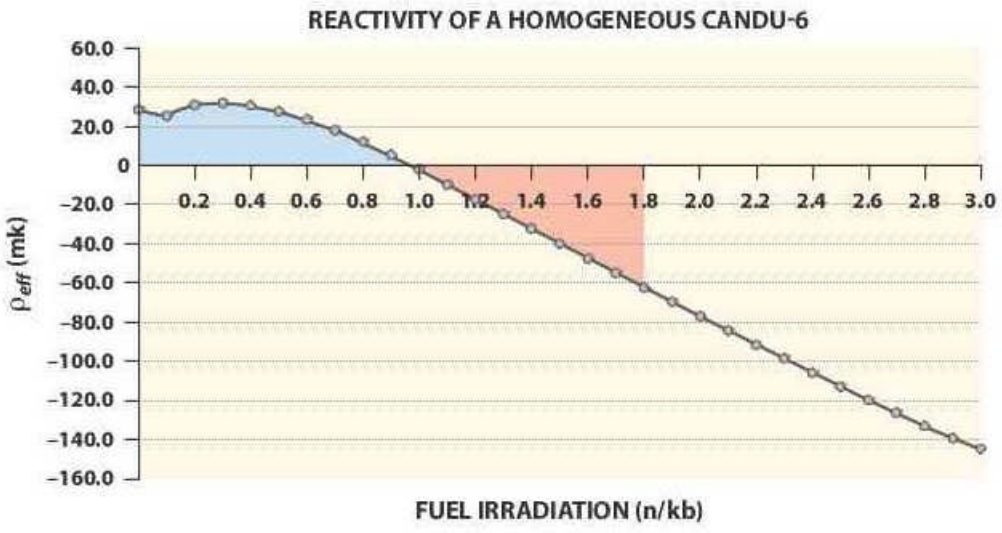

Figure 25 Averaging reactivity with daily refuelling

11 Summary of Relationship to Other Chapters

- The Neutron Physics chapter explains the interactions that neutrons have with matter and defines all the basic quantities needed in the study of the fission chain reaction and the analysis of reactors.
- The present chapter covers mostly the time-independent neutron-diffusion equation and the analysis of steady-state (time-independent) neutron distributions, either in the presence of external sources or in fission reactors. It has not covered time-dependent phenomena, which are left for the following chapter.
- The Reactor Kinetics chapter covers the time-dependent neutron-diffusion equations and

studies the phenomena of fast-neutron kinetics, fission-product poisoning, reactivity coefficients, and others in reactors.

12 Problems

Problem 1

There is an infinite homogeneous non-multiplying medium with diffusion length 8 cm and diffusion coefficient 2 cm. There are four isotropic point sources of neutrons on the *x*-*y* plane:

- Source $S_1 = 10^8$ s^{-1} at (*x, y*) = (10 cm, 0)
- Source $S_2 = 10^8$ s^{-1} at (*x, y*) = (-10 cm, 0)
- Source $S_3 = 10^{10}$ s^{-1} at (*x, y*) = (0, 20 cm)
- Source $S_4 = 10^{10}$ s^{-1} at (*x, y*) = (0, -20 cm)

(a) Find the total flux at (*x, y*) = (0, 0)
(b) Find the magnitude and direction of the total current at (*x, y*) = (0 , 0)
(c) Find the value and the direction of the total current at (*x, y*) = (0, -10 cm).

Problem 2

An isotropic point source of strength *S* $n.s^{-1}$ is located at the origin of axes in a homogeneous non-multiplying material. The material is characterized by an absorption cross section Σ_a and a diffusion constant *D*.

(a) Imagine a sphere of arbitrary radius *R* centred at the origin of axes. Calculate the integrated absorption rate of neutrons (per s) within the sphere.
(b) What is happening to the remaining neutrons (the difference between the number emitted and the number absorbed per s)? Prove this by calculation.

Problem 3

Suppose that you have an infinite plane source of neutrons in the *y*-*z* plane (i.e., at *x* = 0), which emits a total of *N* neutrons per cm^2 per s (half in the positive and half in the negative *x*-direction).

Of course, we can think of the plane source as an infinite number of point sources, one at each point of the plane. Let us take the emission from each point source as isotropic. If the point source actually has differential area *dA* (which can be as small as we want), then the point-source strength will be *NdA* neutrons per s.

Calculate the flux at any point *x* in space by integrating the flux from all point sources (by symmetry, this will of course be the same for any values of *y* and *z*). Show that you get the formula for the flux from the infinite plane source.

Problem 4

This is an exercise on the quantitative aspects of the neutron cycle.

Refer to the figure below which pertains to a critical reactor. Refer also to the notes in the figure. You are asked to calculate how many **thermal** neutrons escape from the reactor per unit time.

Remember that the two main things that can happen when a neutron is absorbed in the fuel

are capture (when the neutron is absorbed and a gamma ray is emitted) and fission (when the neutron is absorbed and fission is induced). Therefore, the ratio of capture to fission, σ_γ/σ_f, is an important parameter. To solve the problem, use the data given and find the right sequence (up and/or down) for filling numbers into the boxes.

Note that numbers need not be exact integers. In each box, retain non-integer numbers to 3 decimal places.

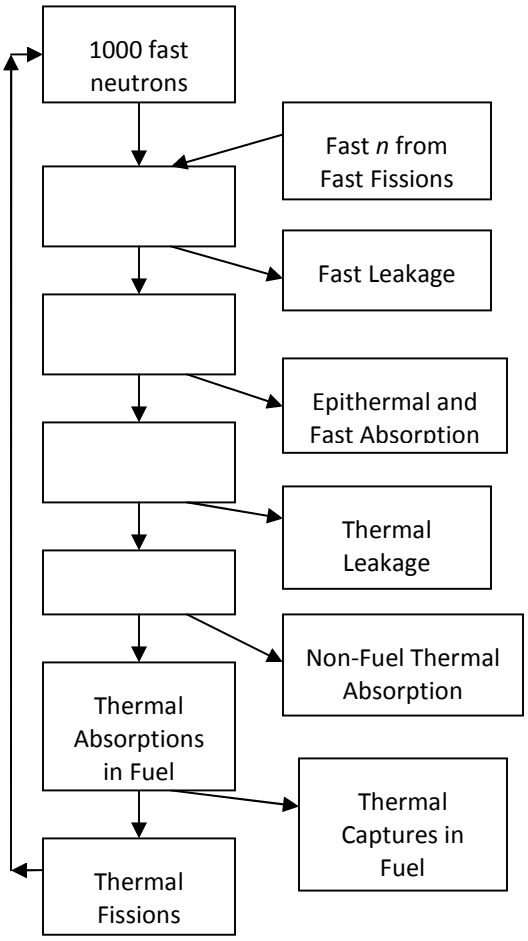

- 1000 fast neutrons are born from thermal fissions
- A thermal fission releases 2.38 fast neutrons
- For the fuel, $\alpha \equiv \sigma_\gamma/\sigma_f$ = 1.059
- 30 fast neutrons are produced by fast fission
- 32 thermal neutrons are absorbed elsewhere than in the fuel
- 9 fast neutrons escape from the reactor
- 95 non-thermal neutrons are absorbed

Problem 5

A homogeneous, bare cylindrical reactor with extrapolated axial length 5.8 m is critical. It is operated at a fission power of 900 MW. In one energy group, the reactor material is known to have ν = 2.38, Σ_f = 0.0042 cm^{-1}, and D = 1.14 cm Σ_a = 0.0099 cm^{-1}.

The leakage is 9.6 mk. [Note: neglect the extrapolation distance.]

(a) Calculate the reactor buckling and the material's absorption cross section.
(b) Determine the reactor's extrapolated diameter.
(c) What is the average flux in the reactor?
(d) What is the ratio of the flux on the cylindrical reactor axis at 50 cm from the reactor face to the maximum flux in the reactor?

Problem 6

Design the proportions of a cylindrical reactor which minimize leakage [neglect the extrapolation distance].

Problem 7

A research reactor is in the shape of a parallelepiped with a square base of side 5.2 m and a height of 6.8 m. The reactor is filled uniformly with a fuel of one-group properties $\nu\Sigma_f$ = 0.0072 cm^{-1} (and ν = 2.45) and Σ_a = 0.0070 cm^{-1}. The reactor operates steadily at a fission power of 15 MW. The average value of energy per fission E_f = 200 MeV, and 1 eV =1.6*10^{-19} J. **[Neglect the extrapolation distance.]**

(a) What is the value of the diffusion coefficient?

(b) What is the average value of the neutron flux?

(c) What is the maximum value of the neutron flux?

(d) At what rate is the fuel consumed in the entire reactor (in nuclides.s^{-1}) **and** at the centre of the reactor (in nuclides.cm^{-3}.s^{-1})?

Problem 8

A critical homogeneous reactor in the shape of a cube loses 4% of produced neutrons through leakage.

a) Calculate k_∞ for an infinite reactor made of the same material.
b) The initial reactor is re-shaped into a sphere. Calculate the new k_{eff} .

NOTE: Use one-group diffusion theory and ignore the extrapolation length.

Problem 9

A reactor is made in the shape of a cone, with the base radius equal to the height and both equal to 3 m. The reactor is homogeneous, with the following properties:

$\nu\Sigma_f$ = 0.002 cm^{-1}
Σ_a = 0.0018 cm^{-1}

Calculate the number of neutrons leaking out of the reactor per second knowing that the reactor is critical and that the average flux in the reactor is 10^{13} n/cm^2/s.

Problem 10

Imagine we have nuclear material with the following properties in two energy groups:

Σ_{a1} = 0.0011 cm^{-1}, $\Sigma_{1\to2}$ = 0.0068 cm^{-1}, Σ_{a2} = 0.0043 cm^{-1}, $\nu\Sigma_{f2}$ = 0.00528 cm^{-1}

D_1 = 1.07 cm, D_2 = 0.92 cm.

(a) Calculate the reactivity of an infinite lattice made of this material.

(b) In this infinite lattice, what fraction of neutrons is captured in resonances?
(c) We are asked to make a critical homogeneous reactor with this material, cylindrical in shape, with a diameter 10% greater than the axial dimension [neglect the extrapolation distance]. What will be this reactor's dimensions?
(d) Calculate the fast and thermal non-leakage probabilities for this reactor. Also, what is the total leakage in mk?
(e) What is the ratio of the group-1 flux to the group-2 flux in the reactor?

13 Appendix A: Reactor Statics

In this Appendix, we derive Fick's Law.

We copy here the angle-integrated version of the time-independent neutron-transport equation:

$$S(\vec{r},E)+\chi(E)\int_{E'}\nu\Sigma_f(\vec{r},E')\phi(\vec{r},E')dE'+\int_{E'}\Sigma_s(\vec{r},E'\to E)\phi(\vec{r},E')dE'-$$

$$\Sigma_t(\vec{r},E)\phi(\vec{r},E)-\vec{\nabla}\cdot\vec{J}(\vec{r},E)=0$$

(presented earlier as Eq. (16)). Our overall objective is to rewrite the last term (the leakage term) in terms of the total flux $\phi(\vec{r},E)$ only.

We first try to obtain an equation for the total current $\vec{J}(\vec{r},E)$ by multiplying the transport equation (7), which depends on angle, by $\hat{\Omega}$ and integrating over it, yielding Eq. (A.1):

$$\frac{1}{4\pi}S(\vec{r},E)\int_{\hat{\Omega}}\hat{\Omega}d\hat{\Omega}+\frac{\chi(E)}{4\pi}\int_{E'}\int_{\hat{\Omega}'}\nu\Sigma_f(\vec{r},E')\phi(\vec{r},\hat{\Omega}',E')d\hat{\Omega}'dE'\int_{\hat{\Omega}}\hat{\Omega}d\hat{\Omega}+$$
$$\int_{\hat{\Omega}}\int_{\hat{\Omega}'}\int_{E'}\Sigma_s(\vec{r},E'\to E,\hat{\Omega}'\to\hat{\Omega})\phi(\vec{r},\hat{\Omega}',E')\hat{\Omega}dE'd\hat{\Omega}'d\hat{\Omega}- \qquad \text{(A.1)}$$
$$\Sigma_t(\vec{r},E)\int_{\hat{\Omega}}\phi(\vec{r},\hat{\Omega},E)\hat{\Omega}d\hat{\Omega}-\int_{\hat{\Omega}}\vec{\nabla}\cdot\vec{J}(\vec{r},\hat{\Omega},E)\hat{\Omega}d\hat{\Omega}=0$$

In the first two terms, which we can call T_1 and T_2, we used the assumption of isotropy in the external and fission sources, so that these terms are proportional to the integral $\int_{\hat{\Omega}}\hat{\Omega}d\hat{\Omega}$. This is a vector quantity; for instance, the *x* component is $\int_{\hat{\Omega}}\hat{\Omega}_x d\hat{\Omega}$. It is clear that this integral (and similarly for the other components) must have a zero value because there are as many positive $\hat{\Omega}_x$'s as there are negative. Therefore, the first two terms drop out of the equation:

$$T_1=T_2=0. \qquad \text{(A.2)}$$

Let us jump to the fourth term, which by definition is:

$$\int_{\hat{\Omega}}\phi(\vec{r},\hat{\Omega},E)\hat{\Omega}d\hat{\Omega}=\int_{\hat{\Omega}}\vec{J}(\vec{r},\hat{\Omega},E)d\hat{\Omega}=\vec{J}(\vec{r},E).$$

Therefore, the fourth term, which we call T_4, becomes:

$$T_4=-\Sigma_t(\vec{r},E)\vec{J}(\vec{r},E) \qquad \text{(A.3)}$$

Let us look at the third term, T_3:

$$T_3=\int_{E'}\int_{\hat{\Omega}'}\int_{\hat{\Omega}}\Sigma_s(\vec{r},E'\to E,\hat{\Omega}'\to\hat{\Omega})\hat{\Omega}d\hat{\Omega}\phi(\vec{r},\hat{\Omega}',E')d\hat{\Omega}'dE'$$
$$=\int_{E'}\int_{\hat{\Omega}'}\int_{\hat{\Omega}}\Sigma_s(\vec{r},E'\to E,\hat{\Omega}'\to\hat{\Omega})\hat{\Omega}\hat{\Omega}'\cdot\hat{\Omega}'d\hat{\Omega}\phi(\vec{r},\hat{\Omega}',E')d\hat{\Omega}'dE'.$$

where we have introduced into the integral the unity factor $\hat{\Omega}'\cdot\hat{\Omega}'\equiv 1$. Also, recall that Σ_s is not

a function of absolute angles, but only of the cosine $\hat{\Omega}\cdot\hat{\Omega}'$.

$$\therefore T_3 = \int_{E'}\int_{\hat{\Omega}'}\hat{\Omega}'\left[\int_{\hat{\Omega}}\Sigma_s\left(\vec{r},E'\to E,\hat{\Omega}\cdot\hat{\Omega}'\right)\hat{\Omega}\cdot\hat{\Omega}'d\hat{\Omega}\right]\phi\left(\vec{r},\hat{\Omega}',E'\right)d\hat{\Omega}'dE'.$$

The integral over $\hat{\Omega}$ can be written as

$$\Sigma_{sa}\left(\vec{r},E'\to E\right) = 2\pi\int_{-1}^{1}\Sigma_s\left(\vec{r},E'\to E,\mu\right)\mu d\mu, \tag{A.4}$$

and

$$\therefore T_3 = \int_{E'}\Sigma_{sa}\left(\vec{r},E'\to E\right)\int_{\hat{\Omega}'}\phi\left(\vec{r},\hat{\Omega}',E'\right)\hat{\Omega}'d\hat{\Omega}'dE' = \int_{E}\Sigma_{sa}\left(\vec{r},E'\to E\right)\vec{J}\left(\vec{r},E'\right)dE'. \tag{A.5}$$

Note that if the scattering cross section were isotropic, Σ_s would not depend on μ, and therefore Σ_{sa} would be 0. Although this is not a good approximation, one that is more reasonable is to neglect the energy change in anisotropic scattering, i.e., to assume that $\Sigma_{sa}\left(\vec{r},E'\to E\right)$ is a delta function $=\delta\left(E'-E\right)\Sigma_{sa}\left(\vec{r},E\right)$, which leads to

$$T_3 = \Sigma_{sa}\left(\vec{r},E\right)\vec{J}\left(\vec{r},E\right), \tag{A.6}$$

where

$$\Sigma_{sa}\left(\vec{r},E\right) = 2\pi\int_{-1}^{1}\Sigma_s\left(\vec{r},E,\mu\right)\mu d\mu \equiv \bar{\mu}\Sigma_s\left(\vec{r},E\right) \tag{A.7}$$

and $\bar{\mu}$ is the average cosine of the scattering angle.

Moving on to the fifth term, T_5:

$$T_5 = -\int_{\hat{\Omega}}\vec{\nabla}\cdot\vec{J}\left(\vec{r},\hat{\Omega},E\right)\hat{\Omega}d\hat{\Omega} = -\int_{\hat{\Omega}}\vec{\nabla}\cdot\phi\left(\vec{r},\hat{\Omega},E\right)\hat{\Omega}\hat{\Omega}d\hat{\Omega}. \tag{A.8}$$

To calculate the integral, we adopt again the assumption of weak angular dependence of the angular flux, which leads to the following approximate expression [Eq. (27)] for the angular flux in terms of the total flux and the total current expression; see derivation in Section 2.3:

$$\phi\left(\hat{\Omega}\right) = \frac{\phi}{4\pi} + \frac{3\vec{J}\cdot\hat{\Omega}}{4\pi}. \tag{27}$$

Substituting this expression into Eq. (A.8), we get

$$T_5 = -\int_{\hat{\Omega}}\vec{\nabla}\cdot\left[\frac{\phi\left(\vec{r},E\right)}{4\pi} + \frac{3}{4\pi}\vec{J}\cdot\hat{\Omega}\right]\hat{\Omega}\hat{\Omega}d\hat{\Omega}. \tag{A.9}$$

Now it can be shown (a reasonable result) that the integral of the product of two components of $\hat{\Omega}$, e.g., $\Omega_i\Omega_j$, is equal to $4\pi/3$ if $i = j$, but 0 if $i \neq j$. Similarly, the integral of the product of three components is 0.

Using these two results, Eq. (A.9) becomes

$$T_5 = -\frac{1}{3}\nabla\phi(\vec{r},E). \tag{A.10}$$

Incorporating all these results for the various terms [Eqs. (A.2), (A.3), (A.6), (A.10)], Eq. (A.1) becomes:

$$0+0+\Sigma_{sa}(\vec{r},E)\vec{J}(\vec{r},E)-\Sigma_t(\vec{r},E)\vec{J}(\vec{r},E)-\frac{1}{3}\nabla\phi(\vec{r})=0, \tag{A.11}$$

which yields the final approximation for the total current:

$$\vec{J}(\vec{r},E)=-\frac{1}{3\left(\Sigma_t(\vec{r},E)-\Sigma_{sa}(\vec{r},E)\right)}\nabla\phi(\vec{r},E), \tag{A.12}$$

which is Fick's Law, giving for the diffusion coefficient,

$$D(\vec{r},E)=\frac{1}{3\left(\Sigma_t(\vec{r},E)-\Sigma_{sa}(\vec{r},E)\right)}. \tag{A.13}$$

The quantity in parentheses in Eq. (A.13) is defined as the transport cross section, $\Sigma_{tr}(\vec{r})$.

14 Acknowledgements

The following reviewers are gratefully acknowledged for their hard work and excellent comments during the development of this Chapter. Their feedback has much improved it. Of course the responsibility for any errors or omissions lies entirely with the authors.

Marv Gold
Ken Kozier
Guy Marleau
Bruce Wilkin

Thanks are also extended to Diana Bouchard for expertly editing and assembling the final copy.

CHAPTER 5

Reactor Dynamics

prepared by
Eleodor Nichita, UOIT
and
Benjamin Rouben, 12 & 1 Consulting, Adjunct Professor, McMaster & UOIT

***Summary**:*

This chapter addresses the time-dependent behaviour of nuclear reactors. This chapter is concerned with short- and medium-time phenomena. Long-time phenomena are studied in the context of fuel and fuel cycles and are presented in Chapters 6 and 7. The chapter starts with an introduction to delayed neutrons because they play an important role in reactor dynamics. Subsequent sections present the time-dependent neutron-balance equation, starting with "point" kinetics and progressing to detailed space-energy-time methods. Effects of Xe and Sm "poisoning" are studied in Section 7, and feedback effects are presented in Section 8. Section 9 is identifies and presents the specific features of CANDU reactors as they relate to kinetics and dynamics.

Table of Contents

List of Figures

List of Tables

1 Introduction

1.1 Overview

The previous chapter was devoted to predicting the neutron flux in a nuclear reactor under special steady-state conditions in which all parameters, including the neutron flux, are constant over time. During steady-state operation, the rate of neutron production must equal the rate of neutron loss. To ensure this equality, the effective multiplication factor, k_{eff}, was introduced as a divisor of the neutron production rate. This chapter addresses the time-dependent behaviour of nuclear reactors. In the general time-dependent case, the neutron production rate is not necessarily equal to the neutron loss rate, and consequently an overall increase or decrease in the neutron population will occur over time.

The study of the time-dependence of the neutron flux for postulated changes in the macroscopic cross sections is usually referred to as *reactor kinetics*, or reactor kinetics without feedback. If the macroscopic cross sections are allowed to depend in turn on the neutron flux level, the resulting analysis is called *reactor dynamics* or reactor kinetics with feedback.

Time-dependent phenomena are also classified by the time scale over which they occur:

- *Short-time phenomena* are phenomena in which significant changes in reactor properties occur over times shorter than a few seconds. Most accidents fall into this category.
- *Medium-time phenomena* are phenomena in which significant changes in reactor properties occur over the course of several hours to a few days. Xe poisoning is an example of a medium-time phenomenon.
- *Long-time phenomena* are phenomena in which significant changes in reactor properties occur over months or even years. An example of a long-time phenomenon is the change in fuel composition as a result of burn-up.

This chapter is concerned with short- and medium-time phenomena. Long-time phenomena are studied in the context of fuel and fuel cycles and are presented in Chapters 6 and 7. The chapter starts with an introduction to delayed neutrons because they play an important role in reactor dynamics. Subsequent sections present the time-dependent neutron-balance equation, starting with "point" kinetics and progressing to detailed space-energy-time methods. Effects of Xe and Sm "poisoning" are studied in Section 7, and feedback effects are presented in Section 8. Section 9 identifies and presents the specific features of CANDU reactors as they relate to kinetics and dynamics.

1.2 Learning Outcomes

The goal of this chapter is for the student to understand:

- The production of prompt and delayed neutrons through fission.
- The simple derivation of the point-kinetics equations.
- The significance of kinetics parameters such as generation time, lifetime, reactivity, and effective delayed-neutron fraction.
- Features of point-kinetics equations and how they relate to reactor behaviour (e.g., reactor period).
- Approximations involved in different kinetics models based on flux factorization.

- First-order perturbation theory.
- Fission-product poisoning.
- Reactivity coefficients and feedback.
- CANDU-specific features (long generation time, photo-neutrons, CANDU start-up, etc.).
- Numerical methods for reactor kinetics.

2 Delayed Neutrons

2.1 Production of Prompt and Delayed Neutrons: Precursors and Emitters

Binary fission of a target nucleus ${}^{A_X}_{Z_X}X$ occurs through the formation of a compound nucleus ${}^{A_X+1}_{Z_X}X$ which subsequently decays very rapidly (promptly) into two (hence the name "binary") fission products A_m and B_m, accompanied by the emission of (prompt) gamma photons and (prompt) neutrons:

$$ {}^{1}_{0}n + {}^{A_X}_{Z_X}X \rightarrow {}^{A_X+1}_{Z_X}X \ , \tag{1} $$

(2)

The exact species of fission products A_m and B_m, as well as the exact number of prompt neutrons emitted, ν_{pm}, and the number and energy of emitted gamma photons depend on the mode m according to which the compound nucleus decays. Several hundred decay modes are possible, each characterized by its probability of occurrence p_m. On average, ν_p prompt neutrons are emitted per fission. The average number of prompt neutrons can be expressed as:

$$ \nu_p = \sum_m p_m \nu_{pm} \ . \tag{3} $$

Obviously, although the number of prompt neutrons emitted in each decay mode, ν_{pm}, is a positive integer (1, 2, 3…), the average number of neutrons emitted per fission, ν_p, is a fractional number. ν_{pm} as well as ν_p depend on the target nucleus species and on the energy of the incident neutron.

The initial fission products A_m and B_m can be stable or can further decay in several possible modes, as shown below for A_m (a similar scheme exists for B_m):

$$ A_m \begin{cases} \xrightarrow{\lambda} & A_{m1} + \gamma & \text{(mode 1)} \\ \xrightarrow{\lambda} & A_{m2} + {}^{0}_{-1}\beta_{HE} & \text{(mode 2)} \\ \xrightarrow{\lambda} & A'_{m3} + {}^{0}_{-1}\beta_{LE} & \text{(mode 3)} \\ & \downarrow \text{(fast)} & \\ & A_{m3} + n \ \text{(delayed neutron)} & \end{cases} . $$

Fission products A_m that decay according to mode 3, by emitting a low-energy beta particle, are

called *precursors*, and the intermediate nuclides A'_{m3} are called *emitters*. Emitters are daughters of precursors that are born in a highly excited state. Because their excitation energy is higher than the separation energy for one neutron, emitters can de-excite by promptly emitting a neutron. The delay in the appearance of the neutron is not caused by its emission, but rather by the delay in the beta decay of the precursor. If a high-energy beta particle rather than a low-energy one is emitted, the excitation energy of the daughter nuclide is not high enough for it to emit a neutron, and hence decay mode 2 does not result in emission of delayed neutrons.

2.2 Prompt, Delayed, and Total Neutron Yields

Although one cannot predict in advance which fission products will act as precursors, one can predict how many precursors on average will be produced per fission. This number is also equal to the number of delayed neutrons ultimately emitted and is called the *delayed-neutron yield*, ν_d. For incident neutron energies below 4 MeV, the delayed-neutron yield is essentially independent of the incident-neutron energy. If delayed neutrons are to be represented explicitly, the fission reaction can be written generically as:

$$n + X \rightarrow A + B + \nu_p n_p + \nu_d n_d + \beta + \gamma \ . \tag{4}$$

The *total neutron yield* is defined as the sum of the prompt and delayed neutron yields:

$$\nu = \nu_d + \nu_p \ . \tag{5}$$

The delayed-neutron fraction is defined as the ratio between the delayed-neutron yield and the total neutron yield:

$$\beta = \frac{\nu_d}{\nu} \ . \tag{6}$$

For neutron energies typical of those found in a nuclear reactor, most of the energy dependence of the delayed-neutron fraction is due to the energy dependence of the prompt-neutron yield and not to that of the delayed-neutron yield. This is the case because the latter is essentially independent of energy for incident neutrons with energies below 4 MeV.

2.3 Delayed-Neutron Groups

Precursors can be grouped according to their half-lives. Such groups are called *precursor groups* or *delayed-neutron groups*. It is customary to use six delayed-neutron groups, but fewer or more groups can be used. For analysis of timeframes of the order of 5 seconds, six delayed-neutron groups generally provide sufficient accuracy; for longer timeframes, a greater number of groups might be needed. Partial delayed-neutron yields ν_{dk} are defined for each precursor group *k*. The partial delayed-neutron group yield represents the average number of precursors belonging to group *k* that are produced per fission. Correspondingly, partial delayed-neutron fractions can be defined as:

$$\beta_k = \frac{\nu_{dk}}{\nu} \ . \tag{7}$$

Obviously,

$$\sum_{k=1}^{k_{\max}} \beta_k = \beta \,. \tag{8}$$

Values of delayed-group constants for ^{235}U are shown in Table 1, which uses data from [Rose1991].

Table 1 Delayed-neutron data for thermal fission in ^{235}U ([Rose1991])

Group	Decay Constant, λ_k (s^{-1})	Delayed Yield, ν_{dk} (n/fiss.)	Delayed Fraction, β_k
1	0.01334	0.000585	0.000240
2	0.03274	0.003018	0.001238
3	0.1208	0.002881	0.001182
4	0.3028	0.006459	0.002651
5	0.8495	0.002648	0.001087
6	2.853	0.001109	0.000455
Total	-	0.016700	0.006854

3 Simple Point-Kinetics Equation (Homogeneous Reactor)

This section presents the derivation of the point-kinetics equations starting from the time-dependent one-energy-group diffusion equation for the simple case of a homogeneous reactor and assuming all fission neutrons to be prompt.

3.1 Neutron-Balance Equation without Delayed Neutrons

The time-dependent one-energy-group diffusion equation for a homogeneous reactor without delayed neutrons can be written as:

$$\frac{\partial n(\vec{r},t)}{\partial t} = \nu\Sigma_f \Phi(\vec{r},t) + D\nabla^2\Phi(\vec{r},t) - \Sigma_a\Phi(\vec{r},t) \,, \tag{9}$$

where *n* represents the neutron density, $\nu\Sigma_f$ is the macroscopic production cross section, Σ_a is the macroscopic neutron-absorption cross section, Φ is the neutron flux, and *D* is the diffusion coefficient. Equation (9) expresses the fact that the rate of change in neutron density at any given point is the difference between the fission source, expressed by the term $\nu\Sigma_f\Phi(\vec{r},t)$, and the two sinks: the absorption rate, expressed by the term $\Sigma_a\Phi(\vec{r},t)$, and the leakage rate, expressed by the term $-D\nabla^2\Phi(\vec{r},t)$. If the source is exactly equal to the sum of the sinks, the reactor is critical, the time dependence is eliminated, and the static balance equation results:

$$0 = \nu\Sigma_f \Phi_s(\vec{r}) + D\nabla^2\Phi_s(\vec{r}) - \Sigma_a\Phi_s(\vec{r}) \,, \tag{10}$$

which is more customarily written as:

$$-D\nabla^2\Phi_s(\vec{r}) + \Sigma_a\Phi_s(\vec{r}) = \nu\Sigma_f\Phi_s(\vec{r}) \,. \tag{11}$$

To maintain the static form of the diffusion equation even when the fission source does not exactly equal the sum of the sinks, the practice in reactor statics is to divide the fission source artificially by the effective multiplication constant, k_{eff}, which results in the static balance equation for a non-critical reactor:

$$-D\nabla^2\Phi_s(\vec{r})+\Sigma_a\Phi_s(\vec{r})=\frac{1}{k_{eff}}\nu\Sigma_f\Phi_s(\vec{r}) \quad . \tag{12}$$

Using the expression for the geometric buckling:

$$B_g^2=\frac{\frac{\nu\Sigma_f}{k_{eff}}-\Sigma_a}{D} \quad , \tag{13}$$

Eq. (12) becomes:

$$\nabla^2\Phi_s(\vec{r})+B_g^2\Phi_s(\vec{r})=0 \quad . \tag{14}$$

Note that the geometrical buckling is determined solely by the reactor shape and size and is independent of the production or absorption macroscopic cross sections. It follows that changes in the macroscopic cross sections do not influence buckling; they influence only the effective multiplication constant, which can be calculated as:

$$k_{eff}=\frac{\nu\Sigma_f}{\Sigma_a+DB_g^2} \quad . \tag{15}$$

Because the value of geometrical buckling is independent of the macroscopic cross section, the shape of the static flux is independent of whether or not the reactor is critical.

To progress to the derivation of the point-kinetics equation, the assumption is made that the shape of the time-dependent flux does not change with time and is equal to the shape of the static flux. In mathematical form:

$$\Phi(\vec{r},t)=T(t)\Phi_s(\vec{r}) \quad , \tag{16}$$

where *T(t)* is a function depending only on time.

It follows that the time-dependent flux $\Phi(\vec{r},t)$ satisfies Eq. (14), and hence:

$$-\nabla^2\Phi(\vec{r},t)=B_g^2\Phi(\vec{r},t) \quad . \tag{17}$$

Substituting this expression of the leakage term into the time-dependent neutron-balance equation (9) the following is obtained:

$$\frac{\partial n(\vec{r},t)}{\partial t}=\nu\Sigma_f\Phi(\vec{r},t)-DB_g^2\Phi(\vec{r},t)-\Sigma_a\Phi(\vec{r},t) \quad . \tag{18}$$

The one-group flux is the product of the neutron density and the average neutron speed, with the latter assumed to be independent of time:

$$\Phi(\vec{r},t)=n(\vec{r},t)\bar{v} \quad . \tag{19}$$

The neutron-balance equation can consequently be written as:

$$\frac{\partial n(\vec{r},t)}{\partial t} = \nu\Sigma_f \overline{\nu} n(\vec{r},t) - DB_g^2 \overline{\nu} n(\vec{r},t) - \Sigma_a \overline{\nu} n(\vec{r},t) \quad . \tag{20}$$

Integrating the local balance equation over the entire reactor volume *V*, the integral-balance equation is obtained:

$$\frac{d}{dt}\int_V n(\vec{r},t)dV = \nu\Sigma_f \overline{\nu}\int_V n(\vec{r},t)dV - DB_g^2\overline{\nu}\int_V n(\vec{r},t)dV - \Sigma_a\overline{\nu}\int_V n(\vec{r},t)dV \quad . \tag{21}$$

The volume integral of the neutron density is the total neutron population $\hat{n}(t)$, which can also be expressed as the product of the average neutron density $\overline{n}(t)$ and the reactor volume:

$$\int_V n(\vec{r},t)dV \equiv \hat{n}(t) = \overline{n}(t)V \quad . \tag{22}$$

The volume-integrated flux $\hat{\Phi}(t)$ can be defined in a similar fashion and can also be expressed as the product of the average flux $\overline{\Phi}(t)$ and the reactor volume:

$$\int_V \Phi(\vec{r},t)dV \equiv \hat{\Phi}(t) = \overline{\Phi}(t)V \quad . \tag{23}$$

It should be easy to see that the volume-integrated flux and the total neutron population satisfy a similar relationship to that satisfied by the neutron density and the neutron flux:

$$\hat{\Phi}(t) = \int_V \Phi(\vec{r},t)dV = \int_V n(\vec{r},t)\overline{\nu}dV = \hat{n}(t)\overline{\nu} \quad . \tag{24}$$

With the notations just introduced, the balance equation for the total neutron population can be written as:

$$\frac{d\hat{n}(t)}{dt} = \nu\Sigma_f \overline{\nu}\hat{n}(t) - DB_g^2\overline{\nu}\hat{n}(t) - \Sigma_a\overline{\nu}\hat{n}(t) \quad . \tag{25}$$

Equation (25) is a first-order linear differential equation, and its solution gives a full description of the time dependence of the neutron population and implicitly of the neutron flux in a homogeneous reactor without delayed neutrons. However, to highlight certain important quantities which describe the dynamic reactor behaviour, it is customary to process its right-hand side (RHS) as follows:

$$\frac{d\hat{n}(t)}{dt} = \left(\nu\Sigma_f - DB_g^2 - \Sigma_a\right)\overline{\nu}\hat{n}(t) \quad . \tag{26}$$

3.2 Average Neutron-Generation Time, Lifetime, and Reactivity

In this sub-section, several quantities related to neutron generation and activity are defined.

Reactivity

Reactivity is a measure of the relative imbalance between productions and losses. It is defined as the ratio of the difference between the production rate and the loss rate to the production rate.

$$\rho = \frac{\text{production rate - loss rate}}{\text{production rate}} = \frac{\nu\Sigma_f\hat{\Phi} - \Sigma_a\hat{\Phi} - DB_g^2\hat{\Phi}}{\nu\Sigma_f\hat{\Phi}} =$$

$$\frac{\nu\Sigma_f - \Sigma_a - DB_g^2}{\nu\Sigma_f} = 1 - \frac{\Sigma_a + DB_g^2}{\nu\Sigma_f} = 1 - \frac{\text{loss rate}}{\text{production rate}} = 1 - \frac{1}{k_{eff}} \quad . \tag{27}$$

Average neutron-generation time

The average neutron-generation time is the ratio between the total neutron population and the neutron production rate.

$$\Lambda = \frac{\text{neutron population}}{\text{production rate}} = \frac{\hat{n}}{\nu\Sigma_f\hat{\Phi}} = \frac{\hat{n}}{\nu\Sigma_f\hat{n}\bar{\mathrm{v}}} = \frac{1}{\nu\Sigma_f\bar{\mathrm{v}}} \quad . \tag{28}$$

The average generation time can be interpreted as the time it would take to attain the current neutron population at the current neutron-generation rate. It can also be interpreted as the average age of neutrons in the reactor.

Average neutron lifetime

The average neutron lifetime is the ratio between the total neutron population and the neutron loss rate:

$$\ell = \frac{\text{neutron population}}{\text{loss rate}} = \frac{\hat{n}}{\left(\Sigma_a + DB_g^2\right)\hat{\Phi}} = \frac{\hat{n}}{\left(\Sigma_a + DB_g^2\right)\hat{n}\bar{\mathrm{v}}} = \frac{1}{\left(\Sigma_a + DB_g^2\right)\bar{\mathrm{v}}} \quad . \tag{29}$$

The average neutron lifetime can be interpreted as the time it would take to lose all neutrons in the reactor at the current loss rate. It can also be interpreted as the average life expectancy of neutrons in the reactor.

The ratio of the average neutron-generation time and the average neutron lifetime equals the effective multiplication constant:

$$\frac{\ell}{\Lambda} = \frac{\dfrac{1}{\left(\Sigma_a + DB_g^2\right)\bar{\mathrm{v}}}}{\dfrac{1}{\nu\Sigma_f\bar{\mathrm{v}}}} = \frac{\nu\Sigma_f}{\Sigma_a + DB_g^2} = k_{eff} \quad . \tag{30}$$

It follows that, for a critical reactor, the neutron-generation time and the neutron lifetime are equal. It also follows that, for a supercritical reactor, the lifetime is longer than the generation time and that, for a sub-critical reactor, the lifetime is shorter than the generation time.

3.3 Point-Kinetics Equation without Delayed Neutrons

With the newly introduced quantities, the RHS of the neutron-balance equation (26) can be written as either:

$$\left(\nu\Sigma_f - DB_g^2 - \Sigma_a\right)\overline{\nu}\hat{n}(t) = \frac{\left(\nu\Sigma_f - DB_g^2 - \Sigma_a\right)}{\nu\Sigma_f}\left(\nu\Sigma_f\overline{\nu}\right)\hat{n}(t) = \frac{\rho}{\Lambda}\hat{n}(t) \tag{31}$$

or

$$\left(\nu\Sigma_f - DB_g^2 - \Sigma_a\right)\overline{\nu}\hat{n}(t) = \frac{\left(\nu\Sigma_f - DB_g^2 - \Sigma_a\right)}{DB_g^2 + \Sigma_a}\left(DB_g^2 + \Sigma_a\right)\overline{\nu}\hat{n}(t) = \frac{k_{eff} - 1}{\ell}\hat{n}(t) \quad . \tag{32}$$

The neutron-balance equation can therefore be written either as:

$$\frac{d\hat{n}(t)}{dt} = \frac{\rho}{\Lambda}\hat{n}(t) \tag{33}$$

or as:

$$\frac{d\hat{n}(t)}{dt} = \frac{k_{eff} - 1}{\ell}\hat{n}(t) \quad . \tag{34}$$

Equation (33), as well as Eq. (34), is referred to as the point-kinetics equation without delayed neutrons. The name *point* kinetics is used because, in this simplified formalism, the shape of the neutron flux and the neutron density distribution are ignored. The reactor is therefore reduced to a *point*, in the same way that an object is reduced to a *point mass* in simple kinematics.

Both forms of the point-kinetics equation are valid. However, because most transients are induced by changes in the absorption cross section rather than in the fission cross section, the form expressed by Eq. (33) has the mild advantage that the generation time remains constant during a transient (whereas the lifetime does not). Consequently, this text will express the neutron-balance equation using the generation time. However, the reader should be advised that other texts use the lifetime. Results obtained in the two formalisms can be shown to be equivalent.

If the reactivity and generation time remain constant during a transient, the obvious solution to the point-kinetics equation (33) is:

$$\hat{n}(t) = \hat{n}(0)e^{\frac{\rho}{\Lambda}t} \quad . \tag{35}$$

If the reactivity and generation time are not constant over time, that is, if the balance equation is written as:

$$\frac{d\hat{n}(t)}{dt} = \frac{\rho(t)}{\Lambda(t)}\hat{n}(t) \quad , \tag{36}$$

the solution becomes slightly more involved and usually proceeds either by using the Laplace transform or by time discretization.

Before advancing to accounting for delayed neutrons, one last remark will be made regarding the relationship between the neutron population and reactor power. Because the reactor power is the product of total fission rate and energy liberated per fission, it can be expressed as:

$$P(t) = E_{fiss}\Sigma_f \hat{\Phi}(t) = E_{fiss}\Sigma_f \hat{n}(t)\overline{v} \quad . \tag{37}$$

It can therefore be seen that the power has the same time dependence as the total neutron population.

3.4 Neutron-Balance Equation with Delayed Neutrons

In the previous section, it was assumed that all neutrons resulting from fission were prompt. This section takes a closer look and accounts for the fact that some of the neutrons are in fact delayed neutrons resulting from emitter decay.

3.4.1 Case of one delayed-neutron group

As explained in Section 2.1, delayed neutrons are emitted by emitters, which are daughter nuclides of precursors coming out of fission. Because the neutron-emission process occurs promptly after the creation of an emitter, the rate of delayed-neutron emission equals the rate of emitter creation and equals the rate of precursor decay. It was explained in Section 2.3 that precursors can be grouped by their half-life (or decay constant) into several (most commonly six) groups. However, as a first approximation, it can be assumed that all precursors can be lumped into a single group with an average decay constant λ. If the total concentration of precursors is denoted by $C(\vec{r},t)$, the total number of precursors in the core, $\hat{C}(t)$, is simply the volume integral of the precursor concentration and equals the product of the average precursor concentration $\overline{C}(t)$ and the reactor volume:

$$\int_V C(\vec{r},t)dV \equiv \hat{C}(t) = \overline{C}(t)V \quad . \tag{38}$$

It follows that the delayed-neutron production rate $S_d(\vec{r},t)$, which equals the precursor decay rate, is:

$$S_d(\vec{r},t) = \lambda C(\vec{r},t) \quad . \tag{39}$$

The corresponding volume-integrated quantities satisfy a similar relationship:

$$\hat{S}_d(t) = \lambda \hat{C}(t) \quad . \tag{40}$$

The core-integrated neutron-balance equation now must account explicitly for both the prompt neutron source, $\nu_p\Sigma_f\hat{\Phi}(t)$, and the delayed-neutron source:

$$\frac{d\hat{n}(t)}{dt} = \nu_p\Sigma_f\overline{v}\hat{n}(t) + \hat{S}_d(t) - DB_g^2\overline{v}\hat{n}(t) - \Sigma_a\overline{v}\hat{n}(t) =$$
$$\nu_p\Sigma_f\overline{v}\hat{n}(t) + \lambda\hat{C}(t) - DB_g^2\overline{v}\hat{n}(t) - \Sigma_a\overline{v}\hat{n}(t) \quad . \tag{41}$$

Of course, to be able to evaluate the delayed-neutron source, a balance equation for the precursors must be written as well. Precursors are produced from fission and are lost as a result of decay. It follows that the precursor-balance equation can be written as:

$$\frac{d\hat{C}(t)}{dt} = \nu_d \Sigma_f \hat{\Phi}(t) - \lambda \hat{C}(t) = \nu_d \Sigma_f \overline{\nu}\hat{n}(t) - \lambda \hat{C}(t) \quad . \tag{42}$$

The system of equations (41) and (42) completely describes the time dependence of the neutron and precursor populations. Just as in the case without delayed neutrons, they will be processed to highlight neutron-generation time and reactivity. Because reactivity is based on the total neutron yield rather than the prompt-neutron yield, the prompt-neutron source is expressed as the difference between the total neutron source and the delayed-neutron source:

$$\frac{d\hat{n}(t)}{dt} = \nu\Sigma_f \overline{\nu}\hat{n}(t) - \nu_d \Sigma_f \overline{\nu}\hat{n}(t) + \lambda \hat{C}(t) - DB_g^2 \overline{\nu}\hat{n}(t) - \Sigma_a \overline{\nu}\hat{n}(t) = \left(\nu\Sigma_f - DB_g^2 - \Sigma_a\right)\overline{\nu}\hat{n}(t) - \nu_d \Sigma_f \overline{\nu}\hat{n}(t) + \lambda \hat{C}(t) \quad . \tag{43}$$

The RHS is subsequently processed in a similar way to the no-delayed-neutron case:

$$\left(\nu\Sigma_f - DB_g^2 - \Sigma_a\right)\overline{\nu}\hat{n}(t) - \nu_d \Sigma_f \overline{\nu}\hat{n}(t) + \lambda \hat{C}(t) = \left[\frac{\left(\nu\Sigma_f - DB_g^2 - \Sigma_a\right)}{\nu\Sigma_f} - \frac{\nu_d \Sigma_f}{\nu\Sigma_f}\right]\left(\nu\Sigma_f \overline{\nu}\right)\hat{n}(t) + \lambda \hat{C}(t) = \frac{\rho - \beta}{\Lambda}\hat{n}(t) + \lambda \hat{C}(t) \quad . \tag{44}$$

The neutron-balance equation can hence be written as:

$$\frac{d\hat{n}(t)}{dt} = \frac{\rho - \beta}{\Lambda}\hat{n}(t) + \lambda \hat{C}(t) \quad . \tag{45}$$

The RHS of the precursor-balance equation can be similarly processed:

$$\nu_d \Sigma_f \overline{\nu}\hat{n}(t) - \lambda \hat{C}(t) = \frac{\nu_d \Sigma_f}{\nu\Sigma_f}\nu\Sigma_f \overline{\nu}\hat{n}(t) - \lambda \hat{C}(t) = \frac{\beta}{\Lambda}\hat{n}(t) - \lambda \hat{C}(t) \quad , \tag{46}$$

leading to the following form of the precursor-balance equation:

$$\frac{d\hat{C}(t)}{dt} = \frac{\beta}{\Lambda}\hat{n}(t) - \lambda \hat{C}(t) \quad . \tag{47}$$

Combining Eqs. (45) and (47), the system of point-kinetics equations for the case of one delayed-neutron group is obtained:

$$\frac{d\hat{n}(t)}{dt} = \frac{\rho - \beta}{\Lambda}\hat{n}(t) + \lambda \hat{C}(t)$$
$$\frac{d\hat{C}(t)}{dt} = \frac{\beta}{\Lambda}\hat{n}(t) - \lambda \hat{C}(t) \quad . \tag{48}$$

3.4.2 Case of several delayed-neutron groups

If the assumption that all precursors can be lumped into one single group is dropped and several precursor groups are considered, each with its own decay constant λ_k, then the delayed-neutron source is the sum of the delayed-neutron sources in all groups:

$$\hat{S}_d(t) = \sum_{k=1}^{k_{\max}} \lambda_k \hat{C}_k(t) \quad , \tag{49}$$

where $\hat{C}_k(t)$ represent the total population of precursors in group *k*.

The neutron-balance equation then becomes:

$$\frac{d\hat{n}(t)}{dt} = \nu_p \Sigma_f \overline{v}\hat{n}(t) + \hat{S}_d(t) - DB_g^2 \overline{v}\hat{n}(t) - \Sigma_a \overline{v}\hat{n}(t) =$$

$$\nu_p \Sigma_f \overline{v}\hat{n}(t) + \sum_{k=1}^{k_{\max}} \lambda_k \hat{C}_k(t) - DB_g^2 \overline{v}\hat{n}(t) - \Sigma_a \overline{v}\hat{n}(t) \quad . \tag{50}$$

Processing similar to the one-delayed-group case yields:

$$\frac{d\hat{n}(t)}{dt} = \frac{\rho - \beta}{\Lambda} \hat{n}(t) + \sum_{k=1}^{k_{\max}} \lambda_k \hat{C}_k(t) \quad . \tag{51}$$

Obviously, k_{max} precursor-balance equations must now be written, one for each delayed group *k*:

$$\frac{d\hat{C}_k(t)}{dt} = \nu_{dk} \Sigma_f \overline{v}\hat{n}(t) - \lambda_k \hat{C}_k(t) \quad (k = 1 \ldots k_{\max}) \quad . \tag{52}$$

Processing the RHS of Eq. (52) as in the one-delayed-group case yields:

$$\nu_{dk} \Sigma_f \overline{v}\hat{n}(t) - \lambda_k \hat{C}_k(t) = \frac{\nu_{dk} \cancel{\Sigma_f}}{\nu \cancel{\Sigma_f}} \nu \Sigma_f \overline{v}\hat{n}(t) - \lambda_k \hat{C}_k(t) = \frac{\beta_k}{\Lambda} \hat{n}(t) - \lambda_k \hat{C}_k(t) \quad . \tag{53}$$

Finally, a system of $k_{max}+1$ differential equations is obtained:

$$\frac{d\hat{n}(t)}{dt} = \frac{\rho - \beta}{\Lambda} \hat{n}(t) + \sum_{k=1}^{k_{\max}} \lambda_k \hat{C}_k(t)$$

$$\frac{d\hat{C}_k(t)}{dt} = \frac{\beta_k}{\Lambda} \hat{n}(t) - \lambda_k \hat{C}_k(t) \quad (k = 1 \ldots k_{\max}) \quad , \tag{54}$$

representing the point-kinetics equations for the case with multiple delayed-neutron groups.

4 Solutions of the Point-Kinetics Equations

Following the derivation of the point-kinetics equations in the previous section, this section deals with solving the point-kinetics equations for several particular cases. The first case involves a steady-state (no time dependence) sub-critical nuclear reactor with an external neutron source constant over time. An external neutron source is a source which is independent of the neutron flux. The second case involves a single delayed-neutron group, for which an

analytical solution can be easily found if the reactivity and generation time are constant. Finally, the general outline of the solution method for the case with several delayed-neutron groups is presented.

4.1 Stationary Solution: Source Multiplication Formula

Possibly the simplest application of the point-kinetics equations involves a steady-state sub-critical rector with an external neutron source, that is, a source that is independent of the neutron flux. The strength of the external source is assumed constant over time. If the total strength of the source is $\hat{S}$ (n/s), the neutron-balance equation needs to be modified to include this additional source of neutrons. The precursor-balance equations remain unchanged by the presence of the external neutron source. Because a steady-state solution is sought, the time derivatives on the left-hand side (LHS) of the point-kinetics equations vanish. The steady-state point-kinetics equations in the presence of an external source can therefore be written as:

$$\begin{aligned} 0 &= \frac{\rho-\beta}{\Lambda}\hat{n}+\sum_{k=1}^{k_{\max}}\lambda_k\hat{C}_k+\hat{S} \\ 0 &= \frac{\beta_k}{\Lambda}\hat{n}-\lambda_k\hat{C}_k \quad (k=1...k_{\max}) \end{aligned} . \tag{55}$$

Equation (55) is a system of linear algebraic equations where the unknowns are the neutron and precursor populations. This can be easily seen by rearranging as follows:

$$\begin{aligned} \frac{\rho-\beta}{\Lambda}\hat{n}+\sum_{k=1}^{k_{\max}}\lambda_k\hat{C}_k &= -\hat{S} \\ \frac{\beta_k}{\Lambda}\hat{n}-\lambda_k\hat{C}_k &= 0 \quad (k=1...k_{\max}) \end{aligned} . \tag{56}$$

The system can be easily solved by substitution, by formally solving for the precursor populations in the precursor-balance equations:

$$\hat{C}_k = \frac{\beta_k}{\lambda_k\Lambda}\hat{n} \quad (k=1...k_{\max}) \tag{57}$$

and substituting the resulting expression into the neutron-balance equation to obtain:

$$\frac{\rho-\beta}{\Lambda}\hat{n}+\sum_{k=1}^{k_{\max}}\frac{\beta_k}{\Lambda}\hat{n} = -\hat{S} . \tag{58}$$

Noting that the sum of the partial delayed-neutron fractions equals the total delayed-neutron fraction, as expressed by Eq. (58), the neutron-balance equation can be processed to yield:

$$\frac{\rho}{\Lambda}\hat{n}-\frac{\beta}{\Lambda}\hat{n}+\frac{1}{\Lambda}\left(\sum_{k=1}^{k_{\max}}\beta_k\right)\hat{n} = \frac{\rho}{\Lambda}\hat{n}-\frac{\beta}{\Lambda}\hat{n}+\frac{\beta}{\Lambda}\hat{n} = \frac{\rho}{\Lambda}\hat{n} = -\hat{S} . \tag{59}$$

The neutron population is hence equal to:

$$\hat{n} = -\hat{S}\frac{\Lambda}{\rho} . \tag{60}$$

Note that the reactivity is negative, and therefore the neutron population is positive. Equation (60) is called the *source multiplication formula*. It shows that the neutron population can be obtained by multiplying the external source strength by the inverse of the reactivity, hence the name. The closer the reactor is to criticality, the larger the source multiplication and hence the neutron population. Substituting Eq. (60) into Eq. (57), the individual precursor concentrations become:

$$\hat{C}_k = \frac{\hat{S}}{-\rho}\frac{\beta_k}{\lambda_k} \quad (k = 1...k_{\max}) \quad . \tag{61}$$

The source multiplication formula finds applications in describing the approach to critical during reactor start-up and in measuring reactivity-device worth.

4.2 Kinetics with One Group of Delayed Neutrons

Another instance in which a simple analytical solution to the point-kinetics equations can be developed is the case of a single delayed-neutron group. This sub-section develops and analyzes the properties of such a solution. The starting point is the system of differential equations representing the neutron-balance and precursor-balance equations:

$$\begin{aligned} \frac{d\hat{n}(t)}{dt} &= \frac{\rho-\beta}{\Lambda}\hat{n}(t) + \lambda\hat{C}(t) \\ \frac{d\hat{C}(t)}{dt} &= \frac{\beta}{\Lambda}\hat{n}(t) - \lambda\hat{C}(t) \end{aligned} \quad . \tag{62}$$

For the case where all kinetics parameters are constant over time, this is a system of linear differential equations with constant coefficients, which can be rewritten in matrix form as:

$$\frac{d}{dt}\begin{bmatrix} \hat{n}(t) \\ \hat{C}(t) \end{bmatrix} = \begin{bmatrix} \frac{\rho-\beta}{\Lambda} & \lambda \\ \frac{\beta}{\Lambda} & -\lambda \end{bmatrix}\begin{bmatrix} \hat{n}(t) \\ \hat{C}(t) \end{bmatrix} \quad . \tag{63}$$

According to the general theory of systems of ordinary differential equations, the first step in solving Eq. (63) is to find two fundamental solutions of the type:

$$\begin{bmatrix} n \\ C \end{bmatrix} e^{\omega t} \quad . \tag{64}$$

The general solution can subsequently be expressed as a linear combination of the two fundamental solutions:

$$\begin{bmatrix} \hat{n}(t) \\ \hat{C}(t) \end{bmatrix} = a_0\begin{bmatrix} n_0 \\ C_0 \end{bmatrix} e^{\omega_0 t} + a_1\begin{bmatrix} n_1 \\ C_1 \end{bmatrix} e^{\omega_1 t} \quad . \tag{65}$$

Coefficients a_0 and a_1 are found by applying the initial conditions.

To find the fundamental solutions, expression (64) is substituted into Eq. (63) to obtain:

$$\frac{d}{dt}\left(\begin{bmatrix} n \\ C \end{bmatrix} e^{\omega t}\right) = \begin{bmatrix} \frac{\rho-\beta}{\Lambda} & \lambda \\ \frac{\beta}{\Lambda} & -\lambda \end{bmatrix} \begin{bmatrix} n \\ C \end{bmatrix} e^{\omega t} \quad , \tag{66}$$

and subsequently:

$$\omega \begin{bmatrix} n \\ C \end{bmatrix} e^{\omega t} = \begin{bmatrix} \frac{\rho-\beta}{\Lambda} & \lambda \\ \frac{\beta}{\Lambda} & -\lambda \end{bmatrix} \begin{bmatrix} n \\ C \end{bmatrix} e^{\omega t} \quad . \tag{67}$$

Dividing both sides by the exponential term and rearranging the terms, the following homogeneous linear system is obtained, called the *characteristic* system:

$$\begin{bmatrix} \frac{\rho-\beta}{\Lambda} - \omega & \lambda \\ \frac{\beta}{\Lambda} & -\lambda - \omega \end{bmatrix} \begin{bmatrix} n \\ C \end{bmatrix} = \begin{bmatrix} 0 \\ 0 \end{bmatrix} \quad . \tag{68}$$

This represents an eigenvalue-eigenvector problem, for which a solution is presented below. First, the system is rearranged so that the unknowns are each isolated on one side, and the system is rewritten as a regular system of two equations:

$$\begin{aligned} \left(\frac{\rho-\beta}{\Lambda} - \omega\right) n &= -\lambda C \\ \frac{\beta}{\Lambda} n &= (\lambda + \omega) C \end{aligned} \quad . \tag{69}$$

Dividing the two equations side by side, an equation for the eigenvalues ω_k is obtained:

$$\frac{\left(\frac{\rho-\beta}{\Lambda} - \omega\right)}{\frac{\beta}{\Lambda}} = -\frac{\lambda}{(\lambda + \omega)} \quad . \tag{70}$$

This is a quadratic equation in ω, as can easily be seen after rearranging it to:

$$\omega^2 - \omega\left(\frac{\rho-\beta}{\Lambda} - \lambda\right) - \lambda\frac{\rho}{\Lambda} = 0 \quad . \tag{71}$$

The two solutions to this quadratic equation are simply:

$$\omega_{0,1} = \frac{\left(\frac{\rho-\beta}{\Lambda}-\lambda\right) \pm \sqrt{\left(\frac{\rho-\beta}{\Lambda}-\lambda\right)^2 + 4\lambda\frac{\rho}{\Lambda}}}{2} \quad . \tag{72}$$

Once the eigenvalues are known, either the first or the second of equations (69) can be used to find the relationship between n and C. In doing so, care must be taken that the right eigenvalue (correct subscript) is used for the right *n* - *C* combination. Note that only the ratio of *n* and *C* can be determined. It follows that either *n* or *C* can have an arbitrary value, which is usually chosen to be unity. For example, if the second equation (69) is used, and if n_0 and n_1 are chosen to be unity, the two fundamental solutions are:

$$\begin{bmatrix} 1 \\ \dfrac{\beta}{\Lambda(\lambda+\omega_0)} \end{bmatrix} e^{\omega_0 t}$$

$$\begin{bmatrix} 1 \\ \dfrac{\beta}{\Lambda(\lambda+\omega_1)} \end{bmatrix} e^{\omega_1 t} \quad . \tag{73}$$

The general solution is then:

$$\begin{bmatrix} \hat{n}(t) \\ \hat{C}(t) \end{bmatrix} = a_0 \begin{bmatrix} 1 \\ \dfrac{\beta}{\Lambda(\lambda+\omega_0)} \end{bmatrix} e^{\omega_0 t} + a_1 \begin{bmatrix} 1 \\ \dfrac{\beta}{\Lambda(\lambda+\omega_1)} \end{bmatrix} e^{\omega_1 t} \quad . \tag{74}$$

4.3 Kinetics with Multiple Groups of Delayed Neutrons

Having solved the kinetics equations for one delayed-neutron group, it is now time to focus on the solution of the general system, with several delayed-neutron groups. The starting point is the general set of point-kinetics equations:

$$\begin{aligned} \frac{d\hat{n}(t)}{dt} &= \frac{\rho-\beta}{\Lambda}\hat{n}(t) + \sum_{k=1}^{k_{\max}} \lambda_k \hat{C}_k(t) \\ \frac{d\hat{C}_k(t)}{dt} &= \frac{\beta_k}{\Lambda}\hat{n}(t) - \lambda_k \hat{C}_k(t) \quad (k = 1,\ldots,k_{\max}) \end{aligned} \quad . \tag{75}$$

As long as the coefficients are constant, this is simply a system of first-order linear differential equations, whose general solution is a linear combination of exponential fundamental solutions of the type:

$$\begin{bmatrix} n \\ C_1 \\ \vdots \\ C_{k_{max}} \end{bmatrix} e^{\omega t} \quad . \tag{76}$$

There are $k_{max}+1$ such solutions, and the general solution can be expressed as:

$$\begin{bmatrix} \hat{n}(t) \\ \hat{C}_1(t) \\ \vdots \\ \hat{C}_{k_{max}}(t) \end{bmatrix} = \sum_{l=0}^{k_{max}} a_l \begin{bmatrix} n^l \\ C_1^l \\ \vdots \\ C_{k_{max}}^l \end{bmatrix} e^{\omega_l t} \quad . \tag{77}$$

4.4 Inhour Equation, Asymptotic Behaviour, and Reactor Period

By substituting the general form of the fundamental solution, Eq. (76), into the point-kinetics equations and following steps similar to those in the one-delayed-group case, the following characteristic system can be obtained:

$$\begin{aligned} \omega n &= \frac{\rho-\beta}{\Lambda} n + \sum_{k=1}^{k_{max}} \lambda_k C_k \\ \omega C_k &= \frac{\beta}{\Lambda} n - \lambda_k C_k \quad (k = 1, \ldots, k_{max}) \end{aligned} \quad . \tag{78}$$

The components C_k can be expressed using the precursor equations in (78) as:

$$C_k = \frac{\beta_k}{\Lambda(\omega+\lambda_k)} n \quad (k = 1, \ldots, k_{max}) \quad . \tag{79}$$

Substituting this into the neutron-balance equation in (78) yields:

$$\omega n = \frac{\rho-\beta}{\Lambda} n + \sum_{k=1}^{k_{max}} \lambda_k \frac{\beta_k}{\Lambda(\omega+\lambda_k)} n \quad . \tag{80}$$

Note that the component n can be simplified out of the above and that by rearranging terms, the following expression for reactivity is obtained:

$$\rho = \Lambda\omega + \beta - \sum_{k=1}^{k_{max}} \lambda_k \frac{\beta_k}{(\omega+\lambda_k)} \quad . \tag{81}$$

Equation (81) is known as the *Inhour equation*. Its $k_{max}+1$ solutions determine the exponents of the $k_{max}+1$ fundamental solutions. To understand the nature of those solutions, it is useful to attempt a graphical solution of the Inhour equation by plotting its RHS as a function of ω and observing its intersection points with a horizontal line at $y = \rho$. Such a plot is shown in Fig. 1 for the case of six delayed-neutron groups.

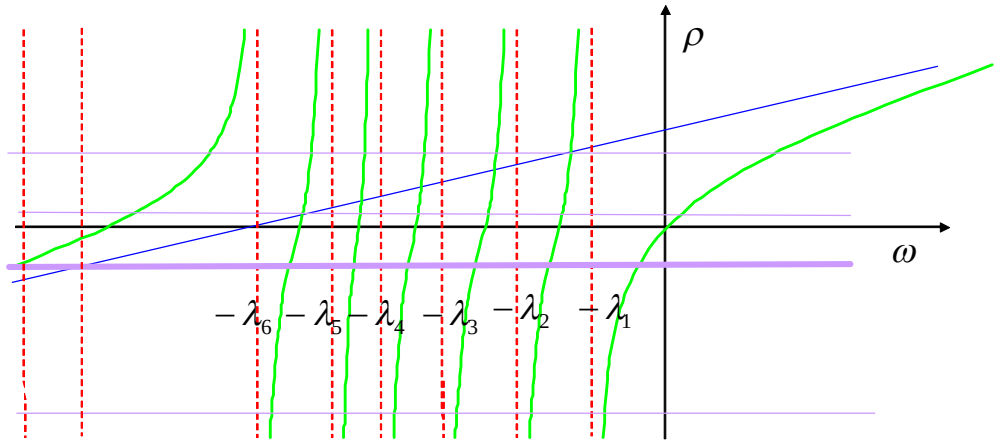

Figure 1 Graphical representation of the Inhour equation

For large (positive or negative) values of ω, the asymptotic behaviour of the RHS can be obtained as:

$$\rho = \Lambda\omega + \beta - \sum_{k=1}^{k_{max}} \lambda_k \frac{\beta_k}{\infty + \lambda_k} = \Lambda\omega + \beta \quad . \tag{82}$$

The resulting oblique asymptote is represented by the blue line in Fig. 1, and the RHS plot (shown in bright green) approaches it at both $-\infty$ and $+\infty$. Whenever ω equals minus the decay constant for one of the precursor groups, the RHS becomes infinite, and its plot has a vertical asymptote, shown as a (red) dashed line, at that value. For $\omega = 0$, the RHS vanishes, as can be seen from Eq. (81), and hence the plot passes through the origin of the coordinate system. Three horizontal lines, corresponding to three reactivity values, are shown in violet. The two thin lines correspond to positive values, and the thick line corresponds to the negative value.

Figure 1 shows that the solutions to the Inhour equation are distributed as follows:

- k_{max} - *1* solutions are located in the k_{max} - *1* intervals separating the k_{max} decay constants taken with negative signs, such that $-\lambda_k < \omega_{k-1} - \lambda_{k-1}$. All these solutions are negative.
- The largest solution, in an algebraic sense, is located to the right of $-\lambda_1$ and is either negative or positive, depending on the sign of the reactivity. It will be referred to as $\omega_{\max}$ or ω_0.
- The smallest solution, in an algebraic sense, lies to the left of $-\lambda_{k_{\max}}$ and will be referred to as $\omega_{\min}$ or $\omega_{k_{\max}}$. It is (obviously) negative as well. Note that because the generation time is usually less than 1 ms, and often less than 0.1 ms, the slope of the oblique asymptote is very small. Consequently, $\omega_{\min}$ is very far to the left of $-\lambda_{k_{\max}}$, and hence $\omega_{k_{\max}} \ll -\lambda_{k_{\max}} < \omega_{k_{\max}-1}$. The importance of this fact will become clearer later, when the prompt-jump approximation will be discussed.

Overall, the solutions are ordered as follows:

$$\omega_{\min} \equiv \omega_{k_{\max}} \ll \omega_{k_{\max}-1} < ..... < \omega_0 \equiv \omega_{\max} . \tag{83}$$

It is worth separating out the largest exponent in the general solution described by Eq. (77) by writing:

$$\begin{bmatrix} \hat{n}(t) \\ \hat{C}_1(t) \\ \vdots \\ \hat{C}_{k_{\max}}(t) \end{bmatrix} = a_0 \begin{bmatrix} n^0 \\ C_1^0 \\ \vdots \\ C_{k_{\max}}^0 \end{bmatrix} e^{\omega_0 t} + \sum_{l=1}^{k_{\max}} a_l \begin{bmatrix} n^l \\ C_1^l \\ \vdots \\ C_{k_{\max}}^l \end{bmatrix} e^{\omega_l t} . \tag{84}$$

Furthermore, it is worth factoring out the first exponential term:

$$\begin{bmatrix} \hat{n}(t) \\ \hat{C}_1(t) \\ \vdots \\ \hat{C}_{k_{\max}}(t) \end{bmatrix} = e^{\omega_0 t} \left(a_0 \begin{bmatrix} n^0 \\ C_1^0 \\ \vdots \\ C_{k_{\max}}^0 \end{bmatrix} + \sum_{l=1}^{k_{\max}} a_l \begin{bmatrix} n^l \\ C_1^l \\ \vdots \\ C_{k_{\max}}^l \end{bmatrix} e^{(\omega_l - \omega_0)t} \right) . \tag{85}$$

Note that because ω_0 is the largest solution, all exponents $(\omega_l - \omega_0)$ are negative. It follows that for large values of *t*, all exponentials of the type $e^{(\omega_l - \omega_0)t}$ nearly vanish, and hence the solution can be approximated by a single exponential term:

$$\begin{bmatrix} \hat{n}(t) \\ \hat{C}_1(t) \\ \vdots \\ \hat{C}_{k_{\max}}(t) \end{bmatrix} \cong a_0 \begin{bmatrix} n^0 \\ C_1^0 \\ \vdots \\ C_{k_{\max}}^0 \end{bmatrix} e^{\omega_0 t} . \tag{86}$$

This expression describes the *asymptotic transient behaviour*.

The inverse of $\omega_0 = \omega_{\max}$ is called the *asymptotic period*:

$$T \equiv \frac{1}{\omega_{\max}} . \tag{87}$$

With this new notation, the asymptotic behaviour can be written as:

$$\begin{bmatrix} \hat{n}(t) \\ \hat{C}_1(t) \\ \vdots \\ \hat{C}_{k_{\max}}(t) \end{bmatrix} \cong a_0 \begin{bmatrix} n^0 \\ C_1^0 \\ \vdots \\ C_{k_{\max}}^0 \end{bmatrix} e^{\frac{t}{T}} . \tag{88}$$

Before ending this sub-section, a few more comments are warranted. In particular, it is worth considering the solution to the *point-kinetics equation* (PKE) for three separate cases: negative

reactivity, zero reactivity, and positive reactivity.

Negative reactivity

In the case of negative reactivity, all exponents in the general solution are negative. It follows that over time, both the neutron population and the precursor concentrations will drop to zero. Of course, after a long time, the asymptotic behaviour applies, which has a negative exponent.

Zero reactivity

In the case of zero reactivity, $\omega_{\max}$ vanishes, and all other ω_l are negative. The general solution can be written as:

$$\begin{bmatrix} \hat{n}(t) \\ \hat{C}_1(t) \\ \vdots \\ \hat{C}_{k_{\max}}(t) \end{bmatrix} = a_0 \begin{bmatrix} n^0 \\ C_1^0 \\ \vdots \\ C_{k_{\max}}^0 \end{bmatrix} + \sum_{l=1}^{k_{\max}} a_l \begin{bmatrix} n^l \\ C_1^l \\ \vdots \\ C_{k_{\max}}^l \end{bmatrix} e^{\omega_l t} . \tag{89}$$

After a sufficiently long time, all the exponential terms die out, and the neutron and precursor populations stabilize at a constant value. Note that these populations do not need to remain constant from the beginning of the transient, but only to stabilize at a constant value.

Positive reactivity

In the case of positive reactivity, $\omega_{\max}$ is positive, and all other ω_l are negative. Hence, after sufficient time has elapsed, all but the first exponential term vanish, and the asymptotic behaviour is described by a single exponential which increases indefinitely.

4.5 Approximate Solution of the Point-Kinetics Equations: The Prompt Jump Approximation

It was mentioned in the preceding sub-section that the smallest (in an algebraic sense) solution of the Inhour equation is much smaller than the remaining k_{max} solutions. This important property will make it possible to introduce the *prompt jump approximation*, which is the topic of this sub-section.

By inspecting the Inhour plot in Figure 1, and keeping in mind the expression of the oblique asymptote given by Eq. (82), it is easy to notice that the oblique asymptote intersects the *x*-axis at:

$$\omega_{as} = \frac{\rho - \beta}{\Lambda} . \tag{90}$$

It is also easy to see that:

$$\omega_{k_{\max}+1} < \omega_{as} . \tag{91}$$

Assuming a reactivity smaller than approximately half the delayed-neutron fraction (equal to 0.0065 according to Table 1), and assuming a generation time of approximately 0.1 ms, the

resulting value of ω_{as} is approximately -32.5 s^{-1}, which is much smaller than even the largest decay constant in Table 1 taken with a negative sign. That value is only -3 s^{-1}. This shows that the following inequality holds true:

$$\omega_{\min} \equiv \omega_{k_{\max}} < \omega_{as} << \omega_{k_{\max}-1} < ..... < \omega_0 \equiv \omega_{\max} . \tag{92}$$

The general solution of the point-kinetics equations expressed by Eq. (77) can be processed to separate out the term corresponding to $\omega_{k_{\max}-1}$:

$$\begin{bmatrix} \hat{n}(t) \\ \hat{C}_1(t) \\ \vdots \\ \hat{C}_{k_{\max}}(t) \end{bmatrix} = e^{\omega_{k_{\max}-1}t} \left(a_{k_{\max}} \begin{bmatrix} n^0 \\ C_1^0 \\ \vdots \\ C_{k_{\max}}^0 \end{bmatrix} e^{\left(\omega_{k_{\max}} - \omega_{k_{\max}-1}\right)t} + a_{k_{\max}-1} \begin{bmatrix} n^{k_{\max}-1} \\ C_1^{k_{\max}-1} \\ \vdots \\ C_{k_{\max}}^{k_{\max}-1} \end{bmatrix} + \sum_{l=0}^{k_{\max}-2} a_l \begin{bmatrix} n^l \\ C_1^l \\ \vdots \\ C_{k_{\max}}^l \end{bmatrix} e^{\left(\omega_l - \omega_{k_{\max}-1}\right)t} \right) . \tag{93}$$

According to Eq. (92), for $l \le k_{\max} - 2$, all exponents of the type $\left(\omega_l - \omega_{k_{\max}-1}\right)t$ are positive. The only negative exponent is $\left(\omega_{k_{\max}} - \omega_{k_{\max}-1}\right)t$, which is also much larger in absolute value than all other exponents. It follows that after a very short time, *t*, the first term of the RHS of Eq. (93) becomes negligible, and the solution of the point-kinetics equations can then be approximated by:

$$\begin{bmatrix} \hat{n}(t) \\ \hat{C}_1(t) \\ \vdots \\ \hat{C}_{k_{\max}}(t) \end{bmatrix} \cong e^{\omega_{k_{\max}-1}t} \left(a_{k_{\max}-1} \begin{bmatrix} n^{k_{\max}-1} \\ C_1^{k_{\max}-1} \\ \vdots \\ C_{k_{\max}}^{k_{\max}-1} \end{bmatrix} + \sum_{l=0}^{k_{\max}-2} a_l \begin{bmatrix} n^l \\ C_1^l \\ \vdots \\ C_{k_{\max}}^l \end{bmatrix} e^{\left(\omega_l - \omega_{k_{\max}-1}\right)t} \right) = \sum_{l=0}^{k_{\max}-1} a_l \begin{bmatrix} n^l \\ C_1^l \\ \vdots \\ C_{k_{\max}}^l \end{bmatrix} e^{\omega_l t} . \tag{94}$$

Concentrating on the neutron population, its expression is:

$$\hat{n}(t) \cong \sum_{l=0}^{k_{\max}-1} a_l n^l e^{\omega_l t} . \tag{95}$$

Substituting this into the neutron-balance equation of the point-kinetics system, the following is obtained:

$$\sum_{l=1}^{k_{\max}-1} \omega_l a_l n^l e^{\omega_l t} = \sum_{l=1}^{k_{\max}-1} \frac{\rho - \beta}{\Lambda} a_l n^l e^{\omega_l t} + \sum_{k=1}^{k_{\max}} \lambda_k \hat{C}_k . \tag{96}$$

Noting that the following inequality holds true:

$$\left|\omega_l\right| << \left|\frac{\rho - \beta}{\Lambda}\right| \quad l = 0, ...k_{\max} - 1 , \tag{97}$$

the LHS of Eq. (96) can be approximated to vanish, and hence the equation can be approximated by:

$$0 = \sum_{l=1}^{k_{\max}-1} \frac{\rho-\beta}{\Lambda} a_l n^l e^{\omega_l t} + \sum_{k=1}^{k_{\max}} \lambda_k \hat{C}_k \quad , \tag{98}$$

which is equivalent to:

$$0 = \frac{\rho-\beta}{\Lambda} \hat{n}(t) + \sum_{k=1}^{k_{\max}} \lambda_k \hat{C}_k(t) \quad . \tag{99}$$

By adding the precursor-balance equations, the following approximate point-kinetics equations are obtained:

$$\begin{aligned} 0 &= \frac{\rho-\beta}{\Lambda} \hat{n}(t) + \sum_{k=1}^{k_{\max}} \lambda_k \hat{C}_k(t) \\ \frac{d\hat{C}_k(t)}{dt} &= \frac{\beta_k}{\Lambda} \hat{n}(t) - \lambda_k \hat{C}_k(t) \quad (k = 1, \ldots, k_{\max}) \end{aligned} \quad . \tag{100}$$

This system of k_{max} differential equations and one algebraic equation is known as the *prompt jump approximation* of the point-kinetics equations. The name comes from the fact that whenever a step reactivity change occurs, the prompt jump approximation results in a step change, a *prompt jump*, in the neutron population. To demonstrate this behaviour, let the reactivity change from ρ_1 to ρ_2 at time t_0. The neutron-balance equation before and after t_0 can be written as:

$$\begin{aligned} &\frac{\rho_1-\beta}{\Lambda} \hat{n}(t) + \sum_{k=1}^{k_{\max}} \lambda_k \hat{C}_k(t) \quad (t < t_0) \\ &\frac{\rho_2-\beta}{\Lambda} \hat{n}(t) + \sum_{k=1}^{k_{\max}} \lambda_k \hat{C}_k(t) \quad (t > t_0) \end{aligned} \quad . \tag{101}$$

The limit of the neutron population as t approaches t_0 from the left, symbolically denoted as $\hat{n}(t_0^-)$, is found from the first equation (101) to be equal to:

$$\hat{n}(t_0^-) = \frac{\Lambda}{\rho_1-\beta} \sum_{k=1}^{k_{\max}} \lambda_k \hat{C}_k(t_0) \quad . \tag{102}$$

Similarly, the limit of the neutron population as t approaches t_0 from the right, symbolically denoted as $\hat{n}(t_0^+)$, is found from the second equation (101) to be equal to:

$$\hat{n}(t_0^+) = \frac{\Lambda}{\rho_2-\beta} \sum_{k=1}^{k_{\max}} \lambda_k \hat{C}_k(t_0) \quad . \tag{103}$$

Taking the ratio of the preceding two equations side by side, the following is obtained:

$$\frac{\hat{n}(t_0^+)}{\hat{n}(t_0^-)} = \frac{\rho_1-\beta}{\rho_2-\beta} \quad . \tag{104}$$

There is therefore a jump $\Delta\hat{n}(t_0)$ equal to:

$$\Delta\hat{n}(t_0) = \hat{n}(t_0^+) - \hat{n}(t_0^-) = \hat{n}(t_0^-)\frac{\rho_1 - \beta}{\rho_2 - \beta} - \hat{n}(t_0^-) = \frac{\rho_1 - \rho_2}{\rho_2 - \beta}\hat{n}(t_0^-) \quad . \tag{105}$$

Of course, the actual neutron population does not display such a jump; it is continuous at t_0. Nonetheless, a very short time Δt after t_0 (at $t_0 + \Delta t$), the approximate and exact neutron populations become almost equal. Note also that Eq. (105) is valid only if both reactivities ρ_1 and ρ_2 are less than the effective delayed-neutron fraction β.

5 Space-Time Kinetics using Flux Factorization

In the previous sections, the time-dependent behaviour of a reactor was studied using the simple point-kinetics model, which disregards changes in the spatial distribution of the neutron density. This section will improve on that model by presenting the general outline of space-time kinetics using flux factorization. The approach follows roughly that used in [Rozon1998] and [Ott1985]. A complete and thorough treatment of the topic of space-time kinetics is beyond the scope of this text. This section should therefore be regarded merely as a roadmap. The interested reader is encouraged to study the more detailed treatments in [Rozon1998], [Ott1985], and [Stacey1970].

5.1 Time-, Energy-, and Space-Dependent Multigroup Diffusion Equation

The space-time description of reactor kinetics starts with the time-, space-, and energy-dependent diffusion equation. An equivalent treatment starting from the transport equation is also possible, but using the transport equation instead of the diffusion equation does not introduce fundamentally different issues, and the mathematical treatment is somewhat more cumbersome. The time-, space- and energy-dependent neutron diffusion equation in the multigroup approximation can be written as follows:

$$\begin{aligned}
&\frac{1}{\overline{\nu}_g}\frac{\partial}{\partial t}\Phi_g(\vec{r},t) = \\
&\nabla\cdot\left[D_g(\vec{r},t)\nabla\Phi_g(\vec{r},t)\right] - \Sigma_{rg}(\vec{r},t)\Phi_g(\vec{r},t) + \sum_{g'\neq g}\Sigma_{sg'\to g}(\vec{r},t)\Phi_{g'}(\vec{r},t) + \\
&\chi_{pg}(\vec{r},t)\sum_{g'}\nu_p(\vec{r},t)\Sigma_{fg'}(\vec{r},t)\Phi_{g'}(\vec{r},t) + \sum_{k=1}^{k_{\max}}\chi_{dg}^k(\vec{r},t)\lambda_k C_k(\vec{r},t)
\end{aligned} \quad . \tag{106}$$

The accompanying precursor-balance equations are written as:

$$\frac{\partial}{\partial t}c_k(\vec{r},t) = \sum_{g'}\nu_{pk}(\vec{r},t)\Sigma_{fg'}(\vec{r},t)\Phi_{g'}(\vec{r},t) - \lambda_k C_k(\vec{r},t) \quad . \tag{107}$$

Equations (106) and (107) represent the space-time kinetics equations in their diffusion approximation. Their solution is the topic of this section.

It is advantageous for the development of the space-time kinetics formalism to introduce a set of multidimensional vectors and operators, as follows:

Flux vector

$$\mathbf{\Phi}\left(\vec{r},t\right)=\left[\Phi_g\left(\vec{r},t\right)\right] \tag{108}$$

Precursor vector

$$\boldsymbol{\xi}_k(\vec{r},t)=\left[\chi_{dg}^k C_k(\vec{r},t)\right] \tag{109}$$

Loss operator

$$\mathbf{M}\left(\vec{r},t\right)=\nabla\cdot\left[D_g(\vec{r},t)\nabla\Phi_g(\vec{r},t)\right]-\Sigma_{rg}(\vec{r},t)\Phi_g(\vec{r},t)+\sum_{g'\neq g}\Sigma_{sg'\to g}(\vec{r},t)\Phi_{g'}(\vec{r},t) \tag{110}$$

Prompt production operator

$$\mathbf{F}_p(\vec{r},t)=\chi_{pg}(\vec{r},t)\sum_{g'}\nu_p(\vec{r},t)\Sigma_{fg'}(\vec{r},t)\Phi_{g'}(\vec{r},t) \tag{111}$$

Precursor production operator for precursor group *k*

$$\mathbf{F}_{dk}(\vec{r},t)=\chi_{dg}^k(\vec{r},t)\lambda_k C_k(\vec{r},t) \tag{112}$$

Inverse-speed operator

$$\mathbf{v}^{-1}=\frac{1}{\overline{\mathrm{v}}_g}\delta_{g'g}, \tag{113}$$

where $\delta_{g'g}$ is the Kronecker delta symbol.

Using these definitions, the time-dependent multigroup diffusion equation can be written in compact form as:

$$\frac{\partial}{\partial t}\mathbf{v}^{-1}\mathbf{\Phi}\left(\vec{r},t\right)=-\mathbf{M}(\vec{r},t)\mathbf{\Phi}\left(\vec{r},t\right)+\mathbf{F}_p(\vec{r},t)\mathbf{\Phi}\left(\vec{r},t\right)+\sum_{k=1}^{k_{\max}}\lambda_k\boldsymbol{\xi}_k(\vec{r},t). \tag{114}$$

The precursor-balance equations can be written as:

$$\frac{\partial}{\partial t}\boldsymbol{\xi}_k(\vec{r},t)=\mathbf{F}_{dk}(\vec{r},t)\mathbf{\Phi}\left(\vec{r},t\right)-\lambda_k\boldsymbol{\xi}_k(\vec{r},t)\quad(k=1,\ldots,k_{\max}). \tag{115}$$

As a last definition, for two arbitrary vectors $\mathbf{\Phi}(\vec{r},t)$ and $\mathbf{\Psi}(\vec{r},t)$, the inner product is defined as:

$$\left\langle\mathbf{\Phi},\mathbf{\Psi}\right\rangle=\sum_g\int_{V_{core}}\Phi_g(\vec{r},t)\Psi_g(\vec{r},t)dV. \tag{116}$$

5.2 Flux Factorization

Expressing a function as a product of several (simpler) functions is known as *factorization*. It is a well-known fact from partial differential equations that trying to express the solution as a product of single-variable functions often simplifies the mathematical treatment. It is therefore reasonable to attempt a similar approach for the space-time kinetics problem. A first step in this approach is to factorize the time-, energy-, and space-dependent solution into a function

dependent only on time and a vector dependent on energy, space, and time. The function dependent only on time is called an *amplitude function*, and the vector dependent on space, energy, and time is called a *shape function*. The sought-for flux can therefore be expressed as:

$$\mathbf{\Phi}(\vec{r},t) = p(t)\mathbf{\Psi}(\vec{r},t) \quad . \tag{117}$$

Such a factorization is always possible, regardless of the definition of the function *p(t)*. In this case, the function *p(t)* is defined as follows:

$$p(t) \equiv \left\langle \mathbf{w}(\vec{r}), \mathbf{v}^{-1}\mathbf{\Phi}(\vec{r},t) \right\rangle \quad , \tag{118}$$

where $\mathbf{w}(\vec{r})$ is an arbitrary weight vector dependent only on energy and position:

$$\mathbf{w}(\vec{r}) = \left[w_g(\vec{r}) \right] \quad . \tag{119}$$

According to its definition, *p(t)* can be interpreted as a generalized neutron population. Indeed, if the weight function were chosen to be unity, *p(t)* would be exactly equal to the neutron population.

From the definition of the flux factorization, it follows that the shape vector $\mathbf{\Psi}(\vec{r},t)$ satisfies the following normalization condition:

$$\left\langle \mathbf{w}(\vec{r}), \mathbf{v}^{-1}\mathbf{\Psi}(\vec{r},t) \right\rangle = 1 \quad . \tag{120}$$

Substituting the factorized form of the flux into the space-, energy-, and time-dependent diffusion equation, the following equations (representing respectively the neutron and precursor balance) result:

$$\frac{dp(t)}{dt}\mathbf{v}^{-1}\mathbf{\Psi}(\vec{r},t) + p(t)\frac{\partial}{\partial t}\left[\mathbf{v}^{-1}\mathbf{\Psi}(\vec{r},t)\right] = -p(t)\mathbf{M}(\vec{r},t)\mathbf{\Psi}(\vec{r},t) + p(t)\mathbf{F}_p(\vec{r},t)\mathbf{\Psi}(\vec{r},t) + \sum_{k=1}^{k_{\max}} \lambda_k \xi_k(\vec{r},t) \quad . \tag{121}$$

$$\frac{\partial}{\partial t}\xi_k(\vec{r},t) = p(t)\mathbf{F}_{dk}(\vec{r},t)\mathbf{\Psi}(\vec{r},t) - \lambda_k \xi_k(\vec{r},t) \quad (k = 1,\ldots,k_{\max}) \quad . \tag{122}$$

The precursor-balance equation can be solved formally to give:

$$\xi_k(\vec{r},t) = \xi_k(\vec{r},0)e^{-\lambda_k t} + \int_0^t e^{-\lambda_k (t-t')} p(t')\mathbf{F}_{dk}(\vec{r},t')\mathbf{\Psi}(\vec{r},t')dt' \quad . \tag{123}$$

By taking the inner product with the weight vector $\mathbf{w}(\vec{r})$ on both sides of the neutron-balance equation and the precursor-balance equation, the following is obtained:

$$\frac{dp(t)}{dt}\left\langle \mathbf{w}(\vec{r}); \mathbf{v}^{-1}\mathbf{\Psi}(\vec{r},t) \right\rangle + p(t)\frac{d}{dt}\left\langle \mathbf{w}(\vec{r}); \mathbf{v}^{-1}\mathbf{\Psi}(\vec{r},t) \right\rangle = - p(t)\left\langle \mathbf{w}(\vec{r}); \mathbf{M}(\vec{r},t)\mathbf{\Psi}(\vec{r},t) \right\rangle + p(t)\left\langle \mathbf{w}(\vec{r}); \mathbf{F}_p(\vec{r},t)\mathbf{\Psi}(\vec{r},t) \right\rangle + \sum_{k=1}^{k_{\max}} \lambda_k \left\langle \mathbf{w}(\vec{r}); \xi_k(\vec{r},t) \right\rangle \quad . \tag{124}$$

$$\frac{\partial}{\partial t}\left\langle \mathbf{w}(\vec{r});\xi_k(\vec{r},t)\right\rangle = p(t)\left\langle \mathbf{w}(\vec{r});\mathbf{F}_{dk}(\vec{r},t)\boldsymbol{\Psi}\left(\vec{r},t\right)\right\rangle - \lambda_k\left\langle \mathbf{w}(\vec{r});\xi_k(\vec{r},t)\right\rangle \quad (k=1,\ldots,k_{\max}) \tag{125}$$

Equations (124) and (125) can be processed into more elegant forms akin to the point-kinetics equations. To do this, some quantities must be defined first which will prove to be generalizations of the same quantities defined for the point-kinetics equations.

5.3 Effective Generation Time, Effective Delayed-Neutron Fraction, and Dynamic Reactivity

The following quantities and symbols are introduced:

Total production operator

$$\mathbf{F}(\vec{r},t) = \mathbf{F}_p(\vec{r},t) + \mathbf{F}_d(\vec{r},t) \tag{126}$$

Dynamic reactivity

$$\rho(t) = \frac{\left\langle \mathbf{w}(\vec{r}),\mathbf{F}(\vec{r},t)\boldsymbol{\Psi}(\vec{r},t)\right\rangle - \left\langle \mathbf{w}(\vec{r}),\mathbf{M}(\vec{r},t)\boldsymbol{\Psi}(\vec{r},t)\right\rangle}{\left\langle \mathbf{w}(\vec{r}),\mathbf{F}(\vec{r},t)\boldsymbol{\Psi}(\vec{r},t)\right\rangle} \tag{127}$$

Effective generation time

$$\Lambda(t) = \frac{\left\langle \mathbf{w}(\vec{r}),\mathbf{v}^{-1}\boldsymbol{\Psi}(\vec{r},t)\right\rangle}{\left\langle \mathbf{w}(\vec{r}),\mathbf{F}(\vec{r},t)\boldsymbol{\Psi}(\vec{r},t)\right\rangle} \tag{128}$$

Effective delayed-neutron fraction for delayed group *k*

$$\beta_k(t) = \frac{\left\langle \mathbf{w}(\vec{r}),\mathbf{F}_{dk}(\vec{r},t)\boldsymbol{\Psi}(\vec{r},t)\right\rangle}{\left\langle \mathbf{w}(\vec{r}),\mathbf{F}(\vec{r},t)\boldsymbol{\Psi}(\vec{r},t)\right\rangle} \tag{129}$$

Total effective delayed-neutron fraction

$$\beta(t) = \sum_{k=1}^{k_{\max}} \beta_k(t) \tag{130}$$

Group *k* (generalized) precursor population

$$\hat{C}_k(t) = \left\langle \mathbf{w}(\vec{r}),\xi_k(\vec{r},t)\right\rangle \tag{131}$$

With the newly introduced quantities, Eqs. (124) and (125) can be rewritten in the familiar form of the point-kinetics equations:

$$\dot{p}(t) = p(t)\frac{\rho(t)-\beta(t)}{\Lambda(t)} + \sum_{k=1}^{k_{\max}} \lambda_k \hat{C}_k(t)$$
$$\frac{\partial}{\partial t}\hat{C}_k(t) = p(t)\frac{\beta_k(t)}{\Lambda(t)} - \lambda_k \hat{C}_k(t) \quad (k=1,\ldots,k_{\max}) \tag{132}$$

Of course, to be able to define quantities such as the dynamic reactivity, the shape vector

$\boldsymbol{\Psi}(\vec{r},t)$ must be known or approximated at each time *t*. Different shape representations $\boldsymbol{\Psi}(\vec{r},t)$ lead to different space-time kinetics models. All flux-factorization models alternate between calculating the shape vector $\boldsymbol{\Psi}(\vec{r},t)$ and solving the point-kinetics-like equations (132) for the amplitude function and the precursor populations. The detailed energy- and space-dependent flux shape at each time *t* can subsequently be reconstructed by multiplying the amplitude function by the shape vector.

5.4 Improved Quasistatic Model

The *improved quasistatic* (IQS) *model* uses an exact shape $\boldsymbol{\Psi}(\vec{r},t)$. By substituting the formal solution to the precursor equations (123) into the general neutron-balance equation (121), the following equation for the shape vector is obtained:

$$\frac{dp(t)}{dt}\mathbf{v}^{-1}\boldsymbol{\Psi}\left(\vec{r},t\right)+p(t)\frac{\partial}{\partial t}\left[\mathbf{v}^{-1}\boldsymbol{\Psi}\left(\vec{r},t\right)\right]=-p(t)\mathbf{M}(\vec{r},t)\boldsymbol{\Psi}\left(\vec{r},t\right)+$$
$$p(t)\mathbf{F}_p(\vec{r},t)\boldsymbol{\Psi}\left(\vec{r},t\right)+$$
$$\sum_{k=1}^{k_{\max}}\lambda_k\left(\xi_k(0)e^{-\lambda_k t}+\int_0^t e^{-\lambda_k(t-t')}p(t')\mathbf{F}_{dk}(\vec{r},t')\boldsymbol{\Psi}(\vec{r},t')dt'\right). \qquad (133)$$

The IQS model alternates between solving the point-kinetics-like equations (132) and the shape equation (133). The corresponding IQS numerical method uses two sizes of time interval. Because the amplitude function varies much more rapidly with time than the shape vector, the time interval used to solve the point-kinetics-like equations is much smaller than that used to solve for the shape vector. Note that, other than the time discretization, the IQS model and method include no approximation. The actual shape of the weight vector $\mathbf{w}(\vec{r})$ is irrelevant.

5.5 Quasistatic Approximation

The quasistatic approximation is derived by neglecting the time derivative of the shape vector in the shape-vector equation (133). The resulting equation, which is solved at each time step, is:

$$\frac{dp(t)}{dt}\mathbf{v}^{-1}\boldsymbol{\Psi}\left(\vec{r},t\right)=-p(t)\mathbf{M}(\vec{r},t)\boldsymbol{\Psi}\left(\vec{r},t\right)+$$
$$p(t)\mathbf{F}_p(\vec{r},t)\boldsymbol{\Psi}\left(\vec{r},t\right)+\sum_{k=1}^{k_{\max}}\lambda_k\left(\xi_k(0)e^{-\lambda_k t}+\int_0^t e^{-\lambda_k(t-t')}p(t')\mathbf{F}_{dk}(\vec{r},t')\boldsymbol{\Psi}(\vec{r},t')dt'\right). \qquad (134)$$

The resulting shape is used to calculate the point-kinetics parameters, which are then used in the point-kinetics-like equations (132). As in the case of the IQS model, Equation (134) is solved in conjunction with the point-kinetics-like equations (132). Aside from the slightly modified shape equation, the quasistatic model differs from the IQS model in the values of its point-kinetics parameters, which are now calculated using an approximate shape vector.

5.6 Adiabatic Approximation

The adiabatic approximation completely does away with any time derivative in the shape equation and instead solves the static eigenvalue problem at each time *t*:

$$\mathbf{M}(\vec{r},t)\boldsymbol{\Psi}\left(\vec{r},t\right)=\frac{1}{k}\mathbf{F}\ (\vec{r},t)\boldsymbol{\Psi}(\vec{r},t) \quad . \tag{135}$$

The resulting shape is used to calculate the point-kinetics parameters, which are then used in the point-kinetics-like equations (132). As in the case of the IQS and quasistatic models, Equation (135) is solved in conjunction with the point-kinetics-like equations (132).

5.7 Point-Kinetics Approximation (Rigorous Derivation)

In the case of the point-kinetics model, the shape vector is determined only once at the beginning of the transient (*t=0*) by solving the static eigenvalue problem:

$$\mathbf{M}(\vec{r},0)\boldsymbol{\Psi}\left(\vec{r}\right)=\frac{1}{k}\mathbf{F}\ (\vec{r},0)\boldsymbol{\Psi}(\vec{r}) \quad . \tag{136}$$

The resulting shape is used to calculate the point-kinetics parameters, which are then used in the point-kinetics-like equations (132). Because the shape vector is not updated, only the point-kinetics-like equations (132) are solved at each time *t*. In fact, they are now the true point-kinetics equations because the shape vector remains constant over time. This discussion has shown that the point-kinetics equations can also be derived for an inhomogeneous reactor, as long as the flux is factorized into a shape vector depending only on energy and position and an amplitude function depending only on time.

6 Perturbation Theory

It should be obvious by now that different approximations of the shape vector lead to different values for the kinetics parameters. It is therefore of interest to determine whether certain choices of the weight vector might maintain the accuracy of the kinetics parameters even when approximate shape vectors are used. In particular, it would be interesting to obtain accurate values of the dynamic reactivity, which is the determining parameter for any transient. The issue of determining the weight function that leads to the smallest errors in reactivity when small errors exist in the shape vector is addressed by *perturbation theory*. This section will present without proof some important results of perturbation theory. The interested reader is encouraged to consult [Rozon1998], [Ott1985], and [Stacey1970] for detailed proofs and additional results.

6.1 Essential Results from Perturbation Theory

Perturbation theory analyzes the effect on reactivity of small changes in reactor cross sections with respect to an initial critical state, called the *reference* state. These changes are called *perturbations*, and the resulting state is called the *perturbed* state. Perturbation theory also analyzes the effect of calculating the reactivity using approximate rather than exact flux shapes. First-order perturbation theory states that the weight vector that achieves the best first-order approximation of the reactivity (e.g., for the point-kinetics equations) when using an approximate (rather than an exact) flux shape is the *adjoint function*, which is defined as the solution to the *adjoint* static eigenvalue problem for the initial critical state at *t*=0:

$$\mathbf{M}^{*}(\vec{r},0)\boldsymbol{\Psi}^{*}\left(\vec{r},0\right)=\mathbf{F}^{*}(\vec{r},0)\boldsymbol{\Psi}^{*}\left(\vec{r},0\right) \quad . \tag{137}$$

The adjoint problem differs from the usual *direct* problem in that all operators are replaced by

their *adjoint* counterparts. The *adjoint* A^* of an operator *A* is the operator which, for any arbitrary vectors $\mathbf{\Phi}(\vec{r},t)$ and $\mathbf{\Psi}(\vec{r},t)$, satisfies:

$$\left\langle \mathbf{\Phi}, A\mathbf{\Psi} \right\rangle = \left\langle A^*\mathbf{\Phi}, \mathbf{\Psi} \right\rangle . \tag{138}$$

The reactivity at time *t* can therefore be expressed as:

$$\rho(t) = \frac{\left\langle \mathbf{\Psi}^*(\vec{r},0), \mathbf{F}(\vec{r},t)\mathbf{\Psi}(\vec{r},t) \right\rangle - \left\langle \mathbf{\Psi}^*(\vec{r},0), \mathbf{M}(\vec{r},t)\mathbf{\Psi}(\vec{r},t) \right\rangle}{\left\langle \mathbf{\Psi}^*(\vec{r},0), \mathbf{F}(\vec{r},t)\mathbf{\Psi}(\vec{r},t) \right\rangle} . \tag{139}$$

The remaining point-kinetics parameters can be expressed similarly using the initial adjoint as the weight function.

An additional result from perturbation theory states that when the adjoint function is used as the weight function, the reactivity resulting from small perturbations applied to an initially critical reactor can be calculated as:

$$\rho(t) = \frac{\left\langle \mathbf{\Psi}^*(\vec{r},0), \delta\mathbf{F}(\vec{r},t)\mathbf{\Psi}(\vec{r},0) \right\rangle - \left\langle \mathbf{\Psi}^*(\vec{r},0), \delta\mathbf{M}(\vec{r},t)\mathbf{\Psi}(\vec{r},0) \right\rangle}{\left\langle \mathbf{\Psi}^*(\vec{r},0), \mathbf{F}(\vec{r},0)\mathbf{\Psi}(\vec{r},0) \right\rangle} , \tag{140}$$

where the δ symbols represent *perturbations* (changes) in the respective operators with respect to the initial critical state. Equation (140) offers a simpler way of calculating the reactivity than Eq. (139) because it does not require recalculation of the shape vector at each time *t*. Note that, within first-order of approximation, the calculated reactivity is also equal to the static reactivity at time *t*, defined as:

$$\rho(t) = 1 - \frac{1}{k_{eff}(t)} . \tag{141}$$

In fact, perturbation theory can also be used to calculate the (static) reactivity when the initial unperturbed state is not critical. In that case, the change in reactivity is calculated as:

$$\Delta\rho = \frac{1}{k_{eff}^0} - \frac{1}{k_{eff}} = \frac{\left\langle \mathbf{\Psi}_0^*, \frac{1}{k_{eff}^0}\delta\mathbf{F}\mathbf{\Psi}_0 \right\rangle - \left\langle \mathbf{\Psi}_0^*, \delta\mathbf{M}\mathbf{\Psi}_0 \right\rangle}{\left\langle \mathbf{\Psi}_0^*, \mathbf{F}\mathbf{\Psi}_0 \right\rangle} . \tag{142}$$

In Eq. (142), the "0" subscript or superscript denotes the unperturbed state. Finally, for one-energy-group representations, the direct flux and the adjoint function are equal. It follows that in a one-group representation, the reactivity at time *t* can be expressed as:

$$\rho(t) = \frac{\left\langle \mathbf{\Psi}(\vec{r},0), \delta\mathbf{F}(\vec{r},t)\mathbf{\Psi}(\vec{r},0) \right\rangle - \left\langle \mathbf{\Psi}(\vec{r},0), \delta\mathbf{M}(\vec{r},t)\mathbf{\Psi}(\vec{r},0) \right\rangle}{\left\langle \mathbf{\Psi}(\vec{r},0), \mathbf{F}(\vec{r},0)\mathbf{\Psi}(\vec{r},0) \right\rangle} =$$

$$\frac{\int_{V_{core}} \Phi^2(\vec{r},0)\left(\delta\nu\Sigma_f - \delta\Sigma_a\right)dV}{\int_{V_{core}} \Phi^2(\vec{r},0)\nu\Sigma_f dV} . \tag{143}$$

More generally, the static reactivity change between any two states, which is the equivalent of Eq. (142), can be expressed using one-group diffusion theory as:

$$\Delta\rho = \frac{1}{k_{eff}^0} - \frac{1}{k_{eff}} = \frac{\int\limits_{V_{core}} \Phi_0^2(\vec{r})\left(\frac{1}{k_{eff}^0}\delta\nu\Sigma_f - \delta\Sigma_a\right)dV}{\int\limits_{V_{core}} \Phi_0^2(\vec{r})\nu\Sigma_{f0}dV} \quad . \tag{144}$$

6.2 Device Reactivity Worth

Reactivity devices are devices, usually rods, made of material with high neutron-absorption cross section. By inserting or removing a device, the reactivity of the reactor can be changed, and hence the power can be decreased or increased. The *reactivity worth* of a device is defined as the difference between the reactivity of the core with the device inserted and the reactivity of the same core with the device removed. Looking at this situation through a perturbation-theory lens, the reactor without the reactivity device can be regarded as the unperturbed system, and the reactor with the reactivity device can be regarded as the perturbed system. Perturbation theory offers interesting insights into reactivity worth. Considering a device that is inserted into a critical reactor and which, after insertion, occupies volume V_d in the reactor, according to the perturbation formula for reactivity, the reactivity worth of the device is:

$$\Delta\rho_d = \frac{1}{k_{eff}^0} - \frac{1}{k_{eff}^d} = \frac{\int\limits_{V_d} \Phi_0^2\left[\frac{1}{k_{eff}^0}\left(\nu\Sigma_{fd} - \nu\Sigma_{f0}\right) - \left(\Sigma_{ad} - \Sigma_{a0}\right)\right]dV}{\int\limits_{V_{core}} \Phi_0^2\nu\Sigma_{f0}dV} \quad . \tag{145}$$

Note that the integral in the numerator is over the device volume only and that the integral in the denominator does not change as the device moves, thus simplifying the calculations. Moreover, if two devices are introduced, their combined reactivity worth is:

$$\Delta\rho_{d1+d2} = \frac{\int\limits_{V_{d1}} \Phi_0^2\left[\frac{1}{k_{eff}^0}\left(\nu\Sigma_{fd1} - \nu\Sigma_{f0}\right) - \left(\Sigma_{ad1} - \Sigma_{a0}\right)\right]dV}{\int\limits_{V_{core}} \Phi_0^2\nu\Sigma_{f0}dV} + \frac{\int\limits_{V_{d2}} \Phi_0^2\left[\frac{1}{k_{eff}^0}\left(\nu\Sigma_{fd2} - \nu\Sigma_{f0}\right) - \left(\Sigma_{ad2} - \Sigma_{a0}\right)\right]dV}{\int\limits_{V_{core}} \Phi_0^2\nu\Sigma_{f0}dV} =$$

$$\Delta\rho_{d1} + \Delta\rho_{d2} \quad . \tag{146}$$

The interpretation of this equation is that as long as devices are not too close together and do not have too large reactivity worths (so that the assumptions of perturbation theory remain valid), their reactivity worths are additive.

7 Fission-Product Poisoning

Poisons are nuclides with large absorption cross sections for thermal neutrons. Some poisons are introduced intentionally to control the reactor, such as B or Gd. Some poisons are produced as fission products during normal reactor operation. Xe and Sm are the most important of these.

7.1 Effects of Poisons on Reactivity

The effect of poisons on a reactor will be studied for a simple model of a homogeneous reactor modelled using one-group diffusion theory. For such a reactor, in a one-energy-group formalism:

$$k_{eff}^0 = \frac{\nu\Sigma_f}{\Sigma_{a0} + DB_g^2} . \tag{147}$$

Uniform concentration

If a poison such as Xe with microscopic cross section σ_{ax} is added with a uniform concentration (number density) *X*, the macroscopic absorption cross section increases by:

$$\Sigma_{aX} = X\sigma_{aX} . \tag{148}$$

The total macroscopic absorption cross section is now:

$$\Sigma_a = \Sigma_{a0} + \Sigma_{aX} , \tag{149}$$

and the new effective multiplication constant is:

$$k_{eff} = \frac{\nu\Sigma_f}{\Sigma_a + DB_g^2} = \frac{\nu\Sigma_f}{\Sigma_{a0} + \Sigma_{aX} + DB_g^2} . \tag{150}$$

Addition of the poison induces a change in reactivity:

$$\Delta\rho = \rho - \rho_0 = \left(1 - \frac{1}{k_{eff}}\right) - \left(1 - \frac{1}{k_{eff}^0}\right) = \frac{1}{k_{eff}^0} - \frac{1}{k_{eff}} =$$
$$\frac{\Sigma_{a0} + DB^2}{\nu\Sigma_f} - \frac{\Sigma_{a0} + \Sigma_{aX} + DB^2}{\nu\Sigma_f} =$$
$$-\frac{\Sigma_{aX}}{\nu\Sigma_f} = -\frac{X\sigma_{aX}}{\nu\Sigma_f} . \tag{151}$$

To calculate the reactivity inserted by the poison, the concentration of poison nuclei, *X*, must first be determined.

Non-uniform concentration

In the case of non-uniform poison concentration, the perturbation formula for reactivity can be

used:

$$\Delta\rho = \frac{1}{k_0} - \frac{1}{k} = -\frac{\int_V \Phi^2(\vec{r})\delta\Sigma_a(\vec{r})dV}{\int_V \Phi^2(\vec{r})\nu\Sigma_f(\vec{r})dV} = \frac{\int_V \Phi^2(\vec{r})\Sigma_{aX}(\vec{r})dV}{\int_V \Phi^2(\vec{r})\nu\Sigma_f(\vec{r})dV} = -\frac{\int_V \Phi^2(\vec{r})X(\vec{r})\sigma_{aX}dV}{\int_V \Phi^2(\vec{r})\nu\Sigma_f(\vec{r})dV} \quad . \qquad (152)$$

It can easily be seen that if the distribution is uniform, the previous formula is recovered:

$$\Delta\rho = \frac{1}{k_0} - \frac{1}{k} = -\frac{\Sigma_{aX}\int_V \Phi^2(\vec{r})dV}{\nu\Sigma_f \int_V \Phi^2(\vec{r})dV} = -\frac{\Sigma_{aX}}{\nu\Sigma_f} \quad . \qquad (153)$$

In the next sub-section, specific aspects of fission-product poisoning will be illustrated for the case of Xe.

7.2 Xenon Effects

7.2.1 ^{135}Xe production and destruction

The mechanisms of ^{135}Xe production and destruction are illustrated in Fig. 2.

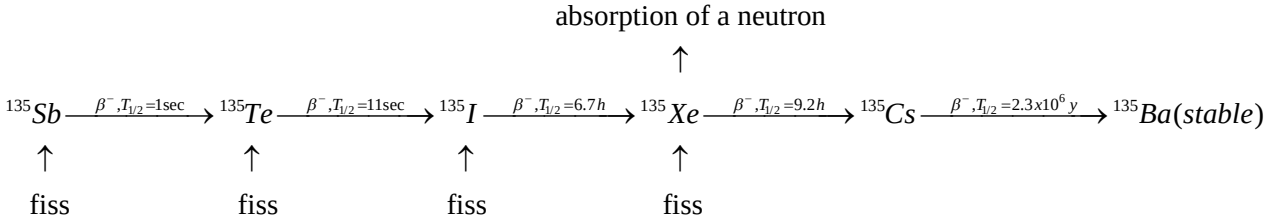

Figure 2 ^{135}Xe production and destruction mechanisms

Because ^{135}Sb decays very rapidly into ^{135}Te, which in turn decays very rapidly into ^{135}I, as an approximation, ^{135}I can be considered to be produced directly from fission. Because ^{135}Cs has a very long half-life, as an approximation, it can be considered stable. As a consequence of these approximations, a simplified ^{135}Xe production and destruction scheme can be used, as illustrated in Fig. 3.

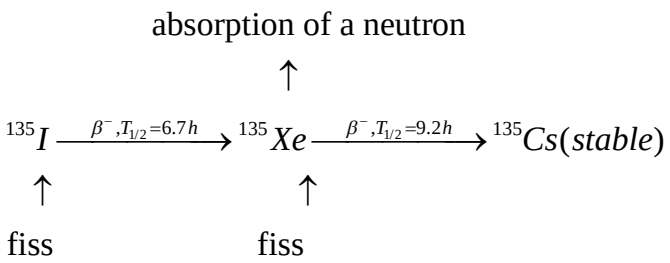

Figure 3 Simplified ^{135}Xe production and destruction mechanisms

7.2.2 Determining the Xe concentration

To find the numerical density of Xe nuclei, the balance equation for iodine nuclei is first written

as:

$$\frac{dI}{dt} = \gamma_I \Sigma_f \Phi \ - \lambda_I I \quad , \tag{154}$$

where γ is called the fission product yield and equals the average number of I nuclides created per fission. The balance equation for Xe nuclei can be subsequently written as:

$$\frac{dX}{dt} = \lambda_I I + \gamma_X \Sigma_f \Phi \ - \lambda_X X - \sigma_{aX} \Phi \ X \quad . \tag{155}$$

Steady-state conditions

Equilibrium conditions are attained after the reactor operates for a very long time (∞) at a steady-state flux level Φ_{ss}. Under equilibrium conditions, the concentration of I nuclei is easily found to be:

$$I_\infty = \frac{\gamma_I \Sigma_f \Phi_{ss}}{\lambda_I} \quad . \tag{156}$$

Similarly, the Xe concentration can be determined as:

$$X_\infty = \frac{\lambda_I I_\infty + \gamma_X \Sigma_f \Phi_{ss}}{\lambda_X + \sigma_{aX} \Phi_{ss}} = \frac{(\gamma_I + \gamma_X) \Sigma_f \Phi_{ss}}{\lambda_X + \sigma_{aX} \Phi_{ss}} \quad . \tag{157}$$

Note that both I and Xe concentrations depend on flux level. However, whereas the I concentration increases indefinitely with flux level, the Xe concentration levels off, and it can, at most, become equal to:

$$X_{\infty - \max} = \frac{(\gamma_I + \gamma_X) \Sigma_f}{\sigma_{aX}} \quad . \tag{158}$$

The Xe macroscopic absorption cross section is:

$$\Sigma_{aX} = X_\infty \sigma_{aX} = \frac{(\gamma_I + \gamma_X) \Sigma_f \Phi_{ss} \sigma_{aX}}{\lambda_X + \sigma_{aX} \Phi_{ss}} \quad . \tag{159}$$

Using the notation:

$$\Phi_X = \frac{\lambda_X}{\sigma_{aX}} = 0.770 \times 10^{13} cm^{-2} \sec^{-1} \quad , \tag{160}$$

the Xe macroscopic absorption cross section can be rewritten as:

$$\Sigma_{aX} = \frac{(\gamma_I + \gamma_X) \Sigma_f \Phi_{ss}}{\Phi_X + \Phi_{ss}} \quad . \tag{161}$$

If Xe is assumed to be uniformly distributed, then its resulting reactivity worth is:

$$\rho_{Xe} = -\frac{\Sigma_{aX}}{\nu\Sigma_f} = \frac{1}{\nu\Sigma_f}\frac{(\gamma_I+\gamma_X)\Sigma_f\Phi_{ss}}{\Phi_X+\Phi_{ss}} = -\frac{\left(\gamma_I+\gamma_X\right)}{\nu}\frac{\Phi_{ss}}{\Phi_X+\Phi_{ss}} \quad . \tag{162}$$

For high reactor fluxes, in the case where $\Phi_{ss} >> \Phi_X$, Φ_X can be neglected in the denominator, and the reactivity becomes independent of the flux level and equal to its maximum value of:

$$\rho_{Xe} \cong -\frac{\gamma_I+\gamma_X}{\nu} \quad . \tag{163}$$

This is to be expected given that the Xe concentration has been found to "saturate" with increased flux. The reactivity expressed in Eq. (163) is nothing but the corresponding reactivity for the maximum Xe concentration shown in Eq. (158).

If, on the contrary, the flux is very low, in the case where $\Phi_{ss} << \Phi_X$, then Φ_{SS} can be neglected in the denominator, and the Xe equivalent reactivity increases linearly with flux level:

$$\rho_{Xe} = -\frac{\left(\gamma_I+\gamma_X\right)}{\nu}\frac{\Phi_{ss}}{\Phi_X} \quad . \tag{164}$$

Xe load after shutdown: reactor dead time

If, the reactor is shut down ($\Phi = 0$), I and Xe production from fission ceases, as well as Xe destruction through neutron absorption. The concentration of I begins to decrease exponentially due to decay. If the I concentration at the time of shutdown is I_0, the I concentration as a function of time can be expressed simply as:

$$I(t) = I_0 e^{-\lambda_I t} \quad . \tag{165}$$

Substituting this expression into the Xe balance equation and setting the flux to zero leads to the following expression:

$$\frac{dX}{dt} = \lambda_I I_0 e^{-\lambda_I t} - \lambda_X X \quad . \tag{166}$$

Denoting the Xe concentration at the time of shutdown by X_0, the solution can be written as:

$$X(t) = X_0 e^{-\lambda_X t} + \frac{\lambda_I I_0}{\lambda_I - \lambda_X}(e^{-\lambda_X t} - e^{-\lambda_I t}) \quad . \tag{167}$$

If the reactor is shut down after operating for a long time at steady state, the resulting Xe concentration is:

$$X(t) = \frac{(\gamma_1+\gamma_X)\Sigma_f\Phi_{ss}}{\lambda_X+\sigma_{aX}\Phi_{ss}} e^{-\lambda_X t} + \frac{\gamma_I\Sigma_f\Phi_{ss}}{\lambda_1-\lambda_X}(e^{-\lambda_X t} - e^{-\lambda_I t}) \quad . \tag{168}$$

The equivalent reactivity for uniformly distributed Xe (and assuming that the reactor was shut down after operating for a long time at steady state) is:

$$\rho = -\frac{1}{\nu}\left[\frac{(\gamma_I+\gamma_X)\Phi_{ss}}{\Phi_X+\Phi_{ss}}e^{-\lambda_X t}+\frac{\gamma_I\Phi_{ss}}{\Phi_I-\Phi_X}(e^{-\lambda_x t}-e^{-\lambda_I t})\right], \tag{169}$$

where:

$$\Phi_I=\frac{\lambda_I}{\sigma_{aX}}=1.055\times10^{13}\,cm^{-2}\,\sec^{-1}. \tag{170}$$

The Xe concentration, and consequently the Xe reactivity worth after shutdown, increases at first because Xe continues to be produced by decay of I, whereas consumption is now reduced in the absence of Xe destruction by neutron absorption. After a while, however, the Xe concentration reaches a maximum, starts decreasing, and eventually approaches zero. This behaviour is shown in Fig. 4, which shows the Xe reactivity worth after shutdown from full power.

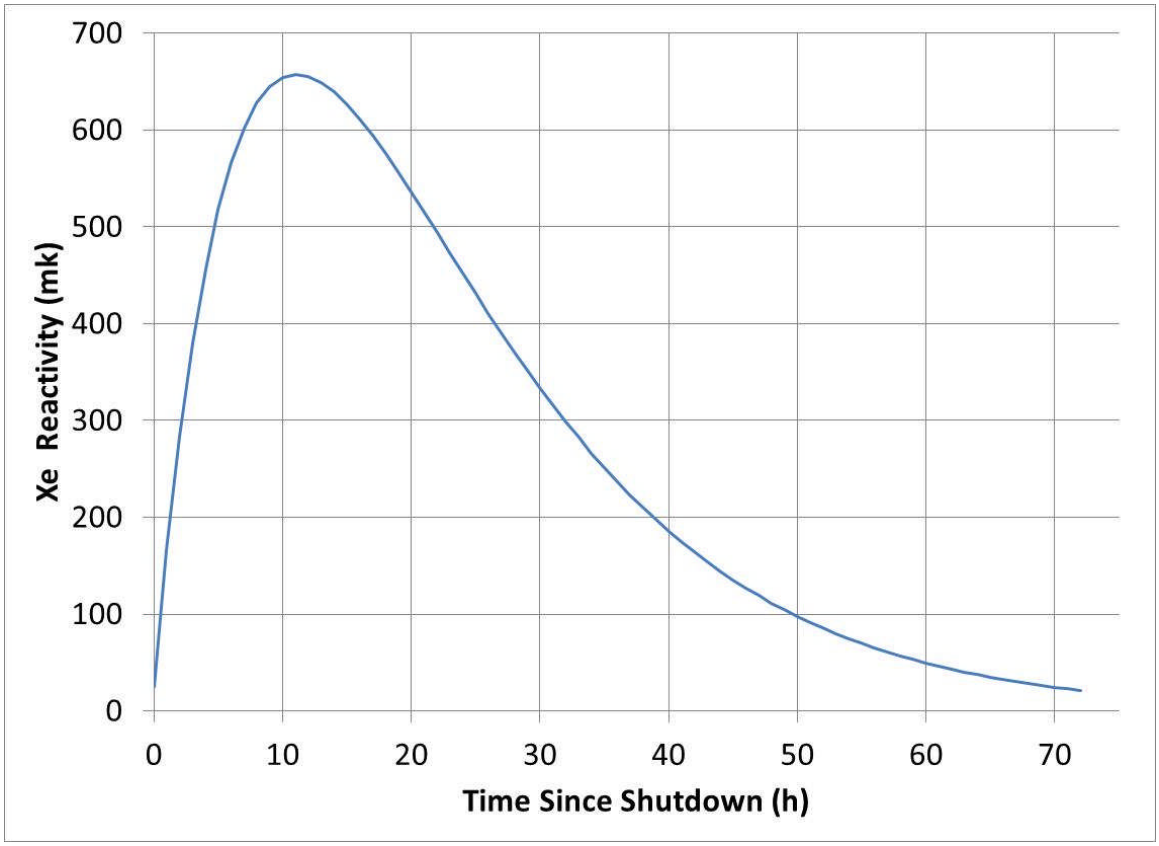

Figure 4 ^{135}Xe reactivity worth after shutdown

Because the Xe reactivity (or *load*) increases after shutdown, a reactor that was critical at the time of shutdown subsequently becomes sub-critical and cannot be restarted until the Xe load drops back to a value close to its steady-state level. The time during which the reactor cannot be restarted due to increased Xe load after shutdown is known as reactor "dead time". Given the Xe half-life of approximately nine hours, the reactor dead time, which spans several half-lives, is of the order of 1.5–2 days. Some reactors have systems to compensate for some of the shutdown Xe load, in the form of reactivity devices that are inserted in the core during normal

steady-state reactor operation. As Xe builds up after shutdown, removal of these devices can counterbalance the Xe reactivity load, enabling the reactor to be brought to critical and re-started. Adjuster rods in the CANDU reactor can serve this purpose, but only up to 30 minutes after shutdown. Beyond 30 minutes, the Xe load becomes larger than the adjuster-rod reactivity worth. Because the Xe load increases with the neutron flux, Xe-poison dead time generally affects only high-power reactors.

8 Reactivity Coefficients and Feedback

Macroscopic cross sections can change as a consequence of various parameters, and in turn, these changes induce changes in k_{eff} and hence in reactivity. The usual parameters that influence reactivity are:

- fuel temperature
- coolant temperature
- moderator temperature
- coolant density.

Changes in reactivity induced by changes in any such parameter are referred to as the *reactivity effect* of the respective parameter. For example, the reactivity change induced by a change in fuel temperature is called the *fuel-temperature reactivity effect*. The derivative of the reactivity with respect to any of the parameters, with the others kept constant (i.e., the partial derivative), is called the *reactivity coefficient* of that parameter. To illustrate this, assume that all parameters are kept constant with the exception of one, e.g., fuel temperature, which is varied. Assume further that reactivity is plotted as a function of the variable parameter, in this case fuel temperature. The plot in question would be a plot of $\rho(T_f)$. If a certain fuel temperature T_{f0} is taken as a reference, then the effect on reactivity of deviations from T_{f0} can be calculated, namely $\Delta\rho(T_f) = \rho(T_f) - \rho(T_{f0})$. $\Delta\rho(T_f)$ is called the *fuel-temperature reactivity effect*. The derivative of the reactivity with respect to the fuel temperature, namely $\alpha_{T_f}(T_f) = \dfrac{d\rho(T_f)}{dT_f}$, is called the *fuel-temperature coefficient*. Of course, because reactivity also depends on other parameters, it becomes clear that this derivative should be a partial derivative. In general, if the reactivity depends on several parameters,

$$\rho = \rho(p_1, \ldots p_n), \tag{171}$$

then the reactivity coefficient with respect to a parameter p_i is defined as the partial derivative of the reactivity with respect to that parameter:

$$\alpha_{p_i} = \frac{\partial\rho(p_1, \ldots p_n)}{\partial p_i}. \tag{172}$$

Of course, in reality, several parameters may vary simultaneously, and their variations may be impossible to decouple. For example, the moderator density also varies when the moderator temperature varies, due to thermal expansion. In this case, the single-parameter reactivity coefficients are somewhat artificial, and additional combined reactivity coefficients can be defined, which are of more practical use. For example, in the case of simultaneous variation of

both moderator temperature T_m and moderator density d_m, a much more useful quantity would be:

$$\alpha_{T_m(d_m)} = \frac{d\rho}{dT_m} = \frac{\partial\rho(T_m, d_m)}{\partial T_m} + \frac{\partial\rho(T_m, d_m)}{\partial d_m}\frac{dd_m}{dT_m}, \tag{173}$$

where the derivative $\frac{dd_m}{dT_m}$ is specified by the thermal expansion law.

Such coefficients are called *combined* reactivity coefficients. One very useful combined coefficient of this kind is the *power coefficient of reactivity* (PCR), which is defined as:

$$PCR = \frac{d\rho}{dP} = \sum_{i=1}^{n} \frac{\partial\rho(p_1 \ldots p_n)}{\partial p_i}\frac{dp_i}{dP}, \tag{174}$$

where the p_i are all the parameters which change with power and on which the reactivity ultimately depends, such as fuel temperature, coolant temperature, coolant density, and so on.

Because the core parameters depend on the flux level and because they influence the reactivity, which in turn influences the flux, the reactivity coefficients are said to express the feedback which describes the connection between the flux level and the cross-section values. When such feedback is accounted for during a transient by recalculating the cross sections and the reactivity as functions of the flux level (and hence of power level), it is said that kinetics calculations with feedback, or *dynamic* calculations, are being performed.

This sub-section will close with a presentation of a few alternate expressions for reactivity coefficients. If reactivity is expressed using the effective multiplication constant, then the reactivity coefficient can be expressed as follows:

$$\alpha_P = \frac{d\rho(p)}{dp} = \frac{d}{dp}\left(1 - \frac{1}{k(p)}\right) = \frac{1}{k^2(p)}\frac{dk(p)}{dp}. \tag{175}$$

For reactors close to critical ($k \cong 1$), this can be processed to yield:

$$\alpha_P = \frac{1}{k^2(p)}\frac{dk(p)}{dp} \cong \frac{1}{k(p)}\frac{dk(p)}{dp}. \tag{176}$$

The last form can also be expressed as:

$$\frac{1}{k(p)}\frac{dk(p)}{dp} = \frac{d}{dp}\ln\left[k(p)\right]. \tag{177}$$

The last two expressions are often used to calculate reactivity coefficients.

9 CANDU-Specific Features

Given the presentation of the basic concepts of reactor kinetics in previous sections, this section will be devoted to presenting how some of these concepts apply to CANDU reactors.

9.1 Photo-Neutrons: Additional Delayed-Neutron Groups

CANDU reactors are heavy-water cooled and moderated. In such reactors, neutrons can be produced by the interaction of gamma rays (with a minimum energy of 2.22 MeV) with deuterium:

$$ {}_1^2D + \gamma \rightarrow {}_1^1H + n \,. \tag{178}$$

Because gamma rays can be emitted by fission products with certain delays, the process is very similar to that through which a "true" delayed neutron is emitted by an emitter which is the daughter of a precursor. However, note than not all gamma rays will interact by photo-neutron emission. Effective precursor concentrations can be defined for the photo-neutrons, such that the photo-neutron production rate density is equal to:

$$ S_{pn} = \lambda_{pn} C_{pn} \,. \tag{179}$$

The term *effective* photo-neutron precursor concentration is used because the *effective* concentrations must also account for the fact that not all emitted gamma rays will result in the production of a photo-neutron and that the fraction of photo-neutrons emitted depends on the geometrical arrangement of the core lattice. Photo-neutron precursors can be grouped by their decay constant, similarly to "real" precursors. It is customary to use 11 photo-neutron groups, for a total of 17 delayed-neutron groups. Once the photo-neutron groups have been defined, photo-neutrons are treated no differently than regular delayed neutrons in the kinetics calculations.

9.2 Values of Kinetics Parameters in CANDU Reactors: Comparison with LWR and Fast Reactors

Deuterium has a much smaller neutron-absorption cross section than hydrogen. Consequently, CANDU reactors have a better thermalized spectrum and hence a much longer generation time (and lifetime) than light-water reactors and even longer compared to fast reactors. The typical generation time of a CANDU core is approximately 1 ms, compared to 0.05 ms for an LWR core. This makes CANDU transients "slower" than LWR transients. Reactivities close in value to the delayed-neutron fraction induce less peak power transients in a CANDU core than in an LWR core. The difference is even larger when comparison is made with fast reactors.

9.3 CANDU Reactivity Effects

CANDU reactivity effects depend on the specific characteristics of the CANDU lattice. Of particular interest is the *coolant density effect*, also known as the coolant void reactivity effect, which is absent in other types of reactors which do not separate the coolant from the moderator. Plots of the various effects are shown in Figs. 5 to 8 for fresh fuel.

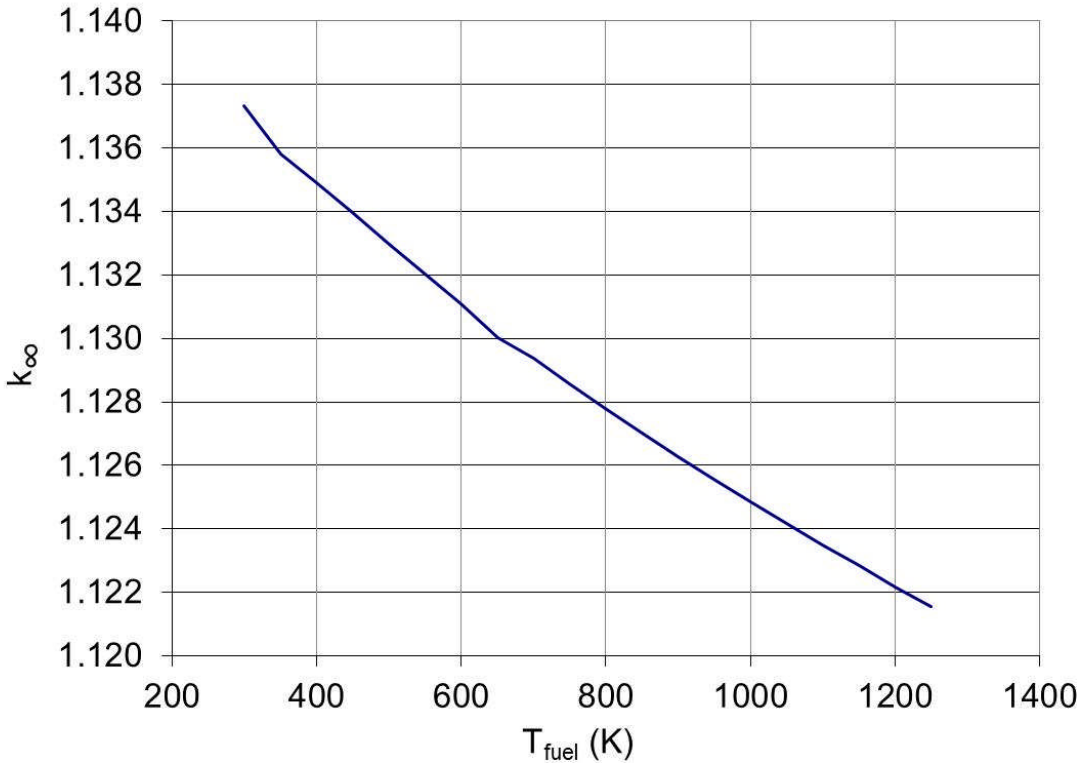

Figure 5 CANDU fuel-temperature effect

The decrease in reactivity with increased fuel temperature is due primarily to an increase in resonance absorption due to Doppler resonance broadening.

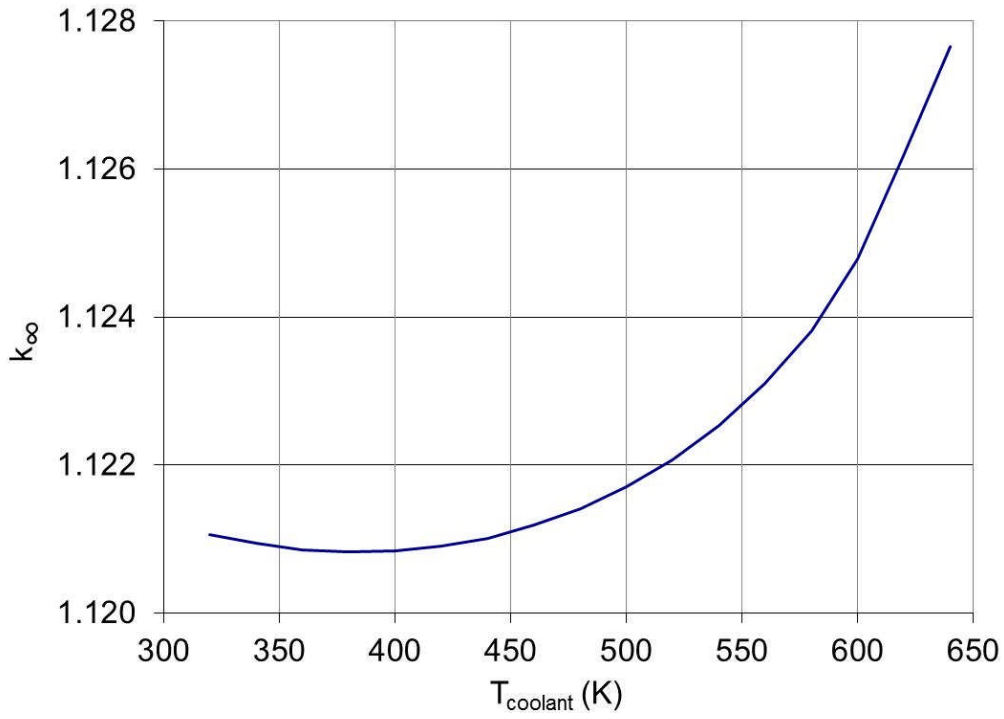

Figure 6 CANDU coolant-temperature effect

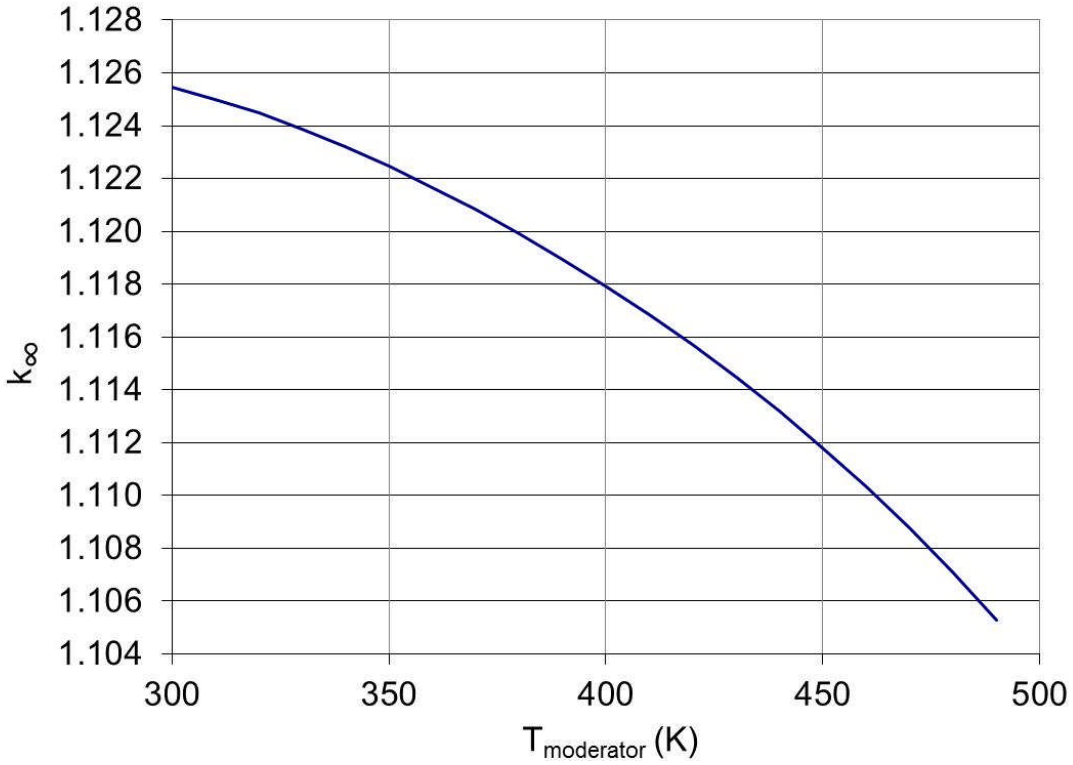

Figure 7 CANDU moderator-temperature effect

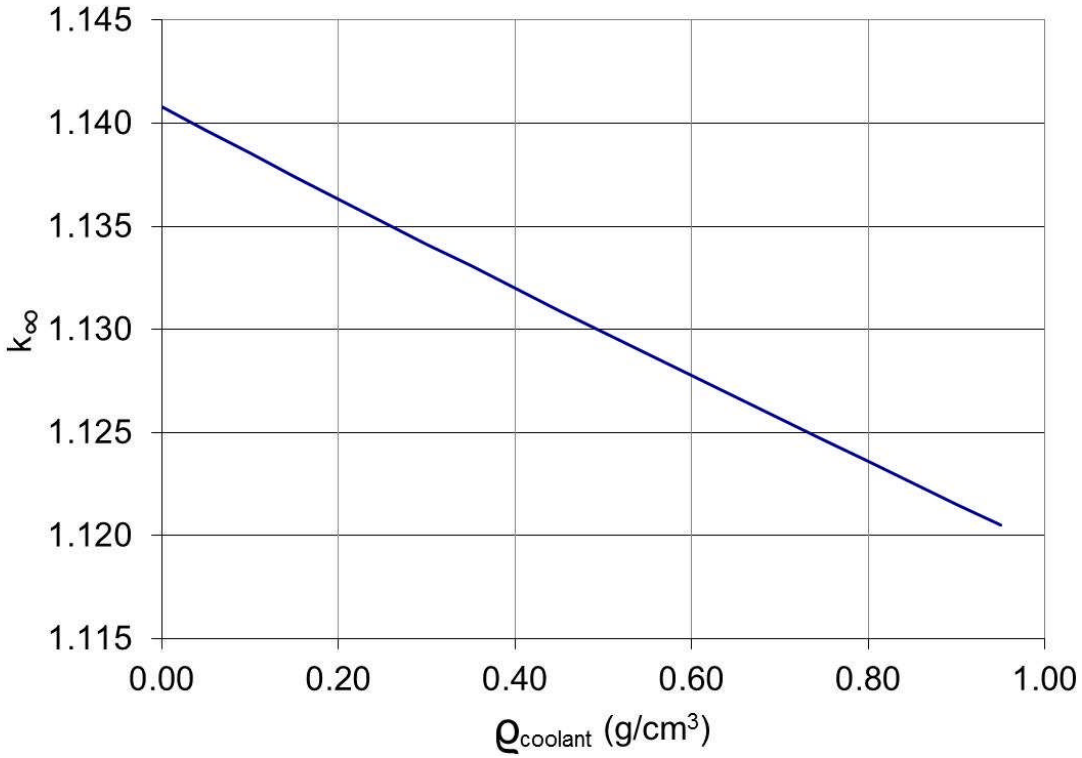

Figure 8 CANDU coolant-density effect

It is apparent that reactivity decreases with coolant density, which means that it increases with void fraction. This effect occurs primarily because when coolant is lost, effective moderation is still possible due to the moderator in the calandria vessel. Overall, the reduced slowing-down in

the coolant leads to reduced resonance absorption and an increased fast fission rate. Both these phenomena increase reactivity when coolant is lost. As fuel burns, a mitigating factor appears in the form of the low-lying Pu fission resonance, which begins to play a role as Pu is created. Reduced upscattering in the coolant reduces fissions in the low-lying Pu resonance and hence reduces reactivity, although not enough to make it negative.

9.4 CANDU Reactivity Devices

As in any reactor, power in CANDU reactors is controlled by controlling reactivity. In turn, reactivity is controlled by means of reactivity devices which can be inserted into or removed from the core. By inserting or removing reactivity devices from the core, the absorption rate is varied; hence, reactivity can be varied, and power can be increased or decreased, or the reactor can be completely shut down. Reactivity devices in CANDU reactors come under the control either of the Reactor Regulating System (RRS) or of one of the two independent shutdown systems (SDS1 and SDS2).

For a CANDU 6, the reactivity devices under the control of the RRS are as follows:

- 14 liquid-zone-control compartments (H_2O-filled)
- 21 adjuster rods
- 4 mechanical control absorbers
- moderator “poison”.

The reactivity devices under the control of the shutdown systems are:

SDS-1: 28 cadmium shutoff rods which fall into the core from above

SDS-2: high-pressure Gd-poison injection into the moderator through six horizontally oriented nozzles.

The reactivity worth of these reactivity devices is shown in Table 2.

Table 2 CANDU reactivity device worth

Function	Device	Total Reactivity Worth (mk)	Maximum Reactivity Rate (mk/s)
Control	14 liquid zone con-trollers	7	± 0.14
Control	21 adjusters	15	± 0.10
Control	4 mechanical control absorbers	10	± 0.075 (driving) -3.5 (dropping)
Control	moderator poison	–	-0.01 (extracting)
Safety	28 shut-off units	80	-50
Safety	6 poison-injection nozzles	> 300	-50

10 Summary of Relationship to Other Chapters

Chapter 5 relies on knowledge acquired from Chapter 4, Reactor Statics and indirectly on knowledge from Chapter 3, Nuclear Processes and Neutron Physics.

11 Problems

1. 10^{20} nuclei of ^{235}U undergo fission with a delayed neutron yield of 0.0125 and a delayed neutron fraction of 0.005.
   a) What is the total neutron yield?
   b) How many precursors are produced?
   c) How many emitters are eventually produced?

2. A radioactive waste site consists of two cylindrical tanks that contain liquid waste in the form of fissile material in an aqueous solution. The tanks are in the form of cubes with the side equal to 1m. The neutronic properties of the radioactive waste are: SA=0.00100cm^{-1}, D=1cm, nu=2.5, SF=0.00158 cm^{-1}, v=2200 m/s. Assume all fission neutrons are prompt.
   a) Calculate the reactivity, generation time and neutron life time for one of the tanks.
   b) The site manager decides to save space and money, by storing the content of both tanks in a larger cubical tank, with side $\sqrt[3]{2}m$. Calculate the reactivity, generation time and neutron life time for the new tank. Comment on the result.

3. A thin foil made of a mixture of isotopes one of which is fissile has a fission macroscopic cross section equal to 0.001 cm^{-1}. When fissioning, the fissile isotope produces two types of precursors: one with yield 0.05 and a half-life of one minute, and another with yield 0.03 and a half-life of two minutes. The sample is subjected to a pulse of neutrons at t=0, and to another pulse of neutrons at t=90s. The first pulse has a fluence of 10^8 n/cm^2, and the second pulse has a fluence of $5x10^7$ n/cm^2. What is the total number of precursors at t=5 minutes?
   Note: Assume that the number of nuclei that react with neutrons (through fission or otherwise) is negligible compared to the original number of nuclei present in the sample, and that neutrons emitted from the sample do not interact in the sample.

4. A thin-foil of fissile material is irradiated uniformly in a neutron flux of 10^8 n/cm^2/s, starting at t=0. There are 10^{22} fissile nuclei in the sample and the fission microscopic cross section is 2000b. There is only one group of delayed neutrons. The total neutron yield per fission is 2.33. The delayed neutron fraction is 0.001 and the half-life of precursors is one minute. The number of neutrons emitted by the sample per second is measured with a neutron detector.
   a) What does the detector indicate 20 minutes after the start of the irradiation?
   b) At 25 minutes the irradiation stops. What does the detector indicate two minutes later?
   Note: Assume that the number of nuclei that react with neutrons (through fission or otherwise) is negligible compared to the original number of nuclei present in the sample, and that neutrons emitted from the sample do not interact in the sample.

5. Consider a homogeneous nuclear reactor for which all neutrons are born prompt. The reactor is cubical, with side equal to 4m. The neutronic parameters of the reactor are:
   $D = 1cm$
   $\Sigma_a = 0.003cm^{-1}$
   $\nu = 2.5$
   $\overline{v} = 2200m/s$
   The reactor is initially critical, operating at 3000 MW fission power. The energy liberated per fission is approximately 200MeV. The extrapolated size of the reactor can be approximated by its physical size.
   a) Find Σ_f.
   b) Calculate the volume-integrated flux in the reactor.
   c) Calculate total neutron population in the reactor.
   d) Calculate the neutron generation time and life time.

6. Consider a slab homogeneous reactor (infinite in the y and z directions and finite in the x direction) extending from -2m to 2m in the x direction, and with the following parameters:
   $D = 1cm$
   $\Sigma_a = 0.003cm^{-1}$
   $\nu = 2.5$
   Assume that the physical length and the extrapolated length of the reactor can be approximated to be equal.
   The reactor is initially critical.
   a) Find the fission cross section.
   b) A control plate, 1 cm thick (and extending to infinity in the y and z directions, just like the reactor) is introduced at x=1m. The neutronic parameters of the control plate are:
      $D = 1cm$
      $\Sigma_a = 0.01cm^{-1}$
      $\Sigma_f = 0cm^{-1}$
   c) Assuming the control plate is thin-enough so that the unperturbed flux across it can be assumed to be constant and equal to the value at the center of the plate, calculate the reactivity of the reactor after the introduction of the control plate.
   d) **Note:** When a plate is inserted in the reactor, its material **displaces** (that is replaces) the unperturbed reactor material at the position of the plate.

7. Consider a reactor with 6 delayed neutron groups, with the following parameters.
   $\bar{v} = 2200\ m/s$
   $\Lambda = 0.001\ s$
   $\rho = 0.000$
   $\nu = 2.5$
   $\beta_1 = 0.0010$
   $\beta_2 = 0.0012$
   $\beta_3 = 0.0008$
   $\beta_4 = 0.0002$
   $\beta_5 = 0.0011$
   $\beta_6 = 0.0014$
   $\lambda_1 = 0.001\ s^{-1}$
   $\lambda_2 = 0.005\ s^{-1}$
   $\lambda_3 = 0.010\ s^{-1}$
   $\lambda_4 = 0.015\ s^{-1}$
   $\lambda_5 = 0.050\ s^{-1}$
   $\lambda_6 = 0.100\ s^{-1}$
   The reactor operates in steady state at 2000 MW. The energy per fission is approximately 200MeV.
   What is the total delayed neutron fraction?
   What is the total delayed neutron yield?
   What is the precursor population for each of the groups 1 to 6?
   What is the total delayed neutron source?

8. Consider a homogeneous nuclear reactor with one delayed neutron group. The reactor is cubical, with side equal to 4m. The neutronic parameters of the reactor are:
   $D = 1cm$
   $\Sigma_a = 0.003cm^{-1}$
   $\Sigma_f = 0.00136cm^{-1}$
   $\nu = 2.5$
   $\bar{v} = 2200m/s$
   $\beta = 0.005$
   $\lambda = 0.2s^{-1}$
   Assume the extrapolated size of the reactor equals its physical size.
   a) Calculate k_{eff}.
   b) The reactor is maintained subcritical by the addition of ^{10}B, which has a microscopic cross section of approximately 4000b. ($1\,barn = 10^{-24}cm^2$). If $k = 0.980$, what is the number density of Boron atoms?
   c) An external neutron source is introduced into the reactor at point b). The neutron balance (point kinetics) equations are thus written:

$$\dot{n} = \frac{\rho - \beta}{\Lambda} n + \lambda C + S$$

$$\dot{C} = \frac{\beta}{\Lambda} n - \lambda C$$

where n is the total neutron population, and S is the strength of the external source (neutrons/s).

If $S = 10^6 \frac{neutrons}{s}$, what is the equilibrium (steady-state) neutron population? What is the equilibrium precursor population?

d) At t=0, the external neutron source is removed from the reactor. What are the neutron population and the precursor population 5 seconds after the removal of the external source?

9. Consider a reactor with six delayed neutron groups, with the following parameters:
   $\Lambda = 0.001s$
   $\beta = 0.005$
   The reactor is initially operating at a steady-state power of 1000MW. A control rod that was initially in the core is accidentally ejected at t=0, yielding a 2mk reactivity increase. What is the reactor power immediately after the rod ejection? Use the prompt jump approximation.

10. Consider a reactor with one delayed neutron group, with the following parameters:
    $\Lambda = 0.001s$
    $\beta = 0.005$
    $\lambda = 0.02s^{-1}$
    The reactor is initially in steady state operation at a power of 1000MW. A control rod with a reactivity worth of 2 mk is inserted in the reactor at t=0. At t=2s, a second, identical, control rod is inserted. What is the reactor power at t=4s?
    Notes:
    Use the prompt jump approximation.
    The prompt jump approximation is also valid when the reactor is not initially critical.

12 References and Further Reading

[Lamarsh2001] Lamarsh, J. R. and Baratta, A. J., *Introduction to Nuclear Engineering* (third edition). Prentice-Hall, 2001.

[Lamarsh2002] Lamarsh, J. R., *Introduction to Nuclear Reactor Theory*. American Nuclear Society, La Grange Park, Illinois, 2002.

[Ott1985] Ott, K. O., Neuhold, R. J., *Nuclear Reactor Dynamics*. American Nuclear Society, Lagrange Park, IL, 1985.

[Rose1991] P. F. Rose (ed.), *ENDF/B-VI Summary Documentation*. Cross Section Evaluation Working Group, Report BNL-NCS-17541 (ENDF-201), 1991.

[Rozon1998] Rozon, D., *Nuclear Reactor Kinetics*. Polytechnic International Press, Montreal, QC, 1998.

[Stacey1970] Stacey, W. M., *Space-Time Nuclear Reactor Kinetics*, Academic Press, 1970.

13 Acknowledgements

The following reviewers are gratefully acknowledged for their hard work and excellent comments during the development of this Chapter. Their feedback has much improved it. Of course the responsibility for any errors or omissions lies entirely with the authors.

Marv Gold
Bruce Wilkin

Thanks are also extended to Diana Bouchard for expertly editing and assembling the final copy.

CHAPTER 6
Thermal-Hydraulic Design

Prepared by
Dr. Nikola K. Popov

Summary

This chapter covers the thermal-hydraulic design of nuclear power plants with a focus on the primary and secondary sides of the nuclear steam supply system. This chapter covers the following topics: evolution of the reactor thermal-hydraulic system; key design requirements for the heat transport system; thermal-hydraulic design principles and margins; design details of the primary and secondary heat transport systems; fundamentals of two-phase flow; fundamentals of heat transfer and fluid flow in the reactor heat transport system; other related topics.

Table of Contents

List of Figures

List of Tables

1 Introduction

Section 1 provides an introduction to thermal-hydraulic design. It defines the expectations and learning outcomes for this chapter and indicates the relationship of this chapter to other chapters in this textbook.

The objective of this chapter is to describe the generic thermal-hydraulic design of nuclear reactors under normal operating conditions, with a specific focus on design details of CANDU reactors.

This chapter covers the thermal-hydraulic design of a CANDU nuclear power reactor, with general comparisons to other reactor types and designs. Thermal-hydraulic design covers the reactor primary and secondary heat transport systems. In fact, the primary heat transfer design defines the maximum power levels (globally and locally) that can be safely generated in the reactor core and thus defines the design characteristics of many systems and components, such as the reactor core physics and the fuel design.

1.1 Overview

This section describes the objectives, principles, and methodologies of reactor thermal-hydraulic design. The thermal-hydraulic design of the reactor process systems that are required to transport heat energy away from the nuclear reactor source and transform this heat energy into useful work (generally electrical energy) are the focus of nuclear engineering and of this chapter.

Section 2 presents the principles of reactor design, with a focus on CANDU reactor design. Designs of other reactor types are described in Appendix A, in which the focus is on providing a historical perspective on reactor thermal-hydraulic and systems design and on pressurized water reactors (PWRs) and boiling water reactors (BWRs).

Section 3 covers the design evolution of the CANDU reactor, including a general description of the overall design of the CANDU heat transport system and the design and evolution of the main components such as primary pumps, steam generators, and the reactor core.

Section 4 defines the thermal-hydraulic design requirements, including fuel cladding (fuel sheath), coolant, fuel, moderator materials, and control materials. Reactor core component materials are discussed and component requirements assessed. This section also discusses various fuel-coolant-moderator arrangements, their optimization, and their performance within the reactor design. Advantages and disadvantages of all the variations are discussed and possible solutions suggested. Finally, the section provides general requirements for the thermal-hydraulic design process.

Section 5 discusses reactor thermal-hydraulic design limits from the perspective of various reactor designs. It explains the concepts of reactor thermal margins and their application to reactor design assessment. Reactor thermal margins are an important parameter in reactor thermal-hydraulic design because they provide assurance that the heat generated by the fuel is removed from the reactor core under all possible operating conditions.

Section 6 covers thermal-hydraulic design fundamentals. The first part of this section presents

the fundamentals of single- and two-phase flow and heat transfer. Two-phase flow and heat transfer present a number of thermal-hydraulic design challenges, which are explained and discussed in this section. In addition, this section covers the thermodynamics of the reactor primary and secondary heat transport systems. The concepts of thermodynamic laws and their application to reactor design are presented. The concept of reactor thermodynamic efficiency is defined and its application to reactor performance assessment explained. Various secondary system designs are discussed, and a description of the secondary side components, such as steam turbines, steam condensers, feedwater systems and pre-heaters, and feedwater pumps, is provided.

Section 7 is the key section in this chapter because it describes the design of reactor heat transfer and fluid flow. This section outlines primary heat transport system behaviour, describes the various mathematical models, and discusses the most important characteristics of the primary heat transport system. The design and operation of the primary pumps is described. The design and operation of the steam generators is covered in detail because this component connects the primary and secondary heat transport systems, and therefore understanding its behaviour is essential for understanding overall reactor thermal-hydraulic behaviour. Flow stability in single-channel and parallel-channel instability situations is explained and its relevance to reactor and pump operation presented.

Also presented in Section 7 are heat transfer in the fuel elements and their heat transfer behaviour and operation in the reactor. Various topics are covered, such as fuel pellet cladding gap heat conduction, variability of heat conductivity in the fuel with temperature, and the influence of other important parameters. Fluid flow fundamentals are also covered, including calculation of pressure drop in the primary heat transport system under single- and two-phase operating conditions, calculation of flow resistance and its impact, and other important aspects.

Heat transfer between fuel and coolant is also discussed in Section 7, including heat transfer regimes in single-phase and two-phase operation, with a particular focus on boiling heat transfer in a CANDU fuel channel. The concept of critical heat flux is defined and discussed, along with various critical heat flux approaches, experimental data, and prediction methods. The impact of critical heat flux on reactor thermal margins is discussed and methods for improvement identified. An important part of the critical heat flux prediction model is the look-up table, which is explained and its application described. Part of this section is devoted to post-critical heat flux heat transfer, i.e., transition boiling and film boiling. Various heat transfer modes are discussed, with particular attention to CANDU fuel bundles. Most of the important heat transfer correlations are listed and explained and their application discussed.

Finally, the last few sub-sections of Section 7 are devoted to special topics in reactor thermal-hydraulic design. One section explains the critical flow phenomenon and its relevance to safety analysis, as well as the water hammer phenomenon. It provides insights on the risk from the water hammer hazard and provides high-level information on preventing this phenomenon in reactor design.

The last part of Section 7 covers natural circulation, which is an important phenomenon because it provides assurance that reactor decay heat will be removed from the core if forced-

flow cooling is lost. This section describes the natural circulation phenomenon and focusses on its application in CANDU reactors. The CANDU-specific phenomena of core cooling in the absence of forced flow and of intermittent buoyancy-induced flow in a CANDU fuel channel are covered.

1.2 Learning outcomes

The goal of this chapter is to help the reader to develop:

- An understanding of the principles and concepts of thermal-hydraulic design of nuclear reactors.
- An understanding of the evolution of the CANDU thermal-hydraulic design.
- Knowledge of general design principles, with a focus on the main parameters, design limits, and thermal-hydraulic margins by which the thermal-hydraulic design is characterized.
- An understanding of the design concepts and key features of the primary and secondary heat transport systems.
- Knowledge of the details of heat transfer and fluid flow and the heat transfer methodology used in the thermal hydraulics of the reactor heat transport system.
- A basic knowledge of unique CANDU thermal-hydraulic features and behaviour.

The reader needs to be generally familiar with other topics and disciplines related to thermal hydraulics. In addition, it is assumed that the reader has a basic understanding of fluid flow and heat transfer phenomena.

1.3 Summary of relationship to other chapters

Thermal-hydraulic design is fundamental to reactor design and behaviour. Therefore, a good understanding of thermal-hydraulic topics is required to understand the other chapters in this textbook.

This chapter is tightly connected to the chapters covering core physics, fuel design, and safety design and analysis. Furthermore, this chapter provides the knowledge base for understanding Chapter 7 on thermal-hydraulic analysis.

1.4 Thermal-hydraulic design

Nuclear reactor thermal-hydraulic design is concerned with designing the process systems required to transport heat (energy) from the nuclear reactor core (i.e., fuel) and to transform this heat energy into useful work (i.e., electrical energy) in the turbine-generator unit.

Thermal-hydraulic design is associated with a number of interrelated systems, including the reactor core, the heat transport system, steam generators, turbines, the pressure control system, the coolant inventory control system, and the power control systems. In addition, a number of components are important, including valves, pumps, pipes, vessels, and heat exchangers, and a number of engineering and scientific disciplines, including reactor physics, heat transfer, fluid mechanics, thermodynamics, chemistry, metallurgy, control, and stress analysis.

The most important role of reactor design from a safety perspective is to ensure that:

- the fission reaction can be achieved and controlled (addressed by the physical core design and fuel design);
- heat can be removed from the core to the ultimate heat sink (addressed by the thermal-hydraulic design);
- the reactor operation can be monitored (addressed by the instrumentation and control design), and
- the radioactive material can be contained within the reactor facility (addressed by the radiation protection and civil engineering design). Among the most important aspects of reactor engineering with respect to safe operation is the heat transfer and fluid flow (i.e., the thermal-hydraulic design).

The basic concept of a nuclear power plant is presented in **Figure 1**; it is similar to that of any other thermal power plant. The overall objective is to produce useful shaft work using a thermodynamic heat engine (a turbine) with a heat source (a reactor) and a heat sink (a lake, the sea, or the atmosphere). Following this basic concept, a number of variations of the nuclear power plant have been designed.

A number of inter-related systems and components are integrated into nuclear power plant design and interact with each other. Understanding their limitations and characteristics is an essential part of reactor design. Consequently, the process designer must appreciate the characteristics and limitations of all the major components and systems to carry out the detailed design of a particular system, i.e., to make intelligent choices. Design is, after all, the process of constraining the possible alternatives (in reaching a design objective) down to one choice. The overall goal is to provide an effective process within the context of the whole operation. This means that the system must perform its process function safely and efficiently at a reasonable cost. The interplay of these key concepts and systems constitutes "the design process".

The final arbitrators in resolving the conflicting demands of each subsystem are: adequate level of safety, low overall cost, material limits (temperature, mechanical stress, erosion, corrosion, etc.), regulations, past experience, standardized design requirements, and quality assurance (QA).

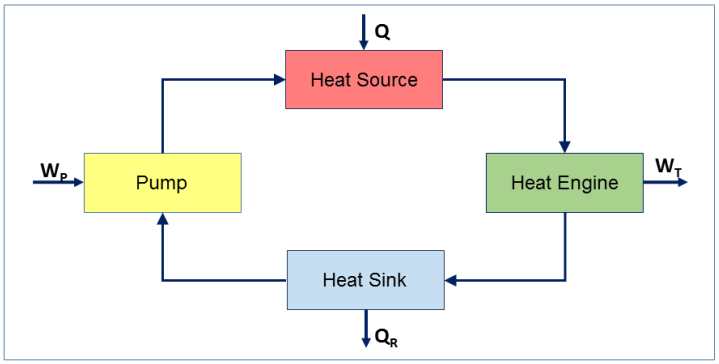

Figure 1 Heat engine concepts

2 Reactor Types

A number of reactor types are operating around the world, and many more have been designed in the past 50+ years of nuclear energy utilization, but never built. Many of these reactor types use very different physical and thermal-hydraulic concepts; however, only a handful have been able to ensure commercial viability over the past 50 years.

A number of these reactor types have proven to be commercially and economically competitive, the most successful of which include [ELW1990]:

- Pressurized water reactors (PWRs)
- Boiling water reactors (BWRs)
- Gas cooled reactors
- Channel type reactors.

Although a detailed discussion of these reactor types is beyond the scope of this text, the general evolution of reactor design and several of these designs are discussed in Appendix A.

The CANDU reactor design is a channel-type reactor, and a general overview, as relevant to the topic of thermal hydraulics, is presented in Section 2.1.

2.1 CANDU reactor design

The CANDU reactor has been designed and built by the Canadian nuclear industry [AECL1978, AECL1997], based on research and development undertaken by AECL, and has been successfully operating for 50 years in Canada and internationally. This is an important reactor type because, unlike other power reactors, it uses natural rather than enriched uranium and therefore offers much flexibility for countries wanting to enter into nuclear programs and fuel fabrication without requiring expensive uranium enrichment services. This section provides a brief description of the thermal hydraulics of CANDU reactors. Other sections in this chapter provide more detailed information about the thermal-hydraulic design of the CANDU reactor and its other systems and components.

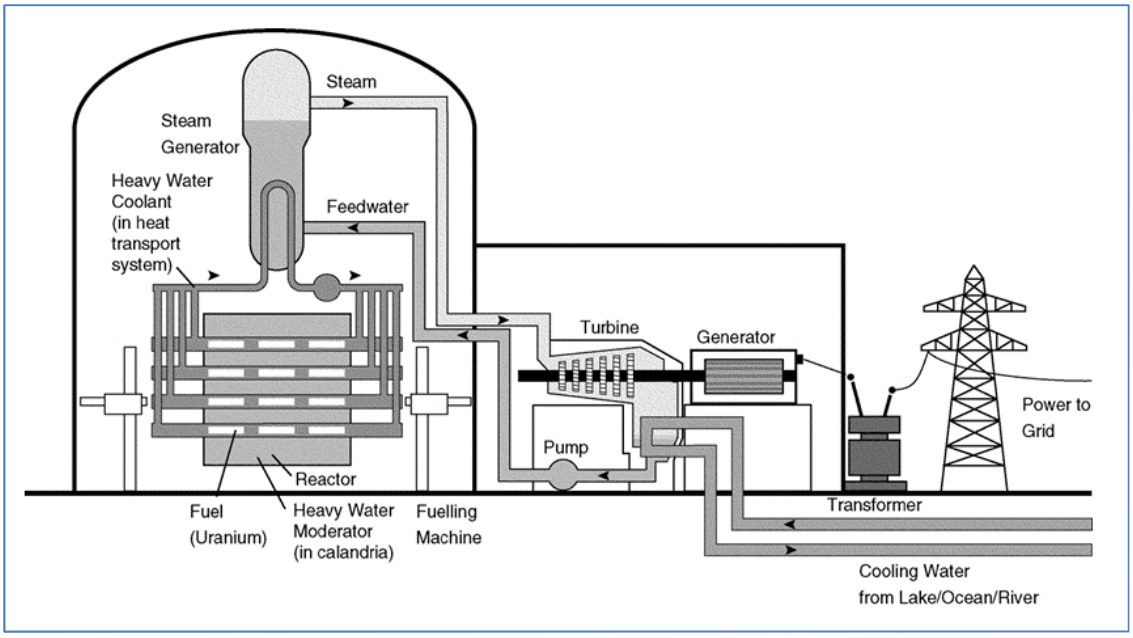

Figure 2 Typical CANDU plant

Figure 2 provides a schematic diagram of a typical CANDU heat transport system.

Figure 3a provides a detailed diagram of the CANDU 6 primary heat transport system (blue solid lines) and the shutdown system (green dashed lines) [AECL1981]. Figure 3b provides a 3D view of the CANDU 6 cooling system layout in the reactor building (the nuclear island) [AECL2005].

A CANDU nuclear steam supply system's power production process starts like that of any other nuclear steam supply system, with controlled fission in the reactor core.

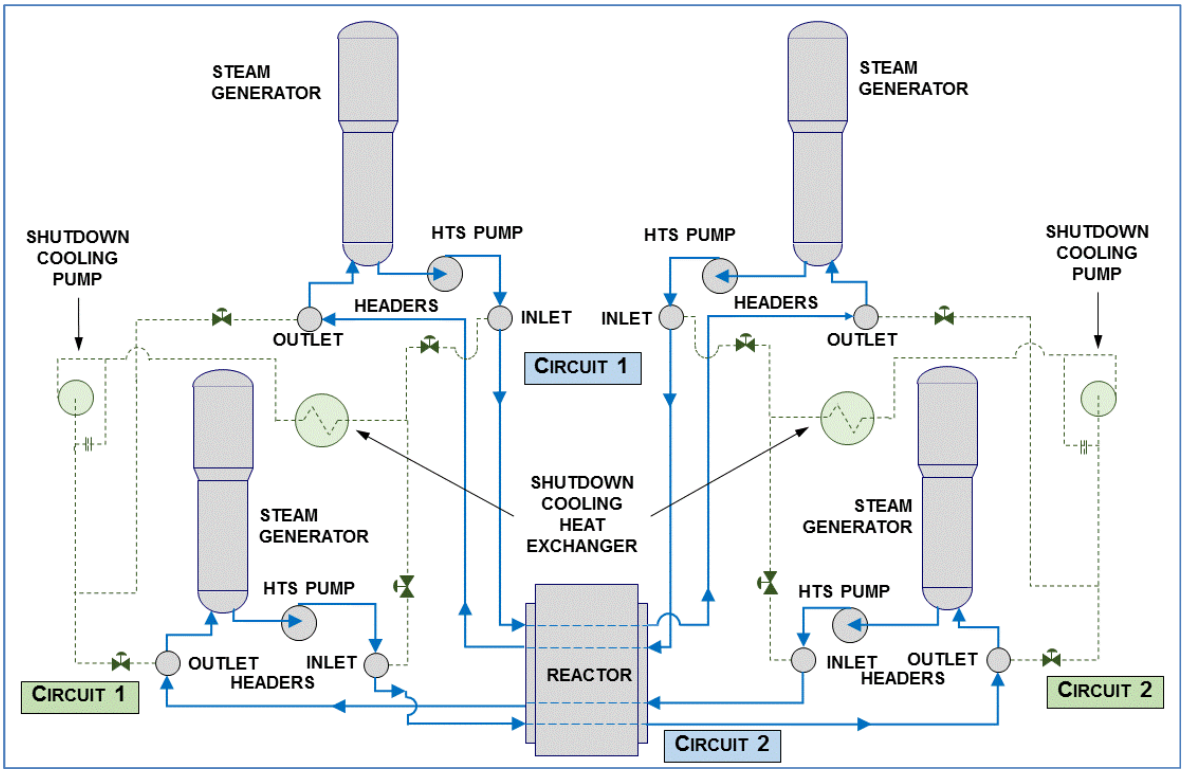

a) CANDU 6 primary and shutdown cooling loops

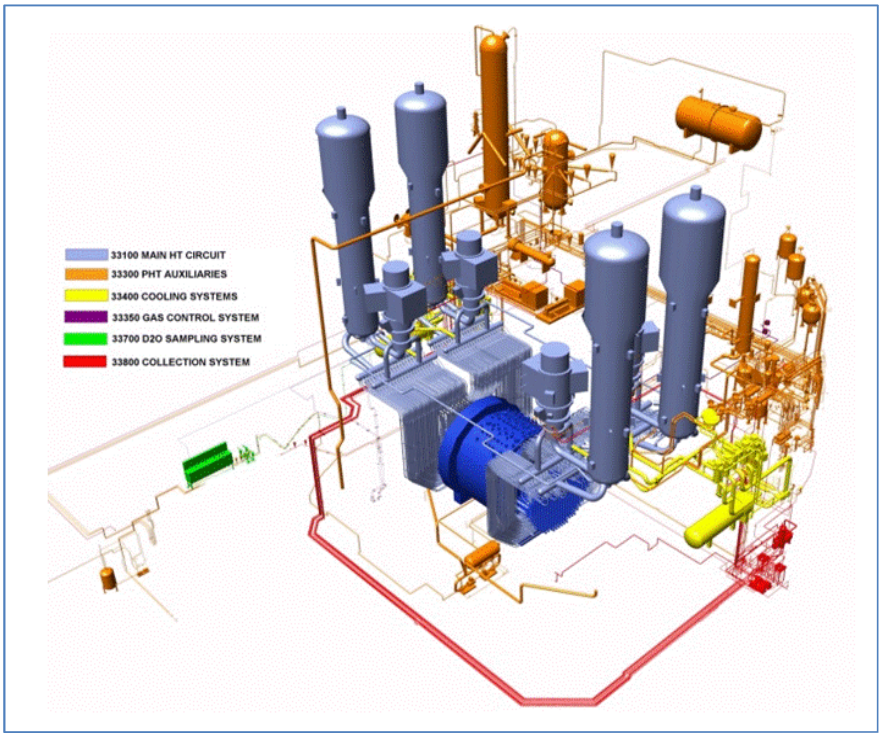

b) CANDU 6 cooling loops in containment – 3D view

Figure 3 CANDU 6 reactor cooling loops

2.1.1 Reactor core and calandria vessel

The core in a CANDU reactor is horizontal (Figure 4), with reactor channels in the core containing the reactor fuel and heavy water coolant, whereas the heavy water moderator is in the calandria vessel surrounding the reactor core [AECL2009a, AECL2010]. The reactor is made up of a stainless-steel horizontal cylinder, the calandria, closed at each end by end shields that support the horizontal fuel channels spanning the calandria and provide personnel shielding. In the CANDU 6 design, the calandria is housed in and supported by a light water-filled, steel-lined concrete structure, the reactor vault, which provides thermal shielding (Figure 5). In the Darlington/Bruce CANDU reactor design, the calandria vessel is housed in a steel shield tank assembly, which performs a similar function to the CANDU 6 calandria vault. The calandria contains heavy water (D_2O) moderator at low temperature and pressure, reactivity control mechanisms, and several hundred fuel channels.

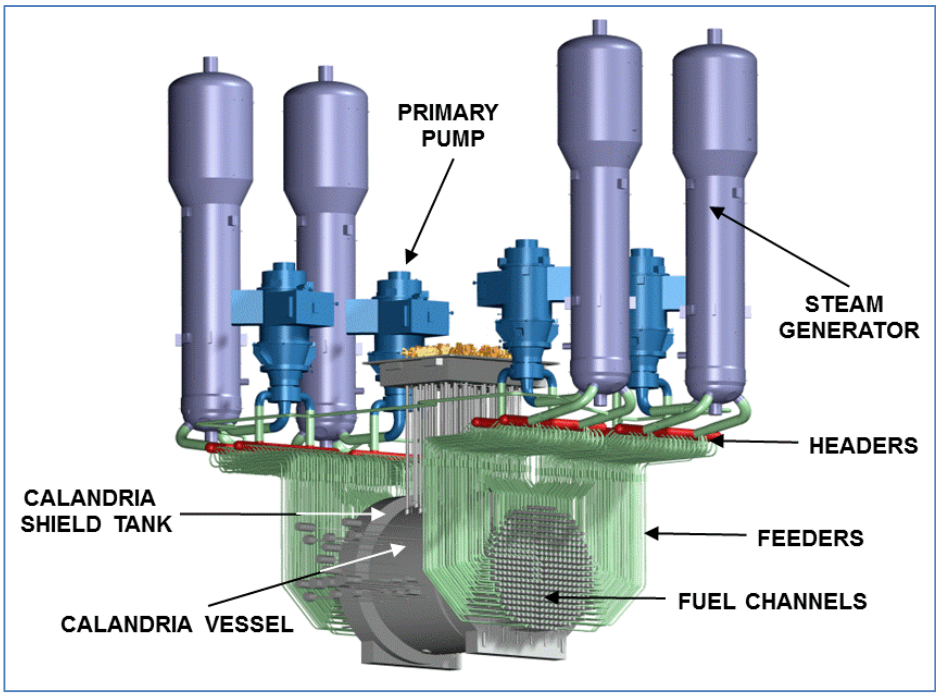

Figure 4a) Typical CANDU reactor and heat transport system

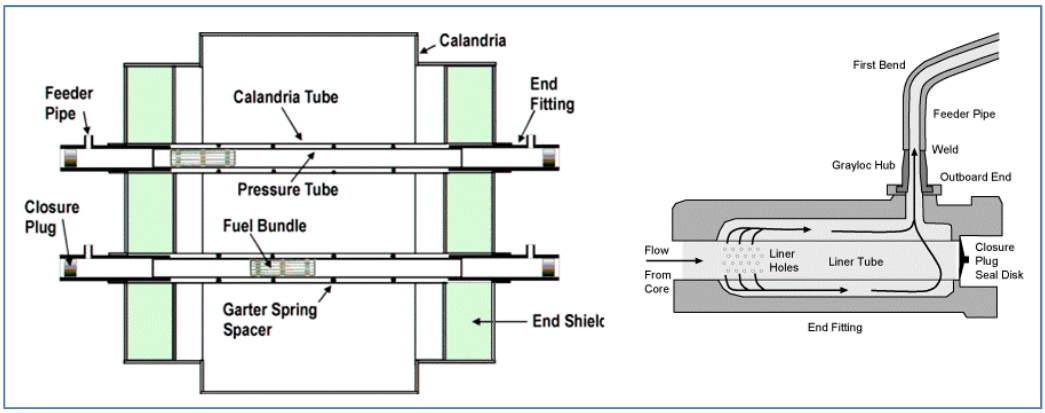

Figure 4b) Typical CANDU fuel channel

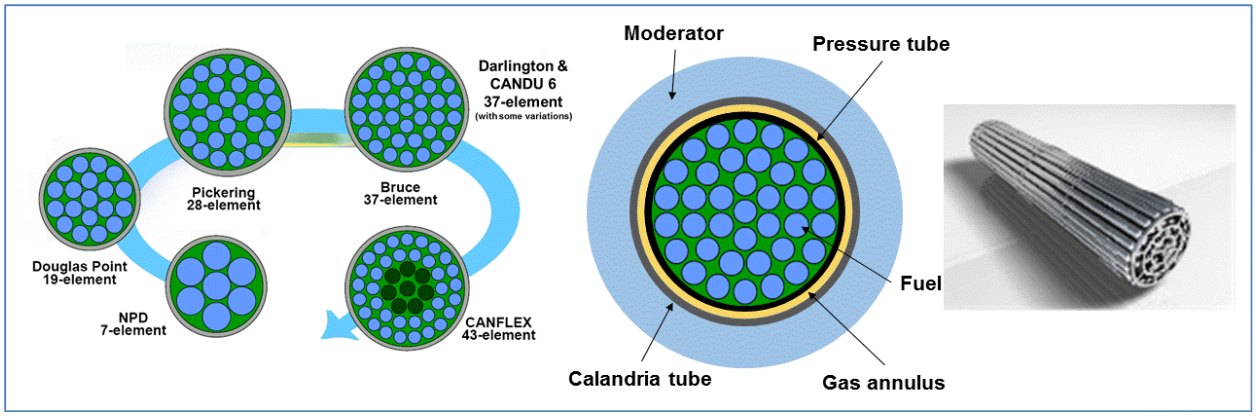

Figure 4c) Typical CANDU fuel bundle

Figure 4 CANDU reactor, fuel channel, and fuel bundle

Neutrons produced by nuclear fission are moderated (slowed) by the D_2O in the calandria. The moderator D_2O is circulated through systems that cool and purify it and control the concentrations of the soluble neutron absorbers used to adjust reactivity.

The fuel channels are also shown in Figure 4c. Each fuel channel supports 12 fuel bundles in the reactor core (13 in the Darlington/Bruce CANDU design). The fuel channel assembly includes a zirconium alloy pressure tube, a zirconium calandria tube, stainless steel end-fittings at each end, and four spacers that maintain separation of the pressure and calandria tubes. Each pressure tube is thermally insulated from the cool, low-pressure moderator by the CO_2-filled gas annulus between the pressure tube and the concentric calandria tube.

The CANDU fuel bundle typically consists of 37 elements (although advanced 43-element designs have been qualified, and 28-element designs are still in service at Pickering station) arranged in circular rings, as shown in Figure 4c.

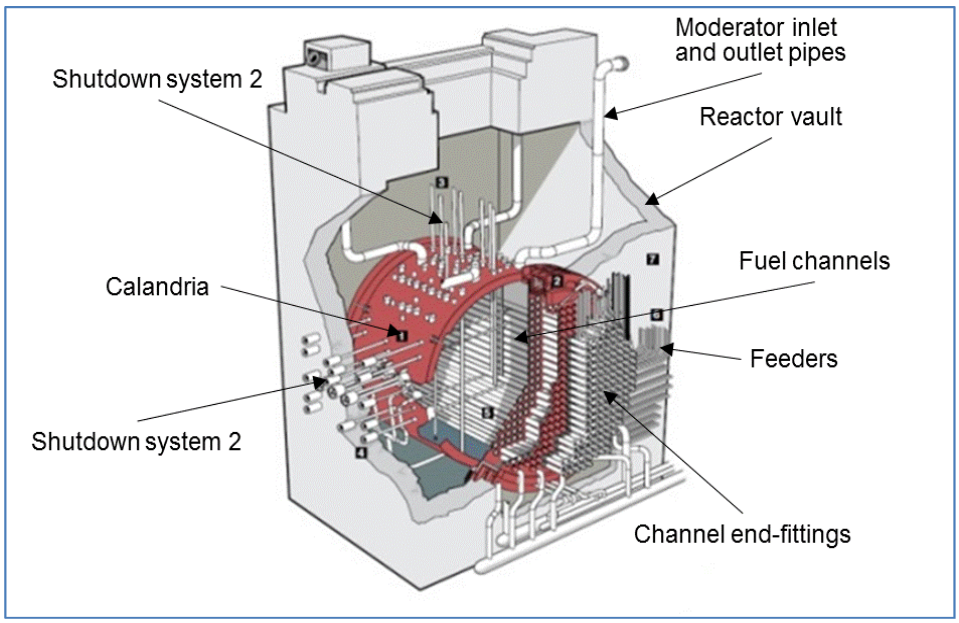

Figure 5 CANDU calandria vessel and reactor vault

Each fuel element consists of natural uranium in the form of cylindrical pellets of sintered uranium dioxide contained in a zircaloy-4 sheath closed at each end by an end cap. The fuel elements are held together by end plates at each end to form the fuel bundle. The required fuel element separation is maintained by spacers brazed to the fuel elements at the transverse mid-plane. The outer fuel elements have bearing pads brazed to the outer surface to support the fuel bundle in the pressure tube.

The CANDU reactor assembly, shown in Figure 5, includes the fuel channels contained in and supported by the calandria. Each end shield consists of an inner and an outer tube sheet joined by lattice tubes at each fuel channel location and a peripheral shell. The inner spaces of the end shields are filled with steel balls and are light water-cooled. The fuel channels, supported by the end shields, are located on a square lattice pitch. The calandria is filled with heavy water moderator at low temperature and pressure.

2.1.2 Primary heat transport system design

The CANDU primary heat transport system consists of primary, secondary, and tertiary loops, as shown in Figure 2 [AECL2009a]. There are several variations of the CANDU heat transport system design, the latest being the Pickering, Bruce/Darlington, and CANDU 6 designs. The CANDU 6 heat transport system design is described in the following sections.

The heat transport system (HTS) circulates pressurized D_2O coolant through the fuel channels to remove the heat produced by fission in the nuclear fuel. The coolant transports the heat to steam generators, where it is transferred to light water to produce steam to drive the turbine. Two HTS coolant loops (one in the Bruce design) are provided in CANDU reactors (Figure 6). Each loop has one inlet and one outlet header, as well as one primary pump and one steam generator at each end of the reactor core. D_2O is fed to each fuel channel through individual inlet feeder pipes from the inlet headers and is returned from each channel through individual outlet feeder pipes to the outlet headers. Each heat transport system loop is arranged in a "figure-of-eight", with the coolant making two passes in opposite directions through the core during each complete circuit and the pumps in each loop operating in series. The coolant flow in adjacent fuel channels is in opposite directions.

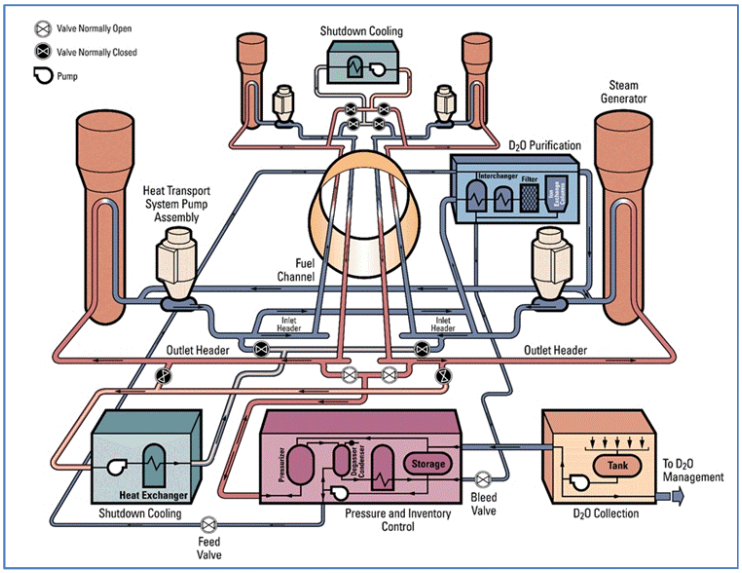

Figure 6 CANDU primary heat transport system

In most CANDU reactors, the pressure in the heat transport system is controlled by a pressurizer connected to the outlet headers at one end of the reactor. Valves provide isolation between the two loops and the pressurizer in the event of a loss-of-coolant accident.

Figure 6 provides a view of the "figure-of-eight" design of the CANDU heat transport system. On the right side, this figure shows the CANDU heat transport system to scale, with all feeders connected to the reactor core. Coolant is transported from the outlet headers to the steam generator by a large steam generator inlet pipe. Primary coolant from the steam generator outlet is transferred to the primary pump by means of a large pump suction pipe and from the pump to the inlet header by means of large pump discharge pipes.

The main components of the reactor primary heat transport system, in addition to the reactor, are the steam generators, primary pumps, connecting piping to each channel, distribution headers, large piping connecting these to the pumps and the steam generators, and the pressurizer. These components are described in the next few sections.

2.1.3 Steam generators

The CANDU steam generators consist of an inverted U-tube bundle within a cylindrical shell. Heavy water coolant passes through the U-tubes [AECL2009a, AECL2010]. The steam generators include an integral pre-heater on the secondary side of the U-tube outlet section and integral steam-separating equipment in the steam drum above the U-tube bundle. A typical steam generator structure is shown in Figure 7.

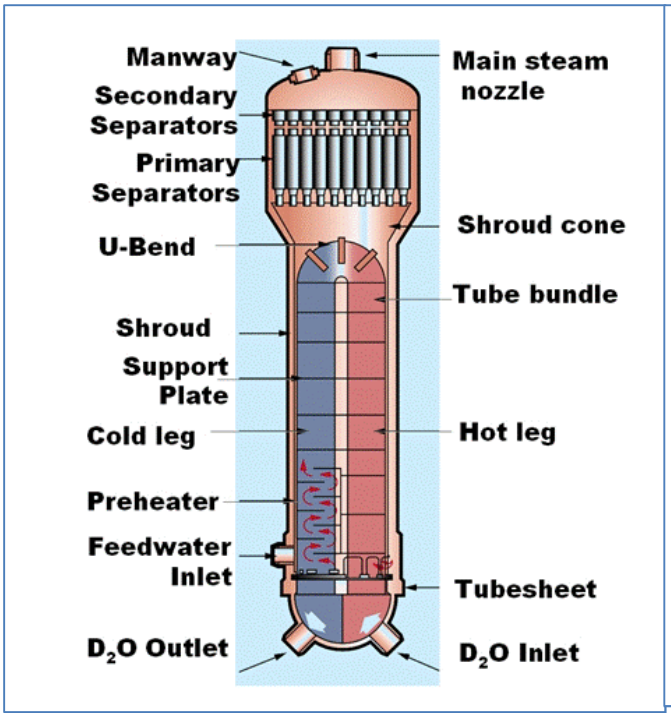

Figure 7 Typical steam generator design

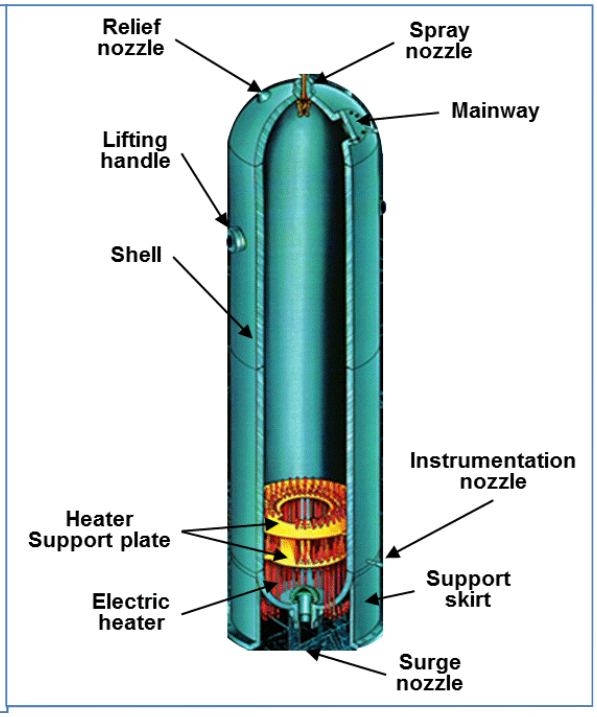

Figure 8 Typical pressurizer design

Operation and design details and calculations for the steam generator are provided in Section 7.3. The steam generator plays an important role in reactor heat transport system operation because it connects the reactor operation with the turbine-generator operation.

2.1.4 Pressurizer

The pressure in the reactor primary coolant system is maintained at a controlled level by a pressurizer. Figure 8 shows a view of a typical pressurizer [AECL2009a, AECL2010]. The pressurizer contains steam in the upper section of its cylinder and water in the lower section. The pressurizer is connected to the primary loop through a surge nozzle at the bottom. Heaters are provided at the bottom of the pressurizer internals, and a spray nozzle, relief nozzle, and safety nozzle are installed at the top of the pressurizer head.

A "positive surge" of water from the primary loop because of increasing loop pressure is compensated for by injecting cold water from the top of the pressurizer, which condenses the steam in the upper portion and thus reduces system pressure.

A "negative surge" of water empties the pressurizer, reducing steam pressure at the top of the pressurizer and thus loop pressure. In this situation, the electrical heaters at the bottom of the pressurizer are automatically activated, converting a portion of the water into steam and resulting in a loop pressure increase. By performing these sequences (i.e., creating steam when the loop pressure is too low or decreasing steam when the loop pressure is too high), the pressurizer maintains loop pressure within a certain design range and also ensures smooth pressure changes in the primary loop.

2.1.5 Primary pumps

The primary pumps used in the CANDU heat transport system are vertical, centrifugal motor-driven pumps with a single suction and a double discharge [AECL2009a, AECL2010]. As shown in Figure 9, the pump impeller is at the bottom of the pump, and the pump shaft extends upward to the pump motor, passing through a number of pump seals and holding the pump flywheel.

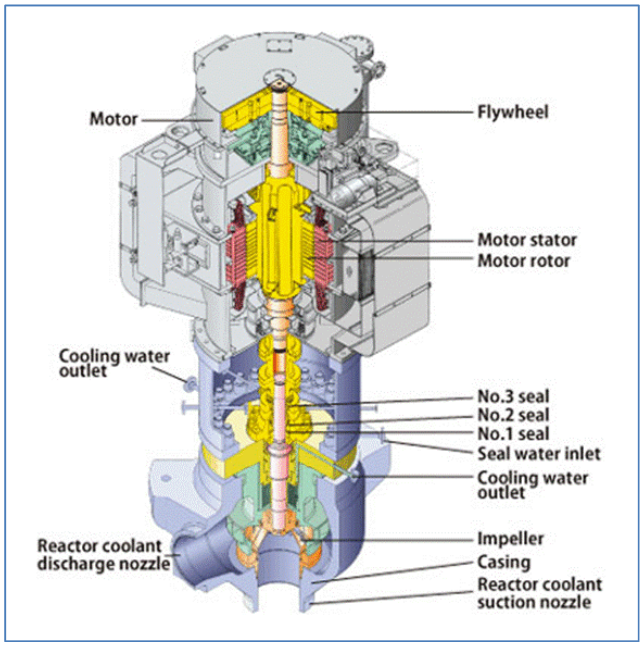

Figure 9 Typical primary pump design

Cooling of the reactor fuel in the event of electrical power supply interruption is maintained by the rotational momentum of the heat transport pumps during reactor power rundown and by natural convection flow after the pumps have stopped. More information on pump function, design, and operation is provided in later sections of this chapter.

2.1.6 Primary heat transport piping

The CANDU reactor contains a relatively large number of pipes, called feeders, and manifolds, called headers, in the primary heat transport system, which are used to distribute coolant to the fuel channels in the core. Although these components have important functions and are mentioned in this chapter, a detailed discussion is beyond the scope of this textbook. Note that feeders are unique to reactor designs with fuel channels and provide a number of design advantages, but are also vulnerable to certain types of accidents and aging effects, as mentioned in other chapters.

2.1.7 Secondary heat transport system design

The NPP secondary heat transport system transfers the generated energy from the primary closed circuit to the secondary, where the heat energy is transferred into mechanical energy of rotation in the turbine and then into electrical energy by the electric generator. The main

components of the secondary heat transport system are the steam turbine, condenser, heat exchangers, feedwater pumps, valves, and piping; these are covered in the next few sections.

2.1.8 Turbine

The CANDU steam turbine is typically a tandem compound unit, directly coupled to an electrical generator by a single shaft. It consists of one double-flow high-pressure cylinder followed by external moisture separators, five steam reheaters, and three double-flow low-pressure cylinders. The turbine is designed to operate with saturated inlet steam. The turbine system includes main steam stop valves, governor valves, reheat intercept valves, and emergency stop valves. All these valves close automatically in the event of a turbine protection system trip.

In the following sections, more details are provided about turbine operation, efficiency, and other relevant parameters.

2.1.9 Condenser

The turbine condenser consists of three separate shells. Each shell is connected to one of the three low-pressure turbine exhausts. Steam from the turbine flows into the shell, where it is condensed by flowing over a tube bundle assembly through which cooling water is pumped. The condenser cooling water typically consists of a once-through circuit that uses water from an ocean, lake, or river or is connected to cooling towers. The condensed steam collects in a tank at the bottom of the condenser called the “hot well”. A vacuum system is provided to remove air and other non-condensable gases from the condenser shell. The condenser is designed to accept turbine bypass steam to permit reduction of reactor power from 100% to 70% if the turbine is unavailable.

2.1.10 Heat exchangers and pumps

On its return to the steam generators, condensate from the turbine condenser is pumped through the feedwater heating system. Typically, it first passes through three low-pressure feedwater heater units, each of which contains two heaters fed by independent regenerative lines. (This arrangement permits maintenance work to be carried out on the heaters with only a small effect on turbine generator output.) Two of the heater units incorporate drain cooling sections and the third a separate drain cooling stage. Next, the feedwater enters a deaerator, where dissolved oxygen is removed. From the deaerator, the feedwater is pumped to the steam generators through two high-pressure feedwater heaters, each incorporating drain cooling sections (see Figure 55).

Several stages of feedwater pumps are installed to raise the pressure from the condenser pressure (vacuum) of 4–6 kPa to the steam generator pressure of 4.7 MPa. More information on heat exchanger design and calculations is provided in later sections of this chapter.

2.2 Problems

1. Name and describe the function of the main components of the CANDU primary heat transport system.

2. Describe the main components of the pressurizer in a CANDU reactor, with a detailed explanation of the method it uses to control the primary heat transport system pressure.
3. Provide a detailed description of the steam generator function, with specific reference to its role in the relationship between the primary and secondary heat transport systems. Comment on the relationship of these systems with the overall size of the steam generators.

3 CANDU Thermal-Hydraulic Design Evolution

To obtain a better understanding of CANDU design concepts, one needs to understand how the design has evolved over the past 50 years [AECL1978, AECL1997]. This section provides information focussing on the reasons why certain evolutionary steps were taken and why certain design solutions were abandoned, based on operating experience and on evolving regulatory requirements. The design evolution is covered from two perspectives: general evolution resulting from nuclear operating and regulatory experience around the world, and CANDU-specific operating and regulatory experience in Canada.

3.1 CANDU reactor evolution

The evolution of the heat transport system is of primary importance in understanding the evolution of power reactor technology. The primary heat transfer system contains the reactor core and the fuel and is therefore an important link between the reactor thermal-hydraulics, physics, and fuel.

The evolution of the heat transport system, which is described in this section, captures the design evolution of the reactor core, the fuel and fuel channels in the CANDU reactor, the type and number of primary heat transfer loops, and the primary pumps and steam generators. Also covered are the evolution of the systems and components on the secondary side of the heat transfer.

The CANDU design had its beginnings in the early 1950s, with preliminary engineering studies on a 20 MWe and a 200 MWe plant [AECL1997]. The design concepts were based on experimental confirmation at the ZEEP, NRX, and NRU experimental reactors at the AECL Chalk River Laboratory facilities. These studies eventually culminated in commitments to the construction of NPD and Douglas Point. NPD began operating in 1962 and Douglas Point in 1966. At the same time, commitments were made to construct Pickering in 1964 and Bruce in 1969. The 1970s witnessed the excellent operating performance of Pickering and Bruce and further commitments to construct the Gentilly-2 (Quebec), Embalse (Cordoba, Argentina), Point Lepreau (New Brunswick), Wolsong (Korea), Pickering B (Ontario), Bruce B (Ontario), and Darlington (Ontario) plants.

In most cases, successive plants have meant an increase in reactor power output. Evolutionary developments have been undertaken to fit the requirements of stricter safety goals, higher ratings and sizes, new regulations, better reliability and maintainability, and lower costs. These evolutionary changes have been introduced in the course of engineering parallel reactor projects with overlapping construction schedules—circumstances which provide close contact with the practical realities of economics, manufacturing, construction activities, and performance in plant commissioning. Features for one project furnished alternative concepts for other plants on the drawing board at that time, and the experience gained in first application yielded a sound basis for re-use in succeeding projects. Thus, the experience gained in NPD, Douglas Point, Gentilly-1, and KANUPP contributed to Pickering and Bruce. In turn, all these plants contributed to the CANDU 6 design (i.e., Gentilly-2, Point Lepreau, Wolsong, Cernavoda, Embalse, and Qinshan). The evolutionary changes that have taken place are discussed in the following sections.

Table 1 provides a general comparison of key design features of other reactor types with those of CANDU [GAR1999, POP2014, POP2015]. Table 2 provides information on the evolution of various key components in CANDU heat transport systems.

Table 1 Typical fuel characteristics for key reactor types

Characteristic	BWR	PWR	AGR	LMFBR	CANDU
Moderator	H_2O	H_2O	Graphite	-	D_2O
Coolant	H_2O	H_2O	CO_2	Molten Salt	D_2O
Neutron Energy	Thermal	Thermal	Thermal	Fast	Thermal
Fuel	Enriched UO_2	Enriched UO_2	Enriched UO_2	PuO_2/UO_2	Natural UO_2
Fuel Geometry	Cylindrical pellet in clad tube	Cylindrical pellet in clad tube	Cylindrical pellet in clad tube	Cylindrical pellet in clad tube	Cylindrical pellet in clad tube
Fuel Assembly	Up to 10 x 10 rod array	Up to 17 x 17 rod array	Concentric circles	Hexagonal rod array	37-element fuel bundles (typ.)

3.1.1 Primary heat transport system

The evolution of the CANDU design has involved a continuing quest for higher reliability, better equipment maintainability, and reduced radiation doses to operating staff. This has been manifested in a dramatic reduction in the number of components, as shown in Table 2. For example, NPD had approximately 100 valves per MW in the nuclear steam supply system. This was reduced to less than 1 valve per MW in the Bruce, Gentilly-2, and Darlington designs. In addition, there are no valves in the large HTS main piping (past the Pickering design). The number of steam generators has gone from 12 in Pickering, to 8 in Bruce, to 4 in the CANDU 6 and Darlington designs. Other evolutionary changes have included improvements in sub-cooling margins, increased gross and channel flowrates, and increases in system pressure and temperature. All materials in the heat transport circuit are now specified for very low levels of cobalt to minimize radiation fields, thus improving CANDU radiation protection robustness.

Table 2 CANDU main process parameters and features

Parameter	Douglas Point	Pickering	Bruce/Darlington	CANDU 6
Power Output MW_e	210	515	750 / 850	700
Number of Channels	306	390	480	380
Number of Pumps	10	16	4	4
Pump Type	Vertical Centrifugal Single Stage	Vertical Centrifugal Single Stage	Vertical Centrifugal Single Stage	Vertical Centrifugal Single Stage
Power per Pump kW	600	1170	> 8250	> 5250
Pump Code	BPVC Sect. VIII	BPVC Sect. VIII	BPVC Sect. III Class 1	BPVC Sect. III Class 1
Pump Seismic Classification	None	None	DBE Category 'A'	DBE Category 'A'
Number of Steam Generators	80	12	4 or 8	4
SG Power MW/boiler	2.5	~ 45	~ 95	150
SG Material	M-400	M-400	I-600	I-800
Number of SG Tubes	196	2600	> 4200	3550

3.1.2 Steam generators

Steam generator size has been generally limited by the industrial capability to produce the generators. Figure 10 [GAR1999] shows the evolution of the steam generator in terms of its size and power. The power of the Darlington steam generators is close to 800 MW. Current CANDU 6 plant designs typically have four steam generators.

Monel was used as the tubing material for Douglas Point, RAPP, KANUPP, and Pickering. This material has proven quite satisfactory for the non-boiling coolant conditions of those plants. Inconel 600 was used in NPD and in Bruce. This is a more costly material than Monel; however, its corrosion resistance in a boiling environment (as in Bruce) is much superior. Currently, Incoloy 800 is used in all 600-MW class CANDU 6 operating reactors. This material is more or less equal in most respects to Inconel 600, has greater resistance to intergranular attack, and is somewhat lower in cost.

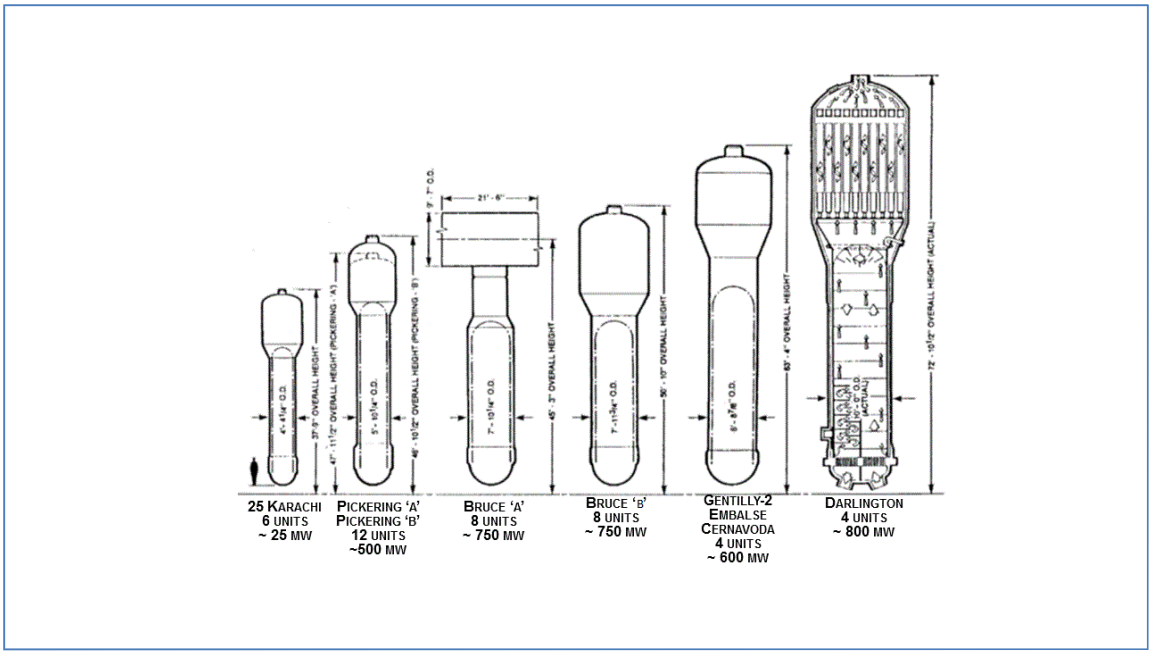

Figure 10 CANDU steam generator design evolution

3.1.3 Heat transport pumps

Pump-motor sets have retained essentially the same configuration in all CANDU stations, i.e., vertical electric motor-driven, centrifugal, volute-type casing, one radial guide bearing in the pump with pumped fluid as lubricant, a tilting pad-type guide and double-acting thrust bearing in the motor, and mechanical shaft seals. Table 2 provides information on the evolution of the primary pump [GAR1999].

Maintainability has been improved by providing interchangeable sub-assemblies. Appropriate shielding placement has made it possible to change a pump motor on Bruce while the reactor continues to operate at 60%–70% power.

There has been a trend away from solid rotor flywheels (Douglas Point to Gentilly-2) to additional packages of rotor laminations located just outboard of the main rotor (Point Lepreau, Bruce 'B'). This manner of fabrication eliminates the requirement for in-service inspection because it is highly unlikely that a defect could grow from one lamination to another.

Regulatory requirements for pumps have grown from minimal at the beginning to the present time, at which the pump pressure boundary is considered in the same way as for nuclear pressure vessels (ASME Section III, Class I). Consequently, non-destructive examination (NDE) and quality assurance requirements have increased considerably.

3.1.4 Reactor core

In 1955, a detailed design of a demonstration natural uranium reactor was carried out. It was called the Nuclear Power Demonstration (NPD) and was based on a vertical pressure vessel concept [AECL1997]. In 1957, this was changed to a horizontal pressure tube configuration—a

configuration which has remained in subsequent heavy water-cooled reactors. The horizontal configuration aided the on-line fuelling scheme by making double-ended fuelling feasible. It also permitted the use of vertical safety control rods, which did not interfere with the pressure tubes and feeders.

Reactor core evolutionary changes have been intended to achieve:

a) large increases in core rating with the minimum increase in reactor size (higher power density enabling reduction in capital cost);

b) reduction in shop fabrication costs through simplification and standardization;

c) reduction in field assembly and shortened construction schedules through more shop fabrication and modularization.

Table 3 Evolution of D_2O content in the core and of power in the fuel channel

Reactor Design	D_2O in Core per MW Thermal [m^3/MWth]	MW Thermal per Metre Length of Fuel Channel [MWth/m]
NPD	0.410	0.163
Douglas Point	0.169	0.453
KANUPP	0.182	0.443
Pickering A	0.157	0.752
Bruce A & B	0.112	0.881
Gentilly-2	0.105	0.931

The major impact of higher power densities on capital costs is to reduce the heavy water inventory. The amount of heavy water in the reactor core per MW produced in the reactor is listed in Table 3. Higher power densities required more MWs of power produced per metre length of fuel channel.

3.1.5 Reduction in radiation exposure

Canada has accepted the recommendations made by the International Commission on Radiological Protection (ICRP) on maximum permitted doses for occupationally exposed persons.

Note that severe accident doses are different from these normal operating doses and that discussion is ongoing about these doses, especially under the influence of the accident in Fukushima, Japan in 2011.

The major factors affecting the radiation dose accumulated by a worker are:

a) Amount of equipment.
b) Frequency of failure.
c) Time required for repair, service, and inspection.
d) Radiation conditions (fields and airborne concentrations).

Because radiation dose is proportional to the product of these four factors, a reduction in any factor will reduce the dose received. The following general classification of some solutions in the design stage has emerged:

1) Avoid adding equipment.
2) Eliminate equipment and remove unnecessary redundancy.
3) Simplify equipment.
4) Provide necessary equipment of high reliability.
5) Relocate equipment to lower radiation fields.
6) Eliminate materials such as cobalt, which could become highly radioactive.
7) Provide better chemical control and purification.
8) Arrange for quick removal for shop maintenance.
9) Extend interval between maintenance periods.
10) Reduce *in-situ* maintenance times.
11) Provide adequate space around equipment.
12) Provide adequate shielding so that maintenance can take place in low fields.

3.2 CANDU reactor types

Over the past 60 years, AECL in Canada has designed many types of CANDU reactors, some of which were built and operated, and some of which were never built or were abandoned. This section provides a brief overview of these past CANDU designs, with a view to understanding the evolution of the CANDU heat transport system and its thermal-hydraulic design [AECL1997].

3.2.1 Nuclear Power Demonstration station

Figure 11 shows the simplified HTS schematic for the Nuclear Power Demonstration (NPD) CANDU design [GAR1999, POP2014]. This was the first reactor design prepared by AECL. The HTS circuit contained in-line isolating valves for maintenance purposes. Pump reliability was enhanced by using three 50%-capacity pumps with check valves to prevent reverse flow through the non-operating pump. The check valves were placed at the pump discharge, of course, rather than at the suction to meet net positive suction head (NPSH) requirements. The 66 inlet and 66 outlet feeders at each end of the core terminated in a reactor inlet and a reactor outlet header respectively. Hence, bidirectional channel flow was used to limit spatial reactivity feedback. Channel flow was trimmed to match the radial power distribution by inserting an orifice plate into the inlet end fittings. All feeders were of the same diameter. Pump flywheels were used to match the power rundown during a Class IV power failure to ensure adequate fuel cooling, as in all CANDU stations. Boilers were placed above the core to enhance thermo-siphoning. Feed and bleed provided pressure and inventory control.

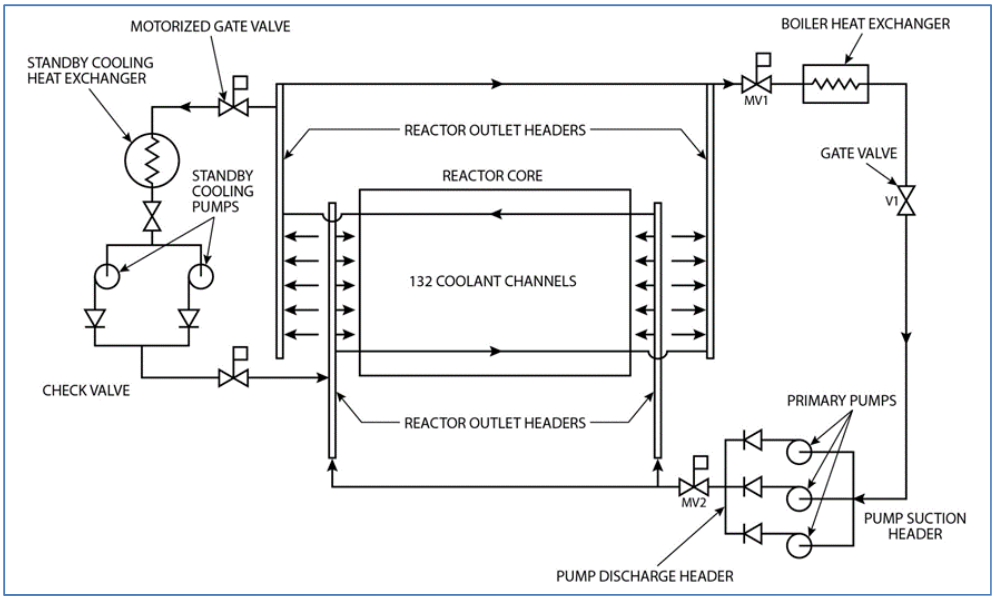

Figure 11 Nuclear Power Demonstration (NPD) heat transport system

The NPD nuclear station had some significant design features that were quite different from other CANDU stations. There was only one set of inlet and outlet headers, with relatively long connecting pipes running from one side to the other of the reactor vessel. The end fittings of the reactor fuel channels did not have shield plugs, leading to a large holdup of heavy water in this region. The core itself consisted of two fuel bundle types. The central region had 19-element bundles, and the outer region had 7-element bundles.

Another difference from later CANDU reactors is that the steam generator was a horizontal U-tube vessel with the steam drum situated above and connected to the steam generator by a series of four-inch risers and downcomers.

3.2.2 Douglas Point

The Douglas Point power plant was the first station to incorporate features typical of later CANDU designs [GAR1999, POP2014]. Figure 12 shows a simplified HTS schematic for the Douglas Point design. This station used the "figure-of-eight" loop layout. This configuration had the advantage of reducing D_2O holdup and pressure drop by eliminating the long piping runs to the far end of the core, which were inherent in the NPD design. This introduced the possibility of east-west (loop end-to-end) imbalances. Redundancy in pumps was required to achieve adequate reliability. As in NPD, bidirectional channel flow, check valves at pump discharges, and isolation valves were used. Channel flow was trimmed to match the radial power distribution using different feeder sizes or orifice plates in inlet feeders and shield plugs.

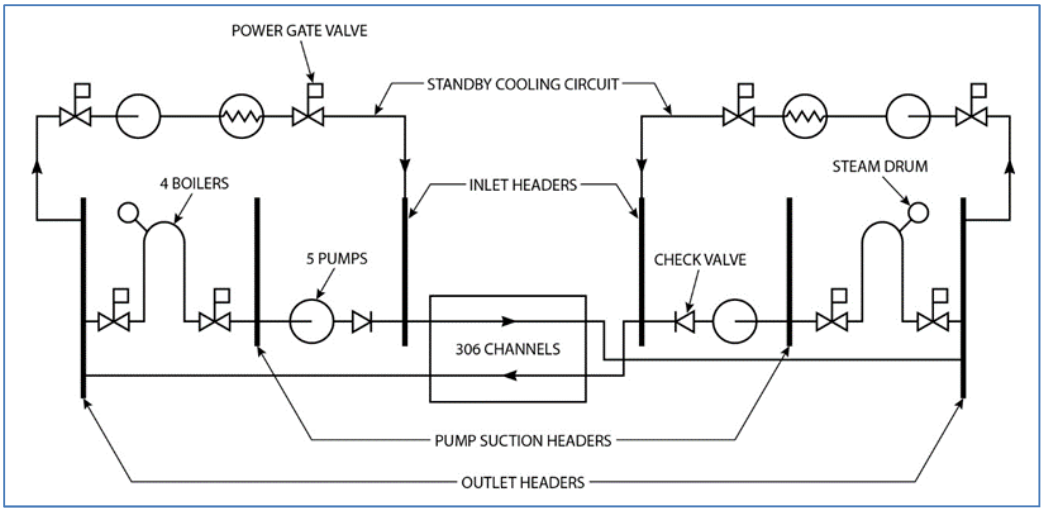

Figure 12 Douglas Point heat transport system

3.2.3 Pickering A and B

The Pickering stations have a similar thermal-hydraulic design to Douglas Point. The Pickering heat transport system is shown in Figure 13 [OPG2000]. Power output was increased to 540 MWe, and two loops were used to reduce the rate of blowdown in the event of a loss-of-coolant accident (LOCA).

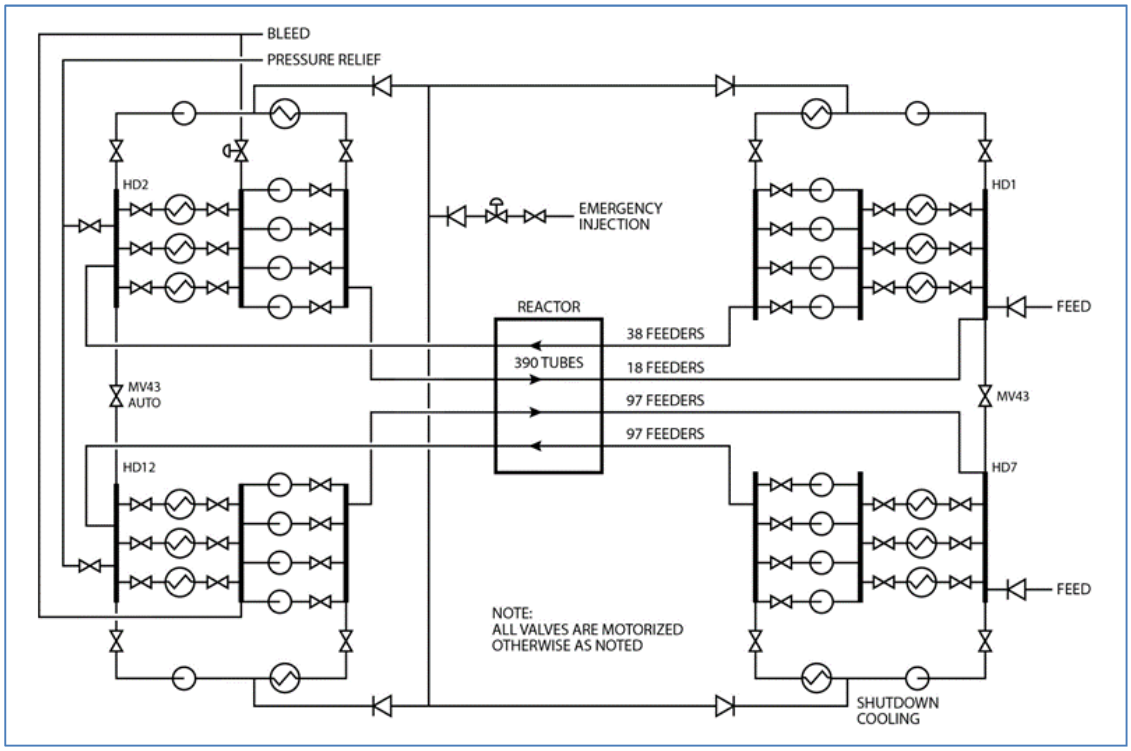

Figure 13 Pickering A heat transport system

A loop interconnect was provided to reduce loop-to-loop imbalance. Manufacturing limits on steam generators and pumps led to the use of 12 operating steam generators and 12 operating

pumps with four reserve pumps. Component isolation was still possible, but check valves were eliminated because of the leakage and poor reliability experienced at the Douglas Point plant. Trimmed channel flow was achieved by varying feeder sizes and inlet feeder orifice plates. The Pickering fuel bundle has 28 fuel elements and is the only CANDU design currently operating with 28-element fuel.

3.2.4 Bruce A and B

Figure 14 shows the simplified schematic of the Bruce HTS system [BPR2000]. It shows a significant difference in layout compared to the Pickering station. For Bruce (and later stations, such as CANDU 6 and Darlington), the reliability experience gained from previous plants justified the elimination of stand-by pumps. For radiation protection and maintenance reasons, valves were eliminated. Manufacturing now permitted larger components, and therefore eight steam generators and four pumps were included. Channel flow was not trimmed to meet power distribution capability as in all other CANDUs. A constant radial flow distribution was maintained by changing feeder sizes to account for geometry and feeder length differences. As in all CANDU designs, fuel channel flow velocity was limited to 10 m/s due to concerns about fretting of the fuel bundle and pressure tubes. The Bruce channel design had thirteen 37-element fuel bundles located in the fuel channel, but the core length was kept the same. Therefore, at each end of the core, half a fuel bundle protruded out of the reactor core region.

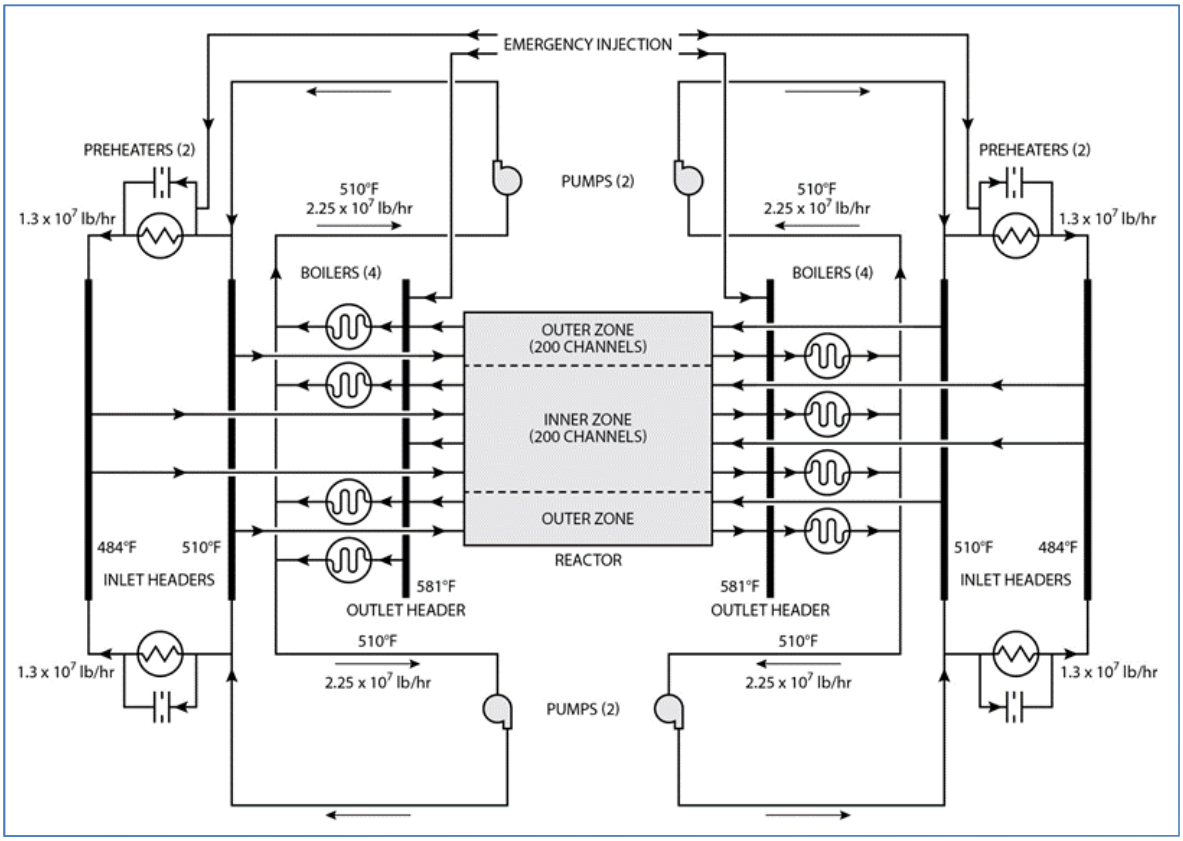

Figure 14 Bruce heat transport system

3.2.5 CANDU 6

The CANDU 6 has been discussed in previous and following sections. The figure-of-eight loop HTS design was adopted as of the Pickering design [AECL2009a, AECL2010]. However, also as in the Bruce design, fewer components were used. Increased confidence in knowledge of two-phase flow led to the use of boiling under normal conditions in the HTS. Erosion and corrosion concerns at the steam generator inlet limited the quality to 4.5% at this position or nominally 4% at the reactor outlet header (ROH). Erosion/corrosion concerns also limited single- and two-phase coolant flow velocities to a maximum value of 15.25 m/s to 16.75 m/s. The presence of boiling required a surge tank or pressurizer to accommodate the larger shrink and swell during transients. The pressurizer was used for pressure control (using heaters and steam bleed valves), whereas inventory control remained as feed and bleed. This is the same approach as in the Bruce design because the Bruce design is nominally single-phase. A heat transport system schematic of the CANDU 6 design is shown in Figure 3.

3.2.6 Darlington

The HTS schematic for the Darlington design, shown in Figure 15, is similar to the CANDU 6 design. The Darlington reactor core design is similar to the Bruce reactor core design (480 fuel channels with 13 bundles per channel) [OPG2002]. The Darlington HTS process conditions were chosen to be very close to those of the CANDU 6 because that was the state of the art at that time. An optimization program showed that higher tube pressures, higher qualities, and higher velocities were economical. However, state-of-the-art engineering limits on pressure tubes, qualities, and velocities forced the optimization to stop at these limits, which were the same as for the CANDU 6 design.

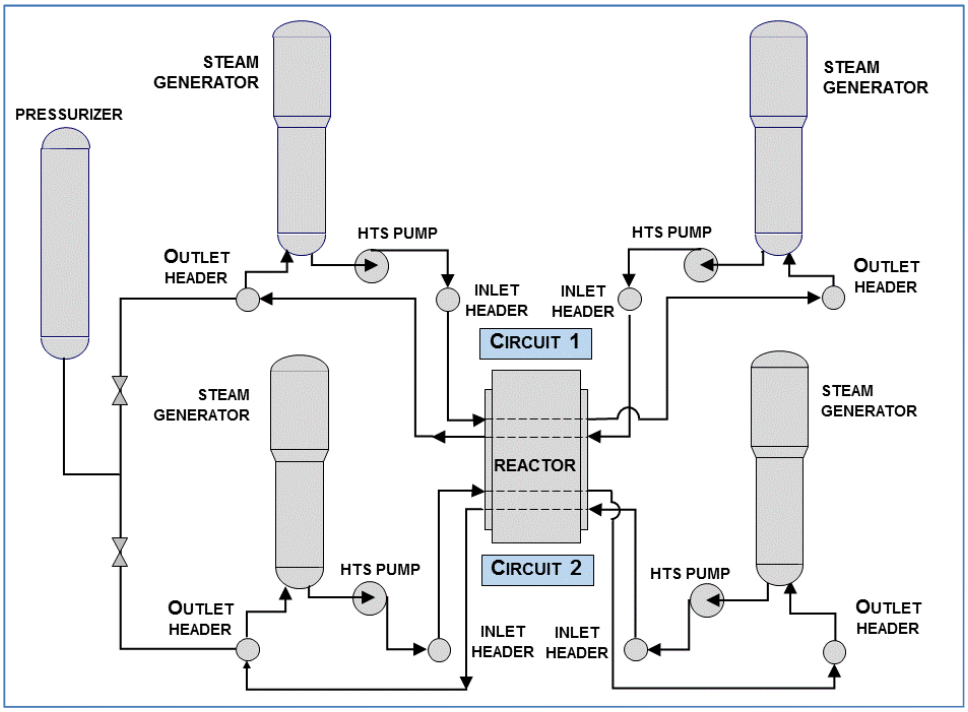

Figure 15 Darlington heat transport system

The HTS for Darlington was designed by Ontario Hydro with design support from AECL. AECL retained responsibility for the primary HTS between the headers (RIH, feeders, end-fittings, fuel channels, and ROH), whereas Ontario Hydro assumed design responsibility for the rest of the system.

The Darlington HTS design has four inlet headers, two on each side of the calandria vessel, and two outlet headers, one on each side of the calandria vessel. This configuration enables mixing in the outlet headers between the two loops, a feature that is useful for balancing the coolant parameters in both loops. However, it also exhibits some weaknesses in achieving isolation of the intact loop when the other loop is exposed to a break and a large LOCA situation.

3.2.7 Advanced CANDU designs

The advanced CANDU designs responded to continuing emphasis on safety, reliability, and maintainability (R&M), quality assurance (QA), reduction in radiation doses, standardization, modularization, and capital cost reduction. The excellent performance record of Pickering and Bruce was maintained through a vigorous R&D program and a common-sense approach to QA. Along with maintaining the above features, some of the high-level design directions were:

a) Reduction of capital cost;
b) Minimization of all areas of cost, from engineering to fabrication, construction, and commissioning; and
c) Shortening of the overall construction schedule.

Heat transport system and process designs also reflected the evolution in the state of the art, notably in the following areas:

1) Critical heat flux;
2) Erosion/corrosion velocity limits;
3) Single- and two-phase pressure drop and heat transfer correlations;
4) Thermo-siphoning;
5) Safety guidelines and requirements;
6) Stability aspects of two-phase flows;
7) Two-phase pump performance requirements;
8) Pump seals;
9) Process modelling (e.g., pressurizer, headers, boilers);
10) Creep of fuel channels;
11) Fuel design (fretting, hydraulic characteristics);
12) Power output and other constraints as required by clients;
13) Feeder sizing criteria.

3.2.7.1 CANDU 3, CANDU 9, and ACR-700

The CANDU 3, CANDU 9, and ACR-700 conceptual and preliminary designs were completed in the 1990s and 2000s to meet a market need for small low-cost power reactors, large natural uranium-fuelled reactors, and customer-specific needs respectively. Each of these reactor types had different heat transport designs; however, no stations were built using these reactor designs, and they were abandoned by AECL.

3.2.7.2 ACR-1000

The ACR-1000 conceptual and preliminary design was completed at the end of the 2000s; however, no station was built using this reactor design. Figure 16 shows the key features of the primary ACR-1000 heat transport system [AECL2009b]. The ACR-1000 reactor uses light water as coolant with a low level of fuel enrichment (around 2.1%). This combination, along with certain fuel design changes, resulted in negative void reactivity. The fuel design consisted of a 43-element bundle (CANFLEX) with low-enriched uranium fuel and with the central and intermediate rings of larger diameter than the outer two rings. The central element did not have fuel in it, and the outer two rings had pins with a certain percentage of neutron absorber to achieve negative void reactivity. The fuel had target burn-up as high as 20,000 MWd/t. Reactor power was about 3200 MWt with 520 fuel channels in the core.

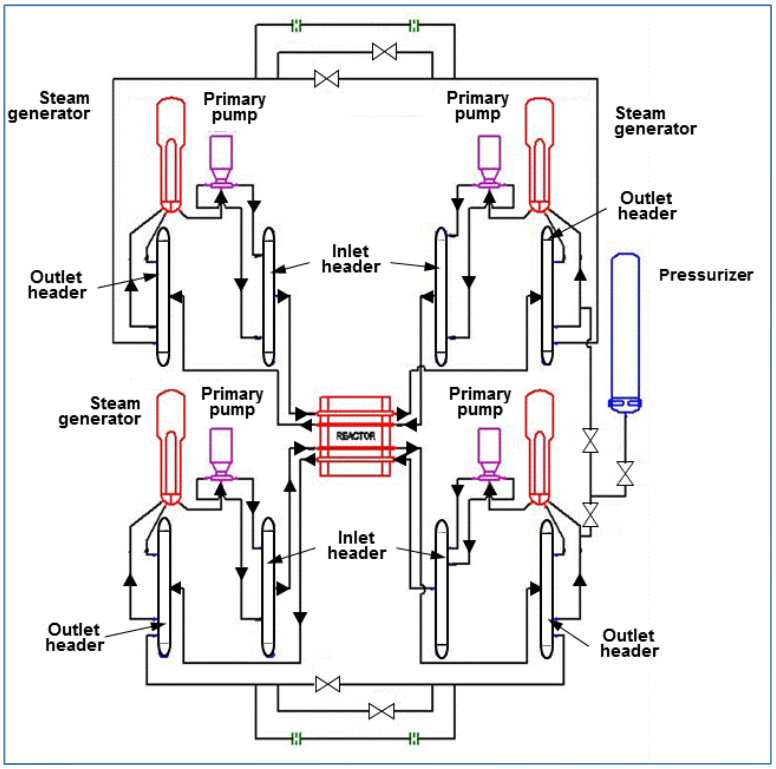

Figure 16 ACR-1000 heat transport system

The heat transport system has two figure-of-eight loops with four steam generators, with four pumps, two pumps, and two steam generators on each side of the loop. Although this reactor design has a negative void reactivity and from this perspective does not need to have two primary loops to reduce the power pulse in a large LOCA, it had two loops for a different reason. Because the reactor power was high, in addition to other reasons, having one loop (as in ACR-700) would require very large steam generators and primary pumps. Hence, splitting the core into two loops brought the scale of the steam generators and primary pumps closer to those readily available on the market.

The reactor pressure was high (about 13 MPa), along with high inlet and outlet temperatures, resulting in better thermal efficiency than earlier models.

3.2.7.3 Enhanced CANDU 6

The Enhanced CANDU 6 (EC6) design followed the CANDU 6 design, but included a number of design changes to enhance safety, operability, maintainability, constructability, and economics [AECL2009a, AECL2010]. Most of these changes were made in the reactor safety systems, with few in the thermal-hydraulic design. The EC6 heat transport system basically followed the CANDU 6 design, which has been covered in previous sections.

3.3 Non-PHWR CANDU designs

A number of CANDU-generic reactor designs were completed that either did not use heavy water coolant or were horizontal. These designs were never used in any CANDU stations, but they present a particular set of design directions that were considered in the past. These designs were later abandoned for various reasons, eventually focussing AECL's design effort on the horizontal heavy water reactor, known as CANDU, which was fuelled, moderated, and cooled in a horizontal direction. Some of these early designs are covered in the following sections.

3.3.1 CANDU-BLW

This was the second version of the basic CANDU concept to reach the prototype reactor stage (the 250 MWe Gentilly-1 plant) [AECL1997]. Its major difference from the others lay in the choice of coolant: boiling light (ordinary) water, hence its name, BLW. Its reactor coolant and turbine systems were fundamentally the same as those of the BWR described earlier, i.e., a direct cycle was used.

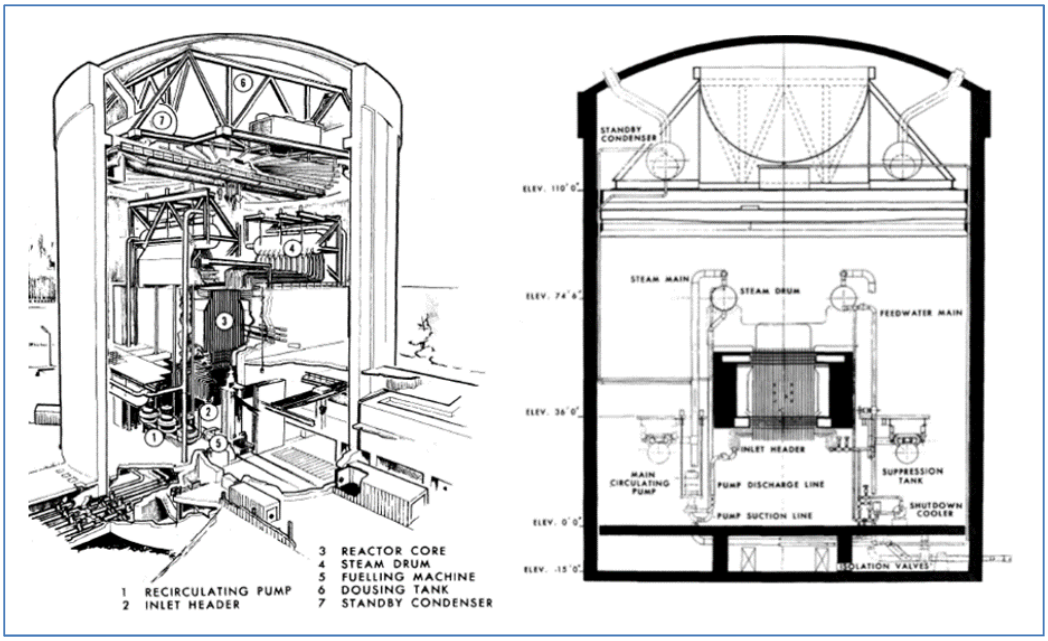

Figure 17 CANDU BLW heat transport system

For this version, a vertical orientation was chosen. A number of detailed considerations relating to the boiling coolant led to this choice.

Figure 17 provides a schematic illustration of the design. Ordinary water is pumped to the bottom of each fuel channel through an individual feeder pipe. As the water passes upwards and absorbs heat from the fuel, a fraction (~18%) is evaporated to steam. The resulting steam/water mixture then flows to a conventional steam drum where the steam and water are separated. The steam then flows to the turbine, and the water, mixed with incoming feedwater in the drum, flows down to the circulating pumps, completing the cycle.

The British developed a similar version, called the SGHWR (steam-generating heavy water reactor). A 100 MWe prototype was built. It differed from the Gentilly-1 design in that it used slightly enriched fuel. This enabled lower-purity heavy water moderator to be used, reducing capital costs. The fuelling costs were, however, somewhat higher.

In Japan, another similar version, called the FUGEN reactor, was developed and operated for about 20 years. The moderator cooling system was similar to the conventional CANDU version.

3.3.2 CANDU-OCR

A third version of the basic CANDU concept used an organic fluid as the coolant [AECL1997]. It would have been similar to the PHWR concept, except that the boilers would likely be of the "once-through" type, with some steam superheating provided. This was made possible because the coolant temperature at the reactor outlet could be ~100°C higher than with heavy water cooling.

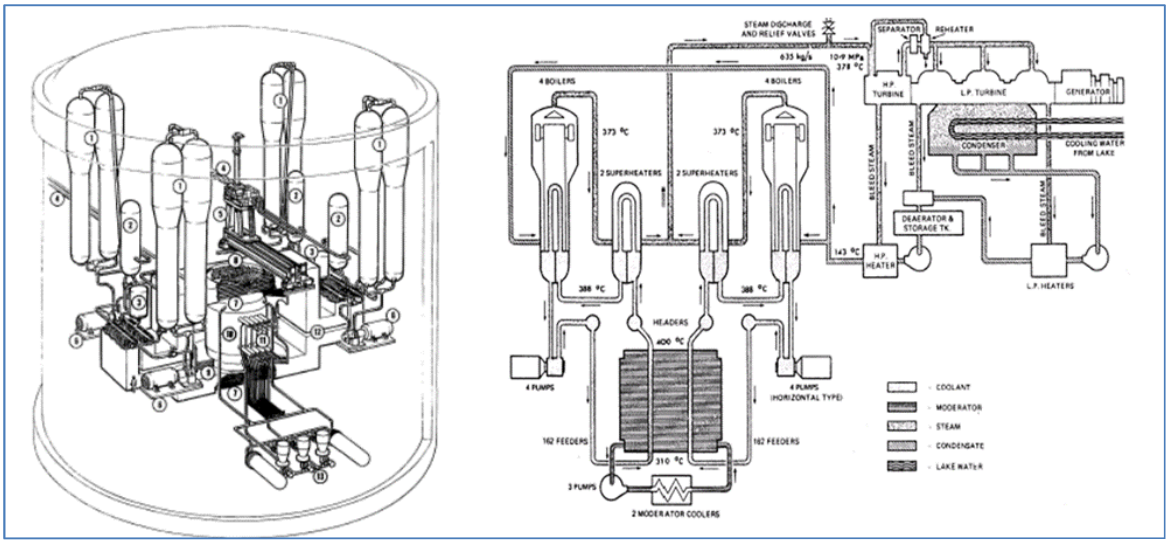

Figure 18 CANDU OCR heat transport system

The Whiteshell Reactor-1 (WR-1) experimental reactor at the AECL Whiteshell establishment used this concept, except that the heat was used only for building heating, i.e., no turbine was provided. The reactor operated under coolant conditions which were the same as those used in a commercial power plant.

Figure 18 shows a design drawing of the CANDU-OCR reactor with the key features explained above. This reactor was never built because this concept was abandoned due to certain weaknesses that were encountered, such as fire protection with coolant that is naturally

flammable, aging of the coolant (which required constant replacement and hence had a negative impact on reactor availability (associated outage frequency)), and radiation protection of the removed aged coolant.

One of the benefits of using organic coolant is that it is a mixture of several components and therefore does not boil completely at a certain temperature. This helps to avoid going through a two-phase region at one pressure and temperature, thus avoiding problems with critical heat flux. Organic coolant also helps to achieve much higher coolant temperatures in the core without the need to elevate the core pressure (as would be necessary for water). This improves thermal efficiency significantly and makes the mechanical design easier and "lighter" because of lower core pressures.

3.4 Problems

1. Describe and contrast the main similarities and differences between a CANDU primary heat transport system and a PWR primary heat transport system design.
2. List three different CANDU reactor designs and explain the differences between each of their heat transport system designs.
3. Identify four impacts of radiation doses on workers and list the general solutions that have emerged at the design stage to mitigate their impacts.
4. Explain the benefits of using organic coolant in the CANDU-OCR design.

4 Thermal-Hydraulic Design Requirements

This section covers power reactor design requirements with a focus on the thermal-hydraulic design of the reactor core [GAR1999, POP2014]. However, it should be kept in mind that the thermal-hydraulic design is tightly linked to and interfaces with other aspects of reactor design, particularly core physics and fuel design. Therefore, in various sections throughout this chapter, these interfaces are mentioned and covered to the extent necessary to obtain a better understanding of thermal-hydraulic design.

Relevant core configurations for various reactor types are covered, with a specific focus on the CANDU design. Requirements for coolant, fuel, moderator, and key materials used for reactor control and construction are covered, typical materials used for these components discussed, options considered, and analysis provided.

When discussing fuel, coolant, and moderator requirements, note that neutron economy is repeatedly mentioned as an important parameter [GLA1967]. This is true even for enriched uranium reactors because the amount of fissile isotope enrichment, and hence the cost of the fuel, is very sensitive to the neutron economy of the reactor. This is particularly so because uranium enrichment is very costly because it involves an isotope separation rather than a chemical separation process. In addition to cost, the fuel enrichment process involves a number of safeguards, regulations, and rules, which make this process politically sensitive.

4.1 Fuel requirements

In all commercial power reactors, fuel is used in solid form and in various geometries such as solid rods (cylindrical), plates, spheres, or annular configurations (see Figure 19). The key parameter governing fuel design, with respect to thermal hydraulics, is the external surface area-to-volume ratio. Good heat transfer to the coolant medium is promoted by high values of this ratio, whereas low fuel manufacturing costs and good neutron economy generally are promoted by low values of this ratio. This presents a “classical” optimization problem during reactor design. Therefore, from this perspective, the annular fuel geometry best meets this requirement; plate fuel is next, and cylindrical fuel is the worst. However, in most power reactors in operation today, cylindrical fuel rods are used, primarily due to lower manufacturing costs.

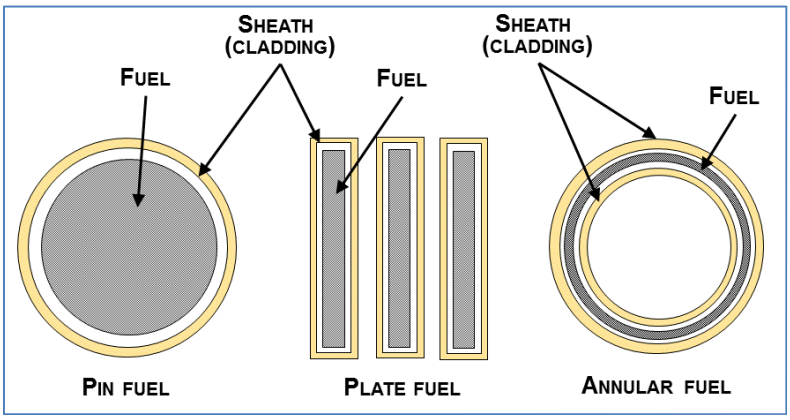

Figure 19 Fuel rod design types

Fuel requirements include (but are not limited to):

a) Low cost – both material and fabrication.
b) Good neutron economy.
c) Good corrosion resistance to coolant.
d) Physical stability under effects of radiation, temperature, and pressure.

Typical uranium-based fuel materials that have been considered or used include:

1) Uranium metal.
2) Uranium / other material alloy.
3) Ceramic uranium dioxide.
4) Uranium carbide.
5) Uranium silicide.

A summary of uranium fuel characteristics is presented in Table 4 [POP2014].

Table 4 Summary of uranium fuel characteristics [POP2014]

U Fuel Form	**Cost**	**Neutron Economy**	**Corrosion**	**Physical Stability**
U Metal	Lowest	OK	Poor	Poor (swelling)
U Alloy	Higher	Lower	OK	OK
UO_2	Higher	Lower	Excellent	Excellent. High T.
UC	Lower than UO_2	UO_2<UC<U Metal	Good, except against water	Good. High T.
US	~UC	~UC	Good even with water	~UC

Among uranium-based fuels, uranium metal is generally lowest in manufacturing cost and highest in neutron economy, the latter because of its high density and the absence of other neutron-absorbing elements. However, it has poor corrosion resistance to most coolants, which is important in the event of fuel cladding failure. Its geometric stability in reactor use is poor, primarily because of the swelling effects of fission products with specific volume greater than that of the parent uranium.

Large quantities of alloying agents, such as zirconium, can be used, which effectively solve the geometric stability and coolant corrosion problems. Unfortunately, both cost and neutron

economy suffer.

Uranium dioxide is the form in which uranium fuel is used in the vast majority of today's power reactors. It is somewhat more expensive to manufacture and less neutron-economical than uranium metal because of its lower density, but possesses excellent corrosion resistance to most coolants and a high degree of geometric stability. Being a ceramic, it can withstand high operating temperatures, which has been the deciding factor.

Uranium carbide may be attractive as a fuel for future reactor designs. It is relatively inexpensive to manufacture (comparable to UO_2) and has somewhat better neutron economy than UO_2 (because of its higher density), but not as good as that of uranium metal. It has good corrosion resistance against many coolants, but unfortunately not to water. Its dimensional stability is good, and it can operate at high temperatures.

Uranium silicide is a more recent development with most of the advantages of uranium carbide and in addition adequate resistance to corrosion by water coolants.

4.1.1 Metallic fuels

Unalloyed uranium metal is a very poor reactor fuel because it exhibits substantial growth under irradiation. Highly irradiated specimens have been known to show axial growth equal to more than 60% of the original sample length.

Uranium metal is highly chemically reactive and can be used at high temperatures with only a few coolants, e.g., carbon dioxide and helium. Low-alloy uranium fuel (with a small amount of alloying material) has been demonstrated to increase corrosion resistance to high-temperature water and to improve irradiation stability. Good results have been obtained with U_3Si (U-3.8 wt.% Si). Irradiation stability is somewhat improved, and corrosion resistance is about 500 times greater than that of unalloyed uranium. More satisfactory fuels can be obtained by addition of alloying materials, for example, 10–20 wt.% Mo or Nb alloys containing 10%–13.5% molybdenum; this option has appeared most promising.

Fuels that are highly satisfactory from both the irradiation-damage and water-corrosion standpoints can be obtained with large additions of alloying material. The only high-alloy uranium fuels in current power-reactor application are alloys of uranium and zirconium because of the good neutron economy features of zirconium.

4.1.2 Ceramic fuels

Uranium dioxide is the most widely used of all reactor materials [POP2014]. It has an irradiation stability far superior to that of metallic fuels and can withstand the high burn-up required for economical power-reactor application. When properly prepared, it exhibits excellent resistance to high-temperature water or sodium.

Uranium dioxide is obtained from the gaseous UF_6 product of the diffusion plant. Hydrolysis of UF_6 produces UO_2F_2, which is reacted in a dilute ammonia solution to form a precipitate of ammonium diuranate. This precipitate is calcined to UO_3, which is then reduced to UO_2 by hydrogen at about 800°C. The oxide is produced as a fine powder, which needs to be pressed

into a high-density compact form followed by sintering at high temperature into cylindrical pellets.

The thermal conductivity of uranium dioxide is quite low. At the high power output required in power-reactor service, this leads to very high temperature gradients across the fuel element. The resulting thermal stresses generally lead to radial cracking of the pellets during operation. However, this cracking does not appear to cause any deterioration in fuel performance, provided that the pellets are suitably restrained by cladding. Fuel element centreline melting does remain a concern and imposes an important safety margin criterion.

The chief limitation on UO_2 fuel performance is the swelling caused by gaseous fission products. At low and moderate burn-up, the swelling is slight and roughly linear with burn-up. Above a critical burn-up, the swelling increases markedly, and continued exposure of the fuel leads to unacceptable dimensional changes. The critical burn-up is primarily a function of fuel density, a value of about 17×10^3 MWd/tHE (heavy elements) being obtained with fuel of 97% oxide density and a value on the order of 42×10^3 MWd/tHE with 93% density fuel.

Thorium dioxide (ThO_2) behaves similarly to UO_2 under irradiation. Thermal stress-induced cracking is also observed in ThO_2 fuels.

Carbide fuels are intended primarily for use in fast-breeder reactors (where they provide better breeding ratios). Because these reactors operate on the U-Pu cycle, the fuel consists of mixed uranium and plutonium oxides. Thermal conductivity of UC is substantially better than that of UO_2. Hence, considerably higher specific powers are possible without risk of centreline melting. However, at higher temperatures, the swelling rate becomes excessive. The higher thermal conductivity of carbide fuel leads to a much lower Doppler coefficient than that obtained with an oxide core (the Doppler effect is the change in frequency of a wave for an observer moving relative to its source). Because the Doppler coefficient in the fuel is the main component of negative reactivity feedback in most accident situations, designing a safe carbide-fuelled core may be more difficult than designing an oxide core.

Nitride fuels have also been considered for use in fast reactor fuel.

4.1.3 Dispersion fuels

In a dispersion-type fuel, particles of fissile material are embedded in a metallic ceramic matrix [POP2014]. Such fuels can generally withstand significantly higher burn-up than alloy fuels. If the fuel particles are separated sufficiently, the areas damaged by fission fragments will not overlap, and a continuous metal phase will remain.

UO_2 and PuO_2 can be dispersed in aluminum, stainless steel, and zirconium alloys. The low-temperature limitation on the use of aluminum eliminates these dispersions from consideration for use in power reactors. Although stainless steel suffers from no such limitation, poor neutron economy eliminates it from consideration in commercial reactors. Dispersion of UO_2 in zirconium alloys forms highly satisfactory fuels if highly enriched uranium is used. Fuel performance is still limited by fuel swelling.

The most important dispersion fuel in use today is the dispersion of mixed uranium-thorium carbides or oxides in graphite. These dispersions are used in high-temperature gas-cooled

reactors. Dispersion is achieved by multiple layers of pyrolytic carbon.

4.2 General fuel sheath (cladding) requirements

During fission, new isotopes of a wide variety of elements are produced. Many of these remain radioactive for a significant time after they are generated and hence constitute a potential radiation hazard to plant operators and the public at large. It is therefore clearly desirable to keep these fission products "bottled up" within the fuel where they are generated. This is the primary function of the fuel sheath (or cladding in light water reactor technology).

The fuel cladding takes the form of an impervious "skin" or "shell" which encloses the fuel material. The most important requirements that cladding material should meet are [GAR1999, POP2014]:

a) Corrosion resistance to coolant.
b) Mechanical durability.
c) High operating temperature capability (high melting temperature).
d) Good neutron economy.
e) Low cost, both material and fabrication.
f) Impermeability to fission products.

The following cladding materials have been considered or are currently used in operating reactors:

1. Aluminum.
2. Magnesium (Magnox).
3. Stainless steel.
4. Ceramics.
5. Zirconium (used in CANDU reactors).

A summary of fuel cladding characteristics is presented in Table **5**.

Table 5 Summary of fuel cladding characteristics [POP2014]

Cladding Type	Corrosion Resistance	Mechanical Durability	High T Capability	Neutron Economy	Cost	FP Containment
Al	Good, except at high T	Low	Low	Good	Low	Good
	~Al, Ok for CO_2	~ Al	> Al	~ Al	> Al	~ Al
Stainless Steel	Good	Good	Good	Poor	Good	Good
	OK	OK	OK	Excellent	High	Good
Ceramic	Good	Brittle	Excellent	OK	OK	OK

4.2.1 Aluminum, magnesium, stainless steel, and ceramic

Aluminum and its alloys possess many attractive properties such as low cost, easy fabrication, high ductility (important in preventing cladding failures), good neutron economy, and

impermeability to fission products. Their major disadvantages for power reactor use are poor mechanical properties at high temperatures and poor high-temperature corrosion resistance with most coolants. Because the latter are temperature-dependent, aluminum alloys are widely used in research reactor fuels where cladding operating temperatures are low, but are not currently used in power reactors.

Magnesium alloys are similar to aluminum alloys in most regards. An alloy called "Magnox" has, however, better high-temperature properties and adequate corrosion resistance to permit its use in some CO_2-cooled power reactors (i.e., Magnox reactors, used in the past and described in Appendix A).

Stainless steel is a very attractive material in all major regards except for its poor neutron economy. It has been and still is used in a number of reactors where its poor neutron economy is somewhat less important because enriched uranium fuel is used. Stainless steels are used as cladding in reactors where high-temperature service is needed. This type of cladding was used in the British high-temperature, CO_2-cooled reactors. Both gas-cooled and sodium-cooled fast-reactor designs use stainless-steel cladding.

Most cladding materials in current use are metals, although ceramic-type materials have seen limited use in certain applications.

4.2.2 Zirconium

Zirconium, in its various low-alloy forms, is by far the most common cladding material in current use. It is the primary material type used for CANDU reactor fuel cladding. Despite its relatively high base material cost, it combines to a large degree all the desirable cladding properties for use with most coolants.

The primary advantage of zirconium as a cladding material is its very low cross section for thermal neutrons, which greatly improves neutron economy. Zirconium has very good water corrosion resistance at high temperatures. Adding tin, iron, and chromium to zirconium greatly improves its mechanical properties. The best-known zirconium alloys are Zircaloy 2, 3, and 4, which have found wide application as cladding for power reactor fuel elements.

Zirconium alloys are unsuitable for use at very high temperatures, even though the melting point of zirconium is 1852°C. At 862°C, zirconium transforms from a close-packed hexagonal structure to one that is body-centred cubic, and it is necessary to stay below this phase change. At these temperatures, a reaction with UO_2 can occur at the cladding inner interface of the zirconium.

Zirconium alloys exhibit significant creep at the temperatures and stresses typical of PWR reactor design. Creep rates increase markedly with temperature and are accelerated by reactor irradiation.

At high temperatures (beginning at above 800°C), zirconium chemically reacts with steam to release hydrogen in an exothermic reaction. This reaction must be considered in evaluating any LOCA event that could expose the fuel elements to steam. Reaction of an appreciable fraction of the cladding could add significantly to the severity of the accident. Moreover, the mechanical properties of ZrO_2 are not as favourable as those of zirconium.

The last point to be made about zirconium cladding is its cost. Zirconium tubes are more expensive than stainless-steel tubes. Fabrication costs are also higher because all welding must be done in an inert atmosphere. However, the decrease in fuel costs more than offsets the increased material and fabrication costs.

Most power reactors in operation today use zirconium alloy as cladding material.

4.3 Reactor coolant requirements

The purpose of reactor coolant is to transport the heat generated in the reactor fuel either to the turbine (direct-cycle reactor) or to intermediate heat exchangers (indirect-cycle reactor). The coolants may be liquids, two-phase liquid/vapour mixtures, or gases.

Reactor coolant must meet the following general requirements [POP2014]:

a) High heat capacity
b) Good heat transfer properties
c) Low neutron absorption
d) Low neutron activation
e) Low operating pressure at high operating temperature
f) Non-corrosive to fuel cladding and coolant system
g) Low cost.

The following coolant materials have been considered or are currently used in operating reactors:

1. CO_2 gas
2. Helium
3. Ordinary water
4. Heavy water
5. Organic fluid
6. Molten salt
7. Liquid metal.

The main commercial power reactor coolant types are described briefly in the following sections.

The CANDU reactor design is the only reactor design that uses heavy water as both a moderator and a coolant and is fuelled by natural uranium fuel.

A summary of coolant characteristics is presented in Table 6.

4.3.1 Ordinary water and heavy water coolants

Of the candidate HTS liquid coolants, ordinary (light) water is by far the most commonly used. It is inexpensive, has excellent heat transfer properties, and is adequately non-corrosive to the zirconium alloys used for fuel cladding and reactor structural components and to ferritic or austenitic steel coolant system materials. Its disadvantages include only moderate neutron economy and relatively high vapour pressure under coolant temperatures at power reactor HTS conditions. It is activated by neutrons in the reactor core, but this activity dies away rapidly,

permitting reasonable access to the coolant system for shutdown maintenance. A further disadvantage is that water transports system corrosion products, permitting them to be activated in the reactor core. These activated corrosion products then create shutdown radiation fields in the coolant system. The water coolant may be used as a liquid in an indirect-cycle system or may be permitted to boil, producing steam in a direct-cycle system.

Table 6 Summary of coolant characteristics [POP2014]

Coolant Type	Cost	Neutron Economy	Corrosive	Heat Capacity	HT Coeff.	HT Coeff.	Activation
CO_2 Gas	< He	Good	OK, except high T	Low	Low	Low	Low
	Higher	Good	Good, if pure	Low	Low	Low	Low
H_2O	Very Low	Moderate	OK	High	Excellent	Excellent	Yes, short $T_{1/2}$
$_2$	High	Excellent	OK	High	Excellent	Excellent	Yes, short $T_{1/2}$
Organic	Moderate	H_2O < organic < D_2O	Excellent	High	Excellent	Excellent	None
	High	Moderate	Select Materials	High	Excellent	Excellent	Yes, long $T_{1/2}$

Heavy water is used as both coolant and moderator in CANDU-type reactors. Its outstanding advantage is much better neutron economy than ordinary water. Its primary disadvantage is its high cost, plus a somewhat higher tendency to activate into tritium. Otherwise, its properties are similar to those of ordinary water.

The relatively ionizing irradiation (including γ's released because of neutron-radiative capture) causes decomposition (radiolysis) of water. Decomposition occurs in both H_2O and D_2O by the same mechanism. The rate of gas evolution (radiolysis) is proportional to radiation flux and decreases with increasing temperature.

Radiolysis of water is an important phenomenon that must be considered in analysis of accident events (as well as in normal operation) in a power reactor. Hydrogen is produced by radiolysis of water discharged from any break and can accumulate in the reactor building. Radiolysis of discharged water can occur because of γ-radiation from the sources within the discharged water (high contribution) or from the reactor fuel (low contribution). Above a certain concentration, hydrogen will burn at an explosive rate, creating a high risk to reactor components and building structures (e.g., in the Fukushima accident). The accumulation of hydrogen produced by radiolysis of discharged water in a LOCA event can be controlled by passive autocatalytic recombiners.

Water circulated through a reactor core exhibits appreciable induced radioactivity. The γ activity induced is primarily due to the 7.4 s half-life ^{16}N produced by fast-neutron interaction with ^{16}O. Additional activity may be introduced by activation of dissolved impurities and dissolved or suspended corrosion products. Hence, water purification is an important process that is continuously performed by dedicated systems.

4.3.2 Gaseous coolants

Two common gaseous coolants are in use: CO_2 and helium. CO_2 has the advantages of low cost, low neutron activation (important in minimizing radiation fields from the coolant system), high allowable operating temperatures, good neutron economy, and for gases, relatively good heat transfer properties at moderate coolant pressures. At very high temperatures, CO_2 tends to corrode neutron-economical fuel cladding materials and the graphite moderator used in most gas-cooled reactors. Its chief drawback, as for all gases, is its poor heat transfer properties relative to liquids. As a result, coolant pumping power requirements tend to be very high, particularly if high reactor power densities are to be achieved (which is desirable to minimize reactor capital costs).

A good gaseous coolant should have a low neutron-absorption cross section, high heat capacity, and high thermal conductivity.

All gaseous coolants have the disadvantage that a significant fraction of the plant energy output must be used to circulate the coolant. Furthermore, the low heat transfer coefficient requires a large heat transfer area. This may require a larger core or the use of extended surfaces (fins).

4.3.3 Liquid metal coolants

Certain liquid metals can be used as coolants. Of these, only sodium and a sodium-potassium eutectic called NaK have achieved significant use. Their advantages include excellent heat transfer properties and very low vapour pressures at high temperatures. Fuel cladding and coolant system materials require careful selection to avoid “corrosion”. Their chief disadvantages include incompatibility with water (the turbine working fluid), relatively high neutron absorption, a relatively high melting point (leading to coolant system trace heating requirements), and high coolant activation with sustained radiation fields after reactor shutdown.

Liquid metal coolants are important only for fast reactors because these metals are poor neutron moderators. Sodium is one of the most suitable liquid-metal coolants.

Sodium becomes radioactive when ^{24}Na is formed by neutron capture. This radioisotope has a 15-h half-life and emits gamma rays of 1.37 and 2.75 MeV [GAR1999]. Hence, shielding of the cooling system is necessary. Care must be taken to ensure a leak-tight system. Sodium is chemically reactive and will burn on exposure to air, evolving the oxide as dense smoke. Furthermore, it reacts violently with water, producing NaOH and hydrogen gas.

4.4 Moderator requirements

Most currently operating power reactors are of the thermal type, i.e., the energy of the neutrons causing fission is in the thermal range. Because the neutrons produced by fission have very high energies, they must be slowed down, or “thermalized”. The medium used for this is called the moderator. It is deployed as a continuous medium surrounding the fuel “cells”. The fuel cells form a geometric pattern, called the reactor “lattice”. The optimum spacing between these fuel cells is a function of several variables, including the mass of fuel per

cell, the mean free path of the neutrons being thermalized, the degree to which the moderator wastefully absorbs neutrons, and the cost of the moderating medium. A summary of moderator characteristics is presented in Table 7 [POP2014].

The best moderator is something that is the same size as a neutron, i.e., the hydrogen atom, $^{1}H_{1}$. However, hydrogen does absorb neutrons as well. The deuterium atom, $^{2}H_{1}$, at twice the mass of hydrogen, is almost as good a slowing-down agent, but because it already has an extra neutron in the nucleus, it has a very low absorption cross section. Therefore, deuterium is a far better moderator overall than hydrogen. By using deuterium in the form of heavy water, natural uranium can be used as a fuel. If ordinary water is used, the fuel must be enriched in ^{235}U.

A good moderator has a high scattering cross section, a low absorption cross section, and slows down the neutron in the least number of collisions (high lethargy, ξ).

The desirable properties of moderators are:

a) High moderating efficiency
b) Low neutron absorption
c) Resistance to irradiation and corrosion
d) Low cost, including material, manufacture, and installation.

The following materials have been considered or are currently used as moderators in operating reactors:

1. Graphite
2. Ordinary water
3. Heavy water.

Graphite has been widely used as a moderator for power reactors. The carbon atom is relatively "light", graphite is relatively inexpensive, and carbon is a relatively weak absorber of neutrons. Nevertheless, the carbon atom is sufficiently large, leading to relatively long neutron mean free paths for thermalization, that graphite-moderated reactors tend to be large. Furthermore, the relatively large amount of graphite required leads to significant neutron wastage through absorption.

Table 7 Summary of moderator characteristics [POP2014]

Moderator Type	Cost	Neutron Economy	Moderator Efficiency	Irradiation Stability	Activation	Mean Free Path
Graphite	OK	H_2O < Graphite < D_2O	Medium	Excellent	Irrelevant	Long
$_2$	Very Low	Moderate	Low	Excellent	Good	Small
D_2O	High	Excellent	Highest	Excellent	Good	Medium

Ordinary water is a much more efficient moderator in terms of the neutron mean free path for thermalization because of its hydrogen atoms. It is also very inexpensive. Unfortunately, however, hydrogen also has a significant "appetite" for absorbing thermal neutrons, which hurts neutron economy. Most of the reactors operating in the world use ordinary water as coolant and moderator.

Heavy water is almost as good as ordinary water in terms of neutron mean free path because the deuterium atoms (which replace the hydrogen atoms in ordinary water) are relatively "light". Its outstanding advantage relative to ordinary water is that it has a very small "appetite" for absorbing neutrons. Hence, it promotes a high level of neutron economy. Its major disadvantages are its high cost and the possibility of its activation into tritium.

4.5 Control material requirements

Reactor control is most commonly accomplished by moving control rods or control mechanisms in the reactor core or by injecting liquid containing material (poisons) with high neutron-absorption cross section in the thermal and near-thermal range [POP2014] into the coolant and/or moderator.

4.5.1 Hafnium

Hafnium is one of the best control-rod materials for water-cooled reactors. It is found together with zirconium and is created as a by-product of the separation process for zirconium. Hafnium is chemically similar to zirconium and shows the same high resistance to corrosion by high-temperature water.

Hafnium consists of four isotopes, each of which has an appreciable neutron absorption cross section. Note that the capture of neutrons in one isotope leads to the production of the next higher isotope, which is also an effective absorber. Therefore, hafnium remains an effective poison for a significant time.

4.5.2 Cadmium alloys

By alloying cadmium, which has a high thermal-absorption cross section, with silver and indium, which have high resonance absorption, a highly effective absorber is produced. The alloy is typically composed of 80% Ag, 15% In, and 5% Cd, can be readily fabricated, and has adequate strength at water-reactor temperatures.

These alloys have exhibited moderate resistance to corrosion by hot water after plating with nickel. Bonding of the base to the nickel was ensured by heating the control rod to an elevated temperature before reactor exposure. Corrosion under reactor conditions was good, but in subsequent use of the alloy, it was encapsulated in stainless-steel tubes so that direct contact with the coolant was eliminated.

Cadmium is typically used in several types of CANDU reactivity mechanism designs. For example, the shut-off rods in CANDU reactors are composed of a thin layer of tubular cadmium sandwiched between stainless steel layers.

4.5.3 Rare-earth oxides

Several of the rare earths (e.g., samarium, europium, and gadolinium) have both high thermal-neutron-absorption cross sections and significant resonances in the epithermal region. The oxides, the only chemical form in which the rare earths have been considered, can be formed into refractory ceramic pellets. Because the oxides hydrate rapidly in hot water with attendant

swelling, their use in water-cooled reactors could lead to difficulties. They may, however, be suitable for use in gas-cooled reactors. Dispersions of rare-earth oxides in metals such as stainless steel have been prepared. Such dispersions, when suitably clad, can be used as water-cooled reactor-control rods because in the event of a cladding fracture, only the oxide particles on the dispersion surface would become hydrated.

4.5.4 Gadolinium nitrate

The CANDU reactor uses a gadolinium nitrate ($GdNO_3$) solution in water as a reactor control (shutdown) poison. Tanks full of concentrated $GdNO_3$ solution are maintained under pressure by helium gas. The solution can be injected into the moderator system at a reactor shutdown trip signal, which provides a fast and effective reactor shutdown mechanism. To restart the reactor, the gadolinium nitrate is removed from the moderator by a purification system. Because the poison is introduced into a low-temperature, low-pressure moderator, there are no corrosion-related concerns.

4.5.5 Boron-containing materials

The very high neutron absorption cross section of ^{10}B and the low cost of boron have led to wide use of boron-containing materials in thermal-reactor control rods and burnable poisons. Unalloyed metallic boron is not suitable for control-rod use.

Boron alloyed or dispersed in stainless steel forms inter-metallic compounds with iron, nickel, and chromium in the metal matrix. The result is a major decrease in ductility. Acceptable materials can be obtained by limiting the boron concentration to 2–3 wt.% B. The boron-stainless steel materials have adequate corrosion resistance in water-cooled reactors.

The performance of boron-stainless steel materials is limited because of the ^{10}B (n, α) reaction, which leads to severe swelling localized at the surface of the element (due to the short travel distance of the alpha particles).

Boron carbide (B_4C) is of much greater interest than elemental boron. Boron carbide can be formed into pellets and effective control elements produced by placing these within stainless-steel tubes. In high-temperature gas-cooled reactor designs, control elements can also be produced by dispersing B_4C in graphite.

In addition to its use in control elements, boron has been used (in PWRs) to control reactivity changes with fuel burn-up by dissolving boric acid in the coolant. Immediately after refuelling, enough boric acid is added to the coolant so that the reactor is just critical with all control rods nearly completely withdrawn. As burn-up proceeds, the boric acid concentration in the coolant is reduced to maintain criticality exactly ("chemical shim control"). However, one significant disadvantage of boric acid in coolant is that it is corrosive to heat transport system and reactor components (i.e., Davis-Besse pressure vessel head corrosion) and must be carefully monitored and mitigated.

Boron may also be used to compensate for the change in reactivity with fuel lifetime through "burnable poison". In this scheme, a small amount of boron is incorporated in the fuel or into special burnable poison rods to reduce the beginning-of-life reactivity. Boron burn-up causes a

reactivity increase that partially compensates for the reactivity decrease due to fuel burn-up and accumulation of fission products. Stainless-steel-boron alloys and dispersions can be used successfully for this purpose because the boron burn-up in such rods can be kept low. Alternatively, pellets of boron-silicate glass encapsulated in hollow stainless-steel tubes may be used.

4.6 HTS design requirements and engineering considerations

This section provides a discussion of design requirements and engineering considerations for the heat transport system and associated systems, which transfer fission heat to the reactor coolant to produce steam in the steam generators.

This sub-section will discuss some of the thermal-hydraulic features that characterize the CANDU system.

The main objectives of the heat transport system are to provide heat transfer at high thermal efficiency and to enable the maximum amount of energy to be extracted from the fuel without surpassing safe operating limits.

The requirements for such a system can be summarized as follows:

a) Due to the decay heat produced by the fuel even when the reactor is shut down, continuous coolant flow must be provided. This leads to requirements for pumps, pump flywheels, stand-by cooling, thermo-siphoning, and various other system functions.

b) Costs should be minimized with due regard for other requirements. This usually leads to trade-offs between, for example, heavy water (D_2O) costs, pumping power costs, equipment and piping size and costs, and layout and engineering constraints.

c) Layout should minimize radiation exposure and maximize maintainability and accessibility within other constraints.

d) Provision must be made for pressure and inventory control of the heat transfer system. Excessively high pressure could damage fluid boundaries (pipes, etc.). Low pressure could lead to high coolant voiding and possible fuel damage as well as pump damage from cavitation. Low inventory jeopardizes coolant circulation and pressure control.

e) The system must be sufficiently reliable because downtime leads to high replacement energy costs, high person-rem exposure, and high repair costs.

f) The design should provide high process efficiency.

g) The system should exhibit ease of constructability to reduce the initial cost and time of construction and to enhance maintainability.

h) The system should meet, and preferably surpass, all safety and licensing requirements.

Various coolants can be used in the CANDU design to achieve these objectives and requirements.

Any nuclear station design involves trade-offs in design features to achieve the lowest-cost power within safety limits.

Another nuclear consideration is that the coolant should have a low induced radioactivity. Both H_2O and D_2O produce ^{16}N and ^{19}O, which emit γ's in the 6–7 MeV range. This leads to reduced accessibility and maintainability while on power. The short half-life (<1 minute) allows shutdown accessibility. Tritium, abbreviated as ^3H or T, has a 12-year half-life and represents a major dose challenge for the CANDU station. Because tritium is a β-emitter, the problem is one of leakage, leading to possible absorption or ingestion by humans. Organic coolant has very little induced reactivity and aids in ease of operation and accessibility.

Coolants should also be stable in a radiation environment. At the high system pressure of the heat transport systems of H_2O and D_2O, radiolysis is not a problem.

The choice of coolant also depends on other factors such as pumping power, heat capacity, heat transfer coefficients, flow rates, pressure drop, boiling point, freezing point, corrosion, flammability, thermal stability, and cost.

Water (both D_2O and H_2O) is an attractive heat transport fluid because it offers a good balance of the considerations described above. In addition, water requires less pumping power for a given amount of heat removal.

For the Bruce reactors (which generate about 750 MWe), approximately 24 MWs of pumping power are required for each reactor. This represents over 2% of the electrical power generated [GAR1999]. Because a MW saved here by reducing pumping power is gained as electrical output, considerable emphasis is placed on lowering pumping power.

Limiting flow rates for coolant water, in addition to ensuring adequate heat transfer rates from the fuel and to the steam generator tubes, depend on many factors such as temperature, the presence of boiling, water chemistry, geometry, and flow regime. Fretting considerations have led to a 10 m/sec limit on fuel channel velocity in single-phase water. Erosion/corrosion considerations have led to limits of 4.3 to 6.1 m/s in the steam generator tubes and 16.8 m/s in heat transport piping.

The fuel distribution in the coolant is designed to maximize the fuel surface-to-volume ratio so that the largest heat transfer surface can be exposed to the coolant for maximum heat transfer without drying out the fuel surface. However, if this approach is carried to extremes, the fuel volume in the core will be less than the optimum, and parasitic neutron absorption by the sheath will increase. Present designs use 37 or 28 elements in a fuel bundle.

Use of boiling in the coolant permits higher heat transfer due to the high heat transfer coefficient of nucleate boiling, but introduces challenges to the attempt to minimize pressure drop and pump size, as well as other two-phase flow effects.

Ideally, the coolant temperature should be as high as possible for maximum overall thermal efficiency. Therefore, a high-boiling-point, low-vapour-pressure liquid is desirable so that the heat transport system can operate at the lowest possible pressure. This reduces the thickness of the pressure boundary and hence is important for reducing parasitic burn-up in the core. Organic coolant is far superior to water from this point of view.

In the case of organic coolant, the secondary-side H_2O pressure is higher than the primary-side pressure. Hence, boiler tube leaks will cause a water leak into the primary coolant system.

Corrosion of heat transport system materials must be minimized because of possible deterioration, flow restrictions, and contamination with active isotopes.

The CANDU-PHW heat transport system has water coolant, low-cobalt carbon steel piping, stainless-steel end fittings, Zircaloy pressure tubes, and Monel or Incoloy steam generator tubes. A pH of 10.2 to 10.8 is maintained by lithium hydroxide and hydrogen gas added to keep the dissolved oxygen content low to help minimize corrosion. The intent is to produce and maintain a continuous and adherent film of magnetite on all carbon steel surfaces. Corrosion with organic coolant is a lesser problem and can be controlled by degassing, using N_2 cover gas, and using a dechlorinator system.

No flammability or thermal stability problems exist with water (except for the possible Zr-water reaction producing H_2 during a LOCA).

The cost of D_2O is high, making it the more expensive coolant. This contributes to a high capital cost for the CANDU-PHW, but a low operating cost due to the efficient use of natural U.

4.7 Problems

1. Identify and explain the primary reasons that natural uranium ceramic is used as the traditional fuel in the CANDU reactor design.
2. Identify and explain the primary reasons that zirconium and zirconium alloys are used as the fuel cladding material in the CANDU reactor design.
3. Identify and explain several advantages and drawbacks of using heavy water as a moderator and coolant in the CANDU reactor design.
4. Summarize and explain the main heat transport system design requirements for the CANDU reactor design, as related to the main objectives of the system.

5 Thermal-Hydraulic Design Limits and Margins

This section covers the basic design principles of power reactor design, including reactor thermal-hydraulic characteristics, along with an overview of these for different reactor types, but with an emphasis on the CANDU design. It also covers the energy production and transfer parameters, the thermal design limits, and the thermal design margins, with a discussion on the reactor thermal-hydraulic figure of merit.

5.1 Heat generation parameter definitions

This section covers the reactor power production parameters generally used in reactor engineering. Energy production in a nuclear reactor is expressed in a variety of terms that are used by various disciplines.

The volumetric energy (heat) generation rate, q‴ (kW/m^3), is mostly used by reactor physicists because they deal with the fission reaction rate that results in a volumetric energy generation rate in the fuel. This term does not provide any information about heat transfer in the core, nor does it indicate any level of core margin.

The surface heat flux, q″ (kW/m^2), is most important to the core thermal-hydraulic designer and is directly related to reactor thermal margins. The thermal-hydraulic engineer deals with heat transfer from the fuel element surface to the coolant.

The linear heat generation rate or power rating, q′ (kW/m), is important to both the thermal/fuel designer and the metallurgical designer because it expresses fuel performance characteristics in terms of linear power rating. Fuel design, testing, and qualification are usually described using this parameter.

The rate of energy generation per fuel element, q (kW), is useful in expressing heat generated separately in each fuel element, which is used in modelling heat transfer phenomena in the core.

The core power, Q (kW), is used in overall calculations of core energy output. Usually, for marketing purposes, this core power is expressed in terms of electrical power delivered by the plant to the grid, or occasionally in terms of net electric power accounting for plant internal energy consumption. However, for thermal-hydraulic design purposes, reactor power is expressed in terms of reactor thermal power. Roughly speaking, reactor electric power is equal to reactor thermal power divided by reactor thermal efficiency.

The core power density, Q‴ (kW/m^3), is used as a figure of merit for core thermal performance. This power level accounts for various materials in the core and thus provides information on reactor core compactness and effectiveness.

The core specific power, *Q/(mass of fissionable atoms)* (i.e., kW/kg), is used as a figure of merit for core thermal performance from the nuclear physics perspective.

5.2 Thermal design limits

Core thermal design limits are expressed in terms of several parameters, including heat flux

from the fuel elements to the coolant, fuel centreline maximum temperature in the core, fuel cladding maximum temperature in the core, bundle maximum power, and channel maximum power.

Figure 20 presents the important concept of reactor thermal limits with respect to the critical heat flux (CHF). The definition, assessment, and calculation of the CHF are covered in the following sections. Reactor thermal-hydraulic design must ensure that the CHF is not reached in any fuel element or bundle in the reactor core. The CHF is the heat flux at the surface of the fuel element that results in a sudden change in heat transfer regime from liquid in good contact with the heated surfaces, to loss of local liquid contact with surfaces because of vapour blanketing the fuel-element surface. This phenomenon leads to severe reduction of the heat transfer coefficient, and for heat flux-controlled surfaces (like fuel rods in a reactor), in a significant increase in fuel temperature as well as damage to or failure of fuel sheaths.

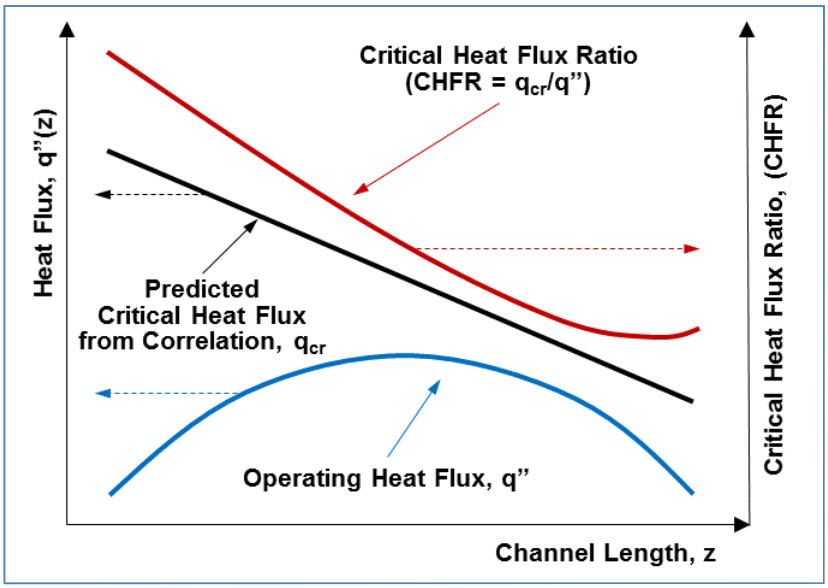

Figure 20 Critical heat flux ratio

Figure 20 shows a typical variation of the heat flux and the critical heat flux along a fuel element. For simplicity, the reactor heat flux in the core is assumed to be represented by a cosine function that peaks at the centre of the core. As will be seen later, the CHF follows a decreasing curve from the fuel channel inlet to the fuel channel outlet. In Figure 20, the ratio of CHF and local heat flux is also illustrated, which is one way to assess how close the reactor is to the occurrence of CHF anywhere in the core.

The key objective of thermal-hydraulic reactor core design, for a desired core power, is to ensure that the heat flux in all fuel elements in the core will remain below the CHF. The CHF is among the important parameters in core thermal-hydraulic design. Note that local power in the core will vary with position along the fuel channel, including the end flux peaking at bundle ends, and from channel to channel in the radial direction of the calandria.

Fuel melting and cladding melting are other important factors and are dealt with in later sections of this chapter.

CANDU reactor design-related CHF phenomena are further described in Section 7.6.4.

5.3 Thermal design margins

This section defines thermal design margins in terms of heat generation rate and the resulting heat flux from the fuel to the coolant. Variation of the reactor parameters in the reactor core is taken into account to define the core average quantities, maximum hot channel quantities, and maximum fuel element quantities that are used in the design space to optimize reactor design options. The heat generation rate during normal operation and the postulated design basis events define the key design limit for which power reactors need to be designed with a certain margin.

Design margins are applied to parameters of primary importance to ensure that the reactor can be safely operated without exceeding important limits. These important operating parameters are assumed to be inside a so-called *safe operating envelope*, which defines the range of values that a particular parameter can take on during reactor operation. The left side of Figure 21 shows a general definition of the safe operating envelope, identifying the optimal operating range, the lower and upper alarm range, the lower and upper buffer zone, and the range where reaching the failure point will be immanent for any of the important thermal margin parameters.

Some of the key operating parameters that are usually considered by thermal-hydraulic designers are:

- Coolant temperature
- Coolant pressure
- Critical heat flux
- Fuel maximum temperature (centreline)
- Fuel cladding maximum temperature
- Bundle maximum power
- Channel maximum power
- Reactor total thermal power.

The thermal design margins function as the most important parameter for demonstrating the robustness, operability, and flexibility of a given reactor design and serve as the main standard of comparison for the safety level of various reactor types. One of the key thermal design margin parameters is the ratio of the critical heat flux to the operating surface heat flux, which must satisfy a reference allowable value that meets economic as well as regulatory requirements.

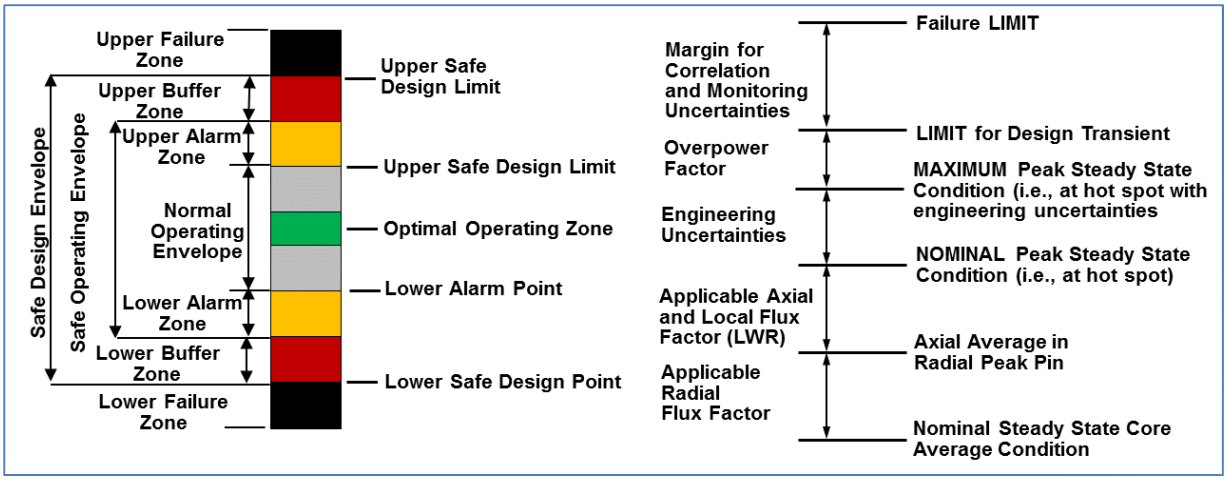

Figure 21 Thermal margins

The required core thermal margins are shown on the right side of Figure 21. Variations in neutron flux and the resulting power generation rate in the core in the radial and axial directions are represented by the corresponding peaking factors. These must be added to the nominal value (the core average value) to obtain the nominal peak steady-state value of the margin parameter. Then uncertainties in the calculated parameters and other engineering uncertainties are "stacked" on top of the peaking factors to arrive at the maximum peak steady-state condition.

During transients, the appropriate overpower factor must be stacked on top of the maximum peak steady-state power to obtain the limit value for design transients. On top of this limit, there should be a margin for all uncertainties in calculating the margin parameter values and the uncertainties in monitoring global and local reactor parameters. This brings the margin parameter to the failure limit.

The left side of Figure 21 indicates that if reactor operation drifts to the lower or upper alarm point, the reactor control systems will provide corrections to certain reactor parameters to bring the reactor operation back within the safe operating envelope. Beyond the safe operating envelope is the safe design envelope. If any of the reactor key safety parameters drifts into this buffer zone, a reactor trip may occur and shut down the reactor. The reactor trip parameters have their own margins, which are required to manage reactor shutdown adequately and to ensure safe reactor shutdown while preventing spurious trips.

5.4 Problems

1. Explain the relationship among the reactor core thermal parameters: reactor core power, core volumetric generation rate, heat flux, critical heat flux, and linear power.
2. Draw a diagram of core thermal margins to explain the relationship among the various elements that must be considered to ensure that appropriate margins are available.

6 Thermal-Hydraulic Design Fundamentals

This section covers the fundamental aspects of thermal-hydraulic design, heat transfer, and fluid flow in the reactor primary and secondary cooling system. It also provides the fundamentals of two-phase flow and the thermodynamics of the nuclear energy conversion process.

6.1 Two-phase flow fundamentals

Heat transfer and fluid flow with boiling water play an important role in nuclear reactor thermal hydraulics. This section discusses two-phase flow definitions and basic theory. It covers flow regimes, experimental observations and data, and application to reactor thermal hydraulics. It also provides a brief description of various two-phase flow models.

6.1.1 Key parameters and definitions

Two-phase flow is encountered in many engineering systems in the chemical, process, power generation, and petroleum industries, including oil-gas pipelines, boilers, heat exchangers, refrigeration equipment, and evaporators, as well as in nuclear reactor applications. Fully understanding the implications and models of two-phase flow is important for proper design of reactor cooling systems and for modelling fluid flow and heat transfer in the reactor under different conditions. Two-phase flow has a profound impact on the ability to remove heat from the nuclear reactor, which is the primary objective of thermal-hydraulic design.

As a simple approximation, two-phase flow can be treated as an extension of single-phase flow. However, in reality, two-phase flow can be very complex due to uncertainty in various interfacial parameters. To simplify the situation, often experimentally obtained correlations are used in design calculations.

Two-phase flow is simultaneous flow of any two phases (liquid-gas/vapour, solid-gas, or liquid-solid) of a single substance. Examples include reactor fuel channels and steam generators. This phenomenon is also referred to as “single-component two-phase flow”. However, two-phase flow can consist of two components, and in this case, it is referred to as simultaneous flow of the liquid and gas phases of two substances, for example in oil-gas pipelines. This is also referred to as “two-component two-phase flow” [HET1982].

The primary parameters used in two-phase flow modelling are:

- Thermal: thermal power, temperature, heat flux, etc.
- Hydraulic: pressure, mass flow rate, fluid temperature, pressure drop, etc.
- Geometric: flow and heated areas, hydraulic and heated equivalent diameters, etc.

Along with these primary parameters, in two-phase flow analysis, the following calculated parameters are commonly used:

- Mass flux, heat flux
- Mass quality, equilibrium quality, thermodynamic quality
- Void fraction.

In addition, two-phase flow calculations require fluid property information such as density, viscosity, enthalpy, thermal conductivity, and heat capacity, which are functions of the primary fluid parameters listed above.

Void fraction is the ratio of the cross-sectional area occupied by vapour and gaseous phases to the total flow area of a pipe [WAL1969]. The opposite of void fraction is the liquid fraction, as given by Eq. (1):

$$\alpha = \frac{A_g}{A}; \qquad (1-\alpha) = \frac{A_f}{A}. \tag{1}$$

Equation (2) defines mass quality as the ratio of vapour mass flow to total mass flow. The opposite is the liquid quality:

$$x = \frac{W_g}{W} = \frac{W_g}{W_f + W_g}; \qquad (1-x) = \frac{W_f}{W} = \frac{W_f}{W_f + W_g}. \tag{2}$$

Mass flux is the mass flow rate per unit flow area and is given by Eq. (3):

$$G = \frac{W}{A} = \rho v = \frac{v}{\upsilon}. \tag{3}$$

Gas and liquid mass fluxes are defined using the steam quality, as in Eq. (4):

$$G_g = G\,x; \quad G_f = G\,(1-x). \tag{4}$$

Volumetric flux (usually referred to as superficial velocity) is the volumetric flow rate over total flow area, as in Eq. (5) [WAL1969]:

$$j = \frac{Q}{A}. \tag{5}$$

The corresponding vapour and liquid volumetric fluxes are given by relationships similar to the void fraction, as in Eq. (6):

$$j_g = \frac{Q_g}{A}; \qquad j_f = \frac{Q_f}{A}. \tag{6}$$

Using the relationships defined in the previous equations, the vapour and liquid phase velocities can be expressed as in Eqs. (7) and (8):

$$v_g = \frac{W_g}{\rho_g A_g} = \frac{Q_g}{A_g} = \frac{G\,x}{\rho_g\,\alpha}, \tag{7}$$

$$v_f = \frac{W_f}{\rho_f A_f} = \frac{Q_f}{A_f} = \frac{G\,(1-x)}{\rho_f\,(1-\alpha)}. \tag{8}$$

These equations assume that no relative motion exists between the two phases. However, if a two-phase mixture is moving, the vapour, because of its buoyancy, density, and different resistance characteristics, tends to move at a higher velocity than the liquid. In a homogeneous

system, a slip ratio *S* is defined as equal to one in the absence of flow or in homogeneous flow and greater than one in non-homogeneous two-phase systems. *S* is defined as the ratio of the average velocity of the vapour to that of the liquid. Hence, the slip ratio is defined as the ratio between the vapour velocity and the liquid velocity, as in Eq. (9) [WAL1969]:

$$S = \frac{v_g}{v_f} = \frac{W_g\ \rho_f\ A_f}{W_f\ \rho_g\ A_g} = \left(\frac{x}{1-x}\right)\left(\frac{\rho_f}{\rho_g}\right)\left(\frac{1-\alpha}{\alpha}\right). \tag{9}$$

Experimental data or theoretical correlations for *S* covering all possible operating and design variables do not exist. In boiling-water reactor studies, values for *S* may be estimated from data that closely approach those of interest. To do this, a certain amount of individual judgment is necessary. Otherwise, experimental values of *S* under conditions similar to a particular design must be obtained. This procedure is usually expensive and time-consuming, but may be necessary in some cases.

The importance of obtaining accurate values of *S* may best be emphasized by the following discussion. One step in the core channel design procedure is to set a maximum value of alpha at the channel exit. This is usually determined from nuclear (moderation) considerations. A corresponding value of *x* at the selected *S* is then determined from the above equations. The latter determines the heat generated in the fuel channel. In design, the usual procedure is to assume a constant value of *S* along the length of the fuel channel. This simplification may introduce error into the results. However, *S* has been observed to be fairly constant over most of the channel length, indicating this assumption to be a good one.

The quality of the flowing liquid-vapour mixture can be expressed using Eq. (2) in terms of liquid and vapour mass flow rates. There is an equivalent quality of a stationary liquid-vapour mixture, which can be expressed by a similar relationship involving liquid and vapour mass. The mass flow quality varies between 0% and 100%, i.e., no vapour to 100% vapour in the flow. Note that mass quality does not carry information about the thermal state of the fluid. However, where appropriate in experimental or theoretical work, if the two phases are in thermal equilibrium (at the same enthalpy or temperature), mass quality can be called equilibrium mass quality.

Often in thermal-hydraulic experiments or calculations, thermodynamic quality is used. It is expressed in terms of a ratio of enthalpies, as in Eq. (10), where h_m is the mixture enthalpy and h_g and h_f are vapour and liquid saturation enthalpies. Thermodynamic enthalpy can be negative when the liquid is below saturation condition (sub-cooled) or greater than one when steam is superheated. From Eq. (10), thermodynamic quality does not carry information about the flows (velocities) of the two phases. Usually, thermodynamic quality is expressed for a mixture at hydrodynamic equilibrium (i.e., both phases travelling at the same velocity) and is sometimes referred to simply as equilibrium quality [COL1972, DEL1981]:

$$x_{th} = \frac{h_m - h_f}{h_g - h_f}. \tag{10}$$

It is very important to understand the relationship between mass flow quality and void fraction. There is no meaningful relationship between thermodynamic quality and void fraction because

void fraction refers to flow geometry, whereas thermodynamic quality refers to the thermal properties of the phases. The relationship between mass flow quality and void fraction is obtained by manipulating the above equations and can be expressed as in Eq. (11) [WAL1969]:

$$\alpha = \frac{x \cdot v_g}{(1-x)v_f + x \cdot v_g} = \frac{1}{1+\left(\frac{1-x}{x}\right)\left(\frac{v_f}{v_g}\right)}. \tag{11}$$

Figure 22 shows the relationship between void fraction and mass flow quality. As expected, at or above the critical pressure of 22.12 MPa, the void fraction and quality are identical because the liquid and vapour phases no longer exist for water regardless of pressure and temperature.

Further examination of Figure 22 shows the following:

1. For constant quality, void fraction decreases with pressure.
2. For any pressure, *dα/dx* decreases with quality.
3. At low quality values, *dα/dx* increases as pressure decreases and becomes very large at low pressure.
4. At atmospheric pressure, a low quality (about 2%) generates almost 100% void fraction because of the low vapour density.

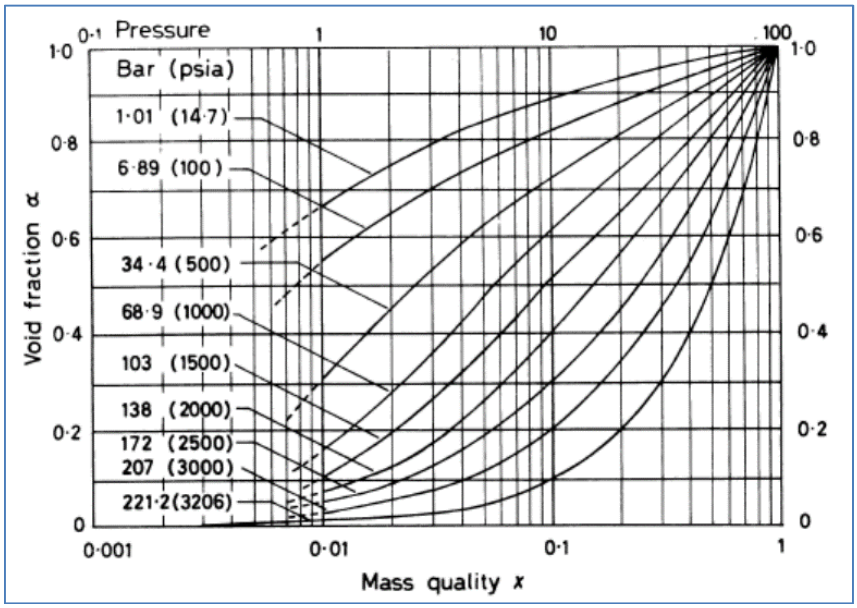

Figure 22 Relationship between quality and void fraction [COL1972]

For CANDU fuel channel exit conditions, because the pressure is approximately 10 MPa and the quality is typically 2%–4%, the void fraction can be as high as 30%.

6.1.2 Non-dimensional numbers

Dimensionless numbers in fluid mechanics are an important tool to capture various parameters and phenomena into a relationship that is applicable to a wide range of parameter values. This section covers the most important dimensionless numbers that are used throughout this

chapter and are important in analyzing mass, momentum, and heat transfer. The most important dimensionless numbers are listed in the following sections.

6.1.2.1 Reynolds number

The Reynolds number (*Re*) is a dimensionless number that measures the ratio of inertial to viscous forces and consequently quantifies the relative importance of these two types of forces under a given flow condition. The Reynolds number can be defined for a number of different situations where a fluid is in motion relative to a surface. These definitions generally include the fluid properties of density and viscosity, plus a velocity and a characteristic length or characteristic dimension. This dimension is a matter of convention; for example, a radius or a diameter is equally valid for spheres or circles, but one is chosen by convention. For flow in a pipe or a sphere moving in a fluid, the internal diameter is generally used today. Other shapes such as rectangular pipes or non-spherical objects have an *equivalent diameter* defined. The velocity may also be a matter of convention in some circumstances, notably stirred vessels. With these conventions, the Reynolds number is defined by Eq. (12) [HET1982, ELW1978]:

$$Re = \frac{\rho \cdot v^2 L^2}{\mu \cdot v \cdot L} = \frac{\rho \cdot v \cdot L}{\mu} = \frac{v \cdot L}{\upsilon}, \tag{12}$$

where:

- v is the mean velocity of the object relative to the fluid (m/s)
- L is a characteristic linear dimension (the length travelled by the fluid; the hydraulic diameter when dealing with river systems) (m)
- μ is the fluid dynamic viscosity (Pa·s or N·s/m² or kg/(m·s))
- υ is the kinematic viscosity ($\upsilon = \mu/\rho$) (m²/s)
- ρ is the fluid density (kg/m³).

For flow in a pipe, the Reynolds number is given by Eq. (13) [WAL1969]:

$$Re = \frac{\rho \cdot v \cdot D_H}{\mu} = \frac{v \cdot D_H}{\upsilon} = \frac{Q \cdot D_H}{\upsilon \cdot A}, \tag{13}$$

where:

- D_H is the hydraulic diameter of the pipe, i.e., its characteristic length travelled (m)
- Q is the volumetric flow rate (m^3/s)
- A is the pipe cross-sectional area (m²).

For shapes such as square, rectangular, or annular ducts where the height and width are comparable, the characteristic dimension for internal flow situations is taken to be the hydraulic diameter D_H as defined by Eq. (14):

$$D_H = \frac{4A}{P}, \tag{14}$$

where A is the cross-sectional area and P is the wetted perimeter. The wetted perimeter for a channel is the total perimeter of all channel walls that are in contact with the flow. This means that the length of the channel exposed to air or steam is *not* included in the wetted perimeter.

6.1.2.2 Nusselt number

In heat transfer at a boundary (surface) within a fluid, the Nusselt number (Nu) is the ratio of convective to conductive heat transfer across (normal to) the boundary, as in Eq. (15) [HET1982, ELW1978]. In this context, convection includes both advection and conduction. Named after Wilhelm Nusselt, it is a dimensionless number. The conductive component is measured under the same conditions as the heat convection, but with a (hypothetically) stagnant (or motionless) fluid.

A Nusselt number close to one, meaning that convection and conduction are of similar magnitude, is characteristic of "slug flow" or laminar flow. A larger Nusselt number corresponds to more active convection, with turbulent flow typically in the 100–1000 range.

The convection and conduction heat flows are parallel to each other and to the surface normal of the boundary surface and are all perpendicular to the mean fluid flow in the simple case:

$$Nu_L = \frac{Convective\,heat\,transfer}{Conductive\,heta\,transfer} = \frac{h \cdot L}{k_f}, \tag{15}$$

where:

- L is the characteristic length (m)
- k_f is the thermal conductivity of the fluid (kW/m °K)
- h is the convective heat transfer coefficient (kW/m^2 °K).

The characteristic length should be selected in the direction of growth (or thickness) of the boundary layer. Some examples of characteristic length are the outer diameter of a cylinder in (external) cross flow (perpendicular to the cylinder axis), the length of a vertical plate undergoing natural convection, or the diameter of a sphere. For complex shapes, the length may be defined as the volume of the fluid body divided by the surface area. The thermal conductivity of the fluid is typically (but not always) evaluated at the film temperature, which for engineering purposes may be calculated as the mean (average) of the bulk fluid temperature and the wall surface temperature.

For relations defined as a local Nusselt number, the characteristic length should be taken as the distance from the surface boundary to the local point of interest. However, to obtain an average Nusselt number, this relation must be integrated over the entire characteristic length.

Typically, for free convection, the average Nusselt number is expressed as a function of the Rayleigh number and the Prandtl number as: *Nu=f(Ra, Pr)* [HET1982]. For forced convection, the Nusselt number is generally a function of the Reynolds number and the Prandtl number, or *Nu=f(Re, Pr).* Empirical correlations are available for a wide variety of geometries that express the Nusselt number in the forms described above.

6.1.2.3 Prandtl number

The Prandtl number (Pr) is a dimensionless number that represents the ratio of momentum diffusivity (kinematic viscosity) to thermal diffusivity [HET1982, ELW1978]. It is named after the German physicist Ludwig Prandtl and is defined by Eq. (16):

$$Pr = \frac{\upsilon}{\alpha} = \frac{viscous\,diffisuion\,rate}{thermal\,diffusion\,rate} = \frac{c_p \mu}{k}, \tag{16}$$

where:

- υ is the kinematic viscosity, $\upsilon=\mu/\rho$ (m^2/s)
- α is the thermal diffusivity, $\alpha=k/(\rho c_p)$ (m^2/s)
- μ is the dynamic viscosity (Pa s = N s/m^2)
- k is the thermal conductivity (W/(m K))
- c_p is the specific heat (J/(kg K))
- ρ is the density (kg/m^3).

Note that whereas the Reynolds number is subscripted with a length scale variable, the Prandtl number contains no such length scale in its definition and is dependent only on the fluid and the fluid state. As such, the Prandtl number is often found in property tables alongside other properties such as viscosity and thermal conductivity.

6.1.2.4 Weber number

The Weber number (We) is a dimensionless number in fluid mechanics that is often useful in analyzing fluid flows with an interface between two different fluids, especially for multiphase flows with strongly curved surfaces. It can be thought of as a measure of the relative importance of the fluid's inertia compared to its surface tension [HET1982, ELW1978]. The quantity is useful in analyzing thin film flows and the formation of droplets and bubbles. It is named after Moritz Weber and can be expressed by Eq. (17) [HET1982, ELW1978]:

$$We = \frac{fluid\,inertia}{surface\,tension} = \frac{\rho \cdot v^2 \cdot l}{\sigma}, \tag{17}$$

where

- ρ is the density (kg/m^3)
- v is the mean velocity of the object relative to the fluid (m/s)
- l is the characteristic length, typically the droplet diameter (m)
- σ is the surface tension (N/m).

6.1.3 Flow patterns

When a liquid is vaporized in a heated tube or a heated channel, the liquid and vapour generated take on a variety of configurations known as flow patterns. The particular flow pattern depends on pressure, flow, heat flux, entrance conditions (i.e., local phase distribution at the inlet), and channel geometry; however, the strongest influences on the flow pattern are the phase mass flow rates or velocities. Because the name given to a flow pattern is largely subjective, many terms exist in the literature which purport to describe the various possible phase distributions. The sequence of flow patterns generally encountered in vertical upwards concurrent flow for increasing levels of thermodynamic quality is shown below. As steam mass flow increases (i.e., velocity increases) and steam temperature increases, the fluid flow

patterns change from single-phase sub-cooled liquid to single-phase steam flow, passing through the flow regimes as indicated from left to right on the diagram below. Indications are provided in this diagram of the values of thermodynamic quality *x* for various flow regimes.

Single-phase sub-cooled liquid flow	*Single-phase saturated liquid flow*	*Bubbly flow*	*Slug flow*	*Churn flow*	*Wispy annular flow*	*Single-phase saturated steam flow*	*Single-phase superheated steam flow*
(x < 0)	*(x = 0)*	*(0 < x < 1)*				*(x = 1)*	*(x > 1)*

Figure 23 shows the flow patterns for vertical flow. These flow patterns are generally symmetrical across the pipe cross section.

In horizontal flow, the flow patterns are similar. However, in horizontal flow, gravity has a different effect, and depending on the mass flow rate in the tube or channel, stratified flow may occur with bubbly flow, slug flow, and wispy annular flow patterns. The flow patterns typical of horizontal two-phase flow are shown in Figure 24. A cross-sectional view of various flow patterns in horizontal flow is shown in Figure 25, in which gravity plays a significant role, so that the combination of gravity and drag force at the liquid-vapour interface can result in various cross-sectional flow patterns.

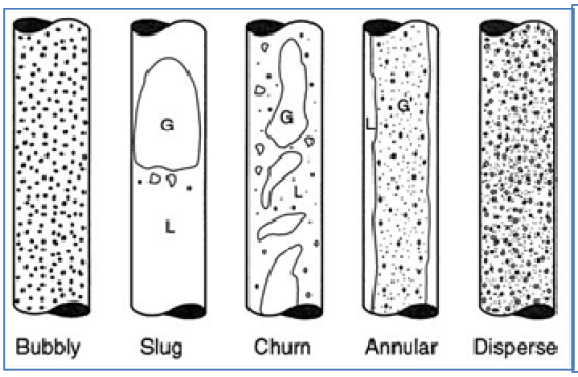

Figure 23 Flow patterns in vertical two-phase flow

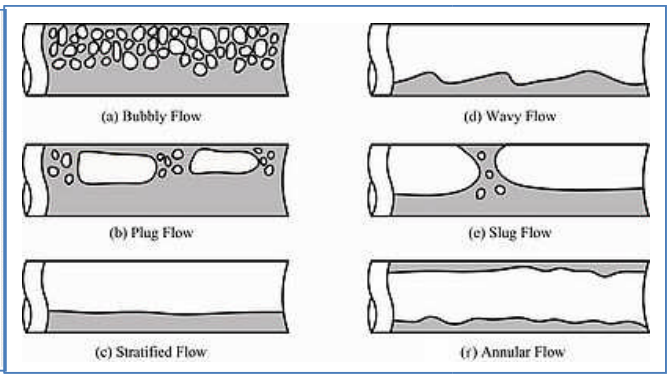

Figure 24 Flow patterns in horizontal two-phase flow

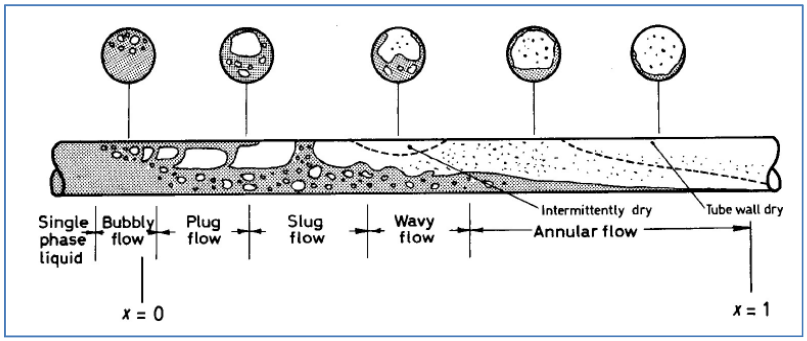

a) Flow regimes in a horizontal heated channel

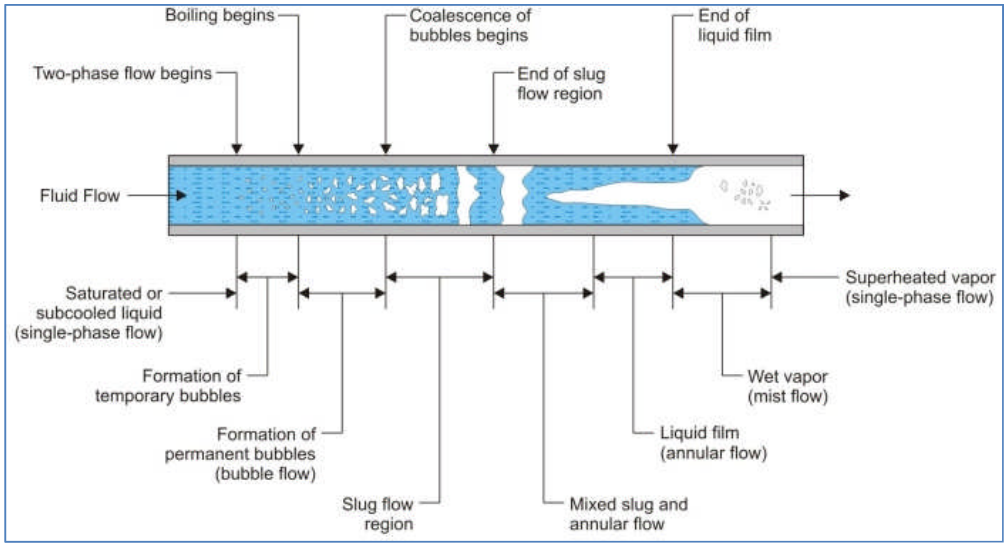

b) Evolution of flow regimes in a horizontal tube

Figure 25 Flow patterns and heat transfer regimes in horizontal heated tubes

The distribution of phases inside a confined area strongly depends on:

- Liquid and vapour velocities.
- Fuel channel geometry and fuel bundle geometry, particularly in reactors where fuel channels are interconnected in the radial direction, like PWRs and BWRs.
- Surface (wall) heating, which influences near-wall flow patterns, resulting in an internal void gradient.
- Appendages, which homogenize flow patterns at downstream locations; the patterns transition back to a basic pattern at locations farther away.

Figure 26 shows the flow patterns and heat transfer regimes for two different situations in vertical flow [DEL1981]. On the left side, a reactor channel is shown with the following parameters: high liquid mass flow rate, high heat flux from the walls, and high water sub-cooling, which is typical of PWRs. To the left of the reactor channels on the first vertical line, corresponding flow patterns are shown for this situation, whereas the leftmost line shows the heat transfer regimes for these flow patterns. Starting from bottom to top, the following pairs of flow pattern and heat transfer regime (note that "film" on this figure refers to steam film next to the heated walls) are typically observed:

a) Single-phase liquid – single-phase forced convection to liquid;
b) Bubbly flow – nucleate boiling;
c) Inverted annular flow – inverted annular flow film boiling;
d) Dispersed droplet flow – dispersed flow film boiling; and
e) Single-phase vapour – single-phase forced convection to vapour.

Note that in Figure 26, the point where the wall loses contact with the liquid is shown at the transition between bubbly flow and inverted annular flow.

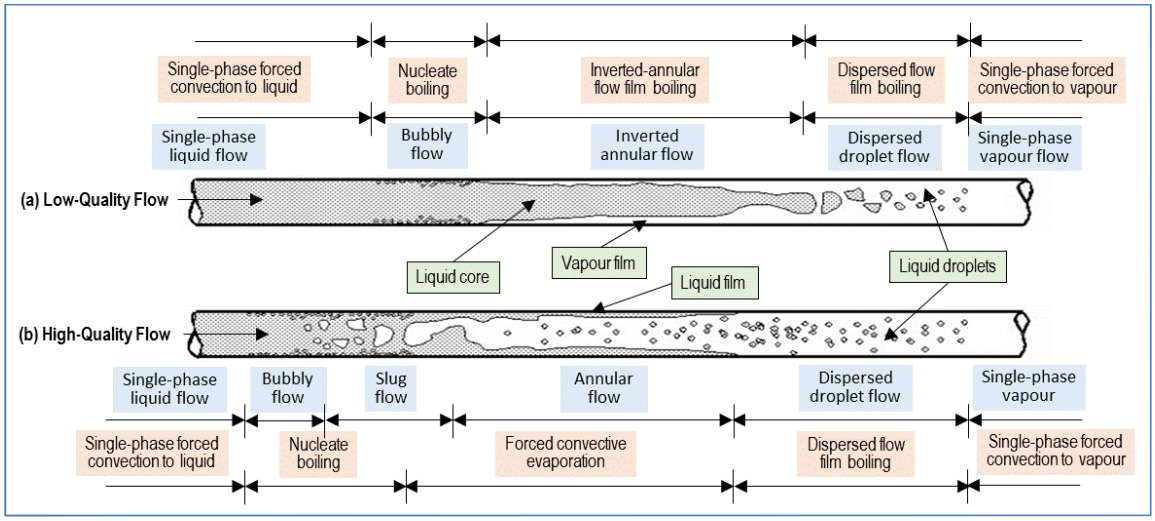

Figure 26 Flow patterns and heat transfer regimes in vertical heated tubes

On the right side of Figure 26, a reactor channel is shown with the following parameters: low liquid mass flow rate, medium heat flux from the walls, and saturated water; this is typical of BWRs. To the right of the reactor channel on the first vertical line, corresponding flow patterns are shown for this situation, whereas the rightmost line shows the heat transfer regimes for these flow patterns. Starting from bottom to top, the following pairs of flow pattern and heat transfer regime (note that "film" in this figure refers to steam film next to the heated walls) can be observed:

a) Single-phase liquid – single-phase forced convection to liquid;
b) Bubbly flow and slug flow – nucleate boiling;
c) Annular flow – forced convective evaporation;
d) Dispersed droplet flow – dispersed flow film boiling;
e) Single-phase vapour – single-phase forced convection to vapour.

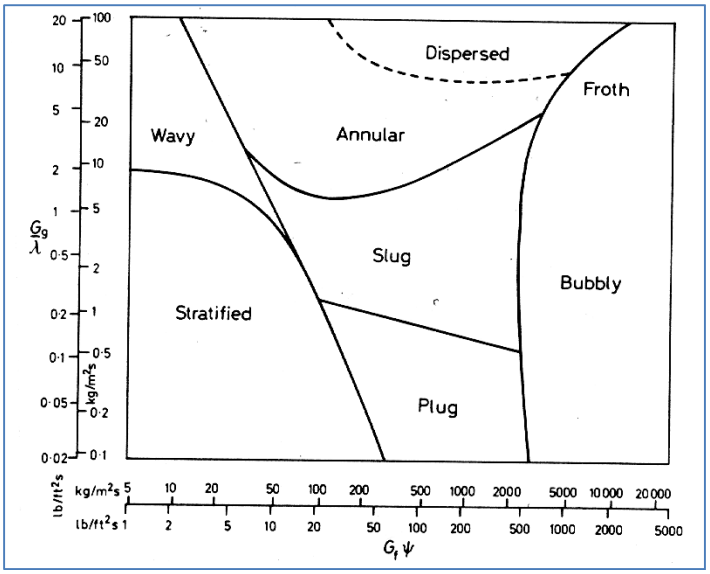

Figure 27 Flow pattern map in vertical flow [HET1982]

Note that in Figure 26, the point where the wall loses contact with the liquid is shown at the transition between annular flow and dispersed droplet flow. Figure 26 indicates that the flow patterns at the entry and exit of the fuel channel are similar for the two cases. The difference is how and where the wall and the liquid lose contact. In addition, the amount of water or the void fraction percentage in the channel does not necessarily determine the contact of liquid with the heated walls. Therefore, as long as the walls are in contact with liquid water, heat transfer is good, and the amount of water in the channel is not important.

Two-phase flow parameters change significantly from one flow pattern to another, in particular the interfacial area between the two phases, and this has a significant impact on the exchange of mass, momentum, and heat between phases. In principle, the degree of thermal and hydraulic disequilibrium between phases has a significant impact on the sustainability of certain flow patterns. Therefore, certain flow patterns, like churn flow, exhibit instability and fast transitions. Various two-phase flow parameters are affected differently by flow patterns, and hence various correlations and models are needed to capture phenomena for each flow pattern. This implies the need for well-defined and predictable flow patterns in two-phase flow modelling.

Many scientists and researchers in recent decades have tried to correlate flow patterns using selected parameters.

Figure 27 shows such an attempt for a vertical flow regime. In this figure, the flow patterns are defined as a function of gas and liquid momentum fluxes. In this example, the flow patterns are correlated by several dimensionless number groups.

6.1.4 The boiling process

Because water as the working fluid in LWRs and CANDUs undergoes a change of phase during heat transfer from the nuclear reactor primary to the secondary cooling system, it is important to understand the boiling process, its phenomena, and its parametric trends.

As liquid is being heated to saturation, with additional heating, boiling starts. Hence, boiling initiation is strongly dependent on pressure, i.e., the saturation temperature. There are two distinctive types of boiling: one is referred to as pool boiling, and the other is forced convective boiling. Vapour formation can take the following forms:

- at the liquid surface to the open environment, when the liquid is superheated;
- homogeneous (internal heating within the fluid at the molecular level); and
- heterogeneous (requires nucleation sites in the fluid or at the heated surface).

Heterogeneous boiling from nucleation sites is a complex boiling mechanism that depends on a number of forces acting on a vapour bubble, including dynamic forces, buoyancy, and surface tension forces. Much research has been devoted to bubble formation at nucleation sites and is presented in a number of two-phase flow textbooks [TON1965, TON1975]. Further discussion of bubble dynamics and formation at nucleation sites is beyond the scope of this textbook.

Figure 28 shows a three-dimensional representation of the two-phase boiling water region as a function of heat flux, temperature, and thermodynamic quality. This figure indicates different flow and heat transfer regimes along the path of changing thermodynamic quality. At high water sub-cooling, the critical heat flux is high, but it diminishes as quality increases. The definition of critical heat flux and its impact on heat transfer in the two-phase region are discussed in Section 7.7.

The boiling process can be analyzed in two distinct situations: pool boiling and forced convective boiling. Pool boiling refers to conditions typical of vessels with unlimited volume and under near-atmospheric pressure. Forced convective boiling refers to boiling in enclosed piping and vessels in which pressure may reach very high values, and in which flow is ensured by an operating pump.

Figure 29 shows a pool boiling process in a diagram relating heat flux to the degree of wall temperature superheating (i.e., the temperature difference between the wall temperature and the saturation temperature). This figure shows a cross section of the 3-D curve in Figure 28 at low quality. Three heat transfer regimes can be seen: nucleate (or sub-cooled) boiling, transition boiling, and film boiling. These three regimes are separated by two important points: the critical heat flux, and the minimum film boiling temperature. The minimum film boiling temperature, sometimes called the Leidenfrost temperature, represents the maximum temperature at which wetting of the heated surface is possible.

Figure 29 also indicates in which direction the process evolves from left to right and vice versa. If heat flux is increasing, then after the CHF point is reached, the surface becomes detached from liquid contact. Beyond this point, heat transfer by liquid evaporation (latent heat of vaporization) is severely reduced. Therefore, because heat transfer to liquid is severely reduced, but heat flux continues to be delivered from internal regions of the wall to the wall

surface, the wall surface temperature significantly increases, as represented by the horizontal dashed line on the diagram from CHF to the film boiling curve (sometimes referred to as the heat flux-controlled region). This significant increase in wall surface temperature can lead to surface damage and melting, which is very troubling in a nuclear reactor where the fuel rod cladding is a major barrier to fission product release.

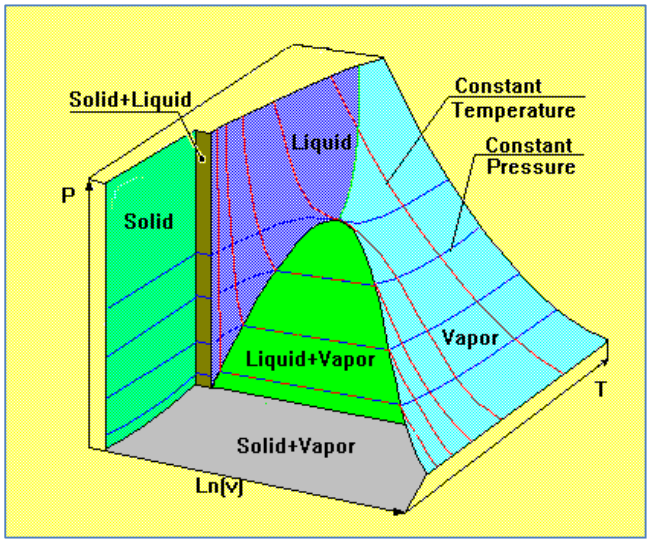

Figure 28 3-D representation of boiling surfaces

On the other hand, as the heat flux is reduced from the region of film boiling back to the CHF point, moving along the bottom part of the curve, it reaches the minimum film boiling temperature. From this point, the heat flux starts to increase in the transition boiling region, during which the heated surface becomes intermittently wetted and dried while the wall temperature is reduced. Once the CHF point is reached by moving from right to left in the diagram, the wall surface is in continued and sustainable contact with the liquid coolant, and heat flux is reduced below the CHF value. This path is sometimes referred to as the temperature control part of the boiling curve.

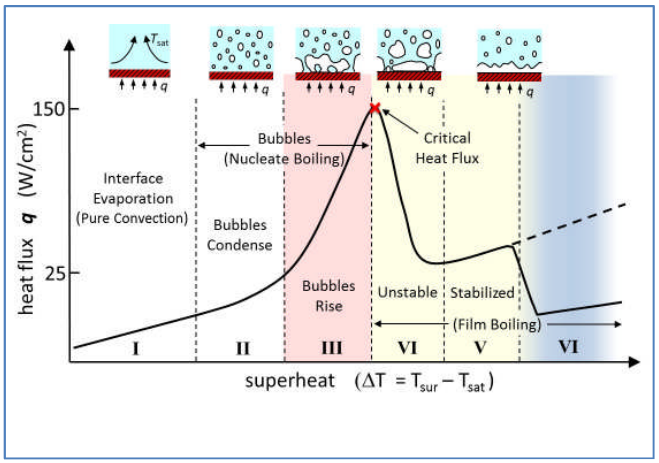

Figure 29 Boiling curve

Figure 29 shows a boiling curve with heat transfer regimes clearly marked. This figure represents one cross section of Figure 28. It shows the heat flux below saturation (in the sub-cooled region), where forced convection to liquid occurs. The transition point between forced convection to liquid and nucleate boiling is called the onset of nucleate boiling and designates the conditions under which the first bubbles start to grow on the wall surface.

Figure 30 shows the parametric trends on the boiling curve [LEU2004, POP2014]. As the mass flux increases in an annular flow regime, the minimum wetting temperature increases, and the boiling curve flattens out. As the mass flux increases in forced convective sub-cooled or low-quality boiling, the CHF and the minimum wetting temperature increase, but the boiling curve retains its shape.

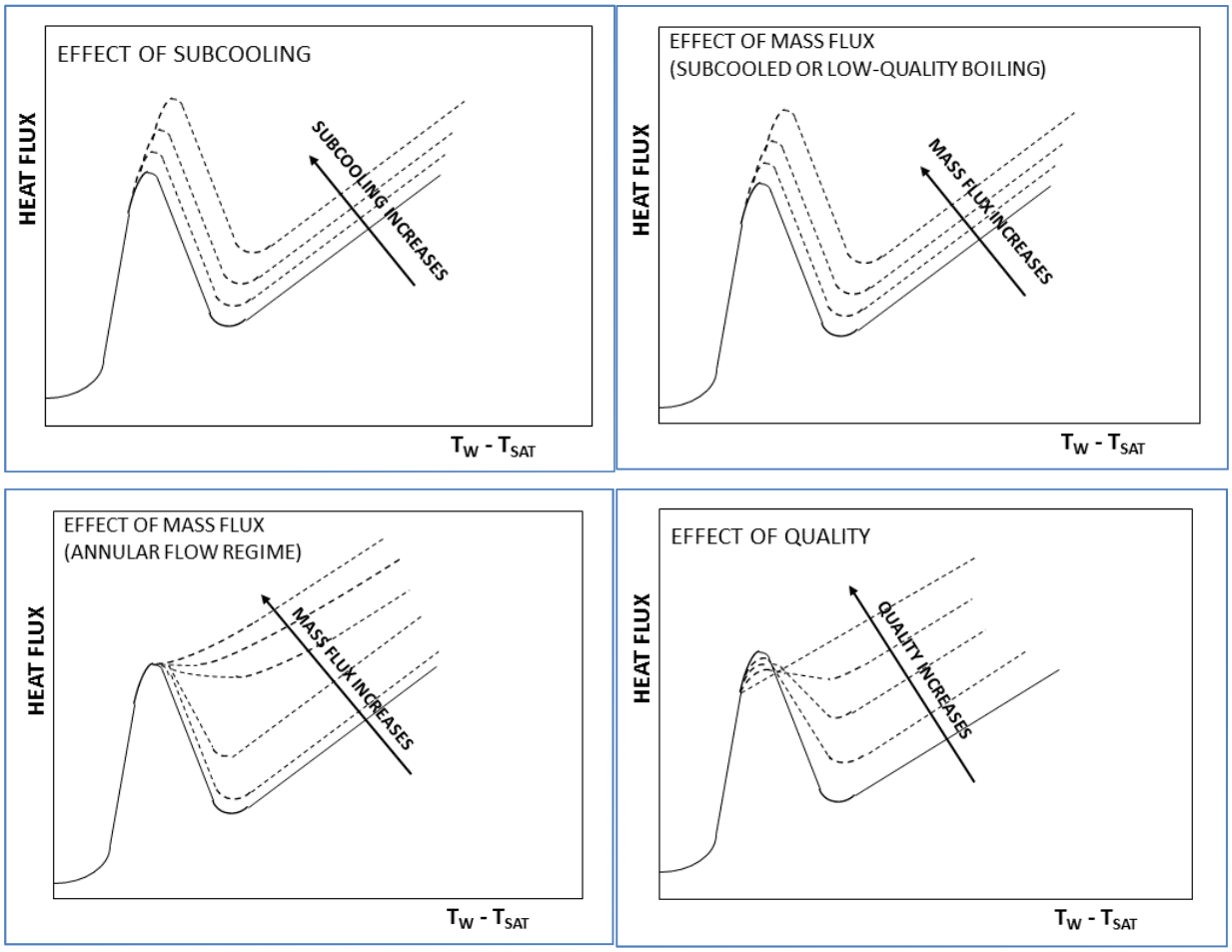

Figure 30 Parametric trends of the boiling curve

A similar effect is seen when increasing the degree of liquid sub-cooling; the CHF point and the minimum wetting temperature increase, but the boiling curve retains its shape. The effect of quality is more complex and is shown in Figure 31.

Figure 31 [LEU2004, POP2013] shows the impact of thermodynamic quality on the boiling curve. For quality equal to or greater than one, the boiling curve is transformed into a straight line, and therefore the CHF concept is not relevant, but the wall temperature increases as the quality increases above one. For saturated boiling ($x = 0$), the boiling curve has the usual S-

shape. As quality increases above zero, the CHF significantly decreases. Moreover, if the quality drops further below zero (i.e., the liquid becomes more sub-cooled), the CHF also increases, and the boiling curve becomes steeper in the nucleate boiling region.

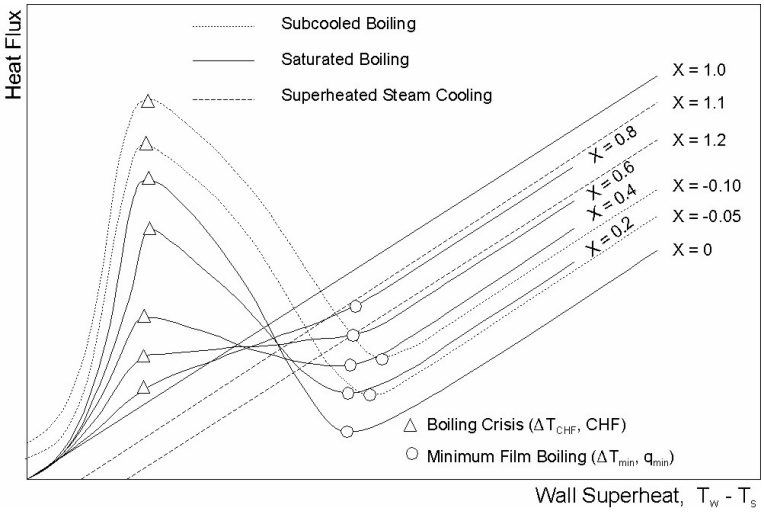

Figure 31 Quality effects on the boiling curve

Figure 32 shows the flow patterns and heat transfer regimes in a boiling channel. In the top part of the figure, the temperature distributions along the heated channel in the coolant and at the wall surface are shown. It is possible to recognize the flow patterns that are most likely to occur given the temperature difference between the coolant and the wall. Note that nucleate boiling starts after the wall surface temperature has risen above the water saturation temperature by a certain amount. Nucleate boiling continues in areas C through F, and then at the point of dryout, when the CHF has been reached, the wall surface temperature exhibits a rapid increase as wall cooling decreases due to loss of contact between the wall and the liquid.

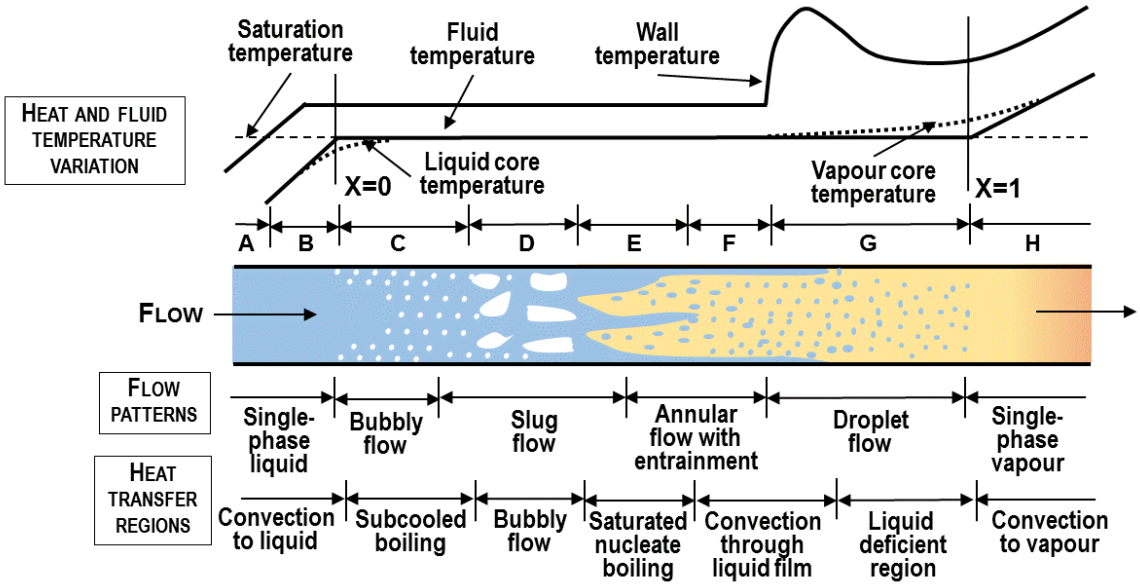

Figure 32 Heat transfer regimes in a boiling horizontal channel

Figure 33 provides model details on the transition from forced convection to liquid and nucleate boiling. It also shows the point of initiation of nucleate boiling, when the first bubbles appear on the wall surface. At the point of net vapour generation, the bubbles can detach from the walls and move to the bulk liquid. A further increase in heat flux at the wall surface happens when the liquid temperature reaches saturation, which creates an opportunity for bubbles to become detached from the wall in great numbers and move with the liquid flow, leading to significant phase separation and disequilibrium.

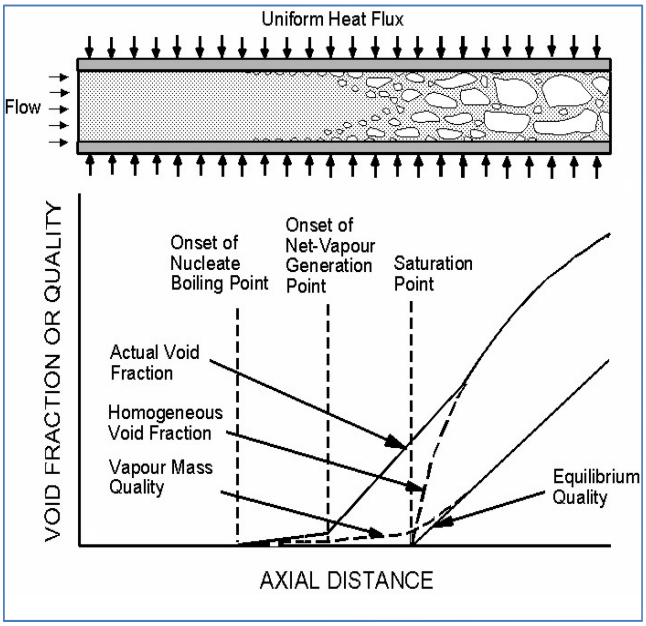

Figure 33 Details of sub-cooled boiling phases in horizontal flow

Three main types of models are used to analyze two-phase flow:

- "homogeneous" flow models,
- "separated" flow models, and
- "flow pattern" or "drift flux" models.

The basic equations are solved within the framework of each of these idealized representations. To apply these models, it is necessary to know when each should be used and to be able to predict the transition from one pattern to another.

6.1.5 Two-phase flow models

The homogeneous model and the separated flow model are the two most widely used and tested models of two-phase flow that are presently available. The homogeneous model considers two-phase flow as a homogenized mixture (pseudo-fluid) possessing average fluid properties. It neglects any local effect that flow patterns may have on two-phase flow and ignores interaction between phases. In other words, the homogenous model considers the phases to be in hydrodynamic and thermodynamic equilibrium.

The homogeneous model is applicable only if the flow parameters do not vary rapidly and thermal disequilibrium has little influence. Although the homogeneous model predicts the

dependence of the two-phase friction multiplier on pressure and quality reasonably well, it has two unsatisfactory features: (a) the friction multiplier is a function of pressure and quality only and is independent of mass flux; and (b) it generally under-predicts low-quality data. Many early software codes used in CANDU design, such as SOPHT [SOP1980], used this type of modelling.

The separated flow model considers the two phases to be segregated into two streams: one of liquid, and one of vapour. Conservation equations are written separately for each phase, and interaction between phases is taken into account by constitutive relationships. The basic equations for the separated flow model are not dependent on the particular flow configuration adopted. The basic assumptions of the separated flow model in analyzing two-phase pressure drop are:

a) The velocities of each phase are constant, but not necessarily equal in any given cross section within the zone occupied by the phase.
b) Thermodynamic equilibrium exists between the two phases.
c) Empirical correlations can be used to relate the two-phase friction multiplier and the void fraction to the dependent flow variables.

Among the various flow patterns, this model would be expected to be most valid for the annular flow pattern. Newer versions of the separate flow model can accommodate both thermodynamic and hydrodynamic disequilibrium between the flow phases.

The drift flux approach satisfactorily accounts for the influence of mass velocity on the void fraction as seen in the separated flow model, and an empirical expression may be used to provide the required relationship between the void fraction and the independent flow pattern.

With the separate flow model and the drift flux model, appropriate void fraction calculations must be performed to ensure model fidelity. Many correlations have been proposed and used in various models; a listing of these correlations is beyond the scope of this handbook (further details can be found in [WAL1969]). Very often used as a void fraction correlation is the homogeneous equation given by Eq. (18):

$$\alpha = \frac{x_a \, \upsilon_g}{(1 - x_a)\, \upsilon_f + x_a \, \upsilon_g}. \tag{18}$$

Another often-used void fraction correlation is the Armand-Massina correlation [LEU2004], which is given by the following equation:

$$\alpha = \frac{(0.833 + 0.167 \, x_a)\, x_a \, \upsilon_g}{(1 - x_a)\, \upsilon_f + x_a \, \upsilon_g}. \tag{19}$$

6.1.6 Two-phase flow in fuel bundles

Two-phase flow in fuel bundles is very complex and requires significant experimental support to understand important phenomena and develop adequate models and correlations. Further information about fuel bundle effects will be given in later sections of this chapter.

The CANDU fuel bundle experimental void fraction database includes data for bundles with 3 to

37 fuel pins, in addition to tube and annulus data. The experimental database includes a wide range of flow conditions with uniformly heated fuel elements or fuel elements with certain radial and axial heating profiles. Figure 34 illustrates that bundle geometries with 6 and 37 fuel elements do not significantly affect the relationship between void fraction and quality [LEU2004, POP2013].

Figure 35 also shows that the impact of the hydraulic diameter of a 7-element bundle does not have a significant impact on the relationship between void fraction and thermodynamic quality, except for very low quality values (representing highly sub-cooled conditions) [LEU2004, POP2013].

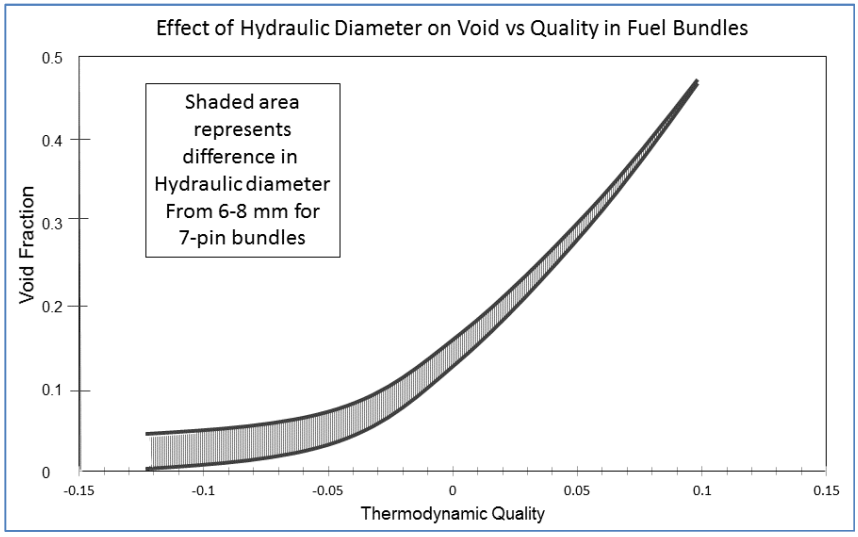

Figure 34 Effect of tube diameter on quality and void fraction

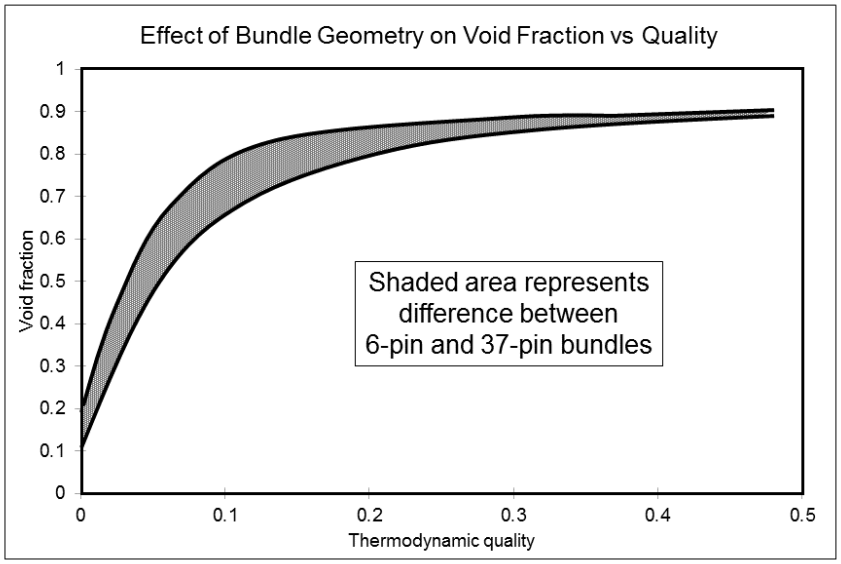

Figure 35 Effect of bundle geometry on quality and void fraction

6.1.7 Problems

1. Explain the relationship between the mass quality and the void fraction in two-phase flow.
2. Explain the difference between the mass quality and the thermodynamic quality in two-phase flow.
3. Explain the main characteristics of the boiling curve, the main parameters that are important for two-phase flow calculations, and the main parameters that influence its shape.
4. Explain the key flow patterns that can occur in vertical and horizontal two-phase flow in heated channels. Explain how the flow regime maps are developed and used in reactor thermal-hydraulic design.
5. Explain the possible models used in two-phase flow calculations, their range of applicability and key features.
6. A BWR reactor operates at a thermal power of 1400 MWt. Water enters the bottom of the reactor core at 275 °C, and passes through the core at a flow rate of 6050 kg/s. the reactor operates at pressure of 7 MPa. Calculate the steam flow rate produced in the reactor.

6.2 Thermodynamics of nuclear energy conversion

This section discusses the thermodynamics of energy conversion in nuclear reactor systems, including a description of the laws of thermodynamics. It provides definitions of basic thermodynamic laws, followed by a description of reactor power cycles, starting with the Carnot cycle, and followed by the Rankine cycle. The definition and analysis of cycle thermal efficiency is discussed, and methods for improving efficiency are described.

6.2.1 Definitions

This section describes the most important concepts and parameters in reactor thermodynamic analysis. Consider a system undergoing a change from state 1 to state 2, as shown in Figure 36. Initially, the system is at energy level E_1. Then, after a certain amount of energy, Q, is added to the system and a certain amount of work, W, is performed by the system, the system is brought to energy level E_2. It would be interesting to discover by what parameters this change is driven and how effective is the energy exchange between the system and its surroundings.

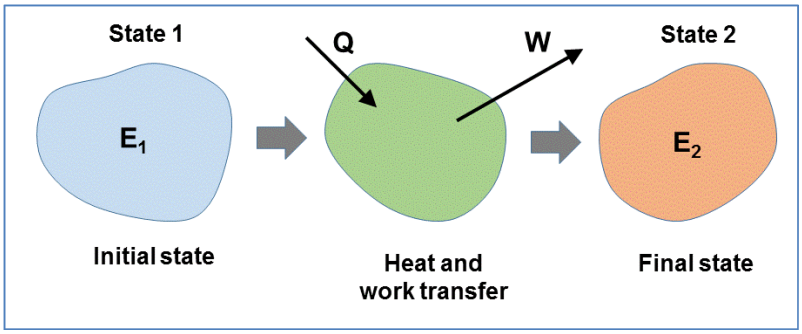

Figure 36 Change of thermodynamic states in a system

6.2.1.1 Work

Figure 37 shows a practical example of the general concept shown in Figure 36. In Figure 37, a piston is moved from a position 1 to a position 2 by sequentially moving small amounts of weight applied at the piston stem. Initially, the piston is under pressure p_1, with volume V_1 and temperature T_1. After moving a certain amount of weight, the piston ends up at pressure p_2, volume V_2, and temperature T_2. The system volume changed by $dV=A \cdot dx$ each time a weight was removed.

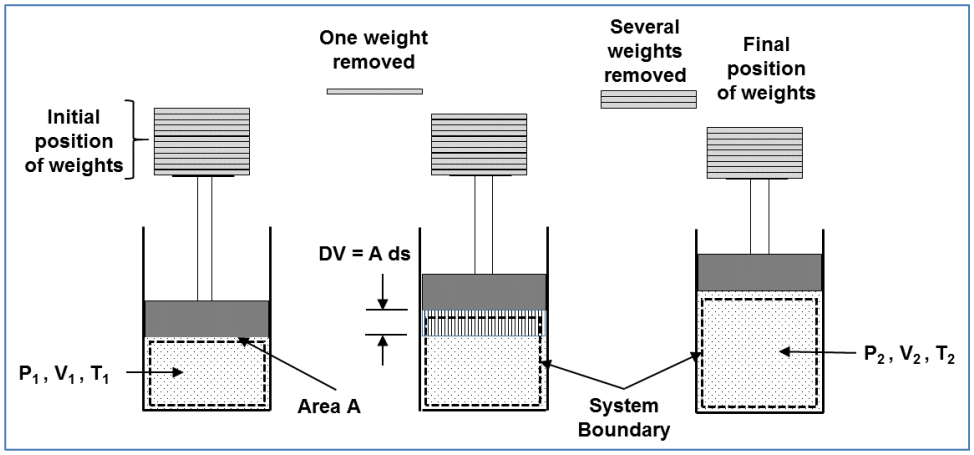

Figure 37 Concept of parameters of thermodynamic state in piston geometry

The infinitesimal amount of work done by the system (shown in Figure 37) is given by Eq. (20) [SAA1966]:

$$dW = f\ dx = p\ A\ dx = p\ dV\ . \tag{20}$$

Assuming that the fluid is an ideal gas and that the above process has been performed at a constant temperature (i.e., is an isothermal process), then the total work performed by weight removal is given by Eq. (21):

$$W_{1-2} = \int_1^2 p\ dV = \int_1^2 mRT\ \frac{dV}{V} = mRT\ \ln\left(\frac{V_2}{V_1}\right). \tag{21}$$

For a constant-pressure process (i.e., an isobaric process), the total work is given by Eq. (22):

$$W_{1-2} = p\int_1^2 dV = p(V_2 - V_1). \tag{22}$$

For a constant-volume process, because the piston does not move, no work is performed, as stated by Eq. (23):

$$W_{1-2} = \int_1^2 p\ dV = 0. \tag{23}$$

One can use the ideal gas law from thermodynamics of gases, as given by Eq. (24):

$$p \cdot V = m \cdot R \cdot T\ , \tag{24}$$

where *P* is pressure [MPa or N/m^2]; *V* is volume [m^3]; *m* is mass [kg]; *T* is temperature [°K]; and *R* is the gas constant [N·m/(kg °K) or J/(kg °K)].

6.2.1.2 Heat

Heat as a form of energy exists in all bodies and is essential for energy transfer. The nature of heat is associated with the movements or vibration of molecules or atoms at the microscopic level in any body, solid, liquid, or gas. Each energy transfer process eventually ends up being a heat transfer process, i.e., it involves transfer of molecular movement or vibration from one body to another. Even the energy exchanged by radiation eventually ends up being transferred

into molecular movement. Transfer of energy as heat is a microscopic process because it represents the microscopic motion and interactions of microscopic constituents such as molecules and photons.

The level of molecular movement in a certain body or system is measured in terms of its temperature. The higher the level of excitement of the microscopic constituents of a system, the higher will be its temperature. Hence, a temperature difference between two bodies or two systems is essential to the heat transfer process because it sets up the potential for energy transfer.

Often assumptions and simplifications are made in heat transfer processes to analyze and understand certain aspects more effectively [BIR1960, ROH1985]. One of these is the assumption of an adiabatic process, which means that during the process, no heat transfer to and from a given system undergoing adiabatic change is made with any surrounding systems. Another important assumption is to treat a system as isolated from the surrounding systems. This means that in addition to no heat transfer with the surrounding systems, there is also no work exchanged with the surrounding systems.

6.2.1.3 Energy

Energy is a conserved property of a physical system, which cannot be observed directly, but can be calculated from the system's state. The energy of a system can present itself in various forms and is therefore difficult to describe by a comprehensive definition. Often, the best description of energy is as "the capacity to perform work".

For the thermal-hydraulic design engineer, three energy components are of most importance [LEU2004, POP2013]:

- Internal energy, E_U [kJ], or specific internal energy e_u [kJ/kg] (internal energy is usually simply expressed in U, or u);
- Kinetic energy, E_K [kJ], or specific kinetic energy, e_k [kJ/kg]; and
- Potential energy, E_P [kJ], or specific potential energy, e_p [kJ/kg].

Internal energy describes the thermodynamic energy of system molecules or atoms (referred to as heat). Kinetic energy is the energy of motion, which is carried by a body or system with a certain mass. Potential energy is energy possessed by a system when moving from one place to another in a force field, such as a gravitational field, an electro-magnetic field, or the nuclear force field in the atom. Most often for a thermal-hydraulic engineer, potential energy denotes the gravitational potential.

The total energy of a system in thermal-hydraulic terms can be expressed as the sum of the above components by Eq. (25) or Eq. (26):

$$E = E_U + E_K + E_P = U + E_K + E_P, \tag{25}$$

$$e = e_u + e_k + e_p = u + e_k + e_p. \tag{26}$$

The energy of a system depends on the temperature, pressure, velocity, and elevation of the system with respect to its surroundings.

6.2.1.4 Enthalpy

Enthalpy is a measure of the total energy of a thermodynamic system. It includes the internal energy, U (or thermodynamic potential) and the volume and pressure (the energy required to make room for a system change). Enthalpy is useful in describing system thermodynamic changes because it simplifies the description of energy transfers and system changes. Enthalpy is a thermodynamic property of a substance.

Consider a system undergoing a change because of addition of heat (energy) to the system at constant temperature; its total energy change can be described in terms of the system's internal energy and the product of the system's pressure and volume, as in Eq. (27):

$$\int_1^2 dQ = \int_1^2 dU + \int_1^2 P \cdot dV \ . \tag{27}$$

The sum of the system's internal energy and the product of its pressure and volume defines its enthalpy level, as shown by Eq. (28):

$$H = U + P\,V \ . \tag{28}$$

On a unit mass basis, the specific enthalpy is shown by Eq. (29), where specific heat is $q = Q/M$, specific internal energy is $u = U/M$, specific volume is $v = V/M$, M is mass, and P is pressure:

$$h = u + P\ v \ . \tag{29}$$

Enthalpy is a state parameter and can be expressed in terms of other parameters. For sub-cooled or super-heated conditions, $h = f(P,T)$, and for saturated conditions, $h = f(P)$ or $h = f(T)$, it is expressed in terms of pressure or temperature. In the two-phase region, the following equation can be used to calculate mixture enthalpy (under homogeneous conditions):

$$h_m = x \cdot h_g + (1-x) \cdot h_f = h_f + x \cdot h_{fg} \ , \tag{30}$$

where h_g is the enthalpy of the saturated gas, h_f is the enthalpy of the saturated liquid, and h_{fg} is the latent heat of vaporization.

6.2.2 First law of thermodynamics

The first law of thermodynamics is one of the most fundamental laws of nature; it simply states that the total energy change in a system is equal to the total energy supplied to the system from surrounding systems minus the energy transferred to the surrounding systems [SAA1966]:

Energy supplied – Energy removed = Change of energy level.

Hence, for a system with a particular mass that remains constant during the process, the first law of thermodynamics can be expressed as in Eq. (31):

$$Q - W = \Delta E = E_2 - E_1 . \tag{31}$$

The above equation written per unit mass becomes Eq. (32):

$$q - w = \Delta e = e_2 - e_1 . \tag{32}$$

With these definitions, it is now possible to define the work performed by a system that goes through an isobaric process as in Eq. (33):

$$W = \int_1^2 P\, dV = P(V_2 - V_1). \tag{33}$$

Using the first law of thermodynamics, as in Eq. (31), and substituting this equation into Eq. (33), one obtains the following equation:

$$Q - P(V_2 - V_1) = U_2 - U_1. \tag{34}$$

Rearranging the terms in Eq. (34) yields Eq. (35), which clearly shows the advantage of using enthalpy because it can provide a better expression of the first law of thermodynamics:

$$\begin{aligned} Q &= U_2 - U_1 + P(V_2 - V_1) \\ &= (U_2 + PV_2) - (U_1 + PV_1) = H_2 - H_1 = \Delta H. \end{aligned} \tag{35}$$

In the case of a system with multiple energy and work inputs and outputs, the first law of thermodynamics must be applied to the sum of these inputs and outputs, as in Eq. (36). Thus, Eq. (37) is obtained as an energy balance equation:

$$\Delta E = 0 = \sum energy\, inflow - \sum energy\, outflow \tag{36}$$

$$\begin{aligned} &= \frac{1}{2} m V_1^2 + m u_1 + Q + P_1 V_1 + m g Z_1 \\ &= -\frac{1}{2} m V_2^2 - m u_2 + W - P_2 V_2 - m g Z_2. \end{aligned} \tag{37}$$

Converting Eq. (37) in terms of specific parameters yields the following equations in terms of internal energy (Eq. (38)) and enthalpy (Eq. (39)):

$$q - w = \left[u_2 + Pv_2 + \frac{1}{2} V_2^2 + g Z_2 \right] - \left[u_1 + Pv_1 + \frac{1}{2} V_1^2 + g Z_1 \right], \tag{38}$$

$$q - w = \left[h_2 + \frac{1}{2} V_2^2 + g Z_2 \right] - \left[h_1 + \frac{1}{2} V_1^2 + g Z_1 \right]. \tag{39}$$

In the case of a turbine, there is no heat addition ($q = 0$) and no change in elevation for a horizontal turbine ($Z_1 = Z_2$), and therefore:

$$w = \left[h_1 - h_2 \right] - \frac{1}{2} \left[V_1^2 - V_2^2 \right]. \tag{40}$$

For a flow through a horizontal nozzle, there is neither heat addition nor work delivered ($q = w = 0$) and no change in elevation ($Z_1 = Z_2$), and therefore:

$$V_1^2 = V_2^2 + 2\left[h_1 - h_2 \right]. \tag{41}$$

Finally, there is a special form of the energy balance equation that is very useful to thermal-

hydraulic engineers for calculating fluid parameters in a pipe flow—the Bernoulli equation—in which neither heat addition nor work is delivered (*q = w = 0*):

$$\left[h_1 + \frac{1}{2}V_1^2 + gZ_1 \right] = \left[h_2 + \frac{1}{2}V_2^2 + gZ_2 \right] = const\,, \tag{42}$$

$$\left[u + Pv + \frac{1}{2}V^2 + gZ \right] = const\,. \tag{43}$$

Equation (43) clearly shows that the key fluid parameters for a flow are connected, so that to add up to a constant, an increase in one parameter must result in a reduction in the other parameters. For example, considering horizontal flow, an increase in fluid velocity results in a decrease in fluid pressure, and vice versa.

6.2.3 Reactor cycles

Nuclear reactors directly or indirectly produce steam that performs a thermodynamic cycle, which is used to convert nuclear energy using the energy conversion chain shown in the diagram below.

Nuclear fission	*Nuclear fuel internal energy*	*Cooling Fluid*	*Steam production*	*Turbine rotational energy*	*Generator magnetic field*	*Electrical energy*
Converts mass into kinetic energy of nuclear particles	*Converts kinetic energy of nuclear particles into molecular motion of the fuel mass*	*Converts fuel internal energy into internal energy of the coolant*	*Converts internal energy of the coolant into steam production*	*Converts steam energy into kinetic energy (rotation) of the turbine shaft*	*Converts the kinetic energy of the turbine shaft into rotation of generator magnetic poles*	*Converts generator magnetic energy into electrical energy*

The shaded area of the diagram represents the thermodynamic cycle that is implemented with the objective of delivering work to the electric generator.

This process leads to rejection of a certain part of the thermal energy into the environment (lake, river, sea, or the atmosphere) to be able to close the cycle; this will be explained in later sections.

With regard to energy generation, the cycle thermodynamic efficiency, η_t, is defined to provide a measure of cycle performance:

$$\eta_t = \frac{W}{Q_{in}}\,. \tag{44}$$

6.2.3.1 Carnot cycle

The Carnot cycle is a theoretical thermodynamic cycle that represents the most efficient way of converting a given amount of thermal energy between two thermal reservoirs into work (turbine work), or conversely the most efficient way of converting a given amount of work into creating a temperature difference between two reservoirs (refrigeration).

Figure 38 shows an ideal Carnot cycle in pressure versus volume and temperature versus entropy diagrams. The Carnot cycle consists of the following processes [SAA1966]:

a) delivering heat to the cycle by a reversible isothermal expansion process (process from points 1 to 2 in Figure 38);
b) delivering work output by isentropic expansion of gas (process from points 2 to 3 in Figure 38);
c) rejecting waste heat from the cycle by reversible isothermal compression of gas (process from points 3 to 4 in Figure 38); and
d) inputting work into the cycle by isentropic compression of gas (process from points 4 to 1 in Figure 38).

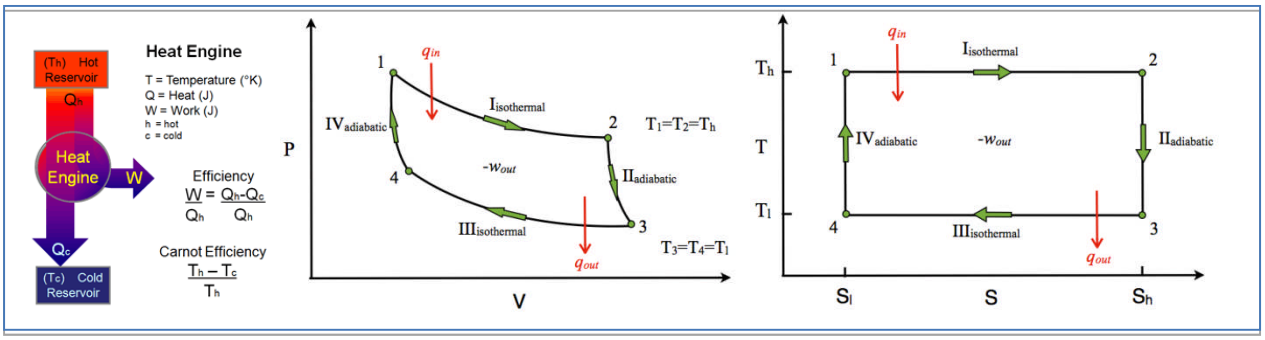

Figure 38 Ideal Carnot cycle

To calculate the thermal efficiency of the Carnot cycle, it is necessary to calculate the total heat delivered and the total work performed and to use these results in Eq. (44).

For the process from points 1 to 2 (at constant temperature, $\Delta U_{1-2} = \int_1^2 m\, c_v\, dT = 0$):

$$W_{1-2} = \int_1^2 p\, dV = m\, R\, T_1 \int_1^2 \frac{dV}{V} = m\, R\, T_1 \ln \frac{V_2}{V_1}. \tag{45}$$

Using the first law of thermodynamics, from Eq. (31), the heat addition can be expressed as:

$$Q_{1-2} - W_{1-2} = \Delta U_{1-2} = 0, \tag{46}$$

$$Q_{1-2} = W_{1-2} = m\, R\, T_1 \ln \frac{V_2}{V_1}. \tag{47}$$

For the process from points 2 to 3 (with no heat addition, $Q_{2-3} = 0$):

$$W_{2-3} = \int_2^3 p\, dV = \int_2^3 C\, V^{-\gamma}\, dV = \frac{p_3 V_3 - p_2 V_2}{-\gamma + 1}, \tag{48}$$

$$\Delta U_{2-3} = \int_2^3 m\, c_v\, dT = m\, c_v (T_3 - T_2). \tag{49}$$

Using the first law of thermodynamics, from Eq. (31), the link between internal energy change and delivered work is:

$$Q_{2-3} = \Delta U_{2-3} + W_{2-3} = 0. \tag{50}$$

For the process from points 3 to 4 (at constant temperature, $\Delta U_{3-4} = 0$):

$$W_{3-4} = m\,R\,T_3 \ln \frac{V_4}{V_3} = Q_{3-4}. \tag{51}$$

For the process from points 4 to 1 (with no heat addition, $Q_{4-1} = 0$):

$$W_{4-1} = \frac{p_1 V_1 - p_4 V_4}{-\gamma + 1}, \tag{52}$$

$$\Delta U_{4-1} = m c_v (T_1 - T_4) = -W_{4-1}. \tag{53}$$

These equations have used the following thermodynamic relationships to calculate the thermal efficiency:

- For a quasi-static adiabatic process:

$$T_2 V_2^{\gamma-1} = T_3 V_3^{\gamma-1} \quad and \quad T_4 V_4^{\gamma-1} = T_1 V_1^{\gamma-1}. \tag{54}$$

- For an isothermal process

$$T_1 = T_2 \quad and \quad T_3 = T_4, \tag{55}$$

$$p_1 V_1 = p_2 V_2 \quad and \quad p_3 V_3 = p_4 V_4. \tag{56}$$

- Volume relation

$$\frac{V_2}{V_1} = \frac{V_3}{V_4}. \tag{57}$$

Hence, the net work done can be obtained by summing up the work in the separate processes described by Eqs. (45), (48), (51), and (52) and using the relationships provided by Eqs. (54), (55), (56), and (57):

$$W_{cycle} = W_{1-2} + W_{2-3} + W_{3-4} + W_{4-1} \tag{58}$$

$$= m\,R\,T_1 \ln \frac{V_2}{V_1} + \frac{p_3 V_3 - p_2 V_2}{-\gamma + 1} + m\,R\,T_3 \ln \frac{V_4}{V_3} + \frac{p_1 V_1 - p_4 V_4}{-\gamma + 1},$$

$$W_{cycle} = mR(T_1 - T_3) \ln \frac{V_2}{V_1}. \tag{59}$$

Now the cycle thermal efficiency can be obtained from Eq. (44):

$$\eta_t = \frac{net\ work\ done}{heat\ input} = \frac{W_{cycle}}{Q_{in}} = \frac{W_{cycle}}{Q_{1-2}} = \frac{mR(T_1 - T_3) \ln (V_2 / V_1)}{mR\,T_1 \ln (V_2 / V_1)} = \frac{T_1 - T_3}{T_1} = 1 - \frac{T_3}{T_1}. \tag{60}$$

One important observation can be made from Eq. (60): the thermal efficiency of the cycle depends on the temperatures of the upper and lower thermal reservoirs. Hence, the higher the temperature at which heat is added to the cycle and the lower the temperature at which heat is extracted from the cycle, the higher will be the thermal efficiency. Therefore, design efforts to improve cycle thermal efficiency are usually directed towards increasing the temperature at which heat is delivered to the cycle. However, it is also evident that this cycle will operate more efficiently if the lower temperature is reduced.

6.2.4 Second law of thermodynamics

The second law of thermodynamics is a very important law of nature and primarily applies to thermodynamics. This law indicates that over time, differences in temperature, pressure, and chemical potential decrease in an isolated physical system, leading eventually, with a time constant that depends on the system thermodynamic inertia, to a state of thermodynamic equilibrium.

There are other definitions of this law, depending on the discipline. The above definition is given in the context of thermodynamics, but this law can also be considered from the perspectives of quantum mechanics or astrophysics, and in such cases, its definition is adjusted to the objectives of the corresponding discipline.

The second law of thermodynamics has many implications, of which a few are stated below:

- Carnot's principle [CAR2015]: The historical origin of the second law of thermodynamics was in Carnot's principle. It refers to the Carnot engine, fictively operating in a very slow mode (quasi-static) so that heat is transferred between two thermal reservoirs that maintain their internal equilibrium. The Carnot principle, which originated at the beginning of the 19th Century, is still valid today. It states that, *"The efficiency of a quasi-static or reversible Carnot cycle depends only on the temperature of the two heat reservoirs, and is independent of the working substance. A Carnot engine operated in this way is the most efficient possible heat engine using these two temperatures".*
- Clausius' statement [CLA2015]: "*It is impossible to construct a device that executes a thermodynamic cycle so that the sole effect is to produce a transfer of heat energy from a body at a low temperature to a body at a high temperature".*
- Kelvin's statement [KEV2015]: *"It is impossible, by means of inanimate material agency, to derive mechanical effect from any portion of matter by cooling it below the temperature of the coldest of the surrounding objects".*
- Kelvin-Planck statement [KPL2015]: *"It is impossible to construct a device that executes a thermodynamic cycle, exchanges heat energy with a single reservoir, and produces an equivalent amount of work".*
- Planck's principle [PLA2015]: *"The internal energy of a closed system is increased by an isochoric adiabatic process".*

Whichever definition is used for the second law of thermodynamics leads to the basic conclusion that any time an energy transfer is performed, from thermal to mechanical to

electrical or vice versa, a penalty is paid in terms of increasing the disorder of the isolated system. In other words, thermal energy cannot be converted into work by a cyclic process with 100% efficiency.

The mathematical formulation of the second law of thermodynamics is best visualized using Figure 39. In this figure, on the left side, a generalized thermodynamic cycle is shown taking place between a hot reservoir at temperature T_H and a cold reservoir at temperature T_C. On the right side, the Carnot cycle diagram is shown between the same boundaries. Therefore, the area in red, labelled as Q_C, is the amount of energy exchanged between the system and the cold reservoir. The area in white, labelled as W, is the amount of work exchanged by the system and its surroundings. The amount of heat exchanged with the hot reservoir, labelled as Q_H, is the sum of the two, Q_C and W. If the system is behaving like an engine, the process moves clockwise around the loop, and if it behaves as a refrigerator, it moves counter-clockwise.

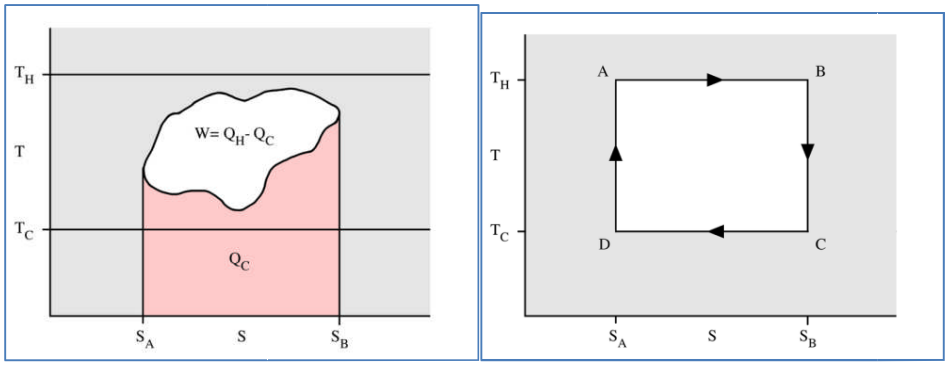

Figure 39 The concept of entropy in closed cycles

From the above, and because the energy addition to the cycle and the energy extraction from it have opposite signs, it follows that:

$$\frac{T_H}{T_C} = -\frac{Q_H}{Q_C} \Rightarrow \frac{Q_C}{T_C} + \frac{Q_H}{T_H} = 0. \tag{61}$$

This can be generalized by splitting the general reversible cycle shown in **Figure 39** into a number of infinitesimally small Carnot cycles. For each small cycle, noting that common boundaries cancel, the following relation can be obtained:

$$\frac{\Delta Q_C}{T_C} + \frac{\Delta Q_H}{T_H} = 0\,. \tag{62}$$

Summing all cycles and performing a circular integration:

$$\sum \frac{\Delta Q}{T} = 0 \;\Rightarrow\; \oint \frac{\Delta Q}{T} = 0\,. \tag{63}$$

The above equation also indicates that the line integral $\int_L \delta Q / T$ is path-independent [SAA1966]. Because the closed integral is equal to zero, *dQ/T* must be an exact differential and

must be a state variable, i.e., a property of the state of the material, like internal energy, pressure, temperature, density (*u, P, T, ρ)*, etc. This differential is defined to be the entropy, *S*.

Because *S* is a system property, it is possible to express any equilibrium state in terms of *S* plus one other state variable (*T*, *P,* or something else):

- In a reversible process (Figure 40), the quantity, *δQ/T*, from point A to point B is the same regardless of the path;
- Hence, the entropy, *S*, can be defined as

$$S_B - S_A = \int_A^B \left.\frac{\delta Q}{T}\right|_{reversible} ; \tag{64}$$

- Specific entropy, *s* (J/kg K).

For a reversible process, heat addition and heat extraction from the cycle are defined as:

$$Q_H = T_H(S_B - S_A), \tag{65}$$

$$Q_C = T_C(S_A - S_B) = -T_C(S_B - S_A). \tag{66}$$

Using Eqs. (65) and (66), the net work done by the cycle is defined as:

$$W_{cycle} = Q_H - Q_C = T_H(S_B - S_A) - T_C(S_B - S_A) = (T_H - T_C)(S_B - S_A). \tag{67}$$

Therefore, the thermal efficiency is defined using Eq. (44) as:

$$\eta_t = \frac{W_{cycle}}{Q_H} = \frac{(T_H - T_C)\,(S_B - S_A)}{T_H\,(S_B - S_A)} = \frac{T_H - T_C}{T_H} = 1 - \frac{T_C}{T_H}. \tag{68}$$

The following relation represents the generalization of the entropy definition for reversible and irreversible processes:

$$\oint \frac{\Delta Q}{T} \le 0 \quad or \quad \Delta S \ge \int \frac{\delta Q}{T}. \tag{69}$$

Hence, for reversible processes, the equality sign applies, whereas for irreversible processes, i.e., realistic processes, the < sign applies. All real processes are considered irreversible. This indicates that for closed systems, any process, regardless of the path, results in an increase in entropy.

6.2.5 Reactor power cycle

Figure 40 shows how an ideal Carnot cycle is applied with water as the working fluid. On the right side, isothermal addition of energy (heat) to the cycle is achieved between the saturated water and saturated steam states. Extraction of waste heat from the cycle is carried out isothermally in the two-phase region.

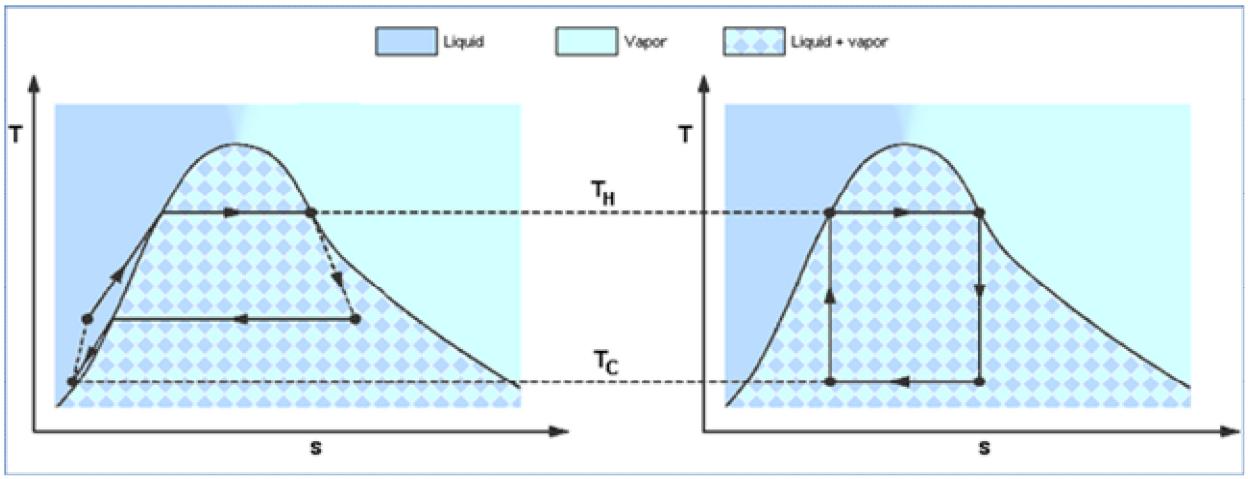

Figure 40 Carnot cycle for steam

The ideal Carnot cycle is impossible to achieve with real turbo machinery. Therefore, a variation of the Carnot cycle, called the Rankine cycle, is shown on the left side of Figure 40 [SAA1966]. This cycle performs complete condensation of the steam at the lower thermal reservoir temperature. Hence, water enters the adiabatic compression in the pump as liquid water. With this modification, more heat rejection is needed to bring the feedwater to saturation, avoiding a liquid-vapour mixture in the pump. This reduces thermal efficiency.

Figure 41 shows the steam-water diagrams used by thermal engineers and designers [WIK2015a]. The first part, Figure 41a, shows the *P-v* diagram, followed by Figure 41b, the *T-s* diagram, and Figure 41c, the *h-s* diagram. The *P-v* diagram is useful for representing changes in volume between different points in the cycle. Note that pressure and temperature are linked parameters at saturation conditions, and hence in the two-phase area, both join in the same straight line. The *T-s* diagram shows temperature changes in the cycle for given entropies. This diagram is useful for the Carnot and Rankine cycles because heat addition and heat extraction are performed as isothermal processes, which are straight horizontal lines in this diagram.

According to the ideal Carnot cycle and the ideal Rankine cycle, isentropic expansion and isentropic compression (no losses) are represented by vertical straight lines, which make the diagram a very easy way to observe heat changes as square areas. On the other hand, the *h-s* diagram is very useful to the turbo machinery designer because each energy change during any of the processes is shown as a vertical increment on the y-axis, whereas reversibility or irreversibility of the cycle is easily observable on the x-axis.

Figure 42 shows an ideal Rankine cycle for a nuclear power plant (ideal because irreversibility is not taken into account). The left side shows the NPP secondary side with the steam generator and other equipment. Certain points in the diagram are labelled on the reactor sketch with numbers.

The separate processes of the cycle as labelled on the left side with their position are:

- Heat supplied: area 6-1-2-2A-3-4-5-6
- Heat removed: area 6-1-4-5-6

- Net work done: area 1-2-2A-3-4-1.

The assumptions of this idealized Rankine cycle are:

- Negligible changes in kinetic energy and potential energy;
- All processes are reversible; and
- Negligible pressure and heat losses.

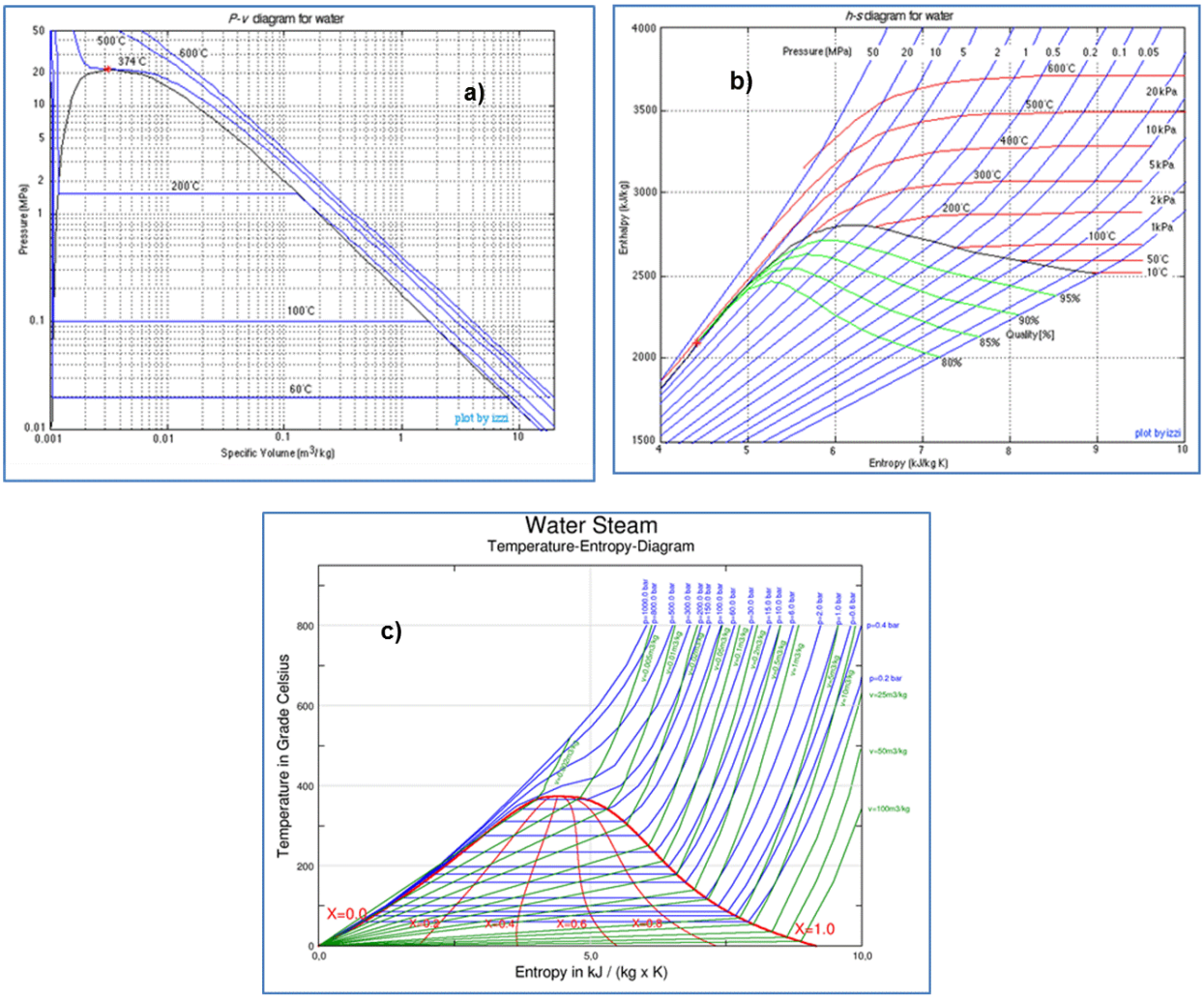

Figure 41 Steam-water diagrams used in thermodynamic analyzes (a, b, c)

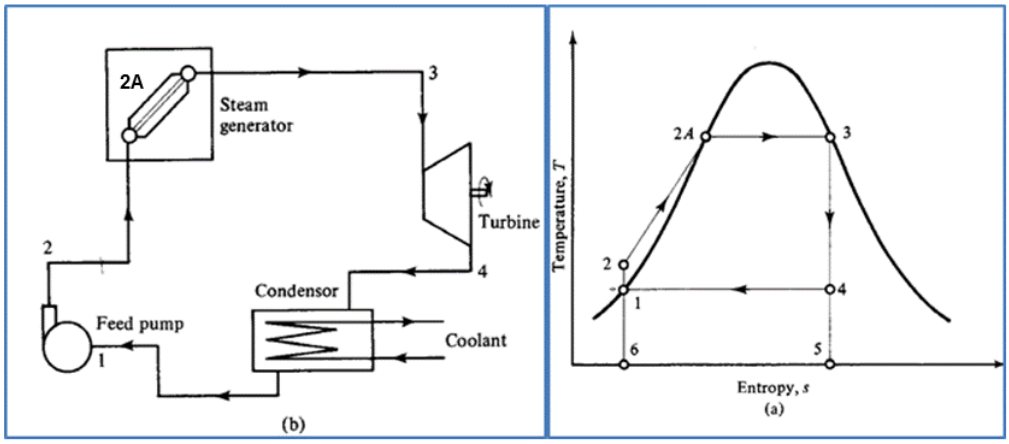

Figure 42 Simplified Rankine cycle in a nuclear power plant

The thermodynamic power cycle in reactor systems is similar to the Rankine cycle. As sketched in Figure 42, the steam generator boils the working fluid (water) isothermally (at saturation temperature), the turbine expands the fluid and performs shaft work, the condenser extracts the reject heat and condenses the fluid, and the feedwater pump returns the fluid to the steam generator at pressure. Of course, the realistic reactor cycle is not reversible, but the principles of the cycle are the same. The typical cycle used in power plants is called the Rankine cycle. The *T-s* and *h-s* diagrams for an ideal simple Rankine cycle are given in Figure 41 and Figure 42.

In the ideal Rankine cycle in Figure 42, saturated steam (point 3) enters the turbine and expands isentropically to position 4. At point 4, the wet steam enters the condenser, where heat is removed until the fluid is condensed to a saturated liquid at point 1. After leaving the condenser at saturation pressure P_2, the fluid is compressed isentropically from pressure P_2 to the boiler pressure P_1. The high-pressure liquid enters the boiler at point 2, where the fluid is first brought to saturation at pressure P_2 (point 2A) and then vaporized to saturated steam at point 3.

In process 1-2 (isentropic compression in the feedwater pump), no heat is exchanged with the surroundings, i.e., $q_{1-2}=0$. Hence, the work input to achieve isentropic compression is given by Eq. (70):

$$-w_{1-2}=-(h_2-h_1)=-\int_1^2 v\,dp\sim -v_1(p_2-p_1)\,. \tag{70}$$

In process 2-2A-3 (heating at constant pressure in the boiler), no work is exchanged with the surroundings, i.e., $w_{2\text{-}3}=0$. Hence, using the *h-s* diagram, the heat addition to the system is obtained as a difference of enthalpies, as given by Eq. (71):

$$q_{2-3}=q_{in}=h_3-h_2\,. \tag{71}$$

In process 3-4 (isentropic expansion in the turbine), no heat is exchanged with the surroundings, i.e., $q_{3\text{-}4}=0$. Hence, the work delivered by the turbine is given by Eq. (72):

$$w_{3-4} = h_3 - h_4 . \tag{72}$$

In process 4-1 (heat removal at constant pressure in the condenser), no work is exchanged with the surroundings, i.e., $w_{4-1} = 0$. Hence, the heat extraction from the system is obtained as a difference of enthalpies, as given in Eq. (73):

$$-q_{4-1} = h_4 - h_1 . \tag{73}$$

The net work performed by this cycle can be obtained as:

$$w_{cycle} = w_{3-4} + w_{1-2} = (h_3 - h_4) - (h_2 - h_1) . \tag{74}$$

The thermal efficiency of the ideal Rankine cycle is obtained by Eq. (75):

$$\eta_{Rankine} = \frac{w_{cycle}}{q_{in}} = \frac{(h_3 - h_4) - (h_2 - h_1)}{h_3 - h_2} = \frac{q_{2-3} - q_{4-1}}{q_{2-3}} . \tag{75}$$

As noted earlier, the thermal efficiency of the ideal simplified Rankine cycle is much less than that of the Carnot cycle because more heat is wasted to the environment. The performance of the Rankine cycle can be improved in practice by:

(1) raising the boiler pressure
(2) lowering the exhaust pressure
(3) using superheat
(4) using reheat.

Options (1), (3), and (4) effectively raise the inlet temperature, whereas (2) effectively lowers the outlet temperature, with a corresponding effect on cycle efficiency.

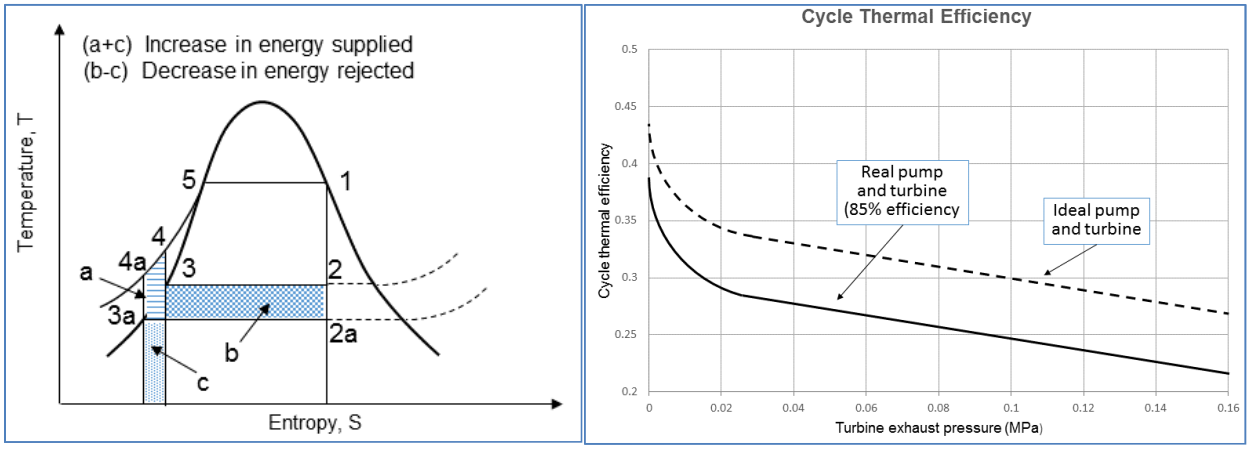

Figure 43 Typical impact of turbine outlet pressure on cycle thermodynamic efficiency

The condenser pressure is limited by the temperature of the available cooling water, the size and cost of the condenser, and the size of the vacuum pumps required to deaerate the condenser. Figure 43 shows the impact of a condenser pressure decrease in a typical PWR nuclear plant. The practical lower limit on condenser pressure is 3–6 kPa(a). Consequently, options (1), (3), and (4) are used to achieve increased efficiency [TOD2011].

The increase in boiler pressure results in an increase in the net work performed by the cycle, with a corresponding decrease in heat rejected. Figure 44 shows the impact of an inlet pressure increase in a typical PWR nuclear plant [TOD2011]. However, for the indirect power cycle, the downside of raising the boiler pressure (and the temperature because the steam is saturated) is that it forces the primary-side temperature to increase to provide sufficient ΔT to transfer the heat from the primary to the secondary side. This higher primary-side temperature requires higher primary-side pressure, which in turn requires thicker pressure vessel walls. In a pressure vessel-type reactor, this can be costly or can lead to reduced plant reliability or life. In pressure tube reactors, the main drawback is the increased parasitic neutron absorption in the pressure tube walls, which need to be thicker, resulting in lower fuel burn-up.

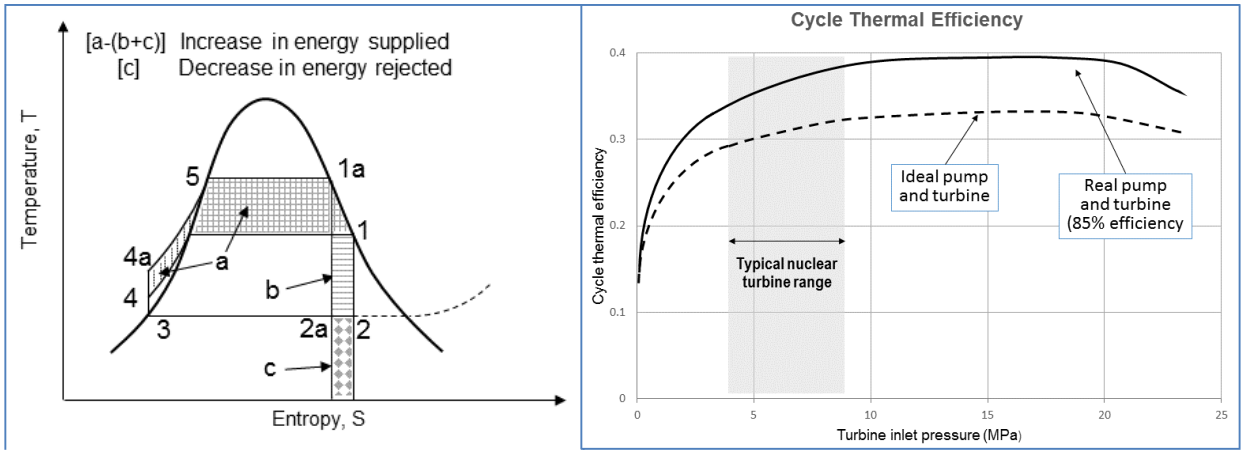

Figure 44 Typical impact of turbine inlet pressure on cycle thermodynamic efficiency

6.2.6 Improvements in reactor cycles

In the following sections, improvements to the Rankine cycle used in power reactors are described, their usefulness discussed, and their consequences analyzed. The improvements described in the following sections are used in power reactors with certain variations and design specifics by various reactor types and vendors. However, they all contribute to higher NPP thermal efficiency, which is considered as an important marketing parameter.

6.2.6.1 Rankine cycle with superheat

Figure 45 illustrates the Rankine cycle with superheat [LEU2004, POP2013]. Superheat causes a net increase in the temperature at which heat is received, with a resulting improvement in cycle efficiency. Another important factor is that the amount of moisture in the fluid leaving the turbine is reduced, which increases turbine efficiency and reduces turbine blade erosion. However, when using superheat, one must have a high-temperature heat source or else reduce boiler pressure. Some recent approaches and ideas include use of traditional gas-fired superheaters in combination with nuclear power reactors.

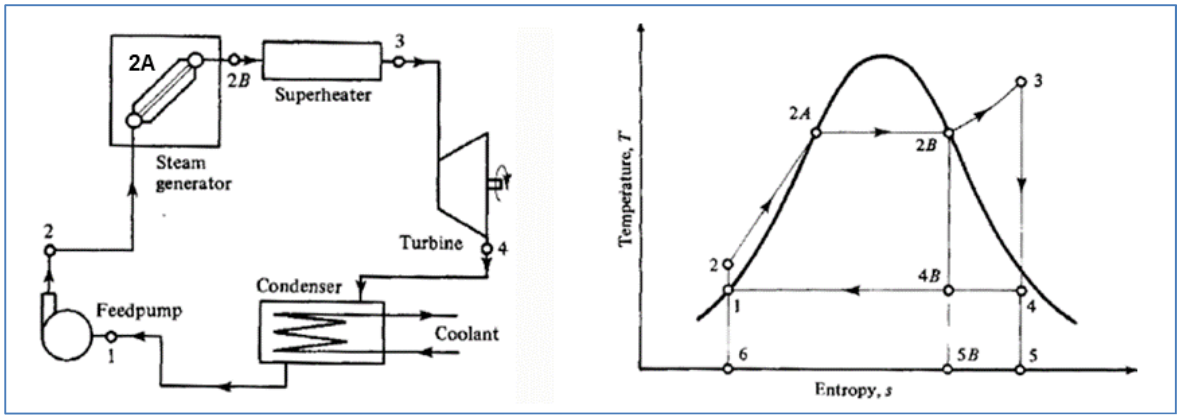

Figure 45 Rankine cycle with superheating

The differences between the cycle with superheat and the simple Rankine cycle are:

- Increased net work output (area 2B-3-4-4B-2B)
- Increased heat supply (area 2B-3-4-5B-2B)
- Increased exhaust steam quality from x_{4B} to x_4.

The thermal efficiency of the cycle with superheat is given by Eq. (76) and is higher than for the simple Rankine cycle:

$$\eta_{Superheat} = \frac{w_{cycle}}{q_{in}} = \frac{q_{2-3} - q_{4-1}}{q_{2-3}} = \frac{(h_3 - h_4) - (h_2 - h_1)}{h_3 - h_2}. \quad (76)$$

6.2.6.2 Reheat cycle

The effective temperature of heat addition is increased and the moisture content further reduced by using reheat in the Rankine cycle. A schematic diagram of the power plant and an appropriate temperature-entropy diagram are shown in Figure 46 [LEU2004, POP2013]. High-pressure, superheated steam is expanded in a high-pressure turbine to an intermediate pressure 4 and the fluid then returned to a second-stage boiler and superheater and reheated to state 3A. The reheated steam is then expanded in a low-pressure turbine to the final exhaust pressure 4A. The moisture content of the working fluid is drastically reduced by use of reheat, and this approach is used in all fossil-fuelled and many nuclear power plants (without the superheating part).

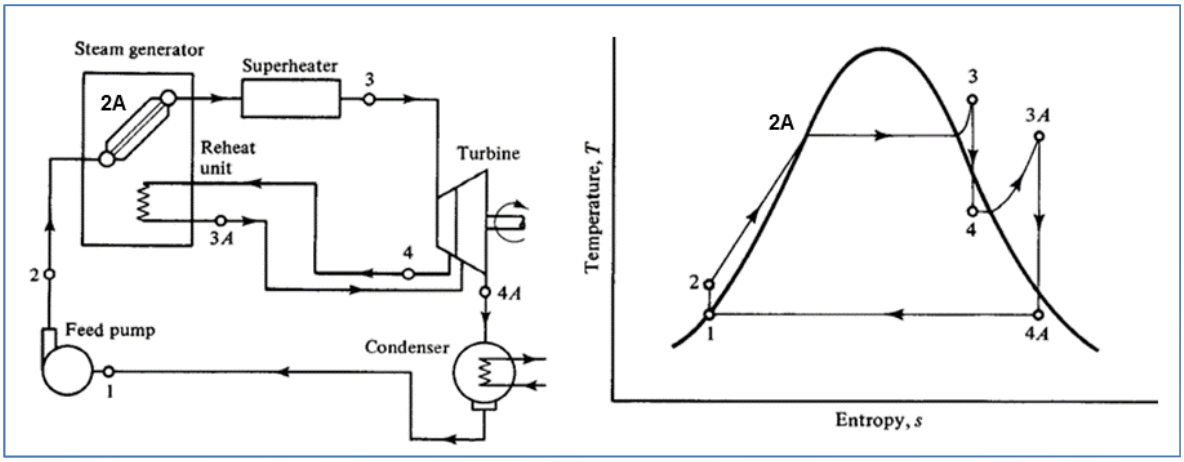

Figure 46 Rankine cycle with superheating and reheating

The approach used to compute the work and the efficiency of reheat cycles is the same as that used in the example problem for the simple Rankine cycle. One calculates the work produced in each turbine separately and the required pumping work. Heat is added to the fluid at two different stages of the cycle and is given by the difference in enthalpy between states 3 and 2 and states 4 and 3A. Wet steam at point 4 is removed after the high-pressure turbine stage, reheated at constant pressure to a superheated state, and admitted to the low-pressure turbine stage. Superheated steam at point 3A is expanded to the design exhaust pressure at point 4A.

The net work performed by this cycle is given by Eq. (77):

$$w_{cycle} = w_{1-2} + w_{3-4} + w_{3A-4A} = (h_1 - h_2) + (h_3 - h_4) + (h_{3A} - h_{4A}). \tag{77}$$

The heat supplied to this system is given by Eq. (78):

$$q_{in} = (h_3 - h_2) + (h_{3A} - h_4). \tag{78}$$

The thermal efficiency of this cycle is given by Eq. (79):

$$\eta_{Reheat} = \frac{(h_1 - h_2) + (h_3 - h_4) + (h_{3A} - h_{4A})}{(h_3 - h_2) + (h_{3A} - h_4)}. \tag{79}$$

6.2.6.3 Regeneration cycle

In theory, modifications to the cycle can be made to reduce cycle irreversibility. One of the principal sources is the sensible heat addition required to bring the boiler feedwater up to saturation temperature. This is accomplished by using some of the flow through the turbine to heat the feedwater. To achieve reversibility, a possible setup is shown in Figure 47, where internal heat from the turbine is used to heat the feedwater in process 2-2A [LEU2004, POP2013]. This cycle could provide the same thermal efficiency as the Carnot cycle. However, this is not a practical modification because it is impossible to design a turbine to serve as both a power-production device and a heat exchanger. Modifications have, however, been designed to make this design change more practical, one of which is presented in the next section.

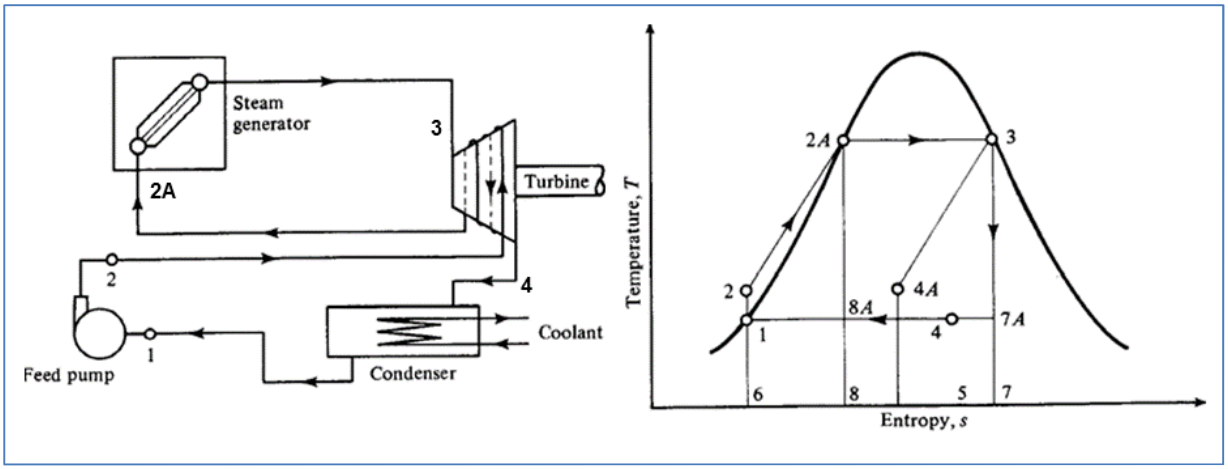

Figure 47 Rankine cycle with regeneration circuit

6.2.6.4 Rankine cycle with feedwater heaters

This improvement is based on the regeneration principle, which was briefly covered in the previous section. This improvement is based on extracting a small amount of steam at an intermediate pressure from the turbine and using it to heat feedwater.

Two types of feedwater heaters exist in practice:

- Open type, in which direct contact between extracted steam and feedwater is achieved, resulting in good heat transfer; and
- Closed type, in which only thermal contact between extracted steam and feedwater is achieved.

For both types, the reheating is usually designed in several stages. The following sections cover both these types in detail.

6.2.6.5 Rankine cycle with open feedwater heater

Figure 48 shows the Rankine cycle with one open feedwater heater (the left side shows the loop and the right side the *T-s* diagram of the cycle) [LEU2004, POP2013].

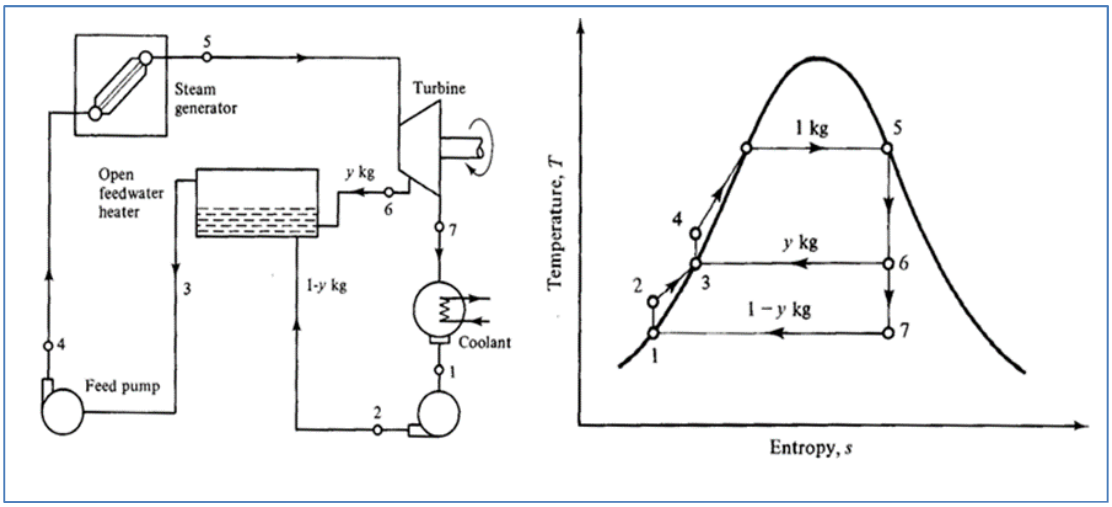

Figure 48 Rankine cycle with open feedwater reheating

The extraction fraction of steam is calculated from an energy balance on the feedwater heater using Eq. (80):

$$\dot{m}(1-y)h_2 + \dot{m}\,y\,h_6 = \dot{m}\left[y+(1-y)\right]h_3,$$

$$(1-y)h_2 + y\,h_6 = h_3. \tag{80}$$

The pump work is obtained by summing the work from both pumps, as given by Eq. (81):

$$w_{pump} = w_{1-2}(1-y) + w_{3-4}. \tag{81}$$

The turbine work is obtained by summing up the two parts of the turbine expansion, one with the full steam flow, and one with the *(1-y)* portion of the steam flow, as in Eq. (82):

$$w_{turbine} = w_{5-6} + (1-y)\,w_{6-7}. \tag{82}$$

The heat supplied to the cycle is not affected by the heater and is given by Eq. (83):

$$q_{4-5} = h_5 - h_4. \tag{83}$$

Usually, operating NPPs have multiple stages of feedwater heating; an example of a plant with two open feedwater heaters is shown in Figure 49.

Using the heat balance at both heaters, one can obtain the enthalpies downstream from the mixing points Z and Y, as shown in Eqs. (84) and (85):

$$h_{4'} = \frac{\dot{m}_{1''}h_{1''} + \dot{m}_4 h_4}{\dot{m}_{1''} + \dot{m}_4} = \frac{\dot{m}_{1''}h_{1''} + \dot{m}_4 h_4}{\dot{m}_1 - \dot{m}_{1'}}, \tag{84}$$

$$h_{5'} = \frac{\dot{m}_{1'}h_{1'} + (\dot{m}_1 - \dot{m}_{1'})h_5}{\dot{m}_1}. \tag{85}$$

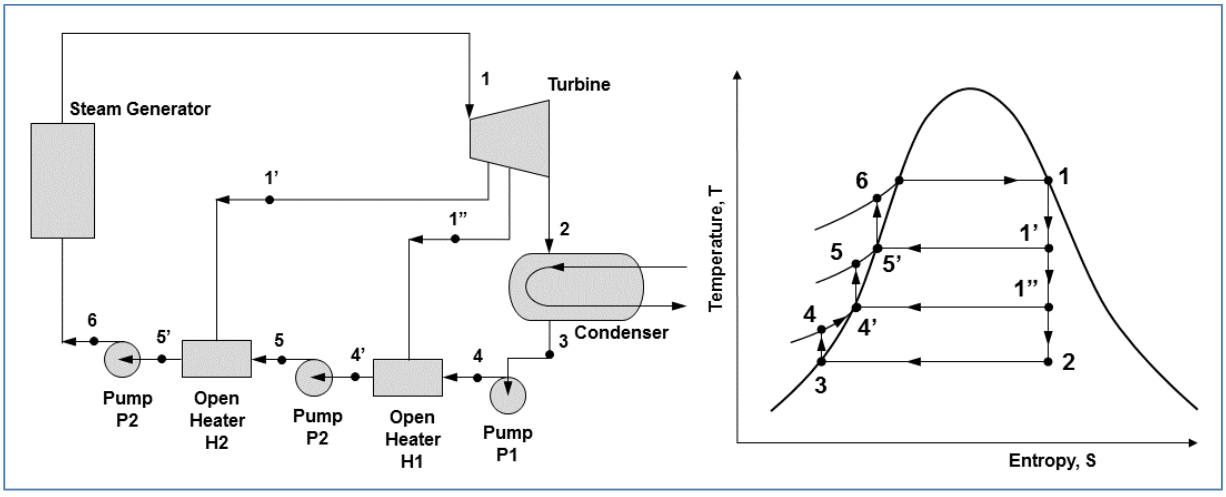

Figure 49 Rankine cycle with multiple open reheaters

The turbine work in this case is obtained by summing up the work at the three parts before and after the steam extractions, as shown in Eq. (86):

$$w_T = \dot{m}_1\left(h_1 - h_{1'}\right) + \left(\dot{m}_1 - \dot{m}_{1'}\right)\left(h_{1'} - h_{1''}\right) + \dot{m}_2\left(h_{1''} - h_2\right). \quad (86)$$

6.2.6.6 Rankine cycle with closed feedwater heater

Figure 50 shows the Rankine cycle with one closed feedwater heater (the left side shows the loop and the right side the *T-s* diagram of the cycle) [LEU2004, POP2013].

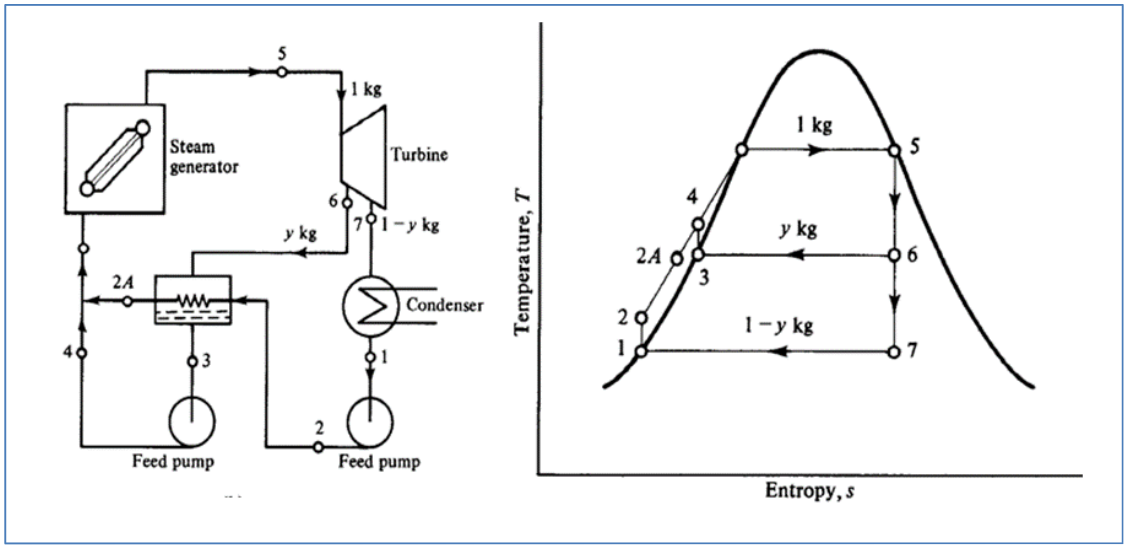

Figure 50 Rankine cycle with closed feedwater reheating

The extraction fraction of steam is calculated from an energy balance on the feedwater heater using Eq. (87):

$$\left(1-y\right)h_2 + y\,h_6 = \left(1-y\right)h_{2A} + y\,h_3. \quad (87)$$

The pump work is obtained by summing the work from both pumps, as given by Eq. (88):

$$w_{pump} = w_{1\text{–}2}\left(1-y\right) + w_{3\text{–}4}. \quad (88)$$

The turbine work is obtained by summing up the two parts of the turbine expansion, one with the full steam flow, and one with the *(1-y)* portion of the steam flow, as in Eq. (89):

$$w_{turbine} = w_{5\text{–}6} + \left(1-y\right)w_{6\text{–}7}. \quad (89)$$

The heat supplied to the cycle is not affected by the heater and is given by Eq. (90):

$$q_{in} = \left(h_5 - h_{2A}\right)\left(1-y\right) + \left(h_5 - h_4\right)y. \quad (90)$$

Usually, operating NPPs have multiple stages of feedwater heating; an example of a plant with two closed feedwater heaters is shown in Figure 51 [POP2013].

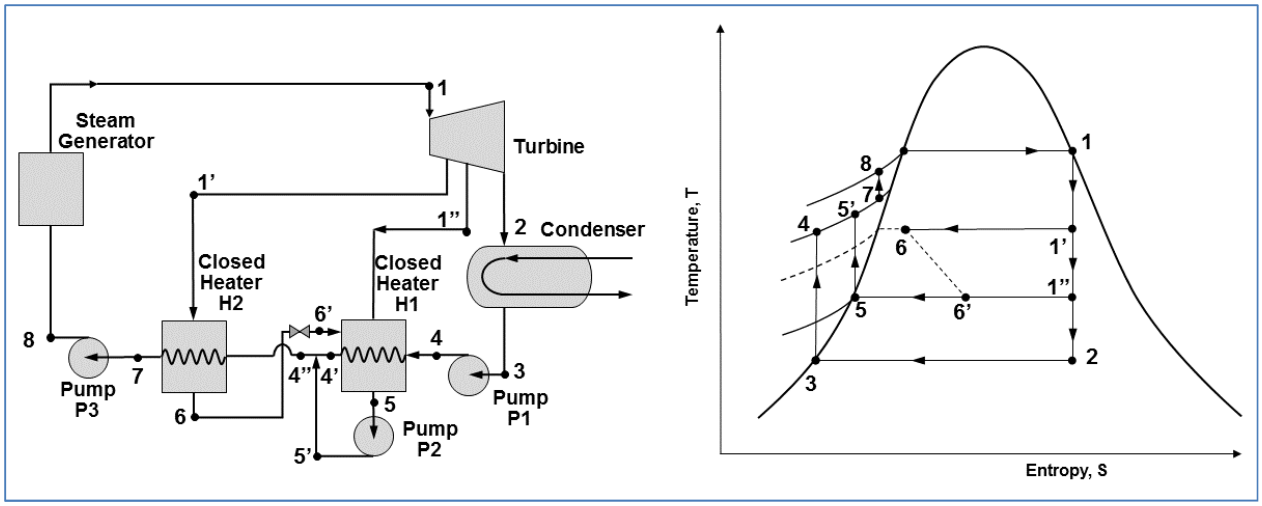

Figure 51 Rankine cycle with multiple closed reheaters

Using the heat balance at both heaters, one can obtain the enthalpies downstream from the exit points 1 and 2, as shown in Eqs. (91), (92), and (93):

$$h_{4'} = \frac{\dot{m}_{1"}h_{1"} + \dot{m}_4 h_4 + \dot{m}_{1'}h_{6'} - \left(\dot{m}_{1'} - \dot{m}_{1"}\right)h_5}{\dot{m}_1}, \tag{91}$$

$$h_{4"} = \frac{\dot{m}_4 h_{4'} + \left(\dot{m}_{1'} + \dot{m}_{1"}\right)h_{5'}}{\dot{m}_1}, \tag{92}$$

$$h_7 = \frac{\dot{m}_{1'}\left(h_{1'} - h_6\right) + \dot{m}_1 h_{4"}}{\dot{m}_1}. \tag{93}$$

6.2.6.7 Thermal efficiency moisture separation

The role of the moisture separator between the high-pressure and low-pressure turbines in the cycle is two-fold:

- to provide feedwater heating, thus improving cycle thermal efficiency; and
- to remove moisture from the steam, enabling dry steam to enter the low-pressure turbine (thus reducing water droplet erosion of the turbine blades).

Figure 52 shows an example of a moisture separator where, using the principle of the open heater, the extracted moisture from the separator is mixed with the feedwater, thus transferring the latent heat of condensation to the feedwater [POP2013].

By defining the parameters at certain points in the *T-s* diagram, $h_{1"} = h_f\left(at\ p_{1'}\right)\ and\ \left(1-x_{1'}\right)\dot{m}_1$ and $h_{1'"} = h_g\left(at\ p_{1"}\right)\ and\ x_{1'}\dot{m}_1$, and by performing an energy balance at the separator, one can obtain the enthalpy after the mixing point using Eq. (94):

$$h_5 = \frac{h_{1"}x_{1"}\dot{m}_{1"} + h_4 x_{1'"}\left(\dot{m}_1 - \dot{m}_{1"}\right)}{\dot{m}_1}. \tag{94}$$

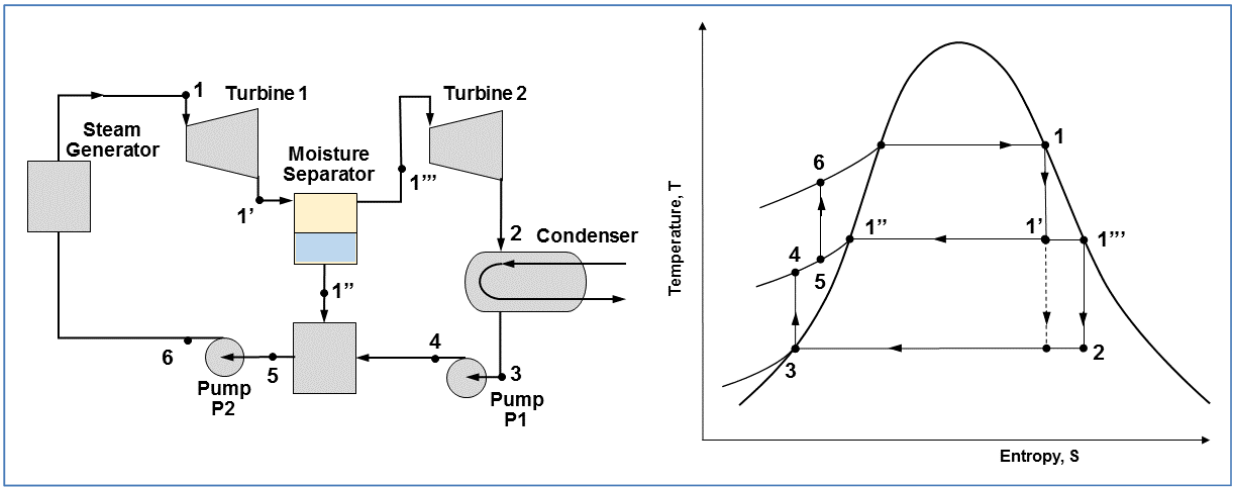

Figure 52 Rankine cycle with dryer

6.2.6.8 Actual Rankine cycle

The real Rankine cycle is not reversible because of various losses that occur in nature and that must be accounted for. Figure 53 shows the real Rankine cycle and the impact of various losses [TOD2011]. The left figure shows the pump losses, the middle figure shows the losses in the steam lines to the turbine, and the right figure shows the losses in the turbine. Some of these losses are listed below:

- Irreversible frictional losses at various places in the turbo machinery;
- Irreversible heat losses from various piping, vessels, etc.;
- Pump losses, in particular:
  - Heat loss to the surroundings;
  - Fluid friction with the pump blades;
  - Mechanical losses due to friction (bearings, gears, etc.);
- Turbine losses, in particular:
  - Pressure drop between the superheater and turbine, which reduces entrance pressure from P_1 to P_2;
  - Heat loss to the surroundings, which reduces the temperature change from point b to point c;
  - Steam expansion inside the turbine, which is irreversibly adiabatic (non-isentropic) and hence reduces efficiency and increases steam quality;
  - Mechanical friction; and
  - Steam bypass outside the turbine blade passages.

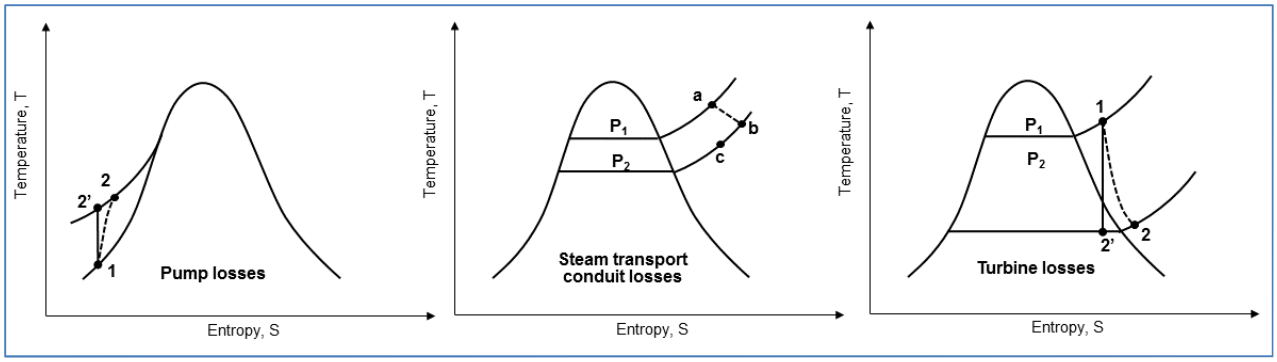

Figure 53 Real Rankine cycle with losses

6.2.6.9 Sample PWR and CANDU 6 cycle diagrams

Figure 54 shows a typical secondary side of an advanced PWR reactor [APR2011]. It is clear that multiple feedwater heaters, one moisture separator, and double reheaters have been designed into the system. The secondary system operates with two feedwater pumps at two different pressures.

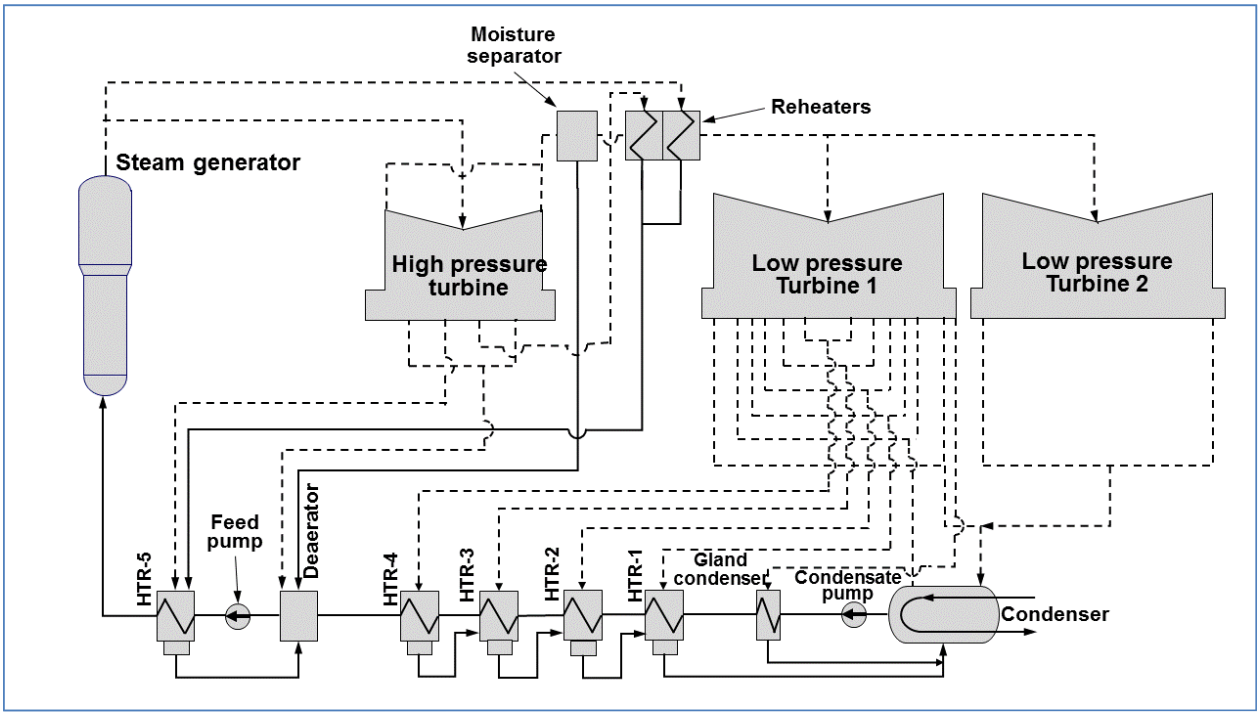

Figure 54 Typical advanced PWR secondary cooling system

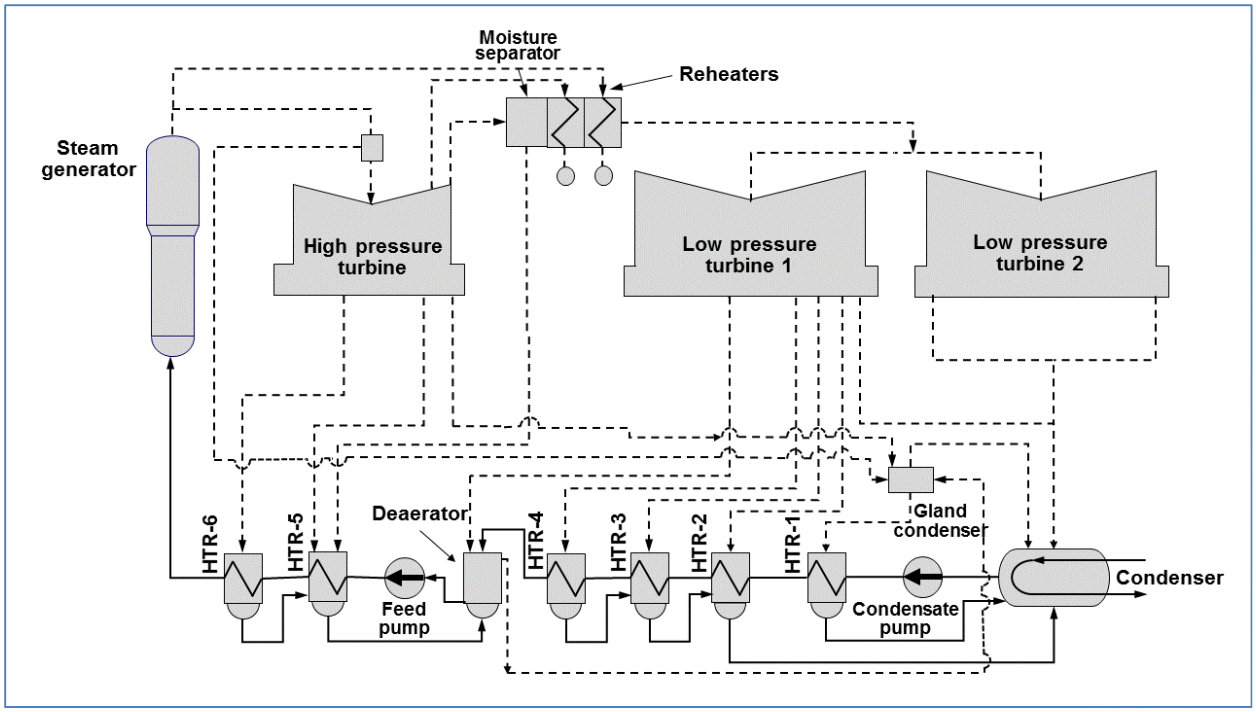

Figure 55 Typical CANDU 6 secondary cooling system

Figure 55 shows a typical CANDU 6 Rankine cycle [AECL2010]. This plant has one double-sided high-pressure turbine and two double-sided low-pressure turbines. On the low-pressure turbine, there is one open feedwater heater and three consecutive closed feedwater heaters. On the high-pressure turbine, there are two closed feedwater heaters. Between the high-pressure and low-pressure turbines, several stages of moisture separators deliver heating to the feedwater heaters. The thermal efficiency of such an arrangement is around 35%.

6.2.7 Entropy and the laws of thermodynamics

Entropy is a state parameter and can be expressed in terms of other parameters. For sub-cooled or superheated conditions, *s=f(P,T)*, and for saturated conditions, *s=f(P)* or *s=f(T)*, it is expressed in terms of pressure or temperature. In the two-phase region, the following equation can be used to calculate mixture entropy (under homogeneous conditions):

$$s_m = x \cdot s_g + (1-x) \cdot s_f = s_f + x \cdot s_{fg}\,, \tag{95}$$

where s_g is the entropy of the saturated gas, s_f is the entropy of the saturated liquid, and s_{fg} is the entropy change during vaporization.

Entropy is a quantitative measure of the microscopic (molecular) disorder of a system. Entropy generated through any process in an isolated system cannot be negative. Moreover, entropy is a non-conserved property (it always increases in isolated systems). In engineering processes, entropy increase is a measure of irreversibility in these processes (a measure of engineering system inefficiency or of system losses).

Entropy change is closely associated with heat transfer. In heat transfer from a hotter to a

colder subsystem, the hotter subsystem exhibits a decrease in entropy, whereas the cold system shows an increase. However, the increase in the cold subsystem is greater, thus making the entropy change of the combined system positive.

Probably the most important outcome of the entropy changes in certain processes is the fact that every process ends up with a certain penalty for moving energy in any direction. In other words, any energy exchange between different systems results in an entropy increase, i.e., there is always a certain cost when moving energy from one place to another, or transferring energy from one form to another. Any conversion of energy in a system from one form to another or any exchange of work with its surroundings must be accompanied by some irreversible dissipation of energy to the surroundings.

Entropy can be seen as the ability to expend energy to carry out a task. For example, a fully charged battery has low entropy, which increases as the battery is used; or a clockwork toy has low entropy when wound up, which increases as it unwinds.

Processes in nature change in the direction of reaching equilibrium. Entropy reaches a maximum value when equilibrium is reached. Entropy is statistical in nature because it explains how phenomena in the micro world affect phenomena in the macro world, capturing the probability of a number of micro events to cause a macro effect.

In modern thermodynamics, the laws of thermodynamics are known as:

- First law – characterizes the energy balance;
- Second law – characterizes cycle/system efficiency;
- Third law – characterizes entropy at near-zero temperatures; and
- Zeroth law – characterizes thermodynamic equilibrium.

The zeroth law of thermodynamics states that if two bodies are in thermodynamic equilibrium (at the same temperature) with a third body, then they are in thermodynamic equilibrium with each other. This is a fundamental law that defines the relationship between different systems (bodies) operating and interacting with each other. This law should have been labelled as the first law, but because it was defined later, it was called the zeroth low to avoid confusion.

The first law of thermodynamics states that the change of internal energy in a system is equal to the amount of heat supplied, minus the amount of work performed by the system on its surroundings. In other words, it states that energy can be converted from one form to another, but cannot be created or destroyed, i.e., everything requires energy to do anything. Different forms of energy must be fed into a system before it can perform any useful work or create any impact on its surroundings.

The second law of thermodynamics states that the entropy of an isolated system never decreases because isolated systems spontaneously evolve toward thermodynamic equilibrium, i.e., the state of maximum entropy. Moreover, it states that a certain cost must always be paid when moving energy from one place to another or transferring energy from one form to another. When it appears that a system's entropy decreases, this generally means that the system is not isolated from its surroundings and that by scaling up to a larger system, it will be

found that the system is a part of a larger system with lower entropy.

The third law of thermodynamics states that the entropy of a perfect crystal drops to zero when the temperature of the crystal is at absolute zero. However, according to quantum theory, because nothing can be considered to be truly at rest, every molecule, atom, or subatomic particle will always have a minimum amount of energy even when cooled to absolute zero (the zero point energy). Hence, one may take the third law as stating the minimum entropy level at a temperature of absolute zero.

6.2.8 Problems

1. Calculate the Rankine cycle thermal efficiency which operates at saturated steam at pressure of 7 MPa, and temperature in the condenser is 30^{o}C. Calculate the steam quality at the exit of an ideal turbine following an adiabatic expansion to condenser pressure for the above conditions, and for the conditions if the turbine has 85% efficiency. Compare the results with the Carnot cycle.
2. A steam generator in a PWR nuclear power plant produces 3200 t/h saturated steam at pressure of 5 MPa. The temperature in the condenser is 35^{o}C. Calculate the ideal turbine power assuming that it operates in Rankine cycle, and the steam quality at the turbine exit.
3. In a Rankine cycle the working fluid enters the turbine at *4.5 MPa* with condenser temperature of *35°C*. Calculate the thermal efficiency of this cycle assuming that:

a. no preheaters are used;
b. one preheater is used to preheat the feed water to *60°C* below the saturation temperature; and
c. the feed water is preheated in 3 preheaters to the same temperature as above.

Given:

a. Turbine inlet pressure, P_i=4.5 MPa
b. Condenser temperature Tc=35 ºC or 308 ºK
c. Feedwater heater outlet temperature, $T_F=T_{sat}$-60 ºC

Assumptions

a. The Rankine cycle described in the problem statement is for a CANDU 6 reactor
b. Steam entering the turbine is saturated
c. Losses in the turbine and pumping losses are the same in all cases, since it is the difference in efficiency that is important here assume these losses are negligible.

4. Consider an emergency water tank that is supposed to deliver water to a reactor following a loss of coolant event. The tank is pressurized by the presence of nitrogen at 1.0 MPa. The water is discharged through a 0.2 m ID pipe. The reservoir has a diameter of 5 m, and the water level is 15 m above the reactor. Calculate the maximum flow rate delivered to the reactor if the water is inviscid and reactor pressure is (a) 0.8 MPa, and (b) 0.2 MPa.
5. Two alternative steam cycles are proposed for a nuclear power plant, as variation of the Rankine ideal cycle, all three operating between the steam temperature of 293^{o}C and condensing temperature of 33^{o}C. The first one operates with condensate in saturated conditions, while the feedwater downstream of the condensate pumps is subcooled.

The steam is saturated at the inlet of the expander. (a) Assuming ideal machinery, calculate the cycle thermal efficiency and steam rate for each cycle.

6. Water at 100 kPa and 20 °C flows through a smooth, circular pipe of 2 cm ID, and length of 3 m. If the flow velocity is 3 m/s, calculate the pressure drop along the pipe and the pumping power necessary to maintain the flow in the pipe.
7. Explain the 1^{st} and 2^{nd} law of thermodynamics and the relationship between these laws. Provide examples of their application in reactor thermal-hydraulics design. Explain the role of entropy in reactor thermal-hydraulics.
8. Develop an expression for thermal efficiency for a secondary heat transport system shown in Figure 55 (CANDU-typical). Show the thermal efficiency in a generic expression by using generic values of key parameters and by making appropriate assumptions.

7 Heat Transfer and Fluid Flow Design

7.1 Heat transfer in the primary heat transfer system

The heat balance in the primary heat transport system is covered in this section, including heat balance in the reactor core and heat balance in a steam generator. An interpretation of the relationship between the primary and secondary loop parameters is provided, and the role of the steam generator as a connection between the primary and secondary loops is explained. Approximations in the steam generator heat transfer model are used to derive trends for various parameters that affect the steam generator design. Analytical and numerical models are developed and used to calculate the distribution of key parameters along the primary and secondary sides of the generator, and the steam generator heat duty diagram is developed and explained.

Figure 56 shows a simplified diagram of the reactor primary heat transport system. The reactor is the heat source, because it is in the reactor that heat is generated. The steam generator is the heat sink, which takes the heat out of the primary heat transport system and transfers it to the secondary heat transport system. The primary pump serves as the driver of the flow in the primary heat transport system by removing heat from the heat source (the reactor) and dumping it into the heat sink (the steam generator).

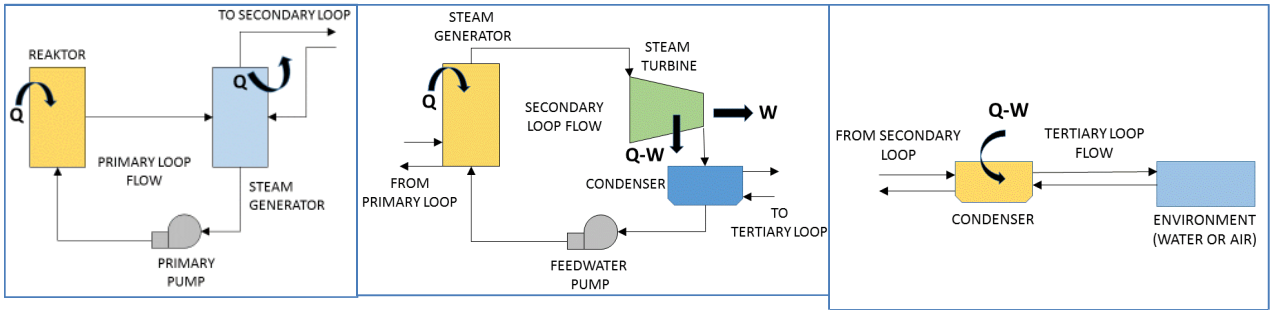

a) Primary b) Secondary c) Tertiary

Figure 56 Reactor cooling systems

The heat balance in the reactor can be described by a simple algebraic equation, Eq. (96), from which the reactor heat production can be expressed by Eq. (97):

$$W_p h_{p,hot} = W_p h_{p,cold} + Q, \tag{96}$$

$$Q = W_p \left(h_{p,hot} - h_{p,cold} \right), \tag{97}$$

where: W_p = primary coolant mass flow rate (kg/s)
$h_{p,hot}$ = core exit enthalpy (hot leg), (kJ/kg)
$h_{p,cold}$ = core inlet enthalpy (cold leg) (kJ/kg)
Q = reactor power transferred to the coolant (kJ/s or kW).

7.2 Primary pumps

The primary pumps are the vital component in the reactor heat transport system (HTS). The primary function of the reactor HTS is to provide continuous heat removal from the reactor core in normal operation, during transients, and during reactor shutdown, and the primary pumps are the essential components that support this function. HTS pump start-up and shut-down are routine operations of the reactor HTS. Pump failures due to loss of power or inadvertent operator action are relatively common events in all nuclear power plants and are considered in the safety case for each reactor type.

The primary side flow is determined by a balance between the head generated by the primary heat transport system pumps (HTS pumps) and the circuit pressure losses due to friction, losses, and other effects.

Figure 57 shows the pressure drop in the loop as a function of mass flow rate in the loop. The pump operating point is indicated at the intersection between the pump head curve and the system flow resistance curve. The system pressure drop curve follows a quadratic law because it depends on the square of the flow velocity, i.e., the square of the mass flow rate (or mass flux), as in Eq. (43). The pump head curve may have various shapes depending on the pump type and design. For "short periods" of time, in transition to the stable operating point, the pump and the system can temporarily operate outside the stable operating point. In this respect, a "short period" of time should be considered in relation to the pump and system hydraulic inertia.

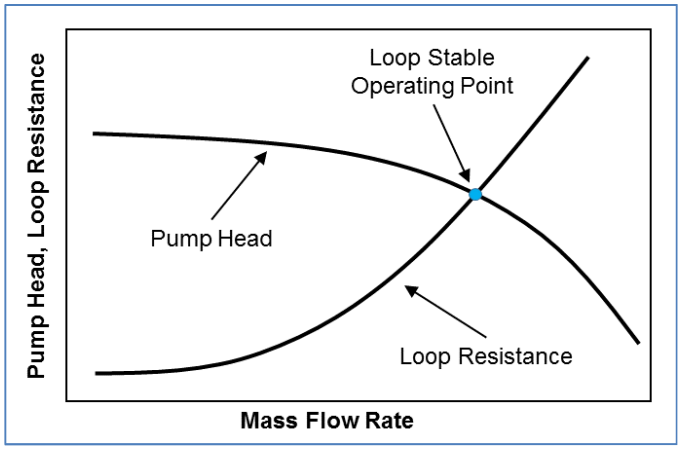

Figure 57 Primary pump flow diagram

Accurate prediction of pump performance includes specification of its head (H), torque (τ), discharge or volumetric flow rate (Q), and rotor speed (ω). The pump motor, by exerting a torque on the rotating shaft, provides energy to the impeller, which creates the flow associated with a head increase from the pump suction to the pump discharge side.

The pump motor provides torque for:

- overcoming frictional resistance and any local losses in the loop (piping, valves, core, etc.);

- overcoming frictional losses in the pump rotating parts;
- acceleration of fluid in the loop; and
- acceleration of pump rotating parts (including the flywheels).

For a pump, only two parameters can be considered independent among *H*, *Q*, *τ*, and *ω*. The other two are determined from the pump characteristics. It is commonly assumed that the pump steady-state characteristics also hold for transient conditions. The pump characteristics are described by specific relationships, called homologous relationships) [TOD1990]:

$$\frac{H_1}{\omega_1^2}=\frac{H_2}{\omega_2^2}, \qquad \frac{Q_1}{\omega_1}=\frac{Q_2}{\omega_2}, \qquad \frac{H_1}{Q_1^2}=\frac{H_2}{Q_2^2}. \tag{98}$$

Pump manufacturers produce realistic relationships from pump tests, for example, relating the head to both volumetric flow and pump angular velocity, as given by Eq. (99):

$$\frac{H_1}{\omega^2}=a_1+a_2\left(\frac{Q}{\omega}\right)+a_3\left(\frac{Q}{\omega}\right)^2. \tag{99}$$

The common approach is to use non-dimensional parameters with respect to the rated pump performance conditions (rated conditions refer to the rated quantities, which represent the point of pump best performance as defined by the manufacturer), as given by Eq. (100):

$$\nu=\frac{Q}{Q_R}, \qquad h=\frac{H}{H_R}, \qquad \alpha=\frac{\omega}{\omega_R}, \qquad \beta=\frac{\tau}{\tau_R}. \tag{100}$$

These non-dimensional parameters are used to express homologous pump relationships in a form similar to Eq. (98), in which the actual parameters are expressed in their non-dimensional forms. Homologous relationships of these forms are used in computer programs describing pump behaviour.

Figure 58 shows the four possible types, i.e., quadrants, of pump operation. Computer models must be able to simulate pump performance in any of the four quadrants, and therefore pump manufacturers must provide information about pump operation in all quadrants [TOD1990]. During a coast-down transient, the pump may pass from the normal pumping region, quadrant I, through the reverse flow but positive rotation region, quadrant II, to reverse flow and rotation, quadrant III, unless the rotor is equipped with an anti-reverse ratchet to avoid this quadrant (such as in most reactor HTS pumps).

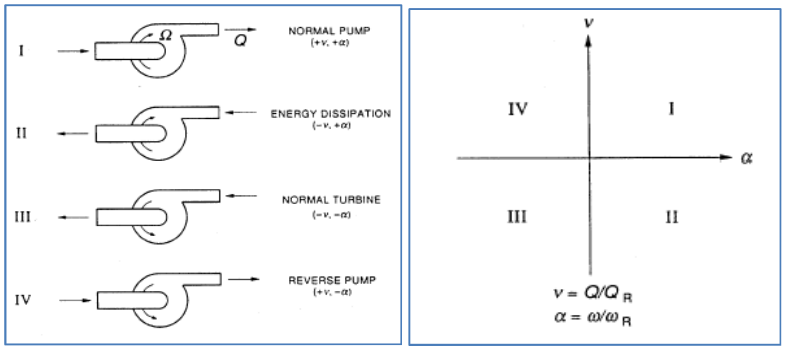

Figure 58 Primary pump operating quadrants

In postulated events with breaks at the pump suction or discharge side and different pump operation control logic, a pump can operate in any of the first three quadrants. Therefore, pump tests are performed to develop pump homologous relationships for all four possible operating quadrants.

Pump characteristics under transient flow conditions have been investigated and tested. One of the most important conditions that must be avoided in operation of reactor HTS pumps is two-phase flow in the bubbly flow regime. Pump characteristics deteriorate significantly following initiation of bubble formation in the pump suction. Moreover, prolonged operation in two-phase flow (the bubbly flow regime) can damage the pump impeller blades.

One of the most important objectives of HTS flow design is to make sure that the pump suction pressure does not fall below the net positive suction head required (NPSHR) [POP2014]. For a pump to deliver its rated output, the absolute pressure (including the velocity head $V^2/2g$) of the fluid at the pump inlet must exceed the vapour pressure by an amount sufficient to overcome any entrance or frictional losses between the point of entry into the pump and the impeller. The NPSH is defined as the absolute pressure at the pump inlet expressed in metres of liquid, plus the velocity head, minus the vapour pressure of the fluid at pumping temperature, and corrected to the elevation of the pump centreline in the case of horizontal pumps, or to the entrance of the first-stage impeller for vertical pumps.

NPSHR (required) is determined by the pump manufacturer and is defined as a function of pump speed and pump capacity. NPSHA (available) represents the energy level of the fluid over the vapour pressure at the pump inlet and is determined entirely by the system preceding the pump. Unless $NPSHA \geq NPSHR$ under any operating condition, some of the fluid will vaporize in the pump inlet, and vapour bubbles will be carried onto the impeller. These bubbles will collapse violently at some point downstream of the pump inlet (usually at some point on the pump impeller blade surface) as the pressure is increased in the pump, producing very sharp, crackling noises accompanied by physical damage to the pump impeller surface. This phenomenon is known as *cavitation* and is highly undesirable (in fact, it represents a micro water hammer effect on the impeller surface). The net mechanical effect of cavitation is pump vibration and impeller damage, whereas the net effect on pump performance is loss of pump efficiency and pump head.

The primary side flow is determined by a balance between the head generated by the primary

pumps and the circuit head losses due to friction:

$$\Delta P_{pump} = \Delta P_{circuit} \,. \tag{101}$$

Normally, the pump head curve is provided in the form of a polynomial such as Eq. (102):

$$\Delta P_{pump} = A_0 + A_1 \cdot W + A_2 \cdot W^2 + ... \tag{102}$$

The hydraulic network losses are proportional to the square of the velocity, i.e., the mass flow rate, along with a loss coefficient, as shown by Eq. (103):

$$\Delta P_{circuit} = K \cdot W^2 . \tag{103}$$

Figure 59 and Figure **60** show the pump curves of two pumps in the CANDU HTS; the first is the primary HTS pump, and the second is the shutdown cooling pump.

These pumps have very different functions. The HTS primary pump operates almost continuously during the operating lifetime of the plant, and therefore the requirements on this pump are very demanding. The shutdown pump operates normally when the reactor is shut down to help remove decay heat from the reactor core. Both diagrams show pump volumetric flow rate on the *x*-axis, pump head on the left *y*-axis, and pump efficiency, pump power, and NPSHR on the right *y*-axis.

Figure 59 and Figure 60 show that pump head declines with increasing volumetric flow, whereas pump power increases [POP2014]. This means that because of momentum balance considerations, if a pump is required to produce higher volumetric flow, its head will be lower. Note that for a pump delivering higher volumetric flow, the pump power must increase. Dotted lines in Figure 59, labelled S1, S2, and S3, show three possible system configurations that impose different flow resistance.

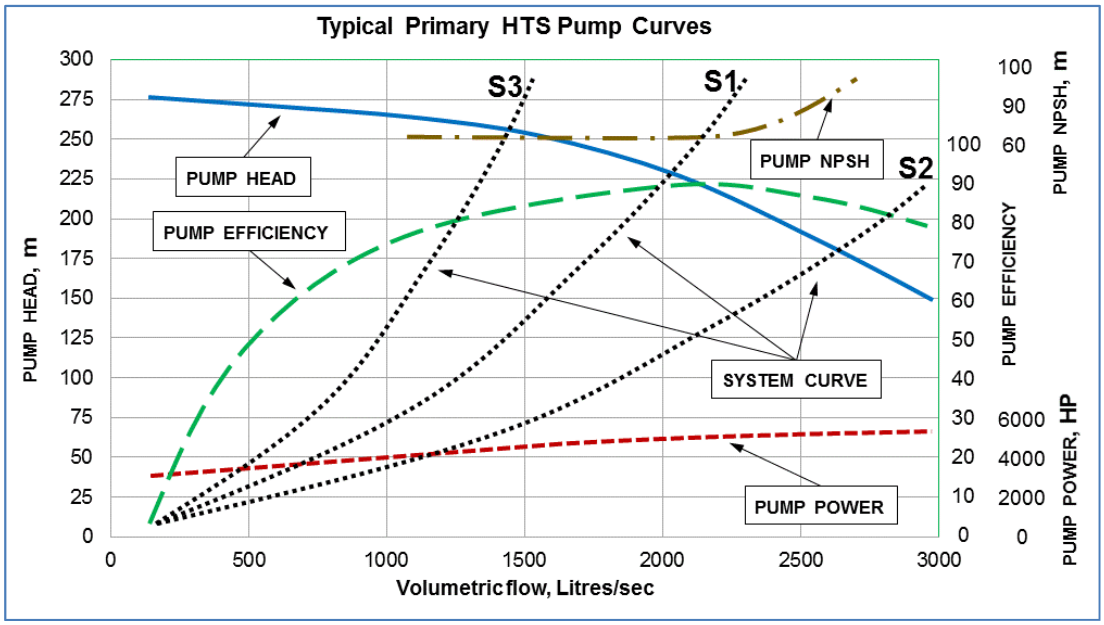

Figure 59 Typical primary pump characteristics

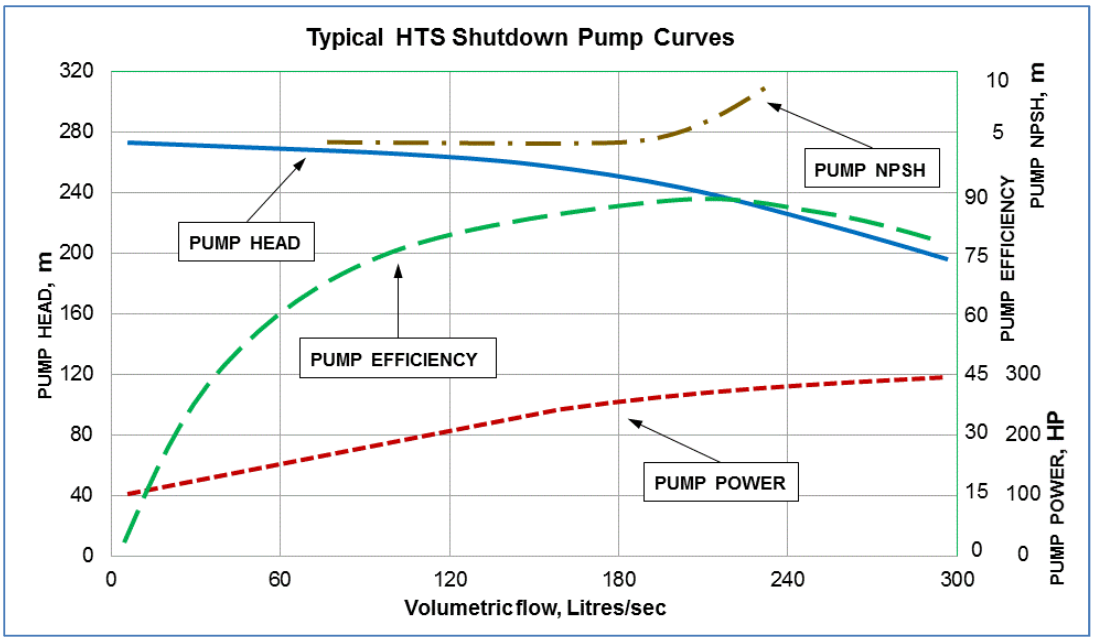

Figure 60 Typical shutdown pump characteristics

The efficiency curve is usually bell-shaped, and it shows that the highest efficiency is achieved in a relatively narrow range of volumetric flow rate. Pump efficiency is very important for the HTS pump because it operates continually over 60 years of plant life, and therefore a small loss of efficiency can result in a relatively large loss of plant earned value. Efficiency drops very sharply if the pump volumetric flow rate moves outside a narrow range.

The NPSHR curve is relatively flat over a wide range of volumetric flow rates. In fact, well-designed pumps should have NPSHR curves as flat as can possibly be obtained. However, when the volumetric flow rate exceeds a certain value, the NPSHR curve starts to increase fast, creating an area of pump cavitation risk.

7.3 Steam generator heat balance

The steam generator has a very important role in energy transport from the reactor core to the turbine and the electrical generator because it connects the primary and secondary loops. Hence, understanding steam generator behaviour is important in understanding plant behaviour.

A simplified steam generator heat balance is shown in Figure 61. The feedwater flow W_{FW} enters the steam generator with enthalpy h_{FW} and exits with enthalpy h_{SAT}. The primary mass flow rate in the reactor is W_p.

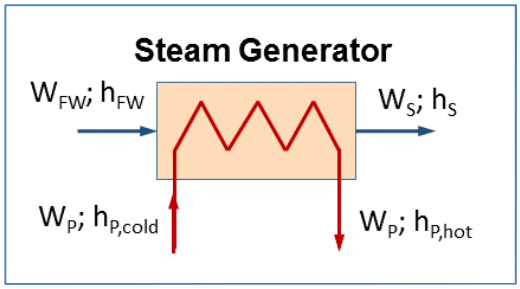

Figure 61 Reactor steam generator loop

The heat transfer from the primary to the secondary steam generator side is expressed by Eq. (104):

$$dQ = U_{SG} \cdot \left(T_p - T_s\right) \cdot dA\,, \tag{104}$$

where U_{SG} is the overall (global) heat transfer coefficient (kJ/m^2-°C),

A is the heat transfer area in the steam generator (m^2),

T_p is the primary-side temperature (°C), and

T_s is the secondary-side temperature (°C).

The total heat transfer in the steam generator can be obtained by integrating the above equation over the length of the steam generator tubes and is given by Eq. (105):

$$Q = \int_Q dQ = \int U_{SG} \cdot (T_p - T_s) \cdot dA\,. \tag{105}$$

Figure 62 shows a general heat-duty diagram for a steam generator with a pre-heater and with saturated primary coolant entering the steam generator U-tubes (i.e., with a certain percentage of quality). The *y*-axis indicates fluid temperatures, and the *x*-axis provides a conceptual representation of space in the steam generator. In this diagram, no heat losses or pressure losses are shown (i.e., an ideal steam generator is assumed).

The primary coolant moves through the U-tubes from right to left in the diagram, starting as saturated with a certain percentage of quality and becoming sub-cooled as it transfers the heat to the secondary side. The secondary coolant (feedwater) enters sub-cooled (zero mass quality, i.e., negative thermodynamic quality) and, as it receives heat from the primary side, heats up to saturation. Thereafter, the secondary coolant boils off as it receives more heat through the steam generator. Note that the point at the primary coolant temperature where the secondary coolant temperature reaches saturation is called the “pinch point” [GAR1999, POP2014].

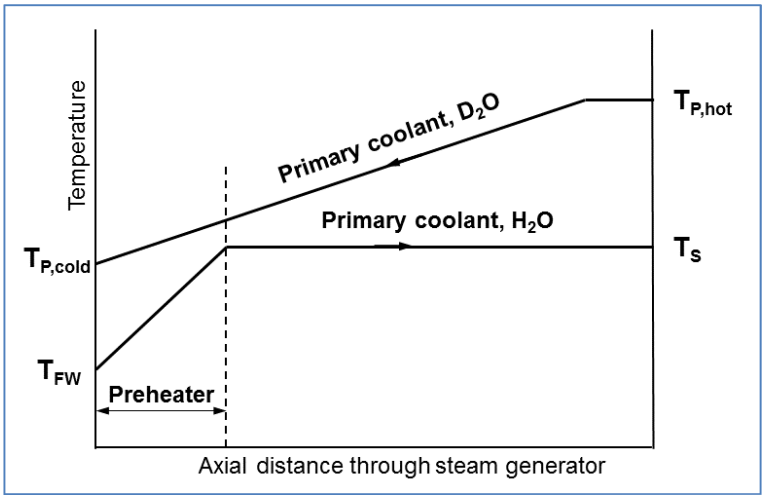

Figure 62 Steam generator simplified heat duty diagram

From the above discussion, it is clear that sufficiently good heat transfer is required to achieve acceptable steam pressure. The steam generator calculation of U-tube length, diameter, and number (i.e., the area used in heat transfer) is carefully performed so that heat transfer from the primary to the secondary side is achieved efficiently with as little heat loss as possible, and so that the economic constraints of manufacturing the steam generator and the system can be satisfied.

7.3.1 Steam generator without a pre-heater region

To achieve a better understanding of the behaviour and design of the steam generator and the impact of its various parameters, it is useful to analyze first a simplified version of the steam generator with no pre-heater, with saturated feedwater entering the steam generator, and with sub-cooled primary coolant entering the steam generator. This simplified steam generator is shown in Figure 63 [GAR1999].

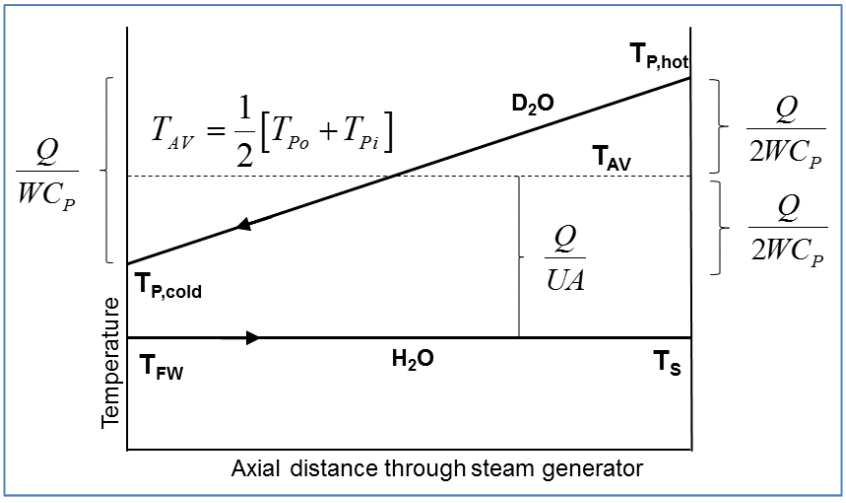

Figure 63 Steam generator heat duty diagram without pre-heating

The primary-side heat balance in the steam generator can be obtained by integrating Eq. (105).

Assuming that the global heat transfer coefficient U_{SG} is constant along the steam generator, the primary coolant temperature variation is linear along the U-tube, and by separating primary and secondary side terms, one obtains Eq.(106):

$$Q = U_{SG} A_{SG} \frac{(T_{p,hot} + T_{p,cold})}{2} - U_{SG} A_{SG} T_s \,. \tag{106}$$

Equation (106) can be further simplified into Eq. (107):

$$Q = U_{SG} A_{SG} \left[\frac{T_{p,hot} + T_{p,cold}}{2} - T_s \right]. \tag{107}$$

The temperatures can be replaced by enthalpies using Eq. (108):

$$h \approx C_p \cdot T + constant \,. \tag{108}$$

Using Eqs. (108) and (107), the heat transferred in the steam generator can be given by Eq. (109):

$$Q = \frac{U_{SG} A_{SG}}{C_p} \left[\frac{h_{p,hot} + h_{p,cold}}{2} - h_s \right]. \tag{109}$$

Using Eq. (96) we find:

$$Q = \frac{U_{SG} A_{SG}}{C_p} \left[\frac{h_{p,hot} + h_{p,cold}}{2} - h_s \right] = W_p \cdot (h_{p,hot} - h_{p,cold}) \,. \tag{110}$$

The secondary side steam flow can be calculated by an energy balance on the secondary side of the steam generator, as given by Eq. (110); using this equation, one can calculate the mass flow rate at the secondary side, as given by Eq. (111):

$$Q = W_s \left(h_s - h_{FW} \right), \tag{111}$$

$$W_s = \frac{Q}{\left(h_s - h_{FW} \right)} \,. \tag{112}$$

7.3.2 Approximate solution to steam generator without a pre-heater region

Combining Eqs. (97), (101), (110), and (112) yields the set of four equations describing the heat transfer in the primary and secondary loops, as shown by Eq. (113) [GAR1999, POP2014]:

$$\begin{aligned} Q &= W_p \left(h_{p,hot} - h_{p,cold} \right) \\ Q &= \frac{U_{SG} A_{SG}}{C_p} \left[\frac{h_{p,hot} + h_{p,cold}}{2} - h_s \right] = U_{SG} A_{SG} \left[\frac{T_{p,hot} - T_{p,cold}}{2} - T_s \right]. \\ \Delta P_{pump} &= \Delta P_{circuit} \\ Q &= W_s \left(h_s - h_{FW} \right) \end{aligned} \tag{113}$$

From the first equation in Eq. (113), one can obtain the reactor outlet (hot) enthalpy:

$$h_{p,hot} = \frac{Q}{W_p} + h_{p,cold} \,. \tag{114}$$

The second equation in Eq. (113) can be transformed into the following equation by dividing it by the primary mass flow rate and using Eq. (114), while also neglecting heat losses between the reactor and the steam generator:

$$\frac{Q}{W_p} = \frac{U_{SG} A_{SG}}{C_p W_p}\left[\frac{Q}{2W_p} + h_{p,cold} - h_s\right] = \frac{U_{SG} A_{SG}}{W_p}\left[\frac{Q}{2C_p W_p} + T_{p,cold} - T_s\right]. \tag{115}$$

Rearranging Eq. (115) in terms of outlet enthalpy at the steam generator and outlet temperature, one can obtain Eq. (116) and Eq. (117):

$$h_{p,cold} = \frac{Q}{W_p}\left[\frac{C_p W_p}{U_{SG} A_{SG}} - \frac{1}{2}\right] + h_s = \frac{QC_p}{U_{SG} A_{SG}} - \frac{Q}{2W_p} + h_s \,, \tag{116}$$

$$T_{p,cold} = \frac{Q}{W_p}\left[\frac{W_p}{U_{SG} A_{SG}} - \frac{1}{2C_p}\right] + T_s \,. \tag{117}$$

From Eqs. (116) and (117), all the parameters Q, W_p, C_p, A_{SG}, U_{SG}, etc., are positive quantities. Therefore, the reactor inlet enthalpy (and temperature) will rise as the primary flow rate increases, will rise as the secondary-side temperature (saturation temperature) and enthalpy increase, and may go up or down as power changes.

Substituting Eq. (116) into Eq. (117),

$$Q = \frac{U_{SG} A_{SG}}{C_p}\left[\frac{h_{p,hot} + h_{p,cold}}{2} - h_s\right] = U_{SG} A_{SG}\left[\frac{T_{p,hot} - T_{p,cold}}{2} - T_s\right]. \tag{118}$$

The enthalpy (and temperature) at the steam generator primary side inlet can be obtained as follows:

$$h_{p,hot} = \frac{Q}{W_p}\left[\frac{C_p W_p}{U_{SG} A_{SG}} + \frac{1}{2}\right] + h_s = \frac{QC_p}{U_{SG} A_{SG}} + \frac{Q}{2W_p} + h_s \,, \tag{119}$$

$$T_{p,hot} = \frac{Q}{W_p}\left[\frac{W_p}{U_{SG} A_{SG}} + \frac{1}{2C_p}\right] + T_s \,. \tag{120}$$

Using Eqs. (116), (117), (119), and (120), one can obtain the following useful relationships [GAR1999, POP2014]:

$$h_{p,aver} = \frac{h_{p,hot} + h_{p,cold}}{2} = \frac{Q}{W_p}\left(\frac{C_p W_p}{U_{SG} A_{SG}}\right) + h_s = \left(\frac{QC_p}{U_{SG} A_{SG}}\right) + h_s \,, \tag{121}$$

$$T_{p,hot} - T_{p,aver} = \frac{Q}{W_p}\left(\frac{W_p}{U_{SG} A_{SG}} + \frac{1}{2C_p}\right) + T_s - \frac{Q}{W_p}\frac{W_p}{U_{SG} A_{SG}} - T_s = \frac{Q}{2W_p C_p} \,, \tag{122}$$

$$T_{p,aver}=\frac{T_{p,hot}+T_{p,cold}}{2} \qquad T_{p,aver}-T_{p,cold}=\frac{Q}{2C_pW_p} \qquad T_{p,aver}-T_s=\frac{Q}{U_{SG}A_{SG}}, \tag{123}$$

$$T_{p,hot}-T_{p,cold}=\frac{Q}{W_pC_p} \qquad T_{p,hot}-T_s=\frac{Q}{U_{SG}A_{SG}}+\frac{Q}{2W_pC_p} \qquad T_{p,cold}-T_s=\frac{Q}{U_{SG}A_{SG}}-\frac{Q}{2W_pC_p}. \tag{124}$$

7.3.3 Calculation of main HTS parameters

From an HTS designer perspective, the key question is how to design the primary heat transport system. As long as the primary flow rate, or the reactor inlet and outlet enthalpies, have not yet been defined, it is necessary to make an assumption about one of these to be able to calculate the other parameters when the desired reactor power is given.

Given a rough estimate of flow for calculating U_{SG} (which is not a strong function of flow because W_p is large and flow is turbulent), T_{aver} can be calculated, as well as an estimate of the spread of $T_{p,aver}$ $(\pm Q/2W_pC_p)$. This gives a good first estimate of temperatures and enthalpies. With the above enthalpy, temperature, and density estimates, the circuit losses can be calculated and compared with available pump head and flow. The flow estimate can be updated and the whole procedure repeated until convergence is reached.

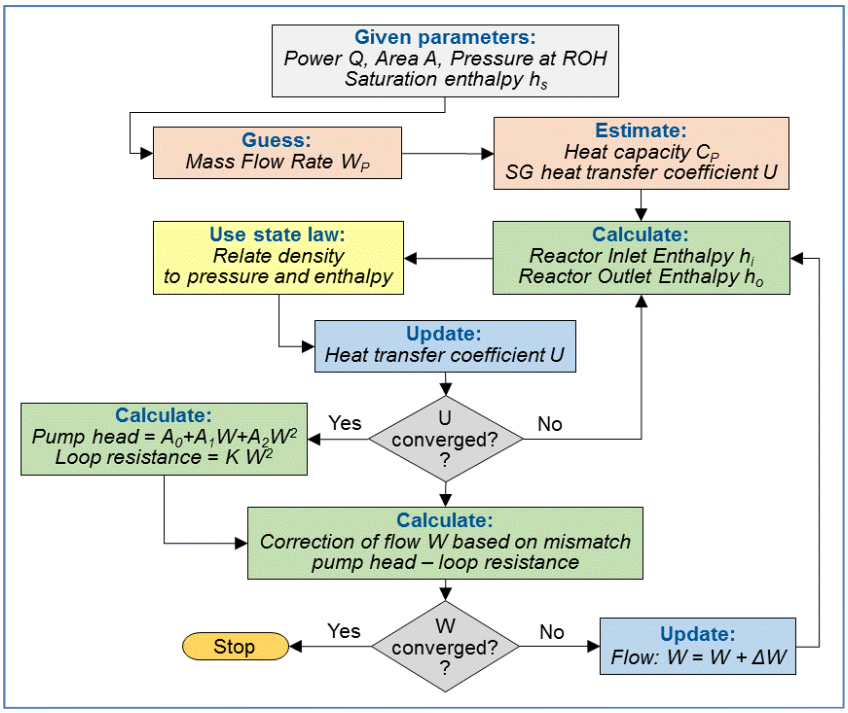

Figure 64 Process for calculating primary loop parameters

Figure 64 illustrates the process used to calculate the primary heat transport system parameters [GAR1999, POP2014]. Note that first the reactor power, the steam generator, and the outlet header pressure and saturation enthalpy are defined. Then the primary flow rate is assumed. This makes it possible to define the steam generator global heat transfer coefficient and the primary fluid heat capacity. Then using Eqs. (116) and (119), the reactor inlet and

outlet enthalpies can be calculated. Once these are defined, the next step is to define other primary fluid state parameters from the state laws, such as the fluid density for the inlet and outlet reactor enthalpy. After these parameters are defined, it is necessary to check whether the assumed U_{SG} has converged. If not, U_{SG} is updated, and another round of these calculations is performed.

After convergence on U_{SG} is reached, the pump head and primary loop resistance can be calculated because the primary flow rate has been defined. The last step is to check whether the pump head and the loop resistance match. If not, then the whole process shown in Figure 64 must be repeated.

Problem 7.3.3.1

To illustrate that this process leads to convergence, a sample calculation will be performed using typical CANDU 6 parameters as given by Eq. (125) [GAR1999, POP2014].

$$\begin{aligned}
&Q \approx 2000\left[MW_{th}\right] \\
&W \approx 8000\left[kg/s\right] \\
&T_s \approx 265\left[°C\right] \;\Rightarrow\; h_s \approx 1150\left[kJ/kg\right] \\
&C_p \approx 5\left[kJ/kg-°C\right] \\
&U_{SG} \approx 5\left[kJ/s-°C-m^2\right] \;\Rightarrow\; \left(C_p W_p / U_{SG} A_{SG}\right) \approx 0.625 \\
&A_{SG} \approx 3200\left[m^2\right]
\end{aligned} \quad . \tag{125}$$

Equation (116) can be expressed in terms of primary flow rate, as shown by Eq. (123):

$$W_p = \frac{Q}{2\left[\dfrac{C_p Q}{U_{SG} A_{SG}} + h_s - h_{p,cold}\right]} . \tag{126}$$

From the above equation, one can define the infinitesimal change in the primary flow rate with the reactor inlet enthalpy as follows:

$$\frac{\delta W_p}{\delta h_{p,cold}} = \frac{Q}{2\left[\dfrac{C_p Q}{U_{SG} A_{SG}} + h_s - h_{p,cold}\right]^2} = \frac{Q}{2\left[\dfrac{Q}{2W_p}\right]^2} = \frac{2W_p^2}{Q} . \tag{127}$$

Substituting the parameters for CANDU 6 from Eq. (125) into Eq. (127),

$$\frac{\delta W_p}{\delta h_{p,cold}} = \frac{2\left(8000\left[\dfrac{kg}{s}\right]\right)^2}{2\cdot 10^6\left[kW \equiv \dfrac{kJ}{s}\right]} = 64\left[\frac{kg^2}{kJ\cdot s}\right] . \tag{128}$$

If Eq. (128) is expressed in terms of the initial values of primary flow rate and reactor inlet enthalpy, the result gives the change in the primary flow rate as a function of reactor inlet

enthalpy with respect to the initial value (a guessed value):

$$\frac{\delta\left(\frac{W_p}{W_{p,o}}\right)}{\delta\left(\frac{h_{p,cold}}{h_{p,cold,o}}\right)} = \frac{\delta W_p}{\delta h_{p,cold}} \cdot \frac{h_{p,cold,o}}{W_{p,o}} = 64 \cdot \frac{1181 \cdot 25}{8000} \cong 9.0 . \tag{129}$$

Therefore, the change in primary flow rate will be nine times the change in reactor inlet enthalpy:

$$\delta\left(\frac{W_p}{W_{p,o}}\right) = 9.0 \cdot \delta\left(\frac{h_{p,cold}}{h_{p,cold,o}}\right). \tag{130}$$

Hence, if we were to guess the reactor inlet enthalpy, and our guess were only 25% wrong, the primary flow rate would be in error by about 225%. This indicates that the process involving assuming reactor inlet enthalpy first is inherently divergent. However, if we were to guess the primary flow rate, and if we were in error by about 25%, the calculated reactor inlet enthalpy would be in error by only 2.8%. Therefore, this process is inherently convergent. This confirms that the process for primary heat transport system design shown in Figure 64 is appropriate.

End of Problem 7.3.3.1.

7.3.4 Steam generator with pre-heater (simplified analytical solution)

Figure 65 shows a simplified heat-duty diagram for a steam generator with a pre-heater for a fully sub-cooled primary side [GAR1999, POP2014]. This figure shows that the secondary-side temperature changes from T_{FW} to T_s (i.e., from feedwater to saturation temperature). The steam generator design may include a section that is targeted to perform feedwater pre-heating, or it may not have a specific section. Whatever the design, steam generator pre-heating will always be relevant because the feedwater enters the steam generator in a sub-cooled state and needs to be heated up to saturation before the steam generator can boil it and generate steam.

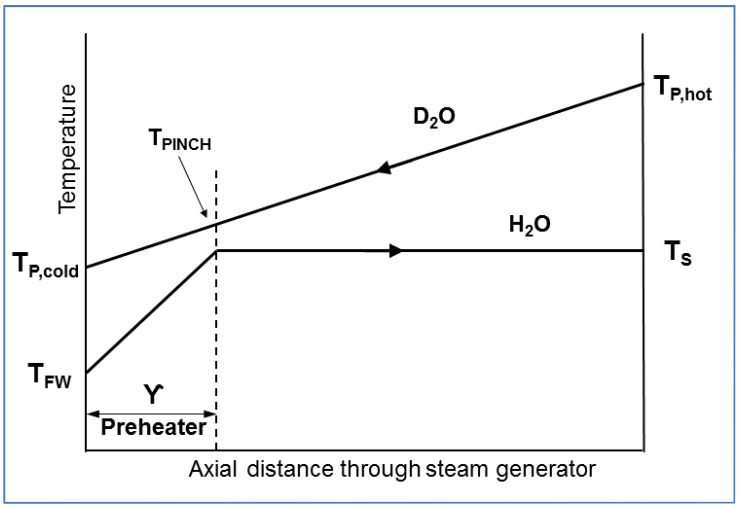

Figure 65 Steam generator heat duty diagram with pre-heating

The reactor heat balance equation is given by:

$$Q = W_p C_p \left(T_{p,hot} - T_{p,cold} \right), \tag{131}$$

where Q is reactor power (or steam generator power), C_p is D_2O heat capacity (assumed constant), $T_{p,hot}$ is ROH temperature, and $T_{p,cold}$ is RIH temperature.

The elementary amount of heat transferred from the primary to the secondary side of the steam generator can be captured using the Fourier law:

$$dQ = U_{SG} \left(T_p - T_s \right) dA_{SG}, \tag{132}$$

where U_{SG} is the overall heat transfer coefficient through the SG piping, dA_{SG} is the incremental heat transfer area from the primary to the secondary side, T_p is the D_2O temperature in the SG tubes, and T_s is the H_2O temperature in the SG shell.

As shown in Figure 65, the secondary side of the steam generator can be split into two parts, the pre-heater part and the boiler part. Therefore, the heat transferred from the primary to the secondary side can also be divided into two parts, as shown in Eq. (133):

$$Q = Q_{PREHEATER} + Q_{BOILER}. \tag{133}$$

The fraction of the steam generator area involved in pre-heating is indicated by γ. The pre-heater part of the steam generator brings the feedwater to saturation. The primary-side temperature at which the secondary side is brought to saturation is denoted as T_{PINCH}.

Using Eq. (113), the total heat exchanged between the primary and secondary sides in the steam generator can be shown by means of the following relation [GAR1999, POP2014]:

$$Q = \gamma U_{SG} A_{SG} \left[\frac{T_{p,cold} + T_{PINCH}}{2} - \frac{T_s + T_{FW}}{2} \right] + \left(1 - \gamma\right) U_{SG} A_{SG} \left[\frac{T_{p,hot} + T_{PINCH}}{2} - T_s \right], \tag{134}$$

where T_s is the saturation temperature at the secondary side and T_{FW} is the feedwater temperature at the inlet of the steam generator secondary side.

The pinch temperature can be expressed in terms of steam generator parameters using Eq. (124):

$$T_{PINCH} = T_{p,cold} + \gamma \left(T_{p,hot} - T_{p,cold} \right) = T_{p,cold} + \gamma \frac{Q}{C_p W_p}. \tag{135}$$

By substituting Eq. (135) into Eq. (134), one can obtain the heat transfer in the steam generator as expressed by the following equation:

$$Q = U_{SG} A_{SG} \left[\left(\frac{T_{p,hot} + T_{p,cold}}{2} \right) - T_s + \frac{\gamma}{2} \left(T_s - T_{FW} \right) \right]. \tag{136}$$

Recall the relationship between the reactor inlet and outlet temperature from Eq. (124):

$$T_{p,hot} = \frac{Q}{W_p C_p} + T_{p,cold} . \tag{137}$$

The reactor inlet and outlet temperatures can be expressed by the following relationship:

$$T_{p,cold} = \frac{Q}{W_p C_p}\left[\frac{W_p C_p}{U_{SG} A_{SG}} - \frac{1}{2}\right] - \frac{\gamma}{2}\left(T_s - T_{FW}\right) + T_s , \tag{138}$$

$$T_{p,hot} = \frac{Q}{W_p C_p}\left[\frac{W_p C_p}{U_{SG} A_{\partial G}} + \frac{1}{2}\right] - \frac{\gamma}{2}\left(T_s - T_{FW}\right) + T_s . \tag{139}$$

By examining Eq. (138), one can evaluate the impact of reactor power on the variation of reactor inlet temperature. The saturation temperature T_s at the secondary side does not depend on reactor power if the pressure on the secondary side is kept constant. The variation in feedwater temperature, T_{FW}, can be assumed to be linearly dependent on reactor power. The primary flow rate W_p, the heat capacity C_P, the area of the steam generator A_{SG}, and the steam generator global heat transfer coefficient U_{SG} exhibit second-order variation with reactor power Q.

To define the dependence of reactor inlet temperature on reactor power, it is necessary to evaluate the impact of the remaining parameter, i.e., the steam generator pre-heater area γ, on reactor power.

The heat addition to the secondary side of the steam generator in the pre-heater area can be calculated as:

$$Q_{PREHEATER} = W_s C_{p,s}\left(T_s - T_{FW}\right). \tag{140}$$

The heat extraction from the primary side of the steam generator can be calculated from Eq. (134) as follows:

$$Q_{PREHEATER} = \gamma U_{SG} A_{SG}\left[\left(\frac{T_{p,cold} + T_{PINCH}}{2}\right) - \left(\frac{T_s - T_{FW}}{2}\right)\right]. \tag{141}$$

Combining Eqs. (140) and (141) leads to the following expression for the steam generator pinch area [GAR1999, POP2014]:

$$\gamma = \frac{W_s C_{p,s}\left(T_s - T_{FW}\right)}{U_{SG} A_{SG}\left[\frac{\left(T_{p,cold} + T_{PINCH}\right)}{2} - \frac{\left(T_s - T_{FW}\right)}{2}\right]} . \tag{142}$$

The most strongly variable parameter in Eq. (142) is the feedwater flow W_{FW}. The heat balance on the secondary side given by Eq. (140) can be rearranged in terms of enthalpies as follows:

$$Q = W_s h_s - W_{FW} h_{FW} . \tag{143}$$

Because $W_s \approx W_{FW}$, it is appropriate to assume that $h_s \approx$ *constant* and $h_{FW} \approx$ *constant*.

Therefore, feedwater flow and steam generator pre-heater area are proportional to reactor power, i.e., $W_{FW} \infty Q$ and $\gamma \infty Q$.

It is normally desirable to describe the pre-heater area in terms of a ratio between the pre-heater area at 100% power and at current power, as follows:

$$\gamma = \frac{\gamma_{100} Q}{Q_{100}}, \tag{144}$$

where γ_{100} is the pre-heating fraction at 100% full power and $Q_{100} = Q$ at 100% full power.

By substituting Eq. (144) into Eqs. (138) and (139), the reactor inlet and outlet temperatures can be obtained as follows:

$$\begin{aligned} T_{p,cold} &= \frac{Q}{W_p C_p}\left[\frac{W_p C_p}{U_{SG} A_{SG}} - \frac{1}{2}\right] - \frac{\gamma_{100} Q}{2 Q_{100}}\left[T_s - T_{FW}\right] + T_s \\ &= \frac{Q}{Q_{100}}\left[\frac{Q_{100}}{W_p C_p}\left(\frac{W_p C_p}{U_{SG} A_{SG}} - \frac{1}{2}\right) - \frac{\gamma_{100}}{2}\left(T_s - T_{FW}\right)\right] + T_s, \end{aligned} \tag{145}$$

$$T_{p,hot} = \frac{Q}{Q_{100}}\left[\frac{Q_{100}}{W_p C_p}\left(\frac{W_p C_p}{U_{SG} A_{SG}} + \frac{1}{2}\right) - \frac{\gamma_{100}}{2}\left(T_s - T_{FW}\right)\right] + T_s . \tag{146}$$

It is clear that the reactor inlet and outlet temperatures are equal to the steam saturation temperature with corrections to capture the primary-side and secondary-side effects. Both these effects are roughly proportional to reactor power. Hence, at 0% full reactor power, $T_{p,cold}=T_s$ and $T_{p,hot}=T_s$.

Problem 7.3.4.1

To illustrate the above analysis and the magnitude of the correction terms, a sample CANDU 6 assessment can be performed with the following given parameters:

- Reactor power $Q_{100} = 2.064\times10^6$ *[kJ/s]*
- Steam generator global heat transfer coefficient: $U_{SG} = 4.5$ *[kJ/sec °C m^2]*
- Steam generator area: $A_{SG} = 3200$ *[m^2]* per steam generator (12,800 [m^2] total for a four-loop reactor)
- Primary flow rate: $W_p = 8250$ *[kg/s]*
- Heat capacity of primary loop: $C_p = 4.25$ *[kJ/kg °C]*
- Steam generator pre-heating portion: $\gamma_{100} = 0.15$ at 100% full power
- Feedwater temperature: T_{FW} = 177 [°C] at 100% full power
- Secondary-side temperature (at saturation): $T_S = 260$ *[°C]*

Using the above parameters, the reactor inlet temperature can be calculated using Eq. (145):

$$T_{p,cold} = \frac{Q}{Q_{100}}\left[58.86\left(0.60 - 0.50\right) - 6.22\right] + 260 = \frac{Q}{Q_{100}}\left[6.32 - 6.22\right] + 260 . \tag{147}$$

Hence, even at 100% full power, the net correction to the reactor inlet temperature $T_{p,cold}$ is less than 0.1°C. Even allowing for large variations in U_{SG} and other parameters, the effect on $T_{p,cold}$ is expected to be small over the full power range. This has been confirmed by detailed calculations. The reactor outlet temperature can be calculated using Eq. (146):

$$T_{p,hot} = \frac{Q}{Q_{100}}\left[64.75 - 6.22\right] + 260 = \frac{Q}{Q_{100}}\left(58.53\right) + 260 . \tag{148}$$

At 100% full power, the reactor outlet temperature T_o is 318.5 [°C], which is greater than the saturation temperature of 310 [°C] at 10 [MPa]. Hence, the assumption of no boiling at the reactor outlet header is not correct. Therefore, the calculation must be repeated with an estimate of the amount of boiling using the following expression:

$$Q = Q_{subcool} + Q_{boil} = W_p C_p \left[\left(T_{p,sat} - T_{p,cold} \right) + \frac{x h_{fg}}{C_p} \right] = W_p C_p \left(T_{p,sat} - T_{p,cold} \right) + W_p x h_{fg} . \tag{149}$$

The power level at which boiling starts is given by Eq. (146), into which the CANDU 6 parameters from Eq. (148) are introduced to obtain the following expression:

$$\frac{T_{p,hot} - 260}{58.53} = \frac{310 - 260}{53.53} = \frac{Q}{Q_{100}} = \frac{50}{53.53} = 0.854 . \tag{150}$$

This means that boiling starts in a CANDU 6 core when the reactor power is at 85.4% of full power. In other words, it means that out of 100% reactor power, 85.4% is used to heat the primary fluid to saturation and 14.6% is used to boil some of the primary fluid.

If this information is used in Eq. (149), the following expression can be obtained for the reactor power split in the primary heat transport system:

$$\frac{Q}{Q_{100}} = \frac{Q_{subcool}}{Q_{100}} + \frac{Q_{boil}}{Q_{100}} = \frac{W_p C_p}{Q_{100}}\left[T_{p,sat} - T_{p,cold} \right] + \frac{W_p x h_{fg}}{Q_{100}} = 0.854 + 0.146 . \tag{151}$$

Hence, using just the boiling part of Eq. (151), the steam quality at the reactor outlet header can be calculated as follows:

$$x = \frac{0.146 Q_{100}}{W_p h_{fg}} = \frac{0.146 \cdot 2.064 \cdot 10^6 \left[kJ / s \right]}{8250[kg / s] \cdot 800[kJ / kg]} = 0.045 . \tag{152}$$

In the above calculation of the steam quality in the reactor outlet header as 4.5%, it was assumed that the value of 85.4% of the total reactor power to onset of boiling as calculated by Eq. (152) remains valid as the power goes up beyond the onset of boiling. Hence, it follows that the parameters that determine the onset of boiling, W_p, C_p, U_{SG}, A_{SG}, T_s, and T_{FW}, have been assumed not to change significantly when boiling starts in the primary heat transport system. This is only approximately true: W_p and U_{SG} are affected by the presence of two-phase flow. However, the approximation used in the above calculation is good enough to illustrate the point.

End of Problem 7.3.4.1

Enough information is now available to sketch out the heat duty diagram as a function of power. Figure 66 presents the impact of reactor power on the heat-duty diagram of the steam generator {GAR1999, POP2014].

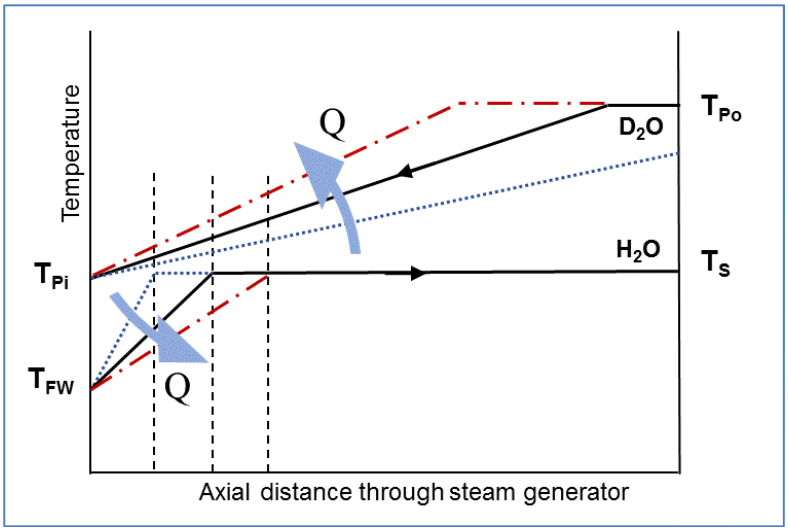

Figure 66 Reactor power versus heat-duty diagram of the SG

It is clear from the figure that the increase of reactor power impacts the primary side in such a way that the primary fluid temperature curve becomes steeper, eventually reaching saturation and starting to boil. The higher the reactor power, the greater will be the quantity of the primary fluid that will be converted to steam, and the higher will be the quality of the primary coolant in the reactor outlet header.

The reactor power also affects the secondary side. The lower the reactor power, the larger will be the pre-heater part of the steam generator, i.e., more of the steam generator heat transfer area will be engaged in pre-heating feedwater, and less will be available to boil the secondary fluid.

7.3.5 Steam generator with pre-heater (numerical solution)

Consider the steam generator to be a counter-current heat exchanger, with the simplified heat-duty diagram shown in Figure 67. For any small segment *dz* of the heat exchanger, according to the figure, the heat transferred from the primary to the secondary side can be calculated using the Fourier law:

$$dQ = U_{SG}\left(T_p - T_s\right)dA_{SG}\,. \tag{153}$$

The primary and secondary temperatures will vary with position in the steam generator. Energy balance on the primary and secondary sides gives the following expressions:

$$dQ = -W_P dh_P\,, \tag{154}$$

$$dQ = W_S dh_S\,. \tag{155}$$

The minus sign indicates a heat flow from the primary to the secondary side, i.e., the enthalpy of the primary fluid decreases, and the enthalpy of the secondary fluid increases.

For a single phase on either side, one can relate enthalpy with temperature as follows: $dh=C_P \cdot dT$.

Therefore, the change in fluid temperatures along the steam generator primary and secondary sides can be expressed as:

$$dT_p = -\frac{U_{SG}\, dA_{SG}\left(T_p - T_s\right)}{C_{p,p} W_p}, \tag{156}$$

$$dT_s = \frac{U_{SG}\, dA_{SG}\left(T_p - T_s\right)}{C_{p,s} W_s}. \tag{157}$$

The steam generator area can be conveniently divided into N segments, each described as $\Delta A_{SG}=A_{SG}/N$. The numerical algorithm for calculating the fluid temperatures simply starts at one end of the heat exchanger with known or assumed temperatures and flows at that boundary and repeatedly applies Eqs. (156) and (157) as it moves forward to the other end of the heat exchanger. The principle of the calculation is shown in Figure 68. If the calculations start at the cold end (where feedwater enters and primary fluid exits), single-phase flow on both sides can be ensured.

At each successive nodal point, the fluid temperatures can be calculated by the following expressions [GAR1999, POP2014]:

$$T_{p,i+1} = T_{p,i} + \frac{U_{SG} A_{SG}}{C_{p,p} N W_p}\left(T_{p,i} - T_{s,i}\right), \tag{158}$$

$$T_{s,i+1} = T_{s,i} + \frac{U_{SG} A_{SG}}{C_{p,s} N W_s}\left(T_{p,i} - T_{s,i}\right). \tag{159}$$

At each nodal point i, the calculated temperature should be compared to the saturation point. Once the saturation temperature is reached, the secondary-side temperature remains at the saturation temperature.

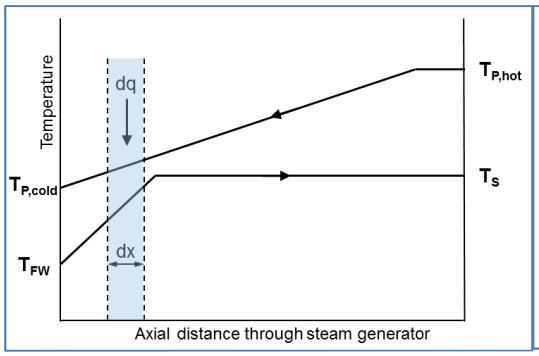

Figure 67 Steam generator numerical calculation concept

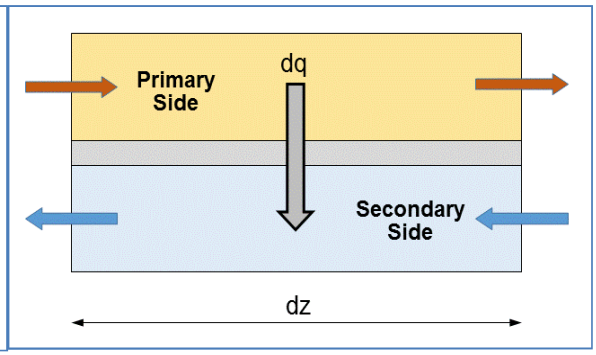

Figure 68 Nodalization concept for steam generator numerical calculation

The result is the temperature profiles for both the primary and secondary sides for the given flow rates, area, heat transfer coefficient, and cold side temperatures. Equation (153) is used to accumulate the total heat transferred by the heat exchanger. If the heat transferred is above or below the desired heat transfer, then iteration is required. Typically, it is desirable to know the primary-side temperature profile for a given set of secondary-side conditions, given the primary-side flow and a given steam generator geometry and heat transfer coefficient. In this case, the primary side inlet temperature is varied until the target Q is met; once again, the primary side "floats" on the secondary side.

The effect of power is seen through W_s, which is proportional to Q. For low Q, T_s will rise rapidly to the saturation temperature. This decreases the effective temperature difference between the primary and secondary sides. Hence, T_p will not rise as quickly as in the high-power case.

7.3.6 Problems

1. Explain the difference in the design of steam generators that have an area designed for preheating of feed water and these that do not. Explain how feed water heating is achieved in both types of design. Explain the role of the pinch point in both types of design.
2. Using the values provided in Problem 7.3.4.1, draw a heat duty diagram of a corresponding steam generator following the format provided in Figure 66.
3. Explain the process for calculating main parameters of the primary heat transport system.
4. Using the values provided in Problem 7.3.4.1, and using the steam generator heat balance template equations, calculate analytically the steam generator parameters. Determine the effect of steam generator fouling on the steam generator performance. Determine the effect of power level on the steam generator performance.
5. Using the values provided in Problem 7.3.4.1, and using the steam generator heat balance equations use numerical technique to calculate steam generator parameters. Determine the effect of steam generator fouling on the steam generator performance. Determine the effect of power level on the steam generator performance. Determine the impact of the numerical calculation increments on the precision of the calculations.

7.4 Heat transfer in the fuel elements

Heat transfer in the fuel, cladding, and coolant is very important from the perspective of adequate thermal design of the reactor core. The most important objective of the thermal designer is to ensure that the heat generated in the reactor at any reactor state is continuously removed from the core within adequate thermal margins.

This section describes the calculation of temperature profiles in the radial and axial directions in the fuel, cladding, and coolant. It also discusses the key parameters and their influence on primary heat transport system design. Note that coolant mixing within the bundle geometry is beyond the scope of this text.

7.4.1 General heat conduction equation

The interface between the fuel and the coolant is centrally important to reactor design because it limits the heat flux that can be removed from the fuel to the coolant, thus limiting the reactor power output.

For a solid body, the general thermal energy balance equation can be written as follows [BIR1960, TOD2011]:

$$\iiint_V \frac{\partial(\rho \cdot e)}{\partial t} dV = \iiint_V q'''(\vec{r},t) dV - \iint_S \vec{q}''(\vec{r},t)\hat{n} dS \,, \tag{160}$$

where ρ is the material density, e is the internal energy, V is the volume, S is the surface area, q''' is the volumetric heat generation, q'' is the heat flux, and $\hat{n}$ is the unit vector on the surface. The term on the left-hand side is the heat storage term, which represents the net change in energy level. The first term on the right-hand side of the equation is the heat generation term, which describes the heat generated at any time and any volume in the solid body. The second term on the right-hand side shows the net energy exchange from the body to the surroundings. The right-hand side shows the net energy exchange from the body to the surroundings. Gauss' Law connects the surface integral to a volume integral of a body that is enclosed by a given surface [BIR1960]:

$$\iint_S \vec{q}''(\vec{r},t)\hat{n} \cdot dS = \iiint_V \nabla q''(\vec{r},t) dV \,. \tag{161}$$

Using Gauss' Law and Eq. (161), the surface integral in the energy balance equation, Eq. (160), can be converted to a volume integral, following which the volume integral can be dropped for all terms in the equation, and the internal energy e can be replaced by the temperature T times the heat capacity c:

$$\frac{\partial(\rho c T)}{\partial t} = q'''(\vec{r},t) - \nabla q''(\vec{r},t). \tag{162}$$

In addition, a relation is needed to specify the heat flux in terms of temperature. In a solid body, Fourier's law of thermal conduction is applicable and can be expressed as follows [ELW1978]:

$$q''\left(\vec{r},t\right) = -k \cdot \nabla T\left(\vec{r},t\right). \tag{163}$$

Hence, substituting Eq. (163) into Eq. (162) leads to an equation describing the temperature distribution in a solid body in which heat generation and conduction take place:

$$\frac{\partial\left(\rho cT\right)}{\partial t} = q'''\left(\vec{r},t\right) - \nabla\left[k\nabla T\left(\vec{r},t\right)\right], \tag{164}$$

where the solid body density ρ is in *[kg/m^3];* the specific heat capacity c is in *[J/(kg ^{o}K];* the heat conductivity k is in *[J/(m ^{o}K sec)]*; the heat flux q'' is in *[J/(m^2 sec) = W/m^2]*; the heat generation rate q''' is in *[J/(m^3 sec) = W/m^3]*; the temperature T is in *[^{o}K]*; and α is defined as *(k/ρc) [m^2/sec].*

7.4.2 Temperature distribution in the radial direction

Consider a typical cylindrical fuel pin composed of a fuel element surrounded by metal cladding, as shown in Figure 69. The fuel pellets are in the fuel element and are surrounded by a small gap between the fuel and the cladding, which offers substantial resistance to heat transfer. The flowing coolant surrounds the pin. This discussion will consider the fuel, gap, cladding, and coolant separately to develop the temperature profile in each material. Then the resulting equations will be combined to yield the full fuel-to-coolant temperature profile. It is sufficient for the present purposes to focus on the steady state to provide an illustration of a fuel temperature distribution and the separate contributions of thermal resistance through various materials. The steady-state version of Eq. (164) will not have the term on the left-hand side, meaning that the heat generated in the fuel is equal to the heat removed by the coolant:

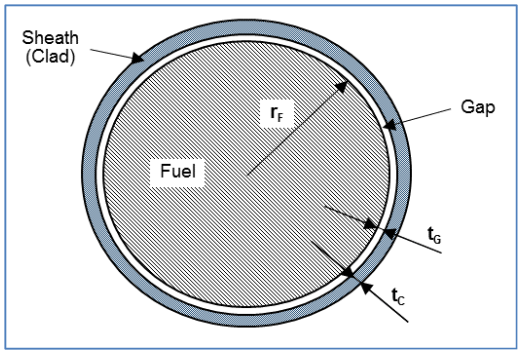

Figure 69 Cross section of a cylindrical fuel pin

$$\nabla\left[k_f \nabla T\left(\vec{r},t\right)\right] = q'''\left(\vec{r},t\right). \tag{165}$$

For a cylindrical fuel pellet, Eq. (165) must be expanded into cylindrical coordinates:

$$\frac{1}{r}\frac{d}{dr}\left(k_f r \frac{dT}{dr}\right) = q'''\left(r\right). \tag{166}$$

Equation (166) must be integrated twice; after the first integration, it is transformed into the following equation:

$$k_f r \frac{dT}{dr} = -\frac{r^2}{2} q'''(r). \tag{167}$$

The constant of integration is zero because the temperature gradient at *r=0* is zero. The thermal conductivity, *k*, is a strong function of *T* in fuel, and therefore its variation needs to be taken into account in the integration process. However, in the first step, its average value $\bar{k}_f$ can be assumed to be within the range of fuel temperature variation. Hence, the second subsequent integration results in the following relation:

$$\int_{T_o}^{T_F} k_f(T) dT \equiv \bar{k}_f (T_F - T_o) = -\frac{r_F^2}{4} q'''(r), \tag{168}$$

where the subscript 0 indicates the centre point and the subscript *F* indicates the fuel pellet radius. Because $T=T_o$ at *r=0*, the constant of integration is again zero. Finally, with the assumption of average fuel conductivity in the fuel pellet, the temperature difference across the fuel pellet has the following form:

$$\Delta T_{fuel} \equiv T_o - T_F = \frac{r_F^2}{4\bar{k}_f} q''' = \frac{q'}{4\pi \bar{k}_f}, \tag{169}$$

where $q' = \pi r_F^2 q''$ is the linear power density. Note that by using linear power density, the same ΔT is obtained for a given q' regardless of the fuel radius.

Problem 7.4.2.1

Calculate for UO_2 ceramic fuel the radial temperature difference in the fuel. For UO_2 ceramic fuel, k_F is typically *0.02–0.03 [W/cm°K]*. At *q'=500 [W/cm]*, ΔT_{fuel} in the fuel pellet is about *1400°C*.

End of Problem 7.4.2.1

In the gap between the fuel pellet and the cladding, no heat is generated. Therefore, for steady-state conditions, Eq. (164) transforms into the following equation:

$$\frac{1}{r}\frac{d}{dr}\left(k_g r \frac{dT}{dr}\right) = 0. \tag{170}$$

This equation can be readily integrated once to yield the following equation:

$$k_g r \frac{dT}{dr} = const. \tag{171}$$

The constant of integration is determined by considering the heat flux q'' at the fuel-gap interface:

$$-k_g \left[\frac{dT}{dr}\right]_{r=r_F} = q'' = \frac{q'}{2\pi r_F}. \tag{172}$$

Substituting Eq. (172) into Eq. (171) yields the following equation:

$$k_g r \frac{dT}{dr} = -\frac{q'}{2\pi} \quad \Rightarrow \quad k_g \frac{dT}{dr} = -\frac{q'}{2\pi r}. \tag{173}$$

Assuming that the gap conductivity does not change significantly with temperature and performing integration, the temperature difference in the gap can be obtained as:

$$k_g \Delta T_{GAP} = k_g \left(T_F - T_C\right) = \frac{q'}{2\pi} \ln\left(\frac{r_F + t_G}{r_F}\right). \tag{174}$$

The subscript *C* indicates the gap-cladding interface. The boundary condition $T=T_C$ at $r=r_F+t_G$ is incorporated into this solution. Finally, the gap temperature difference is obtained as:

$$\Delta T_{GAP} = \frac{q'}{2\pi k_G} \ln\left(\frac{r_F + t_G}{r_F}\right). \tag{175}$$

Because the natural logarithm of a small number can be approximated by the number itself, i.e., $ln(1+x) \approx x$ [GAR1999, POP2014], the gap temperature difference is:

$$\Delta T_{GAP} = \frac{q'}{2\pi r_F}\left(\frac{t_G}{k_G}\right). \tag{176}$$

Problem 7.4.2.2

Calculate for UO_2 fuel the radial temperature difference in the fuel-cladding gap. The gap conductivity k_G is about *0.002 W/cm°*K, but it varies considerably with the amount of fission product gases. For a gap thickness of *0.005 cm*, ΔT_{GAP} is about *300°C* for *q'* of *500 W/cm*.
End of Problem 7.4.2.2

Because with irradiation the fuel will swell to touch the cladding at certain points (because the surfaces have a certain degree of roughness), an effective heat transfer coefficient, h_G, is used:

$$h_G\left(\Delta T_{GAP}\right) = q''. \tag{177}$$

Therefore, taking into account the relationship between heat flux and the linear power $q' = \pi r_F^2 q''$, the temperature difference in the gap can be obtained as follows:

$$\Delta T_{GAP} = \frac{q'}{2\pi r_F h_G}. \tag{178}$$

Problem 7.4.2.3

Calculate for UO_2 fuel the radial temperature difference in the fuel-cladding gap. A heat transfer coefficient of *0.5–1.1 W/cm²°K* gives a ΔT_{GAP} less than *300°C*.
End of Problem 7.4.2.3

For the gap region described above, the steady-state equation for the cladding region, in which there is no heat generation, is similar:

$$\frac{1}{r}\frac{d}{dr}\left(k_c r\frac{dT}{dr}\right)=0. \tag{179}$$

This equation is solved in the same manner as for the gap to yield:

$$k_c\Delta T_{CLAD}=k_c\left(T_C-T_S\right)=\frac{q'}{2\pi}\ln\left(\frac{r_F+t_G+t_C}{r_F+t_G}\right)\Rightarrow\ \Delta T_{CLAD}=\frac{q'}{2\pi k_c}\ln\left(\frac{r_F+t_G+t_C}{r_F+t_G}\right). \tag{180}$$

The subscript *S* indicates the cladding-coolant surface interface. The boundary condition $T=T_S$ at $r=r_F+t_G+t_C$ is incorporated into this solution.

Because the natural logarithm of a small number can be approximated by the number itself, i.e., $ln(1+x) \approx x$ [GAR1999, POP2014], the gap temperature difference is:

$$\Delta T_{CLAD}=\frac{q'}{2\pi\left(r_F+t_G\right)}\left(\frac{t_C}{k_C}\right). \tag{181}$$

Problem 7.4.2.4

Calculate for UO_2 fuel the radial temperature difference in the fuel cladding. The cladding conductivity k_C is about *0.11 W/cm°K*, giving a ΔT_{CLAD} of about *80°C* for a q' of *500 W/cm*.
End of Problem 7.4.2.4

The heat flux from the cladding to the coolant is determined as:

$$q''=h_S\left(T_S-T_{FL}\right), \tag{182}$$

where T_{FL} is the bulk temperature of the coolant fluid. Hence, the temperature drop from the cladding surface to the bulk fluid temperature is:

$$\Delta T_{COOL}=\frac{q'}{2\pi h_S\left(r_F+t_C+t_G\right)}. \tag{183}$$

Problem 7.4.2.5

Calculate for UO_2 fuel the radial temperature difference in the cladding-to-coolant interface. A heat transfer coefficient of *~4.5 W/cm²°K* gives a ΔT_{COOL} of about *10°C–20°C*.
End of Problem 7.4.2.5

By summing up Eqs. (169), (178), (181), and (183), the overall temperature difference between the fuel centreline and the bulk coolant can be obtained according to the following equation:

$$T_o-T_{FL}=\frac{q'}{2\pi}\left(\frac{1}{2\bar{k}_f}+\frac{1}{h_G r_F}+\frac{t_G+t_C}{k_C\left(r_F+t_G\right)}+\frac{1}{h_S\left(r_F+t_G+t_C\right)}\right). \tag{184}$$

The expression in brackets in Eq. (184) is the thermal resistance across the fuel element:

$$R_{th} = \left(\frac{1}{2\bar{k}_f} + \frac{1}{h_G r_F} + \frac{t_G + t_C}{k_C \left(r_F + t_G \right)} + \frac{1}{h_S \left(r_F + t_G + t_C \right)} \right). \tag{185}$$

Hence, the centreline fuel temperature is greater than the coolant temperature by an amount that depends on the amount of heat generated and on various resistances to heat flow. For a given fuel design, most of the parameters are fixed under normal operation. The one exception is the heat transfer coefficient to the coolant, h_S, which is covered in Section 7.6.

Figure 70 shows a radial temperature distribution across the fuel element for two linear power rates [POP2014]. Linear power level *45 [kW/m]* represents full-power operation of the fuel element in the middle of the core. Linear power level *15 [kW/m]* represents operation at full power at the core ends, or at a certain decay power level shortly after reactor shutdown. This figure shows that the highest temperature difference occurs in the fuel pellet (above 1400°C at full power) because UO_2 is a poor heat conductor, but its melting temperature is approximately 2800°C–2900°C. The temperature difference in the gap is significant considering that the gap is very thin. The cladding and the water are very good heat conductors, and therefore the temperature difference is relatively small.

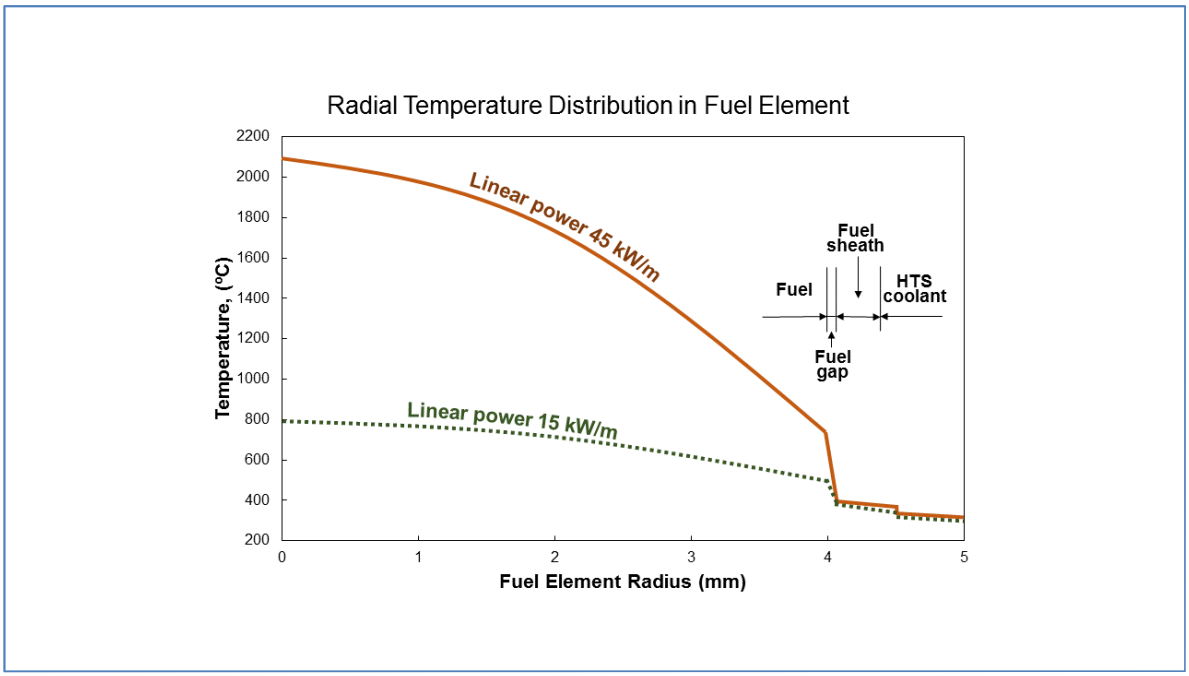

Figure 70 Radial temperature distribution in a fuel element

The fuel element design must ensure that given the coolant pressure and saturation temperature, the fuel pellet centreline temperature avoids exceeding the melting temperature by a good margin. This objective also applies to the temperature transients in design basis events.

Figure 71 shows the temperature gradient for various fuel element materials in absolute terms and per unit thickness [POP2014]. This figure clearly indicates that the highest relative

contribution is from the fuel-cladding gap and the second highest from the fuel pellet.

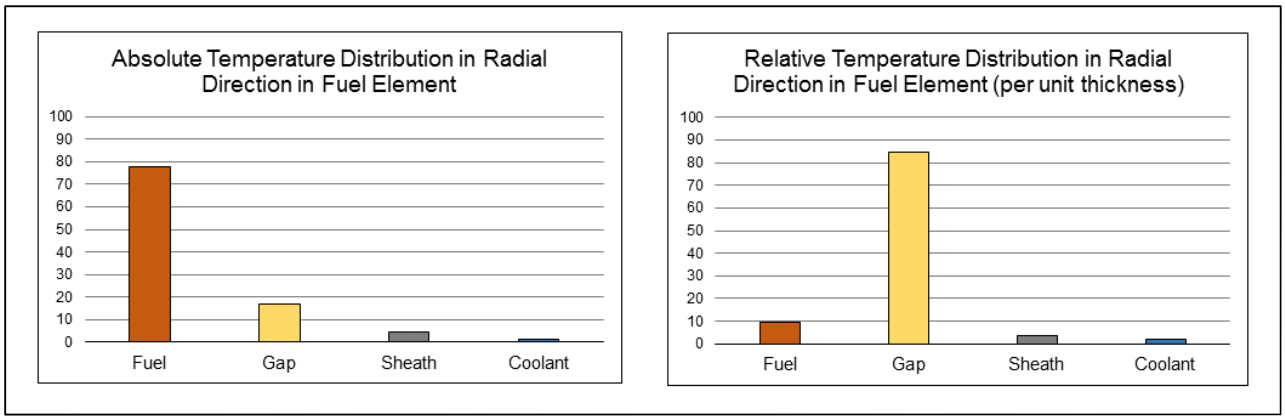

Figure 71 Radial temperature gradient per unit thickness in a fuel pin

7.4.3 Temperature distribution in the axial direction

The fuel and coolant temperature distributions depend on heat transfer in the radial direction at each position in the channel axial direction. The general heat conduction and convection equations for axial heat transfer are covered in Chapter 7.

The amount of heat generated along the fuel channel follows the neutron flux and fission reaction distribution along the fuel channel. Assuming that the reactor core does not use any techniques for balancing (i.e., flattening) the neutron flux and power generation in the axial direction, the natural axial variation of the neutron flux is given by the following relation [POP2014]:

$$\Phi(z) = \Phi_{\max} \cos\left(\frac{\pi z}{L_e}\right), \tag{186}$$

where L_e is the effective core length and Φ_{max} is the maximum neutron flux in the middle of the core.

Axial heat generation follows the neutron flux variation and is given by the following equation:

$$q'''(z) = (q''')_{\max} \cos\left(\frac{\pi z}{L_e}\right), \tag{187}$$

where $(q''')_{max}$ is the heat flux at the middle of the fuel element in the axial direction.

Consider a heat balance for a differential section of a fuel element of length dz, fuel cross section A_f $[m^2]$, and mass flow rate w $[kg/s]$. In a steady-state situation, the sensible heat gain by the passing coolant (assuming no phase change) is equal to the heat generated in the differential fuel element (c_p is the specific heat capacity at a given pressure $[kJ/kg\ ^oC]$):

$$w \cdot c_p dT_c = q''' A_f dz. \tag{188}$$

The axial variation of the fluid temperature T_c can be obtained by substituting Eq. (187) into Eq. (188) and integrating [ELW1978]:

$$wc_p \int_{T_{f1}}^{T_f} dT_c = \left(q'''\right)_{\max} A_f \int_{-L_e/2}^{z} \cos\left(\frac{\pi z}{L_e}\right) dz\,, \tag{189}$$

$$T_c = T_{c,in} + \frac{\left(q'''\right)_{\max} A_f L_e}{\pi w c_p}\left[1+\sin\left(\frac{\pi z}{L_e}\right)\right] = T_{c,in} + \frac{\left(q'''\right)_{\max} V_f}{\pi w c_p}\left[1+\sin\left(\frac{\pi z}{L_e}\right)\right], \tag{190}$$

where V_f *[m^3]* is the volume of the fluid portion of the fuel element. The subscript *"in"* designates the entry point in the channel. In this equation, the equivalent core length is approximated by the actual core length, i.e., $L=L_e$.

The coolant temperature is measured in the middle of the fuel element for *z=0* and has the following form:

$$T_{c,mid} = T_{c,in} + \frac{\left(q'''\right)_{\max} A_f L}{\pi w c_p}. \tag{191}$$

The exit temperature of the coolant from this channel can be obtained by integrating Eq. (189) to the channel exit (labelled as *2*, i.e., at *z=+L/2*):

$$T_{f,out} = T_{f,in} + \frac{2\left(q'''\right)_{\max} A_f L}{\pi w c_p}. \tag{192}$$

This equation shows that the coolant temperature rise in the channel will be greater for higher heat generation rates, larger fuel elements, and longer channels and smaller for higher mass flow rates.

The heat transferred between the cladding and the coolant at any location *z* along the fuel channel, per unit area of cladding surface in contact with the coolant, is given by $h(T_{SH}-T_c)$, where *h* is the heat transfer coefficient. This coefficient can be assumed constant along the fuel channel with no boiling in the channel. Hence, the heat balance between the fuel cladding and the coolant can be expressed by the following equation:

$$hC_{SH}\left(T_{SH}-T_c\right)dz = \left(q'''\right)_{\max} A_f \cos\left(\frac{\pi z}{L}\right) dz\,, \tag{193}$$

where C_{SH} *[m]* is the fuel cladding circumference, T_{SH} *[^oC]* is the cladding temperature, and *h* *[kJ/m^2 ^oC]* is the heat transfer coefficient. Substituting Eq. (190) into Eq. (193) yields the cladding temperature variation along the fuel channel:

$$T_{SH} = T_{c,in} + \frac{\left(q'''\right)_{\max} A_f L}{\pi w c_p}\left[1+\sin\left(\frac{\pi z}{L}\right)\right] + \frac{\left(q'''\right)_{\max} A_f}{hC_{SH}}\cos\left(\frac{\pi z}{L}\right). \tag{194}$$

The temperature variation at the fuel pellet surface along the fuel channel and the temperature of the fuel pellet centreline along the fuel channel can be obtained by means of the following relation:

$$\frac{T_{SH}-T_c}{R_x L} = \left(q'''\right)_{\max} A_f \cos\left(\frac{\pi z}{L}\right). \tag{195}$$

Hence, for fuel pellet surface temperature, the following equations can be developed:

$$\frac{T_{f,S}-T_c}{R_{f,S}L}=\left(q'''\right)_{\max}A_f\cos\left(\frac{\pi z}{L}\right), \tag{196}$$

$$T_{f,S}=T_c+R_{f,S}L\left[\left(q'''\right)_{\max}A_f\cos\left(\frac{\pi z}{L}\right)\right], \tag{197}$$

$$R_{f,S}=\left(\frac{1}{h_G r_F}+\frac{t_G+t_C}{k_C\left(r_F+t_G\right)}+\frac{1}{h_S\left(r_F+t_G+t_{SH}\right)}\right). \tag{198}$$

The fuel pellet centreline temperature variation can be described by the following equations:

$$\frac{T_{f,CL}-T_c}{R_{f,CL}L}=\left(q'''\right)_{\max}A_f\cos\left(\frac{\pi z}{L}\right), \tag{199}$$

$$T_{f,CL}=T_c+R_{f,CL}L\left[\left(q'''\right)_{\max}A_f\cos\left(\frac{\pi z}{L}\right)\right], \tag{200}$$

$$R_{f,CL}=\left(\frac{1}{2\bar{k}_f}+\frac{1}{h_G r_F}+\frac{t_G+t_C}{k_C\left(r_F+t_G\right)}+\frac{1}{h_S\left(r_F+t_G+t_{SH}\right)}\right). \tag{201}$$

Substituting Eq. (190) into Eq. (200) yields the fuel centreline temperature:

$$T_{f,CL}=T_{c,in}+\frac{\left(q'''\right)_{\max}A_f L}{\pi w c_p}\left[1+\sin\left(\frac{\pi z}{L}\right)\right]+\left(q'''\right)_{\max}A_f L R_{f,CL}\cos\left(\frac{\pi z}{L}\right). \tag{202}$$

The location of the maximum cladding temperature can be obtained by differentiating Eq. (194) and equating it to zero, i.e., $dT_{SH}/dz=0$. Hence:

$$z_{SH,\mathrm{m}}=\frac{L}{\pi}\tan^{-1}\left(\frac{hC_{SH}L}{\pi w c_p}\right)=\frac{H}{\pi}\cot^{-1}\left(\pi w c_p R_{SH}\right), \tag{203}$$

$$R_{SH}=\frac{1}{hA_f}=\frac{1}{hC_{SH}L}. \tag{204}$$

The location of the maximum fuel pellet centreline temperature can be obtained by differentiating Eq. (202) and equating it to zero, i.e., $dT_{f,CL}/dz=0$. Hence:

$$z_{f,CL,\mathrm{m}}=\frac{L}{\pi}\cdot\cot^{-1}\left(\pi w c_p R_{f,CL}\right). \tag{205}$$

The maximum cladding temperature can be found by substituting Eq. (203) into Eq. (194):

$$T_{SH,\mathrm{m}}=T_{c,in}+\left(q'''\right)_{\max}A_f L R_{SH}\left[\frac{1+\sqrt{1+\alpha^2}}{\alpha}\right], \text{ where } \alpha=\pi w c_p R_{SH}. \tag{206}$$

The maximum cladding temperature can be found by substituting Eq. (205) into Eq. (202):

$$T_{f,CL,\mathrm{m}} = T_{c,in} + \left(q'''\right)_{\max} A_f LR \left[\frac{1+\sqrt{1+\beta^2}}{\beta}\right], \text{ where } \beta = \pi w c_p R_{f,CL}. \quad (207)$$

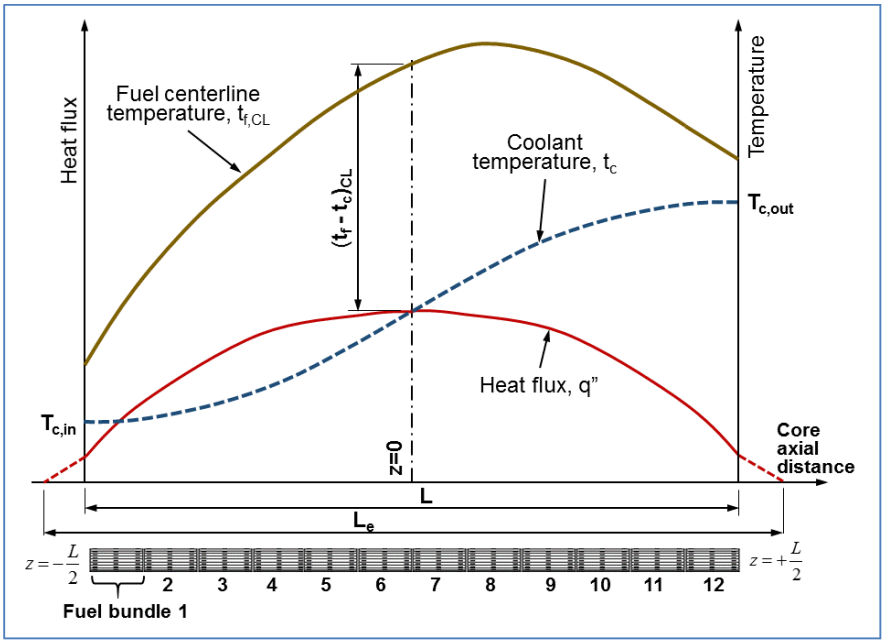

Figure 72 Temperature distribution in the axial direction in a fuel element

Figure 72 shows the temperature distribution in the coolant and the cladding plotted on the same graph with the heat flux distribution along the core [ELW1978]. The heat flux distribution is assumed to have a cosine distribution, which is more pronounced in a core in which no measures have been taken to flatten the neutron flux. In this case, the variations in the coolant and cladding temperatures are more pronounced. Note that the coolant temperature curve is symmetrical. It has a small gradient at the entry and exit parts of the core, where the heat flux is lower. The highest coolant temperature gradient is in the middle part of the core, where the heat flux is substantial. Of course, different core heat flux distributions can have a significant impact on the temperature profile. Moreover, reactivity devices and fuel channel orificing (i.e., channel-to-channel variation of flow rates) can also have significant local effects on the temperature profile.

Figure 73 shows a temperature distribution that includes the coolant (T_c), fuel sheath (T_{SH}), fuel pellet surface ($T_{f,S}$), and fuel pellet centreline ($T_{f,CL}$) temperature profiles. The positions of the maximum values of T_{SH}, $T_{f,S}$, and $T_{f,CL}$ occur at $Z_{SH,m}$, $Z_{f,S,m}$, and $Z_{f,CL,m}$, closer to the fuel element mid-plane [ELW1978].

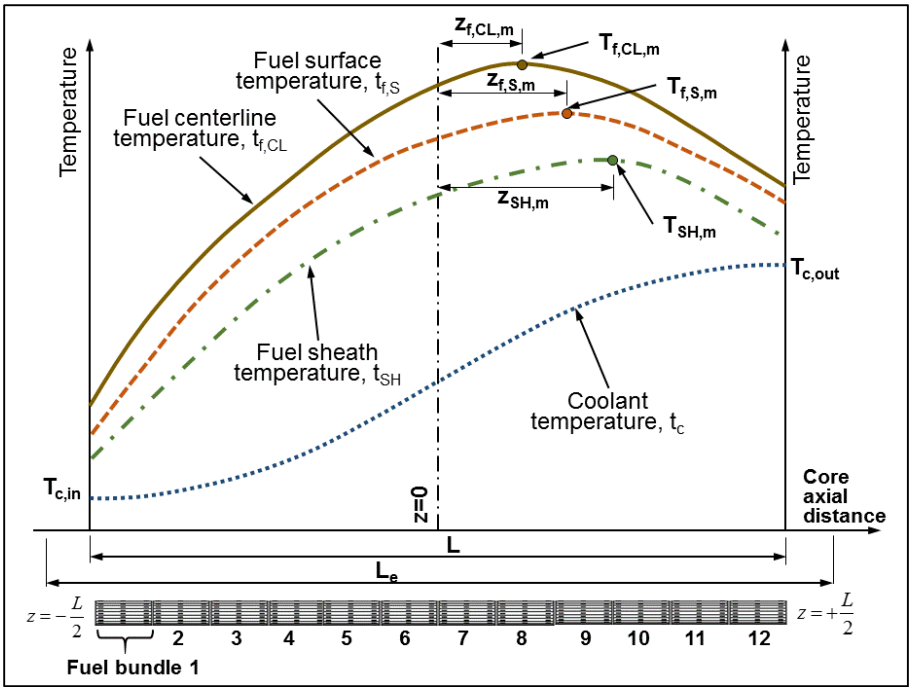

Figure 73 Temperature distribution in the fuel cladding and the fuel element

The reason that the maximum fuel centreline temperature is closer to the fuel mid-plane is that the radial heat flow through the fuel and cladding at any section along the fuel channel is proportional to the heat flux at that location. The temperature differences (T_{SH}–T_c), ($T_{f,S}$–T_{SH}), and ($T_{f,CL}$–$T_{f,S}$) generally follow cosine-shaped functions according to the heat flux cosine profile. The maxima of the cladding and fuel temperatures are affected by the heat flux maximum (at the fuel mid-plane) and the fluid maximum (at the fuel channel exit). Because the cladding is close to the fluid, the impact of coolant temperature is strong, and hence its maximum is pulled away from the mid-plane. Because the fuel centreline temperature occurs inside the fuel, where the heat is generated, its maximum is pulled toward the mid-plane, where the heat flux maximum is located.

7.4.4 Axial distribution of quality

If the coolant boils in a fuel channel, flow quality changes along the channel. It is important in this situation to calculate the change in flow quality and the length of the channel where boiling occurs. The enthalpy of the two-phase coolant is defined using the following relation:

$$h = h_{c,sat} + x h_{fg}\,, \tag{208}$$

where x is the flow quality in the two-phase mixture, $h_{c,sat}$ is the saturated liquid enthalpy, and h_{fg} is the latent heat of vaporization. The heat balance over the differential part of the fuel channel yields the following equation:

$$w_f \left[h(z) - h_{cold} \right] = \int_{-L/2}^{+L/2} q'(z)\,dz\,. \tag{209}$$

In the above equation, h_{cold} is the inlet enthalpy in the channel. If the axial position where the coolant starts to boil (the point where $h(z)=h_{SAT}$) is defined as Z_{BB}, the heat balance equation, Eq. (209), transforms into the following equation:

$$w_f \left[h(z) - h_{c,sat} \right] = \int_{Z_{BB}}^{z} q'(z)dz = x(z) w_f h_{fg} \,. \tag{210}$$

Using the above equation, the flow quality of the two-phase mixture can be expressed by the following equation:

$$x(z) = \frac{1}{w_f h_{fg}} \int_{Z_{BB}}^{z} q'(z)dz \,. \tag{211}$$

7.4.5 Thermal conductivity and fuel element material properties

In developing Eq. (166), it has been assumed that the fuel thermal conductivity can be approximated by an average value that will apply in the range of parameters used in the present calculations. This section covers the effect of various factors on thermal conductivity and other thermal parameters that must be considered when developing a model to calculate fuel-element temperature profiles.

Many factors affect UO_2 fuel thermal conductivity. The major factors are temperature, porosity, oxygen-to-metal atomic ratio, PuO_2 content, pellet cracking, and fuel burn-up.

Figure 74 shows the temperature dependence of UO_2 thermal conductivity [ELW1978]. Experimental measurements have shown that thermal conductivity decreases with increasing fuel temperature (i.e., has a negative slope) until about 1750°C, after which it slowly increases. However, the slope is very steep from 0°C–500°C and very shallow thereafter. Nevertheless, the impact of temperature must be taken into account when calculating fuel temperature profiles, which is routinely done in thermal-hydraulic computer programs. Figure 74 also shows the integral of the thermal conductivity, which monotonically rises with temperature; this is the value to use in solving Eq. (170).

When using experimental values of thermal conductivity, one must be aware of the measurement uncertainties. Note that these uncertainties are significant, particularly at higher temperatures.

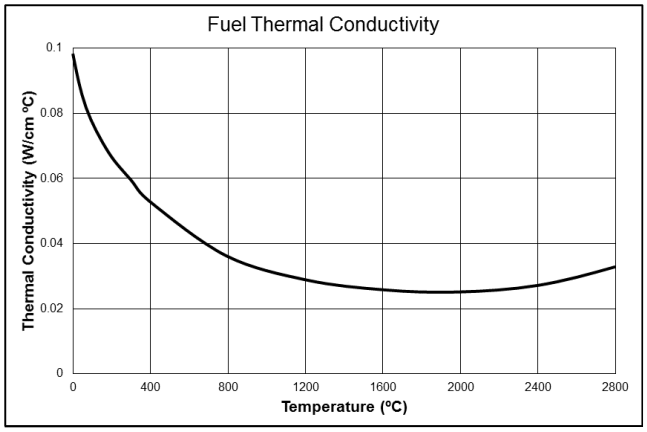

Figure 74 Thermal conductivity in a fuel pin

The oxide fuel is produced by sintering pressed powdered UO_2 or mixed oxide at high temperature. Under such conditions, for any material with a given density, usually only around 90% of the maximum possible (theoretical) density of the solid can be produced.

The thermal conductivity of a solid usually decreases with increasing presence of voids within the structure. Therefore, to maximize thermal conductivity, fuel porosity must be minimized. However, during fuel irradiation, fission gases are produced, resulting in increased internal pressures that may swell and deform the fuel. Hence, a certain degree of porosity is desirable to accommodate the fission gases and limit the possibility of swelling. This is very important for reactor cores that have high power density and therefore produce more gases per unit volume.

The oxygen-to-metal atomic ratio of UO_2 and PuO_2 can vary from the theoretical (stoichiometric) value of 2 because of fuel irradiation and burn-up. A reduction or increase in the oxygen-to-metal ratio results in a reduction of thermal conductivity, as can be clearly seen in Figure 75 for UO_2 and PuO_2 mixtures [TOD2011].

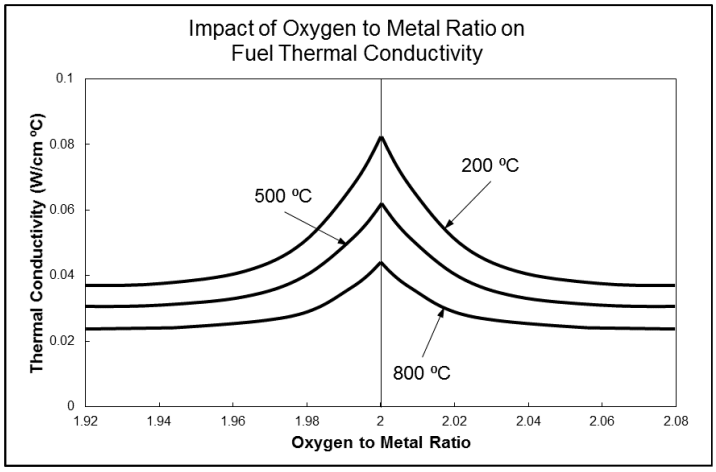

Figure 75 Impact of oxygen-to-metal ratio on the heat conduction coefficient in fuel

The thermal conductivity of mixed fuel decreases as the plutonium oxide content increases. Therefore, as fuel burns up and ages and plutonium content increases, thermal conductivity decreases.

Figure 76 shows the impact of fuel temperature on fuel heat capacity for UO_2 and PuO_2 fuels [TOF2011]. It is evident that heat capacity increases with temperature and decreases with an increase in plutonium content.

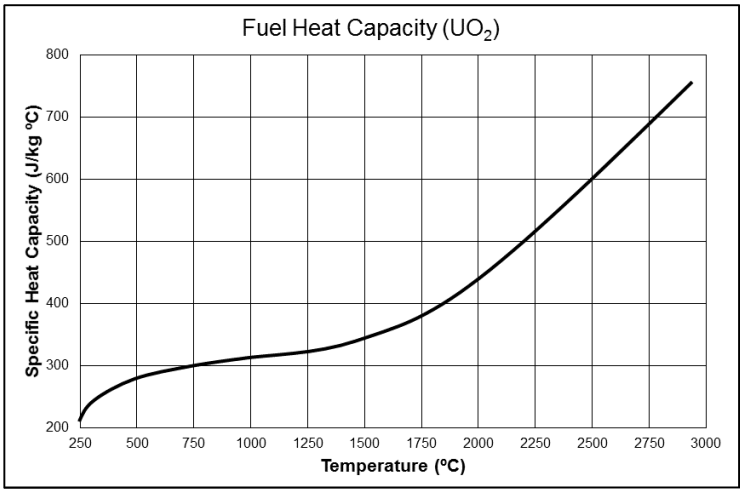

Figure 76 Heat capacity of a fuel pin

The properties of the pellet-to-cladding gap are very important. As shown in Figure 71, its contribution to thermal resistance is substantial. The gap consists of an annular space occupied by gas. Initially, its composition is fill gas, which is usually an inert gas such as helium. With burn-up, the gas composition changes as the gap is penetrated by gaseous fission products such as xenon and krypton, resulting in a gap pressure increase.

Moreover, the fuel pellet cracks with irradiation, leading to circumferential deformation of the gap and fuel pellet swelling. All this causes a reduction of thermal resistance in the gap and increases its thermal conductance with burn-up. Figure 77 shows the effect of burn-up on thermal conductance [TOD2011].

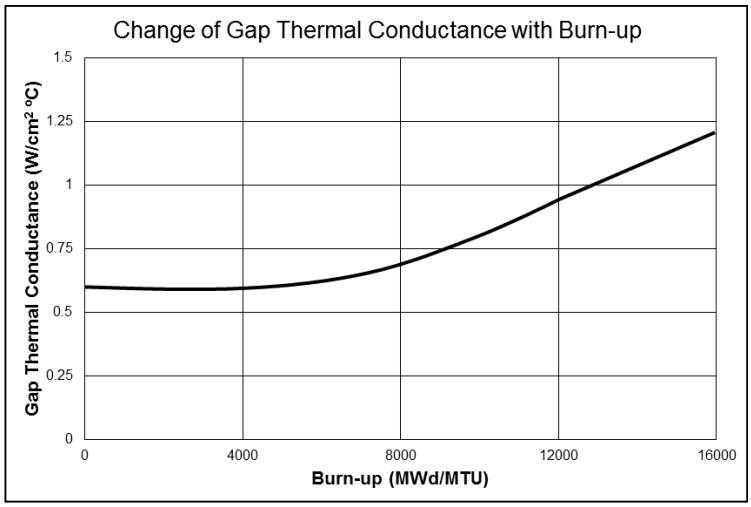

Figure 77 Gap conductance in a fuel pin

The left side of Figure 78 shows the temperature profile in the gap at nominal geometry (fresh fuel). Note that near the walls, there is a mild temperature rise towards the fuel pellet and a reduction towards the cladding because of the smaller number of molecules moving near the walls (the boundary layer effect). The right side of Figure 78 shows the effect of the deformations that occur with fuel burn-up (aging) because of swelling and cracking of the fuel

pellet and cladding. After a certain amount of irradiation, a number of peaks and valleys will develop at the pellet and cladding surfaces. These may eventually produce contact between fuel and cladding, improving thermal conductivity.

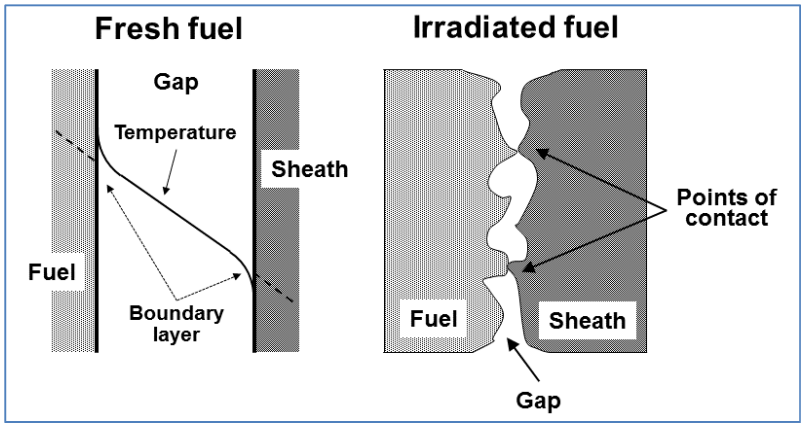

Figure 78 Fuel aging effect on temperature in a fuel pin

Figure 79 shows the typical impact of fuel aging on gap conductance for different linear heat ratings as a function of initial gap thickness [TOD2011]. Note that better thermal conductance is achieved for smaller gap thickness and for higher linear power rates, as could be expected from the above explanation. Therefore, as gap thickness becomes smaller with fuel burn-up, heat transfer is improved. In addition, this figure shows that using a smaller gap thickness for fresh fuel improves heat transfer.

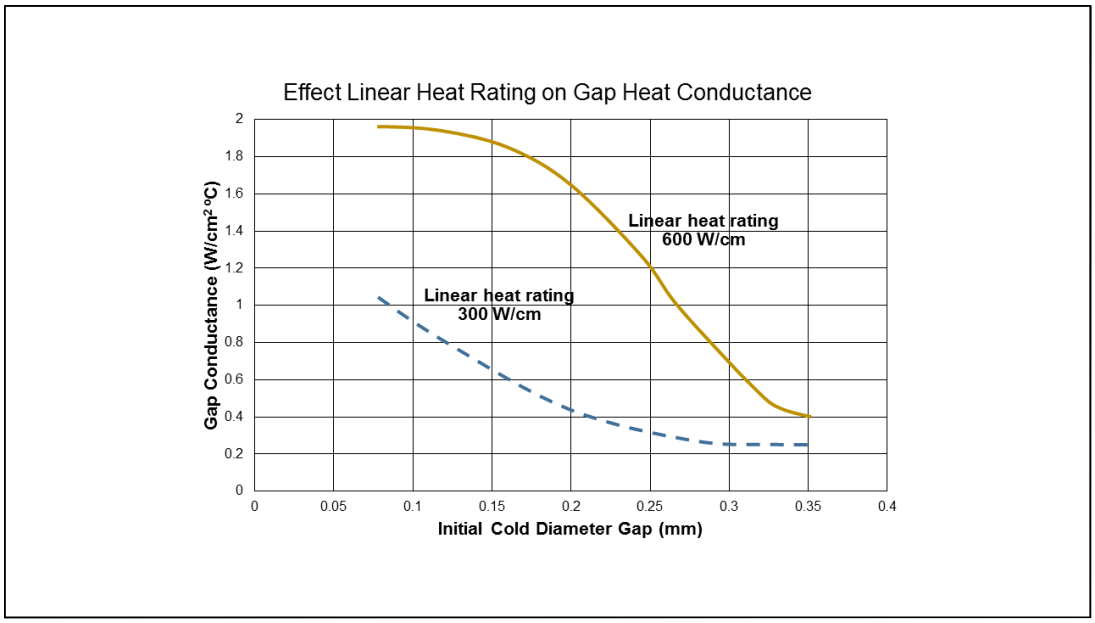

Figure 79 Impact of gap thickness and linear power on heat conductance

The temperature profiles described so far in this section were derived based on the assumption of radial symmetry across the fuel rod. This assumption was a useful way to simplify the derivation of temperature profiles across the fuel element. This assumption is acceptable for vertical reactor cores, such as in LWRs.

However, for horizontal reactor cores, such as CANDU, the assumption of radial symmetry across the fuel rod is not applicable for certain flow regimes. This is relevant for situations in which bubbly flow develops in the upper part of the fuel channel, or even more importantly, when stratification develops (e.g., under accident conditions) in the fuel channel.

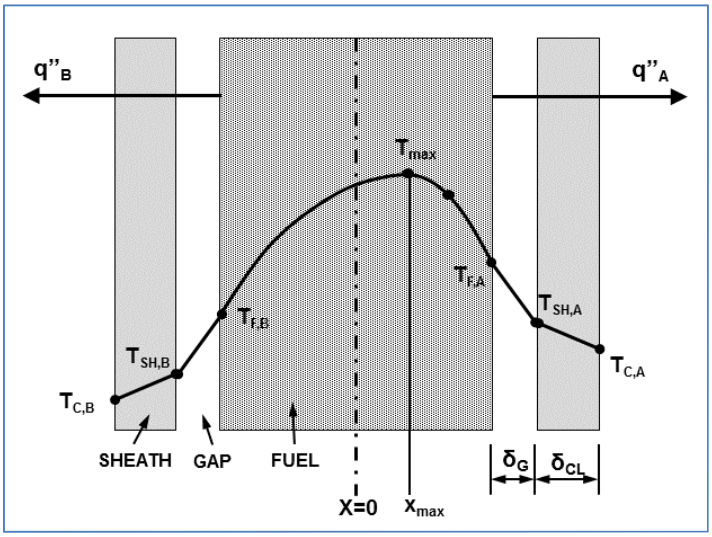

Figure 80 Asymmetric temperature profiles in a fuel pin

In these situations, the heat flux to the upper part of the fuel element could be smaller than to the lower part. This results in a skewed (asymmetric) temperature profile, as shown in Figure 80. In such a case, the maximum fuel pellet centreline temperature will be skewed towards the side with the smaller heat flux. This could also have an important impact on the cladding temperature, and it is particularly relevant to some postulated accidents in which channel stratification occurs.

7.4.6 Problems

1. A PWR reactor produces 2440 MWt with the following core information: UO_2 pellet diameter 0.96 cm; Zr clad inside diameter 0.98 cm; Zr clad outside diameter 1.12 cm; active fuel length 3.7 m. The core contains 220 fuel bundles each with 14 x 14 fuel pins (but 20 positions are used for control elements). The fission energy is distributed uniformly across the fuel pin. and TB=300°C, k_{UO2}=0.050 W/cm°C, h_{cool}=1.8 W/cm^2 °C, h_{gap}=0.57 W/cm^2 °C], k_{clad}=0.12 W/cm°C. Calculate core averaged fuel pin temperature profile.
2. The core of a BWP reactor consists of 764 fuel assemblies, each containing a square array of 49 fuel rods on a 1.9 cm pitch. The fuel rods are 4.4 m long, but fuelled only along over 3.6 m of their length. The outside diameter of the fuel rods is 1.4 cm, the cladding thickness is 0.8 mm, and the fuel pellets are 1.2 cm, thus leaving a gap of 0.2 mm. The UO_2 has average density of 10.3 g/cm^3. The radius of the core is 2.4 m, and the reactor is designed to produce 3300 MWt. The peak to average power density is 2.6. Calculate (a) the maximum heat flux in kW/m^2; (b) the temperature distribution at the location of maximum heat flux ignoring the gap between fuel pellet and cladding; and (c)

the temperature distribution at the location of maximum heat flux taking into account the gap.

3. For PWR cylindrical solid fuel pellet operating ta a heat flux of *1.7 MW/m*^{2} and surface temperature of *400ºC*, calculate the maximum temperature in the pellet for two assumed values of heat conduction: 3 W/mºC, and k = 1 + 3e$^{-0.0005T}$ where T is ºC. The UO2 pellet diameter is *10 mm*, and density is 95% of the theoretical density.
4. A CANDU channel has a typical geometry of 37 fuel elements per bundle, 12 bundles per channel, with power, pressure and inlet and outlet temperature. Assume for this channel linear power rating of *60 kW/m*; burnup at the time of peak rating of *50 MWh/kgU*; sheath-to-coolant heat transfer coefficient *40 kW/m*^{2}*K*; pellet-to-sheath heat transfer coefficient of *60 kW/m*^{2}*K*; and pellet density of *10.6 Mg/m*^{3}. Calculate coolant, cladding and fuel surface and centreline temperatures in radial direction for each bundle in axial direction assuming typical power distribution along the channel with a typical power peaking factor. Draw appropriate diagrams showing the results.
5. A fuel pin with pellet radius of 4.6 mm, clad inner radius of 4.89 mm, and outer radius of 5.46 mm, calculate the maximum liner power that can be obtained from the pellet such that the mass average temperature in the fuel does not exceed 1200 ºC. Take the bulk fluid temperature at 307.5 ºC, and the coolant heat transfer coefficient of 28.4 kW/m2 ºC. In the gap consider only conduction heat transfer. Fuel conductivity is 3 W/m2 ºC; clad conductivity is 18.69 W/m ºC; and helium gas conductivity is 0.277 W/m ºC.
6. Using analytical technique develop equations for calculating temperature distribution in radial direction in the fuel element (fuel pellets, gap, cladding and coolant) calculate temperature distribution in radial direction at heat loading of 40 kW/m. For the thermal conductivity in the fuel pellets assume the distribution shown in the diagram below. To solve the problem approximate the thermal conductivity by a suitably selected quadratic relationship.

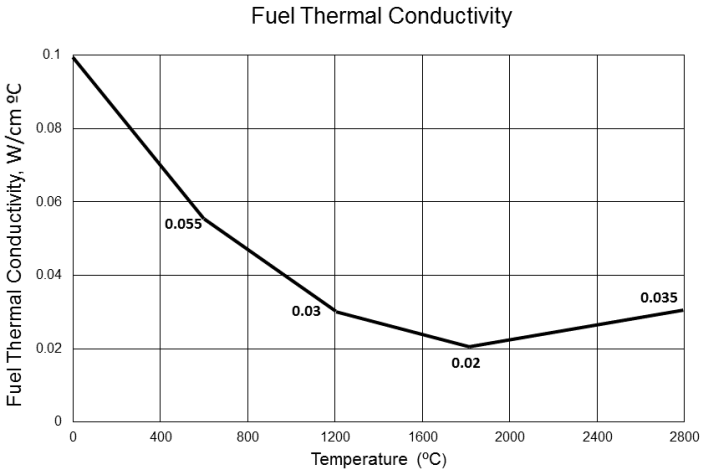

Compare the results with the case assuming constant average heat conductivity in the fuel.

7. Using a numerical technique calculate temperature distribution in radial direction in the fuel element (fuel pellets, gap, cladding and coolant) calculate temperature distribution in radial direction at heat loading of 40 kW/m. For the thermal conductivity in the fuel pellets assume the distribution shown in the diagram above. Compare the results with the case assuming constant average heat conductivity in the fuel (0.03 W/cm^{o}C).

8. Calculate axial temperature distribution of fuel centreline, fuel surface, cladding and coolant in axial direction for a typical CANDU fuel assuming maximum fuel heat load of 50 kW/m, and average fuel load of 25 kW/m. Develop relations for and calculate the positions of maximum temperatures. As per figure below, as a base case assume (1) cosine heat flux distribution, (2) constant heat flux distribution, and (3) asymmetrical linear heat flux distribution (with maximum at bundle 9), and compare the maximum temperatures and their locations in the core.

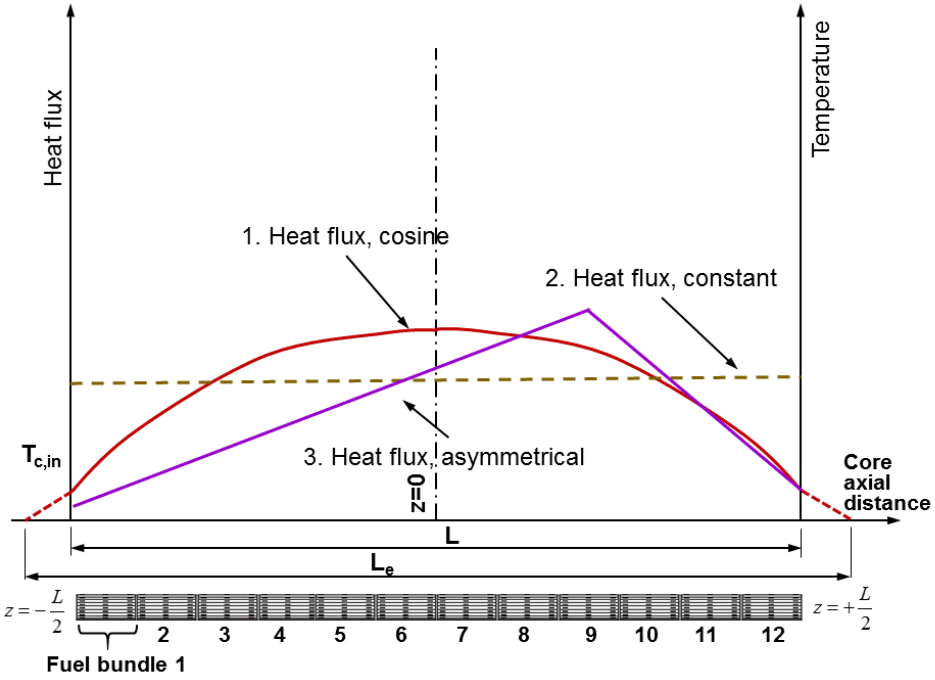

9. Calculate axial temperature distribution of fuel centreline, fuel surface, cladding and coolant in axial direction for a typical CANDU fuel assuming maximum fuel heat load of 50 kW/m, and average fuel load of 25 kW/m. Develop relations for and calculate the positions of maximum temperatures. As per figure below, as a base case assume (1) cosine heat flux distribution, (2) linearly increasing heat flux distribution to the channel exit, and (3) linearly decreasing heat flux distribution to the channel exit, and compare the maximum temperatures and their locations in the core.

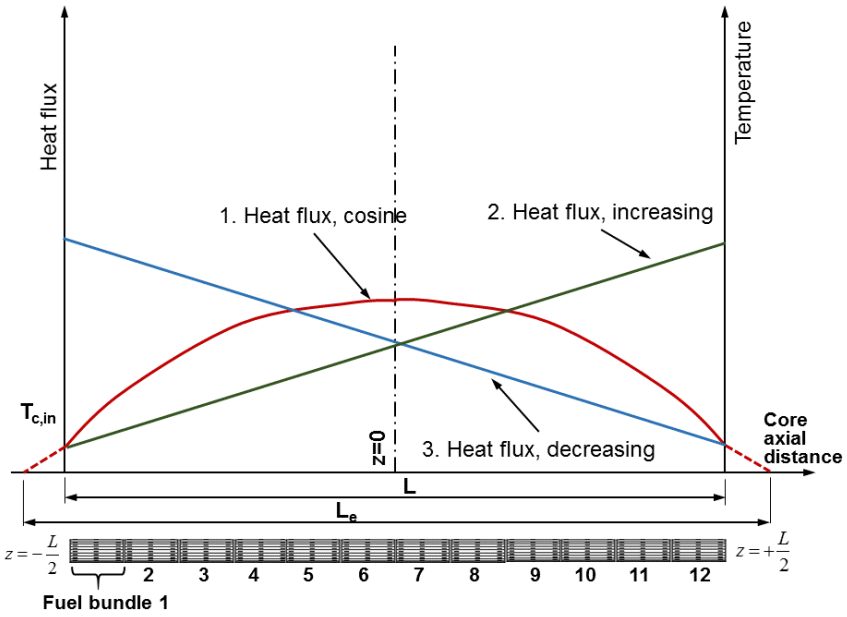

10. Using parameters of a typical CANDU channel, calculate the axial temperature distribution in a fuel channel. Identify the key parameters that affect the calculations, and investigate the sensitivity of the results to these key parameters.

7.5 Fluid flow fundamentals

The flow of coolant in the reactor primary heat transfer system is of key importance for cooling the reactor core under all operational situations, during accidents, and during reactor shutdown. This section provides information on pressure drop calculations and discusses the special topic of flow instabilities.

Design of the primary pump is of critical importance to ensure a robust reactor thermal-hydraulic design. The sources of various friction and local pressure losses around the primary heat transport system are described and compared between PWR and CANDU reactors. Calculation methods used to determine pressure losses around the loop are provided, along with an explanation of the empirical correlations used to calculate pressure losses in single- and two-phase flows in the CANDU primary heat transport system.

The reactor core has a complex geometry, particularly the CANDU fuel channels and the HTS headers and feeders. Moreover, the CANDU reactor primary heat transport system operates partially in two-phase flow. This section describes the type and nature of the experimental tests that were performed to define a number of parameters in the pressure drop calculation.

7.5.1 Introduction to pressure losses

In the nuclear industry, pressure drop calculations are important to determine the appropriate flow rate in the core and the fuel channels, thereby ensuring appropriate heat removal from the core under all possible operating modes. Because almost all reactors under some operating modes operate with two-phase flow, pressure drop calculations in this situation become complex, directly affecting power output and requiring substantial R&D support.

Two-phase pressure drop depends on many parameters, including geometric configuration, mass and volume fractions of the phases, pressure, fluid properties, mass flux, duct orientation, flow direction, and particularly flow patterns. Furthermore, two-phase flow is usually accompanied by heat transfer and changes of phase in multi-component flow. To take into account these many parameters, various empirical correlations have been developed and are used for pressure drop calculations. Mechanistic models also vary in complexity and fidelity, and often they are based on many assumptions to make them workable in a given parameter range.

It is necessary to consider the pressure loss associated with every component in the primary heat transport system. This includes distributed pressure loss due to friction; local pressure losses due to sudden variations in shape, flow area, direction, etc.; and fuel string-related losses and pressure losses due to acceleration (because of flow area variation or fluid density change) and elevation differences (gravity term).

Table 8 shows various components of pressure losses in the reactor heat transport systems in terms of geometry, fluid status, flow nature, flow pattern, flow direction, operating conditions, and driving force [IAEA2001]. Each of these situations introduces major differences in the type and complexity of pressure loss calculations.

Pressure losses must be characterized for a number of components with different geometries.

In addition to frictional pressure losses in the system, Table 9 shows the most important pressure losses in the CANDU reactor core that are specific to CANDU reactors [IAEA2001].

Table 8 Factors affecting pressure drop

Geometry	Basic shapes: Circular pipe, rectangular channel, annulus, etc.
	Other shapes: rod bundle, spacer, valve, orifice, plenum, header, pump, etc.
Fluid status	Single-phase
	Two-phase – one, two, and multiple components.
Flow nature	Laminar
	Turbulent
Flow patterns	Bubbly, slug, annular, etc.
Flow direction	Vertical up-flow
	Inclined flow
	Horizontal flow
Operating Conditions	Steady-state
	Transient
Driving force	Forced convection
	Natural convection

Table 9 CANDU distribution of pressure drop in the primary loop

Pressure Drop in Primary Loop
Entry loss from steam generator outlet pipes to header
Header to feeder entry loss
Inlet feeder bends
Inlet grayloc
Inlet grayloc to liner tube entry
Liner tube to channel entry
Fuel locator
Junction between two bundles
Channel to liner tube entry
Liner tube to outlet grayloc
Outlet grayloc
Outlet feeder bends
Feeder to header entry loss
Header to steam generator inlet pipe entry

The objective of calculating pressure losses with adequate precision is to optimize pump capacity and power requirements, as well as to determine coolant flow rate in the primary circuit, local conditions in bundles and sub-channels, and flow rates across parallel interconnected sub-channels in fuel bundles.

7.5.2 Pressure drop conservation equations

The pressure losses in the primary heat transport system are represented by direct or indirect terms in the conservation equations:

- Mass-balance (continuity) equation;
- Momentum-balance equation; and
- Energy-balance equation.

For design calculations, usually steady-state flow in a channel of uniform flow area in the axial direction is considered. Moreover, negligible variation of fluid properties over the calculation domain is assumed.

The momentum conservation equation is essential to calculate pressure losses along flow paths. The other conservation equations are covered in Chapter 7. The momentum equation can be written for homogeneous or separated flow conditions. Figure 81 shows a calculation domain (control volume) in an inclined flow situation. The forces acting on this control volume are indicated in the figure. Momentum balance over this control volume in fact means a balance of all forces acting on the control volume.

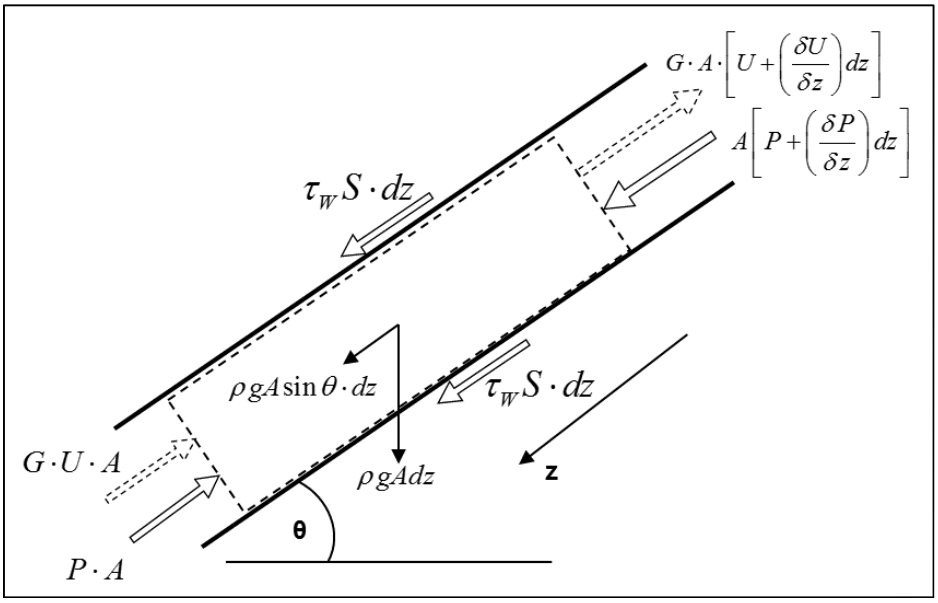

Figure 81 Force-momentum balance in a control volume

Homogeneous flow model

The momentum balance equation over the control volume using the homogeneous flow

assumption is given by Eq. (212) [BIR1960, WAL1969]:

$$\int_A \left[P - \left(P + \frac{dP}{dz}\delta z \right) \right] dA = \int_S \tau_W \delta z dS + \int_A \frac{d}{dz}\left(G u_m \right) \delta z dA + \int_A \rho_H g \cdot \sin\theta \cdot \delta z \cdot dA \,, \tag{212}$$

where P is the pressure, τ_w is the wall friction stress, G is the mass flux, ϑ is the inclination angle, g is the gravity acceleration, dz is the differential axial distance along the channel, δz is the infinitesimal axial distance in the channel, u_m is the mixture velocity, S is the channel circumference, A is the area of the flow channel, and ρ_H is the homogeneous mixture density as a function of flow quality, given by Eq. (213) [WAL1969]:

$$\frac{1}{\rho_H} = \frac{x_e \rho_\ell + (1-x)\rho_g}{\rho_g \cdot \rho_\ell} \,. \tag{213}$$

Equation (212) can be transformed into the following equation after performing some algebraic simplifications and removing the integrals:

$$-\frac{dP}{dz} = \frac{S}{A}\tau_W + \frac{d}{dz}\left(\frac{G^2}{\rho_H} \right) + \rho_H g \sin\theta \,. \tag{214}$$

By substituting the fluid density from Eq. (213), the pressure drop equation can be obtained in the following form:

$$-\frac{dP}{dz} = \frac{S}{A}\tau_W + G^2 \frac{d}{dz}\left(\frac{x_e}{\rho_g} + \frac{(1-x_e)}{\rho_\ell} \right) + \rho_H g \sin\theta \,. \tag{215}$$

Equation (215) contains three pressure drop components on the right side: friction, acceleration, and gravity:

$$-\frac{dP}{dz} = -\left[\left(\frac{dP}{dz} \right)_f + \left(\frac{dP}{dz} \right)_a + \left(\frac{dP}{dz} \right)_e \right]. \tag{216}$$

The negative sign in the above equation indicates that pressure decreases along the flow path.

Separated flow model

In a separated flow model, both flow phases are treated separately, and therefore Eq. (212) takes on the following form:

$$\int_A \left[P - \left(P + \frac{dP}{dz}\delta z \right) \right] dA = \int_S \tau_W \cdot \delta z \cdot dS + \int_A \frac{d}{dz}\left(G_\ell u_\ell + G_g u_g \right) \delta z dA + \int_A \rho_H g \cdot \sin\theta \cdot \delta z \cdot dA \,. \tag{217}$$

The mixture density can be assumed to be a function of the two-phase void fraction as given by the following relation:

$$\rho_{TP} = \alpha \cdot \rho_g + (1-\alpha) \cdot \rho_\ell \,. \tag{218}$$

By substituting Eq. (218) into Eq. (217), the pressure drop equation can be expressed as (in the same form as Eq. (215)):

$$-\frac{dP}{dz}=\frac{S}{A}\tau_W+\frac{d}{dz}\left[\left(1-\alpha\right)G_\ell u_\ell+\alpha\cdot G_g u_g\right]+\left[\alpha\cdot\rho_g+\left(1-\alpha\right)\rho_\ell\right]\cdot g\cdot\sin\theta\,. \tag{219}$$

Further developing the acceleration term using the relationship between the mixture and phasic mass flux leads to the following expression for the separated flow pressure drop:

$$-\frac{dP}{dz}=\frac{S}{A}\tau_W+G^2\frac{d}{dz}\left[\frac{x_a^2}{\alpha\cdot\rho_g}+\frac{(1-x_a)^2}{(1-\alpha)\cdot\rho_\ell}\right]+\left[\alpha\cdot\rho_g+\left(1-\alpha\right)\rho_\ell\right]\cdot g\cdot\sin\theta\,. \tag{220}$$

The frictional pressure loss occurs between the fluid and the channel wall. It depends primarily on the fluid velocity, the tube diameter, and the fluid viscosity.

The acceleration pressure losses occur because of the change in fluid momentum between different locations in the channel. They can be significant in channels with varying flow area and fluid temperature.

The gravity-induced pressure loss in fact occurs because of a change in elevation, i.e., a change of hydrostatic head. Therefore, it is relevant in vertical channels, particularly in piston flow. In single-phase closed loops, the hydrostatic head in sections with upward flow cancels with that in sections with downward flow.

Local pressure losses can result from many different flow obstructions such as valves, orifices, bundle junctions, and appendages. In addition, changes in flow direction in elbows, T-junctions, etc., can result in pressure losses. Significant pressure losses occur with sudden changes in flow area such as sudden contractions, expansions, and orifices.

Using a term for local pressure losses as explained above, Eq. (216) can be written in the following form:

$$-\frac{dP}{dz}=-\left[\left(\frac{dP}{dz}\right)_f+\left(\frac{dP}{dz}\right)_a+\left(\frac{dP}{dz}\right)_e+\left(\frac{dP}{dz}\right)_l\right]. \tag{221}$$

7.5.3 Correlations for calculating pressure losses

Equation (221) has four terms for which correlations must be developed. Before describing these correlations, it is necessary to define them.

Frictional pressure loss

The frictional pressure loss for a single-phase liquid flow is defined by the following relation [IAEA2001]:

$$\Delta p_f=\frac{f\cdot L\cdot G^2}{2D_{hy}\rho_\ell}=\frac{f\cdot L}{D_{hy}}\frac{W^2}{2\rho_\ell A^2}\,, \tag{222}$$

where L is the pipe length, G is the mass flux, D_{hy} is the hydraulic diameter (equal to four times the flow area/the wetted perimeter), ρ_l is the liquid density, W is the mass flow rate, A is the pipe cross section, and f is the friction factor. The frictional pressure drop occurs all along the length and is hence referred to as distributed pressure drop. This equation is applicable for single-phase and homogeneous two-phase flows, although the methods of calculating the

friction factor, f, and the density, ρ, differ in the two cases. Pressure drops across tubes, rectangular channels, bare annuli, and a bare rod bundle (i.e., without spacers) are examples of this component. The challenge in the above equation is to define the appropriate friction factor f for the given flow conditions. This process is described in the following sub-sections.

Acceleration pressure loss

This reversible component of pressure loss is caused by a change in flow area or density. Expansion, contraction, and fluid flow through a heated section are examples. The acceleration pressure loss due to flow area changes can be expressed as [IAEA2001]:

$$\Delta P_a = G^2 \Delta v_\ell \varphi = \frac{\left(1 - A_r\right) W^2 \varphi}{2 A_0^2 \rho_l}. \tag{223}$$

The term Δv_l describes the velocity difference between two points in the channel, A_r is the ratio of the smaller to the larger flow area, A_o is the smaller flow area, and φ is equal to 1 for single-phase flow. For two-phase flow, φ is described by the following relation [IAEA2001]:

$$\phi = \left(\frac{x^3}{\rho_g^2 \alpha^2} + \frac{\left(1-x\right)^3}{\rho_g^2 \left(1-\alpha\right)^2} \right) \left(\frac{\rho_g \rho_l}{x \cdot \rho_l + \left(1-x\right) \cdot \rho_g} \right). \tag{224}$$

The acceleration pressure loss due to density change for single-phase and two-phase flows can be expressed as:

$$\Delta p_a = G^2 \left\{ \left(\frac{1}{\left(\rho_m\right)_o} \right) - \left(\frac{1}{\left(\rho_m\right)_i} \right) \right\}. \tag{225}$$

For single-phase flows, this component is negligible, but it can be significant in two-phase flows. For two-phase flow, the above equation can be used with ρ_m given by [IAEA2001]:

$$\frac{1}{\rho_m} = \left(\frac{x^2}{\rho_g \cdot \alpha} + \frac{\left(1-x\right)^2}{\rho_l \left(1-\alpha\right)} \right). \tag{226}$$

To evaluate acceleration pressure loss due to density change, accurate prediction of fluid density is necessary. For single-phase flow, fluid density can be predicted reasonably well using established relationships for thermo-physical properties of fluids. For two-phase flow, it is necessary to predict the void fraction, and in turn the acceleration pressure loss, accurately to determine density. Hence, the correlation for void fraction must be chosen carefully.

Elevation pressure loss

This reversible component of pressure loss is caused by the difference in elevation and can be expressed as:

$$\Delta p_e = \left[\rho_g \cdot \alpha + \rho_l \left(1-\alpha\right) \right] \cdot g \cdot \sin\theta \cdot \Delta z. \tag{227}$$

Local pressure losses

These are the localized irreversible pressure loss components caused by changes in flow

geometry and flow direction. Pressure drops across valves, elbows, tees, and spacers are examples. The local pressure loss (i.e., the form loss) is defined by the following relation [IAEA2001]:

$$\Delta p_l = K_l \frac{G^2}{2\rho_\ell}, \tag{228}$$

where K_l is the local form loss coefficient, which has different correlations for different geometries, single-phase flows, and two-phase flows. The challenge in the above equation is to define the local friction factor coefficient K_l properly. This topic is covered in the following sub-sections.

7.5.3.1 Frictional pressure drop correlations in single-phase flow

For friction pressure loss correlations, circular pipe, annuli, rectangular channels, and rod clusters are the most common applications. For local pressure loss correlations, spacers, top and bottom tie plates, and locations of flow area changes such as constrictions, expansions, bends, tees, and valves are the most common applications. For CANDU-type fuel bundles, the degree of misalignment of two adjacent fuel bundles is also important in estimating the pressure drop. In addition, in-core effects like radiation-induced creep, blister formation, swelling, and corrosion are also important factors affecting pressure drop, but are not dealt with here.

Figure 82 shows the Moody chart for friction factor as a function of Reynolds number and pipe roughness [MOO1944, IDE1996]. This logarithmic diagram is the basis for calculating friction factors in single-phase flow in pipes. On the left side is the area of laminar flow, represented by a single straight line. Towards the right side, a group of lines is shown that indicate higher friction factors for higher values of pipe roughness and slowly declining friction factors for higher Reynolds numbers.

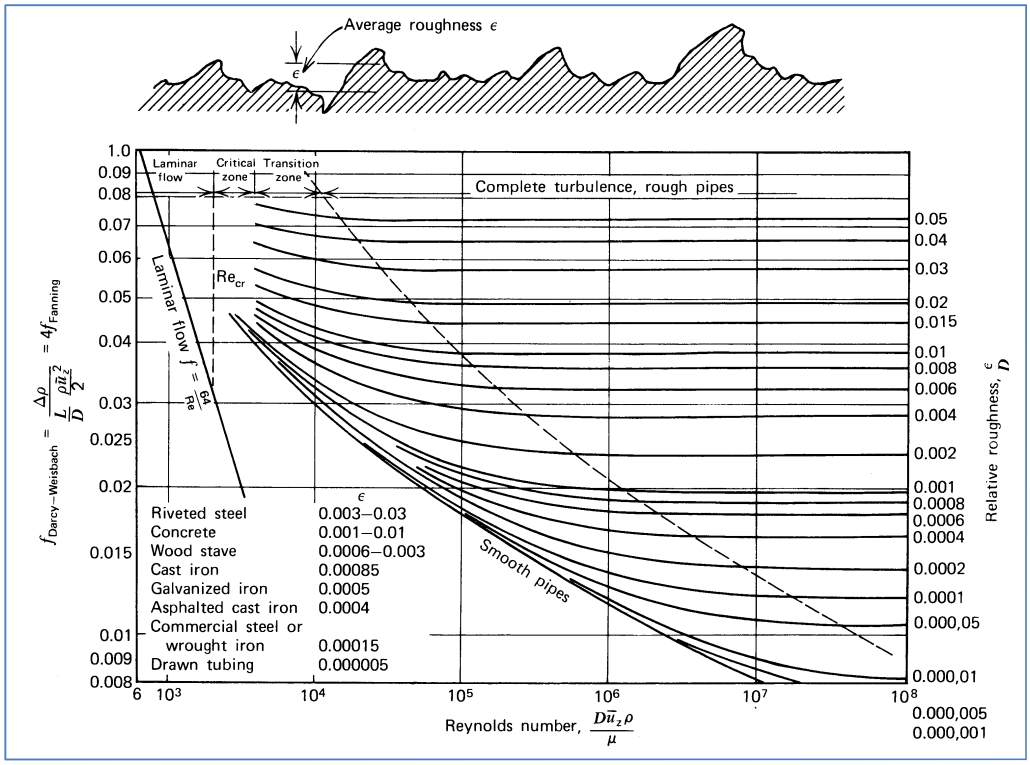

Figure 82 Moody chart for friction factors

For fully developed laminar flow, the friction factor is given by [IAEA2001]:

$$f = \frac{64}{Re}, \tag{229}$$

which is valid for Reynolds numbers less than 2000, as given by Eq. (12). This correlation is shown by a straight line on the left side of Figure 82.

For turbulent flow in smooth pipes, several friction factor correlations have been proposed and are used. A few commonly used correlations for smooth pipe are given below.

The Blasius equation [AECL2001] has the following form:

$$f = 0.316 \cdot Re^{-0.25}, \tag{230}$$

which is valid in the range of $3000 \le Re \le 10^5$.

The following equation, which is valid in the range of $3000 \le Re \le 10^5$, is also often used for design [IAEA2001]:

$$f = 0.184 \cdot Re^{-0.2}. \tag{231}$$

Colebrook-White (1938) proposed the following equation, which is valid for both smooth and rough pipes over the whole range of Reynolds numbers above 3000 [IAEA2001]:

$$\frac{1}{\sqrt{f_{tube}}} = -2 \cdot \log\left(\frac{\varepsilon / D_{tube}}{3.7} + \frac{2.51}{\mathrm{Re} \cdot \sqrt{f_{rube}}} \right). \tag{232}$$

This correlation is often used in computer codes, but it requires several iterations because it is not explicit in terms of the friction factor *f*. Many other correlations attempt to capture different effects such as different parameter ranges or heat transfer effects. These include changes in near-wall velocity gradient due to fluid density changes, bubble formation, sharp variations due to liquid-film thinning, and liquid-surface or vapour-surface contact. These all create different wall heating effects that have a significant impact on the friction factor, even before two-phase flow occurs.

7.5.3.2 Frictional pressure drop correlations in two-phase flow

Many two-phase flow pressure drop correlations can be found in the literature. These correlations can be classified into the following four general categories: (1) empirical correlations based on the homogeneous model; (2) empirical correlations based on the two-phase friction multiplier concept; (3) direct empirical models; and (4) flow pattern-specific models.

In addition, computer codes based on two-fluid or three-fluid models require correlations to partition wall friction among the fluids and to determine interfacial friction correlations.

The most commonly used approach is the two-phase multiplier approach, which is described in this section. In this case, the two-phase pressure drop is calculated by multiplying the single-phase pressure drop by a two-phase frictional multiplier. Equation (233) exemplifies this approach:

$$\Delta p_{f,TP} = \phi_{L0}^2 \Delta p_{f,L0} \quad \text{or} \quad \Delta p_{f,TP} = \phi_L^2 \, \Delta p_{f,L}, \quad \phi_{L0}^2 = \phi_L^2 \left(1-x\right)^{2-b}, \tag{233}$$

where $\Delta p_{f,L}$ is the single-phase pressure drop based on only single-phase liquid in the channel and $\Delta p_{f,L0}$ is the single-phase pressure drop based on total flow as single-phase liquid in the channel. Assuming $f = a \cdot \mathrm{Re}^{-b}$, the relationship between ϕ_{L0}^2 and ϕ_L^2 can be expressed as $\phi_{L0}^2 = \phi_L^2 \left(1-x\right)^{2-b}$.

The two-phase frictional multipliers ϕ_L^2 or ϕ_{L0}^2 are empirical factors based on experimental data and are expressed in the form of graphs or correlations that typically depend on quality and pressure. A mass-flux effect is observed primarily at low flows (and hence is flow-regime-dependent). Surface heating has a strong impact (a near-wall effect) on two-phase multipliers in tubes and annuli, but not in bundles (due to compensating effects).

The correlation for a homogeneous two-phase frictional multiplier in its simplest form can be expressed as:

$$\phi_{L0}^2 = \frac{f_{TP}}{f_\ell} \frac{\rho_\ell}{\rho_{TP}} = \left[1 + x_e \left(\frac{\rho_\ell - \rho_g}{\rho_g} \right)\right] \left(\frac{\mu_\ell}{\mu_{TP}} \right)^{-b}. \tag{234}$$

The two-phase viscosity correlation can have various forms with different degrees of complexity. The simplest correlation was introduced by Cicchitti *et al*. [IAEA2001]:

$$\mu_{TP} = x_a \cdot \mu_g + (1 - x_a)\,\mu_\ell . \tag{235}$$

In general, the following definitions of two-phase frictional multipliers are often used in non-homogeneous two-phase flow:

$$\phi_{LO}^2 = \frac{(dp/dz)_{TPF}}{(dp/dz)_{LO}}, \quad \phi_{GO}^2 = \frac{(dp/dz)_{TPF}}{(dp/dz)_{GO}}, \tag{236}$$

$$\phi_L^2 = \frac{(dp/dz)_{TPF}}{(dp/dz)_{L}}, \quad \phi_G^2 = \frac{(dp/dz)_{TPF}}{(dp/dz)_{G}}, \tag{237}$$

where the denominators refer to the single-phase pressure gradient for flow in the same duct, with mass flow rates corresponding to the mixture flow rate in the case of ϕ_{LO}^2 and ϕ_{GO}^2, and individual phases in the case of ϕ_L^2 and ϕ_G^2. Among these, ϕ_{LO}^2 is the most popular frictional multiplier for steam-water flow. Figure 83 shows a popular form of this two-phase friction multiplier suggested by Nelson-Martinelli [COL1972]. The frictional multiplier is shown as a function of mass quality and pressure. It rises sharply when two-phase flow is initiated (even for very small mass qualities), and its value reaches 10 times the single-phase value even at low quality. Moreover, the friction multipliers are higher at low pressure than at high pressure due to the difference in volumetric and mass flow rates (as shown in Figure 22).

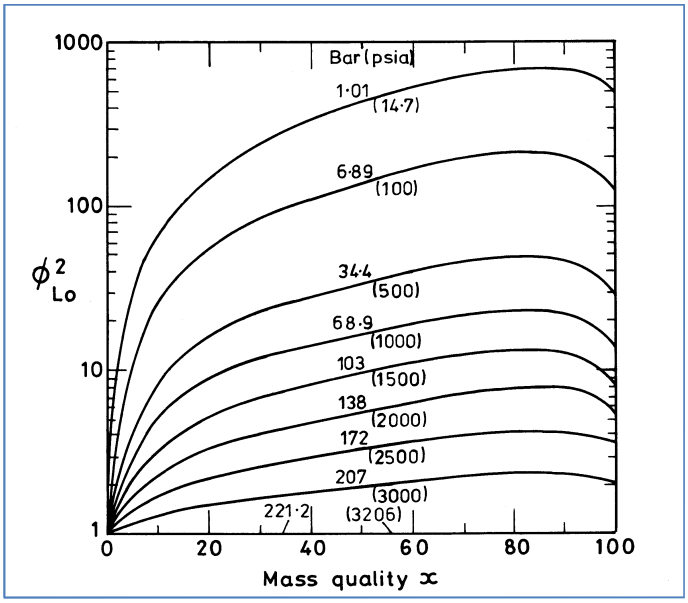

Figure 83 Martinelli-Nelson two-phase multiplier in separated flow

For diabatic two-phase flow (i.e., flow with heat transfer), the quality, void fraction, flow pattern, and other properties change along the heated section. To calculate the pressure drop in such cases, two approaches are usually followed. In the first approach, which is most commonly used, the average ϕ_{LO}^2 is calculated as:

$$\phi_{LO}^2 = \frac{1}{L}\int_0^L \left[\phi_{LO}^2(z)\right] dz \,. \tag{238}$$

The approach can be used in cases where $\phi_{LO}^2(z)$ is a function that can be integrated. Numerical integration is used in other cases.

In the second approach, the heated section is subdivided into a number of small segments. Based on average conditions (i.e., x_i, α_i, and flow pattern) in that segment, the pressure drop is calculated as in adiabatic two-phase flow using one of the models described previously.

7.5.3.3 Local pressure drop correlations

The single-phase local pressure losses are given in Eq. (228). The two-phase local pressure losses are normally obtained using the two-phase multiplier approach. In this case, the two-phase local pressure loss is given by the following relation [IAEA2001]:

$$\Delta P_{l,TP} = \phi_{l,LO}^2 \cdot \Delta P_{l,SP} \,. \tag{239}$$

A simple form of the two-phase local loss multiplier can be obtained by the following relation:

$$\phi_{l,LO}^2 = 1 + x_a \left(\frac{\rho_\ell - \rho_g}{\rho_g} \right). \tag{240}$$

Sudden contraction

Single-phase loss coefficients for sudden contraction can be calculated based on flow-area ratio, according to the following equation [IDE1996]:

$$K_{contr} = 0.5\left(1 - \frac{A_f}{A_0}\right)^{3/4}, \tag{241}$$

where A_f and A_o are smaller and larger pipe cross-sectional areas respectively.

In general, the irreversible pressure two-phase pressure drop due to a flow-area change is estimated from the knowledge of single-phase loss coefficient using an appropriate model.

Sudden expansion

In the case of sudden expansion, the following correlation is used, which is based on the ratio of area changes [IDE1996]:

$$K_{\exp} = \left(1 - \frac{A_f}{A_0}\right)^2 . \tag{242}$$

Fitzsimmons (1964) provides the following equation to calculate the pressure change across an abrupt expansion:

$$\Delta p = \frac{G^2 A_r^2}{\rho_L}\left\{\frac{\rho_l}{\rho_g} x^2 \left(\frac{1}{\alpha_1 A_r} - \frac{1}{\alpha_2}\right)\right\}\left\{(1-x)^2\left(\frac{1}{(1-\alpha_1)A_r} - \frac{1}{(1-\alpha_2)}\right)\right\}, \tag{243}$$

where subscripts 1 and 2 refer respectively to the upstream and downstream locations of the abrupt expansion and $A_r = A_f / A_0$.

Fittings and bends

The single-phase pressure drop due to bends and fittings can be calculated using the appropriate loss coefficients from Idelchik [IDE1996]. For bends, the loss coefficient depends on the bend angle, i.e., on the ratio of pipe diameter to bend radius. Because pressure drop is dependent on piping component geometry, other specific configurations (i.e., end-fitting flow characterization) must be experimentally tested to determine the specific pressure drop correlations.

Orifices

The pressure loss through an orifice can be calculated using the following equation [IDE1996]:

$$\Delta p_{orf} = f_{orf} \frac{\rho W_0^2}{2} \phi_{LO}^2 . \tag{244}$$

The loss coefficient in an orifice depends on the orifice geometry, particularly at the orifice entry. An extensive description of loss coefficients with different orifices in single-phase flow is provided by Idelchik [IDE1996]. For separated two-phase flow (stratified) at an orifice, Beattie [IAEA2001] obtained the following expression for ϕ_{LO}^2 :

$$\phi_{LO}^2 = \left\{1 + x\left(\frac{\rho_L}{\rho_G} - 1\right)\right\}^{0.8} \left\{1 + x\left(\frac{\rho_L \mu_G}{\rho_L \mu_L} - 1\right)\right\}^{0.2} . \tag{245}$$

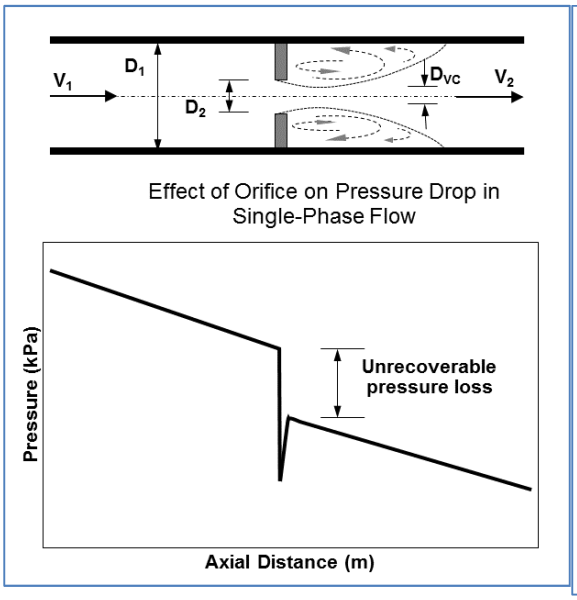

Figure 84 Single-phase pressure distribution over a square-edged orifice

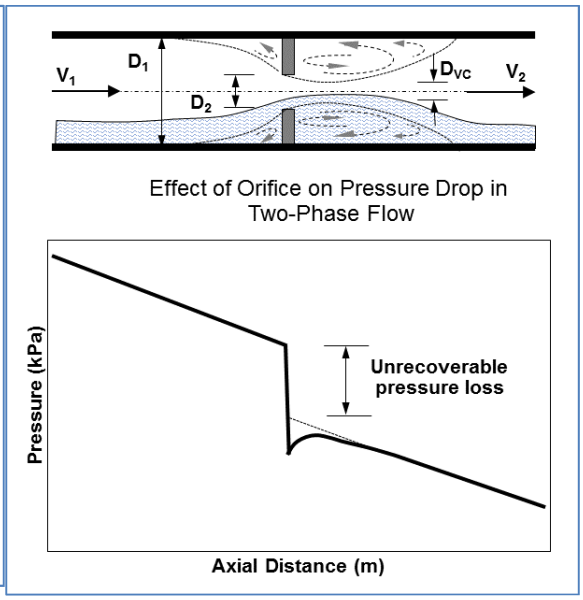

Figure 85 Two-phase pressure distribution over a square-edged orifice

Figure 84 shows a diagram of a pressure loss in a square-edged orifice in a single-phase liquid

flow with 40% blocked area (a blunt-edged orifice). The pressure falls sharply over the orifice because of the sudden increase in velocity (according to the Bernoulli equation, Eq. (43)). Due to turbulence downstream of the orifice, unrecoverable losses occur because mechanical energy is dissipated into thermal energy. Therefore, downstream of the orifice, where the pipe diameter is the same as that upstream of the orifice, the pressure is lower than it would have been without the orifice.

Figure 85 shows the two-phase pressure distribution over the same orifice as in Figure 84. The pressure drop slope is much higher in two-phase flow than in single-phase flow, which signifies an increase in frictional pressure drop. In addition, the unrecoverable losses are much higher, and the pressure recovery occurs over a longer pipe section (pressure recovery is "smoother").

Grid spacers and tie plates

Because of the variation and complexity of their geometry, it is extremely difficult to establish a pressure loss coefficient correlation of general validity for grid spacers. However, calculation methods that are reasonably accurate for design purposes can be achieved. To determine pressure drop across spacers more precisely, experimental studies are required.

Generally, tie plates are used at the ends of rod cluster fuel elements and structurally join all the fuel pins. Unlike spacers, the flow areas on the downstream and upstream sides of tie plates are different. Moreover, they are generally located in the unheated portion of the bundle. An approximate calculation for design purposes can be made using the contraction and expansion model for local pressure losses. In addition, the friction losses over the thickness of the tie plates can be calculated using the hydraulic diameter concept. For two-phase pressure losses, the homogeneous or slip model described above can be used.

7.5.3.4 Pressure losses in CANDU fuel bundles

Several short bundles are stacked end-to-end in CANDU-type PHWRs instead of the long single fuel bundle used in PWRs and BWRs. Due to this basic difference in design concept, some of the issues and geometries are unique to the CANDU design.

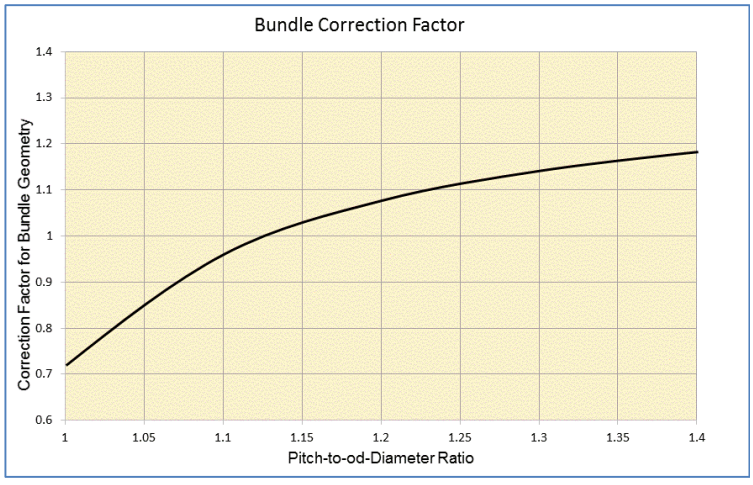

Figure 86 Bundle correction factor (37-element hexagonal bundle)

The pressure losses in CANDU bundles are calculated based on the hydraulic-equivalent

diameter approach using a tube-based equation. Several correction factors are used, including a correction for geometric effects (the differences between tubes and bundles); a correction for eccentricity effects (differences between concentric and eccentric bundles) in crept channels; a correction for channel shape effect (converging and diverging channels) in crept channels; and a correction for surface heating effect.

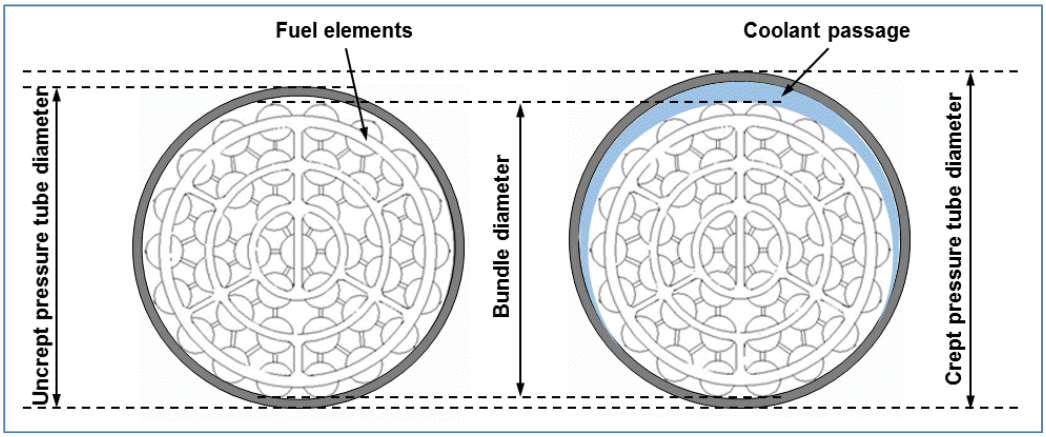

Figure 87 Eccentricity effect

Figure 86 shows a sample of the fuel bundle effect in a hexagonal fuel bundle [LEU2004]. The correction factor is given as a function of the pitch-to-rod-diameter ratio. It is evident from this figure that the correction factor can be greater than or less than one.

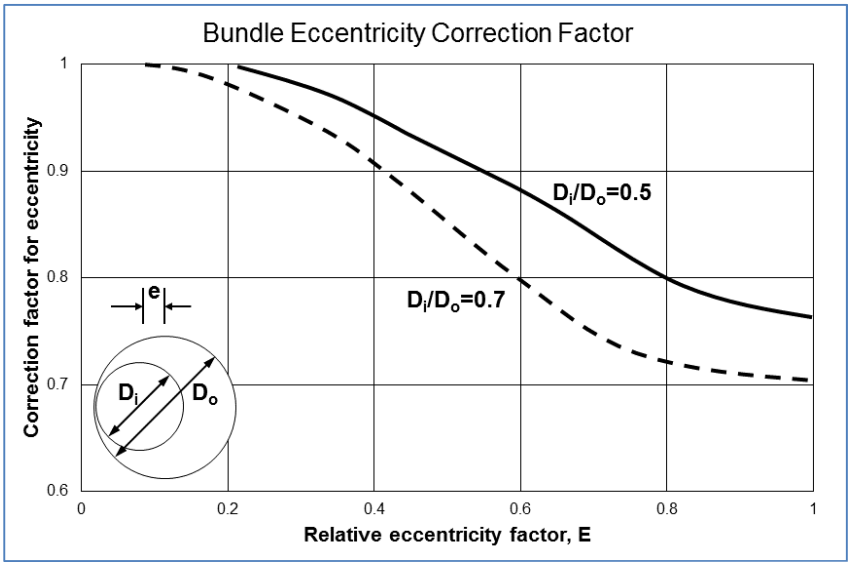

Figure 88 Eccentricity correction factor

Figure 87 shows [LEU2004] on the left side a cross section of the fresh CANDU fuel bundle in an uncrept channel, and on the right side the same bundle in a crept channel, in which the pressure tube diameter has increased after a number of years of irradiation. It is evident that the eccentricity of the irradiated fuel bundle has significantly increased. The effect of eccentricity increase in an annular channel on the friction correction factor is shown in Figure 88. This figure shows that the correction factor for eccentricity decreases from one to a certain

value that depends on the degree of eccentricity and on the ratio of the inner and outer rod diameters. Pressure tube creep and development of significant bundle eccentricity lead more fluid to flow at the top of the bundle where the resistance to flow is lower, thus leaving the bundle with reduced fluid flow. This phenomenon also results in development of a non-uniform velocity distribution in the fuel channel.

The following empirical correlation was proposed by Snoek and Ahmad [IAEA2001] for a friction factor based on experiments on a six-metre long electrically heated horizontal 37-rod cluster (this correlation has not been validated or accepted for a CANDU fuel bundle):

$$f = 0.05052 \cdot Re^{-0.05719} \quad \text{for} \quad 108{,}000 \le Re \le 418{,}000. \tag{246}$$

The following empirical correlations were proposed by Venkat Raj [IAEA2001] based on a set of experiments with prototype horizontal 37-rod clusters for PHWRs with a CANDU-type spacer. They include the junction pressure drop (these correlations have not been validated or accepted for a CANDU fuel bundle):

$$f = 0.22 \cdot Re^{-0.163} \quad \text{for} \quad 10{,}000 \le Re \le 140{,}000, \tag{247}$$

$$f = 0.108 \cdot Re^{-0.108} \quad \text{for} \quad 140{,}000 \le Re \le 500{,}000.$$

However, in addition to the above friction factor, in a CANDU fuel bundle, a number of local pressure losses must be taken into account. The total CANDU bundle pressure losses must include: (1) friction; (2) local resistances from bundle junctions, spacers, buttons (43-element bundle), and bearing pad planes; (3) acceleration; and (4) end fittings.

Various authors have attempted to combine the above effects into a single pressure loss correlation. The friction and form losses have been combined into a bundle loss coefficient given by the following relation [LEU2004, IAEA2001]:

$$\Delta P_{sp,bundle} = K_{sp,bundle} \frac{G^2}{2\rho_\ell} = \left(\frac{f_{bundle} L_{bundle}}{D_{hy}} + K_{junction} + K_{appendage} \right) \frac{G^2}{2\rho_\ell}. \tag{248}$$

The best approach for CANDU fuel bundles is to perform experimental measurements of the pressure losses in a CANDU fuel channel experimental apparatus, i.e., in a so-called fuel bundle or fuel channel flow characterization test. Once pressure losses have been precisely measured for a fuel channel design, they can be tabulated or correlated in a convenient way for use by designers and analysts.

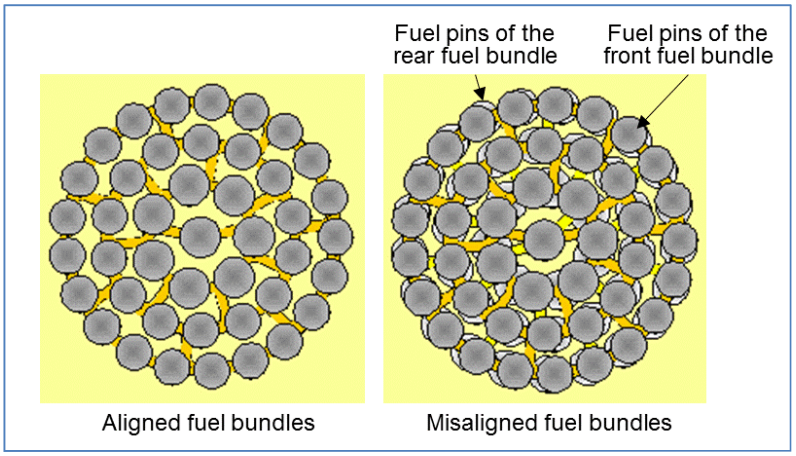

Figure 89 Bundle junction misalignment effect

One of the important contributors to pressure losses in CANDU fuel bundles is fuel bundle misalignment. Figure 89 shows two CANDU fuel channels that visually illustrate this phenomenon [LEU2004]. The channel on the left has all fuel bundles aligned, so that each fuel element is behind the previous fuel element upstream. This perfect alignment achieves the lowest possible pressure loss from local resistance at the bundle end plates. However, in practice, this perfect alignment is not possible because fuelling machines cannot ensure that bundles are always inserted in a channel in the same position. In practice, as fuel bundles are repeatedly inserted into the fuel channel, this misalignment develops a random distribution, as shown on the right side of Figure 89. Pressure loss measurements are therefore performed with various degrees of misalignment to cover all possible situations that can arise in practice.

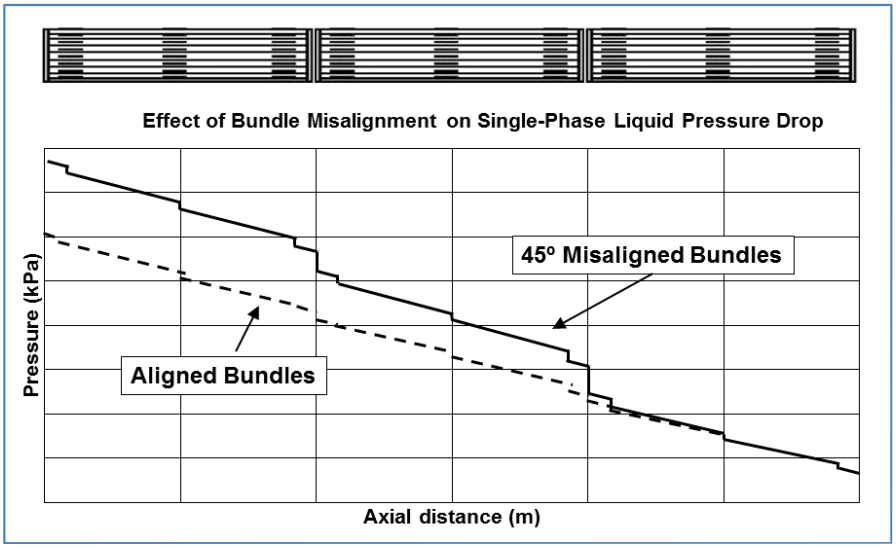

Figure 90 Typical single-phase pressure distribution over misaligned bundles

Figure 90 shows a comparison of typical pressure drops in single-phase flow with three bundles with a misalignment of 45^{o} compared to fully aligned bundles. This figure clearly shows that at each bundle junction, an abrupt local pressure loss can be measured. If the bundles are

misaligned to a greater extent, the abrupt pressure drop at the junction will be larger.

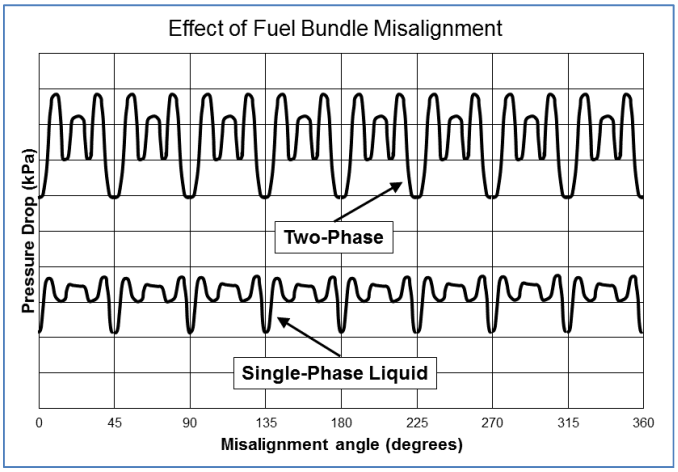

Figure 91 Typical pressure drop in misaligned fuel bundles

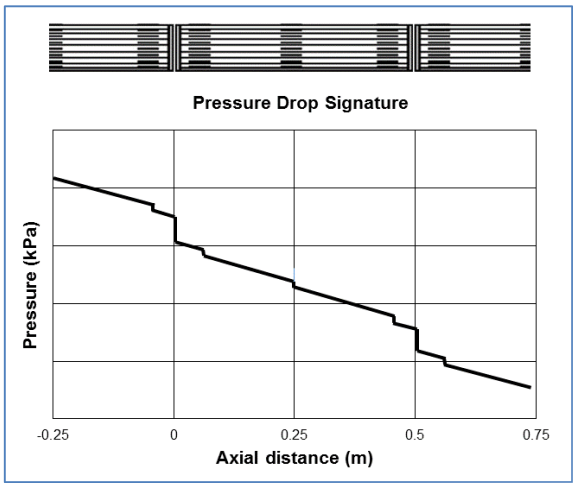

Figure 92 Typical misaligned junction pressure drop signatures

Figure 91 shows a CANDU fuel bundle flow characterization test in which actual pressure measurements were collected along the fuel bundle [LEU2004]. It is evident that each change of flow area along the fuel bundle, such as bundle end plates, spacers, buttons, and bearing pads, creates a clear pressure loss of magnitude proportional to the change in flow area. It is obvious from this figure that the pressure drop variation is symmetrical within a 45 degree cycle.

Figure 92 shows a pressure drop signature from misaligned fuel bundles [LEU2004]. It is clear that the degree of misalignment has a direct impact on the pressure drop measurements. The effect is more pronounced in the case of two-phase flow, in which case the difference in the measured pressure drops is much higher, both in absolute value and in variability with the level of misalignment.

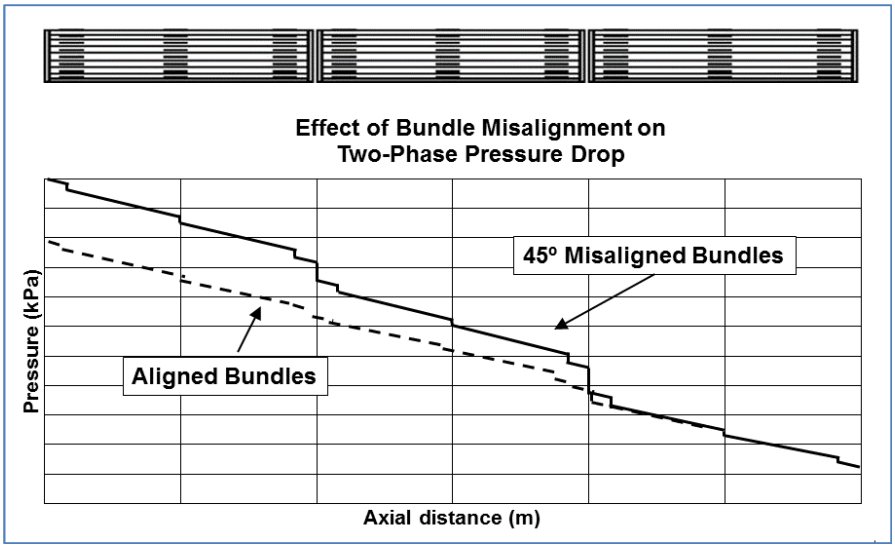

Figure 93 Typical two-phase pressure distribution over misaligned bundles

Figure 93 shows a typical pressure drop effect for misaligned fuel bundles in two-phase flow. This figure should be compared to Figure 90, which shows the same test in single-phase flow. Again, the absolute value of the pressure drop is higher in the case of two-phase flow, and the pressure losses at the bundle end plates are also higher.

7.5.3.5 Use of pressure drop measurements to define the onset of significant void (OSV)

Because pressure drop measurements show such distinctive differences in pressure drop between single-phase and two-phase cases, it has been noted that a sudden increase in pressure drop at a certain location in a thermal-hydraulic network can be used as an indication of the initiation of bulk boiling (i.e., the onset of significant void (OSV)).

Figure 94 shows pressure drop measurements for a crept fuel channel in which three different power rates were applied, resulting in different channel boiling outcomes [LEU2004, POP2014]. The coolant inlet was on the left side and the outlet on the right side. The reference case (dark blue line) is the case of sub-cooled conditions, with outlet thermodynamic quality negative and nominal channel power. When channel power was increased to greater than 200%, the pressure drop increased significantly downstream of the ninth fuel bundle because in this area boiling was initiated, resulting in slightly positive channel outlet thermodynamic quality. When the channel power was increased to three times nominal power, the outlet thermodynamic quality further increased, and the pressure drop as well. Note that when boiling starts at a certain location downstream (in this case, around the eighth fuel bundle), the pressure drop starts to increase, which indirectly indicates the point where OSV occurs in this channel. Hence, pressure drop measurements can reveal where boiling occurs in a fuel channel.

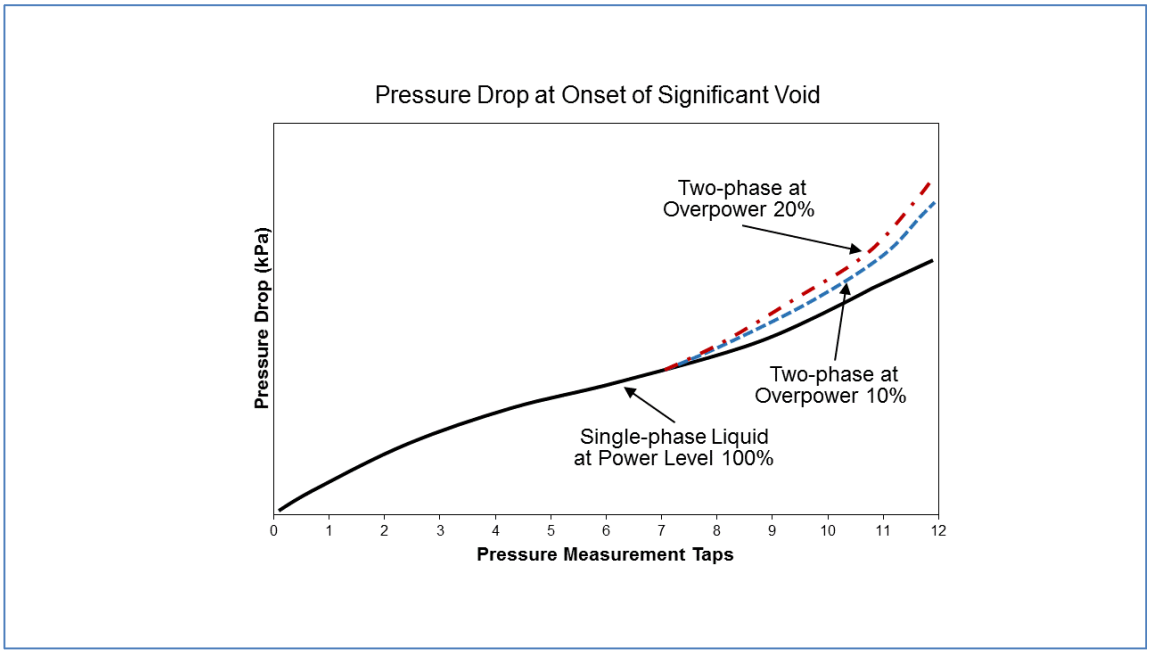

Figure 94 Pressure gradient along a flow channel in boiling

The Saha-Zuber correlation [REL2010, CAT1998, CAT2000, CAT2005] is used to calculate the OSV point in tubes and has the following form:

$$x_{OSV} = -0.0022 \frac{q \cdot D \cdot C_{pf}}{k_f \cdot H_{fg}} \quad \text{for Peclet number } (GDCp/k) < 70{,}000, \tag{249}$$

$$x_{OSV} = -154 \frac{q}{k_f \cdot H_{fg}} \quad \text{for Peclet number} \geq 70{,}000. \tag{250}$$

A modified Saha-Zuber correlation for fuel bundles is based on empirical coefficients using full-scale bundle data.

7.5.3.6 Pressure drop in pipes and orifices

The information covered in the previous sections can now be used to describe pressure drop behaviour in a channel with various changes in geometry. Figure 95 shows such an example, in which fluid comes from a pipe on the left side, flows through a pipe with a different diameter and an orifice, and then into a much larger pipe on the right side. Hence, in this example, major abrupt changes in flow cross-sectional area can be observed.

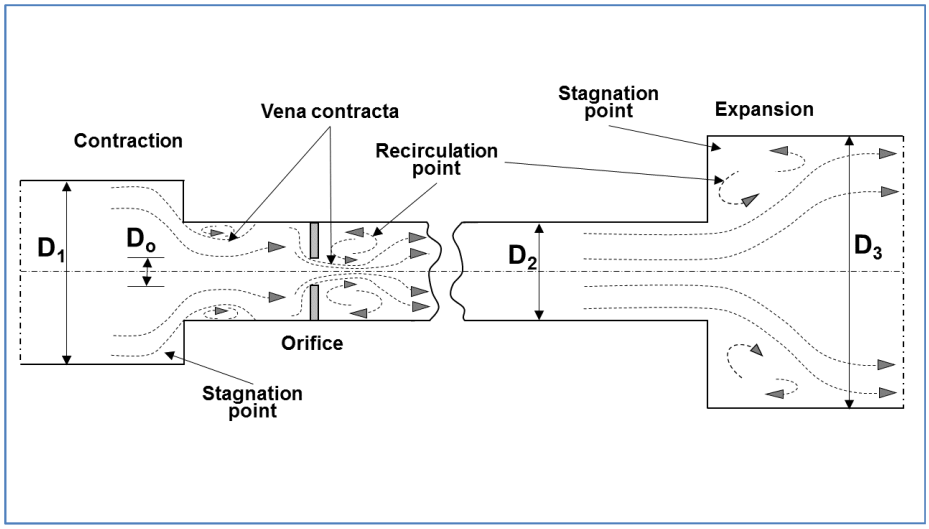

Figure 95 Example of abrupt area changes and orifice

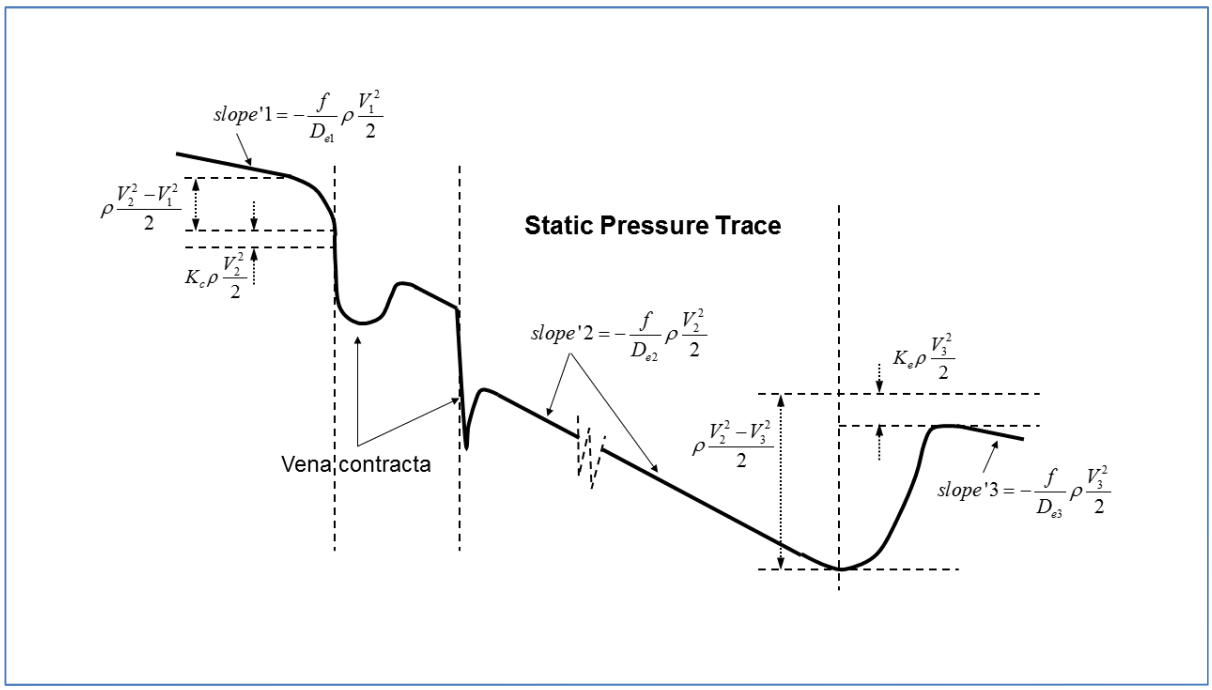

Figure 96 Pressure drop behaviour with abrupt area changes and orifice

The pressure drop diagram for this case is shown in Figure 96. At the transition point between the pipe on the left side (diameter D_1) and the middle pipe (diameter D_2), i.e., at the sudden contraction point, the velocity increases to V_2. As it accelerates, the fluid goes through a vena contracta with eddy flow around the pipe corners. The recoverable pressure loss resulting from the fluid acceleration is equal to $\rho\left(V_2^2 - V_1^2\right)/2$, and the unrecoverable local loss (sudden

contraction) resulting from the turbulence around the vena contracta is $K_e \rho V_2^2 / 2$. The velocity in the vena contracta is higher than the velocity appropriate for the pipe with equivalent diameter D_2. Therefore, the pressure in the vena contracta decreases further around the area occupied by the vena contracta. Downstream of the vena contracta, the pressure recovers where the influence of the vena contracta terminates, and the fluid velocity assumes the value appropriate for a pipe with diameter D_2.

Following the sudden contraction, the flow goes through an orifice with diameter D_o, through another vena contracta, and experiences further unrecoverable pressure loss.

On the other side, where the sudden expansion from the pipe into the larger pipe (diameter D_3) occurs, the reverse happens. The velocity slows down in the larger right-hand pipe from V_2 to V_3. Note that velocity V_3 is different from V_1 because of the different pipe size. At the sudden expansion, the unrecoverable local loss resulting from the turbulence around the vena contracta is $K_e \rho V_3^2 / 2$, and the recoverable deceleration pressure gain is $\rho \left(V_3^2 - V_2^2 \right) / 2$.

Note that the slope of the pressure drop curve in the three pipes is different because of the different hydraulic diameters of the three pipes.

Having defined all the pressure loss terms in a piping configuration, it is interesting to compare their absolute values and to obtain an impression of their relative contribution to the overall pressure drop. This is done in Figure 97, in which typical pressure drop components are shown for a fuel channel in a typical BWR reactor [TOD2011].

Figure 97 shows that for low mass fluxes, the relative contributions of the friction, acceleration, and gravity terms are similar. However, with increased mass flux, the relative contribution of the friction component significantly outweighs the other components. Note that the friction component in the above figure includes both distributed and local losses.

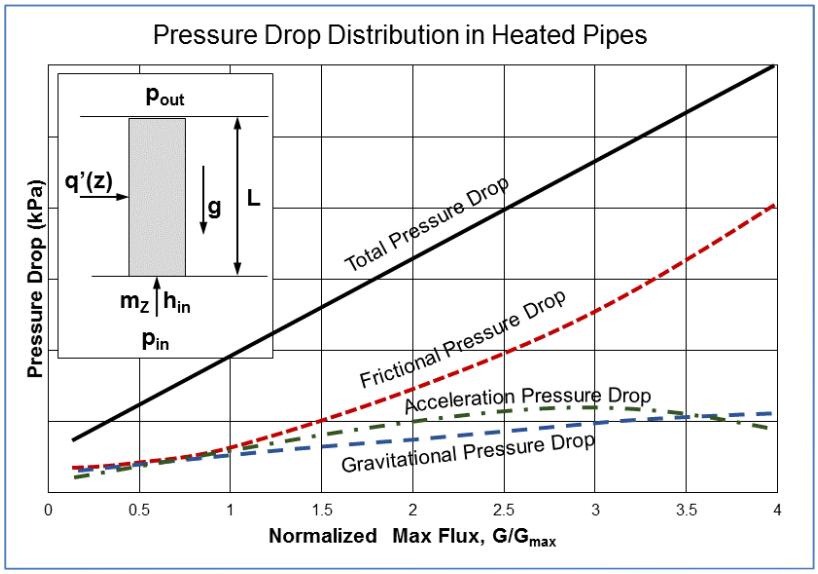

Figure 97 Pressure drop components

7.5.4 Flow Instability

7.5.4.1 Fundamentals of flow instability

Flow instabilities are of particular importance for the reactor core. Under certain flow and heat generation conditions, flow instabilities can cause significant changes in the fluid flow distribution among certain channel groups in the core, thus exposing parts of the core to insufficient cooling and consequent overheating, which can cause fuel damage. Moreover, certain types of flow instabilities can cause pump malfunctions if the pump is not properly selected. This section explains the nature of flow instabilities in the reactor core, provides information on various types of instabilities, and focusses particularly on the Ledinegg instability [TOD2011].

Understanding flow instabilities is instrumental to obtaining a good understanding of the thermal-hydraulic system behaviour of nuclear reactor heat transport systems. A fluid flow in a heated channel with a sub-cooled inlet condition undergoes large volume changes in a non-uniform manner. Because the thermal and hydraulic properties of the flow change continuously along the channel, the flow at any axial point in the channel can never become fully developed thermally or hydrodynamically. Because the flow is not in equilibrium, the flow properties fluctuate upstream and downstream of the point considered, often leading to instability. Flow instabilities are of different types depending on the system configuration and operating conditions. Flow oscillations can dramatically reduce the ability of the coolant to remove heat from the reactor core. On the basis of primary features such as oscillation periods, amplitudes, and relationships between pressure drop and flow rate, flow instabilities have been classified into several types. Flow instabilities in a heated channel are usually caused by two-phase flow and density wave effects. These instabilities are primarily classified as static or dynamic. Some static and dynamic instabilities occur particularly during start-up conditions.

The scale of instability can vary from macroscopic, involving the whole heat transport system, to microscopic, occurring locally in some component or part of the thermal-hydraulic network. In terms of the driving process, instabilities can be grouped into static or dynamic.

A “static instability” occurs when a small perturbation from the original steady-state flow leads to a new stable operating condition that is not close to the original state. The mechanism and the threshold conditions can be predicted using steady-state system characteristics. The pressure drop characteristics, nucleation properties, and flow regime transitions of a flow channel play an important part in characterizing static instabilities. Critical heat flux (CHF), which limits the heat transfer capability of boiling systems, is influenced by static instabilities. Ledinegg instability, flow pattern transition instability, geysering, chugging, and vapour burst are also categorized as static instabilities.

Dynamic instability is caused by dynamic interaction among flow rate, pressure drop, and void fraction. The mechanism involves the propagation of disturbances by pressure and void or density waves. Density wave oscillations (DWOs), parallel channel instability, and pressure drop oscillations (PDOs) are in this group.

Ledinegg instability or flow-excursive instability is characterized by a sudden change in the flow

rate to a lower value or a flow reversal. This instability will be further explained in this section.

Flow pattern transition instability is caused mainly by the different pressure drop characteristics of various flow patterns. For example, if bubbly flow changes to annular flow due to large void generation, the channel pressure drop decreases. For constant pressure drop in a heated channel, when a bubbly flow changes to an annular flow pattern, the flow rate increases, leading to decreased vapour generation. This makes the flow pattern revert to a bubbly or slug flow pattern, and the cycle is repeated.

Geysering occurs at low power and low circulation flow rates. It occurs due to bubble formation, growth, and subsequent collapse during start-up. In vertical channels during start-up, with high inlet sub-cooling, voids are generated, and a large slug of bubbles is formed, which grows due to the decrease in hydrostatic pressure head as it moves toward the exit. The vapour then mixes with the liquid in the sub-cooled riser and becomes condensed there. The condensed liquid re-enters the channel and restores non-boiling conditions. This process repeats periodically and causes flow oscillations.

Vapour burst instability occurs due to sudden vaporization of the liquid phase with a rapid decrease in mixture density. For example, a very clean and smooth heated surface may require high wall superheat for nucleation. The fluid adjacent to the surface is highly superheated, and vapour generation is rapid when nucleation starts. This in turn ejects liquid from the heated channel. Rapid vaporization cools the surface, and the cooler liquid keeps vaporization suppressed until the wall temperature reaches the required nucleation superheat, and the process repeats. Vapour burst instabilities are observed during the reflood phase during re-emergence core cooling of a reactor. Other CHF-related local instabilities are discussed in Section 7.6.

7.5.4.2 Ledinegg flow instability

Ledinegg instability or flow-excursive instability is characterized by a sudden change in the flow rate to a lower value or a flow reversal. This happens when the slope of the channel demand pressure drop vs. flow rate curve (the internal characteristics of the channel) becomes algebraically smaller than that of the loop supply pressure drop vs. flow rate curve (the external characteristics of the channel, or the pump head curve). Physically, this behaviour exists when the pressure drop decreases with increasing flow.

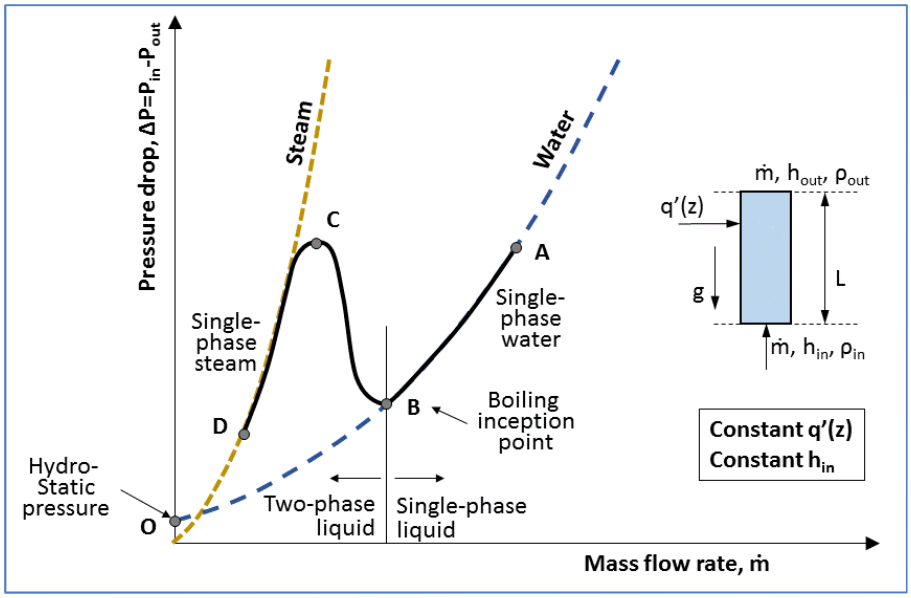

Figure 98 Concept of channel flow instability

Figure 98 shows conceptually the phenomenon of Ledinegg instability [TOD2011]. In this figure, the *y*-axis represents the pressure drop and the *x*-axis the mass flow rate. The figure represents a fuel channel in which the fluid mass flow rate and the heating from the walls are selected so that part of the channel is in sub-cooled flow and part of the channel is boiling. The right curve with a shallower slope represents the channel pressure losses for liquid flow. This curve shows the pressure loss as the square of the mass flow rate (i.e., of the fluid velocity). If the channel did not have heating, this curve would have ended at point O' on the y-axis, representing the hydrostatic head of the stagnant water in the channel.

The left curve shows the pressure drop in the channel when the flow is only gas. This curve is steeper for a given mass flow rate because the difference between the densities of water and gas is almost three orders of magnitude. Therefore, a given mass flow rate of gas results in a much higher volumetric flow of gas compared to liquid, and therefore the velocity of the gas and its associated pressure drop for a given volumetric flow are much greater than those of liquid. The gas pressure drop curve ends almost at the zero point of the *y*-axis because the hydrostatic pressure of gas is negligible compared to that of liquid.

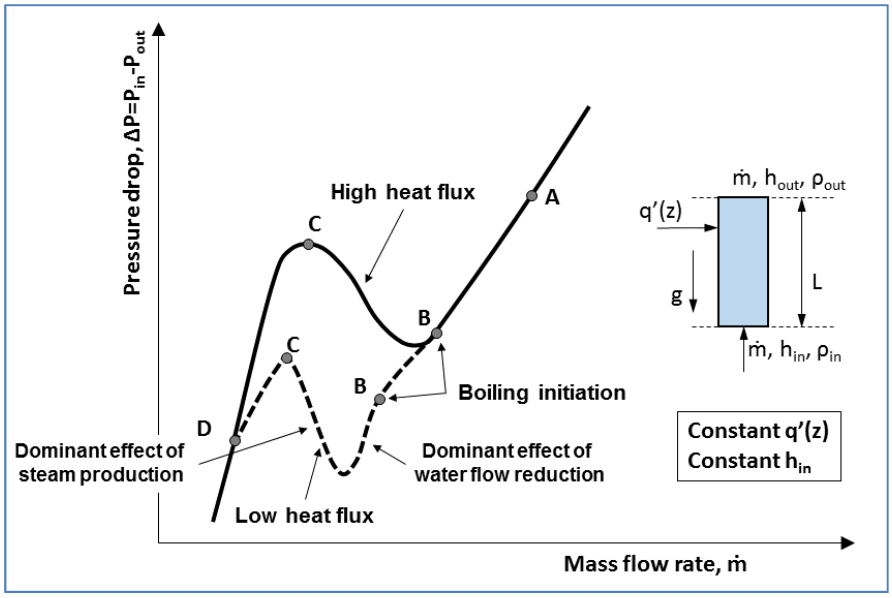

Figure 99 Channel flow instability under low heat flux

With the above explanation, it is possible to analyze the case with heating in the channel and the occurrence of two-phase flow, shown by the thicker solid line in Figure 98. When the mass flow rate is reduced to a point when two-phase flow occurs (consistent with the OSV explanation in Section 7.5.3.5), two phenomena occur:

- the volumetric flow starts to increase for the same mass flow, and therefore fluid velocity is higher for the same mass flow rate; and
- the friction factor becomes higher in two-phase flow (see Section 7.5.3.2).

The net result is that as the mass flow rate decreases, more of the liquid is converted to steam, resulting in higher volumetric flow and higher velocity, and hence the pressure drop increases. This process continues until all liquid is converted to steam, at which point the solid line joins the dashed line representing gas flow. With further reduction of flow rate beyond this point, the pressure drop simply follows the quadratic law of pressure drop vs. velocity, and no more boiling occurs.

Figure 99 shows a comparison of the system pressure drop curve with heat flux as shown in Figure 98, but with a lower heat flux (the lower curve in Figure 99) [TOD2011]. When the heat flux is lower, boiling starts at the lower mass flow rate rather than the higher, except that in this figure, the flow rate is much smaller. This is shown in Figure 99 by having point B occur at much lower mass flow rate. If the heat flux and hence the mass flow rate at boiling inception is very low, then a couple of competing phenomena can create the situation shown by the bottom curve in Figure 99. In this case, because boiling starts at a very low mass flow rate, conversion of liquid into steam results in two phenomena: (1) increase of volumetric flow and hence of liquid velocity, and (2) reduction of hydrostatic head.

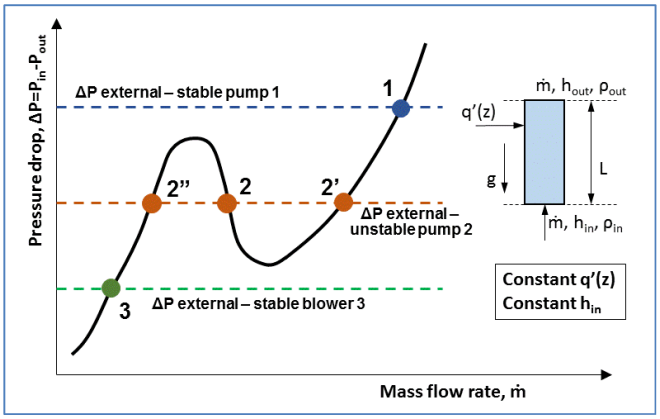

Figure 100 Impact of different pump curves on channel flow instability

After boiling inception at point B at the lower curve, reduction of the hydrostatic head temporarily dominates and creates a reduction in pressure drop. With further decrease in mass flow rate, a large increase in velocity occurs as more of the liquid is transformed into steam, resulting in a pressure drop increase.

Figure 100 shows the external pressure head generated by a pump (dashed lines) superimposed on the system pressure drop curve (solid line) [TOD2011]. It is important to observe in this figure that there are three cases of external pump head. The one on the top has one intersection point 1, at which the pump can sustain a stable operating point with liquid water. In addition, the curve at the bottom has one intersection point 3, at which a blower can have a stable operating point with gas (or steam). The curve in the middle intersects the system pressure drop curve at three points (2, 2', and 2"), and all three are possible operating points for this pump (or blower). At point 2', the pressure head device must be a pump, and at point 2", it must be a blower. At operating point 2, neither a pump nor a blower can operate well because the fluid is in two-phase flow, in which case conventional turbo machinery cannot operate efficiently. Nevertheless, although this operation cannot be achieved by the same device, it is assumed for the moment that it works, and this case and the consequences of this "pump" operation will be further examined.

Figure 101 presents a view of flow excursion instability, continuing the explanation started in Figure 100 [TOD2011]. As explained previously, the unstable operating point is point 1. In this figure, various external pump head curves are plotted through point 1.

Case 1 (positive displacement pump with vertical pump head) represents a pump with a delivery flow that does not change with pump head. This pump is inherently stable, and although it rests on the part of the system curve with negative slope, it intersects the system loss curve at only one point (point 1).

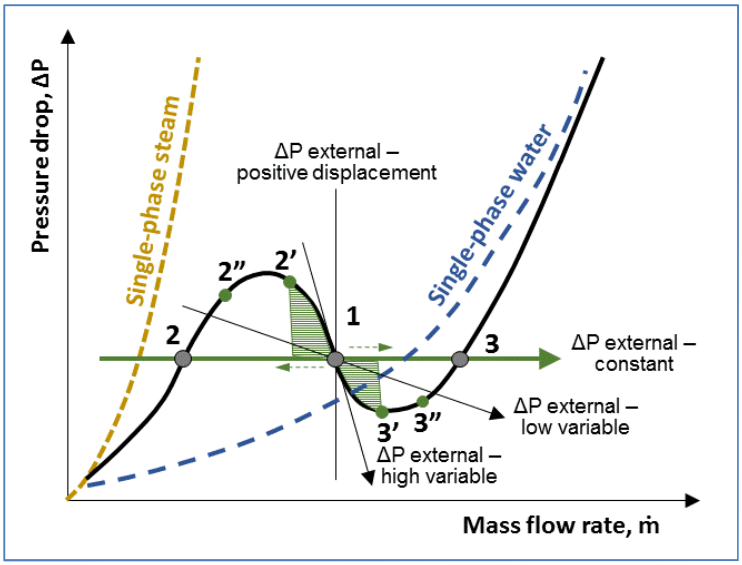

Figure 101 Definition of channel flow excursion instability in a single channel

Case 2 (constant head) represents a situation in which the head from an external pump is delivered to a channel, and hence its curve intersects the system curve at three locations. However, in this case, the pump head is constant irrespective of the flow rate in the channel. This situation can lead to excursion instability because the curve intersects the system loss curve at three points (1, 2, and 3); this will be explained further.

Case 3 (low variable head) represents a centrifugal pump for which the head and flow are related through a polynomial function. This pump head curve also intersects the system loss curve at three points and also leads to Ledinegg instability.

Case 4 (high variable head) represents a pump that is well throttled, so that a small flow change results in a large pump head change. This is a typical situation in operating BWRs, which have well-throttled external circuit pumps. Because the slope of the curve is very steep, the pump head curve intersects the system loss curve at only one point (point 1), and therefore this pump operates in an inherently stable manner regardless of where it intersects the system curve.

From the above examples, a criterion for entering Ledinegg instability can be defined by the following inequality:

$$\frac{\partial\left(\Delta P_{system}\right)}{\partial w} > \frac{\partial\left(\Delta P_{ext}\right)}{\partial w}. \tag{251}$$

This inequality shows that if the pump head curve is $\Delta p_{ext} > \Delta p_{system}$, the pump operation is inherently stable in such a system.

By examining Figure 101 carefully, it is clear that the source of this instability is the negative slope of the system loss curve. This means that if the pump operates at point 1, any small disturbance of the pump flow or head will lead to instability.

For example, at point 1, if pump flow decreases by an infinitesimal amount δW, the pressure

drop in the system will increase by $\delta(\Delta p)$ (the left upper green triangle). This will make the pump further reduce its flow delivery, which in turn will make the pressure drop further increase. Therefore, step by step, the pump operating point will move through points 2' and 2" to point 2.

Inversely, if at point 1, the pump flow increases by an infinitesimal amount δW, the pressure drop in the system will decrease by $\delta(\Delta p)$ (the right lower green triangle). This will make the pump further increase its flow delivery, which in turn will make the system pressure drop further decrease. Therefore, step by step, the pump operating point will move through points 3' and 3" to point 3.

Figure 101 clearly shows that while the pump operating point moves from one point to another, the pump head and the system losses will be in equilibrium for a period of time that depends on the system and the pump hydraulic inertia. However, given enough time, the possible operating points must be at the intersection of the two curves. However, the only sustainable stable operating point must be the intersection point of the two curves that satisfies Eq. (251).

Thermal-hydraulic designers need to examine pump curves and system loss curves carefully to ensure that pump head shape and slope satisfy Eq. (251), thereby ensuring that this type of instability will not occur.

7.5.4.3 Parallel channel flow instability

One aspect of Ledinegg instability (i.e., excursive instability) is the situation that can arise with parallel channels operating under a common pressure drop [POP2014]. This situation can occur in many thermal-hydraulic networks or components. For example, this may occur in a reactor core with two types of channels under the same pressure drop, or in a CANDU fuel channel with crept pressure tubes, in which the flow is split into two flow paths, one in the eccentricity above the fuel bundle, and one through the fuel bundle (see Section 7.5.3.4)

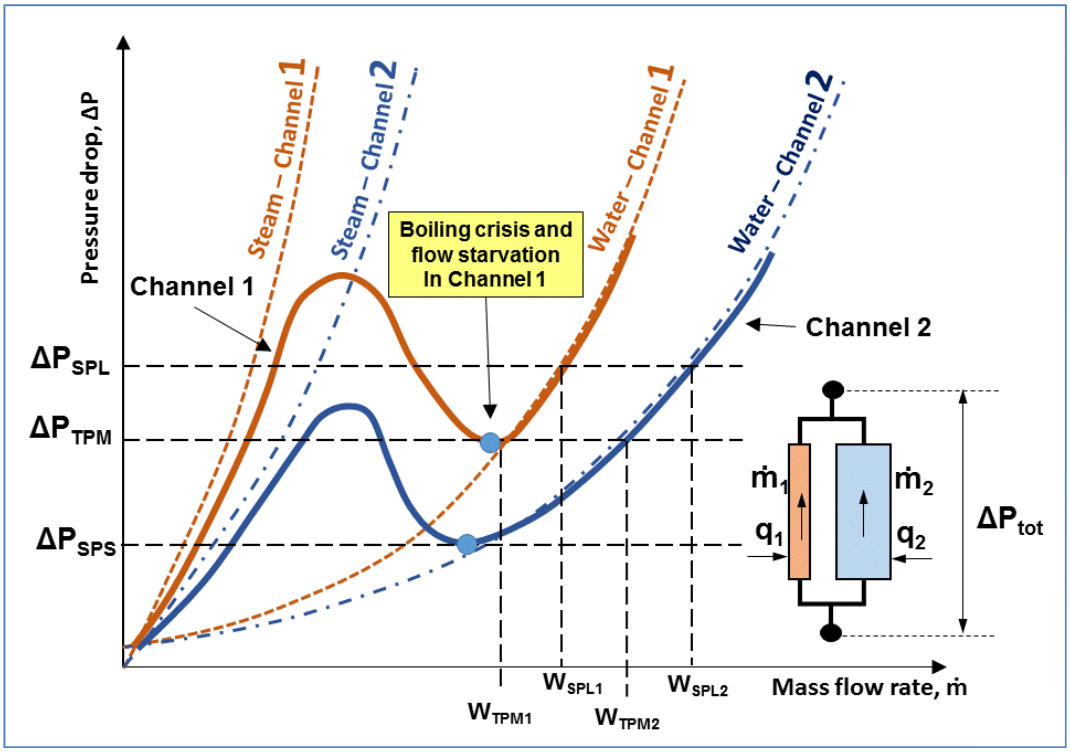

Figure 102 Principles of flow excursion instability in two parallel channels

Figure 102 shows the principles of a two-parallel-channel configuration under the same pressure drop, which is vulnerable to excursive instability. In this configuration, each channel has its own pressure loss curve, but different heat flux, total power, and flow rate. Therefore, each channel will enter the two-phase flow boiling condition at a different flow rate. The first channel that enters two-phase flow will experience an increase in channel pressure drop, which will help divert a portion of its flow to the other channel that remains in single-phase liquid flow. In other words, the channel that first enters two-phase flow will experience successive flow reductions and will eventually overheat as it loses its cooling.

Figure 103 shows an actual calculation of flow instability in a parallel channel configuration in a core with two types of fuel channels using a computer code (a similar geometry to that in Figure 102) [POP2000]. In Figure 103, the mass flow rate is on the *x*-axis and the pressure drop on the *y*-axis. Line 1 represents the total pressure drop across both channels; Lines 2 and 3 represent the pressure drop in each channel, and Line 4 provides the percentage of flow split. It is apparent in this figure that the flow split between the channels changes as the total flow to the two-channel loop decreases. Clearly, the two channels behave differently below a total flow of 0.2 kg/s. At a pressure drop of about 12 kPa, the flow starts to divert from one channel (Line 3) to the other channel (Line 2). Line 3 indicates an increase in pressure drop due to boiling, whereas Line 2 indicates an increase in pressure drop due to higher liquid flow.

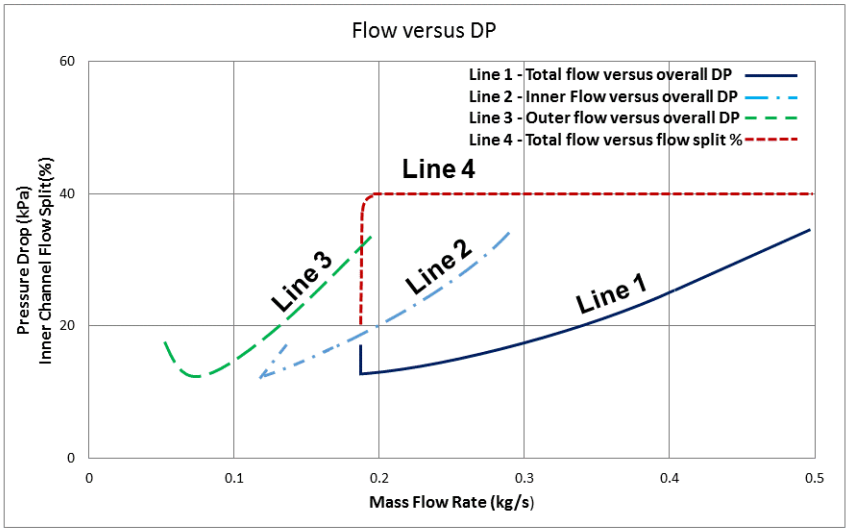

Figure 103 Results of flow excursion instability in two parallel channels

7.5.5 Problems

1. List and explain the most important factors that have significant impact on the pressure drop in the CANDU primary heat transport system. Rank the components in the CANDU primary heat transport system that contribute to the pressure losses in the system. Explain how reactor aging affects pressure drop in the main heat transport system.
2. Explain the components of pressure drop in horizontal channels, and provide information on the parameters that influence their value. Explain the approach used to calculate the pressure drop components in two-phase flow.
3. A mixture of water and steam at mass quality of 30% and temperature of 400^{o}C flows through a 10 m long pipe with diameter of 4 inches. The mass flux in the pipe is 2000 kg/m^2 s. Calculate the pressure drop along this pipe using the most appropriate two-phase flow multiplier.
4. Water flows through an insulated horizontal pipeline 100 m long (no heat losses). Water enters the pipe at temperature of 250^{o}C, and velocity of 3 m/s. Assuming that the pipe is made of carbon steel of commercial quality, calculate the pump power that is required to maintain this flow.
5. Two-phase water-steam mixture at 10% quality flows in thermal equilibrium through a horizontal pipe 6 m long with diameter of 18 mm. The water pressure is 8 MPa. Calculate the two-phase pressure gradient in this pipe, and the total pressure difference between the inlet and the outlet using the Friedel correlation provided below. The total mass flux is 2000 kg/m^2 s.

$$\phi_{\ell o}^2 = E + \frac{3.24FH}{Fr^{0.0454}} We^{0.035} \qquad E = (1-x)^2 + x^2 \frac{\rho_\ell f_{go}}{\rho_g f_{\ell o}} \qquad F = x^{0.78}(1-x)^{0.224}$$

$$H = \left(\frac{\rho_\ell}{\rho_g}\right)^{0.91} \left(\frac{\mu_g}{\mu_\ell}\right)^{0.19} \left(1 - \frac{\mu_g}{\mu_\ell}\right)^{0.7} \qquad Fr = \frac{G_m^2}{gD_e\rho_m^2} \qquad We = \frac{G_m^2}{\sigma\rho_m}$$

$$\rho_m = \left(\frac{x}{\rho_g} + \frac{1-x}{\rho_\ell}\right) \quad \textit{for homogeneous model}$$

$$f_{jo} = \frac{64}{\mathrm{Re}_j} \;\; if \;\; \mathrm{Re}_j \le 1055$$

$$f_{jo} = \left[0.86859 \cdot \ell n\left(\frac{\mathrm{Re}_j}{1.964 \cdot \ell n\,\mathrm{Re}_j - 3.8215}\right)\right] \;\; for \;\; \mathrm{Re}_j > 1055$$

Where: x is quality, ρ is density in (kg/m^3) (g – gas, and l – liquid), f_{go} and f_{lo} are Darcy friction factors, μ is dynamic viscosity in (Pa s), (g – gas, and l – liquid), σ is surface tension in (N/m), and g is acceleration due to gravity (=9.81 m/s^2).

6. Explain the cause and the impact of the Ledinegg flow instability in vertical channels. Explain the importance of this type instability for the process of pump selection.
7. Explain the cause and the impact of flow excursion instability in parallel heated channels, including the applicability and methods for avoiding or mitigating this type of instability.

7.6 Heat transfer between the fuel elements and the coolant

Section 6.1 provides the fundamentals of two-phase flow, which are needed to understand the heat transfer regimes in the reactor core. Section 7 provides the basis for heat transfer in the reactor primary heat transport system. Section 7.4 provides details on heat conduction in the fuel elements. This section now focuses on heat transfer from the fuel to the coolant.

Heat removal from the reactor core is an important issue in reactor design and operation. The main objective of heat transfer analysis for single-phase flow in the reactor is to determine the temperature field in a coolant channel such that the reactor operating temperatures are within the specified limits, including the rate of heat transfer to and from a surface or object. Because reactor power densities are typically much higher than for other conventional heat sources, the heat removal rate from any given reactor core coolant channel is quite large. Heat transfer to the coolant in single phase therefore requires a coolant with a large heat capacity.

The boiling curve shown in Figure 29 provides a good illustration of the boiling phenomenon and the boiling crisis in the fuel channel, which have an important impact on reactor thermal margins. This section discusses the wall heat flux in various heat transfer regimes and the critical heat flux (CHF) in the channel and discusses their importance and the differences between PWR and CANDU reactors. Appropriate diagrams explaining the variation of the critical heat flux with key parameters are shown and discussed. In addition, CHF correlations and calculation methods are described. The CHF is a critical parameter in reactor core thermal-hydraulic design because it sets the primary limitations on reactor thermal margins.

7.6.1 Heat transfer regimes

Various flow and heat transfer regimes that are relevant to heat transfer in the reactor core under various operating modes are illustrated in Figure 32. The heat transfer correlations are important in reactor thermal-hydraulic design because they provide the tools for a designer to calculate various parameters of interest in the design process and to verify that the design can meet the proposed objectives and requirements, primarily the capability to remove generated heat from the core during all possible operating modes.

The heat transfer from any solid surface to a coolant is given by Newton's Law in terms of heat flux:

$$q'' = h \cdot (T_s - T_b), \tag{252}$$

where T_s is the surface temperature, T_b is the bulk temperature of the coolant, and h *(W/m^2 K)* is the heat transfer coefficient. The heat transfer coefficient is dependent on coolant properties, flow parameters such as the velocity field, the temperature fields in the solid surface and the coolant, and solid surface condition and geometry.

A considerable amount of experimental and theoretical research has been published on the heat transfer coefficient for turbulent flow in channels. Although most correlations have been developed based on circular pipes, with appropriate corrective factors, they can be applied to various geometries.

For fully developed turbulent flow of non-metallic fluid, the general heat transfer correlation can be expressed as [ELW1978]:

$$Nu = C \cdot Re^a Pr^b \left(\frac{\mu_w}{\mu} \right)^d , \tag{253}$$

where μ_w is the fluid viscosity at the wall temperature and *a*, *b*, *c*, *d* are constants that depend on fluid and channel geometry.

Heat transport with phase change such as in boiling or condensation is an efficient method to transfer heat because latent heat per unit mass is very large compared with sensible heat. For single-component fluids, the interface temperature difference involved for heat transfer in evaporation and condensation is relatively small. However, when more than one component is present in a system, the temperature difference can be higher. An example is condensation of vapours in the presence of non-condensable gases. The two-phase heat transfer phenomena relevant to reactors include pool boiling, evaporation in vertical or horizontal fuel channels, and condensation inside or outside tubes.

As indicated in Figure 32, many flow and heat transfer regimes are possible in reactor channels in two-phase flow, depending on many parameters. In addition, fuel and channel geometry, heat transport conditions, characteristics, and materials have a significant influence on the type and magnitude of heat transfer from fuel to coolant. As a result, in the literature, many heat transfer correlations have been proposed, adopted, and used by various designers and analysts. This section provides a brief overview of the most important correlations, focussing on the critical heat flux correlations because of their significance for reactor thermal margins.

7.6.2 Convective heat transfer in turbulent forced flow

The convective heat transfer coefficient in turbulent forced flow of non-metallic fluids follows the form given by Eq. (253). The Prandtl number, given by Eq. (16), for non-metallic fluids such as light and heavy water is close to unity. For non-metallic fluids, the Nusselt number given by Eq. (15) is insensitive to wall surface conditions. Moreover, the Nusselt number varies little in the case of constant heat flux and constant mass flux.

Even for this relatively well-known situation, many heat transfer correlation variations have been proposed by different authors. The best-known is the Dittus-Boelter correlation, which is given by the following relation [ELW1978]:

$$Nu = 0.023 \cdot Re^{0.8} Pr^{0.4} . \tag{254}$$

Hence, using the Nusselt number, the heat transfer correlation can be obtained as follows (using a simplified version for plate geometry):

$$h_c = 0.023 \cdot k_f L \cdot Re^{0.8} Pr^{0.4} . \tag{255}$$

This is the best-known correlation used for single-phase convective heat transfer, as shown in the first part of the left side of Figure 29. In this correlation, the physical properties in dimensionless numbers are evaluated at the bulk temperature of the fluid. The correlation does not take into account the effect of temperature variation from the tube wall to the bulk fluid. Clearly, for laminar flow, this correlation does not apply, and other correlations are used.

For forced convection in fuel bundles, the following correlation was proposed by Weisman [ELW1978]:

$$Nu = C \cdot Re^{0.8} Pr^{1/3}, \tag{256}$$

where the constant *C* has the following form for square and triangular lattices respectively (*S* is the fuel rod pitch, and *D* is the fuel rod diameter):

$$\begin{aligned} C &= 0.042\frac{S}{D} - 0.024, \quad 1.1 \le \frac{S}{D} \le 1.3 \\ C &= 0.026\frac{S}{D} - 0.006, \quad 1.1 \le \frac{S}{D} \le 1.5, \end{aligned} \tag{257}$$

7.6.3 Sub-cooled boiling heat transfer in forced flow

Heat transfer from the walls to the liquid at relatively high heat flux, starting from the sub-cooled condition at the entrance of a channel, brings CANDU fuel cladding walls to and beyond saturation somewhere downstream in the reactor fuel channel. When the liquid layer next to the wall and adjacent to the wall becomes superheated, bubble nucleation sites are activated. This point is denoted in Figure 29 as the onset of sub-cooled boiling. Bubbles are generated at the wall cavities by the heat transferred from the wall as latent heat of evaporation. As soon as they depart from the wall, they encounter sub-cooled bulk liquid and condense, releasing the latent heat of vaporization to the bulk liquid. This process helps enhance heat transfer from the wall, partly by evaporation of the liquid and partly by enhancing turbulence near the wall. Note that heat transfer by latent heat of evaporation is much more effective than heat transfer by convective heating of liquid.

The point at which sub-cooled nucleate boiling starts is defined by the following criterion proposed by Bergles and Rohsenow [AHM2009]:

$$q''_{W,SB} = 1082\, p^{1.156} \left[1.799 \left(T_w - T_{sat} \right)_{SB} \right]^{2.3/p^{0.0234}}. \tag{258}$$

Equation (258) is valid for pressures between 0.1 and 13.6 MPa, and *p* is in bar, temperatures in °C, and $q_{W,SB}$ in W/m^2.

For the nucleate boiling heat transfer regime, the best-known and most widely used correlation is the Chen correlation [CAT2005, ELW1978, TOD2011]. This correlation calculates the heat transfer coefficient as a sum of the convective and nucleate boiling parts as follows:

$$h_{SB} = h_C + h_{NB}. \tag{259}$$

The convective heat transfer is calculated using a variation of the Dittus-Boelter correlation given by Eq. (255):

$$h_c = 0.023 \left(\frac{G(1-x)D_e}{\mu_f} \right)^{0.8} Pr^{0.4} \frac{k_f}{D_e} F, \tag{260}$$

$$F = 1.0 \quad for \quad \frac{1}{X_{tt}} < 0.1$$
$$F = 2.35\left(0.213 + \frac{1}{X_{tt}}\right)^{0.736} \quad for \quad \frac{1}{X_{tt}} \geq 0.1 \qquad (261)$$

The Lockhart-Martinelli parameter X_{tt} is defined as:

$$\frac{1}{X_{tt}} = \left(\frac{x}{(1-x)}\right)^{0.9}\left(\frac{\rho_l}{\rho_g}\right)^{0.5}\left(\frac{\mu_g}{\mu_l}\right)^{0.1} . \qquad (262)$$

The nucleate boiling part of the sub-cooled boiling correlation is defined as:

$$h_{NB} = \frac{S\left(0.00122\right)\cdot \Delta T^{0.24}\Delta p^{0.75} c_p^{0.45}\rho_l^{0.49}k_l^{0.79}}{\sigma^{0.5}h_{lg}^{0.24}\mu_l^{0.29}\rho_g^{0.24}} . \qquad (263)$$

The parameter *S* is defined as follows:

$$S = \frac{1}{1 + 2.53\cdot 10^{-6} Re^{1.17}} \quad where \quad Re = Re_l F^{1.25} . \qquad (264)$$

The Chen correlation is valid for pressures of 0.17–3.5 MPa, liquid inlet velocities of 0.06–4.5 m/s, and heat fluxes up to 2.4 MW/m^2.

When the bulk liquid temperature increases to a certain point, as shown in Figure 29, conditions for onset of significant void, i.e., bulk boiling, are established. The criteria that determine the onset of bulk boiling are defined by various correlations, of which the best-known is the Saha-Zuber correlation provided in Eqs. (249) and (250), which is expressed in terms of quality at the OSV point. However, it is useful to express Eqs. (249) and (250) in terms of bulk fluid temperature to estimate the level of coolant sub-cooling at the point of OSV. Figure 32 shows the sub-cooled boiling phases, with OSV labelled as the onset of net vapour generation, which is upstream of the point at which bulk saturation is reached.

Equations (249) and (250) can be transformed into a relation that defines the wall temperature at the onset of bulk boiling:

$$T_{bulk,OSV} = T_{sat} - 0.0022\frac{q''D_e}{k_l} \quad for \quad Pe < 7\cdot 10^4$$
$$T_{bulk,OSV} = T_{sat} - 154\frac{q''}{G\cdot c_p} \quad for \quad Pe > 7\cdot 10^4 , \qquad (265)$$

where the Peclet number is defined according to the following relation:

$$Pe = \frac{G\cdot D_e c_p}{k_l} . \qquad (266)$$

The Saha-Zuber correlation is valid for pressures of 0.1–13.8 MPa, mass fluxes of 95–2760 kg/m^{2}s, and heat fluxes of 0.28–1.89 MW/m^2.

7.6.4 Critical heat flux (CHF)

When the wall surface temperature is further increased beyond the point that results in sub-cooled boiling, as shown in Figure 29, it may reach a value that results in a heat flux referred to as *critical heat flux* (CHF). This is the maximum heat flux at which continuous liquid contact in a tube or fuel channel is maintained. Further increase in the wall heat flux will result in an increase in wall temperature to values that result in a sustained vapour film on the wall surface (along the horizontal dashed line in Figure 29). Usually, for reactors designed to operate with liquid water in contact with the fuel cladding, this large increase in cladding temperature could result in melting and destruction of the cladding. The primary objective of thermal-hydraulic design is to ensure that this does not happen.

7.6.4.1 Outline of CHF phenomena

The CHF is a complex thermal-hydraulic phenomenon that varies with a large number of parameters. This section explains the CHF phenomenon for various combinations of key parameters and provides a discussion of CHF parametric trends. In addition, heat transfer correlations for pre-CHF heat transfer regimes are provided and discussed [IAEA2001, TOD2011, BER1981, DEL1981, COL1972, LWU2004].

Development of the CHF correlation requires a significant amount of experimental testing because of the complex reactor core fuel geometry in PWRs as well as in CANDUs. This section also provides a brief explanation of the experimental tests and their use to develop CHF correlations.

In forced convective boiling, the boiling crisis occurs when the heat flux is raised to such a high level that the heated surface can no longer support continuous liquid contact. This heat flux is referred to as the critical heat flux (CHF). It is characterized either by a sudden rise in surface temperature caused by blanketing of the heated surface by a stable vapour layer, or by small surface temperature spikes corresponding to the appearance and disappearance of dry patches. The CHF normally limits the amount of power transferred, both in nuclear fuel bundles and in conventional boilers. Failure of the heated surface may occur once the CHF is exceeded. This is especially true for highly sub-cooled CHF conditions. At high flows and positive dryout qualities, the post-dryout heat transfer is reasonably effective in keeping the heated surface temperatures at moderate levels, and operation under dryout conditions may be sustained safely for some time, particularly in BWRs or CANDUs.

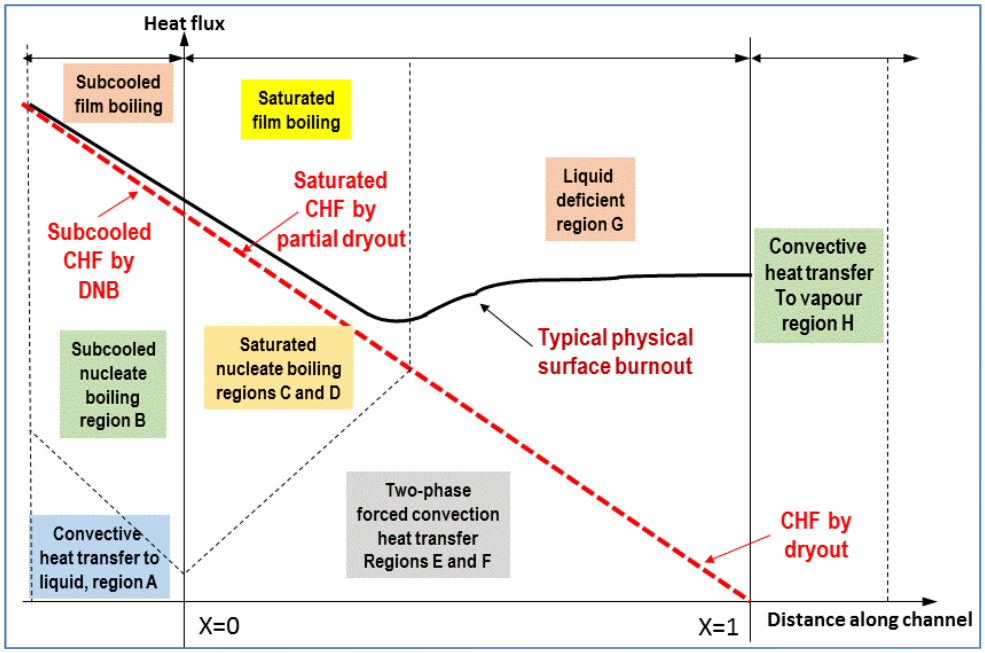

Figure 104 Concepts of CHF, dryout, and burnout

Figure 104 [COL1972] is of key importance in understanding the various mechanisms and the definition of the CHF phenomenon, as well as the consequences of CHF occurrence in a reactor fuel channel (note that this figure is not to scale, values are not shown, and the intent is to illustrate CHF conceptually for various coolant qualities).

Figure 104 shows the basic concept of CHF occurrence and the terms used to describe the various stages and types of the CHF phenomenon. On the *y*-axis, this figure shows the relative value of the heat flux as given, whereas on the *x*-axis, the thermodynamic quality is provided, starting from sub-cooled conditions (negative values), moving to values between 0 and 1 (two-phase flow), and then to values beyond 1 (superheated steam). The straight solid line with a negative slope intersecting the *x*-axis at $x_e=1$ is the locus of CHF. Above this straight line, a line is shown which is labelled as the *burnout locus*—this is the wall heat flux that can destroy the cladding surface under various conditions. On the left side, under sub-cooled conditions, various heat transfer regimes are illustrated moving from bottom to top in the figure: convective heat transfer at the bottom (no boiling), sub-cooled nucleate boiling, and sub-cooled film boiling. In the two-phase region in the middle of the diagram, various heat transfer regimes are shown: two-phase forced convection, saturated bulk boiling, saturated film boiling, and liquid-deficient saturated boiling. On the right side of the diagram, convective heat transfer to steam is shown. These regimes are also illustrated in Figure 26 and Figure 33.

With respect to the diagram in Figure 104, the following terms can be defined. They are related to the CHF, but have a slightly different meaning:

- ***Boiling crisis***. Refers to sub-cooled or saturated boiling when the amount of steam produced by boiling surpasses the amount of steam that can be removed from the wall, thus creating a situation in which heat removal from the wall is limited.
- ***CHF***. Refers to the general condition of limited heat flux in sub-cooled or saturated

boiling; it can include all terms shown on this list.

- ***Dryout***. Refers to conditions at the fuel cladding surface when continuing contact with liquid water can no longer be maintained. Note that under dryout conditions, there may still be abundant liquid water in the pipe or fuel channel (so that the void fraction may be very low), but the cladding surface may still be insulated from the water by a stable steam film.
- ***Departure from nucleate boiling (DNB)***. This term refers to the CHF that occurs under significantly sub-cooled conditions (as in PWRs). In this case, CHF happens when the fuel cladding surface can no longer support sub-cooled boiling.
- ***Burnout*.** This term refers to the destruction of the cladding surface as it begins to melt. This can happen very quickly under sub-cooled conditions after CHF is reached. At saturated conditions (for higher equilibrium quality or void fraction), as shown in Figure 104, burnout can occur only when the heat flux is greater than the CHF (note that the burnout curve moves further away from the CHF curve in Figure 104 as quality rises, particularly for qualities $x > 0$).

Figure 105 [POP2014] shows a different CHF mechanism in a reactor fuel channel superimposed on the CHF diagram from Figure 104. In this figure, heat flux is indicated on the *y*-axis and thermo-dynamic quality on the *x*-axis. There are four distinctive CHF mechanism types: nucleation induced under highly sub-cooled conditions, a bubbly layer induced under sub-cooled conditions, entrainment-induced film depletion at low quality, and deposition-controlled film depletion at very high quality.

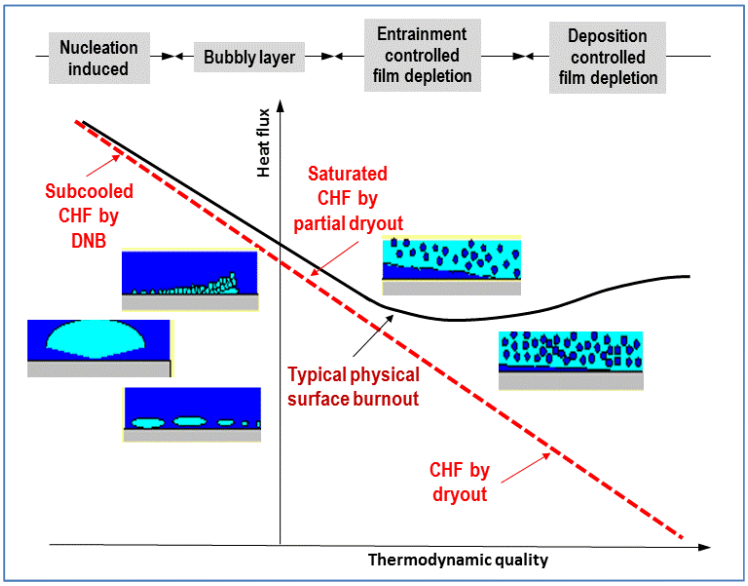

Figure 105 Transitions among CHF mechanisms

Like other thermal-hydraulic phenomena, CHF occurs differently in pool boiling than in forced-flow boiling. In pool boiling, no forced flow is provided to the liquid container. In this situation, CHF usually occurs because of either counter-current flow (Helmholtz) instability or micro-layer evaporation (for highly sub-cooled conditions only).

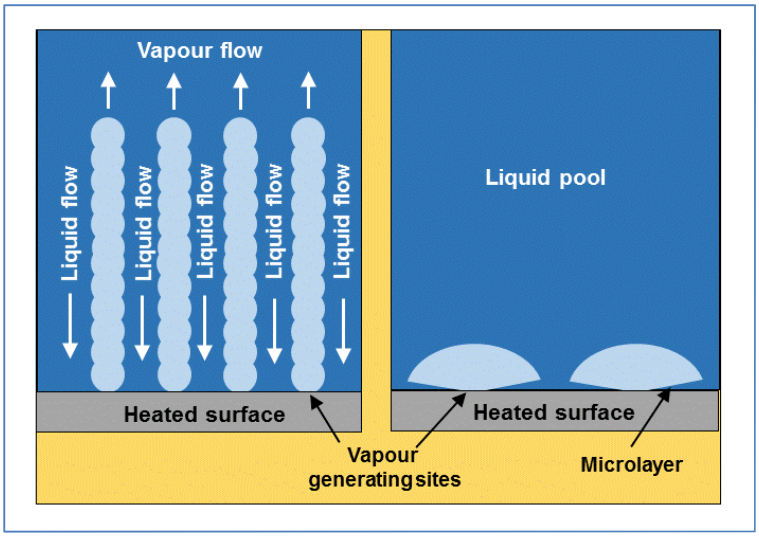

Figure 106 Pool boiling CHF mechanisms

The left side of Figure 106 shows the counter-current flow instability (i.e., the Helmholtz instability) [LEU2004]. In this case, the heated surface is covered by a rising vapour column with counter-current liquid jets flowing downwards due to gravity to compensate for liquid removal by evaporation. Ultimately, at very high heat flux levels (vapour removal rates), the relative velocity between liquid and vapour can be so high that an unstable flow situation is created in which due to interfacial friction, liquid jets cannot penetrate downwards because of the high flow rate of rising bubbles, resulting in a CHF condition. The right side of Figure 106 shows a micro-bubble developed in a cavity on the heated surface. As the bubble grows, a microlayer of thin liquid film develops below the bubble. This microlayer is unstable because of the large heat flux and can break and leave the surface uncovered, i.e., can form a dry patch, leading to CHF.

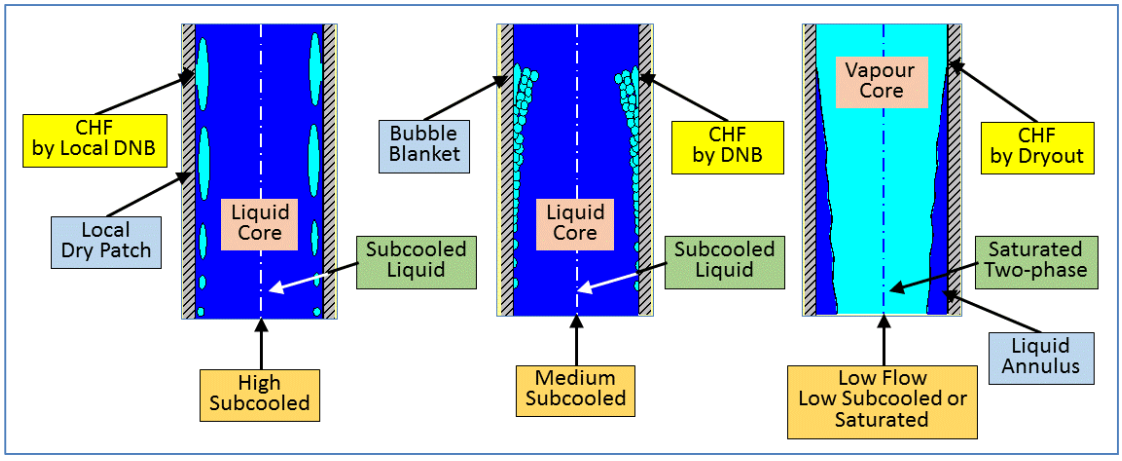

Figure 107 Flow boiling CHF mechanisms

In forced-flow boiling, CHF usually occurs because of one of the following three phenomena: collapse of the liquid sub-layer, bubble crowding, or film depletion. Figure 107 shows these three phenomena [LEU2004]. On the left side of this figure, the collapse of the liquid sub-layer

occurs with highly sub-cooled liquid. CHF occurrence is due to the spreading of a dry patch following microlayer evaporation under a bubble and coalescence of adjacent bubbles. The occurrence of CHF in this case depends on local surface heat flux and flow conditions; it is not affected by upstream heat flux distribution.

Bubble crowding is shown in the middle of Figure 107 for moderate sub-cooling or saturated conditions and high flow rate. The bubble population density near the heated surface increases with increasing heat flux, and a so-called bubble boundary layer often forms a short distance away from the surface. If this layer is sufficiently thick, it can impede the flow of coolant to the heated surface. This in turn leads to a further increase in the bubble population until the wall becomes so hot that a vapour patch forms over the heated surface. This type of boiling crisis is also characterized by a fast rise in heated surface temperature (fast dryout).

At the right side of Figure 107, the film depletion type of CHF is illustrated, which is possible with a relatively low mass flux of saturated liquid in high void fraction flow. In the annular dispersed flow regime (high void fraction and high volumetric flow), the liquid will be in the form of a liquid film covering the walls and entrained droplets moving at a higher velocity in the pipe core. Continuous thinning of the liquid film will take place due to the combined effect of entrainment and evaporation. Near the dryout location, the liquid film becomes very thin, and due to the absence of roll waves (which normally occur at higher liquid film flow rates), entrainment is suppressed. If the net droplet deposition rate does not balance the evaporation rate, the liquid film must break down. The temperature rise accompanying this film breakdown is usually moderate (stable dryout).

Related to the above explanation of dryout resulting from a high void fraction, high flow rate situation in a tube is CHF dryout in a fuel channel. This situation is typical of CANDU reactors in which towards the end of the fuel channels, saturated liquid with significant void fraction and mass flux flows through a densely packed fuel channel. Because the two-phase flow is very well mixed, dryout occurs gradually, and fuel is not exposed to sustained loss of contact with liquid, i.e., slow dryout occurs. During a slow dryout, the heated surface does not experience the usual dryout temperature excursions; instead, a gradual increase in surface temperature with power is observed. A slow dryout is usually encountered in flow regimes where the phases are distributed homogeneously, such as froth flow or highly dispersed annular flow at high mass velocities and void fractions. Under these conditions, liquid-wall interaction is significant, limiting the temperature rise with dryout.

Calculations based on cooling by vapour flow indicate only that post-CHF temperatures are below the minimum film boiling (Leidenfrost) temperature; hence, depositing droplets may wet the surface, increasing the heat transfer coefficient. In a CANDU reactor, because the coolant is close to saturation over most of the channel and at relatively high mass flux and void fraction downstream of the rector mid-plane, the most probable CHF mechanism is slow dryout. Therefore, in a CANDU reactor, the consequences of reaching CHF are not as serious as in a highly sub-cooled PWR because the fuel surface can still be well cooled by passing steam and droplets.

7.6.4.2 CHF parametric trends

As explained above, CHF is a complex phenomenon that depends on many parameters and can be caused by different phenomena. Table 10 shows various parameters that affect the type and intensity of CHF in fuel bundles. Discussion of all these effects is beyond the scope of this textbook; details can be found in the literature [IAEA2001].

Table 10 Separate CHF effects in fuel bundles

GENERAL	DETAILS OF SEPARATE EFFECTS
Global Flow Area Effects	▪ *n*-rod bundle where *n*>>3 and all sub-channels are identical except for corners or cold-wall-adjacent sub-channels (e.g., square or triangular arrays of sub-channels) ▪ *n*-rods where *n*>>3 and adjacent sub-channels are generally not equal (e.g., 37-rod bundle geometries inside round tubes)
	▪ Sub-channel size/shape (similarity to tube) ▪ Cold wall effect ▪ Distorted sub-channels (due to bowing, cladding stain, PT creep) ▪ Misaligned bundles (CANDU case)
Length Effects	▪ Similar to appendage effects
	▪ Mixing grids ▪ Attached spacers/ bearing pads/ endplates (CANDU)
Flow Orientation Effects	▪ Vertically upward ▪ Vertically downward ▪ Horizontal
	▪ Axial flux distribution (flux peaking/global flux distribution) ▪ Radial flux distribution (global RFD effect, cold wall effect, flux tilt across an element)
Flow Parameter Effects	▪ Mass flow (including zero flow or boiling/flow stagnation case)
	▪ Power/flow/pressure transients ▪ Combined transients
Effect of Fluid Type	▪ Light water ▪ Heavy water ▪ Modelling fluids (Freon) in conjunction with a CHF fluid-to-fluid modelling technique

A number of studies have been conducted by various researchers to investigate the effects of various parameters on CHF. An overview of the parametric trends is provided in this section. These parametric trends are provided for two different CHF approaches.

The approach based on fuel channel inlet conditions is very often used in CHF R&D because of the convenience of using inlet conditions because these are easily measured and maintained in CHF experiments. The other method is based on local conditions, i.e., the conditions locally where CHF occurs. This approach is used in computer-based algorithms because a computer program can easily calculate local conditions at the CHF location.

The discussion of parametric trends provided here must be related to the general trends described in Section 6.1, particularly those illustrated in Figure 30 and Figure 31.

The most influential parameters affecting CHF are the fluid pressure, mass flux, level of sub-cooling, and hydraulic diameter [IAEA2001]:

$$CHF = f(P, G, X_{DO} D_{hy}). \quad (267)$$

The general parametric trends on CHF based on inlet conditions are as follows:

1. Heated length has a very high impact on CHF because it affects the amount of heat transferred to the fluid; hence, CHF strongly decreases with increase of heated length and quality.
2. CHF increases with an increase in inlet sub-cooling (a decrease in inlet fluid temperatures).
3. CHF decreases with a decrease in outlet pressure (decrease of channel pressure).
4. For sub-cooled conditions, CHF increases with an increase in mass flow.
5. For saturated conditions, CHF increases with a decrease in mass flow.
6. CHF decreases with a decrease in tube diameter (which decreases the level of mixing and turbulence).

The general parametric trends related to CHF and based on local conditions are as follows:

1. The effect of heated length on local CHF is negligible.
2. Local CHF decreases with an increase in thermodynamic quality.
3. For sub-cooled conditions, local CHF increases with an increase in mass flow.
4. For saturated conditions, local CHF increases with a decrease in mass flow.
5. Local CHF increases with an increase in outlet pressure.
6. Local CHF decreases with an increase in channel diameter.

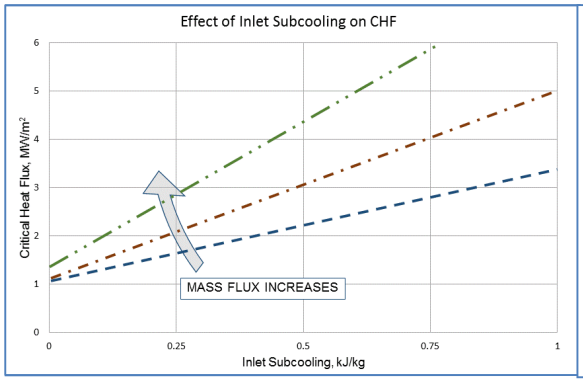

Figure 108 Effect of inlet temperature and mass flux

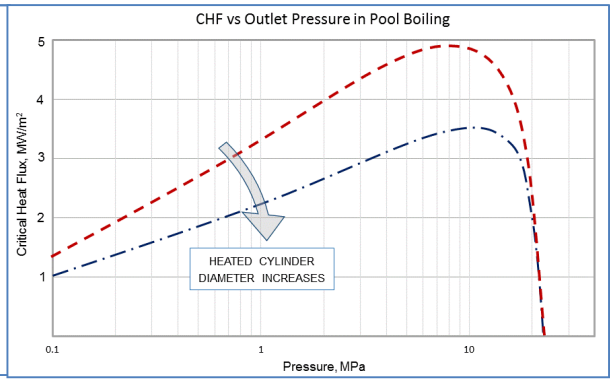

Figure 109 Effect of outlet pressure in pool boiling

Figure 108 shows the relationship between CHF (*y*-axis) and inlet sub-cooling (*x*-axis in enthalpy difference below saturation) for several mass flux values in a straight heated tube [LEU2004]. This figure is drawn in terms of channel inlet conditions. Note that CHF increases with mass flux and with the degree of sub-cooling. In other words, reactors that have more highly sub-cooled coolant and higher mass flux can use higher heat flux before reaching CHF. This is an important fact that demonstrates the strategy of operating PWRs.

In general, pressure has two key effects on heat transfer and CHF, one resulting from a change in the saturation temperature, and the other from a change in the latent heat of vaporization. As pressure increases, the saturation temperature increases, but the latent heat of vaporization

decreases. As a result, CHF increases with pressure, as indicated in Figure 109 [TOD2011]. However, as the pressure approaches the critical pressure, the latent heat of vaporization decreases to zero, reducing the CHF.

Figure 110 shows the effect of coolant outlet pressure (*x*-axis) for several sub-cooling levels for forced flow in a heated tube [LEU2004]. This figure is also drawn for a given level of channel inlet sub-cooling. Again, this figure confirms that higher inlet sub-cooling results in higher CHF. The impact of outlet pressure must be analyzed in combination with the channel inlet pressure, quality, and volumetric flux distribution along the channel (the channel length is 3.658 m).

Figure **111**, Figure 112, and Figure **113** show CHF parametric trends for local conditions in heated pipes [LEU2004].

The effect of heated length is shown in Figure **111**. It is evident that CHF decreases with increasing outlet quality in the channel. Moreover, as the heated length of the channel increases, the CHF value decreases significantly. Hence, for a very short heated length, CHF can be five times larger than for long heated lengths. This is another important observation in terms of CANDU reactor design. Because in CANDU the fuel bundles are relatively short, the bundle endplates and other bundle appendages can significantly improve the CHF value (further explanations in other sections below).

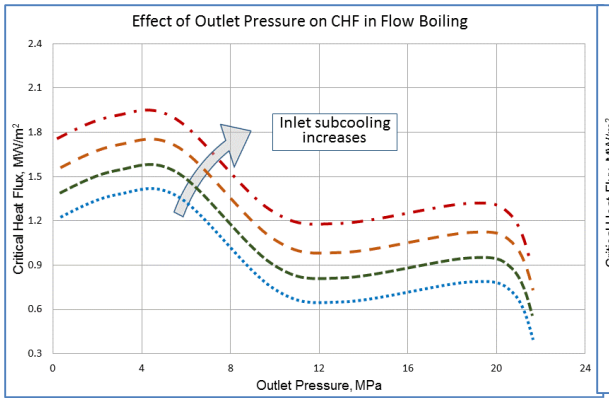

Figure 110 Effect of outlet pressure on flow boiling

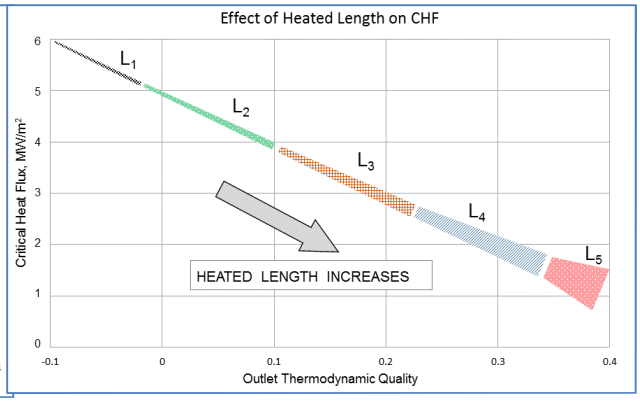

Figure 111 Effect of heated length on local CHF

Figure 112 shows the effect of mass flux under local conditions [LEU2004]. Similar behaviour can be observed with regard to the impact of sub-cooling on heat flux (for negative thermodynamic qualities). For saturated conditions, the effect of mass flux is not as important and should be analyzed in combination with volumetric flux.

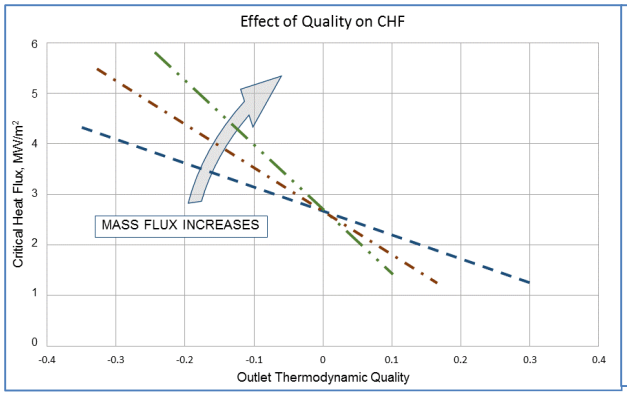

Figure 112 Effect of quality on local CHF

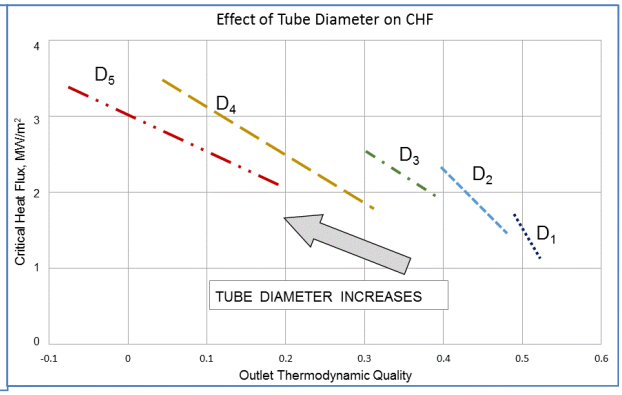

Figure 113 Effect of tube diameter on local CHF

Figure **113** shows, for local conditions, the impact of pipe diameter on CHF for various outlet thermodynamic qualities [LEU2004]. It is evident that larger hydraulic diameters provide a higher value of CHF for a given quality. Moreover, this figure confirms that for a given pipe diameter, CHF decreases with increasing thermodynamic quality.

7.6.4.3 CHF prediction methods

Because of the many possible fuel bundle geometries, the wide range of possible flow conditions, and the various flux distributions for advanced water-cooled reactors, it is impossible to predict the CHF for all cases using a single CHF prediction method and achieve a reasonable degree of accuracy. Over 400 correlations for CHF in tubes are currently in existence [IAEA2001]. The present proliferation of correlations illustrates the complex state of the art in predicting the CHF phenomenon, even for a simple geometry at steady-state flow conditions. The complexity of predicting the CHF increases significantly for fuel bundle geometries during severe transients, when additional parameters characterizing the transient are required. This demonstrates the need to categorize the important CHF-controlling parameters and their ranges of interest.

CHF prediction methods can be conveniently grouped into the following categories:

- Analytical models,
- Empirical correlations, and
- Look-up table methods.

<u>Analytical CHF models</u>

Analytical CHF models are based on physical mechanisms and satisfy the conservation equations [IAEA2001]. They generally require a two-fluid model approach, but occasionally must use a three-field approach (e.g., dispersed annular flow). Although these models have been improved significantly and usually predict the correct asymptotic trends, the evaluation process is complex and time-consuming. Furthermore, because of our limited understanding of the mechanisms involved and the lack of measurements of interfacial parameters, the models are still less accurate than empirical correlations over the range of their database. In addition, the analytical models have limited application because they can be used only in situations that

resemble the conditions upon which the model assumptions are based.

The annular film dryout model is based on a mass balance on the liquid film in annular flow and postulates that CHF corresponds to depletion of this liquid film. Equations for droplet entrainment and deposition have been proposed. The model provides reasonable predictions of CHF for annular flow at medium to high pressures and flows and void fractions exceeding 50%.

The bubbly layer model postulates that CHF first occurs in the lower quality regime when the bubble layer covering the heated surface becomes so thick and saturated with bubbles that liquid mixing between the heated surface and the cooler core liquid becomes insufficient.

The Helmholtz instability model is applicable to pool boiling, where the boiling crisis is reached when the flow of vapour leaving the heated surface is so large that it prevents a sufficient amount of liquid from reaching the surface to maintain the heated surface in the wet condition. The phenomenon that limits the inflow of liquid is the Helmholtz instability, which occurs when a counter-current flow of vapour and liquid becomes unstable.

Empirical CHF prediction methods

Empirical CHF prediction methods can be subdivided into those based on inlet conditions and those based on local cross-sectional average (CSA) conditions [IAEA2001].

The empirical correlations based on inlet conditions (*overall power correlations*) are all in the form of empirical correlations based on CSA inlet conditions (P, G, T_{in}, or ΔH_{in}) and usually assume the "overall power" hypothesis. This hypothesis states that, for a given geometry and set of inlet conditions, the critical power (the power corresponding to the first occurrence of CHF for that geometry) is independent of axial or radial heat flux distribution. This assumption permits the use of CHF correlations derived from uniformly heated bundle data to predict dryout power in non-uniformly heated bundles of identical geometry (i.e., identical cross section and heated length). This technique is a reasonable one for obtaining a first estimate of dryout power; it gives reasonable estimates of dryout power in the annular flow regime for symmetric flux profiles and form factors close to unity. However, it is not recommended for form factors significantly different from unity. This approach can also be used to predict the critical power of fuel channels with a fixed cross section, heated length, axial flux distribution (AFD), and radial flux distribution (RFD), irrespective of the form factor. If the experimental AFD and RFD represent the worst flux shapes from a CHF point of view, then the empirical correlations can be used for lower-bound predictions. The overall power correlations have generally good prediction accuracy. The best examples of this group are the Bowring correlation for tubes and the EPRI-2 correlation for fuel bundles [IAEA2001, TON1996, DEL1981, BER1981, CAT2005].

The overall power correlations have limitations, including applicability only to specific geometries, heated lengths, heat-flux profiles, and the range of conditions in the database. Hence, any variation of these parameters (i.e., extrapolation outside the database) may affect CHF prediction and hence predicted reactor, channel, and bundle power. Moreover, these correlations do not exhibit the correct asymptotic and parametric trends, and the axial and radial CHF locations cannot be predicted.

The local CHF correlations satisfy the local-conditions hypothesis, which states that the local CHF is dependent only on local conditions and not on upstream history. In principle, the local-conditions hypothesis is sound if it is based on true local cross-sectional average conditions. The reference formulation of local correlations is based on the linear trend of CHF with critical quality (transformed from the linear trend of critical power with inlet sub-cooling). Additional terms are included for separate effects (such as axial and radial heat-flux distributions). The local correlations must be used together with the heat-balance equation to determine critical power and CHF location (which requires iteration). The best examples of these correlations are the Biasi correlation for tubes and the Becker correlation for fuel bundles [IAEA2001, TON1996, DEL1981, BER1981, CAT2005].

An important disadvantage of local correlations is a larger prediction scatter than with overall power correlations. They are valid only for specific geometries, heat-flux profiles, and the range of conditions in the database; any variation of these parameters may affect local flow and enthalpy distributions and hence CHF. As with any correlations of this type, extrapolation of the applicability range may result in incorrect predictions. Moreover, these correlations have incorrect asymptotic and parametric trends, and radial CHF location cannot be predicted.

CHF table look-up method

Because most empirical correlations and analytical models have a limited range of application, a more general technique is needed. This approach is based on developing a table of measured values for different geometries and flow conditions and supplementing them in terms of key parameters that affect CHF. This approach has become known as a *look-up table method*. The look-up table includes normalized CHF data banks for reference tubes, triangular-array fuel bundles, and CANDU fuel bundles of natural-uranium fuel in a nominal channel. The look-up table is developed using generalized correlations and trends, and then experimental data are superimposed to improve accuracy and ensure that parametric trends are captured. The look-up table can be statistically extended to table matrix conditions.

The empirical bundle CHF prediction method requires an extensive database with an adequate range of the parameters of interest. It is suitable for design calculations and for reactor power evaluations.

The sub-channel codes predict enthalpy and flow in each fuel sub-channel. They require a sub-channel CHF prediction method (tube-based) and a spacer mixing/enhancement model.

The enthalpy imbalance approach uses enthalpy imbalance (in terms of thermodynamic quality) between the critical sub-channel and the bundle cross-sectional average values. It is used in the tube-data-based CHF prediction method with a modified thermodynamic quality to account for the enthalpy imbalance.

Currently, CANDU 6 design and safety analysis are based on the look-up table prediction method. This method is applicable to other geometries or flow conditions through modification factors embedded in the table. The present CHF values used in design analysis are included in the look-up table for uniformly heated, vertical tubes of 8 mm inside diameter, cooled with an upward flow of water. They cover the widest range of flow conditions (all possible CHF regimes) and exhibit correct asymptotic and parametric trends (smooth transition

between various CHF regimes). In addition, detailed prediction uncertainty is available at sub-region levels. To this point November 13 early afternoon

A sample of the CANDU look-up table is shown in Table 11 [LEU2004, IAEA2001], where CHF values are provided in a table format as a function of pressure, mass flux, and quality. For values of these parameters that fall between the values given in the table, an interpolation is made to calculate the appropriate CHF value.

Table 11 Sample of CHF look-up table

PRESSURE (kPa)	MASS FLUX (kg m^{-2} s^{-1})	QUALITY									
		-0.5	-0.4	-0.3	-0.2	...	...	0.6	0.7	0.8	0.9
...	...	...	...	...	...	...	...	...	...	...	...
...	...	...	...	...	...	...	...	...	...	...	...
7000	2500	10882	9986	8709	7496	...	...	261	204	99	51
7000	3000	11730	10850	9620	8170	...	...	346	263	112	52
7000	3500	12535	11558	10344	8740	...	...	409	317	135	57
7000	4000	13317	12216	10929	9320	...	...	470	317	136	58
7000	4500	14070	12839	11469	9769	...	...	492	317	137	59
7000	5000	14792	13465	11954	10124	...	...	521	326	138	63
7000	5500	15509	14000	12474	10713	...	...	582	348	153	70
7000	6000	16208	14521	12931	11464	...	...	655	379	179	84
7000	6500	16875	15091	13336	12214	...	...	725	422	210	99
7000	7000	17529	15640	13763	12432	...	...	795	476	243	116
7000	7500	18170	16174	14182	12682	...	...	866	530	277	132
7000	8000	18806	16673	14610	12995	...	...	936	581	312	149
8000	0	5101	4795	4484	4175	...	...	542	456	423	364
8000	50	5714	5359	5025	4744	...	...	1183	980	938	720
8000	100	6229	5834	5487	5235	...	...	1678	1457	1449	1050
8000	300	6685	6179	5792	5654	...	...	2144	1877	1538	1083
8000	500	6958	6354	5920	5763	...	...	2068	1858	1427	917
...	...	...	...	...	...	...	...	...	...	...	...
...	...	...	...	...	...	...	...	...	...	...	...

Compared to other available prediction methods, the look-up table approach has the following advantages: (i) greater accuracy; (ii) wider range of application; (iii) correct asymptotic trend; (iv) requires less computing time; and (v) can be easily updated if additional data become available. Applying the tables to transient heat transfer in bundles requires adjustment factors to correct for geometry, flux shape, and possibly transient effects. Here the advantages of the tabular technique (wide range of application, greater accuracy, and greater computing efficiency) are particularly important to the user.

The look-up table approach has some disadvantages: (i) it is a purely empirical prediction method, and hence it does not properly reflect the physics, and (ii) it could introduce erroneous trends if the underlying database were subject to experimental errors.

7.6.4.3.1 CHF correlations in CANDU bundles

Several CHF correlations have been developed for CANDU bundle geometry. These are mainly based on full-scale bundle data and are used for critical channel power calculations.

An example of a general form of a flux-corrected local CHF correlation for uncrept channels is given by [LEU2004, IAEA2001]:

$$CHF_{local} = \left(a_1 P^{a_2} G^{a_3} + a_4 P^{a_5} G^{a_6} x_{cr}\right)\left(\frac{q_{local}}{q_{average}}\right)^{a_7}. \tag{268}$$

An example of a general form of boiling-length-average CHF correlation for uncrept and crept channels is given by [LEU2004, IAEA2001]:

$$CHF_{BLA} = \left(b_1 P^{b_2} G^{b_3} + b_4 P^{b_5} G^{b_6} x_{cr}\right)\left[1 - b_7\left(\frac{q_{local}}{q_{average}}\right)^{b_8}\right]. \tag{269}$$

The values of the parameters in the above equations are of a proprietary nature.

7.6.4.3.2 CHF correlations in fuel assemblies

Providing precise CHF predictions for the fuel bundles of advanced water-cooled reactors is a very difficult task. Advanced water-cooled reactors designs includes a variety of bundle geometries, as well as a variety of element spacer designs.

The basis of almost any generic bundle prediction method is a tube CHF prediction method because (i) parametric trends with pressure, mass flux, and quality are similar in tubes and in bundles, and (ii) tube CHF prediction methods are generally used in sub-channel codes to predict CHF in bundles.

One of the well-known correlations for PWR fuel bundles is the Westinghouse and Tong [IAEA2001, TON1996] correlation, which can be given by the following expression:

$$q''_{cr,DNB} = \frac{q''_{cr}}{F},\ F = \frac{C\int_0^l q''(z')\cdot e^{-C(l-z')}dz'}{q''(l)\left[1-e^{-C\cdot l}\right]},\ C = \frac{4.23\cdot 10^6\left[1-x_e(l)\right]^{7.9}}{G^{1.72}}\ [m^{-1}], \tag{270}$$

$$\begin{aligned} q''_{cr} = &\left[\left(2.022-0.06238\cdot p\right)+\left(0.1722-0.001427\cdot p\right)\cdot e^{18.177-0.5987\cdot p}x_e\right] \\ &\left[\left(0.1484-1.596\cdot x_e+0.1729\cdot x_e\left|x_e\right|\right)\cdot 2.32\cdot G+3271\right]\left[1.157-0.869\cdot x_e\right] \\ &\left[0.2664+0.837\cdot e^{-124\cdot D_h}\right]\left[0.8258+0.0003413\left(h_l-h_{in}\right)\right] \end{aligned}. \tag{271}$$

The critical heat flux at the DNB, $q''_{cr,DNB}\,(kW/m^2)$, is at the local heat flux (for non-uniform heat flux), l (m) is the distance to the DNB, and x_e is the local steam thermodynamic quality. The above correlation is valid for the following parameter ranges: pressures of 5.5–13.8 (MPa), mass fluxes of 1350–6789 (kg/m^{2}s), hydraulic diameters of 0.005–0.0178 (m), thermodynamic qualities of -0.15–0.15, and channel lengths of 0.254–3.658 (m).

Another useful correlation for PWR fuel bundles is given by Bowring [IAEA2001, TON1996]:

$$q''_{cr} = \frac{A - B \cdot h_{lg} x}{C},\ A = \frac{2.317 \cdot \left(h_{fg} D \cdot G / 4\right) \cdot F_1}{1 + 0.0143 \cdot F_2 \cdot D^{1/2} G},\ B = \frac{D \cdot G}{4},$$
$$C = \frac{0.077 \cdot F_3 D \cdot G}{1 + 0.347 \cdot F_4 \left(G/1356\right)^n},\ p_R = 0.145 \cdot p \tag{272}$$

$$F_1 = \left\{ p_R^{18.942} \exp\left[20.89\left(1 - p_R\right)\right] + 0.197 \right\} / 1.917$$
$$F_2 = F_1 / \left(\left\{ p_R^{1.316} \exp\left[2.444\left(1 - p_R\right)\right] + 0.309 \right\} / 1.309 \right) \qquad For\ \ p_R < 1MPa, \tag{273}$$
$$F_3 = \left\{ p_R^{17.023} \exp\left[16.658\left(1 - p_R\right)\right] + 0.667 \right\} / 1.667$$
$$F_4 = F_3 p_R^{1.649}$$

$$F_1 = p_R^{-0.368} \exp\left[0.648\left(1 - p_R\right)\right]$$
$$F_2 = F_1 / \left\{ p_R^{-0.448} \exp\left[0.245\left(1 - p_R\right)\right] \right\} \qquad For\ \ p_R \geq 1MPa. \tag{274}$$
$$F_3 = p_R^{0.219}$$
$$F_4 = F_3 p_R^{1.649}$$

The above correlation is valid for channel lengths of 0.15–3.7 (m), pressures of 0.2–19 (MPa), and mass fluxes of 136–18,600 (kg/m^{2}s).

The CANDU fuel CHF correlation is based on the CHF look-up table and is given by the following expression (note that CANDU 6 uses the look-up table method, whereas the Bruce and Darlington designs use correlations [IAEA2001]):

$$CHF = CHF_{TABLE} K_1 K_2 K_3 K_4 K_5 K_6 K_7 K_8 K_9, \tag{275}$$

where K_1 to K_9 are modification factors to account for sub-channel specific effects (e.g., element gap size, sub-channel equivalent diameter, adjacent heated/unheated surfaces, upstream spacers, etc.) and are defined as: K_1 – tube diameter factor; K_2 – bundle geometry factor; K_3 – spacer-effect factor; K_4 – heated-length factor; K_5 – axial-flux-shape factor; K_6 – circumferential-flux factor; K_7 – horizontal flow factor; K_8 – low-flow factor; K_9 – transient-effect factor.

7.6.4.4 CHF margin evaluation

CHF evaluation in the reactor core is of primary importance for estimating the reactor operating margins with adequate precision and a good understanding of uncertainties. Figure 114 shows the concept of reactor operating margin evaluation as a function of reactor operation (aging) [LEU2004, POP2014].

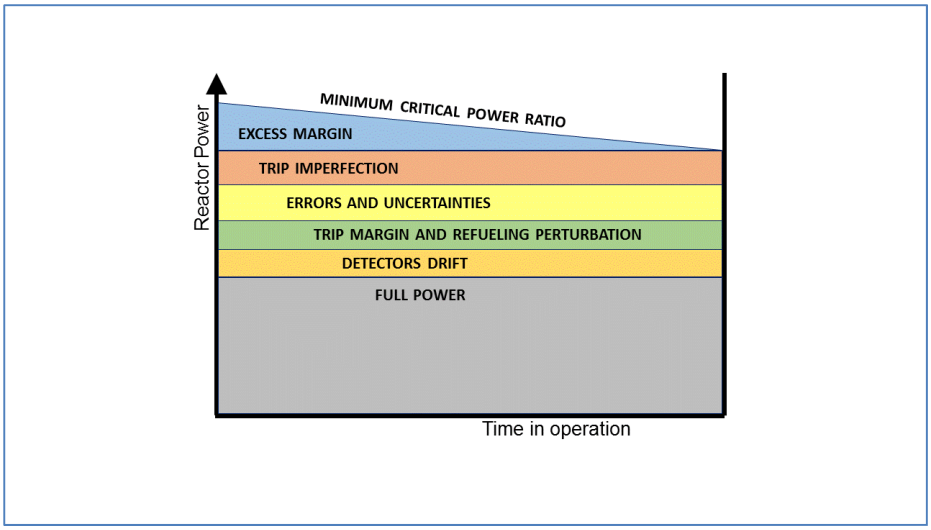

Figure 114 Concept of operating margins

This diagram assumes that the nominal power will remain unchanged during the reactor's life. Above the full nominal power are the detector drift margin and the operator's trip margin/fuelling/operating perturbation margin, which are also assumed to remain unchanged during the reactor life. On top of these are the error and uncertainties margin and the trip imperfection margin, which are also assumed to remain unchanged during the reactor life. However, the excess margin that is embedded in the reactor core design, and which represents all aging mechanisms having an impact on the reactor power margin, such as pressure-tube creep, continually decreases during the reactor life (i.e., the pressure-tube life). When all these margins are evaluated and added on top of the full nominal power, the resulting maximum power should still be less than the reactor critical power at which CHF occurs in some fuel channels.

From the above discussion, it is clear that CHF prediction is an important part of reactor thermal power margin evaluation. Hence, CHF evaluation and application focusses on the following concerns:

i. To set the operating power with a comfortable margin to avoid CHF occurrence, in terms of the following parameters: (a) minimum CHF ratio (MCHFR) at constant pressure, mass flux, and critical quality; (b) minimum CHF power ratio (MCHFPR) at constant pressure, mass flux, and inlet fluid temperature; or (c) minimum power ratio (MCPR) at constant pressure, pump characteristic, and inlet fluid temperature

ii. To evaluate the maximum sheath temperature during LOCA, LOFA, or LORA, which is usually concerned with the first (initial) CHF location;

iii. To evaluate the thermal-hydraulic and neutronic responses to CHF occurrence in a reactor core (trip set points), based on knowledge of how CHF spreads in the reactor core; best-estimate predictions of average CHF and/or area in dryout as a function of power.

For reactor transient (accident) analyzes, it is important to determine sheath and fuel

temperatures. In this case, CHF is considered as the reference point for post-dryout analyzes. The set of transient analyzes includes the following scenarios: loss of regulation, loss of flow, loss of Class IV power, loss of coolant (small and large breaks), etc. More details are provided in Chapter 16.

The following terminology is used when evaluating CHF margins:

1) Dryout (or critical heat flux, CHF) occurs when the fuel sheath can no longer maintain continuous liquid contact. Current licensing criteria are no burnout or dryout at any location in the fuel channel (details depend on whether the first or second trip is considered in the analysis).
2) Critical power (CP) (also known as critical channel power, CCP) is the power corresponding to the first CHF occurrence (at constant pump head). Determining this requires knowledge of various disciplines (physics, fuel, fuel channel, thermal-hydraulics, etc.).
3) Critical power ratio (CPR) is the ratio of critical power to operating power.
4) Regional overpower protection (ROP) or neutron overpower protection (NOP) is aimed at preventing burnout in any fuel assembly during a slow LOR event. It includes full-core analysis of all possible scenarios and establishment of trip set points for various detectors.

Figure 115 shows the concept of critical channel power (CPR) used in the CANDU CHF margin methodology, with channel flow shown on the *y*-axis and channel power on the *x*-axis [IAEA2001, LEU2004, POP2014]. In this diagram, a critical parameter is any parameter associated with the critical heat flux (CHF). Below the diagram, a CANDU fuel channel is shown, with 12 fuel bundles and associated feeders connecting the channel to the reactor inlet and outlet header.

The channel hydraulic curve (blue line) determines the level of channel power that can be removed by a certain flow rate. Therefore, as power rises, the mass quality will also rise (two-phase flow behaviour), which would result in a reduction in the mass flow rate that can be pushed through the channel. To this point November 14 afternoon

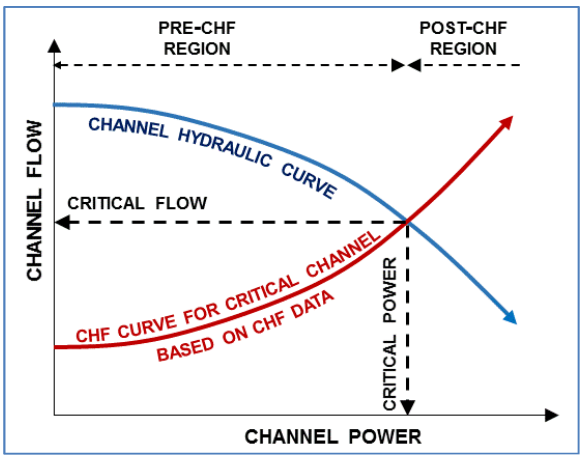

Figure 115 Critical channel power

The CHF curve (red line) shows the CHF values for certain combinations of channel power and flow rate. As explained in previous sections, at higher flow rates, the channel power at CHF will also rise (with the square of the flow rate). The intersection of these two curves shows the actual point at which CHF will be reached in the channel for a given flow rate and power. Hence, the intersection point defines the critical flow and the critical power at CHF. The left part of the diagram for which power is less than the critical power is defined as the pre-CHF region, and the right side of the diagram is the post-CHF region.

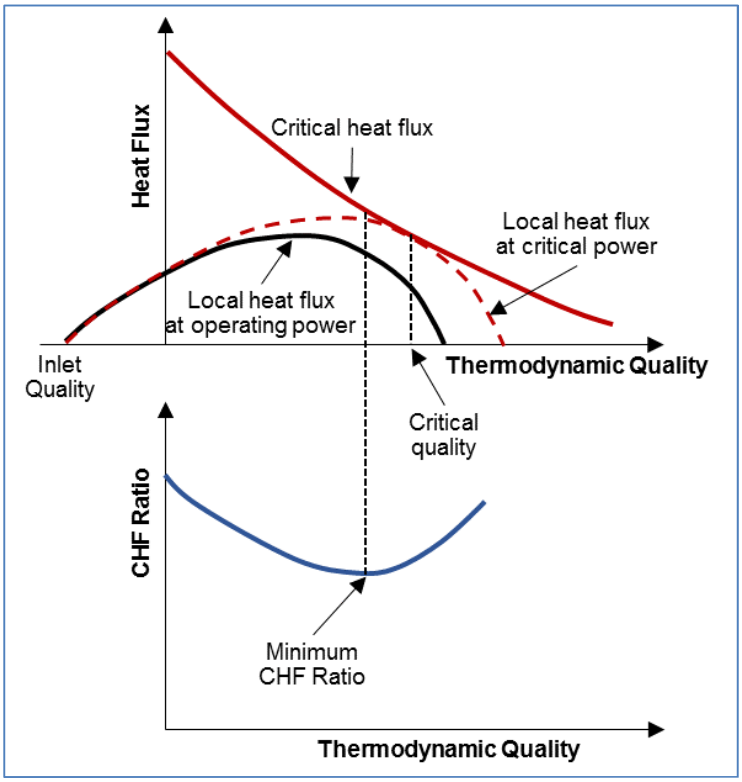

Figure 116 CHF margin definitions

The concept of CHF margin is explained in Figure 116 [IAEA2001, POP2014]. The top diagram on this figure shows heat flux on the *y*-axis and thermodynamic quality on the *x*-axis. The red solid curve shows a prediction of CHF as a function of thermodynamic quality. Of course, thermodynamic quality depends on channel power among other parameters, and therefore in turn, the shape and value of the CHF curve depend on channel power.

The solid black curve shows local heat flux as a function of quality, i.e., axial position in the channel as quality changes along the channel. Normally, under nominal conditions, the heat flux is less than the CHF, and therefore the black curve does not touch the red curve for any quality value. However, if the channel power is increased, the local heat flux along the channel also increases. At a certain value of the channel power, the local heat flux will touch the CHF at a certain position, and this position represents the power value that causes CHF (red dashed line). On the bottom diagram, the CHF ratio is shown, defined by the ratio of the critical heat flux (CHF) to the flux corresponding to the nominal operating power (NOP):

$$CHF_{RATIO} = \frac{CHF}{q_{local}}. \quad (276)$$

The above relation assumes constant inlet thermodynamic quality, constant outlet pressure, and mass flux.

Figure 117 shows a comparison of CHF margin evaluation methods: the CHF ratio, the CHF power ratio, and the critical power ratio [IAEA2001, POP2014]. The above explanation along with Eq. (276) is illustrated on the left side of Figure 117. The MCHFR method is easy to understand and implement. However, it does not provide a clear account of reactor power margins because it uses heat flux instead of channel power, which makes it cumbersome to use for power reactor applications (however, it is often used for research reactor applications).

The CHFPR method is shown on the right side of Figure 117 [IAEA2001, POP2014]. In this method, rather than a ratio of channel heat fluxes, a ratio of channel powers is used that represent a certain value of operating heat flux and CHF. This method provides a better understanding of channel and reactor power margins with respect to CHF. However, it does not provide a clear account of margins because as channel power rises to reach the CHF line, the CHF line will also change position because it indirectly depends on channel power.

The most useful method in CANDU reactor applications is the *critical power* (CPR) method. The principles of this method are explained above and illustrated in Figure 115 [IAEA2001, POP2014]. The critical power ratio is defined by the following relation:

$$CP_{RATIO} = \frac{Critical\ Power}{Operating\ Power}. \quad (277)$$

This relation holds for constant inlet fluid temperature and pressure and a fixed pump curve. As is evident from this diagram, channel flow at point NOP on the hydraulic curve corresponds to NOP power. Keeping the flow at point NOP, the corresponding heat flux that would have resulted in CHF is at point CHF_1 (the top blue point on the CHF curve), corresponding to the critical power. CP_1. The flow at point CHF (lower blue point on the CHF curve) corresponds to the channel power. CP_2.

Hence, the critical power ratio is given by the relation:

$$CPR = \frac{CP_2}{NOP}. \quad (278)$$

The margin to CHF is shown as the distance between points NOP and CP_2, as can be observed on the right side of Figure 117.

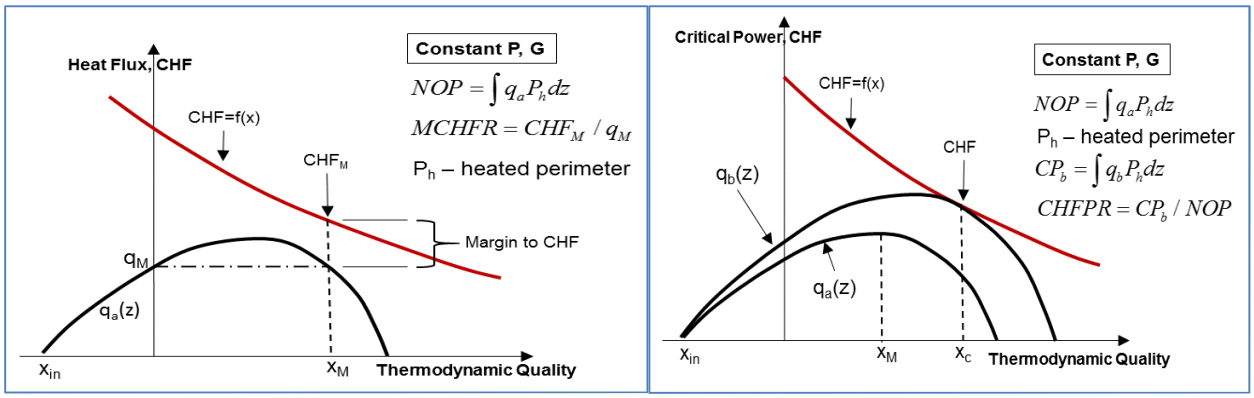

a) Critical heat flux ratio b) Critical heat flux power ratio

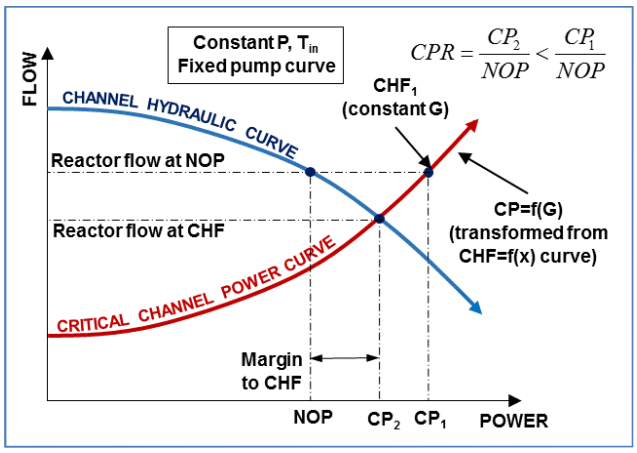

c) Critical power ratio

Figure 117 CHF margin evaluation methods (a, b, c)

There are a number of uncertainties in the development and application of the CHF prediction methods and CHF margin methods covered in this section. These uncertainties need to be well understood, classified, and evaluated and then taken into account in reactor applications. The uncertainties can be broadly grouped into the following categories:

i. Uncertainties in CHF measurements using bundle simulators. These uncertainties can result from errors in flow, power, pressure, and inlet temperature measurements that are caused by (a) inadequate CHF detection methods, (b) variations in flux distribution across/along the bundle, and (c) geometric tolerances;

ii. Prediction uncertainties in CHF correlations or sub-channel codes;

iii. Uncertainties in reactor conditions, including (a) reactor flow, pressure, and temperature (calculated from system safety codes) and (b) reactor power measurements (from detectors); and

iv. Uncertainties in extrapolation to in-reactor conditions resulting from (a) electrical vs. nuclear heating; (b) flux tilts across elements, the bundle, and the core; and reactor aging effects (creep, fouling of pipes, etc.).

7.6.4.5 CHF bundle effects – R&D testing and application

Extensive R&D support is required to gain a better understanding of CHF phenomena, including support for development of CHF correlations and look-up tables and development of computer tools. Any changes in design or operating parameters trigger a need for supporting R&D to provide evidence of the applicability of the current CHF models. The general strategy in performing supporting CHF R&D is to conduct it in an incremental fashion to minimize the cost and optimize the work scope.

CHF experiments are usually based on constant flow conditions (inlet or outlet pressure, inlet mass flow rate, and inlet-fluid temperature) and constant geometric factors (hydraulic diameter and heated length) in each test series. The primary interest in these CHF experiments is measurement of fuel power at CHF. However, determining CHF locations (both axially and radially) is also an objective. The other measurements of interest are circumferential CHF location, subsequent CHF occurrences (CHF spreading, or dry patch spreading), and pressure drops along a channel experiencing CHF.

A number of CHF experiments are performed in a simple geometry consisting of one fuel element simulator. In such case, the experimental setup consists of a pipe in which heating is provided by direct electrical current flowing through the pipe wall and coolant flowing past the pipe outside surface. Another option is to use indirect heating by a coil embedded in the pipe interior. through which electrical current is supplied. In either case, the heat flux from the pipe wall to the fluid is directly proportional to the strength of the electrical current. Axial power profiles can be obtained by varying the pipe wall thickness in direct heating, or by changing the number of coils per unit length in the case of indirect heating.

The pipe is equipped with various instruments to measure important parameters. Stationary or movable thermocouples are used for wall temperature measurements. The stationary thermocouples can measure only temperatures, i.e., burnout/dryout at specific locations in the pipe. Therefore, these may not capture initial CHF value and location. Moreover, no information on subsequent CHF and dry-patch spreading can be obtained with these thermocouples. Moveable thermocouples provide coverage almost over the entire heated length because they are moved during the experiment along the internal wall of the heated pipe. They provide measurements of initial CHF, subsequent CHF occurrences, and dry-patch spreading. However, they are more conservative, expensive, and time-consuming (when scanning the entire pipe surface area).

More complex and sophisticated CHF measurements are performed in CANDU fuel bundle simulators. One such simulator is shown in Figure 118 [LEU2004]. This fuel bundle simulator consists of a 37-element full-scale bundle 6 m long. The bundle is provided with a simulator of junctions and appendages and fully resembles a CANDU fuel channel. The wall heating distribution takes into account bundle endplates and fuel distribution along the string of fuel bundles. This device can simulate non-uniform axial and radial power distribution. Sliding thermocouples are inserted into a number of fuel element simulators that are indirectly heated by coils connected to the electric current source. Figure 119 shows an axial power distribution in such a fuel bundle simulator, and as is evident in the figure, any axial variation in heat flux can easily be simulated. Figure 120 shows a close-up view of one part of a fuel bundle and a

sliding thermocouple moving inside along the fuel element, with a sample of a measured fuel sheath temperature [LEU2004].

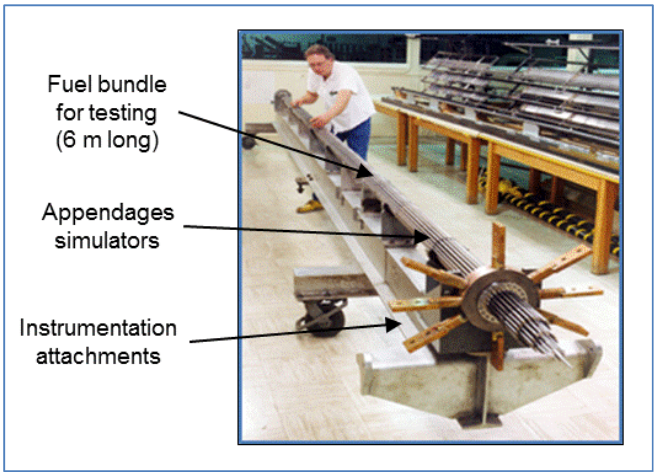

Figure 118 CANDU bundle experimental simulator

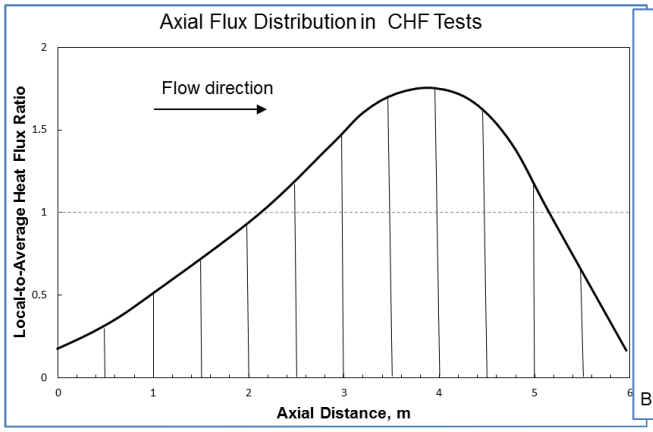

Figure 119 Axial flux distribution in full-scale bundle test

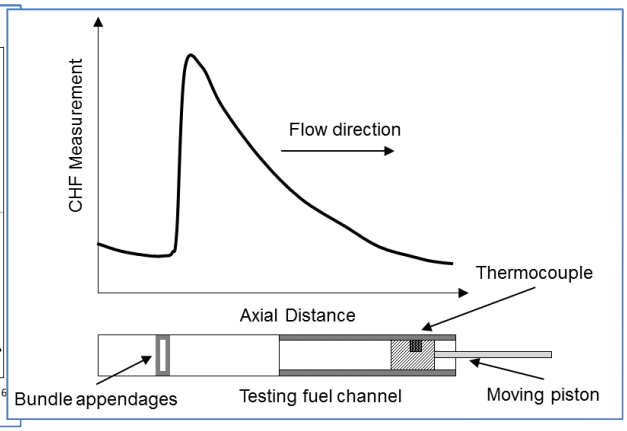

Figure 120 CHF variation along a heated surface

One of the most important aspects and of CHF in fuel bundles is the impact of spacing devices, which enhances CHF as the spacing value increases. In addition, the impact of radial power distribution is important because it can result in asymmetric CHF occurrence in the bundle. However, the 37-element and 43-element CANDU fuel bundle designs have enhanced features that improve CHF design.

Figure 121 shows various spacer devices used in fuel bundle design for various reactor types [IAEA2001]. These devices have a dual purpose: to keep the bundle tight, i.e., to minimize radial vibration, and to enhance turbulence and thus improve CHF robustness (i.e., increase the CHF value). In general, turbulence in pipes and fuel bundles creates better fluid mixing and therefore easier removal of bubbles generated in sub-cooled boiling on the walls. This in turn enables a fuel element to achieve higher heat fluxes without causing CHF by bubble crowding on the fuel sheath surface.

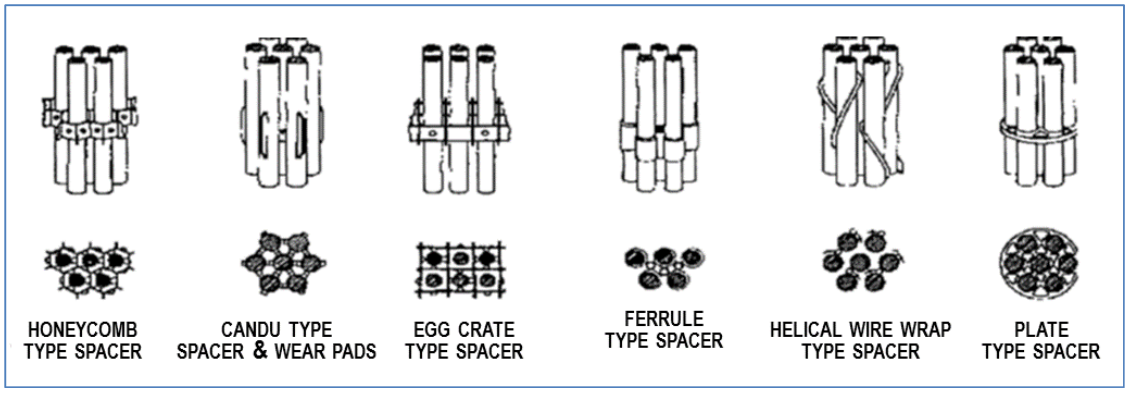

Figure 121 Different types of spacer devices for CHF robustness

Figure 122 presents an illustrative example of the impact of spacer devices on CHF [IAEA2001]. On the *y*-axis, local critical heat flux is shown. The flow along this CANDU channel is from left to right. Because sub-cooling is higher at the inlet, CHF is also higher. As fluid moves along the channel, the pressure decreases, quality increases, and bulk boiling starts. The net effect of these changes is a reduction in the CHF along the channel. However, as fluid approaches a bundle spacer, fluid turbulence increases, causing a sharp CHF increase. If the fuel rods were smooth along the length of the fuel channel and there were no spacers or other appendages, the CHF would have been reduced much faster.

The benefits of more turbulence as a method of enhancing CHF robustness must be weighed against the negative impact of higher turbulence and local pressure losses on the primary pump head. Therefore, having too much turbulence and local pressure loss causes the primary pump head, pump design, and particularly pump operation to become prohibitively expensive, which may outweigh the benefit with regard to CHF.

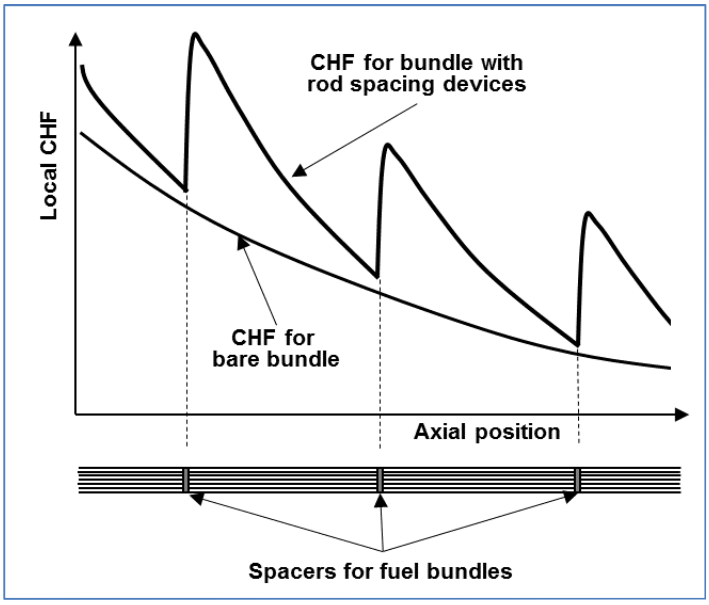

Figure 122 CHF behaviour around fuel bundle spacer devices

CHF data have a wide range of application, and this is one of the most important R&D areas for

reactor design, safety analysis, and licensing. CHF margins are the central issue in the licensing submissions for nuclear reactors, and this application is a strong driver for full-scale fuel bundle data, for quantification of the impact of separate effects, and for assessment of CHF uncertainties.

CHF R&D work is important to reach an adequate understanding of the phenomena involved using fundamental and bundle-specific studies and parametric and separate-effects tests. Certainly, CHF R&D is essential to develop prediction methods, i.e., CHF correlations and models, and to validate these correlations, models, and reactor safety codes. The CHF tests used for this purpose are a combination of bundle and separate-effects tests. The key applications of CHF prediction methods are in ROP (or NOP) and reactor safety codes, fuel channel behaviour codes, and fuel behaviour codes.

Experimentally measured CHF values are based on tests with defined inlet conditions. CHF values based on inlet-flow conditions are limited to a specific channel geometry and heated length. However, reactor safety analyzes use the local-conditions approach based on local pressure, mass flux, and quality to predict local CHF. For given inlet conditions, the local CHF conditions may vary in terms of thermodynamic quality (or enthalpy). In such cases, low quality (or enthalpy) is appropriate for short heated lengths and high quality (or enthalpy) for long heated lengths. It is important to evaluate local thermodynamic quality using inlet flow conditions and power.

When using CHF data, it is important to mention that all CHF data are obtained under steady-state conditions in terms of power, mass flux, and sub-cooling. In safety analysis, CHF prediction tools developed for steady-state conditions are used to simulate reactor transients. If the transient is slow, i.e., longer than 10 s, no significant impact on the models is expected. However, for fast transients (shorter than 1 s), a significant effect on CHF is likely.

Another important CHF application is related to thermal-hydraulic and neutronic responses to CHF occurrence (partial bundle dryout). This application is strongly affected by the level of success in predicting the spread of dryout in a fuel bundle. It has been experimentally observed that the average CHF value that occurs over a large portion of the fuel sheath surface can be much higher than the initial CHF at some cross-sectional locations. To capture such important effects in dryout spreading, sub-channel codes are the most promising tool.

7.6.5 Transition and film boiling heat transfer

Reactor fuel channel operation beyond dryout (beyond CHF) is possible in certain transient and accident regimes. This section provides information on post-dryout heat transfer phenomena and on the correlations used for these heat transfer regimes.

Post-CHF (or post-dryout) heat transfer occurs when the surface temperature becomes too high to maintain continuous liquid contact and the surface becomes covered by a continuous or intermittent vapour blanket. Post-CHF heat transfer includes transition boiling, illustrated in Figure 29 and Figure **123**, where intermittent wetting of the heated surface takes place, and film boiling, where the heated surface is too hot to permit liquid contact. The boundary between these post-CHF heat transfer modes is the minimum film boiling temperature, or T_{MFB}. Due to the poor heat transport properties of vapour, high heated surface temperatures are often encountered during film boiling.

7.6.5.1 Post-dryout phenomena

Several figures presented in previous sub-sections of this chapter are relevant to post-dryout heat transfer. Figure 26 shows heat transfer regimes in vertical fuel channels, with clearly shown areas of post-dryout heat transfer regimes in the upper part of the channel. Figure 28 shows a 3-D representation of the boiling surface for water, with transition and film boiling indicated. Figure 29 shows a conceptual illustration of the boiling curve, again showing post-dryout heat transfer beyond the CHF point. Figure 33 shows temperature profiles along a vertical fuel channel experiencing various flow and heat transfer regimes, including post-dryout heat transfer regimes in the upper part of the figure.

Post-CHF heat transfer is initiated as soon as the CHF condition is exceeded and continues until quenching (rewetting) of the surface is achieved. Depending on the particular scenario and flow conditions present, various heat transfer modes of the boiling curve may be distributed along a heated surface, or a series of heat transfer modes can succeed each other over time at the same location, as is the case during transients.

During sustained post-dryout heat transfer, the heated surface is cooled mainly by vapour flow. Because of the relatively low heat-transfer coefficient for this heat transfer regime, the fuel sheath is exposed to high temperature that may lead to damage. In this respect, it is important to understand and determine the surface conditions and the coolant flow parameters at the time CHF is reached, because these determine the impact of the post-dryout condition on the fuel sheath.

Figure 123 shows various post-dryout flow types and heat transfer regimes on a vertical surface [LEU2004, POP2014]. These are highly similar to those that occur in a horizontal fuel channel. Type I post-dryout identifies a situation in which the heated surface has lost contact with the liquid, but at one location, contact has been re-established, and this point acts as a heat sink. In this case, heat transfer from the internal parts of the wall and from surrounding areas occurs towards this heat sink, thus cooling the wall near the liquid-wall contact and preparing it for quenching.

Type II represents a situation in which a heated surface in post-dryout regime is flooded by

liquid water from the top. This figure clearly shows the quench front moving downward. The upper part of the surface is well cooled, and obviously heat transfer occurs from the lower, hotter portions of the wall upwards towards the cooler area, which therefore acts as a local heat sink, preparing the lower part of the surface for quenching. Type III represents a situation similar to Type II, but in this case, quenching proceeds in an upward direction by flooding from the bottom. Type II and Type III post-dryout regimes combine into one regime for a horizontal surface.

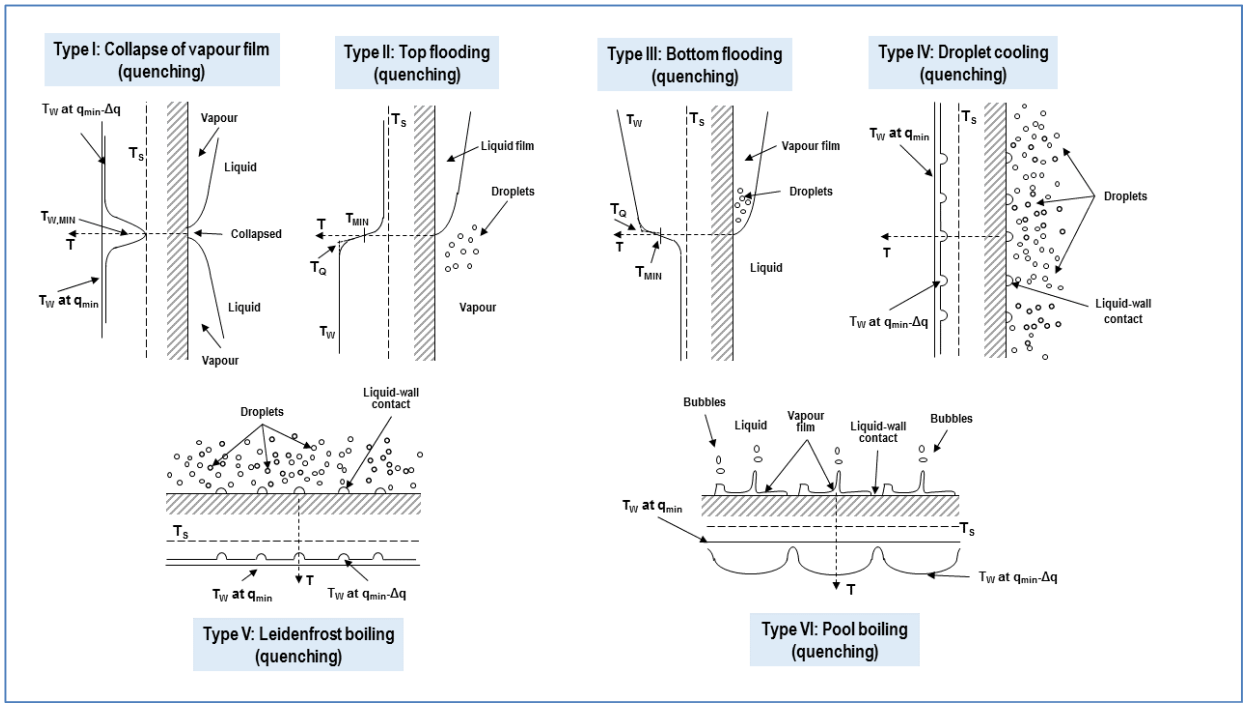

Figure 123 Types of transition boiling and film

Type IV mode occurs when the heated surface in post-dryout regime is cooled by impingement of droplets flowing past the heated wall. Each droplet impingement on the heated surface provides a quick intermittent miniature local heat sink. However, although local surface cooling by one droplet impingement is infinitesimally small, as many droplets impinge on the surface, the integral effect of heat removal is significant, thus preparing the surface for rewetting.

Types V and VI apply to horizontal surfaces in pool boiling. Type V shows droplets impinging on the surface, with an effect similar to Type IV, whereas Type VI represents a regime in which a water layer floats on top of a vapour film, a situation similar to that described for Type I.

Transition Boiling

Berenson [IAEA2001] provides one of the best definitions of transition boiling: a combination of unstable film boiling and unstable nucleate boiling alternately existing at any given location on a heating surface. The variation in heat transfer rate with temperature is primarily the result of a change in the fraction of time that each boiling regime exists at a given location.

Figure 124 conceptually shows transition boiling in a pool boiling regime. Pockets of vapour are

visible on the heated surface and may move intermittently back and forth along the surface, as is typical for this pool boiling situation. At any surface temperature in excess of the CHF temperature, the heated surface is partially covered with unstable vapour patches varying over space and time, with frequent replacement of vapour patches by fluid. Although this may seem similar to transition pool boiling as described above, the introduction of the convective component improves the film boiling component by reducing the vapour film thickness and changing the heat transfer mode, whether dry or wet, from free convection to forced convection.

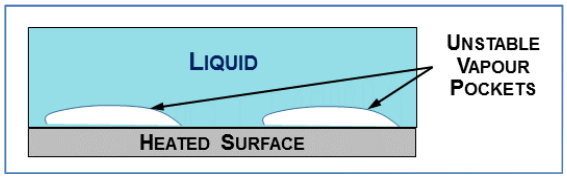

Figure 124 Concept of transition boiling in pool boiling

As shown in Figure 29, the slope of the curve for transition boiling is negative, which means that this is an unstable heat transfer regime. This heat transfer regime can occur on a temperature-controlled surface at conditions beyond CHF. Examples of temperature-controlled surfaces are surfaces with high thermal inertia, surfaces heated by condensing steam (which controls temperature at the saturation point), and fuel element surfaces during fast transients.

A heat-flux-controlled surface at conditions beyond CHF can experience transition boiling only under conditions under which the slope of the transition boiling curve is positive ($dq/dt > 0$), which is possible for mass quality above 50%, as shown in Figure 31. Note that as temperature increases gradually with increasing heat flux, transition boiling intermittently wets and dries the surface. In the case of high quality, even when the surface is continuously dry, the temperature increase is not drastic due to effective convective heat transfer. Examples of heat-flux-controlled surfaces are electric heaters and fuel elements during fast transients.

If the slope of the transition boiling curve is negative ($dq/dt < 0$), a rapid transition from nucleate boiling to film boiling usually occurs, and therefore transition boiling is not encountered (or occurs very briefly).

The periodic contacts between liquid and heated surface in the transition boiling region of the boiling curve result in formation of large amounts of vapour, which force liquid away from the surface and create an unstable vapour film or blanket. Because of this, the surface heat flux and the surface temperature can vary both with time and with position on the heater. The average heat transfer coefficient decreases as the temperature increases because the time of contact between the liquid and the heater surface is decreased.

Heat transfer in transition boiling occurs primarily by liquid-solid contact. At the critical heat flux point, the contact-area (or time) fraction is generally 100%, i.e., most of the surface is in good contact with the liquid. Post-CHF conditions result in a sudden large decrease of the contact fraction between the liquid and the heated wall surface. Thereafter, most of the heat transferred during transition boiling will be due to droplet-wall interaction. Initially, at surface

temperatures just in excess of the boiling crisis temperature, a significant fraction of the droplets deposit on the heated surface, but at higher wall superheats, vapour repulsion forces become significant in repelling most of the droplets before they can contact the heated surface. The repelled droplets contribute to heat transfer by inducing turbulence in the boundary layer to enhance convective heat transfer to the vapour.

Figure 29 shows that transition boiling ends when the heated wall surface temperature drops to a minimum value, called the minimum film boiling temperature, T_{MFB}. Several names are given to the minimum film boiling temperature. They include rewetting temperature, quench temperature, Leidenfrost temperature, film boiling collapse temperature, and others.

During dryout and wall temperature increase, the minimum film boiling temperature separates the high-temperature region, where film boiling or vapour cooling takes place, from the lower-temperature region, where much more efficient heat transfer in transition boiling occurs. Knowledge of the minimum film boiling temperature is particularly important in reactor safety assessments.

During surface quenching (such as emergency core cooling), rewetting commences at the minimum film boiling temperature and proceeds until nucleate boiling is established at a much lower wall temperature. For this reason, predicting the minimum film boiling temperature as a function of the system parameters is very important because heat transfer coefficients on either side of the minimum film boiling temperature can differ by orders of magnitude. Generally, T_{MFB} is defined as the temperature at the minimum heat flux.

In summary, no liquid/sheath contact is possible for $T_W > T_{MFB,}$ but possible liquid/fuel sheath contact exists for $T_W < T_{MFB}$:

$$\Delta T_{W,MIN} = \frac{q_{MIN}}{h_{FB}}. \tag{279}$$

Film boiling

Two theories have been proposed for analytical prediction of the minimum film boiling temperature. One theory says that the minimum temperature is a thermodynamic property of the fluid (i.e., the maximum liquid temperature) and therefore is primarily a function of pressure. According to this theory, the minimum film boiling temperature is associated with the maximum liquid superheat (beyond which the nucleation rate is infinite and liquid cannot exist). This theory comes from the equation of state and from homogeneous nucleation theory.

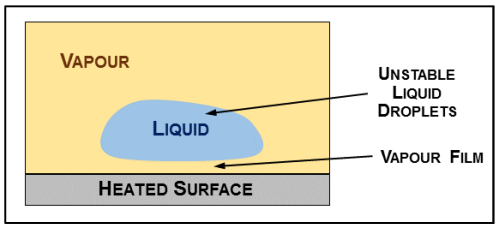

Figure 125 Minimum film pool boiling – Taylor instability

The other minimum film boiling theory suggests that rewetting commences due to hydrodynamic instabilities that depend on the velocities, densities, and viscosities of both phases as well as the surface tension at the liquid-vapour interface. By this theory, the minimum heat flux associated with the minimum film boiling temperature can be predicted from Taylor's instability criterion. Figure 125 illustrates the theory of Taylor's instability [LEU2004, POP2014, DEL1981, BER1981]. This figure shows a chunk of liquid that floats on top of a vapour film above a heated surface. The instability results from gravity acting on the liquid as a heavier phase on the top, and on the vapour as a much lighter phase at the bottom.

During fast transitions, where insufficient time is available to develop hydrodynamic forces fully, rewetting can be expected to be thermodynamically controlled, whereas for low flows and low pressures, where sufficient time is available and the volumetric expansion of the fluid near the wall is large, rewetting is more likely to be hydrodynamically controlled. Once rewetting has occurred locally, the rewetting front can then propagate at a rate controlled primarily by axial heat conduction in the heated wall.

Figure 126 [LEU2004, POP2014] shows various film boiling types in pool boiling and forced convection flow situations.

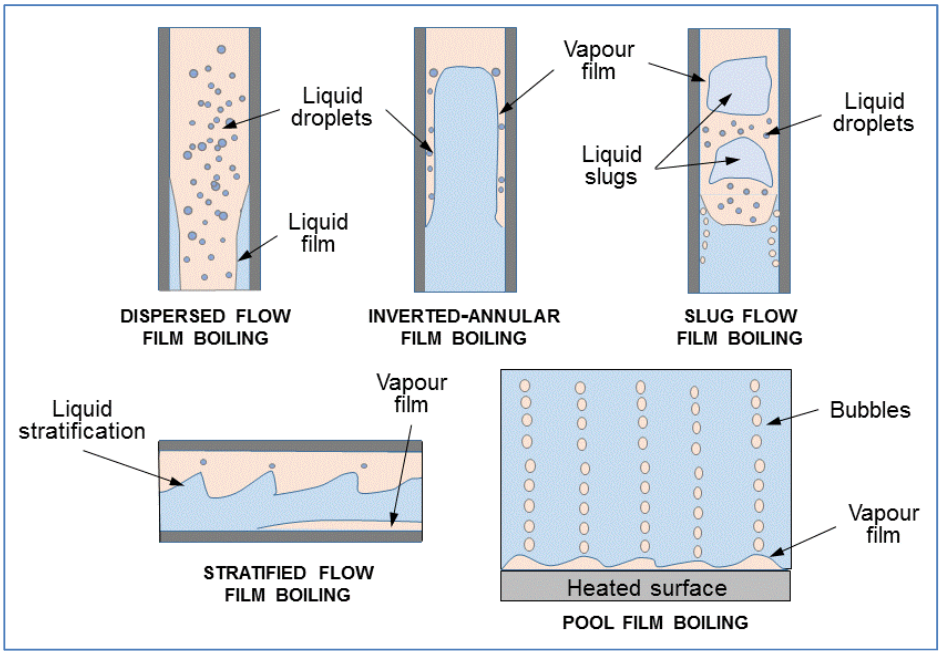

Figure 126 Film boiling types

Film boiling is generally defined as that mode of boiling heat transfer in which only the vapour phase is in contact with the heated surface (see Figure 125 and Figure 126). The term is used in forced convective boiling to refer to conditions under which the liquid does not contact the heated surface, but is usually in one of the following forms (shown on Figure 126 and Figure 32)

a) a dispersed spray of droplets, normally encountered at void fractions in excess of 80% (liquid-deficient or dispersed-flow film boiling regime);

b) a continuous liquid core (surrounded by a vapour annulus which may contain entrained droplets), usually encountered at void fractions below 40% (inverted annular film boiling or inverted annular-flow boiling regime (IAFB)); and
c) a transition between these two cases, which can take the form of an inverted slug flow for low to medium flow.

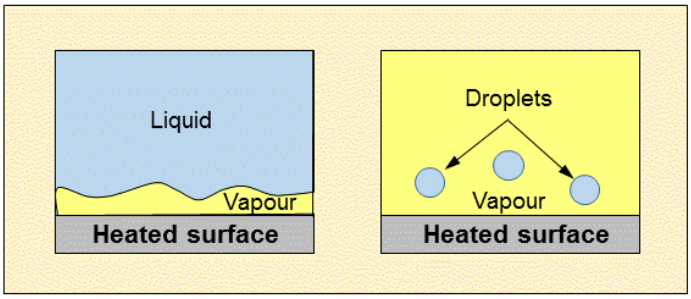

Figure 127 Pool film boiling mechanisms with horizontal heated wall

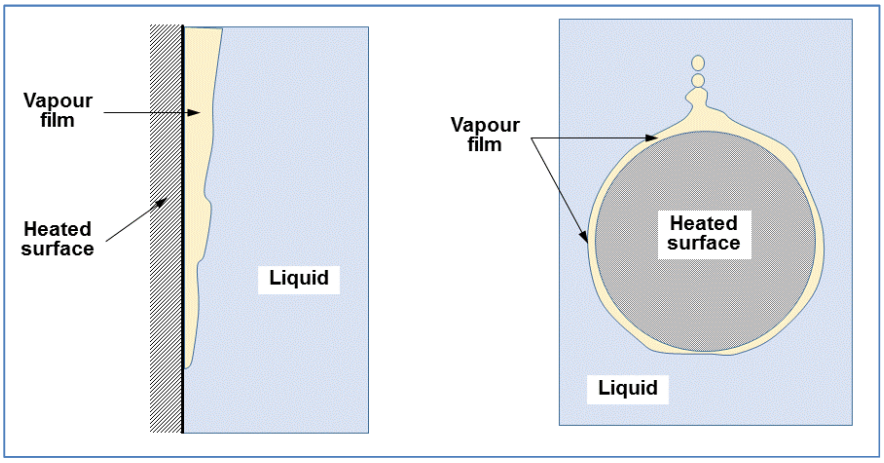

Figure 128 Pool film boiling patterns

The flow and heat transfer regimes types described above are illustrated in Figure 126. This figure also shows an example of stratified flow film boiling that is relevant to CANDU reactor channels. Figure 128 shows pool film boiling at a vertical wall and at a horizontal cylinder in stagnant water.

The dispersed flow film boiling regime, shown in Figure 129 at the bottom, is the most commonly encountered and has been well studied. Its heated surface temperature is moderate. In the inverted annular and inverted slug flow regimes, shown at the top of Figure 129, excessive surface temperatures are frequently encountered (see Figure 104 and Figure 105). Radiation heat transfer, which is unimportant in transition boiling, becomes important in film boiling, particularly at low flows, low void fractions, and surface temperatures in excess of 700°C.

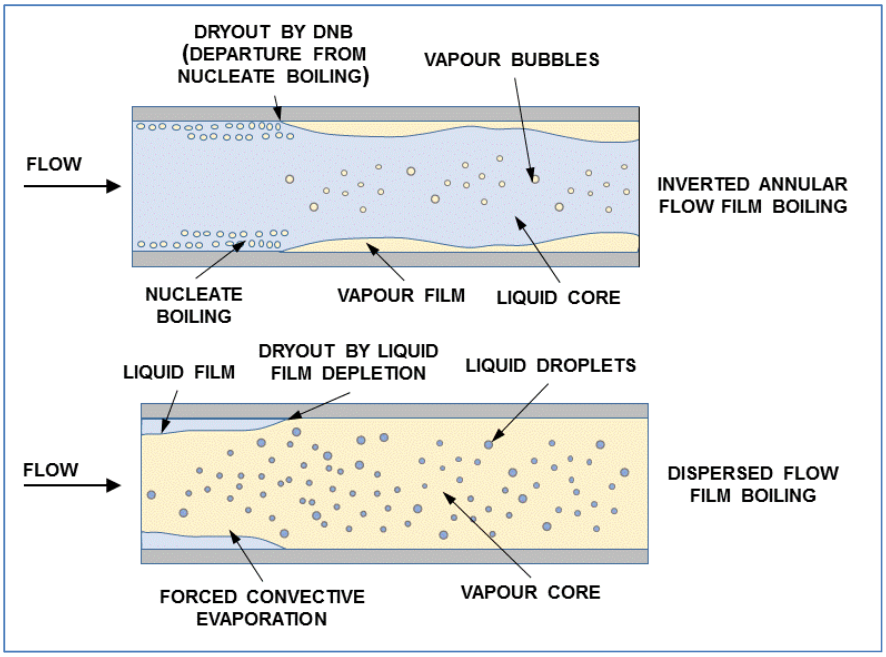

Figure 129 Forced convection film boiling patterns

When the flow and heat transfer regime is film boiling with the presence of liquid, several heat transfer regimes occur, as shown in Figure 130. On the left side of Figure 130, a film boiling regime with droplets in the middle of the pipe is illustrated. On the right side of Figure 130, a film boiling regime with a liquid core in the middle of the pipe is illustrated [POP2014, LEU2004]. These two flow regimes correspond to the regimes shown in Figure 129. The *y*-axis represents temperature or velocity, whereas the *x*-axis represents distance from the heated wall, along with heat flux direction.

In both cases, close to the wall, a gradual change of temperature or velocity is indicated, as appropriate for a boundary layer in a laminar flow regime. On the left side, the liquid droplets are assumed to be small, as is appropriate for dispersed flow. In such a case, the droplets are assumed to be at saturation. Hence, the temperature profile in the channel shows a superheated wall (temperature above the saturation temperature for a given pressure) and superheated steam in the pipe core.

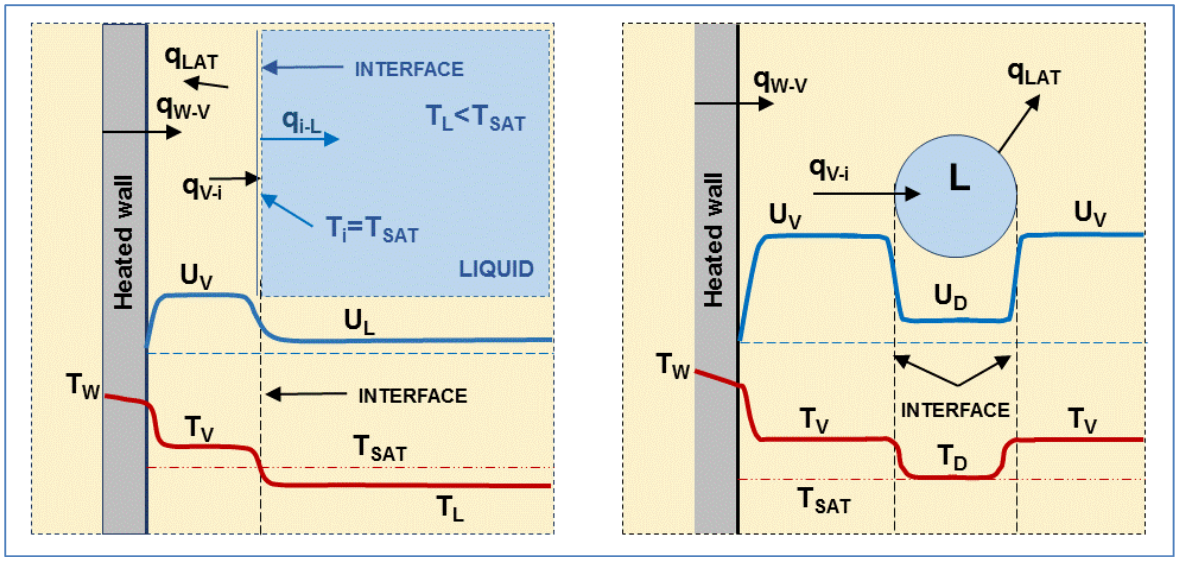

Figure 130 Film boiling heat transfer temperature and velocity profiles

Away from the wall, temperature drops quickly to a lower value in the boundary layer, but still remains above saturation. At the steam-droplet interface, temperature is close to saturation and continues to be at saturation inside the droplet. The velocity is near zero along the wall and rises in the boundary layer to a value representing steam bulk velocity. The steam velocity is higher than the liquid velocity, and this velocity difference, and the associated interfacial friction between the phases, carries the droplets upward. Because water is a much heavier fluid than steam, a large velocity difference between water and steam is needed to produce sufficient interfacial friction to carry the droplets in steam flow.

The heat flux direction on the left side of Figure 130 is from the wall to the vapour, and then from the vapour to the liquid-droplet interface. Because the liquid droplets are saturated, any heat added to the droplets results in a certain mass of liquid evaporating and joining the vapour flow, and therefore liquid droplets continue to lose mass as they flow along the superheated vapour flow. Heat radiation from the wall to the vapour and the droplets is important only if the wall temperature is substantially above the saturation and steam temperatures.

The right side of Figure 130 shows a film boiling regime with a liquid core in the pipe. In this case, the velocity profile is similar to the one on the left, with the vapour velocity being higher than the liquid velocity because the vapour is a much lighter fluid. The temperature profile from the heated wall to the vapour is also similar. However, because the liquid core contains a large volume of liquid, its internal temperature is assumed to be sub-cooled. Hence, the vapour-liquid interface must be at saturation to maintain a continuous temperature profile. A thin thermal boundary layer around the vapour-liquid interface with a steep temperature change is evident.

In the inverted annular flow regime, few entrained droplets can be present in the steam film, whereas the bulk of the liquid is in the form of a continuous liquid core that may contain entrained bubbles. In dryout, the continuous liquid core becomes separated from the wall by a

steam layer that can accommodate steep velocity gradients. As a stable steam blanket is formed, heat is transferred from the wall to the steam and subsequently from the steam to the liquid core. For very thin steam films, heat transfer from the wall to the liquid is primarily by conduction across a laminar steam film. For thicker steam films, turbulent flow occurs in the film, and the liquid-steam interface becomes agitated. Heat transfer across the wavy steam-liquid interface takes place by forced convection. This mode of heat transfer is much more efficient than single-phase convective heat transfer between the smooth wall and the steam. Hence, it is assumed that the bulk of the steam is at or close to the liquid core interface temperature (i.e., the saturation temperature).

The heat flux direction on the right side of Figure 130 is from the wall to the steam, from the steam to the liquid interface, and from the liquid interface to the liquid internal body. Note that the heat flux from the steam to the liquid interface is partitioned into a part that is used to evaporate a portion of the liquid interface and a part that is directed to the internal liquid body as convective heating of the liquid. As mentioned above, heat radiation from the wall to the steam and the liquid core is important only if the wall temperature is substantially above the saturation and steam temperatures.

Heat transfer from the wall to the vapour and from the vapour to the liquid will depend on the conditions of the surfaces, the flow patterns, and other parameters. This topic and the specific heat transfer correlations are described in the section below.

Figure 131 shows various heat transfer regimes in film boiling of a dispersed droplet regime, as described above [POP2014, LEU2004]. Solid lines in this figure indicate heat fluxes and their directions, whereas the dashed line indicates mass transfer by evaporation.

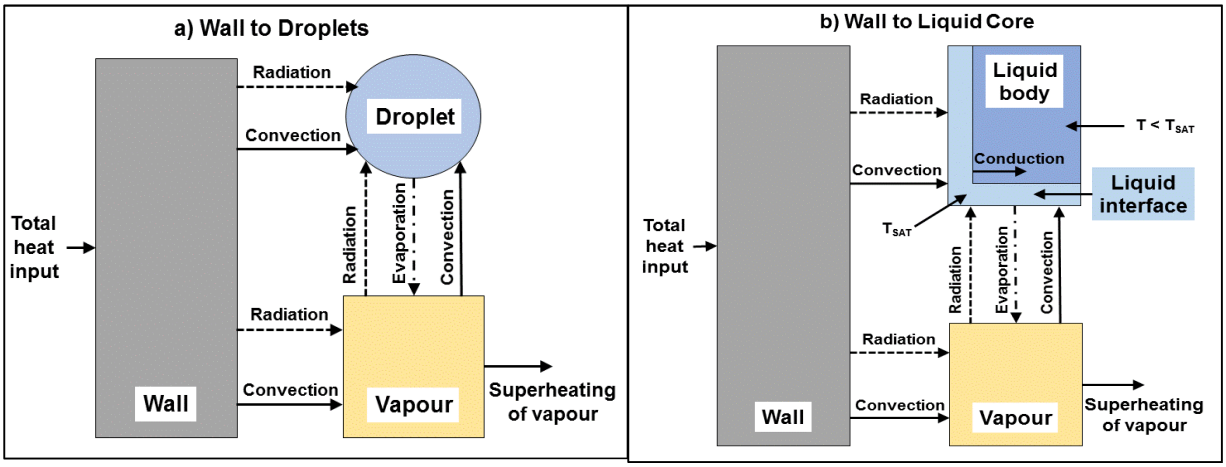

Figure 131 Film boiling heat transfer mechanisms

7.6.5.2 Post-dryout prediction methods and heat transfer correlations

As mentioned before for other heat transfer regimes, many heat transfer correlations have been developed for post-dryout heat transfer regimes. The key correlations and those that are most widely in use are covered in this section.

Accurate prediction of wall temperature in the film boiling regime is of vital importance in accident safety analysis of the core and steam generators of advanced water-cooled reactors.

The following four methods for estimating film boiling heat transfer are commonly used:

i. Semi-theoretical equations for pool film boiling;
ii. Semi-theoretical models to predict flow film boiling. They are based on the appropriate constitutive equations, some of which are empirical in nature;
iii. Purely empirical correlations for flow film boiling, which do not account for any of the physics, but instead assume a forced convective-type correlation; and
iv. Phenomenological equations for flow film boiling, which account for thermal disequilibrium and attempt to predict the "true" vapour quality and vapour temperature.

Transition boiling

The wall temperature at the initiation of transition boiling can be calculated using the CHF correlation (the lower limit temperature) [IAEA2001]:

$$T_{W,CHF} = \frac{q_{CHF}}{h_{NB}} + T_{SAT}\,, \tag{280}$$

where q_{CHF} is the heat flux at CHF and h_{NB} is the nucleate boiling heat transfer coefficient.

The upper wall temperature limit that occurs in transition boiling is the minimum wall film boiling temperature:

$$T_{MFB} = \frac{q_{MFB}}{h_{MFB}} + T_{SAT}\,, \tag{281}$$

where q_{MFB} is the minimum film-boiling heat flux and h_{FB} is the film-boiling heat transfer coefficient. Note that in general, heat transfer coefficients decrease from nucleate boiling to transition boiling and then to film boiling, i.e., $h_{NB} > h_{TB} > h_{FB}$.

Transition boiling is encountered only within a relatively narrow temperature range. For example, for water at 10 MPa, the transition boiling wall temperature range is $300^{o}C < T_{TB} < 373^{o}C$.

Tong [IAEA2001, TON1996] has developed a transition boiling correlation that is frequently used:

$$h_{TB} = 39.75 \cdot e^{-0.144\Delta T} + 2.3 \cdot 10^{-5} \frac{k_g}{D_e} e^{-105/\Delta T} Re_v^{0.8} Pr_v^{0.4}\,. \tag{282}$$

Very often, correlations containing boiling and convective components (valid for transition and film boiling) are used, such as [IAEA2001]:

$$h_{TB} = A \cdot e^{-B \cdot \Delta T_{SAT}} + \left(\frac{k_v}{D}\right) \cdot a \cdot \mathrm{Re}_v^b \cdot \mathrm{Pr}_v^c\,. \tag{283}$$

An example of a phenomenological correlation (valid for transition and film boiling) is the one proposed by Tong & Young and by Iloeje [IAEA2001]:

$$q = q_{dc} + q_{ndc} + q_{conv}. \tag{284}$$

An example of an empirical correlation (valid for transition boiling only) independent of CHF and minimum film boiling has been proposed by Ellion [IAEA2001]:

$$q_{TB} = 4.56 \cdot 10^{11} \cdot \left(\Delta T_{SAT}\right)^{-2.4}. \tag{285}$$

Film boiling

In addition to the above correlations, which are applicable to both transition and film boiling, the minimum film boiling temperature can be given by the following correlation [IAEA2001, DEL1981, COL1972]:

$$\begin{aligned} T_{W,MIN} &= 284.7 + 0.0441\,P - 3.72 \cdot 10^{-6}\,P^2 + \frac{\Delta h \cdot 10^4}{(2.82 + 0.00122\,P) h_{fg}},\ Pressure < 9000\ kPa \\ T_{W,MIN} &= T_{SAT} + \Delta T_{W,MIN,9000\,kPa} \frac{P_{CRIT} - P}{P_{CRIT} - 9000},\ Pressure \geq 9000\ kPa \end{aligned}. \tag{286}$$

There is general agreement that the modified Bromley equation [IAEA2001] for film boiling can be used for horizontal surfaces in pool boiling:

$$h_{FB} = 0.62 \cdot \left[\frac{\lambda_v^3 \cdot \rho_v \left(\rho_\ell - \rho_v\right) \cdot r \cdot g}{\Delta T_s \cdot \mu_v} \cdot \frac{1}{2\pi} \sqrt{\frac{g\left(\rho_\ell - \rho_v\right)}{\sigma}} \right]^{1/4}. \tag{287}$$

This correlation is valid for pressures of 100–9000 kPa, mass fluxes of 50–4500 $kg.m^{-2}s^{-1}$, qualities of 0.15–0.40, sub-cooling of 0°C–50°C, and tube diameters of 9–12 mm.

A general correlation for post-CHF conditions in tubes has been proposed by Groeneveld (1973) [IAEA2001]:

$$\begin{aligned} h_{pcr,ld} &= \frac{a \cdot k_g}{D_e} \left\{ Re_g \left[x + \left(\frac{\rho_g}{\rho_l} \right) (1 - x) \right] \right\}^b Pr_g^c Y^d \\ Y &= 1 - 0.1 \left(\frac{\rho_l}{\rho_g} - 1 \right)^{0.4} (1 - x),\quad Re_g = \frac{G \cdot D_e}{\mu_g} \end{aligned}. \tag{288}$$

For tubes, a=1.09·10^{-3}, b=0.989, c=1.41, d=-1.15. This correlation is valid for equivalent diameters of 2.5–25 mm, pressures of 6.8–21.5 MPa, mass fluxes of 700–5300 kg/m^2s, heat fluxes of 120–2100 kW/m^2, and qualities of 0.1–0.9.

Post-dryout look-up table

The post-dryout bundle look-up table method appears to be a suitable approach for the following reasons:

i. Relatively simple to use;

ii. Provides correct asymptotic and parametric trends;

iii. Uses the most universal method with the best overall fit to the fully developed film boiling data base; and

iv. With embedded modifications for complex geometries, it can be used to account for CANDU fuel bundle effects such as geometry and spacer devices.

Table 12 Sample of PDO look-up table [IAEA2001]

X_e	ΔT_w = 50 K	ΔT_w = 100 K	ΔT_w = 200 K	ΔT_w = 300 K	ΔT_w = 400 K	ΔT_w = 500 K	ΔT_w = 600 K	ΔT_w = 750 K	ΔT_w = 900 K	ΔT_w = 1050 K	ΔT_w = 1200 K
-0.10	1.5664	1.504	1.474	1.358	1.177	1.134	1.280	1.395	1.532	1.705	1.833
-0.05	1.414	1.311	1.275	1.194	1.026	0.981	1.131	1.210	1.356	1.499	1.625
0.00	1.257	1.164	1.106	1.071	1.006	1.048	1.120	1.198	1.283	1.369	1.456
0.05	1.513	1.393	1.223	1.126	1.141	1.270	1.273	1.352	1.371	1.397	1.430
0.10	1.654	1.547	1.318	1.264	1.361	1.476	1.459	1.492	1.483	1.483	1.472
0.20	1.700	1.617	1.427	1.394	1.504	1.655	1.643	1.704	1.704	1.712	1.688
0.40	2.629	2.582	2.547	2.368	2.334	2.393	2.401	2.447	2.456	2.470	2.479
0.60	4.229	4.008	3.750	3.483	3.324	3.285	3.344	3.046	3.119	3.188	3.249
0.80	5.507	5.203	4.488	4.088	3.983	3.936	3.963	3.906	3.955	4.012	4.088
1.00	8.103	7.061	5.500	4.692	4.446	4.605	4.796	5.061	5.264	5.457	5.627
1.20	10.27	8.893	6.784	5.176	5.028	5.471	5.639	6.038	6.296	6.549	6.775
1.40	10.80	9.683	7.906	6.412	5.854	6.206	5.983	6.632	6.846	7.065	7.275
1.60	8.327	8.087	7.856	7.222	6.694	6.780	6.763	6.936	7.107	7.277	7.477

(2001 Film Boiling Table, P=9000 kPa, G=1500kg.m^{-2}, H in kW.m.K^{-1})

A sample extract from a post-dryout look-up table is provided in Table 12. This table provides the heat transfer coefficient for given values of pressure, mass flux, quality, and wall superheat.

Current look-up tables do not yet properly account for developing flow effects, in particular those that usually occur during accident scenarios. This effect is accounted for using specific correction factors. The film boiling look-up table method has been used for the following applications:

i. As a normalized database for validation of film boiling models; and

ii. As an alternative to certain film boiling models which cover only limited ranges of flow conditions.

7.6.5.3 Post-dryout heat transfer R&D in CANDU fuel bundles

Prediction of post-dryout heat transfer in fuel bundles, particularly film boiling heat transfer, is much more complex than that of CHF. Aside from requiring a fourth parameter in the look-up table ("heat flux"), non-equilibrium effects must also be considered, especially in the region just downstream of the quench, near flow obstructions, and at low flows. Fuel bundles are equipped with bundle appendages (as in CANDUs) or grid spacers. These appendages have a CHF- and heat transfer-enhancing effect and also a de-superheating effect, thus reducing the degree of disequilibrium. They can also create multiple quench fronts.

Many experimental tests have been conducted with regard to post-dryout heat transfer to investigate phenomena, develop correlations, and test prediction methods. For such experiments, well-instrumented fuel bundles are required. Figure 132 show a cross section of a fuel bundle with 37 elements at the dryout plane and the appendages plane. A number of fuel element simulators were equipped with movable temperature thermocouples. For each of the

instrumented fuel elements, using different colour codes, dry-patch spreading is indicated by a circular line around the element for each overpower test. Different behaviour is evident for different fuel elements, depending on the flow and heat transfer regimes that occur. These experiments provide very useful information about post-dryout heat transfer in a fuel bundle.

The objective of these experiments is to measure temperature profiles in various flow regimes, such as dispersed flow film boiling, and to measure dryout or dry-patch spreading around the bundle. The sheath temperature in such a heat transfer regime rises gradually with power or decreasing flow, i.e., it is controllable with flow condition variation. Maximum sheath temperature is predictable and occurs at locations just upstream of appendage planes. Dry patches are stable and propagate gradually with flow condition variations, which makes these experiments easily controllable and measurable. In Figure 132, it can be readily seen that at different overpower levels (i.e., power above nominal power), a different extent of wall circumference was in dryout for different fuel pins [LEU2004]. On the left side, a test fuel bundle is shown, with instrumented fuel pins shaded. The right side shows, using different colours, the portions of the circumference of a fuel pin that were measured to be in dryout at different overpower levels. Generally, the higher the power above nominal power, the larger was the portion of the circumference that was in dryout.

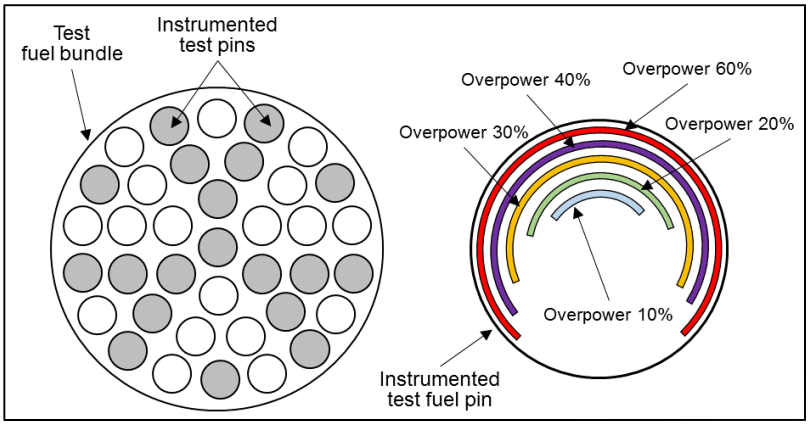

Figure 132 Bundle dry patches in the dryout plane

Two types of tests were conducted, with water and with Freon. The water experiments provided direct confirmation of post-dryout behaviour and closely resembled the phenomena that occur in a CANDU fuel channel. However, these experiments are rather expensive. Freon experiments use a lighter element, Freon R134a, which has a much lower saturation pressure, and therefore these experiments are easier to perform, induce less burden on the survivability of the materials at post-dryout conditions, and enable reuse of the experimental test equipment. However, for these experiments, scaling techniques are needed to convert the collected information to conditions applicable to CANDU.

Many post-dryout water experiments with fuel bundles have used fixed thermocouples attached to the sheath. In these experiments, surface coverage was limited; details of sheath-temperature variation downstream of appendages and spacer grids were not available; and the extent of dry patches, in both axial and circumferential directions, could not be quantified.

Experiments have also been performed with CANDU 37-element bundles in high-pressure

steam-water flow using movable thermocouples. In this case, increased surface coverage was achieved, i.e., more temperature measurements were collected at different places along the fuel element. However, a limited range of powers was applied to avoid damaging the fuel simulator.

A CANDU fuel bundle simulator for post-dryout water experiments is shown in Figure 118. It consists of a 6 m-long full-scale bundle string of fuel elements with junctions and appendages. In these experiments, a uniform axial power profile and a non-uniform radial power profile were used, simulating natural uranium fuel. Sliding thermocouples were installed inside rods at several downstream bundles in the string.

CANDU bundle post-dryout Freon experiments were also performed with movable thermocouples inside the elements of a CANDU 37-element bundle simulator. In these experiments, because of the lower power, temperature, and pressure conditions, fine axial and radial movements were achievable, providing detailed temperature profiles. Freon-134a was used as a coolant, enabling low operating power and sheath temperature and high overpower ratios (i.e., local-to-critical power ratios). With Freon, a relatively wide range of test conditions could be investigated because these experiments were not as expensive as the water experiments.

Figure 133 shows a circumferential distribution of sheath temperatures in a Freon-cooled post-dryout bundle experiment as a function of overpower percentage [LEU2004]. Nominal power means 0% overpower. This figure shows the results of tests on various overpower situations, up to 60% higher than nominal power.

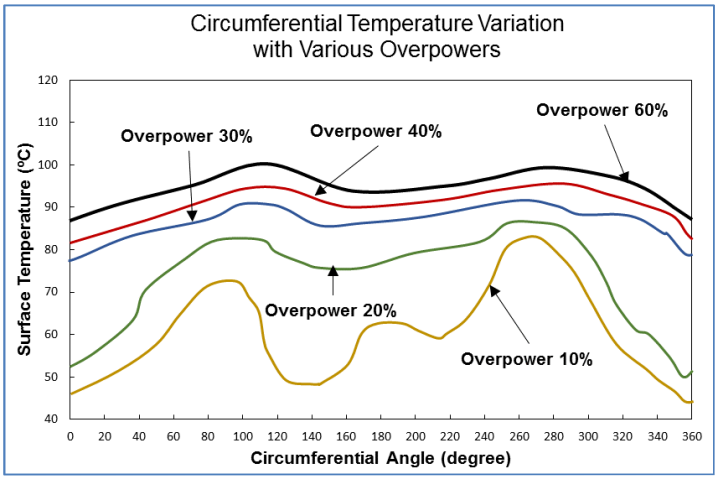

Figure 133 Bundle circumferential temperature profiles

Virtually all film boiling prediction methods are based on correlations derived for tubes. Using them to predict fuel-bundle sheath temperatures is common practice, but the following bundle-specific factors and impacts must be considered:

i. Bundle enthalpy and flow imbalance;

ii. Heat transfer enhancement downstream of grids or spacers;

iii. Adjacent surface wetness or cooling near the pressure tube wall;

iv. Narrow gaps between elements

v. Lower wall friction in dry portions of bundles (resulting in higher flow in dry sub-channels);

vi. Non-circular sub-channel cross-sectional shape;

vii. Presence of axial dry streaks in partially dry fuel bundles.

Reactor safety codes, particularly sub-channel codes that can model variation of flow parameters across a fuel bundle, may account for some, but not all of these effects. When the heat flux of a rod surface facing a given sub-channel exceeds the local CHF, both the wall-fluid heat transfer coefficient and the wall friction factor are reduced drastically. By keeping track of the circumferential dry-patch fraction (CDF) and the axial dry-patch length (ADL) for each rod facing each sub-channel, the flow and enthalpy distribution as well as that of the film-boiling heat transfer coefficient can be evaluated. This enables evaluation of the fuel temperature distribution and prediction of the extent of fuel melting. This approach is now being incorporated in some sub-channel codes to enable detailed prediction of the cladding temperature distribution.

Aside from cross-sectional differences, the global and local effects of the grid or spacers on wall heat transfer, quench behaviour, and interface mass and energy transport are usually not well known, or at best are included by means of an empirical fix for each grid spacer configuration. In general, (grid) spacers can have the following effects:

i. Promote rewetting downstream of the grid due to the higher turbulence level (i.e., can induce multiple quench fronts);

ii. Act as cooling fins;

iii. Cause de-superheating of vapour;

iv. Cause an increase in the liquid-vapour interfacial area by breaking up droplets or liquid core;

v. Homogenize flow by promoting turbulence.

7.6.5.4 Post-dryout applications and analyzes

The application of post-dryout heat transfer is focussed on the safety analysis of postulated events in power reactors, including CANDU. More details about safety analysis of power reactors are provided in Chapter 16, and in this section, these topics are considered only from the perspective of heat transfer.

7.6.6 Single-phase heat transfer to vapour

Single-phase heat transfer to superheated steam is important because it provides an asymptotic value for film boiling heat transfer for cases when the actual quality approached 100%. A number of tube-based correlations have been proposed; all are of the Dittus-Boelter type and give similar predictions. The following equation is frequently used.

Miropolskiy (1975) equation [IAEA2001, DEL1981, BER1981]:

$$Nu_g = h_g D / \lambda_g = 0.028 \cdot Re_g^{0.8} Pr_g^{0.4} \left(\rho_w / \rho_g \right)^{1.15}, \quad (289)$$

where $Re_g = G \cdot X \cdot D / \mu_g$ and ρ_w is vapour density at wall surface temperature. This correlation is valid for pressures of 4–22 MPa, mass fluxes up to 0.42 $Mg \cdot m^{-2} s^{-1}$, ρ_l/ρ_g=0.5–0.9, and Re=10^5–10^6.

7.6.7 Problems

1. Explain the most important aspects of the three approaches of calculating reactor dryout margins: by CHF ratio, by critical CHF power ratio, and by critical power ratio. Provide comments on the applicability of these three approaches.
2. Describe the three main mechanisms that lead to dryout in forced flow in horizontal heated pipes. With respect to these mechanisms, provide explanation on the difference between heated tubes and fuel channels with fuel bundles.
3. Provide explanation about the difference in the following terms boiling crises CHF, dryout, burnout, departure from nucleate boiling, and post-dryout in fuel bundles. Provide examples of conditions where these terms are applicable.
4. Explain the most important parameters that affect CHF, and explain the parametric trends that are used to gain appropriate understanding of the dryout in heated pipes and fuel bundles.
5. Explain the main transition boiling and film boiling types in vertical and horizontal pipes and channels, list the heat transfer modes and provide explanation on the importance of these modes.
6. A PWR reactor uses UO_2 cylindrical fuel pellets, 12.7-mm diameter, with a helium-filled gap of 0.075 mm, and Zr cladding of 0.762 mm. The fuel rods are arranged in a square lattice, with a pitch of 1.8 cm. At a particular section, the bulk water temperature and velocity are 270°C and 4.5 m/s respectively. The volumetric heat generation at this location is 5 x 104 kW/m^3. Calculate (a) the convective heat transfer coefficient using the Dittus-Boelter equation, and (b) the minimum system pressure so that no boiling occurs in the film.
7. Calculate the local CHF for vertical upward flow of water inside a uniformly heated tube (0.012 m ID) at the following conditions: pressure 8200 kPa, mass flux 5000 $kg.m^{-2}.s^{-1}$, and quality 0.175. Use the most appropriate correlation for these flow conditions.
8. Using the most appropriate correlation calculate the post-dryout wall temperature for a vertical water-cooled tube of 0.015 m inside diameter. The following parameters are given: inlet temperature 250°C, inlet pressure 9 500 kPa, mass flux 3961 $kg.m^{-2}.s^{-1}$, local pressure 9400 kPa, local heat flux 1500 kW/m2, local quality 0.225.
9. Evaluate the dryout power for a 3658-m-long tube of 0.0095 m ID, heated with a symmetric-cosine heat flux. The flux profile has been discretized as

Length (m)	0.0	0.051	0.203	0.406	0.607	0.813	1.016	1.219	1.422	1.626	1.829
q_{loc}/q_{avg}	0.3	0.37	0.45	0.66	0.86	1.03	1.17	1.27	1.33	1.38	1.35
Length (m)	2.032	2.235	2.438	2.642	2.845	3.048	3.251	3.454	3.607	3.658	
q_{loc}/q_{avg}	1.38	1.33	1.27	1.17	1.03	0.86	0.66	0.45	0.37	0.30	

More nodes can be introduced to improve the accuracy of the predictions of dryout location and power. Theoretically, an infinite number of nodes should be used for a smooth profile. For a stepped profile, the number of nodes corresponds to the number of steps since dryout generally occurs at the end of a step.

The flow conditions are: pressure 6930 kPa, mass flux 2050 $kg.m^{-2}.s^{-1}$, and inlet subcooling 280.75 kJ/kg.

10. A pressure tube, with inside diameter of 103.86 mm, contains twelve 37-element bundles of the following dimension: bundle length: 495.3 mm, and fuel element outer diameter 13.06 mm.

    Total power generated over the bundle string is 6.3 MW, and the axial power profile is uniform. The channel is cooled with a flow of light water at the following conditions: outlet pressure 9 MPa, mass flow rate: 17 kg/s, inlet fluid temperature 265C.

    Evaluate dryout power ratio for this channel, and surface temperature distribution along the bundle string at an overpower of 10% (overpower is defined as (String-Power/Dryout-Power – 1)*100%).

    Previous research findings appropriate to this problem:

    - Heat-transfer coefficient at nucleate boiling for the 37-element bundle is 120 $kW/(m^{2o}K)$ at the pressure of 9 MPa, mass flux of 5 $Mg/(m^2\ s)$ and quality of 20%.
    - Heat-transfer coefficient at single-phase liquid flow is about 50% of that at nucleate boiling.
    - CHF in the 37-element bundle is 20% lower than that in tubes based on cross-sectional average flow conditions.
    - Heat-transfer coefficient at fully developed film boiling for the 37-element bundle is the same as that for tubes.
    - Overall loss coefficient is 1.7 for a 37-element bundle inside a pressure tube of 103.86 mm.
    - The homogeneous equation is the most appropriate for two-phase multiplier.

    Basic assumptions:

- Nucleate boiling heat transfer coefficient does not vary with flow conditions.
- Fully developed film-boiling heat transfer is reached once local heat flux exceeds CHF.
- Equilibrium flow in the channel.
- Pressure drop due to acceleration is negligible.

11. In the middle of a reactor channel of a PWR reactor the bulk coolant temperature of the turbulent coolant flow is 310^{o}C at pressure of 14 MPa. The heat transfer coefficient in nuclear boiling is 4.44 MW/m^2 ^{o}K. Calculate the minimum heat flux at that location to initiate nucleate boiling.
12. Water enters a heated tube of 2.5 cm diameter at 12 MPa and velocity of 2.5 m/s. The linear heat load in the tube is constant at 100 kW/m. Calculate the distance in the tube at which nucleate boiling starts, and distance at which it converts to bulk boiling. Compare the heat transfer coefficients for forced convective heat transfer with these for nucleate boiling and bulk boiling.
13. A pipe of 15 mm diameter and 3.5 m length is heated with a constant heat flux, and total heat load of 200 kW (appropriately insulated, i.e., no heat losses). The pipe is cooled by water at 150^{o}C and pressure of 2 MPa, which flows through the pipe with enters into the pipe with a velocity of 3 m/s. Calculate the mass flux of the water, and the minimum ratio of the heat flux in the pipe and the critical heat flux.
14. Boiling water reactor operates at average pressure in the core of 8 MPa, and the recirculation ratio of 7:1. The average velocity of the two-phase mixture in the core is 8 m/s. Calculate the critical heat flux at the exit of the reactor core channel.
15. List and explain the most important geometrical factors that have significant impact on CHF in horizontal fuel channels.

7.7 Critical flow

Consider a situation in which fluid discharges from a container at high pressure to a container at lower pressure, or to ambient at lower pressure (back-pressure). When the back-pressure is reduced below a constant upstream pressure in a flow system, flow begins because of the pressure gradient established in the connecting channel between the upstream container and downstream towards the channel exit. The flow increases as the back-pressure is reduced further. When the back-pressure is sufficiently reduced to cause the flow velocity at the channel exit to be equal to the speed of sound at the channel exit temperature and pressure, the mass flow at the exit attains a maximum value. Further reduction in the back-pressure results in no further increase in mass flow rate; the flow remains at the maximum value and is referred to as *"critical"*. The channel, and the flow, are also called *"restricted"* or *"chocked".* Because the back-pressure is less than the pressure resulting in critical flow, free fluid expansion can occur between the exit (at exit pressure) and the ambient (at back-pressure) outside the channel, and the flow takes on a paraboloid shape in this region. This situation can be observed by many flow and measurement systems.

The critical flow phenomenon occurs in both single- and two- phase flow when the velocity of the two-phase mixture is controlled by its upper limit, i.e., the sonic velocity of the mixture. That velocity is a very strong function of quality, varying from ~300 m/s for single-phase steam to ~1400 m/s for single-phase liquid water.

In nuclear reactors, this phenomenon is important for safety analysis of both boiling and pressurized systems. A break in a primary coolant pipe causes two-phase critical flow in either system because even in a pressurized reactor, the reduction in hot coolant pressure from about 10 MPa to near-atmospheric causes flashing and two-phase flow. This kind of break results in a rapid loss of coolant and is considered to be a credible design basis accident in power reactors built to date. This is further explained in Chapter 16.

An evaluation of the flow rate in critical two-phase systems is therefore important for designing emergency cooling systems and for determining the extent and causes of damage in accidents. Further details on modelling critical flow in nuclear reactor primary heat transport systems are provided in Chapter 7.

7.8 Water hammer

Water hammer is an important phenomenon that requires attention by thermal-hydraulic designers and plant operators. This phenomenon can result in equipment damage and can affect the performance or functionality of certain equipment. Therefore, it is important to have a good understanding of this phenomenon so that appropriate prevention, mitigation, and accommodation measures can be undertaken to reduce the risk of its occurrence in nuclear power plant cooling systems.

Detailed coverage of the water hammer phenomenon and its prevention, mitigation, and accommodation are beyond the scope of this textbook, but appropriate information can be found in the literature [EPRI1996] and in the suggestions for further reading at the end of this textbook. This section reviews basic information about water hammer and provides

elementary guidance to thermal-hydraulic engineers and designers.

7.8.1 Types of water hammer

Water hammer events have been observed and reported widely in PWR, BWR, CANDU, and other nuclear power plants in various coolant or support systems. These events have provided valuable information on the types and strength of the water hammer effect, which has been used to develop defensive strategies.

Water hammer events can be classified into two broad groups: water hammer events in single-phase liquid or gas, and two-phase water hammer events.

Most water hammer events in nuclear power plants fall into the first group and are caused by rapid acceleration or deceleration of single-phase liquid flowing in a piping system. Rapid acceleration can be created by rapid valve closure, which results in pressure waves that propagate in the piping system at sonic velocity. Figure 134 shows two examples of single-phase water hammer; Case A shows rapid valve closure causing water hammer. Case B shows check-valve action downstream of a pump triggering water hammer [EPRI1996].

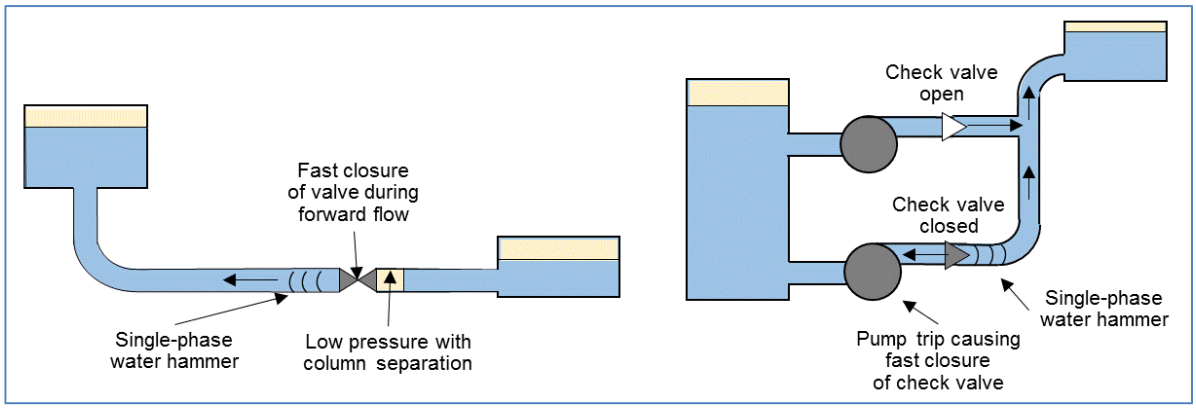

a) Fast valve closure b) Pump check valve closure

Figure 134 Rapid valve operation

The necessary physical and mechanical conditions required for water hammer to occur exist all the time in nuclear power plants. Most nuclear power plants have design and operational provisions to prevent severe water hammer from occurring, but nevertheless, in unanticipated situations, water hammer events do occur. Usually water hammer transients are typically caused by pump start, pump trip, control or isolation valve operation, check valve closure, safety or relief valve operation, main steam turbine trip, and filling of empty systems. All these normally occur in single-phase flow conditions and can be easily predicted by conventional water hammer analysis techniques.

Two-phase water hammer events can be of several types. These events are more complex to analyze, have a strong impact on pump operation, and can cause significant damage to pipe components and pipe supports. Six transient scenarios lead to water hammer events with various probabilities and strengths, with most of them related to steam condensation-induced water hammer.

1. Flow of sub-cooled water with condensing steam in a vertical pipe (Figure 135)

   This type of water hammer is a typical BWR case in which, during a large LOCA event, steam lines discharge water into the suppression pool. If the valve is quickly closed or reduced significantly, a steam pocket remaining in the steam line can condense rapidly, which pulls water from the suppression pool towards the valve, thus creating water hammer [EPRI1996, POP2014].

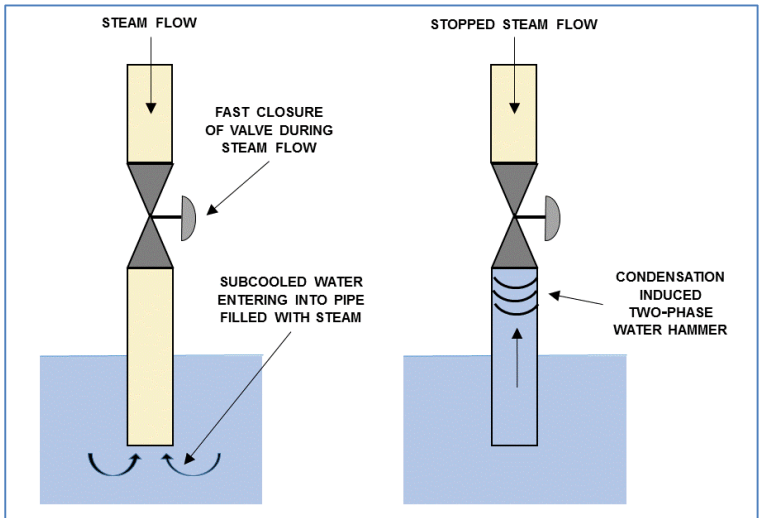

Figure 135 Flow of sub-cooled water with steam condensing in vertical pipe (water cannon)

2. Counter-current flow of steam and water in a horizontal pipe (Figure 136)

   This situation occurs in PWR feedwater lines and in CANDU feeders [POP2014]. In horizontal stratified flow, a large interface area exists between sub-cooled water and steam. Therefore, the steam flow is subjected to fast condensation, which induces an increase in steam flow from the upper pipe. Under certain conditions, the counter-current flow can transition to slug flow and create a steam pocket. When the steam pocket collapses as a result of condensation, severe water hammer can occur. Long feeder sections are particularly vulnerable to steam trapping and this type of water hammer. The advanced CANDU design addresses this problem by having feeders slightly tilted, so that an escape route for steam is provided.

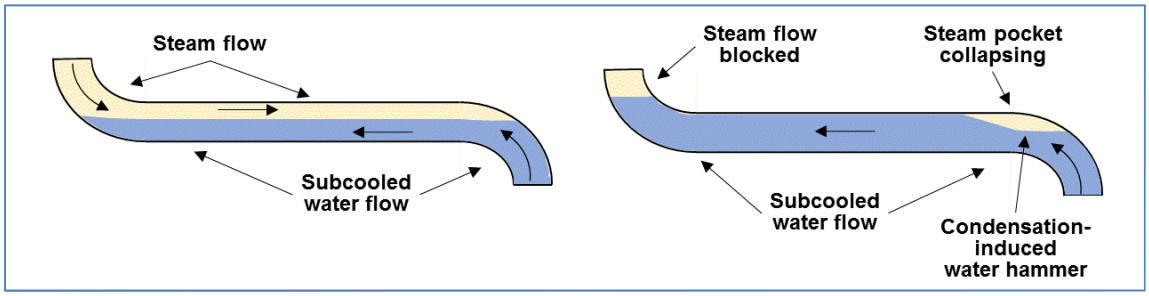

Figure 136 Counter-current flow of steam and water in a horizontal pipe

3. Pressurized water entering a vertical pipe filled with steam (Figure 137)

This type of water hammer can occur in any of the PWR and BWR reactors with refilling of a steam-filled pipe either from the bottom or from the top [EPRI1996]. If pressurized sub-cooled water enters a pipe filled with steam in a piston flow regime, it can create steam trapping. The filling rate for this situation is determined by the inertia of the liquid and the pressure induced by the pump or other refilling device. Water hammer occurs in this situation if the refilling rate is higher than the bubble rise velocity for the top refilling case. This type of water hammer can also occur in CANDU reactors.

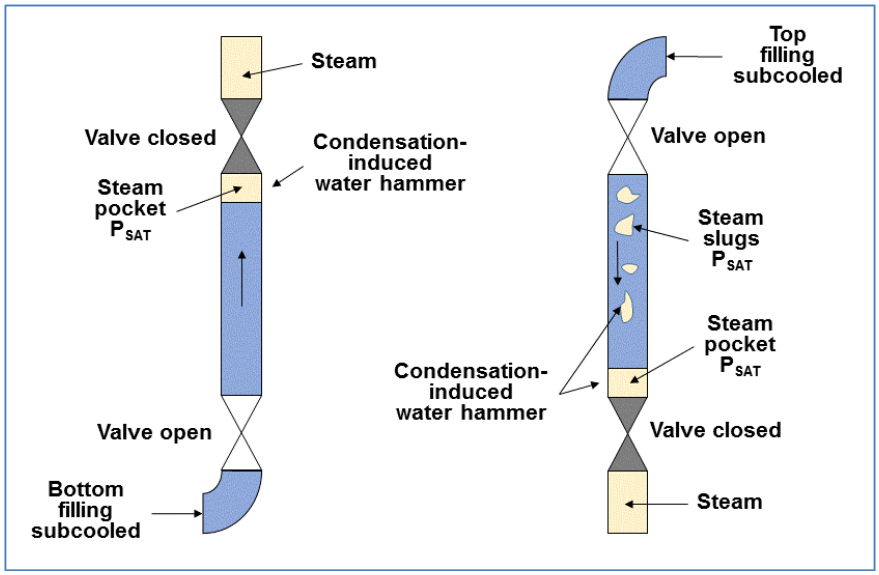

Figure 137 Pressurized water flowing in a vertical pipe filled with steam

4. Hot water entering a low-pressure line (Figure 138)

   This type of water hammer can occur in PWRs, BWRs, and CANDUs. In this case, hot water flowing down the pipe will flash and create a pressure wave flowing upstream, thus creating water hammer on the upstream valve. The cold part of the sub-cooled water that was initially outside and below the pressure vessel can create water hammer on the downstream valve as it enters the steam-filled part of the pipe [EPRI1996].

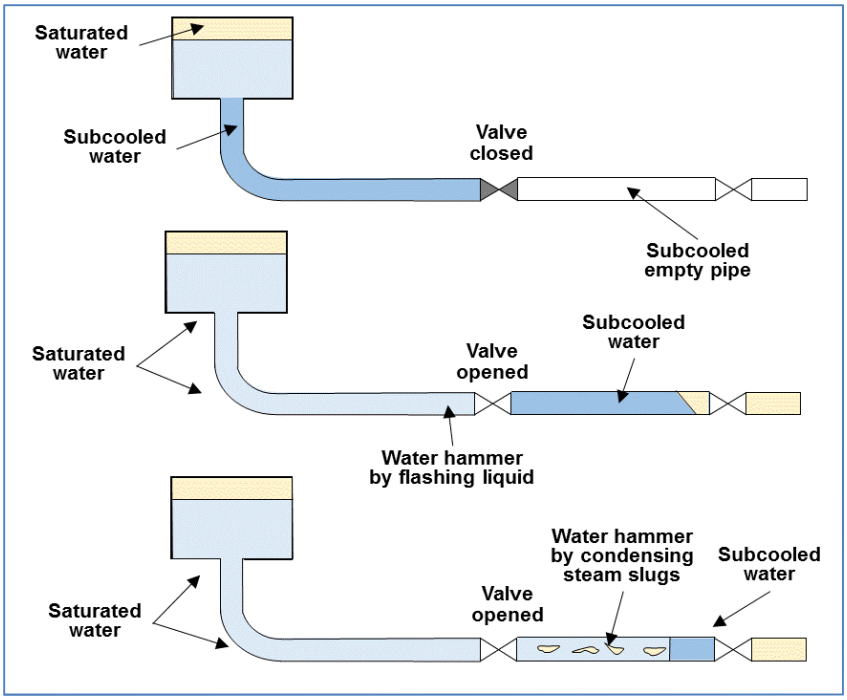

Figure 138 Hot water entering a lower-pressure line

5. Water slug driven by steam (Figure 139)

   This type of water hammer can occur in a piping system that collects condensate upstream of a closed valve or can collect condensate in certain portions of the piping systems that are normally filled with steam. Water hammer can occur when the valve opens and this steam drives the water slug at high speed. The slug can be accelerated significantly and can create a water hammer effect in a restricted part or at the closed end of the pipe [EPRI1996].

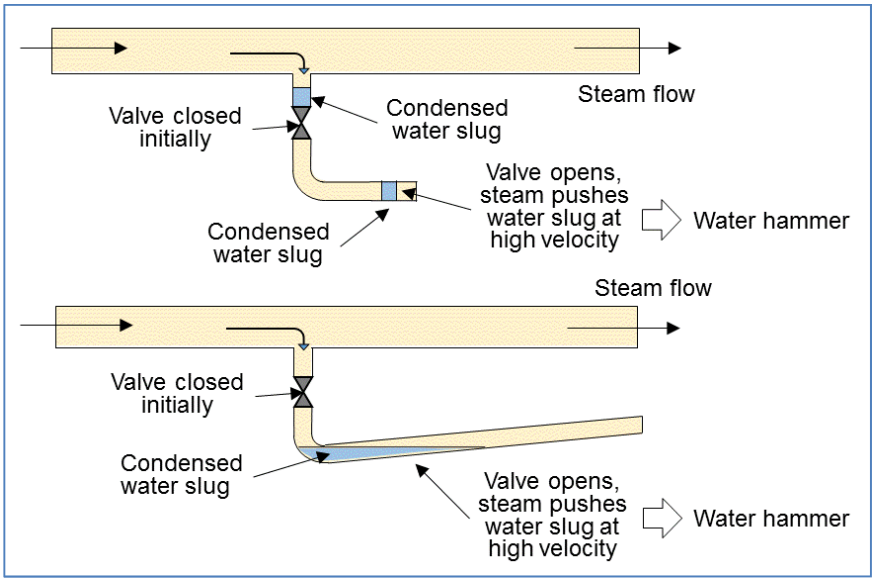

Figure 139 Steam-driven water slug in piping system

6. Water filling a voided pipe line (Figure 140)

   In this situation, as a pump trips, water from the vertical section recedes downwards and creates an empty vacuum-filled space above. When the pump restarts, it will push water to refill the pipe (and perhaps condense some residual steam), thus creating a significant water hammer [EPRI1996].

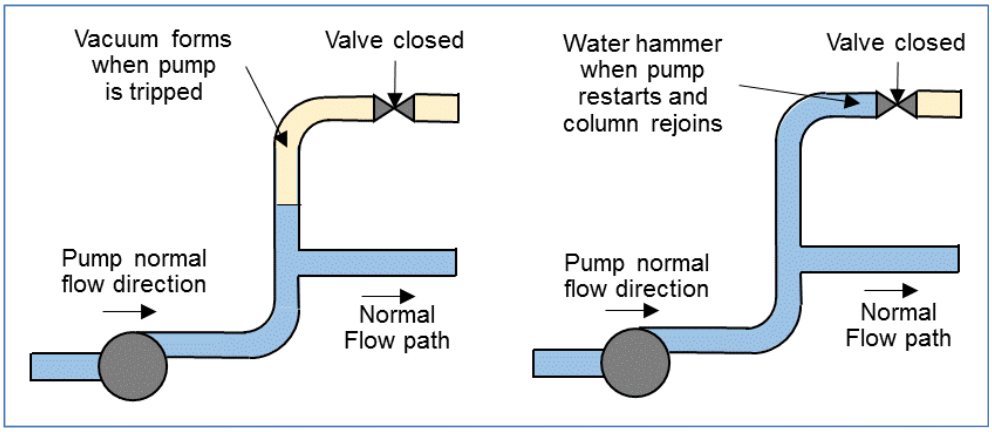

Figure 140 Filling of voided piping system

7.8.2 Analytical models and computer codes for water hammer analysis

Water hammer assessment is performed using analytical models and computer programs designed for this purpose. A detailed discussion of this topic is beyond the scope of this textbook, and hence this chapter provides only a brief summary.

The analytical models consist of governing differential equations for transient single-phase or two-phase flow. Usually, the flow is assumed to be one-dimensional because it describes flow in piping systems. The governing differential equations are solved by appropriate numerical techniques. Then a network model is created in which physical representations of various system components are introduced as boundary conditions. Usually, a number of constitutive correlations are used to cover system-specific phenomena.

Usually, analytical models for liquid, gas, or two-phase mixtures are based on rigid and elastic column theories of the piping system. It is important to recognize that the severity of water hammer is proportional to the level of rigidity of the piping system. Therefore, an increased level of piping elasticity reduces the consequences of water hammer because elastic pipe systems can absorb the energy of the pressure waves traveling through the system.

Software packages vary in complexity depending on the processes modelled. The more sophisticated packages may have one or more of the following features:

- Multiphase flow capabilities;
- An algorithm for cavitation growth and collapse;
- Unsteady-state friction: the pressure waves dampen as turbulence is generated and due to variations in the flow velocity distribution;
- Varying bulk modulus for higher pressures (water becomes less compressible);

- Fluid-structure interaction: the pipeline reacts on the varying pressures and causes pressure waves itself.

Most computer programs that can model water hammer are the same as those used to model general piping networks. However, computer codes may not be completely successful in modelling all types of water hammer, particularly condensation-induced water hammer, which is quite challenging. The RELAP5 code [REL2010] is an example of such a network code that can model certain types of water hammer for PWRs and BWRs. For CANDU reactors, the CATHENA computer code [CAT1998, CAT2000, CAT2005] has been validated for use in analysis of certain types of water hammer.

7.8.3 Diagnostics and assessment of water hammer

Diagnostic and assessment techniques for water hammer consist of systematic review of a thermal-hydraulic network in terms of vulnerabilities to and consequences of water hammer. The assessment principles are based mainly on lessons learned and root cause analysis. Nuclear power plant design features and operating characteristics require specific water hammer inspection processes.

The general diagnostic analysis consists of three major steps: study of deformation evidence, determination of water hammer source, and determination of root causes. Each of these steps consists of several sub-steps as follows:

a) Collect evidence of water hammer impact by field inspections, interviews, and review of operating conditions;
b) Identify pipe network characteristics that may lead to water hammer;
c) Determine water hammer consequences by identifying pipe movement, pipe deformations, and pipe support deformations;
d) Determine the piping or other thermal-hydraulic equipment initial conditions (for example, water-filled or steam-filled piping);
e) Determine the source of water hammer by identifying the origin point of the pressure wave or water slug;
f) Compare the operating conditions and consequences of the various possible water hammer mechanisms;
g) Determine the root causes; and
h) Define possible corrective action in design space and/or procedural space.

The review of systems and equipment susceptibility to water hammer usually consists of the following activities:

i. Collection of plant data to establish plant-specific thermal-hydraulic network configurations and identify component features and functions;
ii. Determine industry practices with respect to thermal-hydraulic network testing, maintenance, and operating procedures that result in water hammer vulnerabilities;
iii. Perform plant assessment with respect to prevention, diagnosis, and assessment of water hammer;

iv. Review plant-specific thermal-hydraulic system operating procedures and designs with respect to water hammer occurrence;

v. Document the findings of the above assessment; and

vi. Develop recommendations for improving plant-specific design features or operating procedures to reduce the probability of water hammer.

7.8.4 Prevention, mitigation, and accommodation of water hammer

This section provides general high-level information on measures taken to prevent, mitigate, and/or accommodate certain types of water hammer events in nuclear power plants. The measures that can be taken can be broadly grouped into design measures and operational (procedural) measures.

Prevention of water hammer is the best option when and where possible. It includes design and operational measures aimed at preventing or significantly reducing the water hammer hazard. However, this option may not be available in many situations, especially in thermal-hydraulic equipment operating in a transient following an accident.

Mitigation of water hammer includes design and operational measures to reduce the impact of water hammer in cases where it cannot be prevented. This technique is mostly used in situations in which prevention is not possible.

If a water hammer hazard cannot be eliminated by design or operational procedure, the next step is to accommodate the residual impact that cannot be mitigated. A number of techniques can be used to achieve this, such as strengthening and reinforcement of pipe support systems, or designing piping systems that take water hammer loads into account.

General recommendations for reducing water hammer hazard are the following:

- Avoid direct contact of steam with sub-cooled water in a horizontal pipe (this is particularly important for CANDU feeder horizontal runs);
- Avoid opening a valve adjacent to a steam pocket (identified or suspected), or ensure that the valve opens slowly to provide an escape path for the steam pocket;
- Open isolation valves slowly where stagnant hot water coexists with hot water in the same line upstream and downstream of the valve;
- Inspect condensate removal systems to avoid accumulation of a water slug in the steam line;
- Inspect check valves routinely, especially those located on a pump discharge line, to ensure that the valve is not stuck open;
- Avoid starting a pump to fill a long line at significantly higher elevation, which could be voided for various reasons (such as leaking valves).

Specific recommendations for reducing each type of water hammer are provided in the following points [EPRI1996].

1. Rapid valve operation

   Rapid valve actuation is defined as rapid closure of a stuck-open check valve or

malfunctioning of a valve actuator. Hence, any system with this type of valve is at risk of experiencing this type of water hammer.

Prevention or mitigation by design involves valve modifications to prevent this type of valve operation. Mitigation or prevention by procedure aims to avoid valve cycling in systems with significant flow, or perhaps uses a special monitoring capability to sense a pressure difference across a valve and to use it as a signal for actuating the valve.

2. Flow of sub-cooled water with condensing steam in a vertical pipe

   This water hammer phenomenon is unique to steam turbine exhaust piping that discharges into a body of water. This happens when reduced steam supply to the turbine traps steam in the exhaust piping.

   The only way to prevent or mitigate this type of water hammer is to install a vacuum breaker with sufficient capacity to replace the condensing steam in the exhaust piping from a tripped turbine.

3. Counter-current flow of steam and water in a horizontal pipe

   This type of water hammer happens in steam generators when a horizontal feedwater pipe is slowly filled in counter-current flow. It can also happen in horizontal sections of CANDU feeders when injecting cold ECC water.

   One design option for mitigation is to shorten the horizontal portions of piping systems, or to have the horizontal piping slightly inclined. A procedural modification may involve better control of the water flow to affected areas.

4. Pressurized water entering a vertical pipe filled with steam

   This type of water hammer can happen unexpectedly due to valve leakage, which can lead to accumulating hot water pockets (which could quickly flash or condense) in the closed parts of piping systems. This kind of water hammer can also occur if high-pressure water is pumped into a system filled with steam (such as injection of ECC into steam-filled CANDU headers or feeders).

   One mitigation design change involves keeping the system full of water and preventing valve leakage. In addition, installation of void detection devices at places where valve back-leakage may occur can be a solution. A procedural modification may involve venting steam pockets before injecting water or starting pumps.

5. Hot water entering a low-pressure line

   This type of water hammer is typical of heater drain systems in cases where a reservoir of hot water is being discharged into low-pressure piping.

   A possible preventative design change is to modify the control system to avoid cyclic dumping of hot water. Installing a flow control valve with slowly increasing flow can also address this problem. A procedural change may involve placing a high-pressure feedwater heater back in operation without inadvertently actuating the emergency dump system.

6. Water slug driven by steam

   This type of water hammer can happen in pipes in which condensate accumulation occurs upstream or downstream of a closed valve.

   A design fix for this water hammer is to ensure proper inclination and condensate drainage from piping systems. Pipes subject to sagging could also be better supported to avoid sags that can collect condensate. A procedural change could involve slowly initiating steam flow after opening a closed valve to ensure gradual acceleration of the condensate pocket.

7. Water filling a voided pipe line

   This type of water hammer happens typically in long piping systems with an elevation change of 10 m or more. In this situation, stopping the water flow can result in formation of a vacuum in the upper parts of the pipe. Restarting the flow leads to refilling the pipe and to interaction of water and steam surfaces.

   A design fix for this kind of water hammer is to keep the system filled with water. Installing a vacuum breaker can also help. A procedural improvement could involve keeping the pump discharge valve closed and then opening it slowly as the pump is restarted.

7.8.5 Problems

1. Explain the reasons and consequences of water hummer in thermal-hydraulic equipment. Provide examples of possible water hummer situations in the CANDU heat transport systems, and indicate the strategies for mitigating the effects.
2. List the types of water hummer in CANDU heat transport system, and for each type list and explain the strategy for avoiding or mitigating it.

7.9 Natural circulation

New generations of nuclear reactor designs under development rely on passive systems, including use of natural circulation. All Generation IV reactors are required to make use of natural circulation as a heat transfer mechanism for removing heat from the reactor core, for some designs even under normal operating conditions. However, currently operating reactors are also required to use natural circulation to remove decay heat in accident situations when forced circulation in the core is lost.

Natural circulation occurs in many different situations, such as a heater immersed into a fluid; an open flame in air; a chimney-driven fire; a surge of hot water into a pool of cold water; a heat source and heat sink connected by piping and located at different elevations; hot steam and cold air mixing in a containment building. In all these situations, natural circulation plays an essential role in transferring heat from one part of a system to another, or between systems.

7.9.1 Natural circulation phenomenon

Natural circulation will occur in a reactor primary loop in the absence of pumped flow whenever buoyant forces caused by differences in loop fluid densities are sufficient to overcome the flow resistance of loop components (steam generators, primary coolant pumps, etc.). Fluid density differences occur as a result of fluid heating in the core region (causing the liquid to become less dense) and fluid cooling in the steam generators (causing the fluid to become denser). Figure 141 shows the principles of natural circulation in a closed loop with a heat source located at a low elevation and a heat sink at a high elevation connected by piping. On the right side of this figure, a similar loop is shown in two-phase operation with a steam drum extracting steam and adding feedwater to the loop. This figure is similar to the situation in a nuclear power plant. Note that in this figure, two-phase flow is indicated out of the reactor, which is typical of BWR and CANDU reactors.

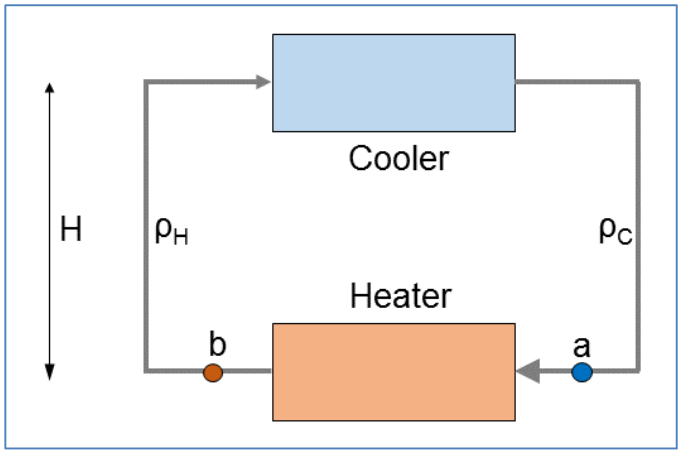

Figure 141 Principles of natural circulation

The buoyancy forces resulting from these density differences cause fluid to circulate through the primary loops, providing a means of removing core decay heat. Depending on the primary loop fluid inventory, natural circulation consists of three distinct cooling modes: single-phase,

two-phase (liquid continuous), and reflux condensation (or boiler-condenser mode for once-through steam generators). Progression from the single-phase mode through the two-phase and reflux condensation modes occurs as primary system liquid inventory decreases, as shown in Figure 142 [IAEA2005, IAEA2012, POP2012a]. Natural circulation flow in a sub-cooled primary heat transport loop (such as in PWRs) is driven by temperature-induced density gradients, enhanced by a thermal centre elevation difference between the hot (core) and cold (steam generator) regions in the primary loop. This density gradient produces a buoyancy force that drives the natural circulation flow. Hence, single-phase natural circulation is the flow of an essentially sub-cooled primary liquid driven by liquid density differences within the primary loop.

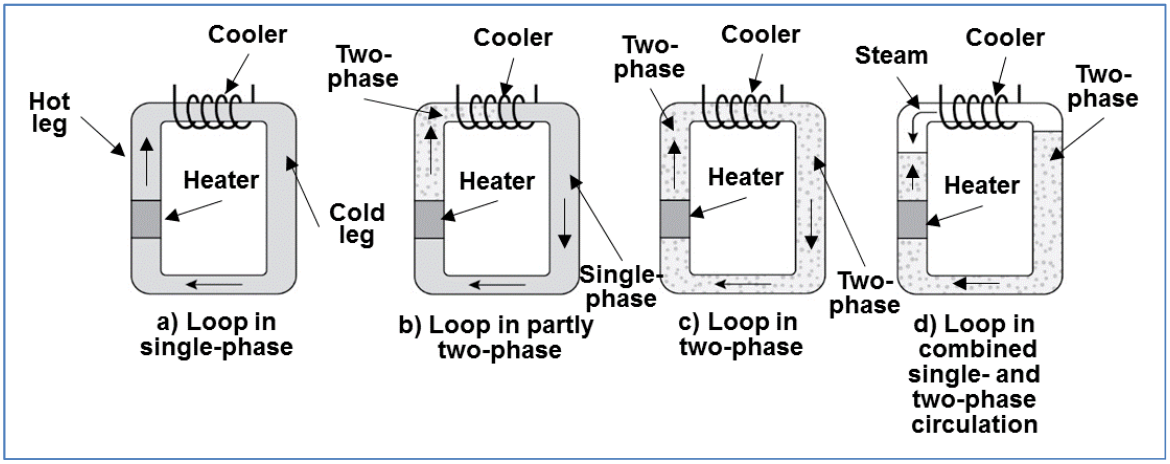

Figure 142 Various types of natural circulation

In a reactor where boiling occurs in the primary heat transport system, vapour generated in the core enters the hot leg and flows along with the saturated liquid to the steam generator, where at least some of the vapour is condensed. Hence, density gradients are affected in two-phase mode, not only by temperature differences, but also by voids in the primary loop. In both single-phase and two-phase natural circulation, the mass flow rate is the most important heat removal parameter.

In reflux condensation, the vapour generated in the core flows through the hot leg, is condensed in the steam generator, and flows back to the core as a liquid. In this mode, the loop mass flow rate has a negligible effect because the primary heat removal mechanism is vapour condensation.

The three modes of natural circulation are distinguishable based upon characteristic mass flow rates, loop temperature differences, and basic phenomenological differences. The dominant heat transfer mechanism in single-phase natural circulation cooling is convection, making the loop flow rate the most important parameter governing heat removal. Heat generated by the core is transported away from the reactor vessel through the hot leg to steam generators (heat sink) by means of the sub-cooled primary liquid.

Advantages of natural circulation

a) Elimination of pumps. Elimination of the primary circulating pumps in some Generation 4 designs not only reduces capital, operating, and maintenance costs, but also eliminates all safety issues associated with circulating pump failure.

b) Better flow distribution**.** Use of pumps can cause misdistributions of pressure in the headers, leading to misdistribution of flow in the parallel channels. Moreover, using pumps requires orificing to provide flow in the fuel channels corresponding to each channel's power. Natural circulation provides a natural channel flow distribution.

c) Flow characteristics. In a natural circulation system, flow increases with power, whereas in a forced-circulation two-phase system, flow decreases with increasing power. This has specific advantages in steam generating power plants.

d) Safety aspects. Because natural circulation is based on a natural physical law, it is not expected to fail, unlike fluid-moving machines such as pumps. This aspect of natural circulation has enabled its application in many safety systems. In all current designs of nuclear power reactors, natural circulation is a backup for decay heat removal in the event of a pumping power failure.

e) Simplicity. Because of the need to minimize pressure losses to enhance flow rates, designers of natural circulation systems tend to eliminate all unnecessary pipe bends, elbows, etc. The result is a system with a simple piping layout that can be fabricated in the factory.

Challenges of natural circulation

a) Low driving force. One of the drawbacks of natural circulation systems is that their driving force is low. The most straightforward way to increase the driving force is to increase the loop height, which may not be economical. In addition, use of tall risers can make natural circulation systems slender in structure and may raise seismic concerns. Due to these reasons, the incremental height of natural circulation systems compared to the corresponding forced circulation systems is often limited to less than 10 m.

   This challenge has a specific impact on channel-type reactors such as CANDU. As explained in this section, at low driving force in a CANDU, certain channels in the core may not sustain forward flow, i.e., channel flow direction cannot be accurately estimated.

b) Low system pressure losses. With low driving force, the only way to obtain reasonably large flow rates is to design for low pressure losses. There are several measures to achieve low system pressure losses:

   i. Use of large-diameter components and pipes. The most straightforward way to reduce pressure losses is to use large-diameter components. However, this also results in increased cost and enhanced system volume, both of which have economic and safety implications.

ii. Simplified system. Generally refers to the simplified piping and equipment layout of the system, such as minimization of U-bends, elbows, loop seals, etc. This not only results in a simplified system, but also results in low pressure losses and prevents phase separation from promoting natural circulation flow.

iii. Elimination of components. An example in this case is the possible elimination of mechanical separators.

c) Low mass flux. Low driving force and the consequent use of large-diameter components result in low mass flux in natural circulation systems compared to forced circulation systems. With low mass flux, the allowable maximum channel power is lower, leading to larger core volume than in a forced circulation system of the same rating.

d) Instability effects. Although instability is common to both forced and natural circulation systems, the latter are inherently less stable than forced circulation systems. This is attributable to the nonlinear nature of the natural circulation phenomenon, where any change in the driving force affects the flow, which in turn affects the driving force, possibly leading to oscillatory behaviour.

e) Low pressure and low flow regime. In natural circulation systems, the flow rate is a strong function of power and system pressure. Moreover, the flow is stagnant when the reactor power is zero during initial start-up. The operating conditions of natural circulation systems can fall into the low-power, low-flow regime, where validated thermal-hydraulic relationships are not readily available.

f) Specification of a start-up and operating procedure. It is well known that most boiling systems exhibit instabilities at low pressures and low qualities. Therefore, natural circulation reactors must be started up from a stagnant low-pressure, low-temperature condition. During the pressure and power raising process, passing through an unstable zone shall be avoided because instability can cause premature CHF occurrence.

g) Low CHF. The basis for thermal margin is the CHF, which depends on geometric and operating parameters. Because flow in natural circulation reactors is less, designers of these reactors tend to use the maximum allowable exit quality to minimize their size. This means that the CHF value of the reactor tends to be significantly lower than in the forced circulation case. This calls for several measures to increase CHF.

As shown on the left side of Figure 141, due to the difference in densities between the vertical legs, a pressure difference is created between stations ‘a’ and ‘b’, which is the cause of the flow. At steady state, the driving buoyancy force is balanced by the retarding frictional force, thus providing a basis for flow rate estimation using the following equation [IAEA2005, IAEA2012]:

$$gH\left(\rho_c-\rho_h\right)=\frac{R\cdot W^2}{2\bar{\rho}}, \tag{290}$$

where g (m/s^2) is acceleration due to gravity, R (m^{-4}) is hydraulic resistance, and W (kg/s) is mass flow rate. Hence, the mass flow rate induced by natural circulation is given by:

$$W = \left[\frac{2\bar{\rho} A^2 \left(\rho_c - \rho_h \right) gH}{R} \right]^{\frac{1}{2}}. \tag{291}$$

Natural circulation flow is enhanced by increasing the loop height *H* and the density difference $(\rho_c-\rho_h)$, as well as by decreasing the hydraulic resistance *R*.

By introducing loop resistance models, the above equation can be further expanded into the following form:

$$W = \left[\frac{2\bar{\rho} A^2 \left(\rho_c - \rho_h \right) gH}{\sum_{i=1}^{N_i} \left(\frac{f_i L_i}{D_i} + K_i \right)} \right]^{\frac{1}{2}}. \tag{292}$$

The natural circulation phenomenon can be classified in terms of the state of the working fluid, the interactions with the surroundings, loop geometry, body force field, system inventory, and number of heated channels. Figure 142 shows certain types of natural circulation in a rectangular geometry.

The state of the working fluid can be single-phase, two-phase, or supercritical. The single-phase natural circulation is important as a decay power removal mechanism in many operating and new designs of nuclear power reactors. Two-phase natural circulation normally occurs in BWRs and CANDUs under certain operating regimes.

In terms of interactions with the surroundings, closed-loop and open-loop natural circulation can be distinguished. The closed loop involves only energy exchange with the surroundings, whereas the open loop involves both energy and mass exchange.

In terms of loop geometry, natural circulation can occur in rectangular, U-tube, toroidal, and figure-of-eight forms (the last being specific to the CANDU design). The body force field has an important impact and can be gravitation (in most cases), centrifugal force, or both for certain specific applications.

In terms of system inventory, natural circulation can occur in full systems (in single-phase mode), in partially filled systems (in two-phase mode), or with boiling in reflux condensation mode. In any of these types, natural circulation can occur in single-channel or parallel-channel loops, as with the CANDU design.

Natural circulation in a containment building is a specific form of single-phase multi-component natural circulation.

7.9.2 CANDU natural circulation

CANDU reactors have a very different design than LWR reactors, and therefore the effectiveness of natural circulation must be carefully assessed. The performance of natural circulation in a CANDU reactor is an important part of reactor safety under certain operating or accident conditions. Therefore, a natural circulation test is performed in each CANDU plant during commissioning to demonstrate that natural circulation works adequately and that the

computer codes predict the observed behaviour sufficiently well.

Figure 143 shows a CANDU primary heat transport system on the left side and a view of the CANDU header on the right side [POP2012a, POP2014]. The CANDU header plays an important role in natural circulation, particularly the outlet header because it contains flows of about 2%–4% quality.

A CANDU reactor cooling system is arranged in a figure-of-eight loop configuration, typically with two loops (i.e., two figure-of-eight loops). Figure 143 shows on the left side an elevation indication for various components. The height difference between the bottom channel and the top of the steam generators is about 22 metres. The height difference between the reactor top channels and the bottom of the steam generators is about 3 metres. Due to the difference in densities between the vertical branches, a pressure difference is created, which creates the potential for natural circulation flow around the loop.

From Figure 143, it is clear that the height difference in CANDU is greater than in PWRs, and according to Eq. (291), this enhances natural circulation. However, flow resistance in the CANDU primary loop is greater than in LWRs because of the relatively small-diameter feeders, channel end-fittings, and shorter fuel bundles, which according to Eq. (291), reduces the natural circulation driving force. In addition, the CANDU core consists of many fuel channels in parallel that have similar geometry, but are at different elevations. This will create differences in the natural circulation driving force.

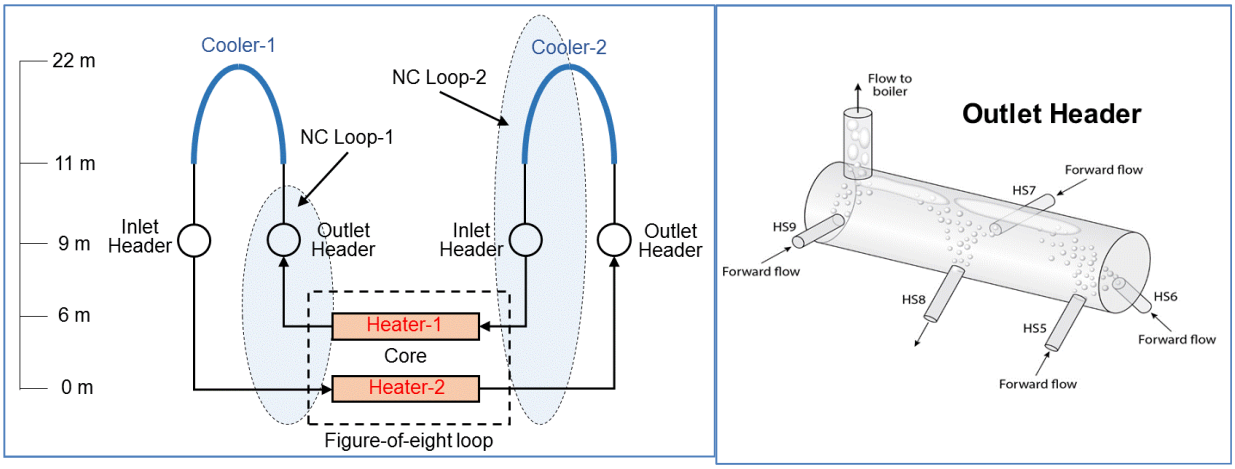

Figure 143 Natural circulation in CANDU

A CANDU header, shown on the right side of Figure 143, has multiple feeder connections at different elevations and angles. When the header is partly voided, this geometry can result in interesting phenomena. One of these is vapour pool-through, in which steam is sucked into the feeder even if the feeder connection to the header is below the collapsed liquid level in the header. Because the scope of this textbook is limited, details of this phenomenon cannot be covered in this section.

At very low pressure drop between inlet and outlet headers, the feeder flow is low and could possibly reverse direction in some feeders and channels. However, flow direction in the channel is not as important as the mass flow rate. Hence, as long as there is sufficient flow in

the feeders and the fuel channel, decay heat generated in the core can be removed effectively, regardless of the flow direction. Experiments have provided information on flow direction in CANDU feeders and core channels under natural circulation and have demonstrated that decay heat removal can be adequate during natural circulation for certain combinations of decay power levels and loop inventory.

The key parameters for CANDU natural circulation are the primary coolant inventory in the core, the secondary pressure, and the primary power. At very low powers in CANDU, two natural circulation loops are created: one between channels and headers, and the other one from headers to steam generators (see Figure 143). This is important because it demonstrates that channel flow direction is not an essential parameter in determining the effectiveness of natural circulation for decay heat removal.

Figure 144 [ING1992, POP2012b]] shows the experimentally observed onset of bi-directional flow in a CANDU core under natural circulation. It is evident that the heat transport system inventory plays an important role, along with channel power and pressure. Figure 145 [POP2012a, POP2012b] shows the criteria for flow reversal in a CANDU core. The upper and lower boundaries are shown in terms of secondary-side pressure and loop-integrated void. It is evident that at higher loop void and lower pressure, the flow reversal band is significantly expanded.

One very specific application of natural circulation in CANDU is heat rejection by the feeders to the containment environment. At very low powers, decay heat can be passively rejected by the feeder pipes directly to the containment atmosphere.

The Canadian Nuclear Safety Commission issued Generic Action Item GAI 90G02 in 1990, requesting utilities to demonstrate reactor cooling adequacy in natural circulation and address uncertainty in the RD-14M experiments with respect to core cooling with reduced loop water inventory in a CANDU loop (LOCA combined with loss of forced circulation). This GAI was closed for all CANDU stations in Canada, thus demonstrating the cooling adequacy of natural circulation in CANDU.

CANDU core cooling in the absence of forced flow (CCAFF), i.e., natural circulation, has been extensively studied over the past 50 years. The CANDU CCAFF terminology defines the following natural circulation modes: a) single-phase thermo-siphoning; b) two-phase thermo-siphoning, c) intermittent buoyancy-induced flow (IBIF), and continuous steam venting.

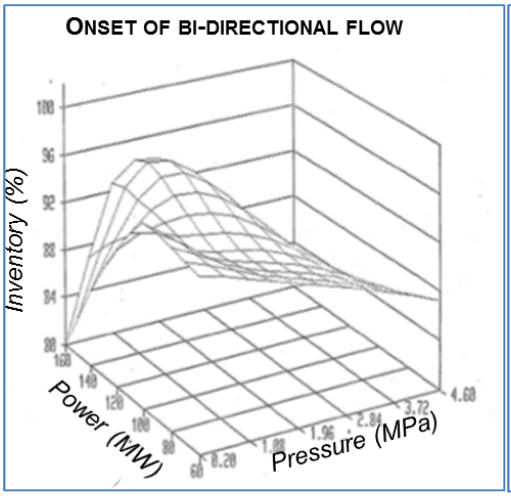

Figure 144 Onset of bi-directional flow in CANDU

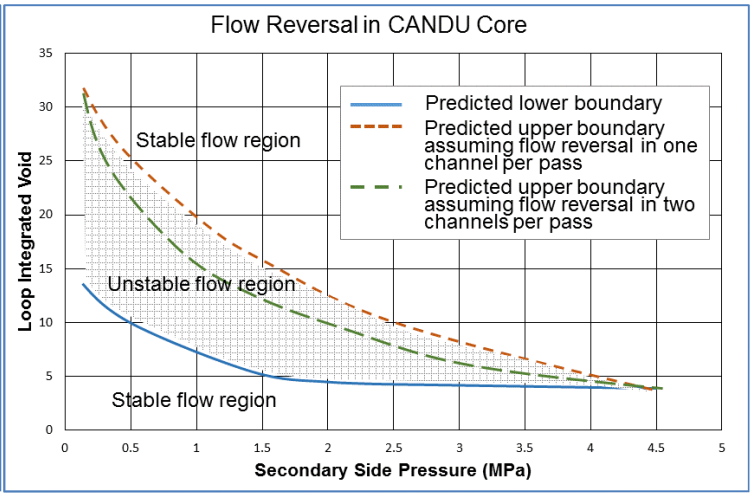

Figure 145 Criteria for flow reversal in a CANDU core

Single-phase thermo-siphoning

In this CCAFF mode, continuous heat input to the coolant raises the temperature in the fuel channel (as shown in Figure 143). This induces a buoyancy force whereby the hot liquid rises to the steam generator and deposits its heat. From the steam generator, a lower-temperature (denser) liquid continues to flow down back to the core. In this case, the buoyancy forces are sufficient to overcome the static pressure caused by the elevation of the boilers with respect to the fuel channels. This is a continuous process and is capable of removing a substantial amount of decay heat indefinitely as long as the loop does not drain beyond about 70%, and as long as the heat is removed from the steam generators.

Two-phase thermo-siphoning

This is a similar phenomenon to liquid thermo-siphoning, but with continuous boiling of the liquid, and thus steam content in the flow provides an additional buoyancy force for heat transfer to the steam generators (resulting from the liquid-vapour density difference). It has been experimentally demonstrated that flow is still continuous in a given direction, with a large quantity of vapour at the channel outlet. For this thermo-siphoning mode, it is important to maintain a certain flow rate rather than a certain flow direction. The flow rate in this type of natural circulation depends on the amount of void in the system and the channel power.

Intermittent buoyancy-induced flow (IBIF)

If the flow rate is reduced to a very small value, or if the fluid stagnates in the channel, the IBIF phenomenon occurs. Numerous analytical and experimental studies of IBIF have been conducted in recent decades to address the Canadian Nuclear Safety Commission-issued Generic Action Item GAI 90G02 on CCAFF. The closure of this GAI provided answers to many issues related to fuel and fuel channel behaviour in a CANDU channel when the flow stops, such as:

- First channel in which boiling occurs;

- Role of static pressure (i.e., channel elevation);
- Location in the channel where boiling occurs;
- Vapour accumulation and outflow from the channel;
- Heat transfer from uncovered fuel elements;
- Impact of void rate generation;
- Fuel sheath temperature for uncovered fuel elements.

Figure 146 shows the four steps in the IBIF cycle, which are explained below [POP2012a, POP2014]. The IBIF cycle repeats itself, providing channel cooling when the flow is stopped. Figure 146a shows a CANDU fuel channel in which flow has stopped and the power profile has a certain cosine shape. As forced circulation is lost, flow almost stagnates in the channel, and therefore heat transfer and removal from the fuel are lost. As a result, because of decay power generation, fuel temperature rises, along with fluid temperature. After some time, the coolant in the channel reaches saturation and thermal stratification. Steam starts to develop at the top of the channel.

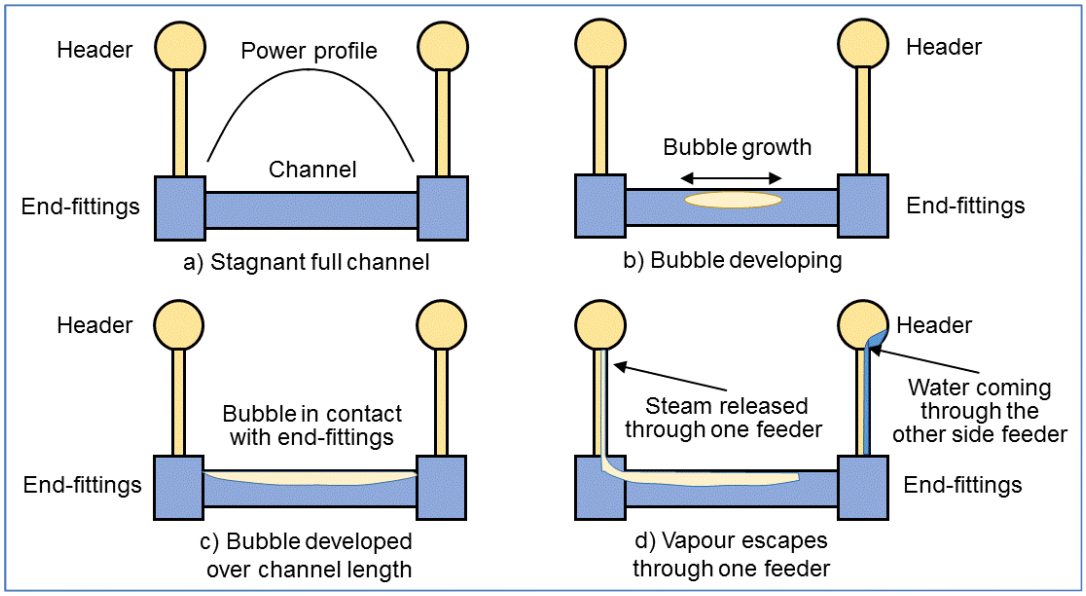

Figure 146 Intermittent buoyancy-induced flow in CANDU

Figure 146b shows a large bubble being generated because of liquid evaporation. The uncovered fuel elements begin to heat up faster (and local heating of the pressure tube occurs). The large vapour bubble grows outward from the centre of the channel towards the end-fittings, and uncovered fuel-element sections stop producing vapour.

Figure 146c shows further progression of an IBIF cycle, as steam reaches and heats up the end-fittings. Because the end-fittings have a very large mass of relatively cold material (during a reactor shutdown, everything approaches 60°C), and it takes a while to heat it up before the bubble can "push" itself by. This delays venting because the longer the fuel is uncovered, the hotter it gets. Before steam can push through, several sub-cycles may occur, with steam condensation at the end-fitting edge. The process continues until the steam creates a flow path to the feeders.

Figure 146d shows the last part of an IBIF cycle, when the steam pushes through to the feeder and the header. Usually steam push-through happens on one side or the other first. It does not necessarily follow the usual flow direction. Once one side starts to "vent" (vapour rushes out of that side of the channel), this creates a pressure force, which sucks in cold liquid from the opposite header.

After venting is completed, the fuel channel refills with sub-cooled or saturated water from the other header. At this point, the previous IBIF cycle is completed, and a new cycle begins.

Figure 147 shows an envelope of CANDU fuel sheath temperature histories during an IBIF cycle [POP2012a, POP2014]. While the channel is full and sub-cooled, the sheath temperatures are below saturation (left part of the diagram). As the channel saturates and remains saturated for a certain time, sheath temperatures remain near saturation. Then, as bubbles are generated in the upper part of the channel and fuel elements are exposed, the fuel sheath temperatures of these fuel elements rise to above 400°C (during the heating period, and depending on fuel element power). When steam venting occurs at the end of an IBIF cycle and the channel is refilled with water from the other header, sheath temperatures fall to and below saturation (the last part of the diagram).

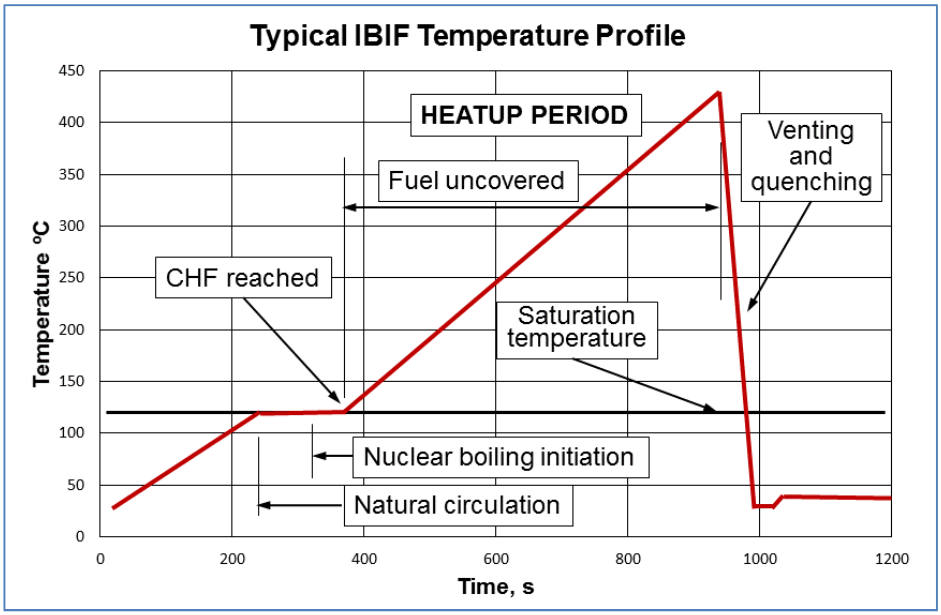

Figure 147 Typical temperature histories in a CANDU channel in natural circulation

7.9.3 CANDU natural circulation experimental studies

In support of natural circulation knowledge base development, numerous experimental tests and assessments have been conducted in Canada on CANDU-typical experimental facilities. The most important experimental facilities in this area are:

- RD-14 natural circulation experiments. RD-14 is a full-scale, full-elevation CANDU-typical experimental facility at AECL with two figure-of-eight passes containing one fuel channel in each loop.
- RD-14M natural circulation experiments. RD-14M is a full-scale, full-elevation CANDU-

typical experimental facility at AECL with two figure-of-eight passes containing five fuel channels in each loop.

- CWIT standing-start experiments. CWIT is a full-scale experimental facility containing two full-scale fuel channels connected to inlet and outlet header at the Stern Laboratories.

More details of these experimental facilities, experimental results, and conclusions are provided in [IAEA2005, IAEA2012]. The experimental work in this area was performed to improve the knowledge base and to provide data for development and validation of computer programs and models.

7.9.4 Natural circulation calculations and predictions

Mathematical modelling of natural circulation is based on several approaches, including empirical models based on experimental data; analytical mechanistic models based on fundamental principles approaches that use conveniently established simplifying assumptions; and general-purpose computer programs based on detailed application of field conservation equations.

CATHENA [CAT2005], TUF [TUF2001], and RELAP [2010] are examples of large one-dimensional two-fluid thermal-hydraulic computer codes used to simulate natural circulation. Recently, more attention has been devoted to use of CFD computer models [HAS2012] for natural circulation analysis in cases where more detailed information is needed. More details about the use of thermal-hydraulic computer programs are provided in Chapter 7.

Various mechanistic models have been proposed in the literature to analyze natural circulation in the CANDU reactor core and feeder system. These models use mass, momentum, and energy conservation accompanied by drift-flux momentum equations. Often, a macroscopic mass, momentum, and energy balance in a six-equation configuration is also used. Details of this topic are beyond the scope of this textbook, but information can be found in the section for suggested further reading. One example of one mechanistic model is provided below.

Algebraic equations or field equations properly solved by simplified numerical models or by complex computer codes can be used to predict natural circulation performance under a wide variety of geometrical conditions and technological systems. The fundamental principles approach is based on the following assumptions: constant core inlet enthalpy; cross-section averaged fluid properties; homogeneous two-phase flow; thermal equilibrium; form losses dominating loop resistance. These assumptions are applied to the mass, momentum, and energy equations for each loop component to obtain the conservation equations. The equations are then integrated over their respective single-phase and two-phase regions to obtain the loop balance equations.

Assuming the natural circulation loop shown in Figure 141, the transient momentum equation can be written as:

$$\sum_{i=1}^{N}\left(\frac{L_i}{A_i}\right)\cdot\frac{dW}{dt}=g\left(\rho_l-\rho_{TP}\right)H_{nc}$$
$$-\frac{W^2}{\rho_l A_c^2}\left\{\sum_{SP}\left[\frac{1}{2}\left(\frac{fL}{D_h}+K\right)_i\left(\frac{A_c}{A_i}\right)^2\right]+\frac{\rho_l}{\rho_{TP}}\sum_{TP}\left[\frac{1}{2}\left(\frac{fL}{D_h}+K\right)_i\left(\frac{A_c}{A_i}\right)^2\right]+\right\}. \quad (293)$$

The energy balance equation for transient natural circulation can be written as:

$$M_{loop}\frac{d\left(e_M-e_l\right)}{dt}=W\left(h_{TP}-h_l\right)-\dot{q}_{SG}-\dot{q}_{loss}. \quad (294)$$

The equilibrium two-phase quality in the core exit can be defined as:

$$x_e=\frac{h_{TP}-h_l}{h_{lg}}. \quad (295)$$

The homogeneous mixture density is defined using the following relation:

$$\rho_{TP}=\frac{\rho_l}{1+x_e\left(\frac{\rho_l-\rho_g}{\rho_g}\right)}, \quad (296)$$

where:

L_i	is the length of a loop component;	K	is the coefficient of local resistance;
A_i	is the area of a loop component;	e_M	is the mixture internal energy;
A_c	is the area of a loop restriction;	e_l	is the liquid internal energy;
H_{nc}	is the elevation difference driving the natural circulation	$\dot{q}_{SG}$	is the steam generator heat sink [kJ/s];
		$\dot{q}_{loss}$	is the loop heat losses;
D_i	is the loop element diameter;	h_{TP}	is two-phase enthalpy;
f	is the friction factor;	h_l	is liquid enthalpy,

These equations can be manipulated to yield the following equations for steady-state mass flow rate in a two-phase natural circulation loop with uniform diameter:

$$W_{ss}=\left[\frac{2}{p}\frac{g\cdot\rho_r\beta_{TP}H_{nc}Q_h D_r^b A_r^{2-b}\rho_l}{\mu_r^b N_G}\right]. \quad (297)$$

The geometric contribution to the friction factor is defined as:

$$N_G=\frac{L_t}{D_r}\left[\sum_{i=1}^{N_{SP}}\left(\frac{l_{eff}}{D_i^{1+b}A_i^{2-b}}\right)+\bar{\phi}_{LO}^2\sum_{i=N_{SP}+1}^{N_B}\left(\frac{l_{eff}}{D_i^{1+b}A_i^{2-b}}\right)_i+\bar{\phi}_{LO}^2\sum_{i=N_B+1}^{N_{TP}}\left(\frac{l_{eff}}{D_i^{1+b}A_i^{2-b}}\right)_i\right]. \quad (298)$$

The Reynolds and Grashoff mixture numbers are defined as:

$$Re_m=\frac{D_r W_{ss}}{A_r\mu_l}\qquad Gr_m=\frac{D_r^3\rho_l^3\bar{\beta}_h g Q_h\Delta z}{A_r\mu_l^3}. \quad (299)$$

In these equations:

β_h	is the thermal expansion coefficient	l_{eff}	is the effective length of a component;
Q_h	(°C)	A	is the flow area (m^2);
Δz	is the total heat input rate (W); is the centreline elevation difference in the loop between cooler and heater	μ	is the dynamic viscosity (Ns/m^2);
		r	is a subscript indicating a reference value.

7.9.5 Problems

1. Explain the importance of natural circulation in the CANDU primary heat transport system, and the design decisions that help to enhance it.
2. Explain the key aspects of the Intermittent Buoyancy Induced Flow (IBIF) in CANDU channels, list and explain the key IBIF parameters.
3. Calculate natural circulation flow in a PWR reactor primary cooling loop assuming typical geometrical and thermal-hydraulic parameters for a PWR reactor (primary loop is in subcooled boiling flow in normal operation, i.e., single phase liquid flow).

8 References

[AECL1978] G.A. Pon, "Evolution of CANDU Reactor Design", AECL-6351, August 1978.

[AECL1981] "CANDU Nuclear Power System", AECL-TDSI-105, January 1981.

[AECL1997] "Canada Enters the Nuclear Age – A Technical History of Atomic Energy of Canada Limited", AECL, McGill-Queen's University Press, Toronto, 1997.

[AECL2005] "CANDU 6 Technical Outline", AECL, September 2005.

[AECL2009a] "Enhanced CANDU 6 Technical Summary", AECL, 2009.

[AECL2009b] "ACR-1000 Technical Description", AECL 10820-01371-TED-001, 2009.

[AECL2010] *"Enhanced CANDU 6 (EC6) Design Description",* IAEA Advanced Water-Cooled Reactors Web-Based Report, 2010.

[AHM2009] R. Ahmadi, A. Nouri-Borujardi, J. Jafari, I. Tabatabari, "Experimental Study of Onset of Subcooled Annular Flow Boiling", Progress in Nuclear Energy Journal, Vol 51, pp.361-365, 2009.

[APR2011] "Advanced Pressurized Reactor (AP1000)", Design Control Document, Rev. 19, Westinghouse, USNRC Website, 2011.

[BER1981] A.E. Bergles, *et al*., Two-Phase Flow and Heat Transfer in the Power and Process Industries, Hemisphere Publishing, 1981.

[BIR1960] R.B. Bird, W.E. Stewart, and E.N. Lightfoot, Transport Phenomena, Wiley, New York, 1960.

[BPR2000] "Bruce: A Safety Report", Brice Power, 2000.

[CAR2015] "Carnot Principle", Wikipedia, Internet, 2015.

[CAT1998] B.N. Hanna, *et al*., "CATHENA: A Thermal-Hydraulic Code for CANDU Analysis", Nuclear Engineering and Design 180 (1998) 113-131, and AECL-1194.

[CAT2000] "CATHENA Mod 3.5c/Mod o Theory Manual", COG-00-008, Nov. 2000.

[CAT2005] "CATHENA Mod 3.5d Theory Manual", AECL, 153-112020-STM-001, Dec. 2005.

[CLA2015] "Clausius Statement", Wikipedia, Internet, 2015.

[COL1972] J.C. Collier, Convective Boiling and Condensation, McGraw-Hill, 1972.

[CRA1957] Flow of Fluids Through Valves, Fittings, and Pipes, Crane, 1957.

[DEL1981] J.M. Delhaye, *et al*., Thermo-Hydraulics of Two-Phase Systems for Industrial Design and Nuclear Engineering, Hemisphere Publishing, 1981.

[ELW1978] M.M. El-Wakil, Nuclear Heat Transport, American Nuclear Society, 1978.

[ELW1990] M.M. El-Wakil, Nuclear Energy Conversion, American Nuclear Society, 1990.

[EPRI1999] Nuclear Reactor Generations, EPRI document EPRI NP-6780-L, Volume 1, 1999.

[EPRI1996] Water Hammer Handbook for Nuclear Plant Engineers and Operators, EPRI Technical Report, Palo Alto, California, 1996.

[GAR1999] B. Garland, "Reactor Thermal-Hydraulic Design", Graduate course EP716 lectures, Engineering Physics, McMaster University, 1999.

[GLA1967] S. Glasstone, A. Sesonske, Nuclear Reactor Engineering, Van Nostrand Reinhold, 1967.

[HAS2012] Y.A. Hassan, Computational Fluid Dynamics for Natural Circulation, Texas A&M University, Texas, USA, for the N.IN.E Nuclear and Industrial Engineering Natural Circulation Course, Beijing, China, 27 July–31 Aug. 2012.

[HET1982] G. Hetsroni, Handbook of Multiphase Systems, Hemisphere and McGraw-Hill, Washington, 1992.

[IAEA2001] Thermal-Hydraulic Relationships for Advanced Water-Cooled Reactors, IAEA TECDOC-1203, Vienna, 2001.

[IAEA2005] Natural Circulation in Water-Cooled Nuclear Power Plants, IAEA TECDOC-1474, Vienna, 2005.

[IAEA2012] Natural Circulation Phenomena and Modelling for Advanced Water-Cooled Reactors, IAEA TECDOC-1677, Vienna, 2012.

[IDE1996] I.E. Idelchik, Handbook of Hydraulic Resistance, 3rd Edition, Begell House, New York, 1996.

[ING1992] P.J. Ingham, Natural Circulation Experiments in the RD_14M Multiple Channel Thermal-Hydraulic Loop, AERCL, Pinawa, Manitoba, Canada, 1992.

[KEV2015] "Kelvin Statement", Wikipedia, Internet, 2015.

[KNI2002] R.A. Knief, Nuclear Engineering—Theory and Technology of Commercial Power, American Nuclear Society, 2008.

[KRI1987] V.S. Krishnan, P. Gulshani, "Stability of Natural-Circulation Flow in a CANDU-Type Fuel Channel", AECL, Pinawa, Manitoba, Canada, in Journal of Nuclear Engineering and Design, Vol. 99, pp. 403–412, 1987.

[KPL2015] Kelvin-Planck Statement, Wikipedia, Internet, 2015.

[KOK2009] K.D. Kok (Ed.), Nuclear Engineering Textbook, CRC Press, 2009.

[LAH1977] R.T. Lahey, Jr., and F.J. Moody, The Thermal Hydraulics of a Boiling Water Nuclear Reactor, ANS&AEC Monograph Series on Nuclear Science and Technology, ANS, 1977.

[LEU2004] L. Leung, Reactor Thermal-Hydraulic Design: CHF, Post-Dryout, and Pressure Drop Lectures, Graduate course UN804 lectures, UNENE graduate courses, Chalk River Laboratories, AECL, 2004.

[MOO1944] L.F. Moody, "Friction in Pipes", Transactions of the ASME, pp. 666-671, 1944.

[OPG2002] Darlington Safety Report, Ontario Power Generation, 2002.

[OPG2000] Pickering: A Safety Report, Ontario Power Generation, 2000.

[PLA2015] Planck Principle, Wikipedia, Internet, 2015.

[POP2000] N.K. Popov, U.S. Rohatgi, H.E.C. Rummens, R.B. Duffy, "Two-Phase Flow Stability in Low-Pressure Parallel Vertical Heated Annuli", ICONE8, Baltimore, MD, USA, April 2–6, 2000.

[POP2012a] N.K. Popov, Natural Circulation Behaviour in PHWRs, Engineering Physics, McMaster University, Hamilton, Canada, for the N.IN.E Nuclear and Industrial Engineering, Natural Circulation Course, Beijing, China, 27 July–31 August 2012.

[POP2012b] N.K. Popov, PHWR Natural Circulation Experimental Program in Canada, Engineering Physics, McMaster University, Hamilton, Canada, for the N.IN.E Nuclear and Industrial Engineering, Natural Circulation Course, Beijing, China, 27 July–31 August 2012.

[POP2013] N. Popov, Reactor Thermal-Hydraulic Design, Graduate course UN804 lectures, UNENE Graduate Courses, 2013.

[POP2014] N. Popov, Reactor Thermal-Hydraulic Design, Graduate course EP716 lectures, Engineering Physics, McMaster University, 2014.

[REL2005] "RELAP5 - A Computer Program for Transient Thermal-Hydraulic Analysis of Nuclear Reactors and Related Systems", INEEL-EXT-98-00834, September 1996.

[REL2010] "RELAP5/MOD 3.3 Code Manual", USNRC, NUREG/CR-5535/Rev P4, October 2010.

[ROH1983] W.M. Rohsenov, J.P. Hartnett, E.N. Ganic, Handbook of Heat Transfer Fundamentals, McGraw-Hill, New York, 1985.

[SOP1975] Y.F. Chang, "The SOPHT Program and its Applications", Proceedings, Simulation Symposium on Reactor Dynamics and Plant Control, May 26–27, CRNL, published as CRNL 1369, 1975.

[SAA1966] M.A. Saad, Thermodynamics for Engineers, Prentice-Hall, 1996.

[SOP1977] Y.F. Chang, A Thermal-Hydraulic System Simulation Model of the Reactor, Boiler, and Heat Transport System (SOPHT), CNS-37-2, Ontario Hydro, September 1977.

[TOD1990a] N.E. Todreas, M.S. Kazimi, Nuclear Systems I—Thermal Hydraulic Fundamentals, MIT, CRC Press, Taylor & Francis, 2011.

[TOD1990b] N.E. Todreas, M.S. Kazimi, Nuclear Systems II—Elements of Thermal Hydraulic Design, MIT, CRC Press, Taylor & Francis, 1990.

[TON1965] L.S. Tong, Boiling Heat Transfer and Two-Phase Flow, Wiley, 1965.

[TON1975] L.S. Tong, Boiling Heat Transfer and Two-Phase Flow, Krieger, 1975.

[TON1996] L.S. Tong, J. Weisman, Thermal Analysis of Pressurized Water Reactors, American Nuclear Society, 1996.

[TUF2010] TUF Thermal-Hydraulics Computer Program, N-REP-06631.02-10010 R00, Ontario Power Generation, October 2001.

[WAL1969] G.B. Wallis, One-Dimensional Two-Phase Flow, McGraw-Hill, 1969.

[WEI1977] J. Weisman, Elements of Nuclear Reactor Design, Elsevier, 1983.

[WIK2015] "Steam-Water Diagrams", Internet, Wikipedia, 2015.

[WNA2009] "Nuclear Reactor Generations", WNA Web site, 2009.

9 Further Reading

[DUD1976] J.J. Duderstadt, L.J. Hamilton, Nuclear Reactor Analysis, Wiley, New York, ISBN 0-471-22363-8, 1976.

[GIN1981] J.J. Ginoux ,Two-Phase Flows and Heat Transfer with Application to Nuclear Reactor Design Problems, Hemisphere, 1981.

[GOV1972] G.W. Govier, K. Aziz, The Flow of Complex Mixtures in Pipes, Van Nostrand Reinhold, 1972.

[HSU1976] Y. Hsu, R. Graham, Transport Processes in Boiling and Two-Phase Systems, Hemisphere, 1976.

[ISH1975] M. Ishii, T. Hibiki, Thermo-Fluid Dynamic Theory of Two-Phase Flow, Springer, 2010.

[LAM1977] J.R. Lamarsh, Introduction to Nuclear Engineering, Addison-Wesley, 2001.

[LEW1977] E.E. Lewis, Nuclear Reactor Safety, Wiley, 1977.

[ROA1976] P.J. Roache, Computational Fluid Dynamics, Hermosa, 1976.

10 Glossary

ACR	Advanced CANDU Reactor
ADL	Axial Dry-Patch Fraction
AECL	Atomic Energy of Canada Limited
AFD	Axial Flux Distribution
AGR	Advanced Gas-Cooled Reactor
BP	Bruce Power
BWR	Boiling Water Reactor
CANDU	CANada Deuterium Uranium
CANFLEX	CANDU Flexible Fuelling
CCAFF	Core Cooling in Absence of Forced Flow
CDF	Circumferential Drypatch Fraction
CHF	Critical Heat Flux
CHFR	CHF Ratio
CHFPR	CHF Power
CP	Critical Power
CPR	Critical Power Ratio
DNB	Departure from Nucleate Boiling
ECC	Emergency Core Cooling
ECI	Emergency Coolant Injection
EPRI	Electric Power Research Institute
GAI	Generic Action Item
HTGCR	High Temperature Gas Cooled Reactor
HTS	Heat Transport System
IAEA	International Atomic Energy Agency
IBIF	Intermittent Buoyancy-Induced Flow
LMFBR	Liquid Metal Breeder Reactor
LOCA	Loss of Coolant Accident
LOFA	Loss of Flow Accident
LORA	Loss of Reactivity Accident
LWR	Light Water Reactors
MCHFR	Minimum CHF Ratio
MCHFPR	Minimum CHF Power Ratio
MCPR	Minimum Power Ration
NPSH	Net Positive Suction Head
NPSHA	Net Positive Suction Head Available
NPSHR	Net Positive Suction Head Required
NOP	Nominal Operating Power
NOP	Neutron Overpower Protection
NPD	Nuclear Demonstration Plant
NPP	Nuclear Power Plant
OCR	Organic Coolant Reactor
OH	Ontario Hydro
OPG	Ontario Power generation
OSV	Onset of Significant Void
PHTS	Primary Heat Transport System
PHWR	Pressurized Heavy Water Reactor
PWR	Pressurized Water Reactor
RBMK	High Power Channel Type Reactor
RCS	Reactor Cooling System
RFD	Radial Flux Distribution
RIH	Reactor Inlet Header
ROH	Reactor Outlet Header
ROP	Reactor Overpower Protection
R&D	Research & Development
R&M	Reliability and Maintainability
SGHWR	Steam Generating Heavy Water Reactor
QA	Quality Assurance
WNA	World Nuclear Association
WWER	Water Cooled and Moderated Power Reactor (from Russian VVER)

11 Nomenclature

A	cross section area, [m^2]
CHF	critical heat flux, [kW/m^2]
c_p	specific heat at constant pressure, [J/(kg K)]
c_v	specific heat at constant volume, [J/(kg K)]
D_H	hydraulic diameter, [m]
d	diameter, [m]
d_h	hydraulic diameter, [m]
dx	axial derivative
E_K	kinetic energy, [kJ]
E_P	potential energy, [kJ]
E_U	internal energy, [kJ]
e	specific energy, [kJ/kg]
f	friction factor
G	mass flux, [kg/s-m^2]
g	gravitational constant, [m/s^2]
H	total enthalpy, [kJ]
H	pump head, [m]
h	specific enthalpy [kJ/kg]
h	convective heat transfer coefficient, [kW/m^2 °K]
h_{fg}	latent heat of vapourization, [kJ/(kg °K)]
j	volumetric flux (superficial velocity) [m/s]
K	concentrated friction factor
k	thermal conductivity, [kW/m °K]
L	length, characteristic linear dimension, [m]
l	characteristic length, typically the droplet diameter, [m]
M, m	mass, [kg]
$\dot{m}$	mass flow, [kg/s]
NOP	neutron over power
Nu	Nusselt number
P	perimeter, [m]
p	fluid pressure, [kPa]
Pr	Prandtl number
Q	Core power, [kW], volumetric flow, [m^3/s]
Q'''	Core power density, [kW/m^3]
q'''	volumetric heat generation rate, [kW/m^3]
q''	surface heat flux, [kW/m^2]
q'	linear power, [kW/m]
q	energy generation per fuel element, [kW]
R	gas constant, [N·m/(kg °K)], [J/(kg °K)]
r	radius, [m]
Re	Reynolds number
ROP	reactor over power
S	slip ratio, S total entropy, [kJ]
s	specific entropy, [kJ/kg]
T	temperature, [°K]
t	time, [s]
t	thickness, [m]
U	steam generator heat transfer coefficient, [$kJ/(m^2$-s)]
U	internal energy, [kJ]
u	specific internal energy, [kJ/kg]
V	volume, [m^3]
ν	fluid velocity, [m/s]
W	mass flow rate, [kg/s], work, [kJ]
w	specific work, [kJ/kg]
We	Weber number
x	mass quality
x_{th}	thermodynamic quality
Z	height, [m]

Greek Symbols

α	void fraction, thermal diffusivity, [m^2/s]
γ	adiabatic exponent, SG pinch fraction
ΔP	pressure drop, [kPa/m^2]σ surface tension, [N/m]
η_t	thermodynamic efficiency
μ	dynamic viscosity of the fluid [Pa·s], [N·s/m²], [kg/(m·s)]
ρ	density [kg/m^3]
σ	surface tension, [N/m]
τ	pump torque, [Nm], friction stress, [N/m^2]
υ	specific volume, [m^3/kg], kinematic viscosity, [m^2/s]
Φ	neutron flux, [neutron/(m^2-s)]
φ	two-phase friction multiplier
ω	pump rotational speed

Subscripts

a	acceleration
C	cold, cladding, fuel sheath
CL	centreline
cold	cold side
CRIT	critical
DNB	departure of nuclear boiling
e	equivalent
G	gap
g	gas, gap
F	fuel
f	fuel, liquid
fg	latent heat of vapourization
FL	fluid
FW	feed water
H	hot, homogenious
Hot	hot side
h	hydraulic
MFB	minimum film boiling
m	mixture
n	vector perpendicular to surface
P, p	primary
S	steam, saturation
SG	steam generator
SH	sheath
TB	transition boiling
w	wall

12 Acknowledgements

I gratefully thank the following reviewers for their hard work and excellent comments during the development of this Chapter. Their feedback has much improved it. Of course, the responsibility for any errors or omissions is entirely the author's.

Bill Garland

Lawrence Leung

Dave Novog

Terry Rogers

Victor Snell

Dave Wright

I also thank Diana Bouchard for expertly editing and assembling the final copy.

13 APPENDIX A – Reactor Types

13.1 General evolution of reactor designs

The categorization of reactor designs into generations was originally suggested by the U.S. DOE and only reflected the technology evolution timeline. The attributes were assigned later, based on observed characteristics.

The nuclear industry typically categorizes nuclear reactors as follows (see Figure 148):

- Generation I – early prototype reactor designs
- Generation II – commercial power reactor designs
- Generation III/III+ – designs with significant improvements in safety and economics
- Generation IV – future designs.

Note that most currently operating reactors are of Gen II design, and reactors currently under construction are of Gen III/III+ design.

As reactor safety and economics became an important benchmark, the Gen III/III+ reactors were given certain attributes to characterize them more fully. Two separate sets of attributes (requirements or guidelines) were developed by EPRI in 1999 and by WNA in 2009.

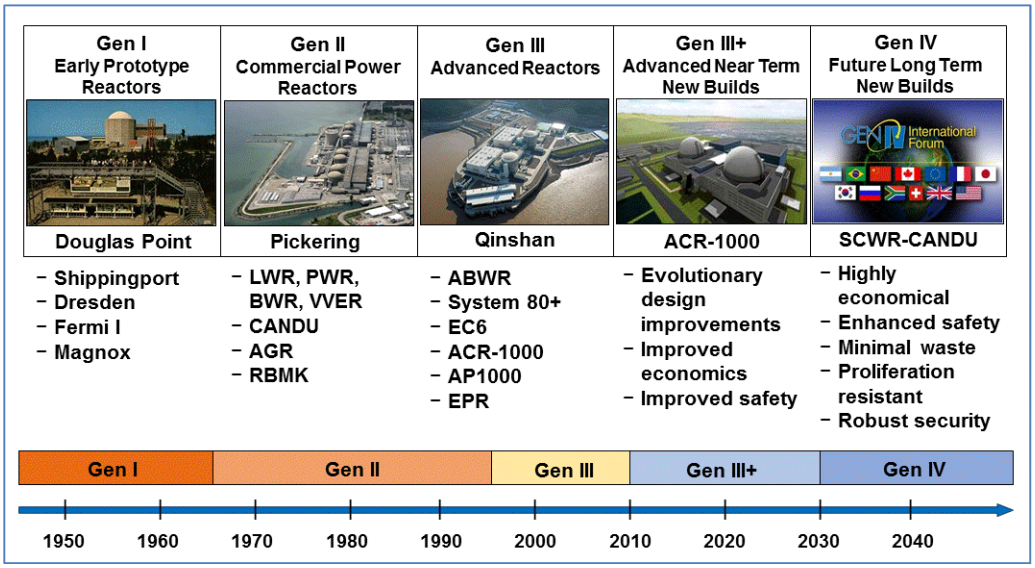

Figure 148 Reactor generations

In the EPRI documentation [EPRI1999], the following attributes are shown to be typically possessed by a Gen III/III+ design:

1. design simplification;
2. design margins;
3. human factors;
4. reactor safety;
5. design basis and safety margin;
6. regulatory stabilization;
7. technology standardization;
8. proven nature of design;
9. enhanced maintainability;
10. enhanced constructability;
11. improved economics;
12. adequate quality assurance;
13. improved security and sabotage protection; and
14. reduced environmental impact.

The WNA definition of the third generation [WNA2009] suggested the following attributes for Gen III/III+ designs:

1. standard design to expedite licensing;
2. reduced cost and construction time;
3. simpler and more rugged design for easier operation and maintenance;
4. higher availability and longer operating life;
5. reduced possibility of core meltdown;
6. resistance to damage;
7. reduced radiation release;
8. higher burn-up;
9. less waste;
10. use of burnable absorbers;
11. more passive systems;
12. load following.

Because the above two sets of guidelines overlap somewhat and expectations are not quantified, it is difficult to compare designs in quantifiable terms. More importantly, there are conflicting expectations, such as expecting changes to improve safety and at the same time expecting the design to be well proven. A detailed discussion of implementation and compliance with these objectives of current advanced design is beyond the objectives of this section, but note that none of the modern advanced designs claims to achieve all the expectations described above.

13.2 Pressurized water reactors

13.2.1 General information

Pressurized water reactors (PWRs) are currently one of the most commercially successful reactor types in operation; they originate from the U.S. nuclear industry. PWRs have been built in large numbers around the world, with many different versions and design variations. However, they all share the common characteristics of a light water coolant and moderator and enriched uranium fuel. This section provides an overview of the PWR reactor type, particularly from the perspective of thermal-hydraulic design of the reactor cooling system (RCS).

The PWR has, to date, been the world's most widely accepted power reactor type [KNI2002, KOK2009, WEI1997, TON1996, APR2011, LAH1977]. It got its start in the development of PWR propulsion reactors for United States (U.S.) nuclear submarines. The first PWR power reactor was designed and built by Westinghouse Electric Company at Shippingport in the United States, followed by a number of designs and units built in the United States by a number of vendors.

In France, during the early stage of development, Framatome designed and built a number of units as a licensee to Westinghouse until 1984. Later, Framatome, presently renamed Areva,

continued the development of PWRs in France. In this way, France became a world leader in PWR development and implementation.

In Japan, Mitsubishi continued development of PWR reactors. In Russia, following submarine and icebreaker design and technology, a similar PWR design, the water-cooled, water-moderated power reactor (WWER), was developed.

Typical PWR reactor thermal-hydraulic parameters are provided in Table 13 [APR2011, POP2014]. To ensure efficient energy conversion from the reactor core to the steam turbine, the primary coolant pressure is typically 10–15 MPa and the primary coolant temperature 290°C–330°C, whereas the secondary loop pressure is typically 5–7 MPa.

In the PWR reactor design, ordinary light water is used both as coolant and moderator. A simplified reactor flow diagram is shown in Figure 149. The reactor coolant loops include primary, secondary, and tertiary loops. In the primary coolant loop, the coolant picks up the heat produced in the core and leaves the reactor at a temperature that is sufficient to generate steam in the steam generator. Then the coolant is returned to the reactor core by means of pumps. In the secondary loop, the steam generated in the steam generator expands in the steam turbine, where its energy is transferred into mechanical energy. In the tertiary loop, the exhaust steam from the turbine is condensed in the condenser, thus transferring heat to the outside heat sink.

Table 13 Typical PWR reactor parameters

Reactor		**Fuel**	
Thermal output, MW_{th}	3800	Fuel pellet material	UO_2
Electrical output, MW_e	1300	Pellet outer diameter, mm	8.19
Thermal efficiency, %	34	Rod outer diameter, mm	9.5
Specific power, kW/kg(U)	33	Zircaloy cladding thickness, mm	0.57
Power density, kW/L	102	Rods per bundle (17 x 17)	264
Ave. linear heat flux, kW/m	17.5	Bundles in core	193
Rod heat flux ave./max, MW/m^2	0.584/1.46		
Vessel		**Core**	
Outer diameter, m	4.4	Length, m	4.17
Height, m	13.6	Outer diameter, m	3.37
Wall thickness, m	0.22	Pressure, MPa	15.5
Steam generator		Inlet temperature, °C	292
No.	4	Outlet temperature, °C	329
Outlet pressure, MPa	6.9	Mass flow rate, kg/s	531
Outlet temperature, °C	284		
Mass flow rate, kg/s	528		

A typical PWR plant and a typical single primary coolant system loop are shown schematically in Figure 149a, and an isometric view with four primary coolant loops is shown in Figure 149b. The number of loops, usually two to four, is determined by the reactor power so that the size of the primary pumps and steam generators is reasonable and obtainable from a commercial vendor. Each primary coolant loop has one primary pump and one steam generator. All loops are

connected through the reactor vessel; one of the loops has a pressurizer connected.

13.2.2 Reactor vessel

Several typical PWR reactor vessel designs are illustrated in Figure 150 [KNI2002, KOK2009, WEI1997, TON1996, APR2011]. Figure 150a shows a quarter section view of the vessel internal structures, in which the reactor core and the fuel elements are also shown. Figure 150b shows a cross section of the reactor vessel body with the internal structures of the core and the control guide tubes above the core. Figure 150c shows an external view of the reactor vessel with a number of inlet and outlet openings for connection to the inlet and outlet piping. The reactor pressure vessel height and diameter depend on the design and the thermal power produced, with a typical height of about 12–14 m and a diameter of 5–7 m. The vessel is constructed of forged low-alloy carbon steel with a wall thickness of 20–25 cm (depending on coolant conditions) and an approximately 3-mm stainless-steel cladding on the inner surface to increase robustness to water corrosion and erosion.

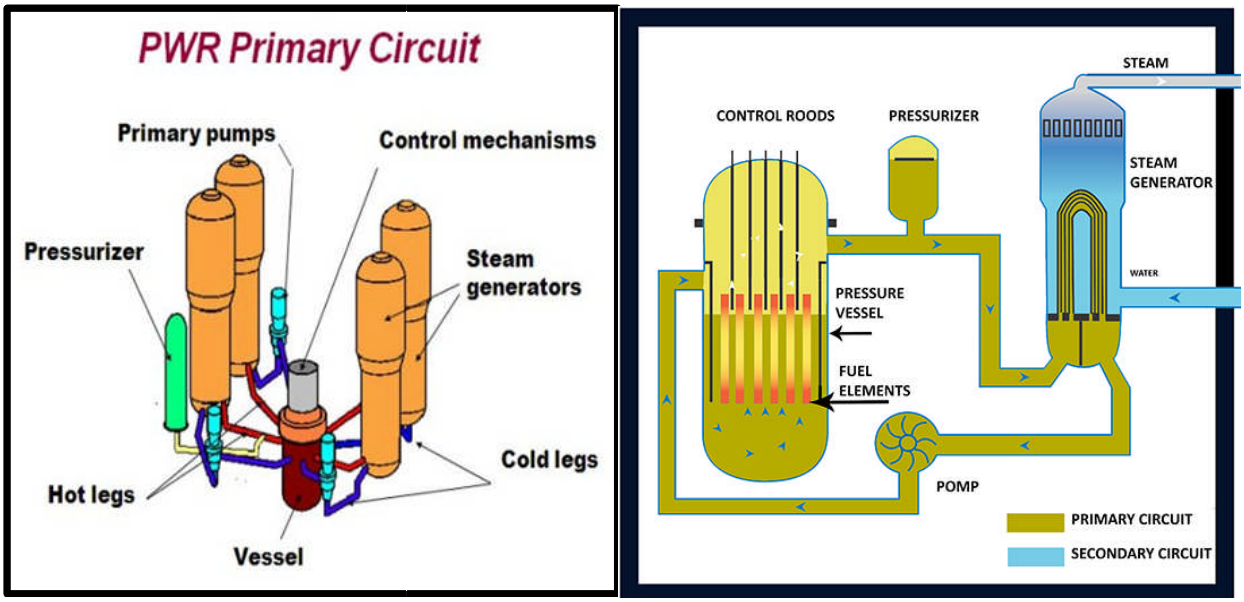

a) PWR four-loop primary system b) PWR primary coolant loop cross section

Figure 149 PWR primary reactor cooling system

As shown in Figure 149a, the nuclear reactor core and fuel assemblies are located in the reactor pressure vessel. The water coolant at high pressure (~14 MPa) is circulated by external pumps into the reactor vessel, flows upwards through the fuel assemblies, out of the vessel to heat exchangers, and from the heat exchangers back to the pumps. The water temperature at the exit of the reactor core is lower than the saturation temperature, i.e., the water is sub-cooled, which has an important impact on reactor thermal-hydraulic margins, as will be explained in later sections of this chapter.

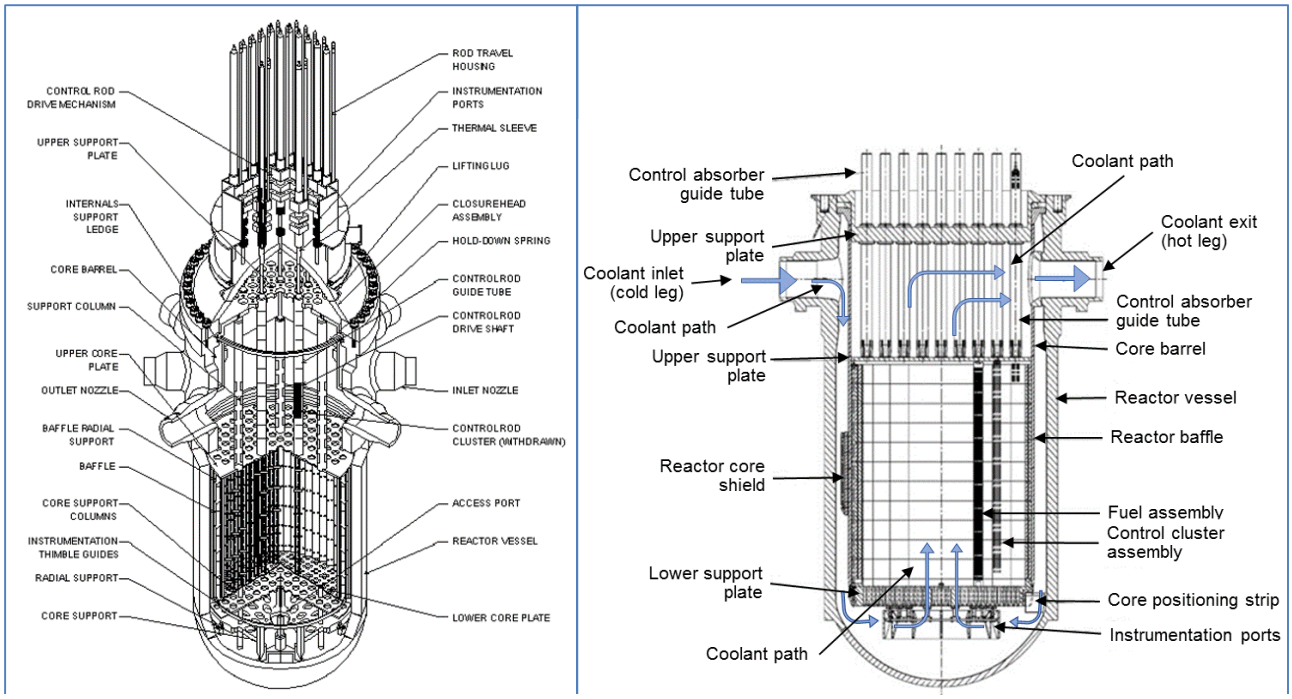

a) PWR vessel internal systems b) PWR vessel cross section

Figure 150 Typical PWR reactor vessel

Figure 150a and Figure **150**b show the internal structures of a typical PWR vessel. The reactor core is located in the lower part of the reactor vessel and is surrounded by a cylindrical inner vessel called the core barrel. On the inner side of the core barrel, the fuel bundles are surrounded by a multi-faced shroud that constrains flow in the radial direction. The bottom of the core barrel has radial sliding pins that give the barrel freedom to accommodate thermal expansion, but do not allow barrel rotation. Around the outside of the core barrel is a metal jacket called the thermal shield (approximately one-third of the core length, situated around the core centre). The role of these thermal shrouds is to absorb core neutron radiation in the radial direction, preventing excessive radiation impact on the reactor vessel and thus reducing radiation aging effects on the vessel.

The top and bottom of the reactor core are supported by the upper core plate and the lower support plate. Both plates support the fuel assemblies in appropriate positions in the core. The reactor control elements and safety shutdown rods pass through the guide tubes that penetrate the upper core plate. The reactor instrumentation typically (in older designs) passes through the lower part of the reactor vessel and penetrates the core through the lower support plate.

The reactor coolant enters the vessel through the inlet pipes (the so-called “cold legs” shown in Figure 149a), then turn downwards in the so-called reactor downcomer and along the outside of the reactor barrel and inside the reactor vessel, thus coming down to the reactor lower plenum. There, the coolant turns upwards, flows through the lower support plate, and enters the core from the bottom. The coolant flows through the core upward and exits in the reactor upper plenum. From there, the coolant flow exits the vessel through the exit pipes (the “hot legs”). The upward flow in the core provides good conditions for thermo-siphoning should primary

pump flow be lost in certain design basis accidents.

13.2.3 Steam generators

Steam generators transfer the heat generated by the reactor in the primary loop to the secondary loop, where the steam turbine transfers the thermal energy into mechanical energy, which in the electric generator is further transferred into electrical energy. Therefore, steam generators are an important part of the heat transfer path connecting the two loops.

Figure 7 shows a typical vertical U-tube steam generator (some PWRs use once-through vertical steam generators, and the Russian WWER design uses horizontal double U-tube steam generators). A typical vertical steam generator is typically 21 m high and 4.5 m wide in the upper portion. Primary coolant enters the steam generator at the bottom inlet chamber and flows upward through the support plate into a U-shaped bundle of small-diameter tubes. Then it flows back down to the outlet chamber at the bottom of the steam generator. Thus, the outside surface of the U-tubes in the steam generators transfers heat from the primary to the secondary side.

On the secondary side of the steam generators, water boils, producing saturated steam that drives the turbine. This steam is generated in the steam generator at ~5–7 MPa depending on the station design. The feedwater coming into the steam generator secondary loop enters at the side, at the bottom above the support plate. It passes through the pre-heater region, where it is heated to saturation temperature and then boils, passes through two sets of steam dryers, and exits the upper plenum, which is located at the top of the steam generator.

The design of the steam generators is similar between the CANDU and the PWR designs. However, some PWR steam generator designs do not have a pre-heater designed at the feedwater entrance to the steam generator secondary side.

13.2.4 Primary pumps

Figure 9 presents a view of a typical PWR primary pump [KNI2002, KOK2009, WEI1997, TON1996, APR2011]. It contains a single-stage impeller and an impeller casing. This is the most important part of the pump because it provides the driving force for the primary flow. Above the impeller casing, the rest of the pump consists of a number of pump seals to insulate the primary flow, a flywheel set to provide inertia for the pump to continue operating for some time after power is lost, and an electric pump motor.

The primary pumps are a vital component in the reactor heat transport system because they drive the coolant flow by forced circulation through the primary heat transport system. Hence, they are essential to fulfill the primary function of the reactor cooling system, to provide continuous cooling of the reactor core in normal operation, during transients, and during reactor shutdown. The pump start-up and shut-down sequences are routine operations of the reactor heat transport system.

Pump failures, whether due to loss of power or inadvertent operator action, are events that must be considered explicitly in the reactor design. The reactor primary cooling system is designed to allow and enhance natural circulation in the absence of pump flow. This is achieved

by placing the reactor core (heat source) at the lowest point in the primary loop and the pumps and steam generators (heat sinks) at the highest point in the primary loop.

The design of the primary pump is similar between CANDU and PWR reactors.

13.2.5 Pressurizer

The pressure in the reactor primary coolant system is maintained at a certain level by a pressurizer. Figure 8 shows a view of a typical pressurizer.

13.2.6 Reactor refuelling and reactivity control

The fuel is in the form of assemblies (or bundles) of enriched UO_2 rods, clad in zirconium alloy (or in some earlier designs, in austenitic stainless steel). As shown in Figure 151, these fuel assemblies are square or hexagonal in shape (depending on the reactor type) and contain an array of fuel rods within each assembly. The fuel assemblies are arranged in a tightly packed lattice configuration, with either square or triangular pitch (depending on the reactor type). Typically, reactors designed by GE-Westinghouse use a square fuel assembly and square lattice pitch, whereas the Russian-designed WWERs use a hexagonal fuel assembly arranged in a triangular pitch.

The fuel assemblies have an open lattice, which enables radial cross flow of the cooling water, i.e., mixing of coolant between adjacent fuel assemblies. The coolant does not boil in the core because its temperature at the core exit is still below saturation.

To refuel a PWR reactor, it must be shut down and the primary loop cooled and depressurized. Several days after reactor shutdown, the decay heat load of the primary loop decreases sufficiently to enable reactor depressurization and the start of refuelling operations. Following cooling and depressurization, the reactor pit (or reactor bunker) is filled with water to at least a 10-m height above the reactor head to provide adequate radiation shielding for the refuelling personnel working at the top of the reactor pit. Then the reactor head is opened and removed, enabling access to the reactor core. The fuel assemblies are individually manipulated underwater, repositioned in the core, fresh fuel assemblies brought into the core, and some irradiated assemblies removed from the core. Typically, the fresh fuel assemblies and irradiated fuel assemblies are positioned and reshuffled in the core in a predetermined sequence. The refuelling crew typically uses computer programs to ensure optimal fuel bundle distribution and to monitor fuel bundle histories in the core.

The irradiated fuel bundles that are removed from the core are transported underwater to the irradiated fuel bay for storage and cooling for a number of years. Removing the fuel from the irradiated fuel bays depends on the national policies of specific jurisdictions for handling highly radioactive irradiated fuel or subjecting it to reprocessing.

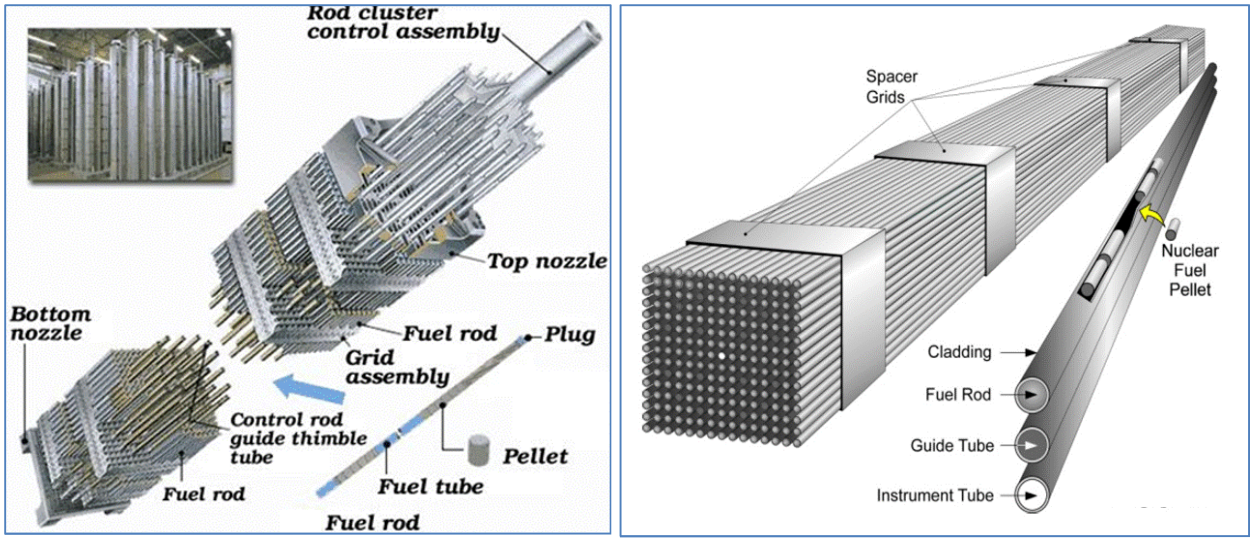

a) Typical fuel assembly structure b) Typical fuel assembly view

Figure 151 Typical PWR square fuel assembly design

Refuelling is normally done on an 18–24 month basis and typically takes 4–5 days. However, refuelling outages in PWRs can last up to one month or sometimes longer when the preparations, cooldown, maintenance activities, and return to full power are taken into account. To operate for long periods without refuelling, the new fuel is enriched in ^{235}U (up to a maximum of 5%). When the fuel is fresh, the excess reactivity in the reactor core is compensated for by a neutron poison dissolved in the coolant/moderator water and by other devices. As the fuel burns up, the dissolved poison in the coolant/moderator is gradually removed by ion-exchange columns.

Reactivity control in a PWR reactor is performed by full-length control rods. Levelling neutron flux and heat generation in the core is performed by various control rod banks of full or partial length, and by other means in newer PWR designs (i.e., burnable absorber material in fuel and in "grey" control rods). Intermediate- and long-term reactivity control in the core is achieved by soluble poison (called "chemical shim"); typically, boric acid is used for this purpose. The critical soluble boron concentration is reduced in the core with core burn-up, i.e., with buildup of ^{135}Xe and ^{149}Sm. Therefore, during the initial burn-up of a few hundred MWd/t, the boron concentration is reduced sharply by up to 40%, followed later by a more gradual reduction to compensate for fuel burn-up and generation of fission products in the fuel.

13.2.7 Fuel assembly and fuel pin design

Figure 151 shows a typical PWR fuel assembly design [KNI2002, KOK2009, WEI1997, TON1996, APR2011]. As shown in Figure 151a, the fuel assembly typically consists of fuel pins (also called fuel rods or fuel elements) arranged in a square pitch with a certain number of grid plates (spacers) that hold the fuel pins in position and constrain them in the radial direction. Other than by the support plates, the PWR fuel bundle does not restrict the coolant flow in the radial direction because there is no flow tube around the bundle. Therefore, all fuel pins in the core create a continuous matrix of fuel pins throughout the core.

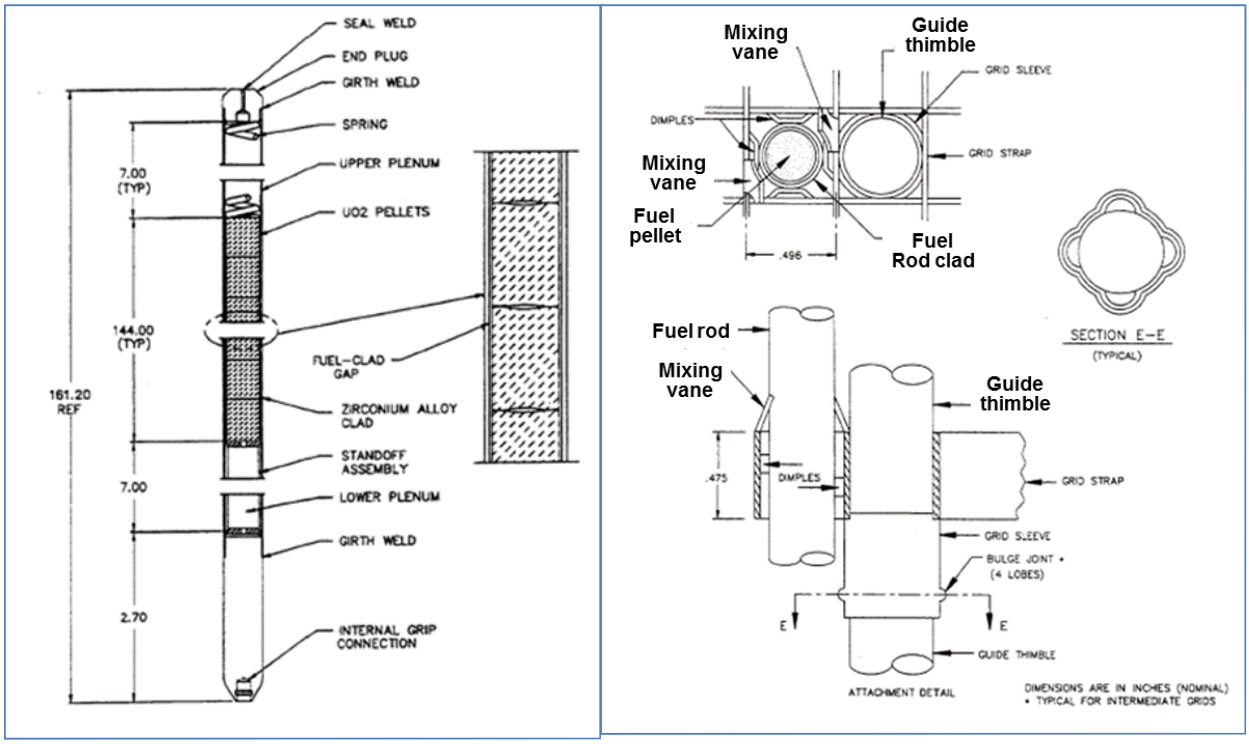

a) Typical fuel rod design b) Typical fuel rod grid design

Figure 152 Typical PWR fuel design

The guide tubes shown in Figure 151a are provided for each fuel assembly. They are intended to receive the control rods (shown in Figure 151a) from the top as a cluster control assembly with a certain number of control rods. Fuel assemblies that do not have control assemblies are plugged from the top by a special plugging device to prevent coolant bypass though them (they have a larger hydraulic diameter than the rest of the fuel matrix).

The top and bottom nozzles are welded with the guide tubes and create a rigid fuel assembly structure. The fuel pins pass though the grid plates, but are not welded to the grid plates to allow for unrestricted thermal expansion. The bottom nozzle contains four openings at the four support legs, which fit into the reactor core bottom plate, and which deliver coolant to the fuel assembly

Figure 152 shows the fuel pin design [POP2014]. The fuel pin design is similar for the LWR and CANDU designs. In fact, all LWRs and CANDUs, regardless of the manufacturer and country of origin, have a similar fuel pin design.

The fuel pin consists of a Zircaloy tube into which fuel pellets are inserted. The tube is then filled with gas and sealed. The fuel pellets have a height-to-diameter ratio of about 1.5 and have dished surfaces on both ends, which help to align them properly in the vertical direction, accommodate fuel swelling, and collect gases generated during fission. Numerous fuel pellets are located in each fuel pin and form a vertical fuel pellet stack within the pin. At the top end of the fuel pin, the fuel pellets are held tightly in a vertical direction by a spring that is installed and sealed in the tube.

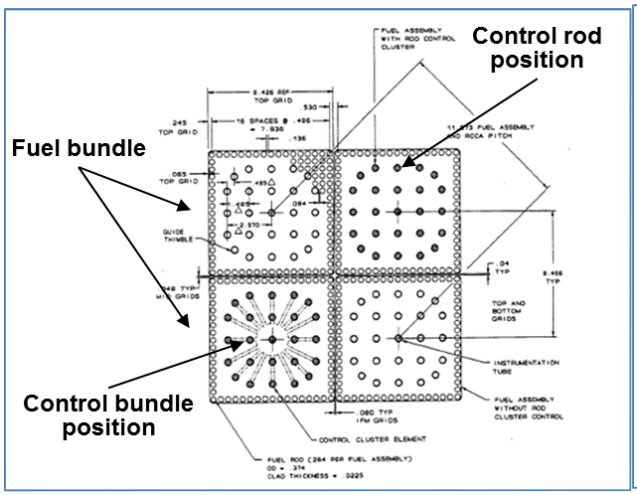

Figure 153 Typical PWR fuel assembly support spacer plates

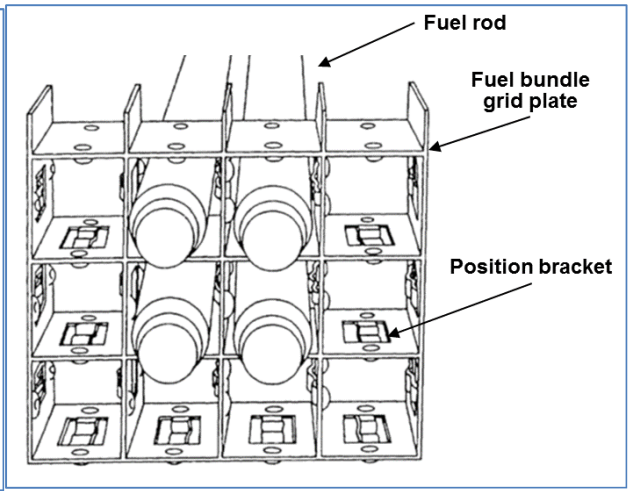

Figure 154 Typical PWR reactor control sites

Figure 153 shows the design of the fuel bundle support plates [POP2014]. Each spacer plate has dimples on each side of the square frame, which hold the fuel pin in the radial direction. The fuel pin can slide along the spacer plates in the vertical direction, thus accommodating thermal expansion. The spacer plates also have mixing vanes in the radial direction that help to enhance turbulence along the fuel pin, resulting in higher thermal margins.

Figure 154 shows cross sections of the fuel bundles and the positions of the 21 control-rod guide tubes [POP2014]. Typically, a number of positions in the fuel assembly are not filled with fuel, but instead with guide tubes that are used as sites for insertion of control rods. Although not all bundles will have control rods inserted in them, they are all made with guide tubes so that they can be installed at any core position regardless of whether they will receive control rods or not. Those assemblies that do not receive control rods will receive plug assemblies, which will insert short plug rods to block coolant bypass through the empty guide tubes (the plug assembly is similar to the assembly shown in Figure 155b, except that its plug pins are shorter).

Figure 155a shows a typical PWR control assembly design. Figure 155b shows one immovable control assembly for long-term reactivity control in certain fixed positions in the core [POP2014]. The movable control-rod assembly consists of 21 control rods held by radial arms, which are connected to the central holding shaft, which in turn is connected to a control drive assembly. The movable control assembly moves up and down vertically as driven by the reactor control system. The immovable control bundle also has 21 control rods, which are connected at the top plate. The top plate has a shaft with a spring to lock the control bundle into position so that it will remain stationary between two fuel replacement cycles.

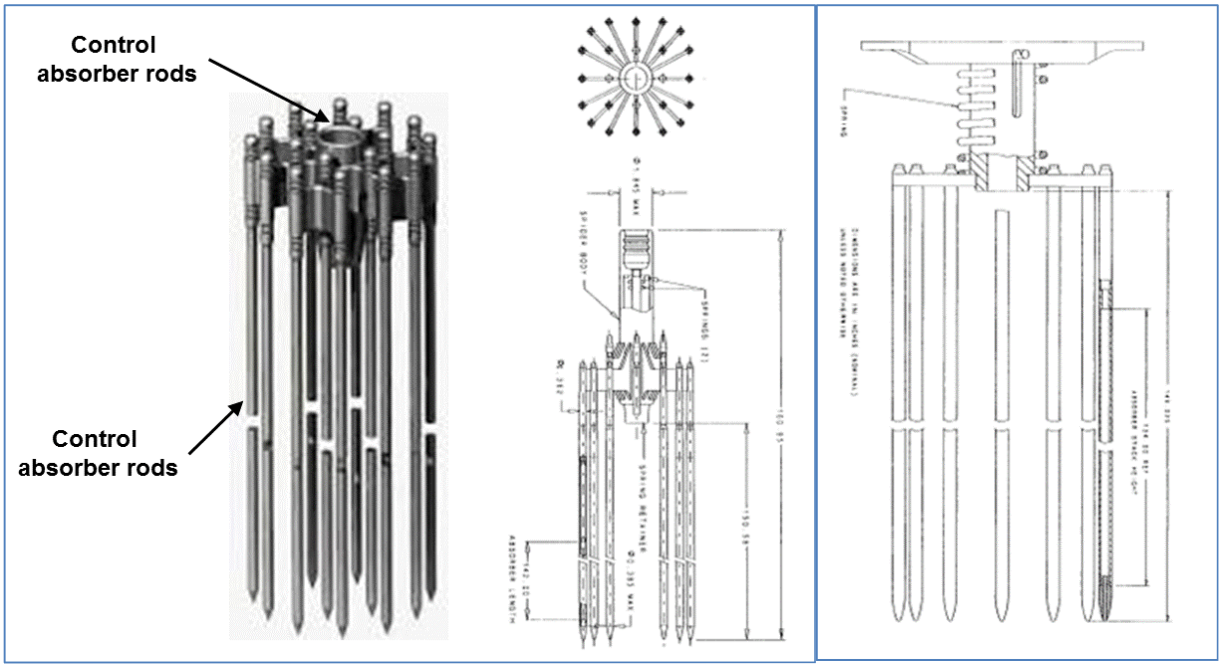

a) Movable control assembly (vertical) b) Immovable control assembly (vertical)

Figure 155 Typical PWR control assembly (cluster) design

Figure 156 shows a typical PWR control rod design [POP2014]. The control rods are of various design and material composition depending on their role in the reactor core. The control rods that are part of the reactor control system are filled with neutron-absorbing material along their full length in the core (usually a mix of 80% silver, 15% indium, and 5% cadmium, which is the material with the largest neutron-absorption capability used in modern reactors). The immovable control rods (Figure 156a) can be filled over their full length or partially filled at the top, bottom, or middle. They can also be filled with neutron-absorbing material of various thicknesses in the annulus (Figure 156a). The immovable control rods are filled with a mix of neutron-absorbing material that reduces absorption capability by neutron capture (diminishing absorption potential per unit volume with radiation exposure), or by materials that retain absorption capability over several control isotope generations.

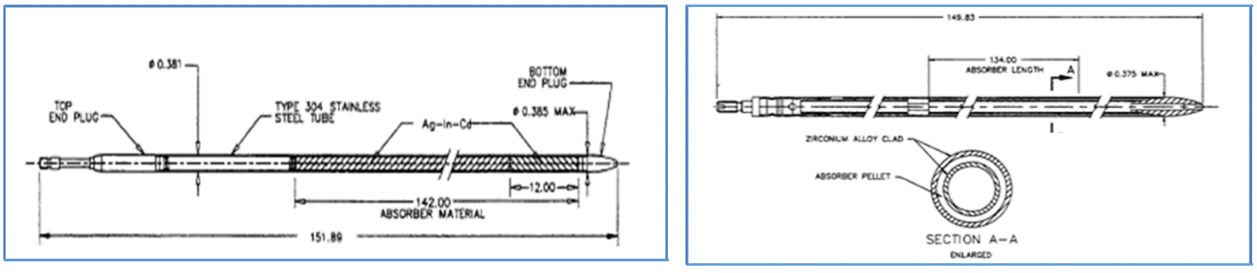

a) Solid control rod (vertical) b) Annular control rod (vertical)

Figure 156 Typical PWR control-rod design

PWR control-rod guide tubes penetrate through the reactor pressure vessel head and hold each

control assembly cluster in place. The control assemblies are driven in and out of the core by control-rod drive devices that are located outside the reactor vessel. The control-rod shaft is located in the guide tubes that extend through the reactor cap, in the space above the core, and holds the control-rod top. Special attention is devoted to the seals of the control-rod guide tubes and assemblies because they are located in the vessel at a pressure of 15 MPa, whereas their shafts and guide tubes are at atmospheric pressure. Because of the large pressure difference between the inside of the vessel and the atmosphere outside of the reactor vessel, special attention is devoted to preventing control-rod ejection from the vessel, which can create a severe large positive reactivity insertion.

13.2.8 Reactor core design

The fuel assemblies in the reactor core are typically 3.6–4.2 m long and have from 14 x 14 to 19 x 19 fuel rod positions. There are typically 120–170 fuel assemblies in the core, depending on the reactor thermal power and reactor type, arranged in a square or hexagonal lattice in the core. The fuel assemblies are enveloped by a metal shroud which follows the core shape at the sides of the peripheral assemblies (see Figure 150a). The metal shroud does not permit fluid movement in the radial direction, but fluid movement in the radial direction is not restricted by the fuel assemblies themselves.

The core flow is in the upward direction, which in the absence of forced circulation (when the primary pumps are off) enhances the potential for natural circulation, thus removing core decay heat.

13.2.9 WWER reactor design

The WWER reactors are of Russian design, and their design follows in principle the original U.S. PWR design [KNI2002, KOK2009,. Figure 157a shows an isometric view of the primary cooling loop and the reactor vessel. The primary cooling system is similar to the PWR primary cooling system, with three or four primary loops depending on reactor power. There are some differences in the fuel assembly design, the most significant being that it is not open in the radial direction because it is surrounded by guide tubes. Figure 157b shows a reactor vessel similar to the American PWR vessel design. Figure 157c shows a WWER steam generator of horizontal design and containing double horizontal U-tube assemblies on the primary side connected at the middle of the steam generator. In addition, steam is collected at the top of the steam generator in a separate steam collector tube.

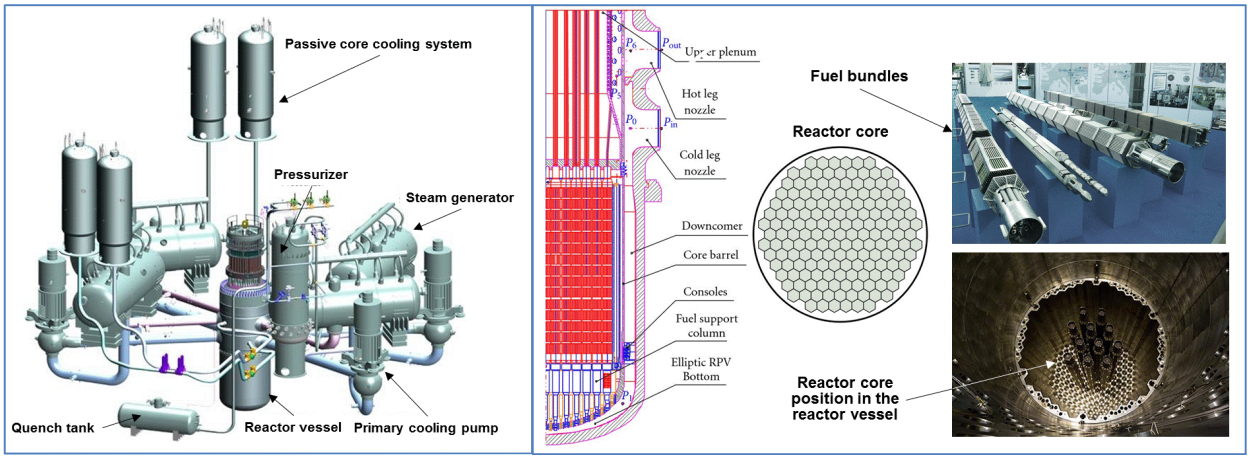

a) Primary loop b) Reactor vessel

Figure 157 Russian WWWR reactor design

13.3 Boiling water reactors

Boiling water reactors (BWRs) also originate from the U.S. nuclear industry, but unlike PWRs, they are designed to allow coolant boiling in the reactor vessel, and hence they do not have a separate heat exchanger (steam generator) for steam production. There are numerous BWRs in operation around the world, although fewer than the PWR designs. BWRs feature a lower primary heat transport system pressure than PWRs for the same power output, which results in decreased thickness of the reactor pressure vessel (which amounts to an economic benefit). Figure 158 shows two BWR reactor versions, BWR/4 and BWR/6 [KNI2002, KOK2009, LAH1977, POP2014].

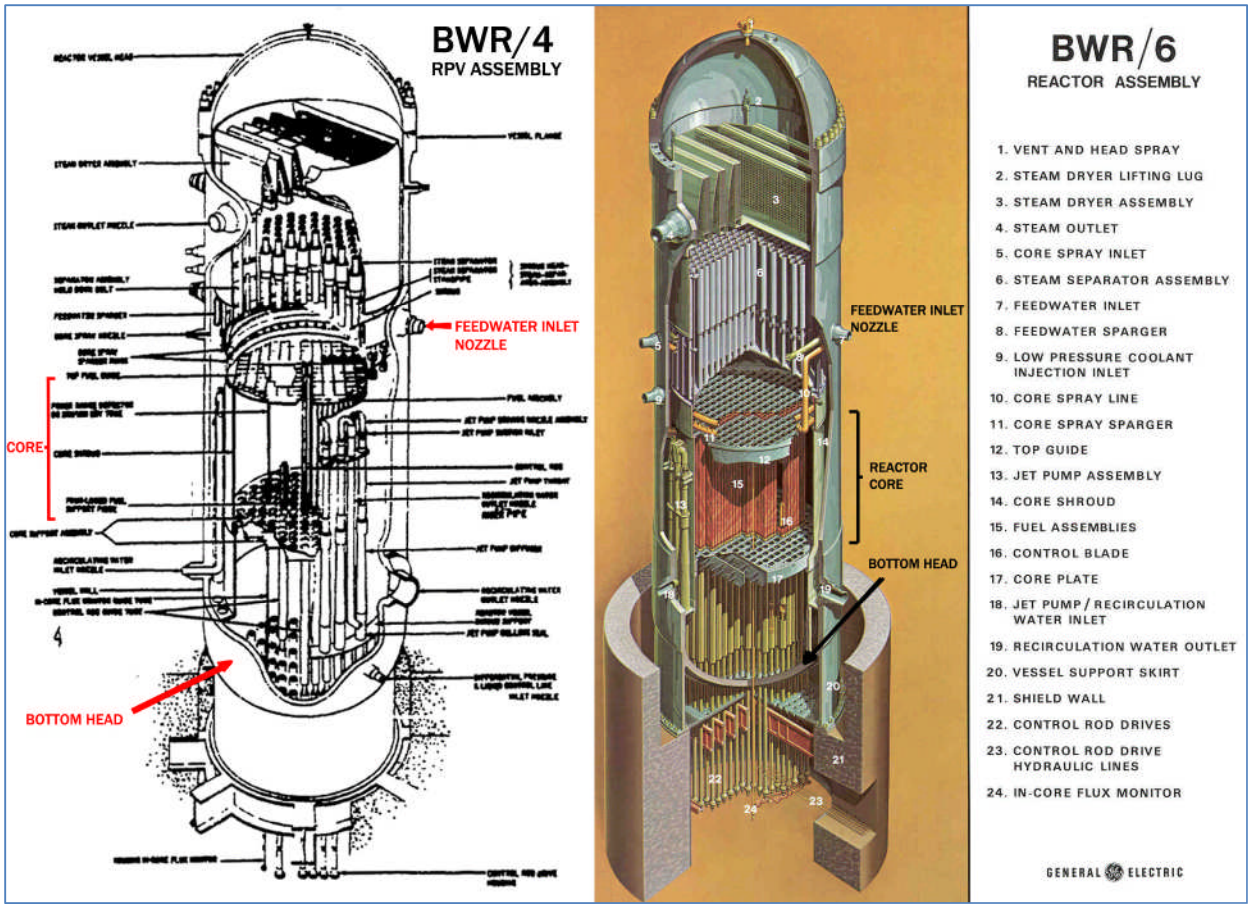

Figure 158 BWR reactor design

BWR plants have been designed in two main design streams: direct-cycle and dual-cycle. In a direct-cycle plant, which is the most common in operation, steam is produced in the steam generator and is moved to the turbine generator as dry steam. In a dual-cycle plant, in addition to steam production in the reactor, steam is also produced in a secondary steam generator fed by saturated water from the moisture separator.

Figure 159 shows a simplified flow diagram of a direct-cycle BWR system [LAH1977]. The direct cycle has the advantages of lower capital cost and simplicity, which increases system reliability. There is no separate steam generator in the cooling system because the reactor generates steam. Older BWR designs could not follow the load, but are to a certain extent self-controlling due to the negative void reactivity. Modern BWR designs are capable of load following by coolant recirculation control.

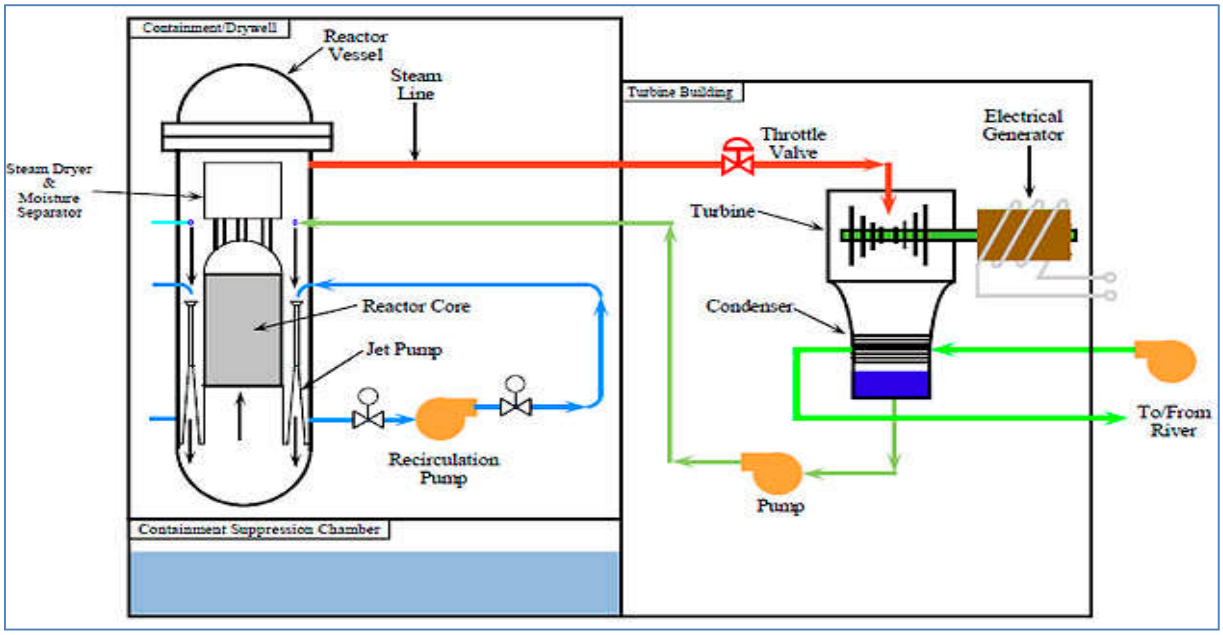

Figure 159 Typical BWR reactor vessel coolant circulation

With this arrangement, the turbine plant is "active" due to activity induced in the reactor coolant (primarily N-16). As a result, the turbine generator plant is less accessible during operation; fortunately, however, this activity decays quickly following shutdown, permitting normal direct access for maintenance.

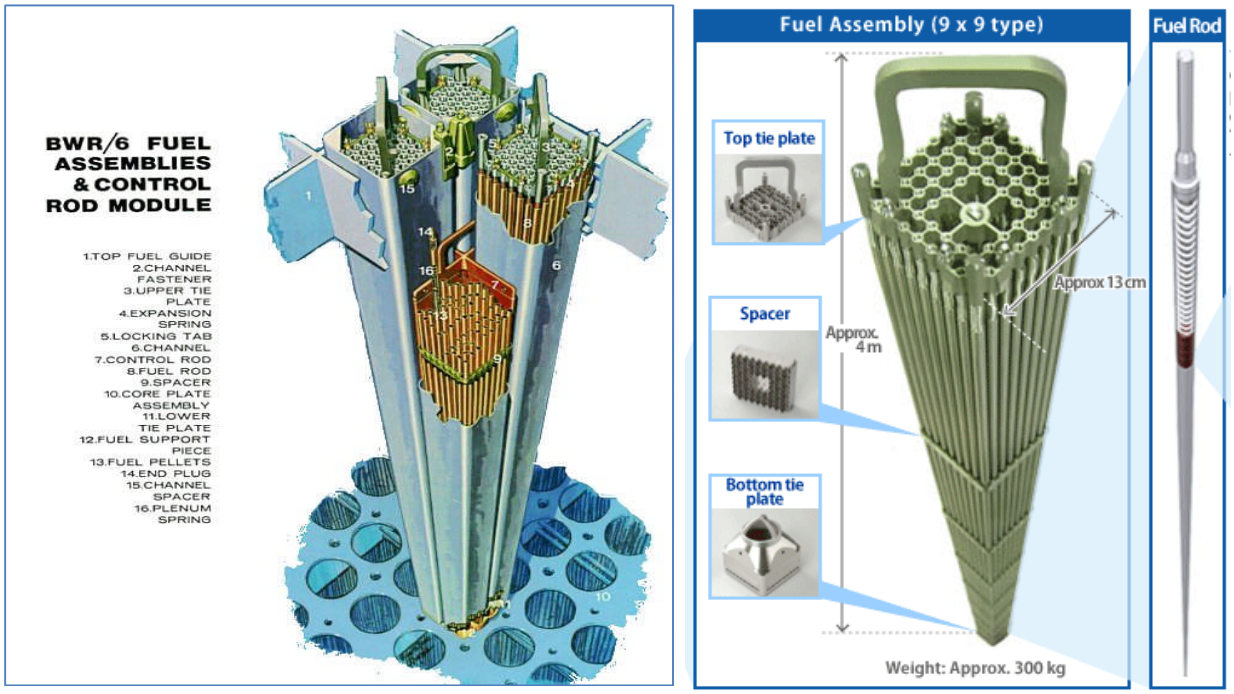

Figure 160 BWR reactor fuel assemblies in the core

The typical BWR reactor vessel, shown in Figure 158, has the steam production and collection part in the upper part of the vessel, the reactor core in the middle of the vessel, and the control

assembly and instrumentation access through the reactor bottom and the lower plenum. The reactor core has an active length of typically 3.5–4 m, similar to PWRs. The core contains between 500 and 800 fuel assemblies, each containing arrays of fuel rods with a similar design to those in PWRs.

Figure 159 shows the coolant circulation in the BWR core. The recirculation system consists of recirculation pump loops located on the sides of the reactor vessel. In the BWR design illustrated, the reactor vessel downcomer jet internal pumps are located on the outer core periphery, arranged in pairs, with each having a common inlet riser. The driving flow from the external pumps passes through the jet pump nozzles and acquires high velocity and momentum. The momentum exchange entrains the recirculation flow, usually called suction flow. The combination of the external pump-driven flow and the suction flow enters the throat of the jet pump, thus ensuring adequate flow through the core. The jet pump design has the advantages of fewer moving parts, higher reliability, and robustness in accident situations. The feedwater inlet is in the upper part of the core, and the coolant falls down by gravity towards the inlet of the jet pumps.

BWR fuel assemblies are typically of square design (see the left part of Figure 160), but the fuel rods are situated in a square flow tube which does not allow flow mixing in the radial direction (see the right part of Figure 160) [KNI2002, KOK2009]. Because the BWR reactor is designed to operate with saturated water that boils in the core, a good level of turbulence is already achieved, and therefore there is no need to promote radial mixing to enhance turbulence, as in the PWR design. The left side of Figure 160 shows a BWR fuel assembly with a square tube and the spacer grids inside holding the fuel pins.

Figure 161 shows a cross section of four fuel assemblies, on the left 10 x 10, and on the right 7 x 7 fuel rod arrays [KNI2002, KOK2009, LAH1977, POP2014]. The cruciform control assembly is located between the fuel bundles. Clearly, between the fuel assemblies, a gap is maintained for the control assembly to move in a vertical direction through the core.

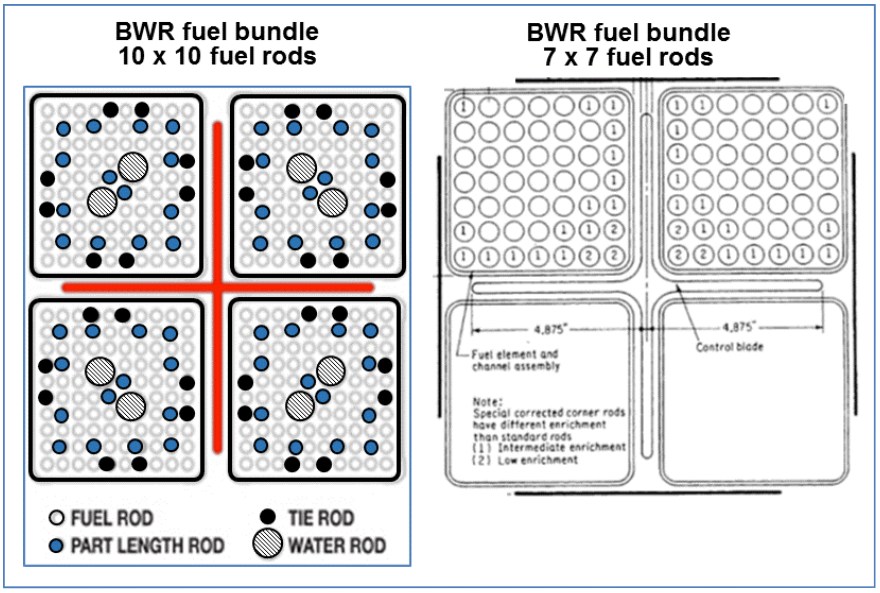

Figure 161 BWR fuel and control assemblies

The control assembly is moved through the core from the bottom of the reactor. Therefore, the control assembly holding the plate and drive mechanisms is at the bottom of the core and needs to work against gravity.

13.4 Gas-cooled reactors

Gas-cooled reactors (AGRs) have been in operation for many years and were promoted by the U.K. nuclear industry due to their potential for higher thermal efficiency and relatively low stored energy in the primary coolant, which reduced containment requirements. AGRs were primarily designed and built in the United Kingdom. They use gas as the reactor coolant and natural or enriched uranium as fuel. In recent years, some of these reactors have been shut down, and others are planned for shutdown soon. The U.K. nuclear industry has abandoned this design and does not plan to use it for future reactors. This section provides a brief overview of the AGR reactor type and a brief history of its development in recent decades.

13.4.1 Magnox reactors

Magnox reactors are graphite-moderated, CO_2 gas-cooled reactors fuelled with natural uranium metal clad with a magnesium alloy called Magnox. They derived their generic name from this last feature. Figure 162 shows a schematic arrangement of one version of this reactor type [POP2014].

This type of reactor was pioneered by the British and French and was a natural outgrowth of earlier air-cooled, graphite-moderated research and plutonium production reactors. A significant number were built in Britain and France, with a few exported to other countries. Early versions used steel reactor pressure vessels with external heat exchangers (boilers) and gas circulating blowers. Later versions, as shown in Figure 163, used pre-stressed concrete pressure vessels incorporating the reactor core, heat exchangers, and coolant circulation blowers. This was primarily a cost reduction measure, although safety advantages in terms of low risk of coolant system rupture were also claimed.

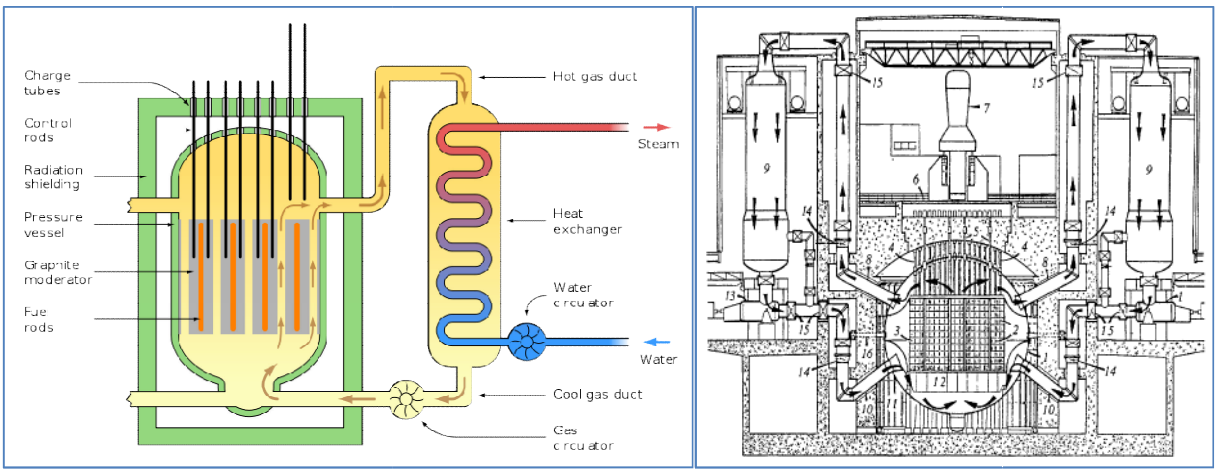

Figure 162 Typical Magnox reactor design

Primarily because of coolant temperature limitations imposed by the uranium metal fuel and the

Magnox cladding, only relatively modest turbine steam conditions are achievable, limiting the station overall efficiency to ~30%.

As is typical of all natural uranium power reactors, the Magnox reactors are fuelled on-load. This is necessary because large quantities of excess reactivity, in the form of additional U-235, are not "built into" the new fuel.

The in-service availability of the Magnox reactors has proven to be relatively good. On-load refuelling helps in this regard. Nevertheless, their relatively high capital cost and relatively modest achievable fuel utilization has led to the abandonment of plans for constructing further reactors of this type. Presently, in the United Kingdom, all Magnox reactors are shut down and undergoing decommissioning.

13.4.2 AGR reactors

The AGR (advanced gas-cooled reactor) was developed in the United Kingdom as a successor to the Magnox line of reactors [POP2014]. A number of these reactors were successfully operating in the United Kingdom, but presently they are aging and require replacement. They differ from the latest Magnox reactors primarily in the fuel used. The fuel is UO_2 clad in stainless steel. This design permits higher fuel temperatures and coolant temperatures to be achieved, leading to conditions similar to those in conventional fossil-fuel steam plants (16.5 MPa, 550°C).

The fuel is designed as a cluster of small-diameter rods, which permits relatively high power levels. This reduces the size of the reactor core relative to the Magnox reactors, where the fuel is in the form of large single elements. However, because of these fuel changes, the AGR requires some fuel enrichment. Figure 163 shows a view of an AGR reactor type diagram.

The British have decided that the AGR is not fully competitive with other types of power reactors. Hence, this design, like the Magnox type, appears to be "dead-ended" and is being replaced by other reactor types, such as advanced PWRs and advanced BWRs.

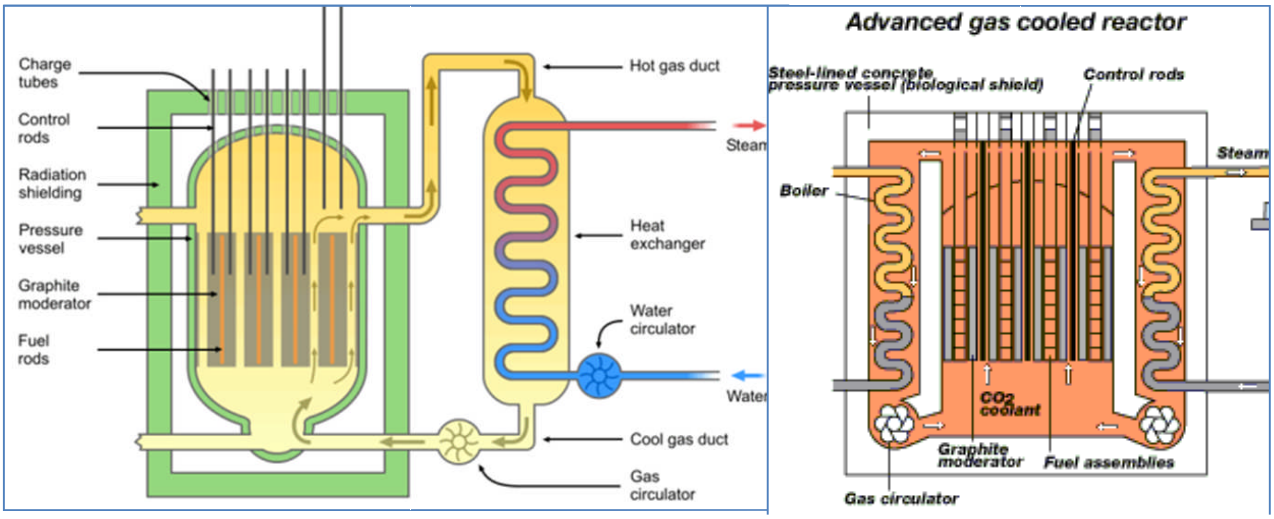

Figure 163 Typical AGR reactor design

13.4.3 HTGCR Reactors

The high temperature gas cooled reactor (HTGCR) differs from the AGR in two major respects [POP2014]. The first is the use of helium as the coolant in place of CO_2. This permits even higher coolant temperatures without inducing a chemical reaction with the graphite moderator. The second relates to the fuel. In very early designs, the fuel was supposed to be fully enriched (93%) U-235 mixed with thorium. Thorium absorbs neutrons and is converted, after a radioactive decay chain, to U-233, which is fissile. As a result, the reactivity of the fuel remains high even after very long irradiation, the U-233 replacing the U-235 as the latter is burned up. The fuel is in the form of mixed carbides. It is manufactured in very small spheres which are coated with pyrolytic graphite, the latter providing the cladding. These spheres are compacted into holes in large graphite assemblies, forming an integral fuel and moderator assembly.

Figure 164 shows an advanced version of the HTGCR reactor design currently being developed as part of the Generation IV development efforts. The very high coolant temperatures achievable lead to high steam cycle efficiencies, or alternatively make possible the ultimate use of gas turbines directly driven by the coolant. The development of the direct-cycle gas turbine version would be particularly attractive in this regard.

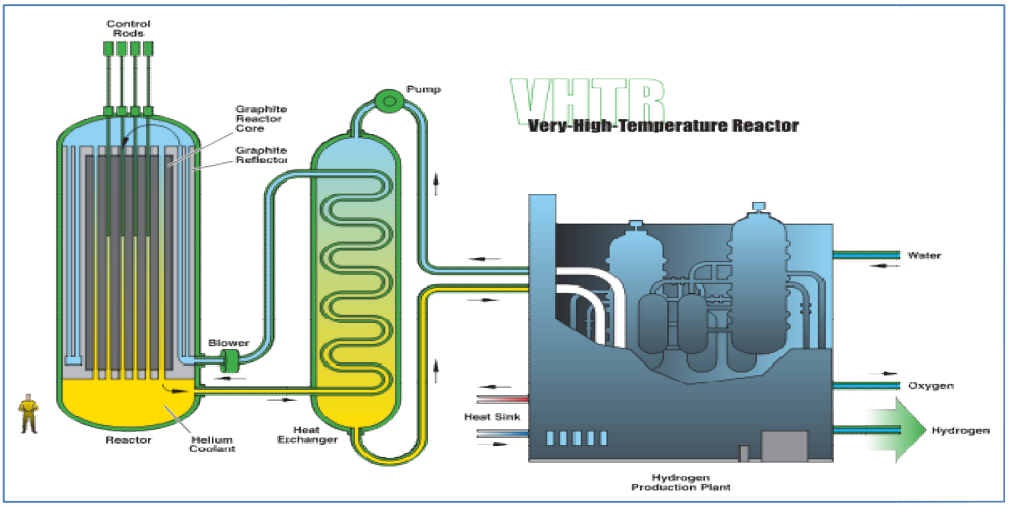

Figure 164 Typical HTGCR reactor design

13.5 Channel-type reactors

13.5.1 SGHWR reactor

The steam generating heavy water reactor (SGHWR) has been developed and operated in the United Kingdom, Japan, and Italy for a number of years. The best example of this reactor type that operated successfully in Japan for more than 20 years is the Fugen reactor (currently decommissioned) [POP2014].

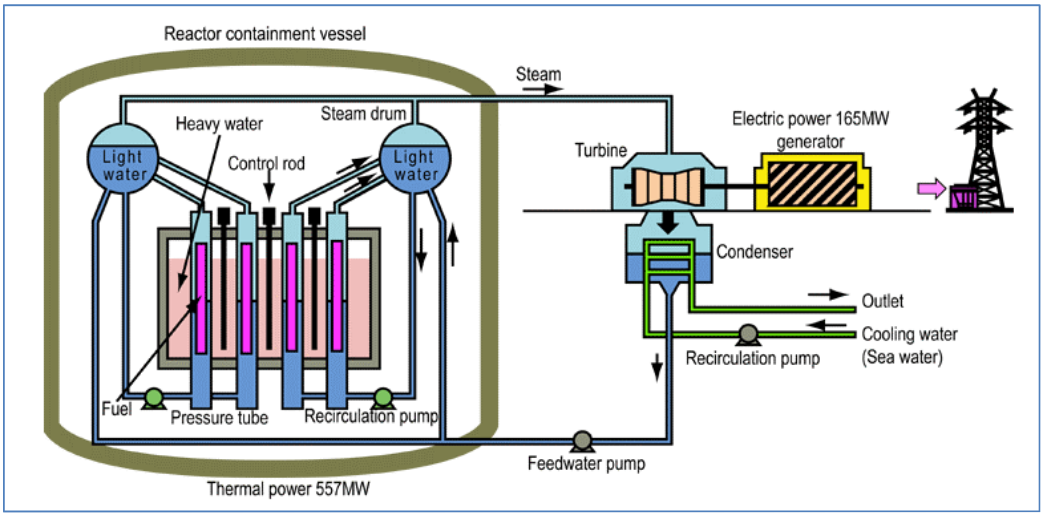

Figure 165 SGHWR reactor

Figure 165 shows a schematic of this reactor type. The heat transport system contains vertical pressure tubes, light water coolant, heavy water moderator in a calandria vessel, and recirculating pumps used to return water from steam drums to the lower end of pressure tubes. The fuel was low-enriched uranium with on-power refuelling. The reactor heat transport system was located in a containment building, thus providing protection during accidents.

Another type of SGHWR design was the CANDU Gentilly-1 reactor, which was shut down and is now decommissioned. It also used vertical pressure tubes with natural uranium, heavy water moderator, and light water coolant.

13.5.2 CANDU reactor

The CANDU fuel channel type reactors have been developed in Canada, have achieved great commercial success around the world, and are being still developed and prepared for new builds in Canada and internationally. Figure 2 shows the CANDU reactor cooling systems and Figure 3 the reactor heat transport system and moderator cooling system.

13.5.3 RBMK reactor

The Russian version of the channel reactor is the RBMK reactor (an acronym for High Power Channel Type Reactor in Russian) [POP2014]. This reactor design was built in Russia and in neighbouring states in the 1980s and 1990s. The RBMK reactors had two basic power levels, one around 1000 MWe, the other around 1400 MWe.

Following the Chernobyl accident, many of these reactors were shut down, and they continue to be shut down, with the exception of a few, such as the Kursk and Leningrad reactors that will continue to operate until the early 2020s. The RBMK design was abandoned by the Russian nuclear industry after the Chernobyl accident. However, many design changes have been implemented in the operating units to improve their safety during their remaining operational life.

Figure 166 shows the reactor cooling systems (primary, secondary, and tertiary), a view of the

reactor core, and a cross section of a RBMK plant. The reactor core is very large (21.6 x 21.6 x 25.5 m). The vessel contains the graphite stack filled with a helium-nitrogen mixture to ensure an inert atmosphere. The reactor fuel is UO_2 with a fuel rod design similar to the LWR design, with 2%–4% enrichment in U-235. Refuelling is performed on-power to achieve a better balance of neutron flux and core utilization and to optimize production of Pu-239.

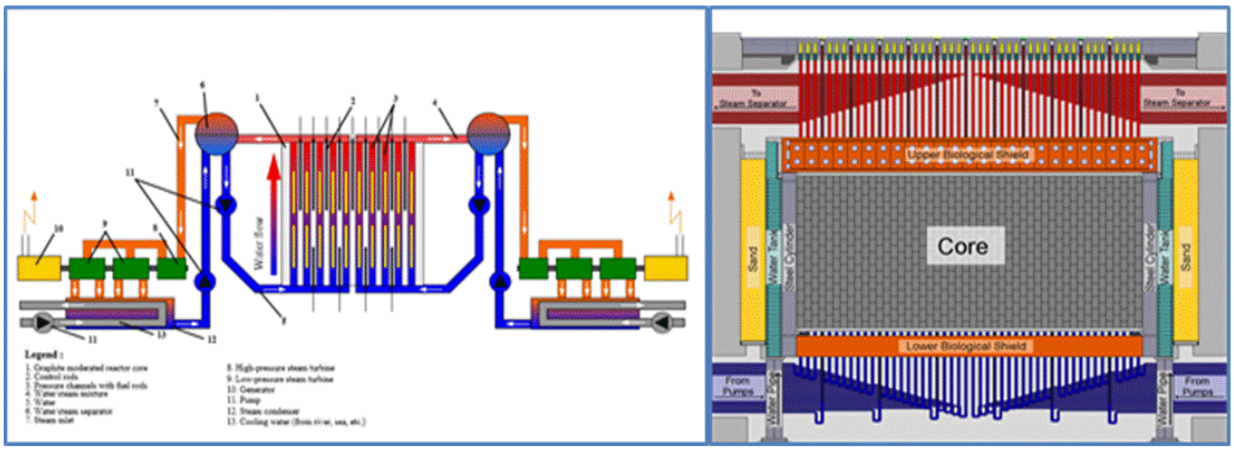

Figure 166 RBMK reactor design

The reactor has two independent cooling circuits, each with four primary circulation pumps (including one stand-by). The cooling water is fed to the reactor through lower water lines to a common header, which is split into 22 distribution headers, each feeding 38–41 fuel channels, in which water boils. The mixture of water and steam is conveyed by the upper steam lines, one for each fuel channel, from the reactor top to the steam separators. Steam with 15% quality is taken from the separators by two steam collectors per separator, combined, and then conveyed to the turbine hall. The nominal total flow through the core is ~46,000–48,000 m^3/h. The nominal temperature of the water at the inlet of the reactor is about 270°C and the outlet temperature 284°C, at a pressure of 6.9 MPa.

The fuel channels consist of Zircaloy pressure tubes that pass through the channels in the centre of the graphite blocks. There are 1661 fuel channels in the core and 211 control channels. There is only a small clearance between each pressure channel and a graphite block, which makes the design vulnerable to damage. If a pressure tube channel deforms due to high internal pressure in an accident situation, the deformation can cause significant pressure straining of the graphite blocks and lead to damage, which can then possibly propagate to neighbouring channels.

Light water was used as coolant and graphite as moderator. This combination of core materials leads to a highly positive void coefficient, which results in high power excursions in the case of a loss of coolant accident.

Because of certain similarities to the CANDU design, and because of the unpopular experience with the RBMK reactors, CANDU has often been criticized as potentially vulnerable in the same way as the RBMK reactors. As described in Chapter 16, many studies have been performed since the Chernobyl accident and have demonstrated that CANDU has different physical

characteristics that make the CANDU design behave quite differently from the RBMK reactors, and that therefore CANDU reactors are not as vulnerable in accidents as RBMK reactors.

13.6 Fast breeder reactors

Liquid metal fast breeder reactors (LMFBRs) were designed many years ago, and some were built as prototype versions in the United States, France, and Russia, and later by other countries as part of pilot programs. These pilot-prototype versions had varying degrees of operational success, and therefore many were shut down or restarted over the past several decades. These reactors use a fast neutron spectrum to maintain the fission chain reaction and are cooled by molten metal coolants. Figure 167 shows the design sketch of a typical pool-type (left) and a loop-type fast breeder reactor [POP2014].

Whereas all the reactors previously described are of the thermal type, i.e., the fissions in the fuel are primarily induced by thermal neutrons, it is also possible to sustain a chain reaction with high-energy neutrons, i.e., fission neutrons, provided that the fuel is highly enriched with fissile material such as U-235 or Pu-239. Furthermore, on average, more than two neutrons are born per fission. One of these neutrons is required to induce the next fission, leaving a surplus of somewhat more than one neutron which can be absorbed by a “fertile” material such as U-238, producing fissile Pu-239. It is therefore possible to produce fissile material as rapidly as it is used up; this is called “breeding”. In fact, it is possible to produce more fissile material than is used because the average number of neutrons produced per fission is greater than 2. The excess is referred to as the “breeding gain”. This can be achieved only if the neutron economy is high, i.e., if relatively few neutrons are wasted.

This possibility of breeding is a very attractive means of extending the power available from uranium because less than 1% of natural uranium is fissile. If a substantial part of the other ~99% could be converted to fissile Pu-239 as a by-product of reactor operation, then the world’s uranium reserves could be stretched enormously. The fast breeder reactor is one way of doing this, which explains the widespread interest in this concept.

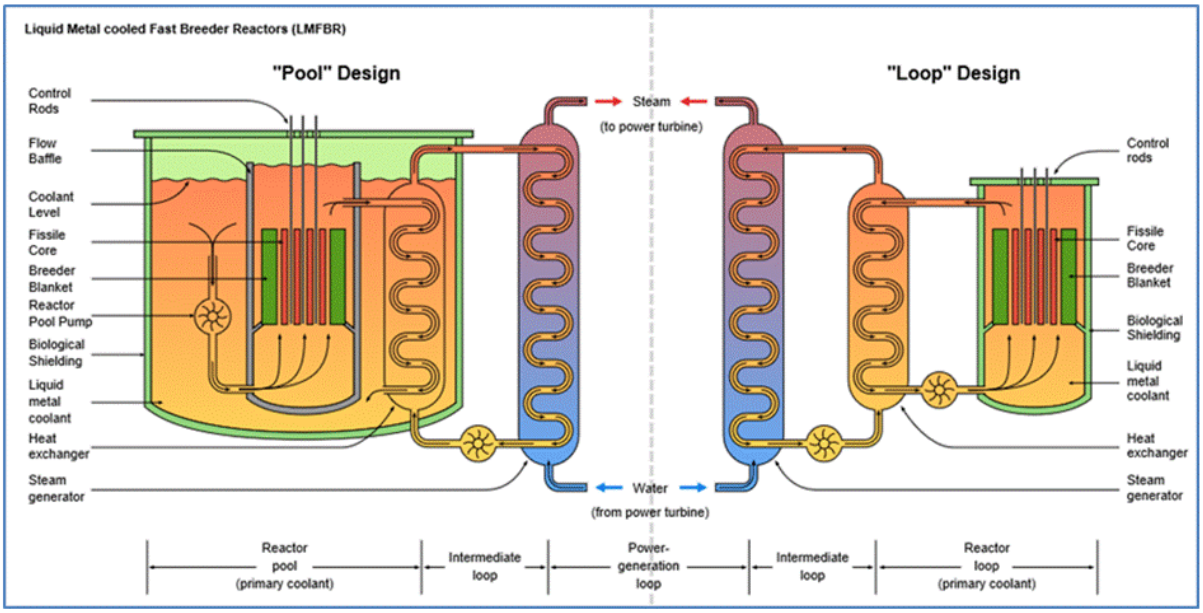

Figure 167 Fast reactor design

The basic arrangement of a liquid metal-cooled fast breeder reactor is shown in Figure 167. The reactor core consists of a closely packed array of highly enriched (U-235 or Pu-239) oxide rods clad in a high temperature-resistant metal. This core is surrounded on all sides by a "breeder blanket" of fertile U-238 rods (also in clad oxide form). The excess fission neutrons produced in the core "leak" out of the core and are absorbed in the blanket rods. Both the core and blanket are cooled by a flow of liquid sodium. This sodium is in turn cooled in heat exchangers and returned to the reactor by more or less conventional centrifugal pumps. The heat exchangers are cooled by a second flow of sodium, which in turn is cooled in a second set of heat exchangers, which produce steam for the turbine. The purpose of this intermediate sodium loop is to provide isolation between the sodium cooling the reactor and the steam and water in the turbine cycle, thereby practically eliminating the in-leakage of water and preventing it from contaminating the reactor coolant.

Despite this intermediate loop, the reactor operating temperature is sufficiently high to permit steam to be produced under modern fossil-fuelled plant conditions (~16.5 MPa with a single reheat to 540°C). There are a number of new Generation IV designs for fast breeder reactors, but none of them has been built yet, even as a prototype.

CHAPTER 7

Thermalhydraulic Analysis

prepared by:
Dr. Wm. J. Garland, Professor Emeritus,
Department of Engineering Physics,
McMaster University, Hamilton, Ontario, Canada

Summary:

This chapter is concerned with thermalhydraulic analysis of the process systems that are required to transport heat energy away from the nuclear reactor source and transform this heat energy into useful work (generally electrical energy. Thermal hydraulic system behaviour is largely determined by the simultaneous solution of the equations that govern the four variables (flow, pressure, density and enthalpy). The general mass, energy and momentum conservation equations are presented in general terms and are simplified to the common approximate forms used in systems modelling. The equation of state that is required for closure is explored with particular emphasis on implementation. Process system solution algorithms are investigated.

Table of Contents

List of Figures

List of Tables

1 Introduction

This chapter is concerned with thermal hydraulic analysis of the process systems that are required to transport heat energy away from the nuclear reactor source and transform this heat energy into useful work (generally electrical energy). Thermal hydraulic design of the process systems is covered in the previous chapter. Design and analysis are, of course, tightly coupled. Nuclear systems design is guided by analysis results. Analysis, in turn, is performed on a specific design to determine its performance. It is a complex, iterative dance. Design and analysis of the reactor process involves a number of interrelated systems:

- reactor core
- heat transport system
- steam generators
- turbines
- pressure control system
- coolant inventory control systems
- power control systems;

a number of system components:

- valves
- pumps
- pipes
- vessels
- heat exchangers;

and a number of engineering and science disciplines:

- reactor physics
- heat transfer
- fluid mechanics
- thermodynamics
- chemistry
- metallurgy
- control
- stress analysis.

The heat transport system (HTS) is of central importance since it is the interface between the heat source and the heat sink. Good HTS performance is essential to reactor integrity, plant performance and safety. Herein, the scope is limited to the modelling tools used in thermal hydraulic analysis of the HTS. This chapter is a systems level chapter, not a components level one. Component modelling is limited to approximate models that are appropriate for systems analysis. Detailed multidimensional modelling of complex components such as steam generators, pumps, calandria vessels, headers, etc., are not attempted.

This chapter is primarily about the interplay the two main actors in hydraulic systems: flow and

pressure. But because we are dealing with systems involving the transfer of heat, local density and enthalpy determine the pressure. Hence, thermal hydraulic system behaviour is largely determined by the simultaneous solution of the equations that govern these four variables (flow, pressure, density and enthalpy).

1.1 Learning Outcomes

The overall objectives for this chapter are as follows:

- The student should be able to explain the roles played by mass, flow, energy and pressure in thermalhydraulic simulation.
- The student should be able to derive appropriate forms of the governing equations, and develop a flow diagram and pseudo-code for a thermalhydraulic system simulator from first principles.
- The student should be able to build a thermalhydraulic system simulator from first principles.
- The student should be able to identify the terms and symbols used in thermalhydraulics.
- The student should be able to distinguish between the differential and integral form and be able to choose, with justification, the correct form to use in various situations.
- The student should be able to recall typical values and units of parameters.
- The student should be able to recognize key physical phenomena.
- The student should be able to recognize the coupling between mass, momentum, energy and pressure in thermalhydraulic systems.
- The student should be able to choose approximations as appropriate (# of dimesions, transient or steady state, averaging, spatial resolution, etc.) with justification.
- The student should be able to develop, with justification, a node-link diagram given a thermalhydraulic system.
- The student should be able to construct the matrix form of the conservation equations for a given node-link structure.
- The student should be able to calculate any dependent thermodynamic property given any two independent state variables using (a) the steam tables, (b) supplied codes, (c) supplied curve fits to the steam tables.
- The student should be able to develop a flow diagram and pseudo-code for the calculation of P and T given density and enthalpy.
- The student should be able to explain the pressure and temperature response of a volume of fluid to perturbations given the F and G functions.
- The student should be able to develop a flow diagram and pseudo-code for the rate method of the equation of state.
- The student should be able to develop a computer code implementing the rate method of the equation of state.
- The student should be able to model a simple thermalhydraulic network using the integral form of the conservation equations and the rate form of the equation of state. The student should be able to check for reasonableness of the answers.

- The student should be able to apply the various numerical methodologies (fully explicit to fully implicit) to special cases of the thermalhydraulic system equations.
- The student should be able to produce a general node-link code based on the cumulative concepts presented in this course.
- The student should be able to evaluate the efficacy of the various numerical algorithms.

1.2 The Chapter Layout

To lay the groundwork for thermal hydraulic systems analysis, Section 2 presents the general mass, energy and momentum conservation equations in very general terms and proceeds to derive the common approximate forms used in systems modelling. Section 3 shows how to model hydraulic piping networks as a system of nodes connected by links and elaborates on the appropriate equation forms for these node-link approximations. The conservation equations requires a relationship between pressure, temperature, density and energy (the equation of state) for closure. In Section 4, the equation of state is explored with particular emphasis on implementation. Sections 5 and 6 cover numerical considerations. Explicit, semi-implicit and implicit techniques are presented. At this point the reader is almost ready to conduct thermal hydraulic simulations. Chapter 6 on Thermalhydraulic design completes the picture by providing heat transfer and hydraulic correlations that are needed for the simulations. A survey of industrial strength tools is outside the scope of this chapter as is a discussion of phenomena identification and evaluation, and code verification and validation.

As with design, there is no one best model for a given analysis task, nor is there even one best solution procedure. Good simulation is evolutionary; we learn from past successes and failures, incorporate the latest experimental, theoretical and numerical results, employ sound engineering principles and a solid understanding of the basics to engineer each and every new simulation tool.

2 Basic Equations for Thermalhydraulic Systems Analysis

2.1 Introduction

This section presents the basic mass, momentum and energy equations used in typical computer codes for thermalhydraulic simulation. The equations are derived from first principles and the necessary approximations lead to the requirements for empirical correlations. Closure is obtained by the equation of state.

The known territory of the basic mass, energy and momentum conservation equations (Bird et al [BIR60]) is explored, herein, from the perspective of thermalhydraulic systems analysis for nuclear reactors. See also [CAR95] for seminal coverage of this topic.

Invariably in the modelling of fluids, the conservation equations are cast in one of two main forms (Currie [CUR74]): integral or distributed approach. The distributed (differential) form sees infrequent use in the analysis of thermalhydraulic systems since the cost and complexity of such a detailed analysis on even a single complex component of a system is enormous, which makes this route to the analysis of systems of such complex components unrealizable. Recourse is generally made to the integral or lumped form so that inter-relationships of various components comprising a system can be simulated. Necessarily, the models used for the individual components are much simpler than that of the detailed models based on the distributed approach. Great care must be taken to ensure that the simpler models of the integral approach are properly formulated and not misused.

It behooves us, then, to develop the models used in thermalhydraulic systems analysis from first principles. This will provide a traceable and verifiable methodology to aid development and validation of system codes, to elucidate the necessary assumptions made, to show pitfalls, to show the common roots and genealogy of specific tools like FLASH [POR69], SOPHT [CHA75a, CHA75b, CHA77a, CHA77b, SKE75, SKE80], RETRAN [AGE82], FIREBIRD [LIN79], CATHENA [HAN95], etc., and to help guide future development.

The exploration proceeds by first establishing and discussing the general principle of conservation. Next, this general principle is applied in turn to mass, momentum and energy to arrive at the specific forms commonly seen in the systems approach. Closure is then given via the equation of state and by supporting empirical correlations. Finally, the ideas developed are codified in a diagrammatical representation to aid in the physical interpretation of these systems of equations and to provide a summary of the main characteristics of fluid systems.

2.2 Conservation

We start, both historically and pedagogically, with a basic experimental observation:

"CONSERVATION".

This was, and is, most easily understood in terms of mass:

"WHAT GOES IN MUST COME OUT UNLESS IT STAYS THERE

OR IS GENERATED OR LOST SOMEHOW".

Although this should be self-evident, it is important to realize that this is an experimental observation.

If we further assume that we have a continuum, we can mathematically recast our basic experimental observation for any field variable, ψ:

$$\frac{D}{Dt}\iiint_V \psi \, dV = \iiint_V \Gamma dV + \iint_S \mathbf{S}\cdot\mathbf{n}\, ds \tag{1}$$

where

D/Dt = substantial derivative[1] = change due to time variations plus change due to movement in space at the velocity of the field variable, ψ,

V = arbitrary fluid volume,

Γ = net sum of local sources and local sinks of the field variable, ψ, within the volume V,

ψ = field variable such as mass, momentum, energy, etc.,

t = time,

s = surface bounding the volume, V,

n = unit vector normal to the surface, and

S = net sum of local sources and local sinks of the fluid variable, ψ, on the surface s.

We can now use Reynold's Transport Theorem [CUR74]:

$$\frac{D}{Dt}\iiint_V \psi \, dV = \iiint_V \frac{\partial \psi}{\partial t}\, dV + \iint_S \psi \mathbf{v}\cdot\mathbf{n}\, ds \tag{2}$$

where

$\partial/\partial t$ = local time derivative, and

v = velocity of the field variable,

to give

$$\iiint_V \frac{\partial \psi}{\partial t}\, dV = -\iint_S \psi \mathbf{v}\cdot\mathbf{n}\, ds + \iiint_V \Gamma\, dV + \iint_S \mathbf{S}\cdot\mathbf{n}\, ds\,. \tag{3}$$

In words, this states that the change in the conserved field variable ψ in the volume V is due to surface flux plus sources minus sinks. We can use another mathematical identity (Gauss'

[1] For a lucid discussion of the three time derivatives, $\frac{\partial}{\partial t}$, $\frac{D}{\partial t}$, $\frac{d}{dt}$, see [BIR60, pp 73-74].

Divergence Theorem):

$$\iint_S \mathbf{A} \cdot \mathbf{n}\, ds = \iiint_V \nabla \cdot \mathbf{A}\, dV\,, \tag{4}$$

where

A = any vector, such as velocity, and

∇ = Del operator (eg. $\nabla = \partial/\partial x\, \mathbf{i} + \partial/\partial y\, \mathbf{j} + ...$) .

Thus equation 3 can be rewritten:

$$\iiint_V \frac{\partial \psi}{\partial t}\, dV = -\iint_S \nabla \cdot \boldsymbol{\psi}\, \mathbf{v}\, dV + \iiint_V \Gamma\, dV + \iiint_V \nabla \cdot \mathbf{S}\, dV\,. \tag{5}$$

If we assume that this statement is universally true, i.e. for any volume within the system under consideration, then the following identity must hold at each point in space:

$$\frac{\partial \psi}{\partial t} = -\nabla \cdot \boldsymbol{\psi}\, \mathbf{v} + \Gamma + \nabla \cdot \mathbf{S}\,. \tag{6}$$

This is the distributed or microscopic form. Equation 3 is the lumped or macroscopic form. They are equivalent and one can move freely back and forth between the two forms as long as the field variables are continuous.

The above derivation path is not unique. One could start with an incremental volume and derive (1) via (6). It is largely a question of personal choice and the end use. One school of thought, attended by most scientists, applied mathematicians and academics, since they usually deal with the local or microscopic approach, focuses on the conversion of the surface integrals to volume integrals using Gauss' Theorem. The volume integrals are then dropped giving the partial differential or microscopic form. This path works well when a detailed analysis is desired, such as subchannel flow in fuel bundles, moderator circulation in the calandria, etc.

The second school, which sees more favour among engineers, particularly in the chemical industry, evaluates the surface integrals as they stand without converting to volume integrals. This leads to a lumped or macroscopic approach useful for network analysis, distillation towers, etc.

There exists a very large number of possible derivations, each with its own advantages and disadvantages. As more and more detail is picked up in each class of models, numerical means have to be used. In the limit of large numbers of nodes or mesh points, etc., both methods converge to the same solution.

Since the above equations are basic to <u>all</u> subsequent modelling of thermalhydraulic systems, one should keep in mind the basis for these equations:

1) Conservation as an experimental observation.

This is usually taken for granted. However, when the conservation equations for separate phases in a mixture are under consideration, the various sinks and sources of mass, momentum

and energy are not entirely known and the interpretation of experimental data can be difficult because of the complexity. It helps to keep in mind the distinctly different roles that we have historically assigned to the players in the conservation process:

a) the local time derivative, $\partial\psi/\partial t$,
b) the advection term (flux), $\nabla\cdot\psi\mathbf{v}$,
c) the local sinks and sources, Γ, within a volume and
d) the local sinks and sources, **S**, on the surface of a volume.

If a clarity of form is adopted by establishing and maintaining a one-to-one correspondence between the form and the physical processes, then a substantial pedagogical tool will have been achieved. This proves invaluable in experimental design (to zero in on a particular process or parameter), model formulation and interpretation, data analysis and presentation, correlation development, etc. A model could lose its generality because, for instance, fluxes across interfaces are written as a term in Γ, thus making the interfacial flux a local phenomena rather than a boundary phenomena. This may be acceptable for a single geometry but causes the model to break down when applied to diverse geometries.

2) The field variables are continuous within the volume V.

This is also usually taken for granted. But care must be exercised in multiphase flow where discontinuities abound. A common approach, taken to simplify the complexity of multiphase flow, is to average the terms in the conservation equations across the cross-sectional area of the flow path. One could speculate that the error introduced in this manner could separate the model from reality enough to make the solutions be "unreal", i.e. complex numbers, singularities, etc. Further, fluctuating parameters are often smoothed by averaging over an appropriate Δt. These averaged parameters and products of parameters are used in models and compared to experiments. But there is no guarantee that, for instance,

$$\frac{1}{\Delta t}\int_{\Delta t}\psi\,\mathbf{v}\,dt = \left(\frac{1}{\Delta t}\int_{\Delta t}\psi\,dt\right)\left(\frac{1}{\Delta t}\int_{\Delta t}\mathbf{v}\,dt\right).$$

Thus the use of time averaged parameters can lead to additional errors. Indeed, because of the possibility of error due to space and time discontinuities, several investigators have offered rigorous treatments for the distributed approach (see, for example, Delhaye [DEL81]). There is no reason why these treatments could not be applied to the lumped approach, as well. But, at this time, there is little incentive to do so since grid coarseness and experimental data are larger sources of error. As always, the operative rule is - BUYER BEWARE.

We now proceed to treat the mass, momentum and energy equations in turn.

2.3 Conservation of Mass

Historically, mass was the first variable observed to be conserved:

$$\iiint_V \frac{\partial}{\partial t}(\gamma_k\ \rho_k)\,dV = -\iint_S \gamma_k\ \rho_k\ \mathbf{v}_k\cdot\mathbf{n}\,ds + \iiint_V \Gamma_k\,dV + \iint_s \mathbf{S}_k\,\mathbf{n}\cdot ds \qquad (7)$$

where

ρ_k = density of phase k (1 = liquid, 2 = vapour),

γ_k = volume fraction of phase, k, in volume V, and

Γ_k, $\mathbf{S}_k$ = phase sinks and sources, including chemical and nuclear effects.

The average density is defined as:

$$\rho = \gamma_1 \rho_1 + \gamma_2 \rho_2 = (1 - \alpha)\rho_1 + \alpha \rho_2 , \tag{8}$$

whereρ = average density, and

α = void fraction.

Adding both phases together, equation 7 becomes:

$$\begin{aligned} \iiint_V \frac{\partial}{\partial t} [(1 - \alpha)\rho_1 + \alpha \rho_2] \, dV &= - \iint_S [(1 - \alpha)\rho_1 \mathbf{v}_1 + \alpha \rho_2 \mathbf{v}_2] \cdot \mathbf{n} \, ds \\ &= + \iiint_V (\Gamma_1 + \Gamma_2) \, dV + \iint_S (\mathbf{S}_1 + \mathbf{S}_2) \cdot \mathbf{n} \, ds. \end{aligned} \tag{9}$$

In our case, $\Gamma_1 = -\Gamma_2$ (liquid boils or vapour condenses) and $\mathbf{S}_k = 0$ (no mass sources or sinks at surfaces). Therefore:

$$\iiint_V \frac{\partial \rho}{\partial t} \, dV = - \iint_S \rho \mathbf{v} \cdot \mathbf{n} \, ds \tag{10}$$

where

$$\rho \mathbf{v} = (1 - \alpha)\rho_1 \mathbf{v}_1 + \alpha \rho_2 \mathbf{v}_2 . \tag{11}$$

If we apply Gauss' Theorem and drop the integrals we have:

$$\frac{\partial \rho}{\partial t} + \nabla \cdot \rho \mathbf{v} = 0 \tag{12}$$

or

$$\frac{\partial}{\partial t} [(1 - \alpha)\rho_1 + \alpha \rho_2] + \nabla \cdot [(1 - \alpha)\rho_1 \mathbf{v}_1 + \alpha \rho_2 \mathbf{v}_2] = 0 . \tag{13}$$

This is the distributed form useful for modelling detailed flow patterns such as in the calandria, vessels, steam generators and headers. Component codes such as THIRST [CAR81a] and COBRA [BNW76] use this approach.

In contrast, system codes such as SOPHT [CHA77a], based on Porsching's work [POR71], use the lumped equations. These codes represent a hydraulic network of pipes by nodes joined by links, discussed in detail in section 3. Mass, pressure and energy changes occur at the nodes. Momentum changes occur in the links. Thus the network is treated on a macroscopic scale requiring an integral approach to the fundamental equations. Flow details in pipes are <u>not</u>

considered. That is, diffusion, dispersion, advection, flow regimes, flow profiles, etc. are not fundamentally accounted for but are covered by empirical correlations. Averaging techniques, commonly used in the distributed approach are not used in the lumped approach mainly because there is little incentive to do so. The main sources of error lie elsewhere, mainly in the coarseness of the discretization in the direction of flow (i.e. node size) and in friction factors and heat transfer coefficients.

Now, $\iiint \rho dV$ is the mass, M_i, in the volume, V_i, of the i^{th} node. Also, for our case, the surface integral can be written as surface integrals over the individual flow paths into and out of the volume or node. That is,

$$- \iint_S \rho \mathbf{v} \cdot \mathbf{n} \, ds = \sum_j \rho_j v_j A_j , \tag{14}$$

where j represents inflow and outflow links with $v_j > 0$ for inflow and <0 for outflow. Inherent in equation 11 is the assumption that the integral, $\iint_S \rho \mathbf{v} \cdot \mathbf{n} \, ds$ can be replaced by the simple product $\rho_j \mathbf{v}_j A_j$. This implies known or assumed (usually uniform) velocity and density profiles across the face of the link (or pipe).

Thus we now have:

$$\frac{\partial M_i}{\partial t} = \sum_j \rho_j v_j A_j \equiv \sum W_j , \tag{15}$$

where W_j is the mass flow. This is the typical representation in system codes. Thus for the node-link type equations, we must add two more assumptions:

i) nodalization, and
ii) assumed velocity and density profile across the cross-section of a pipe.

These assumptions have far reaching ramifications that may not be immediately obvious. This is discussed in more detail in section 3.

To conclude our progressive simplification, we note the steady state form of equation 15:

$$\sum_j \rho_j v_j A_j \equiv \sum W_j = 0 . \tag{16}$$

For a simple circular flow loop, the mass flow rate at steady state is a constant at any point in the loop. Local area and density variations thus give rise to velocity variations around the loop.

Local velocity then is:

$$v = \frac{W}{\rho A} . \tag{17}$$

2.4 Conservation of Momentum

Newton observed that momentum is conserved, i.e. a body moves in a straight line unless

forced to do otherwise. This is equivalent to a force balance if the inertial force (a momentum sink of sorts) is recognized. In the integral sense, the rate of change of momentum is equal to the forces acting on the fluid. Thus:

$$\frac{D}{Dt}\iiint_V \gamma_k\ \rho_k\ \mathbf{v}_k\, dV = \iint_S \boldsymbol{\sigma}_k \cdot \mathbf{n}\, ds + \iiint_V \gamma_k\ \rho_k\ \mathbf{f}_k\ dV + \iiint_V \mathbf{M}_k\, dV, \tag{18}$$

where

σ is the stress tensor (i.e., short range or surface effects including pressure, viscosity, etc.),

f is the long range or body force (i.e., gravity),

and **M** is the momentum interchange function accounting for phase change effects.

Using Reynold's Transport Theorem, we get:

$$\begin{aligned}&\iiint_V \frac{\partial}{\partial t}\ (\gamma_k\ \rho_k\ \mathbf{v}_k)\, dV + \iint_S\ (\gamma_k\ \rho_k\ \mathbf{v}_k)\,(\mathbf{v}_k \cdot \mathbf{n})\, ds \\ &= \iint_S\ \boldsymbol{\sigma}_k \cdot \mathbf{n}\, ds + \iiint_V\ \gamma_k\ \rho_k\ \mathbf{f}_k\ dV + \iiint_V\ \mathbf{M}_k\ dV.\end{aligned} \tag{19}$$

Adding both phases together as per the mass equation, we find:

$$\iiint_V \frac{\partial}{\partial t}\ \rho\,\mathbf{v}\, dV + \iint_S\ \rho\,\mathbf{v}\,(\mathbf{v}\bullet\mathbf{n})\, ds = \iint_S\ \boldsymbol{\sigma}\cdot\mathbf{n}\, ds + \iiint_V\ \rho\,\mathbf{f}\, dV. \tag{20}$$

To get the microscopic form we use Gauss's theorem and drop the volume integral as before to leave:

$$\frac{\partial}{\partial t}\ (\rho\,\mathbf{v}) + \nabla\cdot\rho\,\mathbf{v}\,\mathbf{v} = \nabla\cdot\boldsymbol{\sigma} + \rho\,\mathbf{f}. \tag{21}$$

The stress tensor, **σ**, can be split into the normal and shear components:

$$\boldsymbol{\sigma} = -P\mathbf{I} + \boldsymbol{\tau}, \tag{22}$$

where P is the pressure, **I** is the unity tensor and **τ** is the shear stress tensor. This enables the explicit use of pressure and helps maintain our tenuous link with reality. Of course, it can equally be introduced in the integral form, equation 20, or as a separate pressure for each phase in equation 19. At any rate, equation 21 becomes:

$$\frac{\partial}{\partial t}\ (\rho\,\mathbf{v}) + \nabla\cdot\rho\,\mathbf{v}\,\mathbf{v} = -\nabla P + \nabla\cdot\boldsymbol{\tau} + \rho\,\mathbf{f}. \tag{23}$$

This is the form commonly seen in the literature, useful for distributed modelling as per the mass conservation equation. The term, $\nabla\cdot\boldsymbol{\tau}$, is usually replaced by an empirical relation. For the system codes using the node-link structure, we switch back to the macroscopic form, Equation 20.

If the surface integral for the advective term is performed over the inlet and outlet areas of the

pipe (link) in question, then:

$$\iint_S \rho\mathbf{v}(\mathbf{v}\cdot\mathbf{n})ds = \iint_{Ain} \rho\mathbf{v}(\mathbf{v}\cdot\mathbf{n})ds + \iint_{Aout} \rho\mathbf{v}(\mathbf{v}\cdot\mathbf{n})ds \tag{24}$$

where A_{IN} is the flow inlet area and A_{OUT} is the flow outlet area. If we assume the properties are constant over the areas, then:

$$V\frac{\partial\rho\mathbf{v}}{\partial t} - A_{IN}\rho_{IN}v_{IN}\mathbf{v}_{IN} + A_{OUT}\rho_{OUT}v_{OUT}\mathbf{v}_{OUT} = \iint_S \boldsymbol{\sigma}_k\mathbf{n}\cdot ds + \iiint_V \rho\mathbf{f}dV \tag{25}$$

Alternatively we could perform a cross-sectional average of each term, usually denoted by < >, where $<(\ )> = 1/A\iint_S(\ )\,ds$. If we assume the properties, V, ρ and A are constant along the length of the pipe, then the second and third terms cancel.

Equation 25 can be rewritten as:

$$\begin{aligned} V\frac{\partial\rho\mathbf{v}}{\partial t} &= -\iint P\mathbf{I}\cdot\mathbf{n}ds + \iiint\left(\nabla\cdot\vec{\tau} + \rho\vec{f}\right)dV \\ &= -A_{OUT}\mathbf{P}_{OUT} + A_{IN}\mathbf{P}_{IN} - \frac{V\rho}{L}\left(\frac{fL}{D}+k\right)\frac{\mathbf{v}|\mathbf{v}|}{2g_c} - LA\rho\sin(\theta)\left(\frac{\mathbf{g}}{g_c}\right) \end{aligned} \tag{26}$$

where g_c is the gravitational constant, **g** is the acceleration due to gravity and where $\nabla\cdot\boldsymbol{\tau}$ and ρ**f** evaluated by empirical correlations (the standard friction factor) plus an elevation change term (θ is the angle w.r.t. the horizontal). Note that is $A_{OUT} \neq A_{IN}$ then, even for constant pressure, there is a net force on the volume causing it to accelerate if it were not restrained. In a restrained system such as HTS piping, the piping supports exert an equal and opposite force on the volume. Thus when the area differences are explicitly modelled, the appropriate body forces must be included. Generally, it is simpler to use an average or representative area for the IN and OUT surfaces and to add entrance and exit frictional losses explicitly in the (fl/D+k) term.

Assuming one dimensional flow and defining the mass flow as $W \equiv \rho VA$, and L as the pipe length, equation 26 becomes:

$$\frac{\partial W}{\partial t} = \frac{A}{L}\left[\left(P_{IN} - P_{OUT}\right) - \left(\frac{fL}{D}+k\right)\frac{W^2}{2g_c\rho A^2}\right] - A\rho\frac{g}{g_c}\sin(\theta) \tag{27}$$

which is the form typically used in system codes.

If circumstances require, extra terms can be added. For instance, if a pump is present this can be considered to be an external force acting through head, ΔP_{pump}. Equation 27 would then become:

$$L\frac{\partial W}{\partial t} = -A_{OUT}P_{OUT} + A_{IN}P_{IN} + A\Delta P_{PUMP} \tag{28}$$

The momentum flux terms ($A\rho v^2$) in equation 25 could also be added if large area or property changes were present or the effect could be included in the friction term.

In the steady state, for a constant area pipe with no pump and no elevation change:

$$P_{IN} - P_{OUT} = \rho\left(\frac{fL}{D} + k\right)\frac{V^2}{2g_c} = \left(\frac{fL}{D} + k\right)\frac{W^2}{2A^2\rho g_c} + \Delta P_{PUMP} + \ldots \tag{29}$$

As a final note, the assumptions made for the mixture momentum equation are thus similar to those made for the mixture mass equation and the same comments apply. One cannot hope to accurately model such phenomena as void propagation and other two phase transient flow effects using lumped single phase equations unless a large number of nodes and links are used.

2.5 Conservation of Energy

By the early 1800's, philosophical jumps were made in recognizing that heat was not a substance and in the emergence of electromagnetic theory. The concept of energy as we now think of it was formulated and it was found that energy, too, was conserved, as long as we carefully identify <u>all</u> the different forms of energy (kinetic, chemical, potential, nuclear, internal, electromagnetic, ...).

The mathematical statement of the conservation of energy is:

$$\begin{aligned}\frac{D}{Dt}\iiint_V \gamma_k\ \rho_k\left(e_k + \frac{1}{2}v_k^2\right)dV &= -\iint_S \mathbf{q}_k\cdot\mathbf{n}\,ds + \iiint_V E_k\ dV \\ &+ \iiint_V \gamma_k\rho_k\mathbf{f}_k\cdot\mathbf{v}_k\,dV + \iint_S (\boldsymbol{\sigma}_k\cdot\mathbf{n})\cdot\mathbf{v}_k\,ds,\end{aligned} \tag{30}$$

where

e_k = internal energy of phase k,

q_k = surface heat flux for phase k, and

E_k = internal heat sources and sinks of phase k.

The left hand side is the substantial derivative of the internal plus kinetic energy. The right hand side terms are, respectively:

1) surface heat flux,
2) internal sources and sinks,
3) work due to long range body forces (gravity, etc.),
4) work due to short range forces (surface tension, pressure, etc.).

Using Reynold's Transport Theorem again:

$$\iiint_V \frac{\partial}{\partial t}\left[\gamma_k\ \rho_k\left(e_k + \frac{1}{2}\ v_k^2\right)\right]dV + \iint_S \gamma_k\ \rho_k\left(e_k + \frac{1}{2}\ v_k^2\right)\mathbf{v}_k\cdot\mathbf{n}\,ds$$
$$= -\iint_S \mathbf{q}_k\cdot\mathbf{n}\,ds + \iiint_V E_k\ dV + \iiint_V \gamma_k\rho_k\mathbf{f}_k\cdot\mathbf{v}_k\,dV + \iint_S (\boldsymbol{\sigma}_k\cdot\mathbf{n})\cdot\mathbf{v}_k\,ds. \quad (31)$$

Summing over k, the mixture equation becomes:

$$\iiint_V \frac{\partial}{\partial t}\left[\rho e + \frac{1}{2}\ \rho v^2\right]dV + \iint_S \left[\rho e + \frac{1}{2}\ \rho v^2\right]\mathbf{v}\cdot\mathbf{n}\,ds$$
$$= -\iint_S \mathbf{q}\cdot\mathbf{n}\,ds + \iiint_V E\,dV + \iiint_V \rho\mathbf{f}\cdot\mathbf{v}\,dV + \iint_S (\boldsymbol{\sigma}\cdot\mathbf{v})\cdot\mathbf{v}\,ds, \quad (32)$$

where

$\rho e = \gamma_1\rho_1 e_1 + \gamma_2\rho_2 e_2$ $\quad E = E_1 + E_2$, etc.

Using Gauss' Theorem to change some of the surface integrals to volume integrals:

$$\iiint_V \frac{\partial}{\partial t}\left[\rho e + \frac{1}{2}\ \rho v^2\right]dV + \iint_S \rho e\,\mathbf{v}\cdot\mathbf{n}\,ds + \iiint_V \nabla\cdot\left[\frac{1}{2}\ \rho v^2\ \mathbf{v}\right]dV$$
$$= -\iint_S \mathbf{q}\cdot\mathbf{n}\,ds + \iiint_V E\,dV + \iiint_V \rho\mathbf{f}\cdot\mathbf{v}\,dV + \iiint_V \nabla\cdot(\boldsymbol{\sigma}\cdot\mathbf{v})\,dV. \quad (33)$$

Since

$$\boldsymbol{\sigma} = -P\mathbf{I} + \boldsymbol{\tau},$$
$$\iiint_V \nabla\cdot(\boldsymbol{\sigma}\cdot\mathbf{v})\,dV = \iiint_V \left[\nabla\cdot(\boldsymbol{\tau}\cdot\mathbf{v}) - \nabla\cdot(P\mathbf{v})\right]\,dV.$$

This is the total energy equation, composed of thermal terms and mechanical terms. We can separate the two by first generating the mechanical terms from the momentum equation (equation 20). Forming the dot product with velocity we get:

$$\iiint_V \frac{\partial}{\partial t}\ (\rho\mathbf{v})\cdot\mathbf{v}\,dV + \iiint_V \mathbf{v}\cdot(\nabla\cdot\rho\mathbf{v}\mathbf{v})\,dV = \iiint_V \mathbf{v}\cdot(\nabla\cdot\boldsymbol{\tau})\,dV$$
$$-\iiint_V \mathbf{v}\cdot\nabla P\,dV + \iiint_V \rho\mathbf{f}\cdot\mathbf{v}\,dV. \quad (34)$$

Now

$$\mathbf{v}\cdot(\nabla\cdot\boldsymbol{\tau}) = \nabla(\boldsymbol{\tau}\cdot\mathbf{v}) - \boldsymbol{\tau}:\nabla\mathbf{v}, \quad (35)$$
$$\mathbf{v}\cdot\nabla P = \nabla\cdot(P\mathbf{v}) - P\nabla\cdot\mathbf{v}, \quad (36)$$
$$\mathbf{v}\cdot\frac{\partial}{\partial t}\ (\rho\mathbf{v}) = \frac{\partial}{\partial t}\left(\frac{1}{2}\ \rho\mathbf{v}\cdot\mathbf{v}\right) = \frac{\partial}{\partial t}\left(\frac{1}{2}\ \rho v^2\right) \quad (37)$$

and

$$\mathbf{v} \cdot (\nabla \cdot \rho \mathbf{v}\mathbf{v}) = \nabla \cdot \left(\frac{1}{2} \rho v^2 \mathbf{v} \right). \tag{38}$$

Using these identities and subtracting equation 34 from equation 33, we get:

$$\begin{aligned} \iiint_V \frac{\partial}{\partial t} (\rho e)\, dV + \iint_s \rho e \mathbf{v} \cdot \mathbf{n}\, ds &= - \iint_s \mathbf{q} \cdot \mathbf{n}\, ds \\ + \iiint_V E\, dV + \iiint_V \boldsymbol{\tau} : \nabla \mathbf{v}\, dV &- \iiint_V P \nabla \cdot \mathbf{v}\, dV . \end{aligned} \tag{39}$$

This is the thermal form of the energy equation. This form of the energy equation can be used to generate the thermal conductance equation for solids. By setting fluid velocity to zero and converting surface integrals to volume integrals we get the distributed form:

$$\frac{\partial}{\partial t} (\rho e) = - \nabla \cdot \mathbf{q} + E , \tag{40}$$

where E is the internal energy generation rate term.

From thermodynamics, for solids, we have:

$$\frac{\partial}{\partial t} (\rho e) \geq \rho \frac{\partial e}{\partial t} \geq \rho C_v \frac{\partial T}{\partial t}, \tag{41}$$

and using Fourier's law for heat conduction:

$$\mathbf{q} = - k \nabla T , \tag{42}$$

we have the classical form of the heat conduction equation:

$$\begin{aligned} \rho C_v \frac{\partial T}{\partial t} &= \nabla \cdot k \nabla T + E \\ &= k \nabla^2 T + E \qquad \text{space independent } k . \end{aligned} \tag{43}$$

This is useful for determining the temperature distributions in boiler tube walls, piping walls and reactor fuel pencils. To generate the node-link forms we now turn back to the integral form of equation 39. If we assume that the density and enthalpy are uniform over the node (the volume in question), then

$$\iiint_V \frac{\partial}{\partial t} (\rho e)\, dV = \frac{\partial U}{\partial t}, \tag{44}$$

where

$$U \equiv V \rho e = L A \rho e . \tag{45}$$

The integral of the transport term can be written over the flow surfaces:

$$\iint_S \rho e \mathbf{v}\cdot\mathbf{n}\, ds = \iint_{A_1} \rho e \mathbf{v}\cdot\mathbf{n}\, ds + \iint_{A_2} \rho e \mathbf{v}\cdot\mathbf{n}\, ds + \ldots, \tag{46}$$

where A_1, A_2, etc., are the pipe flow cross-sectional areas. For inflow, $\mathbf{v}\cdot\mathbf{n}$ is negative. For outflow, $\mathbf{v}\cdot\mathbf{n}$ is positive. Assuming uniform velocity, enthalpy and density across the link (pipe) cross-section gives:

$$\iint \rho e \mathbf{v}\cdot\mathbf{n} ds = -\sum_{\text{INFLOW}} \rho e \mathbf{v} A_i + \sum_{\text{OUTFLOW}} \rho e \mathbf{v} A = -\sum W_{IN} e_{IN} + \sum W_{OUT} e_{OUT} \tag{47}$$

The heat flux and generation terms of the thermal energy equation can be lumped into a loosely defined heat source for the volume.

$$-\iint_S \mathbf{q}\cdot\mathbf{n}\, ds + \iiint_V E\, dV \equiv Q. \tag{48}$$

Therefore, the thermal energy equation becomes:

$$\frac{\partial U}{\partial t} = \sum W_{IN} e_{IN} - \sum W_{OUT} e_{OUT} + Q + \iiint \boldsymbol{\tau} : \nabla \mathbf{v} dV - \iiint P \nabla\cdot\mathbf{v} dV \tag{49}$$

The last two terms are the irreversible and reversible internal energy conversion, respectively.

Some system codes track enthalpy rather than internal energy. Defining:

$$h = \text{enthalpy} = e + \frac{P}{\rho} \text{ and } H = V\rho h. \tag{50}$$

we can rewrite equation 39 as follows:

$$\begin{aligned} \iiint_V \frac{\partial(\rho h - P)}{\partial t}\, dV + \iint_s (\rho h - P)\mathbf{v}\cdot\mathbf{n}\, ds &= -\iint_S \mathbf{q}\cdot\mathbf{n}\, ds \\ + \iiint_V E\, dV + \iiint_V \boldsymbol{\tau}:\nabla\mathbf{v}\, dV - \int_V P\nabla\cdot\mathbf{v}\, dV. & \end{aligned} \tag{51}$$

Collecting the pressure terms and simplifying yields:

$$\begin{aligned} \iiint_V \frac{\partial}{\partial t}(\rho h)\, dV + \iint_S \rho h \mathbf{v}\cdot\mathbf{n}\, ds &= -\iint_S \mathbf{q}\cdot\mathbf{n}\, ds + \iiint_V E\, dV \\ + \iiint_V \boldsymbol{\tau}:\nabla\mathbf{v} + \iiint_V \frac{\partial P}{\partial t}\, dV + \iint_S P\mathbf{v}\cdot\mathbf{n}\, ds - \iiint_V P\nabla\cdot\mathbf{v}\, dV. & \end{aligned} \tag{52}$$

The surface integral over P can be transformed into a volume integral using Gauss' theorem and combined with the last term to give:

$$\iint_S P\,\mathbf{v}\cdot\mathbf{n}\,ds - \iiint_V P\,\nabla\cdot\mathbf{v}\,dV = \iiint_V \nabla\cdot(P\,\mathbf{v})\,dV - \iiint_V P\,\nabla\cdot\mathbf{v}\,dV$$
$$= \iiint_V \mathbf{v}\cdot\nabla P\,dV. \tag{53}$$

The enthalpy flux terms can be evaluated in the same manner that the energy flux terms were in equations 46-47. Thus,

$$\iint_S \rho\mathbf{v}\cdot\mathbf{n}\,ds = -\sum W_{IN}h_{IN} + \sum W_{OUT}h_{OUT}. \tag{54}$$

Finally, using equations 48, 50, 53-54, equation 52 becomes:

$$\frac{\partial H}{\partial t} = +\sum W_{IN}h_{IN} - \sum W_{OUT}h_{OUT} + Q + \iiint \boldsymbol{\tau} : \nabla\mathbf{v}\,dV + \iiint\left(\frac{\partial P}{\partial t} + \mathbf{v}\cdot\nabla P\right)dV. \tag{55}$$

The integral term involving pressure is often neglected since it is usually negligible compared to the other terms. For instance, the typical CANDU Heat Transport System operates at a pressure of 10 MPa, a fluid velocity of ~10 m/s, and a pressure gradient of less than 70 kPa/m. This translates into roughly 10 kJ/kg while e is approximately 1000 kJ/kg.

The turbulent heating term is usually approximated by adding pump heat as a specific form of Q.

equation 55 in the steady state, neglecting turbulent heating and the pressure terms, is the familiar:

$$Q = -\sum W_{IN}h_{IN} + \sum W_{OUT}h_{OUT}. \tag{56}$$

For a reactor or a boiler (one flow in, one flow out):

$$Q = W\left(h_{OUT} - h_{IN}\right) = WC_p\left(T_{OUT} - T_{IN}\right) \text{ in single phase.} \tag{57}$$

Another special case of equation 55 is obtained by expanding the term Q as per equation 48:

$$-\iint_S \mathbf{q}\cdot\mathbf{n}\,ds + \iiint_V E\,dV \equiv Q. \tag{48}$$

Using Newton's Law of cooling for convection:

$$\mathbf{q}\cdot\mathbf{n} = h_N(T - T_s), \tag{58}$$

where

$\mathbf{q}\cdot\mathbf{n}$	=	heat flux normal to surface, s,
T	=	Temperature of fluid
T_s	=	Temperature of surface (wall), and
h_N	=	heat transfer coefficient,

Equation 55, neglecting the pressure terms, becomes:

$$V\frac{\partial \rho h}{\partial t} - V\frac{\partial P}{\partial t}\left(\equiv V\frac{\partial \rho e}{\partial t} \approx V\rho C_v \frac{\partial T}{\partial t} \right) = \sum W_{IN} h_{IN} - \sum W_{OUT} h_{OUT}$$
$$-Ah_N (T - T_s) + VE + \iiint \boldsymbol{\tau} : \nabla \mathbf{v} dV \qquad (59)$$

which is useful for accounting for heat transfer between the fluid and the pipe or tube walls (eg: boiler heat transfer).

The heat transfer coefficient, h_N, is supplied through empirical relations. The turbulent heating term $\iiint_V \boldsymbol{\tau} : \nabla \mathbf{v}\, dV$ generally can be neglected or added as a pump heat term.

2.6 The Equation of State

From the conservation equations, we have three equations for each phase (mass, momentum and energy conservation) and four unknowns:

1) density, ρ or mass, Vρ,
2) velocity, v, or mass flow, W, or momentum, ρv,
3) energy, e, or enthalpy, h = e + P/ρ, or temperature, T = fn(e) or fn(h), and
4) pressure, P.

The fourth equation required for closure is the equation of state:

$$P = fn(h, \rho) \qquad \rho = fn(P,T), \text{ etc.} \qquad (60)$$

Thermodynamic equilibrium is usually assumed. For water, H_2O or D_2O, tables of properties give the required functional relationship. Often, a curve fit of the tables is used. This data is input to the computer codes and utilized in table lookup schemes or directly via the parametric curve fits.

The equation of state is discussed in detail in Section 4.

2.7 Empirical Correlations

As previously discussed, supporting relations are required to provide the necessary information for the conservation and state equations. The primary areas where support is needed are:

1) relationship between quality and void fractions, i.e., slip velocities in two phase flow (to link the mass and enthalpy via the state equation);
2) the stress tensor, $\boldsymbol{\tau}$ (effects of wall shear, turbulence, flow regime and fluid properties on momentum or, in a word: friction);
3) heat transfer coefficients (to give the heat energy transfer for a given temperature distribution in heat exchangers, including steam generators and reactors);
4) thermodynamic properties for the equation of state;
5) flow regime maps to guide the selection of empirical correlations appropriate to the flow regime in question;
6) special component data for pumps, valves, steam drums, pressurizers, bleed or degasser condensers, etc; and

7) critical heat flux information (this is not needed for the solution of the process equations but a measure of engineering limits is needed to guide the use of the solutions of the process equations as applied to process design;

The above list of correlations, large enough in its own right, is but a subset of the full list that would be required were it not for a number of key simplifying assumptions made in the derivation of the basic equations. The three major assumptions made for the primary heat transport system are:

1) one dimensional flow;
2) thermal equilibrium (except for the pressurizer under insurge); and
3) one fluid model (i.e. mixture equations).

These are required because of state of the art limitations (however, two fluid models are being used increasingly in recent years.). Empirical correlations were discussed in more detail in Chapter 6.

2.8 Solution Overview

Because of the complexity of solving the mass, momentum and energy equations plus supporting equations of state and empirical correlations all subject to initial and boundary conditions, it is quite easy to "not see the forest for the trees". A skeleton overview may help in this regard. Figure 1 illustrates the equations and the information links between them. In words, the momentum equation gives the flows or velocities from one node to another, or from one grid point to another, based on a given pressure, flow, mass and energy distribution. The updated flows are used by the mass and energy equations to update the mass and energy contents at each location. The new mass and energy are given to the equation of state to update the pressure distribution. The new pressure, along with the new densities and energies are used by the momentum equation, and so on. In this manner, a time history of the fluid evolution is obtained. Of course, only the main variables are noted. The numerous

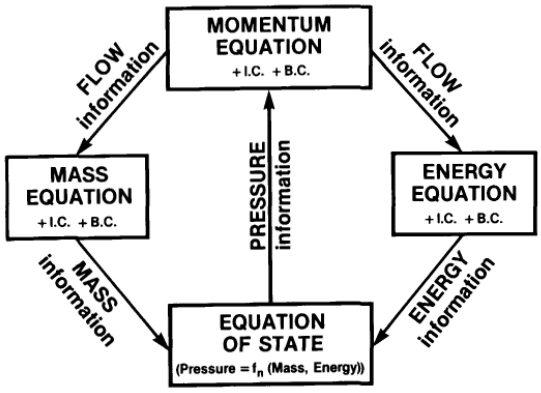

Figure 1 The four cornerstone single phase flow equations and the flow of information between them.

and diverse empirical correlations require updates on the main variables and many secondary variables. This information also "flows" around the calculation.

A further point to note on the solution overview is that each phase in a multiphase flow has a main information flow path as shown in figure 2. In the full UVUEUP (unequal velocity, energy and pressure) model, there are two distinct phases: one for the vapour phase and one for the liquid phase. If a simplified model was imposed, this essentially means that the planes would touch at some point. For instance, if equal pressure in both phases was assumed, then figure 3 would result. Here, the equation of state is common to both planes.

The HEM (homogeneous equilibrium model) is the fully collapsed case where both planes collapse into one (figure 1). You may find these images to be useful in conceptualizing the basic equations and how they fit together.

The precise solution procedure that you might employ is case dependent. At present, no general solution scheme exists because the nuances of specific problems are subtle and because one cannot usually afford to ignore the efficiency and cost savings gained by tuning a method to a particular case. The economics of using a case specific code are changing, however, with developments in the microcomputer field and with the realization that total design and analysis time can often be reduced by using a less efficient but more robust code. Codes such as SOPHT and CATHENA [HAN95] are a direct result of this realization. The near term evolution will likely be affected mostly by microcomputer developments.

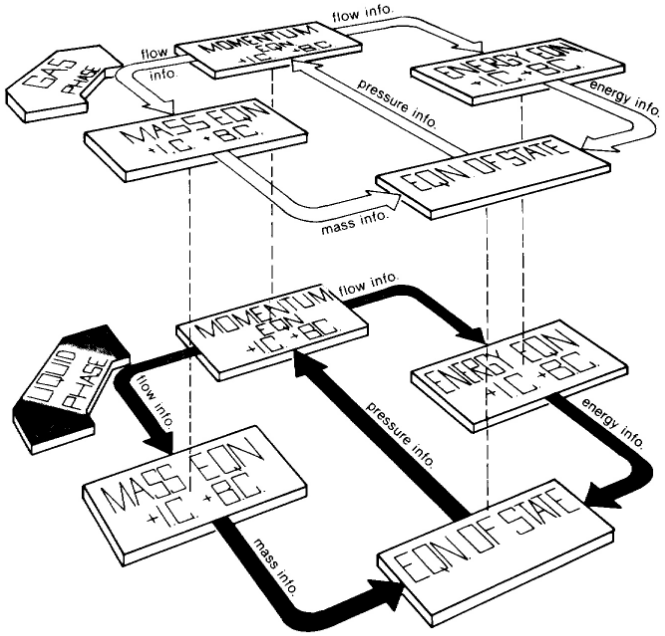

Figure 2 The four cornerstone equations for the two-fluid model.

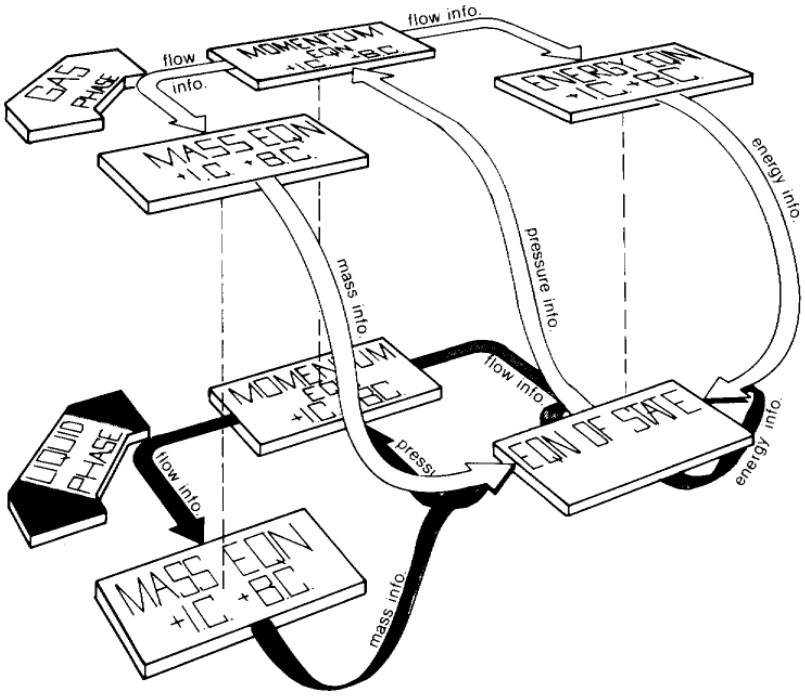

Figure 3 The four cornerstone equations for the full two-fluid model with equal pressure of the two phases.

2.9 Problems

1. Referring to figure 1:

   a. Explain the inter-relationship between the mass, momentum and energy equations and the equation of state.

   b. For the integral form, devise a simple solution scheme for the transient equations. Show what equations are being solved and how they are being solved. Flow chart your scheme.

3 Nodalization

3.1 Introduction

This section focuses on establishing a rationale for, and the setting up of, the geometric representation of thermalhydraulic systems. The hydraulic network is represented by a series of interconnected nodes to form a node-link diagram.

The exploration proceeds by first establishing and discussing the governing rationale. Next, limitations of the approximation are presented and examples are given. Finally, the matrix approach is used to capture the system geometry in a succinct form.

3.2 The Node-Link Concept

From section 2 we have the integral mass, momentum and energy equations for an arbitrary volume, i, with material flow through various surfaces, designated by the subscript j (see figure 4):

$$\frac{\partial M_i}{\partial t} = \sum_j \rho_j v_j A_j \equiv \sum W_j, \tag{61}$$

$$\frac{\partial W}{\partial t} = \frac{A}{L}\left[\left(P_{IN} - P_{OUT}\right) - \left(\frac{fL}{D} + k\right)\frac{W^2}{2g_c \rho A^2}\right] - A\rho g / g_c \sin(\theta) \tag{62}$$

$$\frac{\partial H}{\partial t} = \sum W_{IN} h_{IN} - \sum W_{OUT} h_{OUT} + Q \tag{63}$$

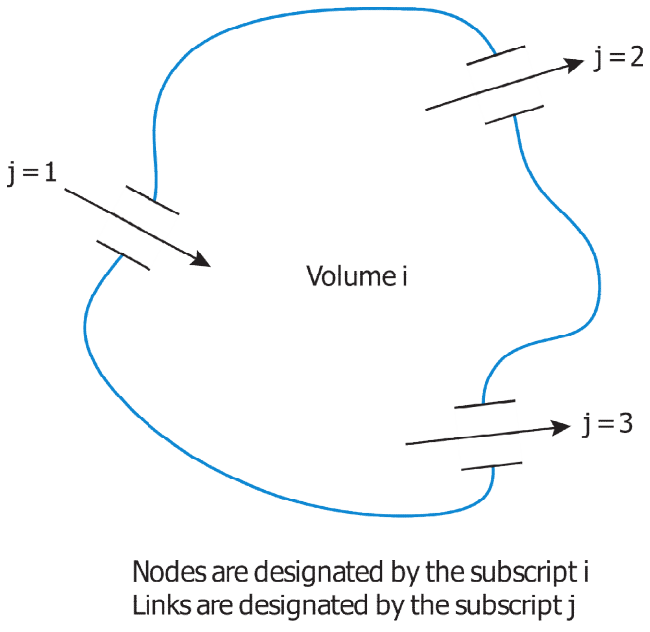

Figure 4 A general node and connecting links.

These mass and energy equations are averaged over the volume in question, hence they do not capture any detail within the volume. Knowing the mass and energy of a volume, the equation of state gives the pressure. Flow, however, is driven by pressure differences. Hence it naturally follows that the momentum equation should be applied between the points of known pressure, ie, between volumes. In the distributed approach, this is called the staggered grid method. In the lumped approach, it is called the node-link method and is illustrated in figure 5. Volumes are represented by nodes, flow paths are represented by links.

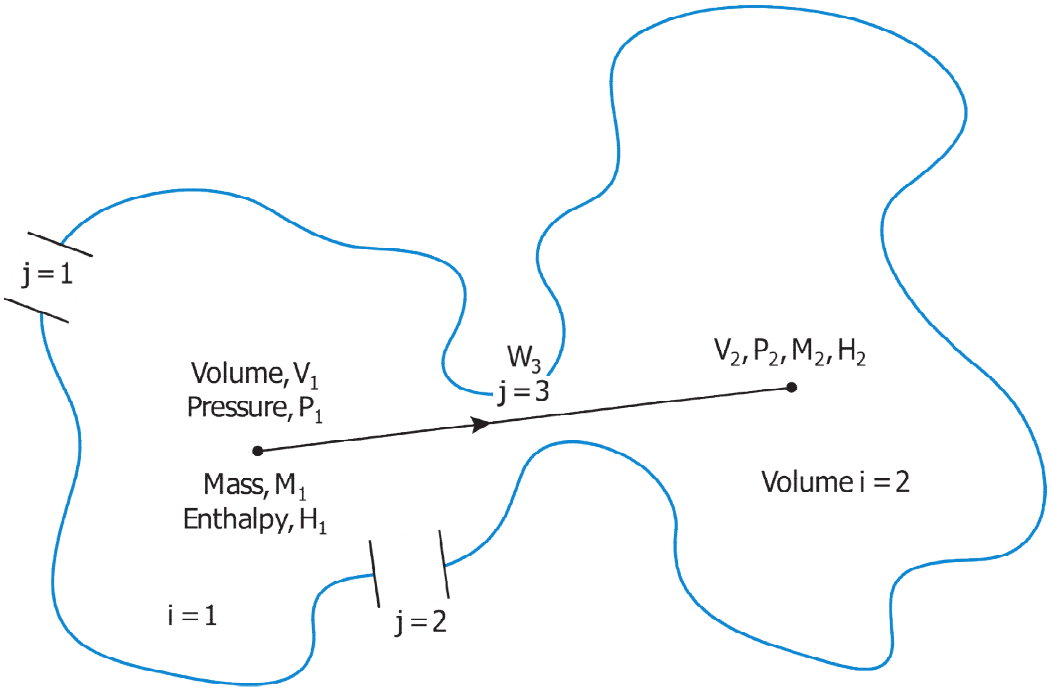

Figure 5 Two connected nodes.

To assign nodes and links to a given piping configuration, say the simple pipe of figure 6, it is best to first focus on the flow modelling. The key question to ask is: Where should the link endpoints (ie the node centres) be placed? The node centre locations define the positions at which the pressure will be evaluated and this is important for correct flow calculations. For constant area pipes, the placement is not critical but at junctions and area changes, modelling is simplified if node centres are placed at junctions and pipe area changes. For the case shown in figure 7 (a), if the flow were going from left to right and the junction resistance were included in link 1, then the pressure at node 2 would be the pressure just downstream of the junction. Carefully plan the node-link configuration to match the problem at hand. If possible, avoid running links across area changes since this inserts ambiguity into the flow area of the link model, as illustrated in figure 7 (b).

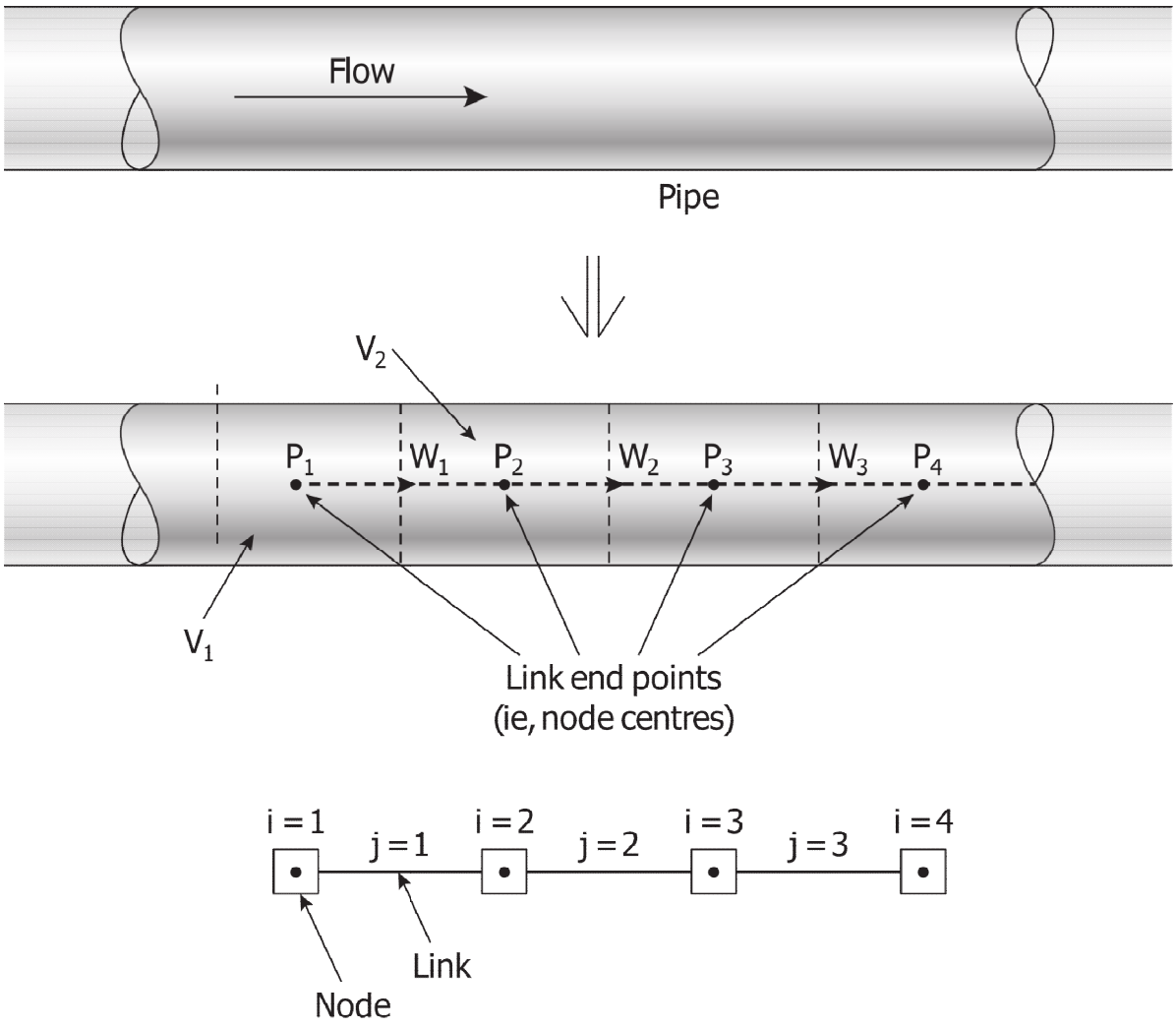

Figure 6 Node-link setup for a simple pipe.

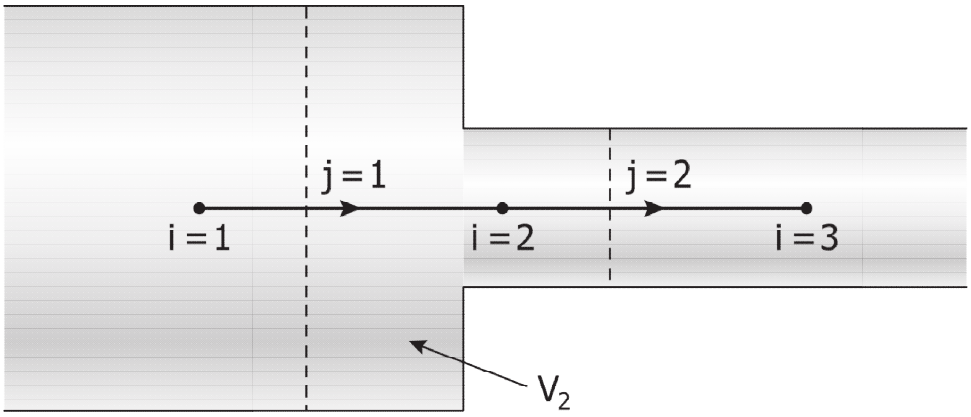

(a) Recommended

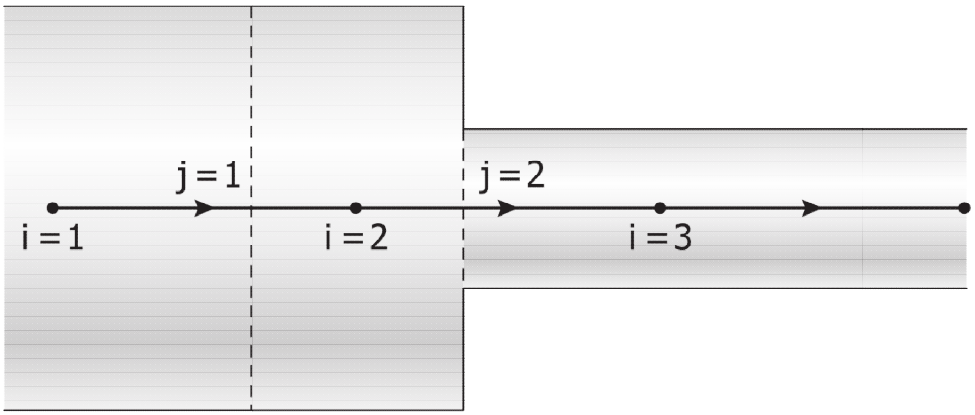

(b) Not recommended

Figure 7 Node-link setup for an area change in a pipe.

Hydraulic friction can be affected by flow direction. Figure 7 illustrates a simple pipe flow situation wherein there is a step change in area. Flow from left to right experiences a different junction resistance than flow going from right to left. Direction dependent resistances are usually modelled explicitly in the system codes. The momentum flux terms, $A\rho v^2$, can either be modelled explicitly or through the resistance coefficient, k. Note that a simple force balance around the junction would show that there is a net lateral force on the pipe. This force imbalance would have to be accounted for by a body force if different inlet and outlet pipe areas were used. This is another reason that links are chosen to coincide with constant pipe length sections.

The properties of the fluid within the link are a result of the properties of the upstream node. As the fluid is transported along a flow path (ie along the link), the link properties will change over time. Naturally there will be a transport delay but given that the nodal properties are themselves average values that change relatively slowly over time, system simulation codes typically assume that the link properties are just the same as the upstream nodal properties. For most purposes this is an acceptable assumption that can be lessened by using more nodes and links in the model. One has to be careful, however, of flow reversal situations that involve two-phase flow since this can lead to rapid and large density changes in the link.

The node volume is usually assigned as the fluid surrounding the node centre as shown in figure 7(a). But this is not a critical assignment; the node "centres" can actually be at the edge of the volume if that proves convenient. From a numerical point of view, it is beneficial to divide the hydraulic network up into volumes of roughly equal size since the properties in small volumes can change very rapidly and thus force the use of correspondingly small time steps. This rationalization of the volume assignments may force the user to take some liberties with the notion of a node "centre".

To recap, the momentum equation is used to solve for W_j in all links, driven by upstream and downstream pressure differences and retarded / accelerated by friction, elevation change, pumps, etc. that appear in the links. This flow transports mass and energy to and from the nodes. Local heat sources and sinks, such as surface heat fluxes, are modelled at the nodes.

3.3 Nodal Diffusion

In the node - link representation of flow in a pipe, no flow detail is considered as the fluid moves along the pipe. Therefore, no diffusion, dispersion, advection, flow profiles or flow regimes are explicitly permitted. This is not too crude an approximation for the calculation of pressure drops and flows but for modelling the propagation of disturbances, this approach is inadequate as it stands unless a large number of nodes and links are used.

To show this, consider a homogeneous or bubbly flow through a pipe, as in the two-phase regions of typical heat transport systems in nuclear reactors, modelled in system codes as nodes connected by links. Perfect mixing at the nodes is assumed. Flow in a pipe, however, has aspects of plug flow. That is, flow is transmitted along the pipe relatively undisturbed. If no diffusion or turbulent dispersion existed, a sharp discontinuity in a property would propagate undisturbed. Figure 8 shows how the discontinuity would move in time and space. The left

to right movement is due to the velocity, v, while the spreading out is due to diffusion. If a single mixing tank (node) represented a section of pipe of volume, V m^3, and volumetric flow, f m^3/s, then a step change to zero in a field property, C, (which could be concentration or density) entering the node would be an exponential by the time it left the node, that is:

$$C_{OUT} = C_{IN} \cdot e^{-\frac{t}{\tau}} \tag{64}$$

where $\tau = V/f$; τ is also the transmission time for the plug flow model. If the pipe were modelled by two nodes in series,

$$C_{OUT\ NODE2} = C_{IN\ NODE1}\left(1+\frac{2t}{\tau}\right)e^{-\frac{2t}{\tau}} \tag{65}$$

and in general, for n nodes:

$$C_{OUT\ NODE2} = C_{IN\ NODE1}e^{-\frac{n\cdot t}{\tau}}\sum_{k=1}^{N}\left(\frac{nt}{\tau}\right)^{k-1}\frac{1}{(n-1)!} \tag{66}$$

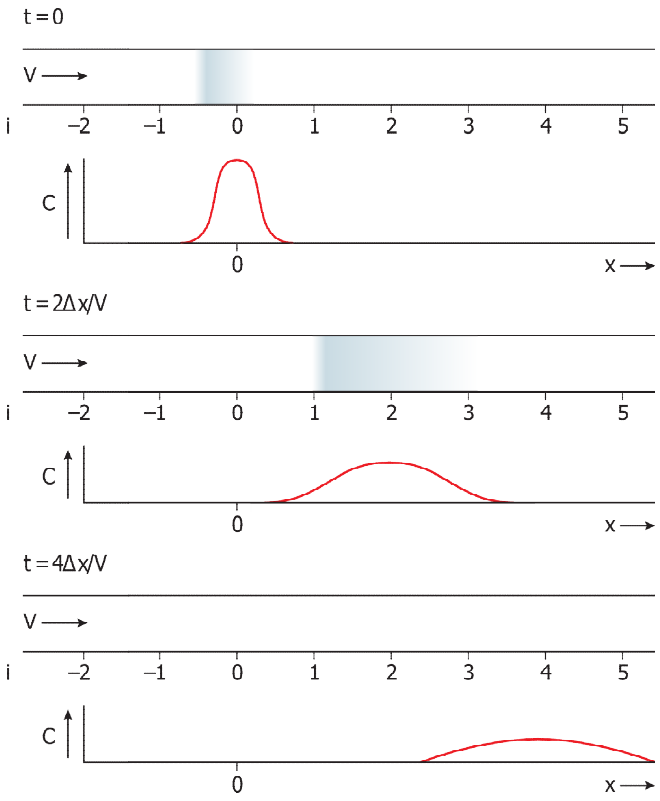

Figure 8 Illustration of convection and diffusion.

Figure 9 compares the transmission of a step change for various numbers of nodes and the plug flow model. It is easy to see why the codes model void propagation poorly. A very large number of nodes are needed to transmit a disturbance without appreciable distortion. The phase relationships or timing, of the propagation is very important in determining the stability of a thermal hydraulic system. A pocket of void reaching a given destination at an earlier or later time may enhance or cancel the phenomenon in question. The smearing of a wave front

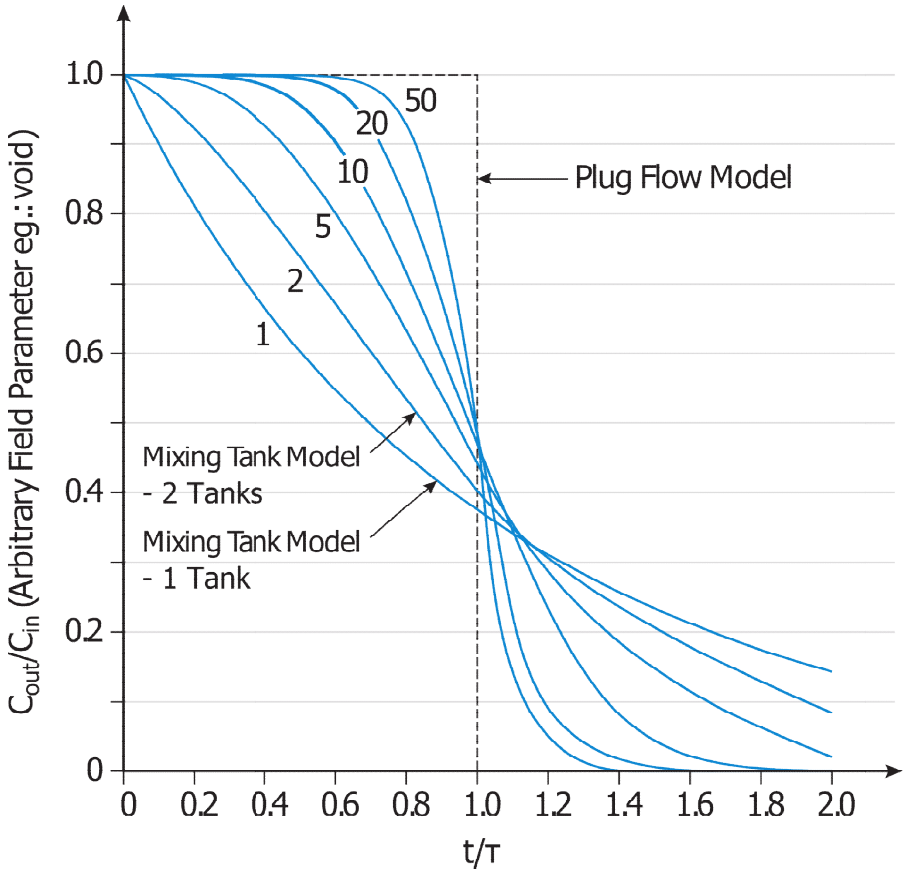

Figure 9 Transmission of a step change using the plug flow model and the mixing tank model (1 to 50 tanks).

alters the timing and gain and hence affects stability. The slow convergence of the mixing model to the plug flow model explains the typically slow convergence of such system codes as more nodes are added to increase accuracy.

Thus, nodalization creates a form of diffusion in much the same manner as finite difference schemes create numerical diffusion (see, for instance, Roache [10]). Attaining convergence in nodalization is, in essence, converging the model to plug flow behaviour. But is the flow in typical heat transport systems plug flow?

Flow in the CANDU feeders (38 to 76 mm) at 15 M/sec may indeed be plug flow. But some turbulent mixing does take place. More importantly, the feeders are of varying length and the flow has a spectrum of qualities. This gives quite a spectrum in transit time. This will skew

the propagation of a disturbance as illustrated in figure 10. Thus, depending on the transit time spectrum, a 5 node approximation (say) may be quite a good representation. The risers and headers may also give more diffusion than plug flow. These pipes are large diameter and the flow is turbulent. Very little is know of flow regimes and propagation properties in these situations.

In short, careful attention should be given to nodalization for meaningful simulation, quite apart from the normal numerical concerns such as the Courant limit, etc.

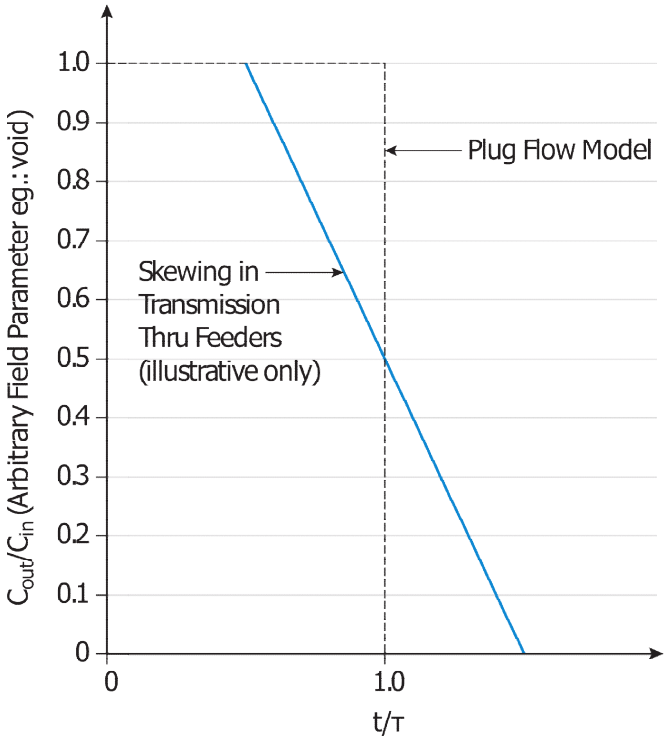

Figure 10 Transmission of a step change using the plug flow model and a feeder model with skewing due to differences in transit times.

3.4 Examples

In figures 11 to 13, some common piping situations are depicted. In figure 11, a simple Tee junction, note that each link has a unique junction resistance associated with the flow path of that link. Note also that a link has a unique upstream node and a unique downstream node. Links are always terminated by nodes at either end; in effect, the nodes provide boundary conditions for the links. There are 2 nodes per link, no more, no less. A node, on the other hand, can have many links connected to it.

The Y junction of figure 12 has a node link structure that is identical to the Tee junction. The differences in the two types of junctions are captured in the details of the correlations for friction, flow regimes, etc.

Figure 13 shows a CANDU HTS header and connecting piping. Note that there is no best or unique node-link representation. The requirements of the problem at hand dictates the number of nodes and links and the layout of the representation. For instance, it is useful to place a node centre at the point of a pressure measuring device so that experimental data can be more readily compared to the simulation results.

Figure 14 shows a typical nod-link diagram for a CANDU Heat Transport System simulation.

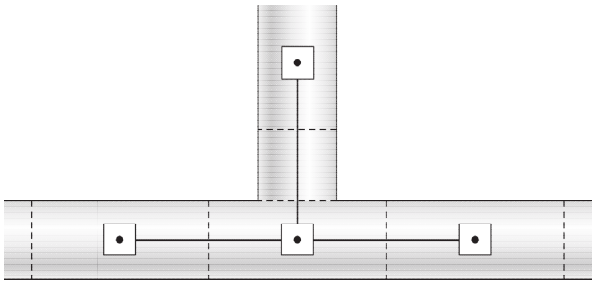

Figure 11 Simple Tee junction.

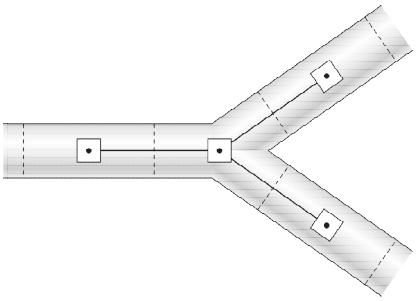

Figure 12 Simple Y junction.

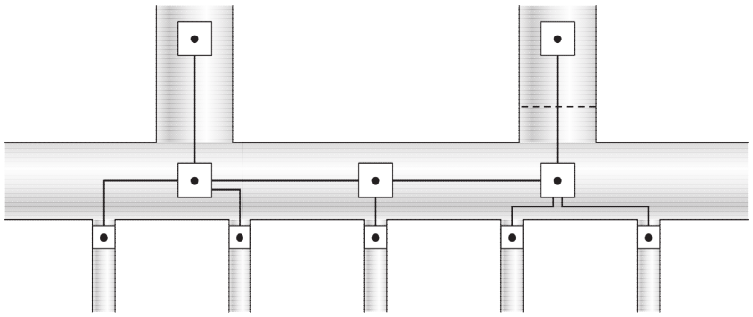

Figure 14 Sample node-link connection for a header.

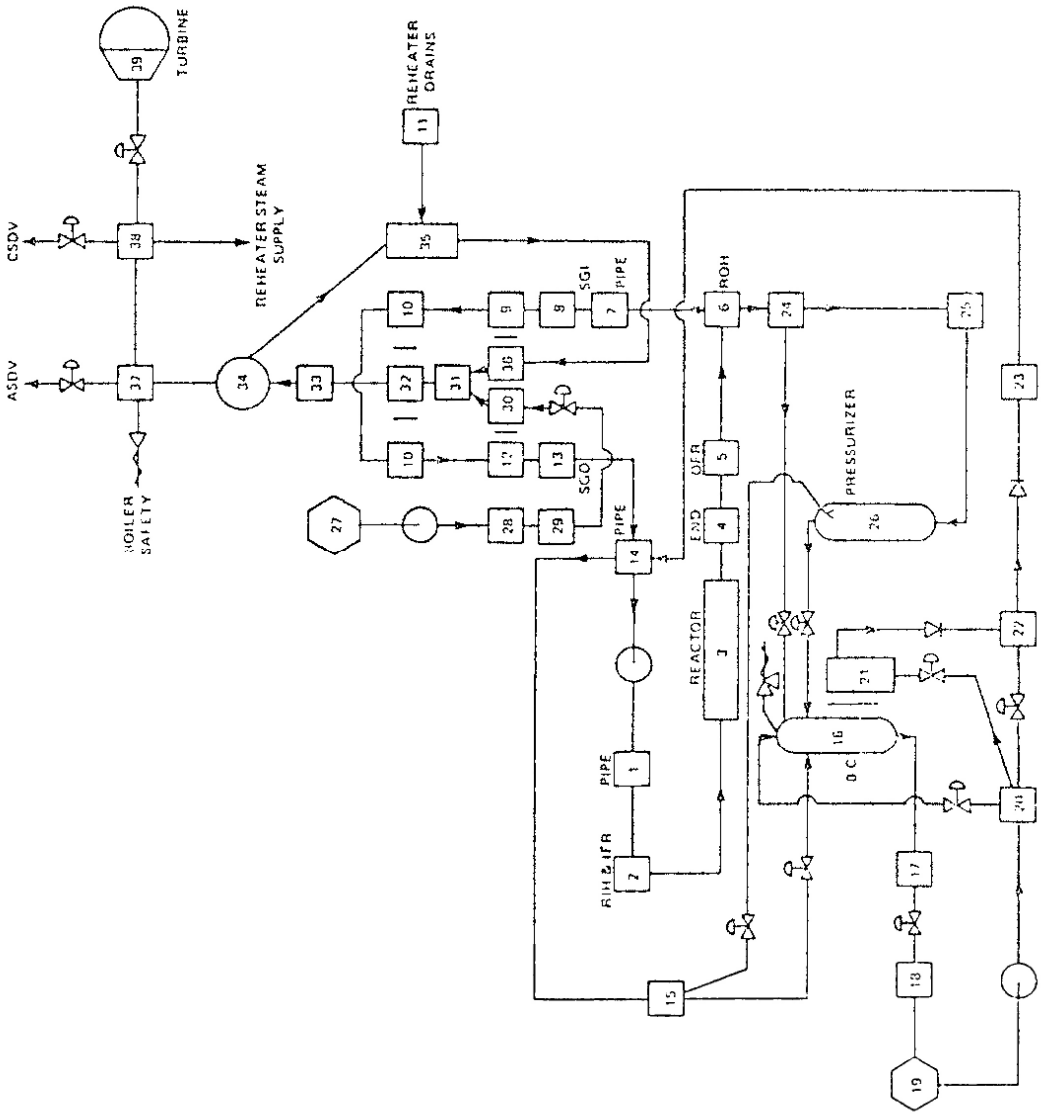

Figure 13 Node-link diagram: ¼ circuit CANDU.

3.5 Matrix Notation

As we shall see, it is sometimes expedient to cast the governing equations in matrix form. To illustrate, consider the node-link network of figure 15. Nominal flow directions are assigned to be positive in the normal flow direction. The mass balance equations for the 4 nodes are:

$$\begin{aligned}
\frac{dM_1}{dt} &= -W_1+W_4 \\
\frac{dM_2}{dt} &= +W_1-W_2+W_5 \\
\frac{dM_3}{dt} &= +W_2-W_3 \\
\frac{dM_4}{dt} &= +W_3-W_4-W_5
\end{aligned} \tag{67}$$

If we define $\dot{M}_i \equiv \frac{dM_i}{dt}$ then the mass balance equations can be written

$$\begin{pmatrix} \dot{M}_1 \\ \dot{M}_2 \\ \dot{M}_3 \\ \dot{M}_4 \end{pmatrix} = \begin{pmatrix} -1 & 0 & 0 & 1 & 0 \\ 1 & -1 & 0 & 0 & 1 \\ 0 & 1 & -1 & 0 & 0 \\ 0 & 0 & 1 & -1 & -1 \end{pmatrix} \cdot \begin{pmatrix} W_1 \\ W_2 \\ W_3 \\ W_4 \\ W_5 \end{pmatrix} \equiv \dot{\mathbf{m}} = \mathbf{A}^{MW} \cdot \mathbf{w} \tag{68}$$

where $\mathbf{A}^{MW}$ is a 4x5 matrix (number of rows = number of nodes N=4, and number of columns = number of links L=5) and **w** is the flow vector. Generally, upper case bold will be used to indicate a matrix and lower case bold will be used to indicate a vector. The superscript ^{MW} denotes that the matrix relates to the mass equation and to the flow vector. It also indicates the size of the matrix (nodes x links)

There can be up to L entries in a row but only 2 non-zero entries in any column - no more, no less. The $\mathbf{A}^{MW}$ matrix uniquely defines the geometry. The matrix is most easily constructed on a column by column basis, ie on a link by link basis: for each link (column vector) place a -1 in the location of the upstream node and a +1 in the location of the downstream node. As we shall see, all other matrices that arise in the solution to the mass, momentum and energy equations can be derived from the structure of $\mathbf{A}^{MW}$. This is very handy for computer coding purposes.

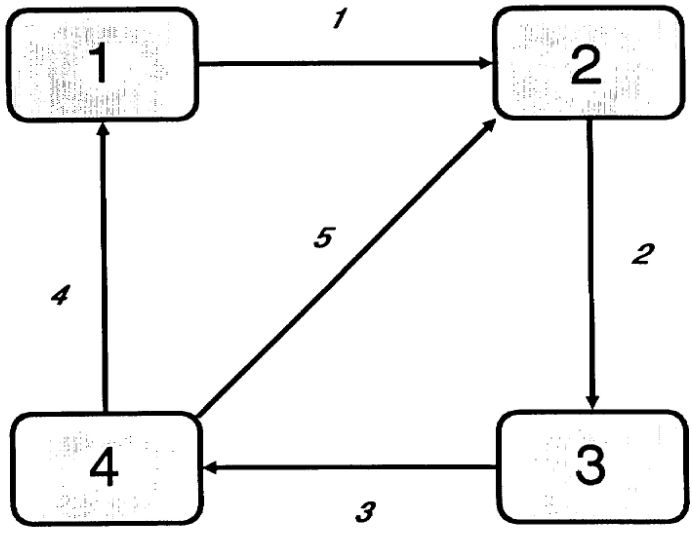

Figure 15 4 Node - 5 link diagram.

3.6 Exercises

1. For the 4 node, 5 link example of section 3.5, write out the flow and enthalpy equations as individual equations and in matrix form. Compare the structure of $\mathbf{A}^{WP}$ and $\mathbf{A}^{HW}$ to $\mathbf{A}^{MW}$, where the superscript ^{WP} denotes that the matrix relates to the flow equation and the pressure vector, and the superscript ^{HW} denotes that the matrix relates to the enthalpy equation and the flow vector.
2. For the case of 2 connected, open tanks of water with surfaces at different elevations, set up the node-link diagram and the mass, momentum and enthalpy equations.
3. What would be different if the tanks in question 2 were closed?

4 Equation of State

4.1 Introduction

As discussed in the previous sections, the momentum equation gives an update on the flows or velocities from one node to another, or from one grid point to another, based on a given pressure, flow, mass and enthalpy distribution. The updated flows are used by the mass and enthalpy equations to update the mass and enthalpy contents at each location. This information is given to the equation of state to update the pressure distribution which, along with the new densities and enthalpies is used by the momentum equation, and so on. In this manner, a time history of the fluid evolution is obtained. Of course, only the main variables are noted. The numerous and diverse empirical correlations require updates on the main variables and many secondary variables. This information also "flows" around the calculation.

The exploration of the appropriate forms of the equation of state to use for systems analysis begins by reflecting on the thermodynamics and the iterative method of finding pressure. Next a non-iterative method is offered as an improvement. This leads naturally to the water property evaluation. Fast, accurate curve fits are presented.

4.2 Thermodynamic Properties

From a thermodynamics viewpoint (see, for instance Sears [SEA75], the equation of state of a substance is a relationship between any four thermodynamic properties of the substance, three of which are independent. An example of the equation of state involves pressure P, volume V, temperature T and mass of system:

$$\pi (P, V, T, M) = 0 \tag{69}$$

If any three of the four properties are fixed, the fourth is determined.

The equation of state can also be written in a form which depends only on the nature of the system and not on how much of the substance is present, hence all extensive properties are replaced by their corresponding specific values. Thus

$$\pi (P, v, T) = 0 \tag{70}$$

is the specific value form of the above equation of state, where *v* is the specific volume. If any two of the thermodynamic properties are fixed, the third is determined.

From a thermodynamic point of view, the appropriate way to present water properties is by tables or formula for each property expressed as a function of the independent parameters P and T, as per Meyer [MEY67 or Haar [HAR84] (figure 16). Thus given values of pressure and temperature, the calculation of other thermodynamic properties is usually straightforward. On the other hand, the determination of pressure from known values of other thermodynamic properties is not direct since interpolation and iteration is required. Unfortunately, T and P are rarely the independent parameters in system dynamics since the numerical solution of the conservation equations yield mass and energy as a function of time. Hence, from the point of view of the equation of state, it is mass and energy which are the independent parameters.

Consequently, system codes are hampered by the form of water property data commonly available.

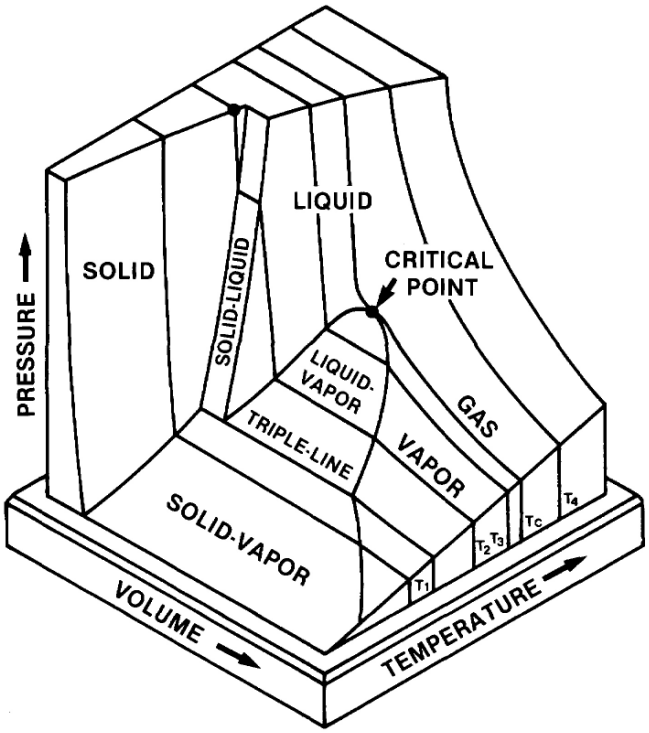

Figure 16 P-v-T surface for water .

A key point to note is that the conservation equations are all cast as rate equations whereas the equation of state is typically written as an algebraic equation. This arises from the basic assumption that, although the properties of mass, momentum and energy must be traced or solved as a function of time and space, the corresponding local pressure is a pure function of the local state of the fluid. Process dynamics are not considered. This is the essence of the equilibrium assumption (in a like manner, of course, we invariably use steady state heat transfer coefficients, etc. in dynamic processes). Historically, this mixture of form arose because thermodynamics endeavours were concerned with equilibrium states and not with system processes. System modellers, on the other hand, emphasized system dynamics and used what was available for constitutive relations. System modellers are more concerned with numerical problems.

But the decisive role of the equation of state in determining system dynamics was recognized early. Paynter [PAY60] identifies the power throughput as being the most important parameter for system dynamics. Power is composed of the product of effort (i.e. force or pressure) and flow. Porsching [POR71] correctly identifies the important role of flow in his work and by keying the formulation of node-link networks to flow, stable, efficient and accurate

solution schemes result. However, the role of pressure has not received the equivalent acknowledgement. Although the system dynamics are captured in Porsching's Jacobian, the essence of the system dynamics is not apparent. Nahavandi [NAH70] comes much closer to recognizing the role of pressure and explicitly casts the equation of state in rate form. Unfortunately, the system essence is again not apparent because Nahavandi's form is very case specific.

Most other popular schemes, for instance, Agee [AGE83], use the algebraic form of the equation of state. This treatment puts the pressure determination on the same level as heat transfer coefficients. Thus, although numerical solution of the resulting equation sets give correct answers (to within the accuracy of the assumption), intuition is not generated and time consuming iterations must be performed to get a pressure consistent with the local state parameters.

We look first at such an iterative scheme and then consider a more efficient alternative (the rate method).

4.3 The Iterative Method

Given the density and enthalpy of a volume of water, the task at hand is to find the associated values of pressure and temperature. Figure 17 shows qualitatively the relation between density, ρ, and enthalpy, h, for a given P. At low enthalpy, the fluid is single phase liquid and the density is high. As heat is added and the fluid reaches saturation temperature, vapour is generated to form a two-phase mixture and the density approaches the vapour density. The curve is well behaved and continuous making it a suitable candidate for numerical search routines.

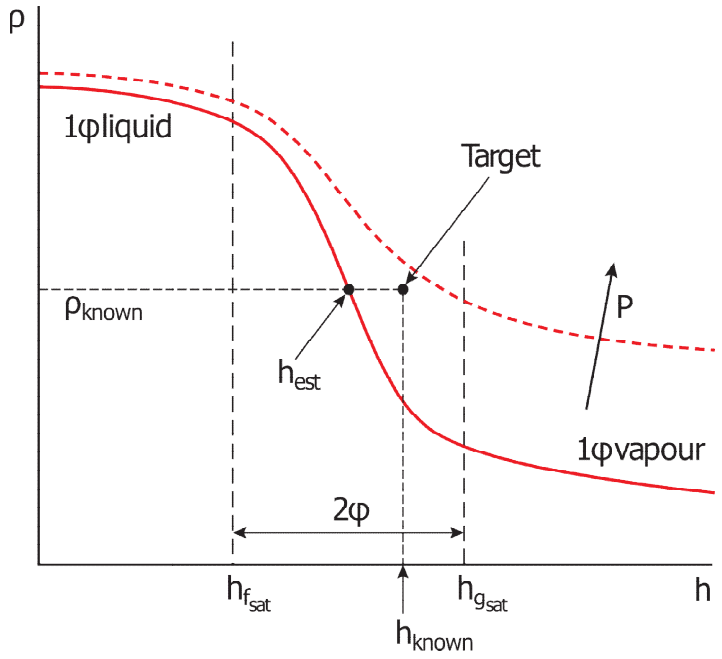

Figure 17 Numerical search for P given ρ and h for a two-phase mixture.

We start the iteration procedure by guessing a pressure. Usually in system transient simulation codes, the value of P at a previous time step is a good choice. Given P we calculate h_{fsat} and h_{gsat}, the saturation enthalpies for the liquid and vapour phases, respectively. If $h < h_{fsat}$ then the fluid is single phase liquid. If $h > h_{gsat}$ then the fluid is single phase vapour. Otherwise the fluid is a two-phase mixture with a quality, $x \in [0,1]$.

The case of two-phase equilibrium is considered first. Subsequently, the equations are extended to cover single phase and two-phase non-equilibrium fluid.

4.3.1 Two-Phase Equilibrium Fluid

For two-phase fluid, the density and enthalpy are functions of the pressure and quality. Since we know the density, ρ, we can estimate the quality (x_{est}) for the guessed P (assuming a homogeneous mixture) since:

$$v = \frac{1}{\rho} = v_f(P) + x_{est}\ v_{fg}(P) \tag{71}$$

and thus calculate the enthalpy based on the guessed P:

$$h_{est} = h_f(P) + x_{est}\ h_{fg}(P) \tag{72}$$

This estimated value of h will differ from the known value of h. This difference is used to drive the iteration, ie, to update the guessed pressure as illustrated in figure 18:

$$\Delta P = \frac{\Delta h}{(\partial h/\partial P)_\rho} \tag{73}$$

The denominator in equation 5 must be evaluated numerically if analytical expressions are not available. The pressure is updated via:

$$P = P + \Delta P \tag{74}$$

and the iteration is repeated until the pressure has converged to some tolerance. The temperature is just the temperature of saturated fluid at that pressure.

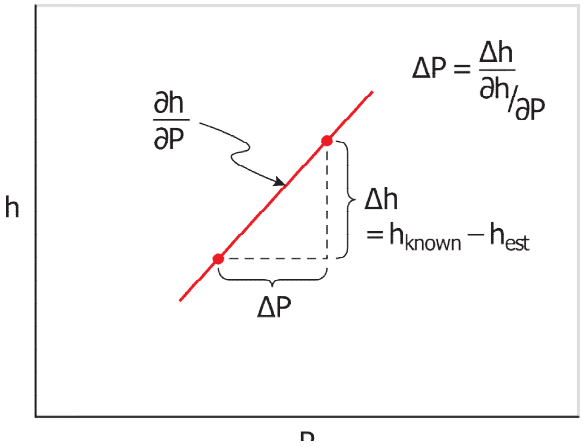

Figure 18 Error correction scheme for pressure in two-phase.

4.3.2 Single-Phase Sub-cooled and Superheated Fluid

For single phase fluid, the density and enthalpy are functions of P and T, ie:

$$\rho = \rho(P, T) \qquad h = h(P, T) \tag{75}$$

For a guessed P and T, ρ and h can be found directly from the water property tables. But this is just an estimate since P and T are guessed. The true values of ρ and h lie some distance away and, to a first approximation, the true values and the estimated values are related by a Taylor's series expansion:

$$\rho = \rho_{est} + \left(\frac{\partial \rho}{\partial T}\right)_P \Delta T + \left(\frac{\partial \rho}{\partial P}\right)_T \Delta P \tag{76}$$

$$h = h_{est} + \left(\frac{\partial h}{\partial T}\right)_P \Delta T + \left(\frac{\partial h}{\partial P}\right)_T \Delta P \tag{77}$$

Defining $\Delta\rho = \rho - \rho_{est}$ and $\Delta h = h - h_{est}$, we solve for ΔP and ΔT:

$$\Delta P = \frac{\left(\frac{\partial h}{\partial T}\right)_P \Delta\rho - \left(\frac{\partial \rho}{\partial T}\right)_P \Delta h}{\left(\frac{\partial \rho}{\partial P}\right)_T \left(\frac{dh}{dT}\right)_P - \left(\frac{\partial \rho}{\partial T}\right)_P \left(\frac{\partial h}{\partial P}\right)_T} \tag{78}$$

$$\Delta T = \frac{\left(\frac{\partial h}{\partial P}\right)_T \Delta\rho - \left(\frac{\partial \rho}{\partial T}\right)_T \Delta h}{\left(\frac{\partial \rho}{\partial T}\right)_P \left(\frac{dh}{dP}\right)_T - \left(\frac{\partial \rho}{\partial P}\right)_T \left(\frac{\partial h}{\partial T}\right)_P} \tag{79}$$

or, more compactly,

$$\Delta P = G_{1P} \Delta\rho + G_{2P} \Delta h \tag{80}$$

$$\Delta T = G_{1T} \Delta\rho + G_{2T} \Delta h \tag{81}$$

The derivatives must be evaluated numerically if analytical expressions are not available.

The pressure and temperature are updated via:

$$P = P + \Delta P \qquad T = T + \Delta T \tag{82}$$

and the iteration is repeated until the pressure and temperature have converged to some tolerance.

4.4 The Rate Method

We next consider a scheme (called the Rate Method) that eliminates the need for iteration with no loss in accuracy. The case of two-phase equilibrium is considered first in order to illustrate the method. Subsequently, the equations are extended to cover single phase and two-phase non-equilibrium fluid.

4.4.1 Two-Phase Equilibrium

For a two-phase homogeneous mixture we have:

$$v = v_f + x v_{fg} \tag{83}$$

$$h = h_f + x h_{fg} \tag{84}$$

where $v_{fg} \equiv v_g - v_f$ and $h_{fg} \equiv h_g - h_f$.

We wish to relate rates of change of pressure to rates of change in ρ and h. Specifically, we desire:

$$dP = G_1 d\rho + G_2 dh \qquad \frac{dP}{dt} = G_1 \frac{d\rho}{dt} + G_2 \frac{dh}{dt} \tag{85}$$

since dρ/dt and dh/dt (or equivalently, dM/dt and dH/dt) are available from the mass and enthalpy conservation equations. First concentrating on the case of constant ρ (or *v*), to obtain G_2, we differentiate equation (16) to gives:

$$\frac{dh}{dt} = \left(\frac{\partial h}{\partial P}\right)_\rho \frac{dP}{dt} = \left[\frac{\partial h_f}{\partial P} + h_{fg} \frac{\partial x}{\partial P} + x \frac{\partial h_{fg}}{\partial P}\right] \frac{dP}{dt}. \tag{86}$$

Using equation (83), holding *v* constant (i.e., ρ = constant):

$$\frac{dx}{dP} = \frac{\partial \left(\frac{v - v_f}{v_{fg}}\right)}{\partial P} = -\frac{1}{v_{fg}} \left[\frac{\partial v_f}{\partial P} + x \frac{\partial v_{fg}}{\partial P}\right]. \tag{87}$$

Substituting this into equation (86) gives:

$$\frac{dh}{dt} = \left\{\frac{\partial h_f}{\partial P} + x \frac{\partial h_{fg}}{\partial P} - \frac{h_{fg}}{v_{fg}} \left[\frac{\partial v_f}{\partial P} + x \frac{\partial v_{fg}}{\partial P}\right]\right\} \frac{dP}{dt} \tag{88}$$

or equally:

$$\begin{aligned} \frac{dP}{dt} &= \frac{v_{fg}}{\left\{v_{fg} \left[\frac{\partial h_f}{\partial P} + x \frac{\partial h_{fg}}{\partial P}\right] - h_{fg} \left[\frac{\partial v_f}{\partial P} + x \frac{\partial v_{fg}}{\partial P}\right]\right\}} \frac{dh}{dt} \\ &= \frac{v_{fg}}{\{\text{DENOMINATOR}\}} \frac{dh}{dt} = G_2 \frac{dh}{dt}. \end{aligned} \tag{89}$$

This gives the pressure rate response due to an enthalpy rate change, holding ρ constant.

If we repeat the above but holding h constant we find:

$$\frac{dP}{dt} = \frac{-h_{fg}}{\{\text{DENOMINATOR}\}} \frac{dv}{dt} = \frac{h_{fg} v^2}{\{\text{DENOMINATOR}\}} \frac{d\rho}{dt} = G_1 \frac{d\rho}{dt}. \tag{90}$$

Note that G_1 and G_2 are functions that depend only on the local saturation fluid properties and their slopes at the local pressure.

Combining equations 89 and 90 to get the total pressure rate response when both h and ρ are varying:

$$\frac{dP}{dt} = G_1(P, x)\frac{d\rho}{dt} + G_2(P, x)\frac{dh}{dt}. \tag{91}$$

This is the rate form of the equation of state for two-phase equilibrium fluid in terms of the intensive rate properties, dρ/dt and dh/dt, which are obtained from the continuity equations.

Equation 91 can be cast in the extensive form by noting that, since ρ = M/V and h = H/M,

$$\frac{d\rho}{dt} = \frac{1}{V}\frac{dM}{dt} - \frac{M}{V^2}\frac{dV}{dt} \tag{92}$$

and

$$\frac{dh}{dt} = \frac{1}{M}\frac{dH}{dt} - \frac{H}{M^2}\frac{dM}{dt}. \tag{93}$$

Substituting into equation 91 and collecting terms:

$$\frac{dP}{dt} = \left(\frac{G_1}{V} - \frac{G_2 H}{M^2}\right)\frac{dM}{dt} + \frac{G_2}{M}\frac{dH}{dt} - \frac{G_1 M}{V^2}\frac{dV}{dt}. \tag{94}$$

After some simplification and rearrangement we find:

$$\frac{dP}{dt} = \frac{F_1\frac{dM}{dt} + F_2\frac{dH}{dt} + F_3\frac{dV}{dt}}{M_g F_4 + M_f F_5} \tag{95}$$

where:

$$\begin{aligned}
F_1 &= h_g v_f - h_f v_g \\
F_2 &= v_g - v_f \\
F_3 &= h_f - h_g \\
F_4 &= \frac{\partial h_g}{\partial P}(v_g - v_f) - \frac{\partial v_g}{\partial P}(h_g - h_f) \\
F_5 &= \frac{\partial h_f}{\partial P}(v_g - v_f) - \frac{\partial v_f}{\partial P}(h_g - h_f) \\
M_g &\equiv x M \\
M_f &\equiv (1 - x) M .
\end{aligned} \tag{96}$$

The F functions are smooth, slowly varying functions of pressure provided good curve fits are used. The latest steam tables [HAA84] were used to fit saturated properties to less than 1/4% accuracy using low order polynomials and exponentials [GAR88]. Considerable effort was spent on obtaining accuracy and continuous derivatives over the full pressure range. The fact that good fits are available means that the F functions are well behaved which in turn makes the rate form of the equation of state extremely well behaved, as shown later.

The G functions are also well behaved for the same reasons.

The F and G functions have direct physical interpretations which aid in generating intuition. The F functions relate changes in the extensive properties, M, H and V, to changes in pressure. The G functions related changes in the intensive properties, ρ and h, to changes in pressure. Often, a simple numerical evaluation of these functions during a simulation aids in developing an appreciation of the changing roles of the key actors in a dynamic simulation.

For instance, because F_1 is negative, we immediately see that adding mass to a fixed volume of liquid with fixed total enthalpy will cause a depressurization (because the specific enthalpy, $h = H/M$, is decreased). But, since G_1 is positive, an increase in density in a fluid of fixed specific enthalpy causes a pressurization.

4.4.2 Single-Phase Sub-cooled and Superheated Fluid

For the single-phase sub-cooled or superheated case, we do not have to account for the sorting out between phases as we did for the two phase case. thus the derivation is more direct and less complex. We could simply use:

$$P = \pi(\rho, h) \quad (97)$$

to give:

$$\frac{dP}{dt} = \left(\frac{\partial P}{\partial \rho}\right)_h \frac{d\rho}{dt} + \left(\frac{\partial P}{\partial h}\right)_\rho \frac{dh}{dt} \quad (98)$$

but, since the steam tables are given as a function of P and T, the slopes in equation (98) are not easily obtained. To cast the pressure rate equation in terms of the independent variables, P and T, consider:

$$\rho = \rho(P, T) \quad (99)$$

and

$$h = h(P, T) \quad (100)$$

Note that the non-equilibrium case requires the explicit tracking of the temperature in addition to pressure. Taking derivatives of Equations (99) and (100):

$$\frac{d\rho}{dt} = \left(\frac{\partial \rho}{\partial P}\right)_T \frac{dP}{dt} + \left(\frac{\partial \rho}{\partial T}\right)_P \frac{dT}{dt} \quad (101)$$

and

$$\frac{dh}{dt} = \left(\frac{\partial h}{\partial P}\right)_T \frac{dP}{dt} + \left(\frac{\partial h}{\partial T}\right)_P \frac{dT}{dt}. \tag{102}$$

But we desire:

$$\frac{dP}{dt} = G_{1P} \frac{d\rho}{dt} + G_{2P} \frac{dh}{dt} \tag{103}$$

and

$$\frac{dT}{dt} = G_{1T} \frac{d\rho}{dt} + G_{2T} \frac{dh}{dt}. \tag{104}$$

This is easily obtained by solving equations (101) and (102) for dP/dt and dT/dt to yield:

$$\frac{dP}{dt} = \frac{\left(\frac{\partial h}{\partial T}\right)_P \frac{d\rho}{dt} - \left(\frac{\partial \rho}{\partial T}\right)_P \frac{dh}{dt}}{\left(\frac{\partial \rho}{\partial P}\right)_T \left(\frac{dh}{dT}\right)_P - \left(\frac{\partial \rho}{\partial T}\right)_P \left(\frac{\partial h}{\partial P}\right)_T} \tag{105}$$

and

$$\frac{dT}{dt} = \frac{\left(\frac{\partial h}{\partial P}\right)_T \frac{d\rho}{dt} - \left(\frac{\partial \rho}{\partial T}\right)_T \frac{dh}{dt}}{\left(\frac{\partial \rho}{\partial T}\right)_P \left(\frac{dh}{dP}\right)_T - \left(\frac{\partial \rho}{\partial P}\right)_T \left(\frac{\partial h}{\partial T}\right)_P} \tag{106}$$

which is the intensive form we desire.

The extensive form is obtained as for the two-phase equilibrium case. Equations (92) and (93) are substituted into equations (105) and (105) and after rearrangement we find:

$$\frac{dP}{dt} = \frac{F_{1P} \frac{dM}{dt} + F_{2P} \frac{dH}{dt} + F_{3P} \frac{dV}{dt}}{M_v F_{4P} + M_l F_{5P}} \tag{107}$$

and

$$\frac{dT}{dt} = \frac{F_{1T} \frac{dM}{dt} + F_{2T} \frac{dH}{dt} + F_{3T} \frac{dV}{dt}}{M_v F_{4T} + M_l F_{5T}} \tag{108}$$

where

$$F_{1P} = \rho \left.\frac{\partial h}{\partial T}\right)_P + h \left.\frac{\partial \rho}{\partial T}\right)_P$$

$$F_{2P} = -\left.\frac{\partial \rho}{\partial t}\right)_P$$

$$F_{3P} = -\rho^2 \left.\frac{\partial \rho}{\partial T}\right)_P$$

$$F_{4P} = 0 \text{ for subcooled, } = \left.\frac{d\rho}{\partial P}\right)_T \left.\frac{\partial h}{\partial T}\right)_P - \left.\frac{\partial \rho}{\partial T}\right)_P \left.\frac{dh}{dP}\right)_T \text{ for superheated}$$

$$F_{5P} = \left.\frac{d\rho}{\partial P}\right)_T \left.\frac{\partial h}{\partial T}\right)_P - \left.\frac{\partial \rho}{\partial T}\right)_P \left.\frac{dh}{dP}\right)_T \text{ for subcooled } = 0 \text{ for superheated}$$

$$F_{1T} = \rho \left.\frac{\partial h}{\partial T}\right)_P + h \left.\frac{\partial \rho}{\partial T}\right)_P$$

$$F_{2T} = -\left.\frac{\partial \rho}{\partial t}\right)_T$$

$$F_{3T} = -\rho \left.\frac{\partial h}{\partial T}\right)_T$$

$$F_{4T} = -F_{4P}$$

$$F_{5T} = -F_{5P}$$

$$M_v = \text{mass of vapour phase } = 0 \text{ for subcooled, } = M \text{ for superheated}$$

$$M_\ell = \text{mass of liquid phase } = M \text{ for subcooled } = 0 \text{ for superheated} \qquad (109)$$

4.4.3 Two-Phase Non-Equilibrium

The rate form for the equation of state for the two-phase non-equilibrium case is a simple extension of the single-phase non-equilibrium case. The liquid and vapour phases are treated independently to give:

$$\frac{dP_k}{dt} = G^k_{1P} \frac{d\rho_k}{dt} + G^k_{2P} \frac{dh_k}{dt} \qquad (110)$$

$$\frac{dT_k}{dt} = G^k_{1T} \frac{d\rho_k}{dt} + G^k_{2T} \frac{dh_k}{dt} \qquad (111)$$

where k represents either l or v for the liquid or vapour phases respectively. In general, the 6 equation model (3 continuity equations for each phase) would be used for the general unequal temperature, unequal velocity, unequal pressure situation. Thus $d\rho_k/dt$ and dh_k/dt are available to the rate form of the equation of state.

4.5 Water Property Fits

To facilitate the calculation of light water properties, the 1984 standard tables were accurately curve fitted as discussed in detail at www.nuceng.ca/water/h2ohome.htm. These fitted functions are supplied in the files H2OPROP.FOR and H2OPROP.C for user convenience. These FORTRAN and C functions cover a wide range of pressures and temperatures and should be sufficient for most nuclear reactor simulations, with the exception of severe accidents that generate extreme conditions. These functions are fast and more than accurate enough given the other errors in system simulation [GAR88, GAR89, GAR92].

Heavy water properties have of course been developed in-house at AECL and Ontario Power Generation for use in their industry computer tool-set. Some tools are available in the public domain; see *www.nuceng.ca/d2o/d2ohome.htm*.

The basic overall approach taken in the curve fitting task was that, since the more difficult region to fit was the transition from single to two-phase and since most power plants operate at or near this region, careful attention would be paid the phase transition region at the expense of accuracy away from the saturation line, if necessary. Thus, the first major step was to accurately fit the saturation lines. Then, since density, enthalpy and other properties vary more strongly with T than with P (as shown in figure 19), the property in question, say density, would be calculated based on the deviation from the saturation value at the given T, ie:

$$\rho(P,T) = \rho_{sat}(T) + \left(\frac{\partial \rho}{\partial P}\right)_T \left(P - P_{sat}(T)\right) \qquad (112)$$

Figure 20 illustrates the strategy. It should be obvious by now that not only the properties need to be fitted but the slopes are needed as well. Both the properties and the slopes of the properties must be free of discontinuities if numerical searches are to converge.

Having derived the desired rate forms for the equation of state, we proceed to section 5 to illustrate the utility of the approach.

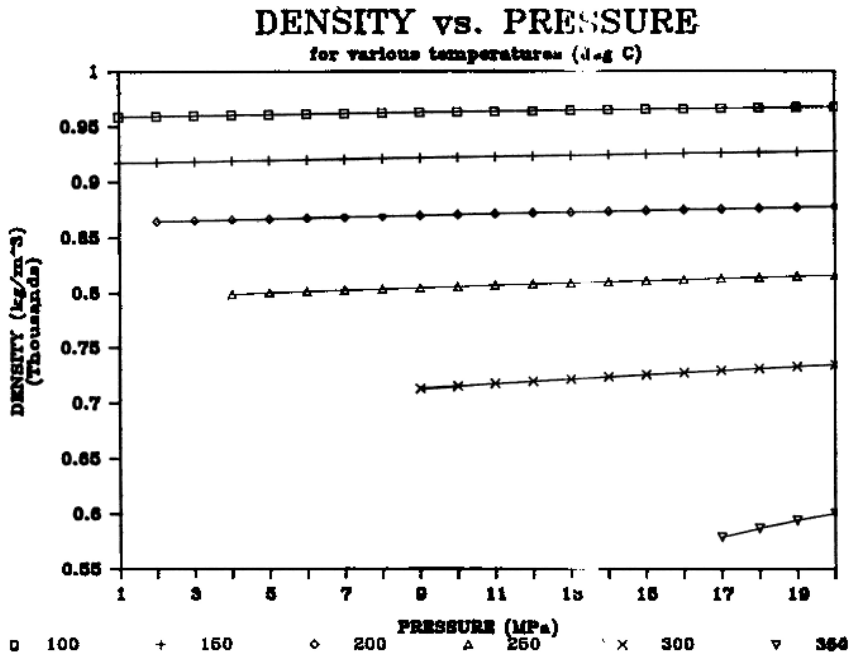

Figure 19 Density vs. pressure at various temperatures in sub-cooled water.

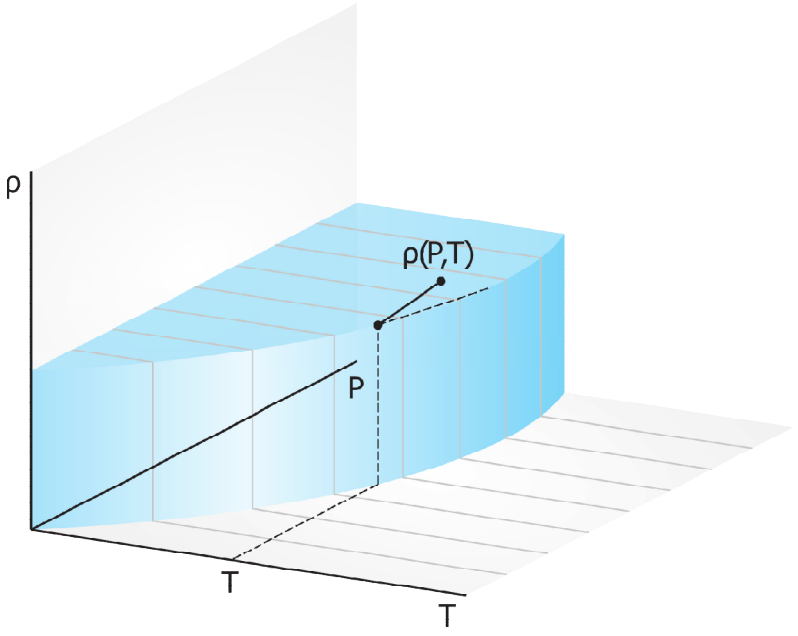

Figure 20 Basis for curve fitting in the subcooled region.

4.6 Problems

4. Using the spread sheet macros for Microsoft Excel supplied by G.R. McGee (as per http://www.nuceng.ca/water/h2ohome.htm), calculate and plot the density, enthalpy, quality and void fraction for a range of pressures (1 to 100 atmospheres) and temperatures(50 °C to 350 °C). Make sure you cover the subcooled, saturated and superheated ranges.

5. Using the code, WATERA.EXE (see http://www.nuceng.ca/water/h2ohome.htm):

   a. Calculate ρ and h for P=10 MPa and T=300 °C. Increase the temperature in steps to see the approach to two-phase.

   b. Using ρ and h slightly different than that found in (a), calculate P and T.

   c. Practice calculating ρ given h and P.

5 The Rate Form of the Equation of State

5.1 Introduction

In conjunction with the usual rate forms of the conservation equations, the time derivative form of the Equation of State is investigated from a numerical consideration point of view. By recasting the equation of state in a form that is on equal footing with the system conservation equations, several advantages are found. The rate method is found to be more intuitive for system analysis, more appropriate for eigenvalues extraction, as well as easier to program and to implement. Numerically, the rate method is found [GAR87a] to be more efficient and as accurate than the traditional iterative method.

First, the derivation of the rate form of the Equation of State is presented. Systematic comparison between the new method and the traditional iterative method is made by applying the methods to a simple flow problem. The comparison is then extended to a practical engineering problem requiring accurate prediction of pressure.

5.2 The Rate Form

Presently, the conservation equations are all cast as rate equations whereas the equation of state is typically written as an algebraic equation [AGE83]. This arises from the basic assumption that, although the properties of mass, momentum and energy must be traced or solved as a function of time and space, the corresponding local pressure is a pure function of the local state of the fluid. Hence the equation of state is considered only as a constitutive equation. This treatment puts the pressure determinations on the same level as heat transfer coefficients. Although numerical solution of the resulting equation sets give correct answers (to within the accuracy of the assumption), intuition is not generated and time-consuming iterations must be performed to get a pressure consistent with the local state parameters.

The time derivative form of the Equation of State is investigated, herein, in conjunction with the usual rate forms of the conservation equations. This gives an equation set with two distinct advantages over the use of algebraic form of the Equation of State normally used.

The first advantage is that the equation set used consists of four equations for each node or point in space, characterizing the four main actors: mass, flow, energy and pressure. This consistent formulation permits the straight-forward extraction of the system eigenvalues (or characteristics) without having to solve the equations numerically.

The second advantage is that the rate form of the Equation of State permits the numerical calculation of the pressure without iteration. The calculation time for the pressure was found to be reduced by a factor of more than 20 in some cases (where the flow was rapidly varying) and, at worst, the rate form was no slower than the algebraic form. In addition, because the pressure can be explicitly expressed in terms of slowly varying system parameters and flow, an implicit numeric scheme is easily formulated and coded.

This section will concentrate on this numerical aspect of the equation of state.

The equation of state has been discussed in section 4 where we saw that the determination of pressure from known values of other thermodynamic properties is not direct. Interpolation and iteration is required because the independent (known) parameters are temperature, T, and pressure, P. Unfortunately, T and P are rarely the independent parameters in system dynamics since the numerical solution of the conservation equations yield mass and energy as a function of time. Hence, from the point of view of the equation of state, it is mass and energy which are the independent parameters. Consequently, system codes are hampered by the form of water property data.

Having derived the desired rate forms for the equation of state in section 4, we proceed to illustrate the utility of the approach.

5.3 Numerical Investigations: a Simple Case

The simple two-node, one-link system is (Figure 21) chosen to illustrate the effectiveness of the rate form of the equation of state in eliminating the inner iteration loop in thermalhydraulic simulations. In general, the task is to solve the matrix equation,

$$\frac{\partial \mathbf{u}}{\partial t} = \mathbf{A}\mathbf{u} + \mathbf{b} \tag{113}$$

over the time domain of interest. The key point that we wish to discuss is the difference in the normal method (where $\mathbf{u} = \{M_1, H_1, W, M_2, H_2\}$) and the rate method (where $\mathbf{u} = \{M_1, H_1, P_1, W, M_2, H_2, P_2\}$). For simplicity and clarity, we first summarize work for a fixed time step Euler integration:

$$\mathbf{u}^{t+\Delta t} = \mathbf{u}^{t} + \Delta t[\mathbf{A}\mathbf{u} + \mathbf{b}] \tag{114}$$

As we shall see, this is sufficient to generate some observations on the utility of the rate method. These observations then guide us in the use of more complicated and efficient algorithms.

5.3.1 Normal Method

The normal method obtains the value of pressure at time, t+Δt, from an iteration (as discussed previously) on the equation of state using the values of mass and enthalpy at time, t+Δt, i.e. the new pressure must satisfy:

$$P^{t+\Delta t} = fn(\rho^{t+\Delta t}, h^{t+\Delta t}) \tag{115}$$

where both ρ and h are pressure dependent functions. Any iteration requires a starting guess and a feedback mechanism. Here, the starting guess for pressure is the value at time, t: P^t. Feedback in the Newton-Raphson scheme is generated by using an older value of pressure, $P^{t-\Delta t}$, to estimate slopes. Since the slope, $\partial h/\partial P$, was readily available from the rate method, we chose to use this slope to guide feedback. Thus, in the comparison of methods, we have borrowed from the rate method to enhance the normal method. This provides a stronger test of the rate method.

Thus we can now generate our next pressure guess from:

$$P_{new} = P_{guess} + \frac{h - h_{est}}{\partial h/\partial P} * ADJ \qquad (116)$$

where h is the known value of h at $t+\Delta t$ and h_{est} is the estimated h based on the guessed pressure as discussed in detail in section 4. ADJ is an adjustment factor $\in [0, 1]$, to allow experimentation with the amount of feedback. This iteration on pressure continues until a convergence criteria, P_{err}, is satisfied. The converged pressure is used in the outer loop in the momentum equation and the time can be advanced one time step. Figure 22 summarizes the logic flow.

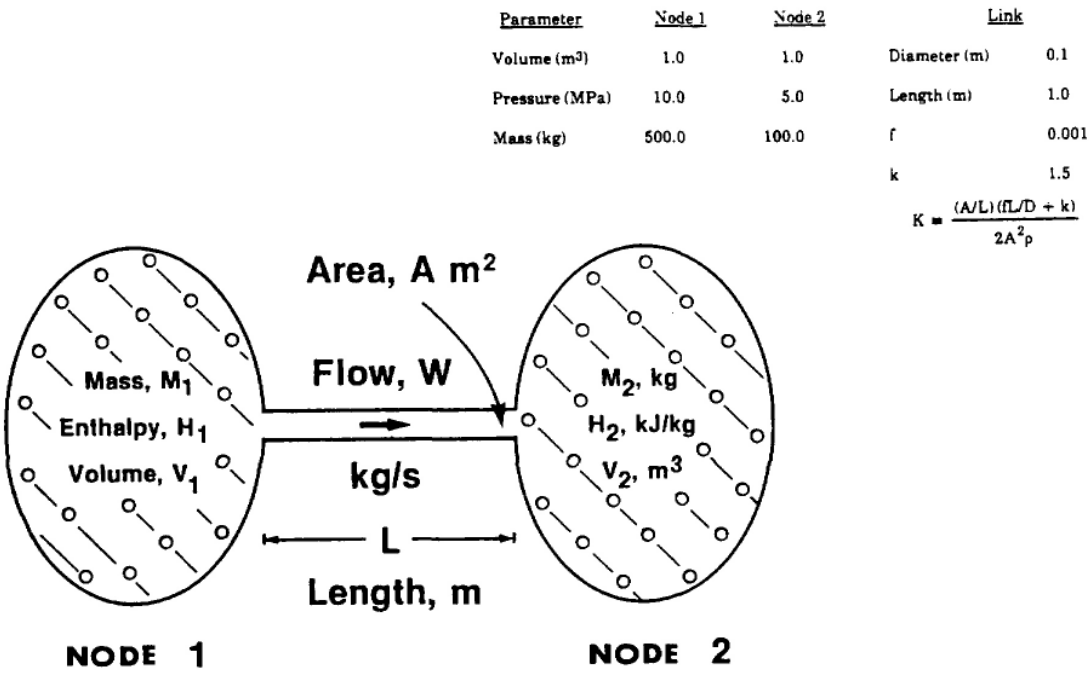

Figure 21 Simple 2-node, 1-link system.

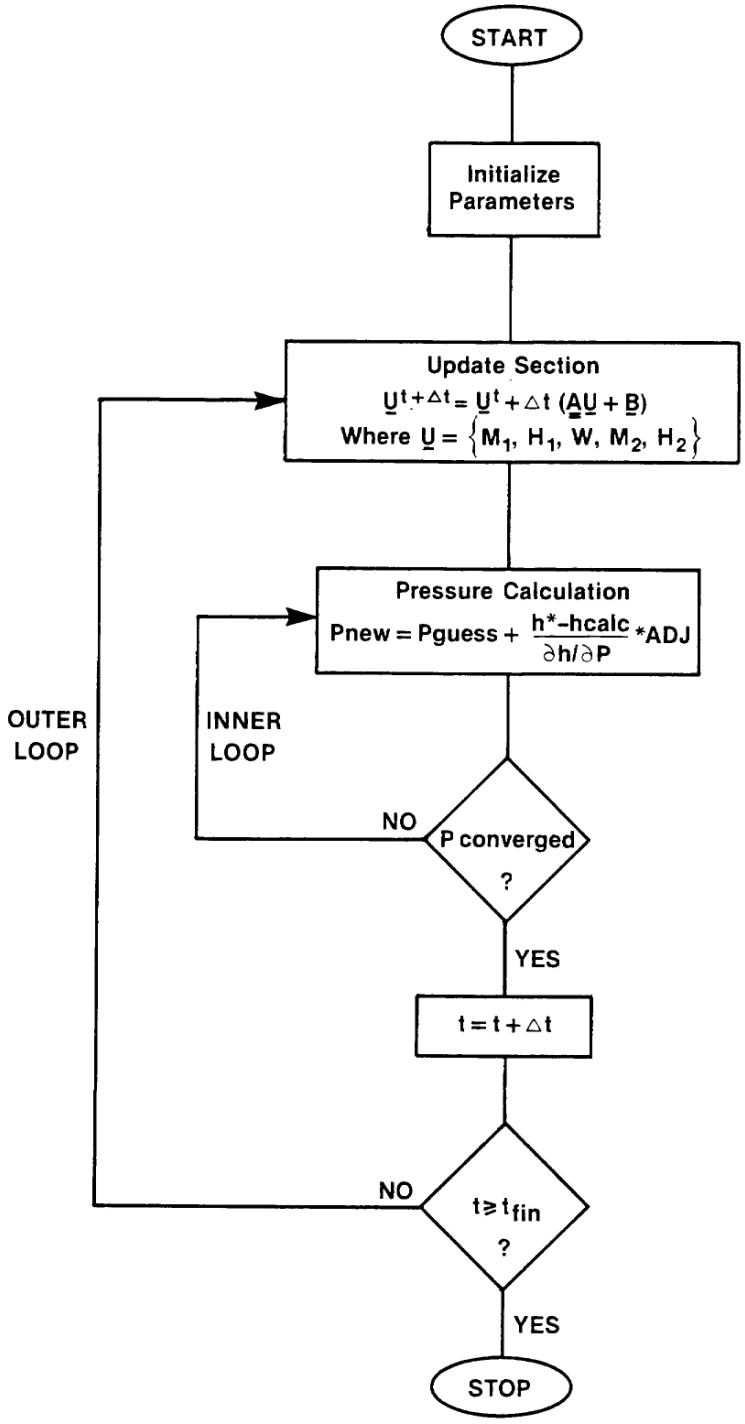

Figure 22 Program flow diagram for the normal method.

5.3.2 Rate Method

The rate method obtains the value of pressure at time, t+Δt, directly from the rate equation as is done for the conservation equations. Equation 95, gives the rate of change of pressure which can be solved simultaneously with the conservation equations if substitutions for dM/dt and dH/dt are made, leading to:

$$\frac{\partial \mathbf{u}}{\partial t} = \mathbf{Au} + \mathbf{b} \tag{117}$$

where $\mathbf{u} = \{M_1\ H_1,\ P_1,\ W,\ M_2,\ H_2,\ P_2\}$.

Thus:

$$\mathbf{P}_i^{t+\Delta t} = \mathbf{P}_i^{t} + \Delta t[\mathbf{Au} + \mathbf{b}]_i \tag{118}$$

No inner iteration is required, as shown in Figure 23.

One problem with this approach is that the pressure may drift away from a value consistent with the mass and energy. This problem does not arise with the conservation equations because the equations are conservative in form, by design. It is not possible to cast the rate form of the equation of state in conservative form since pressure is simply not a conserved property. We can surmount the drift problem by using the feedback philosophy of the normal method. Thus the new pressure is given by:

$$\mathbf{P}_i^{t+\Delta t} = \mathbf{P}_i^{t} + \Delta t[\mathbf{Au} + \mathbf{b}]_i + \frac{h\text{-}h_{est}}{\partial h/\partial P} * ADJ \tag{119}$$

This correction term uses only readily available information in a non-iterative manner.

In essence, the main effective difference between the normal and rate method is that during the time step between t and t+Δt the normal method employs parameters such as density, quality etc. derived from the pressure at time, t+Δt, whereas the rate form employs parameters derived from the pressure and rate of change of pressure at time, t. The normal method is not necessarily more accurate, it is simply forcibly implicit in its treatment of pressure. The rate method can be implicit (as we shall see) but it need not be. Without experimentation it is not evident whether the necessity of iteration in the normal method is outweighed by the possible advantages of the implicit pressure treatment.

The next sections test these issues with numerical experiments.

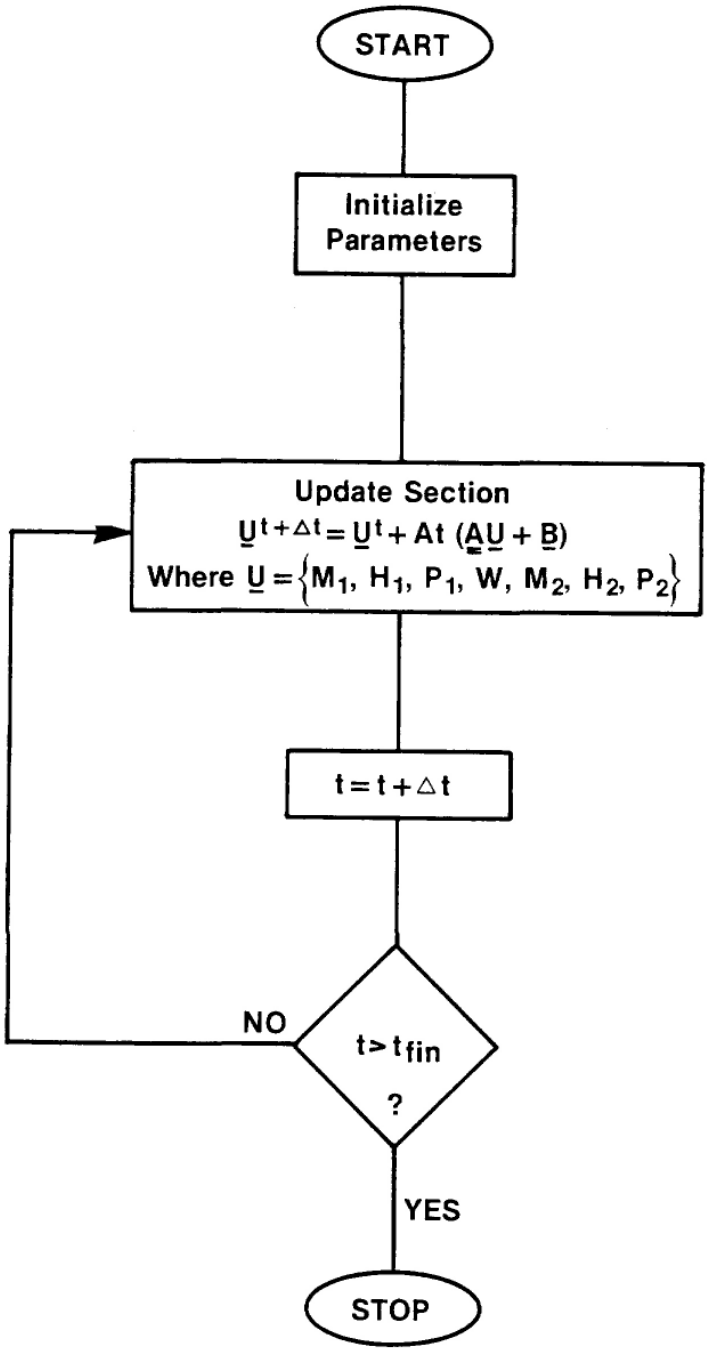

Figure 23 Program flow diagram for the rate method.

5.3.3 Comparison

The two node, one link numerical case under consideration is summarized in figure 21. Perhaps the most startling difference between the normal and rate methods is the difference in programming effort. The rate form was found to be extremely easy to implement since the equation form is the same as the continuity equations. The normal method took roughly twice the time to implement since separate control of the pressure logic is required. This arises directly from the treatment of pressure in the normal method: it is the odd man out.

The second startling difference was ease of execution of the rate form compared to the normal form. The normal form required experimentation with both the pressure convergence tolerance, P_{err}, and the adjustment factor, ADJ, since the solution was sensitive to both parameters. The rate method contains only the adjustment factor ADJ. The first few runs of the rate method showed that since the correction term for drift $(h-h_{est})/(\partial h/\partial p)$ is always several orders of magnitude below the primary update term, $\Delta t\{\mathbf{A}\,\mathbf{u} + \mathbf{b}\}$, the solution was not at all sensitive to the value of ADJ. Thus the rate method proved easier to program and easier to run than the normal method.

We look at the number of iterations required for pressure convergence as a function of P_{err} and ADJ for the normal method without regard to accuracy. For a Δt of 0.01sec, $P_{ert} = 10^{-3}$ (fraction of the full scale pressure of 10 MPa), the effect of ADJ is seen in figure 24. This result is typical: an adjustment factor of 1 gives rapid convergence (one or two iterations) except where very large pressure changes occur. For the case of very rapid changes, the full feedback (ADJ = 1) causes overshoot. Overall, however, the time spent for pressure calculation is about the same, independent of ADJ.

Allowing a larger pressure error had the expected result of reducing the number of iterations needed per routine call. But choosing a smaller time step (say .001) did not have a drastic effect on the peak interations required. The rate method, of course, always used 1 iteration per routine call and the adjustment factor ADJ was found to be unimportant since the drift correction factor amounted to no more than 1% of the total pressure update term.

The integrated error for both methods is shown in figure 25. Both methods converge rapidly to the benchmark. The value of P_{err} is not overcritical. A value of P_{err} consistent with tolerances set for other simulation variables is recommended. The time spent per each iteration is roughly comparable for both methods. The main difference is that the rate method requires the evaluation of the F functions over and above the property calls common to both methods. This minor penalty is insignificant in all cases studied since the number of iterations / call dominated the calculation time.

In summary, to this point, the rate method is easier to implement, more robust and is equal to the normal method at worst, more than 20 times faster under certain conditions. We now look at incorporating a variable time step to see how each method compares.

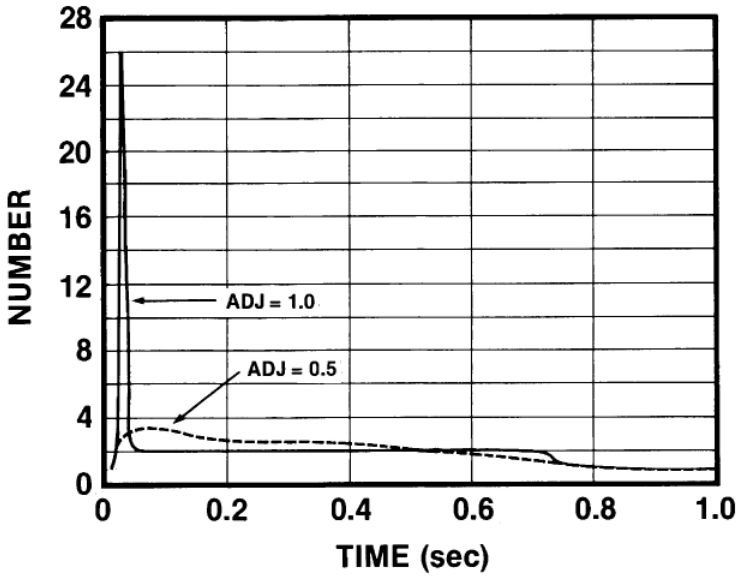

Figure 24 Number of iterations per pressure routine call for the normal method with a time step of 0.01 seconds and a pressure tolerance of 0.001 of full scale (10 MPa).

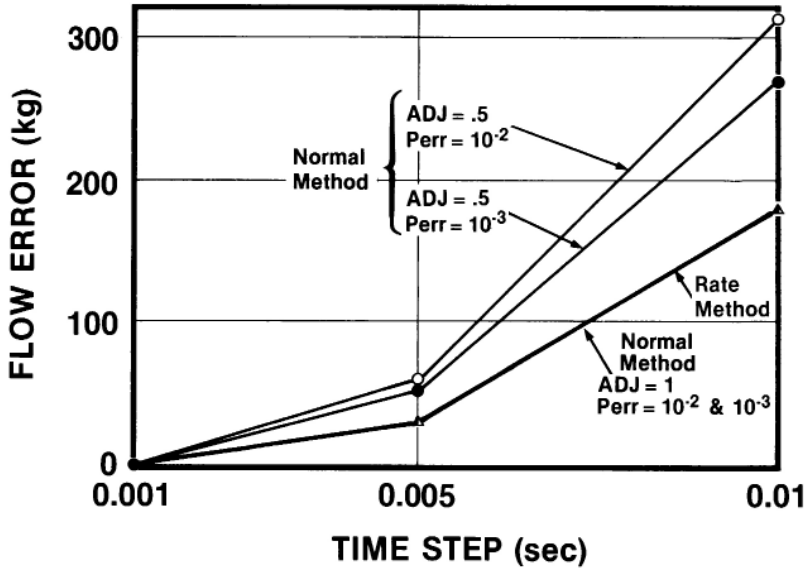

Figure 25 Integrated flow error for the rate method and the normal method for various fixed time steps, convergence tolerances and adjustment factors.

Typical variable time step algorithms require some measure of the rate of change of the main variables to guide the Δt choice. The matrix equation, equation 113, provides the rates that we need. Since the rate method incorporated the pressure into the **u** vector, the rate of change of pressure is immediately available. For the normal method, the rate of change of pressure has to be estimated from previous history (which is no good for predicting the onset of rapid changes) or by trial and error. The trial and error method employed here is to calculate the Δt as the minimum of the time steps calculated from:

$$\Delta t_i = \frac{(\text{fractional tolerance})x(\text{scale factor for } u_i)}{\partial u_i/\partial t} \tag{120}$$

This restricts Δt so that no parameter changes more than the prescribed fraction for that parameter. This can be implemented in a non-iterative manner for the rate method. However, for the normal method, the above minimum Δt based on **u** is used as the test Δt for the pressure routine and the rate of change of pressure is estimated as:

$$\frac{\partial P}{\partial t} = \frac{P^{t+\Delta t} - P^t}{\Delta t} \tag{121}$$

The Δt is then scaled down if the pressure change is too large for that iteration. Then the new Δt is tested to ensure that it indeed satisfies the pressure change limit. This iteration loop has within it the old inner loop.

It is expected then, that the normal method will not perform as well as the rate method primarily because of the "loop within a loop" inherent in the normal method as applied to typical system simulation codes.

A number of cases were studied and the results of the normal method were compared to the rate method. The figure of merit was chosen as

$$\text{F.O.M.} = \frac{10{,}000}{(\text{integrated error})x(\text{total pressure routine time})x(\text{No. of adjustable parameters})} \tag{122}$$

Thus, an accurate, fast and robust method achieves a high figure of merit. Some results are listed in table 1. Derating a method with more adjustable parameters is deemed appropriate because of the figure of merit should reflect the effort involved in using that method. On average, about 6 runs of the normal method, with various P_{err} and ADJ were needed to scope out the solution field compared to 1 run for the rate method. Thus a derating of 2 is not an inappropriate measure of robustness or effort required.

The results indicate that the rate method is a consistently better method than the normal method in terms of numerical performance. We see no reason why this improvement would not exist for any thermal hydraulic system in which pressure field determination is required.

Table 1 Figure of merit comparisons of the normal and rate forms of the equation of state for various convergence criteria (simple case).

Case	Method	Convergence (fraction full scale) Overall	Pressure	ADJ	Integral error	Pressure routine time	AP*	FOM*	Relative* FOM
1	P rate	0.01		0.5	180.39	24	1	2.31	
2	P norm	0.01	0.01	0.5	597.61	25	2	0.33	6.90
3	P rate	0.001		0.5	21.13	96	1	4.93	
4	P norm	0.001	0.001	0.5	79.819	119	2	0.53	9.37
5	P norm	0.001	0.00001	1	22.808	246	2	0.89	5.53
6	P norm	0.001	0.0001	1	22.781	229	2	0.96	5.14
7	P norm	0.001	0.001	1	22.761	140	2	1.57	3.14
8	P norm	0.001	0.01	1	22.847	128	2	1.71	2.88
9	P rate	0.0001		0.5	0.534	736	1	25.44	
10	P norm	0.0001	0.0001	0.5	2.2536	852	2	2.60	9.77
11	P norm	0.0001	0.0001	1	0.4907	894	2	11.40	2.23

* AP = # of adjustable parameters
FOM = Figure of merit
Relative FOM = (FOM for rate method)/(FOM for normal method)

Next we briefly discuss implicit numerical schemes.

The nodal equations are:

$$\frac{dM_1}{dt} = -W \qquad \frac{dM_2}{dt} = +W \tag{123}$$

$$\frac{dH_1}{dt} = -h_1 W \qquad \frac{dH_2}{dt} = +h_1 W \tag{124}$$

$$\frac{dP_i}{dt} = \frac{F_1 \frac{dM_i}{dt} + F_2 \frac{dH_i}{dt}}{M_g F_4 + M_f F_5}, \qquad i = 1,2 \tag{125}$$

Considering just the flow and pressure rate equations, we have (after substituting in for dM/dt and dH/dt):

$$\frac{dW}{dt} = \frac{A}{L}(P_1 - P_2) - \frac{A}{L} K|W|W \tag{126}$$

and

$$\frac{dP_1}{dt} = -\chi_1 W \qquad \frac{dP_2}{dt} = +\chi_2 W \tag{127}$$

where χ_1 and χ_2 are > 0 and are given by:

$$\chi = \frac{F_1 + hF_2}{M_g F_4 + M_f F_5} \tag{128}$$

evaluated at the local property values of nodes 1 and 2.

Employing a scheme that is implicit in flow, the difference equations are cast

$$\frac{W^{t+\Delta t} - W^t}{\Delta t} = \frac{A}{L}(P_1^{t+\Delta t} - P_2^{t+\Delta t}) - \frac{A}{L} K |W^t| W^{t+\Delta t} \tag{129}$$

$$\frac{P_i^{t+\Delta t} - P_i^t}{\Delta t} = \pm\chi_i W^{t+\Delta t} \text{ implies} P_i^{t+\Delta t} - P_i^t = \pm\chi_i W^{t+\Delta t}\Delta t \tag{130}$$

Collecting terms and solving for the new flow:

$$W^{t+\Delta t} = \left[1 + \frac{A}{L} K |W^t| \Delta t + \frac{A}{L}(\chi_1 + \chi_2)\Delta t^2\right]^{-1}\left[W^t + \frac{A}{L}\left(P_1^t - P_2^t\right)\Delta t\right] \tag{131}$$

This is the implicit time advancement algorithm employing the rate form of the equation of state. For the normal method, the pressure rate equation in terms of flow (i.e., equation 130) is not available to allow an implicit formulation of the pressure. Consequently, the implicit time advancement algorithm for the normal method is:

$$W^{t+\Delta t} = \left[1 + \frac{A}{L} K |W^t| \Delta t\right]^{-1}\left[W^t + \frac{A}{L}\left(P_1^{t+\Delta t} - P_2^{t+\Delta t}\right)\Delta t\right] \tag{132}$$

To appreciate the difference between equations 131 and 132, consider the eigenvalues and vectors of

$$\frac{\partial \mathbf{u}(t)}{\partial t} = \mathbf{A}(\mathbf{u},t)\mathbf{u}(t) \tag{133}$$

If we assume, over the time step under consideration, that **A** = constant and has distinct eigenvalues, then the solution to equation 133 can be written as:

$$\mathbf{u}(t) = \sum_{l=1}^{N} \mathbf{u}_l e^{\alpha_l t} \tag{134}$$

where $\mathbf{u}_l$ = eigenvectors

α_l = eigenvalues.

It can be shown that for the explicit formalism, the numerical solution is equivalent to:

$$\mathbf{u}^{t+\Delta t} = \sum_{l=1}^{N}(1+\alpha_l\Delta t)\mathbf{u}_l \qquad (135)$$

while the implicit form is:

$$\mathbf{u}^{t+\Delta t} = \sum_{l=1}^{N}\frac{\mathbf{u}_l}{(1-\alpha_l\Delta t)} \qquad (136)$$

The eigenvalues can often be large and negative. Thus, at some Δt, the factor $(1+\alpha_l\Delta t)$ can go negative in the explicit solution causing each subsequent evaluation of **u** to oscillate in sign and go unstable. For the implicit method, the contributions due to large negative eignevalues decays away as $\Delta t \rightarrow \infty$. Thus the implict formalism tend to be very well behaved at large time steps. Positive eigenvalues, by a similar argument pose a threat to the implicit form. However, this is not a practical problem because $\alpha_l\Delta t$ is kept <<1 for accuracy reasons. Thus, as long as the solution algorithm contains a check on the rate of growth or decay (effectively the dominant eigenvalues) then the implicit form is well behaved.

With this digression in mind, we see that the implicit rate formalism (equation 131) has more of the system behaviour represented implicitly than the normal method (equation 132). Thus, we might expect the rate from to be more stable than the normal form. Indeed, this was found to be the case as shown in figure 26. For a fixed and large time step (0.1sec.) the normal method showed the classic numerical instability due to the explicit pressure treatment. The rate form is well damped and very stable, showing that this method should permit the user to "calculate through" pressure spikes if they are not of interest.

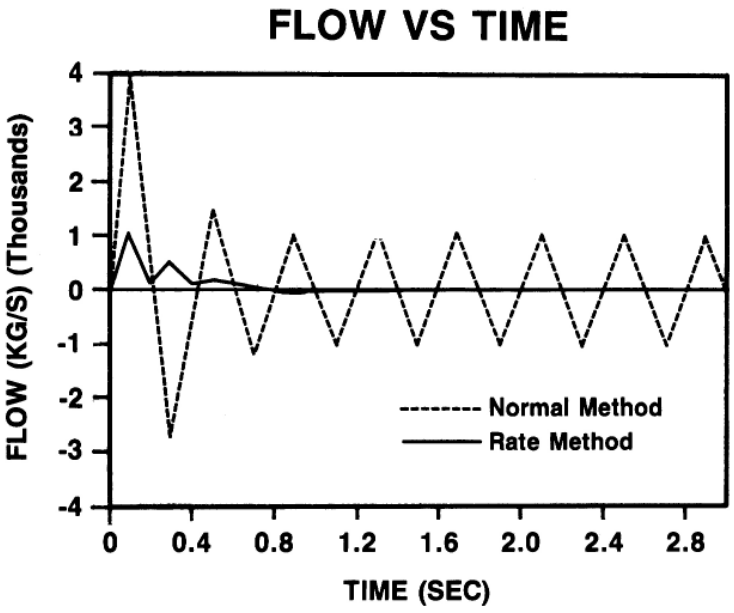

Figure 26 Flow vs. time for the implicit forms of the normal and rate methods.

5.4 Numerical Investigations: a Practical Case

The comparison between the normal and rate methods is extended to a practical application where a two node homogeneous model is used to simulate a transient of a small pressurizer operating at near-atmospheric pressure. The procedure is briefly described in the following [SOL85].

Figure 27 illustrates the problem. Steam and stratified liquid water in the pressurizer are schematically shown as two control volumes (nodes). The nodal fluids are assumed to be at saturated two-phase conditions corresponding to the pressure at their respective control volumes. The overall boundary conditions to the system are the steam bleed flow at the top of the pressurizer, the flow into and out of the pressurizer through the surge line, heat input from heaters at the bottom of the pressurizer and heat loss to pressurizer wall.

The rate of change of mass, M_S in the steam control volume and M_L in the liquid control volume, can be expressed by the following:

$$\frac{dM_S}{dt} = -W_{STB}-W_{CD}-W_{CI}+W_{EI}+W_{BR} \tag{137}$$

$$\frac{dM_L}{dt} = W_{SRL}-W_{EI}-W_{BR}+W_{CD}+W_{CI} \tag{138}$$

where W_{STB} is the steam bleed flow, W_{SRL} is the surge line inflow, W_{CI} is the interface condensation rate at the liquid surface separating the steam control volume from the liquid

control volume, W_{EI} is the interface evaporation rate at the same liquid surface, W_{CD} is the flow of condensate droplets (liquid phase) from the bulk of the steam control volume toward the liquid control volume, and W_{BR} is the rising flow of bubbles (gas phase) from the bulk of liquid volume toward the steam volume.

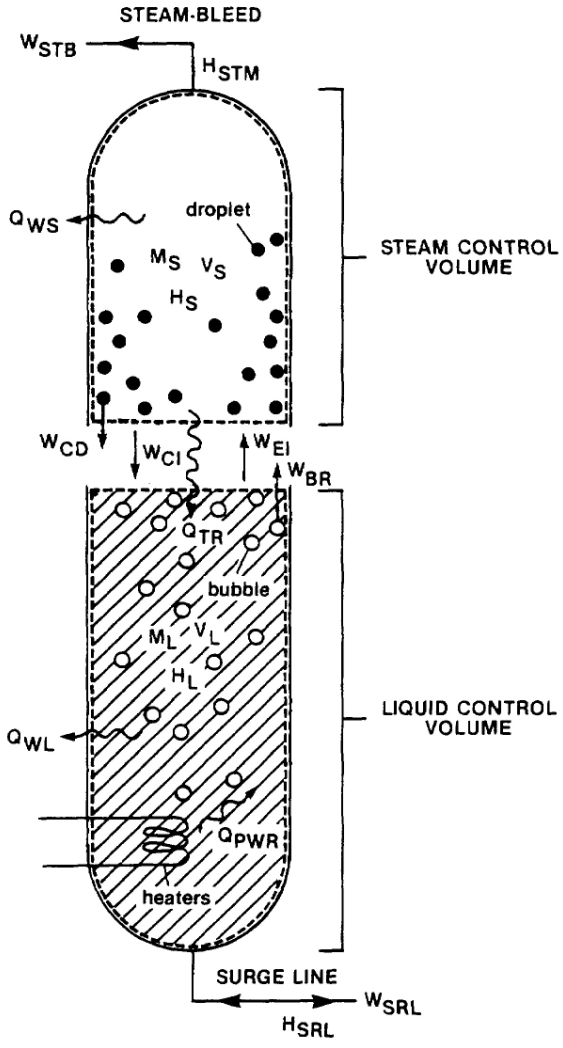

Figure 27 Schematic of control volumes in the pressurizer.

The rate of change of energy in the two control volumes can be expressed by the rate of change in the total enthalpy, H_S and H_L, in the steam and liquid control volumes respectively:

$$\frac{dH_S}{dt} = -W_{STB}h_{gST}-W_{CD}h_{fST}-W_{CI}h_{gST}+W_{EI}h_{sLQ}+W_{BR}h_{gLQ}-Q_{WS}+Q_{TR}-(1-\beta)\left[(1-\delta)Q_{COND}+Q_{EVPR}\right] \quad (139)$$

and

$$\frac{dH_L}{dt} = W_{SRL}h_{SRL}-W_{EI}h_{fLQ}-W_{BR}h_{gLQ}+W_{CI}h_{fST}+W_{CD}h_{fST}-Q_{WL}+Q_{PWR}-Q_{TR}-\beta\left[(1-\delta)Q_{COND}+Q_{EVPR}\right] \quad (140)$$

where h_{SRL} is the specific enthalpy of the fluid in the surge line, h_{gST} and h_{fST} are respectively the saturated gas phase specific enthalpy and the saturated liquid phase specific enthalpy in the steam control volume, h_{gLQ} and h_{fLQ} are respectively the saturated gas phase specific enthalpy and the saturated liquid phase specific enthalpy in the liquid control volume, Q_{WS} and Q_{WL} are the rate of heat loss to the wall in the steam control volume and in the liquid control volume respectively, Q_{TR} is the heat transfer rate from the liquid control volume to the steam control volume due to any temperature gradient, excluding those due to interface evaporation and condensation; Q_{COND} is the rate of energy released by the condensing steam to both the steam and liquid control volumes during the interface condensation process and Q_{EVPR} is rate of energy absorbed by the evaporating liquid from both the steam and liquid control volumes during the interface evaporation process. The constant, β, represents the fraction of these energies distributed to or contributed by the liquid control volume. The ratio δ represents the portion of energy released during the interface condensation that is lost to the wall.

The calculation of swelling and shrinking of control volumes is only done for the liquid control volume and the volume in the steam control volumes will be related to the volume in the liquid control volume, V_L, as:

$$\frac{dV_S}{dt} = -\frac{dV_L}{dt} \quad (141)$$

The swelling and shrinking of the liquid control volume as well as values of W_{STB}, W_{SRL}, W_{CI}, W_{EI}, W_{CD}, W_{BR}, Q_{WS}, Q_{WL}, Q_{TR}, Q_{PWR}, β and δ are calculated using analytical or empirical constitutive equations. The majority of these parameters depend directly or indirectly on pressure. Any inaccurate prediction of pressure during a numerical simulation will result in severe numerical instability. Hence the above problem is a good testing ground for comparing the performances of the two methods.

During the test simulation, the pressurizer is initially at a quasi-steady state. The steam pressure is at 96.3 kPa. The steam bleed flow, W_{STB}, heater power Q_{PWR} and heat losses Q_{WL} and Q_{WS} are at their quasi-steady values, maintaining the saturation condition of the pressurizer. At time = 11 sec., the steam bleed valve is closed and W_{STB} drops to zero while Q_{PWR} is increased to a fixed value of 300 Watts. At time = 16 sec., the steam bleed valve is reopened and its set

point set at 80 kPa.

Since the thermodynamic properties in the steam control volume and the liquid control volume are functions of P_S and P_L (pressures of the respective control volumes), there are seven unknowns, namely: M_S, M_L, H_S, H_L, V_S (or V_L), P_S and P_L. Adding two equations of state, one for each control volume, will complete the equation set:

$$P_S = fn(\rho_S, h_S) = fn\left(\frac{M_S}{V_S}, \frac{H_S}{M_S}\right) \tag{142}$$

$$P_L = fn(\rho_L, h_L) = fn\left(\frac{M_L}{V_L}, \frac{H_L}{M_L}\right) \tag{143}$$

Both the normal iterative method and the rate method are tested to solve. The following observations are made:

1. Using the normal method, the choice of adjusting P to converge on h given ρ or converging on ρ given h is found to be very important in providing a stable numerical result. At time step = 10 msec, no complete simulation result can be generated when ρ was the adjusted variable. An explanation of this can be given by referring to $G_1(P,x)$, or $\partial P/\partial \rho$, This factor is proportional to the square of $[x\, v_g(P) + (1-x)v_f(P)]$. However, the direction of change in the saturated gas phase specific volume with pressure is opposite to that of saturated liquid phase specific volume:
2. $dv_f/dP > 0$
3. $dv_g/dP < 0$
4. Therefore, a fluctuation in the value of pressure during an iteration process will amplify the fluctuation in the value of predicted density when that method is used;
5. Using enthalpy as the adjusted variable to converge on P, simulation results can be generated if an error tolerance E of less than 0.2% is used. The error tolerance is defined as:
6. $E = \dfrac{ABS(h-h_{estimate})}{h} x100\%$
7. Figure 28 shows the transient of P_L and P_S for E = 0.2%. Unstable solutions result for E higher than 0.2%. The average number of iteration is found to depend on the error tolerance as shown in figure 30.
8. On the other hand, the performance of the rate method is much more convincing in both accuracy and efficiency. The transient of P_L and P_S predicted using the rate method is shown in Figure 29.

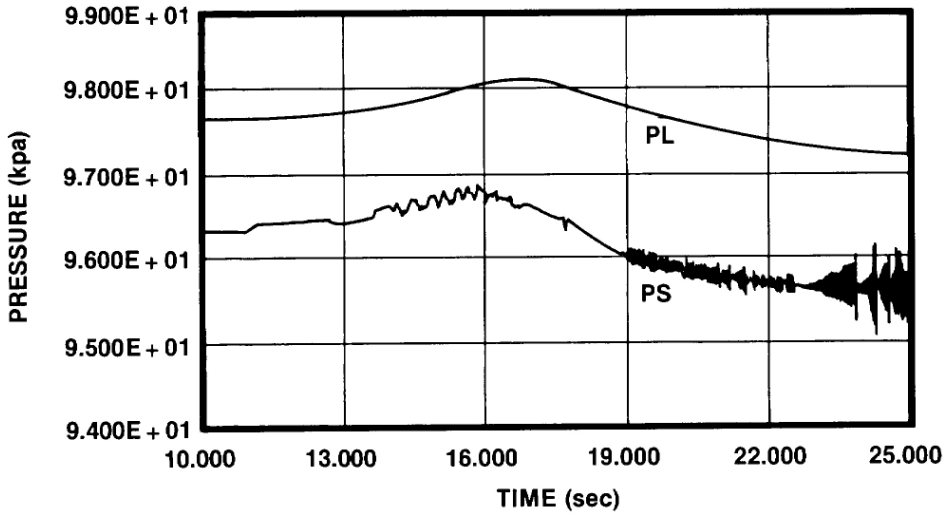

Figure 29 Pressurizer's pressure transient for the normal method with error tolerance of 0.2%.

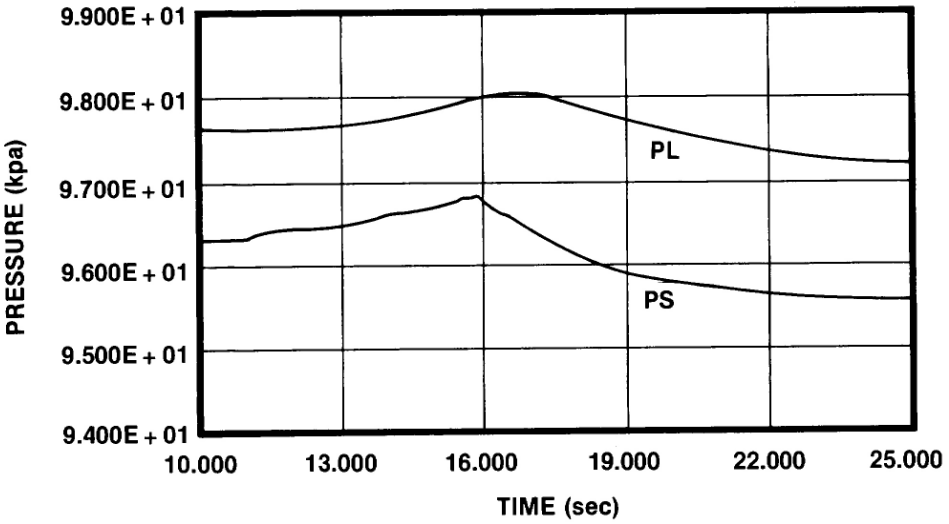

Figure 28 Pressurizer's pressure transient for the rate method.

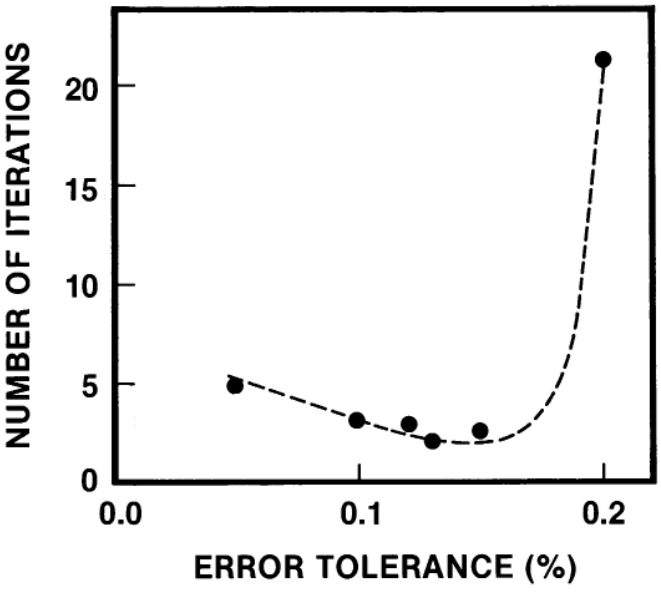

Figure 30 Average number of iterations per pressure routine call for the normal method in simulating the pressurizer problem.

5.5 Discussion and Conclusion

The rate form is a cogent expression of the equation of state that is distinct from the normal algebraic form. The essential difference is that the rate form expresses the relationship between the rates of change of the state variables, while the normal form relates the static values of the state variables. Although this is stating the obvious, the change in viewpoint is revealing.

No barrier is perceived to applying the rate form to the multi-node/link case, to the distributed form of the basic equations, and to eigenvalue extraction (numerical or analytical).

Although we have not made use of it in this work, the non-equilibrium form (equations 110 and 111) is provocative. It entices one to view the non-equilibrium situation as the essentially dynamic situation that it is and helps to focus our attention on the thermal relaxation. Given the temperature rate equations, the non-equilibrium situation should be easy to incorporate without a major code rewrite.

We conclude by restating our major findings. The rate method offers many advantages:

1. It is more intuitive for system work. It permits a proper focus on the two main actors, flow and pressure.
2. The same form is appropriate for eigenvalue extraction as well as numerical simulation. This extends the usefulness of coding.
3. Programs are easier to implement.
4. Programs are more robust and require less hand holding.
5. Time step control and detection of rapid changes (like phase changes) is

improved.

Overall the method is usually faster and more accurate. Time savings peaked at a ratio of 26 for the cases considered.

5.6 Problems

6. Consider 2 connected volumes of water with conditions as shown in figure 21. Model this with 2 nodes and 1 link.
   a. Solve for the pressure and flow histories using the normal iterative method for the equation of state,
   b. Solve for the pressure and flow histories using the non-iterative rate method.
   c. Compare the two solutions and comment.
7. Vary the initial conditions of question 1 so as to cause void collapse in volume 2 during the transient. What problems can you anticipate? Solve this case by both methods.

6 Thermalhydraulic Network Simulation

6.1 Introduction

This section introduces some more advanced numerical algorithms for solving systems of ordinary differential equations such as found in the modelling of thermalhydraulic networks. Explicit algorithms are simple to devise and program but they are restricted in time step so as to ensure stability. The more implicit the formulation, the more stable the solution in most instances. Larger time steps can be used for implicit algorithms but the accompanying matrix manipulation is computationally costly. Herein, we explore the tradeoffs.

Porcsching's method is explored to show the methodology and its limitations. Then the rate form of the equation of state is used with the conservation equations to develop a generalized fully implicit (at least in terms of the main variables) formalism. Porsching's method is a special case of the general method. The section concludes with some programming notes.

6.2 Porsching's Method

One of the more successful algorithms for thermalhydraulic simulation is based on the work of Porsching [POR69, POR71]. This algorithm, involving the Jacobian (derivative of the system state matrix), is used originally in the computer program FLASH-4 [POR69] and subsequently in the Ontario Hydro program SOPHT [CHA77] and evolved into forms used in RETRAN [AGE82].

The strength of Porsching's approach lies in its recognition of flow as the most important dependent parameter and, hence, its fully implicit treatment of flow. This leads to excellent numerically stability, consistency and convergence. Further, the Jacobian permits a generalized approach to the linearization of nonlinear systems. This allows the development of a system state matrix which contains all the system dynamics in terms of the dependent parameters of mass, energy and flow. Back substitution finally gives a matrix rate equation in terms of the system flow (the unknown) and the system derivatives. While this approach is certainly a proven and successful one, it has some disadvantages. The matrix rate equation involving the Jacobian is as complicated as it is general. The resulting expressions are somewhat obtuse and it is difficult to obtain an intuitive feel for the system. This complexity also hinders implementation in a simulation code and makes error tracking a tedious process. The pervasiveness and obtuseness of the algorithm begs a revisit so as to distil the salient features, leaving them exposed for pedagogy and further scrutiny.

Section 5 discussed the use of the Rate Form of the equation of state. This work showed that by casting the equation of state in the form of a rate equation rather than the normal algebraic form, the system state matrix can be more logically formed from the normal conservation rate equations for mass, energy and momentum plus the pressure rate equation. These form the four cornerstone equations in thermalhydraulic systems analysis (figure 1). Numerical implementation of the rate form proved to be very successful, leading to roughly a factor of 10 improvement over the algebraic form of the equation of state, largely due to the iterative nature of the algebraic form. Incorporating the implicit pressure dependency in the numerical

method also drastically improved the numerical stability.

Since Porsching's method also carried the pressure dependency implicitly (via the Jacobian), the question arises as to how the Rate form compares the Porsching's method. This section is devoted to an explanatory derivation of the fully-implicit back-substituted form (FIBS), which is a more general than the Rate form. It is shown that the Porsching form is identical to the Rate form and is a subset of the fully-implicit back-substituted form and is easily derived from it [GAR87b]. The FIBS form thus offers an alternative to Porsching, is found to be of some pedagogical usefulness and is far more intuitive and easier to code.

6.3 Derivation of FIBS

Following Porsching [POR71], the general form of system equations can be written

$$\mathbf{u} = f(t, \mathbf{u}) \tag{144}$$

where **u** is the vector of dependent mass, total enthalpy and flow variables $\{M_i, H_i, W_j\}$ for all nodes i=1..N and all links, j=1..L. Equation 1 is linearized, assuming no explicit t dependence to give:

$$\mathbf{u} = \mathbf{f}^t + \Delta t\, \mathbf{J}\, \mathbf{u} \tag{145}$$

or

$$\Delta\mathbf{u} = \Delta t\, \mathbf{f}^t + \Delta t\, \mathbf{J}\, \Delta\mathbf{u} \tag{146}$$

to give

$$[\mathbf{I} - \Delta t\, \mathbf{J}]\Delta\mathbf{u} = \Delta t\, \mathbf{f}^t \tag{147}$$

where **J** is the system Jacobian, composed of elements $\partial f_k / \partial u_l$.

For typical thermalhydraulic systems using the node-link notation[2]:

$$\frac{dW_j}{dt} = \frac{A_j}{L_J}\left(P_u + S_{WP}\Delta P_u - P_d - S_{WP}\Delta P_d\right) + k_j\left(W_j + S_{WW}\Delta W_j\right)^2 + b_{wj} = \frac{\Delta W_j}{\Delta t} \tag{148}$$

---

[2] Porsching actually uses U, total energy rather than H, total enthalpy in a hybrid form:

$$U_i = \sum_{j\forall d} (H_j/M_j)\, W_j - \sum_{j\forall u} (H_j/M_j)\, W_j + Q_i$$

There is no advantage to tracking both H and U in a simulation; thus in this course, H is used throughout.

Typically $b_{wj} = (A_j/L_j)\,(h_j\rho_j g + \Delta P_{pump})$ where h_j = height.

$$\frac{dM_i}{dt} = \sum_{j\forall d}(W_j + S_{MW}\ \Delta W_j) - \sum_{j\forall u}(W_j + S_{MW}\ \Delta W_j) \geq \frac{\Delta M_i}{\Delta t} \tag{149}$$

$$\begin{aligned}\frac{dH_i}{dt} &= \sum_{j\forall d}(W_j + S_{HW}\ \Delta W_j)\ \frac{(H_j + S_{HH}\ \Delta H_j)}{(M_j + S_{HM}\ \Delta M_j)} - \sum_{j\forall u}(W_j + S_{HW}\ \Delta W_j)\ \frac{(H_j + S_{HH}\ \Delta H_j)}{(M_j + S_{HM}\ \Delta M_j)} + Q_i \\ &= \sum_{j\forall d}\left(\frac{W_j H_j}{M_j} + \frac{S_{HW} H_j}{M_j}\ \Delta W_j + \frac{S_{HH} W_j}{M_j}\ \Delta H_j - \frac{S_{HM}\ W_j\ H_j}{M_j^2}\ \Delta M_j\right) \\ &\quad - \sum_{j\forall u}\left(\frac{W_j H_j}{M_j} + \frac{S_{HW} H_j}{M_j}\ \Delta W_j + \frac{S_{HH} W_j}{M_j}\ \Delta H_j - \frac{S_{HM}\ W_j\ H_j}{M_j^2}\ \Delta M_j\right) + Q_i \\ &\geq \frac{\Delta H_i}{\Delta t}\end{aligned} \tag{150}$$

$$\begin{aligned}\Delta P_i &= \frac{\partial P_i}{\partial M_i}\ \Delta M_i + \frac{\partial P_i}{\partial H_i}\ \Delta H_i + \frac{\partial P_i}{\partial V_i}\ \Delta V_i \\ \frac{\Delta P_i}{\Delta t} &= C_{1i}\ \frac{\Delta M_i}{\Delta t} + C_{2i}\ \frac{\Delta H_i}{\Delta t} \qquad \text{for constant volume.}\end{aligned} \tag{151}$$

where j indicates a sum over all links for which the node i is a downstream (d) or upstream (u) node.

Switches, S, are used to provide user control over the degree of implicitness:

0 = explicit
1 = implicit.

The system unknowns to be solved for are ΔW, ΔM, ΔH and ΔP using equations 5, 6, 7 and 8. The general strategy is to reduce the number of unknowns so that the size of the matrices to be inverted in the simultaneous solution of these equations is reduced. The mass equation 6 is simple and is used to eliminate ΔM in terms of ΔW. Flow is chosen as the prime variable since it is the main actor in thermalhydraulic systems. The enthalpy equation poses a problem as it is too complex to permit a simple substitution. Porsching surmounts this by setting $S_{HH} = S_{HM} = 0$, ie making the solution explicit in specific enthalpy. **However, we need not make this assumption; by casting the equations in matrix notation, the full implicitness can be retained while still allowing the back substitutions to be made.**

Proceeding then, using matrix notation:

$$\Delta \mathbf{M} = \Delta t\, \mathbf{A}^{MW}[\mathbf{W}^{t+S_{MW}}\ \Delta \mathbf{W}] \tag{152}$$

where, for a 4 node - 5 link example (Figure 15):

$$\mathbf{A}^{MW} = \begin{pmatrix} -1 & 0 & 0 & 1 & 0 \\ 1 & -1 & 0 & 0 & 1 \\ 0 & 1 & -1 & 0 & 0 \\ 0 & 0 & 1 & -1 & -1 \end{pmatrix}$$

links ⇨ (columns); ⇩ (rows); nodes (rows) (153)

This matrix contains the total system geometry. It is constructed by the following procedure:

For each column (link), insert -1 for the upstream node and +1 for the downstream node for that link since the link supplies (adds) flow to the downstream node and takes it away from the upstream node. Flow reversal is handled automatically since the sign of W will take care of mass accounting properly.

The form of other matrices in the following are derivable from $\mathbf{A}^{MW}$. This can be used to advantage in coding. The input data for each link need only contain pointers to the upstream node and the downstream node for that link. This allows $\mathbf{A}^{MW}$ to be created. In short, the upstream node and downstream node for each link completely defines the geometry and this can be used to programming advantage.

The flow equation is:

$$\Delta \mathbf{W} = \Delta t\left\{\mathbf{A}^{WP}\left[\mathbf{P}^{t+S_{WP}\Delta \mathbf{P}}\right] + \mathbf{A}^{WW}\left[\mathbf{W}^{t+2S_{WW}\Delta \mathbf{W}}\right] + \mathbf{B}^{W}\right\} \tag{154}$$

Where:

$$\mathbf{A}_m^{WW} = \begin{pmatrix} -k_1|W_1| & 0 \\ -k_2|W_2| & 0 \\ 0 & 0 \\ 0 & 0 \\ 0 & -k_5|W_5| \end{pmatrix} \tag{155}$$

$$\mathbf{A}_m^{WP} = \begin{pmatrix} A_1/L_1 & A_1/L_1 & 0 & 0 \\ 0 & -A_2/L_2 & -A_2/L_2 & 0 \\ 0 & 0 & A_3/L_3 & -A_3/L_3 \\ -A_4/L_4 & 0 & 0 & A_4/L_4 \\ 0 & -A_5/L_5 & 0 & A_5/L_5 \end{pmatrix} \tag{156}$$

note that $\mathbf{A}^{WP}$ is formed easily from $\mathbf{A}^{MW}$ by the following procedure:

First multiply $\mathbf{A}^{MW}$ by $\{-A_1/L_1, -A_2/L_2, \ldots -A_5/L_5\}^{-1}$

Then transpose the resulting matrix to give $\mathbf{A}^{WP}$.

$$\mathbf{B}^{W} = \begin{pmatrix} A_1/L_1(h_1\rho_1 g + \Delta P_{pump1}) \\ A_2/L_2(h_2\rho_1 g + \Delta P_{pump2}) \\ \bullet \\ \bullet \end{pmatrix} \tag{157}$$

Finally:

$$\Delta\mathbf{H} = \Delta t\left(\mathbf{A}^{HW}\left[\mathbf{W}^{t}+S_{HW}\Delta\mathbf{W}\right]+S_{HH}\mathbf{A}^{HH^{*}}\Delta\mathbf{H}^{*} - S_{HM}\mathbf{A}^{HM^{*}}\Delta\mathbf{M}^{*}+\mathbf{B}^{H}\right) \tag{158}$$

where $\Delta\mathbf{H}^{*}$ and $\Delta\mathbf{M}^{*}$ refer to the enthalpy and mass associated with upstream properties of the links (ie the transported properties). Thus

$$\Delta\mathbf{H}^{*} = \begin{pmatrix} \Delta H_1 \\ \Delta H_2 \\ \Delta H_3 \\ \Delta H_4 \\ \Delta H_4 \end{pmatrix}, \qquad \Delta\mathbf{M}^{*} = \begin{pmatrix} \Delta M_1 \\ \Delta M_2 \\ \Delta M_3 \\ \Delta M_4 \\ \Delta M_4 \end{pmatrix} \tag{159}$$

$$\mathbf{A}_m^{HW} = \begin{pmatrix} -H_1/M_1 & 0 & 0 & H_4/M_4 & 0 \\ H_1/M_1 & -H_2/M_2 & 0 & 0 & H_4/M_4 \\ 0 & H_2/M_2 & -H_3/M_3 & 0 & 0 \\ 0 & 0 & H_3/M_3 & -H_4/M_4 & -H_4/M_4 \end{pmatrix} \tag{160}$$

For each link, the elements of the column are formed from the link flow, W_j and the upstream properties (H and M). Each link has a sink and source node.

Similarly

$$\mathbf{A}_m^{HH^*} = \begin{pmatrix} -W_1/M_1 & 0 & 0 & W_4/M_4 & 0 \\ W_1/M_1 & -W_2/M_2 & 0 & 0 & W_5/M_4 \\ 0 & W_2/M_2 & -W_3/M_3 & 0 & 0 \\ 0 & 0 & W_3/M_3 & -W_4/M_4 & -W_5/M_4 \end{pmatrix} \tag{161}$$

$$\mathbf{A}_m^{HM} = \begin{pmatrix} -W_1H_1/M_1^2 & 0 & 0 & W_4H_4/M_4^2 & 0 \\ W_1H_1/M_1^2 & -W_2H_2/M_2^2 & 0 & 0 & W_5H_4/M_4^2 \\ 0 & W_2H_2/M_2^2 & -W_3H_3/M_3^2 & 0 & 0 \\ 0 & 0 & W_3H_3/M_3^2 & -W_4H_4/M_4^2 & -W_5H_4/M_4^2 \end{pmatrix} \tag{162}$$

We wish to write the matrix equations eliminating the * parameters, ie convert $\Delta\mathbf{H}^{*}$ to $\Delta\mathbf{H}$, $\Delta\mathbf{M}^{*}$ to $\Delta\mathbf{M}$. To do this we introduce a transfer matrix, $\mathbf{I}^{LN}$ so that

$$\Delta \mathbf{H}^{*} = \mathbf{I}^{LN} \Delta \mathbf{H} \tag{163}$$

where

$$I_m^{LN} = \begin{pmatrix} 1 & 0 & 0 & 0 \\ 0 & 1 & 0 & 0 \\ 0 & 0 & 1 & 0 \\ 0 & 0 & 0 & 1 \\ 0 & 0 & 0 & 1 \end{pmatrix} \quad \begin{matrix} \text{nodes} \Rightarrow \\ \Downarrow \\ \\ \\ \text{links} \end{matrix} \tag{164}$$

where $\mathbf{I}^{LN}$ is formed by entering 1 for the node that is the upstream or source node for each link. Now, we can define:

$$\mathbf{A}^{HH*} \Delta \mathbf{H}^{*} = \mathbf{A}^{HH*} \mathbf{I}^{LN} \Delta \mathbf{H} \equiv \mathbf{A}^{HH} \Delta \mathbf{H} \tag{165}$$

and

$$\mathbf{A}^{HM*} \Delta \mathbf{M}^{*} = \mathbf{A}^{HM*} \mathbf{I}^{LN} \Delta \mathbf{M} \equiv \mathbf{A}^{HM} \Delta \mathbf{M}. \tag{166}$$

Thus

$$\Delta \mathbf{H} = \Delta t \quad \{\mathbf{A}^{HW} (\mathbf{W}^{t} + S_{HW} \Delta \mathbf{W}) + S_{HH} \mathbf{A}^{HH} \Delta \mathbf{H} - S_{HM} \mathbf{A}^{HM} \Delta \mathbf{M} + \mathbf{B}^{H}\} \tag{167}$$

Substituting in the mass equation 9:

$$\Delta \mathbf{H} = \Delta t \{ \mathbf{A}^{HW} (\mathbf{W} + S_{HW} \Delta \mathbf{W}) + S_{HH} \mathbf{A}^{HH} \Delta \mathbf{H} - \Delta t S_{HM} \mathbf{A}^{HM} \mathbf{A}^{MW} (\mathbf{W}^{t} + \mathbf{W}^{MW} \Delta \mathbf{W}) + \mathbf{B}^{H} \} \tag{168}$$

Solving for $\Delta \mathbf{H}$:

$$\Delta \mathbf{H} = \Delta t[\mathbf{I} - \Delta t S_{HH} \mathbf{A}^{HH}]^{-1} \quad \{\mathbf{A}^{HW} (\mathbf{W}^{t} + S_{HW} \Delta \mathbf{W}) - \Delta t S_{HM} \mathbf{A}^{HM} \mathbf{A}^{MW} (\mathbf{W}^{t} + S_{MW} \Delta \mathbf{W}) + \mathbf{B}^{H}\} \tag{169}$$

So now we have $\Delta \mathbf{M}$ and $\Delta \mathbf{H}$ in terms of $\Delta \mathbf{W}$. Recalling equation 8, in matrix notation, we have:

$$\Delta \mathbf{P} = \mathbf{C}_1 \Delta \mathbf{M} + \mathbf{C}_2 \Delta \mathbf{H}, \tag{170}$$

where

$$C_{m1} = \begin{pmatrix} C_{11} & 0 & 0 & 0 \\ 0 & C_{12} & 0 & 0 \\ 0 & 0 & C_{13} & 0 \\ 0 & 0 & 0 & C_{14} \end{pmatrix} \tag{171}$$

Similarly for $\mathbf{C}_2$.

We can back-substitute $\Delta \mathbf{M}$ and $\Delta \mathbf{H}$ into equation 8 and the result into the flow equation to

leave a matrix equation in $\Delta\mathbf{W}$ only, which can be solved by traditional numeric means. Hence,

$$\Delta\mathbf{P} = \Delta t\, \mathbf{C}_1\, \mathbf{A}^{MW} (\mathbf{W}^t + S_{MW}\, \Delta\mathbf{W}) + \Delta t\, \mathbf{C}_2 [\mathbf{I} - \Delta t\, S_{HH}\, \mathbf{A}^{HH}]^{-1} [\mathbf{A}^{HW} (\mathbf{W}^t + S_{HW}\, \Delta\mathbf{W}) - \Delta t\, S_{HM}\, \mathbf{A}^{HM}\, \mathbf{A}^{MW} (\mathbf{W}^t + S_{MW}\, \Delta\mathbf{W}) + \mathbf{B}^H]$$

$$\equiv \Delta t\, \mathbf{A}^{PW1}\, \mathbf{W}^t + \Delta t\, \mathbf{A}^{PW2}\, \Delta\mathbf{W} + \Delta t\, \mathbf{B}^P \quad (172)$$

where :

$$\mathbf{A}^{PW1} = \mathbf{C}_1\, \mathbf{A}^{MW} + \mathbf{C}_2 [\mathbf{I} - \Delta t\, S_{HH}\, \mathbf{A}^{HH}]^{-1} [\mathbf{A}^{HW} - \Delta t\, S_{HM}\, \mathbf{A}^{HM}\, \mathbf{A}^{MW}] \quad (173)$$

$$\mathbf{A}^{PW2} = S_{MW}\, \mathbf{C}_1\, \mathbf{A}^{MW} + \mathbf{C}_2 [\mathbf{I} - \Delta t\, S_{HH}\, \mathbf{A}^{HH}]^{-1} [S_{HW}\, \mathbf{A}^{HW} - \Delta t\, S_{HM}\, S_{MW}\, \mathbf{A}^{HM}\, \mathbf{A}^{MW}] \quad (174)$$

$$\mathbf{B}^P = \mathbf{C}_2 [\mathbf{I} - \Delta t\, S_{HH}\, \mathbf{A}^{HH}]^{-1}\, \mathbf{B}^H \quad (175)$$

Thus:

$$\Delta\mathbf{W} = \Delta t \{\mathbf{A}^{WP} [\mathbf{P}^t + \Delta t\, S_{WP} (\mathbf{A}^{PW1}\, \mathbf{W}^t + \mathbf{A}^{PW2}\, \Delta\mathbf{W} + \mathbf{B}^P)] + \mathbf{A}^{WW} [W^t + 2S_{WW}\, \mathbf{A}^{WW}\, \Delta\mathbf{W}] + \mathbf{B}^W \} \quad (176)$$

Collecting terms in $\Delta\mathbf{W}$:

$$[\mathbf{I} - \Delta t(2\, S_{WW}\, \mathbf{A}^{WW} + \Delta t\, S_{WP}\, \mathbf{A}^{WP}\, \mathbf{A}^{PW2})]\, \Delta\mathbf{W} = \Delta t \{[\mathbf{A}^{WW} + \Delta t\, S_{WP}\, \mathbf{A}^{WP}\, \mathbf{A}^{PW1}]\, \mathbf{W}^t + \mathbf{B}^W + \mathbf{A}^{WP} [\mathbf{P}^t + \Delta t\, S_{WP}\, \mathbf{B}^P]\} \quad (177)$$

which is of the form

$$\mathbf{A}\, \Delta\mathbf{W} = \mathbf{B}$$

which can be solved by conventional means to yield $\Delta\mathbf{W}$. Then we can directly calculate $\Delta\mathbf{M}$, $\Delta\mathbf{H}$ and $\Delta\mathbf{P}$ using equations 152, 158 (or 167), and 170. Associated changes in temperature can be obtained as for pressure, using the appropriate equation of state coefficients.

6.4 Special Cases

To summarize, the general solution is given by the following equations:

$$\mathbf{A}^{PW1} = \mathbf{C}_1\, \mathbf{A}^{MW} + \mathbf{C}_2 [\mathbf{I} - \Delta t\, S_{HH}\, \mathbf{A}^{HH}]^{-1} [\mathbf{A}^{HW} - \Delta t\, S_{HM}\, \mathbf{A}^{HM}\, \mathbf{A}^{MW}] \quad (178)$$

$$\mathbf{A}^{PW2} = S_{MW}\, \mathbf{C}_1\, \mathbf{A}^{MW} + \mathbf{C}_2 [\mathbf{I} - \Delta t\, S_{HH}\, \mathbf{A}^{HH}]^{-1} [S_{HW}\, \mathbf{A}^{HW} - \Delta t\, S_{HM}\, S_{MW}\, \mathbf{A}^{HM}\, \mathbf{A}^{MW}] \quad (179)$$

$$\mathbf{B}^P = \mathbf{C}_2 [\mathbf{I} - \Delta t\, S_{HH}\, \mathbf{A}^{HH}]^{-1}\, \mathbf{B}^H \quad (180)$$

$$[\mathbf{I} - \Delta t(2\, S_{WW}\, \mathbf{A}^{WW} + \Delta t\, S_{WP}\, \mathbf{A}^{WP}\, \mathbf{A}^{PW2})]\, \Delta\mathbf{W} = \Delta t \{ [\mathbf{A}^{WW} + \Delta t\, S_{WP}\, \mathbf{A}^{WP}\, \mathbf{A}^{PW1}]\, \mathbf{W}^t + \mathbf{B}^W + \mathbf{A}^{WP} [\mathbf{P}^t + \Delta t\, S_{WP}\, \mathbf{B}^P] \} \quad (181)$$

$$\Delta\mathbf{M} = \Delta t\, \mathbf{A}^{MW} [\mathbf{W}^t + S_{MW}\, \Delta\mathbf{W}] \quad (182)$$

$$\Delta\mathbf{H} = \Delta t \{ \mathbf{A}^{HW} (\mathbf{W}^t + S_{HW}\, \Delta\mathbf{W}) + S_{HH}\, \mathbf{A}^{HH}\, \Delta\mathbf{H} - S_{HM}\, \mathbf{A}^{HM}\, \Delta\mathbf{M} + \mathbf{B}^H \} \quad (183)$$

$$\Delta\mathbf{P} = \mathbf{C}_1\, \Delta\mathbf{M} + \mathbf{C}_2\, \Delta\mathbf{H} \quad (184)$$

Special cases of this general algorithm are as follows:

Fully explicit: all S's = 0

$$\mathbf{A}^{PW1} = \mathbf{C}_1\, \mathbf{A}^{MW} + \mathbf{C}_2\, \mathbf{A}^{HW} \quad (185)$$

$$\mathbf{A}^{PW2} = 0 \quad (186)$$

$$\mathbf{B}^P = \mathbf{C}_2\,\mathbf{B}^H \tag{187}$$

$$\therefore\ \Delta\mathbf{W} = \Delta t\,\{\,\mathbf{A}^{WW}\,\mathbf{W}^t + \mathbf{B}^W + \mathbf{A}^{WP}\,\mathbf{P}^t\,\} \tag{188}$$

$$\Delta\mathbf{M} = \Delta t\,\mathbf{A}^{MW}\,\mathbf{W}^t \tag{189}$$

$$\Delta\mathbf{H} = \Delta t\,\{\,\mathbf{A}^{HW}\,\mathbf{W}^t + \mathbf{B}^H\,\} \tag{190}$$

$$\Delta\mathbf{P} = \mathbf{C}_1\,\Delta\mathbf{M} + \mathbf{C}_2\,\Delta\mathbf{H}, \tag{191}$$

as expected.

Porsching's semi-implicit ($S_{HH} = 0$ and $S_{HM} = 0$, all other S's = 1)

$$\mathbf{A}^{PW1} = \mathbf{C}_1\,\mathbf{A}^{MW} + \mathbf{C}_2\,\mathbf{A}^{HW} \tag{192}$$

$$\mathbf{A}^{PW2} = \mathbf{C}_1\,\mathbf{A}^{MW} + \mathbf{C}_2\,\mathbf{A}^{HW} \tag{193}$$

$$\mathbf{B}^P = \mathbf{C}_2\,\mathbf{B}^H \tag{194}$$

$$[\mathbf{I} - \Delta t(2\,\mathbf{A}^{WW} + \Delta t\,\mathbf{A}^{WP}\,\mathbf{A}^{PW2})]\,\Delta\mathbf{W}$$
$$= \Delta t\,\{\,[\mathbf{A}^{WW} + \Delta t\,\mathbf{A}^{WP}\,\mathbf{A}^{PW1}]\,\mathbf{W}^t + \mathbf{B}^W + \mathbf{A}^{WP}\,[\mathbf{P}^t + \Delta t\,\mathbf{B}^P]\,\} \tag{195}$$

$$\Delta\mathbf{M} = \Delta t\,\mathbf{A}^{MW}\,[\mathbf{W}^t + \Delta\mathbf{W}] \tag{196}$$

$$\Delta\mathbf{H} = \Delta t\,\{\,\mathbf{A}^{HW}\,(\mathbf{W}^t + \Delta\mathbf{W}) + \mathbf{B}^H\,\} \tag{197}$$

$$\Delta\mathbf{P} = \mathbf{C}_1\,\Delta\mathbf{M} + \mathbf{C}_2\,\Delta\mathbf{H} \tag{198}$$

Fully Implicit: All S's = 1

$$\mathbf{A}^{PW1} = \mathbf{C}_1\,\mathbf{A}^{MW} + \mathbf{C}_2\,[\mathbf{I} - \Delta t\,\mathbf{A}^{HH}]^{-1}\,[\mathbf{A}^{HW} - \Delta t\,\mathbf{A}^{HM}\,\mathbf{A}^{MW}] \tag{199}$$

$$\mathbf{A}^{PW2} = \mathbf{C}_1\,\mathbf{A}^{MW} + \mathbf{C}_2\,[\mathbf{I} - \Delta t\,\mathbf{A}^{HH}]^{-1}\,[\mathbf{A}^{HW} - \Delta t\,\mathbf{A}^{HM}\,\mathbf{A}^{MW}] \tag{200}$$

$$\mathbf{B}^P = \mathbf{C}_2\,[\mathbf{I} - \Delta t\,\mathbf{A}^{HH}]^{-1}\,\mathbf{B}^H \tag{201}$$

$$[\mathbf{I} - \Delta t(2\,\mathbf{A}^{WW} + \Delta t\,\mathbf{A}^{WP}\,\mathbf{A}^{PW2})]\,\Delta\mathbf{W}$$
$$= \Delta t\,\{\,[\mathbf{A}^{WW} + \Delta t\,\mathbf{A}^{WP}\,\mathbf{A}^{PW1}]\,\mathbf{W}^t + \mathbf{B}^W + \mathbf{A}^{WP}\,[\mathbf{P}^t + \Delta t\,\mathbf{B}^P]\,\} \tag{202}$$

$$\Delta\mathbf{M} = \Delta t\,\mathbf{A}^{MW}\,[\mathbf{W}^t + \Delta\mathbf{W}] \tag{203}$$

$$\Delta\mathbf{H} = \Delta t\,\{\,\mathbf{A}^{HW}\,(\mathbf{W}^t + \Delta\mathbf{W}) + \mathbf{A}^{HH}\,\Delta\mathbf{H} - \mathbf{A}^{HM}\Delta\mathbf{M} + \mathbf{B}^H\,\} \tag{204}$$

$$\Delta\mathbf{P} = \mathbf{C}_1\,\Delta\mathbf{M} + \mathbf{C}_2\,\Delta\mathbf{H} \tag{205}$$

6.5 Programming Notes

It should be noted that the full system geometry is contained in $\mathbf{A}^{MW}$. All other matrices are derived from this matrix and node/link properties. Programming is thus very straightforward. In addition, the switches, S, can be varied at will to control the degree of implications of the system variables, **W**, **M**, **H** and **P**.

The fully-implicit method is more complicated than the semi-implicit method in that it requires the addition and multiplication of more matrices as well as a matrix inversion. The effect of these additional operations is quite costly, especially when a large number of nodes is needed.

In one case study [HOS89], for 9 nodes and links, the cost is a 50% increase in iteration time. But this becomes a 250% increase as one approaches the 36 node/link case. By handling the matrix operations as efficiently as possible, some increase in speed should be attainable for both models. Using efficient assembly routines (rather than FORTRAN) for the matrix operations yielded a 10 to 20% reduction (increasing from 9 nodes to 36 nodes) in the time per iteration for the semi-implicit method and a 15 to 25% reduction in the fully-implicit case.

Usually the matrices contain mostly zeros and, in the case of a circular loop, may be diagonally dominant in nature (i.e. non-zero elements occupy one, two or three stripes through the matrix). By writing routines specific to the nodal layout for handling the matrix operations, significant gains in speed may be possible. However, the simulator will no longer be general in nature and the routines may have to be changed if the nodal layout is altered.

If the multiplication of two large matrices is desired, say NxN in dimension, the time to carry out the operation (N^3 multiplications and N^3 additions) can be very significant. However, it is possible to reduce the number of individual operations without losing the generality of the method. Take, for example, the multiplication of $\mathbf{A}^{WP}$ and $\mathbf{A}^{PW}$. The rows in the former term pertain to links and the columns to nodes. Each row will only contain two terms located in the columns corresponding to the upstream and downstream nodes of that particular link. Thus, knowing which are the upstream and downstream nodes for every link, it is only necessary to do two multiplications and one addition to obtain each element of the product matrix ($2N^2$ multiplications and N^2 additions). By taking advantage of having only two elements in each row of the former term or only two elements in each column of the latter term wherever possible, significant savings in time may be observed. With this improvement in the code, a cut in time by a factor of two for 18 nodes and by a factor of three for 36 nodes, regardless of the method (semi- or fully-implicit) was obtained. The cost of the fully-implicit method is reduced slightly to a 32% increase in iteration time over the semi-implicit method when 9 nodes and 9 links are used. This becomes a 214% increase as one approaches the 36 node case.

Since the focus of this section is to provide a less obtuse and more general derivation of thermalhydraulic system equations than Porsching's method, a full comparison of the performance of the fully- and semi-implicit methods will not be made. Suffice it to say that, in general, the semi-implicit method has a Courant limit on the maximum time step that can be taken in order to ensure stability. The fully-implicit method does not have this limitation. As the Courant time step limit is determined by the nodal residence time, the time step limit is dependant on the node sizes and the flows through the nodes. Practical simulations have a further time step constraints such as: the tracking of movement of valves, the maintenance of accuracy, synchronizing of report times, etc. Thus, the choice between the semi- or fully-implicit method depends on the time per iteration multiplied by the number of iterations required to reach the largest time step permitted by the simulation problem. For example, for a 9 node case, the semi-implicit method required 0.10 seconds per iteration and required 2 iterations to meet the report time of 1.0 seconds. The fully-implicit method meet the report time in one iteration which took 0.14 seconds. At 36 nodes however, the semi-implicit method took 2 x 0.71 seconds while the fully-implicit method took 2.12 seconds. Clearly, one method is not superior to the other in all cases.

Pressure determination involves the use of property derivatives. To avoid the numerical problems associated with discontinuities, smooth functions for properties must be used, such as those derived by [GAR88, GAR89 and GAR92]. These functions and routines permit the quick and fast evaluation of ΔP and ΔT given ΔM and ΔH for all water phases. Automatic adjustment is provided to prevent P and T drift from values consistent with current M and H values. These routines are non-iterative, essential for real-time simulation.

6.6 Conclusion

The FIBS approach for thermalhydraulic system simulation has been compared to the classic work of Porsching. Porsching's algorithm is derived as a subset of the fully implicit approach. Focusing on the system Jacobian, as Porsching did, focuses on the perturbation of the system as a whole. Although general, it tends to obscure the interaction of the main players in typical thermalhydraulic systems: flow and pressure. The FIBS form is shown to be more general than Porsching's method, yet less obtuse. The interplay of flow and pressure is clarified and coding is simplified.

6.7 Problems

1. Rewrite the conservation equations for the 4 node, 5 link case with various explicit / implicit switches set for the following cases:
   a. fully explicit
   b. diagonally implicit
   c. semi-implicit solution scheme (implicit in flow and pressure, explicit in mass and enthalpy)
   d. fully-implicit solution scheme (implicit in flow and pressure, mass and enthalpy).

2. Build a simulation code that solves the thermalhydraulic equations for a general node-link network for the explicit case using the supplied skeleton code as a starting point. Use the node-link diagrams and equations as developed in section 3, the water property routines as developed in section 4, the rate form of the equation of state as developed in section 5 and the explicit solution as developed in this section.

3. Improve upon your solution to question 2 by implementing a diagonally implicit solution procedure. Is the solution more stable? Is there a cost penalty?

4. Implement a semi-implicit solution scheme (implicit in flow and pressure, explicit in mass and enthalpy). Is the solution more stable? Is there a cost penalty?

5. Implement a fully-implicit solution scheme (implicit in flow and pressure, mass and enthalpy). Is the solution more stable? Is there a cost penalty?

7 Case Study: Heat Transport System Stability

As mentioned in section 6.2, Porsching's Method is one of the more successful algorithms for thermalhydraulic simulation. This algorithm was used in the Ontario Hydro program SOPHT to investigate Heat Transport System stability for the CANDU reactors with a figure-of-eight heat transport loop configuration, such as the CANDU 6 and Darlington, since each loop potentially has two-phase water at the outlet headers at high power. Since there are 2 outlet headers per loop (one at each end of the reactor) separated by 2 single phase regions, we have a coupled spring-mass system that, under the right conditions, could give undesirable flow and pressure oscillations. To enhance heat transport system stability, a reactor outlet interconnect was provided in each loop. This is discussed in detail in [GAR84, GAR86] but, of relevance to this chapter, the code predictions based on the best estimate of the heat transport conditions compared well to the plant tests, confirming both the mathematical methodology and the efficacy of the one dimensional homogeneous thermalhydraulic model for overall system simulation.

8 References

AGE82 L.J. Agee, "RETRAN Thermalhydraulic Analyses: Theory and Applications", *Progress in Nuclear Energy*, Vol. 10, No. 1, pp. 19-67, 1982.

AGE83 L.J. Agee, M.P Paulsen and E.D Hughes, "Equations of State for Nonequilibrium Two-Phase Flow Models", *Transient Two-Phase Flow Proceedings of the Third CSNI Specialist Meeting*, Hemisphere Publishing Corporation, 1983.

BAN80 S. Banerjee, "Two-Phase Hydrodynamics: Models and Mechanisms", Keynote Paper, *ANS/ASME Topical Meeting, Nuclear Reactor Thermal-Hydraulics*, Saratoga, New York, October 1980.

BER81 A.E. Bergles et al., Two-Phase Flow and Heat Transfer in the Power and Process Industries, Hemisphere Publishing, 1981.

BIR60 R.B. Bird, W.E. Stewart and E.N. Lightfoot, *Transport Phenomena*, John Wiley and Sons, Inc., New York, 1960.

BLO71 Benjamin S. Bloom, J. Thomas Hastings, George F. Madaus, "Handbook on Formative and Summative Evaluation of Student Learning", McGraw-Hill, Library of Congress 75-129488, 1971.

BNW76 COBRA-IV: An Interim Version of COBRA for Thermalhydraulic Analysis of Rod Bundle Nuclear Fuel Elements and Cores, Battelle Pacific Northwest Laboratories, BNWL-1962, March 1976.

CAR81a M.B. Carver, L.N. Carlucci and W.W.R. Inch, Thermalhydraulics in Recirculating Steam Generators, THIRST Code User's Manual, AECL-7254, April 1981.

CAR81b M.B. Carver, "Numerical Simulation Involving Large Systems of Equations", Keynote Lecture, *United Kingdom Simulation Council, 1981 Conference on Computer Simulation*,

Harrogate, May 1981.

CAR95 M.B. Carver, “Numerical Solution of the Thermalhydraulic Conservation Equations from Fundamental Concepts to Multidimensional Two-Fluid Analysis”, Atomic Energy of Canada report AECL-11387, ARD-TD-550, August 1995, amended January 2017, https://canteach.candu.org.

CHA75a Y.F. Chang, “The SOPHT Program and its Applications”, *Proceedings of the 1975 Simulation Symposium on Reactor Dynamics and Plant Control*, May 26-27, CRNL, published as CRNL 1369, 1975.

CHA75b Y.F. Chang, SOPHT-B Bruce GS A Plant Control Simulation Engineers' Manual and Program Specifications, Ontario Hydro CNS-37.3, June 1975.

CHA77a C.Y.F. Chang and J. Skears, "SOPHT - A Computer Model for CANDU-PHWR Heat Transport Networks and Their Control", *Nucl. Technol*. 35, 591, 1977.

CHA77b Y.F. Chang, A Thermalhydraulic System Simulation Model for the Reactor, Boiler and Heat Transport System (SOPHT), Ontario Hydro CNS 37-2, Sept. 1977.

CHE77 Bindi Chexal, NUCIRC - A Computer Code for Nuclear Heat Transport Circuit Thermohydraulic Analysis, User's Instruction Manual, TDAI-116, AECL, Jan. 1977.

CHO74 W.G. Choe, J. Weisman, Flow Patterns and Pressure Drop in Concurrent Vapour-Liquid Flow, A State-of-the-Art Report, AECL Lib 146648, Sept. 1974.

COL72 J.C. Collier, *Convective Boiling and Condensation*, McGraw-Hill, 1972.

CRA57 Crane, *Flow of Fluids Through Valves, Fittings and Pipe*, 410-C (Engineering Units), 410-m (metric), 1957.

CUR74 I.G. Currie, *Fundamental Mechanics of Fluids*, McGraw-Hill, Inc., 1974.

DEL81 J.M. Delhaye et al., Thermohydraulics of Two-Phase Systems for Industrial Design and Nuclear Engineering, Hemisphere Publishing, 1981.

ELH80 M.A. El-Hawary, Verification of HYDNA-2 and HYDNA-3 Codes against Pertinent Experimental Data, AECL TDAI-231, December 1980.

FIR84 A.P. Firla, “Approximate Computational Formulas for Fast Calculation of Heavy Water Thermodynamic Properties”, *10th Annual Simulation Symposium on Reactor Dynamics and Plant Control*, Saint John, New Brunswick, 1984.

GAR79 W. Garland, *SOPHT-D User's Guide, Revision 3*, Ontario Hydro, Nuclear Systems Department, 1979-03-01.

[GAR84] Wm. J. Garland, W.J.G. Brimley, "CANDU 600 Heat Transport System Flow Stability", l0th Simulation Symposium on Reactor Dynamics and Plant Control, Saint John, N.B., 34 pages, April 9-10, 1984. [www.nuceng.ca/papers/conf.htm, paper C8]

[GAR86] Wm. J. Garland and S. H. Pang, "CANDU 600 Heat Transport Flow Stability", Nuclear Technology, Vol. 75, #, pp. 239-260, December 1986.

[www.nuceng.ca/papers/journal.htm, paper J4]

GAR87a W.J. Garland and R. Sollychin, "The Rate Form of State for Thermalhydraulic Systems: Numerical Considerations", *Engineering Computations*, Vol. 4, December 1987. [www.nuceng.ca/papers/journal.htm, paper J7]

GAR87b Wm. J. Garland, "A Comparison of the Rate Form of the Equation of State to the Jacobian Form", *13th Symposium on Simulation of Reactor Dynamics and Plant Control*, Chalk River Nuclear Laboratories, Chalk River, Ont., 28 pages, April 27-28, 1987. [www.nuceng.ca/papers/conf.htm, C21]

GAR88 W.J. Garland and J.D. Hoskins, "Approximate Functions for the Fast Calculation of Light Water Properties at Saturation", *Int'l J. of Multiphase Flow*, Vol. 14, No. 3, pp 333-348, 1988. [www.nuceng.ca/papers/journal.htm, paper J6]

GAR89 W.J. Garland and B.J. Hand, "Simple Functions for the Fast Approximation of Light Water Thermodynamic Properties", *Nuclear Engineering & Design*, Vol. 113, pp. 21-34,1989. [www.nuceng.ca/papers/journal.htm, paper J8]

GAR92 Wm. J. Garland, R. J. Wilson, J. Bartak, J. Cizek, M. Stasny and I. Zentrich, "Extensions to the Approximation Functions for the Fast Calculation of Saturated Water Properties", *Nuclear Engineering and Design*, # 136, pp. 381-388, 1992.
[www.nuceng.ca/papers/journal.htm, paper J13]

GIN81 Ginoux, Two-Phase Flows and Heat Transfer with Application to Nuclear Reactor Design Problems, Hemisphere Publishing, 1981.

HAA84 L. Haar, J.S. Gallagher, and G.S Knell, NBS/NRC STEAM TABLES: Thermodynamic and Transport Properties and Computer Programs for Vapor and Liquid States of Water in SI Units, Hemisphere Publishing Corporation, 1984.

HAN95 B.N. Hanna and M.E. Laveck, ed., *CATHENA Input Reference*, Atomic Energy of Canada Ltd., RC-982-4 / COG-93-140 (Vol. 4), Rev. 0.4, 1995.

HOS89 J. D. Hoskins, *A Heat Transport System Operator Companion for a CANDU Nuclear Reactor*, Masters Thesis, McMaster University, Hamilton, Ontario, Canada, July, 1989.

HSU76 Y. Hsu and R. Graham, *Transport Processes in Boiling and Two-Phase Systems*, Hemisphere Publishing, 1976.

IDE60 Idel'chik, *Handbook of Hydraulic Resistance - Coefficients of Local Resistance and of Friction*, National Science Foundation, Washington, D.C. (Translation),1960.

ITT73 ITT Grinnel Corp., *Piping Design and Engineering*, Providence, Rhode Island, 1973.

KAY79 R.A. Kay, *AESOP, Atomic Energy Station Optimization Program)*, TDAI-114/Revision 1, AECL-EC, December 1976, revised by M. Gold March 1979.

KIN73 F.K. King, *Steam Generators for CANDU Nuclear Power Stations, Sizing and Cost Analysis Program, User's Instruction Manual*, no file: see N. Subash, Process Systems Development Department, AECL-EC, May 1973, revision 1 by N. Subash, July 1976.

LAH77 R.T. Lahey, Jr., and F.J. Moody, *The Thermal Hydraulics of a Boiling Water Nuclear Reactor*, ANS/AEC Monograph Series on Nuclear Science and Technology, ANS, 1977.

LIN79 M.R. Lin et al., *FIREBIRD-III Program Description*, AECL-7533, September 1979.

MER80 E.E. Merlo, et al, *HYDNA-3 Program Description*, AECL TDAI-205, April 1980.

MEY67 Meyer, C.A. et al., *Thermodynamic and Transport Properties of Steam*, ASME, New York, 1967.

MIL71 D.S. Millar, *Internal Flow, A Guide to Losses in Pipe and Duct Systems*, British Hydromechanics Research Association, 1971.

MUR68 J.H. Murphy and J.A. Redfield, WASP - A Program to Generate Water and Steam Thermodynamic Properties, WAPD-TM-839, 1968.

NAH70 A.N. Nahavandi, and S. Makkenchery, "An Improved Pressurizer Model with Bubble Rise and Condensate Drop Dynamics", *Nuclear Engineering and Design* 12, p135-147, 1970.

PAY60 H.M. Paynter, Analysis and Design of Engineering Systems, MIT Press, 1960.

POR69 T.A. Porsching, J.H. Murphy, J.A. Redfield, and V.C. Davis, FLASH-4: A Fully Implicit FORTRAN IV Program for the Digital Simulation of Transients in a Reactor Plant, WAPD-TM-840, Mar. 1969.

POR71 T.A. Porsching, J.H. Murphy, J.A. Redfield, "Stable Numerical Integration of Conservation Equations for Hydraulic Networks", *Nuc. Sci. and Eng*. 43, p 218-225, 1971.

REL76 RELAP4/MOD5 - A Computer Program for Transient Thermalhydraulic Analysis of Nuclear Reactors and Related Systems, User's Manual, Vol. I: RELAP4/MOD5 Description, Vol II: Program Implementation, Vol. III: Checkout Applications, ANCR-NUREG-1335, Sept. 1976.

ROA76 Patrick J. Roache, *Computational Fluid Dynamics*, Hermosa Publishers, P.O. Box 8172, Albuquerque, NM, 87108, 1976.

SEA75 F.W Sears and G.L. Salinger, *Thermodynamics, Kinetic Theory, and Statistical Thermodynamics*, Addison-Wesley Publishing Company, 1975.

SKE75 J. Skears and T. Toong, *SOPHT Programmers Manual*, Revision 0.0, Ontario Hydro, Engineering Systems Department, May 1975.

SKE80 J. Skears and T. Toong, *SOPHT User's Manual*, Version 2.0, Ontario Hydro, Engineering Systems Department, January 1980.

SOL85 R. Sollychin,, S.A. Adebiyi, and W.J. Garland, "The Development of a Non-Iterative Equation of State for Two-phase Flow Systems", *11th Annual Symposium on Simulation of Reactor Dynamics and Plant Control*, Kingston, Ontario, 1985.

STE48 A.J. Stepanoff, *Centrifugal and Axial Flow Pumps*, John Wiley & Sons, Inc. 1948.

TON65 L.S. Tong, *Boiling Heat Transfer and Two-Phase Flow*, John Wiley and Sons, Inc., 1965.

YAN78 A. Yang, *600MW-SOPHT Control Simulation Manual*, AECL file XX-63330-225-010 and CENI-92, August 1978.

9 Nomenclature

A	area
A	arbitrary vector
C	concentration
C_p	heat capacity at constant pressure
C_v	heat capacity at constant volume
e	specific internal energy
E	internal heat source or sink
f	friction factor
f	long range or body force
g_c	gravitational constant
g	acceleration due to gravity
h	specific enthalpy
h_N	heat transfer coefficient
H	total enthalpy in volume, V
I	unity tensor
k	head loss coefficient
L	length
M	mass in volume, V
M	momentum interchange vector
n	unit vector normal to the surface
P	pressure
q	heat flux
Q	lumped heat source or sink
s	surface bounding volume, V
S	surface sink or source
t	time
T	temperature
U	total internal energy in volume, V
V	arbitrary fluid volume
v	velocity vector
W	mass flow
x	quality (weight fraction)

Greek

α	void fraction
γ	phase volume fraction
Γ	local sink or source
ψ	field variable
ρ	density
σ	stress tensor
θ	angle with respect to horizontal
τ	shear stress tensor

Operators

$\frac{\partial}{\partial t}$	partial time derivative
$\frac{d}{dt}$	total time derivative
$\frac{D}{Dt}$	substantial time derivative
∇	Del operator
$\iiint_V (\,)dV$	volume integral
$\iint_S (\,)ds$	surface integral
$<(\,)>=\frac{1}{A}\iint_S (\,)ds$	cross sectional average

Subscripts

f	liquid (fluid) phase
g	vapour (gaseous) phase
i	summation index for nodes
j	summation index for links
k	1, 2 (1 = liquid, 2 = vapour)
S	surface
SAT	saturated
IN	ingoing
OUT	outgoing

10 Acknowledgements

This chapter is based on a graduate level course given by the author at McMaster University and on research funded by McMaster University and the Natural Sciences and Engineering Research Council of Canada. The author is indebted to Atomic Energy of Canada Ltd. and to Ontario Power Generation since this work is inextricably linked to past involvements with these companies. Special thanks go to students, John Hoskins and Brian Hand, for water property development, and to Raymond Sollychin for his central role in the development of the rate method for the equation of state. A general thanks to all students over the years; their freshness is a constant delight. Their sharp eyes caught many a mistake; of course the responsibility for any errors or omissions lies entirely with the author.

CHAPTER 8

Nuclear Plant Systems

prepared by
Dr. Robin Chaplin

***Summary**:*

This chapter deals with the main components of a CANDU nuclear power plant. It follows the general path of energy production from the nuclear reactor to the electrical generator with descriptions of the systems and equipment essential for the purpose of generating thermal energy, transferring heat and converting heat into mechanical and then electrical energy. Some key auxiliary systems are included where these are an essential part of the energy processes as are the basic control systems which maintain stable operational conditions and ensure safety of the plant. This chapter leads into Chapter 9 which describes how a typical CANDU plant operates.

Table of Contents

List of Figures

List of Tables

1 Introduction

1.1 General Configuration

Specific units in a typical CANDU nuclear plant include a *nuclear reactor* in which heat is generated by nuclear fission, a *heat transport system* to convey this heat from the reactor to the steam cycle, a *steam generator* in which steam is generated, a *steam system* to convey steam from the steam generator to the steam turbine, a *steam turbine* where available heat energy is converted into mechanical energy, a *condenser* where unavailable heat energy is rejected to the cooling water system, a steam *reheating and feedwater heating system* to improve cycle efficiency, an *electrical generator* to convert mechanical energy into electrical energy, and an *electrical system* to generate electrical energy for distribution to consumers. To balance the flow of energy through these components and to regulate plant output, a *control system* is required. Each of these major systems will be described in this chapter.

All thermal reactors have four important components: fuel, moderator, coolant, and control elements. The moderator is that part of the nuclear reactor where neutrons are reduced in energy to increase the probability of fission when they re-enter the fuel. Spacing of the fuel assemblies within the moderator is therefore of key importance. Heat must be removed by the coolant from the fuel assemblies at a high rate without making the fuel sustain excessive temperatures. This is achieved by having multiple small diameter fuel rods (elements) in one fuel assembly. These two requirements dictate the general reactor configuration. A unique aspect of the CANDU reactor is the horizontal arrangement of fuel channels within the reactor calandria. These channels contain the fuel bundles and are surrounded by the heavy water moderator, whereas heavy water coolant flows through the channels.

Heat is generated in the nuclear reactor, and electricity is produced by the electrical generator. The production and discharge of this energy must be perfectly balanced. The steam generator is the key component for maintaining this balance, that is, the rate of steam generation must match the rate of steam flow to the steam turbine, or *vice versa*. Any change in these two energy flows will immediately be reflected as a change in steam pressure in the steam generator. Therefore, steam pressure is a key control parameter for the entire plant under all operating conditions.

2 Nuclear Reactor

2.1 General Arrangement

For all CANDU reactors, the horizontal fuel channels are arranged in a square array across the reactor face, as shown in Figure 1. The calandria, which contains the moderator at essentially atmospheric pressure, contains axial tubes in a similar square array to accommodate the pressurized fuel channels or pressure tubes, which in turn contain the fuel bundles and the primary system coolant. Figure 2 shows a close-up view of the feeder pipes conveying coolant to and from the pressure tubes at one end of the reactor.

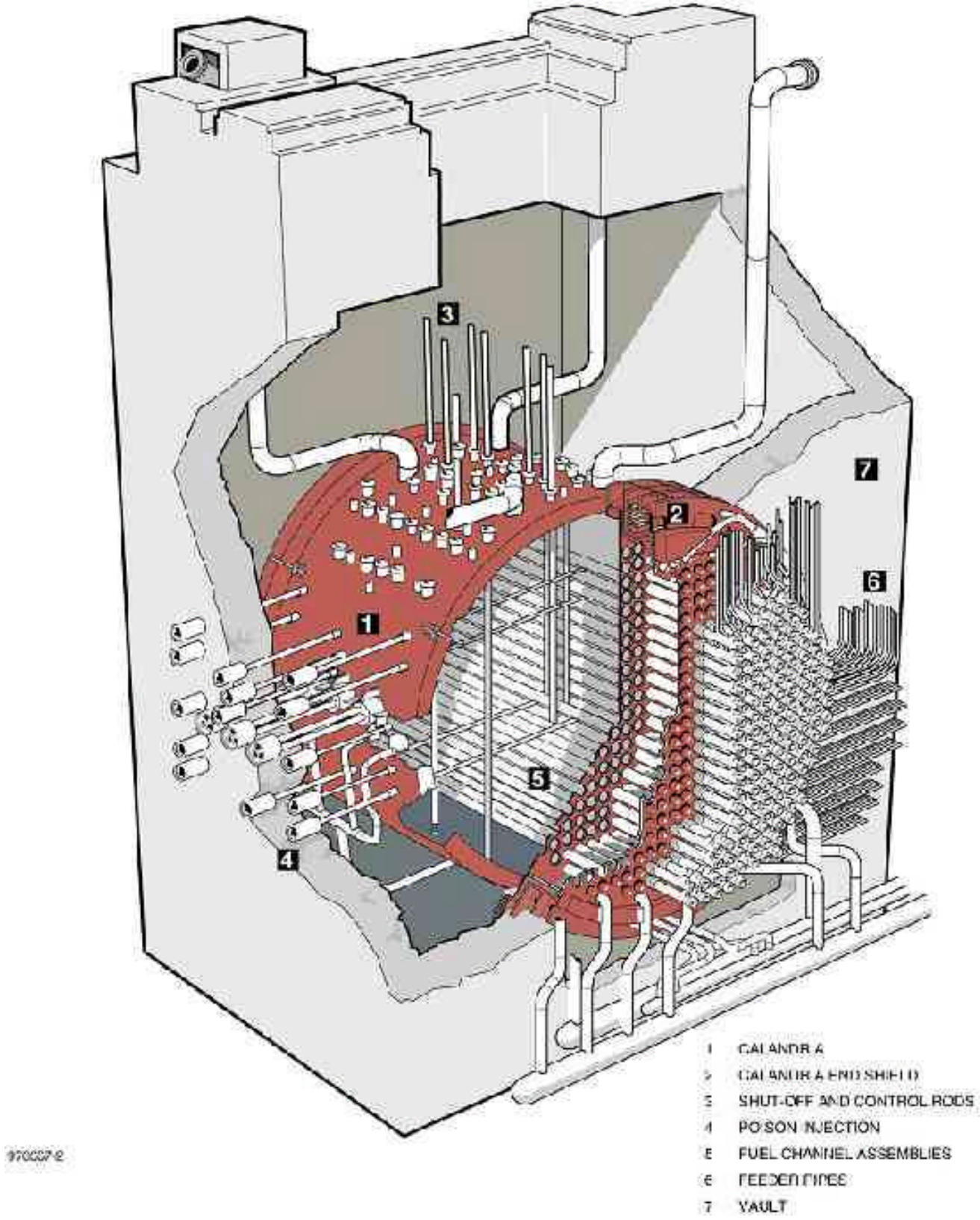

Figure 1 Reactor vault and assembly

Figure 2 Feeder tube assembly on reactor face

2.2 Calandria Arrangement

The calandria contains the moderator for the reactor. It consists essentially of a horizontally mounted cylindrical tank containing many horizontal tubes in a square array. Pressure tubes containing fuel and coolant are fitted inside the calandria tubes, with a small annular gas filled space to provide heat insulation. This annular space is maintained by garter springs which resist sagging of the pressure tubes and thus minimize the risk of contact with the calandria tubes. The gas used is carbon dioxide because it has low thermal conductivity, shows little tendency to promote corrosion, and does not produce significant activation products. The carbon dioxide is circulated in the annular space to cool it and to monitor it for any leakage from the calandria and pressure tubes. The calandria contains heavy water as moderator, which fills the space between the calandria tubes. The spacing of the calandria tubes and hence the fuel channels is greater than optimum with respect to neutron moderation, with the result that the reactor is over-moderated.

2.3 Moderator Temperature Control

Heat is generated in the heavy water moderator by the neutron moderating process, where the kinetic energy of the neutrons is converted into heat energy, and by absorption of gamma radiation. Both these processes intensify with a rise in reactor power. Heat is also transferred to the moderator through the carbon dioxide in the annular space between the pressure tubes and calandria tubes. This process is largely independent of reactor power because the fuel channel temperature is fairly constant at all power levels. The total amount of heat generated in and transferred to the moderator is approximately 5% of total reactor heat production. This heat must be removed to maintain the desired temperature in the moderator.

The moderator temperature is maintained between 60°C and 65°C by an external cooling system, as illustrated in Figure 3. This system includes circulating pumps and heat exchangers, which reject heat to the service water system. Although the relatively large temperature difference between the reactor coolant and the moderator induces some heat loss, the rela-

tively cool moderator can provide some measure of cooling to the fuel in the event of a loss of coolant accident and the coincident failure of the emergency coolant injection system. Because the reactor's configuration makes it over-moderated, any void formation within the moderator would cause an increase in reactivity, leading to unstable reactivity conditions. Hence, it is desirable to maintain an adequate margin below boiling conditions.

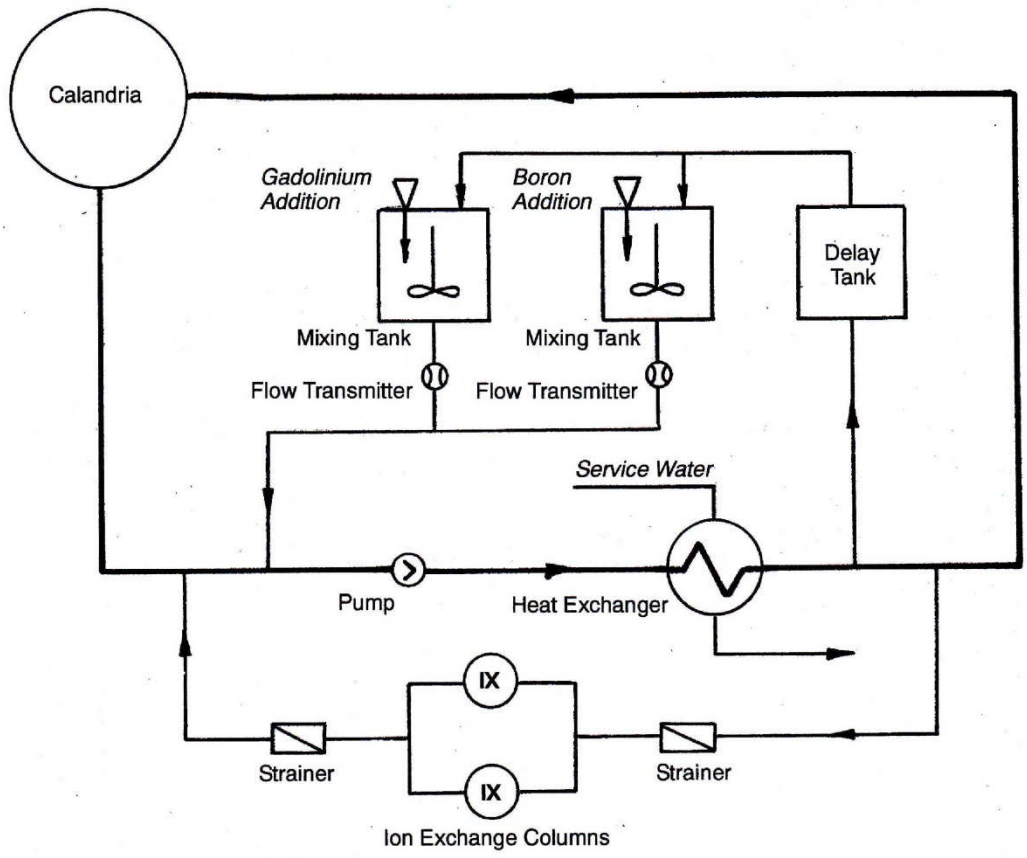

Figure 3 Moderator cooling and purification system

The moderator temperature has an effect on the reactivity of the reactor as its temperature rises from ambient conditions to operating conditions during reactor warm-up. For equilibrium fuel conditions, that is, a mix of used and new fuel that arises after several months of continuous refuelling, the temperature coefficient of reactivity is positive, meaning that the reactivity increases by about 4 mk as the temperature goes from 30°C to 70°C. This phenomenon is due mainly to two factors. One is the lower density of the moderator at higher temperatures, resulting in less neutron absorption. The other is the increased fission cross section of plutonium as the increase in temperature takes the neutron energy into a resonance peak of Pu-239.

2.4 Moderator Reactivity Control

To control moderator reactivity, soluble poisons are added to the heavy water at appropriate concentrations under certain operating conditions through a moderator liquid poison addition system. This system consists of mixing tanks for boron and gadolinium, also shown in Figure 3, where the solutions are formulated, as well as flow transmitters at the circulating pump inlet to measure the amount entering the moderator system.

Both gadolinium and boron have strong neutron absorbing isotopes, namely Gd-155, Gd-157, and B-10. They gradually lose their ability to absorb neutrons as neutrons are absorbed to form a heavier isotope. The burnout rate for boron is slower than that of gadolinium, making it more suitable for longer term operations such as compensation for reactivity loss due to fuel burnup. When a reactor is charged with new fuel, the excess reactivity from the fuel can be balanced by a certain concentration of boron. As the fuel burns up and neutron absorbing fission products are produced, the effectiveness of the boron decreases, making it possible to maintain reasonably constant reactivity with naturally small adjustments. The burnout rate for gadolinium is faster than that of boron, and therefore it is more suitable for short term reactivity adjustments such as those necessary during xenon transients. The xenon concentration in the fuel is lower during periods of low load and builds up following a large power increase. Gadolinium can compensate for this and burns out at a rate roughly corresponding to xenon buildup. Gadolinium can also be used to compensate for a lack of xenon in the reactor during an outage to ensure that the reactor will remain subcritical.

The shutdown system, which will be described later, injects liquid poison directly into the moderator in the event of certain reactor trips. Gadolinium is used at sufficient concentration to ensure an immediate reduction in reactivity to well below critical conditions. Upon reactor restart, it must be removed by the moderator purification system. Gadolinium is easily removed by ion exchange resins, whereas boron, being a weaker ion, is not easily removed. This makes gadolinium better suited for use in the shutdown system, but it still takes several hours to remove it and almost as long as the ensuing outage due to xenon poisoning.

A moderator purification system, also shown in Figure 3, is connected to the moderator cooling system to maintain heavy water purity and to remove or adjust the concentration of soluble poisons such as gadolinium or boron which may have been introduced for shutdown purposes or to assist in reactivity control. The non-active soluble poison (after neutron absorption) must be removed to maintain the general purity of the moderator. The purification system has strainers to remove particulate material such as resin fines from the system, followed by mixed bed ion exchange columns to remove dissolved material in the form of positive and negative ions.

2.5 Core Shielding

The reactor core is shielded at the ends by end shields and around the periphery by a thermal shield to absorb neutron and gamma radiation which would otherwise create excessive radiation fields at the reactor faces and high temperatures in the calandria structure. The shields contain water which is circulated and cooled. The end shields contain steel balls as well to ensure sufficiently low radiation fields during routine maintenance shutdowns. The combination of water and steel balls is very effective in attenuating both neutron and gamma radiation.

2.6 Reactor Control Systems and Devices

Heavy water is a very weak neutron absorber, which is advantageous with regard to fuel utilization. To compensate for reactivity changes in the fuel, the absorption properties of the moderator can be modified by adding a soluble neutron absorber in small concentrations. Gadolinium and boron both have strong neutron absorbing isotopes, namely Gd-155, Gd-157, and B-10. These can be added through the liquid poison system and removed through the moderator purification system using ion exchangers. Light water is a stronger neutron absorber than heavy

water, and therefore the concentration of light water in the heavy water moderator must be limited to avoid excessive neutron absorption. The normal isotopic concentration of D_2O in the moderator is 99.5%. Light water, however, can be conveniently used as a control device within the reactor, where its volume in vertical tubes can be varied.

Reactor power is controlled and maintained at the required level by several devices which absorb neutrons and thereby control the nuclear fission process. These systems and devices are:

- Liquid poison in moderator
- Liquid zone control absorbers
- Mechanical rod control absorbers
- Mechanical rod adjusters.

In addition, a complete reactor shutdown can be achieved by operating one or both of the following devices in addition to those listed above:

- Mechanical rod shut-off absorbers (Shutdown System 1)
- Liquid poison injection system (Shutdown System 2).

Appropriate signals to operate the control systems are obtained from neutron flux detectors within the core and ion chambers alongside the core as well as from other sensors in the steam system and turbine generator. The main control devices are shown as part of the reactor assembly in Figure 4.

The control devices described below are generally applicable to CANDU 6 reactors. The same design philosophy applies to other CANDU reactors, but the number of devices may be different if the reactor core is of different size.

In a CANDU 6 reactor core, there are 26 in-core vertical flux detectors and 7 in-core horizontal flux detectors. Twelve vertically installed detectors provide flux information to Shutdown System 1, while three horizontal flux detectors supply flux data to Shutdown System 2. The remaining vertical flux detectors send information to the liquid zone control absorbers and the solid control rod absorbers. All these in-core flux detectors can provide data for three dimensional flux mapping of the reactor core.

Figure 5, Figure 6, and Figure 7 show three orthogonal views of a CANDU 6 reactor. These show the relative positions and arrangement of various components and devices.

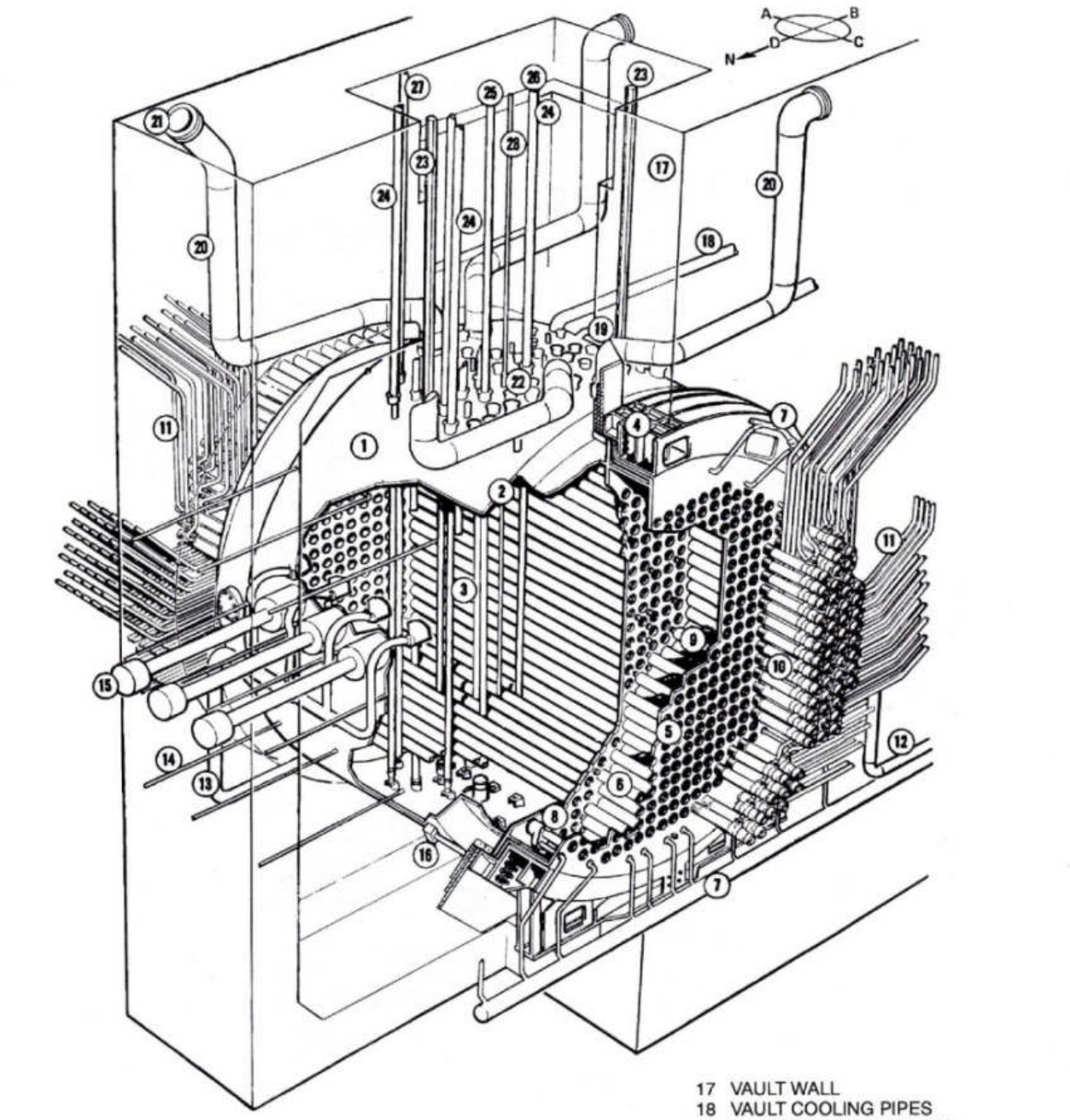

Figure 4 CANDU 6 reactor assembly

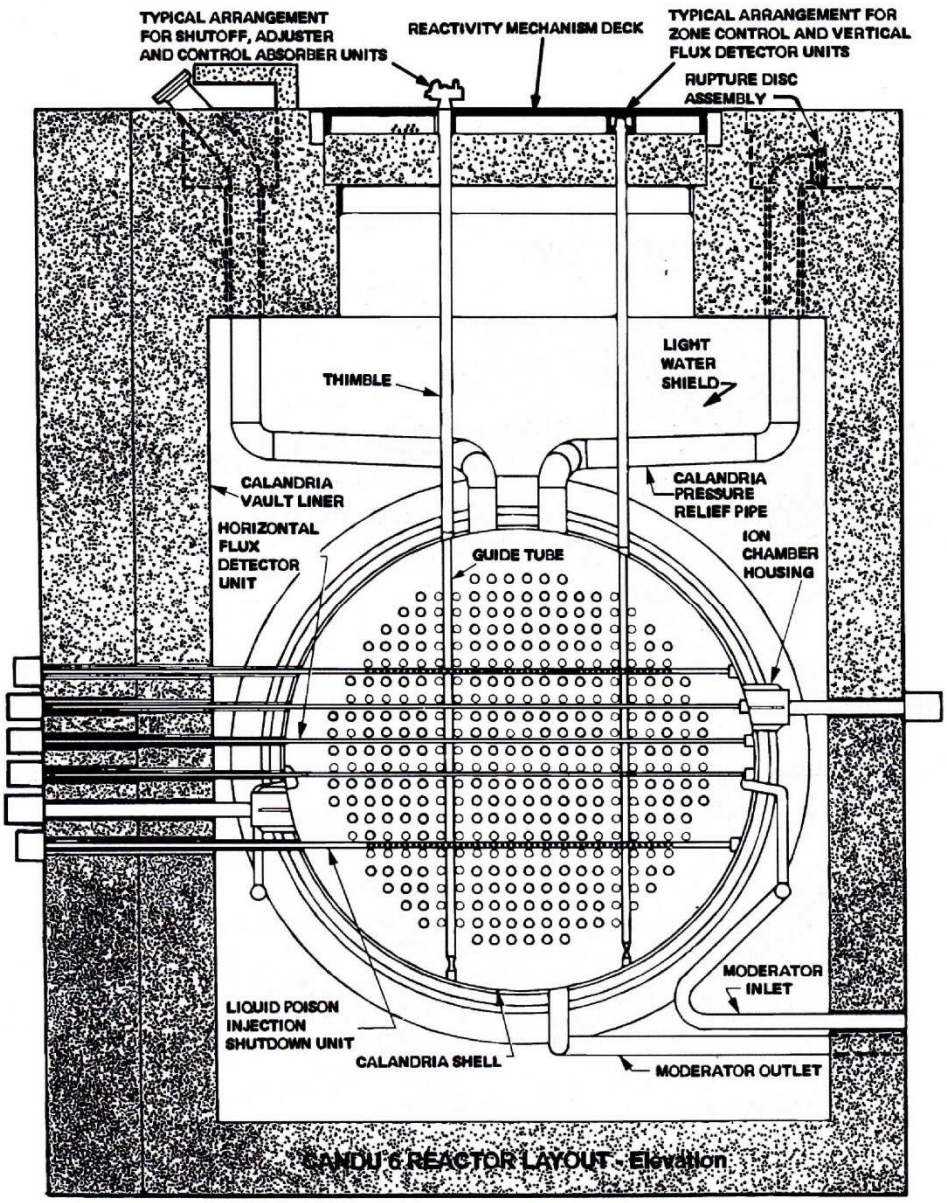

Figure 5 Reactor cross section

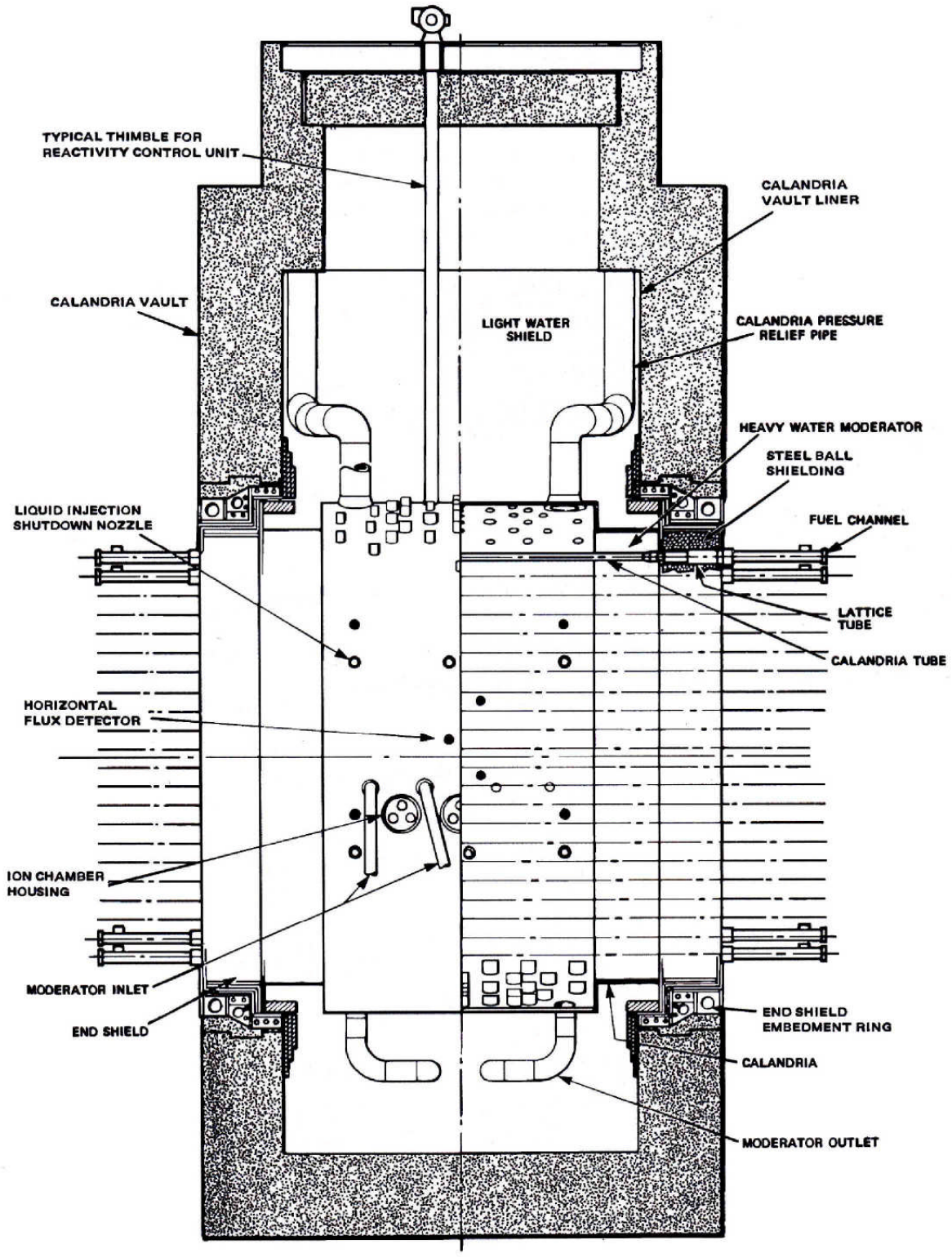

Figure 6 Reactor longitudinal section

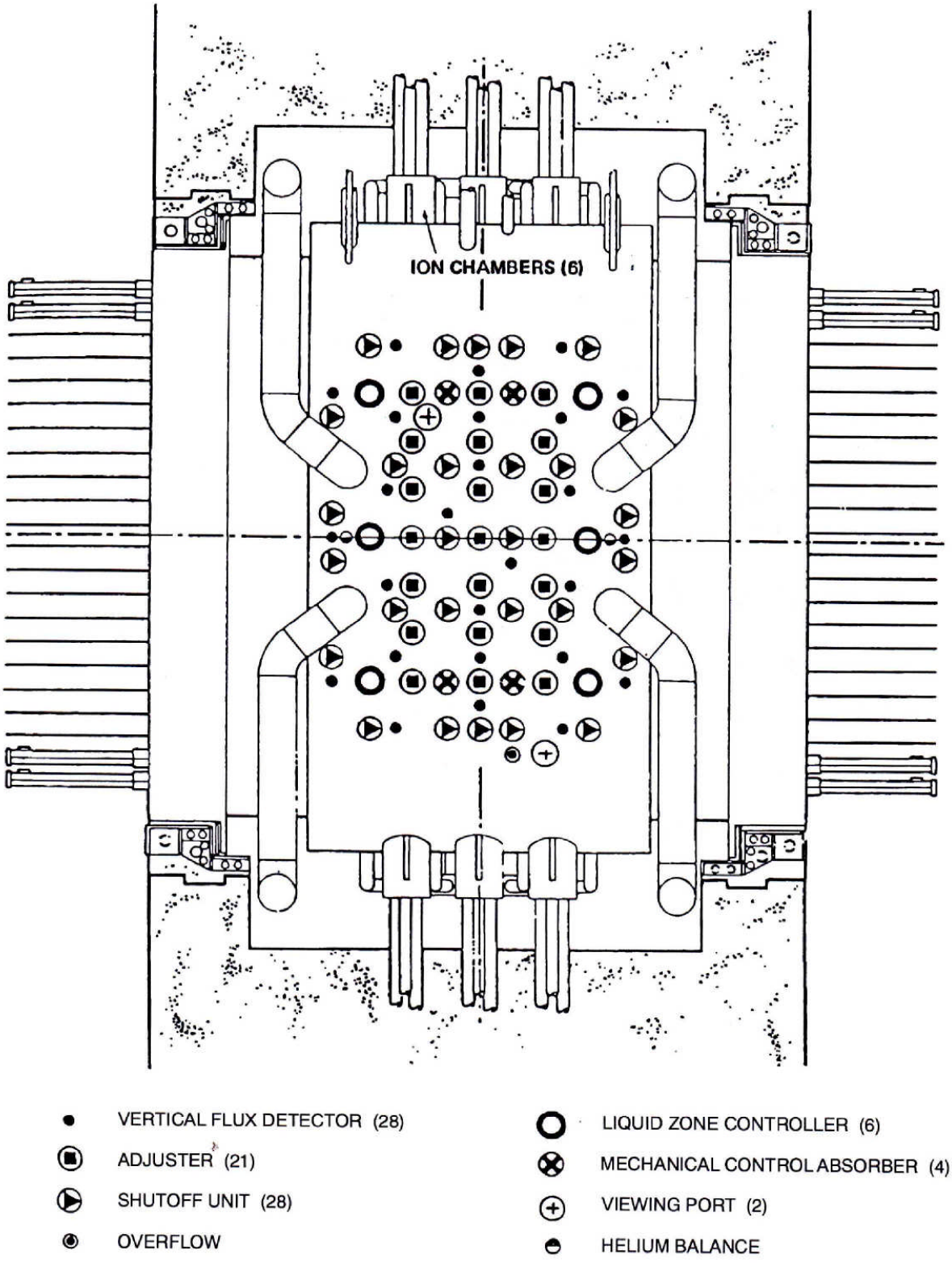

Figure 7 Reactor plan view

2.6.1 Moderator Poison Addition System

Liquid poison such as boron or gadolinium can be added to the moderator to adjust reactor reactivity. Because these are both neutron absorbers, they reduce neutron efficiency and hence adversely affect fuel utilization. However, as described earlier, their use is necessary under certain transient conditions to maintain reactivity within regular control limits. Such conditions arise when a reactor is started with a new charge of fresh fuel, when a significant amount of fresh fuel is added, and during large increases in load when xenon transients need to be accommodated.

2.6.2 Liquid zone control absorbers

Critical reactivity balance is mostly and predominantly maintained by the six liquid zone control absorbers located vertically within the reactor core interspersed among the mechanical control absorbers, adjuster rods, and shut-off rods. These liquid zone absorbers contain light water in two or three separate sections, forming a total of fourteen compartments. These separate and independent absorbers enable spatial control of neutron flux. Light water absorbs neutrons more strongly than heavy water and acts like a control rod as light water is added or removed through inlet and outlet pipes, where a difference in flow rate will vary the level. Helium gas is maintained above the light water, and the difference in pressure between the inlet and outlet, at the bottom and top of the water column respectively, indicates the level of light water. The quantity of water in each compartment is controlled by automated valves receiving signals from the flux detectors through the control computers of the reactor regulating system.

2.6.3 Mechanical rod control absorbers

Besides the liquid zone control absorbers, there are also four mechanical control absorbers made from a variety of alloys, predominantly cadmium encased in stainless steel. These absorbers adjust the flux level when a greater reactivity rate or depth than can be provided with the liquid zone control absorbers is required. They can bring about a fast reactor power reduction such as a reactor stepback. They may be driven in or out of the core at variable speed or dropped into the core by the release of a clutch. The design of these solid control absorbers is virtually identical to that of the shut-off rods described below.

2.6.4 Mechanical rod adjusters

Adjuster rods are used in the reactor to optimize the neutron flux profile for reactor power, compensate for fuel burnup, and provide excess reactivity to overcome Xenon-135 surges following a power reduction. CANDU reactors are designed to develop full power when these adjuster rods are fully inserted into the reactor core. There are 21 adjuster rods arranged in three rows vertically between the other control devices. The adjuster elements are raised or lowered individually by winching drives similar to those described for the shut-off rods, except that these adjusters do not fall into the reactor in the event of a shutdown signal from the flux detectors because they would normally be fully inserted during normal operation. When the adjusters are fully withdrawn, the reactivity gain is about 16 mk, which is sufficient to overcome minor xenon transients during power manoeuvering.

2.6.5 Mechanical rod shut-off absorbers

The signals received from the flux detectors or other plant indicators, which are routed to Shutdown System 1 (SDS1), control a system of 28 vertical shut-off rods. These shut-off rods are composed of cadmium and stainless steel absorber elements and are used to shut the reactor down under normal and emergency conditions. When these rods are inserted into the core, they are aided by perforated guide tubes made of zirconium alloy that are open to the pressure of the moderator. These shut-off rods are inserted into or withdrawn from the core by means of a stainless steel cable which is wound on a drum in the rod drive mechanism. This drum is driven by an electric motor with an electromagnetic friction clutch. When a shut-off signal is received, the clutch de-energizes, and the shut-off rods fall into the reactor core inside the zirconium alloy guide tubes under the influence of gravity. While the clutch is energized, the shut-off rods can be driven into or out of the reactor core by the electric drive motor.

2.6.6 Liquid poison injection system

This system, unlike the *Moderator Poison Addition System*, is a safety system as opposed to a control system. It injects a large quantity of soluble poison into the moderator to reduce reactivity drastically rather than adding a controlled amount to maintain reactivity at the required level.

Shutdown System 2 (SDS2), as illustrated diagrammatically in Figure 8, is activated based on information received from the three horizontal in-core flux detectors or other plant indicators. The poison that is injected into the core is gadolinium nitrate dissolved in heavy water. This poison is contained in six tanks outside the reactor vault in an accessible area for routine maintenance. Each of the six poison tanks is connected to a nozzle pipe in the calandria by stainless steel pipes. These nozzle pipes are oriented horizontally in the reactor core, each with several orifice holes situated to provide maximum negative reactivity changes when the poison is injected. The nozzle pipes themselves are made of zirconium alloy.

The gadolinium nitrate poison is injected into the core by helium under pressure. Pressurized helium in this tank is isolated from the poison tanks by triplicated quick-acting valves. When these valves are opened, the pressure forces the poison into the moderator very quickly. A ball in the poison tanks prevents blowthrough of helium gas and ensures that calandria pressure does not exceed its design value.

SDS2 is typically capable of supplying at least 50 mk of negative reactivity worth, although a negative reactivity of 30 mk is considered adequate to bring about complete and rapid shutdown. This system acts as a backup to SDS1 and should be activated only in the event of a failure of SDS1 or if the initiating event is so severe or so fast that SDS1 has not arrested the transient. Because liquid poison is injected into the moderator, quick recovery from such a trip is not possible.

In the original CANDU design concept, it was decided that there should be two independent and different shutdown systems operated from different sources and configured differently. To achieve this objective, the SDS1 and SDS2 systems inject negative reactivity in different ways and even in different orientations within the reactor, that is, one vertically and one horizontally.

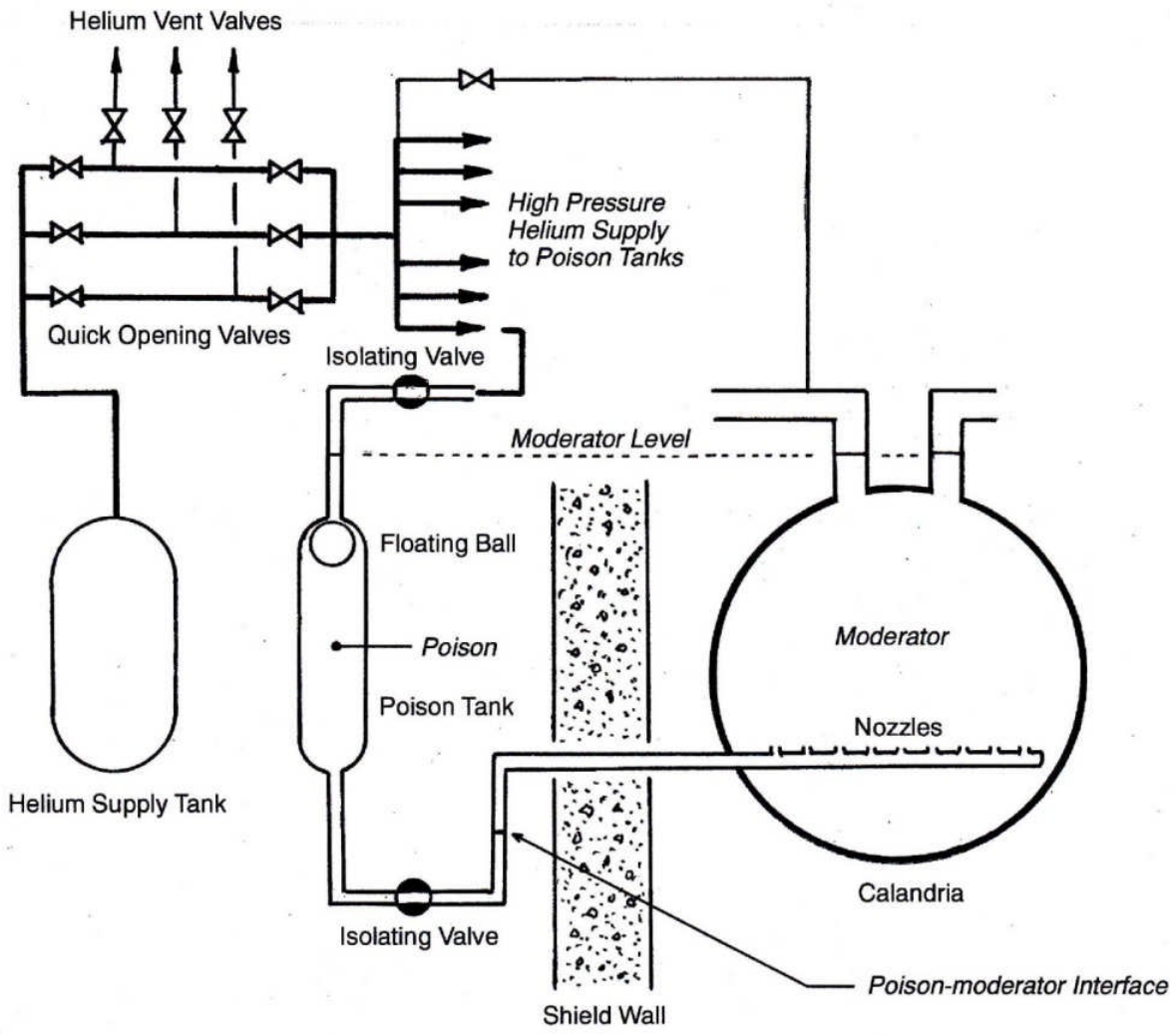

Figure 8 Shutdown System 2 (SDS2)

2.7 Fuel Configuration

In most CANDU reactors, the individual fuel bundles have 37 fuel elements, each containing a stack of natural uranium dioxide fuel pellets. Within each fuel element are approximately 30 fuel pellets, giving an effective stack length of 480 mm. The fuel elements are held in place by end plates which are perforated to enable coolant to flow axially and are prevented from contacting one another or the pressure tube by spacers. The element sheaths are made of zircaloy to minimize neutron absorption. There are 12 fuel bundles in each fuel channel of the CANDU 6 reactor. The configuration of the reactor with horizontal fuel channels enables the reactor to be refuelled while on load and also facilitates partial refuelling of a single channel because the fuel bundles do not have to be linked together as in a vertical channel. A 37-element fuel bundle is shown in Figure 9, while Table 1 gives details of a 37-element fuel bundle.

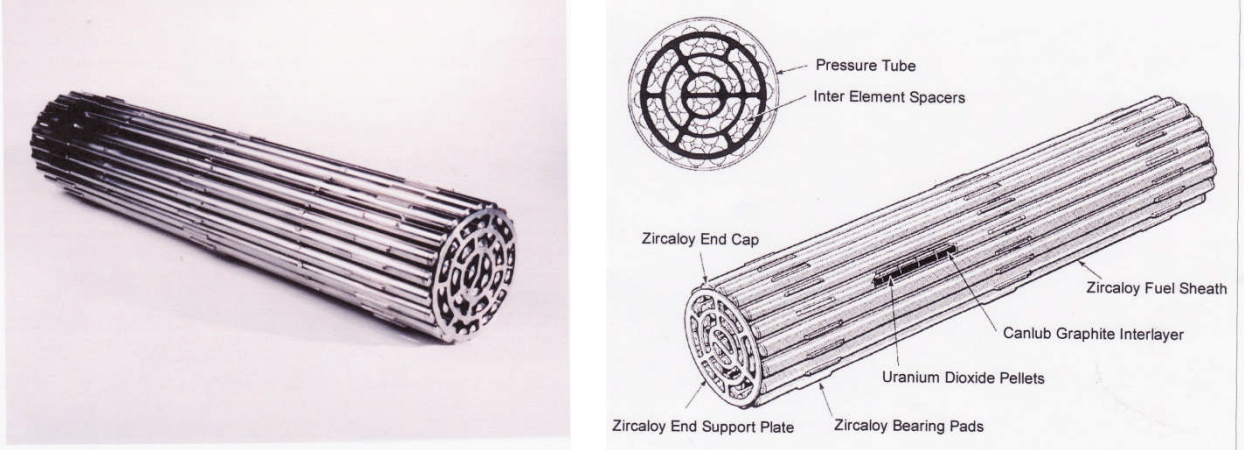

Figure 9 37-element fuel bundle

Table 1 CANDU fuel characteristics

Fuel Type	Sintered natural uranium dioxide
Pellets	Cylindrical with concave dished ends
Number in Elements	30
Elements per Bundle	37
Bundles per Fuel Channel	12
Pellet Diameter	12.16 mm
Pellet Stack Length	480 mm
Cladding	Zircaloy-4
Cladding Outside Diameter	13.08 mm
Bundle Outside Diameter	102.4 mm
Bundle Overall Length	495 mm

2.8 Fuel Channel Conditions

A temperature rise takes place along the fuel channel from the inlet to the outlet until saturation conditions are reached, after which the temperature remains approximately constant. This temperature rise is not linear because the rate of temperature rise depends upon the local rate of heat release and hence on the neutron flux, which drops off towards both the inlet and outlet of the channel. The most severe fuel conditions occur where both the heat flux and coolant temperature are high. This occurs normally somewhat downstream of the channel midpoint. Typical fuel channel conditions are given in Table 2.

Table 2 Fuel channel parameters (CANDU 6)

Fuel Channel Material	Zirconium-Niobium Alloy
Inside Diameter	103.38 mm
Wall Thickness	4.19 mm
Inlet Pressure	11.04 MPa (a)
Outlet Pressure	10.30 MPa (a)
Inlet Temperature	267°C
Outlet Temperature	312°C
Maximum Coolant Flow	24 kg/s
Average Coolant Flow	20 kg/s

2.9 Fuel Handling

Short term reactivity changes occur continuously during normal operation due to load changes or to minor transient conditions. Short term reactivity control is maintained in the reactor core by liquid zone control absorbers (for load changes) and adjuster rods (for transients). Long term reactivity changes occur slowly as fuel is used up and fission products accumulate in the fuel. Long term reactivity control is achieved through on-line refuelling to maintain constant reactivity while fuel is burned. By varying the frequency of refuelling in different areas of the reactor core, the flux and hence the power distribution can be very effectively and accurately controlled.

The CANDU reactor with its horizontal fuel channels has a reactor face at each end, onto which two fuelling machines must attach while maintaining pressure and flow in the channel. Figure 10 shows a typical reactor face with a fuelling machine. This is a larger reactor with 480 fuel channels (Darlington) with a later design of fuelling machine than the one illustrated in Figure 11 and Figure 12.

Fuel is inserted into and removed from the fuel channels by two remotely controlled fuelling machines which attach to the ends of a selected fuel channel. A general view of a typical fuelling machine (Pickering) as seen from the reactor side is shown in Figure 11. These fuelling machines are fully automatic and remotely controlled. The equipment itself consists of a fuelling machine mounted on a suspended carriage. The carriage travels on a track which can be raised or lowered by a gantry so that the fuelling machines can reach any fuel channel. Heavy water and electricity supplies are provided by a flexible catenary which connects the machine to the stationary auxiliary systems.

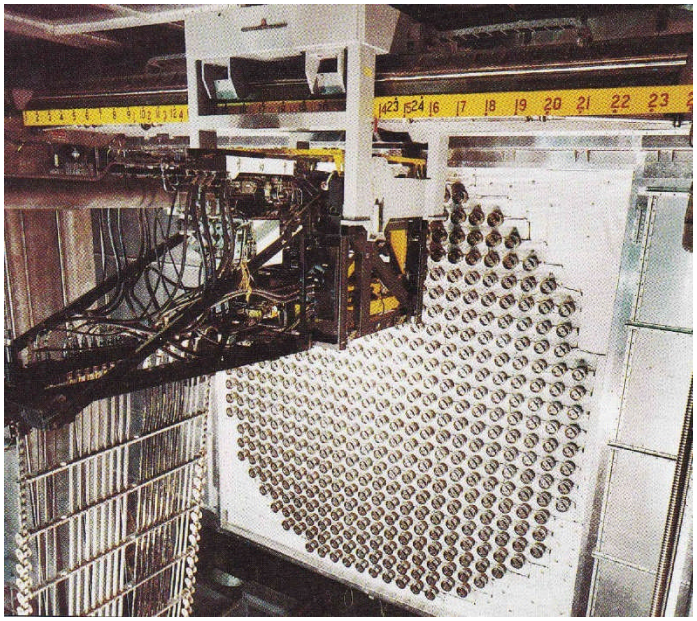

Figure 10 Reactor face with fuelling machine

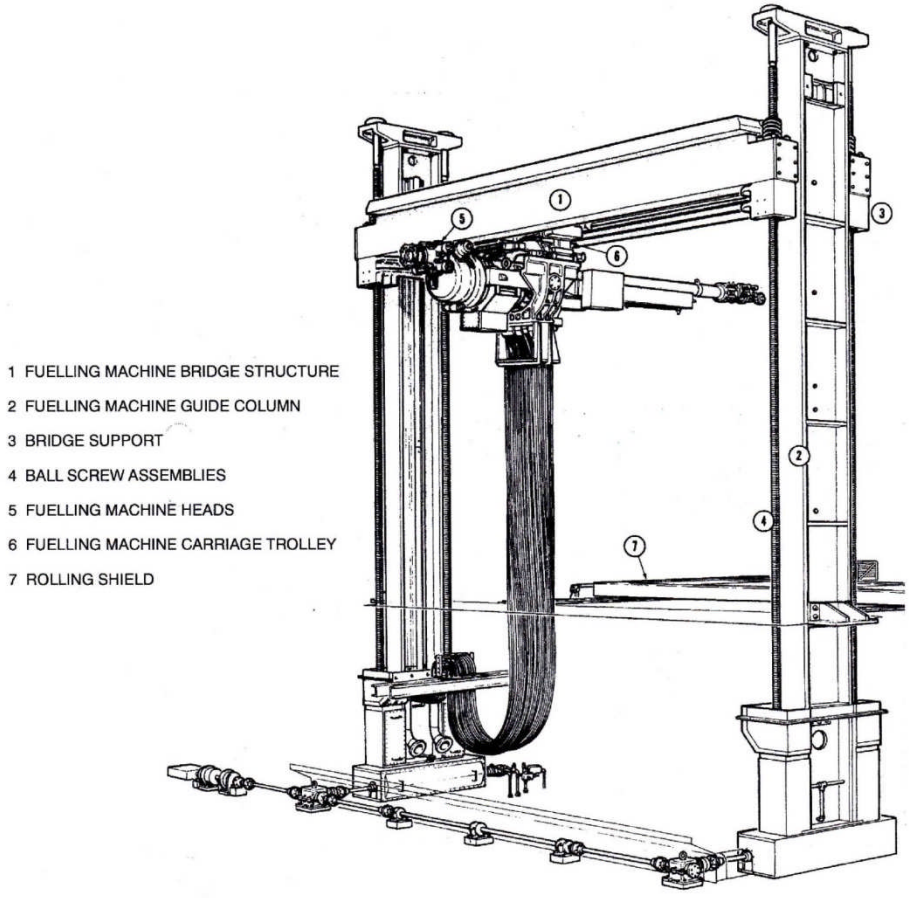

Figure 11 Typical fuelling machine and bridge

The arrangement with respect to the reactor face is shown in Figure 12. By raising or lowering the gantry and traversing the carriage, the fuelling machine can reach any channel. When the gantry is at its lowest point, the machine can turn 90° in the horizontal plane, as shown by the dotted image, to receive new fuel or to discharge spent fuel in the service area. After

attachment to the reactor, the fuelling machines open the fuel channel and remove the shield plug. One fuelling machine carries the new fuel in its magazine, while the other machine at the opposite end of the fuel channel receives and stores spent fuel in its own magazine. Each magazine can revolve and has several slots, each of which can store two fuel bundles. Two new fuel bundles from the fuelling machine are inserted at the coolant inlet end, while two used bundles are removed at the coolant outlet end. Normally, depending on the particular CANDU design, eight bundles are changed during one channel refuelling. In this way, the two bundles at each end where the neutron flux is low spend twice as long in the reactor than those in the high flux zone in the middle. Flow through the channel is maintained, and the pressure difference so derived is used to move the bundles into the channel and to provide a driving force to facilitate their removal. Spent fuel is later transferred to the irradiated fuel bay, where it is stored under water. The average time taken to refuel one fuel channel is about two and one half hours, meaning that the refuelling process is almost continuous during normal working hours.

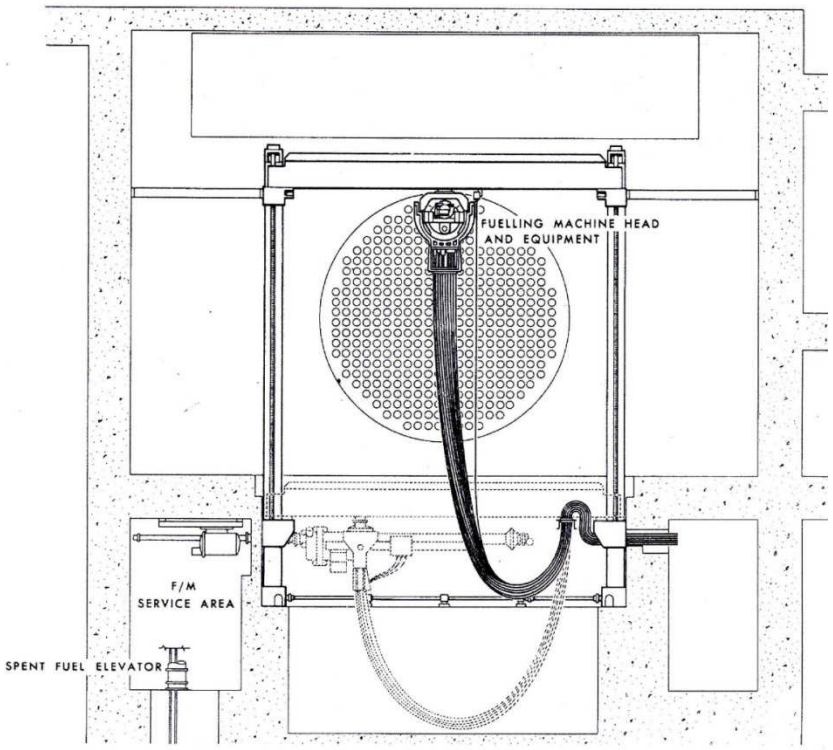

Figure 12 Orientation of fuelling machine with respect to reactor

New fuel is loaded directly into the magazine of the fuelling machine, but irradiated fuel must be remotely handled and transferred under shielded conditions to the irradiated fuel bay for interim storage during its initial cooldown period.

3 Heat Transport System

3.1 General Arrangement

The fundamental function of the primary coolant circuit or heat transport system is to circulate the heavy water coolant and transport heat from the fuel elements to the steam system. The entire circuit consists of pumps, headers, feeder pipes, pressure tubes, and steam generators, as shown in Figure 13. In addition, there is a single pressurizer in the circuit. The coolant used in CANDU

reactors is heavy water to minimize neutron absorption. In the pressure tubes, the coolant flows are in opposite directions in adjacent tubes. Thus the coolant passes from the steam generators at one end of the reactor through half the tubes to the steam generators at the other end of the reactor and back again through the adjacent tubes.

There are two steam generators and two heat transport pumps at each end of the reactor, and therefore the entire system is divided into two independent loops, with each serving half the reactor. They are linked by a balance pipe with restricting orifices so that the same pressure is maintained in each loop and only one pressurizer is required. This arrangement is illustrated diagrammatically in Figure 14. The advantage of this arrangement is that, in the event of a serious loss of coolant accident, only half the reactor will be affected initially, with minimum subsequent loss of coolant from the other half.

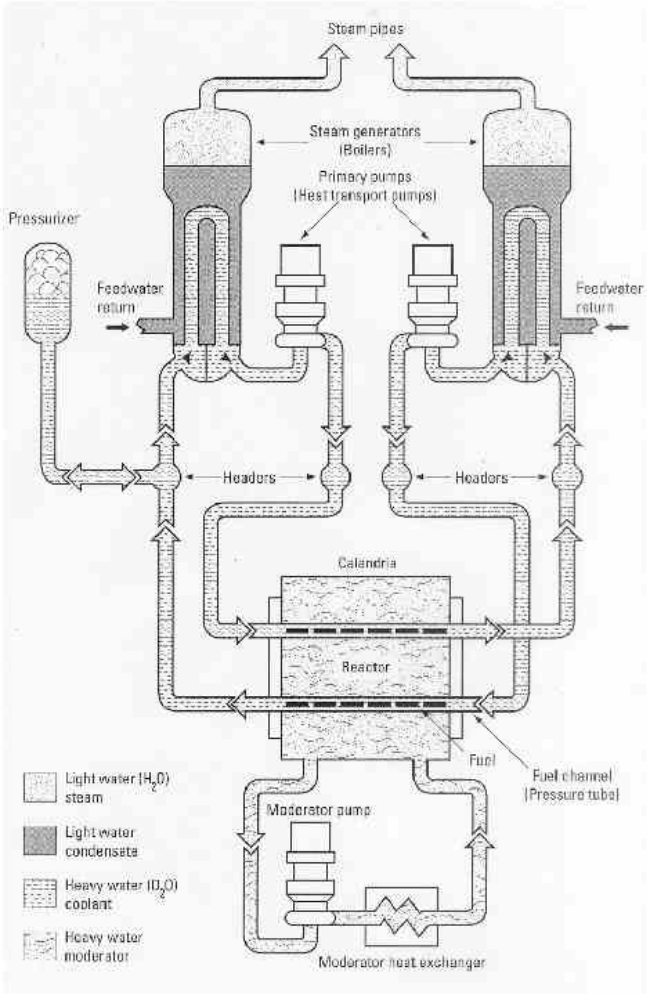

Figure 13 Simplified heat transport and moderator circuits

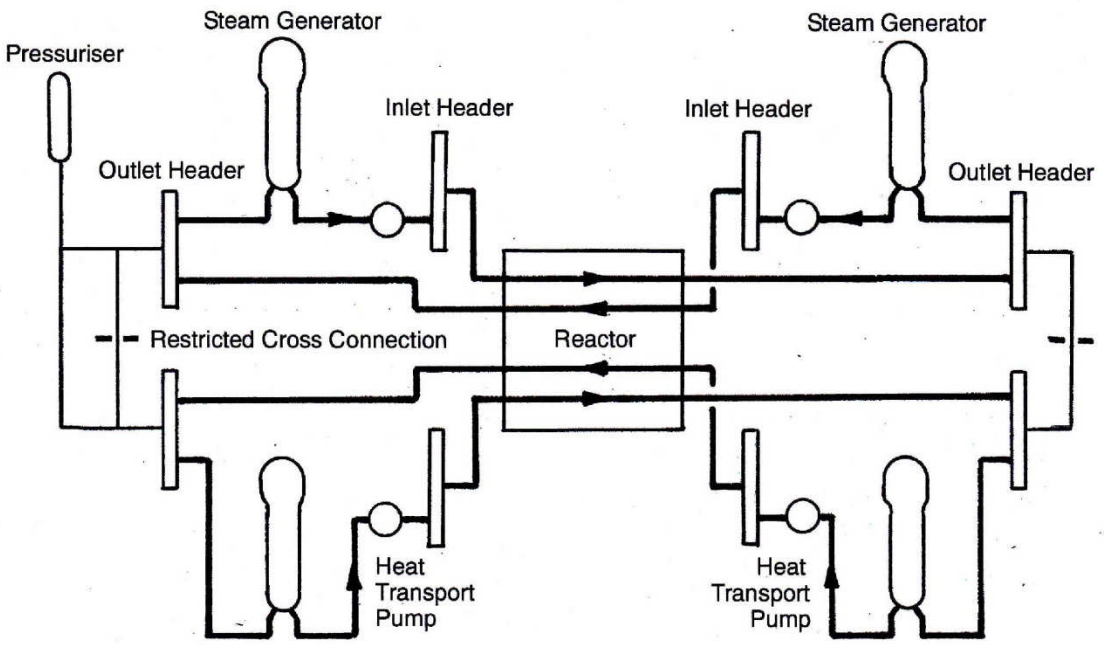

Figure 14 Diagrammatic arrangement of figure-of-eight heat transport system

As coolant leaves the reactor, it passes through the outlet feeder tubes on each reactor face and then to the respective headers. From here, it enters the U-tube steam generators situated at opposite ends of the reactor. In the steam generator, the pressurized heavy water exchanges heat with the light water on the steam side of the steam generator. The now cooled heavy water passes to the heat transport pumps, one for each steam generator, and returns to the reactor core through headers and inlet feeder tubes at each end of the reactor.

The heat transport system serves to remove heat from the reactor under both power producing and shutdown conditions. The flow is maintained by the heat transport pumps under most conditions, but with the steam generators located above the reactor, natural circulation is possible under shutdown conditions.

Pressure in the fuel channels is maintained at about 10 MPa at the outlet end, and the coolant is generally subcooled, although above about 90% full load power, some boiling occurs in the most highly rated fuel channels. At full power, the steam exit quality is typically 3% to 5%, which gives a voidage of 26% to 37% at 10 MPa. This steam is subsequently mixed with sub-cooled coolant from the lower rated channels to give conditions very close to saturation at the steam generator inlet though the flow to the lower rated channels is somewhat reduced to minimize the difference in exit quality.

The heat transport pumps are driven by electrical motors. Should power supply to the motors fail, forcing a reactor trip, the pumps have sufficient built-in inertia to run down over a period of two to three minutes. This allows sufficient time for natural circulation or thermosiphoning to be established.

Pressure in the heat transport circuit is maintained by a pressurizer in most CANDU reactors. This operates at saturation conditions and is approximately half filled with liquid, with the remaining space containing vapour. It is connected to the heat transport system by a pipe which is long enough to maintain its temperature independently of the heat transport system. This enables the reactor outlet header pressure to be controlled regardless of the heat trans-

port system temperature.

There is a feed-and-bleed system to inject or extract heavy water from the heat transport system. This enables the correct inventory to be maintained under transient conditions such as start-up and shutdown and to compensate for leakage. It also enables external clean-up and chemical treatment of coolant under lower pressure and temperature conditions, as well as recovery of leakage and upgrading of heavy water.

3.2 Heat Transport Pumps

Four heat transport pumps circulate heavy water coolant around the system. They are vertical single stage centrifugal pumps driven by induction motors. Mechanical seals prevent leakage of reactor coolant. These seals are supplied with cooled heavy water, some of which leaks outwards and some into the pump, thus maintaining the correct operating temperature at the pump seals and preventing loss of reactor coolant. In the CANDU 6, the pumps each draw approximately 5 MW of electrical power, giving a total of 17 MW of energy input to the heat transport system. This input is used to raise the temperature and pressure of the reactor coolant system during warm-up from cold shutdown conditions.

3.3 Pressurizer

The pressurizer maintains pressure in the heat transport system by maintaining a cushion of vapour above the heavy water in the lower half. Pressure can be reduced by venting vapour at the top or by spraying water into the vapour space and can be increased by heating the water with electric heaters at the bottom. During normal operation, the heaters generally operate periodically because the pressurizer loses heat naturally to its surroundings. Some plants rely on venting vapour only to reduce pressure and do not have water sprays. Level in the pressurizer is ramped up as the temperature of the heat transport system increases to accommodate partially the thermal expansion of the reactor coolant during power raising. Under cold shutdown conditions, the pressurizer is normally isolated from the heat transport system to maintain an elevated temperature in it.

During warm-up, the pressurizer is isolated from the heat transport system, meaning that the system is in the so-called *solid mode* of operation as opposed to the *normal mode* of operation where the pressurizer is connected to the system. In this solid mode, pressure control is by feed and bleed action where the flow rate of heavy water in and out of the system is adjusted to maintain the correct pressure. In the normal mode, the feed and bleed action of the inventory control system adjusts the coolant inventory by maintaining the pressurizer level at its set-point.

To avoid over-pressure conditions in the heat transport system, pressure relief valves on the reactor outlet headers discharge excess coolant to the degasser condenser of the inventory control system. If this action is insufficient to alleviate the over-pressure condition, the control system will step back the reactor to a lower power level, and if this still does not reduce pressure sufficiently, it will trip the reactor.

Note that the steam generators serve as a heat sink for the heat transport system, and therefore reducing pressure and hence temperature in the steam generators will have the effect of reducing temperature in the heat transport system, with a resulting reduction in pressure as well.

3.4 Inventory Control System

The inventory control system serves to maintain pressure in the heat transport system when the pressurizer is isolated and to maintain level in the pressurizer under normal operating conditions. It also serves as a reserve source of heavy water to compensate for minor leakage and to maintain heavy water purity by means of the purification system. This requires continuous bleeding and feeding of heavy water so that it can be treated appropriately. Figure 15 shows a diagrammatic arrangement of a typical inventory control system for purification and feeding of coolant to the heat transport system. The heavy water is at high temperature and pressure upon leaving the system. Therefore, it must be treated under either high pressure or low pressure conditions. Figure 15 shows a system with high pressure purification to minimize pressure reduction and pumping back to pressure, but the feed and bleed operation and heavy water storage are at lower pressure, with the coolant initially passing through a degasser before being pumped back into the system. Furthermore, the ion exchange resins cannot withstand high temperatures, and therefore cooling to about 50°C is required before purification. It is advantageous to use the heat removed from the bleed flow to heat the feed flow before it is returned to the heat transport system. Therefore, the system includes interchangers as well as service water coolers.

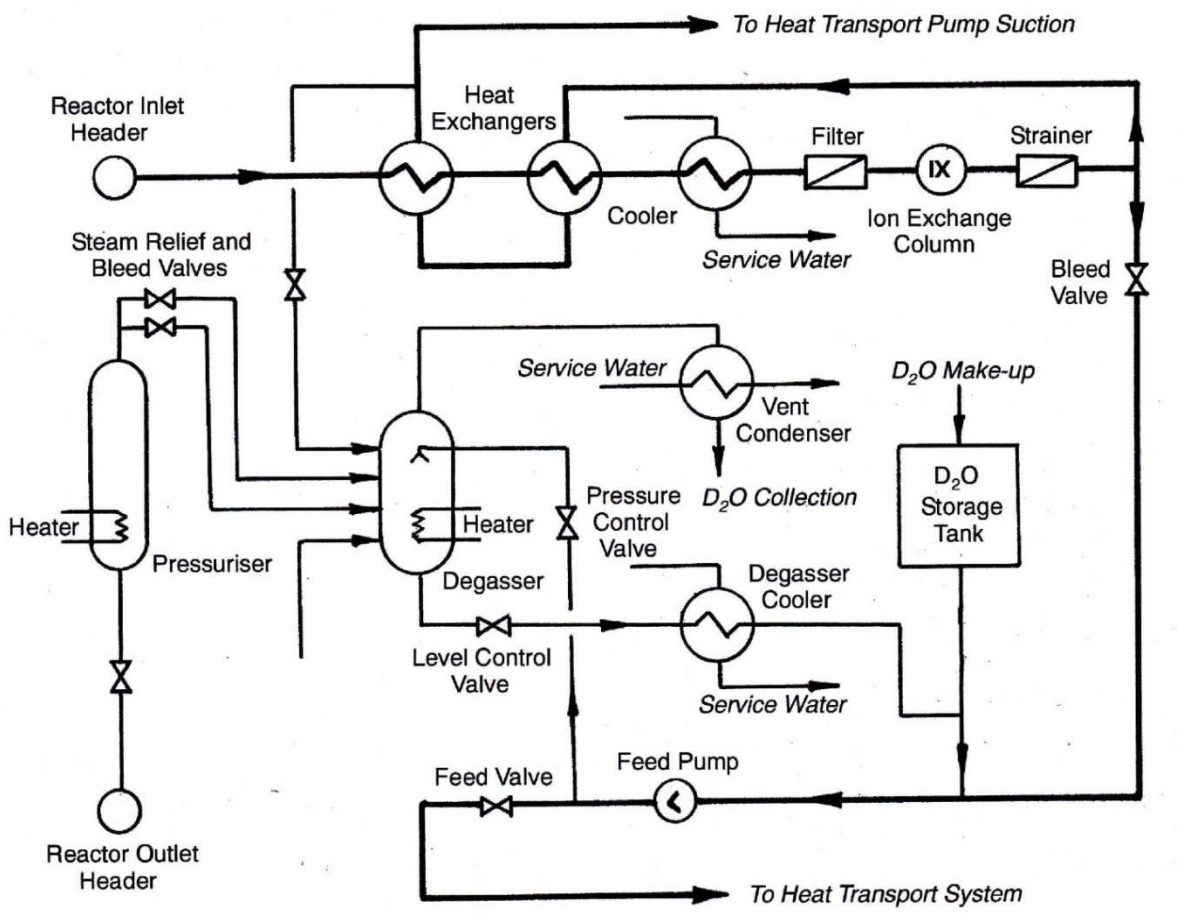

Figure 15 Heat transport purification and feed system

3.5 Shutdown Cooling System

When the reactor is shut down, decay heat is removed through the steam generators and the

steam reject system. If the reactor must be cooled down, the steam reject system can function well until the steam generator pressure drops so low that the volume flow rate through the steam reject or condenser steam discharge valves is insufficient for effective cooling. This occurs at about 150°C to 165°C. Operation of the shutdown cooling system is initiated before this stage is reached and removes heat directly from the heat transport system. A typical system is shown in Figure 16. It can handle about 10% to 15% of the main system flow and is capable of removing 1% to 3% of reactor full power heat.

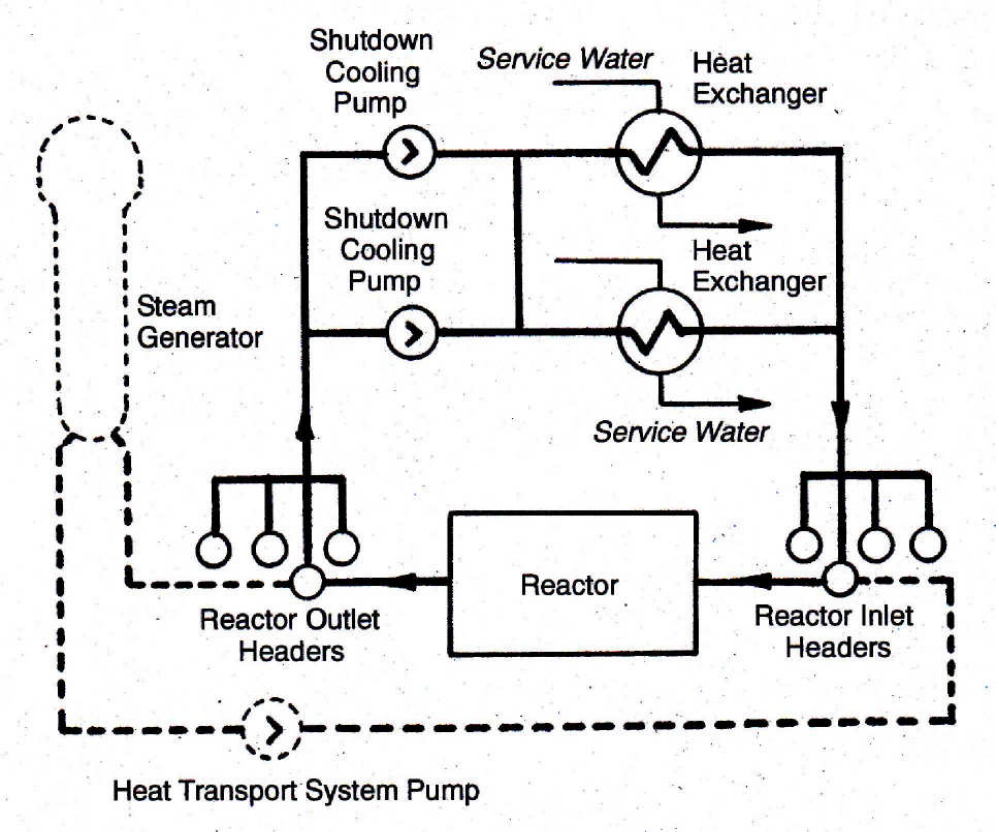

Figure 16 Shutdown cooling system

3.6 Partial Boiling in CANDU Reactors

Although CANDU reactors have pressurized primary coolant systems where boiling is suppressed, local boiling does occur in the highest rated fuel channels. The steam produced is subsequently partially condensed when it mixes with coolant from lower rated fuel channels. This has some definite advantages. Slight boiling enhances the heat transfer coefficient on the fuel element surfaces, thus promoting heat transfer. It also increases the heat removal capacity of the coolant because the enthalpy of the mixture leaving the fuel channel is increased. Thirdly, after mixing with coolant from nonboiling fuel channels, the average coolant exit temperature is at saturated conditions with some vapour present, or at least closer to saturated conditions than it would be if there were no boiling. This means that the coolant entering the steam generators is at as high a temperature as possible considering the prevailing pressure in the system. The degree of boiling is limited to about 3% by weight to avoid flow instability problems and to maintain a sufficient margin to avoid dryout of the fuel elements. This small amount of steam is nevertheless about 25% by volume at prevailing pressures and is not insignificant with regard to reactivity effects because it does provide slight positive feedback.

This occurs because the fuel channel spacing is greater than optimum, resulting in over-moderation of neutrons. Voidage reduces the moderating effect and reduces neutron absorption, creating conditions closer to the optimum.

3.7 Pressure and Level Effects

Pressure in the heat transport system must be maintained within certain limits to avoid over-pressure conditions if it is too high or excessive vapour production and pump cavitation if it is too low. Although these problems can be easily controlled by venting some vapour (if the pressure is too high) or heating the liquid (if the pressure is too low), the required liquid level in the pressurizer must also be maintained, and therefore level and pressure are interdependent, although independently controlled. Level changes occur during warm-up and shutdown and also during power increases and decreases due to changes in average coolant temperature. As the average coolant temperature rises and increases the coolant volume, the excess is pushed into the pressurizer, causing an increase in level. During warm-up from the cold shutdown condition to the hot standby condition, as much as 60 m^3 may be displaced due to swelling. The resulting rise in pressurizer level is accommodated by the feed and bleed system, which temporarily increases the extraction rate. With an increase in power, there is additional swelling due to a further increase in average temperature and the onset of limited vapour generation. Note that the steam generator steam pressure and hence steam temperature are kept constant, and therefore, to achieve an increased heat transfer rate, the temperature difference between the primary side reactor coolant and the secondary side water and steam must increase. Hence, the average reactor coolant temperature in the steam generator must increase, which causes an increase in its specific volume. This last effect accounts for about 10 m^3 to 20 m^3 displacement of reactor coolant. This is accommodated by ramping up the set-point of the pressurizer level control system. Power transients therefore do not force a change in inventory and have minimal impact on the feed and bleed system.

3.8 Temperature and Nuclear Considerations

Temperature and voidage both affect reactor reactivity. Generally, temperature causes a change in reactivity as the coolant goes from cold shutdown conditions to hot shutdown conditions. This leads to a negative coefficient of reactivity with new fuel and a slight positive coefficient with equilibrium fuel. During normal operation, when some boiling occurs in the fuel channels, the effect of voidage becomes significant. Because so little moderator is present between the closest fuel rods, there is little initial moderating of neutrons, and the fast fission factor increases. Moreover, with higher neutron energies, there is less probability of resonance absorption. Both these effects contribute to an increase in reactivity, giving a positive coefficient of reactivity as voidage increases. In the overall design, these effects are compensated for by other negative coefficients and by the reactor regulating system.

During operation of the primary system, the heavy water isotopic concentration is slowly downgraded due to leakage and chemical treatment. The increase in light water increases neutron absorption. This reduces neutron economy and results in an increase in fuel usage. Moreover, with reduced heavy water isotopic concentration, additional reactivity worth must be added to maintain criticality. In the event of a loss of coolant accident and channel void formation, the increase in positive reactivity will be greater. To ensure that this will be controllable, there is a lower limit on heavy water isotopic concentration. This is generally in the range of 97.5% to 98.5%, while the normal value is around 99.5%.

There is also an upper limit on fuel channel heavy water isotopic concentration. It should always be less than the calandria heavy water isotopic concentration by a small margin. This is necessary because, in the event of an in-core loss of coolant accident, the possible penetration of channel coolant into the calandria may displace moderator containing neutron poison. The concentration of light water must therefore be sufficient to absorb at least as many neutrons as the poison and light water in the moderator would have absorbed before the accident.

4 Steam Generators

4.1 Steam Generator Function

The steam generator serves the primary function of supplying energy to the turbine for power production. It also serves the secondary function, but one most important from the safety point of view, of removing energy from the reactor. Immediately after a reactor trip, the decay heat of the fission products amounts to some 7% of full power heat production. The most practical method of removing this heat is through the steam generator. Hence, it is necessary to maintain a certain minimum water inventory in the steam generator and to ensure that adequate reserve supplies of feed water are available.

The steam generator also serves as the main controlling link between the nuclear reactor and the turbine generator. The power flows of the primary coolant system and the secondary steam system must be balanced under all conditions. Any imbalance will cause an accumulation or a depletion of the total heat content of the steam generator inventory, which in turn will result in a rise or fall of steam pressure. Steam pressure is therefore a key parameter in plant control.

The steam generator separates the primary coolant circuit from the secondary steam circuit and hence prevents radioactive products in the reactor coolant from entering the steam turbine and the feedwater heating system. This barrier is an additional safety feature and also minimizes the area over which radiation monitoring is required.

As an example of the importance of the steam generator in performing an essential safety function, consider a nuclear plant with an electrical output of 600 MW. The reactor produces approximately 1800 MW of heat, and the decay heat amounts to about 120 MW immediately after a reactor trip from full power. This is a substantial amount, the removal of which must be guaranteed under all conditions, including for a certain period after shutdown, because it takes almost 10 hours for this heat to fall to a tenth of the initial value, that is, about 12 MW for the example given. Separate smaller capacity heat removal systems can handle these lesser heat flows on their own after the reactor has been shut down for some time, although they are often put into service while the steam generators are still handling the major portion of the heat flow.

4.2 Steam Generator Conditions

The primary coolant enters the steam generators at nearly saturated conditions or saturated with some steam present. As shown in Figure 17, it passes through the inverted U-tubes at high velocity, resulting in high heat transfer coefficients on the inside of the tubes. Water on the outside of the tubes is at lower pressure and therefore boils under the prevailing conditions. This boiling results in high heat transfer coefficients on the outside of the tubes and induces a strong upward convection current which promotes recirculation of the water in the steam generator, while the steam produced is separated for use in the steam system. A feature of the

steam generator is the high heat transfer rate across the tubes compared with other types of heat exchangers. This high heat transfer rate leads to a large temperature difference across the tubes themselves, as well as in the boundary layer on each side of the tubes. Typically, the temperature differences in the two boundary layers and across the tube itself are all approximately the same. This means that the temperature drop across the tubes is about one third of the total temperature difference and cannot be disregarded as in some other heat exchangers such as the main condenser.

Ideally, heat exchangers should be counter-flow to minimize the temperature difference between the hot and cold fluids. This is not possible with a phase change on one side of the heat exchanger. Steam is therefore generated on the secondary side at a somewhat lower temperature than the primary coolant inlet temperature. To maintain good thermodynamic efficiency, a partial counter-flow arrangement is achieved by the subcooled feed water, which enters the steam generator being passed through a preheater section before mixing with the saturated recirculating water. The preheater receives heat from the primary coolant just before its exit to minimize large temperature differences across which heat is transferred. The temperature profile along the length of the tubes is shown in Figure 18. Table 3 gives typical operating parameters of a CANDU 6 steam generator.

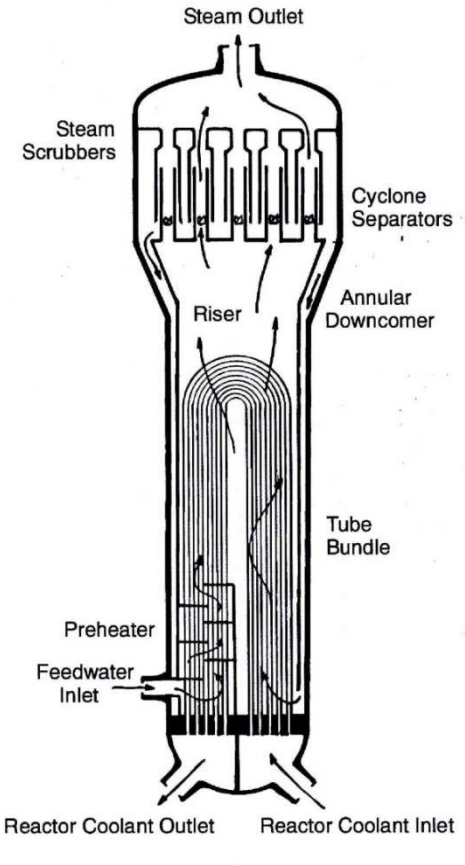

Figure 17 Steam generator for CANDU system

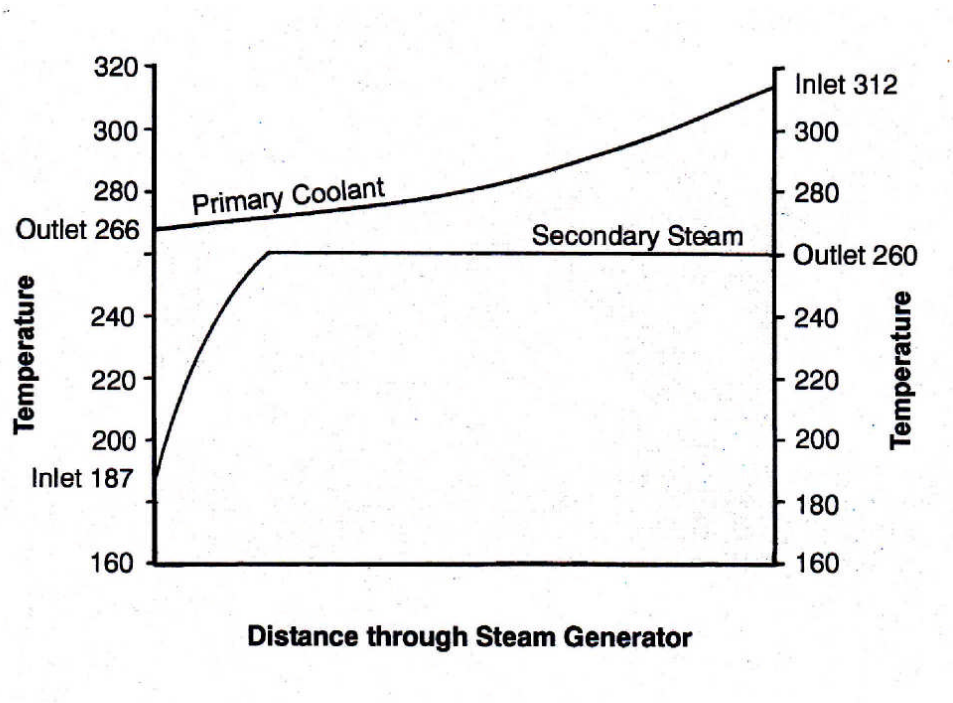

Figure 18 Temperature profiles in steam generator

Table 3 Steam generator conditions (CANDU 6)

Type	Vertical U-Tube with Preheater
Number of Steam Generators	4
Heat Transfer Area (each)	3127 m^2
Heat Transferred (total)	2064 MW
Coolant Flow Rate (total)	7600 kg/s
Coolant Inlet Temperature	312°C
Coolant Outlet Temperature	266°C
Steam Flow Rate (total)	1047 kg/s
Feedwater Flow Rate	959 kg/s
Reheater Return Flow Rate	89 kg/s
Blowdown Flow Rate	1 kg/s
Steam Outlet Pressure	4.69 MPa (a)
Steam Outlet Temperature	260°C
Feedwater Inlet Temperature	187°C
Reheater Drain Inlet Temperature	258°C

4.3 Pressure Control

Any mismatch in the rate of heat flow to the steam generator on the primary side or from it on the secondary side will result in a change in steam pressure. Control of steam generator pressure is therefore achieved by reactor heat input or steam turbine output. It therefore becomes part of overall plant control, which is covered in Chapter 10.

A change in steam pressure in the steam generator affects steam generator water level. A reduction in pressure causes the expansion of existing vapour bubbles in the water and additional evolution of vapour due to the lower saturation conditions. The result is a rise in water level or *swelling* of the inventory. An increase in pressure has the opposite effect, *shrinking* of the inventory. These are *transient* conditions, and the original conditions are restored when steam pressure returns to normal.

A change in load also affects the level. A simultaneous increase in reactor output and turbine generator load will not affect steam pressure, but will result in increased evolution of vapour within the water space. This will in turn cause a rise in water level or swelling of the inventory. The opposite will cause shrinking of the inventory. These are *steady state* effects, and hence there is a relationship between load and level. The level control system takes this into account by ramping up the level set-point as load increases.

4.4 Level Control

Considering the effects described above, it is evident that level control is a critical aspect of steam generator performance. A change in pressure is usually induced by a change in load. An increase in turbine load, for example, will cause a drop in steam pressure as more steam is drawn from the system. This will cause transient swelling, and the rise in water level would indicate that less feed water is required, when in fact more will be required to meet the increased steam demand. Inventory control by level only will result in excessive level fluctuations. To solve this problem, the control system compares steam flow and feedwater flow and combines the result with the level indication. Such a three element level control system gives better control in normal operation, while single element level control using level measurement only is satisfactory for low power operation.

4.5 Comparison of CANDU and PWR Systems

A comparison of steam generators as used in the PWR and CANDU systems is instructive in comparing their relative merits. Both are very similar in construction. Natural circulation drives the flow upwards over the tube bundle and downwards through a peripheral annulus after separation of the steam, which occurs in cyclonic separators. Above the cyclones are steam dryers, so that the steam leaving the steam generator has a moisture content of only about 0.25%. The fundamental difference between the PWR and CANDU steam generators is shown in Figure 19 and Figure 20 respectively. The feed water enters the PWR steam generator at the top near the normal water level and mixes with the recirculating water before passing down the annulus. The recirculating water is therefore somewhat subcooled when it re-enters the tube bundle. In the CANDU steam generator, the feed water enters at the bottom and passes over the outlet side of the tube bundle before mixing with the recirculating water. The feed water is thus preheated by the exiting coolant in a counter-flow arrangement, while the recirculating water within the steam generator is not subject to subcooling. This is an advantage from a thermodynamic point of view because hot and cold fluids are not mixed, but limits must be placed on the feedwater temperature range to avoid thermal shock to the steam generator tubes, and a deaerator with hot storage capabilities is essential. In the PWR, this is not a problem because thorough mixing occurs before the water enters the tube bundle. This means that the PWR steam generator can receive feed water over a much wider temperature range and that hot storage of feed water is not essential.

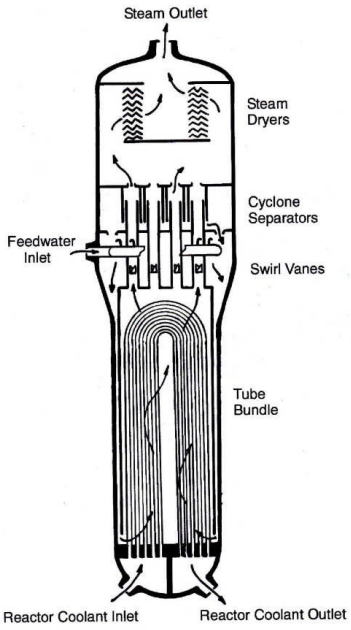

Figure 19 Steam generator for PWR system

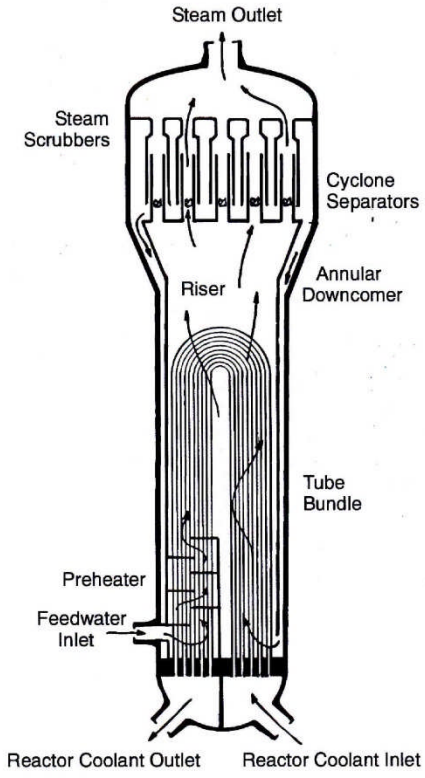

Figure 20 Steam generator for CANDU system

5 Steam System

5.1 General Arrangement

From the steam generators, steam is piped to the high pressure turbine at a temperature of about 260°C, as shown in Figure 21, where it expands partially in the high pressure turbine, yielding some useful work. The steam is then put through a separator and reheater, where moisture in the steam is removed in a cyclonic separator and the steam brought up to higher temperature in a heat exchanger using steam directly from the steam generator. The super-heated steam is then passed in parallel through two or three low pressure turbines where the remaining energy is removed from the expanding steam. The steam is then passed to a con-denser where it is condensed. This condensate is pumped through low pressure feedwater heaters where it is preheated. It is then passed through a deaerator and pumped through high pressure feedwater heaters for further preheating. It re-enters the steam generator at a tem-perature of about 180°C. Table 4 gives typical technical and operating parameters for a CANDU 6 steam turbine.

Table 4 Turbine generator conditions (CANDU 6)

Number of HP Cylinders	1 (double flow)
Number of LP Cylinders	3 (double flow)
Number of Moisture Separators	4
Number of Reheaters	2
Steam Flow Rate (total)	1047 kg/s
Steam Flow Rate (turbine)	957 kg/s
HP Steam Inlet Pressure	4.55 MPa (a)
HP Steam Inlet Temperature	258°C
LP Steam Inlet Pressure	0.588 MPa (a)
LP Steam Inlet Temperature	242°C
Steam Exhaust Pressure	0.0042 MPa (a) (typical)
Steam Exhaust Temperature	30°C (typical)

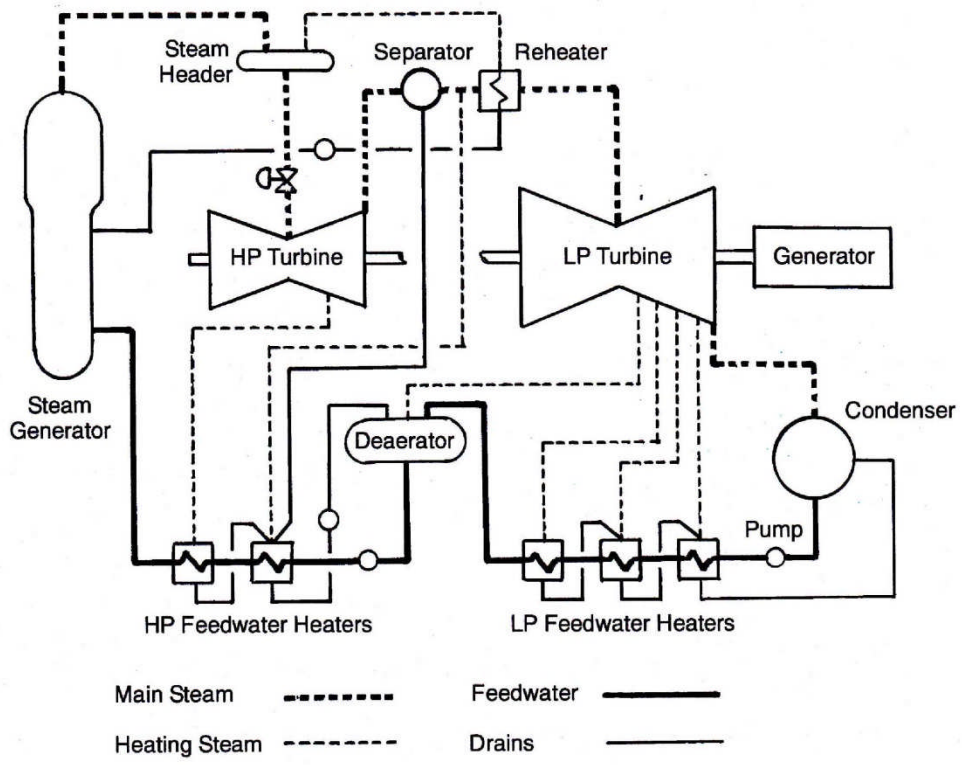

Figure 21 Steam and feedwater system for a CANDU reactor

Control of steam flow is important to protect the steam generators as well as the steam turbine. Provision is therefore made to release excess steam to avoid over-pressure in the steam generators and to stop steam flow to the turbine if electrical output is terminated or if a component or system fails on the turbine generator.

5.2 Steam Bypass System

The main steam system is somewhat more complex than that shown diagrammatically in Figure 21 because provision must be made to discharge excess steam when it is not required or cannot be used. It is advantageous to recover this steam, condense it, and return it to the feedwater system, but if this is not possible, it must be discharged to the atmosphere. Figure 22 shows the steam system for a CANDU 6 unit with the various valves to control steam flow under various conditions.

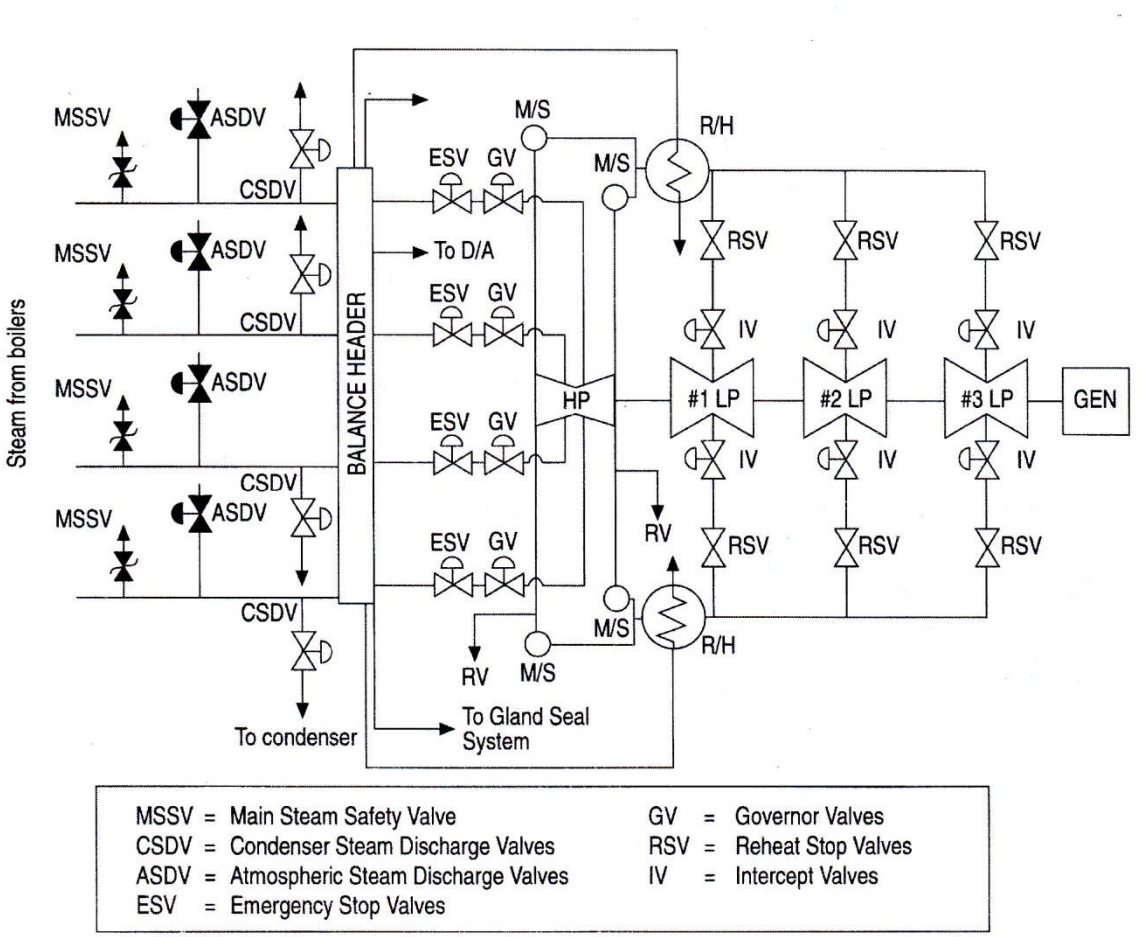

Figure 22 Main steam system (Point Lepreau) (courtesy of NB Power)

As mentioned above, the steam generator has the important secondary function of removing heat from the reactor after a turbine trip. Under such circumstances, the excess steam must be diverted elsewhere. Excess steam may be vented to the atmosphere through *atmospheric discharge valves*. This, however, is wasteful, and it is better to recover the steam in the condenser and to reuse the condensate. All plants therefore have a steam bypass system to enable excess steam to be dumped to the condenser through the *condenser steam discharge valves* and recovered by the condensate system. The condenser bypass system is usually designed to accept the maximum quantity of steam that can be handled by the condenser to enable excess steam to be bypassed under a range of reactor operating conditions. In the event that the atmospheric discharge valves and condenser steam discharge valves are both inoperable, there are conventional *boiler safety valves* on the steam generators to enable discharge of excess steam.

During plant start-up, the reactor load is increased progressively through a series of checks on its operation. During this time, it might not be desirable to run the turbine, and hence excess steam would be discharged to the condenser, bypassing the turbine.

Another situation is a turbine trip or grid system disruption requiring a temporary rejection of load. Such a large load reduction would result in a buildup of neutron absorbing xenon in the

reactor to the extent that it would force a reactor shutdown. To avoid this situation, the reactor load must be maintained at about 60%. By dumping the equivalent quantity of steam into the condenser, reactor load can be maintained at a sufficiently high level to avoid xenon poisoning and a long term forced shutdown. Because the steam cycle has a thermal efficiency of about 30%, almost all the remaining 70% of heat input can be rejected to the environment through the condenser. The maximum heat rejection capabilities of the condenser therefore roughly match the minimum load required by the reactor to avoid excessive xenon buildup and reactor poisoning.

5.3 Condenser Steam Discharge Valves

The condenser steam discharge valves open progressively to control steam generator pressure by discharging an appropriate amount of surplus steam. Under certain circumstances, when the turbine is unavailable and it is desirable to maintain load on a nuclear reactor to prevent poisoning out with xenon buildup, substantial quantities of steam may have to be discharged for an extended period. This steam enters the condenser space at high velocity and in a hot superheated condition. To avoid thermal damage to the condenser structure and tubes and to the condenser neck expansion joint, cool condensate is sprayed into the steam to cool it to normal condenser temperatures. Provision must also be made to avoid flow induced vibration due to the high velocities generated. A typical location of the steam discharge headers is shown in Figure 35 and Figure 36 in the section on the condenser later in this chapter.

Certain limits are imposed on the operation of the condenser steam discharge valves. Under particular circumstances, the condenser steam discharge valves are prevented from opening and discharging steam. Circumstances leading to this are reduced condenser vacuum or high turbine load when the ability of the condenser to absorb additional thermal load is limited.

5.4 Turbine Control Valves

The steam turbine has *stop valves* and *governor valves* on all high pressure turbine inlet pipes. The governor valves control the steam flow to the turbine and hence the turbine output, while the stop valves close in an emergency to stop all flow of steam to the turbine. In the event of a turbine trip, they operate together as a back-up to one another, but during a load rejection, the stop valves stay open. In addition, most turbines have *stop valves* and all have *intercept valves* on all the low pressure turbine inlet pipes to serve the same purpose with regard to the steam trapped in the moisture separator and reheater system. Expansion of this steam could accelerate the turbine generator to overspeed conditions if it were allowed to enter the low pressure turbine. Separate steam *release valves* enable this trapped steam to be released to the condenser.

6 Steam Turbine

6.1 General Arrangement

Steam turbines consist essentially of a casing to which stationary blades are fixed on the inside and a rotor carrying moving blades on its periphery. The rotor is fitted inside the casing, with the rows of moving blades penetrating between the rows of fixed blades. Therefore, steam flowing through the turbine passes alternately through fixed and moving blades, with the fixed blades directing the steam at the correct angle for entry into the moving blades. Both casings

and rotors must be constructed to minimize damaging thermal stresses, and the moving blades must be fitted securely to the rotor to withstand high centrifugal forces.

Where the rotor shaft passes through the ends of the casing, a seal is required to prevent steam leakage and air ingress. In addition, within the casing, seals are required to prevent steam from leaking around the blades rather than passing through them. Turbine seals are of the labyrinth type where there is no mechanical contact between fixed and rotating parts. Leakage is therefore not really eliminated, but merely controlled to minimal amounts.

The rotor shafts are carried on bearings and are linked together and to the electrical generator. Bearings must be properly aligned to accommodate the natural gravitational bending of the shaft. Allowance must also be made for differential expansion between the rotors and the casings during thermal transients. Both must be free to expand without upsetting the alignment, while allowing the rotors to expand more quickly and to a greater degree than the casing. Lubrication is required for the bearings. Multiple pumps driven by alternative power sources ensure adequate lubrication under all operating circumstances.

6.2 Turbine Cylinders

Typical units applicable to CANDU plants have a high pressure cylinder and three low pressure cylinders. These are designed to accommodate the increasing specific volume of the steam as it expands down to subatmospheric pressures. Provision is also made for steam quality improvement by reheating and for the extraction of partially expanded steam for feedwater heating.

To withstand pressure, thick cylinder walls are required, but to minimize thermal stress, abrupt changes in thickness and asymmetrical arrangements should be avoided. This leads inevitably to smooth rounded profiles of the stress bearing components. In addition, uniform heating of components is desirable to avoid differential expansion and undue thermal stress. This requires sections of uniform thickness and provision for steam circulation within the casing, as shown in Figure 23, to promote uniform temperature changes, particularly during unit start-up. Steam access into and out of the cylinder must also be accommodated, which requires special nozzles and casing reinforcement in these areas. Furthermore, overall expansion of the components must be accommodated, and therefore the cylinders must be mounted on sliding pads with keys to maintain alignment.

To assemble the turbine and to disassemble it for maintenance, the casing must be split in some way. The joint is normally horizontal so that the upper half can be removed, leaving the lower half in position along with the rotating parts.

The high pressure turbine is fairly compact due to the low specific volume of steam at this point in the steam cycle. Provision is made to extract steam for feedwater heating and for steam circulation within the casing to promote uniform heating and cooling. Figure 23 shows the high pressure cylinder of a 900 MW turbine for a PWR, which has high pressure steam conditions fairly close to those of a CANDU reactor.

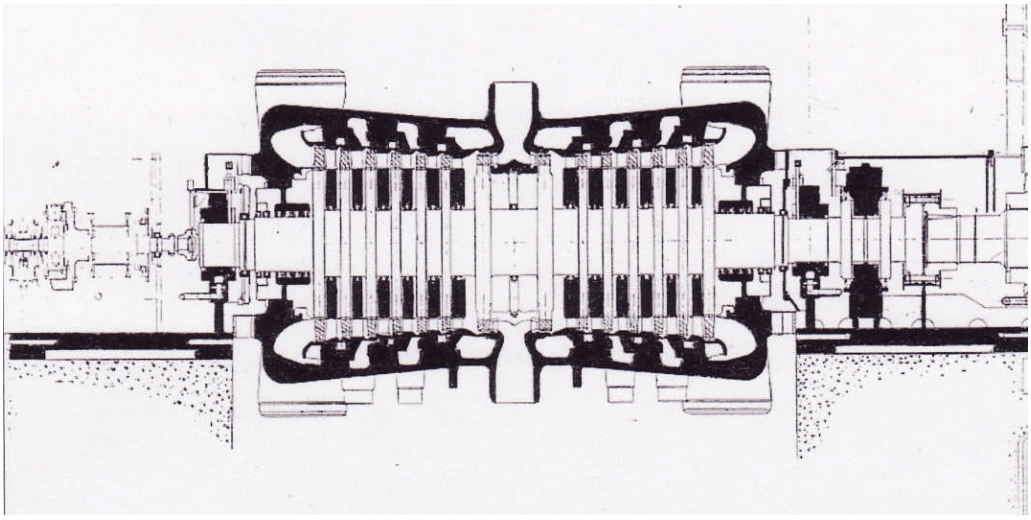

Figure 23 High pressure turbine cross section for nuclear unit (courtesy of Eskom)

Low pressure turbines are very much larger because they must accommodate the increase in specific volume as the steam expands. Low pressure turbines are therefore of different construction. An inner casing supports the fixed blading and has annular channels through which steam is extracted for feedwater heating. Surrounding each entire low pressure turbine is an exhaust hood into which the exhaust steam flows before passing into the condenser below the turbine. Figure 24 shows the low pressure cylinder of a 900 MW turbine for a PWR which has low pressure steam conditions fairly close to those of a CANDU reactor.

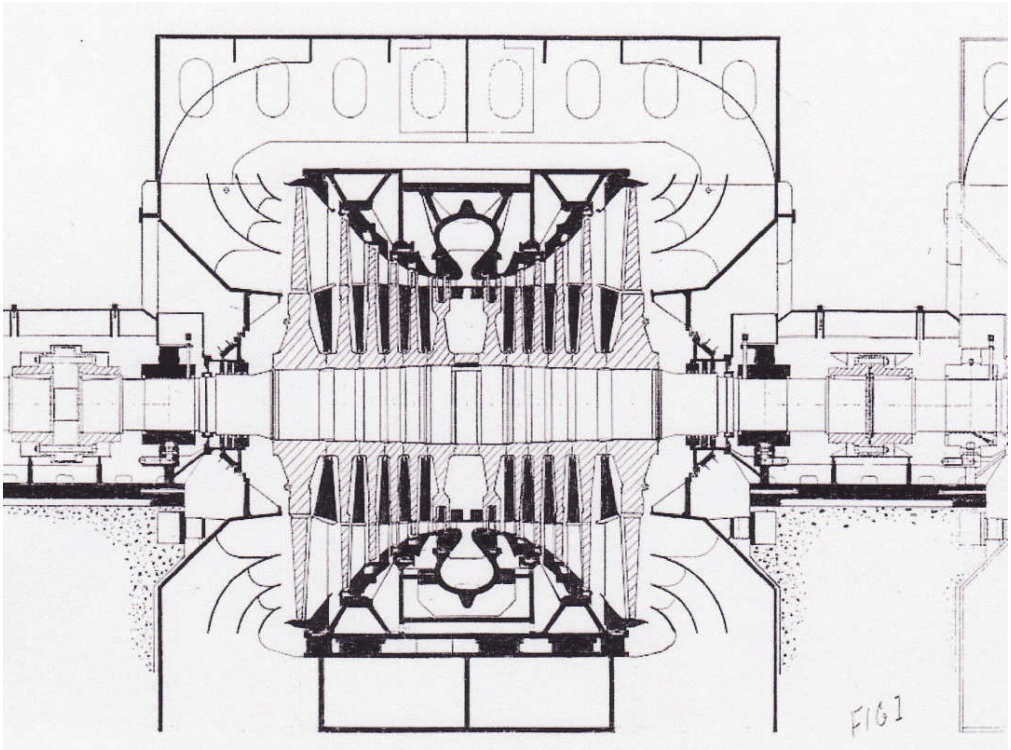

Figure 24 Low pressure turbine cross section for nuclear unit (courtesy of Eskom)

Diaphragms carrying the fixed blades are fixed inside the turbine cylinders. Like the cylinder casings, they are split horizontally to enable assembly around the turbine rotor. Because there is a pressure drop across the fixed blades in both impulse and reaction turbines, sealing must be

provided between the diaphragms and the rotor to minimize steam leakage.

In turbines with reaction blading, significant axial thrust is developed by the steam flow. Double flow turbines are normally used so that this axial thrust is balanced by opposing forces. Turbines with impulse blading do not develop this large thrust, but the low pressure blading near the turbine exhaust must have a reaction component due to the length of the blades. Therefore, all large low pressure turbines are double flow.

6.3 Turbine Rotors

The moving blades are mounted on and transmit power to the turbine rotors. Their shafts are coupled together and drive the generator rotor. Rotors must be able to transmit the applied torque and to withstand the gravitational force due to their mass. As with casings, rotors are subject to high temperatures and must be built to minimize thermal stress during temperature transients. A certain degree of rigidity is important to minimize vibration during full speed operation as well as during run-up and shutdown. Rotors of small turbines are usually machined from solid forgings, but large turbines and especially low pressure turbines are usually built up from discs shrunk onto a stepped shaft.

The blades are attached to the turbine rotors in various ways and in such a pattern as to minimize unbalanced forces. Even with close manufacturing tolerances, there is a slight mass variation between blades. The moment of each blade with respect to the shaft centre is measured and the blades arranged around the circumference to minimize out of balance forces and to ensure uniform stress on the turbine discs. Even so, some imbalance is inevitable, and the turbine rotor must be dynamically balanced, usually at full speed, in a specially designed tunnel or pit.

The generator rotor is invariably the longest of the rotors making up the entire turbine generator. A typical generator is illustrated in Figure 25, which shows the rotor. The rotor carries the field coils which excite the stator coils to produce electric power. Because the field coils carry heavy currents, they must be sufficiently robust and well cooled. The individual current carrying bars must be well insulated and securely mounted to withstand centrifugal forces. Cooling is by hydrogen under pressure circulating through the bars. The hydrogen is driven by fans mounted on the rotor, which contribute to the full speed no-load frictional resistance felt by the machine. More frictional resistance arises from the shaft bearings of all rotors. The stator is also cooled by hydrogen and often by water passing through the windings as well. Electric power is produced at high voltage, and insulation must be designed accordingly.

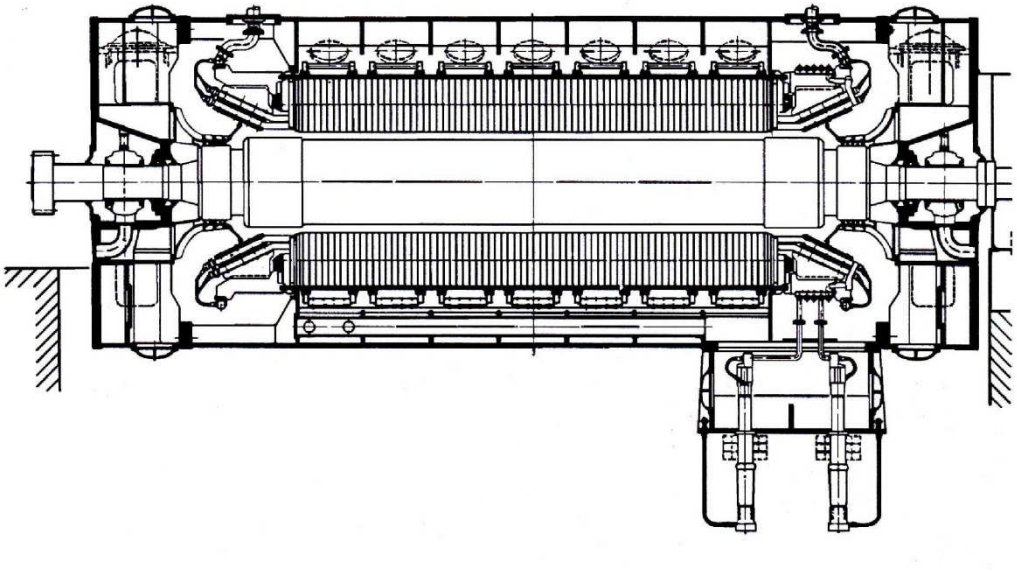

Figure 25 Electrical generator for a large turbine (courtesy of Siemens)

6.4 Turbine Blading

Turbine blades are either fixed or moving and are shaped so that energy transfer takes place by the impulse or reaction principle. The blade design is governed by the steam conditions in the turbine, the desired steam velocities and directions, and the steam forces on the blades. In addition, consideration must be given to geometrical limitations and dynamic forces arising from high speed turbine rotation. The moving blades in particular are subject to very high centrifugal forces and are sensitive to vibration induced by turbine rotation and steam flow.

Figure 26 shows a large nuclear steam turbine under construction. This turbine receives saturated steam at 5.5 MPa from a pressurized water reactor, operates at 1500 revolutions per minute, and has a nominal rating of 900 MW. In the figure, the lower half of a diaphragm containing one row of fixed blades for one low pressure cylinder is seen being lowered into position. Also shown are the moving blades attached to the rotor of another low pressure cylinder. In the background is one complete rotor for a low pressure turbine. It is evident from this photograph that the fixed blades are securely fixed at both ends in a robust diaphragm. The moving blades, however, are attached only to the rotor discs and may or may not have tip shrouding or lacing wires to increase rigidity. Both tip shrouding and lacing wires are used in this machine and can be seen in the picture.

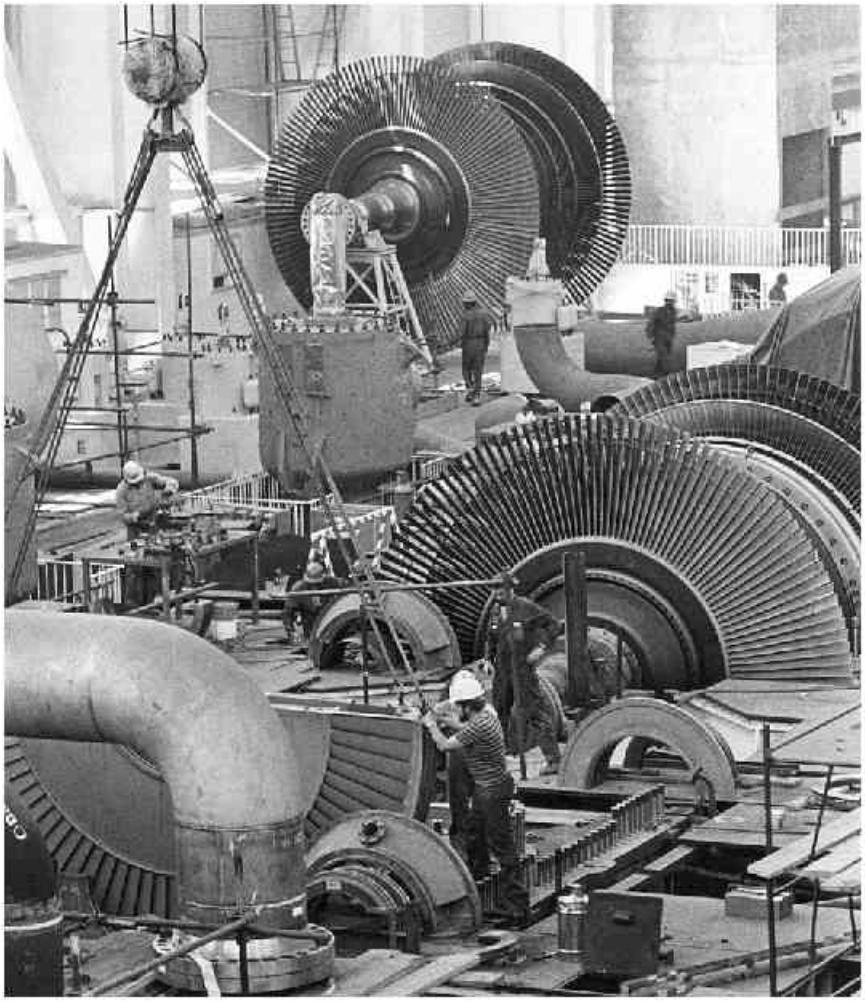

Figure 26 Construction of a 900 MW steam turbine for a nuclear unit (courtesy of Eskom)

The design philosophy for fixed and moving blades is naturally different. All large turbines have pressure compounded impulse blading or reaction blading so that there is a pressure drop across the fixed blading. The blades must withstand this pressure drop, and if the design provides for a large diaphragm, as is usually the case in low pressure turbines, the blades must also support the pressure difference across the diaphragm. The blades may therefore be quite wide (as measured in the axial direction), especially towards the outer diameter. On the other hand, moving blades are subject to high centrifugal forces and have a slender shape decreasing in width towards the outer diameter.

When steam expands below the saturation line, some condensation takes place, and the steam becomes wet. A very fine mist of droplets forms and passes over the blading, and some is deposited on the blades to create a film of water. This film is swept off the blades and entrained by the steam. The size of these entrained drops is governed by surface tension rather than by condensation phenomena. They are therefore somewhat larger than the original condensation droplets and, when travelling at high velocity, can damage any material on which they impinge. Being larger and heavier, they are also separated more easily from the main steam flow during changes in direction. When these larger drops are swept off the fixed blades, their velocity tends to be lower than that of the steam, and the moving blades tend to run into them at high speed. The impact of the drops on the blades (more accurately the blades on the drops) causes material erosion from the blades. Minute amounts of material are removed,

leaving a rough etched like surface. If severe, this material removal can change the blade profile and weaken the blade. After impact on the moving blades, the water film tends to be thrown off towards the periphery by centrifugal action. Turbine blades must be designed to withstand moisture erosion in the affected areas. This is done using inserts of hard erosion resistant material such as tungsten or stellite or by specialized heat treatment to harden the blades in selected areas.

6.5 Turbine Sealing Principles

Steam turbines receive steam at high pressure and discharge it at high vacuum conditions. Provision must therefore be made to prevent steam from leaking out of the turbine where the steam pressure is high and air from leaking into the turbine where the steam pressure is below atmospheric. The turbine casing can be made steam tight with accurately machined flange joints, but where the rotating shaft passes through the stationary casing, leak tight joints cannot be made without direct contact between fixed and rotating parts. Similarly, within the turbine itself, there is a stepwise steam pressure drop through the various stages. Each diaphragm carrying the fixed blades must withstand a pressure differential and have seals around the hole through which the rotating shaft passes. In a reaction turbine, where there is a pressure drop across the moving blades as well, these must have seals around their periphery to reduce steam leakage around the top of the blades.

Various types of glands have been devised, but large steam turbines all use the labyrinth type of seal. The distinct advantage of this type of seal is the lack of direct mechanical contact. Under normal circumstances, this eliminates mechanical friction and wear and heat buildup. The objective is not to eliminate leakage, but to reduce it to manageable proportions. Labyrinth seals are therefore designed to pass steam through the gap between the fixed and moving parts. Abnormal shaft deflection, however, can cause contact between the shaft and seals. The seals are therefore spring mounted so that they can be pushed back and are thin so that they can deform or wear away quickly in the event of contact to avoid overheating and damage to the turbine shaft.

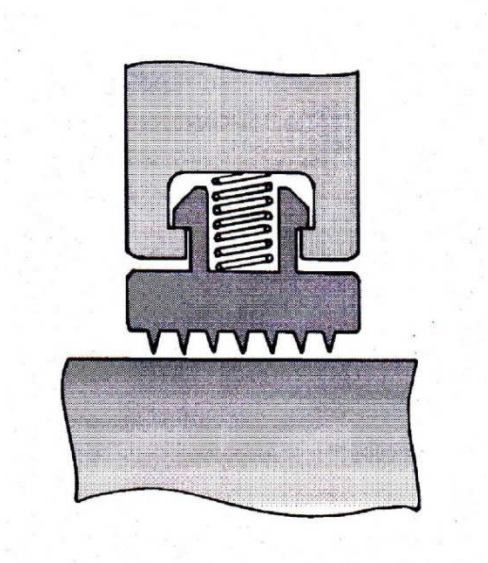

Figure 27 Spring mounted labyrinth seal to accommodate shaft deflection

6.6 Turbine Seals

Pressure in a turbine drops from the inlet to the exhaust, with the exhaust being under subatmospheric conditions. Moreover, as the turbine load changes, so does the steam pressure. The steam flow through the turbine is proportional to the inlet steam pressure. Therefore, as the turbine is throttled and steam flow reduced, the inlet steam pressure drops and, in the limit, will drop to condenser vacuum conditions under no flow. In any case, the entire steam space of the turbine is connected to the condenser, and at start-up, before steam is admitted to the turbine, this space throughout the turbine will be at the same pressure as the condenser, that is, very nearly a complete vacuum. Under these conditions, air will leak into the turbine through the shaft seals, creating difficulty in maintaining the proper vacuum conditions.

To overcome this problem of air in-leakage, provision is made to supply low pressure steam to the shaft seals when they are subjected to subatmospheric internal pressures. This steam is fed into the seals in such a way that some leaks through the labyrinth rings into the turbine and some leaks through the opposite rings to the outside atmosphere, as shown in Figure 28. As long as steam flows outwards, air cannot enter the turbine against this flow, and the condenser is protected against air ingress. The steam that leaks inwards into the turbine space is simply condensed in the condenser and rejoins the steam-water circuit. The steam that leaks out of the turbine to atmosphere is lost unless special provision is made to capture it. With the advent of larger turbines, provision has been made to recover this leakage steam.

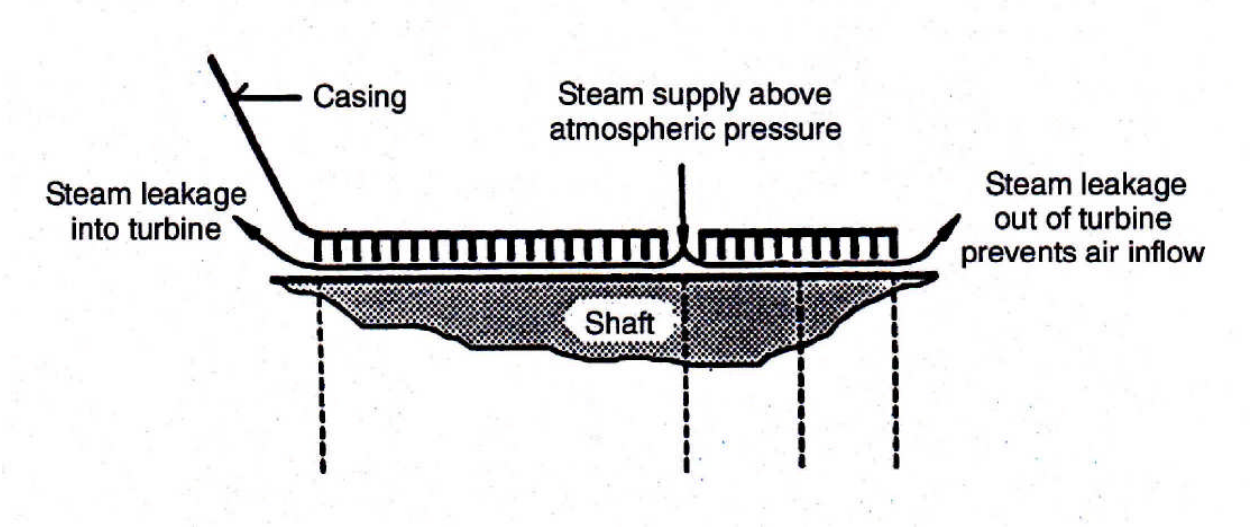

Figure 28 Principle of operation of LP turbine shaft seal (courtesy of NB Power)

6.7 Steam Sealing System

A typical steam sealing system must prevent inward air leakage at all turbine shaft seals during start-up and very low load operation and prevent outward steam leakage at the high pressure turbine and inward air leakage at the low pressure turbine during normal operation. Therefore, auxiliary steam from outside the turbine must be supplied during start-up, but once a certain load has been reached, the steam leaking through the high pressure turbine seals can be directed to the low pressure turbine seals, and the whole system becomes self-sufficient. Figure 29 shows a simplified steam sealing system for a large turbine.

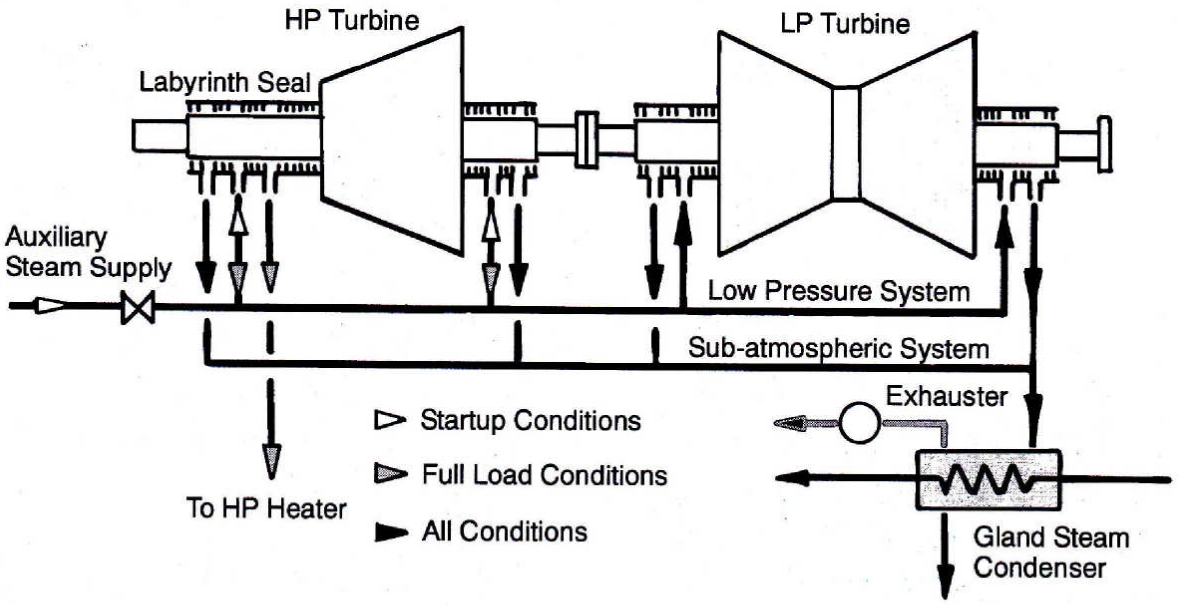

Figure 29 Turbine steam sealing system

6.8 Turbine Bearings

Large steam turbines are made up of several rotating sections, with each section coupled rigidly with the adjacent one. Normally, each rotor is mounted on a pair of journal bearings, one at each end, with the couplings between the bearings of adjacent rotors. The bearings are mounted on foundations to secure the rotating elements in the proper vertical and transverse positions. The bearings are supplied with lubricating oil, and the shaft rides on a hydrodynamic oil film without metal to metal contact. When starting from rest with the oil film having been squeezed out, there is metal to metal contact. To avoid rubbing and scoring of the bearings, high pressure jacking oil is supplied to a point under the shaft to lift the shaft off the bearings before commencing rotation.

To secure the shaft in the proper axial position, a single thrust bearing is provided, usually close to the high pressure turbine, but always in a location that will minimize shaft movement in other parts of the turbine due to thermal expansion. The shaft will naturally expand outwards from the thrust bearing. The turbine casings are also fixed to the foundations in a way that permits free thermal expansion. These fixing points must be positioned to minimize differential movement between the casing and rotor and must maintain proper radial alignment of the rotating parts within the fixed parts. Typical locations of fixing points for a large turbine are shown in Figure 30.

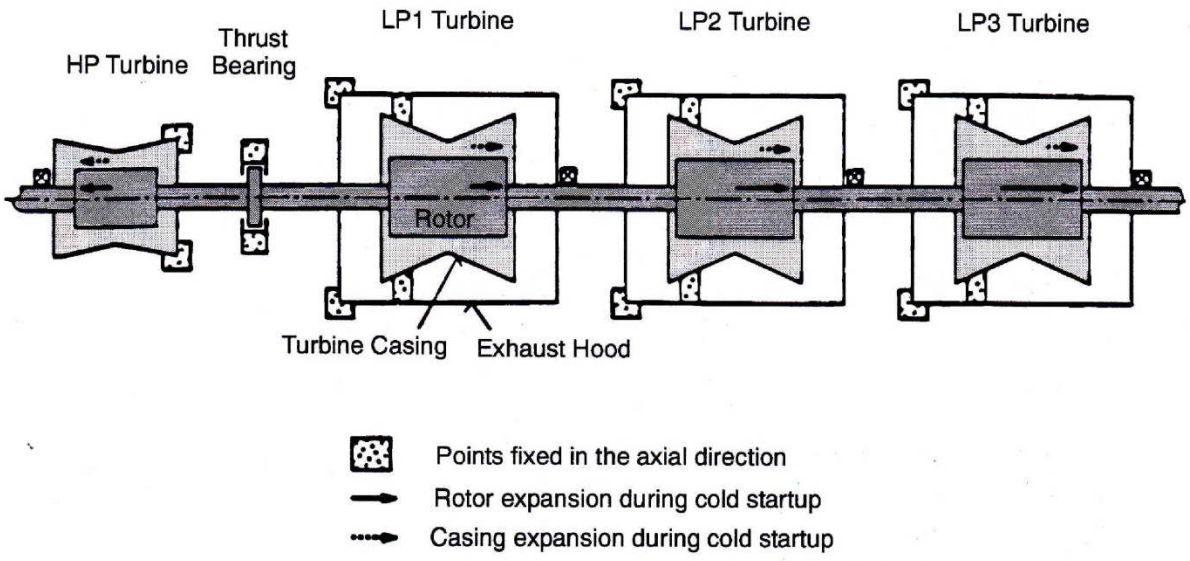

Figure 30 Fixing points for turbine rotors and casings (courtesy of NB Power)

All turbine rotors are slightly flexible due to the elastic nature of the material from which they are made. They therefore bend slightly under the influence of gravity. As they rotate, this bend remains always in the direction of the force of gravity. The couplings are consequently tilted slightly upwards. To ensure proper alignment at the couplings, the adjacent rotors must be installed at a slight upward angle. They in turn deform slightly under gravity, and their outer bearings must be elevated further to compensate for bending. The further a rotor is from the centre, the greater the compensation required. The result is that the entire turbine shaft is mounted along a catenary, as shown in Figure 31. The end points may be some 20 mm to 30 mm higher than the midpoint in a large steam turbine and generator.

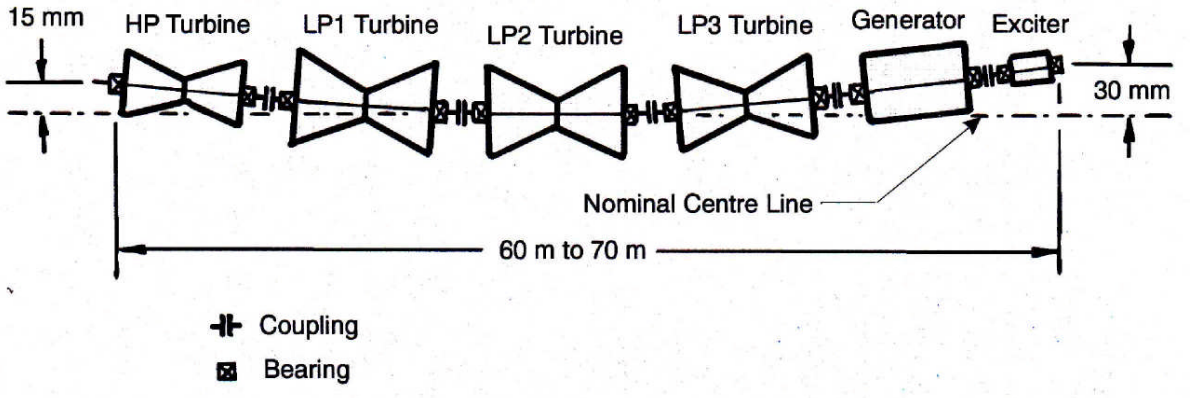

Figure 31 Turbine generator shaft catenary

6.9 Bearing Lubrication

Lubricating oil is supplied to all bearings to maintain hydrodynamic lubrication and to cool the bearings. Heat is generated in the oil by friction in the hydrodynamic oil film and by turbulence within the oil itself. Furthermore, a substantial amount of heat is conducted from the steam in the turbine to the bearing through the shaft.

To ensure continuity of oil supply, there are three or four oil pumps driven by different power sources. The main oil pump is usually driven directly by the turbine through a hydraulic connection to an oil driven turbine and sometimes by an uninterruptable electrical connection from a small separate generator on the turbine shaft. As the turbine runs up to speed, more power is provided to run the pump, which increases its speed, and at some intermediate turbine speed, the main oil pump output reaches the required value.

The auxiliary oil pump is electrically driven and is supplied with power from the station or unit auxiliary electrical systems. It is used during turbine run-up and rundown when the main oil pump does not provide adequate oil pressure. It can also be used as an emergency oil pump at any time, should the main oil pump fail. At low turbine speeds, however, this pump itself could fail, and therefore an emergency pump is required.

At least one electrically driven emergency pump is provided. Its power supply is usually from an uninterruptable electrical source such as the station emergency electrical system, from a DC battery system, or both if two emergency pumps are provided.

There are also jacking oil pumps to lift the shaft off the bearings before rolling the turbine after a shutdown in which the turbine has been stopped. These are positive displacement pumps with a separate pump supplying each bearing to ensure a definite flow to each bearing. Figure 32 shows a typical lubricating oil system for a large steam turbine.

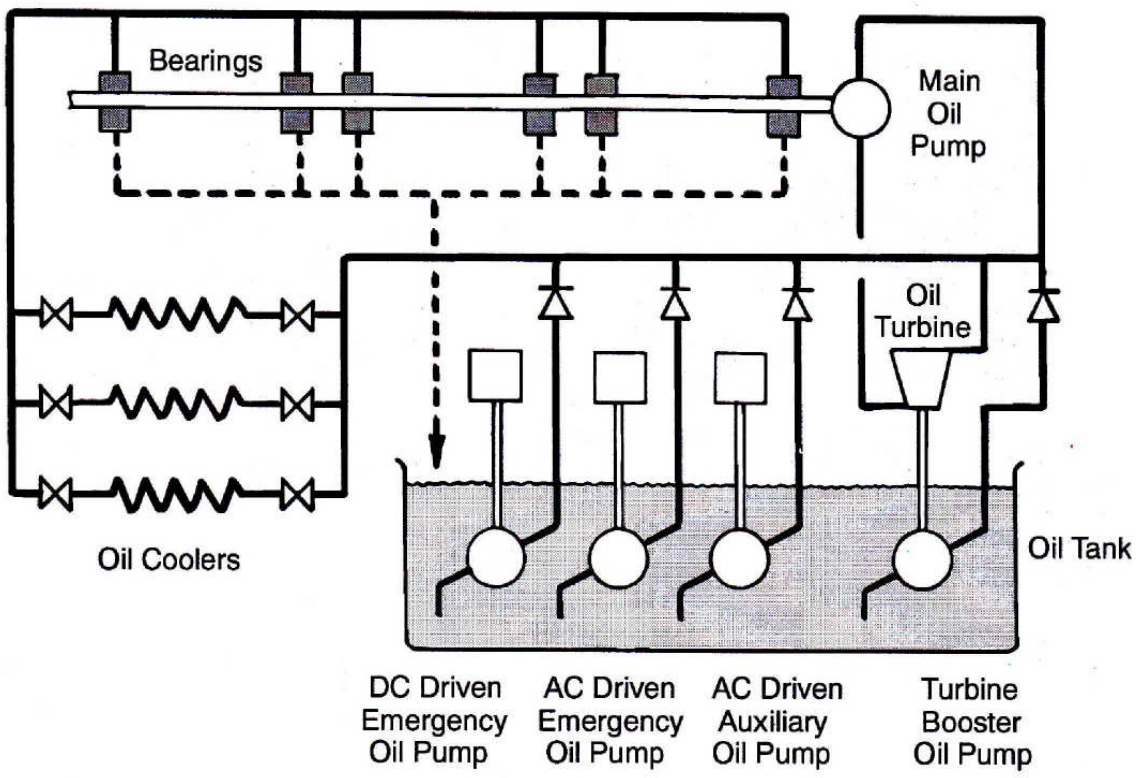

Figure 32 Turbine lubricating oil system

7 Reheating and Feed Heating

7.1 Steam Separators and Reheaters

Reheating is required to ensure adequate steam quality at the turbine exhaust to minimize moisture erosion and is done locally, as part of the steam system, in independent *reheaters* using some high pressure steam. Reheating with high pressure steam limits the maximum temperature of the reheated steam, but sufficient superheat is still present to ensure that the low pressure turbine exhaust steam wetness is not more than about 10%. The reheater generally consists of finned tubes carrying high pressure steam, which condenses fully to water inside the tubes while transferring its heat to the lower pressure steam flowing over the outside. Reheating is preceded by removal of excess moisture from the steam leaving the high pressure turbine in *separators*. The separators may be separate from or integral with the reheaters. If separate, they usually operate using centrifugal principles, where the steam is given a strong swirling motion to throw out the moisture. If integral, sudden changes in the direction of the steam cause moisture to be trapped by chevron type plates.

The flow of reheating steam is governed by the flow of reheated steam. As the reheated steam extracts heat from the reheating steam, the latter condenses. The greater the flow of reheated steam and hence the rate of heat extraction, the greater is the condensation rate and hence the required flow of heating steam to take its place. The system is therefore self-regulating provided that the heating steam is fully condensed in the tubes and that the condensate is released in a controlled manner. It is either pumped back into the steam generator (CANDU) or cascaded into the highest pressure feedwater heater (PWR).

7.2 Deaerator

The *deaerator* is part of the feedwater heating system and receives extraction steam from the turbine. The condensate to be heated and the extraction steam are intimately mixed in the deaerator by a system of spray nozzles and cascading trays between which the steam percolates as shown in Figure 33. The condensate is heated to saturated conditions and the steam condensed in the process. Any dissolved gases in the condensate are released in this process and removed from the deaerator by venting to the atmosphere or to the main condenser. This ensures removal of oxygen from the system particularly during turbine start-up and minimizes the risk of corrosion within the system. Venting to the atmosphere reduces the load on the condenser vacuum pumps, but results in some steam loss unless provision is made to condense it and return it to the condensate system. Venting to atmosphere is only possible if the deaerator pressure is above atmospheric as it is at higher loads. In the CANDU system, auxiliary (pegging) steam is supplied at low loads to maintain elevated temperatures in the deaerator storage tank.

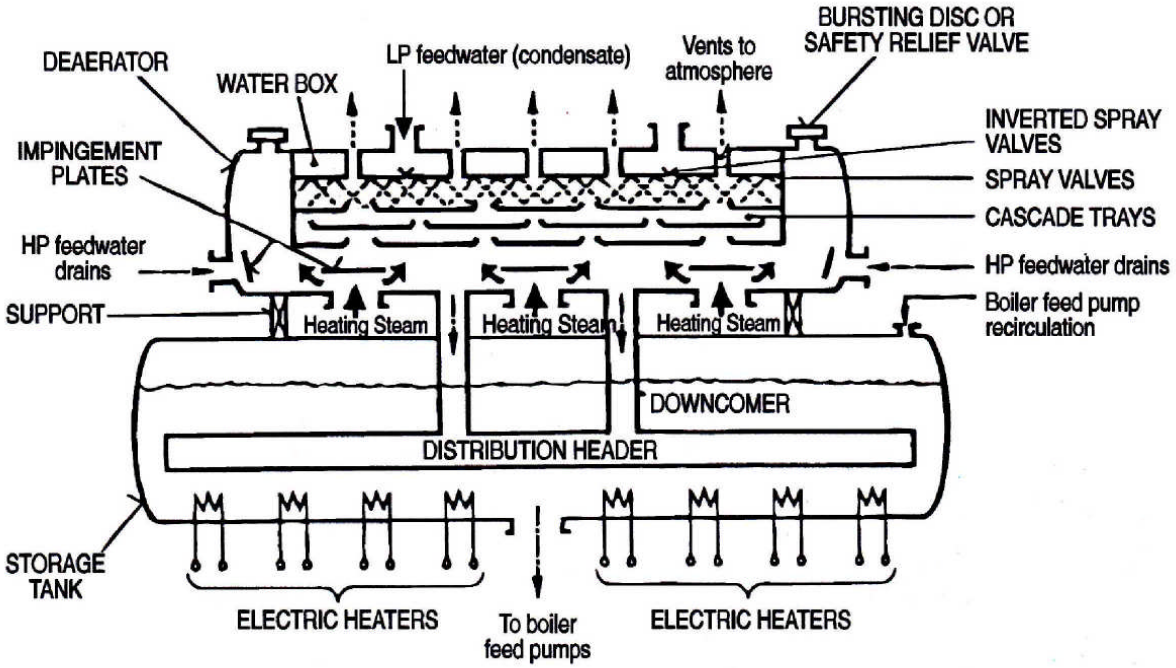

Figure 33 Deaerator and deaerator storage tank (courtesy of NB Power)

Immediately below the deaerator is the *deaerator storage tank*, where a large quantity of feed water is stored at near saturation conditions. In the event of a turbine trip, the steam generator will require an assured supply of feed water to maintain the required water inventory during subsequent stabilizing conditions, during which residual heat must be removed. During such conditions, the loss of extraction steam to the high pressure feedwater heaters renders them ineffective, and water from the deaerator storage tank is pumped into the boiler or steam generator without further heating. If deaerator pressure is maintained between 0.5 MPa and 1.0 MPa, then the corresponding temperature of this stored feed water will be between 150°C and 180°C. With an adequate supply of water at this temperature in the deaerator storage tank, damaging thermal shock to the steam generator can be avoided.

The deaerator storage tank is usually located at a high elevation between the reactor containment and the turbine hall to ensure an adequate net positive suction head at the inlet to the feedwater pumps, thus minimizing the risk of pump cavitation.

7.3 Feedwater Heaters

The *low pressure feedwater heaters* receive extraction steam from the low pressure turbine for heating the feed water. Condensate extraction pumps pump condensate from the condenser hotwell through the low pressure heaters to the deaerator.

The *high pressure feedwater heaters* receive extraction steam from the high pressure turbine. Feedwater pumps pump feed water from the deaerator storage tank through the high pressure heaters to the steam generator.

The conventional design for a feedwater heater is that of a horizontal cylindrical shell inside which is a bank of U-tubes connected to a divided header at one end, as shown in Figure 34. Feed water enters one side of the header, passes through the U-tubes, and leaves from the

other side of the header. Extraction steam from the turbine enters the shell and passes over the outside of the tubes, where it is condensed. The condensed steam collects in the bottom of the shell and is drained away. Generally, the drains from the high pressure heaters are cascaded through lower pressure heaters to the deaerator, and those from the low pressure heaters likewise to the condenser.

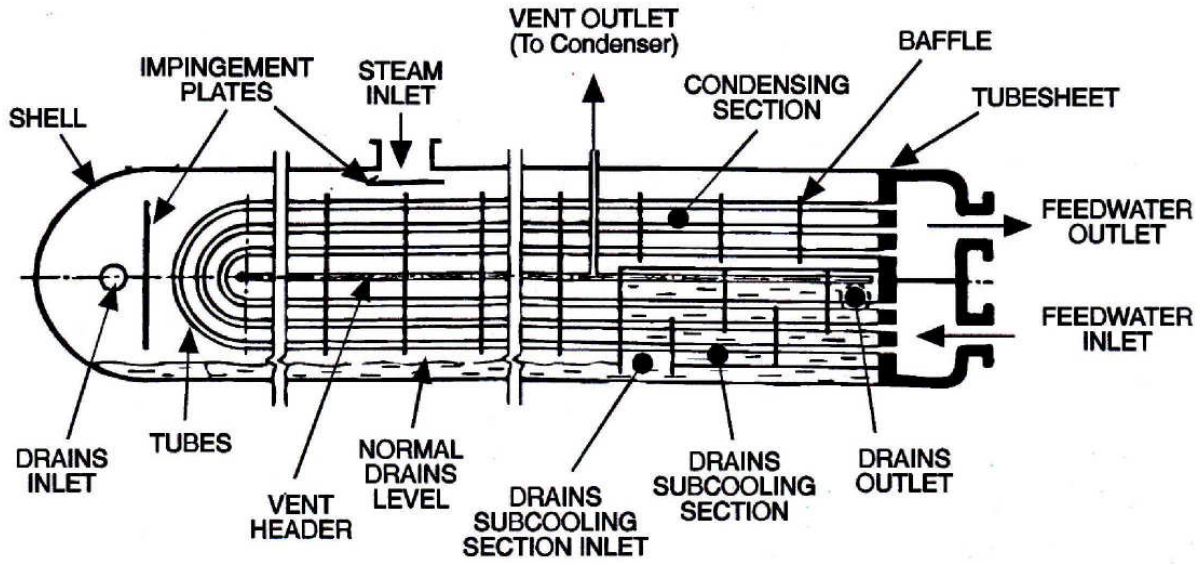

Figure 34 Feedwater heater with integral drain cooler (courtesy of NB Power)

Like the reheaters and deaerator, the feedwater heaters are self-regulating and draw only as much extraction steam from the turbine as they require to heat the feed water. The greater the feedwater flow, the greater is the rate of heat absorption from the steam, and the greater is the flow of extraction steam.

In the event of a turbine trip, the steam supply to the turbine is cut off, and pressures throughout the turbine drop to condenser pressure. Extraction steam pressures follow suit, inducing a reverse flow from the feedwater heaters to the turbine. The low pressure in the feedwater heater shell initiates vigorous flashing of any condensed steam. This may cause some water to become entrained in the reverse steam flow to the turbine. Any water entering the turbine in this way could cause severe damage to the turbine blading. As a precaution, therefore, non-return valves are placed in the extraction steam lines between the feedwater heaters and the turbine. These may be motor assisted to ensure sufficiently rapid closure at the onset of reverse flow.

8 Condenser

8.1 General Arrangement

The purpose of the *condenser* is to condense the exhaust steam from the turbine so that it can be returned to the system for reuse. In the Rankine cycle, the condenser is complementary to the steam generator in that it condenses the steam while the steam generator evaporates the water. Like the steam generator, it has a free water surface that interfaces with the steam, and some form of level control is required. Steam leaving the turbine enters at the top of the

condenser and circulates around the outside of the tubes, where it is condensed by cooling water passing through the tubes. The resulting condensate rains down to collect in a *hotwell* at the bottom of the condenser. Figure 35 and Figure 36 show a typical arrangement for a large condenser.

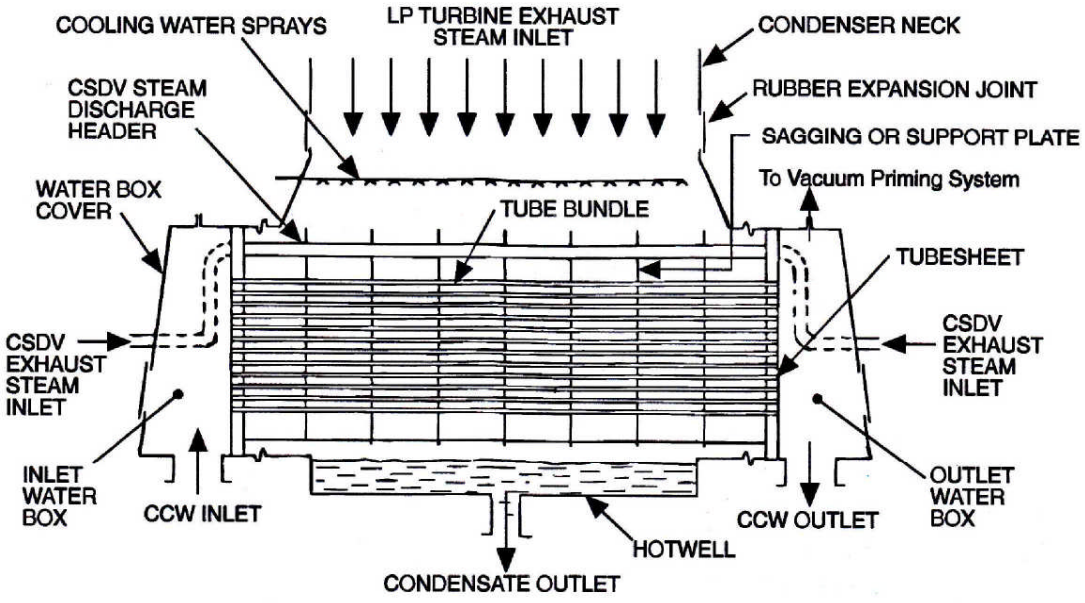

Figure 35 Condenser longitudinal section (courtesy of NB Power)

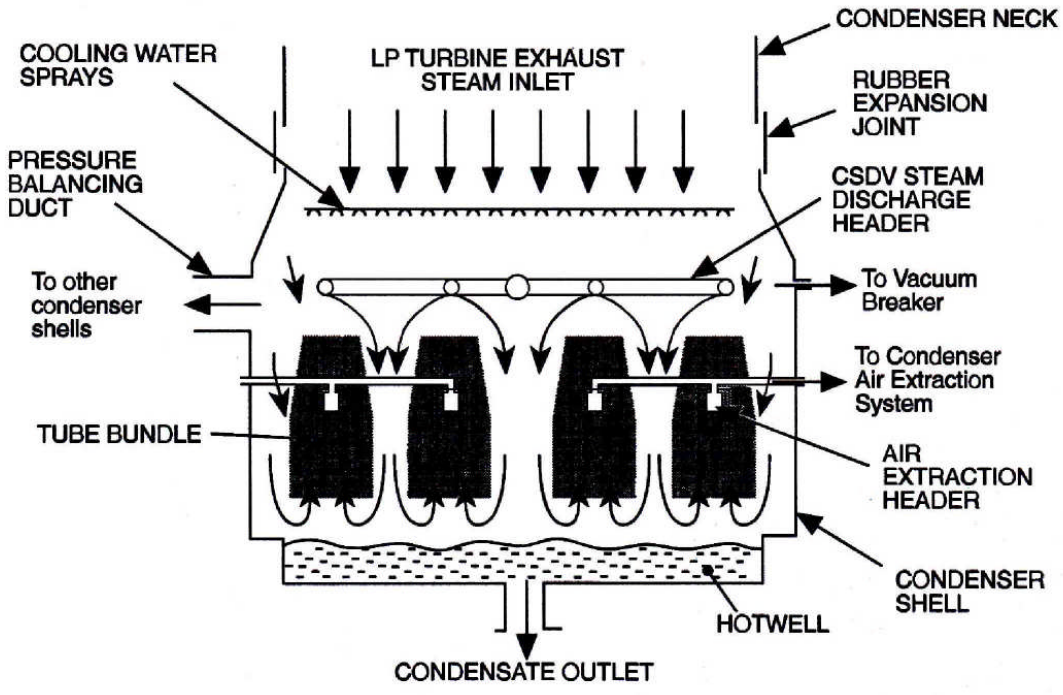

Figure 36 Condenser cross section (courtesy of NB Power)

Cooling water from a lake or ocean is supplied to the condenser by circulating or cooling water pumps and passes through the condenser tubes. The volume circulated is very large and the supply pipes quite long, and therefore damaging inertial effects must be avoided when starting

and stopping the pumps. In the event of a pump trip, vacuum breakers enable the water column to separate at the condenser and provide an air cushion to avoid damaging reverse flow.

The condenser hotwell serves as the entry point for demineralized make-up water, which is required to compensate for leakage losses. Level sensors indicate when there is a need for additional water. Note that the level in the hotwell rises naturally as the system is heated and loaded and water is displaced from other components.

An air extraction system removes air that is in the system before start-up and that may leak into the system during normal operation. This system extracts air from the end of the steam path, that is, at the centre of the condenser tube bundle, where it collects as steam is condensed. Shrouded air cooling tubes in this region reduce the temperature locally to a few degrees below saturation to increase the ratio of air to steam extracted. The air is extracted by vacuum pumps which run continuously to maintain condenser vacuum.

In the CANDU system, water spray pipes and nozzles are located in the condenser shell outside the tube bundle, so that during condenser steam bypass operation, cool condensate can be sprayed into the steam entering the condenser from the bypass system. This steam is at a high temperature and in a superheated condition and therefore must be cooled before it enters the tube bundle.

9 Electrical Generator

9.1 Generator Rotor

The generator rotor is machined from a single long slender forging of high strength steel. Slots are cut on two opposing sides for a two pole rotor and on four sides for a four pole rotor to take the rotor windings. The latter are for large half speed turbine generators used in nuclear plants. The poles between the slots produce the rotating magnetic field as the rotor turns. The copper windings are laid in the slots in pairs so that the current flow in them produces opposite north and south poles in a two pole rotor and alternating north and south poles in a four pole rotor. When rotating, these magnetic poles induce an alternating current in the generator stator. The rotor windings carry a large current at low voltage. Hence, they must be cooled and insulated while being held securely in the slots against very high centrifugal forces.

The individual windings are separated from one another by insulating separators and from the rotor itself by insulating slot liners. These are held in place by insulating blocks and aluminum wedges that fit into tapered grooves at the top of the slots. The windings have spaces between them to allow free flow of hydrogen coolant through the windings. A space is left at the bottom of each slot to create a duct to enable coolant to flow into the rotor from the ends. The flow is driven by centrifugal action, with the rate determined by holes in the wedges. This ensures uniform distribution of coolant and consistent cooling of all rotor windings. Hydrogen under moderate pressure (to increase its density) is a good coolant and very suitable for this application.

The winding connections, which protrude at the ends of the slots, wrap around, and enter slots further around the rotor, are held in place by end bells. These are ring shaped and are shrunk onto the ends of the slotted part of the rotor. They cover the end windings and secure them under the high centrifugal forces arising during operation. Centrifugal or axial flow fans are fitted to the rotor shaft at each end to feed coolant to the ends of the rotor and to ensure

proper circulation of hydrogen through the stator. Each fan serves one half of the generator. Rotor current is provided by an exciter connected to and driven by the generator shaft. Current is transferred to the rotor by fixed brushes and slip rings mounted on the shaft. This current is on the order of 5000 A and the voltage around 500 V for a 660 MW generator.

9.2 Generator Stator

The generator stator, with its laminated iron core and heavy copper windings inside a robust fabricated steel frame, is invariably the heaviest component of the turbine generator. The stator core is made up of laminated steel sheets having low loss magnetic properties and with a thickness of 0.5 mm or less. The sheets are coated with an insulating varnish to prevent circulating currents. Slots are arranged in the core for the stator windings, and provision is made for circulation of hydrogen coolant.

The stator current of a typical 660 MW generator operating at 24 kV and a power factor of 0.85 is on the order of 19,000 A, or about 950 A per bar. The current generates considerable heat, and therefore additional cooling must be provided. Water is an ideal coolant but must be pure enough to be effectively nonconducting. It flows to and from the stator windings through nonconducting polytetrafluorethylene (PTFE) hoses so that the windings remain fully insulated from the coolant pumps and heat exchangers. The water pressure is less than the hydrogen pressure to prevent water ingress to the generator in the event of coolant system leakage. Hydrogen, driven by the fans, circulates over the outside of the windings and then through water coolers mounted longitudinally around the periphery of the stator core or vertically at the corners of the stator core.

9.3 Excitation System

A separate exciter coupled directly to the generator rotor shaft provides excitation current to the rotor through brushes and slip rings. The exciter is, in effect, a small generator, which itself requires a small excitation current. This current in turn is provided by a pilot exciter and delivered to the main exciter rotor through its own brushes and slip rings. The pilot exciter has a permanent magnet on its shaft to provide the necessary rotating magnetic field.

The development of compact rectifiers enabled them to be incorporated into the rotating elements of the exciter. This means that the rotor and stator windings of the main exciter can be interchanged. The resulting brushless excitation system with a rotating armature main exciter is less complex and requires less maintenance than the conventional system.

The further development of thyristors enabled the conventional excitation system to be replaced by a current control system which feeds the required excitation current directly to the generator from an external power source. Although a feed from the generator electrical output circuit through an excitation transformer can be used as this source, it does not have the same intrinsic electrical security as a shaft mounted excitation system.

9.4 Generator Systems

The most important auxiliary systems associated with the electrical generator are those for cooling, sealing, and lubricating.

Virtually all generators of the size used in nuclear power plants are cooled by hydrogen at a pressure of 0.4 MPa to 0.5 MPa. Hydrogen under this pressure, which increases its density, has

good heat transfer properties. Compared with air under similar conditions, it has twice the heat transfer capability and several times the thermal conductivity and specific heat. This makes it ten times more effective at heat removal than air. The hydrogen atmosphere also prevents degradation of insulation and other materials by oxidation processes.

Hydrogen, however, is flammable and explosive in concentrations from 4% to 76% of hydrogen in air. Hence, it must be contained in the generator and maintained at a high purity of about 97%. Special seals are required where the rotor shaft penetrates the casing, and appropriate provisions must be made to prevent any mixing with air during gassing or degassing of the generator. Most seals have a very fine running clearance between the fixed and moving parts, into which seal oil is injected. The seal oil is usually lubricating oil from the main turbine generator oil tank, but is purified and pressurized for this purpose. When gassing the generator before operation, all air is displaced by admitting heavier carbon dioxide at the bottom of the generator casing and allowing the air to escape at the top. Hydrogen is then admitted at the top and, being lighter, displaces the carbon dioxide downwards. When all the carbon dioxide has been expelled, the generator casing is sealed and more hydrogen admitted to pressurize it. Degassing is done by following a reverse procedure, with hydrogen discharged to atmosphere from the top of the generator while being displaced by carbon dioxide admitted at the bottom.

Like the turbine, the generator runs on bearings at each end, with the exciter having its own bearings. These are lubricated by the main turbine oil system. The bearings, however, must be removable because assembly of the generator is different from that of the turbine. Because the generator stator cannot be split horizontally, the rotor must be threaded into the stator from one end of the generator, as shown in Figure 37. Once in place, the bearings are mounted and aligned to ensure that the rigidly bolted generator couplings maintain the required shaft catenary under gravity. This means that the generator bearings must be slightly higher than those of the turbine due to the natural bending of the turbine and generator rotors under the influence of gravity at all times, even at speed. Furthermore, the generator rotor must be able to move axially in the bearings by about 25 mm or more to accommodate axial expansion of the turbine rotors as their temperatures increase to those of normal operation.

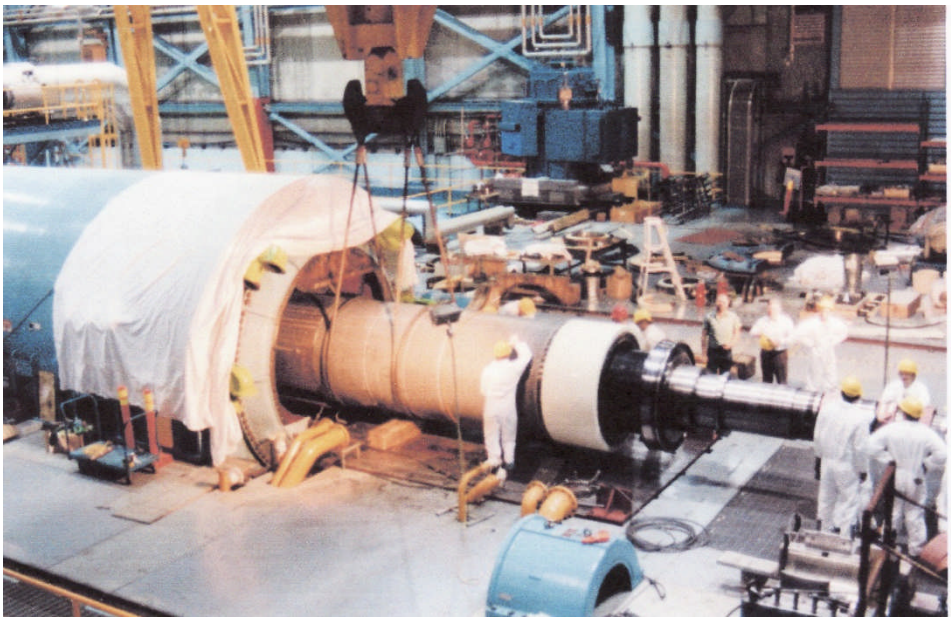

Figure 37 Insertion of rotor into stator of generator (courtesy of NB Power)

10 Power Transmission

10.1 Generator Main Connections

The neutral point of the generator star connection is grounded through a current limiting device to minimize ground fault currents in the generator, should a flashover occur in the stator windings. A convenient manner of providing a low resistance, yet current limiting ground connection is to use a transformer where the inductance limits the current. In the event of a ground fault, the lower voltage secondary side reflects a high current. This signals the fault to the generator protection system, which initiates a trip of the generator circuit breaker.

10.2 Generator Circuit Breakers

Generator circuit breakers are usually provided and located along the busbars between the generator and the tee-off to the unit transformer. They provide the necessary protection to the generator in the event of electrical faults. If not provided in the busbars, they are located on the high voltage side of the generator transformer in the electrical switchyard. The generator circuit breakers must interrupt heavy currents within a fraction of a second, and therefore provision must be made to extinguish the arc which forms as the circuit breaker contacts separate. Usually, this is done with a jet of air in air blast switchgear. A development of this concept is the use of sulphur hexafluoride (SF_6) instead of air. It is odourless, colourless, non-toxic, and nonflammable and has a density five times that of air, a thermal transfer coefficient greater than that of air, and a dielectric strength comparable to oil under moderate pressure. It is therefore ideally suited for use in circuit breakers, particularly where high voltages are used and limited space is available.

10.3 Generator Transformers

Generator transformers are required to increase the voltage before transmission of electrical power through the grid system. By increasing the voltage, the current is correspondingly reduced. Because electrical losses are proportional to the square of the current, there are significant advantages in operating a grid system at high voltages.

10.4 Transformer Connections

Three phase transformers may have star connected or delta connected circuits on the primary and secondary sides. This leads to four possible transformer arrangements between the power source and the load: star-delta, delta-star, star-star, and delta-delta. Practical considerations dictate the use of certain combinations in preference to others. All high voltage three phase circuits require a ground connection. This ensures that the potential differences between lines and grounded structures are maintained at design values. A star connected circuit provides such a connection at the neutral point, whereas a delta connected circuit does not. Furthermore, third harmonic currents are generated by hysteresis in the core. The magnitude of these can be reduced by a delta connected circuit. For this reason, star-star arrangements with star connected circuits on both sides are not common. Hence, it follows that, because most electrical generators have star connected circuits, the generator transformers and unit transformers supplied by the generator have delta connected circuits on the primary side and star connected circuits on the secondary side to provide a new grounded neutral point for the next circuit at a

higher voltage in the case of the generator transformer and at a lower voltage in the case of the unit transformer. In very large generating units, separate single phase transformers are provided for each phase. In such a case, a delta connected circuit may be provided on both primary and secondary sides. The advantage of such a delta-delta arrangement is that one of the single phase transformers can be isolated for maintenance or removed for replacement without disrupting the continuity of the three phase system, as shown in Figure 38. The system can therefore continue to operate, although at a reduced power level which is only about 58 percent of rated power. This is not possible with a star connected secondary circuit.

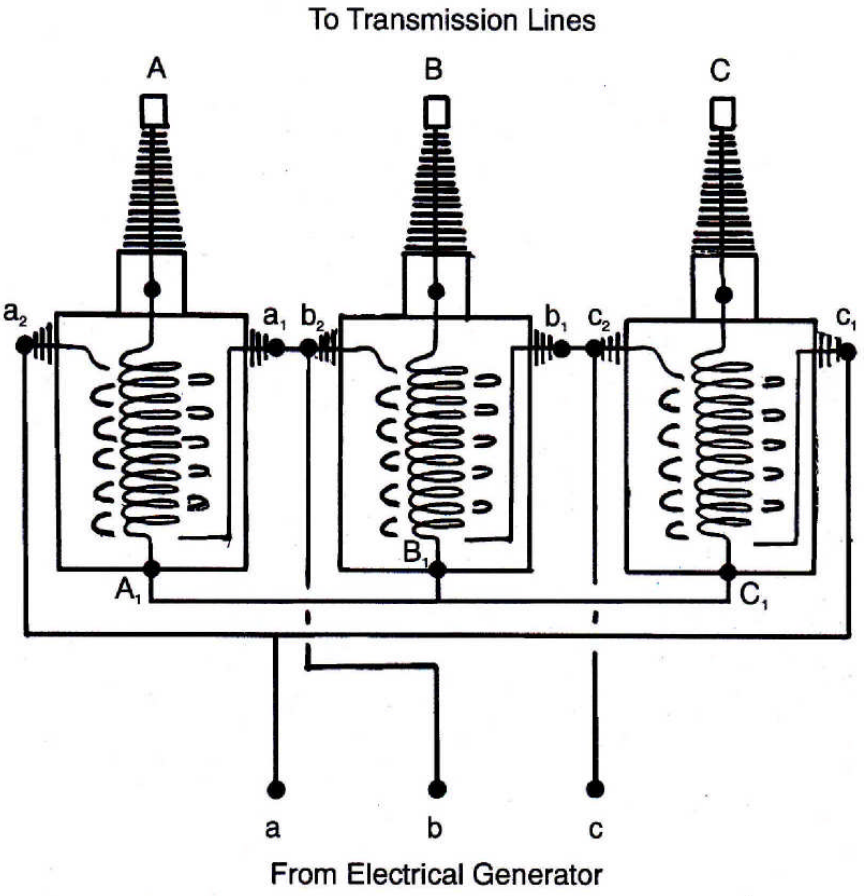

Figure 38 Arrangement of three single phase generator transformers

11 Problems

1. List the reactivity control devices for a CANDU reactor and for each describe briefly its purpose and how it operates.
2. Explain the difference between Shutdown System 1 (SDS1) and Shutdown System 2 (SDS2). Explain how each operates and under what conditions each would operate. Clarify how each would be reset to the primed condition.
3. Explain how the inventory and pressure of the heat transport system are maintained.
4. Describe how heat is removed from the reactor under all operational conditions including the shutdown state.
5. If the exit quality of the steam leaving a fuel channel is 4%, calculate the void fraction at this point assuming no slip (vapour velocity equal to liquid velocity) in the channel. As-

sume that the pressure in the channel at the exit is 10 MPa.

6. Consider heating of the heat transport system from the cold shutdown state at 30°C to the hot zero load condition (assumed to be 260°C) and then power raising to the full load condition.
    a. If, during heating to zero load, the heat transport system inventory is 200 Mg, determine how much heavy water is displaced into the pressurizer during this operation. For a pressurizer 2 m in diameter and 10 m in height, determine the rise in pressurizer level that would occur if heavy water were not bled from the system.
    b. If, during power raising, a further 10 m^3 is displaced into the pressurizer, give and explain two different reasons for this expansion.
7. Determine the percentages of sensible heat and latent heat transferred to the secondary circuit in the steam generator as well as the total rate of heat transfer given the following parameters:
    a. Steam flow rate 1 000 kg/s
    b. Steam pressure 4 MPa
    c. Feedwater temperature 175°C.
8. Suppose that the steam generator has an integral preheater and that during normal full power operation the temperature of the feedwater entering the preheater is 170°C.
    a. Calculate the difference between the temperature in the steam generator and the feedwater inlet temperature (steam generator ΔT) during normal full power operation if the steam generator pressure is 5 MPa.
    b. Calculate the steam generator ΔT during poison prevent operation (turbine tripped) if deaerator pressure is 360 kPa and steam generator pressure is 5 MPa.
9. Suppose that all feedwater flow to the boilers of a CANDU unit is suddenly lost when operating at full power. Explain why this would result in an increase in heat transport system temperature and pressure before the boiler levels would have dropped significantly.
10. In the event of a turbine generator trip or load rejection from full load, the reactor power is decreased to a lower level to prevent xenon buildup in the reactor and the surplus steam is dumped to the condenser.
    a. Explain what limits the maximum amount of steam that can be rejected and state the usual limit. At this limit, state the maximum load that the reactor can sustain.
    b. Explain why water is mixed with the steam before release into the condenser. Give reasons why this must be done.
11. A labyrinth shaft seal is used to ensure proper sealing where the shaft passes through the casing of a low pressure steam turbine.
    a. Explain briefly the design philosophy of such a seal.
    b. Sketch a cross section of the shaft and seal showing labyrinths and external pipe connections. Show the flow of steam and air through the pipes and labyrinths in normal operation.
    c. Sketch the pressure profile across the seal showing clearly the conditions inside and outside the turbine casing.
    d. Explain what would happen to the pressure and flow in the seal if the external steam supply to it should fail. How would this affect the operation of the tur-

bine?

12. Describe, with the aid of a sketch, the arrangement of a typical thrust bearing. Explain the purpose of thrust bearings and state, with reasons, where they are located in a typical large multi-cylinder turbine.
13. Explain, with the aid of a sketch, how the shaft of a large multi-cylinder turbine generator is aligned. Clarify how the bearings are set and what effect would be experienced at the couplings between the rotors if the shaft were not aligned properly.
14. Explain the general philosophy of providing lubrication to the turbine and generator bearings. Explain what pumps are used and how they operate. Clarify how they are driven and what happens should their driving power fail.
15. Explain the purpose of a deaerator and the importance of maintaining its pressure in the event of a turbine trip.
16. Explain the difference between feedwater heating in a deaerator (open heater) and a feedwater heater (closed heater). Consider the temperature differences between the heating and heated fluids and their respective pressures. On this basis, explain why there is usually only one deaerator, but multiple feedwater heaters.
17. Describe the structure of the main condenser and explain the purpose of its key internal components.
18. Explain why hydrogen is used for cooling in the electrical generator and what precautions need to be taken during gassing and de-gassing. Clarify the operational procedure for these processes.

Answer Guide for Chapter 8

1. See Section 2.6 Reactor Control Systems and Devices.
2. See Section 2.6.5 Mechanical rod shut-off absorbers and Section 2.6.6 Liquid poison injection system.
3. See Section 3.3 Pressurizer as well as Section 3.4 Inventory Control System and Figure 15 Heat transport purification and feed system.
4. See Section 3.5 Shutdown Cooling System and Figure 15 Heat transport purification and feed system as well as Section 3.5 Shutdown Cooling System and Figure 16 shutdown cooling system. See also Section 4.1 Steam Generator Function.
5. Use steam tables. Void fraction $\alpha = 0.34$ (using light water steam tables).
6. Use steam tables. (a) Volume displaced $\Delta V = 53\ m^3$ (using light water steam tables). Rise in level $\Delta H = 17\ m$ much greater than available height so some inventory must be bled from the system. (b) Increase in ΔT in steam generator due to increased rate of heat transfer and hence increased average temperature of reactor coolant. Generation of some steam in the fuel channels which has a greater volume than the water from which it was formed.
7. Use steam tables. Sensible heat 17%. Latent heat 83%. Total heat transfer rate $\Omega = 2058$ MJ/s.
8. Use steam tables. (a) Steam generator $\Delta T = 94°C$. (b) Steam generator $\Delta T = 124°C$.
9. See Figure 18 Temperature profiles in steam generator. Consider change and restoration of average temperature difference between primary coolant and secondary steam.
10. See Section 5.2 Steam Bypass System and Section 5.3 Condenser Steam Discharge Valves.
11. See Section 6.5 Turbine Sealing Principles and Figure 27 Spring mounted labyrinth seal to accommodate shaft deflection as well as Section 6.6 Turbine Seals and Figure 28 Prin-

ciples of operation of LP turbine shaft seal. Consider relative pressures and note that flow is always down the pressure gradient.

12. See Section 6.8 Turbine Bearings and Figure 30 fixing points for turbine rotors and casings.
13. See Section 6.8 Turbine Bearings and Figure 31 Turbine generator shaft catenary.
14. See Section 6.9 Bearing Lubrication and Figure 32 Turbine lubrication oil system.
15. See Section 7.2 Deaerator.
16. See Section 7.2 Deaerator and Figure 33 Deaerator and deaerator storage tank as well as Section 7.3 Feedwater Heaters and Figure 34 Feedwater heater with integral drain cooler.
17. See Section 8.1 General Arrangement and Figure 35 Condenser longitudinal section and Figure 36 Condenser cross section.
18. See Section 9.4 Generator Systems.

12 References and Bibliography

Atomic Energy of Canada Limited, *Canada Enters the Nuclear Age*, AECL, McGill-Queen's University Press, 1997.

Chaplin, R. A., "Nuclear Reactor Steam Generation", Chapter 3.10.2.10 in *Thermal Power Plants*, Encyclopedia of Life Support Systems by UNESCO, EOLSS Publishers, Oxford, UK, 2006.

Chaplin, R. A., "Steam Turbine Components and Systems", Chapter 3.10.3.3 in *Thermal Power Plants*, Encyclopedia of Life Support Systems by UNESCO, EOLSS Publishers, Oxford, UK, 2006.

Chaplin, R. A., "Steam Turbine Steam System", Chapter 3.10.3.4 in *Thermal Power Plants*, Encyclopedia of Life Support Systems by UNESCO, EOLSS Publishers, Oxford, UK, 2006.

Chaplin, R. A., "Electric Power Generation", Chapter 3.10.3.9 in *Thermal Power Plants*, Encyclopedia of Life Support Systems by UNESCO, EOLSS Publishers, Oxford, UK, 2006.

13 Acknowledgements

Acknowledgements are extended to Atomic Energy of Canada Limited and to NB Power for the use of information, diagrams, and photographs to support the text of this chapter.

The following reviewers are gratefully acknowledged for their hard work and excellent comments during the development of this Chapter. Their feedback has much improved it. Of course the responsibility for any errors or omissions lies entirely with the authors.

George Bereznai
Simon Pang

Thanks are also extended to Diana Bouchard for expertly editing and assembling the final copy.

CHAPTER 9

Nuclear Plant Operation

Prepared by

Dr. Robin A. Chaplin

Summary:

This chapter deals with the operating concepts of a CANDU nuclear power plant. It combines some theoretical aspects with basic operating procedures to explain how the plant operates. Key aspects related to plant control are addressed. Space allows only the primary energy generation, transport and conversion components to be covered, but there are many other components whose operation is vital for the efficient and safe operation of the plant. There is approximately an equal division of detail between the nuclear reactor, the heat transport and steam systems, and the steam turbine.

Table of Contents

List of Figures

Nomenclature for Equations

A	area	m^2
c_p	specific heat at constant pressure	kJ/kg°C
f	thermal utilization factor	
k	neutron multiplication factor	
M	mass flow rate	kg/s
U	overall heat transfer coefficient	$kJ/sm^2°C$
S_0	number of source neutrons	
S_∞	number of measured neutrons	
p	pressure	MPa
p	resonance escape probability	
v	specific volume	m^3/kg
V	velocity	m/s
Δk	change in neutron multiplication factor	
ΔT	rise in temperature (of fluid)	°C
ε	fast fission factor	

η	reproduction factor	
η	efficiency	
θ	temperature difference (between fluids)	°C
Λ_t	thermal neutron non-leakage probability	
Λ_f	fast neutron non-leakage probability	
ν	neutrons emitted per neutron absorbed	
ρ	density	kg/m^3
Σ_f	macroscopic fission cross section	m^{-1}
Σ_a	macroscopic absorption cross section	m^{-1}
Ω	rate of heat transfer	kJ/s

1 Power Production

1.1 Power Output Regulation

Consider a very simple system with a nuclear reactor, steam generator, and turbine generator supplying electrical power to an isolated electrical grid, as shown in Figure 1. The power must be generated at the moment it is required by the consumers connected to the grid. Power production must follow demand exactly, and any mismatch will cause the grid frequency to fall or rise as demand increases or decreases.

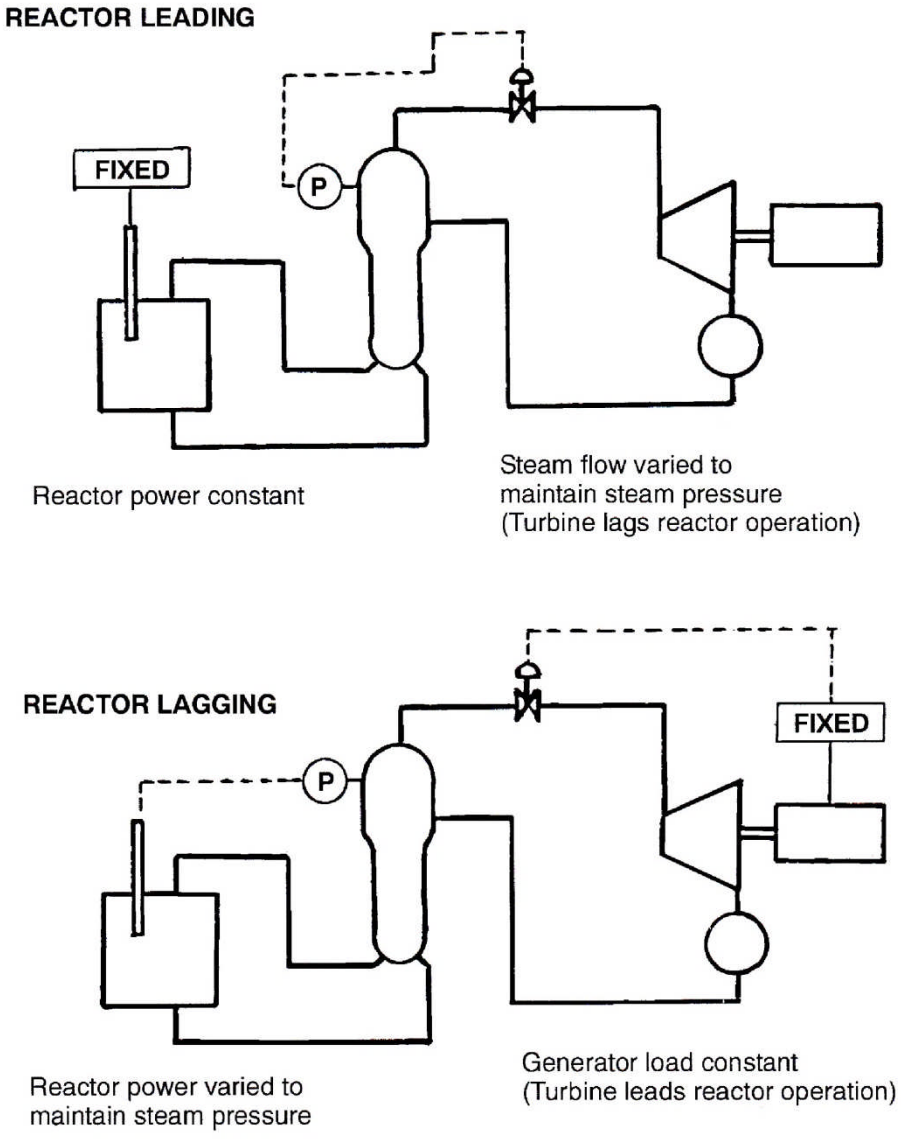

Figure 1 Lagging and leading plant operation

A basic control system works as follows to maintain appropriate power output from the plant. In the event of an increase in demand for electrical power, the mismatch will cause the grid frequency to fall. Because the turbine generator is synchronized to the grid, its speed will drop accordingly. This will be sensed by the turbine governor, which will open the governor valves to

admit more steam to increase the power output of the turbine generator. The additional flow of steam to the turbine will cause a reduction in steam pressure in the steam generator. This in turn will be sensed by the reactor regulating system, which will lower the liquid zones or withdraw control rods from the reactor core until the increased fission rate generates sufficient additional heat to restore the steam generator pressure. In the event of a decrease in demand, the reverse occurs. This is known as the *reactor following* or *turbine leading* mode of operation (or normal mode in some plants because it is a natural way of maintaining stable conditions).

Such a system, however, cannot maintain the specified frequency (60 Hz in North America) exactly without large unstable oscillations, and therefore a certain speed droop is incorporated into the turbine governor. This enables a progressive increase in governor valve opening (steam flow) as the turbine speed (grid frequency) falls. A typical droop setting is 4%, which means that, if the turbine were initially at zero load and at full speed, its speed would have to drop to 96% before the governor valve would be fully open. Such a speed is not acceptable for the turbine due to possible blade vibration, nor to the grid due to loss in speed of connected motors. Therefore, the governor is adjusted to bring the speed back to 100% at full load. In the event of a turbine trip or load reduction to zero under these conditions, the reverse would occur, and the turbine speed would rise to 104% of full speed.

In the operating mode just described, the nuclear reactor output follows the electrical grid demand, and therefore its power level oscillates continuously. This can have certain adverse effects, depending upon the type and design of the reactor. Excessive oscillations impose temperature transients on the fuel, which could cause premature failures of the fuel cladding. Large oscillations near full power could cause power limits to be exceeded, thus tripping the reactor and losing power production as well as imposing restart transients on it and the turbine. Due to high capital cost and low fuel cost, it is desirable to run nuclear reactors at full power most of the time. An alternative mode of operation is therefore often used at nuclear plants, in which reactor power output is fixed. This is known as *reactor leading* or *turbine lagging* operation. To maintain stable operation, reactor power is controlled at a given value by measuring the neutron flux and adjusting the control rods or liquid zones accordingly. Pressure in the steam generator must be maintained at the proper value to ensure stable conditions in the reactor coolant circuit. This is done by opening or closing the turbine governor valves to control the steam flow from the generators. The turbine then delivers power according to the steam flow, and the generator sends this power into the grid system, regardless of the grid frequency. The grid frequency must then be controlled by other turbine generators which feed into the grid system and operate in the turbine leading mode.

By referring to Figure 1 showing the two modes of operation, it can be seen that steam generator pressure is a key controlling parameter in both modes. This highlights the importance of the steam generator, where a balance of heat input and heat output must be maintained to maintain its pressure. Furthermore, the difference in temperature between the primary coolant and the secondary working fluid determines the rate of heat transfer. Hence, the reactor coolant temperature is determined by the saturation temperature and thus by the pressure in the steam generator.

1.2 Operational Constraints

During operation, parts of the reactor, steam system, and turbine are subjected to high temperatures. If these parts have thick walls or a substantial solid mass, they will likely suffer thermal stress during the heating and cooling that arises during start-up and shutdown and also during load transients. If a thick component is heated on one side, this side will tend to expand. If constrained by the still cold base material so that it cannot expand, an internal stress will be set up. The reverse happens during cooling. This means that large rigid components which are subject to transient and uneven heating and cooling will suffer low cycle fatigue damage and may ultimately fail. This effect can be minimized by slow heating and cooling to reduce temperature differences in single components such as reactor pressure vessels, steam generators, steam pipes, turbine casings, and turbine rotors. This means that all these components must be preheated slowly before start-up and the unit loaded slowly. Similarly, load changes on the unit should be done slowly. This imposes operating restrictions on reactors and turbines. Generally, the larger the unit, the longer will be the time to start it up and load it. This makes large units less flexible in operation than smaller units.

In the reactor, temperature transients on the fuel cause structural changes within the fuel and stress on the cladding and therefore must be minimized to avoid premature fuel failures. In the turbine, uneven heating and cooling of the rotor can cause bending, which in turn causes excessive vibration and in the extreme case, contact with the casing. Therefore, heating and cooling must be monitored very carefully.

A nuclear reactor is also subject to xenon transients which may inhibit operation for a period. When the load on a reactor is suddenly reduced, xenon, a fission product that absorbs neutrons very strongly, builds up in the fuel and may force a reactor shutdown. The xenon eventually decays after about 40 hours, and the reactor can be restarted. During this time, there is a loss in electrical power production, and the larger the unit, the more serious will be this loss in revenue generating output.

2 Plant Control and Protection

2.1 CANDU Plant Control Systems

A CANDU nuclear plant can operate as a base load plant or as a load following plant. The latter is the conventional mode because the plant responds naturally to demand changes on the grid system, as explained above. Fossil fuel fired plants operate in this way. In nuclear plants, there are special considerations, the main one being the high capital cost and the low fuel cost compared with conventional plants. Nuclear plants should therefore operate continuously at maximum load to ensure the lowest generation cost. A steady load also avoids thermal transients, prolongs the life of all high temperature components, and minimizes the possibility of premature fuel failures. Hence, most nuclear plants operate as base load plants, and the control system in a CANDU unit provides for this, as shown in Figure 2.

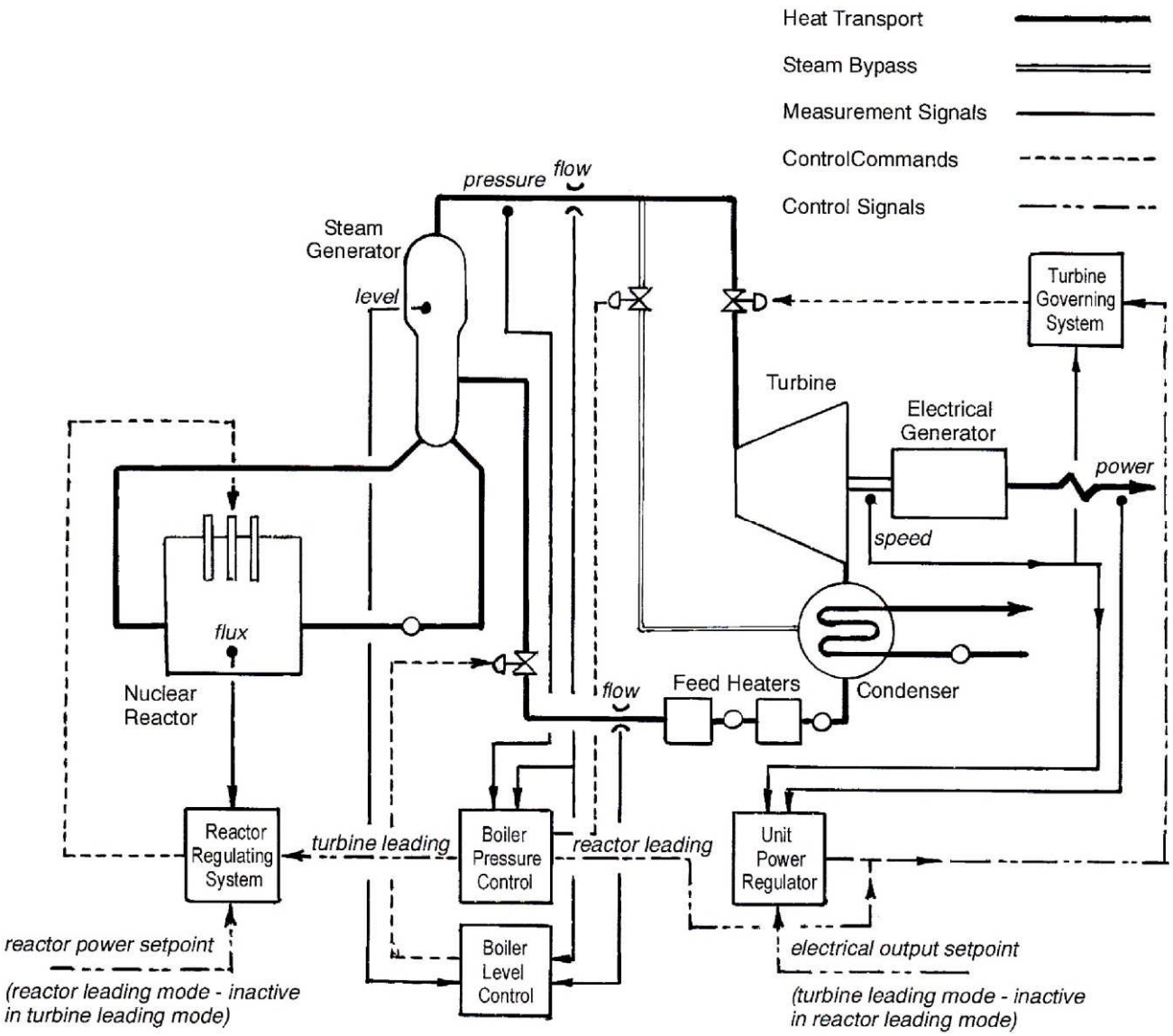

Figure 2 Basic plant control system

The plant can operate as a load following plant where the turbine responds to grid conditions and the reactor follows the turbine to produce the required output (turbine leading and reactor following). In the *alternate mode* the reactor power is fixed, and the turbine follows to produce the equivalent output (reactor leading and turbine following). This alternate mode with reactor power fixed enables the reactor to operate close to its power limits without risk of tripping due to control system oscillations from the turbine or other downstream component perturbations, thus maximizing plant output. In some plants, this *alternate mode* is called *normal mode* because the plant normally operates this way, and load following is the *alternate mode*.

The amount of steam produced in the steam generator depends upon the amount of heat received from the reactor. If the water level and pressure in the steam generator are to remain constant, the heat inflow and heat outflow must be perfectly balanced. Either one may be held constant (leading) and the other varied (lagging) to maintain conditions in the steam generator.

This determines the mode of operation of the plant (turbine leading and reactor lagging, or reactor leading and turbine lagging). Steam generator pressure controls both modes of operation. In turbine leading or reactor following, the steam pressure determines the required reactor output by signalling the reactor regulating system to increase or decrease fission heat release. In reactor leading or turbine following, the steam pressure determines the power output by signalling the turbine governing system to admit more or less steam to the turbine.

2.1.1 Steam generator pressure control

In the turbine leading mode, the steam generator or boiler pressure control (BPC) system measures steam pressure and manipulates reactor power by altering the reactor regulator setpoint. In the reactor leading mode, it measures steam pressure and manipulates steam flow by adjusting the turbine governor speeder gear.

2.1.2 Steam generator level control

The steam generator or boiler level control (BLC) system measures water level, compares steam and feedwater flows, and manipulates feedwater flow. In addition, reactor power or turbine power is measured and the level setpoint ramped up or down accordingly.

2.1.3 Unit power regulator

The unit power regulator (UPR) measures the electrical output and controls this output by manipulating steam flow, which is done by adjusting the turbine governor speeder gear. This is only applicable in turbine leading mode.

2.1.4 Reactor regulating system

The reactor regulating system (RRS) measures reactor neutron flux and thermal power and manipulates the liquid zone control absorbers and adjuster rod positions to control neutron flux.

2.1.5 Heat transport system (not shown in Figure 2)

The heat transport system pressure and level (HTSP&L) control system measures the reactor coolant pressure and pressurizer water level and manipulates the feed and bleed system as well as the pressurizer heaters and water sprays and also the steam release if pressure rise is excessive.

2.1.6 Turbine governing system

The turbine governor senses the turbine speed and adjusts the steam flow to maintain the required speed. This action is applicable only when the turbine generator is not connected to the grid system. Before synchronization, the speed is adjusted by the speeder gear to match the frequency of the grid system exactly. Once synchronized, the turbine generator speed is fixed by the grid frequency. If the speeder gear is then manipulated, it will open or close the governor valves to admit more or less steam and hence increase or decrease the turbine load. Once the load has been set on the turbine, any change in frequency on the grid system will alter the turbine speed, and the turbine governor will respond accordingly and change the governor valve position to adapt to the change in grid demand. This will alter the turbine generator

output according to the speed droop setting. Further manipulation of the speeder gear by the unit power regulator (turbine leading) or the boiler pressure control (reactor leading) will restore the desired power output.

2.2 Reactor Protection Systems

The reactor has protection systems that prevent excessive operating conditions which could cause a reactor trip and that trip the reactor if certain operating conditions are exceeded. A reactor trip is to be avoided if unnecessary because it causes a loss in electric power production and imposes thermal transients on components. Therefore, provision is made for the reactor power to be reduced by a setback or stepback to avoid potential trip conditions. Certain conditions, however, require an immediate reactor trip because continued operation could put the reactor into a dangerous condition. Such conditions require assurance that the reactor will trip, and therefore dual shutdown systems are provided, where each system is completely independent of the other, operates on different principles, and is activated by different inputs.

2.2.1 Reactor setback

A reactor setback reduces reactor power in a ramped manner to a predetermined level. The rate of power reduction and the end point of the power level depend upon the initiating conditions. For example, a high local neutron flux or flux tilts beyond a certain level will trigger a setback to 60% or 20% of full load, depending upon severity, to avoid overrating the fuel locally. A turbine trip or load rejection initiates a setback to 60% of full power because the condenser can absorb this level of heat load. A high steam generator pressure requires a setback to 10% because it indicates an inability of the turbine and condenser to absorb the steam flow adequately. Failure to meet other conditions which are essential for safe reactor operation, but which could be rectified with the reactor on load, requires a setback to 2%.

2.2.2 Reactor stepback

A reactor stepback reduces reactor power immediately to approximately 60% of full power by initiating a drop of the mechanical control absorbers. It is therefore similar to a reactor trip, but does not invoke the reactor shutdown systems, although it is a backup to the shutdown systems. For example, a trip of the heat transport pumps or low steam generator water level will trigger a stepback because these indicate a loss of heat removal capability. A high rate of neutron power increase will also initiate a stepback because it indicates a lack of safe reactor control.

2.3 Reactor Shutdown Systems

The reactor must be protected from the worst type of failure or combinations of failures. A loss of coolant accident is one such scenario. In the event of loss of coolant from one or more fuel channels, the voidage will initially cause an increase in reactivity. This must be counteracted by immediate insertion of a greater amount of negative reactivity to ensure subcritical conditions. There are two independent shutdown systems, SDS1 and SDS2, which are capable of doing this.

2.3.1 Shut-off rod insertion

Shut-off rods controlled by the SDS1 system drop by gravity into the reactor core to absorb neutrons. They are made of hollow cadmium rods encased in stainless steel and are guided into the reactor by vertical guide tubes. Cadmium is a strong neutron absorber and quickly takes the reactor power to a very low level. Activation occurs by release of electrically energized clutches, and the initial fall is accelerated by springs.

2.3.2 Liquid poison injection

Liquid poison controlled by the SDS2 system is injected by pressurized helium into the moderator to absorb neutrons. The gadolinium nitrate solution absorbs neutrons strongly, thus effecting a rapid drop in reactor power to a very low level. To ensure adequate distribution of the liquid poison, it is injected through a pattern of horizontal tubes within the reactor core. Activation occurs by the release of air pressure which holds the helium release valves in the closed position.

Both systems are activated within one second of failure detection, and sufficient negative reactivity is inserted within two seconds. The two systems are entirely independent of one another, and their operation depends on different principles and mechanisms. Although a loss of coolant accident is obviously very serious, there are several other scenarios which could put the reactor at risk, some of which may be transient due to operating disturbances. Several control parameters therefore feed into the SDS1 and SDS2 systems to shut down the reactor if these parameters deviate too far from what is deemed to be a safe operating condition. A dropping steam generator level, for example, will initiate first a stepback, then the SDS1 system, and finally the SDS2 system, so that if the stepback does not arrest the loss in inventory, the first shutdown system should, but if it fails, the second shutdown system will respond accordingly.

Quick recovery after an SDS1 trip is possible because the shut-off rod control mechanism can be reset and the rods withdrawn without residual reactivity effects. However, this is not possible after an SDS2 shutdown because the liquid poison will have thoroughly mixed with the moderator, and it will take several hours for the moderator purification system to remove the gadolinium. The SDS1 system is therefore the first to be actuated, and if this fails to arrest the fault condition, the SDS2 system will follow. Therefore, transient conditions or minor problems which initiate only an SDS1 trip and which can be corrected quickly can be recovered from before the xenon transient causes the reactor to poison out. Major faults or excessive deviations from required parameters would result in both systems tripping in quick succession.

2.4 Emergency Coolant Injection

In the event of a loss of coolant accident, an assured supply of coolant must be supplied to the fuel channels to maintain cooling immediately after the resulting reactor shutdown. This is effected by the emergency coolant injection system, which injects high pressure water into the heat transport system. This water is maintained under pressure in tanks by pressurized nitrogen. After this has been exhausted and the heat transport system pressure has fallen to a lower level, a pump-driven low pressure injection system takes over. Ultimately, lost coolant is recovered, circulated through heat removal exchangers, and returned to the heat transport system to stabilize the situation. Typically, the high pressure system is actuated at a heat transport system

pressure of about 5 MPa to give sufficient margin from normal operating pressure to minimize spurious injections during normal reactor cooldown.

2.5 Turbine Protection System

Like the reactor, the turbine has protection systems to prevent damage to components or catastrophic failure. As with the reactor, avoidance of unnecessary tripping is achieved by a runback to reduce turbine power sufficiently to regain safe operating conditions. In this way, speed and temperature transients on the turbine can be avoided, as well as the risk of faulty synchronization. Serious faults, however, require an immediate turbine trip.

2.5.1 Turbine runback

A turbine runback is the reduction of turbine load at a preset rate to zero load or until the initiating condition has been cleared. The rate is typically in the range of 1% to 10% of full load per second. The rate may be *fast* or *slow* depending upon the condition. A *latched* runback is one in which the governor speeder gear returns the turbine to the no-load speed setpoint. An *unlatched* runback terminates when the initiating condition has been cleared. As an example, a turbine trip would cause a fast latched runback to ensure that the governor speeder gear was reset to its no-load speed condition to avoid rapid reopening of the governor valves when clearing and resetting the trip (after rectifying the fault). A fast unlatched runback would be initiated by high condenser pressure (poor vacuum) because the condenser was unable to handle the exhaust steam flow adequately. This runback would terminate when the pressure had been restored to an acceptable value, and the turbine load would be maintained at this level.

2.5.2 Turbine trip system

In the event of a serious problem on the turbine generator, the turbine is tripped. This action causes a fast runback to the no-load set point on the governor and releases hydraulic pressure from the governor and stop valve actuators. This enables the valves to close rapidly and shut off steam flow to the turbine. Signals causing a trip come from various sources such as excessive rotor vibration, high bearing temperature, a generator electrical fault, and other parameters which have the potential to damage the turbine.

2.5.3 Overspeed governor

A major concern with regard to the turbine generator is the risk of overspeeding. This can happen only when the turbine is disconnected from the electrical grid, which means that critical times are before synchronization and after a turbine generator trip or load rejection. Some degree of overspeeding occurs with a generator trip or a load rejection when the steam valves are still closing after electrical output has been terminated. To provide protection against excessive overspeed, an overspeed governor is mounted on the turbine shaft. This is activated by increasing centrifugal force on overspeed bolts which independently trigger hydraulic pressure release from the steam valve actuators to shut off the steam flow.

3 Nuclear Reactor Operation

3.1 Reactivity Characteristics

To maintain the neutron multiplication factor k equal to unity in an operating reactor, small adjustments must be made continually to one of the factors in the six-factor formula given as follows:

$$k = \varepsilon\, p\, \eta\, f\, \Lambda_f \Lambda_t, \tag{1}$$

where ε is the fast fission factor, p the resonance escape probability, η the reproduction factor, f the thermal utilization factor, Λ_f the fast neutron non-leakage probability, and Λ_t the thermal neutron non-leakage probability. The manipulated factor is usually the factor f, the thermal utilization factor, which includes the neutron absorption in the reactor, Σ_a. This affects the number of neutrons and hence the neutron flux and reactor power.

Control systems must be designed to maintain the desired neutron power following short term changes initiated by natural perturbations or imposed transients. In the longer term, changes occur due to buildup of neutron absorbers and burnup of neutron producers in the reactor core. Because these changes are slow, they do not affect the control system as such, but the overall reactor configuration must be adjusted to maintain the desired balanced condition for a steady neutron chain reaction. The control system then maintains an equilibrium about this balanced condition.

An important consideration is the extremely high velocity of neutrons (2200 m/s when thermalized at 20°C). With the close spacing of fuel elements in the reactor, neutrons do not travel very far. The overall neutron lifetime from production due to fission until absorption to produce fission is therefore extremely short. The average neutron lifetime in a heavy water moderated CANDU reactor is about 1 millisecond, and in a light water moderated reactor such as a PWR or a BWR, it is much less. The complete neutron cycle from one generation to the next takes only this amount of time. It is evident, therefore, that any small deviation from the equilibrium situation, in which the number of neutrons in one generation is equal to that of the previous generation, will very rapidly grow in magnitude.

If all neutrons had a lifetime of about 1 millisecond, it would be almost impossible to design a control system that would be able to sense changes and effect control before the neutron population grew or shrank out of the control range. Fortuitously, some neutrons are produced a short time after the actual fission process. The kinetic behaviour of a reactor is critically dependent upon the existence of these delayed neutrons because they have the effect of increasing the average lifetime of the neutrons arising from fission. This increase in average lifetime to about 1 second because fewer than 1% of the neutrons have much longer effective lifetimes enables control systems to maintain stable operation provided that certain limits are not exceeded.

3.2 Source Multiplication

The delayed neutrons also influence the reactor under shutdown conditions because they are produced by the decay of certain precursors. While the reactor is shut down, this decay process continues, and some neutrons are always present because the decay curve is asymptotic. Both

uranium-235 and uranium-238 are naturally unstable and decay mainly by α-particle emission. Both also fission spontaneously, giving off neutrons in the process. Any fuel, even unused fuel, therefore produces small numbers of neutrons. Furthermore, in heavy water moderated reactors such as the CANDU, neutrons can be created by interaction of high energy γ-rays from certain fission products with deuterium atoms. These are known as photoneutrons. If, after a very long shutdown, these natural sources of neutrons do not produce sufficient neutrons to be detected by the reactor instrumentation, then artificial neutron sources are inserted into the reactor.

These source neutrons can cause fission in fissile fuel, producing more neutrons and establishing a chain reaction. When the reactor is shut down, the neutron multiplication factor k is, however, less than unity. This means that the chain reaction will decay, but in the meantime, other source neutrons will start new chain reactions. The result is that, along with these neutrons, there will be some fission neutrons, so that the total number of neutrons will be greater than would have arisen from the neutron sources only. The factor by which the total number of neutrons S_∞ is greater than the number of source neutrons S_0 is known as the *subcritical multiplication factor.* The relationship between these and the value of k is given by the following formula:

$$S_\infty = S_0 / (1- k) \qquad (2)$$

From the above equation, it can be seen that, as k approaches unity, the measured number of neutrons S_∞ becomes many times greater than the source number of neutrons S_0. Furthermore, it takes longer for an equilibrium condition to be reached. A very simple numerical example for k = 0.5 and S_0 =100 is given in Figure 3 for illustrative purposes.

As long as S_∞ stabilizes at a fixed value after an increase in k, the reactor remains in a *subcritical* condition, with k less than unity. When k is exactly unity, however, the fraction of source neutrons is negligible compared with the total number of neutrons, and the number of neutrons in each generation will be the same. The system is then said to be *critical*.

Source Multiplication

Source strength $S_0 = 100$
Neutron multiplication factor k = 0.5
Measured strength $S_\infty = 199$ [actually 200 since $S_\infty = S_0 / (1 - k)$]
Subcritical multiplication factor = 1 / (k - 1)

Generation	**1**	**2**	**3**	**4**	**5**	**6**	**7**	**8**	**9**	**10**	**11**	**12**
	100	50	25	12	6	3	2	1	..	..	..	..
		100	50	25	12	6	3	2	1	..	..	..
			100	50	25	12	6	3	2	1	..	..
				100	50	25	12	6	3	2	1	..
					100	50	25	12	6	3	2	1
						100	50	25	12	6	3	2
							100	50	25	12	6	3
								100	50	25	12	6
									100	50	25	12
										100	50	25
											100	50
												100
Total	100	150	175	187	193	196	198	199	199	199	199	199

Figure 3 Source multiplication by subcritical multiplication factor

3.3 Approach to Criticality

When a nuclear reactor is started up from the shutdown condition, the neutron flux must be increased by several orders of magnitude. In the shutdown condition, the neutron flux is determined by the intensity of the neutron sources and the subcritical multiplication factor. The value of the neutron multiplication factor k is substantially less than unity, and the reactor is subcritical. When starting up the reactor, the value of k is adjusted to bring it to unity, making the reactor critical and capable of sustaining a continuous fission chain reaction. In so doing, the subcritical multiplication factor increases the neutron flux level because the difference between k and unity, Δk, becomes smaller and smaller:

$$S_\infty = S_0 / (1 - k), \tag{3}$$

$$S_\infty = - S_0 / \Delta k. \tag{4}$$

As Δk approaches zero, the measured neutron flux S_∞ theoretically goes to infinity. This is obviously not practical because critical conditions must be established at a measurable neutron flux level. The real situation is that Δk can only be determined and controlled to a certain

degree of accuracy. Once this limit has been reached, slight perturbations cause control system responses that mask the actual value of Δk, and the reactor can be considered to be oscillating very slightly above and below criticality. Under these conditions, the reactor is considered to be critical, with the average value of k equal to unity.

Even though a nuclear reactor may be shut down, the reactivity within the reactor may change with time due to buildup or decay of fission products. This means that one cannot simply restart a reactor by inserting an amount of positive reactivity equal to the amount of negative reactivity inserted to shut it down. Approach to critical is therefore a delicate manoeuvre, like an approach to a moving and invisible target. At every step, therefore, an assessment must be made of how far from critical the reactor actually is. Each step must also be small enough so as not to overshoot the point of criticality.

While Δk has a large negative value, a change in reactivity will be reflected quickly on the instruments because the fission chain reactions initiated by the source neutrons die away rapidly since the value of k is far below unity. Following insertion of some positive reactivity, the reactor power will rise quickly to a new equilibrium value. When, however, Δk has a small negative value and k is very close to unity, the reactor will respond very much more slowly. Under these circumstances, the fission chain reactions initiated by the source neutrons persist for many generations. Following insertion of some positive reactivity, the reactor power will rise slowly, but more significantly, and take much longer to settle at its new equilibrium value. When the reactor becomes critical due to insertion of additional positive reactivity, the reactor power will rise steadily and continuously without levelling off at an equilibrium value. Because the reactor will be very slightly supercritical, the power will in fact rise exponentially. If power versus time is plotted as shown in Figure 4, criticality will have been achieved when the measured power does not level off, but increases exponentially. Generally, such a crude mechanism of monitoring the approach to criticality is not suitable for commercial reactors.

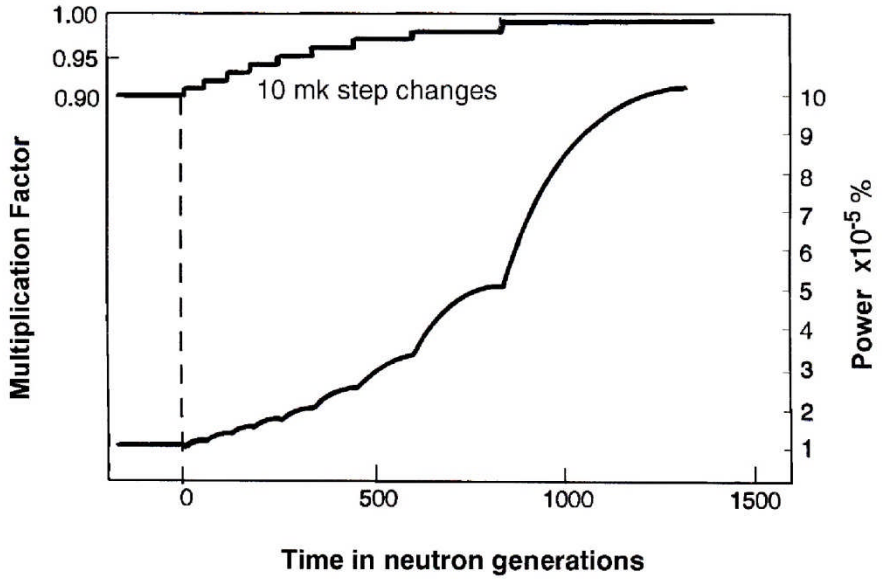

Figure 4 Stabilization time for different subcritical multiplication factors

If it is assumed that the measured reactor power P_∞ (equivalent to S_∞) doubles at each step, then various parameters such as k and Δk can be calculated to show their changes. Figure 5 shows how k and Δk change with each doubling of power from P_∞ = 0.0001 at k = 0.9.

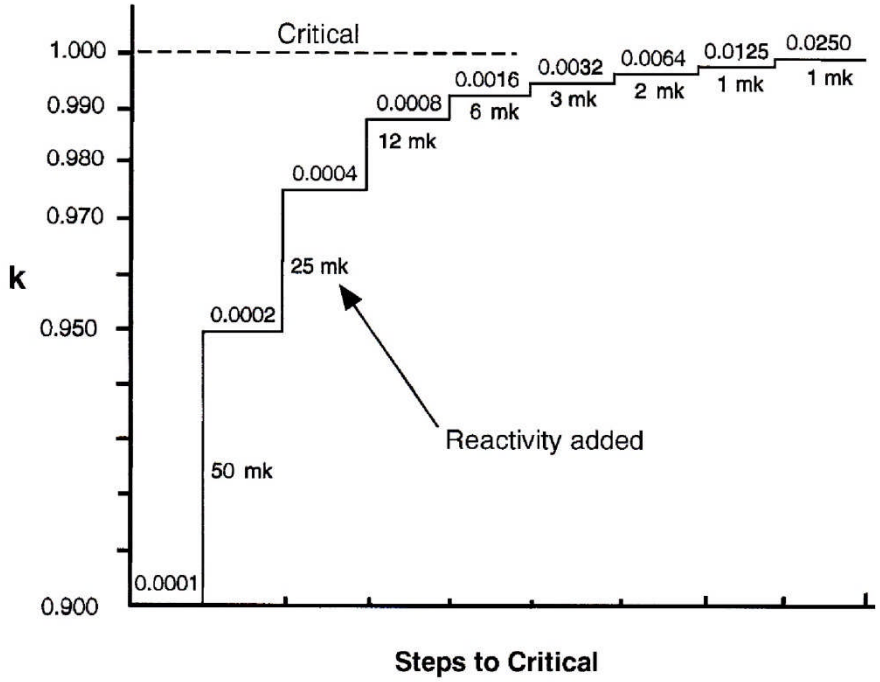

Figure 5 Approach to critical - subcritical multiplication factor change

The neutron count rate on the instruments can be assumed to be proportional to the measured neutron flux S_∞ and the inverse count rate then determined. These changes may be plotted graphically. The most useful plot is the inverse of count rate versus reactivity added, as shown in Figure 6. This shows that criticality is achieved when the inverse of count rate becomes zero. The plot is nearly linear, enabling the amount of reactivity to be added to achieve criticality to be easily determined by extrapolation.

Once the reactor is confirmed to be critical and under control of the reactor regulating system, a specific power level can be set, and the reactor regulating system will reduce the liquid zone levels slightly to insert a little more reactivity and maintain a stable rise in power to the desired level. Typically, the reactor regulating system never needs more than about 0.1 mk of reactivity change to maintain stable conditions or to change the power level.

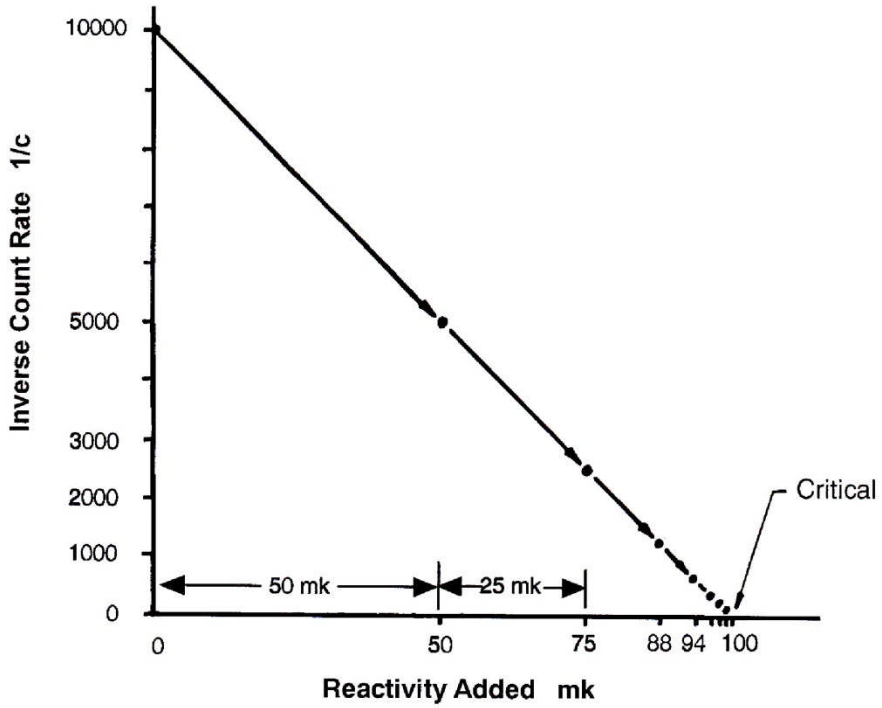

Figure 6 Approach to critical - inverse count rate change

3.4 Approach Technique

The actual process of approach to criticality depends upon how long the reactor has been shut down. After a period of several weeks, the source of neutrons from delayed neutrons and photoneutrons will have fallen to a sufficiently low level so that, even with the subcritical multiplication factor, the reactor regulating system instruments will have drifted off scale and will not be able to measure the neutron flux. Supplementary start-up instrumentation is therefore used as a temporary measure until the regular instrumentation can read the neutron flux. During power raising under these conditions, manual manipulation of reactivity and hence power is required. This requires careful monitoring and plotting of inverse count rate versus reactivity. Once the power is within the range of the regular instruments, they can be relied upon to hold the power at a particular level. The time for power to stabilize becomes longer as the reactor moves closer to criticality, and therefore using the reactor regulating system to maintain a particular power level minimizes the risk of adding more reactivity before the power has stabilized. If the reactor is started up after a short shutdown period, the reactor regulating system will be able to sense the neutron flux and react accordingly.

Assuming that the regular instruments can be used for reactor control, the general procedure is as described below. If not, the same procedure applies, but must be done manually. The reactor regulating system can be used with the reactor in reactor leading mode of operation. With poison removal stopped, the operator requests a doubling of power and monitors the liquid zone control absorber levels. When these have reached about the 20% level, power raising is stopped and the power held at this level by the reactor regulating system. The poison

removal process is then started or restarted with the RRS holding the power level. As the reactivity tends to increase, the liquid zone levels rise to compensate, keeping reactivity and hence power level constant. When the liquid level is high, the poison removal process is stopped. Again the operator requests a doubling of power, and the process is repeated. Because smaller and smaller amounts of reactivity addition are required as criticality is approached, the drop in liquid level becomes smaller and smaller, and after a few iterations, the liquid zone absorber levels can accommodate a full doubling of power. In a typical CANDU reactor, a drop in liquid level from 65% to 20% represents a reactivity change of about 3 mk. If the power were doubled with this change, the reactor would be about 6 mk below criticality. Further iterations of the process can bring the reactor to within 1 mk of criticality. The final step in the process is verification that the reactor is sufficiently close to criticality for the RRS to maintain control of power. Power raising can then follow by the operator adjusting the power setpoint to the required value.

The advantage of this method of approach to criticality is that the reactor does not actually go critical and, when it is nearly critical, power is increased by adjusting power level and not by direct manipulation of reactivity devices.

3.5 Reactor Start-up

A simplified procedure for a reactor start-up is shown in Figure 7. Besides the important process of achieving criticality, all auxiliary systems must be available and in operation as required, and the heat transport system must be pressurized and heated. Auxiliary systems such as the feed and bleed system, moderator cooling system, shutdown cooling system, and emergency core cooling system must be available as required. The emergency core cooling system is disabled during a cold depressurized state to prevent inadvertent initiation in this plant state. The cooling systems, however, will be in operation to remove decay heat under cold shutdown conditions. There is naturally some overlap in these activities, as well as with those of the steam turbine and the steam and feedwater heating systems (which are described later).

Warming up of the pressurizer and degasser can begin before the approach to criticality. Initially, the pressurizer is isolated from the heat transport system and warmed until it reaches a pressure of 4 Mpa while the degasser is warmed to a pressure of 1.1 MPa. At this point, approval is required to proceed with connecting the pressurizer to the heat transport system because plant conditions will be changed during pressurization of the heat transport system. The pressurizer and heat transport system are then pressurized separately to 6.7 MPa by the pressurizer heaters and the feed and bleed system respectively. They are then connected together by opening two motorized isolation valves. Once connected, the main heat transport pumps can be started, and the heat transport system and pressurizer can be warmed together as one system by controlling the shutdown cooling system to remove excess heat as required. Warming of the heat transport system is done using pump heat from the main pumps because their energy is dissipated in the system. Initially, a significant challenge exists for the operator to maintain the heat transport system temperature below 100°C until the emergency core cooling system has been enabled. Normal procedure is to maintain the heat transport system temperature at less than 80°C. Regulations require that the emergency core cooling system be enabled anytime that the heat transport system temperature rises above 100°C. With the heat

transport system temperature at 80°C, the approach to critical would typically commence, along with further warming of the heat transport system.

During the approach to criticality, initiation of reactor power increase by removing moderator poison and continued warming of the heat transport system proceed as parallel activities. The concern about warming the heat transport system during approach to criticality is the effect that it has on core reactivity when reactor power is being increased and criticality has not been achieved. During the approach to criticality, only one reactivity addition mechanism should be in use at any one time. The primary method is moderator purification by removing poison. However, by adding pump heat from the heat transport system pumps, the reactivity is being adjusted due to the temperature coefficients, including those of the fuel, at play during warm-up. This reactivity effect must be considered regardless of whether an equilibrium core or a fresh core is in place. As the heat transport system is warmed, the temperature coefficients add overall positive reactivity to an equilibrium core due to the buildup of Pu-239 which fissions more readily as temperature rises within this range, whereas in a fresh core, this reactivity effect is negative due to the lack of Pu-239. Therefore, warm-up of the heat transport system is stopped when the core is 30 mk subcritical, which is approximately equivalent to the presence of 1 ppm of moderator poison (gadolinium nitrate). This concentration can be confirmed by monitoring the online moderator conductivity, which is proportional to the concentration. A subcritical reactivity balance is conducted at 30 mk to verify the prediction for criticality and to ensure that all reactivity factors have been accounted for. For the remaining approach to criticality, no other actions which adjust reactivity other than that of the operator removing moderator poison by moderator purification are permitted. This guarantees that the core achieves criticality as predicted. In practice, criticality is defined as the point where the reactor regulating system has sufficient positive and negative reactive addition available by means of the liquid zone control absorbers to maintain reactor power at its setpoint**.** This occurs in an equilibrium core when the reactor regulating system can double reactor power within a 10**%** change in liquid zone level.

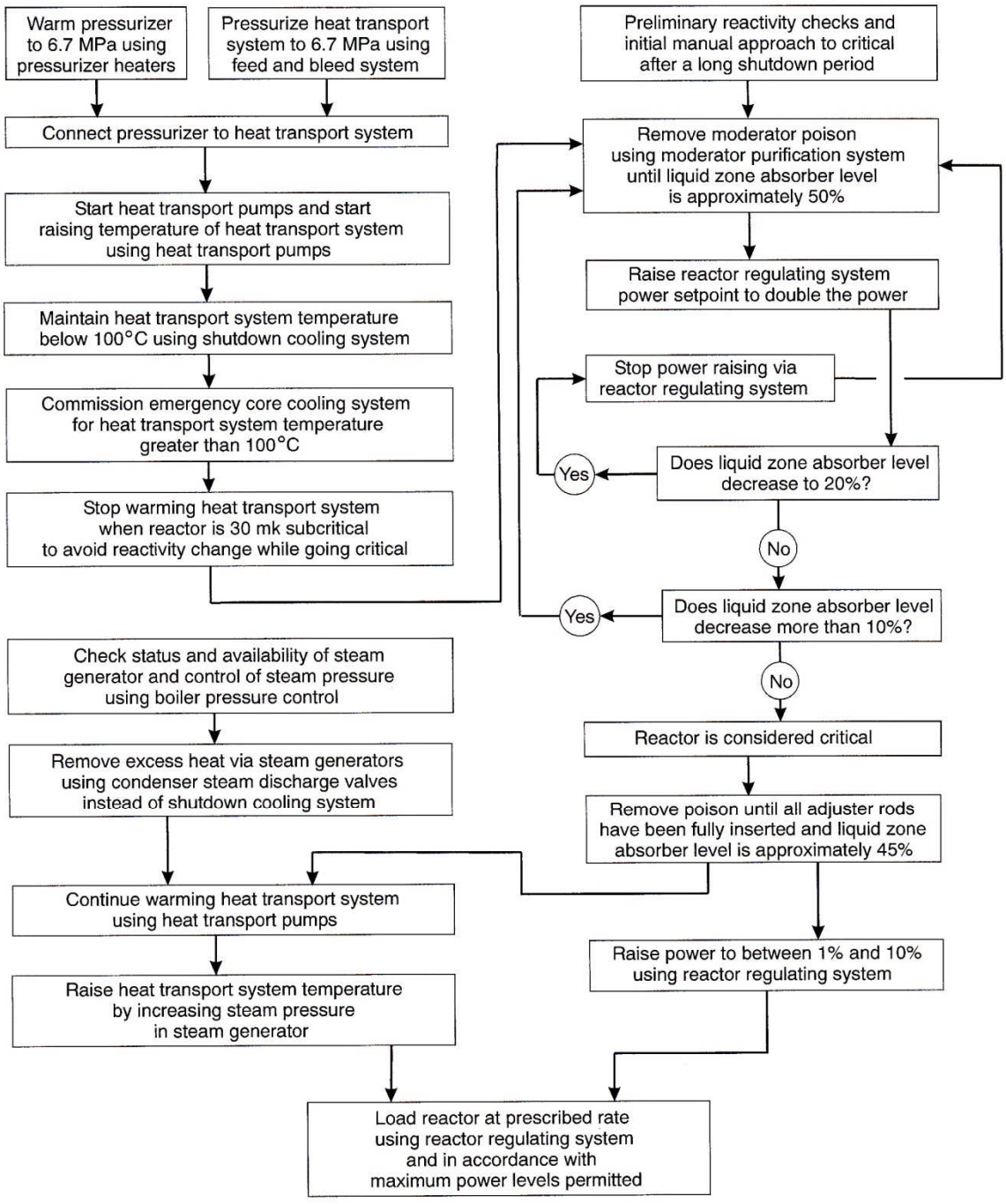

Figure 7 Major activities during start-up and loading

3.6 Reactivity Changes

The previous section considered short term reactivity changes due to operational manoeuvring, including start-up. This requires relatively small changes in reactivity to effect the desired result. In fact, it is important that, except in the case of a reactor trip, such changes be small to ensure proper control of the reactor.

Of further concern, however, are certain other effects which, during normal operation, result in reactivity changes much greater in magnitude than are required for operational control purposes. These occur over a much longer time frame and as such do not upset normal control. They do, however, require significant reactivity adjustment to maintain criticality in the reactor. These effects change one or more factors in the six-factor formula, given again as follows:

$$k = \varepsilon\, p\, \eta\, f\, \Lambda_f \Lambda_t. \qquad (5)$$

The result is a drift of k from unity in a critical reactor. To restore criticality, that factor must be returned to its original value or another adjusted to compensate for the change so as to bring *k* back to unity.

The effects causing these changes fall into three main categories:

Fuel burnup
Xenon transients
Temperature effects.

The fuel effects are due to fuel depletion, buildup of transuranic nuclides, and production of fission products. Eventually, the combination of these factors prevents criticality from being maintained, and refuelling with new fuel is required.

Xenon-135 in particular is troublesome because its equilibrium level in the reactor is maintained by its being destroyed by neutron absorption as fast as it is created. A reduction in reactor power decreases the neutron flux and hence its rate of destruction. This results in a surge of xenon production and an increase in neutron absorption. The consequent reactivity changes may be difficult for the control system to overcome, especially after a significant power reduction.

The temperature effects are related to the neutron absorption characteristics of the fuel and moderator. The temperature of the whole reactor increases from the cold shutdown condition to the hot zero load condition. The temperature of the fuel then increases further as power is raised from the zero load condition to the full load condition. It is desirable that the overall effect on reactivity due to temperature be negative so that the natural tendency of the reactor is to go subcritical (*k* less than unity) during a temperature excursion. This enhances the stability of the reactor, giving it a degree of self-regulation and hence increased safety.

3.7 Fuel Burnup

During operation, fissile fuel such as uranium-235 burns up continuously and eventually reaches a point where it is so depleted that it cannot sustain a nuclear chain reaction. At this time, the fuel is replaced with new fuel and the process continued. As the uranium-235 is burned up, fission products build up in the fuel, and some of these are neutron absorbers. On the other hand, some uranium-238 is converted into plutonium-239 by neutron absorption and two successive β-particle emissions:

Plutonium-239 builds up quite rapidly at first. Some of it absorbs neutrons in two stages to become plutonium-241, another fissile fuel, but the concentration of this never reaches significant proportions within the normal fuel lifetime. Initially, the buildup of plutonium-239 actually causes an increase in core reactivity. This is due to its higher fission cross section as well as the greater number of neutrons produced per fission compared with uranium-235. Ultimately, depletion of uranium-235 and buildup of fission products in the reactor result in a decrease in core reactivity.

The effect of fuel burnup on reactor reactivity is felt primarily through the factor η, which combines the number of neutrons emitted per neutron absorbed ν, the macroscopic fission cross section of the fuel, $\Sigma_{f\ fuel}$, and the macroscopic absorption cross section of the fuel, $\Sigma_{a\ fuel}$:

$$\eta = \nu \Sigma_{f\ fuel} / \Sigma_{a\ fuel}. \quad (6)$$

As the fuel is burned up, $\Sigma_{f\ fuel}$ decreases, and as fission products accumulate, $\Sigma_{a\ fuel}$ increases. The overall effect is that η decreases with time. The effects of samarium-149 and plutonium-239 as mentioned above, together with uranium-235 depletion and fission product buildup, can be shown graphically as in Figure 8 by plotting the value of η with respect to time and noting that the neutron multiplication factor k varies accordingly. At the very beginning, there is a drop in η (and hence k) due to buildup of samarium-149, a neutron absorber. Somewhat later, but still early in the fuel cycle, the value of η (and k) increases and reaches a peak due to formation of plutonium-239. Then the effects of uranium-235 depletion and fission product buildup become significant, and η (and k) falls progressively.

The effects of xenon-135 are not shown on this graph because the associated degree of reactivity change is due mainly to reactor load (neutron flux) and is greater in magnitude than the effects shown here, being as much as -30 mk under full load conditions.

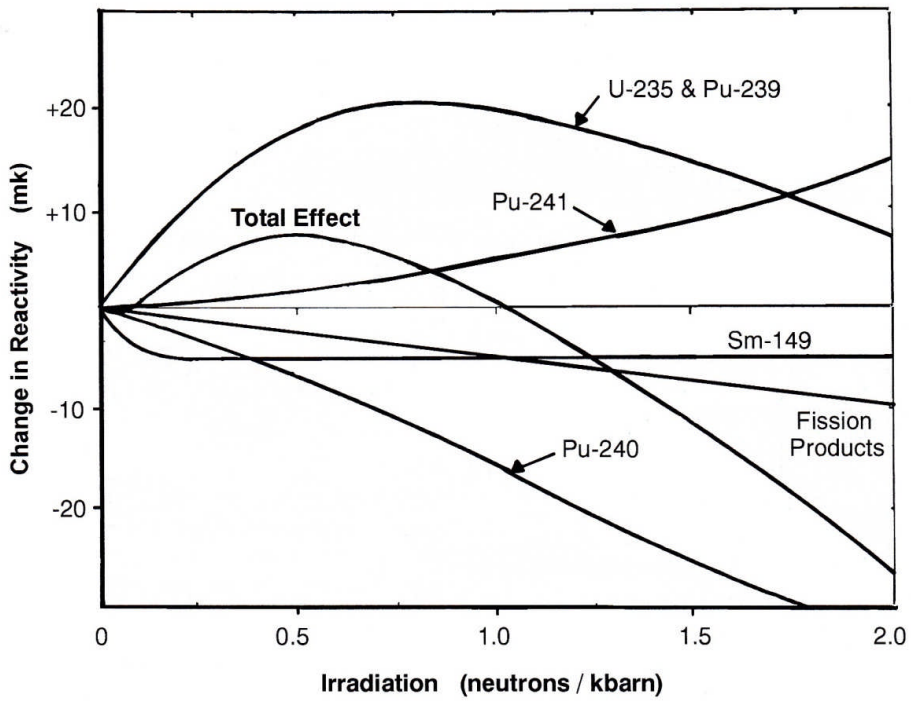

Figure 8 Effects of fuel burnup on reactivity

3.8 Refuelling Considerations

Except when a reactor is loaded with fresh fuel, reactor refuelling is a continuous process, with about a dozen channels being refuelled each week. In selecting the channels to be refuelled, a number of factors should be considered. Channels with the highest burnup should be refuelled first, the reactor power distribution should be kept symmetrical, and the channels with the largest reactivity gain should be selected if the overall core reactivity is low. However, channels close to recently refuelled channels should be avoided, as well as those with known abnormal conditions which could force an unplanned reactor shutdown if a refuelling failure should occur. Any channels containing defective fuel should be refuelled as soon as possible.

The preferred state during refuelling is with the reactor critical, on load, and under control of the reactor regulating system. Control absorbers must not be in the core because this is an abnormal and transient operating condition. There should be no reactivity changes during refuelling, meaning that adjuster positions should not be altered nor poison addition or removal be in progress. This ensures that reactivity changes during refuelling are readily observable.

4 Heat Transport System

4.1 Operational Considerations

When at full power, the reactor derives approximately 92% of its heat from the fission process, 7% from decay of fission products, and 1% from the heat transport system pumps. Immediately after a reactor trip, the heat generated by fission products, even though it decreases rapidly initially, and that generated by the pumps continues. The heat transport system must remove heat at all times through the steam generators. This requires that a temperature difference between the reactor coolant and the steam circuit be maintained. At full load, this temperature difference is large, but at low load and under shutdown conditions, it must be small enough to control the rate of heat discharge, because too high a rate would impose excessive cooling and large thermal transients. Steam generator pressure is the main temperature control parameter.

During warm-up from the cold condition, pump heat input and residual decay heat, even after a long cooldown, are sufficient to bring the system up to the hot standby condition. During shutdown, with a higher decay heat load, steam is discharged from the steam generators under controlled conditions to bring down the pressure and temperature slowly enough to avoid excessive thermal stress on large components. This steam is usually discharged to the condenser through the condenser steam discharge valves. These valves open progressively, but because the steam specific volume increases with decreasing pressure, they eventually reach their fully open condition, and the rate of cooling decreases. Beyond this point, the shutdown cooling system can control the cooling rate. During this cooldown period, one concern is delayed hydride cracking of the zirconium alloy pressure tubes at an intermediate temperature in the range of about 100°C to 200°C, and therefore the system must not be allowed to remain within this temperature range for longer than necessary.

In the event that the condensers are unavailable, steam can be discharged to the atmosphere through the steam reject valves, although this results in loss of treated water. If the steam generators are unavailable or the pressure control system faulty, the heat transport system can be cooled directly by the shutdown cooling system, which has sufficient capacity to handle the decay heat. It can also maintain sufficient flow in the fuel channels under shutdown conditions to remove the heat generated should the heat transport pumps not be available.

The inventory and flow of the heat transport system must naturally be maintained for effective removal of heat from the fuel. Possible failures of various valves which admit or release fluid to and from the system must be considered and allowance made for the system to accommodate such failures without jeopardizing safety. One situation which initially gives a wrong indication is a failed-open pressurizer steam vent valve. This represents a loss of inventory, but the decreased pressure causes boiling in the pressurizer and a consequent increase in level, which indicates excessive inventory. All losses of inventory through valves and fittings can be accommodated by the normal control systems, which either compensate for the problem or reduce reactor power.

An accidental loss of inventory or loss of coolant accident due to a system rupture requires different actions depending upon its severity. A major rupture could result in loss of coolant flow to one or more fuel channels. An emergency coolant injection system is provided to supply water to the reactor under these circumstances. This system, however, operates at a lower

pressure than that of the heat transport system, and therefore rapid depressurization is necessary. This implies reducing temperature and pressure rapidly by discharging steam from the steam generator through the steam reject valves. This procedure, known as crash cooling or crash cooldown, imposes severe thermal stress on the components, which would subsequently require intensive inspection.

The configuration of a CANDU reactor is such that all feeder pipes from the fuel channels are directed upwards to headers, which in turn are connected to the steam generators at an even higher level. Hence, any buoyancy effect due to heating or vapour generation will tend to draw coolant upwards from the reactor to the steam generators, promoting circulation by natural convection. In the event that the heat transport pumps fail, this provision for *thermosyphoning* between the reactor and steam generator is a safety feature of the reactor. The difference in elevation between the reactor and the steam generators promotes natural circulation, and the built-in inertia of the pumps, giving a rundown time of between 2 and 3 minutes, enables this circulation to be established during the initial disturbing transients. This natural circulation is much slower than the normal forced circulation provided by the heat transport system pumps and therefore can be used only under low power conditions.

A typical scenario under which thermosyphoning would be required is in the event of electrical power loss to the heat transport pumps. This would result in an immediate reactor trip. As reactor power drops to about 5% of full power within about 10 seconds (as a result of decay heat), the circulating pumps run down slowly due to built-in rotational inertia, and flow decreases progressively to the point where thermosyphoning takes over naturally and maintains flow in the same direction, but at a much reduced flow rate.

5 Steam Generators

5.1 Plant Control

As is evident from the introduction which deals with power output regulation and from Figure 1, the steam generator is a key component in satisfactory plant control. In both modes of operation, the steam generator pressure is the measured parameter, and the control system acts accordingly.

The rate of heat transfer Ω is governed by the following equation:

$$\Omega = U A \theta, \tag{7}$$

where U is the overall heat transfer coefficient, A is the surface area through which heat is transferred, and θ is the temperature difference between the fluids on each side of the heat exchange surface that exists between the primary side reactor coolant and the secondary side steam-water circuit. Because U and A do not vary much, it is evident that any change in θ will affect Ω, and vice versa. Figure 9 shows typical conditions of the reactor coolant and steam-water mixture in the steam generator under full load.

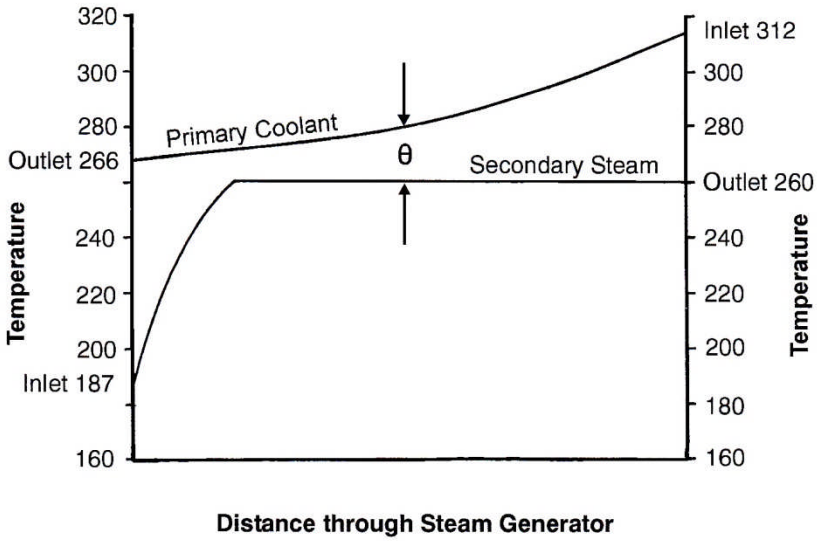

Figure 9 Steam generator temperature profile

The steam pressure affects the saturation temperature of the secondary side steam-water mixture, so the latter can be manipulated by adjusting the steam generator pressure. This in turn will affect the primary side reactor coolant temperature and is an important control parameter in reactor warm-up and cooldown procedures. Under these conditions, the heat transfer rate Ω is very low, although it may be somewhat higher following a trip from a high load condition due to a larger decay heat load.

When supplying power to the grid system under a set steam generator pressure, as load and hence Ω is increased or decreased, the primary side reactor coolant temperature will rise or fall as θ changes.

Steam generator pressure is therefore a key parameter under all operational conditions.

5.2 Steam Generator Pressure Control

Figure 2 shows the basic plant control system. It may be seen that the steam generator pressure is controlled by the boiler pressure control (BPC) system, which senses the steam generator pressure. In the reactor leading mode of operation, the BPC signals the turbine governing system to adjust the governor valves (steam flow) to the turbine to maintain the set pressure. In the turbine leading mode of operation, the BPC signals the reactor regulating system to adjust the neutron flux (heat output) of the reactor to maintain the set pressure.

Under abnormal conditions when there is a mismatch between reactor heat production and turbine power output, such as would occur immediately after an electrical load rejection or turbine trip, boiler pressure is controlled by the condenser steam discharge valves (CSDVs in Figure 16) to be described later in the text. There is also provision for steam discharge directly to the atmosphere through the main steam safety valves and the atmospheric steam discharge valves (MSSVs and ASDVs in Figure 16) to avoid excessive pressure in the steam generator.

These valves are a backup in the event that the CSDVs malfunction or are not available due to condenser restrictions.

5.3 Swelling and Shrinking

It is important to maintain an adequate water level in the steam generators to ensure proper heat transfer and heat removal capability. A further reason to maintain the water level within certain limits is to maintain efficient separation of steam from water in the cyclonic separators. Too high a level can cause flooding of the separation region, and too low a level can result in surging within that region. The water level, however, is affected by the operational conditions within the steam generator and can change markedly without any change in the total water inventory due to the phenomena of swelling and shrinking.

When steam is generated in the steam generator, vapour bubbles are formed on the surfaces of the tubes and rise with the circulating water. These vapour bubbles occupy more space than the water from which they were formed, resulting in an apparent swelling of the total water inventory in the steam generator. The effect of water displaced by the vapour bubbles is seen as an increase in level in the system. This is commonly known as *swelling*, and the converse as *shrinking*. There are steady state and transient effects with regard to swelling and shrinking.

5.3.1 Steady state swelling and shrinking

During steady state operation, the system is in a state of thermal equilibrium, that is, the rate of heat removal from the system by the turbine is equal to the rate of heat input to the system by the reactor. At zero load, no vapour bubbles are formed, and the water level is at a certain point. As load increases, vapour bubbles are formed. These displace water and cause a rise in level, as shown in Figure 10. For each load, there is an appropriate water level in the steam generator corresponding to the number of vapour bubbles in the water. At full load, the water has the highest concentration of vapour bubbles, and the water level is at its highest. This analysis assumes that there has been no attempt to control the water level and that the feed-water flow has matched the steam flow throughout the load change. On a reduction in load, the water level would return to its original value. This increase and decrease in level are respectively known as *steady state swelling* and *steady state shrinking*.

Up to this point in the analysis, it has been assumed that steam generator pressure remains constant under all conditions. This is not necessarily the case. Certain load manoeuvres on the turbine and operation of certain steam valves will cause pressure changes in the steam lines and hence in the steam generator itself. Thus, transient conditions known as *transient swelling* and *transient shrinking* arise.

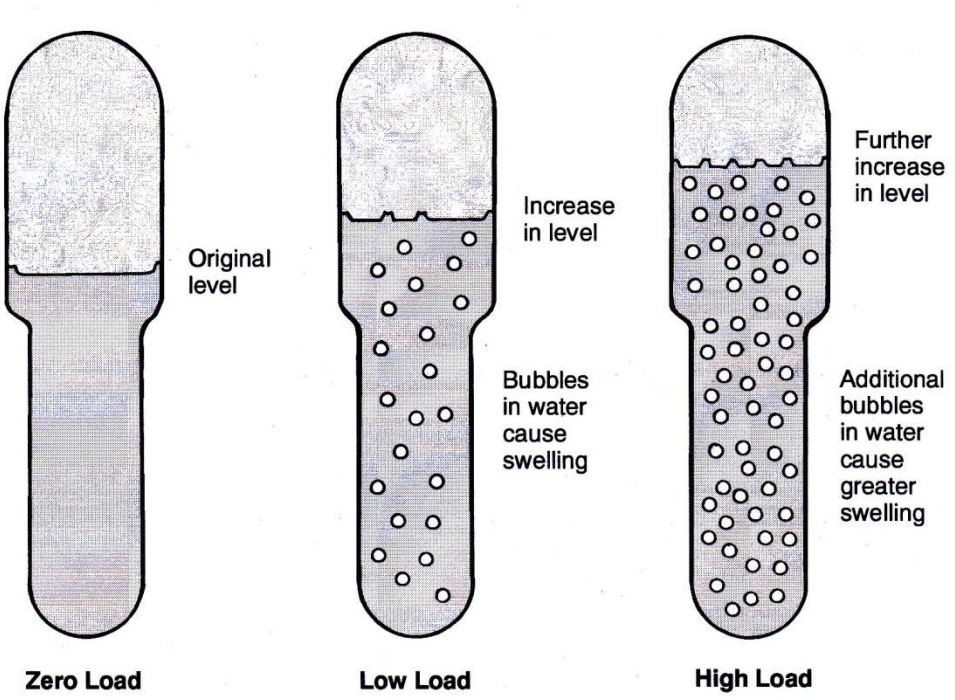

Figure 10 Steady state swelling due to different load conditions

5.3.2 Transient swelling and shrinking

At a particular turbine load there is to a certain rate of steam generation and a certain number of vapour bubbles in suspension in the water. In the event of an increase in power demand, the turbine will require more steam. The increased opening of the governor valves draws additional steam from the steam line and steam generator, causing a temporary pressure drop in the system. The drop in pressure in the steam generator allows the vapour bubbles to expand and increase their volume. In addition, because the new saturation temperature is below that of the water in the steam generator, some water flashes to steam, creating even more vapour volume. The combined effect is reflected as a swelling of the steam generator contents and a rise in water level, as shown in Figure 11. Once the reactor responds to this increased demand for power and thermal equilibrium has been restored, the pressure in the steam generator will return to its set value, and the transient swelling will subside.

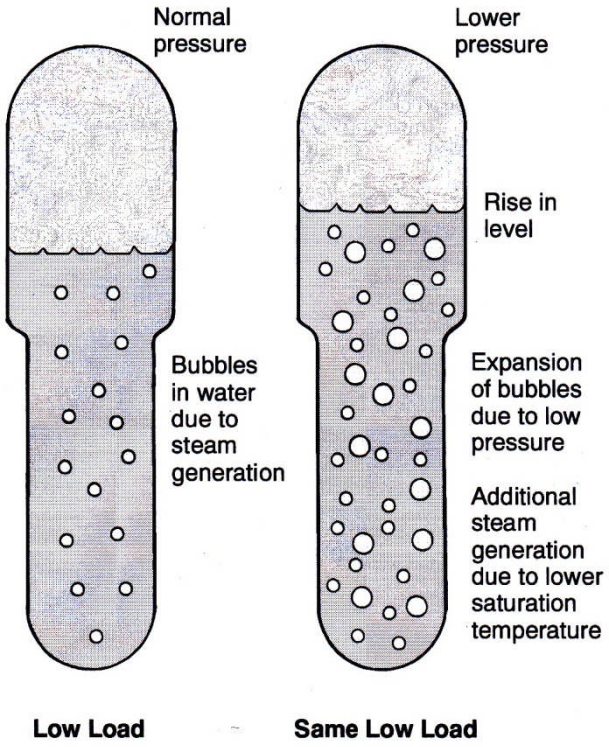

Figure 11 Transient swelling due to changing load conditions

In the event of a decrease in turbine power demand, the effect will be a temporary rise in steam generator pressure. This will be followed by compression of the vapour bubbles and shrinking of the steam generator contents until thermal equilibrium is restored.

A rapid increase in reactor power due to certain manoeuvres, such as recovering from a reactor trip to prevent poisoning out, can also produce transient swelling. The increased power increases the rate of steam generation and vapour production in the steam generator. This causes a temporary swelling effect until the turbine load is matched and thermal equilibrium restored.

A rapid decrease in reactor power, for example following a reactor trip, will reduce vapour production, causing a temporary shrinking effect until thermal equilibrium is restored.

Note that transient swelling and shrinking occur only during rapid load changes. During normal load changes, only steady state effects will be evident, and these will be related to the particular power level. Transient swelling and shrinking effects, when they occur, are superimposed on the steady state swelling and shrinking.

5.4 Steam Generator Level Control

Whenever there is a free liquid surface in a system, the system inventory must be controlled to ensure that the level remains within limits. In the steam generator, this is done by measuring the level and controlling the feedwater flow rate. Any deviation of the actual level from the desired or set level results in a correction to the flow rate.

Swelling and shrinking have an influence on level control in that, for a given water inventory in the steam generator, the level will rise and fall as the load increases or decreases. Alternatively, for a given water level, the inventory will go down or go up as the load increases or decreases. Both situations can lead to difficulties in maintaining desired conditions in the steam generator, particularly during rapid changes in load when transient swelling and shrinking effects are superimposed on the steady state effects.

Consider first the situation in which the water level is to be kept constant, as shown in Figure 12. For fixed level control, a certain margin is required to allow for transient swelling and shrinking because, during rapid load changes, the level control system cannot respond quickly enough to maintain the level. At low load, swelling will occur as load increases, and at high load, shrinking will occur as load decreases. The steam generator must therefore be large enough to accommodate these fluctuations in volume and hence in level. This is done by increasing the diameter of the upper portion and making it tall enough so that there is a margin above and below the desired water level.

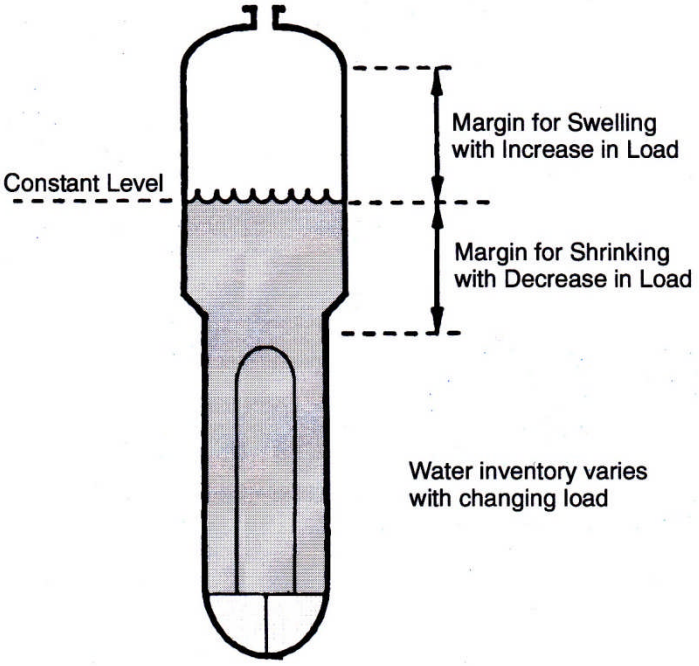

Figure 12 Constant steam generator water level

If, however, the water inventory is maintained at a fixed value and the set level is allowed to rise and fall with load, then this range of level can be used to accommodate transient swelling and shrinking partially, as shown in Figure 13. Transient swelling will occur only from a low load, and hence the required margin must be above this level. Transient shrinking likewise will occur only from a high load and requires a margin below the level at high load. If the set level at high load

is already above the set level at zero load, the margins will overlap, as shown in Figure 13. This enables the vessel to be made smaller while still providing appropriate margins for transient conditions. To achieve this, the desired or set level must be increased with load, resulting in so-called *ramped level control*. This is a more natural method of control because the total inventory remains nearly constant and the control system does not have to drive towards a new inventory every time the load changes.

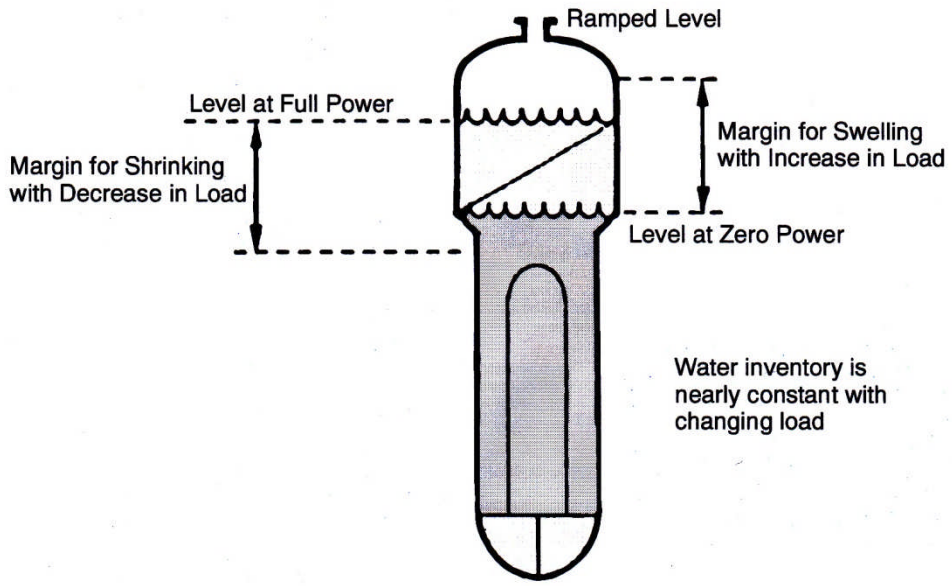

Figure 13 Ramped steam generator water level

Transient swelling and shrinking have influenced the design of level control systems in all types of steam generators and boiler drums. A sudden increase in turbine load will increase steam flow and reduce pressure in the vessel. This will result in transient swelling and a high water level. A controller that responds to water level only will reduce feedwater flow to bring down the water level just at a time when in fact more water is required. After the transient, the steam generator can be left with a severe shortage in inventory. Such a single element controller tends to respond the wrong way during transients. The problem may be overcome by using a *three element controller* which measures steam flow and feedwater flow as well as water level, as shown in Figure 14. This figure is an expansion of the boiler level control (BLC) system shown as part of the overall plant control system in Figure 14, which shows just the inputs and outputs of the boiler level control system. For the case given above, it would sense high steam flow, compare this with feedwater flow, and send a flow error signal to indicate a required increase in feedwater flow. At the same time, the transient swelling would send a level error signal to indicate that a decrease in feedwater flow was required. Initially, the two signals would cancel one another until the transient swelling had subsided, and then the feedwater regulating valve would open to balance the steam and feedwater flows to restore the water level to the setpoint. The level setpoint would in the meantime have been raised by the level control program to correspond to the new turbine load. The use of a three element level

control system in conjunction with a ramped level setpoint results in relatively smooth control of water level during all types of transients.

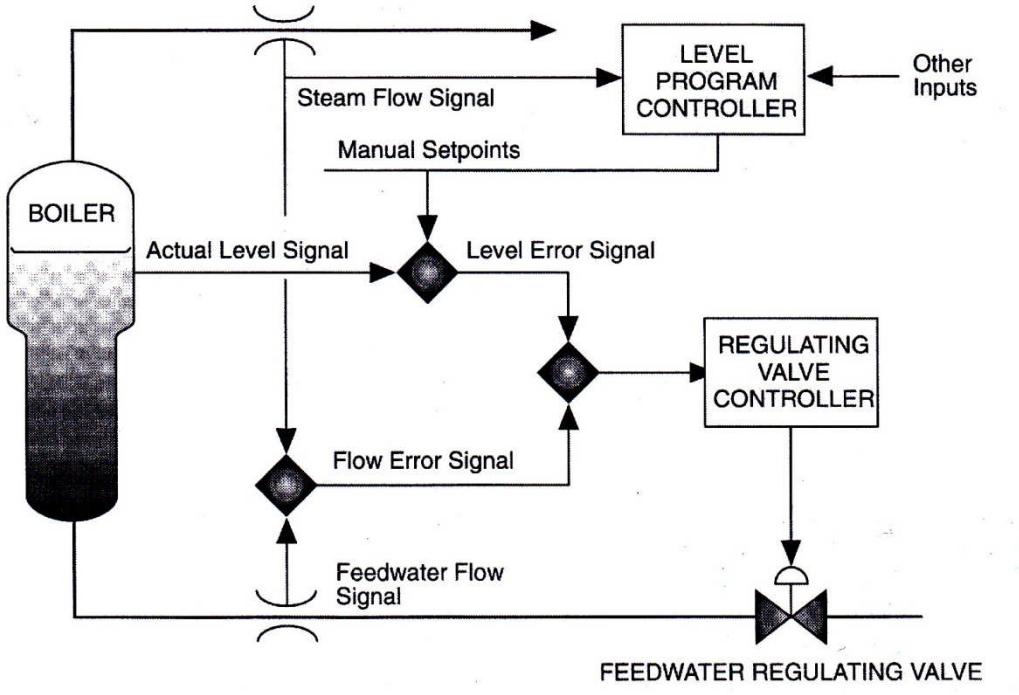

Figure 14 Three element steam generator level control system (courtesy of NB Power)

Figure 15 shows how the level setpoint is ramped up with load. The initial steep slope roughly matches the degree of steady state swelling. This is desirable because the low ratio of throughput to inventory makes the control system take longer to adjust the inventory to correct level errors. Inventory adjustment is faster at higher throughputs, and therefore the level ramp slope can be less steep, as shown in Figure 15. This lesser slope indicates that in fact the steam generator inventory is decreased as load increases in the higher load range. This is desirable with regard to the efficiency of the cyclonic steam separators, which do not operate at optimum efficiency at very high or very low water levels.

Figure 15 also shows how the low level alarm and reactor stepback as well as the SDS1 and SDS2 trips are also ramped with reactor power. The latter slopes are steep to match the degree of swelling or shrinking closely to ensure adequate inventory after a reactor trip from any power level.

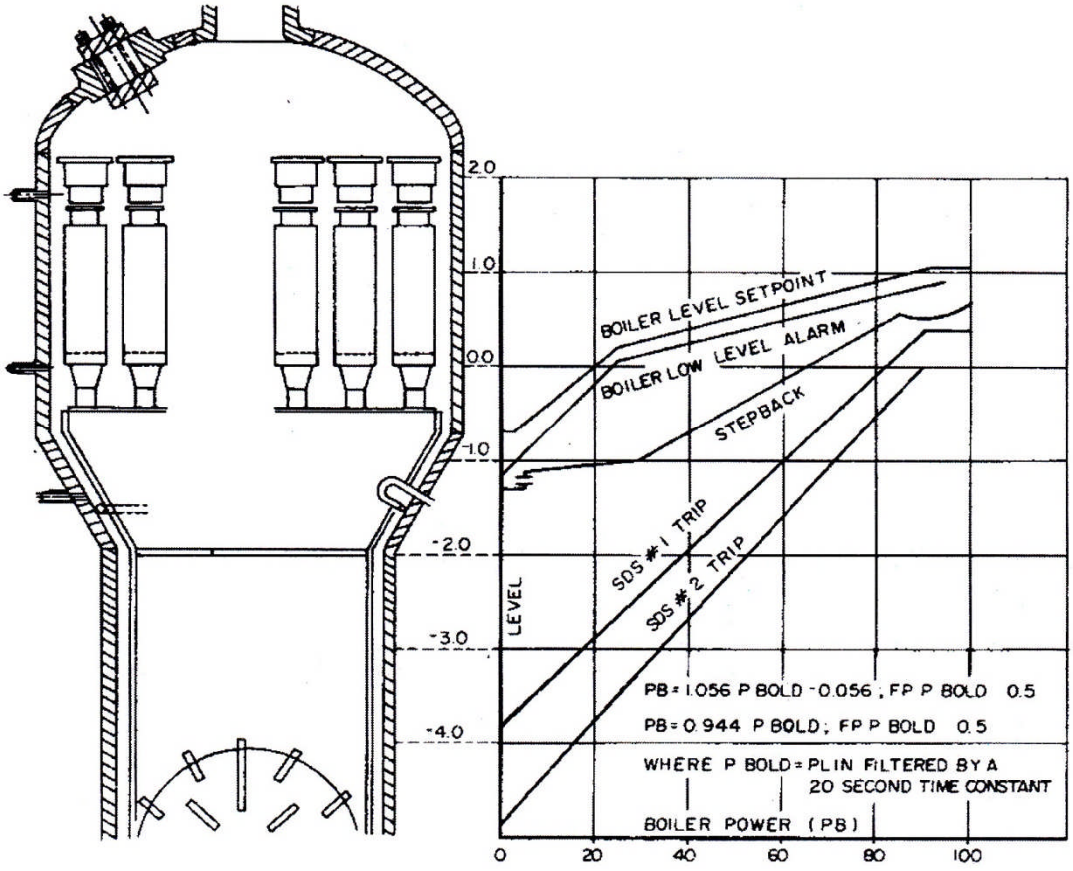

Figure 15 Steam generator level alarms and set points (courtesy of NB Power)

6 Steam System

6.1 Characteristics and Function

The main purpose of the steam system is to convey steam from the steam generators to the steam turbine. In a nuclear plant, the steam generators also serve as a heat sink for the reactor under all operating conditions, and because steam is produced, the steam system becomes the major part of the reactor heat rejection system. Provision must therefore be made to handle steam in large quantities even when not required by the steam turbine.

Steam pressure control in the steam generators is important with regard to their function as a heat sink. As steam pressure varies, so does the prevailing saturation temperature. Because the rate of heat transfer depends upon the difference in temperature between the primary coolant and secondary steam systems, a variation in steam temperature will affect the overall capacity for heat removal. Assuming that the primary coolant pressure is fixed and controlled by the pressurizer, thus limiting the maximum primary coolant temperature, an excessive steam pressure will limit the heat rejection capabilities of the steam generator. However, excessive steam pressures, which would likely arise from insufficient steam discharge, would be prevented by steam discharge through the main steam safety valves. Conversely, an excessively low steam pressure and corresponding temperature will produce excessive heat flow across the

steam generator and pull down the temperature of the reactor coolant. This is done in a controlled manner during a reactor cooldown.

For proper control of the reactor state, the steam system must therefore be able to handle the amount of steam produced under all operating conditions and to control and maintain steam generator pressure within prescribed limits. The steam system must be designed to handle decay heat generation following a reactor shutdown, and it is also desirable that it be able to maintain a high heat discharge rate to prevent xenon poisoning during a short-duration un-planned turbine shutdown.

In the turbine steam cycle, approximately one third of reactor heat is converted into electricity, with the remaining two thirds rejected to the environment through the turbine condenser. The rejection path is a convenient way of disposing of heat when the turbine is unavailable. Thus, if a turbine trip forces a short term shutdown of the turbine generator system, the reactor can be maintained at approximately two thirds power, with the excess steam production dumped to the condenser. Two thirds of full power on the reactor is sufficient to maintain the neutron flux at a high enough level to prevent poisoning out of the reactor and thus permit a restart at any time.

In the event that the turbine condenser is unavailable, an alternative steam discharge path is required. This is directly to the atmosphere, but naturally results in an enormous loss of fluid inventory from the system. For this reason, it is an undesirable mode of operation, but an essential safety feature.

Figure 16 shows a typical steam system with various control, isolation, and relief valves.

6.2 Atmospheric and Condenser Steam Discharge Valves

The atmospheric steam discharge valves (ASDVs) and condenser steam discharge valves (CSDVs) are used to control steam generator pressure rather than to protect against overpressure. For this reason, under certain conditions, the setpoint at which they operate may be lowered to avoid an excessive pressure transient when their operation is known to be inevitable. This lowering of the pressure setpoint occurs upon a turbine trip or load rejection and possible subsequent poison prevention operation. As stated earlier, the atmospheric steam discharge valves and condenser steam discharge valves divert steam from the turbine and respectively discharge excess steam to the atmosphere or dump it to the condenser to balance the heat flow from the steam generators against the heat flow into the steam generators.

Operation of the atmospheric steam discharge valves and condenser steam discharge valves may occur under operational conditions such as a controlled cooldown of the heat transport system, a turbine trip or load rejection followed by poison prevent operation, during start-up conditions when more steam is produced than is required by the turbine, or during any operation when an excess of steam is produced.

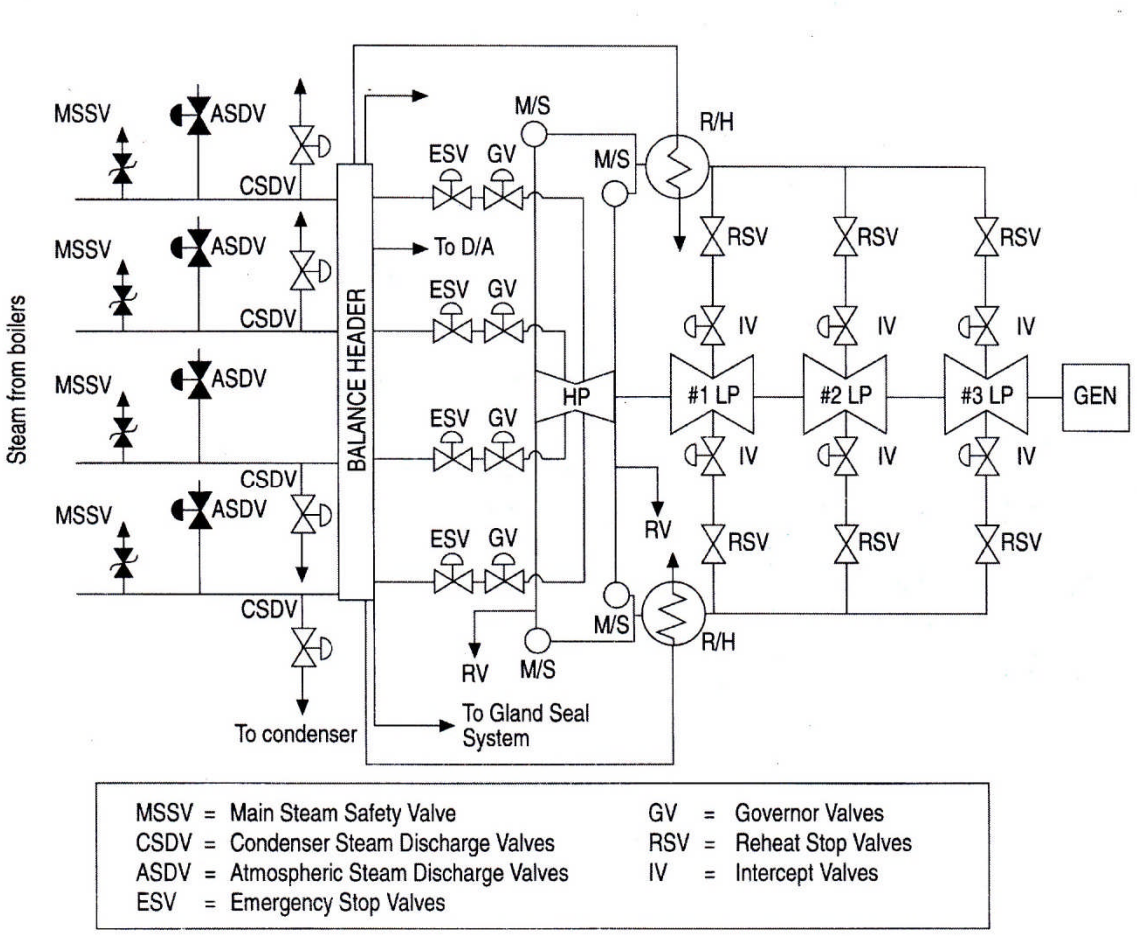

Figure 16 Main steam system (Point Lepreau) (courtesy of NB Power)

Discharge of steam to the atmosphere is of course wasteful because the loss must be made up with appropriately treated water. In any case, the total quantity of steam discharged is limited by the available make-up water capacity. If the condenser is unavailable, this becomes the major path for heat rejection on the steam side. Discharge of steam in this way should be limited to emergency or unusual circumstances.

6.3 Steam System Operation

One important aspect of the steam pipework is valve operation. In the event of a fault on the turbine, generator, or electrical system, the steam supply must be isolated very quickly, usually in a fraction of a second, and therefore the stop valves must operate quickly and reliably.

Another aspect of steam system operation is the possibility of pipe vibration due to sudden changes in steam flow or flow disturbances due to bends and fittings. Steam pipes must be suspended on flexible supports to allow for small changes in length due to thermal expansion. These would permit vibration in the absence of proper restraints and dampers, and therefore their design is an important aspect of steam pipework. Thermal effects are not confined to thermal expansion. To withstand high steam pressures, pipe walls must be thick enough to

ensure a safe working stress. When a pipe is heated from a cold condition with hot steam, the inside wall temperature rises faster than the outside wall temperature. This causes the inside of the pipe to try to expand while restrained by the outside. The inside is therefore subject to a compressive stress and the outside to a tensile stress (in the absence of stress due to internal pressure). If subjected to internal pressure at the same time, parts of the pipe may be subjected to stresses greater than their permissible working stress. The result may be deformation of or damage to the pipe. This can be avoided by limiting the heating rate of the pipe, and all systems therefore have provision for slow heating by admitting a small quantity of steam before subjecting the pipe to full steam temperature and pressure.

During steam line heating, considerable quantities of steam condense on the inside surfaces of the pipes and must be removed through drains at the low points of the system. The drains are open during pipe warming to ensure that collected water is properly drained away and are then closed during normal operation. If not properly drained, water could be entrained with the flowing steam and carried into the turbine, where it could cause severe thermal shock or impact damage to the turbine blading.

7 Main Condenser

7.1 Thermodynamics and Heat Transfer

From a thermodynamic point of view, the steam-water circuit receives heat at a high temperature in the boiler and rejects heat at a low temperature in the condenser. The greater the difference in temperature, the greater will be the drop in enthalpy and the more work produced per kilogram of steam. If the initial steam conditions remain unchanged, it is evident that a reduction in the exhaust temperature will increase the work done in the turbine. This will ultimately improve overall station efficiency. Exhaust conditions are therefore important and have a direct impact on plant performance.

Exhaust steam temperature is determined largely by cooling water temperature. The heat flow per unit time Ω from the exhaust steam to the cooling water is governed by the following equation:

$$\Omega = U A \theta, \tag{8}$$

where U is the overall heat transfer coefficient, A the surface area through which the heat is transferred, and θ the difference in temperature between the water and the steam. Once the condenser has been designed, A is fixed, and, for given flow rates on both steam and water sides, the value of U is unchanged if the condenser tubes remain clean. The amount of heat transferred is therefore proportional to θ, the difference in temperature between the steam and the water.

The cooling water, in passing through the condenser tubes, picks up heat Ω at a certain rate and increases in temperature ΔT according to the following formula:

$$\Omega = M c_p \Delta T, \tag{9}$$

where M is the mass flow rate and c_p the specific heat of water. The outlet temperature of the cooling water is generally some 10°C higher than the inlet temperature for the design mass flow

rate. Note that Ω in this formula is the same as Ω in the previous formula because all the heat transferred across the tubes is absorbed by the cooling water. The result is a temperature gradient in the water along the tubes from one end of the condenser to the other.

On the steam side, there is no temperature gradient because the saturation temperature and pressure are interdependent and the pressure everywhere in the condenser is practically the same. A temperature profile through the condenser illustrating the meaning of θ and ΔT may therefore be drawn, as shown in Figure 17. Note that θ is the average difference in temperature between the steam and the water. More correctly, it should be the log mean temperature difference, but using the average simplifies the analysis.

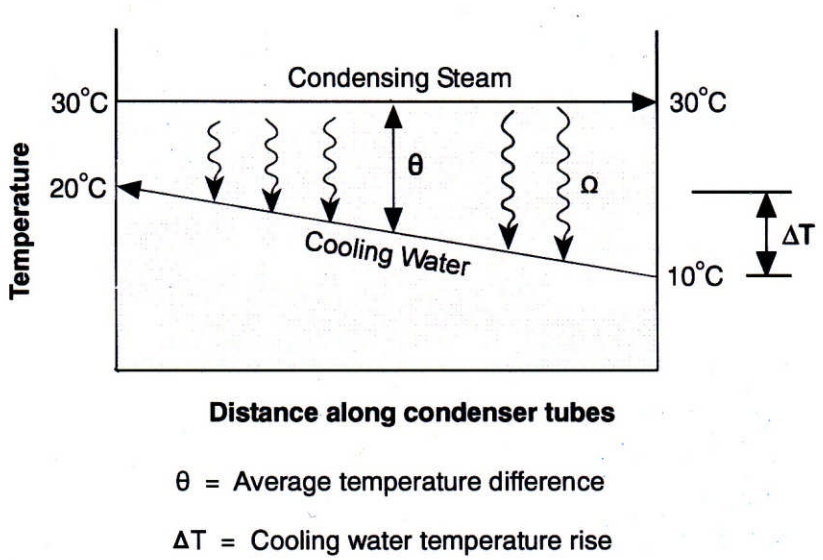

Figure 17 Condenser temperature profile

Figure 18 helps to visualize the effect of various changes. One effect is a change in inlet cooling water temperature. This has a direct and proportional effect on steam temperature. Another effect is a change in turbine load. This in turn changes the rate of heat transferred, Ω, and hence both θ and ΔT. Some simple numerical examples make it possible to verify these effects. Generally, the variation in steam temperature is proportional to load.

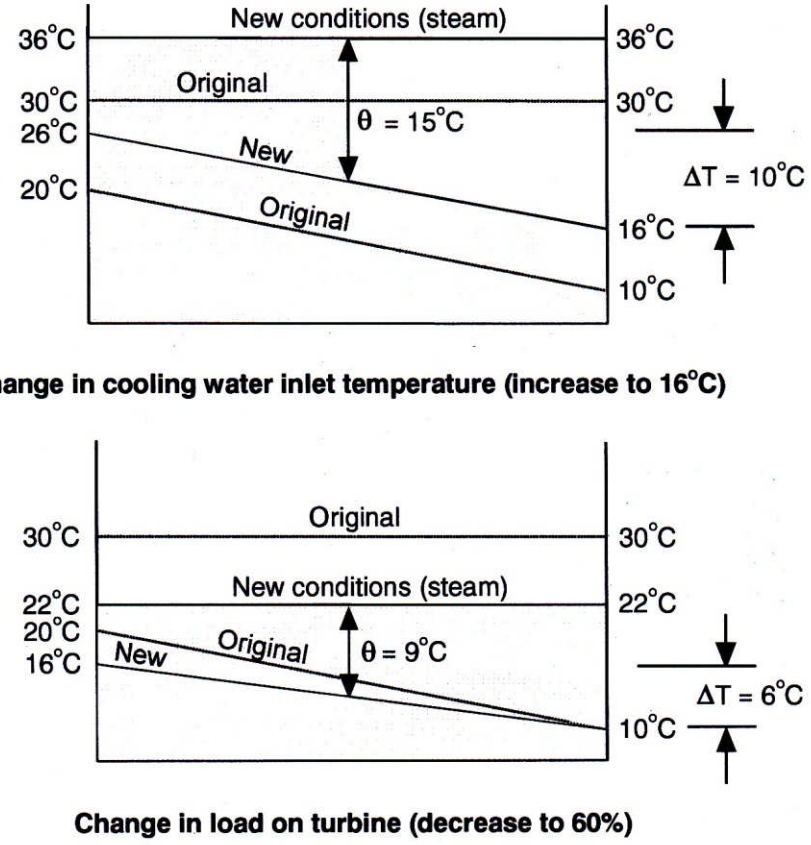

Figure 18 Changes in condenser temperature profile

The steam pressure in the condenser is governed by the temperature of condensation. The steam pressure, however, is not proportional to load because the relationship between saturation temperature and pressure is not linear, as indicated in Figure 19. By combining this variation in steam properties with the temperature variation with load, a condenser performance curve may be obtained, as shown in Figure 20. Using this figure, the pressure in the condenser can be predicted for various cooling water conditions. Superimposed on this figure are the turbine operating limits for a 900 MW nuclear unit.

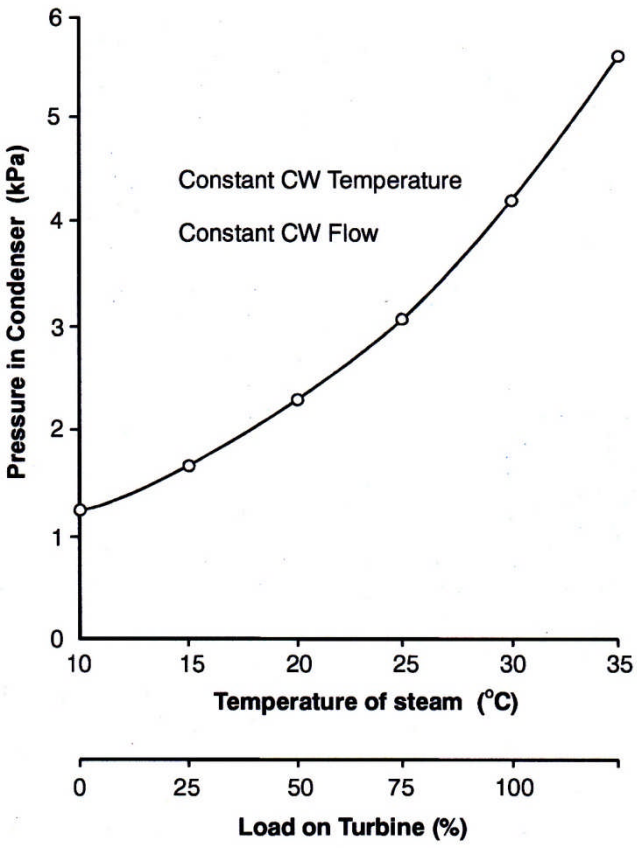

Figure 19 Variation in condenser pressure

7.2 Turbine Limitations

In most power plants, the condenser pressure is governed by the prevailing ambient temperatures. These pressures range from about 0.004 MPa to about 0.005 MPa, corresponding to a range of exhaust steam temperatures from 29°C to 33°C respectively. Steam turbines are designed for this range of backpressures and operate well within this range. If, however, operation is extended outside this range, operating problems may arise. These are primarily due to the change in the specific volume of steam as the pressure deviates from the design value. At high backpressures (high temperatures), steam specific volume decreases, so that the steam passes through the last stage blading at lower velocities. Conversely, at low backpressures (low temperatures), steam specific volume increases, so that the steam passes through the last stage blading at higher velocities. This may be confirmed by reference to the mass flow rate equation:

$$M = \rho V A = V A / v, \quad (10)$$

where the density ρ is the inverse of the specific volume v. For a given mass flow rate M passing through a fixed area A, the velocity V increases as the specific volume v increases, and vice-versa.

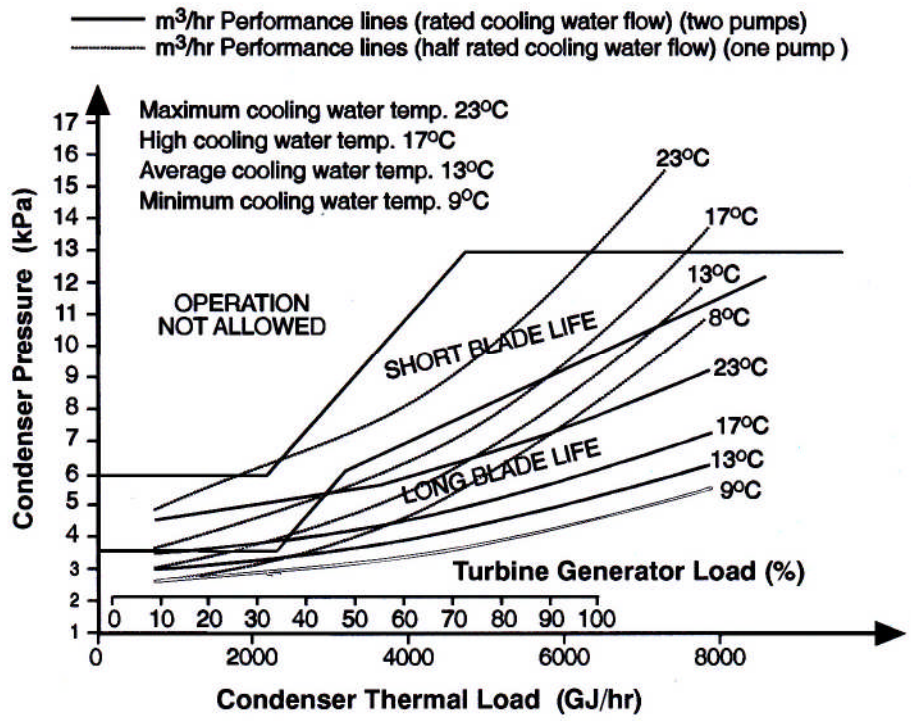

Figure 20 Condenser performance curves (adapted courtesy of Eskom)

The turbine blades are designed only for a certain velocity range. Low velocities (due to high backpressure) result in incorrect blade entry angles and buffeting of the steam on the blades. This causes vibration and high stress (due to increased density) on the turbine blades and shortens turbine life. High velocities (due to low backpressure) result in larger kinetic energy losses in the steam leaving the turbine. This ultimately limits the advantage gained in reducing the backpressure because the increased leaving losses eventually become greater than the increased work done in the blades. High velocities (due to low backpressure) may also result in choking of steam flow due to sonic conditions in the turbine blades. In any case, no additional work is obtained from the turbine once the flow has choked. Figure 20 shows the upper back-pressure limits for a typical large turbine.

7.3 Environmental Limitations

Cooling water leaving the plant carries with it some 2/3 of the heat produced by a nuclear reactor or fossil fired boiler. Most of this is rejected through the condenser and is reflected as a rise in the temperature of the condenser cooling water. The discharged warm cooling water subsequently mixes with that in the environment and may affect aquatic life. For this reason, limits may be imposed on the cooling water temperature rise ΔT and on the effluent temperature T_E.

7.4 Condenser Tube Fouling

Fouling of condenser tubes by material deposition, biological growth, or physical blockage will reduce condenser performance by reducing either the overall heat transfer coefficient U or the

effective surface area A if some tubes are completely blocked. The following equation illustrates these phenomena:

$$\Omega = U A \theta. \quad (11)$$

If either U or A is reduced, then the temperature difference θ between the steam and the cooling water will have to increase to maintain the same total heat transfer rate Ω. The net result is an increase in steam temperature and exhaust pressure and a consequent drop in the work done by the turbine and a loss in plant efficiency.

To avoid fouling, provision is made in most plants to filter the incoming water through screens and in some plants to dose the water with a biological growth inhibitor. Some fouling is inevitable, and condenser tubes must be cleaned periodically either online or offline.

7.5 Cooling Water Circuit

A typical condenser cooling water system consists of an intake structure with suitable rotating or travelling screens, two or three pumps in parallel, ducts to and from the condenser, and an outfall to discharge the water far enough from the intake to prevent external recirculation. Figure 21 shows diagrammatically a system with three pumps and screens, control valves to allow any pair of pumps to be in operation, and isolating gates at the intake and outfall to allow drainage of the system for maintenance. This system supplies three pairs of condensers which are associated with a turbine having three low pressure cylinders. Each pump can normally supply 50% of the design water flow. If only a small derating of the unit is necessary when operating on one pump, then two pumps will suffice, but if a large derating is required, a third pump is usually installed. The former case applies to plants where cooling water temperatures during the year are particularly low, whereas the latter case usually applies to plants using warmer water. The third pump also enables the plant to operate at full power when one pump or screen is out of commission for maintenance.

Generally, some control of condenser conditions is possible by operating one or two condenser cooling water pumps. A change in flow will affect exhaust steam temperature and condenser pressure, as explained in the previous section. At plants operating in areas with particularly cold cooling water, for example, if condenser pressure becomes too low and choking occurs in the turbine blades, one pump can be shut down to raise condenser pressure. This in fact is desirable because it saves auxiliary power and improves overall plant efficiency. At plants operating in areas with high cooling water temperatures, operating limitations are usually at the other end of the scale, and the maximum flow of cooling water is required to avoid excessive condenser pressures.

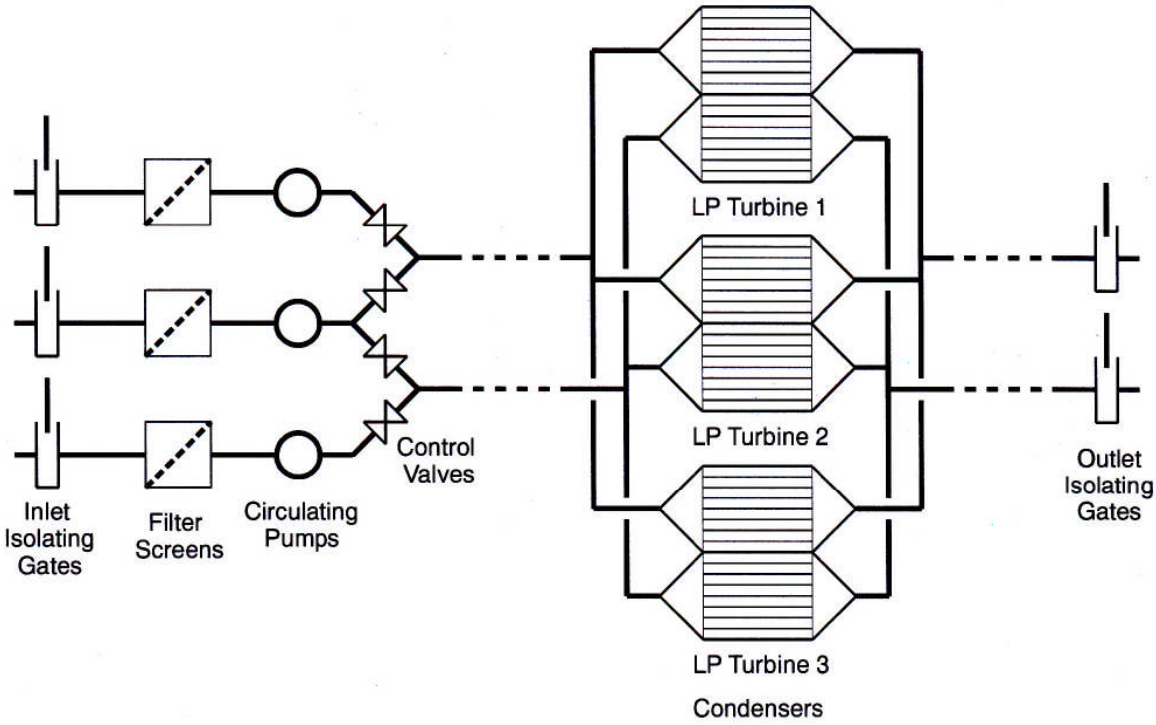

Figure 21 Typical condenser cooling water system

7.6 Flow Transients

The condenser cooling water system has very long and large pipes carrying water at high velocities. Such a large mass of moving water has an enormous amount of kinetic energy. Precautions must therefore be taken when starting and stopping this flow of water. It is important that sufficient time be allowed for the water to accelerate or decelerate before initiating another operation.

The condenser is usually the highest point in the system and operates like a syphon, as shown in Figure 22. In the event of a pump trip, the water upstream of the condenser is retarded by gravity, whereas that downstream of the condenser tends to continue flowing under the influence of gravity. This causes separation of the water column at the condenser due to elevation and pressure drop in the condenser tubes. The resulting vacuum in this part of the system will decelerate the flow downstream of the condenser and eventually suck it back towards the condenser. This reverse flow, on striking the upstream water column near the condenser, will cause severe shock and damage to the condenser or even destroy its tubes and tube plates. Such disastrous consequences can be prevented by incorporating vacuum breakers at the condenser outlet water boxes. These open under the vacuum conditions caused by water column separation and allow air to enter the system and provide an air cushion to prevent or minimize reverse flow of the downstream water column.

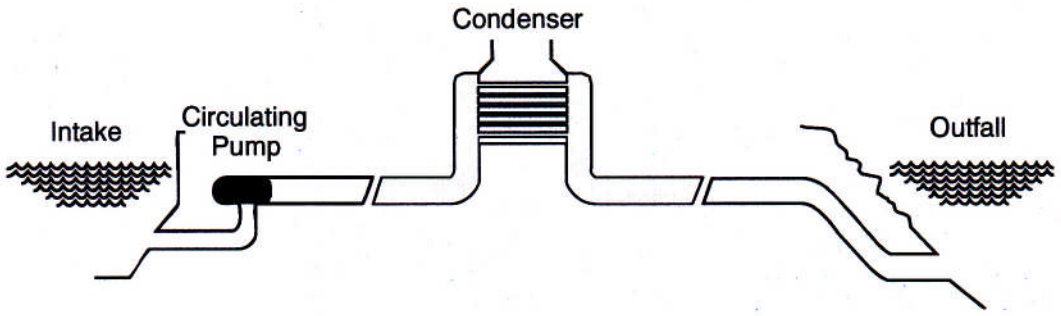

Figure 22 Simplified condenser cooling water system

During a complete system trip, priming may be lost due to admittance of air into sub-atmospheric regions. To restore priming, a vacuum priming system is connected to the condenser water boxes. This draws air out of the system before start-up and ensures that all condenser tubes are filled with water and that there are no air pockets in the water boxes which could persist during normal operation.

7.7 Variation in Condenser Vacuum

An increase in condenser pressure has obvious effects. The enthalpy drop across the turbine is reduced, and the steam flow through the last stage blades departs from the optimum, thus reducing their efficiency. Both these phenomena cause a drop in turbine output and a loss in plant efficiency.

A decrease in condenser pressure has opposite effects on turbine output. A lower pressure causes an increase in the enthalpy drop across the turbine, thus increasing the turbine output. It also causes the steam flow pattern to depart from design conditions, thus decreasing the work done by the turbine. This latter effect is smaller, so that overall there is an increase in turbine output. Other effects, however, become significant at very low pressures. Choking may occur in the last stage turbine blades, thus limiting the increase in turbine output. Even if this does not occur, the increased steam specific volume creates high steam velocities, which increase the kinetic energy loss in the exhaust steam and increase the friction loss in the steam passing through the blades. Both losses increase with the square of the velocity and rapidly overtake the gain due to increased enthalpy drop across the turbine. Beyond a certain point, therefore, the turbine suffers a net loss in output.

Increased steam moisture content at very low condenser pressures can damage the turbine, and certain limits may be imposed on operation under such conditions to avoid excessive blade erosion. Moisture in the steam also affects turbine output because the impact of the moisture drops retards the blades and slightly reduces turbine output.

The net result of these effects is shown in Figure 23. With rising pressure, turbine output decreases almost linearly, but with falling pressure, the increase in turbine output is less, and a maximum is reached. Beyond the maximum, the turbine suffers a decrease in output with falling pressure.

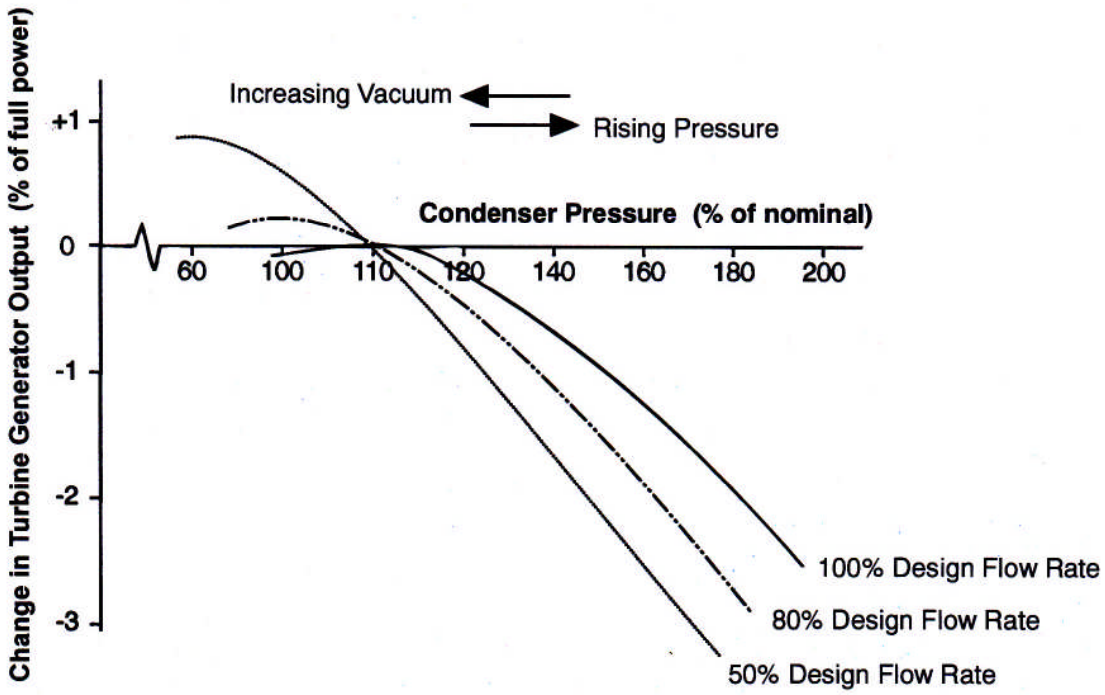

Figure 23 Effect of change in condenser pressure (courtesy of NB Power)

The effects of increased or decreased condenser pressure on the turbine have been discussed. Reference to a Mollier diagram will clarify these effects and enable them to be visualized in conjunction with load changes on the turbine. A change in condenser pressure moves the exhaust point along the turbine expansion line, whereas a change in turbine load moves the exhaust point along a constant pressure line, as shown in Figure 24. Such changes affect the temperature, density, wetness, and enthalpy of the exhaust steam and hence the turbine output.

7.8 Causes of Poor Condenser Vacuum

Cooling water temperature and turbine load variations will drive the condenser pressure one way or the other. Such changes are normal, but may cause the condenser pressure to deviate beyond normal limits. Other causes of rising pressure usually require operator intervention to restore the condition of the system. Condenser tube fouling, for example, will ultimately require that the tubes be cleaned to restore conditions. Tube flooding on the steam side, tube draining on the water side due to air accumulation at high points in the cooling water system, and accumulation of incondensable gases blanketing the tubes in the steam space are further causes of poor vacuum which require an analysis of conditions to determine the reason.

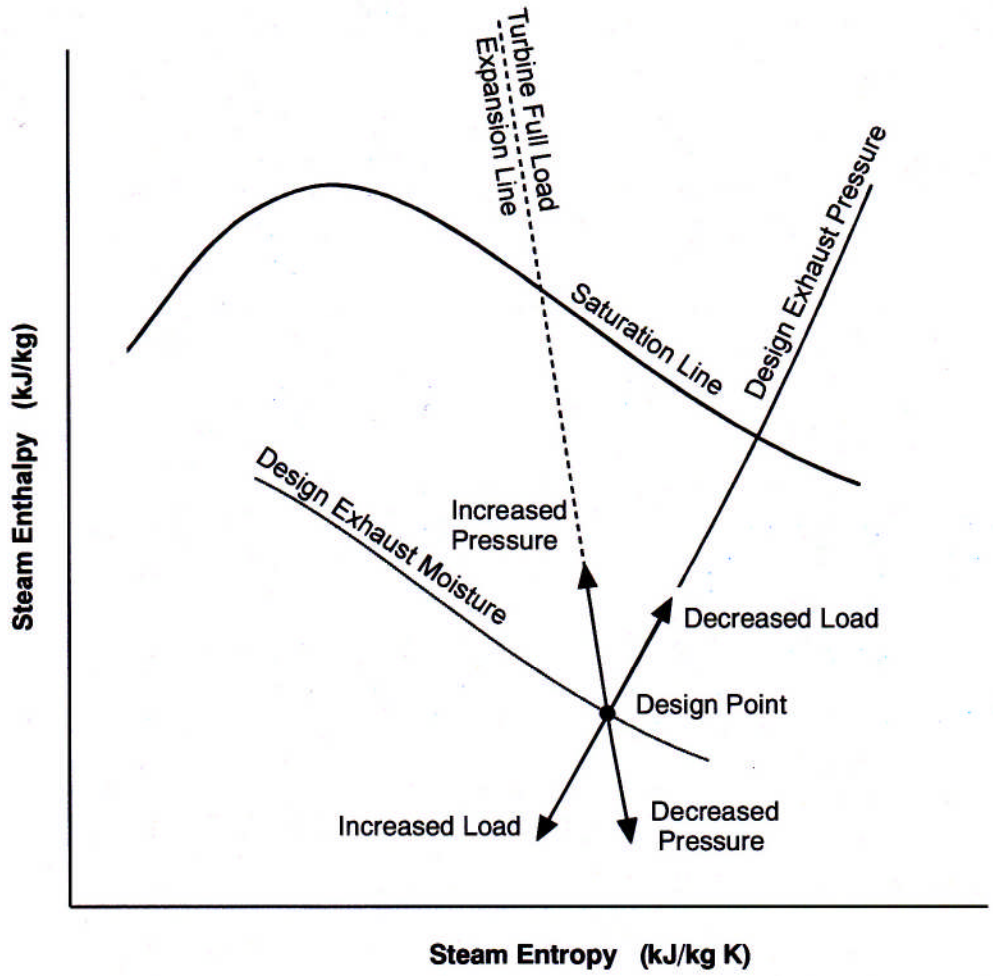

Figure 24 Effect of change in turbine load and condenser pressure

7.9 Condenser Vacuum Raising

On start-up, the entire steam space of the condenser as well as those of the turbine and the separator-reheaters must be evacuated. Initially, the extracted air is of near-atmospheric density, but eventually it is of exceedingly low density as high vacuum conditions are approached. As vacuum raising progresses, the mass flow rate drops as the density decreases. During vacuum raising, therefore, a high flow, low vacuum system is desirable, whereas under normal operating conditions, a low flow, high vacuum system is required. Note that some air leakage into the system always occurs during operation.

Air entering the condenser is carried by the steam until the steam condenses on the tubes. The air cannot flow back against other steam coming in and remains near the tubes at the end of the steam flow path. Obviously, air must be removed from these parts of the condenser. An air removal system is therefore required to pick up air from the appropriate places in the condenser tube bundle. Air extraction efficiency depends upon the partial pressures of air, p_{air}, and steam, p_{steam}, in the condenser. The total pressure, p_{total}, is the sum of these partial pressures:

$$p_{total} = p_{steam} + p_{air}. \quad (12)$$

The total pressure is the prevailing pressure in the condenser as dictated by the saturation conditions. Under these conditions, the partial pressure of air is negligible, and an air extraction system would extract mainly steam, which is not very effective. If, however, the partial pressure of air is increased such that the ratio p_{air}/p_{steam} is increased from near zero to a reasonable value, air removal effectiveness is much increased. This can be done by local cooling within the condenser. Local cooling to a lower temperature will reduce p_{steam} to a pressure corresponding to the saturation pressure at the lower temperature. Because p_{total} is dictated by the overall conditions in the condenser, the value of p_{air} must rise to make up the difference. Thus, the ratio of p_{air}/p_{steam} is increased, and the ratio of air to steam by mass in that area is also increased. The greater the mass of air in the steam, the greater will be the efficiency of air extraction.

Local cooling in the condenser is effected by shielding sections of tubes in the tube bundle from the incoming steam flow. The air extraction points are located in these zones where the partial pressure of air has been increased, as can be seen in Figure 25.

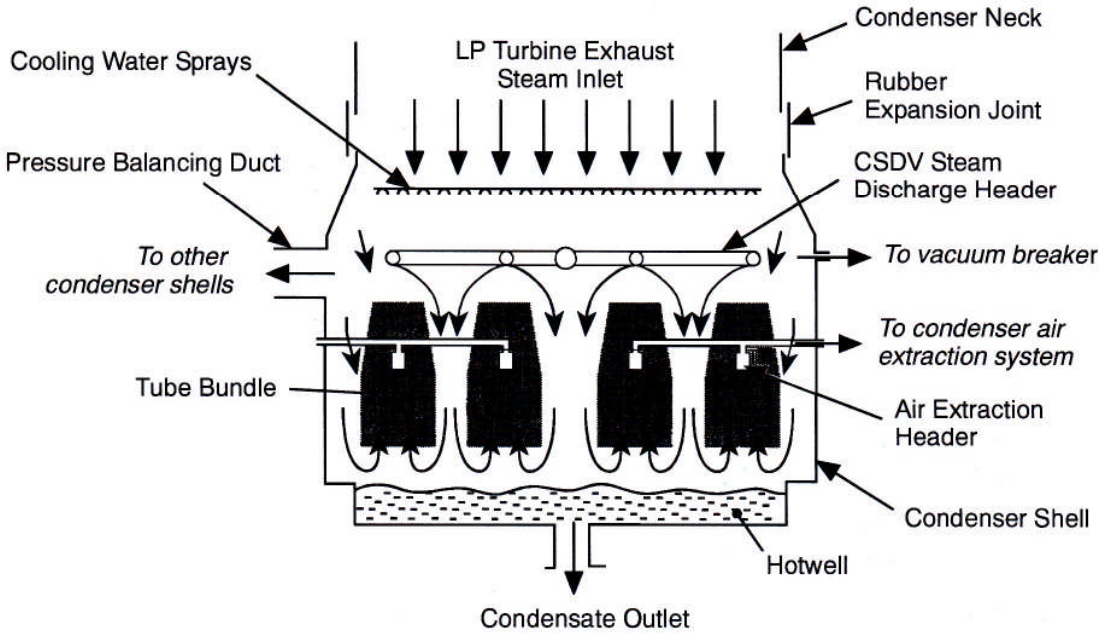

Figure 25 Condenser cross section (courtesy of NB Power)

7.10 Condenser Vacuum Breaking

Condenser vacuum can be relieved on shutdown by condenser vacuum breaking valves which allow atmospheric air to enter the condenser shell and the steam turbine. Vacuum may be broken during or after turbine rundown depending upon operating recommendations and circumstances. When the vacuum breakers are opened, condenser pressure increases rapidly. If the turbine is still rotating, the denser atmosphere around the rotor resists the turbine blade motion, causing the rotor to decelerate quickly. These retarding forces are very high and may stress the blades severely. On the other hand, the rundown time is shortened dramatically, which may be desirable in the event of a turbine fault such as a bearing failure.

8 Steam Turbine

8.1 General Operational Considerations

Steam turbines generally operate very reliably and for lengthy periods between shutdowns for major maintenance. During these periods, however, slow performance degradation may occur due to wear, erosion, or fouling of critical components. This has a slight detrimental effect on overall plant efficiency, but this translates into a loss in electrical power output and loss in revenue, which is significant in the long term, especially in a nuclear plant which normally operates at full load. To optimize plant efficiency, these performance losses must be categorized and monitored with a view to correcting deviations where possible.

Moisture in the steam in the turbine has a detrimental effect, but it tends to decrease as load is decreased. At very low loads, the exhaust steam may actually become superheated, which is even worse. Therefore, slightly wet exhaust steam provides some operating flexibility without changes in exhaust steam temperature.

Turbine back-pressure as determined by condenser conditions is also critical to turbine operation. Deviations in back-pressure affect steam flow through the last stage turbine blades, resulting in various undesirable effects. The turbine must therefore operate within prescribed back-pressure limits, and the condenser must be capable of maintaining these limits.

Steam turbines are also subject to thermal transients, which result in thermal stress and differential expansion. These require monitoring to ensure that they do not exceed prescribed limits and endanger turbine integrity.

The heavy turbine and generator rotors run at high speed, and therefore any slight mass imbalance or shaft bending will cause serious and potentially damaging vibration. When a turbine has been shut down and stationary for a long period, the shafts begin to sag. This *sagging* is in addition to the natural deflection under gravity and is the beginning of creep, but is reversible by slowly rotating the shaft and reversing the sag. This takes time, and, until reversed, the sag bows the shaft, creating an imbalance. When a hot turbine is shut down after a period of operation and comes to rest, the natural cooling process results in a temperature difference between the top and bottom of the casing and rotor. The cooler bottom part of the rotor shrinks slightly relative to the top, bowing the shaft upwards. This *hogging* also creates an imbalance should the turbine be restarted and may in an extreme case jam the rotor against the casing. This can be avoided by putting the turbine onto turning gear and turning the rotor until uniformly cool.

Another critical aspect of turbine operation is governing to maintain speed and load. The turbine is the link between the energy input as steam and the energy output as electricity. Any mismatch between these will cause the turbine to accelerate or decelerate. Uncontrolled acceleration is very dangerous, and precautions must be taken to ensure rapid closure of the steam valves in the event of disconnection from the electrical grid system.

8.2 Turbine Start-up

A simplified turbine start-up procedure is shown in Figure 26. Before turbine runup, several lengthy processes are required, but these can be done concurrently to some degree. The first key operation is to start the lubrication system and to put the turbine onto turning gear to roll out any sag and to ensure uniform heating once steam is admitted. Before any heat can be received, the condensate system and feedwater system must be put into service, followed by the condenser cooling water system to remove reject heat. When steam is available, warming of the steam lines can commence, and the turbine gland sealing system can be put into service. With sealing steam in place, vacuum raising can commence. When sufficient vacuum is available, steam can be admitted to the turbine to commence the runup. The turbine is normally held at a low speed while shaft eccentricity, bearing vibration, etc. are checked and then accelerated to pass quickly through the critical rotor speeds so as not to excite excessive rotor vibration. Full speed must, however, not be reached until full vacuum is available to avoid putting excessive stress on the long low pressure turbine blades due to windage. When at full speed, connection to the grid system can be requested. For satisfactory synchronization, the generator voltage must be the same as that of the grid, the generator frequency, determined by the turbine speed, must be equal to the grid frequency, and the generator phase angle must match the grid phase angle. If synchronization is done manually, it is better to err on the side of the turbine being slightly fast so that it picks up some load immediately as the turbine speed drops to match that of the grid. This avoids an unnecessary reverse torque on the turbine generator shafts, and a small load should immediately be applied to prevent fluctuating torque. Once synchronized, the turbine can be loaded at a rate dependent upon the cylinder temperatures. The initial rate is usually slow to allow metal temperatures to rise slowly to minimize thermal stress due to steep temperature gradients in the cylinders and rotors. The reheaters are valved in above about 25% load, and the loading rate can usually be increased after that, provided that various checks verify that key parameters such as differential expansions are within limits.

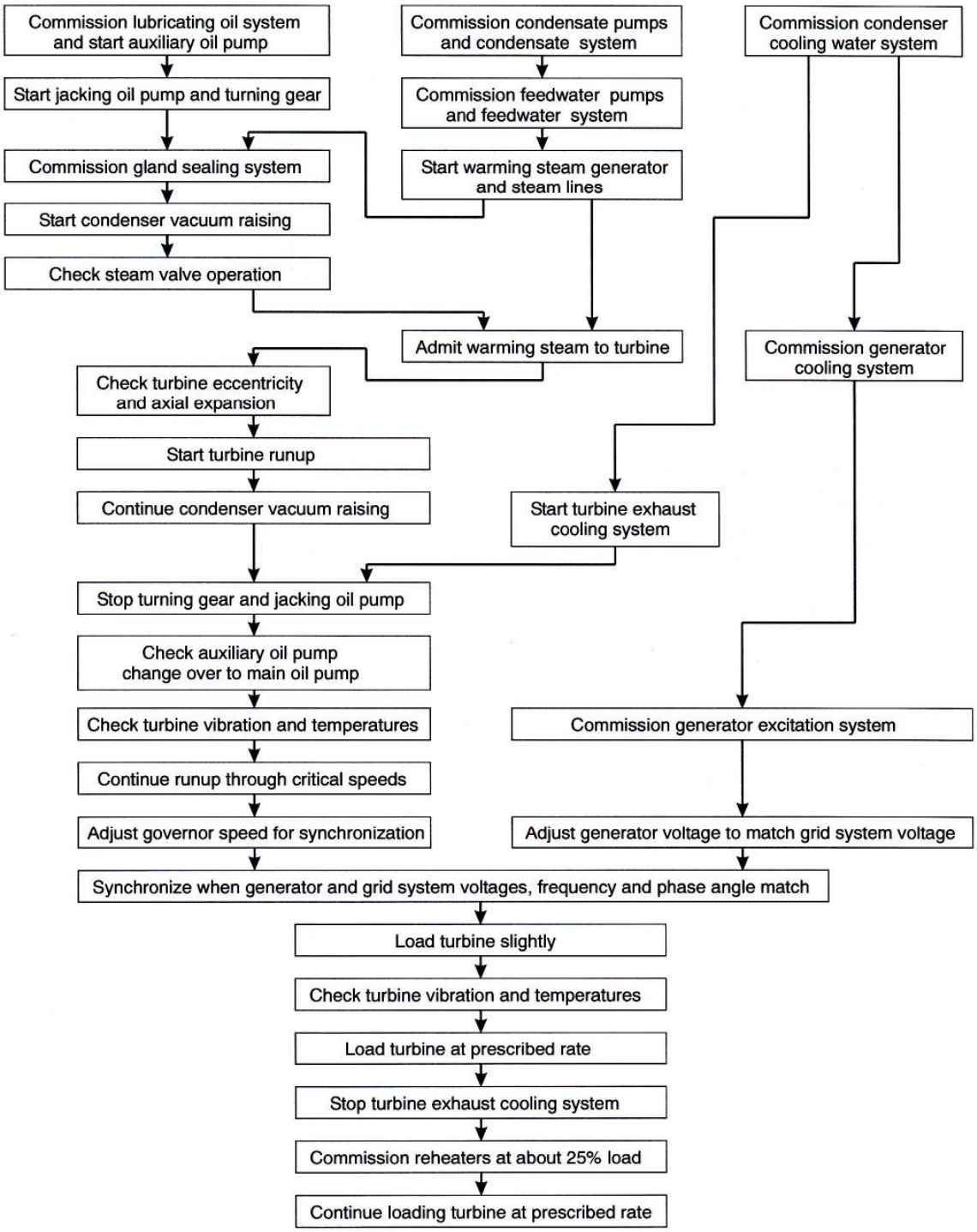

Figure 26 Major activities during start-up and loading

8.3 Turbine Losses

Fluid friction is the most significant of all turbine losses. High velocity steam encounters surface friction and turbulence in passing through the turbine blading. Fluid friction losses amount to about 10% of the total energy input to the turbine. This is a major loss factor which is ultimately reflected in turbine internal efficiency.

Moisture loss occurs when condensed moisture passes through the turbine blades and the moisture drops impinge upon the moving blades. This retards the moving blades, reducing turbine output and efficiency. There is a loss in stage efficiency of about 1% for each 1% moisture content of steam at that point in the machine.

The residual kinetic energy in the steam leaving each stage is usually recovered in the following stage. At the last stage, however, the specific volume of the steam is very large, and to obtain manageable flow areas at the turbine exit, high velocities must be tolerated. This results in a high residual kinetic energy and a significant leaving loss in the order of 2% to 3% of total energy input.

Heat losses occur directly from the turbine. This results in a small overall loss due to convection and radiation to the surrounding atmosphere.

Bearing losses arise due to oil friction in the bearings. Some auxiliaries such as the main oil pump are usually directly driven from the turbine shaft and add to these losses.

Windage loss occurs in the generator where fans mounted directly on the generator rotor circulate the hydrogen coolant within the generator housing.

Some electrical losses occur within the generator windings, but are quite small.

8.4 Turbine Load Variation

As the load on a turbine varies, the pressure profile throughout the turbine changes, as shown in Figure 27. At any one point along the steam flow path, the pressure varies according to steam flow in a linear manner, as shown in Figure 28. This has been demonstrated in practice on a number of machines and is an accepted result. At different points in the turbine, a similar relationship is found. At zero load, however, some steam flow is required to drive the turbine against bearing friction and generator windage. Turbine load (generator output) is therefore not quite proportional to steam flow. The overall result can be summarized as in Figure 29, which shows steam pressure, steam flow, and turbine load or output all on the same plot. Note that in many problems, the zero load steam flow is not known. In such cases, this zero load steam flow may be assumed to be small and the overall steam flow taken to be proportional to turbine load. Note that the value for zero load steam flow is much exaggerated in the diagram.

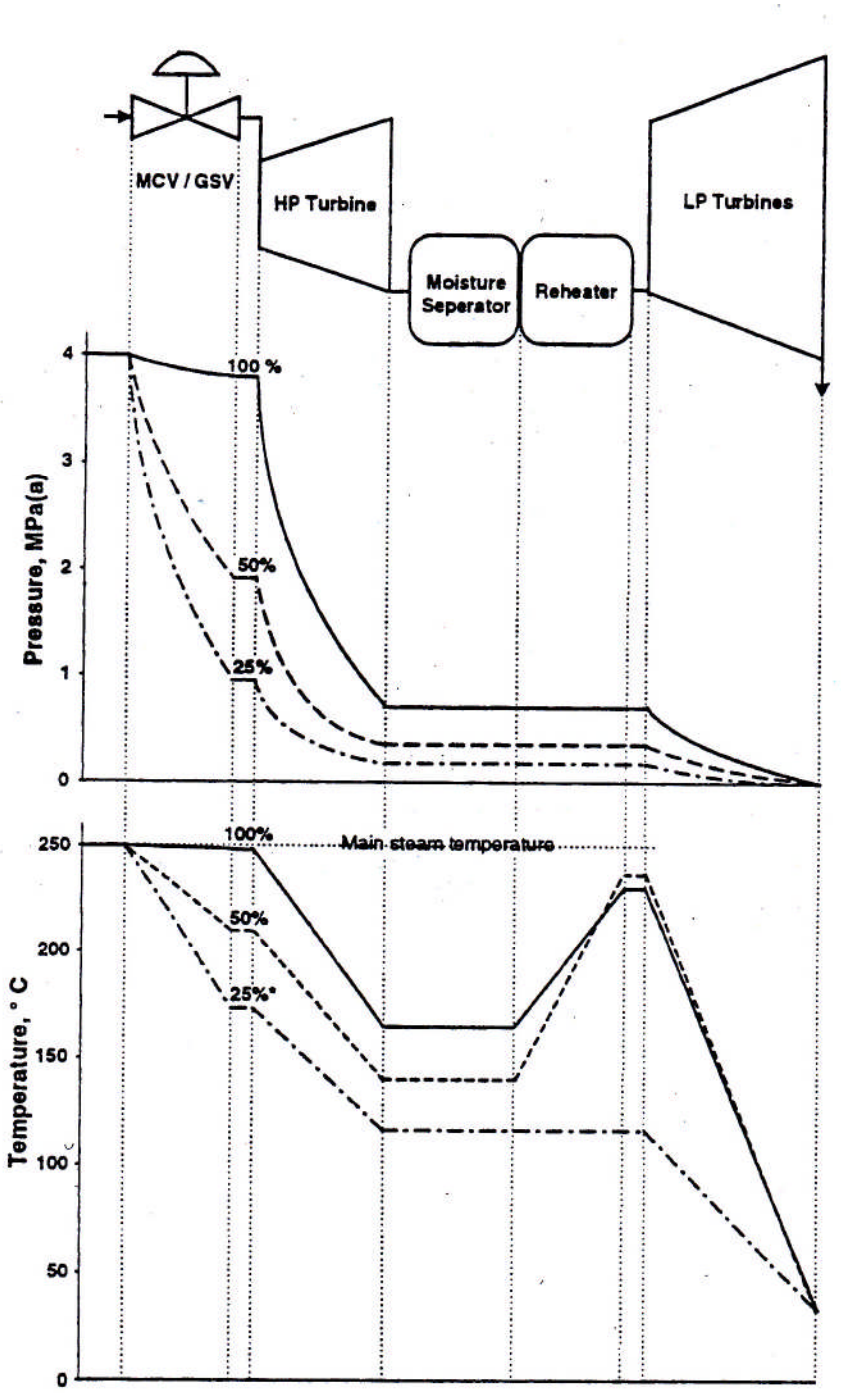

Figure 27 Steam pressure variation through the turbine (courtesy of NB Power)

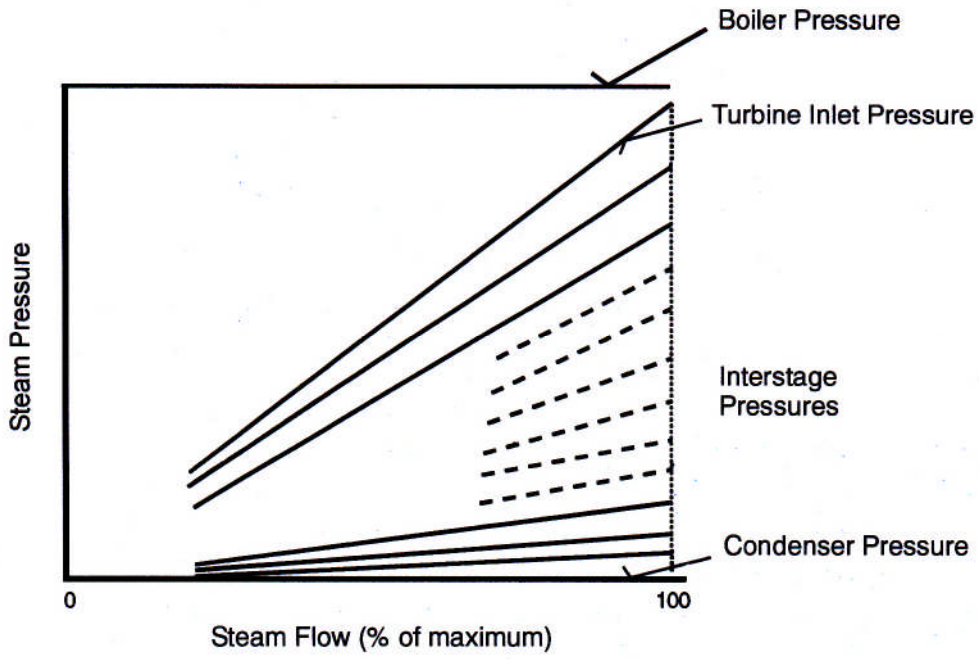

Figure 28 Steam pressure variation with load change

Figure 29 Steam pressure versus steam flow and turbine load

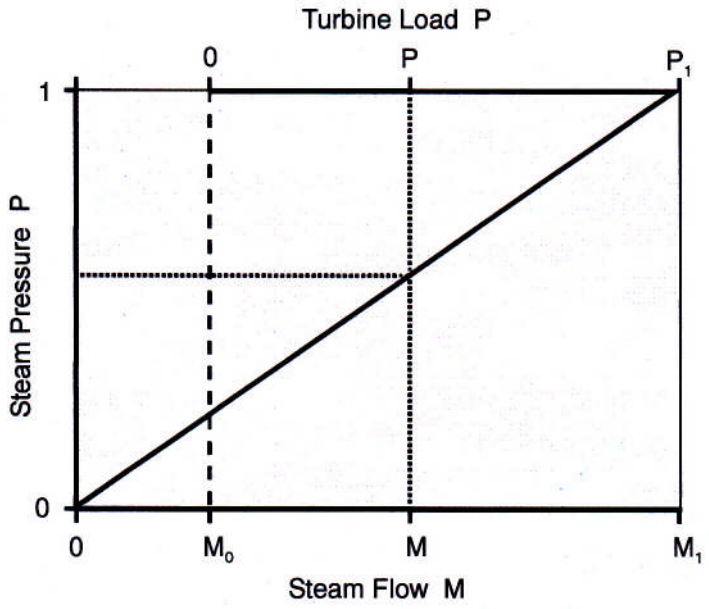

The Mollier diagram is an ideal way to represent varying load conditions. Figure 30 shows the changes in the turbine expansion line for different loads on a large nuclear unit. Some interesting characteristics are apparent in this figure. Because reheating is effected by live steam, the temperature of the reheated steam remains essentially the same with decreasing load. In practice, the reheat temperature actually rises with decreasing flow because the temperature difference for heat transfer becomes less with reduced heat flow. At the low pressure turbine exhaust, the moisture becomes less with reducing load, and eventually the exhaust steam

actually becomes superheated. To avoid this situation, the reheating steam flow is throttled at very low loads to reduce steam temperatures in the low pressure turbine. Even with no reheat, at very low loads, the decrease in internal efficiency due to incorrect steam flow in the blades causes the exhaust temperature to rise to excessive values. This is aggravated by possible recirculation of exhaust steam within the turbine blading.

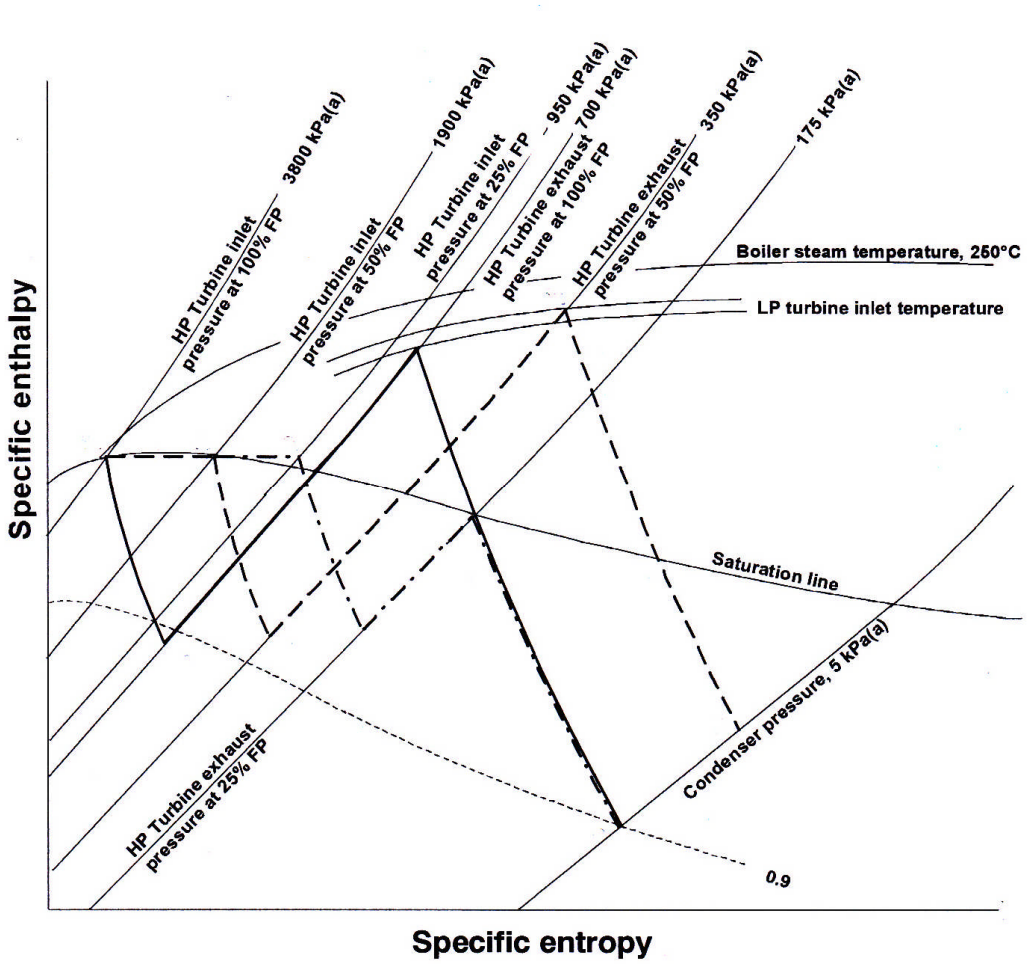

Figure 30 Partial load turbine expansion lines (courtesy of NB Power)

During partial load operation, the incoming steam is throttled to reduce its pressure. As a consequence, the specific volume of the steam increases. Except in the high pressure areas of the Mollier diagram, the constant temperature lines in the superheated regions are nearly horizontal. This means that the throttling process, which is at constant enthalpy, is also almost at constant temperature. Therefore, the expansion index n in pv^n equals a constant is approximately unity. The change in specific steam volume therefore almost exactly offsets the change in pressure. Flow velocities in the superheated region of the turbine are therefore practically constant over a wide range of loads. This means that the velocity triangles are largely unaffected and that the steam continues to pass through the blades at the correct angle. This is fortuitous and promotes high efficiency. In contrast, hydro turbines operating with incompressible water suffer marked losses in efficiency at low loads due to off-design flow directions.

As the steam pressure becomes less in the low pressure parts of the turbine, this no longer applies because the turbine exhausts against a positive (even though very low) absolute pressure. The absolute pressures around the last stages are therefore not quite proportional to steam flow, and the pressure ratio across the last stages (especially the last) drops. This results in reduced steam velocity entering the moving blades.

In large modern turbines, the changes in the velocity diagram at the last stage can be quite significant, as illustrated in Figure 31. Here, the velocity diagram has been redrawn to show the whirl velocity V_W. As long as the whirl velocity is positive, that is, Y is on the right hand side, the steam does work on the blade. At very low loads, the steam incoming velocity V_{S1} is reduced, and at the blade tip, the whirl velocity becomes negative, that is, Y is on the left hand side, indicating that the blade now does work on the steam. Observation of the blade profile at the tip indicates that, once V_{S1} becomes substantially less than V_B, the blades will act as a fan and will drive the steam onwards. This fanning action at low steam flows occurs towards the tips of the blades, that is, around the outer periphery of the turbine rotor. When the fanning action exceeds the normal steam flow, a recirculation in the last stage will be set up, with steam returning through the blades near their roots where the impulse type profile simply plows through the steam at low loads. Such a recirculation is shown in Figure 32. Once set up, this recirculation results in excessive steam heating by friction and turbulence. If no corrective action is taken, steam temperatures can become so high as to cause thermal damage to the turbine.

Two types of corrective action are possible, assuming that the turbine is obliged to continue operation at this abnormally low load. One is simply to displace the recirculating hot steam with a small flow of "cooling" steam through the turbine. The other is to spray cooling water into the recirculating steam at the turbine exhaust so as to reduce its degree of superheat before it circulates back into the turbine blades. Large nuclear units may have to operate at very low loads for extended periods during operating manoeuvres on the reactor. These turbines are usually fitted with exhaust hood sprays or a cooling steam system. Furthermore, a nuclear reactor such as a CANDU may trip inadvertently or be shut down for a quick repair. In this case, it would have to be brought back on load within about 40 minutes to avoid suffering long term (40 hour) unavailability due to buildup of neutron absorbing xenon in the reactor core while off load. During such events, it is desirable to maintain the turbine at full speed and ready to be loaded up once reactor power has been restored. This may be accomplished by keeping the generator connected to the grid system and allowing it to drive the turbine. Such operation is known as *motoring*. When motoring, recirculation of steam in the turbine blades is most severe, and cooling steam and water sprays are required to maintain the temperature of the low pressure turbine blades within limits.

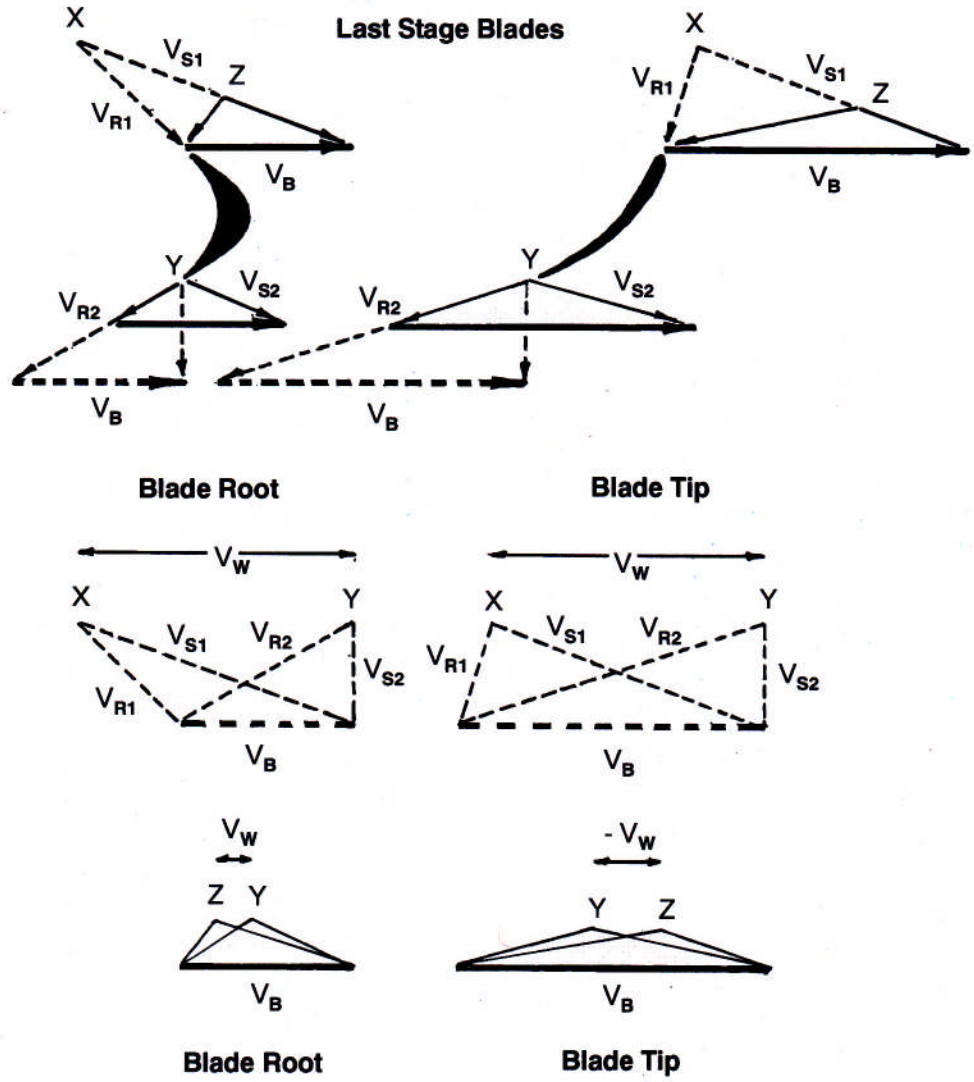

Figure 31 Change in whirl velocity at low loads

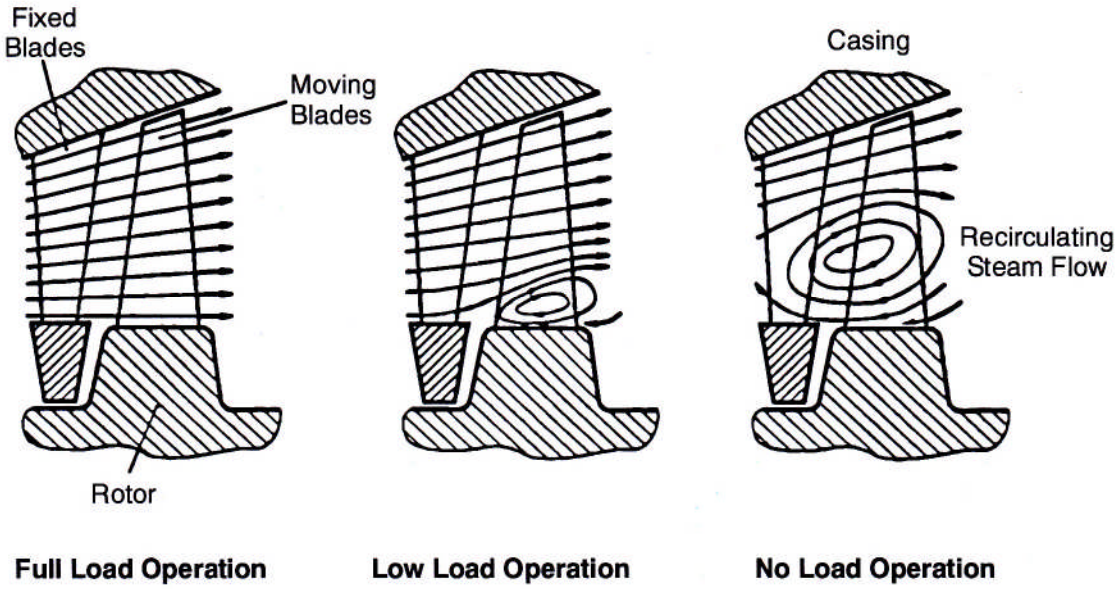

Figure 32 Recirculation of steam at low loads (courtesy of NB Power)

During turbine operation, it is important to minimize thermal transients and to avoid damaging combinations of thermal stress and mechanical stress. For this reason, turbines are warmed thoroughly before being run up to full speed, and, during operation, major load changes are made progressively and slowly so that the turbine casing and rotor can adapt to the changes in internal steam temperatures. Small load changes within certain limits can naturally be made quickly to enable the turbine to follow system load requirements or to control frequency. The turbine may, of course, suffer a trip and immediate initiation of the automatic shutdown sequence. This does not necessarily impose a severe thermal transient because steam flow through the turbine is stopped and it remains hot for an extended period. A restart during this period must, however, be accompanied by rapid loading so as to minimize the period of admission of cooler throttled steam to the turbine casings under low load conditions.

All start-ups, shutdowns, and major load changes subject the turbine to some thermal stress. Such operations reduce the ultimate life of various turbine components and, depending upon their severity, may be considered as equivalent to a certain number of normal steady state running hours on the turbine.

8.5 Differential Expansion

When turbine casings and rotors are heated, they expand generally in all directions. During this expansion, the centre lines of both must remain coincident while the casings and rotors expand in an axial direction, as shown in Figure 33.

The rotor, having less mass than the casing and being surrounded by steam, tends to expand more rapidly than the casing, leading to so-called *differential expansion* between them. This is apparent mainly in the axial direction and blading, and seals must be designed to accommodate this relative axial movement as the temperature changes. Furthermore, each cylinder casing is separately supported on its foundations, but the rotors of all the cylinders are linked together to form a continuous shaft. There is one thrust bearing to locate the shaft in an axial direction, usually near the high pressure cylinder. From this point, the expansion of each rotor contributes to the total expansion, so that there is an additional differential expansion which is cumulative and greatest at the cylinder furthest from the thrust bearings. Such differential expansion must be monitored during warm-up and loading to ensure that there is no risk of contact between the fixed and moving parts.

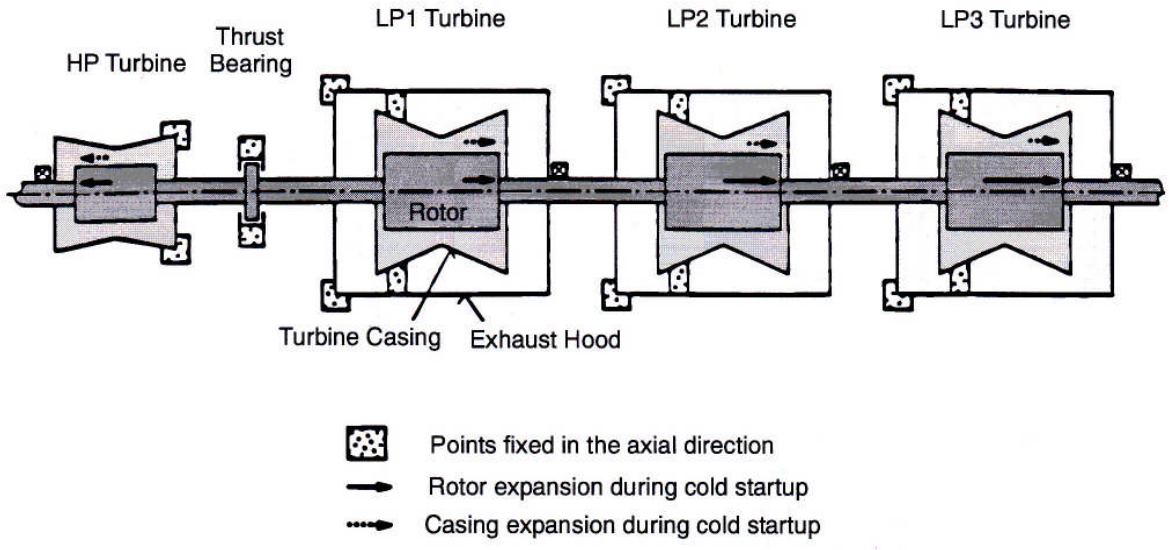

Figure 33 Differential axial expansion of turbine rotors and casings

(courtesy of NB Power)

8.6 Turbine Governing

The turbine governor valves control the flow of steam to the turbine and, as such, are part of the main steam system. As the governor valves are opened from the closed position during start-up, the energy input to the turbine increases. The turbine then accelerates until the energy losses due to windage and friction balance the energy input. Further admission of steam increases the speed of the turbine. Turbine speed is therefore dependent upon governor valve position, and the governor acts to control turbine speed. In this way, the full speed zero load condition can be maintained.

Once the turbine generator has been synchronized to the electrical grid system, the turbine speed is locked to the grid frequency. Additional opening of the governor valves increases the energy input to the turbine, but the speed can no longer increase. At a constant speed, the windage and friction losses remain constant, and therefore the excess energy appears as generator output. Further admission of steam increases the load on the generator. Turbine

load is therefore dependent upon governor valve position, and the governor acts to control turbine generator load.

The main characteristic of the governor is the *speed droop*. This indicates the amount that the speed will change as the load is varied. A speed droop of 5% indicates that, if the speed is 100% at zero load, it will be 95% at full load. Such a change would not normally be permitted, and the speed would be progressively reset as the load increased. The speed droop, however, determines how turbines operating in parallel will maintain stability and share load. With turbines operating in parallel, the speeds must all be the same and match the system frequency. Then, for a given change in frequency, a turbine with a smaller speed droop will change its load by a greater amount.

8.7 Turbine Responses

In the event of various transients and plant upsets, the turbine will respond in different ways to minimize risk to the plant and to facilitate return to normal operating conditions. The following plant upsets are considered:

Reactor trip
Turbine trip
Electrical load rejection.

For each of these, the main steam system valves must operate in an appropriate way to protect the turbine.

Once the generator has been disconnected from the grid system, any mismatch between power input to the turbine and electrical output from the generator will result in a change in speed. In a modern steam turbine, the mechanical inertia of the rotors is relatively small compared with its rated power output. This means that it can accelerate very quickly under an excessive mismatch between power input and power output. Overspeeding is potentially the most dangerous condition that can occur on a turbine because it can have the most disastrous consequences. Past experience has shown that a turbine will literally explode under very high overspeed conditions. The overspeed accident of the 600 MW Unit 4 at Duvha Power Station in South Africa in February 2011 is a stark reminder of this.

8.8 Reactor Trip

In the event of a reactor trip in a nuclear unit, the mismatch in power input to and power output from the steam generators will result in a rapid drop in steam generator pressure and fast cooling of the primary heat transport system. This fast cooling will cause shrinking and reduce pressure in the secondary steam system.

To avoid these adverse consequences, turbine steam flow must be quickly reduced by closing the governor valves. Ideally, steam flow to the turbine should be reduced at the same rate as the reduction in steam generator steam production. The drop in steam generator output slightly lags the drop in reactor fission power because of the heat stored in the primary heat transport fluid and because of decay heat generated in the nuclear reactor.

To ensure a proper response, the boiler pressure control system ensures that the governor valve will be closed progressively and power input from the steam generators to the turbine reduced

to zero while excess steam is diverted to the condenser through the condenser steam discharge valves. When the turbine power falls below that required to overcome windage and friction, the generator will draw the necessary power from the grid system. Under these conditions, the turbine generator is driven at synchronous speed by the electrical grid and is said to be in *motoring* mode. A quick recovery from motoring mode is possible so that, once the reactor trip has been cleared, the unit can be brought up to full power quickly to minimize the effect of the xenon transient. For this reason, other valves in the system, such as the intercept valves, may be automatically positioned in readiness for a turbine restart. The advantage of the motoring mode is to avoid disconnecting the turbine from the grid system, thereby eliminating partial turbine rundown and runup as well as resynchronization, all of which require careful manoeuvring.

Once tripped, however, a reactor requires checking to verify the cause of tripping and careful restart procedures, all of which take time. Therefore, motoring may not be a practical option, and the turbine may need to be tripped automatically in response to a reactor trip.

8.9 Turbine Trip

The purpose of a turbine trip is to protect the turbine in the event of adverse operating circumstances or component malfunction or failure. A turbine trip should be initiated whenever continued operation poses a risk of damage to the turbine.

When a turbine trip occurs, power input and power output must be stopped. On the generator side, power output is stopped virtually instantaneously as the generator circuit breaker opens. On the turbine side, however, the steam valves take a finite time to close. During this brief period, some steam passes through the valves, carrying with it substantial energy. This steam, along with the steam already trapped within the turbine, expands and produces a transient power input to the turbine. The mismatch between power input and power output results in a temporary rise in speed until the effects of windage and friction cause the speed to fall.

This is known as a *non-sequential trip*. The temporary speed rise can be avoided if the trip on the generator side is slightly delayed to balance the power output against the power input. The excess energy in the steam entering the turbine is then passed into the grid system during the tripping process. Once this energy flow ceases, the generator circuit breakers are opened. The turbine then coasts down from its normal running speed under the influence of windage and friction. This is known as a *sequential trip*.

8.9.1 Non-sequential trip

As indicated above, in a non-sequential turbine trip, the generator circuit breakers open at the same time as turbine steam valve closure is initiated. The valves take a finite time (perhaps half a second) to close, and the incoming steam along with the trapped steam in the turbine accelerates the turbine into an overspeed condition (about 10% above normal speed), as shown in Figure 34. Note that the horizontal time scale is not linear. The speed rise is in seconds, and the speed drop is in minutes.

A non-sequential trip must be initiated whenever there is an electrical fault on the generator or generator transformer because the heavy currents arising from faults can cause severe damage very quickly.

8.9.2 Sequential trip

In a sequential trip, the generator circuit breakers remain closed while the turbine steam valves are closing, so that the surplus power from the steam can be passed into the electrical grid. As soon as the electrical power flow from the generator falls to zero or reverses, the generator circuit breakers open. In this way, overspeeding of the turbine is prevented, as shown in Figure 34. This is inherently safer for the turbine generator than a non-sequential trip.

A sequential trip is initiated whenever there is a mechanical fault on the turbine or associated equipment. A sequential trip actually promotes a slightly faster shutdown in an emergency because the overspeed transient is avoided. Moreover, if the mechanical fault is due to bearing problems or excessive vibration, it is highly desirable not to subject the turbine to overspeed conditions.

8.10 Steam Flow Control

Mention has been made of the steam trapped inside the turbine after the steam inlet valves have closed. This steam, on expansion to vacuum conditions in the condenser, will continue to accelerate the turbine. Modern steam turbines contain a large volume of steam in their casings and associated pipework and components such as moisture separator reheaters and feedwater heaters. To minimize the effects of this trapped steam, certain other valves such as the intercept valves and the extraction steam line check valves also close to restrict steam flow into the turbine.

8.11 Load Rejection

A load rejection is, in effect, an electrical trip. In the event of certain external faults on the electrical grid system or transmission line leaving the plant, the generator transformer circuit breaker will open, leaving the unit isolated from the system, but still supplying its own unit service load. Under these circumstances, the unit suffers an instantaneous rejection of virtually its entire load, but it must be kept running and ready for resynchronization with the grid system once the fault has been cleared. A load rejection is therefore not a mechanical trip, and the steam flow must not be cut off permanently. The turbine does, however, suffer the same type of transient as during a non-sequential trip.

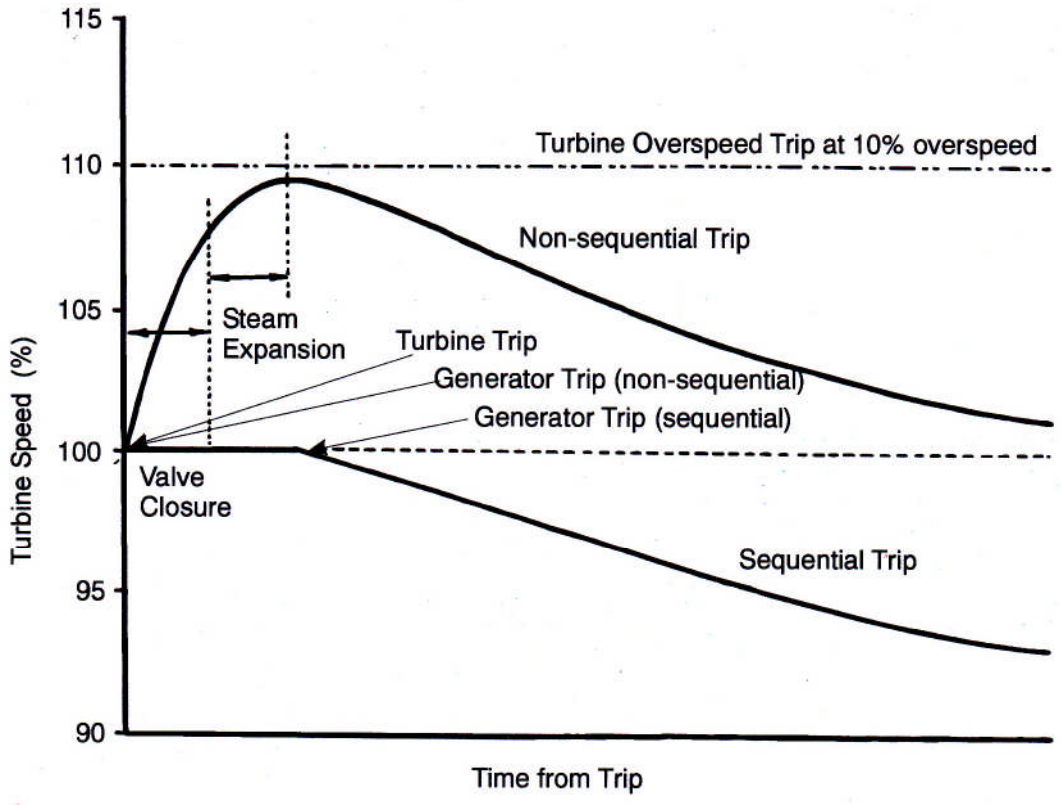

Figure 34 Turbine generator non-sequential and sequential trips

In a load rejection, the power output from the generator is drastically reduced, and closure of the steam inlet valves must be initiated immediately. Even so, the mismatch between power input to the turbine as steam and power output from the generator will accelerate the turbine into an overspeed condition (about 8% above normal speed). This speed transient is not quite as severe as in a non-sequential turbine trip because some surplus power is diverted into the unit services, which account for between 6% and 7% of the full generator power output. Naturally, this speed transient affects the electrical frequency of the supply to the unit services, and the motors of the auxiliaries suffer the same speed transient. Once the speed transient has passed and the turbine speed returned to normal, steam must once again be admitted to the turbine to provide enough power to drive the auxiliaries and to maintain the normal speed condition. The governed speed when supplying only the station load is, however, somewhat above the normal running speed due to the speed droop setting on the governor. The difference between the two speeds is known as the *permanent speed rise*. Returning the speed to normal requires adjustment to the governor. The speed transient arising from a load rejection is illustrated in Figure 35. This assumes no adjustment to the governor settings, but modern control systems initiate a turbine runback to bring the speed back to approximately normal running speed. As before, the speed rise is in seconds and the speed drop in minutes.

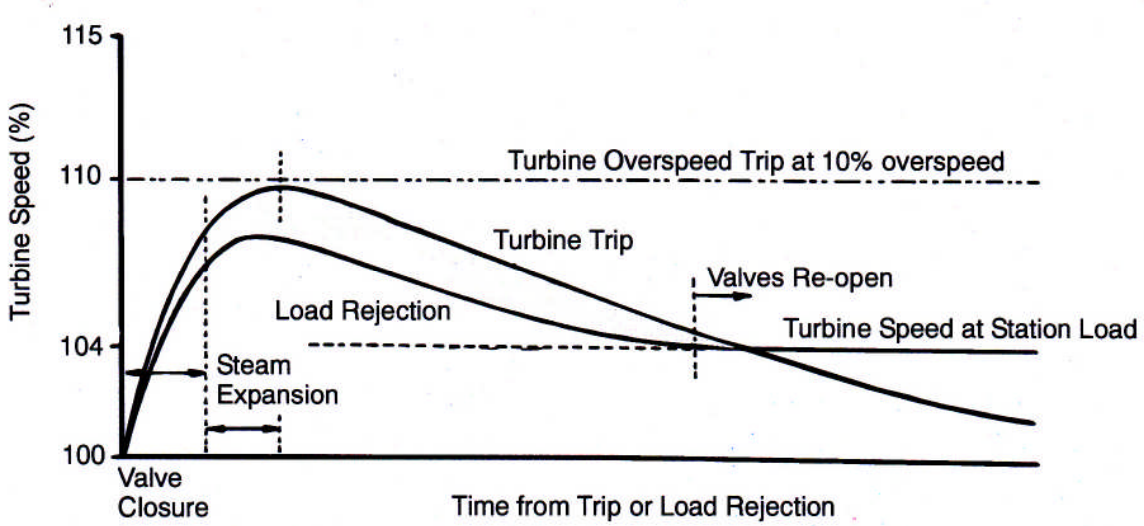

Figure 35 Turbine-generator load rejection

8.12 Turbine Overspeed Protection

All turbines are fitted with direct acting overspeed protection. This usually takes the form of mechanical spring loaded eccentric rings or bolts mounted on the turbine rotor. At an overspeed of about 110% or slightly more of normal speed, they operate and trip the hydraulic circuit of the steam inlet valves. This action is entirely independent of the governing system or other tripping circuits.

In the event of a load rejection and failure of the governing valves to close, the turbine speed would continue to rise. At an overspeed in excess of 110% of normal speed, the overspeed trip would be activated to close the emergency stop valves, and also the governing valves if their failure to close was a governing system failure.

An important aspect regarding the above scenario is that, while a load rejection is initiated at 100% of normal speed, the overspeed trip is activated at about 110% of normal speed. In the event of a governing system failure, the turbine therefore accelerates under full steam flow from 100% to 110% of normal speed before the steam inlet valves begin to close. They take a finite time to close, and after that, the trapped steam expands. During this period, the turbine continues to accelerate into an even higher overspeed condition, as shown in Figure 36. This can be as high as 118% to 120% of normal speed depending upon the turbine design. The turbine overspeed protection does not therefore limit the turbine speed to the settings selected. It is the last line of defence and should be treated accordingly. Any overspeed in excess of the overspeed trip setting should be regarded as dangerous because turbine rotors are overspeeded to only about 125% of normal speed at the manufacturers' facility to confirm their integrity.

The transient overspeed arising from a non-sequential turbine trip or a load rejection should always be below the overspeed trip settings to demonstrate proper operation of the governing system and to avoid a turbine trip following a load rejection.

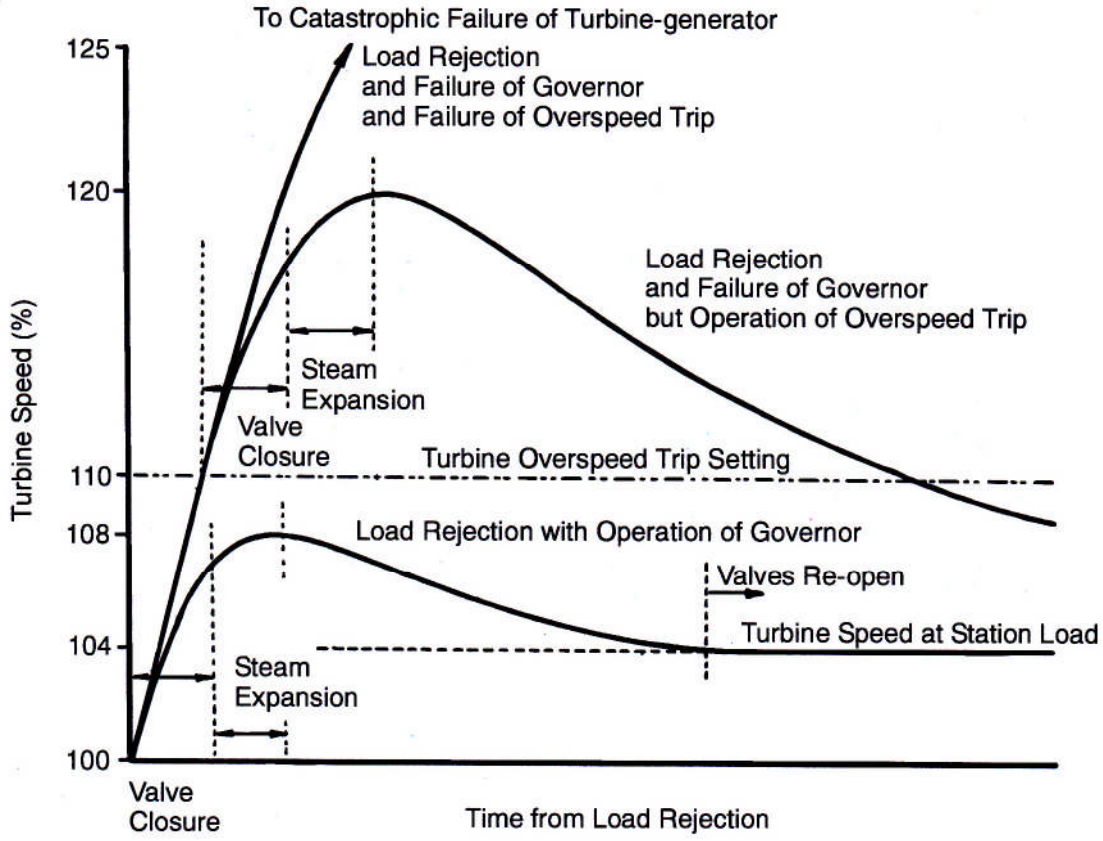

Figure 36 Turbine generator overspeed trip

9 Problems

1. List the key controlling units of a CANDU nuclear plant and explain their function and how they operate. Clarify the difference between normal and alternate modes of operation and explain which controlling units are affected and how they are affected by a change from one mode to the other.
2. Explain how the reactor is protected from abnormal operating conditions and potential accident conditions arising from process excursions or equipment failures.
3. Explain how the turbine is protected from abnormal operating conditions and from potential accident conditions arising from control malfunctions or equipment failures.
4. Explain the theoretical aspects related to the approach to criticality in a reactor, noting in particular the relationship between stabilization time and reactivity added. Explain also how the point of criticality can be predicted and how one knows when criticality has been achieved.
5. Describe the approach to criticality technique used in a CANDU reactor and clarify why this step-wise method has an inherent safety feature.
6. Explain how reactor reactivity changes during operation, noting which key fission products affect reactivity over the life of the fuel. Illustrate these changes in a diagram and

show on the diagram at which point refuelling is necessary. Assume that the reactor initially has new fuel only.

7. Assuming that a hypothetical steam generator operates under the following conditions:

Steam temperature	260°C (saturated steam)
Feedwater temperature	260°C (saturated water)
Steam flow	500 kg/s
Primary coolant pressure	10 MPa
Primary inlet temperature	290°C
Primary outlet temperature	270°C.

   a. Calculate the primary coolant mass flow rate.

   Assuming that the primary coolant mass flow rate is constant and that the heat transfer coefficients remain constant, determine the following:

   b. Primary system temperatures when the steam flow rate is increased to 1000 kg/s, assuming that the steam pressure is kept constant.
   c. Secondary steam pressure when the steam flow rate is increased to 1000 kg/s if a temperature of 300°C in the primary system is not to be exceeded.

   For both (b) and (c) above, sketch the temperature variation along the length of the tube bundle and show terminal temperatures. Assume a linear rise in temperature of the primary coolant.

8. Illustrate the two modes of operation of a typical CANDU unit as follows:
   a. Sketch a typical pressure control system for a steam generator when operating in the reactor leading mode.
   b. Sketch a typical pressure control system for a steam generator when operating in the turbine leading mode.

   Each sketch should show the nuclear reactor, steam generator, and turbine generator as well as the primary sensors and control elements. For each, describe how the system would respond to a transient load condition (increase or decrease in load).

9. Explain the terms “swelling” and “shrinking” when applied to a boiler or steam generator. Clarify the difference between steady state and transient conditions and explain what causes each to occur. As clarification, review the sequence of events following a load change on the system. Explain briefly what effect this has on a single element level control system.
10. If the pressure in the steam generator drops from 4.0 MPa to 3.9 MPa, determine what percentage by mass of the water in the steam generator will immediately be converted to steam. If this steam remains in suspension in the water in the form of bubbles, by what percentage will the water swell (transient swelling)?
11. In large CANDU plants, the steam generator level set point is usually programmed so that the water level is lower at low power levels than at high power levels. Explain why the water level set point is different for different power conditions. Clarify how the water inventory in the steam generator changes as the level set point is ramped up and down.
12. Show in a sketch how steam generator level varies with load in a typical CANDU steam generator. Show also in a separate sketch how steam generator inventory would be expected to vary with load. Discuss the relative merits of maintaining constant level or

constant inventory in the steam generator and clarify to what extent these are achieved with the current arrangement.

13. Consider a typical three element controller for a steam generator.
    a. Sketch the control system used to control the water level. Show what measurements are taken and how the signals are processed by the control system. The diagram must be sufficiently detailed and fully labelled so as to be self-explanatory.
    b. Explain why a three element controller is used instead of a single element (level only) controller. Support the explanation with an example demonstrating when and why a single element controller may give an incorrect response.
14. In the event of a turbine-generator trip or load rejection from full load, the reactor power is decreased and maintained at a certain level to prevent excessive buildup of xenon in the reactor and surplus steam is dumped to the condenser.
    a. Explain what limits the maximum amount of steam that can be rejected and state the usual limit.
    b. Explain why water is mixed with the steam before release into the condenser. Estimate the condition of the steam before mixing with water and hence determine how much water must be added per kilogram of steam.
15. Consider a condenser operating under the following conditions:

Cooling water inlet temperature	10°C
Cooling water outlet temperature	20°C
Steam inlet (saturation) temperature	30°C.

    Sketch the anticipated temperature profiles for both cooling water and steam across the condenser (that is, along the tubes) for each of the following conditions:
    a. Given or normal conditions.
    b. Cooling water inlet temperature increased to 16°C.
    c. Cooling water flow reduced to 1/2 its original value.
    d. Turbine load reduced to 1/2 its original value.

    Assume a linear change in cooling water temperature along the tubes.
16. Consider a condenser which operates at 0.005 MPa and condenses steam with a moisture content of 10% at a rate of 600 kg/s. Cooling water enters the condenser at 13°C and leaves at 23°C. Determine the following:
    a. Temperature profile (sketch) across the condenser (along the tubes from inlet to outlet).
    b. Average temperature difference between steam and cooling water.

    Having established the basic condenser parameters given above, determine what changes in these parameters would occur and what their magnitude would be for the following new conditions:
    c. Cooling water inlet temperature increase to 18°C.
    d. Cooling water flow rate decrease to 50%.
    e. Fouling of condenser tubes which decreases overall heat transfer coefficient by 25%.
    f. Reduction in steam flow to condenser to 400 kg/s.

For each case, sketch the new temperature profile across the condenser, assuming a linear change in cooling water temperature along the tubes and average temperature differences.

17. The condenser of a large steam turbine receives exhaust steam at varying flows depending upon the prevailing turbine output. On axes of condenser pressure versus condenser steam flow, sketch the following:
    a. Variation in condenser pressure with steam flow into the condenser (due to variation in turbine output).
    b. Variation in condenser pressure with steam flow into the condenser at a cooling water temperature higher than that in (a) above.

    Explain why the condenser performance curve has the shape shown and why the variation shown in (b) is different from that shown in (a).
18. Explain how the flow of steam through the turbine is affected by low load operation. Clarify what adverse conditions arise in the last stage blading under low load conditions and how this affects turbine performance. Explain how these adverse effects can be minimized.
19. Describe motoring and explain under what conditions the turbine would be subject to motoring. Give the advantages of motoring and note the precautions that must be taken when motoring.
20. Consider the start-up phase of turbine operation.
    a. Explain in detail the cause of sagging and clarify under what circumstances sagging of the turbine shaft can occur.
    b. Explain in detail the cause of hogging and clarify under what circumstances hogging of the turbine shaft can occur.
    c. Explain why such states are not desirable and the adverse consequences arising from such deformation.
    d. Explain how such states can be prevented from occurring or alleviated if such conditions exist.
21. Explain axial differential expansion in a large steam turbine. Explain how this can be minimized by proper location of the thrust bearing in the case of a large nuclear unit. Support the explanation with a suitable sketch showing the direction of expansion of rotor and casing. Show the fixing points of the casing and the location of the thrust bearing. Clarify under what conditions excessive axial differential expansion can occur. Describe the adverse consequences caused by excessive axial differential expansion.
22. Explain the operation of the following and clarify under what circumstances each would be used:
    a. Regular governor when controlling speed.
    b. Regular governor when controlling load.
    c. Emergency overspeed governor.
23. Describe the sequence of events and the turbine response during the following tripping modes. Clarify under which circumstances each would occur and sketch the speed response of the turbine in each case.
    a. Sequential turbine trip.
    b. Non-sequential turbine trip.
    c. Turbine load rejection.

Show on each sketch the period during which the governor valve closes and the period of steam expansion in the turbine.

24. Explain how a turbine is protected against excessive overspeed. Describe a potential sequence of events with associated physical phenomena that could lead to the total destruction of the turbine.

Answer Guide for Chapter 9

1. See Section 2.1 CANDU Plant Control Systems and Figure 2 Basic plant control system.
2. See Section 2.2 Reactor Protection Systems, Section 2.3 Reactor Shutdown Systems and Section 2.4 Emergency Coolant Injection.
3. See Section 2.5 Turbine Protection System.
4. See Section 3.3 Approach to Criticality as well as Figure 4 Stabilization time for different subcritical multiplication factors and Figure 6 Approach to critical – inverse count rate change.
5. See Section 3.4 Approach Technique and Section 3.5 Reactor Start-up.
6. See Section 3.7 Fuel Burnup and Figure 8 Effects of fuel burnup on reactivity.
7. See Section 5.1 Plant Control and Figure 9 Steam generator temperature profile.
   Use Steam Tables. (a) Flow rate M = 8008 kg/s assuming light water. (b) Inlet temperature t = 290°C. Outlet temperature t = 310°C. (c) Steam Temperature t = 250°C. Steam pressure p = 3.97 MPa.
8. See Section 5.2 Steam Generator Pressure Control and Figure 2 Basic plant control system.
9. See Section 5.3 Swelling and Shrinking as well as Figure 10 Steady state swelling due to different load conditions and Figure 11 Transient swelling due to changing load conditions.
10. Use Steam Tables. Amount of water converted to steam = 0.26%. Degree of swelling = 10%.
11. See Section 5.4 Steam Generator Level Control as well as Figure 12 Constant steam generator water level and Figure 13 Ramped steam generator water level.
12. See Section 5.4 Steam Generator Level Control and Figure 15 Steam generator level alarms and set points.
13. See Section 5.4 Steam Generator Level Control and Figure 14 Three element steam generator level control system.
14. See Section 6.1 Characteristics and Function and Section 6.2 Atmospheric and Condenser Steam Discharge Valves. Use Steam Tables. Assume a steam generator pressure of 5 MPa and a condenser pressure of 0.005 MPa. Water required = 0.10 kg water per kg steam.
15. See Section 7.1 Thermodynamics and Heat Transfer and Figure 18 Changes in condenser temperature profile. (a) Steam temperature = 30°C. (b) Steam temperature = 36°C. (a) Steam temperature = 35°C. (a) Steam temperature = 20°C.
16. See Section 7.1 Thermodynamics and Heat Transfer and Section 7.4 Condenser Tube Fouling as well as Figure 18 Changes in condenser temperature profile. (a) Steam temperature = 33°C. (b) Average temperature difference θ = 15°C. (c) Steam temperature = 38°C. (d) Steam temperature = 38°C. (e) Steam temperature = 38°C. (f) Steam temperature = 26°C.

17. See Section 7.1 Thermodynamics and Heat Transfer as well as Figure 19 Variation in condenser pressure and Figure 20 Condenser performance curves.
18. See Section 8.4 Turbine Load Variation as well as Figure 31 Change in whirl velocity at low loads and Figure 32 Recirculation of steam at low loads.
19. See Section 8.4 Turbine Load Variation.
20. See Section 8.1 General Operational Considerations.
21. See Section 8.5 Differential Expansion and Figure 33 Differential axial expansion of turbine rotors and casings.
22. See Section 8.6 Turbine Governing.
23. See Section 8.9 Turbiine Trip.
24. See Section 8.12 and Figure 36 Turbine generator overspeed trip.

10 References and Bibliography

Bereznai, G., *Nuclear Power Plant Systems and Operation*, Revision 4, UOIT, Canada, 2005.

British Energy International, "Modern Power Station Practice", Volume C, *Turbines, Generators, and Auxiliary Plant*, Third Edition, Pergamon Press, UK, 1991.

Chaplin, R. A., "Fundamentals of Nuclear Energy", Chapter 3.6.1 in *Nuclear Energy and Reactors*, Encyclopedia of Life Support Systems by UNESCO, EOLSS Publishers, Oxford, UK, 2010. [This chapter gives a brief outline of basic nuclear physics and how a reactor operates].

Chaplin, R. A., "Nuclear Reactor Kinetics", Chapter 3.6.1.5 in *Nuclear Energy and Reactors*, Encyclopedia of Life Support Systems by UNESCO, EOLSS Publishers, Oxford, UK, 2007. [This chapter gives the theory related to reactor kinetics and gives simple numerical examples of the effect of delayed neutrons, subcritical multiplication factor and approach to criticality].

Chaplin, R. A., "Reactivity Changes", Chapter 3.6.1.6 in *Nuclear Energy and Reactors*, Encyclopedia of Life Support Systems by UNESCO, EOLSS Publishers, Oxford, UK, 2007. [This chapter gives explanations of the effect of fission products such as xenon and samarium as well as the effect of temperature on the reactivity of the reactor].

Chaplin, R. A., "Nuclear Reactor Steam Generation", Chapter 3.10.2.10 in *Thermal Power Plants*, Encyclopedia of Life Support Systems by UNESCO, EOLSS Publishers, Oxford, UK, 2000. [This chapter gives explanations of the dynamics of steam generators and describes level and pressure control and consequences of inadequate control].

Chaplin, R. A., "Steam Turbine Steam System", Chapter 3.10.3.4 in *Thermal Power Plants*, Encyclopedia of Life Support Systems by UNESCO, EOLSS Publishers, Oxford, UK, 2000. [This chapter describes the steam system and explains the operation of the condenser].

Chaplin, R. A., "Steam Turbine Operational Aspects", Chapter 3.10.3.5 in *Thermal Power Plants*, Encyclopedia of Life Support Systems by UNESCO, EOLSS Publishers, Oxford, UK, 2000. [This chapter describes the thermodynamic phenomena occurring in the turbine which affect its operation as well as the external influences such as those due to the condenser. It also includes thermal effects and governing].

11 Acknowledgements

Acknowledgments are extended to NB Power for the use of information, diagrams and photographs to support the text of this chapter.

The following reviewers are gratefully acknowledged for their hard work and excellent comments during the development of this Chapter. Their feedback has much improved it. Of course the responsibility for any errors or omissions lies entirely with the authors.

George Bereznai
Simon Pang

Thanks are also extended to Diana Bouchard for expertly editing and assembling the final copy.

CHAPTER 10

Instrumentation and Control

prepared by
Dr. G. Alan Hepburn
Independent contractor (AECL Retired)

***Summary**:*

This chapter describes the role of instrumentation and control (I&C) in nuclear power plants, using the CANDU 6 design as an example. It is not a text on the general design of instrumentation and control algorithms, a subject which is well covered by many textbooks on the subject. Rather, it describes the architectural design of these systems in nuclear power plants, where the requirements for both safety and production reliability are quite demanding. The manner in which the instrumentation and control components of the various major subsystems co-operate to achieve control of the overall nuclear plant is described. The sensors and actuators which are unique to the nuclear application are also described, and some of the challenges facing designers of a future new build CANDU I&C system are indicated.

Table of Contents

List of Figures

1 Introduction

This chapter describes the role of instrumentation and control (I&C) in nuclear power plants, using the CANDU 6 design as an example. The scope of I&C includes:

- Implementation of control strategies for those control functions which are automated,
- Presentation of information to the operator and receipt of operator inputs for those functions which are under operator control,
- Initiation of reactor shutdown, emergency coolant injection, and containment isolation in the event of failure of the above control functions, and
- Data acquisition.

The automated functions include:

- Automatic control of the reactor, balance of plant, and auxiliary systems;
- Activation of the special safety systems;
- On-power refuelling (CANDU reactors);
- Human/machine interface.

Virtually all the systems in a nuclear power plant contain an instrumentation and control element.

Although some of the material presented is common to other reactor types, the design details described pertain to the CANDU reactor. The CANDU 6 design as implemented at sites in Canada has been chosen as the reference because it is the most widely deployed CANDU design world-wide. While the implementation of I&C in other plants is broadly similar, the differences between the CANDU 6 and other CANDU stations are significant. These differences will be noted in some cases where they are of particular interest to the understanding of I&C in general.

At the time when the CANDU 6 and many of the world's light water reactors were designed, the process I&C subsystems in nuclear plants were implemented using a combination of individual analog control loops and discrete Boolean logic using relay technology. The design of the analog loops is based on classical linear frequency-domain control theory as described in any textbook on the subject.

As a consequence of the large core of the CANDU reactor and of its many fuel channels, reactor inlet and outlet headers, and other components, the CANDU design is very extensively instrumented. As CANDU reactors began to exceed about 250 MWe, the size of the reactor core and the on-power refuelling combined to make manual supervision of the spatial distribution of power in the core more and more unwieldy. The result was a strong motivation to introduce computer control of the reactor and of key process control loops. The resulting control algorithms are quite complex, with many related inputs and outputs. Implementing such a system using conventional equipment would have been impractical. Therefore, a central dual-redundant digital control computer (DCC) system, in which the control logic is defined by software, was introduced in the CANDU design very early on relative to the I&C industry as a whole, to say nothing of the nuclear power industry. All CANDU reactors, starting with Douglas Point, have used computers in their process I&C systems. At least from Pickering on, the use of this technology was a matter of design necessity.

This chapter is intended to provide an introduction to the role of I&C in nuclear power plant applications and is consequently oriented towards issues that are unique to the nuclear context. It is not a text on the basics of instrumentation and control, nor is detailed knowledge of this field necessary to understand the material presented. The details of the control strategies used in each plant system are not covered. The only detailed discussions of these strategies presented are of the subsystems involved in reactor and overall plant control and of the regional overpower trip logic.

For those interested in studying the individual systems in more detail, there is a plethora of material available on the CANTEACH Web site (https://canteach.candu.org). In reviewing this material, the author noted that it contains many references to design features that are unique to individual sites as if they were part of the generic CANDU design. For those who need to know the details of a specific station, the most reliable source is the system design manuals pertaining to that station.

1.1 Overview

The reliability and availability requirements for nuclear power plants tend to differentiate them from many other applications. The implications of these requirements for the major I&C subsystems are discussed from the point of view of both nuclear safety and plant production. References to current standards and regulatory documentation are provided.

The overall architecture of I&C systems is described, using the reference CANDU 6 design as an example. There are close ties here with the architecture of the electrical power systems described in Chapter 11.

The implementation technologies used in nuclear I&C are also described. As an aid to understanding the design decisions evinced by the design, a brief discussion of the technologies available to the designers in the early 1970s is provided.

To give the reader an insight into the more detailed I&C logic functions typical of the CANDU design, the operation of the main I&C systems involved in overall control of the plant (reactor regulating system, boiler pressure control, and unit power regulation) is described in Section 4. The design of the I&C subsystems of the special safety systems is described in Section 5. The tools and techniques used to verify the design are discussed in Section 8.

I&C technology has arguably experienced the most dramatic change of any of the technologies used in power plant design in the years since most of the world's nuclear fleet was constructed. However, at least in the case of CANDU, although a number of I&C subsystems have been replaced by more modern equipment at various stations over the years, the lack of a truly new build design means that the existing I&C design is now very dated. If and when the next new build is undertaken, the designers will face an extremely challenging task in bringing the design concepts and implementation technologies forward into the 21st century.

Several new-build designs have been initiated in the interim, notably for the CANDU 3, CANDU 9, and the Advanced CANDU reactor, but none of these has been carried out to the point where detailed design documentation was produced and implementation planning was documented, let alone where a reactor had been constructed, commissioned, and licensed. Furthermore, I&C technology moves forward perhaps one generation every ten years, so new designs have a rather limited shelf life.

Given the small number of new builds elsewhere in the world, many plants share this tendency to have outdated I&C technology. A discussion of some of the issues facing the designers of an upcoming new build (as opposed to a new replicate design) is included in Section 9, although, to be sure, any such discussion will be overtaken rather rapidly by technological developments.

1.2 Learning Outcomes

The goal of this chapter is for the student to understand:

- The role of I&C systems in the safety and process systems of the CANDU design,
- The high-level safety and production requirements applicable to these systems,
- The role of system architecture in achieving safety and production reliability,
- The technologies used to implement these systems and the constraints present at the time of their design that influenced the design choices made,
- The unique features of the CANDU I&C design and why they were adopted, and
- Some of the major challenges facing the designers of future CANDU I&C systems.

2 Nuclear Safety and Production Requirements for I&C Systems

A frequent reaction of the general population to the idea of nuclear power is, “What happens if it goes out of control”? They immediately have visions of mushroom clouds and grainy black-and-white movies from the Second World War. In fact, a nuclear explosion of this sort is simply not possible with a power reactor. To create a nuclear explosion requires a small mass of highly enriched uranium to be held very firmly together using conventional explosives for the short time it takes for the chain reaction to go massively supercritical and the consequent release of energy to occur.

In a power reactor, maintaining the configuration of the fissile material is also key to maintaining the chain reaction, but the fuel is not nearly as highly enriched (or in the case of CANDU, not enriched at all), and the fissile material must be maintained at a predetermined separation of the order of a few tens of centimetres, with some moderating material, such as graphite, water, or heavy water in the intervening space. If these conditions are not met, the chain reaction will not be sustained.

In any nuclear reactor at constant power, the rate of production of neutrons by fission is exactly matched by the rate of re-absorption in new fissions and by various losses. The neutron multiplication factor $k = 1$. If $k > 1$ for some time, power will increase rather quickly to the point that so much heat is produced that the fuel melts and the core disassembles, thereby destroying the geometry required for criticality. But there will not be a nuclear explosion. There may be a steam explosion, as happened at Chernobyl, but that, while undeniably violent, is not in the same league as a nuclear explosion.

Although a nuclear explosion is not possible, in the absence of effective process control and other defense mechanisms, the reactor would be destroyed, and radioactive material could be released to the environment, causing an ecological disaster like that which occurred at Chernobyl. Because there is far more fissile material in a power reactor than in a weapon (tonnes vs. kg), the result would be widespread contamination, which is not an acceptable outcome.

For these reasons, a control system is needed to bring the chain reaction to a useful power level and then to hold it there. For thermodynamic efficiency, the hotter the energy source (fuel

elements), the better. However, if dryout is ever allowed to occur, cooling deteriorates quite rapidly, resulting in fuel melting. Therefore, power has to be raised to some point below dryout, then held close to constant by maintaining k = 1. This manoeuvering and control is achieved by adding or removing neutron-absorbing control elements: poison, rods, and in the case of CANDU, light water. Insertion of each reactivity-control mechanism results in a reduction in the neutron multiplication factor. The absorption value of these devices is expressed in milli-k (mk). Insertion of one mk of negative reactivity decreases the neutron multiplication factor by 0.001.

In a light water reactor, fresh fuel requires maximum negative reactivity (rod insertion). As fuel burns up, rods must be gradually withdrawn to sustain the chain reaction. Power distribution within the core is highly predictable because the rods are withdrawn in a predetermined pattern. In CANDU, with continuous refuelling, fuel reactivity can be maintained indefinitely, but local peaks will occur when fresh fuel is inserted. This, together with the larger size of the core, which in the absence of control action can lead to local flux oscillations due to Xe^{135} (a neutron absorber with a fairly short half-life which is produced as a result of the fission process), means that, in a CANDU reactor, flux has to be controlled both as an average value, for the entire core, and spatially, to avoid unwanted flux tilts.

Heat must also be removed from the fuel as it is produced. This is achieved by circulating a heat-transport fluid (e.g., light or heavy water) over the fuel. The energy removed is transferred to the secondary coolant circuit, where it produces steam to drive the turbine. Failure to remove heat can result in damage to the fuel or to heat-transport system components, so control of the heat-transport system is also critical.

The safety role of the process control systems is to keep the various reactor systems operating within predetermined safe limits. Given the potential consequences of process-system failure, however, the defenses against such failure must be extremely robust—much more robust than could credibly be achieved by the process systems themselves. Several additional layers of defense are used in any modern power reactor. The probability that each layer will not be available to accomplish its function is expressed as some unavailability figure, e.g., 10^{-3} years per year. In the case of a defense mechanism, this is equivalent to saying that the mechanism will operate as expected 999 times out of every 1000 challenges.

In any modern reactor design, the additional levels in this defense-in-depth approach are:

- The shutdown systems,
- The emergency core cooling system (ECCS), and
- The containment system.

In CANDU plants, these systems are referred to as the “special safety systems”, while in PWRs, they are referred to as “reactor protection systems” and “engineered safety features”. In the CANDU context, anything else is a “process system”. During plant operation, the special safety systems are poised ready to perform their function when called upon to do so, while the process systems are generally in continuous operation. However, some process-system functions are also normally dormant, but take action to preclude the need for special safety system intervention.

The role of the shutdown system is to stop the chain reaction very rapidly (generally in less than two seconds) if there is an indication that the process parameters are going outside acceptable limits. Shutdown systems achieve their function by rapidly inserting large amounts of negative

reactivity. This is typically done in all reactors by inserting neutron-absorbing rods into the core using a highly reliable power source—the force of gravity (or pressurized gas accumulators, in the case of boiling water reactors), augmented initially by springs in the case of CANDU.

The CANDU core has a slightly positive void coefficient. This means that, as power increases through the point that the primary coolant starts to boil, the reactivity would also increase in the absence of any control-system action. In other words, a positive feedback situation exists. On initial consideration, this does not appear to be a desirable characteristic, because an event that results in a power increase is not self-limiting. The Canadian industry's response to this has been to provide a second separate, diverse shutdown system (SDS2). In all designs from Bruce A on, both shutdown systems are equally capable. The second system injects gadolinium nitrate poison into the moderator, using compressed helium gas as the motivating force.

Every effort is made to ensure that the two shutdown systems are independent (different reactivity mechanisms, different design teams, complete electrical and spatial separation of instrumentation and mechanisms, different I&C devices wherever possible and practical), so that the design unavailabilities of 10^{-3} years per year for each system can be multiplied to achieve an overall unavailability of the shutdown function of 10^{-6} years per year.

Proponents of light water reactors tend to make much of the CANDU's positive void coefficient, but the comparison with respect to inherent power dynamics is not all one-sided. Clearly, in addition to the direction that power tends to move, the rate at which it moves is also important. Although a milli-k may not sound like much, the average lifetime of a neutron is less than one millisecond. Considered simplistically, this would mean that an excess reactivity of only 1 mk would result in an approximate tripling of neutron power within one second. Fortunately, this simplistic approach is not applicable in a power reactor core. Due to the effects of a relatively small number of delayed neutrons (about 6%), the increase in power in one second would, for a CANDU, be around 1%. In a light water reactor, it would be around 10%. This is one key difference between the CANDU core and a typical LWR. For a more complete explanation, see [Rouben2002] and Chapter 5, Section 6. Moreover, once power reduction starts, the strong negative power coefficient of a light water reactor tends to resist the desired power reduction, prolonging heat generation in the fuel. In a light water reactor, the shutdown system alone does not insert enough negative reactivity to shut down the reactor. These reactors also rely on an inherent feature of the physics of the light water core—the Doppler resonance phenomenon—to help terminate the reaction [Rouben2008].

Stopping the chain reaction is necessary, but not sufficient to mitigate the effects of a process-system failure. The decay heat, which initially amounts to about 6% of the pre-shutdown value, still has to be removed. In a fossil-fuel plant, cutting off the source of new energy (the fuel feed) instantly removes the heat source. In a power reactor, even after the chain reaction has been terminated, decay heat could cause the fuel to melt, with the resulting undesirable consequences, for many days after the reactor has been shut down, unless continued cooling of the fuel is provided. Usually, the heat-transport system is available to do this, but to guard against any failures in this system, a backup cooling system is required—the emergency core cooling system, whose role is to provide an alternate path for removal of decay heat from the fuel if there is an indication that the process systems responsible for doing this have failed.

The last line of defense is the containment system, whose role is to provide an envelope around the parts of the plant that contain fission products so that this material will not be released to the environment. The containment system also condenses any steam released into this enve-

lope, thus limiting any upward pressure excursion following such a release.

2.1 Requirements for the Special Safety Systems

Oversight of the nuclear industry in Canada is the responsibility of the Canadian Nuclear Safety Commission (CNSC). The forerunner of the CNSC was the Atomic Energy Control Board (AECB). One of the CNSC's responsibilities is to develop the regulations governing the design and operation of nuclear power plants. The regulatory requirements for nuclear power plant safety in Canada are contained in the AECB Regulatory Documents listed in the references.

The reliability requirements for the special safety systems, which have a dominating influence on both the architecture and detailed design of these systems, are:

- SDS1 and 2: All Canadian power reactors are required to have two independent shutdown systems. As stated earlier, this requirement came about as a result of a design solution to an inherent characteristic of the CANDU core. This is now enshrined in a regulatory requirement, AECB regulatory document R-10 [AECB1977], which requires two shutdown systems "unless otherwise approved by the Board".

The overall unavailability for each of these systems is required to be less than 10^{-3} years per year.

- ECCS and containment: The relevant AECB regulatory documents [AECB1991b, 1991c] require that each of these systems have an unavailability of less than 10^{-3} years per year.

These numerical requirements are derived from the need to achieve what is deemed to be an acceptably low release rate of radioactivity to the public following a number of postulated accidents, or design basis events (DBEs). In other words, these are not just arbitrary numbers.

2.2 Safety Requirements for the Process Systems

The process I&C systems also play a role in plant safety. They have to keep the process systems operating within their designed operating envelope. If a convincing case could be made that the process systems would have an extremely high probability of success in doing this, there would be no need for the special safety systems. However, the reality is that, unless the design of the reactor and its associated process systems is inherently fail-safe, independent special safety systems are the only credible way to achieve an acceptable level of safety.

The unavailability targets for the special safety systems are predicated on their not being challenged very frequently by failure of the process systems. For this reason, the process systems do have some safety requirements, depending on the safety-related role of the process system in question. The system singled out for special mention in the case of CANDU reactors is the reactor regulating system, which has its own CSA Standard [CSA2011a]. The requirement for this system, per 4.3.1.1 of that Standard, is that:

> "The design target for failure of reactor power control shall be established by probabilistic safety analysis methods.
> **Notes:**
> In CANDU nuclear power plants, the design target frequency for loss of regulation is historically less than 1 in 100 years."

> A "loss of regulation" (LOR) is defined to be "a failure resulting in an unplanned increase in bulk reactor power".

Unlike the AECB/CNSC regulatory documents, this CSA Standard has recently been updated to reflect the possibility of non-CANDU designs being licensed in Canada. That "1 in 100 years" number used to be a requirement. Now, whatever design number is used for failures to control reactor power has to be reflected in the overall plant safety analysis.

Because any "unplanned increase in reactor power" should be terminated by the shutdown system, one can conclude that a loss of regulation has by definition occurred if either of the shutdown systems trips, unless it can be shown that the shutdown system itself activated inadvertently. In many cases, it is possible to analyze the event in retrospect and to demonstrate that the shutdown-system intervention was unnecessary, but this analysis still has to be carried out to confirm that the process I&C systems design was not at fault.

In earlier versions of the referenced CSA Standard, which were in force at the time the current Canadian reactors were designed, there was a requirement that "each reactor unit shall be designed and operated such that the combined frequency of all serious process failures does not exceed 1 in 3 years". This number applied to the entirety of all process systems. In an ideal world, the I&C component of each process system would be allocated a portion of that once in three-year budget, and a reliability analysis would be performed as part of the design to demonstrate that this requirement was met.

Because an LOR is by definition attributable to RRS, it is apparent that the Standard has already taken care of the allocation of the RRS portion of the budget—namely 1 in 100 years. This includes the entire RRS, from sensors to reactivity control mechanisms. Breakdown of this 1 in 100-year number to each RRS subsystem, including the I&C subsystem, is quite correctly left to RRS designers.

Systems design in the 1970s and '80s was not pursued in as rigorous a manner as is now considered to be best practice, and the derivation of the safety-related and other reliability requirements for the various process I&C subsystems is typically not fully documented in the design record of CANDU plants. Until recently, design of process systems in the Canadian nuclear industry did not generally follow the detailed process of requirements analysis and allocation which is standard practice in the aerospace and software engineering industries, for example, although these techniques are used in the key areas of plant safety analysis and in the development of safety-critical software.

There are many qualitative requirements included in N290.4, but the reliability requirement quoted above is the only performance parameter stated.

2.3 Production Requirements for the Process Systems

Clearly, for production reasons, quite apart from safety implications, it is desirable that the process systems be sufficiently reliable that they do not result in frequent power reductions or shutdowns. It should be mentioned at this point that the physics of the CANDU reactor are such that, if the reactor is shut down from full power, the buildup of Xe^{135} in the fuel will result in the accumulation of so much negative reactivity that, if the reactor is not restarted within about 30 minutes, it will not be possible to start it up again for about 40 hours. This is known as a "poison-out" and is discussed in more detail in Chapters 5 and 13 (Section 5.3.1). Because many of the control systems must be available if the plant is to run for more than a few seconds, it can

be seen that anything longer than a brief outage of one of these key systems will have a severe economic impact. Poisoning out is not an issue for the PWR/BWR.

Production availability is not, of course, a regulatory requirement, and therefore there are no regulatory documents which pertain to this key attribute. It will be seen in subsequent sections that the control systems are designed to fail safe, which will result in a shutdown of the reactor without the need for special safety-system action. It will also be seen that much of the key process control logic is implemented in a pair of dual-redundant digital control computers (DCCs). Although there is no specific requirement for availability of the process systems in general, these systems were designed to be highly reliable and tolerant of individual component failures. The DCCs were designed not to fail in a manner that leads to a poison-out more than once in three years. Note that, while this reads somewhat like the "serious process failure" requirement described in the previous section, the two requirements are quite distinct because, due to the fail-safe design of the process I&C systems, most process I&C outages will not result in a serious process failure as defined in Section 2.2.

3 Overall I&C Architecture

3.1 Architectural Design of the Special Safety Systems I&C

The architectural design of the special safety systems reflects the requirements for low unavailability discussed in Section 2.1. It was stated earlier that the CANDU design includes two independent shutdown systems. Independence is assured by geographical separation of the systems, including their I&C components, and by equipment and design diversity. For example, nucleonic sensors and actuators for SDS1 penetrate the core vertically from above the reactor, on the reactivity mechanisms deck. Nucleonic sensors for SDS2 are located at the side of the reactor, where the poison injection takes place. The actuation technologies are completely diverse, with mechanical neutron-absorbing rods used on SDS1 and injection of a neutron-absorbing solution into the moderator for SDS2.

To maximize physical separation between systems which must be physically independent, all safety-related systems in the CANDU plant are divided into two groups. Group 1 systems include most process systems and SDS1. Most of the other special safety systems, including SDS2, are allocated to Group 2. Within containment, because both groups must, after all, interface with a single reactor, it is possible to separate systems only by adopting approaches such as the horizontal/vertical separation described in the previous paragraph, but outside containment, the two groups are assigned completely separate locations. SDS1 I&C equipment, for example, is located in the control equipment room, adjacent to the process systems I&C equipment, but SDS2 I&C equipment is located in the secondary control area, on the other side of the reactor building. Penetrations through the reactor building wall for the two groups are separated by 90°. For a more complete discussion of grouping, see Chapter 13, Section 5.2.8.

This physical separation guards against relatively localized common-mode events such as mechanical destruction, fires, and flooding which might otherwise disable equipment in both groups simultaneously.

Not all common-mode events can be addressed by geographical separation and technological diversity. The sensors and actuators must be able to perform their functions during the accident conditions against which they are required to provide protection, which in many cases will

impact both systems simultaneously (e.g., high radiation fields, temperature, and humidity). The equipment must therefore be qualified to function in the anticipated post-accident environment. Equipment must also be qualified to survive and function during more widespread common-mode events such as electromagnetic disturbances and earthquakes, against which only limited physical protection is possible.

The low unavailability of each special safety system is achieved in part by redundancy of the equipment within each system. To ensure independence of the instrumentation, it is channelized. This involves physical separation of the instrumentation, cable routes, logic equipment, and actuators, and the electrical supplies that power them. Typically, the special systems instrumentation and actuation logic is divided into three or more separate channels. The separation of the electrical supplies closely reflects the separation within the I&C systems, as described in Chapter 11.

Channelization minimizes the probability that many classes of events will disable more than one channel at a time. Because safety-system action requires two of the three channels to call for activation of the safety function, the system will continue to perform its design function even if the third channel has failed in an unsafe manner. The design of the individual channel logic is such that unsafe failure of even a single channel is unlikely.

Channelization also enables the logic in each channel to be tested periodically. A channel under test is placed in a state where it votes for safe action. In calculating the system unavailability, each component failure is assumed to be random and is detected by a test carried out at a specific test interval. On average, then, failures may go undetected for one-half this test interval. Therefore,

$$\text{unavailability} = \text{failure frequency} \times \text{test interval} / 2.$$

It can be seen that the test frequency of functions that are normally poised but inactive is a key input to the unavailability calculation. Unless such functions are tested periodically, any system which depends on them must be assumed to be unavailable.

The detailed requirements for channelization in CANDU plants are documented in a series of safety design guides which are not in the public domain.

In PWR plants, a single shutdown system is normally used, with four channels of sensor and actuation logic. A reactor trip will result if any two of the four channels call for a trip. For CANDU plants, two three-channel shutdown systems are used. A reactor trip will result if any two of the three channels in a given shutdown system call for a trip. Either shutdown system will trip the reactor if the logic for any trip parameter calls for a trip in at least two channels. This is known as “general coincidence” logic. It is also possible to design a system in which a trip will occur only if the logic for the same parameter in at least two channels calls for a trip. This design is referred to as “local coincidence logic” and is used in some other CANDU plants. It can be seen that, although local coincidence logic is less prone to spurious trips, it requires more inter-channel communication, which compromises channel separation to some extent and adds complexity, particularly when the logic is hard-wired. In practice, the spurious trip rate has been found to be sufficiently small that the additional complexity of local coincidence logic is not warranted.

3.2 Architectural Design of the Process Systems I&C

The redundancy approach used in the special safety systems to minimize their unavailability is also used in the process systems to enhance the availability of key control functions, thus minimizing losses of production. Key control functions typically use triplicated sensors, with voting logic to reject sensors which have failed. Control logic is duplicated or triplicated, and much of the process equipment itself (pumps, valves, etc.) is either triplicated, using three 50%-capacity units, or duplicated using two 100%-capacity units. However, the separation requirements applicable to special safety systems do not apply to the process systems because the latter are not required to operate following an accident.

The architecture of the power supplies for the process I&C reflects that of the I&C equipment.

3.3 Features of the CANDU DCC Design to Enhance Production

As stated in Section 2.3, the economic penalties of even a brief process I&C outage in a heavy water reactor may well extend far beyond the duration of the equipment outage itself, and therefore, for both safety and production reasons, triplicated or duplicated equipment is extensively used.

The DCCs are a prime example of equipment duplication. The DCCs normally act in a master/standby configuration, with only one DCC in control of a specific function at any given time.

The individual control logic subsystems (or "control programs") running on the DCCs perform their own internal self-checks. Normally, the programs running in the master DCC will be in control of the plant. If a control program in the master DCC determines that it does not have sufficiently reliable input signals to enable it to compute its outputs, that program will stop running, causing control of that specific function to transfer to the standby DCC. Plant control can continue with certain restrictions, with some functions being controlled from the master DCC and some having switched over to the standby machine. This feature is also used to reduce the risk of plant outages when a change is made to the control logic. The new logic can be run in the master DCC only, with the old logic available to take over in the standby DCC at the operator's discretion if problems are encountered.

3.4 Safety-Related Functions of the Process Systems

The frequency of loss-of-regulation events can be reduced by incorporating logic into the process systems design to detect potential loss of control situations and to take action to reduce reactor power independently of the shutdown systems. In the CANDU design, this is accomplished by fail-safe design of the process I&C logic and by two layers of safety-related logic—the setback and stepback functions—implemented in the control computers. "Failing safe" in this context means failing the output devices in the direction of shutting down the reactor and positioning the process systems for post-shutdown conditions.

3.4.1 Setback function

The setback logic continuously monitors a number of process parameters. Typically, these are:

- High local neutron flux;
- Spatial control outside the normal range of operation;
- Low de-aerator level;

- High steam generator pressure; and
- Upsets in moderator temperature or pressure.

If there is an indication that these parameters are straying outside acceptable limits, a reactor power setback is initiated by gradually ramping back the power set-point generated by the set-point logic (see Section 4.1). In many cases, reducing reactor power will return the process system to its normal operating condition. Once a setback is terminated, operator intervention is required before any further automatic adjustment of reactor power set-point is possible.

3.4.2 Stepback function

Some abnormalities in the plant control systems require more rapid action than is available using a power set-point manoeuvre. The following conditions are monitored:

- Reactor trip;
- Turbine trip;
- Loss of line (grid connection);
- Heat-transport pump trip;
- High heat-transport pump pressure;
- High flux power or high flux rate; and
- Low steam generator level.

If any of these conditions is found to be present, an immediate power reduction, or "stepback" in reactor power, is initiated by releasing the clutches that hold the mechanical control absorbers out of the core. The stepback is normally permitted to continue to zero power, but in the cases of turbine trip or loss of line, it is arrested at an intermediate power level by catching the rods in mid-fall. This partial power reduction permits continued reactor operation at a power level that prevents the growth of xenon in the fuel from shutting down the reactor.

Stepback is the exception to the transfer-of-control approach described in Section 3.3. Both DCCs must initiate a stepback before one will take place. This reduces the risk that the stepback function will act spuriously. If a given DCC is shut down or the stepback function is not running on it, then the remaining machine can initiate a stepback on its own.

Although the stepback initiation logic resides in the DCC, it is independent of the RRS logic and therefore can mitigate some high flux power or flux rate events caused by failure of RRS itself. The stepback function reduces the frequency of demands on the two safety shutdown systems, SDS1 and SDS2.

3.4.3 DCC self-check function

Each DCC incorporates self-checking logic to confirm the availability of certain key functions. For minor losses of capability, such as loss of individual instrument measurements, the system will continue to function normally. However, if a major loss of capability is detected, the DCC in question will be shut down by allowing the computer's watchdog timer to time out. This results in all its outputs being de-energized, which, if the DCC in question is the master, transfers control to the standby machine.

An external watchdog timer, which must be reset every few seconds, is incorporated into each DCC. If this fails to happen, as would be the case, for example, if the DCC software got stuck in a loop, the watchdog timer would time out, and the DCC's outputs would again be de-energized.

The sense of the actuation logic for all systems controlled by the DCC is chosen such that de-energization of the DCC outputs will tend to move the affected process system in a safe direction. If both DCCs fail, for example, the mechanical control absorbers will drop into the core, and the light water zones will fill, resulting in a reactor shutdown.

Although the DCC itself is not seismically qualified, this watchdog timer function is. Hence, it is sometimes referred to as a "seismically qualified stepback". This ensures that, the DCCs will be reliably disconnected from the process equipment they control should they fail as a result of a seismic event.

4 Overall Plant Control Functionality

The CANDU approach to overall plant control will now be described as an example of the overall plant control required for a nuclear power plant. Note that CANDU reactors are relatively more manoeuvrable than LWRs because they do not have to respect the rather slow manoeuvring rates imposed by a very thick-walled pressure vessel. The manoeuvrability of LWRs also tends to be restricted at the start and end of their fuel cycle.

Although most of the 200-plus systems in the CANDU plant contain an I&C element, three main I&C subsystems are involved in the control of the nuclear steam supply: the reactor regulating system (RRS), boiler pressure control (BPC), and the unit power regulator (UPR). Due to the complex nature of the control logic used, all three of these functions are implemented primarily in the DCCs. The term "boiler", by the way, was changed at some point to "steam generator", but the name of the DCC program has stuck.

The plant can be operated in two modes, as specified by the operator, the choice being represented by the position of the A/N (alternate/normal) switch shown in Figure 1:

1. In Normal mode, the operator specifies a plant electrical output in megawatts. In this mode, the UPR logic adjusts the governor valves supplying steam to the turbine to maintain the specified electrical output. The BPC function monitors boiler pressure, and any error will result in changing the requested reactor power set-point which is sent from BPC to RRS.
2. In Alternate mode, the operator specifies the reactor power output, in percentage of full power, and a manoeuvring rate. The alternate mode set-point is then moved to meet this request at the specified rate. RRS sets the reactor power, which determines the energy delivered by the primary heat-transport system to the boilers. BPC then manipulates the turbine governor valves to maintain boiler pressure at a fixed set-point. BPC also has control of the condenser and atmospheric steam discharge valves, which can be opened to receive steam if the turbine load is lost, thus isolating the remainder of the system from abrupt changes in generator load and permitting continued reactor operation without the turbine as a load, thus avoiding a reactor shutdown due to buildup of Xe^{135}.

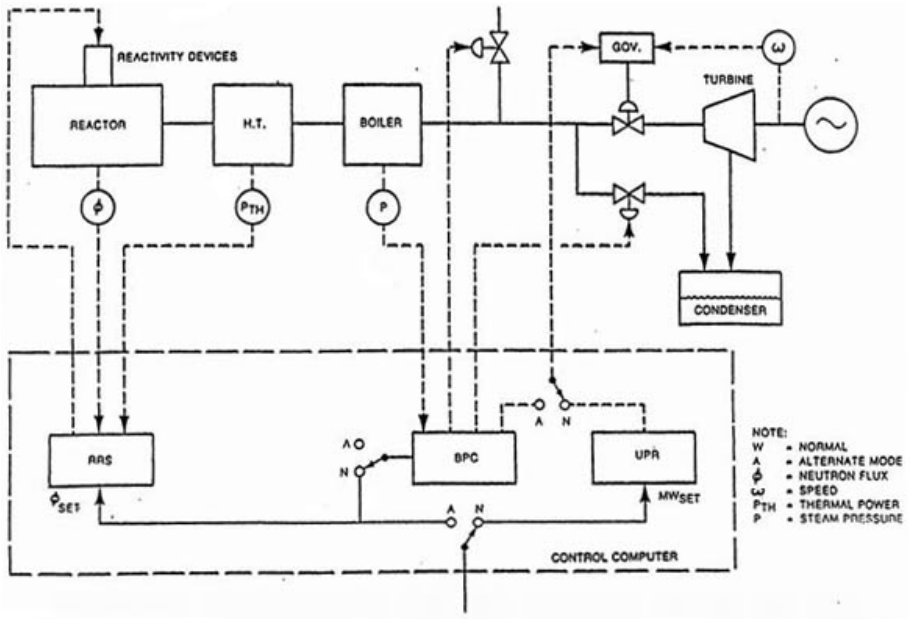

Figure 1 CANDU overall plant control

4.1 RRS control logic

RRS control logic in CANDU accomplishes the following:

1. Because the CANDU core is relatively large and subject to spatial instability due to the dynamic action of Xe^{135}, it has been found necessary to divide the reactor into 14 zones for control purposes (see Figure 2, which shows the arbitrarily labelled “A” and “C” ends of the reactor). There are seven zones at each end of the reactor core.

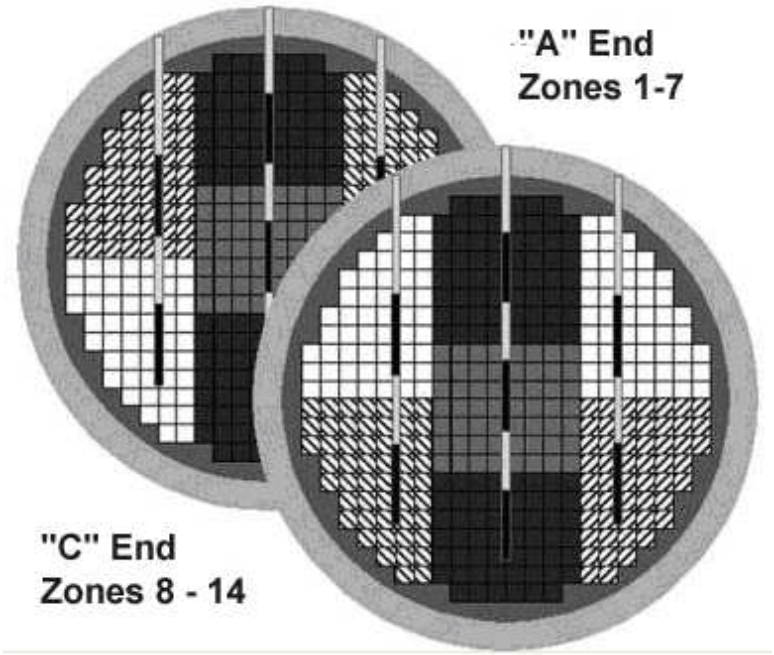

Figure 2 Arrangement of the 14 control zones

The power measurement and calibration logic determines the current reactor power in each of these zones, based on the readings provided by 28 platinum-clad Inconel®

flux detectors (two in each zone) that penetrate the reactor vertically from the reactivity mechanisms deck. The flux power is estimated for each of these 14 zones.

Because the platinum-clad Inconel detectors (see Section 6.1.1) do not provide an absolute value for neutron power, the zone power estimates have to be calibrated against thermal power. This is determined from measurements of temperature rise between the reactor inlet and outlet headers at low power, and from secondary-side measurements of steam flow, feed-water flow, and feedwater temperature at higher power (> 70%), because boiling in the channels renders the primary-side measurements unreliable at these power levels.

2. The appropriate power set-point is selected based on plant mode (Normal/Alternate, see Section 4). This set-point will be overridden if a setback is required (see Section 3.4). In this event, the reactor control mode is automatically switched to alternate mode, and the power set-point is ramped down to a predetermined endpoint. If the operator presses the HOLD POWER button on the RRS panel, automatic adjustment of the power set-point will also be suspended.

3. The demand power logic compares the overall reactor power measured in item (1) above with the required set-point and generates a power error signal E_p, which becomes the basis for the control of the reactivity mechanisms described next.

   Note that internally RRS works with logarithmic power, expressed in decades. This is appropriate because the reactor is a multiplicative device and the reactivity-control mechanisms control the rate of neutron multiplication. The reactivity mechanisms are driven based on E_p, which is also a logarithmic variable, measured in decades. However, in many explanations, and indeed in the displays seen by the operator, the E_p axis is labelled as “Power Error %” (see, for example, Figure 3). What is implied is that the value is a percentage of current power, not of full power.

4. During normal steady-state operation, the reactivity in each of the 14 zones is manipulated by adjusting the level of light water in each of 14 cylindrical compartments, one located in each zone (see Figure 2). In a heavy water reactor, light water is a neutron absorber. Each of the 14 compartments has a fixed outflow and a valve which controls the inflow of light water. These valves are manipulated in response to a combination of the overall power error, E_p, and any deviation of zone flux from the average over all 14 zones. The total worth of all 14 light water zones is about 7 mk. The logic to control overall power is run twice per second. Tilt control is updated every two seconds.

   In a zone where the overall error and the spatial components of the error signal sum to zero, inflow will equal outflow, and the light water level will remain constant at some intermediate level. The level of light water in each zone does not contribute to valve opening. However, as the level approaches either completely full or completely empty, the controlled variable changes from zone power to light water level so that the zones never completely flood or drain. These light water zone controllers are described in Section 6.2.

5. If more negative reactivity is required than the liquid zones are able to provide, as indicated by the zones becoming close to full, then this is accomplished by the me-

chanical control absorber logic, which drives banks of neutron-absorbing rods into the core. These absorber rods are normally located outside the core above the reactor. There are four mechanical control absorbers, with a total worth of 11 mk. The switching logic for them is shown in Figure 3.

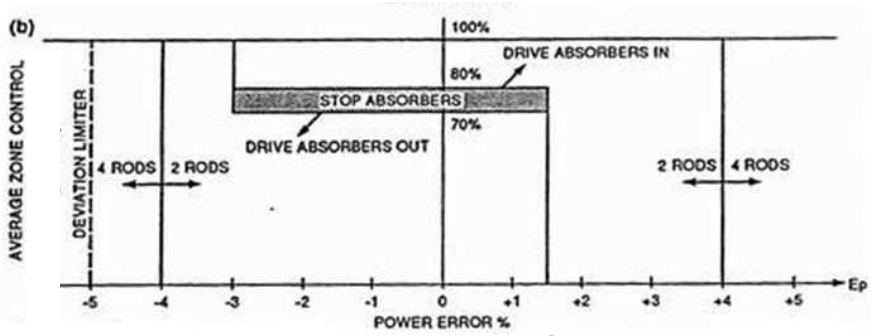

Figure 3 Absorber-rod drive switching

6. Similarly, when there is a lack of positive reactivity, the adjuster control logic can withdraw banks of adjuster rods from the core (see Figure 4). These rods normally reside in the core. There are 21 adjuster rods arranged in seven banks, with a total worth of 15 mk. All adjusters in a given bank are driven simultaneously, but only one bank is driven at a time.

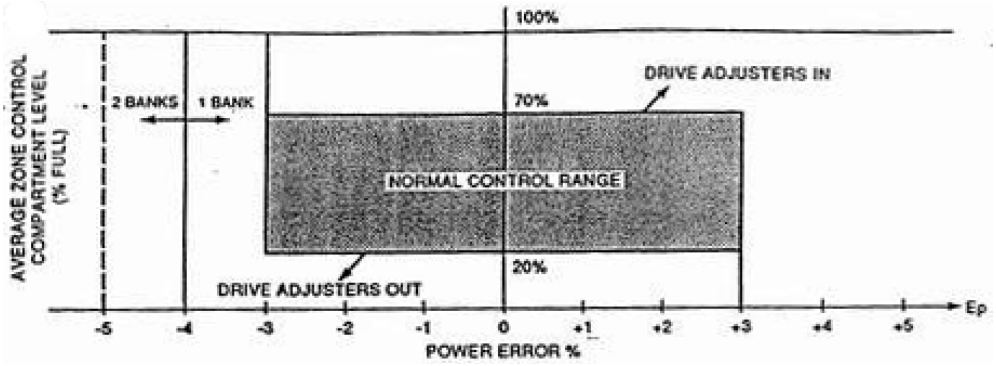

Figure 4 Adjuster-rod drive switching

The speed at which adjuster and absorber rods are driven is determined by a variable-frequency power supply and is a function of power error, as shown in Figure 5.

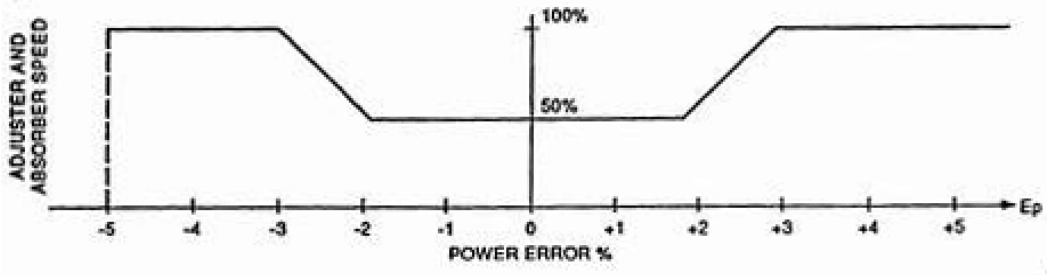

Figure 5 Rod drive speed

Once drive of either adjuster or absorber rods is started, it proceeds to completion to avoid large top-bottom flux tilts.

The absorber rods also incorporate clutches, similar to those used on the SDS1 shutdown rods. When a stepback is required, these clutches are disengaged, allowing

the absorbers to fall into the core under gravity. In this way, a much faster power reduction is achieved than if the rods were driven electrically.

In the long term, if the light water zones tend to move significantly away from the 50%-full point, the operator can adjust the available reactivity by adding poison to or removing poison from the moderator.

4.2 BPC Control Logic

During operation at significant power levels, the goal of BPC is to maintain a constant, predetermined boiler pressure. The BPC program also incorporates logic to handle the warming up and cooling down of the plant, but this will not be discussed here in the interests of brevity.

In Normal mode, BPC will pass a power set-point to RRS to maintain constant boiler pressure despite possible variations in the steam taken by the turbine. Hence, the reactor is said to follow the turbine in this mode. The set-point includes proportional and integral terms based on pressure error.

If boiler pressure becomes excessive, BPC can manipulate a combination of condenser steam discharge valves (CSDVs) and atmospheric steam discharge valves (ASDVs) to control boiler pressure. The CSDVs cause steam to bypass the turbine and go straight to the condenser. The ASDVs discharge steam directly to the atmosphere.

In Alternate mode, BPC also controls the steam fed to the turbine by manipulating the turbine governor. In this mode, the reactor power set-point is specified by the operator, and the resulting thermal power generates steam in the boilers. The objective of BPC is to maintain constant boiler pressure. Any deviation in boiler pressure will result in the governor valves being manipulated to maintain boiler pressure, and hence the reactor is said to lead the turbine in this mode. The algorithm in this case uses proportional and derivative terms based on pressure error, plus a feed-forward term based on the rate of change of reactor power.

In addition to manipulating the governor, BPC drives the turbine load limiter, which reads the current load set-point and drives the load limiter to a point 100 MW above this value.

4.3 UPR Control Logic

When the plant is operating in Normal mode, UPR manoeuvres the turbine load towards the target load specified by the operator. It maintains a variable LR (load reference), which is ramped towards the target load at a rate which is also chosen by the operator. The actual turbine load is compared to this load reference, and the turbine speeder and load limiter are adjusted accordingly.

In Alternate mode, UPR has no control function. It fulfils a monitoring role only.

5 Special Safety Systems Functionality

The four CANDU special safety systems will now be described.

5.1 Shutdown Systems 1 and 2

Safety analysis determines a safe operating envelope for the plant. The values of a number of plant parameters are then monitored in each shutdown-system channel to confirm that this

envelope has not been exceeded. If any parameter exceeds a predefined trip set-point, then the channel votes for a reactor trip. To guard against modelling errors, the CANDU design uses two diverse parameters in each shutdown system where practical to protect against each postulated initiating event. The case of impracticality has been invoked in the regional overpower protection (ROP) logic, which provides the primary defence against a slow loss-of-regulation accident. The ROP sensors use the same technology in both SDS1 and SDS2, and there is no backup nucleonic parameter for a slow loss of regulation, although the heat-transport high-pressure parameter does provide some protection in this case. The log-rate trip provides some diversity for fast LORs.

Most of the parameters that trip the shutdown systems are sensed using conventional process instrumentation, which provides fairly accurate indications of process values. However, in the regional overpower detection function, the platinum-clad Inconel sensors provide a much less direct indication of the physical parameter of interest: the onset of dryout in each bundle in the core. The logic used in the ROP trip will be described in Section 7, after the limitations of the sensors used have been introduced in Section 6.1.1.

5.2 Emergency Core Cooling System

The purpose of the Emergency Core Cooling System (ECCS) is to provide an alternate means of cooling the fuel when a loss-of-coolant accident (LOCA) has occurred. For a discussion of LOCAs of various degrees of severity, see Chapter 13, Section 5.4.

Emergency cooling occurs in two phases:

1. The ECCS monitors heat-transport system pressure and initiates high-pressure coolant injection whenever this pressure drops below the set-point. Valves are opened, which results in light water being forced into the reactor inlet and outlet headers, using pressurized helium as the motivating force. This is followed by a medium-pressure coolant injection phase in which light water from the dousing tank becomes the source of coolant.
2. When the supply of light water is exhausted, low-pressure recovery is initiated. This involves collecting spilled liquid from the reactor-building sump and recirculating it into the core through the reactor inlet and outlet headers. Both medium pressure and low pressure coolant injection are effected by pumps powered by Class III electrical power.

The sensors and logic used by the ECCS are conventional, but must of course be qualified to function in a LOCA environment.

5.3 Containment System

For a full description of the containment system, see Chapter 13, Section 5.5. The containment itself is the envelope designed to contain any release of radioactive material. In normal operation, it is maintained at sub-atmospheric pressure by vacuum pumps which exhaust to the atmosphere through a filtration system. Following a significant release within the reactor building, which is detected by high pressure, radiation, or both, the containment must be isolated. Any ensuing rise in reactor-building pressure is limited to facilitate the task of keeping leakage within allowed limits. On detection of a release, the containment is isolated by means of dual valves or dampers incorporated in every line or duct that penetrates the containment envelope. The dampers isolate the reactor building ventilation ducts and are pneumatically

operated. Examples are the ventilation ducts, the spent fuel port, and the feed-water and steam lines.

The pressure rise is limited by the dousing system. In the upper area of the building, a dousing tank contains water which is released as a spray to condense steam resulting from a heat-transport system or steam-line break. Dousing is initiated by opening a combination of electrically activated and pneumatically actuated valves located beneath the dousing tank. Series valves are used to minimize the probability of inadvertent dosing actuation. Diverse actuation sources enhance the probability that dousing will occur when required. (This applies to single-unit CANDU stations. Multi-unit stations use a vacuum building common to all four units. In the event of a LOCA, the affected containment is connected to this vacuum building, and the steam emanating from the LOCA site is doused there).

A cooling system limits the temperature rise within containment, thus maintaining the integrity of the building in the long term. The cooling system I&C is conventional. A hydrogen ignition system ignites any free hydrogen gas before concentrations can become high enough to be hazardous.

6 I&C Systems Layout and Equipment

In everything that has been said up to this point, the reader may have gained the impression that operation of the nuclear unit is entirely automatic. In the short term (up to about 30 minutes), this is indeed the intent of the design. Experience has shown, however, that there is a role in plant operation for both automated and human control. Humans are not particularly good at performing repetitive, routine tasks without error, and of course most of the control loops involved are simply too fast and have too many interactions with other loops for a human operator to be involved in controlling the loop in real time. However, the human operator has proved to have useful capabilities when things depart from the routine, where perhaps the state of the plant is not completely clear, and when available information is either incomplete or conflicting. He can then assume an overview role and direct the progression of events towards a stable conclusion. To do this, he has to be involved in the operation of the plant in a supervisory role and be presented with available information in a useful way.

The control room is the centralized point for reactor operation. A geographically separate secondary control area is provided to shut down the plant and to provide monitoring of those parameters which confirm safe shutdown following the event, should the main control room become uninhabitable. The Group 2 I&C equipment is located in this area.

The chief operator's station in the CANDU control room is the operator's desk, shown in Figure 6. A separate shift supervisor's office is also provided, but he is not immediately involved in unit operation. The operator's desk is equipped with video display units (VDUs) driven by the DCCs. The operator can select from a large number of displays which provide information on the status of various systems.

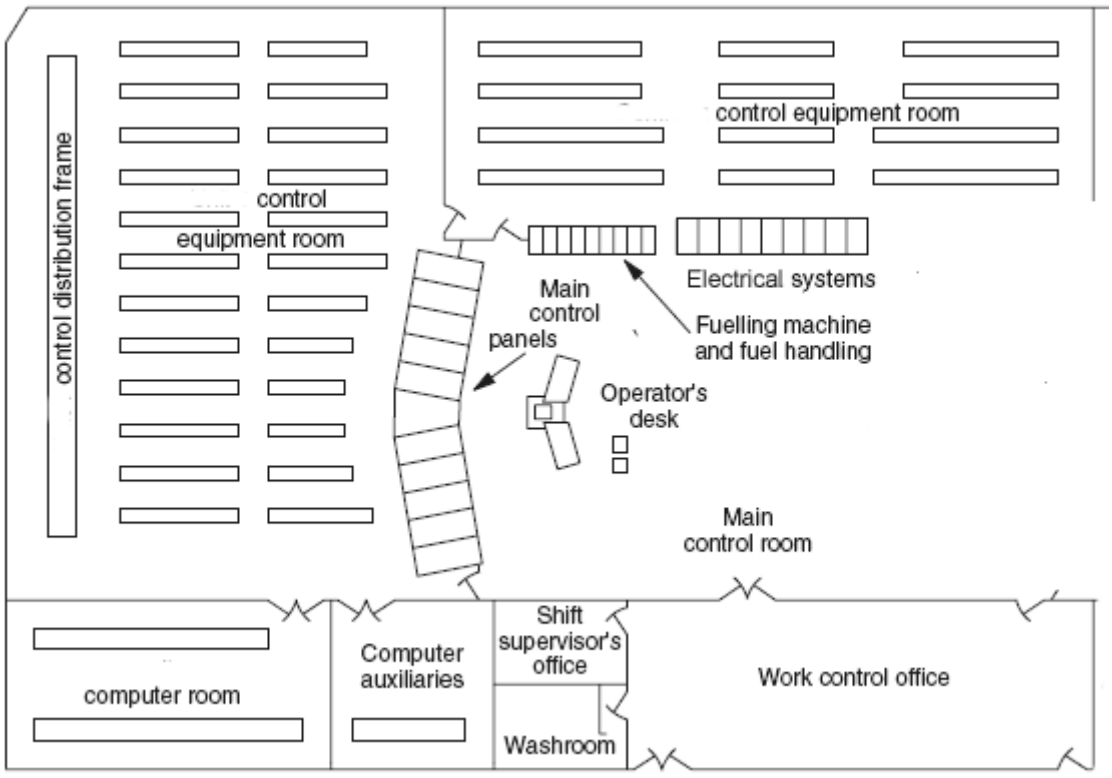

Figure 6 Layout of a CANDU 6 control room

Behind the operators' desk are a number of panels designed for stand-up operation. These panels are organized by system:

1. Containment
2. SDS #2
3. Emergency core cooling
4. SDS #1
5. Moderator
6. Reactor regulation
7. Primary heat-transport system
8. Steam generators
9. Turbine
10. Electrical panels
11. Fuel handling.

Figure 7 shows a view of the CANDU 6 control room, looking from behind the operator's desk. This figure shows a somewhat more modern version of the control room than that depicted in Figure 6. In the centre of the group of stand-up panels are two panels containing large video displays used to display the overall status of the plant. Above these displays are two large monitors which present annunciation information.

Figure 7 Pictorial view, CANDU 6 control room

At the top of each function panel is a matrix of alarm windows, some of which are driven by the DCCs and some of which are hard-wired to so-called “contact alarm units” in the conventional control logic. These are used to provide system-specific indications of alarm conditions and include essential alarms which will be needed should the control computers fail. The stand-up panels themselves contain a mixture of conventional operating controls (switches, lights, meters, and dedicated PID controllers) and VDUs and keyboards interfaced to the DCCs.

Virtually all CANDU stations have been retrofitted with safety-system monitoring computers to give the operator warning of diminishing margin to trip. These computers monitor buffered signals from the shutdown systems and have a dedicated VDU on the operator’s desk. This enables the operator to take steps to avert a reactor trip. For example, the introduction of new fuel can result in an unanticipated reduction in ROP trip margin during refuelling operations. The trip-monitoring computer alerts the operator, who can then manually reduce the RRS set-point if the margin becomes uncomfortably small.

The CANDU 6 control room uses a “dark panel” approach. When no lights are visible, things are normal.

Behind the control panels is the control equipment room, housing the physical I&C for Group 1 I&C equipment (see Figure 6). Separate equipment rooms are provided for the DCCs.

The detailed control logic for each system is subject to change in the early design stages of a new nuclear plant, and therefore a means has been devised to enable much of the required equipment to be installed before these details are available. Much of the logic equipment, as well as the sensors and actuators, can be installed and wired to the control distribution frame (CDF) before details of the interconnecting logic are known. The interconnection logic is implemented later by wiring discrete connecting wires at the CDF. The CDF is, in effect, a giant junction box about two metres high and several tens of metres long and is a major feature in the CANDU control-equipment room (see Figure 6).

Sensors are typically located close to the parameters being measured. This results in a large

number of sensors being located within containment, although the electronics may still be separated from the sensor elements to facilitate maintenance. The electrical signals are taken through the containment wall by penetrations which are designed to preclude leaks from within containment along the cables.

Actuators are likewise close to the process equipment being controlled. They may use electrical power directly or use electrical/pneumatic converters in the case of loads driven by instrument air. Most of the electrical loads are driven by switchgear located in the turbine building.

6.1 Sensors

For the most part, the I&C systems use sensors that are used in other process control applications. However, because the subject of this text is a nuclear reactor, a description of the sensors used for measuring neutron flux is presented below, with particular emphasis on the in-core flux detectors, which are unique to the CANDU reactor. To ensure the necessary independence, the sensors used by each special safety system are dedicated to the system in question and are separate from the sensors, wiring, and associated equipment used by the process systems.

6.1.1 Neutron flux sensors

When starting up and operating a nuclear reactor, it is necessary to measure neutron power over a very wide range, of the order of 10 decades. During start-up, special neutron counters are used to monitor neutron flux as poison is removed from the moderator using ion exchange. After a prolonged shutdown, special fission chambers are also used temporarily. At approximately 10^{-7} x full power, ion chambers located outside the reactor core come on-scale. In the CANDU reactor, control is transferred to the DCCs at this point, and the neutron counters are removed. The ion-chamber readings provide a logarithmic reading of neutron power, which RRS uses for control up to around one decade below full power.

In an ion chamber, two concentric boron-coated cylinders capture thermal neutrons. The resulting alpha emissions cause ionization of hydrogen gas in the space between the cylinders. A high voltage is applied between the cylinders, which captures electrons caused by this ionization. The resulting current (~100 μA at full power) is amplified and provides signals proportional to bulk linear, logarithmic, and log-rate power which are usable over a wide range (10^{-7} to 1.5 x full power).

In the last decade, between 10% and 100% power, the thermal power in the fuel itself is the variable of interest. A prompt measurement of spatial power is required because any control or shutdown action must take place before local fuel damage can occur. Unlike most process variables, there is no single instrument that provides even a close approximation to the power in each channel of the CANDU core. Yet it is crucial to be able to determine this power because the thermal power in each channel determines the point at which dryout will start to occur. Thermal power is closely related to neutron flux, and therefore determining the latter provides a good estimate of the former.

Neutron flux within the core varies continually, even when the reactor is at constant power, due to the rather slow oscillations (in the order of hours) in the distribution of Xe^{135} throughout the core and to local flux peaks resulting from online refuelling. Although it is not possible to control flux down to the location of a few fuel bundles, it is feasible to control flux tilts between the 14 reactor zones. To do this, the flux in each of these zones must be measured locally.

In-core flux detectors are used in the CANDU 6 reactor to measure local flux power for both control and shutdown systems. They resemble coaxial cables with an Inconel sheath and a central core made of either platinum-clad Inconel or vanadium in the sensitive section, as shown in Figure 8.

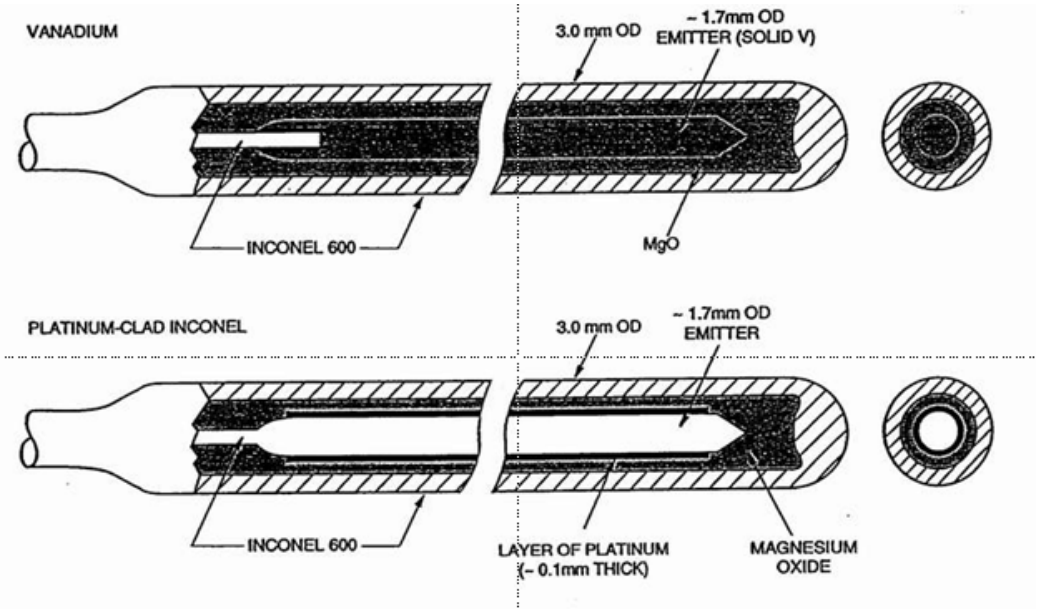

Figure 8 SIR detector geometry.

Vanadium detectors respond primarily to neutrons, but are too slow for either control or shutdown purposes (time constant τ = 335 seconds).

Platinum-clad Inconel detectors provide a signal which is less than fully prompt and varies with age. They respond to both neutrons and γ-rays (proportion approximately 50:50). Because under steady-state conditions γ-flux is proportional to neutron flux, the detector current may be regarded as being proportional to neutron flux. However, although the response of the detector itself to both neutrons and γ-rays is essentially prompt, 30% of the γ-rays which arise indirectly from β-active fission products are delayed, and therefore the overall detector response to a step change in neutron flux is basically about 84% prompt, with the remainder being delayed.

All detectors provide currents of a few microamps and are connected to amplifiers which convert this current to a proportional voltage before passing the signal to the DCCs or to shut-down-system logic. In the case of the SDS detectors, the amplifiers incorporate variable gains, which are adjusted daily to reflect the SDS ROP set-points, and electronic compensation to enable the output signal to compensate for the less than fully prompt detector response (see Section 7).

On Canadian CANDU 6 reactors, all flux detectors are now of the SIR type (straight individually replaceable), incorporating a helium atmosphere. The SIR design facilitates maintenance, and the helium atmosphere has been found to improve reliability.

Neither vanadium- nor platinum-clad detectors provide an absolute response to flux. Their response changes gradually with age and flux exposure in ways that are not yet totally predictable. However, in the short term (e.g., days), their response is repeatable, and therefore if they are calibrated against thermal power, they can provide values which are useful for estimating the thermal power generated in the fuel. This lack of an absolute power measurement contrib-

utes significantly to the complexity of both the ROP protection and power control algorithms. A detailed explanation of this is beyond the scope of this text.

The flux detectors used and their locations are as follows:

- 102 vanadium detectors are inserted vertically from the reactivity mechanism deck. These are used by the flux mapping program in the DCCs. The vanadium detectors are also the basis for the setback on high local neutron flux (see Section 3.4.1)
- 28 platinum-clad Inconel detectors (two for each of the 14 zones) are inserted vertically from the reactivity mechanism deck. In each zone pair, one is in channel A and one in channel C. These are used by the RRS program, the flux mapping program, and the stepback program in the DCCs.
- 34 platinum-clad Inconel detectors are inserted vertically from the reactivity mechanism deck. These are used by SDS1. The detectors are divided between channels D, E, and F.
- 24 platinum-clad Inconel detectors are inserted horizontally and are used by SDS2. The detectors are divided between channels G, H, and J. Future builds are expected to require the same number of detectors as for SDS1.

6.1.2 Other sensors

Most process analog signals are transmitted using 4-20 mA current loops (to help minimize the influence of electrical noise) from the point of measurement to the central control area. Temperatures are measured using resistance temperature detectors (RTDs) and to a limited extent thermocouples.

Given the large ground currents to be expected in generating stations, particular care is needed in sensor wiring to ensure that electrical noise and offset voltages do not corrupt these analog signals.

Contact sensing in the CANDU design uses 48VDC logic, although 24VDC is more common in modern process control equipment. This relatively high voltage has been found to minimize problems with degraded field contacts.

Although some I&C systems have been replaced at various sites with more modern digital equipment, there are still very few, if any, instances in CANDU plants of sensors which use digital communication right from the point of measurement. Because the individual stations make their own design decisions about equipment replacement, they would have to be consulted for accurate information in this regard.

6.2 Actuators

Actuators in CANDU are primarily electrically driven by on/off 48VDC outputs from the control system logic. Small loads may be driven directly, while heavy loads are driven by motor control centres which receive their inputs as 48VDC signals. Some larger valves are pneumatically actuated by electrical-to-air converters, and therefore in addition to the electrical supply system, there is an instrument air system with odd and even channels. Because this system is not described elsewhere, an overview of it is included in Section 6.2.1. Air-driven valves can typically move much more rapidly than electrically driven ones. For example, on CANDU, large air-driven valves are used to isolate containment. Air-driven valves typically use local air accumulators to provide a local power source following loss of the main air supply. This power can

be used to drive air-driven actuators to a predetermined safe position following such an event.

There are a number of proportional actuators, such as the boiler feed-water control valves and the valves which control the flow of light water to the 14 zone controllers.

The CANDU design predated devices that are commanded directly by digital signals sent over a communications network, and therefore such devices will be found only in areas where the original equipment has been replaced.

Although most actuators used in the CANDU design are conventional, the actuators which control spatial power are unique. The reactor is divided for spatial control purposes into 14 zones (see Section 4.1). Each zone contains a cylindrical compartment with a variable amount of light water (see Figure 9). The level of light water in each compartment is controlled by varying the flow of water into it, using a valve whose position is determined by a 4-20 mA controller (normally an output from the DCC). The light water outflow is essentially constant.

The level of water in each compartment is measured by bubbling helium in at the bottom of the compartment and sensing the difference in pressure between the incoming gas and the pressure in the helium balance header connected to the tops of all 14 compartments (see Figure 7).

This system has the advantage of requiring no active components inside the reactor core. It works well as long as no compartment either floods or drains. However, flooding or draining does occur occasionally, and an alternative design which does not have this disadvantage might be worth investigating.

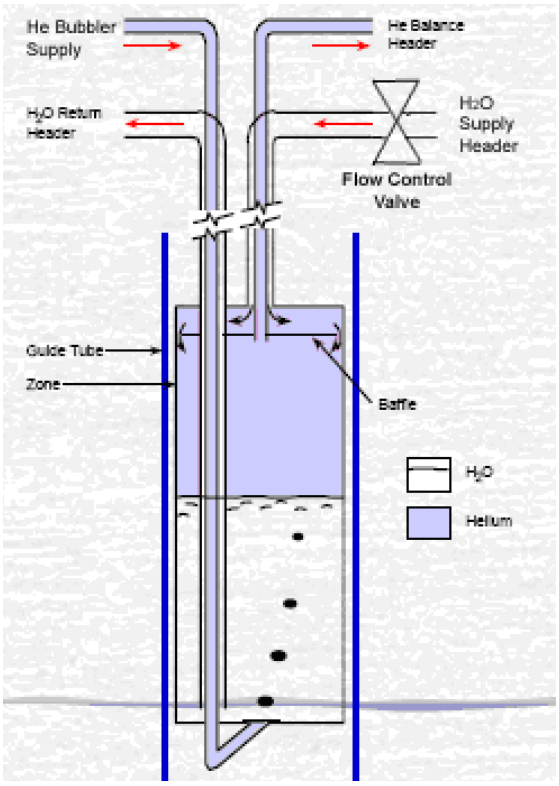

Figure 9 Liquid zone control compartment (simplified).

The absorber rods used for reactor control are very similar to the shut-off rods used on SDS1 (see Section 6.3), except that they are not spring-assisted and use hydraulic damping to limit their rate of movement, allowing them to be caught in mid-fall should a stepback to other than

zero power be required,

The adjuster rods have no rapid movement capability. The winches that control their position are driven by electric motors connected to a variable-frequency supply.

6.2.1 Instrument Air System

Pneumatically operated valves are very common in the process control industry in general. These valves include on/off and continuous control valves and are typically commanded by an electrical signal. Compressed air for these valves is supplied by the Instrument Air System, a service system which, in a manner somewhat analogous to the electrical system described in Chapter 11, distributes compressed air to the numerous end-user devices throughout the plant. Like the electrical system, the instrument air system provides channelized sources and distribution paths to ensure that the appropriate degree of redundancy and separation is available. The compressed air provides a powerful force multiplier, and operation of the end devices also tends to be relatively fast. The requirements for both instrument air and electrical power systems are covered in a common document [CSA2011b].

This description will concentrate on the reactor-building instrument air system because it is of greatest interest in terms of nuclear safety and reliability. Within the reactor building, there are about 130 on/off valves and around 70 continuous-action control valves powered by instrument air. Prominent among the former are the valves which initiate liquid poison injection for shutdown system #2, the dousing valves, the containment isolation dampers, and the moderator temperature-control valves, all of which play significant roles in ensuring plant safety. The reactor-building instrument air system is seismically qualified.

Refer to the greatly simplified schematic in Figure 10.

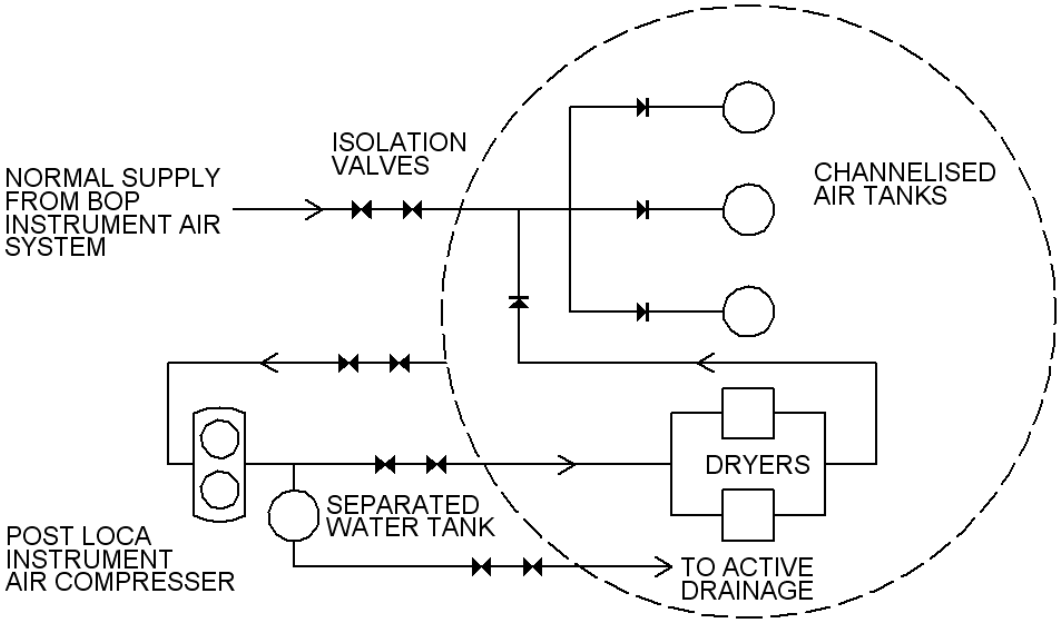

Figure 10 Reactor building instrument air system (simplified).

During normal plant operation, the reactor-building instrument air system receives its supply of compressed air from the same bank of compressors that provide instrument air for the remainder of the plant. These are located in the turbine hall and run off Class 3 electrical power, so that air supply is subject to interruption for a five-minute period in the event of a loss of Class 4

power. The air passes into the reactor building through a single line equipped with two isolation valves in series, which are operable from the control room and provide containment isolation, typically following a LOCA. A number of the pneumatic actuators inside the reactor building are required to operate in the immediate post-LOCA period and must be able to operate during the five-minute interruption caused by loss of Class 4 power. Therefore, a set of three air-storage tanks is provided inside the reactor building to provide the necessary compressed-air reservoir. Note that many of the loads are on/off and have to execute only a single movement in this time frame. The single supply line branches within the reactor building to feed these tanks, each feed being equipped with its own dual isolation valves and a check valve to preclude loss of the tanks' contents in the event of a loss of supply air. Therefore, the three tanks provide a short-term source of triplicated, uninterruptable instrument air within the reactor building. The air, once it has been used, is vented to the reactor-building atmosphere and will eventually be exhausted through the building ventilation system.

Following a LOCA, containment ventilation will be isolated, and continued use of the normal instrument-air source described above would tend to pressurize the reactor building gradually. To address this concern and permit continued long-term use of pneumatic actuators in containment following a LOCA, a separate post-LOCA instrument-air source is provided on recent CANDU 6 plants. This post-LOCA instrument-air (PLIA) system consists of a compressor located outside the reactor building and two redundant dryers located inside the building, together with a number of isolating valves. This equipment is not seismically qualified. The PLIA system feeds the same reactor-building instrument-air tanks described above through appropriate isolating valves. The compressor draws its inlet air supply from within the reactor building, thus avoiding the tendency to pressurize the reactor building. The PLIA compressor will be brought on-line before the valves isolating the supply of normal instrument air to the reactor building are closed. The air handled by the PLIA system is potentially contaminated, and therefore the system components outside containment are located in isolated rooms. Water removed from the flow, which collects in a tank downstream of the compressor, is returned to the reactor building active drainage through an isolated line.

6.3 Actuators for the Special Safety Systems

In the case of SDS #1, 28 cadmium shutoff rods are used, which drop into the reactor core under gravity, assisted initially by springs. They are held out of the core by electromagnetic clutches which are energized by two-out-of-three logic driven by all three channels, as shown in Figure 11. When any two of the three channels vote for a reactor shutdown, the clutches will be de-energized, and a reactor shutdown will take place.

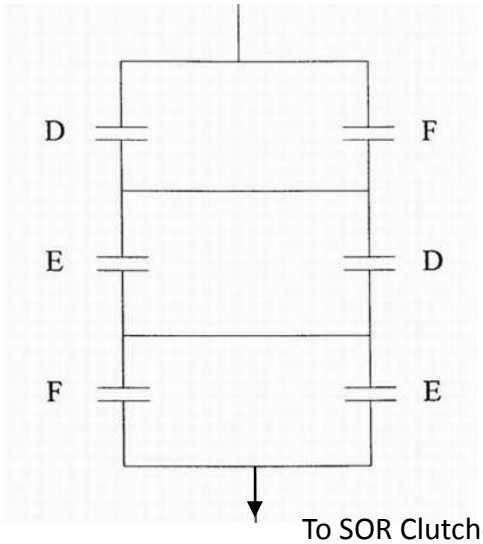

Figure 11 Two-thirds voting logic for SDS1 trip

In the case of SDS2, the contents of six tanks containing gadolinium nitrate/D_2O solution are injected into the moderator using pressurized helium as the motive source. The pneumatically operated valves which connect this pressurized gas to the tanks containing the poison are arranged in a two-out-of-three configuration which is logically similar to that of the electrical contacts shown in Figure 11. Again, a trip in any two of the three SDS2 channels will open the corresponding helium supply valves and trip the reactor.

6.4 Control Logic Technology in the Process I&C Systems

The CANDU design predated the widespread use of digital technology in I&C by perhaps a decade. Nevertheless, the design relies very heavily on digital control technology, which will be described below.

Although the digital control computers (DCCs) are arguably the heart of the CANDU I&C system, they are augmented by a mass of conventional control equipment. For binary control, 48VDC telephone relays were used in the early designs because these were readily available and highly reliable. By the time the detailed design of the CANDU 6 was undertaken, the telephone industry had moved on to solid-state technology, and the telephone relays were replaced by relays designed specifically for the process control industry. By the time Darlington was built, programmable logic controllers (PLCs) were becoming available, and that station used a custom-built PLC to implement much of the Boolean logic.

Much of the closed-loop analog control of the CANDU subsystems is accomplished by general-purpose analog loop controllers for which the parameters are set up as required for the individual application when the plant is commissioned. Because these applications are fairly conventional, they will not be described further here.

6.4.1 Digital I&C technologies in CANDU I&C process systems

The computers used to control the CANDU plant do not use off-the-shelf products designed specifically for digital process control, as is common practice today. At the time of the first CANDU designs, in the mid-1960s to mid-1970s, the number of successful digital control applications world-wide could be counted in no more than double digits, and the available technology was a general-purpose minicomputer with custom-designed process input/output hard-

ware. "Mini" was a relative term. A minicomputer was the size of a small refrigerator and with the associated input/output equipment could well expand to be 10 metres long. These computers were not inexpensive, nor were they noted for their reliability. One did not procure computers in large numbers and deploy them where they were required. Rather, a pair of centrally located computers configured as master and standby was used, and the necessary sensors and actuators were connected to them using discrete pairs of wires (as opposed to communications networks). Networking of computers was unknown. Once the decision was made to use computers, one looked at what other functions, in addition to those that had to be there, could be implemented using this expensive but very flexible resource.

The digital computers on the CANDU 6 implement the following functions:

- Closed-loop control for:
  - the reactor,
  - steam generator level
  - steam generator pressure,
  - turbine loading,
  - heat-transport pressure and inventory, and
  - moderator temperature;
- Control of the fuelling machines, which enable on-power refuelling of the reactor;
- Run-up of the turbine;
- Presentation to the operator of annunciation information for all process systems in the plant;
- Data logging for all process systems in the plant.

A detailed description of the logic implemented in the DCCs is beyond the scope of this text, but as an example, see the description of Overall Plant Control given in Section 4. The architecture of the dual-DCC system is shown in Figure 12.

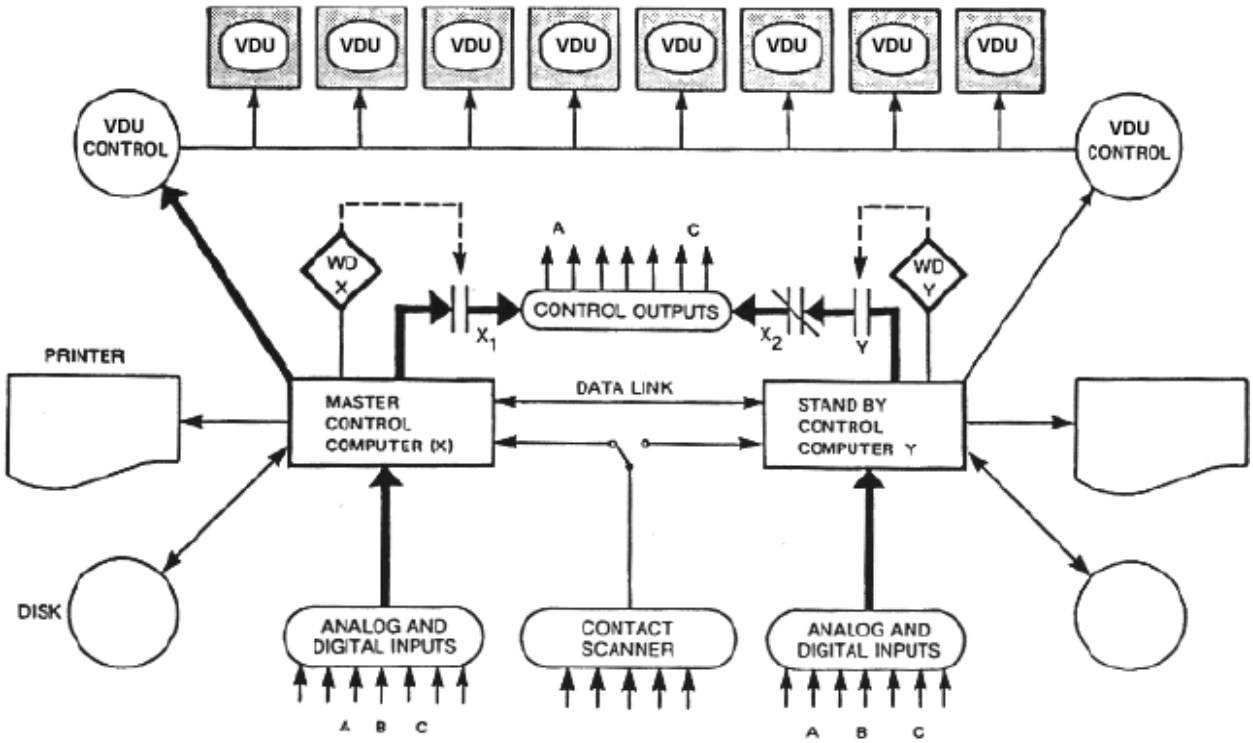

Figure 12 CANDU 6 DCC architecture

All the software was written in assembly language. Although this ensured that the software was as compact and as fast as possible, the result was a program that relied totally on the programmer for its integrity and which was not directly reviewable by other than software cognoscenti.

6.4.1.1 Annunciation and status display

In addition to the inputs needed by the software which controls the plant, several hundred analog and contact inputs are connected to the DCCs to enable alarm information to be presented to the operator and to provide him with status information on the various systems, using the VDU controllers and printers shown in Figure 12.

Alarms are generated within the control logic when abnormal conditions are detected. These conditions are detected either by hardware logic in the control equipment or by tests built into the DCC control software. The alarms are presented to the operator using a combination of illuminated "windows" above the control panels and DCC-driven VDUs in the central area of the stand-up panel. In addition to the alarms generated by the control functions resident in the DCCs, the computers monitor thousands of contact and analog signals, enabling their alarms to be displayed on the VDUs and recorded on a printed log in chronological sequence.

The CANDU alarm annunciation system works well for routine operation and for minor plant disturbances. One can imagine, however, that during major plant disturbances (e.g., loss of Class IV power), the operator is faced with a sudden flood of alarm messages, flashing windows, and horn tones. When Class IV power is lost, many subsystems will no longer be available and will initiate an alarm in consequence, but all that the operator really needs to know is the major event: loss of Class IV power. To mitigate this situation, the CANDU alarm-annunciation scheme uses some very basic prioritization logic. Each alarm is designated as "major" or "minor". When certain predefined plant upset conditions are in progress, minor alarms are temporarily suppressed on the VDUs. Although this does help, there is no doubt that a more intelligent alarm presentation system would be useful. Such schemes have been contemplated in the past and will probably be incorporated in any new CANDU build, but progress has been slow because the conditions under which it is appropriate to suppress any given alarm typically require very careful examination of the operation of the systems involved, meaning that the construction of the database behind such a system would be very labour-intensive. This would appear to be an ideal application for some kind of expert system. However, there is great reluctance to implement any system whose response to a given plant upset is not completely deterministic. The approach to such intelligent annunciation systems has always been very conservative. One can imagine the repercussions if it were determined in some post-event investigation that suppression of a particular alarm had resulted in incorrect operator action.

6.4.1.2 Fuelling-machine control

The on-line refuelling function is unique to the CANDU design. On the CANDU 6 stations, fuelling-machine control is implemented in the DCCs. On many of the Ontario 4 unit stations, this function has separate, dedicated computer controls provided by the fuelling-machine vendor, but again, minicomputer technology is used. Unlike the closed-loop process-system control discussed earlier, control of the fuelling machines is an example of sequential control. The computer carries out a step in a sequence and then checks that the expected feedback indications have been returned from the plant before moving on to the next step. Each step

consists of a single predefined action and a set of post-action checks. A job is made up of a series of steps. Jobs may be executed automatically from start to finish or may progress one step at a time under operator supervision. In any event, if the expected feedbacks do not materialize, execution stops, and the operator is alerted.

The sequential actions required to complete each fuelling activity (i.e., a "job") are defined in an interpretive language developed specifically for the CANDU fuelling application. Although not as readable as a modern sequential control language, this language does provide the reader with some level of isolation from the underlying assembly-language logic. The operator can allow the job to proceed entirely automatically or can elect to require his permission between each step and the next.

Because fuelling is not required on a continuous basis, the fuelling-machine function is only implemented in a single DCC.

6.4.2 Historical perspective

As an indication of how the technology has changed in 40 years, the CANDU 6 DCCs had 64K bytes of memory and a one-megabyte disc drive. The central processor cycle time was around one microsecond. To maximize performance, the machines were programmed in assembly language. Every byte of software was custom developed. A previously developed operating system was not used, for example. The result is a system which, although very flexible, requires outdated skills to maintain and is also particularly prone to errors in software maintenance. However, all attempts to migrate to more modern equipment have been rejected because of the financial consequences of any delays or errors in implementation of a replacement system. Although aging DCC equipment has been replaced, changes have been made at the individual hardware module level, with custom replacements being engineered to match the fit, form, and function of the old equipment, and particularly to have minimal impact on the existing software. The DCC equipment does not support the standard techniques which have evolved over the years for the development of highly reliable computer systems. Standards such as [CANDU1999] would be applied to the systems and software engineering of any new-build design. The replacement of the DCC platform is undoubtedly one of the greatest challenges facing the designers of a new-build CANDU.

6.5 Logic Technology in the Special Safety Systems

On all CANDUs before the CANDU 6, the algorithms for making the trip decision were implemented entirely in hardware (primarily by analog comparators). This tends to mean that the trip set-points for each parameter are constant values because implementation of set-points which are themselves functions of another plant variable becomes rather complex.

6.5.1 Digital I&C technologies in CANDU 6 shutdown systems

With the need to have two diverse trip parameters for each postulated accident, it became difficult to identify suitable parameters with fixed set-points without imposing a large penalty on reactor power or incurring an increased frequency of unnecessary reactor trips. The decision was made to use set-points for some process trip parameters that were functions of other plant variables, notably reactor power. Means of generating these set-points using analog electronic hardware were examined, but ultimately the decision was made to implement the trip logic for process trips (i.e., trips not based on reactor power measurement) using digital computers.

They were not, however, called computers, but were referred to as "programmable digital comparators" (PDCs).

6.5.2 Digital I&C technologies in Darlington shutdown systems

Given the success of the PDCs on the CANDU 6, the decision was made on Darlington to go further. Not only would both nucleonic and process trips be implemented in computers, but separate computers would be added to support automated testing of the shutdown systems. Darlington would be the first reactor in the world to feature completely digital shutdown-system logic. In recognition of this, the term "PDC" was dropped. At Darlington, the equipment was called "trip computers". It was recognized that additional steps would have to be taken to ensure high quality in the software engineering which implemented the trip logic. What was not recognized was just how onerous this process would become.

In the ten years that elapsed between CANDU 6 and Darlington, the software industry had matured immensely, and computers were being used to an increasing degree in applications involving public safety. The experience had not been entirely positive. Lives had been lost as a result of software errors. In fact, one of the landmark case studies cited in software engineering texts involved a radiation-therapy machine engineered by AECL which resulted in several deaths before the software design errors were identified and corrected. Interested readers can Google the "Therac-25".

When the design of the Darlington shutdown-system software was undertaken, it was recognized that there was a problem, but the appropriate systems engineering standards had not yet been written that would establish acceptable ways to address the problem. The Darlington shutdown systems became a stepping stone in the development of these standards, but the program encountered serious delays and cost overruns. A product of this effort was a series of standards written by AECL and Ontario Hydro governing the engineering of software for safety-related applications at various levels of criticality [CANDU1999].

The international safety-related systems industry has since introduced a standard which is applicable not only to software development, but also to systems engineering of safety-related systems using digital technology in general [IEC2001a]. A derivative of this standard applicable specifically to the nuclear industry also exists [IEC2001b], but it has yet to be broadly adopted by the Canadian nuclear industry.

Despite the early experience at Darlington, the end result is a system that is well regarded by operating and regulatory staff.

7 Regional Overpower (ROP) Trip Logic

Description of the ROP logic has been deferred to this point to enable the characteristics of the sensors involved to be discussed before describing how these are accommodated in the design. The following discussion is applicable to both SDS1 and SDS2.

The CANDU 6 ROP systems currently have 34 and 24 flux detectors in shutdown systems 1 and 2 respectively. Hence, there are only 8 to 12 detectors per channel, yet each channel is required to protect against fuel dryout in any one of the 380 channels in the core. As discussed in Section 6.1.1, the detector signals represent only point values in the distribution of flux throughout the core. Moreover, the outputs decline with age and are not completely prompt.

The trip comparator associated with each ROP detector is set to a value determined offline by a computer code "ROVER" to ensure that at least two detectors in each SDS will call for a trip before dryout occurs at any location in the core. The computer code considers a large number of normal and abnormal reactor configurations, but does not account for non-equilibrium fuelling. Typically, with new pressure tubes, this comparator set-point will be around 122%, although it declines as the pressure tubes age. The code is re-run and the comparators are adjusted infrequently (e.g., once every three years) to account for changes that affect thermal hydraulics, such as pressure-tube creep. The comparator setting includes the desired margin to trip.

The RFSP (Reactor Fuelling Simulation Program) code is run frequently (e.g., once every three days). It synthesizes a flux map based on the reactor's power and fuelling history, on reactivity mechanism positions, and on the 102 vanadium detector readings. The power in each channel *j* in the channel-power peaking factor region (all but the outer extremity of the core), CP_j, is then computed and divided by the reference power for that channel, $CP_{ref\ j}$, to yield the normalized channel power:

$$P_{norm\ j} = CP_j/CP_{ref\ j}.$$

The highest $P_{norm\ j}$ becomes the channel-power peaking factor (CPPF, typically around 1.08). Therefore, the CPPF represents the worst-case power peaking factor due to refuelling ripple over all channels. The detector amplifier gains are then adjusted so that they read (current reactor power x CPPF). It can be seen that this approach is quite conservative because it assumes that all detectors will be affected equally by the channel at greatest risk. This purpose of this calibration is to compensate for changes in position of the reactivity mechanisms and for local flux changes due to fuelling. It also incidentally compensates for decreasing detector sensitivity with age. Typically, one or two detectors per channel will be found to be out of limits in any particular adjustment cycle.

Each detector amplifier also includes two filters which compensate for the non-prompt response of the detector itself. These are not normally adjusted. The compensated signals passed to the comparators represent a fairly close approximation to the thermal power in the fuel, which is what causes dryout, and hence is the signal on which the reactor needs to be tripped. The effect of this compensation is shown in Figure 13.

The set-points for both SDS1 and SDS2 are based on the same criteria, including trip margins, and therefore it is a matter of chance which system will trip first. Indeed, in the case of a slow LOR, it is likely that SDS2 will trip first because it has fewer detectors and hence its set-points must be somewhat more conservative. In the past, there was an incentive to arrange things so that SDS1 would trip first because it could be re-poised much more quickly and potentially avoid a reactor poison-out. Nowadays, the analysis associated with restarting the reactor after any trip is sufficiently time-consuming that a poison-out is inevitable in either case.

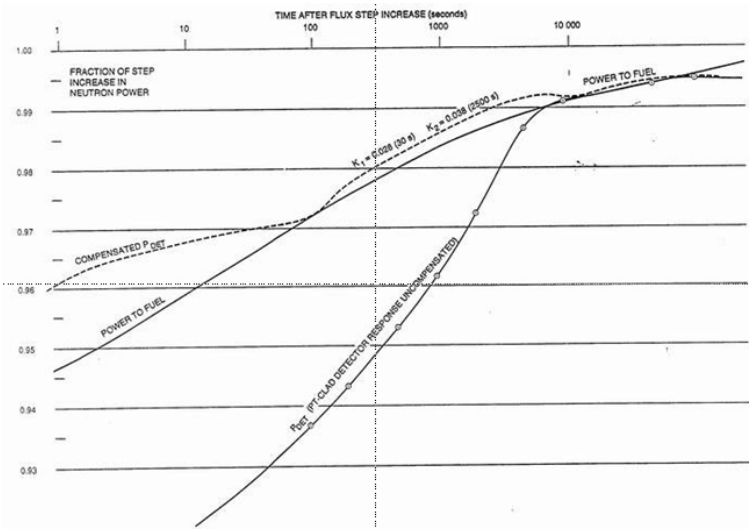

Figure 13 Effect of compensation on Pt-clad detector response

Clearly, there are many uncertainties involved in determining the trip set-points, both in the comparator settings determined by ROVER and in the calibration of the detectors to account for CPPF. Typical uncertainties are:

- simulation uncertainties
- detector uncertainties
- uncertainties specific to a given SDS channel
- common uncertainties
- CCP uncertainties
- refuelling uncertainties
- uncertainties due to the effects of moderator poison.

These uncertainties are combined statistically and incorporated into the comparator settings, the intent being to ensure that at least one detector in each SDS channel will trip in a given shutdown system before dryout occurs, 98% of the time,. As noted in Section 7, two channels must trip before a reactor trip occurs. The CANDU 6 and Ontario reactors use different methods of justifying compliance with this 98% criterion, but achieve similar results.

Uncertainty in any trip set-point results in its being assigned a conservative value. In the case of ROP set-points, this results directly in a loss of plant capacity, and therefore any improvement in understanding the uncertainties is likely to result in higher trip set-points, which will have an immediate economic payoff. Even a 1% increase, for example, results in an increased power capacity of 60,000 MWh per year for a 600-MW station. Depending on the going rate for power, that is worth several millions of dollars every year.

8 Design Verification

All CANDU systems were subject during the design process to a design review carried out by their designers' peers. This review was based on the detailed design documentation produced for the customer. With each succeeding design generation, the documentation became more comprehensive. However, the process-systems review was never based on the detailed comprehensive list of system requirements which is typical of best-practice systems design in a modern engineering context.

In the case of the special safety systems, the situation is better because it was necessary to demonstrate detailed compliance with the safety requirements.

For closed-loop control systems, the dynamic performance of the control algorithms is of major interest because any instability can require close operator attention at best and operator/automatic action up to and including shutting down the plant in the worst case. The design of the CANDU controls was carried out before computers that could simulate plant dynamics in real time were available. The performance of the proposed algorithms was checked using plant models and models of the control algorithms run on a mainframe computer in batch mode. For readers who never knew the days when telephones had wires, a mainframe computer occupied a large room buried in the bowels of the design office, consumed many kilowatts of power, was attended by a staff of dozens of technicians, and executed jobs fed to it in the form of decks consisting of thousands of punched cards. You submitted your job and waited a day or two for the results to be returned. These took the form of endless columns of numbers printed by a line printer on reams of fanfold paper.

The plant models used for such verification were not themselves subject to any formal verification.

In the case of the special safety systems, dynamic performance was of critical interest because any unexpected delays in initiating a trip could lead to fuel damage. In this case, the codes used for verification, such as Cathena, have been subjected to formal validation.

Over the life of the CANDU 6 plants, all sites have added operator training simulators which closely mimic the performance of the subject plant in real time. Although these models have not been formally validated to serve as engineering simulations (i.e., as accurate representations of the process dynamics), it has become common practice to verify any significant control system changes on the operator training simulator before implementation. This not only provides some assurance that the changes to the control algorithms will work, but checks any associated changes to the human/machine interface. The training simulator has been particularly effective in enhancing the level of confidence in changes to the DCC software because the simulators typically emulate the DCC processor, which means that the new DCC software can be loaded and run on the simulator. It should be noted, however, that due to possible lack of fidelity in the plant models used in training simulators, successful operation of the changes on the simulator does not offer a guarantee that the change will be trouble-free on the plant itself.

In the past, no new-build CANDU plant has had a training simulator installed when it was originally commissioned. In today's regulatory environment, availability of an operator training simulator before commissioning has become a requirement. This will lead to a situation where it becomes very important to be able to adapt the operator training simulator rapidly to reflect changes made to the plant design before and during commissioning.

9 Bringing the CANDU I&C Design into the 21st Century

The most advanced CANDU design to be built up to this time is Darlington, which went into service in 1990. Since that time, the instrumentation and control industry has seen a revolution. Key to this change has been the enormous progress in digital electronics and communications. Distributed control system technology is now predominant in I&C system implementation, and standard computer workstations bring almost unlimited computer power to the information management functions supporting plant operation.

During the intervening years, at least three new CANDU designs have been embarked upon, yet none has been developed to the point of implementation. These were the CANDU 3, CANDU 9, and the Advanced CANDU Reactor (ACR). All these featured I&C technology which was current at the time. One might think that, given the advances in computing power, the design of the control systems for these plants would present few problems. Yet this was far from the case.

In a modern distributed control system (DCS), use of which is standard practice in the I&C industry today, the physical inputs are typically digitized close to the field instrumentation. The digital data are then carried over a communications network to one of a number of processing units in which the control algorithms are executed. The control commands are then networked to output stations located near the controlled actuators. The algorithms in the input, processing, and output modules typically run asynchronously, and inter-processor communication is also typically asynchronous. Therefore, the time delays from input to output are no longer deterministic, as is the case for a DCC. If the resulting uncertainties are to be negligible, everything has to run many times faster in a modern system if the same dynamic performance is to be guaranteed in the worst case.

Modern DCS systems have the advantage of being programmed in application-specific high-level languages, frequently using graphical representations of the logic, which make the design much more susceptible to review by outsiders. However, many vendors' products use proprietary languages which are not readily portable to a different vendor's product, should it become necessary to replace the control system at some stage in the life of the plant. An international standard does exist for programmable controller languages [IEC1993], but adoption of this standard has not yet been widespread.

Periodically, the prospect of using some of the more exotic modern I&C technologies such as expert systems, optimal control, neural networks, and fuzzy logic controllers is raised, typically by academics. Many of these techniques have been around since the 1960s, after all. The problem with many of these approaches is that they are typically non-deterministic and therefore difficult to qualify. The regulators quite rightly frown on any design that cannot be guaranteed to produce the exact same response every time it is presented with the same sequence of input conditions.

The old adage, "If it ain't broke, don't fix it", is very good advice. Any change to the existing design must show that it can provide enhanced power output, greater plant availability, and/or lower operating costs if it is to be seriously considered. In this chapter, the author has attempted to point out some features of the existing design that may benefit from re-design in any future CANDU new build.

9.1 Technological Obsolescence

Although Darlington is the last clean-sheet CANDU design developed, there have been several new builds of the CANDU 6, notably in Wolsong, Qinshan, and Cernavoda. Moreover, a number of existing plants have faced the need to replace control equipment as its reliability declined due to age and lack of spare parts.

Perhaps the highest-profile equipment items involved which were not susceptible to plug-in replacement were the shutdown-system computers for the new-build CANDU 6 plants and the DCCs.

The PDCs were replaced with more up-to-date distributed control system hardware. However,

due to the relatively small amount of logic involved and the fact that the PDCs are not geographically distributed, the new design was able to avoid reliance on digital communications. Architecturally, then, the new PDCs were little different from the systems they replaced. The functions of the safety-critical software running on the existing equipment were re-engineered for the new platforms. Although this re-engineering was by no means a trivial task, the existence of well-documented requirements and accepted procedures [CANDU1999] for carrying out this work made it fairly routine.

The replacement approach for the DCC hardware took a very different approach. The obvious approach to DCC replacement is to use a modern DCS, as discussed in the previous section. However, DCC replacement has the potential to lead to a very protracted and costly plant outage if anything goes wrong during the replacement or if the software implementation proves to have defects once the plant is brought back online. To minimize this risk, the fundamental requirement of the plant owners has been to replicate the existing control logic in precise detail.

The existing DCCs contain a large body of purpose-designed software, ranging from the operating system to dozens of applications whose details are specific to each CANDU site. The most reliable definition of the functionality of this software is the program listing itself, which is written in a machine-specific assembly language.

As stated in the introduction, the design and implementation of the analog control loops implemented in the DCCs are based on classical frequency-domain techniques. At a detail level, the control logic consists of an interconnected set of gain elements, integrators, and differentiators. However, because these elements are ultimately implemented in assembly language and are specified in the form of difference equations, the basic structure of the control logic is far from obvious to anybody reviewing the detailed design. Translating the existing control logic into the context of a modern DCS platform with a high degree of confidence that the platform change will not introduce latent errors would be a formidable task. Not only is there a risk of errors in the interpretation of the software functionality, but the different architectures of the two platforms make emulation of real-time performance very difficult to guarantee.

Therefore, if a DCS were used to replace these DCCs, the DCC logic would have to be reverse-engineered and a new DCS-based design developed and re-validated from the ground up. No plant owner or CANDU 6 replication project manager has accepted this risk. The alternative was to custom-build replacement computer equipment which would be fit-, form-, and function-compatible with the existing hardware and which would host the existing software with relatively minor changes.

As it happened, the CANDU industry was not the only one to be confronted with this problem, and replacement computer hardware based on more modern components had been developed for both the Pickering A and CANDU 6 DCCs. These “clone” computers served as a starting point for the refurbishment of these units, a process which is still ongoing.

All this means that all existing CANDUs will run with aging I&C technology for the next couple of decades and that the first CANDU new build, should there be one, will be the proving ground for the design, licensing, and implementation of what is now standard practice for the I&C industry, assuming that the “clone” DCC is not retained.

The design life of a CANDU plant is around 40 years. With refurbishment, this could well extend to 70 years or more. Each generation of I&C technology becomes obsolete in about 15 years,

particularly if one is speaking about digital equipment. The manufacturers of the equipment typically will not guarantee to support their product beyond about 20 years, though if one happens to pick a particularly successful product line, this date might be extended by another 10 years. Therefore, any nuclear plant will have to face replacement of its digital I&C equipment at least twice in the lifetime of the plant. In the case of the original CANDU DCCs, the original equipment was specifically developed in Canada by a custom systems integration supplier who owned much of the design data and was able to purchase the rest from the original equipment manufacturers. Manufacturers of off-the-shelf I&C products are not interested in this kind of re-engineering business. However, by far the most economic and reliable solution in the future will be to base the I&C on off-the-shelf equipment. Design for replacement has not so far been a requirement on next-generation reactors. This is a challenge that should be accepted. The existing refurbished CANDU plants will probably have to face this issue with their DCCs at least once more during their extended lifetimes because it is hard to imagine the present vendor still providing support in 2040. In future replacements, it is unlikely that development of a replacement platform which can run the existing software will be practical, and therefore the issue of rewriting the software when the equipment is replaced will have to be faced. If a hardware platform which supports the industry-standard languages [IEC1993]is used, this offers some hope that the existing software will be portable. However, the industry in general has shown little inclination to adopt these languages, meaning that there is no guarantee that this approach will yield the desired advantages.

10 Summary of Relationship to Other Chapters

By this point, the reader will be aware that the architectural design of the control systems is heavily dependent on the safety requirements that these systems implement, and on the necessity to avoid unnecessary interruptions of the plant's *raison d'être* – the production of electrical power. Chapter 13 provides an excellent description of the safety requirements, and should be read in conjunction with the material presented herein.

Chapter 5 provides a discussion of the reactor physics, including the control actuators which the RRS and shutdown systems use to control reactor flux.

I&C systems are only as good as the motive power sources that drive them—in the case of CANDU, primarily Class I and II electrical power and instrument air. The design of the electrical power distribution system is presented in Chapter 11. A brief description of the instrument air system is included in Section 6.2.1 of the present chapter.

11 Problems

1. Starting with an equilibrium reaction, assume that a control rod is moved out of core by a fixed distance. What form will the curve of reactor power vs. time assume?
2. Given the approximate numbers quoted in Section 2 and assuming that the light-water zone controllers are initially half full, in the absence of any other control or shutdown action, what value would the power in a CANDU reactor reach in one second if all the light-water zone controllers suddenly drained? Assume that initial power = 100% and that the total reactivity worth of the zone controllers = 7 mk.
3. From the point of view of reliability, why is it important in a reactor with two shutdown systems that the two systems be independent?

4. In the CANDU design, what is the probability of occurrence of an uncontrolled increase in reactor power which is not stopped by at least one of the shutdown systems?
5. What is the cost, in lost power production, of an outage leading to a 40-hour poison-out of a CANDU reactor? Assume that the electrical output = 700 MW and that the utility is paid 3.5 cents/ kW hour.
6. The two-out-of-four architecture used on many PWRs has one major advantage over two-out-of-three logic. What is it?
7. Some of the factors that can cause a shutdown system to fail to perform its design function are:

    1. Earthquakes
    2. Flooding
    3. Localized physical damage to the system
    4. Electromagnetic effects
    5. Design/analysis shortcomings.

    Steps which are taken to minimize the impact of these factors on the system as a whole include:

    a) Multiple equipment groups (wide physical separation)
    b) Channelization (physical and electrical separation)
    c) Equipment/technology diversity
    d) Equipment qualification
    e) Multiple activation parameters
    f) Fail-safe design (i.e., the safe state is the de-energized state).

    Prepare a table assigning one or more of these lettered steps to the numbered factors above.
8. Prepare a succinct statement which captures the key differences between a setback and a stepback in the CANDU I&C design.
9. Self-check is not listed as one of the stepback parameters. So why is a self-check sometimes referred to as a "seismically qualified stepback"?
10. If it is assumed that every dual DCC failure leads to a poison-out, that DCC failure is required to lead to a poison-out not more than once in three years, and that, on average, it takes 20 minutes to get a DCC back in operation following a failure, what is the design target for mean time between failures of a single DCC?
11. Name a factor that could cause an MTBF calculation based on hardware failure rates alone to be very optimistic.
12. The logic to avoid flooding of the light water zones precludes filling them beyond about 90%. What action will RRS take if the zones fill, but a positive power error persists?
13. What sensors drive the logic providing primary protection against slow LORs in a CANDU? What is the rationale for not providing diverse logic to protect against this event?
14. What is a key difference between the ECCS and containment systems with respect to continued availability of electrical power?

15. What would be some key requirements for the secondary control area?
16. It has been suggested that the control system be made capable of initiating a power set-back on low margin to trip. What possible objection could there be to such a proposal?
17. What are the potential effects of a failure of the air-conditioning system which services the room housing the DCCs?
18. Why might the CDF be less relevant in the context of modern I&C technology?
19. List some pros and cons of digitizing instrument readings inside containment.
20. When using thermal measurements to calibrate flux-detector readings, what processing will have to be applied to the flux-detector readings before they are compared to thermal power measurements?
21. Why are ion chambers not used for control in the upper decade (10% to 100%) of reactor power?
22. Why do you think digital sensors have seen limited application in retrofit projects on existing CANDU power plants?
23. What would be the most demanding requirement facing a potential replacement for the level measurement in the light-water zone compartments? Suggest some possible technologies which might be used.
24. What long-term factors might require the operator to adjust bulk reactivity using moderator poison?
25. What characteristics of the CANDU design drove the choice to use digital computer control before it was a widely accepted technology?
26. What are some negative consequences of having the control logic defined in software written in assembly language?
27. What would be a major reason that an annunciation scheme based on expert system technology might be difficult to license?
28. Give an example of a non-proprietary language which would be appropriate to the definition of sequential control logic.
29. List some advantages to making shutdown-system testing an automatic function.
30. List two reasons why software is often considered to be particularly prone to design errors.
31. Which ROP adjustment accounts for the changing shape of flux within the reactor core?
32. Why will the ROP trip comparator set-points need to be adjusted downwards as the pressure tubes age?
33. Give an example of a non-proprietary language which would be appropriate to the definition of (a) analog and (b) Boolean control logic.
34. In what way does the architecture of a distributed control system, as opposed to that of a centralized computer system, affect the execution timing of the control logic?

12 References

[Rouben2002] Rouben, B. *Introduction to Reactor Physics*, Atomic Energy of Canada Ltd., September 2002.

[Rouben2008] Rouben, B., *Reactivity Coefficients*, McMaster University course EP 4D03/6D03, September 2008.

[AECB1977] AECB. *Regulatory Document R-10: The Use of Two Shutdown Systems in Reactors*, AECB, January 11, 1977.

[AECB1991a] AECB. *Regulatory Document R-8, Requirements for Shutdown Systems for CANDU Nuclear Power Plants*, AECB, February 21, 1991.

[AECB1991b] AECB. *Regulatory Document R-7, Requirements for Containment Systems for CANDU Nuclear Power Plants*, AECB, February 21, 1991.

[AECB1991c] AECB. *Regulatory Document R-9, Requirements for Emergency Core Cooling Systems for CANDU Nuclear Power Plants*, AECB, February 21, 1991.

[CSA2011a] CSA. *N290.4-11: Requirements for the Reactor Regulating Systems of Nuclear Power Plants*, Canadian Standards Association, October 2011.

[CSA2011b] CSA *N290.5-06: Requirements for Electrical Power and Instrument Air Systems of CANDU Nuclear Power Plants.*

[CANDU1999] CANDU. *Standard for Software Engineering of Safety Critical Software, CE-10010STD, Revision 2*, CANDU Computer Systems Engineering Centre of Excellence, December 1999.

[IEC2001a] IEC. *IEC 61508, Functional Safety of Electrical/Electronic/Programmable Electronic Safety-Related Systems*, International Electrotechnical Commission, June 2001.

[IEC2001b] IEC. *IEC 61513, Nuclear Power Plants – Instrumentation and Control for Systems Important to Safety – General Requirements for Systems*, International Electrotechnical Commission, March 2001.

[IEC1993] IEC. *IEC 61131-3, Programmable Controllers, Part 3: Programming Languages,* International Electrotechnical Commission, March 1993.

13 Acknowledgements

The following reviewers are gratefully acknowledged for their hard work and excellent comments during the development of this Chapter. Their feedback has much improved it. Of course the responsibility for any errors or omissions lies entirely with the authors.

Werner Fieguth
Dave Fournier
Norm Ichiyen
Alek Josefowicz

Thanks are also extended to Diana Bouchard for expertly editing and assembling the final copy.

CHAPTER 11

Electrical Systems

Prepared by
Dr. Jin Jiang[1]
Department of Electrical & Computer Engineering
Western University

Summary

This chapter covers grid requirements, station power systems, and major electrical components in CANDU nuclear power plants (NPP). Grid requirements at an NPP location are discussed in terms of reliability and availability of off-site power, the need for a secure electricity supply for the electrical generation process, and the role of electricity in ensuring the safety of CANDU nuclear power plants. The chapter also describes the operating principles of the major pieces of electrical equipment found in a CANDU plant.

The chapter is divided into four parts. In the first part, general and nuclear safety-based principles and practices for the design of electrical systems in CANDU 6 plants are listed.

In the second part, the main electrical connection to the power grid is explained. The concepts of switchyard, protection schemes, grid connection, and synchronization are also addressed from a CANDU NPP point of view. The chapter considers situations involving electric power production during normal operation, as well as power consumption for maintaining plant safety during shutdowns. The relationship between internal station power, generated power, and grid power is clarified in light of reactor safety.

The third part discusses the internal plant electrical system. The section offers a detailed classification of power sources by their reliability levels and explains the interrelationships among them. The section also provides a justification for the classification of these power sources and introduces the concepts of DC power sources, standby power supplies, and emergency power systems.

The final section briefly introduces the major electrical systems and devices in a CANDU plant, including the generator, transformers, voltage/current transducers, and circuit breakers. The section first explains the operating principles of these systems and devices and then provides their specific ratings and designs in a CANDU plant.

To facilitate learning, a list of exercises has been compiled at the end of the chapter. The reader

1 with contributions of Sections 1.1, 1.2, 3.3, 3.7, 3.8, and 3.9 from Mr. Alek Josefowicz, P.Eng., CANDU Energy (Retired)

should attempt to answer these questions to gain further understanding of the materials presented. Additional information on electrical systems in nuclear power plants can also be obtained through the list of key references provided at the end of the chapter.

It is important to note that electrical systems may vary slightly in different CANDU plants. For example, some diagrams may show elements of shared systems, the CANDU 6, as a single unit design where the design principles exclude sharing except for the switchyard. The main goal of this chapter is to provide a basic knowledge of electrical systems in a CANDU plant, rather than to examine details of a specific plant.

Learning outcomes

- The goal of this chapter is to provide students with a clear understanding of the importance of the availability of electrical power for maintaining the safety of a nuclear power plant under conditions different from the normal mode of operation, but which are, however, within the conditions evaluated in the safety analysis report.

- Students should be able to explain why grid power is as important to the safety of an NPP as the power output from the NPP is to the grid.

- Students should be able to identify any deficiency in the reliability of the power grid at the power station location.

- Students should be able to read the station power distribution diagram by identifying different classes of power sources, i.e., Class I through Class IV. They should also be able to match the names of the safety-related systems with the corresponding power classes.

- Students should be able to describe the relationships among the different classes of power sources.

- Students should be able to explain the functionalities of both standby generators and the emergency power system.

- Students should be able to list the major systems involved in power generation and transmission.

- Students should be able to explain the principles of energy conversion from mechanical energy to electrical energy through synchronous generators.

- Students should be able to describe the functionality and working principles of the excitation and cooling systems of the synchronous generators.

- Students should be able to describe the working principles of transformers and voltage/current transducers, as well as to identify where in the plant they are used.

- Students should be able to identify and describe the different types of circuit breakers and disconnect switches.

- Finally, students should be able to explain how the generated electricity is delivered to millions of customers.

Table of Contents

List of Figures

List of Tables

1 Introduction

1.1 General

Even though the sole objective of a nuclear power plant is to generate electricity, it takes electricity to run the entire plant. The electrical power system in a nuclear power plant is the subject of this chapter. The electrical systems are designed not only for normal plant operation, but also for conditions other than normal operation, so that plant safety can be maintained by ensuring continuity of electrical power supplies regardless of transient disturbances or faults during operation and post-shutdown. The power for an NPP comes from diverse and reliable power sources that are physically and electrically isolated, so that any single failure will affect only one source of supply and will not propagate to alternative sources.

Even after the reactor has been shut down, a significant amount of heat is still being produced by the decay of fission products (decay heat). The amount of decay heat is sufficient to cause fuel damage if not removed effectively. Therefore, systems must be designed and installed in the plant to remove decay heat from the core, even in a plant shutdown condition and in the absence of off-site power sources.

The electrical power distribution system (EDS) is a complete load group distribution system with two independent off-site power sources, the main turbine generator, and on-site standby power sources (standby and EPS diesel generators and, in some cases, a station blackout generator).

1.2 Nuclear Safety-Based Design Principles and Practices for a CANDU EDS

- The EDS needs to be designed in accordance with its safety functional requirements as defined in the safety analysis, including independent and diverse provisions aligned with independent safety functions and including provision to supply electrical power to secure plant safety during both normal operation and accident conditions without losing all on-site power.

- The divisions of the power supply systems should be physically and electrically separated from each other, thus ensuring independence among the divisions as much as possible.

- The Group 1 and Group 2 power supply systems should be physically and electrically separated from each other as much as practically possible.

- The design of the EDS and associated support systems, including I&C, HVAC, and cooling systems, should follow the classification, independence, redundancy, and diversity requirements placed on Structures, Systems, and Components (SSCs).

- The EDS should be designed for a wide range of electrical transients which can be assumed to occur during plant operation and for the assumed environmental conditions.

- The EDS should be designed for or protected from effects of both internal and external hazards, such as short circuits or loss of the power grid.

The EDS uses commercially available conventional hardware with provisions as dictated by the need for seismic qualification (SQ), qualification for operation in a harsh environment (EQ), and radiation hardening. Electrical containment penetrations (ECP) form part of containment.

2 Electrical Power Grids and their Connection with an NPP

2.1 A Holistic View of Electrical Systems between an NPP Station and the Grid

Even though each specific plant may have its own unique characteristics, a typical set of electrical connections between a CANDU station and the power grid is illustrated in Fig. 1.

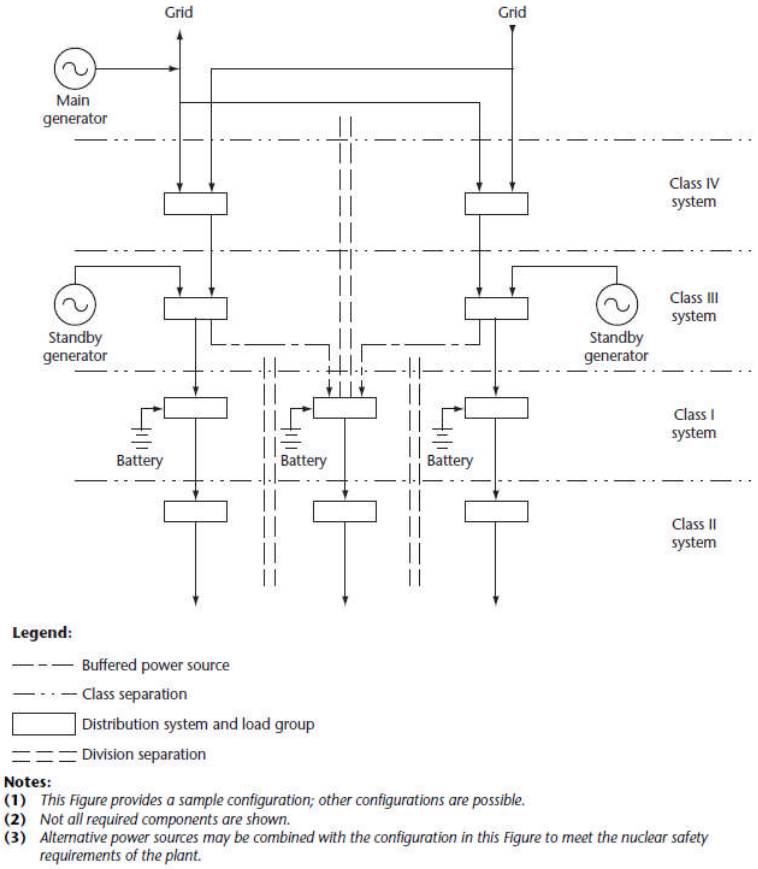

Fig. 1 - Relationships between the station power and the power grid [1].

A station can have either a single reactor unit or multiple reactors. During normal operation, the generated power is fed to the power grid through *main output transformers* (MOTs). In addition, a portion of the generated power is also fed back to the units to support electricity

production through *unit service transformers* (USTs). Furthermore, it is good practice to cross-link multiple units at the switchyard to increase self-reliance within the station, particularly in situations where one shutdown unit may need to draw power from other units within the station to remove decay heat from the reactor, to maintain essential operating services, or to re-start the reactor as long as it has not been poisoned out by xenon.

When the power from the station units is no longer sufficient or available to meet internal demand, the station can draw additional power from the grid through *station service transformers* (SSTs). This is also the case during a start-up process.

It is assumed that the power grid is stable and that there are other power sources connected to the grid, which are available when needed to provide power to the nuclear station site itself. The power flow on the grid can be effectively controlled through grid interconnection and management systems. The NPP may contribute to voltage and power control in the grid. However, most existing CANDU power plants operate in a constant-power output mode to support the base load supplied by the grid.

2.2 Unique Grid Power Requirements for NPP Safety

The main objective of a nuclear power plant (NPP) is to produce electricity to support industrial, commercial, and residential loads. Electricity is therefore the final product for most NPPs. However, it is important to realize that about 8% of the electricity produced by the plant is consumed internally to support power production. This is true for most power plants, such as coal or gas, although their internal consumption may be significantly lower (<4%). NPPs, however, have unique requirements for electric power availability. It is particularly important to have a secure electrical supply when an NPP is in a shutdown state and is not producing any electricity of its own. Even when the fission process in a nuclear reactor stops, a significant amount of decay heat continues to be generated from the fission products. The amount of heat is typically so large that continued cooling is absolutely necessary to protect the fuel sheath from melting. Pumping cooling fluid through the core removes this excess heat, but requires an external electrical power source. Hence, the availability of electrical power (from other units or from the grid) is crucial for the safety of CANDU and other nuclear power plants both under normal operations and in a shutdown state. This includes situations where thermosiphoning is used. Electrical power is required in this case to maintain water in the steam generators, although pumping of primary coolant is not needed.

This unique requirement for electricity requires consideration of different scenarios at the design stage of NPP electrical systems. In CANDU power plant design, the NPP site must be chosen so that the power grid at the site has multiple feeders from different and independent (often geographically separate) sources, as shown in Fig. 1. This requirement ensures that off-site electrical power sources are available to the station for removing decay heat when the reactor is shut down and is no longer producing electrical power of its own. In addition to Canadian standards [1,2] for a CANDU NPP, the International Atomic Energy Agency has also issued guidelines for selecting suitable sites for other types of NPPs based on the reliability and

availability of off-site power [3,4], as has also The Institute of Electrical and Electronics Engineers (IEEE) [5]. As explained in Chapter 13, the availability of off-site electrical power will affect NPP safety analysis.

As a part of the site selection process, the reliability of the grid must be assessed when some of its generating capabilities are assumed to be no longer available. This is often referred to as the (*N*-1) problem [6], where *N* is the number of available units. A desirable site for an NPP is one where power delivery to the NPP site is still guaranteed when only (*N*-1) or (*N*-2) suppliers are available.

The main cause of the 2011 disaster at Japan's Fukushima Daiichi nuclear power plant was a lack of off-site power due to the earthquake and inadequate protection of on-site standby power systems against a tsunami. All the plant's on-site diesel generators operated until they were damaged by the water brought in by the earthquake-induced tsunami. Hence, the leading cause of the disaster was the lack of power after the successful shutdown and an initial period of reactor cooling.

Together with other facilities in a CANDU plant, the electrical systems must also meet the seismic design requirements and qualification processes as outlined in [7] in Canada.

2.3 Switchyard between the Grid and a CANDU NPP Station

Note that even though a single line is used to show the flow of power in Fig. 1, all lines carry three-phase power (except DC power lines). All transformers, circuit breakers, and transmission lines in an AC power grid are three-phase devices. When delivering the generated power to the grid, the station power must be synchronized with the grid, including the phase sequence, voltage levels, and AC power frequency. Voltage and current transducers are used for monitoring and control, and several high-voltage, high-current circuit breakers are placed between the MOT and the grid connection points.

The switchyard contains numerous control and protection devices to ensure that any faults on the grid side will not induce major disturbances to the station, and vice versa. There are also various interlocks to prevent the incorrect operation of power devices, as well as lightning arresters, grounding protection systems, and switchyard control systems.

2.4 Summary

Even though the main function of an NPP is to produce electricity to supply power to the grid, unlike other types of thermal power generation systems, an NPP requires an external power source with on-site backups to remove decay heat from the reactor when the plant is in shutdown mode and is not producing its own electricity. Therefore, significant design considerations have been formulated for the electrical systems within a nuclear power plant. Furthermore, the availability of off-site power also plays a crucial role in nuclear power plant

safety and is one of the most important considerations in the site selection process when constructing a new NPP.

3 Electrical Systems Internal to a CANDU Plant

3.1 Sources of Electrical Power for CANDU NPP Station Use

Almost all systems within an NPP rely on electrical power to operate. A "defence-in-depth" strategy for electrical power supplies is to rely on diverse, multiple, and independent sources. These sources for a CANDU unit are: (1) power generated from the unit itself; (2) power generated from other units within the same station; (3) off-site power obtained from the grid; (4) the emergency power supply; (5) the standby power supply; and (6) batteries. The power sources in a CANDU NPP consist of both AC (alternating current) and DC (direct current) power. "Defence-in-depth" as applicable to the electrical systems can be stated as follows:

- 1st line – normal operation (grid + main generator)
- 2nd line – mitigation (standby generators + batteries)
- 3rd line – station blackout (batteries + designated alternative source(s))
- 4th line – severe accident management (additional, diverse, alternative sources).

These sources are arranged in such a way that they supply power to station systems during normal operation, as well as during emergency conditions to maintain NPP safety. The equipment in the station is also graded according to its importance to safety. In an event that electrical generation is lost, limited alternative power sources will be used first and foremost to keep the essential safety-related systems operating.

A CANDU plant contains several buses at different voltage levels. The selected voltage levels might be different in different plants to meet certain country-specific requirements. One example is shown in Fig. 2, where the output voltage level of the generator is at 22 kV, and the voltages at the unit service transformer (UST) and the station service transformer (SST) are at 11.6 kV and 4.16 kV as secondary voltages. However, in other designs, these voltages could be 13.8 kV and 4.16 kV. Also shown in Fig. 2 are two connections to off-site power at the NPP site, one at 500 kV and the other at 220 kV.

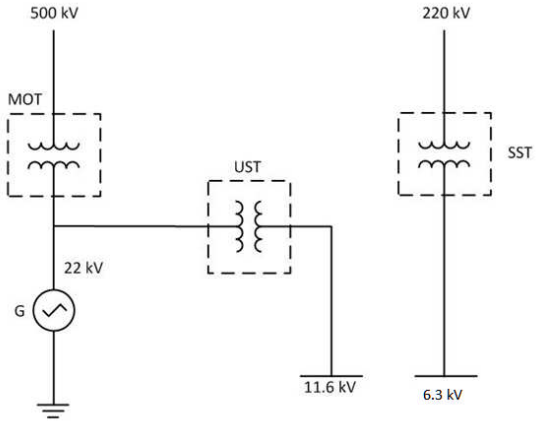

Fig. 2 - Voltage levels within a CANDU plant.

Several other low-voltage buses exist throughout the plant and will be discussed further in the next section.

3.2 Class Definition of Power Sources

Electrical power sources in a CANDU plant can be divided into four levels, according to the allowed duration of voltage interruption that can be tolerated by the loads they supply. Class I power supplies loads that cannot be interrupted. Loads on Class II power can tolerate ~4 millisecond interruptions. Loads on Class III can withstand power interruptions of up to 5 minutes, whereas Class IV loads can tolerate loss of power indefinitely. The most critical and safety-related control and protection systems are powered from Class I and II sources. Different classes of power supplies provide power to different systems, depending on the amount of power the systems require and their relative importance to safety.

Typically, the cost per kW will decrease as the power supplies move from Class I through to Class IV. The power capacities also increase from Class I to Class IV. The allowable interruption times and capacities of the various power sources are summarized in Fig. 3.

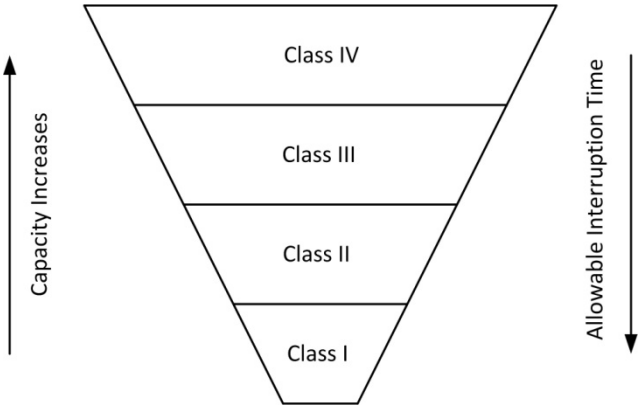

Fig. 3 - Allowable interruption time vs. capacity of the different power classes.

To determine which class of power should be used to supply a specific system, the safety functionalities of the system must be examined, as well as the economic impact if that supply were unavailable. General criteria for matching the class of power supply to the load that it supports are summarized in Table 1. They are expressed in terms of the longest power interruptions that will not affect the safety of either the NPP or its personnel.

Table 1 - Classification of power sources

Class of power	System load characteristics
Class I	Power can never be interrupted under postulated conditions
Class II	Power can be interrupted up to 4 milliseconds
Class III	Power can be interrupted up to 5 minutes
Class IV	Power can be interrupted indefinitely

Different stations may have slight variations in electrical power system configurations. An illustrative diagram showing interconnections in the electrical power system for the different classes of power sources in a CANDU station is presented in Fig. 4.

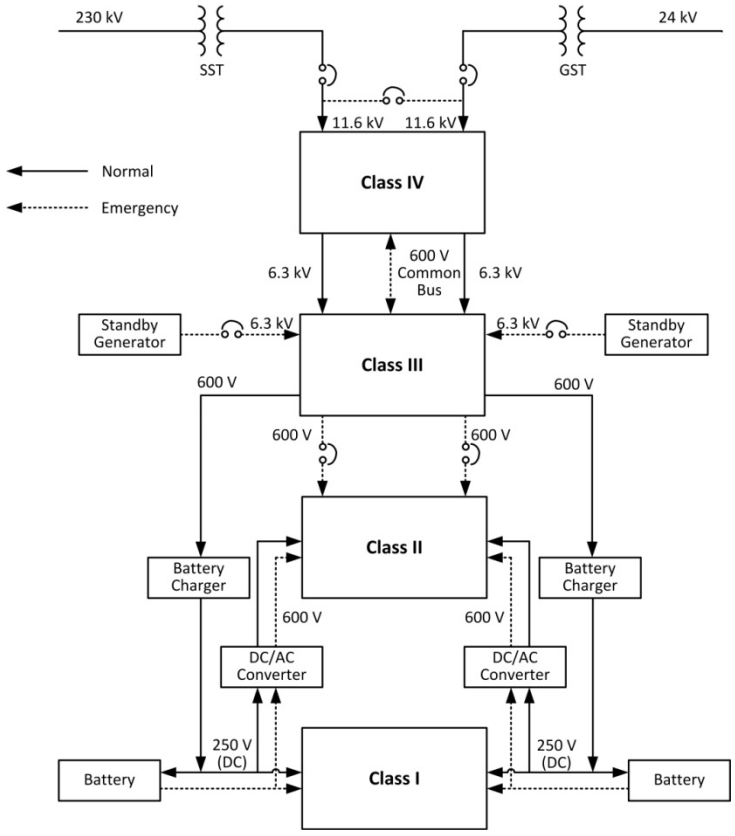

Fig. 4 - Interconnections of different classes of power supplies.

To increase reliability further, Class II, III, and IV power are distributed through two separate

power divisions. If a failure occurs on one division, the equipment connected to the other bus will still be available. In CANDU plants, these two divisions are typically denoted as "Bus A" and "Bus B" or as "Odd Bus" and "Even Bus". During design, loads are distributed evenly between these two divisions.

An example of such a split-bus connection is shown in Fig. 5. A symbol with two circles and an arch over them represents a circuit breaker. Circuit breakers are used to connect or disconnect the systems (denoted as loads) and to protect them whenever a fault occurs. The connection between the Odd and Even buses on the diagram represents two circuit breakers, one on each bus. To accomplish the connection, both breakers must be manually commanded to close.

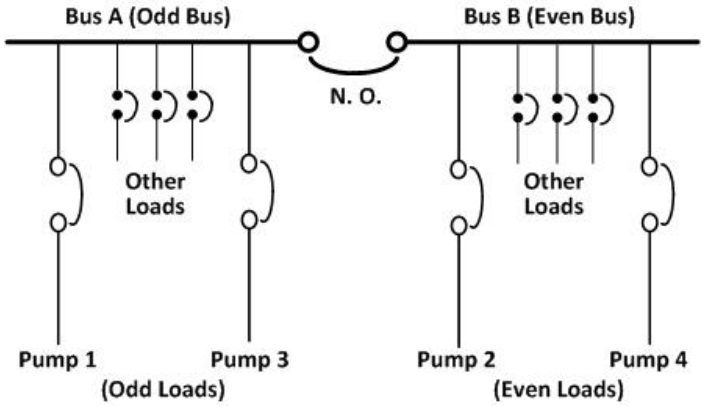

Fig. 5 - Dual-bus configuration for power distribution systems.

3.3 Channelization

Important functions use three instrument channels to provide immunity against single instrument faults. A control channel consists of interconnected hardware and software components that process one of the duplicated or triplicated signals associated with a single parameter. A control channel may include sensors, data acquisition, signal conditioning, data transmission, bypasses, and logic circuits. This defines a subset of instrumentation that can be unambiguously tested or analyzed from end to end. For safety and high-reliability applications, I&C system design uses three instrumentation channels with a two-out-of-three voting strategy (i.e., two of the three channels must be outside the acceptable limits to trip or actuate the system).

To perform on-line tests in such a design, the operator will place the tested channel in a trip state, resulting in the actuation logic performing a one-out-of-two test on the remaining channels. Process and safety systems channels are assigned as shown in Table 2.

Table 2 – Channelization.

System(s)	Safety Group	Odd (**A**) Associated Channels	Third (**B**) Associated Channels	Even (**C**) Associated Channels
RRS and Process	1*	A	B	C
SDS1	1	D	E	F
ECC (NSQ)	1	K	L	M
SDS2	2	G	H	J
ECC (SQ portion)	2	KK	LL	MM
Containment	2	N	P	Q

- The channel association also applies to separation of power supplies and cabling. During normal operation, channels A, B, and C of the UPS supply all their associated channels.

- Group 1 is primarily for power production, and Group 2 is only for safety systems. Physical separation is required between the two groups.

- Group 2 systems can also be powered from the EPS. Functional and physical separation is maintained even though in this situation, only one EPS generator supplies one bus from which the three channelized power sources are derived.

- '1*' denotes non-safety, however, it is associated with Group 1, and

- NSQ means "not seismically qualified", and SQ means "seismically qualified".

3.4 Electrical Power Sources under Different Classes

3.4.1 Class I

Class I power is used to supply loads that cannot be interrupted. It is a DC power source with three independent distribution channels, each backed with battery banks to provide uninterrupted power to critical loads. To maintain adequate charge on the batteries, each bus in Class I is connected to power rectifiers, which convert AC power from Class III power sources to DC to charge the batteries, as shown in Fig. 4. During normal operation, power from the rectifiers is used to support the load on this bus while charging the batteries at the same time. Hence, the batteries always remain fully charged when power is available. DC/AC inverters are also used to convert DC power from Class I to Class II. In the event of a loss of Class III power, batteries provide a seamless transfer to support the loads without any interruption. Note that the batteries are capable of supplying the load on the DC buses for only about 60 minutes, depending on the particular plant design. This is a very critical time window because all Class I and II power would be lost if Class III power could not be restored within the interval provided by the batteries.

The loads supported by the Class I power source are very sensitive and are critical to NPP safety

and operation. A partial list of system equipment powered from Class I is provided in Table 3.

Table 3 - Equipment supported by Class I power supplies.

Class II inverters
DC seal oil pumps for generator
DC lube oil pump for turbine generator bearings
Turbine trip circuits
Turbine turning gear
DC stator cooling pumps
Control and protection systems for station electrical distribution systems
Logic, control, command circuits, and operator interfaces for process and safety systems (48 VDC)

The capacity of the Class I power source is based on the connected load. CANDU plants use several different voltage levels for this DC power supply, including 48V, 220V/250V, and 400V, all to meet the needs of the NPP's various systems. Note that loss of Class I power is one of the conditions that trigger the shutdown systems.

To prevent service interruption caused by a "single line-to-ground" fault, the 48V DC and 250V DC systems are ungrounded. Ground fault detectors, which produce an alarm whenever a ground fault occurs, are provided for each bus.

3.4.2 Class II

Class II power sources are critical to reactor operation. If Class II power is lost, the reactor will be shut down immediately. Under normal operation, Class II power is obtained from Class I sources through power inverters to convert DC power to AC power, as can be seen in Fig. 4. If for any reason the inverters cannot supply a given bus, the Class III power source will be used to support Class II power distribution.

The Class II power source supports those devices and systems that can tolerate power interruptions on the order of milliseconds. Some typical systems supported by Class II power source are listed in Table 4.

Table 4 - Equipment supported by Class II power supplies.

Digital control computers
Reactor regulation instrumentation
Electrically operated process valves (600 V power distribution)
Auxiliary oil pumps on the turbine and generator (600 V power distribution)
Emergency lighting (600 V power distribution)

Three independent channels of single-phase inverters ensure complete supply independence to the triplicated instrumentation and I&C. Class II power sources are relatively low-capacity, have two voltage levels: 120V and 600V, and are available only in AC form.

3.4.3 Class III

Class III power supports large process loads that are unsuitable for Class II power supplies. They are used mainly to maintain fuel cooling when the reactor is in a shutdown state and Class IV power is unavailable. It is important to note that the duration of the loss of Class III power consists of only the time required to start up a standby generator and re-load the Class III power system, which is normally about five minutes.

Class III power is taken from Class IV power. In the event of total loss of auxiliary power from off-site sources, the auxiliary power required for safe shutdown will be supplied from physically and electrically independent diesel generators located on-site. Each power source (the feeds from Class IV and the diesel generators) is physically and electrically independent up to the point of connection to the Class III buses. This improves the reliability of Class III power, making it available even in the presence of partial loss of Class IV power sources.

If the Class IV power source for a unit fails completely, it is still possible to obtain Class IV power from other units in a multiple-unit station. Once the standby generators are started, they will provide power to systems supplied by the Class III power source, ensuring that these critical systems remain functional.

Some typical systems supported by Class III power sources are listed in Table 5.

Table 5 - Equipment supported by Class III power supplies.

Auxiliary boiler feed pumps
Auxiliary condensation extraction pumps
Shutdown system cooling pumps
Turbine turning gear
Heat transport feed pumps
Moderator circulating pumps
Class I power rectifiers
Fire water pumps
Emergency core coolant injection pumps
Instrument air compressors
End shield cooling pumps
Service water pumps

The voltage level of Class III power is 4.16 kV, and its capacity can range from 6 to 8 MWe.

3.4.4 Class IV

Of the four classes of power sources in a NPP, Class IV supplies loads that can tolerate infinite interruption. This power can come from two sources. During normal operation, Class IV power is obtained from the main generator through the unit service transformer (UST). Using power

produced internally by the plant's own generator minimizes the potential impact of disturbances from the grid. Class IV power can also be obtained from the grid through the station service transformer (SST) when the UST becomes unavailable.

It is important to mention that even though Class IV power supplies the entire station during operation, it is not actually required for safe reactor shutdown, although the unit will be shut down immediately upon experiencing the loss of its Class IV power source.

The loads normally supplied by Class IV power are systems which can tolerate long-term power outages without affecting the safety of equipment, personnel, or the public. These loads are not essential to satisfy fuel cooling requirements following a reactor or turbine trip, but are essential for operation of heat sinks above the shutdown level of reactor power. Some typical systems supported by Class IV power sources are listed in Table 6.

Table 6 - Equipment supported by Class IV power supplies.

Main boiler feed pumps
Main heat transport circulating pumps
Condenser cooling water pumps
Generator excitation
Heating and ventilation equipment
Normal lighting systems

As can be seen from Table 6, many important systems in a CANDU plant are supplied by Class IV power sources, and the loss of Class IV power is considered to be a major incident. The preferred voltage levels for Class IV systems are 13.8 kV, 4.16 kV, and 600 V.

3.5 Load Transfer among Different Buses

As shown in Tables 3 to 6, NPP system loads are distributed among the various buses based on their size and importance to system safety. Although a detailed examination of each load is beyond the scope of this chapter, Fig. 6 provides an illustrative load diagram for the Class IV and Class III power buses.

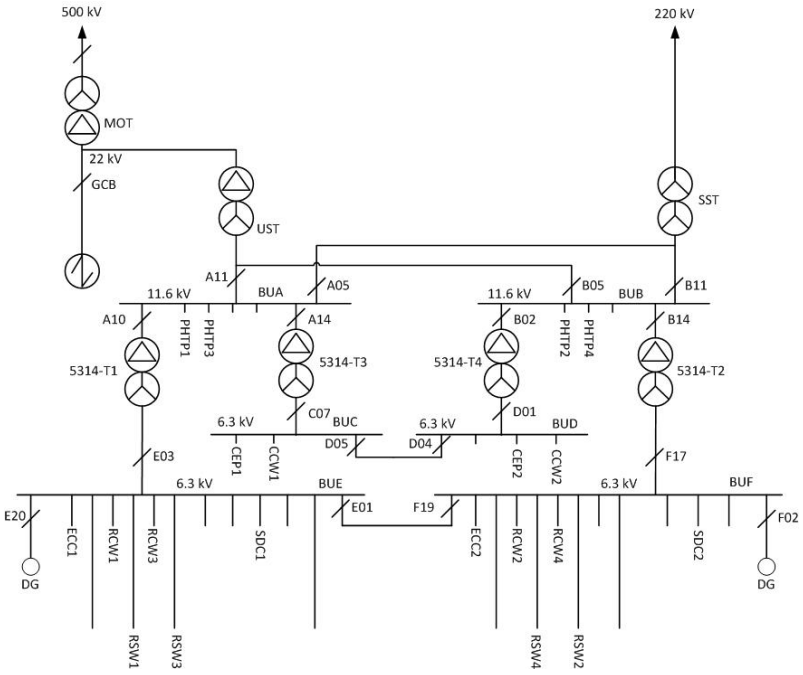

Fig. 6 - Load distribution on the Class IV bus in a CANDU plant.

Under certain circumstances, it is desirable to shift loads from one source to another. There are three modes of load transfer:

- parallel transfer
- fast transfer, and
- slow transfer.

These specific transfer schemes are used at the upper voltage level of Class IV to prevent reactor trip and maintain generation production.

The *parallel transfer* mode consists of two steps: (1) parallel the new power source to the existing one, and (2) remove the existing one to complete the transfer. A *fast transfer* switches the load quickly (within two power cycles) so that little interruption is observed. The *slow transfer* operates after the voltage has decayed to approximately 40% to limit the maximum voltage that could be applied to a connected load upon re-energization and can be used only if the supply transformers can tolerate the inrush currents and if the voltage drop does not prevent loads from being re-accelerated to nominal speeds.

Class IV transfers are manually initiated for normal transfers after start-up or before shutdown and are automatically initiated for reactor trips, turbine-generator trips, or loss of the transmission system. These transfers are accomplished by operating the incoming circuit breakers on the primary Class IV distribution buses to transfer the sources between the unit service transformer and the system service transformer.

Automatic transfer systems are also incorporated into Class II. They monitor the operation of the power inverters and under certain conditions, transfer Class II distribution buses to alternative supplies directly from Class III. These transfers operate within each channel or division of Class II.

There are no transfers in the Class I system because each channel's batteries are charged through two 100%-capacity rectifier-chargers which share the load.

There are no transfers in Class III or in the EPS systems, although it is possible to connect the Odd and Even main distribution buses manually when, following a loss of Class IV power, only one standby generator in the system is operating.

Manual source selection is provided for Class I and II power conversion and distribution to address the condition when, after a loss of Class IV power, only one standby generator is available to power one Class III division.

3.6 Standby Generators (SGs)

To maintain power to safety, safety support, and heat-sink systems following loss of Class IV power sources, CANDU stations contain additional on-site power sources. One type is known as *standby generators*. These generators are not required to be seismically qualified.

This power source is based on two or more generators driven by diesel engines or combustion turbines (in the case of Ontario Power Generation). As shown in Figs. 4 and 6, a generator supplies Class III AC power to each Odd and Even bus at a 6.3 kV level. These generators are supplied with enough fuel to keep the diesel engines running continuously for an extended period of time (up to one week depending on a continued supply of fuel). Standby generator systems have their own compressed air and DC power sources for start-up and will start automatically upon loss of Class IV sources to maintain power to safety and safety support systems. The SGs could form a seismically qualified distribution system, but the design has evolved to create a separate seismically qualified distribution system. The seismically qualified systems are connected to Class III because that is their preferred source of power and are isolated from Class III only when the seismically qualified power sources can provide the required power. The standby generators will also start whenever a loss-of-coolant accident (LOCA) signal is issued, but will not connect to the buses until a loss of Class IV power occurs. Standby generators should be up and running within 30 seconds after receiving a LOCA signal, picking up all designated loads within a further three minutes. One standby generator has sufficient capacity to supply the required loads.

Because of the critical roles played by standby generators, regular maintenance is critically important. This typically consists of starting each diesel generator periodically from the local control panel, paralleling it with the respective division of the Class IV supply, and letting the generators run for a specified minimum period of time.

3.7 Emergency Power Systems (EPS)

The second set of alternative power sources in CANDU plants is known as *emergency power systems*. Unlike standby generator systems, these power sources must be seismically qualified [7], and they function completely independently of other power sources. Similarly to standby generators, the emergency power systems start automatically upon the loss of Class IV power and will also start on a LOCA signal. Under such circumstances, back-up generators provide power to the NPP's critical systems to enable reactor shutdown, monitoring, and decay heat removal. It is expected that the system should be up and running with its intended loads within three minutes.

The following background is relevant to design decisions affecting the EPS:

- Based on plant licensing conditions, a loss-of-coolant accident (LOCA) is a random event because the heat transport system is fully seismically qualified and a seismic event, another random event, is not postulated to occur in the first 24 hours after a LOCA. With 24 hours of operation of emergency core cooling (ECC) and other required safety support systems, a 20–30 minute break can be tolerated in ECC operation. This time is sufficient for the operators to transition from the main control room (MCR) to the SCA and to restart the ECC and the associated systems.

- A total loss of Class IV power coincidental with a subsequent loss of Class III power, both random events (except at Fukushima where Class III was incapacitated by the tsunami, which was induced by the earthquake, but this is a different set of design conditions), but without a LOCA, is a condition in which residual heat is removed from the reactor by means of steam generators and water from the dousing tank. Depressurization of the heat transport system is a precondition for this mode of heat removal. Valves for implementing depressurization and maintaining the required monitoring are powered from a UPS or by compressed air for some valves. There is sufficient time for the operators to initiate the EPS to supplement the dousing tank reserve with an emergency water supply (EWS).

3.8 Grounding and Lightning Protection

The grounding system is required to prevent physical injuries and equipment damage in case of a fault and to minimize electromagnetic effects from ground fault currents as well as to prevent interference and to protect equipment from lightning strikes.

Lightning protection is required so that equipment related to the safety of the nuclear power plant continues to operate and important monitoring devices continue to function when lightning hits facilities or power lines.

3.9 Control of Electrical Loads

Generally, in a typical CANDU power generating station, the electrical loads are remotely controlled using the control logic (relay logic) and interposing circuits, both powered from 48 V DC Class I. The output from the control logic is hard-wired to the switchgear and motor control centre (MCC) control circuits or to the terminals of a solenoid valve when the valve is controlled directly.

Major loads have their mode of operation (ON, AUTO, or STANDBY) selected by the operator from the main control room (MCR) or the secondary control room (SCA). In the AUTO mode, the load will augment the already running load(s) when the process demand exceeds the capacity of the running load(s). In the STANDBY mode, the load will replace the normally running load when the latter fails to operate.

3.9.1 Loads powered from switchgear

Power to the various loads is switched ON and OFF by an individual circuit breaker at the selected voltage level. The circuit breaker protective relays may be mounted within the breaker cell, and the relays interposing between the breaker control circuit and the load's control logic are located in separate cubicles or cells, called the *relay and terminal* (R&T) section, adjacent to each group of circuit breakers.

A typical switchgear control circuit operates from the 250 V DC power source provided by the Class I batteries. The circuit is used to:

- Provide power to the operation of stored-energy devices which operate on the close and trip mechanisms of the circuit breaker.

- Close and trip the circuit breaker in response to commands from the:
  - Unit operator;
  - Process control system;
  - Power circuit protective relays.

Operation of the close and trip circuits requires momentary signals. The circuit breaker controls require manual local reset following a trip due to the operation of power circuit protective relays.

3.9.2 Loads powered from the MCC

Power to these loads will be switched ON and OFF by contactors in individual combination starters. The relays interposing between the contactor control circuit and the load's control logic are located in the relay and terminal (R&T) section adjacent to each group of combination starters.

The circuit breaker in the combination starter is manually operated and, except for

maintenance, remains in the closed position. A typical MCC control circuit operates from the 120 V AC power source provided by the starter's step-down transformer. The circuit is used to energize and de-energize the contactor in response to commands from the:

- Unit operator;
- Process control system;
- Circuit breaker protection and overload relays.

To remain energized, the contactor requires a signal to be maintained. The circuit breaker requires a manual local reset following a trip due to the operation of power circuit protective functions built into the breaker.

3.9.3 Class IV and Class III loads

Typical types of interfacing circuits are:

- MCC and switchgear:
  - Off/On;
  - Off/Auto/On;
  - Off/Standby/On;
  - Off/Standby/Auto/On.
- MCC only:
  - Motorized valve with non-auto control;
  - Motorized valve with auto control.
- Other:
  - Solenoid valve with non-auto control;
  - Solenoid valve with auto control.

3.9.4 Class II and Class I loads

Loads energized from the Class II and Class I (UPS) MCCs or panels perform either special safety-related or personnel/equipment protection-related functions. The control modes are therefore limited to OFF/ON or OFF/AUTO/ON and, in the case of motorized valves, to OPEN/CLOSE or OPEN/AUTO/CLOSE and operate in the same way as the Class III and Class IV loads with the same type of controls.

3.9.5 EPS loads

Loads energized from the EPS are controlled in the same way as when they were energized from Class III, II, and I or will be limited to manual OFF/ON controls.

3.10 Summary

The safety and operating reliability of a CANDU NPP depend heavily on availability of electrical

power to ensure proper operation of its various systems. The electrical power system inside the plant is divided into four classes: Class I, II, III, and IV. Energy for Class I is stored in batteries and can be obtained from the rectified power of Class III sources. Class II power is obtained from Class I through DC/AC inverters or directly from Class III. Standby generators provide alternative power to Class III and EPS systems. Normally, the plant obtains power from its own unit through a UST. It is also possible and permitted to operate the plant with Class IV power supplied through an SST. When a unit stops producing electrical power, power is drawn from neighbouring units through switchyard connections. This may require manual re-configuration (depending on the event) to supply the shutdown unit(s) from the running unit(s) to remove decay heat. When these power sources are not available, grid power can be used to power Class IV through the SST. Once Class IV power is lost, the reactor must be shut down immediately, and heat sink systems are powered from Class III standby generators or the EPS.

In addition, CANDU stations are also equipped with two sets of long-term on-site power supplies, at least one of which is seismically qualified, which are driven by diesel engines. Within the same class, the Class IV, Class III, and some Class II loads in the plant are distributed on multiple and separate buses depending on the number of loads, their power requirements, and the plant's Odd/Even bus philosophy. Class I and Class II power to I&C circuits is supplied through three channelized distribution systems from channelized and independent energy storage and conversion systems. Because Class IV buses are capable of receiving power from either of two supplies and because automatic transfer of supplies is provided on sensing loss of power, reliability of power is ensured, and plant operating safety is increased.

4 Main Electrical Components in a CANDU Plant

4.1 Generators

4.1.1 Basic principle

Electricity output from a CANDU nuclear power plant is generated by a synchronous generator. The generator shaft is directly coupled to that of the steam turbine. The function of the generator is to convert mechanical energy from the turbine to electrical energy to supply electrical loads. A simple illustrative diagram is shown in Fig. 7.

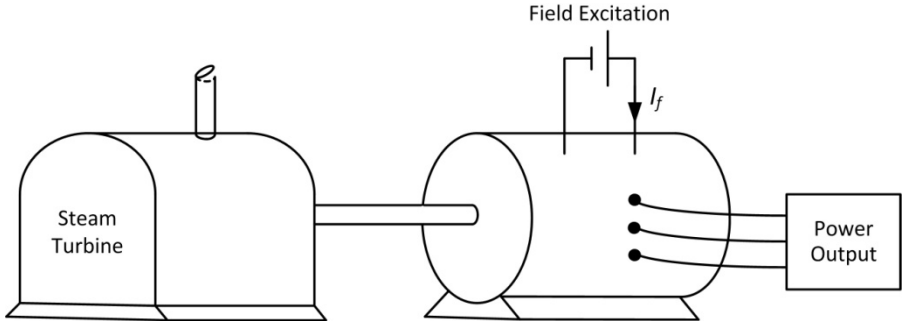

Fig. 7 - Turbine and generator set.

The principle of a generator is based on Faraday's law of electromagnetic induction. The main parts of a generator are a stationary iron core and winding, known as the stator, and a rotating iron core and winding, known as the rotor. When the rotor winding is energized through the field excitation circuit, as the turbine rotates the rotor, a rotating magnetic field is created. The excitation current is supplied to the rotor winding through slip rings. The rotating magnetic flux induces a potential in the stator winding. An illustrative diagram is shown in Fig. 8.

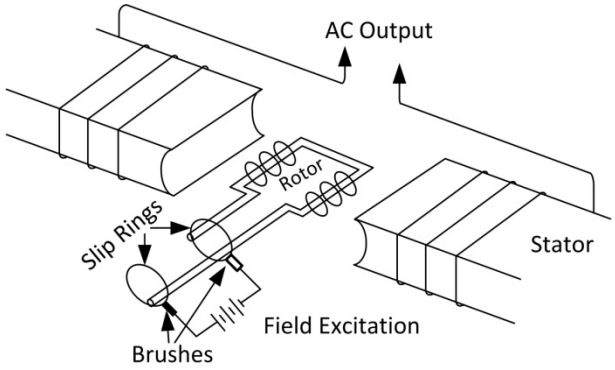

Fig. 8 - Illustrative diagram of a synchronous generator.

Due to the relative positions of the magnetic flux and the stator winding, as the rotor turns, the induced voltage will take on a sinusoidal form. The frequency of the generated voltage will be directly related to the rotational speed. For the two-pole (N-S) machine shown in Fig. 9, one full revolution will produce one full cycle of a sinusoidal wave. If the number of pole pairs on the rotor is increased, a full revolution of the shaft will produce multiple cycles at the electrical output. In other words, it is possible to reduce the rotational speed of the turbine, but still to generate the desired frequency in the electrical output, by increasing the number of pole pairs.

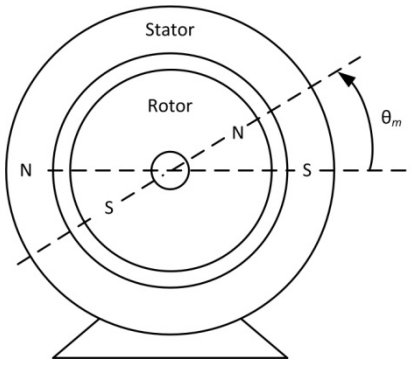

Fig. 9 - A two-pole (one pole pair) synchronous generator.

The relationship among the speed of rotation (n rpm), the output frequency (f Hz), and the number of pole pairs (p) can be stated as follows:

$$n = \frac{60f}{p}.$$

The word *synchronous* means that the magnetic field rotates in synchronism with the rotor. When the stator windings are placed 120° apart as shown in Fig. 10, a three-phase voltage can be generated.

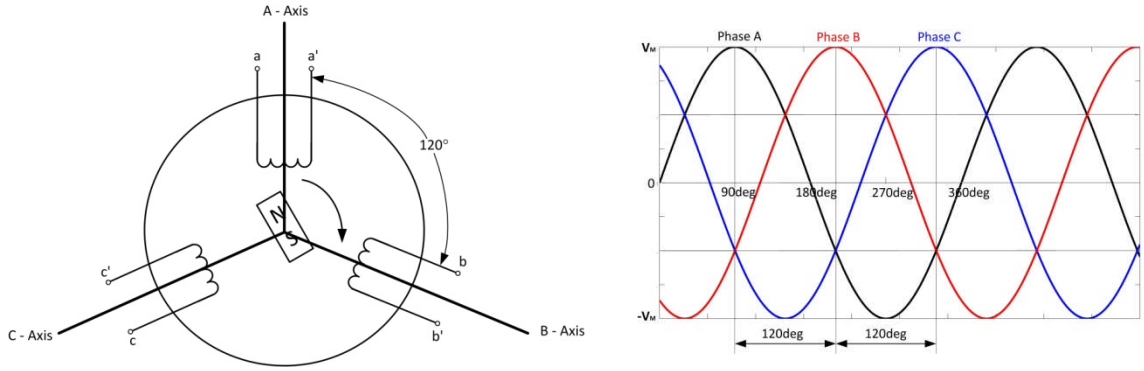

Fig. 10 – Three-phase synchronous generator.

When a load is connected to the output of the stator winding, the generator will transfer the power to the load.

Assume that the currents from each phase can be represented as:

$$i_A = I_M \sin \omega t$$

$$i_B = I_M \sin(\omega t - 120°)$$

$$i_C = I_M \sin(\omega t - 240°).$$

The active power output delivered to the load at each phase can be calculated as:

$$P = i_M v_M \cos \theta_m \quad \text{MW}$$

The reactive power is

$$Q = i_M v_M \sin \theta_m \quad \text{MVar}$$

where i_M and v_M are the phase current and phase voltage.

The angle θ_m is the phase difference between the voltage and the current at the generator output. Hence, the total real and reactive power output from all three phases can be expressed as:

$$P_{total} = 3P = 3 i_M v_M \cos \theta_m \quad \text{MW}$$

$$Q_{total} = 3Q = 3i_M v_M sin\theta_m \qquad \text{MVar}$$

The rated power is

$$P_{rated} = 3i_M v_M \qquad \text{MW}$$

The power factor (*pf*) is

$$pf = cos\theta_m$$

Typically, the power factor is maintained between 0.8 and 0.9. The frequency of the generated power is controlled by a governor on the turbine, and the generator output voltage is controlled by the field excitation through an automatic voltage regulator.

4.1.2 Generators in a CANDU plant

There are several generators in a CANDU plant: (1) the main generator; (2) the standby generators; and (3) the generators in the emergency power system.

The main generator converts the mechanical power from the turbine to electric power that is delivered to the grid to supply power to customers. Typical specifications of a main generator are listed in Table 7.

Table 7 - Characteristics of the main generator in a CANDU plant.

Capacity	817 MVA
Rated output power	728 MW
Output terminal voltage	22 kV
Power factor	0.9 lagging
Frequency	60 Hz
Number of phases	3
Number of poles	4
Rated speed	1800 rpm
Excitation system	Static thyristor exciter
Stator cooling	Water
Rotor cooling	Hydrogen

Typical specifications of the standby generators and the emergency power generators are listed in Tables 8 and 9 respectively.

Table 8 - Characteristics of the emergency power system generator.

Rated output power	1.6 MW
Rated current	183 A
Output terminal voltage	4.16 kV
Power factor	0.8 lagging
Frequency	60 Hz
Number of phases	3
Number of poles	6
Rated speed	1200 rpm

Table 9 - Characteristics of the generator in the Class III power system.

Rated output power	8.2 MW
Output terminal voltage	4.16 kV
Power factor	0.8 lagging
Frequency	60 Hz
Number of phases	3
Number of poles	12
Rated speed	600 rpm

4.1.3 Excitation system

To create a magnetic field inside a synchronous generator, separate windings and an electrical power source must be used. This part of the generation system is known as the *excitation system* and is shown in Fig. 12. The excitation system is essentially a controllable DC source. By adjusting the excitation system output voltage, the output voltage level of the generator can be controlled, and hence the reactive power output. Because the excitation current must be delivered to the windings on the rotor, slip rings are used.

Once the generator is running, power for the excitation system can be obtained from the excitation transformer, which is energized from the Class IV distribution system. The power source can be either the SST or the UST. However, AC power from the generator must be converted to DC before it can be delivered to the rotor windings. In the past, a DC generator coupled to the synchronous generator shaft was used to produce DC power for the excitation system. Nowadays, this conversion is accomplished by a thyristor-based rectifier. Unlike a DC generator, this conversion process has no moving parts; hence, it is often referred to as a *static thyristor-based excitation system*.

During normal operation, the excitation system is often used to (1) control the output voltage level of the generator, and (2) adjust the reactive power output of the generator. A feedback control system, known as an excitation control system, is also used to ensure that adequate excitation voltage is applied to maintain the desired generator output voltage level and the reactive power output. These functionalities are essential to improve the reliability of the generator system.

In the event of an emergency, the excitation system can also be used to provide additional means to improve system stability. For example, when a fault has occurred on the transmission system, the output voltage of the generator can decrease unexpectedly. The excitation system can be used to slow down this voltage collapse, thus improving system stability. If a short circuit in the generator or at the generator output terminal is detected, the excitation system can cut its power immediately to drive the generator output voltage to zero, preventing further damage to the generator.

In a CANDU plant, an excitation transformer is used to step down the generator output voltage from 22 kV to 850 V before sending it to the thyristor-based rectifier. However, different plants may have different output voltage levels. An illustrative diagram of an excitation system is shown in Fig. 11.

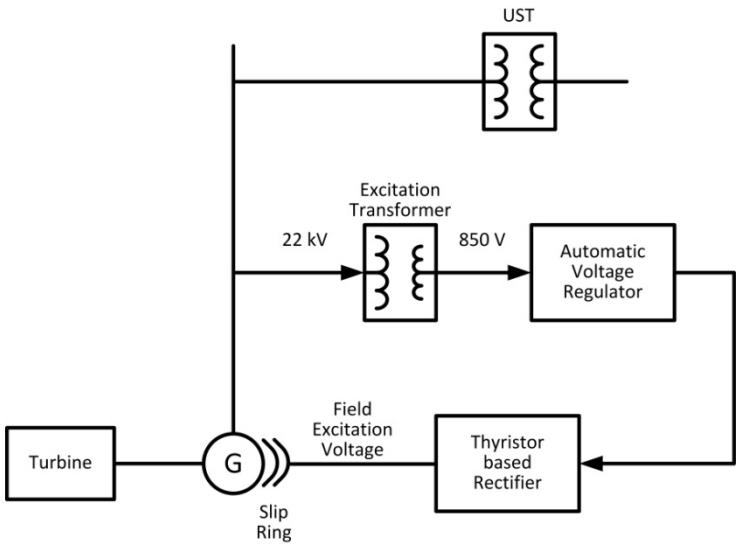

Fig. 11 - Conceptual diagram of a static thyristor-based excitation system.

To start the generator, a separate excitation system must be used. The details will be omitted here. Once the generator starts to operate, a portion of the generated power is used to provide the excitation for its magnetic field. The excitation power is obtained by converting a portion of the 22 kV generator output to 850V AC voltage. This voltage is further regulated through an *automatic voltage regulator* (AVR) and subsequently sent to a thyristor-based static rectifier to convert the AC voltage to DC voltage before sending it to the rotor through the slip ring. The excitation system for the SGs and EPGs is different in that they must start when no additional sources of AC power are present.

4.1.4 Excitation transformer in a CANDU plant

The excitation transformer is a three-phase transformer. Delta (Δ) connections are used on both primary and secondary sides. Specifications of one such transformer are listed in Table 10.

Table 10 - Characteristics of an excitation transformer.

Rated capacity	6,300 kVA
Voltage ratio	22,000 V/850 V
Rated currents	165 A/4,279A
Loss at no load	10,858 W
Loss at full load	46,678 W
Cooling method	Air-cooled

4.1.5 Cooling and protection systems

As electric current passes through the generator windings, heat is produced in both the rotor and the stator. To maintain a safe operating temperature, adequate cooling must be provided. For generators in CANDU plants, water cooling is used for the stator winding, whereas hydrogen is used to cool the rotor winding and the iron cores of both the rotor and the stator.

The main part of the water cooling system consists of two centrifugal pumps and two heat exchangers. The pumps maintain a steady flow of cooling water through the stator windings. The water pressure is controlled by means of a pressure control valve which keeps the loop pressure around 150–200 kPa. The water temperature is adjusted by means of a proportional valve which mixes hot water from the outlet with water cooled by the heat exchanger. The objective is to ensure that the temperature of the water coming out of the stator is around 46°C. The two pumps, rated at 75 kW, are powered by the Class IV electrical system. If cooling water is lost, the generator will shut down immediately. Demineralized water must be used, and dissolved oxygen must be controlled.

The reasons for using hydrogen as a coolant for the rotor and generator are its relatively high thermal conductivity, low density and viscosity. The former property allows effective cooling, and the latter property reduces the windage losses associated with the generator rotor rotation. The main parts of the cooling system are the hydrogen supply unit, the hydrogen cooling heat exchanger units, and the hydrogen leakage detection system. Another critical part is the generator oil seals, which prevent hydrogen from escaping and causing a fire or explosion.

Hydrogen stored at high purity (98%) is injected into the generator air gap between the stator and the rotor. The pressure is controlled through a pressure regulator set at 414 kPa. The humidity of the hydrogen is controlled by a gas dryer heater. Four heat exchanger units are located at the four corners of the generator to maintain the outlet temperature of the hydrogen at 40°C. To prevent leakage, the generator is tightly sealed. Due to the flammable nature of hydrogen, care must be taken to avoid any chance of friction-induced sparks during filling and emptying of hydrogen. Systems removing or adding hydrogen must be grounded (possibly even the individuals using them) to eliminate the potential for sparks due to build-up

of static electricity or from energized equipment. Several hydrogen leakage detectors are installed in the vicinity of the generator.

4.2 Transformers

4.2.1 Basic principles

The main function of a transformer is to convert AC electric energy from one voltage level to another while minimizing the losses in the transformation process. A typical transformer has two independent windings. One is referred to as the primary winding, and the other as the secondary winding. These windings are coupled through a magnetic circuit in the iron core of the transformer. Ferromagnetic materials are used to construct the core to confine the magnetic flux inside. An illustrative diagram of a transformer is shown in Fig. 12. It is interesting to point out that, between the primary and the secondary, there is no direct electrical connection.

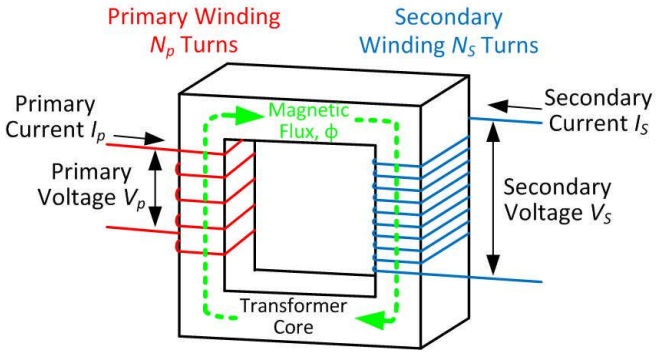

Fig. 12 - Basic operating principle of a transformer.

The operating principle of a transformer can be described as follows: the current in the primary winding creates an alternating magnetic flux, ϕ, inside the core. The strength of this flux is proportional to the current, I_p, as well as to the number of turns in the primary winding, N_p. On the secondary side, based on Faraday's law of induction, a potential, V_s, will be induced in the secondary winding. The level of this induced potential is proportional to the strength of the magnetic flux, ϕ, which is a function of the current, I_p, as well as of the number of turns in the secondary side, N_s. Therefore, if N_s is larger than N_p, the voltage at the secondary will be higher than that at the primary; such a transformer is often referred to as a *step-up transformer*. A transformer with the winding turned the other way around is known as a *step-down transformer*.

Most electrical power systems are three-phase systems. The power generated from a three-phase synchronous generator must be connected to three-phase transmission lines through a three-phase transformer. In fact, a three-phase transformer will have three primary windings and three secondary windings. A three-phase transformer is formed by proper connection of these windings on both the primary and secondary sides. For simplicity, only single-phase

transformers are described in this chapter.

If the circuit in the secondary side is closed (through a load directly, or through transmission lines), a path will be formed for the current, I_s, to flow through. Assume that all the flux serves to couple the primary and secondary windings; therefore, the flux, ϕ, will be equal on both sides:

$$N_p I_p = N_s I_s.$$

Furthermore,

$$V_p I_p = V_s I_s.$$

Therefore, it becomes clear that:

$$\frac{V_p}{V_s} = \frac{N_p}{N_s},$$

or

$$V_s = \frac{N_s}{N_p} V_p.$$

The ratio (N_s/N_p) is known as the *turn ratio*. When the turn ratio is greater than unity, the voltage level on the secondary side will be higher than that on the primary side, and vice versa. Because a transformer is a passive device, the current is inversely related to the turn ratio; the current decreases as the turn ratio increases and increases as the current ratio decreases.

The product of the current and the voltage permitted to be applied to the transformer is known as the *transformer rating*. The rating relates directly to the conductor size, core, and heat dissipation capability.

Like any other electrical apparatus, a practical transformer will be less than 100% efficient. Several sources contribute to these losses. The first is the ohmic losses in both primary and secondary windings due to the resistance of the coils. These are also called copper losses. The second loss occurs as a result of hysteresis and eddy currents in the core. This type of loss is normally independent of the currents in the transformer and is commonly referred to as iron loss. These losses normally take the form of dissipated heat. In practice, the heat must be evacuated through cooling systems. Transformer windings are often submerged in mineral oil to carry away the heat to be dissipated at the fins on the transformer covers. To accelerate the heat dissipation rate further, forced air, forced oil, or water circulation can be used to increase heat transfer effectiveness. However, these added power devices will consume additional energy.

Even though most transformers work under principles similar to those described above, their

appearance can vary greatly. A typical transformer found in a nuclear power plant is illustrated in Fig. 13. The high-power terminals are located at the top of the transformer, where three isolated connections can be seen. Electric fans are used to create forced air circulation to increase the heat dissipation rate.

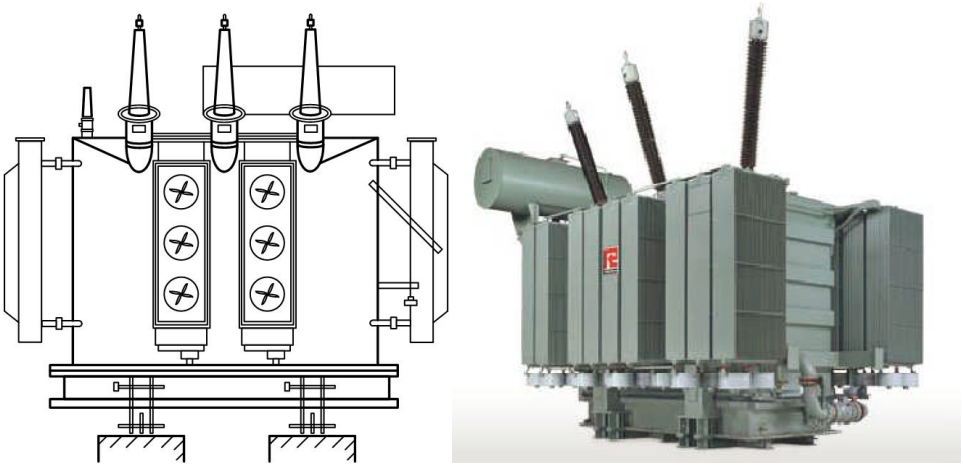

Fig- 13 - External appearance of a typical power transformer.

4.2.2 Major transformers in a CANDU plant

In a CANDU plant, there are many transformers serving different purposes. However, three main transformers deserve special attention:

- Main output transformer (MOT)
- Station service transformers (SSTs)
- Unit service transformers (USTs).

Their functionalities have been explained in Section 2, and their specifications are given in Tables 11 through 13.

Table 11 - Ratings of a main output transformer (MOT).

Rating	3 × 277 MVA
Primary-side voltage	22 kV
Secondary-side voltage	500 kV
Temperature (oil)	45°C
Temperature (winding)	65°C
Cooling method	Forced oil and forced air

Table 12 - Ratings of a station service transformer (SST).

Rating	60 MVA (natural cooling) 80 MVA (forced air cooling)
Primary-side voltage	220 kV
Secondary-side voltage	11.6 kV

Operating temperature range	50°C–75°C
Heat transfer medium	Oil
Cooling method	Natural or forced air

Table 13 - Ratings of a unit service transformer (UST).

Rating	60 MVA (natural cooling) 80 MVA (forced air cooling)
Primary-side voltage	22 kV
Secondary-side voltage	11.6 kV
Operating temperature range	50°C–75°C
Cooling method	Natural or forced air

4.3 Voltage and Current Transducers

4.3.1 Principles

High-voltage, high-current electrical parameters (in the kA and kV range) cannot be directly used for control purposes. To use these parameters in control and monitoring circuits, they must be transformed to a range suitable for these applications, generally in the ampere to milli-ampere and volt to milli-volt range. There are two groups of electrical quantities in a CANDU plant. The second, lower-value group is suitable for monitoring, control, and electrical protection purposes, such as input to a meter displaying the generator power output in the main control room, or input to a data acquisition system which captures the in-rush current of a circulation pump. High-voltage, high-current quantities cannot be directly connected to low-power devices without some type of conversion apparatus. To measure high voltages and large currents effectively, their electrical parameters must be converted to voltage and current ranges which are safe for use by measurement devices and human operators without the need for special protective equipment.

The devices that produce the corresponding low-level signals, which are proportional in value to the original high-power quantities, are known as *transducers*. Because voltages and currents are the two most important electrical quantities in an electrical distribution system, this section will focus mainly on voltage and current transducers. Only AC voltage and current transducers will be discussed because most of the high-voltage, high-current quantities are of this form. An importance difference between power transformers and voltage and current transducers is the requirements for accuracy and linearity. These requirements are much more stringent in the latter case.

A voltage transducer is essentially a transformer with a sufficiently small turn ratio, which converts a high-voltage signal to a low-voltage one. The high-voltage signal is connected to the

primary side, and the low-voltage signal is generated on the secondary side. As discussed in Section 4.2.1, transformers have the unique ability to isolate the high-voltage primary side from the secondary side electrically. The low voltage carries the same amount of information as the high voltage, but at a lower electrical potential, making it safer for maintenance personnel and for equipment designed to operate at lower voltage levels.

An illustrative diagram of a single-phase voltage transducer is shown in Fig. 14(a). When a high voltage, V_1, is applied, the transducer will produce a corresponding low voltage, V_2. The voltage ratio is determined by the turn ratio of the primary and secondary windings, i.e.,

$$V_2 = \frac{N_2}{N_1} V_1,$$

where $(\frac{N_2}{N_1})$ is less than unity and represents the voltage reduction factor.

The principle of a single-phase current transducer is shown in Fig. 14(b). The relationship between the current on the primary side and that on the secondary side can be expressed as follows:

$$I_2 = \frac{N_1}{N_2} I_1,$$

where $(\frac{N_1}{N_2})$ determines the current reduction factor.

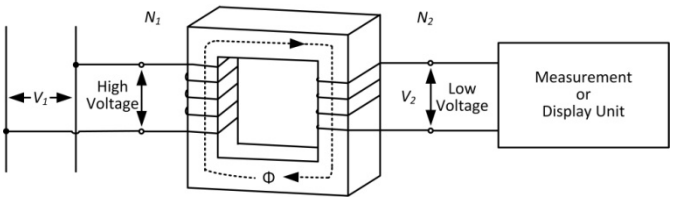

(a)

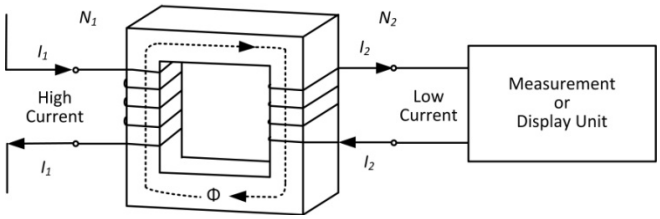

(b)

Fig. 14 - Principles of (a) voltage transducers; and (b) current transducers.

4.3.2 Voltage and current transducers in a CANDU plant

There are many voltage and current transducers throughout the plant that provide information on voltage and current levels in real time for control and monitoring purposes. Four sets of current transducers are located at the generator output, each with a rating of 1,700A / 5A. There are also two voltage transducers at the generator output, both having a reduction ratio of 22kV/100V. Similar devices are also used for electrical protection of major transformers, such as excitation transformers. A capacitor voltage transformer is used for high-voltage measurement at the grid connection point to provide information necessary for plant operation, as well as for protective relaying.

4.4 Switches, Circuit Breakers, and Disconnect Switches

4.4.1 Concepts and operating principles

There are many electrical switches in a CANDU plant. The most common are those used to turn certain pieces of equipment such as lights, pumps, or instruments on and off. A switch that is turned to the on position (closed) allows electricity to pass through, whereas turning it off (opening it) breaks the electrical circuit and stops the flow of electrons. In a low-power environment, the switches are not much different from those in everyday use.

As voltage and current levels increase, the construction and operation of these switches becomes more complex. High-voltage or high-current switches are often known as circuit breakers, disconnect switches, and contactors. As the names imply, one of the important functions of such devices is to conduct or break the current flow in a circuit. There are two main scenarios which call for such actions: (1) to execute a control command, such as to start or stop a load, and (2) to cut off the current flow in an abnormal operating condition such as a short-circuit fault. A circuit breaker must be able to carry and to interrupt current as needed.

An illustrative diagram of an over-current protection circuit breaker is shown in Fig. 15. The breaker is connected in series with the circuit. If there is no manual tripping signal, or if the current is within the operating limit, the breaker remains closed. If either a manual tripping signal is issued (by pushing a button) or if the measured current exceeds the threshold, the tripping coil will generate a trip signal to open the breaker, thereby interrupting the current flow.

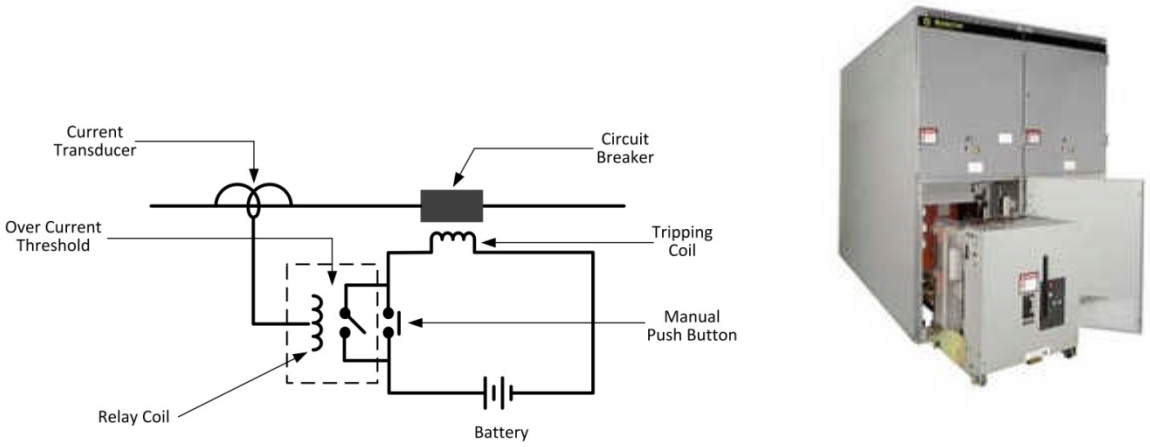

Fig. 15 - An over-current protection circuit breaker.

A significantly high voltage can be induced between the two contacts of the circuit breaker when it interrupts the current flow. As the contacts separate, the resistance between them increases rapidly, producing hot spots between the contacts. The high voltage between the contacts can also form a very strong electrical field. As the particles between the contacts become ionized, electric arcing occurs, which will prolong the time taken for the current to reach zero. To minimize the impact of short circuits and reduce wear and tear on the breaker contacts, the arc must be extinguished quickly. The breaker and bus bars must be designed to withstand the mechanical forces resulting from short-circuit currents. Depending on the duration of the short circuits, the amount of mechanical bracing may need to be increased.

Depending on the method of arc extinction, circuit breakers can be classified as:

- Air-break circuit breakers
- Air-blast circuit breakers
- Vacuum circuit breakers
- SF6 circuit breakers.

An air-break circuit breaker relies on the high-resistance interruption principle by rapidly lengthening the arc through an arc runner. The arc resistance is increased to such an extent that the arc can no longer be sustained. Such types of breakers are mainly used in low- and medium-voltage circuits.

In an air-blast circuit breaker, high-pressure air is blasted into the arc, blowing away the ionized gas between the contacts to extinguish the arc. The voltage and current that can be interrupted by an air-blast circuit breaker are normally higher than in an air-break circuit breaker. As its name implies, the contacts in a vacuum circuit breaker operate in a vacuum interrupter chamber. The arc is generated by ionization of the contact material, whereas in an air breaker, it is generated by the arc material as well as air ionization. Hence, in a vacuum, the arc is immediately extinguished once the voltage can no longer sustain the plasma created at

the contact. The cost of the vacuum circuit breaker is relatively high, and they are often used in circuits at less than 38 kV.

SF6 circuit breakers are the most common for high-voltage and high-current circuits. SF6 is short for sulphur hexafluoride, a gas which satisfies the requirements of an ideal arc-interrupting medium. SF6 gas has high dielectric strength and is colourless, odourless, and non-toxic, with high thermal conductivity. It is also highly stable and non-flammable and does not cause corrosion when in contact with the metallic parts of a circuit breaker. SF6 circuit breakers can be found in circuits with voltages ranging from 3 kV up to 1000 kV.

Circuit breakers should not be confused with disconnect switches. Disconnect switches do not have any arc-extinction capability and therefore cannot be used to interrupt a current flow. Such switches are instead used to provide another layer of protection for repair or maintenance crews, enabling them to isolate the section of a circuit being serviced. Disconnect switches can be operated either manually or automatically (in the case of motorized switches, such as a starter).

4.4.2 Switchgear in a CANDU plant

There are many types of circuit breakers in a CANDU plant that provide control and electrical protection functions. Circuit breakers are installed in the plant to facilitate operation and electrical protection of transformers or electrical distribution bus bars. An illustrative drawing of an arc-extinguishing breaker is shown in Fig. 16. SF6 circuit breakers are used for high-voltage switchyard circuits, whereas vacuum breakers can be used at medium voltage levels (11.6 kV/6.3 kV). These breakers can be operated manually, automatically, or by remote control. The major types of high-voltage circuit breakers in a CANDU plant are described in Tables 14 to 16.

Table 14 - Characteristics of SF6 circuit breakers at the generator output.

Voltage level	24 kV
Rated voltage	30 kV
Rated current	24 kA
Rated capacity	1,000 MVA
Breaker closing time	Less than 42 ms
Breaker opening time	Less than 42 ms
Arc extinction time	Less than 60 ms

Table 15 - Characteristics of vacuum circuit breakers on an 11.6 kV bus.

Voltage level	11.6 kV
Rated voltage	15 kV
Rated current	2,000–3,000 A
Rated capacity	1,000 MVA
Breaker closing time	45–60 ms
Breaker opening time	30–45 ms
Arc extinction time	5–17 ms

Table 16 - Characteristics of vacuum circuit breakers on a 6.3 kV bus.

Voltage level	6.3 kV
Rated voltage	8.25 kV
Rated current	1,200 A
Rated capacity	500 MVA
Breaker closing time	45–60 ms
Breaker opening time	30–45 ms
Arc extinction time	5–17 ms

Disconnect switches are often found in series with circuit breakers to provide additional protection for workers. A disconnect switch is used in series with the circuit breaker at the generator output. The rated voltage of this switch is 24 kV, the current is 24 kA, and the maximum short-circuit current is 160 kA. Note that disconnect switches are not used to interrupt current in circuits. They are used for isolation purposes (worker safety and load isolation), as well as to reconfigure a network. They are installed to provide additional safety measures for maintenance crews working on the power line. There are also fuses installed in many electric systems throughout the plant to isolate short circuits or unforeseen faults.

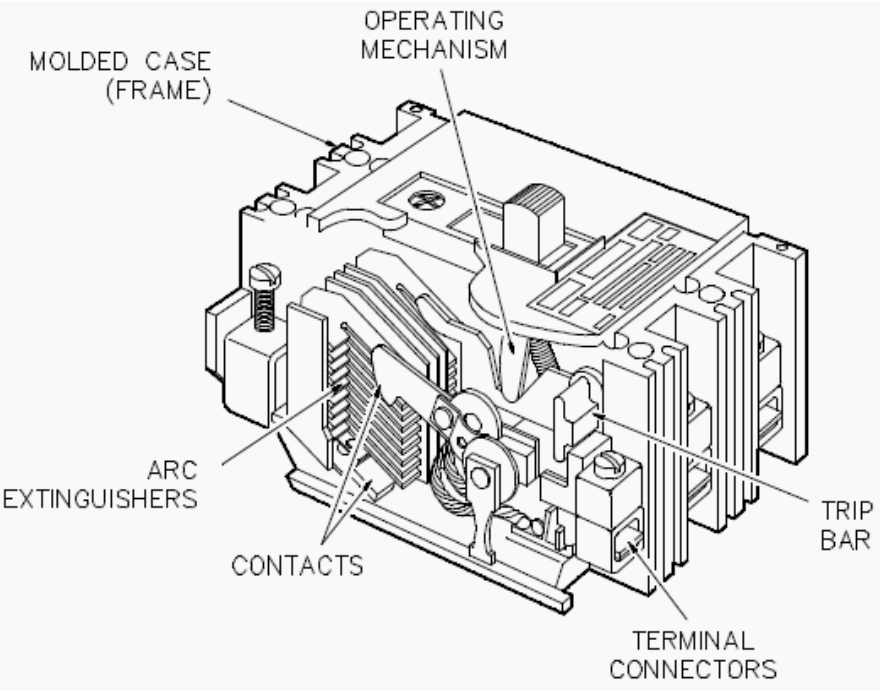

Fig. 16 - An arc-extinguishing circuit breaker.

4.5 Summary

A generator is an energy conversion device that converts mechanical energy from the turbine to electrical energy to supply the load. Together with the generator, there are several other auxiliary electrical systems in an NPP, such as circuit breakers, transformers, and voltage/current transducers. In this section, the general principles of these systems have been first explained, followed by information specific to CANDU NPPs. After completing this section, the reader should have a good understanding of how such systems operate, including knowledge of CANDU-specific applications.

5 Summary and Relationship to other Chapters

Even though the sole objective of a CANDU NPP is to produce electricity, this chapter is relatively independent of the other chapters in this book. To achieve a better understanding of the functionality of the different classes of power sources with respect to safety, the student should read Chapter 13 on Reactor Systems first to learn about the different safety systems and safety functions in a CANDU NPP.

6 Exercise problems

1. State the reasons why an NPP is different from a fossil-fuel power plant in terms of its station power requirements.

2. From a power grid point of view, what criteria are used to select a suitable site for construction of a new NPP?

3. Why is off-site power so important to the safety of an NPP?

4. In your own words, explain the meaning of “odd/even power supplies”.

5. List and define four classes of power used in a CANDU NPP.

6. State the original energy sources of the different classes of power sources.

7. State the sequences under loss of Class III power.

8. State the sequences under loss of Class IV power.

9. Why are batteries used in Class I power supplies?

10. Which class of power is used to charge the batteries in Class I power sources?

11. Explain the sources of power for each power class under both normal and emergency conditions.

12. Explain the role of grid power during the start-up and shutdown of a CANDU reactor.

13. What role do standby generators play in an NPP, and which class of power supply do they support?

14. What are the main differences between standby generators and an emergency power system?

15. Explain the different power sources that a CANDU plant has and the reasons for this.

16. List the main elements inside a generator.

17. Explain the principle of a synchronous generator used in a CANDU NPP.

18. What is the relationship between the number of generator pole pairs, the rotational speed, and the frequency of the voltage at the generator output?

19. Why is excitation important for synchronous generators?

20. How is excitation implemented in a CANDU NPP?

21. What is the function of the excitation transformer?

22. How is a generator cooled in a CANDU plant?

23. Under what conditions can the generator be connected to the power grid?

24. How are current and voltage measured in a CANDU plant?

25. What is the main function of a transformer?

26. Identify step-up and step-down transformers used in a CANDU plant.

27. Why are the coils in large-capability transformers often submerged in mineral oil?

28. What is the main function of the station transformer?

29. Why are protection devices important in a switchyard?

30. Explain the working principle of SF6 breakers.

31. What is the difference between a circuit breaker and a disconnect switch?

32. What is the function of a switchyard?

7 References

[1] Canadian Standards Association (CSA), Requirements for Electrical Power and Instrument Air Systems of CANDU Nuclear Power Plants (N290.5-06), 2011.

[2] CNSC Regulatory Document 2.5 Physical Design, Design of Electrical Power Systems for Nuclear Power Plants and Small Reactor Facilities (Draft stage).

[3] IAEA, Interaction of Grid Characteristics with Design and Performance of Nuclear Power Plants - A Guidebook, 1983.

[4] IAEA, Electric Grid Reliability and Interface with Nuclear Power Plants, No. NG-T-3.8, 2012.

[5] IEEE, Standard for Preferred Power Supply (PPS) for Nuclear Power Generating Stations (NPGS) Standard 765-2012, 2013.

[6] H. Ren, I. Dobson, B.A. Carreras, "Long-Term Effect of the *n*-1 Criterion on Cascading Line Outages in an Evolving Power Transmission Grid", IEEE Trans. on Power Systems, Vol. 23, pp. 1217–1225, 2008.

[7] CSA, General Requirements for Seismic Design and Qualification of CANDU Nuclear Power Plants, N289.1-08, 2008.

8 Further Reading

L.L. Grigsby, Power Engineering Handbook, CRC Press, IEEE Press, 2000 (ISBN-10: 0849385784).

IAEA, Design of Emergency Power Systems for Nuclear Power Plants, NS-G-1.8, 2004 (ISBN 92–0–103504–7).

P. Kiameh, Electrical Equipment Handbook: Troubleshooting and Maintenance, McGraw-Hill, 2003 (ISBN-10: 0071396039).

P. Kundur, Power System Stability and Control, McGraw-Hill Professional, 1994 (ISBN 0-07-035958-X).

J.D. McDonald, Electric Power Substation Engineering (2nd ed.), CRC Press, 2007 (ISBN-10: 0849373832).

9 Acknowledgements

The following reviewers are gratefully acknowledged for their hard work and excellent comments during the development of this Chapter. Their feedback has much improved it. Of course the responsibility for any errors or omissions lies entirely with the author.

Pel Castaldo
Alan Hepburn
Alek Josefowicz

Thanks are also extended to Diana Bouchard for expertly editing and assembling the final copy.

CHAPTER 12

Radiation Protection and Environmental Safety

Prepared by
Dr. Edward Waller, PhD, PEng, CAIH, CHP
University of Ontario Institute of Technology
Faculty of Energy Systems and Nuclear Science

***Summary**:*

Crucial to operation of a CANDU nuclear plant is protection of workers, the public, and the environment. This chapter discusses:

1. *Basic fundamentals of radiation physics as they pertain to radiation interactions that have the potential to cause biological harm in living systems.*
2. *Concepts of regulatory guidance which governs the "as low as reasonably achievable" radiation dose paradigm.*
3. *Radiation detection and monitoring techniques used in CANDU plant environs.*
4. *External and internal radiation hazards, including discussions on shielding and personal protective equipment.*
5. *Radiation management plans, worker dose monitoring, and control and waste management issues.*
6. *Radiation releases to the environment, derived release limits, and environmental protection.*

Table of Contents

List of Figures

List of Tables

1 Introduction

In Chapter 3, the fundamentals of nuclear physics, radioactive decay processes, and radiation interactions with matter were discussed. This chapter expands upon the concepts in Chapter 3 and explores the fundamentals of radiation protection and environmental safety, which are of vital importance to the safe operation of CANDU stations. In a holistic sense, the overarching field that deals with radiation protection and environmental safety is the area of health physics. Health physics is the branch of science that deals with protection of workers, the public, and the environment from potential detrimental effects from exposure to ionizing and non-ionizing radiation. The three primary pillars of health physics in the context of CANDU operations are presented in Figure 1. Radiation shielding is presented as a pillar because it is an important aspect of radiation protection that is often a field in and of itself.

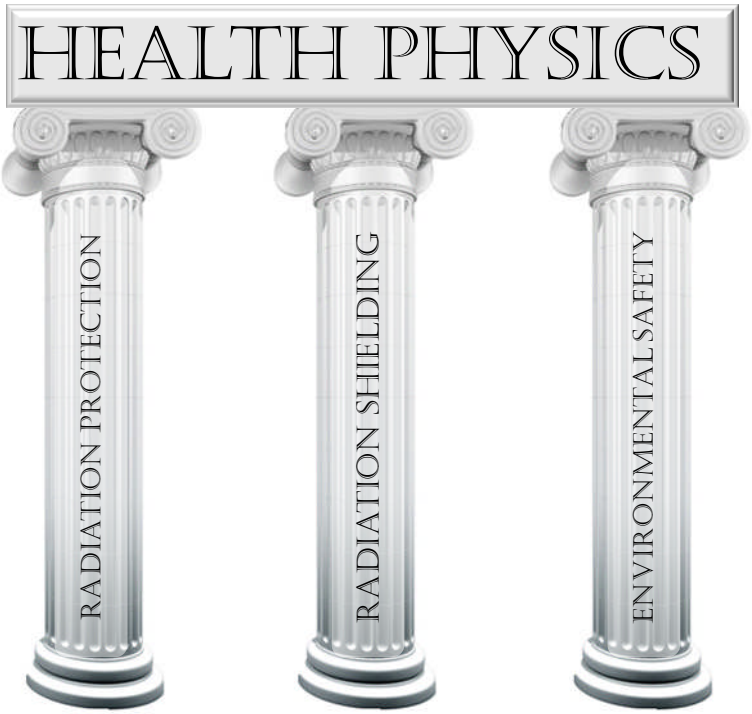

Figure 1 Three pillars of health physics

CANDU stations use experts in health physics, radiation protection, shielding, and environmental safety to ensure that reactor operations comply with Canadian regulations in a safe and controlled manner.

1.1 Overview

Experts in health physics generally require formal training in radiation protection, environmental radioactivity, and shielding design. In this chapter, the concepts of biological effects, radiation protection, health physics, shielding, and environmental safety are discussed with an emphasis on CANDU nuclear plant operations. This chapter represents the principal concepts related to the three pillars (Figure 1) which provide the well-rounded understanding of health physics that is required for a career in CANDU nuclear operations. Specific concepts discussed are: (1) basic fundamentals of radiation biology and the basics for understanding biological harm in living systems; (2) concepts of regulatory guidance which govern the “as low as rea-

sonably achievable" radiation dose paradigm; (3) radiation detection and monitoring techniques that may be used in CANDU plant environs; (4) external and internal radiation hazards, including discussions on shielding and personal protective equipment; (5) radiation management plans, worker dose monitoring, and control and waste management issues; and (6) radiation releases to the environment, derived release limits (DRL), and personnel and environmental protection.

1.2 Learning Outcomes

The goal of this chapter is for the student to understand:

- The biological basis for health impact from radiation exposure
- National and international regulatory guidance principles involving radiation exposure
- Overview of radiation-protection instrumentation used in CANDU plants
- The equations governing external exposure from point and extended sources
- Concepts of radiation shielding of external sources
- The equations governing internal exposure to radiation
- Concepts of radiation protection and management programs for CANDU plants
- Environmental radioactivity from CANDU plants
- Protection of the environment.

2 Biological Effects of Radiation

The principles of radiation biology are germane to background radiation-safety guidance for workers and the public with respect to CANDU operations. Personnel operating in and around CANDU plants, fuel-processing facilities, mining activities, and used nuclear fuel storage must have a fundamental understanding of how radiation may interact with the human body and how protective practices can be used to reduce any potential risk from exposure. In short, radiation biology is the backbone of all radiation protection and health physics.

Before discussing the mechanisms of how radiation affects living organisms, which form the basis of radiation protection, the basics of radiation interactions with matter must be understood. These concepts were discussed in Chapter 3 (Nuclear Processes and Neutron Physics). This section focuses on the fundamentals of how different types of radiation deposit energy in tissue through interactions and the principal target which drives radiation-protection regulation: deoxyribonucleic acid, or DNA. More information on the historical aspects of radiation biology may be found in [Preston2005].

2.1 Basic Radiation Interactions with Tissue

As discussed in Chapter 3, radiation interacts with materials in a variety of ways. Radiation can, for example, scatter, be absorbed, or create secondary particles as it passes through matter. The exact way in which radiation interacts with matter is dictated by the type of radiation and the nature of the matter being traversed. The endpoint(s) of the interaction(s) are dictated by the material being traversed. For example, neutrons impinging upon polymers can have the net effect of creating displaced atoms in the lattice (displacement damage), which can result in embrittlement of the material. The same neutrons impinging upon human tissue can cause changes to the DNA molecules, inducing chromosome aberrations which can lead to cancer. It is worth-while to note here, however, that radiation can also be used to strengthen polymers

and to treat cancer, so that the mode of application of radiation to material becomes important in determining the system endpoint. The fundamentals of radiation interactions with tissue begin with the concept of energy deposition.

Energy that is deposited in biological material can lead to two principal effects on an individual atom: excitation or ionization. Excitation raises an orbital-shell electron to a higher energy state without ejecting it from the atom; radiation can be emitted during this process. Ionization, on the other hand, is the ejection of an electron from an orbital shell of an atom; other kinds of radiation can also be emitted during this process. It is generally the ionization process that causes damage to DNA through direct or indirect action.

If DNA is the primary critical target for radiation-protection applications, then consideration must be given to DNA damage from direct and indirect action of the radiation to which tissue is exposed. DNA is a macromolecule which is the main constituent of chromosomes and the material that contains and communicates genetic information about all life. The DNA molecule is formed as a double helix and is coded with nucleotide base pairs along a twisted backbone of alternating sugar and phosphate groups, as depicted in Figure 2.

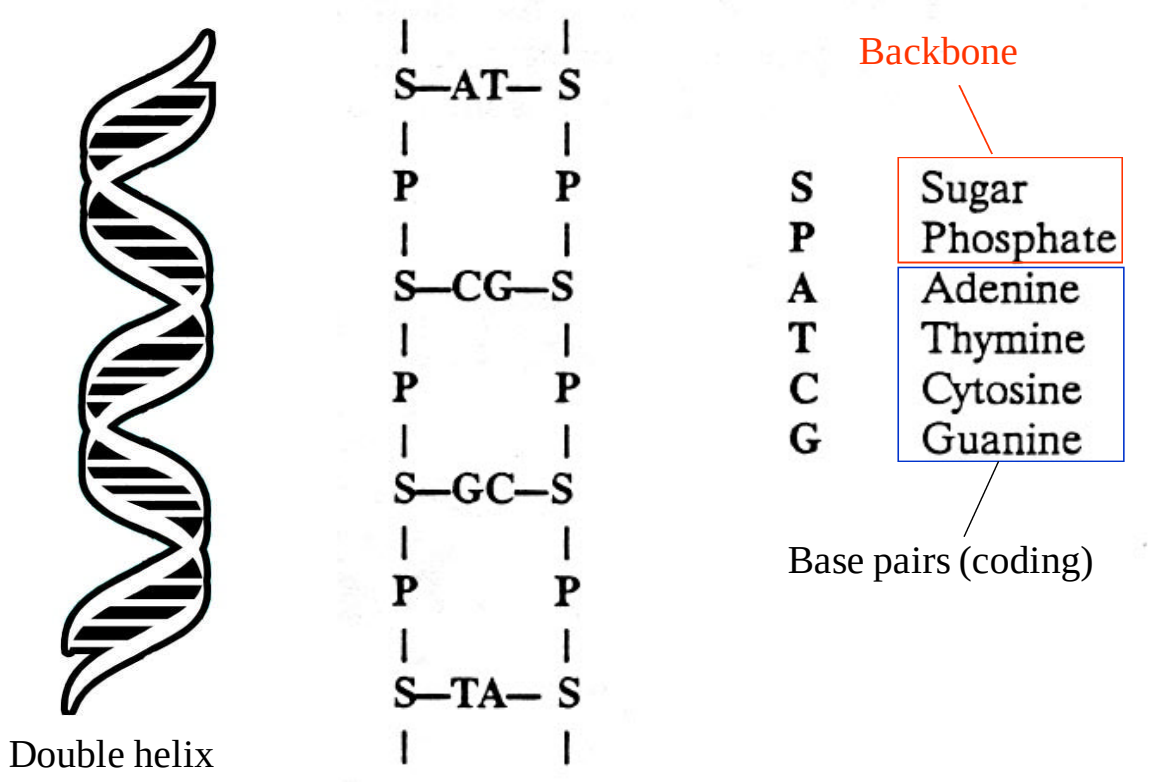

Figure 2 DNA double helix: target for radiation damage

Direct damage to DNA can occur when ionizing radiation interacts directly with the DNA molecule. For example, direct energy deposition on a backbone strand can have the effect of breaking the strand at that location. Direct damage is more probable for high linear energy transfer (LET) radiation, such as α-particles and neutrons. Indirect damage is a more complex process involving radiation interactions with water molecules. On average, the human body is composed of approximately 60% water [Cember2009], which is contained mostly within the body's

cells. Therefore, most direct interactions of all types of radiation on the human body are with water.

The process of indirect DNA damage proceeds as follows: radiation ionizes a water molecule, as described by Eq. (1):

$$H_2O \rightarrow H_2O^+ + e^- . \quad (1)$$

The products of water dissociation, H_2O^+ and e^-, interact further with water molecules. The electron interaction with water yields a hydrogen free radical, $H^\bullet$, and a hydroxide ion, OH^-, as shown in Eq. (2):

$$H_2O + e^- \rightarrow H_2O^- \rightarrow H^\bullet + OH^- . \quad (2)$$

The positive ion undergoes immediate dissociation as described in Eq. (3):

$$H_2O^+ \rightarrow H^+ + OH^\bullet , \quad (3)$$

which yields a positive hydrogen ion, H^+, and a free hydroxyl radical, $OH^\bullet$, the neutral form of the hydroxide ion, OH^-. The free hydrogen radicals tend to form gaseous hydrogen (H_2) which is relatively harmless in the human body. The hydroxyl radical, however, is extremely reactive and can damage DNA. These hydroxyl radicals are, however, short-lived and therefore need to be created in the vicinity of target DNA to do damage. An alternate damage mechanism is for the short-lived hydroxyl radicals to combine to form hydrogen peroxide as indicated in Eq. (4):

$$OH^\bullet + OH^\bullet \rightarrow H_2O_2 . \quad (4)$$

Hydrogen peroxide is a strong oxidizing agent which is fairly stable in the human body and can therefore migrate to distances far from the creation point and damage DNA.

A number of events on varying time scales must occur before deleterious effects from exposure are observed. The complex chain of events from radiation exposure to a biological endpoint is summarized in Figure 3.

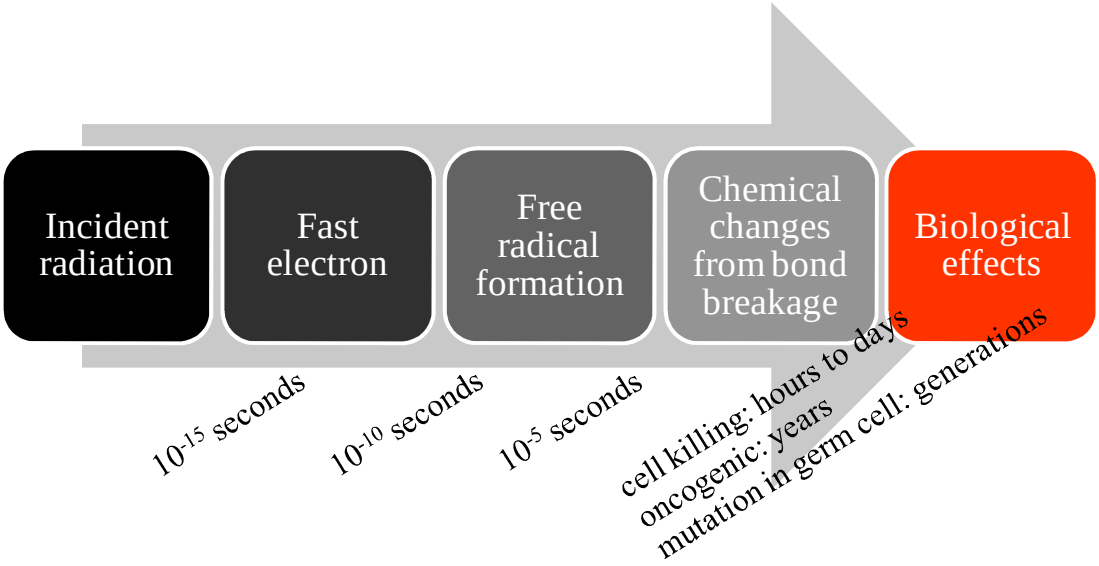

Figure 3 Process chain for radiation interaction with tissue

The time scales extend from femtoseconds for initial ionization, to tens of nanoseconds related to ion-radical lifetimes, to tens of microseconds for free-radical lifetimes, and finally to years post-exposure for onset of cancer.

The dominant modes of interactions for ionizing radiation that are important to CANDU reactors are contrasted in Table 1. The direct and indirect interaction mechanisms of the creation of charged particles by neutral particles are depicted in Figure 4. Dose assessment will be considered in Section 5 for external irradiation and Section 6 for internal irradiation.

Table 1 Radiation-induced DNA damage mechanisms

Radiation	Tissue interaction	Dominant damage mechanism
X- and γ rays	Indirect ionization	Production of fast-moving electrons creating free radicals which induce strand breaks
Neutrons		Production of recoil protons, alpha particles, and heavier atoms, creating free radicals which induce strand breaks
Beta particles (electrons)	Direct ionization	Direct action with DNA, inducing strand breaks. Directly ionizing particles can also generate free radicals.
Alpha particles (helium nuclei)		

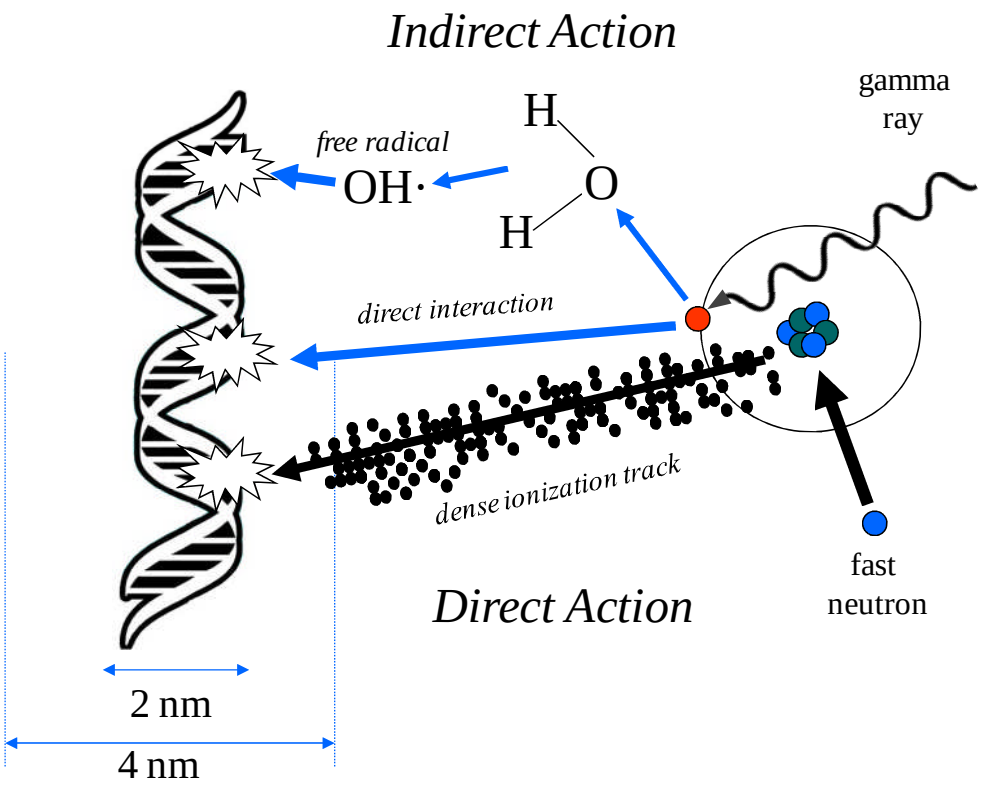

Figure 4 Direct and indirect radiation interaction mechanisms with DNA

2.2 Biological Radiosensitivity

The effect of radiation on living systems varies with the magnitude of exposure, duration of exposure, and region of the body exposed. Responses are characterized as deterministic (threshold) and stochastic (mutagenic, carcinogenic, or teratogenic). The law describing cellular radiosensitivity is attributed to Bergonie and Tribondeau [Bergonie1906] and states that the radiosensitivity of a cell is directly proportional to its reproductive activity and inversely proportional to its degree of differentiation. Cells most active in reproduction and cells not fully mature will be most harmed by radiation exposure. Conversely, the more mature and specialized the cell is, the less sensitive it is to radiation. One of the main reasons for the cause-effect relationship between radiation exposure and rapidly dividing cells is that the effect is essentially seen more rapidly when cells divide more rapidly.

2.2.1 Cell cycle

Cells are made up of various components. The cell membrane is the first line of defence for the cell and regulates what enters or exits the cell. The endoplasmic reticulum provides a transport mechanism from the cell membrane to the cell nucleus. Ribosomes in the cell are producers of proteins, and Golgi apparati store, package, help transmit, and customize proteins. Lysomes break down unwanted material in the cells, and mitochondria generate energy for the cell. For radiation-exposure risk, the most important component is the nucleus, specifically the chromosomes, which are depicted in Figure 5. Chromosomes are made up of DNA segments that code for proteins. Humans have 23 pairs of chromosomes. The DNA, an extremely small molecule in the chromosomes, carries the genetic code for all proteins. There are approximately $3x10^9$ base pairs, but only ~5% are active genes (the other 95% are the “glue” that holds the active genes together). Radiation can do harm when it hits an active gene.

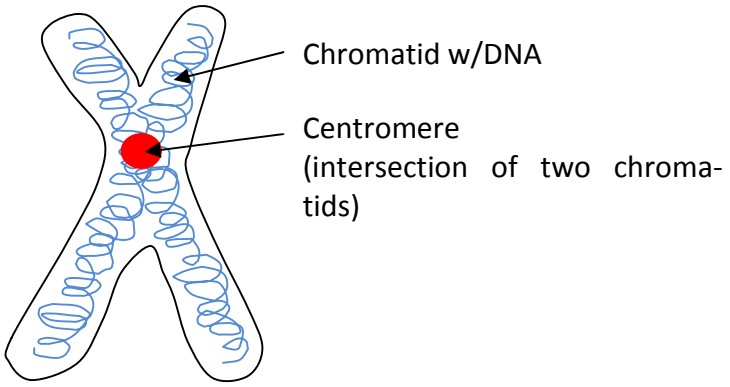

Figure 5 Chromosome

The cell cycle is depicted in Figure 6. The cell progresses from mitosis (cell division) to gap 1 (inactivity) for each divided cell which goes on to its own cycle, then to DNA synthesis, and then to gap 2 (inactivity) before mitosis.

The cell has maximum radiation sensitivity during the mitotic phase of the cell cycle. The cell cycle involves a number of stages before replication, as depicted in Figure 7.

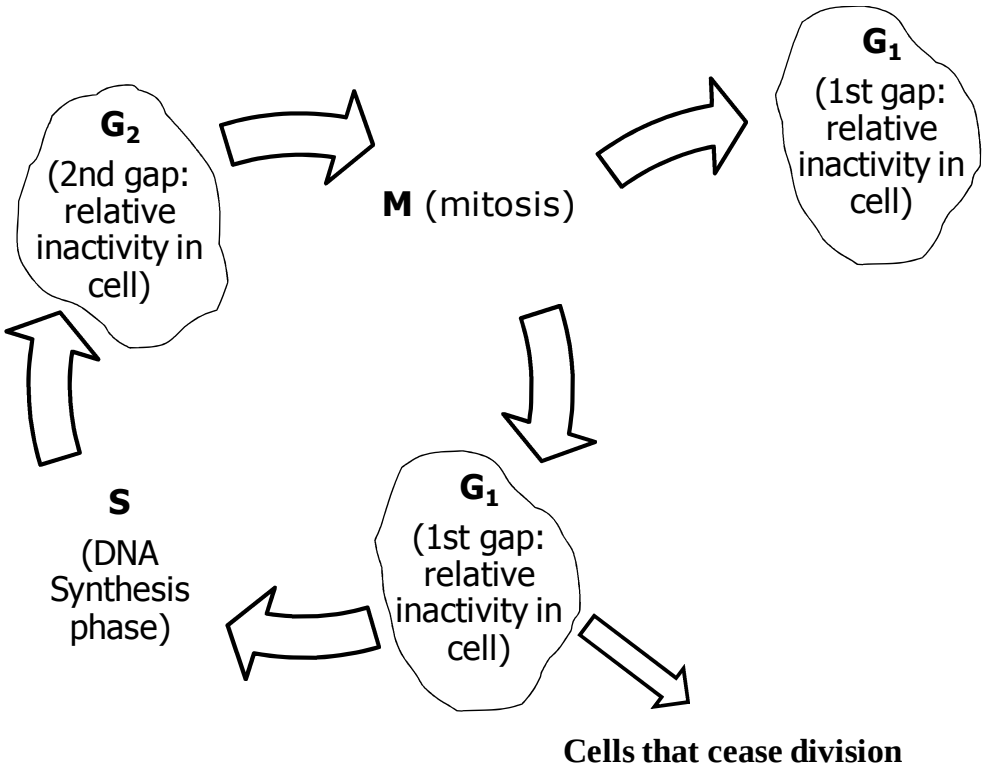

Figure 6 The cell cycle

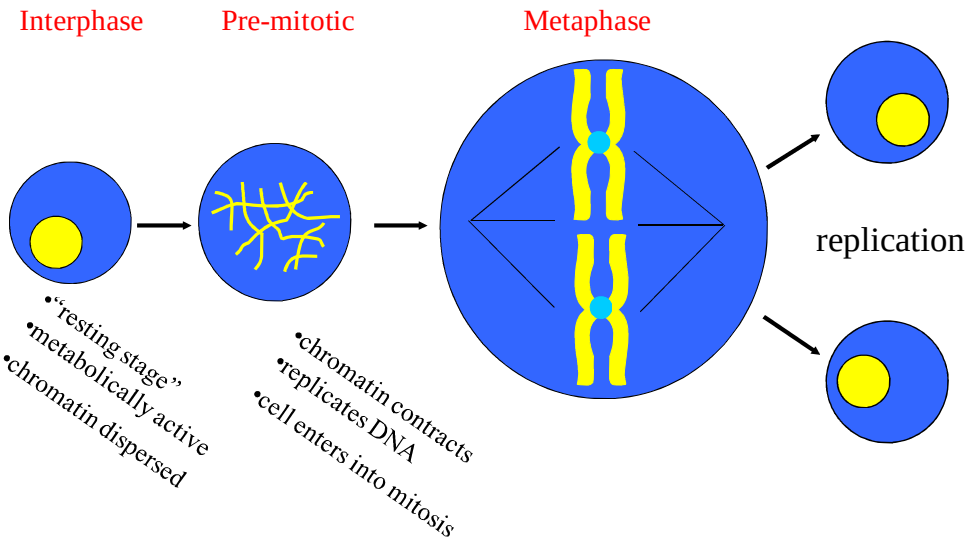

Figure 7 Cell mitosis

2.2.2 DNA damage

As previously stated, the primary target for cell killing is DNA. The primary lesion is the DNA strand break, and in the case of permanent damage, the DNA double-strand break must be considered. A DNA single-strand break is depicted in Figure 8. Radiation or free radicals interact with one of the sugar/phosphate backbone strands. This type of damage is of little risk because the DNA will either repair itself or, at worst, die upon replication.

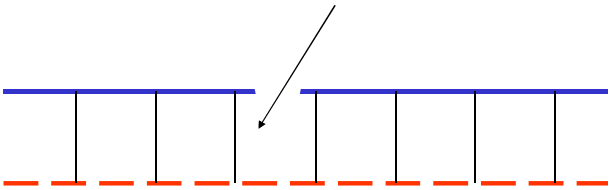

Figure 8 DNA single-strand break

A DNA double-strand break, on the other hand, is depicted in Figure 9. This type of damage can result either from a single, highly ionizing particle interacting with the DNA (such as an alpha particle) or from two events occurring so close in time that they occur, for all intents and purposes, at the same time. In this case, it is also possible for the DNA to repair itself if the strands reattach, but also for the DNA to misrepair itself, either with its own twisted DNA or with another DNA fragment. In this case, genetic coding can be produced that does not die upon replication, yet is not native to normal cellular function. This endpoint can be a precursor to cancer. This type of damage can be observed by examining chromosomes. Radiation damage to DNA can produce aberrations such as rings (a chromosome wrapped upon itself), fragments (small bits of "orphan" chromosomes), or dicentrics (two broken chromosomes which form together to make up a larger macromolecule).

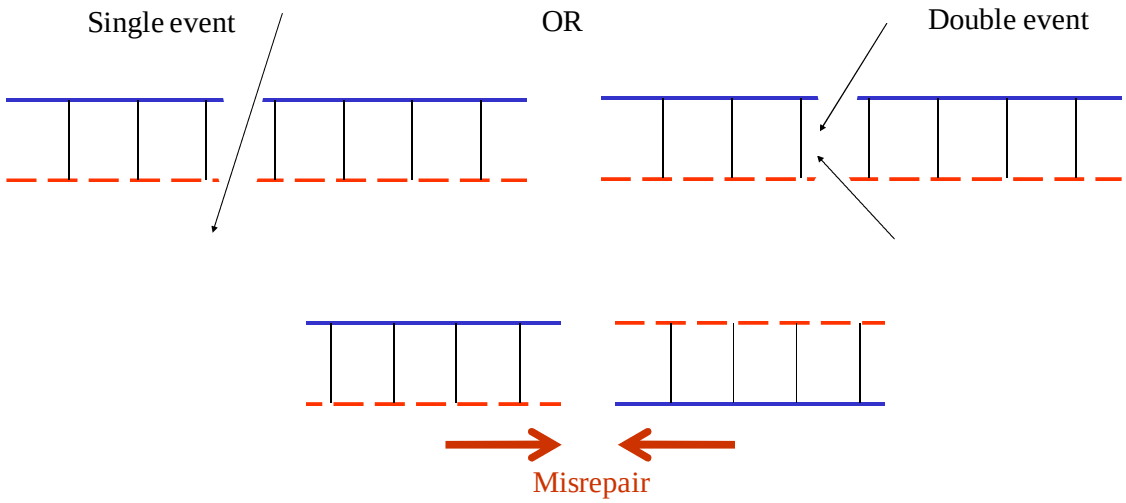

Figure 9 DNA double-strand break

A complete depiction of how radiation damages cells can be seen in Figure 10. During the interphase, radiation-induced strand breaks are generated. This leads to chromosome misrepair and abnormally repaired chromosomes during DNA replication, yielding dicentrics, fragments, (and rings). Note that there is a background level of approximately one dicentric per 1000 lymphocytes in human blood, and therefore excess dicentrics are indicative of radiation damage. During metaphase, the cells divide and can undergo either apoptosis or mutation.

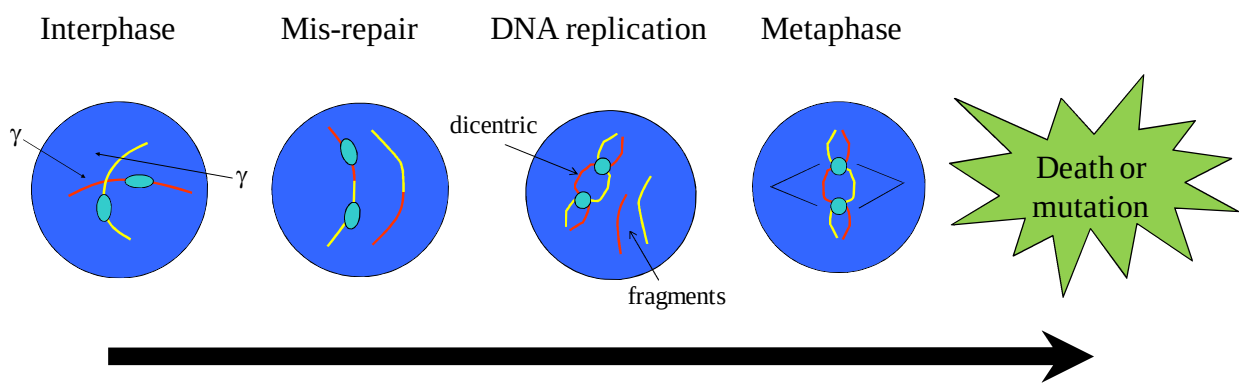

Figure 10 Radiation damage to cells

The possible endpoints of damaged DNA are graphically depicted in Figure 11. Upon DNA damage from ionizing radiation exposure, the DNA may (1) repair itself without coding error (common with single-strand breaks), (2) perform cell "suicide" (apoptosis), or (3) mutate into a viable, yet undesirable, DNA molecule that may have oncogenic (tumour-producing) properties upon cell division.

Various factors can impact the extent of radiation damage at the cellular level, including:

- Dose – generally speaking, as the dose increases, the surviving fraction of cells decreases. In other words, increasing the dose increases the damage.
- Dose rate – as the dose rate increases, the surviving fraction decreases.
- Radiation quality and relative biological effectiveness – for low linear energy transfer (LET) radiation, it requires more than one track to cause a dicentric; for high-LET radiation, one track can cause a dicentric. As a general rule, high-LET radiation is more damaging to cells than low-LET radiation.
- Oxygenation – aerated cells are more radiosensitive. Oxygen reacts with free radicals to produce peroxide, which is highly toxic.
- Radioprotectants – if present, radioprotectors such as aminothiols can scavenge free radicals before DNA damage occurs.

The biological effects of exposure are explored in Section 2.3.

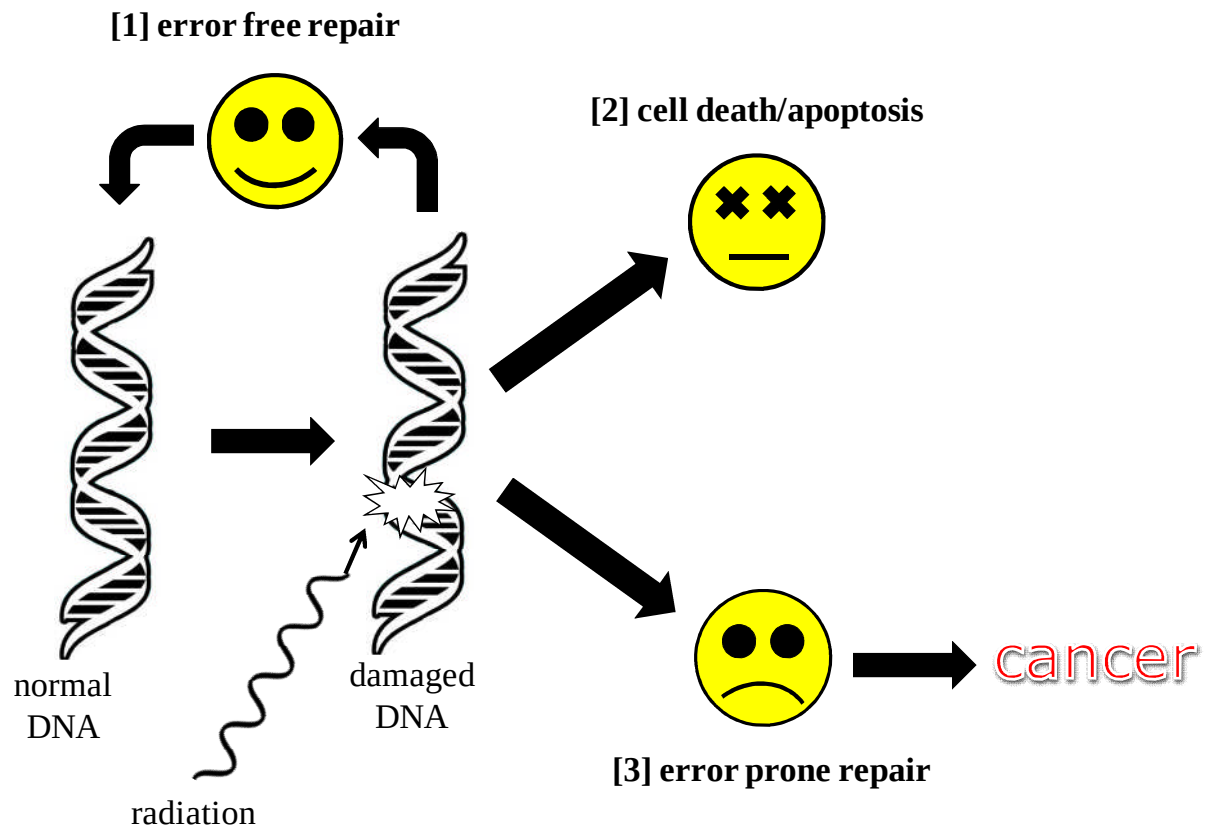

Figure 11 DNA damage endpoints

2.3 Biological Effects of Exposure

In the previous section, factors affecting the extent of radiation damage to cells were explored. A variety of factors that influence the biological effects of exposure must be taken into account, such as:

- Total absorbed energy (dose)
- Rate of dose delivery
    - Acute (seconds-minutes)
    - Chronic (days-years)
    - Type of radiation
- Source of exposure
    - External
    - Internal
- Age at exposure
- Time since exposure
- Area of exposure
    - Localized (cells; organs)
    - Extremities (hands; feet)
    - Whole body
    - Superficial (skin only)
    - Deep tissue.

As presented above, exposure can be categorized in many ways. Two very important concepts related to risk are the rate of dose delivery for exposure and the endpoint.

The rate of dose delivery for exposure is conveniently divided into two principal categories: (a) acute and (b) chronic. Acute exposure is normally considered as a single, large, and short-term whole-body dose, and the effects are observed in a short time frame post-exposure. The effects are categorized by four sequential stages: (i) Initial (prodromal) which lasts approximately 48 hours, (ii) latent, which lasts 48 hours to 3 weeks, (iii) manifest illness, which lasts 6–8 weeks, and (iv) recovery, which can last weeks to months (if death does not occur). Chronic exposure, on the other hand, is typically defined as a lower, protracted dose over a long period of time. The two principal categories describing the endpoint effects of radiation exposure in humans are (a) deterministic effects and (b) stochastic effects. Dose definitions (Gy, Sv, etc.) are provided in Section 3.1.

2.3.1 Deterministic effects

Deterministic effects are those that manifest at some threshold dose, with increasing severity with increasing dose. Some estimated deterministic effects as a function of absorbed dose from X-ray, gamma-ray, and electron exposure of target organs is provided in Table 2 [NCRP2001].

Table 2 Deterministic effects [NCRP2001]

Effect	Target organ	Absorbed dose (Gy)
Sterility (temporary)	Testes	0.15
Nausea	Whole body	0.35
RBC depression	Bone marrow	0.5
Skin reddening (reversible)	Skin	2
Sterility (permanent)	Ovaries Testes	2.5–6 3.5
Vomiting	Whole body	3
Hair loss (temporary)	Skin	3–5
Erythema	Skin	5–6
Death ($LD_{50/30}$)†	Whole body	4

†$LD_{50/30}$ is the Lethal Dose where 50% of an exposed population dies within 30 days. $LD_{50/60}$ is a similar definition at 60 days post-exposure.

There are three general categories of acute radiation sickness, as presented below.

1. Hematopoietic
   - Dose range 3–8 Gy
   - Radiation damages precursors to red and white blood cells and platelets
   - Prodromal phase may occur immediately
   - Symptoms include septicemia
   - Mixed survival
   - Examples include Chernobyl personnel (203 exhibited symptoms; 13 died)

2. Gastrointestinal
   - Dose > 10 Gy
   - Symptoms include abdominal pain/fever, diarrhea, and dehydration
   - Death in 3–10 days (no record of human survivors above 10 Gy)
   - Examples include Chernobyl firefighters
3. Cerebrovascular
   - Dose > 100 Gy
   - Death in minutes to hours
   - Examples include criticality accidents.

Radiation exposure to high doses is well known to induce changes in blood-count levels. There are numerous components of blood and a variety of ways to subdivide blood characteristics. The four factors that are often examined when high radiation exposure is expected are lymphocytes, neutrophils, thrombocytes, and hemoglobin, described below:

- Lymphocytes are white blood cells that govern the body's immune response (directly fighting disease and infection)
- Neutrophils are a subset of white blood cells that fight infection
- Thrombocytes (platelets) are active in blood clotting
- Hemoglobin is the component of red blood cells that carries oxygen.

An example of a hypothetical complete blood count with differential (CBC w/ diff) after exposure to a large dose (insult > 2 Gy whole body) of radiation is provided in Figure 12. It may be seen that immediately after exposure, there is a sharp decrease in lymphocytes, followed by a spike in neutrophils. The neutrophil spike is the body's response to what it believes may be an infection. Three distinct stages of illness are evident through the exposure: (1) latent period from exposure to approximately 20 days, (2) manifest illness, where the exposed person is extremely sick, from day 20 to 35, followed by (3) recovery, assuming the exposed person has survived the blood counts dropping to almost zero. Note that Figure 12 represents a very high whole-body exposure and that the actual blood counts and time frames can vary greatly from person to person. Note also that models have been developed to determine the severity of radiation exposure retrospectively using sequential lymphocyte counts post-exposure [Goans1997].

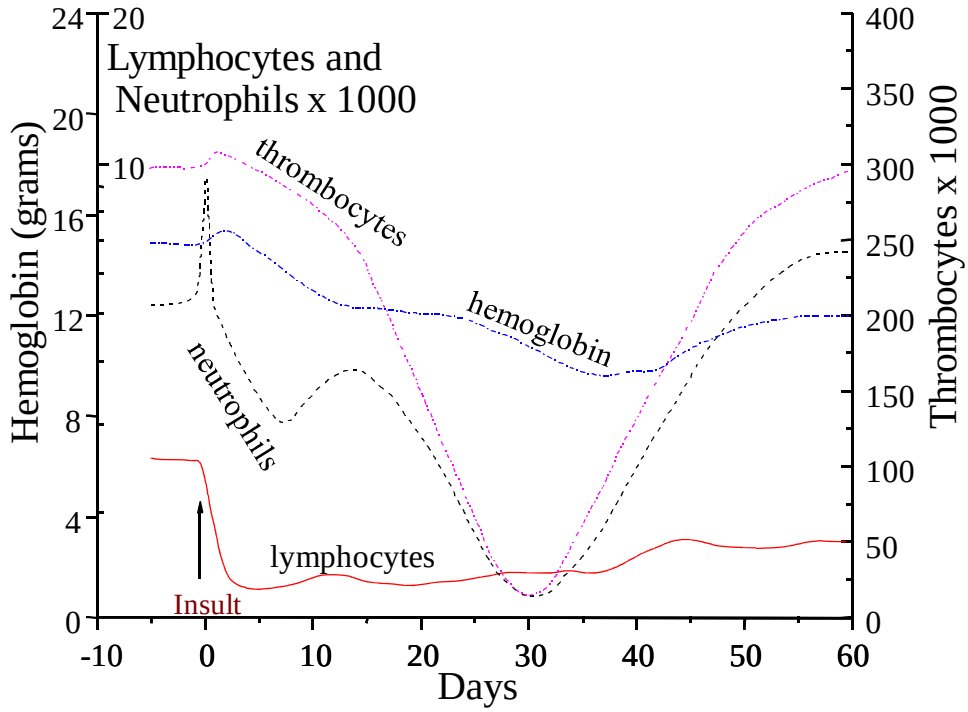

Figure 12 Differential blood count after severe radiation insult (adapted from [Gusev2001] and [Cember2009])

The universal principles of radiation protection dictate that deterministic effects must be avoided in occupational exposure. However, this is not the case with medical exposure because a deterministic-level dose may be required for the medical procedure. A typical example is radiation therapy for treatment of cancer, where deterministic-level doses are routinely applied to treat the cancer.

2.3.2 Stochastic effects

Stochastic effects are those effects which are assumed not to have a threshold dose and for which the severity of the effect is independent of absorbed dose. Stochastic effects may manifest in delayed or late somatic effects. The usual endpoint stochastic effect considered for radiation exposure is cancer induction (for example, leukemia, bone cancer, or lung cancer), which has been inferred at absorbed-dose levels on the order of hundreds of mGy. In addition, genetic and hereditary effects have been observed using animal studies, although these effects have never been observed in human populations exposed to ionizing radiation. Stochastic effects can occur from both acute and chronic exposures.

The often-quoted value for fatal cancer risk as a function of whole-body radiation exposure is 5% per Sv (dose definitions are found in Section 3.1). In other words, if a population of 100,000 were exposed to a 1-Sv whole-body dose, then 5000 excess fatal cancers would be expected (note that there is approximately a 40% baseline fatal cancer incidence across the population). A tabulation of the current ICRP [ICRP2007] guidance on stochastic risk coefficients is provided in Table 3. ICRP recommends continued use of the 5% per Sv value.

Table 3 Stochastic risk coefficients (adapted from ICRP (2007))

Exposed population	Cancer (%/Sv)	Heritable (%/Sv)	Total (%/Sv)
All	5.5	0.2	5.7
Adult only	4.1	0.1	4.2

A study performed by [Brenner2003] indicated that, for doses within a range of 50–100 mSv (protracted exposure) and 10–50 mSv (acute exposure), there was direct epidemiological evidence from human populations to indicate that exposure to ionizing radiation increased the risk of certain cancers. The primary argument to support linear non-threshold response at low dose is not from scientific observation, but from mechanistic arguments and assumptions. Based upon the scientifically observed evidence, there is no conclusive proof of any deleterious endpoint effect below 10 mSv and only weak evidence of an effect below about 50 mSv. In any case, the risk factors below approximately 100 mSv are very low for all exposure scenarios.

Note that effects from radiation exposure cannot be definitively attributed to an individual. That is to say, a deterministic effect that may be observed in an individual at one dose level may not be observed in another individual at the same dose level. This occurs because individuals have different sensitivities to ionizing radiation exposure. Likewise, cancer risk from radiation exposure cannot be extrapolated to an individual for a given exposure. Radiosensitivity is organ-specific because not all organs have the same vulnerability to radiation. Table 4 depicts the relative sensitivity variation among some critical organs.

Table 4 Relative human-organ vulnerabilities to ionizing radiation

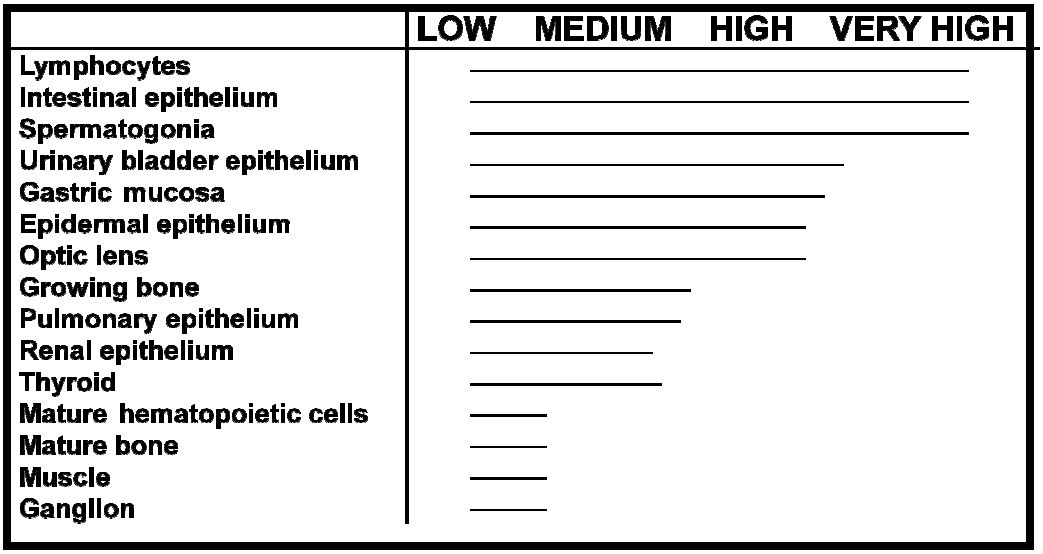

Although cellular and animal studies provide indicators of risk, the primary source of data for radiation-exposure risk modeling is epidemiological studies [UNSCEAR2008]. The primary source of data used for risk models is the Japanese atomic-bomb survivors. Other exposed groups that have contributed data to risk modeling include radiotherapy cancer patients (cervical, endometrial, childhood, breast, Hodgkin's lymphoma, etc.), radiotherapy patients with non-malignant conditions (spondylitis, thymus, tonsils, ringworm, etc.), diagnostic radiology patients (tuberculosis fluoroscopy, pelvimetry, scoliosis, etc.), workers with occupational

exposure (radium dial painters, miners, radiologists, nuclear workers, etc.), and people experiencing environmental exposure (nuclear weapons fallout, Chernobyl, Techa River, etc.).

Radiation is an incredibly weak carcinogen, and as therefore estimation of risk from exposure at low doses requires the use of risk models, which are described in the following section.

2.4 Radiation Risk Models

In the simplest terms, risk may be defined by Eq. (5):

$$\text{Risk} = \left(\text{Probability of occurrence}\right) \times \left(\text{Consequence}\right) \tag{5}$$

Therefore, it is possible to have a low-probability event with high consequence with a low risk factor, or a high-probability event with low consequence with a low risk factor. However, if neither probability of occurrence nor consequence is non-trivial, then it is possible to have a high risk factor. In terms of radiation risk, the BEIR Committee [BEIRVII2006] defines risk as:

> "the chance of injury, loss, or detriment; a measure of the deleterious effects that may be expected as a result of action or inaction".

To understand risk from radiation exposure, a fundamental understanding of what the risk detriment parameter is (for example, cancer) and the background incidence of this detriment is required. Incidence of effect, or endpoint, can be estimated using *in vitro* or *in vivo* studies of humans, animals, or plants (of organisms, components of organisms, or both, down to the DNA level). Risk to populations from exposure can be estimated using the principles of epidemiology, which is the study of the causal factors of the frequency of disease in humans.

Risk from radiation exposure is typically quantified as some probability of endpoint effect (incidence) per unit dose exposure. The relative risk (RR) is a common measure of risk and is defined by Eq. (6):

$$\text{RR} = \frac{\text{Incidence in exposed population}}{\text{Incidence in unexposed population}}. \tag{6}$$

An important metric for risk estimate is based on the increased likelihood of an endpoint (cancer) as a result of exposure to a carcinogen (radiation) and is termed the excess relative risk (ERR), defined by Eq. (7):

$$\text{ERR} = \text{RR} - 1 = \frac{\text{Incidence in exposed population}}{\text{Incidence in unexposed population}} - 1. \tag{7}$$

The excess absolute risk (EAR), sometimes called the attributable risk, is a measure of the discrepancy in incidence rates between exposed and non-exposed populations and is given by Eq. (8):

$$\text{EAR} = \text{Incidence in exposed population} - \text{Incidence in unexposed population}. \tag{8}$$

For example, if the cancer incidence in an exposed population is 0.5 Gy^{-1} and in an unexposed population is 0.4, the RR is 1.25 Gy^{-1}, and the ERR is 0.25 Gy^{-1}. The EAR requires that the incidence in the unexposed population be resolved to a percentage by multiplying by the exposure (Gy). For a 100-mGy exposure, RR = 0.125, ERR = 0.025, and EAR is negative. When RR >1, then

exposure increases the risk, and if RR <1, then exposure does not increase risk. In this hypothetical case, the exposure does not increase cancer risk.

It is often desirable to estimate whether a given exposure is the cause of an observed endpoint (for example, cancer). The metric used for this is the probability of causation (PC), which is given by Eq. (9):

$$\mathrm{PC}=\frac{\mathrm{ERR}}{1+\mathrm{ERR}}. \tag{9}$$

In the example above, the PC is calculated as 0.024.

Understanding the risks of radiation exposure means understanding the cause-effect relationships between endpoints and exposure. Some cancers are more strongly linked to radiation exposure than others. Table 5 presents a variety of cancers in the following categories: (i) strong association with radiation exposure, (ii) moderate association with radiation exposure, although strongly influenced by other risk factors, and (ii) little or no association with radiation exposure.

Table 5 Association of cancers with radiation exposure

Strong	Moderate	Weak to none
Leukemia (excluding chronic lymphocytic)	Childhood leukemia	Bone
Thyroid	Bladder	Brain
	Breast	Esophageal
	Colorectal	Kidney
	Lung	Multiple myeloma
	Stomach	Non-Hodgkin's lymphoma
		Ovarian

Stochastic risk, such as the incidence of cancer, can be plotted as a function of dose to generate a dose-response curve that represents the incidence of an endpoint as a function of increasing dose. There are numerous sources of data for generating risk curves; some major cohorts where data have been obtained are presented in Table 6.

Table 6 Epidemiological categories for radiation risk studies

Population Category	Comments
Japanese atomic bomb survivors	Numerous endpoints studied
Environmental exposures	Events: Chernobyl NPP4 accident Techa River cohort Fukushima disaster Nuclear-weapons fallout Natural background radiation
Occupational exposures	Cohorts: Radium dial painters Miners Radiologists Technologists Nuclear-energy workers Veterans
Radiotherapy cancer treatments	Endpoint cancers: Cervical Endometrial Childhood Breast Hodgkin's lymphoma
Radiation therapies (non-cancer)	Conditions treated: Spondylitis Mastitis Thymus Infertility Tonsils Menstrual disorders Otitis Media Ulcers Ringworm Hemangioma
Diagnostic radiology	Conditions diagnosed: Tuberculosis Scoliosis Pelvimetry All other diagnostic procedures
Radionuclide internalizations	Isotopes of: Th, I, P, Ra, U, Pu

Generally speaking, much of our knowledge about dose response has been obtained from relatively high dose / high dose rate exposure, whereas most non-medical exposure is low dose / low dose rate exposure. Figure 13 depicts a hypothetical, yet realistic, dose response curve (incidence versus dose, where incidence could be relative risk of cancer, for example). The solid

circles represent points for which there are statistically significant data with reasonable confidence levels (for example, data from Japanese atomic bomb survivors). The open circles represent non-statistically significant data with low confidence. “High dose” would generally refer to data obtained above a 1-Gy whole-body dose; “low dose” would generally refer to data below approximately 0.1 Gy. Some risk estimates (for example, leukemia) are generated using a linear quadratic curve [BEIRVII2006] through the data and through the point (0,0), which represents “zero risk at zero dose”. Most risk estimates, however, are generated using a linear curve through the data and through point (0,0). This is termed the linear no-threshold (LNT) hypothesis of radiation risk and is very contentious in the radiation-protection community [Bond1996] [Scott2008] [Siegel2012].

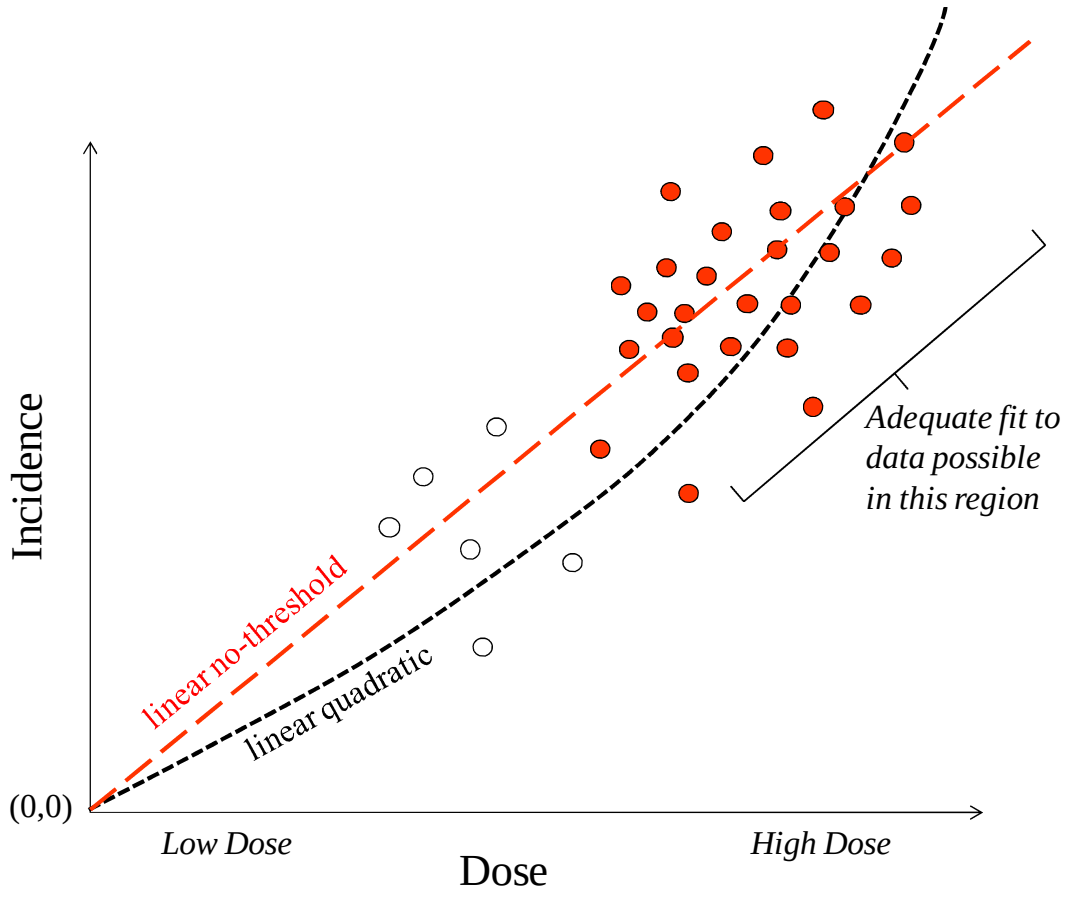

Figure 13 Dose-response curve showing two common models

The primary reason why the linear no-threshold hypothesis of radiation risk is contentious is that, as discussed in Section 2.3, there is no conclusive evidence below approximately 100 mGy to demonstrate deleterious effects of exposure to ionizing radiation. That being said, regulators have adopted the linear no-threshold hypothesis for radiation risk because it is considered conservative (that is, to overestimate the risk from ionizing-radiation exposure).

The various models for dose response [Cember2009] can be represented by a generalized expression given by Eq. (10):

$$f(D) = \left(\alpha_0 + \alpha_1 D + \alpha_2 D^2\right) e^{\left(-\beta_1 D - \beta_2 D^2\right)}, \tag{10}$$

where the dose-response function is given by *f(D), D* is the dose, α_0 is the natural incidence of the effect (for example, spontaneous cancer incidence), α_1 and α_2 are linear and quadratic fitting parameters, and β_1 and β_2 are parameters used in representation of cell killing or mortality only at higher doses (that is, the killing function dominates at high dose).

In terms of relative risk (RR), Eq. (10) becomes Eq. (11):

$$RR = \frac{f(D)}{\alpha_0} = \frac{\left(\alpha_0 + \alpha_1 D + \alpha_2 D^2\right) e^{\left(-\beta_1 D - \beta_2 D^2\right)}}{\alpha_0}. \qquad (11)$$

A graphical representation of the various functions for Eq. (10) is provided in Figure 14. The values for the fitting parameters have been selected arbitrarily, and a background incidence (of a given effect) was arbitrarily selected as 10^{-3}. At low dose, the linear, linear quadratic, and full expressions are basically identical. At high dose, the quadratic function matches the linear quadratic function, and clearly cell killing/mortality attenuates the linear quadratic curve.

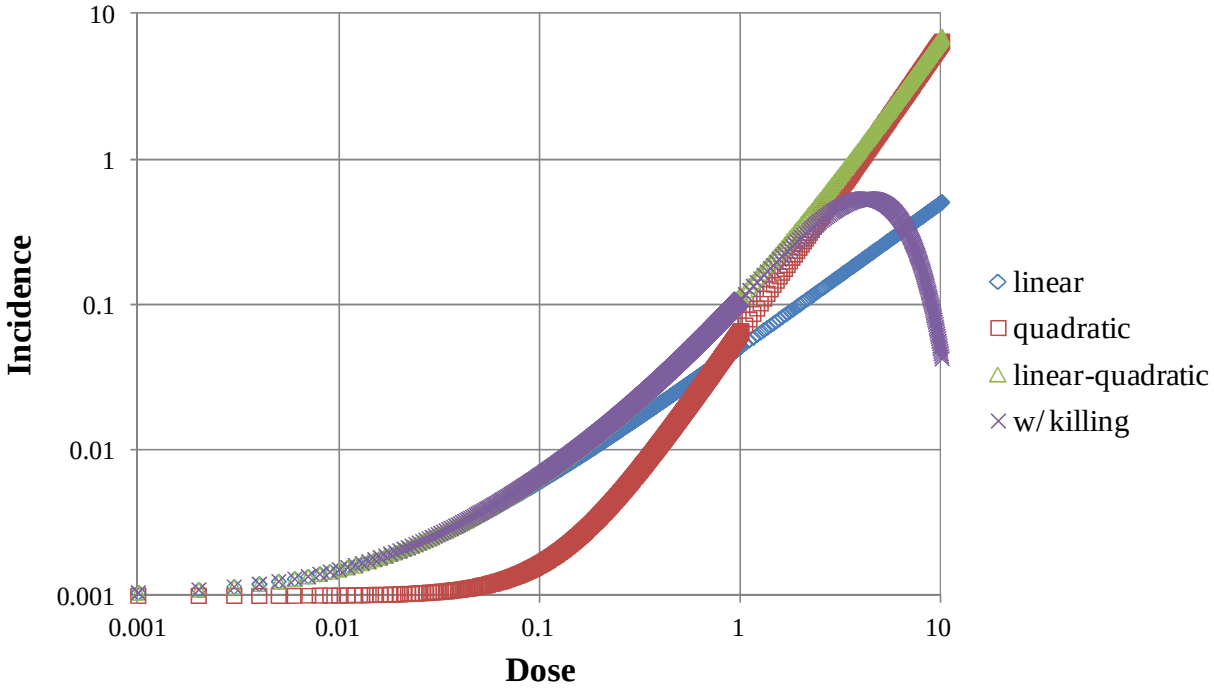

Figure 14 Generalized dose-response curves

Alternative theories of dose response include models that incorporate threshold responses (that is, risk only increases after a threshold dose) and hormetic response (see Figure 15).

Hormesis may be defined as "a process in which exposure to a low dose of a given insult that is damaging at higher doses induces an adaptive beneficial effect on the cell or organism" [Mattson2008]. There has been an abundance of literature published in support of both threshold and hormetic responses (see, for example, the journal Dose-Response [DoseResponse2013]). The relative risk-response curve may be adjusted to compensate for low-dose hormetic effects using Eq. (12):

$$RR = \frac{\left(\alpha_0 + \alpha_1 D + \alpha_2 D^2\right) e^{\left(-\beta_1 D - \beta_2 D^2\right)}}{\alpha_0} \left[1 - B(D) * PROFAC\right], \quad (12)$$

where *PROFAC* is the protection factor, which is the population average probability of cancer prevention given activated natural protection and *B(D)* is the benefit function, which is the probability of activated natural protection [Scott2012], which increases at low doses far more than *f(D)*. At low doses, $f(D)/\alpha_0$ is essentially unity, and at low doses, the relative risk may be approximated by Eq. (13):

$$RR \approx \left[1 - B(D) * PROFAC\right]. \quad (13)$$

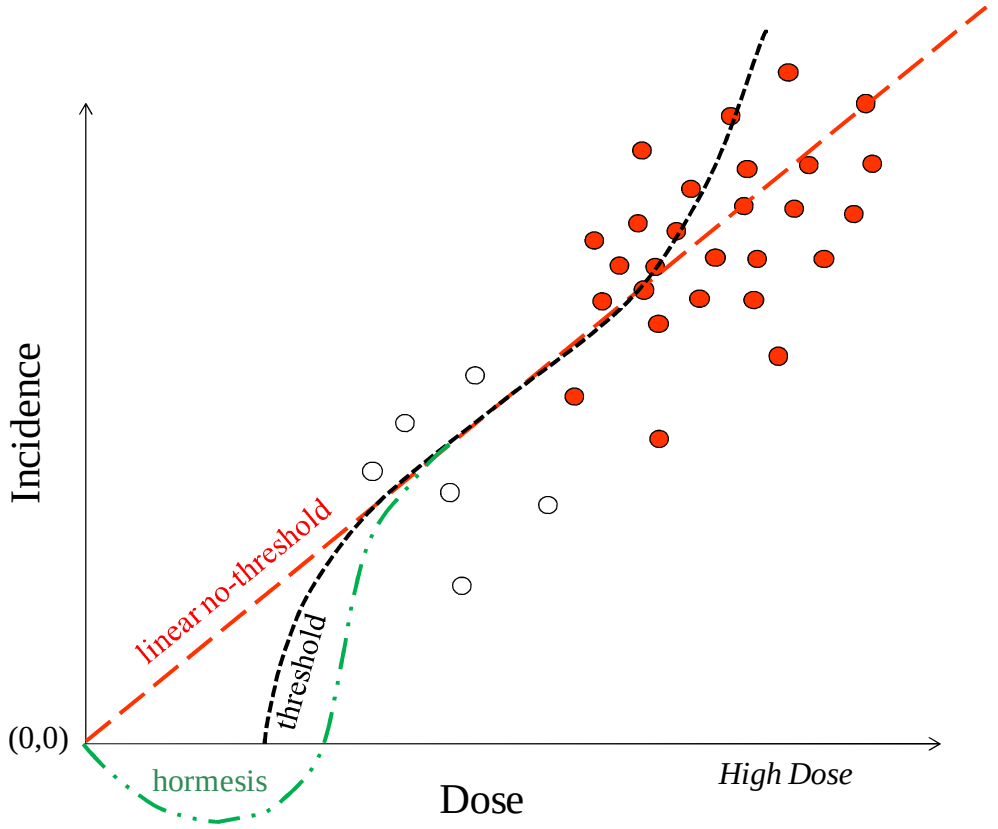

Figure 15 Alternative dose-response curves

2.4.1 Radiation risk controversy

Almost immediately after the discovery of X-rays by Wilhelm Roentgen in late 1895, the emanations were being put to use for therapeutic and diagnostic medical applications. The following year, reports of skin damage due to X-ray exposure were published. Early radiation-protection guidance focused on eliminating deterministic effects such as skin erythema. By the beginning of the 20th century, evidence was appearing that radiation might be responsible for tumours in radiologists, and supporting evidence of cancer induction due to radiation was obtained by studying pitchblende miners and radium dial painters. No formal standards for radiation protection existed until 1913, and at that point, they were established at thresholds for limiting skin erythema and subsequently expanded for internalized radionuclides in terms of maximum permissible body burden. Our current system of understanding of effects of ionizing radiation exposure has been developed over the past 100 years by (a) performing cellular-level studies,

(b) performing animal studies, and (c) performing epidemiological studies on exposed populations [BEIRVII2006].

Scientific debate on low-level radiation effects in the radiation-protection community involves the model used to determine risk from exposure. There is no unanimous agreement on the model of stochastic risk as low doses. There is scientific support for the linear-non-threshold model, threshold dose models, and also hermetic models. Although our current system of radiation-protection guidance is based upon the linear non-threshold model of dose-response, the concept of threshold dose is apparent as early as the writings of Paracelsus (1493-1541), in his famous statement "*What is there that is not poison? All things are poison and nothing is without poison. Solely the dose determines that a thing is not a poison*" [Deichmann1986]. In abbreviated terms, Paracelsus' statement becomes "The dose makes the poison". This suggests that, upon exposure to an anthropogenic chemical, there is a threshold dose above which something becomes poisonous to the body. The concept of threshold dose, established in the 16th century, was abandoned for stochastic-effect radiation-protection purposes in the 20th century. As early as the 1955 Recommendations of the International Commission on Radiological Protection, statements were promulgated that "*no radiation level higher than natural background can be regarded as absolutely 'safe'* " [Clarke2005], despite there being no conclusive proof that low-dose radiation causes any harm, stochastic or non-stochastic. It is this belief, manifest in the so-called linear non-threshold (LNT) hypothesis of radiation risk described above, that has divided public opinion and worker understanding of the effects of ionizing radiation. Various misapplications and misinterpretations of radiation risk using the linear non-threshold hypothesis [Bond1996] [Siegel2012] have made general understanding of the risk of exposure to low-dose radiation confusing and controversial.

2.5 Effects on Pregnancy

In much of the literature, the terms zygote, embryo, fetus, and conceptus are used. Accepted medical definitions are provided as follows [Mosby1990]:

Zygote [Gk *zygon+sporos* seed]: the developing ovum from the time it is fertilized until it is implanted in the uterus.

Embryo [Gk *en* in, *bryein* to grow]: 1. Any organism in the earliest stages of development; 2. in humans, the stage of prenatal development between the time of implantation of the fertilized ovum about 2 weeks after conception until the end of the seventh or eighth week. The period is characterized by rapid growth, differentiation of the major organ systems, and development of the main external features.

Fetus [L, fruitful]: the unborn offspring of any viviparous animal after it has attained the particular form of the species, more specifically, the human being *in utero* after the embryonic period and the beginning of the development of the structural features, usually from the eighth week after fertilization until birth.

Conceptus [L *concipere* to take over]: the product of conception; the fertilized ovum and its enclosing membranes at all stages of intrauterine development, from the time of implantation to birth.

2.5.1 Teratogenesis

The conceptus is a blanket definition which encompasses the zygote, embryo, and fetus stages. Teratogenic insult may be defined as any exposure that is capable of harming the conceptus (for example, inducing birth defects). Radiation is extremely harmful to the conceptus, and to children in general, for two simple reasons: (1) a majority of the cells are in active growth stages in young organisms, and as was demonstrated by the law of Bergonie and Tribondeau, rapidly dividing cells are more radiosensitive; and (2) exposure in the young allows for more time for observable effects to manifest before death.

The human conceptus has an approximate nine-month gestation period, with different radiation sensitivities over this time frame. During the first two weeks of gestation (the zygote stage), the egg is fertilized and implanted in the uterine wall. During this phase, the cells divide at a rapid rate and are highly sensitive to radiation. During this stage, cell killing is the most likely outcome from large doses of radiation. During the following approximately three to seven weeks of gestation (the embryonic stage), differentiated organ development begins, and the embryo is susceptible to cell killing or congenital malformations at moderate to high doses of radiation exposure. From approximately week 8 until birth (the fetal stage), there is rapid growth which makes the fetus susceptible to birth anomalies such as mental retardation. After approximately 17 weeks gestation, all the brain cells have formed and do not further divide, and therefore the most sensitive period for teratogenic effects such as mental retardation is believed to be between 8 and 17 weeks gestation for moderate- to high-dose radiation exposure.

The manifestation of stochastic effects (such as cancer-cell induction) is more probable for *in-utero* exposure. This is recognized by the International Commission on Radiological Protection by suggesting that the risk is a few times that of the population as a whole. Using the value of 5.5%/Sv from Table 3, the cancer-risk coefficient for *in-utero* exposure is estimated at approximately 17%/Sv. Note also that most regulatory agencies have adopted a "balance of pregnancy" dose limit on workers, which is designed to limit *in-utero* exposure. Operationally, when a worker declares a pregnancy to her employer, the dose to the conceptus must be limited to a pre-determined value (in the 2007 ICRP recommendations [ICRP2007], this is 1 mSv).

2.5.2 Perception of risk

Of interest in pregnancy and radiation exposure is the perception of risk by the mother. There is very little scientific evidence that points to increased risk of harm to the conceptus at low doses. To attempt to answer the question, "*How do pregnant women perceive the risk of low-level radiation exposure?*" [Bentur1991] examined the perception of teratogenic risk for exposure to ionizing radiation during pregnancy, specifically considering women who were scheduled to receive diagnostic radiation exams during pregnancy. The control group for the study was women exposed to non-teratogenic drugs and chemicals during their pregnancy. In this study, [Bentur1991] claimed that, *"The two probable factors in creating this misperception of risk are pregnancy-induced anxiety and misinformation. Anxiety is enhanced by the known effects of nuclear disasters and due to continuous flow of information in the medical literature about the long-term effects of therapeutic irradiation on fertility and carcinogenicity".* In the study, women were counselled about the low risk factors for diagnostic radiology procedures. Before counselling, the pregnant women exposed to radiation assigned themselves a higher risk than the non-exposed population, even though their doses from diagnostic procedures would

be extremely low. After counselling, the perception of teratogenic risk did not differ between the groups. This result is very important because it suggests that education and consultation with pregnant women who may be exposed to ionizing radiation can reduce stress and anxiety from the exposure and possibly reduce the risk of the mother selecting therapeutic abortion due to unfounded perceptions of the exposure.

2.6 Summary

From a toxicological standpoint, more is known about the effects of radiation on living organisms than any other insult, including chemicals. As far as carcinogenic toxins go, ionizing radiation is one of the weakest carcinogens on the planet. Effects have been investigated using studies of DNA/molecules/cells, studies on animals, and human epidemiological studies. The time frames for observable effects extend from subseconds (physical) to seconds (chemical) to many years (biological). The endpoints for effects may be (i) radiation enters the body, but misses important targets (a highly likely "endpoint"); (ii) radiation does not cause any damage to the targets; (iii) radiation damages the target, but the target repairs itself; (iv) damaged cells may die; and (v) damage cells may change (mutate). High doses of radiation may cause prompt deterministic effects, such as skin burns. Both high and moderate doses of radiation may increase the risk of stochastic effects such as cancer. Low-dose radiation exposure had not been observed to cause deleterious effects in the populations studied, although the risk of exposure has been extrapolated from high-dose observable effects to the low-dose regime using the linear no-threshold (LNT) dose-response model.

What is known about ionizing radiation exposure can be summarized as:

- Radiation is a very weak carcinogen
- Probability of cancer is a function of dose (increased risk with increased dose; severity of cancer is not a function of dose)
- There is weak-to-no evidence of cancer effects at doses below approximately 100 mSv.

What is NOT known about ionizing radiation exposure:

- Whether there are any negative effects of exposure below approximately 100 mSv
- Whether there are any beneficial effects of exposure below approximately 100 mSv
- Whether there are any effects at low dose other than cancer and leukemia
- Whether there are any inherited effects at any exposure.

Some practical considerations for understanding ionizing-radiation exposure:

- "Normal" cancer incidence is very high (30%–40% over the population)
    - Cause-effect relationships cannot be proven on an individual basis; relative risk can only be established for large exposed groups
- Stochastic effects have a long latent period
    - Leukemia: 2–7 years post-exposure
    - Other cancers: 10–50 years post-exposure
- Exposure must occur to tissue for radiation-induced cancer to form
    - Cancer will not initiate in an organ of the body unless that organ has received a dose
- Certain cancers are not associated with low to moderate doses of ionizing radiation
    - Hodgkin's disease

- Non-Hodgkin's disease
- Chronic lymphocytic leukemia
- Cutaneous malignant melanoma
- Uterine cancer
- Prostate cancer

- Risk from radiation exposure to child and conceptus are enhanced
  - Rapidly dividing cells are radiosensitive
  - Longer lifespan post-exposure enables latent cancers to manifest.

The risks of ionizing radiation exposure have been quantified using a variety of dose-response models. A commonly used model is the linear no-threshold (LNT) model, which is generally considered to be conservative and as such is used extensively by regulators. There are numerous other models, including hormesis models, which are actively debated in the scientific literature and about which scientists have shown evidence for and against. Dose-protection guidance, the LNT approximation, and how the "as low as reasonably achievable, social and economic factors taken into account" (ALARA) mantra is used are discussed in Section 3.

3 Dosimetry, Dose Limitations, and Guidance

The underlying principle of any process that uses ionizing radiation is that the benefit from potential exposure outweighs the potential risk from exposure. Radiation protection is guided by regulations that eliminate deterministic effects and limit stochastic effects from exposure. The relationship between scientific discovery, international synthesis of data, and adoption of national regulations is illustrated in Figure 16.

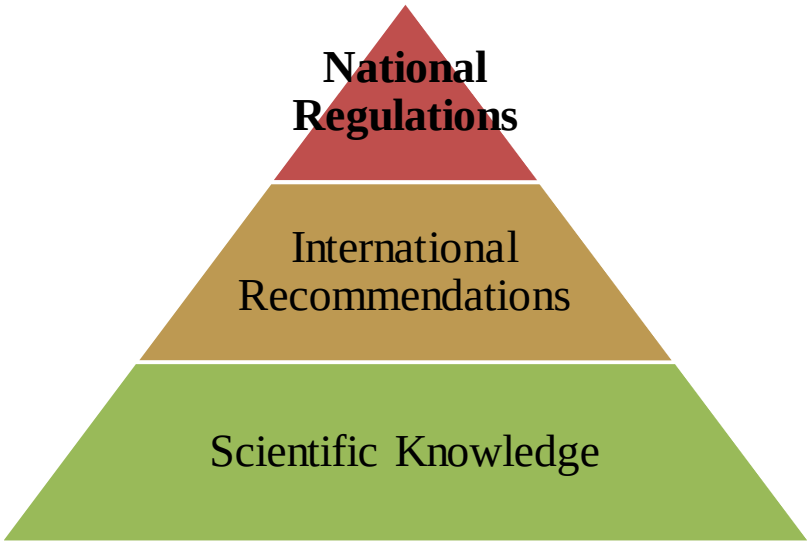

Figure 16 Radiation protection regulation pyramid

Scientific knowledge and discovery is the broad base from which we derive fundamental radiation-protection quantities. This knowledge is disseminated through national reports, industrial reports, peer-review publications, conferences, and many other scientific venues. International bodies periodically synthesize the available data from the scientific literature and produce recommendations on various aspects of radiation protection. International recommendations form the basis of national standards, but are not themselves regulations. National regulations are adopted by government bodies country by country, and although these bodies

tend to follow international recommendations, they are not obligated to do so. In Canada, there are various governmental agencies involved in establishing radiation-protection guidelines, with different areas of responsibility depending upon the source of radiation. For example:

- Nuclear reactor operations – Canadian Nuclear Safety Commission (CNSC)
- Radioactive sources and waste – Canadian Nuclear Safety Commission (CNSC)
- Uranium mining and milling operations – Canadian Nuclear Safety Commission (CNSC)
- High-energy particle accelerators – Canadian Nuclear Safety Commission (CNSC)
- X-ray regulations – each province regulates independently
    - X-ray use – Health Canada (HC) guidelines
- Naturally Occurring Radioactive Material (NORM) - each province regulates independently
    - NORM mitigation – Health Canada (HC) guidelines.

Other agencies that have input into radiation protection regulations include Environment Canada (EC) and Transport Canada (TC). A number of national agencies in Canada are involved in safety and security of radioactive material, including (i) all the above-named agencies, (ii) Public Safety Canada, (iii) Canadian Security Intelligence Service (CSIS), (iv) Department of National Defence, and (v) Canada Border Services Agency (CBSA).

This section discusses fundamental definitions related to ionizing-radiation dose, background radiation, and national/international guidance regarding dose and dose limitations. Background information on the historical development of the radiation protection-system can be found in [Inkret1995] [Lindell1996] [Jones2005] [Clarke2005] [Walker2000].

3.1 Dose Definitions

The concepts of absorbed dose, equivalent dose (radiation weighting factors), and effective dose (tissue weighting factors) are discussed here in relation to risk concepts. In addition, radon guidance will be introduced.

3.1.1 Exposure

Before discussing dose, it is worthwhile to discuss, in a historical sense, exposure. In the early days of X-rays, a common dosimeter was a piece of dental film attached to a paper clip. The daily allowable exposure was an exposure that was just enough so that some "fogging" of the film could be observed on processing. This was known as a "paper-clip unit" of radiation exposure and amounted to an early dosimeter. For larger doses such as might be used in therapeutic medicine, a "skin erythema unit" was used, which was an exposure that would just cause visible reddening of the skin. Neither unit was what could be considered biologically meaningful, although they did provide a measure of protection.

Exposure was defined for X- (and gamma) radiation in terms of air ionization, and the original unit of air ionization established in 1928 was the Roentgen (*R*). The current definition is given as:

$$1R \equiv 2.58 \times 10^{-4}\, C\, kg^{-1}\, of\ air\ .$$

Absorbed dose was subsequently defined as the energy absorbed per unit mass from any kind of ionizing radiation in any target. As such, the absorbed dose is a physical quantity. To calcu-

late the absorbed dose in air from a given exposure, the ionization potential of air (which is 33.7 eV/ion pair or 33.7 J/C) can be used. Using this value, the absorbed dose in air from an exposure of 1 Roentgen can be calculated as:

$$1R \equiv \left(2.58\times10^{-4}\,\frac{C}{kg} \right)\left(33.7\,\frac{J}{C} \right) = 8.7\times10^{-3}\,\frac{J}{kg}\,.$$

A similar calculation of the soft-tissue ionization potential yields $9.5\text{x}10^{-3}$ J kg^{-1}.

Because energy deposition per unit mass was deemed to be close to actual biological damage, a new unit was developed, called the Rad (standing for Radiation Absorbed Dose). The Rad was defined as an energy deposition of 100 erg per gram of material, where 10^7 erg = 1 Joule. The Roentgen could therefore be defined as 87 erg/g in air (or 95 erg/g in soft tissue), and the Rad was defined as 100 erg/g. For regulatory purposes, it was therefore assumed that if one could measure the ionization of air in Roentgen (R), this would be approximately equivalent to the absorbed dose in tissue (Rad_{tissue}). To convert exposure to absorbed dose for any medium, Eq. (14) can be used:

$$D\left(Rad\right) = \frac{87}{100} \times \frac{\dfrac{\mu_m}{\rho_m}}{\dfrac{\mu_a}{\rho_a}} \times E(Roentgen)\ , \qquad (14)$$

where

D = absorbed dose in Rad
E = exposure in Roentgen
μ_m = energy-absorption coefficient for tissue *(or any medium)*
μ_a = energy-absorption coefficient for air
ρ_m = tissue density (or density of any medium)
ρ_a = air density.

Although the historical unit of Rad is still used in some instances, SI units are more common internationally and are promulgated through all major international guidance bodies such as IAEA, ICRP, and UNSCEAR.

3.1.2 Absorbed, equivalent, and effective dose

Three fundamental quantities are required when considering radiation protection:

- Absorbed dose (*D*) is energy absorbed per unit mass. 1 gray (Gy) = 1 joule per kilogram (J/kg)
- Equivalent dose (H_T, units of Sievert, Sv) takes into account the relative biological effectiveness of different radiation types
- Effective dose (*E*, units of Sievert, Sv) takes into account the potential for detrimental effects to the various organs and tissues.

It is important to realize that absorbed dose is a physical quantity, whereas equivalent and effective dose are derived quantities used for radiological-protection purposes. In addition, these derived quantities use reference "individuals" and assigned factors, roughly approximate risk on a population basis, and are not useful for accurate estimation of risk on an individual basis.

The absorbed dose can be expressed as in Eq. (15):

$$D_{T,r} = \frac{E_T}{m_T}, \tag{15}$$

where

$D_{T,r}$ is the absorbed dose to target *T* from radiation *r* (J/kg, or Gy)
E_T is the energy deposited in target *T* (Joule)
m_T is the mass of target *T* (kg).

The equivalent dose is calculated by summing over all different radiations interacting in the target material using Eq. (16):

$$H_T = \sum w_r D_{T,r}, \tag{16}$$

where

H_T is the equivalent dose to target *T* (Sv)
w_r is the radiation weighting factor for the radiation type.

Radiation weighting factors are related to the relative biological effectiveness (RBE) of different kinds of radiation, which is an indication of the relative amount of radiation damage done to tissue for a given absorbed dose. The recommended radiation weighting factors from ICRP103 are provided in Table 7.

Table 7 Radiation weighting factors [ICRP2007]

Radiation	Radiation weighting factor, w_r
Photons (X- and gamma)	1
Electrons (incl. beta)	1
Protons	2
Alpha particles and fission fragments	20
Neutrons (continuous function of energy) N.B.: in ICRP60 [ICRP1990], the centre expression represented all w_r)	$2.5+18.2e^{\frac{-(\ln E)^2}{6}} \quad E<1MeV$ $5.0+17.0e^{\frac{-(\ln(2E))^2}{6}} \quad 1MeV \le E \le 50\,MeV$ $2.5+3.25e^{\frac{-(\ln(0.04E))^2}{6}} \quad E>50\,MeV$

The effective dose, *E*, is calculated using the equivalent dose and tissue weighting factors using Eq. (17):

$$E = \sum w_T H_T \ , \tag{17}$$

where w_T is the tissue weighting factor for target *T*.

Tissue weighting factors have been established as indicators of the relative sensitivities of different tissues to radiation exposure. The ICRP103 tissue weighting factors, along with ICRP60 and ICRP26, are given in Table 8. Blank entries mean that the organ was not uniquely identified in the guide and was included in “remainder”. The sum of tissue weighting factors over all tissues is unity.

Table 8 Tissue weighting factors [ICRP1977,1990,2007]

Organ	Tissue weighting factor, w_T		
	ICRP26 (1977)	ICRP60 (1990)	ICRP103 (2007)
Gonads	0.25	0.20	0.08
Red Bone Marrow	0.12	0.12	0.12
Lung	0.12	0.12	0.12
Breast	0.15	0.05	0.12
Thyroid	0.03	0.05	0.04
Bone surface	0.03	0.01	0.01
Remainder	0.30	0.05	0.12
Colon		0.12	0.12
Stomach		0.12	0.12
Bladder		0.05	0.04
Liver		0.05	0.04
Esophagus		0.05	0.04
Skin		0.01	0.01
Salivary glands			0.01
Brain			0.01
Sum	1.00	1.00	1.00

Unfortunately, ICRP adopted the same base unit (Sv) for both equivalent dose and effective dose, which has the potential to lead to confusion in dose representation.

The equivalencies between classical and SI dose units (and activity, which was discussed in Chapter 3) are provided in Table 9. Dose rate units are the same base units as a function of time (for example, Gy/h).

Table 9 Dose units

Unit	Classical unit	SI unit	Unit conversion
Activity	Curie (Ci)	Becquerel (Bq)	1 Ci = 3.7×10^{10} Bq
Absorbed dose	Radiation absorbed dose (Rad)	Gray (Gy)	100 Rad = 1 Gy
Equivalent dose	Roentgen equivalent man (Rem)	Sievert (Sv)	100 Rem = 1 Sv
Effective dose	Roentgen equivalent man (Rem)	Sievert (Sv)	100 Rem = 1 Sv

In Canada, it is not uncommon to find references to classical units used as operational quantities in nuclear power plants. However, SI units are the approved units of radiation dosage according to the CNSC regulations.

As was discussed in Section 2.3.2 and demonstrated in Table 3, after exposure to low-dose-rate radiation, the ICRP [ICRP2007] suggests detriment-adjusted nominal risk coefficients for cancer and heritable effects in terms of risk per Sv (% per Sv).

The relationship between the various dose quantities and endpoint estimates is depicted in Figure 17. The relative uncertainty in physical and derived quantities is shown by increasing arrow thicknesses, with the uncertainty compounding with each step to calculate the endpoint risk. This demonstrates that, although absorbed-dose estimates may be made with relatively good confidence, the ability to estimate population risk from low dose / dose rate exposure is highly uncertain.

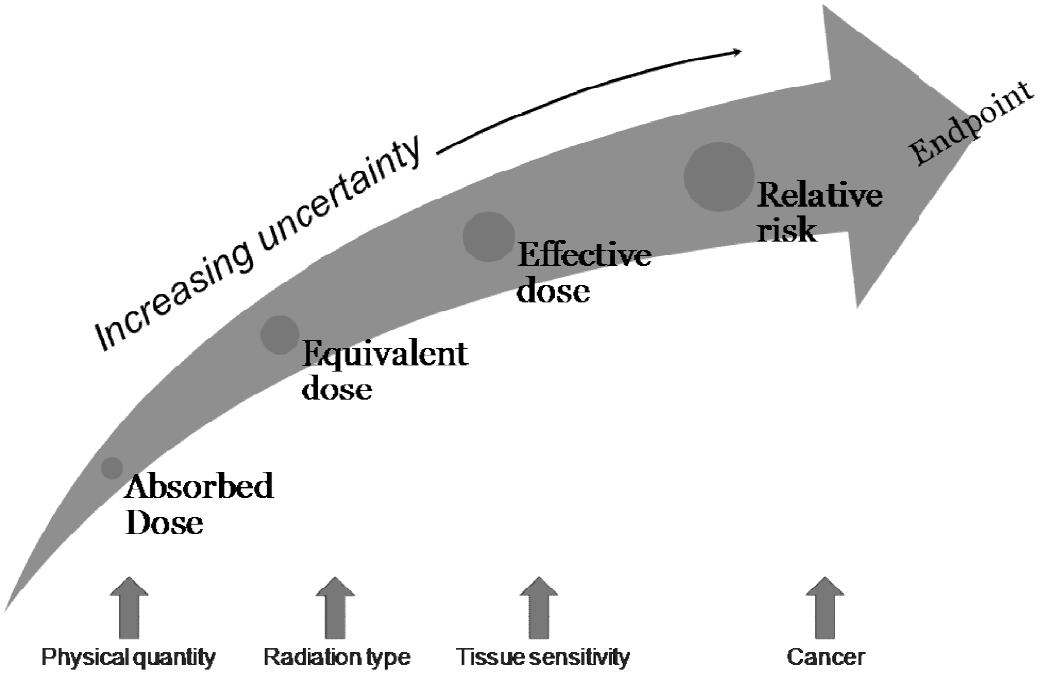

Figure 17 Relationship between dose and endpoint

3.1.3 Committed dose

The committed effective dose (CED) is the effective dose that an individual will eventually receive after having taken a radionuclide into the body (inhalation, ingestion, injection, or skin/wound absorption). Committed usually means to 50 years, although 70 years is used when a childhood intake has occurred.

3.1.4 Collective dose

The collective dose is the sum of individual doses over a population, with units of person-Sv. If the collective dose is divided by the number of persons in the exposed population, then an average individual dose can be estimated. Although this quantity has been used in the literature, ICRP 103 does not recommend the use of collective dose.

3.1.5 Derived quantities

Derived quantities are values or results that are made up, or derived, from other values. Often, derived quantities are made up of other fundamental quantities. Four primary derived quantities are discussed in this section: (i) dose-conversion factors (DCF), (ii) annual limits on intake (ALI), (iii) derived air concentration (DAC), and (iv) radon progeny (WL; WLM).

3.1.5.1 Dose-conversion factors (DCF)

Dose-conversion factors (DCF) are tabulated derived values that enable conversion from one quantity to another. For example, dose-conversion factors are tabulated for inhalation and ingestion for workers in ICRP68 [ICRP1994] and the public in ICRP72 [ICRP1996a]. A dose-conversion factor for an internalized radionuclide typically has units of Sv/Bq committed effective dose (CED), and therefore if the intake (in Bq) is known, the estimated CED in Sv can be immediately calculated. In the case of internalized radionuclides, values are available for inhalation and ingestion, for differing particle sizes, and for the different chemical forms of many radionuclides. Examples of tabulated dose conversion factors for ^{14}C are shown in Table 10.

Table 10 Sample inhalation dose coefficients [ORNL2013]

Inhalation dose coefficients (Sv / Bq) from ICRP 68				
Chemical form=	CO_2	CO	CH_4	Vapour
Effective (ICRP 60)	6.5E-12	8E-13	2.9E-12	5.8E-10

These conversion factors are derived using compartmental biokinetic models for internal dosimetry. Other dose-conversion factors can include external DCFs such as those found in ICRP74 [ICRP1996b] and discussed in Section 5.

3.1.5.2 Annual limit on intake (ALI)

The annual limit on intake (ALI) is the activity (Bq) of a radionuclide which, if taken internally, would result in a dose equal to the annual limit. As such, the ALI is normally defined as the dose limit divided by the effective dose per unit intake. Both equivalent and effective doses are considered; the more restrictive limit is used. Note that simply multiplying the number of ALIs taken in by 20 mSv to calculate committed effective dose may not be a correct estimate because some ALIs are based on effective dose and some on equivalent dose. The ALI is calculated using Eq. (18):

$$ALI\left(Bq\right)=\frac{D_{\text{limit}}\left(Sv\right)}{\sum w_T H_T\left(\frac{Sv}{Bq}\right)}=\frac{0.02\ Sv}{DCF\ \frac{Sv}{Bq}}. \tag{18}$$

3.1.5.3 Derived air concentration (DAC)

The derived air concentration (DAC) is defined as the air concentration (Bq/m^3) that would lead to the inhalation of 1 ALI by a reference person over 2000 hours (50 weeks x 40 h/week)

assuming that the reference person inhales 1.2 m^3/h (light work). The DAC is calculated using Eq. (19):

$$DAC\left(\frac{Bq}{m^3}\right)=\frac{ALI\left(Bq\right)}{2000\,hr\cdot 1.2\,\frac{m^3}{hr}}=\frac{ALI\left(Bq\right)}{2400\,m^3}\ . \tag{19}$$

DACs enable rapid estimation of committed effective dose rate because the DAC represents 1 ALI (in the case of Canadian regulations, 20 mSv) in 2000 h, or stated in another manner, 1 DAC = 10 µSv/h. The number of DAC-h corresponds to the CED.

3.1.5.4 Radon-derived quantities (WL; WLM)

Radon gas (^{222}Rn) is considered harmful primarily because it has numerous short-lived daughters such as polonium, bismuth, and lead which are solids and readily adsorbed on particles of fine dust than can be inhaled. When air containing radon is breathed in, it can be readily expelled without inducing any damage whatsoever. However, the radon daughters, both from gas decay and dust, can be trapped in lung tissue, where they can induce local damage to lung tissue through alpha-particle interactions. The combined alpha energies of the daughters per unit volume of air are the most important parameters to be considered when estimating damage to lung tissue. There is a special unit used to define this quantity, called the working level (WL).

The working level (WL) is defined as any combination of the short-lived decay products of radon (^{218}Po, ^{214}Pb, ^{214}Bi, and ^{214}Po) in one dm^3 (1 litre) that will result in the ultimate emission of $1.3\text{x}10^5$ MeV of alpha energy (or $2.08\text{x}10^{-5}$ J/m^3). An atmosphere containing 3.6 Bq/dm^3 (~100 pCi/L) of radon in equilibrium with its daughters is 1 WL. Note that the short-lived daughters are not necessarily in equilibrium with the radon parent, and for this reason, conversion of radon concentration to daughter concentrations uses a factor of about 0.7 for uranium mines (0.4 for homes). For example, finding 3.6 Bq/dm^3 in a mine is approximately equivalent to 0.7 WL. It is common practice to use an equilibrium factor of 0.5, and therefore a WL would be equal to 100 pCi/L (3.7 Bq/L).

A working-level month (WLM) is defined as the exposure to the equivalent radon daughter concentration of 1 WL for a time period of 170 hours. For regulatory purposes, an abundance of data was obtained from uranium miners, which showed that miners exposed to 100 or more WLM had an increased risk of developing lung cancer. A regulatory limit of 4 WLM per year was therefore set for uranium workers. This was set to correspond to the fact that a 25-year work duration at a level of 4 WLM would lead to a cumulative exposure of 100 WLM. Dose-conversion factors for radon are presented in ICRP50 [ICRP1987]. A worker dose-conversion factor of 5 mSv/WLM is often used for radiation-protection purposes.

3.2 Background Radiation Exposure

The Earth is radioactive and has been since its formation. The Earth contains radioisotopes that originated from planetary formation (primordial radioisotopes) and also from extra-terrestrial origins (cosmogenic radioisotopes produced continuously in the upper atmosphere through cosmic-ray interactions which deposit on Earth through atmospheric dispersion, deposition,

and precipitation). Some important primordial and cosmogenic radioisotopes are listed in Table 11.

Table 11 Primordial and cosmogenic radioisotopes

Primordial			Cosmogenic	
^{40}K	^{142}Ce	^{174}Hf	^{10}Be	^{22}Na
^{50}V	^{144}Nd	^{180}Ta	^{26}Al	^{35}S
^{87}Rb	^{147}Sm	^{187}Re	^{36}Cl	^{7}Be
^{113}Cd	^{148}Sm	^{190}Pt	^{14}C	^{33}P
^{115}In	^{152}Gd	^{204}Pb	^{32}Si	^{32}P
^{123}Te	^{156}Dy	$^{238, 235}$U	^{39}Ar	^{28}Mg
^{138}La	^{176}Lu	^{232}Th	^{3}H	^{24}Na

In addition to the two natural source categories, radioisotopes are introduced into the environment from anthropogenic sources such as nuclear medicine, certain industrial processes, routine nuclear power operations, historical nuclear weapons testing, and nuclear reactor accidents. Theoretically, all radioisotopes on the nuclide chart can be introduced into the environment through anthropogenic processes. In practice, only a few anthropogenic radioisotopes are persistent in the environment, for example, ^{137}Cs. All the above-listed sources contribute to the ubiquitous background that constantly surrounds us [Waller2013].

The most recent analysis of U.S. population dose due to natural and anthropogenic radionuclides was conducted by the NCRP and published in Report No. 160 [NCRP2009]. The report indicated that roughly half the yearly exposure to a member of the U.S. population is from natural background radiation, primarily radon (originating from uranium in the ground) and thoron (originating from thorium in the ground) gases, whereas the other half is from anthropogenic (human-made) sources, of which the majority is due to medical procedures (see Figure 18). In Canada, it can be expected that the ratios will be similar to the U.S. values.

Note that in the U.S. report [NCRP2009], the average estimated yearly dose corresponding to Figure 18 is approximately 6.2 mSv. The data indicated a large increase in average yearly dose, which was exclusively due to medical procedures. Before the release of NCRP Report No. 160, the average yearly dose was estimated to be approximately 3.6 mSv from all sources [NCRP1987]. Therefore, the dose increase of 3.6 mSv to 6.2 mSv (almost 75% greater) due to medical procedures is significant and worthy of increased surveillance.

Because Canada is a country in which advanced medical procedures such as computer tomography (CT) are widely used, it is likely that our yearly average dose is proportionally similar to that shown in Figure 18.

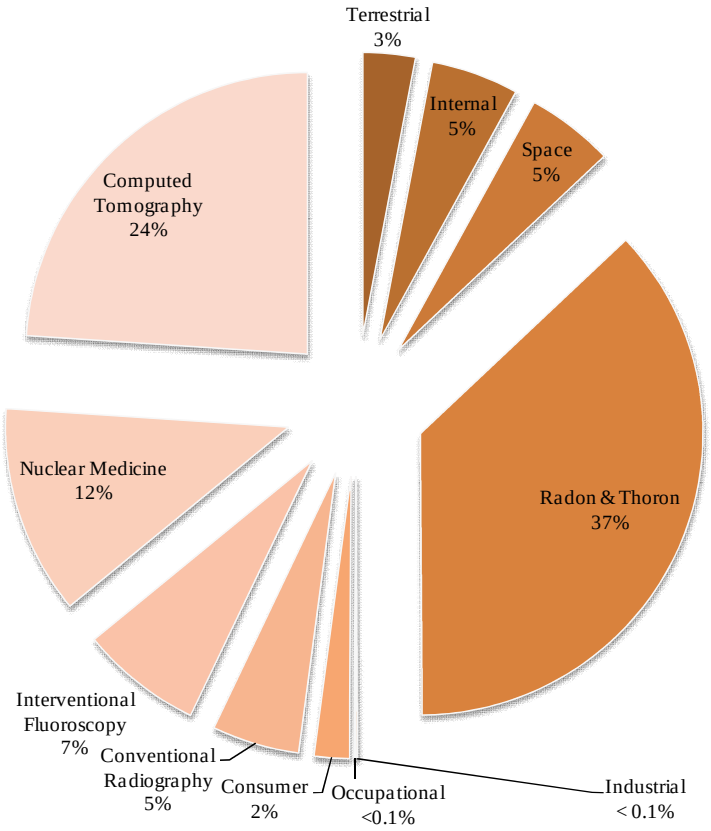

Figure 18 Origin of average yearly radiation exposure (adapted from [NCRP2009])

However, since the use of radiation for medical procedures is more strictly controlled in Canada, it is also likely that the average yearly dose is proportionally smaller that U.S. values, with a correspondingly higher percentage assigned to radon and thoron compared to, for example, CT.

A study done by [Grasty2004] for natural background radiation in Canada indicated that the average annual radon and thoron component of the dose is 926 µSv, compared to the [NCRP2009] U.S. estimate of 2294 µSv. In fact, taking into account all sources of natural (not anthropogenic) radiation, it was found [Grasty2004] that the average yearly effective dose from natural sources was 1769 µSv, which is significantly smaller than the 2422 µSv worldwide average reported by [UNSCEAR2000]. Note, however, that the natural background can vary greatly from location to location in Canada (and, of course, world-wide).

3.3 International Guidance

The history of radiation protection effectively begins in 1895 with the discovery of X-rays by Wilhelm Roentgen (for which he received the Nobel Prize in physics in 1901). Radiation-induced dermatitis was first observed by Emil Grubbé in the U.S. and Henry Drury in the U.K. in 1896. By the end of 1896, within a year of the discovery of X-rays, the first radiation-protection advice was proposed by Wolfram Fuchs in the United States and can be paraphrased as:

- Coat skin with Vaseline™ and leave extra on the most exposed area
- Do not stand within 12 inches of the X-ray tube
- Make exposure as short as possible.

As crude as the above recommendations are, they embody the underlying protective mantra of radiation shielding that we still use today: shielding, distance, and time. As a result, in 1902, a first crude limit corresponding to approximately 100 mGy per day (or 30000 mGy per year) was proposed, corresponding to the lowest radiation exposure that could be detected by fogging on a photographic plate [Inkret1995]. However, despite an acknowledgment of potential detrimental effects, between the time of discovery of X-rays and the mid-1920s, numerous injuries due to radiation exposure were reported (especially among early radiologists). Following increasing radiation-safety concerns by radiologists and the public, the first International Congress of Radiology was held in 1925 in London, England. Until that point, quantification of dose was not consistent and therefore was considered a priority. As a result, the International Commission on Radiation Units and Measurements (ICRU) was formed. In 1928, the second Congress was held in Stockholm, Sweden, which led to the formation of the International X-Ray and Radium Protection Committee, which was the predecessor of the International Commission on Radiological Protection (ICRP). Throughout the years, the trend in radiation protection has involved a lowering of the acceptable radiation dose for workers, and by the 1960s, of limitations on acceptable dose for members of the public. The trend in dose standards is presented in Figure 19.

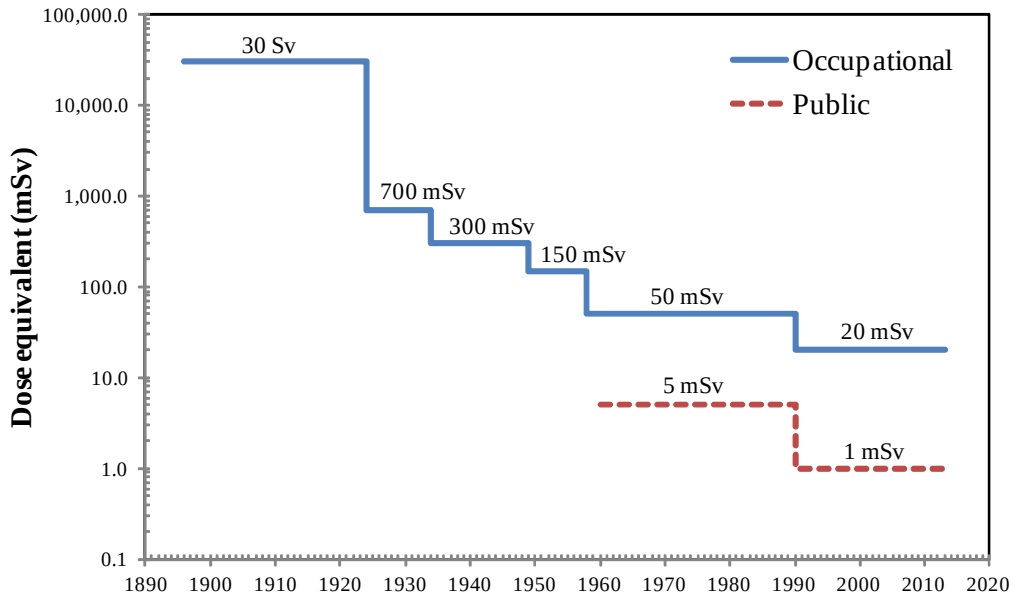

Figure 19 Chronology of radiation-protection guidance (adapted from [Inkret1995])

The change in philosophy for radiation-protection standards has shifted since 1896 as more knowledge about the detrimental effects became known and as more opportunities for population studies of effects (epidemiological studies) became available. A prime example is the paradigm shift from protecting only for deterministic effects (Figure 20, left) to acknowledgement, quantification, and protection standards to minimize risk from stochastic effects (Figure 20, right).

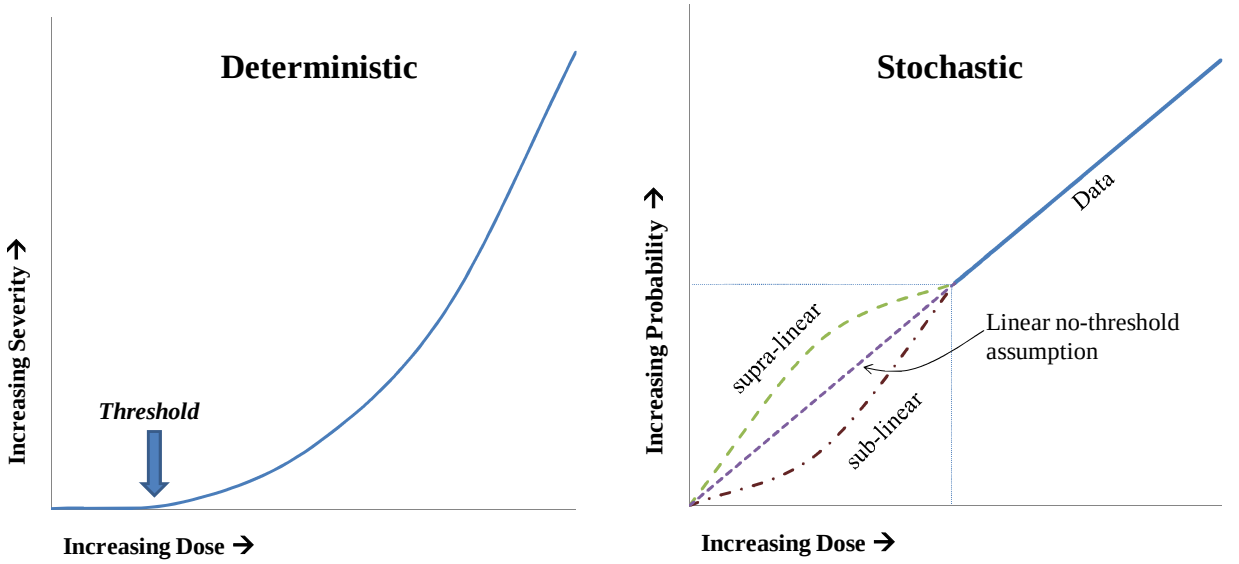

Figure 20 Paradigm shift from deterministic to stochastic effect protection

The paradigm shift in basic radiation-protection philosophy lead to numerous fundamental changes in the way radiation protection was being administered on an international scale. Although the original uses of ionizing radiation were predominantly in medicine, increased non-medical uses became more common throughout the years and were reflected in adaptations of international guidance. Practical guidance shifted to quantified dose limitation and optimization. Although it had always been assumed that if humans were adequately protected from the deleterious effects of ionizing radiation exposure, then the environment was also protected, a change in philosophy moved towards the need for demonstration of adequate environmental protection. Although the concept of the greatest good for the greatest number dominated radiation-protection practice for many years, current philosophy also considers adequate individual protection as well as that of the group. The historical progression of radiation-protection principles is depicted in Figure 21.

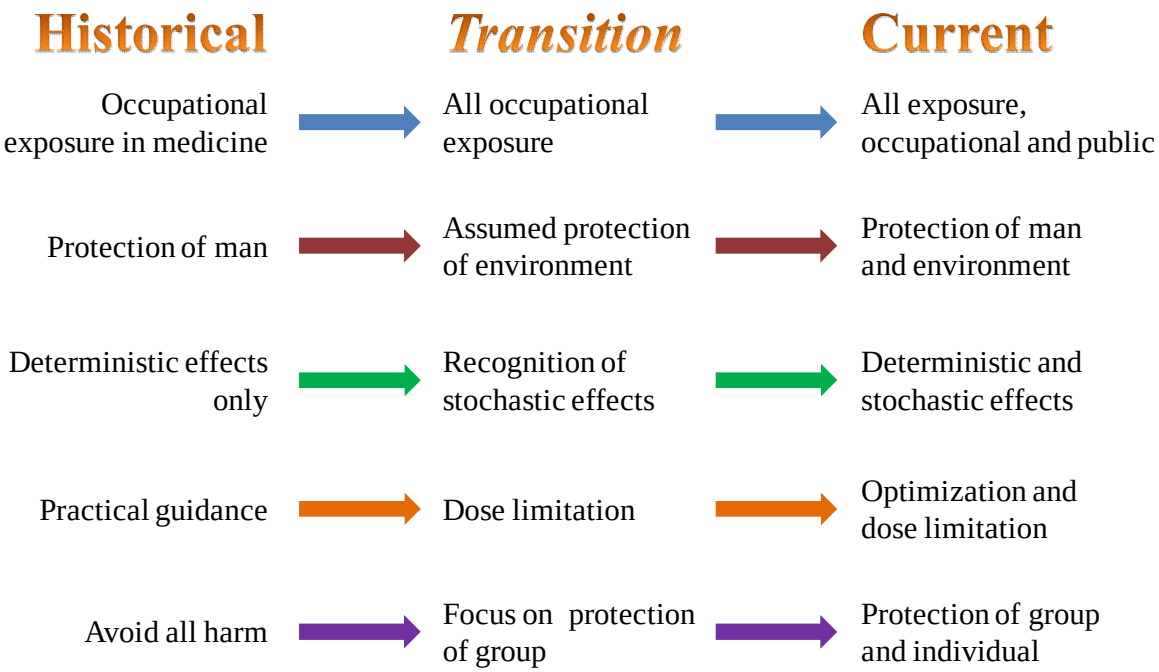

Figure 21 Progression of radiation protection principles (adapted from [Clement2009])

A number of international organizations are pivotal in setting radiological protection standards and providing guidance. The essential organizations that provide input to national regulatory standards are depicted in Figure 22. These organizations are discussed in the following sections.

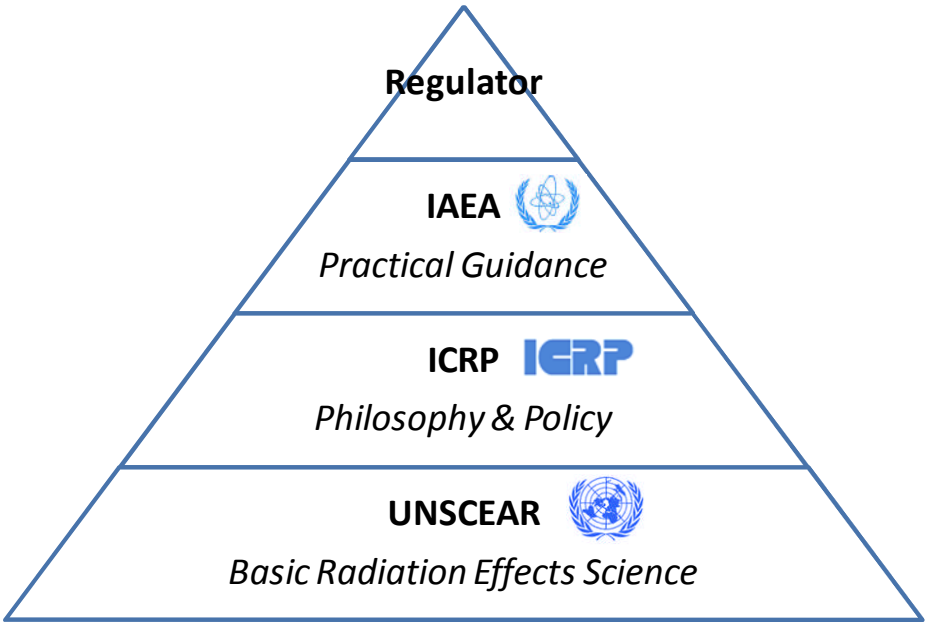

Figure 22 Relationship of international bodies for radiation protection regulations

3.3.1 UNSCEAR

UNSCEAR is the United Nations Scientific Committee on the Effects of Atomic Radiation, which was established by the United Nations in 1955 to assess and report levels and effects of exposure to ionizing radiation and provides the scientific basis for evaluating radiation risk and for

establishing protective measures. UNSCEAR provides the scientific guidance that is consulted when developing ICRP recommendations. UNSCEAR publications can be found online at:

http://www.unscear.org/unscear/en/publications.html .

3.3.2 ICRP

ICRP is the International Commission on Radiological Protection, established in 1928 to advance for the public benefit the science of radiological protection, in particular by providing recommendations and guidance on all aspects of protection against ionizing radiation. The main objective of the Commission's recommendations is to provide an appropriate standard of protection for humans without unduly limiting the beneficial practices giving rise to radiation exposure. The ICRP produces recommendations on radiological protection that are adopted worldwide based on science and value judgements. The ICRP guidance documents form the basis for IAEA regulatory recommendations. ICRP publications can be found online at: http://www.icrp.org/publications.asp.

3.3.3 ICRP 103

The current recommendations of the ICRP [ICRP2007] form the basis for the radiation-protection system. The primary aim of the recommendations is to provide an appropriate level of protection for people and the environment without unduly limiting the desirable human activities that may be associated with radiation exposure. The three primary goals of radiation protection are:

- Justification – more benefit than detriment from exposure
- Optimization – exposure has been optimized to be as low as reasonably achievable
- Dose limitation – limit the dose (except for medical exposures).

The three goals form the core of the radiation-protection system and apply to three different situations:

- Existing situations – natural events, past practices, past events; the situation already exists when a decision on control is required, including natural background and residues from past practices.
- Planned situations – practices, medical exposures; the situation involves planned operation of sources, including decommissioning and disposal of radioactive waste.
- Emergency situations – preparedness, response; the situation is unexpected and requires urgent action to mitigate consequences.

In ICRP103, three exposure types are also considered:

- Occupational exposure - all exposure incurred by workers in the course of their work, with the exception of (i) excluded exposures and exposures from exempt activities involving radiation or exempt sources, (ii) medical exposure, and (iii) normal local natural background radiation.
- Public exposure - exposure incurred by members of the public from radiation sources, excluding any occupational or medical exposure and the normal local natural background radiation.
- Medical exposure - exposure incurred by patients as part of their own medical or dental diagnosis or treatment; by persons, other than those occupationally exposed, knowingly,

while voluntarily helping in the support and comfort of patients; and by volunteers in a programme of biomedical research involving their exposure.

Dose limits corresponding to planned public and occupational exposure are provided in Table 12. Note that the numerical values are essentially the same as reported in ICRP60 [ICRP1990], from which the current CNSC regulations are derived. Note that the dose-limit guidance refers to exposures above background radiation (as discussed in Section 3.2) and as such may be considered as an additional dose over background. It should also be noted that, operationally, action levels are often used that are a fraction of the dose limit. Exceeding an action level would initiate an investigation into the reason for the dose and may initiate a review of procedures to make doses as low as reasonably achievable, social and economic factors being taken into account (ALARA). The ALARA principle is also found in CNSC document G-129, Rev1 [CNSC2004].

Table 12 ICRP103 dose limits for planned exposure scenarios [ICRP2007]

	Occupational	Public
Effective Dose (Whole Body)	20 mSv/a averaged over 5 years (50 mSv/a max)	1 mSv/a
Equivalent Dose (Lens of the Eye)	150 mSv/a	15 mSv/a
Equivalent Dose (Skin)	500 mSv/a	50 mSv/a
Equivalent Dose (Hands and Feet)	500 mSv/a	n/a

ICRP103 also considers the target for exposure in defining a “representative person”. A representative person is an individual receiving a dose that is representative of the more highly exposed individuals in the population. This term is the equivalent of, and replaces the notion of, the “average member of the critical group” described in prior ICRP documents (for example, [ICRP1990]).

Finally, ICRP103 considers explicitly the need for protection of the environment by delineating the requirement for scientific evidence to demonstrate that protection is adequately afforded and the need for improved protection as required. Further guidance is provided by ICRP108 [ICRP2008].

3.3.4 IAEA

The IAEA is the International Atomic Energy Agency, established within the United Nations framework in 1956 as the world’s “Atoms for Peace” organization to promote safe, secure, and peaceful nuclear technologies. The Agency works with its member states and multiple partners world-wide to promote safe, secure, and peaceful nuclear technologies. Three main areas of work underpin the IAEA’s mission: Safety and Security; Science and Technology; and Safeguards and Verification. The IAEA has a wide range of programmes, including development of safety stan-

dards in regulatory language. IAEA Safety Series documents are often used as the principal references for national regulatory policy. The most fundamental IAEA radiation protection standard was the "International Basic Safety Standards for Protection against Ionizing Radiation and for the Safety of Radiation Sources" [IAEA1996], which has been superseded by an interim General Safety Requirements Part 3 report [IAEA2011]. IAEA publications can be found online at: http://www-pub.iaea.org/books/.

3.4 Canadian Guidance

The regulatory body for nuclear power activities in Canada is the Canadian Nuclear Safety Commission (CNSC). The regulatory system is designed to protect people and the environment from licensed sources of anthropogenic radiation resulting from the use of nuclear energy and materials. This is accomplished through a licensing process that requires the licensee to prove that their operations are safe. The basis of the regulatory system is the principle that no technology is fail-proof and that therefore licensees must incorporate multiple layers of protection (defence in depth) whenever radioactive materials are used. The CNSC also licenses the import, export, and transportation of nuclear materials and other prescribed substances, equipment, technology, and dual-use items. CNSC staff evaluates the performance of nuclear power plants and radioactive material users, as well as participating in international activities for non-proliferation of nuclear weapons.

The CNSC operates and enforces regulations under the Nuclear Safety and Control Act (NSCA, 1997). As the Canadian federal regulator, the CNSC executes licensing decisions made by the Commission or its designates continually monitors licensees to ensure that they comply with safety requirements that protect workers, the public, and the environment, and also upholds Canada's international commitments to the peaceful use of nuclear energy. Regulatory requirements are codified in the NSCA, its associated regulations, licences, and directives provided by the CNSC. A number of regulations are referred to under the act and are listed below:

- Canadian Nuclear Safety Commission By-Laws (SOR/2000-212)
- Canadian Nuclear Safety Commission Cost Recovery Fees Regulations (SOR/2003-212)
- Canadian Nuclear Safety Commission Rules of Procedure (SOR/2000-211)
- Class I Nuclear Facilities Regulations (SOR/2000-204)
- Class II Nuclear Facilities and Prescribed Equipment Regulations (SOR/2000-205)
- Directive to the Canadian Nuclear Safety Commission Regarding the Health of Canadians (SOR/2007-282)
- General Nuclear Safety and Control Regulations (SOR/2000-202)
- Nuclear Non-Proliferation Import and Export Control Regulations (SOR/2000-210)
- Nuclear Security Regulations (SOR/2000-209)
- Nuclear Substances and Radiation Devices Regulations (SOR/2000-207)
- Packaging and Transport of Nuclear Substances Regulations (SOR/2000-208)
- Radiation Protection Regulations (SOR/2000-203)
- Uranium Mines and Mills Regulations (SOR/2000-206)

Of significant interest are the Radiation Protection Regulations [NSCA2000], which set limits on the amount of radiation that the public and nuclear energy workers (NEWs) may receive. Canadian regulations are consistent with the most recent recommendations of the International Commission on Radiological Protection (currently adhering to guidance in ICRP60

[ICRP1990]). In Canada, standards and practices to protect people from radiation exposure are also developed by the Federal-Provincial-Territorial Radiation Protection Committee (FPTRPC), which provides a national forum on radiation-protection issues.

The CNSC offers instruction, assistance, and information on these requirements in the form of regulatory documents, such as policies, standards, guides, and notices. Licensee compliance is verified through inspections and reports.

In Canada, the current (2013) radiation-protection regulations are based on ICRP60 [ICRP1990]. However, the numerical values of the dose limits have not been changed in ICRP103 [ICRP2007], and therefore the basic values on which Canadian regulatory guidance is based will continue for many years into the future. The operational values used by the CNSC are provided in Table 12 with the inclusion of a balance-of-pregnancy dose limit for workers of 4 mSv. The effective dose is calculated using Eq. (20) and compared to the dose limit for regulatory purposes [NSCA2000]:

$$E_{total} = E + \left(5\frac{mSv}{WLM} \cdot RnP \right) + \left(20\,mSv \sum \frac{I}{ALI} \right), \tag{20}$$

where

E_{total} is the total effective dose from all sources (mSv)
E is the effective dose from external sources + committed effective dose measured directly or from excreta (mSv)
RnP is the exposure to radon progeny in working-level months (WLM)
I is the intake of radionuclides not already accounted for (Bq)
ALI is the annual limit on intake (Bq to give 20 mSv in 50 years).

3.5 Summary

Radiation-protection standards have evolved over the years to provide increased levels of protection for workers and the public. Dose limits are established on the basis of scientific knowledge which forms policy, best practices and guidance, and then national regulations.

The basic dose quantities used are absorbed dose, equivalent dose, and effective dose. Although nuclear power plant operations often use obsolete units (such as Ci, Rad, and Rem) in their plants, most of the nuclear industry uses SI units. Dose quantities for regulatory purposes, as promulgated through the Nuclear Safety and Control Act, use SI units. Dose limits derived from International Commission on Radiological Protection guidance are established in Canada, and derived quantities are used in operations.

Background radiation is made up of natural and anthropogenic components. Dose limits are established to provide protection above the ubiquitous background level, which has a wide annual dose range world-wide. In Canada, the background dose is estimated to be approximately 3.6 mSv per year. Evidence from U.S. estimates indicates that increased use of advanced medical imaging procedures such as computed tomography is resulting in a larger estimated background dose; however, no such study has indicated that this is the case in Canada.

As research continues into large epidemiological studies and low-dose rate radiation effects, dose-limit guidance may change in the future.

4 Radiation Instrumentation

Detection of ionizing radiation is vitally important to all aspects of the nuclear energy industry. The ability to identify sources of radiation, quantities of radiation, and specific radioisotopes enables the administration of comprehensive radiation protection, environmental monitoring, and security programs.

Before discussing the mechanisms of how radiation interacts with detection materials, the basics of radiation interactions with matter must be understood. These concepts were discussed in Chapter 3 (Nuclear Processes and Neutron Physics). This section considers radiation instrumentation that may be pertinent to CANDU operations. The basics of detection, as well as gas-filled, scintillation, and semiconductor detectors, are discussed. Dosimetry detectors, especially as they relate to CANDU plant operations, are explored.

4.1 Basics of Detection

Ionizing radiation is tasteless, odourless, and colourless and cannot be detected by the human senses. Therefore, devices to aid in detection and identification of ionizing radiation are required for safety purposes. Anything that responds to ionizing-radiation interactions can be considered a radiation detector. In fact, the mechanisms of radiation interactions with tissue and the human body, as discussed in Section 2, are fairly closely related to radiation detectors. The primary differences are in the observable endpoints, where radiation detectors are designed to provide an indication of radiation level through chemical/electric/electronic indications, whereas the endpoints in radiation biology tend to be deterministic or stochastic health effects. That being said, the human body itself is a radiation detector of sorts. The first "radiation dosimeters" used were based on skin reddening (or erythema). The variability in individual human response to radiation (and of course the fact that skin reddening occurs only at unsafe moderate to high radiation doses) makes this type of radiation detector impractical.

Radiation detectors work on one of two basic principles: (i) ionization and (ii) excitation.

Ionization

In an ionization-based detector, electrons bound to the atoms or molecules of the material through which charged particles such as alpha and beta particles pass are released. The separated electrons and ions (Figure 23) can be collected at two electrodes by imposing a potential difference across the detector space; their presence is then measured as pulses or a current. An example of generation of electron-ion pairs in a gas-filled counter (for example, a Geiger-Müller tube) is depicted in Figure 24.

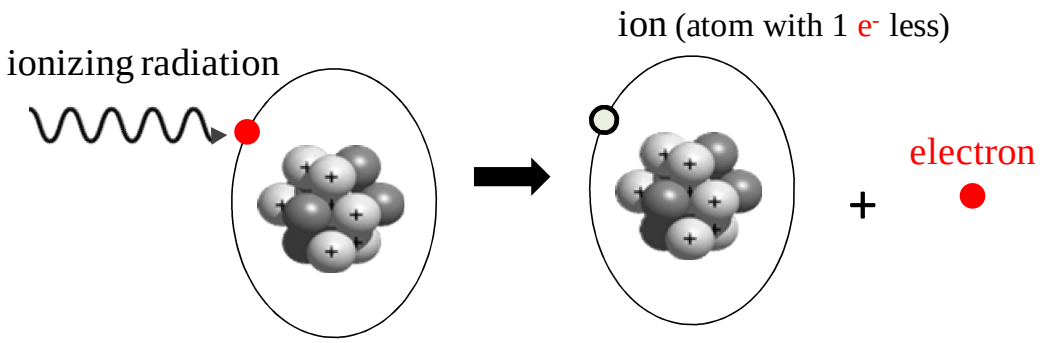

Figure 23 Ionization process

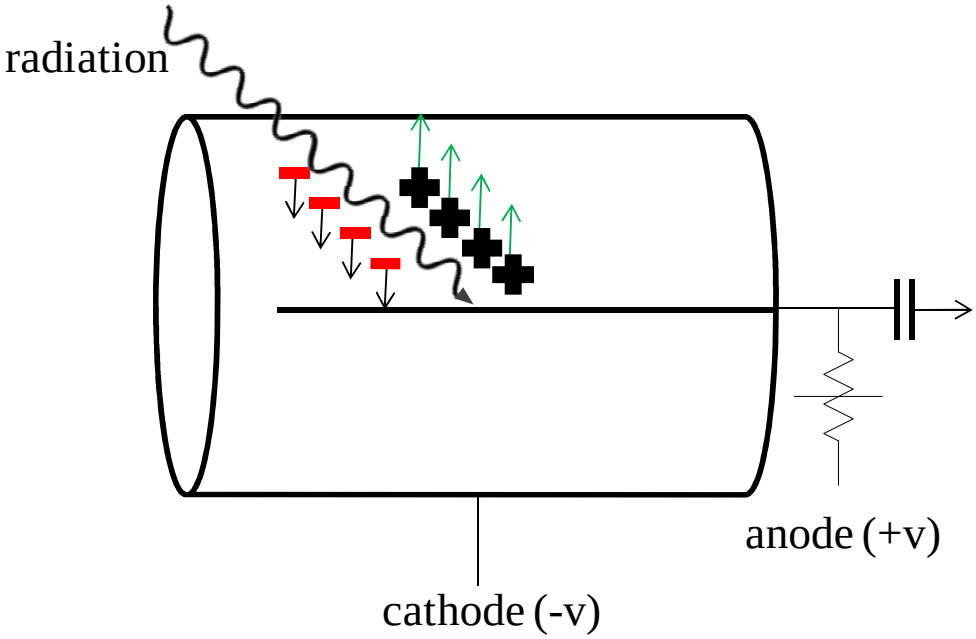

Figure 24 Ionization in a gas-filled tube

Excitation

In an excitation-based detector, part of the radiation energy is transferred to bound electrons and raises them to an excited state in the atom or molecule. When the excited species returns to its ground-state energy level, the excited atom or molecule may emit electromagnetic energy in the ultraviolet to visible region (Figure 25). This light can be detected by a photomultiplier tube (PMT), which generates secondary electrons using a photocathode and multiplies them to generate a detectable signal. This process is depicted in the scintillation-type counter system shown in Figure 26.

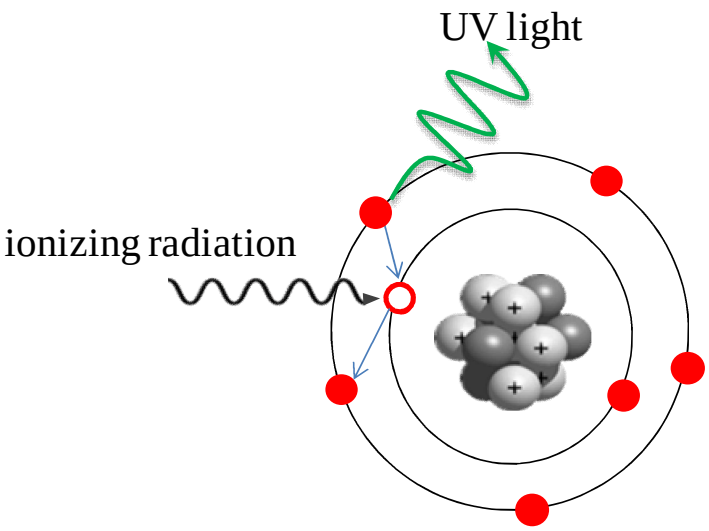

Figure 25 Excitation process

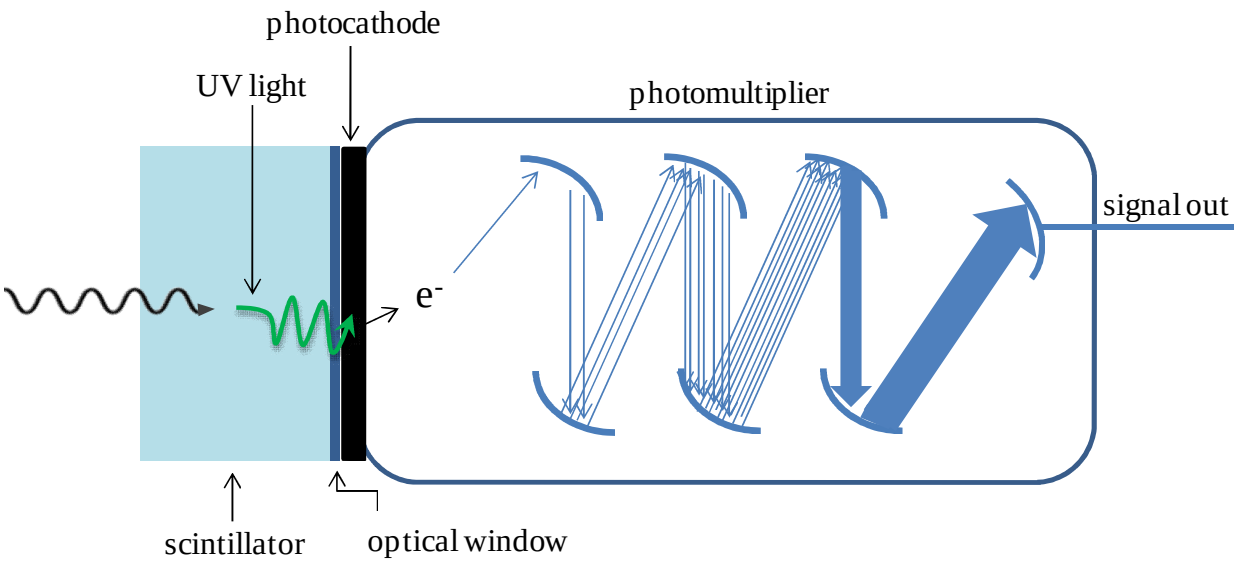

Figure 26 Excitation in a scintillator-type detector

Advances in radiation-detection instrumentation took place in the 1920s and have continued ever since. A concise discussion of the history of radiation-detection instrumentation is provided by [Frame2005]. Important operational characteristics for all detector types include resolving time and efficiency and are discussed below. An excellent reference on particle counting is ICRU Report 52 [ICRU1994].

4.1.1 Resolving time

When ionizing radiation interacts with a detector, a signal in the detector material (whether it be a gas, scintillator, or solid-state device) is produced that is related to the radiation event that generated it. During the time it takes the system to process a pulse that is generated in the detector, the detector may be unavailable to process additional events. For example, during the time it takes for positive ions in a GM tube to reach the cathode, the tube is insensitive to any radiation. During this time, if a second ionizing ray interacts with the detector, it will not be observed because the tube cannot distinguish that there is another electron avalanche present; the system observes only one large electron avalanche until it has been reset after detection. In essence, the counter cannot produce pulses for more than one event because the counter is "occupied" with the first event. This phenomenon is sometimes called coincidence, and as a result, the observed counts are always lower than the true counts. The "resolving time" is often referred to as "dead time", because in essence the detector is "dead" and cannot detect any other radiation in this time window. Note, however, that the resolving time is actually the sum of the dead time and recovery time. In terms of definitions, dead time is the time required in a detector before another unique pulse can form; recovery time is the time required after the dead time until the pulse size is large enough to pass a discriminator; and resolving time is the minimum time from the detection of one interaction until the next detection can occur. True resolving times span a range from a few microseconds to 1000 microseconds, depending on the detector. The loss of particles is important, especially when high count rates are involved and the losses accumulate into large numbers.

For a counting rate, R, from a radioactive source, the presence of coincidence will mean that the rate actually measured, r, will be less than the expected value (r < R). If the detector has a dead time of T, then the true count rate is given by Eq. (21):

$$R = r + rRT \,. \tag{21}$$

The counting rate can therefore be corrected for dead time using Eq. (22):

$$R = \frac{r}{1 - rT} \,. \tag{22}$$

The value of dead time, T, can be determined using a two-source method by measuring the activity from two known sources r_1 and r_2. In theory, the measurement, r_3, should be the simple sum of the two sources as given by Eq. (23):

$$r_1 + r_2 = r_3 + b \,, \tag{23}$$

where b is the background counting rate. If each of these counting rates is corrected for dead time, then Eq. (23) becomes Eq. (24):

$$\frac{r_1}{1 - r_1 T} + \frac{r_2}{1 - r_2 T} = \frac{r_3}{1 - r_3 T} + b \,. \tag{24}$$

Because the background count rate may be considered negligible for this measurement, Eq. (24) can be expressed in the form of a quadratic equation:

$$r_1 r_2 r_3 T^2 - 2 r_1 r_2 T + r_1 + r_2 - r_3 = 0 \,. \tag{25}$$

T should be on the order of microseconds, thereby making T^2 negligible, enabling the simple solution for the dead time, *T*, given by Eq. (26):

$$T = \frac{r_1 + r_2 - r_3}{2 r_1 r_2} \,. \tag{26}$$

The above expressions are useful in the limit of low interaction rates and are considered part of what is known as the non-paralyzable model. If the dead time approaches 30% or more, the above model fails, and the paralyzable model must be used (which is not developed here; the reader is referred to [Knoll2010]. The significance of non-paralyzable versus paralyzable, from a practical perspective, relates to ability to count radiation in extreme fields. An ideal detector will have a linear response of count rate with interaction rate. A non-paralyzable detector will have an increasing count rate with interaction rate (but not necessarily linear at high interaction rate), but will tend to flatten out at high interaction rate. A paralyzable detector is one which has an increasing response at lower interaction rate, a peak response, and then a decreasing response with higher interaction rate. Essentially, in a paralyzable system, an interaction that occurs in the detector during the dead time will extend the dead time. The danger of a paralyzable detector is that if the count rate goes down as the interaction rate goes up, a person entering a progressively higher radiation field will think that he is moving into an area of lower radiation. For example, a GM counter in a high radiation field will tend to become paralyzed and may severely under-predict the radiation hazard.

4.1.2 Energy response and efficiency

All radiation detectors respond to energy deposition differently, based upon the type of radiation interacting with the detector and the energy of the radiation. For example, in a thin-window GM tube, beta particles interact best with the filling gas, followed by alpha particles and then gamma rays. This is due to the range of the respective particles in the gas in relation to the anode and cathode of the GM detector.

No radiation detector counts all the particles which are emitted from a source for various reasons. For example, resolving time affects the registered counts. In addition, many of the particles do not strike the tube at all because they are emitted uniformly in all directions from the source. The combination of effects that prevent the detector from counting all particles is known as the efficiency. Efficiency of a radiation counting system is achieved by comparing the measured count rate in the system to the disintegration rate (activity) of the source when the activity is given in units of disintegrations per second (dps; 1 dps = 1 Bq), where the conversion factor is 1 Ci = 3.7×10^{10} Bq.

The formula for determining the absolute efficiency is straightforward and is given as Eq. (27):

$$\%\,Efficiency = \varepsilon = \frac{C_{measured}}{A} \times 100\%, \tag{27}$$

where $C_{measured}$ is the measured count rate and A is the calculated source activity. Note that the time units of the numerator and denominator must be the same.

In fact, the absolute efficiency is a product of two separate phenomena, known as the geometric efficiency and the intrinsic (or quantum) efficiency. The relationship for absolute efficiency, ε, is given by Eq. (28):

$$\begin{aligned} \varepsilon &= \frac{\text{Number detected}}{\text{Number emitted}} \times 100\% \\ &= \frac{\text{Number reaching detector}}{\text{Number emitted}} \times \frac{\text{Number detected}}{\text{Number reaching detector}} \times 100\%. \end{aligned} \tag{28}$$

$$\begin{array}{cc} \Uparrow & \Uparrow \\ Geometric\ efficiency & Intrinsic\ efficiency \end{array}$$

The intrinsic efficiency is determined by the energy of the particles, atomic number of the detector, density of the detector, thickness of the detector, and other factors. A variety of geometrical efficiency examples are depicted in Figure 27. In the left figure, the source is a certain distance from the detector, and the geometrical efficiency will be low and based upon the angle subtended by the source to the detector edge. In the centre figure, the geometrical efficiency approaches optimal for a planar detector (often called a "2π geometry" because the solid angle of a cone intersecting with the detector is approximately $\Omega = 2\pi(1-\cos(\pi/2)) = 2\pi$). In the right figure, the geometrical efficiency approaches unity because the source is surrounded by detector material. This configuration is called a well detector (often called a "4π geometry" because the solid angle of a cone intersecting with the detector is approximately $\Omega = 2\pi(1-\cos(\pi)) = 4\pi$). In practice, detector efficiencies are specified as a function of radioisotope (or energy) for a given geometry.

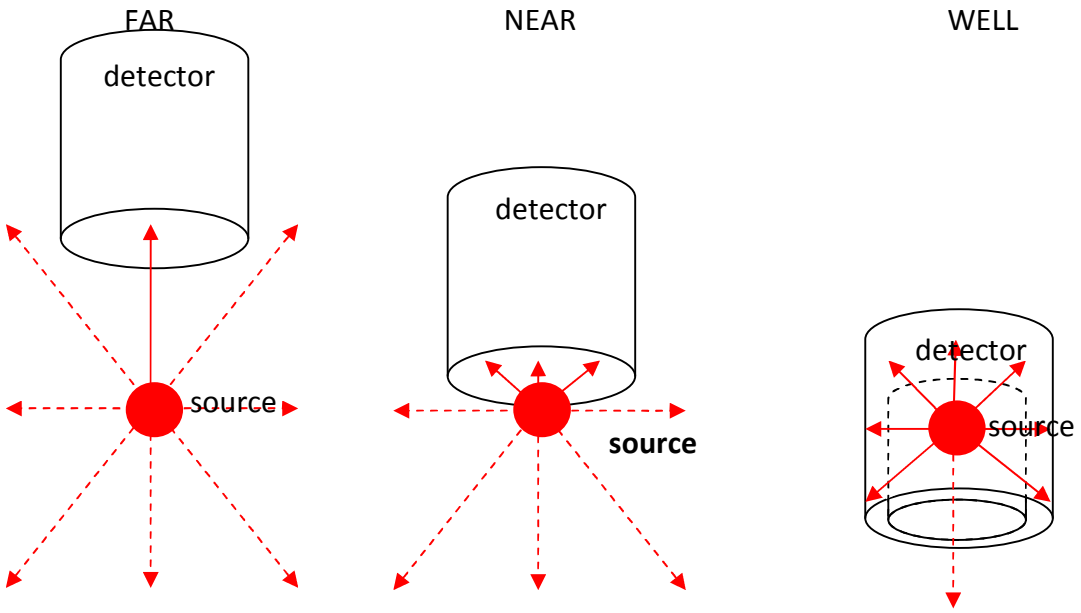

Figure 27 Geometric efficiency examples (far planar, near planar, and well detectors)

For detectors that perform spectroscopy (measurement of incident radiation spectra), both energy and efficiency calibration are generally required. As an example of how this calibration is performed, consider a simple scintillation (sodium iodide) gamma spectroscopy system. When a gamma ray (emitted during a change in an atom's nucleus) interacts with a sodium iodide crystal, NaI(Tl), the gamma ray will frequently give all its energy to an atomic electron through the photoelectric effect (PE). This electron travels a short, erratic path in the crystal, converting its energy into photons of light by colliding with many atoms in the crystal. The more energy the gamma ray has, the more photons of light will be created. A photomultiplier tube (PMT) converts each photon interaction into a small electrical current, and because the photons arrive at the PMT at about the same time, the individual currents combine to produce a larger current pulse. This pulse is converted into a voltage pulse with size proportional to the gamma-ray energy. The voltage pulse is amplified and measured by an analog-to-digital conversion (ADC) process. The result of this measurement is an integer between 1 and 1024 for a 10-bit ADC. One is the measured value for a voltage pulse less than a hundredth of a volt, and 1024 is the measured value for a pulse larger than approximately 8 volts (or the largest voltage pulse in the ADC). Pulses between 0V and 8V are proportionately assigned an integer measured value between 1 and 1024. This measure is called the channel number. The analog-to-digital conversion process is performed, and the computer records the measurements as the number of gamma rays observed for each integer measurement or channel number.

The spectrum is a visual display of the number of gamma rays as a function of the channel number. In the case of known sources (location of the energy peak(s) is well known), then a correlation of channel number with gamma-ray energy can be generated. The result is a graph of the channel number (memory location) as a function of gamma-ray energy (photopeak). The slope of this graph (energy/channel) is the energy calibration (a fitted equation may also be

used if the relationship is not linear over all energy values). An example of energy calibration is shown in Figure 28.

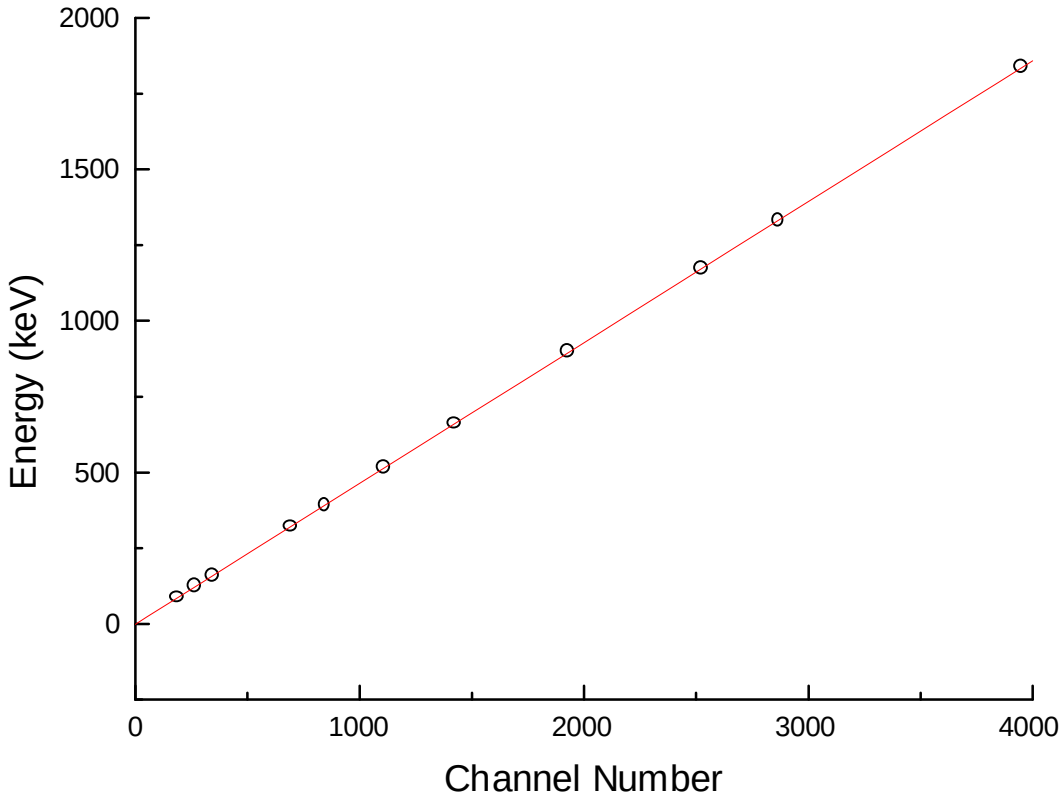

Figure 28 Example energy calibration graph

If the geometry is fixed and the activity of the calibration source is known, the peak area (integral counts) can be correlated with activity to determine the efficiency for each photopeak, as determined by Eq. (27). The efficiency can be plotted as a function of photopeak energy to obtain an efficiency curve, as depicted in Figure 29. This curve enables determination of the activity of an unknown source in a spectroscopic system.

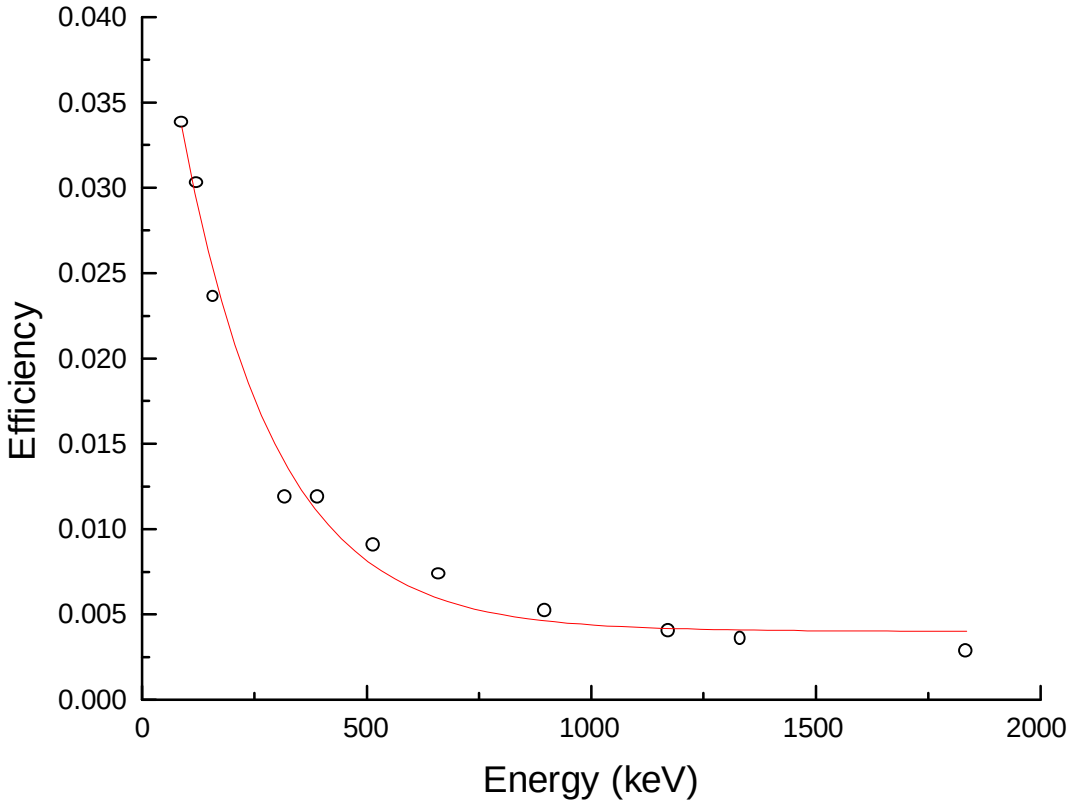

Figure 29 Example efficiency calibration graph

Energy calibration is essential for isotope *identification*, and efficiency is essential for *activity* determination.

4.1.3 Counting statistics and decision levels

Statistics play a very important role in particle counting because atomic concentrations are on the order of Avogadro's number. Therefore, it is impossible to deal with atoms individually, and statistics are used to assist in prediction of behaviour. Statistics uses two main quantities in predicting behaviour, the *mean* and the *standard deviation*.

The mean ($\bar{x}$) is computed as in Eq. (29):

$$\bar{x} = \sum_{i=1}^{N} \frac{x_i}{N}, \tag{29}$$

where the number of measurements (x_i) ranges from 1 to N.

The standard deviation of the data is computed as in Eq. (30):

$$\sigma = \sqrt{\frac{\sum_{i=1}^{N} \left(\bar{x} - x_i\right)^2}{N-1}}. \tag{30}$$

The standard deviation is a measure of the variation of the data without regard to position above or below the mean (that is, an absolute value using the square). Because most measurements tend to follow a Gaussian distribution about the mean (i.e., they are symmetrical),

the mean and standard deviation are widely used measures to predict behaviour. However, particle counting is not symmetrical about a mean. Radioactive decay is a random process that occurs very infrequently for low-activity samples and very frequently for high-activity samples. Three statistical distributions useful in particle counting will be discussed below.

4.1.3.1 Binomial distribution

The binomial distribution is used when there are two possible outcomes of an event. The probability of an outcome is a constant independently of the number of trials, and the selection of either outcome does not affect the outcome of subsequent trials. Assume an experiment where there are only two outcomes: (A) and (B). In a binomial distribution, *p* is defined as the probability of obtaining one of the outcomes (A), and *q* is the probability that the other (B) outcome occurs. Occasionally, statistical references use *1-p* in place of *q* (which is how *q* is calculated). The binomial distribution gives the probability, *P(n)*, that *n* out of *N* objects are A, is given by Eq. (31):

$$P(n) = \frac{N!}{(N-n)!n!} p^n q^{N-n} = \frac{N!}{(N-n)!n!} p^n (1-p)^{N-n} . \quad (31)$$

For this distribution, the mean, *m*, is given by Eq. (32):

$$m = pN , \quad (32)$$

and the standard deviation is calculated using Eq. (33):

$$\sigma = \sqrt{mq} = \sqrt{Npq} = \sqrt{Np(1-p)} . \quad (33)$$

To study radioactive decay, a distribution is required that represents a large number of counts and a small probability of success (large *N* and small *p*). The Poisson distribution is appropriate for this purpose.

4.1.3.2 Poisson distribution

The Poisson distribution is a special case of the binomial distribution given:

1. large number of counts, and
2. small probability of success.

The Poisson distribution, described by Eq. (34), gives the probability, *P(n)*, that *n* out of *N* objects are outcome (A):

$$P(n) = \frac{m^n}{n!} e^{-m} , \quad (34)$$

where *m* is the mean of the distribution (*m = Np*). A primary feature of the Poisson distribution is the ease of calculating the standard deviation using Eq. (35):

$$\sigma = \sqrt{m} . \quad (35)$$

For individual measurements, the standard deviation is the square root of the number of counts, (*N)*, as given by Eq. (36):

$$\sigma = \sqrt{N} \,. \tag{36}$$

For large values of *m* (*m* > 20), a more appropriate distribution, called the Gaussian distribution, is used.

4.1.3.3 Gaussian distribution

The Gaussian (normal, or bell) distribution is used when the sample size is large. An important feature of this distribution is that it uses continuous variables, unlike the Poisson and binomial distributions which use discrete variables. The Gaussian distribution is described by Eq. (37):

$$P(n) = \frac{1}{\sigma\sqrt{2\pi}} e^{-\frac{(x-m)^2}{2\sigma^2}} \,. \tag{37}$$

For a large number of measurements, the data should follow a Gaussian distribution and yield the mean and standard deviation presented by Eqs. (29) and (30).

4.1.3.4 Decision level

An important circumstance involving counting statistics is when low levels of radiation are present (which is often the case, for example, in environmental measurements). When a detector measurement is made at low counts, it must be determined whether the measurement is indicative of anthropogenic radiation or due to fluctuations in the natural background which is also being measured by the radiation-detection system.

The background can be estimated using two approaches. The first is a Poisson approach using Eqs. (29) and (30) for the mean and standard deviation of the measurements and making a judgement as to what multiple of the background measurement indicates a reading that is not due to background radiation. For example, it may be decided that the background mean + 3 standard deviations of the mean is appropriate.

The second, more rigorous approach is to use detection limit statistics. A full discussion is beyond the scope of this chapter, and the user is referred to [Currie1968] and [Chambless1992] for broad discussions of detection limit statistics.

The decision criterion (sometimes called the detection limit, L_D) is a value above some critical level (L_C) in which there is a quantifiable confidence that, if exceeded, you have actually measured radioactivity. The primary indicator is the critical level (L_C), which is defined as the go/no-go value above which a measurement is considered to represent radiation above a blank (or background) sample. The critical level (L_C) is defined by Eq. (38):

$$L_C = \sqrt{2} k \sigma_b \,, \tag{38}$$

where k is the Gaussian parameter related to area under the curve (sometimes termed "z") and σ_b is the standard deviation of the background radiation. Consider a normal distribution of background counts, a 95% confidence level, and the fact that for a normal distribution, the 95% confidence level occurs at k = 1.645; in this case, the critical level is defined as in Eq. (39):

$$L_C = \sqrt{2} \cdot 1.645 \cdot \sigma_b = 2.33 \sigma_b \,. \tag{39}$$

Therefore, the procedure to determine the critical level (the decision criterion) is:

1. Obtain numerous background measurements (for example, 20), spatially and temporally separated, but NOT near contamination or radioactive sources.
2. Determine the mean and standard deviation of the measurements
3. Multiply the standard deviation by 2.33 and add it to the mean to obtain the decision criterion.

For example, if the background-count rate mean is 30 cpm and the standard deviation is 5 cpm, the decision criterion is 30 cpm+12 cpm = 42 cpm. If a measurement above 42 cpm is obtained, it can be attributed to non-background radiation.

4.1.4 Particle counting versus spectroscopy

Generally speaking, gas-filled detectors are used for counting applications. In these, ionizing radiation interacts within the detection material to create a pulse that is counted by an electronic counting system. Scintillation and semiconductor detectors can also be used strictly as particle counters as well. In pulse mode, the signal from each interaction is processed individually. In current mode, the electrical signals from individual interactions are averaged together, forming a net current signal. In current mode, all information regarding individual interactions is lost. If the amount of electrical charge collected from each interaction is proportional to the energy deposited by that interaction, then the net current is proportional to the dose rate in the detector material. This mode is used for detectors subjected to very high interaction rates. The output from a particle-counting system will typically be counts per second (cps) or counts per minute (cpm). It is also possible through calibration to convert the pulses counted to dose rate or to integrated dose (Sv/h; Sv). A simple depiction of a particle-counting system is shown in Figure 30. Radiation interacts in the detector and creates pulses. If the pulses are above a discrimination threshold, they are passed to an integrator or counter circuit, and then if being used with a digital display, through an analog-to-digital converter and digital display. In addition, the count rate may be converted to dose rate using a calibrated radiation source and mapping count rate against known dose rate. The important aspect of a particle-counting system is that single values of count (rate) and/or dose (rate) are presented to the user as a function of time. The user does not generally have any direct information about the radioisotope or the activity being measured. To perform radioisotope identification and quantification, spectroscopy is normally used.

Spectroscopy is strictly defined as the identification of a radioisotope using the energy of emission of the decay particles. Spectrometry, on the other hand, is the quantification (i.e., activity determination) of a radioisotope using the intensity of the decay particle signal. For all practical purposes, spectroscopy is used to denote identification and quantification.

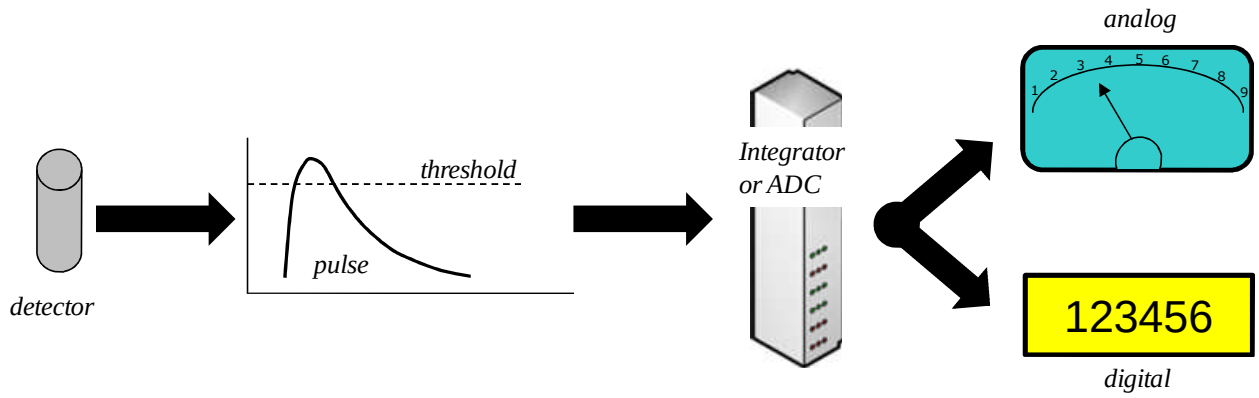

Figure 30 Simple particle-counting system

A simple depiction of a spectroscopy system is provided in Figure 31. In the system, radiation is emitted from the source and interacts with a material that responds to radiation with pulse heights that vary with, and are proportional to, the incident radiation energy. The various pulse heights, which are represented by a range of voltages, are processed in a multi-channel analyzer (MCA). The purpose of the multi-channel analyzer is to process the pulse heights into bins that are determined by memory allocation units (typically called channels). For example, if the pulses are amplified to have a maximum voltage of 10 volts and there are 1024 memory locations, then each memory location is 9.8 mV wide. The first channel is 0–9.8 mV, the second is 9.8–19.6 mV, and so on. It is normal to use a threshold discriminator to eliminate noise that would otherwise be counted as real events, and event logging can be controlled by a lower-level discriminator (LLD) and an upper-level discriminator (ULD). Events that fall within the window will be processed by the multi-channel analyzer. Each pulse is counted within its respective bin (analog-to-digital conversion) and as more counts accumulate, a spectrum is produced which is displayed with counts on the y-axis and channel number on the x-axis. The spectrum produced is characteristic of the radioisotope, and therefore identification is possible.

It can be readily seen that spectroscopy systems can also be used for particle counting. It is not unusual for portable spectroscopy systems to use a scintillation detector for both dose rate and spectral ID functions.

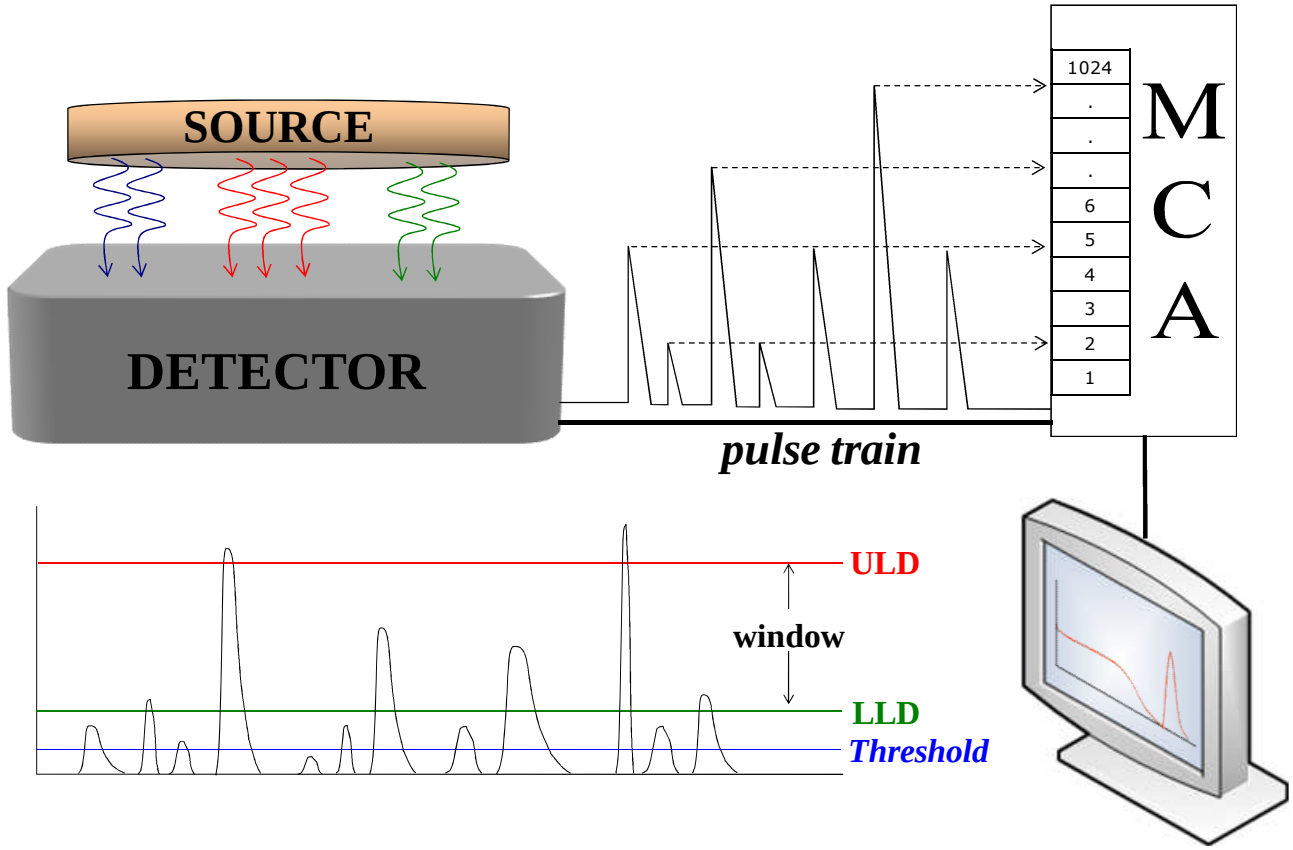

Figure 31 Simple spectroscopy process

Spectrometer systems can be summarized by the following steps:

- When a gamma ray interacts with a detector, a pulse is produced. For gamma spectroscopy, the pulses are produced when gamma rays interacting in the detector create electrons through the photoelectric effect, Compton scattering, or pair production.
- The size of the pulse reflects the energy deposited in the detector.
- An analog-to-digital converter (ADC) sorts the pulses into bins according to size.
- The results of the ADC analysis are displayed. The display, a plot of number of pulses (counts) versus pulse size (channel number), is referred to as a spectrum.
- If a large number of pulses have a similar size, they are sorted into adjacent channels and appear on the spectrum as a peak. A peak represents a number of pulses of similar size.

In an ideal spectrometer system, a peak would be produced that corresponds to the photopeak energy(ies) of the radioisotopes being measured, and the peak would be very narrow (approaching a delta function). In reality, a number of processes can occur within (a) the detector and (b) the shielding that is often present around the system. These processes generally produce undesirable effects in the spectrum, and therefore attempts are made to minimize the impact of these effects. The important aspect of that energy deposited in the detector (which is what the spectrometer measures and displays) is simply the energy in minus the energy out ($E_{dep} = E_{in} - E_{out}$).

4.1.4.1 Detector Interactions

The primary interactions of importance in the detector are as follows:

- **Photopeak.** A photopeak is generated in the spectrum when gamma rays deposit all their original energy in the detector through the photoelectric (PE) interaction. This is the primary signature in a gamma spectroscopy system and is used both to identify and to quantify the radiation.
- **X-Ray Escape Peak.** An X-ray escape peak is generated in the spectrum when gamma rays deposit all their original energy in the detector through the photoelectric effect (PE), except for the energy of an iodine or germanium X-ray that leaves the detector.
- **Compton Continuum.** The Compton continuum is produced when gamma rays interact in the detector through Compton scattering (CS) and then leave the detector.
- **Double Escape Peak.** The double escape peak is produced when gamma rays interact in the detector through pair production (PP) and two 511-keV annihilation photons escape the detector.
- **Single Escape Peak.** The single escape peak is produced when gamma rays interact in the detector through pair production (PP) and one 511-keV annihilation photon escapes the detector.

4.1.4.2 Shield interactions

If there is significant shielding around a spectroscopy system (for example, environmental radioactivity gamma spectroscopy systems often use a scintillator or semiconductor detection system in a lead shield, which is sometimes called a "castle"), then interaction occurring in the shield can produced scattered or secondary radiation in the detector that will be logged in the spectrum.

- **Lead X-Rays.** Lead X-rays are generated in the spectrum when gamma rays interact with a lead shield through the photoelectric effect (PE) and the resulting X-rays produced in the shield interact with the detector. The lead X-rays are around an energy level of 75 keV (73, 75, and 85 keV). If the shield were made of steel, iron X-rays might be seen, but these would be of such low energy that they would probably go undetected.
- **Backscatter Peak.** A backscatter peak is generated in the spectrum when gamma rays interact with the shield through Compton scattering (CS) and the 180^{o}-scattered gamma rays interact with the detector.
- **Annihilation Peak.** An annihilation peak is generated in the spectrum when gamma rays interact with the shield through pair production (PP) and the resulting annihilation photons at 511 keV interact with the detector.
- **Summation Peak.** A summation peak occurs when two gamma rays deposit all their energy in the detector at the same time. The energy of this peak is the sum of the two photopeak energies.
- **Bremsstrahlung.** Bremsstrahlung ("braking" radiation) is observed in the spectrum when high-energy beta particles are produced and slow down in the sample.

4.2 Gas-Based Detectors

The various operating regions for gas-filled detectors are shown in Figure 32.

At low applied voltage, below the ion-saturation region, there is a region called the recombination region. Many electrons and ions produced in the gas recombine because the voltage

applied between cathode and anode is not large enough to collect all the electrons. This region is not useful for counting radiation.

The next region is the ion-saturation region. The potential difference is sufficient to collect all freed electrons. A detector working in the saturation region is called an ionization chamber, and its output is proportional to the deposited radiation energy. Internal or thin-window ionization chambers are used as alpha-particle and fission-fragment detectors.

The next important region is the proportional region. The applied voltage is large enough that the electrons freed by the initial radiation are accelerated, so that they in turn ionize additional atoms or molecules (secondary ionization) to free more electrons. This electron multiplication generates an avalanche toward the anode for each primary electron that was freed. The applied voltage domain is called the proportional region because each avalanche is characterized by the same electron multiplication at a given applied voltage. The output signal is directly proportional to the deposited energy, although each pulse is many times larger than in the ionization region. The limited proportional region is at slightly higher applied voltage, and the proportionality of the output signal to the deposited energy at a given applied voltage no longer applies. Amplification of the greater deposited energy reaches its limit while that for the lesser deposited energy continues to increase. This region is usually avoided as a detection region.

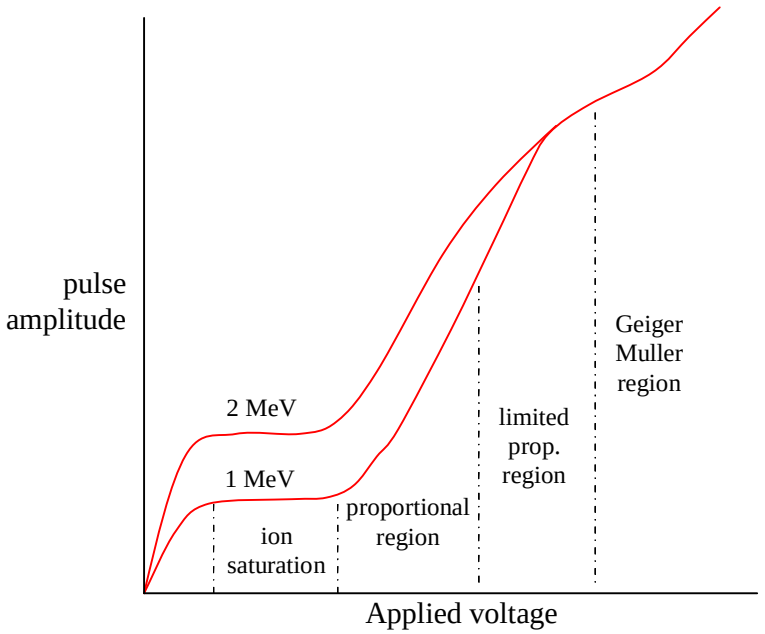

Figure 32 Operating regions of gas-filled counters

The next usable region is the Geiger-Müller region, which is characterized by an applied voltage high enough that any deposited energy produces sufficient secondary electrons to discharge the entire counting gas. A linear amplifier is no longer needed because there is sufficient electron production to generate a usable signal. In this region, it is not possible to distinguish between small and large depositions of energy. At higher applied voltages, electrical discharge occurs between the electrodes. This voltage region, called the continuous-discharge region, has been used for some purposes, but generally is avoided because the discharge can disable the detector.

Details about the two most common types of radiation detectors used in nuclear operations, namely the proportional counter and the Geiger-Müller (GM) counter, are discussed in the following sections.

4.2.1 Proportional counters

The proportional counter is a type of gas-filled detector introduced in the late 1940s. These counters are similar to GM counters in that they rely on gas multiplication to generate a signal. The primary difference between a GM and a proportional counter is that a GM counter produces a pulse when radiation interacts with it, irrespective of incident particle type or energy. A proportional counter generates different-size pulses that are dependent on the incident particle energy. It is, therefore, possible to distinguish between alpha and beta particles using a proportional counter, or between two different energies. Although proportional counters do not have the resolution required to perform spectroscopy, they are extremely useful for discriminating between alpha and beta particles.

The primary use of proportional counters in the nuclear industry is therefore in alpha-beta counters (for example, swipe counters), where it is desirable to discriminate between alpha and beta particles.

4.2.2 Geiger-Müller counters

Geiger-Müller (GM) counters were invented by H. Geiger and E.W. Müller in 1928 and are used to detect radioactive particles (α and β) and rays (γ and x). A GM tube usually consists of an airtight metal cylinder closed at both ends and filled with a gas that is easily ionized (usually neon, argon, or a halogen). One end consists of a "window" made of a thin material, mica, which allows alpha particles to enter (these particles can be shielded easily). A wire, which runs lengthwise down the centre of the tube, is positively charged with a relatively high voltage and acts as an anode. The tube itself acts as the cathode. The anode and cathode are connected to an electric circuit that maintains the high voltage between them.

When the radiation enters the GM tube, it will ionize some of the atoms in the gas. Because of the large electric field created between the anode and the cathode, the resulting positive ions and negative electrons accelerate toward the cathode and the anode. Electrons move or drift through the gas at a speed of about 10^4 m/s, which is about 10^4 times faster than the positive ions move. The electrons are collected a few microseconds after they are created, while the positive ions take a few milliseconds to travel to the cathode. As the electrons travel toward the anode, they ionize other atoms, producing a cascade of electrons called a gas multiplication or avalanche. The multiplication factor is typically 10^6 to 10^8. The resulting discharge current causes the voltage between the anode and cathode to drop. The counter (electric circuit) detects this voltage drop and recognizes it as a signal of a particle's presence. There are additional discharges triggered by UV photons liberated in the ionization process that start avalanches away from the original ionization site. These short-lived discharges are called GM discharges and do not affect performance. Once the avalanche of electrons is started, it must be stopped (quenched) because the positive ions may still have enough energy to start a new cascade. One early method was external quenching, which was done electronically by quickly ramping down the voltage in the GM tube after a particle was detected. This meant that any more electrons or positive ions created were not accelerated towards the anode or cathode. The electrons and ions would recombine and no more signals would be produced. The modern

method is called internal quenching. A small concentration of a polyatomic gas (organic or halogen) is added to the gas in the GM tube. The quenching gas is selected to have a lower ionization potential (~10 eV) than the fill gas (26.4 eV). When the positive ions collide with the molecules of the quenching gas, they are slowed or absorbed by giving their energy to the quenching molecule. They break down the gas molecules in the process (dissociation) instead of ionizing the molecule. Any quenching molecule that may be accelerated to the cathode dissociates upon impact, producing no signal. If organic molecules are used, GM tubes must be replaced periodically because they permanently break down over time (about one billion counts). GM tubes can also use a halogen molecule, which naturally recombines after breaking apart.

Different Geiger-Müller (GM) tubes have varying operating characteristics due to differences in their fabrication. Consequently, each GM counter has a different high voltage that must be applied to obtain optimal performance from the instrument. If a source of ionizing radiation is positioned beneath a tube and the voltage of the GM tube is ramped up (slowly increased by small intervals) from zero, the tube does not start counting right away. The tube must reach the starting voltage where the electron "avalanche" can begin to produce a signal. As the voltage is increased beyond that point, the counting rate increases quickly before it stabilizes. Where the stabilization begins is a region commonly referred to as the knee, or threshold value. Past the knee, further increases in voltage produce only small increases in the count rate. This region is the plateau we are seeking. Determining the optimal operating voltage starts with identifying the plateau. The end of the plateau is found when increasing the voltage produces a second large rise in count rate. This last region is called the discharge region. To preserve the life of the tube, the operating voltage is selected near the middle, but towards the lower half of the plateau (closer to the knee). If a GM tube operates near the discharge region and there is a change in its performance, the tube will operate in a "continuous-discharge" mode, which can damage it. Figure 33 shows a typical plateau shape for a GM tube. Above approximately 1100 volts, the tube enters the continuous-discharge region.

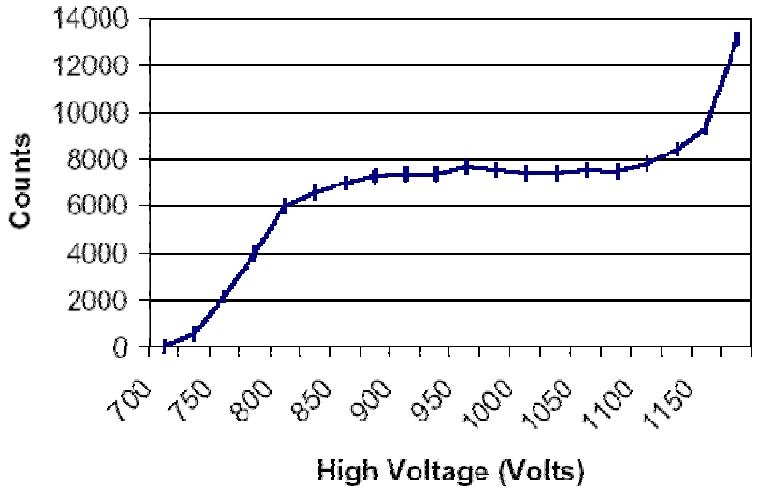

Figure 33 GM counter sample plateau

For hand-held radiation detection instrumentation commonly used in nuclear power operations, GM counters are the most common type of detectors; they can be found in radiation survey instruments, contamination detectors (for example, pancake detectors), and in personal dosimeters.

4.3 Scintillation-Based Detectors

Scintillation detectors are the most commonly used detectors for field applications because they do not require bulky cooling strategies. There are two stages in a scintillation detector unit: the scintillator and the photomultiplier. The scintillation detection process is outlined as follows:

1. Ionizing radiation deposits energy in the scintillator.
2. A portion of the absorbed energy causes electrons in the scintillator to move to a higher energy level.
3. A portion of these electrons immediately fall back down to a lower energy level. As they do, they emit a photon of light. Collectively, the photons of light form a flash, or scintillation.
4. Scintillations are converted into an electronic pulse by a photomultiplier tube (PMT). The brighter the scintillation, the larger is the pulse.

One particle of radiation (alpha, beta, gamma ray, X-ray, or neutron) interacting in the scintillator results in one scintillation (flash) of light and therefore one pulse. The greater the energy transferred to the scintillator, the greater is the number of excited electrons and the greater is the number of photons of light emitted in the scintillation. In other words, the greater the deposition of energy, the brighter is the flash of light and the larger is the pulse.

4.3.1 Scintillators

Scintillators are categorized as fluors as opposed to phosphors. Fluorescence has a lifetime in the excited state from 10^{-7} to 10^{-10} s, whereas phosphorescence has a lifetime in the excited state of 10^{-3} s or longer. It is desirable to have a material with a short excited-state lifetime to achieve a shorter resolving time. Scintillation materials can be classified as solid, liquid, or gas, as detailed below.

- **Gas scintillators:** The radiation energy excites the electrons of the gas molecules, and light photons are emitted when the electrons de-excite. Because these photons are typically in the UV range, a PMT must be chosen that is UV-sensitive. Gas scintillators are extremely fast, but their light output is poor (low efficiency). The most extensively investigated gas scintillators use the noble gases xenon and helium.
- **Liquid scintillators:** Liquid scintillators consist of an organic scintillator dissolved in an appropriate solvent. Normally, the sample to be counted is also dissolved in the scintillator. The advantage of this arrangement is a high counting efficiency for beta particles, even for betas of the lowest energies (e.g., ^{3}H). In some cases, the liquid scintillator is used to measure external radiation sources (e.g., cosmic rays). In such cases, the liquid scintillator is packaged and treated as if it were a solid crystal. One advantage of liquid scintillators is the fact that extremely large detectors can be constructed. This is the basis of the commonly found liquid scintillation counter (LSC).
- **Solid scintillators:** This is the most common type of material used for gamma spectroscopy.

Aside from their physical form, scintillators may also be classified chemically as organic or inorganic:

- **Inorganic:** gas scintillators (e.g., He, Xe), inorganic crystals (e.g., NaI, ZnS, CsI, LiI, BGO), glass scintillators.

- **Organic**: liquid scintillators (e.g., PPO, Bis-MSB, POPOP), organic crystals (e.g., anthracene, stilbene), plastic scintillators.

Two extremely common solid scintillation materials used in the nuclear industry are ZnS and NaI, which are discussed below.

Zinc Sulfide

Zinc sulfide is often doped (activated) with silver in the form of ZnS(Ag). It is typically used in alpha detectors and for heavy-particle detection. In the past, ZnS was combined with ^{226}Ra to form radium paint, which was used to paint clock and aircraft dials so that they would "glow in the dark". ZnS is fairly opaque and has high scintillation efficiency (~40%) with a long decay time.

Sodium Iodide

Sodium iodide is an alkali halide. Its use as a scintillator dates back to the late 1940s, and it is often activated using thallium in the form NaI(Tl). Thallium is added in trace amounts, at a level of approximately one atom in one thousand. NaI is used primarily for photon (X- or gamma) radiation detection. NaI has a high light yield with a scintillation efficiency of approximately 12%. In other words, approximately 12% of the gamma-ray energy deposited in the crystal will be emitted as light. The average energy of a photon emitted by NaI activated with thallium is 3 eV (which has a wavelength of approximately 415 nm, a wavelength readily detected by most photomultiplier tubes). For a hypothetical 1-MeV gamma ray that deposits all its energy in the NaI scintillator, one would expect 120 keV (12% of 1 MeV) to be emitted as light. With an average photon energy of 3 eV, this would be equivalent to 40,000 photons of light. NaI crystals can be grown to relatively large sizes for application in airborne/carborne spectroscopy systems or portal monitors.

Scintillators produce photons of light in the UV to near-visible region and require photomultiplier tubes (PMT) as part of the detection process (Figure 26).

4.3.2 Photomultiplier tubes (PMT)

A photomultiplier tube is used to detect very weak light signals. It is a photoemissive device in which the absorption of a photon results in the emission of an electron. It works by amplifying electrons generated by a photocathode impinged upon by a UV or near-visible light source. Photomultipliers acquire light through a glass or quartz window that covers the photosensitive surface (photocathode), which then releases electrons that are multiplied by electrodes known as metal channel dynodes. At the end of the dynode chain is an anode or collection electrode. The current flowing from the anode to ground is directly proportional to the photoelectron flux generated by the photocathode.

Electrons emitted by the photocathode are accelerated toward the dynode chain, which may contain in excess of 14 elements. Focussing electrodes are usually present to ensure that photoelectrons emitted near the edges of the photocathode will be likely to land on the first dynode. Upon impacting the first dynode, a photoelectron will invoke the release of additional electrons that are accelerated toward the next dynode. Note that photomultipliers produce a signal even in the absence of light due to dark current arising from thermal emissions of electrons from the photocathode, leakage current between dynodes, or background high-energy radiation.

4.4 Semiconductor-Based Detectors

Electrons in a solid can occupy some energy levels, but not others. These levels are not single discrete energies, but ranges of energies called bands. The highest energy band occupied by electrons is referred to as the valence band. The conduction band is of even higher energy than the valence band, but it is normally nearly void of electrons. The range of energies between the valence and conduction bands (forbidden to electrons) is called the band gap (forbidden band).

When the valence band is full, the electrons in the band are essentially fixed in place, i.e., tied to a particular site in the solid. Such a material will not conduct electricity unless electrons in the valence band can be given the energy to reach the conduction band where they would be free to move. If the valence band is not completely full, the electrons in it are free to move, and the solid will conduct electricity.

Solids can be divided into the following three categories:

- **Conductor**. A material in which the valence band is partly, but not completely, full.
- **Insulator**. A material in which the valence is completely full and for which the band gap is greater than 3–5 electron volts.
- **Semiconductor**. A material for which the valence band is completely full and for which the band gap is less than 3–5 electron volts. Semiconductor materials will not normally conduct electricity. However, the band gap is small enough that it is possible to lift enough electrons up into the conduction band for electrical conduction to occur.

When alpha or beta particles enter a semiconductor detector, they create positive and negative ion pairs (electron-hole pairs). Under the influence of an applied electric field, the positive members of the ion pairs (called holes) and the negative members of the ion pairs (electrons) move to the cathode and anode respectively. The result is an electronic pulse.

In the case of gamma detection, the gamma rays must first interact with the solid to produce secondary electrons (through the photoelectric effect, pair production, or Compton scattering). The secondary electrons then move through the detector and create electron-hole pairs which are collected at the electrodes. A semiconductor detector is often considered to be the solid equivalent of an ionization chamber.

Germanium is one of the most common semiconductor detector materials. A very common semiconductor detector used for environmental investigation is the high-purity germanium detector (HPGe). This detector needs to be cooled to near-liquid-nitrogen temperatures (~77°K) to operate. This type of spectrometer is normally found in a health physics laboratory and is used when high-resolution gamma spectroscopy is required. In general, for higher efficiency, scintillation detectors are used because they tend to be much larger-volume detectors, whereas semiconductor detectors are used when higher resolution is required. A typical commercial HPGe spectroscopy system is shown in Figure 34. At the bottom of Figure 34, the details of the opened lead castle can be seen, with the cylindrical HPGe detector element in the castle. The castle is designed to hold cylindrical geometries. For environmental sample analysis, it is very common to use a Marinelli beaker, which is a one-litre geometric design which covers the HPGe detector element for maximum efficiency.

Figure 34 Commercial HPGe system (top) and detail of lead castle (bottom)

4.5 Portable Instrumentation

All nuclear facilities make use of various types of portable instrumentation. Portable or hand-held instruments can be fabricated based on any detector technology, although some are more suited than others to the mission. Broad categories of portable instrumentation include: (a) general-purpose survey meter, (b) area contamination meter, (c) neutron meter, and (d) portable spectrometer.

4.5.1 General-purpose survey meter

A general-purpose survey meter (GPSM) is almost always a gamma detection system using scintillator, GM, or proportional detectors. This type of instrument is often called a gamma survey meter and is used to detect and quantify ambient gamma-radiation fields. The instruments have wide response to both incident photon energy and direction and provide readings

in counts per minute, counts per second, or both. If the instruments are calibrated, readings are in dose rate (μ-, mSv, or Gy per hour) and if they have an integration function, in total dose.

4.5.2 Area contamination meter

An area contamination meter (ACM) is an instrument used to detect and quantify alpha or beta/gamma surface contamination. It must be capable of detecting small quantities of radioactive material, but is not capable of determining whether contamination is fixed to a surface or loose. An ACM must be held very close to the surface to ensure accurate readings; however, there are no suitable portable instruments for detecting small quantities of tritium (^{3}H). A common type of area contamination detector is the pancake probe (see Figure 35), which is a relatively small-area thin-window GM tube that is very useful for frisking personnel for contamination. ACMs are usually based on a GM or other gas-filled tube. A common alpha detector uses a ZnS screen to convert alpha-particle interactions to UV photons, which are then detected by a photomultiplier tube. In this case, no gas is required.

Figure 35 Portable contamination meter with pancake probe

4.5.3 Neutron meter

Portable neutron meters are commonly proportional counters which use neutron detection reactions depending on the filling gas and generate charged particles. Two common reactions (and hence, detection-tube types) are BF_3- and ^{3}He-based respectively according to the reactions in Eqs. (40) and (41):

$$^{10}B + n \rightarrow \begin{matrix} ^{7}Li + \alpha + 2.79\,MeV \\ ^{7*}Li + \alpha + 2.31 MeV \rightarrow {}^{7}Li + \gamma + 0.478\,MeV \end{matrix} \quad (40)$$

$$^{3}He + n \rightarrow {}^{3}H + p + 765 keV\,. \quad (41)$$

These reactions are most likely to occur at low neutron energies, and therefore the counters are wrapped in hydrogenous (neutron-moderating) material. Detector-response functions can be altered using various techniques, such as perforated cadmium sleeves, so that a flat response over a wide energy range of incident neutrons can be achieved. There are also a variety of physical configurations, such as cylindrical, spherical, or even rectangular. Portable neutron detectors have historically been called “neutron REM-meters”, “long counters”, “Bonner spheres” (see Figure 36), “REM balls”, or by other names, depending on their origin and other physical characteristics.

Figure 36 Neutron Bonner sphere

4.5.4 Portable gamma spectrometer

The possibility of portable gamma spectroscopy became a reality as electronics, processors, microprocessors, and computers in general became smaller. Portable gamma spectrometers typically use scintillation-type detectors with small photomultiplier tubes. Some "portable" spectroscopy systems in the past have used semiconductor detectors; however, these are actually quite bulky and heavy, and their true portability is doubtful. Although portable spectroscopy generally cannot give the same performance as a laboratory system, these instruments can perform simplified radioisotope identification and typically offer count, count rate, dose, and dose rate functions.

4.6 Specialized Detectors

A number of specialized detector systems are commonly used in nuclear facilities to process personnel for potential internal or external contamination. These detection systems include portal monitors, whole-body counters, hand/cuff/foot counters, and thyroid counters.

4.6.1 Portal monitors

Portal monitors are used to monitor people in a passive way as they move between areas. They may be used as entrance and exit points from secure areas in nuclear plants or between clean and dirty operational areas. A portal monitor typically is constructed as a tubular frame which houses scintillation detectors (Figure 37). Portal monitors primarily respond to incident gamma radiation that may arise from radioisotope contamination on personnel or equipment. If a person is working in a potentially contaminated (dirty) area and some contamination is transferred to clothing, skin, or equipment, when that person passes through the portal monitor, the

gamma emissions from the contamination should be detected by the scintillators and trigger an alarm on the electronic panel. This will elicit a response from health physics personnel to clean the contamination and generate an incident report.

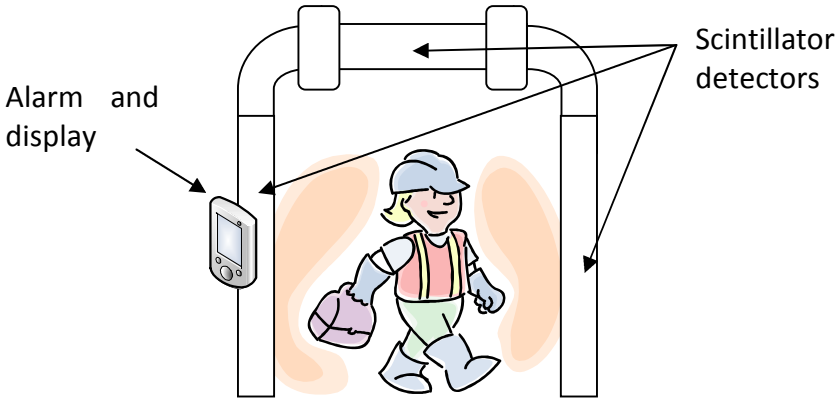

Figure 37 Portal monitor

Portal monitors are passive in that personnel only need to walk through the frame. Although portal monitors cannot readily distinguish between external and internal contamination, some are capable of determining radioisotopes and estimating activity (although this would tend to be a rough estimate). A commercial portal monitor is shown in Figure 38.

Figure 38 Commercial portal monitor

4.6.2 Whole-body counters

Similar to portal monitors (and sometimes synonymous) in that they are often used at entry and exit points, whole-body counters also detect radiation, although their primary mission is to detect and quantify internal contamination (presumably after a person has been externally decontaminated) through gamma emissions. Whole-body counters can use either scintillation or semiconductor spectroscopy detectors. Primary differences from portal monitors are that whole-body counters tend to have extensive shielding to reduce background radiation, they require a dwell time to obtain the measurement, and they may be designed for either standing or prone operation. A commercial whole-body counter is shown in Figure 39. Thin-window detectors can be seen along the length of the body, the head, and the feet.

Figure 39 Commercial whole-body counter

4.6.3 Hand/cuff/foot counters

For radiation workers exiting contaminated areas, it is vital to determine that the extremities, which have the highest probability of becoming contaminated, are adequately monitored. For this purpose, there are specialized hand-, cuff-, and foot-contamination monitoring systems. Generally, the person must stand on a detector and insert or place the hands or cuffs onto or into a detection screen. The detectors may be scintillator or gas-flow proportional counters. These types of counters are effective at detecting both alpha and beta radiation, which have much shorter ranges than penetrating gamma radiation.

4.6.4 Thyroid and lung counters

Thyroid counters, as the name suggests, are specialized detectors used specifically for detecting (principally iodine) radioisotopes in the thyroid (which may be present from fission-product releases that migrate into the coolant system from failed fuel elements). The thyroid counter is generally a scintillation-type detector aimed directly at the neck and thyroid area of the person being monitored. A lung counter is used specifically to detect and quantify radioisotopes that may have been inhaled. The detectors are arranged around the lung area, and due to the geometrical constraints and the longer count times required (especially for actinides), the person being monitored is generally sitting in a reclined seat, with the detectors near the lung region. Detectors are usually scintillation- or semiconductor-based.

4.7 Dosimetry Techniques

This section will consider thermo-luminescent dosimeters (TLD, as dosimeter of record), electronic personal dosimeters (EPD), and liquid scintillation counting (LSC) for bioassay dose estimation.

4.7.1 Thermo-luminescent dosimetry (TLD)

Thermo-luminescence (TL) is a thermally stimulated phenomenon; that is, material absorbs energy from ionizing radiation or light. This energy is stored, and part of it is released in the form of light when the material is heated. This phenomenon was first formally reported by Robert Boyle in his address to the Royal Society of London on October 28, 1663, when he described, "*observation of a glimmering light when he heated a diamond in the dark*" [Uchrin1988]. In the 1950s, research suggested the possibility of applications of thermo-luminescent properties, including radiation dosimetry, which led to development of more sophisticated TL phosphors and commercially available TL readers, making thermo-luminescent dosimetry (TLD) for ionizing radiation widely possible in the 1960s.

The main advantages of thermo-luminescent dosimeters (TLD) are their applicability over a wide dose range (10^{-6}–10^{5} Gy), their usability for various types of radiation including mixed fields, and their small physical size, which enables them to be readily worn as personal dosimeters. One of the fundamental disadvantages of TLDs is that the act of reading the dosimeter effectively "zeros" the dosimeter (through a process called annealing), which means that there is no permanent record of the dose.

The thermo-luminescence mechanism is highly complex and based on solid-state physics. TL materials are insulators with a crystalline structure. In a perfect crystal lattice, the atomic electronic levels are broadened into a series of continuous bands (the conduction band) separated by a several electron volt-wide "forbidden" energy region from the highest filled band, called the valence band. Usually, the conduction band is empty, and the valence band is filled. Crystals always contain imperfections: thermal or intrinsic defects, extrinsic defects, or substitutional impurities and radiation-induced defects [Uchrin1988]. The presence of lattice imperfections and impurities is essential for thermo-luminescent processes. The energy levels presented by them are situated in the forbidden region and act as traps or recombination centres for electrons and holes created in the crystal due to an excitation from interaction with ionizing radiation.

Electrons and holes will remain in traps provided that they do not acquire sufficient energy to escape. The number of trapped states is directly proportional to the number of ionizing-radiation interactions with the material and hence the total dose. When the temperature of the material is raised, the trapped charge carriers are given sufficient energy to escape from their traps to the conduction band, where they recombine at a luminescence centre, and the excess energy is radiated as visible or UV light, which is recorded by a photomultiplier tube (see Section 4.3.2). The TLD reader unit provides a correspondence between the signal generated from the measured light and the radiation exposure of the TL material.

Reading a TLD chip is relatively simple. The TL material is heated from the ambient temperature up to 300°C–400°C, and the emitted light is collected and measured quantitatively. The TLD reader consists of four components: (i) heating unit, (ii) light collection and detection system (PMT), (iii) signal measuring system, and (iv) data recording system. The emission of light from heated TLD material is often called a "glow", and the resulting spectrum from heating the material to release the traps is called a "glow curve". A typical glow curve obtained from a Harshaw model 3500 TLD reader for LiF TLD material irradiated to 500 µSv total dose from a 1 Ci ^{137}Cs irradiator is depicted in Figure 40. The portion of the curve corresponding to the delivered dose is denoted by the region of interest marked with vertical lines.

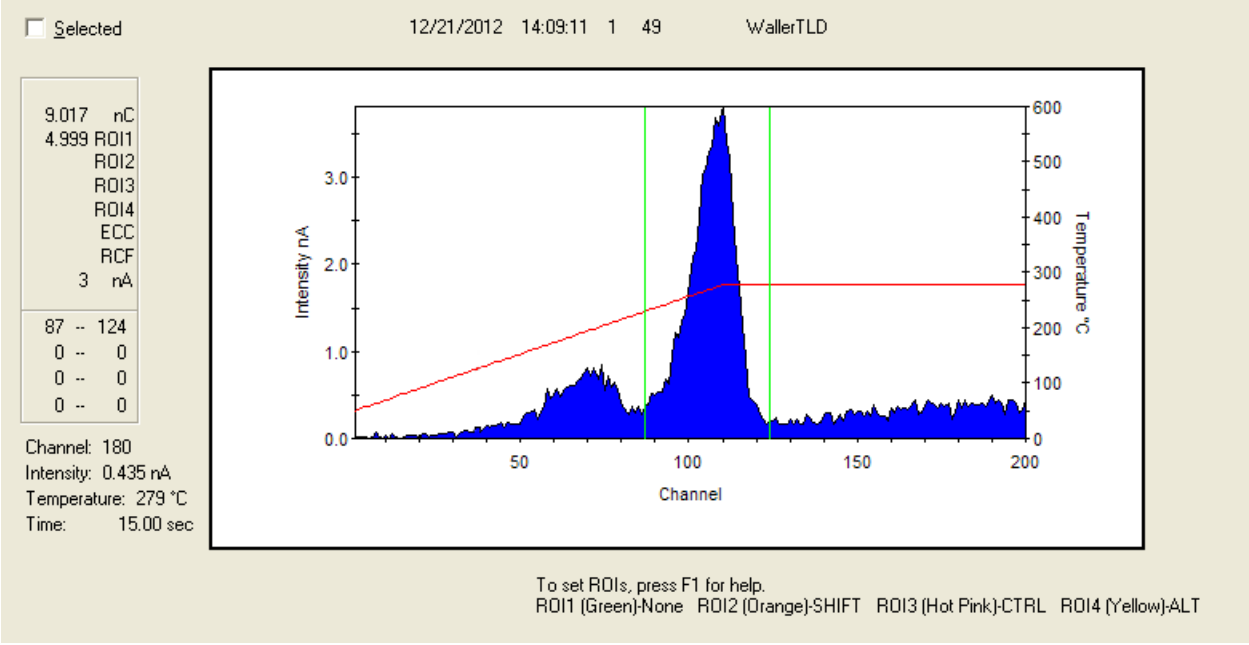

Figure 40 TLD glow curve from irradiated LiF chip

A variety of physical and chemical forms of thermo-luminescent dosimeters are used for different radiations and dose ranges. For example, physical forms of TLDs can include chips, disks, powders, and rods; a subset of materials used as dosimeters include LiF, $Li_2B_4O_7$, CaF_2, $CaSO_4$, and Al_2O_3. TLDs are characterized by their dose-response properties, energy dependence, sensitivity, and fading characteristics (fading is unintentional loss of stored signal due to thermal or optical release of traps). The observed glow curve from reading TLDs may be affected by chemo-luminescence (luminescence due to chemical reactions from material impurities) and tribo-luminescence (luminescence caused by mechanical effects in material preparation). These effects can be greatly reduced by inert gas (typically N_2) flushing. A commercial TLD reader and LiF chips are shown in Figure 41.

Figure 41 Commercial TLD reader (top) and tray of LiF chips (bottom)

The TLD is the dosimeter of record for nuclear energy workers (NEW) in Canada (National Dose Registry, Radiation Protection Bureau, Health Canada), as it is in most countries world-wide. All nuclear energy workers in Canada wear TLD dosimeters if they are working around sources of radiation exposure and as directed by the health physics department.

4.7.2 Electronic personal dosimeter (EPD)

An electronic personal dosimeter (EPD) is a detector calibrated to provide dose rate and dose readings in real time. The readings may be present on a display directly on the dosimeter, stored for later retrieval, or transmitted to a base station. The primary advantage of an electronic personal dosimeter is that it can be set with alarm points to warn the user (through audible and visual alarms) in real time if a dose or dose rate is being exceeded. This makes it a very useful tool for ALARA adherence. Key features of EPDs include: small size, light weight, fast response, continuous update and display, and timer/stay time functions. EPDs are generally

made from small GM tube or semiconductor detectors, and although the most common are sensitive to X- and gamma radiation, some have neutron-detection capabilities.

Although EPDs do not provide a legal dose of record, they are often worn in conjunction with TLDs by personnel working in nuclear-facility radiation environments, especially in non-homogeneous fields or in areas where exposure may be in excess of action or regulatory limits.

4.7.3 Liquid scintillation counting (LSC)

Liquid scintillation counting (LSC) is a radioanalytical technique developed in the 1950s and defined by incorporation of a radioisotope analyte into a scintillating liquid. It is a very sensitive and widely used technique for detection and quantification of radioactivity and is applicable to most forms of nuclear decay emissions (alpha and beta particles, electron capture, and gamma-ray-emitting radionuclides).

Consider the case of a beta-emitting radioisotope in a liquid scintillation material. The beta particle dissipates energy by collisions in the liquid, and the energy is absorbed by the medium in three forms: heat, ionization, and excitation of the molecules in the solution. Excitation of the solution molecules is the mechanism of the liquid scintillation technique. Facilitation of efficient transfer of energy between beta particles and the solution is accomplished using a solvent material and a scintillation solute solution (together called a “cocktail”). The scintillation solute is a fluor, and excited solvent molecules can transfer energy to one another and also to the solute. An excited solvent molecule creates an excited state in the solute, and as the excited orbital electrons of the solute molecule return to the ground state, a photon of UV or near-visible light is generated, which can be detected by a photomultiplier tube. The intensity of light from the scintillation process is proportional to the initial energy of the beta particle.

The detection process for beta decay is summarized in Figure 42.

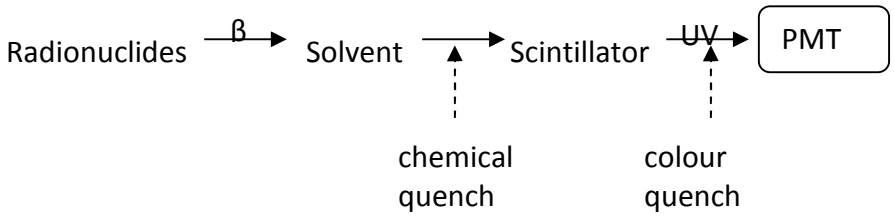

Figure 42 LSC detection process

The counting efficiency of the solvent-scintillator system is affected by many different factors that may reduce detection efficiency. Two dominant factors are: (i) chemical quenching (sometimes called impurity quenching), which causes energy losses in the transfer from solvent to solute, and (ii) colour quenching, which is the attenuation of UV light photons in the solution. Both quench factors can be compensated for through calibration. Other effects that may degrade LSC performance include: (a) thermionic effects, which are noise pulses that are extraneous to the true signal, yet resemble electronic pulses resulting from nuclear decay events; (b) photoluminescence, which results in activation of the cocktail or vial by ultraviolet light, which can occur by exposure to sunlight (LSCs rely on light-tight counting chambers); and (c) static electricity, which is a very common source of counting interference due to buildup and subsequent discharge of static electricity on LSC vials.

The electronic process of light detection and pulse generation in an LSC analyzer is depicted in Figure 43. In most scintillation counters, two photomultiplier tubes collect the total light produced within the scintillation vial that either (a) falls directly onto the two photocathodes or (b) is reflected onto each photocathode by a reflector centrally mounted between the two PMTs. Radioactive decay events produce approximately 10 photons per keV of energy. Beta decay yielding a multiplicity of photons will stimulate both PMTs at the same instant in time, and the signal from each PMT is fed into a summing circuit which produces an output only if the two signals occur simultaneously, which is called coincidence. Because electrical noise from the PMTs is produced randomly over time, it occurs at a sufficiently low rate to be excluded by the coincidence circuit (below the equivalent of 1 keV). The sample in the counting chamber and the PMTs are surrounded by lead, typically about 5 cm in all directions, which generally reduces the background radiation to low levels.

The output from the analog-to-digital converter is processed with a spectrum analyzer calibrated in keV, and regions between 0 and 2000 keV are used for sample analysis. For example, the region of interest for ^{3}H is 0–18.6 keV (^{3}H maximum beta energy = 18.6 keV) and for ^{14}C is 0–156 keV (^{14}C maximum beta energy = 156 keV).

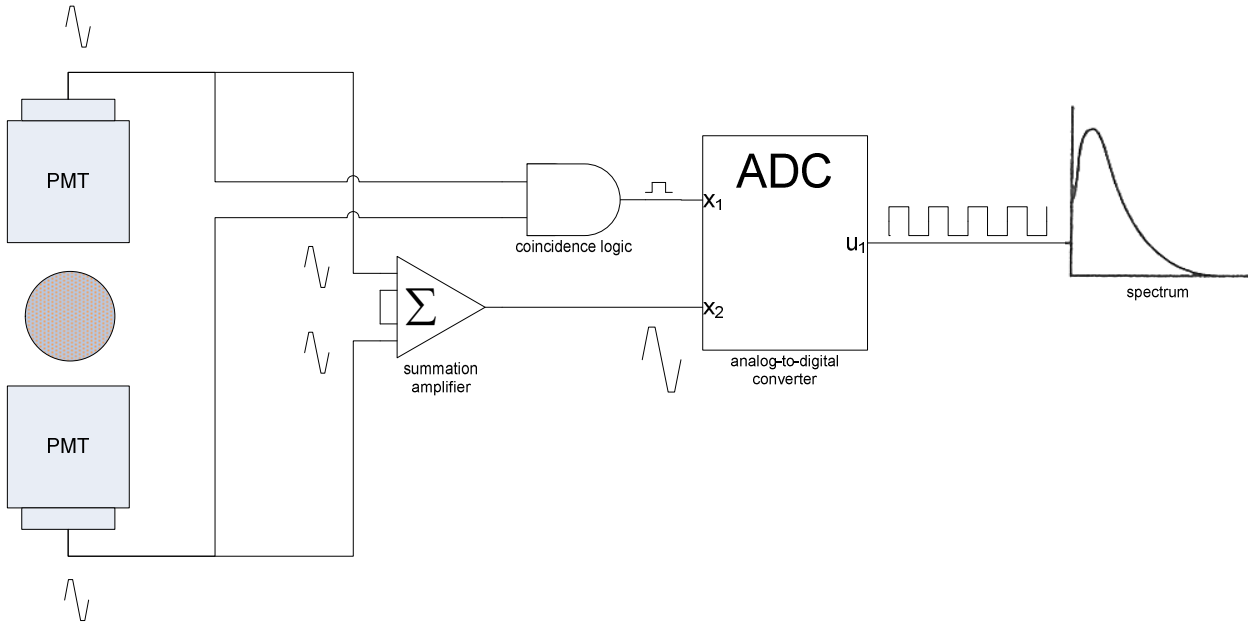

Figure 43 LSC electronics

Liquid scintillation counting is used in the nuclear industry for swipe analysis, environmental sample analysis, and urine (bioassay) analysis. LSC is vitally important to detection of one important radionuclide in CANDU nuclear power stations: tritium (^{3}H). Tritium is extremely hard to detect with field-portable instrumentation because the average energy of the beta particles emitted is very low (5.6 keV). In nuclear plants, LSC is routinely used for determining tritium intake through urine analysis. When tritium contamination is suspected on surfaces, quartz fibre or paper swipes can be used to wipe down a surface and then be analyzed in an LSC. Likewise, when performing environmental sample analysis for tritium, especially on water samples, LSC is the analytical technique of choice for tritium. A commercial LSC (for urine bioassay) is shown in Figure 44.

Figure 44 Commercial LSC counter (top) and detail of trays with vials (bottom)

4.8 Summary

Ionizing radiation cannot be detected by the human senses, and therefore instrumentation is required. A variety of radiation detection instruments is used in nuclear facilities to support routine operations such as dosimetry, radiation protection, and environmental monitoring. Instrumentation is selected by health physics personnel based on its applicability to the mission design. Radiation fields to be measured in nuclear facilities may be in the form of external fields, water effluent, airborne gases, or particulates. Instrumentation is of critical importance for the safe operation of nuclear facilities such as nuclear reactors and therefore is an integral part of the radiation-safety management plan.

5 External Radiation Hazards and Shielding

External radiation hazards from beta, gamma, and neutron sources are discussed in this section, with consideration of the ALARA principle. External radiation fields are always present within nuclear reactors, and therefore consideration of expected doses and strategies to minimize dose are required. Some historical perspective on external dosimetry and on shielding can be found in [Poston2005] and [Shultis2005] respectively.

5.1 External Sources and Dosimetry

The concepts of exposure and dose were explored in Section 3.1. The following subsections discuss the interactions of the primary radiations of concern to CANDU health physics—specifically, light charged particles (such as beta particles and electrons), X- and gamma rays, and neutrons. Note that under normal operating conditions, the primary radiation hazards to personnel expected in a CANDU plant are from gamma, neutron, and beta radiation. Heavy charged particles such as alpha particles are not an external hazard in CANDU plants because they occur only as radioactive decay emissions and because their energy (typically on the order of 4–5 MeV) is not enough to penetrate the outer layer of skin.

Beta radiation exposure is explored as surface contamination, hot particles on the skin, and a submersion dose. Gamma-ray equations for point sources (specific gamma constant), line sources, and volume sources are developed, and fast and thermal neutron-dose calculations are introduced.

5.1.1 Beta radiation

The ways in which an external beta radiation dose can be delivered to human targets are summarized in Figure 45. Generally speaking, it is possible to be submerged in a plume of beta-emitting radioactive material and thereby be exposed in an isotropic field of beta particles (with most radionuclides, there will be a corresponding gamma field that will require analysis). It is possible to be exposed through a plane source of beta particles (for example, a spill of beta-emitting radionuclides) where the target tissue is at some distance from the source, and it is also possible to encounter a contact source of beta-emitting material (for example, by touching a spill or a "hot" particle) that can generate a significant dose. Beta radiation can be significantly attenuated by clothing, boots, gloves, and goggles. Detailed descriptions of charged particle ranges and stopping powers can be found in Chapter 3.

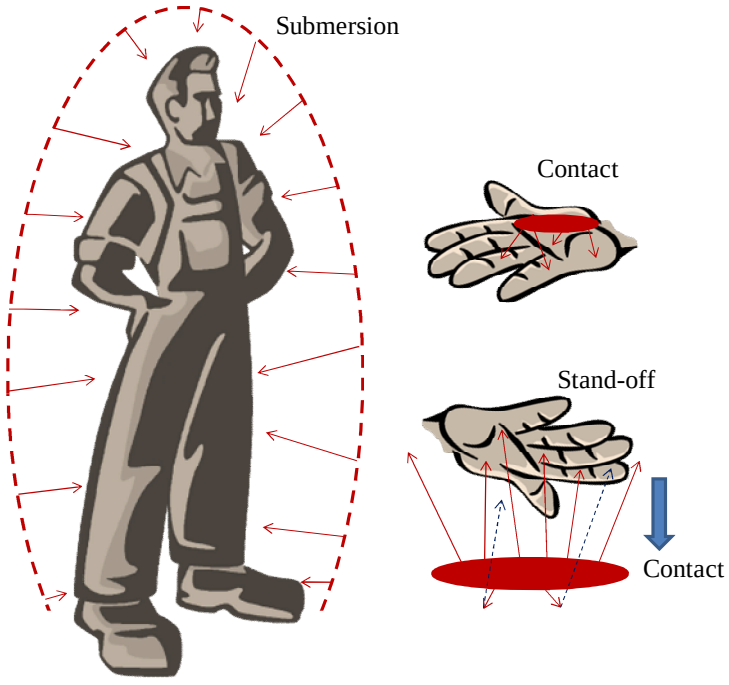

Figure 45 Beta dose delivery geometries

The intensity of beta radiation for depths less than the range of the beta particles can be described by Eq. (42):

$$\phi = \phi_o e^{-\mu_\beta t} \quad , \tag{42}$$

where

φ is the beta intensity at depth t (particle flux, energy flux, etc.)
φ_o is the initial intensity (same units as φ)
μ_β is the beta-ray absorption coefficient (cm^2/g)
t is the depth(density thickness) in material (g/cm^2).

The beta attenuation coefficients for tissue and air are given by Eqs. (43) and (44) respectively:

$$\mu_{\beta,\,tissue} = 18.6\left(E_{\max} - 0.036\right)^{-1.37} \quad \frac{cm^2}{g} \tag{43}$$

$$\mu_{\beta,\,air} = 16\left(E_{\max} - 0.036\right)^{-1.4} \quad \frac{cm^2}{g} \quad , \tag{44}$$

where E_{max} is the maximum beta-ray energy in MeV.

The dead layer of skin provides some beta shielding and is typically represented by 0.007 g/cm^2 density thickness. After the beta particles pass through the dead layer of skin, all beta energy is deposited in living tissue (betas travel no more than approximately 1 cm in tissue), and the energy deposited is essentially equal to the dose.

Beta doses from common industrial scenarios are presented below.

5.1.1.1 Beta dose from a source on a surface

The dose calculated is from a surface contamination scenario with and without a stand-off distance of the tissue from the source. A contaminated surface may be represented by Figure 46. From a dose perspective, this may be considered as a "2π" geometry; half the betas travel up towards the receptor, and half travel down into the surface where the contamination is located.

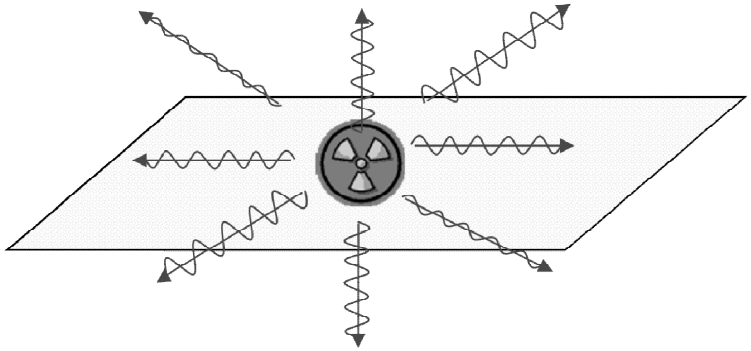

Figure 46 Beta surface contamination

The energy flux at the surface can be represented by Eq. (45):

$$\varphi = 0.5 C_a \overline{E}\,, \tag{45}$$

where

φ is the energy flux at the surface (MeV cm^{-2} s^{-1})
$\bar{E}$ is the average energy per disintegration (MeV)
C_a is the areal activity (Bq cm^{-2}).

The beta surface dose rate, considering the uncollided particles, may be determined using the beta attenuation coefficient as in Eq. (46):

$$\dot{D}_\beta = \phi\ \mu_\beta = 0.5 C_a \bar{E} \mu_\beta \left(\frac{MeV}{g-s} \right). \tag{46}$$

Rewriting Eq. (46) in standard SI dose units yields Eq. (47):

$$\dot{D}_\beta = 0.5 C_a \bar{E} \mu_\beta \left(\frac{MeV}{g-s} \right) = 2.88 \times 10^{-7} C_a \bar{E} \mu_\beta \left(\frac{Gy}{h} \right). \tag{47}$$

Of interest also is the contact dose to the skin (the scenario in which the tissue comes into contact with a surface that has beta-emitting contamination). The dose rate to tissue on contact is represented by Eq. (48):

$$\dot{D}_\beta = \frac{0.5 \times f_\beta \times C_a \frac{Bq}{cm^2} \times \bar{E} \frac{MeV}{transform} \times 1.6 \times 10^{-13} \frac{J}{MeV} \times 3600 \frac{s}{h} \times \mu_\beta \times e^{-\mu_\beta \times 0.007 \frac{g}{cm^2}}}{0.001\ J\ /\ g/Gy}, \tag{48}$$

and the dose rate for tissue on contact with a contaminated surface is given by Eq. (49):

$$\dot{D}_{contact} = \left(3.6 \times 10^{-4}\right) \cdot C_a \left(\frac{Bq}{cm^2} \right) \cdot \bar{E} \left(\frac{MeV}{transform} \right) \cdot \mu_\beta \cdot e^{-0.007 \times \mu_{\beta_{tissue}}} \left(\frac{mGy}{h} \right), \tag{49}$$

which assumes that approximately 25% of the beta particles going down into the contaminated surface are backscattered [Cember2009] towards the dose point (i.e., f_β=1.25) and the exponential represents attenuation through 0.007 g/cm^2 of tissue (the dead tissue-layer density thickness).

For tissue at some distance *d* away from the contaminated surface, air attenuation must also be taken into account, as in Eq. (50). Subsequent layers of attenuating material (such as gloves on hands) may be taken into account using similar exponentials:

$$\dot{D}_{at\ d} = \left(3.6 \times 10^{-4}\right) \cdot C_a \left(\frac{Bq}{cm^2} \right) \cdot \bar{E} \left(\frac{MeV}{transform} \right) \cdot \mu_\beta \cdot e^{-d \cdot \mu_{\beta_{air}}} \cdot e^{-0.007 \times \mu_{\beta_{tissue}}} \left(\frac{mGy}{h} \right). \tag{50}$$

5.1.1.2 Beta dose rate from contamination on skin (or hot particles)

For the case where the beta contaminant is in direct contact with external tissue with no backing material, the beta dose rate is expressed by Eq. (51). Note that no backscatter (f_b) factor is required in this scenario because there is air "behind" the source:

$$\dot{D}_\beta = \frac{0.5 \times C_a \frac{Bq}{cm^2} \times \bar{E} \frac{MeV}{transform} \times 1.6 \times 10^{-13} \frac{J}{MeV} \times 3600 \frac{s}{h} \times \mu_\beta \times e^{-\mu_\beta \times 0.007 \frac{g}{cm^2}}}{0.001\ J/g/Gy} = \left(2.88 \times 10^{-4}\right) \cdot C_a \cdot \bar{E} \cdot \mu_\beta \cdot e^{-\mu_\beta \times 0.007} \left(\frac{mGy}{h}\right) \quad (51)$$

If the beta emitter is not in contact with the external tissue, other attenuating material can be added using exponential attenuation factors with appropriate attenuation coefficients. Some materials that can attenuate betas for skin doses in an industrial setting are listed in Table 13. If the material is hydrocarbon-based, the tissue beta attenuation coefficient may be an appropriate approximation in the exponential.

Table 13 Standard thickness of various beta attenuators (from [Cember2009])

Material	Thickness (mm)	Density (g/cm^3)
Lab Coat (Plastic)	0.1	0.036
Cotton Glove Liner	0.3	0.3
Surgeon's Glove	0.5	0.9
Outer Glove (thick)	0.45	1.1
Ribbed Outer Glove	0.55	0.9
Plastic Bootie	0.2	0.6
Rubber Shoe Cover	1.2	1.0

5.1.1.3 Beta dose from submersion in a plume

In an "infinite" cloud, the rate of energy emission is equal to the rate of energy absorption, and the air dose is given by Eq. (52) for dry air:

$$\dot{D}_{\inf} = \frac{k \cdot C \cdot \overline{E}}{\rho_{air}} = 4.45 \times 10^{-7}\ C\ \overline{E} \quad \left(\frac{mGy}{h}\right), \quad (52)$$

where

k is a constant to yield units in mGy/h (5.76×10^{-7})
C is the air concentration of the radionuclide (Bq m^{-3})
$\bar{E}$ is the average beta energy (MeV)
ρ_{air} is the air density (1.293 kg/m^3).

More interesting is the dose to tissue for a person submerged in an infinite cloud of beta-emitting radionuclide. In this case, the expression given by Eq. (52) is modified by a factor of 1.1 for the approximation that tissue absorbs 10% more energy than air on a per-kg basis and by a factor of 0.5 representing the fact that in the cloud, half the beta particles move inward (towards tissue) and half move outward (away from tissue). Finally, a factor of $e^{-\mu * 0.007}$ compensates for passage through the dead skin layer. Equation (52) therefore becomes Eq. (53):

$$\dot{D}_\beta = \frac{0.5\times 1.1\times C\,\frac{Bq}{m^3}\times 1\frac{tps}{Bq}\times \bar{E}\,\frac{MeV}{transform}\times 1.6\times 10^{-13}\,\frac{J}{MeV}\times 3600\,\frac{s}{h}\times e^{-\mu\cdot 0.007}}{1.293\,\frac{kg}{m^3}\times 1\frac{J/kg}{Gy}} \quad . \qquad (53)$$

$$= 2.45\times 10^{-10}\cdot C\cdot \bar{E}\cdot e^{-\mu\cdot 0.007}\ \frac{Gy}{h}$$

Note that Eq. (53) can be modified for attenuation though clothing by multiplying by an exponential factor $e^{-\mu * t}$, where μ represents the beta-attenuation coefficient for the material and t is the thickness of the material.

5.1.2 Gamma radiation

Gamma rays are neutrally charged quanta of energy (photons). The principal interaction mechanisms for photons, namely the photoelectric effect, Compton scattering, and pair production were introduced in Chapter 3. In addition, photon cross sections and the Klein-Nishina formula for scattering, as well as interaction cross sections, were introduced in Chapter 3.

Some ways in which external neutral particles such as gamma radiation deliver dose are depicted in Figure 47. The exposure can originate from point, area, volume, or distributed source regions.

5.1.2.1 Point source - specific gamma constant (Γ)

A point source may be considered as small with respect to the target (vanishingly small compared to the target). Consider the energy absorbed per unit mass of air at a specified distance from a point source, as given by Eq. (54):

$$\frac{f_i\ (\gamma/t)\times E_i\,(MeV/\gamma)\times 1.6\times 10^{-6}\,(erg/MeV)\times 3.7\times 10^{10}\,(dps/Ci)\times 3600\ (s/h)\times \mu\ (m^{-1})}{4\times\pi\times(1m)^2\times\rho\ (kg/m^3)\times 87.7\ (erg/g/R)}, \qquad (54)$$

where

f_i is the fraction of transformations that yield a photon with energy E_i
μ is the linear energy absorption coefficient for dry air at density 1.293 kg/m^3 (m^{-1}).

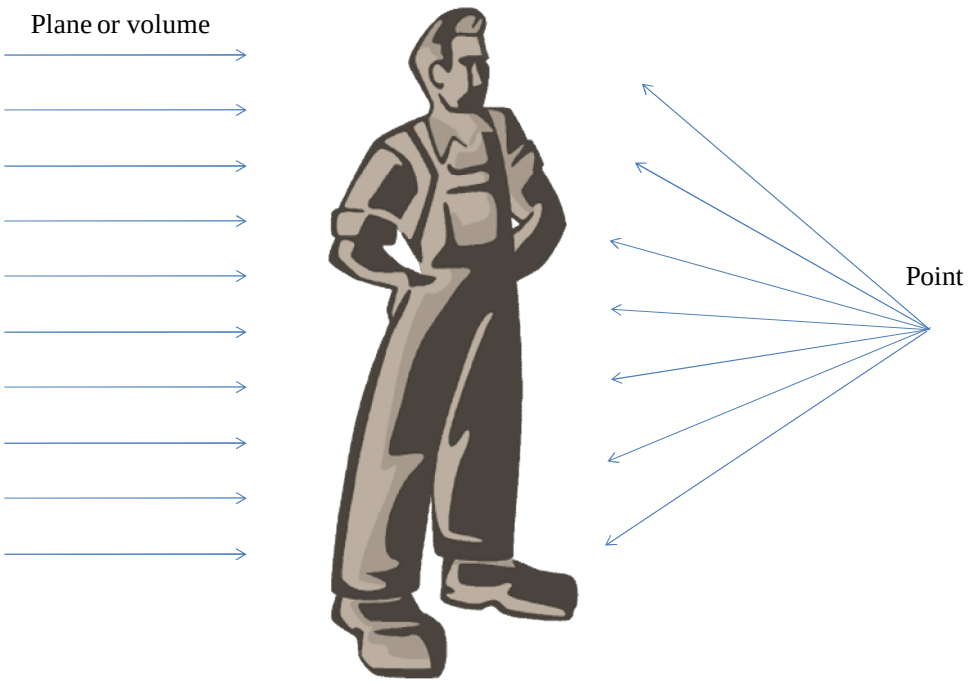

Figure 47 Neutral-particle radiation dose-delivery geometries

By expressing the linear energy-absorption coefficient for air as a constant (which is a good approximation over a large energy range of interest for most radionuclides, as shown in Figure 48), the terms in Eq. (54) can be reduced to a single conversion constant of 0.5, as shown in Eq. (55):

$$\frac{1.6\times10^{-6}\,\frac{\text{erg}}{\text{MeV}}\times3.7\times10^{10}\,\frac{\text{Bq}}{\text{Ci}}\times0.0035\ \text{m}^{-1}\times3600\,\frac{\text{s}}{\text{h}}}{\left[4\times\pi\times(1\ \text{m})^2\right]\times1293\,\frac{\text{g}}{\text{m}^3}\times87.7\,\frac{\text{erg}/\text{g}}{\text{R}}}\simeq0.5\,\frac{R\cdot m^2}{Ci\cdot h\cdot MeV}, \tag{55}$$

which yields the specific gamma constant (Γ) in conventional units as Eq. (56) or in SI units as Eq. (57). The importance of the specific gamma constant in conventional units is that, from an operational perspective, it is much easier to memorize compared to the SI unit form:

$$\Gamma=0.5\sum_i f_i\times E_i\ \ \frac{R\cdot m^2}{Ci\cdot h} \tag{56}$$

$$\Gamma=1.24\times10^{-7}\sum_i f_i\times E_i\ \ \frac{Sv\cdot m^2}{MBq\cdot h}\ . \tag{57}$$

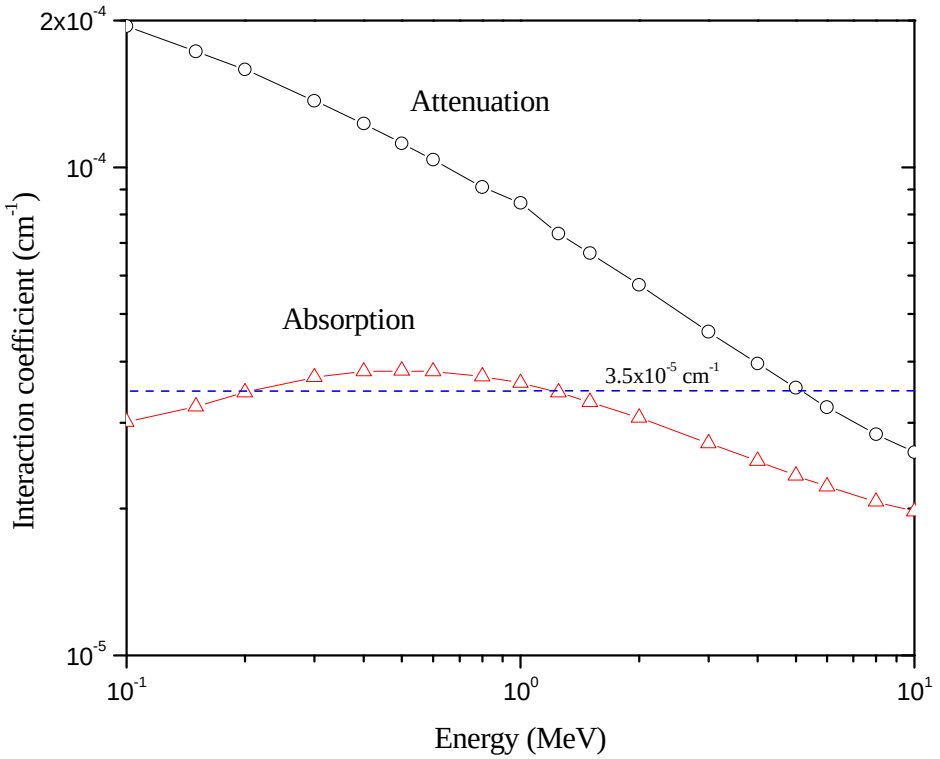

Figure 48 Linear interaction coefficients for dry air

Use of the specific gamma constant (Γ) to determine dose equivalent rate from a point source is straightforward, as shown in Eq. (58):

$$\dot{H}_p = \frac{\Gamma \cdot A}{d^2} \cdot w_r \left(\frac{R \text{ or } Sv}{h} \right), \tag{58}$$

where

$\dot{H}_p$ is the dose equivalent rate (Rem or Sv per hour, depending upon which form of Γ is used) at point p (distance d away from the source)
A is the source activity (Ci or MBq, depending upon which form of Γ is used)
d is the distance from source to receptor (m)
w_r is the radiation weighting factor (=1 for gamma rays).

5.1.2.2 Line source

A line source configuration is one that is infinitely thin but of finite length, such as a pipe carrying contaminated radioactive liquid. The geometry of such a system is described by Figure 49. The receptor is at point *p* at distance *h* from the line, at an arbitrary distance along the line.

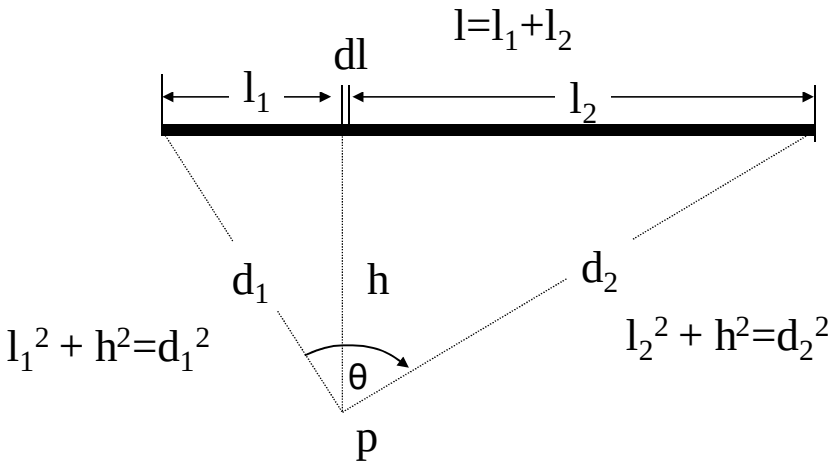

Figure 49 Line-source geometry

For a linear concentration of radioactivity C_i (Ci/m or MBq/m), the dose rate at point *p* can be expressed as a function of the point source-specific gamma constant as defined in Section 5.1.2.1, using Eq. (59):

$$\dot{H}_p = \frac{\Gamma C_l}{h}\left(\tan^{-1}\frac{l_1}{h} + \tan^{-1}\frac{l_2}{h}\right)$$

$$or \qquad , \qquad (59)$$

$$\dot{H}_p = \frac{\Gamma C_l \theta}{h}$$

where

$\dot{H}_p$ is the dose rate (R/h or Sv/h, consistent with Γ)

l_1, l_2, and h are defined in Figure 49 (m)

θ is the opening angle (radians)

Γ is the specific gamma constant for a point source (conventional or SI units)

C_l is the linear activity (Ci m^{-1} or MBq m^{-1}, consistent with Γ).

5.1.2.3 Planar source

A planar source in this case is represented as a disk source which is infinitely thin with area πr^2. This type of geometry could arise, for example, from a spill of radioactive material and is represented by Figure 50.

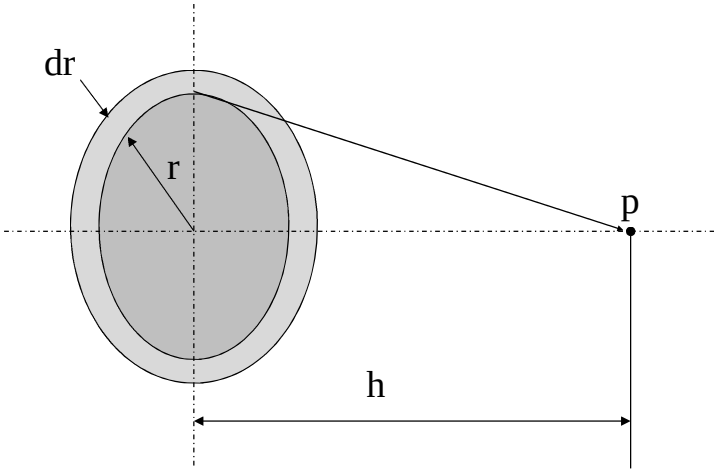

Figure 50 Planar source geometry

For an areal concentration of radioactivity C_i (Ci m^{-2} or MBq m^{-2}), the dose rate at point *p* can be expressed as a function of the point source-specific gamma constant as defined in Section 5.1.2.1, using Eq. (60):

$$\dot{H}_p = \pi \, \Gamma C_a \ln\left(\frac{r^2 + h^2}{h^2}\right), \tag{60}$$

where

$\dot{H}_p$ is the dose rate (R/h or Sv/h, consistent with Γ)

r and *h* are defined in Figure 50 (m)

Γ is the specific gamma constant for a point source (conventional or SI units)

C_a is the areal activity (Ci m^{-2} or MBq m^{-2}, consistent with Γ).

5.1.2.4 Volume source

A volume source is one that has finite dimensions, such as a drum containing radioactive material. The geometry of a cylindrical system used as an example is described by Figure 51. The receptor is at point *p* on the central axis at distance *h* from the surface of the volume.

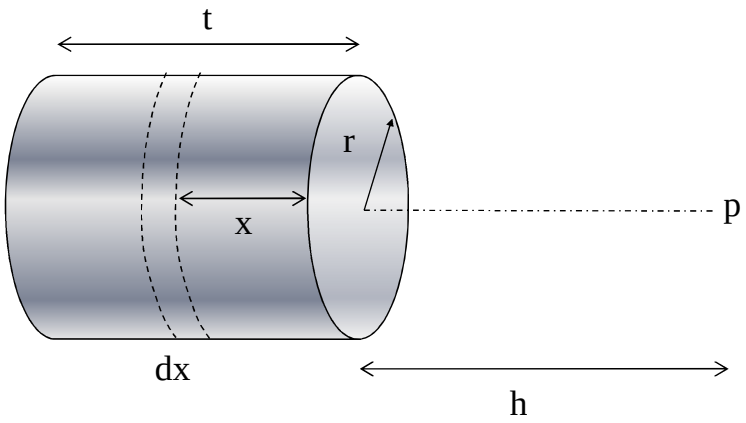

Figure 51 Volume-source geometry

For a uniform volume concentration of radioactivity C_v (Ci m^{-3} or MBq m^{-3}), the dose rate at point *p* can be expressed as a function of the point source-specific gamma constant as defined in Section 5.1.2.1, using Eq. (61):

$$\dot{H}_p = \pi\,\Gamma\frac{C_v}{\mu}\left(1-e^{-\mu\cdot t}\right)\ln\left(\frac{r^2+h^2}{h^2}\right), \tag{61}$$

where

$\dot{H}_p$ is the dose rate (R/h or Sv/h, consistent with Γ)

r, *t,* and *h* are defined in Figure 51 (m)

Γ is the specific gamma constant for a point source (conventional or SI units)

C_v is the volume activity (Ci m^{-3} or MBq m^{-3}, consistent with Γ)

μ is the linear absorption coefficient of the volume source material (cm^{-1}).

It is possible to extend this volume treatment to other simple geometries in a similar manner.

5.1.3 Neutrons

Neutrons can be classified in a variety of ways. The most common way to classify neutrons is by kinetic energy. Thermal neutrons and neutrons in thermal equilibrium with their environment are distributed according to a Maxwell-Boltzmann distribution. Their most probable energy is 0.025 eV at 20°C. At higher energies from 0.01–0.1 MeV, neutrons may be classified as slow, intermediate, or resonance. Fast neutrons have energies from a few MeV up to approximately 20 MeV, and relativistic neutrons have still higher energies. Neutrons are uncharged (neutral) like photons and can travel appreciable distances without interacting. Neutrons are attenuated exponentially under good geometry and do not interact appreciably with electron fields. Neutrons collide with atomic nuclei in elastic and inelastic collisions. With elastic collisions, the total energy is conserved, and the energy lost by the neutron is equal to the total energy of recoil of the nucleus. With inelastic collisions, the nucleus absorbs some of the energy and is left in an excited state, which upon de-excitation can yield neutrons, gammas, and light ions. Fast neutrons undergo a series of primarily elastic scattering reactions, being slowed down in a process called moderation. As neutron energy decreases, scattering continues, but the probability of capture by another nucleus increases. If the neutron reaches thermal energies, it will randomly move around until absorbed by a nucleus.

5.1.3.1 Neutron reactions

A number of reactions important to neutron interactions are listed in Table 14. Some of these reactions are important from a dose-to-tissue perspective, whereas some are important for considering neutron detection.

Table 14 Important neutron reactions

Reaction	Typical use
$^{1}H(n,\gamma)^{2}H$	Dose to tissue
$^{3}He(n,p)^{3}H$	Neutron proportional counters
$^{6}Li(n,T)^{4}He$	Thermal neutron detection
$^{10}B(n,\alpha)^{7}Li$	
$^{14}N(n,p)^{14}C$	Dose to tissue
$^{23}Na(n,\gamma)^{24}Na$	Blood dosimetry
$^{40}Ar(n,\gamma)^{41}Ar$	Internal dosimetry
$^{32}S(n,p)^{32}P$	Neutron spectroscopy
$^{113}Cd(n,\gamma)^{114}Cd$	
$^{115}In(n,\gamma)^{116m}In$	
$^{197}Au(n,\gamma)^{198}Au$	
$^{235}U(n,f)$	Thermal neutron detection

Besides the interactions presented in Table 14, neutron activation of materials can also be a significant source of gamma dose in nuclear plants. Neutron activation is the production of a radioactive isotope by absorption of a neutron and is governed by Eq. (62):

$$\frac{dN}{dt} = \varphi \sigma n - \lambda N$$

$$or$$

$$\lambda N = \varphi \sigma n \left(1 - e^{-\lambda t}\right) \equiv A \quad , \tag{62}$$

where

A is the activity of the radioisotope produced through neutron activation (Bq)
ϕ is the neutron flux (n cm^{-2} s^{-1})
σ is the activation cross section (cm^2)
λ is the decay constant of the produced isotope (s^{-1})
N is the number of produced atoms
n is the number of target atoms.

Although the radioisotopes produced are generally a gamma radiation hazard, activation is an important reaction with respect to this source of gamma (or beta) dose.

5.1.3.2 Neutron dosimetry

The absorbed dose from neutrons, from a biological dose perspective, involves primarily neutron interaction with tissue elements H, C, O, and N and the dose resulting from these interactions. Neutron interactions produce recoil protons and heavy charged particles with short ranges that deposit their energy locally in tissue. Dosimetry estimates may be made empirically be examining separately (i) fast neutrons and (ii) thermal neutrons.

I. Fast neutrons

The dose rate from fast neutrons in a material made up of a number of elements can be estimated using Eq. (63):

$$\dot{D}_n(E) = \frac{\varphi(E) \cdot E \cdot \sum_i N_i \sigma_i f_i}{1 \frac{J}{kg} \Big/ Gy} \quad \left(\frac{Gy}{s} \right), \tag{63}$$

where

$\phi(E)$ is the fast neutron flux (n $cm^{-2}s^{-1}$)

E is the neutron energy (Joules; 1.6E-19 Joules per eV)

N_i is the number of atoms per kg for the i^{th} material element

σ_i is the scattering cross section (cm^2) for the i^{th} material element

f_i is the fractional energy transferred from neutrons for the i^{th} material element, given by $f_i = \frac{2M_i}{(M_i+1)^2}$, where M_i is the atomic mass of the i^{th} material element. f_i represents the average fraction of neutron energy transferred in an elastic collision assuming isotropic scattering.

The fast neutron dose can be calculated as a function of different energy groups (corresponding to the neutron energy spectrum) to determine the total fast neutron dose.

II. Thermal neutrons

The most important specific thermal neutron reactions for tissue dosimetry (hydrogen and carbon) are described below.

Hydrogen capture - $^1H(n,\gamma)^2H$

This is an example of a radiative capture process. The neutron is absorbed, followed by immediate emission of a gamma photon, ${}_0^1n + {}_1^1H \rightarrow {}_1^2H + {}_0^0\gamma$, with photon energy 2.22 MeV. This reaction is of significance when tissue is exposed to thermal neutrons. This reaction yields a uniformly distributed gamma-emitting radioisotope, and therefore initially one must solve for the specific activity (A_s) of this source using Eq. (64)

$$A_s = \varphi N_H \sigma_H \quad \left(\frac{Bq}{kg} \right), \tag{64}$$

where

ϕ is the thermal neutron flux (n $cm^{-2}s^{-1}$)

N_H is the number of hydrogen atoms per kg of tissue (5.98×10^{25} atoms/kg)
σ_H is the absorption cross section for hydrogen (0.33×10^{-24} cm^2).

Knowing the specific activity, it is possible to solve for the internal dose using approaches presented in Section 6.

Nitrogen capture - $^{14}N(n,p)^{14}C$

This reaction has a large thermal cross section of 1.78 barns and an energy release of 0.626 MeV in tissue. This is a significant contributor to dose when tissue is irradiated by neutrons because the proton and the nucleus recoil have limited range and the energy is deposited locally. The dose rate due to the energy released by charged particles for this reaction can be determined by Eq. (65):

$$\dot{D}_{np} = \frac{\varphi \cdot N_N \cdot \sigma_N \cdot Q \cdot (1.6 \times 10^{-13} \frac{J}{MeV})}{1 \frac{J}{kg} \Big/ Gy} \quad \left(\frac{Gy}{s} \right), \tag{65}$$

where

ϕ is the thermal neutron flux (n cm^{-2}s^{-1})
N_N is the number of nitrogen atoms per kg of tissue (1.49×10^{24} atoms/kg)
σ_N is the absorption cross section for nitrogen (1.75×10^{-24} cm^2)
Q is the energy release in tissue (0.626 MeV).

5.2 External Hazards

A variety of potential external radiation hazards are associated with nuclear technology. When a reactor is under power, a variety of areas inside containment can produce significant neutron and gamma radiation fields. Generally speaking, these areas are well characterized, and administrative measures are put in place to minimize any hazard from these fields. When the reactor is on power, there are hazards from fission neutrons, fission prompt gamma rays, and neutron-capture gamma rays, as well as fission-product gamma rays, activation gamma rays, and photoneutrons. When the nuclear chain reaction is halted, the direct neutron component of the hazard rapidly reduces to an insignificant proportion. The hazards that remain are therefore fission-product gamma rays, activation gamma rays, and to a lesser extent, photoneutrons. In an ideal situation, the fission products produced in the fuel would remain in the fuel cladding. However, fuel failure does occur and contaminates water systems, which can lead to deposition of fission products in piping and associated systems. In addition, activation products can migrate away from their original locations due to corrosion processes.

The most common operational hazards from external radiation in a nuclear plant are due to:

(a) Fission-product activity in the core (present regardless of the power condition of the core)
(b) Activation products in the core and surrounding material (including water)
(c) Fission products that migrate and deposit at various locations in the reactor
(d) Activation products that migrate and deposit around various reactor systems

(e) Contamination, in liquid or aerosol form, due to fission and activation products that become inadvertently uncontained (which also may pose a significant external beta hazard and internal alpha/beta hazard if inhaled).

The possible sources of the radiation that may contribute to external radiation dose while a CANDU reactor is operating are depicted in Figure 52. The simplified drawing depicts the biological shield (this shield also encompasses the thermal shield and reflector region), the core (where the fission reaction takes place), and the primary heat transport (PHT) system that circulates the hot pressurized water directly to the steam generators. The reactor operates as a "closed primary circuit", and therefore radioisotopes generated as a result of fission, activation, or other nuclear processes may be circulating in the primary heat transport (PHT) system. The primary circuit is physically separated from the secondary steam-generation circuit at the steam generators. In theory, there should be no sources that migrate from the primary to the secondary side in a CANDU, and therefore no radioactivity at the turbines. Referring to Figure 52, the potential sources may be described as follows (after [Goldstein1962]):

- Prompt fission neutrons – emitted within first few μs after fission
- Delayed fission neutrons – emitted from excited nuclei up to a few minutes after fission
- Activation neutrons – emitted from nuclear reaction products
- Photoneutrons – produced through threshold (γ,n) reactions
- Prompt-fission gammas – emitted in coincidence with fission (< μs)
- Short-period fission gammas – emitted by fission products within a few minutes (~10 min) after fission
- Long-period fission gammas - emitted by fission products after ~10 minutes
- Capture gammas – emitted in (n,γ) reactions
- Inelastic-scatter gammas – emitted from excited nuclei after neutron inelastic scattering
- Reaction-product gammas – emitted from products of charged-particle reactions induced by neutrons
- Activation-product gammas – emitted from radioactive products of nuclear reactions
- Annihilation photons – emitted from positron annihilation due to certain activation or fission products
- Bremsstrahlung photons – emitted from decay electrons (beta particles) slowing down in material.

Note that not all the listed sources are of equal importance, and often their importance is dictated by their physical location in the reactor with respect to receptors (workers). In addition, the importance of sources is affected by the state of the reactor. On shutdown, some of the sources disappear, and the relative importance of the remaining sources changes. There is residual fission power in a CANDU core after shutdown, and therefore there are still prompt fission gammas and neutrons, as well as capture gammas produced in the core. However, they are produced at levels several orders of magnitude lower than during operation. Possible external radiation sources ~10 minutes after shutdown are depicted in Figure 53.

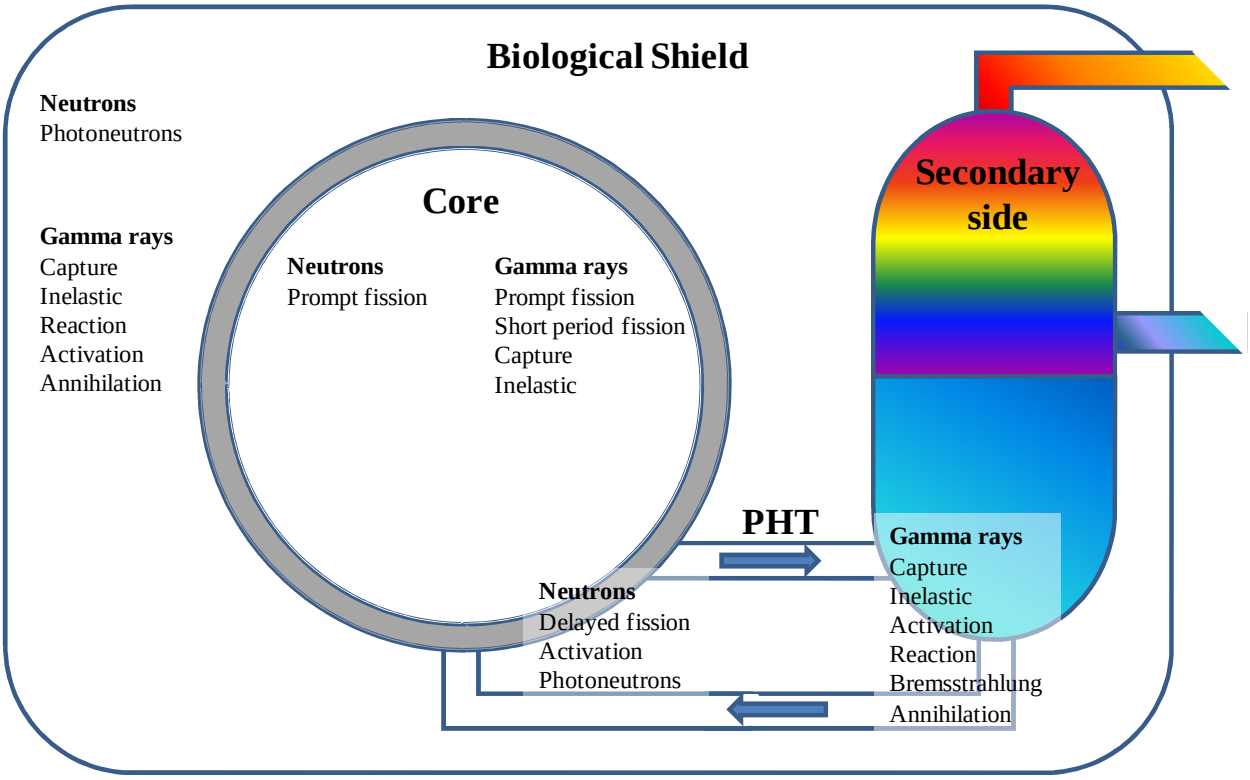

Figure 52 Potential external exposure sources during reactor operation

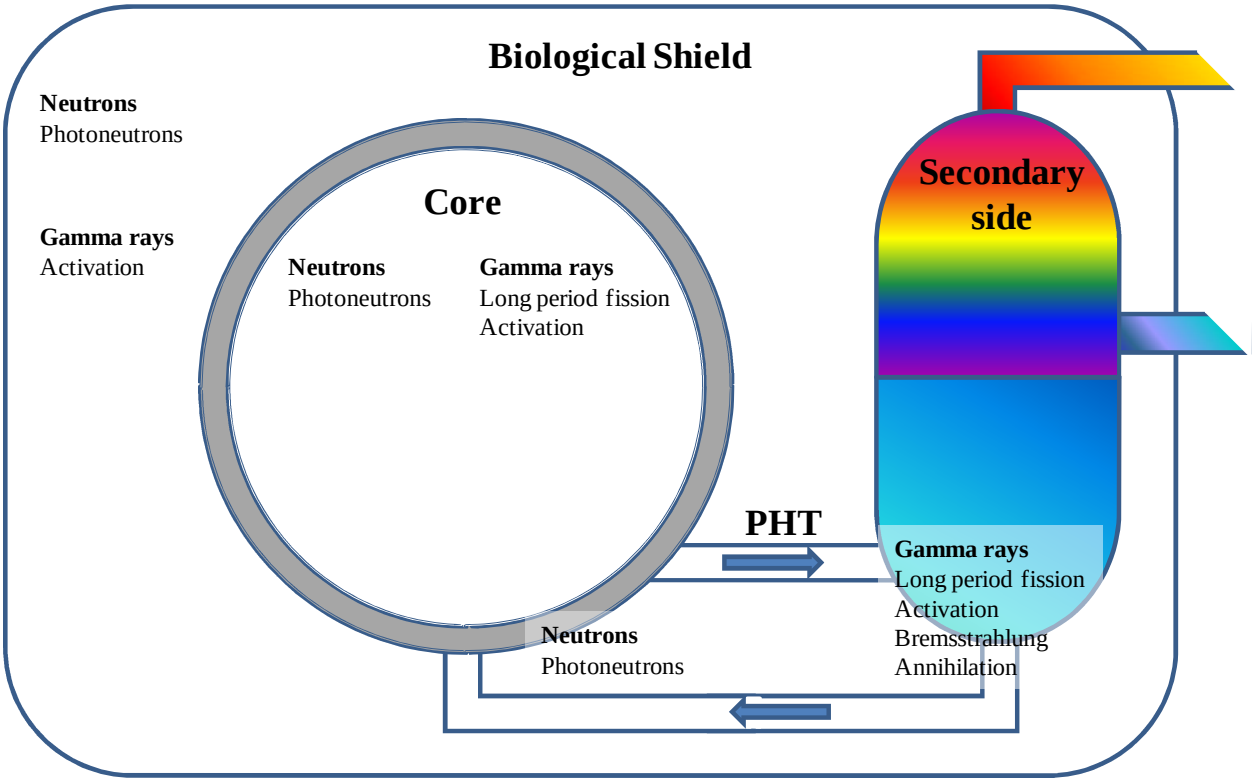

Figure 53 Potential external exposure sources after shutdown (> 10 min)

Some examples of external hazards in a nuclear reactor environment include (but are not limited to) the following:

- Mixed neutron/gamma fields from normal operation (under power or shut down) at various locations around the reactor
- Contaminated coolant in a pipe (circulating or uncirculating)
- Contaminated resin columns
- Fission or activation products that have lodged or attached somewhere unexpectedly in a piping system
- Leakage from a contaminated water system
- Outage activities that may involve opening piping or pump systems, welding and grinding activities on potentially contaminated systems, etc.

Protection against these external hazards includes proper work planning (discussed in Section 7) along with use of the ALARA principle and shielding (discussed in Section 5.3).

5.3 External Protection (Radiation Shielding)

The essential principle of external radiation protection is embedded within the so-called ALARA (as low as reasonably achievable) principle. The ALARA principle was formalized by the ICRP in their 1977 recommendations [ICRP1977] and may be considered as the fundamental philosophy of radiation protection that suggests that no practice dealing with radioactive material should be adopted unless there is a net benefit arising from it. If radiation is to be used, all efforts must be made to ensure that the dose is the lowest absolutely required for the given task. The complete text of the ALARA principle clarifies the context of applicability and has been paraphrased as [ICRP1977] making every reasonable effort to maintain exposures to radiation as far below the dose limits **as is practical**, consistent with the purpose for which the activity is undertaken, taking into account (i) the state of technology, (ii) the economics of improvements in relation to the state of technology, (iii) the economics of improvements in relation to benefits to public health and safety, (iv) other societal and socioeconomic considerations, and (v) relationships to use of nuclear energy and radioactive materials in the public interest.

The typical radiation hazards for CANDU reactor operations are depicted in Figure 54. In applied external radiation protection for CANDU reactors, it is normal to consider gamma, neutron, and beta radiation. Alpha radiation, although a great concern for inhalation dose (considered in Section 6), is of no concern as an external dose because the radiation cannot penetrate the external dead layer of tissue and certainly not any clothing that a person may be wearing. Beta radiation (discussed in Section 5.1.1) can be of concern externally if a worker is not protected and is in contact with a source, submerged in a plume, or gets a “hot” particle on unprotected skin. However, in this type of scenario, there are usually corresponding gamma emitters that require shielding, and therefore the beta particles are generally well shielded as a result. For other applications like nuclear medicine, low atomic number (low-Z) materials can provide effective shielding from beta radiation (while simultaneously yielding less bremsstrahlung radiation compared to high-Z shields). It is common to use Plexiglas™ shielding for beta-emitting radioisotopes. Therefore, for normal shielding, the focus is on gamma and neutron radiation.

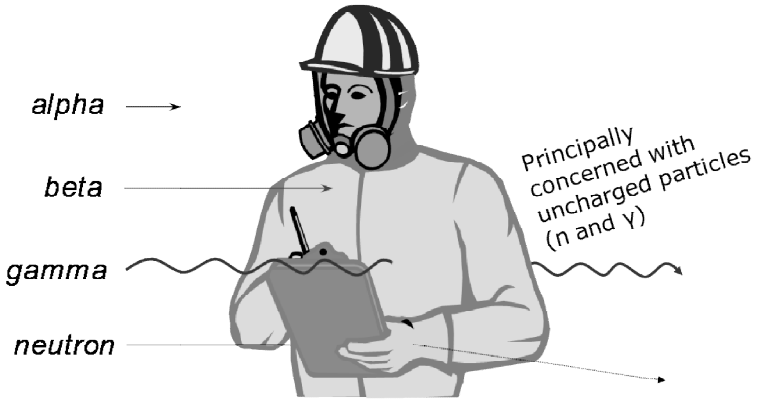

Figure 54 External hazards

The reduction of doses to ALARA for external radiation is primarily accomplished using three principal concepts of radiation protection: shielding, distance, and time. Simply stated, shielding is placing something between the source and receptor that blocks (or attenuates) radiation, distance is keeping space between the source and the receptor, and time is spending as little time around the source as required to reduce exposure. In addition, it is common to use the effect of radioactive decay for short-lived radioisotopes as part of the shielding strategy (for example, delaying entry into an area after shutdown to allow time for radioactive decay).

Time is an obvious dose parameter because dose is accumulated over time and is delivered as a function of time from an external source (dose rate). Therefore, less time = less dose. The role of distance is readily understood by considering the inverse-square law (which is also important in shielding discussions) depicted in Figure 55.

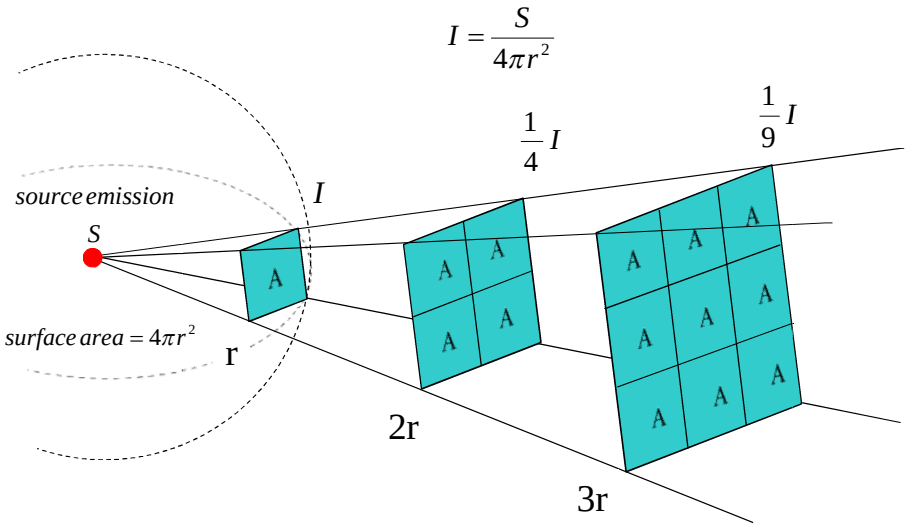

Figure 55 Inverse-square law

The inverse-square law can be readily understood by ray-tracing from a point source outwards and considering the intensity per unit area at the intersection with an arbitrary sphere of radius *r*. For every increase in radius, the intensity decreases by the square of the increased radius because the intensity is propagating outwards across the expanding sphere. For example, twice the radius leads to one-fourth the intensity, three times the radius, one-ninth the intensity, four times the radius, one-sixteenth the intensity, and so on. Because dose is directly proportional to

radiation intensity, this demonstrates that dramatic decreases in dose can be achieved with moderate changes in distance from the source, particularly close to the source.

As discussed earlier, shielding is the act of placing a material between the source of radiation and the receptor, which has the effect of reducing the amount of radiation impinging on the receptor. In radiation protection, shielding is often called biological shielding because its primary purpose is to reduce the biological dose to humans. As such, shielding materials are critically important to the effectiveness of shields. The following sections consider shielding for gamma and neutron radiation.

5.3.1 Gamma shielding

In Section 5.1.2, the principles of gamma dosimetry were discussed. The relationship to determine intensity (fluence, flux, or dose) of radiation after passage through a shield is given by Eq. (66):

$$I = I_0 e^{-\mu x}, \tag{66}$$

where

I is the intensity of the radiation after passing through the shield (fluence, flux, or dose units)
I_o is the intensity of the radiation before passing through the shield (same units as I)
μ is the linear attenuation coefficient for that material (cm^{-1})
x is the thickness of the shield (cm).

Taking into account both the distance from the source and receptor and the influence of the shielding material, the intensity at a point *r* units away from a source shielded by a thickness *x* of material is given by Eq. (67):

$$I = \frac{I_0 e^{-\mu x}}{4\pi r^2}. \tag{67}$$

The physical conditions that describe this type of attenuation are that (i) the radiation is a narrow beam interacting with the shield and (ii) the shield is thin with respect to the mean free path (1/μ) of the gamma radiation in the shield. This scenario is depicted in Figure 56. In this case, the radiation, depicted by the dashed lines, scatters away from the receptor.

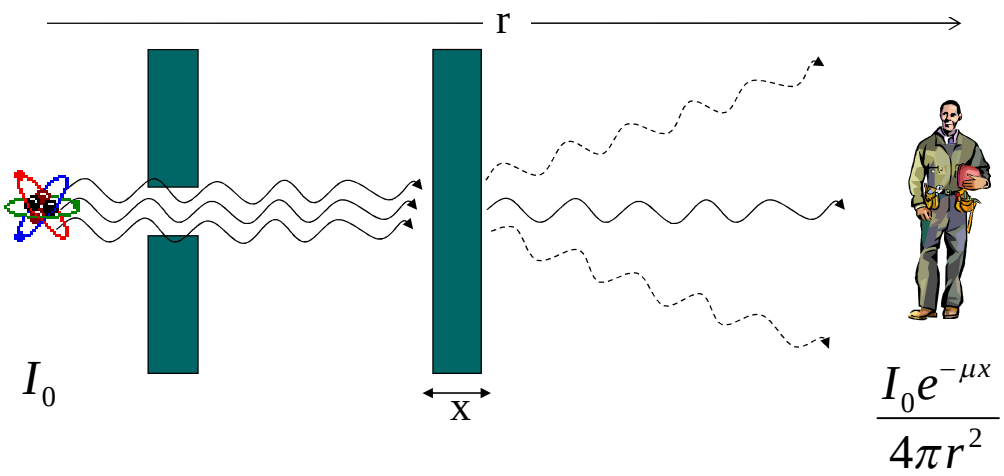

Figure 56 Narrow-beam or thin-shield attenuation

5.3.1.1 Buildup

Although approximation of Eq. (66). may be valid in some cases, there are a number of situations in which the radiation source may be considered a broad beam with respect to the shield or the shield may be thick with respect to the mean free path of radiation in the shield. This case is depicted in Figure 57. It has been observed that in this scenario, some of the radiation that would have scattered away from the receptor actually scatters towards the receptor and contributes additional intensity to the receptor location that is not predicted by Eq. (66). In this case, a factor is used to modify the standard attenuation equation to account for the scattering. This factor is known as the buildup factor (B) and is dimensionless. The intensity equation therefore becomes Eq. (68):

$$I = \frac{I_0 B e^{-\mu x}}{4\pi r^2} \quad . \tag{68}$$

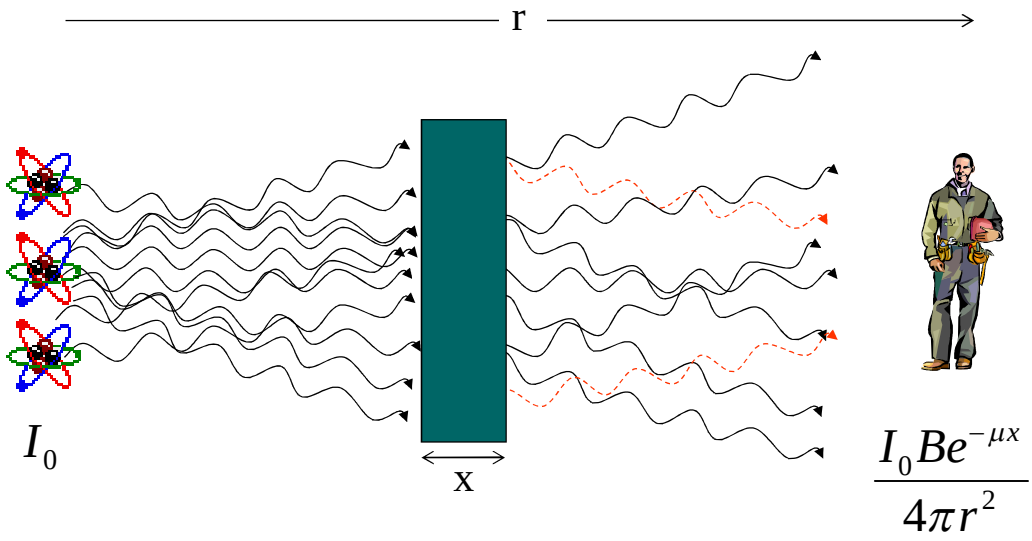

Figure 57 Broad-beam or thick-shield attenuation

The buildup factor is both a function of energy and the shield material (μx, denoted as the optical length, relaxation length, or number of mean free paths) and is given as Eq. (69):

$$B(E,\mu x) \equiv \frac{I_0(E,\mu x)+I_s(E,\mu x)}{I_0(E,\mu x)} = 1+\frac{I_s(E,\mu x)}{I_0(E,\mu x)}, \quad (69)$$

where

B is the buildup factor (dimensionless)
I_0 is the non-collided intensity (fluence, dose, or dose rate) at the receptor
I_s is the scattered (collided) radiation contribution at the receptor.

The buildup factor is the ratio of the radiation intensity, including both primary and scattered radiation, at any point in a beam to the intensity of primary radiation only at that point. The buildup factor accounts for scattering into an area due to poor (broad-beam) geometries and is a function of shield material and shield thickness (*x*). Examining Eq. (69) leads to the conclusion that B is always ≥ 1. Values for B have been experimentally determined; however, the bulk of data available are from calculations, and many evaluations are presented in tables or in a graphical format.

Two common ways of using the buildup factor for solving a shielding problem are: (i) knowing the source and shield, calculate the intensity, and (ii) knowing the desired intensity at the receptor point, determine the amount of shielding required.

Calculating intensity

The steps in calculating intensity (fluence, dose, or dose rate) are given as follows:

1. Look up B for:
   - Material of interest (e.g., lead, iron, etc.)
   - Energy of photons (e.g., 1 MeV)
   - Relaxation length of shield (μx) – Relaxation length is the thickness of shield material that will attenuate a narrow beam to 1/e of its original value.
2. Solve equation: $\mathbf{I=I_0*B*e^{-ux}}$ for fluence, dose, or dose rate.

Calculating required shield thickness

The calculation of the thickness of a shield required for a given desired fluence, dose, or dose rate is difficult because the equation must be solved simultaneously for two variables, *B* and *x*, which can be solved for only by iteration. The steps in calculating the required shielding thickness are the following:

1. Define the target exposure I (fluence, dose, dose rate)
2. Solve the narrow-beam equation $\mathbf{I=I_0*e^{-ux}}$ to obtain an initial shielding thickness *x*. This thickness will be too small.
3. Add one half-value of thickness to *x* ($\mu = (\ln 2) / x_{1/2} \rightarrow x_{1/2} = (\ln 2) / \mu$)
   - (*new* x) = ($x + x_{1/2}$)
4. Look up B for material, energy, (*new* x)* μ.
5. Solve $\mathbf{I=I_0*B*e^{-ux}}$ with new values
   - Check: Is the calculated value of I close to the target I?
6. If the calculated I is still too large, then add another $x_{1/2}$ and recalculate (i.e., go to step 3).

Note that the shield may be placed anywhere between the source and the receptor; however, when the shield is placed closer to the source, it provides the greatest solid-angle protection to the receptor. Tabulated buildup factors can be found in a number of sources including, for example, through the American Nuclear Society [ANS1991] and in work by Shultis and Faw [Shultis2000].

A number of numerical techniques can be used to perform gamma-radiation transport calculations suitable for use in shielding estimates, for example, point-kernel techniques, discrete-ordinate techniques, and Monte Carlo simulation. The need for advanced gamma-shielding approaches arises from requirements to simulate complex geometries, multilayer shields, complex materials, complex source terms, and differing cross-section evaluations.

5.3.1.2 Materials

In general, there are three categories of shield materials: (1) natural materials, (2) construction materials, and (3) special materials. Natural materials include air (insofar as it can be a scattering medium), water, and soil, and often shielding design involves making judicious use of these natural materials. Construction materials are a very advantageous design material from an optimization standpoint because they can serve two purposes, as structural and as shield materials. Construction materials may include concrete, steel, wood, plasterboard, and glass. Special materials for gamma shielding are generally high-atomic-number materials such as steel, iron, lead, tungsten, and uranium. The usefulness of a shield for any given application is related to the mass-attenuation coefficient (directly related to the interaction cross section) and the mass density of the material as a function of the photon energy spectrum. A plot of the interaction cross sections of photons in lead is provided in Figure 58. It can be seen that the photoelectric effect is the dominant interaction at energies below approximately 0.2 MeV, Compton scattering is competing or dominant between approximately 0.2 and 4 MeV, and pair production dominates above 4 MeV (further discussion of photon interactions is provided in Chapter 3).

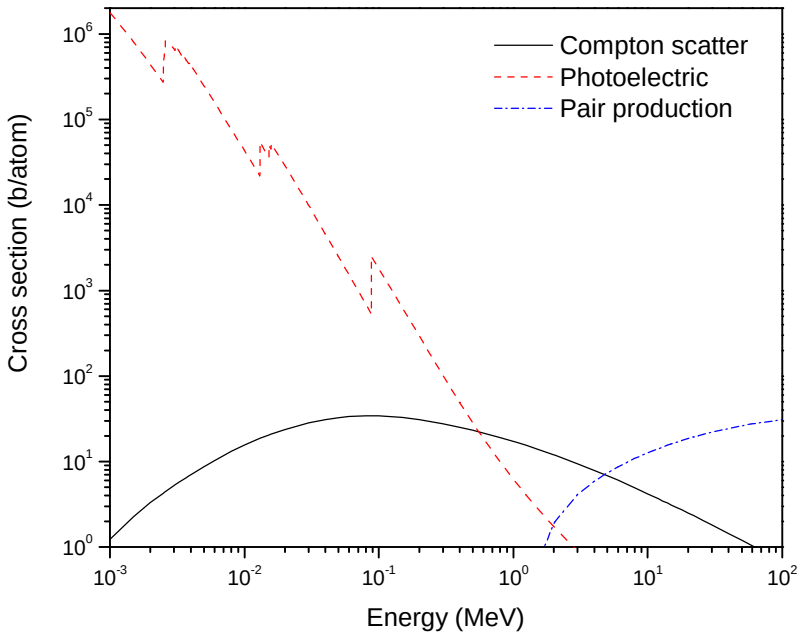

Figure 58 Photon interaction cross sections for lead

Photon total-interaction coefficients for uranium, lead, aluminum, and water are shown in Figure 59. It can be seen that for high-Z materials such as uranium and lead, the interaction mechanisms are very similar. For lower-Z materials such as aluminum and water, the interaction coefficients are significantly lower at most energies. Note that the total interaction coefficients at moderate energies (0.5–3 MeV) are similar for all four materials and that therefore their attenuating power comes primarily from their different mass densities because $\left(\frac{\mu}{\rho}\right)\rho \cdot x$ is the argument of the exponential function when μ is the linear attenuation coefficient.

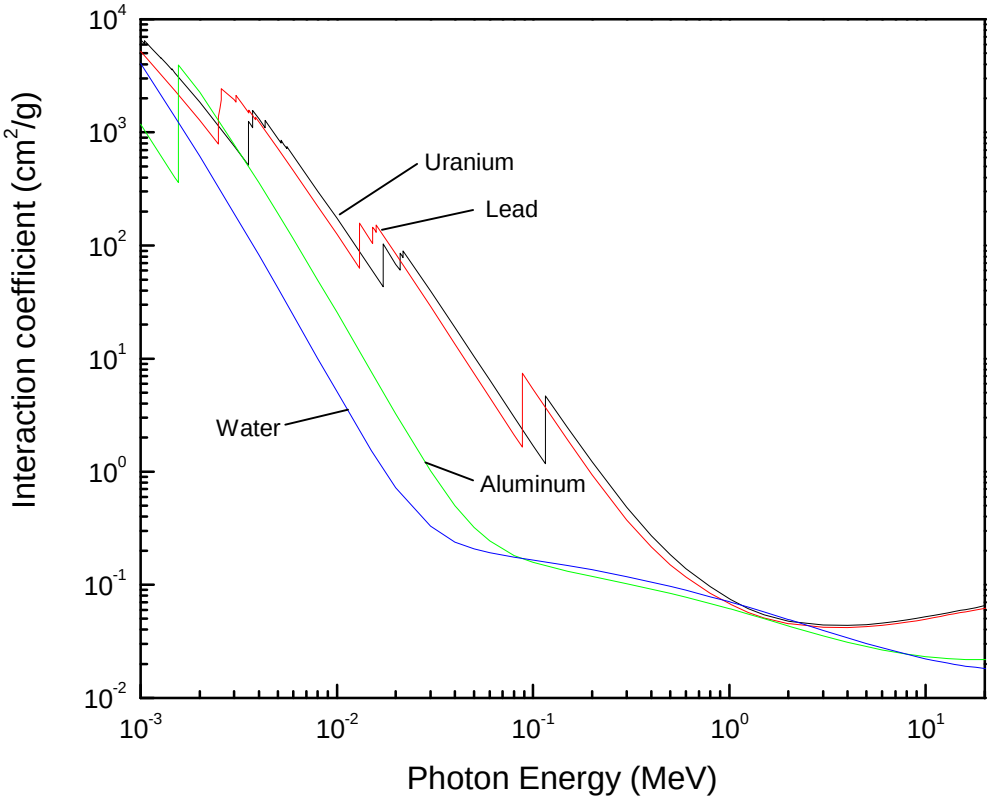

Figure 59 Photon interaction coefficients

5.3.2 Neutron shielding

Compared to the simplified gamma-shielding techniques, fast-neutron shielding is somewhat more complicated. These complications arise from a number of considerations:

- Primary neutrons (usually fast) have a high scattering probability
- Inelastic scattered neutrons produce gamma photons
- Thermal neutrons are produced after slowing down
- Capture gamma photons from (n,*γ*) reactions arise mainly from thermal neutrons
- Secondary neutrons from (n,2n), fission, etc., can be generated
- Neutron production is usually accompanied by primary gamma photons
- Neutron absorption can activate shield material, which in turn emits delayed gamma photons.

Taking all this into account, a simplified approach such as using buildup factors (similar to the approach with photons) is not generally practical for neutron problems because [Shultis2000]:

- Neutrons scatter much more than photons, thereby making B very large
- There is a large buildup of low-energy neutrons because the absorption cross section (σ_a) is small in the slowing-down energy region
- B depends strongly on the
    - Isotopic (material) composition of the shield
    - Physical geometry of the shield
    - Incident neutron-energy spectrum.

Due to the difficulties outlined above, the buildup-factor approach will not be developed for neutrons. However, in addition to the above, because neutrons have radiation-weighting factors that are energy-dependent, the difference between dose conversion factors (response functions) for air kerma, ambient dose, and dose equivalent can be significant, as shown in Figure 60. This can lead to significant differences in dose estimation.

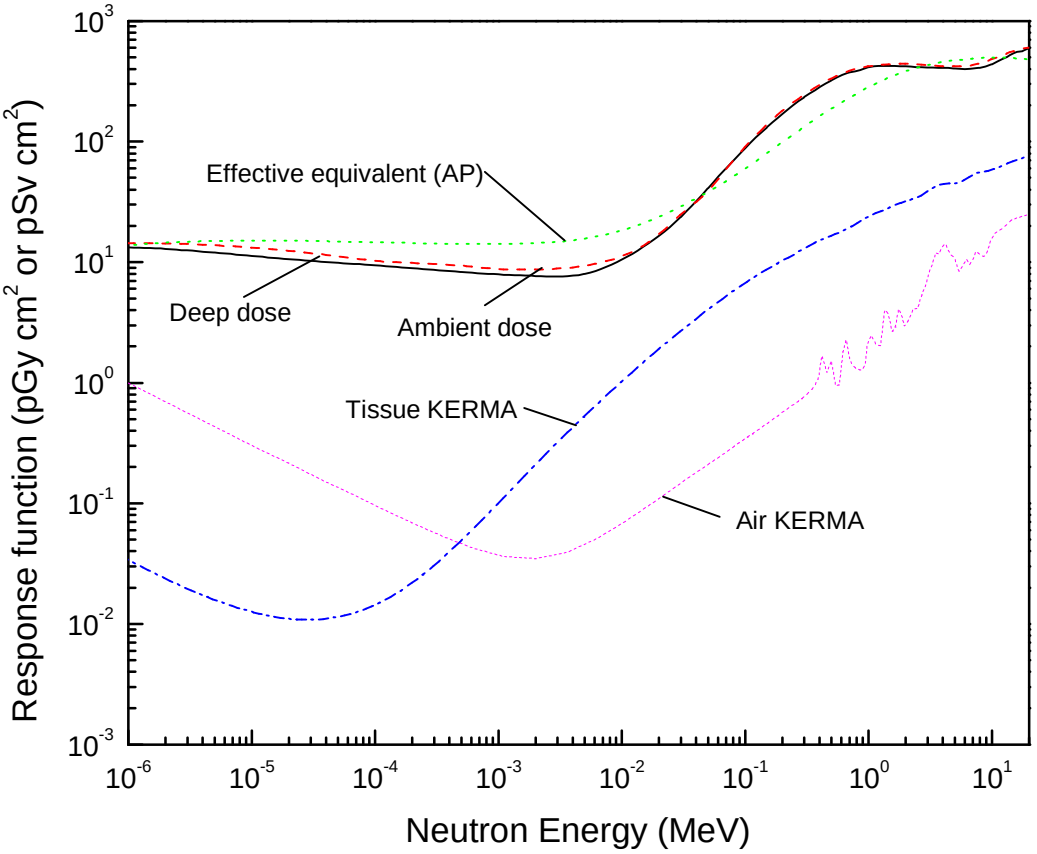

Figure 60 Response functions for neutrons

General considerations with respect to neutron shielding include:

- For biological shields, fast neutrons are of most concern because thermal neutrons are readily absorbed
- Q (w_R) varies with neutron energy and is greatest for 0.1 < E < 2 MeV
- Materials with large σ_a are used to absorb thermal neutrons (e.g., Cd, In, B, Li). However, one must consider the resulting capture gamma radiation

- To stop fast neutrons, they can be thermalized by
    - moderation (low-atomic-number materials) and
    - inelastic scattering (e.g., by iron)

  and then absorbed as thermal neutrons.

Most neutron-shielding analyzes require complex transport calculations. However, a few simplified techniques are available. For example, point kernels can be used for fission neutrons in hydrogenous and non-hydrogenous media, diffusion and removal theories for intermediate energy neutrons, and point kernel techniques for capture gamma photons. In addition, tabulated data for neutron shielding (for example, concrete shields) are often available.

5.3.2.1 Removal techniques

The removal cross section can be used to estimate the flux of fission neutrons in a hydrogenous material (e.g., water) of distance *r* from source to receptor that is shielded by a non-hydrogenous material of thickness *t*. In this case, the flux is given by Eq. (70) [Lamarsh2001]:

$$\begin{aligned} &\phi(r) = S \cdot G(r) \cdot e^{-\Sigma_r t} \\ &where \\ &G(r) = \frac{0.12 \cdot e^{-\Sigma_{r_{water}} r}}{4\pi r^2} \end{aligned}, \tag{70}$$

where

φ is the fission (> 1 MeV) neutron flux at r (n cm^{-2} s^{-1})
S is the source emission rate (n s^{-1})
Σ_r is the macroscopic removal cross section for the shield material (cm^{-1})
Σ_{rwater} is the macroscopic removal cross section for water (0.103 cm^{-1})
t is the thickness of the shield (cm)
r is the distance of the water from source to receptor (cm).

The macroscopic removal cross section can be expressed as a function of the microscopic cross section, as in Eq. (71):

$$\begin{aligned} &\Sigma_r = N\sigma_r \\ &or, \ for\ mixtures \\ &\Sigma_r = \sum_i N_i \sigma_{ri} \end{aligned}. \tag{71}$$

Macroscopic and microscopic cross sections for a variety of elements and mixtures are provided in Table 15 (adapted from [Shultis2005]).

Table 15 Removal cross sections for neutrons

Material	Σ_r (cm^{-1})	σ_r (b)
Aluminum		1.31
Hydrogen		1.00
Deuterium		0.92
Beryllium	0.132	1.07
Boron		1.07
Carbon	0.065	0.81
Oxygen		0.92
Sodium	0.032	1.26
Iron	0.168	1.98
Zirconium	0.101	2.36
Lead	0.118	3.53
Tungsten		3.36
Uranium	0.174	3.60
Zirconium		2.36
Water	0.103	
Paraffin		80.50
Heavy water	0.092	2.76
Concrete (6% water)	0.089	

An approximation for the removal cross section (where $\Sigma_r = \mu_r$) in terms of μ_r/ρ is given by Eq. (72):

$$\frac{\mu_r}{\rho} \simeq 0.206 A^{-1.3} Z^{-0.294} \left(\frac{cm^2}{g} \right). \tag{72}$$

Functionally, the removal technique can be used to estimate the flux at the surface of a shield, and then this flux can be used to estimate the flux at a position outside the shield. Knowing the

fast neutron flux at a receptor point outside the shield, the dose rate can be estimated using Eq. (63). Note that this is a simplified approximation, and a more complex analysis (such as the Monte Carlo technique) is required to determine the intensity accurately.

5.4 Summary

External radioisotope hazards associated with CANDU reactors include hazards directly associated with the nuclear chain reaction (neutron and gamma fields) or indirectly associated as is the case with fission products from fuel (whether intact or defective) and activation products (whether fixed or mobile). Dosimetry can be accomplished from first principles using source activity and geometry or by using dose-conversion factors and fluence measurements.

External hazards in CANDU reactors involve gamma, neutron, and beta fields, and protection of the worker from external hazards is accomplished by adhering to the principles of "as low as reasonably achievable" dose and the concepts of maximum shielding (of source), maximum distance (from source), and minimum time (around source) for any given work function.

6 Internal Radiation Hazards

Internal radiation hazards from alpha, beta, and gamma sources are discussed in this section. Pathways for internal radiation exposure are periodically present within nuclear reactors, and therefore consideration of expected doses and strategies to minimize dose are required. Some historical perspective on internal dosimetry can be found in [Potter2005].

6.1 Internal Pathways and Dosimetry

When a material containing radioisotopes is inhaled, ingested, or absorbed through the skin or a wound, this will lead to an internal dose, as depicted in Figure 61. For an ingestion pathway, typically (1) contamination (for example, a radioactive spill) occurs. If the contamination is touched (whether protected or unprotected), the radioisotope(s) can be either (2a) transferred to the hands or (2b) transferred through a wound if present and directly to the blood. If the hands are contaminated, the radioisotope(s) can be (3) transferred to food or the face directly, from where they can be (4a) transported to the gastrointestinal (GI) tract. Alternately, for an inhalation pathway, if a person is in proximity to airborne radioisotopes, the person may (4b) take in the radiation directly from the plume into the respiratory tract. In both cases, radioisotope(s) will be transported and (5) taken up into the blood and GI tract. From there, they can be transported to target organ(s) and deposit decay energy, or in other words, a dose.

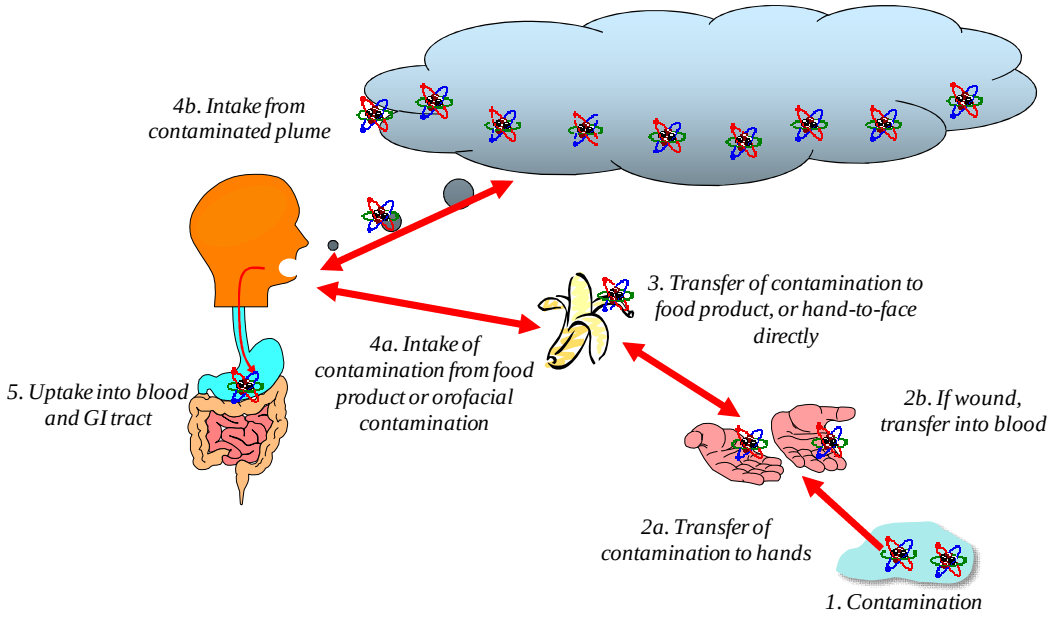

Figure 61 Internal contamination pathways

As was discussed in Section 3.4, the total dose assigned to an individual is the sum of all external and internal exposures. In an industrial environment, the dominant pathway for internal exposure is through inhalation of airborne radioisotopes.

Neutrons are generally not considered when discussing internal dose because the possibility of internalizing a neutron emitter (for example, a spontaneous fission-neutron source) is extremely remote. However, in contrast to external dosimetry, alpha-emitting radioisotopes can be a major contributor to the committed effective dose that a person might receive.

A number of factors affect internal dose, as outlined in Table 16. Note that not only does the type and quantity of radioactive material contribute to dose, but also other factors such as the chemical form of the material and its biological function in the human body.

Table 16 Parameters affecting internal dose

Physical Characteristics	Biological Characteristics
Radionuclide	Metabolic behaviour
Physical half-life	Biological half-life
Chemical & physical form	Chemical toxicity
Emitted radiation	Tissue sensitivity
Intake route	Age of individual
Duration of intake	Individual health
Total intake	Personal habits

The internal dose mechanism can be described as shown in Figure 62. Internal dose is facilitated by basic mechanisms for intake into the body (inhalation, ingestion, or absorption), followed by uptake into extra-cellular fluids for circulation through the body, and finally deposition of radioisotopes into target organs and tissues where decay energy is deposited.

The dominant intake regimes related to transport through the body to excretion are outlined in Figure 63. This is a simple representation of what is called a compartmental model. Dosimetry can be accomplished by solving mathematically for the transport, deposition, and excretion of radioisotopes through “compartments” in the body. Most internal-dosimetry computer codes perform this type of calculation (for example, see [IMBA2010]). Compartmental modelling of internal dose is beyond the scope of this chapter.

Inhalation into the respiratory system can be subdivided into three regions: (i) nasal-pharyngeal (inhalable), (ii) tracheal-bronchial (thoracic), and (iii) pulmonary (respirable, or deep lung). Particle deposition takes place in the three regions with an efficiency based on particle diameter. Generally speaking, particles from submicron to ten microns are considered respirable, whereas larger particles deposit in the upper airway regions. Although upper-airway deposition can lead to dose, the respirable fraction is of primary significance for internal dosimetry. Inhalation leads to deposition in one of the three regions of the respiratory tract, and if deposited in the deep lung, particles can be absorbed into the blood for transport to target organ(s). Inhalation can also lead to a fraction being removed mechanically (by coughing, etc.) from the respiratory tract into the GI tract, where it may be treated as an ingestion and similarly absorbed into the blood for distribution to other organs before excretion. Excretion may occur through urine, feces, sputum, sweat, tears, etc.; however, the dominant modes of biological excretion are through urine or feces. Before radioisotopes are excreted, they will deposit energy in the target tissue(s). The deposition of this energy into a mass of tissue is the definition of absorbed dose.

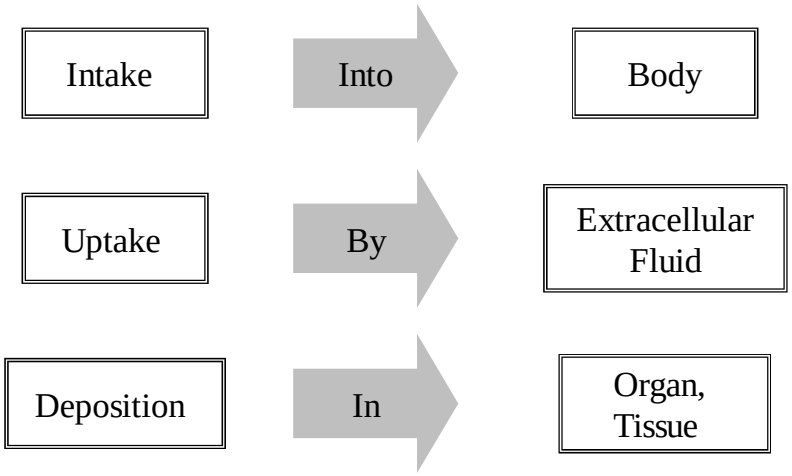

Figure 62 Basic mechanisms for internal dose

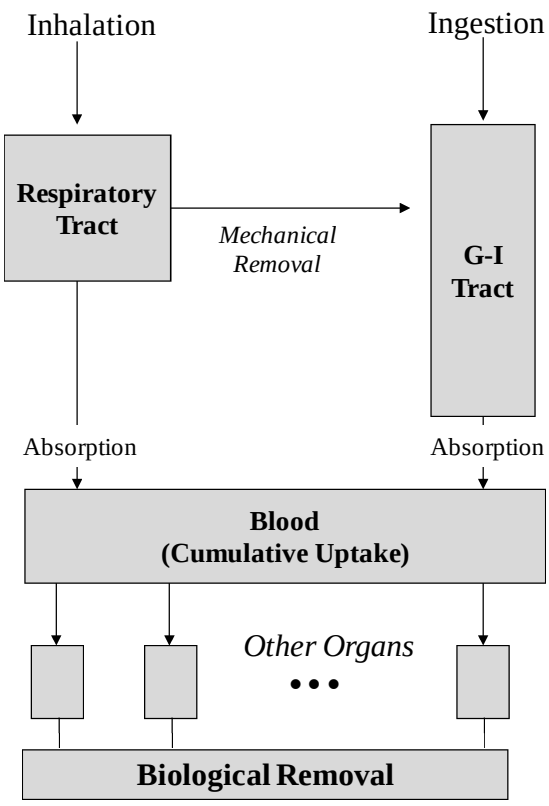

Figure 63 Intake to excretion pathways

The computation of internal dose requires three (3) critical pieces of information:

1. Rate of dose deposition (dose rate in tissue)
2. Elimination of radioactivity from tissue (decay and removal)
3. Total dose "committed" to tissue (committed dose).

In addition, simplified approximations can be made for short-range (high linear energy transfer) particles such as alpha and beta radiation, compared to most penetrating (low linear energy transfer) X- and gamma radiation. These approaches will be developed in Sections 6.1.1 and 6.1.2.

6.1.1 Alpha and beta internal emitters

The determination of absorbed dose from internal emitters follows directly from the definition of dose (J/kg, or Gray). Assumptions of an infinitely large medium and a uniform distribution of radioisotope in tissue are used. "Infinitely large" means that the target-tissue dimensions exceed the range of the radiation. For particles with short ranges (alpha and most beta radiation), the energy absorbed by the surroundings equals the energy emitted by the radioisotope. These assumptions are captured by the concept of specific effective energy (SEE) given by Eq. (73):

$$SEE\left(\alpha \text{ or } \beta\right) = \frac{\overline{E}\left(\alpha \text{ or } \beta\right)}{m} \quad \left(\frac{MeV}{transform \cdot kg}\right), \tag{73}$$

where

$\overline{E}$ is the average energy of the emitted particle per disintegration (MeV per transform)

m is the mass of the target organ or tissue (kg).

The instantaneous dose rate at time=0 from intake of a short-range (charged particle) emitter of activity C_t (Bq) can therefore be calculated from the SEE using Eq. (74):

$$\dot{D}_{\alpha/\beta} = \frac{\left(C_t\ \text{Bq}\right)\left(1\frac{\text{dps}}{\text{Bq}}\right)\text{SEE}\left(\bar{E}\frac{\text{MeV}}{\text{dis}\times\text{kg}}\right)\left(1.6\times10^{-13}\frac{\text{J}}{\text{MeV}}\right)\left(86400\frac{\text{s}}{\text{d}}\right)}{\left(1\frac{\text{J/kg}}{\text{Gy}}\right)}\ \left(\frac{\text{Gy}}{\text{d}}\right), \quad (74)$$

$$= 1.382\times10^{-8}\times C_t\times\text{SEE}\ \left(\frac{\text{Gy}}{\text{d}}\right)$$

where

C_t is the radioisotope activity located in the target tissue (Bq)
SEE is the specific effective activity of the radioisotope contained with mass m_t (MeV/dis-kg).

Radioactivity is removed by the body through two mechanisms: (i) physical decay of the radionuclide, and (ii) biological elimination of the radionuclide. To take into account both processes, the concept of effective half-life is introduced. The effective half-life describes the residence time of a radionuclide in a tissue or an organism and considers both radiological (physical) decay (T_R) and biological elimination (T_B). If biological elimination follows first-order kinetics, then it can be described by a loss-rate constant, λ_B, which is related to half-life by the relation $\lambda_B = (\ln 2/ T_B)$. The biological rate constant can be summed with the radiological rate constant, λ_R, to yield the effective elimination constant, $\lambda_E = \lambda_B + \lambda_R$, which is related to half-life by $\lambda_E = (\ln 2/ T_E)$.

Biological (T_B) and radiological (T_R) half-lives together eliminate a radionuclide from the body faster than either one alone. Combined, they become the effective half-life given by Eq. (75):

$$T_E = \frac{T_B \times T_R}{T_B + T_R}\ . \quad (75)$$

Effective half-lives are generally dependent upon the chemical form of the internal emitter. Note that, although radiological half-lives are well-known quantities, biological half-lives are specific to individuals, and therefore tabulated biological half-lives are approximations for some reference person that may or may not represent any particular individual. With that caveat, some representative examples of radiological, biological, and effective half-lives are given in Table 17.

Table 17 Effective half-life

Radioisotope	half-life		
	radiological	biological	effective
H-3 (tritium)	12 y	12 days	12 days
C-14	5560 years	10 days	10 days
P-32	14 days	257 days	14 days
S-35	87 days	90 days	44 days
Co-60	5 years	10 days	9.5 days
Sr90	28 years	50 years	18 years
I-131	8 days	138 days	7.6 days
Po-210	138 days	60 days	42 days
Ra-226	1620 years	45 years	44 years

Using Eq. (74) as a basis, the estimated dose rate at some time t after intake of a radioisotope is given by Eq. (76):

$$\dot{D}_t = \dot{D}_{\alpha/\beta} e^{-\lambda_e t} = \dot{D}_{\alpha/\beta} e^{-\frac{0.693}{T_E} \times t} . \tag{76}$$

Finally, the dose may be determined by integrating over time as in Eq. (77):

$$\begin{aligned} D &= \dot{D} \int_0^t e^{-\lambda_E t} dt \\ &= \frac{\dot{D}_{\alpha/\beta}}{\lambda_E} \left(1 - e^{-\lambda_E t}\right) , \end{aligned} \tag{77}$$

where D is the dose (Gy), $\dot{D}_{\alpha/\beta}$ is the instantaneous dose rate at time=0 (Gy/d), and λ_E is in units of d^{-1} (any time base will work as long as the dose rate and the effective elimination constant have the same base unit). For long times (on the order of seven half-lives or more), the dose approximation becomes Eq. (78):

$$D = \frac{\dot{D}_{\alpha/\beta}}{\lambda_E} \text{ (Gy)} . \tag{78}$$

For regulatory purposes, t = 50 years is normally used for a committed dose, and the absorbed dose (or dose rate) can be converted to equivalent and effective quantities using the appropriate weighting factors.

6.1.2 Gamma internal emitters

In the previous section, expressions were developed that are appropriate for short-range particles such as alpha and beta particles. Long-range neutral particles such as gamma rays require a different approach because they do not deposit all their energy locally. In other

words, the absorbed dose cannot be calculated by assuming the tissue or organ to be infinitely large because gammas are highly penetrating (unlike alphas or betas). Therefore, only a fraction of the energy carried by photons originating in the tissue containing the radioisotope will be absorbed within that tissue. Therefore, an alternative approach to that used for charged particles is required. For this scenario, the following parameters must be considered in the calculation of absorbed dose:

- Energy per decay
- Total activity
- Mass of tissue or organ (target)
- Fraction of energy emitted which is absorbed in the target
- absorbed fraction, φ
    - φ = (Energy absorbed by target)/(energy emitted by source)
    - φ = 1 for both alpha and beta particles (therefore, this approach will also work for these particles).

The concept of absorbed fraction is illustrated in Figure 64. The absorbed fraction can be calculated as $\varphi = \frac{\Delta E}{E_{in}}$.

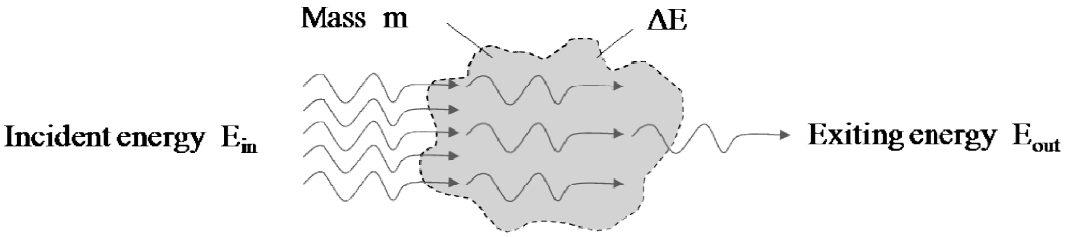

Figure 64 Absorbed fraction in mass

The specific absorbed fraction Φ is defined as the absorbed fraction φ divided by the mass of the target tissue, as given by Eq. (79):

$$\Phi = \frac{\varphi}{m} \quad \left(kg^{-1}\right). \tag{79}$$

Specific absorbed fractions are computed using mathematical phantom calculations (Monte Carlo simulations) and are tabulated as a function of target organ and photon energy for sources in various tissues [MIRD1978]. The generic equation for calculating absorbed dose rate using the absorbed fraction concept is given by Eq. (80):

$$\dot{D} = \frac{k \cdot A \cdot \sum_i n_i E_i \varphi_i}{m}, \tag{80}$$

where

D is the absorbed dose rate (Rad/s or Gy/s)
A is the activity in the source organ (Ci or Bq)
n_i is the yield of particles at energy E emitted per disintegration (also denoted as f_i or Y_i)
E is the average energy per disintegration (MeV per transform)
φ_i is the absorbed fraction

m is the mass of target (kg)

k is a proportionality constant to produce the required dose-rate units. For example, if the desired dose-rate units are Gy/s, the proportionality constant is k = (1.6E-13 J/MeV)(1 dps/Bq)/(1 J/kg/Gy) = $1.6\text{x}10^{-13}$.

The total absorbed dose can be determined using a cumulative activity $\tilde{A}$ which is the integral of the activity as a function of time. The time-dependent activity $A_s(t)$ and the integrated activity $\tilde{A}$ in the source are given, assuming first-order kinetics, by Eq. (81):

$$A_s(t) = A_s(0)e^{-\lambda_E t}$$
$$\tilde{A} = \int_0^\infty A_s(t)\,dt = A_s(0)\int_0^\infty e^{-\lambda_E t}dt = \frac{A_s(0)}{\lambda_E}, \tag{81}$$

where $A_s(0)$ is the activity in the source organ at time = 0. The units of $\tilde{A}$ are activity-time (for example, Ci-h or Bq-s, etc.). The total dose is then given by:

$$\mathrm{D} = \frac{\mathrm{k}\cdot\tilde{\mathrm{A}}\cdot\sum_{\mathrm{i}}\mathrm{n_i E_i}\varphi_{\mathrm{i}}}{\mathrm{m}}. \tag{82}$$

To calculate total dose in the body, consideration must be given to the source (S) and the target (T). The absorbed fractions are usually denoted as $\varphi(T \leftarrow S)$, and if there are multiple sources or targets, this approach can be extended to sum all contributions. For example, for multiple sources (S=1,2,…) contributing to a single target (T=1) of interest, the total-dose equation becomes:

$$D_1 = \frac{k\tilde{A}_1\sum_i n_i E_i \phi_i(1\leftarrow 1)}{m_1} + \frac{k\tilde{A}_2\sum_i n_i E_i \phi_i(1\leftarrow 2)}{m_1} + \cdots. \tag{83}$$

An alternative method of computation, given by [MIRD1978] for the calculation of internal dose, is given by the expressions in Eq. (84):

$$\dot{D}_i = \frac{A_s}{m}\phi_i\Delta_i$$
$$D = \frac{\tilde{A}}{m}\sum\phi_i\Delta_i \quad . \tag{84}$$
$$where$$
$$\Delta_i = \left(1.6\times10^{-13}\right)\cdot n_i\cdot\bar{E}_i$$

Note that consistent base units must be used in the evaluations to achieve the dose or dose-rate units required. Also, as previously discussed, for alpha or beta particles, the absorbed fractions will be equal to unity (φ=1).

6.2 Internal Hazards

A variety of internal hazards are associated with nuclear power plants and nuclear facilities in general, and the dominant pathway to committed dose is through inhalation. The primary hazards with respect to CANDU nuclear power stations under normal operating conditions are tritium, carbon-14, radio-iodines, and short- or long-lived particulates, which are discussed below.

6.2.1 Tritium

Tritium is an isotope of hydrogen with one proton and two neutrons. Tritium may be denoted as ^{3}H, H-3, or T for short. A tritium nucleus decays by emitting a single beta particle with a half-life of 12.3 years. The maximum beta energy is 18 keV (average beta energy ~ 5.6 keV). Tritium can contribute a large portion of the committed dose in a CANDU reactor and has been responsible for 30% to 40% of the radiation dose received by nuclear station staff in the past [Burnham1992]. Tritium, when taken into the body, distributes itself homogeneously throughout the entire body.

Because a beta particle requires at least 70 keV to be able to penetrate the dead surface layer of the skin, tritium is not a significant external hazard; however, it can be a significant internal hazard in large quantities. Tritium is produced through neutron absorption in deuterium ($^{1}n + {}^{2}H \rightarrow {}^{3}H + \gamma$), which is abundant in the moderator and the primary heat-transport (PHT) system of a CANDU reactor core. When neutrons irradiate heavy water (D_2O), some of the deuterium atoms (D) in the D_2O absorb neutrons to become tritium atoms (T) and generate TDO (tritiated heavy water). T_2O will also be produced, but in insignificant amounts.

In the case of heavy water that spends many years in the reactor core (for example, moderator water), after a few years, the tritium content of the D_2O can be on the order of several TBq ^{3}H per kg D_2O. For heavy water that spends most of its time outside the reactor core, for example, the primary heat-transport system water, after a few years, the tritium content of the D_2O can be on the order of a few hundred GBq ^{3}H per kg D_2O. A moderator leak can produce significant committed dose rates if unprotected. For example, for 2 TBq/kg of moderator water that leaks into the vault, an upper estimate of the committed dose rate is approximately 3 Sv/h, or 50 mSv/m [Burnham1992]. Workers around the moderator system must therefore be aware of the enormous tritium risk that can exist there if D_2O leaks are present, and therefore evaluation of the concentration of tritium in air is required before entry. People working with moderator water or performing maintenance on moderator D_2O systems must wear water-resistant (plastic) suits and breathe supplied air.

Because the PHT system operates at high temperature and pressure (300°C / 10 MPa), leaks are inevitable in a CANDU reactor. Each fuelling machine also spills about 1 L of D_2O during each channel visit, the result being that the atmosphere of the fuelling-machine vaults and the boiler room can be expected to have levels of tritiated water vapour up to 50 μSv/h under normal conditions [Burnham1992]. Design improvements to the fuelling-machine (FM) snout assembly to catch D_2O that escapes during re-fuelling operations have been made to reduce tritium-in-air levels in the FM vaults and boiler room [Aydogdu2013]. Any spill or leak of water in any of the CANDU reactor water-handling systems should be assumed to be radioactive, and workers must be aware that high localized levels of exposure may be possible.

Due to the relatively long half-life of tritium, it should be noted that the risk is present whether or not the reactor is on power and remains for a long time after shutdown.

6.2.2 Radio-iodines

Several radioactive isotopes of iodine (I-131, -132, -133, -134, -135) are produced in the fuel as fission products. These are volatile and can easily escape from defective fuel. All radioiodines decay by beta emission with associated gamma emission. Radioiodine is routinely expected to be circulating in the PHT system, and therefore any leakage from the PHT system gives rise to an airborne radioiodine hazard. Radioiodines, when taken into the body, migrate rapidly to, and are taken up by, the thyroid.

Radio-iodines can exist as elemental iodine (I_2 molecules), as organic iodine (frequently as methyl iodide (CH_3I) from ion-exchange resins in the PHT purification circuits), and as volatile hypoiodous acid (HOI). If a leak of PHT steam occurs, the radioiodines enter the air and are picked up by dust particles to exist in particulate form [Burnham1992].

Both tritium and radio-iodines are produced when the reactor operates, and production of both stops when the reactor shuts down. However the radio-iodines, with half-lives on the order of hours to days, decay away over a period of weeks, whereas the tritium does not. Therefore, the radio-iodines are a transient hazard, whereas the tritium is a persistent hazard in a CANDU reactor. There are gaseous fission-product and delayed-neutron monitoring systems in CANDU reactors to detect and locate failed fuel promptly. The FM can then remove the failed fuel from the channel to reduce radio-iodine levels in the coolant. The heavy-water purification system also removes radio-iodines from the coolant. Note that the fuel-failure rate in CANDU reactors is low (<< 0.1%), and therefore, out of approximately 5000 bundles discharged from the core annually, only a few bundles have a single fuel-element defect [Aydogdu2013].

6.2.3 Particulates

Radioactive particulates can be present in CANDU reactors as (i) fission products, (ii) activation products, or (iii) other radioactive volatiles attached to dust particles. Radiation hazard from particulates arises when airborne particulates are inhaled or when “hot” particles come into close proximity to or contact with tissue. There are two general categories of particulates: short-lived and long-lived.

Short-lived particulates, principally fission-product noble gas progeny ^{88}Rb and ^{138}Cs, are not a significant internal hazard due to their short half-lives (18 and 32 min respectively [Burnham1992]).

Long-lived particulates such as ^{141,144}Ce, ^{140}Ba, ^{140}La, ^{134,137}Cs, ^{131}I, ^{103,106}Ru, ^{95}Zr/^{95}Nb, ^{90}Sr, ^{65}Zn, ^{60}Co, ^{59}Fe, ^{54}Mn, ^{51}Cr, and ^{14}C are all beta emitters, and most also emit gamma radiation. These particulates may be found at various locations in a CANDU reactor, essentially anywhere that a leak can occur or maintenance is being done.

6.2.4 Carbon-14

Carbon-14 decays through beta emission with a maximum energy of 156 keV (average ~50 keV) and has a 5730-year half-life. Carbon-14 is generated in CANDU reactors by three processes:

$$^{1}n + {}^{17}O \rightarrow {}^{14}C + \alpha \quad \text{moderator and PHT water}$$
$$^{1}n + {}^{14}N \rightarrow {}^{14}C + p \quad \text{air}$$
$$^{1}n + {}^{13}C \rightarrow {}^{14}C + \gamma$$

About 1985, during a pressure-tube change outage at the Pickering NGS, ^{14}C was found to be widely distributed within the plant. Because of the large volume of moderator (and therefore relatively large quantity of ^{17}O), generation of ^{14}C in CANDU reactors is about an order of magnitude greater than in other pressurized-water reactors. ^{14}C was also generated in large quantities from ^{14}N in the N_2-filled annulus gas spaces of the pre-1985 Pickering A reactors and is also formed in CANDU reactors whenever there is air in-leakage into the core (for example, from the flux detectors). Carbon-14 was primarily a problem in the Pickering A Unit 1 & 2 CANDU station due to the annulus-filling gas and the lack of awareness of the extent of the condition. ^{14}C particulates were released when pressure tubes were replaced at Pickering A in the 1980s and is still present as residuals in the annulus space and in waste from the pressure-tube refurbishment. Although ^{14}C is always present in CANDU reactors, it is less of a hazard in other CANDU reactors than in Pickering A. Since the annulus gas was changed from N_2 to CO_2 in the Pickering A reactors, ^{14}C formation in the annulus gas has been reduced significantly. The production of ^{14}C in the calandria vault air applies to the Pickering A reactors because the vault atmosphere is air. The calandria is inside a water-filled tank in Bruce A, B, and Darlington reactors and inside a water-filled concrete vault in CANDU 6 and Pickering B reactors [Aydogdu2013]. Note, however, that due to its long half-life, ^{14}C can be a persistent problem for operation, shutdown, and subsequent decommissioning and disposal activities.

6.3 Internal Protection

The two primary techniques to prevent internal radiation from entering the body are (1) to block portals of entry into the body (control of the worker), and (2) to interrupt the transmission of radioactivity from the source to the worker (control of the source). Both techniques are standard industrial hygiene practice and are discussed below.

6.3.1 Control of the source

In an industrial setting, the airborne hazard is the most significant. Therefore, it is important to understand and characterize aerosols. Airborne particles are often classified by size and manner of production. Fumes are airborne solid particles formed by vapour condensation with a diameter range of 0.001–1.0 μm. Mists are suspended liquid droplets formed by condensation and can be of any diameter (generally in a range of 0.01–1.0 μm). Dusts are solid particles formed by mechanical action, with a diameter range of 0.1–30.0 μm. Smoke is a product of combustion with a diameter range from 0.1 to 1.0 μm. Inertials are large particles with diameters > 50 μm. In CANDU nuclear plants, particulates are made up of fission products and activation products. Gases are made up of noble fission gases which escape from fuel defects, such as ^{133}Xe, ^{135}Xe, and ^{85}Kr, as well as activation products such as ^{41}Ar. However, these noble gases are more of an external than an internal hazard. Vapours can be present in the form of radio-iodines and tritium and are readily absorbed by the human body.

The primary way to control radioactive emissions from the source is by ventilation. There are two ways to provide ventilation: (1) general exhaust ventilation (GEV), which is the removal of

contaminants by movement of the entire air mass into, around, and out of the workplace [ANSI2007], and (2) local exhaust ventilation (LEV) by systems that remove air at the point where the hazard is generated [ANSI2006,2003] [CSA2004]. The selection of a given ventilation solution depends upon multiple factors. General guidance principles are the following: GEV for non-toxic contaminants, multiple sources, widely distributed sources, and non-contaminated dilution air; LEV for moderately to highly toxic contaminants, one or a few sources, and when there is risk of direct worker exposure. Nuclear facilities use combinations of GEV and LEV with highly monitored and filtered air discharge systems.

6.3.2 Control of the worker

The main method for protecting the worker is the proper use of personal protective equipment (PPE), and for internal dose mitigation, the main protective equipment is respiratory protection appropriately used, although other protective clothing such as suits, gloves, and eye protection will help prevent skin absorption and contamination transfer.

In areas where a worker may be in contact with (or submerged in) radioactive material, plastic or water-resistant protective outer garments are suitable protection from beta emitters (alphas are also blocked). Gamma and neutron radiation will not be attenuated greatly by these garments, hence the need for dose control and shielding (ALARA) for these hazards. A worker performing a radiological survey around contaminated components is shown in Figure 65. The worker is shown wearing a Tyvek^{TM} polyethylene suite with hood, double latex gloves, safety glasses, and a half-face respirator (P100 toxic particulate filter).

Respirators fall into three broad categories: (i) escape, (ii) filtering, and (iii) supplied air. Escape respirators are for emergency purposes and are designed for one use or for one year from placement. Filtering and supplied-air respirators are fit-for-purpose assigned and depend on the nature of the contaminant, the nature of the work, and the level of protection required.

The expression for respirator performance is defined by the ratio of the contaminant concentration outside the mask (C_{out}) to the concentration inside the mask (C_{in}), which is called the protection factor (PF) and is given by Eq. (85):

$$\mathrm{PF} = \frac{C_{out}}{C_{in}} \,. \tag{85}$$

Protection factors are estimated by the manufacturer; however, an accurate protection factor can be determined only after performing a fit test on the respirator [ANSI2001]. Guidance for proper selection, use, and care of respirators is provided by the Canadian Standards Association [CSA2012].

Figure 65 Worker in PPE

Respirators can also be categorized as (i) air-purifying (for particulates only) and (ii) atmosphere-supplying (for particulates, gases, and vapours), which can be further subdivided into (ii-a) air-line respirators and (ii-b) self-contained breathing apparatus (SCBA). Combination-type respirators also exist which incorporate both air purification and atmosphere supply. Respirators are also classified by modes of regulator operation as follows: negative pressure (NP), positive pressure (PP), continuous flow (CF), demand (D), pressure demand (PD), and recirculating pressure demand (RP). The protection factors afforded can range from approximately 5–1000 for air-purifying respirators and 5–10,000+ for atmosphere-supplying respirators, with the largest protection factors being for self-contained breathing apparatus. Although manufacturers state nominal protection factors for respirators, the actual PF for any usage is determined through an individual fit test and check. For internal dosimetry calculations, manufacturer-listed protection factors (assuming that the respirator has been fitted and used properly by the worker) are often sufficient. Air-purifying respirator cartridges are colour-coded by contaminant type and designated by usage type and efficiency, as shown in Table 18.

Table 18 Air-purifying cartridge designations

Contaminant type	Use	Efficiency (%)
White – acid gases	N – Solid and water-based, particulates only (Not oil resistant)	99.97 (denoted as 100)
Black – organic vapours	R – Any particulate; one shift only for oily particulates (oil Resistant)	99
Green – ammonia gas	P – Any particulate (oil Proof)	95
Yellow – acid gases and organic vapours		
Purple – toxic particulates		

For example, the worker depicted in Figure 65 is wearing P100 toxic-particulate cartridges on a half-face air-purifying respirator. The P100 is the most common filter type for work in low-level-contaminated particulate environments. In many environments found in CANDU plants, the contamination is in the form of contaminated water, aerosols, or vapour, and therefore atmosphere-supplying respirators would be required. Air-line supply may be preferable when work will take longer than an SCBA tank full of air will allow, or when complete body coverage is required (such as might be the case in a tritiated water-vapour environment). SCBA may be preferable when increased mobility of the worker is required or when a higher inhalation protection factor is needed. As previously stated, the choice of respirator solution must fit the objectives of the task.

In addition to personal protective gear, another strategy for protection from radio-iodine is to use a thyroid blocker in the form of stable iodine (potassium iodide (KI)). The mechanism of KI is to saturate the thyroid with non-radioactive iodine so that when radioiodine is inhaled, it will be rejected by the thyroid and excreted, primarily through urine. The use of KI is not recommended for routine operations and is therefore only a strategy for emergency response. Charcoal-based cartridges for air-purifying respirators provide radioiodine protection in the absence of atmosphere-supplying respirators.

6.4 Summary

A variety of internal radioisotope hazards are associated with CANDU reactors. Dosimetry methods are well established, either using dose conversion factors on activity estimates (determined from bioassay measurements) or from first principles and compartmental models.

Internal hazards in CANDU reactors involve alpha, beta, and gamma emitters and include ^{3}H (the principal internal hazard), ^{14}C, radio-iodines, and particulates that can be present from leaks of fission products (defective fuel) and activation products (directly or through corrosion). Protection of the worker from internal hazards is accomplished by ventilation systems with filter trains, heavy-water vapour-recovery systems, atmospheric separation and access control features, control of sources of contamination, and judicious selection of personal protective

equipment. Respiratory protection can afford a worker a significant protection factor when used appropriately.

7 Radiation Safety Management

Management of radiation safety programs and actions is essential to the overall effectiveness of CANDU plant operations. Management includes reporting doses and keeping records of dose history for workers, generation of work plans for radiation areas, assignment of personal protective equipment, contamination control principles, waste management, and emergency preparedness. General principles of radiation-protection management can be found in [Miller1992] and details specific to CANDU operations in [Burnham1992].

7.1 Dose Records

Dose records are required by CNSC regulations [NSCA2000] and are maintained by the National Dose Registry, Radiation Protection Bureau, Health Canada. Routine dose monitoring is performed for nuclear energy workers (NEW) as defined under the CNSC Radiation Protection Regulations [NSCA2000], and the dose limits for workers are as defined in Table 12. Nuclear energy workers (NEW) are personnel who have been trained to work around radiation and radioactive materials, who have been educated about the risks (including fetal risks) involved in working around radiation and radioactive materials, who are monitored for dose if they are reasonably expected to be exposed to more than 5 mSv in a one-year dosimetry period and who have been informed in writing that they are designated as nuclear energy workers. Portability of dose records is ensured by coding the records to individual workers' social insurance numbers (SIN). Dose monitoring has a variety of objectives [Miller1992], as listed below:

- Compliance with regulatory limits
- Optimization of radiation protection program
- Assessing adequacy of protective controls
- Detecting changes in work practices
- Transparency in hazard assessment to management and workers.

Dose monitoring is required whenever radiation work is to be performed which can result in significant exposure or contamination. Different organizations can determine what exactly constitutes radiation work. The following are representative of radiation work [Burnham1992]:

- Work with radioactive sources and materials
- Work in external fields greater than 10 μSv/h
- Work in airborne concentrations greater than 10 μSv/h committed effective dose
- Entry into rubber areas (areas where loose contamination is expected and a temporary surface is used in the area with a clean-dirty boundary)
- Any activity in which one expects to receive a dose greater than 0.2 mSv.

Monitoring periods (time between reading dosimeters or bioassays) for CANDU stations tend to be much shorter than for other users (for example, university or medical). A typical monitoring period for a CANDU station may be two weeks or shorter, whereas other users typically submit dosimetry records every three months. Dosimetry estimates may be performed daily depending on the magnitude of the anticipated hazard of the radiation work being performed.

The detection of radiation fields or potential contamination is facilitated by air monitors, area monitors, portal monitors, and hand-held instrument readings. The principal personal exposures in CANDU stations being monitored for are:

- External dose – thermo-luminescent dosimetry (TLD)
    - Whole-body gamma (deep and shallow)
    - Whole-body neutron (could be from instrument reading instead)
- Extremity dose – extremity pack or finger (ring) TLD
    - typically for near-field and contact beta/gamma exposures
- Internal dose - bioassay
    - Tritium
    - Other (^{14}C).

The results of dosimetry estimates at any given time can be used to optimize worker exposure to ALARA levels, or if needed, to remove a worker from further exposure. Yearly reports are provided to NEWs which show their historical dose of record, dose received every year during employment, quarterly dose in the past year, and lifetime occupational dose. These data are maintained locally and are available through the National Dose Registry [NDR2013] upon request.

7.2 Radiation Work Planning

Germane to the effectiveness of work planning is that the persons developing and executing the plans be properly trained. Personnel working in CANDU stations require training to various levels depending on the jobs they will be required to perform. In CANDU operations, workers are categorized by colour scheme as described in the following subsection.

7.2.1 Radiation-worker colour scheme

- **Green**-qualified workers are personnel with sufficient experience and formal training to give them the qualifications to manage themselves and to supervise the radioactive protection of other workers.
- Yellow-qualified workers are trained to manage their own radiation-protection requirements, but not the protection of others.
    - **Orange**-qualified workers have minimal training and radiation work experience, but may perform radioactive work under the direct or indirect supervision of a **Green**-qualified person. They have sufficient qualifications to go into the various areas of the plant that are not posted with radiation hazard signage.
- **Red**-"qualified" persons have no formal radiation work qualifications; however, they can perform work in radiation areas only under the direct supervision of a **Green**-qualified person. The work has hazard limits that must be adhered to.

Whereas **Green-** and Yellow-qualified workers are typically designated as nuclear energy workers (NEWs), **Orange-** and **Red**-qualified workers typically are not designated as NEWs.

7.2.2 Zoning

In addition to categorization of workers, CANDU plants are also categorized by location and potential for radioactive contamination. Although any given CANDU station may have its own zone categories, a typical scheme is presented below [Burnham1992].

- **Unzoned** – areas with absolutely no contamination, generally not within the boundary of a reactor, but within the station boundary (for example, a switchyard).
- **Zone 1** – clean areas where absolutely no contamination is permitted; no radiation training is required to be in these areas (for example, administrative offices).
- **Zone 2** – areas that contain no radioactive systems and are normally free of contamination (although the potential exists for contamination due to ventilation and personnel traffic (for example, a turbine hall).
- **Zone 3** – areas that contain radioactive systems that may act as sources of contamination (for example, a reactor building).

Contamination monitoring stations must be used before crossing the boundary from Zone 3 to Zone 2 or from Zone 2 to Zone 1. A two-zone system is to be introduced in new CANDU reactors: a radiation-controlled area (RCA) and non-RCA spaces [Aydogdu2013]. Zone 3 becomes RCA, and Zones 1 and 2 become non-RCA areas. Work plans must take zoning into account because this impacts the level of qualification required for workers and the PPE or dosimetry that will be assigned.

7.2.3 Work planning

Planning for work in a radiation area goes far beyond categorization of workers. Work planning involves identifying hazards and planning work while acknowledging these hazards. Work planning specifications can be subdivided into approximately 11 steps [Burnham1992]:

1. Identify hazard(s)
2. Control hazard(s), which can be further subdivided into
    a. Elimination of hazard
    b. Minimization of hazard
    c. Install physical barriers
    d. Use warning devices
    e. Minimize human-error potential
    f. Establish procedures commensurate with the hazards
    g. Train and supervise personnel
    h. Accept the hazard and work with it
3. Simplify tasks
4. Verify instruments and assign as appropriate
5. Post signage appropriate to the hazard
6. Identify and issue dosimetry
7. Identify and issue appropriate PPE
8. Identify and assign personnel appropriate to task(s)
9. Perform pre-task briefings and clarify assignments
10. Monitor progress during work
11. Follow up after work.

A radiation-exposure permit (REP) is generated by a qualified person (a responsible health physicist, for example) consistent with the hazard and adhering to the “as low as reasonably achievable” (ALARA) tenet. The work plan takes into account all personnel qualifications and assigns responsibilities accordingly.

7.3 Personal Protective Equipment

- Personal protective equipment is needed for activities in Zones 2 and 3 both from an industrial hygiene and occupational health and safety perspective and a radiation-protection perspective. Normal industrial protective equipment may be required for work in Zone 1 and unzoned areas as well. In Section 6.3, control of the source (i.e., ventilation) and control of the worker (i.e., respirators) were discussed for airborne hazards. Additional routine personal protective equipment includes active work-zone clothing (in CANDU operations, historically called "browns" because the outer garment was a brown-coloured coverall). In fact, personnel working in active areas have a complete change of clothing consisting of coveralls, undergarments, socks, and safety shoes. The important provision is that the active-area clothing remains in the potentially contaminated areas and no personal clothing is allowed in Zones 2 or 3. Besides appropriate respiratory protection commensurate with the task (from cartridge respirator to plastic suit with air-line supply), a worker may also require a hard hat, safety glasses, hearing protection, lab coat, disposable coveralls, appropriate gloves, safety shoes, booties, or any combination of the above.

7.4 Contamination Control

The most effective way to control contamination is at the source, specifically by preventing it from occurring in the first place. However, there are inevitable instances where radioactive contamination will be generated in a CANDU reactor, for example from fuelling-machine visits, primary heat-transport (PHT) system leaks, and shutdown maintenance. Contamination can be present in solid, liquid, and aerosol forms, and may be found near the source or at some distance from the source. Controls are established in CANDU plants in the form of permanent control zones with defined access-control points (Section 7.2.2), and temporary control zones for *ad hoc* decontamination activities (sometimes called "rubber areas").

Personal contamination protection is achieved by proper identification and use of protective clothing (described in Section 7.3) and proper respiratory protection (described in Section 6.3). Spread of contamination is minimized by using proper work planning techniques (described in Section 7.2).

If personnel or equipment become contaminated (as determined by radiation-detection equipment), then decontamination must be performed. Decontamination of equipment can be performed using techniques similar to normal cleaning (washing and scrubbing), although more attention must be given to the waste stream generated (collection and disposal of cleanup waste).

Radiation-detection instrumentation is essential for identifying contamination and determining the efficacy of decontamination. Three distinct limits must be considered with respect to contamination monitoring and decontamination activities: (i) detection limit, (ii) action level, and (iii) regulatory limit. The detection limit is a function of the instrument used to detect radioactive material. The action (or reference) level is established by the licensee (station operator) and is typically some fraction of the regulatory limit. The purpose of this level is to identify potential problems through a comprehensive quality-assurance program and rectify them before contamination approaches the regulatory limit. The regulatory limit is set by a governing body (in Canada, the CNSC) and is a limit which should not be exceeded in normal

operations. The relative relationships, with four different measurement cases, can be seen in Figure 66.

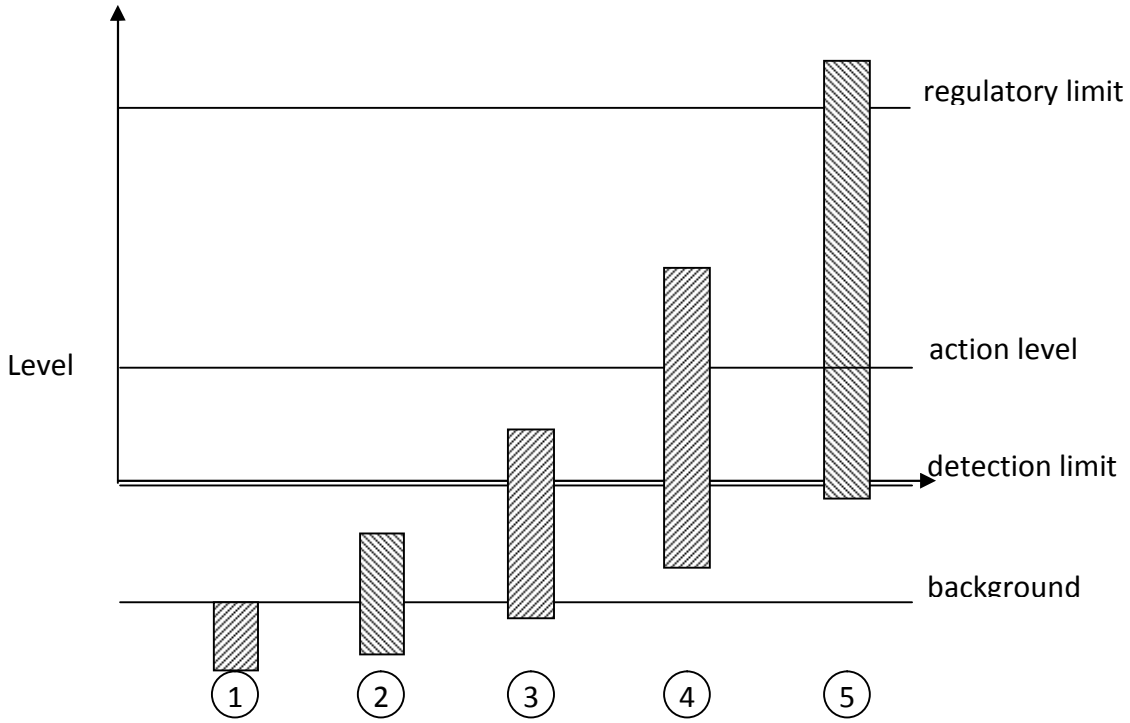

Figure 66 Relationship between background, action level, detection limit, and regulatory limit

In Case 1, the measurement lies at the background level and therefore is considered background. Note that a measurement cannot, by definition, be less than background, although the background level may vary from one place to another. In Case 2, the measurement lies between the background level and the detection limit of the instrument. In this case, with a given confidence, the measurement is below the detection limit of the contamination-survey instrument, and generally no further action is taken. In Case 3, the measurement lies above the detection limit, and radiation has been positively detected with a selected confidence level. This measurement is useful for identifying the presence of radioactive material and may assist in decontamination. In Case 4, the reading has exceeded an action level (as put in place by the station operator), and generally decontamination may be required to mitigate the hazard (although it is not strictly required by the regulations). The location of the detection limit and the action level may be exchanged. In Case 5, the measurement lies above the regulatory limit. In this case, decontamination procedures must be carried out to bring the levels of measured radioactivity to levels below the regulatory limit and as low as reasonably achievable (typically below the action level).

7.4.1.1 Waste management

Radioactive waste is generated in all CANDU plants during routine operations. Waste can originate from contamination sources (Section 7.4) and may include cleanup and laboratory wastes (paper, rags, glassware, etc.), contaminated tools or components, filters, discarded components that have been activated, and ion-exchange resins from process systems. These types of waste are typically called stored wastes. A second source often categorized as waste is

spent (or used) fuel. This material is not really waste as such because there is a strong possibility of reuse (or reprocessing) of the fuel in the future. The International Atomic Energy Agency's philosophy for long-term storage is that future generations should be afforded the same degree of protection as the current population. Spent nuclear fuel will not be considered further in this chapter.

There are two general approaches to radioactive waste management [IAEA1995]:

1. Dilute and disperse
    a. Aerosol: discharge as gases or other fine particulates
    b. Liquid: discharge into marine or fresh-water environments
2. Concentrate and contain
    a. Solid: storage (delay and decay).

Dilution and dispersion occur routinely under the CNSC licence conditions for the CANDU operator. Solid-waste management may be considered in three practical categories for CANDU operations: (i) sources (which may include activated materials or "hot" particles, (ii) loose contamination, and (iii) tritium waste, as discussed in the next subsection.

7.4.1.2 Sources

Sources, including fixed surface contamination, will normally be collected by removing the entire item to solid-waste storage. Efforts to remove sources of radioactive material from the equipment or item to which they belong (such as removing a hot particle from a section of pipe) may not be undertaken depending on the hazard analysis. Measures to ensure the integrity of the source or fixed contamination must be implemented to prevent the spread of contamination while the material is being moved.

7.4.1.3 Loose contamination

For loose contamination, it is first essential to establish contamination-control measures. An appropriate method for removing the contamination will be used. Typically this will include brushing, sweeping, wiping, cleaning, or some combination of these (as discussed in Section 7.4)

In some instances, decontamination may not be practical (e.g., in contaminated piping). Disposal of the entire item (reduced to the smallest practical volume) will then be undertaken. Decontamination efforts must continue until measurement readings are below the detection limit of the instruments, below the action level, and below the regulatory limit. Upon completion of decontamination activities, a thorough survey of the decontaminated location is performed.

7.4.1.4 Special case: tritium contamination

Tritium is a major component of the contamination associated with CANDU plants. Tritium contamination is characterized by the high mobility of tritium, resulting in ready cross-contamination, absorption, and permeation in many materials. Tritium outgassed from surfaces is primarily in the form of tritiated water. The properties of tritium make tritium decontamination more complex than decontamination of other radioisotopes. Surface tritium will generally be found as:

- Removable tritium – tritium near the surface that is easily removed by light washing.
- Fixed tritium – located deep within the surface of the material and not amenable to surface decontamination techniques; and
- Transferable tritium – tritium that is near the surface and acts as a reservoir of tritium to replenish the removable tritium if that layer is significantly diluted.

Accordingly, decontamination only of the removable layer will likely result in reappearance of the tritium after a short time (less than one month) as removable tritium. Repetitive decontamination of the surface layer will eventually reduce the inventory and hence the eventual level of removable tritium on a surface.

The most commonly used methods for tritium decontamination are washing, vacuuming, purging, thermal desorption, and isotopic exchange by adding water or hydrogen gas in the purge gas. These are generally adequate, but are time-consuming. More sophisticated techniques such as chemical or electrochemical etching and plasma can potentially provide high decontamination factors. Baking of the tritium in a contaminated surface is an alternate method for decontamination, but is not normally used.

Tritium contamination of walls and floors, particularly concrete, poses a chronic outgassing problem. Concrete decontamination is very difficult and slow. Covering the surfaces with non-porous covers may be an alternative approach to decontamination. Walls inside a CANDU reactor building are painted with reinforced epoxy-resin paint for ease of decontamination and to reduce tritium contamination.

7.5 Emergency Planning

Besides routine planning functions, health physics/radiation protection also has duties related to emergency planning. Emergencies are classified by the IAEA on the INES Nuclear and Radiological Event Scale [IAEA2009], which outlines methods for assessing releases, estimating doses, and relating these to the INES scale. Emergency planning for different categories of events is critical for protection of workers, the public, and the environment.

Nuclear emergency plans consist of on-site emergency contingency planning as well as off-site planning. In any type of emergency, the top-level management has the ultimate responsibility for emergency response. From a practical perspective, the duty shift supervisor at a CANDU reactor will be responsible for the initial response to an emergency, whether or not it involves radioactive material (for example, emergencies may involve any combination of radioactive material, fire, chemical, medical, and security issues). Emergency response involves activating an emergency response team that is specially trained for a variety of emergencies. If there is an emergency that involves, or may involve, the release of radioactive material from the confines of the station site, an off-site emergency plan will be activated which interfaces with provincial and federal assets. To ensure that emergency plans are relevant to the current plant conditions and that the various assets are prepared for an emergency, periodic training is conducted and emergency-response exercises performed.

7.6 Summary

Radiation-protection program management for CANDU operations is essential for both personnel safety and reactor safety functions. The health physics office will be involved in or responsible for various management aspects including licensing, training, personnel monitoring and

bioassay, work planning and review, surveys and equipment maintenance, inventory control, waste management, emergency preparedness, quality assurance, and audits. Well-defined and well-executed management plans at CANDU plants ensure that the stations operate in the most safe and reliable configuration possible.

8 Radiation and the Environment

CANDU plants routinely release radioactivity to the environment. This section considers releases due to routine CANDU operations and discusses the philosophy behind protection of the environment from these releases. Some historical perspective on environmental radioactivity can be found in [Moeller2005], and guidance on environmental radiological assessment can be found in [Till2008] and [Faw1999].

8.1 Radiological Environmental Monitoring Program (REMP)

There are three general reasons to sample the environment for radioactivity:

1. Establish a baseline level of radionuclides;
2. Show compliance with regulations for some activity; and
3. Track radionuclides in the event of a suspected unplanned release.

There is no essential difference in the sampling strategies for any of the above. In all cases, one is trying to determine a level of radionuclides , biological dose, or both and to define a course of action based upon measurements.

The main differences are the priorities given to various aspects of the sampling:

- For a baseline study, the priority is to determine the levels and the statistical variations to a high degree of confidence;
- For routine environmental sampling, the priority is to determine the lowest minimum detectable activity levels and compare them with what the expected releases might be and what the regulatory criteria demand; and
- For emergency response, the priority is to determine the trends and rough magnitude of the release to provide protective-action guidance to the public.

For routine and baseline sampling, a number of biota that are in the pathway between radiation source and receptor must be sampled. These biota are identified during the planning stage of the environmental monitoring program. Likewise, in a post-accident environment, a number of parameters require monitoring, but their importance has time dependencies because some pathways from radioactive source to human exposure have a longer residency time than others.

The design of an environmental monitoring program and requisite sampling strategies are individually dependent on purposes, goals, and specific locations. However, some general guiding principles for environmental monitoring exist and are presented in the following sections.

8.1.1 Design of a monitoring program

The design of an effective radiological environmental monitoring program requires a thorough understanding of the specific location and the surrounding environment, especially with regard to environmental pathways which lead to human populations.

An environmental radiation monitoring program is normally used to:

- assess independently the actual or potential dose to an average member of a Critical Group resulting from normal operation of a nuclear facility; and to
- provide an independent assessment of the effectiveness of the source and effluent control and effluent monitoring programs.

A Critical Group is made up of individuals in a population which because of habits of lifestyle and diet may be more exposed to radiation than others. Protection of members of the Critical Group ensures that the greater majority of the exposed population will be protected. For example, one such Critical Group is that of one-year-old infants around land-based nuclear facilities where dairy farming is important.

The program can also serve to:

- Validate, as far as possible, the assumptions made in any assessment of derived release (or emission) limits (DRL/DEL) for the facility; and to
- Provide assurance to the regulator and the public that human health and the environment are being monitored and protected.

Normally an operator (licensee) is regulated to develop and implement an approved radiological environmental monitoring program. Elements of an environmental monitoring program can be found in an emergency response program, although their management and deployment will be different.

The primary objective of a long-term radiological environmental monitoring program is to define a regime of both continuous and periodic sampling and analysis to assess those radionuclides which are found in the various identified and sampled pathways. The accumulation of these data over a period of years provides a baseline against which all subsequent variations can be compared and assessed.

8.1.2 CANDU facilities

CANDU facilities have conducted individual radiological environmental monitoring programs for more than 20 years. The rationale for sample collection and the selection of sampling media are discussed below.

There are three significant comparable aspects in the radiological environmental monitoring programs at Canadian utilities which have nuclear reactors. The three aspects are:

(i) source emissions monitoring and control of source emissions;
(ii) derived release (or emission) limits (DRL/DEL) specific to each facility, to define the dose impact to humans of identified radionuclides released into specific pathways; and
(iii) radiological environmental monitoring programs.

These are discussed in the following sections.

8.1.2.1 Source emissions

Source emissions occur into two major pathways from all Canadian facilities: air and water. Continuous monitoring of all airborne radioactive emissions at points of release for the gaseous effluent monitoring (GEM) program alerts station operators to radionuclide releases that may exceed release setpoints defined by derived release (or emission) limit (DRL/DEL) calculations. Radioactive liquid effluent releases from holding tanks are analyzed before pump-out to the environment and are monitored during pump-out to ensure that releases do not exceed setpoints defined (by the DEL calculations) for monthly releases in the liquid effluent monitoring (LEM) program. Such in-plant source-emissions monitoring is the first line of assessment of what is being released on a continuous or interim basis from the facility and forms the basis for control of emissions where possible, for plant shutdown, or for notification of the relevant authorities (for example, advising emergency measures organizations that the emissions exceed the DELs and could lead to exceeding the regulatory dose limits).

Source emissions are controlled at CANDU stations as follows [Aydogdu2013]:

- Airborne and waterborne releases are controlled by limiting releases to 1% of the weekly DRL (see Section 8.1.2.2) for airborne releases and 1% of the monthly DRLs for waterborne releases (these are internal targets); see Section 8.2.
- The gaseous-effluent monitoring system consists of a gaseous-effluent monitor (GEM) which continuously monitors and measures I-131, noble gases, and particulate emissions, and a tritium cartridge and a ^{14}C sampler which continuously monitor tritium and ^{14}C emissions (measurements are made in the laboratory on a daily or weekly basis).
- The reactor-building (RB) ventilation system has filter trains that contain charcoal and HEPA filters to reduce iodine and particulate releases. The off-gas management system in a CANDU reactor is used to reduce noble gas emissions.
- CANDU reactors have liquid-waste decontamination facilities (except Pt. Lepreau Generating Station) to decontaminate liquid waste in high-activity tanks (if necessary) before discharge.

8.1.2.2 Derived release (or emission) limits

Assessment of source radiation releases is gauged against derived release (sometimes called emission) limits (DRL/DEL) calculated for each radionuclide in each source pathway for each facility. The DRL for any radionuclide is derived following a process defined by the Canadian Standards Association in publication N288.1-08 [CSA2008], and guidance has also been provided by the CANDU Owners Group [COG2008]. The DRL is defined as the activity of a particular radionuclide or a group of radionuclides (i.e., noble gases, particulates) that, if released over the course of a year into defined environments, will cause the general public dose limit to be reached. DRLs are calculated in five categories (tritium, I-131, ^{14}C, noble gases, and particulates) for airborne releases and in three categories (tritium, ^{14}C, and gross β/γ) for waterborne releases. This assessment is the means by which human risk from radiation releases from any defined source can be estimated.

8.1.2.3 Radiological environmental assessment

Once releases from a facility have taken place, their impact is assessed by means of a radiological environmental monitoring program. This program is based on site-specific criteria concern-

ing release pathways leading to humans; those humans likely to be most exposed because of specific habits (one or more critical groups); sample types in these pathways; and collection frequency of these sample types. Usually, collection frequency and sample type are based on analyzing those samples that are most likely to provide evidence of specific radionuclides that would be indicative of releases from the facility into the environment. There are constraints on detection because of dispersion (dilution) from the point of release. In most airborne pathways, a dispersion factor of about one million is applied up to the first kilometre. In water effluents, the dispersion factor is a function of cooling-water flow and tidal mixing and may range from a factor of ten to thousands. In addition, radionuclides dispersed into the environment may become concentrated into various biota, making their detection relatively simple. For example, many marine biota concentrate various metals (including radioisotopes of those metals) from seawater. Much of this information is summarized in Canadian Standards Association document N288.4-10, which defines the desirable features of an environmental radiation-monitoring program, and to which Canadian nuclear utilities generally conform.

Table 19 indicates some significant sampling media and their approximate frequency of collection in the two major pathways (air and water) by the various provinces, all of which operate CANDU nuclear reactors. The most significant data outside plant boundaries are obtained from samples gathered close to the point of emission in each of the two major pathways (air and water). The air pathway leads the most directly to humans. Air is monitored by means of continuous sampling for airborne radiation particulates, radioiodines, noble gases, tritium, and carbon-14. Sampling is continuous, and measurements by the GEM of ^{131}I, noble gases, and particulate emissions are also continuous, but measurements of tritium and ^{14}C releases are not; tritium cartridges and ^{14}C samples are taken to the laboratory for tritium and ^{14}C measurements on a regular basis (daily or weekly). Samples which are not amenable to continuous collection (soils, vegetation, vegetables, fruits, milk, and potable water) are taken as grab samples on a monthly or quarterly basis or as the season permits. The effectiveness of air-pathway monitoring relies upon continuous and repetitive sampling of the given media. In the liquid effluent pathway, the primary sample is the water itself. For water which is not used for human consumption, such as seawater, grab samples may be taken quarterly from several locations. In the case of potable lake water from which communities draw their drinking water, for example, water from Lakes Ontario and Huron, daily samples (sometimes several samples per day) may be taken, primarily to monitor for tritium. Less frequently, samples of raw lake water, fish, aquatic plants and sediments may be collected, usually on a quarterly (or less frequent) basis.

Table 19 Example of samples collected by Canadian utilities [Cole1997]

Group	New Brunswick	Ontario	Quebec
Air pathway samples (continuous sampling)	Air particulates (m)	Air particulates (m)	Air particulates (m)
	Air iodine (m)	Air iodine (m)	Air iodine (6m)
(grab samples)	Air tritium (m)	Air tritium (m)	Air tritium (m)
	Air ^{14}C (m)	Air ^{14}C (m)	Air ^{14}C (m)
	Soil (q)	Forage (s)	Vegetation (y,s)
	Fruit (s)	Fruit (s)	Soil (y)
	Vegetation (s)	Vegetables (s)	Vegetables (s)
	Vegetables (s)	Drinking water (m)	Drinking water (q)
	Milk (q)	Milk (w)w	Milk (m)
	Well water (q)	Well water (m)	Farm produce (q,s)
	Surface water (q)	Greenhouse vegetables (q)	
Water pathway samples	Seawater (q)	Lake water (y)	River water (m)
	Mud (q)	Aquaculture fish (m)	Sediment (q)
	Beach sediment (q)	Water treatment plants (d)	Fish (m)
	Seafood (s)	Sediment (y)	Mollusks (m)
		Lake fish (y)	Aquatic plants (a)
Other	Rain water (m)	Rain water (m)	Rain water (m)
	Berries (s)	Honey (s)	Maple syrup (s)
	Lichen (q)	Farm samples (w,s)	TLD (c)
	TLD (c)	TLD (c)	

N.B.: collection frequency is provided in parenthesis. Key: d (daily), w (weekly), m (monthly), y (yearly), c (continuous), s (seasonal), q (quarterly).

Table 20 indicates some of the more significant radionuclides that are characteristic of potential nuclear-reactor releases into the environment because of leakage of either fission or activation

products. Selection of key indicator radionuclides (e.g., ^{131}I, ^{137}Cs, ^{95}Zr, ^{95}Nb, ^{144}Ce, ^{59}Fe, ^{54}Mn, ^{60}Co, etc.) for analysis is sufficient to define whether or not such leakage can be detected and avoids the need to address unusual and difficult-to-analyze radionuclides such as ^{90}Sr (which is a pure beta emitter and is more difficult to identify). If the indicator nuclides are not detected, then it can be assumed that an isotope such as ^{90}Sr is unlikely to be present.

Table 20 Some key fission and activation radionuclides expected from a reactor release

Argon 41	Iodine 131	Krypton 89	Thorium 228
Carbon 14	Iodine 132	Manganese 54	Thorium 234
Cerium 144	Iodine 133	Nickel 63	Tungsten 187
Cesium 134	Iodine 135	Niobium 95	Xenon 131m
Cesium 137	Iron 55	Nitrogen 13	Xenon 133m
Chromium 51	Iron 59	Ruthenium 103	Xenon 133
Cobalt 58	Krypton 83m	Ruthenium 106	Xenon 135m
Cobalt 60	Krypton 85m	Strontium 89	Xenon 135
Hafnium 181	Krypton 85	Strontium 90	Xenon 138
Helium 3	Krypton 87	Tantalum 182	Zinc 65
Hydrogen 3	Krypton 88	Thorium 227	Zirconium 95

Special Cases: ^{131}I and ^{137}Cs

Care must be taken when interpreting results for at least two of the more significant indicator radionuclides (^{131}I, ^{137}Cs) because they can enter the environment from releases other than from nuclear reactors. Iodine-131 is widely used in medical programs at larger hospitals for thyroid diagnosis and therapy. It is readily detectable from time to time in samples taken from the areas surrounding these hospitals, but its existence is not generally publicized. Routine releases of iodine-131 from such medical usage, even from one patient, is generally many thousands of times larger than typical total releases that might be associated with reactor operations. Cesium-137 and ^{90}Sr are associated with hardwood ash. Fallout from the major bomb tests conducted in the 1950s and 1960s resulted in deposition of fission radionuclides in north-eastern North American forests. These radionuclides have relatively long half-lives, are still concentrated in hardwoods in this region, and can still be detected in tree lichens. Careless or inadvertent disposal of wood ash can lead to the detection of ^{137}Cs in many sample types, including milk and soils.

8.1.3 Environmental transfer model

Routine environmental monitoring requires a comprehensive environmental-transfer model which describes the pathways from source to critical group. The principal radionuclides of investigation will be dependent on routine release criteria. For example, in CANDU reactors, ^{3}H, ^{14}C, and noble gases are important environmental radionuclides for monitoring.

By way of comparison, the principal radionuclide releases to the environment under accidental conditions would be, in order of decreasing importance in terms of dose:

- Radioactive particulates, in particular ^{137}Cs, are often released in the form of cesium iodide (CsI) following severe fuel failure and loss of containment. In very severe fuel-melt events, other radioisotopes such as actinides may also be released. However, this is unlikely, and as demonstrated following the Chernobyl accident, actinides would not be the most significant dose contributor; ^{137}Cs and ^{90}Sr would be the most significant dose contributors;
- Radioactive volatiles (mainly radio-iodines) which, along with radioactive noble gases, are the first radioisotopes released from the fuel at the onset of fuel failure; and
- Noble-gas radionuclides (mostly radio-isotopes of krypton and xenon), which may be released following failure of the reactor fuel cladding, even in the absence of reactor fuel melting.

Whether planning for routine monitoring or emergency management, the modelling analysis for pathways is similar. See Chapter 13 for a more in-depth discussion.

8.1.3.1 Modelling

A formal pathways analysis model is required to determine the significant pathways and the types of samples and measurements required for all locations around the source of release. In addition, baseline meteorological data showing long-term weather patterns, especially with respect to prevailing wind directions at different seasons, may or may not indicate that a specific geographical direction should be emphasized for sample collection at each site.

8.1.3.2 Pathways

In pathways analysis, environmental components are analyzed to determine:

- ability to accumulate environmental contaminants;
- relative residence time of contaminants in the medium;
- importance as a food source to humans; and
- suitability for inclusion in a radiation monitoring program.

A generalized environmental transfer model is depicted in Figure 67.

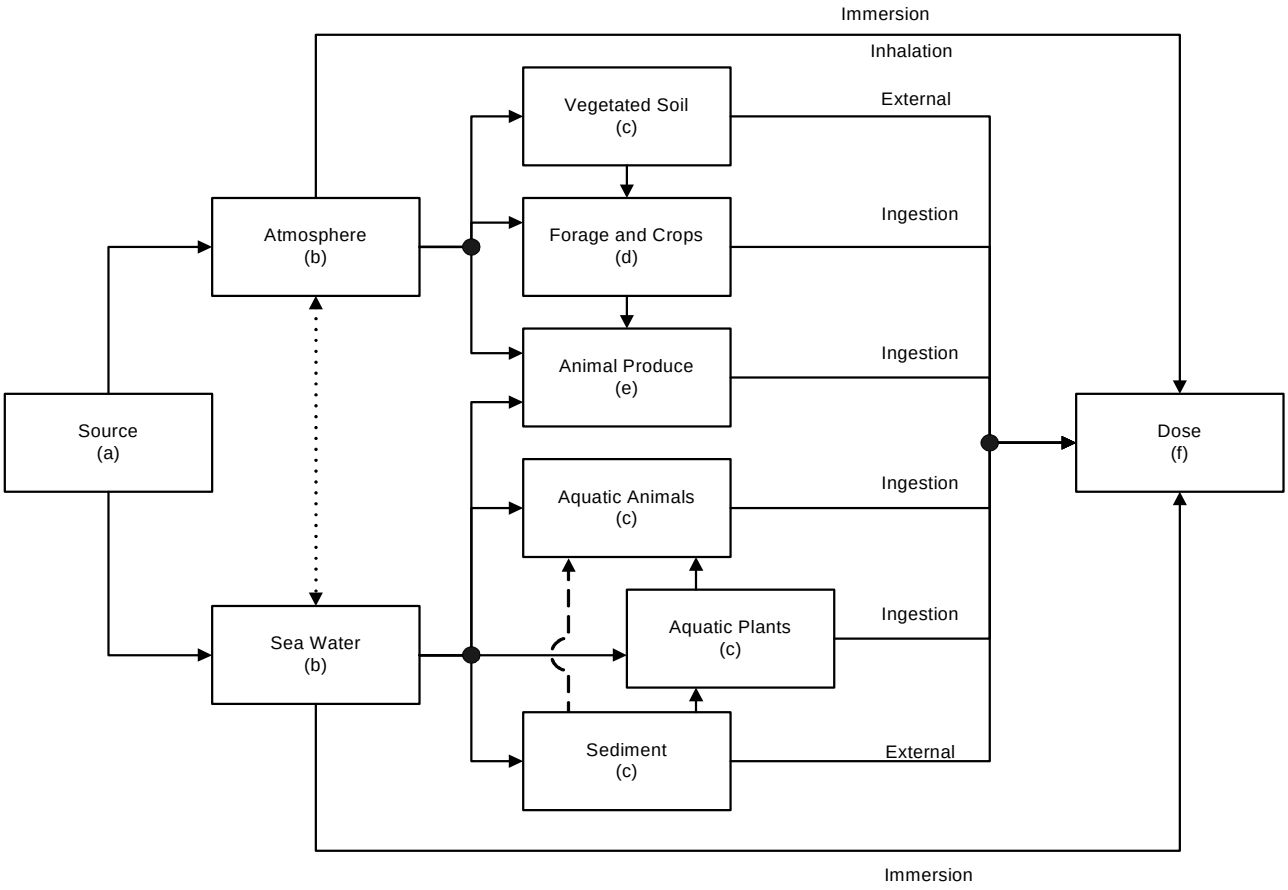

Figure 67 General environmental transfer model

The labels (a) through (f) for each component in Figure 67 may be considered as "levels of desirability" for a given sample from an environmental component. For instance, the most desirable sample for an environmental radiation-monitoring program comes from near the source, whereas dosimetry information at the end of the chain provides inconclusive information about the source of the radiation. The most useful information is, in general, obtained from components (b) through (e). Atmospheric-pathway samples are most useful if obtained from a continuous air-sampling regime because of the temporal variability of these samples. The most useful secondary indicator for the air pathway can be seen to be vegetated soil. For seawater samples, seawater, aquatic animals, plants, and sediments all provide useful data. Note that the environmental-transfer model will change depending on the location where the sampling is taking place. For example, if the sampling locations are not near sea water (as is the case in mainland Ontario), then the sea-water pathway may be replaced by a lake-water pathway. The main point is that the target group must be adequately identified and modelled in the pathways analysis.

8.1.3.3 Indicator species

It is important that food species which constitute critical pathways to humans, including terrestrial and marine organisms, are identified. The uptake through food chains is extremely complex because of the:

- Physical and chemical behaviour of radionuclides;
- Food chain being considered;
- Bio-accumulation factors in different species and foods;
- Seasonal variability; and
- Distance from the source.

The indicator species will vary depending on the individual pathways analysis performed. Some typical indicator species include:

- Cow's milk;
- Beef;
- Vegetables and fruits;
- Soil (vegetation);
- Marine plants; and
- Seafood.

The indicator species will typically be determined by close examination of the critical groups.

8.1.3.4 Seasonality

Time of year (for release and sampling) can have a significant impact on the way in which radionuclides move through the environment, particularly in their use in the various food chains. Although this feature is generally not a primary consideration when performing emergency environmental analysis, it can be extremely important for establishing baseline levels of radionuclides in the environment.

8.1.4 Practical considerations for environmental sampling

When performing sample acquisition during an emergency (such as an unplanned reactor release), care must be taken to prevent over-exposure to radiation. Dosimetry and adherence to dose restrictions will be monitored by the health physics department. A calibrated and functioning field-survey instrument must be used to monitor dose rate and total dose. There will likely be airborne hazards that are not immediately identified and that have implications for personal protective equipment. Generally, the greatest hazards will often be non-radiological hazards (as discussed below).

During routine environmental monitoring, radiation poses no threat to the person obtaining the samples because the work is being undertaken at background levels of radiation. However, there are many non-radiological threats that can pose a hazard to the sampling team. These hazards are generally of the same magnitude of hazard that a person may be exposed to daily.

The following aspects must be considered before performing any environmental survey:

- Is the area to be sampled clear of obvious threats, such as
    - Wild animals
    - Loose terrain
    - Electrical hazards
    - Slippery surfaces?
- Has the owner of the property been contacted, and has approval to sample been obtained? Hazards include:
    - *Agitated* land owners

  - Guard dogs
  - Hunters.
- Is the sampling team prepared *personally* to be out-of-doors?
  - Anti-allergens (EpiPens®)
  - Appropriate footwear
  - Appropriate clothing for time of year, terrain, and weather.

The above is not an exhaustive list, but provides examples of some of the considerations required to ensure safe environmental sampling.

8.2 CANDU Releases

CANDU reactor operators monitor both emissions of radionuclides and quantities in environmental samples. The results from these radiological environmental monitoring programs (REMPs) can be found on utility Web sites, and summaries are available for anyone to review. Detailed analyzes and reports are maintained by the health physics office and are made available to the regulator (CNSC). General emissions monitored and reported by the stations are available in these documents; a representative dataset for a CANDU is provided in Table 21 (adapted from [OPG2012]) along with the order-of-magnitude DRLs and the percentage activity of each DRL . Note that the emissions may vary from year to year, but generally are within an order of magnitude of those presented in Table 21. In addition, note that the emissions are typically much less than 1% of the derived release (or emission) limit for each radionuclide or group of radionuclides.

Environmental samples provide a basis for calculation of dose to critical-group representative persons. The doses estimated from environmental samples from CANDU plants have, up to the time of writing this document, never approached the CNSC public dose limit of 1 mSv/y and have generally been approximately three orders (0.1%) of magnitude below this limit.

Table 21 Order-of-magnitude CANDU radionuclide emissions

Emission	Magnitude of activity (Bq)	Magnitude of DRL	Activity % of DRL
Air			
HTO	10^{14}	10^{17}	0.10
Noble gas	10^{13}	10^{17}	0.01
I-131	10^{8}	10^{12}	0.01
Particulates	10^{7}	10^{11}	0.01
^{14}C	10^{12}	10^{15}	0.01
Water			
HTO	10^{14}	10^{18}	0.01
Gross β/γ	10^{10}	10^{14}	0.01
^{14}C	10^{9}	10^{15}	0.0001

It is clear from Table 21 that tritium and noble gases are the greatest contributors to the emitted activity from CANDU reactors. They are correspondingly the major contributors to

public dose as well (see, for example, [OPG2012]). However, as was previously discussed, the dose attributable to these radionuclides is approximately 1 μSv/y, which is an extremely small fraction of the average person's dose attributable to background radiation exposure.

8.3 Protection of the Environment

The radiological environmental monitoring program is designed to [OPG2012]:

i. demonstrate that radioactive materials are properly controlled at the plant, independently of effluent monitoring results;
ii. enable estimation of annual doses to the public from operation of the nuclear facility;
iii. provide data to be used for calculating derived release (or emission) limits and public doses.

There has always been an underlying assumption that if adequate protection of the public is achieved, protection of the environment and environmental-ecosystem components is *de facto* afforded. For example, in the 1990 recommendations of the ICRP [ICRP1990], it was stated that:

> "The Commission concerns itself with mankind's environment only with regard to the transfer of radionuclides through the environment, since this directly affects the radiological protection of man. The Commission believes that the standards of environmental control needed to protect man to the degree currently thought desirable will ensure that other species are not put at risk."

The underlying assumptions related to ICRP 60 are: (i) the environment is protected through the protection of humankind, (ii) reproductive capacity is the relevant endpoint, and (iii) the appropriate level of protection is to avoid endangering the existence of species or creating ecological imbalances. In the 1990 recommendations, the ICRP has not explicitly stated that the environment should be protected.

In the 2007 recommendations of the ICRP [ICRP2007], this concept is also addressed, and human protection may be considered as an indicator of environmental protection. However, the guidance suggests that it must be demonstrated directly that the environment is not affected by radiological releases. Therefore, protection of the environment shifts the focus from human to non-human biota.

Dose calculations require reference values to describe the anatomical and physiological characteristics of an exposed individual and values for tissues and organs which define a reference individual. A reference individual is not intended to describe an "average" individual, but serves to create a standard and a point of reference for dose-estimation procedures. The concept of a "reference man" is one of the cornerstones of radiological protection [ICRP2003b].

The ICRP has provided guidance on assessment of radiological impact for non-human biota [ICRP2003a]. To this end, the concept of reference animals and plants (RAPs) was introduced to provide a common reference for establishing environmental protection [ICRP2008]. ICRP initiatives include defining a reference set of dosimetric models and environmental geometries that are applied to reference animals and plants (RAP). This enables assessment of the likely consequences for individuals, the population, or the local environment. The common approach in ICRP 103 [ICRP2007] is delineated in Figure 68.

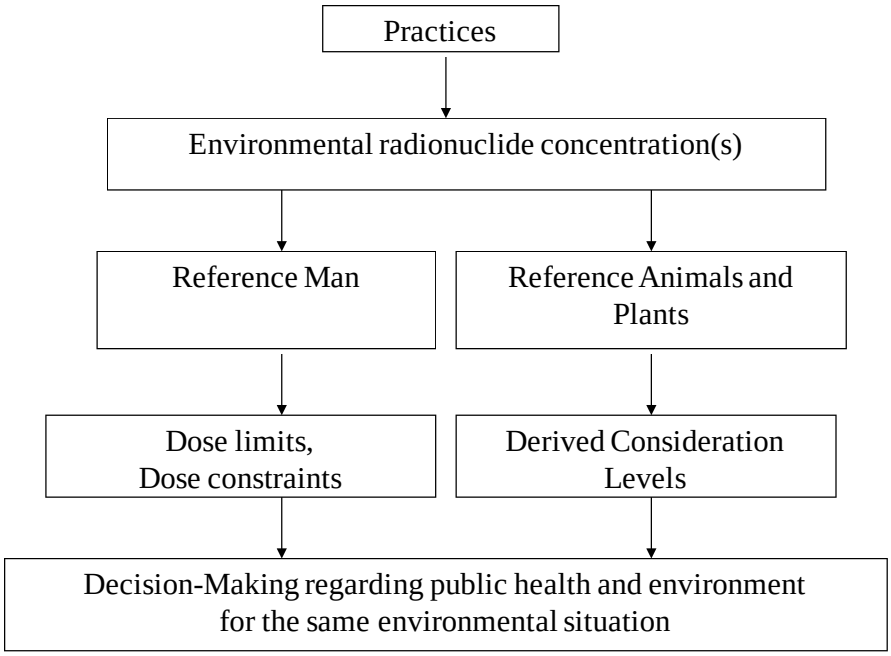

Figure 68 Common radiological assessment approach for human and non-human biota

Whereas assessment of risk for human exposure involves comparison against dose limits and constraints, non-human biota assessment involves comparison against derived consideration levels. The concept of derived consideration levels is depicted in Figure 69.

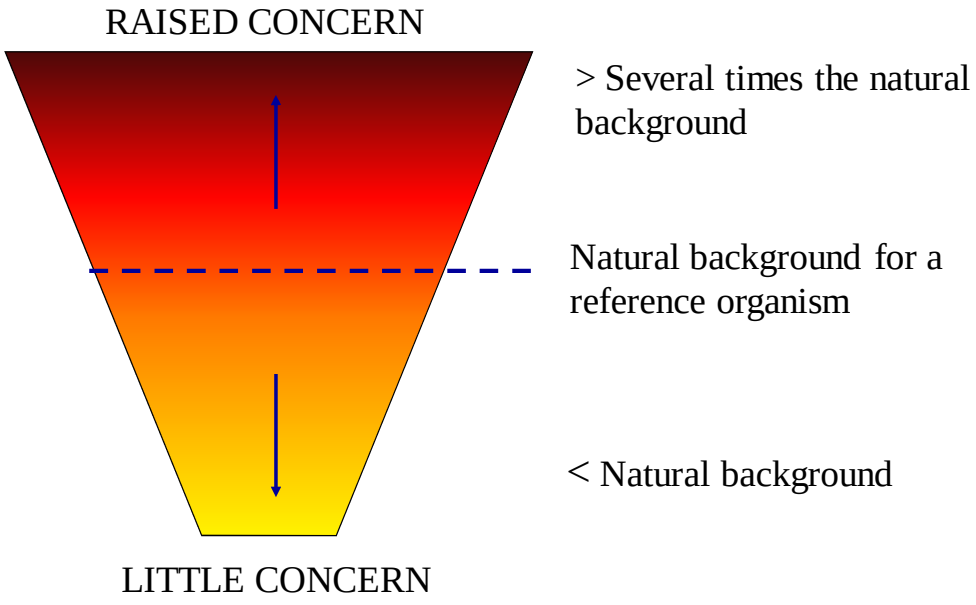

Figure 69 Derived consideration levels

In Figure 69, estimated values of dose to the reference organism that are less than the natural background are of little concern, whereas levels that are several times greater than the natural background do raise concern. The derived consideration level is a band of dose rate for a type of RAP within which there is some chance of deleterious radiation effects.

A reference animal or plant (reference organism) is a hypothetical entity with the assumed basic characteristics of a specific animal or plant, described to the taxonomic level of family,

with precisely defined anatomical, physiological, and life-history properties [ICRP2007]. RAPs are used for relating exposure to dose, and dose to effect, for that type of organism. The ICRP reference animals and plants are presented in Table 22, along with their respective wildlife groups and environments.

Table 22 Reference animals and plants (RAP)

Organism	Wildlife group	Terrestrial	Freshwater	Marine
Deer	Large terrestrial animals	X		
Rodent	Small terrestrial animals	X		
Duck	Aquatic birds	X	X	
Frog	Amphibians	X	X	
Trout	Fresh-water fish		X	X
Flatfish	Marine fish			X
Bee	Terrestrial insects	X		
Crab	Marine crustaceans		X	X
Earthworm	Terrestrial annelids	X	X	X
Pine tree	Large terrestrial plants	X		
Wild grass	Small terrestrial plants	X	X	
Brown seaweed	Seaweeds			X

It is highly likely that the future of radiological environmental monitoring programs will involve incorporating explicit consideration of RAPs to demonstrate protection of both human and non-human biota.

8.4 Summary

CANDU reactors release routine quantities of radioactive material to the environment as permitted under their licensed operating conditions. Radiological environmental monitoring programs are designed to demonstrate that there is a minimal impact of CANDU nuclear reactors as related to human exposure and that the radiological emissions are below derived

release limits established by the federal regulatory body (CNSC). Over the operating lifetime of CANDU reactors, the releases have had minimal impact on the environment, and the dose calculated for critical groups have been generally been orders of magnitude below the limits set by the Canadian Nuclear Safety Commission. The future of environmental protection around nuclear facilities in Canada may involve explicit consideration of reference animals and plants and require demonstration that a high degree of protection is afforded to non-human biota.

9 Summary of Relationship to Other Chapters

Chapter 12 is related to the following chapters in the text:

*Chapter 3 – Nuclear Processes and Neutron Physic*s

This chapter presents background data regarding particles, electromagnetic radiation, and the interactions of ionizing radiation with matter. This background information is germane to understanding the concepts developed in Sections 2 through 6.

Chapter 13 – Reactor Safety Design and Safety Analysis

This chapter discusses radiation hazards, risk, and risk models, which are related to Sections 2.3 and 2.4.

Chapter 16 – Regulatory Requirements and Licensing

This chapter is related moderately to Sections 7 and 8.

Chapter 19 – Interim Fuel Storage and Disposal

This chapter is related to Sections 7 and 8.

10 Problems

Note: Solutions to the problems in this chapter will require reference to other texts, data, materials and/or Web resources.

1. Calculate the individual electron densities and the ratio of the electron densities of a 1.5-cm-thick piece of aluminum to that of the equivalent density thickness of a piece of lead.

2. How much energy does an alpha particle require to penetrate the minimal protective epidermal layer of skin (thickness ~7 mg/cm^2)?

3. How much energy does a beta particle require to penetrate the minimal protective epidermal layer of skin (thickness ~7 mg/cm^2)?

4. Some important reactions in nuclear fuel have implications with respect to nuclear non-proliferation. Two important isotopes are Pu-239 and U-233, which are both fissionable.

a. Starting with a neutron absorption in U-238, write the decay relationship to the endpoint of Pu-239.
b. Assuming that you can have neutron absorptions in both Pu-239 and Pu-240, write down the decay relationships to the endpoint of U-233.

5. A beam of photons is incident on a slab thickness of aluminum shield on one side and exits on the other. Assume that the beam consists of photons at only two energies: 500 keV and 1000 keV, and that the incident intensities of the two energies are equal. Your goal in designing

the shield is that there be 25% intensity of the 500-keV beam component compared to the 1000-keV component on the exit side of the shield. What thickness of shield is required?

6. A primary gamma ray from the decay of K-40 is scattered twice: first, through an angle of 25 degrees, and then through an angle of 130 degrees.

a. What is the energy of the photon after the second scattering? Show intermediate energy.

b. What would the energy of the photon be if you reversed the order of scattering (i.e., first 130, then 25 degrees)? Show intermediate energy.

7. You are designing a slab shield for the outer region of a small light-water-moderated reactor. Assume that the neutron flux is 100% thermal inthe outer reactor region. What thickness of natural cadmium shield is required so that no more than 1% of the thermal flux penetrates the shield? Assume $\sigma_{capture}$ = 2450 barns.

8. Assuming that the specific heat of the body is 1 cal $g^{-1}\,{}^{o}C^{-1}$,

a. Plot the approximate temperature rise as a function of whole-body doses ranging from 100 mGy to 10 Gy;

b. What temperature rise in the body corresponds to an LD50 dose of 4 Gy? Comment on this temperature rise.

c. What whole-body absorbed radiation dose corresponds to a 3 mL sip of 60°C coffee? Show calculations for both males and females.

9. Pocket ionization chambers are built in the form of an electrical capacitor. From previous physics courses, you know that capacitance is equal to a change in charge over a change in voltage, as follows:

$$C = \frac{\Delta Q}{\Delta V},$$

where the capacitance, C, is in Farads (F), the voltage, V, is in volts (V) and the charge, Q, is in coulombs (C). You have a chamber that has a sensitive cylindrical volume with a diameter of 6.35 cm and a length of 63.5 cm. The standard density of the air in the chamber is 0.001293 g/cm^3. The chamber is calibrated so that its quartz fibre has full deflection when there is 100 µC per kg of air. The capacitance of the chamber is 1.2 nF.

a. If it takes 300 volts to charge the chamber, what is the voltage in the chamber at full-scale deflection?

b. To what exposure (in Roentgen) does full-scale deflection correspond? To what absorbed dose in air and in tissue does it correspond?

10. You have 10 GBq of each of Co-60, Cs-137, I-131, and Ir-192 (which you can assume to be point sources of radiation).

a. Compute the exposure rates, in mGy/h, at 25 cm, 50 cm, and 100 cm away from the sources (present your results in a table for full value: rows = isotope; columns = distance)

b. For each isotope at the 1-m distance, how long would it take to get to the public dose limit of 1 mSv/y (assume 1 Sv = 1 Gy)?

11. A standard-size male has an injection of 150 mCi of I-131. Assuming that 90% of this injection goes to, and is retained in, the thyroid, compute the initial dose rate (Gy/h) to the thyroid from the beta radiation.

12. You are working in a nuclear plant, and the area monitors have detected a puff release of CO_2 that has escaped from maintenance being performed on a sealed pressure tube. The only radionuclide identified in the plume is ^{14}C. You are wearing full SCBA (self-contained breathing apparatus), so that you have no possibility of getting an inhalation dose. However, it is later found that you were submerged in the plume for a total of 25 minutes. Using the assumptions listed below, determine your dose from this exposure.

Assumptions:

- ^{14}C activity detected on 1000-L air sample by area monitors = 55 kBq
- Air at STP
- Average material covering the worker has the standard thickness of a thick outer glove (*assume* that the beta attenuation coefficient for tissue will approximate this material).

13. You work in a plant that manufactures sources for radioisotope thermoelectric generators (RTGs). The source is fabricated by pressing and sintering powdered strontium titanate ($^{90}SrTiO_3$). A spill of the powdered material occurred in the plant after a shielded vessel which transports the raw material from shipping and receiving to the handling area fell over and broke open. While the person who was handling the material was trying to find a manager, one maintenance worker (Worker A), who was not wearing personal protective gear, worked near the spill (which was spread out evenly on the floor). You are the health physicist charged with determining the potential exposure to the worker. You interview the worker and co-workers and take measurements near the spill. You gather the following data to use in your analysis:

- Sr-90 contamination measured: 2 MBq cm^{-2} (assume uniform)
- Approximate distance of Worker A's hands from the spill: 1 foot
- Approximate time Worker A's hands spent in the vicinity of the spill: 12 minutes

a. Calculate the dose rate to Worker A's hands using the above data.
During your interview, you also determine that Worker A came into brief contact with the spill and contaminated her hands. She washed her hands immediately after coming in contact with the spill (two hours ago). You estimate that casual hand washing is only 65% effective in removing this type of contamination. You immediately assist her to decontaminate her hands with some strong detergent and a scrub pad.
b. Calculate the dose to Worker A's hands from this contact exposure.

14. A solution is being prepared using 0.835 GBq of Ba-133. The solution spread into a roughly circular area of diameter 50 cm. What is the maximum dose equivalent rate (SI units) 50 cm above the spill?

15. You have the following sources with associated activities:

Bq	Source

5.00E+09	Co-60
7.50E+09	Ir-192
1.00E+09	Na-22
5.00E+10	Tc-99m
7.50E+10	Au-198
1.00E+11	Ra-226

a. Compute the exposure rates, in mGy/h, at 50 cm away from these sources (present your results in a table for full value: rows = isotope; columns = distance)

b. For each isotope at the 50-cm distance, how long would it take to get to the public dose limit of 1 mSv/y (assume 1 Sv = 1 Gy)?

16. You are asked to decommission an old radioactive-waste storage room, and inside you find a large lead pig (sphere). To dispose of the source, you need to know both the radioisotope and the activity. Unfortunately, there is no documentation for this source, and there are no markings on the pig. You take a dose-rate measurement at about 4 feet away from the surface of the lead sphere and find that it is 100 μGy/h. You assume that there is a point gamma source at the centre of the sphere, and using a ruler, you determine the diameter of the sphere to be about 20 cm. Using your portable GR-135 gamma spectrometer, you determine the isotope to be Co-60 by identification of the 1.17 and 1.33 MeV peaks. What do you estimate the activity of this source to be (SI units)? (*Hint: do not neglect buildup*).

17. You are responsible for health physics at a nuclear plant. You have just been told that there are measurable levels of ^{14}C in air in the form of carbon dioxide. This has previously not been a hazard, and therefore there are no derived limits for this radioisotope. Estimate

a. the allowable intake limit (Bq), and

b. the derived air concentration (Bq/m^3) for $^{14}CO_2$ using the stochastic limit for nuclear energy workers at your plant (20 mSv/annum). *Note: Assume that after inhalation, the $^{14}CO_2$ is highly soluble and transfers directly into the blood*.

You have been told that two workers, who did not know there was an airborne $^{14}CO_2$ hazard, performed their duties in a 2-DAC environment. Worker "A" was wearing a half-face air-purifying respirator with P100 (purple) cartridges while performing his duties for three hours in the morning and four hours in the afternoon. A welder (Worker "B") was wearing an air-line, continuous-flow, half-mask respirator while performing her duties for five total hours.

c. Estimate the committed effective dose from this hazard for both Worker A and Worker B (*assume no external hazard*).

18. A standard-size male working in a nuclear plant breathes in 100 mCi of Kr-87. Assuming that 75% of this intake is retained in the lung mass, compute the initial dose rate (Gy/h) to the lungs from the beta radiation (N.B.: only use betas with a probability of emission greater than 1%).

19. Calculate the allowable limit on intake for tritium (HTO vapour) in Bq using the stochastic limit for nuclear energy workers of 20 mSv per annum. Assume that the source is whole-body and the target is whole-body.

20. The DAC value for tritiated water is typically adjusted to allow for the fact that a person working in a tritiated atmosphere will absorb half as much tritium through the skin as through inhalation (factor of 1.5). For example, if a person inhales 100 Bq of tritium, another 50 Bq will have been absorbed through the skin (i.e., 150 Bq total). Using the above, what is the DAC for tritium (Bq/m^3)?

21. A worker is performing his duties in a tritiated atmosphere of 1 DAC for eight hours wearing a positive-pressure (PP) air-purifying full-facepiece respirator. What is the worker's committed dose from his exposure to this environment?

22. You are the health physicist at a nuclear power station. The chemistry manager has asked you to review a purchase requisition that has been initiated for a nitrogen-16 calibration source. The source generates N-16 through an (α,p) reaction involving curium-244 (spontaneous fission radioisotope) and carbon-13. The source gamma-emission strength is 2.2×10^6 γ/s, and the neutron-emission strength is 2.0×10^5 n/s. Assume a gamma energy of 6.1 MeV and an average neutron energy of 2.5 MeV. Data provided are:

- Neutron flux-to-dose equivalent (at 2.5 MeV);
  20 n/cm^2-s = 25 μSv/h.

  a. Write the stoichiometric relationship for the N-16 production reaction.

  b. Calculate the total gamma dose-equivalent rate at 1 foot (μSv/h), assuming 100% emission rate from the principal gamma peak.

  c. Calculate the total neutron dose-equivalent rate at 1 foot (mRem/h).

  Both lead and polyethylene are available to shield the source.

  d. Which shielding arrangement (from the source outward) listed below would be expected to yield the lowest overall dose rate? Explain your answer.

    i. Lead only

    ii. Polyethylene followed by lead

    iii. Polyethylene only

    iv. Lead followed by polyethylene

    v. No shielding is necessary because the 12-inch air gap will sufficiently scatter or attenuate the neutrons.

  e. If the source is surrounded by 3.93 cm of lead, by what percentage will the gamma dose rate at 1 foot be reduced?

23. The radioisotope ^{140}La is a common fission product that requires shielding. For La-140, find the:

- Physical half-life (h)
- Decay scheme, and
- Average beta energy (keV).

a. Calculate the specific gamma constant for La-140 using the four (4) most dominant gamma lines.

24. List the (strongest transition) capture gamma-ray energy (MeV) and capture cross section (barns) for the following isotopes: H-1, B-10, Cd-113, Gd-157. Answer the following questions:

a. Why are cadmium and gadolinium used by control and safety systems in nuclear reactors? Where are they used?

b. With respect to B-10, discuss the principal thermal-neutron capture reactions and discuss the importance of the (n,α) reaction for shielding. What other practical use does the ^{10}B(n,α) reaction have?

25. Derive the working rule for specific gamma constant in classical units (i.e., $\Gamma = 0.5\sum_i E_i Y_i$).

Show all work and units (i.e., be explicit about where the factor of 0.5 comes from).

26. To account for the number of atoms in a material, the density of atoms in the material must be deduced. This is necessary because the interaction cross section for a material depends on the number of atoms that may potentially interact with the transiting radiation per unit path length. The terminology "mixing cross sections" refers to the proportion of the cross section assigned to each element in a material. For example, water has two atoms of hydrogen and one atom of oxygen per molecule in water, and both hydrogen and oxygen have interaction cross sections that are a function of energy and radiation type. The number density of a single-element material is typically expressed as follows:

$$N = \frac{\rho \cdot A_v}{MW},$$

where

N is the atom density (atoms/cm^3)
ρ is the mass density (g/cm^3)
A_v is Avogadro's number (6.02E23 atoms/mole)
MW is the molecular weight of the element (atoms/mole).

For compounds or mixtures, the number density of the i^{th} element in the mixture can be calculated using the weight fraction w_i of the i^{th} element in the mixture. The weight fraction can be determined as:

$$w_i = \frac{n_i A_i}{MW},$$

where

n_i is the number of atoms of element *i* in the mixture;
A_i is the molecular mass of element *i* in the mixture (g/mole); and
MW is the molecule mass of the mixture (g/mole).

The number density of the i^{th} constituent in the mixture is therefore given as:

$$N_i = w_i \frac{\rho \cdot A_v}{MW_i},$$

where N_i is the number density (atoms/cm^3) of the i^{th} constituent in the mixture (atoms/cm^3). It is common to express the number density in terms of (atoms/b-cm), and therefore:

$$N_i = w_i \frac{\rho \cdot A_v}{MW_i} \left(\frac{atom}{cm^3} \right) \cdot 10^{-24} \left(\frac{cm^2}{barn} \right) = w_i \frac{\rho \cdot A_v \cdot 10^{-24}}{MW_i} \left(\frac{atom}{b-cm} \right).$$

Note that atom density is the same thing as number density. The macroscopic cross section for the i^{th} element is:

$$\Sigma_i = N_i \cdot \sigma_i \left(\frac{1}{cm} \right).$$

This is related to material mixing in that the macroscopic cross section for the mixture is proportional to the individual number densities as:

$$\Sigma = \sum_i N_i \cdot \sigma_i \left(\frac{1}{cm} \right).$$

Note that depending on the nomenclature used, $\mu = \Sigma$.

In addition, many computer-based codes require, for material definition, the elemental compositions in terms of weight fraction or number (atomic) density, and therefore it is very useful to know how to compute these (because this is how the computer-based code will use the cross sections!).

a. Show that the weight fraction of oxygen is 0.888 and that of hydrogen is 0.112 in water.

b. Calculate the atom fractions of oxygen and hydrogen in water.

c. Calculate the number densities (atoms/b-cm) of oxygen and hydrogen in water.

27. Using the following absorption and scatter cross sections, determine the macroscopic absorption, scattering, and total cross sections for H_2O. What is the mean free path of neutrons in water based on your calculation?

28. Define and/or briefly explain the significance of the following:

a. ICRP

b. IAEA

c. NCRP

d. WHO

e. MARSSIM

f. MARLAP

g. RESRAD

h. Barriers between outer and inner body

i. Basis for different types of environmental monitoring programs and the concept of an environmental baseline study

j. Three general types of environmental samples

k. Classical method to determine whether a radioactive release has occurred from a nuclear plant accident or a weapon detonation

l. Work disciplines that make up environmental health physics.

29. It is usual to evaluate airborne derived release limits (or derived emission limits) by first evaluating the all-relevant-compartment values in units of $(Sv\ a^{-1})/(Bq\ m^{-3})$ and multiplying the sum by the airborne dispersion factor (P01, in $s\ m^{-3}$) to obtain [X9/X0] in units of $(Sv\ a^{-1})/(Bq\ s^{-1})$. The DRL is then evaluated using the annual dose limit. The applicable transfer factors are given below:

Transfer factor	Description	Value	Units
P(i)19	Dose by inhalation	1.5E-11	$Sv\ Bq^{-1}$
P(e)19	Dose by immersion	Nil	
P49, P59	Dose by ingestion	1.6E-9	$Sv\ Bq^{-1}$
P13, P34	Air to soil to forage, crops	No pathway	
P39	External dose from ground	Nil	
P14	Air to forage	2.75E+3	$m^3\ kg^{-1}$
	Air to crops	3.75E+2	$m^3\ kg^{-1}$
P45	Forage to milk	0.15	$kg\ kg^{-1}$
	Forage to meat	0.64	$kg\ kg^{-1}$
P15	Cow inhalation to milk	4.2	$m^3\ kg^{-1}$
	Cow inhalation to meat	5.1	$m^3\ kg^{-1}$
P01	Source-Atmosphere	2.0E-7	$s\ m^{-3}$

Data are provided as follows:

DRL Data

Parameter	Adult	Infant
Vegetables consumed, fraction grown locally	0.3	0.1
Meat consumed, fraction locally produced	1.0	0.1

Milk consumed, fraction locally produced	1.0	1.0
All vegetables, kg per year	200	84
All meat, kg per year	70	24
All milk, kg per year	170	220
Breathing rate, m^3 per year	8400	1400

Determine the DRL for ^{14}C in the airborne pathway, assuming an infant critical group at 1 km from the nuclear station and all produce and animals at 1 km (i.e., all data apply for 1 km).

30. A nuclear power plant located on Lake Ontario operates an environmental monitoring program which includes annual fish sampling. At the laboratory, the fish are analyzed for the following radionuclides:

- Gamma emitters
- Sr-90/Y-90
- Carbon-14
- Tritium.

One year, some fish samples (lake trout) are found to have the following radionuclide concentrations:

- Cs-137: 3.33 ± 0.19 Bq/kg (wet weight)
- ^{14}C: 250 ± 30 Bq/kgC.
- Tritium: 241 ± 6 Bq/L (free water)
- Sr-90/Y-90: Less than minimum detectable amount.

Relevant data are provided as follows:

Dose factors (Sv/Bq)

	E 10y	E 15y	E Adult
Tritium	2.4E-11	1.8E-11	1.8E-11
^{14}C	8.5E-10	5.6E-10	5.6E-10
Cs-137	1E-8	1.3E-8	1.3E-8
SR-90	5.2E-8	2.6E-8	1.6E-8
Y-90	9E-9	5.4E-9	4.2E-9

Background concentrations:
Tritium in Lake Ontario water: 1.0 Bq/L
Carbon-14 in living material: 24.0 Bq/kgC.
Cs-137 in trout from Lake Ontario: 10. Bq/kg (wet weight)
Station cooling water discharge rate: 10,000 m^3/min
Dilution factor: 30
Cs-137 bioaccumulation factor for Lake Ontario: 10,000
Assume that fish are 90% water
Assume that fish are 45% carbon

Lake Ontario fish consumption by Boy Scouts: 10 kg/y

Calculate the committed dose attributable to radioactivity from the nuclear power plant to Boy Scouts from a nearby camp eating the fish (*assume that any radionuclide concentration above background is due to releases from the nuclear power plant*).

11 Further Reading

F. H. Attix, *Introduction to Radiological Physics and Radiation Dosimetry*. Toronto, ON: Wiley-Interscience, 1986.

V. Baryakhtar, V. Kukhar, I. Los, V. Poyarkov, V. Kholosha, and V. Shestopalov, *Comprehensive Risk Assessment of the Consequences of the Chernobyl Accident. Science and Technology Centre in Ukraine – Ukrainian Radiation Training Centre*. Project No. 369, Kiev, Ukraine, 1998.

R. Bailey, H. Clark, J. Ferris, S. Krause, and R. Strong, *Chemistry of the Environment*, 2nd Edition. New York: Academic Press, 2002.

E. Baum, H. Knox, T. Miller, *Nuclides and Isotopes*, 16th ed. Schenectady, NY: Lockheed Martin, Knolls Atomic Power Laboratory, 2002.

J. J. Bevelacqua, *Health Physics in the 21st Century*. New York: Wiley-VCH, 2008.

A. Brodsky, *Review of Radiation Risks and Uranium Toxicity with Application to Decisions Associated with Decommissioning Clean-Up Criteria*. Hebron, CT: RSA Publications, 1996.

Chernobyl Forum, *Chernobyl's Legacy: Health, Environmental, and Socio-Economic Impacts and Recommendations to the Governments of Belarus, the Russian Federation, and Ukraine*. The Chernobyl Forum: 2003-2005, 2nd revised edition, 2005.

CIBA, *Health Impacts of Large Releases of Radionuclides*. Toronto: John Wiley, CIBA Foundation Symposium 203, 1997.

J. Cooper, K. Randall, and R. Sokhi, *Radioactive Releases in the Environment—Impact and Assessment*. Etobicoke, ON: John Wiley, 2003.

M. Eisenbud and T. Gesell, *Environmental Radioactivity from Natural, Industrial, and Military Sources*, 4th Edition. Toronto, ON: Academic Press, 1997.

M. Gomez, *Radiation Hazards in Mining: Control, Measurement, and Medical Aspects.* New York: Society of Mining Engineers, American Institute of Mining, Metallurgical, and Petroleum Engineers, 1981.

E. M. A. Hussein, *Radiation Mechanics—Principles and Practice*. New York: Elsevier, 2007.

IAEA. *Protection of the Environment from the Effects of Ionizing Radiation—A Report for Discussion*. Vienna, Austria: International Atomic Energy Agency, IAEA-TECDOC-1091, 1999.

IAEA, *Classification of Radioactive Waste*. Vienna, Austria: International Atomic Energy Agency, General Safety Guide GSG-1, 2009.

Journal of Environmental Radioactivity, Elsevier, ISSN: 0265-931X.

R. L. Kathren, *Radioactivity in the Environment—Sources, Distribution and Surveillance*. London, U.K.: Harwood, 1984.

J. Lehr, M. Hyman, T. Gass, and W. Seevers, *Handbook of Complex Environmental Remediation Problems*. Toronto, ON: McGraw-Hill, 2002.

K. H. Lieser, *Nuclear and Radiochemistry—Fundamentals and Applications*, 2nd ed. Toronto, ON: Wiley-VCH, 2001.

J. Louvar and B. Louvar, *Health and Environmental Risk Analysis*. Toronto, ON: Prentice-Hall, 1998.

J. Magill and J. Galy, *Radioactivity, Radionuclides, Radiation*. New York: Springer, 2005.

J. E. Martin and C. Lee, *Principles of Radiological Health and Safety*. Toronto, ON: Wiley-Interscience, 2003.

D. Moeller, *Environmental Health*, 3rd Edition. Cambridge, MA: Harvard University Press, 2005.

T. Moore and D. Dietrich, "Chernobyl and its Legacy", *EPRI Journal,* 5:21 (1987).

G. Paić, *Ionizing Radiation: Protection and Dosimetry*. Boca Raton, FL: CRC Press, 1988.

J. Turner, *Atoms, Radiation, and Radiation Protection*, 2nd Edition. Toronto, ON: Wiley Inter-science, 1995.

R. Tykva and D. Berg (eds.), *Man-Made and Natural Radioactivity in Environmental Pollution and Radiochronology*. Dordrecht, The Netherlands: Kluwer, 2004.

UNSCEAR, *Sources, Effects, and Risks of Ionizing Radiation*. New York: United Nations Scientific Committee on the Effects of Atomic Radiation (UNSCEAR), Report to the General Assembly, with scientific annexes, 1988.

UNSCEAR, *Sources and Effects of Ionizing Radiation*, Volumes I and II. New York: United Nations, 2000.

V. Valković, *Radioactivity in the Environment*. Amsterdam, The Netherlands: Elsevier Science, 2000.

X. G. Xu and F. K. Eckerman, *Handbook of Anatomical Models for Radiation Dosimetry*. Boca Raton, FL: CRC Press, 2010.

12 References

[ANS1991] ANS*, Gamma Ray Attenuation Coefficients and Buildup Factors for Engineering Materials*. La Grange IL: ANSI/ANS-6.4.3-1991.

[ANSI2001] ANSI, *American National Standard – Respirator Fit Testing Methods*. Fairfax, VA: American National Standards Institute, ANSI/AIHA Z88.10-2001.

[ANSI2003] ANSI, *American National Standard – Laboratory Ventilation*. Fairfax, VA: American National Standards Institute, ANSI/AIHA Z9.5-2003.

[ANSI2006] ANSI, *American National Standard – Fundamentals Governing the Design and Operation of Local Exhaust Ventilation Systems*. Fairfax, VA: American National Standards Institute, ANSI/AIHA Z9.2-2006.

[ANSI2007] ANSI, *American National Standard – Recirculation of Air from Industrial Process Exhaust Systems*. Fairfax, VA: American National Standards Institute, ANSI/AIHA Z9.7-2007.

[Aydogdu2013] K. Aydogdu, Personal communication via email with Kam Aydogdu, February 20, 2013.

[BEIRVII2006] BEIR VII, *Health Risks from Exposure to Low Levels of Ionizing Radiation: Phase 2*. Washington DC: National Research Council of the National Academies, National Academies Press, 2006.

[Bentur1991] Y. Bentur, N. Horlatsch, and G. Koren, "Exposure to Ionizing Radiation during Pregnancy: Perception of Teratogenic Risk and Outcome", *Teratology* 43: 109-112 (1991).

[Bergonie1906] J. Bergonie and L. Tribondeau, "De quelques resultats de la radiothérapie et essai de fixation d'une technique rationnelle", *Comptes Rendus des Séances de l'Académie des Sciences* 143: 983-985 (1906).

[Bond1996] V. P. Bond, L. Wielopolski, and G. Shani. "Current Misinterpretations of the Linear No-Threshold Hypothesis", *Health Phys.* 70: 877-882 (1996).

[Brenner2003] D. J. Brenner, R. Doll, D. T. Goodhead, E. J. Hall, C. E. Land, J. B. Little, J. H. Lubin, D. L. Preston, R. J. Preston, J. S. Puskin, E. Ron, R. K. Sachs, J. M. Samet, R. B. Setlow, and M. Zaider, "Cancer Risks Attributable to Low Doses of Ionizing Radiation: Assessing What We Really Know", *PNAS* 100: 13761-13766 (2003).

[Burnham1992] J. U. Burnham, *Radiation Protection*, Rev. 3. Point Lepreau Generating Station, NB: New Brunswick Power Corporation, 1992.

[Cember2009] H. Cember and T. Johnson, *Introduction to Health Physics*, 4th Edition. Toronto, ON: McGraw-Hill, 2009.

[Chambless1992] D. A. Chambless, S. S. Dubose, and E. L. Sensintaffar, "Detection Limit Concepts: Foundations, Myths, and Utilization", *Health Phys.* 63(3): 338-340 (1992).

[Clarke2005] R. Clarke and J. Valentine, "A History of the International Commission on Radiological Protection", *Health Phys.* 88(6): 201-216 (2005).

[Clement2009] C. Clement, *Radiological Protection Standards*. Seminar at University of Ontario Institute of Technology, March 17, 2009.

[CBSC2004] CNSC, *Keeping Radiation Exposures and Doses "As Low as Reasonably Achievable (ALARA)"*. Ottawa, ON: Canadian Nuclear Safety Commission, Regulatory Guide G-129, Revision 1, 2004.

[COG2008] COG, "Derived Release Limits Guidance". In: CANDU Owners Group Document COG-06-3090-R2-1, Hart, D. (ed.), Toronto, ON, 2008.

[Cole1997] D. Cole and E. Waller, *Environmental Radionuclide Baseline Study*. Department of National Defence, Maritime Command Headquarters, prepared by SAIC Canada, 1997.

[CSA2004] CSA, *Fume Hoods and Associated Exhaust Systems*. Mississauga, ON: Standards Council of Canada, Canadian Standards Association, CAN/CSA-Z316.5-04, 2004.

[CSA2008] CSA, *Guidelines for Calculating Derived Release Limits for Radioactive Material in Airborne and Liquid Effluents for Normal Operation of Nuclear Facilities*. Mississauga, ON: Standards Council of Canada, Canadian Standards Association, CAN/CSA-N288.1-08, 2008.

[CSA2010] CSA, *Environmental Monitoring Programs at Class I Nuclear Facilities and Uranium Mines and Mills*. Mississauga, ON: Standards Council of Canada, Canadian Standards Association, CAN/CSA-N288.4-10, 2010.

[CSA2012] CSA, *Selection, Use, and Care of Respirators*. Mississauga, ON: Standards Council of Canada, Canadian Standards Association, CAN/CSA-Z94.4-11, 2012.

[Currie1968] L. A. Currie, "Limits for Qualitative Detection and Quantitative Determination: Application to Radiochemistry". *Anal. Chem.* 40: 586-593 (1968).

[Deichmann1986] W. B. Deichmann, D. Henschler, B. Holmstedt, and G. Kell, "What Is There that is Not Poison? A Study of the Third Defense by Paracelsus". *Arch. Toxicol.* 58: 207-213 (1986).

[DoseResponse2013] Dose-Response, *Dose-Response, an International Journal – Assessing the Nature, Mechanisms, and Implications of Dose-Response Relationships*. ISSN 1559-3258, http://www.dose-response.com/, 2013 .

[Faw1999] R. E. Faw and J. K. Shultis, *Radiological Assessment: Sources and Doses*. La Grange, IL: American Nuclear Society, 1999.

[Frame2005] P. W. Frame, "A History of Radiation Detection Instrumentation", *Health Phys.* 88(6): 97-121 (2005).

[Goans1997] R. E. Goans, E. C. Holloway, M. E. Berger, and R. C. Ricks, "Early Dose Assessment Following Severe Radiation Accidents", *Health Phys.* 72: 513-518 (1997).

[Goldstein1962] H. Goldstein, "Shielding", Vol. III, Part B. In: *Reactor Handbook*, 2nd Edition, E. P. Blizzard and L. S. Abbott (eds.), New York: Interscience, 1962.

[Grasty2004] R. L. Grasty and J. R. LaMarre, "The Annual Effective Dose from Natural Sources of Ionizing Radiation in Canada", *Rad. Prot. Dos.* 108(3): 251-226 (2004).

[Gusev2001] I. A. Gusev, A. K. Guskova, and F. A. Mettler, *Medical Management of Radiation Accidents*, 2nd Edition. New York: CRC Press, 2001.

[IAEA1995] IAEA, *The Principles of Radioactive Waste Management.* Vienna, Austria: International Atomic Energy Agency, IAEA Safety Series No. 111-F, 1995.

[IAEA1996] IAEA, *International Basic Safety Standards for Protection against Ionizing Radiation and for the Safety of Radiation Sources*. Vienna, Austria: International Atomic Energy Agency, IAEA Safety Series No. 115, 1996.

[IAEA2009] IAEA, *INES – The International Nuclear and Radiological Event Scale User's Manual*, 2008 Edition. Vienna, Austria: International Atomic Energy Agency, IAEA-INES-2009.

[IAEA2011] IAEA, *Radiation Protection and Safety of Radiation Sources: International Basic Safety Standards*. Vienna, Austria: International Atomic Energy Agency, IAEA Safety Standards Series No. GSR, Part 3 (Interim), 2011.

[ICRP1977] ICRP, *Recommendations of the International Commission on Radiological Protection*. International Commission on Radiological Protection, ICRP Publication 26; *Annals of the ICRP* 1(3), 1977.

[ICRP1987] ICRP, *Lung Cancer Risk from Indoor Exposures to Radon Daughters*. International Commission on Radiological Protection, ICRP Publication 50; *Annals of the ICRP* 17(1), 1987.

[ICRP1990] ICRP, *Recommendations of the International Commission on Radiological Protection*. New York: International Commission on Radiological Protection, ICRP Publication 60, Permagon, 1990.

[ICRP1994] ICRP, "Dose Coefficients for Intakes of Radionuclides by Workers", ICRP Publication 68; *Annals of the ICRP* 24(4) (1994).

[ICRP1996a]. ICRP, "Age-Dependent Doses to Members of the Public from Intake of Radionuclides: Part 5: Compilation of Ingestion and Inhalation Dose Coefficients", ICRP Publication 72; *Annals of the ICRP* 26(1) (1996a).

[ICRP1996b] ICRP, "Conversion Coefficients for Use in Radiological Protection against External Radiation", ICRP Publication 74; *Annals of the ICRP* 26(3/4) (1996b).

[ICRP2003a] ICRP, *A Framework for Assessing the Impact of Ionizing Radiation on Non-Human Species*. Toronto, ON: International Commission on Radiological Protection, ICRP Publication 91, Elsevier, 2003a.

[ICRP2003b] ICRP, *Basic Anatomical and Physiological Data for Use in Radiological Protection*. Toronto, ON: International Commission on Radiological Protection, ICRP Publication 89, Elsevier, 2003b.

[ICRP2007] ICRP, *Recommendations of the International Commission on Radiological Protection*. Toronto, ON: International Commission on Radiological Protection, ICRP Publication 103, Elsevier, 2007.

[ICRP2008] ICRP, *Environmental Protection: Concept and Use of Reference Animals and Plants*. Toronto, ON: International Commission on Radiological Protection, ICRP Publication 108, Elsevier, 2008.

[ICRU1994] ICRU, *Particle Counting in Radioactivity Measurements*. Bethesda, MD: International Commission on Radiation Units and Measurements, ICRU Report 52, 1994.

[IMBA2010] IMBA, *IMBA Professional Plus Computer Code for Internal Dosimetry Calculations* – Version 4.1.3 HPA. Chilton, UK: http://www.imbaprofessional.com, 2010.

[Inkret1995] W. C. Inkret, C. B. Meinhold, and J. C. Tascher, "A Brief History of Radiation Protection Standards", *Los Alamos Science* 23: 116-123 (1995).

[Jones2005] C. G. Jones, "A Review of the History of U.S. Radiation Protection Regulations, Recommendations, and Standards", *Health Phys.* 88(6): 181-200 (2005).

[Knoll2010] G. F. Knoll, *Radiation Detection and Measurement*, 4th Edition. New York: Wiley, 2010.

[Lamarsh2001] J. R. Lamarsh and A. J. Baratta, *Introduction to Nuclear Engineering*, 3rd Edition. Upper Saddle River, NJ: Prentice-Hall, 2001.

[Lindell1996] B. Lindell, "The History of Radiation Protection", *Rad. Prot. Dos.* 68(1/2): 83-95 (1996).

[Mattson2008] M. P. Mattson, "Hormesis Defined", *Aging Res. Rev.* 7(1): 1-7 (2008).

[Miller1992] K. Miller (ed.), *Handbook of Management of Radiation Protection Programs*, 2nd Edition. Boca Raton, FL: CRC Press, 1992.

[MIRD1978] MIRD, "Estimates of Specific Absorbed Fractions for Photon Sources Uniformly Distributed in Various Organs of a Heterogeneous Phantom". In: Society of Nuclear Medicine, Medical Internal Radiation Dose Committee, MIRD Pamphlet No. 5, W. S. Snyder, M. R. Ford, and G. G. Warner (eds.), New York, 1978.

[Moeller2005] D. W. Moeller, "Environmental Health Physics: 50 Years of Progress", *Health Phys.* 88(6): 160-180 (2005).

[Mosby1990] C. V. Mosby, *Mosby's Medical, Nursing, and Allied Health Dictionary*, 3rd Edition. Toronto, ON: C. V. Mosby, 1990.

[NCRP1987] NCRP, *Radiation Exposure of the U.S. Population from Consumer Products and Miscellaneous Sources.* Bethesda, MD: National Council on Radiation Protection and Measurements, Report No. 95, 1987.

[NCRP2001] NCRP, *Management of Terrorist Events Involving Radioactive Material*. Bethesda, MD: National Council on Radiation Protection and Measurements, NCRP Report No. 138, 2001.

[NCRP2009] NCRP, *Ionizing Radiation Exposure of the Population of the United States.* Bethesda, MD: National Council on Radiation Protection and Measurements, Report No. 160, 2009.

[NDR2013] NDR, *National Dose Registry, Radiation Protection Bureau, Health Canada*. http://www.hc-sc.gc.ca/ewh-semt/occup-travail/radiation/regist/index-eng.php, 2013.

[NSCA1997] NSCA, *Nuclear Safety and Control Act. Government of Canada*, S.C. 1997, c.9. Available at http://laws-lois.justice.gc.ca/eng/acts/N-28.3/. 1997.

[NSCA2000] NSCA, *Radiation Protection Regulations*. Government of Canada, SOR/2000-203. Available at http://laws-lois.justice.gc.ca/eng/regulations/SOR-2000-203/index.html. 2000.

[OPG2012] OPG, *2011 Results of Radiological Environmental Monitoring Programs*. Ontario Power Generation, N-REP-03481-10010. Downloadable at: http://www.opg.com/news/reports/ index.asp. 2012.

[ORNL2013] ORNL, *RadToolbox*. Downloadable from the Centre for Biokinetic and Dosimetric Research, http://ordose.ornl.gov/downloads.html. 2013.

[Poston2005] J. W. Poston, "External Dosimetry and Personnel Monitoring", *Health Phys.* 88(6): 41-48 (2005).

[Potter2005] C. A. Potter, "Internal Dosimetry: A Review", *Health Phys*. 88(6): 49-62 (2005).

[Preston2005] R. J. Preston, "Radiation Biology: Concepts for Radiation Protection", *Health Phys.* 88(6): 29-40 (2005).

[Scott2008] B. R. Scott, "It's Time for a New Low-Dose Radiation Risk-Assessment Paradigm—One that Acknowledges Hormesis", *Dose-Response*, 6: 333-352 (2008).

[Scott2012] B. R. Scott, V. R. Bruce, K. M. Gott, J. Wilder, and T. March, "Small γ-Ray Doses Prevent Rather than Increase Lung Tumors in Mice", *Dose-Response* 10: 527-540 (2012).

[Shultis2000] J. K. Shultis and R. E. Faw, *Radiation Shielding*. La Grange Park, IL: American Nuclear Society, 2000.

[Shultis2005] J. K. Shultis and R. E. Faw, "Radiation Shielding Technology", *Health Phys.* 88(6): 71-96 (2005).

[Siegel2012] J. A. Siegel and M. G. Stabin, "RADAR Commentary: Use of Linear No-Threshold Hypothesis in Radiation Protection Regulation in the United States", *Health Phys*. 102: 90-99 (2012).

[Till2008] J. Till and H. Grogan, *Radiological Risk Assessment and Environmental Analysis*. Toronto, ON: Oxford University Press, 2008.

[Uchrin1988] G. Uchrin and M. Ranogajec-Komor, "Thermoluminescent Dosimetry". In: *Ionizing Radiation: Protection and Dosimetry*, Paić, G., (ed.), Boca Raton, FL: CRC Press, 1988.

[UNSCEAR2000] UNSCEAR, *United Nations Scientific Committee of the Effects of Atomic Radiation – Report to the General Assembly*. New York: United Nations, 2000.

[UNSCEAR2008] UNSCEAR, *Sources and Effects of Ionizing Radiation*. New York: United Nations Scientific Committee on the Effects of Atomic Radiation, Report to the General Assembly (A/63/46), 2008.

[Walker2000] J. S. Walker, *Permissible Dose – A History of Radiation Protection in the Twentieth Century*. Berkeley, CA: University of California Press, ISBN 0-520-22328-4, 2000.

[Waller2013] E. J. Waller, "Sources of Radiation in the Environment, Including Natural Radiation, Naturally Occurring Radioactive Materials (NORM), Technically Enhanced Materials, Weapons Tests, and Nuclear Accidents". In: *Encyclopedia of Sustainability Science and Technology*, ISBN 978-0-387-89469-0, New York: Springer, 2013.

13 Acknowledgements

The following reviewers are gratefully acknowledged for their hard work and excellent comments during the development of this Chapter. Their feedback has much improved it. Of course the responsibility for any errors or omissions lies entirely with the authors.

Kam Aydogdu
Esam Hussein

Thanks are also extended to Diana Bouchard for expertly editing and assembling the final copy.

CHAPTER 13

Reactor Safety Design and Safety Analysis

prepared by
Dr. Victor G. Snell

***Summary**:*

The chapter covers safety design and safety analysis of nuclear reactors. Topics include concepts of risk, probability tools and techniques, safety criteria, design basis accidents, risk assessment, safety analysis, safety-system design, general safety policy and principles, and future trends. It makes heavy use of case studies of actual accidents both in the text and in the exercises.

Table of Contents

List of Figures

List of Tables

1 Introduction

The purpose of this chapter is to describe the safety characteristics of nuclear reactors and how their safety performance is predicted and verified.

1.1 Overview

Figure 1 summarizes the chapter concepts and their logical relationship. We describe each box in turn.

Section 0 (this section) defines risk. The type of risk depends on the activity. Most people want their activities and surroundings to be "safe". However, this is a meaningless ideal, and impossible to achieve in absolute terms, because every activity imposes some risk. Fortunately, risk can be quantified. Then society can set acceptable *levels* of risk in a reasonably objective manner.

The risk from nuclear reactors comes from accidental release of radioactive material. Most of the radioactive material is in the reactor fuel. Therefore, one can postulate accidents which might allow radioactivity to escape and then design systems (called mitigating systems or safety systems) to prevent or control such accidents. These *design basis accidents*[1] (DBA) are covered in Section 2. As well, much knowledge about the risk from nuclear reactors comes from actual experience in both small research and large power reactors. Case histories of the most important events which influenced the development of nuclear power reactor safety are covered in Section 3. Lessons learned from these were extracted in the form of specific *deterministic requirements*, which described the accidents that had to be designed for and the assumptions used in showing the safety systems were effective. These accidents also became design basis accidents.

This approach limits risk, but does not lend itself to quantifying risk because the deterministic requirements and the design basis accidents were chosen "conservatively", i.e., to be worse than what would happen in reality, and with little regard to frequency. In addition, descriptions of these accidents were not complete. A parallel approach is to start off by setting numerical risk targets for the plant as a whole (safety goals). Possible accidents are identified and classified using a frequency-based approach. This probabilistic approach is covered in Section 4. It leads to another list of accidents which overlaps with, but is different from, the list of design basis accidents.

[1] We bow to common practice in using this term. The term was not used in Canada until recently, but has been used for a long time in the United States. It originally implied that as long as the plant was designed to withstand "design basis" accidents, all would be well. The accidents at Three Mile Island and Chernobyl showed the weakness of this concept. At Fukushima, the design basis was wrong (and was known to be – see [IAEA, 2011] p. 75). This means that design basis accidents do not define a strong boundary between possible and "incredible". "Beyond design basis" accidents are now of much interest—indeed, although infrequent, they are the only ones which could have significant consequences.

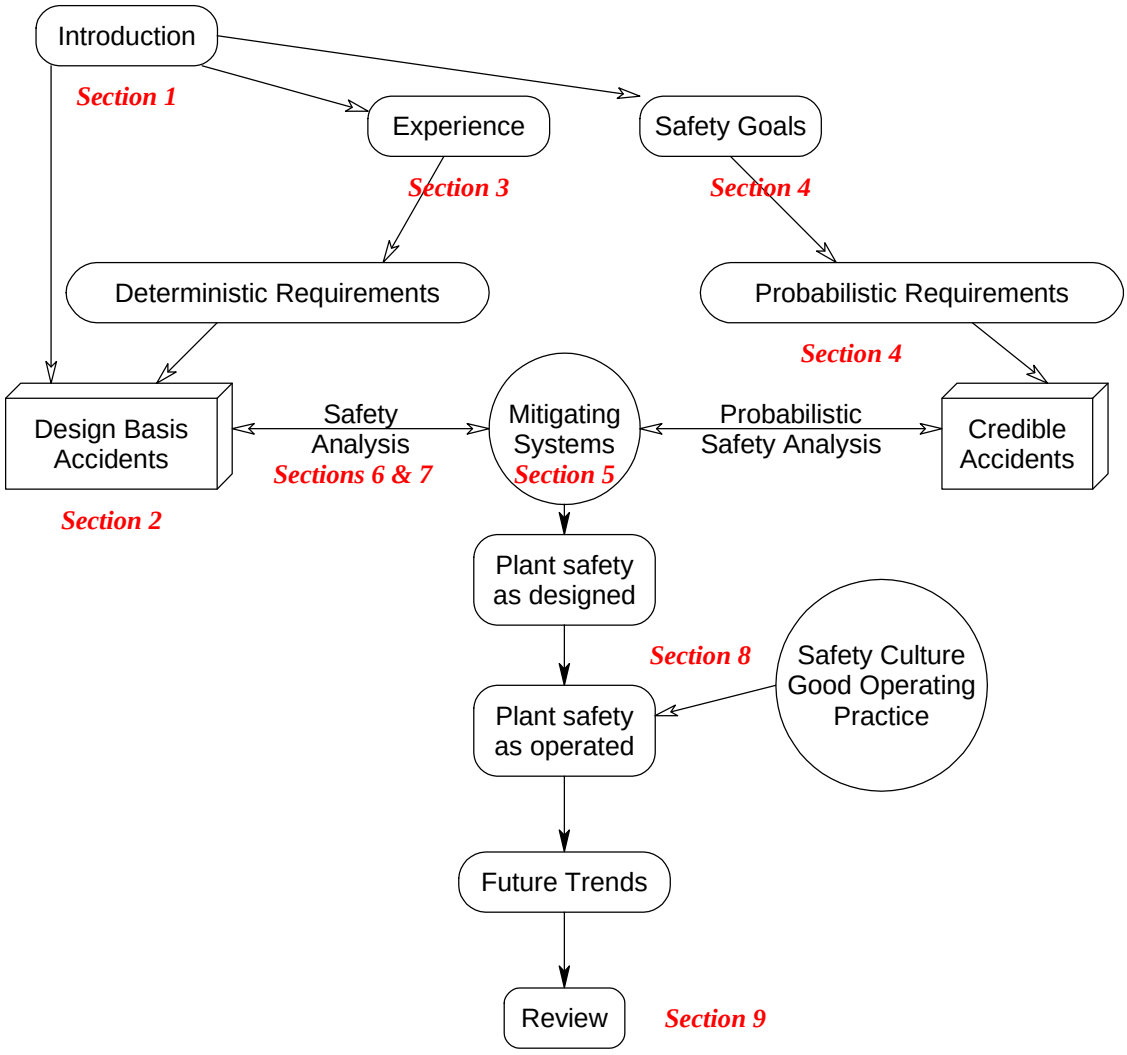

Figure 1 Chapter concept map

The mitigating systems must be able to handle both design basis accidents and accidents identified by the probabilistic approach. They are described in Section 5.

The methods to confirm that the mitigating systems are effective are:

- Probabilistic safety analysis (PSA), which drives design requirements for, and verifies the *reliability* of, normal and mitigating systems. It also ensures to the extent practical that an accident which *requires* a mitigating system does not also *impair* it (Section 4). It uses Boolean algebra to determine the frequencies of initiating events, given the frequency of component failures, and mathematically combines these with the reliability of mitigating systems to determine the frequency of severe accidents, thereby showing that the safety goals have been achieved.
- Deterministic safety analysis, or simply safety analysis, which drives design requirements for, and verifies the *performance* of, mitigating systems. It uses mathematical models of all the key systems in a plant to predict (ultimately) how much radioactive material will

escape from the fuel and where it will be transported. It shows that the deterministic requirements have been met. Section 6 describes the phenomenology of accidents, and Section 7 summarizes the mathematical tools used to predict how they evolve.

Ultimately, the safety of a plant, however well-designed, depends on the people who run it. Section 8 covers safety aspects of operation, including safety culture. A brief summary of innovative designs which promise to deliver increased safety wraps up Section 8.

Section 9 summarizes the key points of the Chapter. Section 10 gives the references used in this Chapter, and Section 11 lists other sources of information on reactor safety. A Glossary in Section 12 is a ready reference for the abbreviations used in this Chapter. Each subsection includes problems for further self-study and the occasional worked example.

1.2 Learning Outcomes

The goal of this Chapter is for the student to develop:

- An understanding of the approach to nuclear reactor safety concepts and safety design
- Familiarity with the hazards involved in nuclear power reactors
- Knowledge of the concepts of risk, risk quantification, and risk optimization
- An understanding of the root causes of key real-world accidents, leading to "respect for the reactor core"
- The ability to develop systematically a list of credible accidents for a nuclear power plant design
- The ability to understand and create simple fault trees and event sequence diagrams
- Familiarity at an overview level with the physical and mathematical models used in safety analysis.

It is assumed that the reader is generally familiar with the material in prior chapters.

1.3 Risk

Risk involves three key ideas:

- all technologies involve risk,
- every endeavour involves a risk/benefit trade-off, and
- risk can be quantified and reduced to an acceptably low level.

Nuclear reactors, hydro dams, and fossil-fuel electrical generating stations are all inherently dangerous. The nature of the hazard in each case is quite different. Hazards can be sudden (acute) or delayed. For hydro dams, an acute hazard is rupture of the dam, causing massive floods downstream. A delayed hazard is build-up of toxic mercury in the water behind the dam due to leaching from the rocks. For natural-gas plants, there is a local acute hazard due to explosion and a global delayed hazard due to climate change from the release of combustion products (greenhouse gases) to the atmosphere. Coal plants are likewise a major source of greenhouse gases and in addition can cause respiratory disease from the combustion and release of toxic chemicals in the coal; see [Inhaber, 1978] and [Rogers, 2004] for Canadian examples. Some coal plants emit more radioactive material to atmosphere in normal operation

than a nuclear power plant. For a nuclear power plant, the hazard of most interest is the release of radioactive material in accidents. Unlike a coal plant, an inadvertent rise in power in a nuclear plant (if it is not stopped) can both drive the release of radioactive material out of the fuel and rapidly cause damage to the reactor and its containment structure.

We "accept" hazards of technologies when they have a benefit which is perceived to offset the risk. Sometimes this decision is made on an individual basis: you may go sky-diving (an activity so objectively risky that you cannot get insurance coverage for it) because you believe that the unique thrill is worth the risk. You accept the hazards of electrical shock and fires for the convenience of using electric lights and appliances. Nothing that we do on a day-to-day basis is as risky as hurtling down a narrow strip of levelled ground at 100 km/h in a thin metal container containing 60 litres of explosive liquid towards someone else in a similar device, using a painted strip as a guide to avoid collision. Yet almost all people believe the benefits of driving are worth the risk.

Sometimes the decision is made on a societal basis: if you live in a city, you cannot easily choose to accept or reject risks such as being hit by a car (even if you choose not to drive one), breathing polluted air, or getting mugged. Activities which pose an involuntary risk are often regulated by law. In our three examples, the respective regulatory devices would be traffic laws, emission controls, and the criminal laws.

The benefits of nuclear power include production of clean electricity. In Ontario, over half the electricity comes from nuclear power; in countries such as France, as much as 80%. Other benefits of nuclear technology are medical and industrial applications, insect control, environmental protection, and scientific research. Canada is the source of much of the world's production of medical isotopes, largely originating from the NRU reactor at Chalk River.

This chapter is concerned with risk to humans. Many technologies also pose risk to other living organisms. For nuclear technology, in general, if radiation risk to humans is acceptable, the risk to other living things will also be acceptable because they are less susceptible to radiation (e.g., they do not live as long (and therefore do not develop cancer as easily) or are inherently more resistant to radiation damage (e.g., insects)). Radioactive elements and compounds can be concentrated as they move up the food chain, and therefore these pathways must be modelled to provide a scientific basis to show that humans are limiting this risk.

Safety can be thought of as the complement to risk; however, usually it is risk that is quantified, and we shall focus on risk in this Chapter.

Because risk cannot be eliminated, it must ideally be optimized. This means a cost/benefit analysis, although such an analysis often looks only at the risk of a technology, without factoring in benefits. At a risk optimum, the additional resources used to provide additional risk reduction would come at a disproportionate cost, and any resources removed from risk reduction would cause a disproportionate increase in risk. This situation is shown in Figure 2. This optimum is never achieved in practice. This is partly because the risk from nuclear power is *perceived* to be greater than that of other technologies, even if the numerical risk is the same, due to social factors such as unfamiliarity with the technology and its association with atomic weapons and cancer. Hence, regulation of nuclear power often includes a penalty on the

allowed risk, called *risk aversion*. Such a topic is beyond the scope of this Chapter; see [Slovic, 1987] or [Siddall, 1981] for examples. However, we still need an objective means of quantifying risk in terms of frequency and consequences. We start with the latter—what are the consequences of a nuclear accident?

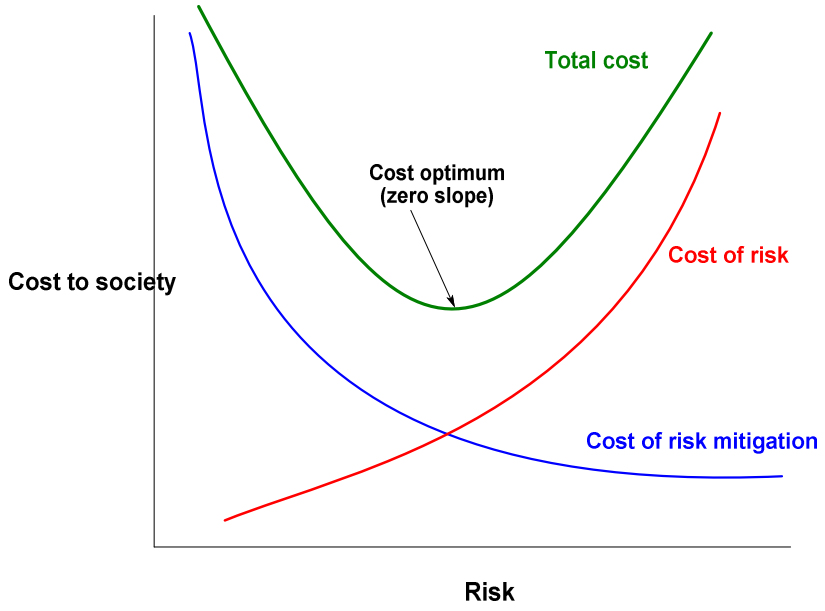

Figure 2 Risk optimization

1.4 Hazards from a Nuclear Power Plant

Most of this chapter covers radiological hazards. However, we will start by systematically listing possible hazards to make sure not to miss one. A hazard in a broad sense can be *physical*, *chemical*, *biological*, or *radiological*.

Nuclear power plants do not pose a *physical* hazard due to the nuclear process—there is no risk of off-site injury due to a *nuclear* explosion (the explosion at Chernobyl was a steam explosion and that at Fukushima a hydrogen one—both with far less energy than a nuclear explosion would have generated).

A simple explanation for this is the following: an atomic (or nuclear) bomb works by making a mass of fissile material supercritical and holding it together long enough to reach very large energies. The hard part is holding it together, which requires three things:

1. banging two sub-critical masses together very fast, so that the supercritical mass formed does not disintegrate due to heating as the pieces approach each other, and
2. ensuring that the source of neutrons that initiates the explosion is located at the centre and is triggered at the right time, and
3. using pure fissile material—U^{235} or Pu^{239}—so that the mass goes critical on fast neutrons. Fast neutrons have very short lifetimes. The basic time unit that bomb designers use is a "shake", or 10^{-8} seconds. It takes only about 50 chain-reaction generations of neutrons to produce enormous nuclear energies in the few shakes before the mass

blows apart and the chain reaction stops.

Most power reactors, however, slow down the neutrons to thermal energies, and thermal neutrons have lifetimes of milliseconds. (In fact, as covered in Chapter 4, a power plant is critical on *delayed* thermal neutrons, with lifetimes of the order of tenths of seconds to several seconds.) This means that if you somehow made a power reactor (e.g., a CANDU) supercritical, the energy doubling time would be the order of hundreds of milliseconds. This is slow enough to stop with mechanical or hydraulic devices, but if these failed, the thermal energy build-up would destroy the fuel and the reactor geometry before the power rose above perhaps ten times normal, ending the chain reaction. The result is not minor (as at Chernobyl), but is not a nuclear bomb. For further detail, assuming you have read the physics Chapter, see Appendix 3 – Why a Reactor Cannot Explode Like an Atomic Bomb.

Most people do not think of a nuclear power plant as posing a *chemical* hazard, but thermal power plants need a large supply of cooling water. Approximately one-half to two-thirds of the energy produced by any thermal power plant is wasted because of the second law of thermodynamics; the waste energy is rejected to a lake, river, sea, or the atmosphere. For many sites near large bodies of water, most of the cooling water is used in once-through mode in the main condenser, and in many plants (fossil-fuel as well as nuclear), it is chlorinated to avoid growth of biological material such as zebra mussels in the plant equipment. It follows that such plants have relatively large tanks of chlorine somewhere on-site. The consequences of rupture of these tanks can be severe off-site contamination (as in the Mississauga train derailment in 1979 [Liverman, 1979], [OMSC, 1981]).

There is no *biological* hazard associated with a nuclear plant because these plants do not contain or produce bacteria[2] or viruses.

A summary of *radiological* hazards is provided in Chapter 15. Key points will be summarized here. The effects can be s*omatic*—affecting the living individual who is exposed to radiation—or *genetic*—appearing in the yet-to-be conceived offspring of that person or in later generations.

- *Somatic* effects can occur:
  - soon after the exposure (*acute*, or *prompt*, or *early*, or *non-stochastic* effects—these terms all mean the same thing) or
  - later (*delayed* or *latent* or *stochastic* effects). The word *stochastic* means random and reflects the fact that if many individuals are exposed to a moderately "high" dose of radiation (above about 0.2 Sv each), one can predict the number of such individuals who will one day get cancer as a result of the exposure, but one cannot predict *which* individuals will be affected.
  - in the fetus of a woman who is exposed while pregnant (*teratogenic).*
- *Genetic* or hereditary effects have been observed in animals, but not in people.

[2] There could be a small biological hazard if the plant uses cooling towers and does not keep them clean, in which case they could become a source of bacterial growth.

[UNSCEAR, 2001].

1.5 Types of Radiation in a Nuclear Power Plant

The radiation in a nuclear power plant comes from fission fragments and from the activation of non-radioactive material. It therefore includes:

- alpha rays, or helium nuclei,
- beta rays, or electrons, and
- gamma rays, or photons.

Neutrons are not normally a concern to the public in reactor accidents because they slow down very rapidly in the reactor structures; however, they can be a concern to workers if local shielding is inadequate, or in non-reactor facilities in case of inadvertent criticality.

1.6 Effects of Radiation

The biological effect of radiation is measured in Sieverts (Sv), a unit which combines the energy deposited in tissue and the effectiveness of that particular form of radiation in causing damage to cells. Chapter 15 provides more detail on this topic. Figure 3 gives a perspective on the range of actual doses, from normal activities to severe accidents. Sources: [CNSC, 2011], [Talbot, 2003], [Lewis, 1999], [TEPCO, 2011], [UNSCEAR, 2000].

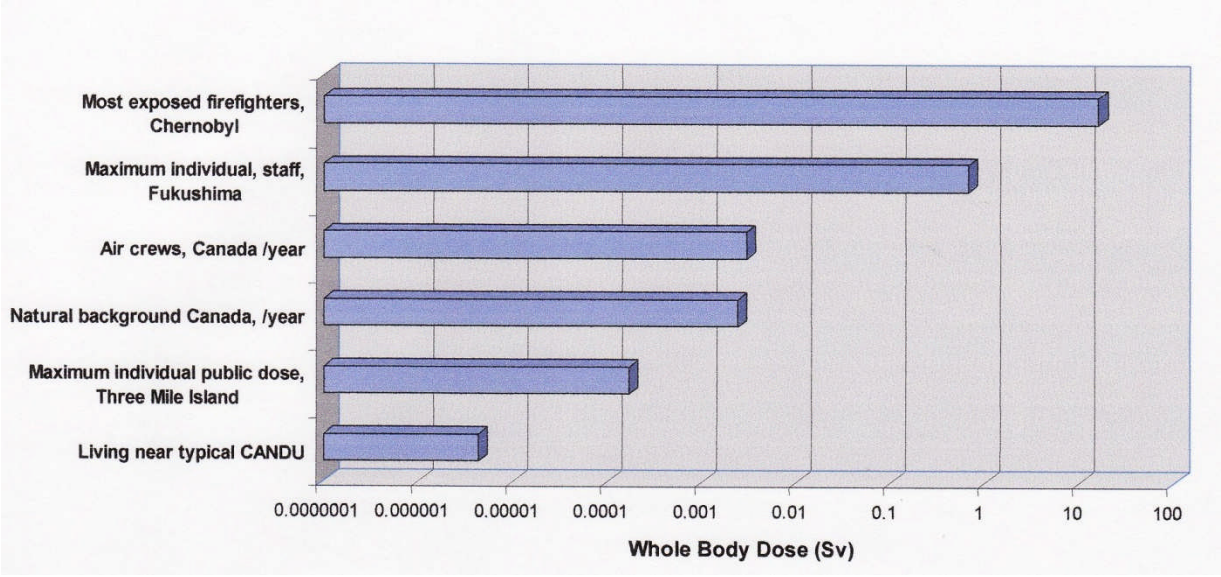

Figure 3 Examples of radiation dose

Below about 0.1 Sv per person in a large human population, there are no observable stochastic effects. Therefore, even the most exposed staff members at Fukushima during the accident are not expected to show symptoms of exposure. One Sv individual dose marks the onset of acute symptoms, and above 5 Sv, as received by the firefighters at Chernobyl, severe illness and death may ensue.

1.6.1 Linear Hypothesis

As discussed in Chapter 15, the *linear hypothesis* is used to extrapolate the observed effects on human populations exposed to high doses of radiation (as in Japanese atomic bomb survivors) to low doses. For large doses in the stochastic range, the linear hypothesis states that [ICRP, 1990]:

100 person-Sv will produce about 5 fatal cancers in the exposed (general) population.

Sample Problem

Rank the magnitude of the following risks to a group of people (express the answers numerically and explain your reasoning):

a. A collective dose of 1000 person-Sv given to 1,000,000 people

b. A collective dose of 1000 person-Sv given to 100,000 people

c. A collective dose of 1000 person-Sv given to 100 people

d. A collective dose of 1000 person-Sv given to 5000 people.

Answer:

According to the linear hypothesis, a collective dose of 1000 person-Sv should result in 50 fatal cancers. However, one must be careful of the range of applicability. For each case in turn:

a) The average dose is 0.001 Sv, which is so small that there is no evidence that the linear hypothesis applies. Incidentally, this is also less than the annual dose in North America from natural background radiation.
b) The average dose is 0.01 Sv, and therefore the linear hypothesis is likely inapplicable.
c) The average dose is 10 Sv, which would cause prompt injury or death, and therefore the linear hypothesis is inapplicable.
d) The average dose is 0.2 Sv, and therefore the linear hypothesis may be used and would predict 50 fatal cancers over time in the exposed population.

1.6.2 Hormesis

The difficulty with the linear hypothesis is that the effects of radiation on humans at low doses (below 0.1 Sv) are so small (or even beneficial—the *hormesis* hypothesis) that the models are very difficult to validate. At the moment, for better or worse, the linear hypothesis is used internationally as the basis for setting regulations for radiation protection. However, the Fukushima accident has led to a rethinking of overly conservative regulations because there is a real risk in evacuating people unnecessarily, which may be greater in some cases than the risk of radiation exposure. Moreover, ICRP has taken great pains to distinguish *a priori* theoretical risks from *a posteriori* predictions of "real" health effects resulting from low radiation doses to many people; see, e.g., [Gonzales, 2013], from which the following is quoted: "Following exposure to low radiation doses below about 100 mSv, an increase of cancer has not been convincingly or consistently observed in epidemiological or experimental studies and will probably never be observed because of overwhelming statistical and biasing factors."

For more details on hormesis, see, e.g., [Cuttler, 2009]. As an example [Chen, 2007], steel containing Co^{60} was used in the construction of 1700 apartments in Taiwan, resulting in an average dose of 0.4Sv to the 10,000 occupants. What was observed was a significant *decrease*, rather than an increase, in cancer deaths.

1.7 Sources of Radiation

Because this chapter will now focus on the radiological hazards of nuclear power plants, we need to know where the radioactive material is normally and how it can escape. There are several repositories of radioactive material (we use CANDU here as an example):

- Most of the radioactive material (fission products) is in the fuel in the core.
- Large quantities of long-lived radioactive isotopes are in the spent fuel, located either in wet pools or in dry shielded concrete containers.
- Tritium (*T*) is produced in the heavy-water moderator and coolant (about twenty times more in the former) through activation of deuterium (D) by neutrons:

$$D(n,p) + n \rightarrow T(2n,p) \xrightarrow{12\,yr} He(n,2p) + e^{-} \quad (1)$$

Figure 4 Fuel element cross section showing location of fission products

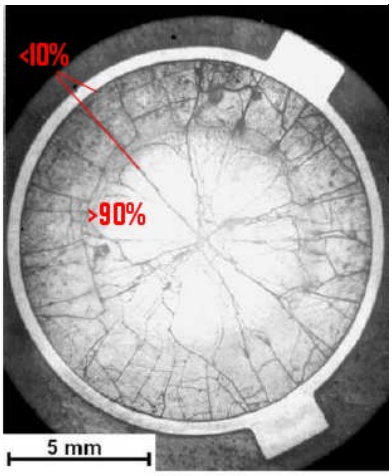

Tritium is radioactive, with a half-life of about 12 years, and decays to helium with emission of an electron. It is hazardous if inhaled or ingested or if it comes in contact with skin, but little shielding is needed to protect a person: beta particles can be stopped by a sheet of plastic.

- Carbon-14 is produced by neutron bombardment of dissolved nitrogen in the moderator.

In terms of public safety, the fission products in the fuel are by far the most significant hazard due to their quantity and their potential to be made mobile or volatile. In normal operation, the radioactive material in the fuel consists of:

- fission products trapped within the ceramic UO_2, and
- fission product gases in bubbles or interlinked spaces within the fuel ceramic, or free between the fuel and the sheath.

These exist in the ratio of about 9:1 for the highest-powered fuel element in a CANDU reactor, as shown in [Ionescu, 2009].

Therefore, accidents which cause perforation of the fuel sheath (but which do not damage the UO_2) have the potential to release only somewhat less than 10% of the gaseous fission products. Sheaths can be damaged mechanically (in fuel-handling accidents) or by overheating: if the sheath overheats from its normal temperature of 300°C to about 600°C–800°C, it will plastically deform because of the pressure of the fission product gases it contains, and eventually rupture. To drive out the remaining gaseous fission products and the solid fission products

such as cesium and strontium, the fuel temperature has to be raised to close to the melting point (2840°C) or the fuel itself must be heavily oxidized by direct exposure to air or steam.

Therefore, accidents which release significant amounts of radioactive material are initiated by:

- overheating the fuel in the core due to a mismatch between power and cooling
- leaks or pipe breaks in the coolant or moderator
- mechanical damage to the fuel
- overheating of the spent fuel in storage due to a power/cooling mismatch.

All accident analyzes reduce to these categories of failures.

It follows that the *fundamental safety functions* that must be carried out after an accident are:

- **Control** the fission reaction (and shut down the reactor)
- **Cool** the fuel (remove the decay heat)
- **Contain** any release of radioactive material
- **Monitor** the state of the plant.

In summary, *control / cool / contain / monitor* is the essence of safety design.

1.8 Risk

Safety concerns are ultimately expressed in terms of *risk*. The risk of a system, which must be specified (e.g., risk of a component failure, of an activity, of a nuclear reactor, of the nuclear fuel cycle) is customarily defined as:

$$Risk = \sum_i f_i c_i \quad , \tag{2}$$

where f_i is the expected frequency of event i and c_i is its consequence; the summation is over all events. Like the risk of betting money, this summation makes sense only for a *large number* of systems over a *long period* of time; it does not apply to a single machine (or a single bet), for which the event outcome is binary (e.g., for one bet, you either win or lose). In nuclear safety, probabilistic risk analysis can be used to quantify the risk posed by a nuclear power plant; more typically, it calculates risk indicators such as severe core-damage frequency or large off-site release frequency. Such indicators can identify potential plant improvements to reduce risk where practical.

Sample problem

The frequency of a (fully-contained) core-damage accident in a certain 1000 MWe nuclear power plant is 10^{-7} per year. If your insurance conglomerate were asked to insure the plant, what premium would you have to charge to break even over the long term?

Answer:

We need to use a common measure of comparison, in this case average cost / year. A contained core melt would require removal of the damaged core, decontamination, and replacement of the reactor. This could take ten years. In addition, the electricity formerly generated by the plant would have to be replaced. Since the accident is stated to be contained, we do not add

costs for off-site decontamination, evacuation, relocation, nor health effects – for an accident resulting in a significant release, these would have to be considered. This means that the average cost / year is (using rough ballpark values—the problem can easily be made very complex if greater sophistication and accuracy is needed):

> {[\$5 × 10^9 for decommissioning / decontamination + \$5 × 10^9 for rebuilding the plant] + [10^6 kW × \$0.06 /kW-hour × 24 hours / day × 365 days / year × 10 years]} × [10^{-7} / year] = [\$1000 + \$526] / year or ~\$1500 /year.

Note the importance of the replacement electricity cost.

Because accidents cannot be prevented in any significant human endeavour, the broad goals of reactor safety analysis are to:

- Show that the frequency and consequences of accidents are within acceptable limits

and/or

- Show that the frequency of an accident is too small to consider.

Acceptable limits are defined (broadly) with respect to the event frequency. For example, frequent occurrences (minor faults such as loss of electrical power) should not stress the system, damage fuel, or invoke protective systems. Very infrequent events, like a large loss of coolant, are permitted to push the physical systems into plastic deformation or damage fuel, but not to allow radioactive release beyond a prescribed limit. Severe accidents may damage the core, but should not fail the containment building. This approach may, but does not necessarily, address the direct economic costs of a severe accident, which can be huge, even if the public safety impact is minimal, e.g., Fukushima.

This framework implies that:

1. We have to know what the possible accidents are.
2. We have to be able to predict their frequency.
3. We have to be able to predict their consequences.

Safety analysis is carried out at several stages in the plant life cycle:

- During preliminary design (design assist), to ensure that the design concepts meet safety requirements.
- During final design, to confirm that safety requirements are met and to include the results as part of the applications for the licences required to construct and operate the plant (see Chapter 16).
- For an operating plant, to incorporate the effects of any changes in the plant, in fundamental knowledge, in operating experience, and in safety analysis methodology.

Three safety-analysis methods are used during some or all of these stages. These are complementary, not mutually exclusive, and in practice all three are used:

1. **Rule** - e.g., use the ASME code for pressure-vessel design. It is implied that following the code or the standard reduces the likelihood of failure of the material to a very low level. This is largely based on long experience, testing, and more recently, analysis.

2. **Deterministic safety analysis** - i.e., assess a prescribed list of failures which are selected based on past experience and judgement. Sometimes these are called "design basis accidents", as discussed in Section **Error! Reference source not found.**. Each accident sequence is chosen to be severe enough that the consequences of a "real" accident should be less; this means that only a subset of possible accidents is analyzed. For example, the Emergency Core Cooling (ECC) system is sized to provide enough flow to refill the core after a break in the heat-transport system that is up to twice the flow area of the largest pipe and on a time scale that prevents excessive fuel damage. The consequences of these stylized accidents are predicted and compared against analysis limits. Such analysis limits can be loosely based on frequency.
3. **Probabilistic safety analysis** - i.e., assess the frequency and consequences of failures, optimizing to deal with the high-risk contributors. PSAs therefore proceed using the following methodology:
    a. define risk-based criteria,
    b. generate a set of accidents to consider,
    c. predict the frequency and consequences of each event,
    d. show that the criteria are met.

Much of the rest of this Chapter covers these three methods.

1.9 Problems

1. International bodies set limits for the dose an individual should receive from all man-made sources. A number of issues exist behind this framework. Discuss the following four questions and draw reasoned conclusions:

    a. How should exposure from radiation used for medical purposes be controlled (i.e., what factors should determine whether or not, and how much, radiation should be used)?
    b. Should large power reactors have the same dose limits as small research reactors such as the McMaster Nuclear Reactor (which also produces medical isotopes)? Why?
    c. You are a safety expert and have been asked to approve a smoke detector. Assume that the smoke detectors give a whole-body dose [USNRC, 2001] of 10^{-5} mSv per year to each of the 35,000,000 people in Canada. What would your decision be, and why? What factors would you look at in normal operation of the detector? What is the most severe accidental exposure that can happen with a smoke detector, and how would you assess its acceptability on a risk basis?
    d. What dose would you accept for voluntary lifesaving (i.e., your colleague is trapped in a very high radiation field and you are asked to go in and save him)? Give reasons.

2. A nuclear designer is trying to optimize his design. He knows of an accident with a frequency of 10^{-7} per year which leads to a contained core melt and causes the following effects:

a. Permanent damage to the plant (i.e., cannot be recovered)
b. Evacuation of nearby people (5,000) for three days
c. No prompt fatalities
d. A collective dose to the closest population of 100 Sv.

He can reduce the frequency (but not the consequences) of this accident by a factor of ten by putting in an extra heat-removal system costing M$10 in capital costs and an extra $100,000 per year in maintenance and operating costs. How would you make this decision in a quantitative way? Hint: Consider expressing *all* accident consequences in terms of dollars. Then calculate the total average annual costs in each scenario. Some organizations assign a cost per Sv of dose—find out typical values. This problem will take you some time.

3. A massive *spontaneous* failure (i.e., due to a material flaw, not as a result of a core melt) in an LWR pressure vessel would simultaneously breach all the physical barriers which prevent radioactive material from escaping: the fuel, the primary-coolant pressure boundary, and the containment. Research and describe the approach taken by LWR designers to show that this is "incredible". Does this issue apply in any way to CANDU?

4. A nuclear regulator is considering a high-level safety goal for new nuclear power plants in Canada. He proposes two requirements:

a. The risk to an individual close to the nuclear power plant of dying immediately from an accident must be less than 10^{-6} per year.
b. The risk to an individual close to the nuclear power plant of getting cancer from an accident must be less than 10^{-5} per year.

Two nuclear power plants apply for a licence. Each has done an accident analysis, and the results are as follows:

1. For plant 1, no significant releases occur for any accident above a frequency of 10^{-7} per year. However, there is a core melt at that frequency which fails containment and gives a dose of 10 Sv to each individual in the nearby population.
2. For plant 2, two accidents are the major contributors to risk. One causes severe fuel damage, but prevents core melt. It occurs at a frequency of 10^{-4} per year and gives a dose of 0.25 Sv to a number of individuals in the nearby population. The other is a core melt, but it is contained—it occurs at a frequency of 10^{-6} per year and gives a dose of 1 Sv to a number of individuals in the nearby population.

Determine numerically whether these plants meet either or both safety goals or neither one. Hint: consider converting average dose to risk.

2 Design Basis Accidents

In Section 1.8, the concept of stylized accidents (design basis accidents) that could be used in designing parts of the plant was introduced. This section shows how to go about defining these.

More specifically, design basis accidents are the set of accidents for which the designer makes explicit provision (defence), while remembering that more severe or peculiar accidents can occur and ensuring that his/her design has some capability to deal with them.

Unfortunately, there is no way of identifying possible accidents beforehand (in any large-scale engineering field) that is guaranteed to be complete. The history of any technology is replete with unpleasant surprises, especially at the beginning—just think of the *Hindenburg* disaster, the Flixborough cyclohexane explosion [Venart, 2004], and of course the *Titanic*. Technologies—if we are fortunate—have their accidents early on, when the scale is small and the lessons learned can be applied to commercial applications.

The best way to obtain a "nearly complete" list of accidents, apart from experience, is to use more than one technique. In the next few subsections, we describe several such techniques.

2.1 Top-Down Approach

One technique is called the "top-down" approach, which starts by specifying an undesired outcome and then asks what the direct and immediate causes of that outcome could be. Then one looks at each cause in turn and asks what are *its* direct and immediate causes, and so on. After a few such cycles, one has generated a list of accidents, from which design basis accidents can be selected.

For a power reactor, the top event could be taken as "unwanted movement of radioactive materials". Because most radioactive materials are in the fuel, the coolant, the moderator, or the spent-fuel bay, we then ask how in each of these cases they could become mobile, i.e., airborne or waterborne. Radioactive material could be released from the fuel by overheating or mechanical damage; from the coolant and moderator, by pipe breaks or overheating (which later then releases the liquid or steam through relief valves); and from the spent-fuel bay, also by overheating. Fuel overheating in the core (power-cooling mismatch) can be caused by loss of heat removal from the coolant (loss of heat sink), loss of the coolant itself, coolant flow impairment, or a loss of reactor reactivity control which causes the power to rise.

Figure 5 illustrates the event-generation sequence graphically. Events in ovals represent possible end-points of the chain, where further detailed decomposition would not add much more information, i.e., the ovals are potential design basis accidents. Once we have reached this reasonable level of resolution, we can sort the events into design basis accidents and *beyond design basis accidents* (BDBAs), using expected likelihood, and possibly consequences, as criteria. Note that the figure is both highly simplified and incomplete, with a number of undeveloped branches.

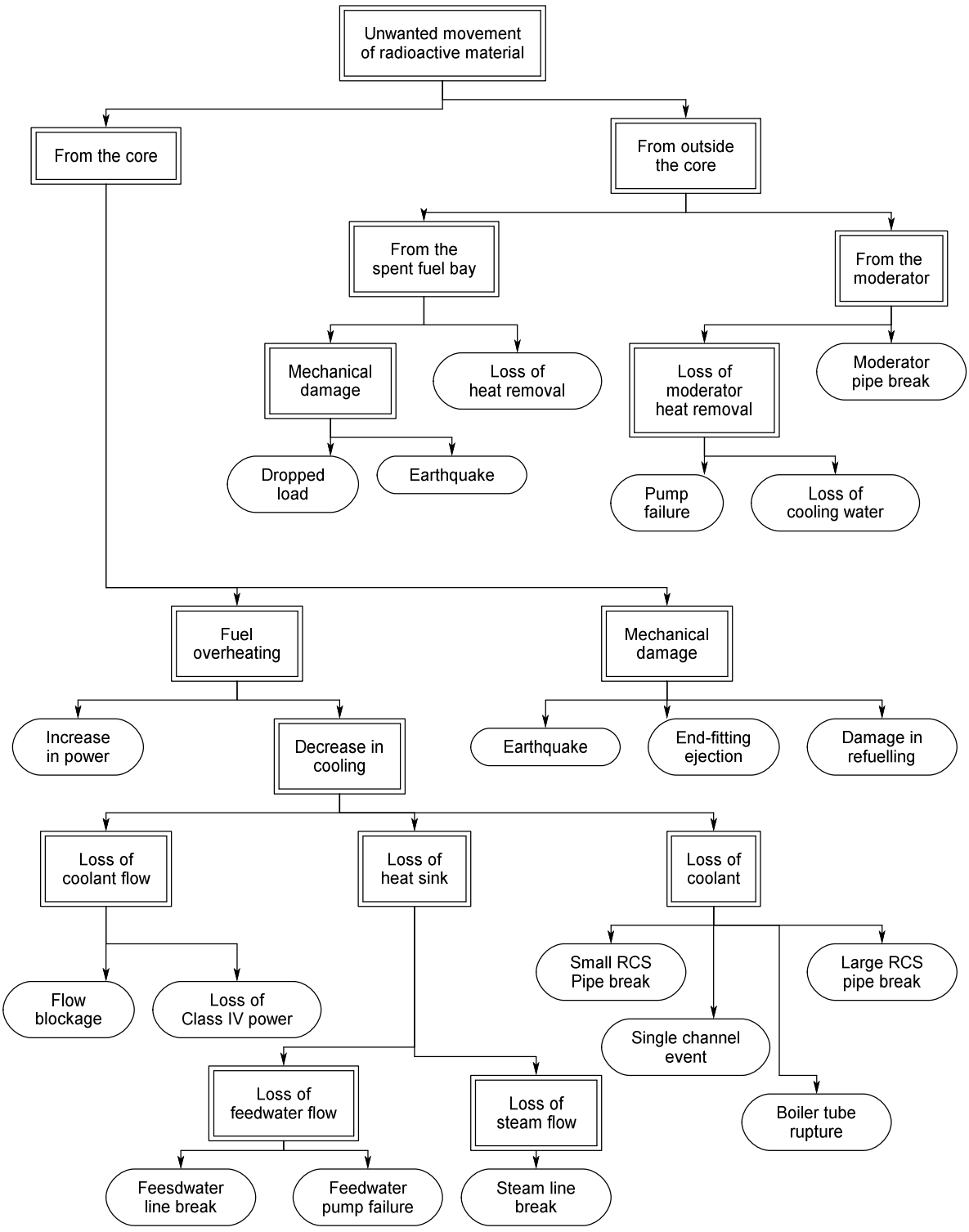

Figure 5 Simplified top-down approach

2.2 Bottom-Up Approach

Another approach is to look at each component of the nuclear power plant and ask what is the consequence if this component fails. If systems exist which are supposed to protect the reactor against such a failure, what are they, and what happens if they also fail? Eventually, if the power plant is well designed, one gets to a very low frequency and draws the boundary between design basis and beyond design basis accidents again. This is called a "bottom-up approach". Another term is FMEA, which stands for "failure modes and effects analysis", although this approach tends to be more limited because it stops after the first failure.

Sample Problem: Do a bottom-up analysis of the feed-water system in a nuclear power plant. (The reader is assumed to be familiar with CANDU design—if not, please consult the earlier Chapters in this book.)

Answer: The feed-water system can fail in a number of ways: power to the pumps may fail, or a feed-water line may break, or the feed-water valve(s) may inadvertently close. Taking each feed-water system component in turn and assuming that it fails, we then identify the systems which are there to protect against such failures—e.g., the auxiliary feed-water system, the shutdown cooling system, and the emergency water system (these are described in Section 5). We then look at the failure of each of these mitigating systems. From these results, using judgment to determine frequencies, we can select likely candidates for DBAs, shown in ovals in Figure 6. The un-terminated arrows represent further development of the diagram.

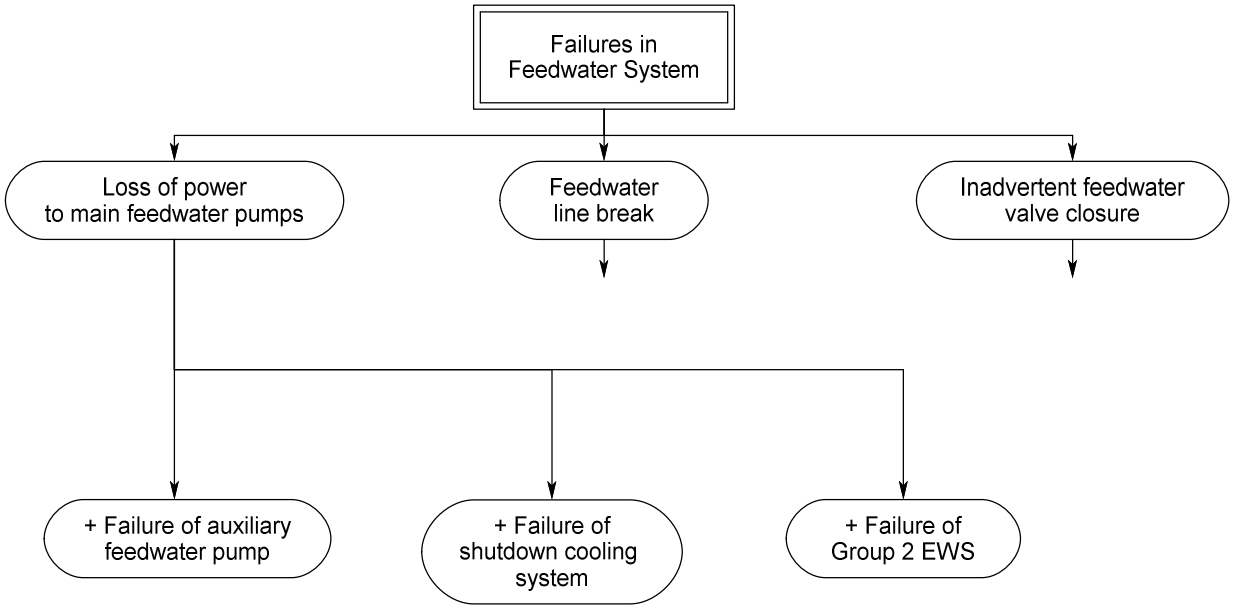

Figure 6 Simplified bottom-up example

A combination of the top-down and the bottom-up methods will give a large number of accidents which cover most possible events. However, the treatment of frequency is not very precise.

2.3 Probabilistic Safety Analysis

Probabilistic safety analysis (PSA) is a rigorous tool for identifying accidents and assigning frequencies to them. PSA uses a top-down approach to generate the failure frequencies of operating systems and the failure probabilities of safety systems (fault trees). It then combines failure of each operating system with successive failures of the required safety systems to obtain a long list of accidents and their frequencies (event trees). One can also select design basis accidents from this list if they have not already been picked up by other techniques. This topic is covered in more detail in Section 4.

2.4 Experience

Design basis accidents may also be added because of experience.

For example, Canadian practice requires that each design basis accident be analyzed assuming complete failure of one shutdown system, no matter how low the frequency. The reason goes back to 1952, when the core of the NRX research reactor in Chalk River, Ontario, was damaged in an accident ([Lewis, 1953] [Hurst, 1953]) in which the power increased and the shutdown system was impaired. One of the causes was a complex control/shutdown system design; the shut-off rods were hydraulically driven, and their performance was sensitive to dirt in the system. The accident resulted in a large subsequent emphasis on shutdown-system reliability, testability, and robustness, to the extent that, even though the shutdown systems in CANDU bear no resemblance to those in NRX (lessons having since been learned about shutdown-system design), the CANDU reactor had to be designed to survive an accident even if the shutdown system failed. Although one could show that the most severe accident without shutdown (a large LOCA) would not release enough energy to break containment, the designers decided (eventually) to add another, fully independent shutdown system, so that even if one shutdown system failed completely, the other could be credited.

The accident at Fukushima in 2011 [JNTI, 2011] is a recent example of a poor choice of the parameters for a design basis accident. Although the plant had a Design Basis Flood level, it was clearly inadequate, and since the accident, all operating plants have had to change their provisions for both Design Basis Floods and Beyond Design Basis Floods. We shall cover key historical events in more detail in Section 3.

2.5 Canadian Approach to DBAs

We do not have space to cover the entire historical development of the Canadian approach to DBAs. See [Snell, 1978] for an overview. Instead, we shall describe the basis for selection of DBAs for currently operating CANDUs and planned future plants.

2.5.1 Siting guide

In 1972, D. G. Hurst and F. C. Boyd of the Atomic Energy Control Board (AECB) — the name at the time of the nuclear regulator (now CNSC) — laid the ground rules for the deterministic licensing guidelines under which all large operating CANDU plants up to but excluding Darlington have been licensed [Hurst, 1972]. The spectrum of possible design basis accidents was

collapsed into two broad categories: *single failures*, or the failure of any one process *system* in the plant, and *dual failures*, a much less likely event defined as a single failure coupled with the unavailability of either a shutdown system, or containment, or the emergency core cooling system: these constituting the so-called *special safety systems*. For each category, a frequency and a consequence limit was chosen that had to be satisfied. In addition, to deal with the siting of a reactor (Pickering A) next to a major population centre (Toronto), population dose limits were defined for each category of accident.

The limits were as follows (sometimes this is called the Siting Guide):

Table 1 Single / dual failure limits

Accident	Maximum Frequency	Individual Dose Limit	Population Dose Limit
Single Failure	1 per 3 years	0.005 Sv	10^2 Sv
		0.03 Sv thyroid	10^2 Sv thyroid
Dual Failure	1 per 3000 years	0.25 Sv	10^4 Sv
		2.5 Sv thyroid	10^4 Sv thyroid

For example, loss of reactivity control, loss of Class IV power, and a loss-of-coolant accident are all single failures; loss of coolant plus failure of the ECC, or loss of coolant with failure of the containment isolation dampers to close, are dual failures. In this framework, both single and dual failures are design basis accidents.

Safety-system demand unavailability can be inferred from the frequency limits in this table: because a dual failure is a single failure plus unavailability of a safety system and must occur no more often than one in 3000 years, each safety system must fail no more often than 1 in 1000 times, and therefore the demand unavailability is 0.001.

This approach had a number of deficiencies, such as lumping events with widely differing frequencies into the same class—e.g., a large pipe break or a loss-of-coolant accident (LOCA) and loss of off-site power both fell into the single-failure category. Combinations of higher-frequency events were also not addressed.

2.5.2 Consultative Document C-6

To address some of the deficiencies in the single-dual failure methodology for design-basis accidents, the AECB issued document C-6 in June 1980 [AECB, 1980]. This retained the concept of classes of events, five in this case. As with the Siting Guide, the classes roughly grouped events based on frequency, but the assignment of events to classes was done by AECB staff based on their beliefs about the likelihood of the event. Design basis accidents included, for example:

Class 1: failure of reactivity or pressure control; failure of normal electrical power; loss of feed-water flow; loss of service-water flow; loss of instrument air; and a number of other events that one might expect to occur occasionally.

Class 2: feeder-pipe failure; pressure-tube failure; channel-flow blockage; pump-seal failure; other events that would not be expected to occur more than once (if that) in a plant lifetime.

Class 3: large LOCA; earthquakes and other events that are rare and could damage the fuel or portions of the plant.

Class 4: Class 1 events + unavailability of a special safety system

Class 5: Class 2 or 3 events + unavailability of a special safety system, e.g., LOCA plus ECC impairment.

Dose limits were defined for individual members of the public only (see Table 2).

Table 2 Consultative document C-6 limits

Event Class	Expected Frequency per reactor-y [Charak, 1995][3]	Whole-Body Dose (Sv)	Thyroid Dose (Sv)
1	$> 10^{-2}$	0.0005	0.005
2	10^{-2} to 10^{-3}	0.005	0.05
3	10^{-3} to 10^{-4}	0.03	0.3
4	10^{-4} to 10^{-5}	0.1	1
5	$< 10^{-5}$	0.25	2.5

2.5.3 RD-337

As the nuclear industry has become more international and more competitive, the Canadian Nuclear Safety Commission (CNSC) has understood the need to align its requirements, especially for new builds, more closely with international ones and has therefore developed top-level design requirements [CNSC, 2008] which align more closely with IAEA standards [IAEA, 2000] and are less technology-specific. Events are divided into three classes: anticipated operational occurrences (AOOs), which are expected to occur at least once in the plant lifetime; design basis accidents; and beyond design basis accidents (BDBAs), including event sequences that may lead to a severe accident. The limits are from [CNSC, 2008] and [CNSC, 2008a].

Table 3 Dose limits

Event	Frequency	Dose Limit (Sv)
Anticipated Operational Occurrence	$\geq 10^{-2}$ / reactor-year	0.0005
Design Basis Accident	10^{-2} to 10^{-5} / reactor-year	0.020

[3] Expected frequency ranges are not part of C-6; they were used by Ontario Hydro in the licensing of Darlington to classify events not listed in C-6.

There are no dose limits for BDBAs, but there are numerical safety goals and specific system design requirements; see Section 4.

2.6 Other Design Basis Events

A complete list of design basis accidents includes external hazards: earthquakes, fires, tornadoes, tsunamis, floods, etc. The magnitude and frequency of each hazard are site-dependent. The unique aspect of these hazards is that they can affect more than one system at the same time.

Design basis accidents also include man-made hazards, both internal (operator error, sabotage) and external (explosions from nearby industrial or transportation facilities, terrorism). Defining what should be the "design basis" and "beyond design basis" for malevolent acts is the responsibility of the national government.

2.7 Problems

The reader should have read and understood Chapters 3, 4, and 5 on reactor physics before proceeding.

1. A laboratory experiment has been set up to determine the critical mass of enriched uranium. Two hemispheres of U^{235} metal are supported in an unshielded facility by one scientist. Other scientists are in the same room, observing. A screwdriver is used to slowly push one hemisphere closer to the other, while a neutron detector measures the increase in neutron flux as they approach each other (Figure 7). (This scenario is modelled on, but is not quite the same as, the Lewis Slotin accident in 1946 [LANL, 2000]). Develop a safety approach using the concept of design basis accidents as follows:

a) Use both "top-down" and "bottom-up" approaches to define a set of accidents. Specifically: What is the "top event" that is to be avoided? What could cause the accidents?
b) How fast do the accidents occur (i.e., what physical process determines the time scale)? What inherently limits the consequences (why don't you get a nuclear bomb)?
c) Compare the nature of the hazard to the scientists with that to the public.
d) How could the consequence of an accident be prevented or mitigated:
   - Without any further equipment, i.e., just after it has occurred?
   - With equipment installed beforehand?

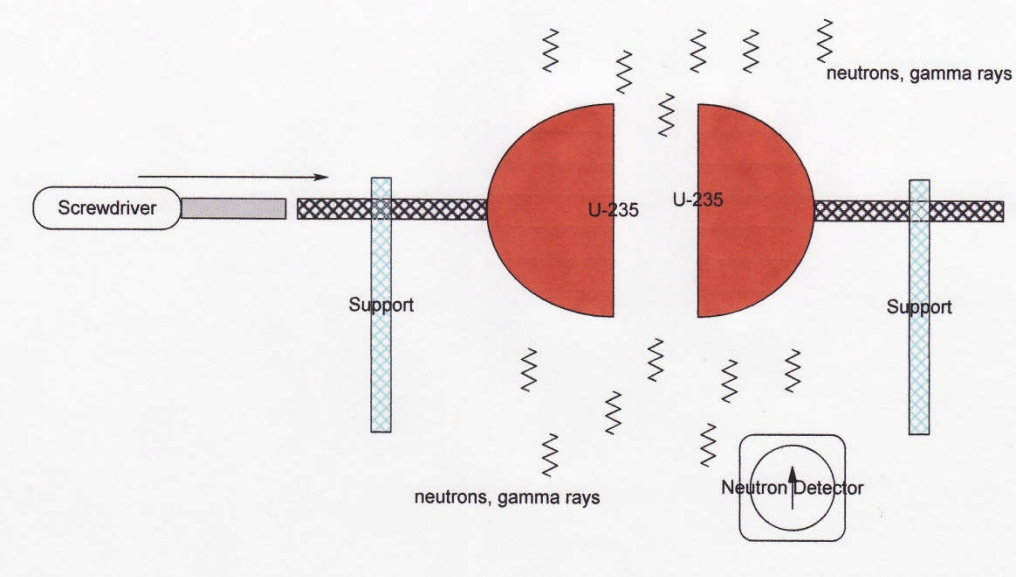

Figure 7 Criticality experiment

2. Calculate the "risk" in Sv/year to an individual at the site boundary from a (not very good) reactor designed and operated so it exactly meets the dose limits in:

a) The two classes of accidents in the single/dual failure approach
b) Event classes 1 to 5 inclusive from Consultative Document C-6
c) The AOO and DBA limits from RD-337.

What conclusions can you draw (if you think the comparison is not meaningful, explain). What relative contribution do the more severe accidents make to the risk?

3. Consider the small reactor for urban district heating shown in Figure 8 [Snell, 1989]. It is intended to be located in urban areas in buildings such as hospitals or universities [Currie, 1985]. Salient safety-related characteristics are:

- pool reactor, natural circulation, atmospheric pressure
- double-walled pool (350,000 litres) with a purification system (small pump and ion-exchange resins, outside the pool)
- 10 MW(th) output
- forced-flow secondary side, with a heat exchanger immersed in the pool
- tertiary heat exchanger connected to the heating grid (why?)
- negative reactivity feedback from fuel temperature, coolant temperature, and coolant void (e.g., an increase in coolant temperature decreases the reactivity)
- active reactor-control devices (rods) with limits on rate (a few mk/hour, compared to, say, CANDU, which can go up to several mk/minute) and worth (no rod in excess of a couple of mk).
- low fuel temperatures, so that there are no free fission products in the fuel
- two shutdown systems—one passive system actuated by a signal (drops the control rods) and one fully passive system (rods within the core which are thermally activated: the absorber material inside the rods, normally above the core, melts and fall

into the core on high coolant outlet temperature)

- a confinement boundary (not shown in the figure) covering the pool top; however, the building is conventional
- no emergency core cooling system (why?)
- a licensed operator is not required to be in the control room. Any upset sounds an alarm which notifies a local attendant (who can shut the reactor down, but not re-start it). Licensed operators can remotely monitor the reactor, but not control it.

Develop a set of design basis accidents for this reactor. It is important to show how you did this, not whether you get the same answer as the designer did (there is not really enough information given in the exercise to get the "right" answer—it's your thinking process that counts). If you are getting design basis accidents which seem inconsistent with an urban location, how could they be made impossible?

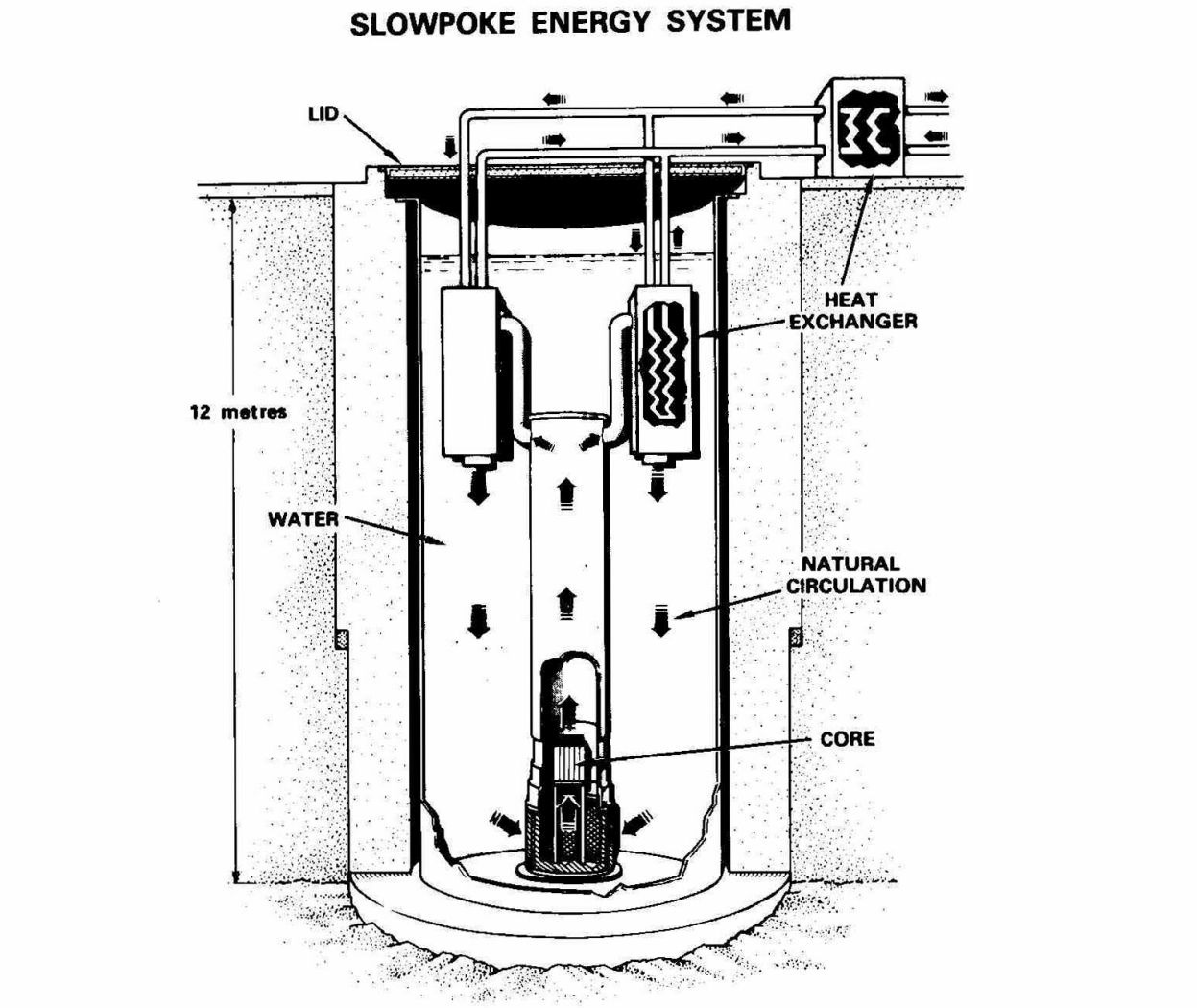

Figure 8 SES-10

4. Consider a low-energy research reactor used to determine fundamental physics parameters. It consists of a vertical cylindrical heavy-water tank in which are suspended fuel assemblies (Figure 9 and Figure 10). Salient safety-related characteristics are (somewhat simplified):

- pool reactor, natural circulation, atmospheric pressure
- nominal zero energy (a few watts), no engineered heat-removal systems
- low fuel temperatures, with very few fission products in the fuel
- fuel rods suspended from hangars which can be arranged manually into different lattice pitches and geometries. Fuel rods are stored beside the pool.
- capability to use fuel with a large range of enrichment ratios (but not highly irradiated fuel)
- provision for insertion of a few channels consisting of fuel inside a pressure tube containing electrically heated coolant at high pressure and high temperature inside a calandria tube (but still nominally ~zero nuclear power)
- control through moderator level (pump-up and drain); pump-up speed limited by pump capacity
- manual start-up and shutdown
- three redundant dump valves which open to trigger a heavy-water dump on high neutron power or high log rate
- no emergency core-cooling system and no containment. A cover provides shielding of operators when the reactor is critical.

a) Develop a set of design basis accidents for this reactor. It is important to show how you did this, not whether you get the same answer as the designer did (there is not really enough information given in the exercise to get the "right" answer, it's your thinking process that counts). Start from a long list developed using at least two of the techniques discussed in this Chapter and then suggest which accidents you would consider too rare to design against, and why. Provide details, e.g., it is not enough to say "increase in power"; list all the ways that this could occur.
b) If you wanted to reduce the risk from this reactor (based on your list of design basis accidents and a judgment about probability), what design changes would you make first?

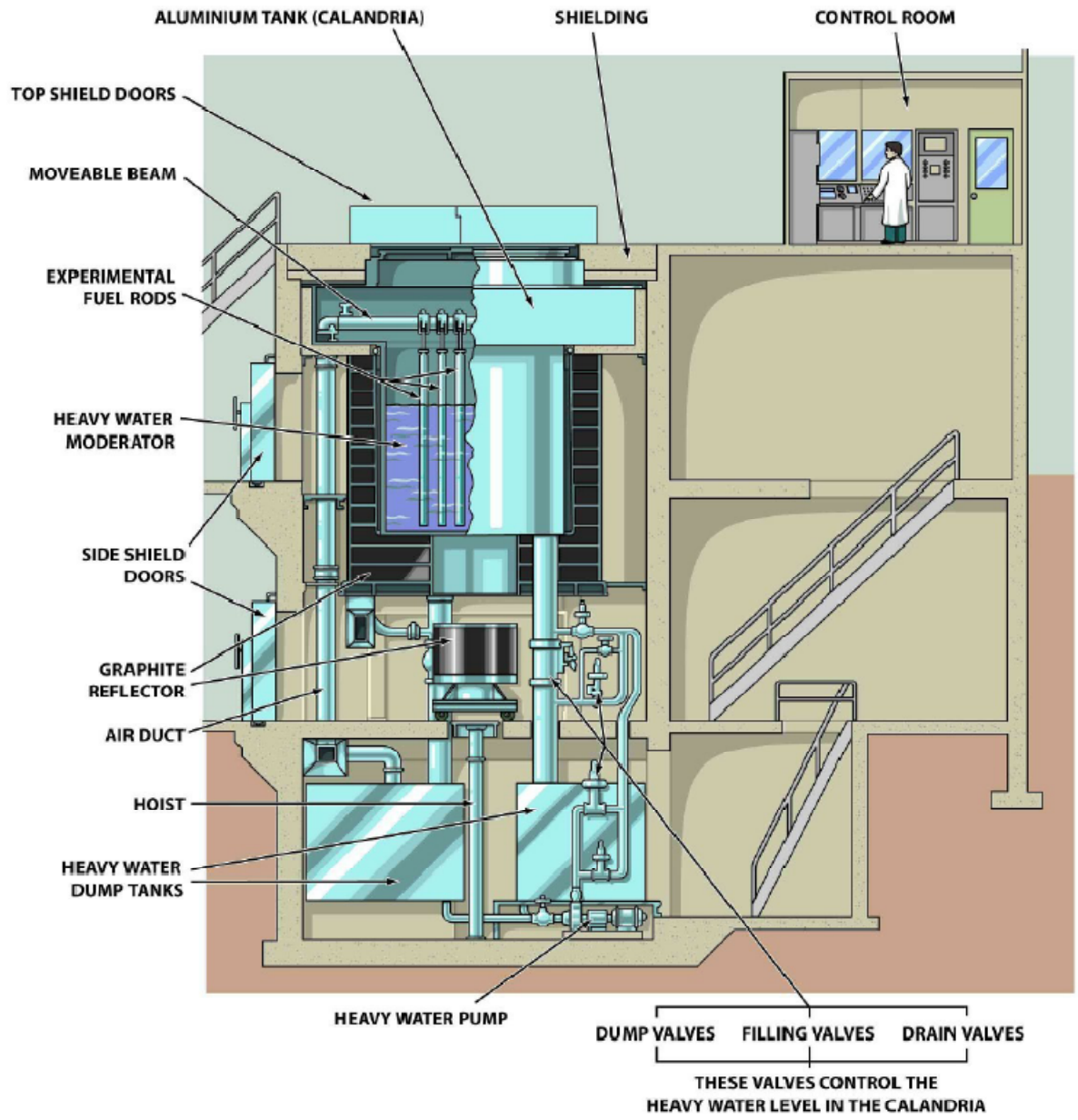

Figure 9 ZED-2 cutaway
[AECL, 2011]

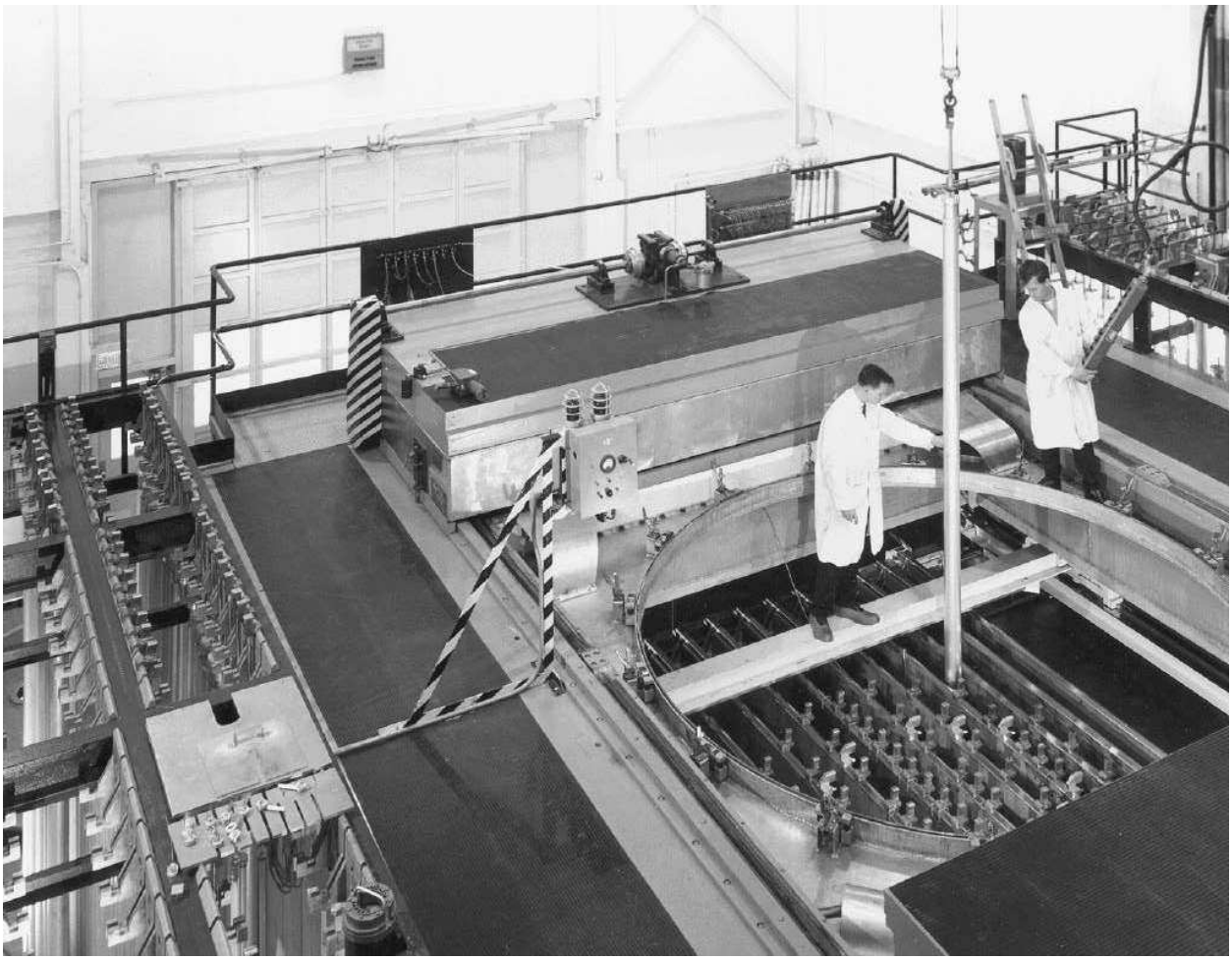

Figure 10 ZED-2 top view

3 Experience

Current power reactor safety design has been powerfully influenced by accidents that happened during the development of the technology. In this Section, we describe a few of them—space constraints do not permit an exhaustive study.

Real accidents almost never follow the simple assumptions in design basis safety analysis. Most real accidents tend to be very complex, have more than one contributing factor, have a high component of human error and extraordinary human recovery, and often leave one wondering, "How did all these things happen together?"

The answer is, of course, that if they didn't happen together, there would be no accident. It is a poorly designed nuclear power plant where a single failure or error causes a catastrophic accident. Most accidents are the end-point of a chain of events, prevention of any one of which would have stopped the accident from happening. We will discuss this later in Section 5.1 (Defence-in-depth).

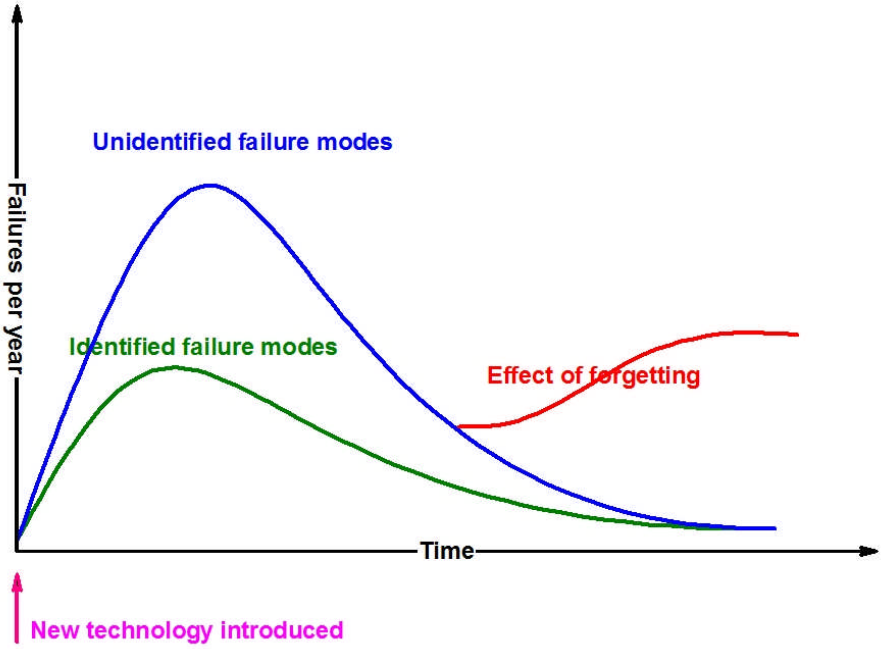

Figure 11 Learning and forgetting

The fact that such chains have occurred provides powerful lessons learned for future designs and current operation.

In general, when any new technology is introduced, its characteristics are not fully known, and there is an early peak in the accident rate. As people learn from mistakes in design and operation, the accident rate declines, as shown in Figure 11. See also [Ott, 1981] for a more detailed discussion. The decline does not, however, account for organizational forgetting, and if nothing is done to preserve corporate or industrial memory, the rate will start to rise again. One of the purposes of case studies is to ensure that past mistakes are not repeated.

What you are expected to obtain from this section is the ability to dissect an accident. What

was its nature? What were the root causes? What were the lessons learned for design? For operation? The exercises at the end of the chapter give you some additional actual incidents to assess.

You should have read and understood Chapters 3, 4, and 5 on reactor physics before proceeding.

Each of the case studies described below gives a brief description of the facility, the event, and lessons learned. These are all of necessity very abbreviated. In particular, of the dozens of lessons learned, only the few most important are listed. The reader should consult the references for more detail.

3.1 Criticality Accidents and Power Excursions

The earliest accidents in nuclear reactors were criticality accidents. This is not surprising because most early reactors were research reactors, which were small enough that if the reactor was shut down, the decay heat could be removed by the water and by structures surrounding the core for long periods of time. Loss of heat sink was not a major issue. Therefore, the main safety concern was avoiding unwanted criticality and shutting down quickly if it occurred. This concern was emphasized by the large worth of some of the reactivity-control devices: because reactors were small, space for control rods was limited, and refuelling was infrequent, the control rods had to compensate for burnup and tended to have high reactivity worth.

A number of reactivity accidents have taken place when the reactor was supposed to be shut down. An initially sub-critical reactor is not as safe as it sounds. The power is fairly constant and proportional to the number of source neutrons divided by the absolute value of the (negative) reactivity [Cameron, 1996]:

$$N_f = \frac{S_e}{-\rho}, \tag{3}$$

where:

N_f is the number of neutrons,
S_e is the source term (neutrons produced per unit of time, either from spontaneous fission, fission product decay, photoneutrons or an artificial neutron source), and
ρ is the reactivity, negative in this case.

However, the reactor is not under active “control”. Detectors are insensitive, and indications that the reactor might be near-critical are not very obvious. In some cases, the reason for the shutdown is to do maintenance on the control or shutdown systems, which means that they are not available. Then safety depends on ensuring an adequate shutdown margin (net negative reactivity) by procedural means, i.e., inserting a number of absorber rods, or removing fuel, or adding a liquid absorber to the moderator or coolant, or removing the neutron reflector surrounding the core. Safety also depends on maintaining the shutdown margin over time. This is the reason for the *guaranteed shutdown state* in CANDUs: to have a large enough negative margin that the reactor is resistant to operator mistakes or equipment failures. It is also good

practice, as we shall see from the case studies, to have an additional means of shutdown always poised, even during shutdown.

You may want to think about whether it is safer to refuel a reactor while it is critical or during a shutdown.

3.1.1 SL-1

3.1.1.1 Description

This summary uses material from [USAEC, 1962], [USAEC, 1962a], [USAEC, 1962b], [Stacy, 2000], and [Thompson, 1965].

The SL-1 (Stationary Low Power Reactor No. 1) was a natural-recirculation pressurized boiling-water military reactor with a thermal power of 3 MW. It was located at the Atomic Energy Commission National Reactor Testing Station in Idaho Falls, Idaho. Figure 12 shows a cutaway of the reactor vessel. At the time of the accident, on January 3, 1961, there were 40 fuel assemblies and 5 control rods in the core.

3.1.1.2 The event

Three operators were engaged in reassembling one of the control-rod drive mechanisms while the reactor was shut down. Part of the assembly process required raising the shaft of the rod a limited amount by hand. This was done by unclamping the rod and raising it; the rod was then re-clamped, and the only remaining task was to unclamp and lower the rod. For some unknown reason, the rod was instead raised rapidly, making the reactor super-prompt critical. The pressure vessel jumped up nine feet, with the chain reaction being compensated for (probably) initially by the negative feedback due to heating of the fuel and moderator and then by the melting and vaporization of the fuel itself.

Two operators were standing on the lid at the moment of the accident. One was thrown to one side as the vessel rose. The other was impaled on a shield plug ejected from the top of the reactor and was carried up to the roof of the reactor room, where he remained suspended. The third man was killed by radiation and flying debris. Table 4 gives a chronology of the events.

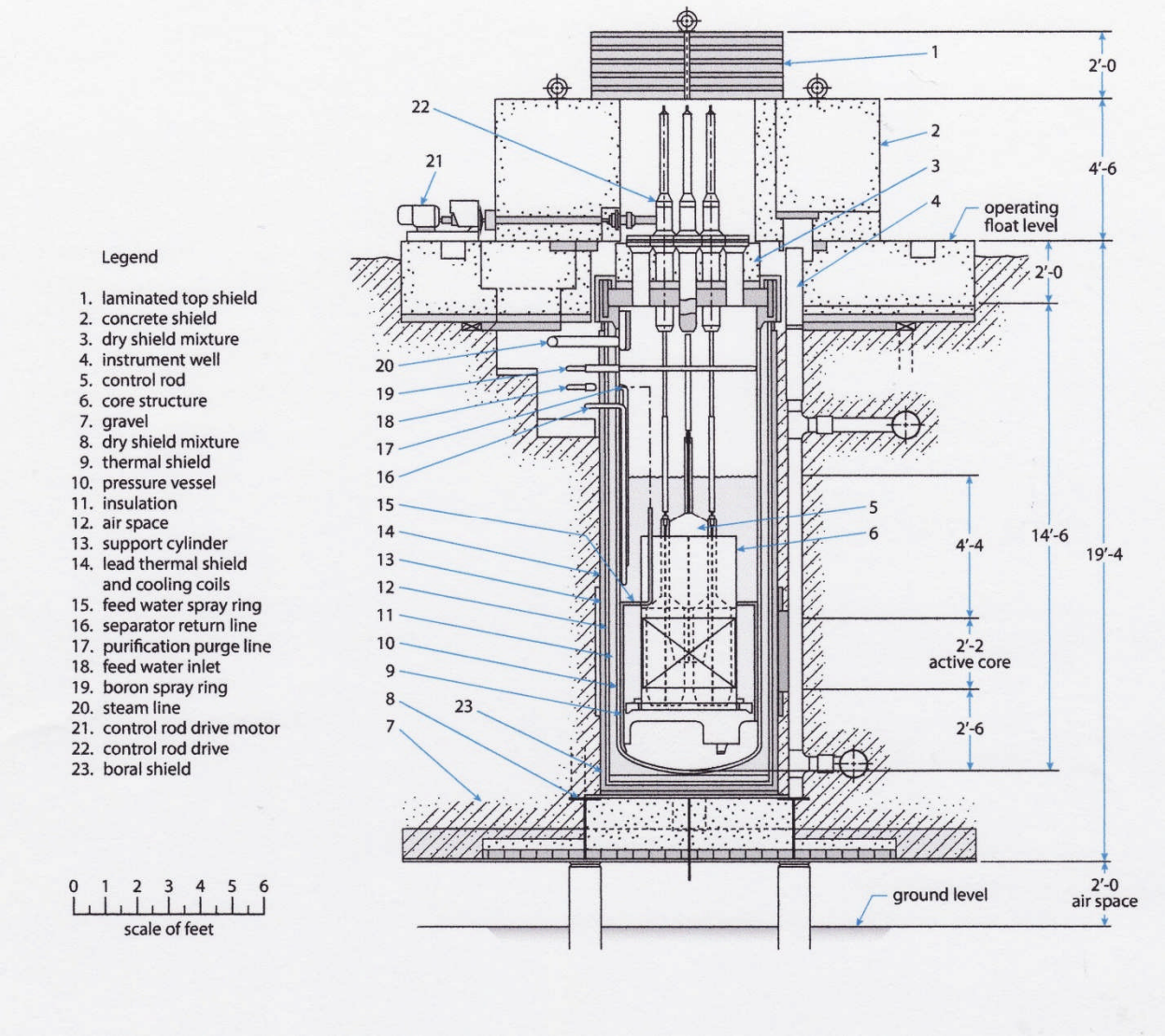

Figure 12 SL-1 cutaway

Table 4 SL-1 chronology

Time	Event
-500 msec	Central control-rod withdrawal starts.
-120 msec	Reactor goes critical with rod at 16.7 in. (40.6 cm).
	Central rod at 20 in. (50.8 cm), period = 3.9 ±0.5 msec, (2.4 ± 0.3)% Δk.
0	Peak power burst (1.9 ± 0.4) × 10^4 MW.
~2 msec	Prompt nuclear energy release ends; total nuclear energy of excursion = (133±10) MW-sec [+(24 ±10) MW-sec in metal-water reaction]. 20% of plate area destroyed; centre 16 elements 50% melted; central shroud and control blade ejected from core. Water column above core accelerated by average pressure (500 psi or 35 atm) to a velocity of 160 ft/sec (49 m/sec).
34 msec	Water slams against lid of vessel. Maximum pressure ≈10,000 psi (~700 atm).
	Head shielding ejected. Plugs ejected with velocity of 85 ft/sec (26 m/sec) or less. Vessel rises, shearing connecting pipes. Guide tubes collapse. Nozzles and vessel expand.
160 msec	First plug hits ceiling.
	Two-thirds of water expelled. 5%–10% of fission products expelled.
	Vessel hits ceiling. Total kinetic energy involved ~1% of total energy released.
	Insulation ripped from vessel.
2000–4000 msec	Vessel comes to rest in support cylinder.

3.1.1.3 Lessons learned

The philosophy of reactivity design is vitally important. The fuel in SL-1 had boron strips attached to the fuel; these were supposed to burn up with the fuel to keep the core reactivity within the control range of the control rods. These strips had burned up faster than planned, and in addition, pieces of boron had fallen off the fuel during operation. The net result was that the core became more reactive to the point that it could be made critical with four rods fully in the core and the central one partially withdrawn. The criticality position of the central rod at the time of the accident was 16.7 inches withdrawn; the extra 4 inches that the rod was withdrawn above this value added more than four times the delayed neutron fraction β, giving a reactor period of 4 msec. Clearly, once the transient had started, no operator action and no

shutdown system could stop it in time.

Many lessons were learned from SL-1; here we summarize the major ones concerning reactivity control:

1. It should be impossible for a reactor to be made critical by withdrawing the single most effective rod. Conversely, it should always be possible to shut down a reactor with the single most effective rod stuck in its outermost position. This so-called "single-rod rule" has been followed ever since in safe reactor design.
2. It should not be possible to withdraw a high-worth rod quickly. It is still unknown why the operator withdrew the rod. In any case, the lesson is that if a reactor requires high-worth rods, there must be mechanical means to prevent their rapid withdrawal.
3. In a reactor where large amounts of reactivity can be added in short times, there must be inherently fast negative reactivity feedback, for example from fuel temperature, so that the transient is stopped short of reactor damage. This lesson was later applied in commercial light-water reactors.

Note that the total worth of reactivity devices in CANDU is quite low because on-power refuelling means that the movable control devices do not have to compensate for burnup. Moreover, the dispersed CANDU core enables the reactivity worth to be spread among many individual reactivity devices.

3.1.2 NRX

3.1.2.1 Description

This summary uses material from [Lewis, 1953], [Hurst, 1953], [Larson, 1961], and [Cross, 1980].

NRX was Canada's first large research reactor, built in 1947 with a thermal power of 30MW. The moderator was heavy water contained in a cylindrical calandria. Cooling was once-through, light-water, taken from and returning to the Ottawa River. Passing through the calandria were vertical tubes open to the air at top and bottom. Each fuel rod, made from metallic uranium sheathed in aluminum, had its own cooling jacket (Figure 13); each rod, with its cooling jacket, was located in one of the vertical tubes (Figure 14). A stream of air passed between each fuel rod and its calandria tube. Twelve boron shut-off rods passed through 12 of these tubes. Start-up was achieved by removing half these rods, after which the reactor was controlled by varying moderator level.

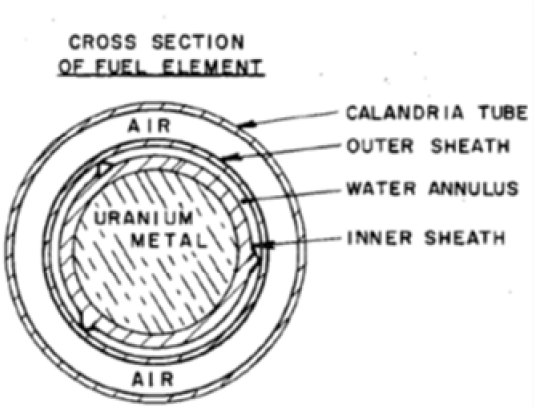

Figure 13 NRX fuel cross section

The shut-off rods could be raised by compressed air and were then held up by an electromagnet. They could be driven back in using high-pressure air, although they would fall more slowly

under gravity if released.

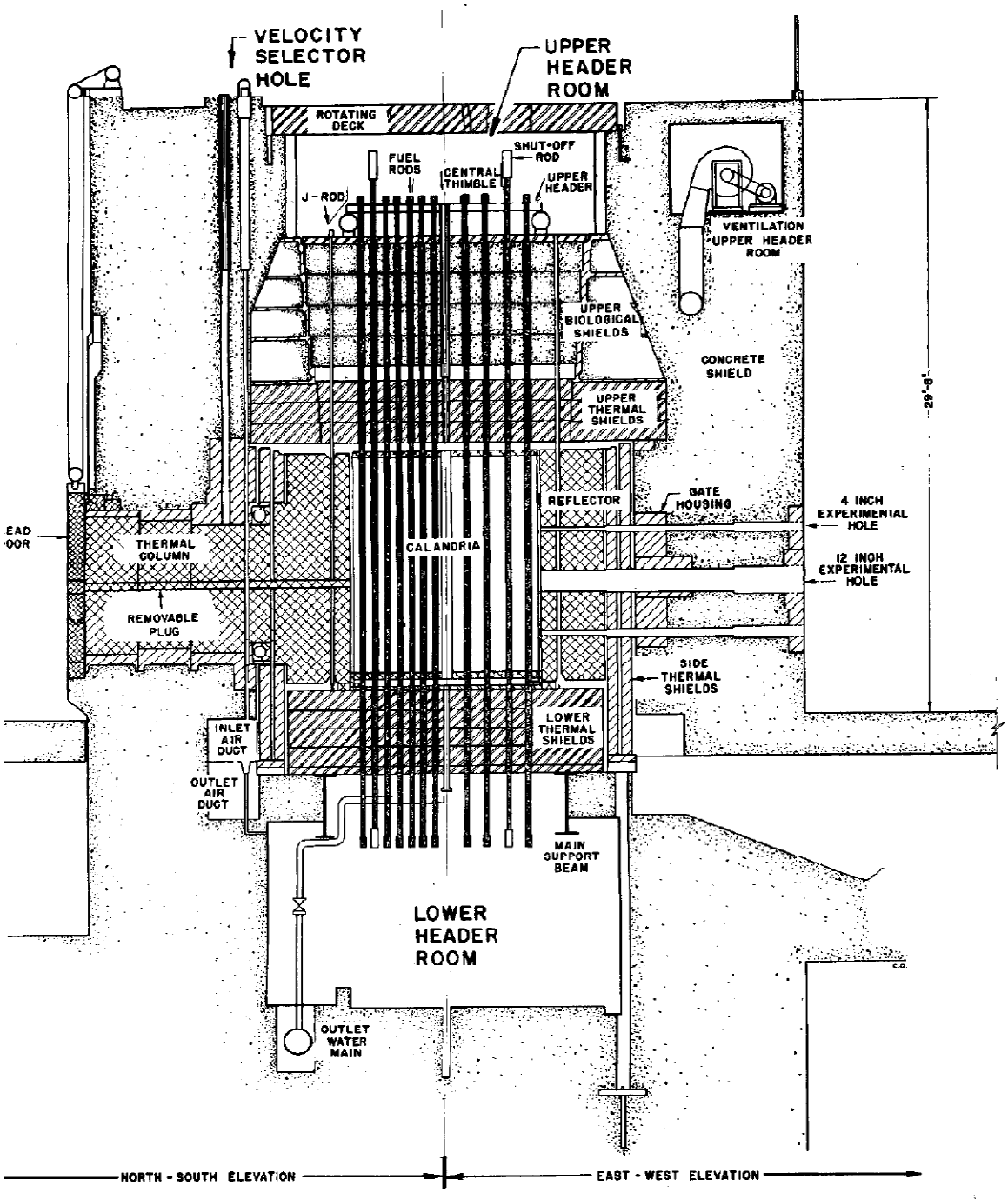

Figure 14 NRX elevation

The 12 rods were divided into six groups, or banks, of rods, ranging from one to four rods per bank. Normally a "safeguard bank" was held in reserve: that is, bank 1 containing four rods was

the first to be removed during a start-up and was designed to overcome any reactivity added if the reactor should go inadvertently critical on removal of any of the remaining banks of rods. Removal of the safeguard bank was prohibited by limit switches on each rod unless all other rods were down; however, the switches had been giving trouble and had been disabled.

To ensure fast start-up after a shutdown (and avoid xenon poison-out), it was possible to drive up the first four rods, worth 30 mk, in a few seconds.

There were four pushbuttons on the control panel. Pushbutton 4 charged air to the heads of the shut-off rods; release of this air drove the rods down. Pushbutton 3 temporarily increased the current in the electromagnet and ensured that the rods were properly seated. Pushbutton 1 raised the safeguard bank, and Pushbutton 2 raised the remaining banks in automatic sequence. Normal operation was to press Pushbutton 3 along with 4, 1, and 2. If 3 was not pressed with 4, air might leak from the head system; if 3 was not pressed with 1 and 2, the shut-off rods might not be drawn fully home, and the safety circuits would prevent start-up from proceeding.

The void reactivity was positive and large; that is, removal of all the light-water coolant would result in an increase in reactivity of 25 mk.

3.1.2.2 The event

At the time of the accident, the reactivity of certain fuel rods was being measured at low power. The cooling to these rods was reduced, and one was being cooled only by air.

The following sequence of events is taken from [Cross, 1980]:

> "The accident occurred during a start-up procedure. Just as the first group of shut-off rods was about to be removed, an operator in the basement of the building (who had nothing to do with the start-up) mistakenly turned some air-valves which caused several shut-off rods to rise. This was immediately shown by the indicator lights in the control room. The reactor supervisor phoned the operator to stop and went down to the basement himself to make sure that the valves were properly reset. When this was done the rods should have gone down into the reactor. In fact, they went down only partway, but far enough that the lights in the control room indicated that they were down."

This failure to reinsert is not explained in any of the published reports. Cross continues:

> "The supervisor in the basement phoned the control room and told his assistant to press two numbered buttons. He gave the wrong number for one of the buttons, and when it was pressed, instead of resetting the air pressure as was intended, it raised four more shut-off rods. If the first group of shut-off rods had been down, as their lights indicated they were, raising four rods was a reasonable thing to do, so the mistake was not recognized."

Specifically, the supervisor asked the assistant to press buttons 4 and 1. This would charge the air to the heads and raises the safeguard bank. He had meant to say 4 and 3, which charges the air to the heads and seats the rods. However, because button 3 was not pressed, the air to the heads brought up by button 4 leaked away, and the safeguard bank (which appeared to have

been up already) was raised. The supervisor realized his mistake, but the assistant in the control room had to leave the phone to use both hands to push the two buttons.

From [Cross, 1980]:

> "It was soon apparent from instruments in the control room that the reactor was above critical and the power level was rising. This was surprising, but not alarming, since the reactor could easily be turned off by dropping the shut-off rods just raised. However, when after 20 seconds, the button was pressed to do this, only one of the four rods actually went down. The power level continued to climb and, after some discussion in the control room, it was decided to dump the moderator into a storage tank. Within less than 30 seconds, the power-level metres were back on scale and the power dropped rapidly to zero."

The removal of the safeguard bank made the reactor supercritical by about 6 mk and started a power rise to about 100 kW. The lone shut-off rod started to fall in at this point, but the power kept rising to about 17 MW. Boiling then occurred in some of the temporarily cooled rods, expelling the light water and increasing the reactivity by another 2.5 mk. Power continued to rise to 60–90 MW, when it was stopped by dumping the moderator.

The power surge melted a number of fuel rods and caused a number of calandria tubes to fail. Eventually, in a major operation, the reactor calandria was removed and buried; the building was decontaminated, and the reactor was replaced.

3.1.2.3 Lessons learned

1. Some negative reactivity should always be held in reserve (safeguard bank). Before a reactor is made critical, the safeguard bank is removed and poised, so that if anything goes wrong, it can be quickly reinserted. In CANDU, both shutdown systems 1 and 2 are poised before the reactor is allowed to go critical using the control devices.
2. The shut-off rods must be of a simple design. After NRX, designers mistrusted shut-off rods as a safety shutdown mechanism; hence, NPD and Douglas Point used moderator dump as their emergency shutdown system and had no safety rods. Pickering had a few safety rods which acted in conjunction with the moderator dump. Only by the time of Bruce A were shut-off rods restored as a primary shutdown mechanism. They were, of course, very different from those in NRX: they consisted of a rod on a cable, which was wound around a pulley and held in place by an electromagnetic clutch. On a shutdown signal, current to the clutch was cut off, and a spring assisted the rod to drop by gravity. It was, and is, a simple and reliable design with large clearances.
3. The control and shutdown systems should be separated and independent, with the latter devices being used only for shutdown and held outside the reactor during critical operation.
4. An accident, even with a shutdown failure, should not be a public-health disaster. This meant that either the reactor containment had to withstand the energy released, or (much later on) two shutdown systems would have to be provided so that failure to shut down after an accident would be a very low-probability event.

3.1.3 Chernobyl

This summary uses material from [USSR, 1986], [USDOE, 1986], [Howieson, 1987], [Chan, 1987], [Rogers, 1987], and [INSAG, 1992].

3.1.3.1 Description

Chernobyl unit 4 was of the RBMK type (Реактор Большой Мощности Канальный, or High-Power Channel-Type Reactor) and the most recent of the 1,000 MW(e) series. It was a graphite-moderated, boiling-light-water-cooled, vertical-pressure-tube design using enriched (2% U^{235}) UO_2 fuel with on-power refuelling. It used a direct cycle to produce electricity from twin turbines (Figure 15, from [INSAG, 1992]). The reactor cutaway is shown in Figure 16, from [Semonov, 1983].

There are two independent primary coolant circuits, each containing about 830 fuel channels, two steam separators, and four pumps (with one normally on stand-by). Refuelling is done during operation from the top of the core. A containment structure encloses the inlet piping in the lower portion of the reactor and provides pressure relief to a water pool located beneath the reactor (Figure 18). Control and shutdown are performed by movable absorbing rods in lattice positions. Emergency core cooling is provided for pipe breaks through a system consisting of a combination of pressurized-water accumulators and electric pumps.

The reactor has a void coefficient which varies from negative to positive according to the operating state. It is limited in normal operation through control of operating conditions.

The containment is a pressure-suppression type (see Section 5) and is compartmentalized (Figure 18). All inlet pipes are enclosed in leak-tight compartments which connect to a bubbler pond or suppression pool below the reactor. Steam discharged from a pipe break is directed to the bubbler pond, where it condenses. Each channel is accessible (for refuelling) from the top through a large cover plate, to which its extension is welded (Figure 16). The (small) outlet pipes above the core are in an enclosure designed for a rupture of up to two channels or their outlet pipes, because rupture of more than one was believed to be highly improbable. As noted in [INSAG, 1992], “Simultaneous failure of a greater number of fuel channels would generate a pressure high enough to fail the containment function by lifting the cover plate, in the process severing the remainder of the fuel channels”.

3.1.3.2 The event

The accident resulted from a test to show that after a main pump trip, the small amounts of steam generated from the low residual reactor power could provide enough electricity through the turbine generators to extend the rundown time of the main coolant pumps. The test was to be done while the reactor was critical. However, shortly after pump trip, the reactor power started to increase rapidly, could not be terminated, and caused the violent destruction of the reactor.

The test was supposed to have been done at a starting power of 700 MW(th). However, it was initiated at a power level of 200 MW(th). The reasons are somewhat lengthy, but during the transfer from the local power control system to the main range automatic power, an unplanned

drop to zero neutron power occurred and lasted for four to five minutes. The operator, instead of aborting the test, then attempted to recover power, but because of xenon decay, had to raise the control rods so that most of them were out of the core. In the end, the reactor never reached the planned initial power level.

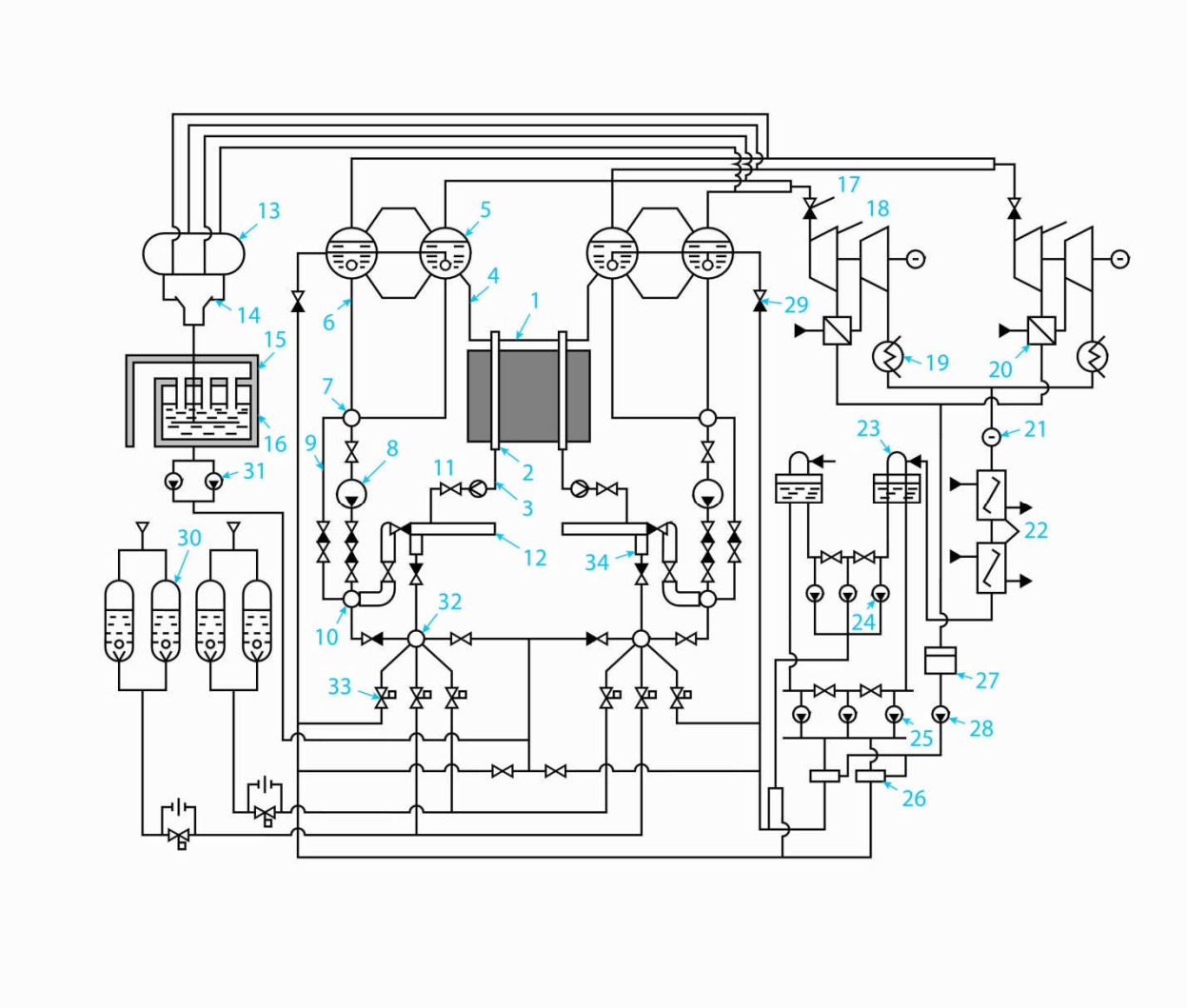

Key: 1: graphite reactor core; 2: fuel channel; 3: in-core instrumentation tube; 4: feedwater pipe; 5: steam separator drum; 6: downcomer; 7: intake header; 8: main circulating pump; 9: bypass; 10: high-pressure header; 11: stop valve; 12: distribution group header; 13: steam header; 14: steam dump valve; 15: accident localization system; 16: ECCS water reserve tank; 17: pressure controller; 18: turbogenerator; 19: condenser; 20: moisture separator/reheater; 21: condensate pump; 22: preheater; 23: deaerator; 24: emergency electric feedwater pump; 25: electric feedwater pump; 26: mixing preheater; 27: condensate collecting tank; 28: moisture separator/reheater condensate pump; 29: level controller; 30: ECCS hydraulic accumulator; 31: ECCS pump; 32: ECCS header; 33: ECCS fast-acting valve; 34: leak limiter.

Figure 15 RBMK schematic diagram

In the immediate aftermath of the accident, the Soviets [USSR, 1986] placed much blame on the operators for not following test procedures and performing the test in an unauthorized reactor configuration. The initial cause of the power rise was stated to be the increase in void reactivity as coolant boiling increased following pump trip. It was implied that because most of the dual control/safety rods were withdrawn, the reactor trip was ineffective in stopping the power rise. Later analysis ([Chan, 1987] and [INSAG, 1992]) indicated that a major cause of the accident was the unexpected behaviour of the shut-off rods, which actually caused an increase in reactor power rather than shutting the reactor down. This surprising design aspect requires more detailed explanation. The absorber rods have graphite displacers or followers attached to their lower ends which are designed to *increase* the absorber reactivity worth. As they are inserted, the absorber rods move into the high-flux region in the centre of the core, which was previously occupied by the graphite, so that the absorber-rod effectiveness is enhanced (see Figure 17). If no graphite were present, the rod would displace water—also an absorber—in which case the change in reactivity with insertion would not be as great.

However, during the accident, most of the absorbers were well removed from the core, which was an abnormal configuration. The flux was peaked at the top and bottom, where most of the reactor power was being generated. Therefore, when absorber insertion first started, the water in the high-flux region at the bottom of the core was first displaced by the graphite follower, leading to a reactivity increase. Therefore, operating the plant in an abnormal condition resulted in an unusually large hold-up of void reactivity, which combined with a deficient shut-down-system design, led to the large power excursion and the resulting core damage. [INSAG, 1992] indicates that this deficiency was known by designers before the event.

The power rise failed a number of fuel channels; the resulting steam release blew off the top cover and severed the remaining fuel channels, effectively exposing the core to the environment and by-passing the containment.

The core damage rendered it subcritical, although to make sure this was the case, the Soviets used helicopters to dump boron into the open reactor structure. The graphite moderator, when exposed to air and heated by the fuel fragments, began to burn and did so for several days until it was smothered by a combination of sand dropped onto the core pit and liquid nitrogen pumped in from underneath. The core melted and flowed into the rooms below the reactor vault, although this was not realized until some years afterwards, when the reactor cavity was inspected remotely and found to be empty. A temporary cover (the sarcophagus) was rapidly built over the damaged structure to prevent radioactive material from escaping and is currently being replaced by a more permanent cover.

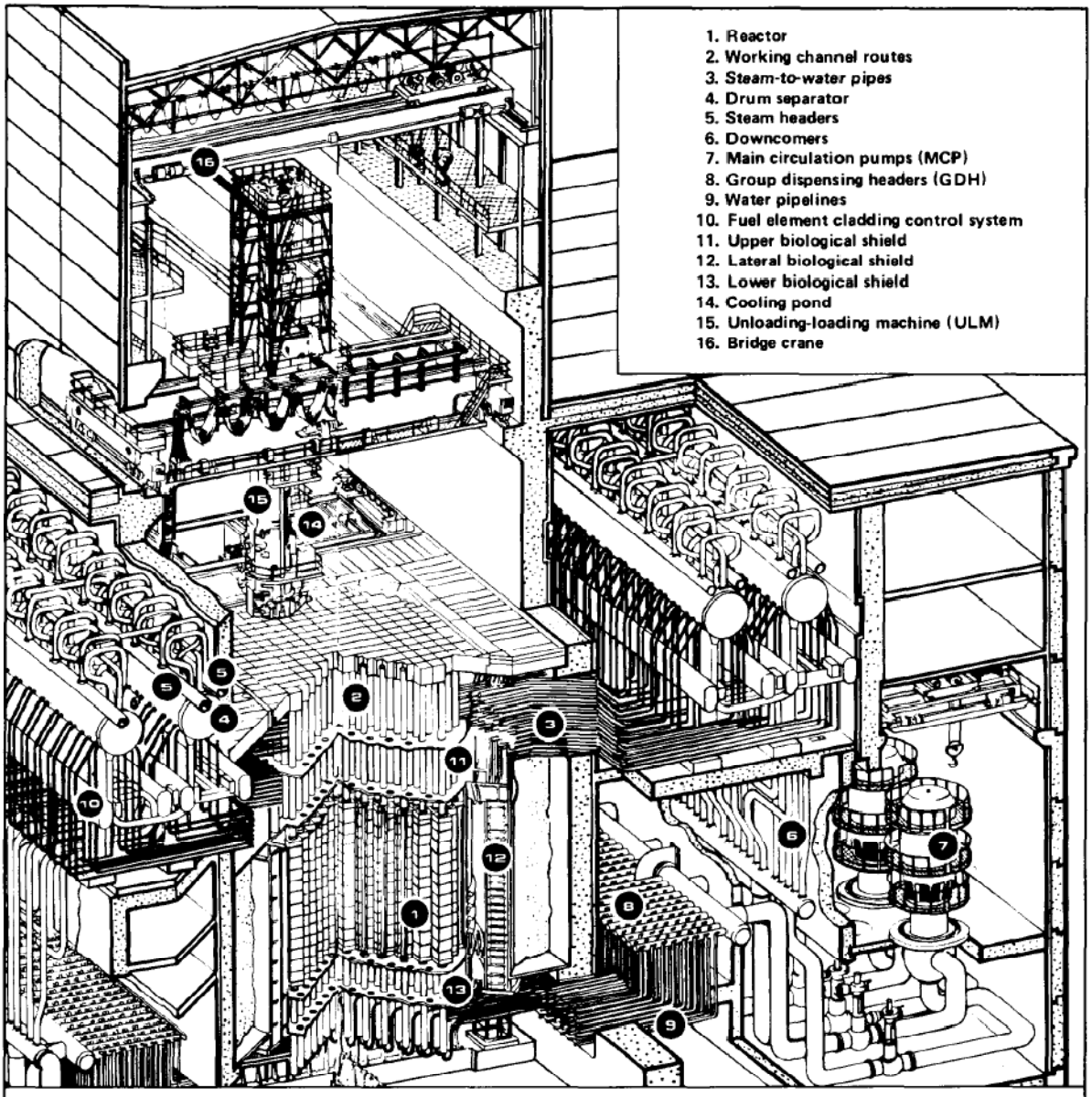

A sectional view of the RBMK-1000 reactor. With an electrical power of 1000 MW, the reactor's thermal power is 3140 MW; the coolant flow is 37.5×10^3 t/h and steam capacity 5.4×10^3 t/h. The reactor inlet water temperature is 270°C and the saturated steam temperature 284°C with a pressure in the separator of 70 kg/cm^2. The initial fuel enrichment is 1.8%.

Figure 16 RBMK reactor

In terms of health effects ([UNSCEAR, 2000], [UNSCEAR, 2008]), 28 prompt deaths occurred among the reactor operators and the firefighters called in to extinguish fires on the turbine-hall roof, arising from the ejected fuel. Some increase in leukemia has been observed among the members of the clean-up crew. Among the public, approximately 6,000 excess thyroid cancers have been observed in children, almost all of which are curable. No other cancers have been observed at statistically significant levels in the population.

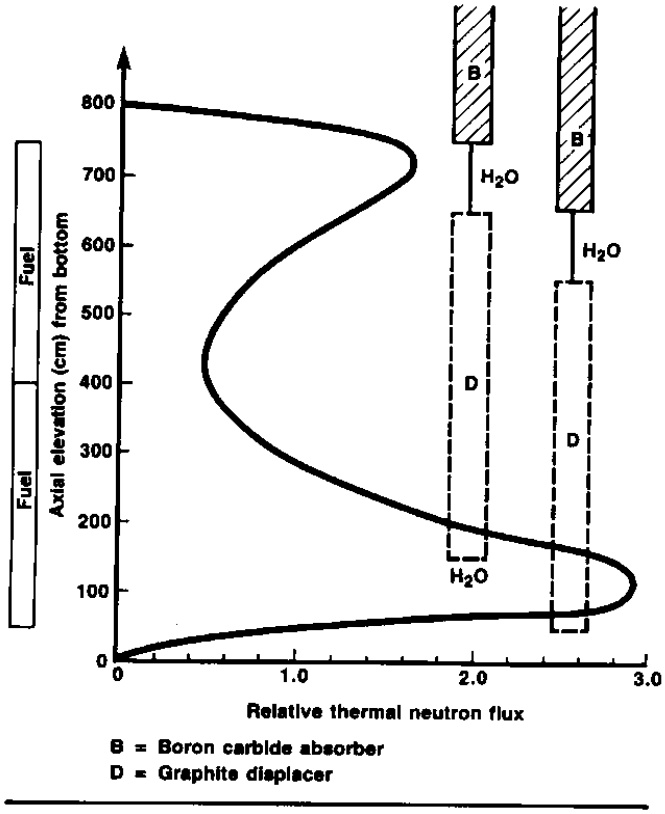

Figure 17 Reverse shutdown in RBMK

3.1.3.3 Lessons learned

1. The effectiveness of shutdown systems should never be impaired by the operating state of the reactor. The shutdown systems should be fast enough and independent enough to overcome any power transient, even from an abnormal operating state.
2. The concept of "safety culture" was used to address inadequacies in the processes of design, operations, and regulation in the USSR, which contributed to the accident. We shall cover this in Section 8. Briefly [INSAG, 1991], "Safety culture is that assembly of characteristics and attitudes in organizations and individuals which establishes that, as an overriding priority, nuclear plant safety issues receive the attention warranted by their significance."
3. Some discussion took place about the role of the containment (Figure 18). It is possible that a complete containment envelope as used in Western PWRs and CANDUs, even if not designed for a reactor runaway, would have mitigated the release of radioactive material, but this has not been demonstrated. At the very least, one can conclude that the upper confinement design basis (rupture of two channels) was not robust in terms of defence-in-depth.

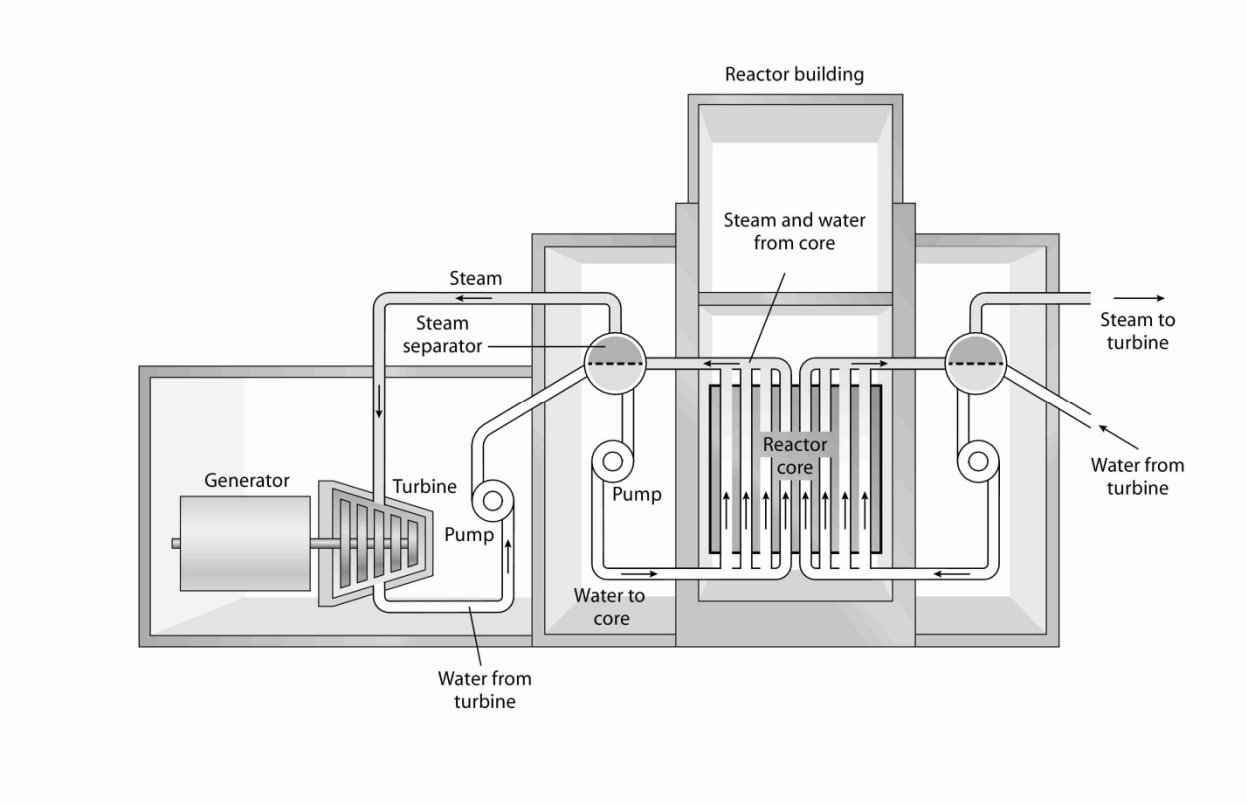

Figure 18 RBMK building cross section

3.2 Loss of Cooling / Heat Removal

Shutting down a power reactor does not eliminate the hazard; the decay heat in the fuel, if not removed, will eventually cause the fuel to melt. We now look at two such events: Three Mile Island and Fukushima Dai-ichi.

3.2.1 Three Mile Island

This summary uses material from [Kemeny, 1979], [Yaremy, 1979], [Rogovin, 1980], and [Brooks, 1980].

3.2.1.1 Description

The Three Mile Island reactor was a conventional pressurized-water reactor; a flow-sheet is shown in Figure 19. The reactor core is inside a large pressure vessel; unlike most CANDUs and BWRs, the coolant is highly sub-cooled and kept so by a pressurizer connected to the pressure vessel. A pressure relief valve on top of the pressurizer provides overpressure protection for the reactor coolant system (RCS).

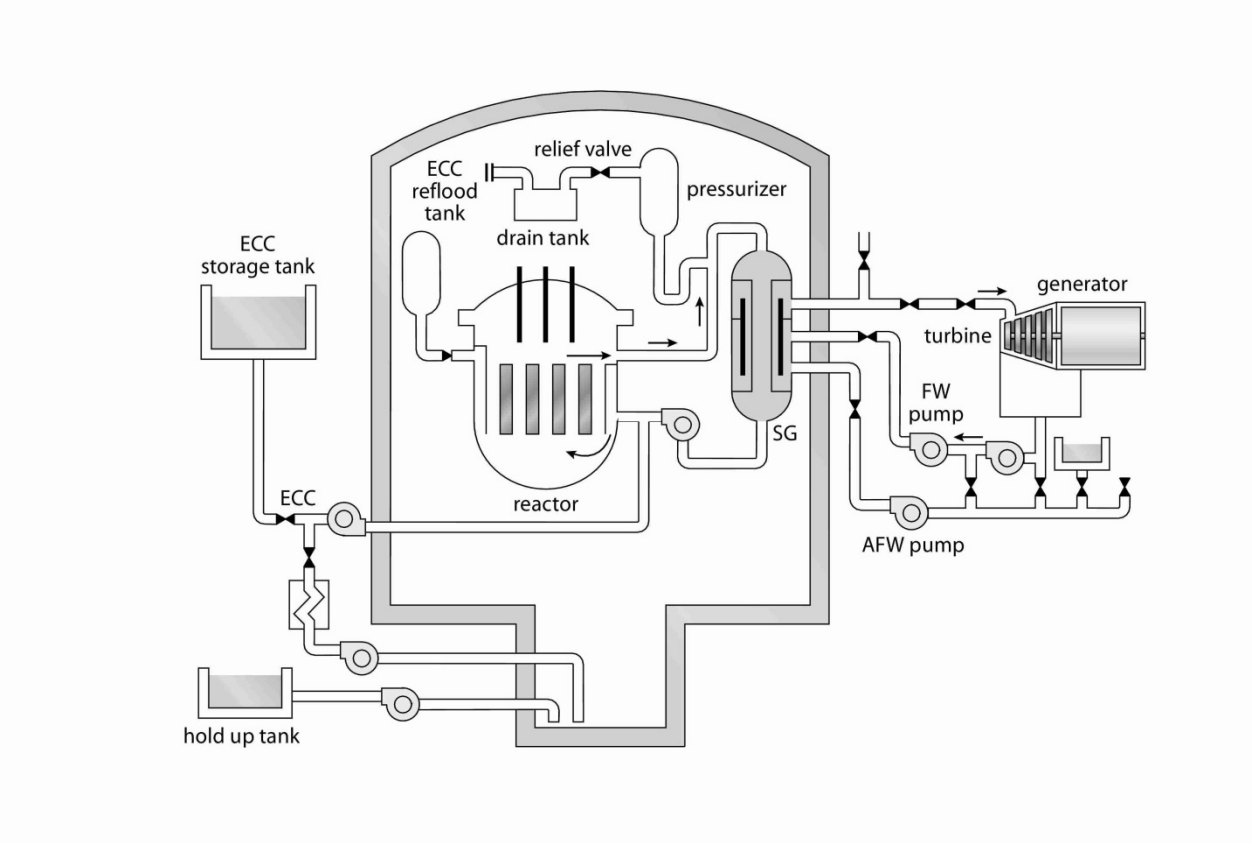

Figure 19 TMI schematic

3.2.2 The event

On March 28, 1979, a maintenance error resulted in loss of feed water to the steam generators when the reactor was on power. Because there was no heat sink for the primary coolant, the coolant pressure began to rise, and the pressurizer relief valve opened to limit the pressure, as it was supposed to do, following which the reactor tripped (shut down automatically). As the pressure fell, the emergency core cooling system activated to make up for lost water, again as designed. The pressurizer relief valve should have re-closed, but did not. This led to a small and continuing loss of coolant through the open valve, which went unrecognized for hours. The result was that the loss of inventory uncovered the core, leading to a partial core melt, hydrogen production from oxidation of the fuel sheaths at very high temperatures, a hydrogen burn inside containment, and a partial melt-through of the pressure-vessel wall at the bottom. However, the wall remained intact. Finally, the failed valve was recognized and then isolated by closing a blocking valve, the main pumps were turned back on to re-pressurize the system, and high-pressure make-up water was added to refill it. Figure 20 shows the end state of the core [Smithsonian, 2004].

A stuck-open pressure-relief valve (PRV) is uncommon, but not rare. What converted this operating transient into a partial core melt was that the operators did not realize that the valve had stuck open, partly because the valve indicator in the control room was derived from the valve actuating signal, not the actual valve-stem position, and partly because the pressurizer level was *rising* due to the loss of coolant from the top—the opposite of what one would expect for loss of coolant elsewhere in the RCS. The operators had been trained when operating a "solid" system (no boiling) to use pressurizer level as a measure of circuit inventory, and they came to the erroneous conclusion that there was *too much* water in the system. If water is added to a sub-cooled system, the pressure can rise very fast indeed when the steam space in the pressurizer is filled up, and the operators were trying to avoid this. Their actions over the next several hours were complex and confused, clearly indicating that they did not understand what was happening and did not have the training or the tools to do so.

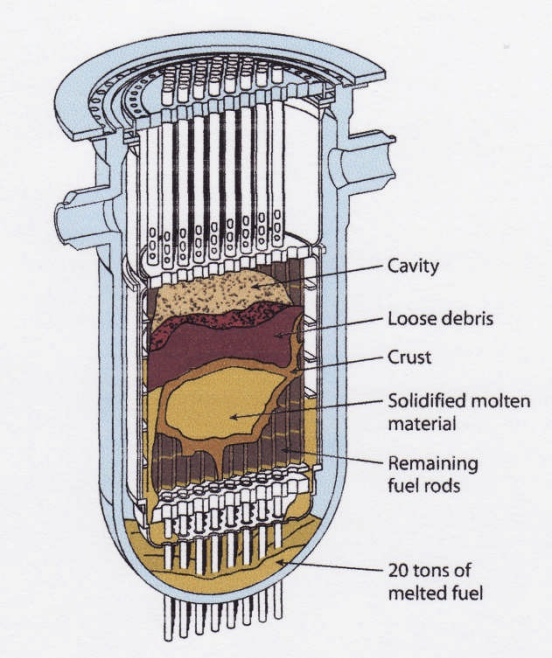

Figure 20 TMI core end state

The containment did its job. Small amounts of noble gases and iodine were released through a leakage recovery system (which could not be isolated because that would also stop primary pump seal cooling) and by venting the make-up tank to control its pressure. It is a credit to the containment design concept that a partial core melt resulted only in very small releases.

In addition, this was a "wet" accident, i.e., the radioactive material had the opportunity to interact with quantities of water in the reactor vessel and containment. This is in contrast to Chernobyl, where the moderator caught fire. Fission products such as iodine and cesium combine when released from overheated fuel to form cesium iodide (an aerosol). However, when CsI meets water, it dissociates:

$$CsI \rightarrow Cs^{+} + I^{-},$$

and is thereafter very difficult to remove (compare this to trying to remove chlorine after dissolving table salt (NaCl) in water). TMI taught that in terms of public safety, "wetter is better".

The lifetime health effects on the surrounding population were predicted to be effectively zero.

3.2.2.1 Lessons learned

1. A number of obvious improvements were needed to valve position indicators, event logging, and alarm prioritization (the printers were swamped by the number of alarms,

running far behind the event), as well as provision of diagnostic aids to the operators.
2. The prescriptive approach to reactor safety in the United States, which was based on regulatory-driven lists of design basis accidents, had focused attention on too narrow a range of accidents, not just because it omitted severe accidents, but also because it focused on bounding design basis accidents and treated superficially the supposedly less-severe DBAs such as a small LOCA.
3. PSA became far more important and more widely used to define and therefore prevent possible severe accidents.
4. Sharing of prior experience with other plants was poor. TMI led to the establishment of the Institute of Nuclear Power Operations (INPO) for industry-wide cooperation in operations and training.

3.2.3 Fukushima Dai-ichi

Much of this material is taken from official reports or presentations by the Japanese Government [Japan, 2011], the Tokyo Electric Power Company (TEPCO) [TEPCO, 2011a], the Japan Nuclear and Industrial Safety Agency (NISA) [NISA, 2011], the International Atomic Energy Agency (IAEA) [IAEA, 2011], and the United States Nuclear Regulatory Commission (USNRC) [USNRC, 2011]. Vast amounts of detailed material exist on this event—it is probably the most photographed accident in history—and many details are still unclear or unknown, e.g., the exact state of the cores in Units 1, 2, and 3 and the containment status.

3.2.3.1 Description

There are six nuclear power reactors at the Fukushima I (Dai-Ichi) site. All are boiling-water reactors (BWRs). There are four more BWR reactors nearby at Fukushima II (Dai-Ini). Figure 21 (from [USNRC, 2011]) shows the overall station layout of Fukushima Dai-Ichi.

Mark 1 type BWRs have an “inverted light-bulb” containment (the drywell) connected to a toroidal suppression pool or chamber (the wetwell), as can be seen in Figure 22. The purpose of the suppression pool is to condense any steam released inside the containment in an accident, such as a loss-of-coolant accident, and also to act as a temporary or permanent heat sink for decay power in case the main heat-removal mechanisms are unavailable. If the suppression chamber (S/C) is to act as a long-term heat sink, it must be cooled by an external circuit, e.g., for Unit 1 (which we shall use as the example), the isolation condenser.

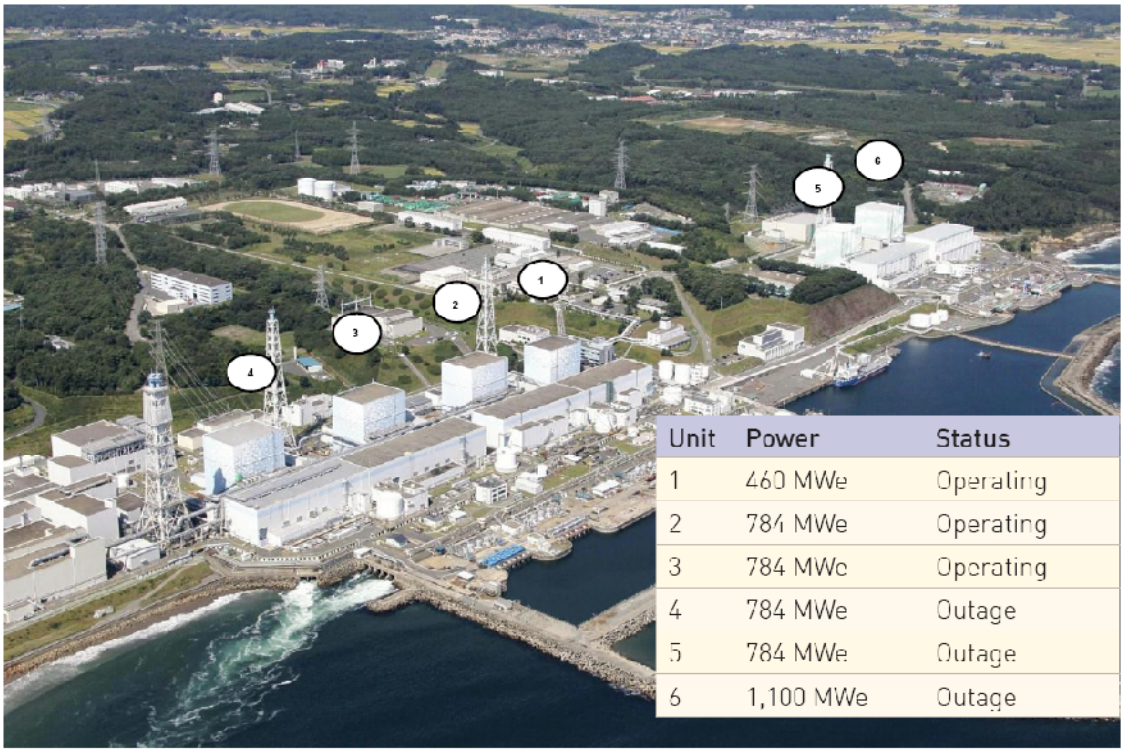

Figure 21 Fukushima Dai-ichi before earthquake

The containment vessel is surrounded by a reactor building, which, among other things, contains and supports the elevated spent-fuel pool. The reactor building is not designed to withstand significant pressure.

The IAEA [IAEA, 2011] notes that:

> "In Unit 1, the Isolation Condenser (IC) is designed to operate through gravity driven natural circulation of coolant from the reactor pressure vessel (RPV) through a heat exchanger immersed in a large tank of water in the reactor building at an elevation above the core. The Unit 1 IC was designed to have a decay heat-removal capacity of about eight hours. A valve must be manipulated to bring the IC into service."

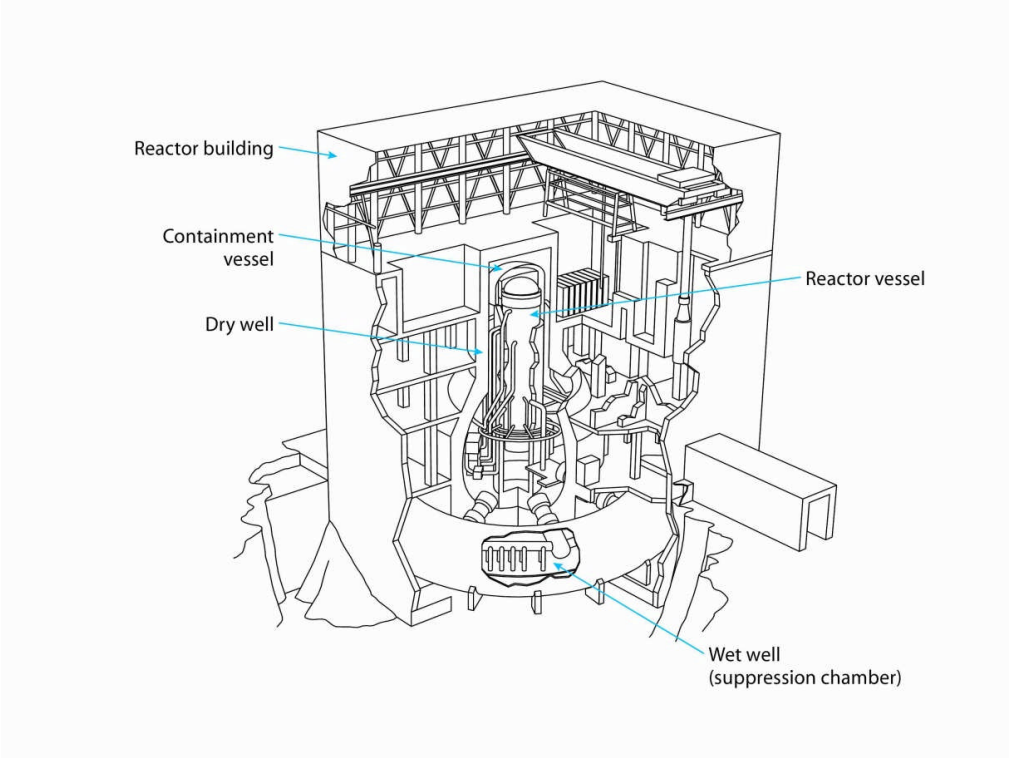

Figure 22 BWR Mark 1 containment

3.2.3.2 The event

At 14:46 on Friday, March 11, 2011, a magnitude 9 earthquake took place off the eastern coast of Japan. The earthquake occurred at a depth of 24 km and initiated a tsunami which was estimated to be 14 m high when it hit Fukushima approximately 40 minutes later, followed by multiple additional waves. The measured on-site accelerations due to the earthquake were greater than the design basis for Fukushima I, but less than the design basis for Fukushima II. Although the earthquake caused significant on-site damage and loss of all off-site electrical power, in both stations, all operating units were automatically shut down, and the emergency diesel generators started and functioned until the tsunami hit.

The design basis tsunami for Fukushima I was O.P. (base level) +5.7m; the actual height was O.P. +14–15 metres. Figure 23 shows a cross section of the station and the flood level.

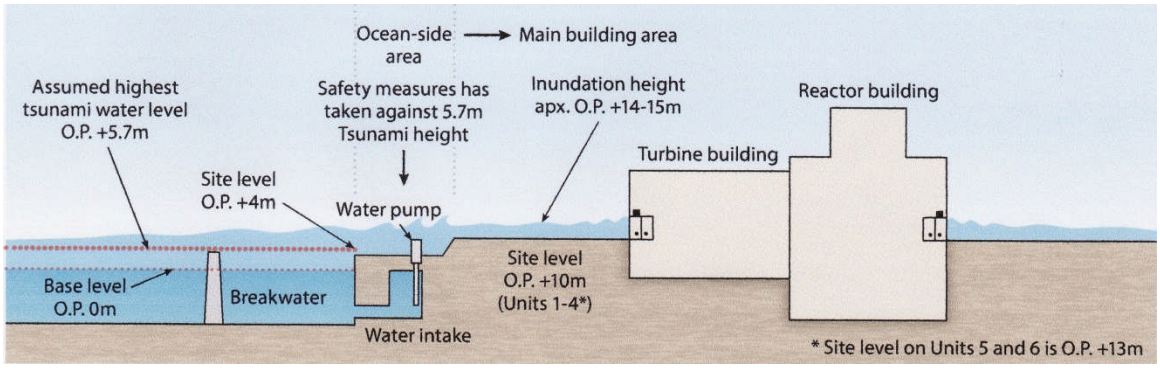

Figure 23 Design basis versus actual flood level

The emergency diesel generators at Fukushima I (which are cooled by sea-water) were all disabled by the flood; because off-site AC power was already lost, the result was a total loss of all AC power at Fukushima I, units 1 through 5; hence, all motor-operated pumps became inoperable. In addition, lighting in the main control room was lost. The sea-water system (used to reject heat to the ultimate heat sink) was likewise inoperable. Unit 6 had one functioning air-cooled diesel generator, which was cross-tied after the flood, with some effort, to Unit 5 and was instrumental in achieving cold shutdown in those units with no fuel damage. In addition, because the emergency batteries could no longer be charged, control and instrumentation power in Units 1–4 was eventually also lost, crippling the ability to monitor the reactor state or to operate motorized valves.

Taking Unit 1 as an example (the sequence of events in other units was similar, but the timing was somewhat prolonged), the isolation condenser was initially used to remove decay heat. However, the isolation condenser stopped operating fairly soon thereafter. With no core heat sink, the water in the vessel began to boil away, with the steam condensing in (and heating up) the suppression pool and the level in the reactor vessel falling, eventually exposing fuel. As the fuel overheated in a steam environment, the zirconium cladding oxidized and produced hydrogen.

The challenges were then:

- to restore water over the fuel
- to prevent containment failure due to over-pressure
- to control and release the hydrogen.

About 15 hours after the earthquake (March 12 at 05:46), the operators managed to inject fresh water using fire pumps, followed about 13 hours later (March 12 ~19:00–20:00) by direct sea-water injection. To control containment pressure, the primary containment vessel (PCV) was apparently vented on March 12 at 10:17. This appears to have allowed the hydrogen in containment to migrate to and accumulate in the reactor building; it exploded at 15:36 on March 12, destroying much of the superstructure of the building.

It appears from analyzes done with severe accident codes that the fuel in Units 1, 2, and 3 melted a few hours after being uncovered and may have penetrated the reactor vessel and the primary containment. (This could also be deduced from fairly simple bounding calculations.)

The current state and location of the core and the integrity of the reactor vessel and the primary containment are not known with certainty, although damage to both is expected.

A further issue was the condition of the fuel in the spent-fuel pools. Normally, the decay heat generated by the fuel bundles in the pools is removed by active systems, which of course were lost when all AC power was lost. In the absence of heat removal, or if water is lost due to leakage, heating of the spent fuel is slower than heating of the core, but if not addressed, will eventually lead to uncovering of the fuel and fuel damage. In Fukushima, the spent-fuel bays are located high in the reactor building to facilitate transfer of fuel assemblies from the core. Spent-fuel cooling was made more difficult by the elevation (and inaccessibility) of the spent-fuel bays, and concerns were voiced about their structural integrity following the earthquake. In the early phases after the accident, water was added manually to the bays (initially from helicopters and later from cranes); stable cooling has since been restored to all pools. Inspection of the bays shows debris from the damaged reactor buildings; TEPCO has stated, "Most spent fuels estimated to be undamaged" based on the radioactive contents of the pool water and remote inspection. As of December 2013, fuel in the Unit 4 pool is now being removed.

Fukushima II was not flooded nearly as severely as Fukushima I and successfully achieved cold shutdown of all units.

The safety goal is to achieve cold stable shutdown, with temperatures below 100°C and any releases of radioactive materials from containment under control.

The injection of sea-water, while presumably stopping further core melting, led to a large accumulation of highly radioactive water in the basement of the buildings because cooling was essentially "once-through". Some of this water intermittently leaked to the sea and to ground. Once-through cooling was later converted to closed-loop cooling and continuously decontaminated using on-line filtration. In addition, to prevent further release of airborne radioactive material from debris or leakage to ground or sea from rain, the reactor buildings are being covered by weatherproof covers.

Finally the large amounts of highly contaminated water on site have to be treated and securely stored.

3.2.3.3 Lessons learned

Although it is still early after the accident to formulate complete lessons learned, it seems reasonable that they will include the following issues:

1. Ensure completeness of design basis accidents, especially external events, and in particular those with a cliff-edge effect like flooding (dramatic worsening of consequences for a small change in the severity of the event).
2. Ensure that resources are available in the long term after a severe event to control, cool, and maintain: for example, portable generators with pre-designed hookups to key equipment, flexible hoses that can be run to sources of water.
3. Ensure prolonged core cooling in the absence of off-site power and failure of on-site diesel generators.
4. Ensure prolonged spent-fuel bay cooling or make-up and monitoring after a prolonged

loss of power.

5. Prevent loss of monitoring (e.g., design the station emergency batteries to last for a significant length of time, protect them against external events, and provide recharging capability). Maintain on-site and off-site communications.
5. Provide facilities on site to deal with physical destruction and high radiation fields (e.g., bulldozers to clear debris).
6. Review lessons learned about institutional behaviour, e.g., the role of the regulator. See Chapter 16 for a case study.
7. Examine the impact on accident evolution of having multiple units at one site.

3.3 Problems

1. Browns Ferry Fire, 1975:
    a. Locate (as a minimum) the following source material (try the USNRC web site): Fire at Browns Ferry Nuclear Plant; Tennessee Valley Authority; March 22, 1975 - Final Report of Preliminary Investigating Committee, May 7, 1975.
    b. Assess the Browns Ferry fire in terms of threats to the ability to *control, cool, contain, and monitor*.
    c. Indicate lessons learned. Describe how you derived these lessons learned. Do not just copy official lessons learned.
    d. Comment on the robustness of the design and indicate whether design or operating changes should have been considered (and why).
2. Tokai-Mura, 1999:
    a. Locate (as a minimum) the following material: International Atomic Energy Agency, Report on the Preliminary Fact Finding Mission Following the Accident at the Nuclear Fuel Processing Facility in Tokaimura, Japan; IAEA report, 1999.
    b. Assess the accident in terms of threats to the ability to *control, cool, contain, and monitor*.
    c. Indicate lessons learned. Describe how you derived these lessons learned. Do not just copy official lessons learned.
    d. Comment on the robustness of the facility design and operation, and indicate whether design or operating changes should have been considered (and why).

4 Safety Goals and Risk Assessment

In this section, we expand on the concept of risk introduced in Section 1.8. We start off by defining *numerical safety goals*, which are a means of quantifying risk, and then present some *probabilistic safety assessment* tools that can be used to calculate whether or not the plant meets the safety goals.

4.1 Safety Goals

A safety goal partially answers the question "how safe is safe enough?" In this sub-section, we will develop a worked example of how a safety goal might be derived and then compare it to safety goals adopted by other organizations. We shall also point out some of the pitfalls of using a safety goal as the only safety criterion. The intent of this section is that the reader should be able to understand how safety goals are derived, what their limitations are, and how they are used in design.

To enable meaningful decisions, a safety goal should be expressed in quantitative terms. A safety goal such as "Make the reactor as safe as possible" will mean different things to different people and provides no guidance to the designer or operator. A goal such as "The reactor must never have a severe accident" is probably physically impossible and sets up expectations that cannot be met.

It is not easy to define a safety goal. Here is a possible starting point for a safety goal which has numerical requirements (and which is often used as the basis for regulatory decision-making):

"The annual risk of death to the most exposed member of the public due to accidents in a reactor should be small in comparison to his/her total risk of premature death."

Some of the aspects of this safety goal are:

- It uses a common risk measure (annual risk of death). Although this is objective, it may not be all that relevant to nuclear accidents: experience has shown that significant public dose from a severe accident develops slowly, giving time to move people out of harm's way. The results of real events have shown few public health effects.
- It compares the risk from a nuclear reactor to all other risks of premature death. This is not at all obvious. One could set up the comparison to all other risks of electricity generation, or all energy generation, or all (average) industrial activity. In fact, the first two would be much more logical because they compare risks of producing the same product (energy).
- No relative benefits are mentioned.
- The safety goal (in this example) is for the most exposed *individual*. It does not consider social effects such as radiation exposure to a *large number* of individuals, evacuation, land contamination, and effects on the environment such as on animals and plants. The assumption in this safety goal is that protection of the most exposed individual member of the public also provides sufficient protection for society at large and for the environment.
- The goal refers to members of the public, not workers in the plant. It is generally ac-

cepted that people will implicitly accept a somewhat higher risk to life and limb if it comes as part of their job, i.e., if a direct benefit is obtained. Attempts have been made (e.g., in the United Kingdom, see [HSE, 2006]) to set (nuclear) safety goals for plant workers in nuclear power plants, but the risk to such workers is dominated by conventional industrial risk, which itself turns out to be less than in comparable non-nuclear industries.

- The goal refers to the risk of nuclear power in isolation. Just as there is a risk to having nuclear power, there is also a risk to *not* having it, because the electricity would then have to be generated from other sources with greater (or lesser) risk.

The goal does not distinguish between prompt and delayed risk of death. We can break down the safety goal proposed above into two sub-goals:

> "The annual risk of prompt death to the most exposed member of the public due to accidents in a reactor should be small in comparison to his/her total annual risk of prompt death due to all accidents",

and

> "The annual risk of fatal cancer to the most exposed member of the public due to accidents in a reactor should be small in comparison to his/her total annual risk of fatal cancer due to all causes."

4.1.1 Risk of prompt death

In Canada in 2009, accidents were the fifth leading cause of death over the whole population, at a rate of 30.4 deaths for every 100,000 people [StatsCan, 2009]. This means that the average person's risk of death from an accident is ~3×10^{-4} per year (note that the rate for males is 50% higher than that for females). We could then say that the risk from a nuclear power plant of premature death to an individual should be small compared to 3×10^{-4} per year, say by a factor of 100 (this may be too conservative, but we will use it for illustration), or 3×10^{-6} per year. Because the only way of causing prompt fatalities to the public in a nuclear accident is through a core melt and failure of containment, and even that will likely not cause prompt public fatalities (given the experience of Chernobyl and Fukushima), this suggests that our safety goal should be:

> "The likelihood of a large release from a nuclear power plant in an accident should be less than 3 per 10^6 reactor years".

(Note that to risk prompt deaths, a large release by itself is not sufficient; it must also be sudden, otherwise people can be evacuated beforehand.) These changes have yielded a goal that can be used in design: it is relatively straightforward using PSA to calculate the likelihood of a large rapid release (core melt plus early failure of containment), to see (if the goal is exceeded) where the dominant contributors are, and to fix them if needed to meet the safety goal.

4.1.2 Risk of delayed death

Cancer fatalities can be considered in a similar fashion. In the same year in Canada (2009), malignant neoplasms were the leading cause of death over the whole population, at a rate of

211 deaths per 100,000 people. Therefore, the average person's risk of dying from cancer is 2.1×10^{-3} per year (or about 16% over a 75-year lifetime). Recall from Chapter 1 that 100 person-Sv will produce about five fatal cancers in the exposed population, or a risk of 5×10^{-2} fatal cancers per Sv. Therefore, using the linear dose-effect hypothesis, 211 cancer deaths per 100,000 people would be induced by a collective dose *D* calculated as follows:

$$D(Sv) \times 5 \times 10^{-2} \text{ (cancers / Sv)} = 211 \text{ cancer fatalities,} \quad (4)$$

which means that D = 4220 Sv, or an average individual dose of 42 mSv. However, *the linear dose-effect hypothesis is not applicable to such low doses*. Regardless, if we divide by 100 again, then the maximum time-averaged individual dose from accidents should be less than 0.4 mSv per year, averaged over a group of people, or about 25% of natural background radiation in Toronto (1.6 mSv / year). The paradox with this safety goal is that it would make nuclear power safer than natural background radiation.

This is not as useful a safety goal as the previous one because it does not tell us anything about the frequency distribution of accidents. However, it can likewise be validated by summing all the events in a PSA which cause a release of radioactive material.

At a more basic level, summing low doses over large numbers of people is incorrect, and a safety goal derived this way is fundamentally flawed.

4.1.3 Safety goals in Canada

The CNSC has recently published safety goals, for new reactors built in Canada. The rationale is similar to our sample case. Specifically, CNSC states [CNSC, 2008]:

> "A limit is placed on the societal risks posed by nuclear power plant operation. For this purpose, the following two qualitative safety goals have been established:
> 1. Individual members of the public are provided a level of protection from the consequences of nuclear power plant operation such that there is no significant additional risk to the life and health of individuals; and
> 2. Societal risks to life and health from nuclear power plant operation are comparable to or less than the risks of generating electricity by viable competing technologies, and should not significantly add to other societal risks."

These are developed into design goals:

1. "*Core Damage Frequency*: The sum of frequencies of all event sequences that can lead to significant core degradation is less than 10^{-5} per reactor year
2. *Low Release Frequency*: The sum of frequencies of all event sequences that can lead to a release to the environment of more than 10^{15} Becquerel of iodine-131 is less than 10^{-5} per reactor year. A greater release may require temporary evacuation of the local population.
3. *High Release Frequency*: The sum of frequencies of all event sequences that can lead to a release to the environment of more than 10^{14} Becquerel of cesium-137 is less than 10^{-6} per reactor year. A greater release may require long term relocation of the local population."

This is largely consistent with international practice for new reactors, with one new concept: the low release frequency. It is intended to address those accident scenarios which may result in small but significant releases. These accidents may require emergency measures such as sheltering or short-term evacuation of an area around the plant, and the low release frequency sets a limit on these [Rzentkowski, 2013].

An approach to safety based *only* on a safety goal has both benefits and limitations. The greatest benefit is that risk-based decisions require greater levels of protection on those areas of greatest risk, and conversely, i.e., they optimize safety resources. Some limitations are:

- To determine compliance with a risk target, all significant events have to be identified and summed. This might be challenging in the early phases of a design.
- Safety goals are meaningful only for events for which frequencies and consequences are reasonably calculable. In practice, this includes most "internal" events for which actual data exist, for which the failure combinations can be calculated, or for which a reasonable extrapolation from the historical record can be made. However, if the design has innovative features, with little operating experience, it may be difficult to support the reliability values and hard to spot the cross-links[4]. Passive safety systems pose a particular challenge in this regard because they can be difficult to test, and therefore it is hard to build up a reliability database.
- Not all (rare) events can be assigned a frequency and consequence with confidence, for example:
    - massive structural failure
    - massive failure of pressure vessels
    - very low-frequency, high-consequence external events such as earthquakes beyond historical record-keeping
    - sabotage, terrorism, and war.

The approach to the first two is usually to design to accepted engineering codes and standards. Then one can infer from experience the likelihood of sudden failure of structures and components so designed. Massive failure of a LWR pressure vessel would be a catastrophic event because it would lead to an immediate release of fission products and probably would damage containment at the same time. Calculations have been done to show that such massive failures are less frequent than 10^{-8} per year, but such low frequencies must be treated with some skepticism. Rare events can happen by unanticipated sneak paths; for example, a precursor to a pressure-vessel boundary failure was the undetected almost-through-wall erosion of the reactor pressure vessel in the Davis-Besse plant [USNRC, 2002]. Similarly, historical records make it possible to define the intensity of earthquakes down to about the ten-thousand-year return frequency, which is taken as the design basis earthquake (DBE) in Canada. More severe but rarer earthquakes are hard to characterize. One can carry out a "seismic margin" analysis to calculate the likelihood of surviving an earthquake somewhat more severe than the DBE; much beyond that, about all one can say is that the effects of damage to the nuclear plant would be

[4] A cross-link is a failure that affects more than one system or component, e.g. a common supply of instrument air.

small compared to the havoc wreaked by such an earthquake on the rest of society, as was the case for Fukushima. Finally for events resulting from hostile human actions, the approach has generally been to design according to rules (e.g., the plant's inherent defences plus the local security force should be able to delay an attack of *x* people armed with *y* type of weapons for *z* minutes); *x*, *y*, and *z* are indeed chosen based on reasonableness (likelihood), but the historical database of hostile acts against nuclear power plants is sparse. In any case, the defences being built into new plants for severe accidents are also helpful against malevolent acts.

For these reasons, those regulators that have safety goals use them *in addition* to whatever deterministic criteria they have developed. This combination is called a *risk-informed* approach, in which the quantified risk provides a powerful rationality check.

4.2 Risk Assessment

This section summarizes the probabilistic safety assessment concepts and tools used to demonstrate numerically that the plant meets its safety goals, as well as for many other purposes. For basic references, see [McCormick, 1981] and [USNRC, 1981].

4.2.1 The basics

First, you may want to refresh your memory by reading Appendix 1 – Basic Rules of Boolean Algebra and the rules about the probability of multiple events. The following text assumes you already know, or have read, all this material.

Sample Problems:

a) A nuclear reactor has two fully independent shutdown systems. The probability that a shutdown system will fail on demand is 1 in 1000. What is the probability that they will *both* fail in an accident?

Answer:

Let A_1 be the event where shutdown system 1 fails and A_2 be the event where shutdown system 2 fails. These are stated to be independent events, so:

$$P(A_1\ A_2) = P(A_1)\ P(A_2) = 10^{-3} \times 10^{-3} = 10^{-6}.$$

(Sometimes it is hard to ensure that redundant systems are *completely* independent).

b) As above, but what is the probability that *either* will fail in an accident?

Answer:

We can use the rare events approximation because $P(A_1)$ and $P(A_2)$ are <<1.

Here, we want $P(A_1 + A_2)$:

$$P(A_1 + A_2) \cong P(A_1) + P(A_2) = 10^{-3} + 10^{-3} = 2 \times 10^{-3}.$$

c) Now consider two independent diesel generators, each with a probability of failure to start of 15%. What is the probability that *either* will fail to start?

Answer:

We cannot really use the rare events approximation here, so:

$$P(A_1 + A_2) = P(A_1) + P(A_2) - P(A_1A_2) = 0.15 + 0.15 - (0.15)*(0.15) = 0.28.$$

4.2.2 Bayes equation

The Bayes equation is typically used in nuclear power applications to predict the likelihood of a rare event given the history of few (or no) such events. We will prove it first and then give some examples which make it clearer.

Given an event or hypothesis, B, and A_n mutually exclusive events or hypotheses (n=1, 2....N):

$$P(A_n B) = P(A_n)P(B \mid A_n) = P(B)P(A_n B), \tag{5}$$

$$\therefore P(A_n \mid B) = P(A_n)\left[\frac{P(B \mid A_n)}{P(B)}\right]. \tag{6}$$

Because the events A_n are mutually exclusive,

$$\sum_{n=1}^{N} P(A_n \mid B) = 1. \tag{7}$$

Multiplying by *P(B)*:

$$P(B) = \sum_{n=1}^{N} P(B)P(A_n \mid B) = \sum_{n=1}^{N} P(A_n)P(B \mid A_n). \tag{8}$$

Substituting (8) into (6)

$$P(A_n \mid B) = \frac{P(A_n)P(B \mid A_n)}{\sum_{m=1}^{N} P(A_m)P(B \mid A_m)}. \tag{9}$$

This is Bayes' theorem. Therefore, if we know $P(B|A_n)$, we can calculate $P(A_n|B)$. A couple of examples will make this clearer.

Sample Problems

Pipe Inspection

Suppose that you are radiographing a Class I pipe for a defect. You know from past experience that the likelihood of a defect is one per 100,000 radiographs. You also know that the likelihood that the instrument indicates a defect when there is *no* defect (false positive) is 1%, and the likelihood that the instrument indicates a defect when a defect in fact exists is 99%. Your test indicates a defect. What is the probability that the pipe actually has a defect when the instrument says it does?

Answer:

Apply Bayes' theorem to two events:

A: pipe has a defect, therefore $P(A) = 0.00001$

B: instrument says that pipe has a defect, therefore $P(B)=0.01$[1]

B|A: instrument says pipe has a defect when it has a defect, therefore $P(B|A) = 0.99$

What we want is $P(A|B)$, the probability that the pipe actually has a defect when the instrument says it has one.

Using Bayes' theorem:

$P(A|B) = P(B|A)[P(A)/P(B)]$

$= 0.99 \times 0.00001 / 0.01$

$= 0.00099$

because the denominator in Equation (9) is just $P(B)$, which in this case is known. The result seems counterintuitive and suggests that the test is not very good in detecting defects, despite the instrument's high accuracy rate. However, the fact that the defect is so rare (we need about a hundred thousand samples before we have a good chance of seeing a real positive) magnifies the small false positive rate, so that most positive tests are false positives.

This is quite important in medical tests; even a very accurate test for a rare cancer will often give far more false positives than real ones.

4.2.2.1 Failure rate estimation when no failures have occurred

We can use Bayes' equation to glean information from non-events as well [Kaplan, 1979].

Large LOCA

There have been 14,800 reactor years of experience without a large break LOCA. What is an upper estimate of the frequency?

Answer

Let B = 14,800 reactor years of experience without a large break LOCA (LBLOCA).

What we do now is take (say) six cases, in each of which we hypothesize the value of the LLOCA frequency. We then use Bayes' theorem to test how good our hypotheses are (i.e., calculate the probability that each hypotheses is correct). We label our hypotheses A_1 to A_6.

---

[1] This is a slight simplification using the fact that $P(A)$ is small. Actually

$P(B) = P(B|A)\,P(A) + P(B|\bar{A})\,P(\bar{A})$

$= 0.99 \times .00001 + 0.01 \times 0.99999$

$= 0.0100098$

or approximately 0.01 as stated.

In words, the first term is the 99% chance of detecting the defect in the one pipe in 100,000 that has the defect; the second term is the 1% chance of indicating a false positive in the remaining 99,999 pipes out of 100,000.

A_1 = LBLOCA probability = 10^{-2} / year
A_2 = LBLOCA probability = 10^{-3} / year
A_3 = LBLOCA probability = 10^{-4} / year
A_4 = LBLOCA probability = 10^{-5} / year
A_5 = LBLOCA probability = 10^{-6} / year
A_6 = LBLOCA probability = 10^{-7} / year

If A_1 were true, then:

$$P(B|A_1) = (1 - 10^{-2})^{14800} = 2.5 \times 10^{-65}.$$

Because we can assume that each reactor-year of experience is independent, the probability of each reactor-year without a LBLOCA is $1 - 10^{-2}$, and $P(B|A_1)$ is just the intersection of 14,800 events.

Likewise, we find that:

$$P(B|A_2) = (1\text{-}10^{-3})^{14800} = 3.7 \times 10^{-7}$$
$$P(B|A_3) = (1\text{-}10^{-4})^{14800} = 0.2276$$
$$P(B|A_4) = (1\text{-}10^{-5})^{14800} = 0.8624$$
$$P(B|A_5) = (1\text{-}10^{-6})^{14800} = 0.9853$$
$$P(B|A_6) = (1\text{-}10^{-7})^{14800} = 0.9985$$

If we knew $P(A_1),...,P(A_6)$, we could calculate $P(A_n|B)$, or the probability that our statement A_n is actually true. But we don't know. Instead, we can make an assumption, called an *a priori* probability: let's just *assume* that $P(A_n) = 1/N = 1/6$, which is the case labelled "uniform prior" in Table 5, i.e., that each hypothesis is equally likely. Then, using Bayes' theorem, we find that $P(A_1|B) = 8.14 \times 10^{-66}$, i.e., A_1 is not very likely. From Table 5, we see that A_2 is more likely than A_1, but that A_4 to A_6 are even more likely. If we use these results to postulate a more likely series of $P(A_n)$, labelled "non-uniform prior" in the table, we can see that $P(A_n|B)$ is further adjusted, and we can conclude that the LLOCA frequency is significantly less than 10^{-3}. The practical application of this is in assigning a reasonable upper limit to a frequency in a probabilistic safety analysis, when no such events have actually occurred and all we have is the number of reactor-years of experience.

Note that one of the criticisms of Bayes' Theorem when used this way is that the answer depends on the appropriateness of the initial hypotheses. If few data are available and you put in strange hypotheses, you get back strange answers. Note also that if no events have occurred, Bayes' Theorem does not give information about the lower limit of the frequency.

Table 5 Bayes' theorem example

n	1	2	3	4	5	6
A_n	10^{-2} / year	10^{-3} / year	10^{-4} / year	10^{-5} / year	10^{-6} / year	10^{-7} / year
$P(B\|A_n)$	2.5×10^{-65}	3.7×10^{-7}	0.2276	0.8624	0.9853	0.9985
Uniform Prior						
$P(A_n)$	0.1667	0.1667	0.1667	0.1667	0.1667	0.1667
$P(A_n\|B)$	8.14×10^{-66}	1.20×10^{-7}	0.0741	0.281	0.321	0.325
Non-Uniform Prior						
$P(A_n)$	0.001	0.01	0.1	0.4	0.4	0.089
$P(A_n\|B)$	2.27×10^{-66}	3.36×10^{-9}	0.0251	0.358	0.394	0.0808

4.2.3 Probability distributions

We will now develop the theory behind failure probabilities, failure rates, and reliability.

Let *p(x)dx* be the probability that an event occurs in an interval *x* to *x+dx*—the probability density function. Let *P(X)* be the cumulative probability that the event occurs somewhere between x_{min} and *X*. Then

$$P(X) = \int_{x_{\min}}^{X} p(x)dx = P(x < X), \tag{10}$$

where *p(x)* is the probability density function. If *p(x)* is a constant, p_o, then $P(X) = p_o(X-x_{min})$, as expected.

There are two types of systems:

1) Those that operate on demand (i.e., safety systems)
2) Those that operate continuously (i.e., process systems).

4.2.3.1 Demand Systems

We define:

D_n = n^{th} demand
$P(D_n)$ = probability of success on demand *n*
$P(\bar{D}_n)$ = probability of failure on demand *n*
W_n = case where system works for each demand up to and including demand *n*

What is the probability that it works for *n-1* demands and fails on demand *n*?

$$P(W_{n-1}) = P(D_1 D_2 ... D_{n-1}) , \tag{11}$$

$$P(\bar{D}_n W_{n-1}) = P(\bar{D}_n \mid W_{n-1}) P(W_{n-1}) . \tag{12}$$

Therefore,

$$\begin{aligned} P(D_1 D_2 ... D_{n-1} \bar{D}_n) &= P(\bar{D}_n \mid W_{n-1}) P(W_{n-1}) \\ &= P(\bar{D}_n \mid D_1 D_2 ... D_{n-1}) \times P(D_{n-1} \mid D_1 D_2 ... D_{n-2}) \times ... \times P(D_2 \mid D_1) \times P(D_1) . \end{aligned} \tag{13}$$

If all demands are alike and independent, this reduces to:

$$P(D_1 D_2 ... D_{n-1} \bar{D}_n) = P(\bar{D}) [1 - P(\bar{D})]^{n-1} . \tag{14}$$

4.2.3.2 Failure dynamics

Failures can be time-dependent.

Let: *f(t)dt* = probability of failure at time *t* in the time interval *dt*

$$\begin{aligned} F(t) &= \text{cumulative failure probability} \\ &= \int_0^t f(\tau) d\tau \end{aligned} . \tag{15}$$

Assuming that the device eventually fails, the reliability, *R(t)* is defined as

$$\begin{aligned} R(t) &= 1 - F(t) \\ &= \int_0^\infty f(\tau) d\tau - \int_0^t f(\tau) d\tau . \\ &= \int_t^\infty f(\tau) d\tau \end{aligned} \tag{16}$$

Therefore,

$$f(t) = -\frac{dR(t)}{dt} = \frac{dF(t)}{dt} . \tag{17}$$

Let *λ(t) dt* = probability of failure at time *t* given successful operation up to time *t* (i.e., the conditional failure rate); then:

$$\begin{aligned} & f(t) dt = \lambda(t) dt R(t) \\ & \text{or} \\ & f(t) = \lambda(t) R(t) = -\frac{dR(t)}{dt} \end{aligned} , \tag{18}$$

and hence

$$\frac{dR(t)}{dt} = -\lambda(t) R(t) . \tag{19}$$

Solving and using the boundary condition $R(0)=1$:

$$R(t) = e^{-\int_0^t \lambda(\tau)d\tau}. \tag{20}$$

If λ is constant, (i.e., random failures):

$$R(t) = e^{-\lambda t}. \tag{21}$$

A typical *λ(t)* is shown in [McCormick, 1981], page 26—the "bathtub" curve (Figure 24).

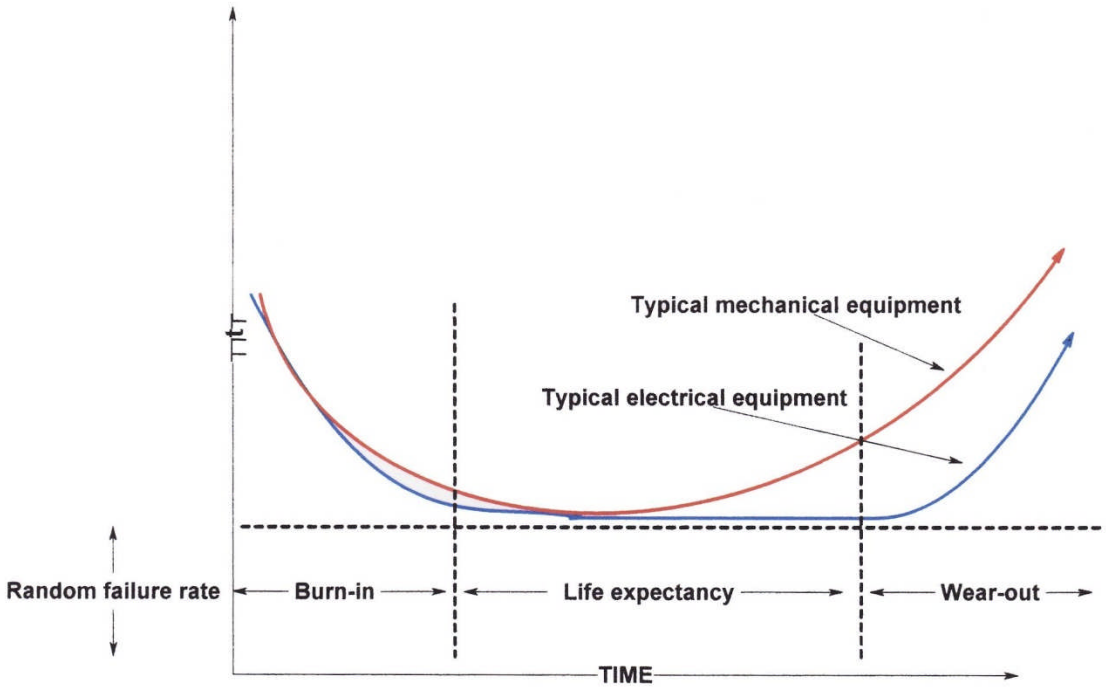

Figure 24 Typical λ(t) versus time

Table 6 summarizes the relationships among these quantities.

Table 6 Reliability terms and relationships

Description	Symbol	=	=	=
Hazard rate	λ(t)	$-\frac{1}{R}\frac{dR}{dt}$	$\frac{f(t)}{1-F(t)}$	$\frac{f(t)}{R(t)}$
Reliability	R(t)	$\int_t^\infty f(\tau)d\tau$	1-F(t)	$e^{-\int_0^t \lambda(\tau)d\tau}$
Cumulative failure probability	F(t)	$\int_0^t f(\tau)d\tau$	1-R(t)	$1-e^{-\int_0^t \lambda(\tau)d\tau}$
Failure probability density	f(t)	$\frac{dF(t)}{dt}$	$-\frac{dR(t)}{dt}$	λ(t) R(t)

4.2.3.2.1 Mean time to failure (MTTF)

This is simply the time-weighted average over all time of the failure probability density:

$$\text{MTTF}=\frac{\int_0^\infty \tau f(\tau)d\tau}{\int_0^\infty f(\tau)d\tau}=\int_0^\infty \tau f(\tau)d\tau \qquad (22)$$

$$\text{since } \int_0^\infty f(\tau)d\tau = 1 \qquad \text{(a component will eventually fail).}$$

If λ is constant, then

$$MTTF=\int_0^\infty \tau\lambda e^{-\lambda\tau}d\tau=\frac{1}{\lambda}. \qquad (23)$$

4.2.3.2.2 Availability, *A*(*t*)

Availability is the proportion of the time that a system is in a functioning condition. If no repairs have been made, it is the same as reliability. If a system has been repaired, then its availability will satisfy:

$$R(t) \le A(t) \le 1.$$

Assume random failures. This implies that λ = constant, and therefore

$$R(t) = e^{-\lambda t} = \text{reliability,}$$

as illustrated in Figure 25. Eventually, the reliability goes to zero for long times.

Conversely, the failure probability is

$$F(t) \equiv 1 - R(t) = 1 - e^{-\lambda t},$$

as illustrated in Figure 25, and goes asymptotically to one for long times.

Let repair occur at some time interval, τ. This resets the failure probability to zero each time the component is repaired, assuming that the repair is perfect and restores the component to its original condition. Then $F(t)$ is a sawtooth curve, as illustrated in Figure 26.

If $\tau << \lambda$, then

$$F(t) = 1 - (1 - \lambda t + \frac{\lambda^2 t^2}{2} - ...) \approx \lambda t \text{ for } t < \tau \text{ in any interval}, \quad (24)$$

with *t* measured after the time of last repair.

Hence:

$$F = \frac{\lambda \tau}{2}, \quad (25)$$

i.e., the failure probability is half the test interval times the failure rate.

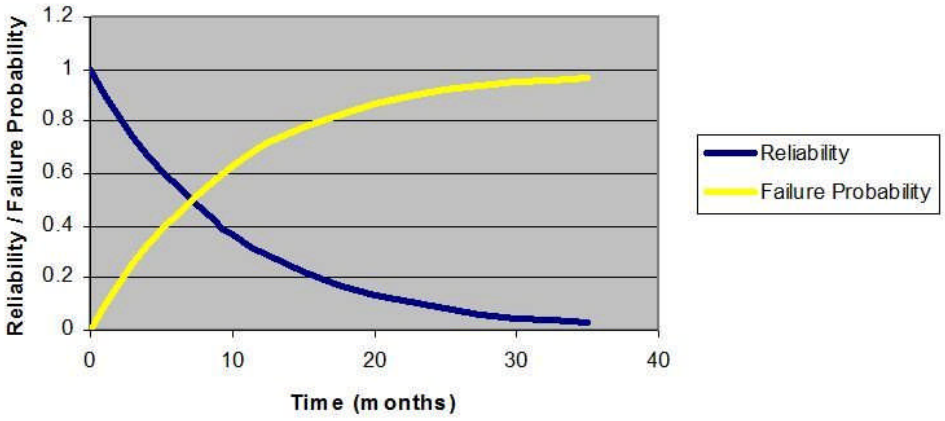

Figure 25 Reliability for constant λ

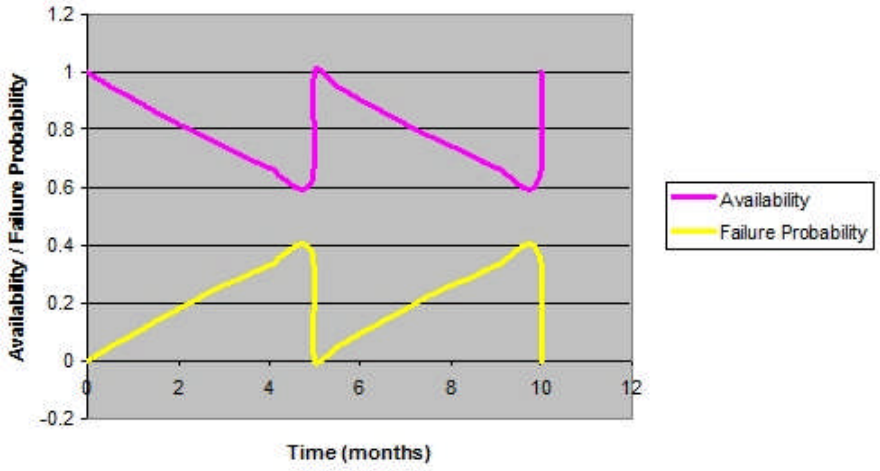

Figure 26 Availability with repair

For constant λ, but τ *not* << λ, the following applies:

$$\langle F \rangle = \int_0^\tau F(t)dt = \int_0^\tau (1-e^{-\lambda t})dt = \frac{\lambda\tau + e^{-\lambda\tau} - 1}{\lambda\tau}. \tag{26}$$

A common task is to design a system (composed of components that have a known failure rate) to meet some target unavailability (1-*A*) or $\bar{A}$. Given a design, the repair interval is the remaining variable. A frequent repair cycle (low τ) gives a low $\bar{A}$, but such frequent repair may be impractical due to excessive cost, radiation exposure, or wearout (i.e., repair does not restore the equipment to an as-built state). In such a situation, alternative designs would have to be considered.

Often repair may not be required to return *F* to zero. It may be sufficient simply to test the components to ensure that they are available. This is usually the case for "demand" systems.

Sample Problem

Consider the case of a single shut-off rod (SOR) for a reactor. Given a failure rate based on previous experience of λ = 0.002/year and a required unavailability of $\leq 10^{-3}$, what is the required test period, τ?

Answer:

$$\bar{A} \approx \frac{\lambda\tau}{2} = 0.001\tau. \tag{27}$$

To meet the $\bar{A}$ target of 10^{-3}, we solve for τ:

$$\tau \leq \frac{10^{-3}}{0.001/yr} = 1 \text{ year}. \tag{28}$$

4.2.3.3 System Unavailability

Of course, a real shutdown system has many more rods, say, *N* in total. Let E_n be the event where all rods except for *n* drop successfully. The system as a whole is designed to meet its requirements for the cases of E_0, E_1, E_2—i.e., if zero, one, or two rods fail to drop. Hence, the system unavailability $\bar{A}$ is the sum of all the failure probabilities:

$$\bar{A} = \sum_{k=3}^{N} P(E_k) = 1 - \sum_{k=0}^{2} P(E_k) . \tag{29}$$

The conversion to the second term makes the calculation much easier because there are fewer terms to sum. Assuming that the rods fail independently and that the failure rate is λ, then the probability of a given rod failing on average is:

$$< F > \approx \frac{\lambda \tau}{2} = p \text{ for conciseness} \tag{30}$$

as before. The success probability is *1-p*. In general, the probability of event E_k is

$$P(E_k) = \frac{N!}{(N-k)!k!} (1-p)^{n-k} p^k . \tag{31}$$

The factor $\frac{N!}{(N-k)!k!}$ gives the number of possible ways for the event to happen, the factor $(1-p)^{n-k}$ is the probability that *N-k* rods all successfully drop, and the factor p^k is the probability that *k* all fail to drop.

4.2.3.4 Fault trees

A more systematic way of calculating system unavailability is through fault trees. One starts at the top with the event of interest, usually a system failure. Then one determines each and every *immediate* cause of such an outcome. If either of several immediate causes is sufficient to cause the top event, then they are joined by an OR gate (please review Appendix 1 – Basic Rules of Boolean Algebra—for a refresher on probability theory).

Conversely, if *all* of several immediate causes must occur to cause the "top" event, then they are joined by an AND gate. Both AND and OR gates can have more than two inputs.

In more detail, the steps in drawing and then calculating a fault tree are:

- Start (at the top) from the undesired event, e.g., loss of feed water.
- Carefully define the boundaries of the system to be evaluated.
- Using the principle of immediate cause, draw the tree downwards using AND, OR, etc. Boolean logic.
- Stop at basic events for which we can no longer decompose the event or when we arrive at a point where we know the probability of failure, e.g., failure of a relay.
- Assign probabilities to each event in the tree.
- Calculate the Boolean algebra to determine the numerical probability of failure of the top event.

The last step is not conceptually difficult, but the amount of arithmetic can be huge. It is almost always done using special-purpose codes for all but the simplest of fault trees.

One test of a properly drawn fault tree is that causality cannot pass through an OR gate—if it does, an AND gate is missing. For an OR gate, the input faults are never the *causes* of the output fault—they are identical to the output, but more specifically defined as to cause. For an AND gate, there *is* a causal relationship between the inputs and the output—the input faults collectively represent the causes of the output fault.

There are additional types of gates which we will not cover here. The *U.S. Nuclear Regulatory Commission Fault Tree Handbook* [USNRC, 1981] is a superb source for learning fault-tree analysis.

Sample Problem

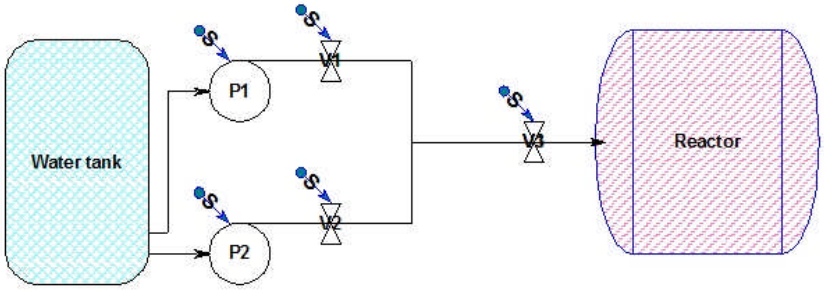

Figure 27 Simple pumped system

Consider a simple (and rather badly designed) pumped system as shown in Figure 27. Each pump can supply 100% of the necessary flow. The demand failure probabilities for each component are:

Pump (P): 0.01
Valve (V): 0.01
Signal (S): 0.001

What is the unavailability of the system?

Answer

The first step is to define the system boundaries carefully. For this example, we will exclude the water tank and the reactor. That means that we will not consider failure modes for the tank (e.g., water freezing, tank drained, line opening blocked); in a real application, these would need to be covered. We also have to define the failure criterion: less than 100% flow to the reactor. We can then draw the fault tree. It may help to think the problem through in words first:

Immediate cause of insufficient flow to reactor = no flow through valve V3
Immediate cause of no flow through valve V3 = (no flow through valves V1 OR no flow through valve V2) OR valve V3 closed
Immediate cause of no flow through valve V2 = pump P2 fails OR valve V2 fails to open
Immediate cause of valve V2 fails to open = valve V2 mechanically fails OR signal S fails,

etc.

This results in the fault tree shown in Figure 28. Note that there are many ways of drawing this; for example, one could recognize that the failure of the signal affects all components and therefore could be in an "OR" gate just under the top event. It is always safer, however, to follow the principle of immediate cause.

Having drawn the fault tree, we now assign labels to each basic event (V1, V2, V3, S, P1, P2), as shown in Figure 28. We can also assign intermediate labels (A, B, C) to help in the calculations. Now we can write out the Boolean algebra, *starting from the bottom*. It is important NOT to assign numerical values immediately to the basic events and work out the final answer before doing the Boolean algebra. In many cases, this will lead to double counting because terms such as S+S will be counted twice. Remember that in Boolean logic, S+S=S, not 2S, and S●S=S, not S^2.

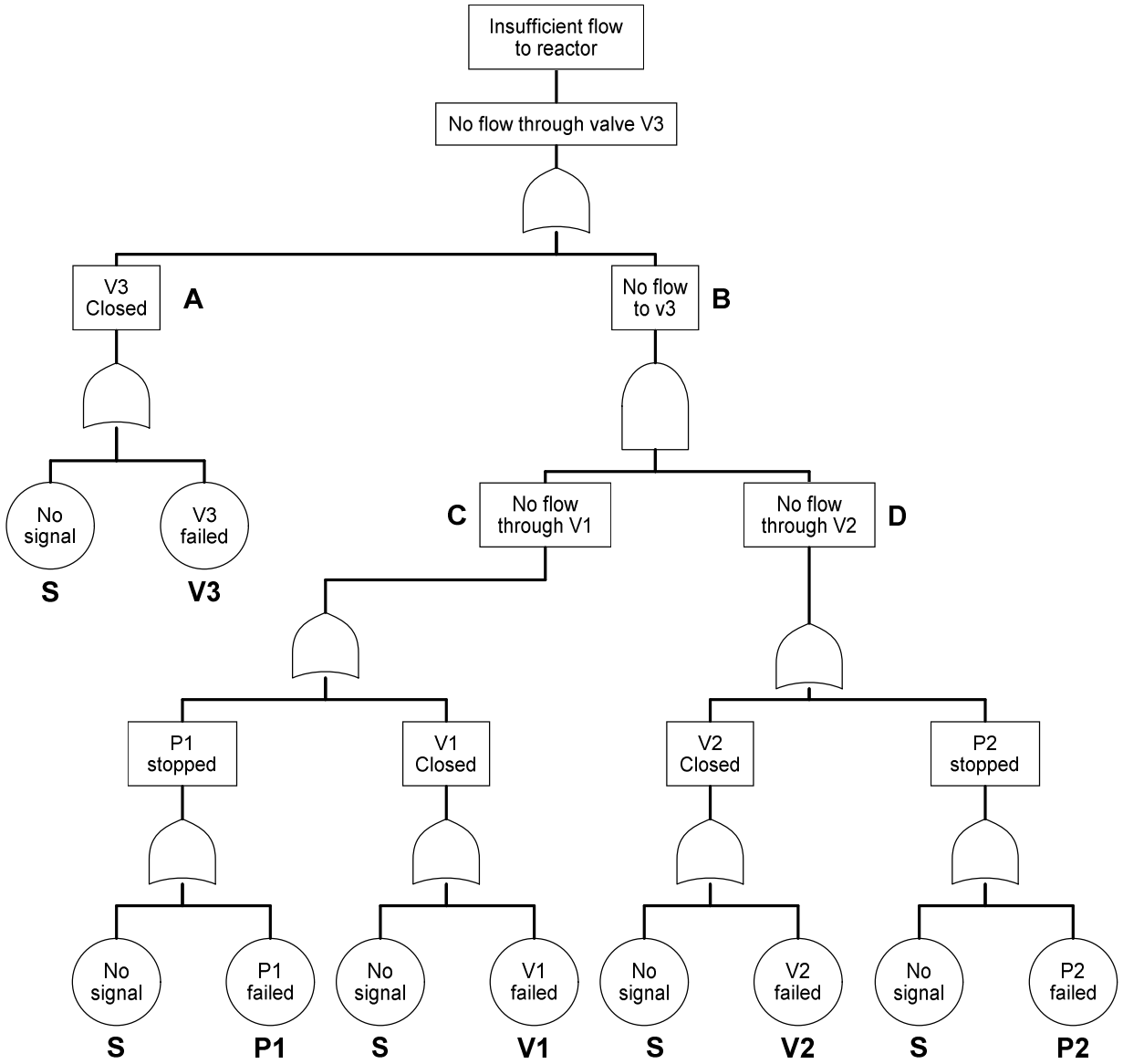

Figure 28 Sample fault tree with labels

Let us calculate the chain up to point C first:

C=(S+P1)+(S+V1).

Similarly,

D=(S+P2)+(S+V2),

B = C●D = ((S+P1)+(S+V1))●((S+P2)+(S+V2)),

A = S+V3.

Top event = A+B

= (S+V3) + [((S+P1)+(S+V1)) ● ((S+P2)+(S+V2))]

= S+V3+(S+P1+V1)●(S+P2+V2) because S+S=S

= S+V3+S●(S+P2+V2)+ P1●(S+P2+V2)+V1●(S+P2+V2)

= S+V3+P1●P2+P1●V2+P2●V1+V1●V2 -- using S●S=S, S+S=S and S● (S+x)=S.

We can see immediately (as is obvious from the diagram) that S and V3 are single points of failure for this poorly designed system.

Now we can plug in the numbers:

Top event = $0.001+0.01+4(0.01)^2 = 0.0114$.

4.2.3.5 Event trees

The companion to a fault tree is an event tree. While a fault tree answers the question "what is the unavailability or failure rate of this system?", an event tree answers the question "what happens after the system fails?" The end result of an event tree is that the plant ends up in one of three main states: stable, core damage, or large release (in practice, these states are often subdivided).

Unlike fault trees, which are written from the top to the bottom of the page, event trees are written from left to right. Here are the steps:

- Start (at left) from the undesired initiating event (e.g., loss of feed water, loss of coolant).
- List the relevant mitigating systems along the top from left to right, in approximate order of actuation.
- At each branch where a mitigating system is called on, assign the probability of success or failure.
- Develop each branch logically to a stable end state, core damage, or a large release.
- Calculate the frequency of each end-point of the branches, starting from the frequency of the initiating event and multiplying by the probabilities of success or failure at each branch.
- Sum these to obtain the frequencies for core damage and large release.

This is a very simplified explanation, and in practice the methods are much more complex—e.g.,

they have to account for a failure in the fault tree (example, loss of instrument air) also occurring in the event tree, or a failure of a mitigating system (e.g., loss of service water) which is common to the failure of other mitigating systems. This topic is well beyond the scope of this section. For more on common-cause failures, see [USNRC, 1981].

A simple example, which should be self-explanatory, is shown in Figure 29, where P1, P2, P3, etc. are the probabilities of success for each mitigating system. Note that if the failure probabilities (1 – *Pi*) are small, the success probabilities can be assumed to be equal to one when calculating each success branch. So, for example, the frequency of core damage in the sequence just below the box labelled "Stable" is:

Small LOCA frequency x (1-P3) x P4,

and one could set P4=1 in calculating this branch, as a good approximation. Note also that even if ECC fails, the moderator will maintain pressure tube integrity and prevent fuel melting by removing heat from the fuel channel, as described in Section 5.3.2.3.

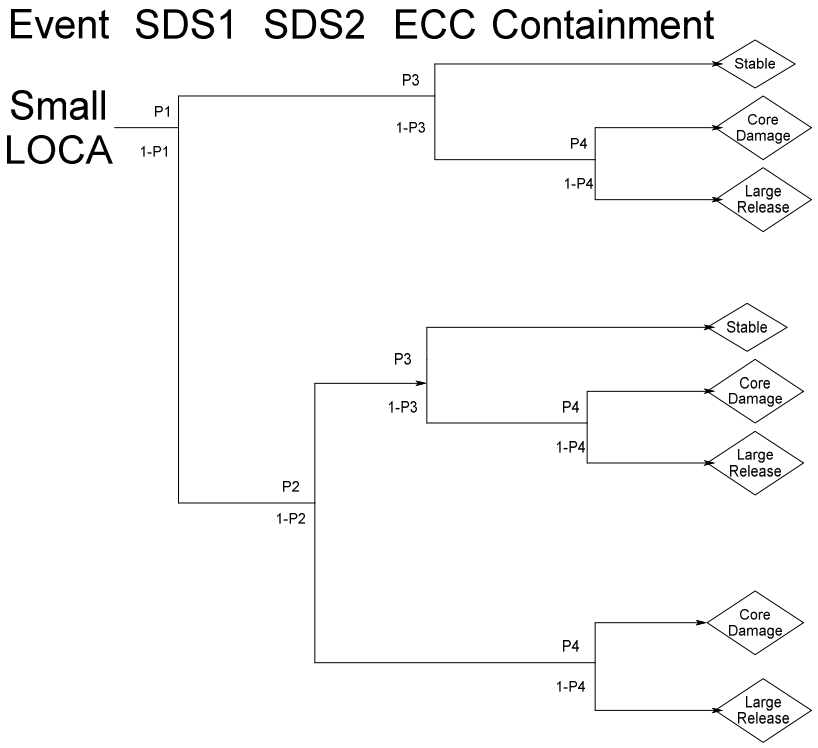

Figure 29 Simple event tree

4.2.3.6 Dormant vs. active systems

So far, we have focused on systems that are normally dormant and are required to operate on demand. Safety systems generally fall into this category. However, some systems, like the Emergency Core Cooling System (ECCS), are required to activate on demand *and* to continue to function for some defined mission time. The normal response of the ECCS to a heat-transport system (HTS) break (loss-of-coolant accident or LOCA) is for the ECCS to detect the event and initiate the injection of high-pressure (HP) cooling water (strictly speaking, the water-injection

function of ECC is called ECI, or Emergency Coolant Injection, because ECC also has other functions such as steam generator cooldown and loop isolation[1]). Then, after the HTS has been depressurized, medium-pressure and finally low-pressure water is injected. The HP water is supplied, for example, from a water tank (accumulator) pressurized by huge gas cylinders. Medium-pressure cooling water can be supplied from a water tank by ECC pumps, and low-pressure water is retrieved from the sumps in the reactor-building basement, cooled, and pumped back into the HTS. For CANDU reactors, an ECC mission time of one to three months has been set[2]. The ECCS is consequently divided into two separate fault trees for the purposes of analysis: dormant ECC and long-term ECC (designated DECC and LTECC respectively). The DECC fault tree focuses on failure to detect the LOCA event, failure to initiate high-pressure (HP) cooling water, failure to distribute the flow, and failure to provide medium- and low-pressure water. The LTECC fault tree focuses on failure to provide long-term low-pressure cooling due to pump failure, valve failure, flow blockage, loss of electrical power, or loss of coolant supply.

4.2.4 Typical results

We have now summarized fault trees and event trees. A PSA is the integrated collection of these across an entire plant. There are three recognized levels of PSA, which can be defined as follows (see, e.g., [IAEA, 2010]):

Level 1 – identifies the sequences of events that can lead to core damage and calculates the core-damage frequency.

Level 2 – uses the information from Level 1 to calculate the magnitude and frequency of releases to the environment of radioactive material.

Level 3 – uses the information from Level 2 to calculate health effects and other consequences such as contamination of food and land.

In practice, Level 1 is used to assess the design and operation of the plant, Level 2 is used to assess the effectiveness of containment, and Level 3 is used in off-site emergency planning.

As an example, we summarize the results of a Level 1 PSA done for an operating CANDU 6 plant [Santamaura, 1998]. The summed severe core-damage frequency (SCDF) was predicted to be 6.1×10^{-6} per year. We have already discussed the underlying reasons that this number is low: redundant shutdown systems mean that accidents with failure to shut down occur at very low frequency, and the moderator, if available, is effective in preventing or arresting severe core damage. Moreover a severe core-damage accident (after shutdown) at high pressure is not possible because failure of a limited number of pressure tubes converts the event inherently to a low-pressure accident. Note that [Santamaura, 1998] covered internal events only; typically, inclusion of external events doubles this value. Also note that accidents in shutdown states

[1]Such a distinction is made in Canada, but most other places just use ECC.

[2]The mission time is defined here as the time beyond which the decay heat can be removed from the fuel to the moderator *without any water in the fuel channel*, so as to prevent any further fuel failures due to overheating. It is a calculated number.

were excluded.

The contributors to the SCDF are shown in Figure 30. Note that it is the high-frequency initiating events, including many AOOs, that dominate the SCDF; the bounding accidents such as large LOCAs contribute very little and hence are much less risk-significant.

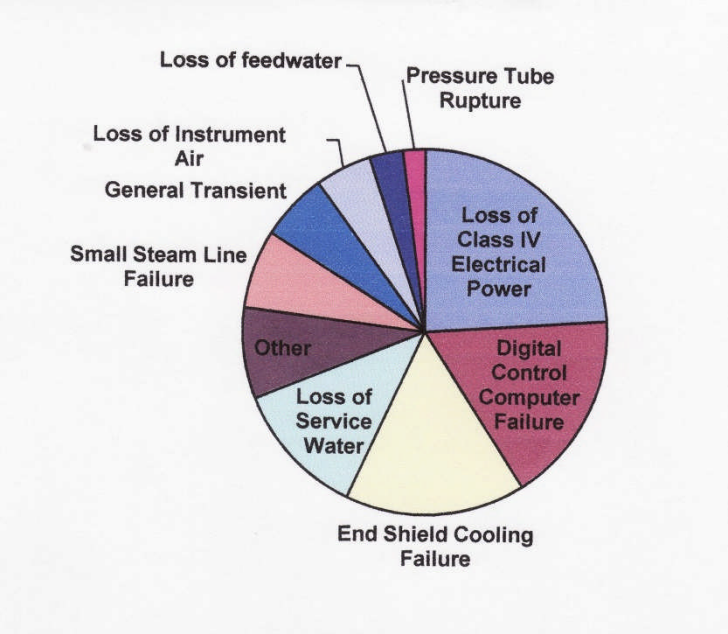

Figure 30 Contributors to SCDF for CANDU 6

4.3 Problems

1. What can you say *quantitatively* about the probability of a pressure-tube/calandria tube failure in a CANDU, based on that fact that only one has occurred? You will need to calculate the number of reactor-years of experience with CANDU operation. Use Bayes' Theorem.

2. Two 100% electrical motor-driven auxiliary feed-water pumps are located in the turbine building and depend on recirculated cooling water and two independent power supplies. They have the flow capability to mitigate steam- and feed water-line breaks. Identify common mode and common-cause failures. The utility wants to extend the life of the plant and is planning refurbishment. What mitigation features or modifications would you include to reduce or eliminate these failures?

3. Develop a set of high-level safety goals for a military-use nuclear submarine. They can be, but do not have to be, numerical. The most important part of your answer is to explain and justify it, not whether or not it matches someone else's "official" goals. Consider any differences due to docked versus at-sea and peacetime versus war.

4. Small reactors could be used in remote northern communities for heating and electricity production. They would replace very expensive diesel generators, the fuel for which has to be flown in, whereas the reactor could be designed to be refueled once in twenty years. Small reactors have also been used for powering unattended remote military installations. Propose

safety goals for each case, with reasons.

5. Assuming that the small LOCA frequency is 10^{-2} per year, work out the frequency of core damage in Figure 29. Use P1=P2=P3=10^{-3}.

6. Simple fault tree

   a. A system consists of two redundant trains as shown in Figure 31 (i.e., 2 × 100%, connected in parallel). If the probability that each component P1, P2, V1, V2 works successfully is 0.9, what is the reliability of the system? Write out the Boolean algebra in full. To achieve a reliability of 0.99, what would the reliability of each component (assumed to be all the same) have to be? List any assumptions.
   b. Now do the same calculation without the cross-tie.
   c. The cross-tie looks like an obvious thing to do. Think of some engineering disadvantages to the cross-tie. Hint: what might happen if one pump fails to start? How would you fix the design? What impact would your fix have on reliability?

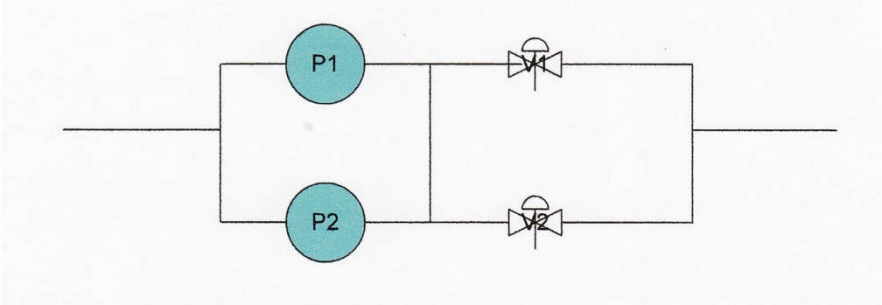

Figure 31 Simple fault-tree exercise

5 Mitigating systems

In previous sections, we have referred to the four safety functions required in a nuclear reactor:

- shut down the reactor
- remove decay heat
- contain any radioactive material
- monitor the state of the plant.

In this section, we shall describe the major systems that perform these functions. We shall concentrate on CANDU for our examples, although other reactor types have similar systems.

First, however, we need to ask how much redundancy and independence we need for each safety function. This concept is called defence-in-depth and is a fundamental underpinning of nuclear safety.

5.1 Defence-in-Depth

The concept of defence-in-depth was developed for military purposes. At one level, it consists of a series of physical barriers, so that breaching any one barrier (or even more) does not lead to disaster. The Krak Castle in Syria is one such example, where an (ancient) intruder would have to breach the moat, the outer wall, the inner wall, and the keep to capture the ruler. More generally, defence in depth requires that a defender deploy his resources, such as fortifications, field works, and military units both at and well behind the front line, so that a breach in the front line does not lead directly to defeat.

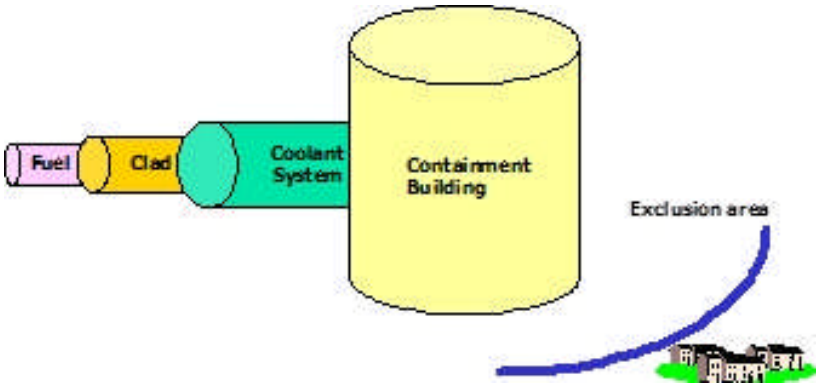

Figure 32 Defence-in-depth: barriers

The analogy for a nuclear power plant involves the physical barriers to release of radioactive material from the fuel, namely the fuel matrix itself (which we have seen is highly resistant to release of fission products except at melting temperatures), the fuel sheath (which prevents the gaseous fission products in the fuel-sheath gap from escaping), the heat-transport system, the containment, and the exclusion zone (which provides dilution rather than a physical barrier); see Figure 32.

A complementary approach to defence in depth is to define a series of five successive levels:

- Prevent abnormal operation and system failures.

- Control abnormal operation and detect further failures.
- Control accidents within the design basis.
- Control severe accidents.
- Apply off-site emergency response.

These are objectives rather than physical barriers. Note that the last is largely independent of reactor design. There are various formulations of these concepts; see [INSAG, 1996], from which the following summary Table 7 is extracted.

Table 7 Levels of defence in depth

Levels of defence in depth	Objective	Essential means
Level 1	Prevention of abnormal operation and failures	Conservative design and high quality in construction and operation
Level 2	Control of abnormal operation and detection of failures	Control, limiting, and protection systems and other surveillance features
Level 3	Control of accidents within the design basis	Engineered safety features and accident procedures
Level 4	Control of severe plant conditions, including prevention of accident progression and mitigation of the consequences of severe accidents	Complementary measures and accident management
Level 5	Mitigation of radiological consequences of significant releases of radioactive materials	Off-site emergency response

Defence-in-depth is fundamental to the achievement of nuclear safety; try Problem 1 in this section.

5.2 Shutdown Systems

Typically, a reactor has one or more systems for each of the four safety functions (control, cool, contain, monitor). Defence-in-depth influences the amount of redundancy provided. For each system, its performance is specified by *design requirements*. These in turn arise from listing and evaluating the challenges that the system must overcome, which make up the *design basis.*

Shutdown is one of the most important safety functions in a reactor because it reduces the amount of energy that has to be removed from the fuel after an accident. It is usually accomplished through rapid insertion of a neutron-absorbing material into the core. Another way is to remove from the core material which is essential to the chain reaction, e.g., the moderator. More radical engineered concepts are possible in principle, such as removing fuel or changing the core geometry, but they are not in widespread use for fast shutdown.

The design bases of the shutdown systems are typically set by those accidents developed using

the various approaches in Section 2, e.g., large loss-of-coolant accident, loss of reactivity control, loss of Class IV power, etc. Each of these accidents contributes to answering the following questions, and the limiting value in each case becomes a design requirement for the shutdown system:

- How is negative reactivity inserted into the core?
- How fast does the system have to act once it receives a signal?
- How much reactivity depth must it have (how many negative milli-k?)
- How reliable must it be?
- What are the analysis limits that describe effectiveness?
- What sorts of signals are available and practical to trigger the shutdown system for each accident?
- What sort of environment must the shutdown system be designed to withstand?
- How do we ensure that a fault does not affect both the control system and a shut-down system? Or both shutdown systems?
- How do we know that the systems will work as designed?
- How does the operator know that the system has been required and that it has worked?

We shall cover these topics in turn. Many of these questions are common to other safety systems, and therefore we shall explore them in detail the first time and simply refer to them later.

5.2.1 Mechanical design

The most basic part of shutdown design is inserting a neutron absorber into the core. Because modern power reactors are large, a single absorbing device is generally not sufficient. Almost all reactor types use some form of absorber rod, multiples of which are inserted vertically into the core. In most reactors in the world, the rods do double duty, being driven in and out of the core for control purposes, and being driven or dropped in rapidly for shutdown purposes. CANDU, however, separates the control rods from the shut-off rods, as one of the lessons learned from the NRX accident.

The first CANDU shutdown system was moderator dump: large valves at the base of the calandria would open, and the moderator would drain out of the calandria vessel under the action of gravity, somewhat like the ZED-2 design. The system would be re-poised by closing the valves and pumping the moderator back into the calandria. NPD, Douglas Point, and Pickering A used this system. Pickering A also used a few shut-off rods which fell in by gravity. The moderator dump system was (and is) highly reliable, but is somewhat slow compared to shut-off rods, especially for larger cores, and in addition removes a source of water surrounding the fuel channels, which could be used in an emergency (we will discuss this later).

Modern CANDUs have two separate shutdown systems: rods and poison injection (Figure 33, from [AECL, 2005]). Specifically, Shutdown System 1 for CANDU consists of 26 or 28 shut-off rods, normally suspended above the core and released on a signal. They act in the moderator, between the rows of pressure tubes, as can be seen in Figure 33. They fall in by gravity and are

spring-loaded, which accelerates them over the first few feet of travel. Mechanically, the rod is suspended on a cable running over a pulley, which is released by a clutch and wound back up by a motor. The rod itself falls into a perforated guide tube within the moderator; the purpose of the guide tube is to make sure that the rod falls straight in and does not tip over or snag.

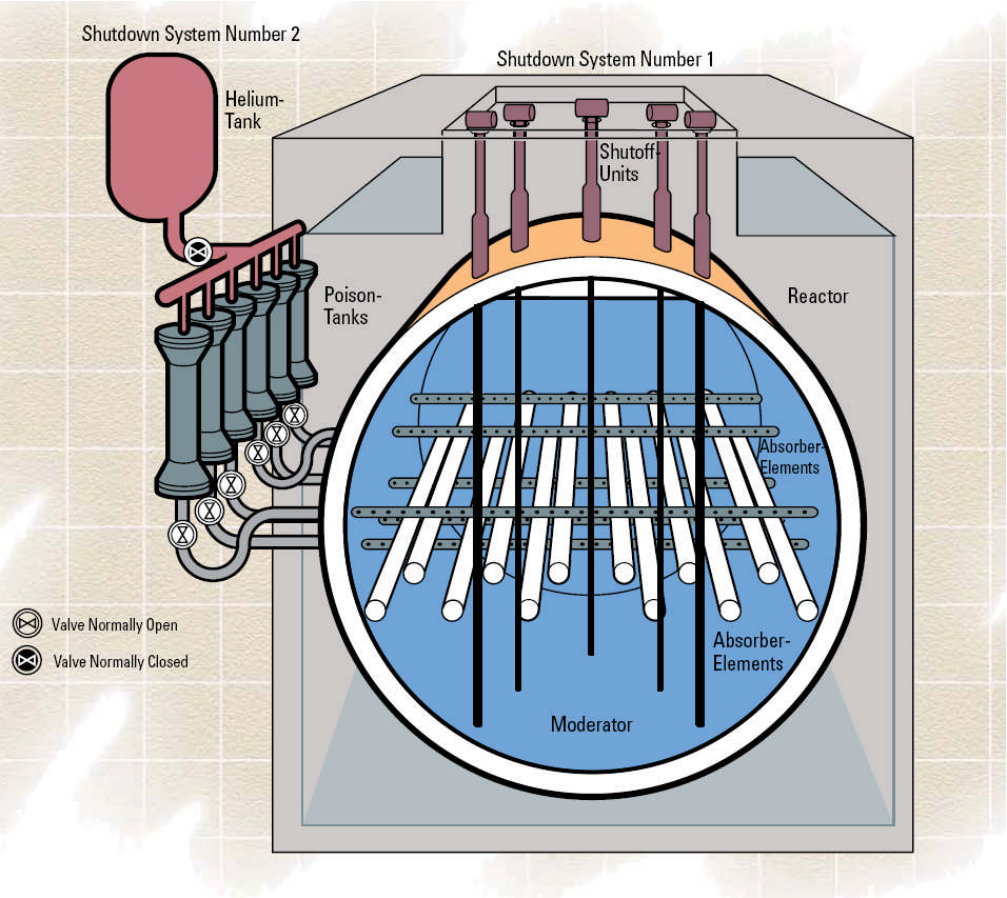

Figure 33 CANDU shutdown systems

Shutdown System 2 consists of a liquid neutron absorber (gadolinium nitrate) which is injected directly into the moderator water through perforated metal tubes. The liquid is accelerated by gas pressure from a common helium tank which pressurizes one poison tank per nozzle, as shown in Figure 33. The system is actuated by opening the fast-acting valves connecting the helium tank to the poison tanks. A disadvantage of this system (in case of a spurious trip) is that because it injects poison into the moderator water, the poison must all be removed chemically (by ion exchange) before the reactor can start up again, a process that takes almost two days. Note that there are no normally closed valves between the poison tanks and the moderator for reliability reasons. As a consequence of this, however, poison gradually diffuses toward the core down the pipe and must be back-flushed from time to time to drive the diffusion front away from the moderator.

5.2.2 Speed

The required speed is set by the fastest accident. In CANDU, this is the large loss-of-coolant accident, where the break is assumed to grow to full size instantaneously—a very pessimistic assumption and inconsistent with what we know of pipe dynamics [Tregoning, 2008]. Core voiding for such a case inserts positive reactivity at a rate of approximately 4 mk/sec. One of the main safety requirements during this phase is to prevent melting of the central part of any fuel pin due to overpower, because significant amounts of molten fuel could risk failure of the nearby pressure tube. As long as the net positive reactivity is kept below approximately 6 mk, depending on the design and the assumptions, the energy is not sufficient to melt the centre of the fuel. This then suggests that the shutdown system has to start to bite (insert negative reactivity) in approximately one second, and that the initial reactivity insertion rate has to overcome the 6 mk already inserted, as well as turning the transient over by 1.5 seconds—in other words, tens of (negative) mk/sec.

5.2.3 Reactivity depth

Reactivity depth means the total negative reactivity inserted once the shutdown system has fully operated. For shut-off rods, this occurs when the rods have been fully inserted; for poison injection, when the poison has been fully injected and mixed with the moderator. The reactivity depth requirement is set by the accident which inserts the greatest positive reactivity. For CANDU, this is not the large LOCA, but a small LOCA, specifically a pressure-tube break followed by an assumed calandria-tube rupture. Why? When a reactor is operating at full power, negative reactivity load is present due to xenon, a neutron absorber which is formed from the decay of iodine, which in turn is formed from the fission product tellurium as follows:

$$^{135}\text{Te} \Rightarrow <1\text{min} \Rightarrow {}^{135}\text{I} \Rightarrow 6.7\text{h} \Rightarrow {}^{135}\text{Xe} \Rightarrow 9.2\text{h} \Rightarrow {}^{135}\text{Cs} \Rightarrow {}^{135}\text{Ba (stable)},$$

where the times represent half-lives. The xenon load in a CANDU at full power is approximately -25 mk and has to be compensated for by positive reactivity from the fuel to keep the reactor critical. When the reactor is suddenly shut down, the xenon decays more slowly than the iodine, so that the absorption due to xenon initially increases to about -40 mk, then decreases as the iodine decays away (Figure 34).

Figure 34 Xenon transient after shutdown and start-up

After a long shutdown, the xenon load is small, so that poison is added to the moderator to compensate for the absent xenon load (because the normal control system does not have the required negative range). As the reactor comes back to power again, the iodine and therefore the xenon gradually build up, and the poison can be chemically removed from the moderator (or a burnable poison is used, i.e., one which is made into a less absorptive species over time by neutron absorption, typically gadolinium). If a pressure-tube break with assumed failure of the surrounding calandria tube occurs during start-up, then the "poisoned" heavy-water moderator can be replaced by non-poisoned heavy-water coolant. The amount of *positive* reactivity that can be added in, say, the first 15 minutes is dependent on:

- coolant void in the fuel channels, from the fraction of coolant that is lost through the break.
- fuel temperature, due to cooldown of the fuel after trip.
- "clean" coolant displacing "poisoned" moderator.
- increase in moderator temperature (albeit small and slow) due to mixing of the hot discharging coolant with cold moderator.
- decay after shutdown of any xenon that has been formed during on-power operation.

Offsetting this is the negative reactivity due to the shutdown systems and eventually the very large negative reactivity due to injection of emergency-coolant light water. The last effect is not credited in licensing analysis for CANDU (although in LWR licensing analysis, the reactivity effect of borated ECC *must be* credited [Westinghouse, 2011a]). For CANDU, the analysis of the reactivity balance is usually done 15 minutes after the first clear signal of a pressure-tube break, when the operator can be assumed to supplement the shutdown-system reactivity (e.g., by manual poison addition). One then designs the shutdown *depth* of the shutdown system to achieve an adequate shutdown *margin* (the net result of the reactivity balance) using conservative assumptions. Physically, one achieves greater shutdown depth by adding more rods (new designs), by putting rods preferentially in the high-flux region of the core, etc. There is a practical space limit, however, on the number and location of rods. The typical shutdown depth for existing CANDU shutdown systems is -70 mk for the shut-off rods and < -200 mk for poison injection. Hence, shutdown margins for the rods are smaller, -5 to -10 mk for existing CANDUs, under the most pessimistic conditions (e.g., assuming that the two most effective rods are unavailable).

5.2.4 Availability

Demand unavailability is expressed in dimensionless units, although it is also written as hours/year or years/year. The required unavailability is set primarily by the safety goals applied to the reactor by the regulator, and for current CANDUs, it is at most one failure per 1000 demands (10^{-3} per demand) for safety systems. Experience has shown that the shutdown systems normally meet approximately 10^{-4} per demand. Unavailability values much lower than this are possible, but are usually not credited for a single system because of:

- the number of tests that would be needed to establish such an unavailability;
- the suspicion that unknown cross-link effects and common-cause failures impose a lower limit on the unavailability of a single system.

If each shutdown system has an unavailability of 10^{-3} per demand, then one is tempted to say that the unavailability of both systems together is 10^{-6} per demand. This is true only if the systems are sufficiently independent and diverse that they are not subject to common-cause failures. See Section 13.

Recent CANDUs have used software for both SDS1 and SDS2. Software can be more reliable than relay logic, but its failure modes can be subtle, so that while testing in operation is important, much more emphasis must be placed on software design to avoid subtle and common-cause failures. Methods include a rigorous development process, diversity in development tools and platforms, simple programming logic, and strict independence between the software engineers responsible for designing each shutdown system. In CANDU, the control-system software is completely independent of and separate from the shutdown-systems software, and in current CANDUs, they run on independent hardware platforms.

5.2.5 Analysis limits

Analysis limits are used to judge the *effectiveness* of shutdown. Trip signals are chosen to reduce the challenge to the fuel and to downstream safety systems—in other words, to prevent or postpone consequences. For example, for accidents which are expected to happen perhaps once or more in the plant lifetime, i.e., anticipated operational occurrences or AOOs, the shutdown systems should act early enough to prevent fuel-sheath failure, thus avoiding any challenge to the HTS and containment as well as the cost of clean-up. This category includes, among others, loss of Class IV power, a very small LOCA, or a failure in the reactivity-control system. In turn, prevention of fuel-sheath failure generates a number of secondary criteria, which we will cover in Section 6. For loss of heat sink accidents, a subsidiary requirement is that the shutdown systems should act soon enough to give the operator adequate time to bring in a backup heat sink—typically 15 to 30 minutes, although new designs aim for at least eight hours before operator action is required. For rare accidents such as a large LOCA, one should limit (but not necessarily prevent) fuel damage (to reduce the challenge to containment) and ensure that the fuel is not made so brittle from the Zircaloy-steam reaction that it forms debris and cannot be cooled by ECC; see Section 6. Limiting fuel damage in a large LOCA is a task shared between shutdown and ECC: the job of the shutdown system is to deliver the fuel to the ECC in reasonable condition so that ECC can remove decay heat from a known fuel geometry. Finally, in any accident, shutdown systems should act early enough so that there is no risk to the pressure boundary (or at least no risk in addition to that from the initiating event).

5.2.6 Signals

A shutdown system must detect an accident soon enough that the analysis limits are met. Some of the commonly used trip signals are listed in Table 8 (this list is illustrative rather than complete).

Manual trip is credited if the time scales are long—typically fifteen minutes from the first clear

signal of the accident in the main control room—and if there is no practical alternative.

Table 8 Typical trip signals for CANDU

Accident	Symptoms	Typical Trip Signals
Loss of reactor power control	Reactor power rises Reactor power rises rapidly Heat-transport system pressure rises	High neutron flux High log rate of neutron flux High heat-transport system pressure
Loss of forced circulation	Coolant flow drops HTS pressure rises Reactor power rises	Low heat-transport system flow Low core pressure drop High heat-transport system pressure High neutron flux
Medium to large loss of coolant	Reactor power rises Reactor power rises rapidly Containment pressure rises Coolant flow drops Coolant pressure drops	High neutron flux High log rate of neutron flux High containment pressure Low heat-transport system flow Low heat-transport system pressure
Small loss of coolant	Pressurizer level drops Coolant flow drops Containment pressure rises Moderator level rises (in-core break) Coolant pressure drops	Low pressurizer level Low heat-transport system flow High containment pressure High moderator level Low heat-transport system pressure
Loss of feed water	HTS pressure rises Feed-water flow drops Steam generator level falls	High heat-transport system pressure Low feed-water flow Low steam generator level
Large steam main failure	HTS pressure falls Pressurizer level falls Steam generator level falls Feed-water pressure falls Reactor power decreases Containment pressure rises[5]	Low HTS pressure Low pressurizer level Low steam generator level Low feed-water pressure High containment pressure

5.2.7 Operating environment

A safety system must be able to function in, or be protected from, the conditions caused by an

[5] For plants where portions of the steam mains are within containment

accident. If it is not possible to meet this requirement, then a redundant system is needed. For example, a major fire in or near the main control room would require shutdown (because it could affect the control computers) and at the same time would *possibly* damage some of the components of Shutdown System 1 so that it would not respond (although it would very likely fail safe)—and therefore SDS2 (which does not depend on the integrity of the main control room) is used as a back-up to perform this safety function.

The shutdown mechanisms in CANDU act mostly within the moderator, which protects them from some of the effects of accidents—but not all. For example, we must design so that:

- no high-energy pipes are within striking distance of the reactivity mechanisms deck on top of the reactor, where the shut-off rod clutches and pulleys are located.
- an in-core break cannot disable shut-off rods to the extent that the system does not meet its reactivity depth requirements (it is not possible to protect *all* the guide tubes and rods from pipe whip and jet forces from an in-core break).
- shutdown-system cables and instruments are separated to the extent practical so that a local fire will not incapacitate both shutdown systems.
- steam, high temperatures, water, and high radiation fields from an accident must not prevent a shutdown system from firing when needed (once it has fired, however, such protection is no longer needed).
- shaking due to an earthquake must not prevent the shutdown system from actuating nor slow it down so severely that it cannot meet its analysis limits.

5.2.8 Common-cause failures

We gave an example earlier where a single cause (fire) could disable more than one system. This is a serious challenge to the protection provided by seemingly independent systems. Known common-cause failures can be "designed out", but to cover the possibility that we cannot anticipate them all, a *two-group* philosophy is followed in CANDU. In summary, this philosophy is:

- for each failure, ensure that there are at least two ways of performing the required safety function.
- separate these two ways geometrically (so that they are not subject to local damaging hazards such as fire, turbine missiles, or aircraft crash).
- use diverse equipment and diverse means of operation.
- protect equipment against the environmental results of the failure.
- qualify or protect at least one of the two systems against plant-wide external events such as tornadoes and earthquakes.

The practical application involves many trade-offs: diversity is not always possible, and there is only so much space within which systems can be separated. Whereas ideally one would like to route control system cables separate from SDS1 cables and SDS2 cables, it would be almost impossible from a plant layout point of view, and therefore grouping of control system and SDS1 cables is allowed, but they must be separated from SDS2. However, all three logic channels (see Section 5.2.9) within any given group must be separated, so that a local cable fire cannot

generally disable all three channels of any one system.

If a compromise in separation must be made, then one must show that one or more of the following applies:

- there is no credible hazard in the area
- another system outside the area will mitigate the event
- the system or component is protected by a barrier
- the system or component is fail-safe
- the component is designed to withstand the hazard.

Table 9 shows an example of how grouping and separation were implemented on CANDU 6.

Table 9 Grouping and separation example

Safety Function	Group 1	Group 2
Shutdown	Reactor Control System Shutdown System 1	Shutdown System 2
Heat Removal From Fuel	Heat Transport System Steam & Feedwater Systems Shutdown Cooling System ECC Moderator	Emergency Water System
Contain Radioactive Material	Reactor building air coolers	Containment & containment subsystems
Monitoring & Control	Main Control Centre	Secondary Control Area

Most safety systems need services such as air, water, and power. These must also be grouped and separated.

5.2.9 Testing

Section 4.2.3.3 discussed the link between testing and availability. It is not practical to test safety systems fully during on-power operation; instead, they are designed to have their components tested in such a way as to preclude actual system operation. Specifically, the testing of the *logic* is separated from that of the final mechanism, and the mechanism is tested in stages, not all at once.

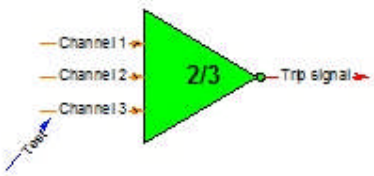

Figure 35 2/3 logic

All safety systems in CANDU have three logic channels, with two out of three being sufficient to initiate the trip or safety-system action (Figure 35). The requirement that two channels must *both* vote for a trip reduces the likelihood of spurious trips due to a single component failure. On the other hand, the reactor will still trip if required even if one channel is unavailable (failed unsafe). Finally, a single channel can be tested without tripping the reactor.

The shut-off rods are designed to be partially dropped individually in a test. In other words, shortly after the clutch has released and the rod begins to fall, the clutch can be re-energized and the rod "caught" before it enters the core. This proves that the rod is not stuck in the first part of its travel. Typically, each rod is partially dropped about once a week.

For Shutdown System 2, Figure 36 shows one way of testing each logic channel and each valve without firing the system, while any two channels which trip *will* fire the system. Testing any single logic channel opens two valves, but does not allow (much) poison to leak into the moderator.

Performance testing is usually done by measuring the speed of actuation of one or more components. Therefore, on a partial rod drop, one can determine how long it takes the rod to reach the point when it is caught, or one can test the valve opening times on SDS2. Before a scheduled shutdown, a full actuation test of the shutdown system measures the rod drop versus time and the actual power rundown.

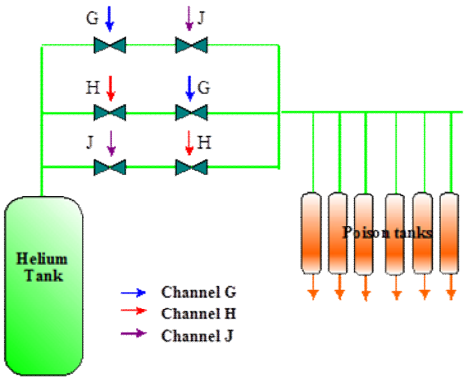

Figure 36 SDS2 testing

5.2.10 Human interface

An operator must:

- Be notified that the shutdown system has tripped
- Be able to confirm that it has actuated correctly
- Have procedures to follow in case it has not.

Normally, notification consists of an alarm window on the SDS panel, showing (for each channel) that a trip parameter has passed its trip set-point and a window showing that the SDS has fired. The latter is *not* sufficient to establish that the system has indeed worked, and an operator will have supplementary information available such as shut-off rod position; he will also check the neutron power measurement to ensure that it is consistent with a shut-down reactor. Finally, should these latter measurements suggest that the system has not fired, he will have and will follow backup procedures such as manually tripping the shutdown system, manually firing the second shutdown system, or dropping the mechanical control absorbers (manual stepback).

We have now covered all the high-level design requirements and design bases of the shutdown systems. Our in-depth example can be extended to the systems responsible for heat removal, containment, and monitoring, but we will cover these more briefly.

5.3 Heat-Removal Systems

The high-level design requirements of the heat-removal systems are determined by the answers to the following:

- How much heat must they remove (full power, decay heat, decay heat after *x* minutes, etc.)?
- Where are they connected (primary side, secondary side, etc.)?
- How are they initiated?
- Under what conditions can they operate (pressure, temperature)?
- What is their reliability?

5.3.1 Heat-removal capability

Heat removal at high power is performed by the primary coolant flowing through the fuel channels and transporting the fuel heat to the steam generators. Coolant is transferred across the steam-generator tubes to the main steam and feed-water systems. The case of a sudden loss of heat removal from the secondary side (e.g., turbine trip with loss of condenser vacuum) must be provided for, so that a capability for 100% steam dump to atmosphere is provided. This is accomplished by banks of main steam-safety valves (MSSVs) on the main steam lines. Full steam flow is needed only until shortly after the reactor has tripped.

For economic reasons, another subsystem is provided which can dump up to 60% steam directly from the steam generators to the condenser. This is used for poison prevention—that is, if the turbine trips, but the operator thinks that he can restart it reasonably soon, instead of shutting the reactor down, he can set back the reactor power to a level just sufficient to prevent a poison-out due to xenon build-up. The heat must still be removed, however, and therefore the design makes it possible to dump the steam directly to the condenser, by-passing the turbine. Because (unlike steam dump to atmosphere) the secondary water is recycled from the condenser back to the steam generators, it is possible to do this for considerable periods of time. This is a big advantage in the case of a prolonged loss of electrical grid power; if the reactor can avoid a trip when the grid is lost (e.g., through stepback to 60% power) and is kept running, it remains ready to supply power as soon as grid stability is restored.

This capability was demonstrated after the power blackout of Thursday, August 14, 2003. When the grid failed at 16:10, all operating reactors in Ontario tripped. The four Bruce Power units and Darlington unit 3 were quickly put into poison-prevent mode, operating at about 60% of full reactor power and by-passing steam to the condensers. These reactors were able to start providing power within a few hours as grid restoration began. For details, see [Rogers, 2004a].

The maximum decay heat immediately after shutdown is approximately 6%. However, we can sometimes design to remove less if the heat sink can be brought on-line later. Figure 37 shows the variation of decay heat with time after shutdown.

The desired end-point of an accident is a *stable cold shutdown*—i.e., the reactor is well subcritical, the decay heat generated by the fuel is being removed, no further release of radioactive material from the fuel is taking place, and the reactor is depressurized and “cold” (i.e., ~100°C or less). Therefore, in addition to removing the decay heat from the fuel as it is generated, there must be some additional heat-removal capability to cool the reactor down.

5.3.2 Location of heat removal

Heat can be removed from the secondary cooling system and from the primary cooling system.

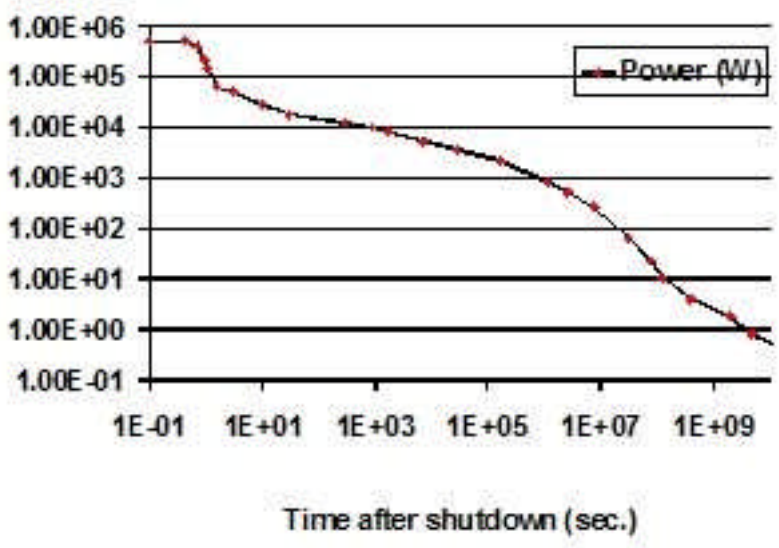

Figure 37 Bundle power after shutdown

5.3.2.1 Secondary-side heat removal

The secondary cooling system is used under the following conditions:

- If all components and systems on the secondary side are working, the main feed-water pumps provide water to the steam generators. The condenser removes heat from the steam and provides a continuous source of cooled water to the feed-water pumps. This relies on the availability of Class IV electrical power to run the main feed-water pumps.
- Alternatively, the task can be undertaken by one or more auxiliary feed-water pumps, sized to remove decay heat. These feed-water pumps are typically powered by Class III electrical power, or directly by a diesel engine, or by a steam turbine connected to the steam generators. It is not necessary to size them for 6% power because they are not needed until some of the water already in the steam generators has boiled away. This takes about half an hour, so that the heat-removal capability of the auxiliary feed-water pumps is typically about 4%. Note that if Class IV power is unavailable, the steam cannot be condensed, and the heat is removed by steaming to atmosphere from the steam generators, either through the atmospheric steam discharge valves (ASDVs), with a capacity of about 10% of full-power steam flow, or through the main steam-safety valves (MSSVs), with a capacity of about 115% of full-power steam flow. After an hour or more, the water in the feed-water train will be used up, and the operator will have to establish another heat sink.
- In some CANDUs, the dousing tank located in the top portion of the containment can supply a long-term source of water by gravity to the steam generators. In others, an elevated tank outside containment (the boiler emergency cooling system, or BECS) per-

forms this function.

- Most recent CANDUs have a seismically qualified source of water (e.g., a large pond) for use after an earthquake. This emergency water system (EWS) has its own seismically qualified power and pumps and can supply water independently to the steam generators for about three days.

5.3.2.2 Primary-side heat removal

Because many of the options for secondary-side heat removal are valid only for a limited period of time after an accident, CANDUs also have a primary-side system to remove decay heat, the shutdown cooling system. It is a closed system connected to the reactor headers with its own pumps and heat exchangers (Figure 38). It can be brought on-line immediately after shutdown at high temperature and pressure.

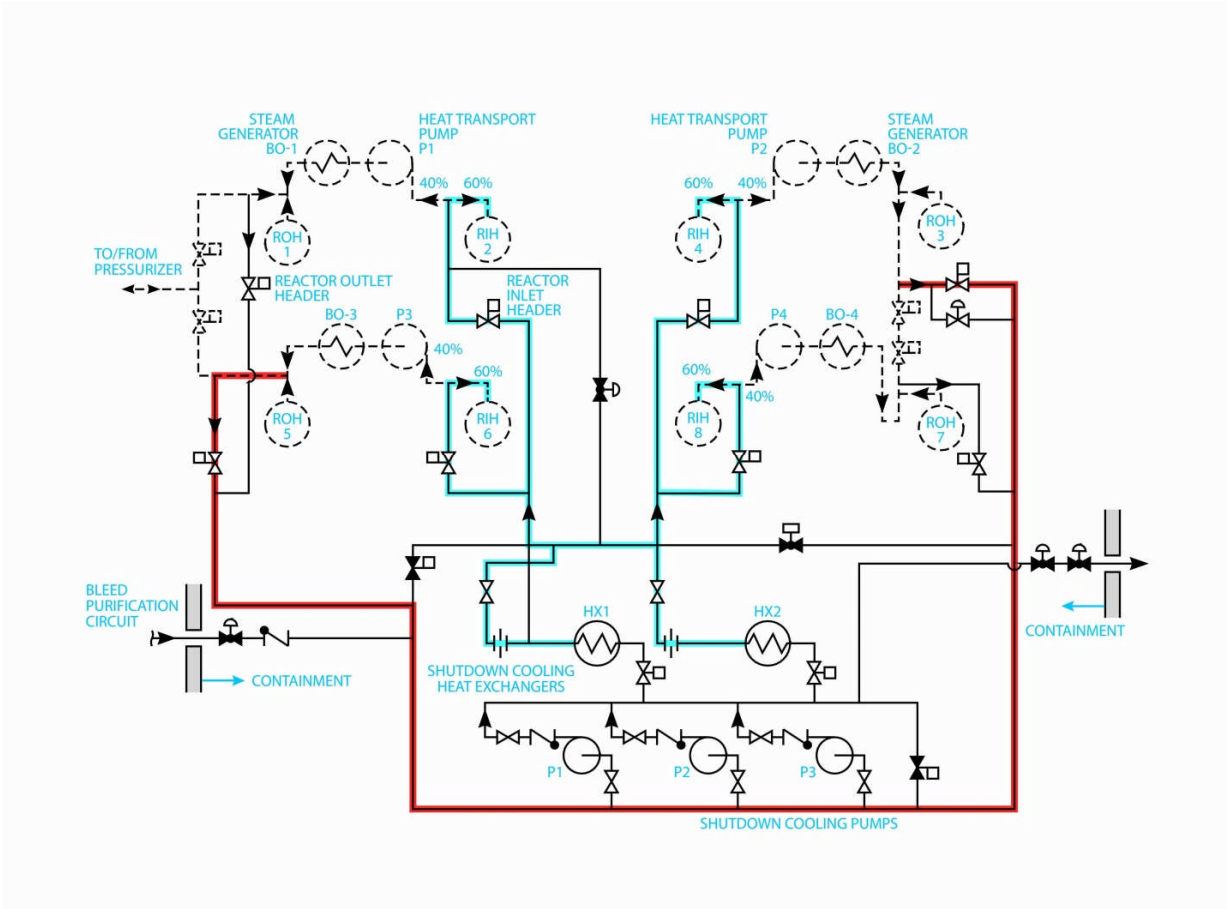

Figure 38 Shutdown cooling system

The emergency core cooling system can be viewed as a decay heat-removal system for the special case of a break in the primary cooling system piping. We shall cover this system later.

5.3.2.3 Moderator and shield tank

The moderator surrounding the fuel channels can be used in a severe accident (LOCA with loss of ECC) to remove decay heat. This heat-removal pathway is efficient enough to prevent fuel

melting, but will not prevent extensive fuel damage and distortion of the fuel channels (Figure 39).

The shield tank surrounding the calandria (see also Figure 39) has its own heat-removal system (pumps and heat exchangers) and can be used in a severe core-damage accident, e.g., if a LOCA plus loss of ECC plus loss of moderator heat removal all occur. In current CANDUs, the shield tank does not have enough heat-removal capability (0.3%) to match that being generated by the fuel; in addition, the causes for the failure of ECC and moderator cooling may also have disabled the heat-removal capability of the shield tank (e.g., loss of electrical power, loss of service water). However, several current CANDUs and all new ones, have installed gravity-driven makeup to the shield tank and/or the calandria to provide a much longer-term heat-removal capability.

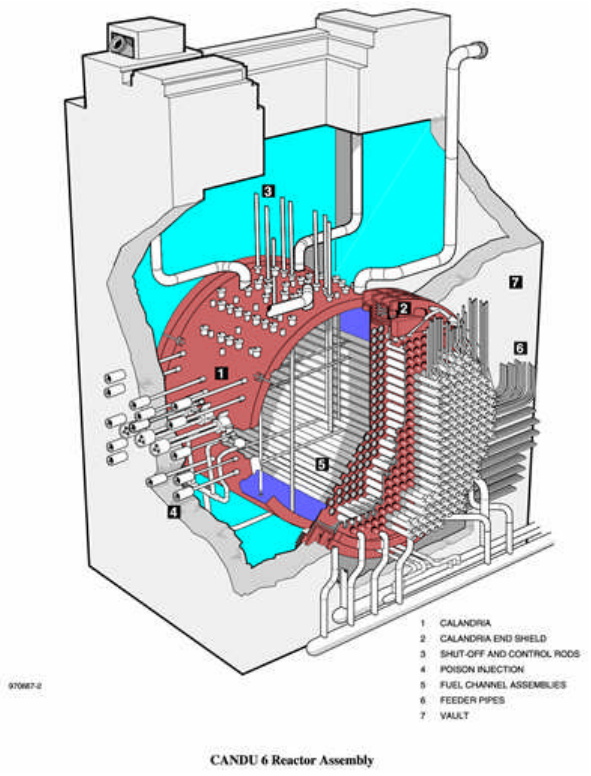

Figure 39 Moderator and shield cooling

5.3.3 Initiation of decay heat removal

Decay heat-removal systems can be either automatic or manual, based on when they are needed. Typically, if they are not needed for 15–30 minutes, they can be manually initiated (e.g., shutdown cooling system, EWS); if they are needed sooner, they must be automatic (e.g., ECC, auxiliary feed-water system).

5.3.4 Operating pressure

A key design choice is the *operating pressure* of the heat-removal system. Table 10 summarizes the advantages and disadvantages of high vs. low pressure. In many cases, the pressure is determined by the nature of the design (e.g., the moderator).

Table 10 Operating pressure of decay heat-removal systems

Operating Pressure	Advantages	Disadvantages
High	Can be brought in at any stage of an accident Components tend to be smaller due to more efficient heat removal (larger ΔT) More easily automated	More stringent requirements on code class of piping and components Need to ensure that it is tolerant if brought on-line when system is at low pressure (e.g., risk of pump cavitation)
Low	Can be simpler and cheaper Can be made more passive	Requires previous depressurization of the system (i.e., depends on another system)

5.3.5 Reliability

Unlike the case of shutdown systems, the mission time of decay heat-removal systems can extend to days or months, and therefore we need to determine both the demand availability (reliability to start) and the running reliability once the system has started. A typical active decay heat-removal system consists of pumps, which require electrical power, and heat exchangers, which require a source of cooling water, which in turn requires electrical power. Unavailabilities in the range of 10^{-2} to 10^{-3} to start and 10^{-1} to 10^{-2} over a specified mission time are typical. Therefore, redundancy in decay heat-removal systems is necessary.

5.4 Emergency Core Cooling System

The functions of the ECCS are to refill the core and to remove decay heat after a LOCA. We now discuss high-level design requirements.

5.4.1 Performance requirements

Sudden large primary pipe breaks have never occurred in a Western nuclear reactor; the probability is less than 10^{-5} per reactor year. A modern CANDU reactor has between 360 and 480 fuel channels and therefore 720 and 960 feeder pipes. The probability of a small pipe break is about 10^{-2} per reactor year based on experience, which is an issue not only for safety but also for plant investment protection. Therefore, the ECCS has safety requirements for both large and small breaks, and in addition, investment protection requirements for small breaks only.

The ECC safety requirements for all breaks are to:

- meet public dose limits by limiting the extent of fuel damage,
- prevent pressure-tube failure,
- ensure that the fuel in the fuel channels retains a coolable geometry,

and for small breaks, in addition, to:

- prevent sheath failure.

5.4.2 Location of water injection

The CANDU ECC injects light water into the reactor inlet and outlet headers in both heat-transport system loops (for reactors which have two loops): eight headers in all in CANDU 6 (Figure 40). Because each channel is connected to two headers and the headers are above the core, this provides a water pathway to every channel in the core. The disadvantages of this scheme are:

- water injected near or at the break discharges without removing heat from the fuel (depending on the break size and location). The design must provide sufficient pressure and water volume that flow of water out of the injection point at or near the break is accounted for.
- the (feeder) pipe to each channel is fairly small in diameter and contains a large amount of stored heat, and the injection water may have to flow countercurrent to the steam exiting the channel as it refills.

Light-water injection also ensures long-term shutdown in CANDU, but is not credited with this function in safety analysis.

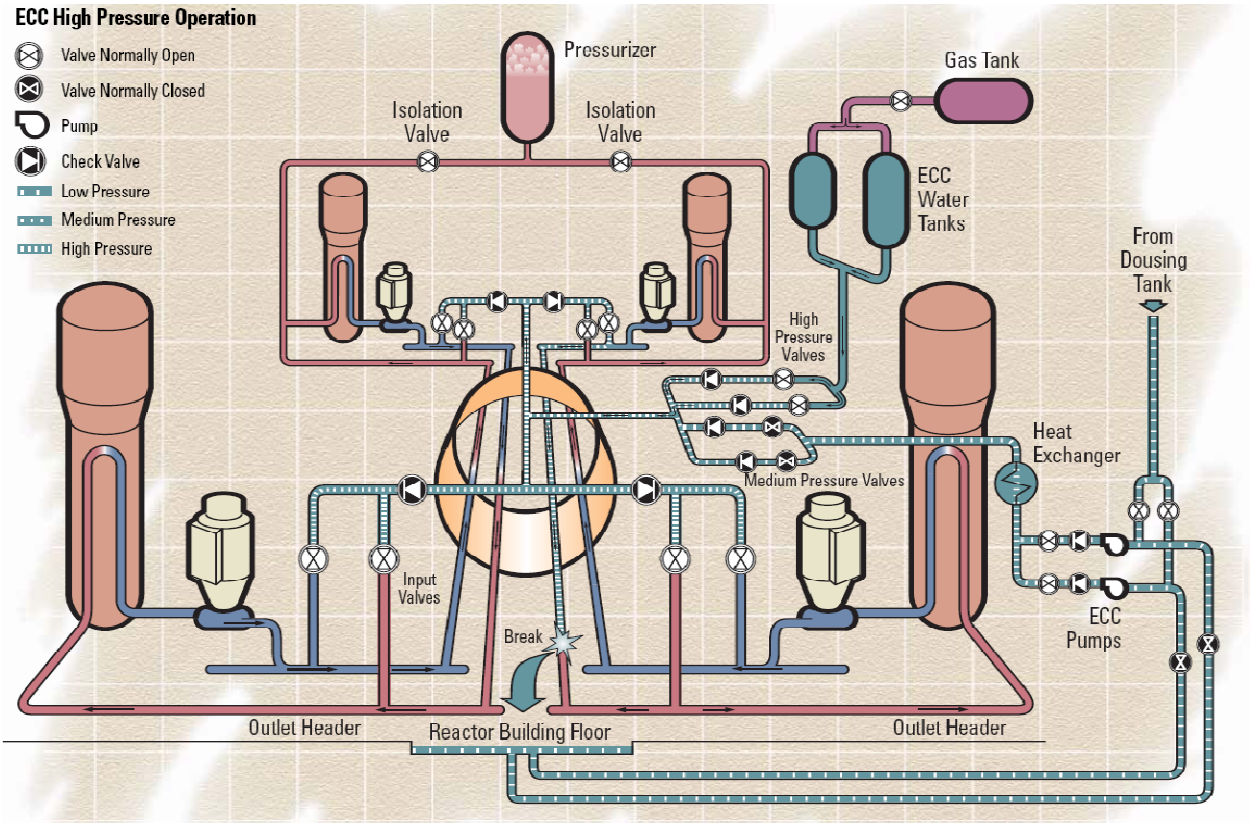

Figure 40 ECC layout

5.4.3 Injection pressure and flow rate

The current design (using CANDU 6 as a model) is a three-stage ECC:

- A high-pressure initial injection phase limits fuel overheating for small breaks and forces early cooling for large breaks (to limit pressure-tube deformation and early fuel damage). Typical injection pressure is 5.3 MPa. In CANDU 6, high-pressure injection comes from two water tanks which are pressurized by gas at the time of a LOCA signal. In some multi-unit CANDU plants, this high-pressure phase is supplied by electrically driven pumps because the reliability of Class IV power tends to be very high (it can be obtained from other operating units as well as the grid).
- Medium-pressure injection takes over when the high-pressure water tanks are nearly empty. It uses medium-pressure (~1 MPa) pumps and draws cold water from the dousing tank or a similar reservoir. It pumps this water into the same locations (all headers) as the high-pressure ECC. The medium-pressure phase ensures that enough water has collected in the basement of the containment building before the next (recovery) phase starts.
- In recovery injection, the medium-pressure ECC pumps are switched over to take water from the sump in the basement. They pump this water through dedicated ECC heat exchangers before returning it to the heat-transport system. This phase is the long-term heat sink.

Figure 41 shows the three phases schematically for a large LOCA.

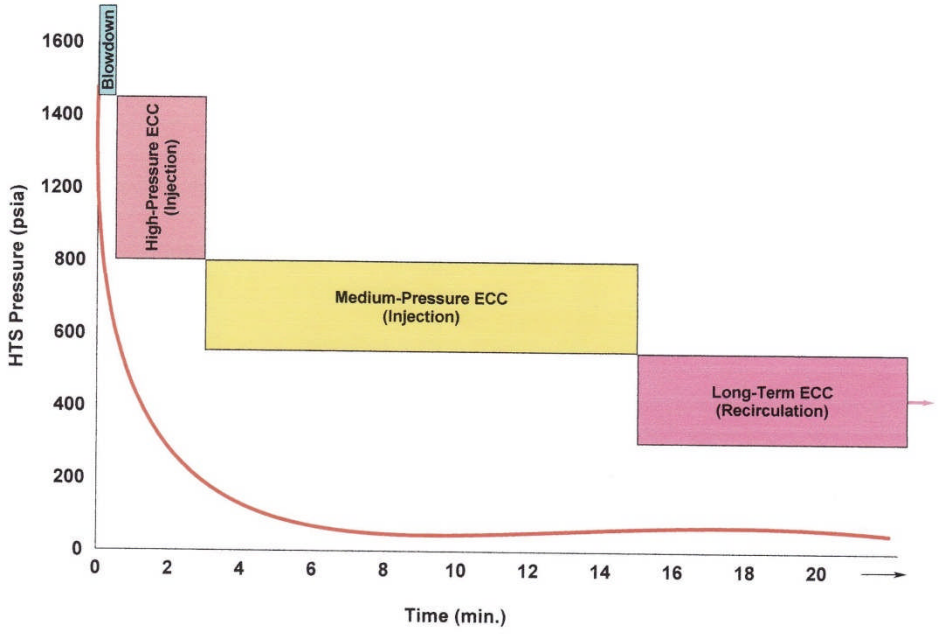

Figure 41 Three phases of ECC

5.4.4 Other Functions

There are two further functions that ECC must perform: loop isolation and crash cooldown.

Loop isolation simply closes the valves connecting the two heat-transport system loops (for some CANDUs which have two loops). It limits (most of) a LOCA to one loop. In addition, for a LOCA with loss of ECC injection, loop isolation (which is an independent signal) limits the possible source of hydrogen.

Crash cooldown is more significant. If a break is small, less than, say, a feeder failure, it is not able to depressurize the heat-transport system down to ECC pressure or to keep it below ECC pressure once injection begins. Crash cooldown opens all the MSSVs on all the steam lines and blows down the steam-generator secondary side to near atmospheric pressure over about 15 minutes. Because the steam generators are still a heat sink for the primary coolant in a small LOCA, this forces the primary-side pressure down over the same time scale. Therefore, it ensures that ECC is not blocked by the heat-transport pressure "hanging up" at secondary-side pressure and that the unfailed loop will also be refilled by ECC. Some CANDUs (Darlington) use high-pressure pumps for a small LOCA and are not as dependent on crash cooldown for this purpose.

5.4.5 Initiation Signals

Clearly, ECC initiation must be automated. The basic signal is low heat-transport system pressure. By itself, this is not unique to a LOCA, and a spurious injection is costly due to heavy-water downgrading, and therefore it is conditioned (ANDed) by one or more of high building pressure, sustained low heat-transport system pressure, and high moderator level (the last is for an in-core break). A separate signal isolates the loops (in some designs) on low pressure. Crash cooldown is part of the ECC signal; however, because of its importance, recent designs have two independent crash cooldown signals.

5.4.6 Reliability

As a safety system, the ECC must meet a demand unavailability of 10^{-3} or less. A running unreliability of 10^{-2} over the three-month mission time has been used as a design target. Availability will be better because fuel will heat up more slowly in the longer term if interruptions in ECC occur; hence, there may be time to repair the fault in ECC before further fuel damage occurs.

5.5 Containment

The important aspects of containment are the following:

1. What is the design pressure?
2. What is the leak rate at design pressure?
3. How is pressure controlled? How is heat removed?
4. How is containment isolation ensured?
5. What is the containment reliability?
6. What other functions must containment perform?

5.5.1 Design pressure and leak rate

Containment is an envelope around those systems containing or potentially containing significant amounts of fission products and is designed to prevent their escape to the environment. Of course any structure will leak, and the leak rate will increase with internal pressure. Typically, containment surrounds at least the reactor core and the primary heat-transport system.

The *design pressure* is chosen to be greater than the maximum pressure reached in any accident

for which a predictable degree of containment leak-tightness is a requirement. To determine the design pressure, all design basis accidents which release significant radioactive material into containment are analyzed, and the peak pressure reached in any one, plus some margin, is chosen to be the design pressure. The important aspect of design pressure is that the leak rate at the design pressure is known. In addition, for severe accidents [CNSC, 2008]:

> "Containment maintains its role as a leak-tight barrier for a period that allows sufficient time for the implementation of off-site emergency procedures following the onset of core damage. Containment also prevents uncontrolled releases of radioactivity after this period."

This requirement may also affect the design pressure.

Leak rate is generally not selected independently in advance, but results from the construction technique. If very low leak rates are required (≤0.2% / day at design pressure), a steel liner is used.

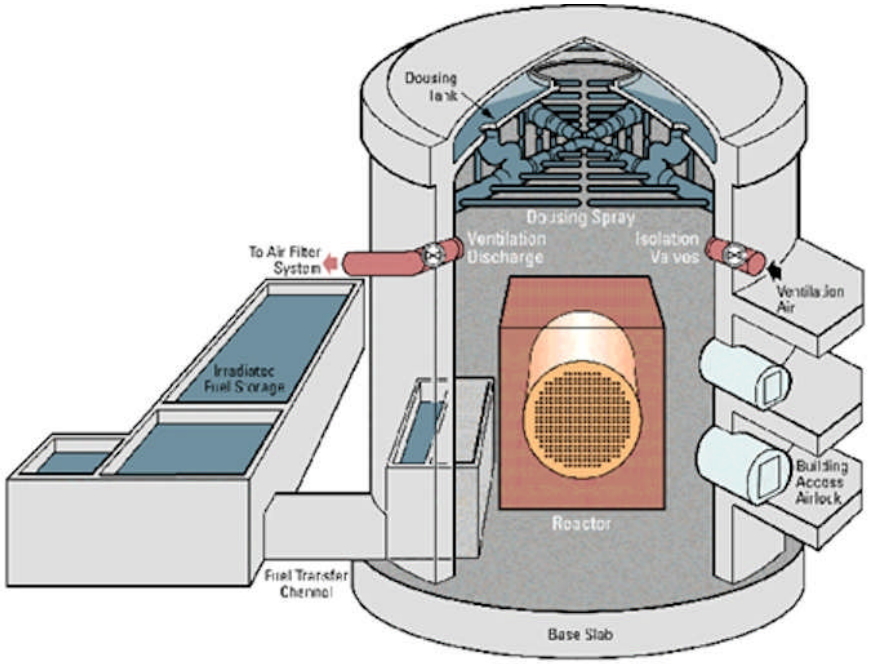

Figure 42 Single-unit containment

For CANDU 6, for example (Figure 42), the design pressure is 124 kPa(g), and the leak rate at the design pressure is 0.5% of the contained volume per day. Vacuum containments have lower design pressures (because the vacuum building terminates the pressure rise), and (after the initial short-term overpressure), leak rates are *negative* (inward) for several days; see Section 5.5.2. For the Darlington containment, for example, the design pressure is +96 kPa(g). The normal operating pressure for the vacuum building is -96 kPa(g) [Huterer, 1984]. Typically, the design pressure is set by the large LOCA because this both causes high short-term pressure and has the potential to release fission products into the containment. The leakage rate at design pressure is confirmed by proof testing before the plant is operational and by periodic testing thereafter.

Should the pressure exceed the design pressure, the building will not explode (typical safety margins on massive failure of the building are a factor of about three over the design pressure; see [Rizkalla, 1984], [Rizkalla, 1986]). However, the leak rate is harder to predict because the leak area may increase. In particular the leak-tightness of any penetrations and seals above design pressure is dependent on their detailed design and will need to be determined on a case-by-case basis. In any event, for an epoxy-lined containment, leakage would increase through penetrations and cracks before the internal pressure reached failure pressure, and therefore it would be very unlikely for the building to fail catastrophically.

5.5.2 Pressure control and heat removal

Without some means of removing heat, the containment pressure in an accident such as a pipe break will rise rapidly as the broken system discharges steam and empties, then more slowly as the decay heat is steamed into containment. It is possible to build a high-pressure containment to withstand this, at least for some time. To date, CANDU containments have had some means of short-term pressure suppression and/or some means of long-term heat removal to provide for these two phases of an accident: the addition of pressure suppression enables a lower containment design pressure.

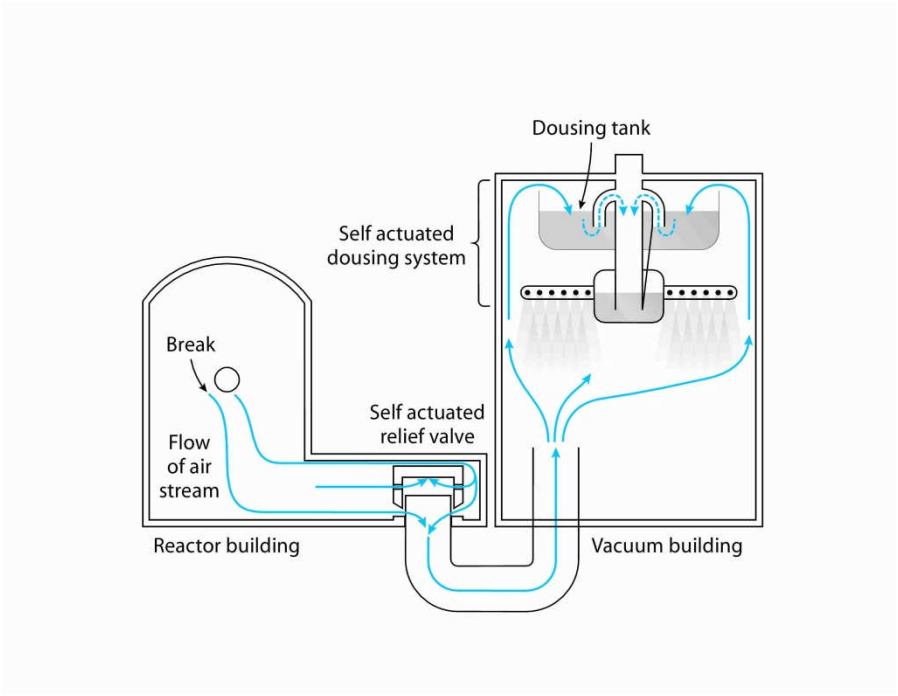

Figure 43 Vacuum containment concept

Large nuclear stations in Ontario use multi-unit containment in which parts of the containment envelope are shared among four or eight units. The individual reactor containment buildings are all connected to a common vacuum building kept at very low pressure. Inside the vacuum building is an elevated water tank; when a LOCA occurs, the vacuum valves open (self-actuated on pressure differential), thereby connecting the vacuum building to the reactor building(s), and the contents of the water tank are sprayed over the vacuum-building volume (Figure 43, from

[Morison, 1987]). The sprays are likewise self-actuated on the pressure differential caused by the LOCA. The water sprays condense the steam and reduce the internal pressure. The containment pressure quickly goes sub-atmospheric and remains so for several days after an accident, meaning that leakage is inward, not outward.

The single-unit CANDU 6 also uses pressure suppression (Figure 42). The sprays and the elevated water tank are located in the reactor building. There are six spray arms, each with spray valves, arranged as two valves in series on each spray arm (to avoid a spurious douse). The valves on three spray arms are pneumatically operated, and for diversity, the valves on the other three are electrically operated. The containment building is made of pre-stressed, post-tensioned concrete with an epoxy liner for leak-tightness. Dousing cycles on and off for small breaks, but for large breaks, it remains on until the dousing water is used up and is all on the basement floor of the reactor building. Dousing does not control pressure in the long term because it is used up in the early part of an accident.

In the longer term, heat can be removed by containment air coolers. These require both water and electrical power. Alternatively, low-flow sprays can also be used, with heat being removed from the spray water by heat exchangers and the cooled water pumped back up to the spray arms.

5.5.3 Isolation

In normal operation, containment is *not* a sealed system. Many fluid lines penetrate the building (e.g., steam lines, feed-water lines, service water lines, instrument lines). For CANDUs, the building is normally ventilated for atmospheric temperature control, especially because personnel access to parts of the building is possible and required during operation. Some penetrations, particularly ventilation, could be pathways for release of radioactive material if an accident should occur, and therefore, on an accident signal, these are automatically isolated.

Steam, feed-water, and service-water lines are not isolated immediately in CANDU practice because continuing to use a running system is more reliable than stopping it and starting up another one. For LWRs, the opposite approach is taken due to a different philosophy of containment isolation [USNRC, 2013] and partly due to the reactivity increase on a steam-line break in LWRs. However, main steam isolating valves (MSIVs) are used in recent CANDUs to prevent leakage to the environment through a pre-existing steam-generator tube failure after an accident, but they are manually operated and slow. Feed water and service water are not normally isolated.

5.5.4 Reliability

As a special safety system, the containment must meet a demand unavailability of 10^{-3} years/year or less. Containment leak-tightness is tested every few years by pressurizing the building and measuring the leak rate. This is an invasive and expensive test, and if the leak rate exceeds the requirement, one must assume that a containment impairment has existed for half the interval between tests. Therefore, on-line leakage monitoring systems are being deployed in existing reactors. The containment isolation system is likewise tested during operation to prove that its unavailability target is not being exceeded.

5.5.5 Other functions

Containment also acts as a barrier to protect reactor systems from external events (tornadoes, turbine missiles, aircraft crashes, and malevolent acts). These may impose additional design requirements on the structure.

Hydrogen can build up in containment after an accident. After a LOCA, hydrogen is formed slowly by radiolysis of the water circulating through the core. A severe accident such as a LOCA plus loss of emergency core cooling can also produce hydrogen early on because of the chemical reaction between the hot fuel sheaths and the steam in the fuel channels (cf. Sections 3.2.2 and 3.2.3.2). The containment building promotes some mixing of hydrogen due to natural circulation. Air cooler fans provide forced mixing. In addition, igniters are placed in various rooms to burn any local hydrogen concentration before it can detonate. Passive autocatalytic recombiners can be used for long-term hydrogen control; they do not need electrical power or controls. They present a catalyst bed to the containment atmosphere, on which the hydrogen recombines with oxygen. The heat of reaction causes a convection flow through the device, which helps mix the containment atmosphere.

5.6 Monitoring

For most accidents, the plant state is monitored from the main control room (MCR), and the safety functions of shutdown, heat removal, and containment can be performed from there. Some accidents, however, can render the MCR uninhabitable or inoperable: for example, earthquakes, fire in the MCR, hostile takeover, aircraft strikes, and high radiation fields. A secondary control area (SCA) is provided for such eventualities; the operators relocate to the SCA and can perform the required safety functions from there.

5.7 Problems

1. Select an accident from the case studies discussed in Section 3 and analyze it in terms of the five levels of defence in depth (both barriers and objectives). Which aspects were present? Which were missing?

2. Consider the ZED-2 reactor described in Section 2.7. What elements of defence in depth are present in this design? What elements are missing? Why might it be acceptable to have missing or weak levels of defence-in-depth?

3. Using the SLOWPOKE 10MW heating reactor described in Section 2.7, describe the possible shutdown-system requirements in terms of design, rate, depth, signals, margins, environment, and independence. Give reasons—do not simply copy existing material.

4. Using the ZED-2 zero-power research reactor described in Section 2.7, describe the possible shutdown-system (moderator dump) requirements in terms of design, rate, depth, signals, margins, environment, and independence. Give reasons—do not simply copy existing material.

5. Look up (e.g., from the USNRC web site) the design of either the EPR or AP1000 decay heat-removal systems. Summarize them and discuss advantages and disadvantages compared

to the CANDU decay heat-removal systems (choose one CANDU plant for your comparison). If you do not have access to CANDU information, simply compare EPR and AP1000 decay heat removal systems.

6. What are the options for heat removal from containment after a severe accident (core damage)? What are the pros and cons of each of these options? Feel free to look up what choices have been made by modern designs.

6 Safety Analysis – Accident Phenomenology

This Section provides a high-level discussion of accident phenomena in CANDUs and how the results are judged. The technical capabilities that computer codes used in CANDU safety analysis should possess are then described. Severe accident phenomena and analysis are summarized, followed by a discussion on uncertainty analysis.

6.1 Accidents by Phenomena

In Section 1.4, we described the hazards posed by a nuclear power plant and the broad classes of events that could cause a release of radioactive material. In Section 2, we discussed how design basis accidents are identified and selected. Based on these concepts, we can describe accidents by major phenomena, as follows (grouped by primary or direct cause):

1. Reactivity accidents
    - Bulk loss of reactivity control
    - Loss of reactivity control from distorted flux shapes
2. Decrease of reactor coolant flow
    - Loss of Class IV power
    - Partial loss of Class IV power
    - Single pump trip or single pump seizure
3. Increase of reactor coolant pressure
    - Loss of primary pressure and inventory control (increase)
4. Decrease of reactor coolant inventory
    - Large heat-transport system LOCA
    - Small heat-transport system LOCA
        - Single-channel events
        - Single steam-generator tube rupture
        - Multiple steam-generator tube rupture
    - Loss of primary pressure and inventory control (decrease)
5. Increase of secondary-side pressure
    - Loss of secondary-side pressure control (increase)
6. Loss of secondary-side heat removal
    - Main steam-line break
    - Feed-water line break
    - Loss of feed-water pumps
    - Spurious closure of feed-water valves
    - Loss of secondary-side pressure control (decrease)
    - Loss of shutdown heat sink
7. Moderator and shield-cooling system failures
    - Pipe break
    - Loss of forced circulation
    - Loss of heat removal
8. Fuel-handling accidents

- Fuelling machine on-reactor
- Fuelling machine off-reactor
- Accidents in the irradiated fuel bay
- Loss of heat removal
- Loss of water

Severe core-damage accidents involving an initiating event and failure of at least two mitigating systems fall into a separate category because the phenomena of severe core damage are not strongly coupled to the initiating event. We will cover these later.

Safety analysis is the method by which we can show that the predicted consequences of a postulated accident meet regulatory and design goals. It involves mathematical modelling of the major systems in the plant to predict the behaviour of their components in an accident. Typically, the focus is on:

- Demonstrating that the physical barriers to release of radioactive material are not further damaged, or have sustained only limited damage, beyond the initiating failure
- Predicting on-site doses to ensure that credited operator actions are feasible in the post-accident environment
- Predicting dose to the public.

In general, in traditional safety analysis for CANDU, the mathematical models are best-estimate, and pessimism is introduced by means of "conservative" assumptions and data. This raises the issue of margins.

6.2 Margins

A discussion of margins must start by defining the essential physical barriers that need to be preserved, or their degradation limited, to meet regulatory dose limits with confidence.

Typically, these barriers are the fuel matrix, the fuel sheath, and the heat-transport system including the pressure tube, the calandria tube, and the calandria shell. To prevent failure of an essential barrier, physically based quantitative *parameter limits* are chosen for each failure mechanism—e.g., $T_{fuel} < 2800°C$ is a parameter limit (no fuel melting) which will prevent one mechanism of failure of the pressure-tube barrier through local strain. More conservative *surrogate criteria* are chosen if the parameter limit is uncertain. *Analysis limits* are chosen to ensure that the parameter limit or surrogate criterion is met. This framework, along with the use of conservative assumptions and data in the safety analysis, gives the margin to the barrier failure point, as shown in Figure 44.

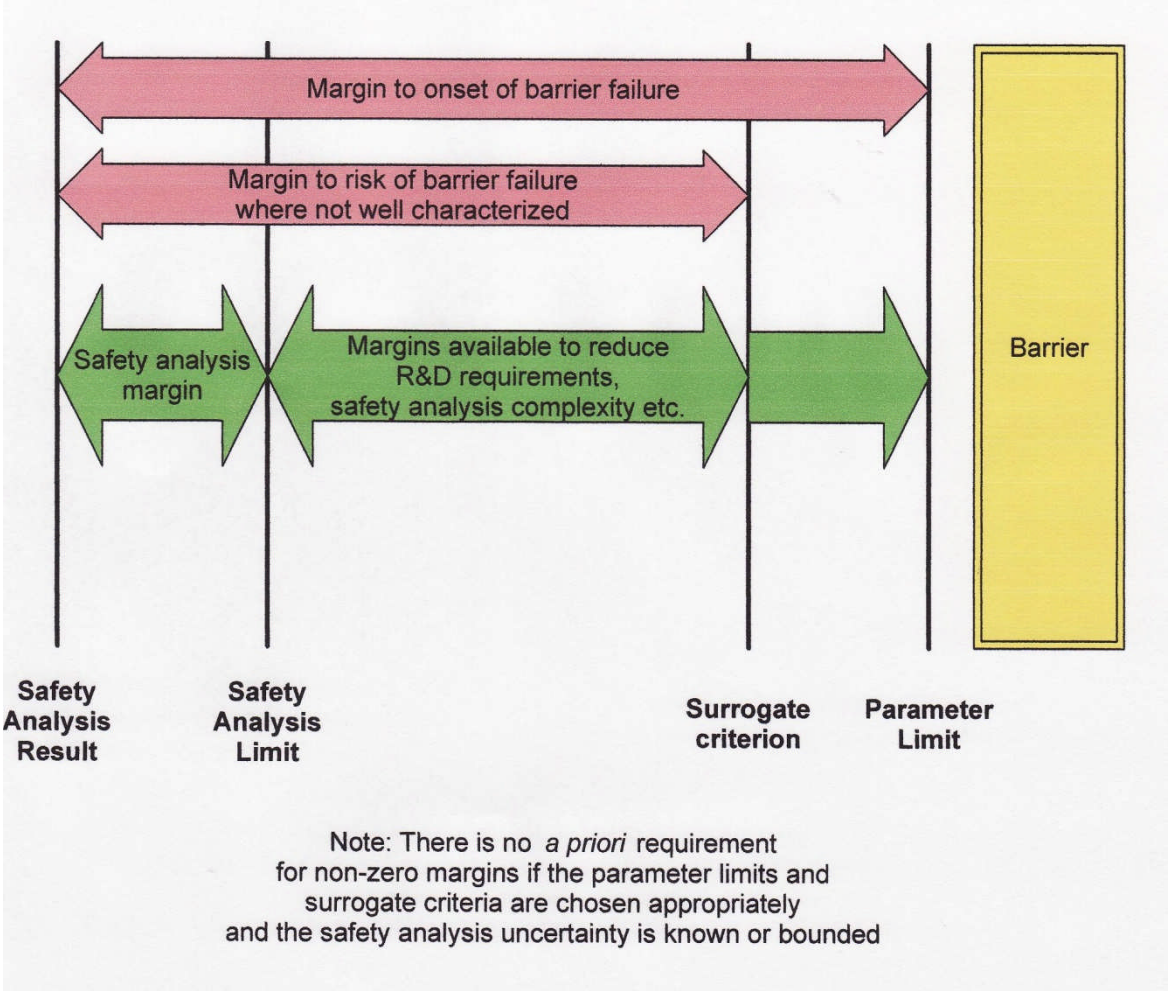

Figure 44 Margins

Of necessity, many assumptions about plant operation are made in safety analysis. These are usually chosen to envelop actual or expected operation—for example, safety analysis will use a maximum bundle power that is greater than that expected in operation. The plant must operate consistently with the assumptions in the safety analysis. The operators therefore define a safe operating envelope (SOE) of parameters under operational control[6]. Operating the plant within this envelope ensures consistency with the safety analysis assumptions and incidentally provides another margin to the results of safety analysis. It is important that the safety analyst not make assumptions that are too restrictive because this will unnecessarily limit operation.

Other methods of safety analysis are best estimate with analysis of uncertainties (BEAU), which we will cover later, and best-estimate analysis, which is used for severe accidents.

[6] In other countries, a set of *Technical Specifications* serves a similar purpose.

6.3 Major Computer Analysis Tools Required for DBAs

CANDU safety analysis requires a comprehensive suite of physical models. The mathematical foundations of these models are presented in simplified form in Section 7. This section lists the capabilities that these codes should have. A detailed description of individual codes is well beyond the scope of this chapter; references are given to enable the student to investigate further any codes of interest.

Reactor physics analysis requires a transient three-dimensional model, especially for larger CANDU cores. The most demanding application is a large LOCA because the positive void coefficient leads to relatively fast kinetics and because of the spatial effects associated with flux tilts and shut-off rod (or liquid absorber) insertion. Three-dimensional effects are also important in slow loss of reactivity control starting from distorted flux shapes. Current codes used [Roy, 2004] include

- WIMS-IST, a two-dimensional lattice-cell code
- RFSP-IST, a reactor code for CANDU full-core 3-D static and dynamic analysis
- MCNP – a "Monte-Carlo" code which tracks large numbers of individual neutron histories to achieve an answer. The accuracy of the answer is limited only by the number of histories and the quality of the input data from experiments which measure nuclear cross sections.

The *system thermo-hydraulics* code is typically a two-fluid, one-dimensional non-equilibrium network code. The two fluids are water and steam; recent codes also incorporate a third non-interacting fluid, e.g., hydrogen, as produced in severe accidents. One spatial dimension suffices for CANDU because the system consists largely of linear flow in pipes (feeders, channels, large pipes above the core) and there are no vessels in which complex three-dimensional behaviour occurs. However, the flow in the headers can be quite complex, and tools based on visualization tests are being developed to model it more accurately. The thermo-dynamic non-equilibrium aspect is important in modelling fuel rewetting and channel refilling after a LOCA because the flow can be stratified (steam and water flowing separately due to the effect of gravity) during that time, and each phase can have its own temperature and flow. Finally, a network capability is clearly a necessity in CANDU, with its multiple parallel paths (e.g., many channels are connected to one header, and ECC is connected through parallel paths to each header). The reactor physics calculations must be coupled with the system thermo-hydraulics code for a large LOCA because the voiding transient determines the power pulse, which in turn has a second-order effect on the voiding transient. Current system thermo-hydraulic codes used are CATHENA [Hanna, 1998] and TUF [Liauw, 1997].

Fuel thermo-mechanical models consist of a code for normal operation, which predicts the initial fuel conditions before the accident (sheath strain, fuel-to-sheath heat-transfer coefficient, fission gas release, initial fuel and sheath temperatures, etc.) and a transient thermo-mechanical code for accidents. The latter includes sub-models for fuel failure mechanisms due to fuel-sheath strain, beryllium braze penetration, sheath embrittlement due to oxidation, athermal strain, and excessive fuel energy content. Because of the need to predict the dose for each accident, the models must be able to estimate the percentage of fuel sheaths that fail in

an accident (if any) and the release of fission products to the fuel channel. Codes used include ELESTRES-IST for initial fuel conditions and ELOCA-IST for transient behaviour [Lewis, 2009].

Under certain circumstances, such as a large LOCA combined with loss of ECC injection, the pressure tube will overheat and (depending on the internal pressure) sag or strain into contact with the calandria tube. This requires models of the *pressure-tube thermal-mechanical* transient behaviour to predict the extent of deformation and the pressure-tube temperature and internal pressure when or if it contacts the calandria tube. Such models are now part of the system thermo-hydraulics code.

The behaviour of a channel subsequent to such contact depends on the heat transfer from the calandria tube to the moderator. Further deformation will not occur if the calandria-tube outer surface does not dry out, or at least does not go into widespread film boiling. This in turn depends on the heat transfer coefficient between the pressure tube and the calandria tube, and the local moderator sub-cooling. For the first, there are theoretical models and comparisons with experiment – see, e.g., [Currie, 1984] and [Currie, 1986]. For the second, a two- or three-dimensional prediction of *moderator temperatures* (and hence flows) is required. Of most interest is the steady-state distribution at the time of contact, although transient calculations are required for in-core breaks. The current industry code is MODTURC-CLAS. See [Xu, 1999] for a brief description of MODTURC-CLAS and a good summary of thermo-hydraulic codes used in CANDU.

Following the release of fission products from the fuel, their movement through the heat transport system to containment and then within containment should be predicted. To date, CANDU safety analysis has not used models for fission-product transport within the HTS and for deposition on surfaces such as end fittings and feeder piping, although this is clearly an area which could be included and has been the subject of intensive R&D over a number of years. However, the partitioning of fission products between steam and water phases at the break and within containment has been modelled, as has long-term formation and transport of organic iodides within and from the water pool. See [Wren, 1999] and [Wren, 2001].

The *containment-pressure* transient calculation uses the transient energy release from the break and includes sub-models for dousing, containment air coolers, fission products, hydrogen transport, and natural and forced circulation. Multi-node, multi-fluid (water, steam, air, hydrogen) three-dimensional containment models are used for this analysis. The GOTHIC international code is used for CANDU; see, e.g., [Andreani, 2010].

The final step is calculation of *dose* to the public. The atmospheric dispersion model typically uses a Gaussian plume model to predict exposure as a function of distance from the station; the input is the predicted transient release of radionuclides from containment for each accident. See [Boss, 2006] for an example. The weather assumed is traditionally the worst weather occurring more than 10% of the time at the site. Exposure-to-dose calculations use standard ICRP-recommended conversion factors ([ICRP, 2010], [ICRP, 2012]).

Figure 45 shows this whole process as a flowchart.

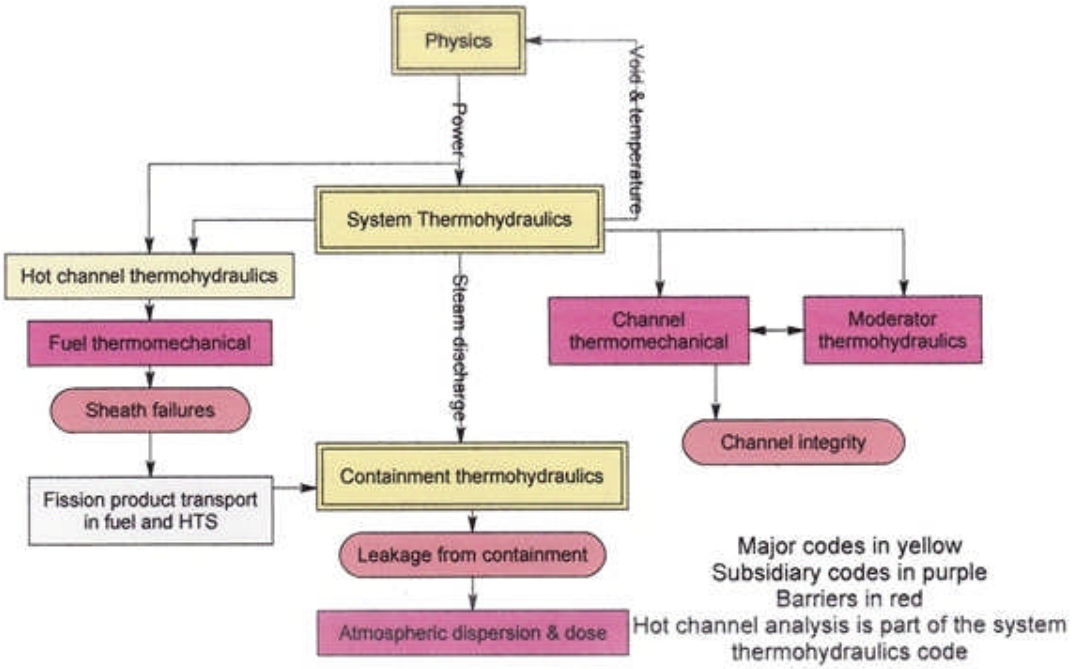

Figure 45 Safety analysis codes

6.4 Code Validation and R&D

It is essential that the results of safety analysis codes reflect reality, or at least a version of reality in which the predictive bias is understood. Extensive R&D is done to support safety analysis codes, in facilities which range from small- to full-scale. The purpose of R&D is *not* to simulate an accident, but to provide the fundamental scientific and engineering data against which the codes can be validated (i.e., their results compared to experimental data). Experiments generate scientific *knowledge* relevant to the phenomena in a nuclear reactor accident. This knowledge is used to build engineering *models*, which in turn are used in digital computer *codes*. The codes are then *validated* against the knowledge (using different data from those used to develop the models). The validation can include comparison against small-scale and integral tests, as well as real nuclear power-plant transients where data are available. The codes are also independently *verified* to confirm that the mathematical and engineering models have been represented correctly in the code language logic. Finally the verified, validated codes are used to prepare the *safety and licensing analysis procedures* for planned or operating plants or to *assist in the design* of advanced plants. This process is shown schematically in Figure 46.

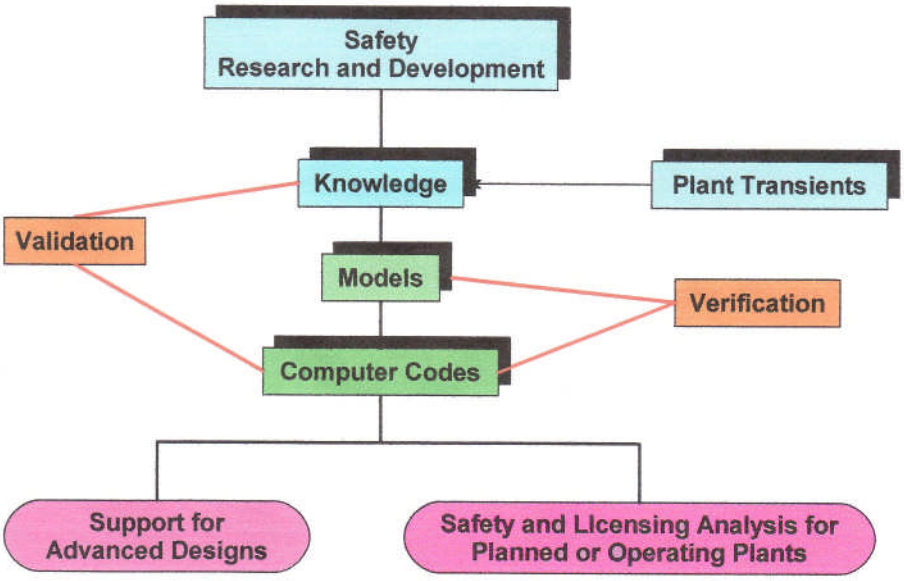

Figure 46 Code validation process

Separate effects must be distinguished from *integral* tests. The former tend to focus on one physical mechanism and are generally small-scale. Integral tests combine many phenomena expected in the reactor and are generally large-scale; however, the interaction among the phenomena can be complex. Hence, integral tests are used in the later stages of validation of system models.

It is not possible within the scope of this Chapter to give a full accounting of all the R&D facilities that support CANDU safety technology. A few of the major facilities are discussed briefly. References are given to enable the student to follow up on any facilities of interest.

6.4.1 Reactor physics

The ZED-2 reactor [AECL, 2011] was described in the problem set in Section 2.7. It is a heavy-water tank reactor used for fundamental physics experiments on natural uranium and advanced CANDU fuels and lattices. It is used for measurements of reactivity coefficients such as coolant void and temperature, and generates basic data for validation of physics codes. At the other end of the scale, real plant transients such as shutdowns are used to validate some aspects of CANDU kinetics at full scale.

6.4.2 Thermo-hydraulics

The major integral facility used for validation of system thermo-hydraulic codes is RD-14M, shown in Figure 47 [Buell, 2003]. It is a full-elevation model of a typical figure-of-eight CANDU reactor heat-transport system, at full pressure and temperature conditions, and with ten full-length electrically heated channels. All HTS components are simulated: channels, end-fittings, feeders, headers, and steam generators. Mass flux, transit times, and pressure and enthalpy distributions are similar to CANDU. Tests cover all phases of a large or small LOCA scenario, including blowdown and refill, natural circulation in single-phase and two-phase, and loss of

shutdown cooling.

6.4.3 Fuel

Separate-effects fuel testing is performed out-of-reactor. For integral tests, the NRU reactor has a vertical in-core loop that can be loaded with CANDU fuel elements and subjected to a LOCA (Blowdown Test Facility). Fuel behaviour during extended post-dryout operation has also been studied in the NRU loops.

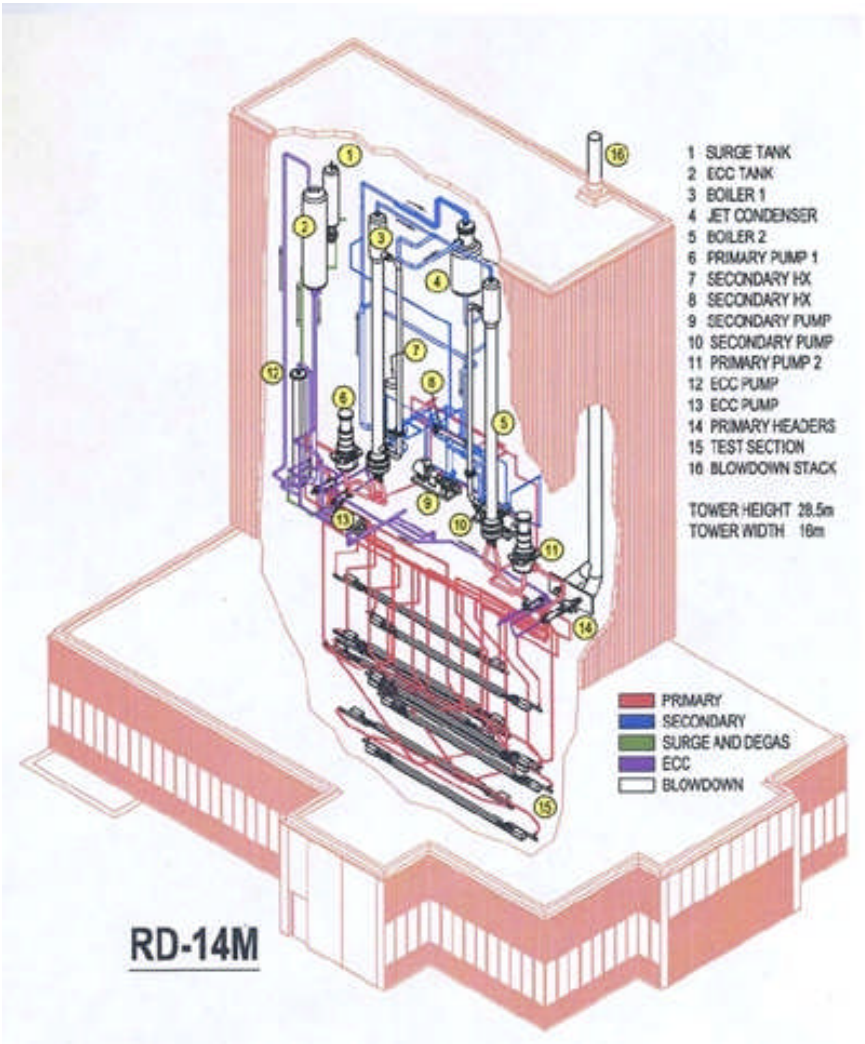

Figure 47 RD-14M schematic

6.4.4 Moderator thermo-hydraulics

The moderator thermo-hydraulic codes have been validated against a wide variety of tests, ranging from pseudo-two-dimensional “slices” of a model calandria to in-reactor probes. The most sophisticated experiments have taken place at Chalk River Laboratories in the Moderator Test Facility, which is a one-quarter scale CANDU calandria containing 480 heaters to represent the 480 channels in the Bruce/Darlington design. The facility can measure a grid of local temperatures and local flow velocities in three dimensions.

6.4.5 Fuel channel thermo-mechanical behaviour

One of the advantages of the pressure-tube concept is that channels can be tested at full diameter. The phenomena exhibited during pressure-tube strain to contact the calandria tube (for large LOCA, or LOCA + LOECC) have been examined using full-diameter channels, in which the pressure-tube is internally heated and expands under pressure. The entire pressure tube / calandria tube assembly is immersed in a water environment which represents the moderator (Figure 48) [Sanderson, 2003].

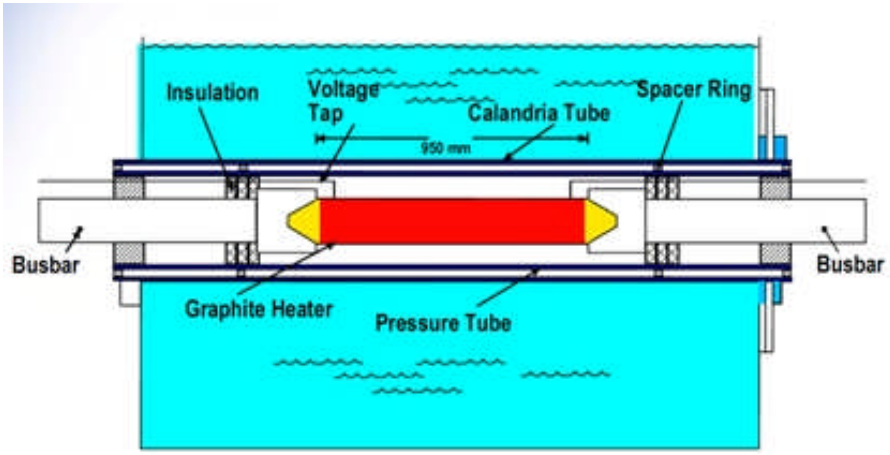

Figure 48 Contact boiling tests

By controlling the internal pressure, heating rate, and moderator temperature, a map can be derived of the regions of heat transfer on the outside of the calandria tube just after pressure-tube contact (Figure 49), which can be used to validate the channel thermo-mechanical codes.

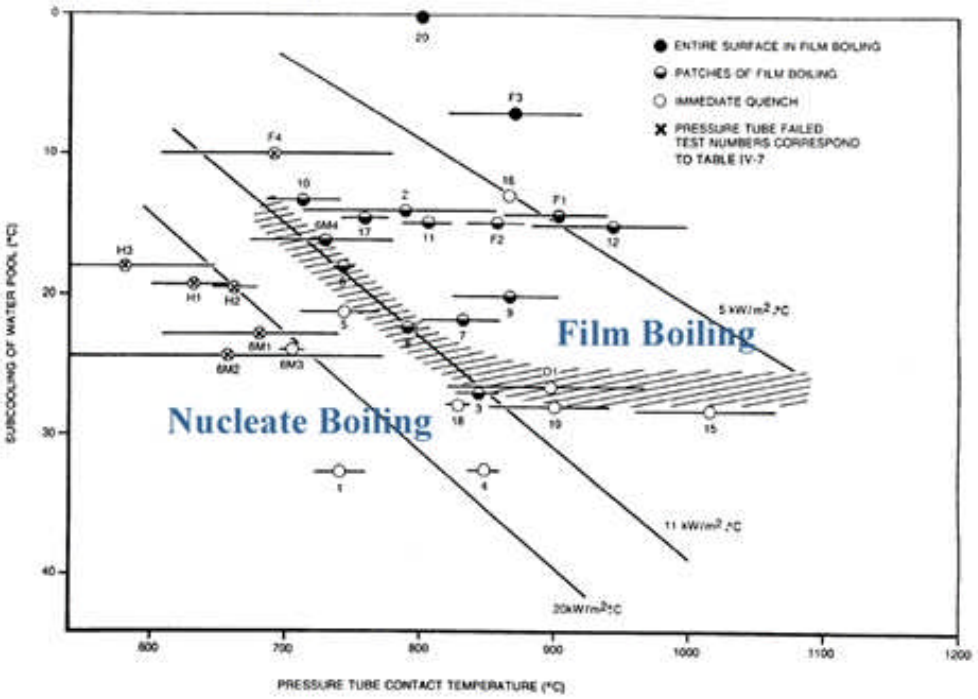

Figure 49 Heat-transfer regimes on outside of calandria tube

6.4.6 Containment thermo-hydraulics

Three large-scale facilities have been used to validate containment codes, particularly hydrogen behaviour (combustion and detonation characteristics and limits) [Krause, 2007].

The Large-Scale Containment Facility at Chalk River Laboratories has a room height of 10 metres with a total volume of ~1,575 m^3. It is used for studying hydrogen mixing behavior at high temperature and high humidity, using helium as a hydrogen simulant. It is also used to study the behaviour of wet aerosols (Figure 50).

The Large-Scale Vented Combustion Facility at Whiteshell (Figure 51) is a rectangular enclosure with an internal volume of 120 m^3 used for studying hydrogen burning in air/steam mixtures at various temperatures. The combustion chamber can be subdivided into two or three compartments, with vent openings of various sizes between the compartments and the outside.

The Containment Test Facility at Whiteshell has also been used to investigate combustion phenomena in single and interconnected vessels, including detonation and the transition to detonation. It consists of a 6 m^3 sphere and a 10 m^3 cylinder, which can be connected by ducts (Figure 52).

Figure 50 Large-scale containment facility

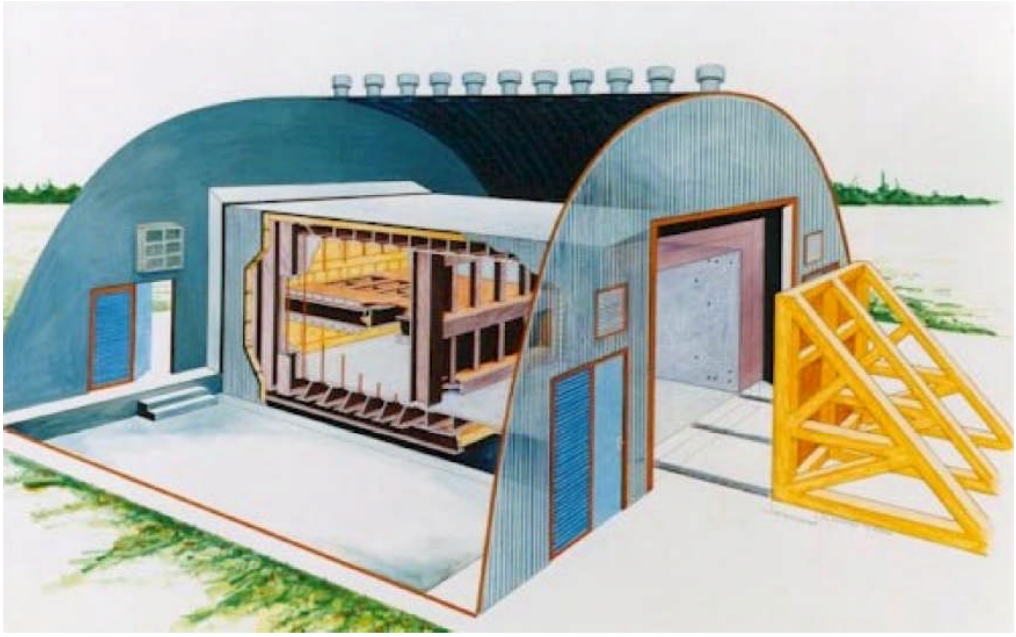

Figure 51 Large-scale vented combustion facility

Figure 52 Containment test facility

6.5 Selection of Initial Conditions

A number of key parameters are chosen in a "conservative" direction for licensing analysis. These include fundamental core property parameters, initial plant conditions, system performance measures, and assumptions on the unavailability of portions of mitigating systems. There is no magic formula for doing this: too much conservatism may require unnecessary design changes or severely limit operation; too little may not cover uncertainties in the models used or the station parameters. This dilemma is largely resolved by a BEAU approach, discussed later, in which all parameters are set at their best-estimate values and the uncertainties are combined and propagated through the calculation.

Table 11 gives a *sample* list of parameters and assumptions and how they might be chosen "conservatively". Note that what is conservative in one application (e.g., minimizing the number of containment coolers credited in calculating peak containment pressure) may be non-conservative in another (calculating high containment-pressure trip effectiveness). Note also that whatever safety analysis *assumptions* are made become *limits* to operation.

Table 11 Some conservative assumptions and parameters

Parameter	Conservative Direction	Rationale
Reactor thermal power	High	Minimize time to use up cooling water inventory, minimize margins to critical heat flux, etc.
Reactor regulating system	Normal operation or inactive, whichever is worse; setback is generally not credited unless it tends to "blind" the trip	Choose so as to delay reactor trip
Radionuclide operating load in the HTS	Highest permissible operating iodine burden (and associated noble gases) plus any "spiking" at the time of reactor shutdown, and end-of-life tritium concentration	Maximize radionuclide release from station and public dose
Pressure-tube radial creep	Highest expected over the time scale over which the safety analysis is to be valid	Reduce margin to critical heat flux (due to flow by-pass around the fuel bundle in a crept tube) and increase value of void reactivity
Steam generators	Clean and fouled cases	Reduce reactor trip effectiveness
Steam-generator tube leak rate	Maximum permitted during operation, plus assessment of any consequential effects due to the accident	Increase radioactive material release

Parameter	Conservative Direction	Rationale
HTS flow	Low	Reduce margins to critical heat flux
HTS instrumented channel flow	High	Reduce low-flow trip effectiveness
Coolant void reactivity coefficient	High;	Maximize overpower transient;
	Low	Delay HTS high-pressure trip
Fuel loading	Equilibrium;	Maximize fuel temperatures, radioactive material releases;
	Fresh	Maximize overpower transient
Shutdown system	Back-up trip on less effective shutdown system using the last of three instrumentation channels to trip	Delay shutdown-system effectiveness
SDS2 injection nozzles	Most effective nozzle unavailable	Reduce shutdown-system reactivity depth
SDS1 shut-off rods	Two most effective rods unavailable	Reduce shutdown system reactivity “bite” and depth
Maximum channel/bundle power	High	Earliest time to dryout and maximize fuel and sheath temperature

Parameter	Conservative Direction	Rationale
Reactor decay power	High	Minimize time to use up cooling water inventory
Initial flux tilt	High	Maximize fuel and sheath temperatures
Moderator initial local maximum sub-cooling	Low	Minimize margin to critical heat flux on calandria tube
Number of operating containment air coolers and other heat sinks	Low;	Maximize containment pressure;
	High	Delay high-pressure trip and maximize likelihood of hydrogen combustion due to rapid condensation of steam
Containment leak rate	High (typically 2× to 10× design leak rate);	Maximize public dose;
	Low	Maximize containment pressure
Containment by-pass leakage	Pre-existing steam-generator tube leak	Maximize public dose
Weather	Least dispersive weather occurring >10% of the time	Maximize public dose

Parameter	Conservative Direction	Rationale
Operator actions	Not credited before 15 minutes after a clear indication of the event, for actions that can be done from the control room; and not credited before 30 minutes, for actions that must be done "in the field"	Ensure adequate time for diagnosis

6.6 Accident Walk-Through: Large LOCA

As an example, we shall walk through the phenomena of a large HTS pipe break. Then we will cover more briefly a few more accidents which are representative, but not exhaustive.

6.6.1 Initiating event

A large LOCA in a CANDU is conventionally defined as one where the break area is larger than twice the cross-sectional area of the largest feeder pipe. Therefore, a large LOCA can be located only in the large piping above the core. There are three representative locations (Figure 53): reactor inlet header (RIH), reactor outlet header (ROH), and pump suction line (PSH). Other possible locations are lines connected to the pressurizer, the shutdown cooling lines, and the header interconnect lines.

It is conventionally assumed that the pipe break is instantaneous, an assumption which bears little relationship to reality, but is selected to ensure conservatism in that it maximizes the predicted coolant voiding rate and hence the coolant void-reactivity insertion and reactor power pulse. This in turn presents the greatest challenge to shutdown-system effectiveness.

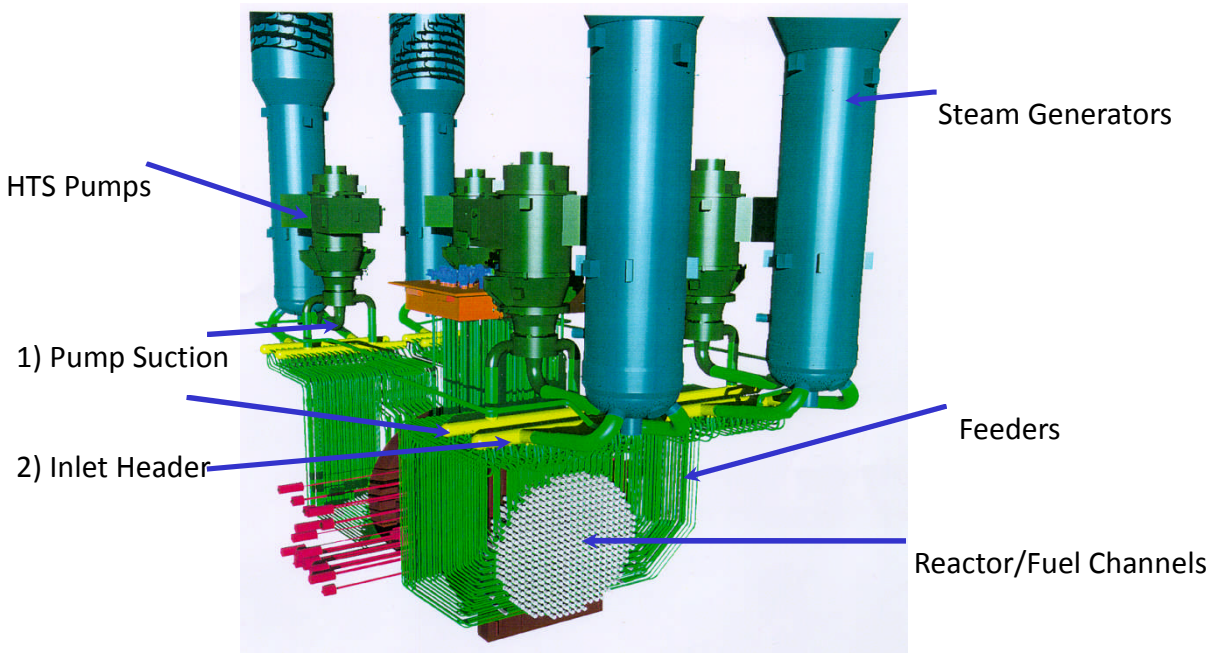

Figure 53 HTS layout

6.6.2 Event sequence (simplified)

- A large HTS pipe break is postulated to occur instantaneously.
- Steam discharges to containment, causing a rise in containment pressure and temperature.
- HTS pressure drops rapidly, causing a rapid decrease in local saturation temperature.
- Fuel channels downstream of the break experience flashing (rapid boiling). Fuel sheaths may dry out.
- The reactor power rises quickly due to the positive void coefficient, causing a rapid increase in fuel and sheath temperatures. Note that there are inherent limits to the speed of voiding, which are set by the subdivision of some CANDUs[7] into two separate PHTS loops, by the fluid inertia in the fuel channels, and by the arrangement of each loop of the PHTS in a "figure-of-eight" configuration. For further reading on this topic, see [Popov, 2013].
- Flow in the downstream channels falls due to the change in pressure drop across the channel (the pressure gradient from the pumps is offset by the pressure gradient due to the break).
- The reactor is shut down by either shutdown system (~2 sec).
- Containment ventilation paths are isolated.
- The fluid inventory in the channels decreases and flow remains low, so that fuel and fuel sheaths continue to rise in temperature. The rise is limited by steam cooling.

[7] Pickering A and B, CANDU 6, and Darlington

- Fuel overheating increases the gas pressure inside the sheath relative to the coolant pressure, which is falling, and can force the sheath to strain. Some fuel sheaths may fail. The temperature excursion depends on the break size, which is traditionally chosen to "stagnate" the flow in the downstream channels, e.g., 30%-40% RIH breaks[8] in Figure 54.

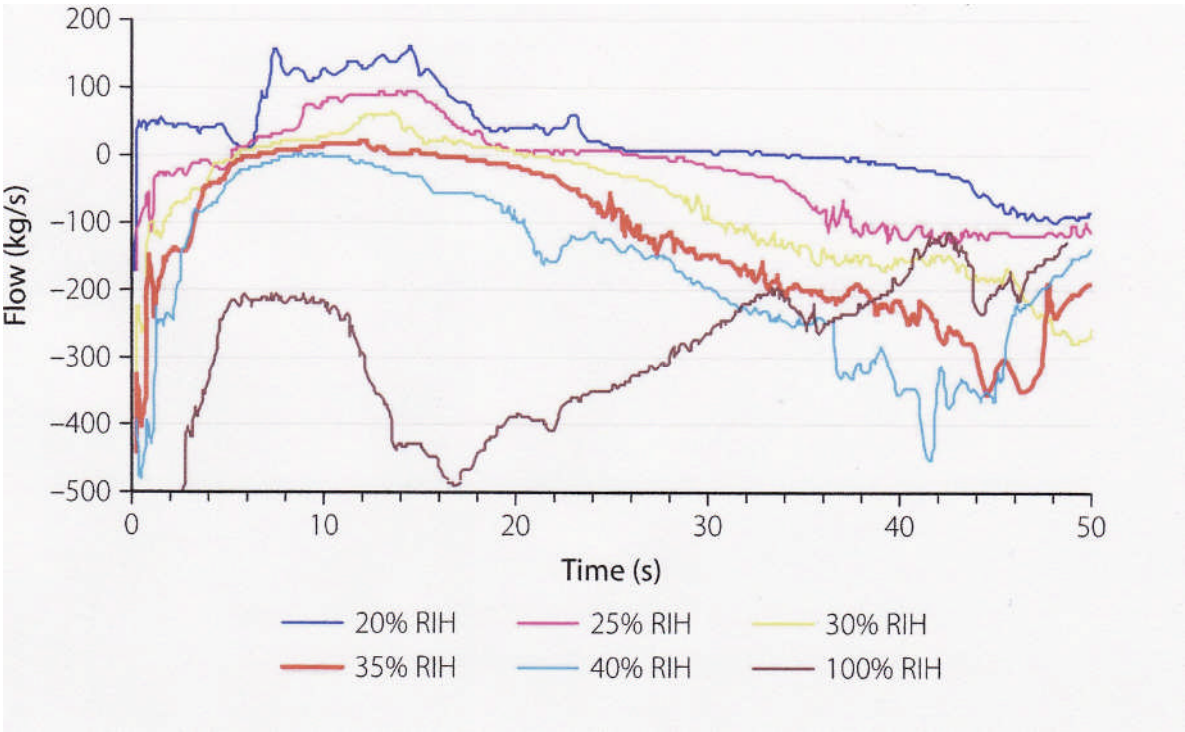

Figure 54 Core flow vs. break size for a group of channels

- Containment dousing is initiated and starts to reduce containment pressure. In multi-unit sites with a common vacuum building, valves to the vacuum building open, and pressure starts to go sub-atmospheric.
- ECC injection is signaled at about 20 seconds. Valves on the gas tanks open to drive water from the accumulator tanks into the HTS (or high-pressure ECC pumps start). Steam-generator rapid ("crash") cooldown is also initiated automatically, and the MSSVs open to discharge secondary-side steam to atmosphere.
- Fuel temperatures stabilize and fall as the headers, and then the channels, refill.
- After the initial injection phase, ECC switches to medium-pressure and then to low-pressure ECC, in which the water from the break is recovered from the building sumps, cooled, and re-injected. This gives a stable end-state which can last for months.

The time scale is shown in Figure 55.

[8] The percentage is *twice* the cross-sectional area of the pipe; hence, a 100% break is twice the cross-sectional area, allowing for discharge of coolant from both ends of the broken pipe. Note that other breaks may also stagnate at different times; which one results in the highest fuel and sheath temperatures is determined by analysis.

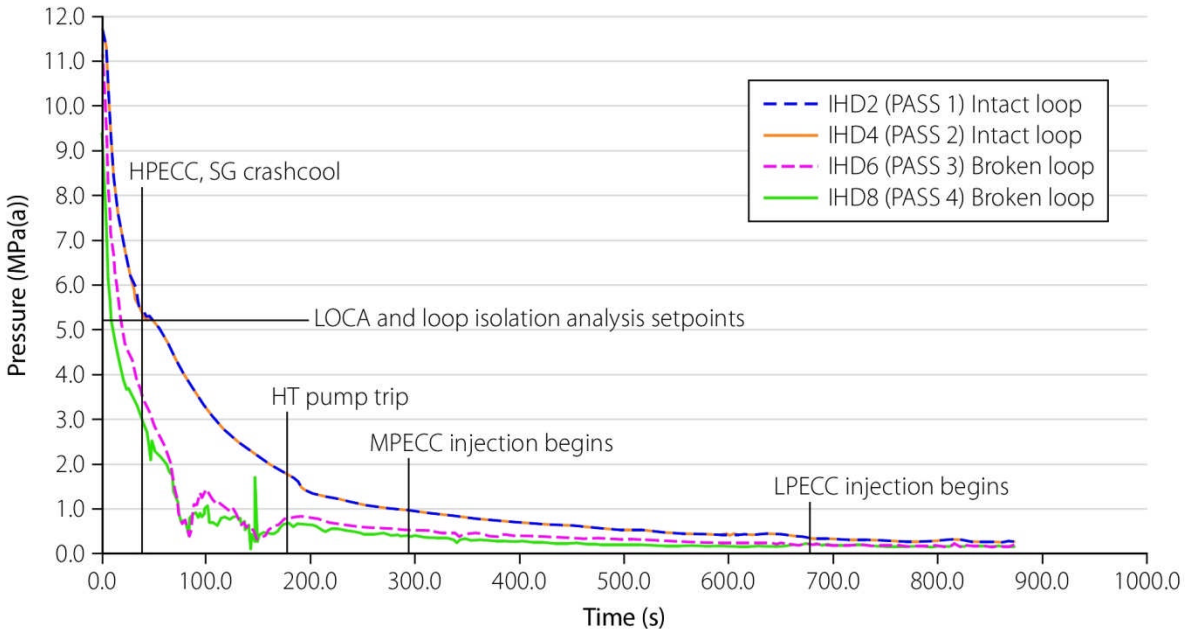

Figure 55 Typical LBLOCA timescale

A typical containment-pressure transient for CANDU 6 is shown in Figure 56. The pressure rises rapidly and is suppressed by dousing sprays. In the long term, the air coolers (and heat removal by ECC) stabilize the pressure. This is quite different behaviour from a vacuum containment, which will go sub-atmospheric once the valves to the vacuum building open and will stay sub-atmospheric for days.

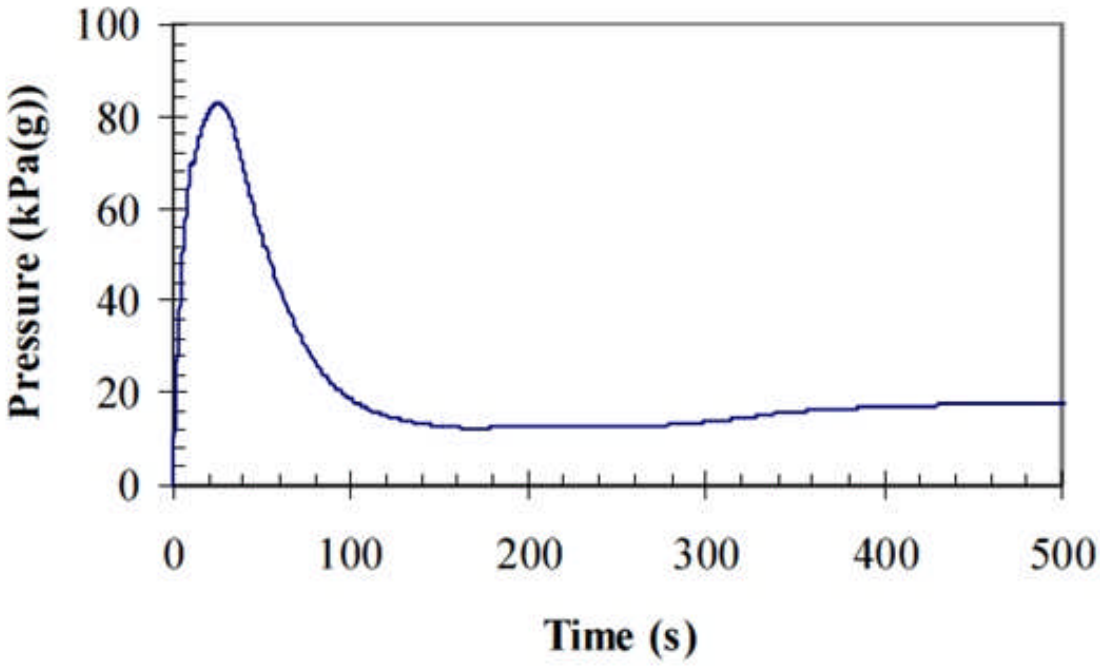

Figure 56 Containment pressure transient for 100% ROH LOCA

6.6.3 Barrier protection

For a LBLOCA, recall that some sheaths may fail, but that the amount of failure must be limited. The fuel barrier may be degraded, but not to the extent that it jeopardizes the pressure-tube barrier. The pressure-tube barrier and the containment barrier must not fail. Further failures in the HTS barrier must be prevented. Moreover, systems which protect these barriers must not fail. This gives rise to the following requirements (simplified—this is not a complete list) for barrier protection, which the safety analysis must demonstrate:

- Fluid from the broken pipe will create jet forces, and reaction forces can cause pipe whip. The effect of these forces on other HTS pipes, on the shutdown systems, on ECC pipes, and on containment must not lead to further barrier failures.
- Continued fuel heating after reactor trip gives a potential for sheath failure due to excessive sheath strain or sheath embrittlement, and for channel flow area reduction due to sheath strain. Sheath failures must be limited to meet public dose limits; sheath failure modes such as embrittlement or severe channel-flow blockage must be prevented to protect the pressure-tube barrier (i.e., to maintain coolable bundle geometry).
- Fuel melting must be prevented to protect the pressure-tube barrier.
- Pressure tubes may overheat and strain or sag until they contact the calandria tube. Failure of the pressure tube before contact with the calandria tube must be prevented. After contact, heat transfer to the moderator must be sufficient to prevent failure of the channel barrier.
- The containment barrier and its internal structures must not be jeopardized by excessive internal pressure.

These requirements for barrier protection can be translated into analysis limits, as discussed earlier. A detailed list of analysis limits is outside the scope of this Chapter.

6.6.4 A note on reactivity coefficients

A large LOCA is the limiting accident in terms of shutdown-system speed. This is due to the positive void coefficient, and more specifically to the rapidity with which void is produced in a large LOCA. CANDU has sometimes been criticized for its positive void coefficient; by contrast, a LOCA in an LWR shuts the reactor down due to loss of the common coolant/moderator. However, a broader perspective is more useful. The following discussion is taken from [Popov, 2012] and [Popov, 2013].

As discussed in Chapters 4 and 5, *reactivity coefficients* measure the amount of change in reactivity per unit of change in the parameter of interest, while other parameters are kept unchanged.

We shall develop three themes:

- all reactors have mechanisms to add positive reactivity
- reactivity changes can be slow or fast
- the reactivity changes of most interest to safety are those that are large and fast. The sign of a reactivity coefficient is less important because the parameter can always be reversed.

The first theme is readily apparent: addition of positive (and negative) reactivity through control rods, for example, is essential in power-reactor operation. Inherent reactivity feedback from fuel temperature, coolant density, moderator density, etc. (see Chapters 4 and 5) can also introduce positive reactivity, with the details depending on the reactor design and the direction in which the particular parameter is changing.

As for the second theme: the speed of reactivity feedback in an accident determines the required countermeasures. Slow reactivity changes are relevant for normal operation in different reactor states and are introduced in the reactor core by: a) burnup and refuelling, b) planned control-device movement, and c) xenon changes in the core during operation. In CANDU, fuelling is done on-line, and therefore the control system does not have to compensate for fuel burnup. In other words, the reactivity worth of control devices is small (the total worth for all devices together is 32 mk, and each device is typically worth less than a mk – see Chapters 4 and 5). Reactivity addition from control devices is inherently slow because they are not subject to pressure-assisted ejection. In PWRs, fuelling is done in batch mode (about every 18 months), and the excess initial reactivity after fuelling is suppressed by a combination of poison in the coolant and fuel, and insertion of control rods. As a result, control rods may have high individual reactivity worth. A typical PWR has a total worth of all control rods of about 110 mk, and the maximum worth of a single rod (using the Westinghouse Advanced Passive 1000 (AP 1000) PWR as an example) can be of the order of 7.5 mk under the most pessimistic conditions (hot zero power in a core just about to be refueled) [Westinghouse, 2011]. This is larger than the delayed neutron fraction, and therefore rod ejection assisted by coolant pressure can result in prompt criticality. This means that whereas in normal operation, control rods add reactivity

slowly, in an LWR accident, reactivity can be added very quickly.

Fast reactivity changes are of interest in accidents. These are induced by fast changes in parameters such as: a) coolant and moderator volume, temperature, or density, b) fuel temperature, c) location of reactivity devices, or d) reactor core geometry. As discussed in Chapters 4 and 5 and in our "lessons learned" from the SL-1 accident (Section 3.1.1.3), the response to a large and fast reactivity addition depends on (1) the reactivity added compared to the delayed neutron fraction β, and (2) the prompt neutron lifetime l_p. PWRs and CANDUs have similar delayed neutron fractions: from 0.0054 to 0.0073 mk in a PWR, depending on core burnup, and 0.0053 for an equilibrium-core CANDU. However, the prompt neutron lifetimes are very different. For a PWR, l_p is typically 20–30 μs; for a CANDU, l_p is about 900 μs, or 30–45 times longer than in a PWR: because heavy water does not absorb neutrons as much as light water, neutron lifetime in CANDU reactors is much longer.

Figure 57 shows the relationship between reactivity ρ and reactor period for various values of prompt neutron lifetime (adapted from [Glasstone, 1994]). For $\rho << \beta$, the period for CANDU and PWR reactors for the same reactivity insertion is approximately the same. As ρ approaches β, the period for PWR reactors decreases sharply, whereas for CANDU, it also decreases, but fairly smoothly. For $\rho > \beta$, the period for PWR reactors is about 40 times shorter (i.e., faster) than for CANDU. Figure 57 also shows typical values of reactivity changes during certain accident classes for a PWR and a CANDU reactor, as shown by the coloured areas.

From [Popov, 2012]:

> "Consider the fastest reactivity accident in PWR, i.e., rapid ejection of the largest-worth control rod in a PWR. Using the value of 7.5 mk for "worst" rod worth, the reactor period can be estimated of the order of a hundredth of a second following rod ejection. It is not practically possible for engineered shutdown systems to stop such a fast rate of rise in power. For PWRs, it is not necessary to have such fast shutdown system because of a strong negative fuel temperature coefficient. Hence, PWRs can partly mitigate this event through negative feedback, but engineered shutdown is still required after the initial transient".
>
> Consider now the fastest reactivity accident in CANDU: the large LOCA. Since there are inherent physical limits to the speed and extent of channel voiding, the net result is that the maximum rate of reactivity addition is approximately 4 mk/sec, and the reactor period is about one second or so. At that rate of reactivity insertion, engineered shutdown systems can be reliably designed to terminate the power rise."

Current CANDU safety analysis does not predict prompt criticality for a large LOCA, but even if it did, the period would not change dramatically. Prompt criticality is not the threshold of a sudden change in behaviour for a CANDU.

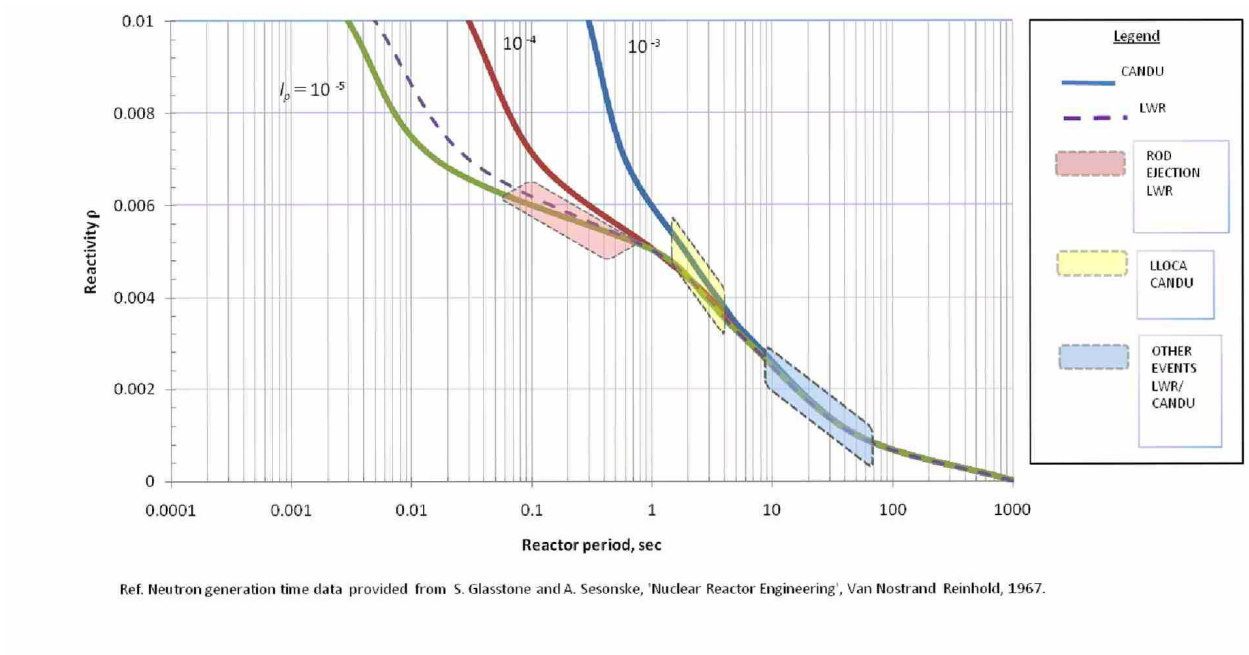

Figure 57 Response of PWR and CANDU to reactivity increase

As for the third theme: ideally, all accidents would induce negative reactivity feedback. However, this is not possible because a large negative coefficient in one event can become a large positive one for the complementary event. In other words, for every physical change that produces a negative reactivity effect, the opposite change produces positive reactivity. For example, insertion of a control rod produces negative reactivity; withdrawal (or ejection) of a control rod produces positive reactivity. Likewise, for a reactor with a positive coolant void (or density) coefficient, a decrease in coolant density produces a positive reactivity, whereas void collapse gives a negative reactivity. Conversely, if the coolant void reactivity is negative, a decrease in coolant density produces negative reactivity, whereas void collapse gives positive reactivity.

Table 12 compares the size and sign of reactivity coefficients in PWR and CANDU.

Table 12 Reactivity effects in PWR and CANDU

Reactivity Effect	PWR	CANDU
Fuel temperature increases	Large Negative (-0.023 to -0.029 mk/^{o}C)	~0
Fuel temperature decreases	Large Positive (+0.023 to +0.029 mk/^{o}C	~0
Coolant voids	Large Negative (-2.5 mk/% void)	Large Positive (+0.15 mk/% void)
Coolant void collapses	Positive (+2.5 mk/% void)	Negative (+0.15 mk/% void)
Coolant temperature increases	Negative (-0.09 mk/°C at BOC to -0.54 mk/°C at EOC)	Small Positive (+0.04 mk/°C)
Coolant temperature decreases	Positive (+0.09 mk/°C at BOC to +0.54 mk/°C at EOC)	Small Negative (-0.04 mk/°C)

We can now summarize the impact on safety of the speed of reactivity feedback and the size and sign of reactivity coefficients:

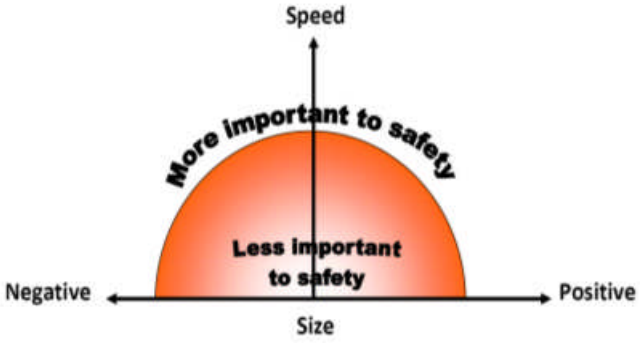

Figure 58 Importance of reactivity effects

- Only reactivity coefficients driven by fast phenomena are highly important to safety; if the phenomenon driving a coefficient acts slowly, whatever its sign or size, its impact can easily be compensated for by reliably engineered reactivity control and shutdown mechanisms.
- The size of the reactivity coefficient is clearly important to safety because it determines the magnitude of inherent effects and the performance of the engineered systems that must control or compensate for them. Generally, a small reactivity coefficient is not important because the amount of compensation needed is also small, regardless of the sign or speed. Conversely, a large reactivity coefficient is important, regardless of the sign.
- The sign of a reactivity coefficient is less important to safety because the physical mechanism can almost always be reversed, as discussed above.

This concept is illustrated in Figure 58.

The use of inherent and engineered safety defences in PWRs and CANDU is summarized for

some typical accidents in Table 13. Relevant coefficients are shown in brackets.

Table 13 Examples of reactivity response to accidents for PWR and CANDU

Accident	PWR	CANDU
Large LOCA	Power decrease, ECC boration required in medium term to ensure shutdown (void reactivity coefficient, fuel temperature reactivity coefficient)	Rapid power increase terminated by engineered shutdown (void reactivity coefficient)
Cold-Water Injection	Power increase, terminated by a combination of inherent feedback and engineered shutdown, e.g., boron addition (moderator/coolant temperature and fuel temperature reactivity coefficients)	Power decrease (coolant temperature and void reactivity coefficients)
Main Steam-Line Break	Power increase, terminated by a combination of inherent feedback and engineered shutdown; possible return to criticality terminated by boron addition (moderator/coolant temperature and fuel temperature reactivity coefficients)	Power decrease, engineered shutdown required in medium term (coolant temperature and void reactivity coefficients)
Control-Rod Ejection	Rapid power increase with local power peaking terminated by combination of inherent feedback and engineered shutdown (delayed neutron fraction, moderator/coolant temperature, and fuel temperature reactivity coefficients)	Not physically possible

For further information, a detailed and quantitative comparison of power transients in LWRs and CANDUs has been given by Meneley and Muzumdar in two papers. The first [Meneley, 2009] gives an overview comparison of positive reactivity insertion accidents, whereas the second [Muzumdar, 2009] looks specifically at large LOCA events in CANDU. These papers are recommended reading for those wishing to understand further the safety differences and similarities between the two reactor concepts.

6.7 Accident Walk-Through: Small LOCA

6.7.1 Initiating event

A CANDU has much more small-diameter piping than large-diameter piping because of the large number of parallel channels, each served by an inlet and outlet feeder. A break in any of these pipes (or a similar-sized break in the larger pipes) is considered a small LOCA. This includes a

break in a steam-generator tube.

6.7.2 Event sequence (simplified)

Generally, the event sequence is similar to a large LOCA, but much extended in time. The rate of rise of void reactivity is slow enough to be compensated for by the control system, and therefore shutdown systems are triggered on process trips (see Table 8) rather than neutronic trips. Typical time scales are a few minutes before the ECC set-points are reached, and similarly the high-pressure and medium-pressure ECC phases are prolonged.

For a steam-generator tube break, the radionuclides contained in the HTS coolant can be released outside containment. The break must be isolated in the longer term because the water lost through the steam generator is unrecoverable. Because the discharge is small, the operator has enough action time to perform HTS cooldown and steam-generator isolation. Back-flow of (light) water from the secondary side to the primary side, after the latter has been cooled down and depressurized, causes negative reactivity and is not a safety concern. Recent CANDUs have manually operated main steam isolation valves which can be used as one of the means to isolate the affected steam generator in the longer term.

6.7.3 Barrier protection

Because a small LOCA may occur during the station lifetime, the safety systems are designed to prevent fuel-sheath failure both before reactor trip (to limit the period of pre-trip overheating due to dryout as the channels void) and afterwards, during ECC.

6.8 Accident Walk-Through: Single-Channel Event

6.8.1 Initiating event

The channel nature of the CANDU design means that certain accidents can affect one channel only, e.g., partial or complete flow blockage due to a foreign object in the HTS, a pressure-tube failure (which may or may not lead to a calandria-tube failure), a break in an individual feeder pipe, or assumed failure of the pressure-tube-to-end fitting rolled joint, which can cause an end-fitting ejection.

6.8.2 Event sequence (simplified)

The last three initiating events listed above behave like a small LOCA as far as the heat-transport system is concerned. The safety systems (shutdown, ECC, and containment) are triggered on small LOCA signals. Flow blockage may not result in a channel failure; for blockages up to about 95% of the channel flow area, the fuel in the channel may fail and could be badly damaged, but the pressure tube will not fail. For more severe blockages, the fuel will melt, and the channel will fail.

Each type of single-channel event has certain unique characteristics in addition to those of a small LOCA. These characteristics are the focus of the safety analysis for these events.

- A break in an inlet feeder of exactly the right size to cause the flow to stagnate tempo-

rarily in a channel can result in channel overheating and failure.

- Any event which leads to channel failure will cause a discharge of the HTS into the moderator. Besides pressurizing the calandria, the discharge can dilute any poison in the moderator used for reactivity suppression, as discussed in Section 5.2.3.
- The jet and pipe-whip forces from an in-core break can damage a limited number of shut-off rod guide tubes, as discussed in Section 5.2.7.
- A severe flow blockage or feeder stagnation break can also cause discharge of molten fuel into the moderator.
- An end-fitting failure can cause discharge of the fuel in the channel into the reactor vault (i.e., directly into the containment).

6.8.3 Barrier protection

A fundamental safety requirement of a channel reactor is that a single-channel failure must not propagate to other channels; otherwise, a relatively benign and moderate-frequency initiating event could cascade to become a severe core-damage accident. This conclusion has been supported for CANDU by years of R&D and code development.

Shutdown depth must remain adequate, accounting for damaged shut-off rod guide tubes.

Moderator pressure increases after an in-core break due to the discharge of high-enthalpy fluid into the moderator. The pressure is relieved by discharge through the four calandria relief pipes, which are designed to prevent structural failure of the calandria shell. Recent work continues to support this conclusion even when significant amounts of molten fuel have been ejected into the moderator after a severe flow blockage.

6.9 Accident Walk-Through: Loss of Reactivity Control

6.9.1 Initiating event

A malfunction in the reactor regulating system (RRS) is assumed to drain zone controllers, drive out absorber/adjuster rods, or both. Two types of accidents are considered: continued increase in reactivity at up to the maximum possible rate and to the maximum degree allowed by the physical configuration of the devices; and a slow power increase from both normal and distorted flux shapes that terminates just below the overpower trip set-points.

6.9.2 Event sequence (simplified)

An increase in reactor power causes a flow/power mismatch which has the potential to damage the fuel. If the ramp is continuous, shutdown-system bulk overpower trips can be designed to prevent fuel damage.

However, an increase in power from a distorted flux shape, which is either very slow or stops at an elevated power, could permit fuel to remain in a dryout condition even if the bulk reactor power is below the average overpower trip set-point. Analysis of such events determines the trip set-points for the spatially distributed regional overpower (ROP) flux detectors on each shutdown system.

6.9.3 Barrier protection

As with a small LOCA, because loss of reactivity control may occur during the station lifetime, the shutdown systems are designed to prevent sheath failure.

6.10 Accident Walk-Through: Loss of Forced Circulation

6.10.1 Initiating event

Loss of Class IV electrical power to the HTS pumps causes them to run down and eventually stop. Partial loss of forced circulation is also possible; particular cases include a partial loss of Class IV power (to two HTS pumps), a single HTS pump shaft seizure, and a single pump trip.

6.10.2 Event sequence (simplified)

The flow reduction causes a mismatch between reactor power and coolant flow that can lead to fuel overheating and HTS pressurization. The power mismatch also causes void formation in the channels, leading to an increase in reactor power. This initial phase is terminated by a reactor trip. In the long term, the fuel decay heat is removed by thermo-siphoning to the steam generators until an alternate heat sink (such as shutdown cooling) can be initiated.

6.10.3 Barrier protection

Because this is an event that is expected to occur during the station lifetime, the shutdown systems are designed to prevent sheath failure and to limit the stress levels in the HTS due to overpressure. Ideally, the fuel temperature excursion should be limited enough that plant operation can be resumed without the need for a fuel inspection.

6.11 Accident Walk-Through: Loss of Secondary-Side Heat Removal

6.11.1 Initiating event

We give a particular case as an example: failure of one of the main steam lines inside or outside the reactor building (or the steam balance header) on the secondary side. This accident is more limiting than feed-water line failures or loss of feed-water pumps.

6.11.2 Event sequence (simplified)

A large steam line break causes a rapid depressurization of the affected steam generator and of the remaining steam generators as well because they are connected at the balance header. Initially, depressurization of the secondary side causes a corresponding depressurization and cooling of the primary side because of enhanced heat transfer through the steam-generator tubes; this causes negative reactivity and power decrease and is not a safety concern. The reactor will trip early in the accident on signals such as high containment pressure (if applicable[9]), low steam-generator level, or low feed-water line pressure. As the steam generators lose

[9] For Bruce and Darlington, the steam line runs entirely outside the containment boundary.

inventory, heat removal from the heat-transport system degrades, and the operator is required to initiate an alternate heat sink such as the shutdown cooling system. Note that because the shutdown cooling system is a high-pressure heat-removal system, the operator does not need to depressurize the HTS before initiating this alternate heat sink in emergencies.

6.11.3 Barrier protection

The safety assessment must demonstrate that three key requirements are met:

- The operator has enough time to initiate an alternate heat sink and maintain fuel-sheath integrity.
- For main steam-line breaks outside containment, in the turbine hall, one must assess the design to show that equipment which is required and assumed to mitigate the event (if located in the turbine hall) is not damaged by the forces, the steam, or the high temperature caused by the break, nor is there damage to the turbine-hall structure.
- For main steam-line breaks inside containment, the containment pressure rises rapidly, and an additional safety aspect is the preservation of building integrity, including the integrity of reactor-building internal structural walls. For new reactor designs, it is a requirement that the peak containment pressure be below design pressure.

Large steam-line breaks are limiting in terms of early containment peak pressure and time available to introduce an alternate heat sink. Small steam-line breaks test the trip coverage and (for designs where part of the steam line is within containment) can lead to long-term containment pressurization after the containment dousing water has been exhausted.

6.12 Accident Walk-Through: Fuel-Handling Accident

6.12.1 Initiating event

A fuelling machine carrying spent fuel may be either on the reactor (attached to a channel), or off the reactor (in transit to the spent-fuel port, or attached to the spent-fuel port and discharging fuel). The spent fuel must be kept cooled, and hoses are attached to the fuelling machine through which high-pressure D_2O cooling water is pumped. Should one or more hoses fail, the integrity of the contained fuel is threatened. The consequences to the reactor of a failure of a fuelling machine on-reactor (e.g., spurious detachment from a channel) are broadly similar to those of a single-channel event, except that more fuel bundles may fail.

6.12.2 Event sequence (simplified)

Assume that the fuelling machine is off-reactor. Following loss of coolant through severance of one or more hoses, the D_2O inventory in the fuelling machine will boil off, the bundles will be uncovered, and fuel may fail, releasing fission products to containment.

6.12.3 Barrier protection

A fuelling-machine failure when off-reactor cannot be mitigated by reactor shutdown or ECC; the only relevant safety system is containment, so that the safety analysis focuses on fission product release from the fuel bundles and containment effectiveness.

6.13 Accident Walk-Through: Loss of Moderator Inventory or Heat Removal

6.13.1 Initiating event

Moderator system failures include moderator pipe break, loss of forced circulation, and loss of heat removal.

6.13.2 Event sequence (simplified)

The moderator does not contain fission products, but does contain activation products (tritium). Failures in the moderator system can therefore release tritium to containment and cause flux distortions if the moderator level falls, leading potentially to excess power in some reactor fuel channels before the reactor is tripped.

6.13.3 Barrier protection

Fuel-sheath failures must be prevented (by tripping the reactor in case of excessive flux distortion). The containment capability is analyzed to show that it can limit dose to the public from tritium.

6.14 Severe Accidents

It is useful on CANDU to distinguish two categories of severe accidents:

1. Severe fuel-damage accidents in which the core geometry is preserved (fuel may be damaged, but remains inside intact pressure tubes). Decay heat is removed from the channels to the moderator. Example: loss of coolant plus loss of ECC with moderator cooling available. A variant on this is “limited core damage”, in which one or a few fuel channels fail, but the others remain intact. Either configuration is unique to a channel reactor where the heat can be removed by the moderator; there is no analogy to this “half-way” point in LWRs, in which a severe accident implies loss of core geometry.
2. Severe core-damage accidents, in which the fuel channels fail and collapse to the bottom of the calandria, i.e., the moderator heat sink is ineffective. Example: loss of coolant plus loss of ECC plus loss of moderator heat removal.

Analyzes of accidents in the first category use similar tools to those for design basis accidents and will not be discussed further.

CANDU is characterized by large volumes of water around the core, consisting of the moderator and the reactor vault or shield tank (Figure 59). Even with no active heat removal from either system, it takes about 20 hours for the water to boil off and for the debris to end up on the vault floor [Snell, 1988].

System	Continuous Heat Removal Capability (% full power)	Time to heat up and boil off, no heat removal
Moderator	4.4%	> 5 hours
Shield Tank	0.4%	10 to 20 hours

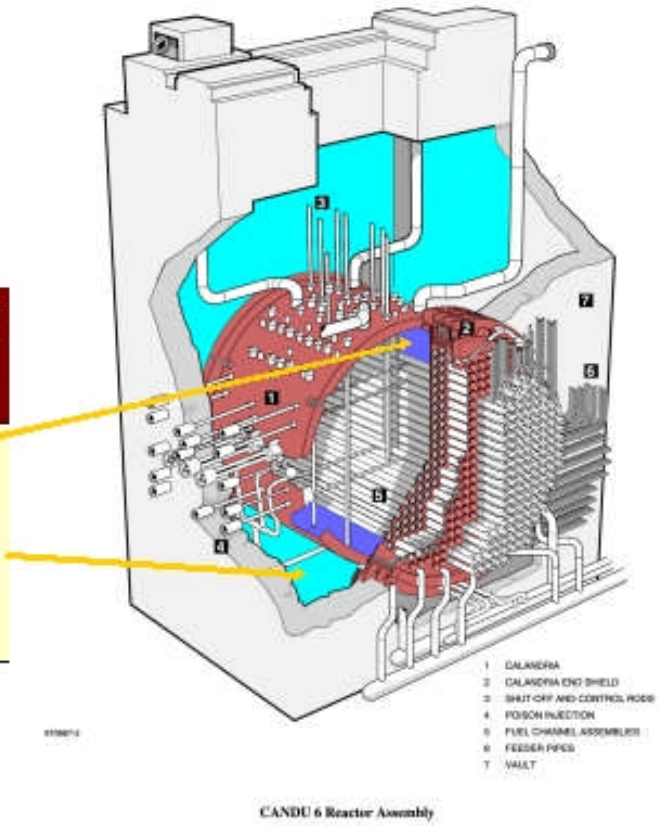

Figure 59 Sources of water near the fuel

Blahnik [Blahnik, 1991], using the MAAP-CANDU code, has characterized the degradation of a CANDU core with no cooling and gradual boiling-off of the moderator. The uncovered channels heat up and slump under their own weight until they are held up by the underlying channels. Eventually, as successive layers of channels pile up, the supporting channels (still submerged) collapse, and the whole core slumps to the bottom of the calandria vessel (Figure 60, Figure 61). See [IAEA, 2008] and [Blahnik, 2012] for further reading.

Details of the channel failure mode are as follows: the axial creep rate of the pressure-tube material (Zr-2.5% Nb) increases rapidly with temperature, and excessive sagging of the channel is expected to occur above ~1200°C. In Blahnik's model, a sagging channel comes into contact with the next lower row of channels. The lower row of channels may or may not be cooled adequately by the moderator, depending on whether it is submerged in the moderator.

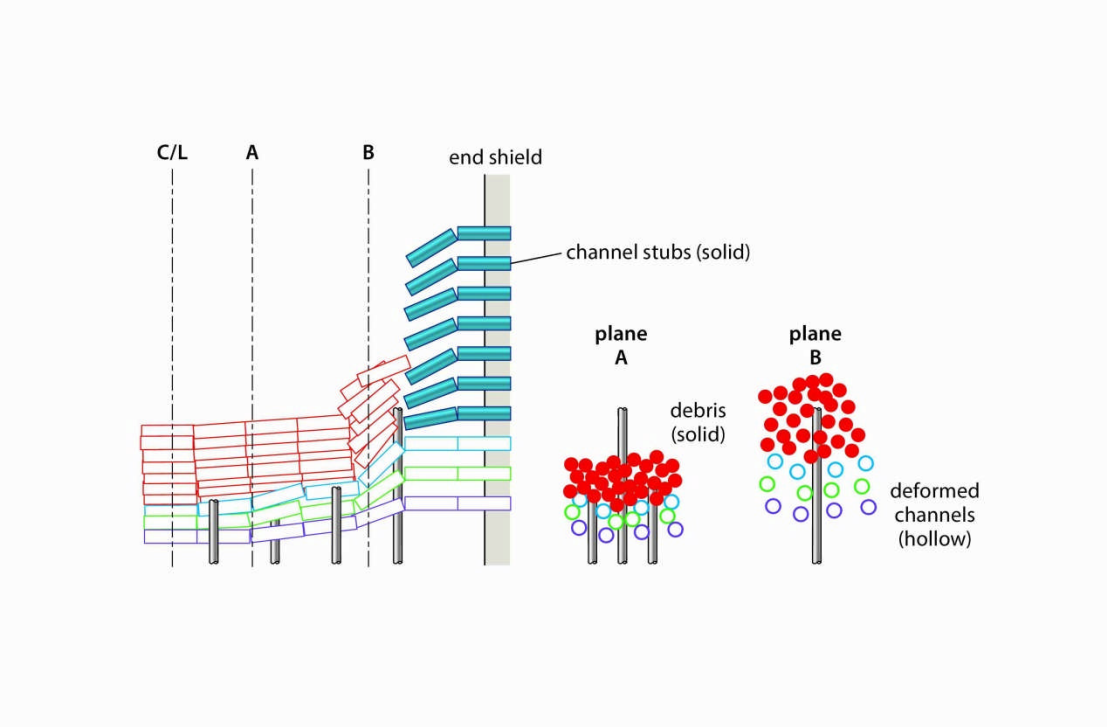

Figure 60 Channel collapse in severe core-damage accident

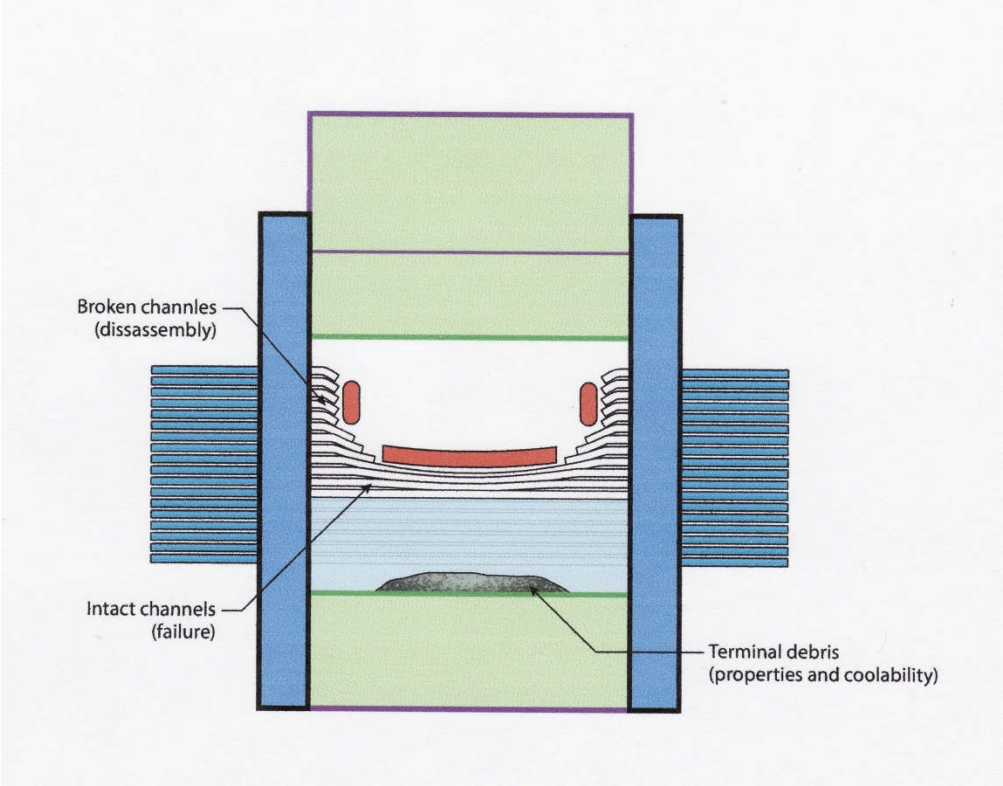

Figure 61 Core collapse

As the moderator level continues to decrease, the lower row of channels is uncovered and sags

under its own weight as well as that of the supported channels [Simpson, 1996]. This process continues as more channels are uncovered. As sagging increases, channel segments separate near the bundle junctions by sag-induced local strain. A suspended debris bed is thus formed which moves downward with the falling moderator level. Because a submerged channel can support only a certain number of channels, the ends of those channels are expected to fail by shear. This process will increase the loading on the channels below, leading to progressive failure of the channels and resulting ultimately in the collapse of the reactor core into the water pool in the bottom of the calandria vessel.

To address the plant state once the debris has collapsed to the bottom of the calandria, Rogers *et al*. [Rogers, 1995] developed an empirically based mechanistic model (Figure 62) of the collapse process, which showed (assuming that the reactor vault is kept full of water) that the end-state consists of a bed of dry, solid, coarse debris irrespective of the initiating event and the core-collapse process. Heating of the debris bed is relatively slow because of the low power density of the mixed debris and the spatial dispersion provided by the calandria shell, with melting possibly beginning in the interior of the bed about two hours after the start of bed

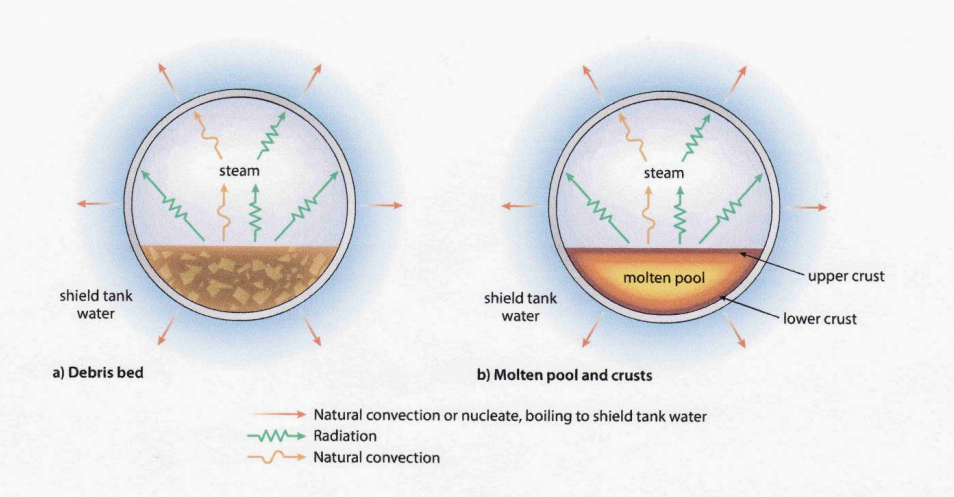

Figure 62 Mechanistic model of channel collapse

heating. The upper and lower surfaces of the debris remain well below the melting point (Figure 63), and heat fluxes to the shield-tank or reactor-vault water are well below the critical heat flux of 200W/cm^2 under existing conditions (Figure 64). The calandria vessel is protected by a solid crust of material on the inside and by water on the outside, and therefore it can prevent the debris from escaping. Should the shield tank or reactor vault water not be cooled or replenished, it will boil off, and the calandria vessel will eventually fail by melt-through, but this will not occur in less than about a day.

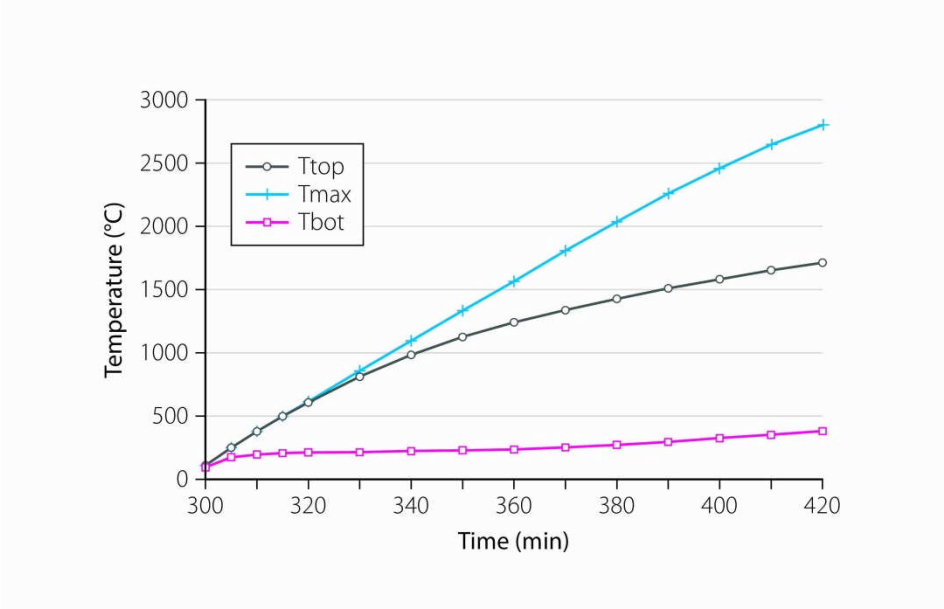

Figure 63 Debris heating transient

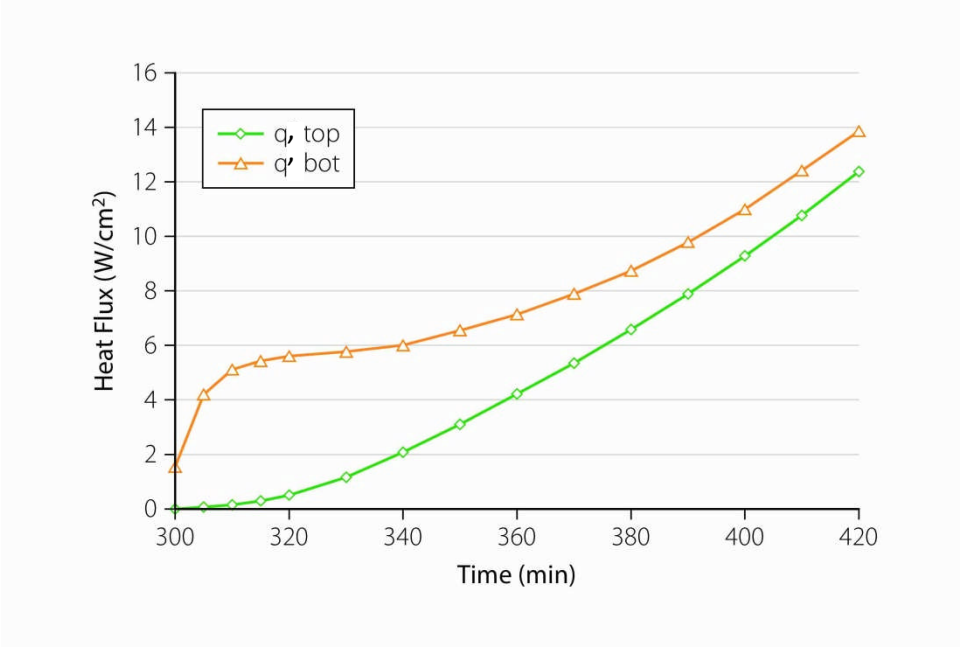

Figure 64 Heat flux on calandria wall

In short, compared to a core melt in an LWR, a severe core-damage accident in CANDU is inherently:

- Slow, because of all the passive heat sinks around the core
- Incoherent, because the channels fail individually over time, forming a coarse debris, rather than rapid "candling"
- In a favourable geometry, either retained in the calandria shell or, should the shell

fail, in the shield tank / reactor vault. Only if these also fail will debris be in contact with the containment boundary
- Subcritical
- Amenable to mitigation by adding water to either the moderator or the reactor vault / shield tank.

Some validation of CANDU severe-accident phenomena has been carried out at both large and small scales. Results obtained from the RASPLAV facility in Moscow have been used to support heat transfer through vessel walls and retention of debris in a vessel: see [Ader, 1998] and [Rogers, 2002]. See [Mathew, 2004] for a summary.

6.15 Problems

1. Consider loss of cooling of the spent-fuel bay due to loss of electrical power to the cooling system. What operating parameters would have the most influence on the outcome, and how would you select conservative values? What tools would you need to analyze the accident (i.e., what capabilities would they have to have)?

2. Estimate the evolution (using hand calculations if necessary) of the following severe accident in CANDU: small loss of coolant plus loss of ECC (assume that crash cooldown is available because it is on a redundant signal) plus loss of moderator cooling. Write down the expected event sequence (based on the list below) and estimate the approximate time of:

- reactor trip
- start of fuel overheating
- failure of first channel
- core collapse
- shield-tank failure
- containment behaviour.

Only an approximate answer is sought (to do this accurately could take weeks). If you cannot obtain the physical data in some cases, especially for the last item, use symbols to show how you would do the calculation. One approach is to use heat balance.

3. Consider a CANDU that has undergone a severe core-damage accident. Assume that the core has collapsed into a debris bed at the bottom of the calandria and is being cooled by boiling of the shield-tank water. Calculate the depth of the debris bed in the calandria (assuming zero porosity) and the average heat flux through the calandria wall. Do the calculation at 12 hours after the event. You will need to look up typical CANDU geometry [AECL, 2005] and calculate the core decay heat. Do not strive for high accuracy.

7 Safety Analysis – Mathematical Models

In this Section, we describe the basic science underlying safety analysis and present in simplified form the types of models used. We shall not derive each model from first principles. The reader is referred to numerous textbooks and reports for details (see Section 11). We borrow heavily from lecture notes by D. Meneley, J. T. Rogers, and W. Garland.

We focus on the large LOCA because it covers most of the disciplines used.

7.1 Reactor Physics

The fundamental equations in reactor physics have been presented in Chapters 3 to 5. The main aspects of physics used in safety analysis are reactor kinetics and diffusion theory. For the kinetics of a (point) reactor:

$$\frac{dN_f(t)}{dt} = \frac{k_\infty(\rho-\beta)}{l_p} N_f(t) + \sum_{i=1}^{M} \lambda_i C_i \,, \tag{32}$$

where:

$N_f(t)$ is the number of neutrons as a function of time t
k_∞ is the multiplication factor for an infinite reactor
ρ is the reactivity
β is the total delayed neutron fraction
l_p is the prompt neutron lifetime
M is the number of delayed neutron groups (chosen by the analyst, typically 6)
λ_i is the decay constant of the ith delayed neutron group
C_i is the number of neutrons of the ith delayed neutron group,
and for each delayed neutron group:

$$\frac{dC_i}{dt} = \frac{\beta_i N_f(t)}{l_p(1-\rho)} - \lambda_i C_i \,, \tag{33}$$

where β_i is the delayed neutron fraction of each group i.

However, a CANDU cannot be considered a point reactor in accidents. Strong spatial effects result from flux tilts (especially for a large LOCA, if only half the core is voided), insertion of shut-off rods from the top of the reactor, or other events. Therefore, in practice, one must use three-dimensional diffusion equations in conjunction with point kinetics. The diffusion model tracks the neutrons as a flow through a medium subject to scattering, absorption, and leakage. The continuity equation, for uniform systems with a single neutron velocity v, becomes the neutron diffusion equation:

$$D\nabla^2\phi - \Sigma_a\phi + s = \frac{1}{v}\frac{\partial\phi}{\partial t} \,, \tag{34}$$

where:

D is the diffusion coefficient

Σ_a is the absorption cross-section
v is the neutron velocity
$\phi(\mathbf{r},t)$ is the neutron flux.
$s(\mathbf{r},t)$ is the *source distribution function*, i.e., the number of neutrons emitted per unit volume per unit time by sources at point $\mathbf{r}$ and time t.

This is very similar to the diffusion of heat through a medium, with the addition of a source term (due to fission).

Transient neutron diffusion plus kinetics is the basis of many of the physics codes used in accident analysis. These equations are solved using spatial finite-difference methods with the reactor core broken up into many nodes, in each of which the diffusion equation is applied at each time step.

For a LOCA, for example, time-dependent cross sections representing coolant voiding transient, fuel temperature transient, reactor control-system action, and shut-off rod movement are the driving functions for the transient in the flux. The average power transient for the reactor is extracted from the calculation, along with peaking factors for the hot channel, hot bundle, and hot element in the loop being analyzed. The system reactivity as a function of importance-weighted void fraction is also calculated. These data are used as input to a system thermo-hydraulics code. This code calculates the distribution of coolant void as a function of time from the pipe break for each pass of the coolant loop. The importance-weighted average void fraction calculated by the thermo-hydraulics code is combined with the previously calculated reactivity function, and the cycle is iterated as necessary. The thermo-hydraulics code and the physics code are combined into one calculation so that manual iteration is not necessary.

7.2 Decay Power

We indicated in Section 3.2 that shutting down a reactor was not sufficient to remove all safety concerns: the *decay heat* must be removed. This heat comes from the radioactive decay of fission fragments and obviously cannot be controlled. In principle, it can be calculated from the power history: the composition of fission products can be predicted at any time, and their half-lives and decay chains are known, so that:

$$P_d(t) = \sum_i n_i(t) E_i \,, \tag{35}$$

where:

$P_d(t)$ is the power produced by all decaying fission products at time t
$n_i(t)$ is the number of atoms decaying per unit time of fission product i at time t
E_i is the average energy produced by the decay of each atom of fission product i.

This is more complex than it seems because $n_i(t)$ will depend on the irradiation history, each fission product may have more than one decay chain (with different energies), and many fission products are generated. In practice, such a fundamental calculation is done as a reference, assuming a rapid shutdown after equilibrium operation. In most cases, the evolution of the accident (because it is short) does not materially change the decay power, so that the results

from the fundamental calculation can be fitted using a series of exponentials, and the curve fit is simply added to the fission power predicted by the physics codes. In exceptional cases, such as an accident occurring during power manoeuvring, the result will not be very accurate, but as with any analysis, an upper bound can be assumed (e.g., assuming the decay power appropriate to prolonged steady-state operation at the maximum operating power level before the accident). Such a trade-off between simplified assumptions which give a conservative bound to an answer, and more realistic assumptions which require more sophisticated analysis tools, is very common in safety analysis. Because safety analysis resources, like all other resources, are finite, part of the art of safety analysis is in judging when to use bounding assumptions and when to use realistic complex models. The difficulty is, of course, that bounding models may lead to unnecessary restrictions on operation, as discussed in Section 6.2.

7.3 Fuel

The key safety parameters related to fuel are:

- fuel-sheath integrity
- fission product inventory in (and release from) the fuel, and
- fuel temperature.

Prediction of fuel temperature in CANDU is important because:

- it drives sheath temperature and hence sheath integrity;
- high fuel temperatures drive pressure-tube deformation rates;
- limited fuel melting can lead directly to fuel-sheath failure;
- extensive melting can lead to pressure-tube failure;
- release of fission products from the fuel increases with fuel temperature;
- reactivity feedback from fuel temperature does occur, although it is small in CANDU.

7.3.1 Fission products in the fuel

During normal operating conditions, all fission products are formed within the fuel grains; they are trapped there (with the exception of a few which recoil directly into inter-grain and gas gaps) until they are released from the grains by diffusion. Those volatile fission products which are released form a gas mixture inside the fuel sheath. It is therefore useful to categorize fission products into three groups: (a) bound inventory, (b) grain boundary inventory, and (c) gap inventory (recall Section 1.7).

The gap inventory includes the fission product gases in the pellet dishes, in the pellet/sheath gap, and in the sheath end cap. If the fuel sheath fails, the gap inventory escapes quickly, the grain boundary inventory much more slowly, and the bound inventory even more slowly. At relatively low fuel temperatures, these diffusion processes are very slow, so that almost all isotopes remain in the grains. (An exception to this occurs when uranium dioxide is exposed to air at moderate temperatures; in this case, oxidation to higher states takes place, and the grain structure is destroyed. Much of the fission products are then released. Such a circumstance could occur after failure of an end-fitting and ejection of the channel contents into the reactor vault). As temperature and fuel burnup increase, the amount of fission gas in the gap increases

to a maximum of about 10% for typical CANDU operating conditions [Lewis, 1990].

At any given burnup, a larger fraction of the fission product gases is released near the centre of the pellet, where the temperature is highest. All volatile fission products tend to migrate down the temperature gradient toward the outside of the pellet. Their diffusion is assisted by the fact that the pellet cracks under the influence of the temperature gradient; this cracking increases with fuel burnup and pellet centre temperature.

In summary:

(a) at low burnup or temperature, nearly all fission products are trapped in fuel grains;
(b) fission products trapped at grain boundaries increase with temperature and burnup;
(c) the gas-gap inventory increases steadily with fuel temperature and burnup.

7.3.2 Fuel temperatures

Consider three-dimensional steady-state heat conduction in a medium. Assuming that energy is being produced in the medium at a volumetric rate *H*, energy conservation can be stated as:

(Rate of change of internal energy) = (rate of energy release into medium) - (rate of energy loss from conduction),

or at any point,

$$\rho c \frac{\partial T}{\partial t} = H + k\nabla^2 T \,, \tag{36}$$

where *T* is temperature, *k* thermal conductivity, *ρ* the density, and *c* the specific heat. Note the similarity to the neutron diffusion Equation (34).

Consider one-dimensional steady-state heat conduction in a cylindrical fuel pin. In cylindrical co-ordinates,

$$\frac{d^2T}{dr^2} + \frac{1}{r}\frac{dT}{dr} = -\frac{H}{k_F} \,, \tag{37}$$

where k_F is the fuel thermal conductivity. Integrating,

$$T(r) = T(0) - \frac{Hr^2}{4k_F} \,, \tag{38}$$

giving the typical parabolic radial distribution of temperatures within an oxide fuel element, as shown in Figure 65.

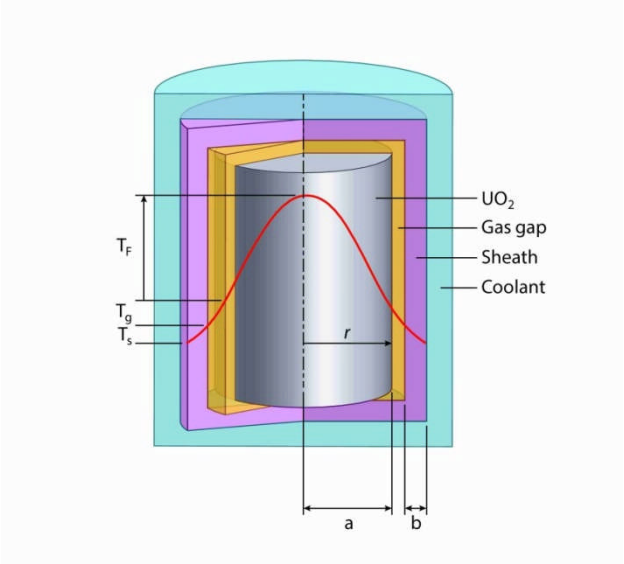

Figure 65 Temperature distribution across a fuel pin

We can apply the same method to the temperature drop ΔT_S across the sheath (for which the internally generated heat H_s=0):

$$\Delta T_S = T_{Si} - T_{So} = \frac{Ha^2 \ln[(a+b)/a]}{2k_S}, \tag{39}$$

where the indices *i* and *o* refer to the inner and outer surfaces of the sheath respectively. It would be tempting to conclude that the temperature drop from the fuel centreline to the outer part of the sheath is simply $\Delta T_F + \Delta T_S$. Not so—the gap between fuel and sheath provides a further thermal resistance, so we can write:

$$q = h_g(T_F - T_{Si}), \tag{40}$$

where h_g is the gap heat-transfer coefficient, which is a very complex function of surface roughness, contact pressure, and temperature and is determined by experiment.

The relationship between sheath and coolant temperature can be again derived from:

$$q = h(T_{So} - T_C), \tag{41}$$

where *q* is the heat flux per unit area to the coolant, T_C is the coolant temperature, and *h* is the convective heat-transfer coefficient. At steady state, all the heat produced in the fuel is transferred to the coolant, so that for a length of element ℓ,

$$q = \frac{H\pi a^2 \ell}{2\pi(a+b)\ell}, \tag{42}$$

so that

$$T_{So} - T_C = \frac{Ha^2}{2h(a+b)}. \tag{43}$$

Typical values in CANDU fuel are (see [Page, 1972] for a summary):

k_F = 0.004 kW/m.°C
k_S = 0.017 kW/m.°C
h_g = 7–60 kW/m^2.°C
a = 6.07 mm
b = 0.42 mm.

Heat capacity, c, does not enter the steady-state equations, but is important in transients. The values for uranium dioxide and Zircaloy-4 are respectively 0.5 and 0.4 J/g-°C. The corresponding heats of fusion are 27 and 42 J/g. The relatively large value of c and the high melting point (2840°C) for UO_2 represent important safety characteristics: typically, one can almost double the stored energy relative to the normal operating point, inside UO_2 before it melts. Metal fuel, on the other hand, has little heat capacity and melts at a lower temperature, but has much higher thermal conductivity, typically ten times more than UO_2.

7.3.3 Internal gas pressure

CANDU fuel has a "collapsible" fuel sheath, which creeps down plastically onto the pellet during irradiation due to the excess external coolant pressure. The small enclosed gas space in the element results in high sensitivity of gas pressure to fuel-sheath geometry. A small amount of fill gas is added to this space on assembly to achieve the proper sheath stress distribution during operation. As burnup increases, gas pressure causes the sheath once again to lift off the fuel; the gap heat-transfer coefficient decreases because the sheath creeps away from the fuel pellet. This decrease leads to higher peak fuel temperature, greater fission gas release from the fuel, and finally higher gas pressure. A new equilibrium point is reached. In an accident, gas pressure is the driving force for sheath strain. Gas pressure can be modelled using the ideal gas law. The volume depends on the transient behaviour of the gas gap, which results from complex models of sheath and fuel behaviour and is beyond the scope of this Chapter.

7.3.4 Sheath strain – large LOCA example

Consider a large LOCA as an example. One of the objectives in LOCA analysis is to predict the number of fuel sheaths which fail; this determines the amount of radioactive material released to the coolant and is input into the calculations of release into containment and public dose.

Because the fuel heats up quickly, the gas pressure inside the sheath increases relative to the coolant pressure and can force the sheath to strain. A uniform strain of at least 5% will not lead to sheath failure; however, greater strains can lead to local instability, ballooning, and failure. The strain-rate equations are complex functions of material composition, material state, temperature, irradiation, and transverse stress and are determined from experiments. Typically, their form is established as follows.

Define the transverse stress σ across the sheath as:

$$\sigma = \frac{Pr}{w}, \tag{44}$$

where:

P is the pressure differential across the tube,
r is the tube radius,
w is the tube thickness.

The strain rate is then expressed in terms similar to the following:

$$\dot{\varepsilon} = \frac{d\varepsilon}{dt} = A\sigma^n e^{-k/T} + B\sigma^m e^{-\ell/T}, \tag{45}$$

where ε is strain, *A, B, k, l, m, n* are determined by experiment, and *T* is temperature.

7.4 Heat-Transport System

The behaviour of the heat-transport system is predicted by solving the equations of mass, energy and momentum conservation for non-equilibrium transient two-phase flow in a network in one dimension. "Two-phase" means that we consider steam and water. "Non-equilibrium" means that the steam and water phases, even in the same location, can have different pressures, temperatures, and flow rates. "Transient" means that the desired behaviour is a function of time. Current CANDU thermo-hydraulic codes are one-dimensional, although sometimes phenomenological two- or three- dimensional models are used for components such as headers and channels. "Network" means that we model parallel paths (e.g., fuel channels, ECC) and several components connected together at the same point (e.g., at the headers).

Codes that model the heat-transport system cover:

- equations of state for the various phases
- component models for steam generators, fuel channels, fuel, headers, secondary side, valves, pumps, etc.
- correlations for pressure drop, heat transfer (including critical heat flux (CHF)), flow regimes
- constitutive relationships: these are equations describing transfers of mass, momentum and energy between the phases. The sets of constitutive relationships depend on the flow regime.
- efficient numerical solution schemes
- plant controllers.

Most thermo-hydraulic simulation codes for reactors break the circuit up into nodes containing mass, and therefore energy, and links joining the nodes, which are characterized by flow, length, roughness, diameter, etc. Mass and energy conservation equations are written for the nodes, and the momentum conservation equation is written for the links. We shall show simplified examples here (one-dimensional flow in a level pipe).

Figure 66 shows two nodes, *i* and *j*, connected by a link *k*.

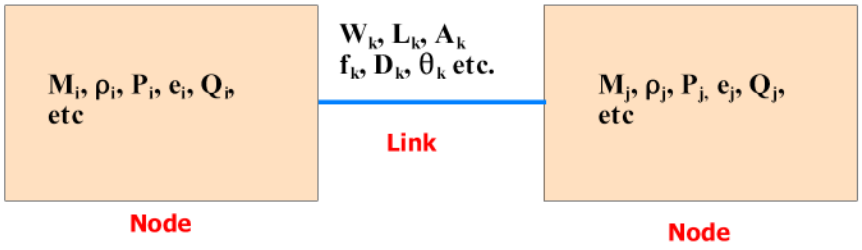

Figure 66 Node/link structure

The mass conservation equation for node *i* is:

$$\frac{dM_i}{dt} = \sum_k W_k \,, \tag{46}$$

where the W_k are all the mass flows into and out of node *i* along links *k*.

The conservation of momentum equation is applied to link *k* and is (ignoring gravity):

$$\frac{dW_k}{dt} = \frac{A_k}{L_k}\left[(P_i - P_j) - \left(\frac{f_k L_k}{D_k} + k_k\right)\frac{W_k^{\,2}}{2g_c \rho A_k^{\,2}}\right], \tag{47}$$

where for the link:

W is the mass flow in link *k* (in Figure 66, between nodes *i* and *j*)
A is the flow area
P is the pressure in the nodes connected to the link
L is the length
D is the hydraulic diameter
f is the friction factor
(fL/D + k) is a pressure-loss coefficient which accommodates changes in flow area, entrance effects, etc.

The first term is simply Newton's law applied to a fluid to which a pressure difference is applied; the second term is the loss due to friction plus other effects that cause pressure loss. Terms for pumps and gravity can be added.

Conservation of energy is applied to each node *i* as follows:

$$\frac{dU_i}{dt} = \sum W_{in} e_{in} - \sum W_{out} e_{out} + Q_i \,, \tag{48}$$

where

U_i is the internal energy of node *i*
Q_i is the heat generated in node *i*.

The summations are the rates of energies coming into and out of node *i* due to mass transfer.

These three equations are applied to each phase. There are four unknowns, e.g., mass, momentum, temperature, and pressure. The fourth equation needed is the *equation of state* for

each fluid, typically in the form

$$\rho = f(P,T) .$$

In safety analysis codes, the equation of state is used in the form of massive detailed tables of water and steam properties or is fitted by correlations.

7.5 Fuel Channels

When we look at the behaviour of fuel channels in accidents, we emphasize three basic disciplines: heat transfer, stress-strain behaviour, and hydrogen chemistry.

7.5.1 Heat transfer

Heat can be transferred from the fluid to the pressure tube by conduction and convection and from the fuel to the pressure tube by conduction (if the fuel sags into contact with the pressure tube) (Figure 67).

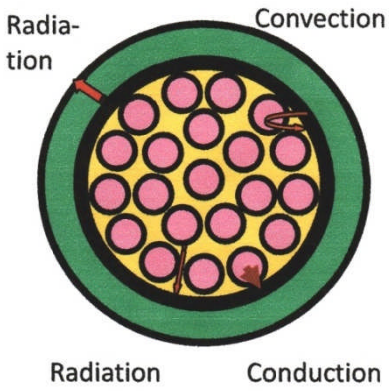

Figure 67 Heat transfer to pressure tube

At high temperatures, the fuel can transfer heat to the pressure tube by radiation, as characterized by the Stefan-Boltzmann law,

$$E = \varepsilon\sigma\left(T_f^4 - T_{PT}^4\right), \tag{49}$$

where

ε is emissivity
T is temperature in degrees Kelvin
σ is the Stefan-Boltzmann constant (1.36×10^{-4} kilo-calories per metre^2-second-°K)
f refers to fuel and *PT* to pressure tube.

A similar equation would apply to radiation from the pressure tube and from the steam itself, although these quantities tend to be small.

In practice, radiation becomes important at sheath temperatures of approximately 800°C or more and is approximately equal to the decay power in the fuel around 1200°C–1400°C. In practice, the hard part is working out the geometry: computer codes break the complex fuel

bundle and pressure tube into smaller pieces, calculate the "view factor" (how much of the pressure tube or neighbouring fuel element each piece can "see") for each piece, and calculate the radiation heat transfer piece by piece.

Heat can also be transferred from the calandria tube to the moderator, which is significant after pressure-tube contact (see below). The heat-transfer characteristics follow a pool boiling curve. Limited patches of film boiling can be tolerated for short periods after contact; lengthy or extensive dryout will lead to calandria-tube (and pressure-tube) failure.

7.5.2 Strain

The pressure tube can be heated by conductive, convective, and radiative heat transfer from the coolant and the hot fuel. If the pressure tube heats up beyond 800°C or so, it will start to deform plastically. If the channel pressure is high (> 6MPa), the strain highly localized, or both, the pressure tube may burst; if not, it will either strain radially or sag under gravity to contact the calandria tube and transfer heat to the moderator water. The equations for pressure-tube strain are, not surprisingly, similar to those for sheath strain.

7.5.3 Hydrogen

At high temperatures, Zircaloy oxidizes in steam to produce heat and hydrogen:

$$Zr + 2H_2O \Rightarrow ZrO_2 + 2H_2 + \ heat\ . \tag{50}$$

This is a quadruple threat:

- hydrogen collects in containment (significant amounts of hydrogen can be produced quickly only by a LOCA with ECC failure or in a severe core-damage accident) and can, under the right circumstances, become flammable or detonate; hydrogen can also be produced slowly over the long term by radiolysis (radiolytic decomposition) of ECC water as it circulates through the core;
- the heat generated by the chemical reaction increases fuel and pressure-tube temperatures;
- the presence of a non-condensable gas in large quantities can impede ECC water if the operator tries to recover from an impairment of ECC by injecting water late[10]; and
- the formation of zirconium dioxide may embrittle the sheaths so that they may fragment and block cooling flow if ECC is eventually restored.

Correlations of the reaction rate of steam and Zircaloy therefore form an essential part of fuel-channel codes.

The reaction rate becomes autocatalytic around 1400°C–1500°C, that is, the heat it generates

[10] This was the fear behind the "gas bubble" within the reactor vessel during the Three Mile Island accident. The concern was not burning within the vessel because no oxygen was present. The hydrogen which escaped to containment, which did contain oxygen, formed a flammable mixture of 9% hydrogen and did indeed burn without serious consequences [Jaffe, 1979].

keeps the chemical reaction going with no further heat input. In light-water reactors, this is a major concern: the fuel elements are close together, so there is no place to which the heat can radiate. Regulatory practice in the United States sets a strict limit on sheath temperature in a design basis accident—namely, 1200°C—which was chosen to allow little possibility of an autocatalytic reaction. In CANDU, the presence of the colder pressure tube less than a few centimetres from each fuel element moderates the reaction. Embrittlement is still a concern, but regulatory practice permits calculation of actual oxidation rates and thicknesses, rather than setting a criterion based on temperature alone; the particular criterion used in Canada is: "the oxygen concentration in the cladding must remain below 0.7 wt.% over at least half of the cladding thickness" (see [Grandjean, 2008] for a broad review).

7.6 Moderator

The modelling requirement for the moderator is to predict the transient local water temperature at each point. The objective is to show that local moderator sub-cooling at any location where the pressure tube contacts the calandria tube in an accident is sufficient to prevent prolonged film boiling on the outside of the calandria tube. The physical problem is therefore solution of three-dimensional fluid flow with heat addition in a porous medium; the medium is not continuous because of the presence of fuel channels, reactivity devices, etc. The mass, momentum, and energy equations described above are therefore generalized to three dimensions. Experimental validation is, of course, a must because of the complex geometry.

7.7 Containment

As far as fundamental equations are concerned, containment behaviour is governed by the same physical phenomena as the heat-transport system, with a few complications:

- the containment volume is compartmentalized, and the flow within the larger compartments is three-dimensional;
- a number of different fluids coexist: air (the normal contents of containment), steam and water from a pipe break, and hydrogen if the sheaths are heavily oxidized;
- heat is added by steam and hot water and also by radioactive decay of any fission products carried into the containment atmosphere by the discharging fluid; heat is removed by water sprays, condensation on containment and equipment surfaces, containment air coolers, and indirectly by ECC in recovery mode;
- pressure can also be influenced by use of the vacuum building (in multi-unit plants), leakage from containment through cracks, and deliberate venting through filters.

Containment codes usually have sub-models for each of these phenomena.

Many containment codes also track the movement of fission products along with other fluids. Fission products can exist as:

- noble gases, which interact very little with water or surfaces;
- tritium oxide (specifically the mixed oxide DTO) from the coolant or moderator.
- iodine, cesium, strontium, etc. which interact strongly with water (dissolve and ionize) and tend to plate out on surfaces;

- actinides such as plutonium. These are released from the fuel in quantity only if the core is massively destroyed.

Generally, iodine-131 is the significant radioisotope of concern because of its short half-life (8.1 days), high-energy gamma emission, and ability to get into the food chain as described in Section 7.8.3.

As long as the pH of water inside containment is high, iodine will stay dissolved in the water. High pH can be engineered through storage of chemicals such as tri-sodium phosphate in areas likely to flood in an accident. However, a fraction of the iodine will react with organic material in containment and form methyl iodide, which is volatile, not very soluble, and hard to capture on filters. In an accident, any iodine-131 which does leak from containment is therefore likely to be in this chemical form.

7.8 Fission Products, Atmospheric Dispersion, and Dose

7.8.1 Fission-product source term

The fission-product inventory in an operating reactor can be estimated as follows. Suppose that the reactor has been operating at a power of *P* MW(th). If the recoverable energy per fission is assumed to be 200 MeV, the total number of fissions occurring per second is

$$\text{Fission rate} = \text{P(MW)} \times \frac{10^6\ joule}{MW - \sec} \times \frac{fissions}{200 MeV} \times \frac{MeV}{1.60 \times 10^{-13}\ joule}. \tag{51}$$

If the cumulative yield of the *i*th fission product (the yield of the fission product itself plus the yields of all its short-lived precursors) is γ_i atoms per fission, then the rate of production of this nuclide is

$$\text{Rate of production} = 3.13 \times 10^{16} P\gamma_i \text{ atoms/sec}. \tag{52}$$

The activity at time *t* of that fission product while in the core of the reactor is

$$\alpha_i = 3.13 \times 10^{16} P\gamma_i (1 - e^{-\lambda_i t}) \text{ disintegrations/sec}, \tag{53}$$

or in Curies,

$$\alpha_i = 3.13 \times 10^{16} P\gamma_i (1 - e^{-\lambda_i t}) \text{Bq} \times \frac{1\text{Ci}}{3.7 \times 10^{10} \text{Bq}}. \tag{54}$$

If the activity is saturated, that is, if λ_i >>1, Equation (54) reduces to

$$\alpha_i = 8.46 \times 10^5 P\gamma \text{ Ci}. \tag{55}$$

Table 14 gives the inventories of the most important noble gases and iodine fission products computed for a typical 1000 MWe (PWR) plant at the end of a fuel cycle. This example is illustrative: the time-average inventory would be different in a 1000 MWe CANDU partly because of on-power fuelling and lower burnup.

7.8.2 Atmospheric dispersion

Consider a reactor containment after an accident in which the concentration of a particular nuclide is *C* Bq/m^3. Assume a leak rate of *V* m^3/ s into the atmosphere at a height of *h* metres, as shown in Figure 68. The release rate *Q* is given by:

$$Q(Bq/Sec) = C(Bq/m^3) \times V(m^3/\sec). \tag{56}$$

This release is dispersed into the surrounding area by the release plume. For given weather conditions with wind velocity *u* and other data, the concentration of radioactive material at some distance and direction from the source can be calculated from the *Gaussian* dispersion model [CSA, 2008]:

$$\chi = \left(\frac{2}{\pi}\right)^{1/2} \frac{Q}{\sigma_z \bar{u}} \frac{f}{\theta x} e^{-h^2/2\sigma_z^2}, \tag{57}$$

where (Figure 68):

χ is the sector-averaged long-term concentration in Bq/m^3 at a distance of *x* metres from the source and will be uniform through the sector
Q is the release rate in Bq/s from a source of height *h* metres
σ_z is the vertical diffusion coefficient in metres
θ is the angle subtended by the sector in radians
f is the fraction of the time that the wind blows into the sector
$\bar{u}$ is the mean wind velocity in m/s.

Table 14 Typical core inventory of volatile fission products

Nuclide*	Half-life†	Fission yield‡	Curies (×10^{-8}§)
^{85m}Kr	4.4 h	0.0133	0.24
^{85}Kr	10.76 y	0.00285	0.0056
^{87}Kr	76 m	0.0237	0.47
^{88}Kr	2.79 h	0.0364	0.68
^{133}Xe	5.27 d	0.0677	1.7
^{135}Xe	9.2 h	0.0672	0.34
^{131}I	8.04 d	0.0277	0.85
^{132}I	2.28 h	0.0413	1.2
^{133}I	20.8 h	0.0676	1.7
^{134}I	52.3 m	0.0718	1.9
^{135}I	6.7 h	0.0639	1.5
* Superscript *m* refers to a nuclide in an isomeric state (see Section 2.8).			

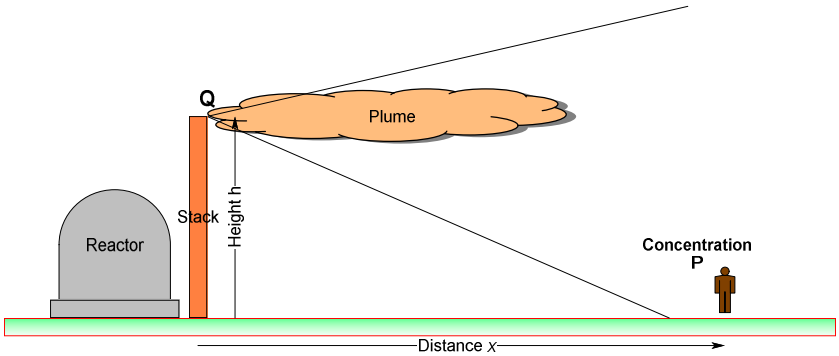

Figure 68 Atmospheric dispersion

7.8.3 Dose

Release of radioactive material from containment leads to an external dose to humans (often called "cloud" dose) which depends on the ambient radiation level and an internal dose which depends on inhaled species (and, in the longer term, ingestion of contaminated foods). External dose is a function of exposure time to an ambient radiation level. Internal dose is a function of radiation uptake and residence time in the body.

For example, the dose from I^{131} can be delivered through the following route:

- released from containment
- deposits on grass
- eaten by cows
- excreted in milk
- drunk by people.

Alternatively, I^{131} can deposit on plants which are eaten directly by people. The external (direct) dose from atmospheric release of I^{131} can also be significant.

Detailed tables have been prepared for each radioisotope which make it possible to convert from external concentration, inhalation, and ingestion to dose. See [ICRP, 2010] for the most recent tables. However, these are given by type of radiation rather than by radionuclide; for an older report that does give the conversion factors by radionuclide, see [EPA, 1993].

Sample Problem

Consider a major release of radioactive Ar^{41} causing an air concentration χ of 10^8 Bq/m^3. A person is immersed in this cloud for an hour. What is his external dose?

Answer

From [EPA, 1993], Table III.1, we see that the effective dose coefficient h_D for air immersion in Ar^{41} is 6.5×10^{-14} Sv/Bq-s-m^3. Hence, the dose D for an immersion of t seconds is:

$$D = h_D \chi t = 6.5\times10^{-14}\,\text{Sv/Bq-s-m}^3 \times 10^8\,\text{Bq/m}^3 \times 3600\,\text{sec} = 0.23\,\text{Sv}\,. \qquad (58)$$

Note that this assumes a continuous release because we have not accounted for decay; the half-life of Ar^{41} is 1.83 hours.

7.9 Problems

1. Calculate the dose to a person due to the release of 1000 Ci/hour of xenon-133 from a CANDU. Assume that the release point is 20 m high and the receptor is 1 km distant. Assume further that the person stays in that location for 15 minutes. Consult CSA-N288.1 for any models you need. You should be able to find dispersion factors in the (public) annual environmental monitoring reports issued, e.g., by OPG.

2. How many grams does 1000 Ci of iodine-131 represent? (Hint: remember or look up the half-life).

3. Calculate the *average* volumetric heat generation of the fuel in a 600MW CANDU at 100% power. At what percentage power (assuming the same heat removal from the fuel as in normal operation) would the centre of the average pin melt?

4. Do the following:

(a) Calculate the amount of hydrogen produced by oxidation of 25% of the Zircaloy in the sheaths in a CANDU (this is not atypical of a severe accident such as a LOCA + LOECC);

(b) Calculate the amount of energy released (you will need to look up the heat of reaction)

(c) Assume that this energy is released starting from 30 minutes after the accident and ending two hours afterwards. Compare the energy to the decay heat produced in the same time.

(d) Now assume that the hydrogen is transported into containment and burns. Calculate the energy produced by the burn.

8 Safety of Operation

In this section, we shall touch briefly on some high-level aspects of safety in operation. No matter how well a plant is designed, in the end, its safety strongly depends on how, and by whom, it is operated. We shall then touch briefly on future trends in safety, notably use of passive systems.

8.1 Safety Culture

The International Atomic Energy Agency (IAEA) was set up in 1957 as the world's "Atoms for Peace" organization within the United Nations family. It had a dual mandate: if nations would eschew the path of nuclear weapons development, those countries which already had nuclear weapons would assist them in developing a civilian nuclear power programme. The objectives were thus: *safeguards*, aimed at preventing the proliferation of nuclear weapons, and *promotion* (including safety), aimed at assisting non-nuclear-weapons states.

The promotional side of the IAEA has been increasingly focussed on safety, especially since the Chernobyl accident. Early on, the IAEA developed a series of Safety Guides, which enunciated good safety practices in all areas of the nuclear fuel cycle, from design to waste management. These Guides were prepared in a collaborative and consensual manner by IAEA members. Because of this, they tended to contain useful advice, but they were not specific enough to affect design and operation in a fundamental way. They were generally adopted by both purchaser and vendor nations. Because safety remains the responsibility of each country, the Guides have no legal force internationally, but tend to be incorporated informally or adopted formally as part of each country's safety regulations.

Chernobyl caused a fundamental rethinking of the effectiveness of the guidance that the IAEA was offering. The first action taken was by an international group of independent experts, who provided advice to the Director-General of the IAEA—the International Safety Advisory Group, or INSAG. They produced a number of key documents which gained widespread international acceptance and have strongly influenced the development of safety since then.

INSAG-1 [INSAG, 1986] initiated safety culture as a meme; however, this report was withdrawn because of deficiencies in the Soviet account of Chernobyl, on which it relied. [INSAG, 1992] entitled *Basic Safety Principles for Nuclear Power Plants*, tried to set down in one place what its title implied: what were the underlying and fundamental safety principles of nuclear power plants. Five levels of safety principles were defined, in a hierarchy going from the general and all-encompassing to specific technical practices. The document was written in the present tense, as if all reactors followed the safety principles—a clear message that if they did not, they should be modifying at least their operating practices. Details are beyond the scope of this Section.

INSAG recognized implicitly that no plant design is so safe that it cannot be damaged by incompetent operation; this is why plant safety is fundamentally the responsibility of the plant operator, not the designer and not the regulator. It is even more important that an unforgiving design requires cautious operation, which in case of uncertainty always opts for the prudent course of action. In this framework, Chernobyl was an unforgiving design run by an organization deficient

in safety culture.

The difficulty with safety culture was that it was hard to "get hold of"—like personal character, one could sense when it was deficient, but it was hard to measure. INSAG therefore hastened to elaborate on the term in a subsequent report [INSAG, 1991] entitled *Safety Culture*. The term was redefined as:

> "Safety culture is that assembly of characteristics and attitudes in organizations and individuals which establishes that, as an overriding priority, nuclear plant safety issues receive the attention warranted by their significance".

The three concepts in this definition are that safety culture is attitudinal as well as structural; that it relates both to organizations and individuals; and that it matches all safety requirements with appropriate perceptions and action. Note that it gives safety a priority to the extent warranted—it is not an absolute.

In simpler terms, the best design and the most carefully written procedures will not help if staff does not place safety first in their thoughts and actions. See [IAEA, 2002] and [INSAG, 1999] for more detail.

Other organizations have used variant definitions. The U.S. Nuclear Regulatory Commission [USNRC, 2011a] defines it as "the core values and behaviors resulting from a collective commitment by leaders and individuals to emphasize safety over competing goals to ensure protection of people and the environment."

Informal but revealing definitions include "Safety culture is what you do when the boss isn't looking", and "Safety culture is the way we do things around here".

To assist in recognizing a lack of safety culture, the IAEA has defined the stages of organizational decline, as shown in Table 15.

Table 15 Stages of organizational decline

Stage	Name of stage	Characteristic of stage
1	Over-confidence	Good past performance leading to self-satisfaction
2	Complacency	Occurrence of minor events that are subjected to minimum self-assessment, and delay in improvement programmes
3	Denial	Number of minor events increases, with possibly a more significant event. These are treated as isolated events. Findings from audits are considered invalid. Root-cause analysis not used.
4	Danger	Several potentially serious events occur, but management and employees reject criticism from audits or regulators by considering their views biased. The oversight function is afraid to confront management.
5	Collapse	Regulator intervenes to implement special evaluations. Management is overwhelmed and may need to be re-placed. Major and very costly improvements need to be implemented.

Audits by organizations such as INPO (Institute of Nuclear Power Plant Operations, an association of operating organizations) have distilled—through auditing utilities which were subsequently forced into extended plant outages due to management deficiencies—a list of symptoms of a poor safety culture [INPO, 2010]. It is the rare organization which does not recognize at least part of itself in the list.

Finally, IAEA Safety Guides are being rewritten to make them more detailed, so that they state the increased safety expectations of the 21st Century. "Requirements" on both design [IAEA, 2012] and operations [IAEA, 2011a] are becoming the *de facto* minimum standard for nuclear power plants. Indeed, the IAEA design "requirements" report is the basis of the current Canadian top-level design requirements for new builds [CNSC, 2008].

8.2 International Nuclear and Radiological Event Scale

No discussion of safety would be complete without a summary of the International Nuclear and Radiological Event Scale (INES). This is a ranking of accidents so that the safety significance of events in nuclear power plants is reported in a consistent way all over the world [INES, 2008]. The seven levels in the scale are shown in Table 16. The table is self-explanatory, but should be read carefully.

Table 16 INES event scale

Description and INES Level	People and the environment	Radiological barriers and controls at facilities	Defence in depth
Major Accident Level 7	Major release of radioactive material with widespread health and environmental effects requiring implementation of planned and extended countermeasures.		
Serious Accident Level 6	Significant release of radioactive material likely to require implementation of planned countermeasures.		
Accident with wider consequences Level 5	Limited release of radioactive material likely to require implementation of some planned countermeasures. Several deaths from radiation.	Severe reactor core damage. Release of large quantities of radioactive material within an installation with high probability of significant public exposure. This could arise from a major criticality accident or fire.	
Accident with local consequences Level 4	Minor release of radioactive material unlikely to result in implementation of planned countermeasures other than local food controls. At least one death from radiation.	Fuel melt or damage to fuel resulting in more than 0.1% release of core inventory. Release of significant quantities of radioactive material within an installation with high probability of significant public exposure.	

Description and INES Level	People and the environment	Radiological barriers and controls at facilities	Defence in depth
Serious Incident Level 3	Exposure in excess of ten times the statutory annual limit for workers. Non-lethal deterministic health effect (e.g., burns) from radiation.	Exposure rates of more than 1 SV/h in an operating area. Severe contamination in an area not expected by design, with a low probability of significant public exposure.	Near accident at a nuclear power plant with no safety provisions remaining. Lost or stolen highly radioactive sealed source. Misdelivered highly radioactive sealed source without adequate radiation procedures to handle.
Incident Level 2	Exposure of a member of the public in excess of 10 mSv. Exposure of a worker in excess of the statutory annual limits.	Radiation levels in an operating area of more than 50 mSv/h. Significant contamination within the facility into an area not expected by design.	Significant failures in safety provisions, but with no actual consequences. Found highly radioactive sealed orphan source, device or transport package with safety provisions intact. Inadequate packaging of a highly radioactive sealed source.
Anomaly Level 1			Overexposure of a member of the public above statutory limits. Minor problems with safety components with significant defence in depth remaining. Low-activity lost or stolen radioactive source, device or transport package.
No safety significance (Below scale/Level 0)			

8.3 Safety Aspects of Future Designs

In the final part of this Section, we shall be discussing some of the safety characteristics of modern advanced designs. These designs fall into two categories: **evolutionary** and **advanced**.

1. *Evolutionary* designs, as their name suggests, build on operating experience in current plants and add those improvements which are warranted by experience.
2. *Advanced* designs use passive concepts in their operation and particularly with respect to safety. The original ideas behind the use of passive safety was to:
   - simplify the design and make it cheaper to build, operate, and maintain
   - increase the *real* safety of the plant through systems which were less complex and more reliable because they used "natural" forces
   - increase the *perceived* safety of the plant for the same reasons.

In its broadest sense, passive safety emphasizes the use of "natural" forces (gravity, self-correcting neutronic feedback) and de-emphasizes systems which require large amounts of electricity (pumps), rapid automatic response, complex logic, or high energy. A clear understanding of the meaning of terms such as "passive" and "inherent" is essential; we shall follow [IAEA, 1991].

8.3.1 Definitions

Inherent safety refers to the achievement of safety through the elimination or exclusion of inherent hazards through the fundamental conceptual design choices made for the nuclear plant. This is impossible for practical reactor sizes because it requires elimination of systems (because they would not be needed) to remove or compensate for decay heat, excess reactivity, and high energy releases. It is possible to have inherent safety for low-energy pool reactors such as the 20kW(th) SLOWPOKE-2 research reactor [AECL, 1976]—the total potential reactivity addition can all be compensated for without fuel damage by the inherent negative feedback from fuel and coolant temperatures, and the power at which this compensation is achieved can be absorbed indefinitely by the pool and the surroundings. For larger reactors, elimination of one or more of these hazards does, however, give a reactor an *inherently safe characteristic*. Note that the hazard must be eliminated deterministically, not probabilistically; for example, a plant is inherently safe against fires if it has no combustible material.

An ideal **passive component** does not need an external input to operate; a passive system is composed of passive components and structures. Ideally a passive system has no reliance on external mechanical or electrical power, signals, or forces. It does rely on "natural" laws, properties of materials, and internally stored energy. Therefore, heat removal from a reactor by thermo-siphoning to an elevated tank of water is passive, at least until the water runs out. In practice, most passive designs do allow active signals because there is usually a need to switch from the active heat-removal systems used in full-power operation to passive decay-heat removal systems after an accident. CANDU shutdown systems are passive in this respect: once they receive a signal, they actuate by gravity or stored energy.

An **active component** or system is one which is not passive.

Fail-safe means that a given failure leads to a safe condition; the component or system is then fail-safe *with respect to that condition*. The fail-safe characteristic is specific to the failure mode: for example, Shutdown System 2 in CANDU is fail-safe with respect to loss of electrical power to the valves, but not to loss of gas pressure.

Grace period is the period of time during which a safety function is ensured after an accident without the necessity for human intervention. Colloquially, it used to be called "walk-away safe" for whatever grace period was involved—this term has unfortunate connotations (operators are not expected to walk away from an accident) and is best not used. A grace period can be achieved through active or passive means; usually, the first line of defence is assumed to function properly in determining the grace period. Therefore, the grace period for loss of feed water in first-generation CANDUs is about 30 minutes because after this period, the operator must manually valve in an alternate heat sink. For new CANDU designs, the grace period is extended to days through use of automatic steam-generator depressurization followed by automatic connection of the elevated reserve water tank to the steam generators. For modern reactor designs, evolutionary or passive, a grace period of three days for most single failures is expected.

8.3.2 Categories of Passive Safety

Very few systems are totally passively safe. To recognize the range of possibilities, the IAEA [IAEA, 1991] defined four categories of passivity, as summarized in Table 17.

Table 17 Categories of passive safety characteristics

Characteristic	Category A	Category B	Category C	Category D
Signal Inputs of Intelligence	No	No	No	Yes
External power sources or forces	No	No	No	No
Moving mechanical parts	No	No	Yes	Either
Moving working fluid	No	Yes	Yes	Either
Example	Barriers such as fuel clad, containment; core cooling relying only on radiation or conduction to outer structural parts	Heat removal by natural circulation to heat exchangers in water pools, from the core or containment	Rupture disk or spring-loaded valve for overpressure protection; accumulator isolated by check valve	Shutdown Systems 1 and 2 in CANDU

For many passive designs, even those for which the "execution" is passive, the actuation may involve an electrical signal. Part of the justification for this is that such signals are highly reliable and can use backup power from batteries if main power fails. Note that even some valves can be actuated on battery power. However, details of how this is implemented are being revisited after Fukushima.

8.3.3 Passive safety desiderata

A passive design strives to ensure that the three major safety functions (other than monitoring)

can be carried out in a passive or pseudo-passive manner. Recall that these functions are to shut down the reactor, to remove decay heat, and to contain any fission products. We describe in general terms how each of these might be accomplished.

8.3.3.1 Shut down the reactor

CANDU shutdown systems are passive in the sense that once they are actuated by a signal, the devices themselves are inserted into the core by gravity (shut-off rods) or stored energy (spring assist to the shut-off rods and gas-driven poison injection). This places them into IAEA Category D above. More passive approaches could be developed based on change in material properties with temperature, e.g., a shutdown system consisting of tubes inserted into the reactor, with a low-melting-point neutron absorber within them, initially located above the core, and which would melt and insert into the core on increasing temperature. This system needs no external "intelligence", but does have a moving fluid, placing it in Category B. Even more basic, fuel with a strong negative temperature-feedback coefficient is certainly a passive form of reactivity compensation. If it truly shut down the reactor, it would be in Category A. However, negative feedback does not shut down the reactor after, say, an inadvertent insertion of positive reactivity (control rod withdrawal); it simply allows the power to rise and then equilibrate at a level where the negative reactivity due to the higher fuel temperature offsets the reactivity addition of the control rod. One still needs to be sure that the power can be removed somehow (by passive means) and that the fuel is not damaged. A strong negative coolant-temperature feedback works the same way, but raises the added concern that fast insertion of cold water could cause a rapid power increase before the negative fuel or coolant temperature had time to compensate for it. The SLOWPOKE 2 reactor dealt with this problem by physically limiting the *amount* of reactivity that it was possible to add; an alternative is to limit physically the *rate* at which it can be added, so that negative feedback has time to take effect. Removal of moderator in LWRs after a LOCA is an example of passive shutdown, but the ECC water that replaces it must be borated to prevent recriticality and therefore is an active means of shutdown.

8.3.3.2 Remove decay heat

In passive designs, removal of decay heat from the fuel is normally done by thermo-siphoning to an elevated heat sink, usually a heat exchanger in a large supply of water high up in the building. Alternatively, the entire core and its surroundings can be flooded by pouring water by gravity from an elevated supply; the core heat is then turned to steam, which flows to and is removed passively from containment. In some, but not all, passive designs decay heat is removed at low pressure; therefore, some means of depressurizing the heat-transport system is required first. This is done using a Category "D" device. CANDU offers inherent characteristics for passive heat removal in severe accidents, as discussed in Section 6.14. Existing and future CANDUs therefore incorporate the features desired in next-generation reactors: spreading of core debris so it can be easily cooled (the calandria shell and/or the reactor vault/shield tank) and passive cooling of the damaged core (moderator and/or reactor vault water).

8.3.3.3 Contain radioactive material

The containment structure is already passive, category A. However, for a number of other

containment functions, a passive approach can be taken.

8.3.3.3.1 Ventilation isolation

The building can simply be sealed during operation, or the isolation system can be Category D (e.g., a spring-loaded valve which fails closed on loss of signal).

8.3.3.3.2 Decay heat removal

This is an extension of core thermo-siphoning. The idea is to move the heat into an elevated tank of water. To achieve this, heat exchangers can be placed in the building, with the tube side connected to the tank and the shell side exposed to containment atmosphere. This requires two natural convection loops: one in the containment atmosphere, transporting heat from the core (e.g., steaming from a LOCA) to the heat exchangers, and one transporting heated water from the heat exchangers to the elevated tank. One variation on this idea is used in the AP1000: the metal shell of the building becomes the heat exchanger, and the elevated tank trickles water down the *outside* [Westinghouse, 2011b].

8.3.3.3.3 Hydrogen removal

Here, passive autocatalytic recombiners can be used. These simply offer a catalyst-coated surface to the containment atmosphere and as the air/steam/hydrogen mixture flows through, the hydrogen and oxygen are catalytically recombined. An alternative is to inert the containment atmosphere, inherently removing the possibility of hydrogen combustion since there will be no oxygen.

8.3.4 Summary

This Section has indicated the direction that safety may take in the future. Passive safety is attractive because of its simplicity, public appeal, and aura of high reliability. Evolutionary designs have also incorporated safety enhancements while both remaining economical and posing less of an "innovation" risk to owners and operators. Once adequate (or even more than adequate) safety is achieved, factors such as economics and proven performance may become the determinants of the choice of technology, particularly as electricity markets become more deregulated.

8.4 Problems

1. Place the following accidents on the International Nuclear and Radiological Event Scale, with brief reasons for your choice. You may need to research some of these if they are not covered in the text:
    1. NRX accident, 1952
    2. SL-1 accident
    3. Pressure-tube failure in Pickering A (G-16)
    4. Fire in Narora plant in India
    5. Chernobyl accident (power runaway)
    6. Three Mile Island accident (core melt)
    7. Fukushima tsunami-induced accident

8. Erosion/corrosion of Davis-Besse vessel head

2. If you work for a design organization or a regulator or a nuclear power plant, evaluate its safety culture in terms of the safety culture framework defined by one or more of INSAG, IAEA, INPO, etc. Give reasons and evidence, not just opinion.

3. Look up information on any two modern designs (e.g., Enhanced CANDU 6, Westinghouse AP1000, EPR). Compare and contrast them as follows: for each of the systems performing the fundamental safety functions (shut down, cool, contain radioactive material), categorize them as active or as passive categories A, B, C, or D (give reasons).

9 Review

This Chapter has summarized the basic concepts of safety for nuclear power plants. Starting with the hazards inherent to nuclear power, it has described tools to identify possible accidents, in particular the top-down and bottom-up approaches. Real experience has been a powerful driver in the approach to nuclear safety, and the Chapter has described seminal historical accidents and lessons learned—and as Fukushima has shown, learning lessons is an ongoing process. We presented risk assessment, first in terms of safety goals for acceptable safety performance, and then developing the probabilistic tools used to show that the goals have been achieved. We then described (for CANDUs) mitigating systems to shut down the plant, remove decay heat, and contain fission products in response to the needs identified by both deterministic and probabilistic analyzes. We looked at accident phenomenology, using a large LOCA as a model, and extended this discussion to CANDU characteristics in severe core-damage accidents. Then we described (at a high level) the mathematical models underlying the safety-analysis codes used to predict plant behaviour in accidents. Finally we looked—all too briefly—at the safety role of the plant operators and indicated the options for the safety characteristics of future designs.

10 References

[Ader, 1998] C. Ader, G. Heusener, and V. G. Snell, "Strategies for the Prevention and Mitigation of Severe Accidents", *IAEA International Symposium on Evolutionary Water-Cooled Reactors: Strategic Issues, Technologies, and Economic Viability*, IAEA Paper No. IAEA-SM-353-16, Korea, 1998.

[AECB, 1980] Atomic Energy Control Board, *Requirements for the Safety Analysis of CANDU Nuclear Power Plants*, Consultative Document C-6, Proposed Regulatory Guide, June 1980.

[AECL, 1976] R. E. Kay, J. W. Hilborn, and N. B. Poulsen, *The Self-Limiting Power Excursion Behaviour of the Slowpoke Reactor*, Atomic Energy of Canada Limited Report AECL-4770, January 1976.

[AECL, 2005] Atomic Energy of Canada Limited, *CANDU 6 Technical Summary*, May 2005 (Primer on CANDU 6 design).

[AECL, 2011], *ZED-2 User Facility Proposal Package*, AECL report ZED2-123110-REPT-001, Revision 0, May 2011.

[Andreani, 2010] M. Andreani and D. Paladino, "Simulation of Gas Mixing and Transport in a Multi-Compartment Geometry using the GOTHIC Containment Code and Relatively Coarse Meshes", *Nuclear Engineering and Design*, Vol. 240, No. 6, pp. 1506–1527 (2010).

[Blahnik, 1991] C. Blahnik, *et al*., "Modular Accident Analysis Program for CANDU Reactors", *Proc. 12th Annual Canadian Nuclear Society Conference*, Saskatoon, Saskatchewan, Canada, June 9-12, 1991, pp. 235-242.

[Blahnik, 2012] C. Blahnik, M. J. Brown, T. Nitheanandan, and S. M. Petoukhov, "Perspective on Analyses of Core Damage in CANDU Reactors", *24th Nuclear Simulation Symposium*, Ottawa, Ontario, Canada, October 14-16, 2012.

[Boss, 2006] K. Aydogdu and C. R. Boss, "Radiation Physics and Shielding Codes and Analyses Applied to Design-Assist and Safety Analyses of CANDU and ACR Reactors", *PHYSOR-2006, ANS Topical Meeting on Reactor Physics*, Vancouver, BC, Canada, September 10-14, 2006.

[Brooks, 1980] G. L. Brooks and E. Siddall, "An Analysis of the Three Mile Island Accident", presented at the *CNS First Annual Conference*, Montreal, Canada, June 1980.

[Buell, 2003] J. Buell, J. D. Dormuth, P. Ingham, and R. Swartz, *RD-14M Facility Description*, 153-112020-UM-001, 2003; also USNRC ML031690499.

[Cameron, 1996] I. Cameron, *Nuclear Physics and Reactor Theory 1.1—Module 9, Source Neutron Effects*, Course given at Chulalongkorn University, Thailand, 1996. See CANTEACH: https://canteach.candu.org.

[Chan, 1987] P. Chan, *et al.*, "The Chernobyl Accident: Multidimensional Simulations to Identify the Role of Design and Operating Features of the RBMK-1000", *Conference on Probabilistic Safety Assessment and Risk Management*, Zurich, Switzerland; September 1987. Also Atomic Energy of Canada report AECL-9246.

[Charak, 1995] I. Charak and P. H. Kier, *CANDU Reactors, Their Regulation in Canada, and the Identification of Relevant NRC Safety Issues*, Argonne National Laboratory report NUREG/CR-63 15 and ANL-9515, April 1995 (prepared for U.S. Nuclear Regulatory Commission).

[Chen, 2007] W. L. Chen, *et al.*, "Effects of Cobalt-60 Exposure on Health of Taiwan Residents Suggest New Approach Needed in Radiation Protection", *Dose Response*, Vol. 5, No. 1, pp. 63–75 (2007).

[CNSC, 2008] Canadian Nuclear Safety Commission, *Design of New Nuclear Power Plants*, Regulatory Document RD–337, November 2008.

[CNSC, 2008a] Canadian Nuclear Safety Commission, *Safety Analysis for Nuclear Power Plants*, Regulatory Document RD–310, February 2008

[CNSC, 2011] Canadian Nuclear Safety Commission, *CNSC Staff Integrated Safety Assessment of*

Canadian Nuclear Power Plants for 2010, INFO-0823, September 2011.

[CSA, 2008] Canadian Standards Association, *Guidelines for Calculating Derived Release Limits for Radioactive Material in Airborne and Liquid Effluents for Normal Operation of Nuclear Facilities*, CSA N288.1-08, 2011.

[Cross, 1980] W. G. Cross, "The Chalk River Accident in 1952", *Historical Perspective on Reactor Accidents*, Seattle, Washington, July 1980.

[Currie, 1984] T. Currie and J. T. Rogers, "Experimental and Numerical Studies of Heat Transfer Through Contact Areas of High Ellipticity", *ASME National Heat Transfer Conference*, Paper 84-HT-85, 1984.

[Currie, 1985] T. C. Currie, J. T. Rogers, and J. C. Atkinson, *A Study of the Technical and Economic Feasibility of Using a SLOWPOKE-3 Nuclear Reactor for Building Heating and Cooling at Carleton University*, Study for AECL; November, 1985.

[Currie, 1986] T. C. Currie and J. T. Rogers, "Heat Transfer between Rough Surfaces in Contact over a Highly Elliptical Contour Area: Comparison of Experimental and Numerical Results", *Proceedings of Eighth International Heat Transfer Conference*, San Francisco, August 1986.

[Cuttler, 2009] J. M. Cuttler and M. Pollycove, "Nuclear Energy and Health: The Benefits of Low-Dose Radiation Hormesis", *Dose Response*, Vol. 7, No. 1, pp. 52–89, 2009.

[EPA, 1993] K. F. Eckerman and J. C. Ryman, *Federal Guidance Report No. 12 - External Exposure to Radionuclides in Air, Water, and Soil*, Environmental Protection Agency report EPA-402-R-93-081, September 1993.

[Glasstone, 1994] S. Glasstone and A. Sesonske, *Nuclear Reactor Engineering*, 4th Edition, Chapman & Hall, 1994.

[Gonzales, 2013] A. J. Gonzalez, *et al.*, "Radiological Protection Issues Arising During and After the Fukushima Nuclear Reactor Accident", *J. Radiol. Prot.*, Vol. 33, pp. 497–571, 2013.

[Grandjean, 2008] C. Grandjean and G. Hache, *A State-of-the-Art Review of Past Programmes Devoted to Fuel Behaviour Under Loss-of-Coolant Conditions, Part 3: Cladding Oxidation, Resistance to Quench and Post-Quench Loads*, Institut de Radioprotection et de Sûreté Nucléaire (IRSN) report DPAM/SEMCA 2008-093, 2008.

[Hanna, 1998] B. N. Hanna, "CATHENA: A Thermal-Hydraulic Code for CANDU Analysis", *Nuclear Engineering and Design*, Vol. 180, 113–131, 1998.

[Howieson, 1987] J. Q. Howieson and V. G. Snell, *Chernobyl: A Canadian Technical Perspective*, Atomic Energy of Canada Limited publication AECL-9334, January 1987. Also *Nuclear Journal of Canada*, Vol. 1, No. 3, September 1987.

[HSE, 2006] Health and Safety Executive (United Kingdom), *Safety Assessment Principles for Nuclear Facilities*, Bootle, 2006 Edition, Revision 1.

[Hurst, 1953] D. G. Hurst, *The Accident to the NRX Reactor, Part II*, Atomic Energy of Canada Limited, Report AECL-233, October 1953.

[Hurst, 1972] D. G. Hurst and F. C. Boyd, "Reactor Licensing and Safety Requirements", Paper 72-CNA-102, *12th Annual Conference of the Canadian Nuclear Association*, Ottawa, Ontario, June 1972.

[Huterer, 1984] J. Huterer, E. C. Ha, D. G. Brown, and P. C. Cheng, "Darlington GS Vacuum Building: Containment Shell", *Nuclear Engineering and Design*, Vol. 85, 131-140, 1985.

[IAEA, 1991] International Atomic Energy Agency, *Safety-Related Terms for Advanced Nuclear Plants*, IAEA-TECDOC-626, September 1991.

[IAEA, 2000] International Atomic Energy Agency, *Safety of Nuclear Power Plants: Design*, IAEA report NS-R-1, 2000.

[IAEA, 2002] International Atomic Energy Agency, *Safety Culture in Nuclear Installations*, IAEA-TECDOC-1329, December 2002.

[IAEA, 2008] International Atomic Energy Agency, *Analysis of Severe Accidents in Pressurized Heavy-Water Reactors*, IAEA-TECDOC-1594, June 2008.

[IAEA, 2010] International Atomic Energy Agency, *Development and Application of Level 1 Probabilistic Safety Assessment for Nuclear Power Plants*, IAEA-SSG-3, April 2010.

[IAEA, 2011] International Atomic Energy Agency, *International Fact Finding Expert Mission of the Fukushima Dai-Ichi NPP Accident Following the Great East Japan Earthquake and Tsunami*, IAEA Report, June 16, 2011.

[IAEA, 2011a] International Atomic Energy Agency, *Safety of Nuclear Power Plants: Commissioning and Operation: Specific Safety Requirements*, IAEA report SSR-2/2, July 2011.

[IAEA, 2012] International Atomic Energy Agency, *Safety of Nuclear Power Plants: Design: Specific Safety Requirements*. IAEA report SSR-2/1, January 2012.

[ICRP, 1990] International Commission on Radiological Protection, *1990 Recommendations of the ICRP*, report ICRP-60, table B.

[ICRP, 2010] International Commission on Radiological Protection, *Conversion Coefficients for Radiological Protection Quantities for External Radiation Exposures*, ICRP Publication 116, Ann. ICRP 40(2–5), 2010.

[ICRP, 2012] International Commission on Radiological Protection*, Compendium of Dose Coefficients based on ICRP Publication 60*, ICRP Publication 119, Ann. ICRP 41 (Suppl.).

[INES, 2008] International Atomic Energy Agency and OECD/Nuclear Energy Agency, *INES - The International Nuclear and Radiological Event Scale - User's Manual, 2008 Edition,* IAEA, Vienna, 2009.

[Inhaber, 1978] H. Inhaber, *Risk of Energy Production*, Atomic Energy Control Board report AECB 1119, March 1978.

[INPO, 2010] Institute of Nuclear Power Operations, *Field Guidance: Organizational Effectiveness Evaluation and Assistance*, INPO report, Revision 2, March 2010.

[INSAG, 1986] International Nuclear Safety Advisory Group, *Summary Report on the Post-*

Accident Review Meeting on the Chernobyl Accident, International Atomic Energy Agency Report 75-INSAG-1, Vienna, 1986.

[INSAG, 1991] International Nuclear Safety Advisory Group, *Safety Culture*, International Atomic Energy Agency Report 75-INSAG-4, 1991.

[INSAG, 1992] International Nuclear Safety Advisory Group, *The Chernobyl Accident: Updating of INSAG-1 – INSAG 7,* International Atomic Energy Agency Report INSAG-7, 1992.

[INSAG, 1996] International Nuclear Safety Advisory Group, *Defence in Depth in Nuclear Safety,* International Atomic Energy Agency Report INSAG-10, 1996.

[INSAG, 1999] International Nuclear Safety Advisory Group, *Basic Safety Principles for Nuclear Power Plants*, International Atomic Energy Agency Report INSAG-12, 1999.

[Ionescu, 2009] S. Ionescu, O. Uta, M. Pârvan, and D. Ohâi, "Pressurized Heavy Water Reactor Fuel Behaviour in Power Ramp Conditions", *Journal of Nuclear Materials*, Vol. 385, 387–391, 2009.

[Jaffe, 1979] L. Jaffe, *Staff Reports to the President's Commission on the Accident at Three Mile Island*, Reports of the Technical Assessment Task Force, Volume II, 1979.

[Japan, 2011] Government of Japan, Nuclear Emergency Response Headquarters, *Report of the Japanese Government to the IAEA Ministerial Conference on Nuclear Safety: The Accident at TEPCO's Fukushima Nuclear Power Stations*, June 2011.

[JNTI, 2011] Japan Nuclear Technology Institute, Examination Committee on Accident at Fukushima Daiichi Nuclear Power Station, *Examination of Accident at Tokyo Electric Power Co., Inc.'s Fukushima Daiichi Nuclear Power Station and Proposal for Countermeasures*, October 2011 (there are many more similar reports from IAEA and others).

[Kaplan, 1979] S. Kaplan and B. J. Garrick, "On the Use of Bayesian Reasoning in Safety and Reliability – Three Examples", *Nuclear Technology*, Vol. 44, 231, 1979.

[Kemeny, 1979] J. G. Kemeny, *Report of the President's Commission on the Accident at TMI*, 1979.

[Krause, 2007] M. Krause, "Hydrogen Program at AECL", *2nd European Review Meeting on Severe Accident Research (ERMSAR-2007)*, Forschungszentrum Karlsruhe GmbH (FZK), Germany, June 12-14, 2007.

[LANL, 2000] Los Alamos National Laboratory, *A Review of Criticality Accidents*, report LA-13638, 2000. (See page 74.)

[Larson, 1961] E. A. G. Larson, *A General Description of the NRX Reactor*, Atomic Energy of Canada Report AECL-1377, 1961.

[Lewis, 1953] W. B. Lewis, *The Accident to the NRX Reactor on December 12, 1952*, Atomic Energy of Canada Limited, Report AECL-232, July 1953.

[Lewis, 1990] B. J. Lewis, C. E. L. Hunt, and F. C. Iglesias, "Source Term of Iodine and Noble Gas Fission Products in the Fuel-to-Sheath Gap of Intact Operating Nuclear Fuel Elements",

Journal of Nuclear Materials, Vol. 172, 197-205, 1990.

[Lewis, 1999] B. J. Lewis, P. Tume, L. G. I. Bennett, M. Pierre, A. R. Green, T., Cousins, B. E. Hoffarth, T. A. Jones, and J. R. Brisson, "Cosmic Radiation Exposure on Canadian-Based Commercial Airline Routes", *Radiat. Prot. Dosim*., Vol. 86, No. 1, pp. 7–24, 1999.

[Lewis, 2009] B. J. Lewis, F. C. Iglesias, R. S. Dickson, and A. Williams, "Overview of High-Temperature Fuel Behaviour with Relevance to CANDU Fuel", *Journal of Nuclear Materials*, Vol. 394, pp. 67–86 (2009).

[Liauw, 1997] W. K. Liauw, W. S. Liu, R. Y. Chan, "TUF Validation against Reactor Trip Data at Darlington NGS", *Canadian Nuclear Society Conference: Powering Canada's Future*, Toronto (Canada), June 8-11, 1997.

[Liverman, 1979] D. M. Liverman and J. P. Wilson, "The Mississauga Train Derailment and Evacuation, 10–16 November 1979", *Canadian Geographer*, Vol. 25, No. 4, pp. 365–375, 1981.

[Mathew, 2004] M. Mathew, T. Nitheanandan, and S. J. Bushby, *Severe Core Damage Accident Progression within a CANDU Calandria Vessel*. AECL Chalk River Laboratories. Reactor Safety Division, Forschungsbericht (2004).

[McCormick, 1981] N. J. McCormick, *Reliability and Risk Analysis*, Academic Press, 1981, ISBN 0-12-482360-2.

[Meneley, 2003] D. A. Meneley, *Nuclear Safety and Reliability*, Lecture notes for a course at the University of New Brunswick, available at the CANTEACH repository, https://canteach.candu.org/Pages/Welcome.aspx, 2003.

[Meneley, 2009] D. A. Meneley and A. Muzumdar, "Power Reactor Safety Comparison – A Limited Review", *Proceedings, CNS 30th Annual Conference*, Calgary, AB, May 31–June 3, 2009.

[Morison, 1987] W. G. Morison, *et al*., "Containment Systems Capability", *Nuclear Journal of Canada*, Vol. 1, No. 1, pp. 53-68, 1987 [from CANTEACH].

[Muzumdar, 2009] A. J. Muzumdar and D. A. Meneley, "Large LOCA Margins in CANDU Reactors: An Overview of the COG Report", *Proceedings, CNS 30th Annual Conference*, Calgary, AB, May 31–June 3, 2009.

[NISA, 2011] Nuclear and Industrial Safety Agency (NISA) and Japan Nuclear Energy Safety Organization (JNES), *The 2011 Pacific Earthquake off the Pacific Coast of Tohoku and the Seismic Damage to the NPPs*, April 4, 2011.

[OMSC, 1981] Ontario Ministry of the Solicitor General, *The Mississauga Evacuation – Final Report*, November 1981.

[Ott, 1981] K. O. Ott and J. F. Marchaterre, "Statistical Evaluation of Design-Error Related Nuclear Reactor Accidents", *Nuclear Technology*, Vol. 52, No. 2, 179-188, 1981.

[Page, 1972] R. D. Page, *Nuclear Power Symposium - Lecture No. 5: Canadian Power Reactor Fuel*, Atomic Energy of Canada Limited, 1972 [from CANTEACH].

[Popov, 2012] N. K. Popov and V. G. Snell, "Safety and Licensing Aspects of Power Reactor Reactivity Coefficients", *Proceedings, 20th International Conference on Nuclear Engineering (ICONE20)*, Anaheim, California, USA, July 30–August 3, 2012.

[Popov, 2013] N. Popov, V. Snell, R. Tran, and G. LeRoy, "Thermo-Hydraulic Aspects of Reactivity Coefficients in CANDU", *15th International Topical Meeting on Nuclear Reactor Thermal-Hydraulics (NURETH-15)*, Pisa, Italy, May 12–17, 2013.

[Rizkalla, 1984] S. H. Rizkalla, S. H. Simmonds, and J. G. MacGregor, "Pre-Stressed Concrete Containment Model", *Journal of Structural Engineering*, Vol. 110, No. 4, pp. 730–743, 1984.

[Rizkalla, 1986] S. Rizkalla, "Limit States Behaviour of Pre-Stressed Concrete Containment Structures", *Proceedings, Second International Conference on Concrete Technology for Developing Countries*, Tripoli, Libya (Splaj), October 27–30, 1986;. Vol. 2, El-Fateh University, Civil Engineering Department, 1986.

[Rogers, 1987] J. T. Rogers, "Insights from Chernobyl on Severe Accident Assessment of CANDU Reactors", *Nuclear Journal of Canada*, Vol. 1, No. 2, pp. 107–118, 1987.

[Rogers, 1995] J. T. Rogers, D. A. Meneley, C. Blahnik, V. G. Snell, and S. Nijhawan, "Coolability of Severely Degraded CANDU Cores", *ICHMT International Seminar on Heat and Mass Transfer in Severe Reactor Accidents*, Cesme, Turkey, May 21–26, 1995. Also Atomic Energy of Canada Ltd. Report AECL-11110.

[Rogers, 2002] J. T. Rogers and M. L. Lamari, "Application of the CANDU Molten Core Model 'DEBRIS.MLT' to RASPLAV Test Results", *22nd Nuclear Simulation Symposium*, Canadian Nuclear Society, Ottawa, November, 2002

[Rogers, 2004] J. T. Rogers, *Options For Coal-Fired Power Plants in Ontario*, monograph at Canadian Nuclear Society, http://www.cns-snc.ca/cns_media, September 27, 2004.

[Rogers, 2004a] J. T. Rogers, "CANDU Power Reactor Behavior Following Reactor Trip", Presentation at *Panel Discussion on Islanding, Cogeneration Conference*, Ottawa, October 26, 2004.

[Rogovin, 1980] M. Rogovin and G. T. Frampton, *Three Mile Island—A Report to the Commissioners and to the Public*, Nuclear Regulatory Commission Special Inquiry Group, January 1980.

[Roy, 2004] R. Roy, *et al.*, "Reactor Core Simulations in Canada", *PHYSOR 2004 -The Physics of Fuel Cycles and Advanced Nuclear Systems: Global Developments*, Chicago, Illinois, April 25-29, 2004, American Nuclear Society, Lagrange Park, IL (2004)

[Rzentkowski, 2013] G. Rzentkowski, Y. Akl, and S. Yalaoui, "Application of Probabilistic Safety Goals to Regulation of Nuclear Power Plants in Canada", *34th Annual Conference of the Canadian Nuclear Society*, Toronto, June 9–12, 2013.

[Sanderson, 2003] B. Sanderson, *Fuel Channel Behaviour*, presented to U.S. Nuclear Regulatory Commission, May 6–7, 2003, USNRC accession ML031340404.

[Santamaura, 1998] P. A. Santamaura, J. G. Tielemans, T. H. Nguyen, H. S. Shapiro, R. E. B. Henderson, and B. A. duQuesnay, "Severe Core Damage Frequency and Insights from CANDU 6 Level 1 Probabilistic Safety Assessment", *Pacific Basin Nuclear Conference (PBNC98)*, Banff, Alberta, Canada, May 1998.

[Semonov, 1983] B. A. Semonov, "Nuclear Power in the Soviet Union", *IAEA Bulletin*, Vol. 25, No. 2, June 1983.

[Siddall, 1981] E. Siddall, *Risk, Fear, and Public Safety*, Atomic Energy of Canada Limited Report AECL-7404, April 1981.

[Simpson, 1996] L. A. Simpson, P. M. Mathew, A. P. Muzumdar, D. B. Sanderson, and V. G. Snell, "Severe Accident Phenomena and Research for CANDU Reactors", *Proc. 10th. Pacific Basin Nuclear Conference*, October 20–21, 1996, Kobe, Japan.

[Slovic, 1987] P. Slovic, "Perception of Risk", *Science*, Vol. 236, No. 4799, pp. 280-285, April 1987.

[Smithsonian, 2004] Smithsonian National Museum of American History, *Three Mile Island: The Inside Story*, 2004.

[Snell, 1978] V. G. Snell, "Evolution of CANDU Safety Philosophy", *Proceedings, Canadian Nuclear Society Symposium on CANDU Reactor Safety Design*, November 1978.

[Snell, 1988] V. G. Snell, S. Alikhan, G. Frescura, J. Q. Howieson, F. King, J. T. Rogers, and H. Tamm, "CANDU Safety under Severe Accidents: An Overview", *IAEA/OECD International Symposium on Severe Accidents in Nuclear Power Plants*, Sorrento, Italy, March 1988. Also Atomic Energy of Canada Ltd. Report AECL-9802.

[Snell, 1989] V. G. Snell, J. W. Hilborn, G. F. Lynch, and S. McAuley, "Safety Aspects of District Heating Reactors", invited paper presented to the *IAEA Workshop on the Safety of Nuclear Installations of the Next Generation and Beyond*, Chicago, August 1989.

[Stacy, 2000] S. M. Stacy, *Proving the Principle*, Idaho Operations Office of the Department of Energy, Idaho Falls, Idaho, report DOE/ID-10799, 2000. This is a history of Idaho Nuclear Laboratories. See Chapters 15 and 16 for SL-1.

[StatsCan, 2009] *Leading Causes of Death, Total Population, by Age Group and Sex*, Statistics Canada, 2009.

[Talbot, 2003] E. O. Talbot, A. O. Youk, K. P. McHugh-Pemu, and J. V. Zborowski, "Long-Term Follow-Up of the Residents of the Three Mile Island Accident Area: 1979–1998", *Environmental Health Perspectives*, Vol. 111, No. 3, March 2003.

[TEPCO, 2011] Tokyo Electric Power Company, *Evaluation Status of Exposed Dose of Employees Engaged in Emergency Work in Fukushima Daiichi Nuclear Power Station*, Exhibit, July 13, 2011.

[TEPCO, 2011a] Tokyo Electric Power Company, *Effects of the Earthquake and Tsunami on the Fukushima Daiichi and Daini Nuclear Power Stations*, May 24, 2011.

[Thompson, 1965] T. J. Thompson and J. G. Beckerley, *The Technology of Nuclear Reactor Safety*, MIT Press, 1965.

[Tregoning, 2008] R. Tregoning, L. Abramson, and P. Scott, *Estimating Loss-of-Coolant Accident (LOCA) Frequencies through the Elicitation Process*, United States Nuclear Regulatory Commission report NUREG-1829, April 2008.

[UNSCEAR, 2000] United Nations Scientific Committee on the Effects of Atomic Radiation, *ANNEX J, Exposures and Effects of the Chernobyl Accident*, UNSCEAR 2000 Report to the General Assembly, 2000.

[UNSCEAR, 2001] United Nations Scientific Committee on the Effects of Atomic Radiation, *Hereditary Effects of Radiation*, UNSCEAR 2001 Report to the General Assembly, with Scientific Annex, 2001.

[UNSCEAR, 2008] United Nations Scientific Committee on the Effects of Atomic Radiation, *ANNEX D, Health Effects due to Radiation from the Chernobyl Accident*, UNSCEAR 2008 Report to the General Assembly, 2008.

[USAEC, 1962] U.S. Atomic Energy Commission, Idaho Operations Office, *Nuclear Incident at the SL-1 Reactor*, report IDO-19302, January 1962.

[USAEC, 1962a] U.S. Atomic Energy Commission, *Final Report of SL-1 Recovery Operation*, report IDO-19311, July 1962.

[USAEC, 1962b] U.S. Atomic Energy Commission, *Additional Analysis of the SL-1 Excursion*, report IDO-19313, November 1962.

[USDOE, 1986] U.S. Department of Energy, *Report of the U.S. Department of Energy's Team Analyses of the Chernobyl-4 Atomic Energy Station Accident Sequence*, DOE/NE-0076, November 1986.

[USNRC, 1981] United States Nuclear Regulatory Commission, *Fault Tree Handbook*, Report NUREG-0492, January 1981.

[USNRC, 2001] United States Nuclear Regulatory Commission, *Systematic Radiological Assessment for Source and By-Product Materials,* report NUREG-1717, June 2001.

[USNRC, 2002] A. Howell, *et al*., United States Nuclear Regulatory Commission, *Degradation of The Davis-Besse Nuclear Power Station Reactor Pressure Vessel Head: Lessons Learned Report*, USNRC report, September 30, 2002.

[USNRC, 2011] United States Nuclear Regulatory Commission, *Recommendations for Enhancing Reactor Safety in the 21st Century: The Near-Term Task Force Review of Insights from the Fukushima Dai-Ichi Accident*, USNRC report, July 12, 2011.

[USNRC, 2011a] United States Nuclear Regulatory Commission, *Final Safety Culture Policy Statement*, USNRC report NRC–2010–0282; see Federal Register / Vol. 76, No. 114 / Tuesday, June 14, 2011 / Notices.

[USNRC, 2013] United States Nuclear Regulatory Commission, *Title 10, Code of Federal Regulations, Part 50*, Appendix A, Criterion 54.

[USSR, 1986] USSR State Committee on the Utilization of Atomic Energy, *The Accident at the Chernobyl Nuclear Power Plant and its Consequences,* Information compiled for the IAEA

Experts' Meeting, Vienna, 25-29 August 1986; Parts I and II, August 1986. Also see *Information on the Accident at the Chernobyl Nuclear Power Station and its Consequences*, prepared for IAEA, translation of *Atomnaya Energiya*, Vol. 61, No. 5, pp. 301-320, November 1986.

[Venart, 2004] J. E. S. Venart, "Flixborough: the Explosion and its Aftermath", *Trans IChemE, Part B*, March 2004; *Process Safety and Environmental Protection*, Vol. 82, Issue B2, pp. 105–127, 2004.

[Westinghouse, 2011] Westinghouse, *AP1000 Design Control Document*, Tier 2, Revision 19, Section 15.4.8.2.1.7, USNRC.

[Westinghouse, 2011a] Westinghouse, *AP1000 Design Control Document*, Tier 2, Revision 19, Section 15.6.5.2, USNRC.

[Westinghouse, 2011b] Westinghouse, *AP1000 Design Control Document*, Tier 2, Revision 19, Section 1, USNRC.

[Wren, 1999] J. C. Wren, J. M. Ball, and G. A. Glowa, "The Chemistry of Iodine in Containment", *Nuclear Technology*, Vol. 129, No. 3, pp. 297-325, 2000.

[Wren, 2001] J. C. Wren and J. M. Ball, "LIRIC 3.2—An Updated Model for Iodine Behaviour in the Presence of Organic Impurities", *Radiation Physics and Chemistry*, Vol. 60, 577–596, 2001.

[Xu, 1999] J. Xu, V. S. Krishnan, P. J. Ingham, B. N. Hanna, and J. R. Buell, "Thermal-Hydraulic Design Methods and Computer Codes", *China Journal of Nuclear Power Engineering*, Vol. 20, No. 6, 1999.

[Yaremy, 1979] E. M. Yaremy, "A Review of the Incident at the Three Mile Island Nuclear Power Plant", presented to the *Canadian Electrical Association Thermal and Nuclear Power Section Meeting*, Calgary, Alberta, October 1979.

11 Further Reading

[Duderstadt, 1976] J. J. Duderstadt and L. J. Hamilton, Nuclear Reactor Analysis, New York, NY: Wiley, 1976. ISBN: 9780471223634.

[IAEA, 2001] International Atomic Energy Agency, Thermo-Hydraulic Relationships for Advanced Water-Cooled Reactors, IAEA-TECDOC-1203, April 2001.

[OECD-NEA CSNI, 1989] Thermo-Hydraulics of Emergency Core Cooling in Light Water Reactors, a State-of-the-Art Report (SOAR) by a Group of Experts of the NEA Committee on the Safety of Nuclear Installations, OECD-NEA report Rep. No. 161, Paris.

12 Glossary

AECB	Atomic Energy Control Board
AECL	Atomic Energy of Canada Limited
AOO	Anticipated Operational Occurrence
BDBA	Beyond Design Basis Accident
BEAU	Best Estimate with Analysis of Uncertainties
BECS	Boiler Emergency Cooling System
BWR	Boiling Water Reactor
CHF	Critical Heat Flux
CNSC	Canadian Nuclear Safety Commission
DBA	Design Basis Accident
DBE	Design Basis Earthquake
DSA	Deterministic Safety Analysis
ECC	Emergency Core Cooling
ECI	Emergency Coolant Injection (a subsystem of ECC)
EPR	European Pressurized Reactor
EWS	Emergency Water System
FMEA	Failure Modes and Effects Analysis
HPECC	High-Pressure ECC
HTS	Heat-Transport System (see also RCS)
IAEA	International Atomic Energy Agency
INES	International Nuclear Event Scale
INPO	Institute of Nuclear Power Operations
INSAG	International Nuclear Safety Advisory Group
LLOCA	Large Loss-of-Coolant Accident
LOCA	Loss-of-Coolant Accident
LPECC	Low-Pressure ECC
LWR	Light-Water Reactor
MCR	Main Control Room
MPECC	Medium-Pressure ECC
MSSV	Main Steam Safety Valve

MWe	Megawatt electric
OPG	Ontario Power Generation
PRV	Pressure-Relief Valve
PSA	Probabilistic Safety Analysis
PWR	Pressurized-Water Reactor
R&D	Research and Development
RBMK	Реактор Большой Мощности Канальный (High Power Channel-Type Reactor)
RCS	Reactor Coolant System (see also HTS)
ROP	Regional Overpower (Protection System)
S/C	Suppression Chamber
SCA	Secondary Control Area
SCDF	Severe Core-damage Frequency
SDS	Shutdown System
SG	Steam Generator
SOE	Safe Operating Envelope
SOR	Shut-Off Rod
Sv	Sievert, a unit of radiation dose
TMI	Three Mile Island
USNRC	United States Nuclear Regulatory Commission

13 Appendix 1 – Basic Rules of Boolean Algebra

This is a quick refresher in the basics of Boolean logic.

Boolean algebra is a set of laws formulated by the British mathematician George Boole. It deals with statements (here represented by A, B, C, etc.) which can be either true or false and are often denoted by the numbers 1 and 0 respectively. So, for example, A=0 means that the statement A is false.

For example, let A represent the statement, "the sun is the centre of the universe". Then A=0.

13.1 Operators

Several operators can act on these statements:

AND is an operator which gives the answer C=1 only if *both* of its inputs are 1, and 0 otherwise. It should be represented as:

A.B or AB or A·B or A$\cap$ B or A.AND.B, or graphically as in Figure 69.

It can be thought of as the intersection of sets A and B.

Examples:

If A is true and B is true, then A$\cap$ B should be true.

If A=1 and B=0, then A.B=0.

Figure 69 AND gate

OR is an operator which gives the answer C=1 only if *either or both* of its inputs are 1, and 0 otherwise. It is represented as:

A+B or A$\cup$ B or A.OR.B, or graphically as in Figure 70.

It can be thought of as the union of sets A and B.

Examples:

If A is true and B is false, then A$\cup$ B is true.

If A=1 and B=0, then A+B=1.

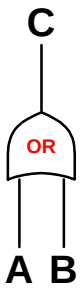

Figure 70 OR gate

NOT is an operator which inverts the input.

It is represented as .NOT.

The output of .NOT.A is denoted as A' or $\bar{A}$.

It is represented graphically as in Figure 71.

It can be thought of as "the opposite of" or "the complement of" set A.

Examples:

If A is true, then .NOT.A is false.

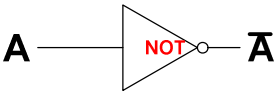

Figure 71 NOT gate

There are also four lesser-used operators (.NAND., .NOR., .XOR., and .XNOR.)

13.2 Basic Principles

A=0 or A=1

(i.e., something can only be true or false, not both)

If A=0, $A \cap A=0$

(i.e., if A is false, and because $A \cap A=A$, then $A \cap A$ is false. Sometimes this is written as 0.0=0)

If A=1, $A \cup A=1$

(i.e., if A is true, and because $A \cup A=A$, then $A \cup A$ is true. Sometimes this is written as 1+1=1. Remember, you are not doing arithmetical addition!)

If A=0, then $A \cup A=0$

(This is obvious if you think of set theory as we did above. Sometimes it is written 0+0=0).

If A=1, then $A \cap A=1$

Again, obvious from set theory; also written 1.1=1

If A=1 and B=0, then $A \cap B = B \cap A = 0$

(i.e., if A is true and B is false, then the intersection of A and B can never be true, and vice versa. Sometimes this is written as 1.0 = 0.1 = 0)

If A=1 and B=0, then $A \cup B = B \cup A = 1$

(i.e., if either one of A or B is true, then the union of A and B (A.OR.B) is always true. This can be written 1+0 = 0+1 = 1)

13.3 Theorems

These sound abstract, but are obvious once you draw Venn diagrams with set-theory symbols. You can substitute the mathematical symbols + and · for $\cup$ and $\cap$ if this is more intuitive for you.

Commutative Law

$A \cup B = B \cup A$

$A \cap B = B \cap A$

Associative Law

$(A \cup B) \cup C = A \cup (B \cup C)$

$(A \cap B) \cap C = A \cap (B \cap C)$

Distributive Law

$A \cap (B \cup C) = (A \cap B) \cup (A \cap C)$

$A \cup (B \cap C) = (A \cup B) \cap (A \cup C)$

Identity Law

$A \cap A = A$

$A \cup A = A$

Completeness

$(A \cap B) \cup (A \cap \overline{B}) = A$

$(A \cap B) \cap (A \cap \overline{B}) = A$

Redundancy

$A \cup (A \cap B) = A$

$A \cap (A \cup B) = A$

Mathematical

$1 + A = 1$

$1 \cdot A = A$

$0 + A = A$

$0 \cdot A = 0$

$A + \bar{A} = 1$

$A \cdot \bar{A} = 0$

$A + \bar{A}B = A + B$

$A(\bar{A} + B) = A \cdot B$

DeMorgan's Theorem

$$\overline{(A+B)} = \bar{A} \cdot \bar{B}$$

$$\overline{(A \cdot B)} = \bar{A} + \bar{B}$$

These will be useful when you work out fault trees mathematically.

13.4 Combining Probabilities

If event A occurs *x* times out of *n* repeated experiments, then:

$$P(A) = \text{Probability of event A} = \lim_{n\to\infty} \frac{x}{n} \tag{59}$$

Obviously:

$$0 \le P(A) \le 1$$
$$P(A) + P(\bar{A}) = 1 \tag{60}$$

In other words, an event must either occur or not occur; there is no third possibility.

13.4.1 Probability of both events occurring

A_1A_2 means that *both* events occur, and therefore $P(A_1A_2)$ is the probability that both events occur. The product rule for probabilities states that:

$$P(A_1A_2) = P(A_1 \mid A_2)\, P(A_2) = P(A_2 \mid A_1)\, P(A_1). \tag{61}$$

For example, if A_1 is the probability that part 1 fails and A_2 is the probability that part 2 fails, then

$P(A_1A_2)$ = probability that both part 1 fails and part 2 fails

= probability that part 2 fails × (probability that part 1 fails, given that part 2 fails)

= probability that part 1 fails × (probability that part 2 fails, given that part 1 fails).

Because probabilities are numbers, the × does mean simple multiplication in these equations. It is conventionally omitted; i.e., $P(A_1)P(A_2)$ is understood to mean $P(A_1) \times P(A_2)$.

The *conditional probability* $P(A_1 \mid A_2)$ means the probability of event A_1 given that event A_2 has

occurred.

Figure 72 shows this graphically; yellow represents all events; green those events with outcome A_1; blue with outcome A_2; red, with outcome *both* A_1 and A_2.

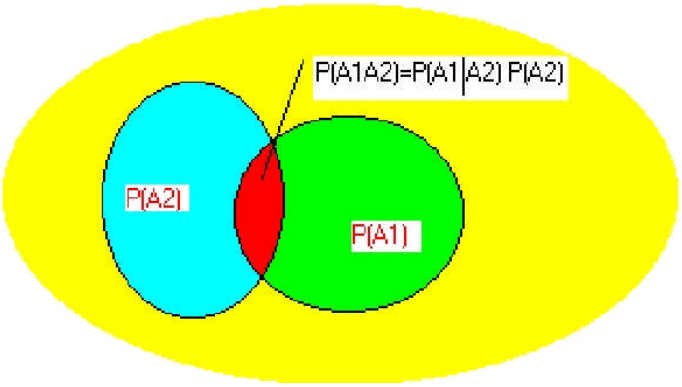

Figure 72 Probability of both of two events

If the events are independent,

$$P(A_2 \mid A_1) = P(A_2). \tag{62}$$

In general:

$$P(A_1A_2...A_N) = P(A_1)P(A_2|A_1)...P(A_N|A_1...A_{N-1}). \tag{63}$$

If events are independent:

$$P(A_1A_2...A_N) = P(A_1)P(A_2)...P(A_N). \tag{64}$$

13.4.2 Probability of either event occurring

The *union* of two events, A_1 and A_2, is denoted as:

$$A_1 \cup A_2 \text{ or } A_1 + A_2 \text{ or } A_1 \text{ OR } A_2.$$

This means the cases where *either* event occurs, including cases where *both* events occur. Note that:

$$P(A_1 + A_2) = P(A_1) + P(A_2) - P(A_1A_2). \tag{65}$$

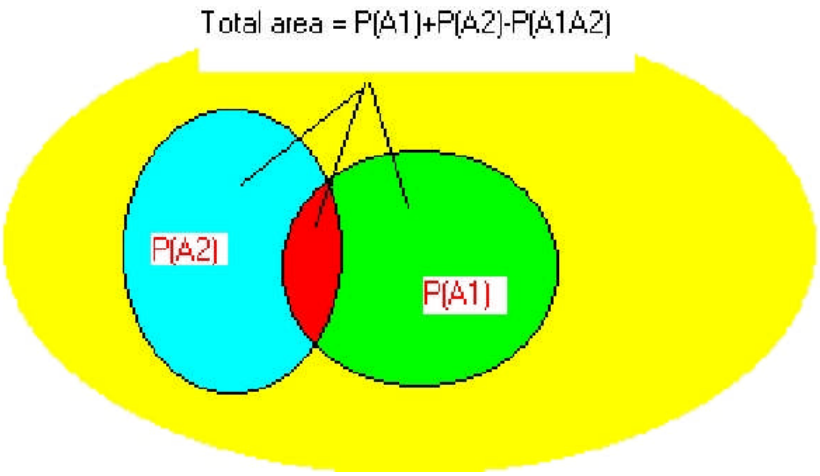

Figure 73 Probability of either of two events

as shown in Figure 73. Note that the + sign on the left of this equation is not the same as the + sign on the right: the former refers to the union of two sets, the latter to arithmetic addition. The reason for subtracting $P(A_1A_2)$ is that what you want is the total area encompassed by the combination of the blue and green ovals in the diagram. If you simply add $P(A_1)$ and $P(A_2)$, you count the intersection where both events occur (in red) twice. Therefore, you have to subtract one of them away.

In general:

$$P(A_1 + A_2 + \ldots + A_N) = \sum_{n=1}^{N} P(A_N) - \sum_{n=1}^{N-1} \sum_{m=n+1}^{N} P(A_n A_m) \pm \ldots + (-1)^{N-1} P(A_1 A_2 \ldots A_N). \quad (66)$$

If events are independent:

$$1 - P(A_1 + A_2 + \ldots + A_N) = \prod_{n=1}^{N} [1 - P(A_N)]. \quad (67)$$

13.4.3 Rare independent events

Assuming (as is often but not always the case for nuclear failure probabilities) that the events are both independent and rare, or $P(A_N) \ll 1$, then:

$$P(A_1 + A_2 + \ldots + A_N) \approx \sum_{n=1}^{N} P(A_N). \quad (68)$$

14 Appendix 2 – Common-Cause Failures – An Example

Consider two shut-off rods, each of which has a probability of failure of 0.001 per demand. What is the probability that they both fail when required?

If they are independent, then P(A1A2) = P(A1)P(A2) = $(0.001)^2 = 10^{-6}$ per demand.

Suppose that a common-cause (CC) failure occurs 10% of the time. That is:

P(A1) = P(A2) = 0.0009 (random) + 0.0001 (CC),

and therefore the probability of one rod failing *given that the other has failed* is 90% random and 10% common cause (with probability 1):

P(A1|A2) = 0.9 * 0.001 + 0.1 * 1 = 0.1009

or

P(A1A2) = P (A_1 | A_2) P (A_2) = 0.1009 * 0.001 = 0.0001009 ~ 10^{-4}.

Therefore, a 10% common-cause probability has increased the combined probability of failure by a factor of 100.

15 Appendix 3 – Why a Reactor Cannot Explode Like an Atomic Bomb

This Appendix provides further technical detail on the difference between a nuclear weapon and a reactor power excursion that is not shut down. It assumes that you have read the reactor physics Chapter. Some material is taken from [Meneley, 2003]. All material is in the public domain.

Assume a pure plutonium core surrounded by a shaped charge of high explosive. The core is initially subcritical and is rendered supercritical by compression from the explosive. The neutron kinetics follows the familiar equation (delayed neutrons are irrelevant here):

$$\frac{dN(t)}{dt} = \frac{\rho - \beta}{\ell} N(t), \tag{69}$$

where *N(t)* is the neutron density, ρ is the reactivity, β is the delayed neutron fraction, and ℓ is the prompt neutron generation time.

Solving,

$$N(t) = N(0)e^{(\frac{\rho-\beta}{\ell})t}. \tag{70}$$

For a weapon, a typical value of ρ - β is ~1.7 (so that β is pretty well irrelevant). Because criticality is achieved by fast, not thermal fission, ℓ is about 10^{-8} seconds or one "shake". The *e*-folding time (when the population of neutrons increases by a factor of 2.7) is therefore 1.7 shakes. After 33 shakes, the number of neutrons is:

$$N(33\times10^{-8}) = 1\times e^{1.7\times10^{8}\times33\times10^{-8}} = 2.3\times10^{24}. \quad (71)$$

Using *very* crude assumptions, such as not adding in the contribution of previous generations of neutrons and not counting energy losses and core expansion, we can estimate the order of magnitude of the energy produced. If each fission event generates 180MeV of usable energy, and if for each incident neutron absorbed in Pu^{239}, two fast neutrons are produced, the number of neutrons in Equation (71) is accompanied by an energy release at 56ns of:

$$E = 2.3\times10^{24}\,neutrons\times0.5\,fissions/neutron\times180Mev/\ fission\times\frac{1kT}{2.6\times10^{25}\,MeV} = 8kT\ , \quad (72)$$

where *kT* is kilotons of TNT equivalent. This is 34×10^6MJ.

The reaction is self-limiting because the thermal energy causes the core to expand rapidly and stops the chain reaction.

By contrast, in a thermal reactor such as CANDU, the largest ρ - β (from a large LOCA) is about 0.011; ℓ is about 0.001 sec. The timescale is measured in tens of seconds rather than nanoseconds, and the reaction is terminated by damage to the core lattice after about ten seconds, with an energy input of ~50 full-power seconds. The total energy produced for an 1800MWth reactor is therefore 9×10^4 MJ, or more than two orders of magnitude smaller than the value for a bomb.

16 Acknowledgments

We gratefully thank the following reviewers for their hard work and excellent comments during the development of this Chapter. Their feedback has much improved it. Of course the responsibility for any errors or omissions is entirely the author's.

Glenn Archinoff
Glen McGee
Dan Meneley
Terry Rogers

We also thank Diana Bouchard for expertly editing and assembling the final copy.

CHAPTER 14

Nuclear Plant Materials and Corrosion

prepared by
Dr. Derek H. Lister and Dr. William G. Cook
University of New Brunswick

Summary:

The choice of materials of construction of a nuclear reactor, while important in terms of plant capital cost, is crucial to the safe and economic operation of the unit throughout its design lifetime; it also affects decisions about plant life extension. Most of the failures of nuclear systems involve the degradation of materials as they interact with their environments, indicating that chemistry control within systems should be formulated as materials are selected. All of the three major process systems of a CANDU reactor – the primary coolant, the moderator and the secondary coolant – have a variety of materials of construction, so the control of system chemistry in each is a compromise based on the characteristics of the interactions between the system materials and the environment, including the effects of irradiation on both the material and the coolant or moderator. Ancillary systems, such as those providing condenser cooling water or recirculating cooling water, have similar constraints on material choice and chemistry control. Components such as concrete structures, cabling and insulation, although not necessarily associated with process systems, may also be critical to safety or plant operation and must have their materials chosen with care. This chapter describes the materials of construction of the main systems and components of a CANDU reactor and shows how they interact with their environments.

Table of Contents

List of Figures

List of Tables

1 Introduction

The performance of power-producing systems has always been limited by the properties of engineering materials and their interactions with the environment. Since the early days of industrial steam generation in the seventeenth and eighteenth centuries, for example, the ever-increasing need for power for new factories created a steady demand for larger boilers and increasingly severe steam conditions. Materials selection was based on limited knowledge of corrosion, especially stress corrosion cracking as the consequence of chloride and oxygen contamination of the water used in the boilers and catastrophic failures of equipment occurred frequently.

As late as the end of the nineteenth century, hundreds of steam plant explosions accompanied by large numbers of casualties were being recorded every year in Europe and North America. The causes were generally linked to the failure of riveted joints or poorly worked steel plate in fire-tube boilers. The innovation of the water-tube boiler and the understanding of localized corrosion of steels in high-temperature water were major factors that led to much safer equipment - even as operating conditions continued to become more severe. The major consequence of these failures was the development of codes and standards for pressure retaining components, the ASME Pressure Vessel Code in North America for example, which dictate the acceptable design and construction practices for materials produced to particular specifications.

Today, the risk of catastrophic failure of a power-producing system is low. This can be attributed to the strict adherence to the standards that are imposed on component designers and manufacturers as well as on plant operators. The setting of these standards clearly involves a thorough knowledge of the properties of the materials of construction and an understanding of their behaviour in the local environment. That environment may itself be adjusted for overall optimum performance by specifying optimum chemistry control strategies. The prime example of such chemistry control is the specification of an alkalinity level in the feedwater systems of steam-raising plants, including nuclear secondary coolants, which is necessary to minimize corrosion of piping and components and to keep systems clean of dissolved and particulate corrosion products and impurities. In a nuclear reactor core, materials must be able to withstand not only the operational conditions (pressure, temperature and water chemistry) but must show minimal degradation from the effects of radiation (high gamma and neutron flux). Radiation effects on materials may include loss of ductility, shape change from radiation enhanced creep and growth and enhanced corrosion resulting from hydrogen ingress (deuterium ingress for the case of heavy water systems).

While the current performance record of power plants is generally good, technology is not standing still. The push for bigger returns on capital investment and the accompanying trends towards higher plant efficiencies and longer component lifetimes lead to even more severe operating conditions in power systems. Inevitably, the demands on the materials of construction escalate. The predominant materials of construction in steam-raising equipment and nuclear systems are the metals and alloys. Their interaction with the operating environment very much dictates the chemistry control to be practised by plant operators.

2 Materials for Nuclear Applications

As described above, materials of construction for nuclear applications must be strong, ductile and capable of withstanding the harsh environment to which they are subjected. Furthermore, for materials used in the core of a nuclear reactor, it is important that they have specific properties such as low neutron absorption and high resistance to radiation-induced creep, hardening and the associated loss of ductility so that reactors can operate for the decades expected by plant owners. Thus, nuclear materials must be selected or specified based upon their strength and interactions with the environment (including the effects of radiation), all of which are dependent upon the metallurgy of the material.

2.1 Metallurgy and Irradiation Effects

2.1.1 Crystal Structure and Grain Boundaries

All metals used in power plant construction are crystalline in nature, meaning that they have a defined and consistent crystal structure. Three of the basic and most observed crystal structures are shown in

Figure 1, namely: face-centred cubic (FCC), body-centred cubic (BCC) and hexagonal close-packed (HCP). Upon cooling from a melt during the production of a metal or alloy, individual crystals nucleate and coalesce as the material solidifies. As the individual crystals grow together they eventually meet and combine as an assemblage of crystal grains, which will likely not have the same orientation of the crystal lattice. This leads to the development of grain boundaries in the material, where the atoms along the boundary between the two grains have elongated metallic bonds leading to slightly elevated boundary energies than those within the bulk of the individual crystal. The grain boundaries are thus slightly more active than the individual grains and can act as diffusion short-circuits or locations for the development of precipitates such as carbides. The materials used in nuclear power plants are thus termed polycrystalline due to the grain/grain-boundary structure.

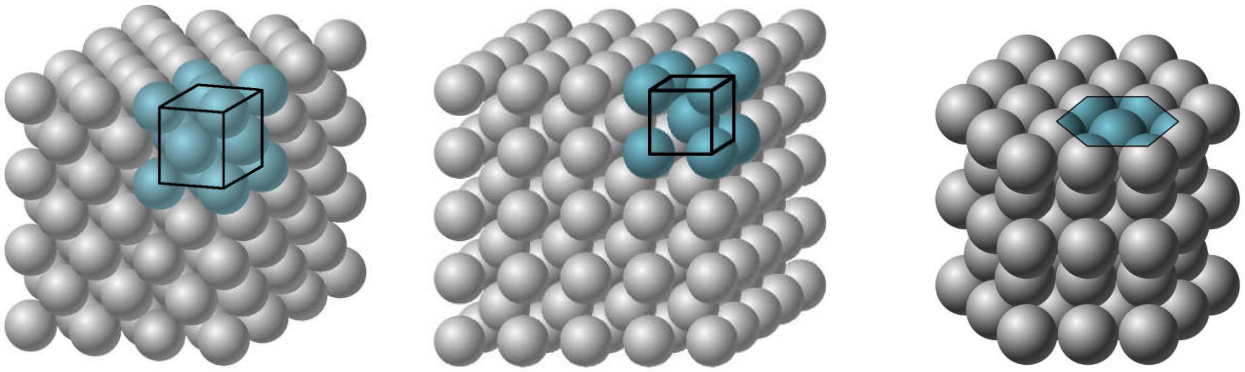

(a) FCC structure (b) BCC structure (c) HCP structure

Figure 1. Unit cell configurations of some common metallic crystal structures (after Callister)

The grains of a metal or alloy may be engineered through appropriate heat treatments (hot and cold working and annealing for example) to be of a specific size and/or orientation to meet a specified purpose. Small-grained metals (1 – 25 μm) will have more grain boundaries and may be more affected by phenomena such as high-temperature creep or radiation-induced creep. Examples of the metallurgy and microstructure of ferritic steel, austenitic stainless steel and zirconium are shown in Figure 2. Note that the grain structure, size and orientation may play significant roles in the specific materials properties such as strength, conductivity and creep resistance.

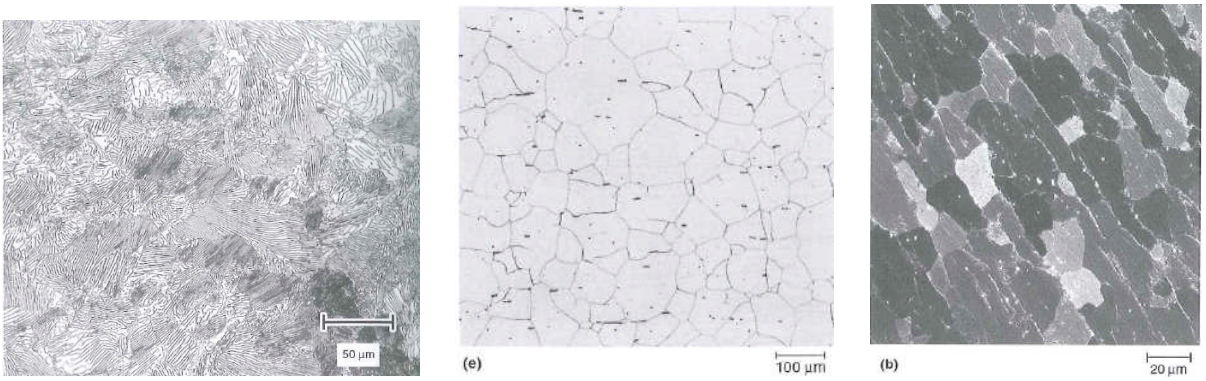

Figure 2. Grain structure for low-alloy (UNS G10800), austenitic (316 SS) steels and Zircaloy 4 (ASM, 2004).

2.1.2 Irradiation effects on materials

The effects of irradiation on materials may be manifest in several ways, the most dramatic being the dislodging or dislocation of a random atom in the crystal lattice to a new location. During neutron bombardment, the energy dissipated by the neutron upon collision with a metal atom can create new defects in the crystal structure, typically "interstitial" sites where the dislocated atoms come to rest between the regular bonding sites in the crystal structure and "vacancy" sites left where the atoms were originally stationed. The pair (interstitial/vacancy) is termed a Frenkel pair and is a key phenomenon associated with radiation damage in polycrystalline materials. The damage induced in the material is additive and substantial, considering that in a CANDU reactor the overall neutron flux may be $2x10^{17}$ neutrons/m^2s and the flux in enriched reactors (light water reactors, breeders etc.) may be several times higher. Radiation damage is typically measured in "displacements per atom" (dpa) and the dose can be as high as 10 – 30 dpa after 30 years of operation.

The fact that neutron bombardment creates interstitials and vacancies within the material gives rise to changes in the physical dimensions and the mechanical properties of the material when placed under stress. The creation of vacancies within the material leads to swelling, elongation and growth whereas production of interstitials can cause the material to shrink. The energy

dissipated by radiation may induce phase changes within the material or promote segregation of alloying constituents, both phenomena will affect the material's strength and ductility. Overall, the mechanical properties and dimensions of a material under irradiation will change and the effect ultimately leads to challenges for the integrity of the components that make up a nuclear reactor. Each mechanical effect is described briefly below, more details can be found in Fundamental of Radiation Materials Science (Was, 2007).

Irradiation Hardening

When a polycrystalline material is placed under stress it will stretch elastically with increasing stress/strain up to the yield point of the material. Additional strain beyond the yield strength leads to plastic deformation whereby the original shape and dimensions of the material can no longer be attained with the relaxation of the strain. Plastic deformation, at the atomic level, is induced when the atoms in the crystal lattice slip, which typically occurs on slip planes in the matrix. When a material is irradiated by particles (neutrons) producing Frenkel pairs, the effect of the interstitital/vacancy sites is to provide barriers to the normal slip planes within the material. This effectively increases the yield strength, which will increase continuously in proportion to the increasing radiation dose (dpa). Figure 3 shows the effect of neutron irradiation on the yield stress/strain for materials with the FCC and BCC crystal structures [Was, 2006].

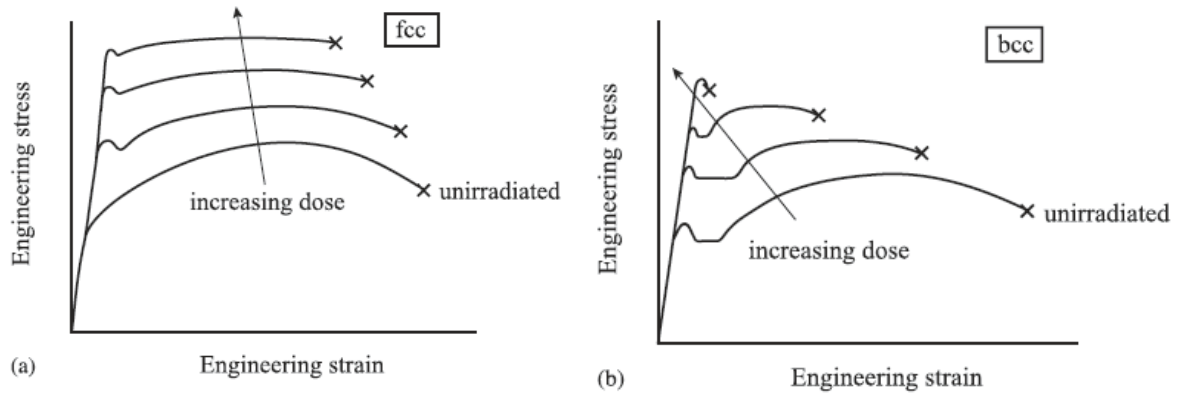

Figure 3. Effect of neutron irradiation on the stress/strain properties of materials with cubic crystal structures (after Was, 2006).

Irradiation Creep and Growth

All metals will exhibit creep over time when exposed at high temperatures and under operational stress. Thermal creep is a diffusion-based migration of atoms and vacancy sites within the metal's lattice, which typically requires a minimum operating temperature before its effects are observed – generally the operating temperature must be greater than $0.3T_m$, where T_m is the melting temperature of the metal. Since diffusion is the primary mechanism at play for thermal creep it typically increases exponentially with increasing temperature following an Arrhenius law. As described above, particle bombardment or irradiation of a metal creates interstitials and vacancies within the metal's lattice, effectively mimicking the effects of thermal creep of the metal only occurring at much lower temperatures than those required for significant thermal

creep alone. Since the diffusion rates of vacancies and interstitials are unaffected by irradiation (diffusion is a temperature dependent phenomenon), irradiation creep is more complex in its mechanism and involves the preferential absorption of interstitials under the action of strain in the material and phenomena such as the "climb and glide" of the dislocations over barriers to the diffusion process. Irradiation creep is preferential in directions perpendicular to the applied stress i.e. pipes will tend to elongate due to irradiation creep.

For materials that do not have a cubic crystal structure (zirconium being the most relevant with an HCP structure below 862^{o}C), grain distribution and orientation (described as the material's texture) play significant roles in irradiation creep and growth. The distinction made between creep and growth is that the former is the elongation of a material under applied stress while the latter occurs even when no external stress is applied. The material's texture gives rise to anisotropy in the preferred crystallographic planes by which the material will stretch under an induced strain as well as grow in a preferred direction during creep. Thus, the creep characteristics of non-cubic crystal materials (zirconium and zirconium alloys) are highly dependent upon the applied stress as well as the operational temperature.

Irradiation Embrittlement

As a metal gains strength upon particle irradiation, it will also tend to lose its ductility, becoming hard and brittle with increasing damage and radiation dose. The material's yield strength increases through build-up of dislocations along barriers to atom migration, but other effects such as the precipitation of secondary and tertiary phases within the material can change the mechanical properties dramatically. Materials that are typically ductile and not susceptible to brittle fracture in an un-irradiated environment may cleave and fracture excessively upon irradiation due to the increasing hardness and loss of ductility.

2.2 Materials of Construction

2.2.1 Zirconium

Zirconium is the eleventh most abundant element in the earth's crust making it more prevalent than the common transition metals copper, lead, nickel and zinc. It occurs naturally as the minerals zircon (zirconium silicate – $ZrSiO_4$) and zirconia (zirconium oxide – ZrO_2) and always in conjunction with 0.5 – 2.5% hafnium (Hf), a metal that has very similar chemical and physical properties making it difficult to separate the two elements. Zirconium or, more specifically, the alloys fabricated from it are the most important of the nuclear reactor materials. They are resistant to corrosion in many process environments, nuclear heat transport systems in particular, and they have excellent nuclear properties making them the predominant materials for construction of in-core components (fuel sheathing, pressure tubes and calandria tubes). Zirconium itself has a neutron absorption cross-section of 0.18 barns, making it nearly transparent to the thermal neutrons in a water-cooled and -moderated reactor. Zirconium alloys used in nuclear reactors must be highly processed to keep the hafnium concentration below 100 ppm since its neutron absorption cross-section is 102 barns, nearly 600 times that of zirconium. Higher concentrations of hafnium would increase the parasitic absorption of neutrons in the

reactor core and reduce the fuel burn-up. Pure zirconium has an HCP structure that transforms to BCC at 862°C before melting at 1850°C. It is a reactive metal that combines easily with oxygen, hydrogen, nitrogen, carbon and silicon and in air retains its metallic lustre because of a very thin but protective zirconia (ZrO_2) oxide layer. A protective but thicker zirconia layer is retained during exposure to high-temperature water, making zirconium alloys ideal for service in water-reactor cores. The pure metal is alloyed with small amounts of elements such as tin, chromium, iron, nickel and niobium to improve mechanical strength, corrosion resistance and to reduce hydrogen pickup. In CANDUs, the alloy Zircaloy-2 is used for the calandria tubes and was the initial choice as the pressure tube material. Zircaloy-2 contains 1.2 – 1.7 weight percent Sn, 0.07 – 0.2 weight percent Fe, 0.05 – 0.15 weight percent Cr and 0.03 – 0.08 weight percent Ni. It is also the material used for BWR fuel cladding. For fuel sheathing in CANDUs and fuel cladding in PWRs, Zircaloy-4 was developed and used because it was observed to have a lower overall corrosion rate and a reduced tendency to pick up hydrogen. It has a similar composition to that of Zircaloy-2 except for the nickel content, which is reduced to a maximum of 0.007 weight percent, and the iron content, which is increased to 0.18 – 0.24 weight percent. The compositions of zirconium alloys used in CANDU reactors are shown in Table 1. Comparatively recent developments in fuel cladding technology for PWRs are the Westinghouse alloy ZIRLO, which contains 0.7 – 1.0 weight percent Sn and 1.0 weight percent Nb, and the Areva variant M5, which has no Sn and 0.8 – 1.2 weight percent Nb. A Zr-1%Nb alloy was developed and used for decades as the fuel cladding material in the Russian VVERs and the Westinghouse and Areva alloys are modifications from the original Russian composition. They are reputedly more corrosion-resistant and have lower hydrogen pick up than Zircaloy-4 under high fuel burn-up. Similarly, for BWR cladding, Westinghouse has developed the alloy ZrSn, which is Zr with 0.25 weight percent Sn. The pressure tubes in CANDUs are made of Zr-2.5%Nb, an alloy of Zr and Nb with the latter within the range 2.4 – 2.8 weight percent. This too is a modification of Russian alloys developed for the RBMK reactors.

Table 1. Compositions of commonly used zirconium alloys in CANDUs.

Common designation	UNS #	chemical composition (wt%)						
		Sn	Nb	Fe	Cr	Ni	O (ppm)	Hf (ppm)
Zr 702	R60702			Fe + Cr < 0.2			< 0.16%	4.5%
Zircaloy 2	R60802	1.2-1.7		0.07-0.2	0.05-0.15	0.03-0.08	1200-1400	100
Zircaloy 4	R60804	1.2-1.7		0.18-0.24	0.07-0.13	0.03-0.08	1200-1400	100
Zr-2.5%Nb	R60901		2.4-2.8				1200-1400	100

2.2.2 Steels

Carbon Steels

The most widely used materials in power-producing systems are the steels, which are basically alloys of iron and carbon but which may also contain other metals as minor or major alloying elements. The alloying elements impart desired properties such as strength, hardness or corrosion resistance to the steel.

Pure iron at ambient temperatures has a body-centred cubic (BCC) crystal structure, in which the atoms making up the unit cell of the crystal lattice are conveniently pictured as occupying the corners of a cube with an atom at the cube centre. Figure 1 shows illustrations of unit cell configurations of typical metals. The BCC phase is called α-iron or ferrite, which in pure iron is stable below 912°C. Above this temperature the γ-iron or austenite phase with a face-centred cubic (FCC) crystal structure is stable up to 1394°C. The FCC unit cell has an atom at each corner of a cube and one at the centre of each face as shown in Figure 1. Above 1394°C another BCC phase, δ-iron, is stable up to the melting point at 1538°C. The relatively small atoms of carbon that can exist in solid solution in these structures are in random interstitial positions between the iron atoms. The carbon concentration determines the stability limits of the phases.

As the portion of the iron-carbon phase diagram that is pertinent to steels indicates, carbon has a low solubility in ferrite. Figure 4 illustrates the iron-carbon phase diagram, in which the regions of stability of the different steel phases are shown in terms of their composition and temperature. The maximum in ferrite is 0.02 weight percent and occurs at a temperature of 727°C. At temperatures much above and below this, the solubility declines to almost zero. The common carbon steels, however, have carbon contents ranging up to about 2.0 weight percent, and they are quite stable at temperatures below 727°C. To accommodate the carbon, these steels are composed of more phases than just the ferrite. As the phase diagram indicates, for carbon contents up to 6.7 weight percent, which is the amount of carbon in the compound Fe_3C (iron carbide or cementite), two distinct phases exist together in equilibrium - ferrite and cementite. The proportions depend upon the overall amount of carbon in the mixture but are not affected much by temperature below the 727°C region.

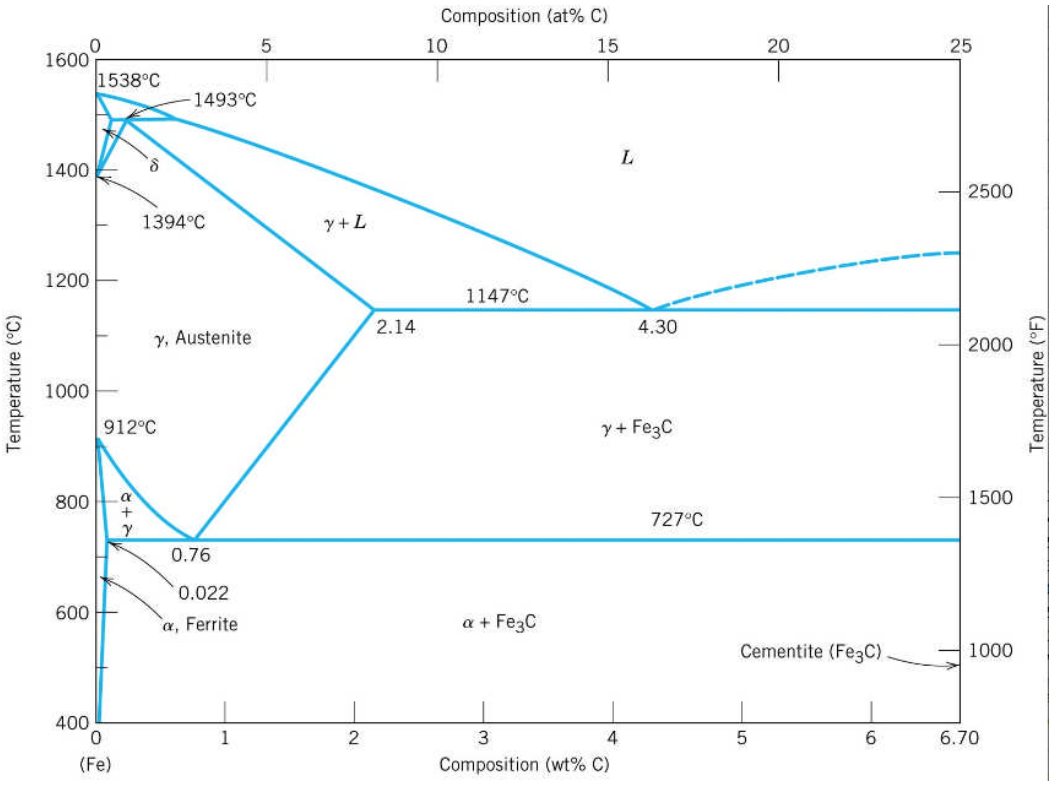

Figure 4. Partial iron-carbon phase diagram (after Callister)

In the aggregate of metal grains and intercalating grain boundaries that make up a carbon steel, some grains may be ferrite or cementite and some will be a two-phase ferrite-cementite composite. The composite grains are formed from alternating microscopic layers or lamellae of ferrite and cementite in a structure called pearlite. The size of the grains, the proportions of the different phases, and the details of the pearlite structure govern the mechanical properties of the steel. In general, higher carbon contents produce steels that can be made stronger and harder by heat treatment and mechanical working to control grain structure and properties. At carbon contents above the 2 weight percent value, however, the material enters the range of the cast irons and starts to become brittle and lose properties such as ductility and toughness that are important for many power plant applications. For most boiler applications and piping in general, steels with carbon contents of 0.20 weight percent or less are employed. Equipment such as pumps, valves, turbine components etc. requiring stronger or harder material commonly use steels with carbon contents up to 0.50 weight percent or more.

The phase diagram in Figure 4 indicates that the high-temperature γ-phase of iron, austenite, can contain a relatively large amount of carbon in solid solution - up to 2.1 weight percent at 1148°C. This is because the FCC structure of austenite, although having a higher atomic packing fraction than the BCC structure of ferrite (0.74 versus 0.68), has more interstitial sites to accommodate the small carbon atoms (by contrast, the more open structure of BCC leads to higher rates of solid-state diffusion). Note that austenite is stable down to the eutectoid temperature 727°C, below which it transforms into the lamellar pearlite. A heat treatment may then consist of heating a carbon steel to a temperature that puts it in the austenite region, where the carbon is completely miscible. Cooling at a controlled rate to below 727°C will then

promote the transformation to pearlite, pearlite-ferrite or pearlite-cementite, depending upon whether the total amount of carbon is respectively equal to, less than or greater than the eutectoid composition of 0.77 weight percent.

If, during the heat treatment, the austenitized steel at high temperature is cooled suddenly or quenched (by plunging into cold water, oil, etc.) rather than cooled in a slow controlled fashion, a different phase called martensite is produced. This has a body-centred tetragonal (BCT) crystal lattice, the unit cell of which can be viewed as a BCC structure stretched in the direction of one of the cube axes as shown in Figure 1. Carbon atoms can then be accommodated in interstitial positions between iron atoms in the direction of elongation or in the centres of the basal planes and can thereby stay in solid solution. Martensite is a very hard, strong but quite brittle material that has a metastable structure (and therefore does not appear on the phase diagram, which shows equilibrium states only). It nonetheless survives indefinitely at ambient temperature.

The formation of martensite can impart very useful properties to steel. Thus, by selective austenitizing, quenching and then tempering for a given period at temperatures near the eutectoid point (727°C), the amount of martensite in a steel can be controlled and a hard, strong material that is not too brittle can be obtained. Other iron-carbon phases called bainite and spheroidite are also formed during selective heat treatments to produce steels with specific characteristics of strength, ductility and toughness.

Alloying elements

Metals other than iron may be added to steel to impart desired mechanical properties or corrosion resistance - particularly useful for service at high temperature. The atoms of alloying metals are generally in substitutional solid solution, meaning that they take the place of iron atoms in the crystal lattice. If the metal addition is less than 5 weight percent what is commonly called a low-alloy steel results, while additions greater than 5 percent produce the intermediate- and high-alloy steels. Note, however, that the plain carbon steels often contain small amounts of elements such as manganese, phosphorus or sulphur - generally less than 1 weight percent - as residuals from the steelmaking process or they may be added for specific reasons such as improved machinability. Manganese in particular can impart desirable mechanical properties to steel and in fact may be added deliberately to form low-alloy manganese steel with a marked resistance to wear. Table 2 shows the typical compositions of various steels and stainless steels commonly used in CANDUs.

Plain carbon steel and manganese steel are used extensively for general construction steelwork in power systems and in non-nuclear boiler construction for tubing and components that experience temperatures below about 500°C. They are also employed in the secondary or steam-raising systems of nuclear power plants and constitute a major proportion of the piping in the primary coolant systems of heavy water reactors such as the CANDU reactor, which operate below about 320°C, and for steam generator tubes and piping in carbon-dioxide-cooled Magnox reactors, which operate below about 360°C. As the service temperature increases the amount of alloying is necessarily increased to impart resistance to creep and scaling. For example, boiler superheater tubes operating at temperature up to 580°C are made of alloys such as 23 weight

percent Cr, 1 percent Mo or even 9 percent Cr, 1 percent Mo. For still higher temperatures, the use of these low- or intermediate-alloy ferritic steels would require excessive wall thicknesses to withstand high pressures and to offset scaling, and their cost advantage would be lost. The highly alloyed materials - in particular, the austenitic stainless steels, "super alloys" and Ni-Cr-Fe alloys such as the Inconels and Incoloys - are therefore employed.

Stainless steels

The addition of small amounts of selective elements such as copper or chromium to steel can impart substantial resistance to corrosion, so that some of the low-alloy steels have superior performance to plain carbon steel in atmospheric environments. True passivity in single-phase water systems, as achieved with the stainless steels, requires at least 12 weight percent of chromium as an alloying element. At least 20 weight percent chromium is required for true passivity in high-temperature gaseous oxidation. [Birks, 2006]

The stainless iron-chromium alloys are basically ferritic with a BCC crystal structure. They typically have chromium contents of 12-25 weight percent with about 1 percent manganese and silicon and up to 0.2 percent carbon, to which other elements such as the strong carbide-formers molybdenum, vanadium and niobium are added to enhance properties such as creep resistance. Like the carbon steels they can be heat-treated and conditioned, depending upon their content of carbon and other elements, to provide desired properties of strength, hardness and toughness. There are also grades that are commonly used in the martensitic condition, which typically contain 12-20 weight percent chromium, up to 1.0 percent carbon and often 1-2 percent nickel or up to 1.0 percent molybdenum.

The stainless steels used for corrosion resistance and for highest temperature service in power systems are the austenitic grades. For example, the cladding for the fuel sheaths in the carbon-dioxide-cooled AGR nuclear reactor, operating at temperatures up to about 650°C, is a 20 weight percent chromium, 25 percent nickel-niobium stainless steel. The Russian design of pressurized water reactor, the VVER, also uses austenitic stainless steel for the steam generator tubes operating below about 320°C. Austenitic steels have the FCC structure, which is stabilized at low temperature by the presence of nickel at concentrations between about 6 and 20 weight percent. Resistance to corrosion is again provided by the chromium, which is added at a concentration between 16 and 30 weight percent. For most power plant applications, stainless steels based on the common 18-8 or 18-12 (18 weight percent chromium and 8 percent or 12 percent nickel) grades are employed. In the designation of the American Society for the Testing of Materials (ASTM) they are types 304 and 320, respectively, of the general 300-series austenitic grades. Manganese is usually present at 2 weight percent and carbon at up to 0.2 percent, though special low-carbon grades with less than 0.03 percent carbon are available when a particular resistance to the deterioration of heat-affected regions such as welds by intergranular attack in corrosive media is required (see intergranular attack Section 4.4). The addition of small amounts of titanium or niobium to form the stabilized grades can also counteract such weld deterioration, which is caused by the removal of the protective chromium from solid solution within the grain boundaries by solid-state precipitation as chromium carbide over a specific temperature range – a process called sensitization. For resistance to pitting corrosion and to

improve creep resistance, molybdenum is added in the range of 2.0 to 3.0 weight percent to form type 316 stainless steel. It should be noted that the austenitic stainless steels cannot be heat-treated like the ferritic steels to improve strength or hardness; however, cold working can change the microstructure and form small amounts of martensite, for example, that change the properties and may even induce ferromagnetism. Annealing at high temperature will relieve the effects of cold-working.

2.2.3 Nickel Alloys

For very high temperature applications (greater than 600°C or so) in power systems where strength, creep resistance and oxidation resistance are required, such as furnace or turbine fittings, or for environments where resistance to aqueous corrosion - particularly localised corrosion - is a major consideration, such as nuclear reactor coolant systems, nickel alloys may be employed.

Elemental nickel has the FCC crystal structure, which it tends to promote in its alloys - austenitic stainless steel being the prime example described above. Oxidation resistance of the nickel alloys is provided by chromium, which is present in the common alloys at concentrations between about 14 and 25 weight percent. For highly aggressive environments, such as strong acid solutions, the so-called “super alloys” with molybdenum additions up to 20 weight percent in alloys of the Hastelloy type, as produced by the Haynes International company, are effective and even higher levels (at about 30 percent with little or no chromium) produce the alloy Hastelloy B2 with superior resistance to concentrated hydrochloric and other reducing acids at all temperatures up to the boiling point. These materials may however have limited application in high-temperature environments in power systems.

Table 2. Standard compositions of commonly used ferritic, martensitic and austenitic steels in CANDUs.

Common designation	UNS #	chemical composition (wt%)								
		C-max	Fe	Cr	Ni	Mn	Mo	Si	P	Cu
Low-alloy steels										
A106 gr.B		0.3	Bal.	< 0.4	< 0.4	0.29-1.06	< 0.15	> 0.1	<0.035	<0.4
A106 gr.C		0.35	Bal.	< 0.4	< 0.4	0.29-1.06	< 0.15	> 0.1	<0.035	<0.4
Martensitic stainless steels										
403	S40300	0.15	Bal.	11.5-13	< 0.6	< 1.0		< 0.5	< 0.04	
410	S41000	0.15	Bal.	12.5		< 1.0			< 0.04	
Austenitic stainless steels										
304	S30400	0.08	Bal.	18-20	8-10.5	< 2		< 1.0	< 0.045	
304L	S30403	0.03	Bal.	18-20	8-12	< 2		< 1.0	< 0.045	
316	S31600	0.08	Bal.	16-18	10-14	< 2.0	2-3	< 1.0	< 0.045	
316L	S31603	0.03	Bal.	16-18	10-14	< 2.0	2-3	< 1.0	< 0.045	

A class of nickel alloys that should be mentioned here, even though they have not achieved wide use in thermal power systems but are extensively employed for gas turbine applications, is that of the super alloys, briefly mentioned above. They have outstanding strength, creep resistance and oxidation resistance at high temperature. Chromium concentrations around 20 weight percent provide their oxidation resistance, which may be enhanced by molybdenum at concentrations up to 10 percent in some cases. Grain-boundary properties, which affect creep, are improved by small additions of metals such as niobium, zirconium or hafnium while strength is imparted by additions of aluminium and titanium. The last two metals, usually present at levels of a fraction of a percent, strengthen the FCC crystal structure by precipitating with nickel as an intermetallic compound called gamma prime (γ'). This precipitation hardening or age hardening process is carried out at temperatures approaching 900°C on material that has been quenched from solution treatment in a high-temperature region where all the constituents are in solid solution. A typical alloy of this type is Inconel X750, as produced by the International Nickel company, which contains 70 weight percent nickel, up to 17 percent chromium, up to 9 percent iron, about 1 percent niobium, 2.25 - 2.75 percent titanium and 0.4 - 1.0 percent aluminium. Alloy X750 in wire form has been used to form toroidal spacers to separate the hot pressure tubes from the surrounding cool calandria tubes. The alloy loses practically all its ductility under neutron irradiation but maintains sufficient strength to carry the necessary loadings. Compositions of some nickel alloys commonly used in nuclear power plants are shown in Table 3.

The most widespread application of nickel alloys in the nuclear industry is for the tubing of steam generators in water-cooled nuclear reactors of the CANDU or pressurized water reactor (PWR) type. In order to ensure resistance to stress corrosion cracking and general corrosion,

Alloy-400, a nickel-copper alloy based on Monel-400 (63-70 weight percent nickel, 28-34 percent copper, with 1-2 percent iron, as produced by International Nickel), was employed in early CANDU reactors. The more rigorous operating conditions in later CANDUs prompted a move to alloys with better resistance to general corrosion in a somewhat oxidizing water coolant, so Alloy-600 (72 weight percent nickel, 14-17 percent chromium and 6-10 percent iron) or Alloy-800 (30-35 percent nickel, 19-23 percent chromium with the balance of iron, which is still classed as a nickel alloy, even though the major constituent is iron) were employed. The last two materials, respectively based on Inconel and Incoloy as produced by International Nickel, are used widely in the PWRs, though Alloy-600 is being replaced with Alloy-690 (61 weight percent nickel, 30 percent chromium and 9 percent iron) as a material more resistant to cracking. It should be noted that the nickel-chromium alloys used for steam generator tubing improve their resistance to cracking when they are thermally treated to relieve the stresses imparted during tube forming.

Table 3. Compositions of commonly used nickel alloys in nuclear power plants.

Common designation	UNS #	chemical composition (wt%)									
		C-max	Fe	Cr	Ni	Mn	Mo	Si	P	Cu	Ti
600	N06600	0.15	6-10	14-17	Bal.	< 1.0	●	< 0.5	●	< 0.5	●
690	N06690	0.05	7-11	27-31	Bal.	< 0.5	8-10	<0.5	<0.015	< 0.05	●
X750	N07750	0.08	5-9	14-17	Bal.	< 1.0	2.8-3.3	< 0.5	●	< 0.5	2.25-2.75
800 NG	N08800	< 0.02	Bal.	19-23	30-35	< 1.5	●	< 1.0	●	< 0.75	0.15-0.6

2.2.4 Copper Alloys

Copper has an important engineering role in electrical equipment and conductors, stemming from its high electrical conductivity (second only to that of silver, which is about 10 percent higher). In addition, its high thermal conductivity, good mechanical properties and corrosion resistance in many environments make it an important material for heat exchangers in the power industry and elsewhere.

The pure metal melts at 1082°C and at all temperatures below this it has an FCC crystal structure as shown in Figure 1. It is readily worked and machined and has good resistance to atmospheric corrosion and corrosion in clean waters. For heat exchanger applications, however, it is alloyed most commonly with zinc - to form the brasses - or with nickel - to form the cupronickels. The alloys are harder and stronger than elemental copper and offer good resistance to aqueous corrosion - particularly in marine environments.

Zinc itself has an HCP crystal structure and it dissolves in copper to a maximum of about 37 weight percent at 500°C without changing the structure from FCC. The resulting solid solutions are in the α phase, which is the basis of the α-brasses. Zinc concentrations above the 37 weight

percent limit precipitate a second phase, the BCC β phase, which becomes the sole equilibrium phase between about 46 and 50 percent zinc. Above this limit another phase, the γ phase, precipitates but forms brittle alloys that are of little commercial utility.

The most widely used brass in the power industry is based on the single-phase 70-30 alloy (70 weight percent copper, 30 percent zinc), since this has the optimum combination of mechanical properties and corrosion resistance and is not subject to the problems of reduced ductility and difficulty of working experienced by the two-phase α-β or the single-phase β brasses. While the α-brasses are easily formed into tubing etc., they tend to lose ductility with increasing cold work and must be annealed at high temperature to avoid stress corrosion cracking (known as season cracking) in service. Brasses are also susceptible in aqueous environments to a type of corrosion called dezincification, in which the alloy is transformed in its original shape to porous copper having little rigidity or strength. This phenomenon is stifled by as little as 0.04 weight percent arsenic, which is a standard additive to α-brasses. A common material for heat exchangers and condensers is Admiralty brass, having 71 weight percent copper, 28 percent zinc, 0.02 to 0.06 percent arsenic and small amounts of lead and iron. Antimony and phosphorus are similar to arsenic in their corrosion inhibition of brass.

Nickel has a similar FCC crystal structure to that of copper, and the two elements are completely soluble in each other in all proportions. The resulting α-phase solid solutions therefore have melting points between that of pure copper (1082°C) and that of pure nickel (1452°C). The cupronickels (so-called when the copper is the major constituent) are tough, readily worked and have a high corrosion resistance. Alloys based on 70 weight percent copper and 30 percent nickel, the 70-30 cupronickels, find widespread use in heat exchangers for sea water service, when additions of iron and manganese to about 2 percent provide extra resistance to erosion-corrosion. The 90-10 cupronickels have better thermal conductivity than the 70-30 alloy and are more resistant to aqueous corrosion at higher temperatures, so they have been commonly used in feedwater heaters in steam-raising systems.

2.2.5 Titanium Alloys

Pure titanium has an HCP crystal structure (the α phase) at temperatures up to 884°C, where it transforms to the BCC β phase, which is stable up to the melting point of 1677°C. Alloying elements stabilize one phase or the other. Aluminum, carbon, oxygen and nitrogen, for example, stabilize the α phase and raise the α-β transition temperature, whereas copper, chromium, iron, molybdenum and vanadium lower the transition temperature and may even stabilize the β phase at room temperature.

The principal titanium alloys are therefore of three types: alpha or near-alpha, alpha-beta and beta. Their high strength-to-weight ratio (especially of the alpha or near-alpha and alpha-beta alloys) has put them in high demand in the aerospace industry, while in the power industry the exceptional resistance to corrosion in a wide range of corrosive waters - particularly sea water - has made titanium an important material for condenser tubes and plate heat exchangers.

Titanium is actually a very reactive metal and must be melted and machined with care. Its resistance to corrosion is afforded by the thin, protective layer of oxide (TiO_2) that spontaneously forms in air to produce an effective barrier against the environment, thereby putting titanium in the class of passive metals. The rather specialized metal refining and component manufacturing process for titanium tubing at one time made the material an expensive proposition for condensers. The growing demand for titanium products, however, has had the effect of lowering the price relative to competitive materials - especially the copper alloys and steels. Also, the development of seam-welded tubing suitable for condenser service and the fact that no thickness allowance need be made for corrosion on the tube wall makes titanium an attractive alternative.

The titanium used mostly in condenser applications is the commercially pure material, which is therefore an alpha-phase material. It exists in five grades distinguished by their impurity content. Thus, the maximum amounts of carbon, nitrogen, hydrogen, iron and oxygen are specified for each grade at levels of the order of 0.01 to 0.1 weight percent, and each grade has particular mechanical properties. Titanium condenser tubing is relatively immune to corrosion in salt or brackish water and in all types of polluted water. Marine organisms stick to its smooth surface with some difficulty and surfaces that do foul or silt are not susceptible to pitting or crevice corrosion. On the condensing steam side of the tubes used for power plant condensers, there is no effect on titanium from common gases such as ammonia, carbon dioxide or oxygen. In fact, the main concern with the use of titanium for condenser tubes is that less noble components of the condenser may suffer galvanically-accelerated corrosion and must be protected either cathodically or by coating or both. It must be borne in mind that in aqueous service the metal absorbs hydrogen readily, so that its exposure as the cathodic component of a metallic couple can promote degradation as the titanium-hydride is formed and the material becomes embrittled.

2.2.6 Concrete

Concrete is an inorganic composite consisting of a coarse aggregate of gravel, crushed rock or slag and a fine aggregate of sand, all held together with a cement. Angular particles or rock fragments are preferred to rounded ones for the aggregate because they tend to interlock and produce a more bonded and therefore stronger structure, although they have more surface defects that can initiate cracks or voids. The larger the aggregate the better in order to minimize the defects, bearing in mind that the size of the particles or fragments should be no more than ~20% of the structure's thickness. The aggregate material can be tailored to the requirements of the structure. Lightweight concrete incorporating steel-making slag as aggregate, for instance, is a better thermal insulator than one incorporating normal silica-based rock, and heavy concrete incorporating dense mineral aggregate such as ilmenite, barytes or magnetite or even metal shot is used for radiation shielding. Ideally, the sand is a silica-based mineral with particle size 0.1 – 1.0 mm. It partially fills the spaces between the coarse aggregate and reduces the porosity of the final concrete, in turn reducing the tendency to disintegrate during alternate freeze-thaw cycles. The cement is a mixture of fine mineral particles that sets and hardens after being made into a paste with water. The most common type of cement is Portland cement, named after the cliffs at Portland in England, which the hardened material resembles. Portland cement is a type

of hydraulic cement, i.e., one that hardens upon reaction with water. It is a mixture of calcium silicate (conveniently designated as 60-65% CaO and 20-25% SiO_2), iron oxide and alumina (7-12%). Adding water hydrates the mixture to produce a solid gel, releasing heat as it does so. The main chemical reactions can be generalized to:

$$2CaO \cdot SiO_2 + xH_2O \rightarrow Ca_2SiO_4.xH_2O + heat \quad (1)$$

$$3CaO \cdot Al_2O_3 + 6H_2O \rightarrow Ca_3Al_2(OH)_{12} + heat \quad (2)$$

$$3CaO + SiO_2 + (x+1)H_2O \rightarrow Ca_2SiO_4.xH_2O + Ca(OH)_2 + heat \quad (3)$$

The hardened cement binds the aggregate particles together, so there must be enough cement added to coat all of the particles completely if a firm composite is to be obtained. A typical cement proportion is 15 vol% of total solids. Both the time to harden and the strength of the final concrete depend on the composition of the initial mixture; a rapid-setting concrete generally is weaker than a slow-setting one. Complete curing is attained after 28 days or so, when concrete reaches its maximum compressive strength.

Like other ceramic-based materials, concrete is strong in compression but weak in tension, so for most construction purposes it has to be strengthened. Reinforced concrete has steel rods ("rebars"), wires or mesh introduced into the structure to take the tensile loads, while the concrete supports the parts under compression. Such a combination is effective for components undergoing bending forces. In prestressed concrete the reinforcing steel is pulled in tension between an anchor and a jack while the concrete is poured and cured. After the concrete has set, the external tension on the steel is removed and as it relaxes the forces are transferred to the surrounding restraining concrete, placing it in compression. The component can now resist higher tensile or bending forces. Post-stressed concrete also has induced compressive stresses, but they are imposed by running steel cables or rods through tubes set in the structure and pulling and maintaining them in tension after the concrete has hardened. Reinforced concrete has many applications in nuclear reactor construction – building foundations, primary containment and shielding, supports for large components such as steam generators, etc. Concrete containment buildings are pre- or post-stressed, and for the LWRs are lined with steel plate. Existing CANDU containment buildings are lined with epoxy.

Concrete structures undergo various modes of degradation. Rebar in civil installations, typically bridges and road overpasses, corrodes in contact with aqueous solutions such as road salt and in time can cause serious deterioration of the structure. Pre- and post-stressing steel can also rust and lose strength and over time the compressive stresses may relax. The concrete itself may be attacked; chlorides, nitrates and sulphates react with the cement and cycles of freezing and thawing can cause cracking. An insidious mode of degradation for concretes with aggregate containing silica in a non-crystalline or glassy form is the co-called alkali-aggregate reaction (AAR). This is an internal process whereby alkaline constituents of the cement react over time with the silica to form a hydrated calcium silicate. This compound has a larger volume than its precursors and the resultant swelling causes the structure gradually to spall and crack. The hydro-electric dam at Mactaquac on the St. John river in New Brunswick has a particularly pernicious form of this degradation. The concrete swelling puts such severe compressive forces on the structure, which is firmly anchored between rock abutments, that the stresses have to be

relieved periodically by sawing vertically through the dam from top to bottom – a process that can continue only for about another decade. The plinth supporting the turbine at the Gentilly-2 CANDU is cracking because of this form of degradation. Concrete used as radiation shielding around a nuclear reactor relies on its water content to maintain not only its strength but also its effectiveness for stopping neutrons. Over time, the absorption of radiation and the resulting heating can lead to dehydration, involving water both bound chemically with hydrous minerals and free as excess molecules. To minimize these losses, reactor shielding structures are continuously cooled, often with cooling water pipes embedded in the structure.

2.2.7 Polymers

Polymers for industrial or domestic consumption are generally called plastics. Because of their ease of manufacture and formation, their physical and chemical properties and their low cost they have a huge number of applications. The transparency of several types makes them useful as substitutes for glass whilst the elasticity of others puts them in the class of elastomers. They can be produced as homogeneous material or as both the matrix and the fibre reinforcement for composites. In reactor systems they are used for electrical insulation, coatings, seals, etc. and occur in a myriad of common articles such as textiles, containers, tools, etc.

Most polymers, and the ones discussed here, are composed of "giant" molecules consisting of chains of simpler units bonded together. They are usually organic carbon-based compounds, although some are inorganic, based on silicone Si-O units. Molecular weights can range from 10^4 to 10^6 g/mol or higher. A linear polymer has its molecules as single strands in a tangled arrangement, rather like a portion of spaghetti. In a branched polymer, each "spaghetti" strand has one or more shorter strands branching off. Linear or branched polymers can be cross-linked, whereby atoms in individual strands are strongly bonded covalently to atoms in other strands, either directly or via linking atoms.

Thermoplastics are composed of linear or branched molecular strands that are weakly connected to each other by van der Waals bonds and that can be partially separated or untangled by applying tensile stress. Thermoplastics therefore are ductile and deform plastically. When heated they at first soften and then melt, making them easily moulded into useful articles and readily recycled. Polyethylene is a common example of a thermoplastic. By contrast, thermosetting plastics have their linear or branched molecular strands strongly bonded covalently to each other in a rigid, three-dimensional network. They are therefore stronger than thermoplastics but more brittle. On heating, they do not melt but decompose, making them difficult to recycle. Polyurethanes are an example of a thermosetting plastic. Elastomers are thermoplastic or lightly cross-linked polymers that have their molecular strands in a folded or coiled configuration. Under stress the molecules deform reversibly, rather like a spring, so that the original form is regained when the stress is relaxed. Natural rubber is the prime example of an elastomer which can be stretched elastically to >200%. The soft, thermoplastic latex from the rubber tree is made into useful rubber by "vulcanising", involving reacting it with sulphur to cross-link the highly folded molecular strands. Depending on the degree of vulcanisation, a tougher and more elastic material is formed, one that does not soften and become sticky when heated to moderate temperatures. Low (1 – 3%) sulphur contents form soft commercial rubber, while high (23-

35%) contents form hard rubber or ebonite.

Polymers are severely degraded by radiation; the familiar embrittlement of polyethylene by prolonged exposure to sunlight is a mundane example. In nuclear reactors, the deterioration of electrical insulation in radiation fields, affecting cable runs and instrument connections, is a burgeoning problem, necessitating frequent inspections and often replacements as plastic components have deteriorated, sometimes to the extent of cracking and disintegrating in-situ. The reactor vault area is especially vulnerable, and when reactor control cabling is affected the deterioration becomes a safety issue. Ion-exchange resins (see Section 2.3 in Chapter 15) in clean-up systems for active circuits such as the moderator (in CANDUs) and the primary coolant are based on polystyrene and are subject to radiation damage as they remove radionuclides from the water. This has been a factor in the decision not to regenerate active resins. Both natural and synthetic rubbers have their tensile strengths reduced but are affected by radiation in different ways. For example, natural rubber is somewhat more resistant to radiation than butyl rubber but is hardened while butyl rubber is softened. Consequently, diaphragms and O-rings made of either material in control valves are replaced frequently to avoid problems arising from radiation-induced deterioration.

The damage mechanism is the radiation-induced rupture of the chemical bonds holding the polymer together, and the subsequent re-forming of the bonds to create an altered structure. Depending on the material, the degree of cross-linking can be increased and polymerization increased or reduced, oxidation in air can be promoted and deterioration with gas evolution may occur. Serious changes in properties such as conductivity, strength, hardness, ductility, etc. result. Table 4 indicates the severity of damage of several common polymers caused by radiation.

Table 4. Severity of radiation-induced damage of common polymers

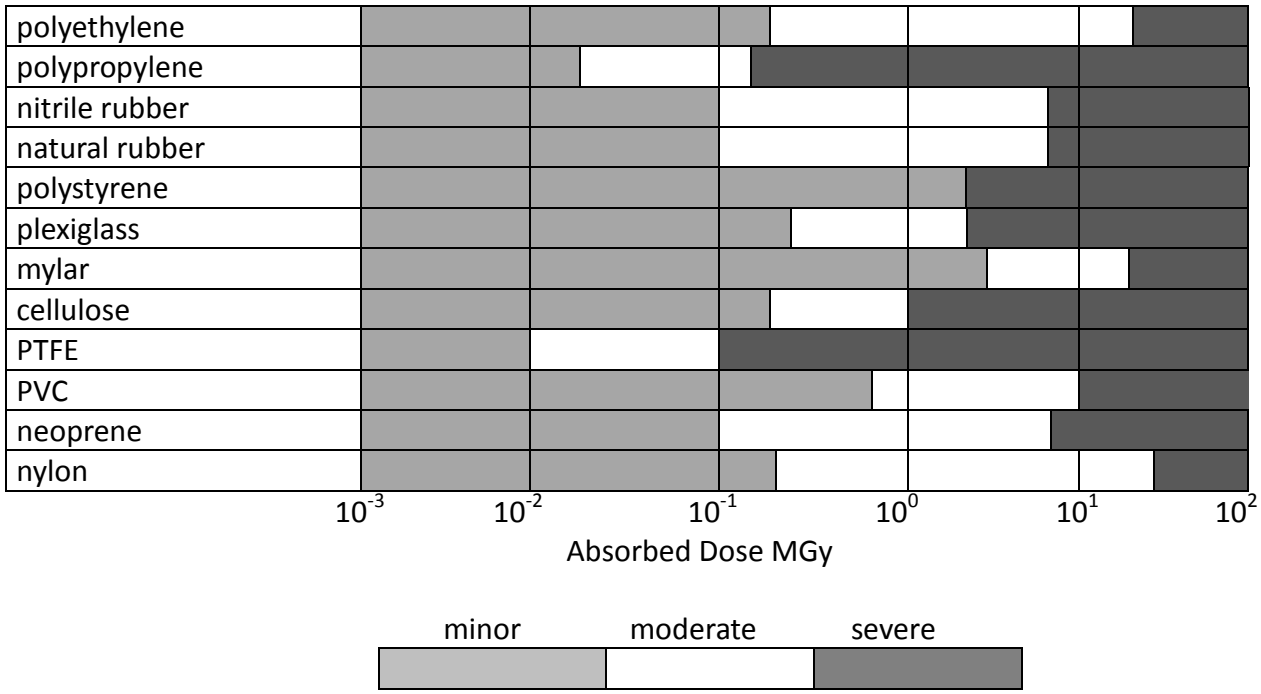

It is noteworthy that polytetrafluoroethylene (PTFE – or the DuPont trade name Teflon®), a most useful product in many domestic and industrial applications because of its non-stick and low friction properties, is the most severely affected by radiation in the list in Table 4 (in any case, its use in reactor systems is proscribed because it tends to release fluorine species as it degrades, and fluorine is particularly damaging to zirconium and its alloys).

3 CANDU Process Systems and their Materials

3.1 Major Process Systems

Diagrams of the various systems are presented in other chapters. The materials of construction of those systems are listed here. Their operating experience has been detailed by Tapping (2008).

3.1.1 Primary Heat Transport System

The primary heat transport system consists mainly of the in-core fuel channels connected to the steam generators by a system of feeder pipes and headers. It has a purification system for the heavy water (isotopic purity ≥95.5wt%) and is connected to a pressurizer.

The fuel channel components in contact with the heavy water primary coolant comprise the pressure tubes of Zr-2.5%Nb, the end-fittings of type 403 stainless steel, the liner tubes of type 410 stainless steel, the shield plugs of ductile iron and the seal plugs of Cr-Fe stainless steel. The fuel bundles are of elements sheathed with Zircaloy-4 that are separated by spacers of Zircaloy-4 that are resistance-welded to the end-plates, which are also made of Zircaloy-4. Bundles sit inside the pressure tubes on bearing pads of Zircaloy-4 which, like the spacers, are attached to the elements with a braze of Zr-Be.

The feeders and headers are made of carbon steel. Originally, when a low cobalt content was specified to minimize radiation-field build-up around the PHT circuit, a low-chromium material (A106 grade B with ~0.02wt%Cr) was selected. As described in Section 4.2 of this chapter and in Section 3.2 of Chapter 15, this gave rise to flow-accelerated corrosion (FAC) of the feeders at the reactor outlet. Replacement outlet feeders are specified as A106C with a chromium level of about 0.3wt%Cr, which, based upon extensive laboratory testing, should be enough to extend the life of the outlet feeders by about 50% and significantly reduce system fouling from transported corrosion products. A degradation phenomenon in some outlet feeders before replacement was a type of cracking, which occurred only at the Point Lepreau CANDU-6. Incidences of feeder cracking at other CANDUs have been extremely low – confined to one repaired field weld – making the Point Lepreau experience unique and rather mysterious. By 2005, nine feeders had been removed because of deep cracks from the inside surfaces, in some cases they were through-wall (Slade and Gendron, 2005), and a total of 12 feeders had been removed and replaced up to the time of the refurbishment shut-down that began in 2008. Cracks were all in the first and/or second tight-radius bends downstream of the fuel channel outlet, where residual stresses were high and where FAC was prevalent. Detailed examination revealed extensive shallow cracks on the outside surfaces also, and these outside-surface cracks were

found to be widespread in feeder bends across the reactor face. The cracking mechanism was not conclusively identified before Point Lepreau was shut down for the refurbishment, which included replacement of the feeders with the A106C material mentioned above and with stress-relieved bends. However, it was postulated that the inside-surface cracks possibly originated from stress-corrosion cracking caused by slightly oxidizing conditions at the reactor outlet due to insufficient suppression of radiolysis and exacerbated at reactor start-up, especially if air ingress had occurred. The outside-surface cracking was possibly low-temperature creep cracking, facilitated by atomic deuterium diffusing through the metal lattice due to FAC (Slade and Gendron, 2005).

The purification is a feed-and-bleed system taken off the connection between the coolant loops or, at Bruce A (which has only one primary loop) directly off the reactor headers. It has heat exchangers with tubes of nickel alloy (e.g., Alloy-600 or Alloy-800) and vessels such as the ion-exchange columns of 300-series stainless steel. The pressurizer, also taken off the connection between the coolant loops, is a carbon-steel vessel with immersion heaters clad with nickel alloy.

The steam generators are tubed with nickel alloy – Alloy-400 at Pickering, Alloy-600 at Bruce and Alloy-800 at the CANDU 6s and Darlington and the refurbished units at Bruce (Units 1 & 2). The replacement units at Bruce, like all the other CANDU steam generators except the original designs at Bruce A, are of the “light-bulb” design (see Figure 17 in Chapter 8) with the steam separator and dryer separate for each unit above the tube bundle (each original Bruce A design has four steam generators connected to an integral steam drum at each end of the reactor). The tube sheets in the primary heads are clad with the tube material, but the heads themselves are carbon steel. The divider plates in the steam generator heads have been replaced with stainless steel to eliminate FAC. All the steam generators except those at Bruce have integral preheaters, but at Bruce the preheaters are separate heat exchangers of carbon steel with tubes of Alloy-600 and tube sheets in contact with the primary coolant clad with the same material (the Bruce preheaters remove heat from the primary coolant serving the inner core fuel channels, which run at a higher power than the outer core ones).

3.1.2 Secondary Heat Transport System

The secondary coolant system consists of the shell side of the steam generators, fed with light-water coolant from the condenser and feed water train and supplying steam to the turbine and thence back to the condenser. CANDUs have been following a policy of eliminating copper alloys from the circuit to avoid corrosion problems from carry-over to the steam generators. The only components remaining with copper alloys are brass-tubed condensers at Gentilly 2 (currently shut down and due for decommissioning), as listed below, although it is of note that Pickering changed its condensers from brass to stainless steel because of release of copper to Lake Ontario.

As mentioned above, steam generator tubing is Alloy-400 at Pickering, Alloy-600 in the original units at Bruce – Alloy-800 in replacement units and at Darlington and the CANDU 6s. The tube supports at Pickering A are lattice bars of carbon steel and at Pickering B are broached plates of carbon steel; at Bruce the original supports are broached plates of carbon steel but, like Darling-

ton and the CANDU 6s (except Embalse, Point Lepreau and Wolsong 1), the replacement units have lattice bars of type 410 stainless steel. Embalse has broached plates of carbon steel, Point Lepreau has broached plates of type 410 stainless steel and Wolsong 1 has lattice bars of Alloy 600. Steam generator shells, shrouds, etc. are of low-alloy/carbon steel.

The feedwater and steam cycle piping is generally carbon steel, although some regions of the system susceptible to flow-accelerated corrosion, such as piping carrying two-phase steam-water mixtures or highly-turbulent feedwater, may have alloy steel or even stainless steel.

All CANDUs except Embalse have a deaerator in the feed water train. These, the high-pressure feedwater heaters and the moisture-separator/reheater in the steam circuit are made mostly of carbon steel, although stainless steel may be employed for some reheater tubes. The low-pressure feedwater heaters are made of stainless steel.

The condensers at Point Lepreau and the Qinshan CANDUs are tubed with titanium since they draw from sea water while the Embalse plant continues to use Admiralty brass (with stainless steel for the outer tubes of the bundles). The remaining CANDUs use Type 304 stainless steel as their condenser tubes, Bruce units 1 & 2 being the most recently converted during their refurbishment project that was completed in 2012.

3.1.3 Moderator

The moderator system is the piping and components containing and processing the heavy water moderator (isotopic purity ≥99.75wt%). It includes the cover gas system containing the helium cover gas and maintaining its content of deuterium and oxygen (formed by heavy-water radiolysis in the reactor) at safe levels of <2wt% via a catalytic recombiner.

All reactors have a calandria vessel made of type 304L stainless steel and calandria tubes made of Zircaloy-2. Most of the rest of the circuits (including the heavy water expansion tank) are of stainless steel, except the heat exchangers, which are nickel alloy – primarily Alloy 800.

3.2 Ancillary Process Systems

3.2.1 Condenser Cooling Water

CANDU condensers are cooled with whatever natural water source is available – sea water at coastal sites or fresh/brackish water at riverside or lakeside sites. Water is drawn into the system through a steel screen arrangement to remove coarse debris, pumped through a circuit of concrete ductwork and steel piping to the condenser, then discharged back to the source. No CANDU to date has employed cooling towers to enable recirculation of condenser cooling water.

The condenser tubing materials have already been listed above. Like the condenser shells, the inlet and outlet “water boxes” are of carbon steel and they may be cathodically protected from galvanic corrosion caused by contact with tube sheets of more noble metals.

3.2.2 Recirculating Cooling Water (RCW)

This system of purified water kept usually at high pH (typically adjusted using the AVT strategy of the steam cycle) and low oxygen with hydrazine additions cools components such as the moderator heat exchangers. It comprises its own heat exchangers of nickel alloy – normally Alloy 800 – and carbon steel piping fed directly from the local water source.

3.2.3 Shield Tank

The shield tank encloses the calandria circumference, providing shielding and cooling for the reactor. In the early reactors it is a water-cooled carbon steel vessel but in the CANDU 6 it is the concrete vault filled with water. The end shields are water-cooled tanks filled with ⅜"- ½" diameter carbon-steel balls that provide shut-down biological shielding for the reactor faces and support for the fuel channel assemblies. They are made of type 304L stainless steel and have lattice tubes (to accommodate the fuel channel end-fittings) of the same material. Like the main shield tank, they are filled with ⅜"- ½" diameter carbon-steel balls. Note that the Pickering reactors have cooled steel slabs as end shields rather than water-cooled tanks.

The purified water, maintained at high pH with lithium hydroxide, is circulated through heat exchangers tubed with nickel alloy or even copper alloy, where it is cooled by plant service water (RCW).

3.2.4 Spent Fuel Bay

The spent fuel bay is the swimming-pool arrangement for accepting and storing spent fuel under water directly from the reactor. About ten-year's accumulation (at ~80% capacity factor of the plant output) of fuel bundles can be stored with about 4m of water above. The water cools the bundles and provides biological shielding. There is an intermediate bay for handling and temporary storage. The construction is reinforced concrete lined with epoxy-coated fiberglass and with a stainless steel floor.

3.2.5 Emergency Cooling

The emergency core cooling system (ECC) is a light-water system designed to supply cooling water to the reactor core via the primary coolant system emergency injection. It is triggered by a loss in pressure following a LOCA (loss-of-coolant accident) and for later reactors with individual containment buildings, is supplied initially from the ECC water tanks which are located outside the containment. For high-pressure operation as occurs with a small leak, the water is injected into the primary coolant headers by automatically pressurizing the ECC tanks with nitrogen (the loop is automatically isolated from the other one). As the system pressure drops, the ECC pumps start and stored water is then injected into the headers from the dousing tank, which is below the roof slab. During these phases, the heat sink is the steam generators. Finally, when the dousing tank is empty and the system pressure has dropped even further, collected water is pumped into the system from the sump via the ECC heat exchanger, which is cooled with service water. This phase is designed to continue indefinitely. The multi-unit stations with a vacuum building have the ECC storage as the dousing tank below the roof slab of the vacuum building.

The dousing tank below the roof slab is made of reinforced concrete and the piping system of carbon steel and stainless steel. In the later reactors the shell-and-tube ECC heat exchangers to reject heat to the outside are alloy-tubed but early designs used titanium plate-type heat exchangers.

3.3 Supporting Structures and Components

3.3.1 Containment

In the four-unit CANDUs at Darlington and Bruce A and B, the reactor of each unit is contained within a reinforced concrete vault, which extends to shielded rooms above containing the steam generators, heat transport pumps and reactivity drive mechanisms. Main steam piping exits the containment for the turbine building. Openings in the floor of the vault allow entry of the fuelling machine, which serves all four units via a duct running below grade for the length of the station and connecting to a fuel handling facility. The overall building for each unit has a flat, steel roof.

The four-unit CANDUs at Pickering A and B, like the CANDU 6 reactors, each have the reactor, steam generators, etc., in a separate containment building of pre-stressed, post-tensioned concrete with a domed roof. The building is lined with epoxy, but future designs could incorporate a steel liner. The main steam pipes exit the containment directly for the turbine building.

3.3.2 Vacuum Building (Multi-unit Plants)

Bruce A and B and Darlington each have the four reactor containments separately connected to a normally sealed building that is kept at about 7kPa absolute pressure. At Pickering, the eight units at the A and B sites are connected to one such vacuum building. In the event of an overpressure in a reactor containment, isolation valves connecting that reactor with a concrete duct running to the vacuum building open and the atmosphere of the containment is vented. A spray from the ECC storage in the vacuum building roof condenses any vapour.

The vacuum building is constructed of reinforced concrete. It is supported inside with an arrangement of columns and beams that also hold up the ECC storage tank and the vacuum chambers.

3.3.3 Fuelling Machine

Each CANDU reactor is served by two fuelling machines, with one machine connecting to each end of a fuel channel that is to be refueled. A machine has a rotating magazine to hold fuel and channel seals and plugs, a snout assembly to lock onto the channel and a ram assembly to remove, store and replace channel seals, plugs and fuel bundles. Figures 10 – 12 in Chapter 8 show the arrangement of the fuelling machine.

The machines simultaneously clamp onto the end-fittings of a channel, unlock, remove and store the seal plugs, remove and store the shield plugs then push new fuel bundles into the pressure tube from one end and remove and store spent fuel bundles from the other end, replace the shield plugs and finally replace and lock the seal plugs. During the operation the machine is in contact with the primary coolant at pressure and sustains a flow of heavy water from the PHT supply tanks. The seal plug sealing faces must be maintained in good condition to prevent expensive heavy water leaks.

Fuelling machines are large pieces of equipment comprising many components that remotely perform a complex series of tasks. They are made of many engineering materials. Of note are the mechanical bearings that support the rotating magazine, which have traditionally been made of the extremely hard-wearing cobalt alloy, Stellite®. This has been responsible for a significant component of out-core radiation fields, since even very small releases of cobalt to the primary coolant during a refuelling operation may give rise to the production of ^{60}Co in the reactor core, and this distributes around the circuit and contaminates out-core components, particularly at the reactor faces and in the steam generator heads. Recent research is identifying alternative materials for the bearings such as silicon nitride (see for example Qiu, L., 2013). Additionally, activation products of antimony (primarily Sb-124) originate from bearings in the heat transport pumps and as impurities in steel and may contribute significantly to the overall activity levels throughout the primary heat transport circuit.

3.3.4 Fuel

The fuel materials in contact with the primary coolant, viz. the element sheaths, end plates, bearing pads, spacers and the braze attaching the appendages to the sheath have already been described. The fuel pellets themselves within a sheath are of high-density, sintered UO_2 of natural isotopic content (0.7% ^{235}U) and the inside surface of the sheath is coated with a thin layer of graphite to reduce sheath-pellet interactions (the CANLUB system). The standard bundle is of 37 similar elements; however, more-efficient designs such as the CANFLEX® bundle with 43 elements of different diameters have been proposed; thus, for future applications, the Advanced CANDU Reactor employs low-enriched uranium (LEU) fuel of UO_2 with 3-4% ^{235}U in a CANFLEX®-type bundle with a central element containing a neutron absorber. Note that the flexibility of the CANDU system makes it suitable for a wide variety of fuel materials, and trials with thorium, recovered uranium (from reprocessing of LWR-type fuel) and plutonium mixed-oxide (with uranium) have been carried out successfully.

3.3.5 Reactor Control Mechanisms

Liquid zone controllers are vertical thimble tubes of type 304 stainless steel attached vertically to the top of the calandria with zone control tubes of Zircaloy extending downwards into the moderator between the calandria tubes. They control reactivity during normal operation. Six of them per reactor contain among them fourteen compartments of circulating light water as the absorber, and the amount of absorber can be controlled by adjusting an overpressure of helium in each compartment and the inlet flow rate.

There are mechanical adjuster rods (21 in the CANDU 6s), also inserted vertically into the moderator, to act as neutron absorbers. They are tubes of stainless steel or Zircaloy containing "shim rods" of steel/cadmium or cobalt that are normally fully inserted to flatten the flux profile but can be withdrawn mechanically via motor-driven winches (sheaves) and cables as override for xenon poisoning following reactor shutdown or a power reduction.

Shut-off rods and mechanical control absorbers are of similar design, penetrating the calandria vertically between the calandria tubes in similar fashion to the adjuster rods. Each employs a cable, winch and clutch to hoist, hold or release an absorber tube containing cadmium as a neutron absorber. They are normally parked in thimbles above the calandria but can be driven vertically downwards into the core to reduce reactivity through perforated guide tubes of Zircaloy that are anchored at the bottom of the calandria. Shutdown System #1 comprises 28 such assemblies arranged throughout the reactor; they release their rods by de-energising the clutch and drive them into the core by spring-assisted gravity to achieve rapid power decrease. Four other assemblies can be used for reactor control to supplement the liquid zone controllers. They are normally parked out of the core but are driven in at variable speeds as required to reduce reactor power.

4 Corrosion and Material Degradation in Nuclear Reactor Systems

As described above and elsewhere in this text, a nuclear reactor is a complex system of different connected materials that must behave optimally in unison to ensure the safe and efficient operation of the plant. Even under the strictest chemistry control practices and careful plant operation, the corrosion and subsequent degradation of the plant components are the inevitable consequences of thermodynamics; the metals that make up the pipes, valves, fittings and vessels all tend to revert back to their thermodynamically stable state – usually an oxide, haematite (Fe_2O_3) for example, the basis of rust on iron and steel. In some cases, the degradation of system components is exacerbated by vibration, fatigue or fretting or by the interaction with high-velocity coolant creating flow-accelerated corrosion (FAC); in all cases, component lifetimes are shortened. Thus, knowledge of the basic forms of corrosion is a prerequisite to understanding the materials selection and chemistry requirements of CANDUs.

4.1 General Corrosion

Metals that are in every-day use for engineering applications are fundamentally unstable. They tend to react with their environment to assume a more stable thermodynamic state, which in the coolant systems of nuclear reactors is normally an oxide. General corrosion is the term for attack that is spread more or less uniformly over the entire component surface; it is driven by an electrochemical reaction in the case of ionic environments such as molten salts or aqueous coolants, or by a chemical reaction in the case of non-ionic coolants such as gases like carbon dioxide. (Note, however, that any oxidation is strictly speaking electrochemical, since it is a chemical reaction involving the transfer of electrons.) The metal thins gradually and may fail if left without being inspected for any length of time, although the rates of such corrosion are low and are generally predictable from tabulated data. Components are designed with adequate

thickness (incorporating a "corrosion allowance") that will last for the desired lifetime; failures are rare.

4.1.1 General corrosion in gas-cooled systems

As an example of a direct chemical oxidation, consider the alloy steel Fe-9%Cr as the boiler-tube material in Advanced Gas-Cooled Reactors (AGRs). In the CO_2 coolant at 580^oC this material corrodes uniformly, forming a duplex film of the oxide Fe-Cr spinel (based on iron chromite, $FeCr_2O_4$) overlaid with the inverse spinel magnetite (Fe_3O_4). Spinels have a crystal structure in which the unit cell contains 32 oxide ions in a face-centred cubic arrangement and 24 metal ions dispersed in the interstices to neutralise the charge. The interstices comprise 64 sites with tetrahedral symmetry and 32 sites with octahedral symmetry. In so-called normal spinels, the eight divalent metal cations (Fe^{2+} in the example of $FeCr_2O_4$) are in tetrahedral sites and the 16 trivalent cations (Cr^{3+} in $FeCr_2O_4$) are in octahedral sites. In inverse spinels, the divalent cations (Fe^{2+} in Fe_3O_4) are distributed along with half the trivalent cations (Fe^{3+} in Fe_3O_4) in octahedral sites, while the remaining trivalent cations are in tetrahedral sites. The relative stabilities of the normal and inverse spinel lattices influence the extent to which magnetite can incorporate Cr^{3+} ions and chromite can incorporate Fe^{3+} ions.

The mechanism for the formation of the duplex oxide film on the AGR steel has been postulated to be the direct reaction of metal with CO_2 that diffuses through pores and microchannels in the growing oxide [Kofstad, 1985]. For example:

$$Fe + 2Cr + 2CO_2 \rightarrow FeCr_2O_4 + 2C \tag{4}$$

The carbon is distributed through the oxide and may carburise the metal. The development of the oxide porosity is governed by stresses created at the metal-oxide interface (M-O) by the difference between the density of the oxide and that of the metal (quantified as the "Pilling-Bedworth" ratio, which is defined as the ratio of the volume oxide formed to the equivalent volume of metal consumed; it is greater than unity for the common transition metals). We note, however, an alternative mechanism [Taylor et al., 1980], whereby corrosion is controlled by the protective nature of the inner layer; thus, the magnetite forms at the oxide-coolant interface (O-C) via direct chemical reaction with CO_2 of Fe that has migrated through the oxide:

$$3Fe + 2CO_2 \rightarrow Fe_3O_4 + 2C \tag{5}$$

although the details will involve reactions with diffused ionic species:

$$Fe^{2+} + 2Fe^{3+} + 2CO_2 + 8e^- \rightarrow Fe_3O_4 + 2C \tag{6}$$

The kinetics of general corrosion governed by the increasing protection afforded by a continuously-thickening oxide film are often described by a parabolic expression, derived from the principle that diffusion rate, and therefore corrosion rate and oxide film growth rate (dm/dt), is inversely proportional to film thickness (m):

$$\frac{dm}{dt} = \frac{k}{m} \tag{7}$$

which integrates to:

$$m^2 - m_o^2 = kt \tag{8}$$

where m_o is the initial film thickness. Modifications of (8) such as (9) are occasionally quoted:

$$m = m_o + kt^{0.5} \tag{9}$$

CANDU reactors have two main gas systems, although several ancillary systems also use inert cover gases to help prevent corrosion and maintain safety envelopes. The two main gas systems include the moderator cover gas system (already described) and the annulus gas system (AGS). The AGS circulates CO_2 through the annulus between the calandria tube and its companion pressure tube. The system is continually monitored for moisture by dew point measurements as a warning of a leak from the PHT system or from the calandria end shield joint. Deuterium produced from the corrosion of the pressure tube on the PHT-side, diffuses into the AGS forming heavy water vapour when combined with oxygen present in the CO_2 so the system needs to be regularly purged to reduce the moisture content. The oxygen added to the CO_2 in the AGS also performs an important role of oxidizing the outside of the pressure tube. By oxidizing the outside pressure tube surface it helps to maintain a barrier to the ingress of deuterium into the pressure tube and promotes oxide formation on the X750 garter-spring spacers.

4.1.2 General corrosion in water-cooled systems

Examples of electrochemical reactions are provided by the general corrosion of metals in water. Thus, carbon steel in contact with high-temperature water develops protective magnetite films according to the overall scheme:

$$3Fe + 4H_2O \rightarrow Fe_3O_4 + 4H_2 \tag{10}$$

The carbon steel feeders in CANDU primary coolant corrode accordingly, except that the coolant is D_2O rather than H_2O and deuterium rather than hydrogen is evolved. Mechanistically, (10) can be regarded as two half-reactions, the anodic or oxidation process:

$$3Fe \rightarrow Fe^{2+} + 2Fe^{3+} + 8e^- \tag{11}$$

and the cathodic or reduction process:

$$4H_2O + 8e^- \rightarrow 4O^{2-} + 4H_2 \tag{12}$$

The half-reactions occur simultaneously and at the same rate. According to the classic Wagner-Traud theory [Wagner and Traud, 1938] it is postulated that the anodic sites on the metal, where metal ions dissolve (reaction (11)), are separate from the cathodic sites, where electrons are discharged, oxide ions form and hydrogen is released (reaction (12)). The electrons are transported between the sites and the metal ions and oxide ions interact and precipitate as magnetite. Clearly, for the oxidation to be uniform, the sites must be mobile across the surface.

In reality, it is understood that in high-temperature water the oxidation at the M-O produces ferrous ions according to:

$$3Fe \rightarrow 3Fe^{2+} + 6e^{-} \tag{13}$$

and that the hydrogen is produced in the accompanying reduction:

$$6H_2O + 6e^{-} \rightarrow 6OH^{-} + 6H \tag{14}$$

where H is in the form of hydrogen atoms that migrate through the metal. It is important to note that if dissolved oxygen is introduced into neutral or alkaline water, reaction (14) is replaced by the more favourable reaction (15):

$$1.5O_2 + 3H_2O + 6e^{-} \rightarrow 6OH^{-} \tag{15}$$

and hydrogen production ceases.

The ferrous ions and hydroxide ions from (13) and (14) or (15) interact to form soluble ferrous hydroxide:

$$3Fe^{2+} + 6OH^{-} \rightarrow 3Fe(OH)_2 \tag{16}$$

but this oxidises and precipitates as magnetite according to the Schikorr reaction [Schikorr, 1928]:

$$3Fe(OH)_2 \rightarrow Fe_3O_4 + 2H_2O + H_2 \tag{17}$$

Again, if oxygen is present, the oxidation of ferrous hydroxide proceeds via the more favourable:

$$3Fe(OH)_2 + 0.5O_2 \rightarrow Fe_3O_4 + 3H_2O \tag{18}$$

There is only room at the M-O (metal-oxide interface) for about half of the ferrous hydroxide to precipitate there as inner-layer magnetite; the other half, along with any hydrogen molecules generated at the M-O by (17), diffuse through the developing magnetite film to the O-C (oxide-coolant interface). There, if the coolant is reducing and saturated in dissolved iron as in the carbon steel inlet feeders of CANDUs, it precipitates as outer-layer magnetite according to (17);

the molecular hydrogen is then dispersed in the bulk of the flowing coolant. In the presence of dissolved oxygen, the outer layer precipitates according to (18) and the magnetite film develops completely without the evolution of hydrogen. In time, it may itself oxidise to the Fe(III) oxide haematite:

$$2Fe_3O_4 + 0.5O_2 \rightarrow 3Fe_2O_3 \quad (19)$$

and if the conditions are oxidising enough haematite may be formed directly without the intermediate formation of magnetite.

The duplex films of magnetite generally consist of a fine-grained inner layer of particles ten or so nanometres in size, overlaid with crystallites of sizes up to about ten micrometres. The outer layer crystallites are generally facetted octahedra, obviously grown from solution (see Figure 5 and 6).

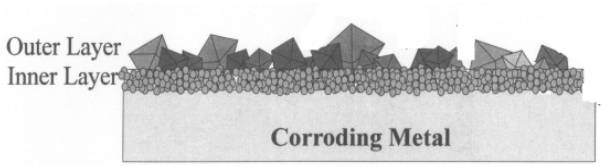

Figure 5. Schematic Cross-Section through Magnetite Film on Carbon Steel [Lister, 2003]

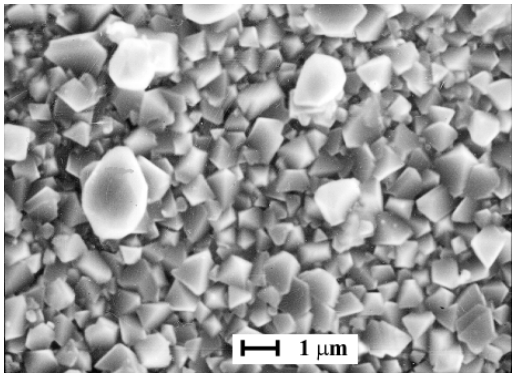

Figure 6. Scanning Electron Micrograph of Magnetite Film formed on Carbon Steel during an 1100-h Exposure in High-Temperature Water [Lister, 2003]

The general corrosion of the higher alloyed materials in widespread use in water reactor systems, such as the stainless steels and nickel alloys, also leads to the development of duplex oxide films. The oxide layers are generally thin and compact, conferring a high degree of corrosion resistance. The precise compositions of the oxides depend on the coolant chemistry, particularly the oxidising propensity. In general, it is the inner layers that "passivate" the alloy; these are based on the normal spinel $FeCr_2O_4$, which has a very stable lattice structure and a low solubility in the chemically reducing coolants of the pressurised water reactors (PWRs) and CANDUs [Lister, 1993]. Variants of the iron chromite structure contain elements arising from other alloy constituents such as nickel, viz. $Ni_xFe_{1-x}Cr_2O_4$, where x depends on the composition of the alloy; small amounts of other metals such as cobalt may also be incorporated and in the

primary coolant this gives rise to radiation fields from ^{58}Co and ^{60}Co. The outer-oxide layers are variants of the inverse spinel magnetite and are designated as $Ni_xFe_{3-x}O_4$; again, x depends on the composition of the underlying alloy but also, since the layer is precipitated from solution, it depends upon the metals dissolved in the coolant and originating in the rest of the circuit [Cook et al., 2000]. In PWRs, the composition of the outer layers on the alloys approximates $Ni_{0.6}Fe_{2.4}O_4$, a variant of nickel ferrite (or trevorite, $NiFe_2O_4$). This also approximates the composition of the particulate matter (called "crud") that circulates in suspension in the primary coolant at concentrations of the order of a ppb (part per billion) or less and that forms deposits on in-core fuel assemblies. In CANDU primary coolants the large surface area of carbon steel feeders makes magnetite the predominant constituent of crud.

The boiling water reactors (BWRs) traditionally operate under conditions of normal water chemistry, NWC, which exposes their alloys to high-temperature water that is slightly oxidising. This favours the formation of soluble Cr(VI) rather than the Cr(III), which is the basis of the chromite oxides that are widespread in the PWRs. Consequently, the stainless steels that constitute much of the BWR circuits develop oxides with less $FeCr_2O_4$; they also contain the Fe(III) oxide Fe_2O_3, haematite. In the move to less-oxidising coolant chemistry in the BWRs, accomplished by adding hydrogen to the feedwater to create hydrogen water chemistry (HWC), the oxides on stainless steel approach those found in the PWRs. It is interesting to note that detailed in-situ studies of corrosion rates on type SA 316L stainless steel indicate that NWC conditions are somewhat less corrosive than HWC conditions [Ishida and Lister, 2012]. The corrosion for the first 100 – 150 h under NWC follows logarithmic kinetics whereas under HWC it follows a joint parabolic-logarithmic law.

4.1.3 Corrosion and degradation of zirconium

In the water-cooled reactors, the major in-core materials in contact with the coolant are alloys of zirconium. The CANDUs have fuel bundles of the dioxide of natural uranium (i.e., 99.3% ^{238}U, 0.7% ^{235}U as UO_2) sheathed in Zircaloy-4 and the bundles are contained in pressure-tubes of Zr-2.5%Nb. Typical fuel burnups in CANDUs are about 7 MWd/kg and on-power refuelling is necessary to maintain the core critical. The PWRs traditionally use Zircaloy-4 to clad their fuel assemblies containing enriched UO_2; however, with the higher enrichment of 3-4% ^{235}U in advanced fuel, which can achieve burnups up to 52 MWd/kg, alloys containing Nb that are more corrosion- and hydriding-resistant, such as Zirlo© , tend to be employed. The BWR fuel assemblies can reach somewhat lower burnups of up to 42 MWd/kg and have their fuel clad with Zircaloy-2. Both types of LWR (light water reactor – PWR or BWR) have batch refuelling.

The corrosion of zirconium alloys has been postulated as occurring in three stages, as shown in Figure 5. The stages have been characterized as [Hillner et al., 2000]:

- Pre-transition, when a thin, black, tightly-adherent oxide thickens according to sub-parabolic (often assumed cubic) kinetics.
- Transitory, apparently corresponding to successive "cubic" periods of decreasing duration, when the thickening film cracks and becomes porous and new oxide grows at the M-O.

- Post-transition, when kinetics become rapid and linear and white or grey oxide is formed.

As indicated in Figure 7, the transitory period was not recognized in early models, although the omission has little effect on the general description. The transition occurs at film thicknesses of 2–5 μm.

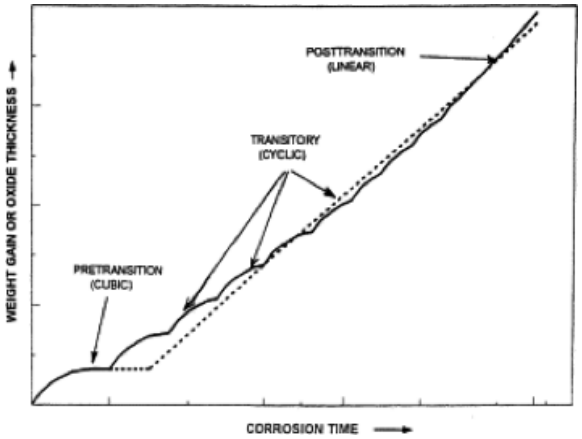

Figure 7. Schematic diagram of Zircaloy corrosion in high-temperature water, showing three regions (dotted line indicates early assumed pre-transition cubic and post-transition linear kinetics) [Hillner et al, 2000]

Much of the early research leading to our understanding of the corrosion and hydriding of zirconium and its alloys was conducted by Cox [Cox, 1976]. The basic electrochemical reaction is the formation of a compact oxide film based on zirconia (ZrO_2) via:

$$Zr + 2H_2O \rightarrow ZrO_2 + H_2 \tag{20}$$

The pre-transition film is adherent and compact zirconia of tetragonal crystal structure that grows via the solid-state diffusion through the oxide of ions/vacancies and electrons/holes. Electron diffusion is rate-determining and drives the cathodic reaction by reducing water to form hydrogen. The hydrogen generated (in overall terms by (20)) enters the metal in atomic form and at high enough concentrations precipitates within the lattice as flakes of hydride of nominal composition between ZrH and ZrH_2, making the material brittle. The post-transition oxide has monoclinic crystal structure and is much less protective than the pre-transition oxide, hence the accelerated corrosion. Since these processes occur with no oxide dissolution or release of cations to the coolant, the weight-gain of laboratory specimens is an accurate gauge of corrosion.

The oxide thicknesses on Zircaloy-4 cladding on high-burnup PWR fuel may reach 100 μm or more but on the advanced alloys are generally less than half that amount. Concentrations of LiOH of more than ~4 ppm (parts per million) may exacerbate corrosion rate. BWR exposures of Zircaloy-2-clad fuel induce nodular corrosion, whereby white spots of thick oxide appear on the underlying black oxide and grow with increasing exposure. The severity of nodular corrosion

depends upon the metallurgy of the alloy and the aggressiveness of the environment, but rarely causes problems (although spalled oxide has occasionally caused abrasion damage in BWR control-rod drive mechanisms). So-called "shadow corrosion", where galvanic effects thicken ZrO_2 films in proximity to components made of non-zirconium alloys such as stainless steel control-blade handles, is an additional mechanism in the low-conductivity and low-hydrogen environment of the BWR. BWR fuel is also subject to increased corrosion when the surface temperature is increased by the deposition of copper-containing crud that impairs the nucleation of steam bubbles. Such "CILC" (crud-induced localized corrosion) has led to fuel failures. These mechanisms of corrosion of zirconium alloys are reviewed in detail in the report of Adamson et al. [2007].

Because of its relatively low burn-up, CANDU fuel sheathing develops a very thin, protective oxide and failures from coolant-induced general corrosion are almost non-existent. The Zr-2.5%Nb pressure tubes in CANDUs and other PHWRs also experience low corrosion rates and their general corrosion over the 20-30-year lifetime in-reactor is acceptable. The oxidation, however, does force hydrogen (actually, deuterium from the heavy-water coolant) into the metal lattice, and this is much aggravated by deuterium that migrates into the pressure-tube ends across the rolled-joint between it and the stainless-steel end fittings, which also experience general corrosion. Hydriding (deuteriding) can then be a problem if concentrations exceed the "terminal solid solubility" (TSS), leading to precipitation of hydride "platelets", brittleness and possible cracking if excessive stresses are experienced [Simpson et al., 1974]. In fact as mentioned earlier, in the past, pressure tubes have failed because of delayed hydride cracking (DHC), so they must be continually monitored for uptake of hydrogen/deuterium during service [Perryman, 1978].

The Zr-Nb alloy of CANDU pressure tubes is subject to several other forms of degradation (growth and creep), and these will be life-limiting for the components in one form or another and are the primary reason a mid-life refurbishment (after approximately 30 years of operation) is required on CANDU reactors. As described in Section 2.1 above, neutron irradiation causes an increase in strength and a loss of ductility (or loss of toughness) in Zr-2.5%Nb alloys (as it does in all metals) but this does not prevent the pressure tubes from performing their role as a pressure boundary. The neutron irradiation causes additional defects (dislocations) to be produced in the metal lattice, which move through the metal's crystal structure either under the action of stress (known as radiation induced creep) or by the action of the neutron flux alone (radiation induced growth). The migration of the dislocations results in extension or contraction of the tube in its three major directions but because of the tube's texture or predominant grain orientation, growth is concentrated in the longitudinal direction. Providing sliding bearings on each end fitting has been demonstrated to accommodate the radiation induced growth and elongation. In early CANDU designs, channel extension was only sufficient to allow for thermal and pressure-based expansion. Design changes have substantially increased the channel extension capability. Fixing one end of the fuel channel now accommodates full-life channel elongation allowing for extension to occur at the opposite, free end of the channel. Typically, at the midway point through the reactor core's operating lifetime, the fuel channel is released at the initially fixed end and then pushed to its maximum inboard position and fixed at the formerly free end, allowing for the full scope of the design extension to be used. Fuel channel elongation is great-

est in the high power channels in the centre of the reactor resulting in a dish-shaped profile of fuel channel extension. Differential elongation could cause feeder pipes at reactor ends to contact and chafe each other, which must be avoided. Because of the material condition of the Zr-2 calandria tubes, they do not elongate to the extent of applying significant loads on the end shields.

The pressure tubes also sag with increased exposure time due to the elongation described above and from diametral creep. The diametral creep meant that fuel channels in the middle of the core, where the combination of neutron flux, pressure and temperature are highest, would suffer from significant portions of the coolant flow by-passing the fuel bundles, reducing the heat transfer efficiency and leading to reductions in the margins to dry-out. The remedy was then to derate – reduce the reactor power. Pressure-tube/calandria-tube sag also meant that the pressure tubes in some reactors approached the calandria tubes closely, and occasionally may have contacted one of the horizontal reactivity mechanism control tubes spanning the calandria. The pressure tube and its matching calandria tube are separated by wire wound toroidal spacers or garter springs that accommodate relative movement between the two. The pressure tube will sag more between the spacers than will the calandria tube due to the higher temperature and pressure operation and the weight of the fuel bundles. Should the spacers move out of position from vibration during operation, there is a risk that the hot pressure tube touchs the cool calandria tube inducing a thermal gradient or “cold spot” on the wall of the pressure tube. The will cause any hydrogen/deuterium in the vicinity to diffuse down the temperature gradient and form a hydride or hydrogen blister at the surface. Above a certain size, the blister will crack to accommodate the volume change and may initiate a delayed hydride crack that could penetrate the tube wall. As these degradation problems worsened with time of operation, pressure-tube rehabilitation programs were undertaken. REFAB (Repositioning End Fitting And Bearing) involved shifting pressure tubes within the core so that they were at the start of their travel on the bearings to accommodate elongation, as described above. SLAR (Spacer Location and Repositioning) involved using electromagnetic induction to find the spacers separating the pressure tubes and calandria tubes and then shift them to their design positions to counteract sag and avoid subsequent contact. Severely affected fuel channels could have their tubes replaced, and in the extreme case LSFCR (Large Scale Fuel Channel Replacement) could be undertaken, in which a full core is replaced. This was done during the early operation at Pickering, when the pressure tubes suffered delayed hydride cracking (DHC) because of faulty installation; it is an integral part of reactor refurbishment to double the operating life of the CANDU plant.

4.2 Flow-Accelerated Corrosion (FAC)

Flow-accelerated corrosion (FAC), sometimes called flow-assisted corrosion, was formerly referred to as erosion-corrosion, but the last term is now usually confined to attack in a corrosive medium aggravated by mechanical forces such as those arising from abrasion by solid particles. FAC is a form of general corrosion, but it is classified on its own here because of its particularly aggressive nature. Attacking the carbon steel piping of feedwater systems, it is one of the most widespread causes of shutdown in all kinds of steam-raising plant and on occasions has led to pipe rupture with accompanying injuries and even deaths of plant personnel. Fatal

accidents due to FAC in condensate systems have occurred in at least two nuclear plants – the Surry PWR in the US in 1986 and the Mihama 3 PWR in Japan in 2004 – and at fossil-fired plants such as the Pleasant Prairie coal-fired station in the US in 1995. Unexpected and sometimes excessive pipe-wall thinning from FAC has also been an endemic problem in the outlet feeders in the primary coolant systems of the CANDU reactors that were in operation before the two CANDU 6 models in Qinshan, China, that went into service in 2002 and 2003. Some feeders have had to be replaced as they reached their minimum wall thickness long before their design lifetime, Although these replaced feeders represent a small fraction of the total number in service, the necessity of regular inspections to ensure suitable margins still remains for the pipe wall thickness; feeder FAC represents a considerable cost to plant operators through planning, conducting and verifying the field inspections in the restricted, high radiation dose area.

The basic mechanism of FAC in power plants is the dissolution and "wearing" of the normally-protective film of magnetite that develops on the corroding steel in high-temperature water. As its title suggests, the phenomenon is exacerbated by fluid flow – specifically, turbulence. As it proceeds, the attack "sculpts" the metal surface into a characteristic pattern of shallow hollows, called scallops, the size of which is governed by the turbulence (see Figure 8). The magnetite dissolves at its interface with the coolant (i.e., at the O-C, by the reverse of Equation 17) and is replenished by corrosion at the metal-oxide interface (M-O) by reactions described above for general corrosion (in overall terms by Equation 7). Also as described above, not all the corroded iron can be accommodated as oxide at the M-O – about half diffuses through the oxide to the O-C. In an FAC environment the coolant is depleted of dissolved iron, no outer layer of magnetite can precipitate and the diffused iron is transported to the bulk coolant along with that produced by the magnetite dissolution. The transport to the bulk is effected by mass transfer, which is governed by the convective processes in the coolant – i.e., by the turbulence. Since the diffusion of iron through the oxide film governs the corrosion rate, the thickness of the film attains a steady-state which then controls the FAC at a constant rate.

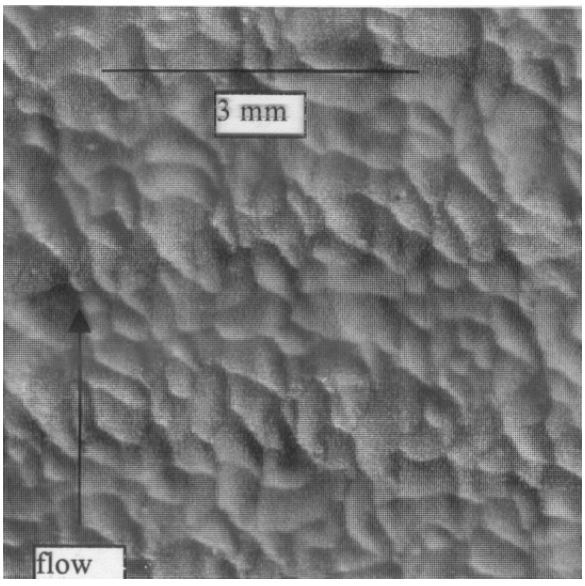

Figure 8. Scalloped surface of outlet feeder from Point Lepreau CANDU

This simple view of FAC, in which there are two processes in series – the dissolution of the magnetite film and the transport of iron to the bulk coolant – has been described by Equation 21 [Berge et al., 1980]:

$$R = \frac{k_m k_d \left(C_s - C_b \right)}{0.5 k_m + k_d} \tag{21}$$

where: R is the FAC rate (gFe/cm^2.s) , k_m is the mass transfer coefficient (cm/s), k_d is the magnetite dissolution rate constant (cm/s), C_s is the magnetite solubility (gFe/cm^3) and C_b is the concentration of iron in the bulk coolant (gFe/cm^3). High alkalinity reduces FAC in feedwater systems by reducing magnetite dissolution (by reducing C_s and k_d) – although at the higher temperatures in primary coolant systems increasing alkalinity tends to increase magnetite dissolution and is expected to increase FAC accordingly. The effects of flow and pH in the mechanism of FAC are shown in Figure 9.

We note that if dissolution controls, $k_d << k_m$ and Equation 21 reverts to:

$$R = 2 k_d \left(C_s - C_b \right) \tag{22}$$

Conversely, if mass transfer controls, $k_m << k_d$ and we have:

$$R = k_m \left(C_s - C_b \right) \tag{23}$$

However, mass transfer cannot be the sole mechanism responsible for FAC, since dependences on flow rate much greater than those conventionally described by empirical mass-transfer correlations are frequently encountered; moreover, FAC often occurs in circumstances where the dissolution of the magnetite is much slower than mass transfer and should control the rate, leading to the untenable situation of the process's being described by Equation 22, which has no flow dependence at all. These observations have led to the postulate of a mechanism for FAC wherein rapidly-flowing coolant that is unsaturated in dissolved iron dissolves the magnetite (as in the conventional description) but the dissolution loosens the nano-crystals of oxide at the O-C which are then stripped from the surface (eroded or spalled) by the force of the fluid shear stress at the pipe wall [Lister and Uchida, 2010]. A schematic view of the overall mechanism, which also involves some of the reactions of magnetite and hydrogen along with the diffusion of dissolved iron through the (now single-layered) oxide film as described earlier for general corrosion, is presented in Figure 10.

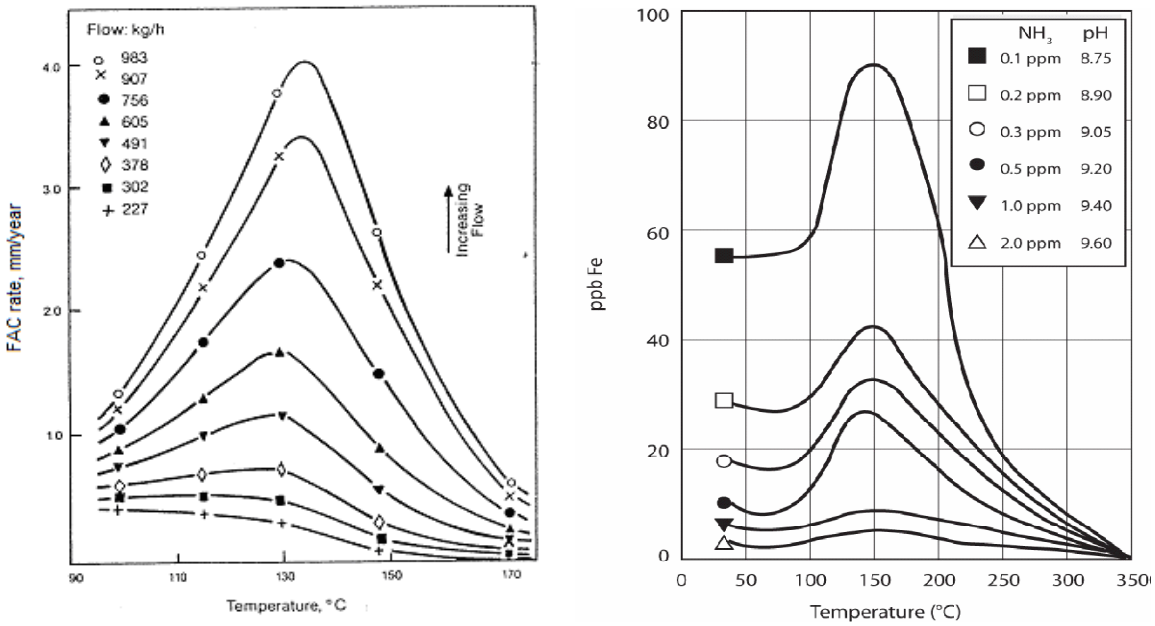

(a) after Bignold et al, 1982 (b) after Sturla, 1973

Figure 9. (a) Effect of temperature and flow on FAC at pH_{25^oC} 9.0 with ammonia; (b) Effect of temperature and pH on the solubility of magnetite.

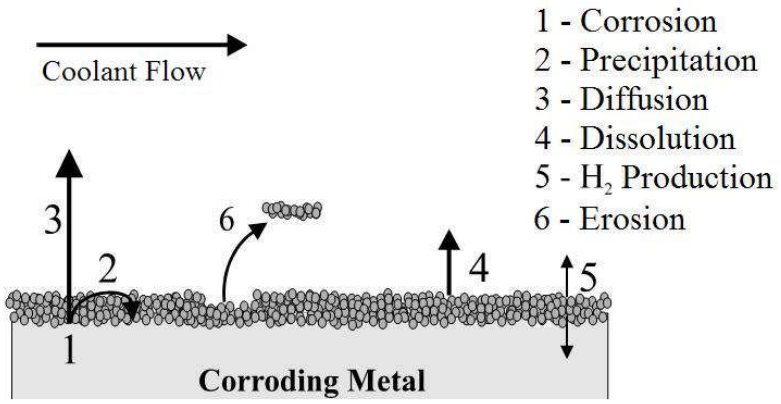

Figure 10. The overall mechanism of flow-accelerated corrosion.

The mathematical model describing this mechanism was first applied to a CANDU primary coolant system, for which measured values of k_d [Balakrishnan, 1977] were so much less than k_m that the conventional explanation of FAC via Equation 21 was clearly inadequate. The FAC in several outlet feeders at the Point Lepreau CANDU was modelled, leading to predictions of wall thinning rate around the first couple of bends downstream of the end-fitting that corresponded very well to plant measurements. At the same time, the oxide spalling terms led to realistic estimates of crud levels (concentrations of suspended oxide particles) in the primary coolant. After replacement of the dissolution terms in the model with precipitation terms and insertion of appropriate coolant flow rates and temperatures, the corrosion and oxide build-up on inlet feeders were also predicted very well, [Lister and Lang, 2002].

Traces of some transition metals (copper, molybdenum and especially chromium) in the carbon steel have long been known to reduce FAC rates; concentrations of Cr as low as a fraction of a percent have been demonstrated to lower FAC rates drastically [Bouchacourt, 1987]. Unfortunately, the existence of a lower limit of Cr content of 0.03 – 0.04%, below which FAC rates are not affected, has been propounded and is apparently incorporated into some examples of FAC software. Recent work, however, has demonstrated a reduction of ~60% in FAC rate between steels containing 0.001% Cr and those containing 0.019% Cr [Lister and Uchida, 2010].

The FAC of CANDU outlet feeders has now been mitigated in replacement piping and in new reactors by specifying a carbon steel with a higher chromium content [Tapping, 2008]. The original material had been specified with a low cobalt content to minimise the build-up of out-core radiation fields from ^{60}Co during reactor operation, and this resulted in a low chromium content since no Cr concentration was specified; for example, the Point Lepreau feeders were made of A106 Grade-B steel with 0.019% Cr. Replacement material has been A106 Grade-C steel with a Cr content of ~0.33% and this has led to a reduction in FAC rate of around 50%, which should be enough to assure the integrity of the piping for the lifetime of the plant.

The lower temperatures in secondary coolants and feedwater systems lead to higher magnetite solubilities and correspondingly higher FAC rates than in primary coolants (both solubility and FAC rate peak at ~130-150^{o}C, irrespective of pH or flow – see Figure 9). Thus, even with a steel containing 0.3% Cr and carrying feedwater dosed with amines, the 56 cm-diameter piping at the Mihama-3 PWR at 140^{o}C corroded at an average rate of 0.3-0.4 mm/year over the 20 years or so of operation before rupturing when the wall thickness reached about 2 mm. The mechanisms of FAC in feedwater systems of Mihama and elsewhere, including the effects of steel composition, have been successfully modelled (Phromwong et al., 2011).

4.3 Galvanic Corrosion

The aqueous corrosion of metals involves the transfer of electrons – it is an electrochemical process. Thus, for the corrosion of iron or steel in pure water, Equation 13 represents the anodic "half-cell" process forming iron ions in solution and electrons that are conducted to adjacent sites and react with water molecules (via Equation 14 – the cathodic "half-cell" process) to form hydroxide ions and hydrogen. The anodic reaction must be balanced by the cathodic reaction. The ions in solution interact and form iron hydroxide that will precipitate as the basis for rust or, at high temperature, will form magnetite.

A metal in contact with a solution establishes an electrical potential with respect to the solution. Such a potential cannot be measured directly, since a conductor introduced into the solution to serve as a measuring electrode to indicate the potential difference with the metal will establish its own potential. The best we can do is then to measure the metal's potential with respect to an electrode that is designated a standard. Such a standard is the "standard hydrogen electrode" (SHE), which is platinum metal in a solution of hydrogen ions at unit activity (i.e., an acid at pH 0) in contact with hydrogen gas at unit activity (i.e., at 1 atm pressure or partial pressure). The SHE is given the potential zero, and the potentials of metals in equilibrium with solutions of their own ions at unit activity are listed against the SHE potential (see Table 5). This list is the

galvanic series for industrially-important metals, and those with high potentials are termed more “noble” than those “active” ones with low potentials. An active metal can displace a more noble metal from solution – so in principle, a metal with a negative potential can displace hydrogen from solution as it dissolves or corrodes; a familiar example is the coating of an iron nail with copper as it is dipped into copper sulphate solution. Note, however, that some active metals such as aluminum and chromium are corrosion-resistant in many aqueous and atmospheric environments. This is because they form a very protective oxide that resists corrosion and makes their behavior more noble (they “passivate”).

Two dissimilar metals in contact in an aqueous environment can therefore act as an electrochemical cell, in which the more noble metal acts as the cathode and the more active metal acts as the anode; i.e., the more active metal dissolves – it corrodes. The greater the difference in the potentials, the greater the reaction rate. This is the principle of batteries such as the Daniel cell, in which electrodes of copper and zinc immersed in sulphate solution generate a potential difference of ~1.1 V as the Zn anode oxidizes and dissolves while Cu species are reduced and precipitated as metal at the Cu cathode. These processes generate an electric current in an external circuit. Galvanic coupling of metals is to be avoided in power plants, otherwise the more active metal will tend to corrode adjacent to the contact point. The severity of the corrosion depends upon the conductivity of the solution and the integrity of the joint between the metals. Oxide films may act as insulators, for example, and reduce the galvanic effect. On the other hand, galvanic processes can be used to protect metals from general corrosion. Galvanising steel by coating with zinc, for example, promotes a galvanic process, since the more active

Table 5. The galvanic series for important metals

Metal-metal-ion Equilibrium		Potential (25°C) Volts vs SHE
$Au^{3+}+3e^- \rightleftharpoons Au$		+1.498
$Pt^{2+}+2e^- \rightleftharpoons Pt$		+1.200
$Pd^{2+}+2e^- \rightleftharpoons Pd$	↑	+0.987
$Ag^{+}+e^- \rightleftharpoons Ag$	More Noble	+0.799
$Hg_2^{2+}+2e^- \rightleftharpoons 2Hg$		+0.797
$Cu^{2+}+2e^- \rightleftharpoons Cu$		+0.377
$2H^{+}+2e^- \rightleftharpoons H_2$		0.000
$Pb^{2+}+2e^- \rightleftharpoons Pb$		-0.126
$Sn^{2+}+2e^- \rightleftharpoons Sn$		-0.136
$Ni^{2+}+2e^- \rightleftharpoons Ni$		-0.250
$Co^{2+}+2e^- \rightleftharpoons Co$	More Active	-0.277
$Cd^{2+}+2e^- \rightleftharpoons Cd$	↓	-0.403
$Fe^{2+}+2e^- \rightleftharpoons Fe$		-0.440
$Cr^{3+}+3e^- \rightleftharpoons Cr$		-0.744
$Zn^{2+}+2e^- \rightleftharpoons Zn$		-0.763
$Al^{3+}+3e^- \rightleftharpoons Al$		-1.662
$Mg^{2+}+2e^- \rightleftharpoons Mg$		-2.363
$Na^{+}+e^- \rightleftharpoons Na$		-2.714
$K^{+}+e^- \rightleftharpoons K$		-2.925
$Li^{+}+e^- \rightleftharpoons Li$		-3.040

zinc becomes the anode when the couple is immersed in a solution and lowers the potential of any areas of exposed steel, protecting them cathodically. Similarly, components prone to corrode in aqueous environments may be protected cathodically by connecting them to an electrical source or by attaching a sacrificial anode of more active metal to lower their potential.

It is important to note that in most galvanic couples it is the cathodic component that controls the reaction rate and therefore the corrosion rate. Consequently, if dissimilar metals must be in contact, the area of the cathode should be small relative to that of the anode. It follows that to protect an active metal in contact with a more noble one by coating, painting, etc., the cathode (more noble component) should be the one coated. Horror stories abound of components such as carbon steel heat exchanger shells corroding rapidly adjacent to tube sheets of more noble metals such as titanium because the steel was coated as a protective measure rather than the titanium.

In summary, measures to minimize galvanic corrosion include: selecting metals as close together as possible in the galvanic series; avoiding small-anode/large-cathode combinations (e.g.,

choosing fasteners of more noble material); insulating dissimilar metals (e.g., sleeving bolts in flanged joints, as well as using insulating washers); applying coatings carefully, and keeping them in good condition (especially those on anodes); avoiding threaded joints where possible; designing for the anodic members (making them thicker, easily replaceable, etc.); and, installing a third metal that is anodic to ***both*** in the couple.

4.4 Stress-Corrosion Cracking & IGA

Stress-corrosion cracking (SCC) occurs in many metals in many environments; even nominally ductile materials can be affected. The attack may be trans-granular or inter-granular, depending upon whether the crack path traverses the metal grains or follows the grain boundaries (see Figure 11).

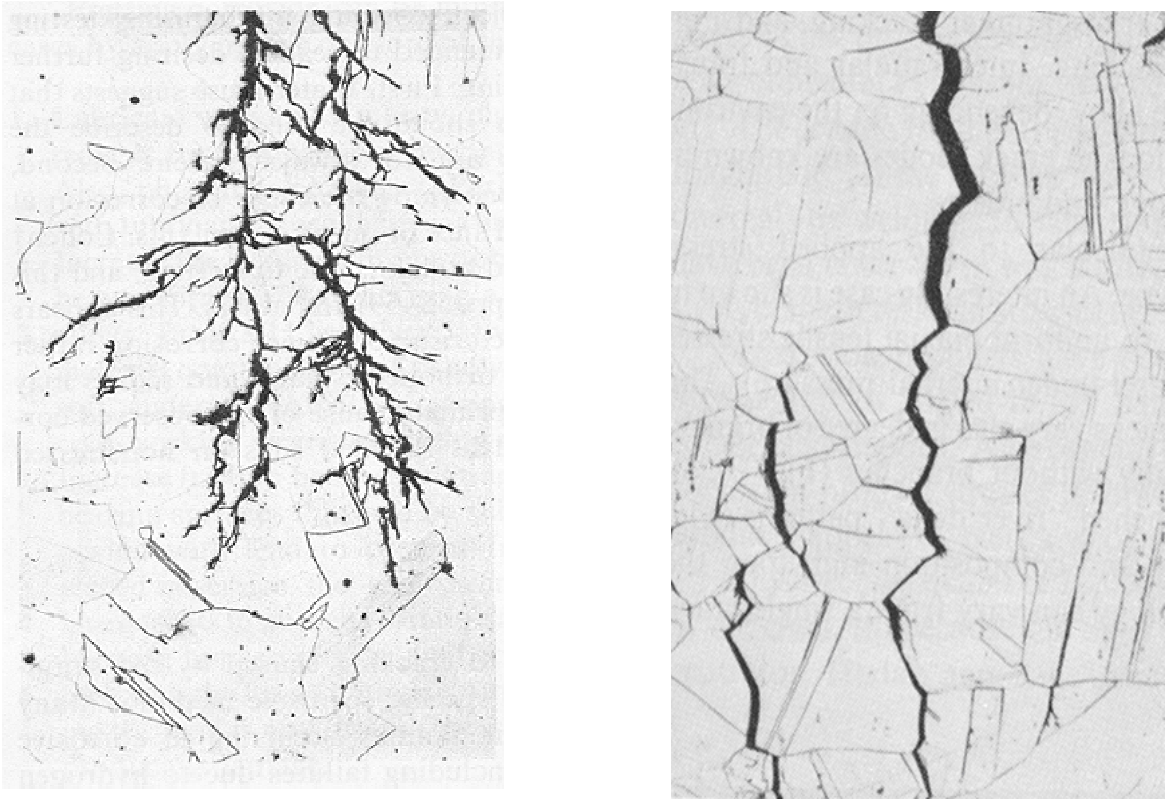

(a) **(b)**

Figure 11. Examples of transgrannular (TGSCC) (a) and intergrannular (IGSCC) (b) stress corrosion cracking in stainless steel and brass respectively (after Fontana 1986)

There are three factors required for inducing SCC: the environment must be sufficiently aggressive, which involves temperature since high temperatures generally increase a material's susceptibility; the composition and microstructure must be susceptible, which includes effects such as sensitisation as discussed earlier; and, the metal must be under tensile stress, which may be residual stress from manufacturing and/or operational stress from contained pressure. Note, however, that threshold levels of these factors do not necessarily exist if there is a long enough

exposure time of the material (Andresen et al., 2000).

The inside surface of Zircaloy sheathing of nuclear fuel elements can crack during operation under the influence of mechanical strain and of fission products, particularly iodine, released during irradiation. The CANLUB process for coating the insides of CANDU fuel sheaths with a thin layer of graphitic material was designed to counteract SCC by acting as a lubricant and to some extent as a getter for iodine. It has made CANDU fuel tolerant to a range of conditions imposed by power ramping and is applicable to both UO_2 and ThO_2 fuels (Hastings et al., 2009).

The alloys most susceptible to cracking in nuclear coolants have been the austenitic steels such as the 300-series stainless steels used for LWR piping and component cladding and the austenitic nickel alloys such as Alloy 600 (Inconel-600) used for steam generator tubing and pressure vessel penetrations. Thus, in the first years of operation of BWRs, the coolant in the reactor recirculating system was treated with "normal water chemistry" – NWC, which was nominally pure water that became oxidizing with ~200 ppb dissolved oxygen because of radiolysis in the core. The recirculation piping (made of type ASA 304 stainless steel) was then found to be prone to IGSCC. Extensive pipe replacements were necessary using, where possible, stress-relieved material containing low amounts of carbon to minimize the presence of sensitized material in service, especially in components where cold work and/or welding were used in fabrication. Lately, to make the coolant less oxidizing and therefore less aggressive to the austenitic steels around the core circuit, the chemistry has been changed to "hydrogen water chemistry" – HWC, which involves injecting hydrogen into the feedwater to counteract the radiolysis in the core. A level of ~2.0 ppm has been used to reduce the electrochemical corrosion potential (ECP) of the steel from the region of +100 to +300 mV with respect to the standard hydrogen electrode (SHE), attained under NWC conditions, to -230 mV (SHE) or lower – the measured threshold for SCC of stainless steel under BWR conditions. To achieve such low ECPs on all susceptible components in the reactor vessel without raising the hydrogen additions to unacceptable levels, General Electric's NobleChem^{TM} treatment has been applied, involving the addition of noble metal salts to the coolant to create a catalytic environment on surfaces (Hettiarachchi, 2005). Note that in CANDU reactors, the main use for the austenitic stainless steels is in the moderator system (the calandria vessel and the piping) and, at the low temperature of the circulating heavy water (<60^{o}C), there have been no incidences of SCC since it was recognized early in the design of the CANDU reactors that the low carbon versions (L-grade) of the austenitic stainless steels were to be specified to avoid known problems associated with sensitization, especially during welding.

Early steam generators in the PWRs and the CANDUs at Bruce A and the demonstration CANDU NPD were tubed with Alloy 600, which was known to be somewhat resistant to TGSCC (transgranular stress-corrosion cracking) from chlorides, although research had indicated that under some circumstances at high temperature it could crack in pure water (Coriou et al., 1960). Unfortunately, most of those tubes had generally received only a cursory heat-treatment during manufacture; they had been "mill-annealed" (MA) and as a result were supplied in a sensitized state that in many instances led to IGSCC during operation. Early failures occurred on the primary side in further-stressed locations such as the tight-radius U-bends and the rolled area near the tubesheet. Also, IGSCC occurred on the secondary side because of contact with high

concentrations of alkaline impurities in crevices with tube support plates and under "sludge piles" on the tube sheet. Full replacement of most of the PWR steam generators tubed with MA Alloy 600 became necessary, so that now only a few remain, the rest having been replaced with those tubed with thermally-treated (TT – to relieve stresses) Alloy 690 – a nickel alloy containing more chromium and less nickel. In CANDUs and several European PWRs, Alloy 800 has been preferred for SG tubing. The Alloy 600 SGs in Units 1 & 2 at Bruce A have been replaced with those tubed with Alloy 800 following the refurbishment projects. This contains more chromium and iron than Alloy 600 and, having less than 50% nickel, is not strictly speaking a nickel alloy, although it is usually classified as such for comparison with the others. It has been relatively resistant to SCC.

Stainless steels and austenitic alloys containing moderate to high concentrations of carbon (i.e., >0.03%) are vulnerable to corrosion of their grain boundaries if they have undergone a heating process such as welding that raises the temperature to the region of 500-800^{o}C. Heating to this range "sensitises" the material by preferentially precipitating the chromium in the grain boundaries as chromium carbide ($Cr_{23}C_6$), thereby leaving the metal surface above the grain boundaries depleted in chromium that would otherwise form the passivating oxide based on Cr_2O_3. As shown in Figure 12, the grain boundaries are then subject to corrosion via intergranular attack (IGA).

In particularly aggressive environments, IGA can be severe enough to loosen metal grains which then fall out, leaving a roughened and even more vulnerable surface exposed. In welded material, the attack is often called weld decay.

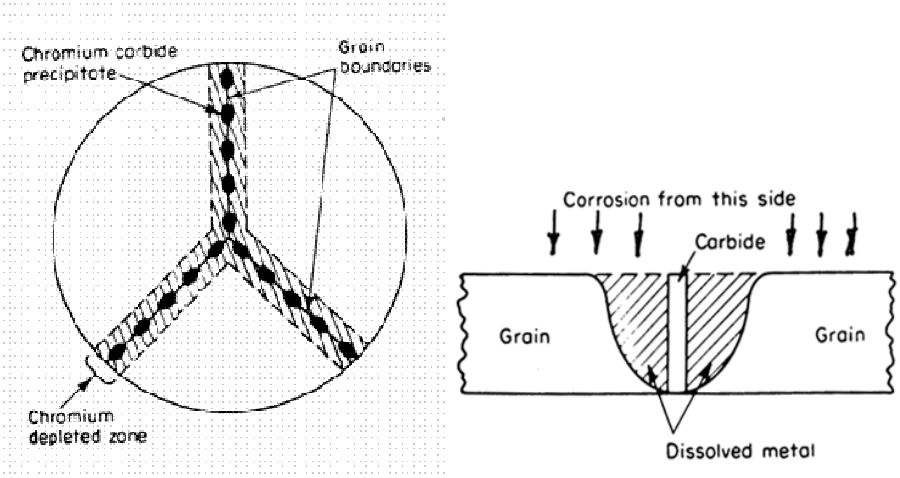

Figure 12. Typical sensitization mode and IGA of Type 304 stainless steel (after Fontana 1986)

Note that some situations may tolerate sensitised material; thus, sensitised stainless steel may be used in non-aggressive environments such as those found in architectural applications. For exposures to potentially aggressive conditions, however, sensitised material should not be used. A low-carbon grade of material (e.g., type ASA 304L stainless steel, with L indicating <0.03% C) is normally specified and since the carbon content is much reduced there is little available to precipitate as the carbide.

Austenitic material in general is usually supplied in the solution-quenched (also called solution-annealed or quench-annealed) condition, indicating that it was heated to above the carbide-precipitation temperature to dissolve the carbides into the metal matrix and then quenched to cool rapidly through the precipitation range of temperature so that carbide has no time to precipitate. Note that subsequent welding can re-sensitise the material, in which case the component must be solution-quenched again. There are also "stabilised" alloys such as type ASA 347 or type ASA 327 stainless steels which, respectively, contain small amounts of the strong carbide formers niobium or titanium. These have been heat-treated to precipitate the carbon as the niobium or titanium carbide at a temperature above the range where the chromium carbide would precipitate, leaving no carbon to combine with the chromium.

4.5 Crevice Corrosion & Pitting

Crevice corrosion and pitting are similar in that each proceeds via an electrochemical mechanism involving the formation of differential concentration cells arising from the occlusion of chemical species within restricted areas. Beneath gaskets in flanged connections, under bolt heads and washers, within riveted and lapped joints and under deposits of sludge or silt are common areas for attack, which can occur in a wide range of environments, including cooling waters, and which is greatly exacerbated by the presence of chloride ions. As with other types of localized corrosion, metals that rely on a passivating oxide for corrosion protection, such as titanium, stainless steel, etc., are especially vulnerable, although active metals such as carbon steel are also affected. In fact, all metals are said to undergo crevice corrosion given the right conditions. The mechanism proceeds as ingress of a corroding solution into a crevice such as a lapped joint in steel, for example, initially causes metal ions (in this example Fe^{2+}) to be released into the restricted space by the straightforward corrosion reaction. If oxygen is present in the solution it is rapidly depleted in the enclosed space and a differential aeration cell between the interior and exterior is established, promoting internal anodic metal dissolution and cathodic reduction of oxygen on surfaces external to the crevice. Even without oxygen present, the accumulated Fe^{2+} ions hydrolyse to $Fe(OH)_2$ and create internal acidic conditions while Cl^- ions are drawn into the space to maintain charge neutrality. Any oxide films within the space are degraded, the anodic processes are accelerated and attack is perpetuated (Figure 13 is a generalized illustration of the development of crevice corrosion in an aqueous environment contaminated with NaCl).

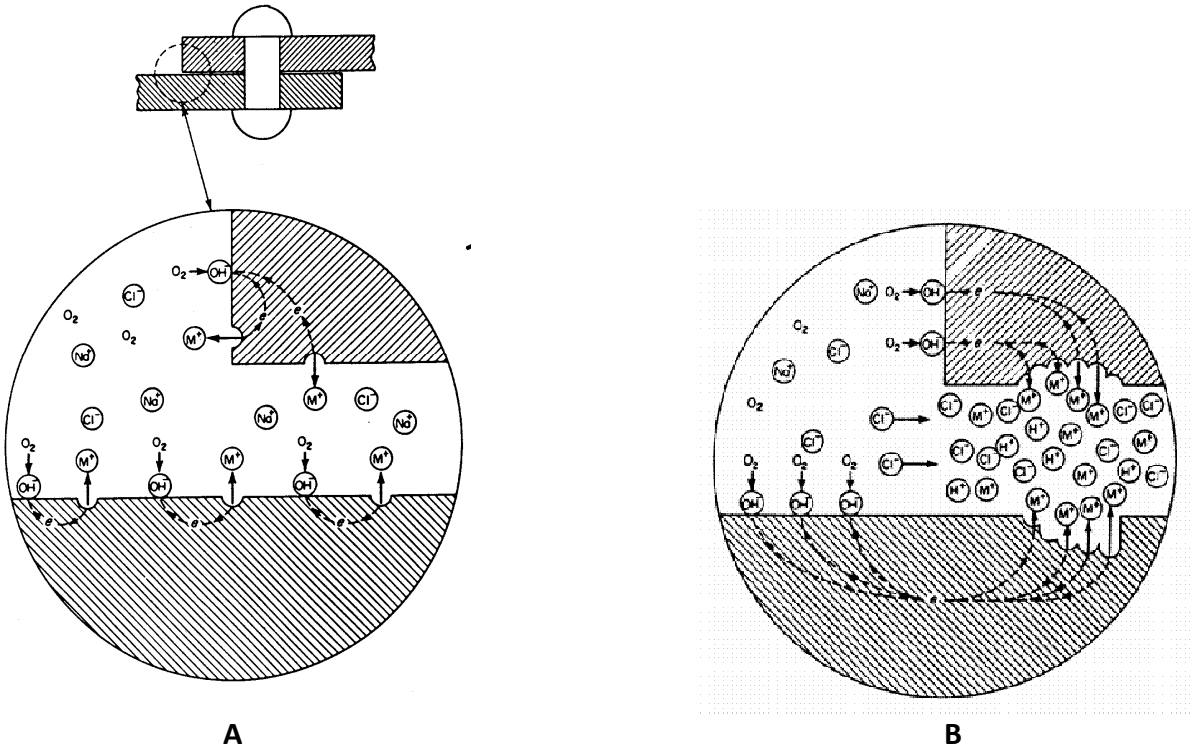

Figure 13. Initial (A) and final (B) stages in the development of crevice corrosion of a metal M (Fontana, 1986)

In the 1980s, the basic mechanism of the denting of the steam generators of Westinghouse design, which had drilled-hole support plates of carbon steel, was the corrosion of the steel forming the continuous crevices around the tubes. The heat transfer and boiling within the crevices drew in impurities such as chlorides and when these concentrated, especially in the presence of oxygen, aggressive acid conditions attacked the steel. The resulting growth of corrosion-product magnetite in the crevices exerted enough force to compress ("dent") the tubes and deform the plate itself. Several steam generators have had to be replaced because of denting. The prime example in CANDUs is the crevice corrosion of the inner surfaces of pressure tubes beneath fuel bearing pads, exacerbated by localized boiling which concentrates solutes such as LiOH and leads to aggressive conditions.

The similarity of the mechanism of pitting with that of crevice corrosion can be seen in the illustration in Figure 14. Note that the precipitation of corrosion products (e.g., hydroxides in the illustrations) can occur at the mouth of the crevice and around the rim of the pit and in the latter example can grow into tubes or tubercules. Pits usually occur on upward-facing surfaces, less frequently on vertical surfaces and rarely on downward-facing surfaces, indicating an effect of gravity on the occluded high-density solution.

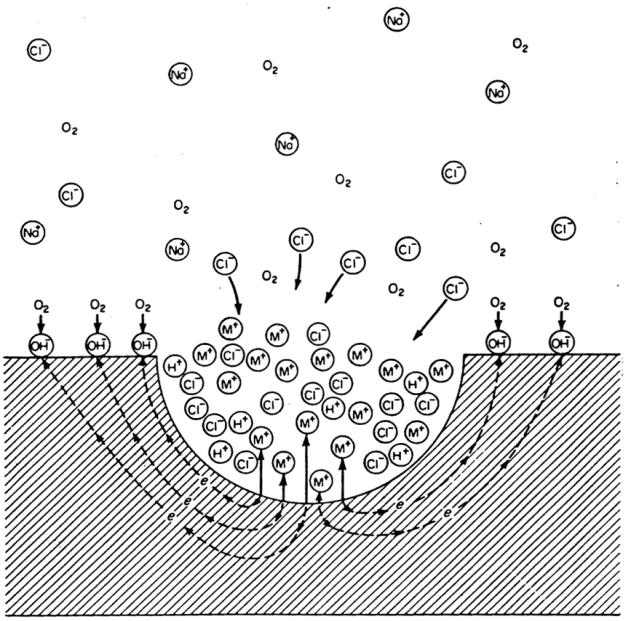

Figure 14. Self-perpetuating corrosion pit (after Fontana, 1986)

Pitting in particular can be extremely damaging. The pit mouths are often quite small and may be accompanied by extensive undercutting, culminating in perforation in severe cases, and pits may run into each other to create a rough surface degradation called general wastage (Figure 15). Beneath deposits, pits can go undetected and escape cursory inspections.

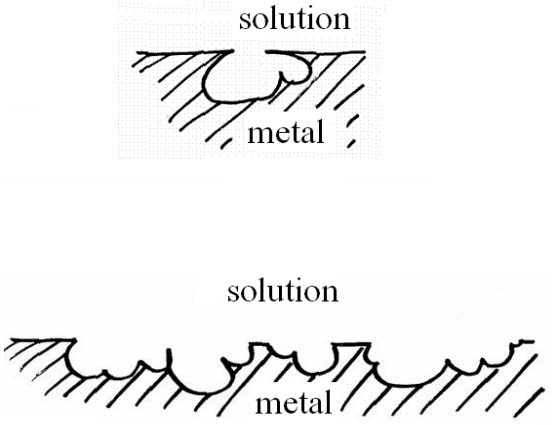

Figure 15. An undercut pit and surface wastage from overlapping pits

The pitting of heat exchanger tubes under silt deposits in an environment of static aerated cooling water polluted with chlorides is a pervasive problem in most industries, including nuclear power generation. Another common example in reactor systems is the pitting of the secondary side of steam generator tubes beneath sludge piles on the tubesheet. This was a particular problem with the German PWRs that had steam generators tubed with Alloy-800 and operated with chemistry controlled with additions of sodium phosphate; the concentration of aggressive species beneath the sludge led to pitting, in some cases extending to wastage. The

steam generators at the CANDU 6 at Point Lepreau, also tubed with Alloy 800, plugged many tubes because of pitting during the period of dosing with phosphate. The change from phosphate to all-volatile treatment seems to have arrested the degradation.

4.6 Fretting Wear & Flow-Induced Vibration

The rubbing of one material against another can damage surfaces; in a corrosive environment the damage is exacerbated. The vibration of foreign objects trapped within components such as heat-exchanger tube bundles (known examples are condensers and steam generators) can cause rapid deterioration of the tubes and loose objects within steam generator channel heads have been known to damage tube sheets. In CANDUs and PWRs the severe conditions of flow of steam-water mixtures in the secondary side of steam generators can create excessive vibrations that cause fretting between the tubes and the tube supports. The U-bend sections of the tube bundles, where the steam quality and coolant velocities are high, are particularly susceptible. Experiments to characterise the fretting behavior of material combinations at various steam generator conditions (temperature, coolant chemistry, etc.) typically record the rate of surface damage, in terms of amount of material removed per unit time, as a function of the work rate, which is the energy dissipated by sliding contact between two surfaces per unit time. The ratio of the two, wear rate V to work rate W, defines the wear coefficient, K:

$$K = \frac{V}{W} \tag{24}$$

K is usually quoted in units of m^2/N, or Pa^{-1}.

AECL at Chalk River performed an extensive series of fretting-wear tests on steam generator tube samples in contact with tube support samples. The factor having the greatest effect on tube damage was temperature; K at a steam generator operating temperature of 265°C was 20 times higher than at 25°C. Other factors, namely chemistry (ammonia, hydrazine, phosphate or boric acid), type of tube support (flat bar or broached hole), tube material (Alloy 800 or Alloy 690) or support material (type 410 or type 321 stainless steel) had relatively little effect. These results led to the suggestion that an average value of K of 20×10^{-15} Pa^{-1} and a conservative value of 40×10^{-15} Pa^{-1} may be used over a range of work rates for typical steam generator geometries and operating conditions (Guérout and Fisher, 1999).

Fretting wear also affects in-core components. In PWRs, it has been estimated that over 70% of fuel leaks are caused by fretting between the Zircaloy fuel rods and support grids – the so-called GRTF, grid-to-rod fretting (EPRI, 2008). The failures usually occur on final-cycle fuel assemblies, which are located at the core periphery. Similar failures occur in the WWER reactors, which have stainless steel grids.

The localized accelerated corrosion of CANDU pressure tubes because of the crevice effect beneath fuel bundle bearing pads has already been mentioned. When there is relative motion between the bearing pad and the pressure tube, resulting from flow-induced vibration for example, fretting can exacerbate the damage. This has rarely been seen except in reactors

having 13 fuel bundles, when significant damage is usually at the end of the pressure tube, where the cross-component of the coolant flow may cause more vigorous vibration. On the other hand, debris caught beneath fuel bearing pads can lead to significant fretting wear anywhere along the pressure tube and objects caught between elements within the fuel bundle can lead to fuel failures.

4.7 Hydrogen Effects

The most common form of hydrogen damage in reactor systems is the degradation of hydride-forming materials, in particular the zirconium alloys. In reactors in general these make up the fuel cladding, but in CANDUs they also make up the pressure tubes and the calandria tubes. As described earlier, delayed hydride cracking (DHC) and hydride blistering have been responsible for major replacements of CANDU pressure tubes in the past. Titanium also can be degraded by hydrogen, so it should be borne in mind that the contact of titanium components (condenser tubes, tube-sheet cladding, etc.) with carbon steel components (condenser shell, tube supports, etc.), which may promote galvanic corrosion of the steel, will drive cathodically-generated hydrogen into the metal. Similarly, hydriding of titanium condenser tubing in contact with a aluminum-bronze tube sheet occurred at the CANDU 6 at Point Lepreau. The condenser was completely re-tubed during the refurbishment outage and the Al-bronze tube sheet replaced with titanium. It follows that cathodic-protection measures such as sacrificial anodes, which lead to the production of hydrogen on cathodic components, can also promote hydriding of susceptible metals.

4.8 Microbiologically-Induced Corrosion (MIC)

Although MIC has been known for over 70 years, it has only been recognized as a serious corrosion mechanism in nuclear and fossil plants for 30 or so years (EPRI, 1988). Early references to the subject were general descriptions of practical situations (Uhlig, 1948) and mechanistic interpretations of observations were attempted from the 1960s onwards (Videla and Herrera, 2005).

There are many types of microbe that influence corrosion and they occur in many environments, especially natural waters. Consuming a variety of nutrients, they can grow under a wide range of temperatures, pressures and alkalinities/acidities. Their spores are even more resistant to adverse conditions and can be transported around systems and lie dormant for years before being revived to germinate, attach to surfaces and create localized colonies that exude corrosive waste matter (Licina and Cubicciotti, 1989). The biofilms created by the colonies consist of the so-called exopolymers, largely consisting of polysaccharides that develop as slimes containing corrosion products and debris carried from elsewhere in the system. They impede the transport of corrosion inhibitors to the metal surface and to some extent they shield the organisms from attack by treatment chemicals such as biocides. They can be tenacious and difficult to remove by fluid forces alone and in some cases – often carbon steel piping systems – can be thick enough to cause severe pressure drops.

The microbial species may exist in anaerobic (e.g., deaerated) conditions or in aerobic (e.g.,

aerated) conditions, and in some situations the one type creates local environments that sustain the other type, giving cycles of corrosion activity. Stagnant or low-flow conditions are conducive to MIC, so components buried in damp or wet soil and water-containing piping such as fire dousing systems are particularly vulnerable. Locally stagnant environments, such as under dirt or deposits and in crevices, also promote MIC. Reactor design features with redundant, static water systems along with long shut-down periods make nuclear plants particularly susceptible. Many materials are attacked, including the common metals in reactor systems such as stainless steels, nickel alloys, carbon steel, copper, and copper alloys. Typical features of attack in carbon steel are corrosion products deposited as tubercles and in stainless steel and nickel alloys are small pits, often stained with rust, that can be deep enough to be through-wall and cause small leaks especially at welds.

Sulphate-reducing bacteria (SRB) are responsible for many failures in water systems. The species *desulfovibrio* and *desulfomaculum* are among the most widespread and economically important organisms causing corrosion. They are anaerobic because their metabolism involves the consumption of the sulphate ion in deaerated waters, especially under deposits, although they can survive limited exposures to aerated conditions. They operate in steel systems by promoting the overall mechanism:

$$4Fe + SO_4^{2-} + 4H_2O \rightarrow 3Fe\left(OH\right)_2 + FeS + 2OH^- \qquad (25)$$

in which the microbes are instrumental in reducing the SO_4^{2-} to S^{2-}. The early postulate that the microbes act by depolarizing the cathodic areas and catalyzing the recombination of adsorbed hydrogen atoms to molecular H_2 has been largely superseded by mechanisms involving the formation of H_2S and the interaction with iron sulphide corrosion products (Videla and Herrera, 2005).

Aerobic species act by creating differential aeration and concentration cells through their biofilms. In seawater-cooled systems, for example, species such as *Pseudomonas* proliferate and can cause extensive damage to carbon steel and stainless steels. Detailed examinations of type 304 stainless steel surfaces pitted by *Pseudomonas* in seawater have shown more localized depletion of chromium in the passive films than similar control surfaces exposed in the absence of the bacteria (Yuan and Pehkonen, 2007).

Counteracting MIC is difficult. System cleanliness is quoted as a desired remedy but it should be noted that deionised water systems are susceptible. Moreover, removing slimes and biofilms by flushing is seldom effective, even with pulsating flows, and mechanical scouring with sponge balls etc. can damage protective films. Biocides are therefore a preferred recourse in many situations. Videla and Herrera (2005) list common biocides in industrial applications:

Table 6. Biocides used in industrial water systems.

Biocide	Properties	Usual concentration (mg/L)
Chlorine	Effective against bacteria and algae; oxidizing; pH dependent	0.1–0.2 (continuous)
Chlorine dioxide	Effective against bacteria, less so against fungi and algae; oxidizing; pH-independent	0.1–1.0
Bromine	Effective against bacteria and algae; oxidizing; wide pH range	0.05–0.1
Ozone	Effective against bacteria and biofilms; oxidizing; pH-dependent	0.2–0.5
Isothiazolones	Effective against bacteria, algae and biofilms; non-oxidizing; pH-independent	0.9–10
QUATs[a]	Effective against bacteria and algae; non-oxidizing; surface activity	8–35
Glutaraldehyde	Effective against bacteria, algae, fungi and bio-films; non-oxidizing; wide pH range	10–70
THPS[b]	Effective against bacteria, algae and fungi; low environmental toxicity; specific action against SRB	

[a]Quaternary ammonium compounds.
[b]Tetrakis-hydroximethyl phosphonium

5 References

R. Adamson, F. Garzarolli, B. Cox, A. Strasser and P. Rudling. Corrosion mechanisms in zirconium alloys. Zirat 12 Special Topic Report. A.N.T. International (2007).

P.L. Andresen, T.M. Angeliu, R.M. Horn, W.R. Catlin and L.M. Young. Effect of deformation on SCC of unsensitized stainless steel. Proc. CORROSION 2000 Conf., Orlando, Fl., USA. NACE Intern. (2000 March 26-31).

ASM International, *ASM Handbook: Volume 9 – Metallography and Microstructures*, GF. Vander Voort, Editor, ASM, Materials Park, Ohio, 2004.

P.V. Balakrishnan. A radiochemical technique for the study of dissolution of corrosion products in high-temperature water. Can. J. Chem. Eng., 55, 357 (1977).

P. Berge, J. Ducreux and P. Saint-Paul. Effects of chemistry on corrosion-erosion of steels in water and wet steam. Proc. 2nd Intern. Conf. onWater Chemistry of Nuclear Reactor Systems, Bournemouth, UK. BNES. (1980 October 14-17).

G.J. Bignold, K. Garbett and I.S. Woolsey. Mechanistic Aspects of the Temperature Dependence of Erosion-Corrosion. Proc. Specialists Meeting on Erosion-Corrosion in High Temperature Water and Wet Steam. *Les Renardières, France. EDF. (*1982).

N. Birks, G.H. Meier, F.S. Pettit, Introduction to the high-temperature oxidation of metals, 2nd Edition, Cambridge University Press, 2006.

M. Bouchacourt. Identification of key variables: EdF studies. Proc. EPRI Workshop on Erosion-Corrosion of Carbon Steel Piping. Washington DC, USA. (1987 April).

W.D. Callister, D.G. Rethwisch, Materials Science and Engineering: An Introduction, 8th Edition, Wiley, 2009.

W.G. Cook, D.H. Lister and J.M. McInerney. The effects of high liquid velocity and coolant chemistry on material transport in PWR coolants. Proc. 8th Intern. Conf. onWater Chemistry of Nuclear Reactor Systems, Bournemouth, UK, BNES, October 22-26, (2000).

H. Coriou, L. Grall, Y. Legall and S. Vettier. Stress corrosion cracking of Inconel in high temperature water. 3e Colloque Metall., Saclay, 1959. North Holland Publ., Amsterdam. p. 161 (1960).

B. Cox. Mechanisms of zirconium alloy corrosion in nuclear reactors. J. Corr. Sci. Eng.,Vol. 6, Paper 14 (2003).

EPRI. Sourcebook for microbiologically influenced corrosion in nuclear power plants. Electric Power Research Institute. Technical Report NP-5580 (1988).

EPRI. Fuel reliability guidelines: PWR grid-to-rod fretting. Electric Power Research Institute, Product ID 1015452. (28th July 2008).

M.G. Fontana. Corrosion Engineering. McGraw-Hill. (1986).

A. Garlick, R. Sumerling and G.L. Shires. Crud-induced overheating defects in water reactor fuel pins. J. Br. Nucl. Energy Soc., 16(1), 77 (1977).

F.M. Guérout and N.J. Fisher. Steam generator fretting-wear damage: a summary of recent findings. Trans. ASME, 121, 304-310 (1999 August).

I. Hastings, K. Bradley, J. Hopwood, P. Boczar, S. Kuran and S. Livingstone. We can use thorium. Nucl. Eng. Intern. (2009 August 28).

S. Hettiarachchi. BWR SCC mitigation experiences with hydrogen water chemistry. Proc. 12th Intern. Conf. on Environmental Degradation of Matls. in Nuclear Power Systems. Salt Lake City, Utah, USA. TMS. (2005 August 14-18).

E. Hillner, D.G. Franklin and J.D. Smee. Long-term corrosion of Zircaloy before and after irradiation. J. Nucl. Matls., 278(2-3), 334-45 (2000).

K. Ishida and D.H. Lister. In-situ measurement of corrosion of Type 316 Stainless Steel in 280ºC pure water via the electrical resistance of a thin wire. J. Nucl. Sci. Tech. 49 (11), (2012 November).

P. Kofstad. On the formation of porosity and microchannels in growing scales. Oxidation of Metals, 24(5-6), 265-276 (1985).

G.J. Licina and D. Cubicciotti. Microbial-induced corrosion in nuclear power plant materials. J. Nucl. Matls., 41(12). 23-27 (1989).

D.H. Lister. Activity transport and corrosion processes in PWRs. Nucl. Energy, 32(2), 103- 114 (1993).

D.H. Lister. Some aspects of corrosion in cooling water systems and their effects on corrosion product transport. Proc. EUROCORR 2003, Budapest, Hungary, (2003 September 28-October 2).

D.H. Lister and L.C Lang. A mechanistic model for predicting flow-assisted and general corrosion of carbon steel in reactor primary coolants. Proc. Chimie 2002; Intern. Conf. Water Chem. Nucl. Reactor Systems. Avignon, France. SFEN. (2002).

D.H. Lister and S. Uchida. Reflections on FAC mechanisms. Proc. Intern. Conf. on Flow-Accelerated Corrosion (FAC) in Fossil and Combined Cycle / HRSG Plants, Arlington, VA, USA. (2010 June 29-July 1).

E.C.W. Perryman. Pickering pressure tube cracking experience. Nucl. Energy, 17, 95–105 (1978).

P. Phromwong, D.H. Lister and S. Uchida. Modelling material effects in flow accelerated corrosion. Proc. Intern. Conf. on Environmental Degradation of Matls. in Nuclear Power Systems, Colorado Springs, CO. TMS. (2011 August 7-11).

E.C. Potter and G.M.W. Mann. Oxidation of mild steel in high-temperature aqueous systems. Proc. 1st Intern. Congress Metallic Corros. London. p. 417 (1961).

Qiu, L. Dissolution of silicon nitride in high-temperature alkaline solutions. Proc. Intn'l. Conf. Props. Water and Steam. IAPWS. Greenwich, London. Sept. 1st-5th (2013).

P.R. Roberge. Handbook of corrosion engineering. McGraw Hill (2000).

G. Schikorr. On the iron-water system. Z. Elektrochem. 35, 62 (1928).

C.J. Simpson and C.E. Ells. Delayed hydrogen embrittlement of Zr-2.5wt.%Nb. J. Nucl. Mater., 52, 289–295 (1974).

J.P. Slade and T.S. Gendron. Flow accelerated corrosion and cracking of carbon steel piping in

primary water – operating experience at the Point Lepreau Generating Station. Proc. Intern. Conf. on Environmental Degradation of Matls. in Nuclear Power Systems, Salt Lake City, UT. TMS. (2005).

P. Sturla. Oxidation and deposition phenomena in forced circulating boilers and feedwater treatment. Proc. Fifth National Feedwater Conf. Prague, Czech. (1973).

R.L. Tapping. Materials performance in CANDU reactors: The first 30 years and the prognosis for life extension and new designs. J. Nucl. Materials. 383, 1-8 (2008).

M.R Taylor, J.M Calvert, D.G. Lees and D.B. Meadowcroft. The mechanism of corrosion of Fe-9%Cr alloys in carbon dioxide. Oxidation of Metals, 14(6), 499-516 (1980).

H.H Uhlig. Corrosion handbook. John Wiley, New York. 466-481 (1948).

H.A. Videla and L.K. Herrera. Microbiologically-influenced corrosion: Looking to the future. Intern. Microbiol., 8. 169-180 (2005).

C. Wagner and W. Traud. On the interpretation of corrosion processes through superposition of electrochemical partial processes and on the potential of mixed electrodes. Z. Elektrochem. Ang. Physik. Chemie, 44, 398 (1938).

G.S. Was, Fundamentals of Radiation Materials Science: Metals and Alloys, Springer, 2007.

S.J. Yuan and S.O. Pehkonen. Microbiologically influenced corrosion of 304 stainless steel by aerobic *Pseudomonas* NCIMB 2021 bacteria: AFM and XPS study. Colloids and Surfaces B: Biointerfaces, 59(1), 87-99 (2007).

6 Acknowledgements

The following reviewers are gratefully acknowledged for their hard work and excellent comments during the development of this Chapter. Their feedback has much improved it. Of course the responsibility for any errors or omissions lies entirely with the authors.

Kit Colman
Mark Daymond
Ed Price
Bob Tapping

Thanks are also extended to Diana Bouchard for expertly editing and assembling the final copy.

CHAPTER 15

Chemistry in CANDU Process Systems

prepared by

Dr. William G. Cook and Dr. Derek H. Lister
University of New Brunswick

Summary:

The efficient and safe operation of a CANDU reactor is highly dependent upon the selection and proper implementation of chemistry control practices for the major and ancillary process systems such as the primary and secondary coolants and the moderator. The materials of construction of the various systems are selected in consideration of the neutron economy while keeping the proper chemical environment in mind in order to keep corrosion and degradation low and to ensure desired plant operating lifetimes. This chapter begins with an overview of the basic chemistry principles required to manage chemistry in CANDU reactors and then provides a detailed description of the chemistry control practices and the reasons behind their use in the major and ancillary process systems. The chapter concludes by examining the current practices of component and reactor lay-up for maintenance shut-downs and refurbishments and a description of heavy water purification and upgrading.

Table of Contents

List of Figures

List of Tables

1 Introduction

1.1 Overview

This chapter explains the current state-of-the-art of CANDU system chemistry. It begins with an overview of the basic chemistry principles, as relevant to the major process systems of a CANDU reactor, and goes on to describe the modes of operation of the primary heat transport circuit, the secondary heat transport circuit, the moderator system and plant auxiliary systems with respect to system chemistry. It draws on knowledge of overall system configuration and materials selection as described in chapters 2 and 11 of this text and, through examples of plant chemistry specifications, creates a detailed knowledge of the reasoning behind the combined selection of materials and chemistry. The necessity of minimizing corrosion and degradation of the auxiliary systems supporting the operation of a CANDU reactor are also highlighted along with a description of current chemistry dosing practices for these systems. Since every reactor undergoes frequent maintenance outages and a mid-life refurbishment, the lay-up practices during these outages are important factors affecting the overall lifetime of the plant; current practices are described. Finally, the isotopic degradation and tritiation of the heavy water coolant and moderator necessitate the use of clean-up and upgrading, issues that are dealt with in the final sections of this chapter.

1.2 Learning Outcomes

The goal of this chapter is for the student to understand:

- The relation between system chemistry conditions and material selection
- The current chemical dosing practices for the various cooling systems
- The primary reasoning behind specific chemistry and materials selection
- The current best practice for system layup during maintenance outages

2 Chemistry Principles Applied to Reactor Coolants

The chemistry of CANDU reactor system coolants is generally kept quite simple with the intent of maintaining highly pure water with low concentrations of chemical additives to maintain low corrosion rates on the materials in the systems. Before the specific chemistry control strategies of the various nuclear and non-nuclear coolant systems are described, it is beneficial to define several basic chemistry concepts that are particularly relevant to chemistry control in the plant. These include a reminder of the measure of acidity/alkalinity (pH) and how it is typically used in heavy water systems as “apparent pH or pH_a”, the definition and calculation of the conductivity of solutions containing dissolved ionic compounds and a discussion of water radiolysis or the breakdown of water when exposed in a radiation field. Each of these topics will be dealt with in turn to begin the chapter and will be used throughout the remainder of the chapter in describing the chemistry of the various reactor systems.

2.1 pH, pD and Apparent pH (pH_a)

The pH in a heavy water system is more correctly the pD, where D is the deuterium isotope. Before the implications of using heavy water in the CANDU systems are discussed, it is beneficial to review some basic chemistry principles. Recall that the definition of pH is:

$$pH = -\log_{10}\left(a_{H^+}\right) \tag{1}$$

where a_{H+} is the activity of the hydrogen ion in the aqueous solution, which is dependent upon the concentration of the hydrogen ion (m_{H+} - mol/kg), the activity of the standard reference state (m^o = 1 mol/kg) and the ionic activity coefficient ($\gamma_{+/-}$) as shown in equation 2.

$$a_{H^+} = \gamma_{\pm}\frac{m_{H^+}}{m^o} \tag{2}$$

Under dilute conditions, the activity of ions in solution can be approximated by their concentration since the mean ionic activity coefficient ($\gamma_{+/-}$) is dependent upon the ionic strength of solution and is nearly unity (1) for concentrations below ~ 10^{-3} mol/kg.

For neutral, light water (H_2O), there is an equilibrium established between the water molecules and the dissociation products H^+ (or H_3O^+) and OH^- as shown in equation 3.

$$H_2O \rightleftharpoons H^+ + OH^- \tag{3}$$

By definition, the equilibrium constant for this chemical dissociation reaction is given by the ratio of the activities (concentrations) of the product species to that of the reactant (H_2O); Equation 4 defines K_w, the dissociation constant or auto-ionisation constant for water, which has a value of 10^{-14} at 25 ^oC [IAPWS, 2007, Bandura & Lvov, 2006]. The activity of water (a_w) is typically regarded as unity in dilute solutions, thus neutral water, defined as the point where the activity of H^+ equals that of OH^-, will give a pH of 7 as calculated through equation 4.

$$K_w = \frac{a_{H^+}a_{OH^-}}{a_{H_2O}} = 10^{-14} \text{ @ } 25^oC \tag{4}$$

Increasing the pH of a solution is as simple as adding hydroxyl anions from a base such as lithium hydroxide (LiOH), which will shift the equilibrium between H^+ and OH^-. Lithium hydroxide is a strong base that is essentially completely dissociated in water up to reactor operating temperatures and thus can be used at low concentrations to achieve considerable changes in pH. Exercise 1 demonstrates the calculation.

The dissociation of water (and other ionic compounds) is dependent upon temperature. The Bandura & Lvov correlation, as recommended by the International Association for the Properties of Water and Steam (IAPWS) is commonly used to relate this temperature dependence, giving the result shown in Figure 1. In the temperature range 0 – 310 ^oC the pK_w (defined as $-\log_{10}K_w$) decreases significantly before starting to increase again around 250^oC. This implies that the

neutral point of water is lowered as temperature is increased, as illustrated by simple calculation – the pH of neutral water at 250°C is ~ 5.57 and at 300°C is about 5.64.

In the heavy water systems of the CANDU reactor, the proper equations describing the dissociation of heavy water would be:

$$D_2O \rightleftharpoons D^+ + OD^- \tag{5}$$

and the pD is:

$$pD = -\log_{10}\left(a_{D^+}\right) \tag{6}$$

where a_{D+} is the activity of the deuterium ion in aqueous solution; this is analogous to the definition of pH in equation 1. As in light water, the activity coefficient under sufficiently dilute conditions is nearly unity so we can consider the activities of D^+ and OD^- to be equal to their molal (mol/kg) concentrations. Unfortunately, the direct measurement of pD is usually not possible since pH electrodes are typically constructed with light-water-based fill solutions and are calibrated using light water buffers. Thus, for heavy water systems, it is standard practice to quote a pH_a or "apparent" pH, which identifies the observed or measured pH value of the heavy water using traditional pH electrodes and buffer solutions. A general relation [Mesmer & Herting, 1978] between the dissociation of heavy water and that of light water leads to the simple correlation shown in equations 7 and 8:

$$pH_a = pD - 0.41 \tag{7}$$

or, when considering an alkaline solution such as CANDU systems adjusted with LiOH:

$$pH_a = pH + 0.456 \tag{8}$$

This equation is the direct result of the difference between the dissociation of heavy water and that of light water when considering that pOD ≈ pOH at room temperature. Also shown in Figure 1 is the pK_D expressing the dissociation equilibrium constant for heavy water [Mesmer & Herting, 1978]. It is apparent that heavy water is less dissociated than light water under equivalent conditions, leading to higher equivalent values of the neutral point of heavy water at the various temperatures. This difference results in the approximate 0.41 unit shift between pH of light water and the pD of heavy water.

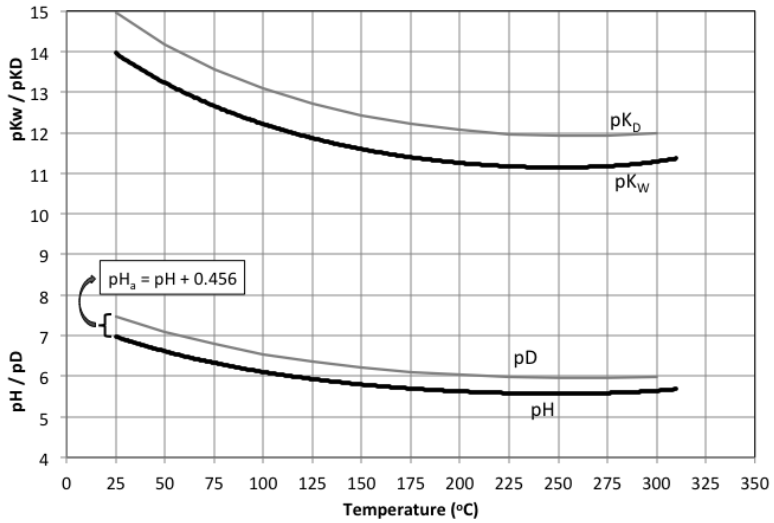

Figure 1. Temperature dependence of pK_w / pK_D and the neutral pH / pD for the dissociation of light and heavy water.

2.2 Solution Conductivity

The fact that water dissociates into H^+ and OH^- ions (equation 3) gives rise to a finite conductivity value, which means that water in its pure state can act as an electrical conductor, albeit a very poor one. We recall that the passage of current or electricity is the movement of charge measured in Amperes (A), which is the movement of one Coulomb of charge per second (i.e. 1 A = 1 C/s). Typically the charge carriers are envisaged as electrons moving down a conducting cable but the migration of ions in solution also carries charge from one point to another down a potential gradient. The conductivity (or inversely, the resistivity) of a solution is dependent upon the concentration of the charge-carrying ions in solution and their overall mobility. Thus, a measurement of the conductivity of an aqueous solution will give an indication about the quantity of the ions that it contains and, in the case of nominally pure CANDU process system water with small concentrations of additives to increase or lower the pH, this measurement should be directly related to the concentration of the specific cations and anions in the solution.

2.2.1 Specific Conductivity

The molar conductivity ($S.m^2/mol$) of an aqueous solution is given by:

$$\Lambda_m = \frac{\kappa}{c} \tag{9}$$

where κ is the specific conductance of the electrolyte (S/m or $1/\Omega.m$) and c is the stoichiometric molar concentration of the solution. Measuring the conductivity (or resistivity) of an aqueous solution is typically accomplished by placing two plate electrodes in the solution having fixed separation between them and with known cross-sectional area and then measuring the absolute resistance between them. The specific resistivity (ρ) follows from the calculation of the cell

resistance shown in equation 10 and specific conductivity (κ) is related through equation 11.

$$R = \frac{\rho \times \ell}{A} \tag{10}$$

$$\kappa = \frac{1}{\rho} \tag{11}$$

The molar conductivity of the solution, and hence the solution specific conductivity, can be broken down into the sum of the individual contributions of the ions, each one of which will be dependent upon its concentration and overall mobility. Essentially, the specific conductivity of the solution is the sum of the specific conductivities of the individual ions:

$$\kappa = \sum_i \kappa_i \tag{12}$$

We define the molar conductivity of the ion in solution (λ_i) in an analogous way as the overall molar conductivity of the solution, thus:

$$\lambda_{m,i} = \frac{\kappa_i}{c_i} \tag{13}$$

In an ideal solution, the molar conductivity would vary linearly with increasing concentration (and specific conductivity); however, in reality the solution molar conductivity has a non-linear dependence on solution concentration, particularly in more concentrated solutions. This stems from the fact that ion-to-ion and ion-to-solvent interactions play larger roles in concentrated solutions. Thus, the molar conductivity for an individual ion in solution may only be truly measured if there are no other interfering ions present, i.e. in an infinitely dilute solution. Inserting equation 13 into 12 and subsequently into 9 yields:

$$\Lambda_m = \frac{1}{c}\sum_i c_i \lambda_i \tag{14}$$

If we note for a $M\nu^+X\nu^-$ electrolyte, where ν^+ and ν^- are the valences of the cation and anion respectively, that the concentration of each ion will depend upon the total concentration of the salt in solution, at infinite dilution this results in the simple relation of equation 15:

$$\Lambda_m^\infty = \nu_+ \lambda_{M^+}^\infty + \nu_- \lambda_{X^-}^\infty \tag{15}$$

The ionic molar conductivities at infinite dilution are tabulated in various sources and allow for the calculation of the solution specific conductivity directly [CRC, 2014]. It should be noted that the above equations apply for solutions at infinite dilution but may be used directly with small error up to total solution concentrations of approximately 10^{-3} mol/L. Table 1 shows the ionic molar conductivity of cations and anions relevant to the operation of CANDU reactors. Note that the ionic molar conductivity of each ion is per equivalent since the total migration of an ion

subjected to an electric field will be dependent upon its charge (valence). Note also the comparatively large conductivities of H^+, D^+, OH^- and OD^-, which is due to the Grotthus "hopping" mechanism for these ions in aqueous solution where the individual ions themselves do not physically migrate but they are exchanged through the interconnecting hydrogen-bonded structure of liquid water. These ions tend to dominate the conductivity of the relatively pure CANDU process solutions.

Table 1. Conductivity at infinite dilution in H_2O [CRC, 2014].

Cations ($S\ cm^2\ mol^{-1}\ eq^{-1}$)		Anions ($S\ cm^2\ mol^{-1}\ eq^{-1}$)	
H^+	349.7	OH^-	198
D^+	249.9	OD^-	119
Li^+	38.7	Cl^-	76.31
Na^+	50.1	½ SO_4^{2-}	80.0
1/3 Gd^{3+}	67.3	HCO_3^-	44.5
NH_4^+	73.5	½ CO_3^{2-}	69.3
½ Fe^{2+}	54	NO_2^-	71.8
$N_2H_5^+$	59	NO_3^-	71.48

Example 15.1- calculating solution conductivity from pH and values at infinite dilution.

Lithium hydroxide is added to the light water in the calandria vault and end shield cooling system to control the pH and minimize corrosion of the carbon steel components. The pH specification is 9.5. Calculate the required lithium ion concentration in the water (in ppm) to attain the pH specification and estimate the solution conductivity assuming no other impurities are present.

Solution

Since the pH specification is given (9.5), the concentration of H^+ and OH^- are readily evaluated from the definition of pH and K_w:

$$pH = -\log_{10}([H^+])$$

thus:
$$[H^+] = 10^{-pH} = 10^{-9.5} = 3.16 \times 10^{-10}\ mol/kg$$

recalling the dissociation of water (K_w, eq. 4), the OH- concentration is:

$$[OH^-] = \frac{K_w}{[H^+]} = \frac{10^{-14}}{3.16 \times 10^{-10}} = 3.16 \times 10^{-5}\ mol/kg$$

In this case, lithium hydroxide is a strong base and completely dissociates into lithium and hydroxyl ions:

$$LiOH \rightleftharpoons Li^{+} + OH^{-}$$

thus, the concentration of lithium must be equal to the hydroxyl concentration in the water, i.e.:

$$[Li+]=[OH-] = 3.16 \times 10^{-5} \text{ mol/kg}$$

Converting to ppm (mg/kg):

$$[Li^{+}] = 3.16 \times 10^{-5} \ \frac{\text{mol Li}}{\text{kg } H_2O} \times \frac{6.94 \text{ g}}{\text{mol}} \times \frac{1000 \text{ mg}}{\text{g}} = 0.219 \text{ mg/kg}$$

Ans.

To calculate the expected conductivity, combining equations 12 and 13 results in:

$$\kappa = \sum_i c_i \lambda_i$$

Conductivity values for Li+ and OH- can be attained from Table 1, and since $[Li^{+}]=[OH^{-}]$:

$$\kappa = c_{LiOH} \left(\lambda^{\infty}_{Li^{+}} + \lambda^{\infty}_{OH^{-}} \right)$$

Since the units of conductivity are in cm^2, the concentration is converted to mol/cm^3 for consistency:

$$c_{LiOH} = 3.16 \times 10^{-5} \frac{\text{mol}}{\text{kg}} \frac{1000 \text{ kg}}{\text{m}^3} \frac{\text{m}^3}{1000 \text{ L}} \frac{\text{L}}{1000 \text{ mL}} \frac{1 \text{mL}}{1 \text{cm}^3} = 3.16 \times 10^{-8} \text{ mol/cm}^3$$

Calculating the conductivity and converting to standard units of mS/m:

$$\kappa = 3.16 \times 10^{-8} \frac{\text{mol}}{\text{cm}^3} \left(38.7 + 198 \frac{\text{S cm}^2}{\text{mol eq}} \right) = 7.48 \times 10^{-6} \text{ S/cm}$$

thus, the conductivity of the cooling water is expected to be 0.748 mS/m. Ans.

2.2.2 Cationic Conductivity or Conductivity After Cationic Exchange (CACE)

While the conductivity of a solution provides an indication of the concentration of impurity ions that are present, it is not species- or ion-specific; thus, there is no way of determing from a conductivity measurement what are the individual dissolved ionic species present in the solution. One way of providing a better indication of the concentration of anionic impurities in an aqueous solution is to use the cationic conductivity (or conductivity after cationic exchange - CACE) [IAPWS, 2012], which gives a direct measure of the anionic impurities in the system that may be aggressive to the corrosion of plant materials. Cationic conductivity is simply the conductivity of an aqueous solution after it has been passed through a strong acid ion-exchange

column to remove the cations (such as Na^+, K^+, Ca^{2+} etc.), which replaces them with the proton (H^+). The solution that elutes from the cation exchange column will contain the same concentration of anions (Cl^-, SO_4^{2-} etc) as the original sample and can provide a rapid and direct indication of the rate of increase of these impurities. This gives a very useful online measurement of impurity ingress, specifically in the case of a condenser leak.

2.3 Purification and Ion Exchange Resin

Filter media and ion exchange resins are used extensively in the nuclear and power generating industry for removing particulate and ionic impurities from a solution. All power plants will have a water treatment plant that includes ion-exchange as a final "polishing" method to ensure extremely pure water is available for use in the various process systems and each process system will contain filters of various configurations to collect suspended solids. Ion exchange media come in many forms and can be tailored for removal of specific impurity cations or anions as appropriate. The main classes of ion exchange media are designated as strong acid, weak acid, strong base and weak base and each may be used in a water treatment plant or a purification stream in the various process systems of a nuclear power plant.

2.3.1 Structure of Ion Exchange Resin

An ion exchange resin consists of a co-polymer, typically polystyrene and divinyl-benzene that have functionalized "exchange" groups attached to each benzene ring in the polymer matrix. A strong acid resin, suitable for removing alkali earth elements and transition metals from a water stream, is typically sulfonated producing an SO_3^-/H^+ functional group on each benzene ring (note that a perfect one-to-one aromatic ring to exchange group ratio is not achievable). The proton is the ion-exchange cation that will be exchanged with other cations from the solution. Strong base resins typically consist of a quaternary ammonium exchange site attached to two or three methyl groups whereby the functional exchange site is a chloride (Cl^-) or hydroxyl anion (OH^-) that acts to exchange with the impurity anions in the process stream to be purified. For nuclear plant process systems, where water purity is paramount, the resins are typically supplied and used in the H^+ and OH^- forms, although different suppliers can provide functionalized exchange groups such a lithiated (Li^+) strong cation resin for use in particular systems such as the primary heat transport system. It is important to note that before use of an ion exchange resin in the D_2O of the primary coolant or the moderator system, resins must be deuterated to the D^+ and OD^- form by plant operators to ensure that the isotopic purity of the D_2O is not significantly affected by H_2O exchange with the resin (see discussion in Section 8.2).

Once fabricated, cation and anion exchange resins appear as small beads (typically ~0.5 – 1.5 mm in diameter) and may be slurried in and out of their process vessels for easy replacement and regeneration. Traditional resins were specified as "gel-type" as they were effectively a wrapped-up sphere of polymer chains with significant porosity and tended to break apart if continuously reused or placed in high flow rate process streams. Newer, "macroporous", resins are much stronger and have shown good resilience in harsh environments.

2.3.2 Ion exchange capacity

The purification of a process water stream depends upon the type and quantity (or volume) of

ion exchange resin used as well as its capacity to remove various ions from the water. Ion exchange capacity is defined as the number of ionic "equivalents" that can be exchanged per litre of resin used. For example, a strong acid resin in the protonated form (H^+) can have an exchange capacity of around 2 eq/L; thus, for every litre of the resin used in a purification vessel two equivalents (or moles) of H^+ cations are available to exchange with cationic impurities in the process stream. If sodium (Na^+) is used as an example, one litre of this strong cation resin may remove 2 mols of Na^+ cations, or effectively 46 grams of sodium.

The exchange capacity is also dependent upon the particular cation being exchanged with higher valence cations showing the greater preference for adsorption on the exchange site. An example of cationic preference is:

$Fe^{3+} > Ca^{2+} > Ni^{2+} > Cu^{2+} > Fe^{2+} > K^+ > NH_4^+ > Na^+ > H^+$

For a strong base ion exchange resin, an example of anionic preference follows:

$SO_4^{2-} > CO_3^{2-} > HSO_4^- > NO_3^- > Cl^- > HCO_3^- > CHOO^- > CH_3COO^- > F^- > OH^-$

Thus, a ferrous or cuprous cation would tend to displace a sodium cation from the ion exchange bed or a sulfate anion would displace a chloride or hydroxyl anion. The capacity of an ion-exchange bed can be described in a manner similar to a chemical equilibrium equation, as shown in equation 17 using the exchange of the sodium cation with the proton as an example.

$$Na^+ + RH \rightleftharpoons H^+ + RNa \tag{16}$$

The equilibrium constant, in this case called the selectivity coefficient, is given by:

$$K_H^{Na} = \frac{[RNa][H^+]}{[RH][Na^+]} \tag{17}$$

where [RNa] and [RH] designate the concentration (mol/L) of the specific cation that is adsorbed on the resin and $[Na^+]$ and $[H^+]$ are the incoming sodium ion and proton concentrations in the solution to be purified. It should be noted that a fresh ion exchange column will have a fixed number of exchange sites based upon the resin's exchange capacity and the amount of resin present; the balance between the [RNa] and [RH] must always be equal to the initial total exchange capacity. Once most or all of the proton exchange sites available have been used or taken up by another cation, the resin will start to "throw" the cations of lowest selectivity back into the process water instead of removing them. This is obviously not a desirable situation as the intent of the purification system is to remove the impurity cations from the process water stream; at this point, the ion exchange column or vessel is said to be "spent".

2.4 Water Radiolysis

The chemistry of CANDU process systems is specified to protect the reactor core and steam generator materials from localized corrosion, minimize deposition of corrosion products on the

fuel and limit the corrosion of system components. The pH of irradiated CANDU process systems is typically adjusted by using lithium hydroxide to produce mildly alkaline conditions and some irradiated systems are kept under reducing conditions by excluding oxygen to prevent elevated electrochemical corrosion potential (ECP) and excessive corrosion. For in-core systems, the water is continuously bombarded by an intense radiation field of high-energy gamma and neutrons, which breaks the chemical bonds and produces highly reactive radical species. This process is known as water radiolysis. The radiolysis of pure water results in the production of hydrogen (H_2) (or deuterium D_2, for heavy water), oxygen (O_2) and hydrogen peroxide (H_2O_2) (or deuterium peroxide D_2O_2 in heavy water) [Spinks & Woods, 1990]. The radiolytic production of these oxidizing species has a direct impact on the corrosion of system components; they elevate the ECP, increasing the possibility of stress-corrosion cracking of the alloy steam generator tubes and, under low-temperature shut-down conditions when the radioactive decay of in-core components and fuel still produces intense gamma radiation, they promote the pitting of carbon steel. Radiolytically generated hydrogen peroxide will also degrade ion-exchange resins.

The radiolytic production of hydrogen, oxygen and hydrogen peroxide can be managed by adding hydrogen to the system. The elementary chemical reactions and kinetics are complicated but the net result is that the added hydrogen molecules react with the radical species and mitigate the radiolytic production of oxygen and hydrogen peroxide. The basic mechanisms for these processes are explained below with the overall result being suppression of the net radiolytic production of oxidizing species. Further details of the radiation kinetics associated with water radiolysis can be found in the AECL report by David Bartels [Bartels, 2009] or in the book chapter by George Buxton [Buxton, 1987].

Upon absorbing the energy dissipated by a particle or photon, water breaks down into several radical species as primary products of the irradiation process; on a timescale of approximately microseconds, the overall result is:

$$H_2O + \text{radiation} \rightarrow e_{aq}^-, H^+, \cdot H, \cdot OH, \cdot HO_2, H_2, H_2O_2 \quad (18)$$

Reactions of these primary products can re-form water, and produce further hydrogen and hydrogen peroxide through equations 19 - 21:

$$\cdot H + \cdot OH \rightarrow H_2O \quad (19)$$

$$\cdot H + \cdot H \rightarrow H_2 \quad (20)$$

$$\cdot OH + \cdot OH \rightarrow H_2O_2 \quad (21)$$

Oxygen is produced as a secondary product through reactions of the radical species with the hydrogen peroxide molecule:

$$\cdot OH + H_2O_2 \rightarrow \cdot HO_2 + H_2O \quad (22)$$

$$\cdot OH + \cdot HO_2 \rightarrow O_2 + H_2O \quad (23)$$

$$\cdot HO_2 + \cdot HO_2 \rightarrow O_2 + H_2O_2 \quad (24)$$

As mentioned above, providing sufficient added hydrogen to the water can mitigate the net production of oxygen and hydrogen peroxide. Hydrogen reacts with the hydroxide radical forming a hydrogen atom that readily combines with hydrogen peroxide and/or oxygen, effectively removing them from the solution and mitigating their overall production as shown in equations 25 - 27. The overall effect is a chain reaction where additional hydroxide radicals are produced (eq. 27) continuing the reaction chain, provided sufficient hydrogen is present. From a kinetic standpoint, the concentration of hydrogen in the water needs to be sufficient to make its rate of reaction with the hydroxyl radical (eq. 25) faster than the rate of reaction of the hydroxyl radical with hydrogen peroxide (eq. 22). This results in the reduction of the concentration of the hydrogen peroxide molecule and effectively suppresses the conversion of hydrogen peroxide to oxygen, removing both species from the solution. When sufficient hydrogen is added to an irradiated aqueous system, the very simplified chemical relation shown in equation 28 is the net result of the radiolysis process.

$$\cdot OH + H_2 \rightarrow \cdot H + H_2O \quad (25)$$

$$\cdot H + O_2 \rightarrow \cdot HO_2 \quad (26)$$

$$\cdot H + H_2O_2 \rightarrow \cdot OH + H_2O \quad (27)$$

$$H_2O + H_2(\text{excess}) + \text{radiation} \rightarrow H_2O + H_2(\text{excess}) \quad (28)$$

The fact that added hydrogen is required in the water to promote the desired recombination reactions implies that there must be a minimum hydrogen concentration by which the overall rate of the reaction in equation 25 is just sufficient to overcome the reaction of the hydroxyl radical with hydrogen peroxide (equation 22) and hence suppress the production of oxygen. This minimum concentration is called the “critical hydrogen concentration” (CHC) and has been measured in flow loops (both fuelled reactor systems and in gamma cells) to be around 0.5 mL/kg (~2×10^{-5} mol/L). [Elliot & Stuart, 2008]. Operating with the hydrogen concentration above the CHC with no oxidants initially present leads to a system in net radiolytic suppression while operation with an initial hydrogen concentration below the CHC (or with the presence of significant quantities of oxidants or impurities in the water) leads to net radiolysis occurring within the system.

Impurities dissolved within water will influence the water radiolysis processes. For example, impurities such as nitrate and nitrite anions will interfere with the water recombination reactions since they tend to react with and consume the hydrogen atoms and hydroxyl radicals [Yakabuskie, 2010], effectively lowering their concentrations and the overall rate of the oxygen and hydrogen peroxide consumption reactions (eq. 26 & 27). This will result in an increase in the quantity of oxygen and hydrogen produced by water radiolysis in the presence of nitrate and/or nitrite ions. Chloride ions interfere with the hydrogen recombination reactions since they readily exchange their outer valence electron with the hydroxyl radicals interfering with the primary recombination reaction (eq. 19). The chloride ion is then regenerated through electron exchange with water molecules and can continuously impede the desired recombination processes. Organic impurities from compressor leaks, oil ingress from pumps or other mechanical systems will break down rapidly in a radiation field. High molecular weight organics undergo polymerization reactions, extending their size and weight leading to plugging of filters and other

flow paths. Lower molecular weight organics decompose producing hydrogen and carbon dioxide that can rapidly lead to hydrogen excursions and reduction in system pH.

The chemistry specifications for a water-filled, irradiated CANDU system must therefore be designed to prevent the build-up of the water radiolysis products in the system, or the effects of water radiolysis must be continuously managed to maintain system chemistry specifications. Some systems, such as the primary heat transport system and the end shield cooling system, are operated under net radiolytic suppression by ensuring the hydrogen concentration in the water is above the CHC. Other systems, such as the moderator, liquid zone control and the spent fuel bay, are operated with net water radiolysis occurring. For these systems, the hydrogen and oxygen produced are managed by ensuring impurity concentrations are kept extremely low and by providing catalytic recombiner units in their cover gas flow paths to ensure flammable concentrations are not exceeded. Further details of the operation of each of these systems are found later in this chapter.

2.5 Solubility of Gases in Water – Henry's Law

Gases are typically sparingly soluble in water due to the vapour-liquid equilibrium established between a gas mixture covering the liquid sample. From thermodynamics, the chemical potential of the chemical species must be equal at the interface between the gas and the liquid meaning that, even though the gas solubility may be low in the liquid phase, it is finite and is an important parameter to consider in nuclear plant process streams. Many CANDU process and auxiliary systems have a head tank and/or a cover gas space that operates at a particular pressure and the solubility of the gas in the liquid phase and its mass transfer and migration to or from the cover gas space needs to be readily monitored. Using the example of hydrogen production by the water radiolysis processes described above, the continuous irradiation of CANDU coolant streams will result in the build up of hydrogen in the water that will equilibrate with its surroundings resulting in hydrogen release to the cover gas space. This needs to be continuously monitored to ensure that the hydrogen concentration is maintained below the flammability limits.

The equilibrium established between a gas dissolved in water and its partial pressure in the gas space above the liquid is given as:

$$k_H = \frac{y_{gas}}{x_{gas}} \approx \frac{p_{gas}}{c_{gas}} \tag{29}$$

where y_{gas} is the mole fraction of the given gas in the vapour space and x_{gas} is the mole fraction in the liquid phase. Since the gases of interest in CANDU process systems are sparingly soluble the mole fractions are typically equated to partial pressure (p_{gas}) and concentration (c_{gas}) for the gas phase and liquid phase respectively giving units of pressure (atm or MPa) per molarity (mol/L). Rearrangement of equation 29 shows that, under low to intermediate partial pressures, there is a linear dependence between the partial pressure of the gas above the liquid and that dissolved in it. Thus, by knowing the equilibrium constant, in this case called Henry's Law constant, the concentration of gas dissolved in water may easily be evaluated as demonstrated in Example 15.2. Henry's law constants at 25^{o}C are shown in Table 2 for some gases commonly

encountered in CANDU process systems. IAPWS has released detailed correlations for determining the Henry's Law constant for various gases as a function of temperature [IAPWS, 2004].

Table 2. Henry's constants for select gases at 25°C (calculated from IAPWS , 2004).

Gas	k_H in H_2O (in D_2O) (atm/M)
O_2	775.7
H_2	1263
N_2	1522
He	2541 (2343)
CO_2	29.40
D_2	(921.0)

Example 15.2 - Henry's law calculation – D_2 in heavy water

The heavy water storage tank for the primary heat transport system contains D_2O at roughly room temperature and is purged with a helium cover gas to maintain the hydrogen concentration below 4% (by volume). The specification for dissolved deuterium in the PHTS is 3 – 10 mL/kg, calculate the equilibrium concentration that would be attained in the cover gas if helium is not frequently added and purged and the dissolved hydrogen is maintained at the upper limit of the specification.

Solution

If 10 mL/kg of dissolved deuterium is maintained in the PHTS, Henry's law can be used to estimate the equilibrium concentration in the storage tank cover gas. First the dissolved deuterium concentration must be converted to consistent units with Henry's law (i.e. Molar or mol/L) using the conversion factor that 1 mol gas = 22.4 L gas at standard temperature and pressure (STP). Thus:

$$c_{gas} = 0.010 \frac{L_{D_2}}{kg_{D_2O}} \times \frac{1 mol_{D_2}}{22.4 L_{D_2}} \times \frac{1000 kg_{D_2O}}{m^3_{D_2O}} \times \frac{m^3}{1000 L} = 4.46 \times 10^{-4} \text{ mol/L} \quad \text{(M)}$$

$$p_{gas} = k_H c_{gas} = \left(921 \text{atm/M}\right)\left(4.46 \times 10^{-4} \text{ M}\right) = 0.411 \quad \text{atm}$$

For a cover gas operating at approximately atmospheric pressure this would amount to a cover gas concentration of 41.1%, well above the flammability limit of about 8% in helium!

3 Primary Heat Transport System

As explained in Chapter 10, the purpose of the Primary Heat Transport System (PHTS) in a CANDU reactor is to remove the heat generated from the fissioning of the reactor fuel and transport it to the steam generator for production of steam in the Secondary System. The materials of construction in the PHTS are numerous due to the different functions of the various components; the particular materials and their properties are described in detail in Chapter 14. The materials with the largest surfaces areas in contact with the heavy water coolant of the PHTS are: zirconium-based alloys in the core of the reactor (Zircaloy-4 fuel cladding, Zr-2.5Nb pressure tubes), nickel alloys for the steam generator tubing (Alloy 400 [Monel] at Pickering, Alloy 600 [Inconel] at Bruce, Alloy 800 [Incoloy] at Darlington and the CANDU-6s), type 410 stainless steel for the fuel-channel end fittings and carbon steel for the feeder pipes joining the fuel channels through the headers to the carbon-steel channel heads in the steam generators. Thus, as with any complex system, the chemistry control practices are a compromise among the optimum chemistries for each of the major materials used.

The Zircaloy-4-clad fuel bundles, Zr-2.5Nb pressure tubes and nickel-alloy steam generator tubes exhibit low general corrosion rates over a wide range of pH and temperature [Cox, 2003]. A major role of chemical control is therefore to protect against localized corrosion, in particular the stress-corrosion cracking of the steam generator tubes and the hydriding and cracking of the pressure tubes. As described earlier in the section on radiolysis, adding hydrogen maintains reducing conditions and this minimizes the possibility of nickel-alloy cracking, but to minimize the potential for hydriding of Zr-2.5Nb the hydrogen is kept within strict limits (3-10 mL/kg).

A further role of the chemical control in the PHTS is the protection of the large surface area of carbon steel. As described in Section 6.1 in Chapter 14, the general corrosion of iron produces mixed and, at low temperature, often hydrated oxides (Fe_2O_3, Fe_3O_4, FeOOH etc.) that become the thermodynamically stable phases at a pH (at room temperature) greater than 9 or so. It is well known that carbon steel corrosion is minimized in mildly alkaline, deaerated water. However, at low temperature with static water that may occur during a shut-down, oxidising conditions can induce severe pitting of carbon steel and should be avoided. Note that during reactor operation the inlet feeders in CANDUs are exposed to coolant saturated in dissolved iron because of the heat transferred producing steam in the steam generators and the consequent drop in iron solubility, so they undergo general corrosion and develop thick magnetite films as the result of magnetite precipitation from the oversaturated coolant. On the other hand, the outlet feeders see coolant undersaturated in iron because of the heating in the core and as a consequence undergo flow-accelerated corrosion (FAC), which leads to very thin magnetite films and loads the system with iron that largely deposits as magnetite in the steam generators. Oxidising conditions tend to mitigate FAC, but the greater need to avoid localized corrosion of the alloy components in the core and the steam generators dictates the use of reducing conditions.

3.1 Chemistry Control in the PHTS

As explained above, one of the primary objectives of chemistry control in the PHTS of a CANDU reactor is to minimize the corrosion of the carbon steel, zirconium and alloy surfaces, which

involves operating under alkaline conditions and mitigating the radiolytic production of oxidizing species. Other objectives include minimizing deposition of corrosion products on the fuel (fouling) and minimizing and controlling the concentration of activiated corrosion products and fission products (both gaseous and dissolved) in the system. These objectives are accomplished through dosing and control of the primary coolant's pH_a and deuterium concentration through regular additions of lithium hydroxide and hydrogen gas. Also, the molecular hydrogen gas exchanges rapidly in the reactor core with deuterium in the D_2O molecules. Although the additions downgrade the heavy water slightly, this is compensated by periodic isotopic upgrading of the system's D_2O (see Section 8.1). Each individual plant maintains its own chemistry practices and operational guidelines but, in general, guidelines for these values are shown in Table 3.

Table 3. Target chemistry parameters in the PHTS.

Parameter	Typical Specification Range
pH_a:	10.2 – 10.4
$[Li^+]$:	0.35 – 0.55 mg/kg (ppm)
$[D_2]$:	3 – 10 mL/kg
conductivity:	0.86 – 1.4 mS/m (dependent upon LiOH concentration)
Dissolved O_2	< 0.01 mg/kg
$[Cl^-]$, $[SO_4^{2-}]$ etc	< 0.05 mg/kg
Isotopic	> 98.65 % D_2O
Fission products	ALARA (< 10^6 Bq/kg D_2O; monitoring I-131 indicative of fuel failure)

During steady-state operation, variations in any of the above parameters are typically small in the absence of system transients or upset conditions. Oxygen concentrations are typically non-detectable. The alkalinity is controlled through periodic additions of LiOH through the sampling system return (for elevating pH_a) or by providing a periodic bleed flow through the purification system using an ion-exchange column containing strong acid cation resins (for lowering pH_a). Lithiated mixed-bed ion-exchange columns (where the strong-acid IX resin D^+ sites have been saturated with Li^+; both acid and base resins are deuterated) are run as normal purification for the PHTS to collect cationic and anionic impurities. A simplified flow diagram for a PHT purification circuit is shown in Figure 2. The purification system keeps particulate concentration low and helps to maintain the anioic impurity concentrations below the specification to minimize the risk of SCC of the stainless steel and alloy components in the system and to minimize the risk of strain-induced cracking of carbon steel components [Turner & Guzonas, 2010]. It also serves to keep the radioacitivity of the PHT coolant low as the filters and ion exchage column may capture activiated corrosion products or ionic fission products released from failed fuel bundles.

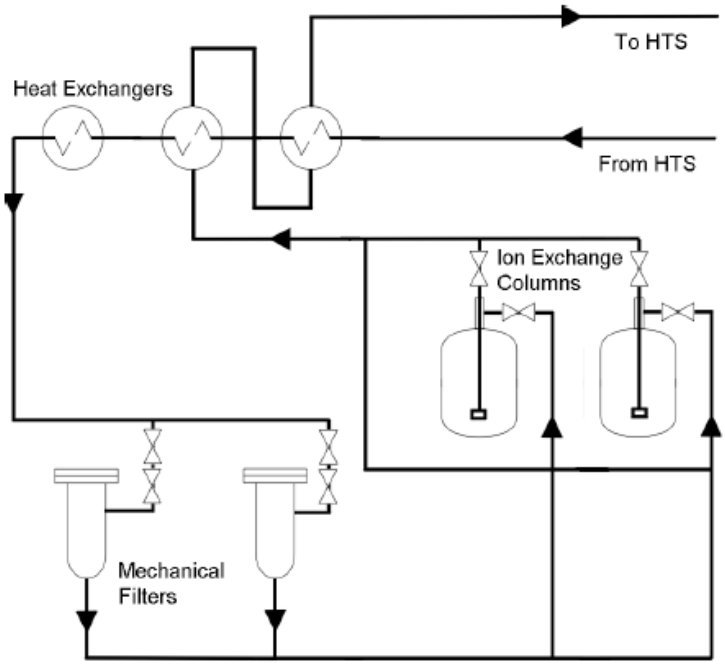

Figure 2. Simplified flow diagram of a PHT purification loop (courtesy of AECL).

Since pH_a and conductivity are directly related to $[Li^+]$, purity of the PHTS coolant is readily observed by comparing the measured values to the theoretical values as calculated using the equations developed earlier in the chapter. If the system is controlled well and has minimal impurities, then the conductivity and pH_a measured should match closely with the calculated values appropriate to the measured lithium-ion concentration. Deviations in the measured-to-theoretical value indicate ingress of ionic impurities or problems with system sampling techniques.

The above discussion seems to imply that sampling the high-temperature PHTS system is routine and simple. While it is routine, collecting and analyzing samples from a high-temperature, high-pressure system is far from simple. Take, for example, the collection of a sample in an open polypropylene jar. The sampled water must first be cooled from the operational temperature and throttled to low pressure. Each of these operations changes the state of the chemical species present in the sample. Once the valve at the end of the sample line is opened, the ideally oxygen-free coolant sample is exposed to the atmosphere and will readily absorb nitrogen, oxygen and carbon dioxide from the air. Thus, this sample is immediately not appropriate for obtaining a dissolved oxygen measurement. Additionally, the absorbed CO_2 dissociates in the sample solution to form carbonate (CO_3^{2-}) and bicarbonate (HCO_3^-) anions, which disturb the equilibrium chemistry established between lithium hydroxide and water. The CO_2 absorption effectively produces carbonic acid and lowers the pH (or pH_a) of the sample, rendering it compromised for system monitoring. Thus, differences in pH_a, conductivity and $[Li^+]$ from PHTS samples may imply improper sampling techniques, not problems with system chemistry and care must be taken to identify the root cause. Several standard methods and recommended practices are available to properly specify and conduct sampling campaigns including the Technical Guidance Document on corrosion product sampling recently released by IAPWS [IAPWS, 2014].

3.2 Corrosion Issues in the PHTS

3.2.1 Feeder Pipe FAC and Cracking

Recent trends for PHTS chemistry practice have focused upon "narrow-band" pH_a control, within the 10.2- 10.4 range, in order to help mitigate excessive FAC on the outlet feeder pipes, which is demonstrated to increase with increasing pH_a (Lister, 2002, Slade & Gendron, 2005). This observation results from the fact that the magnitude of FAC is partially controlled by the degree of corrosion-product under-saturation in the coolant, via processes described by equations 21-23 presented in Chapter 14. Consider the closed-loop PHT system and take the PHT main pump as a starting point. The temperature at this point is typically around 260°C and is considered to be the "cold-leg" of the PHT circuit. In these conditions, the PHT coolant is typically saturated or over-saturated in corrosion-products (mainly dissolved iron), which leads to the precipitation of magnetite on the surfaces up to the inlet of the reactor core and promotes low corrosion rates of the carbon steel inlet feeder pipes (the precipitation actually begins within the steam generator and along the whole inlet section of feeders and headers to the core). Shown in Figure 3 is the calculated solubility of magnetite at a pH of 10.2 and 9.0 (in light water) between the temperatures of 250°C and 310°C, the approximate temperature of the coolant exiting the core. It is seen that for the elevated pH, the solubility increases over this temperature range, which is considered to be beneficial since this will typically prevent deposition of corrosion products in the reactor core. The coolant ultimately leaves the core in an under-saturated condition since most of the in-core surfaces contacting the coolant are zirconium alloys and this leads to a large driving force for magnetite (and metal) dissolution in the end fittings and carbon steel outlet feeder pipes. Compounding the problem is the intricate series of bends that are required for the feeder pipes to connect appropriately to the end-fittings – many outlet feeder pipes can have two tight-radius bends. This acts to increase the fluid turbulence and exacerbates the FAC phenomenon due to the action of fluid shear and mass transfer.

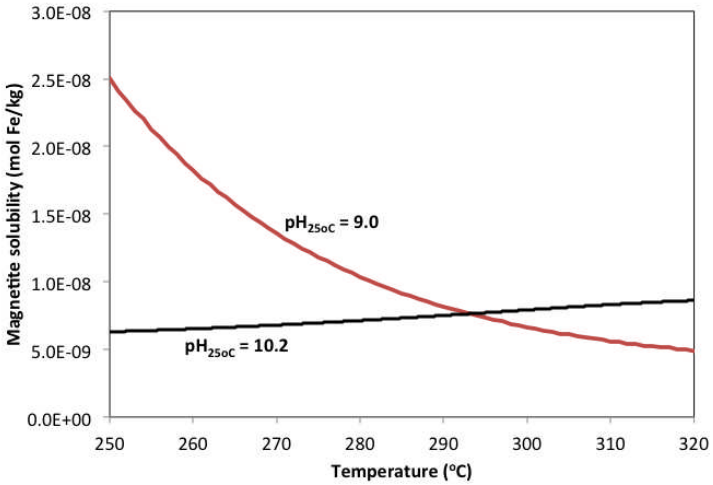

Figure 3. Magnetite solubility calculated from thermodynamic data optimized to the Tremaine & Leblanc data [Tremaine, 1980].

The Point Lepreau CANDU-6 was the first reactor to exhibit FAC of the outlet feeder pipes. The feeders were on average corroding at rates greatly in excess of what was assumed and predicted

in providing a suitable corrosion allowance and many sections of outlet feeders needed to be replaced well before the end of their design lifetime. Unlike other CANDU stations that also observed FAC in the outlet feeder pipes, the Point Lepreau station also had demonstrated cracking, which necessitated many removals and replacements prior to the refurbishment outage that began in 2008. The stress-corrosion cracking (SCC) or environmentally assisted cracking (EAC) observed at Lepreau was very unexpected as carbon steel is not typically susceptible to significant cracking. Theories supporting mechanisms such as hydrogen embrittlement due to the high corrosion rates and hydrogen production associated with the outlet feeder FAC were proposed along with a detailed examination of the construction and operational history [Slade & Genderon, 2005]. Evidence pointed to high residual stresses from the bending, welding and fabrication process as a primary culprit to the cracking mechanism and the fact that none of the bends were stress relieved following fabrication. No direct evidence of a connection with hydrogen embrittlement related to FAC was found, however it is still suspected to have played a factor. The material for replacement sections of pipe, and that used for new construction and refurbishment projects, is now specified to contain a higher chromium content (~0.3 wt%) and has slightly more carbon (~0.35% vs 0.3%) which, in combination act to significantly reduce the FAC issue and increases the yield strength respectively, thereby creating more margin to protect against cracking. All new bends are also fully stressed relieved before being placed into service.

3.2.2 Delayed Hydride Cracking of Zirconium Alloys

Of the corrosion issues of most concern in the PHT system, perhaps the most critical is delayed hydride cracking (DHC) of the Zr-2.5Nb pressure tubes as they represent the physical barrier and pressure boundary of the reactor core. As described in Chapter 10, the pressure tubes in a CANDU reactor are sealed on each end through a rolled-joint connection to the 403SS end-fittings. Deuterium produced through the limited corrosion of the Zr-2.5Nb pressure tubes has been shown to accumulate within the alloy; its accumulation is readily measured through scrape samples obtained during maintenance outages. Over time, should the solution solubility limit of deuterium in the alloy be exceeded, zirconium-hydride platelets may form within the metal's lattice and between grain boundaries. The hydride is a brittle, ceramic-like material that is prone to cracking under stress as was demonstrated on several of the original Zircaloy 2 pressure tubes in the Pickering A station that were replaced as a result of DHC in the period between 1974 – 1976 [Urbanic, 1987]. The most prone locations are at the rolled joint areas on each end of the pressure tube due to the increased deuterium production and migration rate at the galvanic couple between the pressure tube and the stainless steel end-fitting – deuterium produced through corrosion of the stainless steel is free to migrate into the pressure tube due to the intimate contact resulting from the rolled-joint seal. Residual stress due to the rolling process also plays a large role in these locations.

3.3 Activity Transport

The PHTS coolant in a water-cooled reactor such as CANDU may become activated itself through the absorption of neutrons as it passes through the reactor core. This is particularly relevant in CANDU reactors where heavy water is used as the reactor coolant and moderator (in the separate moderator system described in Section 5) since neutron absorption by the deuterium atoms in heavy water will directly produce tritium (T or H_3), which is radioactive and has a 12.3

year half life. Tritium production and decay in the PHTS heavy water means that, even in the absence of particulate or ionic impurities, the coolant will be radioactive and the entire PHTS will have significant concentrations of tritium, typically of the order of 10^4 Bq/kg of heavy water. This is several orders of magnitude lower than the steady state tritium concentrations in the moderator water since only about 3% of the PHTS coolant is in the reactor core at any given time whereas >95% of the moderator heavy water is continuously being exposed to the high neutron flux in the reactor core. Thus, all reactor systems that employ heavy water as their coolant will contain significant tritium activity in all sections of the circuit.

In addition to the production of tritium, the PHTS heavy water coolant will contain trace concentrations of dissolved ions and particulates that are the result of the corrosion and wear of the system materials. These impurities, which include iron, nickel, chromium, cobalt and antimony can deposit in the core and may become activated by neutron absorption. In addition, zirconium alloy wear products released by the movement of fuel inside the fuel channel during refuelling, and fission products and actinides released from the (infrequent) failure of the fuel cladding, can be transported out of the core by the coolant. These species are easily deposited, adsorbed and incorporated into the oxide layers that form on the surfaces of out-of-core components leading to elevated levels of activity on components removed from the direct radiation field of the reactor core, the reactor inlet/outlet headers and feeders and inner surfaces of the steam generator tubes, for example.

Typical activation and fission products observed in the PHT and their half-lives are shown in Table 4. Note the relatively long half-life of Co-60, which is a major contributor to radiation fields in out-of-core components. The fission products are generally kept at very low concentrations in the PHT coolant since they are indicators of failed fuel elements, which are removed as quickly as possible once identified. The radioiodines are of particular concern since they are readily absorbed in the thyroid of humans and must be contained in the system and disposed of appropriately.

Table 4. Common radioactive isotopes and their source in the PHTS.

Activation product	Typical source	Half Life
Cr-51	Alloys	27.7 days
Fe-59	Steels and alloys	44.6 days
Sb-124	Impurity in steels and alloys – bearings and wear surfaces	60.2 days
Co-58	Nickel alloys	70.8 days
Mn-54	Steels and alloys	312.5 days
Co-60	Impurity in steels and alloys – hard-facing materials for wear resistance (e.g. Stellites)	1924 days
I-131	Fission product	8.04 days
Xe-133	Fission product	5.24 days
Xe-135	Fission product	9.1 hours
Kr-85	Fission product	10.73 years
Kr-88	Fission product	2.84 hours

4 Secondary Heat Transport System

The Secondary Heat Transport System (commonly called the secondary system or steam cycle) produces the steam necessary to drive the turbines and electrical generator. The configuration of the secondary system is described in detail in Chapter 8 but in summary it contains the condenser, a series of low-pressure feedwater heaters, a deaerator, a series of high temperature feedwater heaters, the boilers or steam generators, the steam supply piping and control systems, and the high- and low-pressure turbines with a moisture separator and steam reheater in between them. While the secondary system at each plant is unique in terms of its exact configuration and the materials used for the various components there are typically two classifications of system; all-ferrous and copper-containing. The operating chemistry for the secondary system is dependent upon the type of materials from which the plant is constructed. For example, as described in the corrosion section in Chapter 14, it is desirable for iron-based materials to operate with alkaline chemistry to promote the formation of passive oxide films and minimize corrosion. This is often done with the addition of ammonia or other volatile amines and target pH values (measured at room temperature) can be up to 10. In a copper-based system or a system that contains some copper components, copper corrosion is known to be accelerated considerably by ammonia, especially when oxygen is present, and maximum pH's must be kept to about 9.2 – 9.4 and the use of ammonia minimized or excluded all together. Reducing conditions are maintained, mainly to protect the steam-generator alloys from cracking, by the addition of hydrazine.

4.1 Chemistry Control in the Secondary System

In order to protect the entire secondary system from corrosion, a volatile pH-controlling agent is employed, i.e., one that enters the steam phase in the boilers and is carried through the entire system such that it protects the main steam lines, steam extraction lines, moisture separator and reheater and the condenser. Previously, the chemical buffer sodium phosphate was in widespread use for dosing feedwater but was effectively non-volatile and concentrated in the steam generator, where its reactions within crevices and under deposits could lead locally to either highly alkaline or acid conditions if not properly adjusted and monitored. Extended pitting or wastage of nickel-alloy steam generator tubes, especially under the "sludge pile" on the tube sheet, was a not-infrequent occurrence. Nowadays, it is common practice to use "all-volatile" treatment (AVT), with hydrazine for oxygen control and a volatile base such as ammonia to distribute the alkalizing agent around the system. Ammonia, however, is so volatile that it concentrates in the steam phase and can leave the water-touched areas unprotected, so less-volatile amines such as morpholine (the cyclic compound $O(C_2H_2)_2NH$, ethanolamine ($HO(CH_2)_2NH_2$) or cyclohexylamine ($(CH_2)_5CNH_2$) may be used instead of, or in combination with, ammonia. A drawback of these higher-molecular-weight organic compounds is that they break down at high temperature to simpler substances such as acetic acid and eventually carbon dioxide, which may be corrosive; their concentrations therefore have to be limited in the steam generators through strict chemistry control.

Chemistry parameters that are targets for the secondary system chemistry control and are typically measured at the high pressure feed water heater outlet are shown in Table 5.

Table 5. Target chemistry parameters in the secondary system (all-ferrous materials).

Parameter	Typical Specification Range
pH	9.5 < pH < 10 (for all-ferrous systems)
Dissolved O_2	< 0.01 mg/kg (ppm)
Hydrazine	0.020 – 0.030 mg/kg (ppm)
Na^+	< 0.05 μg/kg
Cl^- ; SO_4^{2-}	< 0.05 μg/kg

The distribution of amine retained in the water phase or stripped to the steam phase is described by the distribution coefficient, which is dependent upon both temperature and concentration. The true distribution coefficient is defined as the ratio of the vapour-phase mole fraction of volatile species (y_B) to its liquid phase mole fraction (x_B):

$$D_B = \frac{y_B}{x_B} \tag{30}$$

Note that, in the true distribution coefficient, the measure is per fraction of the volatile species. For ammonia this means the neutral species, NH_3. However, due to the dissociation of ammonia and other amines in water, the true distribution coefficient is not typically what is measured; the measurement is the "apparent" distribution coefficient. The apparent distribution coefficient accounts for the total concentration (or fraction) of ammonia-based species in the liquid phase including the dissociation products as shown in equation 31. For example, the equilibrium established between ammonia and the ammonium cation in water is given by equation 32 and its equilibrium constant in equation 33. If ammonia is stripped to the vapour phase, its liquid phase concentration will be reduced and will subsequently affect the concentration of the ammonium cation retained in solution. As with other equilibrium chemical equations that have been discussed in this chapter, the equilibrium constant for amine dissociation is temperature-dependent, as are the distribution coefficients, thus the apparent distribution coefficient is a complicated function of the true distribution coefficient and equilibrium chemistry.

$$[NH_3]_{Total} = [NH_3]_{(aq)} + [NH_4^+] \tag{31}$$

$$NH_3 + H_2O \rightleftharpoons NH_4^+ + OH^- \tag{32}$$

$$K_{NH_3} = \frac{a_{NH_4^+} a_{OH^-}}{a_{NH_3} a_{H_2O}} \approx \frac{[NH_4^+][OH^-]}{[NH_3]} \tag{33}$$

While protection of the entire secondary system is the goal of the chemistry dosing practices, protection of the materials in the steam generators or boilers is paramount since the boiler tubes represent the physical barrier between nuclear and non-nuclear sections of the plant. A boiler contains an array of 1000's of tubes, tube support plates, tube sheet, and associated steam driers. Since dissolved species, other than the ammonia or the other amines dosed to control pH, represent impurities in the feedwater it is important to minimize (or eliminate if

possible) their concentrations entering the boiler. Some impurities of particular importance in boiler feed water include iron, copper, sodium, chloride and sulphate. The iron (and copper if the system includes some copper-bearing materials) enters the boiler as corrosion products released from the predominately carbon steel components in the feed water train and, since they are not volatile will accumulate in the boiler as steam is produced. Ultimately, boiler sludge (mainly iron oxides or hydrated oxides) will accumulate on the tube sheet and tube support plates and must be periodically removed through a physical or chemical cleaning procedure. This can become difficult if significant copper is retained in the deposits.

Sodium, chloride, sulphate and other inorganic impurities can enter the feedwater system through leaks in the condenser tubes and must be kept at very low concentrations since all non-volatile species will tend to concentrate in the boiler, particularly in crevice regions in the tube sheet or around the tube support plates. The concentration of these species is kept low in the boiler through a continuous blow-down that removes a small fraction of the circulating water in the boiler. Example 15.3 demonstrates the calculation on the effectiveness of blow-down to maintain low levels of contaminants in the boiler. A simple calculation of the feedwater input flow rate divided by the blow-down rate can give a rough indication of the concentration factor (CF) that can be achieved in a steam generator crevice. For example, an individual boiler in a typical CANDU-6 plant will have an incoming flow rate of around 250 kg/s. With a blow-down of approximately 0.5% of the incoming flow (amounting to 1.25 kg/s) this shows a concentration factor of 200, meaning that any impurities entering the boiler from the feedwater will be concentrated 200 times in the bulk water of the steam generator. Regular sampling of the blow-down stream for sodium, chloride, sulphate and other impurities provides a ready indication of poor feedwater chemistry.

Impurities in the boiler cause hide-out, whereby they are absorbed and retained in the boiler crevices or in the deposited sludge piles, which can lead to aggressive chemistry conditions for the boiler tubes. Alloy 800, the choice material for recent CANDU reactor boiler tubes, has shown excellent corrosion resistance and little stress corrosion cracking over a wide range of chemistry conditions. However, if the environment adjacent to the tubes becomes sufficiently acidic or alkaline due to the ingress and hide-out of ionic impurities, chlorides, sulphate or sodium for example, the recommended operating envelope for the boiler tubes may be compromised. This situation has occurred at various nuclear plants, both CANDUs and PWRs, where boiler tubes had to be plugged due to through-wall cracking and leakage of primary system water into the boiler. This is detected by increasing radiation levels in the boiler blow-down or main steam line.

Example 15.3 - Blow-down calculation.

A sketch of a steam generator with feedwater inlet flow rate (F), steam flow rate (S) and blowdown flow rate (B) is shown in Figure 4. Assuming steady state operation, feedwater iron concentration of 5 ppb (mg/kg), feedwater flow rate is 250 kg/s and blowdown rate of 0.5% (1.25 kg/s), calculate the concentration of iron in the bulk boiler water (C_M). If the blowdown rate was reduced to 0.1%, what effect does that have on bulk boiler water iron concentration?

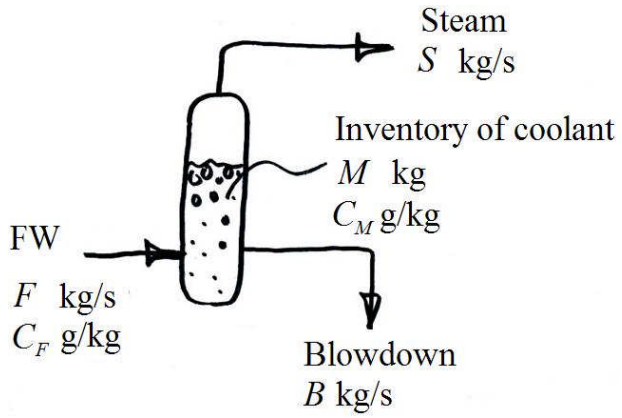

Figure 4. Mass balance on steam generator impurity inventory.

Solution

A steady state mass balance on the iron inventory using the sketch in Figure 4 results in:

$$\text{Fe In} = \text{Fe Out}$$

$$F \cdot C_F = S \cdot C_s + B \cdot C_B$$

We not that the concentration in the bulk boiler water will be the same as the blow-down concentration, hence $C_M = C_B$. Also, the iron in the boiler water is non-volatile so its concentration in the steam line will be zero. Applying these conditions and rearranging results in:

$$C_M = C_B = \frac{F}{B} C_F$$

The term F/B is the concentration factor described above and is the ratio of the feedwater flow rate over the blow-down rate. For the conditions indicated above this results in a concentration factor (CF or F/B) of 200. Thus:

$C_M = 200 \times C_F = 200 \times 0.005$ mg/kg = 1 mg/kg *Ans.*

Reducing the blow-down rate to 0.1% effectively increases the concentration factor by five leading to $C_M = C_B = 5$ mg/kg. Ans.

4.2 Corrosion Issues in the Secondary System

4.2.1 Boiler crevices

As described above, the steam generators represent critical locations in a CANDU plant as the boiler tubes and tube sheets are the physical barriers between the nuclear and non-nuclear sections of the plant. As a result, the operational chemistry practices in the steam generation circuit are targeted primarily at protection of the shell side of the boiler while trying to minimize corrosion issues in the feedwater train and the steam cycle. The recent material of choice for the steam generator tubing is nuclear grade Alloy 800 (~20%Cr, 35% Ni, balance Fe with ~1% each Al & Ti), which has shown excellent corrosion resistance and minimal cracking in well over 30 years of operation in CANDU plants and German PWRs. Earlier CANDUs used Inconel 600 or Monel 400, each showing poorer performance than Alloy 800 in terms of their susceptibility to underdeposit corrosion, SCC, intergrannular attack and fretting wear [Tapping et. al, 2000]. It is, however, imperative to keep the feedwater and hence boiler chemistry within specification limits for pH and oxygen, as these parameters directly affect the electrochemical corrosion potential (ECP) attained on the boiler tubes and have significant influences on corrosion and environmentally-assisted cracking (EAC). During operation, crevices in the steam generator accumulate impurities from the concentrated environment in the bulk boiler water due to the concentration factor (CF) effect as illustrated in the blow-down example above (crevices as defined here are not only the physical crevices between the boiler tubes and the tube sheets and support plates but also the tight-tolerance micro-environments that are created under boiler sludge deposits and along the tube support plates). As the power level is reduced and the CF subsequently lowered, the impurities leach out of the crevices and may be consequently removed via blow-down, a phenomenon known as hide-out return. Failure to keep impurity concentrations low in the bulk boiler water may lead to chemical imbalances in the boiler crevices and promote either acidic or alkaline pH's, both of which are detrimental to the boiler tubes from a general corrosion perspective. The presence of impurity oxygen in the bulk boiler water compounds the effect and may lead to cracking, particularly during transient operations during station run-ups or shut-downs.

AECL has developed a recommended operating environment envelope for Alloy 800 boiler tubes [Tapping, 2012]. The chart, shown in Figure 5, is the result of decades of reactor operating experience and ongoing research at the Chalk River Laboratories and elsewhere to evaluate the cracking and degradation propensity of boiler tubes in out-of-specification chemistry conditions. While a plant may be within the recommended operating envelope for the majority of its operational lifetime, there will be periods of out-of-specification chemistry due to ingress of contaminant ions or elevated concentrations of dissolved oxygen. The effects of these, hopefully short, periods need to be carefully assessed as they may be the initiating events for pitting and cracking later on in the life of the plant.

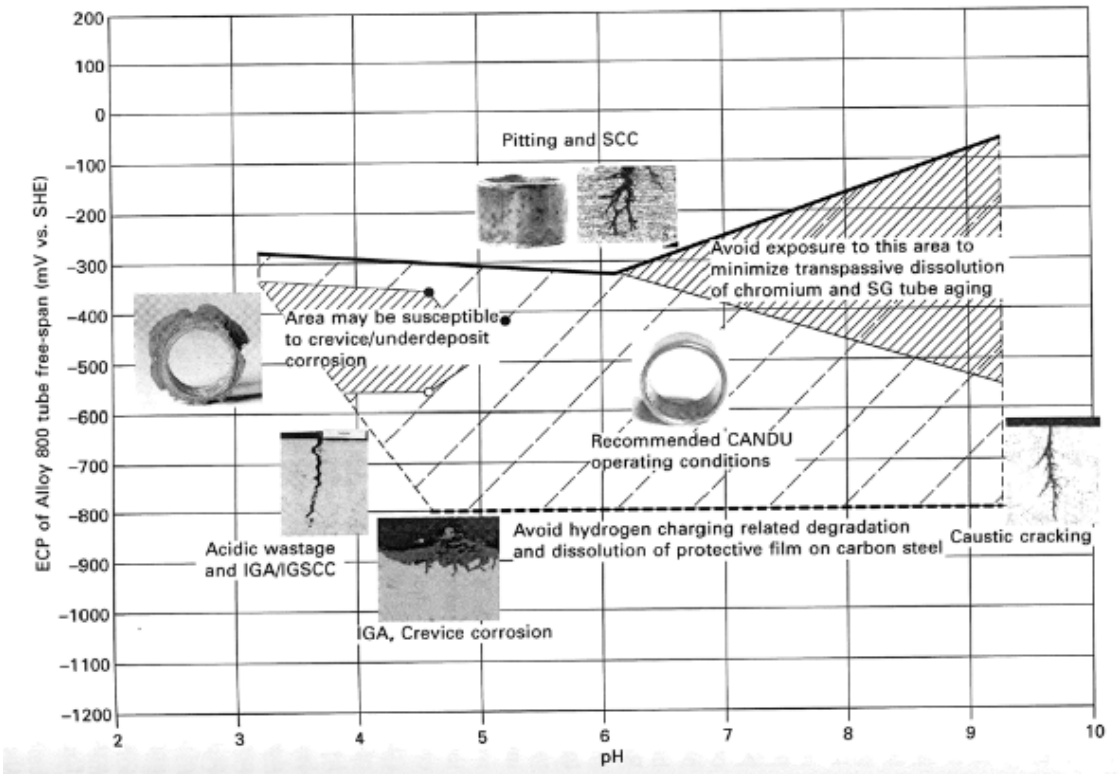

Figure 5. Alloy 800 Recommended Operating Envelope (Tapping, 2012).

4.2.2 Flow-Accelerated Corrosion in the Feedwater and Steam Extraction Piping

Protection of the boiler is the primary objective of the chemistry dosing practices in the secondary system and one of the best ways to accomplish this is to minimize the corrosion of the materials in the feedwater train and regenerative feedwater heaters. Excessive corrosion of the feedwater piping will introduce corrosion products into the boiler water, ultimately dumping the material as sludge that accumulates on the tube support plates and tube sheet in the steam generators. Flow accelerated corrosion (FAC), described in detail in Chapter 14, is prevalent in the feedwater system since the steam that condenses following the low pressure turbines is ultimately pure water with a relatively low concentration of volatile amine that has been carried through the steam cycle. This condensate water is effectively iron-free or fully undersaturated in dissolved corrosion products and is an excellent fluid for promoting FAC of carbon steel piping. The moisture content of wet steam in the moisture separator and turbine steam extraction lines will be effectively pure water and fully undersaturated in corrosion products as well, but have the additional complication of possessing small water droplets that can impinge on piping surfaces, creating a mechanical erosion mechanism compounding the FAC effect. Critical locations for FAC are typically downstream of tight radius bends, orifice plates for flow measurements or any location where turbulence is enhanced and mass transfer from the piping promoted. The solubility of the primary protective oxide film, magnetite, also plays a role in the most affected locations since it is seen to go through a maximum at temperatures between 130-150 ^{o}C as shown in Figure 7 in Chapter 14.

Management of FAC in the secondary circuit of power plants is quite advanced and relies upon

computer model predictions (EPRI's CHECWORKS code for example) to assess critical locations in the plant and frequent inspections. One of the key factors in protecting the secondary side piping from FAC is to maintain a suitable alkalinity level at ***all*** locations around the steam cycle. Magnetite solubility is demonstrated to be at a minimum around a $pH_{25°C}$ of 9.5 or so and maintaining this specification at every location in the steam cycle is highly desirable to minimize pipe wall thinning by FAC. However, this is difficult to achieve in the field since chemical dosing typically occurs at a sole location in the feedwater circuit (usually just downstream of the condensate extraction pump) and the fact that the two-phase sections of the plant can have a significantly different chemical composition from that of the feedwater due to the distribution coefficient of the volatile amine used for plant pH control. In principle, the target is to maintain a delta pH ($\Delta pH = pH_T - pH_{neutral@T}$) greater than 1.0 to ensure that sufficient alkalinity is maintained at each location and the solubility of magnetite is kept to a minimum.

Table 6 shows the results of a calculation for the effect of different chemical dosing strategies on the delta pH throughout a common secondary side feedwater and steam circuit. In case 1, ammonia is used as the pH-controlling chemical and in case 2 morpholine is used, both achieving a final feedwater pH_{25C} of 9.6. Note that in case 2, 1 mg/kg of ammonia is also assumed to be present due to the decomposition of the morpholine (and hydrazine) at the higher temperature locations in the system; such decomposition typically results in a residual ammonium concentration between 0.5-1.1 mg/kg. As is demonstrated in the table, both chemical dosing strategies achieve the same target $pH_{25°C}$ and maintain a sufficient delta pH at the outlet of the HP heater, thus maintaining suitable protection of the feedwater train from FAC. However, due to the differences in volatility and distribution coefficients, the delta pH achieved with the morpholine chemistry in case 2 provides much better protection for the steam extraction lines and moisture separator.

Table 6. Comparison of delta pH for two chemical dosing strategies in a typical steam cycle.

	Case 1: 2.3 mg/kg Ammonia (pH_{25} = 9.6)			Case 2: 25 mg/kg Morpholine + 1 mg/kg Ammonia (pH_{25} = 9.6)		
Location	pH_T	$pH_{neutral}$	ΔpH	pH_T	$pH_{neutral}$	ΔpH
HP heater outlet (final feedwater)	6.71	5.68	1.03	6.87	5.68	1.19
Bulk Boiler water	5.92	5.59	0.32	6.34	5.59	0.74
HP turbine extraction to HPH2	6.29	5.67	0.62	6.80	5.67	1.14
Moisture Separator/Reheater	6.57	5.78	0.80	7.13	5.78	1.35
LP turbine extraction to DA	6.85	5.89	0.96	7.43	5.89	1.54
LP turbine extraction to LPH3	7.11	6.01	1.11	7.73	5.89	1.54
LP turbine extraction to LPH2	7.45	6.16	1.28	8.11	6.16	1.95
LP turbine extraction to LPH1	7.88	6.38	1.50	8.57	6.38	2.20
Condensate	8.73	6.83	1.89	9.49	6.83	2.65

Similar effects are realized with other amines of lower volatility, such as ethanolamine (ETA), which has a relative volatility of about 0.15 at 200°C while that of ammonia is about 5.0. Its

effect on FAC compared with that of ammonia and in neutral chemistry is illustrated in Figure 6, which shows on-line measurements of the FAC rate of carbon steel in an experimental loop. The operating conditions were two-phase steam-liquid flows at 200°C with ammonia and ETA at the same $pH_{25°C}$ (9.2) and with no additive. The effect of the additives on reducing FAC below that of neutral chemistry is immediately realized at zero voidage (% steam by volume) and continues up to 97% voidage. As the voidage increases from zero the FAC rates with the two additives are roughly the same and increase together. At about 80% voidage, the FAC rate with ammonia increases further as the ammonia partitions to the vapour phase, while that for ETA decreases as the ETA partitions to the liquid phase (the FAC occurs in the liquid film on the walls of the pipe or component). The diagram also shows how reducing the flow rate also reduces the FAC rate.

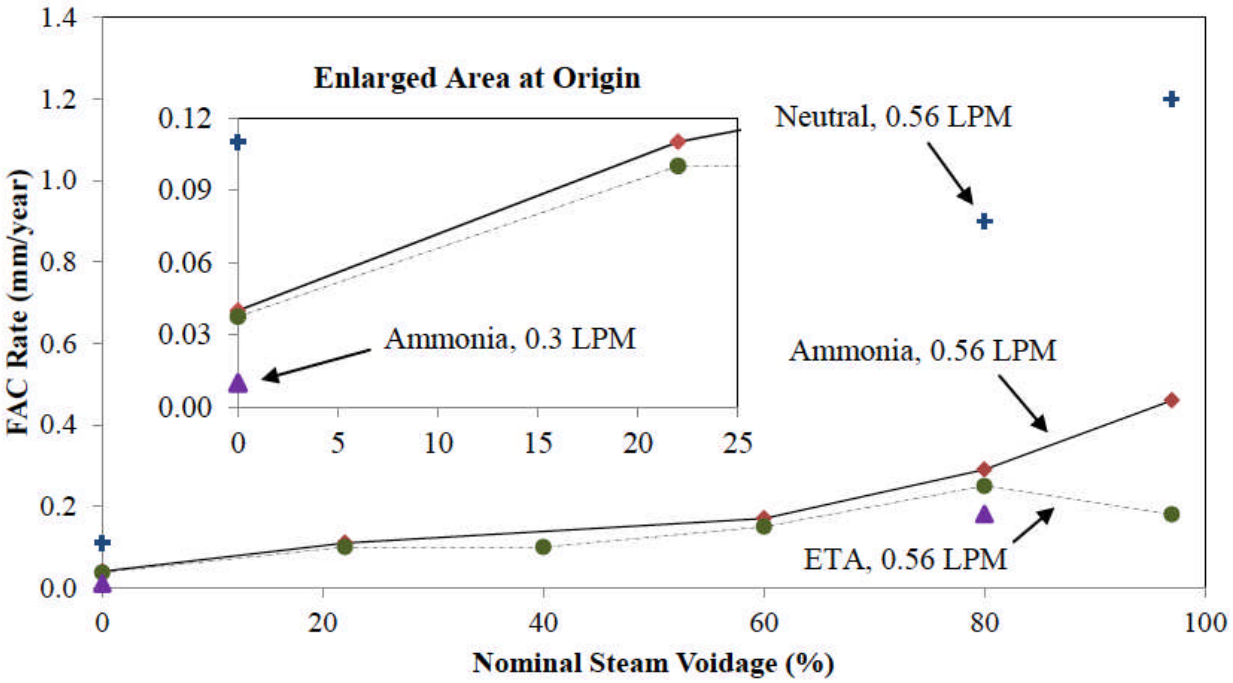

Figure 6. Effect of steam voidage on FAC rate of carbon steel at 200°C under three chemistries (neutral, $pH_{25°C}$ with ammonia and with ETA) at a flow rate of 0.56 L/min (the effect of reduced flow rate on FAC with ammonia also indicated). [Lertsurasakda et al., 2013]

5 Moderator System

As described previously, the main purpose of the heavy water moderator is to slow down or thermalize the high energy neutrons produced through the fission reactions to low, thermal energies so that they more easily induce further fission reactions. A significant amount of heat is produced as a result of the high-energy neutrons losing their kinetic energy and this must be dissipated through the external heat exchanger loops. A secondary purpose of the moderator system is to serve as an additional reactivity control mechanism for the reactor, which is accomplished by dosing the heavy water with low concentrations of neutron-absorbing elements, boron or gadolinium for example. The third purpose of the moderator system is to act as a reactor safety system through rapid additions of high concentration of neutron poisons (known as shut-down system 2 – SDS 2). Thus, the moderator system encompasses a large volume of heavy water contained within the calandria vessel, the associated side recirculation loops for heat removal and purification, the moderator cover gas system for removing deuterium gas produced through the water radiolyisis, and the connections to SDS2. A schematic overview of the moderator systems is shown in Figures 4 and 5 of Chapter 8.

5.1 Chemistry Control in the Moderator System

The materials of construction in the moderator system comprise mainly stainless steel (calandria vessel, heat exchangers, etc), Zircaloy (calandria tubes) and nickel-based alloys, so the chemistry of the moderator is not specified to limit corrosion specifically since the corrosion rates of these alloys at the low temperature and pressure of the moderator system (~60^{o}C and essentially atmospheric pressure) is quite low. Thus, the heavy water in the moderator system is highly purified and the only chemicals added to the system are those used as neutron poisons for excess reactivity control or to guarantee reactor shut-down. Typically, gadolinium nitrate ($Gd(NO_3)_3$) and/or boric acid (H_3BO_3) (alternatively boric anhydride – B_2O_3) are dosed to the moderator system at low concentrations (a few ppm) and these dissolved ions make up the primary contributor to the conductivity of the moderator heavy water – so much so that system conductivity can be translated as a direct measure of reactor negative reactivity. Unlike many of the other reactor coolant systems, the moderator system is not purposely deareated to maintain low dissolved oxygen concentrations. Due to the large radiation fields associated with the reactor core, the heavy water moderator is continuously bombarded with radiation, leading to high production of deuterium and oxygen gases as the net products of water radiolysis. To avoid accumulation of these gases, they are constantly removed through the cover gas system and the deuterium is eliminated by recombination in catalytic re-combiner units, if necessary with oxygen addition.

Typical operating parameters for the moderator system are shown in Table 7. Unlike the heat transport systems where the water is kept alkaline to control and minimize the corrosion of system components, the heavy water in the moderator is kept slightly acidic to ensure that gadolinium hydroxide ($Gd(OH)_3$) will not precipitate on the surfaces of the moderator components and that SDS-2 can function if required.

Table 7. Target chemistry parameters in the moderator system.

Parameter	Typical Specification Range
D_2O isotopic	99.6 – 99.9%
Conductivity	0.005 – 0.1 mS/m
Dissolved D_2	< 3 mL/kg
pHa	4.5 – 6.5
total anions	< 0.2 mg/kg
TIC / TOC*	< 1.0 mg/kg

*Analysis for TIC/TOC has become increasingly important due to concerns for gadolinium oxalate precipitation during guaranteed shut down conditions (see Section 5.1.2).

5.1.1 Reactor shims

Gadolinium Nitrate ($Gd(NO_3)_3$)

Gadolinium has been demonstrated to be an excellent reactor shim and chemical for controlling excess reactivity during refuelling operations and to ensure reactor shut down conditions. The isotopes Gd-155 and Gd-157 are 15 and 16% abundant in nature and have huge neutron absorption cross-sections of 61000 and 255000 barns respectively, which gives them the distinction of being the naturally occurring isotopes with the largest known neutron absorption cross sections. Gadolinium nitrate hexahydrate ($Gd(NO_3)_3.6H_2O$) is easily dissolved in the heavy water moderator. Upon dissolution, the pH of the heavy water will become mildly acidic (pH_a between ~5 to 6) due to the interaction of the nitrate salt dissociation (equation 34). It is important to maintain these slightly acidic conditions within the heavy water moderator because the Gd^{3+} cations will readily hydrolyse at neutral to alkaline pH and precipitate as gadolinium hydroxide (equation 35). This is undesirable since the gadolinium must be homogeneously dispersed in the moderator system to achieve its primary goal of reactivity control.

$$Gd\left(NO_3\right)_3 \rightleftharpoons Gd^{3+} + 3NO_3^- \tag{34}$$

$$Gd^{3+} + 3H_2O \rightleftharpoons Gd\left(OH\right)_3 + 3H^+ \tag{35}$$

Gadolinum concentrations within the moderator system can range from zero to ~ 1 mg/kg under typical reactor operating conditions, leading to water conductivities of ~ 0.005 mS/m to ~ 0.10 mS/m. Care must be taken during normal reactor operation to limit the conductivity, and hence, nitrate concentration in the heavy water to below ~ 0.05 mS/m (corresponding to ~ 1 mg/kg gadolinium nitrate) since the nitrate anions may form reactive intermediate species with the water radiolysis products and promote the formation of deuterium gas (D_2) [Yakabuskie et al., 2010], which can lead to excessive cover gas concentrations and increased workload for the recombiner units (the D_2 concentration in the cover gas must be kept below 4%). Some operating reactors have used gadolinium sulfate ($Gd_2(SO_4)_3.6H_2O$) as their preferred salt, which eliminates the issues of increased deuterium production from interaction of the radiolysis products with the nitrate ion (sulfate ions do not form reactive intermediates with short-lived radiolysis products). However, the sulfate salt is sparingly soluble compared to the nitrate salt thus, if excess reactivity control is required, such as during start-ups with significant amounts of fresh fuel in the core, the preferred reactivity control shim is boric acid. Sulphur species may also promote localized corrosion of alloy components.

Boric Acid

Boron 10 is 20% abundant in nature and has a neutron absorption cross-section of 3838 barns. Boric anhydride or boric acid is soluble in water and can be an efficient alternative to gadolinium as a reactivity control mechanism. Its dissolution, however, is very slow and so boric acid is only employed in the operations of the CANDU plant when necessary. This is typically when concerns of excess deuterium production are encountered through the use of higher concentrations of gadolinium nitrate such as during startups with significant volumes of fresh fuel.

5.1.2 Guaranteed Shutdown State (GSS)

During maintenance shut-downs, the reactor is placed in a guaranteed shut-down state (GSS) whereby a soluble neutron absorbing salt (gadolinium nitrate) is injected into the moderator at high concentrations in addition to having the reactor at zero power with the shut-down rods. This provides redundancy and ensures that the reactor will be maintained in a sub-critical state until the soluble poison is removed via gadolinium and nitrate/nitrite removal in the mixed bed ion exchange columns of the moderator purification circuit, a simplified schematic of which is shown in Figure 3 of Chapter 8.

To ensure a guaranteed shut down state, gadolinium concentrations of greater than 15 mg/kg are typically required and this is the lower limit for gadolinium in the moderator during GSS. Typical concentrations are targeted at greater than 20 mg/kg and assurances must be made to the Canadian Nuclear Safety Commission that GSS is achieved and maintained. This assurance is typically accomplished by manually sampling the moderator and analyzing for gadolinium concentration at least twice per day.

Gadolinium Oxalate

In 2008 during a planned station outage at a unit of the Pickering B plant, while the unit was placed in GSS it was observed that the Gd concentration in the moderator was decreasing at an alarming rate. The over-poisoned condition for the GSS requires assurances that the Gd concentration in the moderator is maintained above 15 mg/kg at all times and the measured loss rate of Gd was approximately 2 mg/kg per day. The utility, with the assistance of experts from AECL Chalk River traced the unexpected Gd depletion to precipitation as gadolinium oxalate ($Gd_2(C_2O_4)_3$), a salt known to be very insoluble in water. Oxalate is normally not present in the moderator heavy water systems and, upon investigation, its formation was attributed to a known leak of CO_2 from the annulus gas system through the rolled joints at one of the end fittings, a condition that had been assessed in 2005 and monitored routinely through measurement of total inorganic carbon (TIC). Elevated CO_2 concentrations in the moderator heavy water produce carbonate anions, which are readily converted to oxalate through combination with primary water radiolysis radicals such as shown in equations 36 & 37.

$$CO_{2(aq)} + e^-_{(aq)} \rightleftharpoons \cdot CO_2 \tag{36}$$

$$\cdot CO_2 + \cdot CO_2 \rightleftharpoons C_2O_4^{2-} \tag{37}$$

Under typical reactor operating conditions, with little gadolinium present in solution, the oxalate

anions would readily decompose back to CO_2. However, under GSS with appreciable concentration of gadolinium in solution and a high enough concentration of TIC (from the ongoing CO_2 leak in the rolled joint), the oxalate anion could readily combine with the gadolinium present as quickly as it was produced, leading to precipitation of the gadolinium oxalate salt throughout the moderator system, as shown in equation 38.

$$2Gd^{3+} + 3C_2O_4^{2-} \rightarrow Gd_2\left(C_2O_4\right)_{3(s)} \quad (38)$$

The Gd depletion is of concern for maintaining the reactor in GSS but the fate of the oxalate precipitate throughout the calandria vessel and on the calandria tubes is of greater concern as it could prevent the reactor from becoming critical upon startup and must be removed. Several research programs were initiated to formulate a chemical cleaning strategy to remove the precipitated gadolinium oxalate; however, none were ultimately needed as the precipitate in-core was found to be readily oxidized and converted to the soluble nitrate salt through action of the shut-down gamma fields and ultra violet radiation (Cerenkov radiation) in the drained (air-filled) and humid calandria vessel. The remaining precipitate from out-core surfaces was easily removed through filtration upon moderator refill and reactor start up [Evans, 2010].

Oxalate production in the moderator system has also been demonstrated to occur by radiolytic processes involving total organic carbon (TOC), primarily from oil ingress. Two operating CANDU units have recently experienced issues with radiolytic decomposition of hydrocarbon lubricants within the moderator system, which will produce decomposition gases such as hydrogen and carbon dioxide as well as create particulate material through polymerization reactions that is highly efficient at plugging filters [Ma, 2010]. These issues with elevated TIC and TOC in the moderator system have led to more strict guidelines and chemistry control practices since the implications of oxalate formation have been realized.

5.1.3 Shutdown System 2 (SDS2)

Gadolinium nitrate is used in the moderator for rapid reactor shut down in the event of a station upset or trip. Shutdown System 2 (SDS2) is described in detail in Chapter 8 and comprises the poison addition tanks which contain approximately 1000 litres each of concentrated gadolinium nitrate solution (~8000 mg/kg). The poison tanks are connected to a high pressure helium gas to rapidly inject the gadolinium solution into the moderator heavy water; the systemis able achieve a reactor shut down in a matter of seconds.

5.2 Moderator Cover Gas

As described above, significant deuterium and oxygen production occurs in the moderator due to the large volume of heavy water that is continuously exposed to high radiation fields associated with the reactor core. The net water radiolysis produces the gases that are initially dissolved in the coolant but diffuse into the moderator cover gas space at the top of the calandria vessel. If the concentration of deuterium gas were not controlled, flammable concentrations would be reached in the cover gas in a matter of hours under normal operating conditions. Flammable concentrations of hydrogen (deuterium) in the helium cover gas are ~ 8%, so upper control limits are set at 4% D_2.

The head space in the calandria vessel is separated from the bulk of the moderator heavy water through a series of calandria relief ducts, as depicted in Figure 7. It is extremely important that the moderator level be maintained within the relief ducts as these provide the conduit for the deuterium and oxygen gases to diffuse into the head-space and to the helium cover gas. Since the surface area for moderator heavy water to cover gas exchange is limited when water level is maintained within the relief ducts, bulk diffusion rates can be minimized and kept within controllable margins. If the moderator level were to fall below the relief ducts a large surface area would then present itself for the D_2 and O_2 to readily migrate into the gas phase, leading to a rapid increase in cover gas concentrations and potential for exceeding flammability limits.

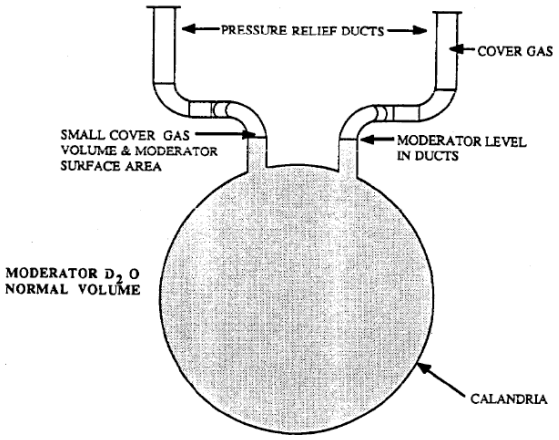

Figure 7. Normal moderator cover gas system volume and relief ducts (CANTEACH)

The helium cover gas is maintained at slightly above atmospheric pressure (~ 110 kPa absolute) and is circulated by several compressors, operating in parallel, through the head-space and on to the catalytic re-combiner units (RCUs). The hydrogen (deuterium) RCUs are usually AECL-patented components that contain a supported platinum or palladium catalyst. The re-combination reaction that ensures deuterium concentrations are kept low in the cover gas follows equation 39. As can be seen, the reaction requires a 1/2x stoichiometric concentration of oxygen in order to fully recombine the deuterium gas to heavy water; however, it is common practice to dose the helium cover gas with oxygen in excess to ensure sufficient recombination occurs. By ensuring the cover gas oxygen concentration is between 1-2%, sufficient excess is continually maintained and deuterium concentrations are kept to very low values and are often undetectable.

$$D_2 + \tfrac{1}{2}O_2 \xrightarrow{\text{catalyst}} D_2O \qquad (39)$$

6 Auxiliary Systems

6.1 Calandria Vault and End Shield Cooling System

The Calandria Vault and End-Shield Cooling system is a light-water system that acts as a biological shield from the gamma radiation and neutrons present in the core of the reactor. In this system, radiation energy is dissipated as heat that is removed from the water in external heat exchangers. Schematic diagrams of the system are shown in Figure 8 and the system is described in more detail in Chapter 8. The system comprises two distinct circuits; the calandria vault that surrounds the reactor calandria vessel, which is enclosed in concrete; and the end shields on either face of the reactor through which the fuel channels protrude. The end shields are packed with carbon steel balls that stop most of the neutrons and gamma emanating from the reactor core (note, in some CANDUs the end shield is a solid carbon steel plate with integral cooling ports). The system operates at nearly atmospheric pressure and contains a circulated nitrogen cover gas. Any gas that is produced from water radiolysis will diffuse into the cover gas, which needs to be purged periodically to avoid the build up of flammable concentrations of hydrogen and oxygen.

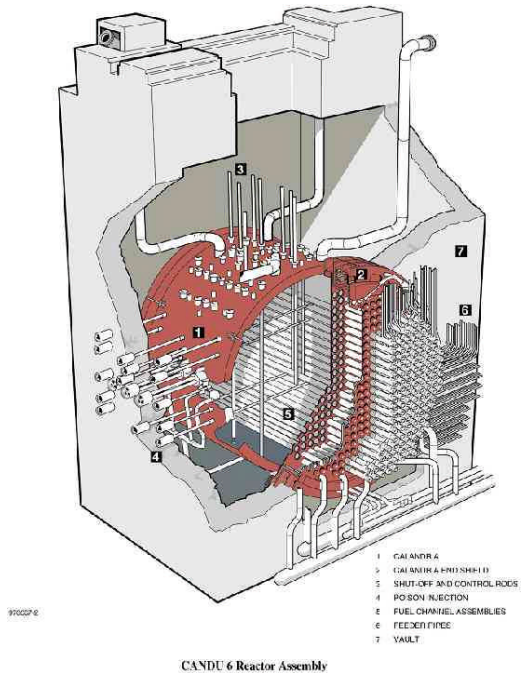

Figure 8. Schematic diagram of the Calandria vault and reactor assembly.

Typical operating specifications for the calandria vault and end shield cooling system are shown in Table 8. Alkalinity is controlled by addition of lithium hydroxide to ensure low corrosion rates of the system materials and the specifications for dissolved hydrogen and dissolved oxygen in the system are set to ensure flammability limits are not exceeded. If the nitrogen cover gas for the system reaches the control limit for hydrogen (4%), the system is purged with fresh nitrogen to ensure safe operation is maintained.

Table 8. Typical Chemistry Parameters of the Calandria Vault and End Shield Cooling System.

Parameter	Typical Specification Range
pH	9.0 – 10.0
$[Li^+]$	0.07 – 0.7 mg/kg
conductivity	0.24 – 2.4 mS/m
Anionic impurities	< 1.0 mg/kg
H_2 (vol. % in cover gas)	< 4%
O_2 (vol. % in cover gas)	< 2%

Under normal circumstances, the end shield cooling system operates with a small excess of dissolved hydrogen produced through the corrosion of system materials. This results in the net radiolytic production of hydrogen and oxygen being suppressed. Some CANDU reactors have had chronic issues with build up of hydrogen in the cover gas, which requires a frequent purging to ensure that flammable concentrations are not reached. The increased hydrogen production has been linked to the presence of dissolved oxygen in the water due to the addition of higher–than-normal quantities of air-saturated make-up water. Dissolved oxygen is consumed through recombination with the dissolved hydrogen, but when there is insufficient dissolved hydrogen net water radiolysis will recommence to produce hydrogen and more oxygen, which exacerbates the process. Once net radiolysis is occurring on a long-term basis, simply addressing the aerated make-up water ingress issue has been shown not to reduce the hydrogen production.

The CANDU industry has investigated the possibility of mitigating excessive hydrogen production in the calandria vault and end shield cooling system and has demonstrated that adding an oxygen scavenger, such as hydrazine, to the system will mitigate the hydrogen production and return the system to net radiolytic suppression [Stuart, 2012]. The dissolved oxygen reacts with hydrazine to form nitrogen and water, which is a process that is fast at low temperatures as it is mediated by the radiation field. Note that simply adding dissolved hydrogen to the water would also promote a radiolysis recombination reaction, however, since the Calandria Vault and End Shield Cooling system operates at atmospheric pressure, this method is not feasible and hydrazine additions are becoming common practice in operating reactors.

6.2 Liquid Zone Control

The liquid zone control system, as described in detail in Chapter 8, is designed to make fine adjustments to the neutron flux profile in the reactor. This is accomplished by varying the water level in each of the liquid-zone control tubes by adjusting the inlet water flow rate to the individual zones. The materials of construction for the liquid zone tubes are primarily Zircaloy 4, with auxiliary components being 300-series stainless steel; thus, the corrosion of the system components is minimal under a wide range of chemistry conditions. Since the purpose of the light water in the liquid zone system is to absorb neutrons to shape the reactor flux, the water is kept nominally pure with a very low conductivity. The cover gas space is occupied with helium and no direct method is used to limit the water radiolysis reactions that produce hydrogen and oxygen. Hydrogen control in the cover gas space is minimized by purging with helium as required and by recombiners. Water purity in the liquid zone system is paramount to minimize the hydrogen produced by radiolysis since impurities such as chlorides or nitrate/nitrites will

interfere with the hydrogen recombination reactions and catalyze oxygen and peroxide production. Thus, nitrogen in the cover gas (indicative of air ingress) is highly undesirable, since it will produce nitrate anions in the presence of a radiation field and subsequently produce nitric acid that can lead to low pH conditions and corrosion of the system materials as well as promote high production rates of hydrogen.

The typical operating specifications for the liquid zone control system are focused on water purity as measured through liquid conductivity. For high purity make-up water, it is often possible to achieve conductivities in the range of 0.006 – 0.008 mS/m, and most utilities will try to keep the system operating within these limits or at least below 0.01 mS/m. By doing so, water radiolysis is minimized and the cover gas purge can be done as frequently as necessary to maintain the cover gas hydrogen concentration below 4%.

6.3 Annulus Gas

The annulus gas system provides a thermal barrier between the Zr-2.5Nb pressure tubes operating at temperatures between 300-310^{o}C and the low temperature (~60^{o}C) calandria tubes that separate the moderator from the primary heat transport system. The annulus space in each fuel channel provides a gap of approximately 5 mm and is continuously purged with carbon dioxide gas, thus purity of the CO_2 is a direct indication of the overall health of the system. Typical impurities in the CO_2 purge gas include deuterium (D_2), which diffuses through the pressure tubes from to the small amount of corrosion occurring on the PHT side of the tube, and water vapour (D_2O). The corrosion of the exterior surface of the pressure tubes and the interior surface of the calandria tubes is not typically an issue when the CO_2 is pure. The presence of heavy water vapour in the gas can indicate leaks from either the PHT or moderator systems. Thus, typical chemistry parameters that are monitored in the annulus gas include the volume percentages of deuterium and oxygen and the dew point (^{o}C). Gradual increases in the dew point are expected in the system since, ultimately, a small amount of heavy water will migrate through the rolled-joint seals at each end of the fuel channel. However, accelerating increases in dew point measurement provide an on-line indication of developing leaks in the system.

Oxygen may also be injected into the CO_2 annulus gas to a concentration of approximately 2-4%. This is beneficial as it promotes protective ZrO_2 films on the pressure tubes and calandria tubes and helps to ensure that the garter springs or calandria tube to pressure tube spacers (Alloy X750 – a nickel superalloy) are maintained in a suitably oxidized state, also promoting passive oxide film formation. If no oxygen is present, the garter springs can become extremely brittle as the reduced oxides or elemental nickel present under these conditions can promote cracking in the material. This is exacerbated by radiation embrittlement due to the high neutron fluxes to which the garter springs are exposed. Oxygen injection to the annulus gas also promotes the recombination with deuterium to form D_2O, helping to ensure the deuterium concentrations are kept below the flammability limits.

6.4 Emergency Core Cooling Systems

The emergency core cooling systems must be ready on a moment's notice in the event of a loss of coolant accident (LOCA) from the PHT, thus it is imperative that the system components do

not corrode excessively and accumulate particulate corrosion products that can accumulate as sludge in the normally stagnant system. Short-term decay heat removal is supplied by the high-pressure and medium-pressure ECC systems that have their own distinct water supplies. For longer-term core cooling, the emergency cooling water is supplied via a tank inside the vacuum building in the multi-unit CANDUs or from the dousing tank in the roof of the containment building of single-unit stations.

In the event of a LOCA, when a reactor PHTS is vented to the building, water from the dousing tank is sprayed into the building to condense the steam and reduce the pressure. The supply tank is connected to the sump below the reactor building that collects water draining from the system for re-injection via the emergency injection pumps. The system chemistry is maintained moderately alkaline and is deoxygenated with hydrazine, which will decompose over time to ammonia producing the alkalinity required to maintain low corrosion rates of the ECC piping and injection nozzles. Recent regulations have focused on ECC chemistry, particularly the effect of debris or corrosion products clogging the strainers of the injection pumps. Of primary concern are high-pH conditions, where the corrosion of aluminum components in contact with the ECC water (the sump strainers for example) has been the focus of considerable research effort [Edwards et al, 2010]. At too high a pH, aluminum components may corrode excessively and form precipitates that could block the strainers. For this reason, an upper limit on dousing system pH is typically set around 9.5.

6.5 Service Water

A nuclear power plant contains many subsystems that act as coolants for the primary process systems. These include auxiliary heat exchangers for the emergency core cooling systems, recirculated cooling water for the turbine/generator lubrication oil, and general service recirculated cooling water (RCW). These systems are chemically-dosed to maintain low corrosion of the piping and heat exchanger tubing by providing an alkaline environment with minimal dissolved oxygen. The RCW and TARCW (turbine & auxiliaries recirculated cooling water) systems are continuously circulated during plant operation, making their chemistry control quite simple; chemicals may be added as required to meet the pH and dissolved oxygen specifications. These auxiliary systems will typically operate with the same chemicals as are used in the feedwater circuit, but care must be taken to limit the operating pH if ammonia is used since the auxiliary systems will typically contain some copper-bearing components. In general, pH is controlled by ammonia and/or morpholine additions to maintain a value of around 9.2. Dissolved oxygen is monitored and managed through hydrazine additions at concentrations between 50 – 100 ppb, ensuring low corrosion of the carbon steel piping. Particulate corrosion products are also monitored to ensure system corrosion is low; higher particulate concentrations can be an indication of out-of-specification chemistry conditions that may be remedied by chemical addition or through a feed-and-bleed procedure to lower overall chemical and impurity concentrations.

7 Lay-up Practices

Inevitably, every power plant needs to be shut down for regular maintenance outages. In the case of a CANDU, a mid-life refurbishment outage (after ~ 25-30 years operation) is required to remove and replace the Zr2.5Nb pressure tubes that tend to stretch and sag due to the operational temperatures and high atomic displacements caused by the continuous neutron bombardment under load. A regular maintenance outage may last from 2 – 8 weeks depending upon the scope of work required and refurbishment outages are planned for at least two years. During any of these plant outages, the systems are typically depressurized and frequently drained to facilitate the required maintenance work and subsequent inspections. These maintenance activities can allow air ingress into the closed-loop systems that are intentionally kept de-aerated to minimize corrosion during operation. The duration and extent of the oxidizing conditions that are produced when the systems are shut down can play large roles in their behaviour during startup and subsequent steady power operation. Thus, it is now considered extremely important to provide a suitable lay-up condition to the plant during regular maintenance outages and is paramount for protecting non-refurbished components during an extended shut down during a mid-life refurbishment. Degradation mechanisms and problem locations in the feedwater and steam circuit of fossil plants are described by Mathews and are shown schematically in Figure 9 [Mathews, 2013]

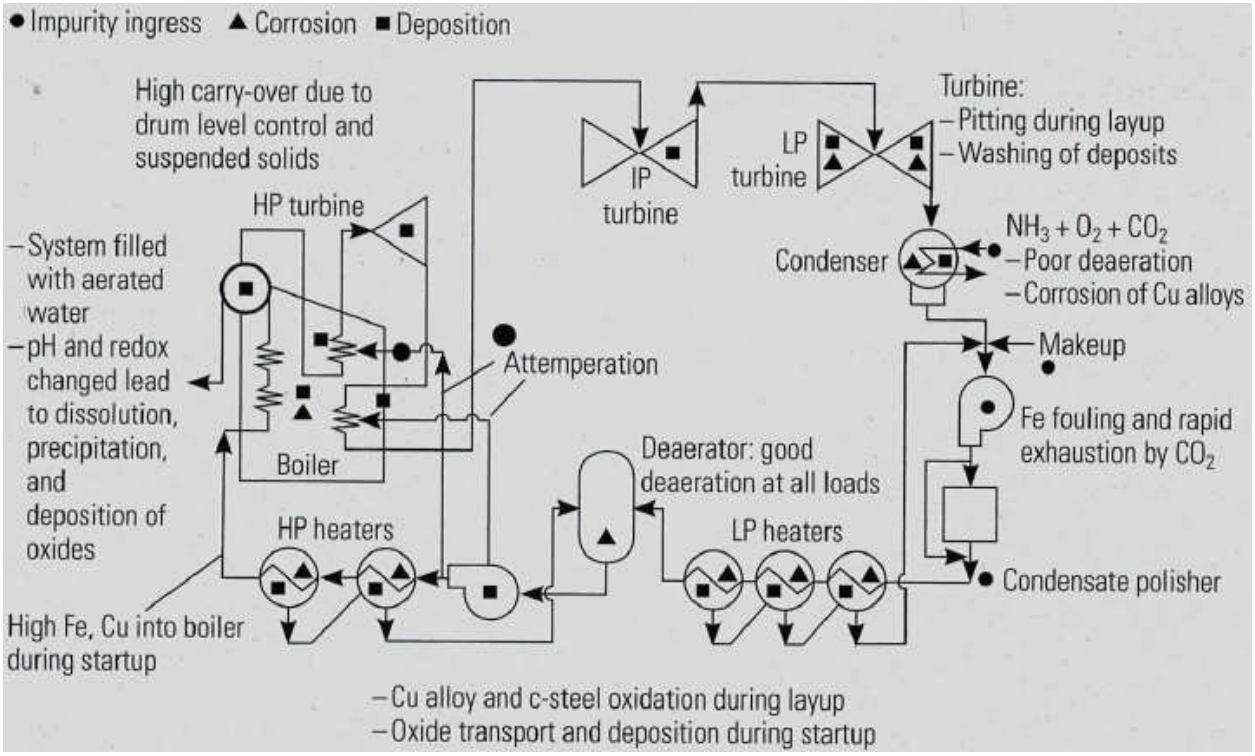

Figure 9. Locations requiring attention during maintenance outages and lay-up of a fossil plant. [after Mathews, 2013]

7.1 Dry Lay-up

It is common practice in the power generating industry to provide, at a minimum, a low humidity environment for systems that are placed in "dry lay-up". This includes the steam-carrying piping and components of the secondary system along with the condenser shells. Depending upon the duration of the maintenance outage it may be desirable not only to circulate low humidity air through the system but also to maintain an inert cover gas, typically nitrogen, to prevent oxidation of the reduced corrosion products present on the piping surfaces. If significant humidity is present, a thin water film will develop on the piping surfaces and this will be fully oxygen saturated, thus promoting general corrosion and pitting on the predominantly carbon steel surfaces in these systems. It will also convert, at least partially, the reduced protective oxide formed on the surfaces during operation (typically magnetite – Fe_3O_4) to a more oxidized form such as hematite (Fe_2O_3). This oxidation process will tend to alter the volume and thickness of the oxide films leading to poor adhesion and spallation during subsequent plant start up. Figure 10 shows the relative oxide/steel volume ratios and it is clear that the further oxidized the corrosion product the larger the volume occupied. Thus, maintaining an oxygen-free, dry environment for all system components during a maintenance outage is seen as the most prudent step in protecting the plant's assets.

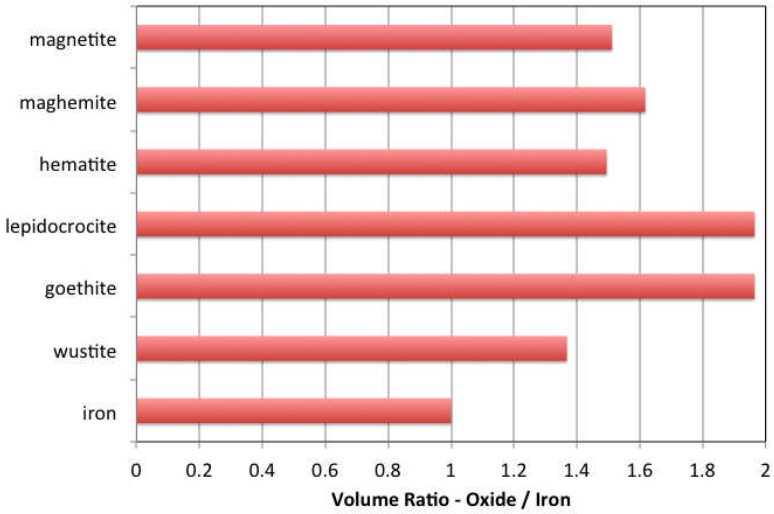

Figure 10. Oxide/steel volume ratios.

7.2 Wet Lay-up

Some systems may not be drained during a maintenance outage if work is not scheduled to be performed on the system or if parts of the system in question can be isolated. Thus, at the start of the lay-up period, the system will have the good chemistry specified for the operational period but this may be difficult to maintain, especially if the outage is extended or if the project is large in scope such as an overall mid-life refurbishment. Under these circumstances, the keys to maintaining low corrosion rates of all system materials are the same as during operation: maintain an alkaline pH condition to promote passivity of the corrosion films and maintain reducing conditions in the fluid by excluding air ingress and, typically, dosing with an oxygen scavenging chemical such as hydrazine (N_2H_4). Frequent recirculation of the laid-up system

volume during the maintenance outage is recommended to promote good mixing and representative sampling.

8 Heavy Water Systems

Heavy water (D_2O) is essential to the operation of a CANDU reactor. It is used in place of light water (H_2O) as a moderator and coolant due to its superior neutron moderating properties (deuterium's neutron absorption cross-section is orders of magnitude lower than hydrogen's) making it feasible to fuel the reactor with uranium containing the natural abundance of the fissile U-235 isotope (~0.7%). Heavy water or, more specifically, the deuterium isotope, is naturally abundant in the environment at about 0.015% (atomic percentage) as both the D_2O and the HDO molecule, all in chemical equilibrium as shown in equation 40. The moderator and PHT systems both require heavy water that is greater than 98% in isotopic for D_2O. For reactor safety purposes in the event of a pressure tube rupture where the PHT water enters and mixes with the moderator, the PHT isotopic content is typically kept slightly lower than the moderator, 98.6% vs > 99% for example, which will dilute the moderator in the accident scenario lowering the overall moderation.

$$H_2O + D_2O \rightleftharpoons 2HDO \tag{40}$$

8.1 Upgrading

Separation techniques are numerous and include fractionation through distillation and various processes involving atomic exchange through chemical sorbants and equilibrium systems. All of these processes rely on the fact that the mass of the deuterium atom is twice that of the hydrogen atom, making properties such as vapour pressure slightly different from those of compounds containing the hydrogen atom alone. The separation factor for the deuterium-hydrogen isotopes is defined as the ratio of the deuterium fraction in the desired phase (liquid, x) over its fraction in the other phase (gas, y), as shown in equation 41. For a light-water/heavy-water mixture, the separation factor can be estimated through the vapour pressure of each of the components as shown in equation 42 for the normal boiling point of natural water [Benedict, 1980].

$$\alpha = \frac{x/(1-x)}{y/(1-y)} \tag{41}$$

$$\alpha_{HD} = \sqrt{\frac{p_{H_2O}}{p_{D_2O}}} = 1.026 \tag{42}$$

The primary method for heavy water production is known as the GS dual-temperature exchange process. It involves the equilibrium exchange of the deuterium atom between water and hydrogen sulfide gas in a staged absorption column as shown in equation 43. Two towers are employed whereby a fresh water feed to the cold tower, which has a higher separation factor for

deuterium ($\alpha_c \approx 2.32$) since it will be retained preferentially in the liquid phase, is stripped of some of its hydrogen content to a deuterium-rich hydrogen sulfide gas (HDS), which is effectively leached of its deuterium content. The feed gas to the cold column is produced in the high temperature column, where the separation factor (ratio of the fraction of D in liquid to D in the gas) is lower ($\alpha_h \approx 1.80$), thereby producing the D-rich gas for feed to the primary, cold exchange column. The basic principles of operation of the GS process are depicted in Figure 11 (from Benedict et al., 1980). With an appropriate number of stages in the absorption columns, water can be fairly economically enriched to about 25% - 30% D_2O. From this concentration, final upgrading using conventional distillation is economically feasible.

$$H_2O + HDS \rightleftharpoons HDO + H_2S \tag{43}$$

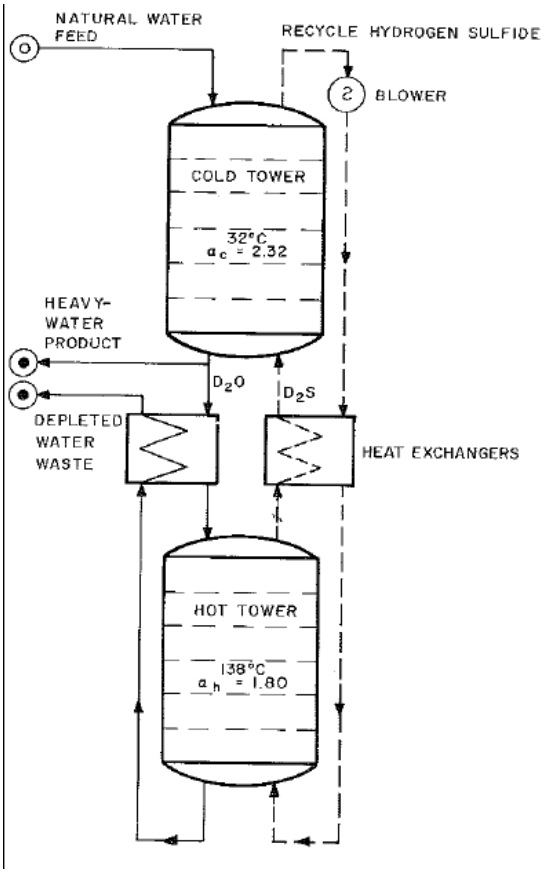

Figure 11. Schematic representation of a GS dual temperature absorption column (Benedict et al., 1980).

The distillation of water to produce a heavy water product is extremely energy intensive, since large volumes are required to compensate for the low isotopic content of natural water. Thus, once primary upgrading has been accomplished from processes such as the GS dual-temperature exchange described above, energy requirements are much reduced, particularly when conducted under vacuum conditions. All CANDU plants will contain a distillation facility for upgrading the D_2O isotopic content since it can be diluted during operation through addition

of chemicals containing the hydrogen atom (H_2, LiOH, N_2H_4, NH_3 etc.) and through neutron absorption producing tritium (H-3 or T). The overall efficiency of the fission process relies upon specified isotopic content in the moderator and coolant thus the process water must be periodically upgraded.

8.2 Clean-up

Like the make-up water that feeds the secondary system and the reactor auxiliaries and is conditioned to ensure low corrosion rates of the materials of construction and adequate system lifetimes, the heavy water used in CANDU plants must be very pure. The basic methods of filtration and ion exchange all apply to heavy water as they do for light water, with the exception that the isotopic content of the heavy water must also be taken into consideration (the H_2O content in the heavy water may be considered an impurity).

As described above, D_2O production and upgrading facilities may produce heavy water at isotopic concentrations greater than 99.5% quite readily. Impurities introduced during the upgrading process may include corrosion products from the materials of construction of the distillation towers and packing columns (Fe, Ni, Cu etc) as well as contaminant cations and anions (Na^+, Ca^{2+}, Cl^-, SO_4^{2-} etc) from ingress of humidity or contamination during transfer operations. These may be removed through ion-exchange; however, it is imperative that the ion-exchange resin first be converted to a deuterated form (exchange of the H^+ sites with D^+) to minimize the downgrading in isotopic from cation exchange.

Tritium Removal

Some plants, notably the Darlington station in Ontario, include a tritium reduction facility in order to ensure low environmental releases and to minimize the tritium activity in the operating plant. Tritium removal plants follow the same isotopic removal principles as upgrading the deuterium content to produce heavy water, except that the separation factor for D/T is very close to unity under near atmospheric and/or vacuum conditions. At the Darlington facility, separation is aided by a series of catalytic exchange columns that facilitate the equilibrium exchange between tritiated heavy water and the carrier deuterium gas. The catalytic exchange process follows equation 44 and typically can reduce the tritium concentration in the input heavy water by a factor of ten [CANTEACH]. The tritium now contained in the deuterium gas stream is concentrated to >99.9% through a series of cryogenic distillation columns operating at temperatures of ~ 25 K absolute. A schematic flow sheet of the Darlington facility is shown in Figure 13. These cryogenic temperatures ensure that any humidity or traces of nitrogen and oxygen are removed (25 K is well below their boiling points) leaving a pure deuterium/tritium gas that is easily separated through the density/buoyancy effects utilized in distillation. The resulting pure tritium gas is encapsulated through reaction with titanium sponge, producing a titanium hydride and immobilizing the radioactivity. The hydride may then be stored until the tritium decays to suitable levels or sold for profit.

$$DTO + D_2 \rightleftharpoons D_2O + DT \qquad (44)$$

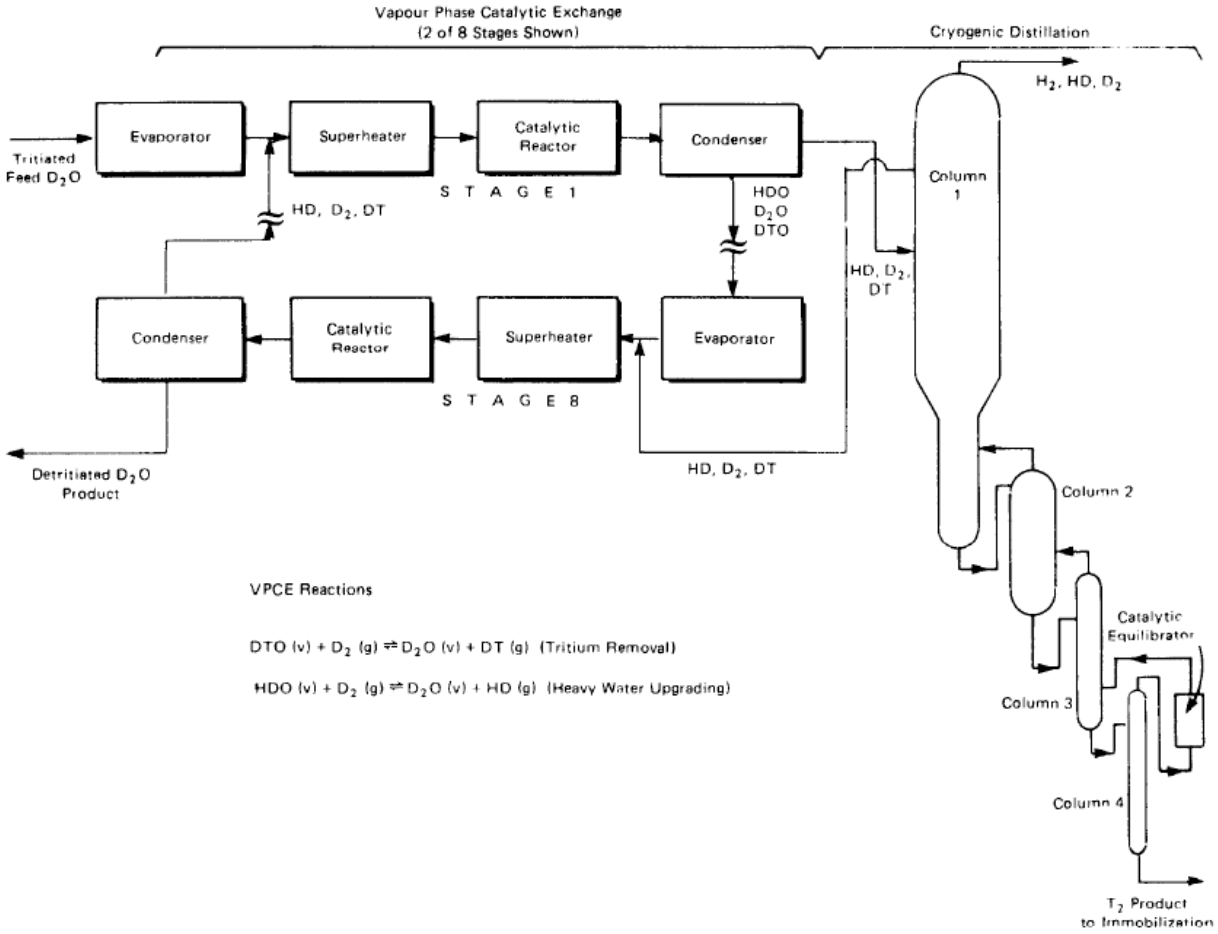

Figure 12. Schematic diagram of the Darlington tritium removal facility. (Busigin & Sood)

9 Summary of Relationship to Other Chapters

The chemistry of process systems is controlled in order to optimize the performance of the variety of materials that make up the systems. There is therefore a strong link to the Chapter 14 on Materials and Corrosion.

10 References

A.V. Bandura & S.N. Lvov, The Ionization Constant of Water over a Wide Range of Temperatures and Densitites, J. Phys. Chem. Data, vol. 25, pp 15-30, 2006.

D.M. Bartels, *The Reaction Set, Rate Constants and g-Values for the Simulation of Radiolysis of Light Water over the Range of 20^{o} to 350^{o}C Based on Information Available in 2008,* AECL Analyses, 153-127160-450-001, Revision 0, 2009.

M. Benedict, T.H. Pigford and H.W. Levi, *Nuclear Chemical Engineering*, Second Edition, McGraw-Hill Book Company, 1981.

A. Busigin and S.K. Sood, Optimization of Darlington Tritium Removal Facility Performance: Effects of Key Process Variables, Nuclear Journal of Canada, 1:4, pp 368-371.

G.B. Buxton, *Radiation Chemistry of the Liquid State: (1) Water and Homogeneous Aqueous Solutions,* in Radiation Chemistry: Principals and Applications, Editors: Farhataziz and M.A.J. Rodgers, VHC, New York, 1987.

CANTEACH, *Introduction to CANDU Process Systems – Heavy Water Production and Management,* available at www.canteach.ca.

CANTEACH, *The Moderator and Auxiliary Systems*, Chemistry Course 224, available at www.canteach.ca.

B. Cox, Mechanisms of Zirconium Alloy Corrosion in High Temperature Water, J. Corr. Sci. & Eng., vol.6, 2003.

CRC, *Handbook of Chemistry and Physics*, 94th Edition, CRC Publishing, 2013-2014.

M.K. Edwards, L. Qui and D.A. Guzonas, *Emergency Core Cooling System Sump Chemical Effects on Strainer Head Loss*, Nuclear Plant Chemistry Conference – NPC 2010, Quebec City, October 2010.

A.J. Elliot and C.R. Stuart, *Coolant Radiolysis Studies in the High Temperature, Fuelled U-2 Loop in the NRU Reactor,* AECL R&D Report, 153-127160-440-003, Revision 0, 2008.

D.W. Evans et al, *Gadolinium Depletion Event in a CANDU® Moderator – Causes and Recovery*, Nuclear Plant Chemistry Conference – NPC 2010, Quebec City, October 2010.

IAPWS, Guideline on the Henry's Constant and Vapor-Liquid Distribution Constant for Gases in H_2O and D_2O at High Temperatures, Kyoto, Japan, available at www.iapws.org, 2004.

IAPWS, *Release on the Ionization Constant of H_2O,* Lucerne, Switzerland, available at www.iapws.org, 2007.

IAPWS, Technical Guidance Document – 2012 Revision: Instrumentation for Monitoring and Control of Cycle Chemistry for the Steam-Water Circuits of Fossil-Fired and Combined-Cycle Power Plants, Boulder, Colorado, available at www.iapws.org, 2012.

IAPWS, Technical Guidance Document: Corrosion Product Sampling and Analysis for Fossil and Combined-Cycle Power Plants, Moscow, Russia, available at www.iapws.org, 2014.

C. Lertsurasakda, P. Srisukvatananan, L. Liu, D. Lister and J. Mathews *The effects of amines on flow-accelerated corrosion in steam-water systems.* Power Plant Chemistry, Vol. 15, No. 3, pp.181-190 (2013)

I.N. Levine, Physical Chemistry, 199??.

D.H. Lister and L.C Lang. *A mechanistic model for predicting flow-assisted and general corrosion of carbon steel in reactor primary coolants*. Proc. Chimie 2002; Intern. Conf. Water Chem. Nucl. Reactor Systems. Avignon, France. SFEN. (2002)

G. Ma et al, *Experience of Oil in CANDU® Moderator During A831 Planned Outage at Bruce Power*, Nuclear Plant Chemistry Conference – NPC 2010, Quebec City, October 2010.

J. Matthews, *Layup Practices for Fossil Plants*, Power, February 2013.

R.E. Mesmer & D.L. Herting, *Thermodynamics of Ionization of D_2O and $D_2PO_4^-$*, J. of Sol. Chem. Vol.7, no.12, pp.901-913, 1978.

J.P. Slade and T.S. Gendron, *Flow accelerated corrosion and cracking of carbon steel piping in primary water – operating experience at the Point Lepreau Generating Station*, Proc. Intern. Conf. on Environmental Degradation of Matls. in Nuclear Power Systems, Salt Lake City, UT. TMS. (2005).

J.W.T. Spinks & R.J. Woods, *An Introduction to Radiation Chemistry,* Wiley, New York, 1990.

C.R. Stuart, *Mitigation of Hydrogen Production in the Shield Cooling System of CANDU Reactors - Recent Changes to Chemistry Control*, 9th International Workshop on Radiolysis, Electrochemistry and Materials Performance, Paris, France, September 2012.

R.L. Tapping, J. Nickerson, P. Spekkens and C. Maruska, *CANDU Steam Generator Life Manage-*

ment, Nuc. Eng. & Design, vol. 197, pp. 213-223, 2000.

R.L. Tapping, Chapter 17: Corrosion Issues in Pressurized Heavy Water Reactor (PHWR/CANDU®) Systems, Nuclear Corrosion Science and Engineering, Woodhead Publishing Limited, London, 2012.

P.R. Tremaine & J.C. Leblanc, The Solubility of Magnetite and the Hydrolysis and Oxidation of Fe^{2+} in Water to 300°C, J. Sol. Chem., vol.9, no.6, pp. 415-442, 1980.

C. Turner & D. Guzonas, *Improving Chemistry Performance in CANDU® Plants*, Nuclear Plant Chemistry Conference – NPC 2010, Quebec City, October 2010.

V.F. Urbanic, B. Cox & G.J. Fields, *Long Term Corrosion and Dueterium Ingress in CANDU PHW Pressure Tubes*, Zirconium in the Nuclear Industry: Seventh International Symposium, ASTM STP939, pp. 189-205, 1987.

P.A. Yakabuskie, J.M. Joseph, J.C. Wren & C.R. Stuart, *Effect of NO_3^- and NO_2^- on Water Radiolysis Kinetics During γ-Irradtiation,* NPC 2010 – Nuclear Plant Chemistry Conference, Quebec City, Quebec, 2010.

11 Acknowledgements

The following reviewers are gratefully acknowledged for their hard work and excellent comments during the development of this Chapter. Their feedback has much improved it. Of course the responsibility for any errors or omissions lies entirely with the authors.

Gordon Burton
Dave Guzonas
Craig Stuart

Thanks are also extended to Diana Bouchard for expertly editing and assembling the final copy.

CHAPTER 16

Regulatory Requirements and Licensing

prepared by
Dr. Victor G. Snell & Dr. Nikola K. Popov

***Summary**:*

This chapter covers the overall aspects of nuclear reactor regulation, with emphasis on Canada, but also covering other regimes such as the United States, the United Kingdom, and Europe. It explains the need for regulation; how regulators work; how they are structured; and the types of requirements they set. Canada, the United States, and the United Kingdom are used as specific examples in these areas, with detailed material on Canadian licensing processes, requirements, and guides.

***Disclaimer:** This Chapter captures the elements of nuclear power reactor regulation as of ~2013, when the Chapter was drafted. Although regulatory concepts change slowly, detailed licensing requirements can change fairly frequently, and some of the details in this Chapter could be superseded by the time the book is used. The reader is advised to consult the most up-to-date regulatory documents if the intended use at the time is critical. The information in this Chapter is current as of late 2012 or early 2013.*

Table of Contents

List of Figures

List of Tables

1 Introduction

The purpose of this chapter is to:

1. describe the need for, and concepts underlying, nuclear regulation
2. cover specific requirements in Canada in some detail, and examples from other jurisdictions where the differences are instructive.

Whereas the first aspect covers "why", the second aspect covers both "why" and "what".

1.1 Overview

Regulatory oversight of nuclear power plants is an essential aspect of the application of the technology, albeit not generally considered a specific engineering discipline. Regulation affects reactor design and operation by setting requirements at both a high level (safety goals, system requirements, operations performance metrics, etc.) and in more detail, and through regulatory review of design and operation.

Section 2 looks at overall regulatory requirements. It begins by explaining the need for regulation. It then looks at generic aspects such as regulatory structure and independence, which tend to be broadly similar in advanced nuclear-power-capable countries. It discusses how a good regulator works through drafting standards and guides and through independent review, but emphasizes that the operator is ultimately responsible for safety. It describes licensing milestones (site licence, construction licence, operating licence, decommissioning licence, and licence to abandon), which are common to most countries.

In Section 3, different regulatory approaches are briefly contrasted, varying from risk- or goal-driven at one end to highly prescriptive at the other.

Section 4 gives a number of case studies of regulatory behaviour (in the same spirit as Chapter 13, of learning from real experience)—not to suggest that the regulator was primarily responsible for an event, but that weaknesses in the overall regulatory approach led to inattention on the part of the industry to certain risks.

Section 5 discusses a recent tool for facilitating the licensing of a new design: a pre-project licensing review.

Section 6 gives some international and national examples of organizations which influence or apply regulatory requirements. Specifically, we summarize the consensus developed by the International Atomic Energy Agency (IAEA) as reflected in its guides and touch briefly on regional organizations. Then we discuss examples of prescriptive (United States) and non-prescriptive (United Kingdom) approaches.

Safeguards are described in Section 7. Security is also covered briefly in Section 8.

Sections 9 and 10 cover the Canadian approach. This can be considered as a balanced approach, mixing prescriptive requirements and overall goals. The mandate and organization of the Canadian Nuclear Safety Commission (CNSC) is presented in Section 9. The structure of Canadian Nuclear Regulations and the CNSC's Regulatory Documents and Regulatory Guides is summarized. Certain key Regulatory Documents affecting design and operation are presented in more detail. The licensing process in Canada for both existing and new nuclear power plants is described in Section 10; this includes a summary of the environmental assessment process.

Three supplementary sections follow. Section 11 gives some problems for the student to work through. Section 12 is an Appendix giving some examples of U.K. Safety Assessment Principles as typical of a non-prescriptive approach. Section 13 is an Appendix listing the information that is typically required in Canada when applying for construction and operating licences for nuclear power plants.

Reactor regulation is a very broad field, and we can cover only the essentials in this chapter. Most sections in the text list references to documents or published papers that the interested reader can pursue for more detail: see Section 14 for the list of references. Section 15 concludes the chapter with a glossary of terms.

1.2 Learning Outcomes

The goal of this chapter is for the student to understand generically:

- The need for regulatory oversight of nuclear technology
- How a regulatory agency is structured
- How it fulfills its responsibilities
- The regulatory process and milestones
- The nature of a regulatory review
- Enforcement of regulatory requirements
- Common threads in international approaches to regulation
- Different approaches to regulation (prescriptive, goal-based, mixed)
- Concepts behind safeguards and security.

In addition, the student will gain a familiarity with the organization and mandate of the Canadian regulatory organization (the Canadian Nuclear Safety Commission, or CNSC). The student will understand the Canadian licensing process for both new and existing reactors, as well as acquiring an overall knowledge of CNSC's most important requirements and guides.

2 Generic Regulatory Requirements

This section covers regulatory requirements and processes in general, supported by selected examples. Later sections give details for Canada.

2.1 Why is a Regulator Needed?

Nuclear power is an inherently hazardous and complex technology. Society regulates such technologies, especially if they are relatively new—non-nuclear examples include prescription drugs and air travel. Regulatory oversight of a technology can encompass most or all of the life cycle, including site selection, design, construction, commissioning, operation, decommissioning, and site abandonment. In addition, fuel fabrication and management of spent fuel (should it leave the plant site) are also regulated, although these aspects are not covered in this chapter.

Regulators are authorized by the government—usually the national one—and have strong legal powers to set requirements and to intervene in the technology they regulate, e.g., to order a drug to be withdrawn from the market, or to order a nuclear power plant to make changes. They can use sanctions (fines or prison) on both corporations and individuals in case of egregious non-compliance.

An "ideal" regulatory framework balances the risk of the regulated technology against those of

similar technologies, so that social risks are rationalized. This hardly ever happens because the mandate of regulators is usually restricted to a specific technology. Nuclear power tends to be regulated more strictly (i.e., lower risks and more risk aversion) than comparable technologies. There are many reasons for this which we do not have space to explore, but which have been touched on briefly in Chapter 13, and which include voluntary versus involuntary risk, perceived risk versus benefit, association of radiation with atomic weapons and cancer (the "dread" factor), and public unfamiliarity with the technology. The interested reader is referred to the literature on this subject. [Starr1969] and [Slovic1987] are good places to start.

One of the key functions of a regulator is that through the *potential* of independent verification of *any* aspects of a licensee's work, the regulator influences *all* a licensee's internal processes, because any piece of safety-related work can be audited. In particular, the simple *existence* of regulatory oversight stops the licensee from internally accepting deficient safety cases or accepting too readily that their assumptions are right and that they have thought of everything. In other words, oversight encourages the building and maintaining of an adequate safety culture. Regulatory oversight provides a critical independent challenge to a licensee's premises, assumptions, and positions and affects far more than the actual items that a regulator reviews.

2.2 What a Regulator is Not

A good regulator does not remove the onus for safe plant design from the designer or that for safe plant operation from the operator. *This is a key concept.* The ultimate responsibility for safe plant operation lies with the licensed operator. A regulator sets the framework and the rules to be followed, but these do not guarantee a safe plant. A deficient regulatory structure, or a regulator that is not sufficiently independent from government, may contribute to an accident by inadequate oversight, or inadequate requirements, or by being so prescriptive that the operator relinquishes the responsibility to maintain a questioning attitude. However, an operator is not absolved by a weak regulator.

Conversely, a good regulatory structure defines a climate of openness, fairness, and high expectations of safe performance that operators will internalize. In addition, a good regulatory structure ensures that international regulatory trends and approaches are readily adopted and implemented by a national regulator.

In any case, it is impossible for a regulator to check everything. This has two implications:

- there is an implicit understanding that once a licence has been given, the licensee will follow the rules and that the regulator is there to verify selected activities from time to time as it sees fit, usually in some risk-informed manner, as discussed in Section 2.5. This is called "trust but verify"[1]. See Section 2.3.3.
- a regulatory "pass" does not guarantee that the plant is safe, just as a corporate audit does not remove the responsibility of the corporation to exercise fiduciary responsibility, and just as such an audit may miss mistakes.

As stated in [IAEA2000]: "The prime responsibility for safety shall be assigned to the operator. The operator shall have the responsibility for ensuring safety in the siting, design, construction,

1 This is a Russian proverb (Доверяй, но проверяй) originally applied to US-USSR relations during the Cold War.

commissioning, operation, decommissioning, close-out or closure of its facilities, including, as appropriate, rehabilitation of contaminated areas; and for activities in which radioactive materials are used, transported or handled." When an operator takes over a plant, it formally assumes most of the responsibility for design safety. In other words, the "design authority" responsibility is transferred from the technology vendor to the operator. In fact, the operator is required to satisfy itself that the design is adequate *before* assuming operating responsibility. Although technical aspects of the design authority can be delegated in part to the vendor, informed oversight cannot be delegated, and the operator must remain at least an "intelligent customer". In any case, this does not absolve the design organization from its safety responsibilities.

2.3 How a Regulator Exercises its Responsibilities

2.3.1 Scope

Generally, the authority of a regulator is enshrined in national legislation, which gives it the ability to permit (or deny) siting, construction, commissioning, operation, decommissioning, and site abandonment of nuclear facilities, and to control the use of radioactive material. Without a licence for a particular activity, it is illegal to proceed.

Typically regulatory authority covers more than just nuclear power plants (NPPs), including any significant nuclear activity (uranium mining, radioactive sources, research reactors, medical and industrial uses of radiation, radioactive waste disposal, etc.). However, this chapter focusses only on NPPs.

Most nuclear regulators also take on enforcement of national policy on safeguards (Section 7) and on security (Section 8) as applied to nuclear power and represent the national government in international fora on nuclear safety.

2.3.2 Nuclear power plant licensing

The steps in the licensing process, through which a regulator can exercise authority, each involve submission by the applicant of information required by the regulations (Section 10). The required information is discussed in more detail in Section 10.1 for Canada; this section gives an overview.

Typically, there are up to eight major approval milestones for a nuclear power plant. In each, the operator submits the required documentation; the regulator reviews this and (normally) grants a licence to start the milestone activity[2]. The regulator continues to review and monitor progress as the milestone is implemented. Typical milestones are:

- Environmental assessment (including site evaluation)
- Site preparation licence
- Construction licence
- Initial fuel loading
- Low-power commissioning

2 Federal, provincial, and even municipal government bodies may require many other regulatory approvals, which are outside the scope of this chapter.

- Operation
- Decommissioning
- Site abandonment (i.e., return to unrestricted usage).

In addition, most regulators perform on request a preliminary review of an NPP design even before a construction licence application, to reduce the risk of licensing issues arising during the project stage when they are difficult and expensive to address. In Canada, this is called a pre-licensing vendor design review [CNSC2012]. In the United States, it is called design certification [USNRC2012], and in the United Kingdom, generic design assessment [HSE2008]. This topic is discussed in Section 5. Note that there are differences in the depth, scope, and implications of these approaches in different countries.

A regulatory review is usually performed against a set of published standards, requirements, and "expectations" (typically through laws, regulations, and guides). Laws are laws of the land, set by the national government; regulations are requirements set by the government (which in some countries are also laws of the land); and guides are non-mandatory "good practices" issued by the regulatory agency. The licence itself is a legal instrument and typically contains additional specific requirements that must be met. In addition, the regulator may require, or the operator may volunteer, compliance with other national standards. In Canada, these are developed by the Canadian Standards Association (CSA). Every country has its own set of requirements, but now there is more and more international coordination, initially after the severe accidents at Three Mile Island and Chernobyl, and now post-Fukushima[3].

Usually, there is some risk basis for regulatory requirements, which are generally a mix of risk-informed and prescriptive requirements based on past experience, as discussed in the accident case studies in Chapter 13.

In many countries, but not all, regulatory deliberations and decisions are made openly, with many opportunities for public input.

Given the power of the regulator, most regulators set up checks and balances to remain fair. Most regulators are structured somewhat like a corporation, with a Commission at the top supported by a small dedicated group of people, and a large separate specialized technical staff which assesses the safety case in detail and presents its conclusions and recommendations to the Commission. The Commission makes the final decision, not the staff. The Commission reports directly to, or is accountable to, the national government in a way that is independent of the proponent. Some regulators have independent advisory committees (e.g., the United States Nuclear Regulatory Commission (USNRC) has an Advisory Committee on Reactor Safeguards (ACRS) consisting of highly respected technical experts). Such committees are independent of the staff, so that technical inputs to the Commission come from more than one source [USNRC2012a]. This is a "typical" description—there are differences in the organization of regulators in different countries because the regulatory structure is the responsibility of each national government.

National and international peer reviews of regulators use the yardstick of international best practices to encourage improvement, e.g., as implemented by the IAEA through its Integrated

3 Post-Fukushima refers to the changes in nuclear safety regulations and requirements in response to the nuclear accident in the Fukushima Dai-ichi NPP in Japan in March 2011.

Regulatory Review Service (IRRS).

2.3.3 Ongoing oversight

Granting of a licensing milestone is only part of a regulator's scope. Regulators also monitor, through documentation review and site inspections, the construction, commissioning, operation, and decommissioning of nuclear power plants. Trend indicators are used as input to decisions to take regulatory action. In particular, assessment of the safety culture in different parts of the nuclear infrastructure is an important indicator of the overall health of the nuclear safety structure and organization (for a discussion of safety culture, see Chapter 13). An operating licence renewal or major plant changes provide opportunities (or requirements) for the operator to perform an in-depth re-assessment of the plant against modern standards and to close any gaps where it is practical to do so.

Internationally, it is becoming common for periodic safety reviews (PSRs) to be performed, typically every ten years [IAEA2013]. The purposes of these are to:

- assess the cumulative effects of plant aging and plant modifications, operating experience, technical developments, and siting aspects, and
- assess plant design and operation against applicable current safety standards and operating practices.

PSRs are particularly useful if the licence renewal period is long (40 years or more in many countries).

More routinely, regulators perform audits on key aspects throughout the nuclear-facility life cycle, effectively "sampling" performance. Negative audit findings in an area will often trigger broader and more intrusive regulatory audits, until the regulator is satisfied that non-compliances are isolated, or conversely that regulatory action is warranted to ensure that any systemic deficiencies are addressed.

2.3.4 Nuclear emergencies

A regulator has a special role in nuclear emergencies. Although practices vary from country to country, the regulator is *not* expected to take control of a station during an emergency or to direct the operators. However regulatory approval may be needed for such things as planned containment venting. Instead, the regulator is often responsible for, or heavily involved in, emergency (off-site) planning and in coordinating the various governmental bodies involved in public notification, sheltering, prophylactic iodine medication, and evacuation. In some cases, the regulator may be either *de jure* or *de facto* the spokesperson to the public.

2.4 How a Regulatory Review is Done

The following are some of the main tools that a (generic) regulator uses to perform an independent review of a licence application[4] [IAEA2002]. They include:

4 Often the Safety Report is equated with the documentation required for a licensing milestone (called the safety case in some countries), but this is not correct—many more documents are reviewed, as described in Figure 14. The Safety Report as a minimum consists of a detailed design description, a deterministic safety analysis, a summary of the probabilistic safety assessment, a description of programmatic aspects such as quality assurance

- Issuing requirements and guidance for the scope, content, and quality of the safety case. This ensures that the licensee or proponent is aware beforehand of what is required and desired. Typical material includes high-level requirements such as safety goals or dose limits ([HSE2006], [CNSC2008]); lower-level requirements such as the scope of safety analysis [CNSC2008b]; and guidance on acceptable methods [CNSC2012b]. Most jurisdictions also issue requirements on design (e.g., [HSE2006], [CNSC2008], [USNRC2012b] with various levels of prescriptive detail.
- Issuing Review Guides for regulatory staff use so that their reviews are consistent and complete. Some of these are published ([HSE2002], [USNRC2012c], [CNSC2013]), while others remain internal.
- Performing an initial acceptance review of the safety case, for completeness.
- Detailed specialist review of the safety case, using such tools as:
  - Line-by-line review using the Review Guides;
  - Independent calculations using the same computer codes as the licensee, or using independent codes;
  - Expert elicitation, including use of outside panels or individuals and independent analysis by consultants;
  - Assessment against written international standards (e.g., IAEA), industry standards (e.g., those from the Canadian Standards Association (CSA)), or against the licensee's own procedures;
  - Quality assurance review and audit, including management and safety culture;
  - Review of the completeness and appropriateness of the research and development support for any step in NPP implementation, including design, site licensing, etc.;
  - Visits to the site;
  - Consultation with international bodies and fellow regulators;
  - Independent experiments or independent analysis of industry experiments;
  - Questions arising from the above to the licensee and discussion and review of the answers.
  - Extensive technical meetings with the proponent.
- The staff review results are consolidated.
- The position is communicated to the Commission in formal meetings, at which the licensee has the opportunity to present its position. The meetings are public, along with the information that is reviewed and discussed at the meetings. It is the Commission that gives the approval to proceed with the relevant milestone.

2.5 Regulatory Independence and Social Policy

Regulatory bodies generally report to a Minister in Cabinet, or to Parliament through a Minister (as is the case in Canada), or to a similar level of the national government. The reporting is usually independent of the industry at the government level [IAEA2000]. Personnel movement between industry and the regulator is fairly common, especially in smaller countries, and is

and human factors, and demonstrations of compliance with regulatory requirements. See [USNRC, 1978] and [IAEA, 2004] for examples of the format of a Safety Report; the former is far more widely used. Details of the probabilistic safety assessment are usually submitted along with the Safety Report.

beneficial because it ensures that regulatory staff have deep hands-on knowledge of the technology they are to regulate. Often personnel movement occurs internationally, which helps internationalize and harmonize regulatory experience.

At the top level of the regulator, the Commission Chairman, and usually the Commission members, are appointed by the government, and therefore the process is political (in the sense of reflecting the will of the people through their elected representatives). The government provides ultimate oversight of the regulatory body, but rarely formally intervenes in licensing decisions.

Regulatory decisions must balance risks, not eliminate them (risk elimination is an impossibility in almost any technology). Moreover, although most regulators say they evaluate only safety and do not explicitly acknowledge benefits, in fact they have a responsibility to account for the fact that an activity may have significant net social benefit. In this sense, regulation sets (or reflects) social policy. Hence, regulatory approval means that the project poses an *acceptable* level of risk. Very few regulators use *only* risk as a regulatory tool (i.e., based just on the probabilistic safety analysis (PSA)); see Chapter 13 for a discussion on PSA. Many regulators use or accept a risk framework to sharpen decisions—this is called *risk-informed decision making* (RIDM) and is a combination of PSA insights and traditional deterministic requirements. This is a broad topic—for more detail, see [Apostolakis2004], [Bujor2010], [CSA1997], and [USNRC2002]. In certain cases, usually when a retrofit is being considered, a cost-benefit case prepared by the proponent may be considered to ensure that the cost is not disproportionate to the benefit; see [HSE2001], [CNSC2000].

Finally, regulators must have adequate resources and experience, but they do not have to replicate all the resources of the designer or operator; cf. our example of a financial audit. To ensure adequate financial resources, regulators are given strong government support at the early stage of their development, whereas later most of their daily operations are on a cost-recovery basis from the licensees.

The above description applies to countries with an established nuclear industry. A country just embarking on a nuclear program, but with no nuclear infrastructure, faces special challenges in developing appropriate expertise and organizations ([IAEA2012b], [Popov2012]).

Four mechanisms have been used. These are not exclusive and are often used in combination.

1. The typical mechanism in the past has been to start with a research reactor and to use it to develop staff for design, operating, and regulatory functions from that base. This route was followed by Canada, where the power reactor program benefited from staff trained in the research reactors (NRU, NRX) at Chalk River. Indeed, the Atomic Energy Control Board (AECB), established in 1946 under the Atomic Energy Control Act, had responsibility for making regulations *and* for the Chalk River research project until Atomic Energy of Canada Limited (AECL) was created in 1952 under the AECB. Two years later, the Canadian Government formalized the separation of the designer/operator of the Chalk River site from the regulatory agency [Sims1980].
2. A second mechanism has been to use the vendor of a power reactor to help create the required infrastructure in the country purchasing the reactor by technology transfer and training of operating personnel. The regulatory staff in the purchasing country are developed under an agreement with the regulator of the vendor's host country. This can go as far as "importing" experienced regulatory staff.

3. A third mechanism is to use IAEA documents and assistance. This organization has developed a comprehensive set of requirements and guides covering all aspects of commercial nuclear applications, including the organization and management thereof. The IAEA also gives assistance to countries developing a nuclear program, such as training courses in nuclear regulation [IAEA2002c].
4. A fourth mechanism is to hire *technical support organizations* (TSOs) to provide technical assistance to the developing regulatory body. These are neutral official organizations which are either part of the regulatory body or are separate, for example a national laboratory. See [IAEA2010] for recent developments.

Figure 1 from [IAEA2011] gives an idea of the steps and timescale involved in a new national nuclear power program.

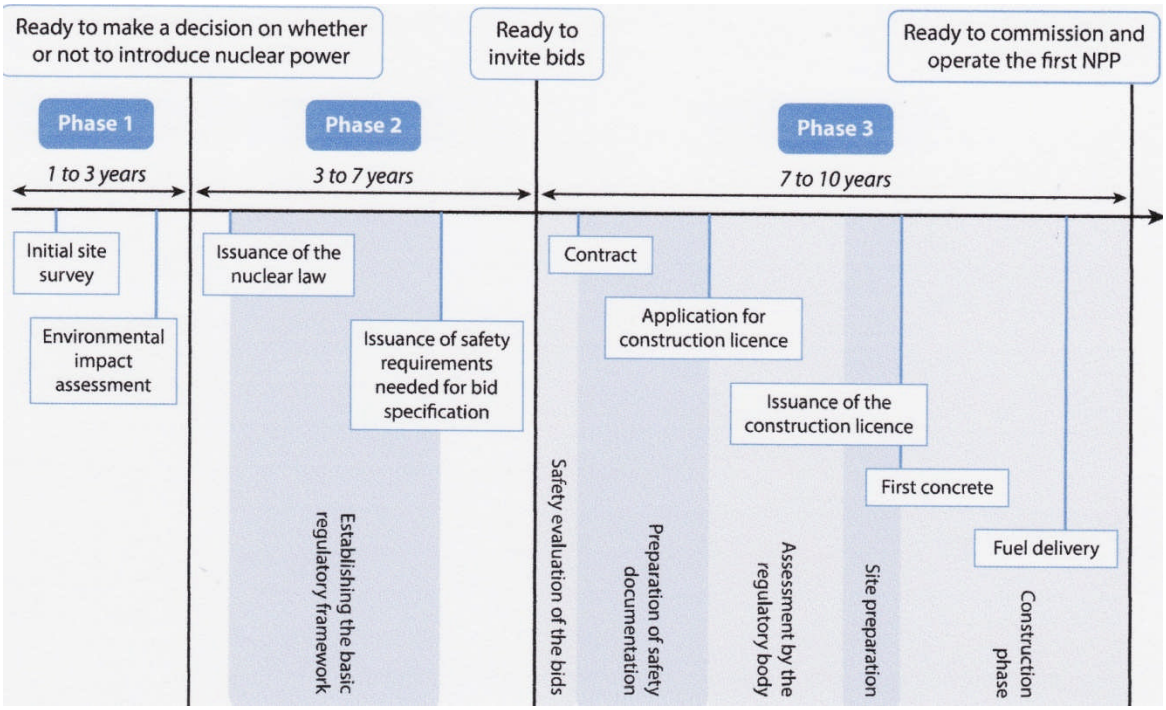

Figure 1 Steps in the development of a nuclear power program

3 Regulatory Approaches

The approaches taken by regulatory agencies across the world tend to fall into four general categories (based on the proven approach used by the regulator in the past; of course, this assertion is oversimplified, and many regulators allow alternative approaches that can be a mix of the four listed below):

1. A largely risk-based approach (e.g., the early U.K. Farmer curve [Farmer1967], and Argentina [Barón1998])
2. A risk-informed, largely non-prescriptive approach with specification of goals or results, not the process (early Canada, some early IAEA, current U.K.);
3. A risk-informed, but more prescriptive approach (current Canada, IAEA);
4. A highly prescriptive approach, with specified detailed requirements (e.g., USNRC and the U.S. Code of Federal Regulations).

Each approach has its advantages and disadvantages.

A risk-based approach is logical, quantifies and balances risk, and leaves major design and operating decisions up to the proponent, who decides how to meet the risk goals. It thereby accommodates and even fosters innovation and evolution. On the other hand, it can lead to uncertainty in licensing because demonstration of numerical risk can be subjective or limited by lack of knowledge. It may not account sufficiently for previously unknown failures, which might be addressed more effectively by a more prescriptive defence-in-depth approach. In particular, cross-linked or common-cause failures (see Chapter 13) are difficult to identify *completely* in a PSA, so that the contribution to risk from these causes can be underestimated.

A mixed approach, which uses both risk-based and prescriptive approaches to various degrees, captures most of the benefits (and some of the disadvantages) of both extremes and generally has served Canada and the United Kingdom well. In particular, it is effective in providing defence against accidents not previously identified, without too much misallocation of resources to truly rare low-risk events.

A highly prescriptive approach in principle leads to well-defined licensing rules and more regulatory certainty and tends to produce an apparently conservative design. However, it can shift the burden of proof of safety from the designer/operator to the regulator. If the designer/operator is required mainly to follow detailed rules set by the regulator, and if the regulator misses something, part of the responsibility for safety has shifted subtly from the proponent to the regulator. Furthermore, de-emphasis of risk leads to some resource misallocation to severe but rare events, as opposed to more frequent ones with *apparently* milder consequences. We shall cover a case study of this situation (Three Mile Island) in the next section.

Much of the world, especially those countries using designs originating from U.S. light-water reactor (LWR) technology, follows the U.S. regulatory approach, largely because the regulatory approach was adopted along with the LWR technology.

4 Case Studies

This section considers a few case studies of regulatory behaviour. Where possible, the regulatory agency's self-evaluation (or that of an independent body) is used, rather than the authors' opinions. The case studies are presented not as a criticism of a particular organization, but as lessons learned about effective regulatory behaviour, as was done for design and operational safety in the case studies in Chapter 13. Some of these examples are also covered in Chapter 13, but with an emphasis on design and operation, rather than regulation.

Success is marked by the *lack* of accidents and "near misses", and just as an accident cannot be laid solely at the feet of a regulator, neither can the lack of accidents be solely ascribed to the quality of regulation. As Three Mile Island, Chernobyl and Fukushima were studied from the technical point of view in Chapter 13, we shall now look at these accidents from the regulatory point of view.

4.1 Three Mile Island

The TMI sequence of events was covered in Chapter 13. A minor event escalated through a small and unrecognized loss of coolant into a partial core melt which was contained in the vessel. Two commissions were struck to carry out an independent review.

The President of the United States appointed a Commission headed by John G. Kemeny. Their report [Kemeny1979] was very broad. Their concentration was on human aspects: "The equipment was sufficiently good that, except for human failures, the major accident at Three Mile Island would have been a minor incident." Of interest here are their findings on the U.S. regulatory structure at the time, which are summarized as follows:

- The regulations were too voluminous and complex, required immense effort for compliance, and equated compliance with safety;
- The preoccupation with the most severe accident (the largest-break LOCA) took attention away from more likely, but slower-developing accidents, which were therefore not analyzed in depth;
- There was too much preoccupation with equipment performance rather than human performance;
- There was no requirement to look beyond the single events specified by the USNRC, for example to multiple failures;
- The role of systems classified as "non-safety-related" in causing accidents was not recognized;
- There was no systematic way of evaluating prior operating experience or looking for patterns;
- There were serious deficiencies in internal communication in the USNRC.

An additional review by the Nuclear Regulatory Commission Special Inquiry Group [Rogovin1980] covered very similar ground, albeit with more comments on the USNRC internal decision-making processes.

Subsequent to TMI, and based on the findings of the Kemeny Commission, severe accidents, emergency preparedness, plant performance monitoring, and human factors were given far more prominence on the regulatory side. Insights from PSA were used more widely, not only to reveal severe accident vulnerabilities, but also to flag requirements that attracted inordinate resources compared to the risk they mitigated. The industry formed cooperative groups such as the Institute of Nuclear Power Operations (INPO) to promote high standards of safety and reliability through plant evaluations, training and accreditation, events analysis, and information exchange and assistance.

4.2 Fukushima

The Fukushima Dai-ichi sequence of events was covered in Chapter 13. A beyond-design-basis tsunami caused a loss of all electrical power in four units, resulting in severe core damage or melting and possible containment failure in the three reactors that contained fuel.

With respect to the Japanese regulator (the Nuclear and Industrial Safety Agency (NISA)), the National Diet of Japan Nuclear Accident Independent Investigation Commission [Japan2012] concluded that "root causes were the organizational and regulatory systems that supported faulty rationales for decisions and actions", and in particular that the inadequacy of the design basis for Fukushima was known to both the utility and the regulator, but was not acted on. The regulator lacked separation from the utility. The Commission recommended formation of a new regulatory body which would be independent, transparent, professional, consolidated, and proactive.

The Japanese Government also established the "Investigation Committee on the Accident at Fukushima Nuclear Power Stations of Tokyo Electric Power Company", an independent committee largely composed of academics. Their final report [Japan2012a], although more technical than the Diet report, raised the same issues and called for reorganization of the regulatory body. They also noted NISA's attention to short-term rather than long-term issues. In addition they focussed on NISA's performance after the event, in emergency measures off-site, and in public communication.

As of this writing (early 2014), the Japanese regulatory body has been reorganized and renamed the Nuclear Regulation Authority (NRA).

Regulators worldwide have applied the technical lessons learned, as outlined in Chapter 13. In terms of national response, in particular, the radiation threshold levels that were used for evacuation were based on the Linear No Threshold (LNT) hypothesis, which implies an unrealistically high level of risk for individual doses of radiation <100 mSv, although no effects on human populations have actually been observed at that level. Although there were no deaths due to radiation from the accident (and there are not expected to be), the evacuation itself resulted in many unnecessary deaths [Tanigawa2012].

4.3 Chernobyl

The Chernobyl sequence of events was covered in Chapter 13. A test which involved running down the main reactor coolant system (RCS) pumps while at low power ended up in a power transient due partly to the voiding of the core, but mainly to the *reverse* action of the shutdown system, destroying the reactor core and bypassing the containment.

The International Safety Advisory Group (INSAG), which provides independent advice to the IAEA Director-General, performed very extensive fuellings of the Chernobyl accident [IAEA1992]. This reference includes as an Appendix the *Report by a Commission to the USSR State Committee for the Supervision of Safety in Industry and Nuclear Power*, which covered the technical facts and the role of the regulatory structure. It noted that:

- There were known violations of the safety standards and regulations in force at the time in the design of Chernobyl Unit 4, but the design was approved and authorization given for construction by all the relevant authorities and regulatory bodies.[5]
- This deficiency resulted from a lack of a well-organized group of experts endowed with its own resources, rights, and responsibilities for its decisions;
- The USSR State Committee for the Supervision of Nuclear Power Safety could not be regarded as an independent body because it was part of the same state authority responsible for the construction of nuclear power plants and for electricity generation.
- The regulatory bodies had no legal basis, no economic methods of control, and no human and financial resources.
- The operating organization did not have ultimate responsibility and decision-making authority for safety.

5 Note added by authors: there are always outstanding regulatory issues when a plant is given a licence—what is important is that the process to determine which issues are acceptable should be an open and robust one.

4.4 Olkiluoto

It is not just accidents than can reveal a regulatory problem. Cost and schedule overruns because of poor communication between the vendor/operator and the regulator can be very damaging to a nuclear build project. This has been exemplified by the construction of the third nuclear power plant unit at Olkiluoto in Finland. The reactor is based on the European pressurized-water reactor (EPR) and is the first of its kind to have started construction. It was meant to start operation in 2009, but as of this writing (early 2014), it is projected to come into service in 2016. This delay has been accompanied by a cost overrun of almost double the turnkey price of ~3.5 billion euros.

Because the matter is currently in legal dispute, the parties have not published much objective analysis of what went wrong. However, the Finnish regulator (STUK) did comment publicly on several occasions, listing lessons learned as follows, from [STUK2006], [Laaksonen2008], [Laaksonen2009], [Tiippana2010], [IAEA2012]:

- "too ambitious original schedule for a plant that is first of its kind and larger than any NPP built earlier;
- inadequate completion of design and engineering work prior to start of construction;
- shortage of experienced designers;
- lack of experience of parties in managing a large construction project;
- world-wide shortage of qualified equipment manufacturers".

The operator TVO, and particularly the vendor AREVA, have offered their own perspective, in which one of the causes mentioned is evolution of Finnish regulations during the construction process, which introduced additional uncertainty into the licensing process.

Of particular interest to the thrust of this chapter is the need for mutual understanding between the regulator and the operator on how the regulatory practices are to be applied:

"The licensee and the regulator need to discuss early enough on how the national safety requirements should be best presented in the call for bids.

- just making reference to national requirements and regulatory guides is not adequate to ensure that requirements are correctly understood by vendors".

With respect to the last point: In Finland, before a project is committed, the Government makes a "Decision in Principle", for part of which the regulator reviews the basic design requirements and main safety features of each proposed alternative design and gives a formal preliminary safety assessment. STUK confirmed in this assessment that "no safety issues can be foreseen that would prevent the proposed plant(s) from meeting Finnish nuclear safety regulations". Although the regulator can apply caveats to this statement in terms of changes that would be required, it is not based on a very detailed review.

5 Pre-Project Licensing Review

The risk to a project from delays associated with uncertainties in the regulatory legal process and requirements has been recognized for decades, spurred by cost and schedule overruns in nuclear plant construction in the United States in the 1970s. The solution adopted in many countries has been a form of pre-project licensing review which is done before project commitment. Typically, a vendor or utility requests a review of a proposed design against the

regulatory requirements of the country in which it is to operate. Such a review ensures that the vendor understands the regulatory requirements and enables regulatory questions to be flushed out and answered earlier. The review is very thorough and is similar in many ways to the construction licence review, but focussing mainly on design details rather than operation. The format of such a review, and the extent to which it is binding on the regulator, depend on national legal and cultural practices. We describe briefly three examples.

In Canada, a designer can request a Pre-Licensing Vendor Design Review, which [CNSC2012]

> "…is to inform the vendor of the overall acceptability of the reactor design…

A Pre-Licensing Vendor Design Review evaluates whether:

- the vendor understands Canadian regulatory requirements and expectations;
- the design complies with, as applicable, CNSC regulatory documents RD-337[6], Design of New Nuclear Power Plants or RD-367, Design of Small Reactor Facilities, and related regulatory documents and national standards;
- a resolution plan exists for any design issues identified in the review".

The review is not binding on the CNSC (i.e., the CNSC can request repeated in-depth reviews on the same topics during construction licence review, and CNSC review results may be subject to change from pre-licensing to the construction licence review).

In the United States, Standard Design Certification is a legal process covered by Part 52 to Title 10 of the Code of Federal Regulations [USNRC2012]. The design submitted and the review are both comprehensive, although some detailed design normally performed in the project phase may be more conceptual (e.g., details of control and instrumentation design). When completed, the product is a standard reactor design certified by the Commission, independent of a specific site, through a rulemaking action (Subpart B of Part 52). This rulemaking action can certify portions of a reactor design for 15 years.

Separately, a licensee can apply for an *early site permit* for approval of a site for one or more nuclear power facilities. This is also separate from the filing of an application for a construction permit or a *combined licence* (see below) for the facility. A specific design is not required for an early site permit, but the design eventually chosen must fit within the safety and environmental parameter envelope requested and specified in the early site permit.

As a third option, a licensee can request a combined licence, which is a combined construction permit and operating licence for a nuclear power facility.

A licensee can use any combination of these tools. For example, a licensee can obtain an early site permit based on the environmental and safety performance envelope of a set of designs; can obtain certification of a specific design that meets the envelope; and can then ask for a combined construction and operating licence for the certified design on the approved site. Standard design certification and early site permits are legally binding, subject to conditions (specified during the certification process) to be met by the detailed project design.

In the United Kingdom, the Office for Nuclear Regulation (ONR) and the Environment Agency

6 Note that the CNSC document titles are in the process of changing; this document has been renamed and revised as REGDOC 2.5.2. Other CNSC regulatory documents are being revised and renamed as REGDOCs.

(EA) offer a *generic design assessment* (GDA) of new reactors. The purpose is [HSE2008] an "assessment of the safety case for a generic design, leading to issue of a design acceptance confirmation if the outcome is positive". It consists of four phases: the first is preparation of the safety case by the proponent, and the next three are reviews by ONR and EA at increasing levels of detail, namely: 1) fundamental safety overview; 2) overall design safety review; and 3) detailed design assessment. A design acceptance confirmation is then issued, subject to possible conditions and exceptions, if the design is considered acceptable. Once completed, a GDA ensures that within the scope of the design, ONR review results are binding. ONR may extend the review during the construction licence review, but the results of the prior GDA remain binding.

6 International and National Examples

6.1 International Organizations

A number of international bodies have a quasi-regulatory role. Regulation is still a *national* legal responsibility, and therefore these organizations do not have formal authority. However, they influence governments, national bodies, and nuclear organizations, and if a country formally adopts their guidance, it takes on the force of national law or regulation.

As before, we give an overview, and the reader may find out more in the references.

6.1.1 IAEA

The origins and purposes of the International Atomic Energy Agency (IAEA) are described in Chapter 13, to which the reader is referred.

Its current document structure with respect to nuclear safety and regulation includes a hierarchy of Principles, Standards, and Guides, as shown in Figure 2, from [IAEA2012a]. Although these have no legal or regulatory force unless they are formally adopted on a national level, they are seen as setting minimum international requirements for safety and regulation. The structure and nomenclature in Figure 2 are self-explanatory, with Safety Fundamentals and Safety Requirements being mandatory (if adopted) and Safety Guides being recommendations and guidance on how to comply with the Requirements. As of this writing (early 2014), they have been formally adopted in countries such as China and the Netherlands; are used directly to establish national requirements in Canada, the Czech Republic, Germany, India, Korea, and the Russian Federation; are used as a reference for review of national standards by most nations; and are also used as inputs by international organizations such as the Western European Nuclear Regulators' Association (WENRA) (Section 6.1.2).

Figure 2 Hierarchy of IAEA safety documents

Of particular relevance to this Chapter, IAEA report GS-R-1 [IAEA2000] deals, among other things, with overall regulatory structure and organization. It is supported by a number of more detailed guides.

Table 1 IAEA guides related to regulation

Report Number	Title
SSG-16	Establishing the Safety Infrastructure for a Nuclear Power Programme (2012)
GS-G-1.1	Organization and Staffing of the Regulatory Body for Nuclear Facilities (2002)
GS-G-1.2	Review and Assessment of Nuclear Facilities by the Regulatory Body (2002)
GS-G-1.3	Regulatory Inspection of Nuclear Facilities and Enforcement by the Regulatory
GS-G-1.4	Documentation for Use in Regulating Nuclear Facilities (2002)
GS-G-1.5	Regulatory Control of Radiation Sources (2004)
GS-G-3.5	The Management System for Nuclear Installations (2009)
SSG-12	Licensing Process for Nuclear Installations (2010)
SSG-16	Establishing the Safety Infrastructure for a Nuclear Power Programme
GS-G-4.1	Format and Content of the Safety Analysis Report for Nuclear Power Plants (2004)

Some of the key principles reflected in these Requirements and Guides are:

- a regulator's purpose is the verification and assessment of safety in compliance with regulatory requirements;
- it has sufficient resources to perform its job;
- it is effectively independent from other organizations that could influence its decisions;
- it has qualified and competent staff;
- its management system is aligned with its safety goals;
- it may solicit expert advice, but does not delegate decisions;
- it communicates professionally with interested parties and with the public;
- regulatory control is stable and consistent;
- it authorizes all facilities unless specifically exempt;
- authorization is supported by a demonstration of safety submitted by the applicant;
- regulatory review occurs before authorization and over the facility lifetime;
- review is commensurate with risks;
- it inspects facilities;
- it has legal enforcement powers and can require corrective action;
- it issues, reviews, and promotes regulations and guides;
- it maintains records;
- it promotes a safety culture (see Chapter 13);
- it ensures that emergency preparedness arrangements and emergency plans are in place.

Finally, there is a growing international consensus on high-level numerical safety goals. Safety goals are defined and discussed in Chapter 13 (Section 4), and the reader is referred there for details. Almost all regulators who specify safety goals do so implicitly or explicitly on the following basis: the goals are set so that the predicted health effects of normal operation and accidents in nuclear power plants are small compared to other social risks. Although IAEA itself has not specified numerical safety goals, its senior advisory body (INSAG, in [IAEA1999]) has proposed the following targets:

- For existing nuclear power plants:
  - Frequency of occurrence of severe core damage < 10^{-4} events per plant operating year;
  - Probability of large off-site releases requiring short term off-site response < 10^{-5} events per plant operating year.
- For future nuclear power plants:
  - Frequency of occurrence of severe core damage < 10^{-5} events per plant operating year;
  - Practical elimination[7] of accident sequences that could lead to large early radioactive releases.

These targets have been used by many other international and national bodies.

7 i.e., if it is physically impossible for the conditions to occur or if the conditions can be considered with a high degree of confidence to be extremely unlikely to arise [IAEA, 2004a]

Note also that the frequency of the design basis earthquake (DBE) has recently been changed in most jurisdictions from 10^{-3} / year to 10^{-4} / year, meaning that the DBE that new plants are required to withstand is significantly more severe.

6.1.2 MDEP and WENRA

There has been an impetus for several years to "harmonize" nuclear regulations, much as aircraft regulations are common internationally. The ideal is that a reactor design licensed in one competent jurisdiction would be licensable anywhere because the requirements would be the same. In practice, licensing requirements are closely linked to design type, and therefore harmonization has made slow progress because of the wide variety of reactor types requiring different regulations at the detail level.

An initiative called the "Multinational Design Evaluation Programme" (MDEP) was established in 2006 to:

- enhance multilateral co-operation within existing regulatory frameworks;
- encourage multinational convergence of codes, standards, and safety goals;
- facilitate the licensing of new reactors.

It currently includes nuclear regulatory authorities from 13 countries. Its work includes co-operation on safety reviews of specific reactor designs. National regulators retain sovereign authority for all licensing and regulatory decisions.

The Western European Nuclear Regulators' Association (WENRA) was formed in 1999 to develop a common approach to nuclear safety and to be able to review nuclear safety independently in countries applying for membership in the European Union (EU).

One of their earliest reports [WENRA2000] surveyed the state of nuclear safety and regulation in countries applying for EU membership. The report covers the status of the regulatory regime and regulatory body and of nuclear power plant safety. For the former, issues such as independence of the regulatory body, resources, and expertise were priority topics.

Because the predominant type of reactor in Western Europe is the LWR, it is somewhat easier to propose harmonized requirements. WENRA has adopted common top-level requirements for any reactor to be built in Western Europe [WENRA2010]. These are largely consistent with the IAEA Safety Fundamentals [IAEA2006a]. More detailed requirements are given in the WENRA "Reference Levels" publications, e.g., [WENRA2007], for reactor safety.

Finally, as requested by the European Union (EU) after the accident at Fukushima Dai-ichi in March 2011, WENRA proposed [WENRA2011] that a series of analytical "stress tests" be done on all EU nuclear power plants to show their robustness against extreme natural events. Unlike the traditional approach of analyzing design basis accidents (DBAs) and beyond design basis accidents (BDBAs) (see Chapter 13), WENRA proposed an analysis assuming:

> "sequential loss of the lines of defence in a deterministic approach, irrespective of the probability of this loss. In addition, measures to manage these situations will be supposed to be progressively defeated."

In other words, design and accident management measures were to be assumed to fail one after the other and the consequences at each step tabulated to understand the plant's robustness. The initiating events conceivable at the plant site included earthquake, flooding and other

extreme natural events. The consequential loss of safety functions included loss of electrical power, including station black-out, loss of the ultimate heat sink, and a combination of both. Each EU country (or country applying for EU membership) completed these stress tests for its own plants and reported the results back to the European Nuclear Safety Regulators' Group (ENSREG), an independent expert body formed by the European Commission, for evaluation.

6.2 National Regulatory Organizations

Although each country operating a nuclear power plant has a national regulatory agency, the overall approach taken generally follows that used in the countries which have designed and deployed the major types of reactors: Canada for pressurized heavy-water reactors (PHWRs), the United States for LWRs, and the United Kingdom for gas-cooled reactors. In this section, we give a brief description of the regulatory approach in the latter two examples; Canada is covered later and in more detail in Sections 9 and 10.

It is impossible in one section of one chapter to cover the full breadth of regulatory philosophy and practices in several jurisdictions. Rather, we focus on the overall philosophy rather than the mechanics of licensing and give references so that the interested reader can find more detail.

6.2.1 USNRC

6.2.1.1 Background

In the United States, the Atomic Energy Act of 1946 established the Atomic Energy Commission (AEC), transferring atomic energy from military to civilian control (see [Buck1983] for a history). Its early years were devoted to nuclear weapons production and research, including the military submarine program, whose reactors became the inspiration for the U.S. PWR commercial power reactor design. The revised Atomic Energy Act of 1954 gave the Atomic Energy Commission the responsibility for regulating and licensing commercial atomic activities. Research, military use, regulation, licensing, and development of the nuclear power industry were all under the same organization, and although it set up separate divisions, the conflicts of interest became more and more apparent, until in 1974 the regulatory functions were transferred to the newly-formed U.S. Nuclear Regulatory Commission (USNRC), which began operations on January 19, 1975.

6.2.1.2 Organization

The USNRC has had enormous influence on regulatory practice in the world because the wide-spread use of LWR technology was accompanied by the LWR regulatory philosophy. Indeed, because almost all the reactors licensed in the United States have been PWRs or BWRs[8], the regulatory requirements tend to be specific to these designs.

The USNRC is headed by a five-member Commission appointed by the U.S. President for staggered five-year terms. The President designates one member to serve as Chairman. The Commission formulates policies and regulations governing nuclear reactor and materials safety, issues orders to licensees, and adjudicates legal matters brought before it. The Executive

8 The United States have also licensed a fast-breeder power reactor (Fermi 1) and high-temperature gas-cooled reactors (Peach Bottom and Fort St. Vrain).

Director for Operations (EDO) carries out the policies and decisions of the Commission and directs the activities of the program offices.

The Commission is supported by a large technical staff, as well as powerful advisory committees who can challenge both the proponent and the staff, e.g., the Advisory Committee on Reactor Safeguards, or ACRS. Typically, the ACRS consists of well-known and respected scientists and experts, often world-renowned professors drawn from universities. It has its own independent support staff. There is no current equivalent in Canada, although at one point the Reactor Safety Advisory Committee (RSAC), which later became the Advisory Committee on Nuclear Safety (ACNS), had a similar role with the then-AECB, albeit on a smaller scale.

The actual trial-level adjudicatory body of the USNRC is the Atomic Safety and Licensing Board Panel (ASLB). The Panel is composed of administrative judges who are lawyers, engineers, and scientists, and administrative law judges who are lawyers. It is chaired by the Chief Administrative Judge. The Panel conducts all licensing and other hearings as directed by the Commission, primarily through individual Atomic Safety and Licensing Boards or single presiding officers appointed by either the Commission or the Chief Administrative Judge. Individual licensing boards conduct public hearings on contested issues that arise in the course of licensing and enforcement proceedings and uncontested hearings on construction of nuclear facilities.

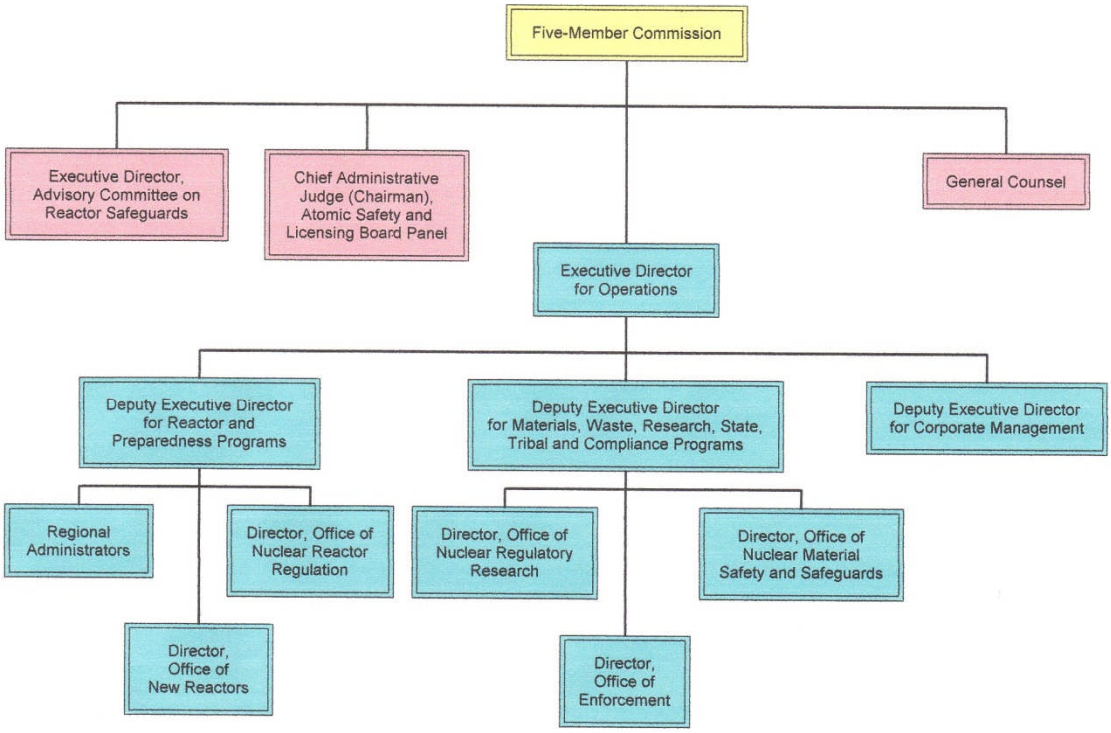

Figure 3 Simplified organization chart of the USNRC

Figure 3 shows a highly simplified organization chart of the USNRC. The five-member Commission (yellow) is supported by the ACRS, the ASLB, and legal counsel, shown in red. The large technical staff (turquoise) is headed by the Executive Director for Operations. For nuclear regulatory purposes, the United States is divided into four regions; the four regional offices conduct inspection, enforcement, and emergency response programs for licensees within their

borders. USNRC also has a large and powerful R&D Division which conducts experimental and analytical work of very broad scope, along with development of their own computer tools, independently of utilities and design organizations.

6.2.1.3 Regulatory approach and documents

As we saw with the IAEA and shall see with other regulators, regulatory documents form a hierarchy, with legislation at the top, government regulations and licences next (both of which are enforceable by law), mandatory regulatory requirements set by the regulator next, then optional regulatory guides provided by the regulator, and finally guidance to regulatory staff themselves on how to review a submission. Figure 4 shows such a generic structure.

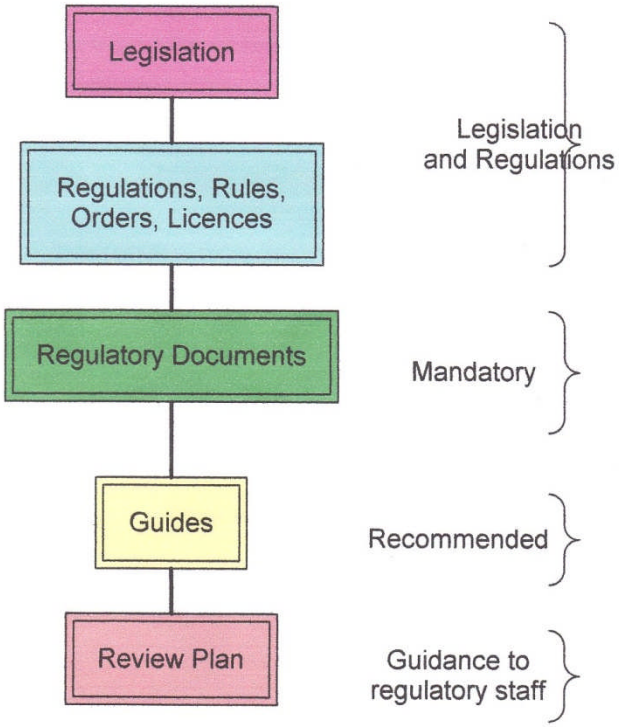

Figure 4 Generic hierarchy of regulatory documents

6.2.1.3.1 Consolidated legislation

In the United States, nuclear energy-related activities are governed by the Atomic Energy Act of 1954, as amended, and the Energy Reorganization Act of 1974, as amended (which created the USNRC). The interested reader is referred to [USNRC2011] as updated, which consolidates all nuclear-related legislation and executive orders and runs well over 1000 pages.

The Nuclear Safety and Control Act in Canada [GovCan2013], by contrast, has 54 pages. [Ahearne1988] is an excellent source of information on the origins of the U.S. regulatory approach and its differences from that used in Canada. Although the work is dated, it is recommended reading to gain an understanding of the differences. One interesting difference in practice is the length of a plant licence; typically, in the United States, it is up to 40 years, whereas in Canada the utility must reapply about every five years.

6.2.1.3.2 Code of Federal Regulations

The technical requirements are covered in the Code of Federal Regulations Title 10 (10CFR), which corresponds to the second box from the top in Figure 4. The requirements are binding on all persons and organizations who receive a licence from the NRC to use nuclear materials or to operate nuclear facilities. Of particular interest are 10CFR Part 50 [USNRC2012d] and 10CFR Part 52 [USNRC2012].

10CFR Part 50 covers requirements for the traditional domestic licensing of production and nuclear power facilities. Much of the main text is legal and procedural, and these aspects will not be discussed further here. Even a detailed technical discussion of 10CFR Part 50 is well beyond the scope of this chapter. We select a few examples to give an idea of the approach.

Section 50.46 states acceptance criteria for emergency core cooling systems for light-water nuclear power reactors. The requirements are in the form of numerical analysis values rather than safety objectives. For example, it is an overall requirement in water reactors to prevent excessive oxidation of the sheath because if it becomes brittle, it can fragment on rewet, and the debris can block fuel cooling. Moreover, at high temperatures, the Zircaloy-water reaction becomes autocatalytic, so that temperature prediction is difficult. Finally the reaction produces hydrogen, which is a source of energy to containment if it burns. In Canada, these requirements are stated as objectives, and it is up to the proponent to justify how they are met. However, in 10CFR Part 50, the acceptance criteria can be quite explicit (from 50.46):

> "(b)(1) Peak cladding temperature. The calculated maximum fuel element cladding temperature shall not exceed 2200° F.
> (2) Maximum cladding oxidation. The calculated total oxidation of the cladding shall nowhere exceed 0.17 times the total cladding thickness before oxidation. As used in this subparagraph, total oxidation means the total thickness of cladding metal that would be locally converted to oxide if all the oxygen absorbed by and reacted with the cladding locally were converted to stoichiometric zirconium dioxide. If cladding rupture is calculated to occur, the inside surfaces of the cladding shall be included in the oxidation, beginning at the calculated time of rupture. Cladding thickness before oxidation means the radial distance from inside to outside the cladding, after any calculated rupture or swelling has occurred, but before significant oxidation. Where the calculated conditions of transient pressure and temperature lead to a prediction of cladding swelling, with or without cladding rupture, the unoxidized cladding thickness shall be defined as the cladding cross-sectional area, taken at a horizontal plane at the elevation of the rupture, if it occurs, or at the elevation of the highest cladding temperature if no rupture is calculated to occur, divided by the average circumference at that elevation. For ruptured cladding, the circumference does not include the rupture opening.
> (3) Maximum hydrogen generation. The calculated total amount of hydrogen generated from the chemical reaction of the cladding with water or steam shall not exceed 0.01 times the hypothetical amount that would be generated if all of the metal in the cladding cylinders surrounding the fuel, excluding the cladding surrounding the plenum volume, were to react."

Although this example illustrates a difference in regulatory philosophy (and not all criteria are this detailed), it is also related to design differences. In PWRs, if the metal-water reaction becomes autocatalytic, there is no nearby heat sink to mitigate it, and it can quickly affect a

large part of the core. In CANDU (as discussed in Chapter 13) the nearby moderator can remove heat from the fuel through the pressure tube and has the effect of tempering the metal-water reaction rate.

As another example, consider Appendix A to 10CFR 50, the General Design Criteria [USNRC2012b]. This Appendix consists of 64 basic requirements which underpin much of the technical approach to safety in the United States. Compliance is mandatory. Although high-level, many are focussed on LWRs, as stated in the introduction:

> "These General Design Criteria establish minimum requirements for the principal design criteria for water-cooled nuclear power plants similar in design and location to plants for which construction permits have been issued by the Commission. The General Design Criteria are also considered to be generally applicable to other types of nuclear power units and are intended to provide guidance in establishing the principal design criteria for such other units."

Many of the GDCs *are* generic; for example

> *"Criterion 16—Containment Design*. Reactor containment and associated systems shall be provided to establish an essentially leak-tight barrier against the uncontrolled release of radioactivity to the environment and to assure that the containment design conditions important to safety are not exceeded for as long as postulated accident conditions require."

Some are clearly specific to LWRs, for example:

> *"Criterion 11—Reactor Inherent Protection*. The reactor core and associated coolant systems shall be designed so that in the power operating range the net effect of the prompt inherent nuclear feedback characteristics tends to compensate for a rapid increase in reactivity."

The underlying purpose of Criterion 11 is that a fast reactivity excursion in an LWR, caused for example by a rod ejection, must be compensated for (not necessarily terminated, as discussed in Chapter 13) by negative (Doppler) feedback since (because of the short prompt neutron lifetime) engineered shutdown systems may not be able to act quickly enough (see Chapter 13). It is often misinterpreted as a blanket requirement for a negative void reactivity.

At the same level in Figure 4 are plant licences, rules (U.S. term for regulations), and orders.

6.2.1.3.3 Commission Policy Statements

Commission Policy Statements are an example of Regulatory Documents (third box down in Figure 4). For example, in 2011, the Commission issued a Policy Statement on Safety Culture, setting forth its expectations for industry to promote a positive safety culture. Such notices are published in the U.S. Federal Register.

Given the detail in 10CFR, USNRC staff have less need to issue *mandatory* regulatory documents.

6.2.1.3.4 Regulatory guides

Regulatory guides (fourth box from the top in Figure 4) provide guidance to proponents on implementing USNRC regulations, on techniques used by NRC staff in evaluating specific prob-

lems or postulated accidents, and on data needed by staff in its review of applications for permits or licences. Although nominally optional, exceptions taken to regulatory guides in the United States (and most other countries) require thorough justification and significant extra regulatory review.

6.2.1.3.5 Standard review plan

Many regulators now have a standard review plan (SRP, bottom box in Figure 4) written by the regulator and aimed at regulatory staff performing reviews of proponent applications. This approach was first developed in the United States and is now being adopted in other countries, including Canada. The purpose of the SRP is to ensure the quality and uniformity of staff safety reviews and to make the review process more transparent. For this reason, the SRP is public in the United States, and proponents can see in advance the criteria against which their submissions will be reviewed and the level of information needed; see [USNRC1987].

6.2.1.4 Licensing process

It is beyond the scope of this chapter to describe the U.S. licensing process in detail. The following description is highly abbreviated; the reader is referred to [USNRC2009] for more detail.

We have already described in Section 5 aspects of an alternative licensing approach in the United States governed by 10 CFR Part 52 that includes options for:

- Early site permits that enable an applicant to obtain approval for a reactor site without specifying the design of the reactor(s) that could be built there;
- Certified standard plant designs which can be used as pre-approved designs;
- A licence which combines a construction permit and an operating licence with conditions for plant operation.

However, at the time this chapter was written (early 2014), all operating plants in the United States have been licensed under a two-step process defined in 10CFR50:

- A construction licence for a particular plant design at a particular site. This process includes submission of relevant information on design, safety analysis, intended operation, the site, the environment, and emergency planning; review by NRC staff, who issue a Safety Evaluation Report summarizing the anticipated effect of the proposed facility on public health and safety; and a public hearing, conducted by the Atomic Safety and Licensing Board (see Section 6.2.1.2).
- An operating licence. This process includes submission of final design and safety information by the applicant and review by the USNRC, who prepare a Final Safety Evaluation Report. A public hearing is not mandatory or automatic, but can be requested by members of the public whose interests might be affected by the issuance of the licence.

In parallel, the licence applications are reviewed by the ACRS (see Section 6.2.1.2), who provide the Commission with independent expert advice.

The entire process is remarkably open, with all documents and correspondence related to the

application placed in publicly accessible paper and electronic repositories[9]. This includes the plant Safety Report, the NRC Safety Evaluation Reports, letters between the NRC and the applicant, records of meetings, and other documents. The NRC also holds numerous public meetings during the licensing process.

In addition, conditions may be placed on the licence, which have the same legal force as the licence itself. A generic set of conditions is described in 10CFR § 50.54, "Conditions of licenses". Many areas are covered, e.g., quality assurance, minimum staffing levels, licence amendment or revocation, responsibility of the operator, process for making changes, security, and emergency planning.

Finally, the USNRC has the authority to impose penalties for violations of regulatory requirements. It uses three primary enforcement sanctions:

1. Notice of Violation: This identifies a requirement and how it was violated and normally requires a written response.
2. Civil Penalties: A civil penalty is a monetary fine up to $130,000 per violation per day.
3. Orders: Orders modify, suspend, or revoke licenses or require specific actions by licensees or persons.

6.2.2 United Kingdom

Unlike the United States, the United Kingdom has a very different legal structure, and the regulator has had to license a wide variety of reactor types (gas-cooled reactors, fast reactors, heavy-water reactors, and light-water reactors). This task has been accompanied by a less prescriptive approach.

6.2.2.1 Organization

The Office for Nuclear Regulation (ONR) is responsible for all nuclear regulation in the United Kingdom. It was formed on April 1, 2011, as an agency of the Health and Safety Executive (HSE). ONR combined the safety and security functions of HSE's former Nuclear Directorate, including Civil Nuclear Security, the U.K. Safeguards Office, and the Radioactive Materials Transport team. In turn, HSE is a non-departmental public body (NDPB), which is defined as a "body which has a role in the processes of national Government, but is not a Government Department or part of one, and which accordingly operates to a greater or lesser extent at arm's length from Ministers" [UK2009]. It is sponsored by the Department for Work and Pensions. At the top level, it has a Board, which also contains its Executive Management Team. The work is organized along program lines, as shown in simplified form in Figure 5.

On April 1, 2014, ONR became a Public Corporation under the 2013 Energy Act. ONR is now the enforcing authority for licensed sites in Great Britain, as well as the licensing authority.

9 Some records are not disclosed, e.g., records which must be kept secret in the interest of national defence or foreign policy; internal personnel records; trade secrets and commercial or financial information; records compiled for law-enforcement purposes. For a comprehensive list, see 10CFR § 9.17, "Agency records exempt from public disclosure".

6.2.2.2 Regulatory philosophy

One of the underpinnings of U.K. nuclear safety philosophy is the concept of "so far as is reasonably practicable", or SFAIRP. This was introduced in the Health and Safety at Work Act of 1974 [UK1974], Section 2-(1), and applies to all industry, not just nuclear:

> 2.-(1) It shall be the duty of every employer to ensure, so far as is reasonably practicable, the health, safety, and welfare at work of all his employees."

For this concept, HSE uses the term As Low as Reasonably Practicable (ALARP) and states that [HSE2006]:

> "for assessment purposes, the terms ALARP and SFAIRP are interchangeable and require the same tests to be applied. ALARP is also equivalent to the phrase 'as low as reasonably achievable' (ALARA) used by other bodies nationally and internationally".

ALARA is discussed in Chapter 12. However, the implementation and emphasis in regulatory practice of ALARA and ALARP can be very different. ALARP places the onus on the nuclear-plant designer and operator to justify why further improvements to all aspects of safety cannot be practicably achieved, and in the authors' experience goes considerably beyond ALARA in its scope.

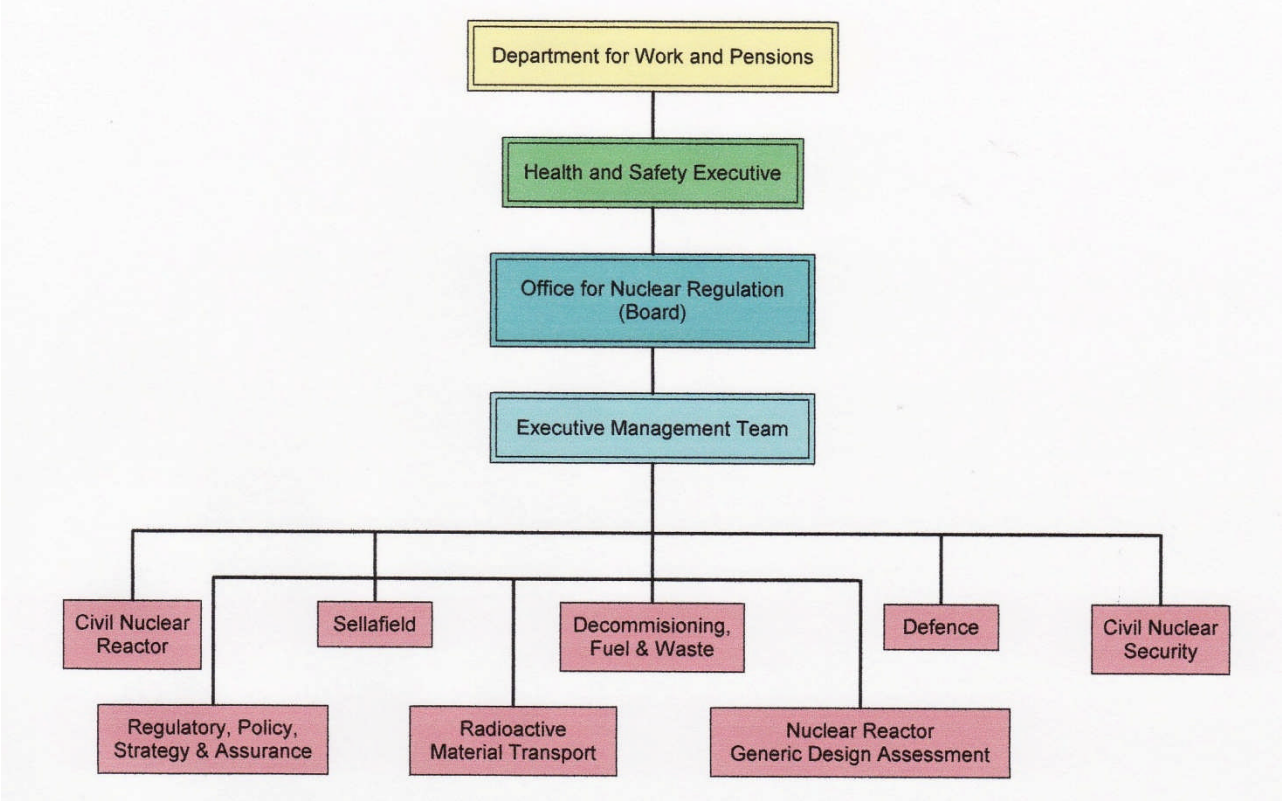

Figure 5 Structure of the ONR

A second underpinning is the concept of acceptable risk. In 1967, Farmer [Farmer1967] proposed a risk-based criterion for use in siting a nuclear reactor. Figure 6 shows his proposed iodine-131 release curve in an accident, versus reactor-years between releases (i.e., the inverse of accident frequency). The basis of the curve was the predicted health effects of an accident, which (if the criterion was met) would be small compared to other social risks. The flattening at the top was to minimize the frequency of small releases due to their nuisance value.

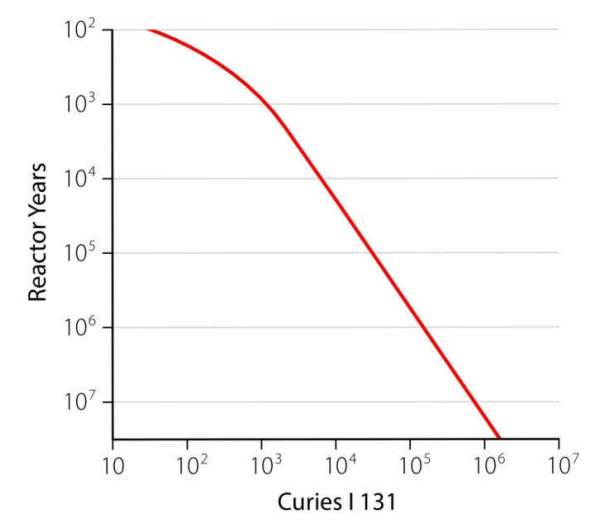

Figure 6 "Farmer" curve

6.2.2.3 Tolerability of risk

This approach developed in the United Kingdom into a risk-based approach along with high-level requirements. These are described in three key documents:

1. The Tolerability of Risk from Nuclear Power Stations [HSE1992];
2. Reducing Risks, Protecting People [HSE2001];
3. Safety Assessment Principles (SAPs) [HSE2006].

The concept evolved from a go/no-go risk line as proposed by Farmer to three distinct regions as shown in

Figure 7. At the top, the risk of the activity is too high regardless of the benefits. At the bottom, the risks are broadly acceptable, and no further reduction is usually required unless reasonably practicable. The middle region of tolerable risk is typical of the risks from activities that people are prepared to tolerate to secure benefits. ALARP would be applied to outcomes in this region.

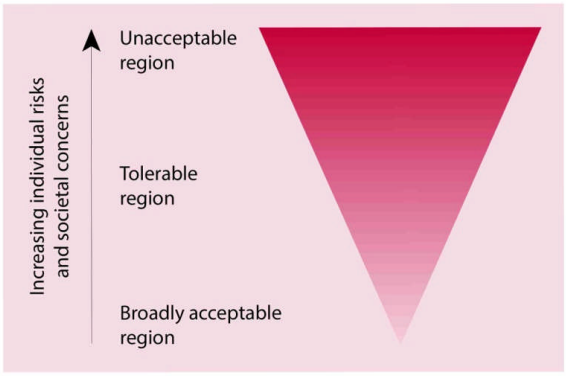

Figure 7 HSE concept of tolerable risk

The risk boundaries are set as follows:

Boundary between "tolerable" and "unacceptable" regions for risk entailing fatality:
Worker: 1 in 1000 /y

Member of the public: 1 in 10,000 /y
This is called the Basic Safety Limit (BSL).
Boundary between "broadly acceptable" and "tolerable" regions for risk entailing fatality:
Worker: 1 in 1,000,000 /y
Member of the public: 1 in 1,000,000 /y
This is called the Basic Safety Objective (BSO).

ALARP is applied in this region between the BSL and the BSO to see if it is reasonably practicable to reduce the risks below the BSO.

These risk targets are applied to all industries in the United Kingdom. For nuclear power, they are translated in the SAPs to BSL/BSOs for normal operation and accidents. The latter become numerical acceptance criteria and targets for the plant PSA. For example, for off-site doses, Table 2 gives typical frequency/dose targets.

Table 2 U.K. frequency / dose targets for accidents off-site

Frequency dose targets for accidents on an individual facility – any person off the site	**Target 8**

The targets for the total predicted frequencies of accidents on an individual facility, which could give doses to a person off the site, are:

Effective dose, mSv	**Total predicted frequency per annum**	
	BSL	**BSO**
0.1 – 1	1	1×10^{-2}
1 – 10	1×10^{-1}	1×10^{-3}
10 – 100	1×10^{-2}	1×10^{-4}
100 – 1000	1×10^{-3}	1×10^{-5}
> 1000	1×10^{-4}	1×10^{-6}

The reader should consult [HSE2006] for the full set of numerical targets.

6.2.2.4 Safety assessment principles

The SAPs consist of a set of high-level principles, followed by a large number of technical principles covering the plant life cycle. Although they are expected to be followed by a proponent, they are not legally mandatory (unless they refer to a legal requirement), and are officially written to guide regulatory staff in their assessment of a safety case. They are generally consistent with IAEA Safety Requirements. Most SAPs are followed by a brief explanation or commentary.

It is outside the scope of this chapter to cover these principles in depth (SAPs consisted of 140 pages as of 2006). Appendix A (Section 12) shows some examples of SAPs.

6.2.2.5 Technical assessment guides

The SAPs are supplemented by a series of Technical Assessment Guides (TAGs), which provide more detailed guidance to regulatory staff and fill a similar role to the U.S. Standard Review Plan. Like the latter, they are public.

6.2.2.6 Nuclear site licence conditions

Finally each licensed plant has a series of 36 Standard Conditions attached to its licence, covering design, construction, operation, and decommissioning [ONR2011]. For example, a number of conditions cover changes to the plant during construction and operation and the need for HSE approvals. Because they are attached to the licence, they give HSE a powerful compliance tool.

7 Nuclear Material Safeguards

IAEA and CNSC material has been used throughout this section and referred to specific documents where appropriate. *Italic* fonts have been used to indicate where statements from IAEA or CNSC documents have been used essentially verbatim.

Previous sections have focussed on the "why" of regulatory approaches and have been relatively high-level. The remainder of this chapter provides more detail on safeguards and security and on the Canadian regulatory approach. It is intended to be a guide to the practitioner in finding and understanding relevant requirements, and for Canada, it provides a concise and unique regulatory roadmap. Because regulatory requirements can affect design and operation in a significant way, regulators and the IAEA spend much time making each sentence as precise as possible, much as one does in drafting legislation. For that reason, we have avoided paraphrasing regulatory requirements as much as practicable, instead quoting directly from the relevant documents.

Nuclear material safeguards are enforced around the world by the International Atomic Energy Agency (IAEA). IAEA safeguards are measures through which the IAEA seeks to verify that nuclear material is not diverted from peaceful uses. States that have signed an agreement with the IAEA (which are then considered to be nations committed to the peaceful use of nuclear energy) accept the application of safeguards measures through the conclusion of safeguards agreements with the IAEA [IAEA2007]. There are various types of safeguards agreements, but the vast majority of countries have agreed not to produce or acquire nuclear weapons and to place all their nuclear material and activities under safeguards to enable the IAEA experts to verify that they are complying with the agreements. The origins of the IAEA and of safeguards are discussed in Chapter 13.

7.1 Objectives and Evolution

IAEA safeguards implementation started more than 50 years ago and has been subject to continuous evolution and improvement [IAEA1998], mainly from lessons learned over time.

Safeguards have gone through three major phases [IAEA1998], [IAEA2002d], [IAEA2007b]. The first phase began in the late 1950s and 1960s as nations started to trade in nuclear plants and fuel. The safeguards at that time were designed mainly to ensure that this trade did not lead to the spread of nuclear weapons. The second phase, from 1971 to 1991, reflected a growing perception that, "pending nuclear disarmament, world security is better served with fewer rather than more nuclear weapons and nuclear weapon states". The third and most recent phase, from 1991 to 1997, consisted of a far-reaching review designed to remedy shortcomings in the 1971 system. The review culminated in approval of a significantly expanded legal basis of IAEA safeguards. Figure 8 shows highlights of safeguards evolution from 1991 to the present time.

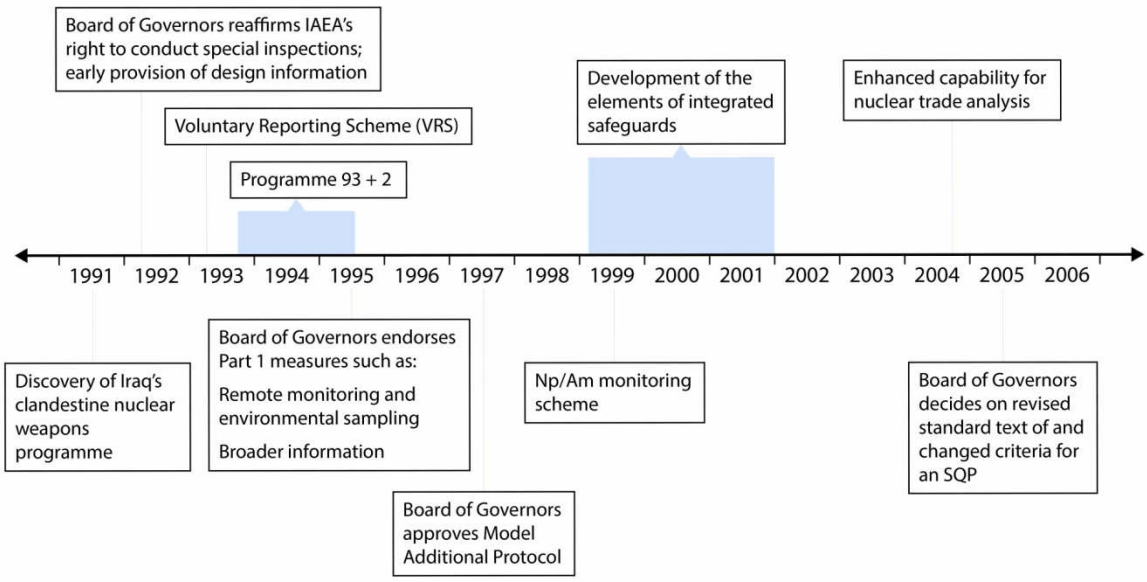

Figure 8 Safeguards state evaluation is a continuous process [IAEA2007b]

One should distinguish between the aims that safeguards seek to achieve in the non-nuclear-weapon and in the declared nuclear-weapon states. The safeguards objectives in the non-nuclear-weapon states are:

- To provide assurance that non-nuclear-weapon states party to comprehensive safeguards agreements are complying with their obligations not to acquire nuclear weapons or other nuclear explosive devices;
- To deter states that have renounced nuclear weapons from acquiring unsafeguarded nuclear material[10]. Safeguards must therefore be effective to detect within a reasonable time the diversion or clandestine production of nuclear material;
- To verify certain facilities and material in some non-nuclear-weapon states with significantly developed nuclear programs, but which have not yet concluded comprehensive safeguard agreements, and therefore are at high risk of proliferation activities. These states are placed under safeguards to prevent them from acquiring nuclear-weapon capability.

The objectives of safeguards related to the formally recognized nuclear-weapon states are:

- To commit not to use nuclear energy to further any military purpose;
- To refrain from any explosive use of nuclear energy;
- To discourage any proliferation of nuclear material that is potentially useful for developing nuclear weapons;
- To encourage widespread acceptance and implementation of safeguards.

10 Note that "nuclear material" includes all fissionable isotopes that can be used as nuclear fuel or explosive material, whereas "non-nuclear material" includes all material of strategic importance, such as heavy water, zirconium tubes, etc.

The technical aim of safeguards is to use technical means to detect and verify safeguards implementation and to provide for reporting of deviations.

For further background, see [IAEA1983], [IAEA1998a], [IAEA2011a], [IAEA2011b], [IAEA2007b].

7.2 Safeguards Treaty Detection Fundamentals

The Treaty on the Non-Proliferation of Nuclear Weapons (the Non-Proliferation Treaty, or NPT) is a cornerstone of the nuclear non-proliferation regime and the basis for implementation of safeguards. It was opened for signature in 1968 and entered into force in 1970. By December 2001, the NPT was in force in 187 states. In 1995, the NPT was extended indefinitely. For details, see [IAEA2002d].

The key requirements of the NPT are:

- Not to receive and transfer any nuclear weapons or nuclear explosive devices, or control of such weapons or devices directly or indirectly;
- Not to manufacture or otherwise acquire such weapons or devices;
- Not to seek or receive any assistance in development or manufacture of such devices;
- To accept IAEA safeguards on all fissionable material in peaceful nuclear activities;
- Not to provide source or special fissionable material, or equipment or material especially designed or prepared for the processing, use or production of special fissionable material to any non-nuclear-weapon State;
- To sign safeguard agreements with the IAEA either individually or together with other States within 18 months of the date on which the State deposits its instruments of ratification of or accession to the NPT Treaty
- Allows each State party to the NPT Treaty to develop research, production, and use of nuclear energy for peaceful purposes and to facilitate and participate in the fullest possible exchange of equipment, materials, and information for the peaceful uses of nuclear energy.

7.3 Safeguard Approaches, Concepts, and Measures

The key requirement for a successful safeguards program is to collect sufficient information from various sources [IAEA2007]. The main sources of safeguards information are:

1. State-supplied information (under the obligation of the safeguards treaties and agreements)
    a. Nuclear material accountancy and facility design
    b. Voluntary reported information
    c. Additional protocol declarations
2. Key results of verification activities
    a. Inspection
    b. Design information verification (DIV)
3. Other information coming from open and other sources

In the first and second phases of the safeguard evolution process (until the early 1990s) the focus of the safeguards program was limited to the Comprehensive Safeguards Agreement protocols, which included:

    a. Fuel enrichment facilities

b. Fuel fabrication facilities
c. Nuclear reactors
d. Spent fuel storage
e. Reprocessing facilities.

The Generic safeguards approach specifies the IAEA goals and safeguard activities for a reference plant. The Facility safeguards approach is prepared for a specific facility, developed and adjusted to specific facility characteristic features and activities. The State-level safeguards approach is developed for a specific state, encompassing all nuclear material, nuclear installations, and nuclear activities.

The integrated safeguards approach, which is a variation of the State-level safeguards approach, was developed as an optimum combination of all safeguards measures available to the IAEA under comprehensive safeguard agreements and additional protocols. Starting in the early 1990s, the safeguards program was extended, and is known today as Broad Overview of Expanded Safeguards Coverage Protocols, which in addition to the above targets, include the following:

a. Equipment manufacturers
b. Mining and milling
c. Conversion facilities
d. R&D centres.

The nuclear material accountancy within the framework of IAEA safeguards begins with the nuclear-material accounting activities by facility operators and the state system of accounting for and control of nuclear materials. *The IAEA implements nuclear accountancy at various levels [IAEA2002d]:*

1) At the Facility Level by:
   a) Dividing operations into nuclear material balance areas (MBAs);
   b) Maintaining records on nuclear material quantities in each MBA;
   c) Measuring and recording all transfers of nuclear material from each MBA to another area or facility;
   d) Periodically determining quantities of nuclear material in each MBA;
   e) Closing the material balance over the period between two successive physical inventory takings and computing the material unaccounted for (MUF);
   f) Providing for a measurement control program to determine the accuracy of calibrations and measurements;
   g) Testing the computed MUF against its limits or errors in the accidental loss of gain;
   h) Analysing the collected accounting information to determine the cause and magnitude, and taking lessons learned for future improvements.
2) At State Authority Level
   a) Preparing and submitting nuclear material accounting reports to the IAEA;
   b) Ensuring that nuclear material accounting procedures and arrangements are adhered to;
   c) Providing for IAEA inspector access and co-ordination arrangements;
   d) Verifying facility operators' nuclear material accountancy performance.
3) At IAEA Level by:
   a) Independently verifying nuclear material accounting information in facility records and State records, and conducting activities as per safeguard agreements signed with the

State;

b) Determining the effectiveness of the State safeguards program;
c) Providing statements to the State about the IAEA verification activities.

7.4 Safeguards Design Implications for Nuclear Power Plants

Most safeguards attention is devoted to nuclear power plants (NPPs) ([IAEA1998a], [IAEA2014]).. NPPs are subject to a large flow of nuclear materials. At both off-load refueled LWRs and on-load refueled PHWRs, the entire facility constitutes one MBA. Therefore, all activities at the NPP site are under the safeguards monitoring program.

Figure 9 shows the elements of safeguards in a generic NPP facility. The top route in Figure 9 shows the real material storage areas and transfer routes, including the possibilities for diversion as dashed lines. The middle route in Figure 9 represents the nuclear-material accounting by the operator concerning the activities that have occurred. If this declared record of storage status and transfers accurately reflects the real inventories and transfers, then there can be a high degree of confidence that diversion activity has not occurred. The bottom route in Figure 9 represents the IAEA activities in monitoring physical activity in the storage and material-transfer areas for accounting verification purposes. Any activity observed that does not correspond to that declared will initiate a pre-planned process to re-establish confidence that the declared record reflects the real inventory. That process might lead to an examination and validation of the entire inventory, an expensive task which should be avoided.

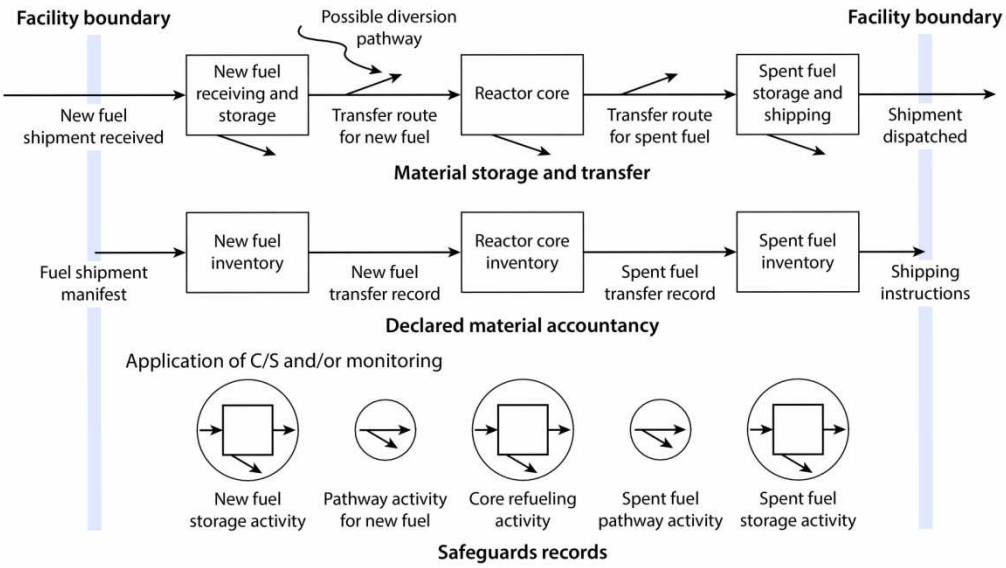

Figure 9 Elements of safeguards [IAEA1998a]

Safeguards approaches, experience, and the associated guidelines vary between off-load and on-load refueled reactors:

a) For off-load refueled reactors, refuelling operations and the associated fuel movements are conducted at low frequency and with large numbers of items moved per refuelling;

b) For on-load refueled reactors, fuel movements and refuelling operations are carried out at high frequency (daily), but with a small number of items moved per refuelling.

LWRs are refueled off-load, refuelling operations occur with an open vessel, and transfers occur in channels filled with transparent water shielding. This design combination permits direct visual observation. Transparent shielding is impractical for refuelling operations in on-load refueled reactors, and therefore observation by other means is required. In these NPPs, detection of variations in radiation fields from continuously operating instrumentation together with optical surveillance provide the information needed on refuelling sequences for safeguard purposes. Regardless of the NPP design, all fuel is properly labelled by visible and non-visible marking to be read by modern optical and laser devices.

Figure 10 shows the position of optical surveillance devices in the reactor building and the fuel-storage pool building in the LWR reactor design.

Application of the general principles for safeguards is common to all pressure-tube PHWRs. Most IAEA experience in handling PHWRs has been obtained on CANDU reactors.

Figure 11 shows the position of optical surveillance devices in the reactor building and the fuel-storage pool building in the CANDU reactor design.

CANDU NPPs have horizontal fuel channels and are heavy-water moderated and cooled. The refuelling system uses two refuelling machines, one at each end of the core, to insert new fuel at one end and to accept spent fuel at the other. CANDU NPPs require appropriate shielding of the refuelling machines and operations to protect personnel. Consequently, the positioning of the fuelling machines in front of the reactor channels, and the refuelling itself, are carried out by remote control.

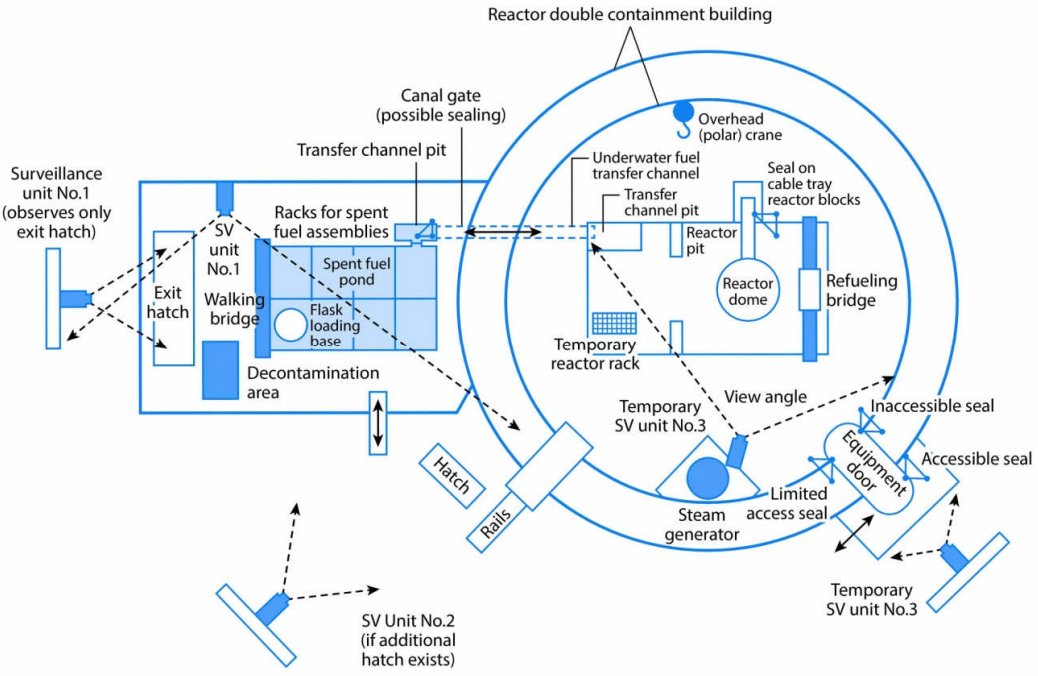

Figure 10 Design aspects of safeguards in LWR reactors (Type II) [IAEA1998a]

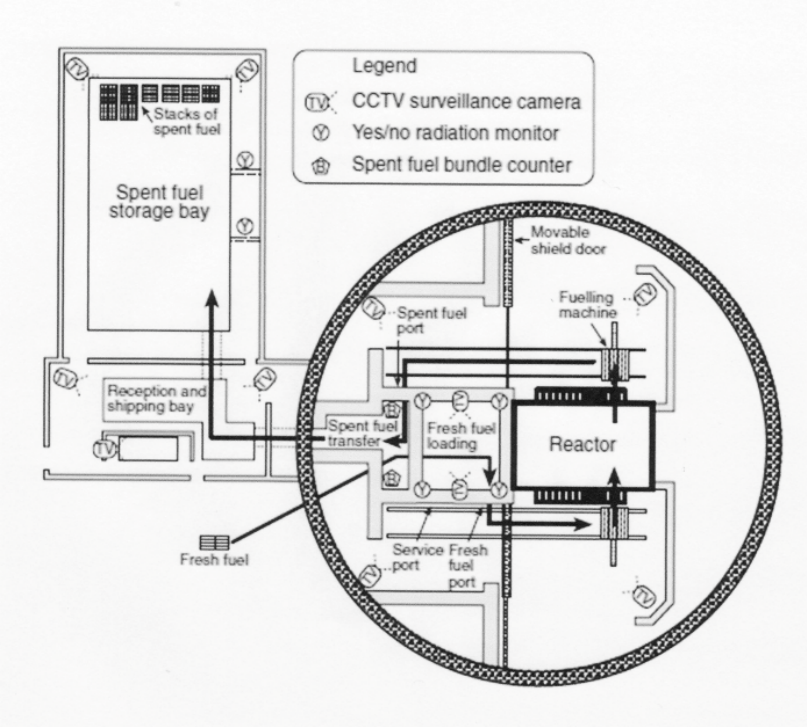

Figure 11 Design aspects of safeguards in CANDU reactors [IAEA1998a]

Item accountancy and maintaining continuity of knowledge using containment and surveillance (C/S) measures form the basis of the CANDU safeguards approach. Direct verification of the operator's declared nuclear material inventory is implemented for fresh and spent fuel. Although fuel bundles in the core remain inaccessible for verification, continuity of knowledge is maintained by a monitoring system when they are discharged. C/S covers the discharge of spent fuel from the reactor and storage in the spent fuel bays to provide continuity of knowledge.

All NPP designer organizations are required to ensure that their designs are safeguards friendly, i.e., the design allows adequate implementation of the safeguards specific approaches. Some of these requirements are listed below (not an inclusive list):

- Requirement for early interaction between the designer and the IAEA;
- Design of barriers which form a part of the C/S system;
- Design of seals for moving nuclear material;
- Design of surveillance techniques;
- Design of fuel identification and fuel verification techniques;
- Detection of unrecorded production or use of nuclear material;
- Transfer for spent fuel from the spent fuel pool to storage or reprocessing.

8 Nuclear Security

Nuclear security has become far more important in the last couple of decades, due largely to changes in the external political environment after the September 11, 2001, terrorist attacks in the United States. Each utility implements security at its sites, and in Canada, regulation of nuclear security is part of the mandate of the CNSC.

Top-level requirements are set by the Nuclear Security Regulations [GovCan2010]. This Act

covers the security of both certain nuclear materials and nuclear facilities.

Nuclear materials are divided into three categories related to their security impact: for example, a quantity of non-irradiated plutonium >2 kg is Category I; between 500 g and 2 kg is Category II; and between 15 g and 500 g is Category III. Possession in each category requires a licence, and the security obligations for each case are defined in the regulations.

For nuclear facilities in Canada, it is up to the CNSC Commission to establish and update the design basis threat which is taken into account by the utility in determining its security provisions. In addition, the utility must conduct an annual facility-specific threat and risk assessment. Nuclear facilities must be located within a protected area enclosed by a barrier. Category I materials are further protected by an inner-area structure or barrier whose function is to detect and delay unauthorized access before the on-site nuclear response force can successfully intervene.

In addition, the operator must identify *vital areas*. These are areas inside the protected area containing equipment, systems, devices, or a nuclear substance, the sabotage of which would or would likely pose an unreasonable risk to the health and safety of persons arising from exposure to radiation. The operator is then required to implement the appropriate physical protection measures.

The Act also sets out requirements for persons authorized to enter protected and inner areas and for security personnel. The CNSC has supplemented and expanded the Nuclear Security Regulations through a number of Regulatory Documents and Guides. Most of those pertaining to high-security sites such as nuclear power plants contain prescribed information and are not publicly available, and therefore they are not referenced here.

Further details of security regulations, implementation techniques, and verification methodologies are beyond the scope of this textbook and are not available to the general public.

9 Canadian Regulatory Process[11]

The Canadian regulatory process is based on over 60 years of CANDU reactor development and operation in Canada and internationally. Canada has been in the forefront of nuclear power development and use since the very beginning, including the development of its nuclear regulatory program.

The Parliament of Canada first established legislative control and federal jurisdiction over the development and use of nuclear energy and nuclear substances in 1946 with the introduction of the *Atomic Energy Control Act* (AECA), which also established the Atomic Energy Control Board (AECB). Fifty years later, the Canadian Government updated its regulatory requirements, and the Canadian Nuclear Safety Commission was established as a successor to the AECB.

CNSC material has been used throughout this section. We refer to specific documents where appropriate. As noted earlier, we do not try to paraphrase carefully developed regulatory texts. *Italic* fonts have been used to indicate where statements from CNSC documents have been used essentially verbatim.

11 Some of the descriptive material has been drawn from the Web site of the CNSC over the period from July 2011 to January 2013.

9.1 The CNSC

The Canadian Nuclear Safety Commission regulates the use of nuclear energy and materials to protect the health, safety, and security of Canadians and the environment, and to implement Canada's international commitments on the peaceful use of nuclear energy.

The CNSC develops, maintains, and revises all regulatory requirements and documents under the authority of the Nuclear Safety and Control Act [GovCan2013], which sets the overall legal framework for regulation.

9.2 CNSC Mandate and Organization

This section covers the mandate and role of the CNSC in the Canadian NPP regulatory process. It also covers the key elements of the CNSC organization, starting with the Commission and continuing with the organization of various departments and their role in Canadian regulatory processes.

As discussed in Section 2.3, the CNSC consists of an appointed Commission supported by technical staff.

The CNSC Commission has up to seven appointed permanent part-time members whose decisions are supported by more than 800 staff. These employees review applications for licences according to regulatory requirements, make recommendations to the Commission, and review (and can be delegated by the Commission to enforce) compliance with the Nuclear Safety and Control Act, regulations, and any licence conditions imposed by the Commission.

Under the NSCA [GovCan2013], CNSC's mandate involves four major areas:

- regulation of the development, production and use of nuclear energy in Canada to protect health, safety and the environment
- regulation of the production, possession, use and transport of nuclear substances, and the production, possession and use of prescribed equipment and prescribed information
- implementation of measures respecting international control of the development, production, transport and use of nuclear energy and substances, including measures respecting the non-proliferation of nuclear weapons and nuclear explosive devices
- dissemination of scientific, technical and regulatory information concerning the activities of CNSC, and the effects on the environment, on the health and safety of persons, of the development, production, possession, transport and use of nuclear substances.

The CNSC organization is shown in Figure 12. Note:

- the Regulatory Operations Branch, which is responsible for NPP licensing in Canada;
- the Technical Support Branch, which is home to all the CNSC discipline specialists and experts who review and assess various reactor designs and all information submitted in support of a licence application.

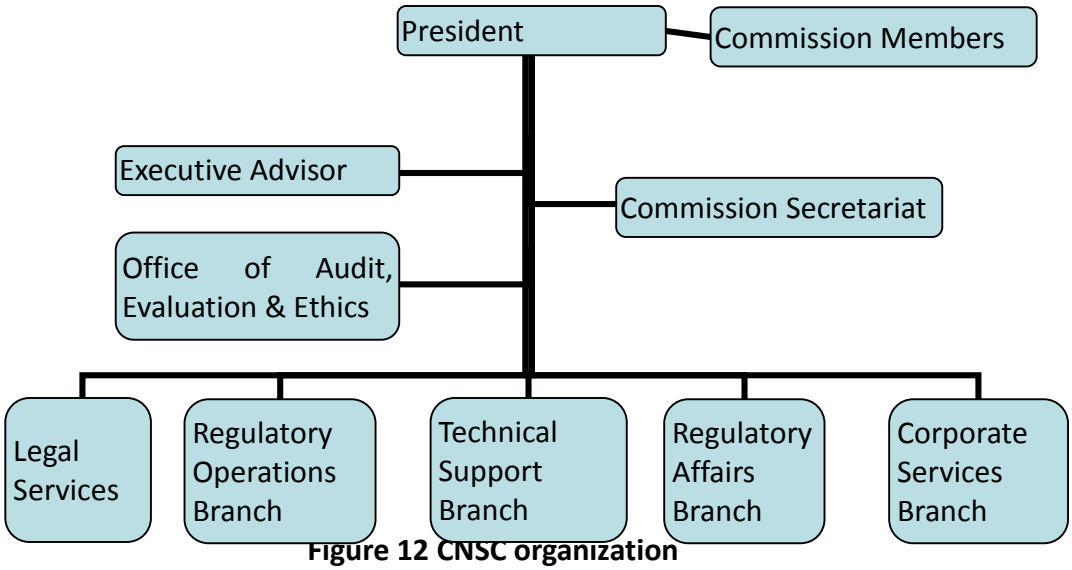

Figure 12 CNSC organization

9.3 Canadian Regulatory Framework and Regulatory Acts

The Canadian regulatory documents are arranged in several levels, as shown in Figure 13, starting at the top level with enabling legislation, then at the middle level with requirements documents, and at the lowest level with guidance documents. The requirements documents can be subdivided into regulations, licences, and regulatory documents (defined in Sections 9.5.1 and 9.5.2).

Three Acts are relevant and are described in the following sub-sections.

9.3.1 Nuclear Safety and Control Act

The Nuclear Safety and Control Act [GovCan2013] is the enabling legislation in Canada, as shown in Figure 13 and as described in Section 9.2.

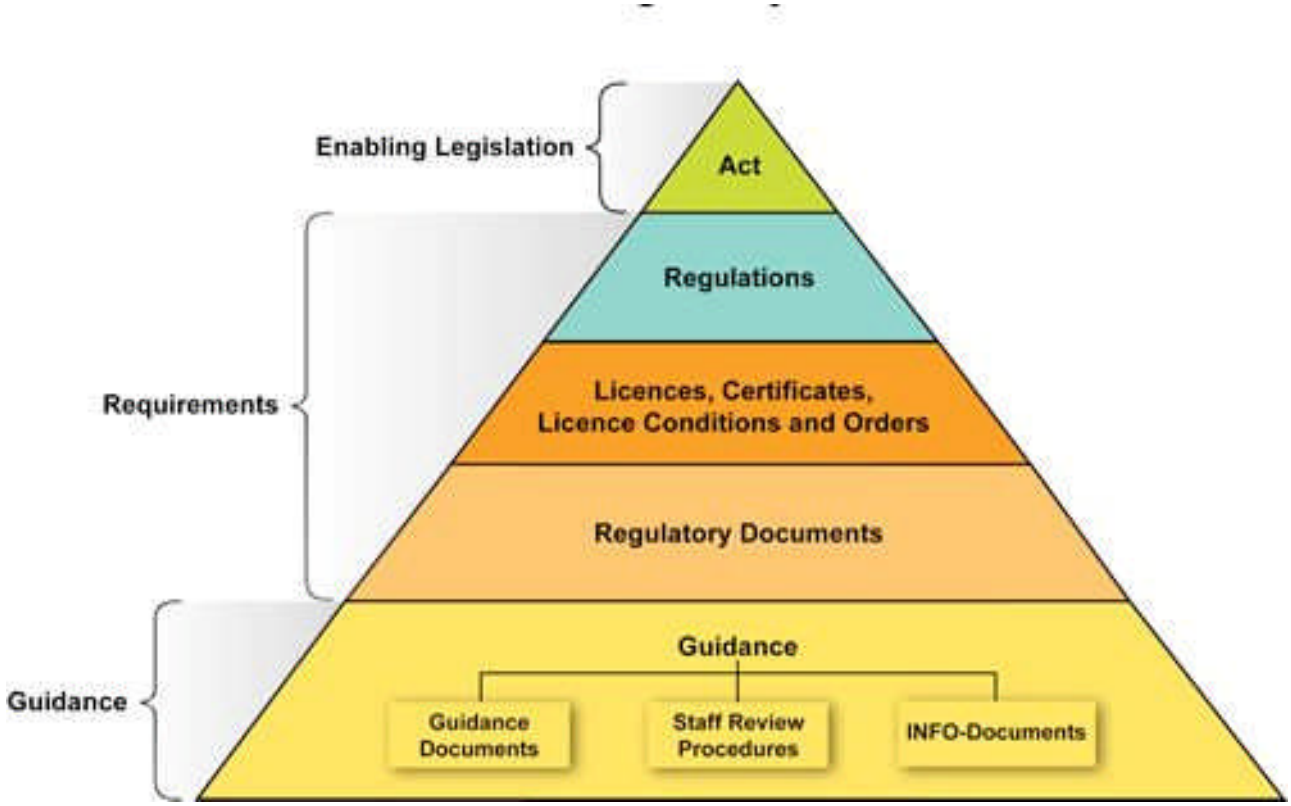

Figure 13 Structure of regulatory documents in Canada

The Act covers the following areas:

- Establishment and organization of the Canadian Nuclear Safety Commission (CNSC);
- Number and role of CNSC members;
- Role, responsibilities, and duties of the CNSC President;
- Directives and powers of the CNSC;
- Use, establishment, and responsibilities of various panels that may be established by the CNSC;
- The decision-making process at the CNSC;
- The scope and process for issuing or revoking various licences to the Canadian industry;
- The responsibilities of the CNSC for maintaining various records and reports;
- Appointment of various specialists, analysts, and inspectors of the CNSC;
- Appointment of designated officers (to whom the Commission can delegate some if its authority to make decisions on its behalf);
- Process for creation of procedures for decisions and orders;
- Process for redetermination and appeal of decisions and orders;
- Scope of regulations and process for their creation and enforcement;
- Provisions for exceptional powers;
- Provisions for offences and punishment;
- Transitional provisions.

Of particular importance is sub-section 24(4) of the Act, which states that:

> "No licence shall be issued, renewed, amended or replaced—and no authorization to

transfer one given—unless, in the opinion of the Commission, the applicant or, in the case of an application for an authorization to transfer the licence, the transferee:
(a) is qualified to carry on the activity that the licence will authorize the licensee to carry on; and
(b) will, in carrying on that activity, make adequate provision for the protection of the environment, the health and safety of persons, and the maintenance of national security and measures required to implement international obligations to which Canada has agreed."

The next level in Figure 13 is *Regulations*, which are published in the Canada Gazette and include:

- General Nuclear Safety and Control Regulations [GovCan2008]
- Radiation Protection Regulations [GovCan2007]
- Class I Nuclear Facilities Regulations [GovCan2012a]
- Class II Nuclear Facilities and Prescribed Equipment Regulations
- Uranium Mines and Mills Regulations
- Nuclear Substances and Radiation Devices Regulations
- Packaging and Transport of Nuclear Substances Regulations
- Nuclear Security Regulations [GovCan2010]
- Nuclear Non-Proliferation Import and Export Control Regulations [GovCan2010a]
- CNSC Cost Recovery Fees Regulations
- Administrative Monetary Penalties Regulations
- Canadian Nuclear Safety Commission Rules of Procedure
- Canadian Nuclear Safety Commission By-Laws

We have provided references above for some of the key Regulations in the nuclear power-reactor field.

In addition, when required, the CNSC puts forward proposals for new regulations or proposed amendments to existing regulations:

- Regulations Amending the Class I Nuclear Facilities Regulations and the Uranium Mines and Mills Regulation
- Amendments to Nuclear Non-Proliferation Import and Export Control Regulations
- Amendment to Class II Nuclear Facilities and Prescribed Equipment Regulations
- Regulations Amending Certain Regulations made under the Nuclear Safety and Control Act (Miscellaneous Program)
- Amendments to the Packaging and Transport of Nuclear Substances Regulations.

9.3.2 Canadian Environmental Assessment Act

The second relevant Act is the Canadian Environmental Assessment Act [GovCan2012], which covers all aspects of the environmental assessment process that must be followed for a new nuclear energy facility of any purpose and type. It sets out the requirements for addressing all important environmental issues, radiological and non-radiological.

9.3.3 Canadian Nuclear Liability Act

The third Act is the Canadian Nuclear Liability Act [GovCan1985], which regulates the nuclear

responsibility of various participants in the Canadian nuclear industry. The underlying purpose of the Act is to require nuclear operators to carry insurance to cover liability should an accident occur. The operator is absolutely liable for damage irrespective of the cause of the accident: that is, claimants do not have to prove negligence on the part of the operator—they need only prove that they have suffered damage. Operators must obtain liability insurance for damages up to a maximum of $75 million (but see next paragraph); if the consequences exceed that amount, the federal government appoints an independent Nuclear Damage Claims Commission that will receive claims, assess damages, and recommend the level of compensation that should be paid. The responsibility to pay claims exceeding $75 million rests with the federal government. The Act does not set a limit on what the government pays.

As of this writing (early 2014), Bill C-22 (the Energy Safety and Security Act) has been tabled in the House of Commons to replace the Nuclear Liability Act. It raises the absolute liability limit to $1 billion for both nuclear energy and offshore oil and gas. It is expected that this bill will be enacted by the House of Commons.

9.3.4 Other acts

Other Acts that pertain to some aspects of nuclear power plants include:

- Canadian Environmental Protection Act
- Fisheries Act
- Species at Risk Act
- Navigable Waters Protection Act
- Transportation of Dangerous Goods Act.

9.4 Licences

The third level in Figure 13 also includes *licences*. These are mandatory legal documents which set forth the requirements and limitations for activities undertaken during the life cycle of a nuclear activity. For example, a Power Reactor Operating Licence typically covers (among other items):

- Authorization to operate the nuclear power plant for a specified period;
- Reporting of events to the CNSC;
- Control of the exclusion zone within which no permanent dwelling is permitted and temporary access is controlled;
- References to some of the CNSC Regulatory Documents listed in Section 9.5, which therefore become mandatory;
- References to some of the CSA Standards listed in Table 6, which therefore become mandatory;
- Maintaining minimum operating-crew size and composition, including obtaining operating licenses for key staff;
- Complying with the requirement to use a set of Operating Policies and Principles, including Operating Limits;
- Complying with reactor power limits, including bundle and channel power limits
- Limits on permissible changes without CNSC prior consent. Specifically, this forbids changes which "introduce hazards different in nature or greater in probability than those considered by the Final Safety Analysis Report and Probabilistic Safety Assess-

ment". Such a clause binds the results of the safety assessment performed by the operator to the licence;
- Using only those fuel-bundle designs approved by the CNSC;
- Complying with requirements for an emergency plan for the facility;
- Complying with the limits on releases of radioactive material in normal operation (derived release limits);
- Following requirements for a maintenance program; and
- Complying with requirements for radiation protection, site security, and safeguards.

The licence is accompanied by, and references, a rather lengthy "Licence Conditions Handbook", which provides:

- compliance verification criteria to meet the conditions listed in the licence;
- information regarding delegation of authority and current versions of documents;
- implementation timelines for specific licence conditions; and
- an explanation of each regulatory requirement specified in the licence.

In effect, the Licence Conditions Handbook extends the scope of the licence.

9.5 CNSC Regulatory Documents

The fourth level in Figure 13 contains the Requirements Documents. They are not *legally* mandatory until and unless referenced in a licence. They are *effectively* mandatory for new designs and are used as an evaluation tool for existing designs.

The fifth level in Figure 13 contains the Guidance Documents. These documents provide direction to licensees and applicants on how to meet the requirements set out in the CNSC's Regulations, regulatory documents, and licences, and the techniques used by CNSC staff to evaluate specific problems or data needed in the review of applications for permits or licences.

The following sub-sections provide a basic explanation of key CNSC regulatory and guidance documents.

9.5.1 Historical classification schemes

The CNSC documents have followed several labelling and numbering schemes that reflect the different periods when these documents were created. We review the historical schemes briefly because many of these documents are still referenced under their original names in licences.

Originally the AECB issued all requirements documents as "R" ("regulatory") documents.

This system was superseded by the following classification:

- "S" ("Standard") documents, which were mandatory
- "G" ("Guidance") documents, which provided guidance
- "P" ("Policy") documents, which provided direction to CNSC staff and information for stakeholders.

More recently, CNSC has used the labels "RD" (Regulatory Document) and "GD" (Guidance Document). Occasionally, CNSC has issued documents as "RD/GD", which means that some parts of the document contain (effectively) requirements and other parts contain guidance. In

such cases, CNSC staff clarifies when information is mandatory.

The “RD” and “GD” labels have now been replaced by “REGDOC”, as discussed in Section 9.5.2.

In CNSC regulatory documents, “shall” is used to express a requirement, i.e., a provision that a licensee or licence applicant is obliged to satisfy to comply with the requirements of the document. “Should” is used to express guidance, or that which is advised, but not required. “May” is used to express an option or that which is permissible within the limits of the document. “Can” is used to express possibility or capability.

9.5.2 Current classification scheme

The CNSC has recently developed a classification scheme (by subject) for its existing and planned regulatory documents. As of April 2013, all these documents are now organized under three key categories and twenty-five series as follows:

1.0 Regulated facilities and activities

1.1 Reactor facilities

1.2 Class IB facilities

1.3 Uranium mines and mills

1.4 Class II facilities

1.5 Certification of prescribed equipment

1.6 Nuclear substances and radiation devices

2.0 Safety and control areas

2.1 Management system

2.2 Human performance management

2.3 Operating performance

2.4 Safety analysis

2.5 Physical design

2.6 Fitness for service

2.7 Radiation protection

2.8 Conventional health and safety

2.9 Environmental protection

2.10 Emergency management and fire protection

2.11 Waste management

2.12 Security

2.13 Safeguards and non-proliferation

2.14 Packaging and transport

3.0 Other regulatory areas

3.1 Reporting requirements

3.2 Public and aboriginal engagement

3.3 Financial guarantees

3.4 Commission proceedings

3.5 Information dissemination

The numbering scheme used in this categorization is "REGDOC-x.yy.zz", where "x" is the number of the key category, "yy" is the number of the series, and "zz" is a number which identifies the document uniquely within that category and series. For example, the design requirements for new reactor designs are documented in REGDOC-2.5.2, where the first "2" means the document is in the "safety and control area"; "5" means it is under the "physical design" series; and the last "2" is a sequence number identifying the specific document.

9.5.3 Licensing basis

Many of these documents form the licensing basis of a regulated facility or activity. The *licensing basis* [CNSC2010a] is a set of requirements and documents consisting of:

a) Regulatory requirements set out in the applicable laws and regulations.
   - Examples: the Nuclear Safety and Control Act, the Canadian Environmental Assessment Act, the Canadian Environmental Protection Act, the Nuclear Liability Act, the Transportation of Dangerous Goods Act, the Radiation Emitting Devices Act, the Access to Information Act, and the Canada/IAEA Safeguards Agreement.

b) Conditions and safety and control measures described in the facility licence and the documents directly referenced in that licence.
   - Examples: the Nuclear Security Regulations, the Nuclear Non-Proliferation Import and Export Control Regulations, the General Nuclear Safety and Control Regulations, the Radiation Protection Regulations, the Uranium Mines and Mills Regulations, the Class I Nuclear Facilities Regulations, the Nuclear Substances and Radiation Devices Regulations, the Class II Nuclear Facilities and Prescribed Equipment Regulations, and the Packaging and Transport of Nuclear Substances Regulations.

c) Safety and control measures described in documents directly referenced in the licence.
   - Examples: regulatory documents (such as RD-204, RD/GD-210, S-294, plus others), industry codes and standards (such as CSA N286-05, CSA N285.4, CSA N290.13), proponent- or licensee-produced documents, and any subsequent changes made to these documents in accordance with a CNSC-approved change control process (such as Management System Manual, Limits and Conditions of Operation).

d) Documents needed to support the licence application.

- Examples are documents describing the design, safety fuellings, and all aspects of operation to which the licensee makes reference; conduct of operations; and conduct of maintenance.

The licensing basis sets the boundary conditions for acceptable performance at a regulated facility or activity and thus establishes the basis for the CNSC's compliance program with respect to that regulated facility or activity.

We now summarize selected regulatory documents. Note that document numbers and titles are shown in terms of the currently issued documents (and not in terms of the new classification scheme shown in Section 9.5.2).

9.5.4 Design of new NPPs in Canada: RD-337

RD-337 [CNSC2008] sets out comprehensive CNSC requirements with respect to the design of new water-cooled NPPs and provides examples of optimal design characteristics[12]. Excerpts follow:

> The information provided in this document is intended to facilitate high quality design, and consistency with modern international codes and standards, for new water-cooled NPPs. It is recognized that specific technologies may use alternative approaches. If a design other than a water-cooled reactor is to be considered for licensing in Canada, the design is subject to the safety objectives, high level safety concepts and safety management expectations associated with this regulatory document.
>
> To a large degree, this document represents the CNSC's adoption of the principles set forth in International Atomic Energy Agency (IAEA) document NS-R-1, Safety of Nuclear Plants: Design, and the adaptation of those principles to align with Canadian practices. The scope of NS-R-1 has been expanded to address the interfaces between NPP design and other topics, such as environmental protection, radiation protection, ageing, human factors, security, safeguards, transportation, and accident and emergency response planning.

The main components of RD-337 are:

i. Safety objectives and concepts
   This section covers safety objectives in Canada (general, radiation protection, and technical), safety goals, radiation dose criteria, accident mitigation and management, and safety concepts (defence-in-depth, physical barriers, and operating limits and conditions).
ii. Safety management during design
   This section discusses safety during the design process. It includes all important aspects of the design process, including design authority, design management, QA, proven engineering practices, design documentation, etc.
iii. Safety considerations
   This section covers all aspects of safety applications in a design, including the application of defence-in-depth, safety functions, accident prevention and plant safety characteris-

12 While this Chapter was being finalized, CNSC issued an update to RD-337 – called REGDOC 2.5.2 – which adds lessons learned from Fukushima. See [CNSC2014].

tics, radiation protection principles and acceptance criteria, exclusion zones, and facility layout.

iv. General design considerations
This section contains general requirements for all technical disciplines and reactor engineering areas. It covers:

- structure, system, and component classifications;
- plant design envelope and operating plant states;
- guidance for consideration of all important hazards and initiating events that need to be considered in the design;
- design rules, limits, and reliability for safety (such as common-cause failures, single failures, fail-safe requirements, etc.);
- pressure-retaining systems and components;
- equipment classification (seismic, fire, environmental, etc.);
- instrumentation and control;
- safety support systems;
- civil structures;
- human factors;
- commissioning;
- security;
- safeguards;
- decommissioning.

v. System-specific requirements
This section covers requirements specific to most important systems and functions, including the reactor core, heat-transport system, steam-supply system, means of shutdown, emergency core cooling system, containment, emergency power supply, heat transfer to an ultimate heat sink, emergency heat-removal system, control facilities, waste management and control, fuel handling and storage, and radiation protection.

vi. Safety analysis
The safety analysis sections cover the most important aspects of safety analysis, namely analysis objectives, hazards analysis, deterministic analysis, and probabilistic analysis. The topic is covered in RD-310 in more detail [CNSC2008b].

vii. Environmental protection and mitigation
This section covers environmental protection design and requirements, as well as requirements for released radioactive and hazardous substances.

viii. Alternative approaches
RD-337 is intended to be technology-neutral for water-cooled reactor designs. It is recognized that specific technologies may use alternative approaches.

The CNSC considers alternative approaches to the expectations in this document where:

- The alternative approach would result in an equivalent or superior level of safety;
- Application of the expectations in this document conflicts with other rules or requirements;
- Application of the expectations in this document would not serve the underlying purpose, or is not necessary to achieve the underlying purpose; or
- Application of the expectations in this document would result in undue hardship

or other costs that significantly exceed those contemplated when the regulatory document was adopted.

One example of an alternative approach is consideration of best estimate and uncertainty analysis instead of a conservative analysis; see Chapter 13.

9.5.5 NPP site evaluation: RD-346

This regulatory document [CNSC2008c] sets out requirements for the evaluation of sites for new NPPs before an application is made for a Licence to Prepare Site and before an environmental assessment determination is initiated.

RD-346 represents the CNSC staff's adoption, or where applicable, adaptation of the principles set forth by the International Atomic Energy Agency (IAEA) in NS-R-3, Site Evaluation for Nuclear Installations. The scope of RD-346 goes beyond NS-R-3 in several aspects such as the protection of the environment, security of the site, and protection of prescribed information and equipment, which are not addressed in IAEA's NS-R-3.

Site evaluation is a process that should precede the submission of an application to prepare a site for the construction of a new NPP. RD-346 is written to serve the broader licensing needs under the Nuclear Safety and Control Act and the Canadian Environmental Assessment Act, and will facilitate a more effective and efficient regulatory review.

The document covers criteria for site evaluation; type and scope of baseline data required in the site evaluation process; evaluation of natural external events; evaluation of external, non-malevolent, human-induced events; security considerations; decommissioning; quality assurance; and the consultation process.

9.5.6 NPP life extension: RD-360

The regulatory document RD-360 [CNSC2008d] covers the regulatory requirements for NPP life-extension programs. The purpose of this regulatory document is to inform licensees about the steps and phases to consider when undertaking a project to extend the life of a nuclear power plant. The main topics are:

- Key elements to consider when establishing the scope of the life-extension project; and
- Considerations to be taken into account in planning and executing a life-extension project.

The document covers the initiation of the life-extension project, preparation of the integrated project plan (which includes environmental assessment, safety assessment, integrated implementation plan and its adequacy, etc.), project execution, and return to service.

A major part of the assessment for life extension requires reviews of the existing plant against modern codes and standards, including, but not limited to, CNSC documents more recent than were in place at the time the plant was originally licensed. Although compliance is not mandatory, gaps must be identified, assessed, and remedied if practical. In addition, the condition of systems, structures, and components (SSC) is assessed, largely to capture the effects of aging and degradation. These assessments may also identify gaps. The entire assessment is collected in a Global Assessment Report (GAR), from which an Integrated Implementation Plan (IIP) is developed. The IIP is a work plan and schedule to fix the identified gaps insofar as is practical

and risk-effective. Such life-extension assessments are similar to, but much broader in scope than, periodic safety reviews.

9.5.7 Safety analysis for NPPs: RD-310 and GD-310

Safety analysis is one of the most important topics in NPP licensing because it provides the assurance that the plant can be operated safely and that the postulated events can be prevented, mitigated, and managed. The CNSC has issued both the requirements document (RD-310 [CNSC2008b]) and the guidance document (GD-310 [CNSC2012b]).

> RD-310 identifies high-level regulatory information for a nuclear power plant licence applicant's preparation and presentation of a safety analysis. In particular, it establishes a more modern risk-informed approach to the categorization of accidents, one that considers a full spectrum of possible events, including the events of greatest consequence to the public. The CNSC expects proponents and applicants for new reactor licences to immediately apply this regulatory document in new-build submissions. In the context of existing reactors, CNSC expects the licensees to apply this document, in a graduated manner, to all relevant programs in future submissions.
> RD-310 explains the objectives of deterministic safety analysis, and in detail covers the requirements for safety analysis. In particular, it covers identification and classification of events following the international practice, i.e., groups them into Normal Operation (NO), Anticipated Operational Occurrences (AOOs), Design Basis Accidents (DBAs), and Beyond Design Basis Accidents (BDBAs), and explains the acceptance criteria. However, most of the details in the document are focussed on the safety analysis methods and assumptions, including methods, data, assumptions, computer code requirements, and required conservatisms in the analysis. The document also covers the required documentation that a licence applicant needs to prepare, and the time line for updating this documentation.

9.5.8 Reliability programs for NPPs: RD/GD-98

Regulatory document RD/GD-98, *Reliability Programs for Nuclear Power Plants* [CNSC2012a], sets out the requirements and guidance of the CNSC for the development and implementation of a reliability program for nuclear power plants in Canada. One of the important aspects of this document is to provide a clear definition of the Systems Important to Safety (SIS) and how these are treated and classified in NPP design.

9.5.9 Reporting requirements for operating nuclear power plants: S-99

The purposes of this Regulatory Standard [CNSC2003] are:

- To help the Canadian Nuclear Safety Commission collect the information that it needs to ensure that a nuclear power plant is operating safely and to verify that the licensee is complying with regulatory requirements;
- To help applicants for operating licences for nuclear power plants design programs for collecting and reporting information in accordance with regulatory requirements; and
- To facilitate CNSC evaluations of the appropriateness, completeness, and timeliness of information reported to the CNSC by operators of nuclear power plants.

This document is a key document for utilities that operate nuclear power plants because it states the requirements for reporting of operational issues. The document groups the requirements into two groups: reporting unscheduled events, and reporting scheduled events.

9.5.10 Pre-licensing review of a vendor's reactor design: GD-385

Guidance document GD-385, Pre-Licensing Review of a Vendor's Reactor Design [CNSC2012], describes the pre-licensing review process provided by the CNSC for assessing a vendor's design for a nuclear power plant or small reactor. The review considers the areas of design that relate to reactor safety, security and safeguards. For this topic, a licensee or licence applicant is not obliged to satisfy any provisions through regulations or licence conditions, and therefore no regulatory document (RD) accompanies this guidance document.

A pre-licensing review is an optional service provided by the CNSC. The objective of a pre-licensing review is to increase regulatory certainty while ensuring public safety. The review can be undertaken by a reactor vendor prior to an applicant's submission of a licence application to the CNSC and can provide early identification and resolution of potential regulatory or technical issues in the design, particularly those that could result in significant changes to the design or safety analysis.

This review does not certify a reactor design and does not involve the issuance of a licence under the Nuclear Safety and Control Act. It is not required as part of the licensing process for a new nuclear power plant or small reactor. The conclusions of a design review do not bind or otherwise influence decisions made by the Commission, with whom the authority resides to issue licences for nuclear power plants and small reactors. It is different in these respects from the U.S. Standard Design Certification.

9.5.11 Licence to construct a nuclear power plant: RD/GD-369

To request CNSC assessment of a request for a construction licence, a formal application must be submitted to the Canadian Nuclear Safety Commission (CNSC) along with appropriate documentation. This CNSC guidance identifies the information that should be submitted to support such an application.

RD/GD-369 [CNSC2012c] applies to applications for a licence to construct a water-cooled nuclear power plant. It does not presuppose or limit an applicant's intention to follow any particular kind of water-cooled reactor technology. This document follows the format of the IAEA Safety Guide No. GS-G-4.1, *Format and Content of the Safety Analysis Report for Nuclear Power Plants*, but is more specific to Canadian regulatory practice. In following these guidelines, an applicant must submit the appropriate information to demonstrate that it is qualified and will make adequate and reasonable provisions to undertake the activity to be licensed, pursuant to sub-section 24(4) of the *Nuclear Safety and Control Act* and associated regulations.

RD/GD-369 is a combined document that lists and explains the requirements, but also provides guidance on how to address them. The document covers plant description; management of safety; site evaluation; general design aspects and support programs; design of plant structures, systems, and components; safety analysis; construction and commissioning; operational aspects; operational limits and conditions; radiation protection; environmental protection; emergency preparedness; radioactive and hazardous waste management; decommissioning and end-of life-aspects; and safeguards.

9.5.12 Severe accident management programs for nuclear reactors: G-306

The CNSC Guide on *Severe Accident Management Programs for Nuclear Reactors* [CNSC2006] describes a typical severe accident management (SAM) program for a nuclear reactor. A person who applies for, or holds, a licence to construct or operate a nuclear reactor can use this guide when developing and implementing measures to help:

a) Prevent the escalation of a reactor accident into an event involving severe damage to the reactor core;
b) Mitigate the consequences of an accident involving severe damage to the reactor core; and
c) Achieve a safe, stable state of the reactor and plant over the long term.

Some severe accidents (in particular dual failures, see Chapter 13) have historically been part of the CANDU design basis. However the spectrum of severe accidents that must be evaluated has broadened in the past few decades due to the maturation of probabilistic safety assessment as an evaluation tool and to the real events at Three Mile Island, Chernobyl, and Fukushima. Because operating plants may not have been explicitly designed against extreme events, in the past, severe accident assessment and management looked at the capabilities of existing plant systems to mitigate such events and developed severe-accident management procedures to take advantage of these capabilities. However, especially post-Fukushima, design measures (retrofits) are being implemented specifically to mitigate a spectrum of severe accidents, for example, filtered containment venting.

A Severe Accident Management (SAM) program provides an additional defence against the consequences of those accidents that fall beyond the scope of events considered in the reactor design basis. The establishment of a SAM program should ensure that personnel involved in managing an accident have the information, procedures, and resources necessary to carry out effective on-site actions.

G-306 provides guidance on the goals and principles of severe-accident management, considerations for program development (risk assessment and accident analysis), determination of high-level accident response (preventive and mitigating actions, evaluation of systems and equipment, and assessment of material resources), and SAM procedures and guidelines.

9.5.13 Containment systems for CANDU nuclear power plants: R-7

This regulatory document [CNSC1991] is one of the original series of AECB documents. It was superseded by RD-337, except in areas in which it is consistent with RD-337, but provides more information.

The document describes the design, operating, and testing requirements for the containment system. It includes definition of the containment envelope, dose limits under accident conditions (see Section 9.5.17), structural integrity, leakage criteria, and requirements in several important areas, such as availability, environmental qualification, shielding, status monitoring, and seismic provisions.

9.5.14 Shutdown systems for CANDU nuclear power plants: R-8

This regulatory document [CNSC1991a] is one of the original series of AECB documents. It was superseded by RD-337 except in areas in which it is consistent with RD-337, but provides more

information.

The document describes the design, operating, and testing requirements for the shutdown systems. It includes definition of the minimum allowable performance standards and requirements in several important areas, such as performance, environmental qualification, availability, separation and independence, actuation instrumentation, status monitoring, and seismic provisions.

9.5.15 Emergency core cooling systems for CANDU nuclear power plants: R-9

This regulatory document [CNSC1991b] is one of the original series of AECB documents. It was superseded by RD-337, except in areas in which it is consistent with RD-337, but provides more information.

The document describes the design, operating, and testing requirements for the emergency core cooling system. It includes definition of the minimum allowable performance standards and requirements in several important areas, such as core cooling, environmental qualification, availability, separation and independence, actuation instrumentation, leakage control, inadvertent operation, shielding, status monitoring, and seismic provisions.

9.5.16 Use of two shutdown systems in reactors: R-10

This regulatory document [CNSC1991b] is one of the original series of AECB documents. It was superseded by RD-337.

The document formalized the requirement for two independent shutdown systems:

“All nuclear power reactors licensed for construction in Canada after January 1, 1977, shall incorporate two independent protective shutdown systems unless otherwise approved by the Board.”

It required that the two shutdown systems be independent, reliable, diverse, and individually capable of meeting regulatory dose limits[13]. Therefore, it could be assumed that at least one system would operate as designed when required (i.e., there was no need to postulate simultaneous unavailability of both systems after an accident).

9.5.17 Classification of systems, design basis accidents, and dose limits

The selection and classification of accidents for safety analysis, or in other words the definition of design basis accidents, is covered extensively in Chapter 13 and is summarized here only for convenience:

The deterministic safety analysis limits under which all large operating CANDU plants up to but excluding Darlington have been licensed can be found in [Hurst1972]. The spectrum of possible design basis accidents was collapsed into two broad categories: *single failures*, or the failure of any one process *system* in the plant, and *dual failures*, a much less likely event defined as a single failure coupled with the unavailability of either a shutdown system, or containment, or the emergency core cooling system, these constituting the so-called *special safety systems*. For each category, a frequency and a consequence limit was chosen that had to be satisfied. In addition, to deal with the siting of a reactor (Pickering A) next to a major population centre (Toronto), population dose limits were defined for each category of accident.

The limits were as follows (sometimes this is called the Siting Guide):

Table 3 Single / dual failure dose limits

Accident	Maximum Frequency	Individual Dose Limit	Population Dose Limit
Single Failure	1 per 3 years	0.005 Sv	10^2 Sv
		0.03 Sv thyroid	10^2 Sv thyroid
Dual Failure	1 per 3000 years	0.25 Sv	10^4 Sv
		2.5 Sv thyroid	10^4 Sv thyroid

For the licensing of Darlington, as discussed in Chapter 13, Consultative Document C-6 was used. This expanded the number of accident classes to five, as follows:

13 This is an oversimplification of R-10. R-10 actually specifies that for single failures, "at least" one shutdown system had to meet dose limits, whereas for dual failures, each shutdown system had to be individually capable of so doing. The distinction was removed in later practice, so that each shutdown system alone had to meet requirements for all design basis accidents.

Table 4 Consultative document C-6 dose limits

Event Class	Expected Frequency per reactor-y [Charak, 1995][14]	Whole-Body Dose (Sv)	Thyroid Dose (Sv)
1	$> 10^{-2}$	0.0005	0.005
2	10^{-2} to 10^{-3}	0.005	0.05
3	10^{-3} to 10^{-4}	0.03	0.3
4	10^{-4} to 10^{-5}	0.1	1
5	$< 10^{-5}$	0.25	2.5

Finally, for new plants (and as an evaluation tool for existing plants), a classification scheme based more on international practice has been used (from [CNSC2008] and [CNSC2008b]):

Table 5 New plants in Canada: dose limits

Event	Frequency	Dose Limit (Sv)
Anticipated Operational Occurrence	$\geq 10^{-2}$ / reactor-year	0.0005
Design Basis Accident	10^{-2} to 10^{-5} / reactor-year	0.020

Plant licences refer to the Final Safety Analysis Report, which in turn references the appropriate classification scheme.

9.6 CNSC Staff Review Procedures

CNSC staff have prepared a set of Staff Review Procedures (SRPs) used during the technical assessment stage of the environmental assessment and site licensing process. They provide instructions to CNSC staff on the conduct of an assessment. They also inform potential applicants and the public about the criteria used to assess environmental impact statements and licence applications for new nuclear power plants. SRPs are not regulatory documents. They are available on the CNSC Web site. Other SRPs are under development.

9.7 CNSC CANDU Safety Issues

All regulators track safety-related issues which are not so pressing as to require immediate regulatory action, but have not been addressed convincingly enough by the operator. Typically, these include knowledge gaps, safety analysis assumptions, and methodologies. Such issues in Canada were formerly called “Generic Action Items” (GAIs); these have now been phased out as a regulatory tool and replaced by the CANDU Safety Issues. Generally, they pertain to more than one operating plant.

14 Expected frequency ranges are not part of C-6; they were used by Ontario Hydro in the licensing of Darlington to classify events not listed in C-6.

The list of CANDU Safety Issues was developed from:

- The IAEA document, Generic Safety Issues for Nuclear Power Plants with Pressurized Heavy Water Reactors and Measures for their Resolution [IAEA2007a];
- Regulatory oversight of currently operating reactors;
- Results of life-extension assessments;
- Safety issues identified in pre-licensing reviews of new CANDU designs.

They are classified into three categories:

- Category 1 means issues that have been satisfactorily addressed in Canada;
- Category 2 identifies issues that are a concern in Canada, but have appropriate measures in place to maintain safety margins;
- Category 3 issues are a concern in Canada and measures are in place to maintain safety margins, but the adequacy of these measures needs to be confirmed.

For the last, the industry and the CNSC have used a risk-informed decision-making (RIDM) process to identify, estimate, and evaluate the risks associated with each and to recommend measures to control these risks. None of these issues has yielded a risk significance level that required immediate corrective action.

As of August 2013 [GovCan2013a], there are 16 Category 3 issues outstanding, including six associated with large-break loss-of-coolant accidents (LBLOCA) and ten other safety issues not associated with LBLOCA.

The current status of each CANDU Safety Issue is reported publicly at International Nuclear Safety Convention meetings [GovCan2013a].

9.8 CNSC Fukushima Action Items

On March 11, 2011, a magnitude 9.0 earthquake, followed by a devastating tsunami, struck Japan. The combined impact of the earthquake and tsunami on the Fukushima Dai-ichi nuclear power plant caused a severe nuclear accident. Details are presented in Chapter 13.

The CNSC established the CNSC Fukushima Task Force to evaluate the operational, technical, and regulatory implications for CANDU nuclear power plants and the capability of CANDU NPPs to withstand conditions similar to those that triggered the Fukushima accident. It issued its recommendations in the Fukushima Task Force Report [CNSC2011]. In response, the CNSC Staff developed an Action Plan [CNSC2011a], which mandates actions both for the utilities and for the CNSC itself. In these documents, CNSC staff requested utilities to conduct certain activities in the following areas:

a) Safety-review criteria, including identification and magnitudes of external events, adequacy of design-basis-accident analysis, consideration of beyond-design-basis accidents, implementation of severe-accident management, licensees' emergency response plans, nuclear emergency management in Canada, and CNSC regulatory frameworks and processes;
b) Strengthening reactor defence-in-depth;
c) Enhancing emergency response; and
d) Improving regulatory framework and licensing.

This work resulted in a number of Fukushima Action Items that the Canadian industry is putting

in place.

9.9 Canadian Codes and Standards

The Canadian Standards Association (CSA) is a not-for-profit membership-based association serving business, industry, government, and consumers in Canada and the global marketplace. CSA develops standards that enhance public safety and health, advance the quality of life, and help to preserve the environment.

The objective of the CSA Nuclear Standards Program is to help promote a safe and reliable nuclear power industry in Canada and to have a positive influence on the international nuclear power industry. Although focussing on nuclear power plants, the program provides guidance for other types of nuclear facilities on selected topics such as radioactive waste management and environmental releases. Compliance with CSA nuclear standards is mandatory for those that are referenced in a plant licence and is *de facto* mandatory for other organizations which contribute to design, analysis, and other aspects of plant construction and operation. Table 6 shows selected CSA Standards relevant to nuclear power plants.

Table 6 Selected key CSA codes and standards

Document number	Title	Creation / Revision or Reaffirmed date
CSA N285.0	General Requirements for Pressure-Retaining Systems and Components in CANDU Nuclear Power Plants/Material Standards for Reactor Components for CANDU Nuclear Power Plants	2008
CSA N285.4	Periodic Inspection of CANDU Nuclear Power Plant Components	2009
CSA N285.5-13	Periodic Inspection of CANDU Nuclear Power Plant Containment Components	1998 (2013)
CSA N285.8	Technical Requirements for In-Service Evaluation of Zirconium Alloy Pressure Tubes in CANDU Reactors	2010
CSA N286-05	Management System Requirements for Nuclear Power Plants	2005 (2010)
CSA N286.7	Quality Assurance of Analytical, Scientific, and Design Computer Programs for Nuclear Power Plants	1999 (2007)
CSA N287.1	General Requirements for Concrete Containment Structures for CANDU Nuclear Power Plants	July 1993 (2009)
CSA N287.7-08 (R2013)	In-Service Examination and Testing Requirements for Concrete Containment Structures for CANDU Nuclear Power Plants	2008 (2013)
CSA N288.4-10	Environmental Monitoring Programs at Class I Nuclear Facilities and Uranium Mines and Mills	2010 (1990)
CSA N288.5-11	Effluent Monitoring Programs at Class I Nuclear Facilities and Uranium Mines and Mills	2011
CSA N288.6-12	Environmental Risk Assessments at Class I Nuclear Facilities and Uranium Mines and Mills	2012
CSA N288.1	Guidelines for Calculating Derived Release Limits for Radioactive Material in Airborne and Liquid Effluents for Normal Operation of Nuclear Facilities	2008
CSA N289.1	General Requirements for Seismic Qualification of CANDU Nuclear Power Plants	2008

Document number	Title	Creation / Revision or Reaffirmed date
CSA N290.1	Requirements for the Shutdown Systems of CANDU Nuclear Power Plants	1980 (2006)
CSA N290.15-10	Requirements for the Safe Operating Envelope of Nuclear Power Plants	2010
CSA N291	Requirements for Safety-Related Structures for CANDU Nuclear Power Plants	2008
CSA N293	Fire Protection for CANDU Nuclear Power Plants	2007
CSA N294	Decommissioning of Facilities Containing Nuclear Substances	2009

10 Reactor Licensing Process in Canada[15]

CNSC material has been used throughout this section and referred to in specific documents where appropriate. *Italic* fonts have been used to indicate where statements from CNSC documents have been used essentially verbatim.

This section covers the licensing process of both new-build NPPs and operating reactors. The emphasis is on new-build NPPs. However, certain aspects of the licensing (relicensing) of operating reactors are also covered. See [CNSC2008a] and [Andrews2012].

The focus is on the Canadian licensing process, but relevant and important aspects of, and differences from, the licensing process in other countries are also covered at a high level.

10.1 Licensing Process

Nuclear power plants are defined as Class I nuclear facilities, and the regulatory requirements for these facilities are found in the *Class I Nuclear Facilities Regulations*. The regulations also require separate licences for each of the five phases in the lifecycle of a nuclear power plant:

i. licence to prepare a site, including the environmental assessment;
ii. licence to construct;
iii. licence to operate;
iv. licence to decommission; and
v. licence to abandon.

There are four major steps in the licensing process:

1. Applicant submits a licence application
2. Environmental assessment

15 Some of the descriptive material has been drawn from the Web site of the CNSC.

3. Licensing technical assessment
4. CNSC renders its decision.

We summarize these in turn.

10.1.1 Licence application

In Canada, the licensing process begins when an application is received by CNSC. All new licence applications or amendments to existing licences require the approval of the Commission or a CNSC Designated Officer. The Commission is notified when an application that requires a decision from them has been filed.

The preparation of a licence application needs to consider all regulatory criteria as defined by the *Nuclear Safety and Control Act*, and *relevant regulations,* CNSC requirements and expectations, international and domestic standards, and applicable international obligations.

For major resource projects such as nuclear power plants, uranium mines, or fuel processing facilities, a project description is sent to Natural Resources Canada's Major Projects Management Office (MPMO). MPMO is responsible for coordinating the work of all the federal departments and agencies that have a role to play in the regulatory process for major resource projects. MPMO offers licensees a single entry point into the federal regulatory system.

For new nuclear power plants in Canada, three licences are initially required:

1. licence to prepare site, including an environmental assessment
2. licence to construct the nuclear power plant, and
3. licence to operate.

The regulatory process in Canada in principle makes it possible to combine these processes, but the normal route is for an applicant to request them sequentially, i.e., each process is completed when the appropriate licence is issued.

Very often, before a formal licensing process is initiated through an application by the NPP owner or operator, a pre-licensing process is performed by the NPP design organization, as explained in detail in Section 5.

The key element of a successful licensing process is to prepare adequate documentation that meets regulatory requirements and expectations. Figure 14 provides a general idea of the level of detail required during different phases of the licensing process. On the left-hand side, the reactor design process is shown, and on the right-hand side, the level of documentation completeness. From top to bottom, the design and documentation move from the initial stage to completeness. The middle of the diagram provides an indication of the percentage completeness of the design. However, the design and documentation completeness level is discussed and agreed in detail with CNSC at the beginning of a licensing process.

The technology vendor must complete a conceptual design and appropriate documentation before engaging in any licensing activity. After the conceptual design has been firmed up, which means that key design options and characteristics have been decided, a basic engineering program begins to develop a preliminary design. During the basic engineering process, at some point, the technology vendor may decide to engage the regulator in performing a non-binding pre-licensing review. This is not a mandatory process, and technology vendors may or may not decide to request it.

As shown in Figure 14, from [CNSC2012], following the preliminary design, detailed design is conducted. After the detailed design and appropriate documentation have been prepared, the licensee applies for a construction licence. During the regulatory review for the construction licence, further detailed design activities related to the construction phase may be conducted. After the regulatory body issues an operating licence, the licensee will continue to provide ongoing design support activities.

Section 13 gives as an example the information that must be submitted in Canada for construction and operating licences.

At any time during operation, if a design or procedural change is considered for implementation which deviates from the safety case or from any prior licence issued by CNSC, an approval process for the particular change must be conducted and CNSC approval obtained before implementing the change.

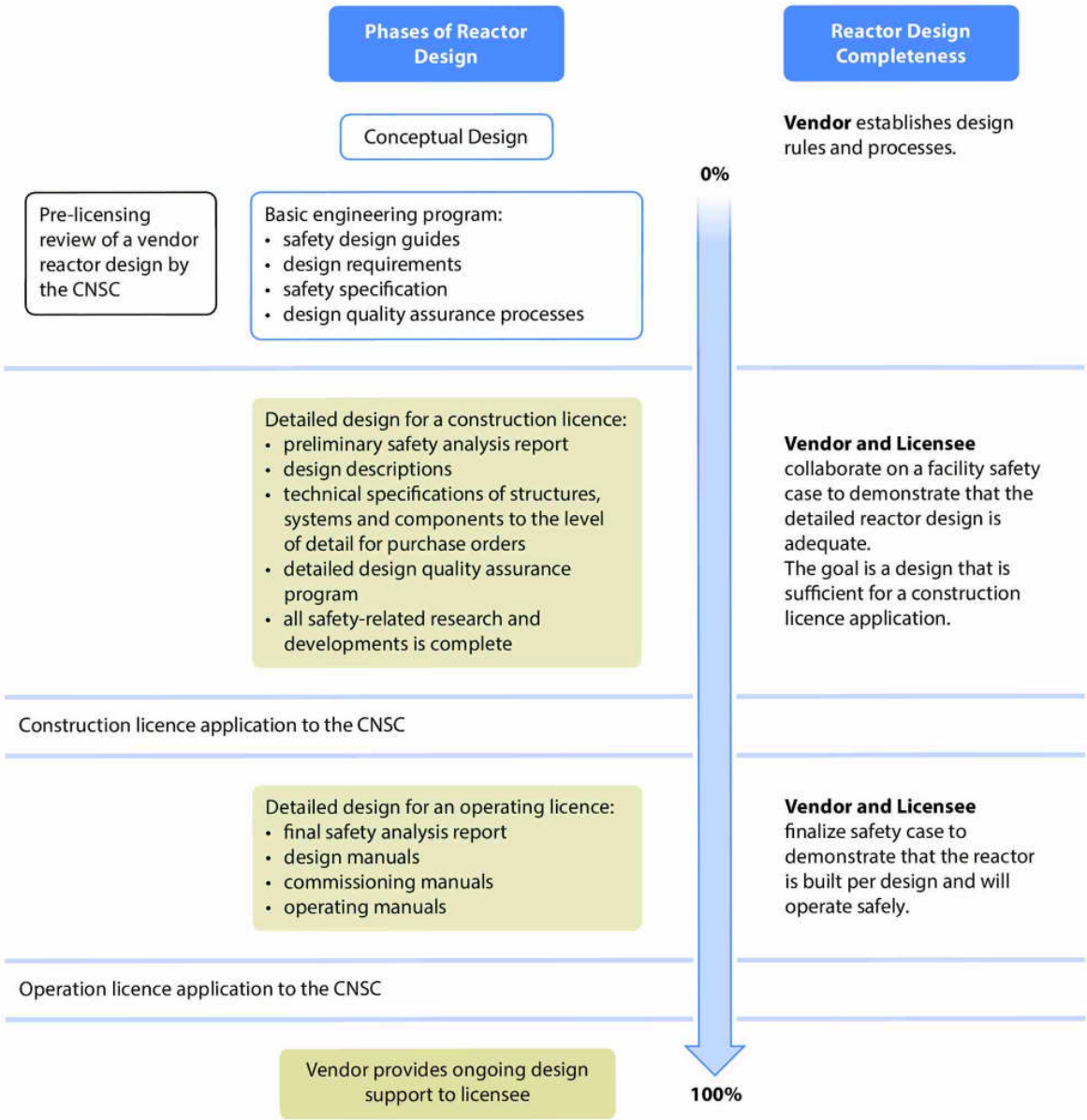

Figure 14 Design and documentation completeness phases

10.1.2 Environmental assessment

CNSC has obligations and responsibilities under the *Canadian Environmental Assessment Act* (CEAA), which is the basis for federal Environmental Assessments in Canada. See [CEAA2012].

During the application review process, CNSC determines whether an environmental assessment (EA) is required for a proposed project. EAs are used to predict the potential environmental effects of a specific project and to determine whether these effects should be mitigated, and by what means, before a project is carried out. EAs consider environmental components such as:

- air, water, and soil quality;
- noise;
- human health;
- aboriginal interest, physical and cultural heritage; and
- use of land and resources.

EAs provide opportunities for public participation in activities undertaken by the potential licensees, the CNSC, or both, including aboriginal consultations.

Under the CEAA [GovCan2012], there are two levels of environmental assessment: a standard environmental assessment and a panel review. The standard environmental assessment is the default level of assessment applicable to a designated project; the second, higher level of environmental assessment is a panel review. The CEAA imposes time limits for environmental assessments. Most standard environmental assessments must be completed within one year, while panel reviews are limited to two years.

At the beginning of an environmental assessment, CNSC provides project-specific advice and guidance about what should be assessed, such as the scope of the project and the factors that apply to each individual project. Further guidance is available from CNSC for conducting these technical studies.

All applications for new nuclear facilities and some amendments to existing licences require the applicant to undertake an EA and technical studies. After technical studies are completed, the applicant can submit an Environmental Impact Statement (EIS) to CNSC, who will assess the EIS and prepare an EA Report. For major new facilities, the assessment of an applicant's EIS, referred to as an EA technical assessment, and is guided by an Assessment Plan and EIS-related *Staff Review Procedures*. The EA report contains recommendations for an EA decision, including all appropriate mitigation measures and the requirements of a follow-up program. Pursuant to the CEAA, the Responsible Authority (the Commission or a delegated officer) must make its EA decision before any licensing action can be considered for the project.

Only one EA is required for a project, even if that project requires separate licences for different phases (i.e., licence to prepare site, licence to construct, etc.). However, additional EAs may be required if a project changes over time. For a new nuclear power plant, if construction is to be performed at a new site, the EA is conducted before a site licence is issued. For a new nuclear power plant where construction is intended on a site that already has other NPP units, the EA is conducted before site preparation can begin for the new NPP addition.

10.1.3 Licensing technical assessment

After receipt of a licence application, CNSC staff undertakes a variety of technical assessments according to a prescribed Assessment Plan and licensing-related Staff Review Procedures to ensure that each application complies with its corresponding regulatory requirements. Peer reviews are sometimes used, when additional rigour is required.

The Licensing Technical Assessment considers all regulatory criteria as defined by the Nuclear Safety and Control Act, relevant regulations, CNSC requirements and expectations, international and domestic standards, and applicable international obligations.

At the end of this process, CNSC staff make a recommendation for a decision on the licence application through an integrated assessment report. A recommended compliance plan for each licence is also developed, and the mitigation measures included in the follow-up program, if applicable, are included in the licence.

10.1.4 CNSC decision

The final decision on a licence is made by either the Commission (e.g., for licences for nuclear power plants) or a CNSC designated officer.

When the decision is to be made by the Commission, public hearings may be held to take into account the views, concerns, and opinions of interested parties, including the applicant and interveners. This is an important part of the process of establishing regulatory policy, making licensing decisions, and implementing programs. CNSC staff recommendations are presented, and the applicant and the public are normally given a chance to make statements.

Most decisions involving major nuclear facilities are made through a two-session[16] public hearing process. The first hearing is for presentations by the applicant and CNSC staff, and the second for intervener presentations. Commission members may ask questions in both cases. The applicant and CNSC staff also attend the second hearing and respond to further questioning by the Commission.

Whether made by the Commission or a CNSC designated officer, the decision will take the form of the granting of a licence or certificate, or else a letter of refusal.

The next section provides more information about the EA process for NPP construction on a new site.

10.2 Site Selection and Site Licensing

This section covers the criteria used for appropriate site selection. A number of regulatory documents in Canada and internationally cover this topic, e.g., [CNSC2008c].

The CNSC must be satisfied that it is feasible to perform the site preparation activities in a manner that will satisfy all health, safety, security, and environmental protection requirements. In addition, the Commission cannot issue a site preparation licence unless a decision as a result of the EA has been made, indicating that the project may proceed; however, these approval

16 The first hearing is known as “Day 1” and the second as “Day 2”, although they may last more than one day each.

processes may proceed in parallel.

The following aspects are considered when evaluating the suitability of a site over the life of a nuclear power plant:

- the potential effects of external events (such as seismic events and floods) and human activity on the site;
- the characteristics of the site and its environment which could influence the pathways of radioactive and hazardous material that may be released; and
- the population density, population distribution, and other characteristics of the region, insofar as they may affect the implementation of emergency measures and the evaluation of risks to individuals, the surrounding population, and the environment.

Under the regulations, an applicant must submit, for any licence, a Project Description of the facility and plans showing the location, perimeter, areas, structures and systems of the facility. An application for a Licence to Prepare Site does not require detailed information or determination of a reactor design; however, high-level design information is required for the environmental assessment that precedes the licensing decision for a Licence to Prepare Site. An application for a Licence to Construct must contain more detailed information about the reactor design and a supporting safety case.

The goal of the CNSC, during the site preparation stage, is to ensure that the site characteristics which may have an impact on health, safety, security, and the environment have been identified, and that these characteristics can and will be taken into consideration in the design, operation, and decommissioning of the proposed nuclear power plant. The technical information arising from the consideration of external events, site-specific characteristics, and supporting assessments is used as input into the design of the nuclear power plant and must be included in the application.

The Canadian Environment Assessment Act, as amended in 2012 [GovCan2012], gives the CNSC decision-making authority on all environmental assessments (EAs) for nuclear projects. Therefore, both environmental assessment and site licensing processes occur concurrently under the authority of the CNSC Commission. This ensures that the information submitted by the proponent can be considered by public and government agencies through a single process and that any appropriate decisions under EA and site licensing can be made by a single body—the CNSC Commission. The Commission process establishes the level of an environmental assessment based on risk and other factors; for example, an application for a site for a new nuclear power plant will almost certainly require a panel review.

The CNSC Commission makes a decision on the EA within the 24-month timeline established for site licensing.

10.3 Construction Licence

During this stage, CNSC undertakes a variety of technical assessments according to a prescribed assessment plan and licensing-related staff review procedures to ensure that each application complies with its corresponding regulatory requirements. The scope and duration of each assessment will vary depending on the type of licence requested. Peer reviews are sometimes used when additional rigour is required.

The licensing technical assessment considers all regulatory criteria as defined by the Nuclear

Safety and Control Act, relevant regulations, CNSC requirements and expectations, international and domestic standards, and applicable international obligations.

The CNSC reviews the submitted application and judges whether the information contained in the application is acceptable and whether the licence applicant is qualified and will make adequate provision for safety, etc., in carrying out the licensed activity (in accordance with 24(4) of the NSCA). If the CNSC accepts this information, it becomes the reference safety case for the plant and will form part of the licensing basis at the construction licence stage. The information provided with the licence application, including the documents to which the application makes reference, constitutes the construction safety case. The requirements for the safety case are listed in detail in [CNSC2012c].

The information required in support of the application to construct a nuclear power plant includes, for example:

- a description of the proposed design for the nuclear power plant, taking into consideration the physical and environmental characteristics of the site;
- environmental baseline data on the site and surrounding area;
- a preliminary safety analysis report showing the adequacy of the design;
- measures to mitigate the effects on the environment and the health and safety of persons that may arise from construction, operation, or decommissioning of the facility;
- information on potential releases of nuclear substances and hazardous materials and proposed measures to control them;
- programs and schedules for recruiting and training operations and maintenance staff;
- and in general, those safety control areas listed in Section 9.5.2.

After the construction licence application has been received, the CNSC performs a comprehensive assessment of the design documentation, the preliminary safety analysis report, the construction program, and any other information required by the regulations. The assessment focusses on determining whether the proposed design and safety analysis, along with other required information, meet regulatory requirements.

Specifically, the evaluation involves rigorous engineering, scientific analysis, and engineering judgment, taking into consideration the CNSC's experience and knowledge of the best practices in nuclear plant design and operation, as gained from existing power plants in Canada and around the world. This review may take place in parallel with the Environmental Assessment and site preparation licensing process. At the end of this process, CNSC staff makes a recommendation for a decision on the licence application, through an integrated assessment report. Occasionally, the recommendations include proposed changes to the regulatory framework to accommodate evolving nuclear technologies. A recommended compliance plan for each licence is also developed, and the mitigation measures included in the follow-up program, if applicable, are included in the licence.

In addition to reviewing the information included in the application, the CNSC also verifies that any outstanding issues from the site preparation stage have been resolved. The CNSC staff's conclusions and recommendations from these reviews are documented in reports submitted to the Commission; the Commission then makes the final decision on the issuance of the construc-

tion licence. As noted earlier, the Commission will not issue a licence unless it is satisfied that the applicant will make adequate provisions to protect health, safety, security and the environment, and to respect the international obligations to which Canada has agreed. As such, it is the responsibility of the applicant to show that there are no major safety issues outstanding at the time the Commission considers the application for a construction licence.

During the construction phase, the CNSC carries out compliance activities to verify that the licensee is complying with the NSCA, with associated regulations, and with its licence. Such compliance activities focus on confirming that plant construction is consistent with the design, that the licensee is demonstrating adequate project oversight and confirming that quality assurance requirements are met, and that the licensee is respecting any requirements of the EA follow-up program.

In the latter part of construction, regulatory attention turns towards the inactive commissioning program (without fuel loaded) and associated activities, whose purpose is to demonstrate to the extent practicable that all systems, structures, and components function in accordance with their design specifications.

10.4 Operating Licence

When applying for a Licence to Operate a nuclear power plant, it is the responsibility of the applicant to demonstrate to the CNSC that it has established the safety management systems, plans, and programs that are appropriate to ensure safe and secure operation. Information required by the CNSC in support of the application for a licence to operate includes, for example:

- a description of the structures, systems, and equipment at the nuclear power plant, including their design and operating conditions;
- the final safety analysis report; and
- proposed measures, policies, methods, and procedures for:
  - commissioning systems and equipment;
  - operating and maintaining the nuclear facility;
  - handling nuclear substances and hazardous materials;
  - controlling the release of nuclear substances and hazardous materials into the environment;
  - preventing and mitigating the effects on the environment and on health and safety resulting from the operation and subsequent decommissioning of the plant;
  - assisting off-site authorities in emergency preparedness activities, including assistance to deal with an accidental off-site release; and
  - nuclear security.

A typical application [OPG2013] would also cover:

- Management system, including safety culture;
- Human performance management;
- Operating performance and corrective action program;
- Fitness for service;
- Probabilistic safety analysis;

- Radiation protection;
- Conventional health and safety;
- Emergency management and fire protection;
- Waste management;
- Safeguards;
- Packaging and transport;
- Community relations and public information;
- Financial guarantees;
- Nuclear liability insurance;
- Open action items.

In addition to assessing the information included in the application to operate the nuclear power plant, the CNSC also verifies that any outstanding issues from the construction licensing stage have been resolved.

The CNSC staff's conclusions and recommendations from these reviews are documented in reports submitted to the Commission, which then makes the final decision on issuance of the operating licence.

The Licence to Operate will enable the operator to begin active commissioning. The purpose of the commissioning activities is to demonstrate that the plant has been constructed in accordance with the design and that the systems, structures, and components important to safety are functioning in accordance with their design specifications. The initial operating licence is typically issued with conditions (hold points) to load nuclear fuel, permit reactor start-up, and operation at power in steps up to the design rating of the plant. All the relevant commissioning tests must be satisfactorily completed before the hold points can be released.

During the subsequent long-term operation of the plant, the CNSC carries out compliance activities in order to verify that the licensee is complying with the NSCA, associated regulations, and its licence terms. If the compliance activities identify any non-compliance or adverse trend, there is a range of possible actions that the CNSC can take, from a request for licensee action to prosecutions.

10.4.1 Ongoing oversight

Operating NPPs are subject to ongoing regulatory monitoring, screening, and inspections. Canadian CANDU plants have resident full-time CNSC inspectors on-site to provide immediate interaction with the operator and to view the station and equipment first-hand.

Aspects of continuing CNSC oversight include:

- Informal information exchange;
- Attending industry working groups as observers;
- Periodic formal audits and inspections of plant operation and management;
- Planned routine assessments and evaluations;
- Reactive inspections following events;
- Formal correspondence;
- Monitoring of progress on CANDU Safety Issues and on specific station action items;
- Conducting an annual review of the safety performance of NPPs;
- Revision to the Licence Condition Handbooks;

- Enforcement actions;
- Orders (legal instruments);
- Licence amendments initiated by CNSC staff;
- Licence amendments or renewals initiated by licensees; and
- Commission meetings and hearings.

10.4.2 Operating licence renewal and refurbishment

There are two longer-term activities which provide an opportunity to ensure that a plant continues to meet regulatory requirements.

Operating licences are typically renewed about every five years in Canada. This requires a review, update, and resubmission of the safety case to reflect changes in plant design and to assess the plant against evolving regulatory requirements. The status of Action Items, CANDU Safety issues, station-specific items, station safety performance, operating experience, quality assurance, and other items are all reviewed at the time of renewal of an operating licence.

CANDU plants can be refurbished by replacement of the fuel channels, typically after about 25 years of operation. This action triggers a much more extensive comparison of the plant against modern standards, as described in Section 9.5.6.

10.5 Licence to Decommission and Return Site to Green Site

At the end of a nuclear power plant's useful life, it will be necessary to decommission the facility. This will require a separate licence from the Commission. Information on decommissioning plans and financial guarantees will, in practice, have been taken into account at all stages of licensing (site preparation, construction, and operation) [CNSC2008a]. Factors taken into account when evaluating an application to decommission a nuclear power plant include, but are not limited to:

- the major components and systems within the facility, which must be properly considered during decommissioning planning;
- the design features that will facilitate decommissioning activities and reduce the spread of contamination during operation;
- the expected levels of activation and contamination within the facility following the end of operation;
- an assessment of structures to ensure that they are capable of being maintained for the proposed period of storage and monitoring;
- the disposal of some of the nuclear materials and radiation devices (e.g., fresh fuel, spent fuel, heavy water, water contaminated with tritium, and other prescribed nuclear materials); and
- the quantities or volumes of wastes of all types (radioactive and hazardous) expected during decommissioning activities.

In addition, the licensees must show that they have sufficient funds to decommission the plant, provide for the long-term management of spent nuclear fuel, and provide continuing environmental monitoring and maintenance of the site for the duration of the licence.

11 Problems

1. Tokai-Mura, 1999: Locate the following material: International Atomic Energy Agency, Report on the Preliminary Fact Finding Mission Following the Accident at the Nuclear Fuel Processing Facility in Tokaimura, Japan; IAEA report, 1999. You may also find or use other documents as well. Assess the accident in terms of regulatory effectiveness, using some of the ideas in this chapter. Propose lessons learned. Which aspects of regulatory performance were also apparent after the Fukushima accident?
2. Compare the approaches taken by the USNRC and the CNSC with respect to large Loss of Coolant Accident (LOCA) regulatory acceptance criteria.
    a. Find out what the acceptance criteria are and where they are documented. Note: not all Canadian criteria are set by the CNSC; you may have to look at CANDU safety reports.
    b. Both Canadian and U.S. practices set limits on sheath oxidation in a LOCA to prevent embrittlement on rewet by Emergency Core Cooling (ECC). Compare the two criteria and explain the rationale in each case.
    c. Find the requirements on shutdown systems for both the United States and Canada. What is the typical reliability of the shutdown system in each case? How are postulated impairments of the shutdown system handled in each case?
3. Review the U.S. General Design Criteria (GDC) in 10CFR, Appendix A to part 50. Which design criteria (if any) would be *intrinsically* difficult for CANDU to meet? If you find any such criteria, what is the safety concern that these GDCs address, and how is that concern addressed in CANDU design?
4. Locate the U.K. Safety Assessment Principles issued by HSE. Compare and contrast the requirements for safety systems with those in CNSC document RD-337. Which ideas are common? Which are different? (Compare the underlying requirement, not the exact wording).

12 Appendix A—Examples of U.K. Safety Assessment Principles

This Appendix lists some examples of U.K. Safety Assessment Principles which illustrate the non-prescriptive technology-neutral approach. The text of the SAP is in **bold** and the commentary in normal typeface.

==========

"Engineering principles: design for reliability Single failure criterion EDR.4

During any normally permissible state of plant availability no single random failure, assumed to occur anywhere within the systems provided to secure a safety function, should prevent the performance of that safety function.

175 Consequential failures resulting from the assumed single failure should be considered as an integral part of the single failure. Further discussion of the single-failure criterion is given in IAEA Safety Standard NS-G-1.2"

==========

"Engineering principles: safety systems: Diversity in the detection of fault sequences ESS.7

The protection system should employ diversity in the detection of fault sequences, preferably by the use of different variables, and in the initiation of the safety system action to terminate the sequences.

342 This principle applies in particular to U.K. civil nuclear power reactor safety systems and in particular to high-integrity safety systems."

==========

"Engineering principles: reactor core Shutdown systems ERC.2

At least two diverse systems should be provided for shutting down a civil reactor.

444 Where a shutdown system is also used for the control of reactivity, a suitable and sufficient shutdown margin should be maintained at all times.

445 Reactor shutdown and subsequent hold-down should not be inhibited by mechanical failure, distortion, erosion, corrosion, etc., of plant components, or by the physical behaviour of the reactor coolant, under normal operation or design basis fault conditions."

==========

This last SAP was part of the basis for fitting a second shutdown mechanism (large-volume boron injection tanks) to the Sizewell-B PWR.

13 Appendix B—Information Required in Licence Applications

(Construction and Operating Licences in Canada, as Examples)

From [GovCan2012a]

Licence to Construct

An application for a licence to construct a Class I nuclear facility shall contain the following information in addition to the information required by section 3:

(a) a description of the proposed design of the nuclear facility, including the manner in which the physical and environmental characteristics of the site are taken into account in the design;
(b) a description of the environmental baseline characteristics of the site and the surrounding area;
(c) the proposed construction program, including its schedule;
(d) a description of the structures proposed to be built as part of the nuclear facility, including their design and their design characteristics;
(e) a description of the systems and equipment proposed to be installed at the nuclear facility, including their design and their design operating conditions;
(f) a preliminary safety analysis report demonstrating the adequacy of the design of the nuclear facility;
(g) the proposed quality assurance program for the design of the nuclear facility;
(h) the proposed measures to facilitate Canada's compliance with any applicable safeguards agreement;
(i) the effects on the environment and the health and safety of persons that may result from the construction, operation and decommissioning of the nuclear facility, and the measures that will be taken to prevent or mitigate those effects;
(j) the proposed location of points of release, the proposed maximum quantities and concentrations, and the anticipated volume and flow rate of releases of nuclear substances and hazardous substances into the environment, including their physical, chemical and radiological characteristics;
(k) the proposed measures to control releases of nuclear substances and hazardous substances into the environment;
(l) the proposed program and schedule for recruiting, training and qualifying workers in respect of the operation and maintenance of the nuclear facility; and
(m) a description of any proposed full-scope training simulator for the nuclear facility.

Licence to Operate

An application for a licence to operate a Class I nuclear facility shall contain the following information in addition to the information required by section 3:

(a) a description of the structures at the nuclear facility, including their design and their design operating conditions;
(b) a description of the systems and equipment at the nuclear facility, including their design and their design operating conditions;
(c) a final safety analysis report demonstrating the adequacy of the design of the nuclear facility;
(d) the proposed measures, policies, methods and procedures for operating and maintaining the nuclear facility;
(e) the proposed procedures for handling, storing, loading and transporting nuclear substances and hazardous substances;
(f) the proposed measures to facilitate Canada's compliance with any applicable safeguards agreement;
(g) the proposed commissioning program for the systems and equipment that will be used at the nuclear facility;
(h) the effects on the environment and the health and safety of persons that may result from the operation and decommissioning of the nuclear facility, and the measures that will be taken to prevent or mitigate those effects;
(i) the proposed location of points of release, the proposed maximum quantities and concentrations, and the anticipated volume and flow rate of releases of nuclear substances and hazardous substances into the environment, including their physical, chemical and radiological characteristics;
(j) the proposed measures to control releases of nuclear substances and hazardous substances into the environment;
(k) the proposed measures to prevent or mitigate the effects of accidental releases of nuclear substances and hazardous substances on the environment, the health and safety of persons and the maintenance of security, including measures to
(i) assist off-site authorities in planning and preparing to limit the effects of an accidental release,
(ii) notify off-site authorities of an accidental release or the imminence of an accidental release,
(iii) report information to off-site authorities during and after an accidental release,
(iv) assist off-site authorities in dealing with the effects of an accidental release, and
(v) test the implementation of the measures to prevent or mitigate the effects of an accidental release;
(l) the proposed measures to prevent acts of sabotage or attempted sabotage at the nuclear facility, including measures to alert the licensee to such acts;
(m) the proposed responsibilities of and qualification requirements and training program for workers, including the procedures for the requalification of workers; and
(n) the results that have been achieved in implementing the program for recruiting, training and qualifying workers in respect of the operation and maintenance of the nuclear facility.

14 References

[Ahearne1988] J. F. Ahearne, "A Comparison between Regulation of Nuclear Power in Canada and the United States", *Progress in Nuclear Energy* 22(3), 215-229 (1988).

[Andrews2012] L. Andrews, "Licensing New Major Facilities", Presentation at the *New Energy Forum*, Toronto, Canada, March 26-27, 2012.

[Apostolakis2004] G. E. Apostolakis, "How Useful is Quantitative Risk Assessment?" *Risk Analysis* 24(3), 515-520 (2004).

[Barón1998] J. H. Barón, C. E. Chiossi, and H. R. Vallerga, "PSA-Based Regulatory Approach in Argentina", Presented to *International Conference on Probabilistic Safety Assessment and Management (PSAM 4)*, New York, USA, September 13-18, 1998.

[Buck1983] A. L. Buck, *A History of the Atomic Energy Commission*, U.S. Department of Energy report DOE/ES-0003/l, July 1983.

[Bujor2010] A. Bujor, G. Rzentkowski, and D. Miller, *Development of Risk-Informed Regulatory Positions on CANDU Safety Issues, Part I: Methodology Development for Risk Estimation and Evaluation*, International Atomic Energy Agency report IAEA-TECDOC-1650, June 2010.

[CEAA2012] First Session, Forty-First Parliament, 60-61 Elizabeth II, 2011-2012; Statutes of Canada 2012, Chapter 19: *An Act to Implement Certain Provisions of the Budget Tabled in Parliament on March 29, 2012 and Other Measures*, assented to June 29, 2012, Bill C-38.

[Charak, 1995] I. Charak and P. H. Kier, *CANDU Reactors, Their Regulation in Canada, and the Identification of Relevant NRC Safety Issues*, Argonne National Laboratory report NUREG/CR-63 15 and ANL-9515, April 1995 (prepared for U.S. Nuclear Regulatory Commission).

[CNSC1977] Canadian Nuclear Safety Commission, *The Use of Two Shutdown Systems in Reactors*, AECB report R-10, January 1977.

[CNSC1991] Canadian Nuclear Safety Commission, *Requirements for Containment Systems for CANDU Nuclear Power Plants,* AECB report R-7, February 1991.

[CNSC1991a] Canadian Nuclear Safety Commission, *Requirements for Shutdown Systems for CANDU Nuclear Power Plants,* AECB report R-8, February 1991.

[CNSC1991b] Canadian Nuclear Safety Commission, Requirements for Emergency Core Cooling Systems for CANDU Nuclear Power Plants, AECB report R-9, February 1991.

[CNSC2000] Canadian Nuclear Safety Commission, *Considering Cost-Benefit Information*, CNSC Regulatory Policy P-242, October 2000.

[CNSC2003] Canadian Nuclear Safety Commission, *Reporting Requirements for Operating Nuclear Power Plants*, CNSC report S-99, March 2003.

[CNSC2006] Canadian Nuclear Safety Commission, *Severe Accident Management Programs for Nuclear Reactors*, CNSC report G-306, May 2006.

[CNSC2008] Canadian Nuclear Safety Commission, *Design of New Nuclear Power Plants*, CNSC

report RD-337, November 2008. Updated in 2014: see [CNSC2014]

[CNSC2008a] Canadian Nuclear Safety Commission, *Licensing Process for New Nuclear Power Plants in Canada,* CNSC report INFO-0756, Rev. 1, May 2008.

[CNSC2008b] Canadian Nuclear Safety Commission, *Safety Analysis for Nuclear Power Plants,* CNSC report RD-310, February 2008.

[CNSC2008c] Canadian Nuclear Safety Commission, *Site Evaluation for New Nuclear Power Plants,* CNSC report RD-346, November 2008.

[CNSC2008d] Canadian Nuclear Safety Commission, *Life Extension of Nuclear Power Plants*, CNSC report RD-360, February 2008.

[CNSC2010] Government of Canada, *Canadian National Report for the Convention on Nuclear Safety, Fifth Report*, Canadian Nuclear Safety Commission report INFO-0805, September 2010.

[CNSC2010a] Canadian Nuclear Safety Commission, *Licensing Basis Objective and Definition*, CNSC report INFO-0795, January 2010.

[CNSC2011] Canadian Nuclear Safety Commission, *CNSC Fukushima Task Force Report*, CNSC report INFO-0824, October 2011.

[CNSC2011a] Canadian Nuclear Safety Commission, *CNSC Staff Action Plan on the CNSC Fukushima Task Force Recommendations*, CNSC report INFO-0828, December 2011.

[CNSC2012] Canadian Nuclear Safety Commission, *Pre-Licensing Review of a Vendor's Reactor Design*, CNSC report GD-385, May 2012.

[CNSC2012a] Canadian Nuclear Safety Commission, *Reliability Programs for Nuclear Power Plants,* Licence Application Guide, CNSC report RD/GD-98, August 2012.

[CNSC2012b] Canadian Nuclear Safety Commission, *Guidance on Safety Analysis for Nuclear Power Plants*, CNSC report GD-310, March 2012.

[CNSC2012c] Canadian Nuclear Safety Commission, *Licence to Construct a Nuclear Power Plant,* Licence Application Guide, CNSC report RD/GD-369, August 2012.

[CNSC2013] Canadian Nuclear Safety Commission, *CNSC Licensing Process,* CNSC web site, January 2013.

[CNSC2014] Canadian Nuclear Safety Commission, *Design of Reactor Facilities: Nuclear Power Plants*, CNSC report REGDOC-2.5.2, May 2014.

[CSA1997] Canadian Standards Association, *Risk Management: Guideline for Decision-Makers,* CSA report CAN/CSA-Q850-97, October 1997.

[Farmer1967] F. R. Farmer, "Reactor Safety and Siting: A Proposed Risk Criterion", *Nuclear Safety*, 8(6), Nov.-Dec. 1967.

[GovCan1985] Government of Canada, *Nuclear Liability Act*, R.S.C., 1985, c. N-28, published by the Minister of Justice.

[GovCan2007] Government of Canada, *Radiation Protection Regulations*, published by the Minister of Justice, SOR/2000-203, last amended on September 18, 2007.

[GovCan2008] Government of Canada, *General Nuclear Safety and Control Regulations*, pub-

lished by the Minister of Justice, SOR/2000-202, last amended on April 17, 2008.

[GovCan2010] Government of Canada, *Nuclear Security Regulations*, SOR/2000-209, published by the Minister of Justice, last amended on May 13, 2010.

[GovCan2010a] Government of Canada, *Nuclear Non-Proliferation Import and Export Control Regulations*, SOR/2000-210, published by the Minister of Justice, last amended on May 13, 2010.

[GovCan2012] Government of Canada, *Canadian Environmental Assessment Act, 2012*, S.C. 2012, c. 19, s. 52, published by the Minister of Justice, last amended on November 25, 2013.

[GovCan2012a] Government of Canada, *Class I Nuclear Facilities Regulations*, SOR/2000-204, last amended on December 14, 2012.

[GovCan2013] Government of Canada, *Nuclear Safety and Control Act*, S.C. 1997, c. 9, published by the Minister of Justice, last amended on July 3, 2013.

[GovCan2013a] *Canadian National Report for the Convention on Nuclear Safety*, Sixth Report, August 2013.

[HSE1992] Health and Safety Executive, *The Tolerability of Risk from Nuclear Power Stations*, The Stationery Office, 1992 ISBN 0 11 886368 1.

[HSE2001] Health and Safety Executive, *Reducing Risks, Protecting People: HSE's Decision-Making Process*, HSE report, 2001.

[HSE2002] Health and Safety Executive, Nuclear Safety Directorate, *Technical Assessment Guide: Foreword*, Issue 002, HSE report T/AST/FWD, July 2002.

[HSE2006] Health and Safety Executive, *Safety Assessment Principles for Nuclear Facilities*, HSE report, 2006 edition, Revision 1.

[HSE2008] Health and Safety Executive, *New Nuclear Power Stations, Generic Design Assessment—Guidance to Requesting Parties*, HSE report, Version 3, August 2008.

[Hurst1972] D. G. Hurst and F. C. Boyd "Reactor Licensing and Safety Requirements", Paper 72-CNA-102, *12th Annual Conference of the Canadian Nuclear Association*, Ottawa, Ontario, June 1972.

[IAEA1983] International Atomic Energy Agency, *IAEA Safeguards: Aims, Limitations, Achievements,* IAEA report IAEA/SG/INF/4, 1983.

[IAEA1992] International Nuclear Safety Advisory Group, *The Chernobyl Accident: Updating of INSAG-1*, IAEA report INSAG-7, November 1992.

[IAEA1998] International Atomic Energy Agency, *The Evolution of IAEA Safeguards,* International Verification Series No. 2, IAEA report, 1998.

[IAEA1998a] International Atomic Energy Agency, *Design Measures to Facilitate Implementation of Safeguards at Future Water Cooled Nuclear Power Plants*, IAEA Technical report Series No. 392, IAEA, 1998.

[IAEA1999] International Nuclear Safety Advisory Group, *Basic Safety Principles for Nuclear Power Plants*, IAEA report INSAG-12, October 1999.

[IAEA2000] International Atomic Energy Agency, *Legal and Governmental Infrastructure for Nuclear, Radiation, Radioactive Waste and Transport Safety*, IAEA Safety Standard GS-R-1, September 2000.

[IAEA2002] International Atomic Energy Agency, *Review and Assessment of Nuclear Facilities by the Regulatory Body*, IAEA Safety Guide GS-G-1.2, August 2002.

[IAEA2002a] International Atomic Energy Agency, *Organization and Staffing of the Regulatory Body for Nuclear Facilities,* IAEA Safety Guide GS-G-1.1, September 2002.

[IAEA2002b] International Atomic Energy Agency, *Regulatory Inspection of Nuclear Facilities and Enforcement by the Regulatory Body*, IAEA Safety Guide GS-G-1.3, September 2002.

[IAEA2002c] International Atomic Energy Agency, *Regulatory Control of Nuclear Power Plants*, IAEA Training Course Series #15, 2002.

[IAEA2002d] International Atomic Energy Agency, *IAEA Safeguards Glossary – 2001 Edition,* International Verification Series No. 3, IAEA report, 2002.

[IAEA2004] International Atomic Energy Agency, *Format and Content of the Safety Analysis Report for Nuclear Power Plants*, IAEA Safety Guide GS-G-4.1, May 2004.

[IAEA2004a] International Atomic Energy Agency, *Design of Reactor Containment Systems for Nuclear Power Plants*, IAEA Safety Guide NS-G-1.10, 2004.

[IAEA2006] International Atomic Energy Agency, *The Management System for Facilities and Activities Safety Requirements*, IAEA report GS-R-3, July 2006.

[IAEA2006a] International Atomic Energy Agency, *Fundamental Safety Principles*, IAEA report SF-1, November 2006.

[IAEA2007] International Atomic Energy Agency, *IAEA Safeguards: Staying Ahead of the Game,* IAEA report, 2007.

[IAEA2007a] International Atomic Energy Agency, *Generic Safety Issues for Nuclear Power Plants with Pressurized Heavy Water Reactors and Measures for their Resolution*, IAEA TECDOC-1554, June 2007.

[IAEA2010] International Atomic Energy Agency, *International Conference on Challenges Faced by Technical and Scientific Support Organizations in Enhancing Nuclear Safety and Security*, Tokyo, Japan, 25–29 October 2010; IAEA report STI/PUB/1519, September 2011.

[IAEA2011] International Atomic Energy Agency, *Establishing the Safety Infrastructure for a Nuclear Power Programme - Specific Safety Guide*, IAEA report SSG-16, STI/PUB/1507, Vienna, December 2011.

[IAEA2011a] International Atomic Energy Agency, *Verifying Compliance with Nuclear Non-Proliferation Undertakings,* IAEA Safeguards and Additional Protocols, IAEA report, September 2011.

[IAEA2011b] International Atomic Energy Agency, *Non-Proliferation of Nuclear Weapons and Nuclear Security—Overview of Requirements for States with Limited Nuclear Material and Activities*, IAEA report, September 2011.

[IAEA2012] International Atomic Energy Agency, *Project Management in Nuclear Power Plant Construction: Guidelines and Experience*, IAEA report STI/PUB/1537, 2012.

[IAEA2012a] International Atomic Energy Agency, *Long-Term Structure of the IAEA Safety Standards and Current Status*, IAEA report from http://www-ns.iaea.org/committees/files/CSS/205/status.pdf, December 2012.

[IAEA2012b] International Atomic Energy Agency, *Licensing the First Nuclear Power Plant*, IAEA report INSAG-26, Vienna, 2012.

[IAEA2013] International Atomic Energy Agency, *Periodic Safety Review for Nuclear Power Plants*, IAEA report SSG-25, Vienna, 2013.

[IAEA2014] International Atomic Energy Agency, International Safeguards in the Design of Nuclear Reactors, IAEA Report NP-T-2.9, Vienna, 2014.

[Japan1948] *The National Government Organization Law* (Law No. 120 of 1948, as amended).

[Japan2012] The National Diet of Japan, *The Fukushima Nuclear Accident Independent Investigation Commission*, Executive Summary, report, 2012.

[Japan2012a] Investigation Committee on the Accident at the Fukushima Nuclear Power Stations, *Final Report,* July 2012.

[Kemeny1979] J. G. Kemeny, *Report of the President's Commission on the Accident at TMI*, 1979.

[Laaksonen2008] J. Laaksonen, "General Overview of Licensing Process and Regulatory Oversight in the Design and Construction Stage of a Nuclear Power Plant", presented at the *Workshop on Licensing and Regulatory Oversight of New Nuclear Builds*, Helsinki and Olkiluoto, September 1–4, 2008.

[Laaksonen2009] J. Laaksonen, "Regulatory Oversight of Olkiluoto 3 (EPR) Construction: Lessons Learnt", presented at *20th International Conference on Structural Mechanics in Reactor Technology*, Otaniemi, Finland, August 9–14, 2009.

[ONR2011] Office for Nuclear Regulation, *Licence Condition Handbook*, October 2011.

[OPG2013] Ontario Power Generation, *Darlington Nuclear Generating Station: Application for Licence Renewal*, December 2013.

[Popov2012] N. Popov, "Licensing Challenges for New Countries Entering Nuclear Power Program", paper ICONE20POWER2012-55244, *Proceedings, 20th International Conference on Nuclear Engineering and ASME 2012 Power Conference (ICONE20 & POWER2012)*, Anaheim, California, USA, July 30–August 3, 2012.

[Rogovin1980] M. Rogovin and G. T. Frampton, *Three Mile Island: A Report to the Commissioners and to the Public*, Nuclear Regulatory Commission Special Inquiry Group, January 1980.

[Sims1980] G. H. E. Sims, *A History of the Atomic Energy Control Board,* AECB Publication INFO-0026, July 1980; Canadian Government Publishing Centre, Catalog CC172-3/1981E.

[Slovic1987] P. Slovic, "Perception of Risk", *Science, New Series*, 236(4799), pp. 280-285 (April 17, 1987).

[Starr1969] C. Starr, "Social Benefit versus Technological Risk*", Science, New Series*, 165(3899), pp. 1232-1238 (Sep. 19, 1969).

[STUK2006] Säteilyturvakeskus, *Management of Safety Requirements in Subcontracting During the Olkiluoto 3 Nuclear Power Plant Construction Phase*, STUK Investigation Report 1/06,

Translation 1.9.2006, July 2006.

[Tanigawa2012] K. Tanigawa, Y. Hosoi, N. Hirohashi, Y. Iwasaki, and K. Kamiya, "Loss of Life after Evacuation: Lessons Learned from the Fukushima Accident", *The Lancet*, 379(9819), pp. 889–891 (2012).

[Tiippana2010] P. Tiippana, "STUK Experience in Licensing and Oversight of New Reactors", presented at the *ELFORSK Conference*, January 21, 2010.

[UK1974] United Kingdom, *Health and Safety at Work*, etc., Act 1974, Legislation.

[UK2009] United Kingdom Cabinet Office, *Public Bodies 2009*. See http://www.civilservice.gov.uk/about/resources/ndpb.

[USNRC1978] United States Nuclear Regulatory Commission, *Standard Format and Content of Safety Analysis Reports for Nuclear Power Plants – LWR Edition*, Regulatory Guide 1.70, Revision 3, November 1978.

[USNRC1987] United States Nuclear Regulatory Commission, *Standard Review Plan for the Review of Safety Analysis Reports for Nuclear Power Plants - LWR Edition*, USNRC report NUREG-0800, June 1987.

[USNRC2002] United States Nuclear Regulatory Commission, *Regulatory Guide 1.174 - An Approach for Using Probabilistic Risk Assessment in Risk-Informed Decisions on Plant-Specific Changes to the Licensing Basis*, November 2002.

[USNRC2009] United States Nuclear Regulatory Commission, *Nuclear Power Plant Licensing Process*, USNRC report NUREG/BR-0298, Rev. 2, July 2009.

[USNRC2011] United States Nuclear Regulatory Commission, *Nuclear Regulatory Legislation - 111th Congress; 2nd Session*, USNRC report NUREG-0980, January 2011.

[USNRC2012] United States Nuclear Regulatory Commission, *Licenses, Certifications, And Approvals For Nuclear Power Plants*, Code of Federal Regulations 10 CFR Part 52, 2012.

[USNRC2012a] United States Nuclear Regulatory Commission, *Advisory Committee on Reactor Safeguards*, Code of Federal Regulations 10 CFR Part 1.13, 2012.

[USNRC2012b] United States Nuclear Regulatory Commission, *General Design Criteria for Nuclear Power Plants,* Code of Federal Regulations 10 CFR Appendix A to Part 50, 2012.

[USNRC2012c] United States Nuclear Regulatory Commission, *Standard Review Plan for the Review of Safety Analysis Reports for Nuclear Power Plants: LWR Edition*, USNRC report NUREG-0800, formerly issued as NUREG-75/087, 2012.

[USNRC2012d] United States Nuclear Regulatory Commission, *Domestic Licensing of Production And Utilization Facilities,* Code of Federal Regulations 10 CFR Part 50, 2012.

[WENRA2000] Western European Nuclear Regulators' Association, *Nuclear Safety in EU Candidate Countries*, WENRA report, October 2000.

[WENRA2007] Western European Nuclear Regulators' Association, Reactor Harmonization Working Group, *WENRA Reactor Safety Reference Levels*, WENRA report, January 2007.

[WENRA2010] Western European Nuclear Regulators' Association, *WENRA Statement on Safety Objectives for New Nuclear Power Plants*, November 2010.

[WENRA2011] Western European Nuclear Regulators' Association, *"Stress Test" Specifications—Proposal by the WENRA Task Force*, April 2011.

15 Glossary

ACNS	Advisory Committee on Nuclear Safety (Canada, historical)
ACRS	Advisory Committee on Reactor Safeguards (USA)
AEC	Atomic Energy Commission (USA)
AECA	Atomic Energy Control Act (Canada)
AECB	Atomic Energy Control Board (Canada)
ALARA	As Low as Reasonably Achievable
ALARP	As Low as Reasonably Practical (UK)
ASLB	Atomic Safety and Licensing Board (USA)
BDBA	Beyond Design Basis Accident
BSL	Basic Safety Limit (UK)
BSO	Basic Safety Objective (UK)
BWR	Boiling Water Reactor
CEAA	Canadian Environmental Assessment Act
CFR	Code of Federal Regulations (USA)
CNSC	Canadian Nuclear Safety Commission
C/S	Containment and Surveillance
CSA	Canadian Standards Association
DBA	Design Basis Accident
DIV	Design Information Verification
EA	Environment Agency (UK)
EA	Environmental Assessment (Canada)
ECC	Emergency Core Cooling
EIS	Environmental Impact Statement
ENSREG	European Nuclear Safety Regulators Group
EU	European Union
GAR	Global Assessment Report
GDA	Generic Design Assessment (UK)
GDC	General Design Criteria (US)
GAI	Generic Action Item

HSE	Health and Safety Executive (UK)
IIP	Integrated Implementation Plan
IAEA	International Atomic Energy Agency
INPO	Institute of Nuclear Power Operations
INSAG	International Safety Advisory Group (IAEA)
IRRS	Integrated Regulatory Review Service (IAEA)
LBLOCA	Large Break Loss of Coolant Accident
LNT	Linear No Threshold (dose response hypothesis)
LOCA	Loss of Coolant Accident
LWR	Light Water Reactor
MBA	Material Balance Area
MDEP	Multinational Design Evaluation Programme
MPMO	Major Projects Management Office
MUF	Material Unaccounted For
NDPB	Non Departmental Public Body (UK)
NISA	Nuclear and Industrial Safety Agency (Japan)
NPP	Nuclear Power Plant
NRA	Nuclear Regulation Authority (Japan)
NRU	National Research Universal (reactor)
NRX	National Research Experimental (reactor)
NPP	Nuclear Power Plant
ONR	Office for Nuclear Regulation (UK)
PHWR	Pressurized Heavy Water Reactor
PWR	Pressurized Water Reactor
PSA	Probabilistic Safety Analysis
PSR	Periodic Safety Review
RCS	Reactor Coolant System
RIDM	Risk-Informed Decision Making
RSAC	Reactor Safety Advisory Committee (Canada, historical)
SAPs	Safety Assessment Principles (UK)
SAM	Severe Accident Management
SER	State Evaluation Report
SFAIRP	So Far As Is Reasonably Practicable (UK)

SIR	Safeguards Implementation Report
SIS	Systems Important to Safety
SRP	Standard Review Plan (US)
SRP	Staff Review Procedure (Canada)
SSC	Systems, Structures and Components
STUK	Säteilyturvakeskus (Radiation and Nuclear Safety Authority, Finland)
Sv	Sievert, a unit of radiation dose
TAG	Technical Assessment Guide (UK)
TOR	Tolerability of Risk (UK)
TSO	Technical Support Organization
TMI	Three Mile Island
USNRC	United States Nuclear Regulatory Commission
WENRA	Western European Nuclear Regulators' Association

16 Acknowledgements

We gratefully thank the following reviewers for their hard work and excellent comments during the development of this Chapter. Their feedback has much improved it. Of course the responsibility for any errors or omissions is entirely the authors'.

Glenn Archinoff
Joe Boyadjian
Dave Newland
Terry Rogers

We also thank Diana Bouchard for expertly editing and assembling the final copy.

CHAPTER 17

Fuel

Prepared by

Mukesh Tayal and Milan Gacesa – Independent Consultants

Learning Objectives

The principal learning objectives of this chapter are:

To gain a general understanding of the major mechanisms affecting fuel behaviour under normal operating conditions;

To understand the underlying sciences of the relatively more important phenomena involving fuel, including fission gas release, internal gas pressure, thermal stresses, element deformation, environmentally assisted cracking, lateral vibrations of fuel elements, and fatigue of the bundle assembly weld; and

To be able to perform calculations in the above subject areas to enable predictions.

Summary

Nuclear fuel, like conventional fuel, is responsible for generating heat and transferring the heat to a cooling medium. Unlike conventional fuel, nuclear fuel presents the additional challenge of retaining all the by-products of the heat-generating reaction within its matrix. Conventional fuel releases almost all its combustion by-products into the environment. Experience has shown that at times the integrity of CANDU fuel can be challenged while performing these roles. Eighteen failure mechanisms have been identified, some of which cause fission by-products to be released out of the fuel matrix. Other chapters in this book deal with preventing fission by-products which escape from the fuel matrix from reaching the public. CANDU reactors can locate and discharge fuel assemblies that release fission by-products into the coolant at power to minimize the effect of fuel defects on plant operation and the public. Acceptance criteria are established against which a fuel design is assessed to verify its ability to fulfill the design requirements without failing. A combination of analyzes and tests is used to complete the verification assessments.

Table of Contents

List of Figures

List of Tables

1 Introduction

The principal roles of fuel are to generate heat and to maintain a reasonable geometry so that the coolant can carry that heat away. In addition, because fuel is a significant source of radiological hazard, appropriate fuel integrity needs to be ensured at all times—including during fabrication, operation, postulated accidents, and storage.

The science of the first two of these aspects, the generation and removal of heat, has been discussed in earlier chapters. In the current chapter, we focus on the science of those aspects of fuel that enable its reasonable integrity during normal operating conditions. Fuel integrity during accidents and during abnormal occurrences is covered in another chapter.

This chapter uses CANDU-6 (also called C6) fuel for illustration, as shown in Figure 1. The figure shows a fuel bundle in which fissile uranium is contained in 37 sealed fuel elements which are held together by two welded endplates. Separation of the hot fuel elements from each other, and from the pressure tube, is maintained by pads that are brazed to the fuel sheaths [Page, 1976].

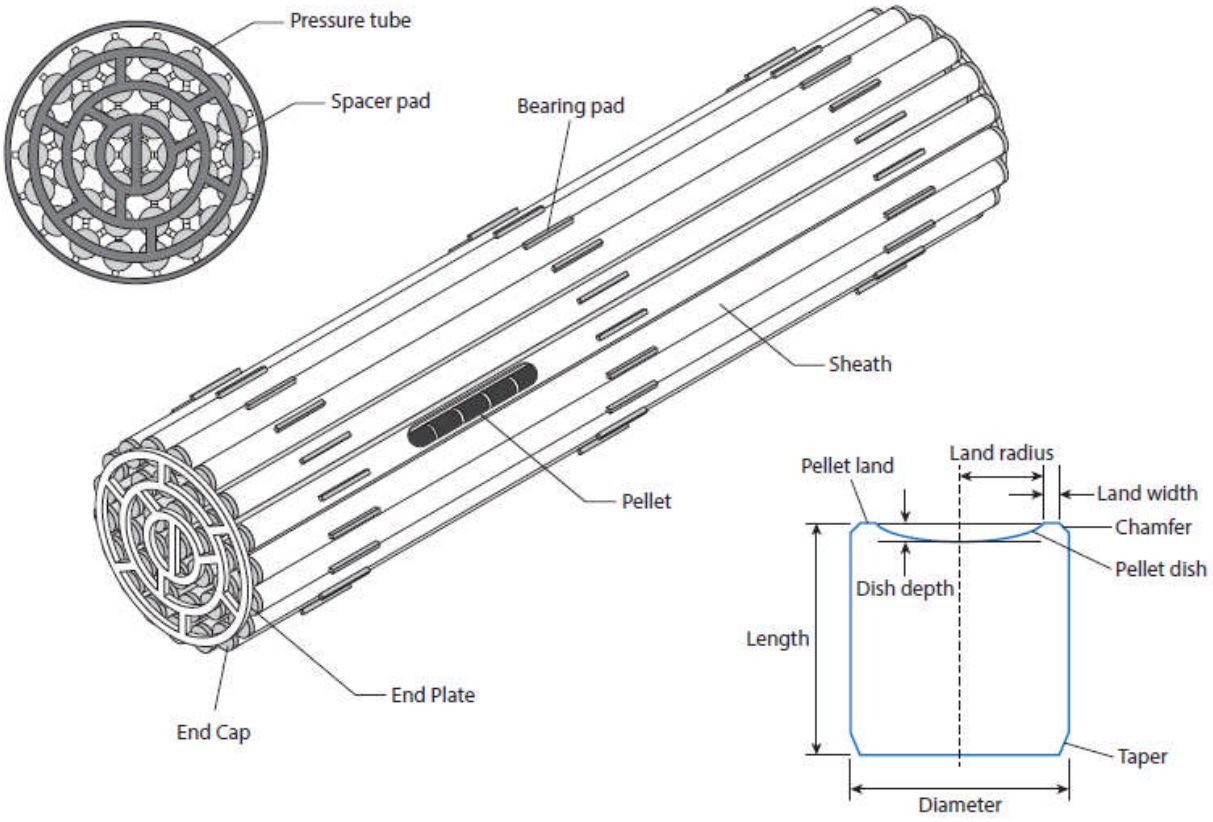

Figure 1 37-element CANDU fuel bundle

Broad overviews of fuel design have been provided in earlier chapters. The focus in this chapter is on the natural-uranium fuel used in current CANDU reactors, using the CANDU-6 reactor for illustration. Chapter 18 covers alternative fuel cycles that have also been considered for application in the CANDU reactor. Chapter 18 also covers, albeit briefly, some aspects of fuel manufacturing, including uranium mining, as part of a discussion on the natural uranium fuel cycle. Chapter 19 describes long-term storage and disposal of irradiated CANDU fuel. Discussion of

radiological hazards is beyond the scope of this chapter and is addressed in another chapter.

2 Overview

Before we can understand the science that underlies fuel integrity and therefore the chosen design, it is important to obtain sufficient background about the operating conditions for which nuclear fuel must be designed and the specific design that has been chosen to operate in them. These factors, in turn, determine which specific scientific disciplines are pertinent to fuel integrity.

2.1 Operating Environment

This section describes certain key illustrative (but not necessarily comprehensive) operating conditions that have major impacts on design choices for fuel and the science that underpins its performance in the reactor.

- Power Intensity: CANDU fuel produces a large amount of power in a small space. In a length of approximately 0.5 m, a fuel element some 13 mm in diameter produces, at its peak, some 30 kW. In comparison, a typical household electrical heater produces approximately 1 kW of heat when it is red hot. Therefore, nuclear fuel is 30 times more intense than the household electrical heater. This high heat intensity is a principal source of thermal and related challenges in nuclear fuel.
- Coolant Temperature: Reactor coolant is at high temperature—about 300° Celsius. This leads to concerns such as corrosion, hydriding, and creep in metals. Corrosion is also influenced by coolant chemistry. Corrosion and hydriding reduce the capability of Zircaloy to carry loads.
- Coolant Velocity: Coolant flows in the pressure tube at high velocity—approximately 10 m/s, or about 36 km/h—and at times this flow is turbulent. This leads to high drag loads and also to a potential for vibration, fatigue, and fretting.
- Embrittlement: Processes such as fast neutrons and hydrogen/deuterium picked up from corrosion tend to embrittle many metals and alloys. Therefore, shortly after insertion in the reactor core, fuel's structural materials have a much diminished capacity to resist tensile strains. These phenomena are important sources of microstructural contributions to structural challenges.
- Fission Products: Fission reaction results in solid and gaseous fission products. These fission products have a larger volume than the original uranium, and their higher volume must be accommodated. Gaseous fission products increase the internal pressure on Zircaloy, and if excessive, this pressure can crack the Zircaloy. In addition, some fission products are corrosive and can aggravate the structural challenges from mechanical loads, especially in materials that become embrittled during irradiation.
- Fuel Management: Natural uranium fuel results in relatively low excess neutronic reactivity; therefore, a CANDU reactor requires frequent addition of new fuel to maintain reactivity (see the earlier chapters on physics). For this reason, a CANDU reactor is refueled on an almost daily basis. Shutting down the reactor every day for refuelling would have a major impact on the total power produced by the reactor. Therefore, CANDU reactors are refueled while they are operating at full power. During on-power fuelling, the reactor coolant carries the new fuel bundle into the C6 fuel channel until it hits an existing bundle in the channel. Therefore, the new as well as the old fuel bun-

dles—the latter potentially more brittle—need to withstand impact loads. On-power fuelling also means that some irradiated fuel bundles are moved from a low-power axial position in the channel to (or through) a higher-powered axial location. This can lead to power-ramp challenges, as described in Section 8.

- Refuelling: The fuel bundle is loaded and unloaded on-power, remotely, through tight spaces, through bends, and sometimes through interrupted (discontinuous) supports. These aspects require tight dimensional control, good dimensional stability, reasonable flexibility, and allowances for wear.
- Power Manoeuvring: The reactor may be required to change its power level periodically to respond to grid demand. Periodic changes in the power extracted from the fuel add another dimension to fatigue considerations.
- Long Duration: A C6 fuel bundle stays in the reactor core for six months to two years. Therefore, the challenging conditions described above must be endured continually for long periods.

2.2 Fuel Design

Fuel is designed to address the operating conditions described above. Each fuel channel of a C6 reactor contains 12 fuel bundles.

Figure 1 shows a typical C6 fuel bundle. Each fuel bundle is made up of 37 fuel elements. Each fuel element consists of a thin cylindrical tube called a sheath, which is made of Zircaloy-4. The sheath encloses about 30 cylindrical pellets of UO_2. A thin coating of a graphite-based compound (called CANLUB) is applied to the inside surface of the sheath to mitigate the harmful effects of power ramps, as described later in Section 8. Each fuel element is sealed at both ends by endcaps that are welded to the sheaths; these welds are called "closure welds". Endplates hold the fuel elements together in the geometric configuration of a fuel bundle. The endplates are welded to the fuel elements; these welds are called "assembly welds". Spacing between individual fuel elements is maintained using spacer pads. Spacing between the fuel bundle and the pressure tube is maintained by bearing pads. The bearing pads and the spacer pads are brazed to the fuel sheaths [Page, 1976; Gacesa *et al.*, 1983].

Figure 1 also shows some key aspects of the internal design of a fuel element. The axial profile of the pellet contains a dish to accommodate thermal expansion of the pellet that occurs because of high temperature during irradiation. To make it easier to insert the pellets into the sheath, (a) a diametric clearance is provided between the pellets and the sheath, and (b) chamfers are provided in the pellets. Axial clearance between the pellet stack and the two endcaps limits or even prevents axial interference between the two. A cavity in the endcap provides space to store fission gas produced during irradiation.

The following are key rationales for some of the chosen features:

- Subdivision of the Bundle: As one illustrative example, a choice was made to subdivide the uranium in the fuel bundle into a number of fuel elements. This permits the coolant to be near the source of the heat at many locations, leading to lower UO_2 temperature and reduced threats from many thermally driven damage mechanisms. At the same time, however, we should avoid excessive subdivision in the form of significantly more numerous but much smaller fuel elements along with additional spacer pads and bearing pads. The latter approach would add zirconium to the bundle, which would, among

other effects, increase parasitic absorption of neutrons; increase fabrication cost; provide additional resistance to flow and hence require bigger and costlier pumps to generate the same flow of reactor coolant; lead to greater potential for fatigue and fretting due to lower resistance of the smaller fuel elements to flow-induced vibrations; and exhibit higher propensity for creep sag of the smaller fuel elements, which could potentially lead to jamming of the fuel bundle in the channel. Increased subdivision also adversely impacts the neutronic-thermal-hydraulic interaction during accidents (coolant void reactivity), and, taken to the extreme, a much smaller element diameter would reduce the available surface area and decrease the efficiency of heat removal by the coolant. Hence, a judicious balance must be struck regarding the degree of subdivision.

- Circular Cross Section of Fuel Elements: As a second illustrative example, the circular cross section of the fuel elements reduces the stress concentration that would otherwise be introduced by non-circular cross sections. This increases the mechanical strength of the fuel elements to resist in-reactor loads.
- Ceramic, High-Density UO_2: A large amount of heat is generated in the uranium fuel under high external coolant pressure; therefore, the uranium must be in a form that will transmit heat efficiently and maintain structural integrity. Ideally, uranium would be used in a metallic form (e.g., uranium-aluminum alloy) to promote better heat transfer. However, uranium metal has two undesirable characteristics: (1) if a fuel sheath were to rupture and hot water from the coolant were to penetrate the fuel element, uranium metal would oxidize rapidly and lose its strength; and (2) uranium metal is also dimensionally unstable because of its anisotropy. Hence, uranium in the form of UO_2 is a good compromise. Although the low thermal conductivity of UO_2 leads to high temperatures in the fuel, its high melting point (about 2840°C) provides a large tolerance to melting. Maximizing the density of UO_2 leads to (1) higher fissile content in the element, hence more energy; (2) improved thermal conductivity and hence lower temperature; and (3) reduced in-reactor densification and hence higher dimensional stability.
- Zircaloy-4: Unlike the enriched uranium used in other types of reactors, CANDU reactors use natural uranium. The latter has much less ^{235}U to undergo fission. Therefore, to sustain the chain reaction, it is essential that neutrons be conserved and that absorption of neutrons by structural materials be minimized. For this reason, the structural components are made from Zircaloy-4, which has a relatively small cross section for neutron absorption. In addition, the structural components are kept as thin as possible, including sheaths that are allowed to collapse if needed under operating pressure and temperature. Zircaloy-4 also has high corrosion resistance, which is important considering the high temperatures and the long residence periods in the reactor. Finally, Zircaloy-4 also has suitable mechanical properties.
- Thin Collapsible Sheaths: As a fifth illustrative example, the sheaths on CANDU fuel are purposely kept very thin, mainly to conserve neutrons. Another benefit of a thin sheath is that it can collapse diametrically under the operating pressure and temperature of the coolant. This improves heat transfer from the pellet to the coolant, which in turn lowers pellet temperature and reduces fission gas release. At the same time, the sheath must be strong enough to carry the in-reactor loads and to avoid forming overly sharp ridges (called longitudinal ridges, described in more detail in a later section of this chapter) which can fail by overstrain or by fatigue.
- Helium Filling Gas: To minimize damage from several mechanisms such as melting, fis-

sion gas pressure, and environmentally assisted cracking, the operating temperature of the pellet should be kept as low as reasonably achievable. Towards that end, empty spaces within a fuel element are filled with gas that has high thermal conductivity. This is called *filling gas*, and helium, or helium mixed with argon and air, is generally used for this purpose. Another advantage of helium is that it has very small atoms that can escape through small faults in joints: if a fuel element is not perfectly sealed by the endcaps during manufacturing, escaping helium can be detected by appropriate sensors during fuel fabrication.

- Internal Shapes and Spaces: Many internal shapes and spaces are carefully chosen to balance a number of conflicting objectives, e.g., to reduce stresses, to provide space for expansion during irradiation, to provide space to store fission gases produced during irradiation, and to promote large-volume, automated, low-cost production. Some such features include the pellet profile, the profile of the sheath/endcap junction, the endcap profile, the diametric clearance between the pellets and the sheath, and the axial clearance between the pellet stack and the endcaps. Several of these aspects are further elaborated upon in later sections of this chapter.
- Manufacturing: Some features are driven primarily by considerations of automation in manufacturing, e.g., resistance welding of endcaps and sheaths and brazing of pads. Both processes enable fast throughputs. Chapter 18 provides additional details of some aspects of fuel manufacturing.
- Ease of Handling: The length of the bundle was chosen primarily to facilitate on-power refuelling, although both the length and weight of the bundle have ergonomic advantages; one individual can lift and carry the bundle by hand.
- Fuel Management: Some important considerations in fuel management are: (a) to maintain neutronic reactivity at the desired level; (b) to achieve reasonable burnup; and (c) to avoid defects due to power ramps. The last aspect is discussed in more detail in a later section.

These configurations were chosen to facilitate the primary objectives of the fuel bundle: to produce heat, to maintain its geometry so that the coolant can carry the heat away, to ensure in-reactor integrity of the fuel elements and the fuel bundle, and to do all this consistently over a lengthy period.

In several other ways as well, the chosen features reflect careful balances among many conflicting requirements, processes, and forces. Fuel design is a complex multidisciplinary optimization process involving reactor physics, thermal-hydraulics, heat transfer, structural mechanics, microstructural processes, geometric stability, and interfacing systems, all under normal, off-normal, and accident conditions.

The choices described above—thin structural materials, high operating temperatures, axial movement of the fuel bundle during on-power fuelling, large in-reactor mechanical forces, and material degradation due to irradiation—all combine to pose unique and significant challenges to the in-reactor integrity of CANDU nuclear fuel under normal operating conditions. An overview of these challenges is given in the next section.

2.3 In-Reactor Challenges

The major challenges to fuel's in-reactor integrity can be grouped into three categories: (1)

thermal challenges, (2) mechanical challenges, and (3) compatibility challenges.

Thermal challenges, if excessive, can potentially cause melting in the pellet or in the structural materials (mainly Zircaloy). Pellet melting can result in (a) escape of additional fission gas from the UO_2 matrix into the pellet-to-sheath gap and (b) thermal expansion of the pellet, causing the sheath to rupture. This combination can send additional radioactive fission products into the coolant. Excessive amounts of radioactive fission products in the coolant could increase the radiological hazard to the health of station staff.

Excessive mechanical damage can potentially cause holes, cracks, or breaks in structural materials, with consequences similar to the thermal challenges described above.

Incompatibility can potentially cause the fuel bundle to jam inside the reactor or in its accessories such as fuel handling equipment, interfering with its proper insertion or eventual removal. Incompatibility can also potentially harm neighbouring or interfacing components through processes such as crevice corrosion.

For these reasons, a major objective in fuel design is to limit the extent of damage from the mechanisms just described. Doing so requires, among other things, assessments of non-linear heat transfer, non-linear stress analyzes, and microstructural processes.

All damage mechanisms are under sufficient control in current CANDU fuels. In most mature CANDU cores, fuel defects typically occur in less than one bundle per year and tend to be caused mostly by fretting due to debris.

The defect rate of CANDU fuel is remarkably low. During 2007–2008, the International Atomic Energy Agency (IAEA) conducted a world-wide survey of fuel defect rates from 1994 to 2006 [IAEA, 2010]. World-wide, water-water energy reactors (WWERs) were found to have a fuel defect rate of 94 defective fuel elements per million discharged (also called ppm, or parts per million). The fuel defect rate was 87 ppm in pressurized water reactors and 65 ppm in boiling water reactors. In comparison, fuel in Canada had a defect rate of 3.5 ppm. The Canadian fuel defect rate is very acceptable—almost in the range of impurities found in most substances—and much lower than for other types of nuclear fuels. This low rate confirms the basic soundness of the practices built into all major aspects of Canadian fuel, from research to development, to design, to fabrication, to operation, and to feedbacks among them.

Nevertheless, several defect excursions have occurred in the past, and it is illustrative to examine the historical causes of significant fuel defects. Figure 2 shows readily available illustrative data on fuel bundles which have been damaged, mostly in defect excursions in power reactors during the first three decades of commercial nuclear power, although the figure also includes some data that would not strictly be considered to represent a major defect excursion.

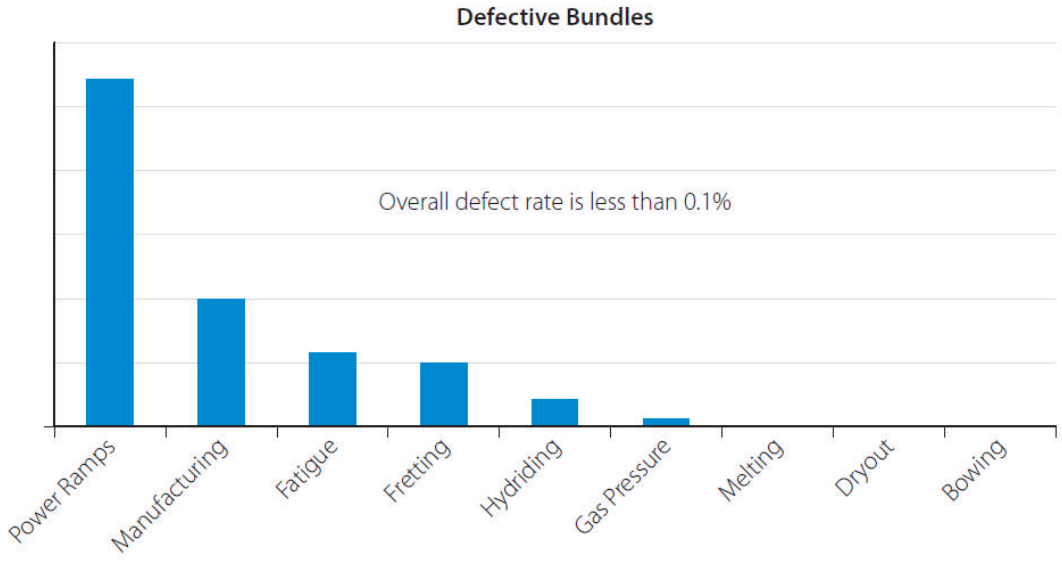

Note: Above data exclude failures due to debris

Figure 2 Causes of defects in CANDU fuel (1967–1996)

The International Atomic Energy Agency has defined a "defect excursion" as one in which 10 or more fuel bundles fail within a 12-month period [IAEA, 2010]. Figure 2 does have limitations: it focusses on defects related to design and/or operation, mostly in Canada, and it excludes defects due to fretting by debris. One can postulate that for any given damage mechanism, the amount of damage is an indicator of how close its failure threshold is to the operating conditions—the closer one operates the fuel to the defect threshold of a specific damage mechanism, the higher will be the likelihood of damage from that mechanism. Figure 2 demonstrates that in the past, power ramps have been a dominant damage mechanism in CANDU fuels.

The underlying science of the relatively more important challenges to fuel integrity is described in later sections of this chapter. Table 1 provides some illustrative design data for C6 fuel. Likewise, Table 2 provides some illustrative data for the physical, thermal, and mechanical properties of CANDU fuel; these can be used for illustrative calculations of fuel performance.

Table 1 Illustrative design data for C6 fuel

[Major Source: Nuclear Engineering International, September 2006]

Parameter	Value	Parameter	Value
Number of elements (rods) per bundle (assembly)	37	Element length (mm)	493
Peak linear fuel element rating (kW/m)	57	Element outside diameter (mm)	13
Average discharge burnup of fuel bundle (MWh/kgU)	170	Sheath (clad) thickness (mm)	0.4
Maximum residence period in the reactor (days)	700	Pellet outside diameter (mm)	12
U weight per bundle (kg)	19.2	Pellet length (mm)	16
Zr weight per bundle (kg)	2.2	Pellet density (g/cm^3)	10.6
Overall bundle length (mm)	495	Endplate width, outer ring (mm)	4.9
Overall maximum bundle diameter (mm)	102	Endplate thickness (mm)	1.6
Average sheath temperature (°C)	340	Diameter of assembly weld (mm)	4

Table 2 Illustrative data for fuel assessments

Parameter	Value	Parameter	Value
UO_2		Zr-4	
Thermo-Physical Data			
Theoretical density (g/cm^3)	10.97	Density (g/cm^3)	6.56
As-fabricated density (g/cm^3)	10.6	Thermal conductivity at 300°C (W/(m.k))	16.4
Thermal conductivity at 1000°C (W/(m.K)	2.8	Specific heat capacity at 300°C (J/(kg.K))	327
Specific heat capacity at 1000°C (J/(kg.K))	328	Melting point (°C)	1850
Melting point at zero burnup (°C)	2840	Sheath-to-coolant heat transfer coefficient (kW/m^2K)	50
Pellet-to-endcap heat transfer coefficient (kW/m^2K) (at high power, hard contact, low burnup)	1	Pellet-to-sheath heat transfer coefficient (kW/m^2K) (at high power, hard contact, low burnup)	80
Mechanical Data			
Young's modulus at 1000°C (GPa) (at 98% theoretical density)	190	Young's modulus at 300°C (GPa)	80
		Shear modulus (GPa)	27
Poisson's ratio	0.316	Poisson's ratio	0.37
Yield strength at 1000°C (MPa) (for grain size of 25 µm)	180	Yield strength at 300°C (78% cold worked and stress relieved at 510°C)	274
Coefficient of linear thermal expansion (µm/(m.K)) (at 1000°C)	12.5	Coefficient of linear thermal expansion (µm/(m.K)) (diametric, at 300°C)	6.72

3 Power and Burnup

Recall from the earlier chapters on physics that the heat output of a fuel element is usually expressed in kW/m. The energy produced by a fuel element per unit mass is called “burnup”. It is also customary to use burnup as an indicator of irradiation time, although strictly speaking, time is equal to energy divided by power. In the CANDU fuel community, burnup is usually measured in MWh/kgU. In other types of fuel, e.g., in PWRs and BWRs, fuel burnup is usually measured in GWd/tU. 1 GWd/tU equals 24 MWh/kgU.

Sometimes "atomic percent" is also used as a unit of burnup. It measures the ratio of the number of fissions to the initial number of uranium atoms. As a working rule, 1 atomic percent equals 240 MWh/kg U.

Exercise: A fuel element is operating at 60 kW/m and contains UO_2 cylinders of 12 mm diameter. What will be the fuel burnup after 30 days?

One meter of this fuel element contains a UO_2 volume of 113 ml. Assuming a UO_2 density of 10.6 g/cm^3, the mass of UO_2 is 1.2 kg. In UO_2, 88% is U. Therefore, one meter of this fuel element contains (1.2 * 0.88) = 1.06 kg of U. This fuel element is producing 60 kW; therefore, in 30 days, it produces (60* 720/1000) = 43 MW•h. Therefore, its burnup is (43/1.06) = 41 MW•h /kgU.

This example illustrates that a typical CANDU fuel element operating at 60 kW/m accumulates about 41 MW•h/kgU of burnup every month.

Recall from the earlier physics chapters that in a CANDU channel, the flux can change significantly from one channel to another and from one axial location in a channel to another. Also recall from the chapters on physics that to maintain reactivity, some fuel bundles are periodically moved from one axial location in the channel to another. These factors produce a variety of power histories in any given bundle.

Figure 3 shows two illustrative power histories for CANDU fuel. The first is called a “declining” power history and would be experienced by a fuel bundle that is loaded in a central axial location of a C6 fuel channel. The second includes a “power ramp” and is experienced by CANDU fuel which is initially loaded in a low-flux axial location of the channel and later shifted to a location of higher flux.

Different types of power histories have different impacts on fuel performance. For example, an element with a declining history generally experiences high power for a long period, which usually results in relatively high gas pressure in the fuel element. On the other hand, a ramped history exposes the fuel element to relatively high risk of “environmentally assisted cracking”. These aspects are illustrated further in later sections.

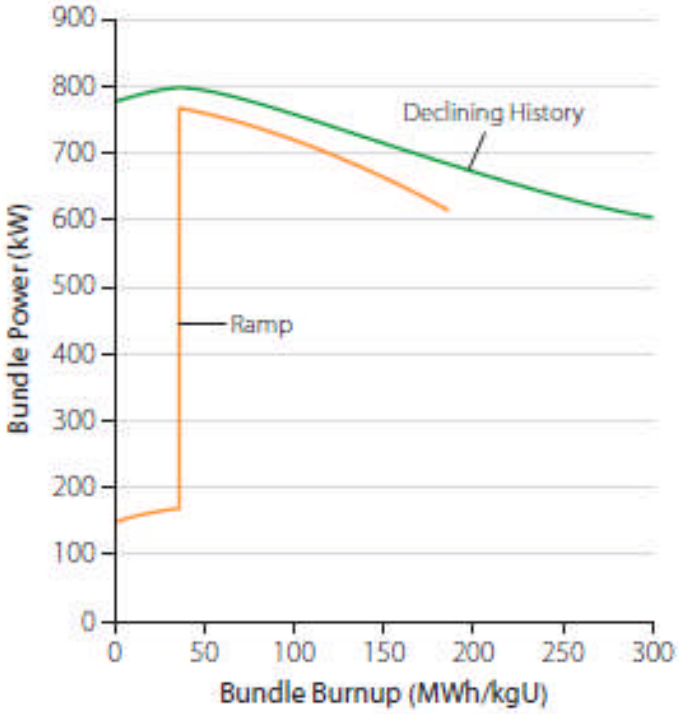

Figure 3 Illustrative power histories

4 Collapsible Sheaths

To minimize unnecessary parasitic absorption of neutrons, CANDU fuel sheaths are kept very thin—so thin that coolant pressure induces high compressive hoop stresses in them. At sufficiently high compressive hoop stress, the sheath will lose its elastic stability and collapse diametrically inwards into the diametric gap between the sheath and the pellet until it is supported by pellets. Figure 4(a) illustrates this phenomenon.

This collapse improves contact between the pellet and the sheath and therefore improves heat transfer between them. This, in turn, lowers pellet temperature and reduces thermally driven processes. Some such processes, such as diffusion and release of fission gas, decrease exponentially with reduced local temperature. Therefore, even a modest decrease in local pellet temperature leads to a disproportionately large reduction in these processes. For this reason, designers of CANDU fuel prefer to promote diametric collapse of the sheath.

At the same time, excessive diametric or axial collapse can risk sheath failure from overly high local strains. These conditions are called longitudinal ridging and axial collapse respectively (see Figures 4(b) and 4(c)) and must be avoided. Therefore, a delicate balance must be struck between promoting sufficient collapse to improve pellet-to-sheath heat transfer and avoiding overstrain due to excessive collapse. This trade-off is explained in the following sections.

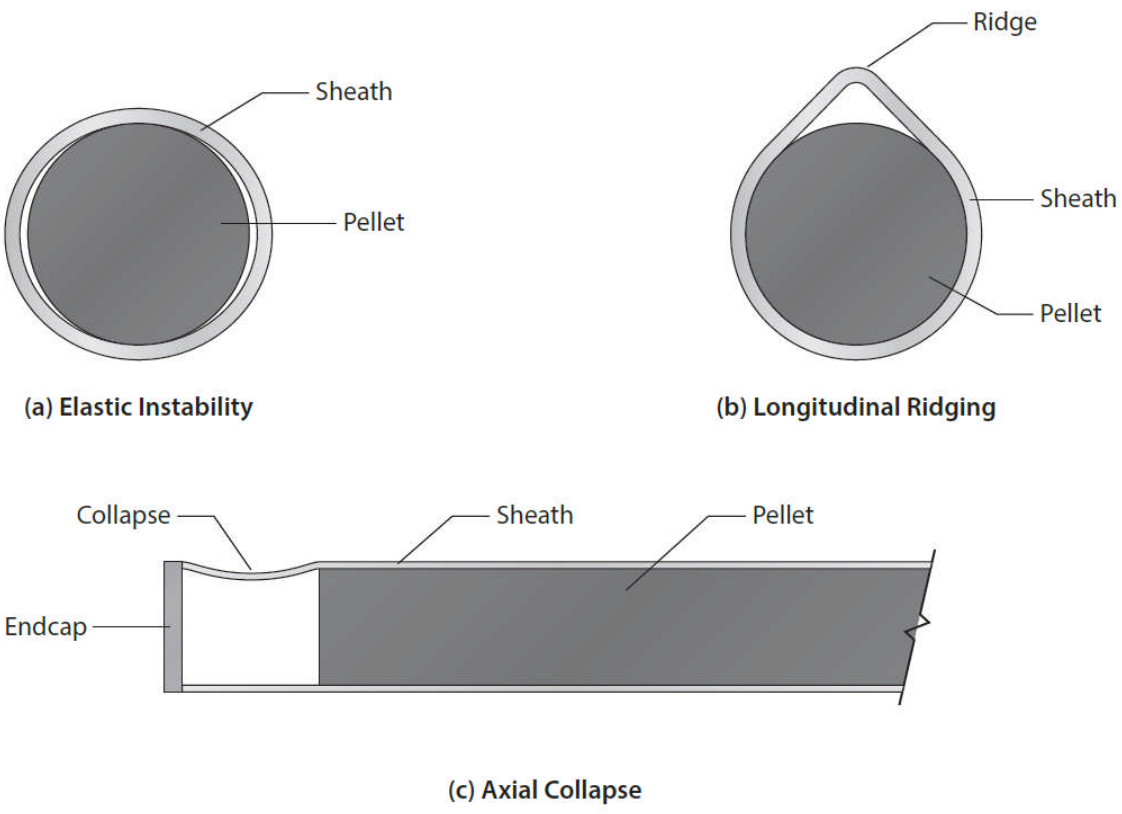

Note: Shapes have been exaggerated for clarity

Figure 4 Sheath collapse: forms and stages

4.1 Diametric Collapse

Elastic instability in a thin circular cylinder can be calculated from Bryan's equation [Bryan, 1888]:

$$P = E\,(t/r)^3/[4(1-\nu^2)],$$

where *P* is the differential pressure (= coolant minus internal), *E* is Young's modulus, *t* is thickness, *r* is radius, and *v* is Poisson's ratio.

Exercise: Consider a fuel sheath with the following properties: diameter, 13 mm; thickness, 0.4 mm; Young's modulus, 80 GPa; and a Poisson's ratio of 0.37. Its collapse pressure is 80,000 * $(0.4/6.5)^3$ / (4 * (1 - 0.37^2)) = 5.4 MPa.

In other words, the sheath just described will become elastically unstable when the differential pressure (coolant minus internal) exceeds 5.4 MPa. By comparison, the coolant pressure is 10 MPa. Therefore, when a C6 fuel element is first loaded into the reactor, the sheath will collapse elastically into the diametric gap.

Internal gas pressure builds up during irradiation (see Section 6). If the internal pressure in the fuel element exceeds about (10 – 5.4) = 4.6 MPa, the differential pressure will drop below the collapse pressure. The sheath will then no longer have much circumferential contact with the pellet, unless by then creep has converted sufficient elastic strain into permanent plastic deformation.

Improved heat transfer from diametric collapse is comparatively more important at high power

because fission gas diffusion increases exponentially with higher temperature. At the beginning of life, the internal pressure is low, the sheath is elastically unstable, the sheath is in contact with the pellet, and pellet-to-sheath heat transfer is good. This helps reduce the diffusion and release of fission gas. By the time internal gas pressure builds up sufficiently to provide elastic stability to the sheath, the element rating has usually decreased with burnup. Therefore, by then, good heat transfer is not as critically important.

4.2 Longitudinal Ridging

If the coolant pressure increases well past the collapse pressure, eventually the sheath starts to wrap itself around the pellet, as shown in Figure 4(b). This eventually creates a sharp ridge that runs along the length of the sheath, called a longitudinal ridge. Depending on how sharp the ridge is, the tip of the ridge can experience high bending strain. In an experimental irradiation, fatigue cracks eventually developed at longitudinal ridges. Some experts have also postulated that hydrogen in the sheath can migrate preferentially to longitudinal ridges, potentially hydriding and thereby embrittling the sheath at that location. For these reasons, strain at longitudinal ridges must be controlled to reasonable levels.

Figure 5 shows a typical development of permanent strain at the tip of a longitudinal ridge when pressure is increased. The two curves in this figure illustrate typical scatter in two different test specimens in this specific experiment.

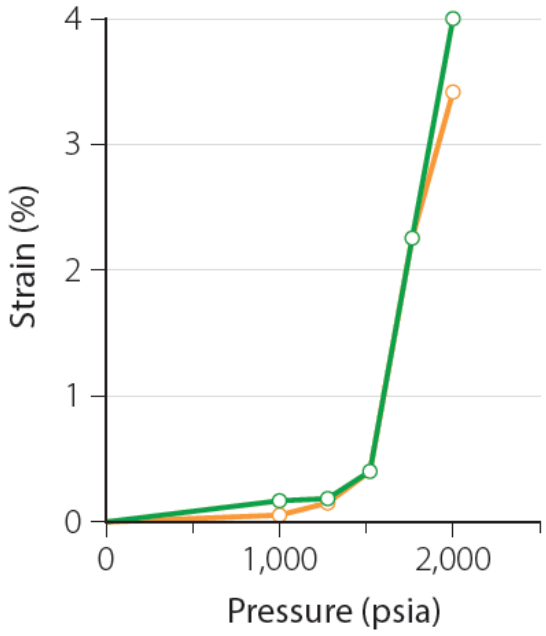

[Courtesy of COG]

Figure 5 Illustrative permanent strain at the tip of a longitudinal ridge

Initially, the strain increases rather gradually. Beyond a critical strain, however, a further increase in pressure increases the sheath strain fairly rapidly. The point at which this occurs is called the critical strain and has been experimentally found to be 0.5%. It is good practice to design CANDU fuel to stay below this strain value at the longitudinal ridge. Fuel designed in this way has never exhibited sheath failures at longitudinal ridges.

Experiments have established that the following parameters are relatively more important in influencing ridge strain: differential pressure, diametric clearance, sheath thickness, sheath diameter, yield strength, and Young's modulus.

4.3 Collapse into the Axial Gap

If the sheath is too thin, or if the axial gap is too long, the sheath can potentially collapse into the axial gap, as shown in Figures 4(c), 6(a), and 6(b). Such a collapse has the potential to crack the sheath, and therefore it is good engineering practice to avoid it.

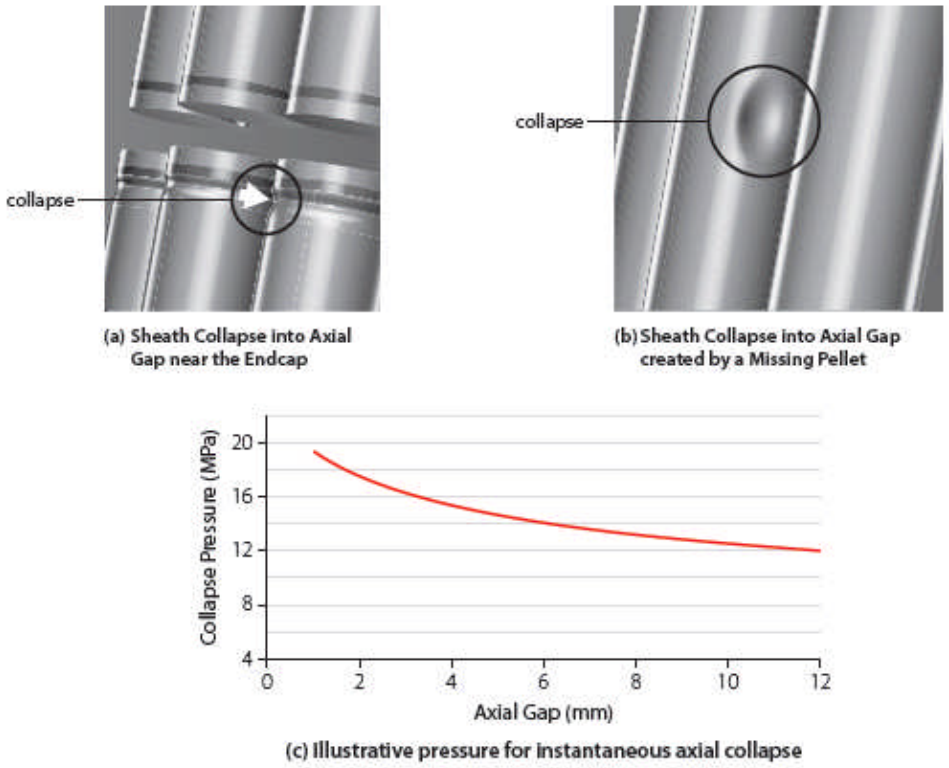

(a) Sheath Collapse into Axial Gap near the Endcap

(b) Sheath Collapse into Axial Gap created by a Missing Pellet

(c) Illustrative pressure for instantaneous axial collapse

[Figure (c) courtesy of COG]

Figure 6 Collapse into axial gap

The following major parameters influence axial collapse: differential pressure, length of the axial gap, radius and thickness of the sheath, and the yield strength, Young's modulus, and Poisson's ratio of the sheath material.

Figure 6(c) shows an illustrative calculation for instantaneous axial collapse in 37-element fuel. Creep collapse can potentially occur at a lower pressure than the instantaneous collapse pressure.

In CANDU fuel, axial collapse has been observed only under unusual situations such as absence of a large part of a pellet or an excursion to unusually high temperature in experimental fuel.

5 Thermal Performance of Fuel

High temperatures in the UO_2 pellet and in the Zircaloy sheath are important drivers for many damage mechanisms. Other chapters discuss the equations that can be used to calculate temperature distributions inside the fuel element.

Table 2 and Figure 7 provide some illustrative data that can be used to assess the thermal performance of fuel.

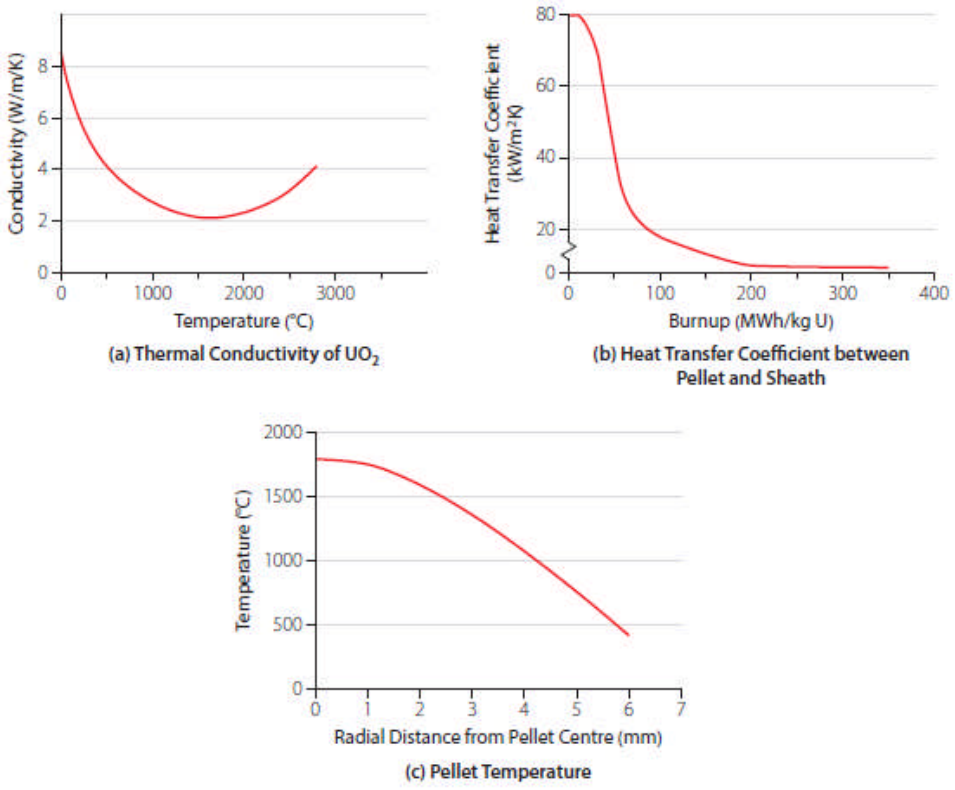

[Source: Tayal *et al*., 1987]

Figure 7 Illustrative heat transfer and pellet temperature in a fuel element

Some parameters are not constant, but depend on other parameters. For example, Figure 7(a) shows that the thermal conductivity of UO_2 depends on local temperature. Likewise, the heat transfer coefficient between the pellet and the sheath changes significantly with time, as shown in Figure 7(b), because of changes during irradiation in factors such as the interface pressure between the pellet and the sheath and the volume and composition of fission and filling gases within the fuel element. In such cases, Table 2 lists an average representative value that can be used for illustrative calculations.

Figure 7(c) illustrates a typical local temperature profile across the pellet radius. Note that (a) the temperature distribution is approximately parabolic, (b) the temperature at the centre of the pellet is about 1,800°C, and (c) the temperature at the surface of the pellet is about 400°C. Needless to say, the absolute values of temperature depend on many parameters, including

element power; Figure 7(c) is merely an illustrative example.

The above absolute temperatures, as well the temperature gradient across the pellet radius, have significant consequences for fuel performance, as discussed in more detail later in this chapter.

6 Fission Gas and Internal Pressure

6.1 Overview

Each fission reaction produces fission products (fission fragments), as described in earlier chapters on physics. Some fission products are solid, whereas others are gaseous. These fission products accumulate over time. The gaseous fission products lead to internal pressure which, if excessive, can potentially create a hole in the sheath, either through mechanical overstrain or through environmentally assisted cracking. A hole can provide a path for radioactive fission products to leach into the coolant and to pose a radiological hazard to operating staff. For this reason, fission gas pressure must be controlled and limited to acceptably low values.

As noted earlier, CANDU fuel is designed to have collapsible sheaths to improve heat transfer to the coolant, which reduces pellet temperature, which in turn reduces the amount of fission gas that can escape from the pellet and contribute to gas pressure in the fuel element. In addition, through appropriate pellet shapes and clearances, empty space—called "open void"—is provided inside a fuel element to keep internal gas pressure below acceptable levels.

Over the years, CANDU reactors have maintained good control of fission gas pressure. In a rare instance, however, control of fission gas pressure was lost for a very brief period in the 1980s in a Bruce reactor in Ontario when unavailability of a fuelling machine prevented timely refuelling of a fuel channel. As a result, some fuel bundles resided in the core for longer durations than designed, resulting in excessive accumulation of fission gas and in high internal pressure. This in turn caused cracks in the sheaths of a few fuel elements. The internal gas pressure can be calculated using a model summarized below [Notley *et al*., 1979].

Figures 8–14 show some processes pertinent to fission gas pressure. Fission produces gas uniformly within the grains of UO_2. However, to exert pressure on the sheath, the gas must first reach the "open space" within the fuel element (Figure 8a). This is the space in the axial and diametric gaps, in the dishes, in the chamfers, in the cracks within the pellets, in the surface roughnesses of the sheath and of the pellets, and in the cavity of the endcap. The movement of gas from within grains to the open space is described below.

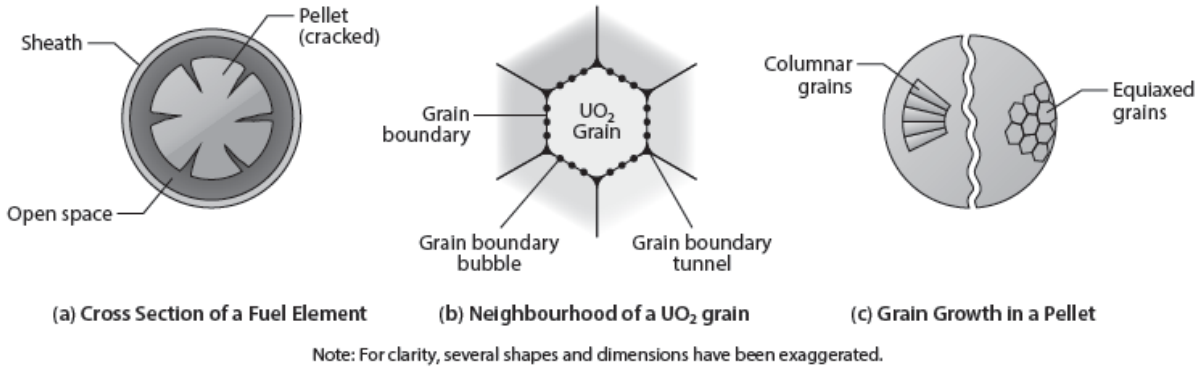

Figure 8 Terms for fission gas release

A number of processes are involved in transporting fission gas from within grains to the open voidage. They include knock-out, recoil, diffusion, grain boundary sweep, storage in grain boundary bubbles, growth of grain boundary bubbles, interlinkage of grain boundary bubbles, and venting of grain boundary bubbles. These are described in the following paragraphs.

Figure 9 is an illustrative example of the steady-state release rate of ^{88}Kr from a single crystal of UO_2 [Carroll *et al.*, 1965].

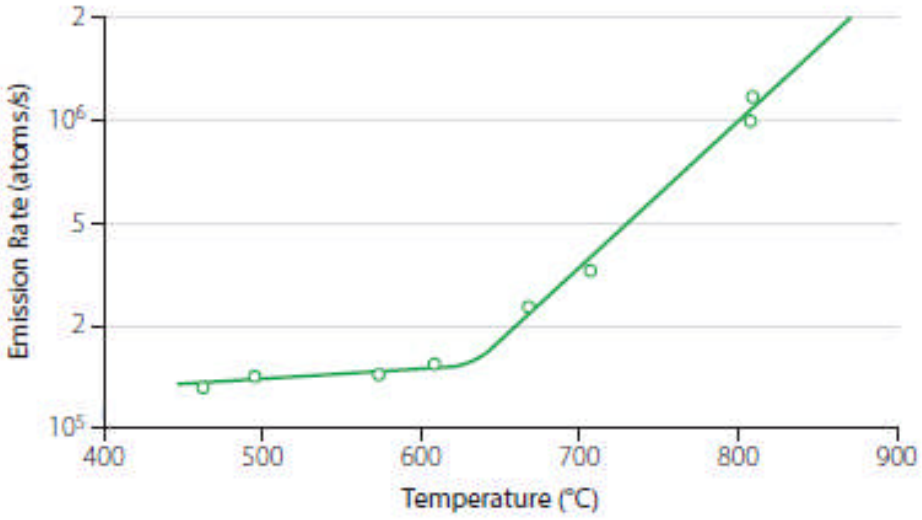

[After Carroll *et al.*, 1965]

Figure 9 Steady-state release of ^{88}Kr from a single crystal of UO_2

Below about 625°C, two thermally-independent processes—recoil and knockout—make significant contributions to total release of fission gas. They are also sometimes called "athermal" release mechanisms.

Above about 625°C, the emission rate increases rapidly with temperature. This is due to diffusion, because diffusivity increases exponentially with temperature. This phenomenon is also sometimes called "thermal" release. If high fission gas pressure does occur in CANDU fuel, it is almost always driven primarily by thermal diffusion.

Fission gas is produced within grains. If the grain boundary acts as a sink, a gradient develops in the concentration of gas across the grain's radius. This concentration gradient drives the rate of diffusion from the grain to the boundary.

At the grain boundary, the gas accumulates in bubbles (Figures 8(b) and 10), which become progressively bigger as more gas reaches the grain boundaries.

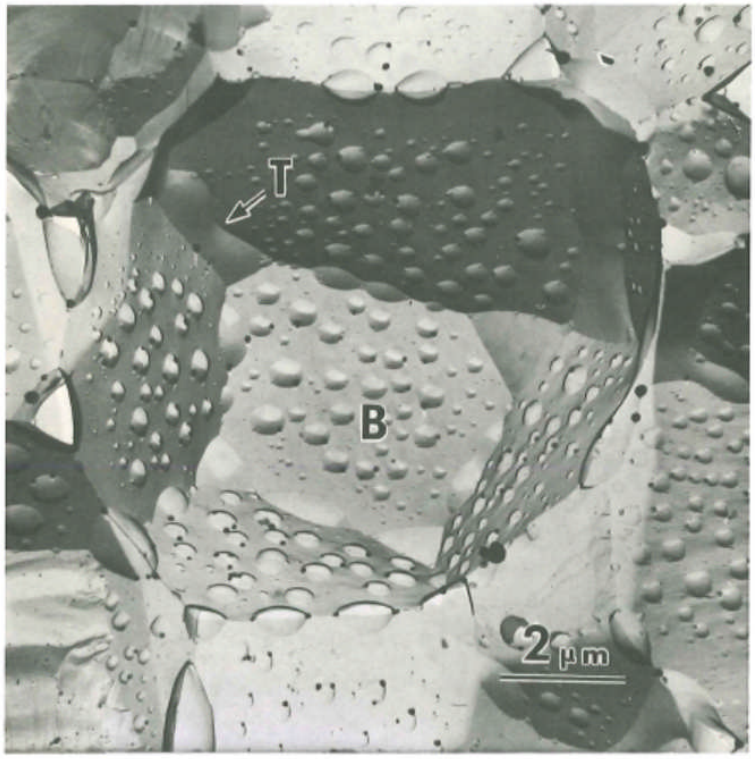

B: Bubbles; T: Tunnels
[Source: Hastings, 1983]

Figure 10 Grain boundary bubbles and tunnels

In parallel, high temperature can also cause the grains to grow (Figures 8(c) and 11), either through equi-axial grain growth (Figure 12) or, at even higher temperatures, through columnar grain growth (Figure 13). The boundaries of the growing grains collect the gas that was previously contained in the areas swept by grain growth. This gas is added to the inventory of gas at grain boundaries. This process is called grain boundary sweep.

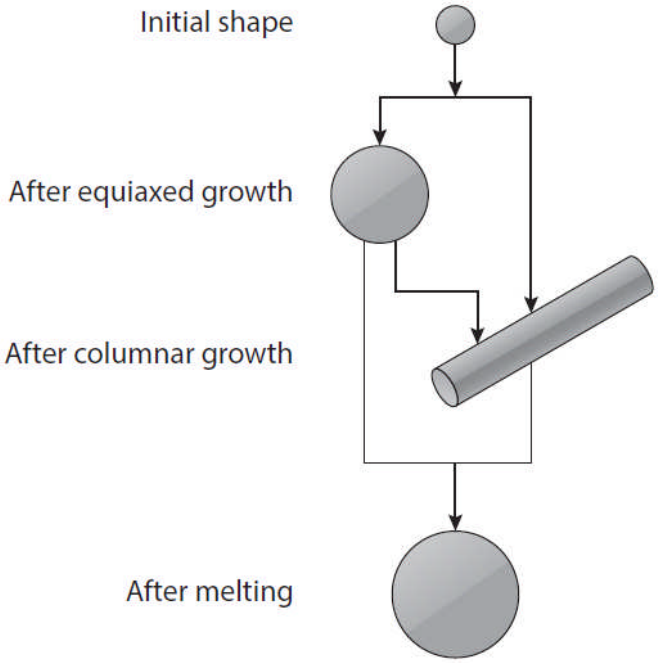

Figure 11 Changes in sizes and shapes of UO_2 grains during irradiation

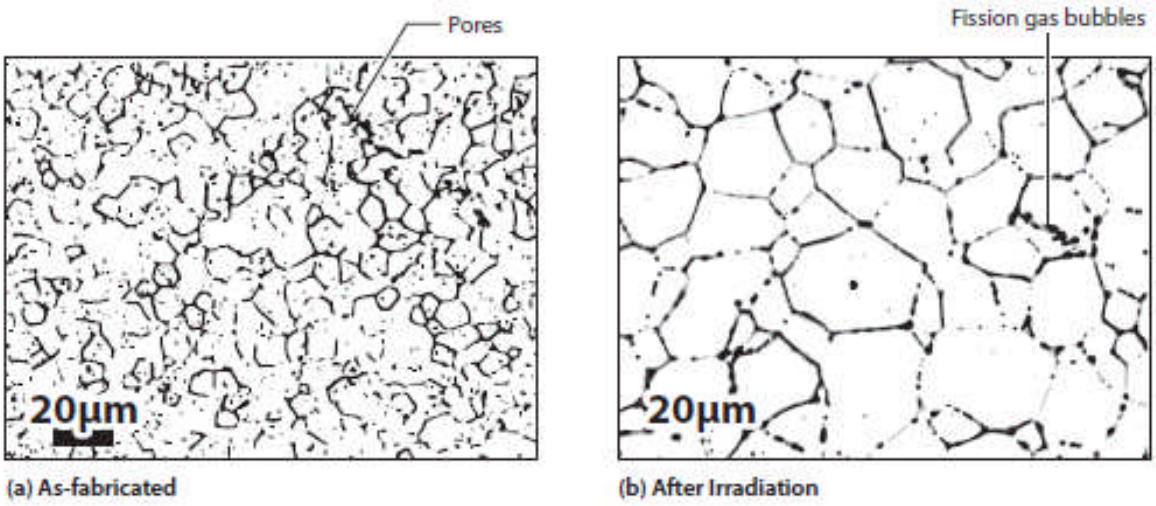

Figure (b) also shows fission gas bubbles at grain boundaries
[Source: Hastings, 1982]

Figure 12 Equiaxial grain growth

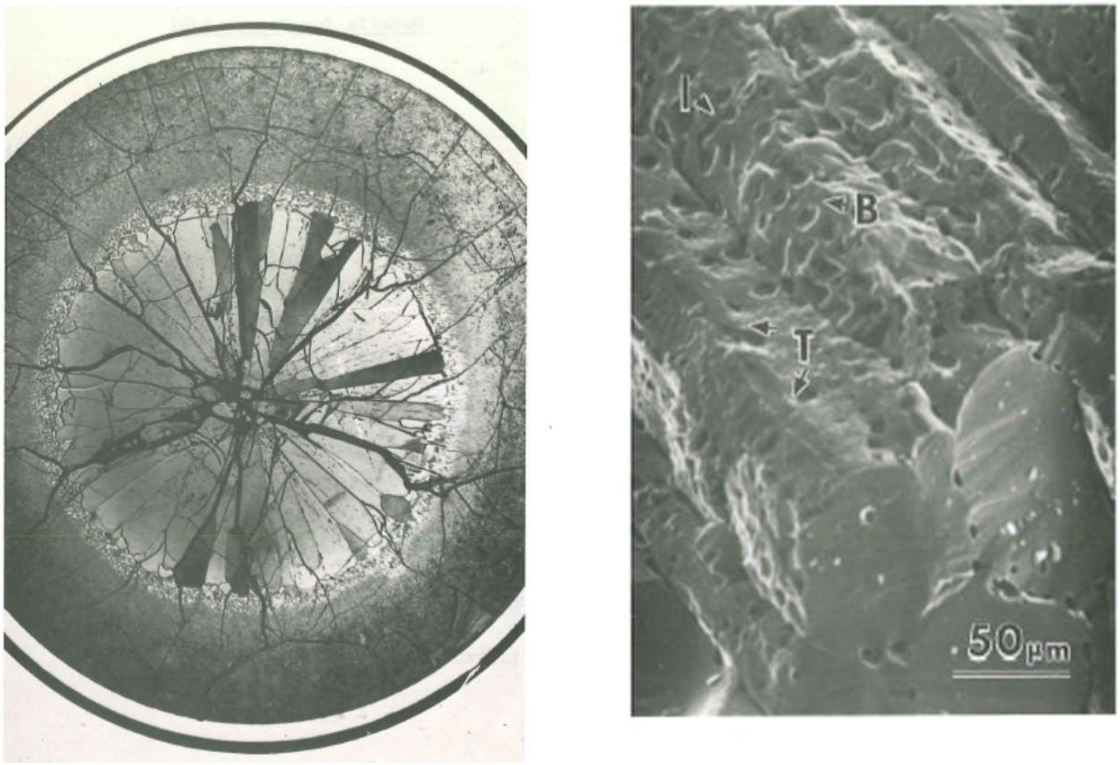

[Source: Hastings, 1983]

Figure 13 Columnar grain growth

As additional gas reaches grain boundaries, the grain boundary bubbles eventually become big enough to touch each other. This is called interlinkage. The volume contained within inter-linked bubbles reflects the storage capacity of the grain boundary bubbles. Any gas that reaches the grain boundaries over and above the bubble capacity is called excess gas.

When fuel power changes, thermal expansions or contractions in the pellet create micro-cracks in the UO_2 ceramic. These provide a pathway for the excess gas in interlinked bubbles to vent to the open space between the pellet and the sheath. This can be deduced from Figure 14, which shows measurements of internal pressure during irradiation [Notley *et al*., 1979].

Figure 14 shows that at high power, internal pressure does not change during constant-power periods, even though fission gas must be produced continually during these periods. Internal pressure increases only immediately after changes in power, suggesting that grain boundary gas escapes to the open space through interconnected micro-cracks formed upon changes in power.

Under the usual operating conditions in CANDU power reactors, only a small fraction (<10%) of the gas produced vents to the open space. Most of the gas stays tied up within the grains of UO_2 and in grain boundary bubbles.

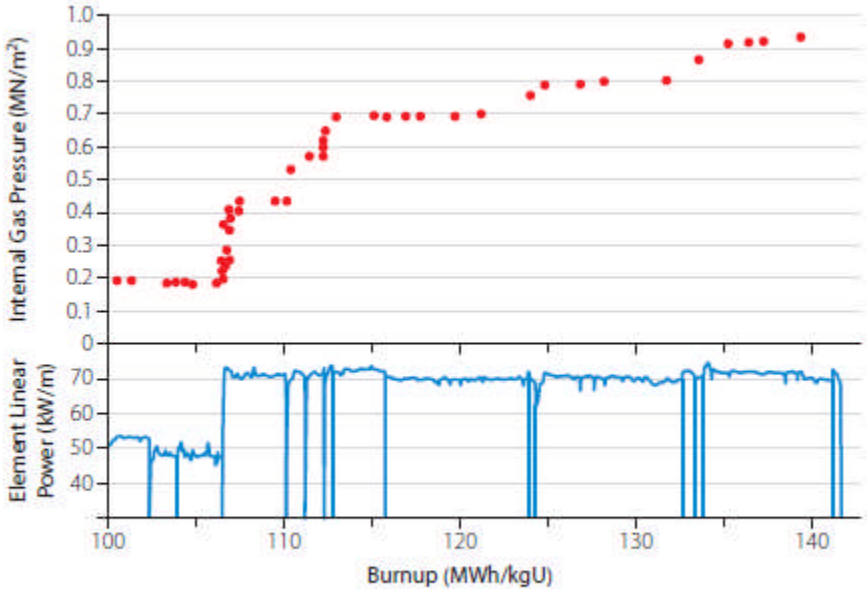

[Source: Notley *et al.*, 1979]

Figure 14 Variation of internal gas pressure during irradiation

The process by which fission gas reaches the open space is called fission gas release. It increases rapidly with higher local temperature, and for a given temperature, it increases with burnup and with smaller grain size.

Later sections of this chapter will describe a simplified model to quantify the amount of fission gas that reaches the grain boundaries through diffusion.

6.2 Recoil

Recoil is one of the mechanisms that releases fission fragments outside the pellet. To a first approximation, fission fragments travel through UO_2 in a straight line. They lose energy as they encounter (primarily) electrons in the material. When the initial kinetic energy of the fission fragment has been fully dissipated in this process, the fission fragment stops as a fission product. This occurs in about 10 µm. However, if the fission fragment reaches a surface of the pellet before expending all its energy, it escapes the pellet. Therefore, recoil is a contributing factor in fission product release from near a surface of the pellet (~10 µm), especially at low temperature [Olander, 1976].

6.3 Knockout

Knockout is another athermal mechanism for fission product release that occurs at low temperature. As a fission fragment travels through the pellet, it may occasionally collide with nuclei of other atoms in the lattice. The latter are called “knock-ons”. Knock-ons are usually uranium or oxygen atoms in the fuel, but occasionally a knock-on can be a fission gas atom lodged in the lattice. A knock-on acquires kinetic energy from the collision, and it also travels in a straight line

and loses energy as it travels. A primary knock-on generally travels a distance of about 200 Å (Angstroms) before coming to rest. If the knock-on reaches a surface of the pellet before stopping, it escapes the pellet. If the knock-on was a fission fragment, this process results in release of fission products [Olander, 1976].

6.4 Diffusion of Fission Gas to Grain Boundaries

As noted earlier, diffusion is a key process that drives the fraction of produced gas that eventually reaches the open space at high operating power. This section discusses the rate of diffusion of stable gases to grain boundaries after a steady-state profile of gas concentration has been built across the grain. This can be calculated from Booth's model [Booth, 1957].

Grains of UO_2 are of irregular shape and size. Nevertheless, this calculation model postulates that gas diffusion out of grains can be approximated by assuming that the pellet consists of a collection of spheres of equal radii. The radius "*a*" of the equivalent sphere is equal to the average grain radius.

To calculate the leak rate at the grain boundary, we first need to know the gas concentration profile across the grain radius. Booth solved Fick's equation for diffusion in a sphere [Fick, 1855] assuming that the surface of the sphere was a sink. This results in a parabolic concentration profile:

$$c(r) = \frac{f\beta}{6D}\left(a^2 - r^2\right), \tag{1}$$

where c is the local concentration, r is the radial distance from the grain centre, a is the grain radius, f is the fission rate, β is the yield, and D is the diffusivity. Concentration means the number of nuclides per unit volume of the grain. By integrating the above equation, we can obtain the volume-average concentration c_{av}.

Diffusion due to a concentration gradient results in the following rate of nuclide flow per unit area of grain surface, q:

$$q = -D\frac{\partial c}{\partial r} \text{ at } r = a\,. \tag{2}$$

The leak rate *LEAK* is defined as the rate of nuclide diffusion from the grains per unit grain volume. Therefore [Tayal *et al.*, 1989],

$$\text{LEAK} = -\frac{3}{a}D\frac{\partial c}{\partial r} \text{ at } r = a\,. \tag{3}$$

By differentiating Equation (1), substituting the results into Equation (3), and then substituting the expression for c_{av} into Equation (3), we get:

$$\text{LEAK} = \frac{15Dc_{av}}{a^2}\,. \tag{4}$$

Equation (4) describes the rate at which fission gas diffuses to the grain boundary during steady state.

6.5 Internal Gas Pressure

As noted earlier, internal gas pressure must be kept within acceptable levels to avoid overstrain

failures. Therefore, internal gas pressure is a consideration in selecting some details of the internal design of a fuel element, such as pellet shape and axial gap.

Internal gas pressure is driven by the combined volumes of filling gas and fission gas. These gases are stored in a variety of locations within a fuel element, e.g., in dishes, in pellet/sheath radial gaps, in axial gaps, in pellet cracks, and in surface roughnesses of the pellet. Furthermore, the local temperature at each storage location differs significantly because of the steep temperature gradients within the fuel element.

To calculate the internal pressure, one usually divides the fuel element into many regions, each with a nearly constant temperature. Then the ideal gas law is used to integrate the impacts on internal gas pressure:

$$p_1 v_1 / T_1 = p_2 v_2 / T_2 \,, \tag{5}$$

where p, v, and T represent pressure, volume, and temperature respectively and subscripts 1 and 2 refer to two different states.

Exercise:

Consider a fuel element which was initially filled with 2 ml of helium at standard temperature and pressure (STP). During irradiation, 10 ml (at STP) of fission gas was released to the open space. Let us assume for simplicity that at operating power, the open space in the fuel can be divided into three zones of essentially constant temperature, each with a volume:

- 0.4 ml at 1,900 K;
- 1 ml at 1,500 K; and
- 0.6 ml at 1,000 K.

This fuel element's internal gas pressure can be calculated as follows. Recall that at STP, the temperature is 273 K and the pressure is 0.1 MPa. Therefore, corresponding to the filling gas volume of 2 ml at STP, the "voidage" (V/T) is (2/273) = 0.00733 ml/K.

On-power, the same gas is now stored at an effective voidage of (0.4/1900 + 1/1500 + 0.6/1000) = 0.00148 ml/K. In other words, the on-power voidage is about (0.00148/0.00733), or one-fifth the off-power voidage. Therefore, from the ideal gas law, the on-power pressure of the filling gas is (0.1 * 0.00733/0.00148) = 0.5 MPa.

Including the fission gas, the total STP volume of gas is (2+10) = 12 ml. On-power, because 2 ml (STP) of filling gas develops a pressure of 0.5 MPa, 12 ml (STP) of filling gas plus fission gas will develop a pressure of (0.5 * 12/2) = 3 MPa.

7 Stresses and Deformations

A variety of mechanical and thermal loads and microstructural changes lead to in-reactor stresses, strains, and deformations in fuel. Excessive stresses and strains can in turn potentially result in a hole in the sheath or in the endcap, which can release radioactive fission products to the coolant. Excessive stresses or strains in the endplate can break it also, which may pose difficulties in discharging the fuel from the reactor. Excessive deformations can potentially jam the fuel in the channel, reduce local cooling, or damage surrounding components through, for example, crevice corrosion.

It would be unrealistic to operate fuel with zero stresses, strains, and deformations, and it

would be very expensive to limit these always to trivial values through massively over-conservative designs. At the same time, it is essential to keep them reasonably below harmful levels. Some such considerations are described in this section.

7.1 Thermal Stresses in Pellets

As noted in an earlier chapter, the radial temperature distribution in an operating fuel pellet is, to a first approximation, parabolic. The temperature gradient is steep, about 1800°C at the centre and about 400°C at the surface, over a radius of only about 6 mm.

Think of a pellet as being made up of many concentric rings (or annuli). Thermal expansion is higher in the inner hotter rings and comparatively lower in the neighbouring, relatively cooler outer rings. Differential thermal expansions lead to dimensional misfits between neighbouring annuli, which in turn lead to stresses. For this reason, operating UO_2 pellets are often found with extensive radial cracks in their outer regions, as shown in Figure 15.

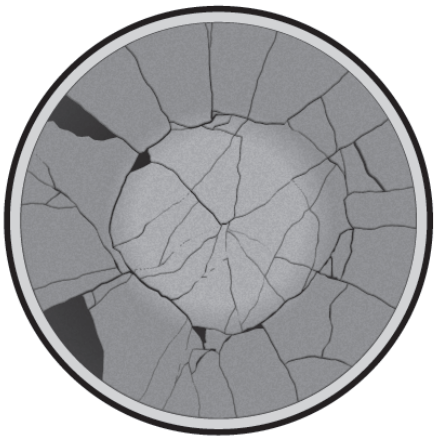

[Source: Hastings, 1983]

Figure 15 Typical cracks in a high-power pellet

Textbooks in mechanics provide a framework of equations which can be used to calculate thermal stresses in a cylinder experiencing parabolic temperature profile across its radius [e.g., see Timoshenko *et al*., 1970]. Figure 16 illustrates a typical result.

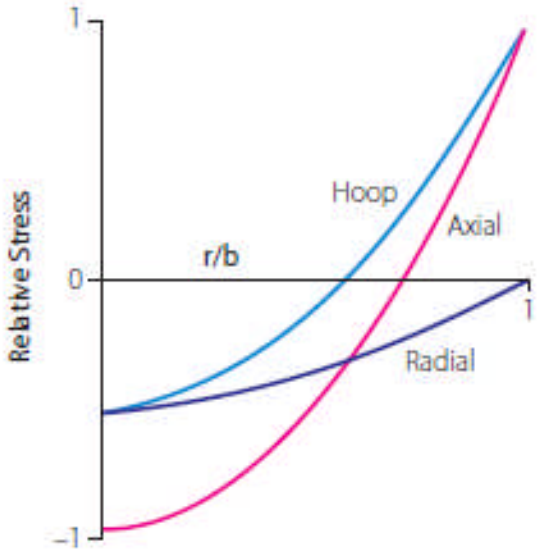

[Courtesy COG]

Figure 16 Thermal stresses in a pellet

Note that the hoop stress is compressive in the inner part of the pellet and tensile in the outer part of the pellet. The tensile hoop stresses lead to radial cracking in the outer parts of the fuel pellet, as can be observed in Figure 15. The radial cracks add to the storage space for fission gas, reducing internal gas pressure. They also increase pellet expansion and hence sheath stress, encouraging detrimental environmentally assisted cracking (described in Section 8).

All three major components of stress are compressive in the central part of the pellet. This leads to compressive hydrostatic stresses, which reduce the size of fission gas bubbles at the grain boundaries. Moreover, the stresses are well into the plastic range. This can potentially lead to permanent deformations in the pellet. High local temperatures plus high local stresses can also lead to high rates of creep, leading to relatively rapid relaxation of stress. High local creep plus local plasticity are also believed to cause "dish filling" at high local temperatures.

7.2 Changes in Element Diameter and Length

During irradiation, several processes affect the diameter and length of the pellet and sheath. Notable among these are densification, swelling, creep, dish filling, thermal expansion, and hourglassing. Brief descriptions of these are given below.

Densification of pellets is caused primarily by irradiation-induced sintering of UO_2 in the reactor. Figure 17 shows an illustrative example of initial as-fabricated pores that have been removed during irradiation, resulting in densification. Although research has identified many factors that can affect densification, the relatively more important primary influences are believed to be temperature, initial density, and duration of high temperature.

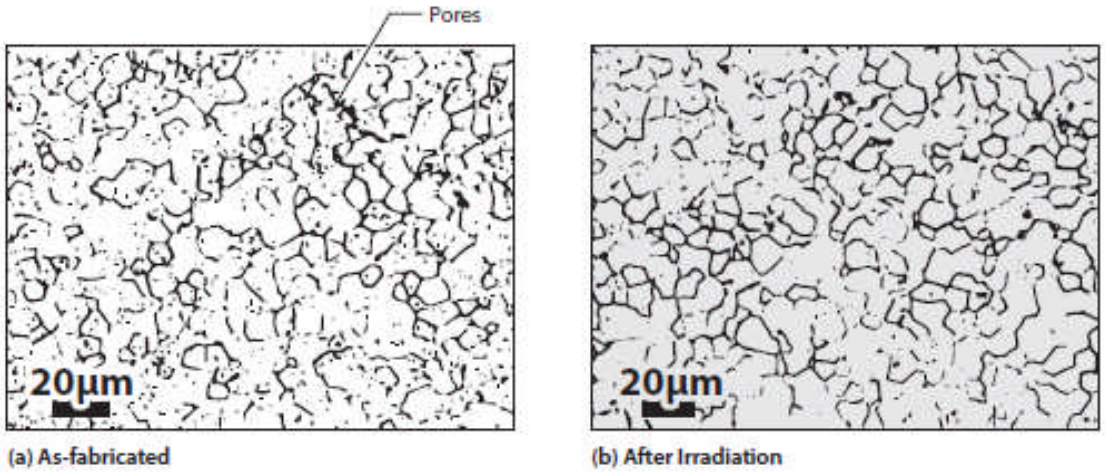

[Source: Hastings, 1982]

Figure 17 Removal of as-fabricated pores during irradiation

Swelling of pellets is caused by fission products—solid as well as gaseous. The combined volume of solid fission products is larger than that of the parent material, resulting in swelling of the pellet. Unreleased fission gases also contribute to pellet swelling. For each percent atomic burnup, solid fission product swelling increases pellet volume by approximately 0.32% [Olander, 1976]. However, this number is subject to large uncertainties. [Note: 1 atomic percent = 240 MWh/kgU].

Creep due to external coolant pressure decreases sheath diameter. However, outward creep of the sheath can be expected if the internal gas pressure exceeds the coolant pressure.

Creep within the pellet is believed to cause axial expansion of the hot inner core of the pellet. This is also the region where dishes are located, as shown in Figure 1. In fuel that is operated at high local temperature, dishes are usually found to have become smaller after irradiation than before. This process is called *dish filling*.

The operating temperatures cause *thermal expansion* in the pellet as well as in the sheath. The pellet operates at much higher temperature than the sheath—for example, the average pellet temperature in the illustration in Figure 7 is about 1000°C, whereas the average illustrative sheath temperature in Table 1 is about 340°C. As well, the coefficient of thermal expansion of UO_2 is about twice that of Zr-4, as can be seen in Table 2. Therefore, the pellet usually expands much more than the sheath. At times, this results in the pellet filling the diametric gap and "pushing" the sheath outward. This in turn creates high tensile stresses in the sheath, often in the plastic range.

Diametric expansion of the pellet is usually much larger at the two ends of the pellet length than at the mid-point, as shown in Figure 18. This is called *"hourglassing"* and is caused by three factors: non-uniform temperature across the radius of the pellet, axial compression, and variations in initial density. These are illustrated in Figure 19 and explained below.

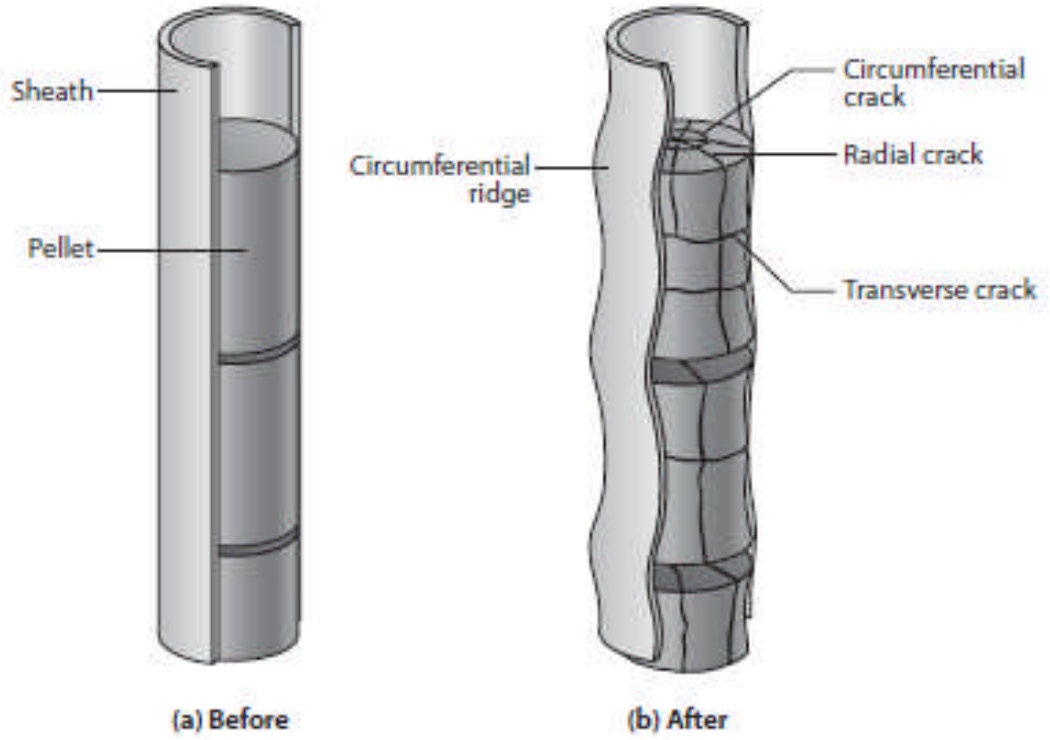

Figure 18 Fuel rod before and after startup

- Non-uniform local stiffness: As noted in Section 7.1, the parabolic temperature profile in the pellet leads to thermal stresses. The net diametric expansion of the pellet is influenced by these thermal stresses. However, these vary from one transverse cross section to the next. At the pellet mid-plane, the deformation of a transverse cross section is resisted, not only by the stiffness of that cross section, but also by the stiffness of the surrounding UO_2. However, at and near the end of the pellet, a transverse cross section is surrounded by less UO_2. Therefore, it can and does expand more than the cross section at the mid-plane of the pellet. This is one reason for pellet hourglassing.
- Axial compression: When the pellet expands axially, there may be axial interference between neighbouring pellets, between the stack of pellets and the endcap, or both. This results in compressive axial forces, which add to hourglassing. Axial compression has a larger influence on hourglassing if the force is applied near the surface of the pellet rather than near the centre.
- Initial variation in pellet density: One step during pellet fabrication is pressing of the pellet at its end (see Chapter 18). This causes the as-pressed densities to be higher near the end than at the centre. The pellet subsequently sinters during fabrication and during in-reactor densification. The resulting densification is higher at the mid-plane than at the ends because of the lower initial density at the mid-plane. This also contributes to hourglassing.

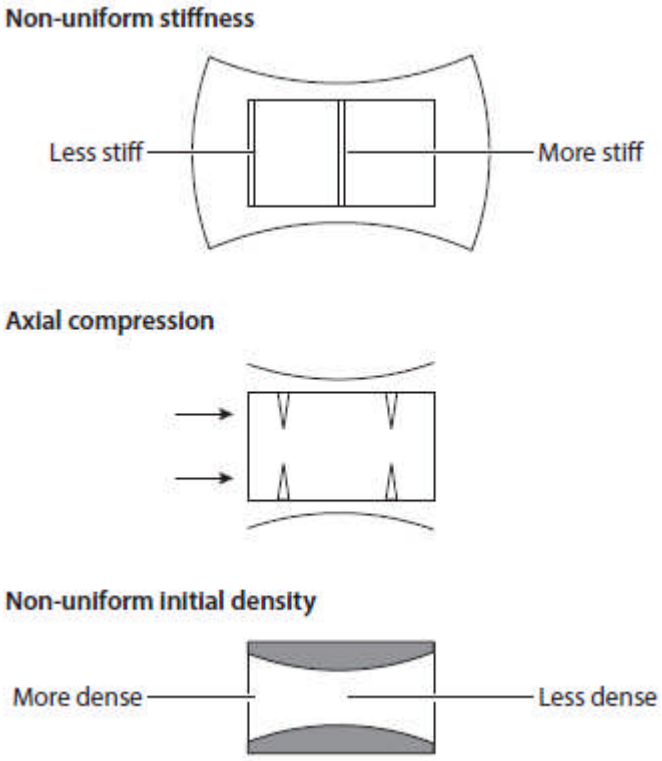

[Source: Tayal, 1987]

Figure 19 Causes of hourglassing in pellets

When an expanded hourglassed pellet pushes against the sheath, it causes *"circumferential ridges"* to be formed in the sheath at the ends of the pellets, giving the sheath the appearance that resembles a bamboo stalk, as shown in Figure 18. The circumferential ridges are locations of high stresses and strains, often well into the plastic range, and are a main location for environmentally assisted cracking, as discussed in the next section.

The pellet and sheath diameters change continually during irradiation in response to the processes described above and to continual changes in element power. This means that the pellet-to-sheath gap and the interface pressure between the pellet and the sheath also change continually during irradiation. These changes feed back to pellet temperature and to fission gas release, which in turn feed back to pellet expansion. Thus, a complex feedback loop is set up.

8 Environmentally Assisted Cracking

Environmentally assisted cracking (EAC) occurs in nuclear fuel when irradiation- and/or hydride-embrittled Zircaloy experiences high tensile stresses and strains in the presence of corrosive agents. These high stresses and strains are usually caused either by changes in power (called power ramps) or by excessive internal gas pressure. Figure 2 demonstrates that in the past, EAC caused by power ramps has been a dominant damage mechanism in CANDU fuels and suggests that CANDU fuels might have relatively low margins to defects from this mechanism.

Furthermore, our experience has been that when conditions are right for power-ramp EAC in a CANDU reactor, a number of fuel bundles tend to fail within a short period of time. As well, multiple fuel elements can often fail in a given fuel bundle. This combination can cause iodine

levels in the coolant to increase quickly. For the above reasons, it is particularly important to have a good understanding of this damage mechanism and of ways to quantify and control it.

To date, EAC has manifested in CANDU fuels through three main routes:

- EAC failures in the sheaths at interfaces between neighbouring pellets (called circumferential ridges) as a result of excessive pellet expansion during increases in power (called power ramps). Figure 20 shows an illustrative example [Penn *et al*., 1977].
- EAC failures in sheaths near their welds with endcaps as a result of excessive pellet expansion during power ramps. Figure 21 shows an illustrative example of a typical crack near the sheath/endcap junction [Floyd *et al*., 1992].
- EAC failures in the sheaths near their junctions with endcap welds as a result of excessive gas pressure accumulated during abnormally long residences of fuel in the reactor [Floyd *et al*., 1992]. Such defects appear similar to those shown in Figure 21.

EAC is also called by other names in the scientific literature. In Canada, it is also called "stress corrosion cracking" (SCC). In the LWR community, it is usually called "pellet/clad interaction" (PCI). Both these names were coined shortly after the initial rash of power-ramp defects and were based on initial understanding of their mechanisms. Subsequently, much additional knowledge about the mechanism has been uncovered in a myriad of tests around the world. As a result, several labels very similar to EAC were proposed in later literature. In light of this additional information, a re-think in the early 2000s concluded that EAC is an appropriate label for this mechanism.

Figure 22 illustrates some key terms associated with EAC during power ramps.

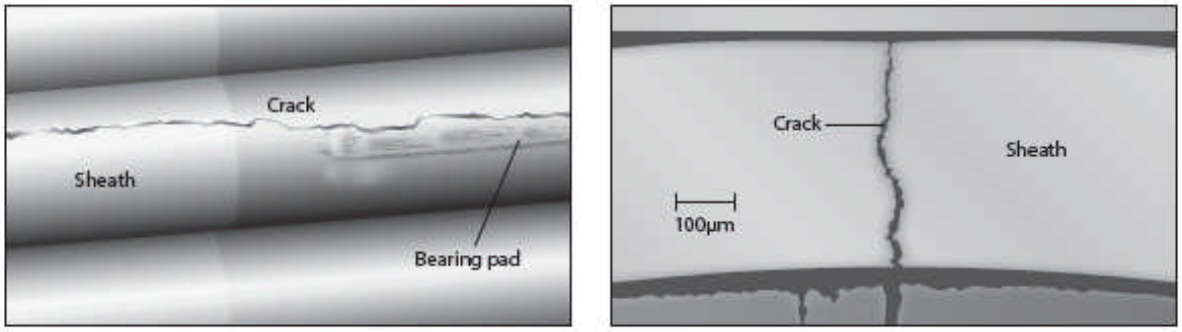

(a) View along the Length of the Sheath (b) View through the Thickness of the Sheath

[Courtesy COG]

Figure 20 Power ramp cracks originating at a circumferential ridge

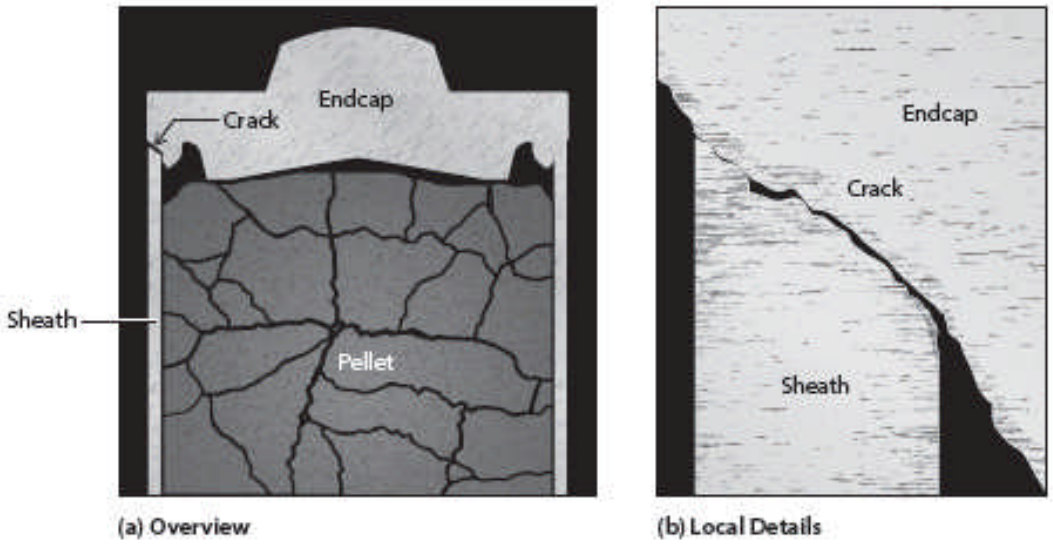

[Courtesy COG]

Figure 21 Power ramp cracks near a sheath/endcap junction

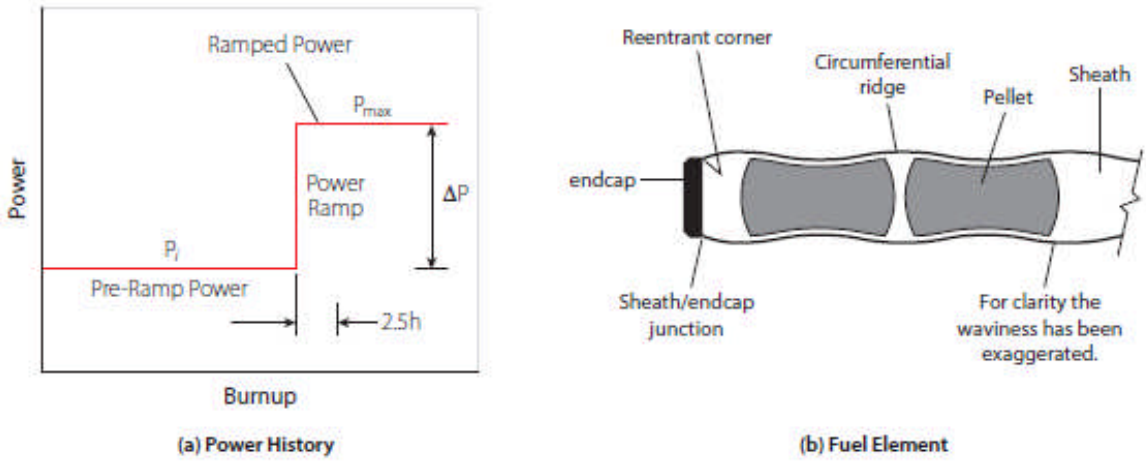

Figure 22 Key terms for environmentally assisted cracking during power ramps

8.1 EAC Processes

To control a CANDU reactor's relative balances of neutronic powers in different parts of the reactor, CANDU fuel bundles can be repositioned in more than one axial location within a fuel channel. This is achieved by on-power refuelling, which is an important and unique feature of CANDU reactors.

Different parts of a fuel channel usually have different neutron fluxes, generally in a cosine

shape over the channel length. Therefore, during on-power refuelling, a previously irradiated fuel bundle can go from a relatively lower initial power to (or through) a relatively higher final or intermediate power. This causes power ramps in irradiated fuel elements.

The resultant pellet expansion strains and stresses the sheath, in the process breaking any protective layer of ZrO_2 that might have built up during initial irradiation. By then, the Zircaloy has also been embrittled by two processes: (a) by fast neutrons experienced during many months of irradiation at the low-power axial position, and (b) by hydrides, which can either promote or hinder initiation and growth of cracks depending on their orientation. In addition, by then, previous irradiation has also released fission products inside the fuel element, some of which are corrosive (such as iodine, cesium, and cadmium). Some fraction of these corrosive fission products is believed to react chemically with the CANLUB layer that is applied on the inside of the sheath, reducing the amount of fission products that are available to attack Zircaloy. The balance of the fission products is available for chemical attack on Zircaloy while the Zircaloy is also experiencing high stresses and strains due to the power ramp. These situations create a potentially potent combination for EAC: high stresses and strains, concurrent with embrittled Zircaloy, and also concurrent with a corrosive internal environment.

Figure 23 provides a specific example of some of the processes described above. It is based on in-reactor measurements of ridge strains during a power ramp to about 55 kW/m [Smith *et al*., 1985]. Specifically, this fuel element was first irradiated in a base irradiation at about 30 kW/m to about 4 MW•d/kgU. Then it was inserted into an experimental rig that could measure sheath diameters during irradiation. The power in the experimental rig was first increased from 0 to about 30 kW/m, where it was held constant for about 30 days. Then the power was increased again, this time to about 55 kW/m.

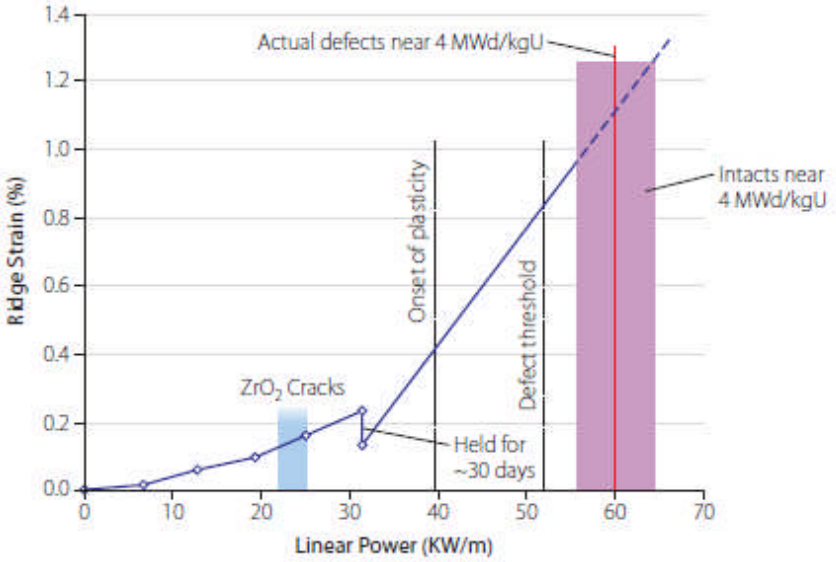

[Source: Tayal *et al*., 2008-2]

Figure 23 Mechanism for power ramp failures

On the plot in Figure 23 for ridge strain vs. element power, we have also superposed the strain at which ZrO_2 breaks and the strain at which Zr-4 becomes plastic [Tayal *et al*., 2008-2]. One can see that ZrO_2 breaks very early during the ramp and therefore is unlikely to play a significant role in protecting the sheath from chemical attack by fission products. We can also see that defects start much later than when the sheath has become plastic. During the plastic part of loading, stresses increase but little, yet significant plasticity is required before EAC failures occur in CANDU fuel. Therefore, the primary mechanical driver of EAC is not stress alone, but rather a combination of stress and strain.

To maintain fuel integrity, the above combination needs to be managed to acceptable levels. This is done in part by designing and operating fuel below defect thresholds for EAC, as described in the next section.

8.2 Defect Threshold

Like many processes, EAC contains some inherent variability. A defect threshold delineates an area below which no fuel defects are expected from EAC. Above the defect threshold, failures may or may not occur. Generally, the farther above a defect threshold the process is, the higher the probability of fuel defects.

An extensive literature of well over a thousand papers suggests that a very large number of parameters can potentially influence EAC. It is not practical to provide here an exhaustive mechanistic treatment of such a large list of parameters. Therefore, the authors have arbitrarily chosen to illustrate key concepts through a relatively recent insight [Tayal *et al*., 2000]. It is acknowledged that other perspectives are also available in the literature, but they are not discussed here for reasons of space.

In the formulation described here, stresses and strains in Zircaloy are represented by the size of the power ramp (ΔP). Corrosive agent concentration is represented by a combination of pre-ramp power (P_i) and burnup (ω) at the time of the ramp. Material degradation is represented by the burnup at the time of the ramp (ω).

Figure 24 shows the empirically obtained defect threshold at 140±20 MWh/kgU for non-CANLUB fuel.

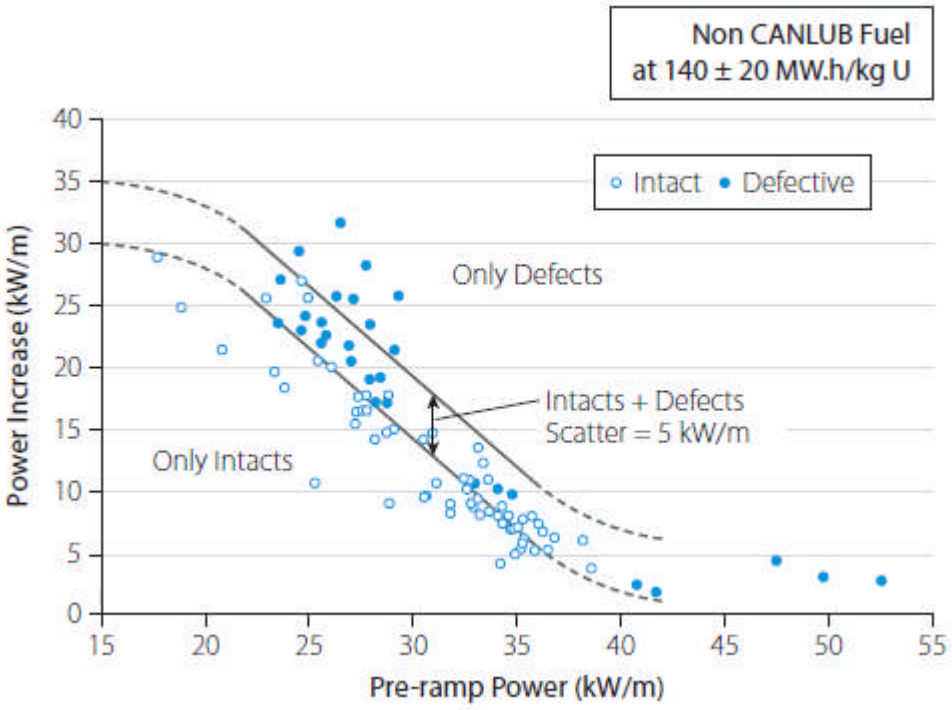

[Source: Tayal *et al*., 2000]

Figure 24 Defect threshold due to power ramp in non-CANLUB fuel at 140±20 MWh/kgU

The figure contains two lines. The lower line is the defect threshold for non-CANLUB fuel. Based on empirically derived curves, the defect threshold for CANLUB fuel is located about 12 kW/m higher than that shown in Figure 24 [Tayal *et al*., 2000].

Exercises:

Consider a non-CANLUB fuel element for which the operator is contemplating a power ramp from 30 kW/m to 50 kW/m for 2 hours at 140 MWh/kgU. Its pre-ramp power, P_i, is 30 kW/m. Its power ramp, ΔP, is (50 – 30) = 20 kW/m. From Figure 24, the fuel element can withstand a power ramp of about 14 kW/m at 140 MWh/kgU. Therefore, the applied power ramp will exceed the defect threshold and expose the fuel element to risk of an EAC defect.

As a second exercise, consider the same ramp being applied to a CANLUB fuel element. Its defect threshold is at (14 + 12) = 26 kW/m. The applied ramp of 20 kW/m is less than its defect threshold, and therefore the fuel can be expected to survive the ramp.

8.3 Defect Probability

The basic rule is always to operate fuel in a region which is safe from EAC defects, i.e., below the defect threshold. Nevertheless, on very rare occasions it may become necessary to operate a small number of fuel bundles slightly above the defect threshold in a one-off situation that might have become unavoidable due to an unusual combination of circumstances, such as during restart under a distorted flux shape after a shutdown. One then needs to consider taking a calculated risk. To develop an effective strategy for such rare occasions, one needs to quantify the risk of fuel failure above the defect threshold. This is done through knowledge of defect probability beyond the defect threshold, as described below.

Figure 24 contains not one, but two lines. As noted earlier, the lower line is called the defect threshold; it is the line below which no defect occurs. The upper line is one above which no fuel bundle stays intact. The region in between contains some scatter: some bundles in that region fail, whereas others stay intact.

Empirical evidence suggests that for all practical purposes, the defect threshold represents a trivial likelihood of defect, essentially zero. Nevertheless, in statistical theory, probabilities usually have asymptotic ends, that is, a probability is never zero, nor is it ever 100%. Therefore, the defect threshold shown in Figure 24 is usually assigned a low arbitrary probability such as 1%. Likewise, the upper line in Figure 24 is usually assigned an arbitrarily high defect probability close to 100%.

Figure 25 shows an illustrative increase in defect probability as a fuel bundle experiences power ramps that exceed the defect threshold [Penn *et al*., 1977]. Theoretically, the probability should be an "S"-shaped curve with asymptotic ends. For practical purposes, however, empirical evidence shows that the asymptotic parts near the two ends are small and that for the most part, the defect probability increases essentially linearly with increasing distance from the defect threshold (see Figure 25).

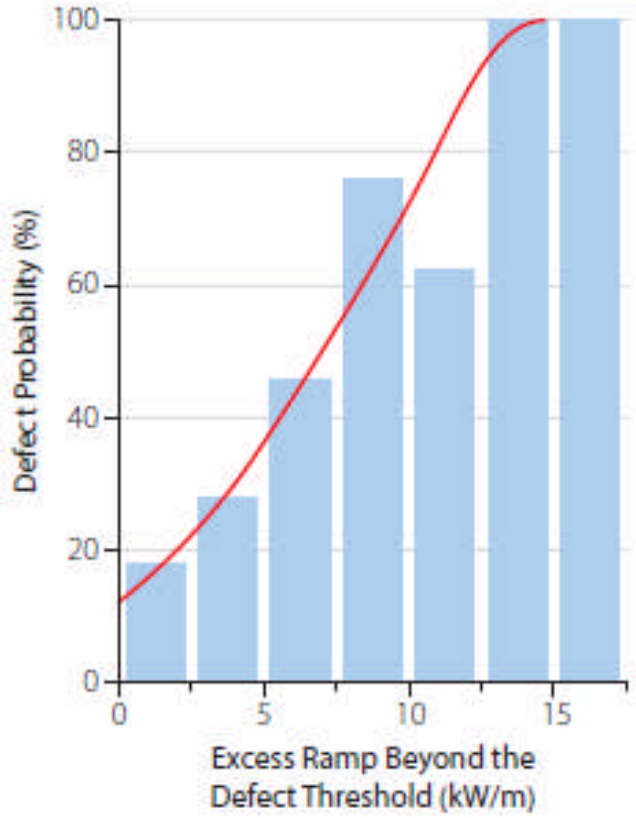

[Source: Penn *et al*., 1977]

Figure 25 Defect probability

The distance between the two lines shown in Figure 24 is about 5 kW/m; however, when the data from other burnups are also considered, the overall separation between the two lines for all burnups is closer to 10 kW/m. Therefore, to a first approximation, and if one ignores small asymptotic regions near the two extremes, for every increment of one kW/m above the defect threshold, the defect probability increases by about 10 percentage points until it reaches 100%.

The portion of the ramp that is above the defect threshold is sometimes also called the "excess ramp". In the illustrative example below, the "excess ramp" is 8 kW/m.

Exercise: Consider a non-CANLUB fuel bundle where the steady-state power in the outer element changes from 35 kW/m to 50 kW/m at 140 MWh/kgU. This gives it a ramp of (50 – 35) = 15 kW/m. From Figure 24, the defect threshold at this initial power is 7 kW/m. Therefore, the actual ramp is (15 – 7) = 8 kW/m above the defect threshold. Therefore, this fuel bundle has a (8*10%) = 80% chance of fuel defects through EAC.

8.4 Mitigation

Based on past experience, the fuel industry has adopted certain strategies to mitigate EAC defects. Some illustrative examples are given below.

- CANLUB: CANLUB significantly increases the defect threshold. It is believed that the effectiveness of CANLUB increases with thickness. However, it is also believed that after a certain thickness, additional increases in CANLUB thickness likely yield diminishing returns. At the same time, there is concern that very thick layers of CANLUB may potentially release excessive hydrogen into the sheath. Therefore, a CANLUB layer of a selected optimal thickness is applied to the inside of the sheath [Wood and Hardy, 1979].
- Fuel Management: The key operating parameters for EAC—size of the power ramp, initial and final powers, and burnup—are all controllable to some degree through refuelling strategy. Therefore, optimal refuelling strategies have been devised to avoid EAC failures in CANDU reactors. A compelling example comes from the Pickering reactors, where early EAC failures were eliminated in part by improved refuelling schemes.
- Sheath/Endcap Junction: A significant contribution to EAC defects at sheath/endcap junctions arises from the stress concentration at re-entrant corners of these junctions. Therefore, the detailed design of the sheath/endcap junction must be carefully controlled, including the radius of the re-entrant corner, the pellet profile at the end of the fuel stack, and the axial distance between the pellet stack and the re-entrant corner.
- Element Rating: Smaller ramps and lower heat generation rates reduce the threat from EAC, as shown in Figure 24. These can be achieved by, for example, spreading a bundle's power among more fuel elements, e.g., by using more but smaller-diameter fuel elements within a fuel bundle. CANDU fuel has indeed evolved in this direction, starting with a fuel bundle that used 19 fuel elements, then moving to one that used 28, to 37 elements, and to the CANFLEX design that uses 43 fuel elements [Hastings *et al*., 1989].
- Detailed Internal Design: Sheath strain and fission gas release can also be influenced by the detailed internal design of the fuel element, such as pellet density and clearances between the sheath and the pellets.

9 Vibration and Fatigue

Fuel elements produce large amounts of heat and therefore must be cooled aggressively. Coolant velocity is usually high (about 10 m/s), and the flow is at least partly turbulent. Moreover, the coolant may sometimes contain standing waves of pressure pulses. The pressure pulses are created when a pump's vanes pass over the pump outlet and may be subsequently amplified by resonance in pipes that carry the coolant. These combinations of conditions can lead to vibrations and rocking in fuel elements and bundles and even in fuel strings. This in turn creates the potential for fatigue and fretting.

In a significant defect excursion, these conditions did indeed occur in 1991 in the Darlington reactors in Canada. This led to excessive axial vibrations in the fuel strings, which cracked endplates in fatigue and also caused significant fretting of spacer pads [Lau *et al*., 1992]. This in turn led to shutdown of the reactors for a few months and significant loss of revenue.

To avoid damage due to fatigue and fretting, one needs to understand the science behind fuel vibrations and the resulting alternating stresses and incorporate appropriate mitigation strategies in the design and operation of the fuel and the plant. The next section describes some aspects of the science of fuel vibration and fatigue.

9.1 Alternating Stresses

Axial flow and turbulence induce lateral vibrations in fuel elements, whereas pressure pulses induce axial vibrations. Both types of vibrations generate alternating stresses in the fuel bundle endplate and in the assembly weld (that is, the weld between the endplate and the endcap).

Quantification of alternating stresses and the resulting fatigue due to lateral vibrations involves a number of calculations, such as the bending moment in the assembly weld and in the endplate due to bending of a fuel element, the resulting alternating stresses, and a comparison of these stresses to the fatigue strengths. Mathematical models to do this are available [Tayal *et al*., 1984] and are summarized below.

9.1.1 Moment Due to Fuel Element Deflection

The overall model is shown in Figure 26. If a fuel element of length ℓ experiences a uniformly distributed load p that deflects it in a direction radial to the fuel bundle, its lateral deflection v is resisted by its own moment of inertia as well as by the stiffness of the two endplates. The endplates are twisted by the fuel element and therefore act as torsional springs in resisting the twisting moment W applied by the fuel element.

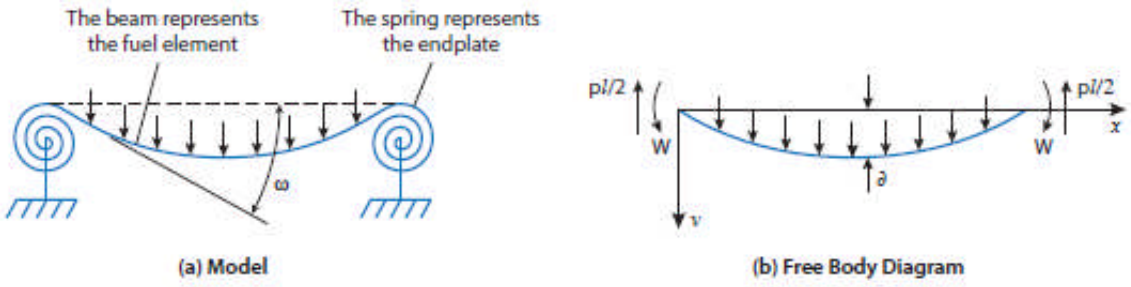

[Source: Tayal *et al*., 1984]

Figure 26 Lateral vibration of a fuel element

If the fuel element's flexural rigidity is J, the classical equation for beam deflection v can be written as [Gere *et al*., 1997]:

$$J\frac{d^2v}{dx^2} = W - px(\ell - x)/2\,, \tag{6}$$

where x represents the distance along the length of the fuel element.

For boundary conditions of:

$$v = 0 \text{ at } x = 0 \text{ and at } x = \ell\,, \tag{7}$$

Equation (6) integrates to:

$$Jv = Wx(x-\ell)/2 + px(x^3 - 2x^2\ell + \ell^3)/24. \tag{8}$$

To derive an expression for the moment transmitted through the assembly weld, consider the relationship between the moment and rotation of the spring:

$$\frac{dv}{dx} = \omega = W/S \text{ at } x = 0\,, \tag{9}$$

where ω represents the rotation of the fuel element.

By differentiating Equation (8) to obtain the fuel element's slope at the end and inserting this into Equation (9), we obtain a relationship for the moment W transmitted by the fuel element to the endplate through the assembly weld [Tayal *et al*., 1984]:

$$W = \frac{p\ell^2}{12}\left[\frac{1}{1+\frac{2J}{S\ell}}\right]. \tag{10}$$

Equation (10) expresses the moment carried by the endplate and the assembly weld in terms of

the uniformly distributed load p. However, p is usually not known. Instead, the mid-span deflection δ can be estimated more easily through other means. Therefore, p can be replaced in Equation (10) by the mid-span deflection δ using the following additional information:

$$\delta = v \text{ at } x = \ell/2 . \tag{11}$$

This results in the following equation for the moment carried by the assembly weld and the endplate as a function of the mid-length deflection of the fuel element:

$$W = 32 J \delta / (\ell^2 + 10 J \ell / S) . \tag{12}$$

To calculate the moment through the above equation, one needs to know the spring constant S of the endplate, which is discussed in the next subsection.

9.1.2 Spring Constant of the Endplate

The moment *W* as calculated above twists the endplate by a force which decays along the circumference of the endplate. As the endplate twists, it forces its own local twist on the fuel elements that are welded to it, which the latter resist. Therefore, the applied twisting moment on the endplate is resisted not only by the torsional rigidity of the endplate, but also by the torsional rigidities of the other fuel elements welded to the endplate. For this reason, the endplate behaves like a beam resting on an elastic foundation. Figure 27 shows such a model.

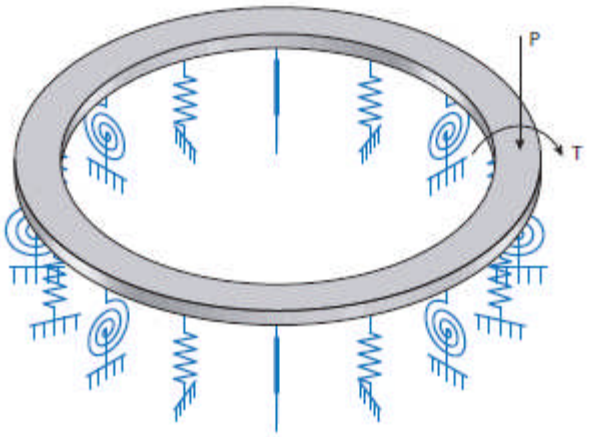

[Source: Tayal *et al*., 1984]

Figure 27 Endplate as a beam on elastic foundations

The endplate rings are circular. Sensitivity studies show that under on-power conditions of CANDU fuel elements, the effect of circularity is small. Therefore, to a good first approximation, the mathematics of the endplate can be simplified considerably by treating it as a straight (rather than circular) beam on elastic foundations. A mathematical model for this can be developed based on the science given in classical textbooks on mechanics of materials [for example, see Timoshenko, 1961].

Let β be the local twist of the beam. A foundation of modulus κ will exert a twisting moment of - κ β per unit length of the beam. If the beam's cross section is assumed to carry only a twisting

moment M_z, then the equilibrium of an infinitesimal length yields:

$$\frac{dM_z}{dz} = GC\left(\frac{d^2\beta}{dz^2}\right) = \kappa\beta\,, \tag{13}$$

where z is the distance along the length of the beam, G is the shear modulus, and C is the twisting moment of inertia.

This second-order differential equation can be integrated to yield the rotation and the twisting moment along the beam's length. The two constants of integration can be obtained by the requirement that the rotation be zero at infinite distance from the origin and that the internal twisting moment at the origin be half the applied twist. This process yields the following equations:

$$\beta = \frac{T\alpha}{2\kappa}e^{-\alpha z}\,, \tag{14}$$

where T is the applied twisting moment and

$$\alpha = \left\{\kappa/(GC)\right\}^{1/2}. \tag{15}$$

If the beam's response to W is represented as a torsional spring, its spring constant S is:

$$S = \left.\frac{T}{\beta}\right|_{z=0} = 2\left(GC\kappa\right)^{1/2}. \tag{16}$$

The above spring constant can be used in Equation (12) to calculate the moment carried by the assembly weld.

9.1.3 Foundation Modulus

Equation (16) requires knowledge of the foundation modulus κ for the endplate.

Let two endplate rings of radius R connected by N fuel elements be twisted by an angle β. The ends of each sheath, which are held perpendicular to the endplate surface by the assembly weld, will also rotate by the same angle β. If W represents the resistive moment applied by each sheath to the endplate, then m, the resistive moment from the sheath per unit endplate length, can be evaluated by spreading the total of such moments over the circumference of the endplate:

$$m = NW/(2\pi R)\,. \tag{17}$$

W is also equal to the bending moment applied by the endplate to the fuel element to rotate its end by β. Therefore, classical beam theory can be used to relate W and β as follows:

$$\beta = W\ell/(2J)\,. \tag{18}$$

Therefore, by combining Equations (17) and (18), the foundation modulus κ can be calculated as:

$$\kappa = m/\beta = JN/(\pi R\ell)\,. \tag{19}$$

To account for the tight contact with the neighbouring fuel bundle under high hydraulic load, it is customary to assume twice the actual number of fuel elements in Equation 19 above.

9.1.4 Cross-Sectional Properties of the Endplate

The equations presented above also require knowledge of the endplate's twisting moment of inertia (C) and the fuel element's flexural rigidity (J).

The twisting moment of inertia C of the endplate can be obtained from the classical equation for a rectangular beam. For the usual shapes of CANDU endplates [Tayal *et al*., 1984]:

$$C = 0.26ct^3, \tag{20}$$

where c is the width of the beam and t its thickness.

9.1.5 Flexural Rigidity of the Fuel Element

At high power, the pellet expands and grips the sheath tightly, often stretching the latter well into the plastic range. Therefore, the flexural rigidity of a fuel element usually contains contributions from the sheath and from the pellets. The concept can be illustrated more simply by examining the experimental results shown in Figure 28.

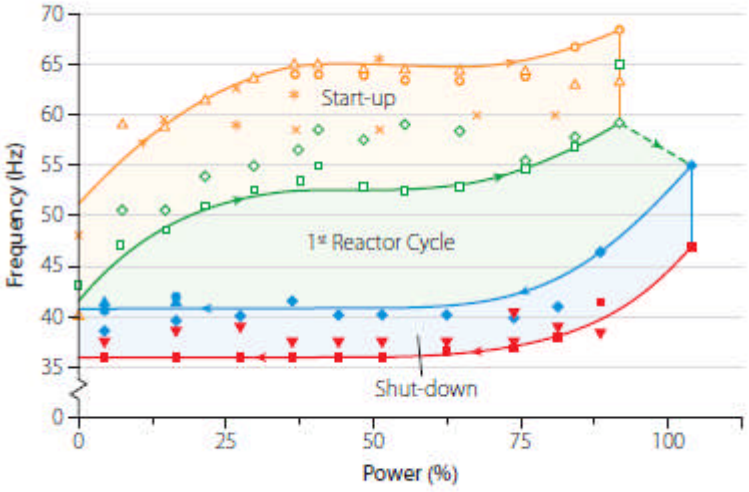

[Source: Pettigrew, 1993]

Figure 28 Stiffening of a fuel element at operating power

When the instrumented fuel element represented in Figure 28 was initially brought to high power, its vibration frequency increased significantly [Pettigrew, 1993]. Frequency of vibration can be related to flexural rigidity through the classical theory of vibration. This suggests that at initial high power, the flexural rigidity of the fuel element is significantly higher than that of an empty sheath. The difference reflects the contribution of the pellet when it is in tight contact with the sheath.

However, the pellet is not always in tight contact with the sheath. With continued irradiation, the interfacial pressure between the pellet and the sheath relaxes due to creep. This in turn lowers the net flexural rigidity of the fuel element and hence decreases its vibration frequency. Lower power also reduces the pellet/sheath interfacial pressure. These dynamics are also reflected in Figure 28. For this reason, we express the flexural rigidity of the fuel element as

that of the sheath plus that of the pellet multiplied by a "pellet interaction factor" *G* which reflects the varying levels of pellet/sheath interaction.

Another complication is that UO_2 is brittle and therefore cannot support significant tensile loads. Therefore, the resulting equation for pellet flexural rigidity is fairly complex, as described for example in [Tayal *et al*., 1984]. For simplicity, here we treat the impact of pellet cracking by means of a pellet cracking factor $\propto$ which reduces the net contribution of the pellet to the overall flexural rigidity of the fuel element. As an illustrative number, the examples below use a pellet cracking factor $\propto$ of 0.1.

Therefore, the net flexural rigidity J of the fuel element can be described as:

$$\begin{aligned} J &= J_s + GJ_p \\ &= E_s\left[\frac{\pi}{4}\left(r_1^4 - r_2^4\right)\right] + \frac{\pi}{4}E_p r_p^4 \alpha G \end{aligned} \tag{21}$$

where J is the flexural rigidity of the fuel element, J_s the flexural rigidity of the sheath, J_p the flexural rigidity of the pellet, E_s the Young's modulus of the sheath, r_1 the outer sheath radius, r_2 the inner sheath radius, E_p the Young's modulus of the pellet, r_p the pellet radius, $\propto$ the pellet cracking factor, and G the pellet interaction factor.

The pellet interaction factor G varies between 0 and 1. Under the conditions of the experiment shown in Figure 28, the pellet interaction factor G is zero when the fuel element is at zero power. When the fuel element is first brought to full power, G increases to 1 because the interfacial pressure between the pellet and the sheath is high. During continued operation at full power, G gradually decreases to 0 as the interfacial pressure between the pellet and the sheath relaxes. Therefore, the pellet/sheath interfacial pressure has a major impact on the pellet interaction factor.

For a given lateral deflection of the fuel element, stresses in the endplate and in the assembly weld are higher for higher levels of pellet/sheath interaction. Therefore, the upper end of the pellet interaction factor range gives conservative results for such stresses.

9.1.6 Stresses

The above Equations (12), (16), (19)–(21) provide all the information needed to calculate the moment carried by the assembly weld and the endplate. This moment can be converted into nominal stresses using the classical equations given below [Timoshenko *et al*., 1970].

Nominal shear stress τ in the endplate:

$$\tau = 1.87\ W / (ct^2). \tag{22}$$

Nominal normal stress σ in the assembly weld:

$$\sigma = 32\ W / (\pi d^3), \tag{23}$$

where d is the weld diameter.

To the nominal stresses given by the above equations, one would need to add the effects of stress concentrations due to the rapid change in geometry near the end of the fuel element. This topic is covered as part of fatigue strength in Section 9.2.

9.1.7 Illustrative Example

As an illustrative example, let us calculate the nominal stresses in the endplate and in the assembly weld when the outer fuel element of a CANDU-6 bundle undergoes lateral vibrations 25 micrometers in amplitude.

Assume that the fuel dimensions and properties are as given in Tables 1 and 2, except that the on-power diametric clearance between the pellet and the sheath is zero. For the remaining inputs, assume that the mean radius R of the endplate's outer ring is 43 mm, the weld diameter d is 4 mm, the pellet cracking factor $\propto$ is 0.1, and the rigidity enhancement factor G is 1.

Equations (20), (21), (19), (16), and (12) yield the following intermediate results: the twisting moment of inertia C of the endplate is 5.2 mm^4, the flexural rigidity J of the fuel element is 46 Nm^2, the foundation modulus κ of the endplate is 25 kNm/(m•rad), the spring constant *S* is 118 Nm/rad, and the bending moment *W* is 0.017 Nm.

Equation (22) gives the nominal shear stress in the endplate as 2.5 MPa. Equation (23) gives the nominal normal stress in the assembly weld as 2.7 MPa.

Because these stresses are due to vibration, they are alternating stresses. Their impacts on fatigue are examined in the next section.

9.2 Fatigue of the Endplate and the Assembly Weld

O'Donnell and Langer recommended 55 MPa as the endurance limit for cold-worked and/or welded Zircaloy-4 at 300°C [see O'Donnell *et al*., 1964]. This assumes that residual stresses are equal to cyclic yield strength, accounts for damage due to irradiation, and includes a safety factor of two to cover miscellaneous effects such as specimen size, environment, surface finish, and data scatter.

The diameter of the fuel element endcap decreases sharply near the weld. Hence, stress concentrations are to be expected in this region. Therefore, the endurance limit specified above should be reduced by the effects of stress concentration. Peterson's ∂ concept can be used for this purpose [see Peterson, 1943]. It states that in a region of sharp stress concentrations, fatigue is best evaluated through stress at a distance ð below the surface. ∂ is a material property.

Based on experimental data, O'Donnell and Langer estimated ∂=50 micrometers for Zircaloy-4. Fatigue strength reduction for this delta can be determined using the results of O'Donnell and Purdy [see O'Donnell *et al*., 1963]. A review of O'Donnell and Purdy's results shows that for a fairly wide range of notch radii (30 to 200 micrometers), the fatigue strength reduction factor *K* is between 2.0 and 2.5 when the section width is 5 mm (close to the CANDU assembly weld). For purposes of illustration, let us conservatively assume a fatigue strength reduction factor *K* of 2.5 for the assembly weld (i.e., the weld between the endcap and the endplate).

There are no major geometric stress raisers in an endplate that would bear significantly on fatigue due to alternating shear stress near the assembly weld. Nevertheless, a small undetected fabrication flaw (e.g., a crack) will act as a notch and reduce local fatigue strength. Such a small crack may exist due to a flaw in the sheet metal used for endplate fabrication or may be introduced during bundle assembly and subsequent handling. Using the curves of O'Donnell and Purdy, the fatigue strength reduction factor for an endplate in the presence of such a small crack can be conservatively estimated as 2. Therefore, the fatigue strength of the endplate is 28

MPa.

Exercise:

Consider the potential of fatigue from lateral vibrations of the fuel element assessed in Section 9.1.6.

Assembly weld: The alternating stress is 2 MPa. The fatigue strength is 22 MPa.

Endplate: For comparison to fatigue strength, the classical von Mises formulation for effective stress tells us that shear stress needs to be multiplied by the square root of 3 to be comparable to normal stress. Therefore, the effective alternating stress in the endplate is (2.5 * √3) = 4.4 MPa. In comparison, the fatigue strength is 28 MPa.

For both the assembly weld and the endplate, the alternating stresses are much lower than the corresponding fatigue strengths. Therefore, the weld and the endplate are not at risk of fatigue failures from this level of vibration.

10 Fuel Design Verification

During design, fabrication, and operation of nuclear fuel, a key objective is to preclude, as a minimum, significant, chronic, systematic fuel failures. This needs to be confirmed up front for credible combinations of the most demanding design, fabrication, and operating conditions that can be expected in the reactor.

During design, likelihood of acceptable fuel performance can be assessed through a mixture of three types of tools: engineering judgment, tests, and analyzes. Each tool has its pros and cons, as explained later in this section, and therefore judicious combinations of them tailored to each specific situation are often used.

Tests can be done on prototype fuels either inside or outside a reactor. In-reactor tests can be done either in a test reactor such as the NRU and NRX reactors in Chalk River, Ontario, or in an operating commercial power reactor. In-reactor tests automatically include the effect of neutrons, which out-of-reactor tests miss. However, out-of-reactor tests can include certain influences that are not available in current in-reactor experimental facilities, such as the effect of gravity (current test loops are vertical) and the effect of the precise support provided to the fuel string by shield plugs, sidestops, or latches (in current test loops, fuel is supported by a central structural tube). In addition, out-of-reactor tests often tend to be significantly less expensive and quicker than in-reactor tests. Judicious choices must therefore be made in each situation.

Tests have a significant advantage over analyzes in that they automatically include all processes encompassed by the test conditions. Therefore, within the parameters of the experiment, there is virtually no risk that an important process has been missed. Table 3 is an illustrative list of tests done on some CANDU prototype fuels.

Table 3 Illustrative list of tests on prototype fuel bundles

Test	Purpose and Configuration
Bent-tube passage	Bench test done at room temperature and atmospheric pressure to verify that a prototype bundle, when not damaged, can pass through the "bent-tube" gauge, which simulates the most restrictive passage in a fuel channel.
Bundle strength – shield plug support	Single-bundle test done in stagnant water at reactor pressure and temperature to verify that a prototype bundle, supported by a simulated shield plug, can withstand the maximum reactor load in the fuel channel under normal conditions without failing. Test bundle failure is indicated when: (1) the bundle fails the bent-tube gauge test and/or (2) shows permanent deformation in any of its components that exceeds the as-built dimensional tolerances for that component and/or (3) develops cracks in any of its structural components or joints between components.
Bundle strength – double side stop support	Single-bundle test done in stagnant water at reactor pressure and temperature to verify that a prototype bundle, supported (normally) by two side stops, can withstand the maximum reactor load in the fuel channel during refuelling without failing. Test bundle failure is indicated when: (1) the bundle fails the bent-tube gauge test and/or (2) shows permanent deformation in any of its components that exceeds the as-built dimensional tolerances for that component and/or (3) develops cracks in any of its structural components or joints between components. Applies to C6-type reactors.
Bundle strength – single side stop support	Single-bundle test done in stagnant water at reactor pressure and temperature to verify that a prototype bundle, supported (abnormally) by a single side stop, can withstand the maximum reactor load in the fuel channel during refuelling without failing. Test bundle failure is indicated when the bundle fails the bent-tube gauge test. Applies to C6-type reactors.
Refuelling Impact	Out-of-reactor test done in a representative full-length fuel channel using circulating light water at reactor operating temperature and pressure, to verify that prototype bundles can withstand the maximum impact loads expected in the fuel channel during refuelling without failing. Test bundle failure is indicated: (1) when the bundle fails the bent-tube gauge test and/or (2) shows permanent deformation in any of its components that exceeds the as-built dimensional tolerances for that component and/or (3) develops cracks in any of its structural components or joints between components. Applies to C6-type reactors.

Test	Purpose and Configuration
Endurance	Out-of-reactor test, done inside a representative full-length fuel channel containing a full complement of prototype fuel bundles, using circulating light water at reactor operating temperature and pressure, in increments of time until the spacer pads of the test bundles cease to exhibit additional wear with increases in test time, to verify: (1) that spacer pad wear on test bundles does not exceed its wear allowance; (2) that bearing pad wear on test bundles, projected over the maximum in-reactor bundle residence time, does not exceed its wear allowance; (3) that test bundles do not show permanent deformation in any of their components that exceeds the as-built dimensional tolerances for those components; (4) that test bundles do not develop cracks in any of their structural components or joints between components; and (5) test bundles do not cause channel damage, projected over the lifetime of the channel, which exceeds the channel's lifetime material loss allowance, also taking into account possible channel damage by other means.
Sliding wear	Single prototype bundle test done in stagnant light water at reactor operating temperature and pressure to verify that: (1) bearing pad wear in the test bundle does not exceed the bearing pad wear allowance and (2) projected lifetime pressure-tube damage, caused by sliding bearing pads of the test bundle, does not exceed the channel's lifetime material loss allowance, also taking into account possible channel damage by other means.
Pressure drop	Out-of-reactor test done in a representative full-length fuel channel, containing a full complement of prototype fuel bundles, using circulating light water at reactor operating temperature and pressure, to verify that the hydraulic pressure drop generated in the portion of the fuel channel that contains fuel bundles does not exceed the pressure drop allowance for the same portion of the channel.
Bundle rotation pressure drop	Out-of-reactor test done in a representative full-length fuel channel and/or a partial-length channel, using circulating light water at reactor operating temperature and pressure and/or at room temperature and low pressure, to determine the variation in hydraulic pressure drop generated across the endplate-to-endplate junction between two abutting prototype bundles as a function of their relative radial (mis)alignment.
Fuelling machine compatibility	Out-of-reactor test done in a representative full-length fuel channel, using circulating light water at reactor operating temperature and pressure, in conjunction with a production fuelling machine, to verify that the fuelling machine can charge and discharge prototype fuel bundles into the channel.
Wash-out	Out-of-reactor test done in a representative full-length (or partial-length)

Test	Purpose and Configuration
	fuel channel, using circulating light water at reactor operating temperature and pressure, in conjunction with apparatus that simulates the relevant functions of the fuelling machine, to determine what malfunctions in use of carrier tubes might cause “wash-out” of the type observed in some power reactors. Applies to CANDU rectors that use carrier tubes during refuelling.
Frequency sweep	Out-of-reactor test done in a representative full-length fuel channel containing a full complement of prototype fuel bundles, using circulating light water at reactor operating temperature and pressure and a pressure pulse generator, to: (1) determine the frequency of pressure pulsations at which the column of test bundles, supported normally inside the channel, may resonate, and (2) verify that the resonant frequency of the column of test bundles is not the same (or nearly the same) as the coolant pump vane passing frequency.
Critical heat flux	Out-of-reactor test done in a representative full-length fuel channel using circulating light water at reactor operating temperature and pressure and electrical heaters to simulate the geometry and power produced by fuel bundles, to determine the spectrum of channel thermal-hydraulic and power conditions in the range of interest to reactor operation, which lead to a step change in heater surface temperature, referred to as “dryout”.
High-power irradiation	Irradiation test done on prototype bundles cooled by circulating water at reactor operating temperature and pressure to verify that a bundle irradiated at power/burnup conditions that encompass the power/burnup conditions of all bundles in the power reactor will be defect-free at the end of the irradiation period. Such a test can be done, for example, in a vertical channel of the NRU test reactor, called a “hot loop”, in which test bundles are cooled by light water; enriched uranium would need to be used to generate the high element ratings expected in a commercial CANDU power reactor.
Power ramp irradiation	Irradiation test done on prototype bundles cooled by circulating water at reactor operating temperature and pressure, to verify that a test bundle can survive, defect-free, the most severe power ramps expected in a reactor. Typically, this would involve: (1) irradiation of a test bundle at relatively low power for some fraction of its residence in the reactor, and then (2) an increase in power for the remainder of its residence in the reactor, such that the burnup accumulated at the initial power and the increased power surpasses the equivalent conditions of all bundles in the power reactor. Using C6 as an illustrative example, the low-power irradiation would reflect power and burnup in positions 1 to 4 in a high-power channel, and the size of the ramp would reflect, in an appropriately conservative manner, the power ramps in bundles 1 to 4 during or after

Test	Purpose and Configuration
	their shift to positions 9 to 12. Such tests can be performed in, for example, the vertical hot loops at NRU in CRL in which test bundles are cooled by light water; enriched uranium pellets would be required to achieve the high element powers expected in a commercial CANDU reactor.
Irradiation of special materials	Irradiation test done on prototype elements which contain the novel material (e.g., an inert matrix for burning of actinides) cooled by circulating water at reactor operating temperature and pressure, to verify that the elements containing the special material will be defect-free at the end of their irradiation period. Such a test can be done, for example, in "demountable" bundles in a vertical channel of the NRU test reactor called a "hot loop", in which test specimens are cooled by light water.

At the same time, fully representative tests are not always practical in some situations, for example because of equipment, cost, schedule, or combinations thereof. As specific illustrative examples, let us consider the following:

- **Comprehensiveness**: As one illustrative example, a CANDU fuel designer needs to confirm, among other aspects, that a fuel bundle has adequate mechanical strength to resist the mechanical loads imposed on it during discharge from the fuel channel. The test facility, to verify this experimentally, would need to provide for all the important effects in this scenario, meaning that (a) the test facility should be shielded so that it can accommodate irradiated fuel so that reduction in ductility due to prior irradiation can be accounted for; (b) it should be long enough to accommodate a string of approximately 12 fuel bundles; (c) it should produce power to simulate the effect of on-power interaction of the pellets and the sheath on load shedding; (d) it should be connected to a pump of sufficiently large capacity to provide the necessary flow for the hydraulic drag load; and (e) it should contain a representative fuel support configuration to simulate the appropriate load concentrations. We currently do not have a shielded facility that meets all these requirements, and building a new one would be very expensive and time-consuming. For this reason, such tests have been done in the past in unshielded out-of-reactor facilities using non-irradiated fuel bundles. Although such tests are useful, they do miss the order-of-magnitude drop in ductility of the fuel bundle's structural materials that occurs during irradiation, and hence they may not always determine the actual adequacy of an irradiated fuel bundle's mechanical strength. Another similar situation that is also not covered by existing test facilities is the effect of gravity on long-term irradiation-enhanced creep sag of fuel in a horizontal orientation. These situations can be rectified through analyzes.
- **Scatter**: As another illustrative example, consider the need to verify whether or not a new fuel design meets the expected power ramp challenges in a new operating envelope for which the EAC defect threshold is not well known ahead of time (*a priori*). For a new operating envelope and fuel design, one would not know *a priori* which specific ramp is the most demanding. Therefore, one would need to test many ramps, and to cover the expected scatter in the results, one would need to test a statistically significant number for each condition. This would require testing many bundles for a large number

of ramps, and for each ramp, significant in-reactor irradiation would be required to accumulate the required burnup. Because only limited facilities for in-reactor irradiation are available, the full test matrix could require large amounts of time and expense. Again, analyzes can help reduce the cost as well as the timeline.

- **Margins**: Knowledge of available margins is needed for a variety of purposes, e.g., to establish a safe operating envelope or to deal quickly with abnormal situations. To determine the margin available in a design solely from tests, one would need to perform a large number of experiments. Again, time and expense for these can be reduced through analyzes.

For these conflicting reasons, some situations are better addressed through tests, whereas others require a judiciously balanced combination of tests and analyzes. Appropriate combinations of tests and analyzes must be tailored to a variety of factors such as (a) features of the specific change in design, (b) completeness and level of knowledge of relevant damage mechanisms, and (c) specific features, capabilities, and capacities of available test facilities and analytical tools. For example, different combinations of tests and analyzes have been used to verify the CANFLEX fuel design [Hastings *et al*., 1989], the ACR fuel design [Reid *et al*., 2008], and the 37M fuel design [Daniels *et al*., 2008]. In the following sections, we describe a fuel design verification process that combines tests and analysis.

To craft an optimal program of comprehensive design analyzes, a sound knowledge is needed of credible damage mechanisms during the conditions for which fuel integrity needs to be ascertained. A few selected damage mechanisms have been described in detail in earlier sections of this chapter. An overview compilation of all currently known credible and significant damage mechanisms is given in the next subsection.

10.1 Damage Mechanisms

Most discussions about fuel damage revolve around two types of damage: primary and secondary. A primary damage mechanism is one that creates the *initial* hole or break in Zircaloy or is an important precursor to it. Secondary damage—usually from zirconium hydrides—is a consequence of primary damage. This section focusses on mechanisms for primary damage. Secondary damage is discussed in Section 12.1.

Based on first principles and confirmed by a comprehensive search of the available literature [Sun *et al*., 2010], 18 primary damage mechanisms have been identified for CANDU fuel [Tayal *et al*., 2008-1], of which only three are described in detail in the preceding sections for reasons of space. All eighteen are, however, listed in the following sections. For simplicity in the following discussion, the primary damage mechanisms are classified into three broad groups: thermal damage, structural damage, and compatibility considerations [Tayal *et al*., 2008-1] and are described below in turn.

10.1.1 Thermal Damage ("T" Series)

Four thermally driven mechanisms can potentially damage the fuel, as described below.

Pellet melting

If the pellet melts, the resulting volumetric expansion of the pellet may potentially push the sheath past its breaking point. Alternatively, molten UO_2 may potentially flow into contact with Zircaloy and melt it by its contained heat.

Zircaloy-UO_2 is another system with a low-melting-point alloy. Hence, strictly speaking, UO_2 does not have to heat the Zircaloy all the way to its melting point to form a liquid alloy.

Melting of Zircaloy or its alloys

Insufficient cooling may potentially melt the Zircaloy, impeding its ability to contain fission products.

The fuel sheath also contains Zircaloy/beryllium eutectic and other alloys in that neighbourhood. Their melting points are lower than that of the parent Zircaloy, and therefore insufficient cooling may potentially melt these alloys. This could detach the pads from the sheaths, destroying their functionality.

Crevice corrosion

Crevice corrosion can potentially occur in crevices such as between bearing pads and the pressure tube or between pads and the sheath. The crevices restrict the flow of coolant. Coolant can boil off in the near-stagnant conditions in the crevice, which in turn can increase the concentration of chemicals such as lithium in the crevice. Lithium, in the form of lithium hydroxide, is added to the coolant to control its pH. The resulting elevated concentration of lithium can potentially accelerate Zircaloy corrosion.

Overheating by contact

If a heated surface such as the sheath contacts a neighbouring surface such as another sheath or the pressure tube, there is potential for reduced local cooling and hence overheating of the fuel, the pressure tube, or both.

10.1.2 Structural Damage ("S" Series)

Structural damage can potentially be caused through nine mechanisms, as described below.

Internal overpressure

In conjunction with a corrosive internal environment and local hydrides, excessive internal pressure in a fuel element can in principle cause cracks at two locations of stress concentration for primary stresses: at the sheath/endcap junction, and at the junction of the sheath and the pad. In practice, to date such cracks have been observed primarily at the sheath/endcap junction.

Environmentally assisted cracking during power ramps

During power ramps, irradiation-embrittled Zircaloy can experience high stresses and strains in the presence of a corrosive internal environment and local hydrides. This combination can potentially crack the sheath at locations of concentration for secondary stresses and strains—at circumferential ridges and at sheath/endcap junctions—through environmentally assisted cracking.

Static mechanical overstrain

During a variety of situations such as refuelling, structural components of the fuel bundle can potentially be exposed to relatively high loads, relatively sparse support, or both, leading to a potential for static mechanical overstrain.

Uncontrolled loss of geometry

This term refers to situations that can potentially lead to buckling, which in turn can lead to uncontrolled loss of geometry.

Fatigue

Alternating stresses caused by vibration (e.g., induced by flow, turbulence, or both), power manoeuvring, and load following can expose the fuel to potential failure through fatigue.

Fuel mechanical rupture due to impact

Situations such as refuelling or starting and restarting of coolant pumps can potentially impose significant impact loads. This is more damaging if it occurs after some amount of irradiation embrittlement of Zircaloy.

Primary hydride failure

A fuel element can pick up hydrogen or deuterium from a variety of sources. The hydrogen and deuterium tend to concentrate at relatively cooler locations and/or at locations of relatively higher stress. Excessive local hydrides and deuterides can reduce the local ductility of Zircaloy, rendering it less capable of carrying its load.

Oxide spalling and hydride lens formation

Some amount of corrosion is unavoidable in Zircaloy at the high temperatures and chemistry of the coolant. If the oxide surface is too thick, it can spall away. This can create local temperature gradients, which can form local hydride/deuteride deposits called “hydride lenses”. Loss of crud from a uniform layer of crud would have a similar effect. A hydride lens embrittles Zircaloy locally, reducing its capacity to carry load.

Insufficient ductility during post-irradiation handling

To enable post-irradiation handling of fuel, it is prudent to limit the amount of hydrides and deuterides in irradiated Zircaloy so that it has reasonable residual ductility to resist its anticipated loads.

10.1.3 Compatibility Considerations (“C” Series)

Five mechanisms can cause potential incompatibilities, as described below.

Interaction loads on the fuel string

This mode of damage refers to the potential expansion of the fuel string to become longer than the available length of the cavity in the fuel channel.

Dimensional incompatibility of a fuel bundle

This mode of damage refers to the possibility of the in-service on-power dimensions of the fuel bundle becoming larger than the available space through processes such as creep and thermal expansion. This can potentially generate unanticipated large stresses that may damage the fuel.

Spacer pad fretting

Excessive fretting of spacer pads due to vibration can potentially rub the corner of a spacer pad into the adjacent sheath, potentially creating a hole in the sheath, or can reduce the gap between elements below the design minimum required for heat removal by the coolant.

Jamming

This mode refers to the possibility that in-service on-power dimensions of the fuel bundle may become such that the fuel bundle cannot pass—easily or at all—through the fuel channel. For example, this can potentially occur due to interlocking of multiple spacers or due to excessive distortion.

Damage to pressure tubes

Bearing pads can cause fretting, sliding wear, and crevice corrosion in pressure tubes.

10.2 Acceptance Criteria and Integration

Acceptance criteria are needed to determine whether or not damage from the above mechanisms is within acceptable limits. Table 4 lists a set of acceptance criteria [Tayal *et al*., 2008-1].

Table 4 Fuel design acceptance criteria for normal operating conditions

[Source: Tayal *et al*., 2008-1]

Damage Consideration	Acceptance Criterion
"T Series": Thermal Integrity	
Fuel element failure due to fuel melting	T1: Local temperature in all parts of the pellet shall stay below the melting point of the pellet, with a minimum acceptable margin.
Fuel element failure due to sheath melting	T2: Local temperature in all parts of the sheath and the endcap shall stay below the local melting point of the material, with a minimum acceptable margin.
Fuel element failure due to crevice corrosion	T3: Underneath a bearing pad or spacer pad, the temperature at the sheath outer surface shall be less than that required to cause crevice corrosion of the sheath, with a minimum acceptable margin.
Fuel or pressure tube failure due to overheating by contact	T4: Fuel bundle dimensional changes (e.g., due to irradiation, loads, creep, bowing, etc.) shall maintain a minimum acceptable clearance between neighbouring sheaths or endcaps and also between the pressure tube and its sheath/endcap.
"S Series": Structural Integrity	
Fuel sheath failure due to	S1: The excess of internal pressure over coolant pressure shall be less than the pressure that causes cracking in the fuel sheath or in

Damage Consideration	Acceptance Criterion
overpressure	the sheath/endcap junction, with a minimum acceptable margin.
Fuel sheath failure due to environmentally assisted cracking due to power ramps	S2: Stresses and strains (or related powers and ramps) during power increases in fuel elements at circumferential ridges and at sheath/endcap junctions shall be less than the appropriate defect thresholds (with a minimum acceptable margin), including the effects of pellet chips, if any.
Fuel failure due to static mechanical overstrain	S3: Local principal strain (elastic plus plastic) shall be less than the available ductility minus the minimum acceptable margin, and local creep strain shall be less than the creep rupture strain, with a minimum acceptable margin.
Fuel failure due to uncontrolled loss of geometry	S4: Axial and related loads on the fuel bundle shall be less than the bundle buckling strength, with a minimum acceptable margin.
Fuel failure due to fatigue	S5: Cumulative fatigue damage from repeated cycles of alternating stresses and strains shall be less than the allowable fatigue life, with minimum acceptable factors of safety on the magnitude of cyclic strain and on the number of cycles.
Fuel mechanical rupture due to impact of loads such as refuelling and/or start/restart	S6: Strain energy density during impact shall be less than that required to crack or break any metallic component of the fuel bundle, with a minimum acceptable margin.
Primary hydride failures	S7: Equivalent concentration of internal hydrogen of an as-fabricated fuel element, from all sources excluding the sheath, shall not exceed the minimum acceptable limit.
Formation of a local hydride lens due to oxide and crud	S8: The combined thickness of oxide and crud on the fuel sheath outer surface shall be less than the amount required for spalling from the surface, with a minimum acceptable margin.
Failure due to insufficient ductility during post-irradiation handling	S9: The volume-average concentration of hydrogen (in the form of soluble atomic hydrogen and equivalent hydrides and deuterides, including their orientation) over the cross section of load-bearing components shall be less than the amount required to retain sufficient ductility, with a minimum acceptable margin.
“C” Series: Compatibility	
Failure due to excessive interaction loads along the	C1: Maximum length of the fuel string (e.g., in the fuel channel) shall be less than the minimum available cavity (e.g., between the

Damage Consideration	Acceptance Criterion
fuel string	shield plug or latches), with a minimum acceptable margin.
Failure from damage by interfacing equipment	C2: Net dimensions, including dimensional changes, throughout fuel bundle residence in the reactor shall be within specified limits for interfacing equipment.
Fuel sheath failure due to fretting of pads	C3: At spacer pads, total wear from all sources such as lateral vibrations, axial vibrations, fretting, sliding, and erosion shall be less than that which brings any part of a spacer in contact with a neighbouring sheath, with a minimum acceptable margin.
Fuel bundle jamming	C4: To enable passage of fuel through the reactor in all fuel handling operations, the axial force required to move the bundle shall be within design allowance, including all pertinent considerations such as on-power deformations, in-service contacts with neighbouring components, and changes in material properties.
Protection of pressure tube from bearing pads	C5: Depth of crevice corrosion, sliding wear, and fretting wear in the pressure tube from fuel bearing pads shall be within specified allowances.

Many complex processes occur in a fuel element. Therefore, in real life, one seldom has complete knowledge of all credible combinations of important variables involving design, manufacturing, and operating conditions that might fail the fuel, nor the luxury of performing an essentially infinite number of experiments that would cover them all. Therefore, in real life, we must deal satisfactorily, not only with what is known, but also with what is not.

In some situations, we know what we don't know—the known unknowns. In other situations, we don't even know what we don't know—the unknown unknowns. "Known unknowns" are usually included in assessments through quantified uncertainties. However, "unknown unknowns" are usually addressed through margins contained within acceptance criteria.

Figure 29 illustrates the concept of margin within an acceptance criterion; the figure labels it as "Minimum Acceptable Margin". Such a margin reflects expert judgment about the "unknown unknowns" in a given technology area. Therefore it can change with time as additional knowledge becomes available and/or as improved technologies for design, production, and/or assessments are developed and incorporated into the product.

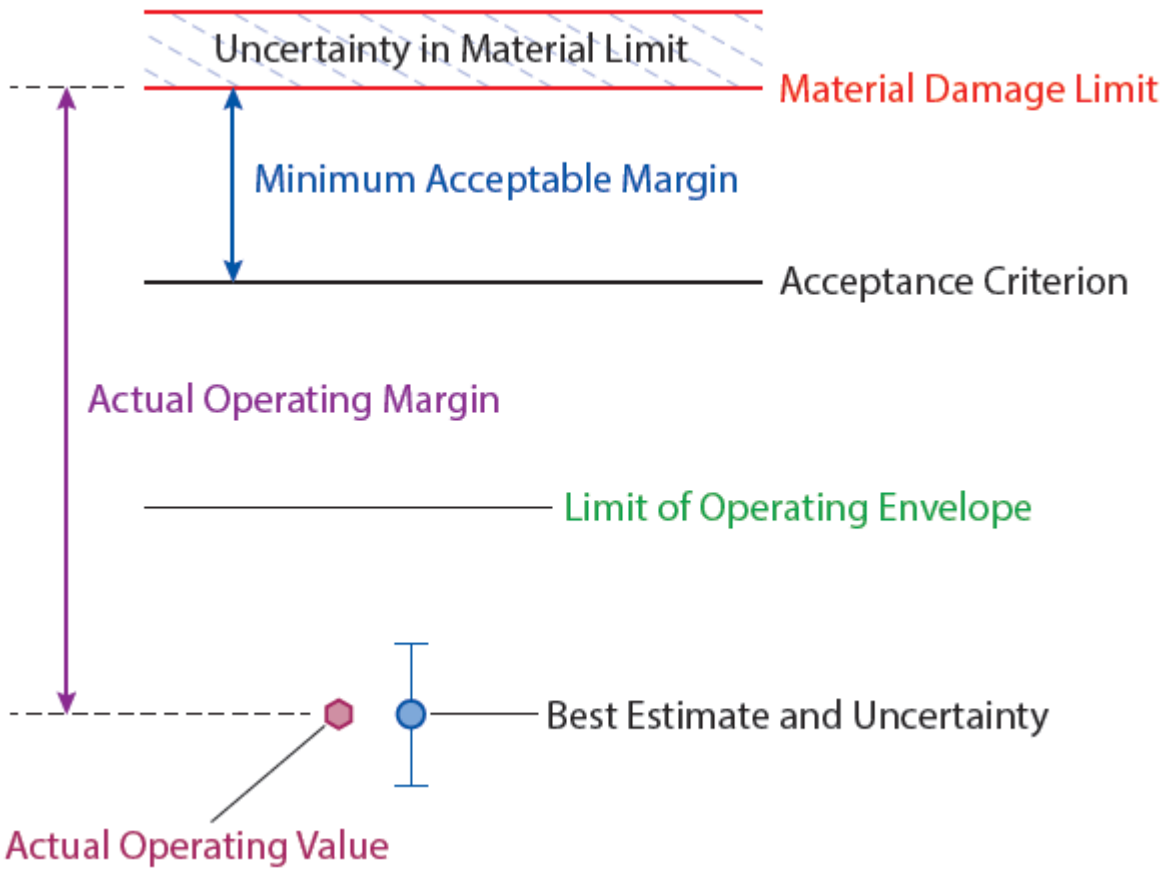

[After Sun *et al*., 2009]

Figure 29 Margins in criteria and analyzes

As noted earlier, a variety of assessment techniques are used to evaluate a product, including engineering judgment, tests, and analyzes. Their combinations are used through a large set of assessments that can potentially be performed as needed to confirm that acceptance criteria have been met. Some illustrative tests for prototype CANDU fuel, shown in Table 3, have already been mentioned.

Most fuel analyzes tend to be highly non-linear and multi-disciplinary. In addition, several analyzes require strong considerations of significant feedbacks among many complex processes. For this reason, the nuclear fuel industry frequently uses a number of computer codes to perform analyzes. An illustrative list is given in Table 5.

Table 5 Illustrative list of computer codes used at AECL for fuel analyzes

Program	Description
ABAQUS	This finite-element code is used for structural analyzes of fuel strings, especially in the presence of non-linearities of intermediate level. Typical examples include: (a) determination of stresses in the fuel string resting on side stops and experiencing hydraulic drag load, and (b) impact stresses during loading of fresh fuel bundles. For an overview and further details of this code, contact Dassault Systèmes, France.
ASSERT	This sub-channel code is used to assess thermal-hydraulic conditions in the fuel channel, including the effects of heat transfer between the fuel and the coolant. Key results include distributions of flow and voids, pressure drop, and critical heat flux. For an overview and further details of this code, contact Atomic Energy of Canada Limited, Canada.
BEAM	This code provides a fast and simple tool to assess several aspects of the mechanical behaviour of a fuel element. Key results include axial and lateral stiffnesses of a fuel element, frequencies of lateral vibrations and resulting elastic stresses, collapse pressure of a sheath, and buckling strength of a fuel element. An overview is available from M. Tayal *et al*., "Assessing the Mechanical Performance of a Fuel Bundle: BEAM Code Description", *Proceedings, Third International Conference on CANDU Fuel*, Canadian Nuclear Society, Pembroke, ON, 1992, October 4-8.
BOW	This finite-element code is used to assess the lateral deformations of fuel elements and bundles, e.g., bow, sag, and droop. An overview is available from M. Tayal, "Modelling the Bending/Bowing of Composite Beams such as Nuclear Fuel: the BOW Code", *Nuclear Engineering and Design*, vol. 116, pp. 149-159 (1989).
ELESTRES	This finite-element code is used to calculate several thermal, mechanical, and microstructural responses of a fuel element. Key results include sheath and pellet temperatures; fission gas release and internal pressure; and sheath strain as a result of expansion, contraction, and hourglassing of pellets and the sheath. An overview is available from M. Tayal, "Modelling CANDU Fuel under Normal Operating Conditions: ELESTRES Code Description", *Report CANDEV-86-110*, published by CANDU Owners' Group; also *Report AECL-9331*, published by Atomic Energy of Canada Limited, February 1987.
FEAST	This finite-element code is used to model detailed local stresses, strains, and deformations such as at circumferential ridges, at sheath/endcap junctions, and in a sheath above an axial gap. An overview is available from M. Tayal, "FEAST: A Two-Dimensional Non-Linear Finite-Element Code for Calculating Stresses", *Proceedings, Seventh Annual Conference of the Canadian Nuclear Society*, Toronto, Ontario, Canada, June 8–11, 1986.

Program	Description
FEAT	This finite-element code is used to model local temperatures such as the effects of end-flux peaking and local temperatures pertinent to crevice corrosion and braze voids. An overview is available from M. Tayal, "The FEAT Finite-Element Code to Calculate Temperatures in Solids of Arbitrary Shapes", *Nuclear Engineering and Design*, Vol. 114, pp. 99-114 (1989).
FEED	This finite-element code is used to model diffusion of hydrogen/deuterium in Zircaloy. Key results include concentrations of hydrogen at various locations. An overview is available from L. Lai *et al*., "A Method to Model Hydrogen Precipitation", *Proceedings, 11th International Conference on CANDU Fuel*, Canadian Nuclear Society, Niagara Falls, 2010.
INTEGRITY	This model uses a semi-mechanistic approach to improve calculations of environmentally assisted cracking due to power ramps by accounting for a variety of effects that are not included in the current database of available empirical correlations, such as varying pellet density, sheath diameter, coolant pressure, and coolant temperature. An overview is available from M. Tayal *et al*., "INTEGRITY: A Semi-Mechanistic Model for Stress Corrosion Cracking of Fuel", *IAEA Technical Committee Meeting on Water Reactor Fuel Element Modelling at High Burnup and its Experimental Support*, Windermere, United Kingdom, AECL-10792, September 19–23, 1994.
LONGER	This code calculates conditions related to sheath collapse. Key results include pressure for elastic instability, critical pressure for excessive longitudinal ridges, and pressure for axial collapse. An overview is available from U. K. Paul *et al*., "LONGER: A Computer Program for Longitudinal Ridging and Axial Collapse Assessment of CANDU Fuel", *Proceedings, 11th International Conference on CANDU Fuel*, Canadian Nuclear Society, Niagara Falls, Ontario, 2010.
LS DYNA	This finite-element code overlaps the functionality of ABAQUS code and can also be used for analyzes of strength, impact, and vibration of fuel strings. For an overview and further details of this code, contact Livermore Software Technology Corporation, U.S.A.
NUCIRC	For purposes of fuel analyzes, this thermal-hydraulic code is used to calculate critical channel power. For an overview and further details of this code, contact Atomic Energy of Canada Limited, Canada.

11 Operating Constraints and Inputs to the Safe Operating Envelope

For a specific project application, one would perform assessments (tests and analyzes) as mentioned above to ascertain that the chosen fuel design meets the specified design requirements without failing (i.e., by showing that the fuel acceptance criteria are met). The assessments would at the same time establish the limits, or constraints, on certain plant parameters such that the specified fuel acceptance criteria are met. These plant operating constraints, as

derived from fuel assessments, and similar constraints derived from assessments of all other systems are then used in safety analysis to establish the plant's safe operating envelope.

12 Removal of Fuel Bundles Containing Defects

CANDU reactors have an enviable record of very low fuel defect rates, as noted in Section 2.3. Nevertheless, defects in fuel bundles do occasionally occur. CANDU reactors also have a unique ability to detect, locate, and discharge fuel bundles which contain defective elements without shutting the reactor down. This capability is described in this section. However, we first give a brief summary of how a small primary defect in a fuel element can grow with time into a bigger hole that releases progressively larger amount of radioactivity to the coolant.

Fundamental aspects of such deterioration have been discussed by Lewis *et al*. [1988]. Section 12.1 below is based largely on a document published by the CANDU Owners' Group (COG). Sections 12.2 and 12.3 below are based on an IAEA document [IAEA NF-T-2.1, 2010].

12.1 Deterioration of Primary Defects in Fuel Elements

As noted in Section 10.1 of this Chapter, there are eighteen mechanisms that can cause a failure (primary defect) in CANDU fuel, some in fuel bundles and some in fuel elements. In this section, we consider only one form of defect, albeit the most important, that of a crack or a hole developing in a fuel element, to illustrate how the defective fuel detection and removal system functions in a CANDU reactor. Detection and removal of fuel bundles that have experienced other types of defects would follow a similar procedure, although some fuel bundle defects (such as a bundle becoming stuck in a fuel channel) may require different or additional steps. Please see Section 10.1 for a description of primary defects and how they are caused.

If a crack or hole in the sheath of a fuel element (a primary defect) permits coolant water to penetrate the fuel element, the hole can grow progressively bigger with time through a process called "post-defect deterioration", resulting in release of progressively larger amounts of radioactive fission products into the coolant. This can eventually pose a health hazard to station staff. Therefore, fuel bundles that contain defective fuel elements must be discharged from the reactor before the crack or hole in the fuel element becomes too big.

As explained below, post-defect deterioration of this type of primary defect in fuel elements occurs due to a combination of three main factors:

- secondary hydriding of the sheath (or "deuteriding" when heavy water is used as a coolant, as it is in CANDU; "hydriding" will be used hereafter in this section for simplicity);
- stresses in the sheath; and
- oxidation and swelling of UO_2.

Secondary Hydriding: Secondary hydriding refers to Zircaloy-hydrogen compounds that are formed in the sheath as a consequence of a primary defect. Water enters the fuel element through the primary crack or hole. At the higher temperature inside the fuel element, the water turns into steam and can better react chemically with Zircaloy and with the UO_2 pellet. The chemical reaction oxidizes some of the Zircaloy and turns some of the UO_2 into higher oxide(s). This chemical reaction also releases hydrogen radicals from steam. Radiolytic decomposition also releases hydrogen radicals from water. The free hydrogen enters the metal matrix of the Zircaloy sheath and migrates by diffusion to areas of higher stress and lower tempera-

ture. Therefore, the hydrogen often accumulates in localized areas such as at the relatively cooler outer surface of the sheath. When the local concentration of hydrogen exceeds the local solubility limit, the excess hydrogen precipitates as hydrides, which are called secondary hydrides. Once hydrides have formed, they can grow by preferentially absorbing additional hydrogen from within the pellet/sheath gap. High levels of hydrides embrittle Zircaloy, leaving it less able to resist stresses and strains.

A number of pertinent factors may vary along the length of the fuel element, for example the local temperature, the local rate of decomposition, and the local oxidation kinetics of UO_2 and of Zircaloy. For this reason, secondary hydriding generally occurs at some distance away from the primary hole.

Sheath Stresses: The volume of compound hydride is about 16% larger than the volume of the parent Zircaloy. This creates geometric incompatibility among neighbouring materials, which in turn leads to large stresses in the hydride and in the Zircaloy surrounding the hydride. When these stresses become high enough, they can cause cracks in the layer of zirconium oxide which exists on the inside surface of the sheath. This in turn enables additional hydrogen to enter the sheath. Moreover, the hydrides can produce cracks that pass—either fully or partly—through the sheath wall. All cracks enable further ingress of hydrogen; through-wall cracks also enable more water to enter the fuel element.

Oxidation and Swelling of UO_2: Reaction of water and UO_2 results in higher concentrations of uranium oxides, commonly labelled $UO_{(2+x)}$. The higher oxides have lower density, and therefore lower thermal conductivity and higher nominal volume, than UO_2. The lower thermal conductivity increases the temperature and hence the thermal expansion of the pellet, which combines with the higher nominal volume to swell the pellet. The expanding pellet then increases the width of the crack in the Zircaloy sheath.

These processes can lead to a hole, often caused by a loss of material from the outside surface of the sheath, called a “blister”. Figure 30(a) provides an illustrative example. Holes due to secondary damage are often much bigger than holes from primary damage and hence can release significant radioactivity, and even some UO_2, into the coolant. For this reason, it is prudent to discharge a fuel bundle that contains a failed fuel element before significant secondary damage to the sheath occurs. Fortunately, the process of forming secondary defects often takes some time, and CANDU reactors are unique in being able to: (1) detect fuel element defects that release radioactive fission products into the coolant, (2) identify the fuel channels that contain bundles with defective fuel elements, (3) discharge these bundles before the defects in the fuel-element sheath become too big, and (4) do all this without shutting the reactor down. The next section summarizes the techniques to do this.

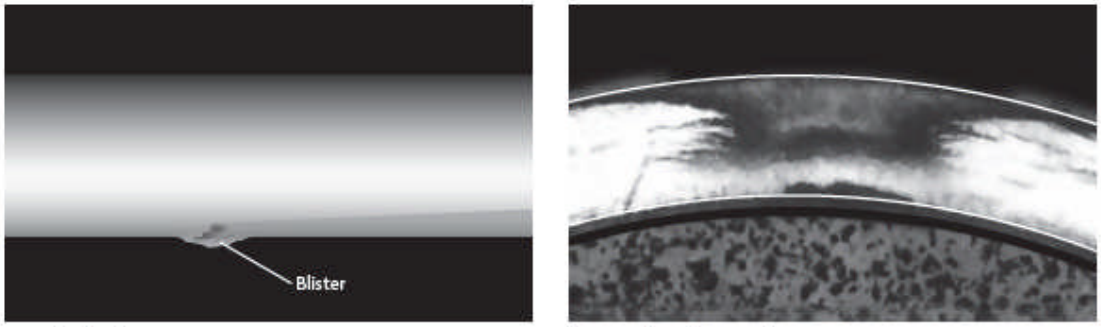

(a) Hydride Blister (b) Typical Sunburst Failure

[Courtesy: COG] [Source: IAEA, 2010]

Figure 30 Secondary hydriding

12.2 Defect Removal Systems

Three systems have been developed to detect and locate defective fuel elements that release radioactive fission products into the coolant: (1) gaseous fission product (GFP), (2) delayed neutron (DN), and (3) feeder scanning (FS) systems.

The GFP system monitors continuously when the reactor is at power and detects a general increase of radioactivity in the coolant when a defect occurs in a fuel element anywhere in the core. This system alerts the operator that a defect has occurred and identifies the coolant loop in which the defect is located, thereby eliminating 50% of fuel channels from the "suspects" list.

The DN system is also used when the reactor is at power, but does not monitor continuously. The activity-sensing portion of the DN system is put into operation after a defect signal is indicated by the GFP system. The DN system is used to identify the fuel channel that contains the defective elements by detecting activity in the coolant at the downstream end of a fuel channel [Manzer *et al.*, 1984]. In a closed-loop configuration, sampling lines attached to outlet feeders continuously carry small streams of coolant to a common room within the reactor building (see Figure 31) and return the streams back into the coolant circuit downstream of the outlet header. In the sampling room, BF3 sensors detect delayed neutrons emitted by short-lived fission-products (^{137}I and ^{87}Br). The lengths of the sampling lines (custom-sized for each channel) are such that the delivery of the sample to the sensor takes advantage of the decay half-life of the delayed-neutron precursors. If neutron activity in a coolant sampling line is higher than normal, the corresponding fuel channel is suspected of containing a fuel bundle with a defective element. The DN system has sufficient sensitivity to locate fuel element defects with very small holes. Bruce and CANDU-6 reactors use the DN system.

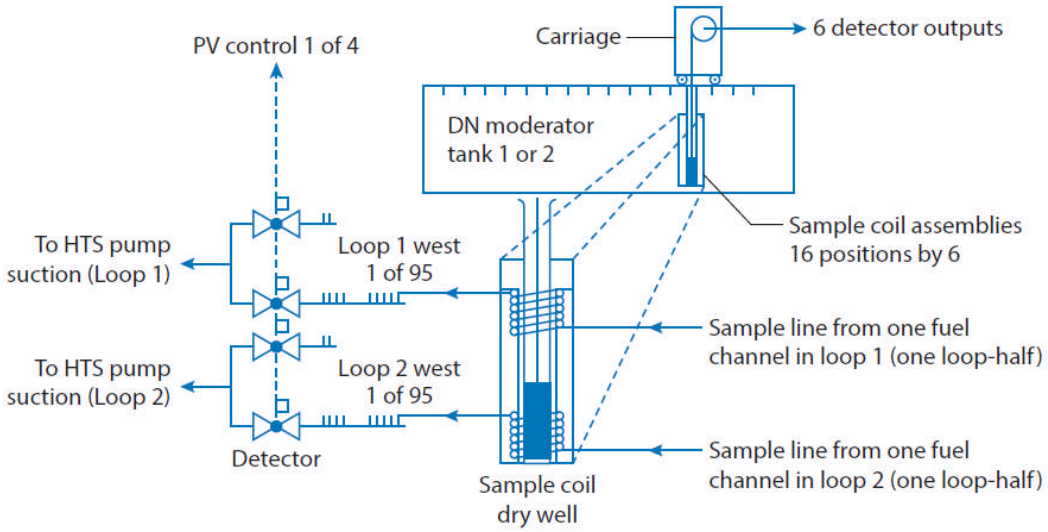

[Source: IAEA, 2010]

Figure 31 Schematic diagram of a delayed neutron monitoring system in a CANDU-6 reactor

The FS system is used when a reactor is shut down. It locates the fuel channel that contains the defective element by scanning for activity on the inside surfaces of the outlet feeders connecting the fuel channels to a common outlet header [Lipsett *et al.*, 1976]. The presence of gamma-emitting fission products inside the channel is detected by Geiger-Muller detectors moving within guide tubes that traverse the outlet feeders. If gamma activity in a specific feeder is higher than normal, then the corresponding fuel channel is suspected of containing a fuel bundle that has a (severely) defective element. The FS system locates only defects that have deteriorated to the point of releasing uranium and fission products which deposit immediately downstream of the defect. The Darlington reactors use the FS system.

12.3 Confirmation of Defect Removal

After the channel which has been identified as containing the defect has been refueled in a CANDU reactor, the defective fuel element is confirmed to have been discharged by various methods, again depending on the station:

- Inspecting the discharged bundles in the bay;
- Monitoring gamma activity near the spent fuel handling system when bundles are en route from the reactor to the fuel bay (wet or dry sipping) and/or when they are residing in the fuel bay (wet sipping);
- Monitoring delayed neutron activity of the coolant at the outlet end of the channel during refuelling.

The first method provides direct confirmation that a bundle that contains a defective fuel element has been removed. Portable underwater TV cameras are used at multi-unit stations operated by Ontario Power Generation, whereas periscopes are used at single-unit CANDU-6 stations [Lipsett, 1976]. Photographs of the defective elements confirm that a defective bundle has been removed.

The second and third methods provide indirect confirmation that a bundle containing a defective element has been removed by monitoring gamma activity near the spent fuel handling system or in fuel bays. At Bruce, dry sipping techniques [MacDonald *et al*., 1990] are used to monitor airborne gamma activity in the air chamber that separates the heavy water side of the spent fuel transfer mechanisms from the light water environment of the fuel bay. A higher-than-normal signal that lingers after bundles have been transferred usually indicates the presence of a defective element.

Two other techniques have also been developed at CANDU-6 stations to confirm that fuel bundles containing defective elements have been discharged from the core. One technique depends on the radiation levels of fission products in the heavy water inside the fuelling machine. Before discharge of irradiated fuel bundles to a bay, heavy water from the fuelling machine is transferred to a nearby drain tank. The presence of a defect is indicated when gamma fields near the tank trigger an alarm that monitors gamma in the area. Another technique developed in the inspection bay at Point Lepreau is based on "wet sipping", or measuring the gamma activity of water samples near recently discharged bundles. Again, a defect is confirmed if gamma activity is unusually high.

Monitoring delayed neutron activity at the outlet end of a fuel channel during refuelling also provides some confirmation that a fuel bundle containing a defective element is being discharged from the core [Manzer, 1985]. At CANDU-6 sites, special refuelling procedures are sometimes used which involve allowing the fuel bundles inside the channel to move slowly with the flow while monitoring the DN signal of the channel. When the signal drops to below "pre-defect" levels, this indicates that the fuel bundle containing the defect has been pushed outside the core boundary.

13 Closure

To restate a point made in Section 2.3, the defect rate is remarkably low in CANDU fuel—almost in the range of impurities found in most substances. An IAEA survey has reported the following world-wide fuel defect rates between 1994 and 2006 [IAEA, 2010]:

- 94 failed rods per million discharged (ppm) in WWERs;
- 87 ppm in PWRs;
- 65 ppm in BWRs; and
- 3.5 ppm in Canada.

These figures affirm the basic soundness of practices built into all major aspects of CANDU fuel—from research to development, design, fabrication, and operation and the feedbacks among them.

14 Problems

Section 2

Q2.1 – Why is a CANDU fuel "element" able to produce 30 times more heat than an electric element of a similar size?

Q2.2 – List at least six conditions that occur during at-power operation of CANDU fuel that challenge the integrity of the fuel.

Q2.3 – Name the components of a typical CANDU fuel bundle.

Q2.4 – Why is the uranium that is used in CANDU fuel bundles in the form of uranium dioxide, rather than uranium metal, for instance?

Q2.5 – Why is helium used to purge the air out of fuel elements during fabrication?

Q2.6 – For a fixed bundle power, the only means that the fuel designer has at his disposal to change the individual element rating is to use more or fewer elements. Using more elements (subdivision) permits the coolant to be nearer the source of the heat at more locations, leading to lower UO_2 temperature and reduced threats from many thermally driven damage mechanisms. What are some of the negative effects of subdivision?

Q2.7 – Experience and fundamental engineering considerations have shown that CANDU fuel bundles can experience 18 different modes of failure in a reactor. Name the three general groups into which the modes are grouped and provide the principal characteristic of each group.

Section 3

Q3.1 – What does "burnup" measure, and what units is it expressed in?

Q3.2 – A CANDU fuel element contains UO_2 pellets 20 mm in diameter and having a density of 10.5 g/cm^3. At 60 kW/m, how long does it need to accumulate a burnup of 40 MWh/kgU? Why does this need so much longer than the fuel element of Section 3?

Section 4

Q4.1 – A fuel element has the following characteristics: diameter = 15 mm; sheath thickness = 0.5 mm; Young's modulus = 80 GPa; Poisson's ratio = 0.37. Is it elastically stable at 6 MPa? At 7 MPa? At 8 MPa?

Section 6

Q6.1 – What is fission gas?

Q6.2 – Why is it important to maintain fission gas pressure as low as possible?

Q6.3 – Describe the processes involved in the generation, accumulation and release of fission gas into "open" spaces inside the fuel sheath.

Q6.4 – What design features does the fuel designer have at his disposal to control or minimize fuel element internal gas pressure?

Q6.5 – Using the equations presented in Section 6.5, determine the effect of storing the fission gas at pellet centreline temperature compared to that of the pellet interface with the sheath.

What do we learn?

Q6.6 – A fuel element's free space is 3 ml, and it contains 15 ml of gas at STP. Assuming that all the gas is stored at a uniform temperature of 1400 K, what is the internal pressure of the fuel element? [Hint: Use Equation 5].

Section 7

Q7.1 – Describe three defect types in CANDU fuel that may be caused by excessive stress.

Q7.2 – Describe in qualitative terms the reasons that cracks develop in uranium dioxide pellets at operating conditions.

Q7.3 – A temperature profile is parabolic in a pellet of radius 6 mm. Is the hoop stress tensile or compressive at: 1 cm? 2 cm? 3 cm? 4 cm? 5 cm?

Section 8

Q8.1 – Describe qualitatively the conditions that might lead to environmentally assisted cracking.

Q8.2 – Provide examples of EAC defects that have been observed in CANDU fuel elements.

Q8.3 – Recognizing the three different effects that can cause EAC defects in CANDU fuel elements, provide a qualitative description of reactor operation that could lead to EAC defects.

Q8.4 – What parameters from operating reactors have been correlated to provide an indication of potential fuel failure due to EAC? Draw a figure to show the relationship.

Q8.5 – Describe the mitigating parameters that have been adopted by CANDU designers and operators to minimize EAC defects.

Q8.6 – A non-CANLUB fuel bundle experiences a power ramp from 25 kW/m to 50 kW/m at 140 MWh/kgU. What is its probability of having a defect? What would the defect probability be if it were CANLUB fuel?

Section 9

Q9.1 – Describe the coolant conditions that may lead to fuel vibration.

Q9.2 – Describe the type of damage that fuel can experience as a result of vibration.

Q9.3 – A C6 fuel element has the same dimensions as in the illustrative example of Section 9.1.6, with the exception that its assembly weld has inadvertently been manufactured with a diameter of 3 mm. Coincidentally, it is also destined to be loaded into a channel where the amplitude of lateral vibration is expected to be 30 micrometers. What nominal stresses are expected in the endplate and in the assembly weld? Are fatigue failures likely by this mechanism?

Section 10

Q10.1 – How many damage mechanisms have been shown to affect CANDU fuel?

Q10.2 – How many thermal damage mechanisms ("T" series) are there? Provide a brief description of each.

Q10.3 – How many structural damage mechanisms ("S" series) are there? Provide a brief description of each.

Q10.4 – How many compatibility damage mechanisms (“C” series) are there? Provide a brief description of each.

Q10.5 – List the design acceptance criteria for CANDU fuel.

Q10.6 – With the aid of a diagram, show the relationship of acceptance criteria to other relevant parameters, e.g., the material damage limit.

Q10.7 – What is the purpose of assigning margins in relation to acceptance criteria?

Q10.8 – List the qualification tests and assessments used to qualify CANDU fuel bundles.

Section 11

Q11.1 – Name at least one plant operating constraint that is related to ensuring fuel integrity. Are there others?

Q11.2 – How are plant operating constraints defined by system designers such as fuel designers used to ensure safe plant operation?

Section 12

Q12.1 – What is the most common defect type that occurs in CANDU fuel during plant operation?

Q12.2 – What are the principal characteristics of the most common defect type that makes its detection possible while the plant is in operation?

Q12.3 – What is secondary hydriding? Explain the mechanism and how it affects the integrity of the fuel element.

Q12.4 – Explain why it is important to remove a defective fuel element from an operating reactor as soon as the defect is detected.

Q12.5 – Name the three systems used in CANDU reactors to assist in the detection and removal of defective fuel while the reactor is at power and explain briefly how each is used.

Q12.6 – Name three techniques used to confirm that a bundle containing a defective fuel element has been discharged from the channel and explain briefly how each works.

15 References

A. H. Booth, "A Method of Calculating Fission Gas Diffusion from UO_2 Fuel and its Application to the X-2-f Loop Test", Atomic Energy of Canada Limited, *Report AECL-496* (1957).

G. H. Bryan, "Application of the Energy Test to the Collapse of a Long Thin Pipe under External Pressure", *Proceedings of Cambridge Phil. Society*, Vol. 6, p. 287 (1888).

R. M. Carroll and O. Sisman, "In-Pile Fission Gas Release from Single-Crystal UO_2", *Nuclear Science and Engineering*, vol. 21, pp. 147–158 (1965).

T. Daniels, H. Hughes, P. Ancker, M. O'Neil, W. Liau, and Y. Parlatan, "Testing and Implementation Program for the Modified Darlington 37-Element Fuel Bundle*", Proceedings, 10th International Conference on CANDU Fuel*, Canadian Nuclear Society (2008).

A. Fick, "Über Diffusion", *Phil. Mag*., vol. 10, pp. 59–86 (1855).

M. R. Floyd, D. A. Leach, R. E. Moeller, R. R. Elder, R. J. Chenier, and D. O'Brien, "Behaviour of Bruce NGS-A Fuel Irradiated to a Burnup of ~500 MWh/kgU", *Proceedings, Third International Conference on CANDU Fuel*, Chalk River, Canadian Nuclear Society, pp. 2-44 to 2-60 (1992).

M. Gacesa, V. C. Orpen, and I. E. Oldaker, "CANDU Fuel Design: Current Concepts", *IAEA/CNEA International Seminar on Heavy Water Fuel Technology*, San Carlos de Bariloche, Argentina, 1983. Also *Report AECL-MISC 250-1 (Rev. 1)*, published by Atomic Energy of Canada Limited, 1983.

J. Gere and S. P. Timoshenko, *Mechanics of Materials*, PWS, Fourth Edition (1997).

I. J. Hastings, "Structures in Irradiated UO_2 Fuel from Canadian Reactors", Atomic Energy of Canada Limited, *Report AECL-Misc-249* (1982).

I. J. Hastings, A. D. Lane, and P. G. Boczar, "CANFLEX: An Advanced Fuel Bundle for CANDU", *International Conference on Availability Improvements in Nuclear Power Plants*, Madrid, Spain. Also *Report AECL-9929*, published by Atomic Energy of Canada Limited (1989).

IAEA, "Review of Fuel Failures in Water-Cooled Reactors", International Atomic Energy Agency, Vienna, *Report NF-T-2.1* (2010).

J. H. K. Lau, M. Tayal, E. Nadeau, M. J. Pettigrew, I. E. Oldaker, W. Teper, B. Wong, and F. Iglesias, "Darlington N12 Investigation: Modelling of Fuel Bundle Movement in Channel under Pressure Pulsing Conditions", *Proceedings, 13th Annual Conference,* Canadian Nuclear Society (1992).

B. J. Lewis, "Fundamental Aspects of Defective Nuclear Fuel Behaviour and Fission Product Release", *Journal of Nuclear Materials*, Vol. 160, pp. 201–217 (1988).

J. J. Lipsett and W. B. Stewart, "Failed Fuel Location in CANDU-PHW Reactors using a Feeder Scanning Technique", *IEEE Transactions on Nuclear Science*, Vol. NS-23, No. 1, pp. 321-324 (1976).

R. D. MacDonald, M. R. Floyd, B. J. Lewis, A. M. Manzer, and P. T. Truant, "Detecting, Locating, and Identifying Failed Fuel in Canadian Power Reactors", *Report AECL-9714*, published by Atomic Energy of Canada Limited, Canada (1990).

A. M. Manzer and R. W. Sancton, "Detection of Defective Fuel in an Operating CANDU-600 MW(e) Reactor", *Proceedings, Conference on Fission Product Behaviour and Source Term Research*, Snowbird, American Nuclear Society, LaGrange Park, Illinois (1984).

M. J. F. Notley and I. J. Hastings, "A Microstructure-Dependent Model for Fission Product Gas Release and Swelling in UO_2 Fuel", *IAEA Specialists' Meeting on Fuel Element Performance Computer Modelling*, Blackpool, UK, 1978. Also *Report AECL-5838*, published by Atomic Energy of Canada Limited, 1979.

W. J. O'Donnell and C. M. Purdy, "The Fatigue Strength of Members Containing Cracks", *Proceedings of ASME Petroleum Division*, ASME Paper 63-PET-1 (1963).

W. J. O'Donnell and B. F. Langer, "Fatigue Design Basis for Zircaloy Components", *Nuclear Science and Engineering*, Vol. 20, pp. 1–12 (1964).

D. E. Olander, "Fundamental Aspects of Nuclear Reactor Fuel Elements", Energy Research and Development Administration, U.S.A., *Report TID-26711-P1* (1976).

R. D. Page, "Canadian Power Reactor Fuel", Atomic Energy of Canada Limited, *Report AECL-5609* (1976).

W. J. Penn, R. K. Lo, and J. C. Wood, "CANDU Fuel—Power Ramp Performance Criteria", *Nuclear Technology*, Vol. 34, pp. 249–268 (1977).

R. E. Peterson, "Application of Stress Concentration Factors in Design", *Proceedings of the Society for Experimental Stress Analysis*, Vol. 1, pp. 118–127 (1943).

M. J. Pettigrew, "The Vibration Behaviour of Nuclear Fuel under Reactor Conditions", *Nuclear Science and Engineering*, Vol. 114, pp. 179–189 (1993).

P. Reid, M. Gacesa, and M. Tayal, "The ACR-1000 Fuel Bundle Design", *Proceedings, 10th International Conference on CANDU Fuel*, Canadian Nuclear Society (2008).

A. D. Smith, I. J. Hastings, P. J. Fehrenbach, P. A. Morel, and R. D. Sage, "Dimensional Changes in Operating UO_2 Fuel Elements: Effect of Pellet Density, Burnup, and Ramp Rate", Atomic Energy of Canada Limited, *Report AECL-8605* (1985).

A. Sun and M. Tayal, "Technical Basis for ACR-1000 Fuel Acceptance Criteria", *Proceedings, 11th International Conference on CANDU Fuel*, Canadian Nuclear Society (2010).

M. Tayal and C. K. Choo, "Fatigue Analysis of CANDU Nuclear Fuel Subjected to Flow-Induced Vibrations", Paper AIAA-84-0959-CP, *25th Structures, Structural Dynamics and Materials Conference*, American Society of Mechanical Engineers, Palm Springs, California, 1984. Also *Report AECL-8331*, published by Atomic Energy of Canada Limited (1984).

M. Tayal, "Modelling CANDU Fuel under Normal Operating Conditions: ELESTRES Code Description", Atomic Energy of Canada Limited, *Report AECL-9331* (1987).

M. Tayal, L. M. MacDonald, E. Kohn, and W. P. Dovigo, "A Model for the Transient Release of Fission Products from UO_2 Fuel: GASOUT Code Description", *Nuclear Technology*, Vol. 85, pp. 300–313. Also *Report AECL-9794*, published by Atomic Energy of Canada Limited (1989).

M. Tayal and G. Chassie, "Extrapolating Power-Ramp Performance Criteria for Current and Advanced CANDU Fuels", *Proceedings, 21st Annual Conference*, Canadian Nuclear Society

(2000).

M. Tayal, P. Reid, M. Gacesa, A. Sun, E. Suk, and D. Gossain, “ACR-1000 Fuel Acceptance Criteria for Normal Operation and for Anticipated Operational Occurrences”, *Proceedings, Tenth International Conference on CANDU Fuel*, Canadian Nuclear Society, Ottawa, Canada (2008-1).

M. Tayal, A. Sun, M. Gacesa, P. Reid, P. Fehrenbach, B. Surette, and E. Suk, “Mechanism for Power Ramp Failures in CANDU Fuel”, *Proceedings, 10th International Conference on CANDU Fuel*, Canadian Nuclear Society (2008-2).

S. P. Timoshenko, *Strength of Materials, Part 2*, McGraw-Hill, Second Edition (1961).

S. P. Timoshenko and J. N. Goodier, *Theory of Elasticity*, McGraw Hill, Third Edition (1970).

J. C. Wood, D. G. Hardy, and A. S. Bain, “Power Ramping Fuel Performance and Development”, Atomic Energy of Canada Limited, *Report AECL-6676* (1979).

16 Further Reading

Design Verification

P. G. Boczar, "CANDU Fuel Design Process", *Ninth International Conference on CANDU Fuel*, Belleville, Canada, Canadian Nuclear Society, 2005.

J. Chang, S. Abbas, A. Banwatt, M. DiCiano, M. Gacesa, A. Gill, D. Gossain, J. Hood, F. Iglesias, L. Lai, T. Laurie, Y. Ornatsky, U. K. Paul, A. Sun, M. Tayal, S. G. Xu, J. Xu, and P. Reid, "Proof of Design Adequacy for the ACR-1000 Fuel Bundle", *10th International Conference on CANDU Fuel*, Ottawa, Canada, October 5-8, 2008.

History (Early)

J. A. L. Robertson, “Fuel for Thought”, *Nuclear Journal of Canada*, Vol. 1, Issue 4; pp 332-341. Also published in *Proceedings of the Engineering Centennial Conference*, Montreal, 18-22 May, 1987.

Irradiation Tests and Performance

F. R. Campbell, L. R. Borque, R. Deshaises, H. E. Sills, and M. J. F. Notley, “In-Reactor Measurements of Fuel-to-Sheath Heat Transfer Coefficients Between UO_2 and Stainless Steel”, Atomic Energy of Canada Limited, Report AECL-5400, 1977.

T. J. Carter, "Experimental Investigation of Various Pellet Geometries to Reduce Strains in Zirconium Alloy Cladding", *Nuclear Technology*, Vol. 45, No. 2, September 1979, pp. 166-176.

M. R. Floyd, J. Novak, and P. T. Truant, "Fission-Gas Release in Fuel Performing to Extended Burnups in Ontario Hydro Nuclear Generating Stations", *IAEA Technical Committee Meeting on Fission Gas Release and Fuel Rod Chemistry Related to Extended Burnup*, Pembroke, Canada. Also Atomic Energy of Canada Limited, Report AECL-10636 (1992).

M. R. Floyd, Z. He, E. Kohn, and J. Montin, "Performance of Two CANDU-6 Fuel Bundles Containing Elements with Pellet-Density and Clearance Variables", *6th International Conference on CANDU Fuel*, Niagara Falls, Canada. Also Atomic Energy of Canada Limited, Report AECL-12033, 1999.

M. R. Floyd, "Extended-Burnup CANDU Fuel Performance", *International Conference on CANDU Fuel*, CNS, Kingston. Also Atomic Energy of Canada Limited, Report AECL-CONF-01135, 2001.

D. G. Hardy, A. S. Bain, and R. R. Meadowcroft, "Performance of CANDU Development Fuel in the NRU Reactor Loops", *ANS Topical Meeting on Water Reactor Fuel Performance*, St. Charles, Illinois, pp. 198-206, 1977.

M. J .F. Notley, A. S. Bain, and J. A. L. Robertson, "The Longitudinal and Diametral Expansion of UO_2 Fuel Elements", AECL-2143, 1964.

Manufacturing and Quality Assurance

C. Ganguly and R. N. Jayaraj (editors), *Characterization and Quality Control of Nuclear Fuels*, Allied Publishers, 2004.

M. Gacesa, G. R. Quarrington, W. R. Tarasuk, I. R. Carrick, J. Pawliw, G. McGregor, H. R. Debnam, and L. Proos, "CANDU Fuel Quality and How it is Achieved", Atomic Energy of Canada Limited, Report AECL-7061, 1980.

R. Sejnoha, "Quality Assurance in CANDU Fuel Design, Development, and Manufacturing", IAEA/INSTN, Saclay (France), October 1992.

Material Science

R. Adamson, B. Cox, J. Davies, F. Garzarolli, P. Rudling, and S. Vaidyanathan, "Pellet-Cladding Interaction", IZNA-6 Special Topical Report, ANT International, 2006.

D. L. Hagrman, G. A. Reyman, and R. E. Mason (editors), "MATPRO-Version 11 (Revision 2): A Handbook of Material Properties for Use in the Analysis of Light Water Reactor Fuel Rod Behaviour", EG&G Idaho, Inc., Report NUREG/CR-0479, TREE-1280, Rev.2, 1981.

A. Sawatzky and C. E. Ells, "Understanding Hydrogen in Zirconium", *Zirconium in the Nuclear Industry: Twelfth International Symposium*, ASTM STP 1354, 2000, pp 32-48.

Modelling and Computer Codes

J. A. L. Robertson, A. M. Ross, M. J. F. Notley, and J. R. MacEwan, "Temperature Distribution In UO_2 Fuel Elements", *Journal of Nuclear Materials*, pp. 225-262, December 1961. Also AECL-1679.

M. Tayal, D. Lim, "Recent Uses of the Finite Element Method in Design/Analysis of CANDU Fuel", *Sixth Annual Conference of the Canadian Nuclear Society*, Ottawa. Also Atomic Energy of Canada Limited, Report AECL-8754, 1985.

17 Relationships with Other Chapters

Chapter 8 provides an overview of fuel bundle configuration. Chapters 3 to 5 explain neutron physics that generates heat in the fuel. Chapters 6 and 7 explain how that heat is removed from the fuel bundle and illustrate the internal temperature distribution within a fuel rod. Chapters 14 and 15 explain chemical and metallurgical aspects that relate to corrosion of the fuel sheath. Chapter 13 explains the performance of fuel during postulated accidents. Chapter 18 discusses advanced fuels and fuel cycles; it also summarizes fuel manufacturing. Finally, Chapter 19

describes interim storage and disposal of used fuel.

18 Acknowledgements

The following reviewers are gratefully acknowledged for their hard work and excellent comments during the development of this chapter; their feedback has much improved it.

Peter Boczar
Lawrence Dickson
Rosaura Ham-Su
Paul Chan
Kwok Tsang

Of course the responsibility for any errors or omissions lies entirely with the authors.

Thanks are also extended to Media Production Services, McMaster University, for producing the figures, and to Diana Bouchard for expertly editing and assembling the final copy.

CHAPTER 18

Fuel Cycles

prepared by

Mukesh Tayal and Milan Gacesa – Independent Consultants

Summary

Most commercial reactors currently use the once-through fuel cycle. However, because there is still a significant amount of useful material (and available energy) in the fuel discharged from these reactors, many fuel cycles are possible in which some fuel components are recycled for further reactor use. In addition, several other fuel cycles are also possible using thorium, which is much more abundant on Earth than the uranium that is the primary source of commercial nuclear power today. The CANDU reactor is designed to use natural uranium fuel, which is less expensive and more efficient in the use of uranium than any known alternative. Some of the features that enable a CANDU reactor to operate on natural uranium also make it eminently capable of using alternative fuels. In spite of increased fuel cost, the use of alternative fuel cycles in a CANDU reactor can lead to benefits such as significant extensions of humanity's energy resources, reduced capital costs of nuclear power plants, reduced volume and duration for long-term storage and disposal of nuclear waste, longer life of some components of nuclear power plants, increased efficiency of the thermal cycle, and reduced severity of some postulated accidents. Several alternative fuel and fuel cycles are described in this chapter, including the enriched uranium fuel cycle, the recovered-uranium cycle, the MOX cycle, the thorium cycle, the DUPIC cycle, the tandem cycle, low void reactivity fuel, and actinide burning fuel. In addition to increasing fuel cost, alternative cycles impose operating requirements that are more challenging than those experienced when using natural-uranium, low-burnup fuel. Incremental technical challenges in the following subject areas are described here: internal gas pressure, power ramps, corrosion, deuterides and hydrides, deposits, end-temperature peaking, bowing, and high burnup structure in the pellet.

Table of Contents

List of Tables

List of Figures

1 Introduction

The term “fuel cycle” commonly refers to all the steps through which the nuclear fuel goes from mining, to use in a reactor, to discharge, possible recycle, and eventual disposal. Therefore, a fuel cycle consists of certain steps in the *front end*, which involves preparation of the fuel; other steps in the *service period*, in which the fuel is used during reactor operation; and still other steps in the *back end* which are necessary to manage, contain, and either reprocess or dispose of spent nuclear fuel safely.

1.1 Overview

This chapter focusses primarily on selected aspects of the “front ends” and the “service periods” of illustrative fuel cycles that use natural uranium, enriched uranium, plutonium, thorium, and their combinations. The discussion covers simplified neutronics, fuel manufacturing, and selected considerations of associated in-reactor fuel performance. The remaining aspects of fuel cycles are covered elsewhere in this book.

The simplest fuel cycle involves a single pass of the fuel through the reactor; this is called the once-through cycle. Current CANDU reactors run on the once-through natural uranium fuel cycle. A significant amount of useful material (and available energy) still exists in the fuel which is discharged from LWR reactors. Therefore, many fuel cycles are possible in which some fuel components are recycled for further reactor use, particularly in a CANDU reactor. In addition, several other fuel cycles are also possible by using thorium, which is much more abundant on Earth than the uranium that is the primary source of commercial nuclear power today.

We can derive a number of benefits by these means, including significant extensions of humanity’s energy resources, reduced capital costs of nuclear power plants, reduced volume and duration for long-term storage and disposal of nuclear waste, longer life of some components of nuclear power plants, increased efficiency of the thermal cycle, and reduced severity of some postulated accidents. However, several other important factors such as cost also need to be considered, as outlined later in Section 6.

1.2 Learning outcomes

The goal of this chapter is for the student to acquire a broad initial overview of some of the more interesting variants of fissile and fertile materials and the associated fuels and fuel cycles. These include fuel cycles based on the use of natural uranium, enriched uranium, plutonium, thorium, and their combinations. The student will also learn how to evaluate some aspects of fuel cycles and the performance of alternative fuels.

2 Neutronics of Fuel Cycles

2.1 Definitions

Fissile Nuclides: Nuclides that have a significant fission cross section at zero energy.

Fissile nuclides can fission by reacting with a neutron of any kinetic energy, including zero or near-zero kinetic energy (i.e., a slow/thermal neutron).

Example of fissile nuclides: ^{235}U, ^{239}Pu, ^{233}U, ^{241}Pu.

^{235}U is the only naturally-occurring fissile nuclide. The interaction of ^{235}U with a thermal neutron gives ^{236}U, which may fission in about 10^{-14} seconds, releasing on average about 2.5 neutrons. Therefore, we can write:

$$n + {}^{235}U \rightarrow \text{Fission Products} + 2.5n + \gamma.$$

Fissionable Nuclei: Nuclides that can undergo fission (either by a slow or by a fast neutron) are called fissionable. Fissile nuclides are therefore a sub-category of fissionable nuclides. Nuclides which can fission only by reacting with a neutron of high kinetic energy (i.e., a fast neutron) are fissionable, but not fissile.

Examples of fissionable nuclides that are not fissile: ^{232}Th, ^{238}U.

In the case of some non-fissile but fissionable nuclides, the energy-dependent fission cross section displays a threshold with incident neutron energy. The cross section is negligible up to the high energy threshold and has a step increase at the threshold.

Fertile Nuclides: Fertile nuclides are nuclides that can capture a neutron and transmute into a fissile nucleus following one or more nuclear decays.

Examples of fertile nuclides: ^{232}Th, ^{238}U (these happen to be fissionable as well).

Conversion Ratio *C*

To yield fissile nuclides, fertile nuclides must be irradiated with neutrons, which are created as a result of fission. Fission, in turn, consumes fissile nuclei, as does capture. We can look at the process of converting fertile nuclides into fissile ones as consuming some fissile nuclides [Lamarsh, 1966].

The *conversion ratio C* can be defined as:

$$C = \frac{rate\ at\ which\ \ fissile\ nuclides\ are\ \ produced\ in\ the\ entire\ reactor\ by\ conversion\ of\ \ fertile\ nuclides}{rate\ at\ which\ \ fissile\ nuclides\ are\ consumed\ (by\ \ fission\ and\ \ radiative\ \ capture)};$$

i.e., *C* is the average number of fissile nuclides produced by conversion per fissile nuclide consumed (by fission and radiative capture).

The total number of fissile nuclides produced starting from *N* initial fissile nuclides can be calculated as:

$$NC + NC^2 + NC^3 + \cdots = \frac{NC}{1-C},$$

where $C < 1$.

Including the initial fissile nuclides, the total number of fissile nuclides available for fission is

therefore:

$$N + \frac{NC}{1-C} = \frac{N}{1-C}.$$

It can be seen that the total number of nuclides available for fission increases with the conversion ratio. Because *C* is a function of the aggregate nuclear properties of fuel which can change with time, the value of *C* can also change with time.

If *C* > 1, more fissile nuclides are created than destroyed. *C* is then called the *breeding* ratio. *Breeding* can therefore be thought of as conversion with *C* > 1. When breeding occurs, the *breeding gain* can be defined as:

$$G = C - 1.$$

Fuel Burnup

The *specific burnup* (sometimes called just *burnup*, ω) equals the fission energy produced per unit mass of heavy elements in the fuel:

$$\omega = \frac{Fission\ Energy\ Generated}{Total\ Initial\ Mass\ of\ Heavy\ Nuclides\ in\ Fuel}.$$

The usual units for fission energy are either MWh or MWd. Because ^{235}U is by far the most frequently used fissile material, initial mass is usually expressed either as kg or T (tonnes) of U. However, if other fissile materials are used, e.g., plutonium or a mixture of uranium and plutonium, then the initial mass is usually expressed as kg or T of HE (heavy elements).

2.2 Dynamics of Depletion

The reactions by which fertile nuclides produce fissile nuclides are, for example:

$$n + {}^{232}Th \rightarrow \gamma + {}^{233}Th \underset{\beta-decay}{\rightarrow} {}^{233}Pa \underset{\beta-decay}{\rightarrow} {}^{233}U \quad (1)$$

$$n + {}^{238}U \rightarrow \gamma + {}^{239}U \underset{\beta-decay}{\rightarrow} {}^{239}Np \underset{\beta-decay}{\rightarrow} {}^{239}Pu \quad (2)$$

and subsequently:

$$n + {}^{239}Pu \rightarrow \gamma + {}^{240}Pu \quad (3)$$

$$n + {}^{240}Pu \rightarrow \gamma + {}^{241}Pu\ . \quad (4)$$

Figure 1 illustrates a more generalized conversion of fertile nuclides to fissile nuclides.

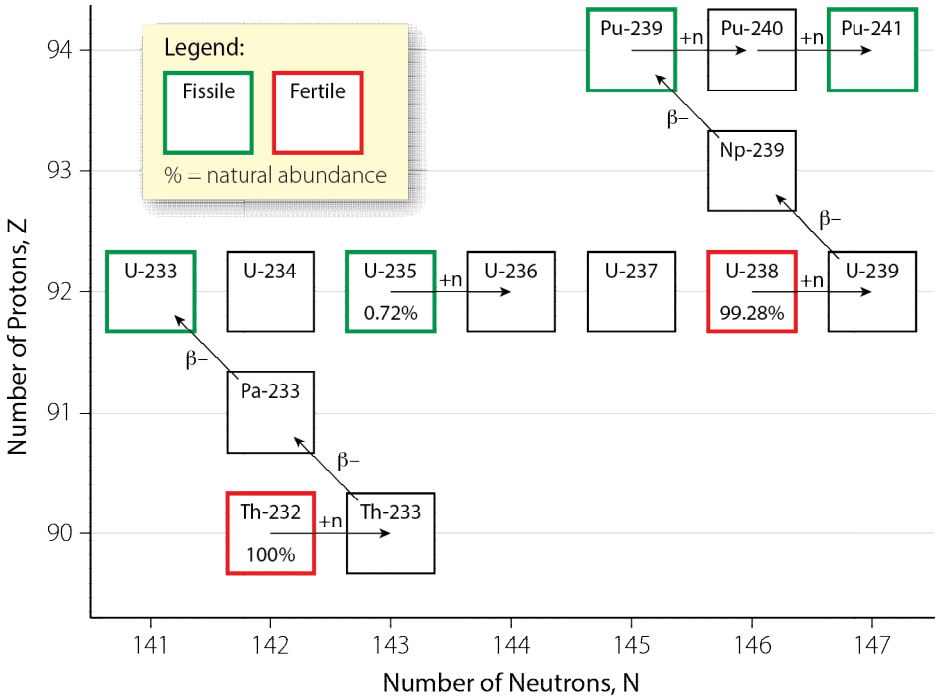

(Courtesy Bill Garland)

Figure 1 Transformation of specific isotopes

Recall from neutron physics that moving to the right in Figure 1 involves adding a neutron (i.e., +*n*), whereas moving left and up involves beta decay (i.e., β-). For clarity, Figure 1 shows arrows and appropriate symbols (i.e., +*n*, β-, etc.) mainly for the key reactions discussed above.

The general nuclide history can be followed by modelling all processes involved [Lamarsh, 1966; Garland, 2005]:

1. loss by decay of the nuclide;
2. loss by neutron capture by the nuclide, which transmutes it into another isotope of the same element;
3. production by decay from a parent nuclide;
4. production by capture transmutation;
5. imposed fuel loading changes.

The first four processes in this list are illustrated in Figure 2.

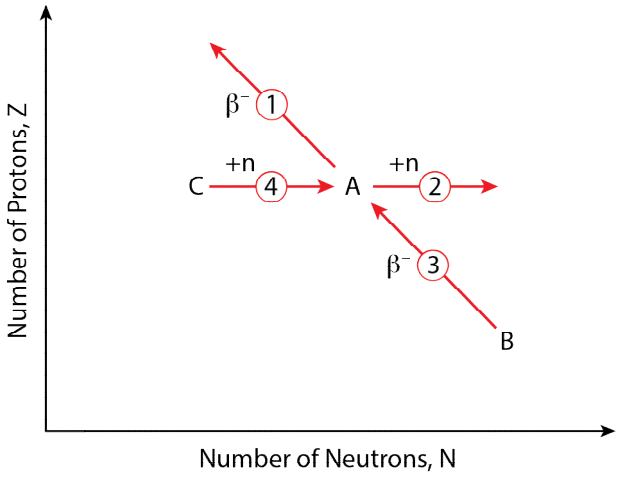

(Courtesy Bill Garland)

Figure 2 Generalized isotope transformation processes

The governing rate equation is:

$$\frac{dN_A}{dt} = \underbrace{-\lambda_A N_A}_{(1)\text{decay}} - \underbrace{\left[\sigma_a^A \phi\right] N_A}_{(2)\text{neutron capture}} + \underbrace{\lambda_B N_B}_{(3)\text{parent decay}} + \underbrace{\left[\sigma_\gamma^C \phi\right] N_C}_{(4)\text{capture transmutation}} + \underbrace{F(t)}_{\text{fuel loading}} . \quad (5)$$

where N_A, N_B, N_C are the number of nuclei (#/cm^3) for isotopes A, B and C respectively, λ is the associated decay constant (sec^{-1}), ϕ is the neutron flux (#/cm^2-sec) and σ_a, σ_γ are the microscopic cross sections (cm^2) for neutron absorption and capture respectively. We can safely assume that the flux is constant over the integration time step and can easily solve this equation numerically. In general, there are many nuclides to track, so they are all solved for simultaneously, thereby tracking the depletion and growth of the various fuel nuclides. Note that the two production processes (3 and 4 above) mean that there is potential for fuel creation, called *conversion* or *breeding* as explained earlier.

The above process yields information on whether or not a given combination and arrangement of materials will achieve criticality and sustain the chain reaction and how much energy can be so produced. The detailed "physics" evaluations of specific fuel cycles use the same general principles that are outlined in earlier chapters on physics and are usually accomplished mainly by changing the inputs of appropriate "generic" physics codes.

3 Overview of Some Possible Fuels and Fuel Cycles

This section outlines some possible fuels and fuel cycles such as the natural uranium cycle, the enriched uranium cycle, the thorium cycle, the breeding cycle, actinide burning fuel, and low void reactivity fuel.

In addition, this section also outlines some interesting and clever fuel cycles that involve extracting significant additional energy from Light Water Reactor (LWR) fuel that would normally be considered as "spent"—that is, fuel that has been discharged from the reactor after having delivered all the energy that is reasonably expected from it. Some cycles that extract additional energy in this manner are: the recovered uranium cycle, the MOX cycle, the

DUPIC cycle, and the Tandem cycle. They are also outlined in this section.

3.1 Reprocessing

Before we delve into various fuel cycles, we first outline reprocessing of LWR fuel as it pertains to this chapter.

Considerable quantities of fission products gradually accumulate inside the fuel element during irradiation. Some fission products are parasitic in that they absorb neutrons without creating proportionate heat. This leaves fewer neutrons to continue the chain reaction, and at some stage, further irradiation of that material risks shutting down the chain reaction. Therefore that fuel is removed from the reactor and is frequently labelled as "spent" or "waste" or "discharged".

Uranium fuel used in LWRs has an initial ^{235}U concentration (enrichment) of between 3% and 5%. After many months (sometimes even a few years) of generating energy in the reactor, most but not all of the original ^{235}U in typical enriched fuels in LWRs is largely used up (e.g., by fission and by radiative capture). Likewise, some fertile nuclides in the fuel, as well as some fissionable nuclides produced by fertile nuclides, are also used up. However, fissionable nuclides are not at zero concentration when the fuel is discharged from the reactor. Spent fuel retains some of the original enriched uranium, and it also contains some fissile plutonium that is produced by the chain reaction (see equations and discussion in Section 2 and in earlier chapters on physics).

The residual fissile content in spent LWR fuel depends on the starting enrichment and the discharge burnup; nevertheless, for illustration purposes, let us say that it is typically in the range of about 1.5% ($^{235}U + ^{239}Pu + ^{241}Pu$). From the perspective of a CANDU reactor, this is a much higher fissile concentration than even the usual fresh (non-enriched) CANDU fuel (0.7%). Even though LWRs cannot continue to "burn" that fuel, CANDU reactors can, due to the latter's superior neutron efficiency. This creates an opportunity to generate additional energy from spent LWR fuel in a variety of ways, as described later in this section.

However, to make effective use of available thermal neutrons, we first need to remove sufficient parasitic neutron absorbers—such as fission products—from spent LWR fuel. This is done through "reprocessing".

Very simplistically, let us think of fuel as having the following initial and final states before and after its irradiation in an LWR:

$$^{235}U\ (3\text{-}5\%) + ^{238}U \rightarrow \{^{235}U + Pu\}\ (\text{about } 1.5\%) + ^{238}U + \text{fission products (FPs)}$$

(fresh LWR fuel) (spent LWR fuel)

Let us next focus only on the right-hand side of this expression. Discussions later in this section use the terms explained below:

- For purposes of this chapter, "conventional reprocessing" or "full reprocessing" means extracting, separating, and purifying uranium (mostly ^{235}U and ^{238}U) and plutonium (mostly ^{239}Pu and ^{241}Pu) in spent fuel. This, however, leads to some concerns that collected plutonium can potentially be diverted towards nuclear proliferation. Full reprocessing generally consists of the following main steps: (Step #1) Irradiated fuel is dissolved; (Step #2) Plutonium and uranium are separated from fission product and then

(Step #3) from each other; and (Step #4) purified for enrichment (in the case of REU) or (Step #5) recycling as MOX.

- In one variant involving partial reprocessing, *all* fission products are removed from spent fuel, but plutonium is neither separated from uranium nor extracted separately, and therefore concerns about proliferation are reduced compared to "full reprocessing". This product is used in the "Tandem cycle" (discussed later).
- In another variant involving partial reprocessing, no dissolution of spent fuel takes place. The gaseous fission products are removed by crushing and heating the spent fuel; the solid fission products are retained in the fuel. The high residual radio-toxicity of this product significantly reduces its attractiveness for potential diversion, which further diminishes concerns about nuclear proliferation. This product is used in the "DUPIC cycle", as described later in this chapter.
- Plutonium recovered from full reprocessing is used to generate electricity in the "MOX cycle".
- Uranium that is collected from full reprocessing is called "recovered uranium" (RU). Its ^{235}U fraction in spent LWR fuel is higher than in natural (as-mined) uranium. RU is used to generate electricity in the "recovered uranium" cycle.

In summary, a variety of fissile and fertile materials are available from different sources in multiple forms such as natural uranium, enriched uranium, thorium, various products of full or partial reprocessing, and others (e.g., dismantled nuclear weapons). This presents opportunities to design a variety of fuels and fuel cycles in neutron-efficient CANDU reactors, some of which are outlined in the following sections.

3.2 Natural Uranium Fuel Cycle

In this cycle, the initial fissile nuclide is ^{235}U as found in mined (natural) uranium. This yields an inexpensive fuel which is the staple of the current generation of CANDU nuclear power plants.

Fission of initial ^{235}U is subsequently augmented by plutonium, produced by neutrons captured in ^{238}U. By the time the fuel is discharged from the reactor, almost half the fissions come from plutonium.

3.3 Enriched Uranium Fuel Cycle

This cycle uses ^{235}U as the initial fissile nuclide that has been enriched, typically to less than 5%.

Enriched uranium fuels are the staples of a variety of reactor types, such as pressurized water reactors (PWRs), boiling water reactors (BWRs), and Russia's VVER/RBMK reactors. In these reactors, enrichment is used to provide an abundance of fissile atoms, which (1) increases the probability of neutron fission and decreases the importance of moderator efficiency, and (2) prolongs the period before fissile atoms must be replenished in the reactor.

During the late 1900s and early 2000s, CANDU reactor designers seriously considered using enriched fuels in designs such as the Advanced CANDU Reactor (ACR) [Reid *et al*., 2008] and in low void reactivity fuels [Boczar *et al*., 2004]. In CANDU reactors, the additional neutrons

generated by enrichment can be used for a variety of purposes such as: (1) using less expensive coolant (i.e., light water) to reduce capital cost; (2) enabling use of thicker pressure tubes to reduce their creep rate and thus to extend their service life; (3) enabling use of burnable neutron absorbers which can reduce the magnitude of a power pulse during a postulated accident; and (4) reducing the volume of spent fuel through extended burnup.

Enriched uranium fuel could also be used in existing CANDU reactors to achieve other benefits such as higher reactor power (through a flatter radial channel power profile).

3.4 Recovered-Uranium Cycle

This is a variant of the enriched uranium fuel cycle. In this cycle, LWR fuel is reprocessed to recover unused uranium. The recovered uranium is reused to make new uranium-based fuel (if necessary, with the addition of fresh uranium).

Thanks to superior neutron efficiency, the CANDU reactor can use RU fuel from LWRs as-is, without additional enrichment, to achieve the benefits mentioned above for enriched uranium fuel.

A number of publications have described the salient attributes of RU fuel, for example Boczar *et al.* [1993 and 2010]. Briefly, the ^{235}U content of RU depends mainly on initial enrichment and discharge burnup of LWR fuel. Conventional reprocessing yields very pure RU with very few contaminants from fission products.

In principle, residual fissile material is also available in used CANDU fuel. However, used natural-uranium (NU) fuel's residual fissile content is much lower than that of used enriched fuels from LWRs. Hence, recovery of residual fissile material for re-use would be significantly more expensive from used NU fuel than from used enriched fuel [Boczar *et al*., 2010].

Significant amounts of high-grade highly enriched uranium (HEU) can also be obtained from dismantled nuclear warheads for use in power reactors.

3.5 MOX Cycle

In this cycle, plutonium recovered through reprocessing LWR fuel is mixed with either fresh or depleted uranium (from enrichment tails) to make mixed uranium- and plutonium-oxide fuel (MOX). The plutonium concentration is adjusted to give the required enrichment and burnup.

Significant amounts of high-grade plutonium can also be obtained from dismantled nuclear warheads for use in power reactors.

3.6 Thorium Cycle

^{232}Th is fertile and can be used to produce ^{233}U, which is fissile and is used *in situ* as it is produced. In the CANDU reactor, a once-through thorium cycle is economically viable, which enables energy to be derived from ^{233}U without reprocessing and recycling. Full benefit from the thorium cycle would require reprocessing of the used fuel to recover and recycle the ^{233}U at an appropriate concentration as new reactor fuel.

Thorium cycles are important because thorium is much more abundant on Earth than uranium. Some countries or regions have thorium resources, but lack plentiful uranium. They

can extend the energy from natural uranium (which is the source of the only natural fissile material) by using the thorium cycle. In addition, thorium cycles provide other benefits, such as in fuel performance and fuel safety, as explained in a later section devoted specifically to thorium.

3.7 DUPIC Cycle

This is one of the cycles that can use discharged LWR fuel in CANDU reactors after partial reprocessing. In the DUPIC cycle, the LWR fuel is reprocessed using dry thermal or mechanical methods to remove gaseous fission products [Boczar *et al*., 1996]. This yields a fuel that neutron-efficient CANDU reactors can use.

Uranium and plutonium are not separated during this operation, and therefore this fuel is attractive from the perspective of nuclear non-proliferation. Irradiation tests have confirmed satisfactory performance of DUPIC fuel [Karam *et al*., 2010(a)].

3.8 Tandem Cycle

This is another cycle based on the use of discharged LWR fuel in CANDU reactors after partial reprocessing. In this cycle, the plutonium and uranium in LWR fuel are separated from all the fission products, but are not separated from each other, as is done in conventional LWR fuel reprocessing operations [Hastings *et al*., 1991]. Therefore, the extraction of fissile materials is more attractive from the non-proliferation perspective than the full reprocessing operation, but less attractive than DUPIC, as explained at the beginning of this section.

3.9 Low Void Reactivity Fuel

One important aspect of CANDU reactor safety is its *coolant void reactivity* (CVR). If a significant volume of the coolant were to be lost in an accident, a complex change in the neutron spectrum would initially rapidly increase the reactivity in the affected reactor core. This would automatically trigger corrective action(s) by the reactor's shutdown system(s), which would quickly decrease the reactivity again. Therefore, the affected core's reactivity would peak for a very short duration. The initial increase in reactivity is called "positive coolant void reactivity". In CANDU reactors, the magnitude of the CVR during postulated loss of coolant accidents sets several requirements for the shutdown system, such as speed, redundancy, and depth. A smaller value of CVR (including a negative value) could loosen these performance requirements and/or increase the safety and/or licensability of the reactor.

One option to reduce such reactivity is the appropriate use of a very small amount of burnable neutron absorber (BNA) in the fuel bundle. The low void reactivity fuel (LVRF) bundle uses a burnable neutron absorber (BNA) such as dysprosium and locates it strategically in the centre element. Enriched uranium is used in the outer elements to compensate for neutrons absorbed by the BNA. The amount of neutron absorber and the level of enrichment can be varied to give the desired values of coolant void reactivity and burnup, although the decrease in void reactivity is at the expense of uranium utilization [Boczar *et al*., 2004]. Such a fuel design has been developed and successfully tested in the reactor [Boczar *et al*., 2004].

3.10 Actinide Burning Fuel

The back end of the fuel cycle continues to attract considerable public scrutiny. A potential amelioration involves reducing the duration for which used fuel remains a radioactive hazard. This could potentially be achieved by fissioning some of the long-lived actinides from used LWR fuels in fast reactors. In a variant of this concept, actinides can first be removed from used LWR fuel (through an enhanced reprocessing route) and blended with a fuel matrix such as uranium, thorium, or a neutronically inert material such as zirconia and used as fuel in a CANDU reactor. The resulting waste would have significantly lower decay heat and radiotoxicity. These actinide-burning CANDU reactors could be used on their own to dispose of spent fuel or in conjunction with fast burner reactors. Use of the CANDU burner reactor would significantly reduce the number of fast reactors that would need to be built for ultimate destruction of LWR actinide waste [Hyland *et al*., 2010; Bhatti *et al*., 2013].

As a by-product, this process would also create many rare earths, which are economically very valuable.

3.11 Breeding Cycles

In fast reactors, breeding cycles are possible: more fissile fuel is produced from fertile nuclides than the amount of fissile fuel destroyed. This cycle in fast breeder reactors can then be used multiple times to increase the use of nuclear-fuel resources. For example, ^{238}U is one of the possible fertile fuels for breeder cycles. This nuclide makes up most of mined uranium—over 99%—compared to 0.7% of ^{235}U. Although current thermal reactors do also convert a tiny fraction of the original ^{238}U into energy, designs of thermal reactors are tailored primarily towards extracting energy from the relatively miniscule fraction of ^{235}U that exists in mined uranium. Through breeder cycles, we can produce energy from a far greater fraction of the much more abundant ^{238}U, thus increasing humankind's nuclear-fuel resources by factors of 50–100 compared with their use in thermal reactors.

4 Key Drivers for Advanced Fuel Cycles

This section provides a broad overview of some of the more significant advantages of alternative fuel cycles.

4.1 Increase the Sustainability of the Nuclear Fuel Cycle

Energy resources can be expanded, sometimes dramatically, through the following methods individually or in combination:

- By using thorium, which is much more abundant than uranium. Thorium fuel has other advantages as well in safety, in-reactor performance, and long-term waste reduction, as discussed in Section 9.3;
- By using plutonium, which can be obtained from a variety of sources such as dismantled warheads or by reprocessing used fuel, as discussed in Section 9.4;
- By using enriched uranium, which can be obtained from a variety of sources such as dismantled warheads or by reprocessing used LWR fuel, as discussed in Section 9.2;
- By using used LWR fuel, which has been reconfigured (but not reprocessed), in a CANDU

reactor;

- By using a breeder reactor to extract energy from ^{238}U, which constitutes over 99% of natural uranium, as discussed in Section 9.5.

Section 5 gives a more detailed discussion of resource extension.

4.2 Improve Fuel Cycle Economics

The natural uranium (NU) fuel cycle, which is currently used in CANDU power reactors, provides low-cost fuel and the highest uranium utilization (energy derived from mined uranium) of any current commercial reactor. The fuel bundles for this cycle are also relatively easy to manufacture. Nevertheless, the economics of the CANDU reactor can be further improved by using enriched uranium. Enriched fuel can be used to:

- Reduce the initial capital cost of a CANDU reactor by enabling the use of lower-cost light water coolant.
- Safely uprate reactor power: Enriched uranium fuel can also be used to uprate reactor power (if allowed by the rest of the plant) by flattening the radial channel power distribution across the core. This means that the channels produce close to the same amount of power and that about 15% more power can be extracted from the same number of fuel channels in a given size of reactor.
- Safely increase bundle power: Different amounts of power are produced in different rings of fuel elements. By adding different degrees of enrichment to the fuel elements that produce low power in different rings, their heat output can be raised without exceeding the safe limits of local power (including considerations of heat removal).
- Increase the lifetime of plant components by measures such as thickening the pressure tubes, thus reducing their creep rate and increasing their service life. The enriched fuel compensates for the increase in parasitic material in the core. Longer service life means that mid-term replacement of pressure tubes can be delayed, thus extending the total life of the plant.
- Increase the efficiency of the steam cycle. Thicker pressure tubes also permit operation at higher coolant pressure and hence at higher outlet temperature. At the higher temperature, steam converts a higher fraction of its thermal energy into electricity. This in turn increases the overall efficiency of the steam cycle.
- Reduce the frequency of on-power fuelling. Higher burnup means a longer residence period of the fuel in the channel. This, in some cases, translates into less frequent channel fuelling and hence a decreased number of duty cycles on the fuelling machines. This in turn may potentially also increase the time available for maintenance of these machines.
- Reduce the volume of spent fuel by extending the burnup. The cost of storage, however, may not be reduced proportionally due to other considerations.
- Reduce the cost of the long-term disposal of spent fuel through the transmutation of hazardous fuel components such as long-lived actinides.

4.3 Improve the Health and Environmental Impacts of the Fuel Cycle

The health and environmental impacts of nuclear power can be improved by using enriched uranium in CANDU reactors and by transmuting hazardous components of the fuel, such as long-lived actinides, in a reactor. This reduces the mass of these materials that requires long-term disposal. This in turn reduces the size of the repositories that will be required and reduces potential impacts on human health and the environment.

4.4 Improve Safety Characteristics

Additional neutrons produced by enriched fuel can be used to offset the reactivity reduction when burnable neutron absorbers are used to reduce coolant void reactivity, as discussed in the section on low void reactivity fuel.

4.5 Improve the Proliferation Resistance of Fuel Cycles

The proliferation resistance of used nuclear fuel can be improved by irradiating derivatives in CANDU reactors, as follows:

- Burn both weapons plutonium and plutonium from used reactor fuel, thereby reducing the inventory of material for potential use in a nuclear explosive device.
- Use new fuel types (such as thorium denatured with ^{238}U) which create spent fuel that is unattractive for use in nuclear explosives.

5 Resource Extension: A Major Incentive

This section expands on one benefit of alternative fuel cycles noted in the section above: extension of world-wide resources for fission energy. Although the subject has been considered by many analysts, the discussion below is based largely on Meneley's analysis [2006] of the world energy situation over the next 100 years, focussing largely on oil and nuclear.

As the world's population and living standards continue to rise, demand for energy is also likely to increase, despite conservation. Oil supply analysts agree that world oil production must decline at some time during the 21st Century; some say that we can expect to see the peak of world oil production very soon. Therefore, there could be a substantial long-term gap (demand minus supply) in availability of primary energy. If nuclear energy is used to fill a significant fraction of the expected energy gap, would it also soon run into resource limitations?

Table 1 summarizes the energy requirements of various fuel cycles in thermal reactors. For a given amount of mined uranium, the fuel cycle that is neutronically the most efficient—1.2% enriched uranium in a CANDU reactor—produces about 90% more energy than the cycle that is neutronically the least efficient.

Table 1 Energy output per megagram of mined uranium

	MWy(e)/Mg
Enriched U in PWR, BWR	4.61
Pu Recycle in PWR, BWR	5.41
DUPIC (PWR → CANDU reactor)	6.37
Natural U in CANDU reactor	6.37
1.2% Enriched U in CANDU reactor	8.77

[Source: D. Meneley, 2006]

Based largely on the projections of the International Energy Agency (IEA) supplemented as required by assumptions, Meneley deduced that to fill the projected world-wide gap in primary energy, we would need some 6,000 nuclear reactors, each with a capacity of 1 GWe. This is significantly more than the currently installed nuclear capacity world-wide.

Table 2 summarizes Meneley's results for years of uranium availability for the above scenario, i.e., a nuclear capacity of 6 TWe. It suggests that if enriched ^{235}U were used to fuel pressurized water reactors (PWRs) or boiling water reactors (BWRs), the planet's identified uranium resources would last about 30 years. If the same ^{235}U were instead used in natural-uranium CANDU reactors, the uranium resources could be extended to last about 42 years. If 1.2% enriched uranium were used in CANDU reactors, these uranium reserves would last about 58 years. The extension from about 30 years in LWRs to about 58 years in CANDU reactors is largely due to the superior neutron efficiency of the latter.

If plutonium is recovered from used fuels and reused in LWRs, reactors can be run for 36 years. Alternatively, if used LWR fuel is reused in CANDU reactors in a DUPIC cycle along with top-up enriched uranium, reactors can be run for 42 years—even without the expensive intermediate step of extracting plutonium.

Note, however, that when uranium eventually becomes scarce, prices will likely increase, exploration will be spurred, and additional reserves can be expected to be discovered.

Table 2 Years of uranium availability

	Megawatt-Years per Tonne	Years of Uranium Availability for 6000 1000-MWe Units
Enriched U in PWR, BWR	4.61	30
Pu Recycle in PWR, BWR	5.41	36
DUPIC (PWR → CANDU Reactor)	6.37	42
Natural U in CANDU Reactor	6.37	42
1.2% Enriched U in CANDU Reactor	8.77	58
Fast Reactor	1,000	6700
Fast Reactor using Seawater*	1,000	>100,000

* Seawater contains about 0.003 ppm of uranium, for a total of over 4 billion tons of uranium.

[Courtesy D. Meneley; Extracted from a presentation to Canadian Nuclear Society by D. Meneley, 2006]

A more dramatic way to extend our energy resources is to breed fissile materials from fertile materials. This can usually be done in two ways: one, fertile ^{232}Th can be converted into fissile ^{233}U; and two, fertile ^{238}U can be converted into fissile ^{239}Pu, as summarized below.

"The absorption cross-section for thermal neutrons of ^{232}Th (7.4 barns) is nearly three times that of ^{238}U (2.7 barns). Hence, a higher conversion (to ^{233}U) is possible with ^{232}Th than with ^{238}U (to ^{239}Pu). Therefore, ^{232}Th is a better 'fertile' material than ^{238}U in thermal reactors, but ^{232}Th is inferior to ^{238}U as a 'fertile' material in fast reactors. For the 'fissile' ^{233}U nuclide, the number of neutrons liberated per neutron absorbed is greater than 2.0 over a wide range of the thermal neutron spectrum, unlike ^{235}U and ^{239}Pu. Therefore, contrary to the ^{238}U-to-^{239}Pu cycle in which breeding can be obtained only with fast neutron spectra, the ^{232}Th-to-^{233}U fuel cycle can operate with fast, epithermal, or thermal spectra" [IAEA, 2005].

Thorium resources have not yet been explored as extensively as uranium; nevertheless, experts estimate that thorium in the Earth's crust is some three to four times as abundant as uranium [IAEA, 2005]. Boczar *et al*. [2010] have estimated that "if all the plutonium from used natural uranium fuel from existing CANDU reactors operating over their lifetime were to be used in a mixed thorium/plutonium cycle, two to three times the existing nuclear capacity in Canada (currently about 15 GWe) could be sustained indefinitely" in a self-sufficient thorium cycle in a CANDU reactor, e.g., a near-breeder. With a breeder, an expanding nuclear system could be fueled essentially indefinitely (depending on the breeding ratio).

Other experts have estimated that ^{238}U in "waste" CANDU fuel alone that has already been accumulated in Canada can, after reprocessing and recycling in fast breeder reactors, produce some 4,000 years of electricity at today's consumption rates [Ottensmeyer, 2012].

Moreover, additional ^{238}U is available underground. Therefore, in principle, fast breeder reactors can provide energy for millennia to come, as shown in Table 2.

At this time, these are only theoretical possibilities. Many technical, economic, and practical concerns remain about fast breeder reactors, such as the very large fissile inventory needed to start a fast reactor and the very daunting concerns about proliferation.

6 Other Considerations

In addition to the drivers described above, various other technical and non-technical factors should be considered in deciding on the most appropriate fuel cycle for a specific power plant, utility, or country. Although a detailed discussion of this subject is beyond the scope of this book, five major aspects are summarized below: energy independence, resource utilization, resistance to nuclear proliferation, fuel performance, and cost.

Energy Independence

Plants that enrich large quantities of uranium are very expensive and are operational in only a few nations. Fuel cycles based on natural uranium do not require a nation to build a plant to enrich uranium, nor do they require a nation to rely on a few other nations for continual supply of enriched uranium over a very long period. Therefore, natural uranium cycles promote national energy independence.

Resource Utilization

To produce a given amount of energy, some fuel cycles require less mined uranium than others. For example, the combination of heavy water and natural uranium used in current CANDU reactors requires some 40% less mined uranium per unit energy than fuel cycles that use light water and enriched uranium. This can be a consideration in countries that do not have much uranium and would like to stretch their domestic uranium to the extent practical.

Resistance to Nuclear Proliferation

There is concern in some quarters that during reprocessing, potent fissile material can potentially become accessible and hence available for diversion to uses other than electricity generation. Some fuel cycles such as DUPIC are comparatively more resistant to nuclear proliferation.

Fuel Performance

Overall, current fuels perform very well in current fuel cycles, as noted in Chapter 17. In fuel cycles that differ significantly from current cycles, satisfactory fuel performance must be designed and demonstrated. Depending on the specific cycle, new R&D may potentially also be required.

Cost

Generally, enriching and reprocessing fuel is expensive, and the radioactivity and radiotoxicity of spent enriched fuel tends to be higher than that of natural uranium. At the same time, enriched fuel generally yields higher burnup, which tends to reduce fuelling cost (within a range) and also reduces the volume of spent fuel to be stored. Therefore, this is a complex topic, and its impact also changes with local conditions and with time.

In summary, the choice of a specific fuel cycle must consider not only the drivers discussed earlier, but also other techno-commercial and geo-political aspects, some of which are noted above.

7 Pertinent Features of the CANDU Reactor

A number of features of a CANDU reactor enable it to use alternative fuel cycles more effectively than other reactor types, mainly through higher neutron efficiency and also through easier processing and fabrication of recycled fuel. These features are explained below.

Higher Neutron Efficiency

Natural uranium has low fissile content. To enable fission in a sustained chain reaction, CANDU reactors are, of necessity, designed with high neutron efficiency. This in turn makes CANDU reactors attractive for using other low-fissile materials in alternative fuel cycles.

The following main features contribute to the high neutron efficiency of CANDU reactors [Boczar, 2012]:

- CANDU reactors use heavy water (D_2O) as both moderator and coolant. This reduces parasitic absorption of neutrons compared to light water.
- The moderator, which is separate from the coolant, is at low temperature. This promotes neutron efficiency.
- In CANDU reactors, a small cluster of fuel elements (i.e., a fuel bundle) is surrounded by a large amount of low-temperature moderator. This thermalizes a higher fraction of neutrons.
- The principal structural components inside the core, e.g., the calandria tubes, pressure tubes, and fuel bundle, are made from zirconium alloys. This reduces parasitic absorption of neutrons, for example in comparison to components made of stainless steel.
- CANDU reactors use relatively thinner structural materials. For example, as a proportion of fuel element diameter, sheaths are significantly thinner in CANDU reactors than in LWRs, reducing parasitic absorption of neutrons in the former.
- CANDU reactors are refueled on-power, as necessitated by the use of NU. This has a consequential benefit in that the reactor can be operated effectively with low excess reactivity in the core, obviating the need for burnable neutron absorbers and minimizing neutron absorption in control materials.
- CANDU reactors contain equipment for on-power refuelling, which provides flexibility in accommodating alternative fuels.

The resulting high neutron economy of a CANDU reactor enables high fuel utilization regardless of the fissile material (^{233}U, ^{235}U, or plutonium). About 90% more energy can be extracted from a particular fissile material than in an LWR reactor [Boczar *et al*., 1996], as shown in Table 1.

Easier Fabrication and Reprocessing of Fuel

The simple, small fuel bundle design of a CANDU reactor (see Chapters 8 and 17) facilitates remote processing and fabrication for highly radioactive recycled fuels.

A key “enabler” of these advantages is the separation of moderator and coolant in a CANDU reactor through pressure/calandria tubes. This separation permits the reactor designer to

adjust the moderator and the coolant independently to exploit neutronic characteristics more effectively. For example, the moderator can be kept at low temperature to promote neutron efficiency, while the coolant can simultaneously be kept at high temperature to promote the thermal efficiency of the steam cycle. In another example, the choice of coolant fluid and the moderator-to-coolant-volume ratio can potentially be fine-tuned to reduce capital cost without adversely affecting fuel cooling, as is done with the Advanced CANDU Reactor. CANDU reactors are unique among successful contemporary reactor systems in offering this important flexibility to designers.

8 Natural Uranium Fuel Cycle

The front end of the NU cycle starts with mining, refining, and conversion of uranium into ceramic UO_2 powder. The next segment of the front end is fuel manufacturing, including the procurement and processing of Zircaloy components. These front-end segments are described below.

8.1 Production of Ceramic UO_2 Powder

The steps involved in production of reactor-grade ceramic UO_2 powder include mining, refining, and conversion, as summarized below.

There are four methods of obtaining uranium from ores:

- Open-pit mining;
- Underground mining (the main method until the recent past);
- *In-situ* leaching (currently the leading method);
- Recovery from mining of other minerals such as copper, phosphate, or gold.

Regardless of how the uranium is obtained, it cannot be fed directly into a nuclear power station because it contains mineral and chemical impurities, including radioactive daughter products of uranium. Processing is required before uranium can be used efficiently to generate electricity.

If uranium is obtained by open-pit or underground mining, the first process after mining is crushing (milling) of the ore, followed by dissolution in an acid or alkaline medium to separate the uranium metal from unwanted rock and purification with chemicals which selectively leach out the uranium. The uranium-rich solution is then chemically separated from the remaining solids and precipitated out of solution. Finally, the uranium is dried. The resulting powder is uranium oxide concentrate, U_3O_8, commonly referred to as “yellowcake” due to the bright yellow colour that it frequently, but not always, exhibits. The unwanted solids, called “tailings”, are stored at the mine site for safe disposal.

If the *in-situ* leaching method is used, an acidic or alkaline mining solution is passed directly through the underground ore body by means of a series of bores or wells, and uranium is brought to the surface in a dissolved state for purification. The uranium-rich solution is treated as described above, the principal difference being that no tailings are produced by this method.

Uranium meeting nuclear-grade specifications is usually obtained from yellowcake through a

tributyl phosphate solvent-extraction process. First, the yellowcake is dissolved in nitric acid to prepare a feed solution. Uranium is then selectively extracted from this acid feed by tributyl phosphate diluted with kerosene or some other suitable hydrocarbon mixture. Finally, uranium is stripped from the tributyl phosphate extract into acidified water to yield highly purified uranyl nitrate, $UO_2(NO_3)_2$. Uranyl nitrate is the starting material for conversion to uranium dioxide (UO_2) powder or to uranium hexafluoride (UF_6). Both these conversion routes conventionally begin with calcining the nitrate to UO_3.

A large percentage of the UO_3 produced in Canada is converted to uranium hexafluoride (UF_6) destined for enrichment plants for use in LWRs, and the remainder is converted to natural uranium dioxide (UO_2) ceramic-grade powder for use in CANDU reactors. The processes involved in producing natural uranium (NU) UO_2 powder for CANDU fuel pellets are described in more detail below. The UO_3 is dissolved in nitric acid, and the resulting solution is diluted and reacted with ammonium to precipitate ammonium diuranate (ADU). The liquid is decanted, and the ammonium diuranate slurry is dried to remove the water. The resulting ammonium diuranate powder is dried in a rotating kiln in hydrogen gas to produce UO_2 powder. The powder may then be subjected to further physical "conditioning" to improve its mechanical "reactivity" during pellet sintering. Small batches of each powder lot may be subjected to sintering trials as part of the final QA acceptance test before it is sent to manufacturers of CANDU fuel bundles.

At each production stage mentioned above, the uranium compound is subjected to stringent quality control surveillance to ensure that the final product meets industry technical specifications with respect to the content of specified impurities as well as certain physical characteristics related to subsequent manufacturability. In-reactor behaviour of CANDU fuel bundles has demonstrated that some aspects of fuel performance (e.g., fission product behaviour) are related not only to powder characteristics, but also to the process parameters used in producing the powder.

8.2 Fuel Bundle Manufacturing

A simplified CANDU fuel bundle manufacturing flow sheet is shown in Figure 3.

Manufacturing of bundles starts in two separate production streams: production of UO_2 pellets (left-hand side (LHS) of Figure 3), and production of sheath sub-assemblies and other Zircaloy components (right-hand side (RHS) of Figure 3). These two production streams require such diverse processes and expertise that they are not only carried out in separate production lines, but also may be carried out at different geographical locations.

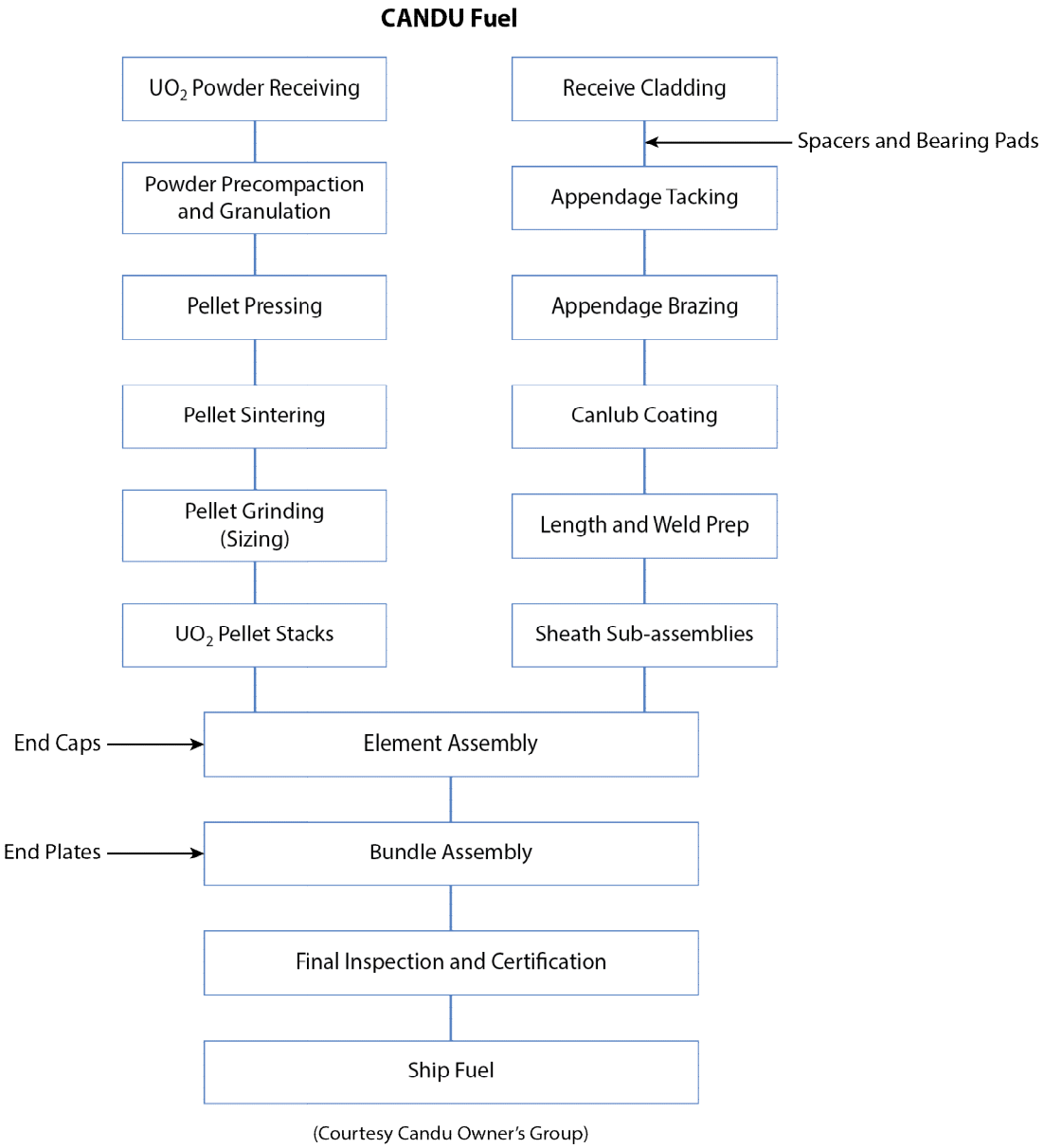

Figure 3 CANDU fuel manufacture: assembly flow chart

The UO_2 pellet production stream starts with receipt of UO_2 powder (Step 1, LHS of Figure 3). As received, the powder consists of very fine particles that tend to agglomerate and impede rapid and consistent filling of the pellet pressing dies. To improve the "flow" of the powder, it is subjected to two physical processes: compaction and granulation (Step 2). During this step, a lubricant is also added to aid pellet pressing (Step 3), which is followed by pellet sintering (Step 4). Sintering is one of the most critical steps in pellet production and requires precise control of temperature, time, and the atmosphere used during the sintering cycle. Pellet density and density distribution as well as physical integrity (no cracks or "chips") are critically dependent on proper control of this process step.

As sintered, the pellets are hourglass-shaped (see Chapter 17 for additional discussion of this phenomenon). The sintered pellets are ground (Step 5) in a "centreless" grinder to (1) remove the hourglass shape and produce a straight cylindrical pellet shape, (2) size the pellet

to the desired diameter, and (3) impart a fine finish to the cylindrical pellet surface.

The ground pellets are sorted by diameter and placed into stacks (Step 6) ready for insertion into sheath sub-assemblies, which come from the second stream. Pellet stack length is controlled to tight tolerances because it is the principal means for ensuring adherence to the required axial clearance within the fuel element. Pellet stacks and sheath sub-assemblies are sorted by diameter and matched to satisfy the diametric clearance requirements. In addition, to prevent interference with the sheath, the pellets at both ends of the stack may be tapered, or their diameter may be reduced. Additional discussion on this topic is provided below.

Some of the greatest challenges in CANDU fuel production occur in the UO_2 pellet production stream. These challenges derive from the pellet technical specifications, some of which are unique to CANDU fuel. A few of the major challenges are high pellet density; precise dimensional control, especially of pellet diameter; small size of permissible visible surface flaws, referred to as "chips"; and high quality of surface finish, especially the pellet cylindrical surface (see Chapter 17 for additional discussion on pellet/sheath interaction). These challenges have been successfully met by manufacturers of CANDU fuel. This is substantiated by the almost complete absence of defects ascribed to pellet manufacturing deficiencies, the only notable exception being failures observed in "overstuffed" fuel elements, which were intentionally manufactured to challenge the extreme limits of the relevant parameters: maximum pellet density, minimum diameter clearance, and minimum axial clearance. Once defects were witnessed in "overstuffed" elements, the practice was subsequently discontinued.

The second manufacturing stream, the production of sheath sub-assemblies, starts with receipt of tubes finished to the required diameter and cut to length (Step 1, RHS of Figure 3). Some manufacturers (including both Canadian manufacturers) have "vertically integrated" Zircaloy tubing production into this stream, so that the stream actually starts with receipt of zirconium tube hollow (TREX), which undergoes several stages of reduction and associated processing (not shown in Figure 3), culminating in cut-to-length tubes.

In parallel with receipt of tubes, Zircaloy sheet/strip, bar/rod, wire, graphite slurry, and beryllium are also received. The sheet (or wire) is used to manufacture spacers and bearing pads (appendages). When manufactured from sheet, the appendages are punched and "coined" into their final shape from the sheet after it is coated with beryllium. When manufactured from wire, the appendages are cut to length, coined, and subsequently coated with beryllium. The appendages are "tacked" to the tubes with spot welds (Step 2) and heated until the beryllium coating and the Zircaloy metal in the appendage and tube form an alloy, i.e., "braze" (Step 3). Appendage dimensions, the shape of the coined surfaces, the thickness of the brazing metal, and the location and tacking of the appendages on the tube must be controlled to tight tolerances to enable the manufacturer to achieve the required dimensional tolerances for the assembled bundle. The manufacturers have successfully met the challenges of this part of the manufacturing process, as evidenced by the absence of any fuel failures caused by detached appendages or appendages causing bundle incompatibility within the fuel channel.

Graphite slurry is diluted with water or an industrial alcohol, applied to the inside of the tube sub-assemblies, and dried to form a coating of precisely controlled thickness and hydrogen

content referred to as "CANLUB" (Step 4). The effect of CANLUB on in-reactor performance of fuel elements is discussed in Chapter 17. The ends of the sheath sub-assemblies are machined (Step 5) to (1) achieve the required final length, and (2) produce the profile required for end-cap welding. In addition, CANLUB and any debris are removed from the end of the sub-assembly lest they interfere with the subsequent welding process.

The two process streams (LHS and RHS in Figure 3) come together at the element assembly step, i.e., the insertion of pellet stacks into the sheath sub-assemblies and the welding of element end closures (endcaps). Endcaps are machined from bar or rod to match the sheath sub-assembly weld preparation and to include other features (internal and external) which are crucial to the final configuration of the element assembly. They are then welded to the sheath using resistance welding, which is a thermo-electric process.

During resistance welding, the sheath is held by a collet. Heating during resistance welding softens the sheath locally. The combination of the heating and cooling cycle that occurs during the welding cycle and the restraint provided by the collet causes the sheath diameter to shrink immediately adjacent to the weld. To maintain the minimum required diametric clearance in this region of the element, the pellets at both ends of the stack have a reduced diameter (usually tapered to mimic the sheath diameter profile).

After insertion of the pellet stack into the sheath sub-assembly, and before welding of the end caps, the air trapped inside the sheath sub-assembly is purged with helium (or a mixture of helium and argon). The end cap is then welded while the weld region is blanketed by inert gas.

Similarly to the pellet production stream, the Zircaloy component stream has its own unique CANDU-related challenges, the most unique and critical being the dimensional and process parameters related to welding of endcaps to sheath sub-assemblies. To appreciate the importance of this operation more fully, it is useful to remember that the largest CANDU reactors have close to one-half million of these welds in the active part of the core and that one defective weld is cause for concern, requiring urgent action to remove it from the core. In comparison, LWR reactors have no discontinuities or joints of any type in fuel cladding within the active part of the core. To make sure that the contribution of endcap welding to defect statistics in CANDU reactors remains insignificant, defects due to endcap welding must be maintained at or below the part-per-million (ppm) level, which is extremely challenging. Careful examination of the fuel manufacturing flow chart, including the relevant component design and process parameters, reveals more than 15 design and process parameters which must be maintained within control limits and must come together at the precise moment the weld is made. It is not surprising that of the very few defects in operating CANDU fuel which have been ascribed to manufacturing causes, more than 90% are related to endcap welding. Fuel integrity statistics for CANDU reactors and LWRs are discussed in Chapter 17; notwithstanding the contribution from endcap welding to defects in CANDU fuel, defects in CANDU fuel from all causes are significantly fewer than defects in LWR fuel (see Chapter 17).

Following endcap welding, the fuel elements are inserted into an assembly jig and the element ends resistance-welded to endplates to form the final fuel assemblies, i.e., the fuel bundles. End plates are stamped out of an incoming strip. Although this final process in itself is not as challenging as some of the processes described above, it is important to note

that some of the dimensional requirements on the bundle assembly are equivalent in precision to those which are normally associated with machined components. To achieve this, manufacturers must have stringent control, not only of the final assembly process, but also of the processes used to produce the component parts, particularly element sub-assemblies and endplates.

Manufacturing is the final step in the realization of a product, converting the intent specified in the design drawings and technical specifications into functioning hardware. For one unit of energy produced, current CANDU reactors use five to six times the mass of fuel used in LWRs. Despite this relative disadvantage, fuelling cost per unit energy has always been much lower for CANDU than for LWR. This can be attributed mainly to three factors: (a) CANDU reactors avoid the high cost of enrichment, (b) CANDU reactors use 40% less mined uranium per unit of energy produced than LWRs, and (c) CANDU fuel manufacturers have managed to keep their fabrication costs very low while keeping fuel reliability very high. In addition, Canadian fuel manufacturers have also been very successful in transferring access to their technology to all non-Canadian manufacturers of CANDU fuel.

9 Details of Selected Alternative Fuels and Fuel Cycles

From the ten possible alternative fuel cycles summarized in Section 3, selected five alternative cycles are described in greater detail in the sections below.

9.1 Natural Uranium Equivalent (NUE) Fuel

In all respects other than the sourcing of the fissile material (^{235}U) and the starting amount of fissile material (%^{235}U in total U), this "cycle" is essentially the same as the natural uranium (NU) cycle. The starting feedstock (UO_2 ceramic-grade powder) for this cycle is a blend of recycled enriched uranium (REU) and depleted uranium (DU) from enrichment plant tails. The proportion of each component is determined by the respective content of ^{235}U in each. For instance, if the ^{235}U content of REU is 0.9% ^{235}U in total U and that of DU is 0.2% ^{235}U in total U, then the proportion of the two components per unit weight of the blend, with an enrichment of 0.71% ^{235}U in total U, can be calculated as follows:

If x is the fraction of REU in the blend, then the fraction of DU is $(1 - x)$. If the enrichment of the final mixture is 0.71%, then:

$$x*0.9 + (1 - x)*0.2 = 0.71. \quad (7)$$

By solving Equation (7) for x, one can conclude that the blend needs to consist of 73% REU and 27% DU. Similar calculations can also be performed for other combinations of starting ^{235}U contents of the constituent components. It is likely that the blended ^{235}U fissile content for this cycle will have to be very slightly higher than for NU to compensate for impurities in the REU and DU, which are expected to be higher than the respective impurities in NU. The exact ^{235}U content in the blend would be determined for each batch of fuel procured, based on the measured amount of impurities in each component.

Once the NUE powder has been obtained, the fuel bundle is manufactured using the same processes that are used to produce NU fuel bundles, as described earlier.

Satisfactory performance of NUE fuel has been confirmed in "demonstration" irradiations in a commercial power plant in China [Jioa *et al*., 2009].

9.2 Extended Burnup Fuel

As noted in Section 3, enriched uranium can be used for several purposes in a CANDU reactor. One of them is to increase significantly the discharge burnup of CANDU fuel. This means that a given amount of energy can be produced by fewer fuel bundles, reducing the amount of spent fuel (i.e., high-level waste) that needs to be stored and disposed of.

To balance the above, one must consider (a) the increased cost of fuel, because enrichment is expensive, (b) technical considerations in several key areas of fuel performance, such as internal gas pressure, power ramps, corrosion, hydriding, deposits, end-temperature peaking, bowing, high burnup structure, and (c) other effects related to plant operation, such as the effect of enriched uranium on coolant void reactivity (CVR) and on refuelling operations.

Explanations of how fuel integrity is affected by some of these mechanisms have already been discussed in Chapter 17 from the perspective of normal CANDU burnup. High burnup exacerbates some of these, especially those discussed below. The sub-sections that follow provide additional science that can aid in developing successful fuel designs for extended burnup, which is a common feature of many of the alternative fuel cycles described in Section 3.

From the perspective of maximum utilization of mined uranium, the optimal enrichment (and hence burnup) for a CANDU reactor is around 1.2%, which is much lower than the typical enrichments in LWRs. Therefore, many of the performance challenges discussed below for extended burnup fuel are significantly lower in CANDU fuel than in high-burnup LWR fuels.

However, in CANDU fuel, the high burnup occurs in conjunction with high element power, which frequently exacerbates the challenge to fuel integrity. On the other hand, in CANDU reactors, on-line fuelling provides a measure of flexibility in shaping the axial and radial power profiles throughout the core. This can be used to help keep peak element ratings within limits and reduce the size of power ramps resulting from refuelling.

9.2.1 Internal Gas Pressure

Extended burnup has the potential to increase, among other things, the internal gas pressure within a fuel element (see Chapter 17). If excessive, the higher gas pressure can potentially overstress and crack the fuel sheath. Some CANDU fuel elements indeed failed in the Bruce reactor when they stayed in the reactor for unusually long periods and their internal pressure inadvertently exceeded failure limits. Likewise, excessive internal pressure has also failed a few fuel elements in experimental fuels as well [Floyd, 2001].

Three techniques are available to avoid such failures. First, fission gas release can be reduced, e.g., by reducing element ratings. Second, the void space in the element can be increased, e.g., by using bigger chamfers, gaps, or plena [Floyd, 2001]. Third, stress concentrations at critical locations can be reduced by using a larger notch radius at the sheath/endcap junction [Tayal *et al*., 1993], see Figure 4.

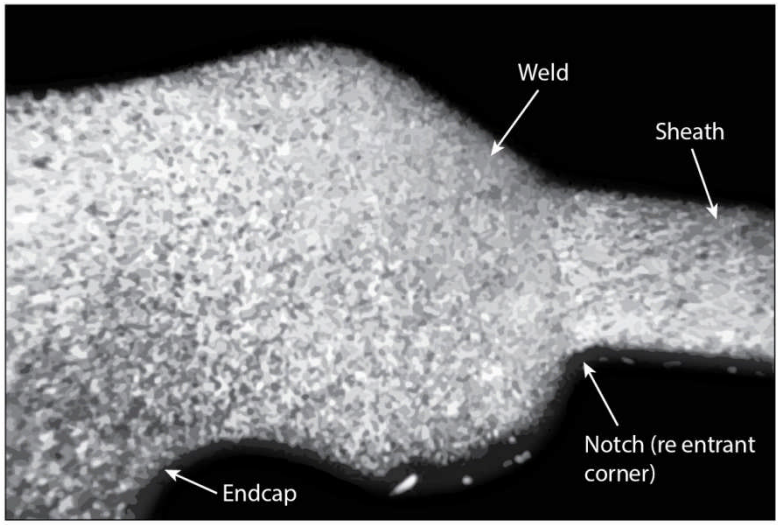

[Source: Page, 1976]

Figure 4 Illustrative notch at the sheath/endcap junction

9.2.2 Zircaloy ductility and power ramp

As noted in Chapter 17, a power ramp causes thermal expansion of a pellet, which in turn pushes the sheath. The sheath can crack if its strain exceeds its ductility in the corrosive environment of fission products.

Irradiation reduces the ductility of Zircaloy significantly, as illustrated in Figure 5 [Tayal *et al*., 1995]. For example, Figure 5 suggests that irradiation to 200 MWh/kg reduces the ductility of Zircaloy by a factor of three to four compared to its initial as-fabricated value.

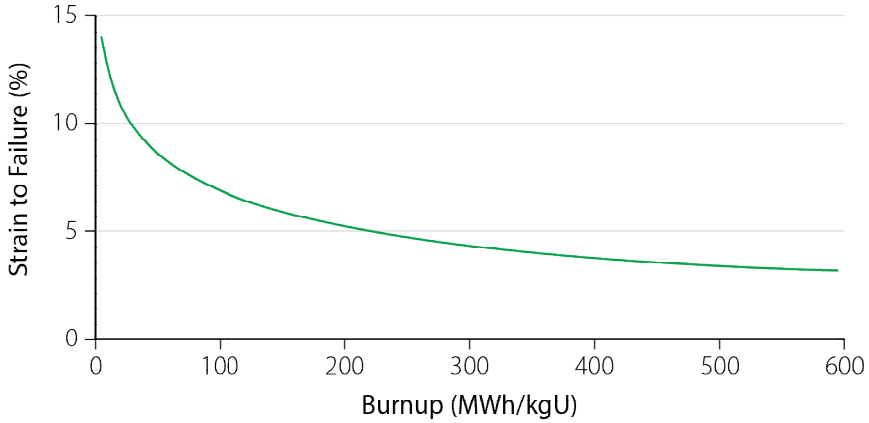

[Source: Tayal *et al*., 1995]

Figure 5 Illustrative effect of irradiation on ductility of Zircaloy

Decreased ductility leads to lower tolerance to power ramps at extended burnups. In Chapter 17 (Section 8.2), the power ramp defect threshold of the sheath was considered in a narrow burnup range of 140 ± 20 MWh/kgU. Fuel can be operated to much higher burnups, especially LWR fuel and extended burnup CANDU fuel. To design safe operating conditions for such fuel, we need to know the power ramp defect thresholds at the higher burnups. To obtain an illustrative idea, let us use Figure 5 of this chapter to extend the defect threshold

curve of Figure 24 in Chapter 17 to other burnups. The result, Figure 6, illustrates how higher burnups can decrease resistance to power ramps in non-CANLUB fuel. The decrease is initially rapid, but slows down after burnup of about 100 MWh/kgU. Similar trends are expected in CANLUB fuel as well.

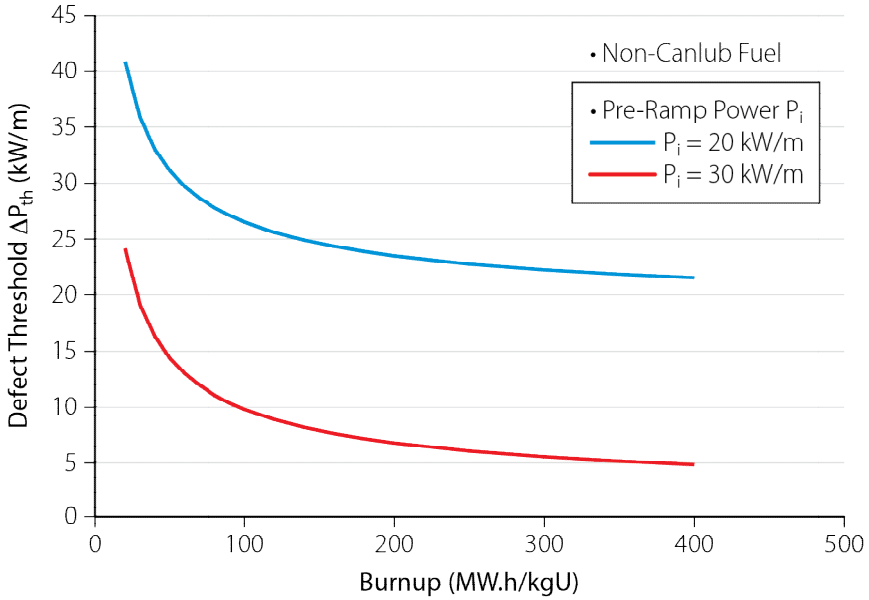

Figure 6 Illustrative effect of burnup on power ramp defect threshold

Exercise: As an illustrative example, assume that a power ramp of 10 kW/m is being considered in non-CANLUB fuel at a burnup of 300 MWh/kgU. Before the ramp, the fuel is operating at 20 kW/m. (a) Will the fuel survive this ramp? (b) Will the fuel survive the same ramp if its pre-ramp power is 30 kW/m?

Figure 6 shows that the first ramp is below the defect threshold, and therefore the fuel will survive it. The second ramp, however, is above the defect threshold; therefore, the fuel will have a non-zero probability of developing defects.

If the fuel's expected ramps are significantly higher than the defect threshold, appropriate steps must be taken to increase the sheath's tolerance to power ramps. These could include, for example, optimizing the shape of the pellet to decrease its thermal expansion; a thicker coating of CANLUB to reduce the concentration of aggressive species of fission products at the sheath surface; or even an entirely new CANLUB formulation.

The decreased ductility of Zircaloy at extended burnup also affects several other areas of fuel performance, for example the mechanical strength of the endplate during discharge. These factors must all be considered carefully during the design process.

9.2.3 Corrosion

Higher burnup is usually associated with longer residence periods. The latter can potentially increase sheath corrosion. This tends to be much more pronounced at the outer surface of the sheath, which is in contact with water.

When part of the sheath corrodes, its ability to carry mechanical load decreases. Strength assessments must account for this loss, and therefore we need to quantify sheath corrosion. Furthermore, very thick layers of oxide tend to flake, causing a potential for debris and deposits in the heat transport system. In addition, flaking often leaves behind non-uniform patches of oxides. These cause significant axial and circumferential variations in sheath temperature, which in turn cause hydrogen and deuterium to diffuse and concentrate at local peaks. The shape of the resulting hydrogen- (and deuterium)-rich areas often resembles a lens, and therefore the product is often called a "hydrogen lens". If local peaks of hydrogen, hydrides, deuterium, and deuterides become pronounced, they can embrittle the sheath, which in turn can significantly challenge its mechanical integrity. For all the above reasons, the extent of corrosion must be kept within acceptable limits.

In CANDU reactors, lithium hydroxide (LiOH) is added to maintain coolant pH in the 10.5 range, which is intended to minimize deposition of iron-based system corrosion products ("crud") on both fuel surfaces and steam generator tubes [Barber *et al*., 1982]. From out-of-reactor autoclave tests, several investigators have determined that oxidation of zirconium alloys is not affected by the LiOH concentrations that are required to maintain coolant pH near 10.5. Similarly, in-reactor, no acceleration of zirconium-alloy oxidation has been observed in the pre-transition oxidation period, with additions of lithium hydroxide to control pH in the 10.5 range. However, under very long exposures and high burnups which develop relatively thick post-transition oxide films, some acceleration of oxidation has been observed on fuel elements in light water reactors [Garzarolli *et al*., 1982; Cox, 1985]. The latter has been attributed to possible concentration of the lithium hydroxide within the thick oxide films due to temperature rise during heat transfer [Courtesy COG].

Waterside corrosion has indeed been identified in LWRs as a process that warrants the use of more corrosion-resistant materials in the sheaths of very high burnup fuels. In CANDU reactors, however, the burnup, and therefore the residence period, is far less, and therefore current CANDU reactors are still quite far from requiring such an expensive change. Even in enriched CANDU fuel with burnup of about 30 MWd/kg, corrosion is not expected to be a problem.

In summary, there are many detailed nuances in sheath corrosion. Nevertheless, for purposes of this initial introduction, Figure 7 shows an illustrative progression of sheath corrosion with burnup. Note the large scatter in the data, which is typical. Also note that the overall trends are similar in CANDU and PWR sheaths.

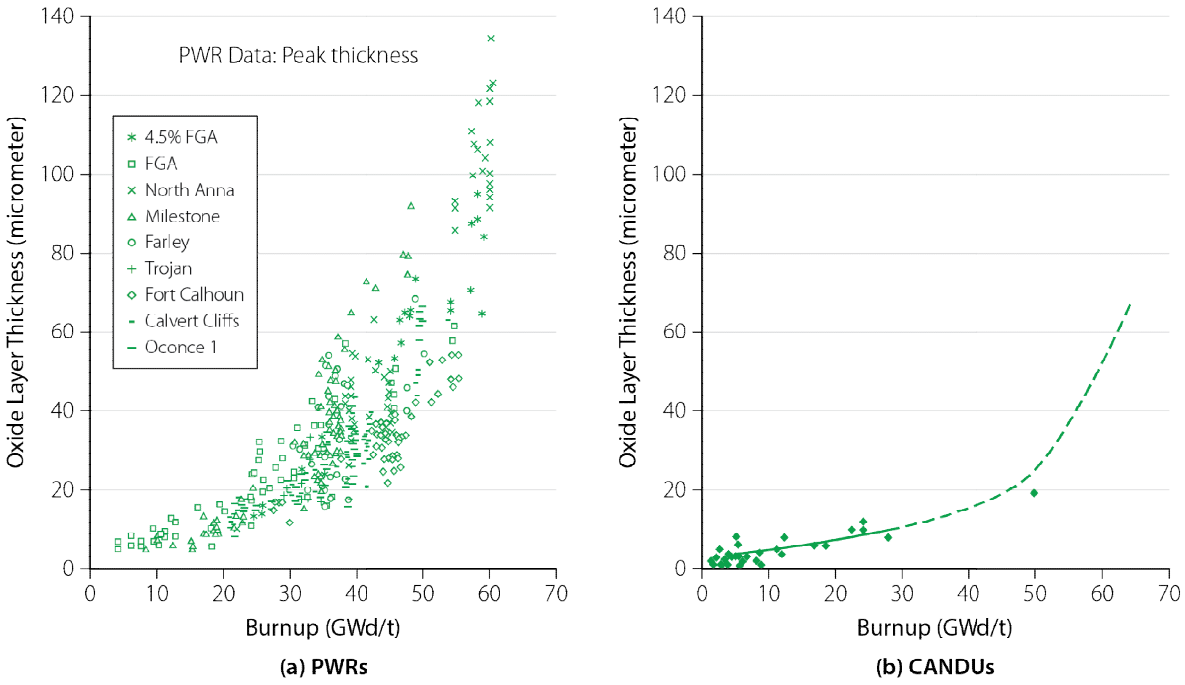

[Source: Tayal *et al*., 1995]

Figure 7 Waterside corrosion in the sheath

Example: How much corrosion can be typically expected in a CANDU sheath (a) at 240 MWh/kgU; (b) at 480 MWh/kgU?

From Figure 7(b), we would expect an oxide layer of about 5 µm at 240 MWh/kgU and one of about 15 µm at 400 MWh/kgU. These are both very thin layers and pose no risk of flaking. Note the disproportionate increase in oxidation with burnup.

9.2.4 Deuterides and hydrides

Waterside corrosion liberates deuterium or hydrogen:

In heavy water: $Zr + 2D_2O = ZrO_2 + 2D_2$ (8)

In light water: $Zr + 2H_2O = ZrO_2 + 2H_2$. (9)

In this section, for simplicity, we will use the terms “deuterium/deuteride” to include generically “hydrogen/hydride” depending on context.

Some fraction of the liberated deuterium is dissolved in the sheath, a process sometimes also called “uptake”. Over time, the deuterium diffuses due to gradients of concentration, temperature, and stress and can accumulate preferentially at a few spots. When the local concentration exceeds the solubility limit, deuterium precipitates in the form of deuteride platelets, referred to as “deuterides”. The solubility limit decreases with lower temperature, and therefore deuterides tend to precipitate preferentially in relatively colder regions.

Depending on their orientation, deuterides can embrittle Zircaloy, thereby reducing its ability to carry tensile loads. For this reason, deuteride levels must be maintained within acceptable limits.

If the coolant is light water rather than heavy water, the same qualitative assessment applies,

except that instead of deuteride platelets, hydride platelets (referred to as "hydrides") are formed. Figure 8 shows an illustrative example of hydrides in a sheath that was irradiated to a burnup of about 600 MWh/kg HE in light water coolant. Note the relatively higher concentrations of hydrides near the outer surface because that surface is cooler than the inner one.

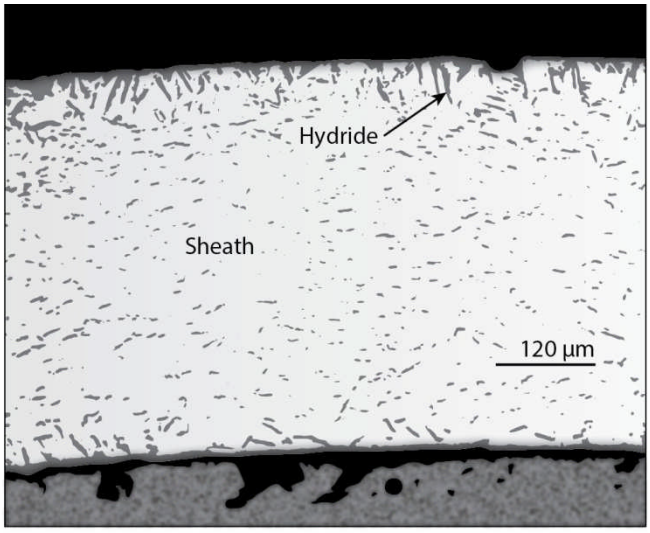

[Source: Karam *et al*., 2010(b)]

Figure 8 Illustrative distribution of hydrides in the sheath at about 25 MWd/kg HE

There is no evidence that excess hydrogen in the coolant causes primary defects in fuel-bundle metallic components, or that it participates in the formation of secondary damage in fuel metallic components. This may be because there is no thermodynamic mechanism for excess H^+ (or H_2) to enter the matrix of metallic components. The mechanism for introducing deuterium (not hydrogen) into the matrix of CANDU-bundle metallic components is dependent on D_2O coming into contact with an unoxidized metallic component, at which point oxygen, having a greater affinity for the metal than deuterium, combines with the metal, causing the D_2O molecule to dissociate and leaving the liberated D^+ radical (or D_2) inside the matrix of the metallic component. D^+ radical (or D_2) then dissolves within the metal matrix. Excess D^+ (or D_2) within the metal then precipitates to form deuterides in the coldest part of the metallic component, as explained earlier.

Typical values of hydrogen/deuterium (H/D) pickup in extended-burnup CANDU sheaths are available from a compilation presented by Floyd [2001]. For comparison purposes, sheath D concentrations are expressed in terms of equivalent H (=D/2). With the exception of siloxane-coated fuels, equivalent H concentrations up to 200 µg/g are widely observed, with most of the data bounded by 150 µg/g. The data contain large variability with respect to burnup. This suggests that besides burnup, other parameters such as coolant chemistry, neutron fluence, coolant/sheath temperatures, and sheath properties exert significant influence on H/D pickup.

9.2.5 Deposits

[This section was contributed primarily by John G. Roberts, JGRChem Inc. and Dr. Craig R. Stuart, Canadian Nuclear Laboratories].

Deposits are sometimes observed on the external surfaces of fuel bundles and are sometimes also called "crud". Most deposits on CANDU fuel tend to be magnetite-based compounds. In BWRs, "scale-type" crud contains high concentrations of copper, up to and sometimes even in excess of 50%. In PWRs, deposits tend to be compounds based mainly on nickel ferrite. Deposits on LWR fuels can also incorporate lithium and boron.

Deposits on fuel are undesirable because they can potentially impede heat transfer. In BWRs, they have sometimes even caused through-wall holes in the sheath [IAEA, 2010].

Deposits on fuel are very rare in CANDU reactors, but relatively more frequent and also thicker in BWRs [IAEA, 2010]. The causes of these deposits are rooted mainly in materials and coolant chemistry, which differ in different types of reactors. This is a very complex subject, and its detailed treatment is beyond the scope of this chapter. However, pertinent experts have identified the following four significant differences between the various reactor types that affect in-core deposits:

a) different materials among reactor types, e.g., carbon steel in the CANDU heat transport system and stainless steels in LWRs;
b) presence of boron in PWR coolant and its absence in CANDU coolant;
c) higher degree of success in CANDUs in maintaining consistent chemistry over time in the primary heat transport system (PHTS); and
d) much longer fuel residence period in an LWR (usually a few years) than in a CANDU reactor (usually less than two years).

As for boron in the coolant, recall that CANDU reactors separate the coolant from the moderator using pressure tubes and calandria tubes. This enables CANDU designers to maintain separate chemistries in the coolant and in the moderator. Each system can then be focussed on optimally addressing its own respective needs. For instance, in a CANDU reactor, the additives required for neutron management are injected into the moderator, not the coolant, and therefore the chemistry of the PHTS is not affected. In contrast, when boron is added in an LWR's moderator-cum-coolant to manage the neutronics, it also has a chemical impact on the entire primary heat transport system (PHTS), including the steam generators and all the pipes. If this promotes crud in the PHTS of an LWR, it is then carried by the coolant into the core, where it can deposit on fuel surfaces. In this way, separation of moderator and coolant in separate systems is one aspect that contributes to fewer crud deposits on CANDU fuel.

In summary, the lesser quantities of deposits on CANDU fuel than on PWR fuel are due principally to different materials in the coolant circuit, lack of boron in the coolant, higher consistency over time in coolant chemistry, and shorter fuel residence period.

9.2.6 End-temperature peaking

Consider two neighbouring fuel bundles in a CANDU channel. Their fuel stacks do not abut each other; they are separated by the two endplates, endcaps, and axial gaps, as shown in Figure 9. Because of the absence of UO_2 in this region of bundle-to-bundle contact, neutron

absorption cross sections are smaller here than in the bulk of the fuel bundle. Some fraction of the unabsorbed neutrons from the bundle-to-bundle junction—the "excess" neutrons—becomes available for capture by neighbouring UO_2. This results in an increase in neutron flux in this region; the flux is higher a few centimetres into the fuel pellets on either side of this junction than in the axial centre of the bundle. This is called *end-flux peaking* (EFP) and is illustrated schematically in Figure 9.

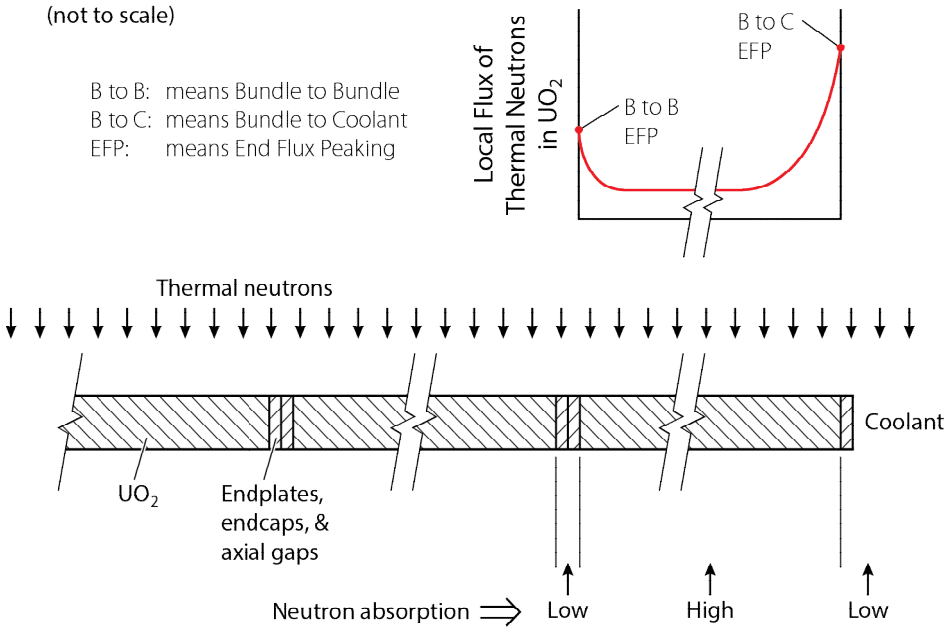

Figure 9 Concepts for end-flux peaking

End-flux peaking is even more severe at the very end of the fuel string because of the larger step change in absorption cross section at that location, the "bundle-to-coolant contact".

The *end-flux peaking factor* is defined as the ratio of the local thermal flux at the end of the fuel rod to the thermal flux at the centre of the rod. Figure 10 illustrates typical magnitudes of end-flux peaking. For bundle-to-bundle contact, thermal flux at the end of the pellet stack can be about 20% higher than that at the centre of the rod. For bundle-to-coolant contact, the local flux at the end can be considerably higher—some 80% higher than the flux at the centre [Roshd *et al*., 1978].

Flux peaking in UO_2 fuel leads directly to higher local heat generation and potentially also to higher local temperature, depending on heat transfer in the end region of the fuel element. This is called *end-temperature peaking*. The higher temperature in turn is associated with other detrimental effects such as higher thermal expansion and increased surface heat flux.

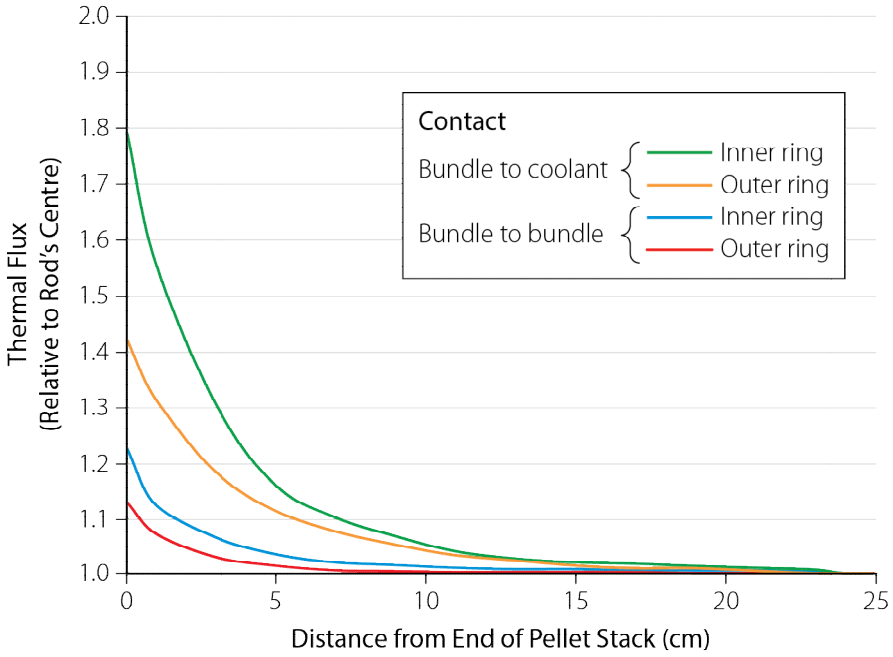

[After Roshd *et al*., 1978]

Figure 10 Illustrative peaking of flux at the end of a 28-element fuel bundle

From the perspective of local temperature, increased local heat generation can be partially, or even wholly, offset by better heat transfer in the end region. The area near the end of the pellet stack is not only cooled by radial transfer of heat, as in other locations, but also by axial transfer of heat through the endcap, as shown in Figure 11.

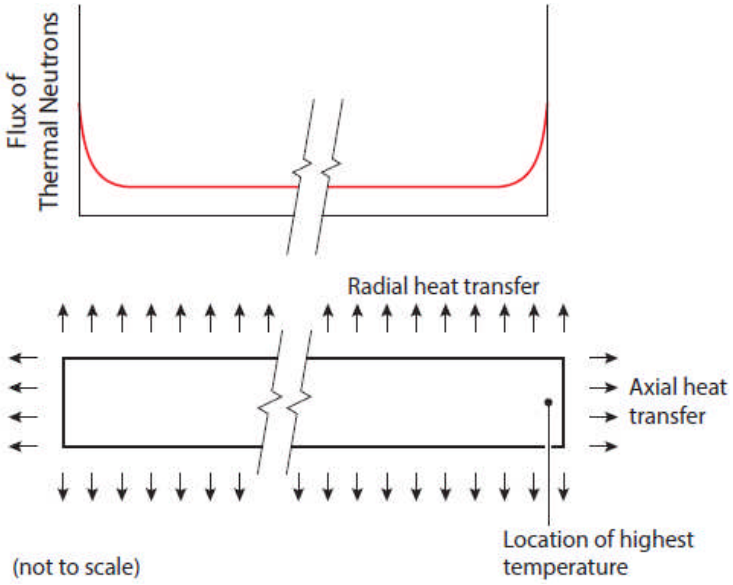

Figure 11 EFP: neutron flux and heat transfer

During bundle-to-bundle contact, the strong axial heat transfer usually depresses the local temperature at the very end of the pellet stack, despite EFP. For this reason, the peak local temperature occurs not at the very end of the fuel stack, but a short axial distance inward of it, as shown in Figure 11. Therefore, although at high power levels, the local temperature in

the end region does tend to increase due to end-flux peaking, it increases less than would be expected from the amount of end-flux peaking alone.

Figure 12 illustrates a typical temperature distribution at high power in the end region during bundle-to-bundle contact [Tayal, 1989(a)]. Isotherms in the end region are shaped like teardrops, a shape determined by the net balance between local generation and local transfer of heat. Teardrop-shaped voids are indeed observed in UO_2 pellets that are irradiated at very high power levels. In Figure 12, the local thermal flux in the end region is about 10% higher than at the element's mid-point. Due to axial heat transfer, the increase in peak local temperature is limited to about 150°C in this case.

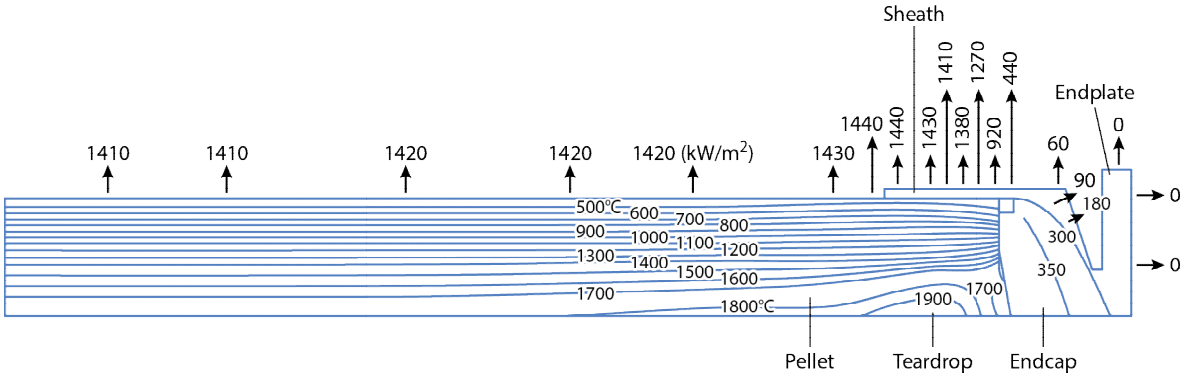

[Source: Tayal, 1989(a)]

Figure 12 End-temperature peaking: illustrative isotherm

In contrast, at low power levels and for small values of end-flux peaking, e.g., during bundle-to-bundle contact, axial transfer of heat is stronger than the local increase in heat flux. Under such conditions, the local pellet temperature does not peak at all in the end region; instead, it decreases only near the very end of the pellet stack [Tayal, 1989(a)].

Enrichment increases the degree of end-flux peaking and hence also the amount of end-temperature peaking. This tends to decrease the margin to melting in enriched fuel [Girgis *et al*., 1990].

9.2.7 Bowing

Bowing means lateral deformation. It is of two kinds: element bowing and bundle bowing. Element bowing refers to lateral bending of individual fuel elements. Bundle bowing refers to lateral bending of the fuel bundle as a whole or of a number of elements acting in concert.

In an experiment in Ontario, intentional local dryout in a fuel element led to excessive local bowing, which led to contact between the fuel sheath and a neighbouring component. The latter in turn led to local overheating and therefore significant local oxidation in the region of contact. Failures of fuel sheaths due to bowing have also been reported in the WR1 experimental reactor in Manitoba [Veeder *et al*., 1974].

Excessive outward bowing in the outer ring of elements has also led to "sticking" of the fuel bundle in the channel of Manitoba's WR1 reactor, creating difficulties in removing the fuel bundle [Veeder *et al*., 1974]. The WR1 reactor was cooled by organic oil which dissociated into components, some of which were solids at operating temperature. Some of the solids deposited on the bundle surfaces, including the surfaces of matching element spacers. This increased the overall diameter of the fuel bundle and caused it to stick in the WR1 reactor

channel.

In another experiment in a reactor in Ontario, excessive element bowing caused many central bearing pads to press tightly against the pressure tube for a significant duration. This trapped some coolant water between the bearing pad and the pressure tube. With time, the trapped, stagnant water boiled off. This increased the local concentration of LiOH in the coolant (LiOH is used to control coolant pH). At high concentration, an LiOH-water solution is corrosive. This led to local corrosion in the bearing pads and also likely in the pressure tube. This process is called *crevice corrosion*. There is always a potential for crevice corrosion at the bottom bearing pads; excessive bowing can lead to crevice corrosion at other locations around the bundle circumference if the bearing pads come into contact with the pressure tube. Although a small amount of crevice corrosion is acceptable, its extent needs to be limited to reasonable levels lest it threaten the integrity of the pressure tube.

Excessive bowing can also alter the thermal hydraulics in the channel, which in turn can complicate the evaluations and confirmations of heat transfer coefficients between the sheath and the coolant. In light water reactors, excessive bowing of a fuel assembly has led to concerns about control rod movements and dryout. Therefore, bowing and dryout also have a mutual feedback cycle. For these reasons, it is important to limit bowing to acceptable levels. Bowing can increase with time, and therefore it needs to be addressed in high-burnup fuels.

When CANDU sheaths do bow, spacer pads prevent them from touching each other at their mid-planes. Likewise, bearing pads at three axial locations reduce the likelihood of a sheath touching the pressure tube in the absence of a severe local dry patch.

Major Driving Forces

Fabricated fuel elements are not necessarily perfectly straight, i.e., they may be bowed. In addition, during normal operations, fuel elements initially bow due to non-uniform temperature around the circumference of a fuel element and also because of mechanical loads (a list of causes of bowing is given later in this section).

Circumferential variations in temperature lead to differences in thermal expansion around the sheath circumference. The hotter side of the fuel element becomes relatively longer than the colder side. The fuel element then deforms laterally (bows) towards the longer side to accommodate the extra length. Bowing due to thermal effects is illustrated schematically in Figure 13(a).

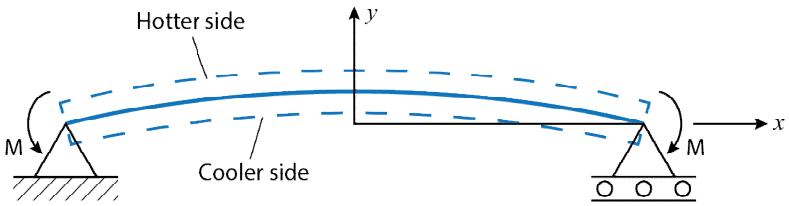

(a) Idealization for Free Bowing

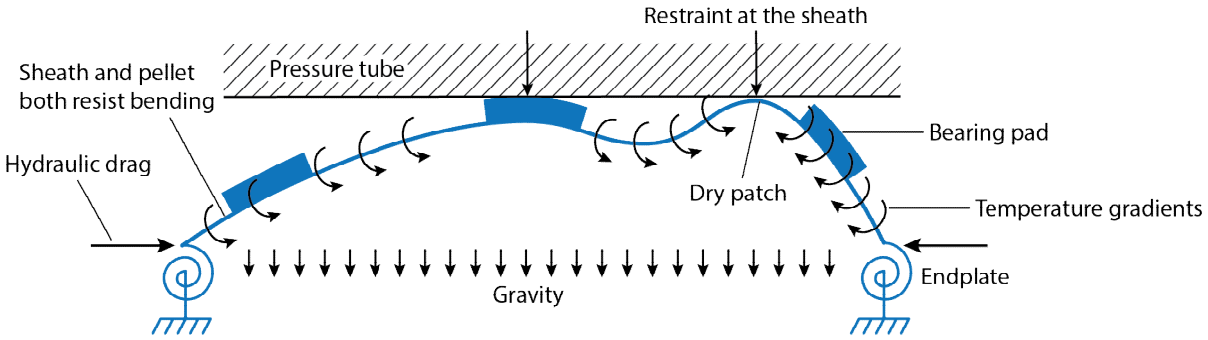

(b) Major Forces

[Source: Tayal, 1989(b)]

Figure 13 Model for element bowing

Gravitational pull also acts to bend a horizontal fuel element. Once a fuel element has bowed, a moment-arm is available to the axial forces generated by hydraulic drag; this magnifies the amount of bow. Therefore, the initial bow is the net result of the following major influences:

- initial as-fabricated bow;
- thermal effects, e.g.,
    - non-uniform heat transfer between the sheath and the coolant due to variations in sub-channel geometry and local flow conditions;
    - non-uniform coolant temperature due to imperfect mixing among sub-channels; local hotspots, if any (such as a dry patch);
    - asymmetric heat production due to neutron flux gradients.
- mechanical effects:
    - gravitational pull;
    - axial load, e.g., hydraulic drag.

Across the diameter of a CANDU fuel bundle, the flux profile is approximately parabolic, as shown in Figure 14. That means that in any given fuel element, heat production may not always be centred at the geometric centre of the fuel element. Figure 15 provides an illustrative example of this: the centre of grain growth has shifted in the direction of maximum neutron flux. Asymmetric heat production will necessarily set up circumferential temperature variations in the pellet and in the sheath, contributing to their bowing.

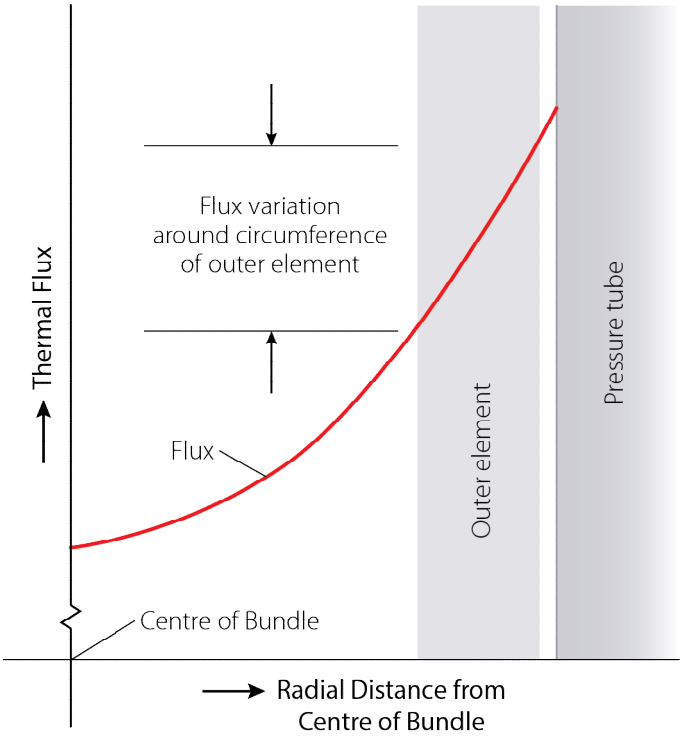

[After Veeder *et al*., 1974]

Figure 14 Illustrative circumferential variation in flux of thermal neutrons

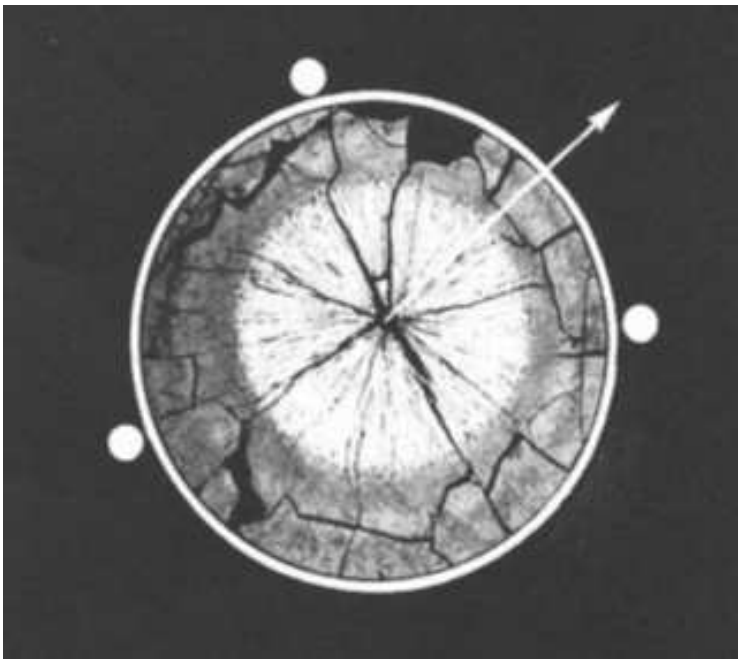

[Source: Veeder *et al*., 1974]

Figure 15 Off-centre grain growth

The loads mentioned above are resisted mainly by the flexural rigidities of the sheath and of the pellets, by endplates, and by lateral restraints (if any) from the pressure tube and from neighbouring fuel elements. Most of these loads as well as the major restraints are shown

schematically in Figure 13(b).

After initial bowing has occurred, creep, additional deposits on spacer pads, or both can increase the bow further over time. For example, Figure 16 shows post-irradiation bow in a fuel element measured after 100, 240, and 304 days in the reactor under similar irradiation conditions. Note the significant increases in bow with continued irradiation. Therefore, the design process needs to consider the potential for additional bowing in extended-burnup fuels.

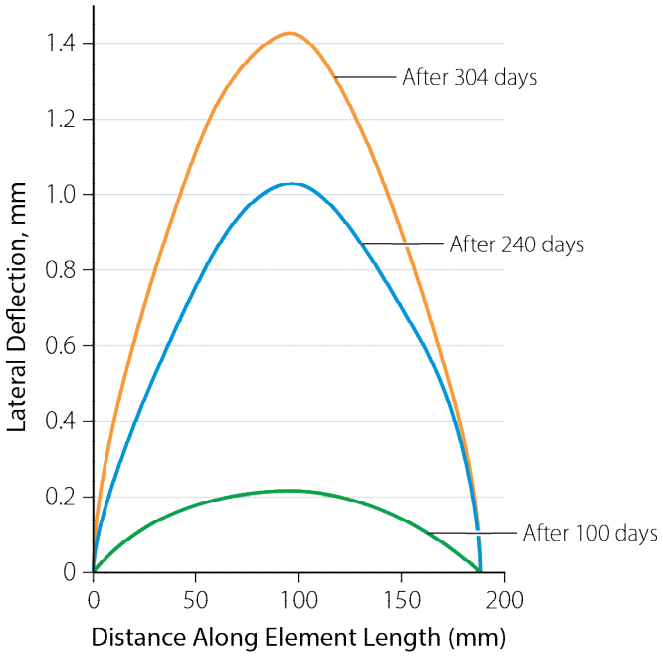

[Source: Veeder *et al*., 1974]

Figure 16 Increase of bowing during continued irradiation

Simplified Model for Initial Thermal Bowing

Veeder *et al*. [1974] and Tayal [1989(b)] have outlined models for bowing calculations. As a simplified illustrative example, let us consider the empty fuel sheath shown in Figure 13(a) that experiences a linear variation in temperature around its circumference and uniformly along its length. In the absence of hydraulic drag load and gravity, the equation for thermal bending of this beam can be written as [Gere *et al*., 1997]:

$$d^2y/dx^2 = \alpha\, \Delta T/d, \qquad (10)$$

where y is the transverse deflection, x is the axial distance, α is the coefficient of linear thermal expansion of the sheath in the axial direction, ΔT is the difference in temperature across the diameter, and d is the diameter.

Furthermore, let us assume for simplicity that neighbouring fuel elements or pressure tubes do not impede lateral deflection of the fuel elements and that the endplates provide simple supports to the fuel element. Under these assumptions, the boundary and symmetry conditions simplify to:

$$y = 0 \text{ at } x = l/2, \text{ and } dy/dx = 0 \text{ at } x=0. \qquad (11)$$

Equation (10) can be integrated under boundary and symmetry conditions (11) to yield the

following equation [Gere *et al*., 1997] for unconstrained thermal bowing at the mid-plane, δ:

$$\delta = \alpha \, \Delta T \, l^2/(8d). \quad (12)$$

As a specific example, let us consider an empty sheath with a diameter of 13 mm, a length of 500 mm, and a coefficient of linear thermal expansion of 6.72 µm/(mm•°C). It experiences a thermal variation of 5°C around its circumference. Equation 12 predicts that in the absence of mechanical loads, its initial mid-span thermal bow would be about 0.08 mm.

The pellet operates at a much hotter temperature than the sheath, and its coefficient of thermal expansion is about twice that of Zircaloy. Hence, a pellet can have a significant impact on the thermal bow of a fuel element, especially if it is in tight diametric contact with the sheath. Mechanical loads can also have a significant impact on element bow. Their quantitative treatments are complex and beyond the scope of this chapter; interested readers can explore several detailed papers that have been published on this subject, e.g., Veeder *et al*. [1974] and Tayal [1989(b)].

9.2.8 High burnup structure

Very high local burnup can cause the formation of "high burnup structure" (HBS) at the periphery of the pellets [Baron *et al*., 2009, 2012], also called the "rim effect" and "cauliflower structure". To date, this has been observed mainly in LWR fuels because their burnups tend to be significantly higher than those of current CANDU fuels. The discussion below is based largely on Baron *et al*. [2012].

Figure 17 shows a typical HBS. It is believed to be formed by subdivision of pellet grains when the local burnup typically exceeds 55–60 MW•d/kg (or 1300–1400 MW•h/kg).

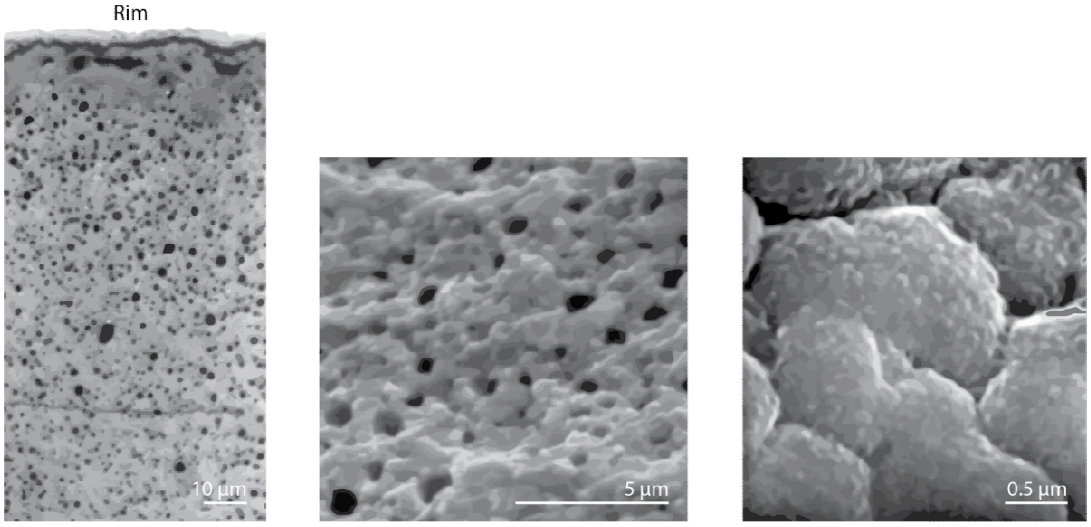

[Source: Baron *et al*., 2009, 2012]

Figure 17 High burnup structure near the rim of a pellet

In UO_2 fuels, the local burnup has a sharp peak at the radial periphery of the pellet due to "neutronic self-shielding" (also called the "skin effect"), as shown in Figure 18. Therefore, in UO_2 fuels, HBS tends to be confined to a very narrow shell at the pellet's radial periphery.

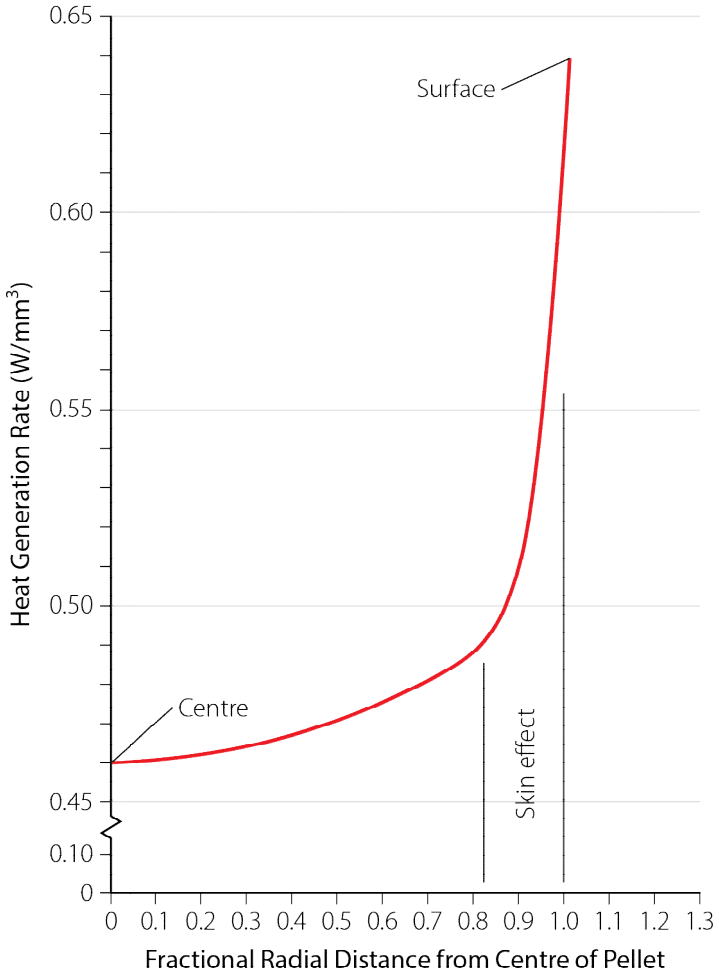

[Source: Tayal, 1987]

Figure 18 Illustrative heat generation rate across the radius of the pellet

Generation of HBS is a complex process and is described in detail in many publications such as Baron *et al*. [2012]. At a very simplified level, irradiation produces, among other things, point defects and dislocation loops in the pellet. They do recover thermally, but the recovery is relatively slow in the comparatively colder regions near the periphery of the pellet. Therefore, the dislocations gradually become denser (more numerous) and more tangled. This eventually causes the crystalline structure of the pellet to become unstable, initiating a restructuring driven by the energy stored in the material. This in turn results is subdivision of grains, often into range of 0.2 to 0.5 µm diameter.

In comparison, typical grain diameter is about 10 µm in as-fabricated CANDU pellets. By considering the ratio of volumes of as-fabricated vs. subdivided grains, i.e., (about 10 µm / (0.2 to 0.5 µm))^3, one can deduce that HBS subdivides a typical grain into a few thousand smaller grains.

Compared to the parent material, UO_2 restructured by HBF is typically less dense and more viscous.

9.3 Thorium Fuel

[Main source: World Nuclear Organization, WNA, 2014]

Thorium does not have a fissile isotope, which means that it does not undergo fission by thermal neutrons. It is, nevertheless, a fertile material. This means that thorium absorbs thermal neutrons to create, or "breed", ^{233}U, which in turn undergoes fission by thermal neutrons.

Section 2.2 summarizes the neutronics of how fertile ^{232}Th converts to fissile ^{233}U. Fission of a ^{233}U nucleus releases about the same amount of energy (200 MeV) as that of ^{235}U.

During the early years of nuclear power development, interest in thorium was prompted by a concern that economically available uranium resources would not be sufficient to support the ambitious nuclear program then envisioned. Subsequently, new uranium resources have been discovered that are thought to be sufficient to support the currently envisioned nuclear program for at least a few decades. Development aimed at exploiting the natural advantages of thorium and demonstrating the feasibility of its introduction into all known types of thermal reactors (and breeder reactors) has continued, with considerable success. Some countries are planning to introduce commercial thorium-fueled reactors, mainly for strategic reasons of energy independence. A comprehensive review of the work done internationally is provided in [IAEA, 2005], which is recommended for additional reading.

Experts estimate that thorium is about three to four times as abundant as uranium. Therefore, thorium can significantly moderate the cost of nuclear fuel in the future if it can be used to generate electricity. In addition, thorium and uranium are distributed differently among the various geographic locations on Earth. For example, countries such as India, China, and Turkey have comparatively little uranium, but substantial amounts of thorium. Such countries may potentially find thorium especially attractive for power generation.

The preferred method of using thorium is in the form of thorium dioxide, also called thoria, which is a ceramic. The reasons are analogous to those for using uranium in the form of UO_2 (see Chapter 17). The following properties of thorium dioxide pellets contribute to improving various aspects of their in-reactor performance (compared to UO_2 pellets) [Boczar, 2012]:

- Figure 19 shows that for a wide range of temperatures, the thermal conductivity of unirradiated thoria is about 25–35% higher than that of unirradiated UO_2 [Pillai *et al*., 2000; MacDonald *et al*., 1976]. Therefore, for a given power level, thorium pellets operate at lower temperatures;
- The lower temperature of ThO_2 reduces fission gas release, which reduces internal gas pressure, which in turn helps achieve higher burnup;
- The melting temperature of unirradiated ThO_2 is about 3350°C [IAEA, 2005], which is among the highest of any oxide. This compares with a melting point of about 2840°C in non-irradiated UO_2. This increases the margin to melting in ThO_2. It also introduces challenges in pellet production, requiring a higher sintering temperature;
- Thorium has only one oxidation state; therefore, it has a higher resistance to oxidation;
- Thorium is chemically inert. Therefore, it can be expected to yield a more stable form of waste that is expected to be more resistant to leaching.

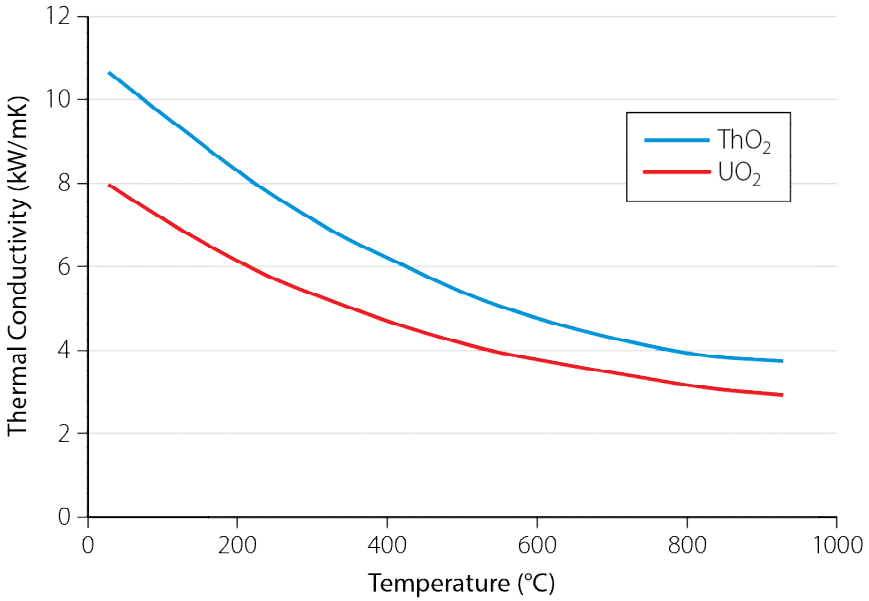

Sources: [UO_2: MacDonald *et al*., 1976] [ThO_2: Pillai *et al*., 2000]

Figure 19 Thermal conductivities of unirradiated pellets

Test irradiations to date have confirmed the beneficial impacts of these properties. Compared to UO_2 fuel irradiated under similar conditions, (Th, Pu)O_2 fuel has exhibited minimal grain growth (as shown in Figure 20), benign fission gas release, and low sheath strain [Karam *et al*., 2010(b); Livingstone *et al*., 2013; Kupferschmidt *et al*., 2013]. All these observations suggest that thorium pellets indeed operate at considerably lower temperature.

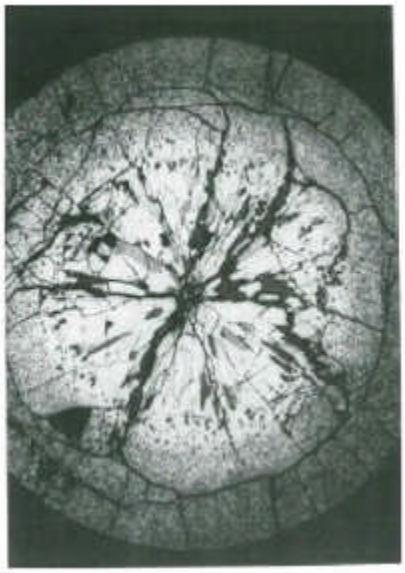

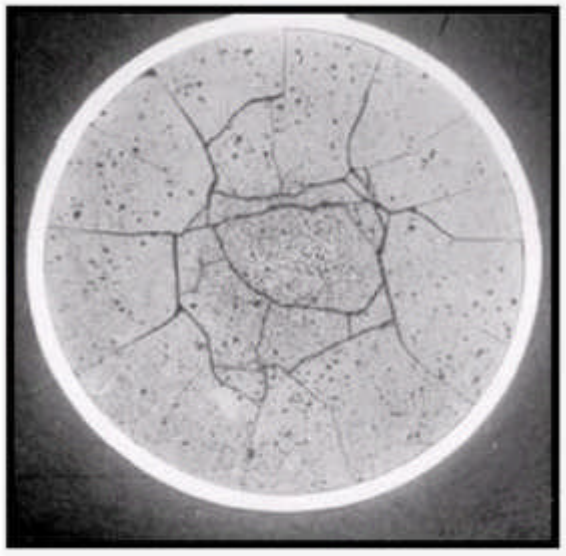

Extensive Columnar Grains — Equiaxed Grains
(a) UO_2 (65 kW/m) — (b) $(Th,Pu)O_2$ (67 kW/m)
[Source: Kupferschmidt, 2013]

Figure 20 Illustrative structures in irradiated pellets

9.3.1 Energy from thorium

The paragraphs below are based largely on and/or reproduced from Boczar et al. [2012], IAEA [2005], and WNA [2014].

As illustrated in Section 2.2 , ^{232}Th must first be converted into ^{233}U for use in power generation. "Therefore, thorium fuel concepts require that ^{232}Th be first irradiated in a reactor before fissile material can be made available. The ^{233}U that is produced can either be chemically separated from the parent thorium fuel and recycled into new fuel, or the ^{233}U may be usable *in-situ* in the same fuel form".

"Thorium fuels therefore need a fissile material as a 'driver' so that a chain reaction can be initiated and maintained. The only fissile driver options are ^{233}U, ^{235}U, or ^{239}Pu, none of which is easy to supply".

A number of configurations are possible for arranging thorium and a fissile driver in a reactor; some have been used successfully to demonstrate the feasibility of thorium implementation. In a CANDU reactor, three illustrative configurations are the following [Boczar, 2012]:

- Homogeneous fuel. In this option, each pellet contains a mixture of thorium and the fissile material.
- Heterogeneous "mixed bundles". Such bundles contain thorium and the fissile material in separate fuel elements.
- Heterogeneous "mixed channels". In this option, each bundle contains either only thorium or only the driver fuel. Each channel contains only one type of bundle.

"In the heterogeneous fuel arrangements, the high fissile (and therefore higher-power) fuel

zone is called the *seed* region, and it is physically separated from the fertile (low-power) thorium part of the fuel, called the *blanket*".

"It is possible—but quite difficult—to design thorium fuels that produce more ^{233}U in thermal reactors than the fissile material they consume. Thermal breeding with thorium is only really possible if neutron economy in the reactor is very good (i.e., low neutron loss through escape or parasitic absorption). The possibility to breed significant amounts of fissile material in slow (thermal) neutron systems is unique to thorium-based fuels and is not possible with uranium fuels. Irrespective of whether breeding is achieved, more practical thorium fuel cycles in a CANDU reactor offer a significant reduction in uranium requirements".

"Another distinct option for using thorium is as a 'fertile matrix' for fuels containing plutonium (and even other transuranic elements like americium). No new plutonium is produced from the thorium component, unlike for uranium fuels, and so the level of net consumption of this metal is rather high".

"In fresh thorium fuel, all the fissions (thus power and neutrons) derive from the driver component. As the fuel operates, the ^{233}U content gradually increases, and it contributes more and more to the power output of the fuel. The ultimate energy output from ^{233}U (and hence indirectly from thorium) depends on numerous fuel design parameters, including fuel burnup attained, fuel arrangement, neutron energy spectrum, and neutron flux (affecting the intermediate product protactinium-233, which is a neutron absorber)".

Specific thorium cycles can be designed to suit a country's specific circumstances.

9.3.2 Margin to melting

As an illustrative example, consider two neighbouring fuel elements, one fueled with UO_2, the other with ThO_2. Both are operating at 60 kW/m; the coolant temperature is 300°C. If end-temperature peaking is ignored, what are the margins to melting in the two fuel elements?

To work this out, we can use the theoretical background given in Chapters 6 and 7 about the temperature distribution within a fuel element, along with some assumptions to simplify this illustrative calculation. Recall that if other parameters are the same, to a first approximation, the temperature difference between the centre and the surface of the pellet is inversely proportional to the thermal conductivity of the pellet.

Guided by the previous illustrative examples in this book, assume that the UO_2 fuel element has a central temperature of about 1900°C and that the melting point of unirradiated UO_2 is about 2840°C. Therefore, in the UO_2 fuel element, the thermal margin is about 2840 – 1900 = 940°C.

The peak operating temperature in the ThO_2 pellet can be approximated as follows:

- Guided by the previous illustrative examples, assume that the temperature increase between the coolant and the pellet surface is about 100°C.
- Therefore, the temperature at the surface of the pellet is: 300 + 100 = 400°C.
- In the UO_2 pellet, the temperature increase from the surface to the centre of the pellet is 1900 – 400 = 1500°C.
- Guided by Figure 19, assume that to a first approximation, the thermal conductivity of ThO_2 is about 30% higher than that of UO_2. Therefore in a thoria pellet operating at the

same power, the temperature increase from the surface to the centre of the pellet is about 1154°C (=1500°C / (1 + 0.3)).

- Therefore, the temperature at the centre of the thoria pellet is 400 + 1154 = 1554°C.
- The melting point of ThO_2 is about 3350°C [IAEA, 2005], and therefore the margin to melting in the ThO_2 pellet is about 3350 – 1554 = 1796°C.

Therefore, for the same operating power of about 60 kW/m, the margin to melting in ThO_2 fuel is 1796°C, which is significantly higher than in UO_2 fuel.

9.3.3 Internal gas pressure

Pellet temperature is a main driver of fission gas release. Above a threshold temperature, fission gas release increases rapidly with local temperature.

In the preceding illustrative example, the UO_2 fuel operates a few hundred degrees above the threshold temperature for fission gas release. This results in significant fission gas release in UO_2 fuel.

Assuming that the threshold temperature is similar in ThO_2 and UO_2, the ThO_2 fuel described above operates much closer to the threshold temperature for fission gas release. This means that the ThO_2 pellet will release much less fission gas.

The above illustrative examples point to some of the large benefits in operating performance that are possible with thorium. Along with thorium's impressive benefits, we do also need to consider, as noted earlier, the higher costs of some thorium cycles.

9.4 Mixed Oxide (MOX) Fuel

MOX stands for Mixed Oxide, which means that the fuel contains a mixture of uranium and plutonium (Pu).

Section 2.2 summarizes the neutronics of Pu generation and fission. A slow neutron can fission ^{239}Pu into mainly barium and strontium. This releases 207 MeV of energy, which is very similar to the energy released by fission of ^{235}U (202 MeV).

In a real-world application of "swords-to-plowshares", plutonium extracted from dismantled nuclear warheads can be used to generate electricity as MOX fuel. Plutonium can also be obtained by reprocessing used LWR fuel. Although feasible, reprocessing of used CANDU fuel is seen as impractical because of the relatively small quantity of plutonium (and fissile uranium) contained in used CANDU fuel. LWRs are already being used to dispose of military plutonium, and MOX is a commercial reality in European LWRs. More detailed overviews of the MOX cycle are described in many publications such as [Boczar, 2012; Dyck *et al*., 2005].

One interesting aspect of the common variant of MOX fuel is its tendency to form "agglomerates" arising out of non-homogeneities in the mixture of UO_2 and PuO_2. The amount of agglomerates depends on the specific manufacturing process, as explained below.

Reasonably homogeneous mixtures of UO_2 and PuO_2 can be produced by vibratory milling of UO_2 and PuO_2 powders in the proportions desired in the final fuel. The resulting homogeneity is expected to yield the best performance in MOX fuel. However, this process is quite time- and resource- consuming. Alternative manufacturing processes which produce less

homogenous mixtures require less effort, but they also contain agglomerates, meaning that trade-offs must be considered [Harrison *et al*., 2010].

For purposes of illustration, two such alternative processes are: [Harrison *et al*., 2010]:

Alternative Method # 1: A master mix with high Pu concentration is prepared by vibratory milling of the UO_2 and PuO_2 powders together. The required amount of this "master mix" is added to additional UO_2 powder to achieve the desired final Pu concentration. This approach results in discrete "islands"—also called agglomerates—of master mix contained in the UO_2 matrix.

Alternative Method # 2: Same as Alternative Method # 1 above except that only PuO_2 is milled (rather than a mixture of PuO_2 plus UO_2). The resulting powder is then added to UO_2, resulting in nearly pure PuO_2 "islands" distributed within the UO_2 matrix.

The two alternative fabrication processes above create islands of relatively higher plutonium concentration. The islands undergo relatively higher amounts of fission and produce correspondingly higher quantities of fission gases. Figure 21 shows a typical island in a fuel element that was fabricated using Alternative Method # 1. The arrow points to the area of high fission. Similar areas were also observed in pellets produced by the second alternative method.

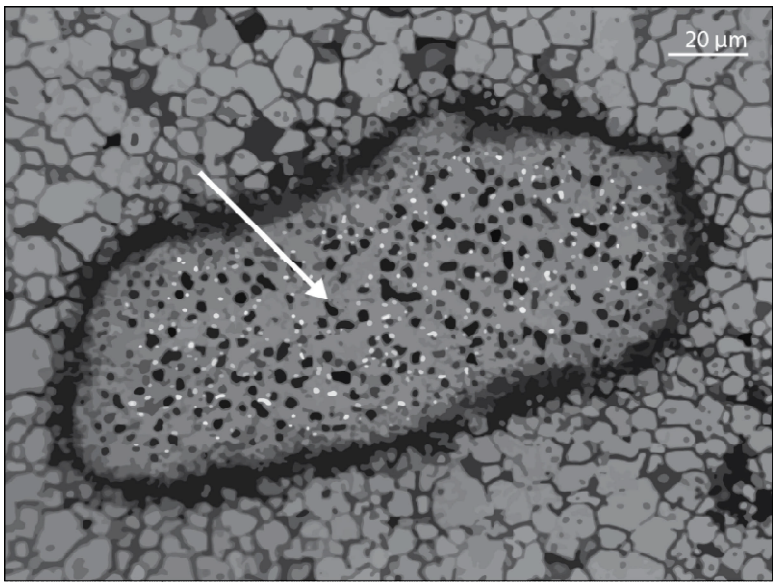

Arrow points to the high fission area.

[Source: Harrison *et al*., 2010]

Figure 21 High fission area (HFA) in an irradiated MOX fuel pellet

Within an island, the pellet behaves as if it were operating at significantly higher local power. This results in larger local fission gas release. This is partly offset in the remaining parts of the pellet, which behave as if they are operating at a lower local power. Because fission gas release increases non-linearly with local temperature, the overall fission gas release from non-homogeneous pellets is greater than from homogeneous pellets. However, there is significant scatter in both the UO_2 and the MOX data, and the limited MOX data to date in Canada are in the general range of scatter of the UO_2 data.

Non-homogeneous MOX fuel also shows larger post-irradiation sheath strain than homoge-

neous fuel.

Note that despite the higher gas release and strain noted above, the overall performance of MOX fuel is quite acceptable in many LWRs worldwide [IAEA, 2003].

9.5 Breeder Fuel

[Main source: Wikipedia, 2015]

In a typical thermal reactor fuel cycle, energy is extracted from ^{235}U as well as from ^{239}Pu, the latter being bred from ^{238}U. Because some fraction of the starting ^{235}U remains unused when the fuel is discharged, less than 1% of the available energy is currently extracted from mined uranium.

The dominant isotope—over 99%—in natural uranium is ^{238}U, which is not fissile. However, it is fertile, which means that it can be converted into a fissile isotope (^{239}Pu) through fast neutrons, and energy can then be extracted from it as well.

^{238}U can be sourced from virgin uranium, from the recycled uranium from reprocessing irradiated fuel, or from depleted uranium from enrichment plant tails.

As noted earlier, some amount of fertile ^{238}U is routinely converted to fissile ^{239}Pu in CANDU reactors. One measure of a reactor's performance is the *conversion ratio*—the ratio of the rate at which fissile nuclides are produced in the entire reactor by conversion, to the rate at which fissile nuclides are consumed through radiative capture and fission. All practical nuclear reactor fuels experience some degree of conversion.

As long as any amount of a fertile material exists within the neutron flux of the reactor, some new fissile material is always being created. For example, commonly used light water reactors have a conversion ratio of approximately 0.6. Pressurized heavy water reactors (PHWR) running on natural uranium have a conversion ratio of 0.8. In a breeder reactor, the conversion ratio is greater than one. "Breakeven" occurs when the conversion ratio is exactly one, and the reactor produces exactly as much fissile material as it uses. (This is the basis of the so-called self-sufficient equilibrium thorium CANDU reactor, which at equilibrium contains as much ^{233}U in the used fuel as is in the fresh fuel, accounting for reprocessing losses.)

Historically, breeder reactor development has focussed on reactors with low breeding ratios, from 1.01 for the Shippingport reactor running on thorium fuel and cooled by conventional light water to over 1.2 for the Russian BN-350 liquid-metal-cooled reactor. Theoretical models of breeders with liquid sodium coolant flowing through tubes inside fuel elements ("tube-in-shell" construction) show that breeding ratios of at least 1.8 are possible.

Some experts have estimated that thousands of years' worth of ^{238}U is available world-wide for use in fast breeder reactors.

10 Synergy between CANDU Reactors and LWRs

As mentioned in previous sections, the superior neutronic characteristics of CANDU reactors can be used for a variety of synergies with LWRs, e.g.:

- extracting additional energy from used LWR fuel, e.g., through RU/NUE, through ex-

tended burnup, through DUPIC, or through plutonium recycling (e.g., MOX), and/or
- destroying some of the long-lived actinides removed from spent LWR fuels through reprocessing.

Based on the fissile content of used LWR fuel, one can calculate the number of LWRs from which the used fuel can be used as fuel by a single CANDU reactor [Boczar *et al*., 1996].

The quantities used in the example below are not necessarily actual values for a specific CANDU or LWR reactor, although they are reasonably representative of the two reactor types and are used to illustrate how the actual quantities would be used to determine the synergy between an actual LWR and an actual CANDU reactor by substituting real, specific values.

LWR reactor:

- capacity: 1000 MW(e)
- total uranium in core: 80,000 kgU
- amount of U refueled annually: 20,000 kg (one-quarter of the core replaced annually)
- ^{235}U contained in spent fuel (annually): 180 kg (0.9% ^{235}U in total U).

CANDU reactor:

- capacity: 1000 MW(e)
- total uranium in core: 120,000 kg (6000 bundles containing 20 kg U each)
- annual requirements:
  - annual refuelling: 140,000 kg of U (7000 bundles);
  - annual ^{235}U requirements: approximately 1,000 kg ^{235}U (0.71% ^{235}U in total of 140,000 kg U).

Synergy:

- annual ^{235}U arising from spent LWR fuel: 180 kg
- annual ^{235}U requirements for CANDU reactor of equal electrical capacity: 1,000 kg
- proportion of ^{235}U used in CANDU fuel that is derived from LWR arising: 0.73% (see Section 9.1 above); the remainder of ^{235}U is derived from depleted U from tails of enrichment plants.
- CANDU reactor's annual ^{235}U requirements supplied by LWR: 730 kg (73% of 1,000).
- Number of LWRs required to supply ^{235}U for CANDU reactors of equal electrical capacity (rounded to the nearest whole number): 4 (= 730/180).

The example above assumes that only ^{235}U arisings would be used. If plutonium were also used, the proportion of LWR per CANDU reactor would be accordingly reduced.

11 Closure

In summary, some illustrative fuels and fuel cycles are the natural uranium cycle, natural-uranium equivalent fuel, extended burnup fuel, thorium, mixed oxide fuel, DUPIC fuel, low void reactivity fuel, actinide burning fuel, and breeder fuel.

The natural-uranium fuel cycle that is currently used in CANDU power reactors is simple, reliable, and low-cost. It is also very amenable to localization, which promotes national energy independence.

Alternative fuel cycles offer several potential strategic advantages, such as significantly ex-

tending humanity's energy resources, reducing the initial capital cost of a power plant, increasing the lifespan of a CANDU power plant, increasing the thermal efficiency of the steam cycle, reducing the coolant void reactivity, reducing the volume of spent fuel, and increasing the power output from a fuel bundle and the reactor.

Many alternative fuel cycles result in more expensive fuel, additional challenges in the front end, enhanced challenges during the service period, and reduced challenges in the back end.

Therefore, a careful assessment of net benefit is required before implementing any particular fuel cycle.

12 Problems

Section 1 – Introduction

Q1.1 – Why would one consider fuel cycles other than the once-through cycle?

Section 2 – Neutronics of Fuel Cycles

Q2.1 – Define fissile nuclides and give examples. Which is the only naturally occurring fissile nuclide?

Q2.2 – Define fissionable nuclide and provide examples.

Q2.3 – Define fertile nuclides and provide examples.

Q2.4 – What is the conversion ratio as related to nuclides?

Q2.5 – In the context of conversion ratio, what is breeding and breeding gain?

Q2.6 – What is burnup as applied to nuclear fuel?

Section 3 – Overview of Some Possible Fuels and Fuel Cycles

Q3.1 – List the fuel cycles which are used, or can be considered for use, in CANDU rectors and provide a brief rationale for using each.

Section 4 – Key Drivers for Advanced Fuel Cycles

Q4.1 – List the principal advantages of the once-through natural uranium (NU) fuel cycle used in CANDU compared to fuel cycles using enriched uranium.

Q4.2 – With reference to the three parts of the fuel cycle, provide a general assessment of the advantages or disadvantages of alternative cycles compared to the once-through CANDU-NU fuel cycle.

Q4.3 – Compared to the NU fuel cycle used in CANDU, many alternative fuel cycles tend to increase the cost of fuel and also pose various degrees of additional technical challenge. Nevertheless, they are considered for use in CANDU because they offer other advantages. List these advantages and provide a brief explanation of each.

Section 5 – Resource Extension: A Major Incentive

Q5.1 – Compared to LWRs, CANDU reactors can better use alternative fuel cycles, principally because of their superior neutron efficiency. How much more efficient is CANDU than an LWR in the use of uranium?

Q5.2 – In current CANDU reactors, peak neutron efficiency occurs at about 1.2% enrichment. If 1.2% enriched uranium is used in CANDU reactors, how long will the planet's identified uranium resources (mentioned above) last?

Section 6 – Other Considerations

Q6.1 – List the considerations that have to be taken into account when deciding whether or not to "recycle" spent fuel.

Section 7 – Pertinent Features of the CANDU Reactor

Q7.1 – CANDU reactors can use alternative fuel cycles principally because of their superior neutron efficiency. List the seven features of the CANDU reactor that enable it to have superior neutron efficiency.

Q7.2 – Explain how the design of CANDU fuel facilitates the adoption of alternative fuel cycles.

Section 8 - Natural Uranium Fuel Cycle

Q8.1 – List the four methods by which natural uranium can be obtained.

Q8.2 – Unlike other types of fuels (e.g., coal, gas, or oil), as-mined uranium ore cannot be fed directly into a nuclear power station. Explain why.

Q8.3 – Produce a simplified flow sheet of the processes involved in the manufacture of CANDU fuel bundles.

Q8.4 – Why is as-received uranium powder subjected to two physical processes, compaction and granulation?

Q8.5 – What are the three process parameters that the operator controls during pellet sintering?

Q8.6 – Why are pellets ground after sintering?

Q8.7 – Pellet stack length is the principal means by which axial clearance is maintained inside the finished fuel element. What are the other means?

Q8.8 – Why do the pellets at the ends of the pellet stack have a reduced diameter?

Q8.9 – List the four features of uranium dioxide pellets that render their production challenging.

Q8.10 – Similarly to the pellet production stream, the Zircaloy component stream has its own unique CANDU-related challenges, the most unique and critical being welding of endcaps to sheath sub-assemblies. Explain why endcap welding is a critical and challenging process.

Q8.11 (a) – Identify five design and/or process parameters that must be controlled to achieve a good endcap weld; **Q8.11 (b)** for bonus marks, identify an additional five parameters; **Q8.11 (c)** for additional bonus marks, identify five more parameters.

Q8.12 – For one unit of energy produced, current CANDU reactors use five to six times the mass of fuel as is used in LWRs. Despite that relative disadvantage, fuelling cost per unit energy has always been much lower for CANDUs than for LWRs. List the three reasons for this.

Section 9 – Details of Selected Alternative Fuels and Fuel Cycles

Q9.1 – A fuel manufacturer has purchased REU fuel containing 1% ^{235}U and DU fuel containing 0.4% ^{235}U. He wishes to blend them to obtain NUE fuel. What should be the fraction of REU fuel in the blend?

Q9.2 – List the benefits which can be derived from using enriched fuel in a CANDU.

Q9.3 – List the commercial and technical aspects that must be considered in increasing element rating, burnup, and bundle power by using enrichment.

Q9.4 – Why is it important to control fuel-element internal gas pressure, and what can fuel designers do to achieve this?

Q9.5 – A power ramp of 15 kW/m is contemplated in CANLUB fuel at a burnup of 400 MWh/kgU. The pre-ramp power is 20 kW/m. Is this fuel element expected to survive the power ramp?

Q9.6 – List at least two reasons for keeping sheath corrosion below the allowable limit.

Q9.7 – List the reasons for the reduced amount of corrosion on CANDU fuel compared to PWR fuel

Q9.8 – In the example of Section 9.2.3, what is the expected thickness of waterside corrosion in a CANDU sheath at 800 MWh/kgU?

Q9.9 – What causes end-flux (and end-temperature) peaking?

Q9.10 – Pellet/sheath interaction causes an unrestrained thermal bow of 0.6 mm in a fuel element that has a diameter of 13 mm and a length of 500 mm. What is the equivalent temperature variation around its circumference?

Q9.11 – What are the two main reasons for considering the use of thorium in place of uranium?

Q9.12 – Which is the fissile isotope in thorium?

Q9.13 – The preferred method of using thorium is in the form of thorium dioxide, also called thoria, which is a ceramic. The reasons are analogous to those for using uranium in the form of UO_2 (see Chapter 17). List the properties of thorium dioxide pellets that contribute to improving their in-reactor performance compared to UO_2 pellets.

Q9.14 – Describe three ways that thorium and the fissile driver can be arranged to power a CANDU reactor.

Q9.15 – (a) What are the two possible sources of plutonium that can be used in CANDU? (b) Is reprocessing of spent CANDU fuel a likely source of plutonium?

Q9.16– What is a common challenge in the production of MOX?

Q9.17 – Why are "agglomerates" undesirable in MOX pellets?

Section 10 – Synergy between CANDU Reactors and LWRs

Q10.1 - Assume that the waste of LWRs contains 0.9% ^{235}U and 0.6% Pu. Further assume that DU can be procured with ^{235}U content at any value in the range from 0.2%^{235}U to 0.4%^{235}U. We wish to use the ^{235}U and Pu from LWR to feed a CANDU of equal capacity, after blending with DU. If each CANDU and each LWR is 1000 MW(e), determine the required content of ^{235}U in DU, such that a single LWR will feed one CANDU of equal capacity. Solving this problem highlights and reinforces six (6) aspects covered in this chapter. What are they?

13 References

D. Barber, D. H. Lister, 1982. "Chemistry of Water Circuits in CANDU Reactors", Proceedings, Symposium on Water Chemistry, Report IAEA-SM-264/15 and AECL-8217, 1982.

D. Baron, M. Kinoshita, P. Thevenin, R. Largenton, 2009. "Discussion about HBS Transformation in High-Burnup Fuels", Nuclear Engineering and Technology, Vol. 41, No. 2, pp. 199-214, March 2009.

D. Baron, L. Hallstadius, 2012. "Fuel Performance of Light Water Reactors (Uranium Oxide and MOX)"; Chapter 40 in "Comprehensive Nuclear Materials", book edited by R. Konings, Elsevier, ISBN-9780080560274, 2012.

Z. Bhatti, B. Hyland, G. Edwards, 2013. "Minor Actinide Transmutation in Thorium and Uranium Matrices in Heavy Water Moderated Reactors", Proceedings, Global 2013, Salt Lake City, Utah, U.S.A., September 29–October 3, 2013.

P. G. Boczar, J. D. Sullivan, H. Hamilton, Y. O. Lee, C. J. Jeong, H. C. Suk, C. Mugnier, 1993. "Recovered Uranium in CANDU—A Strategic Opportunity", Proceedings of International Nuclear Conference and Exhibition (INC 93), Toronto, Ontario, Canada. October 3-6, 1993.

P. G. Boczar, P. J. Fehrenbach, D. A. Meneley, 1996. "CANDU Fuel Cycle Options in Korea", Proceedings, KAIF/KNS Annual Conference, Seoul, Korea, April 1996; also Atomic Energy of Canada Limited, Report AECL-11586, 1996.

P. G. Boczar, J. D. Sullivan, 2004. "Low Void Reactivity Fuel", Proceedings, 25th Annual CNS Conference, Toronto, 2004.

P. G. Boczar, J. T. Rogers, D. H. Lister, 2010. "Considerations in Recycling Used Natural Uranium Fuel from CANDU Reactors in Canada", Proceedings, 31st Annual Conference of the Canadian Nuclear Society, Montreal, Quebec, Canada, May 24–27, 2010.

P. Boczar, 2012. "CANDU Nuclear Reactor Design, Operation, and Fuel Cycles", Chapter 11, "Nuclear Fuel Cycle Science and Engineering", Woodhead, 2012.

B. Cox, 1985. "Assessment of PWR Waterside Corrosion Models and Data", EPRI Report NP-4287, 1985.

G. R. Dyck, T. Mochida, T. Fukasawa, 2005. "Application of Fluoride Volatility to the Recycling of LWR Spent Fuel into CANDU", Proceedings, Global 2005, Paper number 493, Tsukuba, Japan, October 9–13, 2005.

M. R. Floyd, 2001. "Extended-Burnup CANDU Fuel Performance", Proceedings, International

Conference on CANDU Fuel, CNS, Kingston. Also Atomic Energy of Canada Limited, Report AECL-CONF-01135, 2001.

W. J. Garland, 2005. EP4D03 course notes, Chapter: Core Composition Changes, McMaster University, http://www.nuceng.ca/ep4d3/ep4d3home.htm, 2005.

F. Garzarolli, W. Jung, H. Schoenfeld, A. M. Garde, G. W. Parry, P. G. Smerd, 1982. "Waterside Corrosion of Zircaloy Fuel Rods", Electric Power Research Institute, U.S.A., Report EPRI-NP-2789, 1982.

J. M. Gere, S. P. Timoshenko, 1997. "Mechanics of Material", PWS, 4th edition, 1997.

S. Girgis, N. Singhal, M. Tayal, 1990. "Influences of Load Following Partial Dryout and End-Flux Peaking on Temperature Distributions in CANDU Fuel", Proceedings, 11th Annual Conference, Canadian Nuclear Society, June 3–6, 1990.

N. F. Harrison, T. Janathasing, F. C. Dimayuga, 2010. "Post-Irradiation Examination of MOX Fuel with Varying Plutonium Homogeneity", Proceedings, 11th International Conference on CANDU Fuel, Sheraton Fallsview Hotel and Conference Centre, Niagara Falls, Ontario, Canada, CW-124920-CONF-004, October 17–20, 2010.

I. Hastings, P. G. Boczar, C. J. Allan, M. Gacesa, 1991. "Synergistic CANDU-LWR Fuel Cycles", Korea Nuclear Society, Annual Conference, 1991. Also Atomic Energy of Canada Limited, Report AECL-10390, 1991.

B. Hyland, B. Gihm, 2010. "Scenarios for the Transmutation of Actinides in CANDU Reactors", Proceedings, 18th International Conference on Nuclear Engineering (ICONE18), Paper ICONE18-30123, Xi'an, China, May 17–21, 2010.

IAEA, 2003. "Status and Advances in MOX Fuel Technology", International Atomic Energy Agency, Vienna, Austria, Technical Report Series, Report TRS 415, 2003.

IAEA, 2005. "Thorium Fuel Cycle", International Atomic Energy Agency, Report IAEA-TECDOC-1450, 2005.

IAEA, 2010. "Review of Fuel Failures in Water-Cooled Reactors", International Atomic Energy Agency, Vienna, IAEA Nuclear Energy Series, report number NF-T-2.1, ISBN 978-92-0-102610-1. 2010.

Y. Jioa, D. Li, M. Chen, Z. Meng, J. Wang, C. Cottrell, S. Kuran, 2009. "Test Irradiation of Recycled Uranium in Chinese CANDU Reactors", Proceedings, 30th Annual Conference of the Canadian Nuclear Society, Calgary, Alberta, Canada, May 31–June 3, 2009.

M. Karam, N. Harrison, J. Montin, 2010(a). "Post-Irradiation Examination of DUPIC Fuel", Proceedings, 11th International Conference on CANDU Fuel, Sheraton Fallsview Hotel and Conference Centre, Niagara Falls, Ontario, Canada, October 17–20, 2010.

M. Karam, F. C. Dimayuga, J. Montin, 2010(b). "Post-Irradiation Examination of CANDU Fuel Bundles Fueled with (Th, Pu)O_2", Proceedings, 11th International Conference on CANDU Fuel, Sheraton Fallsview Hotel and Conference Centre, Niagara Falls, Ontario, Canada, October 17–20, 2010.

W. C. H. Kupferschmidt, 2013. "Advanced Fuel Development at AECL: What does the Future

Hold for CANDU Fuels/Fuel Cycles?", Proceedings, 12th International Conference on CANDU Fuel, Canadian Nuclear Society, Kingston, Ontario, Canada, September 15–18, 2013.

J. R. Lamarsh, 1996. "Introduction to Nuclear Reactor Theory", Addison-Wesley, 1966.

S. J. Livingstone, M. R. Floyd, 2013. "Thoria Irradiation and Post-Irradiation Examination Experience at AECL", Proceedings, 12th International CANDU Fuel Conference, CNS, Kingston, 2013.

P. E. MacDonald, L. B. Thompson (eds.), 1976. "A Handbook of Materials Properties for Use in the Analysis of Light Water Reactor Fuel Rod Behaviour", MATPRO-Version 09, TREE-NUREG-1005, 1976.

D. A. Meneley, 2006. "Transition to Large-Scale Nuclear Energy Supply", Proceedings, 27th Annual CNS Conference, Toronto, 2006.

P. Ottensmeyer, 2012. "CANDU Fuel Waste Re-Used, Recycled, Eliminated: $48 Trillion Carbon-Free Electricity via Fast-Neutron Reactors", Engineering Dimensions, Professional Engineers of Ontario, Volume 33, No. 4, July/August 2012.

R. D. Page, 1976. "Canadian Power Reactor Fuel", Atomic Energy of Canada Limited, Report AECL-5609 (1976).

C. G. S. Pillai, P. Raj, 2000. "Thermal Conductivity of ThO_2 and $Th_{0.98}U_{0.02}O_2$", Journal of Nuclear Materials, Vol. 277, pp. 116-119, 2000.

P. Reid, M. Gacesa, M. Tayal, 2008. "The ACR-1000 Fuel Bundle Design", Proceedings, 10th International Conference on CANDU Fuel, Canadian Nuclear Society, 2008.

M. H. M. Roshd, H. C. Chow, 1978. "The Analysis of Flux Peaking at Nuclear Fuel Bundle Ends using PEAKAN", Atomic Energy of Canada Limited, Report AECL-6174, 1978.

M. Tayal, 1987. "Modelling CANDU Fuel under Normal Operating Conditions: ELESTRES Code Description", Atomic Energy of Canada Limited, Report AECL-9331, February 1987.

M. Tayal, 1989(a). "The FEAT Finite Element Code to Calculate Temperatures in Solids of Arbitrary Shapes", Nuclear Engineering and Design, Vol. 114, pp. 99–114, 1989.

M. Tayal, 1989(b). "Modelling the Bending/Bowing of Composite Beams such as Nuclear Fuel: The BOW Code", AECL-9792, Nuclear Engineering and Design, Vol. 116, pp. 149–159, North-Holland, Amsterdam, 1989.

M. Tayal, K. D. Hallgrimson, R. Sejnoha, P. N. Singh, R. DaSilva, 1993. "Elastic-Plastic Stress Distributions near the Endcap of a Fuel Element", Proceedings, 4th International Conference on Simulation Methods in Nuclear Engineering, Canadian Nuclear Society, Montreal, Canada. Also Atomic Energy of Canada Limited, Report AECL-10646, June 1993.

M. Tayal, B. Wong, Y. Shudoh, 1995. "Effect of Radial Power Profile on Endplate Integrity", Proceedings, 4th International Conference on CANDU Fuel, Canadian Nuclear Society, Pembroke, Canada. Also Atomic Energy of Canada Limited, Report AECL-Conf-00452, 1995.

J. Veeder, M. H. Schankula, 1974. "Bowing of Pelletized Fuel Elements: Theory and In-Reactor Experiments", Nuclear Engineering and Design, Vol. 29, pp. 167–179, 1974.

Wikipedia, 2015. "Breeder Reactor", http://en.wikipedia.org/wiki/Breeder_reactor, January 2015.

WNA, 2014. “Thorium”, World Nuclear Association, http://www.world-nuclear.org/info/inf62.html, September 2014.

14 Relationships with Other Chapters

Chapter 8 provides an overview of fuel bundle configuration. Chapters 3 to 5 explain neutron physics that generates heat in the fuel. Chapters 6 and 7 explain how that heat is removed from the fuel bundle and illustrate the internal temperature distribution within a fuel rod. Chapters 14 and 15 explain chemical and metallurgical aspects that relate to corrosion of the fuel sheath. Chapter 13 explains the performance of fuel during postulated accidents. Chapter 17 describes the design and performance of fuel, focussing on the current natural-uranium cycle (i.e., low burnup). The current chapter (#18) describes a few selected fuel cycles, summarizes key aspects of fuel manufacturing related primarily to the natural-uranium fuel cycle, and explains a few selected aspects of fuel performance that become relatively more important for advanced fuel cycles. Finally, Chapter 19 describes interim storage and disposal of used fuel.

15 Acknowledgements

The authors thank Dr. Peter Boczar for permission to borrow heavily from his extensive publications on fuel cycles. Sections 2.1 and 2.2 of this chapter were provided by Dr. Dorin Nichita, Dr. Ben Rouben, and Dr. William Garland. Dr. William Garland also contributed Figures 1 and 2. Dr. D. Baron (EdF, retired) graciously provided material on high burnup structure. John Roberts and Dr. Craig Stuart contributed key material on fuel deposits. The above contributions are gratefully acknowledged with thanks.

In addition, the following reviewers are gratefully acknowledged for their hard work and excellent comments during the development of this chapter; their feedback has much improved it:

Peter Boczar

Bronwyn Hyland

Geoff Edwards

William Garland

Of course the responsibility for any errors or omissions lies entirely with the authors. Thanks are also extended to Simon Oakley and Media Production Services, McMaster University, for nicely drawing the figures, and to Diana Bouchard for expertly editing and assembling the final copy.

CHAPTER 19

Storage and Disposal of Irradiated Fuel

prepared by

Mukesh Tayal and Milan Gacesa – Independent Consultants

Summary

Nuclear wastes, in particular irradiated nuclear fuel, must be handled, stored, and placed into permanent disposal facilities safely to prevent harm to people and the environment. Radioactive wastes can be grouped into four classes: (i) low-level radioactive waste, (ii) intermediate-level radioactive waste, (iii) high-level radioactive waste such as irradiated nuclear fuel, and (iv) uranium mine and mill waste. Storage and disposal of irradiated fuel in Canada follows a three-step process: storage in water-cooled pools, storage in air-cooled storage cylinders, and final disposal. The two stages of storage (the first two steps above) are fully proven and have been in practical operation for some time. The associated technical challenges that must be addressed and the engineered solutions are discussed in this chapter. Several configurations for final disposal have been shown to be technically feasible. Public acceptance and implementation remain to be achieved; ongoing work aimed at achieving these goals is discussed. Nature's "reactors" that existed billions of years ago are examined for useful analogies that can be applied to engineered disposal facilities.

Table of Contents

List of Figures

1 Introduction

This chapter focuses mainly on the challenges that must be met during storage and disposal of high-level nuclear waste, specifically storage and disposal of irradiated fuel (also called “spent” fuel or “used” fuel). Some illustrative potential solutions are also summarized.

To this end, Sections 2 to 5 describe the types of wastes, the overall strategy to manage them, the associated design considerations, and the potential mechanisms for damage to fuel integrity. Then each major phase of managing irradiated fuel is described: initial wet storage at reactor sites (Section 6), followed by dry storage at reactor sites (Section 7) and final disposal (Section 8). IAEA [2003] provides an extensive glossary of relevant terms.

This chapter draws heavily from previous publications. Significant passages that have been copied verbatim from other sources are enclosed within quotes “...”.

1.1 Learning Outcomes

The goal of this chapter is for the student to acquire a broad initial understanding of the main challenges that must be considered in designing facilities to store irradiated fuel (also called "spent" fuel), the evaluations performed, and the safety and other criteria used for selecting the principal features of the facilities for initial wet storage of irradiated fuel at reactor sites, subsequent dry storage of irradiated fuel at reactor sites, and the current Canadian concepts for eventual disposal of irradiated fuel (e.g., geological isolation).

2 Types of Waste

All biological life forms produce waste as part of their normal cycle of existence. Within the biosphere, dissimilar life forms (e.g., plants and animals) have evolved to exist in harmony and dependence on exchange of wastes. All human activity, starting with the most primitive prehistoric activity associated with subsistence, up to and including the most sophisticated industrial activity of today, produces waste. Regulations for managing all aspects of human-generated wastes have evolved from “non-existent” for most of human existence to the comprehensive and sophisticated regulations of today. Human industrial activity has not been in existence sufficiently long to test the ability of ecological systems to create synergies, interdependency, or both. Indeed, some industrial wastes are known to be detrimental to people and the environment. Such wastes must not be left untreated or allowed to enter the biosphere. Some nuclear wastes also fall into this category.

Under the terms of its statute, the International Atomic Energy Agency (IAEA) has a mandate to establish or adopt safety standards to protect people and the environment from the harmful effects of ionizing radiation. IAEA identifies six classes of nuclear waste ranked in order of their harmful radiological effects (from the lowest to the highest) and the escalating requirements for their safe disposal, as follows [IAEA, 2009]:

- Exempt waste
- Very short-lived waste

- Very low-level waste
- Low-level waste
- Intermediate-level waste
- High-level waste.

The crafters of the IAEA standard provided this list of waste classes as an aid to individual users, recognizing that it may not be necessary or suitable for all users to adopt the list explicitly. Users have the option of adopting the list literally or adapting it to their own needs, particularly users who have had prior experience with managing radioactive waste.

The Canadian Standards Association (CSA), in collaboration with industry, government, and the Canadian Nuclear Safety Commission (CNSC), has developed the "Radioactive Waste" standard [CNSC, 2015a] that recognizes four main classes of radioactive waste:

- Low-level radioactive waste
- Intermediate-level radioactive waste
- High-level radioactive waste
- Uranium mine and mill waste.

Although these two lists of radioactive waste classes are not identical, it can be readily discerned that the Canadian standard is not inconsistent with that of the IAEA. The Canadian standard omits "exempt" waste and combines the three classes of "low-level" waste into a single class. The two standards are explicitly consistent with respect to "intermediate" and "high-level" waste. The Canadian standard adds a separate class for "uranium mine and mill" waste, which reflects the importance of uranium mining in Canada. Every existing source of radioactive waste in Canada and its class is listed, and the entity responsible for its management is identified. Some entities may be responsible for managing more than one class of waste.

3 Strategies to Manage Radioactive Waste

Low-Level and Intermediate-Level Wastes

Radioactive waste has been produced in Canada since the early 1930s; see, for example, "Historic Nuclear Waste" [CNSC 2015a], which describes the period when radium and uranium were mined in the Northwest Territories and transported to Port Hope, Ontario, for refining. Subsequently, uranium in much greater quantities has been mined and milled, most notably in northern Ontario and Saskatchewan, and transported to Port Hope for refining and subsequent use in nuclear fuel.

The following steps are taken to manage low-level and intermediate-level radioactive wastes [CNSC, 2015b]:

- Decontamination and clean-up;
- Long-term storage and management by the user;
- Return to the manufacturer for long-term storage and management;

- Storage and management at large central facilities such as those operated or proposed by Ontario Power Generation and Canadian Nuclear Laboratories.

The remainder of this chapter deals with the management of irradiated CANDU fuel.

Irradiated Fuel

Irradiated fuel continues to produce power and emit radiation after it is removed from the reactor. The power and radiation decay with time, and therefore the need to cool the fuel and to monitor its activity also decrease with time. For this reason, irradiated nuclear fuel passes through two phases of storage before final disposal in the third phase, as follows:

- Immediately after its discharge from reactors, the fuel is stored for several years in deep cooling pools adjacent to the reactor.
- After several years of forced-circulation cooling in water, the fuel is transferred to concrete containers which are air-cooled by natural convection. The fuel can reside in these storage cylinders for up to 100 years before its ultimate disposal.
- In the third phase, irradiated fuel is intended to be permanently sequestered in specially designed facilities. As an illustrative example, one concept is to put the fuel in a sealed container which is surrounded by clay and placed in a room that is built deep underground in impervious rock.

Examples of these facilities, particularly as they apply to CANDU irradiated fuel, are described later in this chapter.

Irradiated CANDU fuel may well be commonly considered "waste" to be (eventually) permanently sequestered in specially designed facilities. At the same time, it also has the potential to be recycled to generate significant energy through advanced fuel cycles in the future (see Chapter 18), and therefore it can also be rightly considered as an asset worth a few trillion dollars. Therefore it is prudent to adopt a flexible approach. On the one hand, the disposal facility should safely isolate the irradiated fuel from the human population and the environment with minimal ongoing expense, and on the other hand, the disposal facility should permit its retrieval at a later date if appropriate and if so chosen.

IAEA [2012] provides guidance and recommendations for design, safe operation, and safety assessments of fuel storage facilities, both wet and dry.

4 Irradiated Fuel Storage and Disposal: Main Considerations

The main features that irradiated fuel storage and disposal facilities must incorporate are listed below. Other more detailed design and jurisdictional requirements exist, but are not covered in this book. The relative importance of a specific feature may differ from one facility to the next; therefore, an individual feature listed below may or may not be absolutely essential in a given facility.

(i) Avoid overheating of irradiated fuel

Even after discharge from the reactor, fuel continues to produce power, as explained in more detail in other chapters. Both the fuel and the materials used in storage and disposal structures

and facilities have their respective temperature limits for safe operation. Therefore, the potential temperature increase caused by decay power must be controlled effectively to prevent overheating.

(ii) Limit chemical and metallurgical damage to irradiated fuel bundles

A variety of factors can damage stored and disposed fuel, e.g., chemical, metallurgical, and mechanical. Damaged fuel can release highly radioactive substances into the irradiated fuel bay and also potentially into the air above. Such radiological contamination must be controlled to acceptably low levels to protect the workers and the general public. Therefore, degradation and damage to bundles must also be limited to acceptably low levels.

(iii) Avoid mechanical damage to irradiated fuel bundles

Irradiated fuel bundles are handled remotely by fuelling machines (pre-programmed robots) during their removal from the reactor into the irradiated fuel pool, and by operators using remotely operated tools for subsequent transfers. These tools must be designed and operated so that the irradiated bundles are not damaged.

(iv) Avoid irradiated fuel configurations that could achieve criticality

CANDU fuel is made of natural uranium oxide and Zircaloy. Therefore, whether it is new or irradiated, it cannot be put into a configuration that will achieve criticality in ordinary water [Tsang, 1996]. This is not true, however, of LWR irradiated fuel, which contains higher levels of fissile isotopes than CANDU irradiated fuel.

(v) Protect workers and public from radiological exposure

Adequate shielding must be provided to protect the workers and public from the radiotoxicity of nuclear fuel. Whereas the cooling challenge reduces very quickly, shielding requirements last longer because some long-lived isotopes (particularly the transuranics) take thousands of years to decay. Nevertheless, the radioactivity of irradiated fuel does decrease with time, and therefore so does the radiological threat. Hence, the most demanding conditions exist when the fuel is handled during the initial wet and dry storage phases; special shielding must be designed to protect workers from radiation exposure.

(vi) Adequately safeguard irradiated fuel against proliferation

IAEA takes proactive measures to observe and record movements of nuclear fuel at reactor sites wherever practical. CANDU reactors are refuelled essentially continuously. This presents unique safeguards (tracking) challenges, particularly during discharge and initial storage of irradiated fuel in water-cooled bays. Continuous refuelling makes in-person monitoring impractical; hence, IAEA-approved monitoring by remote means is used. Several monitoring devices positioned at a number of locations in the reactor are used [Feiveson et al., 2011]. For example, neutron and gamma radiation detectors are used in the reactor vault and in the transfer port between the vault and the irradiated fuel bay (see Section 6.2); closed-circuit video cameras are used in the irradiated fuel bays; and tamper-indicating enclosures that have been inspected and sealed by IAEA are installed within the irradiated fuel bay.

(vii) Provide appropriate retrievability of irradiated fuel

Irradiated fuel may need to be retrieved from storage, especially after the fuel completes its designated storage periods in phases 1 and 2.

However, during phase 3—disposal/isolation—a nation may or may not choose to incorporate fuel retrievability into the design of its disposal facility, as explained in Section 3. Therefore, a reasonable balance must be struck regarding ease of access to irradiated fuel: access must be made quite difficult for a member of the general public, but not prohibitively so for an approved, legitimate, large, organized agency. The desired duration for such retrievability must also be chosen. These conscious choices influence the final configuration of the disposal facility. Canada's choice is described in a later section.

(viii) Avoid damage to facilities that interface with irradiated fuel

Similarly to the requirement for protection against damage to irradiated fuel, interfacing equipment must also be adequately protected, e.g., from corrosion.

5 Fuel Integrity

The above considerations promote safety during storage. Even though this section lists a number of items that focus on fuel integrity, several other aspects of storage also contribute significantly to overall safety; some of these are discussed in later sections.

As with safety of the reactor core, safety during storage and disposal must be confirmed during normal situations, during anticipated operational occurrences, and during postulated accidents. For brevity, this chapter focusses largely on normal situations. Broader discussions of safety during accidents are given elsewhere; see, for example, OPG [2009].

Recognizing that there will invariably be significant uncertainties in projections involving such long time periods, it is also common practice to vary a number of important parameters and assumptions and to perform bounding assessments. Furthermore, a number of hypothetical "what if" scenarios are usually also developed to explore the influence of parameters and scenario uncertainties in assessing long-term safety [NWMO, 2012a].

The remainder of this section provides some details on one aspect of safety during storage—fuel integrity.

5.1 Requirements

IAEA [1994] outlines, among other aspects, requirements for fuel integrity during storage. Lian [2010] cites the following two illustrative requirements from this IAEA document:

> "The spent fuel cladding shall be protected during storage against degradation that leads to gross ruptures, or the fuel shall otherwise be contained in such a manner that degradation of the fuel during storage will not pose operational problems" (Article 223),

and:

> "The heat removal capability shall be such that the temperature of all fuel (and fuel cladding) in a storage facility does not exceed the maximum temperature recommended or approved by the national nuclear regulatory body for the type and condition of fuel to be stored" (Article 225).

Furthermore, from IAEA [2002]: "The prediction of the integrity and retrievability of spent fuel constitute the main discussion topics for spent fuel behaviour regardless of the storage system and time period envisaged." Therefore, fuel integrity is an important consideration in the overall design of storage facilities.

As well, some fuel bundles do occasionally develop defects during operation in the reactor, i.e., before they are brought to storage facilities (see Chapters 17 and 18). Their pellets may well undergo faster degradation than those of intact fuel due to, for example, exposure of pellets to air, which would increase the rate of oxidation of UO_2. Therefore, the impact of fuel with defects on safety during storage must also be considered.

To quantify up-front the expected degradation of fuel in any given design or scenario, one must first identify credible damage mechanisms. Towards this end, the authors have culled from the literature some illustrative fuel damage mechanisms pertinent to storage and disposal and their key precursors and drivers. These are discussed in the next two sections.

5.2 Key Drivers and Precursors

Decay Power

As noted earlier, even after discharge from the reactor, nuclear fuel continues to produce power.

Standard methods are available to quantify decay power; for example, see Garland [1999], ANS [2014], and Glasstone [2014] for illustrative examples. Figure 1 shows how power decays with time in typical irradiated CANDU fuel. The figure shows power decay in a fuel bundle that produced 493 kW in the reactor just before its discharge. Immediately upon removal from the reactor core, an irradiated CANDU fuel bundle generates less than 10% of the power that it produced in the core. This figure drops to less than 1% in only a day after removal and to about 0.013% after a year has passed. The average power generated in a bundle at this point (one year) is less than 100 W, which is comparable to a household light bulb. This keeps dropping substantially with time, e.g., to about 5 W after 10 years and to about 1 W after 100 years, as shown in Figure 1. Hence, the decay power is small compared to the power produced by the fuel in the reactor; nevertheless, the fuel's temperature increase must be controlled effectively to avoid overheating the fuel and the storage structures.

Fuel Temperature

As an illustrative example of how fuel temperature depends on decay power, Figure 2 shows temperature decay in LWR[1] fuel and in its storage canister after emplacement in a long-term

Note 1: LWR means Light Water Reactor

repository for permanent disposal [Rothman, 1984]. In the repository, LWR fuel temperature peaks at about 330°C and then declines. For much of the latter half of the first millennium after emplacement, maximum LWR fuel temperature ranges from 90°C to 150°C. CANDU fuel temperature is expected to be comparatively lower due to its lower burn-up and therefore lower decay power.

Changes in UO_2 composition and microstructure

In the dry sealed environment inside containers, there are few processes that would significantly alter the local composition and microstructure of UO_2. Over long periods, however, some changes are likely to develop by processes such as ongoing decay, diffusion of radionuclides, and damage from alpha radiation.

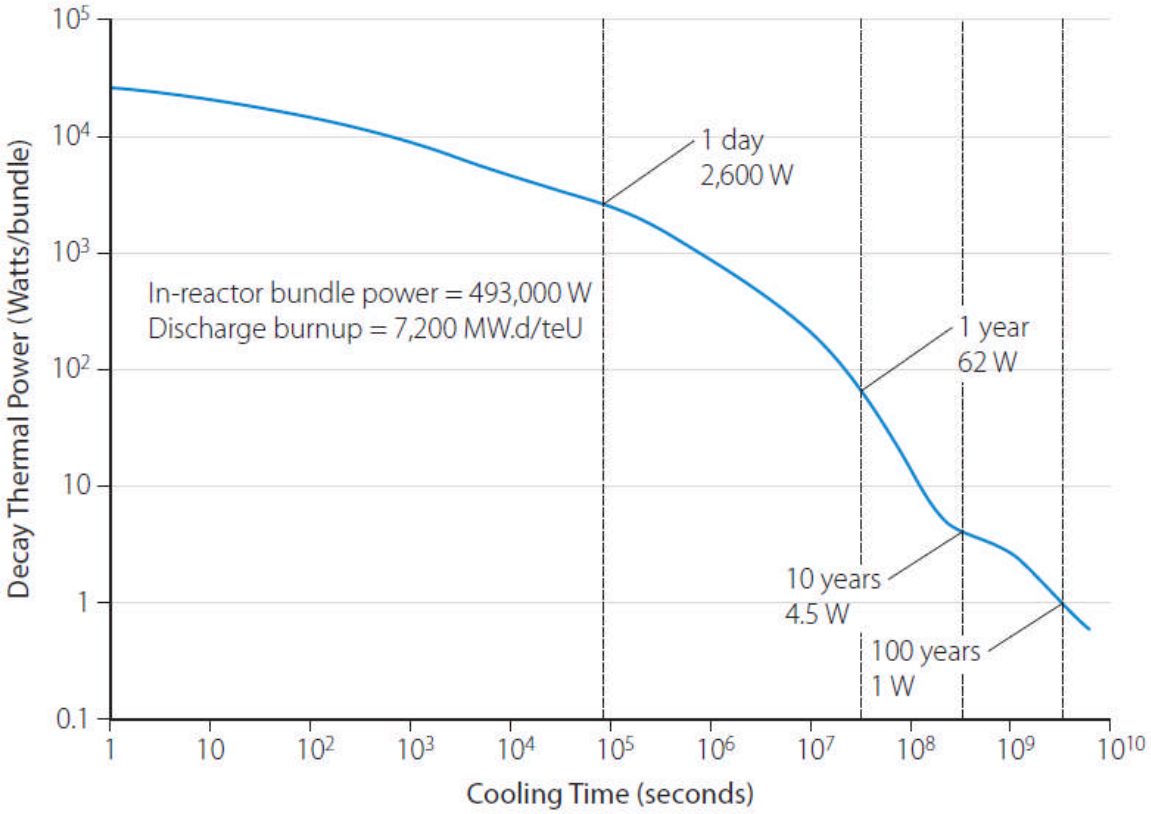

[Illustrative Example; Courtesy Kwok Tsang]

Figure 1 Decay power of an irradiated fuel bundle

Build-Up of Helium Gas and Internal Gas Pressure

As explained in Chapter 17, fuel elements contain: (a) initial filling gas that is added inside a fuel element during fabrication and (b) fission gas that is generated during irradiation. In addition, alpha decay during storage generates helium (He) gas. All three components together can create internal pressure that can frequently be higher than atmospheric pressure. The excess pressure (=internal minus external pressure) can create tensile stresses in the fuel element's

Zircaloy, which can persist over significant durations. If stress is excessive, even nominally slow mechanisms can potentially threaten fuel element integrity over the long periods pertinent to storage and disposal.

The following description has been reproduced largely from NWMO [2012a]. Helium is stable (i.e., not radioactive) and does not react chemically with other elements. Therefore, the total amount of helium gas in the fuel elements would be expected to increase with time during storage. Figure 3 gives an illustrative example, assuming that all fission-generated gases escape the UO_2 matrix into the open space inside the fuel element (see Chapter 17 for explanations of these terms). Fission gases are formed in the reactor, and therefore, except for radioactive decay, their amount would not change significantly during storage and disposal. In contrast, after about 30,000 years, the amount of helium would be equal to that of fission gases, so that the total amount of gas present would be double that under initial conditions. After about one million years, the rate at which helium is produced would slow down due to changes in the composition of the decay chain, but the total amount of helium within the fuel element would continue to increase.

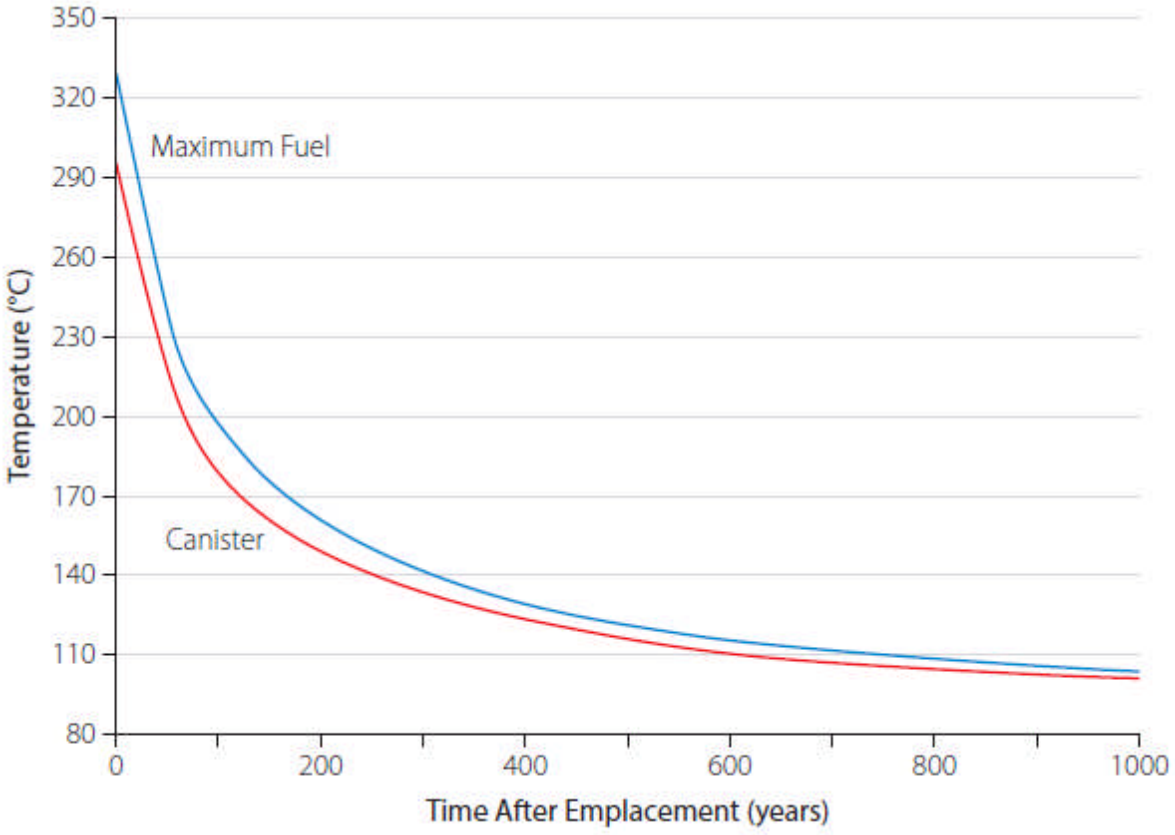

[Source: Rothman, 1984]

Figure 2 Illustrative temperatures in an LWR fuel and canister

Figure 3 illustrates the amount of helium produced within grains of UO_2. Before it can contribute to internal gas pressure, this helium would need to reach the open void inside the fuel element. Pertinent processes that enable this are described in Chapter 17 and consist

mainly of diffusion to grain boundaries, storage within grain boundary bubbles, inter-linkage of bubbles, and micro-cracking in grains. See Chapter 17 for more detailed descriptions of these phenomena.

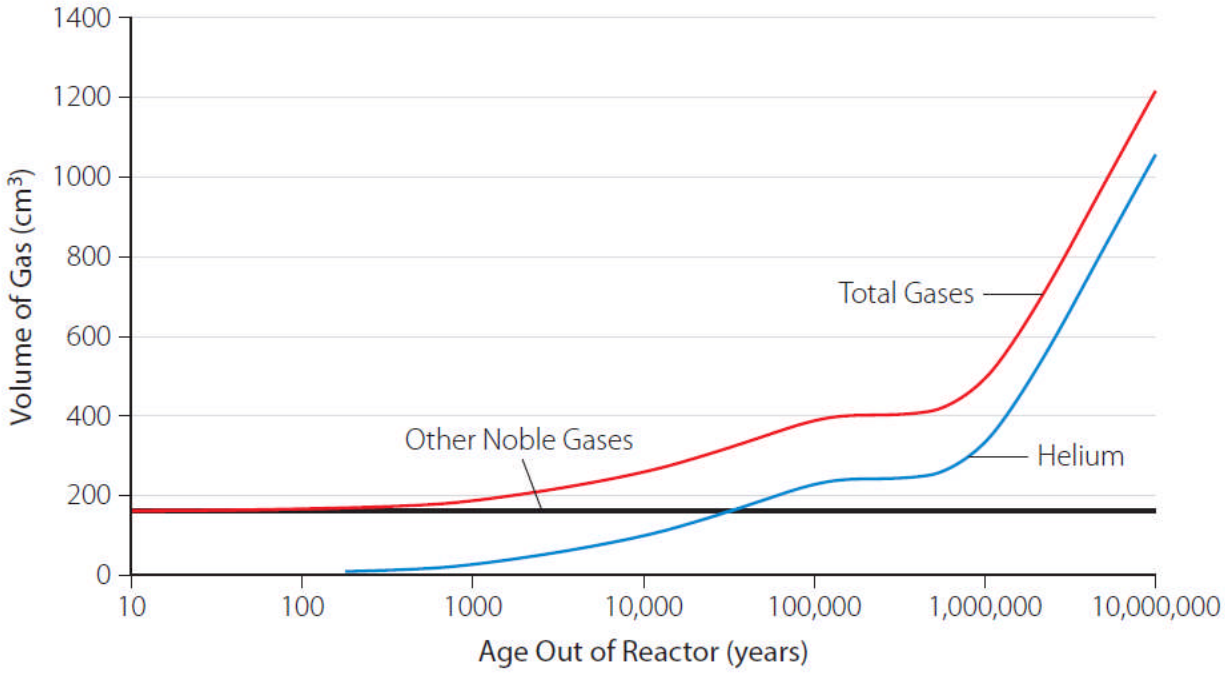

[At normal temperature and pressure. Source: NWMO, 2012]

Figure 3 Gas volume inside a fuel element

5.3 Fuel Damage Mechanisms

Over extended periods of time, fuel temperatures generated as described above can lead to mechanisms for fuel damage during storage and disposal, as documented in a number of publications such as Rothman [1984], IAEA [2002], McMurry et al. [2003], Lian [2010], and NWMO [2012a]. Some illustrative damage mechanisms are summarized in the following paragraphs, mainly from NWMO [2012a].

Zircaloy Corrosion

Obviating excessive corrosion is a generic design requirement for fuel. This topic is addressed in Chapter 17 in the context of fuel residence in the reactor. In addition, during storage, sheath corrosion must be limited to acceptable levels.

Zircaloy is relatively resistant to pitting corrosion in the pure chloride-free water encountered in the fuel bay, and pitting does not occur in the atmosphere provided during dry storage.

Hydrogen Absorption and Zircaloy Embrittlement

As noted in Chapter 18, fuel sheaths can contain hydrogen and deuterium from several sources, mainly residual hydrogen produced during fabrication, hydrogen or deuterium picked up from the coolant during irradiation, and hydrogen or deuterium generated by in-reactor corrosion of

the sheath. Still more hydrogen can enter the Zircaloy as a result of radiolysis in the storage pool; this can be limited by chemistry control and by purification of pool water. If quantities are excessive, some hydrogen and deuterium may precipitate in the Zircaloy as zirconium hydride or deuteride, especially at the relatively cooler temperatures of storage after removal from the reactor. These hydrides and deuterides result in more brittle (less ductile) Zircaloy that is more susceptible to fracturing from the mechanical loads imposed on it, for example during fuel transfers and/or during fuel extraction from or loading into a disposal container.

Delayed Hydride Cracking (DHC)

DHC is similar to the process mentioned above (embrittlement of Zircaloy caused by hydrogen), but occurs after a time delay, as explained below.

In some situations, this hydrogen or deuterium may be distributed fairly uniformly. In such situations, their local concentrations could be acceptably low. However, if the material is under significant temperature and/or stress gradients for a significant duration, hydrogen and deuterium can migrate and concentrate preferentially at locations of relatively lower temperature and higher stress. Over time, this can potentially lead to excessive local hydride and deuteride concentrations and therefore to higher susceptibility to brittle fracture.

Sheath Creep and Rupture

Internal gas pressure can lead to long-term creep of Zircaloy. If excessive, this can potentially rupture the Zircaloy.

Stress Corrosion Cracking (SCC)

As noted in Chapter 17, SCC (also called environmentally-assisted cracking, or EAC, in Chapter 17) occurs when irradiation-embrittled Zircaloy experiences sufficiently high tensile stresses in the presence of a corrosive environment for a sufficiently long duration. Depending on the magnitude of stress and of intensity of the corrosive environment, through-wall cracks due to SCC can occur quickly, or slowly, or not at all. During storage, long-term stresses are provided by internal gas pressure. A corrosive internal environment is provided by fission gases that were released during irradiation in the reactor.

Mechanical Overstress

From NWMO [2012a]: "As long as the fuel bundles are supported by baskets in intact containers, they are not subjected to significant load-bearing stresses. If tremors associated with earthquakes caused the fuel bundles to vibrate sufficiently, presumably some of the fuel pellets or the cladding could be damaged. The damaged material would remain in an intact container, and the overall evolution of the used fuel bundles would not be significantly changed."

Fatigue

This would be a consideration mainly during transportation of irradiated fuel bundles, e.g., to sites for dry storage and/or long-term disposal or isolation.

Defective Fuel

Sometimes fuel can develop defects in the reactor, that is, the Zircaloy develops a hole or a crack. Detailed discussions of this phenomenon are provided in Chapters 17 and 18.

A hole or crack in Zircaloy will allow oxygen-containing air to come in contact with UO_2. This, over time, can potentially oxidize the pellet to higher states of oxygen, such as U_3O_8. The latter is less dense than the former, and therefore the pellet can swell. Excessive swelling of the pellet can potentially split the sheath. Under these conditions, in addition to the original hole or crack, the Zircaloy can develop further splits during storage.

Other Effects and Remarks

The literature also mentions other mechanisms pertinent to potential fuel damage, for example, hydraulic processes and biological processes. They are not covered in this chapter for the sake of brevity. Combinations of these various mechanisms are also possible.

These fuel failure mechanisms during storage have been postulated partly from first principles and partly from exploratory experiments. Because several of these mechanisms are thermally activated and increase non-linearly with temperature, it would be good design practice to keep storage temperatures reasonably low. Design studies as well as experience to date indicate that under realistic as-designed operating conditions, the actual risk of fuel failure from any of these postulated mechanisms is negligibly small. Some of these aspects are illustrated in the following sections.

6 Wet Storage at Reactor Sites

Storage of irradiated fuel entails engineered facilities that can and must be monitored for the entire time that the fuel is stored and that make retrieval and movement of irradiated fuel to other facilities readily feasible.

6.1 Flow of Fuel Bundles Through a CANDU

Because CANDUs use natural uranium fuel, they need to be refuelled essentially continuously to maintain the required level of reactivity within the core. From practical considerations of work scheduling and equipment maintenance, refuelling is not done continuously, but rather during parts of each day. The flow of fuel through a CANDU is shown in Figure 4.

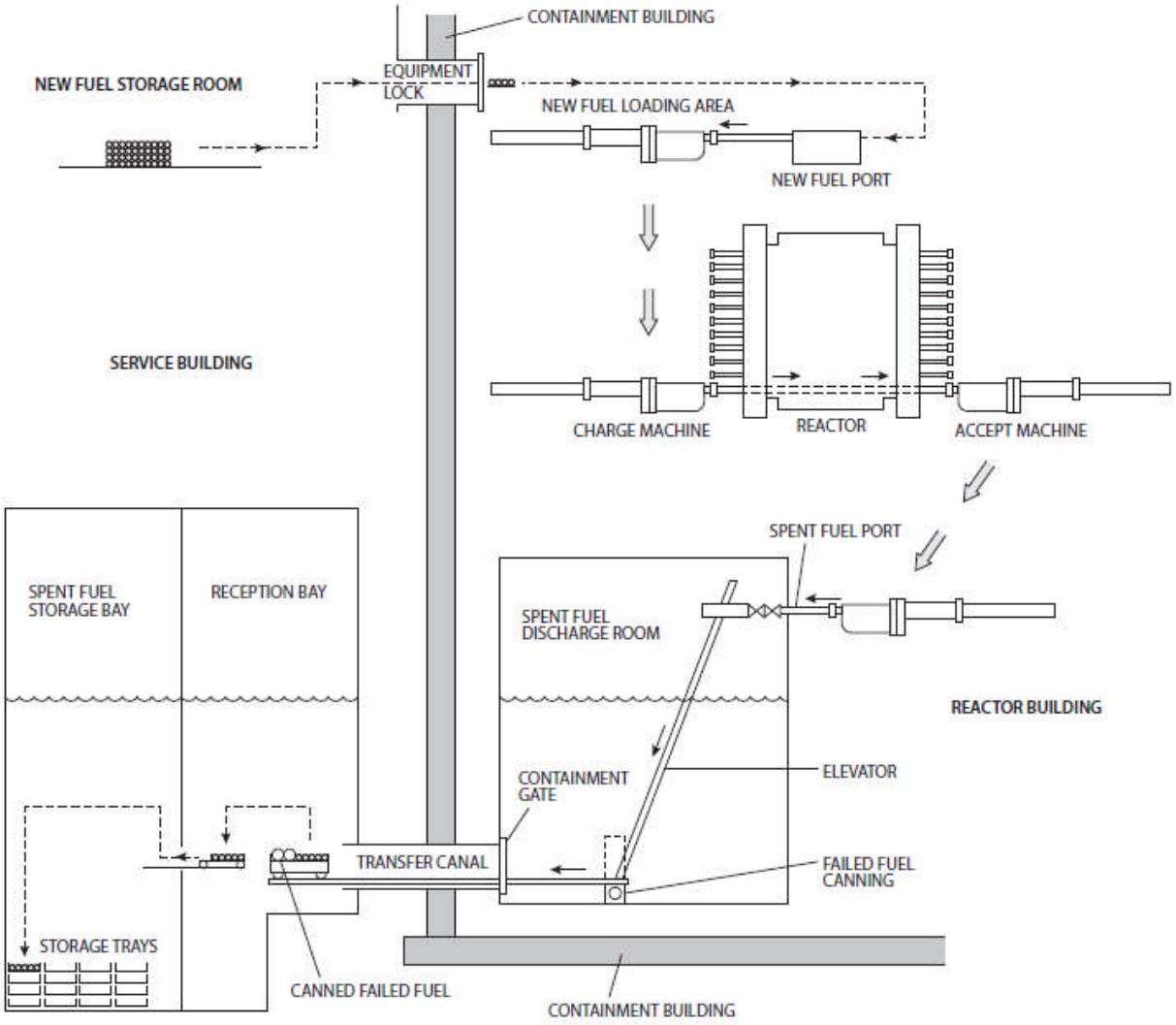

[Courtesy Ralph Granz]

Figure 4 Flow of fuel through a CANDU reactor

Inside the core, fuel bundles reside in horizontal fuel channels and are cooled by high-pressure heavy water. During refuelling, new fuel bundles are inserted into a fuel channel (usually in the same direction as the coolant flow), and irradiated bundles are removed from the same fuel channel by two fuelling machines operating in tandem. One machine, labelled as the "charge" machine in the figure, inserts new fuel bundles at one end of the channel, and the other, labelled the "accept" machine, removes irradiated bundles from the other end. The two machines reverse charge/accept roles depending on the channel being fuelled (i.e., the flow direction in the channel being fuelled). Fuelling machines, when connected to the fuel channel, act as extensions of the fuel channel pressure boundary and provide the required cooling for irradiated fuel bundles while they are inside the fuelling machine. The "accept" machine delivers the irradiated bundles to the irradiated fuel (spent fuel) port. From there, the bundles are moved by other remotely operated means to the irradiated fuel discharge room, which contains ordinary water at atmospheric pressure.

During their residence in the reactor, and during all movements within the reactor and the irradiated fuel storage bay, the bundles are oriented in the horizontal position. This is the orientation for which the bundles are designed when they are subjected to the flow and power conditions inside the reactor fuel channel (Chapter 17), and therefore this would be the preferred orientation for the bundles throughout their storage and disposal life. However, a single tier of vertical bundles supported on their end plates is also an acceptable configuration, provided that the bundles are not required to support more than their own weight.

6.2 Irradiated Fuel Bundles Temporarily in Air

At the spent fuel port (Figure 4), the irradiated fuel bundles transit from the fuelling machine, which contains heavy water, through an air-cooled interlock and elevator at atmospheric pressure, and are then deposited in the spent fuel discharge room, which contains ordinary (light) water. CANDU designs that use enriched fuel and ordinary water for coolant, such as the ACR [AECL, 2007], obviate the passage of irradiated fuel through air, and the transfer of the bundles can be performed underwater from the fuelling machine to the spent fuel discharge room (or possibly directly to the reception bay). In existing CANDUs, movement of bundles through the air interlock and elevator is timed so that irradiated bundles do not overheat while in air.

As an illustrative exercise, you are encouraged to determine the maximum length of time that the bundles can safely stay in air. Start with the information on decay heat given in Section 5. Assume power equivalent to zero time after discharge and no heat removal by air. Use the standard equation for adiabatic heat-up and apply it to a fuel element. How long does it take for the sheath temperature to reach the melting point of Zircaloy?

CANDU plants are equipped with water spray nozzles to cool the bundles if their residence in air exceeds the maximum permissible time.

6.3 Throughput of Irradiated Fuel Bundles

From the spent fuel discharge room (Figure 4), irradiated bundles are moved to the spent fuel reception bay through the water-filled transfer canal. From the reception bay, the bundles are

moved to the spent fuel storage bay, where they are loaded underwater by a remotely controlled bundle loading apparatus into storage trays that rest on storage racks. More recently, consideration has been given to replacing the storage trays or racks with storage baskets which are directly transferrable to dry storage containers. Both the trays or racks and the baskets are designed to ensure:

- adequate cooling of the bundles in the storage bay,
- avoidance of damage to bundles during their residence in the pool,
- avoidance of damage to pool components,
- compliance with safeguards monitoring requirements (e.g., bundle serial numbers are readily visible),
- direct transfer of bundles (baskets only) into dry storage containers, and
- use of the most compact arrangements of bundles in the pool.

As an illustrative exercise, one can determine the number of bundles discharged from a CANDU 6 reactor in one year, assuming the following:

- The plant's electrical output is 600 MW(e).
- The plant overall efficiency of conversion of thermal power to electricity is ~30%.
- Capacity factor (fraction of time the plant is running at full power) is 90%.
- Each bundle contains approximately 19 kg of U and produces thermal power (average discharge burn-up) of 6,500 MWd(th)/teU.

Using the above parameters, one can determine:

- Total thermal energy produced in one year: 657,000 MWd(th) (=600x0.9x365/0.3).
- Average thermal energy produced by an individual fuel bundle: 123.5 MWd (th) (=6500x19/1,000).
- Number of bundles required to produce the reactor's annual power: 5,320 bundles (=657,000/123.5).

The storage pool is designed to accommodate the spent fuel generated from 10 years of operation (~53,200 bundles in this example) plus one full core-load of bundles (4560 bundles in this example; 380 channels containing 12 bundles each). The additional capacity of one core-load provides for the possibility of having to unload the entire core to accommodate refurbishment. In practice, bundles could begin to be removed from the pool as early as seven years after their placement into the pool, reducing the risk that pool capacity would be reached anytime during reactor life.

6.4 Irradiated Fuel Bay: Typical Dimensions

In Canada, there are several locations where irradiated fuel is either currently stored in fuel bays or has been stored in the past. Some of these locations are: Chalk River Laboratories (CRL) at Chalk River, ON; Whiteshell Laboratories (WL) at Pinawa MN; McMaster Nuclear Research Reactor, Hamilton, ON; Point Lepreau Nuclear Power Plant at Point Lepreau, NB; Gentilly

Nuclear Power Plant at Trois-Rivières, QC; Darlington Nuclear Power Plant in Darlington ON; Pickering Power Plant at Pickering ON; and Bruce Power Plant at Tiverton ON.

Designs, layouts, and dimensions of irradiated fuel bays (IFBs) differ from one station to another. As an illustrative example, the following discussion concerns an IFB with three sections: a reception bay; a long-term (or main) storage bay; and a transfer bay.

Irradiated fuel is received in the reception bay and stored there for one to two weeks (Figure 4). Then it is transferred to the long-term storage bay and stored there for a few years. The long-term storage bay usually also has a fuel inspection station where fuel can be inspected underwater, for example to monitor and assess fuel performance. Finally, in the transfer bay (not shown in Figure 4), fuel is loaded (underwater) into storage baskets en route to placement in dry storage

Figure 5 illustrates a typical irradiated fuel storage bay. The sizes of the bays differ in different stations, e.g., as small as 20 m x 12 m or as large as 34 m x 17 m [OECD/NEA, 2015]. These have a surface area similar in size to an Olympic-size swimming pool, but the IFBs are constructed of double-walled reinforced concrete and are much deeper. To provide sufficient radiological shielding to workers above, water in IFBs is usually 6–8 m deep. Typically, the volumes of water in C6 IFBs are: reception bay, 700 m^3, and main storage bay, 2,000 m^3.

6.5 Irradiated Fuel Bay: Heat Removal

Heat must be removed from the fuel bay to maintain water at a predetermined temperature and to continue to provide cooling to the fuel. Generally, an irradiated fuel bay with 10-year storage is maintained at <38°C; with 10-year storage plus one full core load, the pool is maintained at <49°C. Major elements of the cooling system are a pump, a heat exchanger, and a resin bed.

As industrial installations go, incorporating the required heat removal capability into the irradiated fuel pool cooling system is not a significant challenge for the designer. However, in case of impaired heat removal capability, it is important for safety reasons to determine how much time may be allowed to elapse before auxiliary cooling must be provided. In the example above, the reader is encouraged to determine how much time is required for the cooling water to evaporate and the fuel bundles to be exposed to air, and how that time changes with the number of bundles in the bay.

In the post-Fukushima era, factors such as available response time based on pool size and the availability of off-site emergency cooling have achieved heightened prominence.

[Source: Villagran, 2014]

Figure 5 A typical irradiated fuel bay

6.6 Corrosion of Irradiated Fuel in the Pool

Corrosion of CANDU fuel during its residence in the reactor is covered in Chapter 18. To in-reactor corrosion, any additional corrosion occurring during the residence of the fuel in storage pools must be added. To help reduce the latter, demineralized water is used in the pool.

Because CANDU fuel's residence time in the reactor is relatively short (especially compared to LWR fuel), the resulting in-reactor corrosion is very low (see Chapter 18). Experience to date has been that additional corrosion during storage is trivial compared to the corrosion picked up during residence in the reactor. Hence, the total corrosion in-reactor and during pool storage is very small and does not significantly reduce the fuel bundle sheath thickness.

6.7 Shielding of Irradiated Fuel in the Pool

For shielding to protect workers and the public, irradiated fuel storage pools typically contain about 7 m of water above the last rack of fuel.

6.8 Criticality Not an Issue for CANDU Irradiated Fuel

The IAEA (and CNSC) design guidelines for irradiated fuel storage and disposal include a need to assess conditions that could lead to criticality. There are no criticality-based restrictions on proximity of irradiated CANDU bundles in the pool because the remaining fissile content in irradiated bundles is low. Bundles can be placed into the most compact configuration (based on heat transfer considerations only) and do not need to be "re-racked" during their residence in the pool.

7 Dry Storage at Reactor Sites

As noted earlier, after a few years in water pools, fuel bundles are transferred to dry storage because it is a comparatively less expensive method of storing large quantities of fuel and because after a few years out of the reactor, fuel requires much less cooling.

A variety of options are available for dry storage. As one illustrative example, *dry storage containers* are used at the Pickering and Bruce plants [OPG, 2015]. As another illustrative example, Atomic Energy of Canada Limited (AECL) has developed *concrete canisters* that are used at some C6 plants and decommissioned prototype plants. These are described in the following sections.

7.1 Dry Storage Containers

Each dry storage container (DSC) can store a few hundred fuel bundles [OPG, 2015]. It is made of reinforced high-density concrete approximately 51 cm thick and is lined inside and outside with 12.7 mm-thick steel plate. The thick concrete provides an effective barrier against radiation. Irradiated fuel bundles are loaded into a DSC within the IFB. The DSC is then sealed, dried, and moved indoor into a secure storage building.

7.2 Concrete Canisters

AECL has developed modular "concrete canisters" such as CANSTOR and MACSTOR [CANDU Energy, 2014]. The two are similar in concept, but MACSTOR is significantly bigger. A brief overview of the latter is provided here; Figure 6 illustrates its principal features.

In the MACSTOR design, many fuel bundles are stored in a "storage basket"; many baskets are in turn placed in a steel "storage cylinder". A large number of storage cylinders are inserted into a concrete labyrinth called MACSTOR. Shielding is provided by the concrete of the module, and heat removal is achieved by air circulation due to natural convection. In Figure 6, note the staggered openings at the bottom and top of the module; they allow air circulation, but do not provide a direct line of sight through the concrete to the storage cylinder. Three barriers prevent escape of radionuclides from the fuel: the fuel sheath, the sealed basket, and the storage cylinders. Irradiated bundles can be retrieved using appropriate shielded equipment.

The cross section of each module is about 8 m wide and about 7 m high. Each MACSTOR unit can store about 12,000 CANDU fuel bundles.

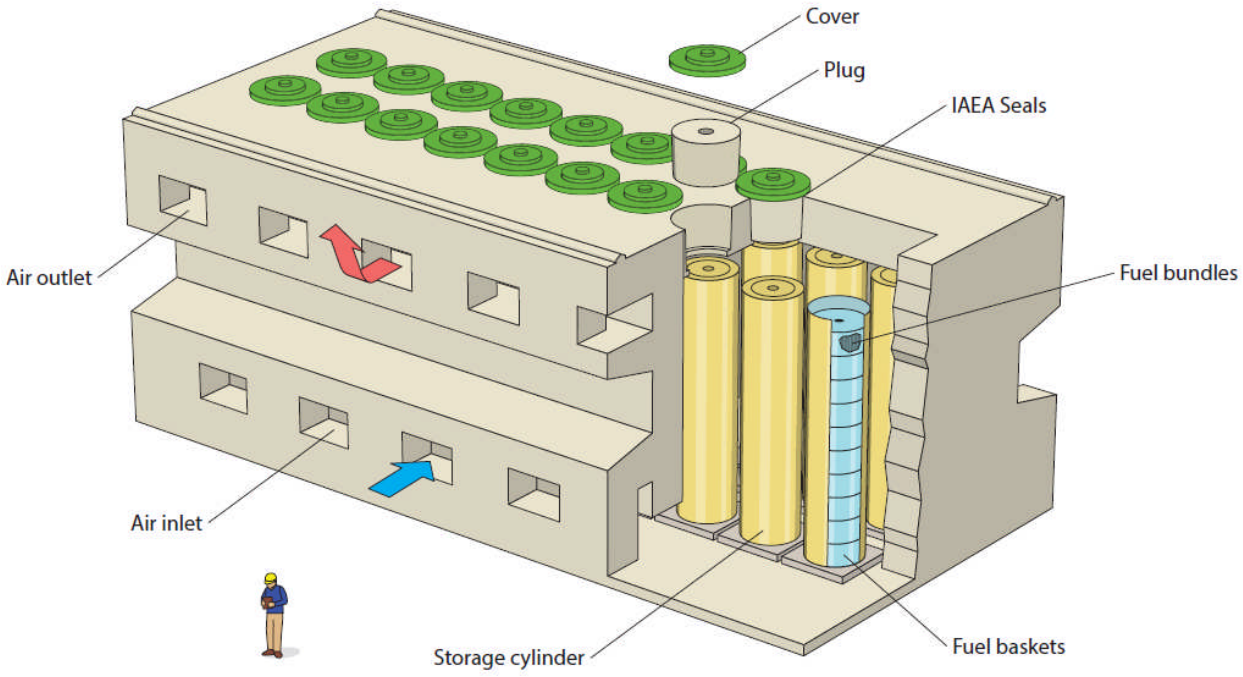

[Courtesy Jim Lian]

Figure 6 Overview of MACSTOR

7.3 Storage Baskets

Figure 7 [OPG, 2009] illustrates the main features of a typical storage basket used in MACSTOR. Fuel bundles are loaded into baskets underwater in the fuel transfer bay, dried and weld sealed inside the baskets, then moved in shielded flasks and loaded into storage cylinders. Bundle orientation is changed from the normal horizontal orientation in the reactor and the irradiated fuel storage bay to the vertical orientation during the basket loading process. In this design, the basket is typically designed to hold 60 CANDU fuel bundles oriented vertically. Ten such baskets are loaded into a metal storage cylinder.

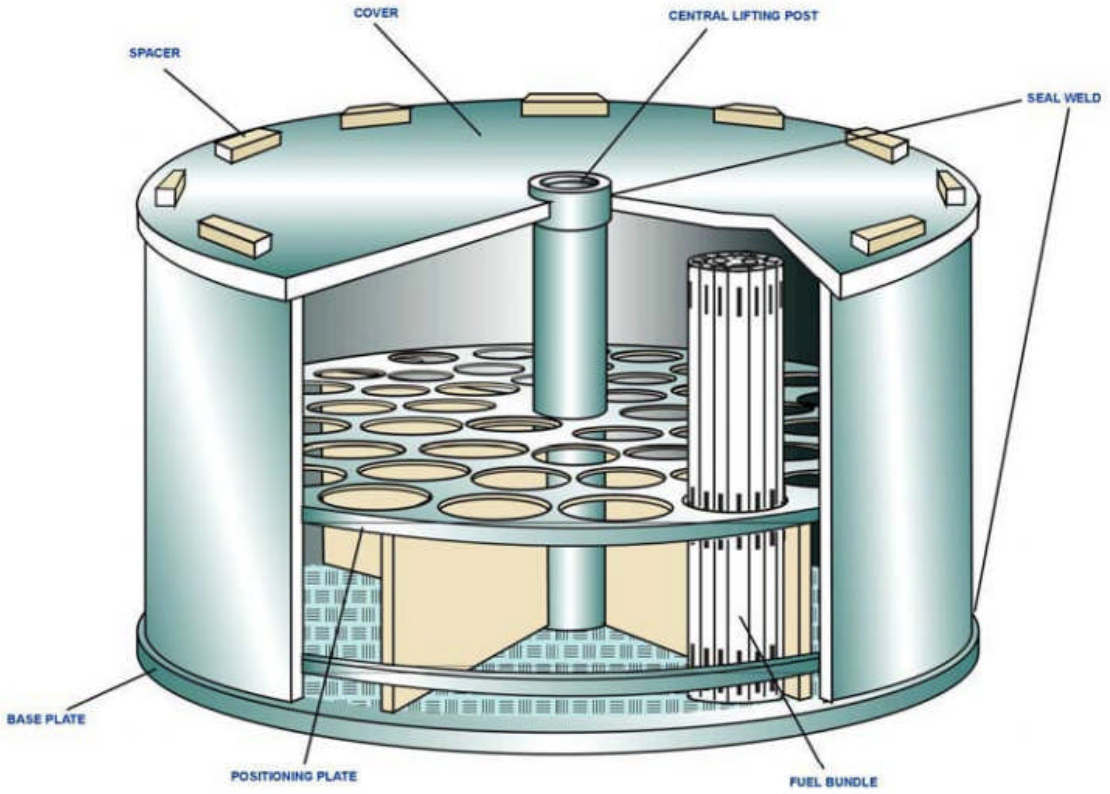

[Source: OPG, 2009]

Figure 7 Basket for dry storage of fuel

7.4 Transfer of Bundles from the Pool into Baskets

Shielding requirements dictate that bundles must be loaded into dry storage baskets underwater using remotely operated equipment. Design and process details differ from one station to another.

7.5 Heat Transfer

MACSTOR facilities enable dry storage of fuel bundles with up to about 6 W of power per bundle. This is typical of C6 fuel that has been cooled for six years.

Considering the size and good heat transfer configuration of the fuel elements, it can be easily recognized that effective dissipation of this amount of heat from CANDU fuel can be achieved by heat transfer through convection, conduction, and/or radiation without any parts of the element or the bundle becoming overheated. Ultimately, the heat is passively transferred from the storage cylinder to the atmosphere through natural convection.

7.6 Fuel Integrity

For dry storage, the target criterion is to limit sheath failures to within 1% of fuel rods during 100 years of storage [Lian, 2010].

Lian [2010] provides an overview of the integrity of irradiated CANDU fuel during interim dry storage in MACSTOR and the associated research and development. Lian concludes the following:

- Highest fuel temperature is less than 150°C; and
- Maximum sheath hoop stress is less than 4 MPa.

The above conditions are less demanding than those experienced by LWR fuel during dry storage. Therefore, based on detailed assessments of LWR fuels done by the Electric Power Research Institute in the United States, Lian [2010] concluded the following for CANDU fuel stored in MACSTOR:

- Creep-rupture and external oxidation should not cause failure at storage below 300°C;
- For storage temperatures below 300°C, stress-corrosion cracking (SCC) is the most likely mode of fuel failure, but even it is unlikely to occur to any significant extent during dry storage;
- Fatigue is not a limiting failure mechanism for stored fuel sheaths; and
- Sheath splitting by UO_2 oxidation is a limiting mode only for fuel rods that have already developed defects.

Based on the above discussion, Lian [2010] projects that the failure rate in CANDU fuel during dry storage in MACSTOR would likely be in the neighbourhood of 0.001% of fuel rods in 100 years. This is 1,000 times lower than the criterion noted earlier.

7.7 Shielding

As also noted in Section 5, radiation (i.e., the shielding requirement) does not diminish proportionately as much as heat generation and requires continuing attention in handling of irradiated fuel. As an illustrative example, nominal wall thickness in MACSTOR is approximately one metre of ordinary concrete to control direct radiation exposure at the outside wall. This is an indication that significant radiation can be expected from stacks of irradiated fuel bundles, even six years after discharge.

8 Final Disposal or Isolation

As of 2014, Canada had about 2.5 million irradiated fuel bundles in storage [Garamszeghy, 2014]. Following the two interim phases of irradiated fuel storage described above, the irradiated fuel may be either reprocessed or placed into permanent disposal or isolation facilities. This section touches upon the following aspects of Canada's current concept for permanent disposal or isolation of irradiated fuel: approach and strategy; repository design; container design; and health protection.

The remainder of this section has borrowed heavily from lectures delivered by J.E. Villagran at a course sponsored by the Canadian Nuclear Society [Villagran, 2013, 2014].

8.1 Strategy

Several options are available for permanent disposal or isolation of irradiated nuclear fuel,

including isolation in stable geological formations or emplacement in abandoned salt mines. After many decades of research [Boulton, 1978], detailed evaluations, and public consultations [Seaborn, 1998], Canada has opted for centralized containment and isolation of irradiated nuclear fuel in a deep geological repository (DGR) [NWMO, 2015a]. Several other nuclear countries are also inclined towards geological repositories, e.g., Finland, Sweden, France, Germany, Japan, Switzerland, and the United Kingdom.

> "The goal of (Canada's) plan is to place the (irradiated) fuel deep underground in rock where it will be constantly watched to make sure it is secure and not affecting anything around it. Then at some point in the future, people can decide if they want to close the facility and return the ground to its natural state" [NWMO, 2015b]. This approach includes an optional step of interim shallow underground storage.

A key aspect of the current concept is to surround the irradiated fuel by multiple barriers, as explained later in this section. This minimizes the potential for release of radionuclides should any individual barrier fail.

The Canadian strategy for long-term waste fuel management is called "adaptive phased management" (APM) [NWMO, 2015a] and is being administered by the Nuclear Waste Management Organization (NWMO). APM covers all phases of high-level waste management, including dry storage of fuel at the reactor site; the end result is final disposal (e.g., isolation in a DGR).

8.2 Phases of Disposal

One can define two distinct phases in the life of a disposal or isolation facility:

- The initial, operational period during which the facility is constructed, filled with fuel, and closed; and
- The long period of isolation of irradiated fuel after closure of the facility.

Initial operational period: Canada's strategy and design preserves the retrievability option and provides for continuous monitoring. Thus, APM engenders flexibility in design and promotes ongoing technical and sociological research, enabling continuous learning and adaptation. The process is collaborative, open, inclusive, and transparent, and decision-making is phased. The current expectation is that this phase will last a few decades.

Isolation period after closing the facility: The facility's closure is a few decades away, and society's needs and preferences that far away cannot be reasonably anticipated at this time with sufficient certainty. Therefore, it is best to be flexible for now about the facility's configuration after closure. NWMO's intention is to "remove underground equipment and backfill and seal the access tunnels and shafts. Surface facilities will also be dismantled at a pace and in a manner determined collaboratively with the community, regulators, and other interested individuals" [NWMO, 2012b]. In this sense, there is an option, even an intention, eventually to "entomb" the fuel.

From "first principles" many factors can be postulated as important for detailed quantitative assessment of repository and container design. The following sub-sections highlight a few such factors. Experience and actual analyzes have shown that some are relatively more important

than others.

8.3 Repository

Figure 8 shows a conceptual design of an illustrative repository. The overall concept starts with placing many fuel bundles inside a sealed, corrosion-resistant container called a "used fuel container" (UFC). This step isolates the fuel bundles from groundwater and delays release of radionuclides into the environment.

The containers in turn are surrounded by a buffer material, bentonite clay, which possesses two physical characteristics that enhance its function of isolating the fuel. First, this natural clay can absorb up to 10 times its weight in water. If moisture were to approach the containers filled with used fuel, the bentonite clay would absorb the water and swell up, forming a seal around the container. This would delay the groundwater from reaching the container. Second, this clay has low permeability. Therefore, should the container fail, the clay would slow the diffusion of radionuclides out of the repository.

Many such containers would be placed in a horizontal position inside placement rooms in the repository, at a depth of some 500 m. Other concepts are also being considered, such as vertical placement of containers in boreholes.

Thus, multiple barriers isolate the fission products from the biosphere: the UO2 matrix; the Zircaloy sheath; the sealed copper containers; bentonite clay; and rock.

Current projections are that by their end of life, CANDU power reactors will irradiate some 4.6 million fuel bundles. To dispose of these, a typical repository would require an area of about 2 km x 3 km, or about 600 Ha or 1,480 acres.

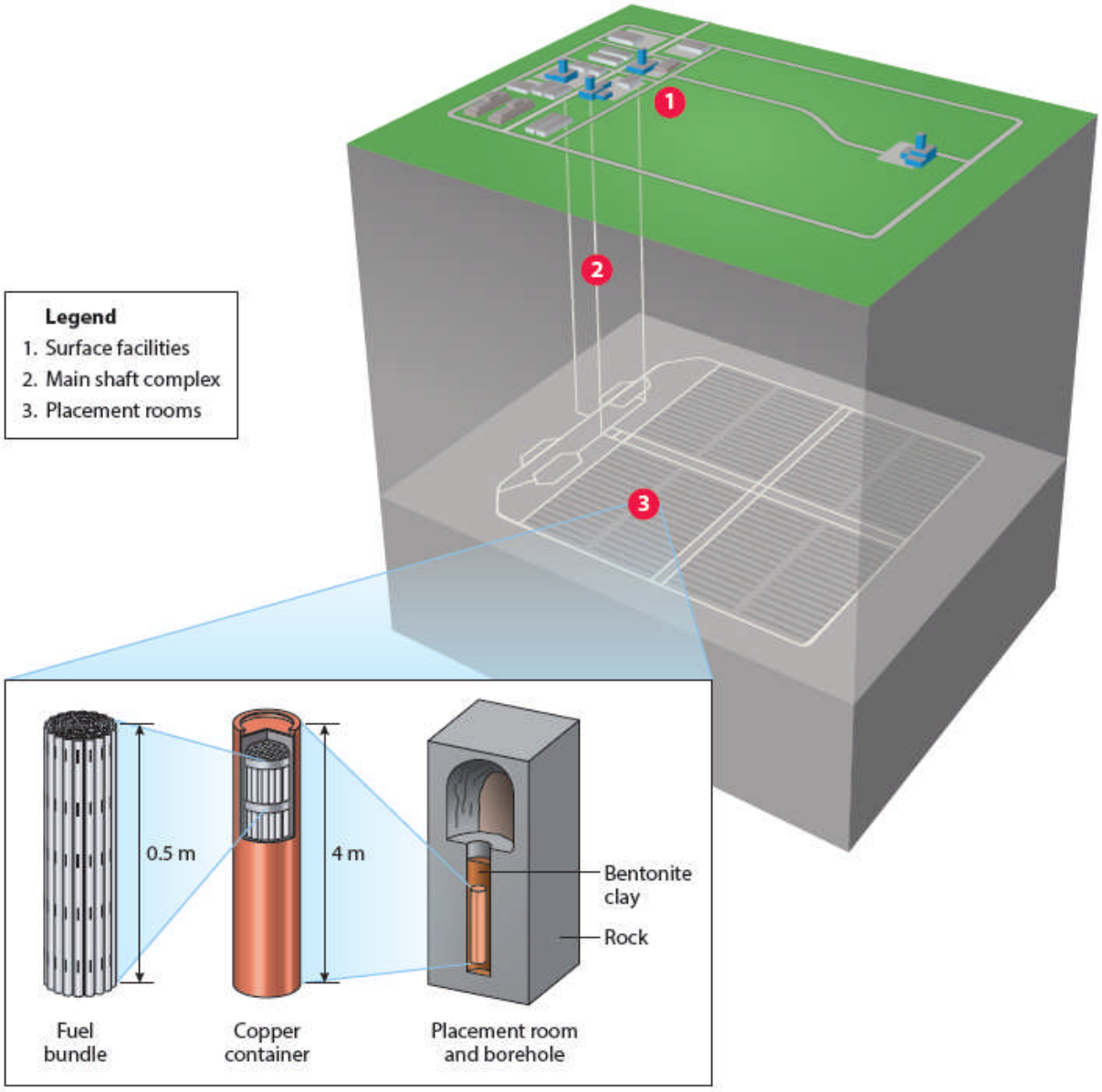

[Illustrative concept; Source: Villagran, 2014]

Figure 8 Concept of a deep geological repository

8.4 Used Fuel Containers

This section illustrates the main features of two designs of used fuel containers (UFCs) that use a copper shell.

8.4.1 Conceptual designs

Figure 9 shows two slightly different container concepts; each container can hold many CANDU fuel bundles. In the first concept, an important barrier to corrosion is provided by a shell made from oxygen-free phosphorus-doped (OFP) copper 25 mm thick. Structural support is provided by an inner liner made of carbon steel 96 mm thick. In the second concept, the copper shell is replaced by a copper coating about 3 mm thick [Hatton, 2015].

The number of UFCs in a typical repository depends on the detailed design of the UFC. For example, about 100,000 UFCs of Concept # 2 (as shown in Figure 9) would be needed to accommodate some 4.6 million fuel bundles.

8.4.2 Container lifetime

The major damage mechanisms are expected to be uniform corrosion and pitting of the copper shell or coating. Corrosion in turn can be driven by two major environmental factors [Villagran, 2014]:

- By initially trapped oxygen: the resulting corrosion is equivalent to about 0.080 mm of wall penetration;
- By chloride and/or sulphide from groundwater, from pyrite impurities in the clay, or by microbial activities. These cumulative corrosive interactions can cause additional wall thickness loss of about 0.27 mm over a period of one million years.

After increasing nominal estimates by applying conservative factors, the total potential loss of container wall thickness is estimated to be about 1.7 mm over one million years. Therefore, depending on the thickness of copper, a typical UFC should stay intact for over one million years.

8.5 Buffer Material

Main design requirements for the buffer material (bentonite clay in the above example) include preventing groundwater migration to the disposal container, slowing migration of radionuclides away from the container, and maintaining the long-term integrity of the chemical and mechanical properties of clay.

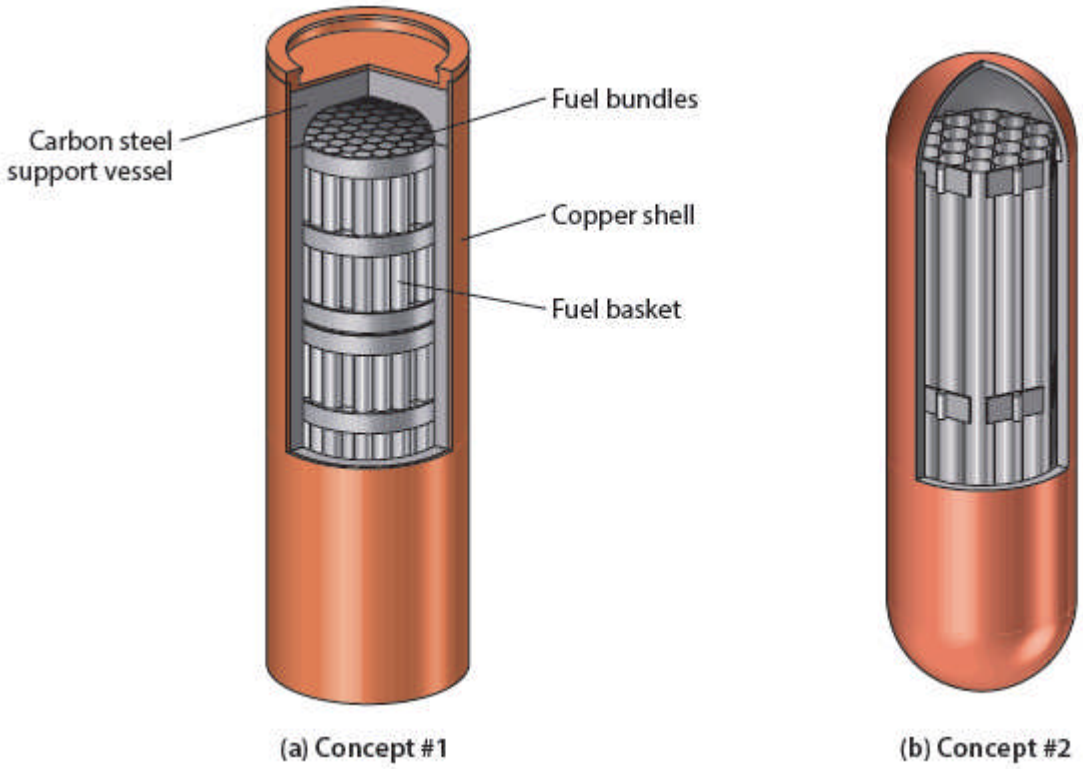

[Source: Villagran, 2013, 2014]

Figure 9 Containers for Permanent Disposal of Irradiated Fuel

8.6 Rock Temperature

The power generated by the fuel mass will increase its temperature, which will cause heat to be transferred from the fuel to the surrounding rock mass. Therefore, the temperature of the disposal vault is a design criterion for a repository. For hard-rock (granite, sedimentary rock, clay) geological disposal facilities, the temperature must remain below 90°C–100°C, but for salt repositories (such as the Asse facility in Germany or the WIPP facility in New Mexico), a higher temperature of up to 250°C may be acceptable. The higher-temperature facilities are more appropriate for disposal of reprocessed waste, which has a higher short-term heat load.

Consequently, the thermal calculations revolve around geometry: how much fuel can be placed into each container and how close to each other the containers can be placed to maintain a temperature below the design requirement. The limiting parameters for heat transfer to the rock vault are usually the surface temperatures of the container and the vault, rather than the maximum fuel temperature in the container.

Initial calculations indicate that it takes between 25 and 40 years for the temperature of a fully filled vault to go from ambient to 90°C, which would be a rather high temperature for workers. Hence, one might need to consider potential arrangements for cooling the vault during the waste emplacement period.

The rock temperature will be higher near the fuel and lower further away. This will lead to non-uniform local expansion of the rock, which in turn will lead to thermal stresses. From "first principles", one can postulate that if the temperature gradients and the resulting thermal stresses are large, the rock can potentially crack locally. However, are the thermal gradients expected to be large enough to crack the rock?

As an illustrative example, let us assume that the rock temperature inside the repository is 100°C. The minimum temperature in the Earth's crust at the depth of the repository must be greater than the freezing temperature of water (because otherwise leaching and migration would be impossible). Therefore, the maximum temperature gradient in the rock is ~100°C. Considering that it takes at least 25 years for the vault temperature to increase by 70°C (see the discussion earlier) provides a strong indication that the heat flux into the rock is extremely small and therefore that the local stress anywhere in the rock due to the temperature gradient is also very small.

8.7 Health Protection

8.7.1 Radioactivity and relative toxicity

Figure 10 [Boulton, 1978] illustrates the typical decay of radioactivity of irradiated nuclear fuel for up to ten million years after discharge. Shortly after 100,000 years, the radioactivity of irradiated fuel is very similar to that of natural uranium plus its decay chain.

The only credible escape route of radioactivity from disposed fuel to the biosphere is by transport through groundwater. Therefore, an illustrative perspective on the potential hazard of nuclear waste can be obtained by comparing its toxicity in water with that of naturally occurring materials.

The International Commission on Radiological Protection (ICRP) has defined a "relative toxicity index" as the ratio of the volume of water needed to dilute the radionuclides in waste material to drinking water standards to the volume of water needed to dilute an equal weight of 0.2 percent uranium ore to the same standards [Boulton, 1978]. Figure 11 shows some illustrative results of these relative toxicity calculations [Boulton, 1978]. The calculations necessarily contain some assumptions, but nevertheless, for purposes of an initial illustration, the figure suggests that after about a century following removal from the reactor, the relative toxicity of used nuclear fuel (in groundwater) is similar to that of a naturally occurring ore of mercury which contains 2.6% mercury. Within another century, the radiotoxicity of irradiated nuclear fuel becomes similar to that of naturally occurring ores of lead (of 5.8% concentration) and of uranium (3% concentration).

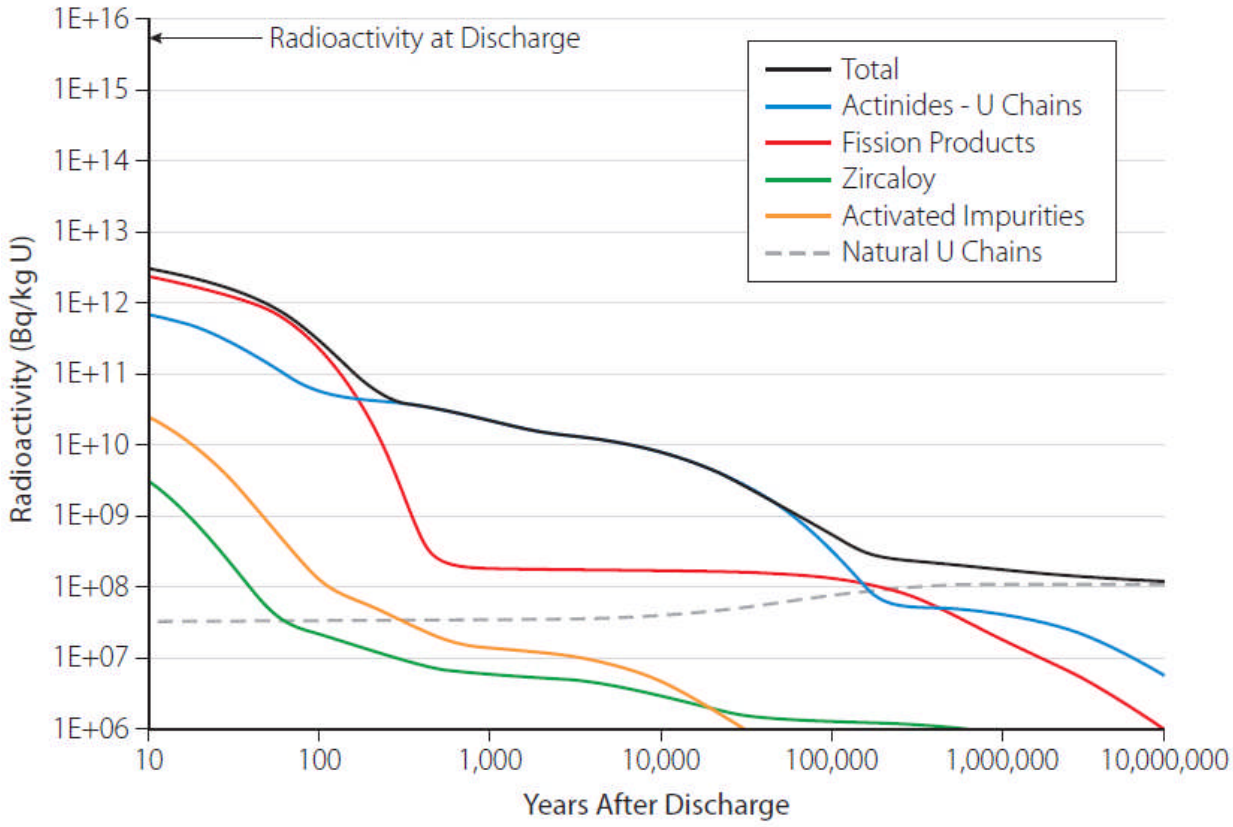

[Illustrative example; Fuel burnup: 220 MWh/kgU]

[Source: Villagran, 2014]

Figure 10 Decay of radioactivity in CANDU fuel

In a repository, access of groundwater to radionuclides is delayed by the engineered barriers described earlier. It must, however, be recognized that some engineered barriers may eventually fail, and therefore it is of key importance to ensure that significant time has elapsed by the time groundwater gains access to radionuclides and carries them to the biosphere. If so, the radionuclides would have decayed to harmless levels by the time they reach the biosphere (as illustrated in Figures 10 and 11). Therefore two important aspects of a safe disposal facility are orderly failure of barriers and the specific sequence of events. Hence, performance modelling is a critical component of the safety case and is explicitly dealt with in the CNSC Regulatory Guide G320 [CNSC, 2006].

Discussions on safety can be conveniently classified into two broad categories: (i) safety during the phase of waste emplacement in the facility, and (ii) safety during the post-closure and entombment phase.

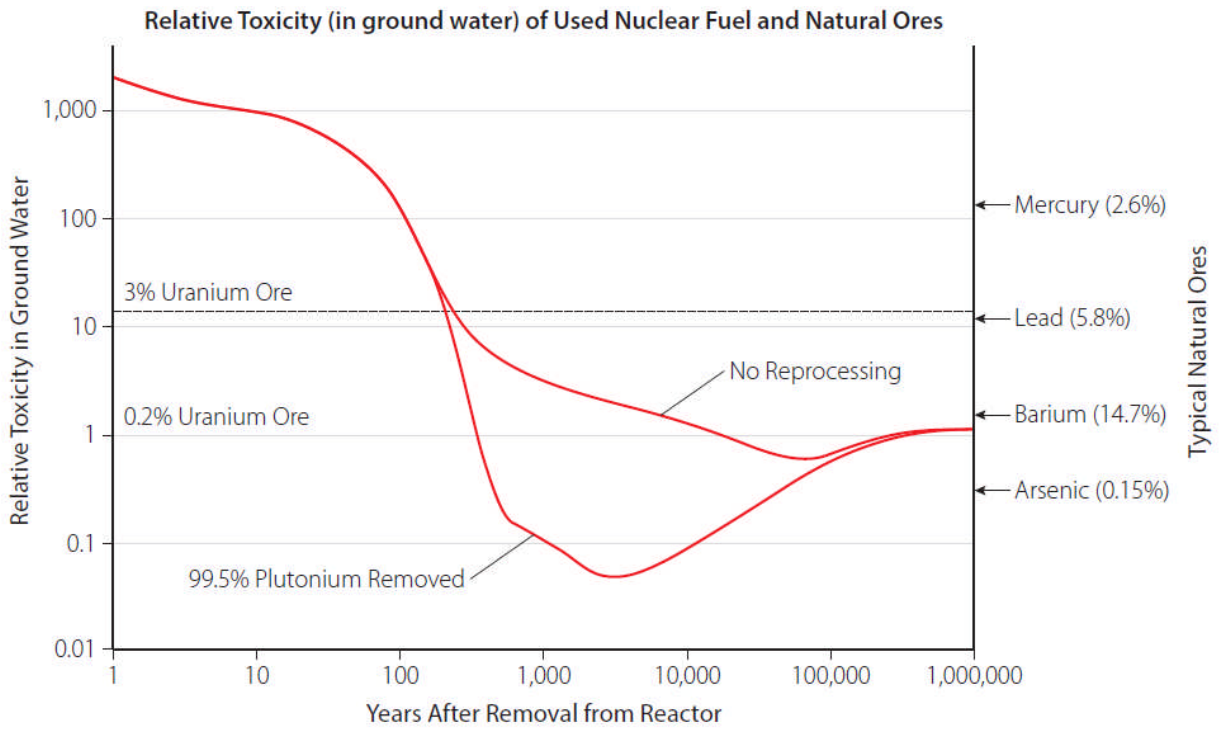

[Illustrative example; Source: Boulton, 1978]

Figure 11 Toxicity in ground water

8.7.2 Operational Phase

The relatively more important aspects of worker safety during this period are:

- radiation dose,
- rock falls,
- container stability during transport,
- hazards and difficulties in retrieval, and
- accident analysis.

8.7.3 Post-closure phase

In any disposal system, potential release of pathogens to the public is the main health concern.

Two important health protection objectives are that the committed dose be negligible and that the risk of increased cancer be negligible. Therefore, an important element of public health protection is provided by making the fuel inaccessible. This is enhanced by entombment of the fuel.

In general, the relatively more important aspects of a disposal facility are container lifetime, radionuclide diffusion, groundwater chemistry, vault sealing, and performance modelling.

It must also be ascertained that the Earth provides sufficient radiological shielding to humans on the surface. Figure 12 shows the results of illustrative dose rate calculations at the surface of

a conceptual repository at a hypothetical site. The predicted dose rates provide good margins of safety compared to the natural background dose rate and also compared to the acceptance criteria recommended by the International Commission on Radiological Protection (ICRP).

8.8 Breach of Containment

Write-ups in this and the following sections are based heavily on a variety of previous publications, mainly Whitlock [2015].

"In the design of Canadian technology, one aspect that was seriously considered was: 'what if both the copper container and the Zircaloy sheaths are breached?' Would the radioisotopes in used fuel reach the biosphere and pose a significant hazard to human health?"

If both fuel containers were breached, migration through groundwater is the one credible mechanism through which harmful radionuclides from the used fuel could be transported to the food chain and/or to water reservoirs accessible to humans.

Extensive experiments and detailed computer simulations have established that in the current design, transport times to the surface are in the hundreds of thousands of years. In that time, the radionuclides would decay to harmless levels (see Figure 10), and therefore the effects of used fuel on the biosphere would be negligible. In fact, after a few hundred years of decay, the actinide content in the used fuel repository is comparable to that of naturally occurring high-grade uranium deposits found in Canada, as well as those of other toxic ores such as lead and mercury. This period—a few hundred years—is well within human experience for safe design of engineered structures.

Although this science is based on extensive experiments and detailed computer modelling, its complete verification over the timescales of interest is obviously not possible through laboratory experiments alone. Therefore, this technological solution has also been verified using "natural analogues". Natural analogues are systems that occur naturally and possess key attributes that are very similar to components of the used fuel disposal system. They are described next.

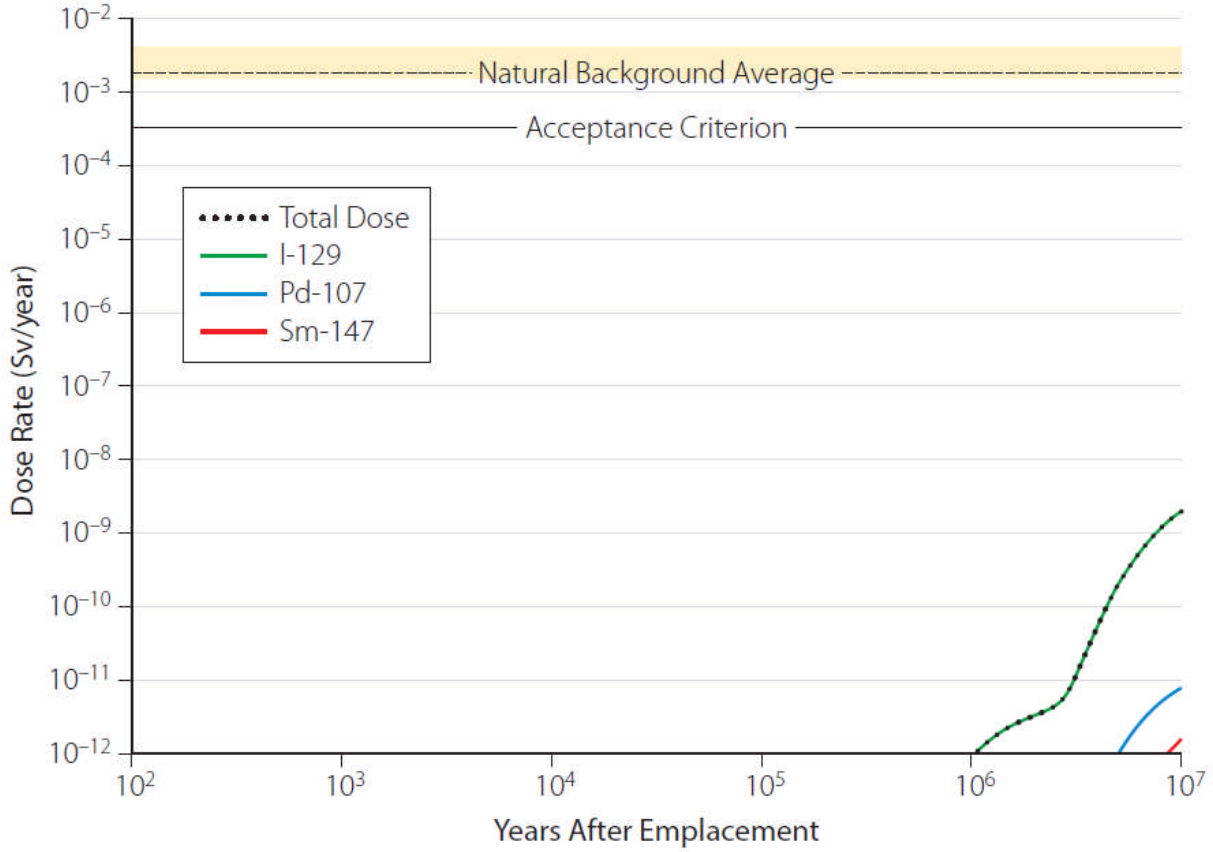

[Illustrative calculations; Source: Villagran, 2014]

Figure 12 Dose rate at the surface of a repository

8.9 Nature's Analogues for a Waste Repository

From the discussion above, it should be clear that the two aspects of the Canadian disposal strategy that are most critical to its success and that would benefit from having natural analogues to demonstrate their viability are a demonstration that radionuclide migration through groundwater is equal to or less than that used in the assessment models, and a demonstration that the effectiveness of the buffer material (bentonite clay) is as good as or better than that assumed in the assessment models.

- **Migration of plutonium and uranium**

In 1972, a French uranium mining company deduced that a natural "chain reaction" existed on earth some 2 billion years ago, long before the first chain reaction was demonstrated by human beings. These "natural reactors" existed at Oklo in Gabon, Africa. The key ingredient that made these natural reactors possible at that time is that natural uranium contained a significantly higher proportion of ^{235}U than it does today. At this higher enrichment level, natural uranium, with access to ordinary water, could be configured to constitute a critical mass. In fact, about 16 such "reactor" locales were identified at Oklo. It is postulated that these natural reactors "operated" intermittently for nearly a million years, with their power being regulated by access

to water. When the reactor power increased, groundwater heated up and evaporated; this caused the reactor to shut down. When the water cooled down and flooded the uranium deposit, the power started up again, and so on. These reactors shut down permanently when the concentration of ^{235}U became depleted to a value that could no longer sustain a chain reaction. However, the groundwater that had made the chain reaction possible continued to flow over the ore body until it was discovered 2 billion years later.

Unfortunately, by the time the phenomenon of "natural reactors" was understood, most of the locales where these natural reactors operated had been mined and the evidence of radionuclide migration 2 billion years earlier destroyed. Fortunately, some sites were undisturbed, which provided evidence that neither the plutonium (now totally decayed) nor the uranium had migrated from the location in the grain where they existed when fission occurred. This is powerful evidence that the model used for radionuclide migration in the Canadian waste disposal assessments (which assume that the radionuclides percolate to the surface of the repository together with groundwater) is extremely conservative.

- **Effectiveness of the buffer material**

The most direct natural analogue that provides evidence of the effectiveness of the buffer material is the uranium deposit in the Athabasca Basin of northern Saskatchewan, known as Cigar Lake. This deposit was discovered in 1981 and, after a lengthy period fraught with production difficulties unrelated to its geology, came into production in 2014. It is one of the richest (average ore grade of 20%) and largest deposits of uranium in the world. It occurs at a depth of about 500 metres as a contiguous deposit about 2000 m long, 100 m wide, and 20 m thick. A well-defined ridge of basement rocks about 2 billion years old underlies the mineralized zone over its entire length.

The most remarkable feature that has relevance to the effectiveness of the buffer material is the clay deposit that completely covers the ore deposit, on top of which there is an overburden of sandstone. The fact that the ore deposit has survived undisturbed for about 2 billion years speaks to the effectiveness of the clay barrier in preventing water from reaching the ore deposit and leaching out uranium atoms. The effectiveness of this entombment is further verified by the fact that the ore deposit provides no chemical or radioactive signal of its existence that can be detected at the surface. The age of the ore deposit and the traumatic geological events that have occurred during that time, and which events the clay barrier has survived intact, provide indisputable evidence for the effectiveness of the clay barrier. Finally, it must be remembered that the buffer material designated for use in the Canadian disposal facility will be superior to the Cigar Lake clay, and that the host rock in the disposal facility will be far less permeable than the sandstone of the Cigar Lake deposit. Additional thoughts on natural analogues can be found in Whitlock [2015].

9 Problems

Section 2

Q2.1 – Why is it necessary to regulate and control storage and disposal of nuclear waste?

Q2.2 – Why do regulatory bodies such as the IAEA classify nuclear wastes?

Q2.3 – Which Canadian agency is responsible for regulating the manner in which nuclear wastes are to be handled in Canada, and how many classes of nuclear waste are designated?

Section 3

Q3.1 – What are the two stages of nuclear fuel storage that are generally accepted and used in Canada?

Q3.2 – Why is nuclear fuel stored in water-cooled pools immediately after discharge from the reactor and for several years thereafter?

Q3.3 – After being stored in a water-cooled pool for several years, why is it acceptable and desirable to remove irradiated CANDU fuel bundles from the pool and store them in air-cooled storage cylinders?

Section 4

Q4.1 - Designers of storage facilities must be mindful of a number of design requirements that must be met to ensure the integrity and security of irradiated fuel while it is being stored. List them.

Section 5

Q5.1 – What are the two overriding requirements specified by the IAEA that must be met to ensure the integrity of spent fuel while it is being stored?

Q5.2 - Whether stored in water-cooled pools or air-cooled storage cylinders, irradiated fuel and its surroundings are potentially susceptible to a number of damage mechanisms and other challenges. List them.

Section 6

Q6.1 – What is the preferred orientation for CANDU fuel bundles in-reactor and in storage facilities?

Q6.2 – Why are irradiated CANDU fuel bundles required to reside temporarily in air as they pass from the fuelling machine to the irradiated fuel discharge room?

Q6.3 – How are the irradiated bundles, when residing in air, prevented from overheating?

Q6.4 – How much water is contained in a typical irradiated fuel storage pool?

Q6.5 – What can the operators of irradiated storage pools do to minimize oxidation of fuel Zircaloy components?

Q6.6 – How are the workers inside irradiated fuel storage facilities protected from radiation produced by irradiated bundles?

Q6.7 – What is the optimum stacking arrangement of irradiated CANDU bundles to prevent criticality in the irradiated fuel bay?

Section 7

Q7.1 – Describe the main features of a storage cylinder.

Q7.2 – Although the thermal power of the irradiated bundles decreases dramatically while the bundles are stored in water-cooled pools, the bundles' emission of ionizing radiation remains high (due to decay of long-lived isotopes and elements). How are people and the environment protected from radiation when bundles are stored in concrete casks?

Section 8

Q8.1 – What types of geological formations are thought to be suitable for final entombment of irradiated fuel (or fuel waste)?

Q8.2 – What is the proposed method in Canada for permanent disposal of high-level radioactive waste?

Q8.3 – What is "adaptive phased management" and how does it influence Canada's high-level waste disposal program?

Q8.4 – What are the two distinct phases in the "life" of a disposal facility?

Q8.5 – Describe the main components of a disposal facility.

Q8.6 – What are the two physical properties of bentonite clay that make it eminently suitable for sealing storage containers inside rock caverns?

Q8.7 – Once the irradiated bundles have been placed into containers and the containers sealed inside the vault, how many barriers are at work to prevent the radioactivity from affecting people and the environment? Name the barriers.

Q8.8 – What are the life-limiting factors for a storage container, and what is the container's expected lifetime?

Q8.9 – What is the principal characteristic of the Deep Geological Repository that provides shielding protection to people and the environment from the radiological effects of irradiated fuel?

Q8.10 – The initial three barriers to release of radiologically harmful effects of irradiated fuel to people and the environment are UO_2 pellets, Zircaloy sheaths, and steel/copper containers, which can delay the release of radioactivity for several million years and are assumed (conservatively) to do so for 10^5 years. If these three barriers were accidentally breached immediately after the fuel was entombed, how would the effects of radiation on people and the environment be affected?

Q8.11 – Empirical verification of the efficacy of the proposed disposed concept would require several hundred years, if not hundreds of thousands of years, which is not feasible. Therefore, verification to date has been based on short-term experiments, computer modelling, and natural analogues. Name and describe the natural analogues that have produced information that provides direct support (verification) of the design of the disposal facility proposed in Canada.

10 References

AECL, 2007. "ACR-1000 Technical Summary", Atomic Energy of Canada Limited. http://www.uea.ac.uk/~e680/energy/energy_links/nuclear/ACR1000-Tech-Summary.pdf

ANS, 2014. "Decay Heat Power in Light Water Reactors", American Nuclear Society, Publication ANSI/ANS-5.1-2014.

J. Boulton, 1978. "Management of Radioactive Wastes: The Canadian Disposal Program", Atomic Energy of Canada Limited, Report AECL-6314.

CANDU Energy, 2014. "MACSTOR: Modular Air-Cooled Storage", published by CANDU Energy, 1016/2014_05. http://www.candu.com/site/media/Parent/CANDU%20brochure-MACSTOR-0618B.pdf.

CNSC, 2006. "Assessing the Long-Term Safety of Radioactive Waste Management", Canadian Nuclear Safety Commission, Regulatory Guide G-320.

CNSC, 2015a. "Historic Nuclear Waste", Canadian Nuclear Safety Commission, Web site, http://nuclearsafety.gc.ca/eng/waste/historic-nuclear-waste/index.cfm.

CNSC, 2015b. "Radioactive Waste", Canadian Nuclear Safety Commission, http://nuclearsafety.gc.ca/eng/waste/index.cfm.

H. Feiveson, Z. Mian, M.V. Ramana, and F. von Hippel (editors), 2011. "Managing Spent Fuel from Nuclear Power Reactors Experience and Lessons from Around the World", International Panel on Fissile Materials, ISBN 978-0-9819275-9-6, http://fissilematerials.org/library/rr10.pdf.

M. Garamszeghy, 2014. "Nuclear Fuel Waste Projections in Canada – 2014 Update". Nuclear Waste Management Organization, Report NWMO TR-2014-16. http://www.nwmo.ca/uploads_managed/MediaFiles/2471_nwmo_tr-2014-16_nuclear_fuel_waste_projections_201.pdf.

W.J. Garland, 1999. "Decay Heat Estimates for the McMaster Nuclear Reactor", McMaster University Nuclear Reactor, Technical Report MNR-TR 1998-03, 11 pages.

S. Glasstone, A. Sesonske, 2014. "Nuclear Reactor Engineering: Reactor Design Basics / Reactor Systems Engineering", Springer, ISBN-13: 978-1-4615-7527-6 / 978146157276, ISBN: 0-442-02725-7, Fourth Edition.

C. Hatton, 2015. "Development of the Canadian Used Fuel Repository Engineered Barrier System", 35th Annual Conference of the Canadian Nuclear Society, St. John, NB, Canada.

IAEA, 1994. "Design of Spent Fuel Storage Facilities", International Atomic Energy Agency, IAEA Safety Series No. 116.

IAEA, 2002. "Long-Term Storage of Spent Nuclear Fuel: Survey and Recommendations", International Atomic Energy Agency, Report IAEA-TECDOC-1293.

IAEA, 2003. "Radioactive Waste Management Glossary", International Atomic Energy Commission, STI/PUB/1155 ISBN 92–0–105303–7.

IAEA, 2009. "Classification of Radioactive Waste", General Safety Guide GSG-1, International Atomic Energy Agency, Vienna.

IAEA, 2012. "Storage of Spent Nuclear Fuel", International Atomic Energy Agency, Specific Safety Guide, Number SSG-15.

J. Lian, 2010. "Integrity Assessment of CANDU Spent Fuel During Interim Dry Storage in MACSTOR", IAEA International Conference on Management of Spent Fuel from Power Reactors, Vienna, May 31–June 4, 2010.

J. McMurry, D.A. Dixon, J.D. Garroni, B.M. Ikeda, S. Stroes-Gascoyne, P. Baumgartner, T.W. Melnyk, 2003. "Evolution of a Canadian Deep Geological Repository: Base Scenario", Ontario Power Generation, Nuclear Waste Management Division, Report 06819-REP-01200-10092-R00.

NWMO, 2012a. "Used Fuel Repository Conceptual Design and Post-Closure Safety Assessment in Crystalline Rock", Nuclear Waste Management Organization, Toronto, Canada. Report NWMO TR-2012-16.

NWMO, 2012b. "Description of Canada's Repository for Used Nuclear Fuel and Centre of Expertise", Nuclear Waste Management Organization, Toronto, Canada. http://www.nwmo.ca/uploads_managed/MediaFiles/2011_projectdescriptionbrochure-english.pdf.

NWMO, 2015a. "Implementing Adaptive Phased Management, 2015 to 2019", Nuclear Waste Management Organization, Canada.

NWMO, 2015b. "Managing Canada's Used Nuclear Fuel", Nuclear Waste Management Organization, Toronto, Canada. http://www.nwmo.ca/aboriginalbrochure.

OECD/NEA, 2015. "Status Report on Spent Fuel Pools under Loss-of-Cooling and Loss-of-Coolant Accident Conditions", Nuclear Energy Agency, Report NEA/CSNI/R(2015)2.

OPG, 2009. "Darlington Environmental Assessment", Ontario Power Generation, Nuclear Waste Management, Technical Support Document, New Nuclear, Report NK054-REP-07730-00027 Rev 000.

http://www.ceaa.gc.ca/050/documents_staticpost/cearref_29525/0104/nwm.pdf.

OPG, 2015. "Pickering Waste Management Facility", Ontario Power Generation, Brochure. http://www.opg.com/generating-power/nuclear/nuclear-waste-management/Documents/PWMFbrochure.pdf.

A.J. Rothman, 1984. "Potential Corrosion and Degradation Mechanisms of Zircaloy Cladding on Spent Nuclear Fuel in a Tuff Repository", Lawrence Livermore National Laboratory, Report UCID-20172.

B. Seaborn (Chair), 1998. "Environmental Assessment Panel: Review of Nuclear Fuel Waste Management and Disposal Concept", Report to Canada's Ministers of Environment and of Natural Resources, published by Minister of Public Works and Government Services Canada. Catalogue No. EN-106-30/1-1998E, ISBN: 0-662-26470-3.

http://www.ceaa.gc.ca/default.asp?lang=En&n=0B83BD&printfullpage=true.

K. Tsang, 1996. "Storage of Natural Uranium Fuel Bundles in Light Water: Reactivity Estimates", Proceedings of the CNS Simulation Symposium, Montreal, Quebec.

J.E. Villagran, 2013 and 2014. "Long-Term Management of Canada's Used Nuclear Fuel", CANDU Fuel Technology Course, Canadian Nuclear Society.

J. Whitlock, 2015. "The Canadian Nuclear FAQ, Section E: Waste Management", http://www.nuclearfaq.ca/cnf_sectionE.htm#v2.

11 Further Reading Material

F.K. Hare (Chair), A.M. Akin, and J.M. Harrison, 1977. "The Management of Canada's Nuclear Wastes", Energy, Mines, and Resources Canada, Report EP77-6.

A. Porter (Chair), 1978. "A Race Against Time", Interim Report on Nuclear Power in Ontario (Ontario), Royal Commission on Electric Power Planning, Queen's Printer for Ontario.

A. Porter (Chair), 1980. "The Report of the [Ontario] Royal Commission on Electric Power Planning: Vol. 1, Concepts, Conclusions, and Recommendations", Queen's Printer for Ontario.

P.K. Kuroda, 1982. "The Origin of the Chemical Elements and the Oklo Phenomenon", Springer, ISBN 978-3-642-68667-2.

12 Relationships with Other Chapters

Chapter 8 provides an overview of fuel bundle configuration. Chapters 3 to 5 explain the neutron physics that generates heat in the fuel. Chapters 6 and 7 explain how that heat is removed from the fuel bundle and illustrate the internal temperature distribution within a fuel rod. Chapter 13 explains fuel performance during postulated accidents. Chapters 14 and 15 explain chemical and metallurgical aspects that relate to fuel sheath corrosion. Chapter 17 describes fuel design and performance, focussing on the current natural-uranium cycle (i.e., low burnup). Chapter 18 describes a few selected fuel cycles, summarizes key aspects of fuel manufacturing related primarily to the natural-uranium fuel cycle, and explains a few selected aspects of fuel performance that become relatively more important for advanced fuel cycles. Finally, the current chapter (#19) describes interim storage and disposal of irradiated fuel.

13 Acknowledgements

The following reviewers are gratefully acknowledged for their contributions, hard work, and excellent comments during the development of this chapter; their feedback has much improved it.

- Jim Lian
- Brian Ikeda
- Kwok Tsang
- Jennifer Noronha

Of course the responsibility for any errors or omissions lies entirely with the authors.

Thanks are also extended to J. Villagran for providing many figures; to Jeremy Whitlock for providing initial write-ups on natural analogues and breach of containment; to Simon Oakley and Media Production Services, McMaster University, for nicely drawing the figures; and to Diana Bouchard for expertly editing and assembling the final copy.

CHAPTER 20

Fuel Handling and Storage

prepared by

Diane Damario P. Eng,
Senior Engineer – Mechanical, Fuel Handling, Nuclear Power,
SNC-Lavalin Nuclear Inc., Candu Energy Inc.

Summary:

CANDU® reactors are fuelled on a somewhat continuous basis while on-power. This fuelling capability is mainly performed by two remotely operated fuelling machines. CANDU®[1] 6 fuelling machines are part of the fuel handling and storage system, which is divided into three main sub-systems. New fuel transfer and storage involves the receipt, handling and storage of palletized crates of unirradiated, or new, fuel, the inspection and handling of individual new fuel bundles and the transfer of this fuel into a fuelling machine via a new fuel port. Fuel changing involves a pair of fuelling machines transporting new fuel from a new fuel port to the reactor face, loading and unloading fuel from a reactor fuel channel and transporting discharged irradiated fuel from the reactor face to a spent fuel port. Spent fuel transfer and storage involves the discharge of irradiated fuel from a fuelling machine and the transfer and storage of this irradiated fuel in water-filled bays until the fuel is transferred to dry storage.

Table of Contents

1 CANDU® (CANada Deuterium Uranium) is a registered trademark of Atomic Energy of Canada Limited (AECL) used under exclusive licence by Candu Energy Inc.

List of Figures

1 Introduction

1.1 Overview

This chapter provides an overview of a typical CANDU 6 fuel handling and storage system handling natural uranium fuel. It does not address the potential use and handling of alternative fuels. Although the fuel handling and storage systems of different CANDU 6 stations are almost identical to each other, there are some differences resulting from evolution over time. As a result, some of the equipment described herein, may not be applicable to all CANDU 6 stations. Although this chapter does not address the fuel handling and storage system of CANDU stations other than CANDU 6, the equipment and processes described herein share many similarities with their equipment and processes.

This chapter explains how the fuel handling and storage system is divided into three main sub-systems: new fuel transfer and storage, fuel changing and spent fuel transfer and storage. It discusses the structures, equipment and purpose for each sub-system, and provides descriptions of major components and system processes.

Section 3 covers the new fuel transfer and storage system, Section 0 covers the fuel changing system and Section 5 covers the spent fuel transfer and storage system.

1.2 Learning Outcomes

The principal learning objectives of this chapter are to gain a general understanding of the following aspects of a typical CANDU 6 fuel handling and storage system:

- The purpose of this system and that of its three main sub-systems: new fuel transfer and storage, fuel changing and spent fuel transfer and storage;
- The main structures and equipment of these sub-systems;
- The operation of these sub-systems.

2 Fuel Handling and Storage System Overview

The purpose of the fuel handling and storage system, depicted in Figure 1, is to provide on-power fuelling capability at a rate sufficient to maintain continuous reactor operation at full power. While fulfilling its purpose, the fuel handling and storage system is also required to maintain all fuel sub-critical outside the reactor core and in conditions preventing fuel damage and contamination by foreign materials. Refer to Chapter 8 for information on the main components of a CANDU nuclear power plant and Chapter 9 for information on the operating concepts of a CANDU nuclear power plant.

The main equipment necessary to achieve on-power refuelling capability, together with associated services and controls, includes:

- New fuel transfer and storage;
- Fuel changing; and
- Spent fuel transfer and storage.

On-power refuelling, which involves replacing discrete amounts of fuel in the core as required while the reactor is operating, is a major contributor to the high capacity factor of existing CANDU reactors. Other advantages of on-power refuelling include the following:

- Optimized burnup of natural uranium fuel and, therefore, lower fuelling costs.
- Low excess reactivity available, which reduces the requirement for reactivity control during operation.
- Flexibility to plan scheduled shutdown activities that do not have to include fuelling operations.
- Low levels of fission products in the heat transport system, by early detection and removal of failed fuel bundles.

The sequence of movements for typical fuel handling and storage operations is illustrated in Figure 2. The average equilibrium fuelling rate in the CANDU 6 reactor at full power is approximately 112 fuel bundles per week.

New fuel transfer and storage, described in Section 3, involves new, or unirradiated, fuel being received and stored in the new fuel storage room in the service building. New fuel is transferred to the new fuel loading room in the reactor building as required. There, fuel is loaded into one of two new fuel transfer mechanisms for transfer into one of the fuelling machines via the new fuel ports.

Fuel changing, described in Section 0, involves new fuel being received by a fuelling machine via one of the new fuel ports, fuelling machines travelling to the reactor face, new fuel being inserted into and irradiated fuel being removed from one of the 380 fuel channels by the fuelling machines, fuelling machines travelling from the reactor face, and irradiated fuel being discharged via one of the spent fuel ports.

Spent fuel transfer and storage, described in Section 5, involves irradiated fuel being received from fuelling machines via spent fuel ports and placed in water-filled fuel storage bays.

The fuelling machines, the new fuel transfer equipment and the spent fuel discharge equipment are normally operated remotely and automatically from the fuel handling control console in the control room. The automatic control system for the fuel handling and storage system uses one of the station computer-controllers and includes the fuel handling control console in the Main Control Room and local control panels specific to the fuel handling system.

Personnel are normally only required to enter the reactor building to load new fuel and to maintain the fuel handling system components. . Regular and frequent maintenance of fuel handling equipment, particularly the fuelling machines, is required to prevent or minimize unexpected breakdown of fuel handling equipment and to maintain or achieve station target capacity factors. Breakdown of fuel handling equipment at the reactor face and/or while manipulating irradiated fuel is particularly undesirable and problematic due to very high radiation fields.

The term ‘irradiated fuel’, which is common in the industry and is more precise, is used when referring to the fuel itself; however, the term 'spent fuel' is used when referring to applicable fuel handling subsystems and components per traditional fuel handling naming conventions for these subsystems. Refer to Chapter 17, for information about the fuel.

Note that the figures provided are for illustrative purposes only. Actual fuel handling and

storage equipment may vary in appearance.

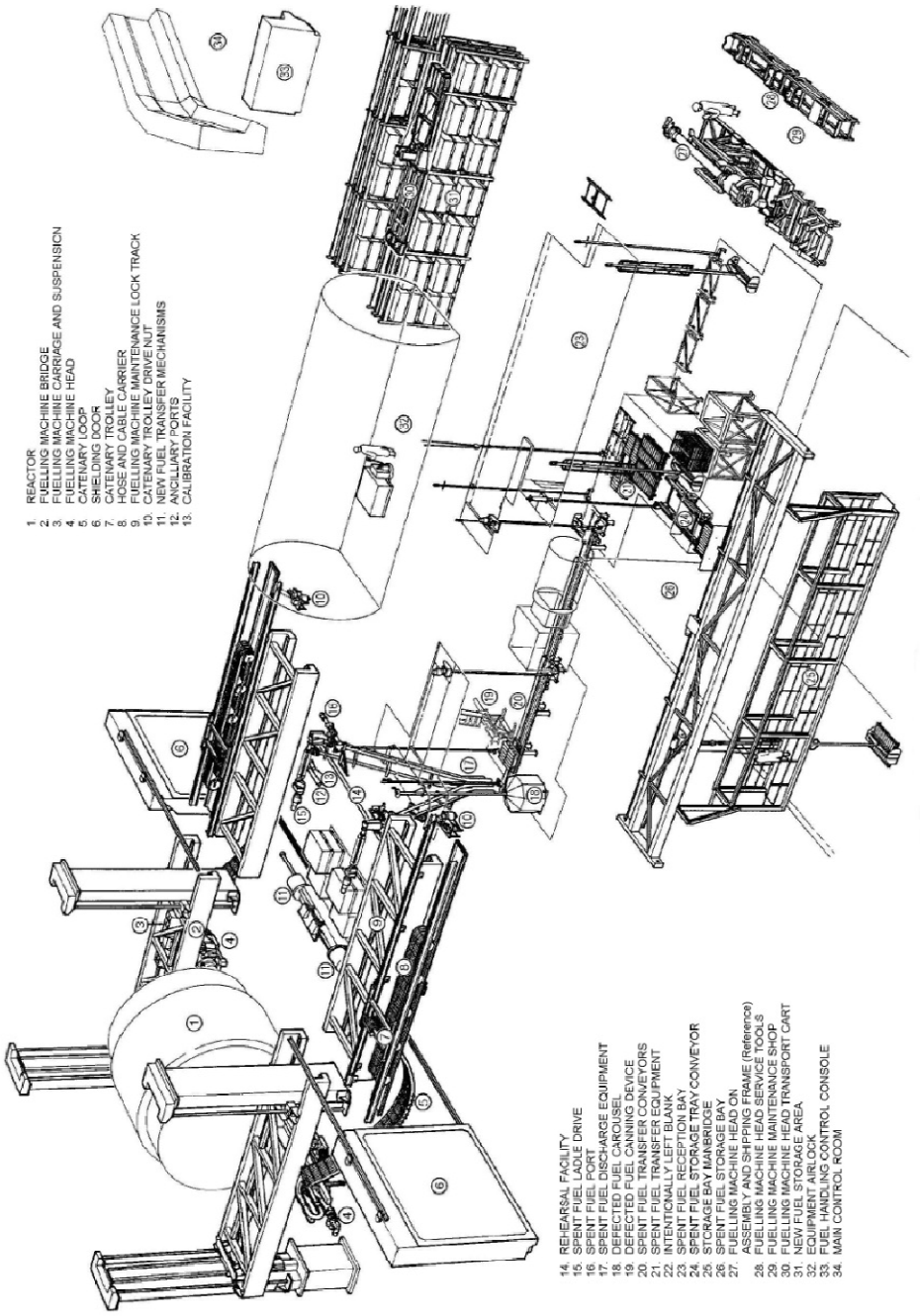

Figure 1 Fuel handling and storage system

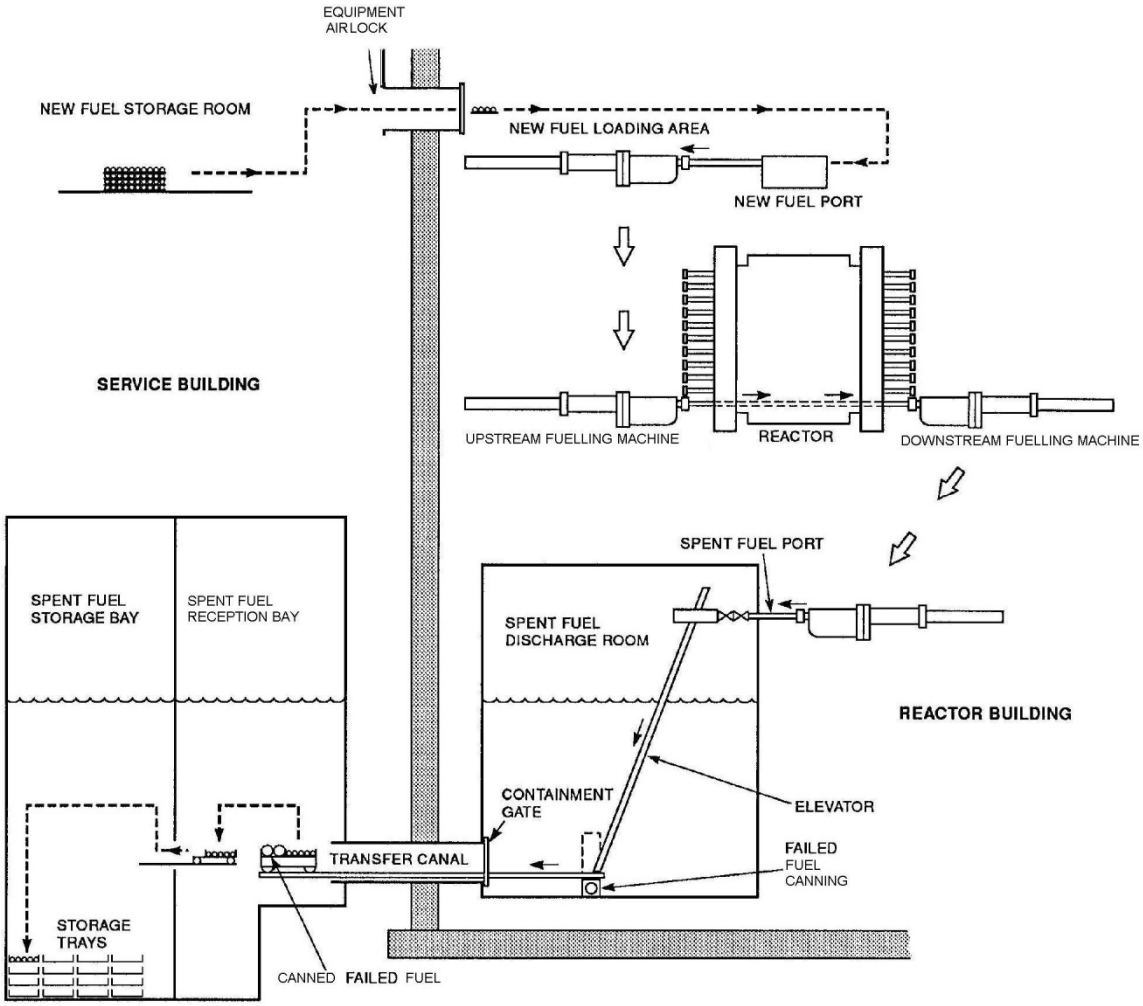

Figure 2 Fuel handling and storage sequence

3 New Fuel Transfer and Storage

3.1 System Description

The new fuel transfer and storage system covers the structures and equipment involved in receiving, handling and storing palletized crates of new fuel, inspecting and handling individual new fuel bundles and transferring these new fuel bundles into the fuelling machine.

New fuel transfer and storage equipment, shown on Figure 1, includes racks in the new fuel storage room, a fork lift truck, crane lifting attachments, a pallet cart and new fuel transfer equipment located in the new fuel loading room in the reactor building, just adjacent to the reactor vault and in between the two fuelling machine maintenance locks. The new fuel transfer equipment, shown on Figure 3, and located in the new fuel loading room, includes an air balance hoist, jib crane, fuel bundle lifting tool and fuel spacer interlocking gauge for handling and inspecting fuel bundles, and two new fuel transfer mechanisms for transferring fuel bundles into a fuelling machine magazine. Each new fuel transfer mechanism, shown on Figure 4, includes a new fuel port, a loading trough and loading ram, an air lock valve, a magazine, a shield plug, a transfer ram and drive and a magazine/port adapter. New fuel transfer auxiliaries use instrument air to power the new fuel transfer equipment. They also connect the new fuel transfer mechanism to the vapour recovery system and provide drainage for it. A local control panel located on each new fuel transfer mechanism allows semi-automatic control of the process for loading new fuel into the new fuel transfer mechanism magazine.

Up to 144 pallets each containing 36 fuel bundles can be stored on racks in the new fuel storage room as part of the normal storage capacity, which accommodates more than eight months of operation at equilibrium. Additional pallets of fuel can also be stored on the floor as part of the abnormal storage capacity.

3.2 Component Description

Major new fuel transfer and storage components are as follows.

New Fuel Storage Room Racks

Racks are available in the new fuel storage room in the service building for storing palletized crates of new fuel. Some of the racks are fixed while some of them are movable.

New Fuel Storage Room Lift Truck

A fork lift truck is available in the new fuel storage room to move the pallets of new fuel. It is an electrically operated, stand-up rider type, and has a capacity of one fuel pallet. This fork lift truck is also used to transport the pallets to the pick-up point for the service building crane during transfer to the new fuel loading room in the reactor building.

Crane Lifting Attachment

Two fork lifting crane attachments are available; one located in the service building for use with the service building crane, and one in the reactor building for use with the reactor building crane. Two pallets can be lifted at one time with these attachments.

Cart

A powered, pallet cart is available at the equipment airlock level to transfer up to two pallets at a time between the service building and the reactor building through the equipment airlock.

Air Balance Hoist and Jib Crane

The air balance hoist is mounted on a jib crane. This crane is pivoted from the building wall above the two new fuel transfer mechanisms and covers the area of the new fuel loading room through which new fuel bundles have to be moved. The air balancing hoist is free to travel along the length of the jib. It is air-powered and can be adjusted to balance the load from a control on the operator's handgrip.

Fuel Bundle Lifting Tool

The fuel bundle lifting tool is used with the air balance hoist to manually load fuel bundles into the new fuel transfer mechanism loading trough. The bundle lifting tool is a manually operated device which clamps around the end plates of the fuel bundles, through lifting adaptors. When the bundle is suspended, it is clamped securely by the toggle action of the tool linkage. The lifting adaptors are mounted on spherical bearings which allow the adaptors to align with the bundle end plates and permit the bundle to be rotated for inspection. The air balancing hoist used with the bundle lifting tool allows the operator to transfer the fuel bundles without damage and with a minimum of effort.

Fuel Spacer Interlocking Gauge

The fuel spacer interlocking gauge is used for checking the diameter of each fuel bundle over the central spacers before the bundles are loaded into the new fuel transfer mechanism magazine. This gauge is used while the fuel bundle is supported on the fuel bundle lifting tool. This gauge consists of two pivoted segments and a dial gauge having a shaded area which indicates the go/no-go range. The dial gauge is used to verify that the bundle has not changed shape during transit and that the pencil spacers have not interlocked. This is to verify that the bundle diameter has not expanded and that it will pass through the fuel handling tubes and the reactor channel without interference.

Loading Trough and Loading Ram

The loading trough and loading ram are provided for moving the new fuel into the magazine of the new fuel transfer mechanism. Two fuel bundles are normally loaded into the trough, and after the bundles are loaded, the lid is closed and the bundles pushed into the magazine by the loading ram. The trough is provided with a hinged lid which is interlocked to prevent operation of the ram unless the lid is closed. Limit switches are mounted in the trough and provide an indication to the control system when a fuel bundle is placed in the trough. The loading ram is in line with the top magazine station of the new fuel transfer mechanism. The ram is an oil/air operated, double acting cylinder, supplied from the new fuel transfer auxiliaries. Oil pressure is used to extend the ram to provide smooth ram operation and adequate lubrication.

Air Lock Valve

The air lock valve is pneumatically operated and is installed between the loading trough and the new fuel transfer mechanism magazine, to seal off the magazine whenever fuel is not being loaded into the magazine. This valve prevents the spread of contamination from the fuelling

machine head, the maintenance lock or the fuelling machine vault, into the new fuel loading room. Limit switches indicate when the valve is in the open and closed positions.

New Fuel Transfer Mechanism Magazine

The new fuel transfer mechanism magazine assembly consists of a leak-tight housing, a rotor, and a drive unit. The magazine housing is a drum-like enclosure with a normally closed drain connection to the active drainage system and a vent to the reactor building vapour recovery system to remove any contamination through purging. The magazine rotor contains seven tubular channels, six for accommodating the fuel bundle pairs and one for the new fuel transfer mechanism shield plug.

New Fuel Transfer Mechanism Shield Plug

The shield plug, which is normally installed in the new fuel port except when new fuel is being transferred to the fuelling machine, reduces radiation streaming into the new fuel loading room when a fuelling machine containing irradiated fuel passes the end of the new fuel port in the fuelling machine maintenance lock.

Transfer Ram and Drive

The function of the transfer ram is to remove and install the shield plug between the new fuel port and the transfer mechanism magazine and to push the new fuel bundles from the new fuel transfer mechanism magazine into the fuelling machine. The openings for the transfer ram on the magazine front and rear covers are located at a bottom position, in line with the respective magazine station. The ram head incorporates a latch assembly for engagement with the shield plug. Ram position, for control of ram stopping and speed changing operation, is detected by a shaft encoder mechanically connected to the chain drive sprocket shaft.

Magazine/Port Adapter

An adapter assembly is bolted to the new fuel transfer mechanism front cover, at a bottom position in line with the respective magazine station and the fuel transfer ram. The adapter connects the magazine to the new fuel port and consists of a spool piece with two double-acting pneumatic cylinders. Its function is to hold the shield plug in position in the new fuel port.

New Fuel Ports

The new fuel ports are mounted in embedments in the walls between the new fuel loading room and the fuelling machine maintenance locks. Each port is a tubular connection with an end fitting at one end extending into the fuelling machine maintenance lock and the other end engaging with the fuel transfer mechanism port adaptor. When loading fuel into a fuelling machine, the new fuel port becomes the passageway for bundle movement from the fuel transfer mechanism to the fuelling machine.

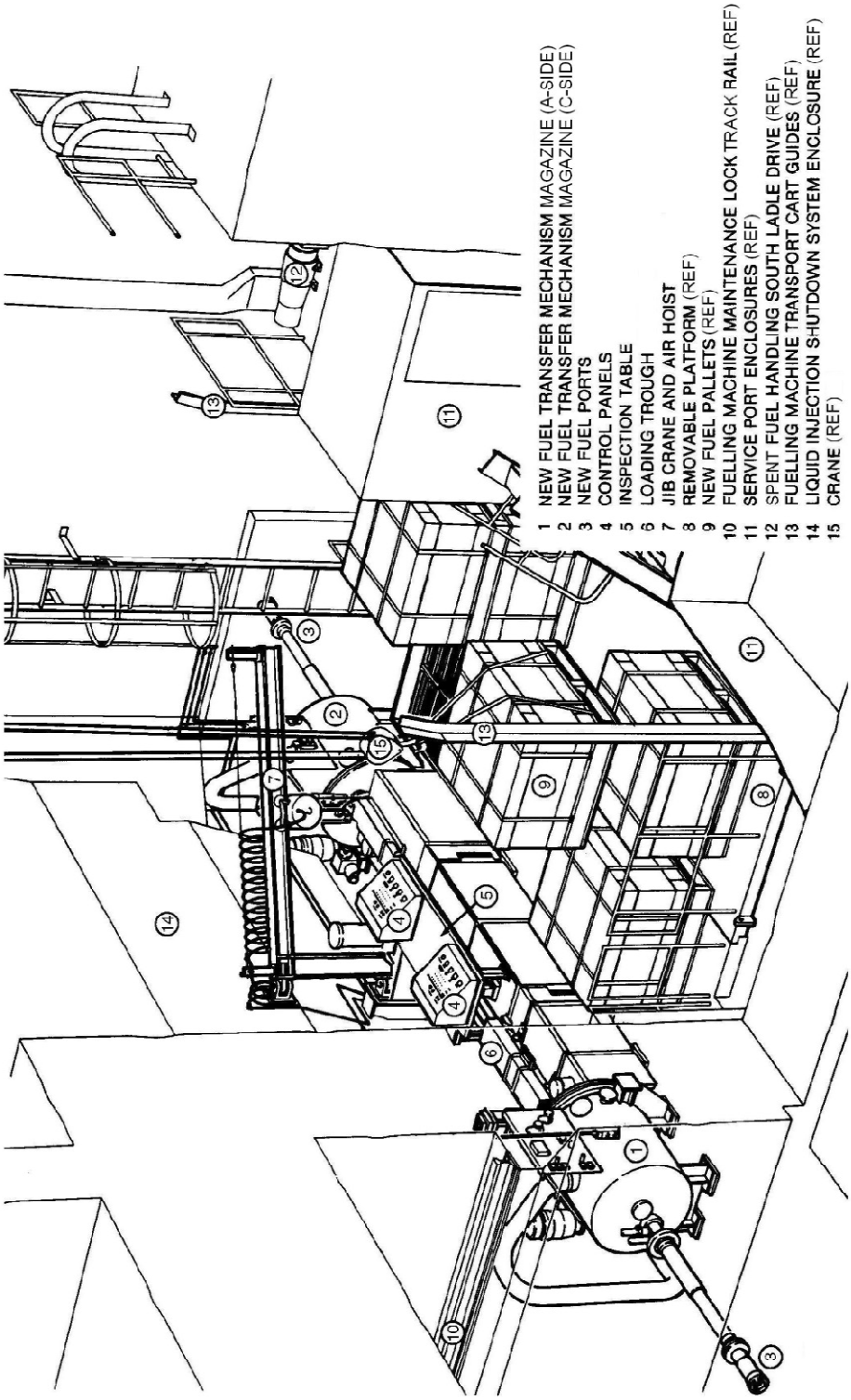

Figure 3 New fuel transfer equipment

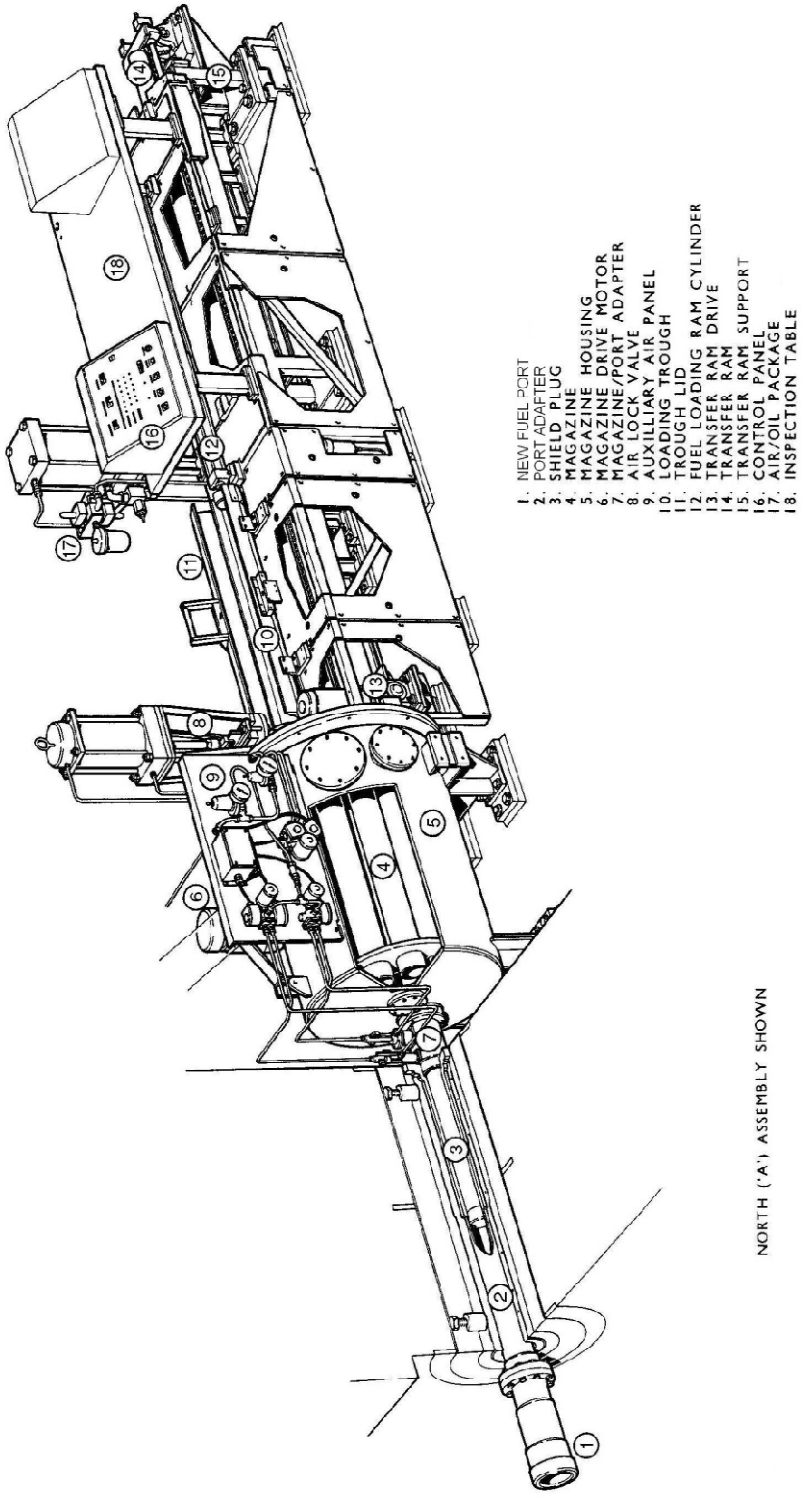

Figure 4 New fuel transfer mechanism

3.3 System Operation

New fuel is received on pallets and stored on racks in the new fuel storage room in the service building. When required, one or two pallets of new fuel are transferred to the new fuel loading room in the reactor building.

1) One new fuel pallet is removed from the new fuel storage room and transferred to the service building crane using the new fuel storage room lift truck. This is repeated for the second pallet.
2) Then the two new fuel pallets are lifted from the crane hall floor elevation and set on the floor of the equipment airlock using the main service building crane.
3) The two new fuel pallets are transported through the equipment airlock into the reactor building with the new fuel pallet cart.
4) From the air lock floor elevation, the two pallets are then lifted using the reactor building crane and set in the new fuel loading room.

Keeping the new fuel bundles on the new fuel pallet protects the new fuel from damage and contamination during transportation from the fuel supplier, during storage at the station and during transfer from storage to the new fuel loading room. The new fuel pallet has slots the fork lift has to engage into prior to lifting and thereby eliminates the chance of dropping the entire pallet.

The new fuel storage room is kept locked and access to fuel is restricted to people who have a valid reason to access or handle fuel. Security procedures are to be followed and the key to the new fuel storage room is controlled by the shift supervisor who authorizes all access to it. The serial number of each fuel bundle is recorded prior to loading into the new fuel transfer mechanism.

In the new fuel loading room, the new fuel pallet is opened and individual fuel bundles are manually unwrapped. One fuel bundle at a time is then picked up and moved onto the inspection table via the bundle lifting tool which clamps around the end plates of the bundle and which is attached to the air-balance hoist. The bundle size (the bundle diameter over the centre bearing pads) is carefully inspected with the fuel spacer interlocking gauge to ensure that it will pass smoothly through the fuel handling system. Each fuel bundle is checked to be free of abnormalities, damage or foreign matter prior to loading into one of the two new fuel transfer mechanisms. Experience from operating CANDU plants indicates that very few new fuel bundles have been rejected because of damage.

The new fuel loading room is heavily shielded and the spread of contamination, from the fuelling machine and the fuelling machine maintenance locks into the new fuel loading room, is prevented by the air lock valve, the shield plug, by maintaining a negative pressure at all times in the magazine of the new fuel transfer mechanism through a duct connected to the vapour recovery system, and by draining into the active drainage system any liquid which may accumulate in the magazine. The shield plug is not removed from the new fuel port unless the air lock valve is closed, and the air lock valve is not opened unless the shield plug is installed in the new fuel port.

New unirradiated fuel bundles, which are made up of natural uranium, have a very low level radioactivity, and can be handled safely by personnel without protective clothing (Note: gloves are normally worn).

Once the operator has manually placed two fuel bundles in the loading trough and closed the trough lid, the fuel bundles are pushed into the new fuel transfer mechanism magazine by the loading ram. The magazine is indexed, using the local control panel mounted on the new fuel transfer mechanism. This process is repeated until the magazine contains the required number of fuel bundles.

The transfer of fuel bundles from the new fuel transfer magazine to the fuelling machine magazine is normally performed under complete computer control, using a series of steps. Confirmation of the successful completion of each step, which is indicated by either a limit switch or a shaft encoder, is required prior to starting the following step. Prior to beginning the transfer sequence, the fuelling machine is clamped onto the new fuel port and its heavy water[2] level is lowered to just below the snout.

To ensure that the system is ready to begin the sequence, the computer memory is checked to confirm that the fuelling machine snout plug is stored in its magazine station and that the guide sleeve has been installed in the snout. Feedback must indicate that all rams are retracted to their home positions, that the air lock valve is closed, that there is new fuel in the new fuel transfer mechanism magazine, and that the new fuel transfer mechanism magazine is not in use. All conditions being satisfactory, the new fuel magazine is rotated to the shield plug station, the ram is advanced to remove the shield plug from the port, and then retracted to deposit the shield plug in the magazine for storage. The commands are then given to rotate the fuelling machine magazine to an empty station and the new fuel magazine to a full station. The new fuel transfer ram is then fully advanced to push two new bundles into the fuelling machine magazine station. The rams are retracted to their respective home positions, the fuelling machine and new fuel magazines are rotated to the next stations, and two more fuel bundles are transferred. This process is repeated until the fuelling machine magazine contains the required number of bundles. After completion of the fuel bundle transfer, the shield plug is re-installed into the new fuel port and locked in place. The fuelling machine then removes the guide sleeve from the new fuel port, installs its snout plug, raises its heavy water level and is unclamped from the new fuel port in order to traverse to the reactor face.

Normal handling of new fuel in air or light water does not pose criticality problems for natural uranium.

Note: New fuel bundles for the initial core are manually loaded into the fuel channels. Visual inspections of these new fuel bundles are performed on a loading platform at the reactor face.

2 Heavy water (D_2O) has deuterium atoms instead of hydrogen atoms and is approximately 10% heavier than light or regular water.

4 Fuel Changing

4.1 System Description

Fuel changing, depicted in Figure 5, involves the structures, equipment and activities required to transport new fuel from the new fuel port to the reactor, to load and unload fuel from the fuel channel, and to transport the discharged fuel from the reactor to the spent fuel port. This is mainly performed by two fuelling machine heads remotely operated from the Main Control Room.

Each fuelling machine head is suspended on a carriage, which moves horizontally along bridge rails in its respective fuelling machine vault and on tracks in its respective fuelling machine maintenance lock. A bridge assembly, adjacent and parallel to each reactor face, provides for vertical movement of the fuelling machine head and its carriage. Each bridge and carriage assembly allows a fuelling machine to access all 380 reactor fuel channels at the respective reactor face. The maintenance lock tracks align with the lowest bridge position to allow transfer of the fuelling machine and carriage between the fuelling machine vault and the maintenance lock.

The fuelling machine D_2O system supplies the fuelling machines with heavy water to cool irradiated fuel temporarily stored in the fuelling machines, operate associated fuelling machine mechanisms and generate injection flow. The oil hydraulic system supplies the fuelling machines and carriages with oil to operate and lubricate associated mechanisms. The catenary system conveys heavy water, hydraulic oil and electrical power and control signals to and from the mobile fuelling machine heads and carriages.

The fuelling machine heads are normally stored in two maintenance locks, where they can lock onto the new fuel ports to accept new fuel, onto the service ports for maintenance and rehearsal, or onto the spent fuel ports to discharge irradiated fuel.

Powered shielding doors separate the fuelling machine vault and the reactor from the maintenance locks and, when closed, provide shielding that allows personnel access to the fuelling machines in the maintenance locks while the reactor is operating.

The on-channel fuel changing operations are performed in the direction of coolant flow in the channel. Each fuel channel contains 12 fuel bundles. Typically, eight new fuel bundles are inserted at the upstream end of a fuel channel, and eight irradiated fuel bundles are removed at the downstream end. Since the coolant in adjacent fuel channels flows in opposite directions, for reasons of reactor symmetry, each fuelling machine is an upstream machine (carrying new fuel) and a downstream machine (carrying irradiated fuel) at different times.

4.2 Component Description

4.2.1 Fuelling Machine Head

The fuelling machine is a pressure vessel that comprises five major sub-assemblies, the snout, the magazine, two separators and the ram, which are necessary for it to perform its required functions. The fuelling machine head, shown on Figure 6, includes the fuelling machine mounted and supported in a cradle assembly as well as the guide sleeve and tool, and the ram adapter. The fuelling machine heads engage the end fittings at opposite ends of the same

channel assembly for the purpose of fuel changing. The fuelling machine head contains heavy water and is designed to form an extension of the heat transport system pressure boundary to enable refuelling operations to be carried out with the reactor at full power.

Snout Assembly

The snout assembly, located at the front of the fuelling machine and shown in Figure 7, enables the fuelling machine head to clamp onto any reactor fuel channel and to seal the connection at high pressure and temperature. To achieve loading of new fuel bundles and the discharging of irradiated fuel bundles from the fuelling machine, the snout assembly is capable of locking onto the new fuel port and the spent fuel port. It is also capable of connecting to the service ports as required.

The snout assembly includes the centre support, the clamping mechanism, the snout emergency lock assembly, the head antenna and the snout probes. The clamping mechanism is engaged by oil hydraulic pressure. The snout emergency lock, a passive safety lock, prevents inadvertent removal of the snout assembly from an end fitting when the channel closure is not installed. When the fuelling machine is not attached to a fuel channel or port, the snout is sealed with a snout plug.

Magazine Assembly

The magazine assembly, as shown on Figure 7, includes a twelve-chamber rotor inside a pressure-retaining housing assembly for storing fuel bundles, channel closures, shield plugs, a snout plug, a ram adapter, a guide sleeve and tool, and a flow assist ram extension (FARE) tool.

It also includes a drive system, comprising an indexing mechanism driven by an oil-hydraulic motor for turning the magazine rotor, and the magazine emergency drive, a manual drive facility to rotate the magazine rotor if the oil hydraulic motor becomes disabled.

Ram Assembly

The ram assembly, shown in Figure 8, provides the necessary axial movements and forces required for the transfer and discharge of the fuel bundles, or the installation and withdrawal of various tools and plugs such as the guide sleeve, the channel closure plug, the shield plug, and the snout plug. The ram assembly consists of a B ram, a latch ram and a C ram. These rams are essentially concentric tube assemblies supported within a pressure-retaining ram housing. Each ram has a different head assembly to perform the necessary plug or fuel changing operation. Both the B ram and the latch ram are driven by oil hydraulic motors through a gear system and ball screws. The C ram acts as a multi-stage hydraulic cylinder and is powered by the fuelling machine D_2O system.

Separators

For each fuelling machine head there are two separator assemblies which perform identical functions and operate in synchrony. They are mounted in penetrations through the magazine front cover at points just forward of the magazine tubes and each assembly is oriented at 67.5° from the vertical. The separators sense the gaps between two fuel bundles or between a fuel bundle and ram adapter or FARE tool, provide a signal to the computer to stop the fuelling machine ram at the correct position, restrain the axial motion of the fuel column due to hydraulic forces from the fuel channel flow, push the bundles that have been separated from the fuel column into the magazine to allow clearance for magazine rotation, and verify the presence of

the shield plug and the FARE tool during the refuelling operations. High pressure heavy water from the fuelling machine D_2O system is used to operate the separators.

Ram Adapter

The ram adapter, shown in Figure 9, attaches to the C ram head to provide a flat face for contacting the end plate of a fuel bundle and to centralize and support the C ram, which minimizes sagging of the ram. The ram adapter consists of five parts: the body, the sleeve, the stem, the inner spring and the outer spring. The ram adapter body provides the contact face with the fuel. The face is machined to simulate the end face of a fuel bundle, so that the gap between the ram adapter and the fuel is identical to the gap between two fuel bundles. The body is also machined to allow adequate cooling flow. The stem is screwed into the bore of the body and is contoured to connect with the C ram. The sleeve is spring-loaded by the concentric inner and outer springs and locks the C ram to the stem.

Guide Sleeve and Tool

The channel closure seal face in each fuel channel end fitting forms a step in the fuel channel, the bore of the channel being smaller than the bore of the end fitting. This discontinuity forms an obstruction to the smooth passage of fuel bundles and shield plugs. The guide sleeve provides a smooth bore for the passage of fuel bundles and shield plugs between the fuel channel and the fuelling machine.

The guide sleeve is moved between the fuelling machine magazine and the fuelling machine snout by the fuelling machine ram using a guide sleeve insertion tool. The guide sleeve and the insertion tool are locked together except when the guide sleeve is in position in the snout and end fitting. When not in use, they are stored together in the fuelling machine magazine and are held in the magazine tube by a locating tube and spacer.

Snout Plug

The snout plug, shown in Figure 10, is used to seal the fuelling machine snout when the fuelling machine is not attached to a fuel channel or port. It allows the interior of the fuelling machine to be maintained full of water at a controlled temperature and pressure, to maintain cooling of the irradiated fuel while in transit from the reactor fuel channel to the spent fuel port. The fuelling machine snout plug is composed basically of two parts, the latching mechanism and the seal assembly. The latching mechanism which makes up the rear half of the plug has four jaws which are extended by a spider mechanism. These four jaws locate the plug in a groove in the fuelling machine snout centre support. The front end of the snout plug is comprised of the seal assembly, which is screwed onto the latch assembly. The seal assembly contains a large elastomer O-ring seal and the associated mechanism required to expand and retract it.

4.2.2 Fuelling Machine Bridge and Carriage

Two fuelling machine bridge and carriage assemblies are provided, one at each reactor face. As shown in Figure 5, each bridge spans the face of the reactor and supports a carriage assembly, when the carriage is in the fuelling machine vault. The carriage assembly supports a fuelling machine head. Each bridge moves vertically on two guide columns, to provide vertical motion (y-motion) of the fuelling machine head. Carriage wheels ride on rails mounted on the bridge (when in the fuelling machine vault) and on the maintenance lock tracks (when in the maintenance lock) to provide horizontal motion (x-motion) of the fuelling machine. With the bridge in

its lowest position, the rails on the bridge are aligned with matching rails on the maintenance lock tracks, enabling the carriage, with the fuelling machine head, to transfer between the fuelling machine vault and the maintenance lock.

Each carriage assembly consists of a drive unit assembly, and upper and lower gimbal assemblies, as shown in Figure 11. In addition to horizontal motion along the bridge and maintenance lock rails, the carriage assembly also provides fine vertical motion and motion toward and away from the reactor (z-motion) and allows a controlled amount of rotation of the head. It also provides a termination point for the catenary system.

The carriage also includes clamping mechanisms, which securely anchor the carriage to the bridge rails when the fuelling machine head is clamped to a reactor end fitting, to prevent excessive loads from being applied to the end fitting by the fuelling machine head during a seismic event.

4.2.3 Fuelling Machine D_2O System

The D_2O system supplies the fuelling machine with heavy water compatible with the heat transport system, and regulates the pressure and flow of heavy water to and from the various parts of the fuelling machine. Heavy water is used in the fuelling machine for the following functions:

- Cooling irradiated fuel stored in the fuelling machine magazine.
- Operating the C ram.
- Operating the separators.
- Preventing high temperature heat transport system water from entering the fuelling machine when the fuelling machine is coupled to a fuel channel.

The fuelling machine D_2O system is divided into the following major parts:

- Two valve stations that contain most of the control components of the stationary portion of the system.
- The mobile portion of the system located on each fuelling machine head.
- Catenary hoses that connect the stationary portion of the system with the mobile portion located on the fuelling machine head.

4.2.4 Fuelling Machine D_2O Supply System

The fuelling machine D_2O supply system can be divided into three subsystems:

1. The supply subsystem, which supplies pressure regulated, filtered heavy water, drawn from the primary heat transport system storage tank and/or the D_2O return subsystem, to the two D_2O system valve stations.
2. The D_2O return subsystem, which accepts the D_2O discharge from the fuelling machine head via the D_2O System, and cools and purifies it before returning it to the supply subsystem.
3. The D_2O leakage collection system, which collects the D_2O from all drain, leak and vent points in the system into two tanks.

4.2.5 Oil Hydraulic System

Each of the two fuelling machines is operated by an individual oil hydraulic system. The oil hydraulic system provides a continuous oil supply, at controlled conditions of flow, pressure and temperature, to the mobile fuelling machine head and carriage, via a catenary system. This oil supply is used to operate associated actuators on the fuelling machine head and carriage.

4.2.6 Fuelling Machine Head Accessories

Fuelling machine head accessories include the FARE tool, the pressure tube seal and latch assembly and the fuel grapple system.

FARE Tool

The FARE tool provides a restrictive element in low flow fuel channels, which develops the necessary coolant flow drag force to overcome the frictional resistance of the fuel bundles in the channel, in order to push the fuel column downstream when the fuelling machine ram cannot provide this force without entering the core. The FARE tool has an overall length of two fuel bundles and is handled like a pair of fuel bundles. For simplicity, it can be considered as a piston in a cylinder with a large amount of leakage.

The FARE tool is carried in the fuelling machine magazine and is pushed into the fuel channel in the same manner as the fuel bundles after the last new fuel bundle is inserted in the fuel channel.

After the irradiated fuel bundles are discharged from the fuel channel and the fuel string is returned to its normal in-core position, the C ram attaches to the FARE tool for its removal and return to the fuelling machine magazine.

Pressure Tube Seal and Latch Assembly

The pressure tube seal and latch assembly can be inserted into a fuel channel by the fuelling machine so that it stops the channel flow, thus enabling ice-plugs to be formed in the channel feeders by means of a freezing operation. This channel flow blockage is sometimes required to allow inspection of the channel or other possible fuel handling recovery scenarios. It is only used during reactor shut downs at low pressures. The pressure tube seal and latch assembly consists of a seal assembly with a mechanism for radially expanding an O-ring to seal the bore of the pressure tube and a latch assembly which is similar to a fuel channel shield plug.

Fuel Grapple System

The fuel grapple system enables the fuel channel to be defuelled from one end using a single fuelling machine when the other fuelling machine is disabled or when a channel is to be defuelled. It includes a fuel grapple assembly, for latching onto a fuel bundle; grapple extensions, which attach to the grapple assembly or other extensions for grappling fuel bundles beyond the reach of the fuelling machine rams; a ram grapple adaptor, which allows the fuelling machine to operate latches on the extensions; and a grapple reset tool for releasing irradiated fuel bundles from the fuel grapple.

4.3 System Operation

To begin the fully automated fuel changing process, one of the two fuelling machines clamps onto the new fuel port, its water level is lowered to just below the fuelling machine snout, its

snout plug is removed, the guide sleeve is installed and the fuelling machine typically accepts eight new fuel bundles from the new fuel port. The guide sleeve is removed, the snout plug re-installed and the water level is raised. Fuel bundles are received and stored in pairs.

With the shielding doors open, both fuelling machines travel along the maintenance lock tracks onto the fuelling machine bridges at each face of the reactor. The bridges are then raised and the fuelling machines positioned on the bridge so that the fuelling machines are located at opposite ends of the selected fuel channel. The fuelling machine with the new fuel is at the upstream end while the other fuelling machine, which contains no fuel, is at the downstream end of the same fuel channel.

Each fuelling machine then moves forward to home and lock onto the fuel channel end fitting to form a secure and pressure-tight joint with the channel. Figure 12 depicts a typical eight-bundle refuelling sequence.

The fuelling machines remove their snout plugs followed by the fuel channel closures. At this point, the fuelling machines become part of the heat transport system pressure boundary. The fuelling machine at the upstream end of the fuel channel removes the shield plug and typically inserts eight new fuel bundles, two at a time, into the channel. The downstream fuelling machine removes the shield plug and typically receives eight irradiated fuel bundles, two at a time, into its magazine. The remaining twelve-bundle fuel string is then moved back to the correct in-reactor position and the shield plugs and channel closures are re-installed in the fuel channel. The fuelling machines re-install the snout plugs in their snouts, the channel closures are checked for leaks and the fuelling machines are then retracted from the end fitting.

The fuelling machine containing irradiated fuel returns to the maintenance lock and discharges the irradiated fuel through the spent fuel port.

An eight-bundle refuelling sequence, from the time that one fuelling machine clamps onto the new fuel port to accept new fuel to the time that the other fuelling machine unclamps from the spent fuel port after discharging irradiated fuel, as described above, typically takes approximately two hours. This includes approximately 30 minutes at the new fuel port, a little over 50 minutes at the reactor face and approximately 35 minutes at the spent fuel port.

Other fuelling schemes are also possible. For example, an alternate scheme is available for the first refuelling visit to a fuel channel; it involves the fuelling machine at the upstream end of a fuel channel inserting eight new fuel bundles as usual, and the fuelling machine at the downstream end of this fuel channel receiving ten irradiated fuel bundles and returning the first bundle pair removed to the fuel channel. Although refuelling fewer than eight bundles at a time is favourable with respect to improving fuel economy; it increases wear and tear on fuel handling equipment, particularly on the fuelling machines. A fuelling machine can accommodate up to eight fuel bundles when carrying a FARE tool, up to ten fuel bundles without a FARE tool, and up to twelve fuel bundles when the reactor is shut down. Refuelling uneven numbers of fuel bundles is expected to be limited to abnormal situations.

Bundle movement is controlled by the downstream fuelling machine, assisted by the coolant flow inside the channel which moves the string of fuel bundles due to hydraulic drag.

The channel flow, however, varies depending on location. In the outer zone fuel channels where the flow is lower, a FARE tool is used to provide sufficient hydraulic drag force to move the fuel string under the reduced channel flow condition. The FARE tool is loaded at the end of

the fuel string after new fuel bundles have been inserted by the upstream fuelling machine. The FARE tool is removed after the required number of irradiated fuel bundles is received by the downstream machine and the fuel bundle string is moved back to its correct in-reactor position. The FARE tool is used rather than the upstream machine ram so that the latter does not enter the core to become activated and contribute to the dose rate to maintenance personnel working on the machine. The FARE tool (which also becomes activated when it passes into the core) is discharged from the machine in the same manner as irradiated fuel bundles before maintenance work is started. The FARE tool is not required on inner zone channels.

The failed fuel detection and location system, which is part of reactor instrumentation and control, is used to detect and identify failed fuel in the reactor core. Its gaseous fission monitoring system detects the reactor loop in which the fuel failure has occurred. Its failed fuel location system, also referred to as the delayed neutron monitoring system, is then used to identify in which channel of the particular coolant loop, the fuel failure occurred and to find, in this particular channel, which bundle pair contains the failed bundle(s). It does this by monitoring delayed neutrons via a sample station. The delayed neutron count rate decreases sharply when a failed fuel bundle leaves the channel flow. Failed fuel bundle(s) are then identified via their fuelling machine magazine position. They are otherwise handled by the fuelling machine in the same way as undamaged fuel bundles.

The fuel changing system maintains irradiated fuel, temporarily stored in its magazine, at acceptable temperatures by keeping it submerged and accommodating adequate heavy water circulation in the fuelling machine magazine, except for the short period of time when fuel bundles are exposed to air for discharge via the spent fuel port. The temperature of the water in the fuelling machine magazine is monitored.

In order to prevent damage to fuel:

- Fuel changing mechanisms are normally operated automatically according to pre-defined sequences.
- Interlocks inhibit mechanism operations unless the configuration is acceptable.
- Fuel changing components that interface with the fuel such as the ram adapter and the separator assemblies are designed to limit the stresses in the fuel bundle to acceptable levels.
- When handling fuel, the ram forces are limited to prevent unacceptable axial forces on the fuel bundles.

The geometry of the fuelling machine maintains the fuel subcritical even with heavy water present.

Fuel changing operations are performed remotely to limit radiation exposure of site personnel. The fuelling machine shielding doors provide radiation shielding and a ventilation barrier between the fuelling machine vaults and maintenance locks when the fuelling machine heads and their carriage and suspension are in their maintenance locks to permit personnel access for their maintenance. The atmosphere in the maintenance locks can be purged.

Prior to the start of maintenance work on the fuelling machine, plugs and tools, such as the shield plug, ram adapter and FARE tool, which become activated when they enter the core, are discharged from the fuelling machine.

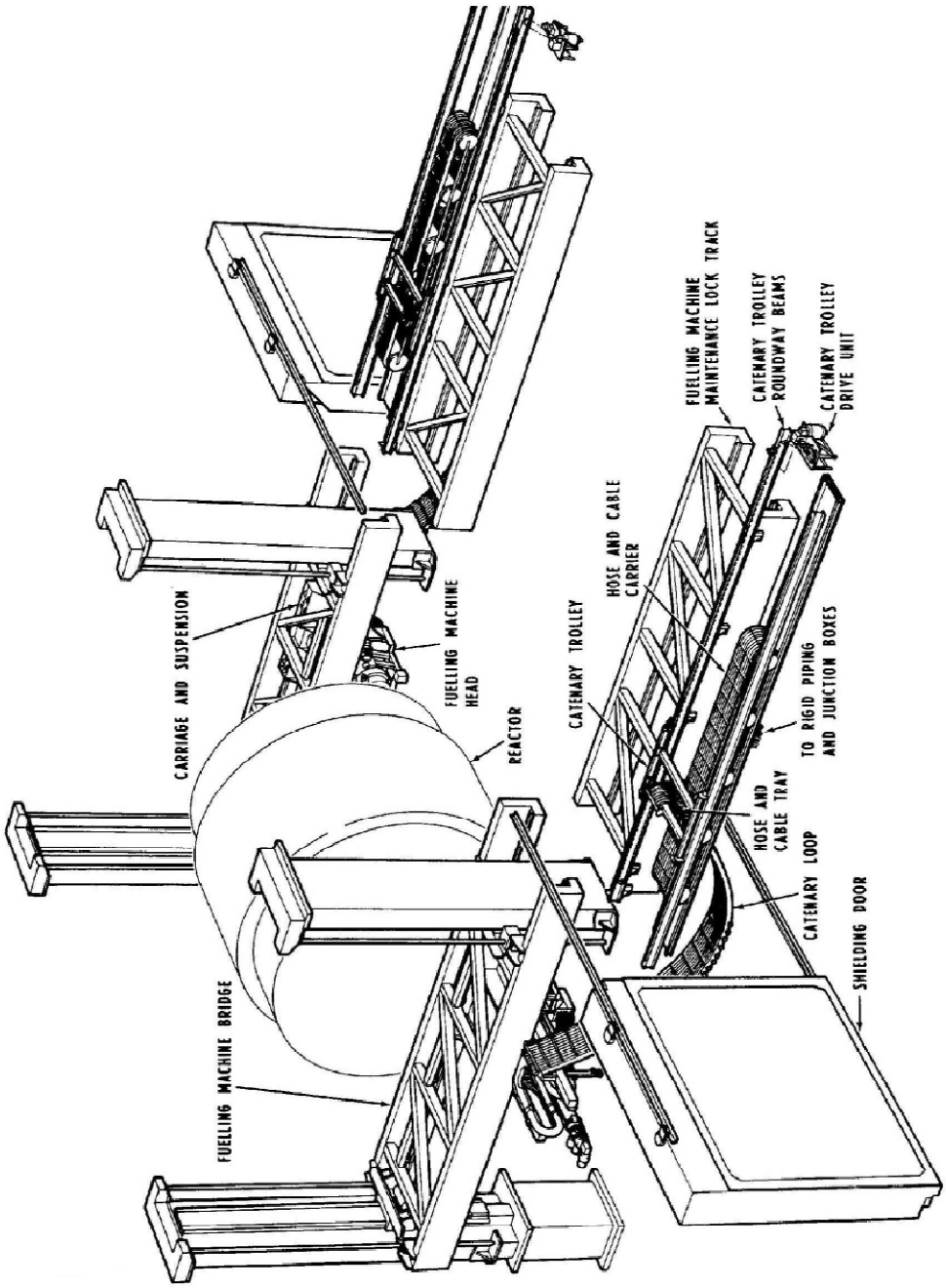

Figure 5 Fuel changing equipment

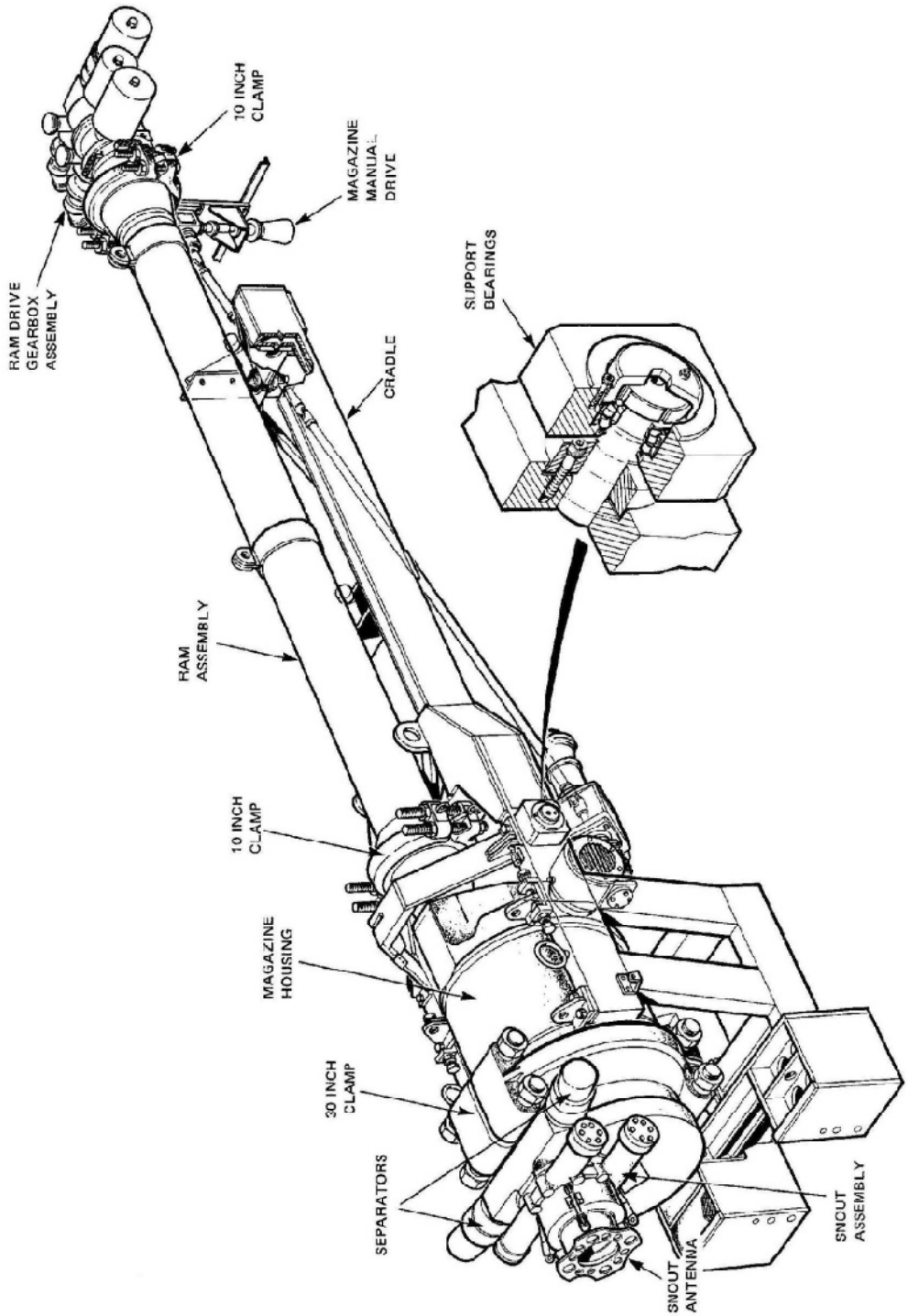

Figure 6 Fuelling machine head

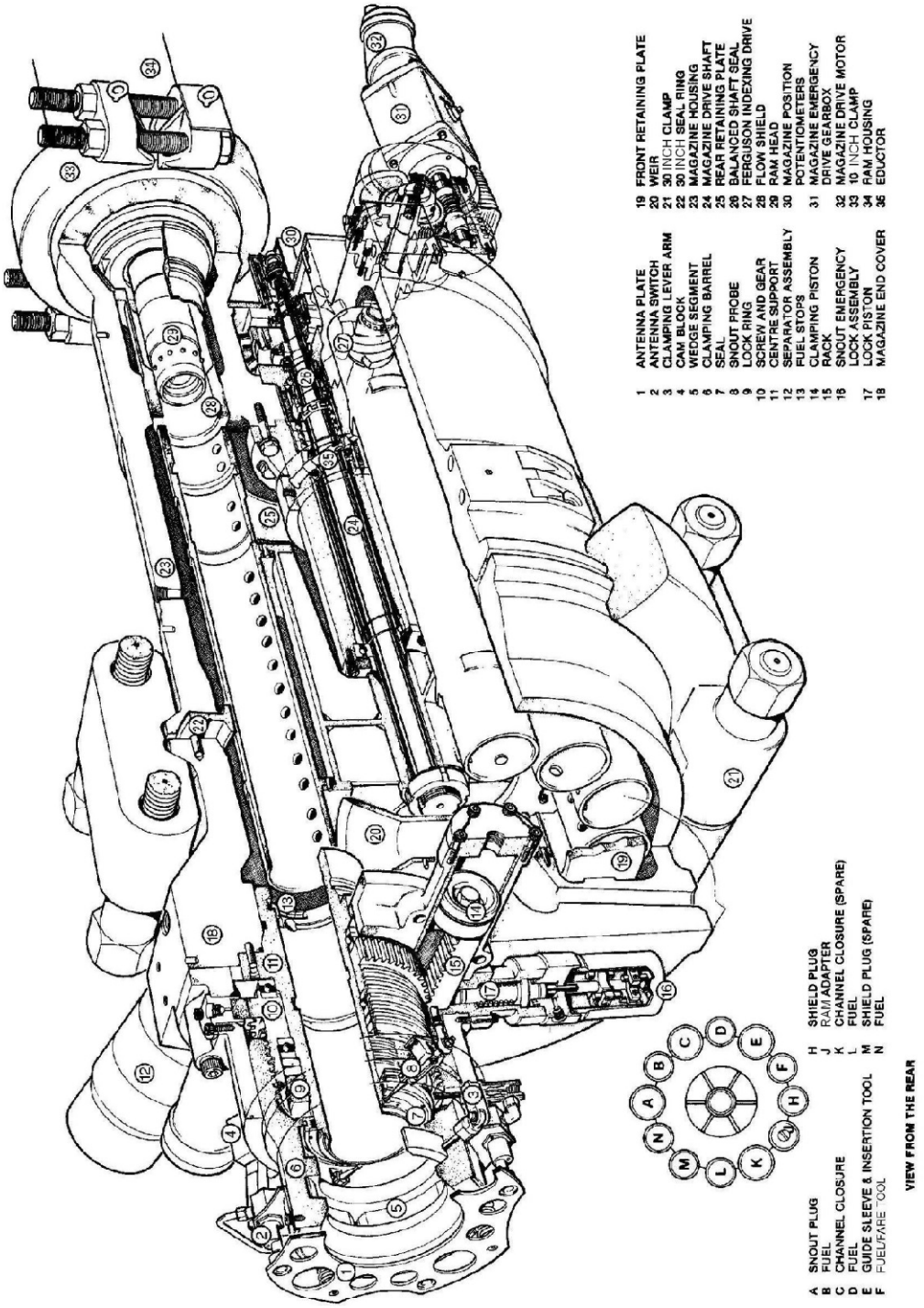

Figure 7 Front end of fuelling machine

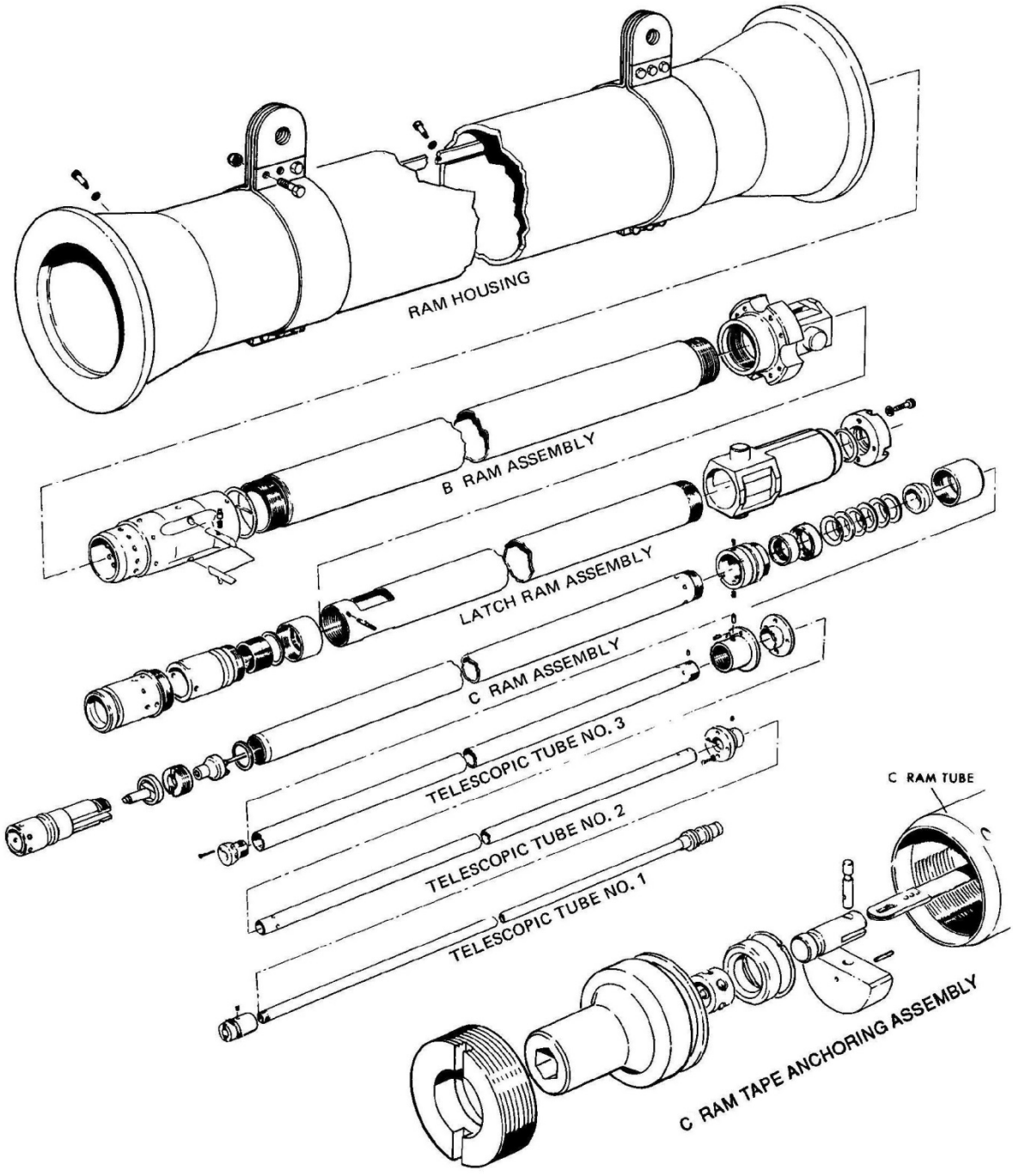

Figure 8 Ram assembly – exploded view

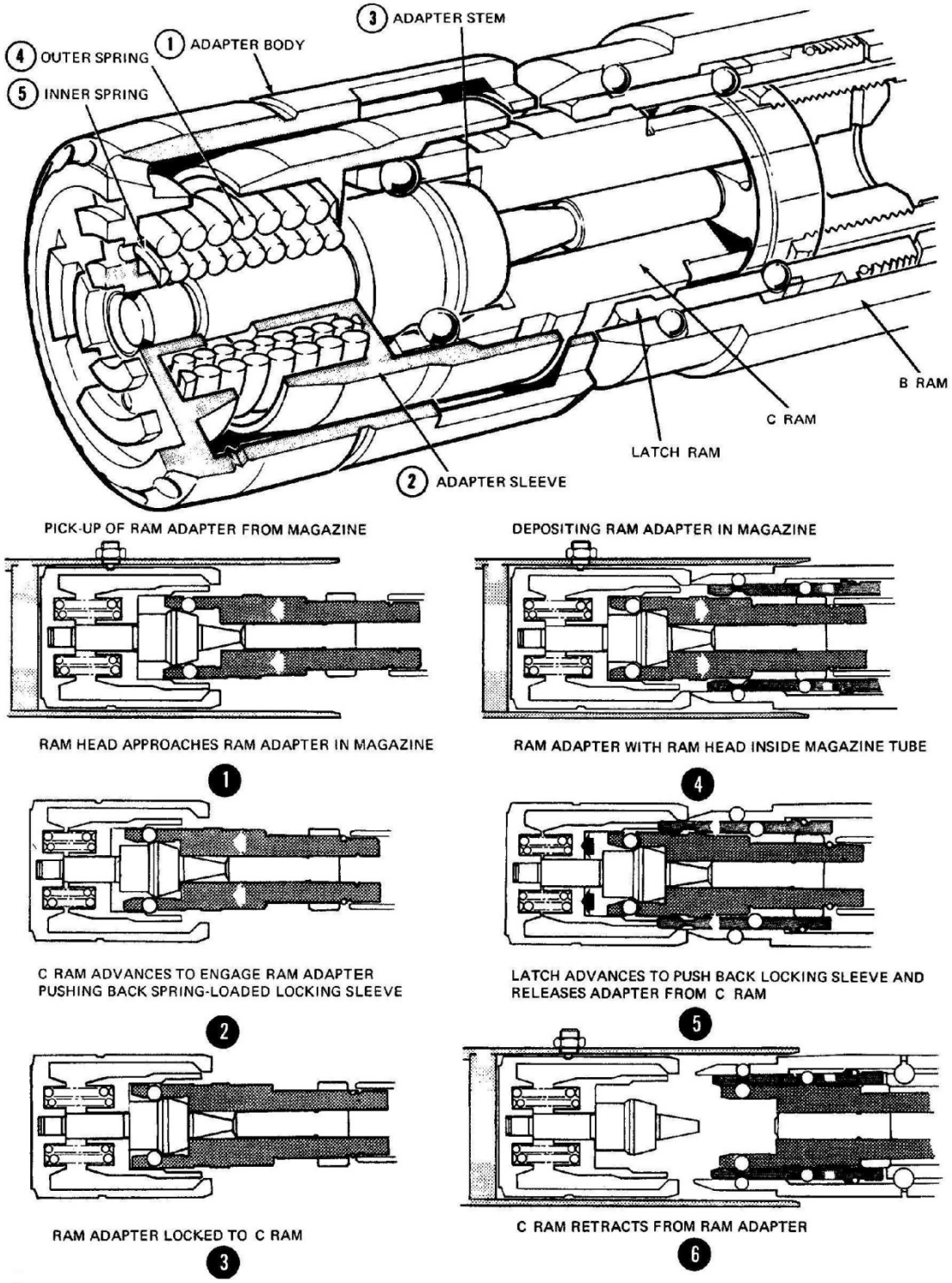

Figure 9 Ram adapter and operation

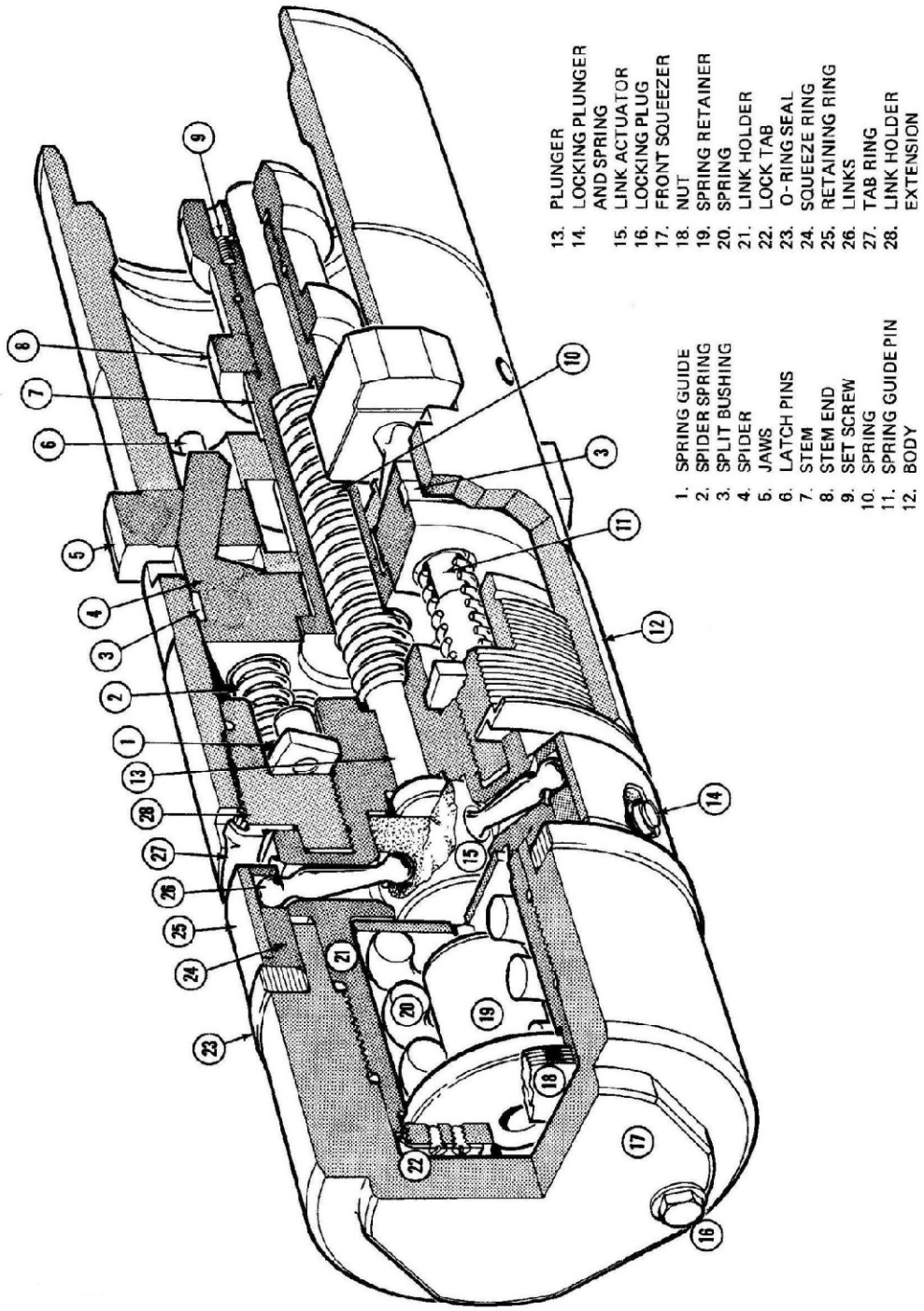

Figure 10 Fuelling machine snout plug

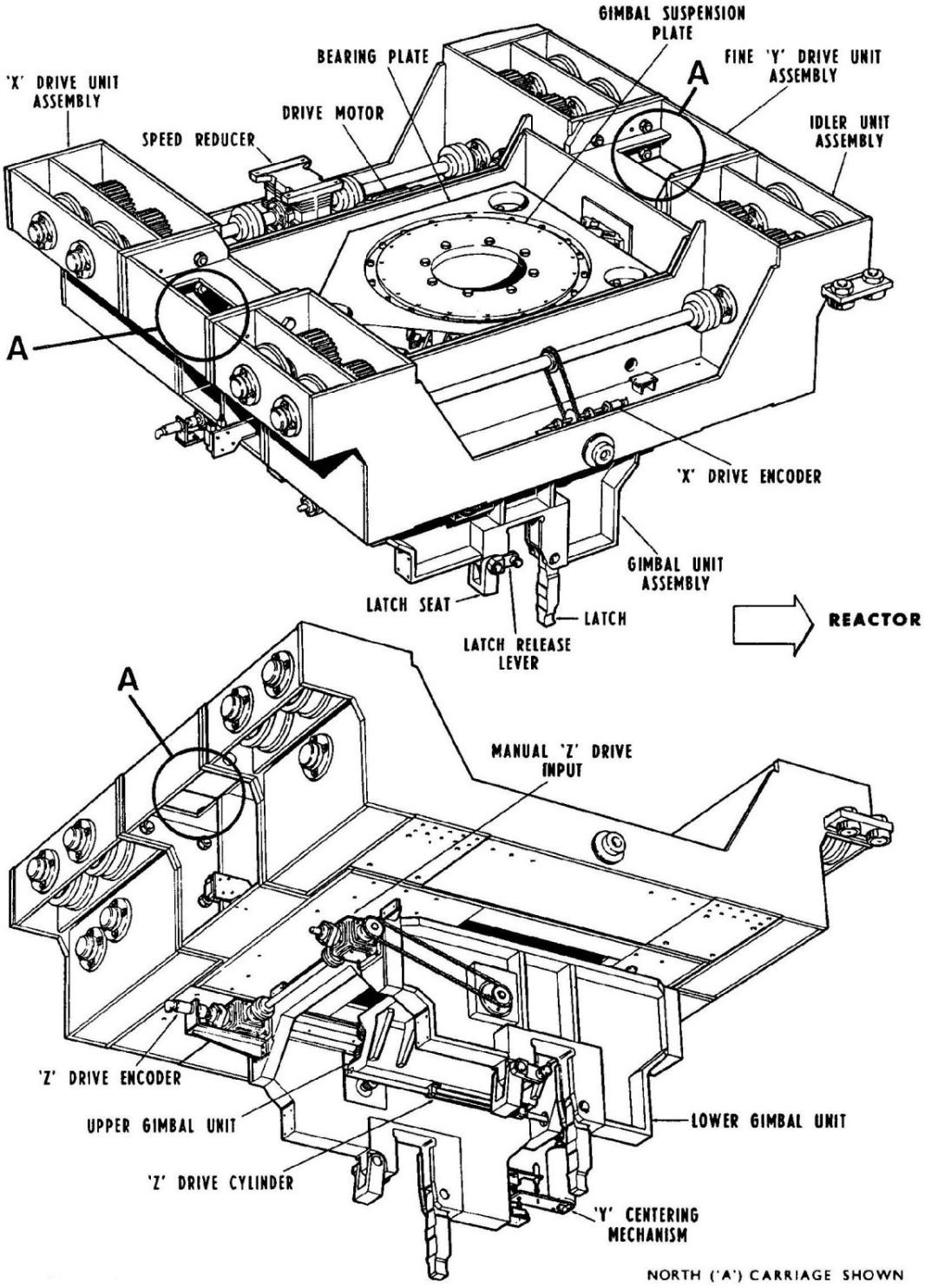

Figure 11 Carriage assembly

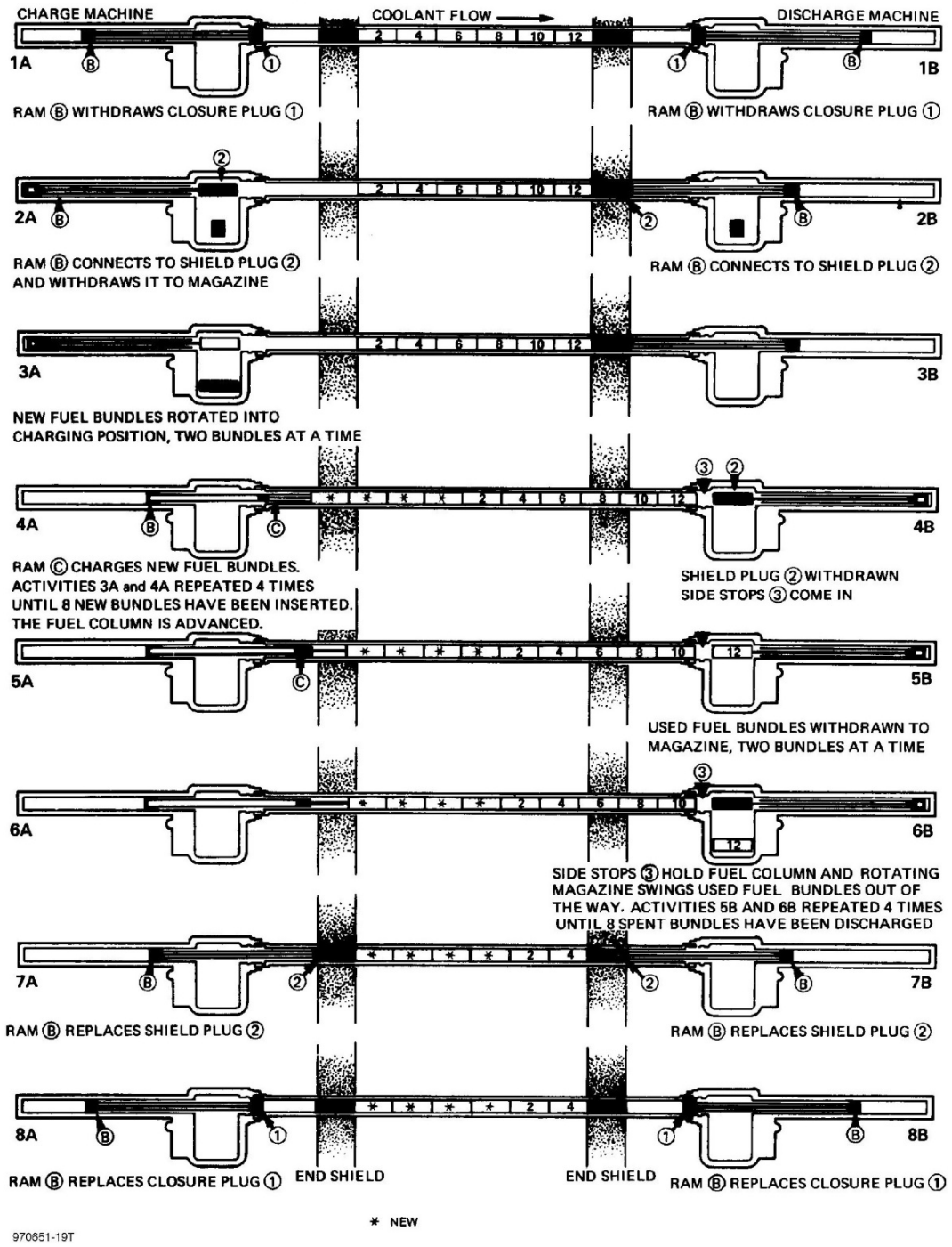

Figure 12 Fuel changing sequence

5 Spent Fuel Transfer and Storage

5.1 System Description

Spent fuel transfer and storage, which can be seen on Figure 1, covers the structures and equipment involved in the discharge of irradiated fuel from the fuelling machine and the transfer and storage of this irradiated fuel in bays until the fuel is transferred to dry storage. It consists of spent fuel discharge equipment, shown in Figure 13, spent fuel transfer auxiliaries, spent fuel transfer equipment, shown in Figure 14, and storage bay equipment. It also includes failed fuel canning equipment, shown on Figure 15, which is a subset of the spent fuel discharge equipment, and failed fuel handling equipment, which is a subset of the storage bay equipment. Spent fuel transfer and storage involves three bays filled with light, or regular, water: the spent fuel discharge bay, spent fuel reception bay and spent fuel storage bay (also referred to as the main storage bay).

The discharge equipment, which is located in the reactor building, receives irradiated fuel from the fuelling machines and lowers it into the discharge bay. It includes spent fuel ports that interface with the fuelling machines, and elevators to lower the fuel bundles into the water. It also includes the failed fuel canning equipment in the discharge bay, for handling and canning the small quantity of failed fuel.

The spent fuel transfer auxiliaries provide the fluid flows (air and water) for the spent fuel discharge mechanisms. They include a standby cooling system, D_2O leak collection system, fuel stop actuating system, port relief system, fuelling machine overflow detection system and port valve actuating system.

The spent fuel transfer equipment provides for the transportation of irradiated fuel from the discharge bay in the reactor building to the reception bay and the storage bay in the service building. It includes the discharge and transfer canal conveyors, the storage tray conveyor, a conveyor rack and cart, as well as tools and accessories for manipulating the fuel in the reception bay. The transfer of irradiated fuel between buildings is under water through a containment gate and a transfer canal, which connects the reception and storage bays under water. The reception bay is connected under water with the main storage bay by the penetration for the storage tray conveyor.

The storage bay equipment provides for the storage of irradiated fuel in the reception and storage bays. It includes the storage bay man-bridge, the storage trays and their supports, a storage tray lifting tool and the failed fuel handling equipment for handling and storing canned failed fuel in the reception bay.

An irradiated fuel channel shield plug (with its jaws retracted by a locking mechanism) or FARE tool can be received from either fuelling machine and accommodated similarly to fuel bundles. Irradiated elements of the reactivity control mechanisms can be accommodated in the storage bay for underwater storage.

5.2 Component Description

5.2.1 Spent Fuel Discharge Equipment

Spent fuel discharge equipment, shown in Figure 13, includes the components described as follows, in addition to the failed fuel canning equipment described in Section 5.2.5.

Spent Fuel Ports

Spent fuel ports are mounted in port sleeves embedded in the walls between the spent fuel discharge room and the fuelling machine maintenance locks. Two ball valves are mounted in series on the bay end of each port to seal the port and maintain the containment boundary.

The ports are cantilevered from the discharge room end, via a flange on the port housing, to provide the degree of flexibility necessary for fuelling machine lock-up. A detachable stainless-steel liner tube is installed in the bore of the port housing, forming an annulus between the liner and the housing, for emergency cooling of irradiated fuel, if required. The liner has a row of 10 holes along the top and 5 holes radially around the fuelling machine end. The annulus connects to the standby cooling system water supply to provide adequate cooling water through the liner holes for cooling of any irradiated fuel bundles, which may, inadvertently, be held up in the port.

Elevators

Two elevator ladles accept the fuel bundles from the spent fuel ports and are electrically driven to lower them onto a conveyor rack on a conveyor at the bottom of the discharge bay. The two elevators consist of ladles running on tubular and angle rails. The 30° inclination of the rails allows both elevators to terminate at the single conveyor at the bottom of the discharge bay. The two elevators are interlocked so that only one ladle can be driven down to the unloading position at any one time. Each ladle accommodates two fuel bundles and is suspended and driven by a stainless steel cable from a drum mounted above the rails.

5.2.2 Spent Fuel Transfer Auxiliaries

The spent fuel transfer auxiliaries comprise a series of systems, which provide the fluid flows (air and water) for the spent fuel discharge mechanisms. The systems include a standby cooling system, a D_2O leak collection system, a fuel stop actuating system, a port relief system, a fuelling machine overflow detection system and a port valve actuating system.

Standby Cooling System

The standby cooling system can be initiated to provide cooling water to the spent fuel port via its liner tube and/or to the length of travel to the bay water via spray headers mounted parallel to the elevator ladle rails, to provide cooling to exposed irradiated fuel if the discharge process is delayed.

D_2O Leak Collection System

The D_2O leak collection system collects heavy water that leaks past the inner ball valve seals into the spent fuel port cavity between the inner and outer valves, during fuelling machine operations at the spent fuel port, when the fuelling machine and spent fuel port are filled with heavy water and pressurized. The D_2O leak collection system includes a pneumatically operated drain valve, which is connected to the cavity between the port valves and is opened to

drain any heavy water into the D_2O system. At the same time, the cavity is supplied with air to assist in clearing any heavy water from the cavity.

Fuelling Machine Overflow Detection System

The fuelling machine overflow detection system includes a D_2O collection container located below the discharge end of the spent fuel port, and connected to the port. The container is drained into the spent fuel discharge bay through a removable orifice. If the level of heavy water in the fuelling machine fails to be lowered, a liquid level detector probe in the container actuates a transmitter.

Port Valve Actuating System

The port ball valve actuating system is used to operate the spent fuel port ball valves via pneumatic actuators.

5.2.3 Spent fuel transfer equipment

Spent fuel transfer equipment, shown in Figure 14, includes the following components.

Conveyor Rack

Each conveyor rack (also referred to as a transfer rack) can receive up to 12 fuel bundles from the spent fuel discharge elevator in two rows of 6; although 8 are normally carried. A conveyor rack can also accommodate canned failed fuel bundles.

Conveyor Cart

The conveyor cart (also referred to as a transfer cart) supports the conveyor rack and travels between the discharge bay and the reception bay on conveyors. The cart runs on eight stainless steel wheels which enable it to traverse the gap between the two conveyors. The cart engages drive chains on each conveyor.

Discharge Bay and Transfer Canal Conveyors

Two conveyors, the discharge bay and transfer canal conveyors (also referred to as spent fuel transfer conveyors), allow the conveyor cart to travel between the discharge bay and the reception bay. The transfer canal conveyor is sometimes also referred to as the reception bay conveyor.

The conveyors are of similar construction and consist of a welded stainless steel frame with a flat upper surface on which the cart runs. A rectangular guide rail on the upper surface mates with three sets of rollers on the cart to provide lateral guidance for the cart. A mechanical stop is mounted at each end of cart travel. The two conveyors are driven by electrical motors mounted above water on the discharge bay walkway floors, and vertical shafts used to drive the underwater gearboxes, conveyor sprockets and chain.

The discharge bay conveyor is mounted on a series of supports secured to embedments in the bottom of the reception bay. The conveyor is secured to the supports by captive screws and tapered alignment pins which facilitate conveyor removal and installation. The conveyor is also provided with lifting lugs.

The transfer canal conveyor is mounted on supports in the bay and also sits directly on the concrete in the transfer canal. It is located laterally and vertically by a slotted bracket assembly

at the discharge bay end of the canal and is secured by captive screws and tapered alignment pins only at the reception bay end to facilitate removal and installation.

Fuel Transfer Canal Containment Gate

The fuel transfer canal containment gate is located at the entrance to the fuel transfer canal in the spent fuel discharge bay. The stainless steel gate is raised and lowered by a pneumatic actuator and includes a safety latch actuated by a second pneumatic actuator. It is closed and becomes part of the containment boundary when the spent fuel port ball valves are open during the discharge of irradiated fuel from the fuelling machine and through the spent fuel port. Otherwise the gate is normally open to permit water circulation between the bays. The containment gate opening permits passage of the conveyor cart with a full load of fuel.

Storage Tray Conveyor

The storage tray conveyor transports spent fuel storage trays, in any state of loading, between the reception bay and the storage bay. The manually driven storage tray conveyor has three superimposed frames, capable of telescopic extension. The bottom frame is bolted to the floor of the reception bay, while the other end extends into a rectangular opening in the wall between the reception bay and storage bay. The storage tray conveyor is manually operated from a handwheel located on the reception bay walkway and extended or retracted to the limit of its travel as required.

Tools and Accessories

Spent fuel transfer equipment tools and accessories are located in the reception bay. They enable fuel bundles to be transferred from the conveyor rack to a storage tray.

5.2.4 Storage Bay Equipment

Storage bay equipment, which can be seen in Figure 1, includes the following components in addition to the failed fuel handling equipment described in Section 5.2.6.

Storage Bay Manbridge

The spent fuel storage bay manbridge consists of an over-running, electric, travelling crane to which an under-slung walkway is attached. A hoist with an electrically driven trolley provides the lifting capability. The walkway spans the width and runs the full length of the storage bay to provide a working platform for operating personnel engaged in handling irradiated fuel or other active reactor components. The crane and hoist are controlled from a single pendant control station suspended from the hoist so that an operator can manipulate the crane from the walkway or the side of the bay.

Storage Trays

Each storage tray can hold 24 fuel bundles in two rows of 12 each. The trays are of stainless-steel welded construction, with contoured cradle strips to support and separate the fuel bundles. The trays are stackable. Each tray is provided with two lifting plates corresponding to the pins on the storage tray lifting tool. Each tray is also provided with two tapered locating pins and two slots, the pins engaging with the slots of the next-higher tray in the stack.

Storage Tray Supports

Storage tray supports are provided in the reception bay, and in the main storage bay, to support the stacks of trays. Each support consists of a diagonally braced, stainless-steel frame, supported on raised pads.

Storage Tray Lifting Tool

This tool is similar to the storage tray lifting tool used in the reception bay, except for the length of the tool and the orientation of the handle to the head.

5.2.5 Failed Fuel Canning Equipment

The following failed fuel canning tools and equipment, shown on Figure 15, are available in the spent fuel discharge bay.

Carousel

A carousel provides temporary storage for failed fuel, for a decay period of up to two months after the bundle has been discharged from a fuelling machine. The carousel base is a weldment of angles bolted onto the bay floor. The outside walls consist of an octagonal lower section open at the bottom, with a removable conical hood also of octagonal shape covering the top of the tray. The 360° tray is divided into 12 sections, with each section capable of holding one failed fuel bundle. The maximum capacity of the carousel is 11 bundles, to allow an empty section to line up with the open portion of the carousel canopy. The carousel is manually operated from a handle located on the discharge bay walkway. A ventilation pipe connects the hood to the radioactive off-gas waste management system, to collect and purge active gases released by the failed fuel bundles in the carousel.

Failed Fuel Can

Each stainless steel failed fuel can is able to accommodate one failed fuel bundle after the necessary decay period in the carousel. The can has one open end for the bundle insertion, while other end is blanked and punched with a small hole to prevent pressure building up inside the can, during and after canning operations. The can is sealed by a lid, after the failed fuel bundle has been pushed into it.

Canning Device

The canning device consists of a can storage rack, a can support, a fuel bundle trough, and a bundle transfer ram. All these components are submerged and mounted on the canning device support frame.

Failed Fuel Bundle Lifting Tool

The failed fuel bundle lifting tool enables failed fuel bundles to be lifted from the conveyor rack into the carousel, and from the carousel to the canning device.

Lid Rack Handling Tool

The lid rack handling tool is used to transfer full lid racks from the ladle onto the canning device, and move empty lid racks back to the elevating table.

Elevating Table

The elevating table is a carbon-steel rectangular table, which can be hooked onto either of the elevator ladles. A rack of can lids can then be loaded onto the table and lowered into the bay by the elevator.

Can Handling Tool

This tool is used to move empty failed fuel cans between the elevator ladle and the can storage rack, between the rack and the trough, and to move full cans between the trough and conveyor rack.

Lid Handling Tool

This tool allows the failed fuel can lids to be picked up from the storage rack and placed in position in the canning equipment ram. The tool consists of a length of pipe, with a hook at the top and a contoured fork at the bottom.

5.2.6 Failed Fuel Handling Equipment

The following failed fuel handling tools and equipment are available in the reception bay.

Transition Table

The transition table is used to provide a transition point between the reception bay and the failed fuel storage area, which is lower, and to accommodate the tools of different lengths.

Can Handling Tool

Two can handling tools are provided for handling cans of failed fuel in the reception bay. These tools are similar to the can handling tool used in the discharge bay. Each tool consists of a handle connected to a double lifting hook by a length of pipe.

Failed Fuel Handling Storage Tray

These trays are of similar construction to the main storage trays, but can only hold 10 canned fuel bundles in a single row. These trays are also stackable.

5.3 System Operation

5.3.1 Normal Operation

Irradiated fuel bundles removed from the reactor remain immersed in heavy water within the fuelling machine until the fuelling machine magazine rotates to align the first pair of bundles with the spent fuel port. This raises the two bundles above the heavy water level inside the fuelling machine head and exposes them to air. This rotation starts a timer to measure the time the fuel bundles are exposed to air. The irradiated bundles will normally be exposed to air for less than two minutes.

After irradiated fuel is received, two bundles at a time from the fuelling machine via the spent fuel port, the elevator lowers the bundles into the water of the discharge bay, and deposits them on the conveyor rack, supported by the conveyor cart and correctly indexed under the elevator by the discharge bay conveyor drive, in position to receive pairs of fuel bundles.

If, due to a delay, the irradiated fuel remains in air longer than a predetermined time, an alarm is provided to the operator. In such a case, the operator would then select one of the following

options to supply cooling water to the exposed fuel bundles, to prevent fuel bundle overheating and possible subsequent bundle failure.

If the fuel bundles are stuck in the port and the outer ball valve can be closed, the level of heavy water in the fuelling machine can be raised to flood the port with heavy water and cool the fuel.

The standby cooling system can be initiated to provide cooling water to the spent fuel port via its liner tube if fuel is stuck in the port such that the outer ball valve cannot be closed, and/or to the length of the elevator travel to the bay water via spray headers mounted parallel to the elevator ladle rails, if fuel is stuck on the elevator.

Once all fuel bundles are discharged onto the conveyor rack, the containment is sealed by closing the spent fuel port globe valves, and the containment gate is then opened. The conveyor cart then travels on the discharge bay conveyor up to the containment gate. Once the cart reaches the space between the two conveyors, one slotted bracket on the cart disengages the pins of the chain as the pins go around the sprocket of the first conveyor. This automatically aligns the other slotted bracket of the cart to engage the pins of the reception bay conveyor chain, which then moves the cart to the reception bay.

The fuel bundles are then transferred individually to a spent fuel storage tray. Full storage trays are moved onto the extendable storage tray conveyor for transfer to the storage bay via an opening in the wall between the two bays. Once in the storage bay, individual trays are lifted by a hoist on the storage bay manbridge and placed in stacks on a storage tray support. The storage tray conveyor then retracts until it closes the opening in the wall with its flow obstruction plate. This minimizes the movement of water between the two bays.

An operator on the manbridge manoeuvres all storage trays, and stacks them, using an electrical hoist and storage tray handling tool.

Irradiated fuel bundles are typically stored in the spent fuel bays for a minimum of six years prior to transfer to dry storage; this allows the heat of a natural uranium fuel bundle with maximum burnup to decay enough to allow for dry storage. The typical transfer of irradiated fuel to dry storage involves transferring irradiated fuel from storage trays into a storage basket, drying and seal welding the basket, transferring the basket, via a transfer flask, to one of the multiple storage cylinders within a concrete storage module. Fuel transfers are typically carried in batch processes where the inventory from approximately one year of irradiated fuel production is transferred to dry storage. The quantity of fuel baskets transferred to dry storage is selected to completely fill the storage cylinders involved. Refer to Chapter 19 for additional information on the dry storage of irradiated fuel.

The spent fuel storage bay can accommodate the storage of irradiated fuel in stacked spent fuel storage trays, in addition to the space required for equipment to prepare the fuel for dry storage. The storage capacity of the spent fuel storage bay accommodates the storage of irradiated fuel for a minimum of six years of wet-storage after removal from the reactor, the accumulation of inventory from at least one year of irradiated fuel production for transfer to dry storage, plus a half-core off-load (sometimes referred to as one loop) for emergency purposes.

Normal handling of irradiated fuel bundles in air or light water does not pose criticality problems for natural uranium fuel.

Operations are carried under water as much as possible and the amount of time irradiated fuel spends in air is minimized to maintain acceptable temperatures for the irradiated fuel and prevent fuel damage.

During handling, the fuel bundle is supported on at least two bands of its wear pads. Minor axial forces only are directly applied to the fuel sheaths via the endplates and endcaps.

Discharge operations are controlled remotely and the spent fuel discharge room is inaccessible to personnel while irradiated fuel is being discharged or when there is a high radiation field. The depth of water in the spent fuel bays has been calculated to limit exposure to any personnel in the area to well below allowable levels. Long-handled manual tools have markers to show safe operating lift heights. Fixed area monitors are permanently installed in the spent fuel transfer and storage areas and provide safe notification to personnel when radiation levels exceed allowables. Consequently, operators do not normally require personal protective equipment for radiation protection when handling irradiated fuel during normal operation.

5.3.2 Failed Fuel Handling

Once a failed fuel bundle has been detected, identified and removed from the reactor, it is discharged from the fuelling machine head and lowered on the spent fuel elevator in the same way as a normal fuel bundle. However, in the case of a failed fuel bundle, the conveyor rack is indexed two positions and the failed fuel bundle is removed from the rack and inserted into the carousel using the failed fuel bundle lifting tool suspended from the discharge bay monorail hoist. The carousel is then indexed to position the bundle under the carousel canopy.

The failed fuel bundle is retained in the carousel, where its radioactive gases are captured and directed to the radioactive offgas waste management system, for a period of up to two months, during which time radioactive gases will have decayed to safe levels.

Protective equipment is required when handling the small quantity of failed fuel.

If necessary, the failed fuel bundle is canned; otherwise, it is further handled as a normal bundle. A fuel bundle requiring canning is lifted from the carousel and placed in the trough of the canning device. A manually driven ram is then actuated to push the bundle into the can. A lid handling tool is then used to position the lid such that the ram can drive the lid into the tapered open end of the can.

The canned fuel bundle is then transferred via the discharge bay and transfer canal conveyors into the reception bay.

Canned failed fuel bundles are handled with a can handling tool and stored on failed fuel storage trays in a deeper area of the reception bay specially designated for failed fuel storage. A failed fuel storage tray lifting tool is used to maneuver and stack these trays. The failed fuel area of the reception bay can accommodate the small quantity of failed fuel.

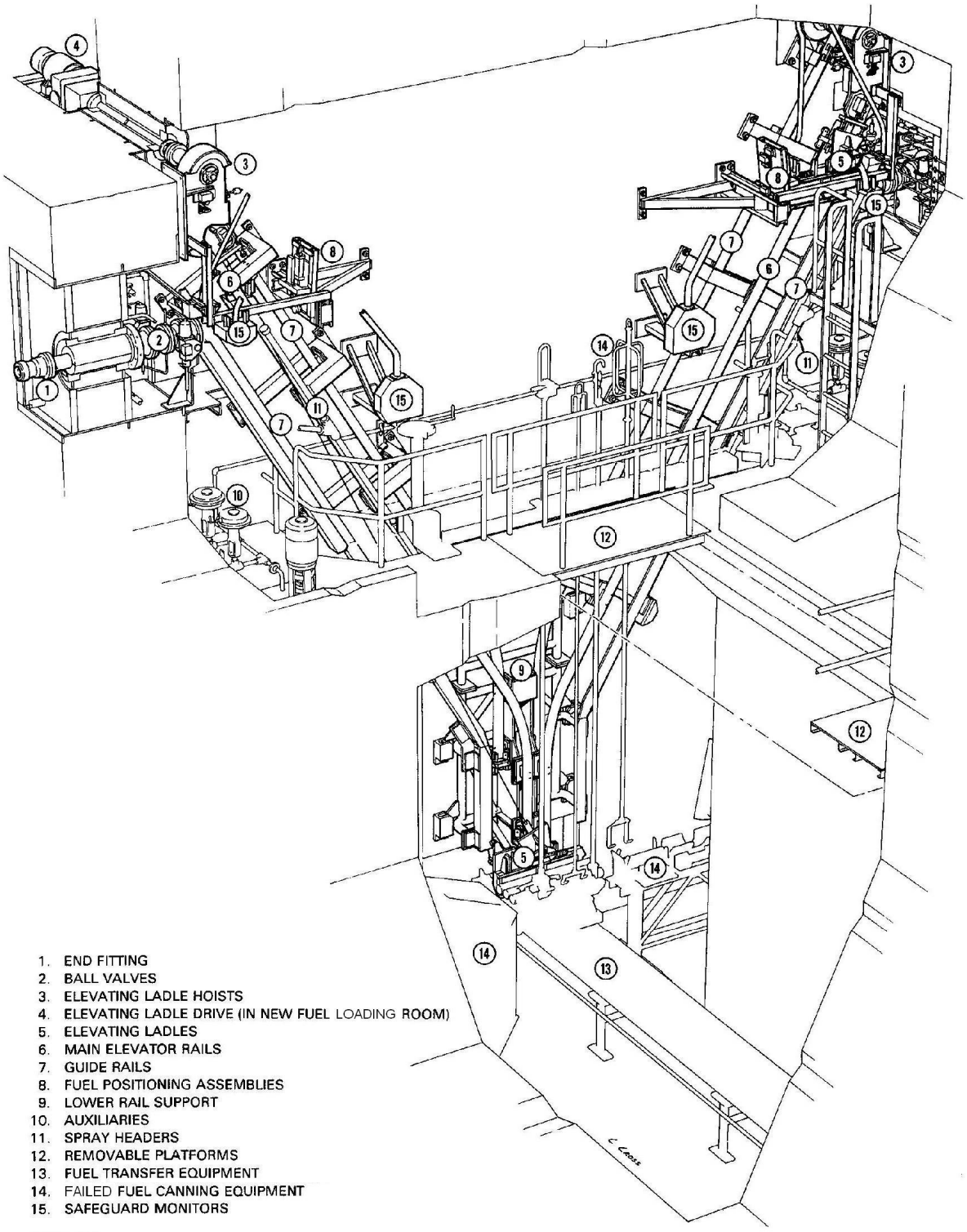

Figure 13 Spent fuel discharge equipment

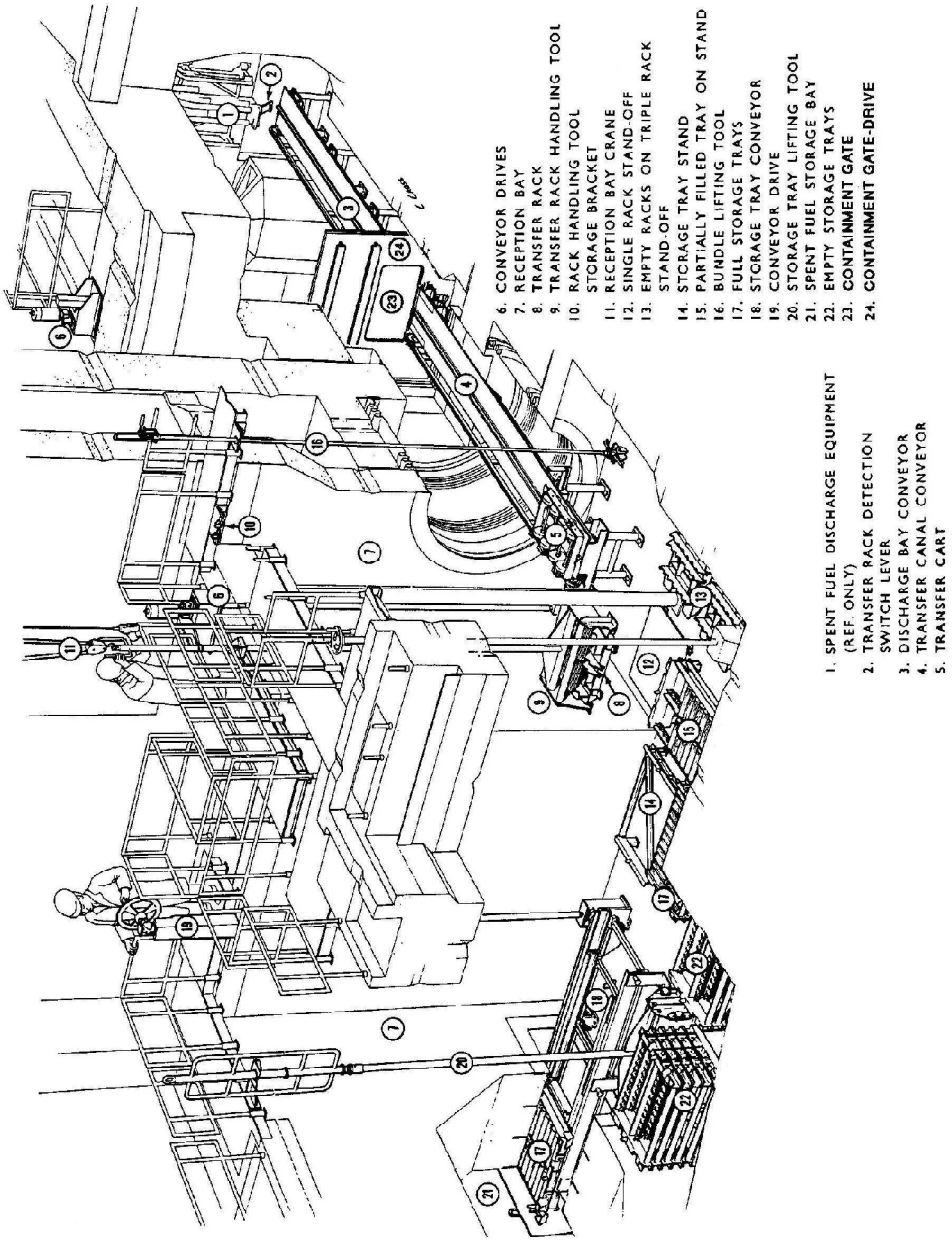

Figure 14 Spent fuel transfer equipment

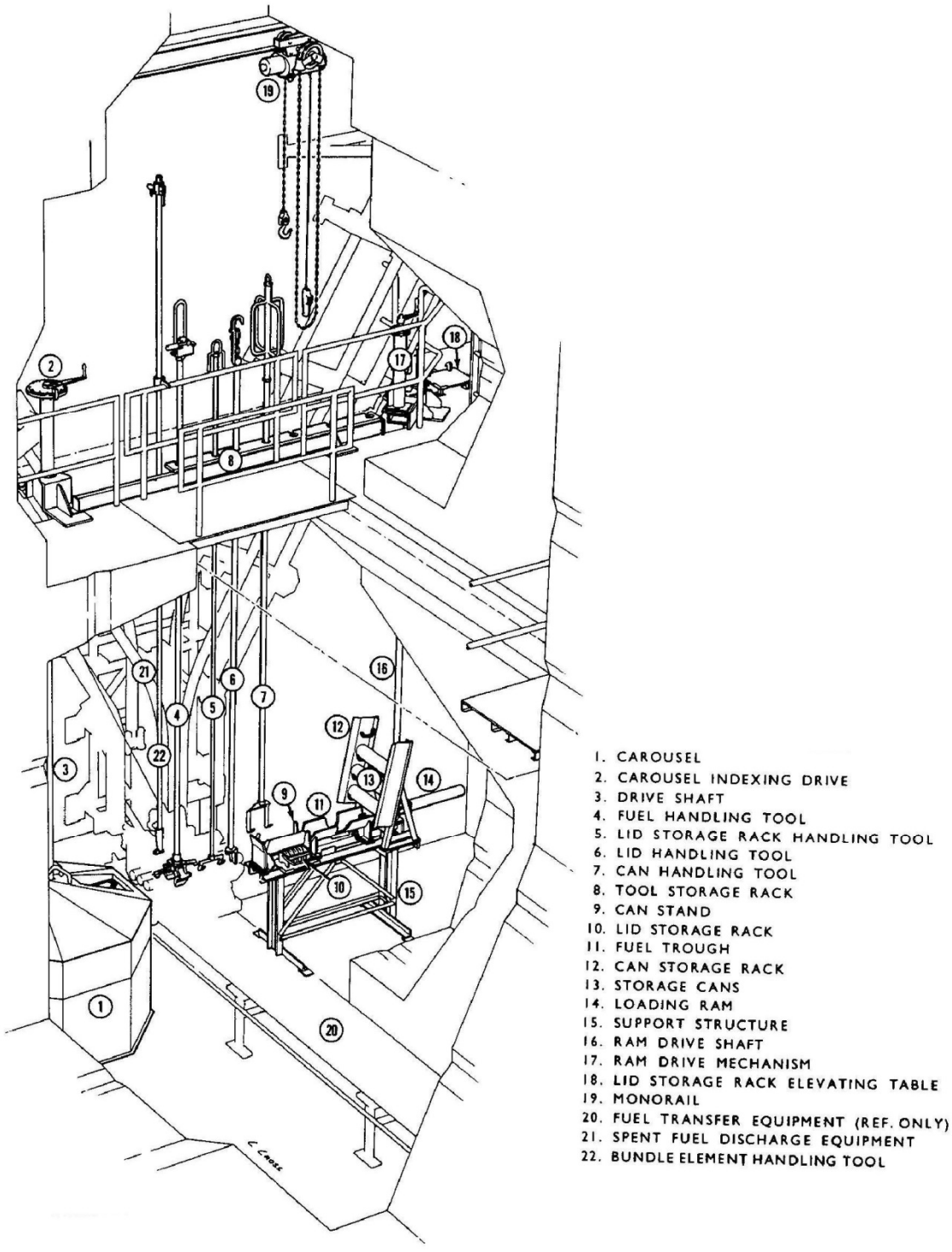

Figure 15 Failed fuel canning equipment

6 Problems

1. To accommodate eight months of reactor operation at equilibrium,
   a. Approximately how many channels are required to be refueled by the fuelling machines?
   b. Approximately how many fuel bundles need to be stored in the new fuel storage room?
   c. How many pallets of new fuel are required?
2. Estimate the minimum number of fuel trays that the spent fuel storage bay needs to accommodate, assuming that fuel is transferred to dry storage when an accumulation of fuel from approximately one year of production has decayed adequately for dry storage?
3. Describe the typical direction of on-channel fuel changing operations and the benefit(s) of operating in this direction.
4. Why does the level of water in the fuelling machine need to be lowered below its snout level for the transfer of fuel bundles to the spent fuel port and from the new fuel port?
5. What measures can be taken if a fuel bundle(s) is (are) stuck during spent fuel transfer?
6. What is the purpose of the snout emergency lock?

7 Further Reading

[ISA1984] P. Isaac, “Evolution of On-power Fuelling Machines on Canadian Natural Uranium Power Reactors”, AECL-8337, October 1984

[JAC2004] W.H. Jackson, “Design of On-Power Fuelling Machines”, *CNS Bulletin*, Vol. 25, No. 3, September 2004

[STE2006] R.G. Steed, *Nuclear Power in Canada and Beyond*, General Store Publishing House, ISBN-13: 978-1-897113-51-6, 2006

8 Acknowledgements

The following reviewers are gratefully acknowledged for their hard work and excellent comments during the development of this Chapter. Their feedback has much improved it. Of course the responsibility for any errors or omissions lies entirely with the author.

George Ilich
Benjamin Rouben

Thanks are also extended to Bill Garland for expertly editing and assembling the final copy.

CHAPTER 21
CANDU In-Core Fuel-Management

prepared by

Dr. Benjamin Rouben, 12 & 1 Consulting, Adjunct Professor,

McMaster University & University of Ontario Institute of Technology (UOIT)

Summary:

This chapter describes the physical and mathematical models and the computational methods used in the management of fuel in CANDU nuclear reactors. The concepts important to the topic of fuel management are explained: fuel irradiation (fluence), fuel burnup, cross-section averaging. The various levels of physics models used in fuel management are presented in quantitative detail: these are the continuous refuelling model, the time-average model, patterned-age snapshot models, and core-follow models. The typical reactivity curve for the CANDU lattice is presented, and a method to estimate the average attainable fuel burnup from the reactivity curve is explained. The CANDU initial core and the first few months of operation are discussed. Finally, the chapter gives a short qualitative survey of advanced fuel cycles which could be exploited in CANDU reactors.

Table of Contents

List of Figures

List of Tables

1 Introduction

1.1 Overview

CANDU Refuelling is carried out with the reactor at power. This feature makes the in-core fuel management substantially different from that in reactors that must be refuelled during shut-downs. The capability for on-power refuelling means that excess reactivity requirements are at a minimum: only a few milli-k are necessary for continuous and short-term reactivity control. This leads to excellent neutron economy and low fuelling costs.

The primary objective of CANDU in-core fuel management is to determine fuel-loading and fuel-replacement strategies to operate the reactor in a safe and reliable fashion while keeping the total unit energy cost low. Within this context, the specific objectives of CANDU in-core fuel management are as follows:

- Adjust the refuelling rate to maintain the reactor critical
- Control the core power to satisfy safety and operational limits on fuel and channel power, thus ensuring that the reactor can be operated at full rating
- Maximize burnup within operational constraints, to minimize fuelling cost
- Avoid fuel defects, to minimize replacement fuel costs and radiological occupational hazards.

To refuel a channel, a pair of fuelling machines latches onto the ends of the channel. A separate chapter in this book describes the fuelling machine and the related fuel handling [Damario 2016]. An even number of fresh fuel bundles are inserted into the channel by the machine at one end, and an equal number of irradiated fuel bundles are discharged into the machine at the other end of the channel. For symmetry, the refuelling direction is opposite for next-neighbour channels. In the CANDU-6 reactor, the refuelling direction is the same as that of coolant flow in the channel.

Several refuelling operations are normally carried out daily, so that refuelling is almost continuous. CANDU reactors offer extreme flexibility in refuelling schemes:

- The refuelling rate (or frequency) can be different in different regions of the core, and in the limit can in principle vary from channel to channel. By using different refuelling rates in different regions, the long-term radial power distribution can be shaped and controlled.
- The axial refuelling scheme is not fixed;
- A channel can be refuelled without delay if failed fuel exists or is suspected;
- The fuel can be removed completely from a few channels, in order for example to limit the channel axial growth.

This chapter will cover the topics relevant to the management of nuclear fuel in CANDU reactors. Fuel management in CANDU has both design and operations aspects; both are covered in this chapter. The concepts important to in-core fuel management will be explained: fuel irradiation (fluence), fuel burnup, cross-section averaging. The various levels of physics models which are used to carry out fuel-management calculations will be presented: these are the continuous-refuelling model, the time-average model, patterned-age snapshot models, and core-follow

models. The purpose and use of the various calculations will be explained. Additional information can be obtained from [Rouben 2003].

1.2 Learning Outcomes

The goal of this chapter is to help the student understand:

- The basic concepts of fuel irradiation (fluence), fuel burnup, and fuel isotopic changes
- The reactivity curve of the fuel lattice and its importance
- The refuelling process in CANDU
- The significance of the flux and power shapes in reactor
- How to control the flux shape, the means to flatten the flux distribution (adjuster rods, differential fuelling)
- Time-average, snapshot, and core-follow models for CANDU reactors, and their use.

2 Definition of Concepts

Fuel irradiation (also known as fluence) and fuel burnup are separate but related concepts. Both are in a way a measure of the "age" of the fuel in the reactor.

2.1 Fuel Irradiation

Let us use the symbol $\Phi_F(t)$ for the neutron flux in the fuel in a certain fuel bundle, where *t* is the time measured from the moment when the bundle entered the reactor core. The irradiation (or fluence) of the fuel in the bundle, denoted $\omega(t)$, is defined as the time integral of the flux to time t:

$$\omega(t) = \int_0^t \Phi_F(t)\,dt \tag{1}$$

This definition is not quite complete, since the flux is a function of neutron energy *E*. We must remove the vagueness and make the definition complete by specifying which flux is to be used. The usual choice is to select Φ_F as the **thermal** flux in the fuel. Excluding for now the time variable, we can write Φ_F as the integral of the flux as a function of energy:

$$\Phi_F = \int_0^{E_{th}} \Phi_F(E)\,dE \tag{2}$$

where E_{th} is the upper bound of the thermal energy interval. Note: Since the thermal energy interval may be defined differently in different computer codes, the fuel irradiation may vary from code to code, and caution must therefore be exercised when comparing irradiation values using different codes.

Having settled on the definition of fuel flux, let us return now to Eq. (1) and note that fuel irradiation (fluence) is a monotonically increasing function of time, since flux is never negative. The irradiation starts at 0 when the fuel bundle enters the core, and increases up to the time when the fuel bundle exits the core. The value of the irradiation when the bundle exits from the core is then called the **exit** or **discharge** irradiation.

The units of irradiation are units of flux multiplied by units of time. This gives for example $n.cm^{-2}.s^{-1}*s$, i.e., $n.cm^{-2}$. But a much more appropriate (microscopic) unit for area is the barn ($b = 10^{-24}$ cm^2) or kilobarn ($kb = 10^{-21}$ cm^2). Thus, the common unit for irradiation is n/kb.

2.2 Fuel Burnup

The fuel burnup of a given fuel bundle, denoted *B(t)*, is defined as the total **fission energy** (note: not thermal or electric energy) released in the fuel bundle since the moment when it entered the reactor core, divided by the initial mass of heavy element in the bundle. (In the case of the CANDU reactor, where the only initial heavy element in the fuel is uranium, the initial mass of heavy element is the mass of uranium in the bundle.)

Since the energy release depends on the fission rate in the bundle, we can write

$$B(t) = \frac{\int_0^t E_R \Sigma_f(t) \Phi_f(t) dt}{M} \tag{3}$$

where *M* is the mass of uranium in the bundle, Σ_f is the fission cross section in the bundle, and E_R is the fission energy release per fission (~200 MeV).

In contrast to that of fuel irradiation, the definition of fuel burnup does not suffer from vagueness, since energy is a measurable, well-defined quantity. For this reason, if comparisons are to be made between different computer codes, it is much easier, and preferred, to compare on the basis of fuel burnup rather than of irradiation.

Similarly to fuel irradiation, fuel burnup is a monotonically increasing quantity, since the fuel continues to fission and release energy with time. The burnup of the fuel in the fuel bundle starts at 0 when the fuel bundle enters the core, and increases up to the time when the fuel bundle exits the core. The value of the fuel burnup when the bundle exits from the core is then called the **exit** or **discharge** burnup.

The units of fuel burnup are units of energy divided by units of mass. The most commonly used burnup units are megawatt-days per megagram of uranium (MW.d/Mg(U)) or megawatt-hours per kilogram of uranium (MW.h/kg(U)). The typical average exit discharge burnup in existing CANDU reactors varies depending on the design of the core, and may range between 180 and 225 MW.h/kg(U) (or, equivalently, between 7,500 and 9,375 MW.d/MgU).

2.3 Relationship Between Fuel Irradiation and Fuel Burnup

Both fuel irradiation and fuel burnup increase with time and reflect therefore in a way the "age" of the fuel. Of course, fuel "ages" faster in a high neutron flux, since the flux appears in the integrand of both Eqs. (1) and (2).

In a given nuclear lattice, fuel burnup and fuel irradiation have a one-to-one relationship which depends on the fission cross section Σ_f and its variation with time. In the CANDU lattice, there is a relatively small variation in Σ_f (and in E_R) over the typical residence time of a fuel bundle in core, so the relationship between irradiation and burnup is almost linear. For example, the old lattice code POWDERPUFS-V [Rouben 1995] gives the following relationship for fuel burnup as a function of irradiation:

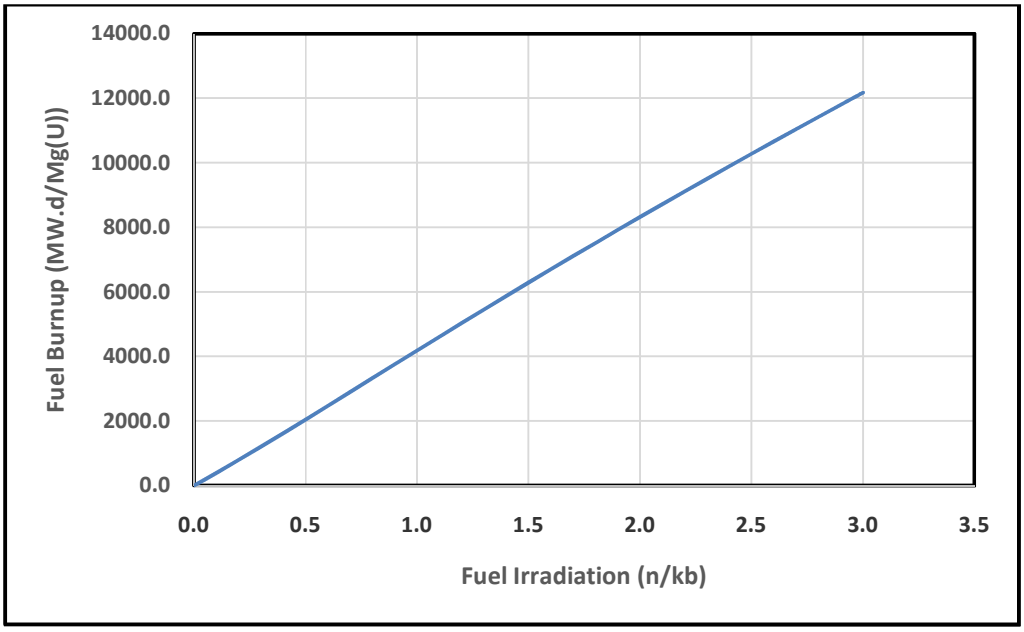

Figure 1 Relationship of Fuel Burnup and Irradiation from POWDERPUFS-V Code

3 CANDU Reactor Physics Computational Scheme

To properly manage the nuclear fuel in the core, one must be able to calculate the neutron flux and power distributions in space and in time. The most accurate computational tool for CANDU neutronics is the Neutron Transport equation (see Section 2.1 of Chapter 4, Reactor Statics). However, solving this equation over the full core on a routine basis demands too much computational effort. Therefore, a 3-stage process involving the Neutron Transport equation and the simpler Neutron Diffusion equation, which involves some approximation (see Section 2.2. of Chapter 4), has been developed for CANDU neutronics. By experience, this 3-stage computational system has been found to give generally very good results. It has been described in Chapter 4 and is reviewed here.

3.1 Lattice Calculation

The first stage involves solving for the flux distribution in the fundamental unit of the CANDU reactor, i.e., the basic lattice cell, which is defined to consist of the fuel, coolant, pressure and calandria tubes, and moderator, but no reactivity devices (see face view in Figure 2; in the third dimension the basic lattice cell is one bundle-length deep).

The lattice calculation is performed using a lattice code. For many years, the lattice calculation was performed with the code POWDERPUFS-V, which was developed specifically for CANDU reactors and which makes use of computational “recipes” to incorporate experimental results obtained with heavy-water lattices. More recently, deterministic multi-group neutron transport codes with a strong mathematical and theoretical basis, such as WIMS-IST [Irish 2002] or DRAGON [Marleau 1999], have been adopted in place of POWDERPUFS-V for lattice calculations. The DRAGON code is currently freely available from École Polytechnique de Montréal.

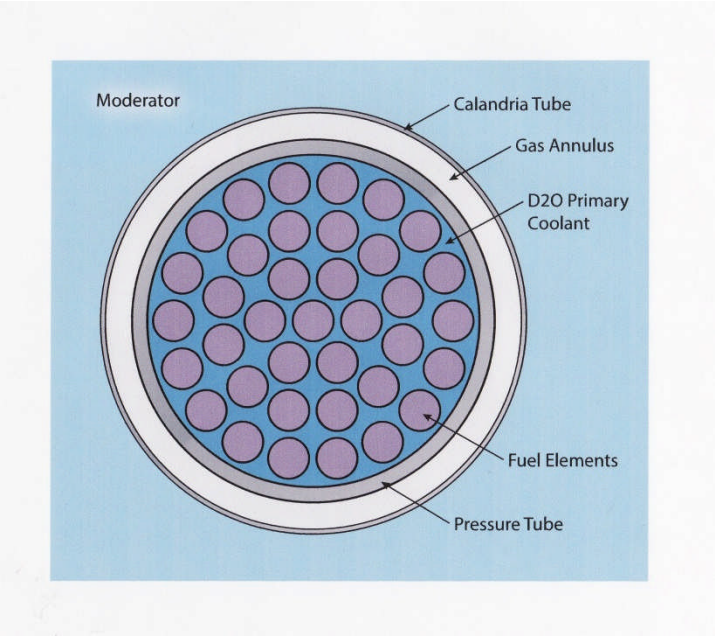

Figure 2 Face View of the CANDU Basic Lattice Cell

The deterministic transport code uses the geometry and properties of materials in the lattice cell to do a very accurate calculation of the flux distribution over the lattice cell. It uses a large or very large number (tens or even hundreds) of neutron energy groups in this calculation, to take account of the neutron moderation accurately. It then averages the nuclear properties (for absorption, moderation, fission, etc.) over the cell according to the calculated reaction rates in each sub-region of the lattice cell to determine the effective neutronic properties of the whole cell. This averaging (homogenization) of the properties of the basic lattice cell dilutes the strong absorption of the fuel with the much weaker absorption in the moderator. The code also "collapses" the cell properties over a very small number of neutron energy groups. Most often in CANDU neutronics, the collapsing is done over 2 energy groups (a thermal group and a slowing-down group). This is sufficient since only about 2% of all fissions are induced by non-thermal neutrons. With these homogenized properties, Fick's Law (see Section 2.2 of Chapter 4) becomes a good approximation over most of the reactor, and the diffusion equation can be used to calculate the neutron flux over the full core.

The lattice code must do one more thing, a "depletion" calculation: Here the code updates the composition of the fuel over a time step, using the various reaction rates that it has determined, and then recalculate the homogenized cell properties. Repeating this over many time steps, the code evolve the lattice-cell neutronic properties to reflect the changes in the nuclide composition of the fuel with time (irradiation/burnup).

The output of the lattice code is then a table of the basic-cell (lattice) nuclear properties as functions of fuel irradiation or burnup. For example, POWDERPUFS-V gives the properties in the 2-energy-group formalism, but in the approximation that the fast-fission and upscattering cross sections are assumed to be 0. A typical fuel table would then appear as in Table 1. Note that the lattice code must also in addition provide the nuclear properties (cross sections) of the

moderator, to be applied outside the fuelled region of the core.

Table 1 Sample Lattice Nuclear Cross Sections versus Fuel Irradiation

Irradiation ω(n/kb)	Fast Diffusion Coefficient D1 (cm)	Thermal Diffusion Coefficient D2 (cm)	Fast Absorption Cross Section Σa1 (cm^-1)	Thermal Absorption Cross Section Σa2 (cm^-1)	Yield Cross Section νΣϕ2 (cm^-1)	Downscattering Cross Section νΣϕ2 (cm^-1)	Ratio of Fuel Flux to Cell Flux
0.00	1.269	0.936	7.68E-04	3.79E-03	4.52E-03	7.40E-03	0.383
0.10	1.269	0.936	7.68E-04	3.82E-03	4.56E-03	7.40E-03	0.380
0.20	1.269	0.936	7.68E-04	3.89E-03	4.66E-03	7.40E-03	0.374
0.30	1.269	0.937	7.67E-04	3.95E-03	4.73E-03	7.40E-03	0.369
0.40	1.269	0.937	7.67E-04	3.99E-03	4.78E-03	7.40E-03	0.365
0.50	1.269	0.937	7.67E-04	4.03E-03	4.81E-03	7.40E-03	0.361
0.60	1.269	0.937	7.66E-04	4.07E-03	4.83E-03	7.40E-03	0.359
0.70	1.269	0.937	7.66E-04	4.10E-03	4.83E-03	7.40E-03	0.356
0.80	1.269	0.937	7.66E-04	4.12E-03	4.83E-03	7.40E-03	0.354
0.90	1.269	0.937	7.66E-04	4.14E-03	4.82E-03	7.40E-03	0.352
1.00	1.269	0.937	7.65E-04	4.15E-03	4.81E-03	7.40E-03	0.351
1.10	1.269	0.937	7.65E-04	4.17E-03	4.78E-03	7.40E-03	0.350
1.20	1.269	0.937	7.65E-04	4.18E-03	4.76E-03	7.40E-03	0.349
1.30	1.269	0.937	7.65E-04	4.19E-03	4.74E-03	7.41E-03	0.348
1.40	1.269	0.936	7.64E-04	4.20E-03	4.71E-03	7.41E-03	0.348
1.50	1.269	0.936	7.64E-04	4.20E-03	4.68E-03	7.41E-03	0.347
1.60	1.269	0.936	7.64E-04	4.21E-03	4.65E-03	7.41E-03	0.347
1.70	1.269	0.936	7.63E-04	4.22E-03	4.62E-03	7.41E-03	0.346
1.80	1.269	0.936	7.63E-04	4.22E-03	4.59E-03	7.41E-03	0.346
1.90	1.269	0.936	7.63E-04	4.22E-03	4.56E-03	7.41E-03	0.346
2.00	1.269	0.936	7.63E-04	4.23E-03	4.53E-03	7.41E-03	0.345
2.10	1.269	0.936	7.62E-04	4.23E-03	4.50E-03	7.41E-03	0.345
2.20	1.269	0.936	7.62E-04	4.23E-03	4.47E-03	7.41E-03	0.345
2.30	1.269	0.936	7.62E-04	4.24E-03	4.45E-03	7.41E-03	0.345
2.40	1.269	0.936	7.62E-04	4.24E-03	4.42E-03	7.41E-03	0.344
2.50	1.269	0.936	7.61E-04	4.24E-03	4.39E-03	7.41E-03	0.344
2.60	1.269	0.936	7.61E-04	4.25E-03	4.37E-03	7.41E-03	0.344
2.70	1.269	0.936	7.61E-04	4.25E-03	4.35E-03	7.41E-03	0.344
2.80	1.269	0.936	7.60E-04	4.25E-03	4.33E-03	7.41E-03	0.343
2.90	1.269	0.936	7.60E-04	4.26E-03	4.30E-03	7.41E-03	0.343
3.00	1.269	0.936	7.60E-04	4.26E-03	4.28E-03	7.41E-03	0.343
3.10	1.269	0.936	7.60E-04	4.26E-03	4.27E-03	7.41E-03	0.343
3.20	1.269	0.936	7.59E-04	4.26E-03	4.25E-03	7.41E-03	0.342
3.30	1.269	0.936	7.59E-04	4.27E-03	4.23E-03	7.41E-03	0.342
3.40	1.269	0.936	7.59E-04	4.27E-03	4.21E-03	7.41E-03	0.342
3.50	1.269	0.936	7.59E-04	4.27E-03	4.20E-03	7.41E-03	0.342
3.60	1.269	0.936	7.58E-04	4.28E-03	4.18E-03	7.41E-03	0.341
3.70	1.269	0.936	7.58E-04	4.28E-03	4.17E-03	7.41E-03	0.341
3.80	1.269	0.936	7.58E-04	4.29E-03	4.16E-03	7.41E-03	0.341
3.90	1.269	0.936	7.58E-04	4.29E-03	4.15E-03	7.41E-03	0.340
4.00	1.269	0.936	7.57E-04	4.29E-03	4.13E-03	7.41E-03	0.340

3.2 Reactivity-Device Calculation

The CANDU basic lattice cell contains, by definition, no reactivity devices. Neither does it contain any structural material other than the fuel channel itself (i.e., the pressure tube and calandria tube). However, there are reactivity devices in appropriate locations in the core. Therefore, the effect of the reactivity devices, their guide tubes and other structural material on the nuclear properties in their vicinity needs to be taken into account. This effect is expressed in the form of homogenized "incremental" cross sections which are added to the (unperturbed) homogenized properties of neighbouring lattice cells in a modelled volume around the device, called a "supercell"; see an example in Figure 3, although the supercell is often defined as having half the width shown, i.e., with only half the width on either side of the device. The incremental cross sections are calculated with a transport code, most often DRAGON; they are identified with the differences in the supercell homogenized properties between the case where the device is inserted into the supercell and the case where it is withdrawn from it. The incremental cross sections are added to the lattice-cell cross sections in the modelled volume around the device's position in the reactor core, when that particular device is inserted.

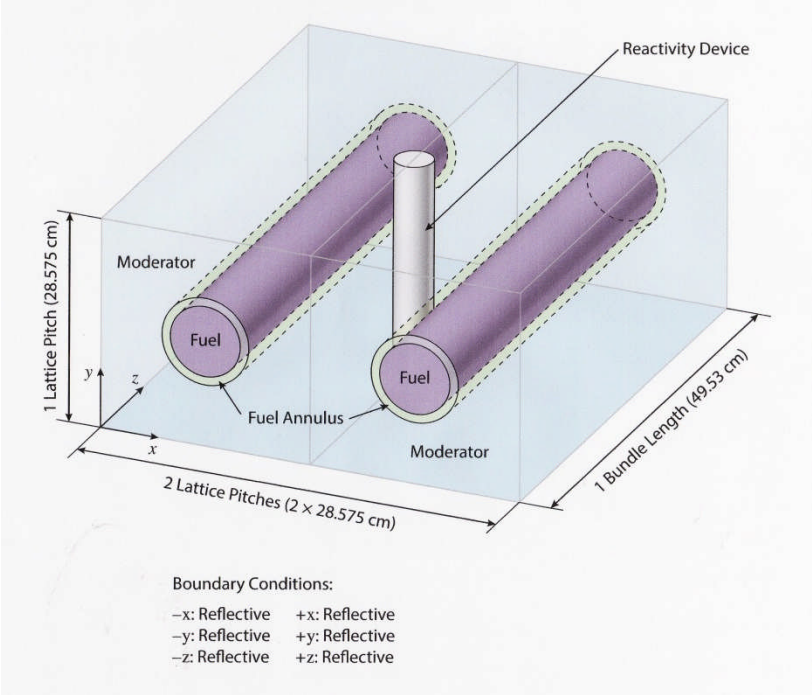

Figure 3 Supercell for Calculation of Device Incremental Cross Sections

3.3 Full-Core Calculation

In the final stage, a full-core reactor model is assembled. As explained above, because homogenized cell and device properties are used, few-group (most often 2-group) diffusion theory can be applied with this model. The full-core model must incorporate, for each cell in the reactor, the homogenized unperturbed-lattice-cell cross sections which apply there, together with the incremental cross sections of nearby reactivity devices in their appropriate locations. The model therefore consists of homogenized basic-lattice-cell properties in the appropriate locations, on which are superimposed reactivity-device properties in the devices' modelled

volumes.

A typical full-core 3-d CANDU reactor model for use with finite-difference diffusion theory is shown in Figure 4 (face view, showing adjuster modelled volumes) and Figure 5 (top view, showing adjuster and liquid-zone-controller modelled volumes).

The full-core flux and power distributions are calculated in CANDU with the finite-difference diffusion-theory code Reactor Fuelling Simulation Program RFSP-IST [Rouben 2002], or for example with DONJON [Hébert 2012]. The DONJON code is currently freely available from École Polytechnique de Montréal.

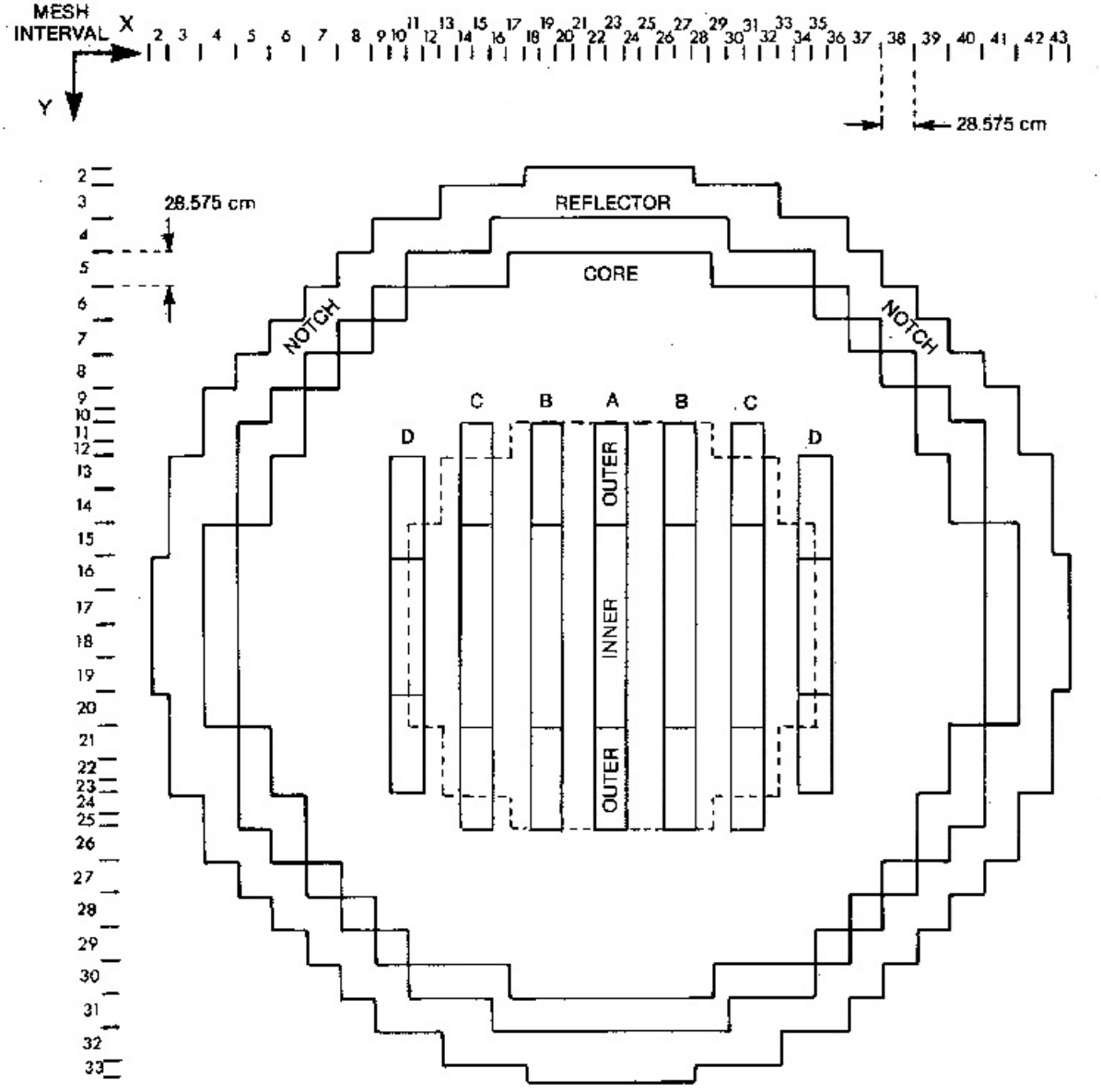

Figure 4 Face View of a Typical CANDU-6 Full Reactor Model

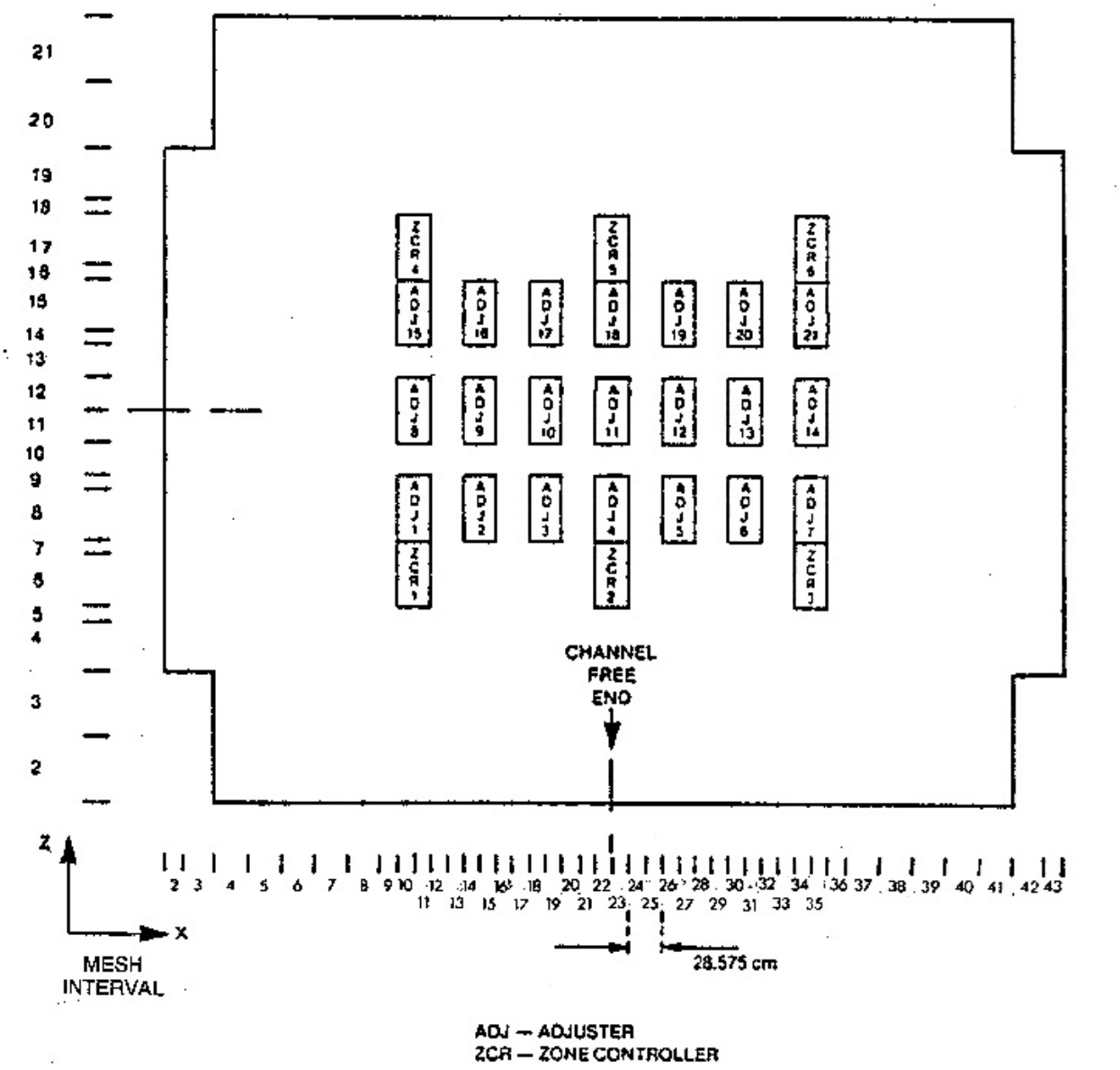

Figure 5 Top View of a Typical CANDU-6 Reactor Physics Model

4 Averaging Nuclear Cross Sections

There are many situations in which one wishes to average nuclear cross sections in space or in time. For example, we have already seen in Section 2.1 that the lattice code averages (homogenizes) the nuclear properties within the basic lattice cell. In the finite reactor also, we may wish to average the properties of a region of the core. How to do this is explained here.

The overarching aim in reactor physics is to calculate reaction rates, because from a knowledge of reaction rates we can derive the values of the important quantities in the system, for example the core reactivity or the power distribution in the core, etc.

A reaction rate *RR* at a point, corresponding to a process with cross section Σ, is calculated as the product of the cross section with the neutron flux:

$$RR = \Sigma\Phi \tag{4}$$

These point reaction rates can then be integrated over space or time. Since the total reaction rate is the quantity of interest, then we must ensure that this is conserved in any averaging.

4.1 Averaging Over Space

Suppose we consider a non-uniform reactor subdivided into a number of regions with different values of the cross section, and we would like to know the "average" cross section for the whole reactor. Let's take a very simple example of a reactor with 2 regions, with uniform cross section value Σ_1 and Σ_2 respectively (see Figure 6).

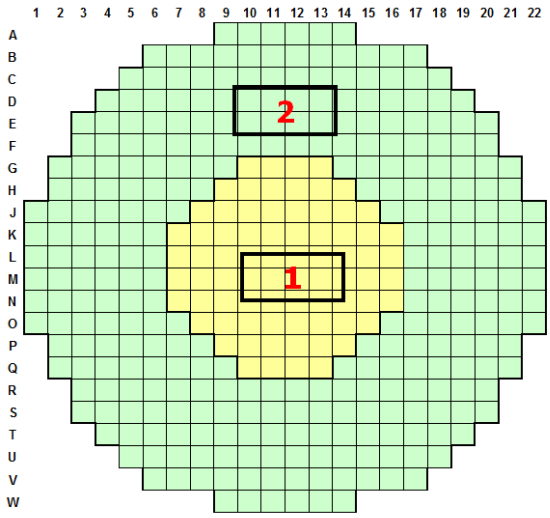

Figure 6 Averaging the properties of a 2-region core

The flux is Φ_1 and Φ_2 in the two regions, and is a function of space in each region. How would we calculate the overall average cross section $\overline{\Sigma}$?

We want to conserve the total reaction rate, which is

$$RR_{total} = \int_{V_1} \Sigma_1\Phi_1 dV + \int_{V_2} \Sigma_2\Phi_2 dV \tag{5}$$

Therefore $\overline{\Sigma}$ should satisfy

$$\int_{V_1} \overline{\Sigma}\Phi_1 dV + \int_{V_2} \overline{\Sigma}\Phi_2 dV = RR_{total}$$

which gives

$$\overline{\Sigma} = \frac{\int_{V_1} \Sigma_1\Phi_1 dV + \int_{V_2} \Sigma_2\Phi_2 dV}{\int_{V_1} \Phi_1 dV + \int_{V_2} \Phi_2 dV} \tag{6}$$

This shows that the proper definition of the average cross section is obtained by averaging the cross section with flux and volume weighting.

If we define also the average flux

$$\bar{\Phi} = \frac{\int_{V_1} \Phi_1 dV + \int_{V_2} \Phi_2 dV}{\int_{V_1} dV + \int_{V_2} dV} = \frac{\int_{V_1} \Phi_1 dV + \int_{V_2} \Phi_2 dV}{V} \tag{7}$$

where $V = V_1 + V_2$ is the total volume, then we can also write

$$\bar{\Sigma} = \frac{\int_{V_1} \Sigma_1 \Phi_1 dV + \int_{V_2} \Sigma_2 \Phi_2 dV}{\bar{\Phi} V} \tag{8}$$

or

$$\bar{\Sigma}\bar{\Phi}V = \int_{V_1} \Sigma_1 \Phi_1 dV + \int_{V_2} \Sigma_2 \Phi_2 dV = RR_{total} \tag{9}$$

4.2 Averaging Over Time

Now let's think about averaging over time at a given point or region (say, for a fuel bundle). Here the properties will vary with time, i.e., with fuel irradiation or burnup. The reaction rate which we must conserve is the time-integrated reaction rate $\int \Sigma(t)\Phi(t)dt$.

The average cross section over a time interval t_1 to t_2 is then defined by

$$\bar{\Sigma} = \frac{\int_{t_1}^{t_2} \Sigma(t)\Phi(t)dt}{\int_{t_1}^{t_2} \Phi(t)dt} \tag{10}$$

Now let's change variables to ω, using $d\omega = \Phi dt$, and we get

$$\bar{\Sigma} = \frac{\int_{\omega_1}^{\omega_2} \Sigma(\omega)d\omega}{\int_{\omega_1}^{\omega_2} d\omega} = \frac{\int_{\omega_1}^{\omega_2} \Sigma(\omega)d\omega}{\omega_2 - \omega_1} \tag{11}$$

i.e., $\bar{\Sigma}$ is basically the average of the cross section over irradiation on the irradiation interval.

5 The Fuel Reactivity Curve

The reactivity of the fuel lattice versus irradiation (or burnup) is provided by the lattice code, together with the lattice properties. For any lattice design, the fuel reactivity curve is a fundamental piece of knowledge for fuel management. A typical reactivity curve for the CANDU lattice is shown below (Figure 7):

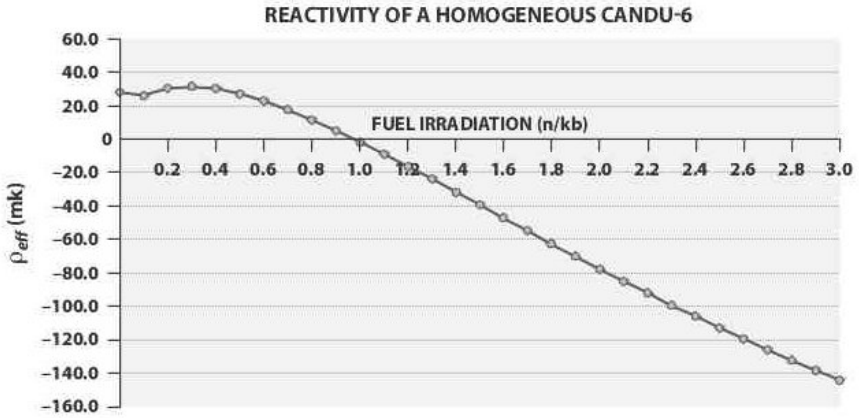

Figure 7 The Reactivity of the CANDU Lattice

The reactivity curve has several interesting features:

- The reactivity at zero irradiation (fresh fuel) is quite high, ~76 mk. It is to be noted that this value is calculated assuming that the saturating fission products (xenon, samarium, etc.) are already at equilibrium, even though the fuel is fresh. To run the infinite lattice in steady state, the positive reactivity would have to be cancelled by adding poison to the moderator, for example ~9.5 ppm of boron in the initial core (assuming a boron reactivity coefficient of -8 mk/ppm).
- The reactivity reduces slowly at first, then increases to a maximum, called the plutonium peak. This behavior is due to the combined effects of the start of U-235 depletion and the start of Pu-239 production. The latter is a slightly better fuel than U-235, and consequently increases reactivity as it is produced, following a short time lag due to the ~2.5-day half-life of Np-239, the immediate parent of Pu-239.
- Following the plutonium peak, the reactivity decreases in a monotonic fashion indefinitely. This is due to the continued net depletion of fissile nuclides and accumulation of fission products. The plutonium peak, however, does not mark the maximum in plutonium concentration. In fact the latter keeps increasing, however it does so more and more slowly, since Pu-239 participates in fission at the same time as it is produced.
- Hypothetically, if the infinite lattice could be run in steady state as the fuel gained irradiation, the boron concentration would have to be adjusted continuously to reflect the positive reactivity.
- In Figure 6, the reactivity reaches a value of zero at an irradiation of ~1.6 n/kb. This would mark the exit irradiation of the infinite lattice. At this point the boron concentration required would of course be 0.

6 Exit-Burnup Estimation from Lattice Calculations

The fuel-reactivity curve above gave us the discharge irradiation attainable for the infinite lattice. Even before doing fuel-management calculations for the full core, we can devise a way to make a fairly good estimate of the average attainable discharge irradiation for the real CANDU reactor, if we have an estimate of the leakage and in-reactor-device worth.

For the CANDU-6 reactor, good estimates of the leakage and of the device worth (adjusters and zone-controller water) are 30 mk and 18 mk respectively. If we subtract a total of 48 mk from the fuel-reactivity curve, we get a curve (Figure 8) which the full reactor would follow if all parts of it advanced in irradiation at the same rate. While this is obviously not exactly the case, we will still get a fairly good approximation of the reactivity curve for the full reactor as per Figure 8, which shows that the CANDU 6 core would initially reach 0 ppm of boron at an irradiation of about 1.0 n/kb (a burnup of ~4,000 MW.d/Mg(U)). This would be the exit irradiation if the CANDU were refuelled in batch mode. [Note that in practical applications, the excess reactivity of the fresh core is reduced with the use of depleted fuel, and the refuelling is started gradually before the excess reactivity of the core reaches decreases to 0.]

However, CANDU can be - and is - refuelled on line. This means that when the moderator poison runs out, daily refuelling can be started, replacing just enough fuel each day to cancel the loss of reactivity due to the increased overall irradiation.

By repeating this day after day, we eventually reach a state where there is approximately an equal amount of fuel at all irradiations, from 0 to a maximum value which determines the attainable discharge irradiation with daily refuelling. This value is obtained by doing a “rolling average” of the reactivity starting from an irradiation of 0, up to the point where the rolling average is 0. It is clear that the 0 rolling average is obtained when the positive area to the left of the point where the reactivity is 0 is exactly cancelled by the negative area beyond that point. By doing the rolling average numerically, we find that the average attainable exit irradiation is ~1.8 n/kb (burnup ~7,500 MW.d/Mg(U)) – see Figure 8. Thus daily refuelling has almost doubled the average exit burnup, compared to batch refuelling!

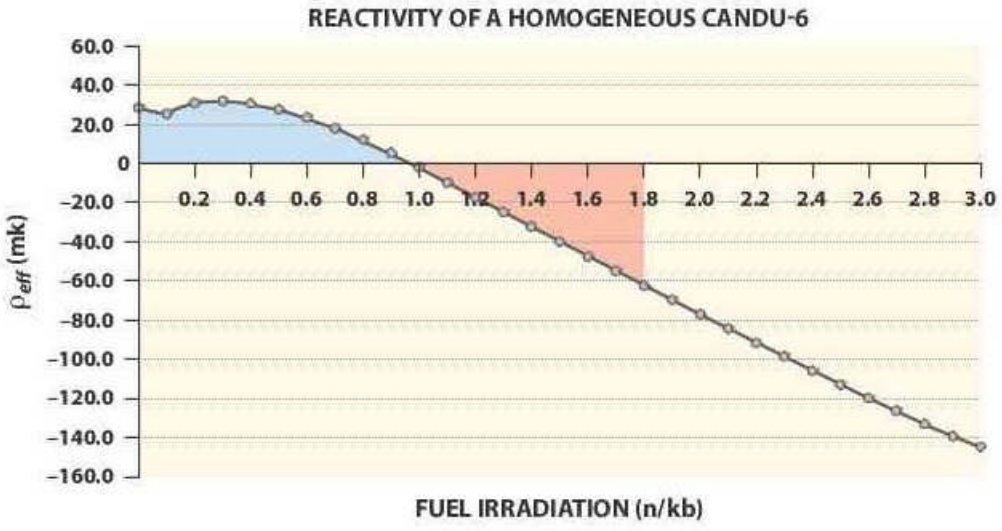

Figure 8 Average Exit Irradiation Attainable with Daily Refuelling

Note of course that all the above analysis, in the previous and current sections, depend on the specific values assumed for various lattice parameters, such as heavy-water purity, fuel and moderator temperatures, etc. A higher value of moderator purity, most importantly, can raise the reactivity curve and consequently increase the attainable exit burnup: a 0.1% increase in moderator purity is estimated to increase the exit burnup by ~360 MW.d/Mg(U). Values around 99.9% for the moderator isotopic purity are common.

7 Flattening the Power Distribution

The reactivity curves in the previous sections provide information on the "local" reactivity in bundles according to their irradiation level. And we have up to now used these figures in the approximation of uniform irradiation throughout the core.

However, of course, fuel in different locations in core actually picks up irradiation at different rates, depending on the local flux. Chapter 4 of this book has shown that the flux distribution in a uniform reactor has a J_0 (Bessel function) shape and a cosine shape in the radial and axial directions respectively. CANDU reactors are not homogeneous, and so the flux distribution will be different. In addition, we may **deliberately** want to change the power distribution.

One reason we may want to change the power distribution is that the J_0 and cosine shapes are "peaked" flux shapes. This means that the power decreases relatively quickly from the maximum value. Now, a peaked flux shape may create a conflict between the reactor power and peak local powers (channel or bundle power). The plant's operating license typically puts limits not only on the total reactor power, but also on the maximum channel and bundle powers. With these restrictions, it may not be possible with a peaked flux shape to generate the reactor power desired without exceeding the licensed maximum channel and bundle powers. For this reason, most power reactors in fact operate with a flattened power distribution, in which the power is redistributed so that the peak is reduced and more channels (radially) and bundles (axially) generate more power. In this way, the desired total power can be generated while

complying with the peak local limits.

In CANDU reactors, power flattening is done in two ways:

1) By placing some absorbing rods in the central area of the core. In CANDU reactors, these are the adjuster rods.
2) By differential fuelling. This means deliberately running the fuel in the central region of the core to a higher discharge irradiation than fuel in the peripheral region. The higher irradiation reduces the local reactivity and therefore the local flux.

Differential fuelling of a core region (it could even be a single channel) in CANDU can also be thought of as being produced by varying the region's refuelling frequency. This can be seen from the following relationship between exit burnup and refuelling rate.

Let P be a region's fission power, B be the average exit burnup in the region, and r_m be the refuelling rate in the region (in mass of uranium per unit time). It is easy then to derive the relationship

$$B = \frac{P}{r_m}, \; also \; written \; as \; r_m = \frac{P}{B} \tag{12}$$

If for example P is given in MW and r_m in MW(U)/d, then the units of B are MW.d/Mg(U). If a CANDU bundle contains a mass M of uranium, then we can write the above relationship in terms of the bundle refuelling rate, r_b:

$$B = \frac{P}{Mr_b} \; or \; r_b = \frac{P}{BM} \tag{13}$$

The most convenient units for r_b are bundles/d, obtained for example from P in MW, B in MW.d/Mg(U), and M in Mg(U)/bundle.

From this analysis we can see that by controlling the refuelling rate one can control the average exit burnup. In fact, in this way we can control the reactivity of the fuel in each region. If we run the fuel in a certain region to a higher burnup, we decrease the region's reactivity, and consequently lower the region's power, as we will see in greater detail further below.

8 Fuel-Management Calculations for Core Design

CANDU reactors are refuelled on-line. Refuelling operations are typically performed every day, or a few times per week. A very small fraction of the fuel in core (typically ~8 fuel bundles, representing something of the order of 0.1-0.2%) is replaced at each refuelling operation. Also, because refuelling is performed on a quasi-continuous basis, the excess reactivity of the core is always very low (except at the very start of the core life, or after a long shutdown).

On account of these features, the overall global power distribution in a CANDU core operated in a well-thought-out manner remains largely constant in time, with relatively small variations ("power ripples") superimposed locally as individual bundles and channels go through their normal burnup cycles from one of their refuellings to the next. Thus, it is meaningful and

useful to want to calculate this long-term average.

In this Section we start to look at fuel-management models which are used at the core-design stage. They represent the reactor in the average over a long period of time, not on any particular day. Such models can then be used to perform diffusion calculations (for example, with full-core codes such as RFSP-IST) to obtain the expected spatial distribution of flux and power in the long term; these distributions will eventually be used as basis for running the reactor over time.

8.1 The Axially-Uniform Model Based on Continuous Refuelling

The first model which we will develop is the Axially-Uniform Model of nuclear cross sections. We start by visualizing the reactor as being continuously refuelled, meaning that fuel is pushed continuously and simultaneously through every fuel channel at a certain speed υ. If channels have length *L*, then the time *T* it takes fuel to traverse the entire channel length is $T = \frac{L}{\upsilon}$.

Let $\Phi(x)$ be the axial flux distribution in a fuel channel, from $x = 0$ to $x = L$ (channel inlet to outlet). Suppose as a first approximation we would like to use the average value $\overline{\Sigma}$ of a basic-lattice cross section $\Sigma(x)$ over the channel [this can be the fission cross section, or absorption cross section, or any other). We can get this average value by applying Eq. (5) to our specific case:

$$\overline{\Sigma} = \frac{\int_0^L \Sigma(x)\Phi(x)\,dx}{\int_0^L \Phi(x)\,dx} \tag{14}$$

Now change variables from x to t by using $x = \upsilon t,\ dx = \upsilon dt$, which gives

$$\overline{\Sigma} = \frac{\int_0^T \Sigma(t)\Phi(t)\,dt}{\int_0^T \Phi(t)\,dt} \tag{15}$$

Now we make a second change of variable, from *t* to fuel irradiation ω:

$$\omega(t) = \int \Phi(t)\,dt,\ \ d\omega = \Phi dt \tag{16}$$

And if we define ω_{exit} as the value of the fuel irradiation at the exit of the fuel channel (but note that we are not limited to using the same value of exit irradiation in all channels), we get

$\therefore$

$$\overline{\Sigma} = \frac{\int_0^{\omega_{exit}} \Sigma(\omega)\,d\omega}{\int_0^{\omega_{exit}} d\omega} = \frac{\int_0^{\omega_{exit}} \Sigma(\omega)\,d\omega}{\omega_{exit}} \tag{17}$$

Thus we would use the average values $\overline{\Sigma}$ calculated as per Eq. (16) (for the various cross-section types) at all bundle positions within each individual fuel channel. Note that actually Eq. (16) is

just another manifestation of Eq. 10). [Once again, note that we can select different values of ω_{exit} in different channels. Another way to visualize this is to realize that we have the option of selecting different speeds υ of the fuel in different channels.]

Once all cross sections are defined for each position in core, and the incremental cross sections of in-core devices are added, then we have a full axially-uniform reactor model for use with the diffusion equation. The solution of that equation will be the core reactivity and the 3-dimensional flux distribution in core, from which all powers, etc., can then be calculated.

Of course this is a simplified model of the properties in the reactor, since in each channel the properties are modelled as uniform and we are losing the axial variation of lattice properties over the channel. This is actually not as bad an approximation as may be thought, because it can be shown that the bi-directional refuelling in CANDU reactors leads to approximately constant lattice properties when these are averaged over 2 neighbouring channels (with the same ω_{exit}). Thus, the axially-uniform model was used extensively in the early stages of CANDU design development and analysis. However, eventually a model which better models the variation of lattice properties in each individual channel was developed. This is the time-average model, described in the next subsection.

8.2 The CANDU Time-Average (Equilibrium-Core) Model

The time-average model [Rouben 2007] is the next, more realistic effort to take into account the spatial distribution of properties over time, arising from different fuel irradiations in different fuel bundles. As opposed to the axially-uniform model, the time-average model does not average lattice properties along a channel. Instead, it takes into account the fact that individual fuel channels are refuelled once in a while, and that fuel bundles remain in a certain location in the channel until the channel is refuelled. It models the effect of the axial refuelling scheme (e.g., 8-bundle-shift (8-bs), 4-bundle-shift (4-bs), etc.) used in each channel on the average lattice properties at each bundle location in the channel.

8.2.1 Degrees of Freedom in CANDU Operation

Let us look at the breadth of freedom in operating a CANDU reactor. The following are "degrees of freedom" available to the operator:

- The fuel type used (e.g., the fuel enrichment or the fuel-bundle geometry, that is 28-element, 37-element, etc.)
- Which channel to refuel on any given day
- Which channel to refuel after the previous one refuelled, and which channel to re-fuel after that one (i.e., ultimately, the sequence of refuellings)
- The "axial" refuelling scheme to be used (i.e., the number of bundles to change at each channel refuelling), e.g., 8-bundle shift, 4-bundle shift, 2-bundle shift, or other, more complicated scheme. In addition, this axial refuelling scheme may vary from core region to core region, or even in principle from channel to channel. [Note that refuelling schemes where bundles are reshuffled from one channel to another are not considered in the current discussion.]
- The refuelling frequency of each channel – the average frequency will depend on the

fuel type(s), on the refuelling scheme, and on the overall core-reactivity decay rate.
- The desired discharge (exit) burnup for the fuel, as an overall average and even by core region
- The power desired for each core zone or region – yes, this is something that can be set at design time (of course the sum of the region powers must be equal to the total core power).

These degrees of freedom are not all independent of one another: refuelling frequencies, discharge burnup, and region powers are all interrelated. Nonetheless, it is clear that there is a very broad range of possibilities available to the operator, even if a single fuel type is used. Therefore, rational and orderly operation of the reactor really requires following guidelines in terms of the average refuelling frequency of each channel.

8.2.2 Definitions

Let us start with some notation and some definitions:

Let *c* be a label for channel number, *c* = 1 to *M*, where *M* is the total number of channels in core

- Let *b* be a label for a bundle-position number within a channel, *b* = 1 to N_c, where N_c is the total number of bundles per channel
- Then we can use *cb* as a label for a specific individual bundle position in core
- Let *x* be a label for a type of nuclear cross section, e.g., absorption, fission, etc.
- Let $\phi_{cb}(t)$ and $\Phi_{cb}(t)$ be respectively the **fuel flux** and the **cell flux** at position cb at some time t. These fluxes are actually multigroup quantities (2-group in the current RFSP-IST). $\phi_{cb}(t)$ and $\Phi_{cb}(t)$ are related by the so-called "F-factor", ratio of flux in fuel to average flux in cell; this is calculated by the lattice code.
- Let $\phi_{tav,cb}$ and $\Phi_{tav,cb}$ be the corresponding **fuel and cell fluxes** in the time-average model. Because the time-average model does not have time as an independent parameter, these fluxes are not functions of time.
- Let D_c be the average time interval between refuellings of channel *c*; this is also known as the **dwell time** for channel *c*. [Note: This is not the same as the average residence time of a bundle in core, since in most refuelling schemes some bundles remain in core for more than 1 cycle.]
- Let $\omega_{entr,cb}$ be the fuel irradiation at the time of entrance of the fuel at position *cb*, and
- Let $\omega_{exit,cb}$ be the fuel irradiation at the time of exit of the fuel from position *cb*.
- Also, let E_c be the total number of bundles which leave channel c on a refuelling operation; these bundles will be labelled β, β = 1 to E_c. For example, in the 8-bs refuelling scheme, we have E_c = 8, and the bundles β are bundles 5 to 12 from the channel inlet end.
- Let $\omega_{exit,c}$ be the **channel exit irradiation** of the fuel from channel *c*, i.e., it is the average of the exit burnup over the bundles β = 1 to E_c which leave the core on a refuelling.
- Let $\Sigma_{x,cb}(\omega)$ be the macroscopic cross section for cell *cb* for reaction type *x*. This is a function of the fuel irradiation ω.

- Then let $\Sigma_{x,cb,tav}$ denote the time-average cell cross section for cell *cb* and reaction type *x*; this will be calculated in the time-average model.

8.2.3 The Selectable Quantities

We shall take the channel exit-irradiation values $\omega_{exit,c}$ values as the essential degrees of freedom, i.e., as the ones most easily selected by the designer. These $\omega_{exit,c}$ values will be dependent on the dwell times D_c, and vice versa. Both of course will depend also on the fuel-flux distribution $\phi_{tav,cb}$, which depends on the core flux distribution $\Phi_{tav,cb}$, which will be determined as the solution of the neutron diffusion equation. The relationship between the fuel and cell fluxes comes from the lattice (or cell) calculation.

Note that in addition the axial refuelling scheme is also a degree of freedom which can be selected a priori by the designer, for each fuel channel (or region) in core.

8.2.4 Relationships Between Bundle and Channel Irradiations and Dwell Times

For positions *cb* in core where a refuelling introduces fresh fuel:

$$\omega_{entr,cb} = 0 \tag{18}$$

For positions *b* to which a bundle moves from a position *b'* in the same channel upon refuelling,

$$\omega_{entr,cb} = \omega_{exit,cb'} \tag{19}$$

Now, since

$$\omega \equiv \mathit{Irradiation} = \mathit{Flux} \times \mathit{Time}(19) \tag{20}$$

then

$$\mathit{Incremental\ irradiation\ accumulated\ by\ fuel\ at\ cb\ between\ refuellings} = \varphi_{tav,cb} \times D_c \tag{21}$$

and we can use this to relate the exit irradiation to the entrance irradiation:

$$\omega_{exit,cb} = \omega_{entr,cb} + \varphi_{tav,cb} \times D_c \tag{22}$$

We can now relate the average channel exit irradiation $\omega_{exit,c}$ to the fuel flux at the various bundle positions in the channel, as follows.

By definition,

$$\omega_{exit,c} = \frac{1}{E_c} \sum_{\beta=1}^{E_c} \omega_{exit,c\beta}$$

(23)

and, using Eq. (22)

$$\omega_{exit,c} = \frac{1}{E_c} \sum_{\beta=1}^{E_c} \left(\omega_{entr,c\beta} + \varphi_{tav,c\beta} \times D_c \right) \tag{24}$$

The bundle positions β are those from which bundles leave the channel on refuelling. Some of these positions may at the same time be positions into which bundles enter as fresh bundles, e.g., bundle positions 5 to 8 for an 8-bundle-shift refuelling scheme. For these bundles, the

term $\omega_{entr,c\beta}$ is zero and does not contribute in Eq. (24).

On the other hand, some β may be positions where bundles come from a previous location in the channel, e.g., bundles 9 to 12 in the channel for the 8-bundle-shifts refuelling scheme. For these bundles, the term $\omega_{entr,c\beta}$ is **not** zero, but can be equated (see Eq. (19)) to $\omega_{exit,c\beta'}$, where β' is the position from which the bundle at β came on the previous refuelling. In this way, it can be seen that the sum of terms in ϕ_{tav} in Eq. (24) now extends over bundles β **and** β'.

In fact, by repeating the exercise for bundles β' and examining from which position **they** came, we see that eventually all the terms $\omega_{entr,cb}$ disappear and are replaced by terms in ϕ_{tav}, with the sum in Eq. (24) covering **all** bundles b in the channel:

$$\omega_{exit,c} = \frac{1}{E_c} \sum_{b=1}^{N_c} \left(\varphi_{tav,cb} \times D_c \right) \tag{25}$$

Since D_c is a channel quantity and is independent of the bundle position *b*, we can take D_c out of the sum. We can also turn the equation around to isolate D_c on one side:

$$D_c = \frac{E_c \times \omega_{exit,c}}{\sum_{b=1}^{N_c} \varphi_{tav,cb}} \tag{26}$$

Eq. (26) links the channel dwell time to the channel average exit irradiation, the refuelling scheme (via E_c), and the total fuel flux in the channel.

8.2.5 Relationships Between Time-Average Cross Sections and Irradiation Values

For any bundle position *cb* in core and any cross section of type x, we can write the time-average cross section during the bundle's residence time at that location using Eq. (11) derived earlier:

i.e.,

$$\Sigma_{x,cb,tav} = \frac{\int_{\omega_{entr,cb}}^{\omega_{exit,cb}} \Sigma_{x,cb}(\omega)\, d\omega}{\omega_{exit,cb} - \omega_{entr,cb}} \tag{27}$$

The integral in Eq. (27) can easily be computed using the cell cross section obtained as a function of irradiation with the cell code.

Using the values selected for the entrance and exit irradiations at each position, the $\Sigma_{x,cb,tav}$ can be computed for all positions in core. These nuclear lattice properties can then be entered into the diffusion core model, and the neutron-diffusion equation can be solved by the usual means to find the time-average flux distribution $\Phi_{tav,cb}$.

8.2.6 Summary of Computational Scheme

The computational scheme for the time-average model is now complete. It consists of the neutron-diffusion equation plus Eqs. (18), (19), (22), (24)-(27).

Remember that:

- The flux distribution $\Phi_{tav,cb}$ depends on the time-average cross sections $\Sigma_{x,cb,tav}$ through the diffusion equation;
- The time-average cross sections $\Sigma_{x,cb,tav}$ depend on the entrance and exit irradiation values via Eq. (27);
- The entrance and exit irradiation values $\omega_{entr,cb}$ and $\omega_{exit,cb}$ depend on the fuel flux in the channel (which will be calculated from the time-average flux $\Phi_{tav,cb}$) and the dwell-time D_c via Eqs. (18), (19) and (22);
- The dwell-time D_c depends on the flux and on the channel-average exit irradiation $\omega_{exit,c}$ via Eq. (26).

It is clear then that this equation set must be solved as a self-consistency problem. An iterative solution scheme is applied until satisfactory self-consistency is attained.

The basic independent data which needs to be input to the time-average model consists of:

a) the axial refuelling scheme for each channel (for instance, 8-bs, 4-bs, 10-bs, etc.). Note that this may vary from channel to channel, i.e., one may choose 8-bs for some channels and 4-bs for others. Typically, however, the axial refuelling scheme must be selected taking into account also non-physics considerations, e.g., fuelling-machine utilization.
b) the channel-average exit irradiations $\omega_{exit,c}$. These are the main degrees of freedom in the problem. While there are in principle as many degrees of freedom as there are channels, the core is usually divided into a small number of relatively large regions, in each of which ω_{exit} is taken as uniform, to reduce the number of degrees of freedom. Figure 9 illustrates a possible time-average model with 8 irradiation regions, for fine control over the target power distribution; note in particular the regions at the bottom and far right-hand side, which represent areas in the calandria with much hardware (to hold device guide tubes in position) and consequently for which different exit irradiations are needed.

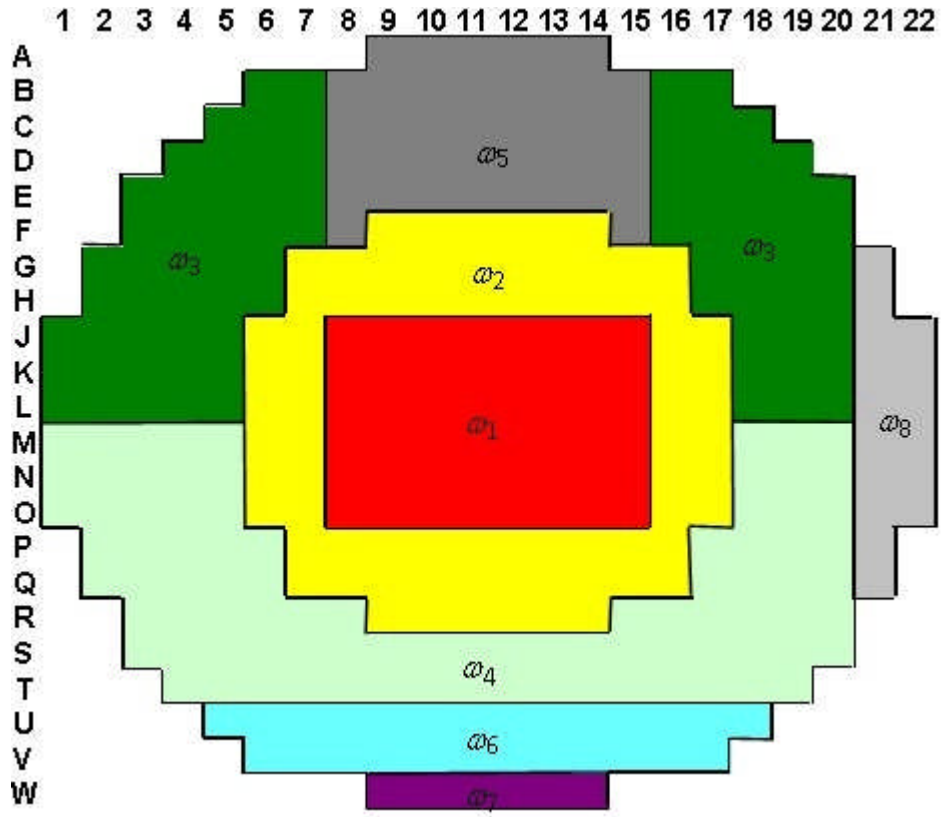

Figure 9 Example of Possible Time-Average Model, with Eight Irradiation Regions

A very important point to note is that there are constraints on the degrees of freedom:

- First, reactor criticality is required. That is, the value obtained for the reactor multiplication constant k_{eff} when solving the diffusion equation must be unity (or close to unity, if we know that the model does not include all material in core, for instance detector material, in which case a small bias is required) – otherwise, the results obtained cannot be expected to represent a realistic time-average picture.
    - Secondly, the absolute and relative values of the channel-average exit irradiations $\omega_{exit,c}$ have a significant impact on the radial power distribution, and in turn on the refuelling frequencies and the attained discharge burnup. Increasing the exit irradiation in a region tends to decrease the local reactivity of the region, leading to a lower power. Decreasing the exit irradiation has the opposite effect.
    - Thus, the channel exit irradiations need to be selected judiciously to achieve both criticality and the desired degree of radial flattening of the power distribution and of consequent burnup and refuelling rates.

The flow chart for the iterative calculation for the time-average flux and power distribution is

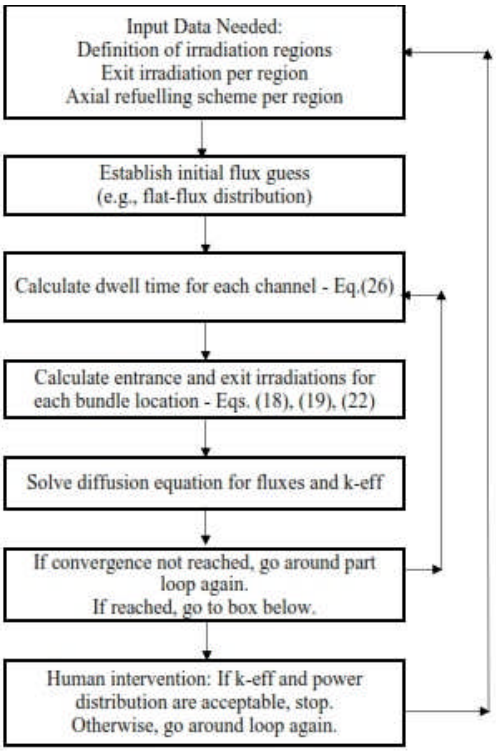

Figure 10 Flow Chart of Time-Average Calculation

shown in Figure 10. First, the user selects the axial refuelling scheme(s) and the core regions with the corresponding values of $\omega_{exit,c}$. Using an initial guess for the flux distribution, the program determines the channel dwell times D_c and the entrance and exit values of irradiation $\omega_{entr,cb}$ and $\omega_{exit,cb}$. It then determines the time-average cross sections $\Sigma_{x,cb,tav}$. The program then proceeds to solve the neutron diffusion equation. The flux distribution thus obtained is used to repeat the cycle, until consistency is attained in all the parameters.

At that point, the user must intervene (outside the code) and examine the results obtained for k_{eff} and for the power distribution. If k_{eff} is not equal (or at least close) to unity, the exit irradiations selected must be adjusted. A standard way of doing this is to increase or decrease all the $\omega_{exit,c}$ values uniformly, depending on whether the k_{eff} is too high or too low. Also, the radial power distribution must be examined (this can be done at this time, or after another cycle of iterations with the new $\omega_{exit,c}$ values).

If the radial power distribution is not satisfactory, e.g., if the degree of radial flattening is not the desired one, or if peak channel powers are too high (or too low), or if the rate of refuelling in certain regions is too high, then the regions and/or exit irradiation values must be "manually" adjusted to move the results in the desired direction. Then another cycle of iterations is started.

This process is repeated until a critical reactor (or the required bias) and a satisfactory power distribution are obtained, at which point the time-average model has been established. In practice, for operating reactors some additional conditions may be imposed when designing the

time-average model, such as matching time-average channel powers determined from relevant operating histories. This is obtained by varying the individual channel exit irradiations; in such instances Figure 9 may be replaced by a map with more irradiation regions, or even by a full map of 380 individual exit irradiations, one for each channel.

8.2.7 Output of Time-Average Calculation

The calculations described above provide or can provide a number of time-average outputs, which are useful as design outputs and also as targets for the reactor operator. These outputs include:

- The reactor multiplication constant (k_{eff})
- The 3-dimensional time-average neutron-flux distribution. From this, the time-average zone fluxes can be obtained, for use as the target distribution by the Reactor Regulating System.
- The channel and bundle powers. Note that these are the time-average values; they do not include the instantaneous ripple corresponding to the stage in the refuelling cycle. The maximum time-average channel power in a CANDU-6 reactor is typically about 6.6-6.7 MW.
- The entrance and exit irradiation values for each bundle position in core.
- The channel dwell times (intervals between refuellings of the individual channels). Figure 11 shows dwell times from a CANDU-6 time-average calculation. One-cycle residence time of bundles at a given position in a CANDU-6 reactor typically range between 160 and 360 full-power days (FPD).
- The refuelling rates in the various irradiation regions.
- The reactivity decay rate in mk/Full-Power Day. This can be determined in the time-average model from the change in reactivity (as obtained from the change in k_{eff}) for an overall change in the exit irradiation in all regions and linking that to the change in residence time corresponding to the change in irradiation. The reactivity-decay rate per FPD is useful in gauging the expected variation in zone-control-compartment fill per FPD if there were no refuelling. [Note that the same quantity can also be calculated by doing 2 core snapshots 1 FPD apart (see next Section) without refuelling any channels.]

See some of these results from a particular time-average calculation for a CANDU-6 reactor in Table 2 below.

Table 2 Example of Summary Results from a CANDU-6 Time-Average Calculation

Total Reactor Power (MW)	2061.4
Total Fission Power (MW)	2158.5
Average Channel Power (kW)	5425
Average Bundle Power (kW)	452
Uranium Mass per Bundle (kg)	19.1
Maximum Channel Power (kW)	6604 (N-6)
Maximum Bundle Power (kW)	805 (O-5, Bundle 7)
k_{eff}	1.00250
Average Exit Burnup	3272 MW.h/Bundle 171.3 MW.h/kg(U) 7139 MW.d/Mg(U)
Avg. Channel Dwell Time (FPD)	192
Feed Rate	1.98 channels/FPD 15.83 bundles/FPD
Reactivity Decay Rate (mk/FPD)	-0.385
Average Zone Fill (%)	50.0

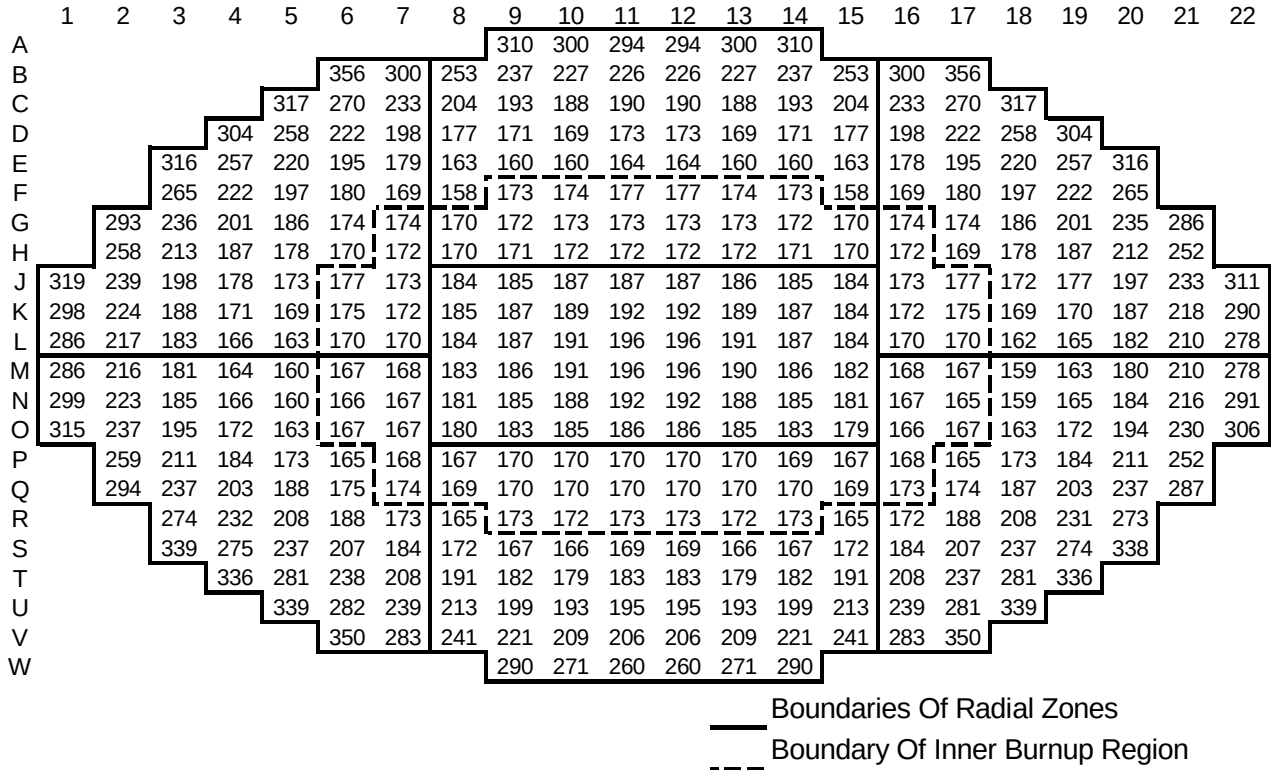

Figure 11 Dwell Times (in FPD) from a Time-Average Calculation for the CANDU 6

9 More Design Calculations: Snapshots Based on the Time-Average Model

In this section we look at another type of design calculations, intended to look ahead at power and overpower results which may be expected during reactor operation.

An important point to remember about the time-average core is that it features no refuelling ripple: all properties are averaged over residence time, no channel is near the beginning or end of its refuelling cycle. However, at the core design stage it is important to be able to collect possible and realistic snapshots of the reactor power distribution during actual reactor operation, without actually following the history of the reactor. We can obtain snapshots of the power distribution if we can define instantaneous distributions of bundle irradiation to calculate instantaneous lattice properties, based on which the diffusion equation can be solved.

On way to obtain instantaneous lattice properties is to create a map of "channel ages". To define channel ages let us first consider a typical "channel-irradiation-and-power cycle".

9.1 Channel-Irradiation-and-Power Cycle

The channel-irradiation-and-power cycle may be described as follows.

- When a channel is refuelled, its local reactivity is high, and its power will be several percent higher than its time-average power.
- The fresh fuel in the channel then initially goes through its plutonium peak as it picks up irradiation. The local reactivity **increases** for ~ 40-50 FPD, and the power of the channel tends to increase further.
- Following the plutonium peak, the reactivity of the refuelled channel starts to decrease as the irradiation increases further, and its power drops slowly.
- The reactivity of the channel and its power then continue to drop. Eventually, the channel becomes a net "sink" (absorber) of neutrons, the time since the channel's last refuelling approaches the channel's "dwell time" D_c (as defined in the time-average model), and the fuel irradiation in the bundles which will be discharged at the channel's next refuelling increases towards the discharge value, and the time comes around when the channel must be again refuelled. At this time the power of the channel may be 10% or more below its time-average power. When the channel is refuelled, its power may jump by 15 to 20% or even more.

In on-going reactor operation, the power of each channel therefore goes through an oscillation about the time-average power during every cycle. This cycle repeats - not in exactly the same quantitative detail each time- at every refuelling of the channel. This is illustrated in Figure 12.

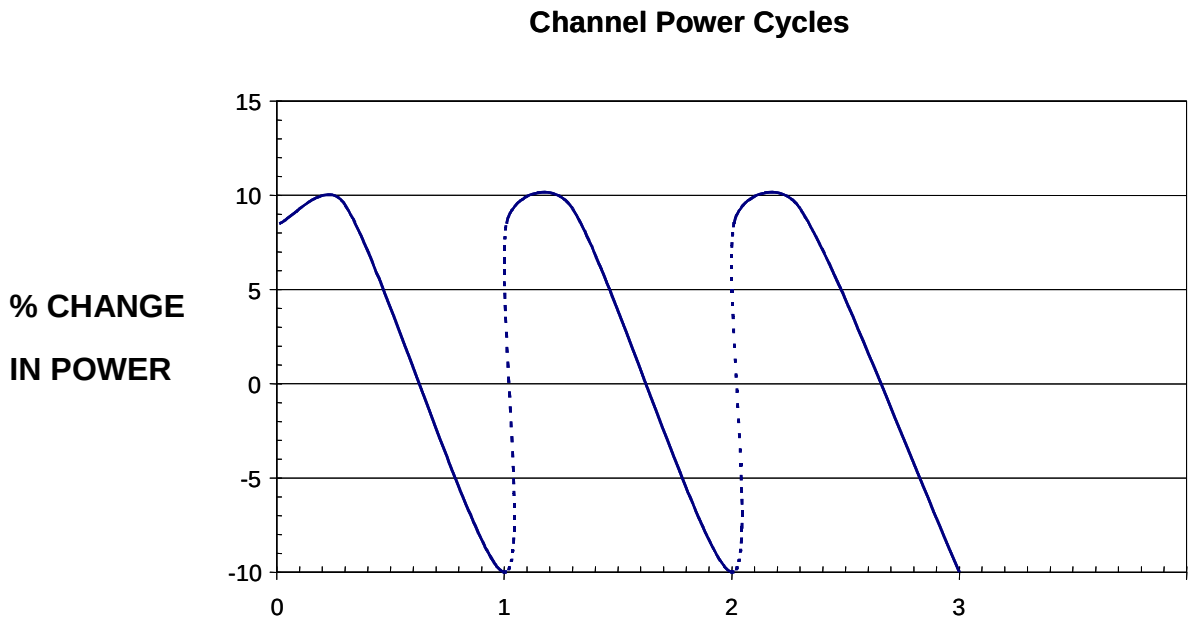

Figure 12 Channel-Power Cycle During On-Going Reactor Operation

9.2 Channel Ages

On any day of operation, we can define the "age" a_c of channel *c* as the instantaneous fraction that it has achieved in its irradiation cycle since its last refuelling. On any given day different channels will of course have different ages: channels which were refuelled recently have a low age (a number close to 0.0), whereas those which were refuelled quite a while ago have a "high" age (a number close to 1.0). The channel ages a_c will be numbers between 0 and 1, although it is possible for a given channel to have an age somewhat higher than 1, if it has not been refuelled for a time longer than its dwell time.

From the meaning of the channel's age, we can define a value for the instantaneous irradiation of all bundles in the channel. For channel *c* and bundles *b*, using the entrance and exit irradiation values for bundle positions (from the time-average model), we can write for bundle's *cb* instantaneous irradiation

$$\omega_{inst,cb} = \omega_{entr,cb} + a_c \times \left(\omega_{exit,cb} - \omega_{entr,cb} \right) \tag{28}$$

The lattice properties for position c_b can then be determined from the instantaneous irradiation value.

9.3 Snapshot with Patterned Ages

To model the core on a given day, we can define a core snapshot by assigning to each channel *c* in core an age value a_c.

We could select random values (between 0 and 1, or slightly higher than 1) for the a_c. However, random selection of ages may easily result in low age values for close-neighbour channels (i.e., clusters of low ages). This would not be very realistic, because low ages in close proximity can

lead to "hot spots" in channel power, and a good operator will consciously avoid refuelling close-neighbour channels very closely in time, so as to avoid low ages close to one another.

It is therefore more desirable to use some "intelligence" in assigning channel ages. One way which has been found to do this is to start by defining an "intelligent pattern" in the order in which channels would be refuelled in a relatively small region of the core, e.g., 6-channels-by-6-channels (see Figure 13). The next step is to subdivide the entire core into 6 x 6 regions and to define a core "refuelling sequence" by selecting channels intelligently in sequence from one region to region to another, making sure that whenever revisiting each 6 x 6 region the order within the region follows the pattern defined for the 6 x 6 square. One obtains (see [Rozon and Shen 2001] a core refuelling sequence such as shown for example for the CANDU 6 in Figure 14, with numbers n_c from 1 to 380 assigned to the channels. The age assigned to channel c can then be defined as

$$a_c = \frac{380.5 - n_c}{380}, \quad n_c = 1,...,380 \tag{29}$$

Once the snapshot model with lattice properties derived using Eqs. (29) and (28) is solved with the diffusion code, useful results are obtained for the maximum channel and bundle powers and, also very importantly, for the Channel Power Peaking Factor (see further below, Section 11.3) and for the overall channel-power, bundle-power, and region-power distributions which can be expected during on-going reactor operation.

From the one snapshot, many others can be obtained by "massaging" the core refuelling sequence, for example by reflecting it horizontally or vertically, or alternatively by redefining each n_c as modulo (n_c + N), where N is a number which can be selected at will. In this manner many sets of results and good statistics can be obtained for maximum channel and bundle powers and the CPPF. This can be very useful in determining rules for selecting channels for refuelling.

22	29	8	17	14	27
7	16	23	34	9	4
30	11	28	19	24	35
3	20	33	2	21	6
12	25	10	15	26	31
5	36	13	32	1	18

Figure 13 Possible Pattern for Order of Refuelling in a 6 x6 Region of Core

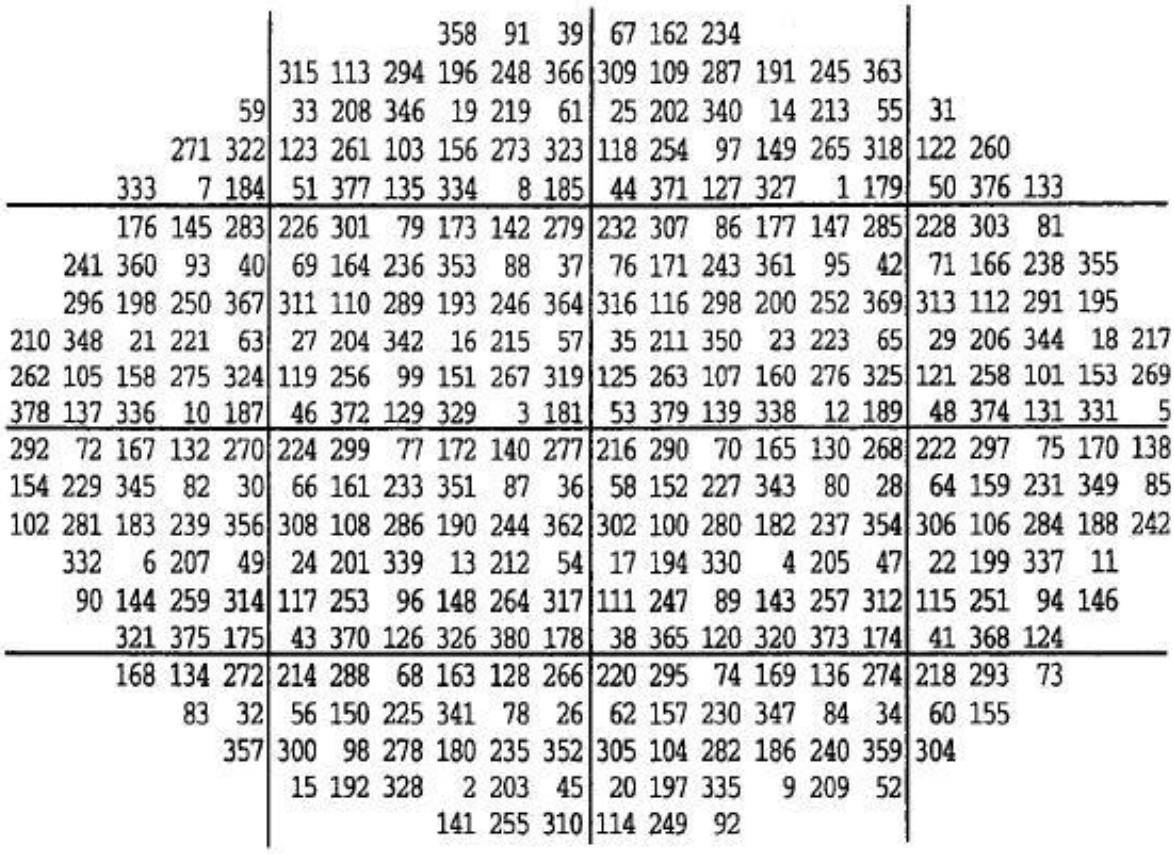

Figure 14 Possible Core Refuelling Sequence for the CANDU 6

10 Design of the CANDU Initial Core

The CANDU initial core is the state of the reactor as it starts life. This is a very specific state, in which the fuel throughout the core is fresh (unirradiated). At zero irradiation, the CANDU lattice has high reactivity. Of course this high reactivity must be cancelled in order to allow for the reactor to be run in steady state.

There is no differential burnup which can assist in flattening the power distribution. Consequently, the power of the central core region would be unacceptably high if no alternate means of flattening the radial power distribution were provided.

Two means are available in CANDU to cancel the high reactivity of the initial core and to flatten its power distribution. These are the use of moderator poison (boron, or possibly gadolinium) and the use of depleted fuel (fuel at an enrichment around 0.48-52% of U-235).

Advance calculations are needed to design how exactly to use these two means to render the core critical and to provide appropriate power flattening. Design calculations are done with various concentrations of poison and various numbers and locations of depleted-fuel bundles until a desirable/attractive result is achieved.

The solution is not unique. There are many ways to design the poison concentration and

depleted-fuel assignment for the initial core. However, note:

- using only depleted fuel and no moderator poison would result in having to initiate refuelling very early, the consequence being that too much fuel would be removed with very low burnup – an economic penalty, whereas
- using only boron and no depleted fuel would not achieve sufficient power flattening.

In the first design of the CANDU-6 initial core, the solution which was adopted used two depleted-fuel bundles (of 0.52 atom percent ^{235}U content) in each of the innermost 80 fuel channels, with the depleted-fuel bundles located in positions 8 and 9, numbered from the channel refuelling end. In these axial positions, the depleted-fuel bundles are removed from the core in the first refuelling visit of each of these channels. The boron concentration in this design turns out to be about 2 ppm at full CANDU-6 power. In recent years some operators have redesigned the initial core loading to factor in the impact of the required initial poison concentration on the safety analysis.

11 Fuel-Management Calculations for Reactor Operation

Once the reactor is operating, it is important to follow the reactor history. This is called a core-follow calculation. It involves calculating updates of the core's power and burnup distributions at specific instants in the reactor's operating history, usually at time intervals of 1 or a few FPD. The objective is to have good knowledge of the state of the core at all times, to be able to confirm compliance with the maximum channel and bundle powers allowed by the operating licence.

Note that the core-follow calculations described here can also be done for a simulated core history, with simulated channel refuellings and device positions. This is to demonstrate how a reactor would/could be operated.

11.1 From Initial Core to Onset of Refuelling

At the very start of reactor operation, the entire initial fuel load goes through the plutonium peak at about the same time (about 40-50 FPD). At this juncture, the core reaches its global plutonium peak and the core reactivity is the highest it will ever be. Following the plutonium peak, the plutonium production can no longer compensate for the depletion of ^{235}U and the build-up of fission products, and the excess core reactivity decreases. Also at this time moderator poison must be removed as the excess reactivity drops gradually to zero, at about FPD 120.

During this entire first period in the reactor life, refuelling is not necessary since there is already excess reactivity. The core-follow for this period is therefore rather simple. It is a matter only of simulating the core every few days with instantaneous reactivity devices and a poison concentration which yields a critical reactor.

When the excess core reactivity has fallen to a small value, actually, about 10 or 20 FPD before it reaches 0 (i.e., typically around FPD 100), refuelling operations start. It is best not to wait until excess reactivity is exactly 0, because the initial refuelling rate would prove too high.

11.2 After Onset of Refuelling

When on-power refuelling starts, it becomes the primary means of maintaining a CANDU

reactor critical. During the transitional period which follows the onset of refuelling, the reactor gradually approaches the equilibrium core, with the refuelling rate rapidly tending to the time-average value (for example, approximately 15-16 bundles per FPD in the CANDU 6).

When refuelling starts, it is channels in the inner core which tend to be refuelled first, because this region has achieved the highest burnup (on account of its higher flux values). As time goes on, more channels in the peripheral regions of the core will be refuelled.

Approximately 400 to 500 full-power days (FPD) after initial start-up, a CANDU reactor has reached an "equilibrium core" state. The overall refuelling rate, the in-core average burnup, the burnup of the discharged fuel, and the refuelling rates in different core regions have become essentially steady with time. A number of channels are refuelled every day, **on the average**. However, note that refuelling is not necessarily done **every** calendar day; some stations prefer to concentrate all refuelling operations to 2 or 3 days within each week.

Doing core-follow calculations at short intervals (1 to a few FPD) then becomes crucial in running the reactor in a steady and effective manner, to comply with licence limits, to ensure that there are no "hot spots" or large power tilts.

Each run of the diffusion code in the core-follow requires inputting the instantaneous 3-dimensional irradiation/burnup distribution. This of course comes from the output of the preceding run. In addition, each run of the core-follow requires modelling all channel refuellings which have occurred since the previous run (and their timing). This allows modelling bundle movements and the entry of fresh-fuel bundles in appropriate locations. The instantaneous positions of reactivity devices are also input. From the power calculated and the time step used, the fuel irradiation in each individual bundle are updated, and the lattice properties updated.

The output of the current run is then obtained and becomes the starting point for the calculation at the next time step. The current 3-dimensional power and fuel-irradiation distributions obtained serve then specifically as the basis on which intelligent selections of channels to refuel are made (see second section below).

In addition, another very significant output of core-follow calculations is the determination of the Channel Power Peaking Factor, which is used in the calibration of in-core protection-system (Regional Overpower/Neutron Overpower) detectors. This is defined in the next Section.

11.3 Channel-Power Peaking Factor

At any given time, there are several channels in the core which are at or near the maximum power in their power-and-irradiation cycle. Therefore, the maximum instantaneous channel power is always higher than the maximum channel power in the time-average model.

The Channel-Power Peaking Factor (CPPF) quantifies the degree by which the instantaneous power distribution peaks above the time-average distribution:

$$CPPF = \underset{c}{Max}\left[\frac{Channel-Power_{instantaneous}(c)}{\underset{c}{Channel-Power}_{time-average}(c)}\right] \tag{30}$$

where *c* runs over channels in the core.

The exact value of the CPPF (which varies from day to day) is extremely important because it is used to calibrate the in-core protection (ROP/NOP) detectors. The protection system(s) are designed to actuate a shutdown system in a power increase before any fuel channel risks reaching a "critical channel power" (e.g., a power at which there would be fuel dryout somewhere in the channel). The CPPF has therefore important safety implications.

Hundreds of flux shapes are used in the design of the ROP/NOP detector system to determine detector positions and setpoints. These flux shapes are calculated in the time-average model, assuming many different core configurations. But because the real instantaneous channel powers are higher than the time-average powers, channels would reach their "critical channel power" earlier than predicted in the time-average model. To take this into consideration and ensure proper safety coverage in the instantaneous power shape, the in-core detectors are calibrated each day to the instantaneous value of CPPF.

On the other hand, a high CPPF value could cut into the reactor's operating margin, i.e., the CPPF has economic implications. It is therefore important to keep the CPPF as low as possible.

The competing safety and economic considerations mean that a careful selection of channels to be refuelled needs to be made always. Determining the daily CPPF value, selecting channels to keep it low, and ensuring detectors are calibrated to the correct value, are on-going duties of the fuelling engineer or reactor physicist at a CANDU nuclear generating station.

11.4 Criteria for Selecting Channels for Refuelling

One of the main functions of the fuelling engineer or reactor physicist is to establish a list of channels to be refuelled during the following period (few days) of operation. For instance, for a 5-FPD period, a list of approximately 10 channels must be prepared. To achieve this, the current status of the reactor core is determined from computer simulations of reactor operation, the on-line flux mapping system, the ROP and RRS in-core detectors, and zone-control-compartment water fills. The computer simulations of reactor operation provide the instantaneous 3-dimensional flux, power and burnup distributions.

Good combinations of channels selected for refuelling in the few days to follow will typically contain:

- channels "due to be refuelled", i.e., channels for which the time interval since the last refuelling is approximately equal to the channel dwell time (from the time-average calculation)
- channels with high current value of exit burnup, relative to their time-average exit burnup
- channels with low power, relative to their time-average power
- channels in (relatively) low-power zones (compared to the time-average zone-power distribution)
- channels which, taken together, promote axial, radial and azimuthal symmetry and a power distribution close to the reference power shape
- channels which provide sufficient distance to one another and to recently refuelled channels (to avoid hot spots)

- channels which will result in acceptable values for the individual zone-controller fills (20%-70% range), and
- channels which, together, provide the required reactivity to balance the daily reactivity loss due to burnup (and which will, therefore, tend to leave the zone-controller fills in the desired operational range: average zone fill between 40 and 60%) .

Note that channel selections for refuelling are seldom unique. Many options are available. A good way of being confident about a channel selection is to perform a **pre-simulation** of the core following the refuellings. This pre-simulation, especially if the code can predict the resulting zone-control-compartment fills (i.e., the bulk-control and spatial-control responses of the Reactor Regulating System), will show whether the various power, burnup, and zone-fill criteria are likely to be satisfied, or whether a different channel selection should be made. In fact, CANDU operators employ pre-simulations routinely to ensure optimum fuelling selections, including achieving low CPPF values, i.e., good operating margins.

12 Advanced Fuel Cycles

On account of the high neutron economy provided by heavy-water moderation, the CANDU reactor can run on natural-uranium fuel (unlike Light-Water Reactors). But this also means that the CANDU reactor can run on fuels which have higher effective enrichments than natural uranium. This allows a number of Advanced Fuel Cycles to be adopted in CANDU reactors in the future. Many of these cycles illustrate the great synergy possible between CANDU and PWRs, as CANDU can in some way re-use PWR fuel and extend the achievable burnup and reduce waste volumes.

Fuel-management simulations for Advanced Fuel Cycles would proceed in essentially the same manner as for the once-through natural uranium (NU) cycle. Of course the calculation of lattice properties would have to reflect the presence of different nuclides and/or of different nuclide concentrations.

In many cases the Advanced Fuel Cycles can be adopted in CANDU reactors without any changes to the reactor or the control devices. In other cases it may be necessary to adopt different axial refuelling schemes (replacing fewer bundles per visit to a channel). Or it may be appropriate to alter or remove some reactivity devices to optimize reactivity and burnup considerations.

Some examples of Advanced Fuel Cycles in CANDU are:

- The use of Slightly Enriched Uranium (SEU). In this cycle uranium with enrichment in the range 0.9% to, say, 1.2% is used instead of NU. The discharge burnup can be increased significantly, with a consequent significant decrease in the volume of irradiated fuel replaced per year.
- The use of recycled uranium (RU). This uranium would be recovered from the reprocessing of irradiated fuel from CANDU, or more likely, from PWRs. In this case, the presence of certain concentrations of other isotopes of uranium in the fuel has to be recognized in the calculation of lattice properties.
- The MOX (Mixed Oxide) Fuel Cycle, where fuel would be produced from a mixture of uranium and plutonium separated in the reprocessing of PWR fuel. Here again a

range of fissile fractions can be accommodated in the MOX fuel.

- The DUPIC Cycle (Direct Use of PWR Fuel in CANDU). This cycle also uses fuel made from reprocessed PWR fuel, however in this case dry reprocessing is used which does not separate the plutonium from the uranium. A typical fissile fraction in irradiated PWR fuel is about 1.5% (0.9% uranium and 0.6% plutonium). Studies of the DUPIC cycle made from this fuel have shown that the **additional** burnup obtainable in CANDU can be about double the burnup achieved in the original Pressurized Water Reactor.
- The Thorium Cycle. Although Th-232 is not fissile, it is a fertile nuclide: Upon absorption of a neutron and two beta decays it becomes (via Pa-233) the fissile fuel U-233. This cycle draws a lot of interest, as thorium is roughly 3 times as abundant as uranium in the earth's crust, so its use would significantly increase our nuclear natural resources. The thorium cycle requires mixing uranium with a "driver" fuel which provides the neutrons to be absorbed by the thorium. The driver fuel can be uranium or plutonium. In CANDU, the thorium and the driver fuel can be placed in different core regions or different channels, or can even be mixed within the same fuel bundle. The U-233 can be burned in situ or can be separated by reprocessing the fuel after it has been sufficiently irradiated. Much study of the thorium cycle is ongoing currently.

13 Summary

This Chapter has summarized the concepts, models and calculations involved in the management of nuclear fuel in CANDU reactors.

Fuel management in CANDU has both design and operations aspects.

The design component consists of establishing:

- the desired time-average power distribution for the equilibrium core, which will be used as the target power shape by the site fuelling engineer, and
- the configuration of depleted fuel in the initial core.

The design of the time-average distribution is facilitated by the flexibility in selecting region-specific (or, in the limit, channel-specific) target exit-irradiation values and axial refuelling schemes, allowed by the CANDU on-power-refuelling feature.

The operations component is the responsibility of the site fuelling engineer or reactor physicist. It involves:

- core-follow calculations, typically performed 2 or 3 times per week to keep close track of the in-core flux, power, and burnup distributions and of the discharge burnup of individual bundles,
- the selection of channels for refuelling, based on the current core state, power and burnup distributions and zone-control-compartment water fills, and
- the determination of the CPPF (channel-power-peaking factor) value, used as a calibration factor for the ROP/NOP detectors.

14 References

[Damario 2016] D. Damario, "The Fuelling Machine", chapter in *The Essential CANDU*, edited by W. Garland, 2016.

[Hébert 2012] A. Débert, D. Sekki and R. Chambon, "A User Guide for DONJON Version4", Technical Report IGE-300, École Polytechnique de Montréal, 2012.

[Irish 2002] J.D. Irish and S.R. Douglas, "Validation of WIMS-IST", in Proceedings of the 23rd Annual Conference of the Canadian Nuclear Society, Toronto, Ontario, Canada, 2002 June.

[Marleau 1999] G. Marleau, "DRAGON, Theory Manual", Technical Report IGE-236, Institut de Génie Nucléaire, École Polytechnique de Montréal, 1999 February.

[Rouben 1995] B. Rouben, "Description of the Lattice Code POWDERPUFS-V", AECL-11357, 1995 October.

[Rouben 2002] B. Rouben, "RFSP-IST, The Industry Standard Tool Computer Program for CANDU Reactor Core Design and Analysis", in Proceedings of PBNC-2002 (13th Pacific Basin Nuclear Conference), Shenzhen, China, 2002 October.

[Rouben 2007] B. Rouben, "Review of the CANDU Time-Average Model and Calculations", in Proceedings of the 28th Annual Conference of the Canadian Nuclear Society, Saint John, New Brunswick, Canada, 2007 June 3-6.

[Rozon and Shen 2001] D. Rozon and W. Shen, "A Parametric Study of the DUPIC Fuel Cycle to Reflect Pressurized Water Reactor Fuel Management Strategy", Nucl. Sci. Eng. 138, 1-25 (2001)

15 Acknowledgements

The following reviewers are gratefully acknowledged for their hard work and excellent comments during the development of this Chapter. Their feedback has much improved it. Of course the responsibility for any errors or omissions lies entirely with the author.

Richard Chambon
Ovidiu Nainer

Thanks are also extended to Bill Garland for expertly editing and assembling the final copy.

Author Biographies

Table of Contents

1 Dr. Robin A. Chaplin (chapters 1, 2, 8, 9, appendix Basic Electrical Theory)

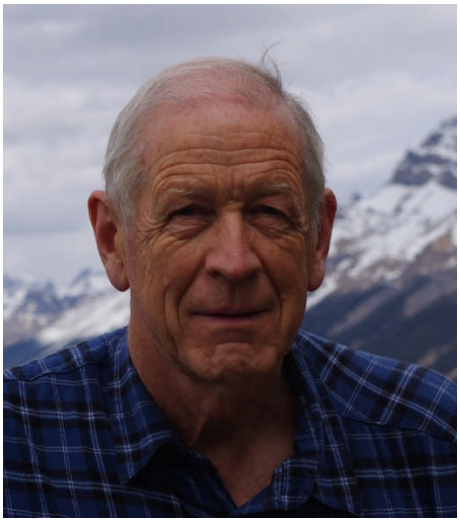

Robin Chaplin obtained a B.Sc. and M.Sc. in Mechanical Engineering from University of Cape Town in 1965 and 1968 respectively. Between these two periods of study he spent two years gaining experience in the operation and maintenance of coal fired power plants in South Africa. He subsequently spent a further year gaining experience on research and prototype nuclear reactors in South Africa and the United Kingdom and obtained an M.Sc. in Nuclear Engineering from Imperial College of London University in 1971. On returning to South Africa and taking up a position in the head office of Eskom he spent some twelve years initially in project management and then as Head of Steam Turbine Specialists. During this period he was involved with the construction of the 3 x 80 MW Ruacana Hydro Power Station in Namibia and the 2 x 900 MW Koeberg Nuclear Power Station in South Africa being responsible for the underground mechanical equipment and civil structures and for the mechanical balance-of-plant equipment at the respective plants. Continuing his interests in power plant modeling and simulation he obtained a Ph.D. in Mechanical Engineering from Queen's University in Canada in 1986 and was subsequently appointed as Chair in Power Plant Engineering at the University of New Brunswick. Here he has taught thermodynamics and fluid mechanics and specialized graduate level courses in nuclear and power plant engineering in the Departments of Chemical Engineering and Mechanical Engineering. An important function was involvement in the plant operator and shift supervisor training programs at Point Lepreau Nuclear Generating Station. This included the development of material and the teaching of courses in both nuclear and non-nuclear aspects of the program. He has also been involved with the UNESCO sponsored Encyclopedia of Life Support Systems (EOLSS) as Honorary Theme Editor and primary author of the theme on Thermal Power Plants and has also assisted with the theme on Nuclear Energy and Reactors. Altogether he has contributed some three dozen chapters to this major source of international knowledge. As an adjunct professor at Waterloo University he has established and taught a graduate course in power plant thermodynamics to engineers in the nuclear industry as part of the UNENE masters program in nuclear engineering. He has served as Acting Chair and Chair in the Department of Chemical Engineering at University of New Brunswick and has been a consultant for Canadian Power Utility Services.

2 Dr. Willy Cook (chapters 14, 15)

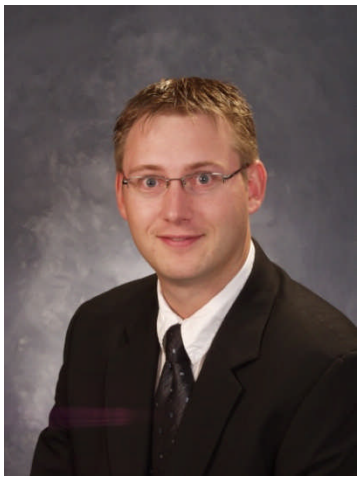

Willy Cook is an Associate Professor in the Department of Chemical Engineering at the University of New Brunswick (UNB). He is a professional engineer with consulting and research interests in power plant chemistry and corrosion control and teaches courses related to these topics and global energy issues. Willy earned his BSc and MSc degrees in Chemical Engineering at UNB in 1997 and 1999 where he completed option programs in Power Plant and Nuclear Engineering. He worked as the research engineer and laboratory manager for the Chair in Nuclear Engineering at UNB until 2004 where he supervised the academic research and industrial contracts undertaken by the Chair. He completed his PhD in 2005 (UNB) and has since been actively involved in the Generation IV International Forum (GIF) evaluating materials and chemistry control regimes for a supercritical water-cooled reactor. The restart of the CANDU-6 plant at Point Lepreau following its refurbishment outage in 2012 coincided with a sabbatical leave from UNB and Willy spent nine months during this time as a technical consultant for the chemistry department at the station during the restart activities. In the Fall of 2014, he was appointed as the Scientific Director of the Centre for Nuclear Energy Research, an Institute on UNB's campus that undertakes research and provides consulting to the power generating industry and develops commercial products for corrosion measurement and control.

3 Ms. Diane Damario (chapter 20)

Diane is a registered professional engineer in the province of Ontario. She earned a B.A.Sc. in Mechanical Engineering at the University of Toronto in 1990. After completing her studies, she joined AECL at Sheridan Park. She has been involved in fuel handling at Sheridan Park ever since, transitioning to Candu Energy Inc., a member of the SNC-Lavalin Group, when the commercial division of AECL was privatized in 2011. Diane's fuel handling experience has mainly been based on the CANDU 6 station design, particularly for the Qinshan and Wolsong 2, 3 and 4 stations. Over the years, she has delivered training on fuel handling at Sheridan Park and Chalk River.

4 Mr. Milan Gacesa (chapters 17, 18, 19)

Independent consultant - nuclear fuel and project management. Milan earned his BASc and MAsc in Mechanical Engineering at the University of Windsor and is a registered professional engineer in the province of Ontario. He worked at Westinghouse Canada Ltd. for 7 years, initially performing tests and developing design/analysis tools used for CHF and thermal-hydraulic stability analysis, and later leading the nuclear fuel design section where the design of C6 fuel was produced. At AECL he continued to work on C6 fuel design, testing, and verification until its successful launch in the first generation C6 reactors. As manager of the fuel branch Milan broadened the branch's participation in all aspects of the CANDU fuel industry, in particular fuel design, testing, development of analytical tools, assessment of plant performance feedback (especially as related to defective fuel), and assistance to operators. As Engineering and Project Manager of CIRENE Technical Assessment (Italian BWR similar to Gentilly 1) he led a group of selected AECL specialists to a successful completion of an independent evaluation of CIRENE design and, in particular, safety. Following CIRENE, Milan completed a number of other projects, including an extensive multi-disciplinary study of alternative fuel cycles in CANDU for a Japanese client, before his overseas assignment as Manager of Engineering at KAERI (Republic of Korea) where he led an expat group of AECL senior technical specialists and Korean engineers in completing the design packages for a number of C6 NSSS systems. For the past 14 years Milan has provided consulting services to a number of clients, including AECL where he worked for a number of years as the senior fuel specialist on the ACR project. In addition to producing the fuel bundle configuration for ACR, the fuel team spearheaded a number of methodology changes, including the adoption of fuel acceptance criteria, development of design verification strategy and plan, and standardization of verification assessments, which can be used on any future CANDU project.

5 Dr. William J. Garland (editor in chief, prologue, chapter 7)

Bill Garland is Professor Emeritus of Nuclear Engineering in the Department of Engineering Physics at McMaster University (Ontario, Canada). He specialized in reactor physics and thermalhydraulics. Since 2000, he has been Academic Director of CANTEACH, the public on-line library for technical information on CANDU reactors. On partial and full secondment from McMaster from 2004 to 2008 he served in various capacities within the University Network of Excellence in Nuclear Engineering (UNENE), namely Secretary / Treasurer, Program Director, and Executive Director. Since retiring from McMaster he served as UNENE President until September 2009. From October 2009 to September 2011 he was Academic Consultant to UNENE with Knowledge Management as the primary duty.

He served as Department Chair in the Department of Engineering Physics at McMaster from 1988 to 1994 and was Director of MNR (McMaster Nuclear Reactor) for 1994 to 1995 leading up to the decision to revitalize reactor operations. Subsequent to that he is took a lead role in MNR safety analysis and operational support analysis.

From 1975 to 1983, he worked in the Canadian Nuclear Industry specializing in CANDU heat transport system analysis and design (Darlington and CANDU 6). The major effort from early 1980 to mid 1983 was in heat transport system stability investigations leading up to the now standard header to header interconnection. This included pre- and post-test analysis, coordination of AECL's process team, test planning, and liaison.

While on research leave at Harwell Nuclear Labs in England, Bill conducted knowledge engineering for heat exchanger selection and developed a heat exchanger selection computer code which became a commercial product distributed through the international company HTFS. In addition, computerized water property functions developed at McMaster are in use in about 13 countries by over 120 users in 51 institutions and major engineering firms worldwide.

Bill received the CNS Education and Communication Award in 2001 and became a CNS fellow in 2006.

William J. Garland, P. Eng., FCNS (B. Eng. Phy. 1970, M. Eng. Phy., 1971, Ph.D. Chem. Eng. 1975, McMaster University, Canada)

6 Dr. George Alan Hepburn (chapter 10)

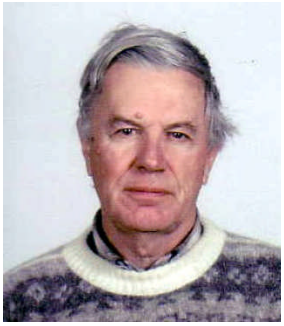

Alan Hepburn earned his B.Sc. in Electrical Engineering at the University of Glasgow in 1966. After a further four years study in the field of automatic control, he obtained a Ph.D. in Electrical Engineering in 1970. During his postgraduate work, he had the use of an early prototype computer which had been developed to demonstrate that semiconductors were a practical replacement for vacuum tubes in digital computers.

Despite the assurance of the Canadian embassy that there were "no jobs for Ph.D.s in Canada", Alan emigrated to Canada in the fall of 1970, where he obtained a position in a small company applying minicomputers to data acquisition.

Alan joined the Plant Computer Systems Branch at AECL in Mississauga in 1972. He was the first employee of the branch to have had experience with computers prior to joining the company. His first task at AECL was to write the Reactor Regulating System program for Bruce A. In 1974, he was posted to Bruce "A" NGS, where he was AECL's representative on the Digital Control Computer (DCC) commissioning team.

Following his return to Sheridan Park in 1976, Alan continued his work in real time computer systems development for Bruce B, the early CANDU 6's, and Darlington, including involvement in the development of the world's first fully computerized shutdown systems for Darlington GS. He became a section head, followed by branch manager of the Plant Computer Systems Branch, then Department Manager of the Instrument and control systems Department at Sheridan Park.

In 1987, Alan left the nuclear industry and moved to the aerospace, where he managed the Engineering Sciences group at Garrett Canada, primarily responsible for the development of software for the environmental control systems on many of the western world's larger civil and military aircraft. After four years at Garrett, he transferred to TRW who were subcontracted to the Systems Engineering group of CDC in Nepean to develop a major communications system for the Canadian Army. Just two years later, the project was transferred to Calgary, and after a further two years, TRW's contract was cancelled.

Rather than move to Washington with TRW, Alan decided to see if there was still a position for him back at AECL, and as a result, found himself working as a contractor on the development of a modern distributed control system for the CANDU 3, and subsequently CANDU 9 reactors in Saskatoon. This was followed by four years at Bruce A as AECL's on-site representative on replacement project.

In 2000, Alan moved to Chalk River to head the Control and Operations Technology Branch, whose responsibilities included the early development work on a distributed control system for the Advanced CANDU Reactor. He retired from this position in 2006.

Alan's only teaching exposure has been as a flight instructor, in which capacity he is still active.

7 Dr. Jin Jiang (chapter 11)

Professor, Western University

An NSERC/UNENE Senior Industrial Research Chair Professor, in the Department of Electrical and Computer Engineering, Western University in Canada. His research interests are in the areas of fault-tolerant control of safety-critical systems, instrumentation and control of nuclear power plants, and control of electrical power plants and power systems.

He is a fellow of Canadian Academy of Engineering, a fellow of IET (formally IEE), and a fellow of ISA. He is also a member of International Electrotechnical Commission (IEC) 45A subcommittee to develop industry standards on instrumentation and control for nuclear facilities. He also works closely with International Atomic Energy Agency (IAEA) on modern control and instrumentation for nuclear power plants.

8 Dr. Derek Lister (chapters 14, 15)

Derek Lister is Professor Emeritus in the Department of Chemical Engineering at the University of New Brunswick in Fredericton, where he continues to hold the Research Chair in Nuclear Engineering. He has a BSc and an MSc in chemical engineering from the University of Manchester and a PhD in physical chemistry from the University of Leicester. He entered the nuclear industry after graduation as an R&D Engineer with the English Electric Co. in the UK, where he worked on Magnox fuel systems and was on the commissioning team for the Hinkley Point A reactor. He joined AECL at Chalk River to develop CANDU fuel but soon moved to the Chemical Engineering Branch to work on coolant chemistry and corrosion, specialising first of all in activity transport. His research broadened over the years to cover many aspects of primary and secondary coolant chemistry and corrosion and in 1992, when Manager of the System Chemistry and Corrosion Branch, he accepted the appointment of Industrial Research Chair in Nuclear Engineering at UNB. His research still involves coolant chemistry and corrosion and besides his Chair research he manages a number of research contracts dealing specifically with power-plant corrosion. He serves on a number of national and international advisory committees. He is a Fellow of the Chemical Institute of Canada and as a Member of the Institution of Chemical Engineers in the UK he is a Chartered Engineer. He is a member of the Nuclear Institute and of the Canadian Nuclear Society, which presented him with an Outstanding Contribution Award in 2011.

9 Dr. Guy Marleau (chapter 3)

Professor, Department of Engineering Physics, École Polytechnique de Montréal.

Guy earned his BSc (1977) in physics from the University of Ottawa and his MSc (1979) and PhD (1983) in physics from McGill University. In 1983, he joined École Polytechnique de Montréal as a research scientist where he became a professor of nuclear engineering and engineering physics in 2006. From 2007 to 2013 he served as the director on the Institut de Génie Nucléaire at École Polytechnique de Montréal. For the last 30 years, he has been involved in the development of reactor physics simulation codes being one of the co-developers of the well known lattice code DRAGON that is used to solve the neutron transport equation for general 2D and 3D geometry. Over the years, he taught several courses in nuclear engineering including reactor statics, reactor simulation, radiation and radioprotection as well as nuclear technology. He received in 2010 the WB Lewis medal from the Canadian Nuclear Association and the Canadian Nuclear Society for his contribution to the development of advanced computational methods in reactor physics.

courriel/email: guy.marleau@polymtl.ca, Tel: (514)-340-4711 x 4204

addresse: Institut de genie nucleaire, Ecole Polytechnique de Montreal, C.P. 6079, succ. Centre-ville, Montreal, QC, H3C 3A7, Canada

10 Dr. Eleador Nichita (chapters 4,5)

Dr. Eleodor Nichita, Associate Professor, Faculty of Energy Systems and Nuclear Science, University of Ontario Institute of Technology.

Eleodor holds a B.Sc. in Engineering Physics from the University of Bucharest, a M.Sc. in Health Physics from Georgia Institute of Technology, a M.Sc. in Medical Physics from McMaster University, and a Ph.D. in Nuclear Engineering from Georgia Institute of Technology. He is a Licensed Professional Engineer in the Province of Ontario. He has extensive nuclear-industry experience, beginning at the Institute for Nuclear Research in Pitesti, Romania, and continuing at Atomic Energy of Canada Ltd., where he worked on analysis and code development for the neutronic core-simulator, RFSP. In 2004 Eleodor joined the University of Ontario Institute of Technology where he is currently an Associate Professor and Director of the undergraduate Nuclear Engineering Program. He teaches courses in Reactor Physics, Transport Theory and Medical Imaging, and performs research in Nuclear Reactor Modelling and Simulation, Computational Particle Transport and Computational Medical Physics. Eleodor held the presidency of the Canadian Nuclear Society between 2009 and 2010.

11 Dr. Nik Popov (chapters 6, 7, 16)

Dr. Popov has over 35 years of experience in the nuclear industry in Canada and internationally in various disciplines including thermal-hydraulics, safety analysis, licensing, computer codes development and validation, and severe accident analysis. He worked at the University Cyril & Methodius at Skopje, Macedonia as lecturer and assistant professor (1978-88). Then he worked 23 years at the Atomic Energy of Canada (1988-2011), the last 3 years as the Director for Safety and Licensing. He also worked at SNC-Lavalin-Nuclear as Director of Safety and Licensing (2011-2014). He is the owner of DENIPO Consulting Ltd., which provides nuclear engineering consulting and educational services.

Dr. Popov was involved and managed various projects at AECL, such as the licensing of advanced CANDU reactor in Canada, USA, UK, and other countries. He was involved in international projects at AECL, such as serving as the Canadian representative in the G-8 safety review of the Kursk 1 RBMK nuclear power station in Russia (2001-2002); and leading the AECL team that interfaced with the European Commission Panel safety review to obtain approval to proceed with the Cernavoda 3-4 CANDU project in Romania (2009-2010). At COG he was the lead of the Severe Accident Working Group of the joint project JP-4426 working on the update of the Severe Accident Management Guidance documentation (2012-2014).

Dr. Popov is an Adjunct Professor at McMaster University, Engineering Physics (since 2000), where he teaches graduate courses at McMaster and the UNENE program (reactor thermal-hydraulics design and reactor thermal-hydraulics analysis). He is also an Adjunct Professor at the University Cyril and Methodius, Electrical Engineering, in Macedonia, where he teaches graduate courses (reactor engineering, nuclear energy industrial applications, and environmental aspects of power engineering). Dr. Popov is a lecturer of an international team organized by the University of Pisa, Italy (since 2006), delivering 3D-SUNCOP courses at annual international seminars. He teaches best-estimate and uncertainty assessment, safety culture in safety analysis, and development and validation of computer programs.

Dr. Popov participated in the preparation of over 200 publications and industrial reports.

Nikola K. Popov (B. Mech. Eng., 1976, M. Sci. Nucl. Eng., 1983, Ph.D. Mech. Eng. 1988, University of Zagreb, Croatia).

12 Dr. Benjamin Rouben (chapters 4, 5, 21)

Ben Rouben holds an Hons. B.Sc. from McGill University in Physics and Mathematics, and a Ph.D. in Nuclear Physics from the Massachusetts Institute of Technology. After pursuing research at the Université de Montréal for several years, he joined Atomic Energy of Canada Limited (AECL) in 1975, where he worked in many areas of reactor physics. From 1993 to 2006, Ben served as Manager of the Reactor Core Physics Branch at AECL.

Ben was President of the Canadian Nuclear Society (CNS) in 1997-98, and is currently its Executive Director. He was elected CNS Fellow in 1999. He is also a member of the American Nuclear Society (ANS), where he is active on the Reactor Physics Standards Committee and on the ANS International Committee.

Ben retired from AECL in 2007 February. He is currently a consultant, and an Adjunct Professor at McMaster University and at the University of Ontario Institute of Technology. He teaches courses on Reactor Physics, Reactor Dynamics, Nuclear Fuel Management, Power Plant Operation, and Nuclear Concepts for Scientists and Engineers. He teaches also in the M. Eng. Program offered by UNENE, the University Network of Excellence in Nuclear Engineering, where he also serves as Secretary/Treasurer.

roubenb@alum.mit.edu

13 Dr. Victor G. Snell (chapter 13, 16)

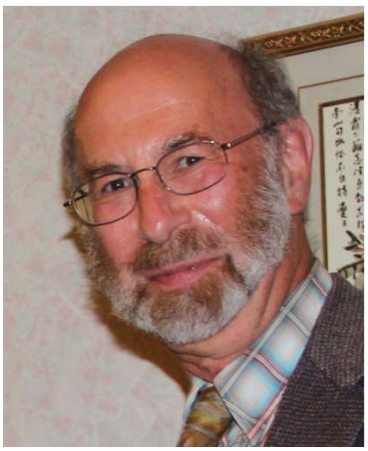

Dr. Snell is the owner of VGSSolutions, a nuclear safety consulting and education firm. He has 38 years of nuclear experience, largely in the area of safety and licensing. As a member of the Senior Global Assessment Team in 2010-11, he helped review the Global Assessment of the NRU reactor. As Enhanced CANDU 6 Licensing Manager for AECL in 2008-9, he was responsible for obtaining a positive conclusion by the Canadian Nuclear Safety Commission for the Phase 1 pre-project design review. For ten years, as Director of Safety and Licensing at AECL, he had overall responsibility for interaction with regulatory agencies on AECL's product line of reactors. This included obtaining a favourable AECB report on licensability of CANDU 9; initial licensing of Wolsong 2 with KINS in Korea; negotiating licensing requirements for an unattended urban heating reactor (SES-l 0); and managing licensing for CANDU 3U with the USNRC, to the point of submittal of an application for Standard Design Certification. Other major projects included responsibility for pre-project licensing, safety design and Probabilistic Safety Analysis of AECL' s Advanced CANDU Reactor (ACR) design; responsibility (for two years) for the safety analysis and licensing of the MMIR Project; participation in an IAEA-sponsored design review of a district heating nuclear plant in Gorky (the first mission of its kind in the Soviet Union); and team leader of a design review of CANDU & Chernobyl. In the nuclear education area, he is currently Programme Director, University Network of Excellence in Nuclear Engineering (UNENE), responsible for course development and deployment and administration of the nuclear M.Eng. programme. He has over fifty publications on Reactor Safety and Licensing.

Contact: Email: vgssolutions@rogers.com, Phone: (905) 824-6236

14 Mr. Mukesh Tayal (chapters 17, 18, 19)

Mukesh is an independent consultant in nuclear fuel. He has 37 years of nuclear experience in areas of nuclear fuel, safety analysis, stress analysis, and heat transfer. He has developed a criterion-based approach to qualify fuel designs which significantly increases the robustness of design verification while reducing its cost and schedule. He has performed, and provided technical leadership to, design, testing and analytical verification of fuels such as 37-element fuel for C6, Bruce, and Darlington stations; 43-element fuel for ACR (Advanced CANDU Reactor); and 61-element fuel for HAC (Highly Advanced Core) CANDU reactor. He has played key roles in developing several computer codes used by Atomic Energy of Canada Limited (AECL) for design assessments of nuclear fuels. These include: ELESTRES code for thermo-microstructural-mechanical performance of fuel under normal operating conditions; ELOCA-A code for accident analysis of fuel; FEAT code for non-linear thermal analysis; FEAST code for non-linear stress analysis; BOW code for non-linear lateral deflection; LONGER code for ridging and collapse; BEAM code for rigidity and vibration; FEED code for diffusion; and GASOUT code for transient release of fission gas. He has also developed science and models for several phenomena such as environmentally-assisted cracking (stress corrosion cracking), bowing, longitudinal ridging, and endplate fatigue. Mukesh has also worked on advanced fuel cycles such as thorium fuel and enriched high-burnup fuel. Mukesh received the CNA/CNS award for Innovative Achievement in 2007 and has authored/co-authored well over 200 technical documents in the area of nuclear fuel.

Mukesh Tayal, P. Eng., (B. Tech., Mech. Engg., 1970; M. Sc., Mech. Engg., 1973, Univ. of Sask., Canada).

15 Dr. Edward J. Waller (chapter 12)

Faculty of Energy Systems and Nuclear Science, University of Ontario Institute of Technology

Ed earned his BSc in Physics and MScE in Chemical Engineering at the University of New Brunswick (UNB) and his PhD in Nuclear Engineering at Rensselaer Polytechnic Institute, New York (RPI). He worked for over 15 years in industry for Science Applications International Corporation, primarily in threat assessment, health physics and applications of radiation. In 2003 he joined the University of Ontario Institute of Technology. He is currently an NSERC Industrial Research Chair in Health Physics and Environmental Safety. Ed is a Professional Engineer (PEng), Certified Associate Industrial Hygienist (CAIH) and Certified Health Physicist (CHP). He teaches radiation protection, health physics, environmental effects of radiation, Monte Carlo methods and nuclear forensics at UOIT, and performs research in areas of emergency response, radiation dosimetry, applied health physics, radiation safety, and threat assessment.

Abbreviations

ACNS	Advisory Committee on Nuclear Safety (Canada, historical)
ACR	Advanced CANDU Reactor
ACRS	Advisory Committee on Reactor Safeguards (USA)
AEC	Atomic Energy Commission (USA)
AECA	Atomic Energy Control Act (Canada)
AECB	Atomic Energy Control Board (Canada)
AECL	Atomic Energy of Canada Limited
AESOP	Atomic Energy Simulation of Optimization (computer code)
ALARA	As Low as Reasonably Achievable
ALARP	As Low as Reasonably Practical (UK)
AOO	Anticipated Operational Occurrence
ASDV	Atmospheric Steam Discharge Valve
ASLB	Atomic Safety and Licensing Board (USA)
ASSERT	Advanced Solution of Subchannel Equations in Reactor Thermalhydraulics (computer code)
ASTM	American Society for and Testing Materials
BDBA	Beyond Design Basis Accident
BDBA	Beyond Design Basis Accident
BEAU	Best Estimate with Analysis of Uncertainties
BECS	Boiler Emergency Cooling System
BLC	Boiler Level Control
BLW	Boiling Light Water
BPC	Boiler Pressure Controller
BSL	Basic Safety Limit (UK)
BSO	Basic Safety Objective (UK)
BWR	Boiling Water Reactor
C/S	Containment and Surveillance
CANDU	CANada Deuterium Uranium – the generic name for Canadian heavy water power reactors
CATHENA	Canadian algorithm for thermal hydraulic network analysis (computer code)
CCP	Critical Channel Power
CEAA	Canadian Environmental Assessment Act
CFR	Code of Federal Regulations (USA)
CHF	Critical Heat Flux
CNSC	Canadian Nuclear Safety Commission
CPR	Critical Power Ratio
CRL	Chalk River Laboratories
CRT	Cathode Ray Tube
CSA	Canadian Standards Association
CSDV	Condenser Steam Discharge Valve
CSNI	Canadian Standards for the Nuclear Industry; also Committee on the Safety of Nuclear Installations
DBA	Design Basis Accident
DBE	Design Base Earthquake
DCC	Digital Control Computer

DF-ET	Drift Flux-Equal Temperature
DF-UT	Drift Flux-Unequal Temperature
DIV	Design Information Verification
DNB	Departure from Nucleate Boiling
DSA	Deterministic Safety Analysis
EA	Environment Agency (UK)
ECC	Emergency Core Cooling
ECI	Emergency Coolant Injection (a subsystem of ECC)
EFPH	Effective Full Power Hours
EIS	Environmental Impact Statement
ENSREG	European Nuclear Safety Regulators Group
EPR	European Pressurized Reactor
EU	European Union
EVET	Equal Velocity Equal Temperature
EVUT	Equal Velocity-Unequal Temperature
EWS	Emergency Water Supply
FBR	Feed, Bleed and Relief; also Fast Breeder Reactor
FMEA	Failure Modes and Effects Analysis
FP	Full Power
GAI	Generic Action Item
GAR	Global Assessment Report
GCR	Gar Cooled Reactor
GDA	Generic Design Assessment (UK)
GDC	General Design Criteria (US)
HEM	Homogeneous Equilibrium Model
HPECC	High-Pressure ECC
HSE	Health and Safety Executive (UK)
HTS	Heat-Transport System (see also RCS)
HWP	Heavy Water Plant
HYDNA	Hydraulic Network Analysis (extinct computer code)
I&C	Instrumentation and Control
IAEA	International Atomic Energy Agency
IBIF	Intermittent Buoyancy Induced Flow
ICRP	International Commission on Radiological Protection
IIP	Integrated Implementation Plan
INES	International Nuclear Event Scale
INPO	Institute of Nuclear Power Operations
INSAG	International Nuclear Safety Advisory Group (IAEA)
IRRS	Integrated Regulatory Review Service (IAEA)
LBLOCA	Large Break Loss of Coolant Accident
LGR	Liquid Graphite Reactor
LLOCA	Large Loss-of-Coolant Accident
LMFBR	Liquid Metal Fast Breeder Reactor
LNT	Linear No Threshold (dose response hypothesis)
LOC	Loss of Coolant
LOC/LOECC	Loss of Coolant with Coincident Loss of Emergency Core Cooling
LOCA	Loss of Coolant Accident

LOP	Loss of Pumping
LOR	Loss of Regulation
LPECC	Low-Pressure ECC
LWR	Light-Water Reactor
MBA	Material Balance Area
MCCR	Ministry of Consumer and Commercial Relations
MCR	Main Control Room
MCS	Maintenance Cooling System
MDEP	Multinational Design Evaluation Programme
milli-k	Unit of reactivity for reactor physics
MPECC	Medium-Pressure ECC
MPMO	Major Projects Management Office
MSSV	Main Steam Safety Valve
MUF	Material Unaccounted For
MWe	Megawatt electric
NDPB	Non Departmental Public Body (UK)
NISA	Nuclear and Industrial Safety Agency (Japan)
NPD	Nuclear Power Demonstration
NPP	Nuclear Power Plant
NPSH	Net Positive Suction Head
NRA	Nuclear Regulation Authority (Japan)
NRU	National Research Universal
NRU	National Research Universal (reactor)
NRX	National Research Experimental Research Reactor
NUCIRC	Nuclear Circuits (computer code)
OECD	Organization for Economic Co-operation & Development
OH	Ontario Hydro (now OPG)
ONR	Office for Nuclear Regulation (UK)
OPG	Ontario Power Generation
PNGSA	Pickering Nuclear Generating Station A
PHTS	Primary Heat Transport System
PHW	Pressurized Heavy Water
PHWR	Pressurized Heavy Water Reactor (CANDU)
PRESCON2	Pressure Containment (computer code)
PRV	Pressure-Relief Valve
PSA	Probabilistic Safety Analysis
PSR	Periodic Safety Review
PWR	Pressurized-Water Reactor
QA	Quality Assurance
R&D	Research and Development
R&M	Reliability and Maintainability
RAMA	Reactor Analysis Implicit Algorithm
RB	Reactor Building
RBMK	Реактор Большой Мощности Канальный (High Power Channel-Type Reactor)
RCS	Reactor Coolant System (see also HTS)

rem	röentgen equivalent man (radiation dose)
RIDM	Risk-Informed Decision Making
RIH	Reactor Inlet Header
ROH	Reactor Outlet Header
ROP	Regional Overpower (Protection System)
RSAC	Reactor Safety Advisory Committee (Canada, historical)
RTD	Resistance Temperature Detectors
S/C	Suppression Chamber
SAM	Severe Accident Management
SAPs	Safety Assessment Principles (UK)
SCA	Secondary Control Area
SCDF	Severe Core-damage Frequency
SDM	Safety Design Matrix
SDS	Shutdown System
SER	State Evaluation Report
SFAIRP	So Far As Is Reasonably Practicable (UK)
SG	Steam Generator
SGHWR	Steam Generating Heavy Water Reactor (United Kingdom)
SIR	Safeguards Implementation Report
SIS	Systems Important to Safety
SOE	Safe Operating Envelope
SOPHT	Simulation of Primary Heat Transport (computer code)
SOR	Shut-Off Rod
SRP	Staff Review Procedure (Canada)
SRP	Standard Review Plan (US)
SRV	Safety Relief Valve
SSC	Systems, Structures and Components
STUK	Säteilyturvakeskus (Radiation and Nuclear Safety Authority, Finland)
Sv	Sievert, a unit of radiation dose
TAG	Technical Assessment Guide (UK)
TUEC	Total Unit Energy Cost
TMI	Three Mile Island
TOFFEA	Two Fluid Flow Equation Analysis (computer code)
TOR	Tolerability of Risk (UK)
TSO	Technical Support Organization
USNRC	United States Nuclear Regulatory Commission
UVUEUP	Unequal Velocity, Unequal Energy, Unequal Pressure (thermalhydraulic model)
UVUT	Unequal Velocity Unequal Temperature (thermalhydraulic model)
VB	Vacuum Building
VC	Vacuum Chamber
WENRA	Western European Nuclear Regulators' Association
WRE	Whiteshell Research Establishment
ZEEP	Zero Energy Experimental Pile